

As peak D only appeared in crystals C1 and C9 and as these crystals were of type I, level β is suggested to be that level which causes the secondary absorption edge (Clark, Ditchburn and Dyer 1956). Tentatively it is suggested that this level is identical with the deep-lying donor level due to substitutional nitrogen suggested by Kaiser and Bond (1959) and discussed by Elliott (1960). In crystal CIIa the density of states in this level is assumed to be much smaller, and therefore no peak has been observed. However, the slight shift of the peak C towards higher energies with this crystal may well have been caused by a small, but unobservable peak in position D. Peak E was rather weak with crystal C9, but most predominant with crystal CIIa. It did not occur with crystal C1. It is suggested that this is due to a high density of states in level β in this crystal. This high density gives rise to such large optical absorption that the photoconductive current is reduced by the large annihilation rate of the free charge carriers in the thin surface layer of the crystal penetrated by the light.

4.3. Optical Absorption

The density of states in a level required to produce a detectable optical absorption is several orders higher than that needed for an observable photoconductive response. Therefore it appears most appropriate to consider the level structure in relation to a typical absorption spectrum for crystals of type I, which are supposed to have the largest number of impurities (Kaiser and Bond 1959). Such a spectrum has been reported by Clark, Ditchburn and Dyer (1956). The absorption coefficient shows a rise at about 1.5 eV, a very small rise at about 2.1 eV, a larger one at about 2.6 eV, a band centring at about 3.3 eV and a large increase beginning at 3.74 eV which is known as the secondary absorption edge.

The absorption was not measured in the region below 1.2 eV. On the other hand, it is very improbable that an absorption corresponding to the peak A could have been found, as this peak only appeared after prolonged irradiation with energetic ultra-violet light or after bombardment with beta particles. The rise at 1.5 eV may be ascribed to transitions between the valence band and level β . The rise at 2.1 eV is so small that no firm conclusion can be drawn from it. As the effects of green light became stronger when the energy of the light was increased beyond 2.1 eV it is tentatively suggested that the rise near 2.5 eV nevertheless arises from transitions between level γ and the conduction band. A further support for this model is provided by the fact that the absorptions at 2.6 eV and 3.3 eV are due to the same centres in the crystal, whereas the secondary absorption edge is due to another kind of centre. The absorption near 1.5 eV was too weak to be definitely assigned to one of the centres.

§ 5. CONCLUSION

From beta-particle counting experiments under various conditions, total charge measurements and photoconductivity measurements, an electronic energy level scheme consisting of three levels in the forbidden gap of insulating diamonds has been found. The measurements did not provide any data on the density of states in the levels. The occupation of the states in a level could be deduced from the experiments, but only in so far as they were fully, partly, or not occupied. Differences in the experimental results obtained from different diamonds could be attributed to different degrees of occupation of the same levels and to different absolute numbers of states in the levels.

ACKNOWLEDGMENTS

We wish to thank Messrs. Industrial Distributors (1946) Limited for financing this research and for providing a maintenance grant for one of us (R. R. U.), and the Council of the University of the Witwatersrand for making certain grants available. Thanks are also due to Dr. J. F. H. Custers, Director of Research, Diamond Research Laboratory, Johannesburg, for supplying the diamonds and for helpful discussions.

REFERENCES

- ALLEN, J. W., 1960, *Nature, Lond.*, **187**, 403.
BULL, C., and GARLICK, G. F. J., 1950, *Proc. Phys. Soc. A*, **63**, 1283.
CHAMPION, F. C., 1956, *Proc. Roy. Soc. A*, **234**, 541.
CHAMPION, F. C., and DALE, B., 1956, *Proc. Roy. Soc. A*, **234**, 419.
CLARK, C. D., DITCHBURN, R. W., and DYER, H. B., 1956, *Proc. Roy. Soc. A*, **234**, 363.
COTTINI, C., GATTI, E., GIANELLI, G., and ROZZI, G., 1956, *Nuovo Cim.*, **3**, 473.
CUSTERS, J. F. H., 1952, *Physica*, **18**, 489.
ELLIOTT, R. J., 1960, *Proc. Phys. Soc.*, **76**, 787.
FREEMAN, G. P., 1952, *Thesis*, Utrecht.
GUDDEN, B., and POHL, R. W., 1923, *Z. Phys.*, **17**, 331.
HECHT, K., 1932, *Z. Phys.*, **77**, 235.
KAISER, W., and BOND, W. L., 1959, *Phys. Rev.*, **115**, 857.
KLICK, C. C., and MAURER, R. J., 1951, *Phys. Rev.*, **81**, 124.
KOJIMA, S., and KONO, S., 1952, *J. Phys. Soc. Japan*, **7**, 84.
LENZ, H., 1925, *Ann. Phys., Lpz.*, **77**, 449.
MCKAY, G. K., 1950, *Phys. Rev.*, **77**, 816.
MENDELSSOHN, T., and DEMBER, H., 1942, *Rev. Fac. Sci. Univ. Istanbul A*, **6**, 18.
NEWTON, R. R., 1949, *Phys. Rev.*, **75**, 234.
REDFIELD, A. G., 1954, *Phys. Rev.*, **94**, 526.
STÖCKMANN, F., 1956, *Photoconductivity Conference* (edited by BRECKENRIDGE, R. G., RUSSELL, B. R., and HAHN, E. E.) (New York: John Wiley), p. 269.
—— 1957, *Z. Phys.*, **147**, 544.
TAYLOR, K. W., 1956, *Thesis*, University of London.
TROTT, N. G., 1953, *Proc. Roy. Soc. A*, **220**, 498.
WARTENBERG, H., 1912, *Phys. Z.*, **13**, 1123; see also MOSS, T. S., 1952, *Photoconductivity in the Elements* (London: Butterworths), p. 100.
WILLARDSON, R. K., and DANIELSON, G. C., 1950, *Phys. Rev.*, **77**, 300.
—— 1952, *J. Opt. Soc. Amer.*, **42**, 42.

Quantum Theory of Magnetoresistance—I: Low Fields

By R. B. STINCHCOMBE†

Department of Mathematical Physics, University of Birmingham

Communicated by R. E. Peierls; MS. received 9th February 1961

Abstract. The conventional treatment of magnetoresistance is based upon the Boltzmann equation for a distribution function $f(\mathbf{k})$, and an equation which gives the average current in terms of $f(\mathbf{k})$. With the usual definition of $f(\mathbf{k})$ neither equation is exact: the derivation of the Boltzmann equation requires $\omega\tau < 1$ where ω is the cyclotron frequency and τ is the relaxation time. In this paper a representation is proposed which exploits the properties of homogeneous systems in a uniform magnetic field. We redefine $f(\mathbf{k})$ as the diagonal element of the density matrix in the new representation. Then the usual equation for obtaining the current becomes exact. Proceeding from the equation of motion of the density matrix we then give a weak-coupling derivation of the Boltzmann equation in the manner used by Kohn and Luttinger in 1957 for field-free systems. The derivation is restricted to the case of non-interacting carriers elastically scattered by impurities or lattice vibrations, and moving in a lattice which in the absence of the magnetic field gives rise to non-overlapping bands. The conductivity yielded by this method is found to be accurate as long as $\hbar\omega$, \hbar/τ are small compared with the Fermi energy, and $\hbar\omega$ is less than the thermal energy. The condition $\omega\tau < 1$ does not arise.

§ 1. INTRODUCTION

THE usual treatment of magnetoresistance is based upon the application of the Boltzmann equation

$$\frac{1}{\hbar} \frac{\partial f(\mathbf{k})}{\partial k} \cdot \left(e\mathcal{E} + \frac{e}{c\hbar} \frac{\partial E_{\mathbf{k}}}{\partial \mathbf{k}} \wedge \mathbf{H} \right) + \frac{2\pi}{\hbar} \sum_{\mathbf{k}'} W_{\mathbf{k}\mathbf{k}'} [f(\mathbf{k}') - f(\mathbf{k})] = 0 \quad \dots\dots (1.1)$$

to the Bloch independent-electron model of a metal, together with the prescription for obtaining the total current

$$\bar{j}_{\mu} = \frac{e}{\hbar} \int \frac{\partial E_{\mathbf{k}}}{\partial \mathbf{k}_{\mu}} f(\mathbf{k}) d^3\mathbf{k}. \quad \dots\dots (1.2)$$

In Eqns (1.1), (1.2) e and m are respectively the charge and mass of the electron, \hbar is Planck's constant divided by 2π , \mathcal{E} is the electric field and \mathbf{H} is the magnetic field. $W_{\mathbf{k}\mathbf{k}'}$ is the probability per unit time that the scattering should in the absence of the fields cause a transition from state \mathbf{k} to state \mathbf{k}' , and $E_{\mathbf{k}}$ is the Bloch energy of an electron in state \mathbf{k} .

† Now at Physics Department, Cornell University, Ithaca, N.Y., U.S.A.

$f(\mathbf{k})$ is usually defined for a one-band model as the probability that the Bloch state $\psi_{\mathbf{k}}$ will be found occupied by an electron: if the exact electron wave function Ψ is expanded in terms of the Bloch waves,

$$\Psi = \int \alpha(\mathbf{k}) \psi_{\mathbf{k}}(\mathbf{r}) d^3\mathbf{k}$$

then $f(\mathbf{k}) = |\alpha(\mathbf{k})|^2$. With this definition of $f(\mathbf{k})$ Eqn (1.2) is not exact since the three components $j_{\mu} = (e/m)(p_{\mu} - (e/c)A_{\mu})$ of the current operator are not all diagonal in the Bloch representation. They do not even commute with each other. Furthermore in the derivation of the Boltzmann equation (1.1) for $|\alpha(\mathbf{k})|^2$ the 'repeated random phase assumption' was required in the treatment of the collision term, and $|\alpha(\mathbf{k})|^2$ could only be shown to change under the influence of the fields according to

$$\left[\frac{\partial |\alpha(\mathbf{k})|^2}{\partial t} \right]_{\text{fields}} = \frac{1}{\hbar} \left(e\mathcal{E} + \frac{e}{c} \frac{\partial E_{\mathbf{k}}}{\partial \mathbf{k}} \wedge \mathbf{H} \right) \cdot \frac{\partial |\alpha(\mathbf{k})|^2}{\partial \mathbf{k}}$$

for times small compared with mc/eH . The derivations were therefore subject to the condition $\omega\tau \ll 1$ where τ is the relaxation time and $\omega = eH/mc$ is the cyclotron frequency. It should be understood that the derivations which treat the system classically are not open to this objection (Peierls 1931, 1932). In these treatments f is a function of the velocity and its rate of change under the influence of the electromagnetic field is given exactly by the Lorentz force equation.

The purpose of this paper is to justify the usual prescription (1.1), (1.2). We shall give a definition of $f(\mathbf{k})$ which makes (1.2) exact. By considering a simple model in which electrons move independently through a perfect periodic lattice and are elastically scattered by randomly distributed impurities we shall then show without the use of the random phase assumption that the new function satisfies the Boltzmann equation (1.1) for magnetic fields small enough to eliminate quantum effects but for which $\omega\tau$ may be arbitrarily large.

We thereby give some justification for the recent theories of magnetoresistance proposed by Lifshitz and Peshanskii (1959, 1960) and by Ziman (1958). Here the two equations (1.1) and (1.2) are applied for $\omega\tau \gtrsim 1$ to models in which the important features of the metal structure are included. The theories predict for single crystals that the dependence of the magnetoresistance ratio on the magnetic field should vary with the orientation of the crystal with respect to the field, saturating in high fields for certain orientations and increasing without limit as H^2 for others. These phenomena have since been observed by Alekseevskii and Gaidukov (1959). The field dependence in polycrystalline specimens is the result of averaging these different field dependences, and for filamentary specimens at least the linear law of Kapitza (1924) can be accounted for.

There have recently been attempts to provide a new basis for the treatment of high field magnetoresistance (see for instance Argyres 1958a, b). These attempts have all treated the simple model of free electrons for which the exact field-dependence can be retained by using the Landau states of an electron in a uniform magnetic field. The generalization to more realistic models of a metal is of course extremely difficult: for this one requires the wave function of the electron in the lattice in the magnetic field. This difficulty does not arise in the method presented in this paper. We do not attempt to derive an equation of

motion valid for arbitrarily high fields but instead demonstrate that (1.1) and (1.2) can be used whenever quantum effects are unimportant. For the application of (1.1), (1.2) one needs only the wave functions of the electron in the perfect lattice in the absence of the field.

The new $f(\mathbf{k})$ is defined as the diagonal element of the density matrix in a non-orthogonal representation (Dirac 1947). We select this representation by requiring that it should diagonalize any operator which is the sum of functions of the separate current components and any periodic function of the coordinates. (1.2) follows at once. Also because the scattering interaction is on the average homogeneous, its matrix elements in the new representation will have certain diagonality properties. We exploit these by writing the quantum mechanical equation of motion of the density matrix in the new representation. It is then possible to show that in a consistent limiting procedure certain terms are small and can be eliminated. The remaining terms furnish an equation of motion for the diagonal elements of ρ alone, which is just the Boltzmann equation (1.1).

In §2 the non-orthogonal representation is established and its properties demonstrated. The Boltzmann equation is derived in §3 by considering the lowest order terms in the limiting procedure. In §4 some of the higher order terms are investigated and the corrections they give rise to are estimated. These corrections are small provided

$$\hbar\omega \ll \zeta \quad \hbar/\tau \ll \zeta \quad \dots\dots (1.3)$$

where ζ is the Fermi energy and kT is the thermal energy. These are the conditions under which the Boltzmann equation (1.1) is valid.

§ 2. THE NEW REPRESENTATION

In the absence of a magnetic field the systems encountered in transport problems have the following property, called by Van Hove (1955) "the diagonal singularity property":

$$\langle E\alpha|WAW|E'\alpha'\rangle \sim \delta_{EE'}\delta_{\alpha\alpha'}\langle E\alpha|WAW|E\alpha\rangle. \quad \dots\dots (2.1)$$

Here W is the scattering interaction and A is any operator diagonal in a representation E, α which diagonalizes the Hamiltonian of the unperturbed system. For the free electron model of a metal this representation is the momentum representation, and the property (2.1) is sufficient to establish the Boltzmann equation for the diagonal matrix elements $\langle \mathbf{k}|\rho|\mathbf{k}\rangle$ of the density operator.

When, however, a magnetic field is imposed no orthogonal representation is known which diagonalizes the unperturbed Hamiltonian exactly except in the case of free electrons. In this case the representation is based on the Landau states and the matrix elements of the scattering interaction no longer have the diagonal singularity property.† However the average translation invariance of the field-free system, reflected in (2.1) when we identify $|E\alpha\rangle$ with $|\mathbf{k}\rangle$, is not completely destroyed by the magnetic field. The overall invariance to translations in a plane containing the field direction can be maintained with a suitable choice of gauge. Making transformations between the gauges corresponding to different

† An exception is the special case which has been treated by Argyres (1958 a, b) in which the scattering is caused by a random array of zero-range scatterers.

planes we shall show in this section that a non-orthogonal representation can be found which diagonalizes the unperturbed Hamiltonian and in which the matrix elements of the scattering interaction have the required property. Moreover this representation exists whether or not we assume the electrons to be free. It can be chosen in such a way that with $f(\mathbf{k})$ equal to the diagonal matrix element of ρ in this representation, (1.2) is an exact equation for computing average currents. For this we require that the representation diagonalizes all operators of the type

$$D = \alpha(\mathbf{r}) + \sum_{\mu} \beta_{\mu}(j_{\mu}) \quad \dots\dots (2.2)$$

where β_{μ} is any function of the μ th component of the current, and α is any function of the coordinates which has the periodicity of the lattice. Consider

$$\langle \mathbf{r}_1 | D | \mathbf{r}_2 \rangle = \alpha(\mathbf{r}_1) \delta(\mathbf{r}_1 - \mathbf{r}_2) + B(\mathbf{r}_1, \mathbf{r}_2) \quad \dots\dots (2.3)$$

where

$$B(\mathbf{r}_1, \mathbf{r}_2) = \langle \mathbf{r}_1 | \sum_{\mu} \beta_{\mu}(j_{\mu}) | \mathbf{r}_2 \rangle \quad \dots\dots (2.4)$$

and suppose that the magnetic field is in the z direction. The value of B depends on the choice of gauge. Two possible choices for the vector potential are:

$$\mathbf{A}_1: (0, Hx, 0) \quad \dots\dots (2.5 a) \quad \mathbf{A}_2: (-Hy, 0, 0). \quad \dots\dots (2.5 b)$$

In the first gauge B becomes B_1 , the matrix element in configuration space of an operator that commutes with p_y and p_z . Therefore B_1 depends only on x_1, x_2 and the differences of y_1 and y_2 and of z_1 and z_2 :

$$B_1 = B_1(x_1, x_2, y_1 - y_2, z_1 - z_2). \quad \dots\dots (2.6 a)$$

Similarly in the second gauge B becomes

$$B_2 = B_2(x_1 - x_2, y_1, y_2, z_1 - z_2). \quad \dots\dots (2.6 b)$$

Now we could write

$$B_1 = \sum_{\beta} \langle \mathbf{r}_1 | \beta \rangle_1 \beta \langle \beta | \mathbf{r}_2 \rangle_1 \quad \dots\dots (2.7 a)$$

where $\langle \mathbf{r}_1 | \beta \rangle_1$ is the eigenfunction of the operator $\sum_{\mu} \beta_{\mu}(j_{\mu})$ expressed in the first gauge. The eigenvalue of this operator in this state is β . Corresponding to this eigenvalue there will be another function $\langle \mathbf{r}_1 | \beta \rangle_2$ which is the eigenfunction of $\sum_{\mu} \beta_{\mu}(j_{\mu})$ expressed in the second gauge:

$$B_2 = \sum_{\beta} \langle \mathbf{r}_1 | \beta \rangle_2 \beta \langle \beta | \mathbf{r}_2 \rangle_2. \quad \dots\dots (2.7 b)$$

Now under a change of gauge

$$\mathbf{A} \rightarrow \mathbf{A}' = \mathbf{A} - \nabla f \quad \dots\dots (2.8)$$

the wave function changes according to

$$\langle \mathbf{r} | \beta \rangle \rightarrow \langle \mathbf{r} | \beta \rangle' = \langle \mathbf{r} | \beta \rangle \exp\left(+\frac{ie}{\hbar c} f\right) \quad \dots\dots (2.9)$$

(Pauli 1933). It follows that

$$\langle \mathbf{r}_1 | \beta \rangle_2 = \langle \mathbf{r}_1 | \beta \rangle_1 \exp(+i\epsilon x_1 y_1) \quad \dots\dots (2.10)$$

where $\epsilon = eH/\hbar c$. Hence

$$B_2 = \exp\{+i\epsilon(x_1 y_1 - x_2 y_2)\} B_1. \quad \dots\dots (2.11)$$

Let us write

$$B_1 = \exp(-i\epsilon X y) G(x_1, x_2, y, z) \quad \dots\dots (2.12)$$

where

$$\mathbf{R}: (X, Y, Z) = \frac{1}{2}(\mathbf{r}_1 + \mathbf{r}_2) \text{ and } \mathbf{r}: (x, y, z) = \mathbf{r}_1 - \mathbf{r}_2.$$

Then

$$B_2(x, y_1, y_2, z) \exp(-i\epsilon Yx) = G(x_1, x_2, y, z). \quad \dots (2.13)$$

The left-hand side depends only on x , not on both x_1 and x_2 . The right-hand side must therefore also depend only on x . That is: $G = G(x, y, z)$. Hence

$$B_1(\mathbf{r}_1, \mathbf{r}_2) = \exp(-i\epsilon Xy)G(\mathbf{r}). \quad \dots (2.14)$$

In the new variables $\alpha(\mathbf{r}_1)\delta(\mathbf{r}_1 - \mathbf{r}_2)$ is $\alpha(\mathbf{R})\delta(\mathbf{r})$, and α is periodic with the lattice periodicity. Therefore with the first choice of gauge the matrix element of D has the form

$$\langle \mathbf{r}_1 | D | \mathbf{r}_2 \rangle = \exp(-i\epsilon Xy) \mathcal{D}(\mathbf{r}, \mathbf{R}) \quad \dots (2.15)$$

where $\mathcal{D}(\mathbf{r}, \mathbf{R})$ has the periodicity of the lattice with respect to its \mathbf{R} -dependence. From now on we shall use only the first form (2.5a) of the vector potential. Eqn (2.15) can now be used to find a non-orthogonal representation in which D is diagonal. We define $\{l_1 | D | l_2\}$ by

$$\{l_1 | D | l_2\} = \int \int \exp(+i\epsilon yX) \langle \mathbf{r}_1 | D | \mathbf{r}_2 \rangle \psi_{l_1}^*(\mathbf{r}_1) \psi_{l_2}(\mathbf{r}_2) d^3\mathbf{r}_1 d^3\mathbf{r}_2 \quad \dots (2.16)$$

where $\psi_l(\mathbf{r}) = \exp(i\mathbf{k} \cdot \mathbf{r}) u_{\mathbf{k}l}(\mathbf{r})$ is the Bloch wave function for the electrons in the perfect lattice and l denotes the complete label (\mathbf{k}, ν) in the reduced zone scheme. If in (2.16) we change the integration variables to \mathbf{R} and \mathbf{r} , since we have shown that $\exp(+i\epsilon yX) \langle \mathbf{r}_1 | D | \mathbf{r}_2 \rangle$ has the periodicity of the lattice with respect to its dependence on \mathbf{R} , $\exp[i(\mathbf{k}_2 - \mathbf{k}_1) \cdot \mathbf{R}]$ is the only factor in the integrand which does not depend in this way on \mathbf{R} . The integration with respect to \mathbf{R} therefore gives zero unless \mathbf{k}_1 and \mathbf{k}_2 differ only by a vector of the reciprocal lattice. Thus in the reduced-zone scheme

$$\{l_1 | D | l_2\} = \delta_{\mathbf{k}_1 \mathbf{k}_2} \{ \mathbf{k}_1 \nu_1 | D | \mathbf{k}_1 \nu_2 \}. \quad \dots (2.17)$$

Functions of the type (2.2) are therefore diagonal within a band, in the new representation defined by (2.16). For simplicity we shall limit ourselves from now on to a single band, when \mathbf{k} labels the state completely. The treatment of the more general case is quite straightforward.

As an example of (2.17) suppose that for D we take the unperturbed Hamiltonian

$$\mathcal{H}_0 = \frac{1}{2m} \left(\mathbf{p} - \frac{e}{c} \mathbf{A} \right)^2 + V_0(\mathbf{r}), \quad \dots (2.18)$$

where V_0 is the lattice potential. Substituting into (2.16) one finds that

$$\{ \mathbf{k}_1 | \mathcal{H}_0 | \mathbf{k}_2 \} = E_{\mathbf{k}_1} \delta_{\mathbf{k}_1 \mathbf{k}_2}. \quad \dots (2.19)$$

In the new representation the matrix elements of the scattering interaction have the diagonal singularity property for all values of the magnetic field. For if

$$\langle \mathbf{k} | W A W | \mathbf{k}' \rangle = \delta(\mathbf{k} - \mathbf{k}') \langle \mathbf{k} | W A W | \mathbf{k} \rangle \quad \dots (2.20)$$

when A is diagonal in the Bloch representation, it follows that

$$\{ \mathbf{k} | W B W | \mathbf{k}' \} = \delta_{\mathbf{k} \mathbf{k}'} \{ \mathbf{k} | W B W | \mathbf{k} \} \quad \dots (2.21)$$

when $\{ \mathbf{k} | B | \mathbf{k}' \} = \delta_{\mathbf{k} \mathbf{k}'} \{ \mathbf{k} | B | \mathbf{k} \}$. Here we have labelled matrix elements in the

orthogonal (Bloch) representation by the bracket notation of Dirac, and matrix elements in the non-orthogonal representation are denoted by a curly bracket.

The representation (2.16) is therefore entirely analogous to that used by Van Hove (1955) and Kohn and Luttinger (1957) in the field-free case. We shall now show that the diagonal elements of the density matrix in this representation provide a function suitable for averaging all components of the current. The average value of the μ th component of the current j is $\text{Tr} [\rho j_\mu]$. Taking the trace in \mathbf{x} -representation the density matrix can be written in terms of $\{\mathbf{k}|\rho|\mathbf{k}'\}$ by using the inverse of the transformation (2.16):

$$\langle \mathbf{r}_1 | \rho | \mathbf{r}_2 \rangle = \exp(-i\epsilon y X) \iint d^3\mathbf{k}_1 d^3\mathbf{k}_2 \psi_{\mathbf{k}_1}(\mathbf{r}_1) \psi_{\mathbf{k}_2}^*(\mathbf{r}_2) \{\mathbf{k}_1 | \rho | \mathbf{k}_2\}. \quad \dots\dots (2.22)$$

The properties of the Bloch functions and current operators are such that the trace reduces exactly to the very simple form:

$$\bar{j}_\mu = \int d^3\mathbf{k} \{\mathbf{k} | \rho | \mathbf{k}\} \frac{e}{\hbar} \frac{\partial E_{\mathbf{k}}}{\partial \mathbf{k}}. \quad \dots\dots (2.23)$$

Hence (1.2) is exact if $f(\mathbf{k})$ is the diagonal element of ρ in the new representation, or any quantity that differs from $\{\mathbf{k}|\rho|\mathbf{k}\}$ only by a part which contributes zero to the integral in (2.23).

The averaging properties of $\{\mathbf{k}|\rho|\mathbf{k}\}$ are striking. When integrated with respect to the parameters k_x, k_y connected with the other components of the current, it gives the correct quantum mechanical probability for any value $\partial E_{\mathbf{k}} / \partial k_\mu$ of the μ th component of the current. This suggests that $\{\mathbf{k}|\rho|\mathbf{k}\}$ is closely connected with the distribution function defined by Wigner (1932). The correspondence with the Wigner function is complete if in transforming the density matrix according to (2.16) we do not perform the integrations $\iint d^3\mathbf{r}_1 d^3\mathbf{r}_2$ but instead integrate with respect to \mathbf{r} only. For when $\mathbf{l}_1 = \mathbf{l}_2 = \mathbf{k}$, the function $g(\mathbf{k}, \mathbf{R})$ so obtained gives for the sum of a function α of coordinates and functions β_μ of the separate current components the correct expectation value by the normal probability calculation:

$$\overline{\alpha + \sum_\mu \beta_\mu} = \int d^3\mathbf{R} d^3\mathbf{k} \left[\alpha(\mathbf{R}) + \sum_\mu \beta_\mu \left(\frac{\partial E_{\mathbf{k}}}{\partial k_\mu} \right) \right] g(\mathbf{k}, \mathbf{R}). \quad \dots\dots (2.24)$$

§ 3. THE DERIVATION OF THE BOLTZMANN EQUATION IN A MAGNETIC FIELD

The treatment presented here is a generalization of the method of Kohn and Luttinger (1957) and of Greenwood (1958) to the case when a uniform magnetic field is present. The essential difference is that we use the non-orthogonal representation discussed in § 2 rather than the usual Bloch representation.

The system considered is one of non-interacting electrons moving in a perfect periodic lattice under the influence of an external electric and magnetic field. The electrons are scattered by a random array of static impurity centres. The total Hamiltonian of each electron is

$$H_T = \mathcal{H}_0 + W + H_F. \quad \dots\dots (3.1)$$

Here W is the interaction with the static impurities, H_F is the interaction with the electric field \mathcal{E} and \mathcal{H}_0 is defined by (2.18). Suppose ρ_T is the density

matrix of the complete system. Its equation of motion is

$$i\hbar\dot{\rho}_T = [H_T, \rho_T]. \quad \text{..... (3.2)}$$

We assume that in the infinite past the system was in equilibrium in the absence of the electric field. Then $\rho_T(-\infty) = \rho_0(\mathcal{H}_0 + W)$ is the Fermi function of $(\mathcal{H}_0 + W)$. If the electric field is switched on in the following manner:

$$\mathcal{E}^t = \mathcal{E}e^{st}, \quad s > 0, \quad \text{..... (3.3)}$$

we may write

$$\rho_T(t) = \rho_0 + \rho_F(t) \quad \text{..... (3.4)}$$

where ρ_F is the change in the density matrix due to the electric field, and so $\rho_F(-\infty) = 0$. For the Ohmic conductivity we need ρ_F only to first order in \mathcal{E} . To this order (3.2) becomes

$$i\hbar\dot{\rho}_F = [\mathcal{H}_0 + W, \rho_F] + [H_F, \rho_0]. \quad \text{..... (3.5)}$$

Since

$$H_F = H_1 e^{st} \quad \text{where} \quad H_1 = -e\mathcal{E} \cdot \mathbf{x} \quad \text{..... (3.6)}$$

the above equation and initial condition are satisfied if

$$\rho_F = f e^{st} \quad \text{..... (3.7)}$$

where f is time-independent. f is the correction to the density matrix at time $t=0$, when the field has reached the value \mathcal{E} . From Eqn (3.5) we find that

$$i\hbar s f = [\mathcal{H}_0 + W, f] - C \quad \text{..... (3.8)}$$

where $C = [\rho_0, H_1]$ and is in principle known.

Using the representation defined by (2.16) and again considering only a single band we can write Eqn (3.8) as

$$i\hbar s \{ \mathbf{k}_1 | f | \mathbf{k}_2 \} + \{ \mathbf{k}_1 | C | \mathbf{k}_2 \}$$

$$= \int d^3 \mathbf{r}_1 d^3 \mathbf{r}_2 d^3 \mathbf{r}_3 d^3 \mathbf{k}_3 d^3 \mathbf{k}_4 \exp(i\epsilon y_{12} X_{12}) \psi_{\mathbf{k}_1}^*(\mathbf{r}_1) \psi_{\mathbf{k}_2}(\mathbf{r}_2) \{ \mathbf{k}_3 | f | \mathbf{k}_4 \} \\ \times \left\{ \begin{aligned} &\langle \mathbf{r}_1 | \mathcal{H}_0 + W | \mathbf{r}_3 \rangle \exp(-i\epsilon y_{32} X_{32}) \psi_{\mathbf{k}_2}(\mathbf{r}_3) \psi_{\mathbf{k}_1}^*(\mathbf{r}_2) \\ &- \langle \mathbf{r}_3 | \mathcal{H}_0 + W | \mathbf{r}_2 \rangle \exp(-i\epsilon y_{13} X_{13}) \psi_{\mathbf{k}_3}(\mathbf{r}_1) \psi_{\mathbf{k}_4}^*(\mathbf{r}_3) \end{aligned} \right\}, \quad \text{..... (3.9)}$$

where

$$\mathbf{r}_{ij} = \mathbf{r}_i - \mathbf{r}_j, \quad \mathbf{R}_{ij} = \frac{1}{2}(\mathbf{r}_i + \mathbf{r}_j).$$

Since the new representation is equivalent to that used in the field-free case by Kohn and Luttinger (1957) we expect that the properties of the scattering should produce a sharp distinction between $\{ \mathbf{k}_1 | f | \mathbf{k}_2 \}$ and $\{ \mathbf{k}_1 | f | \mathbf{k}_1 \}$. We therefore split Eqn (3.9) into diagonal and off-diagonal equations. These are

$$i\hbar s \{ \mathbf{k}_1 | f | \mathbf{k}_1 \} + \{ \mathbf{k}_1 | C | \mathbf{k}_1 \}$$

$$= \int d^3 \mathbf{r}_1 d^3 \mathbf{r}_2 d^3 \mathbf{r}_3 \sum_{\mathbf{k}_3} \exp(i\epsilon y_{12} X_{12}) \psi_{\mathbf{k}_1}^*(\mathbf{r}_1) \psi_{\mathbf{k}_1}(\mathbf{r}_2) \{ \mathbf{k}_3 | f | \mathbf{k}_3 \} \\ \times \left\{ \begin{aligned} &\langle \mathbf{r}_1 | \mathcal{H}_0 + W | \mathbf{r}_3 \rangle \exp(-i\epsilon y_{32} X_{32}) \psi_{\mathbf{k}_3}(\mathbf{r}_3) \psi_{\mathbf{k}_1}^*(\mathbf{r}_2) \\ &- \langle \mathbf{r}_3 | \mathcal{H}_0 + W | \mathbf{r}_2 \rangle \exp(-i\epsilon y_{13} X_{13}) \psi_{\mathbf{k}_3}(\mathbf{r}_1) \psi_{\mathbf{k}_1}^*(\mathbf{r}_3) \end{aligned} \right\} \\ + \int d^3 \mathbf{r}_1 d^3 \mathbf{r}_2 d^3 \mathbf{r}_3 \sum_{\mathbf{k}_3} \sum_{\mathbf{k}_4 \neq \mathbf{k}_3} \exp(i\epsilon y_{12} X_{12}) \psi_{\mathbf{k}_1}^*(\mathbf{r}_1) \psi_{\mathbf{k}_1}(\mathbf{r}_2) \{ \mathbf{k}_3 | f | \mathbf{k}_4 \} \\ \times \left\{ \begin{aligned} &\langle \mathbf{r}_1 | \mathcal{H}_0 + W | \mathbf{r}_3 \rangle \exp(-i\epsilon y_{32} X_{32}) \psi_{\mathbf{k}_3}(\mathbf{r}_3) \psi_{\mathbf{k}_4}^*(\mathbf{r}_2) \\ &- \langle \mathbf{r}_3 | \mathcal{H}_0 + W | \mathbf{r}_2 \rangle \exp(-i\epsilon y_{13} X_{13}) \psi_{\mathbf{k}_3}(\mathbf{r}_1) \psi_{\mathbf{k}_4}^*(\mathbf{r}_3) \end{aligned} \right\}, \quad \text{..... (3.10)}$$

$$i\hbar s\{\mathbf{k}_1|f|\mathbf{k}_2\} + \{\mathbf{k}_1|C|\mathbf{k}_2\}$$

$$= \int d^3\mathbf{r}_1 d^3\mathbf{r}_2 d^3\mathbf{r}_3 \sum_{\mathbf{k}_2} \exp(i\epsilon y_{12} X_{12}) \psi_{\mathbf{k}_1}^*(\mathbf{r}_1) \psi_{\mathbf{k}_2}(\mathbf{r}_2) \{\mathbf{k}_3|f|\mathbf{k}_3\} \\ \times \left\{ \langle \mathbf{r}_1 | \mathcal{H}_0 + W | \mathbf{r}_3 \rangle \exp(-i\epsilon y_{32} X_{32}) \psi_{\mathbf{k}_3}(\mathbf{r}_3) \psi_{\mathbf{k}_2}^*(\mathbf{r}_2) \right. \\ \left. - \langle \mathbf{r}_3 | \mathcal{H}_0 + W | \mathbf{r}_2 \rangle \exp(-i\epsilon y_{13} X_{13}) \psi_{\mathbf{k}_1}(\mathbf{r}_1) \psi_{\mathbf{k}_2}^*(\mathbf{r}_3) \right\} \\ + \int d^3\mathbf{r}_1 d^3\mathbf{r}_2 d^3\mathbf{r}_3 \sum_{\mathbf{k}_2} \sum_{\mathbf{k}_4 \neq \mathbf{k}_1} \exp(i\epsilon y_{12} X_{12}) \psi_{\mathbf{k}_1}^*(\mathbf{r}_1) \psi_{\mathbf{k}_2}(\mathbf{r}_2) \{\mathbf{k}_3|f|\mathbf{k}_4\} \\ \times \left\{ \langle \mathbf{r}_1 | \mathcal{H}_0 + W | \mathbf{r}_3 \rangle \exp(-i\epsilon y_{32} X_{32}) \psi_{\mathbf{k}_3}(\mathbf{r}_3) \psi_{\mathbf{k}_4}^*(\mathbf{r}_2) \right. \\ \left. - \langle \mathbf{r}_3 | \mathcal{H}_0 + W | \mathbf{r}_2 \rangle \exp(-i\epsilon y_{13} X_{13}) \psi_{\mathbf{k}_1}(\mathbf{r}_1) \psi_{\mathbf{k}_4}^*(\mathbf{r}_3) \right\} \dots \dots \dots (3.11)$$

Since these equations are complex and we are only concerned with their structure we shall write them in the following way:

$$i\hbar s f_d + C_d = (\mathcal{H} + \mathcal{W})^d_d f_d + (\mathcal{H} + \mathcal{W})^d_{nd} f_{nd} \dots \dots \dots (3.12)$$

$$i\hbar s f_{nd} + C_{nd} = (\mathcal{H} + \mathcal{W})^{nd}_d f_d + (\mathcal{H} + \mathcal{W})^{nd}_{nd} f_{nd} \dots \dots \dots (3.13)$$

The subscripts d, nd denote diagonal and non-diagonal parts of $\{f\}$ or $\{C\}$ and the definition of the integral operators \mathcal{H} and \mathcal{W} and their kernels $\mathcal{H}(\mathbf{k}_1\mathbf{k}_2|\mathbf{k}_3\mathbf{k}_4)$ and $\mathcal{W}(\mathbf{k}_1\mathbf{k}_2|\mathbf{k}_3\mathbf{k}_4)$ follows by comparison with Eqns (3.10), (3.11).

We cannot hope to solve these coupled equations exactly. We can however simplify them in the weak scattering limit. In the treatment by Kohn and Luttinger (1957) of the field-free case, it is shown that in this limit the equations have a solution which is independent of the rate s at which the electric field is switched on provided $s \ll 1/\tau$. We shall take the weak scattering limit in such a way that s is about equal to $1/\tau$ or less (τ depends inversely on the strength of the scattering) and only later make use of the fact that in practice the rate of application of the electric field is always such that $s\tau \ll 1$. We shall find however that the restriction $s \sim 1/\tau$ is not the only one that has to be imposed; in a similar way the size of the magnetic field has to be introduced into the limiting process. To show this we demonstrate how an attempt to solve the equations in the weak scattering limit for arbitrary fields fails.

We replace W by $\lambda_w W$ where λ_w is a dimensionless parameter measuring the strength of the scattering interaction. Since $\tau \propto \lambda_w^{-2}$ our restriction on s requires that $s = \lambda_s^2 s_0$ where $\lambda_s \sim \lambda_w$ and s_0 is some reference frequency independent of λ_w . A short calculation shows that for $\lambda_w \ll 1$, \mathcal{H}^d_d , \mathcal{H}^{nd}_d , \mathcal{H}^d_{nd} , \mathcal{H}^{nd}_{nd} , $C_d \sim \lambda_w^0$ and \mathcal{W}^d_d , \mathcal{W}^{nd}_d , \mathcal{W}^d_{nd} , \mathcal{W}^{nd}_{nd} , $C_{nd} \sim \lambda_w$. Suppose that to leading order, f_d is of order λ_w^r , where r is not necessarily positive, or even an integer. Taking the terms of lowest order in λ_w from Eqn (3.13) the following equation is obtained for f_{nd} in terms of f_d :

$$\mathcal{H}^{nd}_{nd} f_{nd} = \begin{cases} C_{nd} & \text{if } r > 1 \\ C_{nd} - \mathcal{H}^{nd}_d f_d & \text{if } r = 1 \\ -\mathcal{H}^{nd}_d f_d & \text{if } r < 1 \end{cases} \dots \dots \dots (3.14)$$

Substituting this back into (3.12) we find that the only consistent choice of r is $r=0$ with f_d given by the equation

$$\mathcal{H}^d_d f_d = C_d + \mathcal{H}^d_{nd} (\mathcal{H}^{nd}_{nd})^{-1} \mathcal{H}^{nd}_d f_d, \dots \dots \dots (3.15)$$

where the existence of the operator inverse to \mathcal{H}^{nd}_{nd} has been assumed. Now

in the limit of zero field the integral operators $\mathcal{H}^{\text{d}}_{\text{d}}$, $\mathcal{H}^{\text{nd}}_{\text{d}}$, $\mathcal{H}^{\text{d}}_{\text{nd}}$ and $\mathcal{W}^{\text{d}}_{\text{d}}$ vanish. For in this limit the general kernel becomes

$$\begin{aligned} & [\mathcal{H}(\mathbf{k}_1\mathbf{k}_2|\mathbf{k}_3\mathbf{k}_4) + \mathcal{W}(\mathbf{k}_1\mathbf{k}_2|\mathbf{k}_3\mathbf{k}_4)]_{\text{zero field}} \\ &= \langle \mathbf{k}_1 | \mathcal{H}_{0H=0} | \mathbf{k}_1 \rangle \delta_{\mathbf{k}_1\mathbf{k}_2} \delta_{\mathbf{k}_3\mathbf{k}_4} - \langle \mathbf{k}_2 | \mathcal{H}_{0H=0} | \mathbf{k}_2 \rangle \delta_{\mathbf{k}_1\mathbf{k}_2} \delta_{\mathbf{k}_3\mathbf{k}_4} \\ &+ \langle \mathbf{k}_1 | W | \mathbf{k}_3 \rangle \delta_{\mathbf{k}_2\mathbf{k}_4} - \langle \mathbf{k}_4 | W | \mathbf{k}_2 \rangle \delta_{\mathbf{k}_1\mathbf{k}_3} \dots\dots (3.16) \end{aligned}$$

since $\mathcal{H}_{0H=0}$ is diagonal in the Bloch representation. If either $\mathbf{k}_1 = \mathbf{k}_2$ or $\mathbf{k}_3 = \mathbf{k}_4$ the kernel $\mathcal{H}_{\text{zero field}}$ vanishes, and if both $\mathbf{k}_1 = \mathbf{k}_2$ and $\mathbf{k}_3 = \mathbf{k}_4$, $\mathcal{W}_{\text{zero field}} = \mathcal{W}^{\text{d}}_{\text{zero field}}$ vanishes. Hence in zero field the coefficient of f_{d} in Eqn (3.15) is zero. Thus this equation only gives a solution valid in the weak scattering limit provided the field \mathbf{H} is not too small, and when this is so f_{d} becomes independent of the strength of the scattering. This is to be contrasted with the behaviour of f_{d} in zero field when $f_{\text{d}} \sim \lambda_w^{-2}$ as $\lambda_w \rightarrow 0$ (Kohn and Luttinger 1957). These different dependences reflect the different mechanisms which limit the momentum acquired by the electrons under the influence of the electric field: when $\mathbf{H} = 0$ the scattering is entirely responsible; if there is a magnetic field perpendicular to the electric field the electrons execute circular motion under the influence of the Lorentz force and this mechanism dominates in the weak scattering limit. This limiting process ($\lambda_w \rightarrow 0$) can therefore provide a basis for the calculation of the transverse magnetoconductance in high fields. A high field theory of this type will be developed in a second paper. For low fields a different method of attack has to be devised.

The method we use takes into account the vanishing of $\mathcal{H}^{\text{d}}_{\text{d}}$, $\mathcal{H}^{\text{d}}_{\text{nd}}$, $\mathcal{H}^{\text{nd}}_{\text{d}}$ as the field goes to zero. This is accomplished by ordering the Eqns (3.12), (3.13) not only with respect to λ_w , but also with respect to a parameter λ_H measuring the size of the field. We assume that each of λ_w and λ_H is small compared with unity. The limiting process $\lambda_H \rightarrow 0$ is the extra condition referred to earlier. The exact nature of this will be made clear subsequently. We define the parameter λ_H by the equation $\hbar\omega = \lambda_H^2 E$ where E is an energy independent of λ_w . The possible energies are ζ , kT and a screening energy giving the range of the potential of a single scatterer.

It can be shown that to leading order in λ_H , $\mathcal{H}^{\text{nd}}_{\text{nd}}$, $\mathcal{W}^{\text{d}}_{\text{nd}}$, $\mathcal{W}^{\text{nd}}_{\text{d}}$, $\mathcal{W}^{\text{nd}}_{\text{nd}}$ are of order λ_H^0 while $\mathcal{H}^{\text{d}}_{\text{d}}$, $\mathcal{H}^{\text{nd}}_{\text{d}}$, $\mathcal{H}^{\text{d}}_{\text{nd}}$, $\mathcal{W}^{\text{d}}_{\text{d}}$ go linearly with the field to zero, that is they are of order λ_H^2 . To leading order $C_{\text{d}} \sim (\lambda_w^0) \lambda_H^0$ and $C_{\text{nd}} \sim (\lambda_w) \lambda_H^0$. From Eqns (3.12), (3.13) it is now possible to deduce the leading order of f_{d} , f_{nd} . From (3.12)

$$f_{\text{nd}} = [i\hbar s - \mathcal{H}^{\text{nd}}_{\text{nd}} - \mathcal{W}^{\text{nd}}_{\text{nd}}]^{-1} [(\mathcal{H}^{\text{nd}}_{\text{d}} + \mathcal{W}^{\text{nd}}_{\text{d}})f_{\text{d}} - C_{\text{nd}}]. \dots\dots (3.17)$$

In the inverse operator $i\hbar s$ and $\mathcal{W}^{\text{nd}}_{\text{nd}}$ can at once be discarded since λ_s^2 , λ_w are each very much less than one. Inserted into (3.13) this gives an equation for f_{d} :

$$\begin{aligned} i\hbar s f_{\text{d}} + C_{\text{d}} &= (\mathcal{H}^{\text{d}}_{\text{d}} + \mathcal{W}^{\text{d}}_{\text{d}})f_{\text{d}} \\ &+ (\mathcal{H}^{\text{d}}_{\text{nd}} + \mathcal{W}^{\text{d}}_{\text{nd}})(-\mathcal{H}^{\text{nd}}_{\text{nd}})^{-1}[(\mathcal{H}^{\text{nd}}_{\text{d}} + \mathcal{W}^{\text{nd}}_{\text{d}})f_{\text{d}} - C_{\text{nd}}]. \end{aligned} \dots\dots (3.18)$$

In the limit $\lambda_H \rightarrow 0$, λ_w , $\lambda_s \rightarrow 0$ with $\lambda_w/\lambda_s \rightarrow \text{a constant}$, the coefficient of f_{d} reduces to $i\hbar s - \mathcal{H}^{\text{d}}_{\text{d}} - \mathcal{W}^{\text{d}}_{\text{nd}}(-\mathcal{H}^{\text{nd}}_{\text{nd}})^{-1}\mathcal{W}^{\text{nd}}_{\text{d}}$ and the inhomogeneous term to \hat{C}_{d} . Here the circumflex means that the integral operators and inhomogeneous term

are to be evaluated to leading order in λ_w, λ_H . So far nothing has been said about the relative order of λ_w and λ_H . Now $i\hbar s \sim \lambda_s^2$, $\mathcal{H}_{\text{d}}^{\text{d}} \sim \lambda_H^2$ and $\mathcal{W}_{\text{nd}}^{\text{d}} (-\mathcal{H}_{\text{nd}}^{\text{nd}})^{-1} \mathcal{W}_{\text{nd}}^{\text{nd}} \sim \lambda_w^2$. We have already supposed that $\lambda_s \sim \lambda_w$. If we further assume that $\lambda_w \sim \lambda_H$ the terms in Eqn (3.18) of leading order in both the field and the scattering are retained. In any other limiting process some of these terms disappear. For instance for the high field approach already mentioned we would assume $\lambda_w/\lambda_H \rightarrow 0$ and the scattering interaction would disappear from Eqn (3.18).† We therefore impose the limiting process

$$\lambda_s \rightarrow 0, \quad \lambda_w \rightarrow 0, \quad \lambda_H \rightarrow 0 \quad \text{..... (3.19)}$$

in such a way that $\lambda_w/\lambda_s, \lambda_w/\lambda_H$ each tends to a finite limit.

Then

$$f_{\text{d}} \rightarrow f_{\text{d}}^{\text{f}} \sim \lambda_w^{-2} \text{ function of } (\lambda_H/\lambda_w, \lambda_s/\lambda_w) \quad \text{..... (3.20)}$$

$$f_{\text{nd}} \rightarrow f_{\text{nd}}^{\text{f}} \sim \lambda_w^{-1} \text{ function of } (\lambda_H/\lambda_w, \lambda_s/\lambda_w). \quad \text{..... (3.21)}$$

These are consistent with the results obtained by Kohn and Luttinger (1957) in zero field. Under the limiting process (3.19) the Eqns (3.12), (3.13) are to be replaced by

$$i\hbar s f_{\text{d}} + \hat{C}_{\text{d}} = \mathcal{H}_{\text{d}}^{\text{d}} f_{\text{d}} + \mathcal{W}_{\text{nd}}^{\text{d}} f_{\text{nd}}^{\text{f}} \quad \text{..... (3.22)}$$

$$i\hbar s f_{\text{nd}} = \mathcal{W}_{\text{nd}}^{\text{nd}} f_{\text{d}}^{\text{f}} + \mathcal{H}_{\text{nd}}^{\text{nd}} f_{\text{nd}}^{\text{f}}. \quad \text{..... (3.23)}$$

The term $i\hbar s f_{\text{nd}}$ is of higher order than the other terms in the second equation but it cannot be discarded as it later appears in a limiting form for a delta function. The discussion of the other higher order terms is left to the next section.

We shall solve Eqn (3.23) for f_{nd} in terms of f_{d} . For this the integral operators $\mathcal{W}_{\text{nd}}^{\text{nd}}, \mathcal{H}_{\text{nd}}^{\text{nd}}$ are required. These are just the zero field values of $\mathcal{W}_{\text{nd}}^{\text{nd}}, \mathcal{H}_{\text{nd}}^{\text{nd}}$ which from (3.16) are non-vanishing. The kernels are

$$\mathcal{H}_{\text{nd}}^{\text{nd}}(\mathbf{k}_1 \mathbf{k}_2 | \mathbf{k}_3 \mathbf{k}_4) = \delta_{\mathbf{k}_1 \mathbf{k}_3} \delta_{\mathbf{k}_2 \mathbf{k}_4} [E_{\mathbf{k}_1} - E_{\mathbf{k}_3}] \quad \text{..... (3.24)}$$

and

$$\mathcal{W}_{\text{nd}}^{\text{nd}}(\mathbf{k}_1 \mathbf{k}_2 | \mathbf{k}_3 \mathbf{k}_4) = \langle \mathbf{k}_1 | W | \mathbf{k}_2 \rangle \delta_{\mathbf{k}_1 \mathbf{k}_3} - \langle \mathbf{k}_1 | W | \mathbf{k}_2 \rangle \delta_{\mathbf{k}_1 \mathbf{k}_4}. \quad \text{..... (3.25)}$$

For Eqn (3.22) $\mathcal{W}_{\text{nd}}^{\text{d}}$ will also be needed. This has the kernel

$$\mathcal{W}_{\text{nd}}^{\text{d}}(\mathbf{k}_1 \mathbf{k}_1 | \mathbf{k}_3 \mathbf{k}_4) = \langle \mathbf{k}_1 | W | \mathbf{k}_3 \rangle \delta_{\mathbf{k}_1 \mathbf{k}_4} - \langle \mathbf{k}_4 | W | \mathbf{k}_1 \rangle \delta_{\mathbf{k}_1 \mathbf{k}_3}. \quad \text{..... (3.26)}$$

Using (3.24) and (3.25) in Eqn (3.23), the solution f_{nd} is easily obtained:

$$\{\mathbf{k}_1 | f | \mathbf{k}_2\} = \frac{\langle \mathbf{k}_1 | W | \mathbf{k}_2 \rangle [\{\mathbf{k}_2 | f | \mathbf{k}_2\} - \{\mathbf{k}_1 | f | \mathbf{k}_1\}]}{i\hbar s - [E_{\mathbf{k}_1} - E_{\mathbf{k}_2}]} \quad \text{..... (3.27)}$$

This checks the statement that $f_{\text{nd}} \sim \lambda_w f_{\text{d}}$. Together with (3.26), (3.27) gives the last term in Eqn (3.22):

$$\sum_{\mathbf{k}_3 \mathbf{k}_4} \mathcal{W}_{\text{nd}}^{\text{d}}(\mathbf{k}_1 \mathbf{k}_1 | \mathbf{k}_3 \mathbf{k}_4) \{\mathbf{k}_3 | f | \mathbf{k}_4\} = \sum_{\mathbf{k}_3} [\langle \mathbf{k}_1 | W | \mathbf{k}_3 \rangle^2 \{\{\mathbf{k}_3 | f | \mathbf{k}_3\} - \{\mathbf{k}_1 | f | \mathbf{k}_1\}\} \\ \left\{ \frac{1}{E_{\mathbf{k}_1} - E_{\mathbf{k}_3} - i\hbar s} - \frac{1}{E_{\mathbf{k}_3} - E_{\mathbf{k}_1} + i\hbar s} \right\}]. \quad \text{..... (3.28)}$$

The importance of retaining the small imaginary terms $i\hbar s$ in the denominators is now apparent. Recognizing now that these are of smaller order than the

† The restriction $\lambda_H \rightarrow 0$ is not required for the high field approach.

other terms, the factor becomes properly ordered in the limit $s \rightarrow 0$. In this limit it is $2\pi i \delta(E_{\mathbf{k}_1} - E_{\mathbf{k}_2})$. Then the right-hand side of (3.28) becomes:

$$\mathcal{W}_{\text{nd}}^{\text{d}} = 2\pi i \sum_{\mathbf{k}_2} [\langle \mathbf{k}_1 | W | \mathbf{k}_3 \rangle]^2 [\{ \mathbf{k}_3 | f | \mathbf{k}_3 \} - \{ \mathbf{k}_1 | f | \mathbf{k}_1 \}] \delta(E_{\mathbf{k}_2} - E_{\mathbf{k}_1}). \quad \dots (3.29)$$

Using (3.29) Eqn (3.22) becomes an equation for f_{d} alone. The inhomogeneous term \hat{C}_{d} and the integral operator \mathcal{H}_{d} of this equation can be put into very simple forms. To zero order in λ_w the inhomogeneous term is

$$\{ \mathbf{k}_1 | C | \mathbf{k}_2 \}_{w=0} = \int \int d^3 \mathbf{r}_1 d^3 \mathbf{r}_2 \exp(i\epsilon y X) (-e \mathcal{E}) \cdot \langle \mathbf{r}_1 | [\rho_0(\mathcal{H}_0), \mathbf{r}] | \mathbf{r}_2 \rangle \psi_{\mathbf{k}_1}^*(\mathbf{r}_1) \psi_{\mathbf{k}_2}(\mathbf{r}_2). \quad \dots (3.30)$$

Now

$$\exp(i\epsilon y X) \langle \mathbf{r}_1 | [\rho_0(\mathcal{H}_0), \mathbf{r}] | \mathbf{r}_2 \rangle = -\mathbf{r} \exp(i\epsilon y X) \langle \mathbf{r}_1 | \rho_0(\mathcal{H}_0) | \mathbf{r}_2 \rangle.$$

Writing this to the leading order in λ_H we therefore have for \hat{C}_{d}

$$\{ \mathbf{k}_1 | \hat{C} | \mathbf{k}_1 \} = \int \int d^3 \mathbf{r}_1 d^3 \mathbf{r}_2 e \mathcal{E} \cdot \mathbf{r} \langle \mathbf{r}_1 | \rho_0(\mathcal{H}_{0H=0}) | \mathbf{r}_2 \rangle \psi_{\mathbf{k}_1}^*(\mathbf{r}_1) \psi_{\mathbf{k}_1}(\mathbf{r}_2). \quad \dots (3.31)$$

Using the properties of the Bloch functions (3.31) can be reduced to

$$\{ \mathbf{k}_1 | \hat{C} | \mathbf{k}_1 \} = i e \mathcal{E} \cdot \frac{\partial}{\partial \mathbf{k}_1} f_0(\mathbf{k}_1, \mathbf{k}_1) \quad \dots (3.32)$$

where

$$f_0(\mathbf{k}_1, \mathbf{k}_1) = \langle \mathbf{k}_1 | \rho_0(\mathcal{H}_{0H=0}) | \mathbf{k}_1 \rangle. \quad \dots (3.33)$$

The form of $\mathcal{H}_{\text{d}}(\mathbf{k}_1 \mathbf{k}_1 | \mathbf{k}_3 \mathbf{k}_3)$ is derived in the Appendix, where it is shown that \mathcal{H}_{d} is identical with \mathcal{H}_{d} , that is \mathcal{H}_{d} only contains terms linear in the magnetic field, and

$$\sum_{\mathbf{k}_2} \mathcal{H}_{\text{d}}(\mathbf{k}_1 \mathbf{k}_1 | \mathbf{k}_3 \mathbf{k}_3) \{ \mathbf{k}_3 | f | \mathbf{k}_3 \} = -\frac{ie}{\hbar c} \left(\frac{\partial E_{\mathbf{k}_1}}{\partial \mathbf{k}_1} \wedge \mathbf{H} \right) \cdot \frac{\partial}{\partial \mathbf{k}_1} \{ \mathbf{k}_1 | f | \mathbf{k}_1 \}. \quad \dots (3.34)$$

This has the form of the usual Lorentz force acting on a charged particle moving with velocity $\mathbf{v} = \hbar^{-1} \partial E_{\mathbf{k}} / \partial \mathbf{k}$.

The equation obtained by inserting the detailed forms (3.29), (3.32) and (3.34) of the kernels and inhomogeneous term into (3.22) contains the square modulus of the matrix element $\langle \mathbf{k}_1 | W | \mathbf{k}_3 \rangle$ of the interaction of an electron with all the impurities. Kohn and Luttinger (1957) obtained a similar result in their treatment of the zero field equation and were able to show that this collision term could be reduced to its usual form provided there were no correlations between the positions of the impurities. Then the collision term (3.29) can be written in its customary form

$$i\hbar \sum_{\mathbf{k}_2} [W_{\mathbf{k}_1 \mathbf{k}_3} \{ \mathbf{k}_3 | f | \mathbf{k}_3 \} - W_{\mathbf{k}_1 \mathbf{k}_1} \{ \mathbf{k}_1 | f | \mathbf{k}_1 \}]$$

where $W_{\mathbf{k}_1 \mathbf{k}_3}$ is the probability per unit time that in the absence of the field the electron should make a transition from the Bloch state \mathbf{k}_1 to the state \mathbf{k}_3 . Recognizing that for the physically interesting rates at which the field could be

applied s is in fact very much less than the inverse of the relaxation time, we may discard the term $i\hbar s\{\mathbf{k}_1|f|\mathbf{k}_1\}$ in the detailed form of Eqn (3.22) and the final equation is obtained:

$$e\mathcal{E} \cdot \frac{1}{\hbar} \frac{\partial}{\partial \mathbf{k}} f_0(\mathbf{k}, \mathbf{k}) + \frac{e}{c} \left(\frac{1}{\hbar} \frac{\partial E_{\mathbf{k}}}{\partial \mathbf{k}} \wedge \mathbf{H} \right) \cdot \frac{1}{\hbar} \frac{\partial}{\partial \mathbf{k}} \{\mathbf{k}|f|\mathbf{k}\} \\ + \sum_{\mathbf{k}'} [W_{\mathbf{k}\mathbf{k}'}\{\mathbf{k}|f|\mathbf{k}\} - W_{\mathbf{k}\mathbf{k}'}\{\mathbf{k}'|f|\mathbf{k}'\}] = 0. \quad \dots\dots (3.35)$$

This is the usual Boltzmann equation (Jones and Zener 1934, Peierls 1931, 1932).

§ 4. CORRECTIONS TO THE BOLTZMANN EQUATION

In this section we shall investigate the corrections that appear when the magnetic field and scattering potential are included to higher order than that required to give the Boltzmann equation (3.35), and in this way deduce the conditions under which this equation is valid.

We shall solve the exact equations (3.12), (3.13) for f_d and f_{nd} in ascending powers of λ_H and λ_w . We assume that

$$f_d = f_d^{(-2)} + f_d^{(-1)} + f_d^{(0)} + \dots \quad \dots\dots (4.1)$$

$$f_{nd} = f_{nd}^{(-1)} + f_{nd}^{(0)} + \dots \quad \dots\dots (4.2)$$

where

$$f_d^{(n)} \sim \lambda_w^n \text{ function of } (\lambda_H/\lambda_w) \quad \dots\dots (4.3)$$

and f becomes $f_d^{(-2)}$ in the limit $s \rightarrow 0$. λ_s has here been treated as small compared with λ_w , and from now on s is only retained to define the path of integration near the poles caused by the energy denominators, as in the derivation of (3.29). This procedure is a valid one as long as s is sufficient to fix the sign of the imaginary part of the energy denominators. If in higher order the energy denominator is modified in the following manner:

$$\frac{1}{i\hbar s - \Delta} \rightarrow \frac{1}{i\hbar s + i\alpha\hbar\omega - \Delta}$$

where α is real and about unity, but of unknown sign, the path is not defined unless $\hbar\omega \lesssim \hbar s$. Since we here want $\lambda_s \ll \lambda_w$ we would then require $\omega\tau \ll 1$. It will be seen however that such a situation does not arise.

By writing f_d as a power series in λ_H and λ_w we have eliminated any part of f_d which may have the form $\exp(-\pi^2 kT/(\hbar\omega))$, for this cannot be expanded in powers of λ_H . Such a term is expected to account for the de Haas-Schubnikov oscillations of the conductivity, which therefore cannot be treated by this method.

All inhomogeneous terms and integral operators are expanded in the same way. For example

$$C_d = C_d^{(0)} + C_d^{(1)} + \dots \quad \dots\dots (4.4)$$

while

$$\mathcal{W} \equiv \mathcal{W}^{(1)} \equiv \hat{\mathcal{W}}; \quad \mathcal{H}^d_d \equiv \mathcal{H}^d_d^{(2)} \equiv \hat{\mathcal{H}}^d_d. \quad \dots\dots (4.5)$$

Then the first three equations for the successive parts of f_d can be shown to be

$$C_d^{(0)} = \mathcal{H}^d_d^{(2)} f_d^{(-2)} + \mathcal{W}^{nd}_{nd^{(1)}} \frac{1}{i\hbar s - \mathcal{H}^{nd}_{nd^{(0)}}} \mathcal{W}^{nd}_{nd^{(1)}} f_d^{(-2)}, \quad \dots\dots (4.6)$$

$$C_d^{(1)} = \mathcal{H}_d^{(2)} f_d^{(-1)} + \mathcal{W}_{nd}^{(1)} \frac{1}{i\hbar s - \mathcal{H}_{nd}^{(0)}} \left[\mathcal{W}_{nd}^{(1)} f_d^{(-1)} + \mathcal{W}_{nd}^{(1)} \frac{1}{i\hbar s - \mathcal{H}_{nd}^{(0)}} \mathcal{W}_{nd}^{(1)} f_d^{(-2)} \right] \dots (4.7)$$

$$C_d^{(2)} = \mathcal{H}_d^{(2)} f_d^{(0)} + \mathcal{W}_{nd}^{(1)} \frac{1}{i\hbar s - \mathcal{H}_{nd}^{(0)}} \left[\mathcal{W}_{nd}^{(1)} f_d^{(0)} - C_{nd}^{(1)} + \mathcal{H}_{nd}^{(2)} \frac{1}{i\hbar s - \mathcal{H}_{nd}^{(0)}} \mathcal{W}_{nd}^{(1)} f_d^{(-2)} \right] + \mathcal{W}_{nd}^{(1)} \frac{1}{i\hbar s - \mathcal{H}_{nd}^{(0)}} \left\{ \mathcal{W}_{nd}^{(1)} f_d^{(-1)} + \mathcal{W}_{nd}^{(1)} \frac{1}{i\hbar s - \mathcal{H}_{nd}^{(0)}} \times \mathcal{W}_{nd}^{(1)} f_d^{(-2)} \right\} \dots (4.8)$$

Equation (4.6) is the Boltzmann equation (3.35). The higher order equations can be simplified by a convenient choice of the zero point of potential, and by the use of the diagonal singularity property (2.1). For $\langle \mathbf{k} | W | \mathbf{k} \rangle = \int W(\mathbf{r}) d^3\mathbf{r}$ can be chosen to be zero. $C_d^{(1)}$ contains this as a factor and is then zero. The diagonal singularity property can be used to eliminate any term containing

$$\dots \mathcal{W}_{nd}^{(1)} \frac{1}{i\hbar s - \mathcal{H}_{nd}^{(0)}} \mathcal{W}_{nd}^{(1)} \dots$$

which written in detail is

$$\dots \sum_{\mathbf{k}_1 \mathbf{k}_2} \langle \mathbf{k} | W | \mathbf{k}_1 \rangle \left\{ \frac{\delta_{\mathbf{k} \mathbf{k}_2} - \delta_{\mathbf{k}_1 \mathbf{k}_2}}{i\hbar s - (E_{\mathbf{k}_1} - E_{\mathbf{k}'})} + \frac{\delta_{\mathbf{k}_1 \mathbf{k}_2} - \delta_{\mathbf{k} \mathbf{k}_2}}{i\hbar s - (E_{\mathbf{k}_1} - E_{\mathbf{k}'})} \right\} \langle \mathbf{k}_1 | W | \mathbf{k}' \rangle \dots$$

where $\mathbf{k} \neq \mathbf{k}'$. This factor vanishes because of (2.1). The inhomogeneous term of Eqn (4.7) therefore vanishes and we may take $f_d^{(-1)}$ equal to zero. Eqn (4.8) then simplifies to

$$I_w^{(2)} + I_H^{(2)} = \mathcal{H}_d^{(2)} f_d^{(0)} + \mathcal{W}_{nd}^{(1)} \frac{1}{i\hbar s - \mathcal{H}_{nd}^{(0)}} \mathcal{W}_{nd}^{(1)} f_d^{(0)} \dots (4.9)$$

where the two parts of the inhomogeneous term are

$$I_w^{(2)} = C_d^{(2)} + \mathcal{W}_{nd}^{(1)} \frac{1}{i\hbar s - \mathcal{H}_{nd}^{(0)}} C_{nd}^{(1)}, \dots (4.10)$$

$$I_H^{(2)} = -\mathcal{W}_{nd}^{(1)} \frac{1}{i\hbar s - \mathcal{H}_{nd}^{(0)}} \mathcal{H}_{nd}^{(2)} \frac{1}{i\hbar s - \mathcal{H}_{nd}^{(0)}} \mathcal{W}_{nd}^{(1)} f_d^{(-2)}. \dots (4.11)$$

Since $C_{nd}^{(1)}$ depends only on the scattering perturbation the second part of $I_w^{(2)}$ is independent of the magnetic field. $C_d^{(2)}$ also has this property, for the part of $C_d^{(2)}$ due to the magnetic field is

$$[C_d^{(2)}(\mathbf{k})]_{\text{field}} = ie\mathcal{E} \cdot \frac{\partial}{\partial \mathbf{k}} f_H^{(2)}(\mathbf{k}) \dots (4.12)$$

where

$$f_H^{(2)}(\mathbf{k}) = \epsilon \left[\frac{i}{2} \langle \mathbf{k} | y \rho_0 x - x \rho_0 y | \mathbf{k} \rangle - \hbar \langle \mathbf{k} | \frac{\partial \rho_0}{\partial \mathcal{H}_0} v_y x | \mathbf{k} \rangle \right]_{H=0, W=0} \dots (4.13)$$

the two parts of which cancel for the one-band model. Hence $I_W^{(2)}$ is a correction due to the scattering only, and is given in detail by Kohn and Luttinger. $I_H^{(2)}$ contains all the corrections caused by the magnetic field. A detailed analysis shows that

$$I_H^{(2)}(\mathbf{k}) = 2i\mathcal{R} \sum_{\mathbf{k}_1} \langle \mathbf{k} | W | \mathbf{k}_1 \rangle \frac{1}{i\hbar s - (E_{\mathbf{k}_1} - E_{\mathbf{k}})} \frac{e}{\hbar c} \mathbf{H} \cdot \left(\frac{\partial E_{\mathbf{k}_1}}{\partial \mathbf{k}_1} - \frac{\partial E_{\mathbf{k}}}{\partial \mathbf{k}} \right) \wedge \left[\left(\frac{\partial}{\partial \mathbf{k}_1} - \mathbf{J}(\mathbf{k}_1) \right) - \left(\frac{\partial}{\partial \mathbf{k}} - \mathbf{J}(\mathbf{k}) \right) \right] \frac{1}{i\hbar s - (E_{\mathbf{k}_1} - E_{\mathbf{k}})} \langle \mathbf{k}_1 | W | \mathbf{k} \rangle [f^{(-2)}(\mathbf{k}) - f^{(-2)}(\mathbf{k}_1)] \dots (4.14)$$

where $\mathbf{J}(\mathbf{k})$ is defined by Eqn (A 5) of the Appendix.

In order to investigate the accuracy of the conductivity derived from the Boltzmann equation it is necessary to solve Eqns (4.6), (4.9) for $f_d^{(-2)}$, $f_d^{(0)}$ and estimate the ratio of the current components caused by a given electric field:

$$\frac{j_\mu^{(0)}}{j_\mu^{(-2)}} = \frac{\int \frac{\partial E_{\mathbf{k}}}{\partial k_\mu} f_d^{(0)} d^3 \mathbf{k}}{\int \frac{\partial E_{\mathbf{k}}}{\partial k_\mu} f_d^{(-2)} d^3 \mathbf{k}} \dots (4.15)$$

The solution of the equations requires a knowledge of the inverse operator

$$\left[\mathcal{H}_d^{(2)} + \mathcal{W}_{nd}^{(1)} \frac{1}{i\hbar s - \mathcal{H}_{nd}^{(0)}} \mathcal{W}_{nd}^{(1)} \right]^{-1}.$$

This we know explicitly for a simple case, and our detailed arguments from now on concern this case though they may be applicable generally.

We consider the simple case where the energy surfaces are spherical. Here $\mathcal{H}_d^{(2)}$ is a simple multiple of the z component of the angular momentum operator and if the scattering is spherically symmetric depending only on the angle of scattering, it is advantageous to expand the transition probability per unit time in terms of spherical harmonics:

$$W_{\mathbf{k}\mathbf{k}'} = W(\Theta) = \sum_l \frac{w_l}{2l+1} P_l(\cos \Theta) \dots (4.16)$$

where Θ is the angle between \mathbf{k} and \mathbf{k}' . Then one can show that the harmonic Y_{lm} is an eigenfunction of the integral operator, with eigenvalue $i\hbar(\frac{1}{2}m\omega + w_l - w_0)$:

$$\left[\mathcal{H}_d^{(2)} + \mathcal{W}_{nd}^{(1)} \frac{1}{i\hbar s - \mathcal{H}_{nd}^{(0)}} \mathcal{W}_{nd}^{(1)} \right] Y_{lm} = i\hbar(\frac{1}{2}m\omega + w_l - w_0) Y_{lm} \dots (4.17)$$

Hence the solutions of Eqns (4.6), (4.9) are in this case easily obtained in terms of the expansions of the inhomogeneous terms in spherical harmonics. The corresponding contributions to the current are

$$j_\mu^{(r)} = \frac{e\hbar}{m} \sum_{lm} \frac{k_{\mu lm} I_{lm}^{(r+2)}}{\frac{1}{2}m\hbar\omega + i\hbar(w_l - w_0)} \quad r = -2, 0 \dots (4.18)$$

where

$$I_{lm}^{(r)} = \sum I^{(r)} Y_{lm}, \quad \dots\dots (4.19)$$

$$k_{\mu lm} = \sum k_{\mu} Y_{lm}. \quad \dots\dots (4.20)$$

$I^{(0)}$ is given by Eqn (3.23) and since $I^{(2)}$ consists of the two parts $I_w^{(2)}$ and $I_H^{(2)}$ we split $j_{\mu}^{(0)}$ into corresponding parts $j_{\mu w}^{(0)}$ and $j_{\mu H}^{(0)}$. We consider in turn the ratio of each of these to $j_{\mu}^{(-2)}$, using dimensional arguments.

(i) $j_{\mu w}^{(0)} / j_{\mu}^{(-2)}$

$$= \frac{\sum_{lm} \sum_k \frac{k_{lm} Y_{lm}}{\frac{1}{2} im \hbar \omega + i \hbar (w_l - w_0)} \left\{ C_d^{(2)} + \mathcal{W}_{nd}^{(1)} \frac{1}{i \hbar s - \mathcal{H}_{nd}^{(0)}} C_{nd}^{(1)} \right\}}{\sum_{lm} \sum_k \frac{k_{lm} Y_{lm} ie \mathfrak{E} \cdot (\partial / \partial \mathbf{k}) f_0(E_k)}{\frac{1}{2} im \hbar \omega + i \hbar (w_l - w_0)}} \quad \dots\dots (4.21)$$

This ratio differs only by the terms $\frac{1}{2} im \hbar \omega$ in the denominators from a correction evaluated by Chester and Thellung (1959) for the field-free case. It is easy to verify that there are no singular points in the summation in $j_{\mu w}^{(0)}$ and that the sum converges at large energies. The only fast-varying factors in the sum are energy denominators, and derivatives of Fermi functions. We replace the latter by their values at absolute zero, with errors of the order kT/ζ . We now write all wave vectors in terms of the Fermi wave number. Then

$$\frac{j_{\mu w}^{(0)}}{j_{\mu}^{(-2)}} = \frac{\hbar / \tau}{\zeta} \frac{\sum_z \sum_{z'} \phi_1(z, z') \alpha(z, \omega, \tau)}{\sum_z \phi_2(z) \alpha(z, \omega, \tau)} \quad \dots\dots (4.22)$$

where

$$\alpha(z, \omega, \tau) = \sum_{lm} \frac{z_{lm} Y_{lm}}{m \hbar \omega + \hbar (w_l - w_0)} \quad \dots\dots (4.23)$$

and ϕ_1 and ϕ_2 are functions of the dimensionless variables z, z' . τ is some mean value of the relaxation times $\tau_l = (w_l - w_0)^{-1}$. The dependence of α on ω or τ can be factored out when either $\omega \tau \ll 1$ or $\omega \tau \gg 1$ and the ratio of the currents is then of the order $(\hbar / \tau) / \zeta$ since each of the integrals over z, z' then yields a number about unity. For intermediate values of $\omega \tau$ the integrals in the numerator and denominator of (4.22) are different functions of $\omega \tau$. These functions are slowly varying and because of their similar limiting behaviour their ratio is never likely to differ appreciably from one.

(ii) We may write the ratio of $j_{\mu H}^{(0)}$ to $j_{\mu}^{(-2)}$ in the following way:

$$\begin{aligned} \frac{j_{\mu H}^{(0)}}{j_{\mu}^{(-2)}} &= \left[\sum_{lm} \sum_k \frac{ie \mathfrak{E} \cdot (\partial / \partial \mathbf{k}) f_0 Y_{lm} k_{lm}}{\frac{1}{2} im \hbar \omega + i \hbar (w_l - w_0)} \right]^{-1} \\ &\times \sum_{lm} \sum_{l'm'} \frac{ie \mathfrak{E} \cdot (\partial / \partial \mathbf{k}) f_0 Y_{lm}(k) Y_{l'm'}(k')}{\frac{1}{2} im \hbar \omega + i \hbar (w_l - w_0)} \mathcal{W}_{d}^{nd(1)} \frac{1}{i \hbar s - \mathcal{H}_{nd}^{(0)}} \mathcal{H}_{nd}^{nd(2)} \frac{1}{i \hbar s - \mathcal{H}_{nd}^{nd(0)}} \\ &\times \mathcal{W}_{d}^{nd(1)} \frac{k_{l'm'} Y_{l'm'}}{\frac{1}{2} im' \hbar \omega + i \hbar (w_{l'} - w_0)}. \quad \dots\dots (4.24) \end{aligned}$$

Again we approximate the derivatives of Fermi functions by their values at absolute zero. Introducing dimensionless variables leads to

$$\frac{j_{\mu H}^{(0)}}{j_{\mu}^{(-2)}} = \frac{\hbar \omega}{\zeta \tau} \frac{\sum_{zz'} \phi_3(z, z') \alpha(z', \omega, \tau) \beta(z, z', \omega, \tau)}{\sum_z \phi_2(z) \alpha(z, \omega, \tau)} \quad \dots\dots (4.25)$$

where

$$\beta = \sum_{lm} \frac{Y_{lm}(z)Y_{lm}(z')}{m\hbar\omega + \hbar(w_1 - w_0)}. \quad \dots\dots(4.26)$$

In the limits $\omega\tau \gg 1$ it is possible to factor out the dependence of α, β on ω, τ and the ratio (4.25) becomes approximately $(\hbar/\tau)/\zeta$ for $\omega\tau \gg 1$, and approximately $\hbar\omega/\zeta$ for $\omega\tau \ll 1$. A slowly varying function of $\omega\tau$ with this limiting behaviour is $\hbar\omega/\zeta(1 + \omega\tau)^{-1}$ and the ratio should differ little from this value.

The correction $j_\mu^0 = j_{\mu_v}^{(0)} + j_{\mu_H}^{(0)}$ is therefore small compared with $j_\mu^{(-2)}$ provided $\hbar\omega, \hbar/\tau \ll \zeta$. However, we expect $j_\mu^{(-2)}$ to differ appreciably from the total current if $\hbar\omega \gtrsim kT$ because of the inability of the expansion method to treat the de Haas-Schubnikov terms in the conductivity. The Boltzmann equation therefore only gives a good approximation to the conductivity if (1.3) is satisfied.

§ 5. CONCLUSION

It has been shown that in the presence of a magnetic field the Boltzmann equation for a simple distribution function can be derived by a weak coupling approach which proceeds from the equation of motion of the quantum mechanical density matrix. The analysis was made convenient by the use of a representation in which it was expected on the grounds of invariance arguments that the diagonal elements of the density matrix would be much larger than the off-diagonal elements. Thus the analysis is similar to the treatment of the field-free problem where it was possible to use the momentum representation. The representation we have employed is of the Wigner type and the diagonal elements of the density matrix in this representation are all that are required for computing the average values of the three operators j_x, j_y, j_z . It is remarkable that the Boltzmann equation satisfied by this distribution function is identical with that derived by Jones and Zener (1934) on the basis of wave-packet analysis. We have therefore clarified the usual idea that individual electrons can be regarded as localized in \mathbf{k} -space, and that the Lorentz force equation is valid for them.

At no point in the analysis is it necessary to assume $\omega\tau < 1$ and the corrections estimated in §4 are all small provided $\hbar\omega, \hbar/\tau \ll \zeta, \hbar\omega \lesssim kT$. Thus the application of the Boltzmann equation for arbitrary $\omega\tau$, required in the recent theories of the linear law, has been justified. Of the remaining limitations on the magnetic field, $\hbar\omega \lesssim kT$ ensures that the border region of the Fermi distribution extends over several energy levels, and $\hbar\omega \ll \zeta$ implies that states with high quantum numbers are occupied. These conditions remove any quantum effects associated with the magnetic field.

ACKNOWLEDGMENTS

The author wishes to express his sincere appreciation of the guidance and encouragement provided by Professor R. E. Peierls who suggested the problem, and to thank Dr. G. V. Chester for his constant help during the course of this work.

The award of a research studentship by the Department of Scientific and Industrial Research is also gratefully acknowledged.

REFERENCES

- ALEKSEEVSKII, N. E., and GAIDUKOV, I. U., 1959, *Soviet Physics-JETP*, **35**(8), 383.
 ARGYRES, P. N., 1958 a, *J. Phys. Chem. Solids*, **4**, 19.
 — 1958 b, *Phys. Rev.*, **109**, 1115.
 CHESTER, G. V., and THELLUNG, A., 1959, *Proc. Phys. Soc.*, **73**, 745.
 DIRAC, P. A. M., 1947, *The Principles of Quantum Mechanics*, 3rd Edn (Oxford: Clarendon Press).
 GREENWOOD, D. A., 1958, *Proc. Phys. Soc.*, **71**, 585.
 JONES, H., and ZENER, C., 1934, *Proc. Roy. Soc. A*, **144**, 101.
 KAPITZA, P., 1924, *Proc. Roy. Soc. A*, **105**, 691.
 KARPLUS, R., and LUTTINGER, J. M., 1954, *Phys. Rev.*, **95**, 1154.
 KOHN, W., and LUTTINGER, J. M., 1957, *Phys. Rev.*, **108**, 590.
 LIFSHITZ, I. M., and PESCHANSKII, V. G., 1959, *Soviet Physics-JETP*, **35**(8), 875.
 — 1960, *Soviet Physics-JETP*, **38**(11), 137.
 PAULI, W., 1933, *Handb. d. Phys.*, Vol 24, 2nd Edn (Berlin: Springer).
 PEIERLS, R. E., 1931, *Ann. Phys., Lpz.*, **10**, 97.
 — 1932, *Ergebn. exakt. Naturw.*, **11**, 264.
 VAN HOVE, L., 1955, *Physica*, **21**, 517.
 WIGNER, E., 1932, *Phys. Rev.*, **40**, 749.
 ZIMAN, J. M., 1958, *Phil. Mag.*, **3**, 1117.

APPENDIX

The Evaluation of \mathcal{H}_d

The term in (3.10) giving $\mathcal{H}_d(\mathbf{k}; \mathbf{k}|\mathbf{k}_1; \mathbf{k}_1)$ contains the matrix element in configuration space of \mathcal{H}_0 :

$$\langle \mathbf{r}_1 | \mathcal{H}_0 | \mathbf{r}_3 \rangle = \frac{1}{2m} \left\{ -\hbar^2 \frac{\partial^2}{\partial \mathbf{r}_1^2} - \frac{2e\hbar}{ic} \mathbf{A}(\mathbf{r}_3) \cdot \frac{\partial}{\partial \mathbf{r}_1} + \frac{e^2}{c^2} A^2(\mathbf{r}_1) + 2mV_0(\mathbf{r}_1) \right\} \delta(\mathbf{r}_1 - \mathbf{r}_3) \quad \text{..... (A1)}$$

where V_0 is the lattice potential. Inserting this expression into (3.10) and performing partial integrations with respect to \mathbf{r}_1 :

$$\begin{aligned} \mathcal{H}_d(\mathbf{k}; \mathbf{k}|\mathbf{k}_1; \mathbf{k}_1) &= \mathcal{J} \frac{1}{m} \int d^3\mathbf{r}_1 d^3\mathbf{r}_2 d^3\mathbf{r}_3 \delta(\mathbf{r}_1 - \mathbf{r}_3) \\ &\times \left\{ -\hbar^2 \left[\frac{\partial}{\partial \mathbf{r}_1} + \left(\frac{i\epsilon}{2} \right) \mathbf{d}_{12} \right]^2 - \frac{2e\hbar}{ic} Hx_1 \left[\frac{\partial}{\partial y_1} + i\epsilon X_{12} \right] + \frac{e^2 H^2}{c^2} x_1^2 + 2mV_0(\mathbf{r}_1) \right\} \\ &\times \psi_{\mathbf{k}}^*(\mathbf{r}_1) \psi_{\mathbf{k}}(\mathbf{r}_2) \psi_{\mathbf{k}_1}(\mathbf{r}_3) \psi_{\mathbf{k}_1}^*(\mathbf{r}_2) \quad \text{..... (A2)} \end{aligned}$$

where \mathbf{d}_{12} is the vector with components $(y_{12}, 2X_{12}, 0)$ produced by the action of the differential operators on the phase factors $\{\exp[y_{12}X_{12} - y_{32}X_{32}]\}$. The phase factors can be replaced by unity after the differentiation since $[y_{12}X_{12} - y_{32}X_{32}]$ vanishes when $\mathbf{r}_1 = \mathbf{r}_3$. The term in (A2) independent of the magnetic field can be written as the zero field limit of $2\mathcal{J} \langle \mathbf{k} | \mathcal{H}_0 | \mathbf{k}_1 \rangle \delta_{\mathbf{k}\mathbf{k}_1}$, which vanishes. The term proportional to H^2 is a linear combination of terms like $\mathcal{J} \langle \mathbf{k} | x^2 | \mathbf{k}_1 \rangle \delta_{\mathbf{k}\mathbf{k}_1}$ and terms like $\mathcal{J} |\langle \mathbf{k} | y | \mathbf{k}_1 \rangle|^2$. Both types vanish. Hence \mathcal{H}_d contains only the term linear in the magnetic field. This can be reduced to

$$\begin{aligned} \mathcal{H}_d(\mathbf{k}; \mathbf{k}|\mathbf{k}_1; \mathbf{k}_1) &\equiv \mathcal{H}_d(\mathbf{k}; \mathbf{k}|\mathbf{k}_1; \mathbf{k}_1) \\ &= \frac{eH}{mc} \left\{ \begin{aligned} &\langle \mathbf{k} | p_y | \mathbf{k}_1 \rangle \langle \mathbf{k}_1 | x | \mathbf{k} \rangle - \langle \mathbf{k} | x | \mathbf{k}_1 \rangle \langle \mathbf{k}_1 | p_y | \mathbf{k} \rangle \\ &- \langle \mathbf{k} | p_x | \mathbf{k}_1 \rangle \langle \mathbf{k}_1 | y | \mathbf{k} \rangle + \langle \mathbf{k} | y | \mathbf{k}_1 \rangle \langle \mathbf{k}_1 | p_x | \mathbf{k} \rangle \end{aligned} \right\} \quad \text{..... (A3)} \end{aligned}$$

where \mathbf{p} is the momentum operator. Now

$$\langle \mathbf{k} | \mathbf{r} | \mathbf{k}_1 \rangle = i \frac{\partial}{\partial \mathbf{k}} \delta_{\mathbf{k}\mathbf{k}_1} + i \mathbf{J}(\mathbf{k}) \delta_{\mathbf{k}\mathbf{k}_1} \quad \dots\dots (A 4)$$

where

$$\mathbf{J}(\mathbf{k}) = \int u_{\mathbf{k}}^*(\mathbf{r}) \frac{\partial}{\partial \mathbf{k}} u_{\mathbf{k}}(\mathbf{r}) d^3\mathbf{r} \quad \dots\dots (A 5)$$

and the diagonal matrix elements of the velocity operator can be written simply as

$$\langle \mathbf{k} | \mathbf{v} | \mathbf{k} \rangle = \frac{1}{\hbar} \frac{\partial E(\mathbf{k})}{\partial \mathbf{k}} \quad \dots\dots (A 6)$$

(Jones and Zener 1934, Karplus and Luttinger 1954). The contribution of \mathbf{J} to the right-hand side of (A 3) vanishes identically leaving

$$\sum_{\mathbf{k}_1} \hat{\mathcal{H}}_d(\mathbf{k}; \mathbf{k} | \mathbf{k}_1; \mathbf{k}_1) \{ \mathbf{k}_1 | \hat{f} | \mathbf{k}_1 \} = - \frac{ie}{\hbar c} \left(\frac{\partial E_{\mathbf{k}}}{\partial \mathbf{k}} \wedge \mathbf{H} \right) \cdot \frac{\partial}{\partial \mathbf{k}} \{ \mathbf{k} | \hat{f} | \mathbf{k} \}. \quad \dots\dots (A 7)$$

The Possibility of Negative Resistance Effects in Semiconductors

By B. K. RIDLEY AND T. B. WATKINS

Mullard Research Laboratories, Salfords, Nr. Redhill, Surrey

MS. received 22nd February 1961

Abstract. The possibility of obtaining negative resistance effects in a new way in semiconductors is discussed. The principle of the method is to heat carriers in a high mobility sub-band with an electric field so that they transfer when they have a high enough 'temperature' to a higher energy low mobility sub-band. The conditions required for negative resistance are discussed generally and more specific conditions are obtained for some simple cases of spherical and ellipsoidal bands by solving the Boltzmann equation. It is shown that the most favourable case is when the sub-bands are sufficiently separated in energy for the emission of optical phonons to be the dominant mechanism for energy relaxation in both sub-bands. Ge-Si alloys and some III-V compounds may have suitable sub-band structures in the conduction bands. The case of p-type uniaxially strained silicon appears to be marginal in the region where the current is proportional to the square root of the electric field. The electrical instability of a crystal with a differential negative resistance is briefly discussed and it is pointed out that some sort of 'electrical domain' formation may establish itself and inhibit the observation of negative resistance. Side effects which can influence the condition for negative resistance such as specimen heating, which is advantageous, and impact ionization, which is deleterious, are also discussed.

§ 1. INTRODUCTION

IT has recently been proposed by Krömer (1958) that certain energy band structure properties giving rise to a negative effective mass may be used to obtain negative resistance effects in semiconducting crystals. The chief difficulty appears to be finding a means of making a sufficiently large proportion of the carriers have negative mass.

In this paper the possibility of using other band structure properties to produce negative resistance effects is considered. The approach taken is to study means of varying the average effective mass of the carriers.

The conduction and valence bands in semiconductors consist of a number of sub-bands, and for normal conduction only the sub-bands with lowest carrier energy are effective. The next highest sub-band may be separated from the lowest sub-band by a large fraction of an electron volt. Sub-bands with very much smaller separation in energy can sometimes be produced by the effects of strain. For example, in germanium the conduction band has four sets of ellipsoidal constant energy surfaces in the [111] direction in k space, while the valence band is doubly degenerate at $k=0$, the two bands giving light and heavy holes. In both cases a strain will produce separate sets of sub-bands. In the conduction band two valleys go down and two rise in energy, and in the valence band the degeneracy is removed and two sub-bands separated in energy result.

According to the curvature of the bands and the direction of the applied electric field the carriers in the sub-bands will have different resultant effective masses. The average effective mass and hence the conductance of the crystal will depend on the relative populations of each sub-band, and this will be a function of carrier temperature. This may be varied with an applied electric field, and in what follows we shall see that under certain conditions it may be possible to use this effect to make the semiconducting crystal exhibit negative resistance effects.

§ 2. THE VARIATION OF CURRENT WITH FIELD

Let us consider the conduction band to consist of two sub-bands which may be represented in the (ϵ, k) diagram, as shown in Fig. 1. The lower band is denoted 'a' and the upper 'b'. The energies of the minima are $\epsilon_{a,b}$ and their

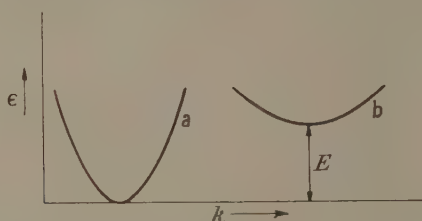


Fig. 1. Two sub-bands in a semiconductor.

energy difference E . Their effective density of states are $N_{a,b}$. We assume that the k direction is along a principal axis which is parallel to the electric field F and the effective masses and mobilities are $m_{a,b}$ and $\mu_{a,b}$. The numbers of electrons per cubic centimetre in the bands are $n_{a,b}$. The conductivity is then given by

$$G = e(\mu_a n_a + \mu_b n_b). \quad \dots (1)$$

When a sufficiently high electric field is applied to the crystal the electrons are accelerated and their effective temperature rises above the lattice temperature, and in general we must also expect the lattice temperature to increase. The effect of this will be not only to alter the mobilities but also to alter the electron densities in the bands. The incremental variation of conductivity with field may be written

$$\frac{dG}{dF} = e \left(\mu_a \frac{dn_a}{dF} + \mu_b \frac{dn_b}{dF} \right) + e \left(n_a \frac{d\mu_a}{dF} + n_b \frac{d\mu_b}{dF} \right)$$

or, putting $n_a + n_b = n$, where n is constant, and taking $\mu_a, b \propto F^p$,

$$\frac{dG}{dF} = e(\mu_a - \mu_b) \frac{dn_a}{dF} + e(\mu_a n_a + \mu_b n_b) \frac{p}{F}. \quad \dots (2)$$

Since the current density

$$J = GF$$

and

$$\frac{dJ}{dF} = G + F \frac{dG}{dF},$$

the condition for negative resistance is

$$-\frac{dG}{dF} \bigg/ \frac{G}{F} > 1$$

or, from Eqns (1) and (2) with $f = n_b/n_a$,

$$\left[\left(\frac{\mu_a - \mu_b}{\mu_a + f\mu_b} \right) \left(-\frac{F}{n_a} \frac{dn_a}{dF} \right) - p \right] > 1. \quad \dots\dots(3)$$

In the next section we will examine the conditions for negative resistance by solving the Boltzmann equation for particular simple cases to gain a more detailed insight into the effect. Here we wish to limit ourselves to some general observations concerning the inequality expressed above.

The field exponent p is a function of the scattering mechanism and should be negative and large. This makes impurity scattering quite undesirable since when this is dominant the mobility rises with increasing field and thus p is positive. When lattice scattering is dominant, however, p is negative and will depend on the lattice and carrier temperatures. When the lattice temperature remains constant there are three distinct regions in the current-voltage relationship for hot electrons at low lattice temperatures ($\lesssim 20^\circ\text{K}$).

(i) The $F^{1/2}$ region where acoustic phonon collision scattering is dominant, $p = -0.5$.

(ii) The $F^{1/3}$ region where the emission of acoustic phonons is the dominant scattering mechanism, $p = -0.8$ (e.g. Stratton 1957, Conwell and Brown 1960).

(iii) The F^0 region where optical phonon scattering is dominant, $p = -1.0$. We see immediately that any contribution from the first term of Eqn (3) in region (iii) will give negative resistance. Such a contribution will arise when electrons become hot enough to spill over into the upper band, providing the upper band has a lower mobility.

(iv) Another case may be considered in which the lattice temperature is allowed to increase with field. To see the effect of this we imagine a one band case in which the lattice temperature is predominantly determined by the heat produced per unit volume Q , due to the current, but is still small compared with the electron temperature, so that

$$T \propto QF \propto F^2 \mu.$$

In the $F^{1/2}$ region $\mu \propto F^{-1/2} T^{-3/4}$ (Eqn (7); also Yamashita and Watanabe 1954), so $\mu \propto F^{-8/7}$, that is, $p = -8/7$, giving negative resistance without any contribution from the band structure. This is an extreme case, but it illustrates that Joule heating is generally advantageous to negative resistance.

The first bracket in Eqn (3) is straightforward—we must have $\mu_a > \mu_b$. Electrons must begin in a low mass band and transfer to a high mass band when they are heated by the field. The maximum value of this term is unity, i.e. when $\mu_a \gg \mu_b$.

The second bracket is not so easy to deal with. It represents the rate with field at which electrons transfer to the upper band and this will depend upon differences between the bands of effective density of states, electron temperature, and the energy gap between the sub-bands. To obtain an idea of its value let us assume a common electron temperature T_e and a Maxwell-Boltzmann distribution. If we have $T_e \propto F^q$ then

$$-\frac{F}{n_a} \frac{dn_a}{dF} = -q \frac{T_e}{n_a} \frac{dn_a}{dT_e}.$$

If E is the band separation it may be shown that with $f = (N_b/N_a) \exp(-E/kT_e)$

$$-\frac{T_e}{n_a} \frac{dn_a}{dT_e} = \frac{f}{1+f} \left(\log \frac{N_b}{N_a} - \log f \right),$$

where $N_{a,b}$ are the effective densities of states, which has a maximum value when

$$\log \frac{N_b}{N_a} - \log f = 1 + f.$$

As an example, let us consider the $F^{1/2}$ region and take the first bracket to be unity. Although the distribution is not Maxwellian let us nevertheless take our electron temperature to have the same dependence on the field as is obtained in the actual case, namely $T_e \propto F$. Thus q is also unity. Since $p = -0.5$ we must have $f > 0.5$ and $-(T_e/n_a)(dn_a/dT_e)$ at a maximum to obtain negative resistance. For the limiting case of $f = 0.5$, $N_b/N_a \sim 2.25$ and $E = 1.5kT_e$. Such requirements are not obviously impracticable. The condition for E is not very sensitive to the ratio N_b/N_a . When $N_b/N_a = 1$, $f = 0.3$ and $E = 1.3kT_e$. The more detailed calculations of the next section show that negative resistance, if possible, occurs at values of kT_e which are somewhat less than the band separation, in agreement with this estimate.

§ 3. NEGATIVE RESISTANCE IN PARTICULAR CASES

To clarify ideas it is worth while to consider a particularly simple model of two spherical energy bands displaced from one another by an energy E at $k=0$ (Fig. 2), the lower band having the lower effective mass. Such a situation is unlikely to occur naturally but if the spherical bands are replaced by suitably oriented ellipsoidal bands we come nearer to a practically realizable state, e.g. uniaxially strained p-type germanium. But to continue with the simple case, we assume that the dominant scattering is due to the interaction with a fully

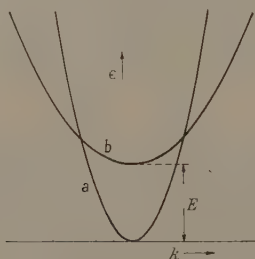


Fig. 2. Two spherical sub-bands with minima at $k=0$.

excited distribution of longitudinal acoustic phonons and that the matrix element governing interband transitions is of the same form as that governing intraband transitions. The first assumption means that we are dealing with conditions which in a single band would give rise to the $F^{-1/2}$ factor in the mobility law for hot electrons.

The Boltzmann equation for the lower band is

$$\left(\frac{\partial f_a}{\partial t}\right)_{\text{field}} + \left(\frac{\partial f_a}{\partial t}\right)_{\text{intra}} + \left(\frac{\partial f_a}{\partial t}\right)_{\text{inter}} = 0$$

and a similar equation exists for the upper band. The individual terms can be obtained in the usual way by expanding the electronic distribution function f_a in spherical harmonics and taking the phonon energy to be small compared with the

electron energy. Only the first two terms of the spherical harmonic expansion need be used, i.e.

$$f_a = f_{a0} + f_{a1} \cos \theta$$

where θ is the angle between k and the electric field F . After some manipulation we obtain the energy and momentum relaxation equations:

$$\begin{aligned} & \frac{2}{3} \frac{(eF)^2}{m_a} \frac{\epsilon}{S_a \epsilon^{1/2} + S_{b1}(\epsilon - E)^{1/2}} \frac{d^2 f_{a0}}{d\epsilon^2} + \left[\frac{2}{3} \frac{(eF)^2}{m_a} \frac{1 - \frac{1}{2} S_{b1} E / \epsilon^{1/2} (\epsilon - E)^{1/2}}{S_a \epsilon^{1/2} + S_{b1}(\epsilon - E)^{1/2}} \right. \\ & \left. + \frac{2m_a c^2}{kT} S_a \epsilon^{3/2} \right] \frac{df_{a0}}{d\epsilon} + \frac{4m_a c^2}{kT} S_a \epsilon^{1/2} f_{a0} + [S_{b1}(\epsilon - E)^{1/2} (f_{b0} - f_{a0}) + O(2)] = 0, \quad \epsilon > E \end{aligned}$$

..... (4)

and

$$f_{a1} = - \frac{2^{1/2} eF}{m_a^{1/2}} \frac{\epsilon^{1/2}}{S_a \epsilon^{1/2} + S_{b1}(\epsilon - E)^{1/2}} \frac{df_{a0}}{d\epsilon}, \quad \epsilon > E \quad \text{..... (5)}$$

where ϵ is the energy measured from the bottom of the lower band,

$$S_a = \frac{\mathcal{E}_a^2 (2m_a)^{3/2} kT}{2\pi \rho c^2 \hbar^4}, \quad S_{b1} = \frac{\mathcal{E}_i^2 (2m_b)^{3/2} kT}{2\pi \rho c^2 \hbar^4},$$

\mathcal{E}_a and \mathcal{E}_i are deformation potentials associated with intraband and interband scattering respectively, ρ is the density and c is the velocity of the acoustic waves. $O(2)$ stands for second-order interband scattering terms which cannot be neglected in general but with which we will not be concerned in the approximations to follow. Two other similar equations occur for the upper band but these are omitted for brevity. It may be noted that the mean free path, which is the factor multiplying $eF df_{a0}/d\epsilon$ in Eqn (5), is dependent on electron energy, for energies greater than E .

3.1. Intraband Scattering Dominant

To find f_{a0} and f_{b0} we must solve two coupled second-order differential equations. We can simplify the problem, however, by taking the case of weak interband scattering and assuming that the distribution functions are determined solely by the electric field and intraband scattering. This is analogous to having a high thermal resistance between the bands so that the electrons in the lower band will differ in 'temperature' from those in the upper band. The solutions are now straightforward and we obtain

$$f_{a0} = A \exp(-\alpha_a \epsilon^2) \text{ and } f_{a1} = -2^{1/2} \frac{eF}{m_a^{1/2} S_a} \frac{df_{a0}}{d\epsilon} \quad \text{..... (6)}$$

and

$$f_{b0} = B \exp[-\alpha_b (\epsilon - E)^2] \text{ and } f_{b1} = -2^{1/2} \frac{eF}{m_b^{1/2} S_b} \frac{df_{b0}}{d(\epsilon - E)},$$

where

$$\alpha_a = \frac{3 \mathcal{E}_a^4 m_a^5 kT}{\pi^2 \rho^2 c^2 \hbar^5} \frac{1}{(eF)^2},$$

and similarly for α_b .

To obtain the constants A and B we evoke the particle balance equations

$$n_a + n_b = n, \quad dn_a/dt = 0,$$

where n is the total density of conduction electrons and n_a, n_b are the densities in

the two bands. In terms of the distribution functions these equations become

$$A \frac{4\pi(2m_a)^{3/2}}{h^3} \int_0^\infty \epsilon^{1/2} \exp(-\alpha_a \epsilon^2) d\epsilon + B \frac{4\pi(2m_b)^{3/2}}{h^3} \times \int_0^\infty (\epsilon - E)^{1/2} \exp[-\alpha_b(\epsilon - E)^2] d(\epsilon - E) = n$$

$$- A \int_E^\infty \epsilon^{1/2} (\epsilon - E)^{1/2} \exp(-\alpha_a \epsilon^2) d\epsilon + B \int_E^\infty \epsilon^{1/2} (\epsilon - E)^{1/2} \exp[-\alpha_b(\epsilon - E)^2] d\epsilon = 0.$$

In the latter equation we have neglected the second-order interband terms. This is permitted since $f_{0a} \neq f_{0b}$. Solving these equations for A and B gives us the explicit distribution functions from which the current-field relationship can be deduced in the usual way. The electron densities are given by

$$\frac{n_a}{n} = \frac{1}{1 + \beta r^3 \gamma^{9/4}}, \quad \frac{n_b}{n} = \frac{\beta r^3 \gamma^{9/4}}{1 + \beta r^3 \gamma^{9/4}}$$

where $\gamma = m_a/m_b$, $r = \mathcal{E}_a/\mathcal{E}_b$,

$$\beta = \frac{\int_1^\infty [x(x-1)]^{1/2} \exp(-\alpha_a E^2 x^2) dx}{\int_0^\infty [x(x+1)]^{1/2} \exp(-\alpha_b E^2 x^2) dx}.$$

They depend upon the field through β , which derives from the interband scattering and increases in value as the field increases. Thus as the field rises electrons spill over into the upper band. The current-field relationship is

$$J = neF\mu_a \frac{1 + \beta r^4 \gamma^{7/2}}{1 + \beta r^3 \gamma^{9/4}}, \quad \dots (7)$$

where J is the current density and the mobility μ_a is given by

$$\mu_a = \frac{2^{1/2} \pi}{3^{3/4} \Gamma(3/4)} \frac{e^{1/2} \rho^{1/2} \hbar^2 c^{3/2}}{\mathcal{E}_a m_a^{1/4} (kT)^{3/4}} \frac{1}{F^{1/2}}.$$

Equation (7), in dimensionless form, is plotted in Fig. 3 for various values of the ratio of effective masses assuming equal deformation potentials. Negative resistance is just evident for $\gamma = 0.4$ and is well established for $\gamma = 0.2$.

When we turn to the more realistic case of ellipsoidal bands we realize that three different masses arise in our equations. One is the density of states effective mass ($m_\perp m_\perp m_\perp$),^{1,3} which appears in, for example, S_a in Eqn (4), a second average mass appears in the mc^2/kT terms in the same equation, and the third is the mass in the direction of the field (the mass in the $(eF)^2/m_a$ terms in Eqn (4)). In the spherical band case the ratio of each of these masses contributes to produce negative resistance. To be now more pessimistic let us consider the case of two identical ellipsoids oriented such that their major axes are at right angles to one another and the major axis of the upper band is parallel to the electric field. This is close to the condition of the valence band in uniaxially strained p-type germanium or silicon near $k=0$. Since the ellipsoids are identical the average masses are the same and we have to rely on the ratio m_\perp/m_\parallel , i.e. the ratio of masses in the direction of the field, to give us negative resistance. Under the same conditions as before we obtain for the current

$$J = neF\mu_a \frac{1 + \beta \gamma^{3/2}}{1 + \beta \gamma^{3/4}},$$

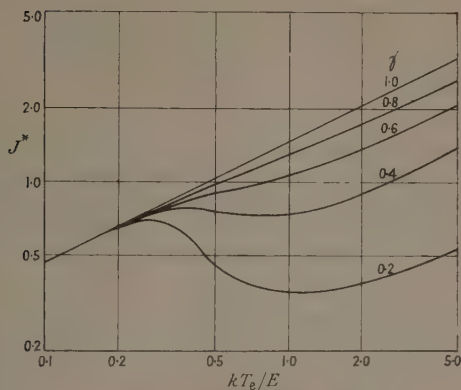


Fig. 3. Variation of current with voltage for two spherical sub-bands with minima at $k=0$, where E is the energy separation at $k=0$ and $\frac{3}{2}kT_e$ is the mean electron kinetic energy in the lower band. The dominant scattering mechanism is assumed to be collisions with longitudinal acoustic phonons with the same deformation potential operative for both bands.

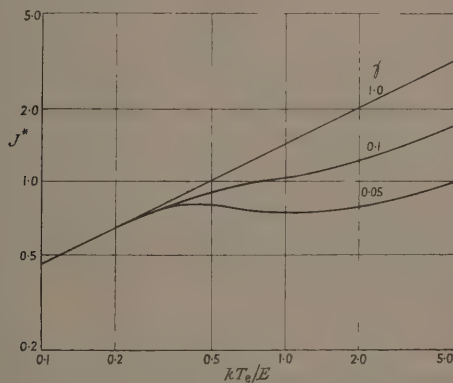


Fig. 4. Variation of current with voltage for two identically shaped ellipsoidal sub-bands with minima at $k=0$ and their major axes mutually perpendicular. The electric field is parallel to the major axis of the upper band. E is the energy separation at $k=0$ and $\frac{3}{2}kT_e$ is the mean electron kinetic energy in the lower band. The dominant scattering mechanism is assumed to be collisions with longitudinal acoustic phonons with the same deformation potential operative for both bands.

where now $\gamma = m_{\perp}/m_{\parallel}$ and μ_a is the same as before except that $m_a^{5/4}$ is replaced by $m_{\perp}^{3/4}\bar{m}^{1/2}$ where \bar{m} is an average mass. In dimensionless form this is plotted in Fig. 4 and the conditions for negative resistance are shown to be much more stringent.

3.2. General Remarks

The case just considered has been one in which the bands developed independent distribution functions, just as though they had been thermally insulated

from one another. What happens when there is no insulation? The interband scattering is now appreciable and Eqn (4) is governed by the first-order interband scattering terms so that

$$f_{a0} = f_{b0},$$

which means that the bands are at the same 'temperature'. Thus for energies below E the distribution function for the lower band will still be given by Eqn (6), since there is no interaction between the bands, but for energies above E there will be a common distribution function f_0 which will be some sort of mixture of the f_{a0} and f_{b0} of Eqn (6). Obviously, for energies just above E the density of states in the lower band is greater than that in the upper band, and $f_0 \sim f_{a0}$ for any mass ratio. For spherical bands with $\gamma < 1$ it is also clear that well above a critical energy ϵ_c the situation will be reversed and $f_0 \sim f_{b0}$; ϵ_c is the energy at which the densities of states are equal.

This case is more difficult to treat than the previous one and no attempt to do so will be made here, concerned as we are primarily with the principles behind this method of achieving negative resistance. However, there is probably very little difference in behaviour between the two cases under steady state conditions since the steady state densities of electrons in the bands are mainly governed by the densities of available states and not by the rate of transition from one band to the other. The remarks of the previous paragraph also indicate the similarity between the two cases. In fact the two cases become identical when $\gamma \ll 1$.

It should be noted that implicit in this treatment is the condition that the energy gap between the bands be large enough to ensure that no significant interaction between the bands occurs before the field is great enough to heat the upper band electrons. There is also an implicit upper limit to the energy gap defined by the condition that significant interaction between the bands is completed before the electrons in the lower band become so hot that phonon emission or optical phonon scattering becomes important. Breakdown of this condition over the critical range of field when band-to-band transitions become important can enhance the possibility of negative resistance, since the lower band mobility begins to drop more rapidly with field just at the point where electrons are lost from the lower band.

If the energy gap between the bands is large enough it is possible to make the electrons so hot before interband processes occur that optical phonons are excited and the drift velocity saturates with field. Since the saturation drift velocity is inversely proportional to the square root of the effective mass in the direction of the field (see, for example, Reik, Risken and Finger 1960), the condition for negative resistance is just $\gamma < 1$, a condition which is certainly a practical one. What is not so easy to obtain is the large energy gap.

At low lattice temperatures the scattering of hot electrons can be by emission of acoustic phonons ($J \propto F^{1.5}$). Conditions for negative resistance in this range will lie between those for the optical phonon range and the $F^{1.2}$ range.

3.3. *The Band Separation and Lattice Temperature*

It was mentioned in § 3.2 that the band separation had to be enough to allow the upper band electrons to become hot before appreciable interaction between the bands occurred. The critical field F_c for the upper band is given by $F_c \sim c/\mu_{01}$, where μ_{01} is the low field mobility. Defining an electron temperature T_e for

the lower band by

$$\frac{3}{2}kT_e = \frac{\int_0^\infty \epsilon^{3/2} \exp(-\alpha_a \epsilon^2) d\epsilon}{\int_0^\infty \epsilon^{1/2} \exp(-\alpha_a \epsilon^2) d\epsilon} = \frac{\Gamma(5/4)}{\Gamma(3/4)} \alpha_a^{-1/2},$$

we obtain the condition $kT_e/kT \gtrsim \frac{1}{3}\mu_{0a}/\mu_{0b}$. Interband interaction becomes important when $E \sim 3kT_e$, therefore the required condition is $E/kT \gtrsim \mu_{0a}/\mu_{0b}$. For spherical bands with equal deformation potentials this becomes $E/kT \gtrsim \gamma^{-5/2}$. For 'insulated' bands the highest value of γ giving negative resistance was 0.4, hence $E/kT \gtrsim 10$. $10kT$ is therefore the smallest separation between the bands for which it is possible to observe negative resistance.

§ 4. INSTABILITY

It has been pointed out by Reik (private communication) that a crystal under conditions in which it exhibited negative resistance should be electrically unstable. At any point in the crystal a random fluctuation of carrier density can produce a momentary space charge which, in the direction of the particle current, decreases the electric field on one side and increases the field on the other. When the resistance is positive a smaller current flows into the space charge region than that which flows out, and consequently the space charge decays and a uniform field is established once more. The reverse will occur when the resistance is negative, the space charge increasing until the fields on either side of it are high and low enough respectively to make the resistance positive and the currents into and out of the space charge equal. The result is a stable situation but with markedly inhomogeneous fields set up in the crystal. The process is like a separating out of two phases, one phase characterized by a higher electric field, the other by a lower electric field, giving rise to a kind of electrical domain structure throughout the crystal.

A consequence of electrical domain formation would be to reduce or, more likely, eliminate the possibility of obtaining a finite differential negative resistance in the current-voltage curve, though abrupt transitions are not ruled out. It is also possible that some sort of hysteresis may occur as the field is cycled over the negative resistance region. What is certain is that the electrical state of a crystal with negative resistance bears close theoretical, as well as experimental, scrutiny.

§ 5. DISCUSSION

Although we have discussed the conditions for negative resistance in two-band models only, it is obvious that what has been said can apply equally well to a single band if above an energy E from the band minimum the effective mass increases fairly suddenly to a new value. The single band in this case becomes very similar to two bands, one vertically above the other in energy, so we can limit our discussion to two-band models.

The requirements of a material to show negative resistance may be broadly divided into two categories, one containing intrinsic and one containing extrinsic properties. The intrinsic requirements concern the band structure and the scattering mechanisms in the material. It is apparent from what has gone before that the band structure should be such that hot electrons (or holes) move sufficiently quickly from a high mobility state to a low mobility state as the field is increased.

The higher energy band should therefore have a high density of states or, if ellipsoidal, at least have a very high effective mass in the field direction relative to the lower band.

It is possible that uniaxially strained p-type germanium or silicon has the necessary structure. Under uniaxial strain the degeneracy of the 'light' and 'heavy' valence bands at $k=0$ is removed and two ellipsoids with their major axes at right angles to one another appear separated in energy at $k=0$ (Fig. 5).

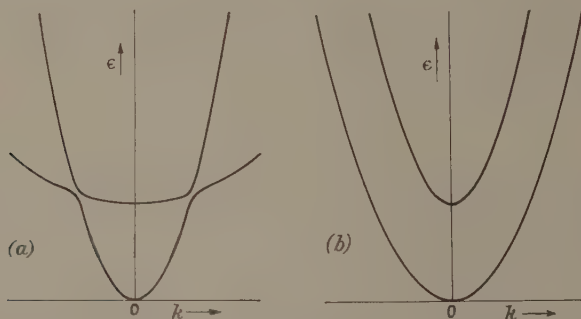


Fig. 5. Schematic (ϵ , k) diagram for the valence bands in uniaxially strained germanium; (a) for k parallel to the strain, (b) for k perpendicular to the strain.

Holes becoming hot will tend to move from the lower ellipsoid into the 'heavier' upper ellipsoid. Hensel and Feher (1960) have measured inverse-mass parameters in silicon for strains in the [001] and [111] directions; so taking their interpretation of the band structure as being reasonable and assuming that the ellipsoids actually intersect one another in the strain direction, we can make an estimate of the possibility of negative resistance. For the lower energy ellipsoid with the strain in the [111] direction $m_{\perp}/m=0.401$ and $m_{\parallel}/m=0.128$, where m_{\perp} is the mass perpendicular to the direction of the strain, and m_{\parallel} is the mass parallel to the direction of the strain. For the upper ellipsoid $m_{\perp}/m=0.166$ and $m_{\parallel}/m=1.408$. The density of states effective masses are $0.274m$ and $0.339m$ respectively, giving an effective mass ratio of 0.806 . This value coupled with the ratio of masses in the field direction of 0.091 when the field is in the same direction as the strain means that marginal negative resistance effects may be observable in the $F^{1/2}$ region. The condition for the energy separation is $E \gtrsim 13kT$. For strains of the order of 10^{-3} , and assuming a rate of band separation of about 10 eV per unit strain, the lattice temperature must be about 12°K or less. At these temperatures the $F^{1/5}$ region will be reached rapidly by the holes in the lower ellipsoid and this can enhance the negative resistance. The case of p-type silicon uniaxially strained in the [111] direction therefore appears to be marginal as far as the band structure goes.

Since negative resistance occurs most easily when the carriers are scattered by optical phonons, it is useful to consider materials which have naturally occurring sub-band separations of $\sim 0.03\text{ eV}$ and greater since such separations are difficult to produce by strain. (Strain, however, can be used to modify a natural energy gap.) Such separations occur in the conduction valleys in the III-V

compounds and also in Ge-Si alloys. These materials are therefore well worth investigating.

Given a promising band structure we must look critically at the scattering mechanism. First of all, impurity scattering must be negligible so that the density of ionized impurities must be kept low (an 'extrinsic' condition). More serious is the fact that the ratio of the deformation potentials and/or optical scattering constants of the two bands is important (e.g. Eqn (7)) since this affects the mobility difference between the bands. It is advantageous to have a lower acoustical deformation potential and a higher optical scattering constant for the lower band.

The extrinsic requirements concern the carrier density in the main. Certainly any process which increases the density as the field is increased jeopardizes the achievement of negative resistance. Impact ionization and injection from the contacts are two such processes. Ohmic contacts are certainly desirable. Impact ionization of shallow impurities can occur at quite low fields in germanium at 4°K, but how near to complete ionization one gets at high fields is not well known. If saturation in the ionization can be obtained before the negative resistance region occurs, or if the electrons are mainly thermally ionized already, the effect of impact ionization should not be serious. Alternatively, the onset of ionization can be delayed to higher fields by replacing shallow level impurities by impurities having a level near the middle of the band. This may mean that at the low working temperature conduction via the band is negligible compared with impurity conduction, in which case it would be essential to optically excite enough of the electrons in the impurity level to the lower band to ensure normal conduction. The case of hot photoelectrons has not been studied yet, but the use of light to generate electrons obviously complicates matters since the steady state density of electrons depends upon the trapping time which will be governed by the mean velocity of the electrons and hence the electric field. If the capture cross section is independent of electron energy then the trapping time will decrease as the electrons become hotter and hence the density of electrons will go down. Not only would this be an advantage for negative resistance, as hitherto envisaged, it would mean that negative resistance would occur in a single simple band at fields high enough to evoke optical scattering. Most of the measured cross sections, however, decrease with increasing temperature (see, for example, Lax 1959). If this is taken as an indication of how the cross section varies with electron energy the tendency will be to inhibit negative resistance.

It must not be forgotten that a rise in lattice temperature with increasing field is advantageous. Since a trend in this direction is inevitable anyway it is gratifying that its effect is in the right direction.

§ 6. CONCLUSIONS

It has been shown that negative resistance effects can occur in a semiconductor if a suitable band structure is available, and that the conditions which determine the suitability of a band structure are not so severe as to make it improbable that the effect will be observed in some existing semiconductors. In fact, the main hurdle to be jumped may not be the discovery of a suitable band structure but rather the elimination of the effects of impact ionization. The existence of a negative resistance region in the current-voltage characteristic of a crystal may give rise to interesting effects due to electrical instability.

ACKNOWLEDGMENTS

We would like to express our thanks to Professor H. B. G. Casimir, Dr. H. J. G. Meyer, Dr. H. G. Reik, and Mr. K. Tweedale for many invigorating discussions and also to Drs. J. Ross MacDonald and R. Stratton of Texas Instruments for pointing out an error in the earlier work. Mrs. E. Keeble's assistance with the calculations was invaluable.

REFERENCES

- CONWELL, E. M., and BROWN, A. L., 1960, *J. Phys. Chem. Solids*, **15**, 208.
HENSEL, J. C., and FEHER, G., 1960, *Phys. Rev. Letters*, **5**, 307.
KRÖMER, H., 1958, *Phys. Rev.*, **109**, 1856.
LAX, M., 1959, *Advances in Semiconductor Science* (London: Pergamon), p. 66.
REIK, H. G., RISKEN, H., and FINGER, G., 1960, *Phys. Rev. Letters*, **5**, 423.
STRATTON, R., 1957, *Proc. Roy. Soc. A*, **242**, 355.
YAMASHITA, J., and WATANABE, M., 1954, *Progr. Theor. Phys.*, **12**, 443.

LETTERS TO THE EDITOR

The Effect of Absorption in the β Filter on the Mean Wavelength of X-ray Emission Lines

The effect of absorption on the mean wavelength of x-ray emission lines has been investigated theoretically by Wilson (1958). This note describes an experimental investigation of the effect of absorption in the β filter on the mean wavelength for the case of copper K_{α} radiation.

The investigation was carried out using a Philips PW 1050/30 diffractometer, together with the recording apparatus of Pike and Hughes (1959). The diffractometer was used with 4° divergence and anti-scatter slits, two sets of Söller slits with an angular aperture of 4.5° , a 0.1 mm receiving slit and North American Philips Type 62019 Geiger counters as detectors.

Measurements were made on the 321 line of a tungsten specimen, firstly with no filter and then with three normal β filters placed in the diffracted beam from the specimen. The specimen of tungsten was obtained in connection with the International Lattice Parameter Project (Parrish 1960). The 321 line was recorded in steps of 0.02° (2θ) over an angular range of 3.6° (2θ). The position of the centroid of the line thus detected was calculated for four angular ranges by a method previously described (Pike and Wilson 1959).

The temperature of the specimen was noted at intervals during each run and the position of the centroid corrected to 18°C , assuming the linear expansion coefficient of tungsten to be 4.3×10^{-6} per deg c. The actual temperatures on different days were all in the range 16 – 20°C . Systematic errors, introduced in resetting the diffractometer arm, were avoided, as the step scanning mechanism is such that the diffractometer arm can be, and was, reset without unlocking the gears. The effect of any variations with time was minimized by alternating the two sets of experimental conditions.

Nine measurements were made of the 321 line with no foil and eight with three foils, and the mean position of the centroid calculated in each case. The standard deviation of the mean was calculated both from the experimental results and directly from the line profile. The values calculated by the two methods were very closely similar. The results thus obtained and the corresponding values of $\Delta\lambda/\lambda$ are shown in the Table.

Results of Measurements on 321 Line of Tungsten, corrected to 18°C				
Range ($^{\circ}2\theta$)	3.6	3.2	2.8	2.4
No foil				
Mean position of centroid ($^{\circ}2\theta$)	130.6121	130.6120	130.6110	130.6082
S.D. of mean ($^{\circ}2\theta$)	0.0010	0.0006	0.0005	0.0006
3 foils				
Mean position of centroid ($^{\circ}2\theta$)	130.6075	130.6063	130.6051	130.6027
S.D. of mean ($^{\circ}2\theta$)	0.0011	0.0011	0.0010	0.0008
Difference caused by insertion of foils				
Change in centroid ($^{\circ}2\theta$)	0.0046	0.0057	0.0059	0.0055
$\Delta\lambda/\lambda$ (units of 10^{-6})	18	22	23	21
S.D. of $\Delta\lambda/\lambda$ (units of 10^{-6})	6	5	4	4

For the case of absorption in the β filter, with μ varying as λ^3 , Wilson (1958) gives the result

$$\frac{\Delta\lambda}{\lambda} = - \frac{3V\mu t}{\lambda} \quad \dots\dots(1)$$

where V is the variance of the wavelength, μ the linear absorption coefficient and t the thickness of the filter. For the particular case investigated here the value of μt was 2.2 and the fractional change in wavelength is calculated to be 1.8×10^{-5} , assuming the variance to be one third of the square of the separation of the α_1 and α_2 peaks. The mean of the experimentally observed values of $\Delta\lambda/\lambda$ is $2.1 \pm 0.4 \times 10^{-5}$, which is in good agreement with the calculated value.

No correction has been made for truncation error in these experimental results. The effect of truncation is negligible in the present application, as can be seen from the fact that $\Delta\lambda/\lambda$ remains effectively constant with variation of the range over which the centroid is calculated.

The diffractometer was purchased with the aid of a grant from the Department of Scientific and Industrial Research. The author is grateful to Professor A. J. C. Wilson for his encouragement.

Viriamu Jones Laboratory,
University College,
Cathays Park, Cardiff.

B. W. DELF.

PARRISH, W., 1960, *Acta Cryst.*, **13**, 847.

PIKE, E. R., and HUGHES, J. W., 1959, *J. Sci. Instrum.*, **36**, 212.

PIKE, E. R., and WILSON, A. J. C., 1959, *Brit. J. Appl. Phys.*, **10**, 57.

WILSON, A. J. C., 1958, *Proc. Phys. Soc.*, **72**, 924.

Thermoelectricity in Metals at Normal Temperatures—A Query

It is believed that thermoelectric power S in metals may arise in two primary ways: first, because of electron thermal diffusion, involving essentially the electronic specific heat† so that

$$S_e \sim \frac{c_{e1}}{e} \sim \frac{k}{e} \left(\frac{T}{T_0} \right) \quad \dots\dots(1)$$

(cf. for example Mott and Jones 1936, Wilson 1936, 1953) where c_{e1} is the electronic specific heat per conduction electron, and T_0 is the electron degeneracy temperature; secondly, due to 'phonon drag' when the lattice specific heat is primarily responsible and

$$S_g \sim \frac{c_g}{e} \frac{\tau_{p-p}}{\tau_{p-p} + \tau_{p-e}} \quad \dots\dots(2)$$

(MacDonald 1954, Sondheimer 1956) where c_g is the lattice specific heat per conduction electron, τ_{p-e} is the phonon-electron relaxation time, and τ_{p-p} is the phonon relaxation time due to all other phonon scattering processes.

† We exclude specifically 'mutual electron-drag' found at low temperatures in certain metals containing transition elements as solutes (cf. for example de Vroomen, van Baarle and Cuelenaere 1960, Guénault and MacDonald 1961).

Equation (1) evidently predicts $S \propto T$ essentially at all temperatures, while, if $T \gtrsim \theta$ so that $c_g \sim k$ (assuming the order of one free electron per atom), τ_{p-e} is constant, and $\tau_{p-p} \propto T^{-1}$ arising from anharmonic lattice interactions (phonon-phonon collisions), then from Eqn (2) $S_g \propto T^{-1}$. Rough estimates (e.g. Sondheimer 1956, p. 1249, MacDonald 1961) indicate that, to quote Sondheimer: " S_g may be expected to be comparable in magnitude with S_e at ordinary temperatures". Thus far, we would expect that neither S_g could be neglected in comparison with S_e at room temperature in typical metals nor, moreover, that the observed thermoelectric power $S_e + S_g$ would be even approximately proportional to the absolute temperature. Figs 1 and 2 are quite

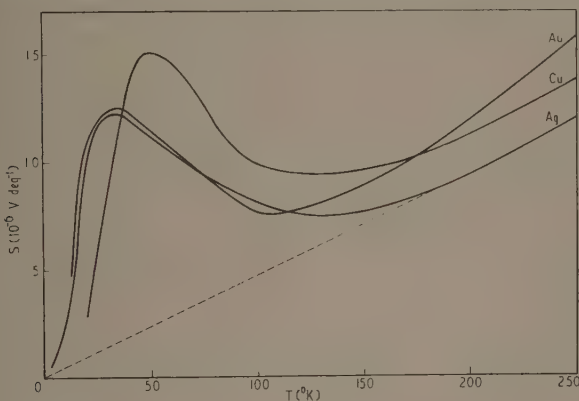


Fig. 1. Absolute thermoelectric power of 'pure' samples of Cu, Ag and Au as a function of temperature.

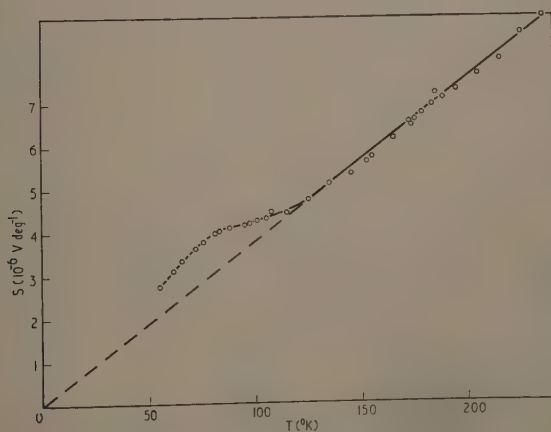


Fig. 2. Absolute thermoelectric power of 'pure' lithium as a function of temperature. Unpublished data of J. N. Mundy.

typical of experimental results in many metals: the obvious 'hump' at lower temperatures is now generally recognized as arising from phonon drag, and indeed this contribution clearly decays progressively at higher temperatures in qualitative agreement with Eqn (2). However, in all the cases illustrated it appears experimentally that S_g has become essentially *negligible* by room temperature so that in each case the overall thermoelectric power is reasonably proportional to the absolute temperature.

Although the theoretical estimates mentioned above do *not* take specific account of *Umklapp* processes in electron-phonon scattering, one might have surmised that in conduction phenomena at high temperatures one could ignore to a first approximation the finer details of scattering processes. To quote Mott (1956, p. 1341): "At high temperatures the resistance can well be calculated from an Einstein model. The analyses into phonons, *Umklapp* processes, etc., are not important. . . ." On the other hand a detailed calculation of thermoelectric power by Bailyn (private communication†) for the particular case of sodium, taking specific account of *normal* and *Umklapp* electron-phonon processes, indicates that around room temperature S_g would not be more than a few per cent of S_e (Bailyn estimates about $0.2 \mu\text{v deg}^{-1}$ for S_g).

This result is thus in welcome agreement with the general experimental findings and Bailyn agrees that it must involve some rather precise cancellation of the contributions to S_g from *normal* and *Umklapp* processes. However, at present there appears no particular reason why such a cancellation should be a *general* feature in metals, and we are now anxious to know whether a general theoretical reason can be offered for a more or less universal neglect of S_g in comparison with S_e at higher temperatures. Furthermore, if such a reason *can* be found it would appear to be of considerable importance showing that even at 'high' temperatures a rather detailed analysis of collision processes is very essential for electron transport phenomena.

We are grateful to Drs. J. S. Dugdale and J. N. Mundy for supplying us with unpublished data on lithium (Fig. 2).

Division of Pure Physics,
National Research Council,
Ottawa,
Canada.

D. K. C. MACDONALD,
W. B. PEARSON.

9th May 1961.

GUÉNAULT, A. M., and MACDONALD, D. K. C., 1961, *Phil. Mag.*, in the press.

MACDONALD, D. K. C., 1954, *Physica*, **20**, 996.

— 1961, *Principles of Thermoelectricity: an Introduction* (New York: John Wiley), in the press.

MOTT, N. F., 1956, *Canad. J. Phys.*, **34**, 1341.

MOTT, N. F., and JONES, H., 1936, *Theory of the Properties of Metals and Alloys* (Oxford: Clarendon Press).

SONDHEIMER, E. H., 1956, *Canad. J. Phys.*, **34**, 1246.

DE VROOMEN, A. R., VAN BAARLE, C., and CUELENAERE, A. J., 1960, *Physica*, **26**, 19.

WILSON, A. H., 1936, 1953, *The Theory of Metals* (Cambridge: University Press, 1st Edn 1936, 2nd Edn 1953).

† We are most grateful to Dr. Bailyn for correspondence on this problem.

A Study of Superconducting Niobium by Electron Tunnelling

Giaever (1960) and Nicol, Shapiro and Smith (1960) have reported current-voltage characteristics of sandwiches composed of two metals separated by a thin insulating oxide film. By observing the deviation from linearity of these characteristics with one, or both, of the metals in the superconducting state, they have obtained conclusive proof that the predominant conduction mechanism is quantum mechanical tunnelling through the potential barrier afforded by the oxide. Under certain conditions, the superconductor-oxide-superconductor system resulted in a negative resistance region from which the energy gaps of the two superconductors were obtained directly. The superconducting energy gaps of Al, In and Pb have been reported and, together with the general features of the characteristics, have been interpreted in terms of the Bardeen-Cooper-Schrieffer (BCS) theory of superconductivity (1957).

With the exception of a report of tunnelling through niobium oxide by Sherrill and Edwards (1961), the requirements that the oxide be continuous at thicknesses of about 20 Å and of high resistivity have limited measurements to Al-Al₂O₃-metal sandwiches. The aluminium system suffers from the disadvantage that direct measurement of energy gaps can only be obtained below the transition temperature of Al, which for evaporated films varies from 1.2°K to 1.8°K. For most superconductors, therefore, it is not possible to explore the temperature dependence of the energy gap near the transition temperature, and it is in this region that the BCS theory predicts the greatest variation. The development of sandwiches using a superconductor with a higher transition temperature than that of Al would therefore bring about a considerable improvement.

Bulk niobium ($T_c = 9.2^\circ\text{K}$) and niobium oxide, have been investigated at these laboratories and found to fulfil the requirements outlined above. Their use should allow the measurement of the temperature dependence of the energy gaps of the majority of elemental superconductors up to their transition temperatures. In this Letter, current-voltage characteristics of Nb-Nb oxide-Pb sandwiches are reported as a function of temperature and magnetic field.

The sandwiches were prepared as follows. Strips of zone refined niobium were vacuum outgassed at about 2000°C to remove surface impurities. Oxide films, estimated to be 20 Å thick, were grown on the surface of the niobium by heating it to 40°C in pure oxygen for about 2 hours. The oxidized strips were mounted on glass substrates and lead cross strips, about 1000 Å thick, evaporated across them to give nominal tunnelling areas of 1 mm square.

Initial specimens of Nb-Nb oxide-Pb at 4.2°K showed current-voltage characteristics indicative of electron tunnelling between superconducting lead and normal niobium. The value of $2\epsilon_{\text{pb}} = (2.7 \pm 0.1) \times 10^{-3} \text{ eV}$ given by the voltage at which

$$\left(\frac{dI}{dV}\right)_{\text{normal}} / \left(\frac{dI}{dV}\right)_{\text{superconducting}} = 1,$$

obtained from this characteristic, was in good agreement with that obtained from Al-Al₂O₃-Pb sandwiches at the same temperature. The bulk niobium, however, was shown to be superconducting and the normal surface was ascribed to

the presence of impurities. When a more stringent outgassing procedure was adopted results indicated that both metal surfaces were superconducting and typical characteristics are shown in Figs 1 and 2.

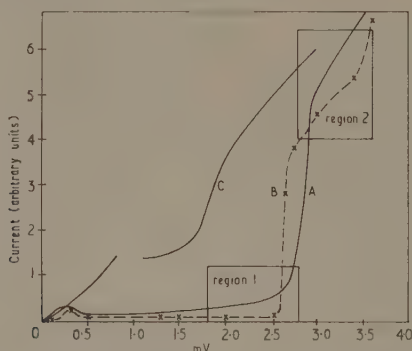


Fig. 1. Characteristic curves for Nb-Nb oxide-Pb sandwich: curve A measured at 4.18°K; curve B calculated from BCS theory ($T=4.2^{\circ}\text{K}$); curve C measured at 6.5°K.

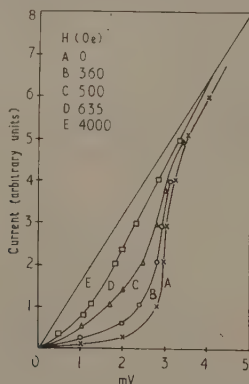


Fig. 2. Tunnel current through a Nb-Nb oxide-Pb sandwich at 4.18°K as a function of magnetic field.

Figure 1, curve A, shows the characteristic of a Nb-Nb oxide-Pb sandwich at 4.18°K. Curve B, the theoretical characteristic at 4.2°K, has been evaluated from the equation

$$I = \text{const} \int \rho_1(E) \rho_2(E - V) [f(E - V) - f(E)] dE, \quad \dots (1)$$

where ρ_1 and ρ_2 are the density of states functions for the two superconductors, f is the Fermi function, V the applied voltage and E the energy measured from the Fermi level. The density of states was calculated from the BCS function

$$\rho = \frac{n_s}{n} = \frac{E}{(E^2 - \epsilon^2)^{1/2}}, \quad \dots (2)$$

where 2ϵ is the superconducting energy gap at 0°K and is given by

$$2\epsilon = 3.5kT_c. \quad \dots (3)$$

The deviation of the experimental and theoretical curves in region 1 is assumed to be due to the presence of domains of normal and varying transition temperature niobium, i.e., the niobium surface is a non-homogeneous superconductor. The deviation in region 2 results from the methods used in the evaluation of Eqn (1). The integral is particularly sensitive to the variation of the density of states near the band edge, and when the current-voltage characteristics have been evaluated by computer it should be possible to check the validity of Eqn (2) directly.

The initial peak is not very pronounced because at 4.2°K there are few thermally excited carriers. However, preliminary values of $2\epsilon_{\text{pb}} = (2.4 \pm 0.3) \times 10^{-3} \text{ eV}$ and $2\epsilon_{\text{Nb}} = (2.8 \pm 0.3) \times 10^{-3} \text{ eV}$ were obtained. At higher temperatures, the accuracy is considerably improved and curve C shows a characteristic obtained at 6.5°K . Experiments are in progress to measure the detailed variation of the energy gaps of lead and niobium with temperature.

Figure 2 shows the effect of a magnetic field applied parallel to the tunnelling area. The variation of characteristic shape with field is most rapid near the critical field for lead, and a value of $H_c = 630$ oersteds was obtained.

The Nb-Nb oxide-Pb sandwich would seem to be ideally suited to the detection of microwave radiation as suggested by Burstein, Langenberg and Taylor (1961). At 4.2°K it should be possible to detect radiation of wavelength less than 0.46 mm .

We would like to thank the Admiralty and the Plessey Company Ltd. for permission to publish this Letter.

Plessey Company, Ltd.,
Caswell Research Laboratories,
Towcester,
Northants.

P. TOWNSEND.
J. SUTTON.

2nd June 1961.

- BARDEEN, J., COOPER, L. N., and SCHRIEFFER, J. R., 1957, *Phys. Rev.*, **108**, 1175.
BURSTEIN, E., LANGENBERG, D. N., and TAYLOR, B. N., 1961, *Phys. Rev. Letters*, **6**, 92.
GIAEVER, I., 1960, *Phys. Rev. Letters*, **5**, 147, 464.
NICOL, J., SHAPIRO, S., and SMITH, P., 1960, *Phys. Rev. Letters*, **5**, 461.
SHERRILL, M. D., and EDWARDS, H. H., 1961, *Phys. Rev. Letters*, **6**, 460.

The Application of Onsager's Theory to Dielectric Dispersion— A Correction

In a previous publication (Hill 1958) the behaviour of Onsager's model of a dielectric (Onsager 1936) in the region of dielectric dispersion was considered. It was pointed out that previous generalizations of Onsager's theory to this case (e.g. Cole 1938) were incorrect, because the reaction field produced by the permanent dipole moment is not dependent on the frequency of the applied field, since the motion of the dipole is of thermal origin.

Unfortunately the derivation of the equation for the high frequency case contains an error. It was assumed that the reaction field \mathbf{R} remains parallel to the total moment \mathbf{m} , which is not the case since

$$\mathbf{m} = \mu_0 + \gamma \mathbf{F}$$

but

$$\mathbf{R} = \frac{(2\epsilon_0 - 1)\mu_0}{2\epsilon_0 + 1} \frac{1}{a^3} + \frac{2(\epsilon - 1)\gamma \mathbf{F}}{2\epsilon + 1} \frac{1}{a^3}$$

where μ_0 is the permanent moment, γ the polarizability, \mathbf{F} the internal field, ϵ_0 and ϵ the static and high frequency dielectric constants.

The couple tending to turn the molecule was therefore given incorrectly. It should be

$$\mathbf{C} = \mathbf{m} \times \mathbf{F} = g \frac{\mu_0 \times \mathbf{E}}{1 - r\gamma/a^3}$$

$$\left(g = \frac{3\epsilon}{2\epsilon + 1}, \quad r = \frac{2(\epsilon - 1)}{2\epsilon + 1} \right).$$

The final equation then becomes

$$\epsilon - \epsilon_\infty = \frac{\epsilon_0 - \epsilon_\infty}{1 + j\omega\tau} C_1 C_2$$

where

$$C_1 = \frac{\epsilon(2\epsilon_0 + \epsilon_\infty)}{\epsilon_0(2\epsilon + \epsilon_\infty)}$$

as before but

$$C_2 = 1 + \frac{6(\epsilon_\infty - 1)}{(\epsilon_\infty + 2)(2\epsilon_0 + 1)} \frac{\epsilon_0 - \epsilon}{2\epsilon + 1}$$

which is the square root of the factor previously found.

The values of C_1 and C_2 and the dielectric constants ϵ_1 and ϵ_2 , obtained by applying first C_1 alone and then C_1 and C_2 together for the case $\epsilon_\infty = 2.5$, $\epsilon_0 = 12.5$ previously considered, then are:

$\omega\tau$	C_1	C_2	ϵ_1	ϵ_2	ϵ_{Debye}
0	1.000-0.0000j	1.000+0.0000j	12.50-0.00j	12.50-0.00j	12.50-0.00j
0.2	0.999-0.0145j	1.000+0.0059j	12.11-2.06j	12.12-2.00j	12.11-1.92j
0.4	0.997-0.0288j	1.002+0.0117j	10.99-3.69j	11.04-3.59j	11.12-3.45j
0.6	0.993-0.0425j	1.004+0.0174j	9.61-4.69j	9.71-4.58j	9.85-4.41j
0.8	0.988-0.0555j	1.008+0.0229j	8.05-5.18j	8.39-5.07j	8.60-4.90j
1.0	0.982-0.0677j	1.012+0.0281j	7.07-5.25j	7.24-5.15j	7.60-5.00j
1.2	0.974-0.0788j	1.017+0.0330j	6.11-5.10j	6.31-5.03j	6.60-4.91j
1.5	0.962-0.0935j	1.026+0.0396j	5.03-4.73j	5.25-4.69j	5.58-4.62j
2.0	0.939-0.1121j	1.043+0.0488j	3.93-3.98j	4.16-4.01j	4.50-4.00j
3.0	0.893-0.1307j	1.081+0.0600j	3.00-2.81j	3.19-2.90j	3.50-3.00j
5.0	0.823-0.1271j	1.147+0.0634j	2.57-1.64j	2.68-1.75j	2.89-1.92j
∞	0.733-0.0000j	1.280+0.0000j	2.50-0.00j	2.50-0.00j	2.50-0.00j

The correction C_2 does not compensate so completely for C_1 as the previous calculation suggested, consequently the Cole-Cole plot consists of an arc which lies slightly outside the Debye semi-circle, the maximum loss being 3% higher than the simple Debye relation implies. The conclusion that the maximum loss occurs almost exactly at $\omega\tau=1$, where τ is the microscopic relaxation time (i.e. that the microscopic and macroscopic relaxation times are almost identical), remains unchanged.

Bedford College,
Regent's Park, N.W.1.
12th June, 1961.

NORA E. HILL*

COLE, R. H., 1938, *J. Chem. Phys.*, **6**, 385.

HILL, N. E., 1958, *Proc. Phys. Soc.*, **72**, 532.

ONSAGER, L., 1936, *J. Amer. Chem. Soc.*, **58**, 1486.

Hyperfine Structure in Terbium Metal

The hyperfine contribution to the specific heat of terbium metal, measured by Kurti and Safrata (1958), was found to be slightly smaller than that expected from the electron paramagnetic resonance experiments of Baker and Bleaney (1958) on terbium ethyl sulphate. It was suggested that the discrepancy might be due to a reduction in the mean value of $\langle r^{-3} \rangle$ for the 4f electrons in the metal compared with the salt; however, the nuclear resonance measurements of Hervé and Veillet (1961) on the metal show that this explanation is not correct. The purpose of this Letter is to show that the discrepancy may be resolved when the electric quadrupole interaction with the terbium nucleus (^{159}Tb) is taken into account.

Terbium metal is hexagonal in structure, and the electron moments in the ferromagnetic state are directed along the hexagonal axis (the z axis). The appropriate Hamiltonian for the hyperfine structure is then

$$\mathcal{H} = a \langle J_z \rangle I_z + P \{ I_z^2 - \frac{1}{3} I(I+1) \}, \quad \dots\dots (1)$$

where $I = \frac{3}{2}$ and $\langle J_z \rangle$ is the time-averaged value in the ferromagnetic state. At temperatures well below the Curie point $\langle J_z \rangle$ is expected to be close to $J = 6$, a value consistent with the measured saturation moment. The electron paramagnetic resonance measurements on Tb^{3+} of Baker and Bleaney (in lanthanum ethyl sulphate) and Hutchison and Wong (1958) (in lanthanum trichloride), after allowing for crystal field effects, both give $a = 0.0177 \pm 0.0002 \text{ cm}^{-1} = 530 \pm 5 \text{ Mc/s}$. If we write $a \langle J_z \rangle = a'$, the eigenvalues of this Hamiltonian become $\frac{3}{2}a' + P$, $\frac{1}{2}a' - P$, $-\frac{1}{2}a' - P$, $-\frac{3}{2}a' + P$; the allowed transitions are between successive values and therefore fall at $a' + 2P$, a' and $a' - 2P$, respectively. Hervé and Veillet (1961) have observed only a single transition at $3190 \pm 15 \text{ Mc/s}$ (extrapolated to $T = 0^\circ\text{K}$); this may be identified as the central $+\frac{1}{2} \longleftrightarrow -\frac{1}{2}$ transition at a' , giving very good agreement with the value $a' = 3180 \pm 30 \text{ Mc/s}$ (assuming $\langle J_z \rangle = 6$) expected from the paramagnetic resonance measurements on the two salts. This close agreement is remarkable, since in the metal either there is no change in $\langle r^{-3} \rangle$ or in the core polarization contribution (estimated by Baker and Bleaney as 6%) and no contribution from conduction electrons, or the changes accidentally cancel.

From the theory of Elliott and Stevens (1953), Baker and Bleaney estimated the value of P for $\langle J_z \rangle = 6$ to be $+0.020_6 Q$ °K, where Q is the nuclear electric quadrupole moment in barns. No experimental determination of Q exists for ^{159}Tb , but it would be expected to be of order 1 to 2 barns. From the Coulomb excitation cross section, Alder, Bohr, Huus, Mottelson and Winther (1956) deduce a value of the intrinsic quadrupole moment of $Q_0 = 6.9$ barns, which corresponds to a value of $Q = 1.4$ barns. This leads to a value of $P = +0.02_9$ °K $\simeq 600 \text{ Mc/s}$, which may be taken as $a'/5$ within the uncertainties of our estimate.

The nuclear specific heat given by Kurti and Safrata (1958) can be written as $CT^2/R = (24.8 \pm 1.2) \times 10^{-3} \text{ deg}^2$, which is noticeably smaller than that of $(29.1 \pm 0.6) \times 10^{-3}$ obtained from the electron paramagnetic resonance and nuclear magnetic resonance data when P is ignored, and the specific heat is evaluated only as far as the T^{-2} term. A general series expansion for the specific heat is†

$$\frac{C}{R} = \sum_{n=2}^{\infty} c_n T^{-n}, \quad \dots\dots (2)$$

† We have given the formulae for the specific heat in some detail as they can be used in a number of other cases, both nuclear and electronic.

where

$$c_n = n(n-1) \left\{ b_n - \frac{1}{2} \sum_{p=1}^{n-1} b_{n-p} b_p + \frac{1}{8} \sum_{p=1}^{n-2} \sum_{q=1}^{n-2} b_{n-p-q} b_p b_q + \text{etc.} \right\}$$

$$b_p = \frac{(-1)^p \langle W^p \rangle}{p!} \quad \dots\dots(3)$$

Here $\langle W^p \rangle$ is the mean of the p th powers of the energy levels, measured in temperature units. If the origin is chosen to make $\langle W \rangle = 0$, considerable simplification is obtained and the leading coefficients are (first in general and second for ^{159}Tb):

$$c_2 = \langle W^2 \rangle = \frac{5}{4} a'^2 + P^2$$

$$c_3 = -\langle W^3 \rangle = -3a'^2 P$$

$$c_4 = \frac{1}{2!} (\langle W^4 \rangle - 3\langle W^2 \rangle^2) = -\left(\frac{17}{16} a'^4 + P^4\right)$$

$$c_5 = -\frac{1}{3!} (\langle W^5 \rangle - 10\langle W^3 \rangle \langle W^2 \rangle) = \frac{25}{6} a'^4 P + \frac{10}{3} a'^2 P^3$$

$$c_6 = \frac{1}{4!} (\langle W^6 \rangle - 15\langle W^2 \rangle \langle W^4 \rangle - 10\langle W^3 \rangle^2 + 30\langle W^2 \rangle^3) = \frac{65}{96} a'^6 - \frac{15}{4} a'^4 P^2 + \frac{2}{3} P^6.$$

The presence of P in the first term appears to accentuate the discrepancy, since for $P = a'/5$ the first term increases to 30.1×10^{-3} , but the higher terms are by no means negligible in the relevant temperature range, which was about 0.6 to 1.0°K . Substitution of our values for a' and P gives

$$\frac{CT^2}{R} = (30.1 - 2.13T^{-1} - 0.58T^{-2} + 0.071T^{-3} + 0.0067T^{-4}) \times 10^{-3}$$

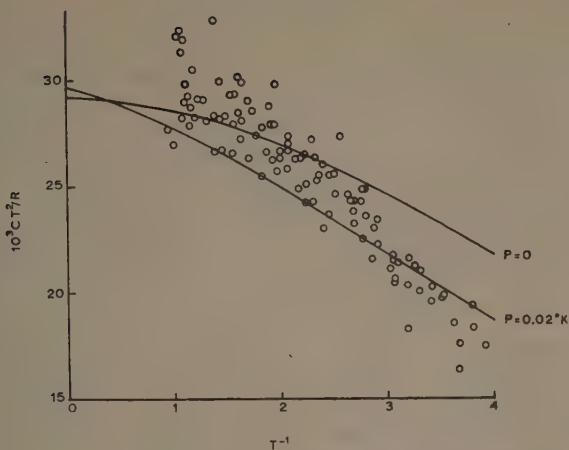
$$\dots\dots(4)$$

the mean value of which over the temperature range 0.6 to 1.0° is 26.3×10^{-3} , which agrees well with the value given by Kurti and Safrata (1958).

At this point we received a preprint from Heltemes and Swenson (1961), giving details of their specific heat measurements on terbium metal down to 0.25°K . They have kindly allowed us to publish these data, which are shown as a plot of CT^2/R against T^{-1} in the Figure. Near 1°K the points lie rather higher than the results of Kurti and Safrata, through a reduced estimate for other contributions. This uncertainty is least at the lowest temperatures, where the specific heat is noticeably smaller than that calculated from the nuclear magnetic resonance results, assuming $P=0$. At this temperature a series expansion is no longer sufficiently accurate, and the following (exact) expression has been used

$$\frac{CT^2}{R} = \left\{ \left(\frac{1}{2} a'^2 + 2P^2 \right) \cosh \frac{2a'}{T} + (2a'^2 + 2P^2) \cosh \frac{a'}{T} \right. \\ \left. - 2a'P \sinh \frac{2a'}{T} - 4a'P \sinh \frac{a'}{T} + \frac{1}{4} a'^2 \left[9 \exp \left(\frac{-2P}{T} \right) + \exp \left(\frac{2P}{T} \right) \right] \right\} \\ \times \left\{ \exp \left(\frac{-P}{T} \right) \cosh \frac{3a'}{2T} + \exp \left(\frac{P}{T} \right) \cosh \frac{a'}{2T} \right\}^{-2} \quad \dots\dots(5)$$

The two curves drawn are for $P=0$ and for $P=0.02^\circ\text{K}$, which gives the best fit at $T=0.3^\circ\text{K}$. The fit is not so good elsewhere, though the discrepancy is not perhaps outside the experimental error, but there appears to be definite evidence for a quadrupole interaction whose size is of the order assumed.



Plot of CT^2/R against T^{-1} for terbium metal. The experimental points are from Heltemes and Swenson (1961), and near 1°K lie higher than the data of Kurti and Safrata (1958) through a difference in the estimates for contributions from non-nuclear effects (the uncertainty in these may amount to 2 or 3 units in the ordinate). The full curves are calculated from the nuclear magnetic resonance data of Hervé and Veillet (1961), with $P=0$ and 0.02°K respectively.

Work is planned to measure the specific heat of the metal down to lower temperatures, and the quadrupole interaction in a terbium salt by means of ENDOR. In the metal it may be possible to determine the quadrupole interaction by nuclear magnetic resonance, but Dr. R. A. Kamper (private communication) has suggested that transitions at $a' \pm 2P$ are likely to be broadened by strains, especially as the nuclei observed in this method are those in the domain walls; a more promising experiment would be to use the Mössbauer method. The quadrupole interaction should be of particular interest, since P varies as $\{3\langle J_z^2 \rangle - J(J+1)\}$, and should be a somewhat different function of temperature from a' , which varies as $\langle J_z \rangle$. This may give an indication of the contribution from electrons other than $4f$ (for example, s -electrons might contribute to a' but not to P). It should be noted also that the axis of the quadrupole interaction is primarily determined by the direction of the spontaneous magnetization, and only indirectly by the crystal field. Such nuclear electric quadrupole interactions should exist in all rare earth metals which exhibit spontaneous magnetization, whether ferromagnetic or antiferromagnetic.

Clarendon Laboratory,
Oxford.

15th June 1961.

B. BLEANEY.
R. W. HILL.

ALDER, K., BOHR, A., HUUS, T., MOTTELSON, B., and WINTHER, A., 1956, *Rev. Mod. Phys.*, **28**, 432.

BAKER, J. M., and BLEANEY, B., 1958, *Proc. Roy. Soc. A*, **245**, 156.

ELLIOTT, R. J., and STEVENS, K. W. H., 1953, *Proc. Roy. Soc. A*, **218**, 553.

HELTAMES, E. C., and SWENSON, C. A., 1961, *J. Chem. Phys.*, in the press.

HERVÉ, J., and VEILLET, P., 1961, *C.R. Acad. Sci., Paris*, **252**, 99.

HUTCHISON, C. A., and WONG, E., 1958, *J. Chem. Phys.*, **29**, 754.

KURTI, N., and SAFRATA, R. S., 1958, *Phil. Mag.*, **3**, 780.

The Hall Effect in Monovalent Metals at Low Temperatures

In a previous paper (Simons 1960) the thermal resistance tensor was considered for a dielectric at low temperatures where N -type collision processes predominate. The variational approach used there will now be employed to obtain, for a metal under the same conditions, the change in the electrical resistance tensor brought about by an applied magnetic field.

It is shown by García-Moliner (1958) that the relevant variational principle for the Boltzmann equation in the presence of a magnetic field, yields the electrical conduction tensor σ_{ij} in the form

$$\sigma_{ij} = \frac{e^2}{4\pi^3} S_{pi} S_{qj} R_{pq}^{-1}, \quad \dots\dots(1)$$

Here we suppose that the existing distribution function $f(\mathbf{k})$ is given by $f = F - (\partial F / \partial E) \phi$, where F is the Fermi-Dirac equilibrium distribution and E is the energy of an electron of wave number \mathbf{k} . The deviation from equilibrium $\phi(\mathbf{k})$ is expanded in the form $\phi(\mathbf{k}) = \sum_p U_p \phi_p(\mathbf{k})$ for a given set of $\phi_p(\mathbf{k})$ and

$$R_{pq} = \sum_i \int L_i [\phi_p]_i [\phi_q]_i d\mathbf{k} + \frac{e}{\hbar c} H \int \phi_p \frac{\partial F}{\partial E} \left(v_2 \frac{\partial}{\partial k_3} - v_3 \frac{\partial}{\partial k_2} \right) \phi_q d\mathbf{k} \quad \dots\dots(2)$$

where $[\phi]_i$ is the linear combination of ϕ 's relevant to the i th type of electron collision process and L_i is the corresponding collision operator. H is the magnetic field, applied along the x axis, and \mathbf{v} is the velocity of an electron,

$$S_{pi} = \int \frac{\partial F}{\partial E} \phi_p v_i d\mathbf{k}. \quad \dots\dots(3)$$

We now wish to apply these results to a metal in which both electron scattering and phonon scattering are dominated by electron-phonon N processes. A necessary condition for this to be so, is that the Fermi surface should not touch the surface of the first Brillouin Zone, since if this were the case, U processes of a frequency comparable with that of the N processes would occur at any temperature. This means that we are immediately restricted to a consideration of monovalent metals. For these, it is then necessary that the temperature should be sufficiently low, so that the frequency of 3-particle U processes of the type electron + phonon \rightleftharpoons electron is negligibly small. Assuming that the amount of impurity scatter and the effect of the magnetic field is also much less than the contribution of the N processes, we may then adequately represent $\phi(\mathbf{k})$ by a linear combination of the three independent resolutes of \mathbf{k} ; that is,

$$\phi_p(\mathbf{k}) = k_p, \quad p = 1, 2, 3 \quad \dots\dots(4)$$

(Ziman 1956). This is so, since the effect of N processes acting alone is to impress this form on the distribution function $\phi(\mathbf{k})$, and to produce a similar displacement of the phonon distribution function. In the absence of other scattering processes the collision integral and the resistivity will then vanish (Peierls 1955). The presence of such processes will lead to a non-zero resistivity, but if they are much less frequent than N processes, the change in the distribution function from the form given by Eqn (4) will be very small, and may be neglected for present purposes. Substituting from Eqn (4) into Eqn (3), it is readily shown by an approach similar to that of Simons (1960) that

$$S_{pi} = -4\pi^3 \hbar^{-1} N \delta_{pi}, \quad \dots\dots(5)$$

where N is the total number of electrons. From Eqn (2) it is seen that

$$R_{pq} = R_{pq}' + R_{pq}'' \quad \text{where} \quad R_{pq}' = \sum_i \int L_i[k_p]_i[k_q]_i d\mathbf{k}$$

is the contribution to R_{pq} arising from the electron collisions, and

$$R_{pq}'' = \frac{e}{\hbar c} H \int \mathbf{k}_p \frac{\partial F}{\partial E} \left(v_2 \frac{\partial}{\partial k_3} - v_3 \frac{\partial}{\partial k_2} \right) k_q d\mathbf{k} \quad \dots\dots (6)$$

is the contribution arising from the magnetic field. It may be shown that R_{pq}'' is an antisymmetric matrix (García-Moliner and Simons 1957), and from Eqn (6) it is clear that it is zero if $q=1$. Thus the only non-zero components are $R_{23}'' = -R_{32}''$, and from Eqns (3), (4) and (5) we have

$$R_{32}'' = 4\pi^3 e H N / \hbar^2 c. \quad \dots\dots (7)$$

Substituting this into Eqn (1), it follows that the resistance tensor $r_{ij}(=\sigma_{ij}^{-1})$ is given by $r_{ij} = r_{ij}' + r_{ij}''$, where r_{ij}' is the resistance tensor in the absence of an applied magnetic field, and

$$r_{ij}'' = \begin{bmatrix} 0 & 0 & 0 \\ 0 & 0 & -\gamma \\ 0 & \gamma & 0 \end{bmatrix} \quad \text{with } \gamma = H/Nec.$$

Since the magnetic field is applied along the x axis, we see that this form for r_{ij}'' implies the absence of any magnetoresistance. In fact, it is clear that the only non-zero change in the resistance tensor arises when the magnetic field, electric field and current are mutually perpendicular. This is just the condition for the Hall effect, and it is seen from the above results that the Hall coefficient is given by $R=1/Nec$. This is, of course, the same result as is given by the elementary theory of the Hall effect, but there it is derived subject to certain assumptions, among which are the following: (i) an effective mass exists, (ii) the electron gas is degenerate, (iii) an isotropic relaxation time exists. Since for real metals, these approximations may be somewhat in error, experimental deviations from the $R=1/Nec$ result would not have been unexpected. However, we now see that if experiments are performed at low temperatures with low magnetic field on monovalent metals of increasing degree of purity, we might reasonably expect the results to tend to $R=1/Nec$, independent of the crystal orientation with respect to the magnetic field.

Queen Mary College,
University of London.

S. SIMONS.

23rd March 1961, in revised form 2nd June 1961.

GARCÍA-MOLINER, F., 1958, *Proc. Roy. Soc. A*, **249**, 73.

GARCÍA-MOLINER, F. and SIMONS, S., 1957, *Proc. Camb. Phil. Soc.*, **53**, 848.

PEIERLS, R., 1955, *Quantum Theory of Solids* (Oxford: Clarendon Press).

SIMONS, S., 1960, *Proc. Phys. Soc.*, **76**, 458.

ZIMAN, J. M., 1956, *Canad. J. Phys.*, **34**, 1256.

The Magnetic Susceptibility of Manganese Zinc Fluoride Solid Solutions

The change in the antiferromagnetic transition resulting from the dilution of the magnetic ion has been the subject of considerable theoretical investigation (see references in Baker, Lourens and Stevenson 1961). All models predict that the Néel temperature will fall rapidly with dilution, and that no long range order will exist if the concentration of the magnetic ion is less than a certain value. There is little experimental evidence, but early work by Bizette and Tsai (1943) on MnO-MgO and FeO-MgO suggests such behaviour, and recently Baker, Lourens and Stevenson (1961) have reported on the disappearance at low temperatures of the nuclear magnetic resonance line of manganese zinc fluoride mixed crystals. From this they deduce the dependence of the Néel temperature on concentration. The variation is in qualitative agreement with the predictions of Sato, Arrott and Kikuchi (1959) for a model in which the local fluctuations in the density of magnetic ions are accounted for. It may be noted, however, that the agreement is much more complete with the results obtained from a model in which every magnetic ion is surrounded by a density of magnetic ions equal to the average density.

The variation in magnetic susceptibility in magnetically dilute systems will not give a particularly satisfactory measure of the Néel temperature, as the maximum in the susceptibility may be ill defined. However, the susceptibility variation below the Néel temperature, as predicted by different models, is widely different. Measurements on $\text{MnF}_2\text{-ZnF}_2$ down to 90°K have already been published by Corliss, Delabarre and Elliott (1950). In the present work the measurements were extended below the Néel temperatures where the influence of the ordering process is marked.

The preparation and analysis of the single crystal specimens has already been described (Finlayson *et al.* 1960). A fine powder was prepared for this experiment and immobilized by paraffin wax in a small silica cup suspended by a silica rod from a Sucksmith balance (Finlayson, Llewellyn and Smith 1959). Thermal contact between specimen and thermometer was maintained by introducing a few millimetres of helium into the sample chamber. Correction was made for the deflection of the silica cup, and the absolute value of the susceptibility was obtained by calibration of the balance with a water sample. The diamagnetic correction for the zinc and fluorine ions is less than the experimental error, and has not been included.

In the higher temperature region, the reciprocal susceptibility varies linearly with temperature (Figure) and can be represented by

$$\chi_M = \frac{C_M}{T + \Delta}$$

where Δ is the asymptotic Néel temperature. The magneton values p_B can be obtained from

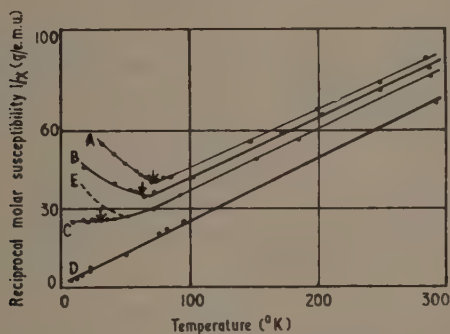
$$p_B = 2.828\sqrt{C_M}$$

and values of both p_B and Δ are given in the Table.

Specimen	C_M	Δ	p_B
MnF_2	4.37	100	5.91
$Mn_{0.87}Zn_{0.13}F_2$	4.36	80	5.90
$Mn_{0.61}Zn_{0.39}F_2$	4.23	58	5.88
$Mn_{0.11}Zn_{0.89}F_2$	4.19	8.0	5.86

These data agree with the results of Corliss, Delabarre and Elliott (1950) in giving a value of p_B rather lower than the free ion value of 5.92 for a $^6S_{5/2}$ state. Also the asymptotic Néel temperature is proportional to the concentration of the manganese ion.

It can be seen from the Figure that the linear section of the $(1/\chi, T)$ plot extends to lower temperatures as the concentration is reduced. Below this section a minimum in the inverse susceptibility is found for the higher concentrations and this corresponds with the temperature (indicated by arrow on graph) at



Inverse molar susceptibility variation with absolute temperature: A, experimental curve for MnF_2 ; B, experimental curve for $Mn_{0.87}Zn_{0.13}F_2$; C, experimental curve for $Mn_{0.61}Zn_{0.39}F_2$; D, experimental curve for $Mn_{0.11}Zn_{0.89}F_2$; E, calculated curve for $Mn_{0.61}Zn_{0.39}F_2$.

which the nuclear magnetic resonance line disappears (Baker, Lourens and Stevenson 1961). For the medium concentration a departure from linearity is found 20° above the temperature at which the resonance line disappears, and there is no minimum in the inverse susceptibility at any temperature. For the lowest concentration there is no departure from a linear variation over the temperature range investigated.

A broadening of the minimum in dilute antiferromagnetics has been found by other workers (Bizette and Tsai 1943, Bizette 1946). However, the absence of a minimum in the intermediate concentration curve would not be expected from the simplest models. Thus, the treatment given by Sato *et al.* (1959), which gives a qualitative prediction of the variation of the Néel temperature with concentration, leads to a clearly defined minimum in the inverse susceptibility (see Figure).

It can be seen, therefore, that susceptibility measurements below the Néel temperature provide a useful test of the adequacy of any model of the ordering processes in a dilute antiferromagnetic.

Department of Natural Philosophy,
Marischal College,
University of Aberdeen.
13th June 1961.

D. M. FINLAYSON.
I. S. ROBERTSON†.
T. SMITH.
R. W. H. STEVENSON.

- BAKER, J. M., LOURENS, J. A., and STEVENSON, R. W. H., 1961, *Proc. Phys. Soc.*, **77**, 1038.
BIZETTE, H., 1946, *Ann. Phys., Paris*, **1**, 88.
BIZETTE, H., and TSAI, B., 1943, *C. R. Acad. Sci., Paris*, **217**, 444.
CORLISS, L., DELABARRE, Y., and ELLIOTT, N., 1950, *J. Chem. Phys.*, **68**, 1256.
FINLAYSON, D. M., LLEWELLYN, J. P., and SMITH, T., 1959, *Proc. Phys. Soc.*, **74**, 75.
FINLAYSON, D. M., ROBERTSON, I. S., SMITH, T., and STEVENSON, R. W. H., 1960, *Proc. Phys. Soc.*, **76**, 355.
SATO, H., ARROTT, A., and KIKUCHI, R., 1959, *J. Chem. Phys.*, **68**, 1256.

† Now at the Department of Physics, The University, Hull.

REVIEWS OF BOOKS

Time Series Analysis, by E. J. HANNAN. Pp. vi+152. (London: Methuen; New York: John Wiley, 1960.) 21s.

The history of time-series analysis may be traced back to two distinct sources. On the one hand, the statistician's approach via autocorrelation analysis has proved useful in the analysis of, for example, econometric data. Here, the object is to fit a 'finite-parameter' model (i.e. an autoregressive or moving-average scheme) to the data in order to make short term predictions. Physicists and engineers, however, have developed the method of spectral analysis to investigate problems in, for example, communication engineering and noise in electronic circuits. In recent years the development of the theory of stationary stochastic processes has provided a common meeting ground for these two approaches. In fact, in the light of such results as the Wiener-Khinchine theorem, autocorrelation and spectral analysis are seen to be complimentary concepts, and the statistical approach to spectral analysis (commencing with the work of Bartlett and Tukey) has considerably increased the scope and usefulness of this method.

In his monograph, Professor Hannan gives a very elegant account of the statistical approach to time-series analysis, treating both autocorrelation and spectral analysis with equal weight. However, the book is written primarily for the mathematical statistician, and physicists will no doubt find the style rather formal.

The work is divided into five chapters. Chapter I presents a fairly theoretical introduction to the spectral theory of discrete stochastic processes, based on the theory of finite dimensional vector spaces, and chapter II deals with the application of autocorrelation analysis to the problem of estimating the parameters of a finite parameter model. Chapter III contains the most recent developments in time-series analysis concerning the estimation of a continuous spectral density function. The author discusses the work of Grenander and Rosenblatt and Parzen on the statistical errors of spectral estimates, but due, no doubt, to restrictions of space, the very important problem of practical analysis is only briefly outlined. However, it should be pointed out that, given only a sample record, the problem of constructing an estimate of a continuous spectrum which has a prescribed error and prescribed resolvability is still unsolved. From the point of view of the physicist or engineer, this is perhaps the most important aspect of spectral analysis, and one which requires urgent theoretical investigation.

In chapter IV the author considers a variety of problems under the heading 'Hypothesis testing and confidence intervals'. The situation is roughly that one wishes to test whether an empirical autocorrelation function (i.e. a 'correlogram') or spectrum is consistent with an assumed model of the original time-series. Most of the standard 'goodness of fit' tests for the correlogram are neatly presented, and recent work on similar types of tests for the spectrum is also included. A brief discussion is presented of the problem of 'mixed spectra', i.e. estimating the spectrum of a process which contains a number of sine waves with different amplitudes and frequencies (corresponding to spectral 'lines') superimposed on a component with a purely continuous spectrum. This is, perhaps, the most difficult problem in statistical spectral analysis, and one which also requires further theoretical investigation.

The final chapter deals with regression analysis and the elimination of non-stationary trends, and contains some of the author's own original work on time-series analysis. It should be noted that most of the theoretical distributions which arise in this type of analysis usually involve the covariance structure of the residual process. However, in many practical applications this covariance structure is unknown. The chapter concludes with an investigation of the effects of trend removal on the analysis of the residual process.

On the whole, the author is to be highly complimented on achieving a truly comprehensive survey of time-series analysis in such short space. The book may be confidently recommended both to physicists who are familiar with the practical side of spectral analysis and wish to acquaint themselves with the mathematical theory, and to mathematical statisticians who wish to be brought up to date with the statistical analysis of time series.

M. B. PRIESTLEY.

Variational Principles in Dynamics and Quantum Theory, 2nd Edn, by W. YOURGRAU and S. MANDELSTAM. Pp. xi + 180. (London: Sir Isaac Pitman, 1960.) 32s. 6d.

The first edition of this little book which appeared in 1955 was highly praised for its soundness as philosophy as well as physics (see, for example, Professor Salam's review in this journal, 1955, A, 68, 659). This new edition which has been revised and enlarged retains the original character. We are presented not merely with formal mathematics but with a critical analysis of the ideas underlying the formulation of variational principles in physics.

Several additions have been made. Two postscripts, resulting from correspondence with Professor Schrödinger, deal with the fine-structure formula and with the correct replacements of curvilinear coordinates by operators in quantum mechanics. There is a new Appendix on the application of variational methods to chemical reactions. By far the most important addition is a new chapter on the Feynman and Schwinger principles in quantum mechanics. Instead of the Hamiltonian formalism, these principles employ a Lagrangian formulation directly. This chapter gives a lucid account of the Feynman principle (including a very clear discussion of integrals over paths), its classical limit and its relationship to the Schwinger principle and to the conventional formulation of quantum mechanics. The Feynman and Schwinger principles have played a prominent part in the development of quantum field theory. A readable account of these ideas represents a most worth-while addition to this excellent book.

F. MANDL.

Nuclear Photodisintegration, by J. S. LEVINGER. Pp. viii + 144. (Oxford: University Press, 1960.) 15s.

Workers in the field of nuclear photodisintegration who have awaited eagerly the publication of this work by J. S. Levinger, who has made so many theoretical contributions to the development of the subject, will not be disappointed. The author leads into the theory by analogy with the atomic photoeffect, the transition probabilities here being calculated by perturbation theory. The experimental physicist will be able to follow this treatment including the derivation of the dipole 'sum-rules' which occupies the first 36 pages of the book. The dispersion theory application to the nuclear photoeffect is also indicated in this first chapter.

Subsequent chapters deal with the photodisintegration of the deuteron (12 pages), sum-rule calculations (16 pages), discrete transitions (12 pages), total

cross section for photon absorption discussed from the point of view of various models (20 pages) and a final chapter of 30 pages on the products of photo-disintegration.

The experimental work is not discussed in detail although the difficulties associated with the use of continuous bremsstrahlung spectra are indicated.

The main features of the nuclear photoeffect are discussed in terms of several different models. Many of them are model-independent and it is clear that more precise detail in the experimental measurements is needed. Thus, structure in the 'giant resonance' is now beginning to emerge and much more should be known about this in the near future.

It is perhaps a pity that the flair that the author obviously possesses of explaining theoretical calculations in simple terms was curbed by the limited size of the book, but the 130 pages of text collect much information not elsewhere available in a single publication and despite the compression the experimentalist will find the theoretical treatment invaluable.

E. H. BELLAMY.

High Energy Nuclear Physics, by W. O. LOCK. Pp. xi+190. (London: Methuen; New York: John Wiley, 1960.) 18s.

There has been a growing demand during the last few years for a book to serve as an introduction to nuclear physics below 1 GeV for the research student. This small but compact book easily fills this demand and, more importantly, should give the student a genuine appreciation of the subject.

The introductory chapters set the level of the book by using mathematical equations together with reasoning to show the physical concepts behind the common glibly used symbols. In the following chapters on scattering and photoproduction of pions the experimental results are analysed theoretically and explained phenomenologically, the result again producing a genuine understanding of the topics. Nucleon-nucleus and nucleon-nucleon interactions are then discussed and finally the two sections combined in the production of pions in nucleon-nucleon collisions.

Of course there are complaints: in such a small book some arguments must be curtailed and some results omitted, but surely energies below 1 GeV are not called high nowadays! Here, in effect, is the one main fault: the book is badly dated in the middle of 1959. To take two examples: the discussion of the Panofsky ratio implies that a discrepancy between theory and experiment needs further investigation, and the section on p-p scattering at 310 MeV gives five phase-shift solutions; whereas at that time the discrepancy was reasonably well explained and only two phase-shift solutions remained. However, these and other points can easily be removed in the next edition, and one hopes that this will not be long delayed.

R. T. TAYLOR.

Soviet Research in Geophysics, Vol. 3, *Microstructure and Macrostructure*, by B. N. IVAKIN. Pp. xiii+113. (New York: Consultants Bureau, 1960.) \$ 6.00.

The volume *Microstructure and Macrostructure of Elastic Waves* can be gauged for both form and content and on the first count it must be rated negatively. The volume is a translation of a monograph, No. 39, of the *Transactions of the Geophysical Institute of the Academy of Science*, from the original Russian into English. The quality of the translation is, at best, amateurish and the author's work has suffered because of the abuse by the translator. We have all

seen examples in the popular literature of the raw output to be expected from machine translation devices; this volume has many of these properties. I do not know if the monograph in question has been subject to machine or manual translation but it shows the lack of both literary and scientific editing. As an example, the following quotation is offered (page 5): "In the latter case†, the wave properties of waveguides have some asymptotic state to which the wave properties of a waveguide fed by an abruptly connected source with a periodic (e.g. sinusoidal) form of oscillations tends."

This is not the first example of a published translation from the Russian; we have a right to expect greater literacy and less literality. We also expect a use of proper English scientific terminology.

Ivakin considers the problem of the multiple reflections of sinusoidal waves from a multiply layered or one-dimensional, continuously inhomogeneous medium. His special device is to convert all the quantities involved, reflection coefficients, propagation constants, etc., into terms encountered in electrical engineering, a discipline where the problem has been discussed in the literature. He treats the problem by describing a series of transmission lines with different lengths and characteristic impedances. A number of examples are solved. The people most concerned with multiple reflections from one-dimensional media having many layers, the petroleum exploration geophysicists, are now able to synthesize seismograms corresponding to impulsive excitation of layered media using computing machinery. The Ivakin scheme is good and well known to electrical engineers; the problem of sinusoidal excitation is not particularly pertinent to current geophysics. There are more significant works in the Russian geophysical literature appropriate to the early translations into English.

Readers interested in a more sophisticated treatment of reflections in multiply layered media, including the difficult problems of oblique incidence, should refer to the recent translation of the Russian volume *Waves in Layered Media* by Brekhovskikh; this has been done in comparatively good scientific and grammatical English.

L. KNOPOFF.

Ionization Phenomena in Gases, by GORDON FRANCIS. Pp. vii + 300. (London: Butterworths Scientific Publications, 1960.) 60s.

The rapid progress that has been made since the end of the last war in the study of gas discharges, particularly at very high current densities, and the growing importance in so many fields of physics of the plasma state of matter has made clear the need for a monograph that discusses developments in this field from a modern standpoint. Dr. Francis has succeeded in writing a book that should fill this need admirably. The subject matter is well chosen, particular attention being devoted to those topics that are most rapidly developing and of greatest current interest. A great deal of it has not previously been brought together into a monograph. The elucidation of the physical principles underlying the phenomena observed in ionized gases is maintained as the primary aim of the book and is not allowed to become obscured with technical detail.

After a short and scarcely necessary introductory chapter on atomic structure and spectral notation, which this reviewer found the least satisfactory part of the book, a very condensed chapter follows on fundamental physical processes of importance in the gas discharge. A short but lucid chapter on the applications

† Steady state oscillations.

of the similarity principle follows. Alternating and high frequency discharges are treated in considerable detail in chapter 4. This chapter possibly goes into somewhat greater detail than is the case in the other chapters, but since this is a field in which the author has made important contributions he can be forgiven for being a little expansive. After a short chapter on the upper atmosphere an interesting account of high current discharges, including the pinched discharge and applications to thermonuclear reactions, follows. The final chapter contains a useful account of plasma oscillations and waves.

In his preface the author states that the book is intended mainly for those finishing their degrees or about to begin research, but there is no doubt that many who are already active workers in plasma physics or related topics will find the book of value. A high standard is maintained throughout on the technical side of the production.

E. H. S. BURHOP.

Resonance Absorption in Nuclear Reactors, by L. DRESNER. Pp. x+131. (Oxford, London, New York, Paris: Pergamon Press, 1960.) 40s.

In early discussions of the feasibility of self-sustaining chain reactions based on natural uranium fuel, it was recognised that the unknown extent of resonance absorption introduced an important uncertainty. Although it was known that resonance absorption could be reduced by lumping the uranium, little quantitative discussion appeared in the open literature until the first Geneva Conference in 1955. At this stage it became apparent that Western and Russian physicists had approached the topic from fundamentally different viewpoints.

The Conference therefore stimulated further and more penetrating study of the subject in which Dr. Dresner has played an important part. His monograph provides a comprehensive survey of the present position and is of particular value to the newcomer to the field, since care has been taken to derive important results from first principles with a clear indication of the assumptions involved. The theory of resonance absorption in homogeneous media is first developed and then generalized to cover other situations of practical interest. This includes a discussion of the wide and narrow resonance approximations in heterogeneous systems formed from relatively isolated lumps, regular lattices or fuel clusters. More study is evidently required on clusters since no improvement on Hellstrand's semi-empirical method has yet been devised. The value of the work is enhanced by the inclusion of chapters on relevant topics in slowing down and transport theory, a historical introduction and a critical comparison of the theory with experimental data. It is apparent that present understanding of the subject is such that it is entirely feasible to calculate resonance escape probabilities from the measured resonance parameters.

One small criticism must be made. On page 89 there appears the following statement, which might prove misleading to a reader unfamiliar with water-moderated reactor calculations: "In practical examples of tight lattices such as occur with homogeneous moderation the Dancoff correction is relatively small, the surface being decreased by the order of 5%." It is quite true that the mutual shielding of a single pair of fuel pins will be approximately 5%, but in a conventional square lattice each fuel pin has 8 near neighbours. The Dancoff correction therefore amounts to 40–50% of the effective surface and gives rise to very significant changes in the resonance integral, resonance escape probability and effective reproduction constant.

The book can be thoroughly recommended in view of the importance of the subject matter and the absence of comparable works; it should be studied carefully by all interested in low-enrichment reactor physics. D. HICKS.

Imperfections in Crystals, by H. G. VAN BUEREN. Pp. xviii + 676. (Amsterdam: North-Holland, 1960.) 110s.

This book is about atomic defects such as dislocations, vacancies, interstitials and F-centres, in crystals. Despite the intense interest now being shown in these defects by metallurgists and solid state physicists it is surprising that, until this book appeared, there existed no published introductory account of the whole field of crystal imperfections; only special accounts of particular parts such as dislocation theory or radiation damage. The author is to be congratulated on having recognized this gap; on having realized the exceptional timeliness of the present moment for such a book, when the basic theory has become stable and so much direct evidence for the structure and properties of the defects has appeared; and on having filled the gap with such a pleasant and useful book.

The treatment throughout is fairly elementary and this, together with the readable style, should make the book useful for students of physics and metallurgy who are interested in this branch of solid-state theory. The complete and impartial review of all the various contributions to the subject, including some that have undeservedly been forgotten in much of the recent research work, will also make the book valuable as a work of reference to more advanced readers.

The range of topics covered is extremely wide and complete. To take some examples, work hardening and alloy hardening of metals, creep, recrystallization, observations of lattice defects, radiation damage, diffusion and phase changes, internal friction, nuclear resonance, scattering of electrons and electromagnetic waves by defects, fatigue and fracture, optical and electrical properties of non-metallic crystals, and movements of lattice defects in non-metallic crystals. Naturally the treatment in most places is introductory rather than definitive but nevertheless it is rarely superficial; and on topics which touch on the author's own research interests, for example the dislocation structure and plastic properties of silicon and germanium, it is quite authoritative.

This book can be strongly recommended to those who seek a readable, thorough, and reliable introduction to this branch of solid-state physics and physical metallurgy. A. H. COTTRELL.

Cartesian Tensors: an Introduction, by G. TEMPLE. Pp. vii + 92. (London: Methuen; New York: John Wiley, 1960.) 12s. 6d.

Anything written by Professor Temple is expected to be interesting and provocative. But we need not always agree with his own reasons for finding his material interesting. Here he gives an account of cartesian tensors defined as invariant multilinear functions of direction. He considers this definition to give 'a new unity to the subject'. However, the unity is rather formal at this level; I think that it does not compensate for the severe limitations of cartesian tensors compared with general tensors. I always find that students learn general tensor calculus very quickly. It appeals to them because of its naturalness and usability, whereas I believe they would find this treatment of cartesian tensors to be artificial in itself and to be confusing when they proceed to general tensors. Professor Temple says that his book is for first-year students; I think

it is likely rather that lecturers preparing courses in tensor calculus will find it useful on account of some of its more subsidiary topics such as isotropic tensors (chapter VI) and spinors (chapter VII) of which such simple accounts are probably not available elsewhere. Also, anyone who knows a little about tensor calculus in general will find the 'Bourbaki treatment' given by Temple to be entertaining for its own sake. The reader must be warned, however, that he has to do some of his own proof-correcting!

W. H. MCCREA.

Nuclear Fusion—The Second Geneva Series on the Peaceful Uses of Atomic Energy, edited by W. P. ALLIS. Pp. viii + 488. (New York, London: Van Nostrand, 1960). 94s.

In this book Professor Allis has brought together a number of selected papers on thermonuclear research delivered at the International Conference at Geneva in 1958. He has grouped them into chapters, each preceded by a short explanation, a page or two long, of the principles concerned. He has cut the papers, sometimes considerably. The result is rather surprisingly successful as an exposition of the state of the subject at the time of Geneva. It would, however, be hard reading for anyone hitherto unacquainted with the subject, but if he has read, for example, Spitzer's admirable little book in *Interscience Tracts*, or its equivalent, he will find this book most helpful. Partly because of the self-contained character of the individual papers it is convenient for reference.

G. P. THOMSON.

Royal Society Mathematical Tables, Vol. 7, *Bessel Functions*, Part III, *Zeros and Associated Values*, edited by F. W. J. OLVER. Pp. ix + 79. (London: Cambridge University Press, 1960.) 50s.

New methods have been developed in the presentation of this book of tables of Bessel Functions which is the third in the series of three undertaken by the Royal Society of the Mathematical Tables Committee. In an interesting introduction the new method is described and its debt to the present day automatic electronic computing machine acknowledged.

Annual Reports on the Progress of Chemistry, Vol. LVI, 1959. Pp. xiv + 476. (London: The Chemical Society, 1960.) 40s.

Among the articles contained in Volume LVI of the *Annual Reports on the Progress of Chemistry* 1959 are some which will interest physicists; these include The physical properties of some simple fluids, by J. S. Rowlinson, and Nuclear magnetic resonance, by J. A. Pople.

Full reviews of the volume will be found in the various chemical journals.

Solid State Physics, Vol. 11, edited by F. SEITZ and D. TURNBULL. Pp. xvi + 438. (New York: Academic Press, 1960.) 89s. 6d.

This, the eleventh volume of the series *Solid State Physics*, edited by F. Seitz and D. Turnbull, contains the following articles: Semiconducting properties of gray tin; Physics at high pressure; The effects of elastic deformation on the electrical conductivity of semiconductors; Imperfection ionization energies in CdS-type materials by photoelectronic techniques; Cyclotron resonance. It contains also a cumulative subject index for Volumes 1-10. A list of articles planned for future volumes is also given and covers some thirty further articles by a wide range of well-known authors.

Neutron Detection, by W. D. ALLEN. Pp. viii + 260. (London: Newnes, 1960.) 45s.

Dr. Allen has packed an amazing amount of information about the methods of detecting neutrons into 250 pages. Obviously he was unable to go into considerable detail in a book of this size, but each technique which he mentions carries references, and an extensive bibliography is included at the back for good measure.

My objection (and it is a small one) is that he has stuck so closely to his title. I should like to have seen a few more numbers quoted in the section on neutron sources, for example, a graph of the deuteron-triton cross section as a function of energy, and energy-angle graphs or nomograms for the neutrons arising from this process, and from other common processes for neutron production. More details on the shielding of neutron detectors also would have been acceptable. Finally, far more useful range-energy curves exist than that given in appendix IX(a), for research workers using nuclear emulsions to detect neutrons.

I recommend this book to anyone working in the field of neutron physics, and also to experimenters who are bothered by neutron backgrounds.

W. H. R. F. MUIRHEAD.

Stochastic Processes, Problems and Solutions, by L. TAKÁCS. Pp. xi + 137, (London: Methuen; New York: John Wiley, 1960.) 18s.

This book is one of the first of a new series of monographs on applied probability and statistics, edited by M. Bartlett. It is not a textbook in the usual sense of the word but rather a collection of problems and their solutions for readers who are already familiar with probability theory. The fundamental notions and theorems of the theory of stochastic processes which are needed for dealing with the special problems are only given in a condensed but precise and lucid form. The complete solutions of all the problems are given and the ways to find them are clearly indicated though, of course, not in all mathematical detail.

The first two chapters of the book deal with Markov chains and Markov processes which are stochastic sequences or processes in which the future behaviour of a system depends only on its present state but not on its past. The third chapter is devoted to non-Markovian processes, in particular to stationary, recurrent (or regenerative) and secondary processes. Most of the theorems and problems of this chapter have not been treated in other books, and a considerable part of them is the result of the author's own scientific work.

The problems are chosen from a wide field of pure and applied science and engineering, like random walk and Brownian motion, nuclear processes and their recording, cosmic rays, birth and death processes, problems of renewals (e.g. of machine parts), theory of queues and waiting times, linear prediction of stochastic series, etc.

The book will be of great interest and value to all those mathematically minded scientists who work on phenomena which have stochastic features.

R. FURTH.

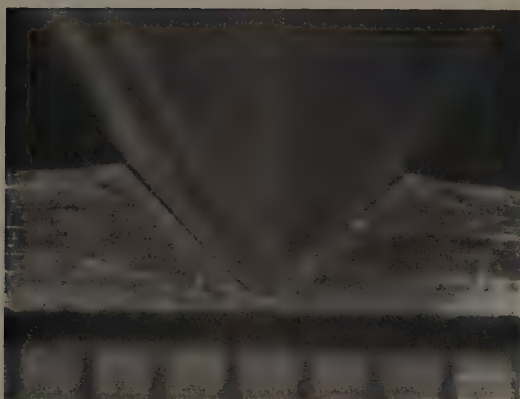


Fig. 2. Cross section of recovered indentation formed in duralumin, with indenter lying within it. The walls of the recovered indentation are almost straight. Each division is 1 mm.

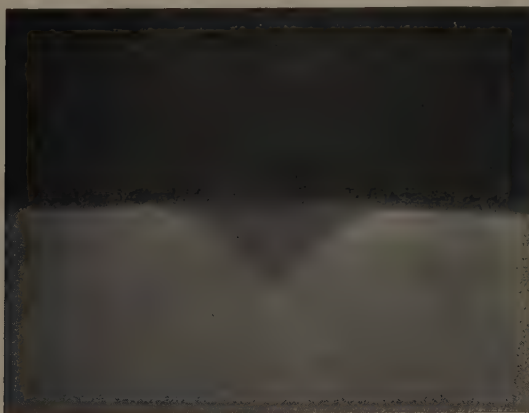
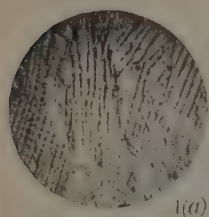
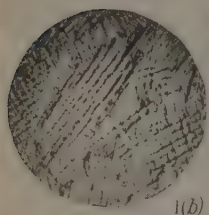


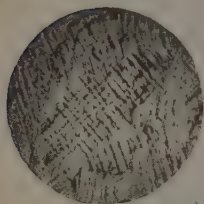
Fig. 7. Cross section of recovered indentation formed in a polymeric solid. When recovery is large the walls of the indentation are not straight.



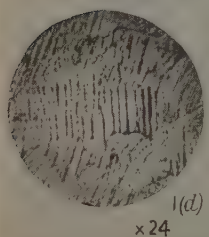
1(a)



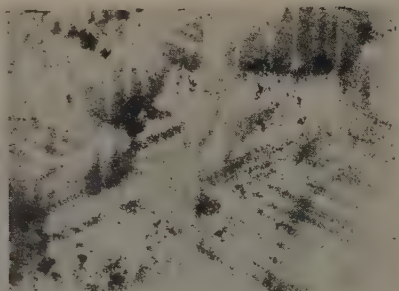
1(b)



1(c)

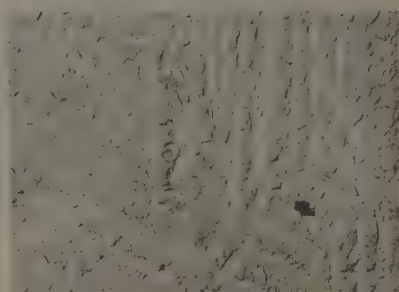


1(d)
×24



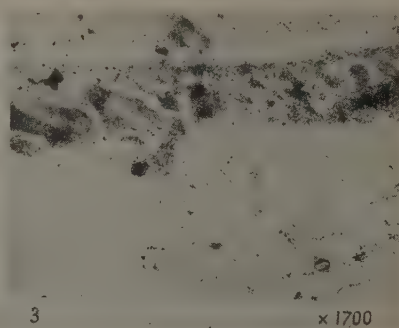
2(a)

×5100



2(b)

×5100



3

×1700

- Fig. 1. Patterns on a mechanically polished surface of platinum-cobalt as the specimen was turned through 90° with respect to a high field (horizontal in the figure).
 Fig. 2. (a) Details of patterns shown in Fig. 1; (b) etch pattern corresponding to (a) (carbon replica).
 Fig. 3. Pattern on an annealed surface showing clear structures along a grain boundary.
 Figs 1 to 3 refer to specimens with low coercivity, $H_c \approx 35$ Oe.

Fig. 4.

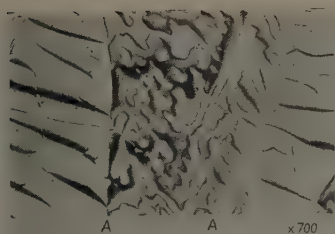


Fig. 7.

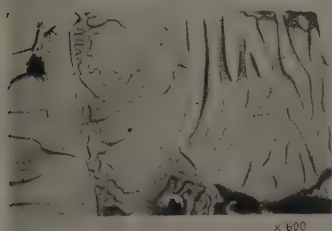


Fig. 6.

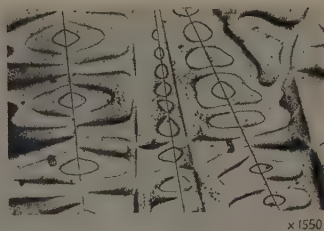


Fig. 8.

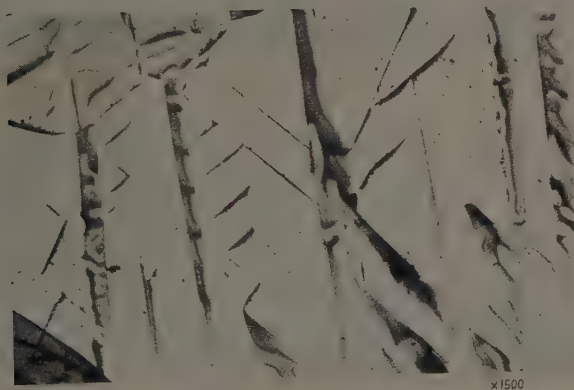
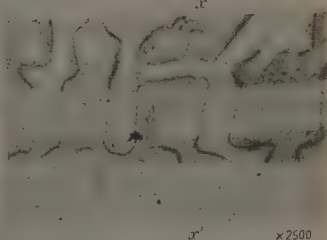
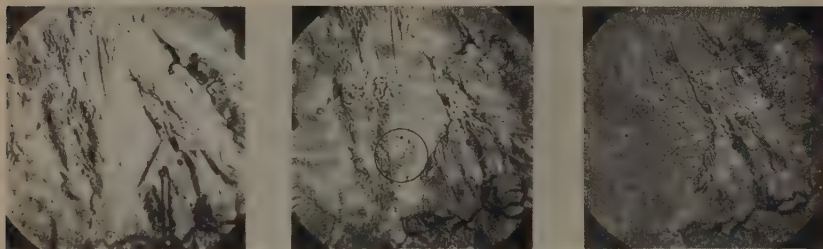


Fig. 9.

- Fig. 4. Patterns on three ordered regions, in two of which the easy axes are parallel.
 Fig. 6. Six ordered lamellae having easy axes oriented alternately in one of two directions.
 Fig. 7. Three ordered regions with mutually perpendicular easy axes.
 Fig. 8. Lamellae with easy axes alternately parallel and normal to the surface.
 Fig. 9. Very fine lamellae, uniformly magnetized or with very simple domain structures.



(a)

(b)

(c)

Figs 10
(a-f).

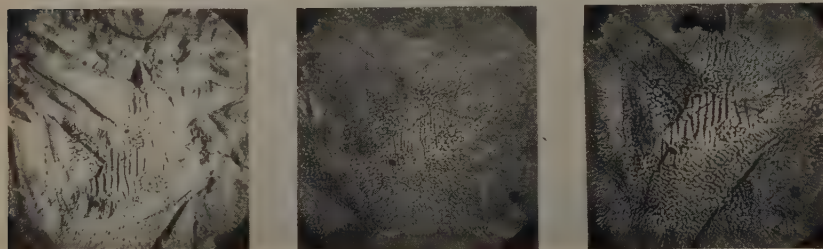


(d)

(e)

(f)

Figs 12
(a-c).



(a)

(b)

(c)

Figs 10 (a-f). The nucleation and movement of domain walls in a region with easy axis, parallel to the direction of an applied field (horizontal with respect to this figure and to Fig. 12). The values of the internal fields are given by Fig. 11.

Figs 12 (a-c). The behaviour of the domains in a region having its easy axis perpendicular to the direction of an applied field: (a) 17 000 oersteds, (b) 600 oersteds, (c) -500 oersteds.

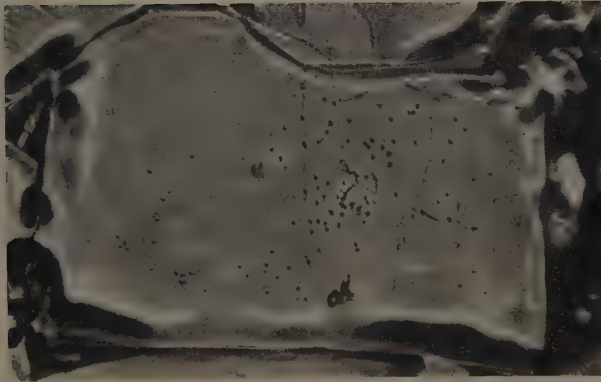


Fig. 1. A grain of 'square loop' ferrite with two 180° domain walls.



Fig. 3. A mosaic photograph of a grain of 'square loop' ferrite showing a 180° domain wall and Neel spike domains around the pores.

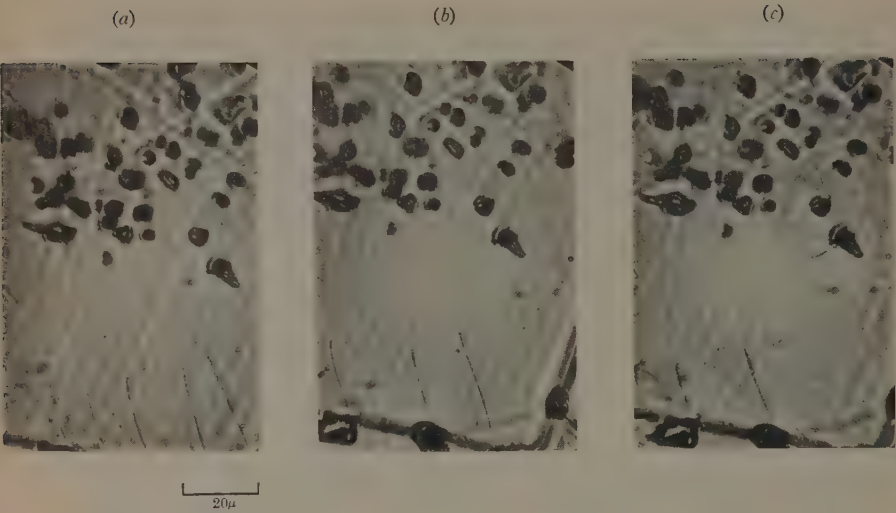


Fig. 5. The transit of a domain wall through the encircled pore of Fig. 3.



Fig. 6. The nucleation and reversal process in a grain of 'square loop' ferrite. (Retouched.)

The Scattering of Low-energy Ortho-positronium by Hydrogen Atoms

By P. A. FRASER

Department of Physics, University of Western Ontario, London, Canada

Communicated by Sir Harrie Massey; MS. received 7th December 1960

Abstract. When ortho-positronium collides with a hydrogen atom not only may it be scattered, but there is also the possibility of conversion of the ortho-positronium to para-positronium by electron exchange. The total elastic cross section and the conversion cross section have been calculated for positronium kinetic energies 0 to 9.8 eV, for the $l=0$ partial wave only. A particular choice of trial wave function explicitly satisfying the Pauli principle and a variational argument lead to integro-differential equations, with no 'ordinary force', from which the phase shifts have been obtained by a numerical method. The cross sections are very strongly energy dependent: the total cross section ranges from $192\pi a_0^2$ at zero energy to $2.92\pi a_0^2$ at 6.8 eV, while the (conversion)/(total) ratio ranges from 0.176 to 0.070 over these energies. These ratios are well below the value $1/4$ expected at high energies from the Born approximation. The total cross section results of Massey and Mohr for this problem using Born approximation were $230\pi a_0^2$ at zero energy and $25\pi a_0^2$ at 6.8 eV, with the (conversion)/(total) ratio $1/4$.

§ 1. INTRODUCTION

MASSEY AND MOHR (1954) have surveyed, using Born approximation methods, the processes involved in the fate of positrons slowed down in atomic hydrogen gas. These processes included the formation of positronium and the slowing down of ortho-positronium and the ortho-para conversion by collisions with the hydrogen. This paper reports a more detailed calculation of the cross sections for elastic collisions of slow ortho-positronium with hydrogen atoms and for the quenching of ortho-positronium by electron exchange and conversion to para-positronium in collisions with hydrogen atoms. It is assumed throughout that the positronium has a stable existence; that is, that its life time against spontaneous decay by annihilation is long enough to make the notion of a collision meaningful. Further, the possibility of annihilation of the positron with the atomic electron during the collision has been neglected in this calculation (Deutsch 1953, p. 148). Only s-scattering has been considered, and at the low energies of interest (generally < 5.1 eV) the neglect of higher order partial waves should not be serious. Spin-orbit effects have been neglected (Massey and Mohr 1954).

§ 2. SCATTERING AND CONVERSION CROSS SECTIONS

The Schrödinger equation for the system of ortho-positronium and the hydrogen atom is (assuming infinite mass for the proton):

$$H\Psi = E\Psi \quad \dots\dots(1)$$

where

$$H = -\nabla_p^2 - \nabla_1^2 - \nabla_2^2 - \frac{2}{r_{1p}} - \frac{2}{r_{2p}} - \frac{2}{r_1} - \frac{2}{r_2} + \frac{2}{r_p} + \frac{2}{r_{12}}.$$

\mathbf{r}_1 and \mathbf{r}_2 are the position vectors of the two electrons, \mathbf{r}_p that of the positron. Units in which $\hbar = 1$, $m_e = \frac{1}{2}$ and $e^2 = 2$ are used; in this system, similar to atomic units, the unit of length is a_0 (the Bohr radius) and the unit of energy is the binding energy of the hydrogen atom, 13.6 eV. Writing

$$\boldsymbol{\sigma}_1 = (\mathbf{r}_1 + \mathbf{r}_p)/2; \quad \boldsymbol{\rho}_1 = (\mathbf{r}_1 - \mathbf{r}_p),$$

the 'positronium portion' of the Hamiltonian (the positron and electron 1, say) may be written

$$-\nabla_p^2 - \nabla_1^2 - \frac{2}{r_{1p}} \equiv -\frac{1}{2}\nabla_{\sigma_1}^2 - 2\nabla_{\rho_1}^2 - \frac{2}{\rho_1}.$$

The positronium ground state wave function $\phi(\rho_1)$ binding energy $\frac{1}{2}$, satisfies

$$\begin{aligned} \left(-2\nabla_{\rho_1}^2 - \frac{2}{\rho_1}\right)\phi(\rho_1) &= -\frac{1}{2}\phi(\rho_1) \quad \dots\dots (2) \\ \phi(\rho_1) &= \left(\frac{1}{8\pi}\right)^{1/2} \exp(-\rho_1/2) \quad (\text{normalized}). \end{aligned}$$

The ground state hydrogen atom wave function $\psi(r_2)$, binding energy 1, satisfies

$$\begin{aligned} \left(-\nabla_{r_2}^2 - \frac{2}{r_2}\right)\psi(r_2) &= -\psi(r_2) \quad \dots\dots (3) \\ \psi(r_2) &= \left(\frac{1}{\pi}\right)^{1/2} \exp(-r_2) \quad (\text{normalized}). \end{aligned}$$

It is convenient to write

$$E = \frac{1}{2}k^2 - \frac{3}{2} \quad \dots\dots (4)$$

where $\frac{1}{2}k^2$ is the kinetic energy of the positronium; k is the magnitude of the momentum.

Solutions $\Psi^{(-)}(\mathbf{r}_p, \mathbf{r}_1, \mathbf{r}_2)$ and $\Psi^{(+)}(\mathbf{r}_p, \mathbf{r}_1, \mathbf{r}_2)$ of (1) are sought, respectively antisymmetric and symmetric in the electron coordinates \mathbf{r}_1 and \mathbf{r}_2 , with asymptotic forms ($\sigma_1 \rightarrow \infty$)

$$\begin{aligned} \Psi^{(+)} &\sim \left(\exp(ik\sigma_{1z}) + F(\theta_1) \frac{\exp(ik\sigma_1)}{\sigma_1}\right) \phi(\rho_1)\psi(r_2), \\ \Psi^{(-)} &\sim \left(\exp(ik\sigma_{1z}) + G(\theta_1) \frac{\exp(ik\sigma_1)}{\sigma_1}\right) \phi(\rho_1)\psi(r_2), \quad \dots\dots (5) \end{aligned}$$

where θ_1 is the scattering angle (the angle the positronium position vector $\boldsymbol{\sigma}_1$ makes with the z axis). We do not consider the possibility of excitation of the positronium or hydrogen atoms, which is of course impossible below $\frac{1}{2}k^2 = 0.375$ (5.1 eV). The differential elastic scattering cross section, including the ortho-para conversion, is given by

$$\sigma(\theta) = \frac{3}{4}|G|^2 + \frac{1}{4}|F|^2.$$

The differential cross section for the ortho-para conversion or the differential quenching cross section is given by

$$\sigma_p(\theta) = \frac{1}{18}|G - F|^2$$

as may be seen as follows:

The system of three spin $\frac{1}{2}$ particles forms quartet or doublet states. With the quartet spin functions, which are, in particular, symmetric in the spin coordinates of the electrons, must be associated $\Psi^{(-)}$. There is no possibility of ortho-para conversion in a quartet state.

The doublet states may be divided into two classes: those symmetric in the spins of the electrons and those antisymmetric in these spins. For the case $m = \frac{1}{2}$ these may be taken to be

$$\chi_{1/2}^{1/2}(\mathbf{p}, \overline{1}, \overline{2}) = \frac{1}{\sqrt{6}} \left\{ -2\beta(\mathbf{p})\alpha(1)\alpha(2) + \alpha(\mathbf{p})\alpha(1)\beta(2) + \alpha(\mathbf{p})\beta(1)\alpha(2) \right\},$$

$$\chi_{1/2}^{1/2}(\mathbf{p}, \widetilde{1}, \widetilde{2}) = \frac{1}{\sqrt{2}} \left\{ \alpha(\mathbf{p})\alpha(1)\beta(2) - \alpha(\mathbf{p})\beta(1)\alpha(2) \right\};$$

where the bar over 1 and 2 denotes symmetric, and the tilde denotes antisymmetric. Together with the $m = -\frac{1}{2}$ states, these form a complete set of doublet states.

The linear combination

$$\Psi = \frac{\sqrt{3}}{2} \Psi^{(+)}(\mathbf{p}, 1, 2) \chi_{1/2}^{1/2}(\mathbf{p}, \widetilde{1}, \widetilde{2}) + \frac{1}{2} \Psi^{(-)}(\mathbf{p}, 1, 2) \chi_{1/2}^{1/2}(\mathbf{p}, \overline{1}, \overline{2})$$

satisfies the Pauli principle, and also corresponds to an incoming wave of ortho-positronium alone. For the doublet spin functions may be written

$$\chi_{1/2}^{1/2}(\mathbf{p}, \widetilde{1}, \widetilde{2}) = \frac{\sqrt{3}}{2} \sqrt{\frac{2}{3}} \left\{ \chi_1^1(\mathbf{p}, 1)\beta(2) - \frac{1}{\sqrt{2}} \chi_1^0(\mathbf{p}, 1)\alpha(2) \right\} - \frac{1}{2} \chi_0^0(\mathbf{p}, 1)\alpha(2),$$

$$\chi_{1/2}^{1/2}(\mathbf{p}, \overline{1}, \overline{2}) = \frac{\sqrt{3}}{2} \chi_0^0(\mathbf{p}, 1)\alpha(2) + \frac{1}{2} \sqrt{\frac{2}{3}} \left\{ \chi_1^1(\mathbf{p}, 1)\beta(2) - \frac{1}{\sqrt{2}} \chi_1^0(\mathbf{p}, 1)\alpha(2) \right\},$$

where $\chi_1^1(\mathbf{p}, 1)$ and $\chi_1^0(\mathbf{p}, 1)$ are triplet functions of the positron and electron spins, and $\chi_0^0(\mathbf{p}, 1)$ is the singlet function of these spins. Thus Ψ has the asymptotic form

$$\Psi \sim \phi(\rho_1)\psi(r_2) \left\{ \left[\exp(ik\sigma_{1z}) + \left(\frac{3}{4}F + \frac{1}{4}G \right) \frac{\exp(ik\sigma_1)}{\sigma_1} \right] \right.$$

$$\times \sqrt{\frac{2}{3}} \left\{ \chi_1^1(\mathbf{p}, 1)\beta(2) - \frac{1}{\sqrt{2}} \chi_1^0(\mathbf{p}, 1)\alpha(2) \right\}$$

$$\left. + \frac{\sqrt{3}}{4} (G - F) \frac{\exp(ik\sigma_1)}{\sigma_1} \chi_0^0(\mathbf{p}, 1)\alpha(2) \right\},$$

which explicitly describes a plane wave of unit amplitude of ortho-positronium incident on hydrogen atoms with a scattered wave, in the doublet eigenstate

$$\sqrt{\frac{2}{3}} \left\{ \chi_1^1(\mathbf{p}, 1)\beta(2) - \frac{1}{\sqrt{2}} \chi_1^0(\mathbf{p}, 1)\alpha(2) \right\},$$

together with an outgoing wave of para-positronium of amplitude $\sqrt{3}(G - F)/4$.

Taking into account the quartet scattering we have then that

$$\sigma(\theta) = \frac{1}{6} [4|G|^2 + 2\{\frac{3}{4}F + \frac{1}{4}G\}^2 + \frac{3}{16}|G - F|^2]$$

$$= \frac{3}{4}|G|^2 + \frac{1}{4}|F|^2,$$

as could have been expected; and clearly the part of the total scattering that corresponds to conversion is

$$\sigma_p(\theta) = \frac{1}{16}|G - F|^2.$$

This result has also been obtained by Field (1958) in connection with the essentially similar problem of the conversion of ground state hydrogen atoms in a hyperfine triplet state to the hyperfine singlet state by electron collisions. Ferrell (1958) has made similar considerations.

s-scattering alone is considered in this paper. The s-parts of $F(\theta)$ and $G(\theta)$ are respectively

$$\frac{1}{k} \exp(i\eta^+) \sin \eta^+ \quad \text{and} \quad \frac{1}{k} \exp(i\eta^-) \sin \eta^-$$

where η^+ and η^- are the s-phase-shifts obtained from wave functions $\Psi^{(+)}$ and $\Psi^{(-)}$ respectively. Considering then that it is sufficient to consider $l=0$ scattering alone, the total scattering and conversion cross sections (integrated over 4π) are

$$\sigma = \frac{4\pi}{k^2} \left\{ \frac{3}{4} \sin^2 \eta^- + \frac{1}{4} \sin^2 \eta^+ \right\}, \quad \dots\dots (6)$$

$$\sigma_p = \frac{4\pi}{k^2} \frac{1}{16} \{ \sin^2 \eta^- + \sin^2 \eta^+ - 2 \sin \eta^+ \sin \eta^- \cos(\eta^- - \eta^+) \}, \quad \dots\dots (7)$$

For zero energy

$$\frac{\tan \eta^+}{k} \rightarrow -A^+ \quad \text{and} \quad \frac{\tan \eta^-}{k} \rightarrow -A^-$$

where A^+ and A^- are scattering lengths. The cross sections become

$$\sigma = 4\pi \left\{ \frac{3}{4} (A^-)^2 + \frac{1}{4} (A^+)^2 \right\}$$

$$\sigma_p = 4\pi \frac{1}{16} \{ A^- - A^+ \}^2.$$

§ 3. THE SPATIAL WAVE FUNCTIONS

Wave functions $\Psi^{(-)}(\mathbf{r}_p, \mathbf{r}_1, \mathbf{r}_2)$ and $\Psi^{(+)}(\mathbf{r}_p, \mathbf{r}_1, \mathbf{r}_2)$, respectively antisymmetric and symmetric in \mathbf{r}_1 and \mathbf{r}_2 , and satisfying asymptotic conditions (5), are to be found. The exact wave functions have the property that

$$I^{(\pm)} = \int d\mathbf{r}_1 d\mathbf{r}_2 \Psi^{(\pm)}(H-E)\Psi^{(\pm)} = 0.$$

If $\Psi^{(\pm)}$ be taken as having asymptotic form (writing a^\pm for $\tan \eta^\pm$)

$$\Psi^{(\pm)} \sim \phi(\rho_1) \psi(r_2) \frac{1}{\sigma_1} [\sin k\sigma_1 + a^\pm \cos k\sigma_1],$$

that is considering only the $l=0$ parts† and also changing the amplitude at infinity, then for variations $\delta\Psi^{(\pm)}$, with

$$\delta\Psi^{(\pm)} \sim \phi(\rho_1) \psi(r_2) (\delta a^\pm) \frac{\cos k\sigma_1}{\sigma_1},$$

about the exact solution,

$$[\delta I^{(\pm)} - 4\pi k (\delta a^\pm)] = 0. \quad \dots\dots (8)$$

† Throughout this paper only s-scattering is considered; higher order partial waves could of course be considered by similar means, but at the expense of complicating the presentation.

The approximate calculation of $\Psi^{(\pm)}$ is based on the following considerations. Form trial functions

$$\Psi_t^{(\pm)}(\mathbf{r}_p, \mathbf{r}_1, \mathbf{r}_2) = \phi(\rho_1)\psi(r_2) \frac{1}{\sigma_1} f^{(\pm)}(\sigma_1) \pm \phi(\rho_2)\psi(r_1) \frac{1}{\sigma_2} f^{(\pm)}(\sigma_2) \quad \dots\dots (9)$$

which have explicitly the appropriate symmetries, and where

$$f^{(\pm)}(\sigma) \underset{\sigma \rightarrow \infty}{\sim} \sin k\sigma + a_t^{\pm} \cos k\sigma$$

$$\text{with} \quad f^{(\pm)}(0) = 0.$$

Form

$$I_t^{(\pm)} = \int d\sigma_1 d\rho_1 d\mathbf{r}_2 \Psi_t^{(\pm)}(H-E)\Psi_t^{(\pm)} \quad \dots\dots (10)$$

and calculate $\delta I_t^{(\pm)}$ for variations $\delta f^{(\pm)}(\sigma)$ with

$$\delta f^{(\pm)}(\sigma) \sim (\delta a_t^{\pm}) \cos k\sigma. \quad \dots\dots (11)$$

The calculation of $\delta I_t^{(\pm)}$ is fairly straightforward and certainly lengthy and is outlined in appendix A. It is found that

$$\begin{aligned} \frac{1}{2} [\delta I_t^{(\pm)} - 4\pi k(\delta a_t^{\pm})] = \int d\sigma_1 \frac{\delta f^{(\pm)}(\sigma_1)}{\sigma_1} \left\{ (-\nabla_{\sigma_1}^2 - k^2) \frac{f^{(\pm)}(\sigma_2)}{\sigma_2} \right. \\ \left. \pm \int d\sigma_2 K(\sigma_1, \sigma_2) \frac{f^{(\pm)}(\sigma_2)}{\sigma_2} \right\} \quad \dots\dots (12) \end{aligned}$$

with

$$\begin{aligned} K(\sigma_1, \sigma_2) = (4)^3 \int d\mathbf{r}_p \phi(2|\sigma_1 - \mathbf{r}_p|)\psi(|2\sigma_1 - \mathbf{r}_p|)\phi(2|\sigma_2 - \mathbf{r}_p|)\psi(|2\sigma_2 - \mathbf{r}_p|) \\ \times \left\{ -k^2 - 5 + \frac{2}{|2\sigma_1 - \mathbf{r}_p|} + \frac{2}{|2\sigma_2 - \mathbf{r}_p|} + \frac{4}{r_p} \right. \\ \left. + \frac{2}{|\sigma_1 - \sigma_2|} - \frac{2(2\sigma_1 - \mathbf{r}_p) \cdot (\sigma_1 - \mathbf{r}_p)}{|2\sigma_1 - \mathbf{r}_p||\sigma_1 - \mathbf{r}_p|} \right. \\ \left. - \frac{2(2\sigma_2 - \mathbf{r}_p) \cdot (\sigma_2 - \mathbf{r}_p)}{|2\sigma_2 - \mathbf{r}_p||\sigma_2 - \mathbf{r}_p|} \right\}. \quad \dots\dots (13) \end{aligned}$$

It is noted that $K(\sigma_1, \sigma_2)$ is symmetric in σ_1 and σ_2 .

The requirement that

$$\delta I_t^{(\pm)} - 4\pi k(\delta a_t^{\pm}) = 0$$

leads to integro-differential equations for $f^{(\pm)}(\sigma)$:

$$\frac{1}{\sigma_1} \left\{ \frac{d^2 f^{(\pm)}(\sigma_1)}{d\sigma_1^2} + k^2 f^{(\pm)}(\sigma_1) \right\} = \pm \int d\sigma_2 K(\sigma_1, \sigma_2) \frac{f^{(\pm)}(\sigma_2)}{\sigma_2}. \quad \dots\dots (14)$$

Writing

$$\Psi_t^{(\pm)} = \Psi^{(\pm)} + \Delta \Psi^{(\pm)},$$

to first order in $\Delta \Psi^{(\pm)}$ (the 'error' in $\Psi_t^{(\pm)}$), one obtains from (8)

$$I_t^{(\pm)} = 4\pi k(\Delta a^{\pm})$$

where

$$a_t^{\pm} = a^{\pm} + \Delta a^{\pm}.$$

A presumably better approximation to a^\pm is thus given by

$$a_1^\pm = a_t^\pm - \frac{I_t^{(\pm)}}{4\pi k}.$$

It is shown in appendix B that

$$I_t^{(\pm)} = 0$$

for $f^{(\pm)}(\sigma)$ satisfying (14). Thus a_t^\pm is an approximation to a^\pm accurate to second order in the difference between the trial function and the exact function. The apparent success of the exchange approximation, which employs a trial function of similar form to that above, for electron-hydrogen atom elastic scattering at low energies (Bransden *et al.* 1958, Brackmann *et al.* 1958), would suggest that the approximation used here is quite good. The most serious source of error is likely to be neglect of such virtual processes as the formation, during the impact, of H^- and a free positron or the excitation of higher states of positronium or hydrogen.

§ 4. THE KERNEL

The angle integrations in the integro-differential equations (14) may be carried out. Consider, for example, the term on the right-hand side proportional to k^2 (the subscript on \mathbf{r} will now be dropped):

$$f^{(\pm)}(\sigma_1) = \int d\sigma_2 \int d\mathbf{r} \phi(2|\sigma_1 - \mathbf{r}|) \psi(|2\sigma_1 - \mathbf{r}|) \phi(2|\sigma_2 - \mathbf{r}|) \psi(|2\sigma_2 - \mathbf{r}|) \frac{f^{(\pm)}(\sigma_2)}{\sigma_2}$$

with

$$\phi(\rho) = \left(\frac{1}{8\pi}\right)^{1/2} \exp\left(-\frac{\rho}{2}\right)$$

and

$$\psi(r) = \left(\frac{1}{\pi}\right)^{1/2} \exp(-r).$$

Now

$$|\sigma - \mathbf{r}| = (\sigma^2 + r^2 - 2\sigma r \mu)^{1/2}$$

and

$$|2\sigma - \mathbf{r}| = (4\sigma^2 + r^2 - 4\sigma r \mu)^{1/2}$$

with

$$\mu = \frac{\sigma \cdot \mathbf{r}}{\sigma r}.$$

The products of exponentials may be expanded in series of Legendre polynomials:

$$(\exp[-|\sigma - \mathbf{r}|])(\exp[-|2\sigma - \mathbf{r}|]) = \frac{1}{\sigma r} \sum_{l=0}^{\infty} (2l+1) G_l(\sigma, r) P_l(\mu)$$

with

$$G_l(\sigma, r) = \frac{\sigma r}{2} \int_{-1}^1 d\mu P_l(\mu) (\exp[-|\sigma - \mathbf{r}|])(\exp[-|2\sigma - \mathbf{r}|]).$$

..... (15)

With such expansions for both σ_1 and σ_2 dependent factors, and making use of the addition theorem for the spherical harmonics, and further carrying out the angle integrations $d\Omega_{\sigma_1}$ and $d\Omega_r$ inside the summations, one obtains

$$f^{(\pm)}(\sigma_1) = \frac{2}{\sigma_1} \int_0^\infty d\sigma_2 \int_0^\infty dr G_0(\sigma_1, r) G_0(\sigma_2, r) f^{(\pm)}(\sigma_2).$$

The remaining terms may be similarly treated; the result is that the integro-differential equations for $f^{(\pm)}(\sigma)$ become

$$\left\{ \frac{d^2}{d\sigma_1^2} + k^2 \right\} f^{(\pm)}(\sigma_1) = \pm \int_0^\infty d\sigma_2 \left\{ \frac{k^2}{2} K^{(1)}(\sigma_1, \sigma_2) + K^{(2)}(\sigma_1, \sigma_2) \right\} f^{(\pm)}(\sigma_2) \quad \dots (16)$$

with

$$f^{(\pm)}(0) = 0$$

and

$$f^{(\pm)}(\sigma_1) \underset{\sigma_1 \rightarrow \infty}{\sim} \sin k\sigma_1 + a^\pm \cos k\sigma_1,$$

$$K^{(1)}(\sigma_1, \sigma_2) = -(256) \int_0^\infty dr G_0(\sigma_1, r) G_0(\sigma_2, r)$$

with $G_0(\sigma, r)$ given by (15) with $l=0$;

$$\begin{aligned} K^{(2)}(\sigma_1, \sigma_2) = (256) \int_0^\infty dr \bigg\{ & -\frac{5}{2} G_0(\sigma_1, r) G_0(\sigma_2, r) + \frac{2}{r} G_0(\sigma_1, r) G_0(\sigma_2, r) \\ & + G_0(\sigma_1, r) J_0(\sigma_2, r) + J_0(\sigma_1, r) G_0(\sigma_2, r) \\ & + \left(\sum_l \gamma_l(\sigma_1, \sigma_2) G_l(\sigma_1, r) G_l(\sigma_2, r) \right) \\ & - G_0(\sigma_1, r) [(2\sigma_2^2 + r^2) K_0(\sigma_2, r) - 3\sigma_2 r K_1(\sigma_2, r)] \\ & - G_0(\sigma_2, r) [(2\sigma_1^2 + r^2) K_0(\sigma_1, r) - 3\sigma_1 r K_1(\sigma_1, r)] \bigg\} \end{aligned}$$

where

$$\begin{aligned} \gamma_l(\sigma_1, \sigma_2) &= \frac{1}{\sigma_2} \left(\frac{\sigma_1}{\sigma_2} \right)^l, \quad (\sigma_1 \leq \sigma_2) \\ &= \frac{1}{\sigma_1} \left(\frac{\sigma_2}{\sigma_1} \right)^l, \quad (\sigma_1 \geq \sigma_2) \end{aligned}$$

(arising from the expansion of $1/(|\sigma_1 - \sigma_2|)$) and where

$$\begin{aligned} J_0(\sigma, r) &= \frac{\sigma r}{2} \int_{-1}^1 d\mu \exp(-|\sigma - r|) \frac{\exp(-|2\sigma - r|)}{|2\sigma - r|} \\ K_0(\sigma, r) &= \frac{\sigma r}{2} \int_{-1}^1 d\mu \frac{\exp(-|\sigma - r|)}{|\sigma - r|} \frac{\exp(-|2\sigma - r|)}{|2\sigma - r|} \\ K_1(\sigma, r) &= \frac{\sigma r}{2} \int_{-1}^1 d\mu \mu \frac{\exp(-|\sigma - r|)}{|\sigma - r|} \frac{\exp(-|2\sigma - r|)}{|2\sigma - r|}. \end{aligned}$$

The $G_l(\sigma, r)$ are given by Eqn (15).

While the integrals $G_l(\sigma, r)$ etc., could be expressed as series of products of Bessel functions, it was decided to evaluate them numerically, this being a more straightforward process. These integrations were carried out on the first University College (London) Electronic Computer for a net of σ and r . The time available on the machine demanded some economy in the numerical work: the integrals were thus computed along rays of constant σ/r to cut down the time spent in the exponential sub-routine.

The net of points covered the ranges $0 \leq \sigma \leq 10$ and $0 \leq r \leq 16$, and because of the ray technique was necessarily rather sparse for large arguments. Some of the integrals could be evaluated in closed form for an irrational (σ/r) ratio,

$(\sigma/r) = (1/\sqrt{2})$, and this possibility was used to check the accuracy of the numerical procedure. It was found that the results were accurate to a fixed *decimal place*, with 5 figures accurate in the largest values. The values for large arguments were exponentially smaller and hence relatively not as accurate. However, their final contribution is small. The r -integration was subsequently carried out on a desk machine, and the results for $K^{(1)}(\sigma_1, \sigma_2)$ and $K^{(2)}(\sigma_1, \sigma_2)$, Eqn (16), are displayed in Table 1. $K^{(2)}(\sigma_1, \sigma_2)$ is made up of several contributions: the summation over l in one term was cut off at $l=6$, which was consistent with the overall accuracy of the kernel.

§ 5. SOLUTION OF THE INTEGRO-DIFFERENTIAL EQUATIONS

The integro-differential equations (16) with the conditions on the solutions may be transformed into integral equations by means of the appropriate Green's function. That is the systems

$$\begin{aligned} \left\{ \frac{d^2}{d\sigma_1^2} + k^2 \right\} f^{(\pm)}(\sigma_1) &= \pm \int_0^\infty d\sigma_2 K(\sigma_1, \sigma_2) f^{(\pm)}(\sigma_2) \\ f^{(\pm)}(0) &= 0 \\ f^{(\pm)}(\sigma) &\sim \sin k\sigma + a^\pm \cos k\sigma \\ &\quad \sigma \rightarrow \infty \end{aligned} \quad \dots\dots (16)$$

become

$$f^{(\pm)}(\sigma) = \sin k\sigma - \int_0^\infty d\sigma' L(\sigma, \sigma') \int_0^\infty d\sigma'' [\pm K(\sigma', \sigma'')] f^{(\pm)}(\sigma'') \quad \dots\dots (17)$$

with

$$\begin{aligned} L(\sigma, \sigma') &= \frac{1}{k} \sin k\sigma' \cos k\sigma \quad (\sigma' \leq \sigma) \\ &= \frac{1}{k} \cos k\sigma' \sin k\sigma \quad (\sigma' \geq \sigma). \end{aligned} \quad \dots\dots (18)$$

The approximations a^\pm to the tangents of the phase-shifts are given by

$$a^\pm = -\frac{1}{k} \int_0^\infty d\sigma' \sin k\sigma' \int_0^\infty d\sigma'' [\pm K(\sigma', \sigma'')] f^{(\pm)}(\sigma''). \quad \dots\dots (19)$$

If the range of the kernel be considered finite, the integral equations (17) may be approximated by systems of simultaneous algebraic equations, the unknowns being the values of $f^{(\pm)}$ at selected points, and the integrations approximated by standard numerical rules. This method of solution was ideally suited for the present problem where it was impractical to compute the kernel $K(\sigma', \sigma'')$ at many regularly spaced points. The $f^{(\pm)}(\sigma)$ need only be known within the range of the kernel (indeed need not be very well known where the kernel is small), for the a^\pm may be obtained from the integrals (19). A survey of the application of this method of solution of scattering problems has been given by Fraser (1958). It has been found that use of the simple trapezoidal rule for the σ' -integration gives satisfactory results; indeed it gives better results than more refined rules blindly applied. The reason is the discontinuity in slope of the Green's function $L(\sigma, \sigma')$. Simpson's or other appropriate rules may be used for the σ'' -integration. It is of course possible to use better integration rules, taking careful account of

Table 1. The Kernel Equation (16)
 Above lines: $-(\frac{3}{8})^2 K^{(1)}(\sigma_1, \sigma_2)$, below lines: $(\frac{3}{8})^2 K^{(0)}(\sigma_1, \sigma_2)$

σ_1 σ_2	0	1/4	1/2	3/4	1	5/4	3/2	2	5/2	3	4	5
0	0	0	0	0	0	0	0	0	0	0	0	0
1/4	0	$\frac{0.0144}{0.0837}$	0.0225	0.0238	0.0207	0.0161	0.0116	0.0052	0.0020	0.00071	0.00008	0.00001
1/2	0	0.0734	$\frac{0.0371}{0.1213}$	0.0412	0.0374	0.0302	0.0224	0.0104	0.0041	0.00151	0.00017	0.00001
3/4	0	0.0454	0.0802	$\frac{0.0487}{0.0960}$	0.0472	0.0403	0.0316	0.0158	0.0066	0.00251	0.00029	0.00002
1	0	0.0208	0.0397	0.0536	$\frac{0.0490}{0.0624}$	0.0458	0.0372	0.0204	0.0092	0.00374	0.00048	0.00005
5/4	0	0.0056	0.0124	0.0204	0.0297	$\frac{0.0455}{0.0372}$	0.0391	0.0242	0.0122	0.00543	0.00076	0.00008
3/2	0	-0.0017	-0.0024	0.0001	0.0077	0.0158	$\frac{0.0366}{0.0227}$	0.0250	0.0136	0.00648	0.00108	0.00013
2	0	-0.0041	-0.0087	-0.0116	-0.0113	-0.0076	-0.0020	$\frac{0.0216}{0.0081}$	0.0145	0.00848	0.00171	0.00028
5/2	0	-0.0027	-0.0060	-0.0088	-0.0105	-0.0110	-0.0095	-0.0035	$\frac{0.0117}{0.0031}$	0.00805	0.00214	0.00045
3	0	-0.00121	-0.00270	-0.00419	-0.00590	-0.00699	-0.00705	-0.00554	-0.00086	$\frac{0.00672}{0.00155}$	0.00262	0.00069
4	0	-0.00019	-0.00038	-0.00065	-0.00105	-0.00159	-0.00180	-0.00221	-0.00183	-0.00123	$\frac{0.00163}{0.00018}$	0.00067
5	0	-0.00002	-0.00005	-0.00007	-0.00012	-0.00021	-0.00028	-0.00053	-0.00063	-0.00070	-0.00036	$\frac{0.00038}{-0.00001}$

the discontinuity in slope of $L(\sigma, \sigma')$, but such refinement was not felt to be necessary here. The integral equation may be modified for the case of zero energy (Fraser 1958).

Appendix C gives further details of the numerical calculation as well as the results of applying the method to a similar problem solvable in closed form given by Buckingham and Massey (1941-42). Judging from the results of applying the method to the exactly solvable case it would appear that for the present problem, with the net of points shown in Table 1, the error in the cross sections is at most about 5%. In principle, at least, the method is capable of considerable refinement, but may not be practical beyond a certain stage of required accuracy. With the rather sparse and irregular net of points available in this problem it would seem ideal. The 11 simultaneous equations for each energy and symmetry were set up and solved on a Bendix G-15-D Computer.

The results of applying this numerical method to the present problem are given in tabular and graphical form in the following section.

§ 6. RESULTS AND DISCUSSION

The s-cross sections (6) and (7) may be recast in terms of the quantities $k \cot \eta^+$ and $k \cot \eta^-$:

$$\sigma = (4\pi) \left\{ \frac{3}{4} \frac{1}{k^2 + k^2 \cot^2 \eta^-} + \frac{1}{4} \frac{1}{k^2 + k^2 \cot^2 \eta^+} \right\} \quad \dots\dots (20)$$

$$\sigma_p = (4\pi) \frac{1}{16} \frac{(k \cot \eta^- - k \cot \eta^+)^2}{(k^2 + k^2 \cot^2 \eta^-)(k^2 + k^2 \cot^2 \eta^+)}. \quad \dots\dots (21)$$

Table 2 presents the calculated values of $(k \cot \eta^\pm)$ and η^\pm as functions of k^2 and k , and the cross sections σ and σ_p in units of a_0^2 obtained from Eqns (20) and (21). The assignment of the value π to the phase shifts at zero energy was made on the basis of the behaviour of curves of (η^\pm, k) (Fig. 1). Results for higher

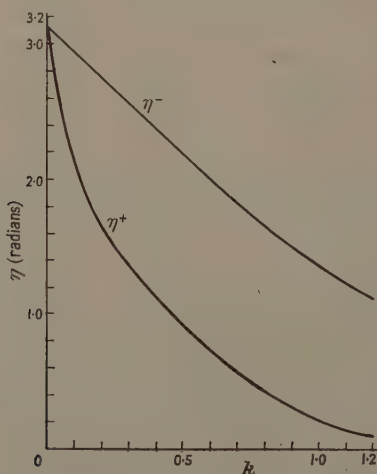


Fig. 1. The phase-shifts η^+ and η^- as functions of k .

energies than those presented here indicated that the η^+ curve crossed the axis at $k \approx 1.4$ while that for η^- showed no sign of crossing. The Born approximation would indicate that the phase shifts are equal and opposite at high energies. However the assignment is unimportant as the cross sections may be expressed in terms of $k \cot \eta^\pm$. (The results for $k > 1.2$ have not been given as they were felt to be relatively inaccurate, and as the corresponding energies are well above the limit of elastic scattering alone.) Also in Table 2 are shown some cross sections obtained by interpolation.

Table 2

The total elastic cross section and the conversion cross section in units of a_0^2 (respectively σ and σ_p from Eqns (20) and (21)) and related quantities, as functions of the ortho-positronium kinetic energy: $\frac{1}{2}k^2$ in units of 13.6 ev.

k	k^2	$k \cot \eta^+$	$k \cot \eta^-$	η^+	η^-	σ	σ_p	σ_p/σ
0	0	-0.0742	-0.543	π	π	603	106	0.176
0.1	0.01	-0.0594	-0.536	2.107	2.957	265	44.6	0.169
0.2	0.04	-0.0137	-0.514	1.639	2.771	109.3	16.1	0.147
0.25	0.0625	0.022	-0.498	1.483	2.676	79.2	10.7	0.135
0.4	0.16	0.194	-0.428	1.119	2.390	43.4	4.48	0.103
0.5	0.25	0.382	-0.363	0.918	2.199	32.6	2.88	0.088
0.6	0.36	0.661	-0.283	0.737	2.011	25.4	2.00	0.079
0.7	0.49	1.082	-0.185	0.574	1.829	19.9	1.45	0.073
0.8	0.64	1.727	-0.0696	0.434	1.658	15.5	1.08	0.070
0.85	0.7225	2.173	-0.0048	0.373	1.576	13.6	0.95	0.070
0.9	0.81	2.729	0.0646	0.319	1.499	12.0	0.84	0.070
0.95	0.9025	3.423	0.138	0.271	1.426	10.5	0.73	0.070
1.0	1.0	4.290	0.215	0.229	1.359	9.2	0.64	0.070
1.1	1.21	6.793	0.376	0.161	1.241	7.0	0.51	0.072
1.2	1.44	11.46	0.537	0.104	1.150	5.5	0.41	0.075

Interpolated values (from $k \cot \eta^\pm$ curves and from η^+ curve)

0.0707	0.005	-0.0667	-0.5395			364	62.8	0.172
0.141	0.02	-0.0442	-0.5285			175	28.0	0.160
0.173	0.03	-0.0292	-0.5215			133	20.4	0.153
0.316	0.1		-0.471	1.31		58.6	7.03	0.120

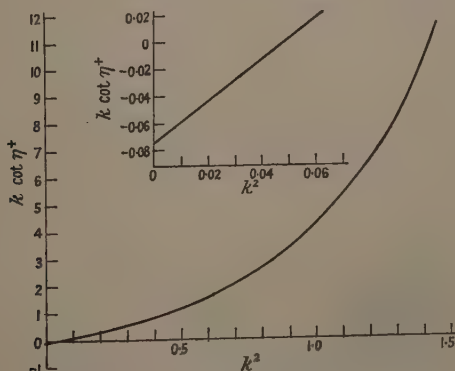
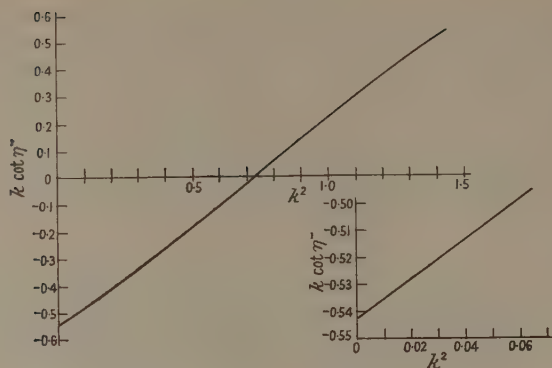


Fig. 2. $k \cot \eta^+$ as a function of k^2 .

Fig. 3. $k \cot \eta^-$ as a function of k^2 .

Figs 2 and 3 show the $(k \cot \eta^\pm, k^2)$ curves, with insets showing the expected straight line behaviour for very small energies. Effective ranges may be deduced from the slopes at low energies:

$$r_0^+ = 3.00a_0$$

$$r_0^- = 1.44a_0.$$

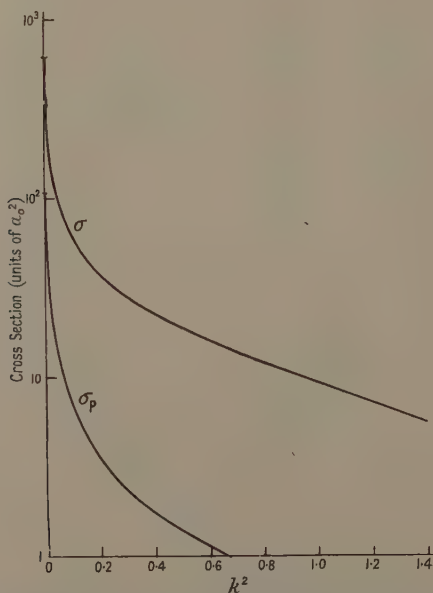


Fig. 4. Semi-logarithmic plots of the scattering and conversion cross sections σ and σ_p (in units of a_0^2) as functions of k^2 . The positronium kinetic energy is $\frac{1}{2}k^2$ in units of 13.6 ev.

The cross sections (Table 2 and Fig. 4) are seen to be strongly energy dependent and very large at very low energies, as was indicated by the Born-Oppenheimer approximation results of Massey and Mohr (1954). It is interesting but probably coincidental that the Massey and Mohr value for the elastic cross section at zero energy is $230\pi a_0^2$, while the present work leads to the value $192\pi a_0^2$. The disagreement at higher energies is considerable; at $k^2 = 1$ (6.8 eV) the Massey and Mohr value is $25\pi a_0^2$ while the present work gives $2.92\pi a_0^2$. Over the range of energies here considered the ratio of the quenching and elastic cross sections is substantially lower than the value $1/4$ expected at higher energies.

A more accurate calculation of the elastic scattering of ortho-positronium by helium atoms is well in hand, and will shortly be completed. The results will be applicable to the problem of the moderation of ortho-positronium by helium gas, and the wave functions obtained will be used in a calculation of the quenching rate by annihilation on collision with the atomic electrons.

ACKNOWLEDGMENTS

The author is grateful to the National Research Council of Canada for an Overseas Post-Doctoral Fellowship (1954-56) held at University College, London, during the tenure of which this work was started, and acknowledges the partial support since that time of the Defence Research Board of Canada, The Department of Defence Production, the Geophysics Research Directorate of the U.S. Air Force Cambridge Research Center, and the National Research Council of Canada.

The author's thanks are due to Professor Sir Harrie Massey for suggesting the problem and for his continued interest throughout. He also wishes to thank Mr. W. Lawson for his help with the operation of the computer at the Physics Department of University College London, Mrs. Joyce Walton of Computing Devices of Canada for her assistance on the G-15-D, and Dr. M. A. Preston of McMaster University for making available the G-15-D at that University.

APPENDIX A

THE CALCULATION OF $\delta I_t^{(\pm)}$

From (9), (10) and (11) one obtains after slight reduction (the \pm superscripts are omitted in this appendix):

$$\begin{aligned} \frac{\delta I_t}{2} &= \iint \int d\sigma_1 d\rho_1 d\mathbf{r}_2 \phi(\rho_1) \psi(r_2) \frac{\delta f(\sigma_1)}{\sigma_1} (H-E) \Psi_t \\ &+ \iint \int d\sigma_1 d\rho_1 d\mathbf{r}_2 \Psi_t (H-E) \phi(\rho_1) \psi(r_2) \frac{\delta f(\sigma_1)}{\sigma_1} \\ &= A + B. \end{aligned}$$

Now

$$(H-E) \phi(\rho_1) \psi(r_2) \frac{f(\sigma_1)}{\sigma_1} = \phi(\rho_1) \psi(r_2) \left\{ \left(-\frac{1}{2} \nabla_{\sigma_1}^2 - \frac{1}{2} k^2 \right) - \frac{2}{r_1} + \frac{2}{r_p} - \frac{2}{\rho_2} + \frac{2}{r_{12}} \right\} \frac{f(\sigma_1)}{\sigma_1},$$

where use is made of (2), (3) and (4). Similar results may be obtained for

$$(H-E) \phi(\rho_1) \psi(r_2) \frac{\delta f(\sigma_1)}{\sigma_1}$$

and for

$$(H-E)\phi(\rho_2)\psi(r_1)\frac{f(\sigma_2)}{\sigma_2}$$

with a rewriting of the Hamiltonian appropriate for electron 2 being 'in the positronium' and electron 1 'in the atom'. Further

$$\begin{aligned} & \int \int d\boldsymbol{\rho}_1 d\mathbf{r}_2 \phi(\rho_1)\psi(r_2) \left\{ \frac{2}{r_p} - \frac{1}{r_1} + \frac{2}{r_{12}} - \frac{2}{\rho_2} \right\} \phi(\rho_1)\psi(r_2) \\ &= \int \int d\boldsymbol{\rho}_1 d\mathbf{r}_2 \phi(\rho_1)\psi(r_2) \left\{ \frac{2}{|\boldsymbol{\sigma}_1 - \boldsymbol{\rho}_1/2|} - \frac{2}{|\boldsymbol{\sigma}_1 + \boldsymbol{\rho}_1/2|} \right. \\ & \quad \left. + \frac{2}{|\mathbf{r}_2 - \boldsymbol{\sigma}_1 - \boldsymbol{\rho}_1/2|} - \frac{2}{|\mathbf{r}_2 - \boldsymbol{\sigma}_1 + \boldsymbol{\rho}_1/2|} \right\} \phi(\rho_1)\psi(r_2) \\ &= 0; \end{aligned}$$

the result corresponds to the statement that in first approximation there is no direct interaction between the positronium and the atom (Massey and Mohr 1954).

Thus

$$\begin{aligned} A &= \int d\boldsymbol{\sigma}_1 \frac{\delta f(\sigma_1)}{\sigma_1} \left\{ -\frac{1}{2}\nabla_{\sigma_1}^2 - \frac{1}{2}k^2 \right\} \frac{f(\sigma_1)}{\sigma_1} \\ & \quad \pm \int d\boldsymbol{\sigma}_1 \frac{\delta f(\sigma_1)}{\sigma_1} \int \int d\boldsymbol{\rho}_1 d\mathbf{r}_2 \phi(\rho_1)\psi(r_2) \left\{ -\frac{1}{2}\nabla_{\sigma_1}^2 - \frac{1}{2}k^2 - \frac{2}{r_2} \right. \\ & \quad \left. + \frac{2}{r_p} - \frac{2}{\rho_1} + \frac{2}{r_{12}} \right\} \phi(\rho_2)\psi(r_1) \frac{f(\sigma_2)}{\sigma_2} \\ &= C \pm D. \end{aligned}$$

Similarly

$$\begin{aligned} B &= \int d\boldsymbol{\sigma}_1 \frac{f(\sigma_1)}{\sigma_1} \left\{ -\frac{1}{2}\nabla_{\sigma_1}^2 - \frac{1}{2}k^2 \right\} \frac{\delta f(\sigma_1)}{\sigma_1} \\ & \quad \pm \int \int \int d\boldsymbol{\sigma}_1 d\boldsymbol{\rho}_1 d\mathbf{r}_2 \phi(\rho_2)\psi(r_1) \frac{f(\sigma_2)}{\sigma_2} \left\{ -\frac{1}{2}\nabla_{\sigma_1}^2 - \frac{1}{2}k^2 - \frac{2}{r_1} + \frac{2}{r_p} \right. \\ & \quad \left. - \frac{2}{\rho_2} + \frac{2}{r_{12}} \right\} \phi(\rho_1)\psi(r_2) \frac{\delta f(\sigma_1)}{\sigma_1} \\ &= E \pm F. \end{aligned}$$

Making use of Green's theorem and the asymptotic forms of $f(\sigma)$ and $\delta f(\sigma)$ one may easily show that

$$E = A + 2\pi k(\delta a_t).$$

It is convenient to transform the integrations in D and F from $(\boldsymbol{\sigma}_1, \boldsymbol{\rho}_1, \mathbf{r}_2)$ space to $(\boldsymbol{\sigma}_1, \boldsymbol{\sigma}_2, \mathbf{r}_p)$ space. The Jacobian of the transformation has the value $(4)^3$. In terms of $\boldsymbol{\sigma}_1, \boldsymbol{\sigma}_2$ and \mathbf{r}_p :

$$\begin{aligned} \boldsymbol{\rho}_1 &= 2(\boldsymbol{\sigma}_1 - \mathbf{r}_p); & \boldsymbol{\rho}_2 &= 2(\boldsymbol{\sigma}_2 - \mathbf{r}_p) \\ \mathbf{r}_1 &= 2\boldsymbol{\sigma}_1 - \mathbf{r}_p; & \mathbf{r}_2 &= 2\boldsymbol{\sigma}_2 - \mathbf{r}_p, \end{aligned} \quad \dots\dots (22)$$

and these expressions will be understood in the following.

The terms in D and F that need consideration are those involving ∇_o^2 . For D , this part is

$$\begin{aligned} (4)^3 \int d\sigma_1 \frac{\delta f(\sigma_1)}{\sigma_1} \int \int d\sigma_2 d\mathbf{r}_p \phi(\rho_1) \psi(r_2) \phi(\rho_2) \psi(r_1) \left\{ -\frac{1}{2} \nabla_{\sigma_1}^2 \right\} \frac{f(\sigma_2)}{\sigma_2} \\ = (4)^3 \int d\sigma_1 \frac{\delta f(\sigma_1)}{\sigma_1} \int \int d\sigma_2 d\mathbf{r}_p \frac{f(\sigma_2)}{\sigma_2} \left\{ -\frac{1}{2} \nabla_{\sigma_1}^2 \right\} \phi(\rho_1) \psi(r_2) \phi(\rho_2) \psi(r_1). \end{aligned}$$

For F , this part may be transformed into

$$(4)^3 \int d\sigma_1 \frac{\delta f(\sigma_1)}{\sigma_1} \int \int d\sigma_2 d\mathbf{r}_p \frac{f(\sigma_2)}{\sigma_2} \left\{ -\frac{1}{2} \nabla_{\sigma_1}^2 \right\} \phi(\rho_1) \psi(r_2) \phi(\rho_2) \psi(r_1).$$

Now,

$$\begin{aligned} \nabla_{\sigma_1}^2 \phi(\rho_1) \psi(r_1) &= \nabla_{\sigma_1}^2 \phi(2|\sigma_1 - \mathbf{r}_p|) \psi(|2\sigma_1 - \mathbf{r}_p|) \\ &= \phi(\rho_1) \psi(r_2) \left\{ 5 - \frac{8}{r_1} - \frac{4}{\rho_1} + 4 \frac{\mathbf{r}_1 \cdot \boldsymbol{\rho}_1}{r_1 \rho_1} \right\}, \end{aligned}$$

and similarly for $\nabla_{\sigma_2}^2 \phi(\rho_2) \psi(r_2)$.

Combining D and F , using the intermediate results and expressing the coordinates in terms of σ_1 , σ_2 and \mathbf{r}_p one obtains

$$D + F = \int d\sigma_1 \frac{\delta f(\sigma_1)}{\sigma_1} \int d\sigma_2 K(\sigma_1, \sigma_2) \frac{f(\sigma_2)}{\sigma_2},$$

with $K(\sigma_1, \sigma_2)$ given by (13).

Finally one obtains, from $\frac{1}{2} \delta I_t = A + B = (C + E) \pm (D + F)$,

$$\begin{aligned} \frac{1}{2} (\delta I_t - 4\pi k(\delta a_t)) &= \int d\sigma_1 \frac{\delta f(\sigma_1)}{\sigma_1} \left\{ (-\nabla_{\sigma_1}^2 - k^2) \frac{f(\sigma_1)}{\sigma_1} \right. \\ &\quad \left. \pm \int d\sigma_2 K(\sigma_1, \sigma_2) \frac{f(\sigma_2)}{\sigma_2} \right\}, \end{aligned}$$

which is Eqn (12) of the text.

APPENDIX B

THE VANISHING OF $I_t^{(\pm)}$

Many of the steps required to show the vanishing of $I_t^{(\pm)}$ are similar to those in appendix A, and will not specifically be pointed out. Again the (\pm) superscripts are suppressed, and the vectors are often written in their simplified form with Eqns (22) understood. In Ψ_t , $f(\sigma)$ now satisfy (14).

$$\begin{aligned} \frac{I_t}{(4)^3} &= \int \int \int d\sigma_1 d\sigma_2 d\mathbf{r}_p \Psi_t (H - E) \Psi_t \\ &= 2 \int \int \int d\sigma_1 d\sigma_2 d\mathbf{r}_p \Psi_t (H - E) \phi(\rho_1) \psi(r_2) \frac{f(\sigma_1)}{\sigma_1} \\ &= 2 \frac{1}{(4)^3} \int d\sigma_1 \frac{f(\sigma_1)}{\sigma_1} \left\{ -\frac{1}{2} \nabla_{\sigma_1}^2 - \frac{1}{2} k^2 \right\} \frac{f(\sigma_1)}{\sigma_1} \\ &\quad \pm \int \int \int d\sigma_1 d\sigma_2 d\mathbf{r}_p \frac{f(\sigma_2)}{\sigma_2} \phi(\rho_2) \psi(r_1) \frac{f(\sigma_1)}{\sigma_1} \phi(\rho_1) \psi(r_2) \\ &\quad \times \left\{ -\frac{5}{2} - \frac{1}{2} k^2 + \frac{2}{r_1} + \frac{2}{\rho_1} - \frac{2}{\rho_2} + \frac{2}{r_{12}} + \frac{2}{r_p} - \frac{2\mathbf{r}_1 \cdot \boldsymbol{\rho}_1}{r_1 \rho_1} \right\}. \end{aligned}$$

Table 3. Comparison of Approximate and Exact Results for the Kernel $\mu\sigma\sigma' \exp[-b(\sigma+\sigma')]$, Eqns (24) and (25) with $b=2$, $\mu=\pm 100$.

	$k=0$		$k=0.5^\dagger$		$k=1$		$\mu=-100$		$\mu=100$		$\mu=-100$		$\mu=100$		$\mu=-100$		$\mu=100$	
	$\mu=100$		$\mu=100$		$\mu=100$		$\mu=100$		$\mu=100$		$\mu=100$		$\mu=100$		$\mu=100$		$\mu=100$	
	Approx.	Exact	Approx.	Exact	Approx.	Exact	Approx.	Exact	Approx.	Exact	Approx.	Exact	Approx.	Exact	Approx.	Exact	Approx.	Exact
0	0	0	0	0	0	0	0	0	0	0	0	0	0	0	0	0	0	0
1/4	-0.060	-0.058	-0.270	-0.270	-0.035	-0.034	-0.035	-0.034	-0.035	-0.034	-0.035	-0.034	-0.035	-0.034	-0.035	-0.034	-0.035	-0.034
1/2	-0.073	-0.071	-0.460	-0.464	-0.040	-0.039	-0.040	-0.039	-0.040	-0.039	-0.040	-0.039	-0.040	-0.039	-0.040	-0.039	-0.040	-0.039
3/4	-0.028	-0.026	-0.554	-0.561	-0.008	-0.007	-0.008	-0.007	-0.008	-0.007	-0.008	-0.007	-0.008	-0.007	-0.008	-0.007	-0.008	-0.007
1	0.069	0.071	-0.559	-0.568	0.057	0.058	0.057	0.058	0.057	0.058	0.057	0.058	0.057	0.058	0.057	0.058	0.057	0.058
5/4	0.210	0.211	-0.493	-0.503	0.147	0.148	0.147	0.148	0.147	0.148	0.147	0.148	0.147	0.148	0.147	0.148	0.147	0.148
3/2	0.382	0.385	-0.373	-0.383	0.255	0.257	0.255	0.257	0.255	0.257	0.255	0.257	0.255	0.257	0.255	0.257	0.255	0.257
2	0.797	0.796	-0.016	-0.032	0.500	0.501	0.500	0.501	0.500	0.501	0.500	0.501	0.500	0.501	0.500	0.501	0.500	0.501
5/2	1.258	1.256	0.419	0.400	0.743	0.744	0.743	0.744	0.743	0.744	0.743	0.744	0.743	0.744	0.743	0.744	0.743	0.744
3	1.741	1.739	0.890	0.871	0.953	0.955	0.953	0.955	0.953	0.955	0.953	0.955	0.953	0.955	0.953	0.955	0.953	0.955
4	2.733	2.728	1.877	1.853	1.202	1.204	1.202	1.204	1.202	1.204	1.202	1.204	1.202	1.204	1.202	1.204	1.202	1.204
5	3.733	3.727	2.876	2.850	1.160	1.164	1.160	1.164	1.160	1.164	1.160	1.164	1.160	1.164	1.160	1.164	1.160	1.164
-A	-1.254	-1.274	2.101	-2.151	-0.694	-0.705	-0.694	-0.705	-0.694	-0.705	-0.694	-0.705	-0.694	-0.705	-0.694	-0.705	-0.694	-0.705
tan η																		

† For this value of k , a different set of integration weights was used. This set was based largely on the $3/8$ rule; for other values of k , the results using these weights were very slightly better for $\mu=100$, and rather worse for $\mu=-100$.

On replacing

$$\left\{ -\frac{1}{2}\nabla_{\sigma_1}^2 - \frac{1}{2}k^2 \right\} \frac{f(\sigma_1)}{\sigma_1}$$

by

$$\pm \int d\sigma_2 K(\sigma_1, \sigma_2) \frac{f(\sigma_2)}{\sigma_2}$$

from (14), one obtains, after some cancellation of terms,

$$\begin{aligned} \frac{I_t}{(4)^3} = \mp \int \int d\sigma_1 d\sigma_2 d\mathbf{r}_p & \frac{f(\sigma_1)}{\sigma_1} \frac{f(\sigma_2)}{\sigma_2} \phi(\rho_2) \psi(r_2) \phi(\rho_1) \psi(r_1) \\ & \times \left\{ -\frac{1}{|2\sigma_1 - \mathbf{r}_p|} + \frac{1}{|2\sigma_2 - \mathbf{r}_p|} + \frac{1}{|\sigma_1 - \mathbf{r}_p|} - \frac{1}{|\sigma_2 - \mathbf{r}_p|} \right. \\ & \left. + \frac{(2\sigma_1 - \mathbf{r}_p) \cdot (\sigma_1 - \mathbf{r}_p)}{|2\sigma_1 - \mathbf{r}_p||\sigma_1 - \mathbf{r}_p|} - \frac{(2\sigma_2 - \mathbf{r}_p) \cdot (\sigma_2 - \mathbf{r}_p)}{|2\sigma_2 - \mathbf{r}_p||\sigma_2 - \mathbf{r}_p|} \right\}. \end{aligned}$$

Thus $I_t = 0$, since the quantity in braces is antisymmetric in σ_1 and σ_2 .

APPENDIX C

THE NUMERICAL SOLUTION OF THE INTEGRAL EQUATIONS FOR $f^{(\pm)}(\sigma)$

This appendix gives further details of the numerical method of solution of the integral equations, which was briefly outlined in the text. Also, some results of applying the method to a similar problem solvable in closed form are presented. Consider the integro-differential equation, with conditions on the solution,

$$\begin{aligned} \left\{ \frac{d^2}{d\sigma^2} + k^2 \right\} f(\sigma) &= \int_0^\infty d\sigma' M(\sigma, \sigma') f(\sigma'), \\ f(0) &= 0; \quad f(\sigma) \sim \sin k\sigma + a \cos k\sigma. \end{aligned}$$

$\sigma \rightarrow \infty$

These may be transformed into the integral equation

$$f(\sigma) = \sin k\sigma - \int_0^\infty d\sigma' L(\sigma, \sigma') \int_0^\infty d\sigma'' M(\sigma', \sigma'') f(\sigma''),$$

with the Green's function $L(\sigma, \sigma')$ given by (18), and with

$$a = -\frac{1}{k} \int_0^\infty d\sigma' \sin k\sigma' \int_0^\infty d\sigma'' M(\sigma', \sigma'') f(\sigma'').$$

It is presumed that the kernel $M(\sigma', \sigma'')$ vanishes sufficiently fast for large argument that the integrations may be cut off at some finite value of σ . The integrals are then approximated by some numerical rule, and this procedure leads to simultaneous algebraic equations with the unknowns being the values of $f(\sigma)$ at a set of discrete points:

$$f_i = s_i - \sum_{jk} L_{ij} \beta_j' M_{jk} \alpha_k'' f_k$$

or

$$\sum_{jk} (\delta_{ik} + L_{ij} \beta_j' M_{jk} \alpha_k'') f_k = s_i \quad \dots\dots (23)$$

where $f_i = f(\sigma_i)$ etc. The numbers β_j' and α_k'' are the appropriate numerical integration weights for the σ' and σ'' integrations respectively. These have been

discussed in the text. Solution of (23) leads to values of f_i which are then used to compute a through

$$a = -\frac{1}{k} \sum_{jk} s_i \alpha_i M_{ij} \alpha_j f_j.$$

Buckingham and Massey (1941-42) have given the solution for the case of

$$M(\sigma, \sigma') = \mu \sigma \sigma' \exp[-b(\sigma + \sigma')]:$$

$$f(\sigma) = \sin k\sigma + a \cos k\sigma - a \left\{ 1 + \left(\frac{b^2 + k^2}{2b} \right) \sigma \right\} \exp(-b\sigma) \dots\dots (24)$$

with

$$\frac{1}{a} = \frac{-4b^3(b^2 + k^2)^4 + \mu(-5b^6 + 15b^4k^2 + 5b^2k^4 + k^6)}{16kb^5\mu} \dots\dots (25)$$

The choice of $b=2$ and $\mu = \pm 100$ gives kernels $M(\sigma, \sigma')$ approximating in behaviour and magnitude the kernels of the present problem. Accordingly this soluble problem was attacked by the numerical method, and the approximate results compared with the exact ones. The set of points used was that available for the present problem:

$$\{\sigma\} = \{\frac{1}{4}, \frac{1}{2}, \frac{3}{4}, 1, \frac{5}{4}, \frac{3}{2}, 2, 2\frac{1}{2}, 3, 4, 5\}.$$

The integration weight factors used were

$$\{\beta\} = \{\frac{1}{4}, \frac{1}{4}, \frac{1}{4}, \frac{1}{4}, \frac{1}{4}, \frac{1}{8} + \frac{1}{4}, \frac{1}{2}, \frac{1}{2}, \frac{1}{4} + \frac{1}{2}, 1, \frac{1}{2}\},$$

which arise from the use of the trapezoidal rule for the Green's function integration as discussed in the text, and

$$\{\alpha\} = \{\frac{1}{3}, \frac{1}{6}, \frac{1}{3}, \frac{1}{6}, \frac{1}{3}, \frac{1}{12} + \frac{3}{16}, \frac{9}{16}, \frac{9}{16}, \frac{3}{16} + \frac{1}{3}, \frac{4}{3}, \frac{1}{3}\},$$

which arise from the use of the $\frac{1}{3}$ and $\frac{3}{8}$ rules. Values for the point $\sigma=0$ are, of course, unnecessary.

Table 4

Values of $(\cos \eta^\pm) f^{(\pm)}(\sigma)$ (for $\sigma=5$) for the positronium problem obtained (i) from the solution of the simultaneous equations and (ii) by substitution into $\sin(k\sigma + \eta^\pm)$ of the computed phase-shifts (for $k=0$, into $\sigma - A^\pm$).

k	$f^{(+)}$		$f^{(-)}$	
	(i)	(ii)	(i)	(ii)
0	-8.58	-8.48	3.12	3.16
0.1	0.515	0.510	-0.307	-0.310
0.2	0.485	0.481	-0.585	-0.588
0.25	0.399	0.397	-0.704	-0.707
0.4	0.020	0.022	-0.953	-0.949
0.5	-0.280	-0.273	-1.010	-1.000
0.6	-0.572	-0.561	-0.970	-0.956
0.7	-0.817	-0.803	-0.833	-0.816
0.8	-0.972	-0.961	-0.601	-0.586
0.85	-1.003	-0.996	-0.453	-0.441
0.9	-0.998	-0.994	-0.287	-0.280
0.95	-0.952	-0.966	-0.105	-0.156
1.0	-0.867	-0.870	0.085	0.076
1.1	-0.582	-0.583	0.466	0.442
1.2	-0.184	-0.178	0.787	0.762

The results for this 'test-case' kernel are presented in Table 3 for $k=0.5$ and 1, and are compared with the exact solutions. The method may also be formulated for $k=0$ in terms of

$$\Phi(\sigma) = \lim_{k \rightarrow 0} \left(\frac{f(\sigma)}{k} \right)$$

with

$$\Phi \sim \sigma - A,$$

A being the scattering length (Fraser 1958). The results for $k=0$ are also presented in Table 3.

Finally, as an indication of the consistency of the results of applying this method to the positronium problem, Table 4 shows values of $f^{(\pm)}(\sigma)$ (normalized to unit amplitude at infinity) for $\sigma=5$ obtained in two ways: (i) from the solution of the simultaneous equations and (ii) by substitution into the expression $\sin(k\sigma + \eta^\pm)$, the phase-shifts being obtained from the integrals (19), or into $\sigma - A^\pm$ for $k=0$.

REFERENCES

- BRACKMANN, R. I., FITE, W. L., and NEYNABER, R. H., 1958, *Phys. Rev.*, **112**, 1157.
 BRANDSEN, B. H., DALGARNO, A., JOHN, T. L., and SEATON, M. J., 1958, *Proc. Phys. Soc.*, **71**, 877.
 BUCKINGHAM, R. A., and MASSEY, H. S. W., 1941-42, *Proc. Roy. Soc. A*, **179**, 123.
 DEUTSCH, M., 1953, *Progress in Nuclear Physics*, Volume 3 (Ed. O. R. Frisch), pp. 131-158 (London: Pergamon).
 FERRELL, R. A., 1958, *Phys. Rev.*, **110**, 1355.
 FIELD, G. B., 1958, *Proc. Inst. Radio Engrs*, **46**, 240.
 FRASER, P. A., 1958, *Scientific Report No. 4*, Contract No. AF 19(604)1718, Department of Physics, University of Western Ontario.
 MASSEY, H. S. W., and MOHR, C. B. O., 1954, *Proc. Phys. Soc. A*, **67**, 695.

Infra-red Emission and Electroluminescence in Zinc Sulphide Phosphors

By D. W. G. BALLENTYNE

University of Hull

MS. received 8th March 1961

Abstract. It is shown that the infra-red emission of zinc sulphide phosphors is dependent upon the copper concentration. Infra-red emission occurs after simultaneous excitation by ultra-violet and infra-red in phosphors containing less than 5×10^{-4} g atoms Cu per mole ZnS. For greater concentrations of copper infra-red emission does not occur but such phosphors are electroluminescent.

§ 1. INTRODUCTION

IN 1954 Garlick and Dumbleton first observed infra-red emission bands in zinc sulphide phosphors. In 1956 Browne showed that infra-red emitting phosphors belong to two classes. The infra-red emission of class I phosphors is excited by illuminating the phosphor with infra-red radiation of the correct wavelength. Class II phosphors require simultaneous excitation by ultra-violet radiation as well as infra-red. Class II phosphors were shown to contain copper impurities but the emission of class I phosphors was believed to depend upon non-stoichiometry. The origin of infra-red emission can be explained by reference to Fig. 1 which shows a simple band model for a crystalline phosphor. The green and blue emissions are the emission bands usually associated with zinc sulphide phosphors. The infra-red excitation bands correspond to the transitions I and II whilst the emission bands correspond to the transitions III and IV. The difference in class I and class II phosphors depends upon the occupancy of these levels. If the levels are normally unoccupied then infra-red alone will cause the necessary electron transitions. If, however, electrons are usually present in these levels infra-red emission can only occur if holes are trapped from the valence band or generated by the direct transitions V and VI. These transitions are, of course, in the ultra-violet.

Apple and Prener (1960) have studied infra-red emission in aluminium co-activated ZnS(Cu) phosphors. The emission is greatly increased by allowing the phosphor to anneal in a high sulphur pressure thereby reducing the anion vacancies to a very low concentration. The phosphors prepared in this way are class I phosphors, and the intensity of the emission is proportional to the concentration of copper added. It was assumed that the gas-solid reaction can be represented by the equation



where $\text{V}_{2\delta}^{++}$ represents a sulphur vacancy doubly charged with respect to the sulphur in the solid. Cu^0 is a copper ion with a hole in the ground state which is neutral with respect to the copper for which it substitutes and Cu^- is a copper ion with the states occupied by electrons making it negatively charged with respect

to zinc. This equation explains the observation that the fourth power of the brightness of emission is proportional to the sulphur pressure. The addition of aluminium to the system which can act as a singly ionized donor allows replacement of V^{++} by Al^+ so that the charge balance is

$$Cu^- = V^{++} + Al^+.$$

It is shown that when the aluminium concentration is much smaller than the copper concentration the infra-red intensity is almost constant but as it approaches that of copper the infra-red emission should drop rapidly to zero. This behaviour is not observed and it was concluded that not all the aluminium goes into solution.

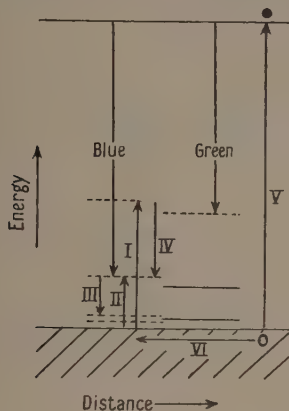


Fig. 1.

The present work was undertaken to determine whether infra-red emission occurred during electroluminescence. As a preliminary the emission of the series of phosphors previously studied was investigated under ultra-violet and infra-red excitation. The correlation of electroluminescence and infra-red emission was then investigated.

§ 2. EXPERIMENTAL

The phosphors were prepared as previously described. The zinc sulphide used was freed from gross contamination with chlorine by washing with distilled water until the filtrate gave no precipitate with silver nitrate and was then fired for two hours at $800^{\circ}C$ in a stream of dry H_2S . The chlorine content of the final product was of the order of parts per million. The activator, copper, and the co-activator, aluminium, were added to a slurry of the zinc sulphide as the sulphates. After drying at $110^{\circ}C$ the phosphors were fired for half-an-hour in a stream of wet hydrogen sulphide. These phosphors appear to have reached equilibrium with the surrounding atmosphere, as increasing the length of the firing time had no effect. X-ray diffraction studies show that phosphors containing less than 6×10^{-4} g atom Cu per mole ZnS are hexagonal in structure whilst phosphors with greater concentrations of copper are mixtures of the cubic and hexagonal phases, although preponderantly cubic in structure (Ballentyne 1960).

The infra-red emission was detected using a lead sulphide cell with a silicon filter. A 60 w tungsten lamp was focused on the phosphor in a holder, the construction of the holder being such that the phosphor tube could be removed and replaced at the same place in the system. The desired excitation band was isolated by filters. In three experiments a 0.700μ , a 0.903μ interference filter and a Wratten 29 filter were used. The form of the curves was not affected although the intensity of emission was greatest with the last filter. The ultra-violet radiation was filtered through a 2 cm CuCl_2 filter to remove infra-red. The emitted radiation was focused on to the lead sulphide cell through an 800 cycle chopper disk. In order to reduce reflection of the exciting radiation the emergent light passed through a Wratten 89 filter.

In order to investigate the phenomenon under field excitation of the phosphor the holder was replaced by an electroluminescent cell. The chopper disk was removed and the phosphor was excited by a 400 c/s 800 v alternating field. The fact that the emission is modulated at twice the frequency of the applied field means that the light arriving at the lead sulphide cell is modulated at the correct frequency for acceptance by the amplifier.

§ 3. RESULTS

3.1. Effect of Copper Concentration on Infra-red Emission during Photoluminescence

The variation of copper concentration had a marked effect on the infra-red emission. In Fig. 2 the intensity of infra-red emission in arbitrary units is plotted against the copper concentration for a constant aluminium concentration of 3.5×10^{-4} g atoms Al per gramme ZnS. The reflection of the exciting radiation from an MgO sample is also shown so that emission and absorption of the sample may be differentiated on the assumption that MgO is a perfect reflector. The integrated infra-red emission is constant for phosphors prepared from pure zinc sulphide ($\text{Cu} < 1$ part per million), up to 3.0×10^{-4} g atom Cu per mole ZnS.

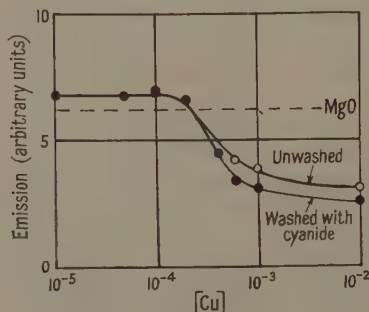


Fig. 2.

For copper concentrations above this value infra-red emission does not occur. The phosphors with these larger copper concentrations have a layer of copper sulphide precipitated on to the crystallites. In order to test whether the decrease in emission was due to the absorption of this layer, the phosphors were washed in hot 10% KCN which dissolves the excess copper sulphide. The washed phosphors still did not emit infra-red although the reflectance of the powder increased.

3.2. Effect of Aluminium Concentration

It appears from Fig. 2 that the emission of infra-red only occurs when the molar concentration of the activator is less than the molar concentration of the co-activator (see above). Experiments with variation of aluminium concentration indicates that this result is fortuitous. In Fig. 3 the effect of aluminium concentration on an emitting phosphor containing 1.5×10^{-4} g atom Cu per mole

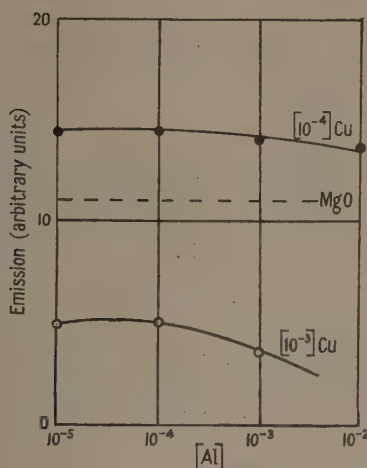


Fig. 3.

ZnS and a non-emitting phosphor with 1.5×10^{-3} g atom Cu per mole ZnS is shown. Over a large range of concentrations the effect is small but at large aluminium concentrations the intensity of both the emission and reflectance decreases. This may probably be attributed to the precipitation of increasing concentrations of Al_2O_3 oxide in the phosphors (Fröhlich 1953) due to a limit of solubility of aluminium in the phosphor.

3.3. Infra-red Emission and Electroluminescence

In Fig. 4 the variation of electroluminescent brightness with copper concentration is given. Electroluminescence occurs in those phosphors which do not emit infra-red. The concentration of co-activator does not appear to effect the appearance of electroluminescent emission. There is a precipitation of copper sulphide on to the grains of the phosphor and the crystal structure changes from predominantly hexagonal to predominantly cubic. It has been argued that the electron-rich layer of copper sulphide is the source of electroluminescence. The fact that cyanide washed phosphors from which superficial copper sulphide has been dissolved are brighter electroluminescent phosphors seems to indicate that the copper in the bulk of the crystal is more important than the surface layer.

No infra-red emission can be detected from electroluminescent phosphors under the joint action of infra-red or ultra-violet with the electric field.

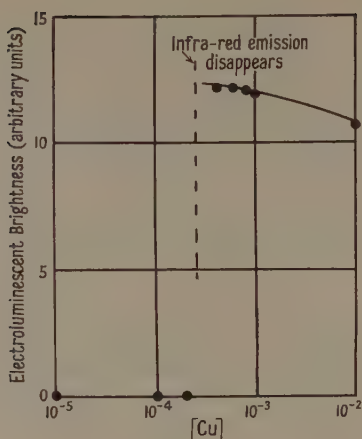


Fig. 4.

§ 4. DISCUSSION

The observation that the intensity of infra-red emission is independent of the copper concentration indicates that these phosphors differ markedly from those prepared by Apple and Prener. Their phosphors belonged to class I whilst the phosphors studied here are class II. It is well known that blue and green emission bands can be observed in phosphors containing no copper whatsoever (Garlick 1958). The emission in these cases is attributed to cation vacancies which, after capturing an electron, can be equated to the Cu^0 ions described above. The number of cation vacancies which can be generated will depend upon the total charge equality. It can be seen that

$$\text{Cu}^- + V_{\text{C}} = \text{Al}^+ + V_{\text{A}}$$

where V_{C} and V_{A} are the anion and cation vacancies. Thus if the cation vacancies are greatly in excess of the copper centres then the emission will be virtually independent of the copper and aluminium concentrations as found above.

The discontinuity in the curve may be attributed to the precipitation of copper. Thus the solubility of copper in zinc sulphide is independent of the co-activator concentration. When copper sulphide precipitates out it causes a major change in the crystal structure of the zinc sulphide host crystal (Ballentyne 1960). Although the powder has been fired at 1100°C (above the wurtzite sphalerite transition temperature of 1024°C) the phosphor is found to be predominantly cubic in structure with a slight inclusion of the hexagonal form.

Copper sulphide is cubic in form and if we assume that the substitutional solubility of copper in zinc sulphide is low and that a concentration of interstitial copper has gradually built up, then when the concentration of copper reaches a certain level (i.e. 1 Cu for 10–20 atoms in the lattice) it causes nucleation of a new phase in which a high concentration of copper is present substitutionally in the lattice thereby modifying the crystal form. Infra-red emission due to cation vacancies is now no longer a possibility. Charge compensation of these centres by means of the aluminium co-activator is not possible and the copper ions must be uncompensated unless a large number of anion vacancies are generated.

This is not probable as the firing atmosphere is rich in free sulphur. It is possible that the copper ions are auto-compensated. Under these conditions it is possible that necessary electrons are found from the inner shell of the copper. The transitions from the normal levels into the d shell of the copper ion may account for the appearance of the red emission band. The luminescent centre will now consist of three levels whose kinetics may differ widely from the two-level centres and this may account for the disappearance of the infra-red emission. The situation can also be affected by the fact that the concentration of copper ions is so high that these are in close spatial proximity. It is to be expected that the wave functions will overlap and the levels will become continuous forming a pseudo-conduction and valence band in the forbidden region. Such an effect has been observed by Woods (1958†) in cadmium sulphide which, with high copper doping, has been shown to be p-type.

Electroluminescence is usually attributed (Zalm 1956) to impact ionization of the luminescent centres by electrons accelerated to sufficiently high energies in the large electric field in an exhaustion barrier at the interface between a semi-conducting phosphor and an electron-rich layer. The effect of the concentration of copper on the crystal structure and the infra-red emission of these phosphors indicates that the role of copper may be more complicated than providing a source of electrons. A pseudo-conduction band due to the high concentration of copper atoms in the crystal could lead to a p-type material in contact with the normal n-type ZnS phosphors. A recombination effect at the p-n junction so formed may be responsible for electroluminescence. The possibility of such a mechanism is being investigated further using copper doped single crystals.

§ 5. CONCLUSION

It has been shown that infra-red emission in ZnS [Cu](Al) phosphors does not occur in the materials containing high copper concentrations. The copper concentration in these cubic materials is large and most of the ions will be uncompensated. The conditions of preparation are such that the presence of sulphur vacancies is unlikely but the inclusion of the ion can possibly be explained by autocompensation (i.e. by withdrawing an electron from an inner shell of the copper ion). The kinetics in the three-level centre so formed may well be different from the two-level centre. Under these conditions infra-red emission is not to be expected. The proximity of the copper centres may lead in fact to impurity bands whose formation may be connected with the appearance of electroluminescence. During electroluminescence processes infra-red emission was not detected.

ACKNOWLEDGMENTS

My thanks are due to Miss J. B. Bleackly for the preparation of the phosphors used in this work and to the University of Hull for the facilities for the work.

REFERENCES

- APPLE, E. F., and PRENER, J. S., 1960, *J. Phys. Chem. Solids*, **13**, 81.
- BALLENTYNE, D. W. G., 1960, *J. Electrochem. Soc.*, **107**, 807.
- BROWNE, P. F., 1956, *J. Electronics*, **2**, 1.
- FRÖHLICH, H. C., 1953, *J. Electrochem. Soc.*, **100**, 496.
- GARLICK, G. F. J., 1958, *Handb. d. Phys.*, **26**, 34.
- GARLICK, G. F. J., and DUMBLETON, M. J., 1954, *Proc. Phys. Soc. B*, **67**, 442.
- ZALM, P., 1956, *Phillips Res. Rep.*, **11**, 417.

† *Dielectric Device Conference Birmingham*, unpublished.

Temperature Variation of Optical Energy Gap for GaSb-InSb Alloys

BY J. C. WOOLLEY AND J. A. EVANS†

Department of Physics, University of Nottingham

MS. received 6th March 1961

Abstract. Reasonably homogeneous, polycrystalline, solid ingots of GaSb-InSb alloys have been produced by slow directional freezing techniques, as described previously. For alloys of various compositions, normal absorption measurements have been made to determine the variation of optical energy gap E_g with temperature in the range 100–800°K. It is found that alloys show a linear variation of E_g with temperature, and values of extrapolated absolute zero energy gap and energy gap temperature coefficient are obtained. These results are compared with the data from electrical measurements described previously and the question of the variation with composition of the band form of the alloys is discussed.

§ 1. INTRODUCTION

SINCE the results of Goryunova *et al.* (Goryunova and Fedorova 1955, Goryunova and Gorshkov 1958) and Woolley *et al.* (Woolley, Smith and Lees 1956, Woolley and Smith 1958) showed that single-phase solid solution could be obtained at all compositions of GaSb-InSb alloys, considerable work has been carried out to determine the electrical and optical properties of these alloys. On the optical side, the variation of optical energy gap E_g as a function of composition has been determined by Woolley, Evans and Gillett (1959, to be referred to as I) and by Ivanov-Omskii and Kolomiets (1959a). Determination of electrical parameters have been made by Ivanov-Omskii and Kolomiets (1959b, 1960) on the equimolecular alloy GaSb-InSb and by Woolley and Gillett (1960, to be referred to as II) for the complete range of alloy composition. The present work is an extension of the optical investigation described in I, and the determination of the variation of E_g with temperature allows a comparison to be made between the optical results and the electrical data given in II.

§ 2. PREPARATION OF SPECIMENS AND METHODS OF MEASUREMENT

The preparation of the ingots from which the specimens were taken for the present work has already been described in I and II, the same ingots being used for all three sets of measurements. The compounds were prepared from elements of 99.999% purity and the InSb was further purified by normal zone refining techniques. Three ingots containing (a) 70 mol. %, (b) 30 mol. % and (c) 10 mol. % GaSb respectively were made up and equilibrium conditions obtained

† Now at Standard Telephones and Cables Ltd., Footscray, Kent.

by slow directional freezing. Cross sections from various points on these ingots provided specimens covering the range of composition from 0-94 mol. % GaSb, the degree of homogeneity being as described in I.

The optical measurements were made by normal transmission methods using the apparatus described in I, specimens of thickness somewhere in the range 60-160 μ being used. For measurements below room temperature the specimen holder was made of steel and the specimen attached to it with Durofix. The specimen and holder were contained in an evacuated chamber, the holder making good thermal contact with the top plate of the chamber which was of brass. This top plate formed the bottom of a metal Dewar which could be filled with liquid air or solid carbon dioxide in ether. Conduction through the brass holder enabled the specimen to be held at a steady temperature while the transmission measurements were made, the temperature of the specimen being determined by a chromel-alumel thermocouple placed close to it. The infra-red beam entered and left the chamber through arsenic trisulphide windows.

For temperatures above room temperature, the specimen was clamped at the centre of a long steel holder, and around each end of the holder was wound a small insulated tubular heating element. This holder was again mounted in an evacuated chamber and conduction along the holder enabled the specimen to be held at the required temperature, a Pt-PtRh thermocouple being used for temperature determination in this case. This system allowed measurements to be made up to temperatures of approximately 800°K.

§ 3. RESULTS

For various alloys throughout the composition range, measurements were made of relative transmission I/I_0 as a function of wavelength at temperatures at approximately 100°K intervals from 100°K upwards. In the case of the InSb-rich alloys measurements were made up to only approximately 400°K, this limit being set by the wavelength range of the apparatus ($\sim 8 \mu$) since for these alloys at high temperature the absorption edge had moved outside this wavelength range. Since, however, the electrical results in II had indicated no anomalous behaviour in this composition range, it was assumed that measurements up to 400°K were sufficient to allow the values of E_{0g} (the energy gap E_g at absolute zero) and β (the temperature coefficient of E_g) to be determined. For the GaSb-rich alloys, where the electrical results of II showed anomalous behaviour, measurements were made up to the temperature limit of the apparatus, which was approximately 800°K.

The method of determining E_g from the transmission data on polycrystalline specimens of unknown reflectivity is somewhat arbitrary. In I the value of λ corresponding to the energy gap was obtained by estimating the apparent onset of transmission from $(I/I_0, \lambda)$ graphs. In an attempt to obtain a more consistent set of values, particularly as specimens of different thickness were used, a different method of interpretation, described previously for other similar alloy systems (Woolley and Ray 1960, Woolley, Gillett and Evans 1960), was used in this case. The results have been plotted as $\log(I_0/I)$ against λ and some of the curves for an alloy containing 78 mol. % GaSb are shown in Fig. 1. Assuming that for specimens of thickness d the approximate equation $I = I_0 C \exp(-Kd)$ can be used for the transmitted intensity and that over the range concerned C is reasonably

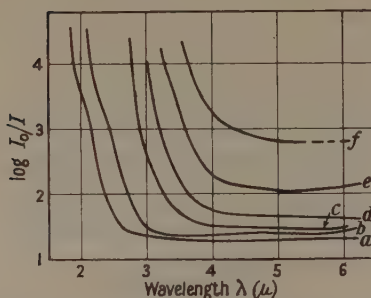


Fig. 1. Variation of $\log(I_0/I)$ with wavelength for the alloy 78 mol. % GaSb 22 mol. % InSb. Curve *a*, 103°K; curve *b*, 291°K; curve *c*, 499°K; curve *d*, 599°K; curve *e*, 685°K; curve *f*, 718°K.

independent of λ , this gives

$$\log\left(\frac{I_0}{I}\right)_E - \log\left(\frac{I_0}{I}\right)_B = \frac{K_E - K_B}{2 \cdot 303} d$$

where the subscript *E* indicates values at the wavelength λ_E , corresponding to the energy gap E_g , and the subscript *B* the background values. A choice of definition of λ_E was made by putting $K_E - K_B = 300 \text{ cm}^{-1}$, as this choice gave a value of E_g for InSb close to the generally accepted value for the compound. Using this criterion the values of E_g obtained for the alloys were reasonably close to those quoted in I. By this method, values of E_g were obtained as a function of temperature for each specimen and these are plotted in Fig. 2. It is seen that in each case E_g is found to vary linearly with temperature over the temperature range considered, and hence E_g can be represented by the equation $E_g = E_{0g} + \beta T$.

From the results in Fig. 2 the values of E_g at 300°K have been taken for the various compositions and compared with the room temperature results given in I and also with the values quoted by Ivanov-Omskii and Kolomiets. All of these results are collected in Fig. 3. It is seen that there is good agreement over the whole range of composition between the results given in I and the present results. The values of Ivanov-Omskii and Kolomiets, however, while showing reasonable agreement in the range 0–20 mol. % GaSb, lie well below the other results over the rest of the composition range. It is to be noted that preliminary values of E_g given by Woolley, Smith and Evans (1960) for material showing some inhomogeneity tend to agree with the results of Ivanov-Omskii and Kolomiets for alloys in the range 85–100 mol. % GaSb. It is thus possible that the presence of some inhomogeneity may be responsible for the disagreement in the results in Fig. 3, but it is not possible to consider this further as Ivanov-Omskii and Kolomiets do not indicate the degree of homogeneity of their specimens.

By extrapolating the graphs in Fig. 2 to $T=0$ a value of E_{0g} can be obtained for each composition, and the values of E_{0g} are plotted as a function of composition in Fig. 4. Also shown by the broken line in Fig. 4 are the values of E_0 determined by electrical measurements and given in II. The form of these curves is discussed below. The slopes of the lines in Fig. 2 give the values of energy gap temperature coefficient β and these are plotted as a function of composition in Fig. 5. This graph also is discussed below.

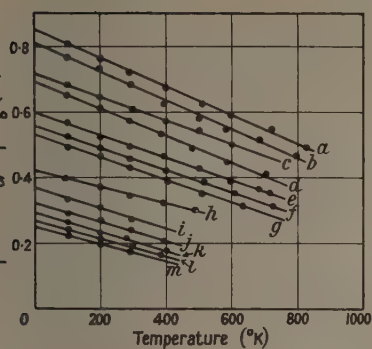


Fig. 2. Variation of optical energy gap E_g with absolute temperature for alloys of various compositions.

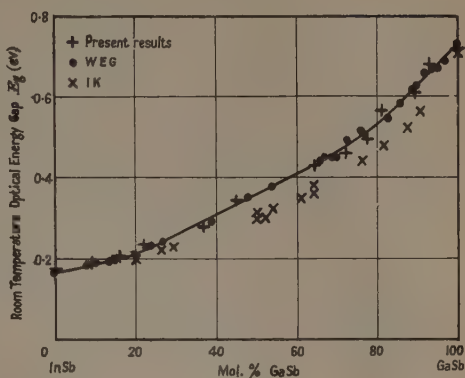


Fig. 3. Variation of room temperature optical energy gap E_g with composition. WEG, Woolley, Evans and Gillett (1959); IK, Ivanov-Omskii and Kolomiets (1959 a).

Curve	Mol. % GaSb	Mol. % InSb
a	100	0
b	93	7
c	89.5	10.5
d	81	19
e	78	22
f	73	27
g	64.5	35.5

Curve	Mol. % GaSb	Mol. % InSb
h	45	55
i	37	63
j	22	78
k	16	84
l	9.5	90.5
m	0	100

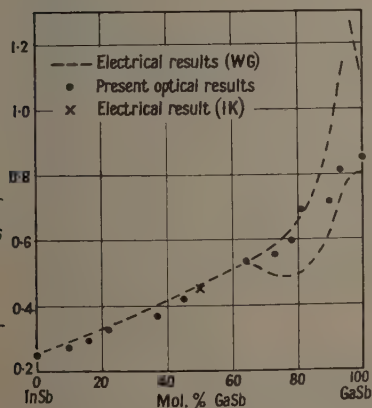


Fig. 4. Variation of extrapolated absolute zero energy gap values E_0 with composition. WG, Woolley and Gillett (1960); IK, Ivanov-Omskii and Kolomiets (1960).

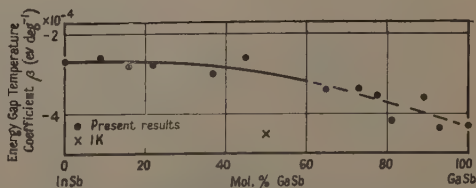


Fig. 5. Variation of energy gap temperature coefficient β with composition. IK, Ivanov-Omskii and Kolomiets (1959 b).

§ 4. DISCUSSION

The electrical results given in II indicated that for compositions between 0 and 60 mol. % GaSb the behaviour of the alloys was normal and that the addition of GaSb to InSb progressively changed the value of the extrapolated energy gap E_0 without causing any changes in the general form of the band structure. The present values of E_{0g} and β shown in Figs 4 and 5 reinforce this suggestion. Over this range of composition the values of E_{0g} are in good agreement with the electrical values of E_0 , particularly as the absolute values of E_g depend to some extent on the arbitrary choice of definition of E_g from the optical data. Also the value of β changes very little over this range of composition. It thus appears most probable that the band form of InSb with the conduction band minimum at 000 in k -space is retained by the alloys in this composition range. For the composition range 60–100 mol. % GaSb the results obtained so far have been anomalous. Thus the values of optical energy gap E_g given in I indicated the possibility of a discontinuity in the slope of the curve of E_g against composition at about 73 mol. % GaSb. The electrical data presented in II gave two values of E_0 in this composition range, a lower value E_{01} being obtained at low temperatures, and a higher value E_{02} at higher temperatures, the transition temperature T_c lying in each case in the temperature range 650–800°K. The variation of E_{01} and E_{02} with composition is shown in Fig. 4. When these values are compared with the values of E_{0g} presented here, it is seen that over the approximate composition range 60–85 mol. % GaSb E_{0g} agrees with E_{02} , but in the range 95–100 mol. % GaSb E_{0g} shows some agreement with E_{01} .

In II it was suggested that the form of the electrical results could be explained by one of two possible alternatives, i.e. the anomalous behaviour in the range 60–100 mol. % GaSb was due to either (a) band changes occurring in this range of composition or (b) ordering, possibly relatively short range, occurring in the composition range around 75 mol. % GaSb, the transition temperature T_c being in fact the ordering temperature. In order to explain the electrical results in terms of a band change, it is necessary to postulate a change in band form not only with composition, but also with temperature, in the anomalous range. Owing to the difficulties of making the detailed electrical results for each specimen fit with the idea of a change of band minimum with temperature, it was suggested that possibly ordering effects were a more likely explanation.

This view must be modified however in the light of the present results. The observed values of E_{0g} show a monotonic variation from InSb to GaSb. Bearing in mind the fact that in both InSb and GaSb the conduction band minimum occurs at 000 in k -space (Zwerdling *et al.* 1959, Sagar 1960, Moss 1960), it appears probable that at every composition the measured E_{0g} corresponds to a direct transition which is what is observed in the absorption measurements. The smooth variation of β in Fig. 5 supports this suggestion. Since all the optical measurements were made at temperatures below 800°K, these represent conditions below the transition temperature T_c . The lower values of E_{01} could not then correspond to a direct transition but would correspond to indirect transitions not observed in the present optical work. And since in the composition range 60–85 mol. % GaSb the high temperature electrical E_{02} corresponds with the low temperature optical E_{0g} , the idea that ordering takes place and gives two entirely different sets of conduction band minima above and below T_c seems to be ruled out.

In an explanation in terms of a band change, it is seen that since in this composition range $E_{02} = E_{0g}$, E_{02} would correspond to a direct transition. Thus here the 000 minimum would be the lowest minimum in the conduction band at temperatures down to T_c , but below this temperature some other conduction band minimum would be the lowest, resulting in indirect transition begins observed by the electrical measurements at these lower temperatures. Such an effect would occur if the minima had different temperature coefficients, and were at the same energy at the temperature T_c . There is some support for this suggestion in the form of the $(\log(I_0/I), \lambda)$ curves for the alloy containing 78 mol. % GaSb as shown in Fig. 1. The curves corresponding to low temperatures, i.e. below approximately 500°K, show a slight kink in the absorption edge whereas at higher temperatures no such kink was observed. Such a kink could be due to the effect of an indirect transition of lower energy than the direct transition becoming noticeable at lower temperatures. Effects of this type were observed for various alloys in the range 73–89 mol. % GaSb.

It is still not clear however how the relatively sharp discontinuities at a temperature T_c which occur in the $(\log(np/T^3), 1/T)$ graphs (II) can be correlated with such a band change. It is of interest to note that even in this case if the values of E_{01} are explained as being due to an indirect transition to a conduction band minimum with an anomalous temperature coefficient, this effect occurs only over a limited range of composition centred on 75 mol.% GaSb which is the optimum ordering composition for these alloys. Thus some structural effect such as short range ordering could still play a part and be responsible for the anomalous values of β in this composition range.

The form of the various E_0 curves (Fig. 4) in the range 85–100 mol.% GaSb would still appear anomalous and it is not possible at this stage to account for their form. The values of β shown in Fig. 5 as a function of composition are considerably scattered about the mean line (shown broken) in this anomalous range, and it is felt that these deviations are greater than would be expected from the estimated accuracy of the determinations. The deviations may be significant and reflect the more complex behaviour of the band structure in this composition range. More detailed data are required before explanations can be attempted, and it is hoped in particular to carry out a more detailed investigation of the optical absorption edge for alloys in the range 60–100 mol.% GaSb, and to extend the temperature range of observations from the present limit to values well above T_c .

ACKNOWLEDGMENTS

The authors are indebted to Professor L. F. Bates for the facilities of his laboratory. The work described forms part of an investigation carried out for the Admiralty.

REFERENCES

- GORYUNOVA, N. A., and FEDOROVA, N. N., 1955, *Ź. Tech. Phys., Moscow*, **24**, 1339.
GORYUNOVA, N. A., and GORSHKOV, I. E., 1958, *Zh. Neorg. Khim.*, **2**, 668.
IVANOV-OMSKII, V. I., and KOLOMIETS, B. T., 1959 a, *Dokl. Akad. Nauk., S.S.S.R.*, **127**, 135.
— 1959 b, *Soviet Physics Solid State*, **1**, 512.
— 1960, *Soviet Physics Solid State*, **2**, 363.

- MOSS, T. S., 1960, *Progress in Semi-conductors*, Vol. 5 (London: Heywood), p. 189.
- SAGAR, A., 1960, *Phys. Rev.*, **117**, 93.
- WOOLLEY, J. C., EVANS, J. A., and GILLETT, C. M., 1959, *Proc. Phys. Soc.*, **74**, 244.
- WOOLLEY, J. C., and GILLETT, C. M., 1960, *J. Phys. Chem. Solids*, **17**, 34.
- WOOLLEY, J. C., GILLETT, C. M., and EVANS, J. A., 1960, *J. Phys. Chem. Solids*, **16**, 138.
- WOOLLEY, J. C., and RAY, B., 1960, *J. Phys. Chem. Solids*, **15**, 27.
- WOOLLEY, J. C., and SMITH, B. A., 1958, *Proc. Phys. Soc.*, **72**, 214.
- WOOLLEY, J. C., SMITH, B. A., and EVANS, J. A., 1960, *Solid State Physics in Electronics and Telecommunications*, Vol. 2 (London: Academic Press), p. 802.
- WOOLLEY, J. C., SMITH, B. A., and LEES, D. G., 1956, *Proc. Phys. Soc. B*, **69**, 1339.
- ZWERDLING, S., LAX, B., BUTTON, K. J., and ROTH, L. M., 1959, *J. Phys. Chem. Solids*, **9**, 320.

The Electrical and Magnetic Properties of the Uranium-Niobium System

By L. F. BATES AND R. D. BARNARD†

Department of Physics, University of Nottingham

MS. received 3rd March 1961

Abstract. The magnetic susceptibilities and electrical resistivities of a series of γ -phase uranium-niobium alloys were measured over the temperature ranges 293–1200°K and 90–1200°K, respectively. The form of the resistivity-temperature-concentration relations is abnormal, especially at low temperatures, where negative temperature coefficients of resistivity occur in the uranium-rich alloys, and no explanation can be found in terms of localized moments on either U or Nb atoms. Comparison is made of the same properties of the γ U-Mo alloys and particular attention is directed towards the electronic band structure of niobium. A rigid band model is shown to be appropriate for dilute solid solutions of uranium and molybdenum, but such a model is not applicable to the uranium-rich γ U-Mo and the U-Nb alloys.

§ 1. INTRODUCTION

RESEARCH on the physical properties of the U-Mo and U-Nb alloys has received impetus in recent years, following the discovery by Bleiberg, Jones and Lustman (1956) that some of the metastable γ body-centred cubic alloys possess small negative temperature coefficients of resistivity below room temperature. More recently, Chandrasekhar and Hulm (1958) studied the electrical resistivity and superconductivity of a series of α (orthorhombic) and γ (body-centred cubic) binary alloys of uranium with molybdenum and niobium between 1° and 295°K. All the quenched γ alloys in the range 15–30 at. % were found to exhibit anomalous negative temperature coefficients of resistivity. Magnetic susceptibility and electrical resistivity measurements on the γ U-Mo alloys were made (Bates and Barnard 1961) over an extended temperature range in order to include the stable γ region, and it was concluded that no explanation of the results could be given in terms of localized electrons on either the molybdenum or uranium atoms.

In spite of these and other investigations (Loasby 1958, Blatt 1961, Berlincourt 1959), the origin of the unusual behaviour has not been completely explained. It was therefore thought that more light might be shed on the problem by studying the electrical and magnetic properties of the U-Nb system, where the γ phase could be retained in metastable equilibrium over a much larger composition range than in the U-Mo system. In addition, it was hoped that a comparison of the properties of the γ U-Mo and γ U-Nb alloys would provide information on the electronic structure of γ uranium, particularly on the density of states-energy distribution.

† Now at Research Laboratories of Electrical and Allied Industries Research Association, Leatherhead, Surrey.

No previous extensive investigation into the physical properties of the U-Nb alloys has been made, but the phase diagram of the system is well established (Pfeil, Brown and Williamson 1958). There is complete solubility above 950°C of γ uranium and niobium, although with intermediate compositions below 950°C the state exists in two body-centred forms, γ_1 and γ_2 . The γ phase of samples of composition greater than 20 at. % Nb can be retained at room temperature by quenching.

§ 2. EXPERIMENTAL PROCEDURE

The alloys were prepared at the Atomic Energy Research Establishment, Harwell, in an argon arc furnace from 99.9% pure uranium (see Bates and Barnard 1961), and spectroscopically standardized niobium, supplied by Johnson Matthey and Co. Ltd. The ingots were wrapped in molybdenum foil, sealed in quartz capsules under a pressure of less than 10^{-4} mm Hg, and annealed for two weeks at 1000°C. The ingots were afterwards machined to give cylinders 4 cm long and 5 mm in diameter, which were resealed, heated in the capsules, and quenched in water from 1000°C with fracture of the quartz. Microscopic inspection of the specimens kindly performed at the Atomic Energy Research Establishment, Harwell, showed for compositions above 30 at. % Nb the existence of the γ body-centred cubic phase in metastable equilibrium; but, like the alloys of similar composition in the U-Mo system, between 20 and 30 at. % Nb there was established a distorted γ body-centred tetragonal phase whose axial ratio was so close to unity that the tetragonality was not observable by x-ray techniques. In addition, the investigation showed that the alloys were not completely homogeneous despite the long time of anneal, the inhomogeneity being more marked in the 20–70 at. % Nb range of composition. No observations of the lattice parameters were made, as these were being performed concurrently at Harwell by Pfeil, Brown and Williamson (1958). The parameters were found to obey Vegard's law fairly accurately, the addition of niobium contracting the lattice of γ uranium.

The experimental arrangements for the measurement of magnetic susceptibility between 293 and 1200°K and for electrical resistivity between 90 and 1200°K together with a discussion of the experimental limitations have been described elsewhere (Bates and Barnard 1961).

Alloys in the composition range 20–80 at. % Nb were first measured in the metastable γ state with rise in temperature until the γ phase began to decompose. This was manifested by marked discontinuities in the slopes of the susceptibility-temperature and of the resistivity-temperature curves, at which juncture measurements were discontinued until further rise in temperature took the specimens into the stable γ region. Having once in these alloys established the γ phase, which is stable only at very high temperatures, it was possible to make measurements with decrease in temperature into the $\gamma_1 + \gamma_2$ phase region; for precipitation of γ to $\gamma_1 + \gamma_2$ is so slow that the γ phase does not decompose at temperatures near 700°C, even after several days. Above 800°C, Pfeil, Brown and Williamson (1958) reported that the transition from single phase γ to $\gamma_1 + \gamma_2$ does not occur even after anneals of eight weeks duration. Each of the curves for these alloys thus had a temperature region where no observations of the γ phase could be made, but it was possible to interpolate between the observations in the metastable and stable γ regions and so estimate with reasonable accuracy the form of

the curves where the γ phase was decomposing. For compositions above 80 at. % Nb, the alloys were stable in the body-centred cubic modification for all temperatures up to their melting points.

§ 3. EXPERIMENTAL RESULTS

3.1. Magnetic Susceptibility

The molar susceptibilities against temperature of the U-Nb alloys in both metastable and stable γ states are shown in Figs 1 and 2. In view of the inhomogeneity of some of the specimens, two values of the room temperature susceptibility were obtained for each specimen (one in the inverted position) and the

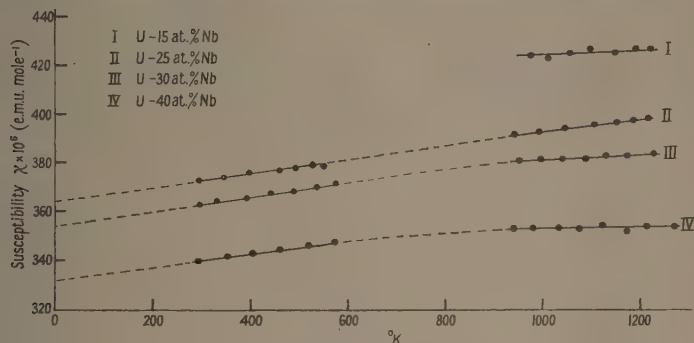


Fig. 1. Susceptibility plotted against temperature for γ U-Nb alloys.

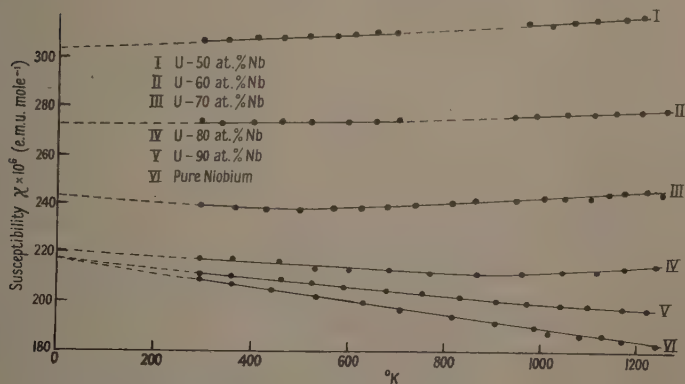


Fig. 2. Susceptibility plotted against temperature for γ U-Nb alloys.

mean taken as the correct value. With no specimen was a difference of more than 2% found between measurements when the specimen was inverted, to bring another portion of the specimen into the region of maximum field gradient.

It is clear that the addition of niobium to γ uranium gives a general reduction, not only of the magnitude of the susceptibility, but also of the temperature coefficient. The temperature coefficient of susceptibility of U-25 at. % Nb is positive, as in the U-Mo system, and gradually decreases with increasing niobium

concentration until it is negative as with pure niobium. The results for pure niobium are in close agreement with those previously recorded (Kriessman 1953), the variation with temperature being fairly linear over the range of temperature investigated. The absolute value at room temperature was $2.29 \pm 0.02 \times 10^{-6}$ e.m.u. g⁻¹, a value rather higher than that recorded by Kriessman, but in close agreement with that recorded by Williams (1960 unpublished), viz. 2.3×10^{-6} e.m.u. g⁻¹.

Two of the niobium-rich alloys, U-70, 80 at. % Nb, exhibited shallow susceptibility minima at about 500°K and 900°K, respectively. This tendency for a minimum to exist and for it to shift towards higher temperatures with increasing concentration of niobium is most unusual, but it is interesting that Kriessman observed a minimum in observations on pure niobium at about 2000°K.

The isothermal susceptibilities at 0°K and 1100°K are shown as functions of composition in Fig. 3. The 0°K values were obtained by extrapolation from the

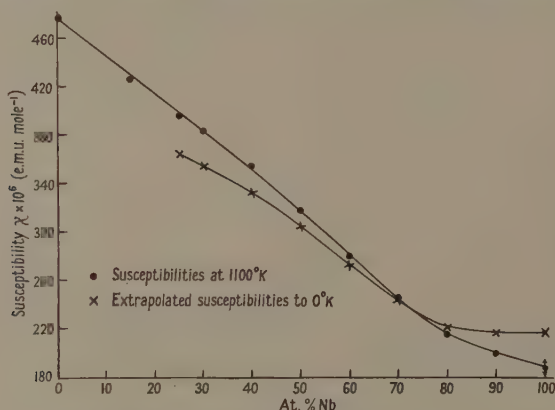
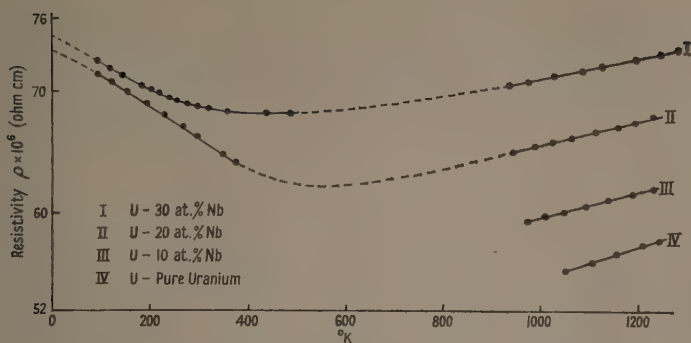
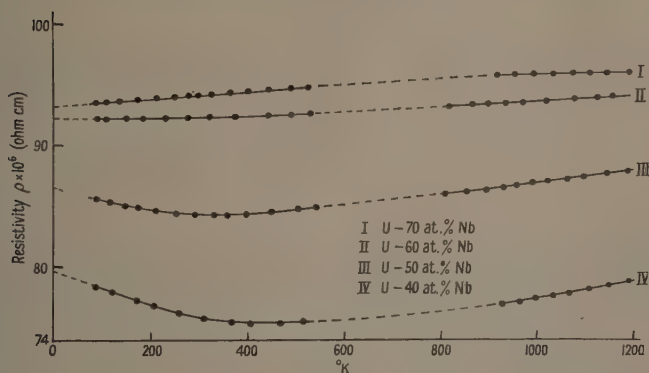
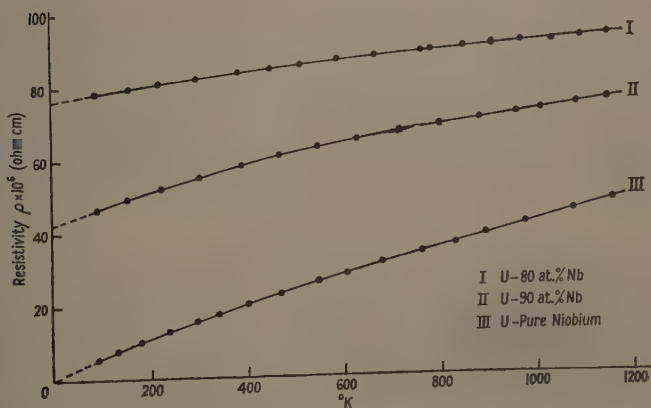


Fig. 3. Susceptibility plotted against composition for γ U-Nb alloys.

observations above room temperature shown in Figs 1 and 2. They are particularly interesting; firstly, because small additions of uranium to niobium did not alter the susceptibility, and secondly, because the susceptibility curve when extrapolated to zero niobium content yields a value in close agreement with that obtained from work on the U-Mo alloys (Bates and Barnard 1961). The constancy of the susceptibility of the niobium-rich alloys is very remarkable, especially in view of the different, conventional valencies of uranium and niobium. This point is considered in greater detail in the discussion below.

3.2. Electrical Resistivity

The resistivity-temperature curves for uranium-rich alloys, shown in Fig. 4, are characterized by behaviour very similar to that of uranium-rich U-Mo alloys; i.e. by a negative temperature coefficient of resistivity for the quenched alloys. Increasing concentrations of niobium reduced the magnitude of the negative temperature coefficient and the magnitude of the positive coefficient in the stable γ region. This abnormal behaviour persisted to 60 at.% Nb, Fig. 5, and then more or less normal behaviour prevailed, Fig. 6, to pure niobium.

Fig. 4. Resistivity plotted against temperature for γ U-Nb alloys.Fig. 5. Resistivity plotted against temperature for γ U-Nb alloys.Fig. 6. Resistivity plotted against temperature for γ U-Nb alloys.

The resistivity curves of pure niobium and the niobium-rich alloys show, like those of many other transition elements, temperature coefficients which decrease with temperature. This effect is considered below in greater detail in the discussion of the density of electron states against energy curve for pure niobium.

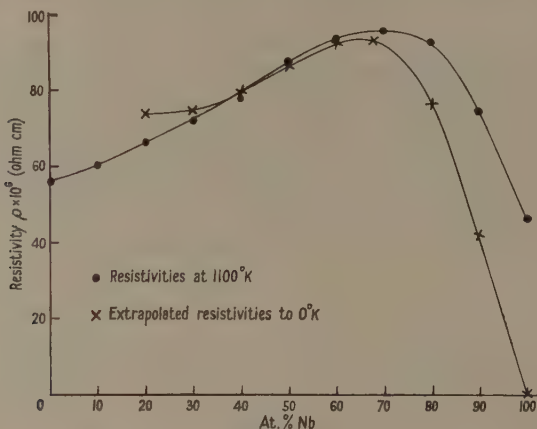


Fig. 7. Resistivity plotted against composition for γ U-Nb alloys.

The resistivity with composition curves, shown in Fig. 7, exhibit deviations from normal alloy behaviour. The curve for the resistivities at 0°K, obtained by extrapolation of the resistivity-temperature curves indicates an extremely high value for the resistivity of pure γ uranium when the curve is extended. This is, of course, unacceptable; in addition, the variation with composition at 1100°K is concave upwards at the uranium-rich end, in contrast with the concave downwards curve given by the equation

$$\rho_0 \propto x(1-x) \quad \dots\dots (1)$$

Here ρ_0 is the residual resistivity and x the concentration of one element in the other. Eqn (1) gives a maximum in the residual resistivity curve at 50 at. % Nb; the maximum observed here is at about 64 at. % Nb.

No previous work on the magnetic susceptibilities of these alloys has been recorded, and only the low temperature resistivities of the uranium-rich alloys have received attention, through the work of Chandrasekhar and Hulm (1958). Their numerical results are in excellent agreement with those presented above.

§ 4. DISCUSSION

Striking similarities exist between the present results for the U-rich U-Nb alloys and those for U-Mo alloys (Bates and Barnard 1961). These are essentially (1) strong positive temperature dependence of susceptibilities in the case of the metastable alloys and almost no temperature dependence in the stable γ regions; (2) negative temperature coefficients of resistivity in the case of the metastable γ alloys, and weak positive dependence in the stable γ regions; (3) similar resistivity-concentration and susceptibility-concentration curves.

The similarities in the results would seem to indicate that an explanation like that for the γ U-Mo alloys is appropriate, although there is no indication as to why Nb and Mo behave in the same manner in γ uranium. Briefly, then, the susceptibility results for the U-rich U-Nb alloys are compatible with the Fermi surface lying in each case in an energy region for which

$$A - B > 0 \quad \text{.....(2)}$$

where
$$A = \left(\frac{1}{N} \frac{d^2 N}{dE^2} \right)_{E=E_0} \quad \text{and} \quad B = \left(\frac{1}{N} \frac{dN}{dE} \right)^2_{E=E_0}$$

Here, N is the density of states per unit energy per mole, and E_0 is the Fermi energy measured from the band edge. The density of states against energy curves for these alloys are thus concave upwards at the Fermi surface. The failure of the susceptibilities to give T^2 variations, especially at high temperatures, may be due to the failure of the degeneracy condition

$$E_0 \gg kT. \quad \text{.....(3)}$$

The susceptibility results, Fig. 2, further indicate that at about 60 at. % Nb the inequality (2) becomes $A - B = 0$, to change to $A - B < 0$ at higher concentrations of niobium.

As in the discussion of the U-Mo alloys one notes that a negative temperature coefficient of resistivity may arise if

$$3B - A > 0, \quad \text{.....(4)}$$

and if the residual resistivity is large compared with the thermal resistivity given by the Grüneisen expression. The latter condition is, of course, likely to be satisfied at fairly low temperatures where the unusual behaviour is in fact observed. Further, the residual resistivities are large, Fig. 7, for the U-rich alloys, and the weak concentration dependence is indicative of a large increase in the effective number of free electrons with composition. It is thus evident from the present discussion that the Fermi surfaces in both the U-rich U-Mo and U-Nb alloys lie in regions where the density of states-energy curves possess finite gradients of strong positive curvature.

Since in the uranium-rich U-Nb alloys the addition of Nb with five valency electrons depletes the band of the solvent, the application of a rigid band model should lead to a curve of the variation of the density of states with solute concentration which is concave upwards. The variation of susceptibility at 0°K with composition shown in Fig. 3 may be taken to represent the variation of the density of states with niobium content provided that the empirical relation (Childs, Gardner and Penfold 1960)

$$K = \frac{C}{N(E_0)} \quad \text{.....(5)}$$

is valid, where K is the exchange interaction and C is a constant. This variation is concave downwards for the low niobium content alloys, and so it appears that the addition of Nb to U in concentrations greater than 20 at. % not only alters the degree of occupation of the bands but also their $(N(E), E)$ relation. It should be remarked that values of K and $N(E_0)$ for both the γ U-Mo and pure niobium obey the relation (5) fairly accurately.

In a discussion of the magnetic properties of the transition elements, Kriessman and Callen (1954) concluded that, if the Pauli susceptibility decreased with temperature, the Fermi surface was near a maximum in the density of states curve. Such susceptibility behaviour is exhibited by pure niobium, and thus little change of susceptibility should result when uranium, which enhances the degree of occupation of the bands of niobium, is added in small quantities. This argument is clearly supported by the susceptibility-composition curves shown in Fig. 3, and also by similar results on the Nb-Mo system (Matthias *et al.* 1960). Additional evidence that this band shape is correct for pure niobium was obtained by calculations of A and B from the susceptibility and resistivity data.

Values of $A - B$ and $3B - A$ were obtained from the linear regions of plots of the Pauli susceptibility against T^2 and of $\rho(E, T)/T$ against T^2 , where $\rho(E, T)$ is the resistivity. That these plots should be straight lines is evident from the formulae

$$\chi_M' = 2\mu^2 N(E_0) \left[1 + \frac{\pi^2 k^2 T^2}{6} (A - B) \right]_{E=E_0} \quad \dots\dots (6)$$

for the molar Pauli susceptibility χ_M' and

$$\rho(E, T) = \rho(E_0 T) \left[1 - \frac{\pi^2 k^2 T^2}{6} (3B - A) \right]_{E=E_0} \quad \dots\dots (7)$$

for the resistivity, where $\rho(E_0 T)$ is the Grüneisen expression which is proportional to T in the temperature range under consideration. Above the Debye temperature ($\sim 254^\circ\text{K}$), and below 500°K , the plot of $\rho(E, T)/T$ against T^2 was linear. The values of A and B thus obtained were

$$A = \left(\frac{1}{N} \frac{d^2 N}{dE^2} \right)_{E=E_0} = -2.2 (\text{eV})^{-2}$$

and

$$B = \left(\frac{1}{N} \frac{dN}{dE} \right)_{E=E_0}^2 = 9.0 (\text{eV})^{-2}.$$

The negative value for A clearly supports the previous discussion, as this condition is essential for the Fermi surface to be near a maximum in the $(N(E), E)$ distribution. No great accuracy is claimed for these values of A and B , especially as the Pauli susceptibility was calculated on the assumption of a temperature independent exchange interaction. It may well be that when consistent data is available for the temperature dependence of the thermoelectric power and Hall coefficient, the values will need modification.

ACKNOWLEDGMENTS

The authors are indebted to Dr. G. K. Williamson, formerly of the Metallurgy Division, Atomic Energy Research Establishment, Harwell, and Dr. W. E. Gardner, for the provision of the alloys and also for much valuable discussion, and to the Director, Atomic Energy Research Establishment, for permission to publish the results.

REFERENCES

- BATES, L. F., and BARNARD, R. D., 1961, *Proc. Phys. Soc.*, **77**, 691.
 BERLINCOURT, T. G., 1959, *J. Phys. Chem. Solids*, **11**, 12.
 BLATT, F., 1961, *J. Phys. Chem. Solids*, **17**, 177.
 BLEIBERG, M. L., JONES, L. J., and LUSTMAN, B., 1956, *J. Appl. Phys.*, **27**, 1270.
 CHANDRASEKHAR, B. S., and HULM, J. K., 1958, *J. Phys. Chem. Solids*, **7**, 259.
 CHILDS, B., GARDNER, W. E., and PENFOLD, J., 1960, *Phil. Mag.*, **5**, 1267.
 KRIESSMAN, C., 1953, *Rev. Mod. Phys.*, **25**, 122.
 KRIESSMAN, C., and CALLEN, H., 1954, *Phys. Rev.*, **94**, 837.
 LOASBY, R. G., 1958, *Proc. Phys. Soc.*, **72**, 429.
 MATTHIAS, B. T., PETER, M., WILLIAMS, H. J., CLOGSTON, A. M., CORENZWIT, E., and
 SHERWOOD, R. C., 1960, *Phys. Rev. Letters*, **5**, 542.
 PFEIL, P. C. L., BROWN, J. D., and WILLIAMSON, G. K., 1958, *A.E.R.E. Report M/R 2498*.

Exchange Effects and Anisotropy Broadening of the Hyperfine Spin Resonance Spectrum of the Biphenyl Negative Ion in Solution

By J. G. POWLES AND M. H. MOSLEY

Physics Department, Queen Mary College, University of London

MS. received 27th January 1961

Abstract. The electron spin resonance absorption spectrum of the biphenyl negative ion has been measured at 9.5 mm wavelength in solution in tetrahydrofuran and in diethylene glycol dimethyl ether (DGDE) over the temperature range -90°C to $+70^{\circ}\text{C}$ and for concentrations from 1.94×10^{-3} to 4.35×10^{-3} M. The normal nine line hyperfine spectrum loses its structure with falling temperature for solution in DGDE at about -70°C independent of concentration. It is thought that this is due to a decrease in motional narrowing of an anisotropic hyperfine interaction comparable in magnitude with the isotropic hyperfine interaction. With rising temperature the hyperfine structure again disappears. This occurs at -34°C for a concentration 4.35×10^{-3} M and increases with falling concentration to $+37^{\circ}\text{C}$ at 1.94×10^{-3} M. After loss of structure the line continues to narrow with increasing temperature. Similar but less extensive measurements have been possible for solution in tetrahydrofuran. This effect is thought to be due to exchange, i.e. perturbation of the electron spins at encounters between the radicals which are diffusing through the solvent. An analysis is carried out using a theory proposed by Pake and Tuttle in 1959 in which a quantity related to the ratio of exchange frequency to collision frequency is derived and which should be constant and of order unity. We find this quantity to be indeed of order unity over a wide range of temperature and for the two solvents but that it varies significantly nevertheless. These variations have not been explained and show that a more elaborate theory even than that proposed by Kivelson in 1960 is required.

§ 1. INTRODUCTION, EXPERIMENTAL ARRANGEMENT AND RESULTS

WE have measured the electron spin resonance absorption line for the biphenyl ($\text{C}_6\text{H}_5\text{C}_6\text{H}_5$) negative ion in solution in tetrahydrofuran ($(\text{CH}_2)_4\text{O}$) and in diethylene glycol dimethyl ether ($\text{CH}_3\text{O}[(\text{CH}_2)_2\text{O}]_2\text{OCH}_3$, which we call DGDE) over the temperature range -90°C to $+70^{\circ}\text{C}$ and over a range of concentration from 1.94×10^{-3} M to 4.35×10^{-3} M (2×10^{-3} M corresponds to one ion to 7×10^3 solvent molecules for tetrahydrofuran). The spectrometer operates at 9.5 mm wavelength, and has been briefly described elsewhere (Powles and Mosley 1961). The derivative absorption signal as a function of field is obtained, as shown for instance in Fig. 1.

The biphenyl negative ion was prepared from pure biphenyl using potassium metal and specially purified and degassed solvents (Balk, Hoijsink and Schreurs 1957). The concentration of free radical, which is not readily controlled in the method of preparation, was calculated from the optical absorption using a Unicam SP.500 spectrophotometer and using the results of Balk *et al.* (1957)

for calibration. The solutions remained stable for at least several days at room temperature depending on concentration. They could be heated to 60°C for up to thirty minutes without appreciable degradation.

The viscosity of tetrahydrofuran was only available above 0°C (Timmermans 1950) and that of DGDE was not available. The viscosities, given in Fig. 2, were measured using a thermostatted Ostwald viscometer. The values are thought to be accurate to $\pm 5\%$ and they agree with Timmerman's quoted values to this accuracy where the comparison is possible.

Tetrahydrofuran and DGDE show no apparent freezing point in the temperature range covered and none is reported in the literature. We believe DGDE forms a supercooled liquid and eventually a glass although the glassy state was probably not attained in our measurements. The usual hyperfine spectrum of biphenyl approximates to a nine line spectrum with a spacing of approximately 2.9 gauss (8.1 Mc/s) between lines. This is as reported by De Boer (1956) and is shown in Fig. 1(c). The spectrum is only apparently nine line, some structure is not resolved, and so the spacing 2.9 gauss is not the hyperfine interaction parameter.

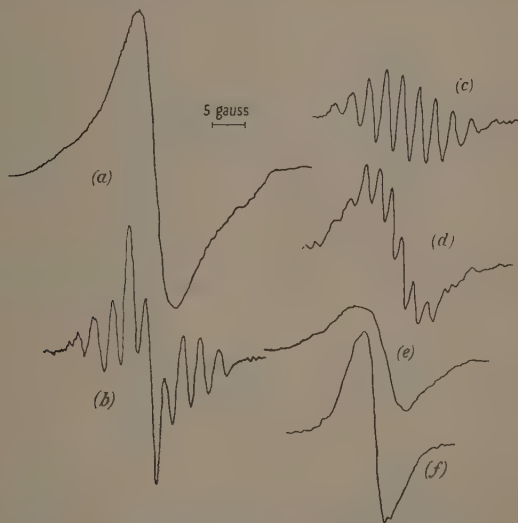


Fig. 1. Experimental absorption derivative curves for the biphenyl negative ion in diethylene glycol dimethyl ether at various temperatures and concentrations illustrating the various line shapes: (a) anisotropy broadening, -90°C , $2.37 \times 10^{-3}\text{M}$; (b) partial anisotropy broadening, -62°C , $3.12 \times 10^{-3}\text{M}$; (c) normal hyperfine splitting, -33°C , $3.12 \times 10^{-3}\text{M}$; (d) onset of exchange broadening and loss of structure, -28°C , $3.04 \times 10^{-3}\text{M}$; (e) exchange broadened, -23°C , $4.35 \times 10^{-3}\text{M}$; (f) exchange narrowed, 0°C , $2.46 \times 10^{-3}\text{M}$.

For rising temperature we have observed a loss of the hyperfine structure (Figs 1(d) and (e)) and finally a continued narrowing of the line (Fig. 1(f)). This is similar to the effect noted by Pake and Tuttle (1959) for a solution of diphenyl picryl hydrazil (DPPH) in toluene and by Hausser (1959) for α , γ -bisdiphenylene β -phenyl allyl (BPA) in ethyl alcohol.

The temperature at which the hyperfine structure just disappears, which we call the exchange temperature (say between the two spectra of Figs 1 (*d*) and (*e*)), depends markedly on concentration in DGDE as indicated in Table 1.

The effect of concentration at room temperature only, for DPPH in benzene, was studied by Hutchison, Pastor and Kowalsky (1952).

Table 1. The Effect of Concentration on the Exchange Temperature and Values of the Quantity F (Eqn (2))

	(1)	(2)	(3)	(4)
Solution in DGDE				
1.94		+37	0.83	0.67
2.37		-2	1.65	1.24
2.46		-12	2.16	1.62
3.04		-22	3.1	1.95
4.35		-34	4.7	2.17
Solution in tetrahydrofuran				
3.3		+50	0.47	0.21

(1) Concentration $C \times 10^3(\text{M})$; (2) exchange temperature ($^{\circ}\text{C}$); (3) viscosity (cp); (4) value of F .

The same effect is observed in tetrahydrofuran but for one concentration only (Table 1). For lower concentration in tetrahydrofuran the structure persists until the rise in temperature causes excessive decomposition. For higher concentration the line is narrow over the whole temperature range, but the line width varies with temperature as shown in Table 2. Table 2 also shows the

Table 2. The Effect of Temperature on the Line Width for Narrowed Lines and the Values of the Quantity F using Eqns (2) and (3)

(1)	(2)	(3)	(4)	(5)
Solution in tetrahydrofuran				
4.3	-62	6.2	1.35	1.6
"	-55	5.9	1.18	1.4
"	-42	5.6	0.91	1.1
"	-17	4.9	0.67	0.8
"	+3	4.6	0.60	0.7
"	+13	4.3	0.57	0.7
Solution in DGDE				
2.46	0	4.2	1.57	3.4
3.04	-16	8.0	2.44	2.4

(1) Concentration $C \times 10^3(\text{M})$; (2) temperature ($^{\circ}\text{C}$); (3) line width $\delta H(\text{gauss})$; (4) viscosity (cp); (5) value of F .

variation in width of the narrowed, i.e. structureless, line for two solutions in DGDE.

On lowering the temperature for solutions in DGDE the structure again disappeared (Figs 1 (*a*) and (*b*), note the difference between Figs 1 (*b*) and (*d*)). A similar effect has been reported by Hausser (1959) for BPA in ethyl alcohol and by the authors (Powles and Mosley 1961) for peroxyamine disulphonate in water/glycerol. The temperature at which this occurs is not readily defined but

the general effect is shown by the sequence of Figs 1 (a), (b) and (c). This change seems to be independent of concentration over the range measured (see Table 1) and it occurs at $-70 \pm 15^\circ\text{C}$. It is not clear why some variation in the results from sample to sample, run to run and concentration to concentration occurred.

§ 2. INTERPRETATION OF THE RESULTS

We wished to study further the presumed exchange narrowing effects for free radicals in solution discussed by Pake and Tuttle (1959) and to extend the results of Hausser (1959). The system biphenyl negative ion in tetrahydrofuran, the usual solvent, was not sufficiently flexible. We considered this to be due to the rather small variation of viscosity of tetrahydrofuran over the liquid temperature range and to the fact that the viscosity was too low. De Boer (1956) used tetrahydrofuran or 1,2-dimethoxyethane which has a similar viscosity range to tetrahydrofuran. It is not easy to find a suitable solvent in which the biphenyl radical can be formed in a suitable range of concentration and in which it is stable over a wide temperature range. DGDE has proved very suitable.

2.1. Exchange Effects

Pake and Tuttle (1959) proposed a rather crude theory, as they admit, for the effect of exchange narrowing as a result of perturbation of the electron spins during encounters between the ions. The problem has two parts: one is to calculate how frequently in a given concentration in a given solvent the ions meet, and the other to calculate the probability of an interaction on collision sufficiently strong to cause loss of hyperfine structure or the number and frequency of weak collisions required to give the same effect (Kivelson 1960). The former is essentially a problem of diffusion of the ion in the solvent. In the absence of self-diffusion data Pake and Tuttle removed the self-diffusion constant D by the Stokes-Einstein relation

$$D = kT/6\pi a_r \eta, \quad \text{.....(1)}$$

where η is the shear viscosity and a_r is an effective radius of the diffusing ion. They find for the frequency of phase interrupting collisions f_e ,

$$f_e = \frac{N_r kT}{\eta} \left[\frac{4zpa_s^3}{3\lambda^2 a_r} \right] = \frac{N_r kT}{\eta} F, \quad \text{.....(2)}$$

where N_r is the radical concentration in cm^{-3} (which is readily related to the molar concentration C); z is the number of new molecular neighbours encountered per diffusion step; p is the probability of a collision being effective in causing spin dephasing; a_s is the solvent molecular radius introduced via $N_s^{-1} = 4\pi a_s^3/3$ (it would probably be slightly better to use $N_s^{-1} = 8a_s^3$), where N_s is the number of molecules of solvent per cm^3 ; λ is the elementary jump step in the diffusion process. Rather similar formulae are obtained by Kivelson (1960) if the parameters are interpreted slightly differently. Pake and Tuttle point out that the quantity in the square brackets (which we will call F) should be approximately unity. This is seen by taking the plausible values, $z=6$, $p=\frac{1}{2}$, $\lambda=2a_s$ so that $F=a_s/a_r$, and if $a_s \simeq a_r$, $F \simeq 1$.

The experimental results in Table 1 determine a particular value of f_e . At the temperature at which the hyperfine structure is removed by exchange the exchange rate f_e must be comparable with the hyperfine splitting frequency.

In this case there are three sources of hyperfine splitting due to the three types of protons. It would be pointless to try to account for this in detail with the present theory and we shall use the apparent experimental splitting 8.1 Mc/s. With Pake and Tuttle we assume that f_e is about half this, i.e. 4 Mc/s. Hence at the temperature at which the structure disappears f_e is 4 Mc/s, and we calculate $f_e\eta/N_TkT$ and obtain the estimate of F given in Table 1 using Fig. 2.

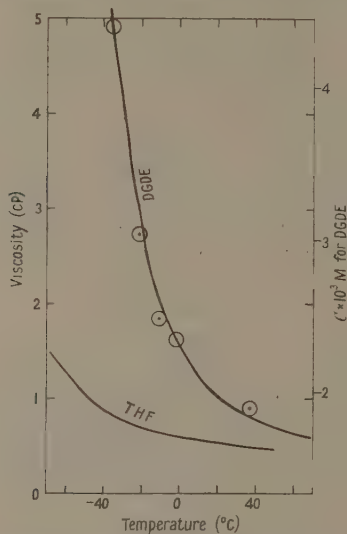


Fig. 2. The curves represent measured viscosity (left-hand ordinate) as a function of temperature for tetrahydrofuran and DGDE. The points show the exchange temperature (abscissa) as a function of ion concentration (right-hand ordinate) in DGDE.

F is indeed close to unity but it varies considerably with concentration although not as much as the viscosity itself. For solution in tetrahydrofuran F is considerably smaller than in DGDE. This difference is not explained by the change in the ratio a_s/a_r which we estimate from molecular volumes of the liquids to change only by the factor 0.75 from DGDE to tetrahydrofuran. It might be regarded as due to appreciable solvation in tetrahydrofuran giving an unexpectedly high a_r in this solvent. Pake and Tuttle find for DPPH in toluene $F=0.08$, whereas in this case $a_s/a_r \approx 0.6$. However, high concentrations of radical were used (140×10^{-3} M) and the possibility of multiple collisions cannot be excluded. For BPA in ethyl alcohol, Hausser's results give $F=8$, assuming the exchange temperature is -40°C , and his concentration is exactly 10^{-3} M—we suspect it might have been higher which would lower F .

According to Eqn (2) $\eta \propto CF$ at the exchange temperature where $C \propto N_T$ is the molar concentration. In fact, as shown in Fig. 2, the experimental relation between η and C for DGDE is $\eta = 1.6C - 2.1$. Unfortunately for tetrahydrofuran there is only one pair of values of η and C .

As pointed out by Pake and Tuttle, it is also interesting to study the narrowed line with hyperfine structure well removed since then we can again estimate f_e

through the relation (Kubo and Tomita 1954)

$$f_e \simeq \frac{\gamma}{2\pi} \frac{\Delta H_2^2}{\delta H}, \quad \dots\dots(3)$$

where γ is the electron spin gyromagnetic ratio, ΔH_2^2 is the second moment of the spectrum before exchange narrowing and δH is the line width. Thus a study of δH as a function of temperature also gives f_e , and hence together with η another check on the theory. We take $\Delta H_2^2 = 16$ gauss² for biphenyl, the experimental second moment of the hyperfine line before narrowing. F is given in Table 2. The value is again of order unity but higher than in Table 2. Part of the discrepancy may reside in the approximate relation (3) which, as shown by Kivelson (1960), depends on the situation by a factor 2 or more. Pake and Tuttle found $F = 0.13$ for DPPH in toluene at 28°C. The results of Hutchison, Pastor and Kowalsky (1952) for DPPH in benzene correspond to $F = 0.6, 2.9$, and 4.2 for 0.2, 0.02, and 0.0093 M respectively. We note that in our results F varies to a considerable extent with temperature, about as much as the viscosity itself. The change in F with solvent is in the correct direction and nearer to the expected change than found from the 'exchange temperature' (Table 1).

The estimated value of f_e from the exchange narrowing even at -62°C for the 4.3×10^{-3} M solution in tetrahydrofuran is 8 Mc/s. This is larger than the critical f_e of 4 Mc/s and so makes it clear why the hyperfine structure is still exchange narrowed even at this low temperature. It is also consistent with the observation of hyperfine structure over the whole temperature range below +50°C for a concentration of 3.3×10^{-3} M since f_e is sufficiently lower.

We conclude from the variation in the value of F , using our results as well as those of others, that the theory leaves a lot to be desired, as no doubt Pake and Tuttle would admit. Any attempt to put the theory on a sounder basis, particularly as regards the effectiveness and nature of the encounters in causing exchange narrowing, introduces considerable difficulties, as we see from Kivelson's (1960) rather inconclusive analysis of earlier results.

It ought to be less difficult to reduce the uncertainties associated with the calculation of the frequency of encounter by use of a measured self-diffusion coefficient and a closer study of the diffusion process. Alternatively the rate of radical motion might be more directly obtained from dielectric loss measurements of the polar solvents, as has been found profitable for the peroxyamine disulphonate ion in solution (Powles and Mosley 1961).

2.2. Anisotropy Broadening

The loss of hyperfine structure in the region of -70°C for solution in DGDE, as shown in Fig. 1(a), is we believe due to the anisotropic hyperfine interaction which above about -70°C is motionally averaged out to reveal the isotropic interaction only. Pake and Tuttle (1959) have explained similar effects observed by Hausser (1959) in this way. We have already (Powles and Mosley 1961), discussed a similar but rather more elaborate effect.

Following a similar motional narrowing calculation given by Bloembergen, Purcell and Pound (1948), we find for the anisotropic contribution δH_{aniso} to the line width arising from a rigid lattice contribution $\delta H_{\text{r.l.}}$ which is motionally narrowed by radical reorientation at rate ν_e ,

$$\delta H_{\text{aniso}} \simeq \delta H_{\text{r.l.}}^2 \frac{\sqrt{3}}{\pi^2} \gamma \nu_e^{-1}, \quad \dots\dots(4),$$

An independent estimate of ν_c is obtained by use of the formula for the Brownian reorientational motion of a spherical molecule in a viscous medium,

$$\nu_c = \frac{3kT}{8\pi^2\eta a_T^3} \quad \dots\dots (5)$$

Hence, using $\eta = 55$ *cp* (Fig. 2, extrapolated) at -70°C and $a_T \approx 3.2 \text{ \AA}$ (from the molecular volume of liquid biphenyl), we obtain $\nu_c \approx 60$ Mc/s at -70°C . When, as at this temperature, the isotropic hyperfine structure is just appearing we may assume $\delta H_{\text{anis.}} = \frac{1}{2}\delta H_{\text{iso}}$ and we recall that $\delta H_{\text{iso}} \sim 2.9$ gauss. Substituting these values in Eqn (4) gives $\delta H_{\text{t.t.}} \sim 4.3$ gauss. In other words the anisotropic and isotropic hyperfine interactions are comparable in magnitude. This seems a reasonable result.

§ 3. CONCLUSION

It is shown that the observed loss of structure at low temperatures of the hyperfine spin resonance spectrum of the biphenyl ion in DGDE, which is independent of ion concentration, may be due to anisotropic hyperfine interaction which suffers motional averaging and which is comparable in magnitude with the isotropic interaction. The loss of structure and the subsequent continued narrowing at high temperatures which are very concentration dependent are thought to be due to exchange effects. The results are broadly in agreement with the theory of Pake and Tuttle but show significant departures which have not been satisfactorily explained.

ACKNOWLEDGMENTS

The magnet used in these experiments was provided by the Department of Scientific and Industrial Research. Some of the microwave components were loaned by the Services Electronic Research Laboratory. Mr. J. Blackwell of our Chemistry Department suggested using DGDE.

REFERENCES

- BALK, P., HOLTHUIS, G. J., and SCHIFFERS, J. W. H., 1957, *Rec. Trav. Chim. Pays-Bas*, **76**, 813.
 BLOEMBERGEN, N., PURCELL, E. M., and POUND, R. V., 1948, *Phys. Rev.*, **73**, 679.
 DE HOER, W., 1956, *J. Chem. Phys.*, **25**, 190.
 HAWESER, K. H., 1959, *Nature*, **14a**, 428, and *Report of the 8th Colloque IMPERE*, p. 195.
 HUTCHINSON, C. A., PASTOR, R. C., and KOWALSKY, A. G., 1952, *J. Chem. Phys.*, **20**, 534.
 KAYLORON, D., 1960, *J. Chem. Phys.*, **33**, 1094.
 KURO, R., and TOMITA, K., 1954, *J. Phys. Soc. Japan*, **9**, 888.
 PAKE, G. E., and TUTTLE, T. R., 1959, *Phys. Rev. Letters*, **3**, 423.
 POWLES, J. G., and MOSLEY, M. H., 1961, *Proc. Phys. Soc.*, **77**, 729.
 PLYUNOVASS, L., 1950, *Physico-Chemical Constants of Pure Organic Compounds* (London: Elsevier).

Multiple Proton Magnetic Resonance Relaxation in a Number of Molecular Liquids

By J. G. POWLES AND D. J. NEALE

Physics Department, Queen Mary College, University of London

MS. received 1st February 1961

Abstract. Experimental results are given for the proton spin-lattice relaxation times T_1 at 47.5 Mc/s for liquid ethyl benzene, bromobenzene, chlorobenzene, fluorobenzene, benzene, aniline, paraxylene, mesitylene and methyl alcohol over the whole liquid range including some supercooling. Where more than one chemical type of proton is present the distinct T_1 values have been measured by a method described earlier this year by Powles and Neale. In ethyl benzene the ring proton T_1 has a minimum but the ethyl proton T_1 does not (as reported by Powles and Neale for toluene), thus emphasizing the difference in their nature. Motional correlation frequencies are deduced from the T_1 values. In ethyl benzene and aniline the substituent correlation frequency agrees with the dielectric correlation frequency. Methyl alcohol is different. The predicted ring proton correlation frequencies are lower to an extent which depends on the particular molecule and on the interpretation adopted. The results are related to shear viscosity data. $\eta T_1/T$ should not depend on temperature but does, in a way depending on the molecule and on the individual value of T_1 . Thus the introduction of the viscosity in this way is not very helpful.

It is concluded that in these liquids composed of non-spherical molecules the thermal molecular motions are complex, including motion about different axes at different rates. This complexity should be borne in mind when considering other motionally dependent properties of liquids.

§ 1. INTRODUCTION

NUCLEAR magnetic resonance relaxation times can give information about thermal motions. This is because the relaxation is often due to direct dipolar interactions between the magnetic nuclei which are modulated by the random thermal motions. For two or more magnetic nuclei in a molecule the internuclear distance is usually fixed, but the reorientational molecular motion varies the angle which the line joining them makes with the externally applied static magnetic field. In some cases the molecule also has internal flexibility, and then intramolecular magnetic interactions are modulated in this way also. The latter affects the relaxation times in ethyl benzene for instance. Interactions between magnetic nuclei in different molecules also contribute to the relaxation, and so diffusional or translational molecular motion can be investigated. It is desirable in interpreting magnetic resonance data in terms of molecular motion to have independent information, and we use, where appropriate, the dielectric loss correlation frequencies. These indicate directly

the motion of the electric dipolar vector. We also consider the relation of our results to shear viscosity data.

We have again (Powles and Neale 1961) taken molecules with more than one chemical type of proton and the several relaxation times must be interpreted. It is necessary to postulate rather complex motions of the molecules in the liquid.

§ 2. EXPERIMENTAL TECHNIQUE AND RESULTS

The proton magnetic resonance spin-lattice relaxation times T_1 have been measured by a method described earlier (Powles and Neale 1961, to be referred to as I). In this method the proton resonance signal in a moderately high resolution apparatus is saturated by a strong radio-frequency field at resonance, and the recovery after removal of this field is monitored by means of a weak radio-frequency field and appropriate field sweep. When only one chemical type of proton is present the method has no particular advantage over pulse methods (Carr and Purcell 1954), but we have nevertheless used it to measure benzene and its monohalogen derivatives (Fig. 4). When more than one type of chemically shifted proton is present the method has considerable advantage over other transient methods since the signal from each type of proton may be observed separately and its relaxation behaviour studied. As for toluene (see I), we find in all cases that the relaxation of chemically different sets of protons is distinct in the sense that the recovery of one set appears to be independent of what is done to any other, and it is in all cases exponential. We therefore report a T_1 value as a function of temperature for each type of proton. In many cases the several T_1 's are very different in magnitude and behave differently with temperature.

The measurements were made at 47.5 Mc/s. The accuracy of measurement of T_1 is to about $\pm 7\%$ for the longer T_1 's, depreciating to about $\pm 15\%$ for the shorter ones. The materials were Analar grade and were fractionally distilled and purified. Dissolved atmospheric oxygen was removed by a freeze-pump-thaw technique or by a sintered disk method. Contamination by oxygen is readily detected (see I). Measurements were made to within a few degrees of the boiling point at atmospheric pressure and in most cases well below the melting point by careful supercooling. The actual T_1 values varied from 0.2 to 50 seconds.

Shear viscosity values over the required temperature range were not available in the literature. The literature values were checked and the temperature range extended where necessary by means of a thermostatically controlled Ostwald viscometer. Our values agreed with the literature values to $\pm 5\%$ but at low temperatures they are less accurate, possibly to $\pm 10\%$.

§ 3. DISCUSSION OF THE RESULTS

There is little doubt that the observed spin-lattice relaxation times are mainly due to direct magnetic dipole-dipole interaction modified by the thermal motion. The results are analysed in much the same way as for toluene (see I) but in less detail since the procedure and its limitations were discussed for that liquid.

Valuable auxiliary information about molecular motion is obtainable from dielectric relaxation correlation times. However, for most of our substances this information is lacking or fragmentary and we shall use shear viscosity data to some extent. The latter are more readily available but are less desirable, shear

viscosity being a rather indirect method of obtaining information about molecular motion as is magnetic resonance itself.

A satisfactory study of molecular motion by magnetic resonance demands more information than we have, for example, T_1 as a function of resonance frequency and the T_2 values, but it is worth making a preliminary analysis with the present data.

Present theories of magnetic resonance relaxation are not adequate to deal with the complex situations encountered here but we use the following formula (based on Bloembergen, Purcell and Pound 1948, Solomon 1955, Kubo and Tomita 1954, Skrotskii and Kokin 1959, Powles and Neale 1961)

$$\frac{1}{T_1} = \frac{3}{10} \frac{1}{2\pi\nu_r} \gamma^4 \hbar^2 \left[\frac{2}{n_g} \sum_{i>j} d_{ij}^{-6} + \frac{6}{5} \pi \frac{n_m}{2} N_0 a^{-3} \right] f\left(\frac{\nu_r}{\nu_c}\right), \quad \dots\dots (1)$$

where

$$f\left(\frac{\nu_r}{\nu_c}\right) = \frac{\nu_r/\nu_c}{1 + (\nu_r/\nu_c)^2} + \frac{4\nu_r/\nu_c}{1 + (2\nu_r/\nu_c)^2},$$

ν_c is the motional correlation frequency, $1/(2\pi\tau_c)$, ν_r the resonant frequency (47.5 Mc/s), γ the proton gyromagnetic ratio, d_{ij} the interproton distances within a molecule, N_0 the number of molecules per cubic centimetre, n_m the number of protons per molecule, n_g the number of protons in the group being considered, and a an effective radius of the diffusing molecule. According to Skrotskii and Kokin (1959) the second term in square brackets in (1) is only valid for $\nu_c > \nu_r$, but this condition will usually be satisfied and in any case it is only applicable to pairs of protons. We have generalized this term from a pair to n_m protons by the factor $n_m/2$ which is no doubt inexact but makes some allowance for the fact that there are more than two protons per molecule. It will be shown that this external term is usually smaller than the first, although by no means negligible, in the present substances. It is more important for the ring than for the substituent protons.

The first term in Eqn (1) for a pair of protons at fixed separation d is known to be d^{-6} (Solomon 1955), and to a good approximation for a trio of protons disposed on an equilateral triangle of side d (Hubbard 1958) it is $2d^{-6}$. For four protons arranged tetrahedrally it is $\frac{3}{2}d^{-6}$. In other cases we use the expression $(2/n_g)\sum_{i>j} d_{ij}^{-6}$ which gives the above particular results and which appears in the computation of the rigid lattice second moment for a 'powder' sample (Van Vleck 1948). It surely shows the correct trend. An alternative formula proposed by Gutowsky and Woessner (1956) has $\frac{1}{2}\sum_{ij} r_{ij}^{-6}$ in place of $(1/n_g)\sum_{i>j} r_{ij}^{-6}$. This has the disadvantage that it depends on the nucleus chosen for groups where all r_{ij} are not equal.

We have in addition to allow for different magnetic nuclei, e.g. ^{19}F in fluorobenzene, by additional terms which however will prove to be small. We have also to allow for the effect of non-resonant protons when two or more chemically shifted sets are present. It is suggested in I that their contribution to relaxation is reduced as compared with that from resonant nuclei. It is necessary, further, to allow for complex molecular motion not described by a single ν_c , and then Eqn (1) will be generalized as in I. Also the correlation frequency for intermolecular interaction is not necessarily the same as for intramolecular since it depends more on translational than reorientational motion.

In the absence of better information we shall usually assume that the two correlation frequencies are the same, to the extent implied by Eqn (1).

We first establish the order of magnitude of the terms in Eqn (1). In benzene and the benzene derivatives studied here N_0 ranges from $7 \times 10^{21} \text{ cm}^{-3}$ for benzene to $4 \times 10^{21} \text{ cm}^{-3}$ for mesitylene. We shall assume that $(2a)^3$ is the available volume per molecule, i.e. $(2a)^3 = N_0$. Hence

$$\frac{6}{5} \frac{\pi n_m}{2} N_0 a^{-3} \simeq 3 \times 10^{-3} \text{ \AA}^{-6}.$$

For a methyl group $(2/n_g) \sum_{i,j} d_{ij}^{-6} = 63 \times 10^{-3} \text{ \AA}^{-6}$ and for the six protons in benzene $9.2 \times 10^{-3} \text{ \AA}^{-6}$. Hence the external term is less than the internal although its exact value is rather uncertain. This external term should also probably suffer reduction by a factor for molecules with more than one type of proton (see I). The argument that the intermolecular contribution is the minor one is somewhat reinforced by measurements on proton containing molecules in solution in a proton-free solvent. However, solution may change the molecular correlation frequencies and even the type of motion. The former may be allowed for to some extent by use of shear viscosity (see §3.1). An analysis by Bovey (1960)[†] suggests that the intermolecular contribution is probably not more than 50% of the total interaction even in the case of benzene where inter- and intramolecular proton distances are comparable. Our rough calculation based on Eqn (1) gives 30% for benzene. A rather more elaborate analysis of solution results by Mitchell and Eisner (1960) using viscosity still, in our opinion, does not clear up this difficulty. A more reliable test would be to compare the pure liquid T_1 's with those for dilute solution in the perdeutero compound. It would then be reasonable to suppose that the molecular motion and the correlation frequencies would be little affected, and so parameters for the pure normal liquid would be obtained.

In the absence of anything better, we shall usually suppose the external interaction to make a minor contribution to $1/T_1$. In that case Eqn (1) can be written

$$\frac{1}{T_1} = \frac{I}{\nu_r} \frac{1}{1.42} f\left(\frac{\nu_r}{\nu_c}\right), \quad \dots\dots (2)$$

where

$$I = 1.42 \times \frac{3}{10} \frac{1}{2\pi} \gamma^4 \hbar^2 \frac{2}{n_g} \sum_{i>j} d_{ij}^{-6}$$

and hence $I/\nu_r = 1/T_{1 \text{ min}}$. The symbol I is introduced to express the theoretical interaction and distinguish it from the experimental quantity $1/T_{1 \text{ min}}$ which may or may not be available and is not always to be taken as I/ν_r . Also, of course, I/ν_r may depend on temperature.

3.1. Ethyl Benzene

We consider ethyl benzene ($\text{C}_6\text{H}_5\text{C}_2\text{H}_5$) first since its molecular structure is rather similar to that of toluene ($\text{C}_6\text{H}_5\text{CH}_3$, see I). It will also facilitate the interpretation of the results for the monohalogen substituted benzenes which

[†] N.B. The title of this article is a statement of the problem, not the conclusion reached.

might appear to be simpler cases to deal with first. The T_1 values for ethyl benzene in Fig. 1 are similar to those of toluene in that the ethyl group signal

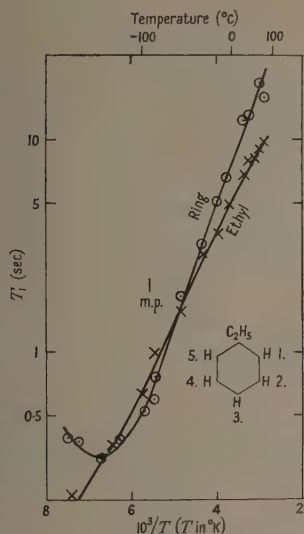


Fig. 1. Proton spin-lattice relaxation times at 47.5 Mc/s for the ethyl and ring protons in liquid ethyl benzene.

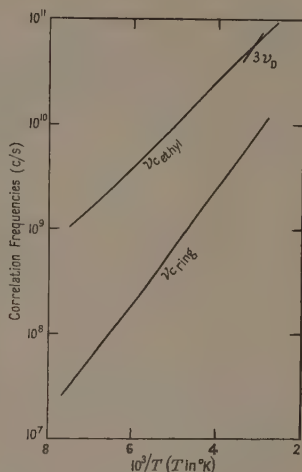


Fig. 2. Correlation frequencies for ethyl benzene deduced from the proton magnetic relaxation times, as described in the text. ν_D is the dielectric correlation frequency (Petro and Smyth 1957).

has no minimum in the available temperature range whereas the ring proton signal does. We were not able to resolve the methyl and methylene proton signals and so $T_{1\text{ethyl}}$ is a composite T_1 . Probably $T_{1\text{methyl}}$ and $T_{1\text{methylene}}$ do not differ much. The minimum of $T_{1\text{ring}}$ is 0.32 sec whereas it was 1.42 sec in toluene. Neglecting the external interaction we find from $T_{1\text{min}}$ and Eqn (2), $I/\nu_r = 3.1 \text{ sec}^{-1}$ and $\nu_c = 1.62\nu_r = 77 \text{ Mc/s}$ at 148°K. Using this value of I in Eqn (2) and assuming that I is independent of temperature, we find $\nu_{c\text{ring}}$ as a function of temperature as shown in Fig. 2.

For $T_{1\text{ethyl}}$ we must calculate I . The weighted mean value of $(2/n_g)\sum_{i>j} d_{ij}^{-6}$ for the two groups is $50.3 \times 10^{-3} \text{ Å}^{-6}$, so that $I/\nu_r = 41 \text{ sec}^{-1}$ and $\nu_{c\text{ethyl}}$ obtained from Eqn (2) is given in Fig. 2. The dielectric correlation frequency ν_D is also given in Fig. 2 (Petro and Smyth 1957) plotted as $3\nu_D$ which is probably to be compared with ν_c (Bloembergen, Purcell and Pound 1948). ν_D is only available over the temperature range 20°C to 60°C.

When $\nu_c \gg \nu_r$ we expect $T_1 \propto \nu_c$ from Eqn (1) and possibly $T/\eta \propto \nu_c$ in view of the Stokes-Einstein relation (see Eqn (3)). Some authors therefore consider whether $\eta T_1/T$ is independent of temperature. This function is given in Fig. 3 for the T_1 's of ethyl benzene and shows a considerable variation with temperature,

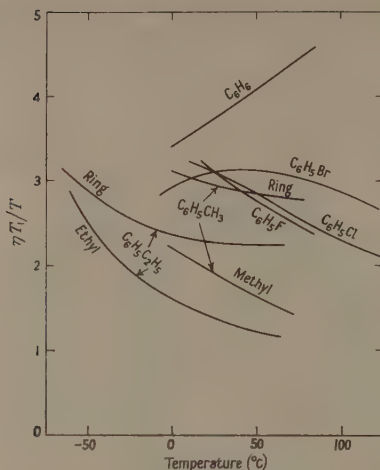


Fig. 3. The dependence of $\eta T_1/T$ on temperature for ethyl benzene for the ring and ethyl protons. Also similar data for toluene (from I), benzene, fluorobenzene, chlorobenzene and bromobenzene (using Fig. 4). η is the shear viscosity, T the absolute temperature.

especially at low temperatures. This may be contrasted with the case of *n*-octyl bromide (Powles and Hartland 1960) and with water (Simpson and Carr 1958) where $\eta T_1/T$ varies much less. It is well known that this use of viscosity tends to be more valid for low viscosity liquids than for high viscosity, and the tendency for $\eta T_1/T$ to vary less with temperature at high temperatures may be related to this fact. The greater constancy of $\eta T_1/T$ for the ring protons could mean that the ring motion is the more closely related to viscosity.

An apparent radius of the moving entity may be deduced from the viscosity and the nuclear correlation time through the appropriate Einstein-Stokes formula,

$$a^3 = \frac{3k}{8\pi^2\nu_c} \frac{T}{\eta}. \quad \dots\dots(3)$$

This gives at 25°C, $a = 1.8 \text{ \AA}$ from $\nu_{c \text{ ethyl}}$ and $a = 3.5 \text{ \AA}$ from $\nu_{c \text{ ring}}$. The effective molecular radius deduced from the density is 3.0 \AA . The van der Waals dimensions of the ethyl group and of benzene are approximately 1.8 \AA and 2.3 \AA assuming approximate enclosing ellipsoids (Perrin 1934). There is a temptation therefore to think that the ethyl group and the whole molecule move almost independently as bodies of appropriate size. However, a similar calculation for toluene gives similar results, but it is not reasonable that the motion of the methyl group and the molecule should be independent (except for methyl C_3 reorientation which has special effects). For this reason this explanation of the difference in correlation frequencies was not proposed in I and is not considered a likely explanation here.

Figure 2 shows that there is a close correspondence between $3\nu_D$ and $\nu_{c \text{ ethyl}}$. This is very satisfactory since the ethyl group carries the electric dipole. We

doubt if the difference in rate of variation of $3\nu_D$ and $\nu_{\text{c ethyl}}$ with temperature seen in Fig. 2 is significant since the results of Petro and Smyth (1957) showed a similar divergence for toluene and differed in this respect from other dielectric measurements.

It seems unlikely that $\nu_{\text{c ethyl}}$ should fall at a lower rate with falling temperature. The low temperature value is perhaps beginning to be affected by the methyl C_3 reorientation as well as that of the ethyl group as a whole. This would be readily investigated by an extension of the dielectric loss measurements to lower temperatures. A similar but not identical conclusion was reached for toluene and an analysis similar to that given here could be carried out.

As with toluene, $\nu_{\text{c ring}}$ is considerably less than $\nu_{\text{c ethyl}}$ over the whole temperature range. For the ring protons, even without external interactions, $I/\nu_r = 6.0 \text{ sec}^{-1}$ whereas the experimental value from the minimum of $T_{1 \text{ ring}}$ and Eqn (2) is 3.1 sec^{-1} . To explain a similar but much larger discrepancy in I/ν_r for the ring protons in toluene as well as a similar but larger difference between $\nu_{\text{c substituent}}$ and $\nu_{\text{c ring}}$, we suggested a rather complex motion of the toluene molecule. We suggest that for ethyl benzene we ought to consider the two most important motions to be firstly reorientation of the ethyl group about the bond joining it to the ring and secondly reorientation of the ring about its ' C_2 ' axis. Reorientation about a ' C_6 ' axis (perpendicular to the ring) may be relatively less important than in toluene owing to the obstruction of the much larger ethyl group. These assumptions explain the basic facts. The agreement of $3\nu_D$ and $\nu_{\text{c ethyl}}$ is expected because the motion of the dipole is essentially the same as that of the ethyl protons. The slower motion C_2 and possibly C_6 will not affect either to any extent. If the C_2 motion controls $\nu_{\text{c ring}}$ the theoretical value of I/ν_r is smaller than that given above because the interactions of ring protons 1 and 2 and 4 and 5 in Fig. 1 are not modulated by the motion and so contribute little to T_1 . Interactions 1 and 3 and 1 and 4 are reduced in effective contribution to T_1 . A revised estimate of I/ν_r is 4.2 sec^{-1} which is closer to the observed value 3.1 sec^{-1} . This argument demands some reconsideration of the external interaction since it could be that the translational motion of the molecules is associated with $\nu_{\text{c ring}}$ rather than $\nu_{\text{c ethyl}}$. This is only important for $\nu_{\text{c ethyl}}$ and increases the contribution from the external interaction by $\nu_{\text{c ethyl}}/\nu_{\text{c ring}} \simeq 6$ at 25°C (since $\nu_{\text{c}} \gg \nu_r$). The two terms in Eqn (1) would therefore be 50.3 and 18, so that the external interaction is still the less important one for the ethyl protons within the approximation of this analysis. The comparison for the ring protons remains unaffected. Even a serious underestimation of the external interaction for the ring protons could not explain the difference between $\nu_{\text{c ethyl}}$ and $\nu_{\text{c ring}}$.

The difference between $\nu_{\text{c ethyl}}$ and $\nu_{\text{c ring}}$ can be explained in a number of ways. We have already mentioned the viscous reorientation of a quasi-independent ethyl group. We have given a detailed discussion of the difference in the ν_{c} 's for toluene (I). Since the present case is no more conclusive we shall not reproduce the arguments here. A worth-while analysis awaits a much more thorough knowledge of liquids and a more detailed knowledge of the nuclear resonance parameters.

We emphasize that the motions we consider are a first approximation to the actual motion of the molecules but that they should be seriously considered in any explanation of transport, and possibly other, properties of this liquid.

3.2. Fluorobenzene, Chlorobenzene and Bromobenzene

The T_1 values for the ring proton are given in Fig. 4. Although the liquids were supercooled to a considerable extent no minimum in T_1 was attained.

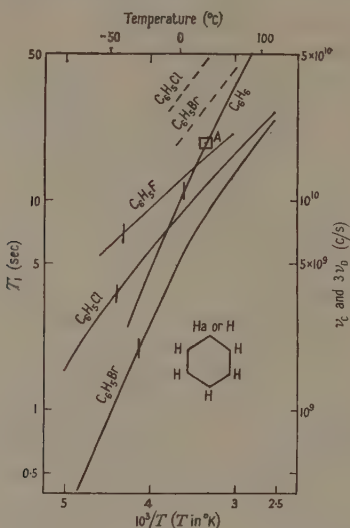


Fig. 4. Proton spin-lattice relaxation times for liquid benzene, fluorobenzene, chlorobenzene and bromobenzene. The right-hand scale indicates estimated values of ν_c (except for benzene). Values of $3\nu_D$ (broken lines) are also given for chlorobenzene and bromobenzene. $T_1 = 19$ sec at 25°C for benzene (A) is widely reported in the literature. Vertical bars on curves indicate the melting temperature.

We therefore assume $\nu_c \gg \nu_r$ and take the calculated value (§ 3.1) $1/\nu_r = 6.0 \text{ sec}^{-1}$. Hence from Eqn (2), $\nu_c = 10^9 T_1$ and this scale is given on the right-hand ordinate in Fig. 4. Since all three molecules are polar we can again compare ν_c and $3\nu_D$, although ν_D is only available in a small temperature range near room temperature. Values of $3\nu_D$ for bromo- and chlorobenzene (Branin and Smyth 1952, Hennelly, Heston and Smyth 1948) are given in Fig. 4. The only available value for fluorobenzene is $3\nu_D = 8.6 \times 10^{10} \text{ c/s}$ at 21°C (Poley 1955). $3\nu_D$ is much larger than $\nu_{c \text{ ring}}$. At 21°C in particular, $3\nu_D/\nu_c = 5.5$, 4.0 and 3.3 for fluoro-, chloro- and bromobenzene respectively. In view of the analysis presented for toluene and ethyl benzene and remembering that ν_D refers to the reorientation of the ring to halogen bond while ν_c refers to the reorientation of the ring, we conclude that these differences are significant. (For toluene and ethyl benzene where a minimum is attained, the experimental value of $1/\nu_r$ is less than 6.0 sec^{-1} . For the benzene ring protons and monohalogen benzenes with a lower density of protons it should be even lower. The difference between $3\nu_D$ and ν_c may therefore be even greater than given above.) We conclude that the motion of these molecules is also complex, although the data given here hardly warrant an elaboration of this statement.

Chlorobenzene should perhaps be rather similar to toluene in view of the comparable size of the chlorine atom and the methyl group. We were unable

to supercool chlorobenzene sufficiently to attain a minimum of $T_{1\text{ ring}}$. However, the lowest observed value of $T_{1\text{ ring}}$ is 1.5 sec and so the minimum must certainly be below the value 1.4 sec observed in toluene, in spite of the lower proton concentration. Toluene and chlorobenzene do not therefore seem obviously similar. For bromobenzene the lowest value of T_1 is 0.45 sec, i.e. well below the minimum value for toluene and only just above the minimum for ethyl benzene. Bromobenzene may therefore be comparable with ethyl benzene and it may be the bulky substituent which gives this result.

Further information about fluorobenzene is obtainable from a study of the relaxation of the ^{19}F nucleus. Owing to the weakness of the signal we were unable to do more than confirm that T_1 for ^{19}F does not differ greatly from the proton T_1 .

3.3. Benzene

We also give in Fig. 4 our results for benzene itself. One might have expected a uniform gradation from bromobenzene through chlorobenzene and fluorobenzene to benzene, but in fact benzene is very different. This is not due specifically to the effect of the extra proton since this only increases I/ν_r by the factor 1.25, but it may well be associated with the increase in symmetry. This peculiarity of benzene as compared with substituted benzenes does not appear in the shear viscosity. $\eta T_1/T$ for benzene in Fig. 3 shows a strong *rise* with temperature. To our knowledge this has not been reported before. Bromobenzene shows a maximum of $\eta T_1/T$. Chlorobenzene and fluorobenzene show a fall with temperature. Such behaviour emphasizes the lack of direct correlation between T_1 and η and is no indication of where the peculiarity lies. It should be recalled that for benzene the external interaction makes a large contribution to T_1 and so the relaxation may be controlled to a much greater extent by the translational motion. If this is so it is even more surprising that $\eta T_1/T$ should be anomalous since the viscosity is surely more dependent on translational than reorientational motion. Our experience with toluene suggests that the C_6 motion of benzene is faster than the C_2 motions but the present results hardly warrant an elaboration of this point of view.

3.4. Aniline

In aniline ($\text{C}_6\text{H}_5\text{NH}_2$) the substituent carries only a pair of protons and the dipole moment partially reorients with them. The T_1 values are quite different from those of toluene and ethyl benzene in that the substituent T_1 is lower than the ring T_1 over the whole temperature range. Proceeding as usual we take $I/\nu_r = 40 \text{ sec}^{-1}$ for the NH_2 group, assuming $\text{H-H} = 1.64 \text{ \AA}$ and $I/\nu_r = 6.0 \text{ sec}^{-1}$ for the ring protons, which gives $\nu_{\text{amide}} = 6.7 \times 10^9 T_{1\text{amide}}$ and $\nu_{\text{ring}} = 10^9 T_{1\text{ring}}$ since evidently $\nu_{\text{e}} \gg \nu_r$. From Fig. 5 $T_{1\text{ring}}/T_{1\text{amide}} = 2.8$ at -15°C and 1.5 at $+107^\circ\text{C}$. Hence $\nu_{\text{amide}} \simeq 3\nu_{\text{ring}}$ over the whole temperature range. At 20°C $\nu_{\text{amide}} = 1.3 \times 10^{10} \text{ c/s}$ and this agrees quite well with the dielectric correlation frequency, $3\nu_{\text{D}} = 2.4 \times 10^{10} \text{ c/s}$ at 20°C , the only value available (Fischer 1949). The rather small factor between ν_{amide} and ν_{ring} and the uncertainty in the I/ν_r values we have used makes the simplest interpretation that the ring and amide group motions are essentially similar. Rapid reorientation of $-\text{NH}_2$ may be inhibited by weak hydrogen bond formation. The latter may be associated with the unusually high viscosity of this liquid.

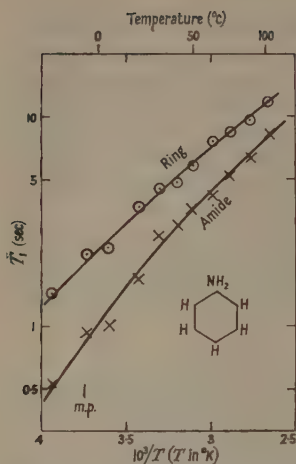


Fig. 5. Ring and substituent proton spin-lattice relaxation times for liquid aniline.

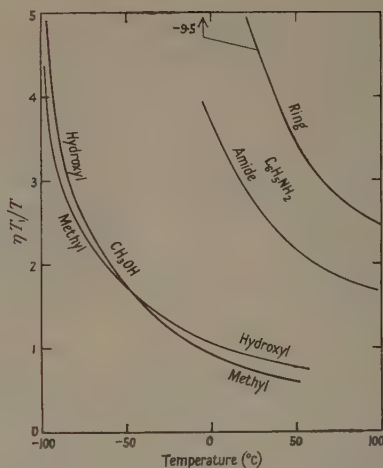


Fig. 6. $\eta T_1/T$ as a function of temperature for aniline and methyl alcohol.

An alternative explanation is that the dielectric correlation frequency corresponds to reorientation of the NH_2 group about the C-N bond. Suppose also that the molecule as a whole reorients and then the appropriate I/ν_r value for the NH_2 group would be reduced by a factor about $\frac{1}{4}$ and $T_{1\text{amide}}$ is then controlled by the molecular motion. In that case we find $\nu_{\text{amide}} \simeq \nu_{\text{ring}}$ together with $3\nu_D \simeq 7\nu_{\text{amide}}$ in agreement with the hypothesis. A choice between these alternative explanations is difficult. It is again unfortunate that the lack of a minimum prevents an experimental evaluation of the magnetic interaction. $\eta T_1/T$ is given in Fig. 6 and shows a strong dependence on temperature.

3.5. Paraxylene and Mesitylene

The results for paraxylene ($\text{C}_6\text{H}_4(\text{CH}_3)_2$) and mesitylene ($\text{C}_6\text{H}_3(\text{CH}_3)_3$) are shown in Figs 7 and 8. (Note the difference in temperature scale.) Our values agree with those of Nederbragt and Reilly (1956) at 25°C. Both molecules have zero dipole moment and so dielectric correlation frequencies are not available.

The results for paraxylene are more like those for ethyl benzene than those for toluene, while those for mesitylene are similar to those for aniline. In paraxylene the behaviour of the ring and methyl protons is very different and we feel must correspond to different correlation times and different motions. In view of the symmetry of the molecule it is tempting to suppose that the ring proton T_1 is related to reorientation about what may be called the C_2 axis. This corresponds to a weak interaction since the ring proton's principal interactions are not modulated by this motion.

In contrast with ethyl benzene and toluene (Fig. 3) the value of $\eta T_1/T$ is less dependent on temperature for substituent rather than the ring proton T_1 (Fig. 9). The latter is like that of benzene.

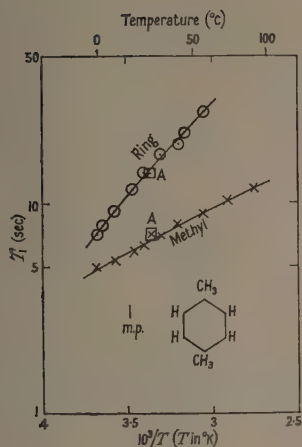


Fig. 7. Proton spin-lattice relaxation times for liquid paraxylene. A, results due to Nederbragt and Reilly (1956).

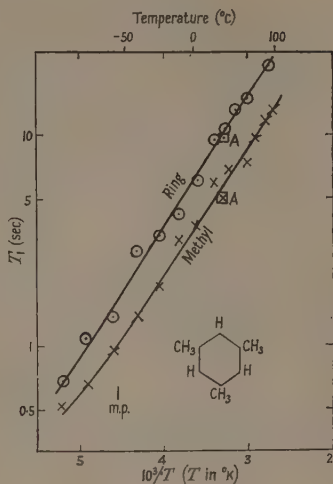


Fig. 8. Proton spin-lattice relaxation times for liquid mesitylene. A, results due to Nederbragt and Reilly (1956).

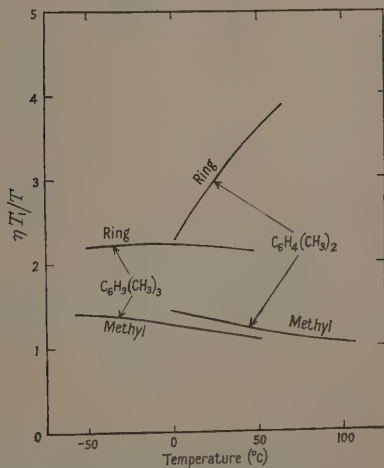


Fig. 9. $\eta T_1/T$ as a function of temperature for paraxylene and mesitylene.

For mesitylene there is even greater difficulty in estimating the interaction of the ring protons. For the methyl protons the I/ν_r value associated with the isolated methyl group is 52 sec^{-1} . In this molecule the interaction between ring and methyl protons in the same molecule must surely be important although

we have not observed any interaction between the relaxation of the two systems of protons (see I and Solomon 1955). The sum $(2/n_g)\sum_{i>j} d_{ij}^{-6}$ for the ring protons, including interactions with methyl protons, is $11 \times 10^{-3} \text{ \AA}^{-6}$; without the methyls it is only $1.5 \times 10^{-3} \text{ \AA}^{-6}$. Thus if the ring and methyl protons are affected by the same motion and interact like resonant systems we would expect $T_{1 \text{ ring}}/T_{1 \text{ methyl}} \simeq 52/11 = 4.7$. Experimentally (Fig. 8) this quantity varies between 1.4 and 1.8. We suggest therefore that the ring and methyl proton correlation times do not differ substantially. This does not exclude a complex motion for the molecule but the nuclear resonance parameters are not sensitive to it.

It is tempting to favour easy reorientation about an axis perpendicular to the ring but there is no direct evidence for this.

3.6. Methyl Alcohol

We give finally some results for a sample of methyl alcohol. These are of interest because although the T_1 values for the hydroxyl and the methyl protons

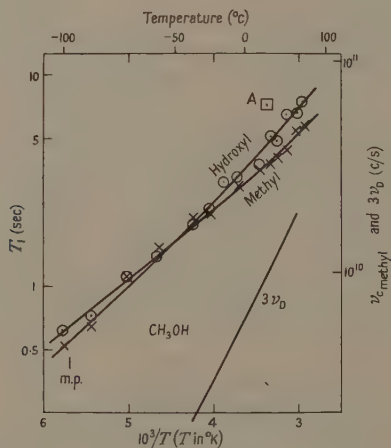


Fig. 10. Proton spin-lattice relaxation times for a sample of liquid methyl alcohol. The right-hand ordinate shows an estimate of $\nu_{\text{c methyl}}$ and provides a scale for the dielectric correlation frequency $3\nu_D$ (Poley 1955). A, value reported by Bonera *et al.* (1960).

are very close they are nevertheless different. The largest ratio of the two which we find is 1.3 and would be extremely difficult to detect by the usual transient methods (see for example Bonera *et al.* 1960). In this liquid we have hydroxyl proton exchange and a J-type interaction between the two sets of protons, which at low temperatures is not averaged out in this sample (Powles and Hartland 1961). These may be rather dependent on sample purity. The result of Bonera *et al.* (1960) at a single temperature differs from ours.

Because of the strong interaction within the methyl group we consider using the I/ν_I value for an isolated methyl group, i.e. 52 sec^{-1} , and hence

$\nu_{\text{cmethyl}} = 8.6 \times 10^9 T_1$ (since $\nu_e \gg \nu_r$). This scale is indicated on the right-hand ordinate of Fig. 10. Hence ν_{cmethyl} is greater than $3\nu_D$. On the other hand if we assume fast reorientation of the methyl group, the interaction parameter for reorientation of its axis is a factor approximately $\frac{1}{4}$ smaller and so ν_{cmethyl} is brought closer to $3\nu_D$ at least at high temperatures. However, then the large external interaction of about 11 sec^{-1} (see below) becomes important. The divergence at low temperatures may be associated with the modulated J-type interaction and should be investigated in conjunction with the high resolution spectrum.

For the hydroxyl proton, in view of the exchange, the interaction might be given by the external interaction term only of Eqn (1). For methyl alcohol the proton density is high and this gives $1/\nu_r = 11 \text{ sec}^{-1}$. Hence $\nu_{\text{c hydroxyl}}/3\nu_D \sim 1$ at 25°C which is satisfactory since the main electric dipole moves with OH. However this agreement is again lost with falling temperature possibly because of the J interaction with the methyl group.

For *n*-octyl alcohol it has been suggested (Powles and Hartland 1960) that the hydroxyl proton moves more slowly than the chain because of hydrogen bonding. A similar argument could be used here but the faster motion of the methyl group would be C_3 reorientation. No higher frequency secondary dielectric relaxation has been observed in methyl alcohol which could be associated with our ν_{cmethyl} .

§ 4. CONCLUSIONS

We have shown that the differences between the spin-lattice relaxation times for different chemical types of proton in the same molecule in several liquids are quite marked. Their interpretation forces us to the conclusion that the thermal motions of non-spherical molecules in these liquids are not simple and that the rate of motion about different axes may be very different. Little information is obtained about translational molecular motion. In some cases the molecule has internal flexibility, and the effect of this on the relaxation times has been discussed. The motional parameters obtained agree where expected in a satisfactory way with the dielectric correlation frequencies except in the case of methyl alcohol. These measurements show the way for a more extensive study of molecules of various shapes and flexibilities. They show in particular the value of being able to study the motion of different parts of a complex molecule in elucidating its mode of motion in the liquid state.

ACKNOWLEDGMENTS

The magnet used in these investigations was provided by the Department of Scientific and Industrial Research who also provided a grant for one of us (D. J. N.). The Central Research Fund of the University of London provided a pen-recorder.

REFERENCES

- BLOEMBERGEN, N., PURCELL, E. M., and POUND, R. V., 1948, *Phys. Rev.*, **73**, 679.
BONERA, G., CHIODI, L., LANZI, G., and RIGAMONTI, A., 1960, *Report of 9th Colloque AMPERE* (Geneva: Institut de Physique), p. 445.
BOVEY, F. A., 1960, *J. Chem. Phys.*, **32**, 1877.
BRANIN, F. H., and SMYTH, C. P., 1952, *J. Chem. Phys.*, **20**, 1121.

- CARR, H. Y., and PURCELL, E. M., 1954, *Phys. Rev.*, **94**, 630.
FISCHER, E., 1949, *Z. Phys.*, **127**, 49.
GUTOWSKY, H. S., and WOESSNER, D. E., 1956, *Phys. Rev.*, **104**, 843.
HENNELLY, A. D., HESTON, W. M., and SMYTH, C. P., 1948, *J. Amer. Chem. Soc.*, **70**, 4102.
HUBBARD, P. S., 1958, *Phys. Rev.*, **109**, 1153.
KUBO, R., and TOMITA, K., 1954, *J. Phys. Soc. Japan*, **9**, 888.
MITCHELL, R. W., and EISNER, M., 1960, *J. Chem. Phys.*, **33**, 86.
NEDERBRAGT, E. W., and REILLY, C. A., 1956, *J. Chem. Phys.*, **24**, 1110.
PERRIN, F., 1934, *J. Phys. Radium*, (7), **5**, 497.
PETRO, A. J., and SMYTH, C. P., 1957, *J. Amer. Chem. Soc.*, **79**, 6142.
POLEY, J. P., 1955, *Appl. Sci. Res., Hague*, **4B**, 337.
POWLES, J. G., and HARTLAND, A., 1960, *Proc. Phys. Soc.*, **75**, 617.
— 1961, *Proc. Phys. Soc.*, **77**, 273.
POWLES, J. G., and NEALE, D. J., 1961, *Proc. Phys. Soc.*, **77**, 737.
SIMPSON, J. H., and CARR, H. Y., 1958, *Phys. Rev.*, **111**, 1201.
SKROTSKII, G. V., and KOKIN, A. A., 1959, *Soviet Physics-J.E.T.P.*, **36**, (9), 335.
SOLOMON, I., 1955, *Phys. Rev.*, **99**, 559.
VAN VLECK, J. H., 1948, *Phys. Rev.*, **74**, 1168.

The Magnetoelastic Constants of Nickel

By E. W. LEE† AND R. R. BIRSS‡

† Department of Physics, The University, Sheffield

‡ Department of Physics, Imperial College, London, S.W.7 §

M.S. received 17th March 1961

Abstract. The magnetoelastic constants of nickel are calculated from the magnetostriction constant measured by Birss and Lee in 1960 and elastic constants measured by Alers, Neighbours and Sato in 1960. It is shown that the temperature variation of these magnetoelastic constants is in good agreement with the theory proposed by Kittel and Van Vleck in 1960. According to this theory the magnetoelastic constants depend upon the magnitude of the spontaneous magnetization. This may be increased slightly by a large magnetic field and it is shown that the theory explains, in principle, the origin of the forced magnetostriction.

§ 1. INTRODUCTION

IN a recent paper (Birss and Lee 1960) we reported measurements of the magnetostriction constants of nickel from the liquid nitrogen temperature up to the Curie point. As we remarked at the time, the magnetostriction constants by themselves do not provide information likely to be of interest to the theorist. What is really required is information on the magnetoelastic constants, which can be derived from the magnetostriction constants only if the elastic constants are also known. At the time our paper was written these were not known for nickel except at room temperature and the discussion of our results was necessarily limited. Since then a paper by Alers, Neighbours and Sato (1960) has appeared which contains, *inter alia*, the measured values of the three elastic constants of nickel from 0°K to 760°K. In this paper we present values of the magnetoelastic constants of nickel, derived from the two sets of results. The temperature variation of these constants is examined in the light of the theory of Kittel and Van Vleck (1960).

§ 2. THEORETICAL BACKGROUND

Although the calculation of the magnetoelastic constants is simple it is necessary to write down the basic equations since they will be required later.

The fourth-order equation for the spontaneous magnetostriction λ of a cubic crystal is (see, for example, Birss 1959)

$$\lambda = A_0 + A_1 S(\alpha_1^2 \beta_1^2) + A_2 S(\alpha_1 \alpha_2 \beta_1 \beta_2) + A_3 S(\alpha_1^2 \alpha_2^2) \\ + A_4 S(\alpha_1^4 \beta_1^2) + A_5 S(\alpha_1 \alpha_2 \alpha_3^2 \beta_1 \beta_2). \quad \dots (1)$$

In this equation, which ignores terms involving powers of α higher than the fourth, $\alpha_1, \alpha_2, \alpha_3$ and $\beta_1, \beta_2, \beta_3$ are the directions of the spontaneous magnetization

§ Now at Department of Electrical Engineering, Imperial College.

and of measurement respectively with reference to the cubic crystal axes, and the operator $S()$ denotes the sum of three quantities obtained by cyclic permutation of the suffixes on the expression within the brackets.

To derive Eqn (1) the magnetic energy V is expanded as a Maclaurin series in the strain A_{ij} . Thus

$$V = V^0 + V_p^0 E_p + V_{pq}^0 E_p E_q, \quad \dots (2)$$

In this expression the suffixes p, q, \dots run from 1 to 6 and the A_{ij} are related to the E_p in accordance with the scheme $A_{11} = E_1, A_{22} = E_2, A_{33} = E_3, A_{23} = A_{32} = \frac{1}{2}E_4, A_{31} = A_{13} = \frac{1}{2}E_5$ and $A_{12} = A_{21} = \frac{1}{2}E_6$. The association of the subscripts p, q, \dots with V indicates successive partial differentiation with respect to E_p, E_q, \dots and the zero superscript indicates that these quantities are to be evaluated at zero lattice strain. If the elastic energy $U = \frac{1}{2}C_{pq}E_p E_q$ is added to Eqn (2) and the quantity $U + V$ is minimized with respect to all E_p , then it may be shown (Birss 1959) that, taking only the first two terms in Eqn (2), the equilibrium strains are

$$E_p^V = -S_{pr}V_r^0, \quad \dots (3)$$

where the S_{pr} are the elastic compliance moduli. For a cubic crystal in which there are only three independent elastic moduli Eqn (3) reduces to

$$\left. \begin{aligned} E_p^V &= -(S_{11} - S_{12})V_p^0 - S_{12}(V_1^0 + V_2^0 + V_3^0) \quad \text{for } p = 1, 2, 3 \\ E_p^V &= -S_{44}V_p^0 \quad \text{for } p = 4, 5, 6. \end{aligned} \right\} \quad \dots (4)$$

The V_p^0 must depend upon α_i in such a way as to satisfy the lattice symmetry, and it may be shown that for a cubic crystal they must have the form

$$\begin{aligned} V_1^0 &= L_0 + L_1\alpha_1^2 + L_2\alpha_1^4 + L_3\alpha_2^2\alpha_3^2 + L_4\alpha_1^6 \\ &\quad + L_5\alpha_1^2\alpha_2^2\alpha_3^2 + \dots, \end{aligned} \quad \dots (5)$$

with corresponding expressions for V_2^0 and V_3^0 , and

$$V_4^0 = \alpha_2\alpha_3(M_0 + M_1\alpha_1^2 + M_2\alpha_1^4 + M_3\alpha_2^2\alpha_3^2 + \dots), \quad \dots (6)$$

with corresponding expressions for V_5^0 and V_6^0 . The constants L_0, L_1, \dots and M_0, M_1, \dots are the magnetoelastic constants, which are related to the

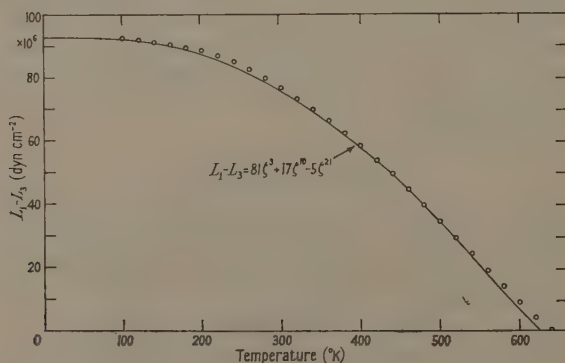


Fig. 1. Magnetoelastic constant $L_1 - L_3$ as a function of temperature. The circles represent experimental values deduced from the magnetostriction constant A_1 and the elastic constant $C_{11} - C_{12}$. The full line is that calculated from Eqn (11).

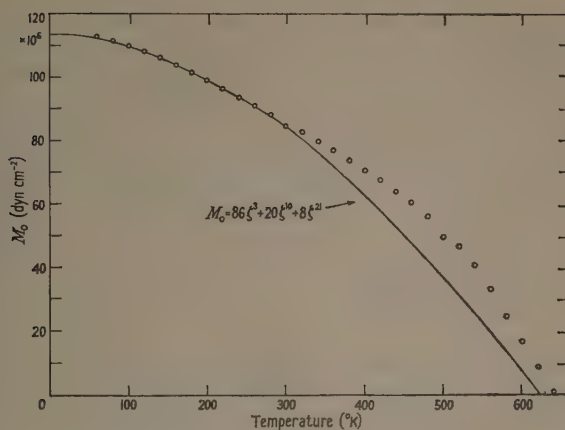


Fig. 2. Magnetoelastic constant M_0 as a function of temperature. The circles represent experimental values deduced from the magnetostriction constant A_2 and the elastic constant C_{44} . The full line is that calculated from Eqn (12).

magnetostriction constants in Eqn (1) by

$$\begin{aligned}
 A_0 &= -L_0 S_{11} - (2L_0 + L_1 + L_2 + L_4) S_{12}, \\
 A_1 &= -(L_1 - L_3)(S_{11} - S_{12}), \quad A_2 = -M_0 S_{44}, \\
 A_3 &= -L_3 S_{11} + (2L_2 + 3L_4) S_{12}, \\
 A_4 &= -(L_2 + L_3)(S_{11} - S_{12}), \\
 A_5 &= -M_1 S_{44}, \dots \dots \dots (7)
 \end{aligned}$$

Thus from our own measurements of A_1 and A_2 and the elastic constant data of Alers, Neighbours and Sato (1960) the magnetoelastic constants $L_1 - L_3$ and M_0 may be determined. The results are shown in Figs 1 and 2.

§ 3. DISCUSSION

In the first place we notice that the magnetoelastic constants drop sharply to zero at the Curie point. There is no evidence of any 'tail' such as is frequently exhibited by the spontaneous magnetization. At low temperatures both constants appear to be varying continuously towards their value at absolute zero. The observation by Corner and Hutchinson (1958) that the magnetostriction constant A_1 is virtually independent of temperature between 20°K and about 200°K must be ascribed to a fortuitous combination of circumstances in which the rates of change with temperature of the coupling constants and the elastic constants are the same.

In the previous paper we observed that, although the magnetostriction constant A_2 appears to approach its value at absolute zero monotonically, A_1 does not seem to vary with temperature in the same manner but reaches a (numerical) maximum at about 120°K. This behaviour we formerly attributed to the possibility of incomplete saturation in the magnetically difficult [100] direction at low temperatures. We are now inclined to reject this explanation for the following reasons: (a) the magnetoelastic constants $L_1 - L_3$ and M_0 do approach their

absolute zero values monotonically; (b) even if this were not so the theory of Kittel and Van Vleck would provide a natural explanation; and (c) the incomplete saturation hypothesis seems to be untenable. The saturation field for magnetization in a [100] direction is $2K_1/I_s$ oersteds (Fowler 1936). According to Bozorth (1951), K_1 for nickel at 77°K , the lowest temperature at which our measurements were made, is approximately $650\,000\text{ erg cm}^{-3}$. Taking $I_s = 500\text{ e.m.u.}$ allows us to estimate the saturation field at 77°K as 2700 Oe , which is considerably less than the 5000 Oe actually employed.

§ 4. COMPARISON WITH THE THEORY OF KITTEL AND VAN VLECK

A theory of the temperature variation of the magnetoelastic constants has recently been given by Kittel and Van Vleck (1960) in which the observed variation is explained in terms of a dependence of the magnetoelastic constants upon the spontaneous magnetization. The problem is thus reduced to that of finding the form of this dependence and to this end the theory proceeds along the lines of the conventional theory of the anisotropy constants.

The theory of Kittel and Van Vleck (1960) is, in fact, based on a theory due to Van Vleck (1959) of very general validity. It starts from an expression for the magnetoelastic energy which is, to second-order terms, essentially our Eqn (2) and which they write in the form

$$\begin{aligned}
 V_A = & \beta'_0 [E_1 + E_2 + E_3] \\
 & + \beta'_1 [(\alpha_1^2 - \frac{1}{3})E_1 + (\alpha_2^2 - \frac{1}{3})E_2 + (\alpha_3^2 - \frac{1}{3})E_3] \\
 & + \beta'_2 [\alpha_1\alpha_2E_6 + \alpha_2\alpha_3E_4 + \alpha_3\alpha_1E_5] \\
 & + \beta'_3 s' [E_1 + E_2 + E_3] \\
 & + \beta'_4 [p_4(\alpha_1)E_1 + p_4(\alpha_2)E_2 + p_4(\alpha_3)E_3] \\
 & + \frac{1}{2}\beta'_5 [(7\alpha_1\alpha_2\alpha_3^2 - \alpha_1\alpha_2)E_6 + (7\alpha_2\alpha_3\alpha_1^2 - \alpha_2\alpha_3)E_4 \\
 & + (7\alpha_3\alpha_1\alpha_2^2 - \alpha_3\alpha_1)E_5], \quad \dots\dots (8)
 \end{aligned}$$

with

$$p_4(\mu) = \frac{8}{35} P_4(\mu) = \mu^4 - \frac{6}{7}\mu^2 + \frac{6}{70}$$

and

$$s' = S(\alpha_1^2\alpha_2^2) - \frac{1}{3}.$$

This grouping of terms is employed instead of the usual arrangement in ascending powers of α_i in order that each magnetoelastic constant $\beta'_0, \beta'_1, \dots$ (not to be confused with the β_1, β_2 and β_3 in Eqn (1)) shall be the coefficient of a homogeneous surface harmonic, of degree 4 for β'_3, β'_4 and β'_5 , and of the second degree for β'_1 and β'_2 . The basis of the theory is then that whilst the spin moments are aligned parallel at saturation, there is nevertheless, at any finite temperature, an angular spread amongst the local units so that, locally, Eqn (8) is true where the β' 's are temperature independent. Instead the temperature variation of the magnetoelastic energy is ascribed to local variations in the α 's and the problem is to determine the angular averages for a given angular distribution. Kittel and Van Vleck relate these angular averages to the reduced spontaneous magnetization $\zeta = I_s/I_0$, and show that the effective value of each β' at a finite temperature depends on ζ in a way that is determined by the order of surface harmonic with which it is associated. Experimentally it is essential that the magnetostriction constants, and hence the magnetoelastic coupling constants derived therefrom,

should be associated with ascending powers of the α 's, since, in this way, the various constants can be distinguished by their different angular dependences. Thus the experimentally determined constants A_1, A_2, \dots will, in general, each consist of terms having different modes of temperature variation and it is not to be expected that the constants A_1, A_2 , etc. will show a simple or even similar dependence upon temperature. It is necessary therefore to relate the β 's occurring in Eqn (8) to the measured quantities.

It may be shown that the constants L_1, \dots , in Eqn (5) and M_1, \dots , in Eqn (6) are related to the β 's in Eqn (8) by,

$$\begin{aligned} L_0 &= \beta_0' - \frac{1}{3} \beta_1' - \frac{1}{5} \beta_3' + \frac{3}{35} \beta_4' \\ L_1 &= \beta_1' + \beta_3' - \frac{6}{7} \beta_4' \\ L_2 &= \beta_4' - \beta_3' \\ L_3 &= \beta_3' \\ M_0 &= \beta_2' - \frac{1}{2} \beta_5' \\ M_1 &= \frac{7}{2} \beta_5'. \end{aligned} \quad \dots\dots(9)$$

According to Kittel and Van Vleck the β 's depend upon temperature through the reduced spontaneous magnetization ζ according to the scheme

$$= \frac{\beta'(l)}{\beta'(l)_0} = \zeta^{l(l+1)/2}$$

in which $\beta'(l)$ is a coefficient of a homogeneous surface harmonic of degree l . Thus $\beta_1'/\beta_{1,0}' = \beta_2'/\beta_{2,0}' = \zeta^3$ and $\beta_3'/\beta_{3,0}' = \beta_4'/\beta_{4,0}' = \beta_5'/\beta_{5,0}' = \zeta^{10}$.

Before expressing the measured constants $L_1 - L_3$ and M_0 as functions of ζ it is necessary to enquire into the effect of including terms in α^6 in Eqn (8). If these are also grouped so as to form homogeneous surface harmonics of degree $2n$ then one can predict that higher terms will vary with temperature as $\beta_6'/\beta_{6,0}' = \beta_7'/\beta_{7,0}' = \dots = \zeta^{21}$ and that these terms will appear in the expressions for L_1, \dots , and M_0, \dots , given in Eqn (9). Consequently these constants will in general vary as

$$L_i \text{ (or } M_i) = A_i + B_i \zeta^3 + C_i \zeta^{10} + D_i \zeta^{21} + \dots \quad \dots\dots(10)$$

To investigate whether our experimentally determined constants $L_1 - L_3$ and M_0 could be fitted to an expression of this form, we first made a logarithmic plot of $L_1 - L_3$ and M_0 against ζ^3 which confirmed the general dependence of the constants upon ζ^3 . Further analysis shows that $L_1 - L_3$ can be represented by the equation

$$L_1 - L_3 = 81\zeta^3 + 17\zeta^{10} - 5\zeta^{21}, \quad \dots\dots(11)$$

assuming that this quantity is not vitiated by the effect of non-saturation, and that M_0 may be expressed as

$$M_0 = 86\zeta^3 + 20\zeta^{10} + 8\zeta^{21}. \quad \dots\dots(12)$$

These equations are plotted in Figs 1 and 2 together with the experimental points. Eqn (11) fits the experimental points rather well over the entire temperature

range. Eqn (12) on the other hand fits the experimental data extremely well at low temperatures but breaks down just above room temperature. It is evident, though, that the magnetoelastic constants may be represented fairly accurately by Eqn (10) and that the constants A_i , B_i , etc. do, in fact, converge respectably.

§ 5. CALCULATION OF FORCED MAGNETOSTRICTION CONSTANTS

It is observed experimentally in all magnetic materials that above the point of technical saturation the magnetostriction exhibits a weak dependence upon the applied magnetic field H . The variation of λ with H is a linear one and is known as the forced magnetostriction. Although the effect was, for a long time, regarded as a pure volume effect, measurements by Calhoun and Carr (1955) showed the forced magnetostriction of iron to be anisotropic. The effect is small, usually of the order 10^{-10} Oe $^{-1}$, and has so far been analysed only in terms of the second-order equation for the spontaneous magnetostriction

$$\lambda = C_0 + C_1 S(\alpha_1^2 \beta_1^2) + C_2 S(\alpha_1 \alpha_2 \beta_1 \beta_2). \quad \dots (13)$$

The forced magnetostriction is, by definition, $d\lambda/dH$ and the second-order forced magnetostriction constants are C_0' , C_1' and C_2' , the prime denoting differentiation with respect to field. The work of Calhoun and Carr showed that, in iron, C_1' and C_2' are not negligible in comparison with C_0' . Experimentally it is observed that, for a given material, there is no constant proportionality between the C 's and the corresponding C'' 's. Thus, for example, for iron $C_1 = +31.1 \times 10^{-6}$, $C_1' = 0.94 \times 10^{-10}$ Oe $^{-1}$; $C_2 = -63.6 \times 10^{-6}$, $C_2' = -0.34 \times 10^{-10}$ Oe $^{-1}$, and in certain aluminium-iron alloys C and C' do not even have the same sign (Hall 1957).

These observations may be explained as follows. Above technical saturation the spontaneous magnetization I_s is slightly field dependent. The increase of I_s with H is linear and small. Values of the quantity dI_s/dH for a given substance differ widely from one source to another, and almost the only certain thing about it is that it decreases with decreasing temperature. The forced magnetostriction arises because the magnetoelastic constants depend upon ζ and at finite temperatures $d\zeta/dH (\equiv \zeta')$ is finite. Since the magnetoelastic constants are given by Eqn (10) the forced magnetoelastic constants must depend on ζ as

$$L_i' \quad (\text{or } M_i') = \frac{dA_i}{dH} + (3B_i\zeta^2 + 10C_i\zeta^3 + 21D_i\zeta^{20} + \dots)\zeta', \quad \dots (14)$$

and the forced magnetostriction will have the same kind of dependence. Thus the C 's and the corresponding C'' 's will not bear any simple relation to each other. In particular, since the latter quantities depend much more strongly on terms involving higher powers of ζ than the former, there appears to be no compelling reason for the two quantities even to have the same sign. Although it would be possible in principle to compute the forced magnetoelastic constants for nickel from Eqns (11), (12) and (14), very little purpose would be served thereby because any values of ζ' employed would be little more than a guess and probably uncertain to an order of magnitude; in addition there appear to be no experimental determinations of the forced magnetostriction constants of nickel.

§ 6. DISCUSSION

There seems little doubt that the temperature variation of the magnetoelastic constants of nickel is correctly given by Eqn (10). Thus the observation by Döring (1936) that the polycrystalline magnetostriction constant of nickel is proportional to I_s^2 can only be regarded as fortuitous and well illustrates the dangers of drawing conclusions from the magnetostriction constants alone. However, the very success of Eqn (10) raises a problem, for the theory which predicts it also predicts that the first anisotropy constant of nickel K_1 should vary as $K_1/K_{1,0} = \zeta^{10}$, whereas the experimental data imply a more rapid variation.

Thus the question of a temperature variation of both the anisotropy and magnetoelastic constants whose origin is different from that considered in this paper must be considered. One rather obvious mechanism is through the agency of thermal expansion, and Carr (1960) has shown that if the expression for the variation of the anisotropy constant K_1 with temperature, namely $K_1 = K_{1,0}\zeta^{10}$, is regarded as being correct for constant volume then when the thermal expansion of the lattice is taken into account the exponent becomes $10 - \kappa\omega A^{-1}T^{-3/2}$, in which ω is a volume strain, $\kappa = (1/K_{1,0})(dK_{1,0}/d\omega)$, A is the constant in the Bloch spin-wave equation, $\zeta = 1 - AT^{3/2}$, and T is the absolute temperature. Brenner (1957) identified $K_{1,0}\kappa$ with the constant A_3 in Eqn (1), and Carr showed that for iron $10 - \kappa\omega A^{-1}T^{-3/2}$ is almost independent of temperature and equal to 8.2 over the small range of temperature where the spin-wave equation $\zeta = 1 - AT^{3/2}$ is applicable. For iron the recent experimental results of Graham (1958) obey the law $K_1 = K_{1,0}\zeta^5$ quite closely. Thus it is clear that when allowance for thermal expansion is made the agreement between theory and experiment is improved although it is still far from perfect. An analysis similar to that of Carr can be carried out for the magnetoelastic constants. Assume for the time that a particular magnetoelastic constant may be expressed as $L(T) = L_0(\omega)\zeta^3$ in which $L_0(\omega)$ is regarded as being volume dependent. Then, from the spin-wave equation and a Taylor expansion of $L_0(\omega)$ it follows that

$$L(T) = L_0(0) [1 + \kappa'\omega - 3AT^{3/2}]$$

where

$$\kappa' \equiv \frac{1}{L_0} \frac{dL_0}{d\omega}.$$

This may be written in the form

$$L(T) = L_0(0) [1 - (3 - \kappa'\omega A^{-1}T^{-3/2})AT^{3/2}]$$

whence $L(T) = L_0(0)\zeta^n$ where $n = 3 - \kappa'\omega A^{-1}T^{-3/2}$. Now κ' may be related to a magnetostriction constant in a term which is of the sixth order in α_i . If Eqn (1) is to be of any use at all such a constant must be very small indeed at all temperatures, and since the effect of thermal expansion in higher order terms in Eqn (10) will involve magnetostriction constants of even higher orders than the sixth it would seem that the temperature variation of the magnetoelastic constants is not significantly affected by thermal expansion of the lattice.

An intrinsic effect of temperature on the magnetoelastic constants is, however, not ruled out by the preceding analysis, nor is such an effect wholly unexpected as the following considerations show. The constant β_0' in Eqn (8) and the related magnetostriction constant A_0 in Eqn (1) are due to the effects of exchange. They represent a pure volume effect and give rise to the anomaly in the thermal

expansion near the Curie temperature. Now the very existence of such an anomaly indicates that A_0 and β_0' must be strongly temperature dependent, at least in the neighbourhood of the Curie temperature. Nevertheless the theory of Kittel and Van Vleck gives the unequivocal result $\beta_0'/\beta_{0,0}' = 1$, independent of ζ . The reason for this is that this theory does not cover the temperature variation of the magnetoelastic constants as such. It relates the value of each magnetoelastic constant at a finite temperature to the average value of the angular spread of the spins about a definite crystallographic axis. This average value, and through this the temperature variation of the magnetoelastic constants, is uniquely related to the order of the harmonic of which each β' is a coefficient. It follows from the theory that the coefficient of the zeroth-order harmonic β_0' must vary with temperature as ζ^0 . But this is merely a restatement of the fact that β_0' does not depend on the angle the spin moments make with a crystal axis, i.e. on spin-lattice alignment. β_0' can, and indeed does, vary with the average angle that one spin makes with another, i.e. on spin-spin alignment, but this is outside the scope of the theory of Kittel and Van Vleck. Now it is clear that if β_0' depends on spin-spin alignment the other β' 's may do so as well, and although there will in general be some correlation between spin-spin and spin-lattice alignment it is very difficult to predict what form it will take. The rather good agreement we have found between our experimental results for nickel and the theory of Kittel and Van Vleck suggests that the intrinsic temperature dependence of the magnetoelastic constants other than β_0' through spin-spin angular variation is considerably less than that due to the spin-lattice angular variation.

REFERENCES

- ALERS, G. A., NEIGHBOURS, J. R., and SATO, H., 1960, *J. Phys. Chem. Solids*, **13**, 40.
 BIRSS, R. R., 1959, *Advanc. Phys. (Phil. Mag. Suppl.)*, **8**, 252.
 BIRSS, R. R., and LEE, E. W., 1960, *Proc. Phys. Soc.*, **76**, 502.
 BOZORTH, R. M., 1951, *Ferromagnetism* (New York: Van Nostrand).
 BRENNER, R., 1957, *Phys. Rev.*, **107**, 1539.
 CALHOUN, B. A., and CARR, W. J., 1955, *Conference on Magnetism and Magnetic Materials, Pittsburgh, Pennsylvania* (New York: Amer. Inst. elect. Engrs), p. 107.
 CARR, W. J., 1960, *J. Appl. Phys.*, **31**, 69.
 CORNER, W. D., and HUTCHINSON, F., 1958, *Proc. Phys. Soc.*, **72**, 1049.
 DÖRING, W., 1936, *Z. Phys.*, **103**, 560.
 FOWLER, R. H., 1936, *Statistical Mechanics* (Cambridge: University Press).
 GRAHAM, C. D., 1958, *Phys. Rev.*, **112**, 1117.
 HALL, R. C., 1957, *J. Appl. Phys.*, **28**, 707.
 KITTEL, C., and VAN VLECK, J. H., 1960, *Phys. Rev.*, **118**, 1231.
 VAN VLECK, J. H., 1959, *J. Phys. Radium*, **20**, 128.

Franck-Condon Factors and r -Centroids for the Triplet Band System of CO Molecule

BY N. L. SINGH AND D. C. JAIN

Department of Spectroscopy, Banaras Hindu University, India

MS. received 28th February 1961

Abstract. It has been verified that the Morse potential function is a good approximation for the representation of the potential energy curves of $d^3\pi$ and $a^3\pi$ electronic states of the CO molecule. The Franck-Condon factors for the triplet band system have been computed by the direct method of numerical integration of the Morse wave functions. The r -centroids for this band system have been calculated by (i) the direct method of numerical integration and (ii) the quadratic equation method of Nicholls and Jarman. A close agreement is obtained between the values of r -centroids evaluated by both the methods.

Assuming that the electronic transition moment is approximately constant, the relative population of the vibrational levels of the $d^3\pi$ state of the CO molecule has been calculated using Herman and Rakotoarijimy's experimental data on the relative intensity measurement of the triplet bands developed in the presence of xenon.

§ 1. INTRODUCTION

HERMAN AND RAKOTOARIJIMY (1960) have made a quantitative study of the spectrum of CO in the presence of rare gases and have obtained evidence of a marked selective excitation in the triplet band system of CO in the presence of xenon. They have calculated the relative population of the vibrational levels in the $d^3\pi$ electronic state of the CO molecule in the presence of xenon by making use of the Franck-Condon factors, evaluated by Pillow's 'distortion method' (Pillow 1951). We have already reported the Franck-Condon factors for this band system evaluated by the method of numerical integration using Morse wave functions. In the present paper the details of the calculations of the Franck-Condon factors and r -centroids for this band system are presented. Using Herman and Rakotoarijimy's experimental data on relative intensity measurement, we have calculated the relative population of the vibrational levels of the $d^3\pi$ state of CO in the presence of xenon, assuming the electronic transition moment approximately constant. These results will have to be further considered in the light of the variation of electronic transition moment to be reported in a subsequent paper.

§ 2. COMPUTATIONAL PROCEDURE AND RESULTS

2.1. Evaluation of Franck-Condon Factors

As the form of the wave functions involved in the overlap integrals is very much determined by the potential function used, the ability of the Morse potential function to represent the 'true' potentials of both the electronic states involved

in the CO triplet band system had to be checked. This was done by determining the 'true' potential curves by the Klein-Dunham-Jarmain method (Jarmain 1959) using data from Herzberg (1950) and comparing the corresponding points on the Morse potential curves. The values of r_{\min} and r_{\max} for the different vibrational levels of the two electronic states are given in Table 1.

Table 1. 'True' and 'Morse' Potential Curves for $d^3\pi$ and $a^3\pi$ Electronic States of CO

$d^3\pi$ state					$a^3\pi$ state				
v'	$r_{\min}(\text{\AA})$		$r_{\max}(\text{\AA})$		v''	$r_{\min}(\text{\AA})$		$r_{\max}(\text{\AA})$	
	True	Morse	True	Morse		True	Morse	True	Morse
0	1.3348	1.3339	1.4666	1.4657	0	1.1594	1.1594	1.2662	1.2661
2	1.2706	1.2663	1.5690	1.5644	2	1.1060	1.1058	1.3480	1.3478
4	1.2367	1.2291	1.6424	1.6334	4	1.0770	1.0766	1.4065	1.4061
6	1.2125	1.2020	1.7073	1.6931	6	1.0559	1.0555	1.4578	1.4575
8	1.1936	1.1804	1.7684	1.7477	8	1.0390	1.0387	1.5059	1.5056

The straightforward method of Jarmain and Nicholls (1952) has been used for computing the Franck Condon factors. The Morse wave functions have been calculated on a desk calculator at intervals of 0.02\AA over the range of r within which they are significant. For higher vibrational quantum numbers, as there is a large cancellation in the Laguerre polynomials, we have carried as many significant figures in the computation as possible. Stirling's approximation to a gamma function of large argument has been employed. The values of wave functions have then been interpolated at intervals of 0.01\AA by means of sufficiently large scale graphs. All the wave functions have been checked for normalization to unity.

The overlap integrals have been evaluated numerically by applying trapezoidal and Simpson rules and the values of Franck Condon factors obtained by both the methods are in good agreement with a maximum difference of 0.001 . This shows that the interval of integration is sufficiently small. The Franck-Condon factors are entered in Table 2.

Table 2. Franck-Condon Factors for the Triplet Band System of CO Molecule

$v' \backslash v''$	0	1	2	3
0	0.007	0.043	0.120	0.201
1	0.031	0.114	0.162	0.091
2	0.068	0.145	0.074	0.000
3	0.107	0.113	0.004	0.057
4	0.133	0.051	0.018	0.079
5	0.141	0.008	0.061	0.030
6	0.132	0.002	0.073	0.000
7	0.113	0.022	0.045	0.020
8	0.086	0.055	0.017	0.043

2.2. Evaluation of *r*-Centroids

The *r*-centroids have been evaluated by two different methods: (i) the direct method of numerical integration, and (ii) the quadratic equation method of Jarman and Nicholls.

The Direct Method. The integrals

$$\int \psi_{v'} r \psi_{v''} dr$$

have been evaluated numerically using the Morse wave functions by applying Simpson's rule, and $\bar{r}_{v', v''}$ have been calculated by the relation

$$\bar{r}_{v', v''} = \frac{\int \psi_{v'} r \psi_{v''} dr}{\int \psi_{v'} \psi_{v''} dr} \quad \dots\dots (1)$$

The Quadratic Equation Method. The *r*-centroids of molecular band systems can be evaluated by solving the approximate equation, given by Nicholls and Jarman (1956),

$$E_{v'} - E_{v''} = D_1' [1 - \exp \{-\alpha(\bar{r}_{v', v''} - r_{e1})\}]^2 - D_2' [1 - \exp \{-\alpha(\bar{r}_{v', v''} - r_{e2})\}]^2, \quad \dots\dots (2)$$

where α is the mean of the Morse constants α_1 and α_2 of the potential curves of the two electronic states and the primes over the various quantities indicate that these have been adjusted with respect to the chosen mean value of α (Fraser and Jarman 1953).

Equation (2) is a quadratic equation in $\kappa (= \exp \{-\alpha \bar{r}_{v', v''}\})$ having two roots. out of which the one that gives real physical meaning to $\bar{r}_{v', v''}$ has been used in the calculation. The Morse constants used are: $\alpha_1 = 1.761057 \times 10^8$, $\alpha_2 = 2.426142 \times 10^8$, mean $\alpha = 2.093600 \times 10^8$. Results of both the methods of calculation of $\bar{r}_{v', v''}$ are given in Table 3.

§ 3. DISCUSSION

It is seen from Table 1 that the Morse potential function is a very close approximation to the 'true' potential of the $a^3\pi$ state of the CO molecule. The 'true' potential of the $d^3\pi$ state is also adequately represented by the Morse potential function in the region of lower vibrational levels. There is, however, some discrepancy in the region of higher vibrational levels due to the comparatively large value of $w_e y_e$ (-0.1125) for the $d^3\pi$ state. Nicholls (1960) has reported a similar discrepancy in the $B^3\Sigma_u^-$ state of O_2 . On account of this fact the values given in Table 2 may be slightly different from the exact Franck-Condon factors corresponding to the wave functions appropriate to the 'true' potentials of both the electronic states.

It is seen from Table 3 that there is a fairly good agreement between the *r*-centroids calculated by the two methods, showing that the quadratic equation method is a good approximation up to $v' = 8$, $v'' = 3$. Tawde and Murthy (1960) have drawn similar conclusions in the case of BeO ($B \rightarrow X$ system) up to $v' = 3$, $v'' = 5$.

Nicholls and Jarman (1956) have shown that under certain approximations $\Delta \bar{r} (= \bar{r}_{v'+1, v''+1} - \bar{r}_{v', v''})$ in a sequence remains constant. In the case of the CO triplet band system such a regularity is exhibited if we determine $\Delta \bar{r}$ from the values of $\bar{r}_{v', v''}$ calculated by the quadratic equation method. This is because the approximations used in deducing the difference $\Delta \bar{r}$ are the same as applied in the

Table 3. r -Centroids for the Triplet Band System of CO

$v' \backslash v''$	0	1	2	3
0	1.298	1.321	1.346	1.371
	1.296	1.319	1.342	1.366
1	1.282	1.305	1.328	1.351
	1.282	1.304	1.327	1.350
2	1.267	1.289	1.311	—
	1.268	1.290	1.312	—
3	1.252	1.274	1.286	1.323
	1.255	1.276	1.298	1.320
4	1.238	1.259	1.287	1.305
	1.242	1.263	1.284	1.306
5	1.225	1.243	1.269	1.289
	1.230	1.250	1.271	1.292
6	1.212	1.241	1.254	—
	1.218	1.238	1.259	—
7	1.200	1.220	1.252	1.267
	1.207	1.227	1.247	1.267
8	1.186	1.211	1.238	1.240
	1.197	1.216	1.235	1.255

Upper figure: numerical integration method

Lower figure: quadratic equation method

quadratic equation method. Values of $\Delta\bar{r}$ determined from the values of $\bar{r}_{v', v''}$ calculated by the numerical integration method, however, show some increase for higher bands in each sequence.

The Franck-Condon factors entered in Table 2 have been used for calculating the relative intensities of a few bands of $v''=0$ progression. The intensity of the (0, 0) band has been taken as unity and it has been assumed that (a) all the vibrational levels of the excited state have equal population (i.e. $T \rightarrow \infty$), and (b) the electronic transition moment is approximately constant. Then by making use of Herman and Rakotoarijimy's experimental data on relative intensities of CO triplet bands in the presence of xenon, the relative population of the vibrational levels of $d^3\pi$ state of the CO molecule has been calculated. The results are shown in Table 4. For comparison, Herman and Rakotoarijimy's results are also entered in the Table.

Herman and Rakotoarijimy have concluded that the population of the fifth vibrational level is much increased due to resonance excitation by collisions of CO molecules with metastable xenon (3P) atoms. Their conclusion is supported by our calculations of the relative population of the vibrational levels based on the more accurate values of the Franck-Condon factors obtained by us by the method of numerical integration using Morse wave functions.

Table 4. Relative Population ($N_{v'}$) of the Vibrational Levels of $d^3\pi$ State of CO in Presence of Xenon

(1)	(2)	(3)	(4)	(5)	(6)
2,0	16	16.2	17.0	0.99	0.94
3,0	46	34.8	35.1	1.32	1.31
4,0	115	61.6	56.3	1.87	2.04
5,0	400	90	75.3	4.44	5.31
6,0	81	99	87.7	0.82	0.92

(1) v', v'' ; (2) $I(v', v'')$ experimental (Herman and Rakotoarijimy); (3) $I_{\infty}(v', v'')$ calculated by Pillow's method (Herman and Rakotoarijimy); (4) $I_{\infty}(v', v'')$ calculated by us by the method of numerical integration; (5) $N_{v'}$ (Herman and Rakotoarijimy); (6) $N_{v'}$ (our calculations).

ACKNOWLEDGMENTS

The authors are grateful to Dr. P. Shah, Department of Mathematics, Banaras Hindu University, for many invaluable discussions in connection with this work. One of us (D.C.J.) is indebted to the Government of Madhya Pradesh for financial assistance.

REFERENCES

- FRASER, P. A., and JARMAIN, W. R., 1953, *Proc. Phys. Soc. A*, **66**, 1145.
 HERMAN, L., and RAKOTOARIJIMY, D., 1960, *J. Phys. Radium*, **21**, 629.
 HERZBERG, G., 1950, *Molecular Spectra and Molecular Structure I*, 2nd edn (New York: Van Nostrand).
 JARMAIN, W. R., 1959, *J. Chem. Phys.*, **31**, 1137.
 JARMAIN, W. R., and NICHOLLS, R. W., 1952, *Scientific Report No. 4*, Contract No. AF 19 (122)-470 (London, Canada: University of Western Ontario).
 NICHOLLS, R. W., 1960, *Canad. J. Phys.*, **38**, 1705.
 NICHOLLS, R. W., and JARMAIN, W. R., 1956, *Proc. Phys. Soc. A*, **69**, 253.
 PILLOW, M. E., 1951, *Proc. Phys. Soc. A*, **64**, 772, 779.
 TAWDE, N. R., and MURTHY, N. S., 1960, *Bull. Soc. Sci. Liège*, **29**, 325.

The $^{55}\text{Mn}(\text{d}, \text{p})^{56}\text{Mn}$ Reaction

BY A. W. DALTON, G. PARRY, H. D. SCOTT AND
S. SWIERSZCZEWSKI

Department of Physics, University of Liverpool

MS. received 15th February 1961

Abstract. The energy spectra of the protons emitted from a manganese target when bombarded with 8.9 mev deuterons have been measured by magnetic analysis at angles of observation between 5 and 60°. Angular distributions of a number of proton groups have been obtained and compared with theoretical stripping curves to obtain information on parities, spins and reduced widths. The results have also been compared with those of Schiffer, Lee and Zeidman on gross structure in the proton spectra.

§ 1. INTRODUCTION

THE energies of many of the excited states of ^{56}Mn have been determined by Green, Smith, Buechner and Mazari (1957) from a high resolution study of the $^{55}\text{Mn}(\text{d}, \text{p})^{56}\text{Mn}$ reaction using 6.6 and 7.0 mev deuterons. The same reaction has been studied in the present investigation using 8.9 mev deuterons. Angular distributions were obtained for a number of proton groups. These were fitted with Butler type stripping curves to obtain information on parities, spins and reduced widths. The results have also been compared with those of Schiffer, Lee and Zeidman (1959) on gross structure in proton spectra from reactions using 10 mev deuterons.

§ 2. EXPERIMENTAL AND RESULTS

Using the techniques described previously (Dalton, Kirk, Parry and Scott 1960) with a target 0.27 mg cm^{-2} and exposures up to $900 \mu\text{C}$, measurements were made at angles from 5 to 60° to the incident beam.

In Fig. 1 is shown the proton energy spectrum obtained at 20° to the beam direction. The groups which have been identified with transitions to states of ^{56}Mn are labelled with their excitation energy in mev. Detailed measurements were made on groups corresponding to states with excitation energies up to 3.03 mev and Fig. 2 gives their angular distributions while the information obtained for the transitions is contained in the Table.

Measurements were made on nineteen groups up to this excitation. Eight of these corresponded to single levels as observed by Green *et al.* and were fitted by $l=1$ curves. The other eleven were composite groups and each one corresponded to two or more levels. Five of these distributions were fitted with $l=1$ curves, two with $l=2$ curves and three with curves for $l=1$ or 2. The remaining distribution at 2.12 mev excitation was too complex for a single l -value to be

assigned. Possibly it contains an $l=0$ component and undoubtedly it contains components up to $l=2$. No obvious $l=3$ distributions were observed although most of the experimental distributions had appreciable yields at the larger angles of observation.

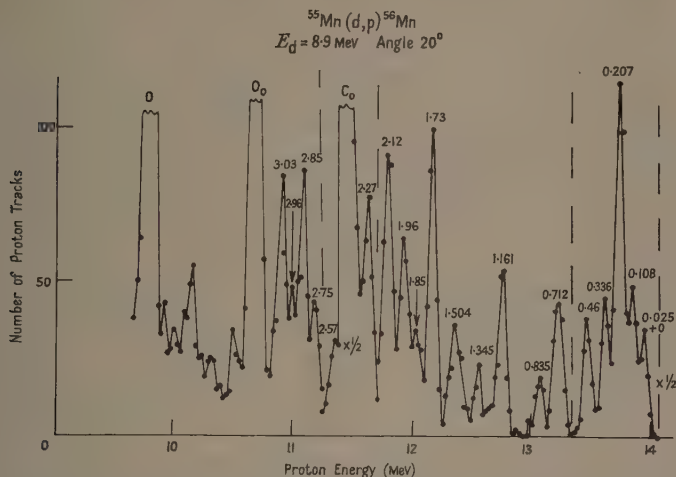


Fig. 1. Proton spectrum observed at an angle of 20° from a target of ^{55}Mn bombarded by 8.9 mev deuterons.

The spectra became rather complicated at higher excitations but to enable a comparison to be made with the work of Schiffer *et al.* they were examined for possible $l=0$ transitions, particularly in the region corresponding to $Q=1$ mev where the oxygen impurity gives rise to a group with an $l=0$ distribution. Two strong forward peaking groups were observed corresponding to transitions with Q -values of 0.71 and 1.32 mev, that for $Q=0.71$ mev being three times the stronger. The cross section at 5° for the transition with $Q=0.71$ mev was about $11 \text{ mbnsterad}^{-1}$. The angular distributions of the two groups can be fitted approximately with either $l=0$ or $l=1$ curves. The group with $Q=0.71$ mev is possibly better fitted by the $l=0$ curve and that at $Q=1.32$ mev by the $l=1$ curve.

As the ground state spin of ^{55}Mn is $5/2$ (Mack 1950) unique spin assignments to the states of ^{56}Mn cannot be made. For those states reached by $l=0$ transitions the spin is 2 or 3, for $l=1$ transitions 1 to 4 units and for $l=2$ transitions 0 to 5 units.

§ 3. DISCUSSION

The results of the angular distribution measurements may be compared with those of Schiffer *et al.* In Fig. 3 is shown a gross structure spectrum with impurity contributions removed. Averaging has been performed over an energy interval of about 200 keV. There is considerable similarity between the spectrum and the one shown by Schiffer *et al.* These authors assign the states $s_{1/2}$, $d_{5/2}$, $p_{1/2}$ and $p_{3/2}$ at positions corresponding to Q -values of 0.4, 2.3, 3.1 and 4.6 MeV respectively, corresponding to transitions with $l=0, 2, 1$, and 1 for the ingoing

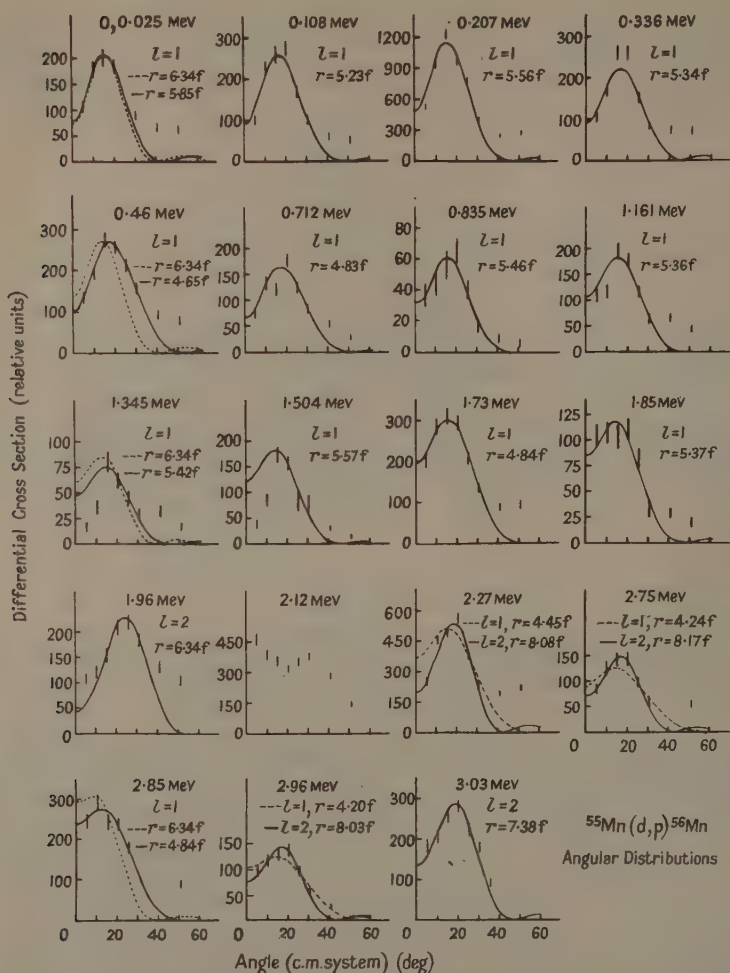


Fig. 2. Angular distributions of proton groups from the $^{55}\text{Mn}(d, p)^{56}\text{Mn}$ reaction. The distributions are labelled by the excitation energy of the corresponding final state. 100 units of relative cross section are equivalent to $0.71 \text{ mbn sterad}^{-1}$.

neutron. From our results it is clear that there is a strong $l=1$ group centred round the Q -value of 4.84 MeV , and there is probably a strong $l=0$ group centred round the Q -value 0.71 MeV . These two broad groups could correspond to the $p_{3/2}$ and $s_{1/2}$ states assigned by Schiffer *et al.* The association of other single particle states with broad groups between these extremes is not at all obvious. Following on the broad $l=1$ group centred round $Q=4.84 \text{ MeV}$ there is a run of $l=1$ transitions with Q -values down to 3.20 MeV . These transitions do not produce, when summed, one broad group which can obviously be identified with a single particle $p_{1/2}$ state at about 3.1 MeV . In addition there are in the lower

of one l -value to each group is not possible. This may be due to lack of experimental resolution or to defects in the simple stripping theory. Nevertheless there appear to be two distinct regions where $l=2$ transitions are a strong possibility. The Q -values at the centres of these groups of levels are about 2.90 and 2.05 mev. It is not obvious that these two groups should be combined in order that the resultant might be identified with the single particle $d_{5/2}$ state assigned by Schiffer *et al.* at about 2.3 mev.

REFERENCES

- DALTON, A. W., KIRK, A., PARRY, G., and SCOTT, H. D., 1960, *Proc. Phys. Soc.*, **75**, 95.
GREEN, J. W., SMITH, A. J., BUECHNER, W. W., and MAZARI, M., 1957, *Phys. Rev.*, **108**, 841.
MACK, J. E., 1950, *Rev. Mod. Phys.*, **22**, 64.
SCHIFFER, J. P., LEE, L. L., and ZEIDMAN, B., 1959, *Phys. Rev.*, **115**, 427.

An Analogue Solution of the Continuity Equation of the Ionospheric F Region

By B. H. BRIGGS AND H. RISHBETH†

Cavendish Laboratory, Cambridge

MS. received 6th March 1961

Abstract. It is shown that the continuity equation for the electron density in the F region of the ionosphere can be solved by the use of an electrical analogue. The equation which is solved in this way takes account of the rates of production and loss of electrons, and of vertical diffusion, but other types of movement are not included. The rates of production, loss and diffusion are assumed to vary with height in a manner appropriate to a particular model of the atmosphere, based on rocket and satellite data.

The analogue computer is first used to find how the electron density at a series of heights varies with time due to the diurnally varying rate of production. The time of maximum production is at noon, but the time of maximum electron density occurs some time after noon, and the variation of this time lag with height is studied. Near noon, the electron density is found to be a maximum at a height of 250 km. In the evening, the height of the maximum rises to about 300 km, and remains constant during the night. Above the level of the maximum, the ionization is controlled by diffusion and the ionization density falls off exponentially with increasing height; its time variation follows closely the time variation at the maximum.

In other experiments, the production function is modified so as to represent a solar eclipse which occurs near noon. Diurnal curves of electron density are obtained at a series of heights, and the results show how the time of maximum electron density and the percentage decrease of electron density vary with height.

In another type of experiment, the diffusion and recombination of a slab of ionization introduced at a fixed height are studied. It is shown that the slab spreads out to form a 'layer' which eventually assumes a certain fixed shape with a maximum at a fixed height of 300 km, and that this 'shape-preserving' layer then decays with a time constant determined by the rate of recombination at the level of maximum ionization density. The final form of the layer is independent of the height at which the slab of ionization is introduced. These results may be relevant to the behaviour of the F layer at night when production is absent, and diffusion and recombination are the controlling factors.

§ 1. INTRODUCTION

THE electron density in the F region of the ionosphere is thought to depend largely on the production of ionization by solar radiation, loss by recombination and vertical transport by plasma or ambipolar diffusion. If these three processes only are considered, the continuity equation for the electron density $N(h, t)$ is a partial differential equation, being second-order in height h and first-order in time t .

† Now at the Department of Scientific and Industrial Research, Radio Research Station, Ditton Park, Slough.

This paper describes how solutions of this equation may be obtained by the use of an analogue computer. This employs a series of condensers, the charge on any one of which represents the electron density at a certain height. The condensers form part of a network which contains resistors whose values are related to the diffusion and loss coefficients. The diurnal variation of production of ionization is represented by the supply of current from potentiometers, varied periodically by an assembly of cams. The voltage on each condenser is recorded by a pen-recorder, and represents the variation of electron density at the appropriate height. Daytime quasi-equilibrium conditions can be studied by stopping the cams at 'noon' or any other desired position. With the addition of another cam the effects of a solar eclipse can be investigated.

The behaviour of a slab of ionization under the influence of diffusion and loss alone may be investigated by disconnecting the 'production' circuits, giving an initial charge to one of the condensers and recording the voltage as a function of time on each condenser.

In addition to the processes mentioned above, there may exist motions of the ionization caused by electromagnetic forces and diurnal temperature changes. The effects of these are complicated and it is of interest to solve the differential equation which applies if they are neglected. Comparison of the solutions with the actual ionosphere may show the extent to which these movements are important.

It is hoped to present more detailed results in a later paper, and the account given here is mainly concerned with the assumptions made about the ionosphere (§2) and the equations governing the circuits (§3). A few samples of the results obtained with the first model are presented in §4.

§ 2. IONOSPHERIC PROCESSES

The equation of continuity satisfied by the electron density N may be written

$$\frac{\partial N}{\partial t} = q - \beta N - \frac{\partial}{\partial h}(Nw_D) \quad \dots\dots(1)$$

in which the production rate q is a function of height and of the solar zenith angle $\chi(t)$, and the loss rate β is a function of height. The vertical drift velocity of diffusion w_D depends on the plasma diffusion coefficient D , which is also a function of height, and on gravity.

For the purposes of the model, the neutral constituents of the F region are taken to be atomic oxygen and molecular nitrogen. In the equations which follow the symbols n_j , H_j , A_j denote concentration, scale height and ionization cross section; the suffix $j=1$ is used for O and $j=2$ for N_2 . The cross sections A_j are assumed to be independent of wavelength.

The processes envisaged are as follows:

- (i) Electrons are produced by the photo-ionization of atomic oxygen at a rate $q(h) = A_1 n_1(h) S(h)$, where $S(h)$ is the flux of ionizing photons at height h .
- (ii) A proportion of the ionizing radiation is absorbed by N_2 and does not contribute to the observable ionization because the N_2^+ ions recombine rapidly. The ratio of the flux $S(h)$ at height h to the flux S_∞ incident at the top of the atmosphere (which is assumed to be horizontally stratified) thus depends on the distribution of both gases along the path traversed by the radiation.

(iii) The loss process involves an atom-transfer reaction between O^+ ions and N_2 molecules, the resulting NO^+ ions being rapidly lost by dissociative recombination (Bates and Massey 1948). The loss rate is thus $\beta = \lambda n_2$ where λ is the rate coefficient of the transfer reaction, which is assumed independent of height. (iv) At the top of the F region, the ionization is in diffusive equilibrium.

Low down in the F region, the loss rate is not directly proportional to the electron density as assumed in (iii) because the recombination of NO^+ ions does not proceed rapidly in comparison with the transfer reaction. This circumstance is thought to be responsible for the presence of two peaks of electron density in the F region by day, the F1 and F2 layers (Ratcliffe 1956 a, Hirsh 1959). This bifurcation cannot be reproduced by the analogue, which solves only the linear equation (1) in which the loss rate is proportional to the electron density. In the lower F region the linear equation applies to the concentration of O^+ ions, and the additional electrons associated with molecular positive ions are not represented in the analogue.

With sufficient accuracy for present purposes, the production function given by (i) and (ii) may be written as

$$q = S_{\infty} A_1 n_1 \exp \{ -Ch \chi (n_1 A_1 H_1 + n_2 A_2 H_2) \}, \quad \dots (2)$$

in which $Ch \chi$ is the function defined by Chapman (1931 a, b) and approximates to $\sec \chi$ for $\chi < 85^\circ$.

The plasma diffusion coefficient D is assumed to be given by the relation

$$\frac{1}{D(h)} = \left[\frac{n_1}{b_1} + \frac{n_2}{b_2} \right] \left[\frac{T + 187^\circ}{T^{3/2}} \right]. \quad \dots (3)$$

The dependence of D upon the absolute temperature T is that suggested by Ferraro (1945) and takes account of attractive intermolecular forces. According to Dalgarno (1958), O^+ ions diffuse more slowly in the parent gas than in other gases, and it is later assumed that $b_1 = \frac{1}{4} b_2$. Shimazaki (1957) has shown that if μ is the ratio of the molecular weight of the plasma to that of the neutral atmosphere, and H the atmospheric scale height, then the velocity of diffusion w_D is given by

$$-w_D = D(h) \left[\frac{1}{N} \frac{\partial N}{\partial h} + \frac{1}{T} \frac{\partial T}{\partial h} + \frac{\mu}{H} \right]. \quad \dots (4)$$

The differential equation obtained by combining Eqns (1) and (4) may be transformed into a type suitable for analogue solution by means of two changes of variable, which remove terms due to gravity and temperature gradients. A limiting height h_a is chosen, at the bottom of the F region, and two new variables x and X are introduced, defined by the equations

$$x = \frac{T_a}{T} \exp \left[- \int_{h_a}^h \frac{\mu}{H} dh \right] \quad \dots (5)$$

$$X = \int_{h_a}^h x dh. \quad \dots (6)$$

The variable x is dimensionless, and decreases from unity at $h = h_a$ to zero at infinite height; it is approximately proportional to the gas pressure. X has the dimensions of length and increases from zero at $h = h_a$ to a finite value X_∞ as $h \rightarrow \infty$. X is termed 'analogue height' and it naturally depends upon the model atmosphere employed.

The dependent variable employed is v , where

$$N(h, t) = x(h)v(h, t). \quad \dots\dots (7)$$

The assumption of diffusive equilibrium of ionization at the top of the atmosphere implies that $NT \sim \exp(-\mu h/H)$ as $h \rightarrow \infty$, so that $N \propto x$. At any height δX represents the number of electrons in a unit column of extent δX in 'analogue height' X , and of extent $\delta h = \delta X/x$ in 'real height' h .

Table 1. Some Numerical Data

(i) Atmospheric model

Top	$h = 735$ km,	$H = 78$ km,	$X = 40.94$ km,	$x = 0.0057$
Bottom	$h = 140$ km,	$H = 20$ km,	$X = 0.00$ km,	$x = 1$
Interval			$\Delta X = 0.89$ km	
Composition	$n_1/n_2 = 0.76$ whence (above 250 km) $\mu = 0.35$			
Diffusion	$b_2 = 4b_1 = 2.5 \times 10^{18} \text{ cm}^{-1} \text{ deg}^{-1/2}$			
Loss	$\lambda = 1.75 \times 10^{-13} \text{ cm}^3 \text{ sec}^{-1}$			
Production†	$S_\infty = 7.9 \times 10^8 \text{ cm}^{-2} \text{ sec}^{-1}$			
	$\bar{A} = \frac{n_1 A_1 + n_2 A_2}{n_1 + n_2} = 1.3 \times 10^{-17} \text{ cm}^2$			

Function	Peak value	Height	Nearest source	Nearest condenser
q	$400 \text{ cm}^{-3} \text{ sec}^{-1}$	200 km	$i = 5$	$n = 25$
q/x	$3050 \text{ cm}^{-3} \text{ sec}^{-1}$	228 km	$i = 6$	$n = 29$

(ii) Circuit

Period of revolution of cams = 24 sec

Whence time-scaling factor = $\tau = 3600$

13 cams at heights h_i of 150(10)180(20)280(40)400 and 480 km

47 condensers, $4 \mu\text{F}$ (within 3%)

Typical values of resistors:

Feeding (r_n) 2 M Ω ($n < 40$) 10 M Ω ($n \geq 40$)

Loss (ρ_n) 4.5 k Ω ($n = 0$), increasing to 5 M Ω ($n = 42$); omitted for $n > 42$

Diffusion (R_n) greatest value 8.9 k Ω at $n = 25$, decreasing to 4.8 k Ω at $n = 1$ and to 1.3 k Ω at $n = 46$

(iii) Calibration

The greatest noon voltage is 6.7 v on source $i = 6$. By substitution in Eqn (11), it is found that:

$$F = 1.3 \times 10^7 \text{ cm}^{-3} \text{ v}^{-1} = 1.8 \times 10^8 \text{ cm}^{-3} \text{ per division on chart}$$

† Calculated for sunspot minimum conditions at equinox, latitude 52° .

The variations of n_1 , n_2 , H and T with height have been taken from a model atmosphere computed by Dr. K. Weekes and based on rocket and satellite data (see Rishbeth and Barron 1960, Fig. 8). In that model, complete mixing of O and N₂ at all heights is postulated, so that the ratio n_1/n_2 is independent of height.

This is admittedly unrealistic but greatly simplifies the calculation of $q(h, t)$ and of $D(h)$. The limit h_a is taken at 140 km, low enough to include all levels at which the rate of production of ionization is appreciable. From 560 km to the upper limit of the model, at 735 km, the scale height is assumed to be independent of height. A few numerical values are shown in Table 1, and the variation with height of x and X plotted in Fig. 1. The production functions are computed for equinox in latitude 52° .

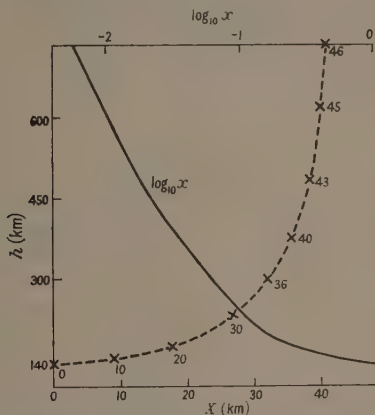


Fig. 1. Variation with height of the coordinates x and X , calculated from Weekes' data by Eqns (5) and (6). The locations of a few condensers are marked.

The value of μ depends on the composition of the neutral atmosphere and the nature of the positive ions. In the F region, above 250 km, nearly all the ions are thought to be O^+ , and if the atmosphere consisted entirely of atomic oxygen μ would be $\frac{1}{2}$, a value often used in theoretical work. With the model used here, in which $n_1/n_2 = 0.76$, it is found that $\mu = 0.35$. Below 250 km, however, the relative abundance of different kinds of ion varies with height, and so μ has been estimated from the results of Johnson, Meadows and Holmes (1958) obtained with a rocket-borne ion spectrograph. The uncertainties introduced by this procedure should not be serious near the level of maximum ionization of the F region, and the present results are mainly concerned with the behaviour at this level and above it.

With the substitutions and transformations outlined above, the continuity equation (1) becomes an equation for v , namely

$$\frac{\partial v}{\partial t} = \frac{q}{x} - \beta v + \frac{\partial}{\partial X} \left[Dx^2 \frac{\partial v}{\partial X} \right]. \quad \dots (8)$$

This transformed equation contains a modified production rate q/x . The diffusion term is now of the standard form appropriate to a straightforward diffusion equation with a diffusion coefficient Dx^2 and the additional terms in the original equation, which represented the effects of gravity and vertical temperature gradients, have disappeared.

§ 3. THE CIRCUIT

A section of the network is shown in Fig. 2. The charge $C_n V_n$ on the n th condenser represents the electron density at one height. This charge is dissipated by leakage through the resistance ρ_n , which represents the 'loss' of ionization by recombination. Charge can also be transferred between condensers by the resistances R_n , and this corresponds to 'vertical diffusion' in the ionosphere. The applied voltage Q_n is varied periodically and simulates the diurnally varying 'rate of production' of ionization. Because the time variation of the production function is different at different heights, the voltages Q_n are controlled by a number of cams cut to the appropriate profiles and mounted on a common shaft.

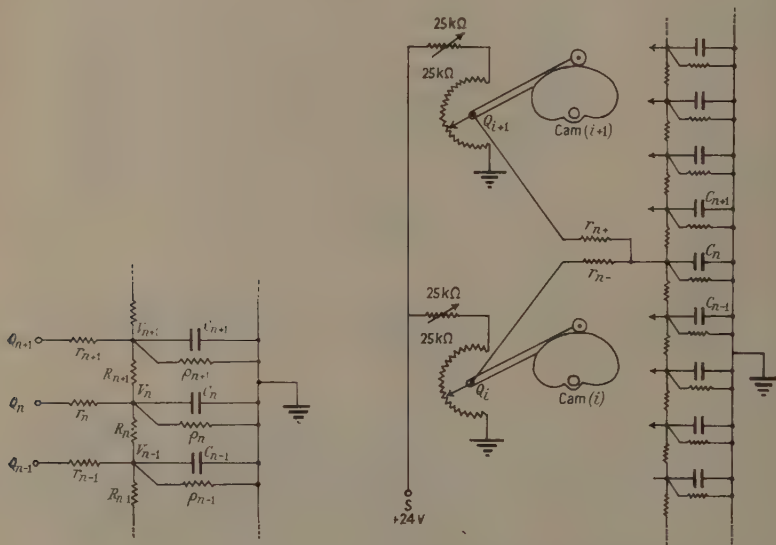


Fig. 2. Section of idealized circuit.

Fig. 3. Diagram of voltage supply, showing how the potential applied to each condenser C_n is derived by interpolation from two cam-controlled voltages Q_i , Q_{i+1} . The special 'eclipse' cam (not shown) varies the voltage supplied at S.

The equation satisfied by the voltage V_n is

$$C_n \frac{\partial V_n}{\partial t} = \frac{Q_n - V_n}{r_n} - \frac{V_n}{\rho_n} + \frac{V_{n+1} - V_n}{R_{n+1}} - \frac{V_n - V_{n-1}}{R_n}. \quad \dots\dots (9)$$

This may be rewritten by expressing the finite differences of neighbouring voltages in terms of differentials, and becomes

$$\frac{\partial V_n}{\partial t} = \frac{Q_n}{C_n r_n} - \frac{V_n}{C_n} \left[\frac{1}{\rho_n} + \frac{1}{r_n} \right] + \frac{\partial}{\partial n} \left[\frac{1}{C_n r_n} \frac{\partial V_n}{\partial n} \right], \quad \dots\dots (10)$$

This equation is similar to (8), and with a suitable choice of parameters the condensers C_n may be 'labelled' with corresponding heights h_n , which are spaced at equal intervals ΔX in analogue height. A time-scaling factor τ must also be chosen; it is the ratio of the periods of the solar production function (one day) and of the revolution of the cams (twenty-four seconds). Another scaling factor F is required to convert the voltage V into the independent variable v ; this is expressed in units of $\text{cm}^{-3}\text{v}^{-1}$, and must be determined in each experiment. It then follows that at the height h_n ,

$$q(h_n)/x_n = FQ_n(C_n r_n \tau)^{-1} \quad \dots\dots (11)$$

$$\beta(h_n) = (C_n \rho_n' \tau)^{-1} \quad \dots\dots (12)$$

$$D(h_n) = (\Delta X)^2 (C_n R_n' \tau x_n^2)^{-1}, \quad \dots\dots (13)$$

where

$$R_n' = \frac{1}{2}(R_n + R_{n+1}) \quad \dots\dots (14)$$

$$(\rho_n')^{-1} = \rho_n^{-1} + r_n^{-1}, \quad \dots\dots (15)$$

Some numerical data concerning the circuit are given in Table 1. It is not necessary to construct a separate cam for each of the forty-seven condensers because the shape of the production function changes quite slowly with height. In practice thirteen cams are provided, and each condenser is fed by two resistors from adjacent potentiometers as shown in Fig. 3. By choosing these two resistors suitably it is possible to interpolate between the two cams.

In general, a condenser C_n at height h_n is connected through a resistance r_{n-} to the source Q_i at height h_i , and through a resistance r_{n+} to the source Q_{i+1} at height h_{i+1} , where $h_i < h_n < h_{i+1}$. The resistances r_{n-} and r_{n+} present a combined parallel resistance r_n , and their ratio depends on the analogue heights X_i , X_n , X_{i+1} . If

$$\theta = (X_n - X_i)/(X_{i+1} - X_n), \quad \dots\dots (16)$$

then

$$r_{n-}/r_n = \theta + 1, \quad r_{n+}/r_n = (\theta + 1)/\theta \quad \dots\dots (17)$$

and

$$r_n^{-1} = r_{n-}^{-1} + r_{n+}^{-1}. \quad \dots\dots (18)$$

The camshaft is driven by an electric motor, and the cams operate the potentiometers through gears so that a larger angular movement can be obtained. The output of the i th potentiometer varies with time in accordance with the ratio $q(h_i, t)/q(h_i, 12^h)$. Each potentiometer is connected to a fixed voltage through a variable resistor which is adjusted to give the correct output at 'noon', and not afterwards changed. The total resistance in each potentiometer circuit ($\sim 50 \text{ k}\Omega$) is small compared with the resistances r_n ($\geq 2 \text{ M}\Omega$).

To investigate the effects of a solar eclipse, another potentiometer is used, operated by a cam mounted on the same camshaft. This 'eclipse cam' is cut to give the required obscuration function appropriate to the eclipse which is being studied. The output of the potentiometer is used to feed all the other potentiometers, in place of the fixed voltage normally used. A change-over switch can be arranged so that the main bank of potentiometers can be fed from either the fixed voltage or the 'eclipse potentiometer'; in this way, results for an 'eclipse day' and a 'control day' can be obtained in rapid succession. In this method of

simulating an eclipse it is assumed that the time variation of the eclipse function has the same form at all heights; this is not strictly accurate but it is a good approximation for an eclipse which takes place near noon.

The voltages $V_n(t)$ are recorded one at a time by connecting the condensers to a cathode-follower followed by an amplifier, whose output operates a pen-recorder. The scale of the chart is calibrated in terms of the variable v by recording the production voltages $Q_i(t)$ on the chart (Fig. 4); this enables the calibration factor F to be computed from Eqn (11). The electron density at any height h_n is then found by multiplying the deflection by $x(h_n)$. Another pen on the same recorder is used for timing purposes. The time constant of the recorder is about $\frac{1}{2}$ sec.

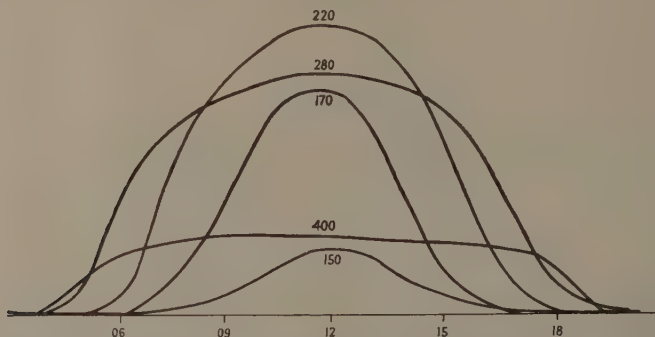


Fig. 4. Outputs of five of the 'production' potentiometers, as functions of apparent time. The height represented, in kilometres, is marked on each curve.

Figure 4 shows the curves obtained by recording the outputs $Q_i(t)$ of a few potentiometers, and so demonstrates the well-known characteristics of the production functions. At great heights, production is small and approximates to an 'on-off' function. The amplitude of $Q_i(t)$ increases with decreasing height and reaches its greatest amplitude for the sixth source at $h = 220$ km. Below this, the amplitudes of the production curves decrease rapidly with decreasing height, and Q is only appreciable for a few hours around noon.

In a different kind of experiment, which will be called a 'pulse' experiment, the behaviour of a slab of electrons injected at a certain height is investigated with the use of a network of condensers and resistors alone. For this purpose, the resistances r_{n-} , r_{n+} are connected to ground instead of to the potentiometers and a $4\mu\text{F}$ condenser is charged to a suitable voltage and momentarily connected across one of the condensers C_n ; a timing pulse is simultaneously fed to the timing pen. The voltage-time curve on each condenser is recorded and converted to an electron density curve as described above.

§ 4. DISCUSSION OF RESULTS

4.1. Introduction

Three kinds of $N(t)$ curves are obtained with the analogue computer, namely 'diurnal', 'eclipse' and 'pulse' curves. In each case a set of curves can be used to find how the electron density varies with height at fixed times. Examples will be given in §§ 4.2–4.4.

In considering the experimental results, it is necessary to bear in mind the limitations of the method. The accuracy is mainly determined by the finite number of condensers, which determines the step length ΔX in the integration by the circuit of the differential equation. The error in the determination of the level of maximum electron density, for example, is of the order of one step (i.e. about 10 km at $h = 250$ km). In addition, there is some uncertainty in the reading and calibration of the chart; an accuracy of about 5% is attempted.

It should be emphasized that the diffusion coefficients (b_1, b_2) used for these initial investigations are larger, by a factor of about five, than those which may be appropriate to the actual F region. Consequently, the results presented here may be thought of as showing the maximum possible effects of diffusion in the F region. Further experiments with smaller values of diffusion coefficient are in hand.

4.2. Diurnal Variations

A set of $V(t)$ curves is shown in Fig. 5, and the derived $N(h)$ curves in Fig. 6. In general, the level h_m of maximum ionization is found to lie in the region where the 'diffusion rate' D/H^2 and the loss coefficient β are comparable, as

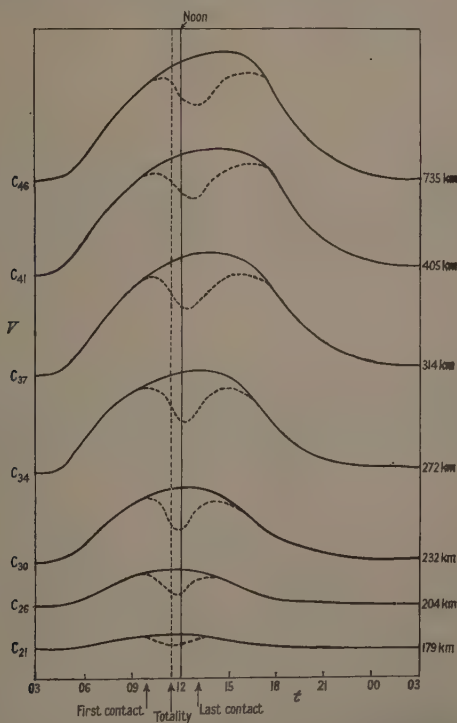


Fig. 5. 'Diurnal' $V(t)$ curves for seven condensers, whose serial numbers and heights in kilometres are shown on the left. The dashed curves refer to an 'eclipse' the timing of which is shown by the arrows below the scale of hours. The centre arrow marks the time of 'totality'; the others show 'first contact' and 'last contact'.

suggested by Rishbeth and Barron (1960). During the night, h_m approaches a constant level and the ionization at all heights decays with approximately the loss coefficient appropriate to that level. By day, the bulk of the production of ionization takes place well below the level h_m , which is lower than it is at night. In the following description of results the level of maximum ionization h_m will for brevity be called the 'F2 peak'.

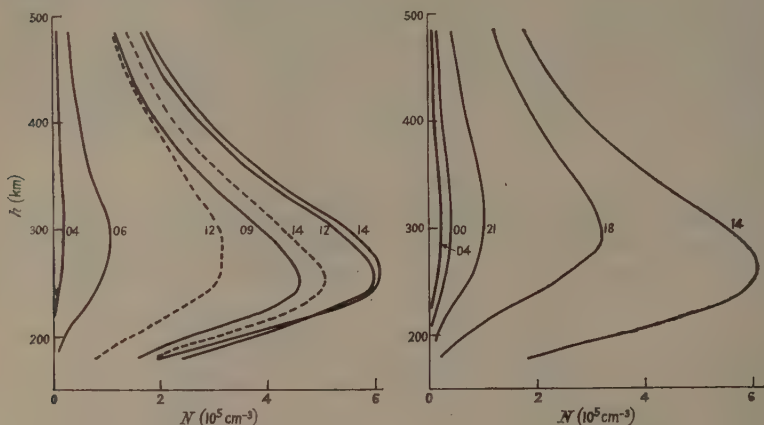


Fig. 6. Electron density distributions, or (N, h) curves, calculated from the (V, t) curves of Fig. 5. The left-hand diagram shows the increase of electron density, from 04^h 'apparent time' (before sunrise) to 14^h; the 'eclipse' (N, h) curves for 12^h and 14^h are shown dashed. The right-hand diagram shows the decrease of electron density during the afternoon and night.

It is interesting to consider the times of maxima of the (V, t) curves at different heights (Fig. 5). These are shown in Table 2 and compared with the values of $1/\beta$ at each height. Below the level of the F2 peak the maximum electron density at a height h occurs at a time of the order of $1/\beta(h)$ after noon, as would be expected if only production and loss processes were important (Appleton 1953). Above the peak production and loss are both small, and the variation of electron density is controlled by diffusion and closely follows the variation at the peak. This is manifested in the circuit by the form of the voltage-time curves, which are almost identical for all condensers above the peak ($n > 35$). In terms of the circuit this is because the top condensers are effectively connected in parallel and have negligible leakage. The time constant for the equalization of charge between neighbouring condensers is very short; for example, $C_n R_n = 0.016$ sec for $n = 40$, representing a scale time in the ionosphere of only one minute.

Another way of showing the effect of diffusion is to plot measured voltages as a function of condenser number n , at fixed times (Fig. 7). Near the top, V is independent of height and so the corresponding $N(h)$ curve is exponential (Fig. 8).

The equilibrium $N(h)$ curve for noon (obtained with the cams stationary) is compared in Fig. 8 with the function $q(h)/\beta(h)$ to show how a peak is produced by the action of diffusion. Below the peak, the electron density is not very

different from the ratio q/β , and diffusion has little effect. The peak occurs at 250 km, at which height the ratio $\beta H^2/D = 1.1$; this agrees well with the results of Rishbeth and Barron (1960) which were based on the assumption of equilibrium (i.e. $\partial N/\partial t = 0$). The $N(h)$ curve for 14^h in the time-varying solution is copied from Fig. 6, to show how the F2 layer approaches equilibrium conditions in the afternoon.

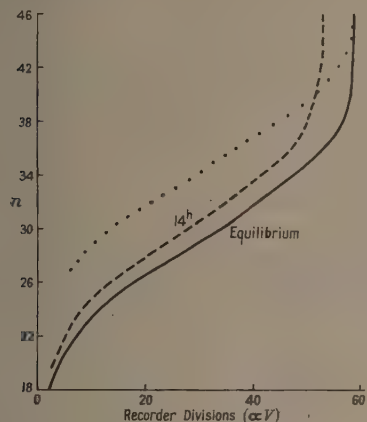


Fig. 7. Distributions of voltages on condensers C_n . Full curve, equilibrium, cams stopped at noon. Broken curve, time 14^h of diurnal variation, from Fig. 5. Dotted curve, pulse experiment of § 4.4; the 'shape-preserving' distribution (scaled to coincide at the top with the full curve).

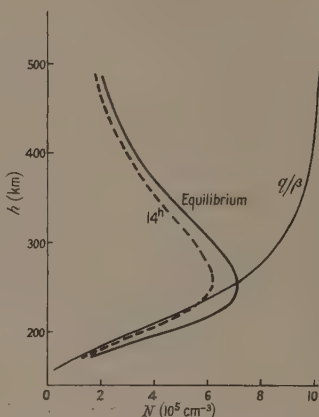


Fig. 8. (N, h) distributions derived from Fig. 7 for noon equilibrium (continuous line), and for the diurnal variation at 14^h (broken line) from Fig. 6. The thin continuous line shows the 'equilibrium' electron density distribution $N = q/\beta$ which would be obtained if there were no diffusion and if $\partial N/\partial t$ were negligible.

The $N(t)$ curves are similar to those obtained by Gliddon and Kendall (1960). These authors assumed an isothermal atmosphere and obtained a solution of the continuity equation in terms of analytic functions, which were evaluated with a digital computer.

4.3. Eclipse Effects

An initial study of eclipse effects has been made with the special cam set to give an eclipse near noon. The results are not meant to represent any particular eclipse, but to indicate the kind of effects produced. In this example, 'first contact' occurs at 10^h apparent time, 'totality' at 11^h30^m, and 'last contact' at 13^h, so that the duration of the whole eclipse is three hours.

The effects observed are illustrated by the dotted curves of Fig. 5 and summarized in Table 2. The greatest reduction of electron density varies from 38% at the top of the F region to 70% at 180 km, and occurs later than totality; the time lag is comparable with $1/\beta$ at heights below the peak, but above the peak the variation of electron density is controlled by diffusion and closely follows that at the peak. This is consistent with the behaviour noted in connection with the diurnal $N(t)$ variation.

Two $N(h)$ curves are shown in Fig. 6. At 12^h the effect of the eclipse is near its maximum; the $N(h)$ curve is flat near the peak, and it is possible that more accurate measurements would show an 'F1₂' stratification' of the type suggested by Ratcliffe (1956b). By the time of the next $N(h)$ curve plotted, at 14^h, the effect of the eclipse has diminished, and it disappears before 18^h.

Table 2

(1)	(2)	(3)	(4)	(5)	(6)
21	179	70	0.2	0.2	0.12
26	204	60	0.3	0.4	0.25
30	232	53	0.6	0.8	0.5
34	272	48	0.9	1.5	1.2
37	314	42	1.1	2.0	2.6
41	405	38	1.3	2.4	12.8
46	735	38	1.4	2.6	1000

(1) Condenser number; (2) height (km); (3) percentage reduction in electron density due to eclipse; (4) delay in time of minimum electron density after totality (hours); (5) delay in time of maximum electron density after noon for normal day (hours); (6) value of $1/\beta$ at each height (hours).

4.4. The Pulse Experiment

Figure 9 shows the $V(t)$ curves for a 'pulse' experiment, in which the condenser C_{46} , corresponding to the 'top' of the F region, was suddenly given a charge. For condensers near to the point of entry of the pulse the response is immediate, but the response at more distant points in the circuit is delayed.

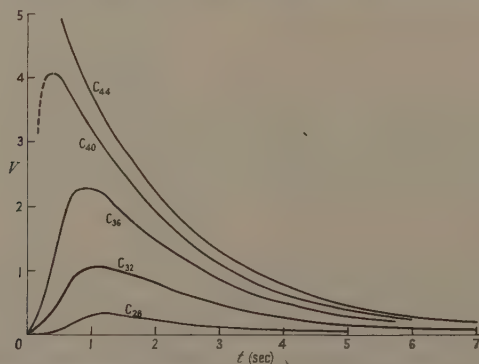


Fig. 9. (V, t) curves for several condensers, obtained by injecting a pulse at the 'top' of the circuit. The initial response is somewhat influenced by the recorder characteristics. The unit of the time scale is 1 second, representing 1 hour in the ionosphere.

After the initial rise, the voltage on all condensers decays with approximately the same time constant. From the voltage distributions at selected times $N(h)$ curves may be constructed (Fig. 10), and these show that the ionization spreads out into a distribution which after about two hours maintains a constant shape.

and decays with a time constant which is approximately the time constant $C_{ii}\rho_{ii}$ appropriate to the level of the peak of N . It is found that wherever the pulse is introduced, the same shape-preserving distribution is finally obtained. Since the circuit is linear, this result may be generalized to the conclusion that any initial distribution of voltage on the condensers will evolve into this particular form.

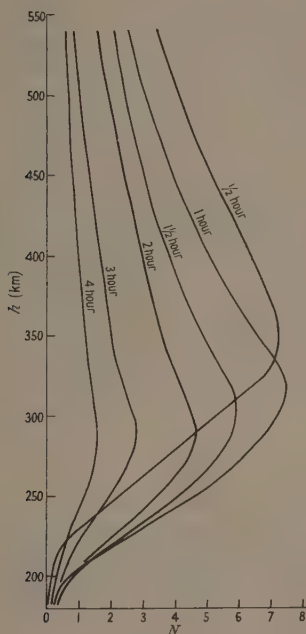


Fig. 10. (N, h) curves for the 'pulse' experiment at times of $\frac{1}{2}$, 1, $1\frac{1}{2}$, 2, 3 and 4 seconds after the injection of the pulse at the 'top' of the circuit (i.e. $\frac{1}{2}$, 1, $1\frac{1}{2}$, 2, 3 and 4 hours in the ionosphere). The curves show the development of the 'shape-preserving' distribution. The scale of N is arbitrary.

The 'shape-preserving' distribution of voltage is shown in Fig. 7, its amplitude having been chosen for comparison with the 'noon equilibrium' distribution discussed in §4.2. The decrease of voltage with increasing distance from the 'top' of the circuit is slower in the case of the 'noon equilibrium' distribution because of the steady supply of current at lower levels.

The results of the 'pulse' experiment are of interest in connection with the behaviour of ionization in the F region at night, when production is absent. The observed changes of the distributions are not unlike those described by Shimazaki (1957).

It has been shown (Dungey 1956, Duncan 1956, Martyn 1956) that in an isothermal atmosphere an ionized layer would develop into a certain form, under the influence of diffusion and loss, and would then decay without change of shape.

In the special case in which the loss coefficient β decreases exponentially upward with a scale height equal to that of the neutral atmosphere, the shape-preserving solution is a 'Chapman alpha' layer, with its peak at the level where $\beta H^2/D = \frac{1}{4}$, and it decays with the loss coefficient appropriate to this level.

The model atmosphere used for the first version of the analogue computer does assume this variation of β with height, but it is not isothermal. The shape-preserving layers which are formed are very like 'Chapman alpha' layers; their peak is at the level where $\beta H^2/D = 0.3$, and they decay with an apparent loss coefficient which is approximately 0.6 times the value of β at this level. There is thus a qualitative agreement with theory, satisfactory in view of the experimental accuracy and the fact that the model atmosphere used is not isothermal.

§ 5. CONCLUSION

The previous discussion shows that interesting results can be obtained by using an electrical analogue to solve the continuity equation for the F region. The analogue demonstrates results obtained by several theoretical investigators, and shows how diffusion may control the top of the ionosphere. In some ways the method is limited, in that many important factors (such as electromagnetic movements) must be omitted, and that changes of parameters involve the replacement of numerous components and are thus laborious to carry out. In other ways it is versatile, as it need not be limited to any special, mathematically simple model of the atmosphere.

ACKNOWLEDGMENTS

The authors are indebted to Mr. P. Noble and to Mr. G. D. Stubbings who carried out most of the constructional work; to Mr. J. P. Dougherty, who suggested the transformations of Eqns (5) and (6); and to Mr. J. A. Ratcliffe for his interest in the investigation and his comments on the manuscript of this paper. The atmospheric model adopted was computed from rocket and satellite data by Dr. K. Weekes.

Part of this work was carried out during the tenure by H. R. of a Senior Research Fellowship, for which he is indebted to the Civil Service Commission.

REFERENCES

- APPLETON, E. V., 1953, *J. Atmos. Terr. Phys.*, **3**, 282.
 BATES, D. R., and MASSEY, H. S. W., 1948, *Proc. Roy. Soc. A*, **192**, 1.
 CHAPMAN, S., 1931 a, *Proc. Phys. Soc.*, **43**, 26.
 ——— 1931 b, *Proc. Phys. Soc.*, **43**, 483.
 DALGARNO, A., 1958, *J. Atmos. Terr. Phys.*, **12**, 219.
 DUNCAN, R. A., 1956, *Aust. J. Phys.*, **9**, 436.
 DUNGEY, J. W., 1956, *J. Atmos. Terr. Phys.*, **9**, 90.
 FERRARO, V. C. A., 1945, *Terr. Magn. Atmos. Elect.*, **50**, 215.
 GLIDDON, J. E. C., and KENDALL, P. C., 1960, *J. Geophys. Res.*, **65**, 2279.
 HIRSH, A. J., 1959, *J. Atmos. Terr. Phys.*, **17**, 86.
 JOHNSON, C. Y., MEADOWS, E. B., and HOLMES, J. C., 1958, *J. Geophys. Res.*, **63**, 443.
 MARTYN, D. F., 1956, *Aust. J. Phys.*, **9**, 161.
 RATCLIFFE, J. A., 1956 a, *J. Atmos. Terr. Phys.*, **8**, 260.
 ——— 1956 b, *Solar Eclipses and the Ionosphere* (London: Pergamon), p. 1.
 RISHBETH, H., and BARRON, D. W., 1960, *J. Atmos. Terr. Phys.*, **18**, 234.
 SHIMAZAKI, T., 1957, *J. Radio Res. Lab.*, **4**, 309.

Electrical Breakdown of Liquid Dielectrics

By D. W. SWAN

Queen Mary College, London, E.1

MS. received 7th October 1960, in revised form 17th March 1961

Abstract. Assuming that electron emission from the cathode and collision ionization in the liquid are both necessary for the electrical breakdown of liquid dielectrics, a criterion for breakdown is developed in which the cumulative effects of the applied field and the space-charge field of the positive ions produce a continuously increasing electron current at the cathode. The present theory differs from earlier similar theories in that the ionization occurring in the liquid is considered to be very small even at breakdown, in agreement with recent conduction measurements. The breakdown criterion shows clearly how the measured electric strength can depend on either the cathode or the liquid. The influence on the breakdown measurements of dissolved oxygen is also discussed, and the quantitative predictions of the theory are compared with measurements of the electric strength of liquid argon.

§ 1. INTRODUCTION

THE possible importance of space-charge distortion in electrical breakdown of liquid dielectrics has been realized previously (Macfadyen 1955, O'Dwyer 1954), and a theory has been developed (Goodwin and Macfadyen 1953) in which ions produced in the liquid by collisions between electrons and liquid molecules move to the cathode and enhance the field there to give increased electron emission. At a certain critical field strength this feedback process becomes unstable and breakdown follows. Possibly the most serious objection to the theory is that there is little evidence for collision ionization in liquids, and very large electron multiplication is necessary to satisfy the breakdown criterion. The most recent measurements of conduction in *n*-hexane with pulsed fields up to $1.3 \times 10^6 \text{ v cm}^{-1}$ have indicated that there is practically no ionization occurring even at field strengths just below breakdown (Watson and Sharbaugh 1960), and consequently the theory in its present form is not applicable.

It is the purpose of this paper to derive a criterion for the breakdown of a liquid subject to a steady electric field assuming, as in earlier theories, that space-charge distortion at the cathode is important, but that the ionization taking place in the liquid is small. As a result of this small degree of ionization the magnitude of the field distortion is small also, and this enables certain simplifying assumptions to be made. In the derivation of the theory of Goodwin and Macfadyen (1953), it was assumed that the ionization coefficient was constant at all points in the gap, but since a large multiplication rate was necessary to satisfy their breakdown criterion considerable field distortion would have resulted. O'Dwyer (1954) attempted to improve on this by allowing for non-uniformity of the field in the

basic equations, but he only shows that a cathode effect may be expected in breakdown measurements, the equations being too complicated to take the theory further.

As a basis of the theory it is necessary to assume some law for the emission of an electron current from the cathode as a function of the cathode field. Conduction measurements at fields below breakdown may be described either by a field emission law (Green 1955, Goodwin and Macfadyen 1953) or by a Schottky-type emission law (House 1957), and the recent pulse conduction measurements of Watson and Sharbaugh (1960) are found to give a good fit to both laws. In the following theory it will be assumed that a simple field emission law adequately describes the current-field relationship, but this does not imply that the mechanism of emission is true field emission. Other laws could equally well be used.

§ 2. THEORY

The emission of electrons from the cathode when subject to a field E_c may be described by an equation of the form

$$j_e = A\mu^2 E_c^2 \exp\left(-\frac{B}{\mu E_c}\right) \quad \dots\dots (1)$$

in which j_e is the electron current density, μ is the local field enhancement factor (Lewis 1955) and A and B are constants depending on the cathode surface. It will be assumed that the cathode field is composed of the applied field E_0 and the field E_+ ($\ll E_0$) due to the positive ions produced in the liquid. If j_0 is the electron current density in the absence of space-charge ($E_c = E_0$ in Eqn (1)), then replacing E_c by $E_0 + E_+$ in (1) gives

$$j_e = j_0 \left(1 + \frac{2E_+}{E_0}\right) \exp\left(\frac{BE_+}{\mu E_0^2}\right). \quad \dots\dots (2)$$

It is assumed that μ is independent of field.

If the electronic and ionic mobilities are denoted by k_- and k_+ respectively, and if the ionization coefficient corresponding to a field E is denoted by α , then it may be shown that the field at a distance x from the cathode of a gap of width d is given by (Loeb 1939)

$$\frac{d}{dx}(E^2) = -\frac{8\pi j_e}{\epsilon} \left\{ \frac{1}{k_+} \exp\left(\int_0^d \alpha dx\right) - \left(\frac{1}{k_+} + \frac{1}{k_-}\right) \exp\left(\int_0^x \alpha dx\right) \right\} \quad \dots\dots (3)$$

in which ϵ is the dielectric constant of the liquid. If the distortion due to space-charge is small throughout the whole gap, then E may be replaced by $E_0 + \Delta E$ ($\Delta E \ll E_0$) and little error will be introduced by assuming that the value of α at every point in the gap is that corresponding to the applied field E_0 , denoted by α_0 .

Integrating (3) and writing $E^2 = E_0^2 + 2E_0\Delta E$ leads to the following expression for the field enhancement,

$$\Delta E = \frac{1}{2\epsilon E_0} \left\{ C - \epsilon E_0^2 - 8\pi j_e \left[\frac{x}{k_+} \exp(\alpha_0 d) - \left(\frac{1}{k_+} + \frac{1}{k_-}\right) \frac{1}{\alpha_0} \exp(\alpha_0 x) \right] \right\}.$$

The constant of integration C may be evaluated by noting that

$$\int_0^d \Delta E dx = 0,$$

and an equation for the cathode field distortion E_+ is obtained by setting $\alpha = 0$. After some rearrangement this gives

$$E_+ = G j_e \quad \dots\dots (4)$$

where

$$G = \frac{4\pi d}{\epsilon k_+ E_0} \left[\frac{1}{2} \exp(\alpha_0 d) - \left(\frac{1}{k_+} + \frac{1}{k_-} \right) \frac{k_+}{\alpha_0^2 d^2} \{ \exp(\alpha_0 d) - \alpha_0 d - 1 \} \right]. \quad \dots\dots (5)$$

If the rate of ionization occurring in the liquid is small, then $\alpha_0 d$ is small and (5) may be simplified to give

$$G = \frac{2\pi d}{\epsilon k_+ E_0} \left(\alpha_0 d - \frac{k_+}{k_-} \right). \quad \dots\dots (6)$$

The sign of the cathode field distortion is therefore determined by the magnitude of $\alpha_0 d$ and the ratio k_+/k_- . The minimum value of $\alpha_0 d$ required to give a positive field enhancement at the cathode will therefore be different for different liquids, since the ion mobilities may differ widely from one liquid to another.

Much of the experimental work on the breakdown of liquid dielectrics has been concerned with the paraffin hydrocarbons, and of these *n*-hexane has been studied most extensively. This liquid may therefore be considered as representative of the normal liquids used in breakdown experiments. The mobility of the negative ion in *n*-hexane has been investigated in some detail (LeBlanc 1959, Chong and Inuishi 1960, Gzowski and Terlecki 1959), but in recent years there has only been one report of the mobilities of both positive and negative ions (Gzowski and Terlecki 1959). These latter measurements were taken with electric fields less than 1 kv cm^{-1} , and the ratio k_+/k_- was found to be 0.308. While there is evidence that the negative ion mobility is independent of field up to 500 kv cm^{-1} (Chong and Inuishi 1960) it has been suggested that at fields near to the normal breakdown level (about 1 MV cm^{-1}) an increase in mobility may be expected if the electron can be stripped from the hexane molecules by the high fields (Crowe 1956, LeBlanc 1959). The large conduction currents measured by Watson and Sharbaugh (1960) and by Macfadyen and Helliwell (1959) are suggestive of a high mobility ion. Direct measurements of the ion mobilities at breakdown field strengths in these hydrocarbons are necessary before the predictions of the present theory may be compared quantitatively with the existing breakdown measurements, but if it is assumed that k_- may increase from the low field value by a factor of ten at breakdown fields, then k_+/k_- would be only about 0.03. Thus even in the complex liquids $\alpha_0 d$ required for a positive cathode field enhancement can be small, and the theory to be developed here could then be applicable to these dielectrics.

However, it has been established that electrons in liquid argon remain free even at very low fields (Williams 1957), and the ratio k_+/k_- at a field of 100 kv cm^{-1} is about 10^{-4} . Consequently, even for very small $\alpha_0 d$ the factor k_+/k_- in Eqn (6) may be neglected and G may be simplified further to give

$$G = \frac{2\pi\alpha_0 d^2}{\epsilon k_+ E_0}. \quad \dots\dots (7)$$

The electric strength of liquid argon has been reported recently (Swan and Lewis 1960), and it is therefore an ideal liquid for comparison between the

present theory and experiment. During breakdown no solid deposits are formed on the electrodes, and this has enabled a thorough investigation of electrode effects to be made. For the hydrocarbon liquids many of these effects may be obscured by deposits on the electrode surfaces. Further calculations will therefore be concerned principally with liquid argon, but the same reasoning may be applied to other liquids, bearing in mind that the important parameters are the positive ion mobility k_+ and the ratio k_+/k_- at breakdown.

The factor G in Eqn (7) contains the ionization coefficient α_0 , and it is necessary to specify the form of the variation of this coefficient with field. There are no measurements of α in liquids and the choice of the function $\alpha(E)$ is purely arbitrary. In the absence of evidence to the contrary it seems reasonable to assume that the same law for the gas phase may be extended into the liquid phase. Ward (1958) has found that over a very wide range of E/p the variation of α_0 for argon may be expressed as

$$\alpha_0 = C \exp\left(-\frac{D}{E_0^{1/2}}\right) \quad \dots\dots (8)$$

where the constants C and D involve the gas pressure.

Introducing this into (7), and combining with (4) allows the cathode field E_c to be expressed as

$$E_c = E_0 + \frac{2\pi j_e c d^2}{\epsilon k_+ E_0} \exp\left(-\frac{D}{E_0^{1/2}}\right) \quad \dots\dots (9)$$

Figure 1 shows the cathode emission current j_e plotted as a function of cathode field E_c from both Eqns (1) and (9). The ionization and emission constants are given on the diagram together with the values of the other parameters used in the calculation. For low applied fields the characteristics intersect in two places. The smaller of the two intersections represents the stable conduction current finally established, while the second represents an unstable state analogous to many other physical problems, and has no practical significance. For very large applied fields there is no intersection of the characteristics and consequently

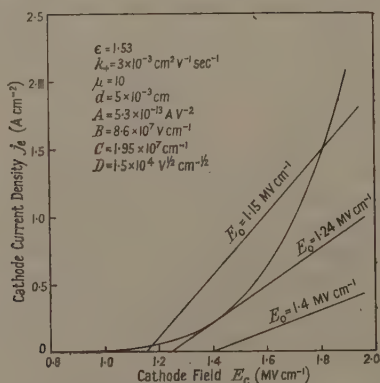


Fig. 1. Graphical representation of Eqns (1) and (9). The curve represents the cathode emission (Eqn 1), while the straight lines show the cathode field-emission current relationship due to the space-charges (Eqn (9)).

there is no stable emission current. Physically this means that the number of ions produced in the liquid causes the cathode field, and therefore the emission current, to increase continuously. The condition for which the two characteristics are tangential therefore represents the state where a stable emission current will be established, but where a slight increase of E_0 will cause this current to increase indefinitely. This is taken to represent the breakdown condition. It is clear that when the breakdown criterion is satisfied the emission current is not infinite, and the cathode current density at breakdown may be conveniently evaluated from Eqns (4) and (2).

Combining these gives

$$j_e = j_0(1 + Pj_e) \exp(Qj_e) \quad \dots\dots (10)$$

where

$$P = 2G/E_0 \quad \text{and} \quad Q = BG/\mu E_0^2.$$

This equation has two roots for small j_0 , the smaller one corresponding to the stable conduction current as before. At breakdown these roots are coincident and therefore $\partial/\partial j_e$ of both sides of (10) must be equal. The quantities P and Q depend on the applied field E_0 , and before differentiating (10) these must be examined in more detail. Using Eqns (7) and (8), and the constants as given on Fig. 1, the quantities P and Q are found to increase by a factor of about ten when the applied field is increased from 0.8 MV cm^{-1} to 1.5 MV cm^{-1} . For the same field change at the cathode Eqn (1) predicts that j_e is increased by a factor of 10^3 , and thus P and Q are only weak functions of j_e and may be considered as constants in Eqn (10). Any realistic form of α_0 as a function of field would lead to a similar result. Differentiating (10) and solving for j_e at breakdown gives

$$j_e^* = E_0^* \Omega / 4G \quad \dots\dots (11)$$

where $\Omega = [1 + (8\mu E_0^* / B)]^{1/2} - 1$, and the asterisk denotes the values of the parameters at breakdown. Introducing (11) into (2) gives the breakdown criterion

$$\Omega = 2GA\mu^2 E_0^* (2 + \Omega) \exp[-(4 - \Omega)B/4\mu E_0^*].$$

Clearly an explicit expression for E_0^* is not possible, but if G is replaced by (7) and α_0 by (8) an explicit relationship for d^* may be obtained in the form

$$d^* = \left[\frac{\Omega \epsilon k_+}{4\pi\mu^2 AC(2 + \Omega)} \right]^{1/2} \exp \left[\frac{D}{2E_0^{*1/2}} + \frac{B(4 - \Omega)}{8\mu E_0^*} \right]. \quad \dots\dots (12)$$

If the cathode constants are known, and α_0 is a known function of E_0 , then d^* may be calculated for a given applied field and the breakdown voltage determined.

§ 3. APPLICATION AND DISCUSSION

Equation (12) shows how the liquid and the cathode can both influence the breakdown voltage at a given gap setting. The first term in the exponential is the ionization term and therefore represents liquid properties, while the second term contains the constants of the cathode. Clearly, depending on the relative magnitudes of these two terms, the cathode may be important or the ionization term may completely mask any cathode changes. For example, if D is very large and the first term predominates, the ionization occurring is small (from (8)), and the field necessary to give breakdown is set by a certain degree of ionization,

there being ample electrons available from the cathode by virtue of the smaller term in B . Under these conditions changes in B are not important and the breakdown voltage would not depend on cathode material. On the other hand, if the term in B were predominant the breakdown voltage would depend critically on the cathode, the actual breakdown being governed by the availability of electrons, and not greatly by the ionization rate. Such a balance between two processes, one at the cathode and one in the liquid, has been proposed by Lewis (1953a), and evidence from breakdown measurements using point-plane electrode configurations in n -hexane suggest that this idea is correct.

Figure 2 shows the breakdown voltage-gap width characteristic as calculated from Eqn (12) for two values of the cathode constant B . The ionization and emission constants are as given on Fig. 1. Because of the lack of experimental information on emission and ionization in liquids choice of the constants A , B , C and D is arbitrary, but an attempt has been made to use realistic values. Also shown on Fig. 2 is a typical characteristic obtained experimentally in liquid argon using gold electrodes. Good agreement could be obtained over the whole curve by adjusting the constants, but exact agreement is meaningless in view of the uncertainties involved. Increase of B in Eqn (1) will reduce the emission at a given field, and consequently a higher field is required to cause the breakdown instability. The criterion for breakdown as expressed by Eqn (12) is very sensitive to changes in B or D .

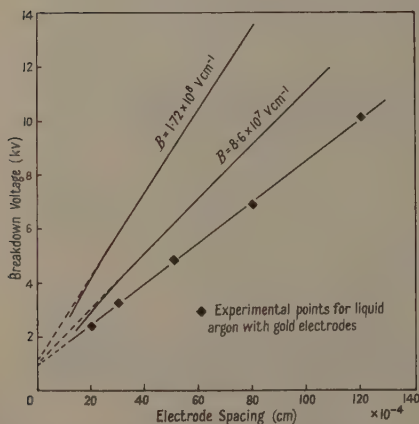


Fig. 2. Breakdown voltage-electrode spacing characteristics calculated from Eqn (12).

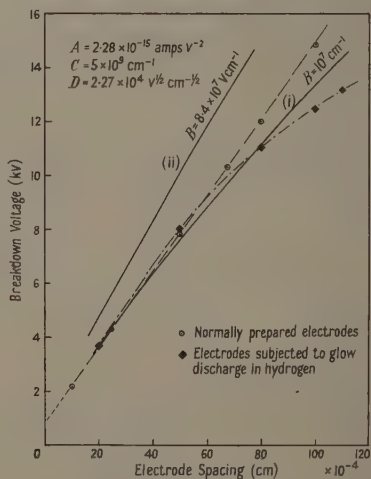


Fig. 3. Breakdown voltage-electrode spacing characteristics calculated from Eqn (12) and compared with measurements in liquid argon.

The shape of the breakdown voltage-gap spacing characteristic depends on which term of the exponential in Eqn (12) is dominant and on the functional relationship of these terms with E_0 . With the forms of emission and ionization laws assumed in the derivation of (12) the characteristic can take two distinctly

different forms depending on whether the term in $E_0^{-1/2}$ or in E_0^{-1} is of greater importance. It is obvious that the term involving $E_0^{-1/2}$ will result in a more non-linear characteristic than the term in E_0^{-1} . This is illustrated in Fig. 3, where curve (i) has been calculated from (12) with a value of B small enough to make the emission term unimportant. It is seen to exhibit considerable curvature and shows that if the electron supply just prior to breakdown is plentiful the actual breakdown voltage depends strongly on the ionization law. A change in the field dependence of α would change the degree of curvature. With the same ionization constants as before curve (ii) of Fig. 3 has been calculated with B increased until the contribution of the emission term became significant. The introduction of a term in E_0^{-1} reduces the curvature, and the characteristic becomes practically linear.

Results of experiments with liquid argon are again in agreement with this theory. Also shown in Fig. 3 are experimentally determined breakdown characteristics for liquid argon using stainless steel electrodes which were prepared by a normal buffing procedure (Swan and Lewis 1960), but which in one case were used directly and in the other were subjected to a glow discharge in hydrogen prior to the breakdown test. With the normally prepared electrodes the characteristic obtained was linear within the experimental error, while with electrodes that had been subjected to a glow discharge in hydrogen there was considerable curvature. In the light of the theory developed above, this suggests that the normally prepared electrode was not emitting strongly and that the breakdown occurred when a certain level of cathode emission was obtained. A glow discharge in hydrogen would reduce much of the oxide on the cathode surface and an increased electron emission would result. The term involving the ionization could now become significant and the curvature of the characteristic would become appreciable depending on the form of α as a function of field. The constants A , C and D were chosen to make the experimental curve and the theoretical curve with small B in reasonable agreement.

In many experimental determinations of the electric strength of liquids it has been found that the breakdown voltage-gap width characteristic does not pass through the origin when extrapolated to zero gap but that there appears to be an intercept on the voltage axis of about 1000 v. It is significant that for electrode spacings in excess of about 2×10^{-3} cm the characteristics calculated from (12) and shown in Fig. 2 are almost linear, and extrapolation of this linear portion back to the voltage axis shows an intercept of about 1000 v. Large changes of the coefficient B do not appreciably alter this voltage. The characteristic obtained with $B = 10^7$ v cm $^{-1}$ in Fig. 3 is not linear in the range of electrode spacings of interest ($d < 10^{-2}$ cm), but for the smaller gap widths a linear approximation also gives an intercept of about 1000 v. Since it is usual to determine the breakdown voltage at only four or five gap widths in the range up to 10^{-2} cm slight curvature may not be noticed and the characteristic assumed linear, showing the same intercept as is obtained when the term in B is predominant. However, if the breakdown is dependent on the ionization term the introduction of an impurity may change the functional form of α with E , which will alter the curvature and possibly also the apparent intercept. The rapid increase in electric strength as the gap becomes smaller (which gives rise to the apparent voltage intercept) could therefore be attributed to the increase in E_0 required to maintain the necessary degree of ionization.

In *n*-hexane which is free of dissolved oxygen, breakdowns can occur with steady voltage stresses as low as 500 kv cm^{-1} . The recent pulse conduction data of Watson and Sharbaugh (1960) have shown that a measurable α process becomes significant only for fields in excess of 1.2 mv cm^{-1} , so that at first sight it would appear that the theory given here can not be applied to the hydrocarbon liquids. However, there is strong evidence to suggest that these low breakdown strengths are caused by spurious effects. Sletten (1960) has examined the behaviour of particles in *n*-hexane under the influence of electric stress, and has found that it is impossible to remove all particles from the gap and electrode surfaces, even with vigorous flushing and careful filtration of the liquid. These particles oscillate between the electrodes, and under certain conditions the arrival of a positively charged particle from the anode on to the cathode surface has been observed to cause the steady conduction current to increase by a factor in excess of 10^5 . Clearly, under these circumstances the mechanism of breakdown might be entirely different.

If short duration impulses are used, the particles do not have time to pass between the electrodes and a higher breakdown strength results. As long as the pulse length is sufficient to allow the positive ion space-charge to accumulate near the cathode without appreciable particle movement the above space-charge theory could hold. For very short impulses the temporal development of the space-charge becomes important.

With air-saturated *n*-hexane the particles do not seem so effective, and in fact are often ejected from the gap after a breakdown (Sletten 1960). Under these circumstances the breakdown strength with direct voltage is found to be about 1.2 mv cm^{-1} , which corresponds to the stress where a measurable α appears. As for measurements in liquid argon, the breakdown voltage-electrode spacing characteristics for the hydrocarbon liquids containing dissolved air exhibit an intercept of about 1 kv (Lewis 1953 b). In liquid argon it is well known that oxygen as an impurity is very efficient in trapping free electrons to form stable negative ions (Davidson and Larsh 1950), and it is possible that this could also occur in *n*-hexane, although the impulse electric strength of this liquid is not affected by the presence of dissolved oxygen, which suggests that attachment may not be important. The breakdown theory developed above could be modified to include electron attachment, but for the present qualitative discussion it is sufficient to note that the loss of electrons to negative ions may be considered as a reduction in α , and that a higher electric field would be necessary to give the required degree of ionization. It is likely that the introduction of oxygen into the liquid will also have an effect at the electrodes where a double layer can be formed due to the chemisorption of the oxygen. This will reduce the emission and change the cathode emission constants.

§ 4. CONCLUSIONS

The theory developed in § 2 differs from previous theories involving a positive ion space charge in that the ionization occurring in the liquid is assumed small, and that the field distortion in the gap is assumed small in comparison with the applied field. From Eqns (4) and (11) the cathode field enhancement is $E_0^* \Omega/4$, and for the two characteristics shown in Fig. 2 the ratio E_+^*/E_0^* is found to be about 0.1. From the definition of Ω in Eqn (11) it is clear that a very low value

of B will give rise to a larger cathode field distortion. The values of $\alpha_0 d$ at breakdown corresponding to the two curves in Fig. 2 are found to be between 0.1 and unity, while the theories of Goodwin and Macfadyen and of O'Dwyer would require $\alpha_0 d$ to be about 10^2 . With such small values of $\alpha_0 d$ it is unlikely that an α process would be observed in conduction measurements at field strength much below breakdown, in agreement with recent pulse conduction measurements (Watson and Sharbaugh 1960).

The electron emission current density as calculated from Eqn (11) is also of a reasonable magnitude, being less than 1 A cm^{-2} in most cases; and if it is assumed that the discharge develops in a filamentary channel of about 10^{-4} cm diameter, the current at breakdown would be approximately 10^{-9} A . The arbitrary choice of constants involved makes exact calculations unnecessary, but the examples given appear to indicate that the theory derived is consistent with the assumptions made.

The electric strength of liquid argon containing small quantities of oxygen in solution has been found to depend strongly on the anode surface condition and material (Swan and Lewis 1960). This may be explained in terms of a space charge of negative ions near to the anode surface which can lead to a degree of ionization greater than that corresponding to the applied field. The space-charge formed at the anode depends on the insulating properties of that electrode and hence on the surface condition. A full discussion of the anode effects and anode space-charge is to be given in another paper (Swan and Lewis 1961). A few additional ions produced in the enhanced field near the anode would alter the breakdown voltage from the value predicted by Eqn (12) for the case where the anode was not important by effectively changing the ionization coefficients C and D .

While space-charge distortion at the cathode combined with an ionization process in the liquid predicts an instability in the current growth, the final development of the discharge is not explained. A possible explanation is that once the instability criterion is satisfied the current density at the cathode spot increases very rapidly, and the energy liberated there vaporizes the liquid to form a bubble. Any pressure dependence of breakdown must in some way be due to changes in the development of the discharge prior to the attainment of the current instability, and it is reasonable to assume that a change in hydrostatic pressure will alter the gas in equilibrium at the cathode surface, which in turn will change the emission constants.

ACKNOWLEDGMENTS

The author would like to thank Professor M. W. Humphrey Davies for facilities provided, and Dr. T. J. Lewis for helpful discussion and supervision during the experimental investigation. The work was performed during the tenure of a maintenance grant by the Department of Scientific and Industrial Research, which is gratefully acknowledged. Thanks are also due to the British Electrical and Allied Industries Research Association for financial assistance in the purchase of equipment.

REFERENCES

- CHONG, P., and INUISHI, I., 1960, *Technology Reports of the Osaka University*, **10**, 545.
- CROWE, R. W., 1956, *J. Appl. Phys.*, **27**, 156.
- DAVIDSON, N., and LARSH, A. E., 1950, *Phys. Rev.*, **77**, 706.
- GOODWIN, D. W., and MACFADYEN, K. A., 1953, *Proc. Phys. Soc. B*, **66**, 85, 815.
- GREEN, W. B., 1955, *J. Appl. Phys.*, **26**, 1257.

- GZOWSKI, O., and TERLECKI, J., 1959, *Acta Phys. Polon.*, **18**, 191.
HOUSE, H., 1957, *Proc. Phys. Soc. B*, **70**, 913.
LEBLANC, O. H., 1959, *J. Chem. Phys.*, **30**, 1443.
LEWIS, T. J., 1953 a, *Proc. Phys. Soc. B*, **66**, 425.
—— 1953 b, *Proc. Instn Elect. Engrs*, **100**, Pt II A, 141.
—— 1955, *J. Appl. Phys.*, **26**, 1405.
LOEB, L. B., 1939, *Fundamental Processes of Electrical Discharges in Gases* (New York: John Wiley).
MACFADYEN, K. A., 1955, *Brit. J. Appl. Phys.*, **6**, 1.
MACFADYEN, K. A., and HELLIWELL, G. C., 1959, *J. Electrochem. Soc.*, **106**, 1022.
O'DWYER, J. J., 1954, *Aust. J. Phys.*, **7**, 400.
SLETTEN, A. M., 1960, *Ph.D. thesis*, University of London.
SWAN, D. W., and LEWIS, T. J., 1960, *J. Electrochem. Soc.*, **107**, 180.
—— 1961, *Proc. Phys. Soc.*, **78**, 448.
WARD, A. L., 1958, *Phys. Rev.*, **112**, 1852.
WATSON, P. K., and SHARBAUGH, A. H., 1960, *J. Electrochem. Soc.*, **107**, 516.
WILLIAMS, R. L., 1957, *Canad. J. Phys.*, **35**, 134.

The Determination of m/e for Free Electrons by Momentum Transfer

By H. A. DAW† AND F. S. HARRIS, JR.

Department of Physics, University of Utah, Salt Lake City

MS. received 25th January 1961

Abstract. A new method for measuring m/e for free electrons has been developed by using momentum transfer. A Faraday cage mounted on a torsion device collects electrons from an electron gun. The change in maximum angular displacement of the fibre with electron beam on and off together with the measured current gave a value of m/e of $5.82 \times 10^{-12} \text{ kg C}^{-1}$ compared to the accepted value of $5.6854 \times 10^{-12} \text{ kg C}^{-1}$.

§ 1. INTRODUCTION

SHORTLY before the turn of the twentieth century a significant physical constant was measured, the ratio of the mass to charge for cathode rays. (Thomson 1897). It has been estimated since, that at least forty-three different methods have been used in making this determination (Hoag and Korff 1948). All of these methods involve however only four basic principles. The four principles may be written as follows in equation form (the symbols have their usual meanings)

$$v = E/B, \quad \dots\dots (1)$$

$$v = s/t, \quad \dots\dots (2)$$

$$Bev = mv^2/r, \quad \dots\dots (3)$$

$$\frac{1}{2}mv^2 = eV. \quad \dots\dots (4)$$

The first equation represents the velocity filter consisting of crossed electric and magnetic fields as used by Thomson. The second equation determines the same information as the first but is a direct measurement on the time of flight of the electronic stream. This principle was incorporated in the experiments of Wiechert and others (Wiechert 1899, Kirchner 1931, Perry and Chaffee 1931). The latter two equations connect the electrical and inertial properties of the electronic stream. The third equation relates the momentum of the stream to the magnetic field strength, while the fourth equation relates the energy of the stream to the applied voltage. Instances where these principles have been used are numerous (Hoag and Korff 1948, Gerlach 1933).

Of the four principles only the time-of-flight velocity determination is independent of the nature of the electromagnetic field interaction of charged particles. Since for a determination of m/e any two of the principles may be used, the combination of (1) with (2) excepted, no determination of this ratio is independent of the nature of the electromagnetic interactions. The nature of the interaction however may be side-stepped if one introduces a new measurement which is independent of the fields, but connects the inertial and electrical properties of the stream. Two solutions suggest themselves: one is to measure

† Now at Department of Physics, New Mexico State University, University Park, New Mexico.

electron beam momentum directly as a function of beam intensity, and the second is the measurement of the power directly as a function of beam intensity. The direct measurement of the momentum transferred per unit time by the cathode ray stream is the subject of this paper. Momentum transfer has been used for ions (Lamar 1933).

§ 2. ELECTRON BEAM MOMENTUM METHOD

Consider a current I crossing the boundary x_0 from the left in Fig. 1. The current is carried by a stream of free electrons from the boundary x_0 to the boundary x_2 . Here the current I moves away from the boundary to the right.

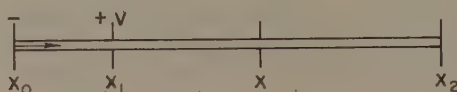


Fig. 1. Electron path in acceleration region and field-free region.

During a portion of the path the stream may suffer an acceleration due to an applied electric field. Let us for convenience suppose this to occur between x_0 and x_1 due to a potential V between these two points, and that the stream then moves in field-free space over the remaining path. The momentum per unit time crossing the boundary x is then given by

$$F = \frac{m}{e} I v \quad \dots\dots (5)$$

where I is the beam current and m/e is the ratio of the mass to charge for electrons. Making use of Eqn (4) to eliminate the velocity from Eqn (5) one obtains

$$m/e = \frac{F^2}{2VI^2} \quad \dots\dots (6)$$

If one makes use of Eqn (2) the resulting equation would be simply

$$\frac{m}{e} = \frac{F\Delta t}{I\Delta s} \quad \dots\dots (7)$$

This latter equation would permit an absolute determination of m/e .

The nature of the field interactions with moving charged particles is dependent on the speed of the particles, and of particular interest is the relativistic region. In this region Eqn (6) becomes

$$\frac{m_0}{e} = \frac{F^2}{I^2 V} - \frac{V}{c^2} \quad \dots\dots (8)$$

where c is the speed of light. The purpose of this study was to apply the principle stated by Eqn (5) and to determine if the momentum transferred by a moving charged stream could be used to determine m/e with reasonable accuracy.

§ 3. EXPERIMENTAL

Careful consideration was given to the design of suitable measuring equipment. The problems of target weight, detector sensitivity, secondary electron emission, electrostatic forces, etc. were solved by means of the tube design shown in Fig. 2. The body of the tube was made of a one-litre boiling flask. A round glass joint

put into the tube wall permitted the insertion of an electron gun. A torsion device was used as the detector and this effectively eliminated gravitational forces. Secondary electron emission was controlled by completely capturing the electron beam in a Faraday cage mounted at the bottom of the torsion fibre, see Fig. 2.

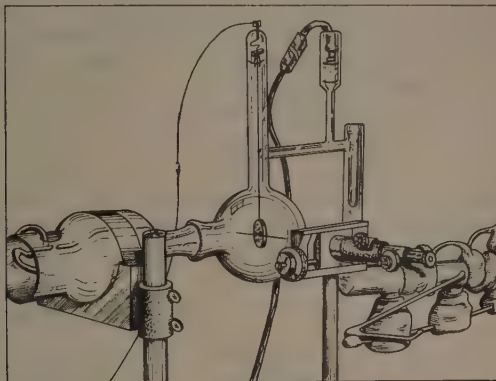


Fig. 2. Vacuum tube showing the Faraday cage and torsion suspension. The focus and deflection coils are at the left, the travelling microscope is in the foreground, and the vacuum system to the right.

The torsion fibre was a 1 mm tungsten wire, spot welded at the lower end to the cage, and attached to a rotatable support at the upper end. The upper support enabled one to adjust the cage position by means of an external magnet. The torsion constant of the suspension fibre was determined by measuring the period of oscillation with a body of known moment of inertia suspended from the fibre. The suspended body was in this case the cage itself. All of its components were carefully massed and measured.

The following values were determined for the detector suspension:

Cage moment of inertia	$31.9 \times 10^{-7} \text{ kg m}^2$
Period	67.7 sec
Torsion constant	$27.3 \times 10^{-9} \text{ kg m}^2 \text{ sec}^{-2}$

The cage was constructed of brass with a tungsten pointer passed horizontally through a diameter. The semi-length of the tungsten pointer was $5.75 \times 10^{-2} \text{ m}$. Target holes were drilled in the cage $1.45 \times 10^{-2} \text{ m}$ from the suspension and the cage face coated with willemite. The interior of the tube was completely coated with a semi-transparent coat of silver by means of the Rochelle salt process so that electrostatic charges could not disturb the detector.

The tube was evacuated by means of a fore vacuum pump and a three stage oil diffusion pump, DPIGF 25W. All measurements were made with a vacuum of approximately 10^{-3} micron. The deflections produced by the electron stream were measured in the following manner. A travelling microscope was mounted near the tube wall and focused on the end of the tungsten rod pointer. The microscope was adjusted to the position of maximum (positive) deflection with

the electron beam turned off. The oscillations were timed, and after one-half cycle had elapsed from the position of maximum deflection, the electron beam was turned on. The beam had been previously directed to and focused on a hole in the target. The change in the maximum positive displacement was then measured by means of the microscope. The electron beam was turned off after it had been on for one complete cycle and a second reading was made on the maximum positive displacement. The positions were very reproducible. In general five independent readings were made of the deflection produced at each electron beam intensity. There are several factors to note: the damping of the system was negligibly small, the deflection as measured was twice the value one would obtain with a static measurement, and the overall deflection angles were very small.

§ 4. RESULTS

The measured values of deflection as a function of beam current are plotted in Fig. 3. All of the readings were taken at 5000 volts. The slope of the solid

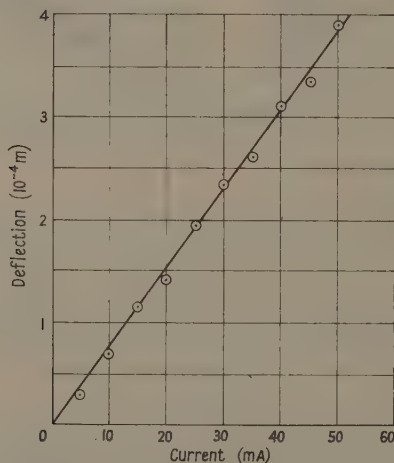


Fig. 3. Deflection of the pointer as measured by the travelling microscope plotted against the beam current for a potential of 5000 v.

line together with the measured values for the instrument were combined to yield F in Eqn (6) which there becomes

$$\frac{m}{e} = \frac{k^2}{2S^2Vl^2} \left(\frac{d}{I} \right)^2 \quad \dots\dots (9)$$

where s is the distance from axis to target hole centre, l the semi-length of pointer, k the torsion constant, V the voltage and d/I the ratio of deflection to current. Upon substitution in Eqn (9) one obtains $5.82 \times 10^{-12} \text{ kg c}^{-1}$ which agrees favourably with the results of other measurements (Cohen, DuMond, Layton and Rollett 1955, $5.6854 \times 10^{12} \text{ kg c}^{-1}$).

§ 5. CONCLUSIONS

This method of determining m/e has been demonstrated to be practical. The experiment was not designed to yield a precise result and refinements in this direction will require considerable ingenuity. This is a new application of Newton's second law to measurements in the field of electron physics. Aside from its restricted application here, it may find application to measurements in other areas of physics, such as in the measurement of scattering and capture cross section. Measurements are currently being made on relativistic electrons by one of the authors at New Mexico State University.

ACKNOWLEDGMENT

The authors wish to acknowledge the support of the University of Utah where this investigation was conducted. Acknowledgment is also made to Milton Marshall who originally suggested that the momentum of electron streams might be measurable (Marshall 1935, private communication).

REFERENCES

- COHEN, E. R., DUMOND, J. W. M., LAYTON, T. W., and ROLLETT, J. S., 1955, *Rev. Mod. Phys.*, **27**, 363.
GERLACH, W., 1933, *Handb. d. Phys.* (Berlin: Springer), **22**, 1.
HOAG, J. B., and KORFF, S. A., 1948, *Electron and Nuclear Physics*, 3rd edn (New York: Van Nostrand).
KIRCHNER, F., 1931, *Ann. Phys., Lpz.*, **8**, 975.
LAMAR, E. S., 1933, *Phys. Rev.*, **43**, 169.
PERRY, C., and CHAFFEE, E., 1931, *Phys. Rev.*, **36**, 904.
THOMSON, J. J., 1897, *Phil. Mag.*, **44**, 293.
WIECHERT, E., 1899, *Ann. Phys., Lpz.*, **69**, 739.

Measurement of Ionization and Attachment Coefficients in Carbon Monoxide in Uniform Fields

By M. S. BHALLA AND J. D. CRAGGS

Department of Electrical Engineering, The University of Liverpool

MS. received 6th February 1961

Abstract. Measurements of pre-breakdown currents in uniform field conditions, in carbon monoxide at different pressures, in the E/p range of 36 to 200 $\text{v cm}^{-1} (\text{mm Hg})^{-1}$ indicate the presence of electron attachment. It is suggested that the mechanism of negative ion formation is due to dissociative attachment, therefore values of α and the dimensionally equivalent attachment coefficient η have been computed from the semi-logarithmic plots of current against electrode separation, by employing the modified Townsend equation for the growth of current. Static breakdown potentials have been measured up to $pd \sim 1050 \text{ mm Hg cm}$ (where p is the pressure and d the gap length) and show that Paschen's law is obeyed. Further, the values of secondary coefficient γ have been computed from upcurving of the semi-logarithmic plots of current against electrode separation. The values of breakdown potential calculated from the breakdown criterion are in good agreement with the measured values, showing that the static breakdown in carbon monoxide is brought about by the Townsend build-up mechanism.

The mean cross sections for ionization and attachment have been calculated for various electron mean energies from the mean values of α/p and η/p obtained from the present study and compared with the values computed from low pressure single collision data, by assuming either a Maxwellian or a Druyvesteyn distribution of electron energies. It is concluded that the Maxwellian distribution is satisfactory to explain the results but the Druyvesteyn distribution does not seem to apply. Calculations show that the electron attachment observed in this study is due to resonant attachment processes occurring at about 10 eV and the contributions due to processes of a continuous nature at about 21 and 23 eV are negligible.

§ 1. INTRODUCTION

THE attachment processes occurring in carbon monoxide when submitted to bombardment by low-energy electrons of well-defined energy, at low pressures, have been studied by Tate and Smith (1932), Lozier (1934) and Hagstrum and Tate (1941). Accurate measurements of attachment and ionization cross sections in carbon monoxide under single collision conditions have been made by Craggs and Tozer (1958) in these laboratories, using a Lozier apparatus.

Earlier workers were unable to observe electron attachment in carbon monoxide in swarm conditions (Bradbury 1934, Loeb 1956). It therefore seemed desirable in view of the single collision data (Craggs and Tozer 1958) to study attachment in carbon monoxide in swarm conditions and to measure the attachment and ionization coefficients for various values of the parameter E/p (E is the field strength and p the gas pressure) in uniform fields.

It has been shown (Harrison and Geballe 1953, Geballe and Reeves 1953) that when electron attachment of the type



occurs in the growth of the electron avalanche the equation for the current flowing in a uniform field gap is given by

$$\frac{I}{I_0} = \left[\frac{\alpha}{\alpha - \eta} \exp [(\alpha - \eta)d] - \frac{\eta}{\alpha - \eta} \right] / \left[1 - \frac{\gamma\alpha}{\alpha - \eta} (\exp [(\alpha - \eta)d] - 1) \right] \quad \dots\dots(2)$$

where α is Townsend's primary coefficient, η the attachment coefficient, γ the secondary coefficient, d the electrode separation and I_0 the initial electron current at the cathode.

Provided only those current measurements are considered in which contributions due to secondary processes are negligible then Eqn (2) is reduced to

$$\frac{I}{I_0} = \left[\frac{\alpha}{\alpha - \eta} \exp [(\alpha - \eta)d] - \frac{\eta}{\alpha - \eta} \right] \quad \dots\dots(3)$$

Equation (3) indicates that the semi-logarithmic plot of $(I/I_0, d)$ is not linear and that curve fitting techniques are necessary to evaluate α and η accurately.

When α is large compared with η the curvature of the $(\log I, d)$ plots ceases to be apparent and the latter becomes linear. It has been shown by Prasad (1960) that under these conditions the exponential term in Eqn (2) tends to dominate the subtractive term particularly at large values of d ($d > 0.5$ cm) and the current growth in the gap can be approximated by

$$\frac{I}{I_0} = \frac{\exp [(\alpha - \eta)d]}{1 - \gamma' (\exp [(\alpha - \eta)d] - 1)} \quad \dots\dots(4)$$

where $I_0' = I_0\alpha/(\alpha - \eta)$ and $\gamma' = \gamma\alpha/(\alpha - \eta)$. If further $\alpha/(\alpha - \eta)$ is close to unity, then Eqn (4) can be approximated to

$$\frac{I}{I_0} = \frac{\exp [(\alpha - \eta)d]}{1 - \gamma' (\exp [(\alpha - \eta)d] - 1)} \quad \dots\dots(5)$$

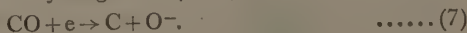
as in a non-attaching gas. This shows that the mean slope of the $(\log I, d)$ plot under these conditions would yield an 'apparent' value of $\alpha/p \simeq (\alpha - \eta)/p$ and the value of the secondary coefficient γ would be in error by a factor of $(\alpha - \eta)/\alpha$.

It follows from Eqn (5) that the criterion for breakdown at which current I becomes self-maintained and independent of I_0 is

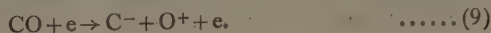
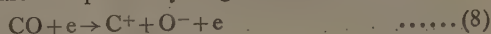
$$\gamma (\exp [(\alpha - \eta)d_s] - 1) = 1 \quad \dots\dots(6)$$

where d_s is the breakdown sparking distance (cm).

Studies by earlier workers, working under single collision conditions, show that a resonant attachment process occurs in carbon monoxide at about 10 eV. The process has been interpreted by Hagstrum (1955) as



Further processes occur at about 21 and 23 eV and are of a continuous nature involving ion pairs. These are interpreted by Hagstrum as



In the present study it was not possible to observe attachment for the parameter $E/p > 56 \text{ v cm}^{-1} (\text{mm Hg})^{-1}$ corresponding to the mean electron energy of approximately 4 eV because the curvature of the $(\log I, d)$ plots ceased to be apparent. Energy considerations indicate that under these conditions, i.e. for mean electron energies less than 4 eV, the possibility of reactions (8) and (9) contributing to the negative ion formation to any appreciable degree can be ruled out (cf. § 5). Thus reaction (7) is the only one that need be considered for mean electron energies less than about 4 eV. However the formation of negative ions at higher pressures where three-body processes must be considered will presumably comprise



(CO^{*-} denotes an excited state of CO^-) together with reaction (7). The degree of branching between (7) and (10) is not known.

Consequently values of α , η , apparent α , γ and the breakdown sparking distance d_s have been calculated in carbon monoxide by employing Eqns (3), (5) and (6). The authors find that the measurements of pre-breakdown currents conform to the above theory over a wide range of pressures.

From the mean values of α/p and η/p so obtained the mean cross sections for ionization and attachment have been calculated for various electron mean energies and an attempt has been made to compare these values of cross sections with the values computed from the low pressure single collision data by assuming either a Maxwellian or a Druyvesteyn distribution of electron energies.

§ 2. EXPERIMENTAL PROCEDURE

A detailed description of the apparatus and the modifications made to improve its performance and accuracy have been published earlier (Hopwood, Peacock and Wilkes 1956, Bhalla and Craggs 1960) and will not be dealt with here. In the present study the ionization chamber was always evacuated to better than $5 \times 10^{-6} \text{ mm Hg}$ with an apparent leak of less than $0.4 \mu \text{ h}^{-1}$, before the gas was admitted. The gas used in the experiments up to 100 mm Hg pressure was spectroscopically pure and supplied by British Oxygen Gases Ltd., but preliminary measurements up to 100 mm Hg pressure and the final measurements at 300 mm Hg pressure were made in cylinder gas (97.3% carbon monoxide, 1.7% nitrogen, 0.8% carbon dioxide, 0.2% oxygen) obtained from the Imperial Chemical Industries Ltd. Each gas filling from the cylinder was passed very slowly through a trap maintained at -78°C by using a mixture of solid carbon dioxide and acetone.

The gas pressures were measured (corrected to 20°C) either on an oil manometer using silicone oil of specific gravity 1.09 to within $\pm 0.05 \text{ mm Hg}$ or on the micromanometer (cf. Hopwood, Peacock and Wilkes 1956) to within $\pm 0.5 \text{ mm Hg}$. A platinum coated cathode was used throughout this study and its distance from the dural (aluminium alloy) anode was measured to within $\pm 0.005 \text{ mm}$. The voltage applied to the ionization chamber, variable in steps of 0.2 volt (0 to 50 kV) was known to within $\pm 0.3\%$ and the ionization currents produced could be determined to an accuracy better than 1.5%. The overall error in the measurement of α/p should therefore be not greater than 3%. It is very difficult to assess the

errors in η/p , since they depend on curve fitting but it is estimated that in the most favourable conditions (medium values of E/p) they are about $\pm 5\%$ increasing to perhaps $\pm 15\%$ for low and high values of E/p .

§ 3. DATA AND RESULTS

The experiments were conducted over a pressure range of 2.5 to 300 mm Hg (corrected to 20°C) and a range of E/p from 36 to 200 $\text{v cm}^{-1} (\text{mm Hg})^{-1}$. Some of the typical ($\log I, d$) plots at 25 and 100 mm Hg pressures are shown in Fig. 1. All these plots exhibit curvatures characteristic of Eqn (3), thus justifying the assumption made regarding the mechanism of negative ion formation. It was observed, however, that, beyond a particular value of the parameter E/p , for each pressure the curvature of the plots ceased to be apparent and the latter became linear.

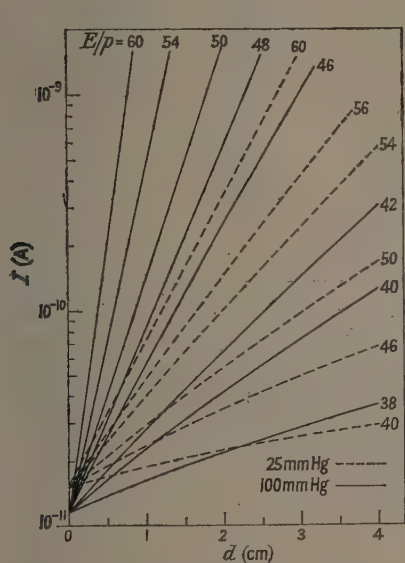


Fig. 1. Ionization currents in carbon monoxide at 25 and 100 mm Hg pressures for various constant values of the parameter

$$E/p \text{ (v cm}^{-1} (\text{mm Hg})^{-1}\text{)}.$$

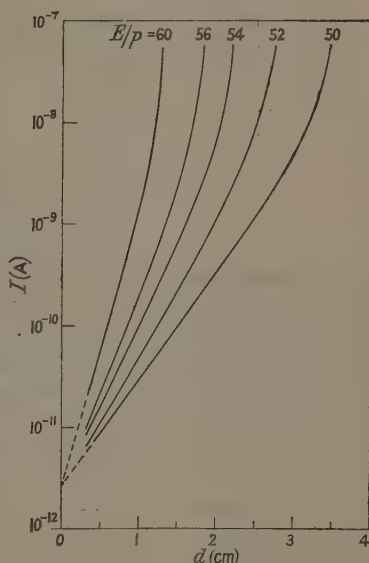


Fig. 2. Ionization currents in carbon monoxide at 100 mm Hg pressure for various constant values of the parameter

$$E/p \text{ (v cm}^{-1} (\text{mm Hg})^{-1}\text{)}.$$

Figure 2 shows the upcurving of ($\log I, d$) plots indicating the presence of secondary ionization processes. For the sake of brevity only typical plots for 100 mm Hg pressure are shown, for which the initial photoelectric current I_0 from the cathode was reduced by adding a fine wire gauze filter in the path of the ultra-violet radiation, from the low pressure mercury discharge lamp, incident on the cathode. This enabled pre-breakdown currents to be measured sufficiently close to the sparking distance without causing space-charge distortion of the electric field due to unnecessarily large values of anode current.

3.1. Evaluation of α and η

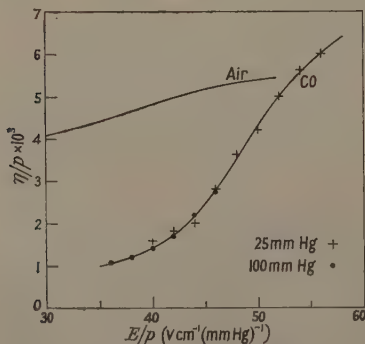
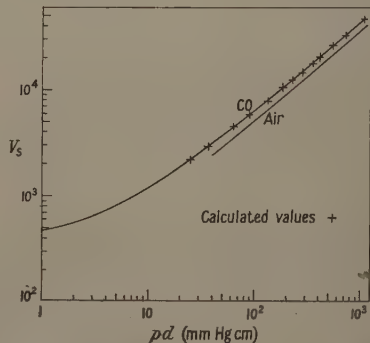
The values of α and η have been computed from the above-mentioned curves by a careful process of curve fitting employing Eqn (3). The values of α/p and η/p obtained in the range $E/p = 36$ to $60 \text{ v cm}^{-1} (\text{mm Hg})^{-1}$ at 25 and 100 mm Hg pressures are given in Table 1 and the values of η/p are plotted as a function of E/p in Fig. 3, which also includes Prasad's (1960) data in dry air for comparison. Values of α/p and η/p obtained at 300 mm Hg pressure are not included, since they are considered only to be of sufficient accuracy to measure γ and breakdown potentials because of impurities present in the gas (cylinder gas).

Table 1. Values of α/p and η/p for CO at 25 and 100 mm Hg Pressure

E/p	25 mm Hg		100 mm Hg	
	α/p	η/p	α/p	η/p
36	—	—	0.0033	0.0011
38	—	—	0.0048	0.0012
40	0.0070	0.0016	0.0068	0.0014
42	0.0094	0.0018	0.0094	0.0017
44	0.0124	0.0020	0.0128	0.0022
46	0.0164	0.0028	0.0169	0.0027
48	0.0212	0.0036	0.0195†	—
50	0.0266	0.0042	0.0245†	—
52	0.0330	0.0050	0.0303†	—
54	0.0400	0.0056	0.0368†	—
56	0.0480	0.0060	0.0445†	—
60	0.0615†	—	0.0616†	—

† 'Apparent' values.

'Apparent' values of α/p (cf. § 1) for the parameter $E/p > 56 \text{ v cm}^{-1} (\text{mm Hg})^{-1}$ at 25 mm Hg pressure and $E/p > 46 \text{ v cm}^{-1} (\text{mm Hg})^{-1}$ at 100 mm Hg pressure were calculated from the linear ($\log I, d$) plots employing Eqn (5). Table 1 shows that these 'apparent' values of α/p at 100 mm Hg pressure are consistently below the true values of α/p but agree within 10% to the $(\alpha - \eta)/p$ values obtained from the non-linear plots at 25 mm Hg pressure for the corresponding values of E/p .

Fig. 3. Values of η/p as a function of E/p in carbon monoxide and in dry air for comparison.Fig. 4. Observed breakdown potentials as a function of pd in carbon monoxide and in dry air for comparison.

3.2. Breakdown Measurements and γ

Breakdown potentials V_s were measured over a pressure range of 2.5 to 300 mm Hg (corrected to 20°C) up to $pd \sim 1050$ mm Hg cm and are plotted (in volts) as a function of pd in Fig. 4, which includes Prasad's (1959, 1960) data in dry air for comparison. Results showed no pressure dependence (within 2% for spectroscopically pure gas and 2.5% for the cylinder gas) for any particular value of pd , thus indicating that Paschen's law is obeyed in this region.

Values of the secondary coefficient γ have been computed from the upcurving of linear ($\log I, d$) plots (cf. Fig. 2) at various pressures employing Eqn (5) and are plotted as a function of E/p in Fig. 5. These values of γ have been used to

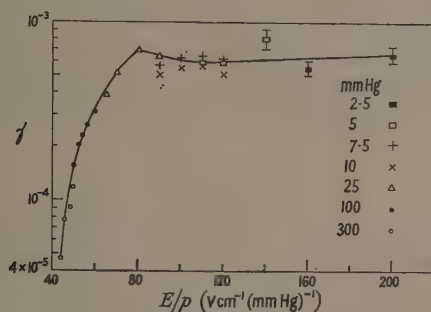


Fig. 5. Values of γ as a function of E/p in carbon monoxide, for a platinum surface.

calculate the sparking distances d_s and consequently the breakdown potentials V_s from the breakdown criterion (6). Table 2 summarizes the values of α/p (apparent values), γ , d_s and calculated V_s , together with measured V_s for different values of the parameter E/p at various pressures. Calculated values of the

Table 2

p (mm Hg at 20°C)	E/p	α/p^\dagger	$\gamma \times 10^4$	d_s (cm)	V_s (kv)	
					Calc.	Meas.
25 (Spec. pure)	90	3.04×10^{-1}	6.3	0.97	2.18	2.18
	80	2.01×10^{-1}	6.9	1.45	2.90	2.90
	70	1.21×10^{-1}	5.1	2.51	4.39	4.39
	65	8.9×10^{-2}	3.8	3.54	5.75	5.77
100 (Spec. pure)	60	6.16×10^{-2}	3.1	1.31	7.86	7.92
	56	4.45×10^{-2}	2.6	1.86	10.42	10.42
	54	3.68×10^{-2}	2.3	2.28	12.31	12.26
	52	3.03×10^{-2}	2.0	2.81	14.61	14.66
	50	2.45×10^{-2}	1.55	3.58	17.9	18.0
300 (Cylinder)	50	2.20×10^{-2}	1.17	1.37	20.6	20.7
	48	1.72×10^{-2}	0.90	1.81	26.1	26.1
	46	1.30×10^{-2}	0.77	2.43	33.5	33.7
	44	9.4×10^{-3}	0.47	3.53	46.6	46.3

† 'Apparent' values.

breakdown potential agree with the measured values to within 1% (cf. Table 2) and are indicated in Fig. 4. The good agreement between the measured and the calculated values of breakdown potential shows that the static breakdown in carbon monoxide is brought about by the Townsend build-up processes up to a pd of 1050 mm Hg cm.

§ 4. CORRELATION OF RESULTS WITH LOW PRESSURE EXPERIMENTS

Calculated values of mean cross sections for ionization $\bar{\sigma}^+$ and for attachment $\bar{\sigma}^-$ employing the cross section data from low pressure experiments in carbon monoxide (Craggs and Tozer 1958) are compared with the values obtained from the present study, using the electron drift and agitation velocity data from the diffusion experiments (Skinker and White 1923) for the Maxwellian and Druyvesteyn distributions.

The earlier work of Deas and Emeléus (1949), Tozer, Thorburn and Craggs (1958) and Thompson (1959) shows that the mean cross section for any particular collision process for the mean energy \bar{E} of a given energy distribution is given by the equation

$$\bar{\sigma}_{\bar{E}} = \int \sigma_E v_E dN_E / \int v_E dN_E \quad \dots\dots (11)$$

where σ_E is the cross section for this process for electrons of energy E ev and v_E is the velocity and dN_E the number of electrons in the range E to $E + \delta E$ of the distribution in the swarm. Further, swarm constants α/p and η/p can be converted into a mean cross section for any particular value of E/p from the knowledge of the drift velocity W , the mean velocity of agitation U and mean energy \bar{E} of the electrons as functions of E/p by using the equation

$$\bar{\sigma}_{\bar{E}} = \frac{1}{N} \frac{W\theta}{U} \frac{\theta}{p} \quad \dots\dots (12)$$

where N is the number of molecules per cm^3 at 1 mm Hg at the appropriate temperature and θ represents α or η . However it is to be noted that when employing the data from the diffusion experiments the various quantities should be corrected for the different energy distributions assumed (Healey and Reed 1941, Huxley and Zaazou 1949).

The $\bar{\sigma}^+$ and $\bar{\sigma}^-$ values thus obtained by using the ionization and attachment cross sections from Craggs and Tozer's (1958) low pressure data employing Eqn (11) and the mean values of α/p and η/p from the present measurements employing Eqn (12) are represented in Figs 6 and 7 for both the Maxwellian and the Druyvesteyn distributions.

§ 5. DISCUSSION

The double sets of values at 25 and 100 mm Hg pressures given in Table 1 show that the measured values of α/p and η/p for different gas fillings are consistent and the 'apparent' values of α/p (cf. § 1) agree with the true values of α/p to within 10%. However, for the values of the parameter $E/p > 60 \text{ v cm}^{-1} (\text{mm Hg})^{-1}$ contributions due to the attachment processes decrease rapidly (cf. Fig. 8) and the 'apparent' values of α/p approach the true values of α/p .

Further, the values of α/p obtained at different pressures in the range E/p where the results overlap, also showed good agreement within the experimental

limits ($\pm 3\%$). These considerations suggest that α/p and η/p are not pressure dependent and are therefore functions of E/p . The values of α/p and η/p do not depend on the ionization current, which can be seen by a careful consideration of the experimental data such as those, for example, plotted in Fig. 1. However no accurate measurements could conveniently be made at pressures higher than 100 mm Hg because the quantities of spectroscopically pure gas required were prohibitively great.

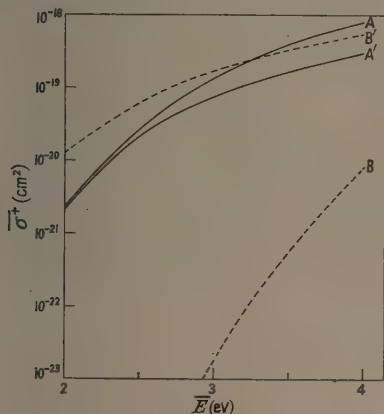


Fig. 6. Mean ionization cross sections in carbon monoxide as a function of mean electron energy. A, calculated from Craggs and Tozer's low pressure data, for a Maxwellian distribution of electron energies; A', calculated with the data from the present study, for a Maxwellian distribution of electron energies; B and B', as for A and A' but with a Druyvesteyn distribution.

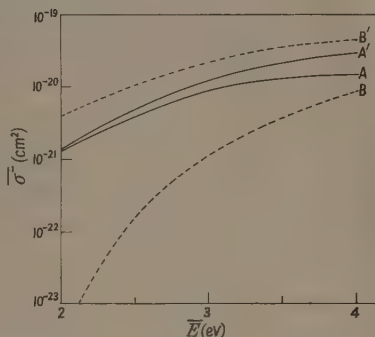


Fig. 7. Mean attachment cross sections in carbon monoxide as a function of mean electron energy. A, A', B, B', as in Fig. 6.

Figures 6 and 7 show respectively for ionization and attachment the comparisons between the mean cross sections deduced from α/p and η/p measurements and from the low pressure single collision work of Craggs and Tozer (1958) assuming either a Maxwellian or a Druyvesteyn distribution of electron energies. The results obtained by using the Maxwellian distribution show satisfactory agreement whereas it seems that the Druyvesteyn distribution does not apply. It was therefore decided to use the Maxwellian distribution and extend the calculations for the mean attachment cross sections to 10 eV mean electron energy and estimate theoretically the contributions made by reactions (8) and (9) to the negative ion formation. The mean ionization and attachment cross sections, calculated from the low pressure data as well as from the present measurements, are shown in Fig. 8 as a function of mean electron energy (2 to 10 eV). The mean attachment cross sections are represented by the curve F when contributions due to reactions (8) and (9) are ignored and by the curve G when these are taken into consideration. This indicates that the contributions made by reactions (8) and (9) to the negative ion formation for mean electron

energies less than 4 eV are negligible. As mentioned earlier, no attachment could be observed in this study for the parameter $E/p > 56 \text{ v cm}^{-1}(\text{mm Hg})^{-1}$, i.e. mean electron energy $\approx 4 \text{ eV}$, because the curvature of $(\log I, d)$ plots ceased to be apparent. These considerations justify the use of Eqn (2) to represent the attachment processes in the present study. Fig. 8 also includes the mean ionization cross sections calculated from the low pressure data of Tate and Smith (1932). These show slightly better agreement than those calculated from the low pressure data of Craggs and Tozer (1958) when compared with the mean ionization cross sections obtained from the present α/p measurements.

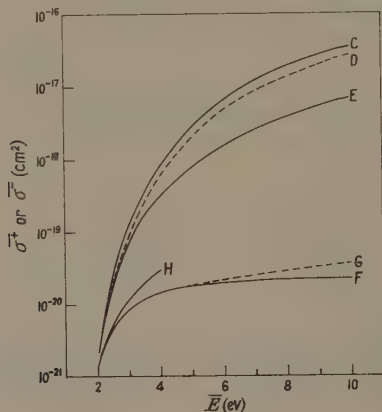


Fig. 8. Mean ionization and attachment cross sections in carbon monoxide as a function of mean electron energy, for a Maxwellian form of electron energy distribution. C, D and E, mean ionization cross sections; F, G and H, mean attachment cross sections. C, F and G, calculated from Craggs and Tozer's low pressure data; D, calculated from Tate and Smith's low pressure data; E and H, calculated with the data from the present study; F and G, see text for details.

It is found that the 'apparent' values of α/p , i.e. $(\alpha - \eta)/p$ in dry air are higher than those in carbon monoxide for the corresponding values of the parameter E/p , e.g. approximately a factor of 3 at $E/p = 50 \text{ v cm}^{-1}(\text{mm Hg})^{-1}$. The secondary ionization coefficient γ in dry air (Prasad 1959) as well as in carbon monoxide is of the same order, e.g. $\gamma \sim 10^{-4}$ at $E/p = 50 \text{ v cm}^{-1}(\text{mm Hg})^{-1}$. Therefore breakdown potentials in dry air should be lower than those in carbon monoxide for the same values of pd . Breakdown potentials in carbon monoxide and dry air are indicated in Fig. 4 as a function of pd and it shows that the curve for dry air is lower than that of carbon monoxide as expected.

ACKNOWLEDGMENTS

One of us (M. S. B.) is indebted to the Electrical Research Association for financial support and permission to publish this paper. We are grateful to Dr. A. N. Prasad for many discussions and advice.

REFERENCES

- BHALLA, M. S., and CRAGGS, J. D., 1960, *Proc. Phys. Soc.*, **76**, 369.
BRADBURY, N. E., 1934, *J. Chem. Phys.*, **2**, 827.
CRAGGS, J. D., and TOZER, B. A., 1958, *Proc. Roy. Soc. A*, **247**, 337.
DEAS, H. D., and EMELÉUS, K. G., 1949, *Phil. Mag.*, **40**, 460.
GEBALLE, R., and REEVES, M. L., 1953, *Phys. Rev.*, **92**, 867.
HAGSTRUM, H. D., 1955, *J. Chem. Phys.*, **23**, 1178.
HAGSTRUM, H. D., and TATE, J. T., 1941, *Phys. Rev.*, **59**, 354.
HARRISON, M. A., and GEBALLE, R., 1953, *Phys. Rev.*, **91**, 1.
HEALEY, R. H., and REED, J. W., 1941, *The Behaviour of Slow Electrons in Gases* (Sydney: Amalgamated Wireless (Australasia)).
HOPWOOD, W., PEACOCK, N. J., and WILKES, A., 1956, *Proc. Roy. Soc. A*, **235**, 334.
HUXLEY, L. G. H., and ZAAZOU, A. A., 1949, *Proc. Roy. Soc. A*, **196**, 402.
LOEB, L. B., 1956, *Handb. d. Phys.* (Berlin: Springer), **21**, 460.
LOZIER, W. W., 1934, *Phys. Rev.*, **46**, 268.
PRASAD, A. N., 1959, *Proc. Phys. Soc.*, **74**, 33.
——— 1960, *Ph.D. Thesis*, University of Liverpool.
SKINKER, M. F., and WHITE, J. V., 1923, *Phil. Mag.*, **46**, 630.
TATE, J. T., and SMITH, P. T., 1932, *Phys. Rev.*, **39**, 270.
THOMPSON, J. B., 1959, *Proc. Phys. Soc.*, **73**, 821.
TOZER, B. A., THORBURN, R., and CRAGGS, J. D., 1958, *Proc. Phys. Soc.*, **72**, 1081.

The Influence of Cathode and Anode Surfaces on the Electric Strength of Liquid Argon

BY D. W. SWAN AND T. J. LEWIS

Electrical Engineering Department, Queen Mary College,
Mile End Road, London, E.1

MS. received 13th March 1961

Abstract. The electric strength of liquefied argon is found to depend to a marked degree on the nature of both cathode and anode. This effect has been investigated systematically. The cathode is thought to influence the strength through the process of electron emission into the liquid, whilst the anode becomes important only if the rate of emission from the cathode exceeds that at which the anode can accept charge. In this case a high space charge field is set up near the anode which can lower the applied field necessary for breakdown. By measuring the electric strength of liquid argon containing various concentrations of oxygen, it has been shown that probably the anode space charge is formed only when part of the current before breakdown is carried by negative oxygen ions. The electric strength is found to be very sensitive to small concentrations of oxygen.

§ 1. INTRODUCTION

MEASUREMENTS of the electric strengths of liquefied argon, oxygen and nitrogen have been reported in an earlier paper (Swan and Lewis 1960) and it was shown that for argon in particular, the strength was greatly influenced by the nature of the cathode and anode surfaces and by the presence of dissolved oxygen. The experiments reported here are a continuation of that work in which these effects have been studied in more detail. Hancox (1957) has already reported that the degree of cathode surface oxidation can influence the impulse electric strength of transformer oil, and Sletten (1959) has demonstrated that dissolved oxygen increases the strength of *n*-hexane. Both these effects are found to a marked degree with the inert liquid argon, which is ideal for such studies since a minimum of damage occurs to the liquid and electrodes when a discharge takes place. It has been found possible to separate the roles of cathode and anode in determining the strength of liquid argon and to advance reasons for the unusual control exercised by the anode.

The apparatus and experimental techniques were the same as those described in the earlier paper (Swan and Lewis 1960). The electrodes were 5 mm diameter spheres and the electrode spacing could be adjusted externally by means of a micrometer. The procedure for obtaining reproducible surface oxide conditions on the electrodes was simple. Freshly polished electrodes were allowed to oxidize freely in dry air in a desiccator for pre-determined times and the oxide growth was then arrested by immersion in *n*-hexane. This procedure had previously been found to give reliable control of the surface oxide in the measurements

reported by Hancox (1957). Except for the experiments using spectroscopically pure argon and mixtures of argon and oxygen, commercial grade argon has been used having a purity of 99.95%; the significant impurities being nitrogen (<500 parts per million), oxygen (<20 parts per million), and hydrogen (<10 parts per million).

§ 2. EXPERIMENTAL RESULTS

2.1. Influence of Electrodes

For each sample of liquid and set of electrodes the breakdown voltage was obtained at a number of electrode spacings ranging from 2×10^{-3} cm to 10^{-2} cm. The electric strength was then determined as the slope of this characteristic, which was usually a straight line within experimental error with an intercept of approximately 1 kv if extrapolated to zero electrode spacing. A similar intercept was found in previous measurements with liquefied gases (Kronig and Van der Vooren 1942, Blaisse, van den Boorgaart and Erne 1958) and in measurements on hydrocarbon liquids (Lewis 1953). The reason for this intercept is not fully understood at the moment but in a recent study (Swan 1961) it has been shown that a mechanism of breakdown involving a small degree of ionization in the liquid could account for it (see § 3). At each electrode spacing it was found necessary to record about twenty values of the breakdown voltage in order to

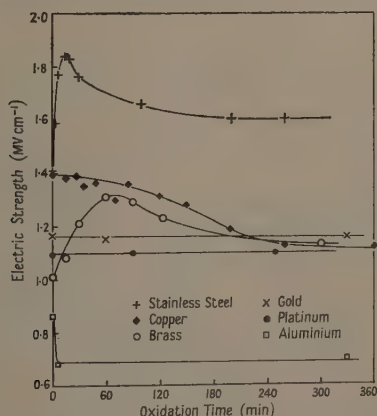


Fig. 1. Electric strength of liquid argon with oxidized electrodes.

obtain a reliable average. Fig. 1 shows the results obtained for a number of electrode materials, and in every case both anode and cathode were treated identically. The results for platinum and gold show that contact with air in the desiccator did not influence the strength. This is consistent with the idea that the surface change for the other metals produced by exposure to air in the desiccator is due to oxidation, since neither platinum nor gold forms oxides at room temperatures. For stainless steel, brass, copper and aluminium electrodes there is a considerable change in electric strength with increasing oxidation time. Maxima occur in the strength for both stainless steel and brass electrodes

but copper and aluminium do not produce an increase in the initial stages of oxidation, the strength falling throughout the entire range of oxidation times. The points on the curve for copper electrodes are seen to be more scattered at the shorter oxidation times than the points obtained with other electrode materials. This is thought to be due to the very temperature-dependent rate of oxide growth on copper, the heating produced during the final stage of polishing being sufficient to cause appreciable variations in the surface conditions from one test to another. Aluminium electrodes produce quite a different characteristic which can be explained in terms of the very rapid initial oxidation of that metal which does not continue at longer times.

Initially (Swan and Lewis 1960), these effects were attributed to the combined but opposing influences of the increasing effective barrier to emission at the cathode due to the growth of the oxide, and the subsequent decrease due to positive ions from the liquid forming a double layer there (Green 1955). If the electric strength were directly related to the emission then a plausible explanation of the results would be possible. The absence of an initial increase of strength when using copper or aluminium electrodes could be attributed to the thickness and nature of the oxide present at 'zero oxidation time' since, in the preparation, a thin layer of oxide will form even when the time in the desiccator is zero. For copper this layer may contain the highly insulating cupric oxide (Ronnquist and Fischmeister 1960) and thus the positive ion layer could form readily, resulting in an increased emission. Aluminium would behave in a similar manner.

Table 1. Electric Strength of Liquid Argon with Anode and Cathode of Different Materials

Cathode material		Anode material	Electric strength (mv cm^{-1})
Aluminium	(15)	Aluminium (15)	0.69
Aluminium	(15)	Stainless steel (15)	1.44
Stainless steel	(15)	Aluminium (15)	0.88
Stainless steel	(15)	Stainless steel (15)	1.86
Stainless steel	(0)	Gold	1.22
Stainless steel	(17)	Gold	1.26

The period of oxidation in minutes is indicated in brackets.

However, experiments performed with anode and cathode of different materials show that the state of the anode surface also influences the strength, so that these suggestions are not correct. Table 1 gives results for stainless steel and aluminium electrodes and it can be seen that, with an aluminium cathode of 15 minutes' oxidation time, the strength is 0.69 mv cm^{-1} when the anode is aluminium and 1.44 mv cm^{-1} when it is stainless steel. On reversing the aluminium-stainless steel pair, the strength fell to 0.88 mv cm^{-1} , and with both electrodes of stainless steel the strength was 1.86 mv cm^{-1} . As a further check on the influence of the cathode, a gold anode was selected because of its inactivity with oxygen, and the strength determined for changes of oxidation time of a stainless steel cathode (Table 1). There was only a slight increase in strength as the cathode was oxidized to the point corresponding to the peak

strength obtained with two stainless steel electrodes (Fig. 1), in fact the strength (1.26 MV cm^{-1}) is little greater than that for two gold electrodes (1.16 MV cm^{-1}). It is concluded that the gold anode is exerting a much greater influence than the cathode in this case.

2.2. Separation of Cathode and Anode Effects

In order to obtain results showing cathode effects without anode influence it was necessary to substitute a stainless steel electrode of zero oxidation time for the unsuitable gold anode. As described below, such an electrode will exhibit the least anode influence. With this arrangement curve A of Fig. 2 was obtained.

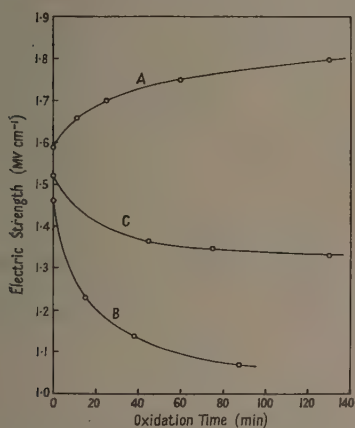


Fig. 2. Influence of anode and cathode on the electric strength of liquid argon. A, Cathode stainless steel, various oxidation times; anode stainless steel, zero oxidation time. B, Cathode gold; anode stainless steel, various oxidation times. C, Cathode stainless steel, 24 hour oxidation time; anode stainless steel, various oxidation times.

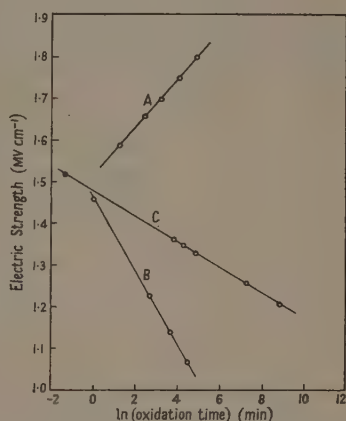


Fig. 3. Influence of cathode and anode oxidation on the electric strength of liquid argon. The electrode conditions are as given for Fig. 2.

The strength is seen to increase continuously for oxidation times up to 140 minutes and there is no tendency for a peak strength at about 15 minutes as occurs when both electrodes are oxidized for the same period. This is considered to be good evidence that the cathode oxidation was responsible for the initial increase of strength when using stainless steel electrodes. A similar cathode oxidation could also produce the increase observed with brass electrodes. To demonstrate that the anode determines the decline in strength for oxidation times beyond the peak in Fig. 1 a gold cathode was employed with stainless steel anodes of different oxidation times. The strength declined continuously with increasing anode oxidation time in the manner shown in curve B of Fig. 2. A similar result shown as curve C was obtained by using a stainless steel cathode which had been

oxidized for 24 hours (thus giving a maximum strength due to the cathode) and a stainless steel anode with oxidation times up to 120 hours. The complete characteristic is given in logarithmic form in Fig. 3 together with the results of Fig. 2 curves A and B. The plots are good straight lines showing that the strength varies exponentially with oxidation time, but due to the overall complexity of the relationship between strength and oxide growth, it is not possible to explain why this should be so.

2.3. Oxygen in Solution

From the fact that curves B and C of Fig. 3 have different slopes for the anode effect in spite of identical stainless steel anodes, it may be deduced that the cathode can control the degree of anode influence. A possible way by which this could occur would be for the emission from the cathode to determine the degree of negative space charge at the anode and this in turn to determine the strength. This space charge would be most effective if oxygen (or other electron-attaching impurity) were capable of producing, in the body of the liquid, negative ions which would be transported to the anode. This possibility was investigated by modifying the system so that a given sample of argon gas with small admixtures of oxygen could be retained under pressure and condensed into the cell many times without appreciable change in composition. Some preliminary tests with gold electrodes showed that the addition of oxygen resulted in an increased strength, and because gold should not be directly influenced by oxygen, it may be assumed that part of the increase in strength was due directly to the oxygen in the body of the liquid. With electrodes that form oxides some change in the surface oxide conditions may also occur to alter the strength, particularly as each discharge could momentarily expose fresh metal at a high temperature. The anode effect in the argon-oxygen mixtures was examined more carefully using a platinum cathode together with anodes of either aluminium or stainless steel of zero oxidation time. It had been observed before that these latter two metals behave very differently as anodes and, since a platinum cathode should not be influenced by oxygen concentration, changes in strength due to the anode effect should show clearly. Table 2 gives the results obtained for argon containing various percentages of oxygen. The quantities of oxygen recorded are approximate only but the general trend of results is not affected by this. Oxygen above a concentration of about 0.002% increases the strength of the liquid but does not

Table 2. Electric Strength of Liquid Argon-Oxygen Mixtures with Aluminium and Stainless Steel Anodes and a Platinum Cathode

Liquid	Electric strength (mv cm^{-1})		Difference in strength (mv cm^{-1})
	Aluminium anode	Stainless steel anode	
Commercial A 20%	1.35	1.71	0.36
Commercial A 1%	1.33	1.68	0.35
Commercial A 0.002%	0.686	1.07	0.384
Spectroscopic A 0.0002%	0.764	0.888	0.124

The quantity of oxygen in the mixture is given as a percentage in each case.

change the difference in strengths due to the different anodes. With very small oxygen concentrations the influence of the anode is reduced, the difference for spectroscopic grade argon being only 30% of the difference for commercial argon. A significant effect shown by the results of Table 2 is that with an aluminium anode the strength of the mixture first decreases as the oxygen content is increased and then increases in the same way as observed with the stainless steel anode. It might be expected from the earlier results that addition of oxygen should increase and not decrease the strength. The decrease found can be associated with space charge distortion of the field (§3).

It is clear from the foregoing results that the 'intrinsic strength' of liquid argon is not a meaningful quantity, but in order to obtain a reliable value for the electric strength of liquid argon a measurement was made using spectroscopically pure argon and gold electrodes. By using these electrodes contamination from oxygen absorbed on the electrode surfaces was reduced, and the percentage of oxygen in the argon itself was very small. The results of the measurement,

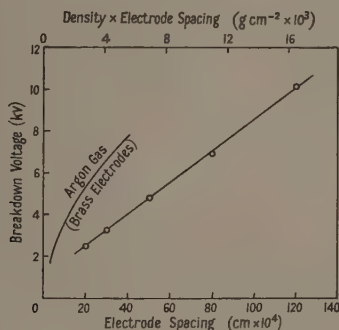


Fig. 4. Breakdown voltage as a function of electrode spacing for spectroscopic grade argon. Gold electrodes.

shown in Fig. 4, are compared with the characteristic of breakdown voltage against the product of gap width and density for gaseous argon given by Kachikas and Fisher (1953) using brass electrodes. The strength of the liquid is found to be 750 kv cm^{-1} . It is seen that for a given value of density times gap-width the breakdown voltage of the liquid is considerably lower than that of the gas. The implications of this will be discussed in §3. Other measurements for spectroscopically pure argon have been given in Table 2 and in each case the strength is considerably less than 1 mv cm^{-1} .

§ 3. DISCUSSION

3.1. The Breakdown Instability

To explain the results obtained, certain breakdown processes are suggested which allow the roles of anode, cathode and the bulk liquid to be distinguished. It is generally accepted that, at the fields existing when breakdown occurs in liquid dielectrics (approximately 1 mv cm^{-1}), there will be significant electron emission from the cathode and that this emission will be field dependent.

It is obvious from the complex nature of the metal-liquid interface that the emission will not occur strictly according to the Fowler-Nordheim law as for a metal-vacuum interface but, nevertheless, available evidence suggests that a relationship with that form of field dependence is adequate for the present purposes (Watson and Sharbaugh 1960, Green 1956), particularly at low temperatures. The electrons emitted drift through the liquid, and if the field is high enough ionizing collisions (α process) could occur, producing positive ions which, moving towards the cathode, enhance the field there, so producing increased emission. This feedback process could cause the emission to increase progressively and so lead to breakdown as a result of high local heat input and vaporization of the liquid at the cathode. The concept of breakdown resulting from vaporization at the cathode has been suggested recently by Watson and Sharbaugh (1960). It should be emphasized that the degree of ionization required in the bulk of the liquid may be very small and not normally detectable at fields below breakdown if the increase of emission with cathode field is very rapid, so that only a small number of positive ions is necessary. Boyle and Kisliuk (1955) have examined the influence of small numbers of positive ions on emission and have used the idea to explain the breakdown phenomena in air at small electrode spacings when the chance of an ionizing collision is very small. Kisliuk (1959) has also considered the emission caused by a single ion acting alone. The number of electrons emitted as a result of one ion returning to the cathode depends on the number of ions already present and on the field and may be much greater than unity. Swan (1961) has recently investigated a similar effect for liquids, and choosing arbitrary but realistic laws for the emission and for the field dependence of ionization in the gap, has set up an equation for current instability as a breakdown criterion. It has been possible to reproduce theoretically the relationship between breakdown voltage and electrode spacing for liquid argon using values of αd (where d is the electrode spacing) much less than unity. With such a small number of ionizing collisions it is unlikely that an α process would be observed in conduction experiments. The necessity for sufficient although very small ionization gives rise to the increase of electric strength observed at small electrode spacings (Swan and Lewis 1960). In a liquid all these processes may well be confined to narrow filaments between cathode and anode (Goodwin 1956) and involve the single ion and the collective ion processes discussed by Kisliuk (1959) and by Boyle and Kisliuk (1955).

3.2. The Role of the Cathode

Due to surface dislocations, patches having low work function, and geometrical irregularities, a freshly prepared cathode surface will always be non-uniform in structure and certain sites will be able to emit more freely than others (Lewis 1955). The probability of breakdown being initiated at one of these sites is therefore high. On exposure to air oxidation will commence and this will occur first at those sites where the emission would be greatest (Cabrera 1957). On most metals after the initial preferential oxidation the whole surface will oxidize more slowly and uniformly (Mott 1947). The growth of an oxide layer will decrease the emission by raising the potential barrier at the surface; consequently a correlation between cathode oxidation and the breakdown instability outlined above might be expected. This is supported by the evidence of curve A of Fig. 2, and is in agreement with the work of Hancox (1957) who

found similar results with oxidized stainless steel cathodes when measuring the impulse strength of transformer oil. In some experiments the strength did not attain a steady value until several discharges had occurred, and this was probably due to the preferential removal of sites of abnormally high emission. The patchy nature of the surface would give greater scatter in measurements than if it were microscopically uniform and would account for the coefficient of variation of 10% found in nearly every case.

The strong influence of a cathode-dependent field-emission process for breakdown of liquid argon would also account for the difference in breakdown voltage between the gaseous and liquid phases (Fig. 4), because Paschen's law is valid only when the processes of breakdown depend on the ratio of the field strength to density and not on field strength alone.

3.3. The Effect of Dissolved Oxygen

After emission from the cathode, electrons will suffer collisions with argon atoms and with impurity molecules as they move to the anode. The measured drift velocity of electrons in liquid argon is about 10^6 cm sec⁻¹ for fields above about 5 kv cm⁻¹ (Williams 1957, Malkin and Schultz 1951) and this value indicates that the electrons remain free in the liquid at these stresses. The presence of very small concentrations of molecular impurities can influence the motion of electrons (Swan 1960) and oxygen and nitrogen will produce stable negative ions (Davidson and Larsh 1950). There is no direct evidence for collision ionization in the liquid, but the mean electron energy in a field of 10^5 v cm⁻¹ is likely to be only about 1 ev (Stacey 1959, Swan 1960). It has been suggested by Swan (1960) that the transport of electrons in liquid argon can be described by classical kinetic theory, in which case a field of 1 mv cm⁻¹ would give an electron energy distribution of mean value 5.5 ev. This value is large enough to suggest that there would be sufficient electrons in the high energy tail of the distribution to produce the small degree of ionization required.

If oxygen is present in the argon a strong electron attachment process could exist having a maximum cross section at about 1 ev (Biondi 1960) in which stable O_2^- ions are formed by three-body collisions. In oxygen gas the three-body attachment process is pressure dependent and a second oxygen molecule stabilizes the excited ion. Argon atoms are not efficient in stabilizing the molecular ion since they cannot absorb quanta of vibrational energy and for this reason the concentration of oxygen in the liquid argon will be very important. If the stabilizing collision occurs with a third body capable of resonant absorption, as would be the case when both the ion and the third body were identical molecules, the cross section for the transfer of the excess energy can be quite large. If n is the percentage concentration of oxygen in the liquid argon, N the number density of argon atoms and Q the cross section for the attachment process, the mean free path for attachment λ is given by $\lambda = (nNQ \times 10^{-2})^{-1}$. For liquid argon N is 2×10^{22} cm⁻³, and if Q is taken to be 10^{-14} cm² (Massey 1938) the mean free path for attachment at an oxygen concentration of 0.001% is 5×10^{-4} cm. Clearly, since the electrode spacing is normally much larger than this many of the electrons will be attached to form negative ions at some point in the gap even at this low concentration. Another attachment process occurring at about 7 ev (Hurst and Bortner 1959) has a much smaller cross section but its influence on

the number of electrons reaching higher energies may be very important. Thus both attachment processes could reduce the number of electrons making ionizing collisions. A greater electric field is then necessary to produce the required ' α ' coefficient for breakdown.

3.4. The Anode Process

For breakdown measurements with steady voltage, the voltage is increased slowly over a period of time and many ions could be formed even at the lowest oxygen concentrations. These ions drift to the anode and, unless instantaneous neutralization of charge is possible there, a space charge will be formed. On a clean surface it is likely that neutralization can occur without difficulty, but if there is a semiconducting or insulating layer on the anode it is possible for this layer to acquire negative charge and prevent further neutralization of ions.

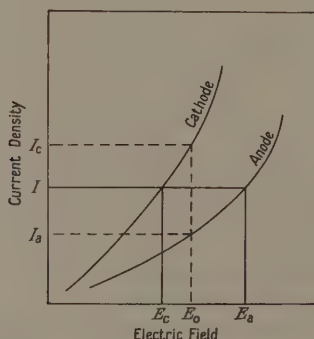


Fig. 5. Hypothetical representation of field-current characteristics for cathode and anode.

A space charge formed at the anode will enhance the field there as can be seen by considering a simple model in which the rates of charge emission from the cathode I_c and neutralization at the anode I_a are field dependent (Fig. 5). If, for a given mean applied field E_0 , I_a would be less than I_c at that field, then a space charge will be produced to reduce the applied field at the cathode to E_c and raise it at the anode to E_a until $I_c = I_a = I$ (Fig. 5). A problem of this type but with different boundary conditions has been examined by Fan (1948). An analysis of the present situation including the effects of diffusion of the ions shows that the cathode field is practically undistorted whilst the anode field is increased until the current taken at that electrode is equal to that emitted from the cathode. This is a consequence of the large value of E_0 applied near to breakdown which causes the diffusion layer of ions to be very compact and against the anode surface. The growth of an insulating oxide layer on the anode surface will increase the blocking properties of the anode and alter the law relating I_a to the anode field. This will lead to a greater anode space charge field.

Thus, when the anode is blocking, the emitted charges will cross the gap in a field that is practically undistorted by space charge until they are very near to the anode surface. Here the field can increase rapidly, and an enhanced

ionization rate α will occur. Since the space charge layer is small, the increased number of ionizing collisions will not be large, but only a few additional ions are necessary to cause an instability in the current from the cathode (Swan 1961). If the number of additional positive ions is small and they are removed rapidly from the space charge region by the high field, they will have a negligible effect on the field distribution.

The experimental curves in Fig. 1 can now be explained as follows. For zero oxidation time with stainless steel and brass electrodes the anode is not important in the breakdown process since the surface layer is not sufficiently insulating to prevent ion neutralization. This results in practically no anode space charge and the actual breakdown strength is determined by the emission properties of the cathode and by the positive ion space charge set up there by ions produced uniformly in the bulk of the liquid. As the oxide layer on the electrodes increases in thickness the cathode emission is reduced, and if the anode space charge is still insignificant a rise in the electric strength will result. When the electrode layers are sufficiently thick the emission from the cathode could exceed that accepted by the anode, resulting in an anode space charge field enhancement and an increased α value. The strength now depends more upon the anode surface condition than upon the cathode. Further increase of oxide layer increases simultaneously the space charge field at the anode and the production of positive ions in that region. The mean electric field required for breakdown is therefore reduced. Curves A and B of Fig. 2 can be explained in similar terms. The absence of the initial cathode-dependent range when using copper and aluminium electrodes (Fig. 1) can be explained if it is assumed that even at zero oxidation time the anode surface is sufficiently insulating to set up an appreciable space charge. With platinum and gold electrodes it is not possible to deduce whether the anode or the cathode is predominant since no variation with oxidation time was observed. However, the last two results in Table 1 suggest that a gold anode can give rise to a space charge since if the cathode had been the controlling electrode in these experiments the measured electric strength should have been much greater in magnitude. The existence of an insulating surface layer on gold has been proposed by Green (1955), who found that his results for the conduction current in *n*-hexane with gold electrodes could be explained in terms of an adsorbed hydrocarbon layer. It is quite possible that during electrode preparation a chemisorbed hydrocarbon layer could have been formed, thus giving rise to the observed effects.

If it is assumed that the law relating I_a to anode field is some rapidly increasing function of field, then, once a space charge has been established for a given pair of electrodes and a fixed applied field, the magnitudes of the space charge field will not be very dependent on oxygen concentration. An increase in the rate of arrival of negative ions will be compensated for by a small change in anode field. Consequently, in this case, the influence of the anode on the measured breakdown strength will be almost independent of oxygen concentration. The results in Table 2 confirm this. For commercial argon and argon with greater concentrations of oxygen, the strength increases with increasing oxygen content but the difference in strength due to different anode materials remains the same. The increase in strength with increasing oxygen content can, in this range, be attributed to a reduction in the number of electrons as a result of attachment in the liquid as discussed earlier. When the oxygen concentration is

very small and ion formation in the liquid is less probable, no appreciable space charge is formed and the influence of the anode is reduced. From Table 2 it can be seen that for the spectroscopically pure argon the change in strength due to the different anodes was reduced to 30% of that observed at large oxygen concentrations. That a difference was still found suggests that, even in the purer argon, electron attachment was occurring, although at a very much reduced rate. For a stainless steel anode the strength increases continuously with increasing oxygen content, but with an aluminium anode there is a reduction in strength for very small oxygen concentrations which is followed by a continuous increase with the addition of more oxygen. This behaviour suggests that a stainless steel surface of zero oxidation time does not give rise to an anode space charge, so that the continuously increasing strength observed with increasing oxygen content and a stainless steel anode can be attributed to progressively increased electron attachment in the liquid. Aluminium, however, forms a highly insulating surface layer immediately on exposure to air. It is to be expected, therefore, that a space charge would form even at very low oxygen concentrations when only a small percentage of the electrons emitted form ions, and as a result of this an appreciable anode field enhancement could be set up during the period of voltage increase prior to breakdown. In this situation the α process would increase and the strength decrease with increasing oxygen concentration until attachment in the body of the liquid became predominant. At this point the effective reduction in α outweighs the increase due to the anode space charge, and the strength increases in a similar way to that observed with a stainless steel anode.

§ 4. CONCLUSIONS

As far as the authors are aware, this is the first time that the influence of the anode material on the electric strength of liquids has been examined in detail, although Sharbaugh, Crowe, Cox and Auer (1956) did observe a 9% reduction in the impulse strength of *n*-hexane when the anode surface was roughened. It is possible that for hydrocarbon liquids and oils which contain dissolved oxygen an anode influence may still be important, but that the solid deposits and adsorbed surface layers completely mask any variations in the properties of the underlying surface. With liquid argon, however, the absence of solid deposits allows slight changes of the electrode surfaces to be effective, and the influence of the cathode and anode may be investigated separately.

The formation of an anode space charge depends on the ease with which negative charge can be accepted at that electrode, and it is to be expected that negative ions in which the excess electron is more strongly bound would give rise to a greater space charge distortion than free electrons or ions on which the electron is only weakly attached. The much reduced anode influence observed with spectroscopic grade argon suggests that oxygen as an impurity is particularly important in this respect.

The mechanism postulated for the anode behaviour requires the establishment of a space charge at the anode surface, and is time dependent therefore. By using pulse fields of short duration it should be possible to prevent the development of the space charge, and the electric strength measured in this way should be independent of the anode. Work is now in progress to check this.

ACKNOWLEDGMENTS

The authors are grateful for generous financial assistance from the British Electrical and Allied Industries Research Association for the purchase of equipment. They would also like to thank Professor M. W. Humphrey Davies for facilities provided, and the Department of Scientific and Industrial Research for a maintenance grant to one of us (D. W. S.).

REFERENCES

- BIONDI, M. A., 1960, *Proc. 4th International Conf. on Ionization Phenomena in Gases*, Vol. I, 72 (Amsterdam: North Holland).
- BLAISSE, B. S., VAN DEN BOOGAART, A., and ERNE, F., 1958, *Institut International du Froid, Annexe 1958-1*, 333.
- BOYLE, W. S., and KISLIUK, P., 1955, *Phys. Rev.*, **97**, 255.
- CABRERA, N., 1957, *Semiconductor Surface Physics*, Ed. by R. H. Kingston (Oxford: University Press).
- DAVIDSON, N., and LARSH, A. E., 1950, *Phys. Rev.*, **77**, 706.
- FAN, H. Y., 1948, *Phys. Rev.*, **74**, 1505.
- GOODWIN, D. W., 1956, *Proc. Phys. Soc.*, **69**, 61.
- GREEN, W. B., 1955, *J. Appl. Phys.*, **26**, 1257.
- 1956, *J. Appl. Phys.*, **27**, 921.
- HANCOX, R., 1957, *Brit. J. Appl. Phys.*, **8**, 476.
- HURST, G. S., and BORTNER, T. E., 1959, *Radiation Research, Suppl.*, **1**, 547.
- KACHICKAS, G. A., and FISHER, L. H., 1953, *Phys. Rev.*, **91**, 775.
- KISLIUK, P., 1959, *J. Appl. Phys.*, **30**, 51.
- KRONIG, R., and VAN DER VOOREN, A. I., 1942, *Physica*, **9**, 139.
- LEWIS, T. J., 1953, *Proc. Instn Elect. Engrs*, **100**, Pt. IIA, 141.
- 1955, *J. Appl. Phys.*, **26**, 1405.
- MALKIN, M. S., and SCHULTZ, H. L., 1951, *Phys. Rev.*, **83**, 1051.
- MASSEY, H. S. W., 1938, *Negative Ions* (Cambridge: University Press).
- MOTT, N. F., 1947, *Trans. Faraday Soc.*, **43**, 429.
- RONNQVIST, A., and FISCHMEISTER, H., 1960, *J. Inst. Metals*, **89**, 65.
- SHARBAUGH, A. H., CROWE, R. W., COX, E. B., and AUER, P. L., 1956, *Annual Report 1955 Conf. on Electrical Insulation* (Washington: National Research Council), p. 16.
- SLETTEN, A. M., 1959, *Nature, Lond.*, **183**, 311.
- STACEY, F. D., 1959, *Aust. J. Phys.*, **12**, 105.
- SWAN, D. W., 1960, *Proc. Phys. Soc.*, **76**, 36.
- 1961, *Proc. Phys. Soc.*, **78**, 423.
- SWAN, D. W., and LEWIS, T. J., 1960, *J. Electrochem. Soc.*, **107**, 180.
- WATSON, P. K., and SHARBAUGH, A. H., 1960, *J. Electrochem. Soc.*, **107**, 516.
- WILLIAMS, R. L., 1957, *Canad. J. Phys.*, **35**, 134.

The Electronic Structure and Spectrum of Nitrobenzene

BY T. E. PEACOCK

Chemistry Department, Kings College, Strand, London, W.C.2

MS. received 27th March 1961

Abstract. The self-consistent field molecular orbital theory has been used to calculate the π electronic structure and spectrum of nitrobenzene.

§ 1. INTRODUCTION

THE self-consistent field molecular orbital theory (Roothaan 1951), as applied to π electron systems (McWeeny 1956, McWeeny and Peacock 1957), has been used to calculate the π electron charge distribution and spectrum of nitrobenzene. The matrix elements of the self-consistent field Hamiltonian are given by (McWeeny 1956)

$$h_{ii}^F = \omega_i + \frac{1}{2}P_{ii}\gamma_{ii} - \frac{1}{2}\gamma_{ii}^C + \sum_j (P_{jj} - Z_j)\gamma_{ij}$$

and

$$h_{ij}^F = \beta_{ij} - \frac{1}{2}P_{ij}\gamma_{ij}$$

where the $\omega_i - \sum_j Z_j\gamma_{ij}$ (Z_j is the number of π electrons supplied by atom j) and the β_{ij} are the elements of the 'bare' framework Hamiltonian. The P_{ij} are the elements of the 'charge and bond order' matrix and the

$$\gamma_{ij} = \langle i(1)j(2) | \tau_{12}^{-1} | i(1)j(2) \rangle$$

are the two-electron interaction integrals. γ_{ii}^C is the one-centre two-electron integral for an atomic orbital centred on carbon atom i .

For a heterocyclic molecule the equation for h_{ii}^F , corresponding to a heteroatom, is (McWeeny and Peacock 1957)

$$h_{ii}^F = \omega_i + \delta\omega_i + \frac{1}{2}P_{ii}\gamma_{ii} - \frac{1}{2}\gamma_{ii}^C + \sum_j (P_{jj} - Z_j)\gamma_{ij}.$$

We choose $\omega_i + \frac{1}{2}\gamma_{ii}^C$ as the energy zero, and then the h_{ii}^F vanish for alternant hydrocarbons. The energy unit β , is chosen to have the value of the resonance integral for nearest neighbours in benzene, i.e. -4.79 eV (McWeeny and Peacock 1957). For a nitrogen atom contributing two π electrons $\delta\omega_i = 2.80\beta$ (Peacock 1959c) and for an oxygen atom contributing one electron $\delta\omega_i = 0.8\beta$ (Sidman 1957). β_{ij} for N-O bonds was given the value 0.570β and for C-N bonds 0.538β . The electron interaction integrals have the values assigned in previous calculations (McWeeny and Peacock 1957, Peacock 1959a, b, c). In particular $\gamma_{ii}^C = -2.380\beta$ and $\gamma_{ii}^N = -2.672\beta$. γ_{ii}^O is given the value -3.060β (Sidman 1957). The Hamiltonian and the charge and bond order matrix are made self-consistent using McWeeny's iterative procedure (McWeeny 1956). The electronic spectrum was then calculated as in previous work (McWeeny and Peacock 1957, Peacock 1959a, b, c).

Table 1

M.O.	Symmetry	Energy β	ϕ_1	ϕ_2	ϕ_3	ϕ_4	ϕ_5	ϕ_6	ϕ_7	ϕ_8	ϕ_9	ϕ_{10}
E	A	2.6100	0.0493	0.0817	0.1667	0.3131	0.3755	0.7692	0.3131	0.1667	0.0817	
D	A	1.9116	0.4458	0.4228	0.3557	-0.1650	0.2577	-0.2640	-0.1650	0.3557	0.4228	
C	B	1.3374	0.0000	0.4931	0.5011	-0.0755	0.0000	0.0000	0.0755	-0.5011	-0.4931	
B	A	1.2727	0.5318	0.2607	-0.2992	0.1917	-0.5526	0.1533	0.1917	-0.2092	0.2607	
A	B	0.8334	0.0000	0.0679	0.0397	0.7028	0.0000	0.0000	-0.7028	-0.0397	-0.0679	
B'	A	-0.7342	0.3155	-0.0854	-0.2950	-0.4887	0.3066	0.3739	-0.4887	-0.2950	-0.0854	
C'	B	-1.0242	0.0000	0.5025	-0.4972	-0.0206	0.0000	0.0000	0.0206	0.4972	-0.5025	
D'	A	-1.2029	0.5014	-0.2886	-0.1427	0.2992	0.4666	-0.3805	0.2992	-0.1427	-0.2886	
E'	A	-1.7246	0.4063	-0.3947	0.3859	-0.0981	-0.4190	0.1749	-0.0981	0.3859	-0.3947	

§ 2. RESULTS

Nitrobenzene was considered as a π electron system containing ten electrons; one from each carbon and oxygen atom and two from the nitrogen atom.

The self-consistent field molecular orbitals together with their energies are given in Table 1. The numbering of the atoms in the molecule is given in Fig. 1. The molecule has the symmetry C_{2v} and the molecular orbitals are given the symbols A and B, depending upon whether they belong to the symmetric or antisymmetric representation of the point group. The self-consistent charges and bond orders (for nearest neighbours) are shown in Fig. 2. From this charge distribution the π dipole moment is estimated to be 3.06 D.

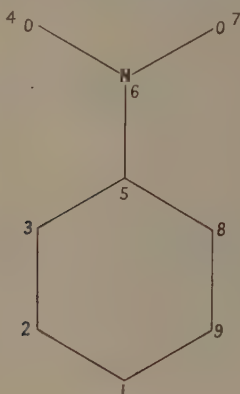
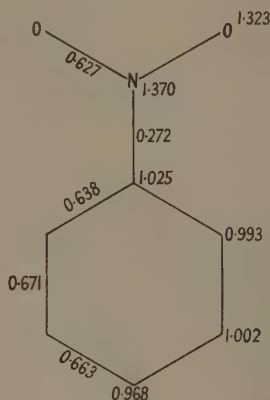


Fig. 1. The nitrobenzene molecule.

Fig. 2. π electron charges and bond orders.

For the calculation of the excited states, all of the configurations involving the molecular orbitals C, B, A, B' and C', in which one electron has been excited, were used. For completeness the ground state configuration was included; although as expected its interaction with the excited states was negligible. The symmetries of the configurations which arise are given in Table 2. The wave functions for the excited states in terms of the interacting configurations are given in Table 3.

Table 2

A	$\Phi(0)$	$\Phi(B \rightarrow B')$	$\Phi(C \rightarrow C')$	$\Phi(A \rightarrow C')$
B		$\Phi(A \rightarrow B')$	$\Phi(B \rightarrow C')$	$\Phi(C \rightarrow B')$

Table 3

	Energy ($\bar{\nu}$)
$\Psi_{B1}^* = 0.9723\Phi(A \rightarrow B') - 0.0504\Phi(B \rightarrow C') - 0.2282\Phi(C \rightarrow B')$	31000
$\Psi_{B2}^* = 0.1704\Phi(A \rightarrow B') - 0.5152\Phi(B \rightarrow C') + 0.8400\Phi(C \rightarrow B')$	36500
$\Psi_{B3}^* = 0.1599\Phi(A \rightarrow B') + 0.8556\Phi(B \rightarrow C') + 0.4923\Phi(C \rightarrow B')$	52800
$\Psi_{A0}^* = 0.9993\Phi(0) + 0.0377\Phi(B \rightarrow B') + 0.0059\Phi(C \rightarrow C')$	0
$\Psi_{A1}^* = 0.0379\Phi(0) - 0.9572\Phi(B \rightarrow B') - 0.2870\Phi(C \rightarrow C')$	37000
$\Psi_{A2}^* = \Phi(A \rightarrow C')$	40500
$\Psi_{A3}^* = 0.0052\Phi(0) - 0.2871\Phi(B \rightarrow B') + 0.9579\Phi(C \rightarrow C')$	51200

§ 3. DISCUSSION

The observed spectrum of nitrobenzene has three main bands (Wolf and Strasser 1953) at $40\,000\bar{\nu}$, $36\,000\bar{\nu}$ and $30\,200\bar{\nu}$. These bands can be interpreted in terms of the excited states listed in Table 3. The $30\,000\bar{\nu}$ transition can be identified with the state in which $\Phi(A \rightarrow B')$ is prominent. The $36\,000\bar{\nu}$ transition is associated with the $\Phi(C \rightarrow B')$ and $\Phi(B \rightarrow B')$ states. Finally, the band at $40\,000\bar{\nu}$ can be associated with $\Phi(A \rightarrow C')$. From an examination of the orbital coefficients, the $30\,000\bar{\nu}$ is confined to the nitro-group. Both the A and B' orbitals are fairly well localized on the nitro-group and this transition will therefore be characteristic of the nitro-group. Furthermore it is a $\pi \rightarrow \pi^*$ transition and not $n \rightarrow \pi$ as previously assigned. A recent interpretation of the experimental data confirms this (Godfrey and Murrell 1961).

Similarly the $36\,000\bar{\nu}$ transition will be expected to be benzene-like in character. $\Phi(C \rightarrow B')$ and $\Phi(B \rightarrow B')$ are the analogues of the benzene α and p bands, but they are heavily perturbed by the nitro-group. This leads to considerable charge transfer from ring to nitro-group (about $\frac{1}{2}$ electron in each case). Observations of the crystal spectrum should indicate that this band is both long and short axis polarized. The $40\,000\bar{\nu}$ band involves the transfer of almost a whole electron from the nitro-group to the ring. The A orbital is localized on the nitro-group, whereas the C' orbital is concentrated in the ring. This band will be characteristic of benzenoid nitro-groups.

The observed behaviour of the three bands is in agreement with this interpretation. The model used gives a satisfactory interpretation of the spectrum of nitrobenzene.

ACKNOWLEDGMENTS

The author wishes to thank Professor D. P. Craig of University College London for many helpful discussions on the interpretation of the spectrum. He also wishes to thank Messrs. Shell Research Ltd. for financial support whilst he was at University College London, during which time this work was commenced.

REFERENCES

- GODFREY, M., and MURRELL, J. N., 1961, *Proc. Chem. Soc.*, p. 171.
MCWEENY, R., 1956, *Proc. Roy. Soc. A*, **237**, 355.
MCWEENY, R., and PEACOCK, T. E., 1957, *Proc. Phys. Soc. A*, **70**, 41.
PEACOCK, T. E., 1959 a, *J. Chem. Soc.*, 2308.
— 1959 b, *J. Chem. Soc.*, 3241.
— 1959 c, *J. Chem. Soc.*, 3645.
ROOTHAAN, C. C. J., 1951, *Rev. Mod. Phys.*, **23**, 69.
SIDMAN, J., 1957, *J. Chem. Phys.*, **27**, 429.
WOLF, K. L., and STRASSER, O., 1933, *Z. Phys. Chem. B*, **21**, 389.

LETTERS TO THE EDITOR

**A Corrigendum to the Article 'Double Beta Decay' by
H. Primakoff and S. P. Rosen in *Reports on Progress in Physics***

The following corrections should be made to Eqn (44) of the article mentioned in the title (Primakoff and Rosen 1959): in the coefficient of

$$|\langle \Psi_f^* | \sum_{n,m} \tau_n^{(\pm)} \tau_m^{(\pm)} \sigma_n \cdot \sigma_m / r_{nm} | \Psi_i \rangle|^2 \equiv |M_2|^2 \quad \dots\dots (1)$$

replace f_i by $\frac{1}{3} f_i$ for $i=1, 2, 3$, and in the coefficient of

$$2\mathcal{R} \langle \Psi_f^* | \sum_{n,m} \tau_n^{(\pm)} \tau_m^{(\pm)} / r_{nm} | \Psi_i \rangle \langle \Psi_f^* | \sum_{n,m} \tau_n^{(\pm)} \tau_m^{(\pm)} \sigma_n \cdot \sigma_m / r_{nm} | \Psi_i \rangle^* \\ \equiv 2\mathcal{R}(M_1 M_2^*) \quad \dots\dots (2)$$

replace f_i by $\frac{1}{3} f_i$ for $i=1, 2, 3, 6$; all other terms remain unchanged. Eqn (44) is now positive definite and in agreement with earlier, independent calculations of both authors (Primakoff 1952, Rosen 1957). Moreover the numerical estimates of no-neutrino $\beta\beta$ decay lifetimes (Eqn (54)) do not involve M_2 and are unaffected by these corrections.

At first sight, the corrected form of Eqn (44) does not appear to include, as a special case, the results of Greuling and Whitten for $m_\nu = V=0$ (Greuling and Whitten 1960, Eqns (35)–(38)); in particular it does not contain the matrix element

$$M_3 \equiv \langle \Psi_f^* | \sum_{n,m} \tau_n^{(\pm)} \tau_m^{(\pm)} (\sigma_n \cdot \mathbf{r}_{nm})(\sigma_m \cdot \mathbf{r}_{nm}) / r_{nm}^3 | \Psi_i \rangle. \quad \dots\dots (3)$$

The discrepancy can be resolved, however, by observing that the passage in our paper from Eqn (36) to Eqn (41) involves an average over the direction of \mathbf{r}_{nm} . This procedure automatically eliminates the matrix element

$$\left. \begin{aligned} M_4 &\equiv \langle \Psi_f^* | \sum_{n,m} \tau_n^{(\pm)} \tau_m^{(\pm)} T_{nm} / r_{nm}^3 | \Psi_i \rangle \\ &\equiv 3M_3 - M_2 \\ T_{nm} &\equiv \frac{2}{3} \sum_{\lambda, \mu=1}^3 (\sigma_{n\lambda} \sigma_{m\mu} + \sigma_{n\mu} \sigma_{m\lambda} - \frac{2}{3} \delta_{\lambda\mu} \sigma_n \cdot \sigma_m) \\ &\quad \times (2(\mathbf{r}_{nm})_\lambda (\mathbf{r}_{nm})_\mu - \frac{2}{3} \delta_{\lambda\mu} r_{nm}^2) \end{aligned} \right\} \dots\dots (4)$$

from our expression and replaces M_3 by $\frac{1}{3} M_2$ in the results of Greuling and Whitten. It then follows that Eqn (44) does contain their results as a special case, except for a difference in the sign of M_1 .

The average over the direction of \mathbf{r}_{nm} is a good approximation only if the initial and final 0^+ nuclear states are, to a large extent, spherically symmetric in ordinary space (i.e. $1S_0$). Therefore, within the limits of this approximation,

our results agree with those of Greuling and Whitten, except for the sign of M_1 . Since our independent calculations (Primakoff 1952, Rosen 1957) agree on this sign, we believe ours to be correct.

† The University of Pennsylvania,
Philadelphia,
Pennsylvania, U.S.A.

H. PRIMAKOFF†.
S. P. ROSEN†.

‡ Midwestern Universities Research Association,
Madison, Wisconsin, U.S.A.
3rd July 1961.

GREULING, E., and WHITTEN, R. C., 1960, *Ann. Phys., N.Y.*, **2**, 510.

PRIMAKOFF, H., 1952, *Phys. Rev.*, **85**, 888.

PRIMAKOFF, H., and ROSEN, S. P., 1959, *Rep. Progr. Phys.*, **22**, 121.

ROSEN, S. P., 1957, *D. Phil. Thesis*, University of Oxford.

LETTERS TO THE EDITOR

We should like to draw readers' attention to the publication of Letters to the Editor in this journal. We have arranged with our printers to publish letters six to seven weeks after receipt, provided they are reported upon favourably by our referees. For example, items for publication in the November issue of the journal should be received in the office not later than 20th September. This also applies to the other two journals of The Institute of Physics and The Physical Society, i.e. the *British Journal of Applied Physics* and the *Journal of Scientific Instruments*.

REVIEWS OF BOOKS

Angewandte Gitterphysik, 3rd Edn, by W. KLEBER. Pp. xii+291. (Berlin: Walter de Gruyter, 1960.) DM 38.

This book makes an introductory survey of the whole field of crystal properties and their relation to lattice structure. Dr. Kleber is Professor of Mineralogy and Crystallography in the Humboldt University of Berlin, and has the primary aim of giving students who are only moderately equipped in mathematics an understanding of the fundamentals of crystal lattice theory and its applications. This aim determines the scope of the book, which is mainly concerned with the general properties of crystals at medium and high temperatures and says comparatively little either about low temperatures or about refined theories.

After an introductory section on the principles of crystal structure and its experimental determination, the greater part of the book deals with physical and physical chemical properties (both bulk and surface) of ideal crystals, and how they can be at least partly understood in terms of crystal structure and intermolecular binding. A final section discusses the real structure of crystals and properties dependent on lattice imperfections.

The book is clearly written, and avoids most of the complicated mathematical detail that so often obscures physical significance to the common reader. In places, however, it could have been improved by referring some of the sections to specialists for comment. The discussion of thermal properties, which is particularly interesting to the present reviewer, is probably one of the worst examples: it has no references after 1939, contains several inaccuracies and betrays an odd emphasis in its selection of topics. Zero-point energy is not mentioned, and the lattice is stated to be at rest at $T=0$; the cyclic boundary condition is stated to be physically equivalent to holding the end atoms of a chain fixed; and the coefficient of linear expansion (denoted by γ !) is continually confused with the coefficient of volume expansion, so that two different values for NaCl are even quoted on the same page (p. 160). A rather unrealistic model proposed by Klemm in 1928 for the vibrations and melting of NaCl is treated in considerable detail, but Lindemann's simple treatment is not mentioned. No indication is given of what the frequency distributions of crystals are really like (and hence why Debye's approximation is so good), and it is implied that the anharmonic contribution to the specific heat is necessarily positive. Nevertheless, even this section will give many students a clearer idea of thermal properties of crystals than they would get from trying to study the usual treatises.

In short, this is a good book, but a thorough critical revision could make it much better. Naturally it is rich in German references, which English readers should find refreshing. It is very well printed and bound. T. H. K. BARRON.

Atomic Theory for Students of Metallurgy, by WILLIAM HUME-ROTHERY.
Pp. viii+418. (London: Institute of Metals, 1960.) 50s.

Since it was first published in 1946 this book has been revised and reprinted several times and has become firmly established as an introduction to modern physical ideas on the structure and properties of metals and alloys, not only for the 'Students of Metallurgy' to whom it is addressed but also for

physicists and chemists with an interest in the metallic state. The title has always been misleading and does the book less than justice for it deals with far more than atomic theory as such, three-quarters of it being an account of the properties, mainly electronic, of bulk metals and alloys.

The present edition is considerably enlarged (by 85 pages) and many chapters have been rewritten to take into account recent advances in knowledge. In particular there is a useful new chapter summarizing the experimental methods that are available for investigating electronic structure. The arguments are presented in a delightfully clear and usefully critical manner and the book contains probably as complete an elementary account of the electronic properties of metals as is to be found anywhere. Those familiar with earlier editions will welcome this more up-to-date treatment and to those coming new to the subject it may be warmly recommended as an excellent introduction to it. The book is well produced and the price is not unreasonable.

A. D. L.

Physics of the Upper Atmosphere, ed. J. A. RATCLIFFE. Pp. xi+586. (New York, London: Academic Press, 1960.) \$14.50.

The investigation of the upper atmosphere of the earth has long been the concern of physicists, radio scientists, astronomers and magneticians, and workers in the field have to be familiar with a correspondingly wide range of studies. In recent years the intensive measurements made during the International Geophysical Year, and the remarkable developments in space research, have both enhanced the importance of the subject and accelerated the study of it. The publication of this comprehensive and authoritative survey is thus very timely and greatly to be welcomed.

This volume is a co-operative effort on the part of a team of workers under the general editorship of Mr. J. A. Ratcliffe, formerly of the Cavendish Laboratory, Cambridge, and now Director of the Radio Research Station, Slough. Each of the contributing authors is an acknowledged authority in the branch of the subject concerned, and each chapter is, in effect, a monograph critically surveying the present state of knowledge and including a list of the more important references. The individual topics and authors are: The thermosphere—the earth's outermost atmosphere (S. Chapman); The properties and constitution of the upper atmosphere (M. Nicolet); The upper atmosphere studied by rockets and satellites (Homer E. Newell, Jr.); The sun's ionizing radiations (H. Friedman); The airglow (D. R. Bates); General character of aurorae (D. R. Bates); The auroral spectrum and its interpretation (D. R. Bates); Radar studies of the aurora (H. G. Booker); The ionosphere (J. A. Ratcliffe and K. Weekes); The upper atmosphere and geomagnetism (E. H. Vestine); The upper atmosphere and meteors (J. S. Greenhow and A. C. B. Lovell). The book was in preparation at the time of the International Geophysical Year and since the upper atmosphere was the subject of very intensive study during that period, it is fitting that in the final chapter of the book the authors have taken the opportunity of summarizing the significant advances in this field which occurred during the I.G.Y. and details of which had been published up to December 1959.

The planning and production of the book are of the highest quality and there can be no doubt that it will prove to be of the utmost value to all workers in this field.

W. J. G. BEYNON.

High Energy Electron Scattering Tables, by R. HERMAN and R. HOFSTADTER. Pp. ix+278. (Stanford, California: University Press, 1960.) 68s.

The study of high-energy electron scattering has made rapid progress in the past few years and an increasing number of laboratories are taking part or planning to take part in this work. In this book much of the information needed for the planning and interpretation of experiments is assembled, and it will surely take its place not only on the library shelves but also in the research rooms of these laboratories.

It deals essentially with the elastic scattering of electrons from nucleons and nuclei and is divided into two parts. The first 70 pages, which form an introduction to the tables, are also an excellent survey of the theoretical and experimental results in this field.

The second part, occupying about 200 pages, contains the following main groups of tables: (1) Nuclear charge density distributions for eleven different models. (2) The nuclear form factor for these tabulated against qa , where q is the momentum-energy transfer parameter and a is the root mean square radius. (3) The Rosenbluth scattering cross sections for point protons and neutrons from 50 mev to 10 000 mev, and the coefficients of the form factors F_1 and F_2 used in extending the Rosenbluth formula to nucleons of finite size. Values of q are also tabulated and these can be readily applied to the previous sets of tables. (4) Tables relating to scattering from the deuteron, in particular the cross section for inelastic scattering according to the point proton and neutron theory of Jankus and some sets of values from an extension of the theory to finite nucleons.

These are the chief contents. There are also graphs based on the tables, lists of kinematic relations, information on electron-electron and muon-nucleus scattering and much more.

Some of the material in this book may well become obsolete in a few years and in fact the authors say that they intend it as a preliminary handbook to be brought up to date as occasion demands. Nevertheless, it contains sufficient basic information to make it extremely useful for some time to come.

J. R. HOLT.

Graphite and its Crystal Compounds, by A. R. UBBELOHDE and F. A. LEWIS. Pp. xii+217. (Oxford: Clarendon Press, 1960.) 35s.

Graphite is a material of great interest to the pure scientist, and of considerable and growing importance to technologists in many fields of activity. The authors have done a useful service to workers in both categories by bringing together much of the information available about graphite and related substances in a way that certainly fulfils their aim, that of giving descriptive access to current lines of research.

Inevitably, no single viewpoint can be used as a starting point for the discussion of properties as various as the thermoelectric power, the mechanical properties, and the oxidation of even pure, defect-free graphite; and an extension to compounds ranging from dilute solid solutions to materials behaving like organic macromolecules must introduce further complexities. The authors have shown great flexibility in adjusting their terminology to the topic under discussion, and are rightly aware of the part that can be played by defects of various types in rendering interpretations of a given property uncertain.

Some of the discontinuous impressions one receives, however, might surely have been avoided by a more logical arrangement of the material of the book, and by the inclusion in the earlier sections of some brief account of the theoretical models for metals and semiconductors, with which comparisons are often made. If a description of the structures of graphite and its compounds (including for this purpose boron nitride, the structure of which is described in the chapter on the thermal properties of graphite) had been followed at once by an account of models for their electronic structures, the discussion of individual properties in later sections could be handled more conveniently. As it is, the electron band structure of graphite is dealt with towards the end of the chapter on electronic properties, and after reference has been made in earlier sections to electronic contributions to the specific heat and transport properties, while a discussion of changes in energy band populations in the compounds comes three chapters later.

There can be no doubt however that this book will prove very useful to the growing number of people who are concerned with graphite and related materials; and its extensive bibliography provides convenient access to specialized accounts of the many theoretical, experimental, and technological points referred to.

B. R. COLES.

From Dualism to Unity in Quantum Physics, by ALFRED LANDÉ. Pp. xvi + 114. (London: Cambridge University Press, 1960.) 18s. 6d.

The main theses of this book are roughly as follows. Statistical behaviour is a *fundamental* characteristic, both of classical and of quantum phenomena. Hence no distinction should be made between accidental and essential indeterminacy. This is supported by the following arguments: (a) absolute determinism can never be established as a physical doctrine; (b) it is a known fact (not logically impossible) that in many physical situations specific causes lead to randomly distributed effects; (c) this randomness is intrinsic, a fact supported by the conformity, or harmony, between *a priori* mathematical probability theory and statistical observed behaviour.

Though randomness is intrinsic, it is no mere *ad hoc* brute fact but can be shown to follow from the application of the principle of continuity. Randomness then is due to transitions between causally determined states.

The transition may be considered in connection with an important conceptual unit, the filter, leading to the definition of statistical passing fractions (of the passage of particles in a given state passing through a filter itself being in some state or other), using the principle of symmetry. Given the additional postulate of reproducibility, the passing fractions become transition probabilities. These may be expressed through matrices for which certain mathematical correlation laws hold, in particular a triangular matrix multiplication law, the law of unitary transformation, which turns out to be identical with the law of interference of probabilities. With the addition of the postulates of the homogeneity of space (q) and momentum space (p variable) together with the assumption of the dependence of transition values of observables on p - and q -intervals only, the author deduces the wave function $\psi(q, p) = \text{const. exp}(2iqp/\hbar)$.

This is a unitary theory because it insists that "particles are real things, ψ -waves are not" (p. 73), i.e. there is no need to invoke a principle of complementarity. Instead of wave-theory, we need no more than the concept of

statistical frequency applied to the transition probabilities of particles subjected to some physical process of interference. The dualistic wave-particle ideas of the Copenhagen School as well as recent attempts at a determinist substructure for quantum mechanics (Bohm etc.) are both rejected.

Professor Landé is particularly concerned to show that the rules of quantum mechanics are not merely *ad hoc* but "can be understood as necessities rather than as oddities under certain simple ground postulates" (pp. 49-50). Actually, however, his argument for basic universal indeterminacy seems itself to involve a brute fact, viz. the harmony between statistical experienced behaviour and *a priori* probability theory. More specifically, even if the principle of continuity bestows rationality upon statistics, the statement that if the ratio of the number of particles blocked by a filter to that passed "is not to be quite erratic, *it can only be a definite statistical ratio*" (p. 19, italics mine) is certainly far from being transparently "self-evident" (p. 41). Further, Landé admits that he possesses no proof of the *uniqueness* of the "unitary transformation law" (p. 46), limiting himself to the statement that "it seems *inconceivable*" that another could be constructed, though quoting Eddington's remark, "The building at this point shows some cracks".

Still, his attempt to "dispel the aura of incomprehensibility" of quantum mechanics by "simple, almost self-evident physical ground axioms, so that we can recognize it as a necessity rather than an oddity" (pp. 41, 42) is courageous, refreshing, and curiously harks back to seventeenth and eighteenth century modes of physical thought—indeed, Descartes is quoted approvingly on p. xv!

Although the author displays verbally hostility to "positivism" (pp. xi, 97), its essential approaches are fortunately frequently retained; thus we find on page 31 that the definition of the state of a system "has no concrete meaning unless it is (observationally) substantiated". But one wonders how strictly the author has applied the principle himself? Well-defined states must be reproducible. But though "position x of a particle is not a well-defined state, . . . position x at a certain time instant t is" (p. 29). Now how can the latter be reproduced?

This is a most important and stimulating volume. It breaks fresh ground in fundamentals and one can only hope that it will be followed by more work on the explication of the simple meanings of quantum mechanics, in lieu of the "semantic tricks" (p. 72) with which only too much recent exploratory literature has been burdened.

GERD BUCHDAHL.

The Hydrogen Bond, by G. C. PIMENTEL and A. L. McCLELLAN. Pp. xii + 475. (San Francisco, London: W. H. Freeman, 1960.) 82s.

This work represents the first survey in book-form of the hydrogen bond in all its manifestations. About 2250 references to publications covering research done in the main in the last thirty years, testify to the growing interest in this field. The investigation of the hydrogen bond has for a long time been considered as a byway of physics and chemistry; with the increasing success in the elucidation of the structure of proteins and nucleic acids it has, however, become apparent that hydrogen bonds play a decisive role in the configuration of these spiral structures. A real understanding of this curious effect to which we may owe our very existence, becomes of increasing importance to the biochemist and biologist, quite apart from its intrinsic interest to the student

of the nature of chemical bonding. This book will therefore fulfil a very useful function. It provides a detailed and complete discussion of the various phenomena produced by the presence of hydrogen bond such as anomalies in the pressure-volume-temperature curves, in the values of dielectric constants, the shifts and widths of infra-red and Raman spectra, in the spacings observed in the x-ray spectra of crystals, in the fine structure of nuclear magnetic resonance spectra and in neutron diffraction. So far, the last two methods have not come up to expectation; infra-red spectroscopy provides still the most accurate criterion for the presence of hydrogen bonds. The work done in this field is mainly, in spite of the great number of publications, in the qualitative stage; it lacks systematic attack and careful quantitative determinations are confined to Professor Mecke's admirable studies. Two chapters are devoted to the role of hydrogen bonds in the configuration of proteins, nucleic acids, industrial substances and the human body. The various attempts at a theory of the hydrogen bond are discussed. They have so far been unsuccessful. The experimental results are summarized in a great number of tables and diagrams illustrate the text.

The authors have been extremely thorough in the treatment of their subject but not very critical. The over emphatic presentation of the material is not quite in keeping with its general importance.

L. KELLNER.

Field Theory of Guided Waves, by R. E. COLLIN. Pp. xiii + 606. (London: McGraw-Hill, 1960.) 128s.

The propagation of waves in transmission lines, waveguides and free space is studied in most honours degree courses in physics and electrical engineering. The engineer approaches the subject most readily through the distributed circuit concepts of transmission lines in terms of voltages, currents and impedances. He then discovers the limitations and finds that further progress requires the field approach using Maxwell's equations. For the physicist, on the other hand, Maxwell's equations frequently provide the starting point for the transmission and propagation of electromagnetic waves. Although this approach is more fundamental and more rigorous the ideas of equivalent circuits and impedances are most powerful in solving many problems, and it is most desirable that the serious microwave experimenter should be well versed in both methods.

The book under review is concerned with postgraduate study, and it is based almost entirely on field concepts though occasionally it uses equivalent circuits. It is assumed that the reader has a previous knowledge of microwave theory such as would be covered in a first course in physics or electrical engineering. The chapter headings are: Basic electromagnetic theory, Green's functions, Transverse electromagnetic waves, Transmission lines, Propagation in cylindrical waveguides, Inhomogeneously filled waveguides, Excitation of waveguides, Variational methods for waveguide discontinuities, Periodic structures, Integral transform and function theoretic techniques, Surface waveguides, Artificial dielectrics. There is a mathematical appendix and there are sets of problems at the end of each chapter. It will be seen that this is a fairly advanced text and it requires some mathematical ability in the reader. The coverage is wide and much of the material has not previously been collected together in one volume. The general presentation is first class. The book can be thoroughly recommended for reference purposes in all microwave laboratories.

M. R. GAVIN.

Théorie des Groupes en Physique Classique et Quantique, Vol. 1, *Structures Mathématiques et Fondements Quantiques*, par TH. KAHAN. Pp. xxiv + 664. (Paris: Dunod, 1960.) 75 n fr.

The theory of the physical applications of groups and their representations is certainly a sufficiently large and well established subject to warrant up-to-date and unified treatment in a printed book. At present the student has at his disposal one or two excellent but old textbooks, a few key published papers, and a medley of mimeographed notes. The present attempt to give a complete account of the entire field of group theory in physics is therefore welcome. There is to be a second volume dealing with particular applications of groups. The first volume is largely of a mathematical nature. It is in seven parts, by different authors, each of which is nearly self-contained.

Part 1, by Cavaillès and Kahan, is the longest and also the most unusual. Its aim is to provide a thorough and rigorous understanding of all the mathematical notions directly or indirectly involved in group theory. This is done by a formal series of definitions and theorems, starting from the elements of mathematics, together with a few illustrative examples about rotation groups and spinors.

It seems to the reviewer that this was a misguided effort. The theoretical physicist will normally prefer a less formal treatment; or else he will do better to turn to an actual mathematics textbook. The physicist confronted with a mathematical term he does not understand may, however, find this part useful to refer to.

Part 2, by T. D. Newton, is about the inhomogeneous (and extended) Lorentz group and its unitary representations. Whilst chiefly concerned to recover the classic results of Wigner, the author combines this with some other material and presents it in a unified way which is nowhere else available in book form.

Part 3, by Gouarné, is on the theory of abstract groups; and Part 4, by Rideau, on group representations. Part 5 is also by Rideau and is about permutation groups and their representations. Part 7, by Nataf, deals with the three-dimensional notation group. This part contains the results most familiar to ordinary physicists, on angular momentum, Clebsch-Gordan coefficients, tensor operators, and so on. These four parts give straightforward and useful accounts of important topics, but they are portions of the theory already quite well covered by existing books.

Part 6, by Kahan, is on the axiomatic foundations of quantum theory, and does not seem to occupy a very natural place in the book.

The book as a whole suffers greatly from being by several different authors. There is considerable overlapping between different parts, and unity of presentation is not achieved. For example, rotation groups are mentioned in several places in unconnected ways. The work cannot help but be a useful source of reference, but a judgment on the value of the project must await the publication of the second volume.

J. C. TAYLOR.

The Energy Levels of the Magnesium Isotopes of Mass 25 to 28

By S. HINDS, H. MARCHANT AND R. MIDDLETON

Atomic Weapons Research Establishment, Aldermaston, Berks.

Communicated by K. W. Allen; MS. received 7th March 1961

Abstract. The energy levels of the magnesium isotopes of mass 25 to 28 inclusive have been measured with a broad-range magnetic spectrograph using a variety of deuteron and triton induced nuclear reactions. The following is a list of the reactions used to study each magnesium isotope together with the number of levels observed below a particular excitation energy:

^{25}Mg	$^{24}\text{Mg}(\text{d}, \text{p})^{25}\text{Mg}$	54 levels below 7.64 meV
	$^{27}\text{Al}(\text{d}, \alpha)^{25}\text{Mg}$	54 levels below 7.64 meV
^{26}Mg	$^{25}\text{Mg}(\text{d}, \text{p})^{26}\text{Mg}$	49 levels below 8.617 meV
	$^{24}\text{Mg}(\text{t}, \text{p})^{26}\text{Mg}$	63 levels below 9.370 meV
	$^{27}\text{Al}(\text{t}, \alpha)^{26}\text{Mg}$	87 levels below 10.515 meV
^{27}Mg	$^{26}\text{Mg}(\text{d}, \text{p})^{27}\text{Mg}$	18 levels below 5.017 meV
	$^{25}\text{Mg}(\text{t}, \text{p})^{27}\text{Mg}$	42 levels below 7.031 meV
^{28}Mg	$^{26}\text{Mg}(\text{t}, \text{p})^{28}\text{Mg}$	19 levels below 6.759 meV

The ground state Q -values of the above reactions were also measured.

§ 1. INTRODUCTION

THE work described in this communication originated as a study of the energy levels of ^{25}Mg using the $^{24}\text{Mg}(\text{d}, \text{p})^{25}\text{Mg}$ and the $^{27}\text{Al}(\text{d}, \alpha)^{25}\text{Mg}$ reactions. However, due to the presence of small amounts of ^{25}Mg and ^{26}Mg in the enriched ^{24}Mg target it was also thought desirable to study the $^{25}\text{Mg}(\text{d}, \text{p})^{26}\text{Mg}$ and the $^{26}\text{Mg}(\text{d}, \text{p})^{27}\text{Mg}$ reactions. This greatly assisted in the analysis of the ^{25}Mg data and also provided much new information about the nuclei ^{26}Mg and ^{27}Mg . Recently, when tritium was accelerated in the Aldermaston 6 meV electrostatic generator, it was possible to confirm the latter results with measurements made using a number of triton induced reactions. Thus, ^{26}Mg was further studied using the $^{24}\text{Mg}(\text{t}, \text{p})^{26}\text{Mg}$ and the $^{27}\text{Al}(\text{t}, \alpha)^{26}\text{Mg}$ reactions and ^{27}Mg using the $^{25}\text{Mg}(\text{t}, \text{p})^{27}\text{Mg}$ reaction. Some energy levels of ^{28}Mg have also been measured from the $^{26}\text{Mg}(\text{t}, \text{p})^{28}\text{Mg}$ reaction but it was not possible to confirm these because of the lack of convenient reactions proceeding to this nucleus.

The energy levels of ^{25}Mg have previously been measured, below 4.2 meV excitation energy, by Endt, Enge, Haffner and Buechner (1952), Enge (1954) and Sheline, Nielson and Sperduto (1959). In all of these investigations high resolution magnetic analysis was used to study the $^{27}\text{Al}(\text{d}, \alpha)^{25}\text{Mg}$ reaction and in the case of Endt, Enge *et al.*, also the $^{24}\text{Mg}(\text{d}, \text{p})^{25}\text{Mg}$ reaction. Recently,

the well-known state at 3.40 meV has been shown to consist of two groups by Hinds, Middleton and Litherland (1961) having components at 3.398 and 3.407 meV. A few states have also been reported above 4.2 meV by Hinds, Middleton and Parry (1958) from a low resolution study of the $^{24}\text{Mg}(\text{d}, \text{p})^{25}\text{Mg}$ reaction. Two neutron resonance levels have also been reported at 7.411 and 7.581 meV and have recently been confirmed by Newson, Block, Nichols, Taylor, Furr and Merzbacker (1959).

The energy levels of ^{26}Mg have previously been measured by Endt, Haffner and Van Patter (1952) from a magnetic analysis study of the $^{25}\text{Mg}(\text{d}, \text{p})^{26}\text{Mg}$ reaction. Blair and Hamburger (1960) have studied this reaction and also the $^{26}\text{Mg}(\text{d}, \text{d}')^{26}\text{Mg}$ reaction and report an additional level at 3.614 ± 0.020 meV which was not observed by Endt, Haffner and Van Patter.

The energy levels of ^{27}Mg are not accurately known and only the first excited state has been precisely measured. This was done by Endt, Haffner and Van Patter (1952) who employed magnetic analysis to study the $^{26}\text{Mg}(\text{d}, \text{p})^{27}\text{Mg}$ reaction. Several higher excited states have also been reported by Hinds, Middleton and Parry (1958) from a low resolution study of the same reaction. A neutron resonance level, at 6.726 meV and having a natural width of greater than 75 keV, has also been reported by Newson *et al.*

The authors are unaware of any previous measurements of the energy levels of ^{28}Mg .

§ 2. EXPERIMENTAL PROCEDURE

Thin aluminium and enriched magnesium isotope targets were bombarded with 5.5 to 6.0 meV deuterons and tritons from the Aldermaston electrostatic generator and the charged reaction products analysed with a broad-range magnetic spectrograph. The latter instrument has previously been described, see Hinds and Middleton (1959a). Prior to striking the target, the ion beam from the accelerator was defined to an area of 0.25 mm by 1.5 mm and this bombarded portion of target served as an object for the spectrograph. In general several exposures were made at different angles of emission for each target and frequently two exposures were made at one angle with different field strengths. The latter was done to increase the effective energy range of the instrument which is normally restricted by the length of the nuclear plate. Exposure strengths were about 500 to 3000 μC depending upon the target thickness, the angular acceptance of the spectrograph and the reaction cross section.

Normally 100 μ thick Ilford C2 nuclear plates (recently replaced by K2) are used in the spectrograph to record all types of particles. However, trouble has been experienced when exposing at small angles of emission. This arises from the spurious scattering of the primary particles and in a (d, p) reaction, for example, results in a dense continuous background of deuteron tracks which makes the counting of proton tracks difficult. In this example, the background can be effectively prevented by placing an absorber in contact with the emulsion of sufficient thickness to stop the deuterons while still permitting the protons to pass through into the emulsion. This is clearly not possible in the case of a (d, α) or a (t, α) reaction because the range of the α -particle is generally less than that of the deuteron or triton. A very satisfactory solution has been found to

this problem by using Ilford K minus 1 nuclear plates. These record α -particle tracks clearly but little more than a few grains are produced by protons, deuterons and tritons of more than 2 or 3 mev. They also have the advantage of being less sensitive to γ -rays and are almost completely insensitive to neutrons.

The magnesium isotope targets were prepared from enriched magnesium oxide supplied by the Atomic Energy Research Establishment, Harwell. This was evaporated from a tantalum boat directly on to a thin carbon film (about $10 \mu\text{g cm}^{-2}$) which had previously been mounted on a target frame. Tantalum was used as a boat material because it reduces the magnesium oxide to basic metal and since this is more volatile than either tantalum or its oxide, only the magnesium metal evaporates. Relatively pure targets of ^{24}Mg , ^{25}Mg and ^{26}Mg were prepared in this way ranging in thickness from about 20 to $40 \mu\text{g cm}^{-2}$. The aluminium targets consisted of self-supporting films of about 10 to $30 \mu\text{g cm}^{-2}$ and were also prepared by the evaporation process. Some difficulty was experienced with the thinner aluminium targets since they were extremely fragile and rarely permitted more than a single exposure to be made before breaking.

§ 3. RESULTS AND DISCUSSION

3.1. The Energy Levels of ^{25}Mg

The energy levels of ^{25}Mg were measured using the $^{24}\text{Mg}(\text{d}, \text{p})^{25}\text{Mg}$ and the $^{27}\text{Al}(\text{d}, \alpha)^{25}\text{Mg}$ reactions, the latter being preferred and generally considered to yield the more consistent results. This preference was based on the general observation that individual α -particle groups from a (d, α) reaction are usually of comparable intensity (neglecting isotopic spin considerations) while the proton groups from a (d, p) reaction frequently differ very strongly in intensity. Thus, in a (d, p) study there is a greater probability of missing a group, particularly if weak and neighbouring a strong group. The energy resolution, however, is generally less in the (d, α) reaction because of the greater loss of energy of the α -particle in traversing the target. In principle this can be compensated for by using a thinner target but in practice generally only partial compensation can be achieved because thin targets are extremely fragile and will not withstand prolonged ion bombardment.

Two typical spectra from the $^{24}\text{Mg}(\text{d}, \text{p})^{25}\text{Mg}$ reaction are shown in Fig. 1. The upper was measured at an incident energy of 5.721 mev and with the spectrograph at a laboratory angle of 30° and a magnetic field strength of 8690 gauss. The lower spectrum was obtained at an incident energy of 5.60 mev, an angle of 31° and with a field of 6576 gauss. Other energy spectra were measured at 60° and 90° with the higher field setting and at 20° and 60° with the lower field. The proton groups corresponding to states in ^{25}Mg were identified by their characteristic variation of energy with angle and are labelled numerically, with '0' referring to the ground state. Groups arising from target impurities of ^{12}C , ^{14}N , ^{16}O and ^{28}Si are labelled by the symbols of their residual nuclei with a subscript referring to the appropriate excited state. It will be noticed that the groups arising from ^{14}N and ^{28}Si are very weak and only the more prominent groups have been labelled. Identification of groups from the latter impurity was greatly facilitated by a previous study of the $^{28}\text{Si}(\text{d}, \text{p})^{29}\text{Si}$ reaction (unpublished).

The incident deuteron energy for each exposure was computed from the measured energy of the ground state proton group from the $^{16}\text{O}(\text{d}, \text{p})^{17}\text{O}$ reaction and the known Q -value of this reaction. A value of 1.917 MeV was assumed for the latter which was derived from the recent compilation of nuclear masses by Everling, König, Mattauch and Wapstra (1960). This method of determining the beam energy was preferred to the more direct method dependent on measuring the energy of the elastically scattered deuterons since it is almost completely independent of target thickness. Beam energies measured in this way are thought to be accurate to within ± 10 keV. The Q -value of the $^{24}\text{Mg}(\text{d}, \text{p})^{25}\text{Mg}$ reaction has been computed, from several such measurements, to be 5.096 ± 0.012 MeV which is in good agreement with the value of 5.097 ± 0.007 MeV reported by Endt, Enge, Haffner and Buechner (1952). Agreement is not quite so good, but within the experimental error, with the value of 5.106 MeV obtained from the masses reported by Everling *et al.* (1960) (N.B. The mass data reported by Everling *et al.* were used to obtain all other mass Q -values referred to in this communication).

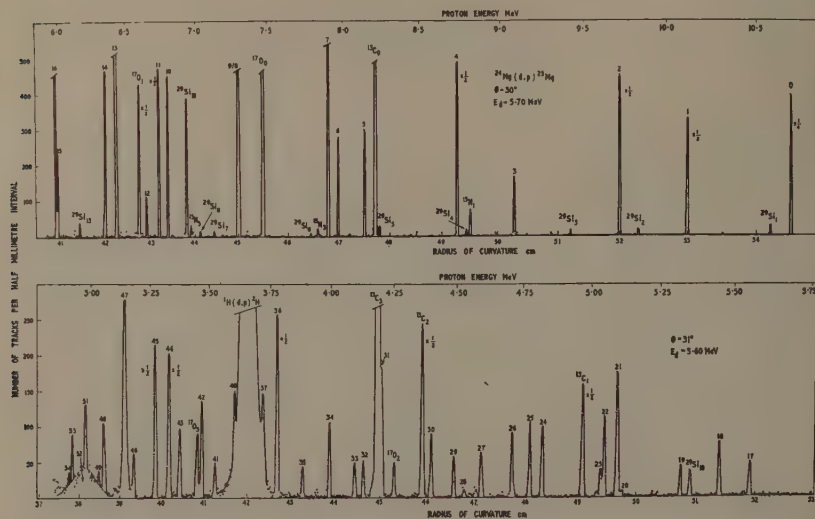


Fig. 1. Proton energy spectra measured from the $^{24}\text{Mg}(\text{d}, \text{p})^{25}\text{Mg}$ reaction. The upper spectrum was obtained at an angle of observation of 30° using deuterons of 5.721 MeV and the lower spectrum at 31° with deuterons of 5.60 MeV.

The mean values of the energy levels of ^{25}Mg , determined from the $^{24}\text{Mg}(\text{d}, \text{p})^{25}\text{Mg}$ reaction, are listed in column (1) of Table 1. The levels above 7.331 MeV are virtual, but of these only the 7.399 and the 7.57 MeV states were observed to have appreciable natural widths. These were measured to have widths respectively of 13 ± 3 keV and 80 ± 20 keV and are to be compared with the values of 7.8 ± 0.5 keV and 75 ± 15 keV reported by Newson *et al.* from neutron scattering measurements.

Table 1. The Energy Levels of ^{25}Mg (mev)

Group number	(1)	(2)	(3)	(4)	(5)	(6)
0	0	0	0	0	0	
1	0.579	0.583	0.581	0.583	0.586	
2	0.973	0.979	0.976	0.976	0.975	
3	1.609	1.609	1.609	1.611	1.608	
4	1.962	1.958	1.960	1.957	1.963	
5	2.564	2.564	2.564	2.562	2.568	
6	2.737	2.731	2.734	2.736	2.741	
7	2.800	2.795	2.798	2.799	2.806	
8	—	3.398	3.398	—	—	
9	3.407	—	3.407	3.405	3.404	
10	3.900	3.902	3.901	3.898	3.915	
11	3.965	3.966	3.965	3.969	3.975	
12	4.054	4.057	4.055	4.055	4.061	
13	4.268	4.269	4.268	4.265	4.280	
14	4.351	4.350	4.350			
15	4.701	4.706	4.704			
16	4.711	4.714	4.712			4.72
17	5.004	5.006	5.005			
18	5.108	5.108	5.108			
19	5.243	5.245	5.244			5.27
20	5.454	5.453	5.454			
21	5.465	5.51	5.465			5.49
22	5.511	5.514	5.512			
23	5.52	5.523	5.523			
24	5.738	5.738	5.738			
25	5.786	5.785	5.785			5.79
26	5.851	5.851	5.851			
27	5.969	5.965	5.967			
28	6.04	6.032	6.032			
29	6.074	6.073	6.074			
30	6.159	6.159	6.159			
31	6.350	6.349	6.350			
32	6.423	6.423	6.423			
33	6.458	6.456	6.457			
34	6.558	6.558	6.558			
35	6.668	6.669	6.668			
36	6.768	6.769	6.768			
37	6.825	6.826	6.825			6.80
38	6.871	6.872	6.872			6.85
39	6.903	6.899	6.901			
40	6.944	6.944	6.944			
41	7.026	7.023	7.025			
42	7.078	7.075	7.076			
43	7.170	7.172	7.171			7.18
44	7.215	7.214	7.215			7.23
45	7.271	7.270	7.270			
46	7.364	7.365	7.365			(7)
47	7.399	7.400	7.400			7.411
48	7.490	7.482	7.486			
49	7.513	7.510	7.512			
50	—	(7.538)	(7.538)			
51	7.563	7.564	7.564			
52	7.57	—	7.57			7.581
53	7.623	7.623	7.623			
54	7.640	7.640	7.640			

(1) Measured from the $^{24}\text{Mg}(\text{d}, \text{p})^{25}\text{Mg}$ reaction; (2) measured from the $^{27}\text{Al}(\text{d}, \alpha)^{25}\text{Mg}$ reaction; (3) mean values of (1) and (2); experimental error is ± 10 kev, except for 7.538 ± 0.015 and 7.57 ± 0.02 mev; (4) measurements of Endt, Enge *et al.* (1952) and Enge (1954); (5) measurements of Sheline, Nielsen and Sperduto (1959); (6) measurements of Hinds, Middleton and Parry (1958); (7) neutron resonance scattering measurements of Newson *et al.* (1959).

Alpha-particle energy spectra, from the $^{27}\text{Al}(\text{d}, \alpha)^{25}\text{Mg}$ reaction, were measured at laboratory angles of 15° , 30° and 60° at incident energies of 5.60, 5.70, 5.72 and 6.01 mev. Most of these exposures were made with relatively low magnetic field strengths and were primarily intended to study the higher excited states and only two exposures were made which included the ground state. One of these, obtained at an incident energy of 5.704 mev, a laboratory angle of 30° and with a field strength of 9169 gauss is shown in the upper half of Fig. 2. The lower spectrum was also obtained at 30° but with an incident energy of 6.01 mev and a field of 8455 gauss.

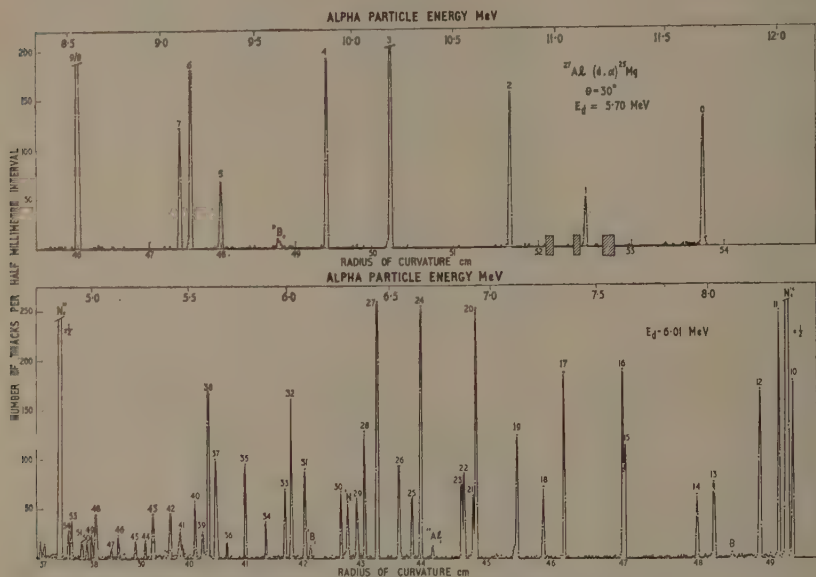


Fig. 2. Alpha-particle energy spectra from the $^{27}\text{Al}(\text{d}, \alpha)^{25}\text{Mg}$ reaction measured at an angle of 30° . The upper and lower spectra were obtained with spectrograph magnetic field strengths of 9169 and 8455 gauss using 5.704 and 6.01 mev deuterons respectively.

The α -particle groups corresponding to states in ^{25}Mg were identified by their characteristic variation of energy with angle and are labelled numerically. Several groups were also identified as arising from target impurities of ^{13}C , ^{16}O and ^{28}Si and these are labelled by their symbols for the residual nuclei. It is notable that two strong groups were observed from the $^{16}\text{O}(\text{d}, \alpha)^{14}\text{N}$ reaction corresponding to the ground and second excited states of ^{14}N and also a weak group proceeding to the $T=1$ first excited state. The latter transition can only proceed by violating the isotopic spin selection rule (see Browne 1956). Alpha-particle groups were observed corresponding to all the states of ^{25}Mg excited in the (d, p) reaction except for the broad state at 7.57 mev. A weak group of α -particles was also observed corresponding to a state at 7.538 mev. This may have escaped detection in the (d, p) reaction because of the masking effect of the broad 7.57 mev group.

The energy of the incident deuteron beam was calculated from the measured energy of the ground state α -particle group from the $^{16}\text{O}(\text{d}, \alpha)^{14}\text{N}$ reaction and the mass Q -value of 3.110 mev. From this the mean Q -value of the $^{27}\text{Al}(\text{d}, \alpha)^{25}\text{Mg}$ reaction was calculated to be 6.691 ± 0.012 mev which is in good agreement with the value of 6.694 mev reported by Endt, Enge *et al.* Both these values agree, within the experimental errors, with the mass Q -value of 6.700 mev.

The mean values of the energy levels of ^{25}Mg , measured from the $^{27}\text{Al}(\text{d}, \alpha)^{25}\text{Mg}$ reaction, are listed in column (2) of Table 1. In column (3) are the weighted mean values from both reactions which are subject to an experimental error of ± 10 kev except for the levels at 7.538 and 7.57 mev for which errors of ± 15 and ± 20 kev respectively are possible. Columns (4) and (5) of the Table contain respectively the aforementioned results of Endt, Enge *et al.* and Sheline *et al.* Agreement between the three sets of measurements is good and particularly so in the cases of the present results and those of Endt, Enge *et al.* where the maximum deviation is only 4 kev. In column (6) are the levels reported by Hinds, Middleton and Parry from a low resolution study of the $^{24}\text{Mg}(\text{d}, \text{p})^{25}\text{Mg}$ reaction. It is of interest to note that although many states were missed in this investigation, most of these were weakly excited and a recent study of the proton angular distribution (Middleton and Hinds, to be published) revealed that most of these were formed by processes other than stripping.

3.2. The Energy Levels of ^{26}Mg

The energy levels of ^{26}Mg have been measured using three independent nuclear reactions and a typical energy spectrum from the $^{25}\text{Mg}(\text{d}, \text{p})^{26}\text{Mg}$ reaction is shown in Fig. 3. This was obtained at a laboratory angle of 50° , an incident deuteron energy of 6.020 mev and with a spectrograph magnetic field of 10100 gauss. Similar energy spectra were measured at angles of 31° , 40° and 60° at a slightly lower bombarding energy. Groups corresponding to states in ^{26}Mg were identified as previously described and are labelled numerically, with '0' referring to the ground state. Strong impurity groups were observed arising from ^{12}C and ^{16}O and these are labelled in Fig. 3, using the same notation as previously. It should be noted that several weak groups were also observed arising from ^{24}Mg but only the ground state is labelled in the figure. Also at the particular angle illustrated groups 22 and 37 are masked respectively by the intense proton groups corresponding to the ground and first excited states of ^{17}O .

The incident deuteron energy was calculated for each angle of observation from the measured energy of the ground state proton group from the $^{16}\text{O}(\text{d}, \text{p})^{17}\text{O}$ reaction and the mass Q -value. From these the mean Q -value of the $^{25}\text{Mg}(\text{d}, \text{p})^{26}\text{Mg}$ reaction was calculated to be 8.861 ± 0.012 mev. This is to be compared with the value of 8.880 ± 0.012 mev reported by Endt, Haffner and Van Patter and with 8.873 mev expected from nuclear mass data. Agreement between these values is not very good.

A more convenient and reliable reaction for studying the energy levels of ^{26}Mg is the $^{27}\text{Al}(\text{t}, \alpha)^{26}\text{Mg}$ reaction. This has the advantage of proceeding from a target of a 100% isotopic abundance and thus the probability of incorrectly assigning a group is considerably reduced. Alpha-particle energy spectra have been measured at laboratory angles of 30° , 40° and 50° at an incident energy of 5.95 mev and in Fig. 4 is shown a typical spectrum obtained at 40° with a

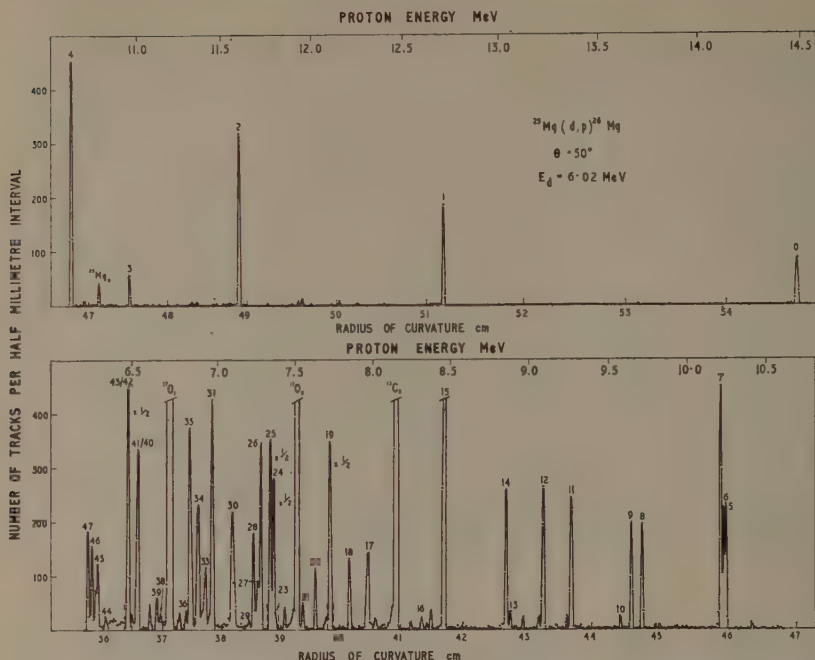


Fig. 3. An energy spectrum of the protons from the $^{25}\text{Mg}(d, p)^{26}\text{Mg}$ reaction obtained at an angle of observation of 50° with incident deuterons of 6.020 MeV.

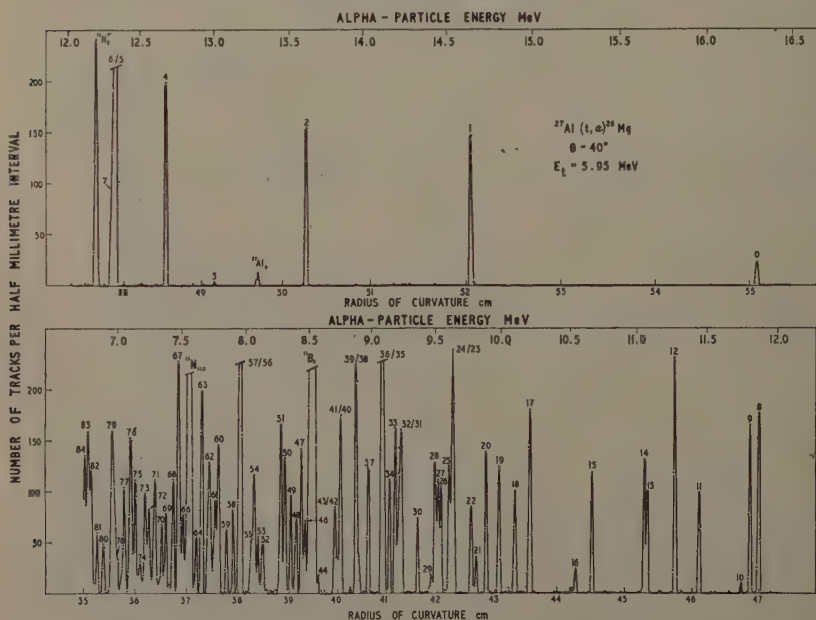


Fig. 4. A typical alpha-particle energy spectrum from the $^{27}\text{Al}(t, \alpha)^{26}\text{Mg}$ reaction. This was measured at an angle of observation of 40° at an incident triton energy of 5.95 MeV.

spectrograph field of 10569 gauss. Groups were identified and are labelled as previously described. Strong impurity groups were observed arising from ^{12}C and ^{18}O and also a weak group from the $^{28}\text{Si}(t, \alpha)^{27}\text{Al}$ reaction corresponding to the ground state of ^{27}Al .

The incident triton energy was determined by measuring the energy of the ground state α -particle group from the $^{16}\text{O}(t, \alpha)^{15}\text{N}$ reaction and by assuming a Q -value of 7.687 mev for this reaction. The latter value was obtained from nuclear mass measurements. This led to a triton energy of 5.951 ± 0.010 mev and from this the Q -value of the $^{27}\text{Al}(t, \alpha)^{26}\text{Mg}$ reaction was determined to be 11.541 ± 0.012 mev. This is in excellent agreement with the value of 11.540 mev expected from nuclear mass data. We are not aware of any previous direct measurements of this Q -value.

The third reaction used to study ^{26}Mg was the $^{24}\text{Mg}(t, p)^{26}\text{Mg}$ reaction and a typical energy spectrum is shown in Fig. 5. This was obtained at a laboratory

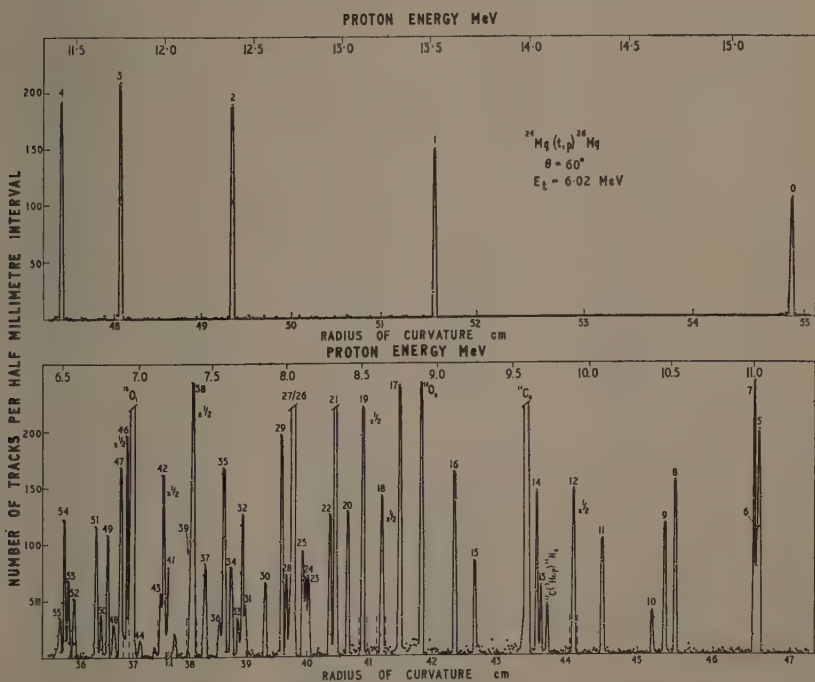


Fig. 5. A proton energy spectrum from the $^{24}\text{Mg}(t, p)^{26}\text{Mg}$ reaction measured at an angle of observation of 60° and at a bombarding energy of 6.015 mev.

angle of 60° , an incident energy of 6.015 mev and with a spectrograph magnetic field of 10334 gauss. Similar spectra were measured at the same incident energy at angles of 30° and 45° . Groups corresponding to states in ^{26}Mg and those arising from impurities were identified and labelled as previously described. It will be noticed that a weak group of protons was observed arising from the

$^{12}\text{C}(^3\text{He}, \text{p})^{14}\text{N}$ reaction, indicating the presence of a small percentage of ^3He in the triton beam. However, since we had previously studied the $^{24}\text{Mg}(^3\text{He}, \text{p})^{26}\text{Al}$ reaction (Hinds and Middleton 1959b) we were able to verify that none of the proton groups appearing to correspond to states in ^{20}Mg did in fact correspond to states in ^{26}Al .

The incident triton energy was determined from measurements made on the $^{16}\text{O}(\text{t}, \text{p})^{18}\text{O}$ reaction and by assuming the mass Q -value of this reaction to be 3.706 mev. From this the Q -value of the $^{24}\text{Mg}(\text{t}, \text{p})^{26}\text{Mg}$ reaction was determined to be 9.930 ± 0.012 mev which is to be compared with the mass Q -value of 9.946 mev.

The energy levels of ^{20}Mg measured from the $^{25}\text{Mg}(\text{d}, \text{p})^{26}\text{Mg}$, the $^{27}\text{Al}(\text{t}, \alpha)^{26}\text{Mg}$ and the $^{24}\text{Mg}(\text{t}, \text{p})^{26}\text{Mg}$ reactions respectively are listed in columns (1), (2) and (3) of Table 2. In column (4) are the weighted mean

Table 2. The Energy Levels of ^{20}Mg (mev)

Group number	(1)	(2)	(3)	(4)	(5)
0	0	0	0	0	0
1	1.807	1.800	1.803	1.805	1.825
2	2.941	2.938	2.944	2.941	2.972
3	3.591	3.571	3.588	3.584	—
4	3.945	3.944	3.938	3.943	3.969
5	4.321	4.316	4.318	4.319	—
6	4.331	—	4.332	4.331	4.353
7	4.353	—	4.348	4.350	—
8	4.829	4.834	4.828	4.830	4.863
9	4.896	4.900	4.892	4.896	4.924
10	4.968	4.976	4.966	4.970	5.270
11	5.287	5.290	5.285	5.287	5.322
12	5.474	5.471	5.468	5.472	5.502
13	5.687	5.684	5.686	5.686	—
14	5.711	5.709	5.711	5.710	—
15	6.121	6.120	6.118	6.120	6.147
16	6.252	6.259	6.249	6.253	—
17	6.617	6.617	6.614	6.616	—
18	6.738	6.740	6.734	6.737	—
19	6.866	6.871	6.872	6.870	—
20	6.967	6.971	6.972	6.970	—
21	7.053	7.058	7.055	7.056	—
22	7.096	7.092	7.097	7.095	—
23	7.237	7.241	7.238	7.239	—
24	7.251	7.252	7.249	7.251	—
25	7.273	—	7.270	7.272	—
26	7.338	7.338	7.341	7.339	—
27	—	7.352	7.364	7.355	—
28	7.383	7.377	7.383	7.382	—
29	7.414	7.40	7.417	7.413	—
30	7.528	7.531	7.535	7.531	—
31	7.668	7.670	7.667	7.668	—
32	—	—	7.680	7.680	—
33	7.714	7.716	7.712	7.714	—
34	7.761	7.762	7.761	7.761	—
35	7.808	7.816	7.807	7.810	—
36	7.842	—	7.834	7.837	—
37	7.945	7.948	7.940	7.944	—
38	8.020	8.030	8.022	8.023	—

Table 2. The Energy Levels of ^{26}Mg (mev)—(continued)

Group number	(1)	(2)	(3)	(4)	(5)
39	8.040	—	—	8.040	
40	8.175	—	8.169	8.172	
41	—	8.189	(8.186)	(8.188)	
42	—	—	(8.215)	(8.215)	
43	8.243	8.233	(8.235)	8.237	
44	8.388	8.384	8.386	8.386	
45	8.451	8.448	8.446	8.449	
46	8.494	8.488	8.491	8.491	
47	8.524	8.518	8.521	8.521	
48	8.565	8.566	8.567	8.566	
49	8.617	8.611	8.615	8.614	
50		8.660	8.658	8.659	
51		8.694	8.694	8.694	
52		8.849	8.853	8.851	
53		8.889	8.891	8.890	
54		8.917	8.920	8.918	
55		—	8.950	8.950	
56		9.031	9.034	9.033	
57		—	9.045	9.045	
58		9.101	9.102	9.101	
59		9.157	9.155	9.156	
60		9.225	9.224	9.225	
61		9.242	9.246	9.244	
62		9.294	9.296	9.295	
63		9.366	9.370	9.367	
64		9.415			
65		9.461			
66		9.528			
67		9.564			
68		9.615			
69		9.674			
70		9.707			
71		9.760			
72		9.814			
73		9.841			
74		9.895			
75		9.931			
76		9.970			
77		10.028			
78		10.090			
79		10.118			
80		10.213			
81		10.272			
82		10.316			
83		10.358			
84		10.40			
85		10.419			
86		10.483			
87		10.515			

(1) Measured from the $^{26}\text{Mg}(\text{d}, \text{p})^{26}\text{Mg}$ reaction; (2) measured from the $^{27}\text{Al}(\text{t}, \alpha)^{26}\text{Mg}$ reaction; (3) measured from the $^{24}\text{Mg}(\text{t}, \text{p})^{26}\text{Mg}$ reaction; (4) weighted mean values of (1), (2) and (3); (5) reported by Endt, Haffner and Van Patter (1952).

Experimental error: ± 10 kev for levels 1 to 49, in column (4); ± 12 kev for levels 50 to 63, in column (4); ± 15 kev for levels 64 to 87, in column (2).

values which are subject to an experimental error of ± 10 kev for groups 1 to 49, ± 12 kev for groups 50 to 63 and ± 15 kev for groups 64 to 87. The energy levels in parentheses are doubtful and were in general observed only with one nuclear reaction. It may be noted that although according to the Table groups 32 and 39 were observed only with one reaction their existence was supported by one or both of the other reactions studied.

In column (5) of Table 2 are listed the energy levels of ^{26}Mg reported by Endt, Haffner and Van Patter (1952) from a magnetic analysis study of the $^{25}\text{Mg}(d, p)^{26}\text{Mg}$ reaction. These are not in good agreement with the present values but if allowance is made for the omission of certain levels the remainder are found to be consistently greater than the present values by about 25 kev. This suggests that an error may have been made in the determination of the ground state Q -value. Blair and Hamburger (1960) also report a level at 3.614 ± 0.020 mev which was not observed by Endt, Haffner and Van Patter but which may be identified with our level at 3.584 ± 0.010 mev.

3.3. The Energy Levels of ^{27}Mg

The energy levels of ^{27}Mg have been measured using the $^{26}\text{Mg}(d, p)^{27}\text{Mg}$ and the $^{25}\text{Mg}(t, p)^{27}\text{Mg}$ reactions and a typical proton energy spectrum from the former reaction is shown in Fig. 6. This was measured at an angle of 31° using

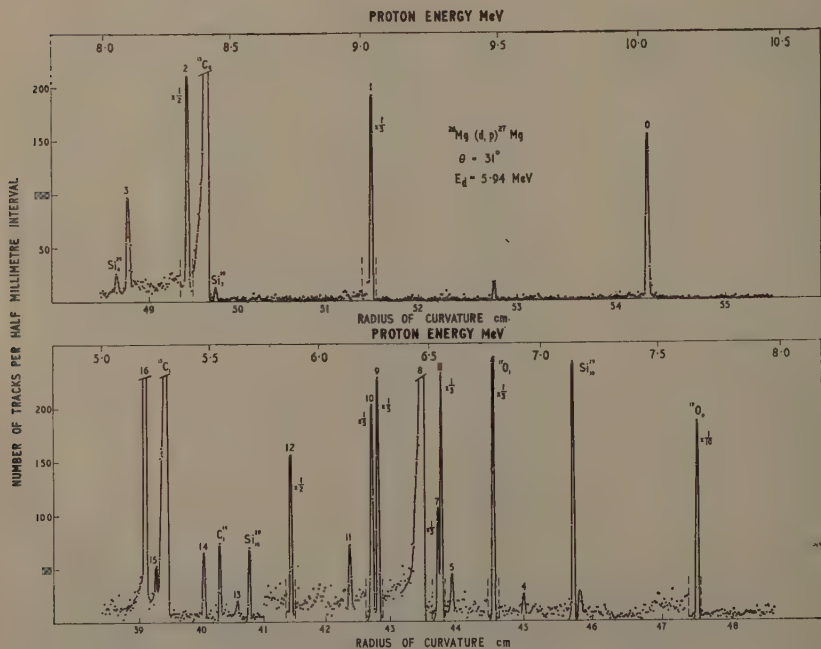


Fig. 6. Energy spectrum of the protons from the $^{26}\text{Mg}(d, p)^{27}\text{Mg}$ reaction measured at a laboratory angle of 31° and at an incident deuteron energy of 5.937 mev.

deuterons of 5.937 meV and with a spectrograph magnetic field of 8455 gauss. Energy spectra were also measured at angles of 25, 40 and 60° using deuterons of slightly lower energy. The various proton groups were identified in the manner previously described and those corresponding to states in ^{27}Mg are labelled numerically. Strong impurity groups were observed arising from carbon and oxygen and several weak groups from ^{13}C and ^{28}Si . The groups arising from the latter impurity were difficult to identify by their characteristic variation of energy with angle from those arising from ^{26}Mg . Identification, however, was simplified by comparison with previously measured proton energy spectra obtained at a similar deuteron energy with a target of ^{28}Si .

The incident deuteron energies were determined individually at each angle in terms of the accurately known Q -value of the $^{16}\text{O}(\text{d}, \text{p})^{17}\text{O}$ reaction. From these the mean Q -value of the $^{26}\text{Mg}(\text{d}, \text{p})^{27}\text{Mg}$ reaction was calculated to be 4.213 ± 0.012 meV which is in excellent agreement with the mass Q -value of 4.212 meV. Agreement is also good with the previous measurement of Endt, Haffner and Van Patter who reported a value of 4.207 meV.

Proton energy spectra from the $^{26}\text{Mg}(\text{t}, \text{p})^{27}\text{Mg}$ reaction were measured at angles of 30, 45 and 60° at incident triton energies of 6.024, 6.017 and 6.014 meV respectively. The 30° spectrum is shown in Fig. 7 which was obtained with a spectrograph magnetic field of 10 100 gauss. Groups were identified following our usual procedure and those corresponding to states in ^{27}Mg are labelled numerically using the same notation as was used in the $^{26}\text{Mg}(\text{d}, \text{p})^{27}\text{Mg}$ reaction. As is evident from the spectrum a fairly strong proton group was observed arising

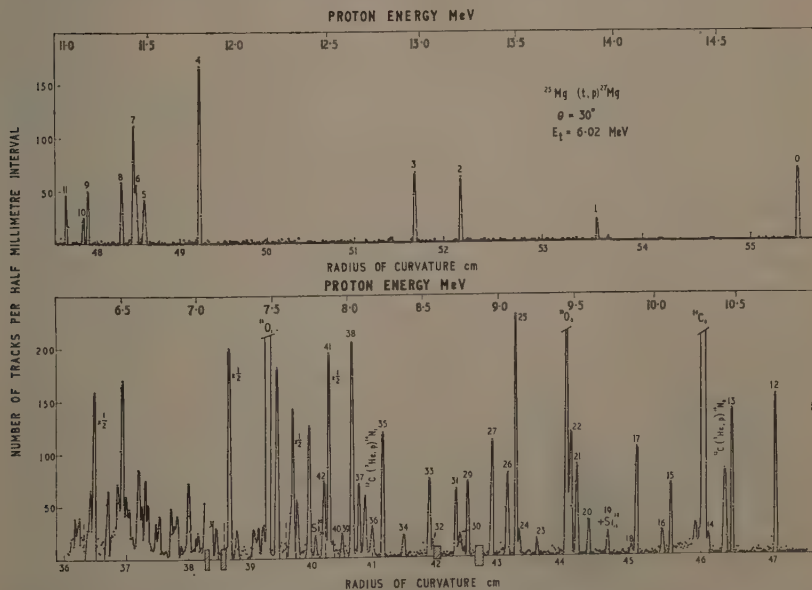


Fig. 7. A proton energy spectrum, obtained at an angle of 30° and with incident tritons of 6.024 meV, from the $^{26}\text{Mg}(\text{t}, \text{p})^{27}\text{Mg}$ reaction.

from the $^{12}\text{C}(^3\text{He}, \text{p})^{14}\text{N}$ reaction indicating that our triton beam contained a significant contamination of ^3He ions. This was particularly disturbing since it is kinematically impossible to distinguish between a $(^3\text{He}, \text{p})$ and a (t, p) reaction proceeding from the same target nucleus and some of the groups attributed to states in ^{27}Mg might be due to the $^{25}\text{Mg}(^3\text{He}, \text{p})^{27}\text{Al}$ reaction. To eliminate this possibility repeat exposures were made at 30° and 45° using carefully purified tritium gas in the ion source. Neither of these spectra exhibited a group corresponding to the $^{12}\text{C}(^3\text{He}, \text{p})^{14}\text{N}$ reaction and from them we were able to confirm that our previous assignments to states in ^{27}Mg were correct. It may also be noted that the ^3He contamination of the beam obtained with the purified gas was measured to be less than 0.1% by observing the elastically scattered groups from an aluminium target.

Strong impurity groups were observed in all exposures arising from ^{12}C and ^{16}O and also a significantly strong group from the $^{28}\text{Si}(\text{t}, \text{p})^{30}\text{Si}$ reaction corresponding to the 39th excited state of ^{30}Si . The latter assignment was possible because the authors had previously studied the $^{28}\text{Si}(\text{t}, \text{p})^{30}\text{Si}$ reaction (to be published). Other impurity groups from this reaction are of negligible intensity except for that leading to the 15th excited state of ^{30}Si . Unfortunately this group coincides at most angles of observation with group 19 from the $^{25}\text{Mg}(\text{t}, \text{p})^{27}\text{Mg}$ reaction. Group 19 is tentatively assigned to ^{27}Mg because it was consistently observed to be too strongly excited to be entirely accounted for by the $^{28}\text{Si}(\text{t}, \text{p})^{30}\text{Si}$ reaction.

The energy of the incident triton beam was determined for this exposure in terms of the Q -value of the $^{16}\text{O}(\text{t}, \text{p})^{18}\text{O}$ reaction in the manner described in the study of the $^{24}\text{Mg}(\text{t}, \text{p})^{26}\text{Mg}$ reaction. From this the mean Q -value of the $^{25}\text{Mg}(\text{t}, \text{p})^{27}\text{Mg}$ reaction was calculated to be 9.045 ± 0.012 MeV which is in good agreement with the mass Q -value of 9.052 MeV.

In Table 3 are listed the energy levels of ^{27}Mg determined from the two reactions and also the weighted mean values for the first 18 states. The experimental error for the latter values is ± 10 keV and for the higher levels, which were determined only from the $^{25}\text{Mg}(\text{t}, \text{p})^{27}\text{Mg}$ reaction, is ± 15 keV. The assignment of group 19 is doubtful and this value is shown in parentheses. Several groups were observed corresponding to higher excited states than group 43 but due to the complexity of the spectrum, precise analysis was not possible. Nevertheless, two strong groups were consistently observed corresponding to levels in ^{27}Mg at 7.240 ± 0.015 and 7.676 ± 0.015 MeV.

The excitation energy of the first excited state is in good agreement with the value reported by Endt, Haffner and Van Patter (column (4) of Table 3). The levels reported by Hinds, Middleton and Parry from a study of the $^{26}\text{Mg}(\text{d}, \text{p})^{27}\text{Mg}$ reaction are also in fair agreement with the more intense groups observed in the present investigation with the same reaction. The resonance level at 6.726 MeV reported by Newson *et al.* to have a natural width greater than 75 keV was not observed. This is not surprising since such a wide level, particularly if weak, might easily have been mistaken for background.

3.4. The Energy Levels of ^{28}Mg

The $^{26}\text{Mg}(\text{t}, \text{p})^{28}\text{Mg}$ reaction was used to measure the energy levels of ^{28}Mg up to an excitation energy of 6.8 MeV. Exposures were made at an incident triton energy of 5.957 MeV at laboratory angles of 30° , 45° and 60° . In Fig. 8

Table 3. The Energy Levels of ^{27}Mg (mev)

Group number	(1)	(2)	(3)	(4)
0	0	0	0	0
1	0.981	0.982	0.982	0.987
2	1.690	1.694	1.692	1.66
3	1.934	1.939	1.936	
4	3.112	3.106	3.109	
5	3.426	3.420	3.423	
6	3.471	3.470	3.470	
7	3.483	3.485	3.484	3.50
8	3.554	3.556	3.555	3.56
9	3.758	3.756	3.757	3.76
10	3.782	3.782	3.782	
11	3.880	3.879	3.880	
12	4.145	4.147	4.146	4.13
13	4.398	4.391	4.394	
14	4.550	4.548	4.549	
15	4.767	4.759	4.763	4.75
16	4.816	4.817	4.816	
17	4.982	4.982	4.982	
18	5.016	5.017	5.016	
19	(5.169)			
20	5.292			
21	5.365			
22	5.405			
23	5.618			
24	5.742			
25	5.762			
26	5.817			
27	5.922			
28	6.005			
29	6.074			
30	6.122			
31	6.152			
32	6.306			
33	6.327			
34	6.499			
35	6.643			
36	6.712			
37	6.807			
38	6.846			
39	6.912			
40	6.978			
41	7.007			
42	7.031			

(1) Measured from the $^{26}\text{Mg}(t, p)^{27}\text{Mg}$ reaction; (2) measured from the $^{26}\text{Mg}(d, p)^{27}\text{Mg}$ reaction; (3) weighted mean values of (1) and (2); (4) first excited state measured by Endt, Haffner and Van Patter (1952), other levels are measurements of Hinds, Middleton and Parry (1958).

Experimental error: ± 10 kev for levels in column (3); ± 15 kev for levels above 19 in column (1).

The figure consists of two vertically stacked plots. Both plots show the 'NUMBER OF TRACKS PER HALF MILLIMETRE INTERVAL' on the y-axis, ranging from 0 to 200.

The top plot has 'PROTON ENERGY MeV' on the x-axis, ranging from 9.0 to 12.0. It shows several sharp peaks labeled with ion species and their atomic numbers: $^{16}\text{O}_8$, $^{28}\text{Si}_{14}$, $^{12}\text{C}_6$, 1 , $^{28}\text{Si}_{14}$, and 0 . Text in the upper right corner of this plot specifies: ^{24}Mg (t.p) ^{28}Mg , $\theta = 45^\circ$, and $E_t = 5.96 \text{ MeV}$.

The bottom plot has 'PROTON ENERGY MeV' on the x-axis, ranging from 5.0 to 9.0. It shows numerous sharp peaks labeled with ion species and their atomic numbers: $^{16}\text{O}_8$, $^{15}\text{O}_7$, $^{14}\text{O}_7$, $^{13}\text{O}_7$, $^{12}\text{O}_6$, $^{11}\text{O}_6$, $^{10}\text{O}_5$, 9 , 8 , 7 , 6 , 5 , 4 , 3 , 2 , 1 , and 0 . There are also labels for $^{28}\text{Si}_{14}$ and $^{24}\text{Mg}_{12}$ near the baseline.

As for the other (t, p) reactions the beam energy was measured in terms of the $^{16}\text{O}(\text{t}, \text{p})^{18}\text{O}$ ground state Q -value. From this the mean Q -value of the $^{26}\text{Mg}(\text{t}, \text{p})^{28}\text{Mg}$ reaction was calculated to be 6.466 ± 0.012 mev, which is in good agreement with the mass Q -value of 6.460 mev. No previous direct determinations have been made of this Q -value. The energy levels of ^{28}Mg are shown in Table 4 where the experimental error is ± 12 kev for levels 1 to 4 and ± 15 kev for the remainder. These errors are slightly larger than usual since they are the means of only three determinations and it was not possible to verify them using another reaction.

The ground state Q -values reported in this communication are such that their internal consistency may readily be verified. This is illustrated in Table 5 by comparing the ^{25}Mg - ^{26}Mg mass excess difference, which may be calculated in four independent ways from the present results. The first two columns of the

Table 4. The Energy Levels of ^{25}Mg

Group number	Level energy (mev)	Group number	Level energy (mev)
0	0	10	5.652
1	1.468	11	5.695
2	3.861	12	5.910
3	4.014	13	6.135
4	4.553	14	6.416
5	4.874	15	6.516
6	5.169	16	6.539
7	5.177	17	6.599
8	5.264	18	6.708
9	5.463	19	6.759

Experimental error: ± 12 kev for levels 1 to 4; ± 15 kev for levels 5 to 19.

Table contain respectively the reaction and its measured Q -value. From the latter the mass excess differences between the initial and final nuclei have been determined and these are listed in column (3). By subtracting successive pairs of values from column (3), three independent values of the ^{25}Mg - ^{26}Mg mass excess difference were obtained and these are listed in the fourth column together with the directly determined value from the $^{25}\text{Mg}(\text{d}, \text{p})^{26}\text{Mg}$ reaction.

The four independent determinations of the ^{25}Mg - ^{26}Mg mass excess difference agree with each other within the stated experimental errors. The mean value of the ^{25}Mg - ^{26}Mg mass excess difference is 3.023 ± 0.008 mev which is in good agreement with the mass value of 3.026 ± 0.003 mev. All mass excess values are referred to the scale where ^{12}C has zero mass excess.

Table 5

(1)	(2)	(3)	(4)
A. $^{24}\text{Mg}(\text{d}, \text{p})^{25}\text{Mg}$	5.096 ± 0.012	$^{24}\text{Mg}-^{25}\text{Mg} = -0.751 \pm 0.012$	3.021 ± 0.017
$^{24}\text{Mg}(\text{t}, \text{p})^{26}\text{Mg}$	9.930 ± 0.012	$^{24}\text{Mg}-^{26}\text{Mg} = 2.270 \pm 0.012$	
B. $^{26}\text{Mg}(\text{d}, \text{p})^{27}\text{Mg}$	4.213 ± 0.012	$^{26}\text{Mg}-^{27}\text{Mg} = -1.634 \pm 0.012$	3.019 ± 0.017
$^{25}\text{Mg}(\text{t}, \text{p})^{27}\text{Mg}$	9.045 ± 0.012	$^{25}\text{Mg}-^{27}\text{Mg} = 1.385 \pm 0.012$	
C. $^{27}\text{Al}(\text{d}, \alpha)^{25}\text{Mg}$	6.691 ± 0.012	$^{27}\text{Al}-^{25}\text{Mg} = 4.019 \pm 0.012$	3.036 ± 0.017
$^{27}\text{Al}(\text{t}, \alpha)^{26}\text{Mg}$	11.541 ± 0.012	$^{27}\text{Al}-^{26}\text{Mg} = -0.983 \pm 0.012$	
D. $^{25}\text{Mg}(\text{d}, \text{p})^{26}\text{Mg}$	8.861 ± 0.012	$^{25}\text{Mg}-^{26}\text{Mg} = 3.014 \pm 0.012$	3.014 ± 0.012

Mean value of ^{25}Mg - $^{26}\text{Mg} = 3.023 \pm 0.008$.

^{25}Mg - ^{26}Mg calculated from the masses of Everling *et al.* = 3.026 ± 0.003 .

(1) Reaction; (2) measured Q -value (mev); (3) mass excess difference (mev);
(4) mass excess difference of ^{25}Mg - ^{26}Mg (mev).

ACKNOWLEDGMENTS

We would like to thank Dr. K. W. Allen for his continued interest in this work, Mr. A. H. F. Muggleton for preparing the targets and Mr. V. Shepherd and his staff for operating the Van de Graaff accelerator.

REFERENCES

- BLAIR, A. G., and HAMBURGER, E. W., 1960, *Bull. Amer. Phys. Soc.*, [II], **5**, 247.
BROWNE, C. P., 1956, *Phys. Rev.*, **104**, 1598.
HINDS, S., and MIDDLETON, R., 1959 a, *Proc. Phys. Soc.*, **74**, 196.
—— 1959 b, *Proc. Phys. Soc.*, **73**, 501.
HINDS, S., MIDDLETON, R., and LITHERLAND, A. E., 1961, *Nucl. Phys.*, **24**, 510.
HINDS, S., MIDDLETON, R., and PARRY, G., 1958, *Proc. Phys. Soc.*, **71**, 49.
ENDT, P. M., ENGE, H. A., HAFFNER, J. W., and BUECHNER, W. W., 1952, *Phys. Rev.*, **87**, 27.
ENDT, P. M., HAFFNER, J. W., and VAN PATTTER, D. M., 1952, *Phys. Rev.*, **86**, 518.
ENGE, H. A., 1954, *Univ. Bergen Årb. Naturv. R.*, **1**.
EVERLING, F., KÖNIG, L. A., MATTAUCH, J. H. E., and WAPSTRA, A. H., 1960, *Nucl. Phys.*, **18**, 529.
NEWSON, H. W., BLOCK, R. C., NICHOLS, P. F., TAYLOR, A., FURR, A. K., and MERZBACKER, E., 1959, *Ann. Phys., N.Y.*, **8**, 211.
SHELIN, R. K., NIELSEN, H. L., and SPERDUTO, A., 1959, *Nucl. Phys.*, **14**, 140.

Twinning in a Cation-deficient Spinel Structure

BY J. GOODYEAR AND G. A. STEIGMANN

Physics Department, University of Hull

MS. received 28th March 1961

Abstract. Crystals of $\beta\text{-In}_2\text{S}_3$ have been studied under the polarizing microscope and by x-ray diffraction. Optical examination has shown that the crystals are twinned, and the relative orientations of the twin components have been determined by rotation and oscillation x-ray photographs. The diffraction data have also confirmed the body-centred tetragonal cell proposed by Rooymans. Assuming that the material has a spinel structure, deficient in cations, it follows that twinning takes place when a redistribution in the tetrahedrally occupied sites occurs.

§ 1. INTRODUCTION

THE structure of $\beta\text{-In}_2\text{S}_3$ has been studied by Rooymans (1959) using an x-ray powder technique. The powder pattern contained a large number of weak reflections which were attributed to a superlattice based on a cation-deficient spinel structure. Rooymans found that the supercell was body-centred tetragonal with $a = a'/\sqrt{2} = 7.62 \text{ \AA}$ and $c = 3a' = 32.32 \text{ \AA}$, a' being the parameter of the spinel-type cell from which the structure was derived. The absence of $00l$ reflections with $l \neq 4n$ (n being an integer), and the assumption that the structure is essentially that of a spinel with 4 tetrahedrally coordinated cation vacancies per supercell, suggested that the space group was $I4_122$, the four vacancies being located at the equivalent positions of the 4_1 screw axes of the space group. However, Rooymans also mentioned that the structure might possibly have a lower symmetry because of the observation of a weak reflection at about 3.6 \AA which was not reconcilable with a tetragonal lattice.

Single crystals of $\beta\text{-In}_2\text{S}_3$ have recently been prepared in this department for infra-red luminescence study. Equivalent amounts of indium and sulphur were placed separately in silica boats in a sealed evacuated tube. The portion of the tube containing the sulphur was heated at 600°C and that containing the indium at 1060°C , indium sulphide forming in the boat containing the indium. Plate crystals were found on the edges of the boat containing the indium, and although only about 10μ in thickness, were quite extensive (as much as several millimetres) in their dimensions parallel to their flat faces. When examined

under the microscope the crystals showed three directions of growth edge at 60° to each other, and were found to be birefringent and twinned on a macroscopic scale.

The purpose of the present study is to check Rooymans' cell using single crystal diffraction data, and to examine the nature of the twinning phenomenon in relation to the crystal structure.

§ 2. OPTICAL AND X-RAY DATA

Crystals of $\beta\text{-In}_2\text{S}_3$ were examined between crossed polaroids with their flat faces lying parallel to the microscope stage. With most of the crystals it was observed that different parts of the specimen were extinguished in turn as the stage was rotated, in one direction, through multiples of 30° . This suggested that there were three twin components oriented at 120° to each other. Some of the crystals were lath-like in shape showing well-defined growth edges parallel to the elongated axis, and one such crystal was selected for x-ray examination. Figs 1(a), (b) and (c) (Plate 1) show the extinction positions for the twin components in such a specimen. For convenience the components will be labelled types (a), (b) and (c) depending on whether extinction occurs when the specimen axis is parallel, at 30° or at 60° respectively, to the vertical crosswire when the microscope stage is rotated in a clockwise direction.

An x-ray rotation photograph of type (a) material, taken with the elongated axis parallel to the rotation axis, showed layer lines corresponding to an identity period of about 7.6 \AA parallel to the specimen axis. Corresponding rotation photographs of type (b) and (c) specimens were identical, with layer line spacings corresponding to an identity period of about 22.9 \AA . In terms of Rooymans' cell these correspond to the following axes: type (a) to the $[100]$ axis, types (b) and (c) to the $[331]$ axis. Oscillation photographs taken about each specimen axis, with the flat face of the crystal approximately perpendicular to the x-ray beam, revealed that the crystal face of each component was the (013) or ($0\bar{1}3$) face. When these observations are considered in relation to the optical data, the extended face of each individual of the twin can be taken as the (013) face with specimen axes as $[100]$ for a type (a) crystal, $[\bar{3}31]$ for type (b) and $[\bar{3}3\bar{1}]$ for type (c).

At this stage it seemed worth while to check Rooymans' cell using both single crystal and powder diffraction data. Oscillation photographs, about both the a and c axes, yielded reflections which could be accounted for by Rooymans' cell, the only systematic absences being of the type $h+k+l=2n+1$ and, for $00l$ reflections, $l \neq 4n$ (where n is an integer in each case). The space group is thus $I4_122$, $I4_1/a$ or $I4_1$. Fig. 2 (Plate II) shows a c axis rotation photograph and, as one would expect, the principal (non-superlattice) reflections occur on layer lines with $l=0$ or a multiple of 3.

Powder photographs of the material were taken with a crystal-focusing camera, of effective diameter 22.9 cm , employing $\text{CuK}\alpha$ radiation. The cell parameters, calculated from the powder data, are $a=7.62_3\text{ \AA}$ and $c=32.3_6\text{ \AA}$, and a comparison between the observed and calculated lattice spacings is given in the Table. The agreement with Rooymans' parameters is within the experimental error, and it can be concluded that Rooymans' cell is correct. It thus seems most probable that the extra reflection observed by Rooymans was due to some impurity in his powder specimen.

Comparison of Observed and Calculated Lattice Spacings of $\beta\text{-In}_2\text{S}_3$

I/I_0	d_{obs}	hkl	d_{calc}	I/I_0	d_{obs}	hkl	d_{calc}
W	8.12	004	8.09	VVS	3.252	213	3.252
W	7.43	101	7.42	WM	3.114	206	3.113
S	6.23	103	6.23	W	3.017	215	3.017
MS	5.12	112	5.11	W	2.775	208	2.774
W	4.942	105	4.934	W	2.744	217	2.744
W	4.046	008	4.045	S	2.695	220	2.695
W	3.952	107	3.953	VW	2.558	224	2.557
MS	3.812	200	3.812	W	2.534	301	2.533
W	3.450	204	3.449	W	2.472	303	2.473
W	3.389	211	3.390				

§ 3. A STRUCTURAL INTERPRETATION OF THE TWINNING PHENOMENON

In discussing the twinning in terms of the crystal structure, it is convenient to consider an alternative unit cell whose base is parallel to the (013) face of the tetragonal cell. This secondary cell is side face-centred monoclinic and its relation to the more fundamental tetragonal cell is shown in Fig. 3 (a). Fig. 3 (b) shows the orientation of the secondary cell in the three components of a lath-like crystal. These orientations are possible because the identity periods along the specimen axis of type (b) and (c) crystals are each exactly three times that along the axis of a type (a) specimen.

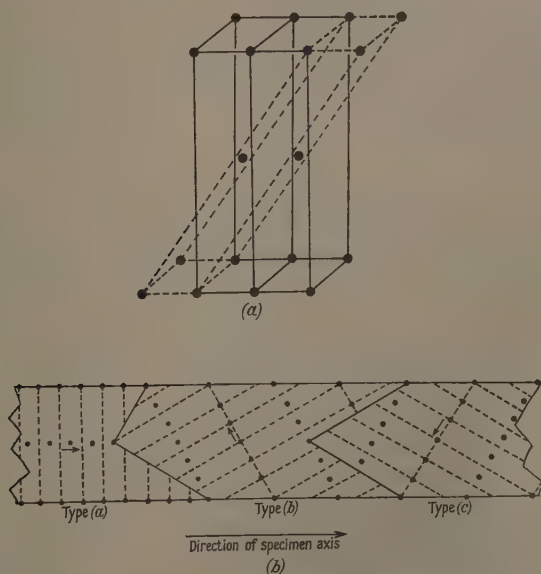


Fig. 3. (a) Secondary unit cell (dotted outline) having a centred base parallel to the (013) face of the tetragonal cell (full outline). (b) Orientation of the secondary cell in the three twin components; in each component the arrow represents the direction of the tetragonal *a* axis.

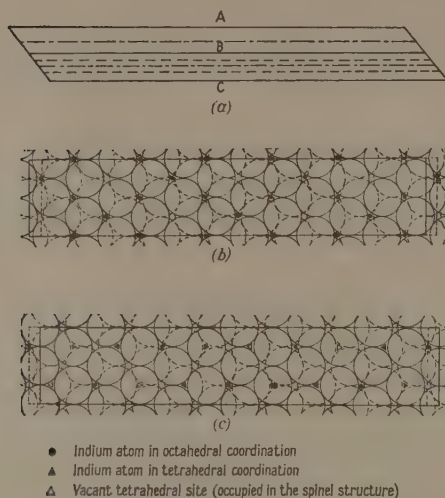


Fig. 4. Atomic arrangement within the secondary cell. (a) Sequence of atomic sheets which are parallel to the centred base. Full lines A, B and C represent sheets of close-packed sulphur atoms, chain lines sheets of octahedrally co-ordinated indium atoms, and broken lines sheets of tetrahedrally co-ordinated indium atoms. (b) Octahedrally co-ordinated indium atoms between sheets A (dotted circles) and B (full circles) of close-packed sulphur atoms. Full line is outline of top cell; broken line is cell perimeter in plane of octahedral sites. (c) Octahedrally and tetrahedrally co-ordinated indium atoms between sheets B (dotted circles) and C (full circles) of close-packed sulphur atoms. Full line is outline of base of cell; broken line is cell perimeter in plane of octahedral sites.

If one assumes the very plausible structure proposed by Rooymans, i.e. a cation-deficient spinel, then 16 molecules are required per unit cell giving a calculated density of 4.60 g cm^{-3} , which agrees well with a value of $4.55 \pm 0.02 \text{ g cm}^{-3}$ found by a pycnometer method. In this structure the sulphur atoms would be in approximate positions of cubic close packing in layers parallel to the (013) face of each twin component, i.e. parallel to the centred faces of the secondary cell of Fig. 3(a). The arrangement of the atoms within a secondary cell is shown in Figs 4(a), (b) and (c); there are two close-packed layers of sulphur atoms per cell with indium atoms octahedrally co-ordinated between two sulphur layers and indium atoms, both octahedrally and tetrahedrally co-ordinated, between the next two sulphur layers. Four of the tetrahedral sites, normally occupied in a spinel structure, are now vacant. The symmetry of this structure conforms with the space group $I4_122$, with the vacancies located at equivalent positions of the 4_1 screw axes of the space group.

From the standpoint of the structure, no change in the disposition of the sulphur atoms or of any of the octahedrally co-ordinated indium atoms is required in crossing the boundary between one twin component and the next. Twinning takes place when the pattern of vacancy sites changes. This feature is clear if

Fig. 5, showing the slight change in the occupied tetrahedral sites at the twin boundaries, is considered in relation to Fig. 4 (c). In fact, if all the vacant sites normally occupied in a spinel were filled with indium atoms there would be no

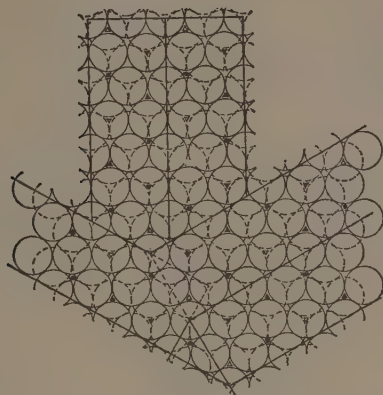


Fig. 5. Changes in the pattern of occupied tetrahedral sites at the twin boundaries.

twinning phenomenon. This structural interpretation explains why only three components are found and also their relative orientation. Finally, as is actually observed, one would not expect to find a well-defined plane between two components because of the relative ease with which one individual could encroach on the domain of the other.

ACKNOWLEDGMENTS

The authors are indebted to Miss J. Bleackley for preparing the specimens of $\beta\text{-In}_2\text{S}_3$ examined in this work.

One of the authors (G. A. S.) is indebted to the Department of Scientific and Industrial Research for the award of a research studentship.

REFERENCES

- ROOYMANS, C. J. M., 1959, *J. Inorg. Nucl. Chem.*, **11**, 78.

The Manchester High Energy Magnetic Cosmic Ray Spectrograph

By J. E. R. HOLMES†, B. G. OWEN‡ AND A. L. RODGERS§

Department of Physics, University of Manchester

*Communicated by J. G. Wilson; MS. received 16th May 1960,
in revised form 10th April 1961*

Abstract. Modifications to the Manchester counter spectrograph are described which have permitted the momentum measurement of single cosmic ray particles to a maximum detectable momentum of 1000 gev/c . The measured output of the instrument was 20 particles per day of which approximately 50% had momentum exceeding 10 gev/c and 2% exceeding 100 gev/c .

§ 1. INTRODUCTION

THE counter spectrograph at Manchester, described by Hyams *et al.* (1950) attained a maximum detectable momentum of about 20 gev/c , a limit mainly set by the 4 cm diameter of a single counter. With this instrument Owen and Wilson (1955) measured the momentum spectrum of μ -mesons arriving vertically at sea level in the range 0.5 gev/c to 20 gev/c .

Consideration of counter spectrographs show that it is not easy to increase the maximum resolution by more than an order of magnitude by the use of smaller counters or by methods involving the overlapping of counters. To gain a greater increase in the momentum resolution suggests a different method of measuring the deflection of a particle trajectory. If cloud chambers are used for the purpose, it is possible to locate the particle trajectory to the order of the track width.

With this in mind, during 1952 flat horizontal cloud chambers were introduced at each of the three measuring levels of the Manchester spectrograph. The Geiger counter was thus replaced by a cloud chamber track as the fundamental mode of location of a particle trajectory. The counter trays were retained, although vertically displaced to make room for the cloud chambers, and served in a secondary role as the control system of the instrument. The particle trajectory at each horizontal measuring level was located with respect to a centimetre graticule ruled over the inner surface of the top glass plate of each cloud chamber. This surface formed one of the strict measuring planes and was coincident in each case with the original plane occupied by the counters, thus leaving the dimensions of the spectrograph unchanged.

We attempted to reach a maximum detectable momentum of about 1000 gev/c . From the geometry of the spectrograph this implied measurement of particle deflections of about a third of a millimetre.

† Now at Atomic Energy Research Establishment, Winfrith, Dorset.

‡ Now at Atomic Energy Research Establishment, Risley, Lincs.

§ Now at Atomic Weapons Research Establishment, Aldermaston, Berks.

§ 2. THE SPECTROGRAPH CHARACTERISTICS

2.1. Principle of the Spectrograph

The spectrograph consists of a symmetrical arrangement of two deflecting magnetic fields and three horizontal measuring levels, symmetry being established about the middle measuring level.

The schematic representation of the instrument is shown in Fig. 1. A fast charged particle moves in a vertical plane through the horizontal magnetic fields having significant values of field only in the restricted similar regions H_1 and H_2 .

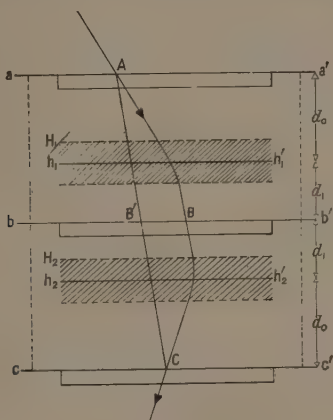


Fig. 1. The principle of trajectory deflection measurement.

The deflection of the particle trajectory is described by reference to the intersections A, B and C of the trajectory with the horizontal lines aa' , bb' , cc' which are symmetrically placed relative to the field regions H_1 and H_2 . The angular deflection θ of the particle trajectory in each magnetic field is given by

$$\theta = \int \frac{dl}{\rho} = \frac{300 \int H dl}{\hat{p}} \quad \dots\dots (1)$$

where ρ is the radius of curvature in centimetres from point to point of the trajectory of a singly charged particle of momentum \hat{p} ev/c. The line integral of the magnetic field $\int H dl$ is taken throughout the whole of the region H_1 or H_2 from which significant contributions arise.

The momentum \hat{p} of the particle is therefore given by

$$\hat{p} = \frac{300 d_0 \int H dl}{\Delta} \quad \dots\dots (2)$$

where $BB' = \Delta = d_0 \theta$ is the deflection in centimetres referred to the middle measuring level.

The above expression assumes that the whole of the deflection θ occurs at the median lines $h_1 h'_1$ and $h_2 h'_2$ respectively, a description which is true only for a vertical trajectory and a symmetrical field distribution about the median line. The effect of departures from the ideal conditions is investigated in § 4.1, but it may be stated here that to within the precision of the present measurements the lines $h_1 h'_1$ and $h_2 h'_2$ are adequately defined by the horizontal planes of symmetry of the magnetic fields.

2.2. Description of the Spectrograph

The general features of the instrument are discussed here in so far as they are relevant to spectrum measurements at momenta exceeding the upper limit of the counter work. A more complete description of the design and performance is given in Hyams *et al.* (1950).

The three cloud chambers which are each enclosed in a light-tight box determine the points of intersection of the particle trajectory with the three planes aa', bb', cc' respectively. Immediately below are the three counter layers which form the control system of the spectrograph. Counter alignment is achieved by a hanging plumb-line method. The two supported electromagnets of the Blackett type have vertical rectangular pole faces of 30 cm × 40 cm, with the smaller dimension vertical, which are separated by a distance of 9.5 cm. The characteristics of the magnets are described by Hyams *et al.*

'Defining' counters of cathode length 30 cm are placed in, and fill about 80% of, the gap width. The purpose of the counters is firstly to ensure that each accepted particle trajectory is totally described in air, minimizing the effect of particles being scattered in the iron, and secondly to exclude vertical particle trajectories which pass through the edges of the pole gap where $\int H dl$ falls rapidly. At full magnet excitation the defining counters exclude vertical particle trajectories whose integrated field value is more than 8% below that of the value corresponding to the central point of the pole gap. It may be shown that for all straight, i.e. high energy, tracks accepted by the aperture of the spectrograph and the defining counters, the root mean square deviation in $\int H dl$ is less than 1.5%. Since the present paper is concerned only with these 'straight' tracks, it may be concluded that, to within the accuracy of the present observations, all particles of a given momentum recorded by the chambers suffer the same deflection characterized by a unique value of $\int H dl$.

The weighted mean value of the magnet current over the duration of the spectrum determination (Holmes, Owen and Rodgers 1961) was 29.2 ± 0.4 A and corresponded to an integrated field of $(5.97 \pm 0.05) \times 10^5$ gauss cm. The value of d_0 is 149 cm and the equation relating the particle momentum p to the deflection Δ in the central plane of the spectrograph is

$$p = \frac{26.8 \pm 0.2}{\Delta} \text{ GeV/c}, \quad \dots\dots (3)$$

where Δ is measured in centimetres.

The deflection of the particle trajectory is defined in two stages. (i) At each measuring level the cloud chamber track is located with respect to a centimetre graticule ruled over the inner surface of the top plate of each chamber at a ruling pressure sufficient to provide adequate scattering of light by the chamber grid lines. This location establishes the point of intersection of the particle trajectory with each chamber grid. (ii) The three chamber grids are aligned with respect to one another thus establishing a three-dimensional coordinate system.

2.3. Characteristics of the Cloud Chambers

The design of the cloud chambers is governed by the necessity of keeping the additional scattering material in the particle beam at the measuring levels to a minimum, of conforming to the general geometry of the spectrograph, and of retaining sufficient accessibility. Further requirements are the reduction of gas motion and the production of comparable tracks in each of the three chambers.

The chambers are of light construction, the material in the particle beam consisting of 0.6 cm of plate glass (the top plate of the chambers) and 0.9 cm of Perspex which constitutes the material of the base and walls of the chamber. In addition the chambers are pressure controlled and require no back plate or piston.

The internal dimensions of each chamber are such as to provide adequate coverage of the respective counter trays. For the two extreme chambers the overall dimensions are 48 cm \times 17 cm \times 4.8 cm and cover the middle 14 of the 16 counters in the tray. The dimensions of the middle chamber are 32 cm \times 15 cm \times 4.8 cm and it spans the eight counters in this tray.

Consistent with their purpose the chambers are shallow, of sensitive depth 3.5 cm, and the gas expansion is downwards through a velvet covered perforated Perspex plate to the base of the chamber. The measuring plane adopted has the advantage that because the expansion is downwards, and therefore in the direction of the particle trajectory, this plane is one of zero movement at expansion.

To produce comparable tracks the chambers are connected in parallel to a common supply of gas. The gas used is saturated air produced by passing air through a mechanical filter to a large reservoir where it stands over distilled water. A fresh supply of gas is used after each expansion. The cloud chamber tracks are 1.10 ± 0.25 mm in width and correspond to an expansion time of 15 msec.

Satisfactory backgrounds of less than 10 drops per square centimetre of chamber grid may be obtained by using two cleaning expansions and a waiting interval of approximately 4 minutes. The total insensitive time is thus about 8 minutes, which is entirely permissible for the rate accepted by the geometry of the instrument in the momentum region investigated.

2.4. Photography

Figure 2 shows the photographic and illumination system of a single measuring unit which is comprised of a chamber CH and a horizontal layer of Geiger counters C. For compactness, and to keep associated apparatus out of the particle beam the chamber CH is photographed stereoscopically by the open shutter camera

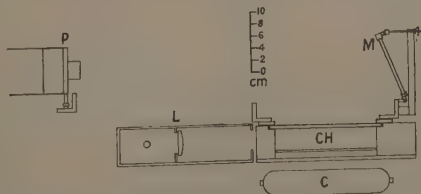


Fig. 2. Section through a single cloud chamber unit.

P through the plane mirror M inclined at $22\frac{1}{2}^\circ$ to the vertical. Chamber illumination is provided by a line source of light at the focus of a cylindrical lens contained in the lamp box L. A parallel beam of light enters the chamber immediately below the top plate, of width sufficient to provide adequate illumination over the sensitive depth. Light scattered through 45° is used. The length of the projected track is about 2 cm and the juxtaposition of the stereoscopic photographs gives a mean angle between the projected tracks of about 10° .

The point of intersection of the particle trajectory with the chamber grid is determined by finding the coordinate of the point of intersection of the stereoscopic tracks.

2.5. *Alignment of Chambers*

An optical method is used to align the three chambers with respect to each other. The top plate of each chamber extends beyond the sensitive chamber region in the 'longitudinal' direction (parallel to the pole faces of the magnets). For the chambers at the top and middle measuring levels brass plugs are cemented into the glass, one on each extension. For the top chamber a hole of 0.5 mm diameter is drilled into each plug and accurately located on the extension of the central line of the chamber grid whereas for the middle chamber there is a 5 mm aperture again located on the central line. A subsidiary grid is ruled on the bottom chamber glass.

Monochromatic light is passed through the small holes of the top level which then act as point sources of light. The light is diffracted by the 5 mm hole in the middle chamber extension and a Fresnel diffraction pattern is projected on to the subsidiary grid of the bottom chamber. The lines defined by the centre of the diffraction patterns and the point source of light are used as the reference lines from which all track locations are measured, in effect establishing a three-dimensional coordinate system.

The chambers are first mounted horizontally and an approximate alignment is achieved by hanging plumb-lines. The three chambers are then each adjusted the extra small amount until the centre of each diffraction pattern coincides with the central line of the bottom chamber. Subsidiary cameras photograph the diffraction patterns.

The system allows two degrees of freedom, one a translation of one chamber with respect to another and secondly a skewness of the chambers with respect to one another. It may be shown that the effect on the measured deflection of a particle trajectory by a pure translation is nullified by the symmetrical arrangement of measuring levels, and that in the general case where both conditions may exist, the effect is again zero for vertical particle trajectories. It is therefore only necessary to investigate the error introduced in the deflection as a function of the inclination of the particle trajectory. It may be shown that providing the angle of skewness is small (and in our instrument this is certainly less than 10^{-3} radian), and for a maximum inclination of 10° , then the maximum error introduced in the longitudinal deflection of a particle is of the order of 10^{-3} mm whilst that in the transverse direction is about 0.5 mm. The arrangement gave an alignment accuracy to 50μ .

The equation for the deflection of a particle is now related to the intersections A, B, C (Fig. 1) of the trajectory by the relation

$$\Delta = BB' = \frac{1}{2}(T+B) - (M + M_0), \quad \dots\dots (4)$$

where T , M , and B , refer respectively to the distances measured from the first grid line of the top, middle and bottom chambers and M_0 is a correction factor relating the chamber grids with the three dimensional coordinate system defined by the diffraction alignment.

Equation (4) is combined with Eqn (2) to define the momentum of the incident particle.

§ 3. SELECTION OF EVENTS

A single event is characterized by the discharge of a set of three Geiger counters, one in each measuring level, which assigns each particle to a particular momentum category (Hyams *et al.* 1950), and by the particle deflection as measured by the cloud chambers. Strict criteria are applied to the acceptance of a particle trajectory in order that background effects may be reduced to a minimum. These considerations reduce the possibility of spurious observations below the already small value ($\sim 0.1\%$) determined by Hyams *et al.* for the counter spectrograph.

3.1. General Criteria of Acceptance

That the expansion of the chambers is initiated by the discharge of a single counter in each of the measuring counter trays implies that a particular counter defines a region of the chamber where the track must be found. Tracks which lie outside this region are rejected, and only one track must lie within it. In addition the track width must be of the order of 1 mm, that is, its passage through the chamber must be contemporary with the expansion; furthermore the inclination of the track must not be greater than 10° to the vertical in the spectrograph.

3.2. Selective Criterion

In the plane parallel to the magnetic field the particle has nominally zero deflection. However, because of observational errors, scattering in the spectrograph and possible chamber distortion, the distribution of particle deflection in this direction is Gaussian of measured standard deviation ± 3.0 mm. Deflections of more than three times this standard deviation are rejected as arising from a spurious identification.

§ 4. FACTORS AFFECTING THE ACCURACY OF THE MEASURED PARTICLE DEFLECTION

The performance of the spectrograph is limited by errors which occur in the determination of particle momenta; in the paper by Holmes, Owen and Rodgers (1961) it is shown how these modify the measured sea level μ -meson spectrum at very high momenta.

The various sources of uncertainty in the spectrograph may be classified as follows.

4.1. Geometrical Errors

It was stated in §2, that Eqn (2) is true only for a vertical trajectory and a symmetrical magnetic field distribution about the median line.

Measurements show that the magnetic fields are symmetrical about the median planes to within 2%. As the order of accuracy in the present measurements is never better than about 7%, only movements of h_1h_1' and h_2h_2' which arise from the inclination of the trajectory in the magnetic fields are considered. It may be shown that the vertical displacement of h_1h_1' from the plane of symmetry is given (Hyams *et al.* 1950) by

$$\delta = \frac{\int H dl}{2H_{\max}} \tan \frac{1}{2} \theta \sin \alpha, \quad \dots (5)$$

where H_{\max} is the almost uniform field which extends over the major part of the pole gap, and where α is the inclination to the vertical of the incident trajectory.

In the present measurements $\int H dl = 6 \times 10^5$ gauss cm, $H_{\max} = 12\,500$ gauss and the maximum inclination of the particle trajectory is 10° . This leads to a maximum uncertainty in the location of $h_1 h_1'$ of 0.014Δ where Δ is the longitudinal deflection. The corresponding uncertainty in the longitudinal deflection is $0.005\Delta^2\%$ and is negligible compared with the observational errors of measurement. To the precision of the present measurements therefore, the lines $h_1 h_1'$, $h_2 h_2'$ are adequately defined by the horizontal planes of symmetry of the magnetic fields.

Departure from the general symmetrical arrangements, either of measuring levels, or of inequality in deflecting magnetic fields, introduces an error in the measured particle deflection.

It may be shown that if the angular deflections in the two magnetic fields are θ and $\theta + \phi$ respectively and the middle measuring level is displaced by ϵ from the position of symmetry, then to the first order the error $\delta\Delta$ in the measured particle deflection is given by

$$\delta\Delta = \epsilon(\alpha - \theta) + \frac{1}{2}\phi d_0. \quad \dots\dots (6)$$

The first term in the above expression represents the departure from geometrical symmetry whilst the second refers entirely to the inequalities in the angular deflections in the magnetic fields; the two terms are independent.

In the present work it has been possible to define the middle measuring level to within 0.7 mm from the plane midway between the top and bottom levels. For a particle incident at maximum inclination 10° and momentum greater than 10 gev/c, the corresponding uncertainty in the particle deflection is 0.15 mm.

The difference in the field exciting current in each magnet may be controlled to less than 1%, corresponding to an uncertainty of 0.25% in the particle deflection, an amount small compared with the error introduced by the departure from geometrical symmetry.

Thus, within the accuracy of work undertaken, the measuring grids in each chamber are coincident with the symmetrical measuring levels aa' , bb' and cc' of Fig. 1, and a particle experiences equal deflections in the two magnetic fields.

4.2. Scattering in the Spectrograph

Following Eqn (15) of Hyams *et al.* (1950) the root mean square scattering deflection $(\delta\Delta)_s$ is proportional to the particle deflection, where both quantities are measured at the middle measuring plane of the spectrograph. A direct experimental determination of the scattering deflection has been derived from measurements of the half-width of the distribution of transverse deflections as a function of increasing particle momentum. For about a quarter of the period of the observations the spectrograph was run without any other scattering material in the particle beam than was necessary to determine the particle momentum. For the remainder of the time a subsidiary experiment involved the positioning of ancillary apparatus in the spectrograph. The experimental determination gives ratios for $(\delta\Delta)_s/\Delta$ of 0.022 ± 0.007 and 0.045 ± 0.005 respectively under these two conditions. The ratios of the experimental scattering contribution to the expected scattering based on the William's formula are 0.85 ± 0.27 and 0.9 ± 0.1 respectively.

4.3. *Observational Errors*

Measurement errors are determined mainly by the geometry of photography. The errors in the point of intersection of the stereo-tracks projected on to the longitudinal and magnetic field directions vary over a single chamber with the angle made by the tracks to the chamber grid lines. For all cases the uncertainty in the location of a particle with respect to a chamber grid is greater in the magnetic field direction than in the longitudinal direction. The error in a particle deflection is calculated as a function of the trajectory displacement in the spectrograph. The measured distribution in deflections in the plane parallel to the magnetic field is used as an independent check on the calculated values.

For a particle which passes centrally through the spectrograph the error in measurement of the longitudinal deflection is 0.25 mm and corresponds to a maximum detectable momentum of 1000 GeV/c, whereas for the most unfavourable case of a particle which traverses vertically through the edge of the instrument the deflection error is 1.4 mm. The mean error averaged over the total aperture of the spectrograph is 0.9 mm and 70% of the particle deflections are subject to errors within the range 0.6 mm to 1.2 mm.

4.4. *Convective Gas Distortion*

An attempt has been made to determine the magnitude of the effect due to chamber gas movement before photography. Experimentally this may be indirectly inferred from the distribution of particle deflections in the direction parallel to the magnetic field. No great statistical accuracy may be placed on the conclusions, but it seems probable that convective gas distortion has a negligible effect on the measured particle momentum at least up to 300 GeV/c above which the paucity of measured particles becomes the controlling feature in spectrum determinations.

4.5. *Systematic Errors*

To provide an overall check on the presence of systematic errors in the measurement of particle deflections, observations were made both on zero magnetic field and of positive and negative deflections on reversed fields. These investigations showed that systematic effects were of negligible consequence compared to the observational errors of measurement.

§ 5. APPLICATION TO SPECTRUM DETERMINATIONS

It is for energetic particles that the additional information of the cloud chamber spectrograph is most important. There was, therefore, incorporated in the apparatus an electronic 'momentum selector', a device which in effect carries out the analytic operation by which particle momenta are determined in the counter spectrograph, and only passes an operating pulse to the cloud chamber system when the traversing particle falls into a desired momentum category. With the counter instrument statistical errors of 3% were achieved for momenta less than 10 GeV/c and thus it was unnecessary to re-investigate this momentum region. It was therefore important to record all particles of momentum appreciably greater than 10 GeV/c accepted by the geometry of the instrument, together with a sufficient number of particles of lower momentum to provide an overlap of the new data with the existing counter-determined spectrum. The selector bias was accordingly adjusted so that the selector only passed an operating pulse to the

cloud chamber system when the traversing particle was recorded in momentum categories 0, 1, 2, and 3 (see Hyams *et al.* 1950, Table 4). Under these conditions the lower momentum limit of the cloud chamber spectrograph is approximately 3 GeV/c and effectively all particles of momentum greater than 10 GeV/c are recorded.

The rate of collection of particles accepted by the chambers is about 20 per day, of which 8 are of momentum greater than 10 GeV/c. Over an effective running period of 14 months, 4566 particles were recorded of which approximately 1800 were of momentum greater than 10 GeV/c and 70 were in excess of 100 GeV/c. The operating efficiency over this period, including maintenance time, was 70%.

REFERENCES

- HOLMES, J. E. R., OWEN, B. G., and RODGERS, A. L., 1961, *Proc. Phys. Soc.*, **78**, 505.
HYAMS, B. D., MYLROI, M. G., OWEN, B. G., and WILSON, J. G., 1950, *Proc. Phys. Soc. A*, **63**, 1053.
OWEN, B. G., and WILSON, J. G., 1955, *Proc. Phys. Soc. A*, **68**, 409.

Measurements of the Momentum Spectrum and Charge Ratio of Cosmic Ray Muons at Sea Level in the Momentum Range 10 GeV/c–1000 GeV/c

By J. E. R. HOLMES†, B. G. OWEN‡ AND A. L. RODGERS§

Department of Physics, University of Manchester

*Communicated by J. G. Wilson; MS. received 16th May 1960,
in revised form 10th April 1961*

Abstract. The momentum spectrum of single cosmic ray muons arriving at sea level in the north-south plane at 57° N geomagnetic latitude has been measured for near vertical incidence. Results are given which cover the momentum range $5 \text{ GeV/c} < p < 1000 \text{ GeV/c}$, and together with the earlier work of Owen and Wilson form a continuous spectrum from 0.5 GeV/c to 1000 GeV/c . The high momentum work is based on 1800 particles of momentum greater than 10 GeV/c .

The charge ratio of single muons arriving at sea level has been measured, for near vertical incidence, to an upper momentum limit of 100 GeV/c . The measurements are compared with those of other workers and together show evidence for a maximum in the sea level charge ratio in the momentum range 3 GeV/c to 7 GeV/c .

§ 1. INTRODUCTION

A PARTICULAR application of the cloud chamber spectrograph, described in Holmes, Owen and Rodgers (1961), is to investigate the near-vertical sea-level spectrum and charge ratio of cosmic ray muons at appreciably higher momenta than could be attained using the original counter spectrograph of Hyams *et al.* (1950). With the counter instrument statistical errors of 3% were achieved in spectrum measurements for momenta less than 10 GeV/c and it was unnecessary to re-investigate this momentum region. It was therefore important to record effectively all particles of momentum greater than 10 GeV/c accepted by the aperture of the instrument together with a sufficient number of particles of lower momentum to provide an overlap of the new spectrum data with the existing counter spectrograph measurements of Owen and Wilson (1955). To achieve this performance the 'momentum selector' bias was adjusted so that the cloud chambers operated only when the traversing particle was recorded in counter momentum categories 0, 1, 2 and 3. Under these conditions the lower momentum limit of the cloud chamber spectrograph was approximately 3 GeV/c and all particles of momentum appreciably greater than 10 GeV/c were recorded. Over an effective running period of 14 months, during the years 1953–55, 4566 particles were recorded of which 1800 have momenta greater than 10 GeV/c and 70 momenta greater than 100 GeV/c .

All particles were collected within 10° from the vertical in the north-south plane, and within 2° in the east-west plane.

† Now at Atomic Energy Research Establishment, Winfrith, Dorset.

‡ Now at Atomic Energy Establishment, Risley, Lancs.

§ Now at Atomic Weapons Research Establishment, Aldermaston, Berks.

§ 2. THE PRINCIPLE OF SPECTRUM MEASUREMENTS

A particle traversal is characterized by the discharge of three Geiger counters which assign the particle to a momentum category covering a relatively wide momentum range, Hyams *et al.* (1950). Within the category n of nominal deflection Δ_n , defined by the measured deviation for a trajectory passing through the axes of the three counters concerned, the deflection spectrum $S_n(\Delta)$ is the product of the incident deflection spectrum $S(\Delta)$ and the quantity $P(\Delta - \Delta_n)$ which is a purely geometrical expression for the relative collecting efficiency of a set of three counters as a function of the difference of deviation from the nominal deflection of the counter geometry. The particle deflections measured by the use of the three cloud chambers consist of observations of $S_n(\Delta)$ within the separate momentum categories.

The relative efficiency of collection K_n for particles of a given momentum category is a factor which is defined by the aperture of instrument. The total counting rate in a single momentum category is composed of counts from a number of 'channels' each of which is defined by the three Geiger counters concerned in a single event. Essentially the unit of counting is such a channel, and the differing relative efficiencies of collection K_n from one momentum category to another arise because different numbers of unit channels are available for the various momentum categories.

In the present instrument a further channel bias is produced by the operation of the 'momentum selector'. Ideally the selection output pulses should be constant in the same momentum category, but in practice the actual selection pulses are distributed about the nominal pulse for the category and those categories whose output selection pulses are near to the chosen bias value are in part rejected. There is thus no sharp cut off in momentum category selection, and for the fixed value of bias used during the present investigation, whilst appreciably all category 0 particles were recorded, the acceptance factors R_n for categories 1, 2 and 3 were 85%, 50% and 20% respectively. Under these conditions the normalized deflection spectrum is

$$S_n(\Delta) = K_n R_n S(\Delta) P(\Delta - \Delta_n). \quad \dots\dots (1)$$

The momentum spectrum $S(p)$ is related to the incident deflection spectrum by

$$S(\Delta) \sim p^2 S(p). \quad \dots\dots (2)$$

§ 3. CALCULATION OF THE SEA-LEVEL SPECTRUM

3.1. *Methods of Spectrum Determination*

It is apparent from Eqn (1) that if observations are made within a single momentum category, the incident particle deflection spectrum may be calculated in arbitrary units independently of the category normalization factors, as both K_n and R_n affect a single momentum category as a whole.

Following Owen and Wilson (1955) the incident spectrum is derived by comparing the observed distribution of particle deflections in a single momentum category with the expected distribution of deflections in that category for an assumed incident spectrum. The comparison spectrum used is identical with the one used in the Owen and Wilson investigation and refers to a muon differential generation spectrum for a unique height of production and given by

$$S(p) dp \sim p^{-2.85} dp.$$

Whilst the application of the comparison spectrum in the present investigation is somewhat different from that in the earlier work, this spectrum was found still to be a convenient approximation.

Measured particle deflections are allocated to their respective counter categories and are grouped into suitable deflection ranges. The deflection distribution in a counter category is normalized to the intensity per unit of deflection, giving a differential deflection distribution for each category. The distribution expected on the basis of the incident comparison spectrum is calculated for each counter category and normalized to the same number of observations. The errors in normalization in no case exceed 1%. Fig. 1 shows the observed distributions for categories 0, 1, 2 and 3 together with the smoothed expected distribution for the comparison spectrum.

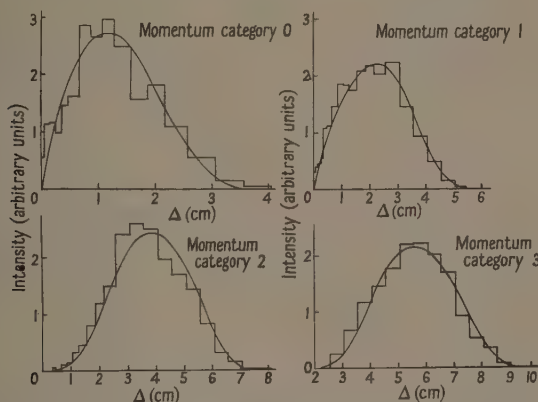


Fig. 1. The measured deflection distributions within momentum categories. The expected distributions for the comparison spectrum are shown by the full lines.

As each momentum category has considerable overlap with neighbouring categories, more than one comparison may be made for a particular deflection range. The method established a series of slowly varying differences between the measured incident spectrum and the comparison spectrum for successive deflection ranges.

Two methods are used to calculate the incident spectrum and these afford a convenient check on the interpretation of the measured data. In the first method the ratio of the observed number of particles to the integrated product of the comparison spectrum and the efficiency factor in a deflection range is multiplied by the integrated area of the comparison spectrum. This gives the incident spectrum in terms of the numbers of particles observed in a deflection range, and thus the corresponding momentum range. The observed intensities are normalized to unit momentum interval and give the differential momentum spectrum in histogram form and arbitrary units. The derived spectrum is fitted to the original counter spectrum of Owen and Wilson by normalizing to the same number of particles over the whole region of overlap. The statistical error in this normalization is 2.5%.

The second method of deriving the incident spectrum is to assume that the ratio of the observed number to the expected number of particles in a deflection range may be defined at a particular deflection in the range. This ratio is multiplied by the comparison spectrum at the chosen deflection to give the incident differential deflection spectrum. Conversion to the differential momentum spectrum is made by Eqn (2).

The choice of the deflection at which the whole of the contribution in a deflection range is plotted requires knowledge of the mean slope of the spectrum over the deflection interval considered. A method of successive approximations is used and the deflection is chosen so that the area under the histogram cell is equal to that under the smoothed curve of known slope which is assumed constant over the deflection interval considered. It may be shown that because of the shape of the incident spectrum the procedure is only important for particle deflections less than 0.5 cm, i.e. momenta greater than 50 GeV/c.

Table 1. Derivation of the Vertical Intensity of Cosmic Ray Muons at Sea Level as a Function of Momentum

(1)	(2)	(3)	(4)	(5)	(6)	(7)	(8)
0.23	0.23	1.71†	0.39	0.022	4.8×10^{-13}	48	1160
1.0	0.80	1.64†	1.31	1.27	2.8×10^{-11}	20	271
2.0	1.40	1.14	1.60	6.40	1.42×10^{-10}	18	134
3.0	2.00	1.10	2.19	19.7	4.38×10^{-10}	16	89
4.0	2.50	0.97	2.44	39.0	8.65×10^{-10}	15	67
5.5	3.12	0.97	3.00	91.0	2.02×10^{-9}	10	49
7.5	3.91	1.18	4.60	259	5.75×10^{-9}	7	36
9.5	4.55	1.15	5.24	470	1.04×10^{-8}	7	28
11.5	5.05	1.13	5.69	753	1.67×10^{-8}	7	23
14.0	5.54	0.97	5.35	1.05×10^3	2.33×10^{-8}	5	19
17.0	5.98	0.97	5.76	1.66×10^3	3.68×10^{-8}	5	16
20.0	6.35	1.05	6.68	2.66×10^3	5.90×10^{-8}	5	13
23.5	6.64	0.97	6.40	3.55×10^3	7.88×10^{-8}	4	11
28.0	6.86	1.13	7.76	6.07×10^3	1.35×10^{-7}	5	9.6
33.0	6.99	1.08	7.56	8.25×10^3	1.83×10^{-7}	5	8.2
38.0	6.97	1.00	6.97	1.01×10^4	2.24×10^{-7}	5	7.1
43.0	6.90	0.86	5.90	1.10×10^4	2.44×10^{-7}	6	6.2
48.0	6.77	0.87	5.85	1.34×10^4	2.98×10^{-7}	9	5.6
53.0	6.61	0.97	6.40	1.79×10^4	3.98×10^{-7}	9	5.1
58.0	6.39	0.94	5.97	2.00×10^4	4.44×10^{-7}	10	4.6
63.0	6.13	0.94	5.72	2.28×10^4	5.06×10^{-7}	11	4.3

† Corrected for a total random error of 0.9 mm, $\alpha_T = 0.75$.

(1) The mean deflection in the deflection range concerned Δ (mm), (2) The corresponding value of the comparison spectrum $S(\Delta)$, (3) The measured conversion factor including correction due to observational errors, (4) Differential deflection spectrum, i.e. product of (2) and (3), $S(\Delta)$, incident, (5) Differential momentum spectrum in arbitrary units $S(p)$, incident unnormalized, (6) Differential momentum spectrum in particles $\text{cm}^{-2} \text{sec}^{-1} \text{sterad}^{-1} (\text{MeV}/c)^{-1}$ normalized to Rossi, $S(p)$, incident, (7) Statistical uncertainty: standard deviation of $S(p)(\%)$, (8) Mean momentum p (GeV/c).

The measured data derived by this method are presented in Table 1. The spectrum is normalized to the counter spectrum of Owen and Wilson over the whole region of overlap by comparing the observed points with the smoothed curve of these workers. The comparison is displayed in Fig. 2 where the observed

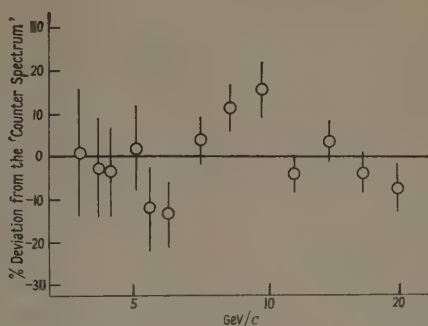


Fig. 2. Comparison with the counter spectrum of Owen and Wilson (1955).

points are expressed as a percentage difference from the counter spectrum. A χ^2 -test gives a goodness of fit $P(\chi) = 0.20$, and it is concluded that there is satisfactory agreement over the region of overlap.

3.2. The Effect of Random Errors on the Observed Spectrum

The presence of spurious errors in the measurement of particle deflections modifies the measured spectrum in the region where the magnitude of these errors becomes comparable with the particle deflection. The degree of modification is a function of the shape of the incident spectrum and the magnitude of the total random errors. In the present work the effect is to produce a net transfer of particle deflections to regions of lower deflection and results in a measured momentum spectrum which contains an excess of particle over the true incident spectrum at high momenta.

The effect of the observational error of measurement is negligible for particle deflections greater than 1.5 mm, i.e. for momenta less than 200 GeV/c. At this value the correction term is less than 1%. Beyond 200 GeV/c, a comparison is made between the observed numbers of particles collected in a deflection interval with the number expected from an assumed incident spectrum and the observational error of measurement.

Over the error-sensitive range it is assumed that the true differential spectrum $S(\Delta_T)$ of particles may be represented by a simple power law of the form

$$S(\Delta_T) d\Delta_T = K \Delta_T^{\alpha_T} d\Delta_T$$

where Δ_T is the true deflection and α_T is the true exponent in this range. K is a constant of normalization. The observation that over a relatively large range at higher deflections (lower momenta) the differential spectrum may be represented by a simple power law allows confidence to be placed in this assumption. A further assumption is that the random errors are normally distributed. This is in part justified by the observation that the residual particle deflections parallel to the magnetic field direction also follow such a distribution. Under these conditions the observed differential deflection spectrum $S(\Delta_0)$ is related to the true differential spectrum $S(\Delta_T)$ by

$$S(\Delta_0) = k \int_0^\infty S(\Delta_T) \exp \frac{1}{2} \left(- \frac{\Delta_0 - \Delta_T}{\sigma} \right)^2 d\Delta_T \quad \dots\dots (3)$$

where σ is the total root mean square error, and equals 0.9 mm (Holmes, Owen and Rodgers 1961), and k is a constant of normalization. A normalization point in the spectrum is taken where the effect of random errors is negligible. The actual choice of this point is insensitive for the statistical accuracy of the present observations in the momentum range concerned. In practice numerical integration of Eqn (3) is carried out. The ratio of the observed number of particles in a deflection interval to the number expected as a function of the exponent α_T and the mean square error σ is derived for various values of α_T . The most probable value of α_T is deduced by the χ^2 -test applied to the comparison.

The conclusions of the analysis are that the most probable value of α_T is not significantly different from the exponent at higher deflections, and corrections to the measured spectrum in the error sensitive range are relevant to a true exponent $\alpha_T = 0.75 \pm 0.03$.

The uncertainty in the correction term due to a corresponding uncertainty in the total root mean square error is in no case greater than the statistical uncertainty in the groups affected, and only in the highest momentum group does the absolute correction exceed the statistical uncertainty.

The method is of course insensitive to any singularities in the spectrum which may occur at momenta greater than 200 GeV/c. It is however, commensurate with the paucity of events recorded in the error sensitive region.

§ 4. SEA-LEVEL CHARGE RATIO OF HIGH ENERGY MUONS

4.1. Introduction

Extended measurements of the momentum variation in the charge ratio of muons arriving vertically at sea level have been made by Owen and Wilson (1951) using the Manchester magnetic spectrograph described in Hyams *et al.* (1950), by Caro, Parry and Rathgeber (1951) and Moroney and Parry (1954) from observations on the Melbourne spectrograph, by Filosofo, Pohl and Pohl-Ruling (1954) from measurements using a magnetic lens at various depths underground, and by Pine, Davisson and Greisen (1959) who have used a cloud chamber magnetic spectrograph.

The results of Owen and Wilson, and those of Filosofo, Pohl and Pohl-Ruling, show that the charge ratio increases with meson momenta from about 1.17 at 1 GeV/c to about 1.26 at 5 GeV/c and that at higher momenta a slight decrease seems to occur. The results of Pine, Davisson and Greisen show stronger evidence of a decrease for momenta greater than 20 GeV/c. The observations of Caro, Parry and Rathgeber and Moroney and Parry, though statistically inferior to those of Owen and Wilson and Filosofo, Pohl and Pohl-Ruling corroborate an increase in the charge ratio at low meson momentum for the vertical muon component and are not inconsistent with a decrease at higher momenta.

The use of Geiger counter spectrographs and depth methods to study the behaviour of the charge ratio at momenta considerably greater than 10 GeV/c is limited by the maximum resolution of counter spectrographs and by the rate of collection of data at great depths. A further limitation with counter spectrograph measurements is that because particles are assigned to counter categories it is only possible to examine the general behaviour of particles over a relatively broad momentum range. In the Manchester counter instrument, because of the variation of the geometrical efficiency factor over a single category, the observed

spectrum of particle deflections in category 1 contains a 3% contamination of particles of opposite sign of appreciably higher (70 gev/c) mean momentum. A correction must therefore be made which depends upon the mean value of the charge ratio corresponding to this high momentum group, and an extrapolation of the charge ratio to momenta considerably in excess of the maximum detectable momentum must be inferred.

The increased resolution of the modified system allows an investigation of the charge ratio to be made to meson momenta of 100 gev/c and the limit is imposed by the rate of collection of particles which is small at momenta greater than this value. Relatively small momentum ranges may be investigated and the limit to which the sign of the particle may be detected is set by the observational error in the location of the particle trajectory defined by reference to a set of three measuring cloud chambers in the instrument.

4.2. Measurements with the Spectrograph

The application of the instrument to charge ratio measurements is relatively simple since the ratio of the numbers of particles of opposite sign collected in a given time is independent of the variation of instrumental efficiency with momentum. Charge ratio observations were recorded continuously and concurrently with the collection of spectrum data and the direction of the magnetic field was reversed at frequent intervals to ensure that equal numbers of deflections of opposite sign were recorded. It is expected that the particles recorded were essentially muons, the proton component being negligible at the energies under consideration.

4.3. Factors affecting the Observed Charge Ratio

A correction to the observed charge ratio of the highest momentum group is imposed by the limit to which the sign of a measured particle deflection can be detected. This leads to an analogous correction to that of the earlier counter work, and depends upon the value of the charge ratio at the limits of measurement. As such a correction is uncertain to an extent to which the charge ratio at the limit of measurement is uncertain, two extreme possibilities are taken, i.e. that either the charge ratio at the higher momenta remains appreciably the same as the last measured point, or that it falls to unity at higher momenta. No evidence exists for an increase in the charge ratio and it is assumed that the true value lies between the two limits. It may be shown that the true value of the charge ratio in the highest momentum group is greater than the observed value by 0.6% if the charge ratio at high momentum is assumed to remain at the value of the last measured point, and is within 0.1% of the observed value if the charge ratio falls to unity. Both corrections are negligible compared with the statistical accuracy of the measured ratio.

The possibility of an electronic bias associated with the operation of the momentum selector was investigated and it was concluded that within the momentum categories used in the measurements the effect of such a bias would have negligible effect on the measured values of the charge ratio.

4.4. Experimental Results

Observations were collected within separate momentum categories for reversed magnetic fields and the measured values of the charge ratio are presented in Table 2. Columns (3) and (4) of this table show the charge ratios in the

Table 2. Measured Charge Ratios

(1)	(2)	(3)	(4)	(5)	(6)	(7)
0-5	0	1.07 ± 0.28	0.87 ± 0.26	1.02 ± 0.14	203	98
	1	1.02 ± 0.26	1.14 ± 0.36			
5-9	0	1.61 ± 0.34	1.08 ± 0.25	1.29 ± 0.14	328	36
	1	1.01 ± 0.22	1.43 ± 0.33			
9-20	0	1.32 ± 0.18	1.04 ± 0.16	1.29 ± 0.08	1133	18
	1	1.34 ± 0.15	1.21 ± 0.15			
21-30	0	1.52 ± 0.37	1.50 ± 0.38	1.35 ± 0.08	1060	11
	1	1.15 ± 0.13	1.25 ± 0.15			
	2	1.85 ± 0.30	1.28 ± 0.22			
31-50	0	1.47 ± 0.20	1.51 ± 0.22	1.39 ± 0.08	1272	6.7
	1	1.46 ± 0.15	1.15 ± 0.13			
	2	1.60 ± 0.35	1.10 ± 0.29			

(1) Deflection range (mm); (2) momentum category number; (3), (4) observed charge ratios on reversed fields: (3) H^+ , (4) H^- ; (5) weighted mean charge ratio N^+/N^- ; (6) total particles; (7) mean momentum (GeV/c).

relevant categories for reversed magnetic fields and column (5) is the weighted mean value for the momentum range concerned.

It has further been possible to check experimentally the numbers of particles of opposite sign which, because of the geometrical efficiency factor, appear in category 1 (Hyams *et al.* 1950). Reversed field observations show this fraction to be 2.86% and 2.78% respectively and give a mean value of $2.8 \pm 0.4\%$ which agrees well with the expected value.

§ 5. CONCLUSIONS

The description of the measured spectrum in terms of the comparison spectrum used by Owen and Wilson is given in Fig. 3 in an extended form of Fig. 2 of their paper (Owen and Wilson 1955, p. 413). The adopted form of the

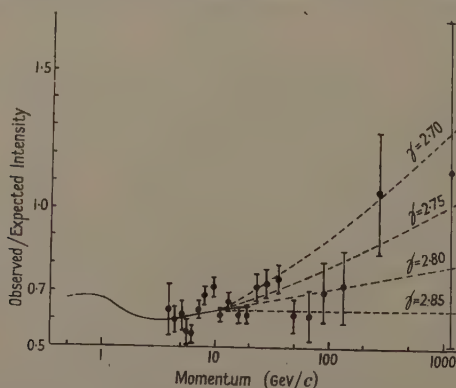


Fig. 3. Ratio of the observed intensity to the intensity expected based upon a muon differential generation spectrum $S(p) dp \sim p^{-\gamma} dp$. The full curve represents the counter spectrum of Owen and Wilson (1955).

differential spectrum of single muons arriving vertically at sea-level at 57° N geometric latitude is shown in Fig. 4, where the present results are combined with those of Owen and Wilson to form a continuous spectrum for

$$0.5 \text{ GeV}/c < p < 1000 \text{ GeV}/c.$$

The corrections to the measured spectrum arising because particles are in general collected from a direction inclined to the vertical, which varies for different momentum categories, are negligible in the present work where the lowest momentum particles are recorded in category 3 of mean zenith angle 3° .

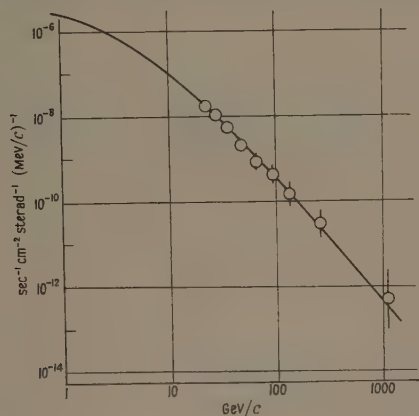


Fig. 4. The differential momentum spectrum of vertically incident muons at sea level.

The spectrum is essentially composed of muons. The electron component is eliminated as in the work of Owen and Wilson (1955), and the evidence on the proton component (Mylroie and Wilson 1951 and Barrett *et al.* 1952) indicates that the sea level proton flux in the momentum range investigated is less than 0.1% of that of the total sea level flux. From the expected form of the pion spectrum at sea level it is concluded that unless the pion cross section for nuclear interaction falls to a very small fraction of the geometric value, pions contribute a negligible proportion of the total sea level flux up to the highest measured momentum.

The fact that the spectrum described here is composed of single unaccompanied muons does not exclude the possibility of there existing a high momentum bias, which would act to reject an increasing fraction of the sea level component if the probability that a muon is accompanied by a shower increases with momentum. No experimental information may be gained from the records because of the impossibility of identifying the muons in such cases. The chance that two muons arising by decay of parents produced in the same primary collision and arriving simultaneously within the aperture of the spectrograph is negligibly small at the energies considered. It is further expected that the density of the soft component at sea level is low enough to make no substantial corrections to the observed rates at the highest momentum recorded.

Compared with the results of other workers the measured spectrum is in agreement with the more recent investigations of Ashton *et al.* (1960) and of

Pine, Davisson and Greisen (1959) over the whole of the momentum range below 200 gev/c . It does not agree however with the earlier work of Caro, Parry and Rathgeber (1951), particularly above a momentum of 20 gev/c .

In relation to charge ratio measurements the emphasis of the present work is primarily to study the behaviour at momenta in excess of 10 gev/c . In Fig. 5 the present measurements are displayed together with the results of Owen and Wilson and those of later workers.

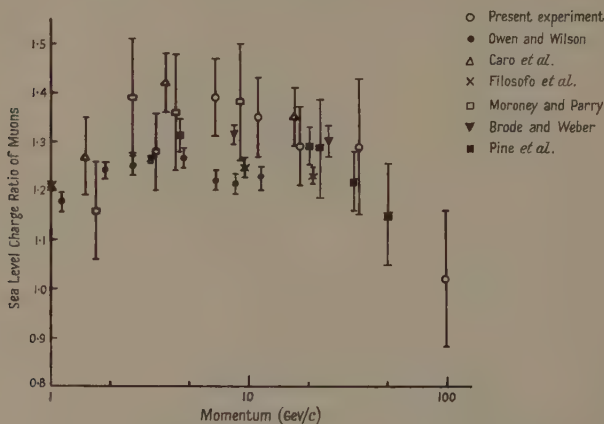


Fig. 5. Collected observations of the charge ratio of muons arriving vertically at sea level.

Taken alone the present investigation suggests that the sea-level charge ratio of vertically incident muons decreases with increasing momentum greater than 7 GeV/c . The measured points are in reasonable agreement with the observations of Pine *et al.* and of Brode and Weber (1955) above a momentum of 20 GeV/c , but are however approximately 10% greater than the Owen and Wilson and the Filosofo work.

On the basis of the evidence presented in Fig. 5 it would appear that the sea-level charge ratio passes through a broad maximum in the momentum range 3 GeV/c to 7 GeV/c but that only the general shape of the curve may be inferred.

ACKNOWLEDGMENTS

The authors wish to thank Professor P. M. S. Blackett and Professor G. D. Rochester for the support given and the facilities provided, Dr. A. W. Wolfendale for his interest and advice and Dr. D. A. Eyeions for help in the routine testing of the spectrograph. They are grateful to the technical staff of the Physical Laboratories, in particular to Mr. R. E. Bradford for the construction of parts of the apparatus and to Mrs. S. Holden for assistance in the measurement of track records.

One of us (A. L. R.) is indebted for a Further Education Training Scheme grant enabling him to do part of the work.

REFERENCES

- ASHTON, F., BROOKE, G., GARDENER, M., HAYMAN, P. J., JONES, D. G., KISDASAMYS, LLOYD J. L., TAYLOR, F. E., WEST, R. H., and WOLFENDALE, A. W., 1960, *Nature, Lond.*, **185**, 364.
- BARRETT, P. H., BOLLINGER, L. M., COCCONI, G., EISENBERG, Y., and GREISEN, K., 1952, *Rev. Mod. Phys.*, **24**, 133.
- BRODE, R. B., and WEBER, M. J., 1955, *Phys. Rev.*, **99**, 610.
- CARO, D. E., PARRY, J. K., and RATHGEBER, H. D., 1951, *Aust. J. Sci. A*, **4**, 16.
- FILOSOFO, L., POHL, E., and POHL-RULING, J., 1954, *Nuovo Cim.*, **12**, 809.
- HOLMES, J. E. R., OWEN, B. G., and RODGERS, A. L., 1961, *Proc. Phys. Soc.*, **78**, 496.
- HYAMS, B. D., MYLROI, M. G., OWEN, B. G., and WILSON, J. G., 1950, *Proc. Phys. Soc. A*, **63**, 1053.
- MORONEY, J. R., and PARRY, J. K., 1954, *Aust. J. Phys.*, **7**, 423.
- MYLROI, M. G., and WILSON, J. G., 1951, *Proc. Phys. Soc. A*, **64**, 404.
- OWEN, B. G., and WILSON, J. G., 1951, *Proc. Phys. Soc. A*, **64**, 417.
- 1955, *Proc. Phys. Soc. A*, **68**, 409.
- PINE, J., DAVISSON, R. J., and GREISEN, K., 1959, *Nuovo Cim.*, **14**, 1181.

Low Temperature Electric Field Effects in Semiconductors†

By V. V. PARANJAPÉ

Department of Theoretical Physics, University of Liverpool

Communicated by H. Fröhlich; MS. received 30th August 1960, in final form 10th April 1961

Abstract. Germanium shows at liquid helium temperature a very strong rise in conductivity with field strength at about 2 v cm^{-1} . This process has been investigated theoretically on the basis of electron temperature concept. The variation of the density of electrons with field is calculated considering excitation of donors into the conduction band by impact ionization and phonon absorption as well as reverse processes. It is shown that the current, though strongly field dependent, is always stable and an expression for current density as an explicit function of the field strength is obtained. Good agreement with experiments supports the validity of this theory.

§ 1. INTRODUCTION

THE variation of current with electric field in germanium has been a subject of extensive experimental investigation in recent years (Ryder 1953, Gunn 1957, Bray and Mendelssohn 1957). In general it is observed that the current obeys Ohm's law up to a certain value of the field strength, but deviations occur beyond this value. Shockley (1951) has proposed a theory and has shown that the mobility μ_L of the current carriers in a covalent semiconductor varies with the field F , according to the law

$$\mu_L = \mu_L(T_0) \left[\left(\frac{32}{3\pi} \right)^{1/2} \frac{s}{F\mu_L(T_0)} \right]^{1/2} \dots\dots (1.1)$$

where $\mu_L(T_0)$ is the mobility of the current carriers at vanishing field and s is the velocity of sound in the crystal, provided the scattering of the current carriers is due to the acoustical modes of the lattice vibrations and the field F satisfies the condition $F\mu_L(T_0) \gg s$. If the density of the current carriers $n(T_0)$ is independent of the electric field the expression for the current density J in view of (1.1) is

$$J = Fen(T_0)\mu_L(T_0) \left[\left(\frac{32}{3\pi} \right)^{1/2} \frac{s}{F\mu_L(T_0)} \right]^{1/2} \dots\dots (1.2)$$

where e is the charge of a current carrier.

Ryder (1953) investigating experimentally the field effects in a fairly pure n-type germanium at temperature 77°K and above found that the current density is proportional to $F^{1/2}$ as is predicted by the theoretical relation (1.2). However, the constant of proportionality was not in agreement with this relation. On the other hand Sclar and Burstein (1957) working at liquid helium temperatures observed that the current variation with the field was completely different from (1.2). These authors have reported that for a fairly pure n-type germanium at

† Based on report L/T 406 of the British Electrical and Allied Industries Research Association.

liquid helium temperature the current obeys Ohm's law up to a field strength of about 2 v cm^{-1} while for a small increase in the applied voltage above 2 v cm^{-1} the current increases by several orders of magnitude. This rapid increase ceases at about 4 v cm^{-1} and for higher values of the field strength the current is proportional to $F^{1/2}$. Sclar and Burstein refer to this behaviour as 'low temperature breakdown' because of its similarity with the rising current observed in semiconductors at intrinsic breakdown fields. These authors have also estimated theoretically, on the basis of a simple model, the magnitude of this breakdown field at which a steep rise in the current is observed. In the opinion of the present author however, this field dependence of the current at low temperatures cannot be denoted as a breakdown process. We emphasize this point because the processes involved in the low temperature field dependence and in intrinsic breakdown are quite distinct. Intrinsic breakdown results from a state of instability of the current carriers under the action of the breakdown field, whereas in the case of low temperature field dependence the current though strongly field dependent, is always stable. Furthermore at intrinsic breakdown, in view of the instability of the current, no theoretical expression for the current density can be obtained. It is the object of the present paper to provide a theoretical explanation for this low temperature field dependence and obtain an expression for the current density as a unique and continuous function of the field strength.

The basic idea of our theory lies in the use of electron temperature concept first introduced by Fröhlich (1947 a, b). He has shown that electrons in a semiconductor under the action of a field can establish among themselves an equilibrium energy distribution corresponding to an electron temperature T , which is always greater than the lattice temperature T_0 . Making use of this idea, Shockley calculated the effect of the field on the mobility of electrons and obtained the relation (1.1). The consequent expression (1.2) for the current density J follows if the density of electrons is constant. At liquid helium temperatures however we cannot expect the density of the free electrons to remain constant with the field as may be seen from the following argument. Consider a crystal† of n-type germanium having a donor impurity concentration of about 10^{14} cm^{-3} . At these low temperatures the number of free electrons will be small, about 10^7 – 10^8 cm^{-3} , whereas the number of electrons bound to the donor sites will be of the order of 10^{14} cm^{-3} . Under the action of an electric field the free electrons would assume a Maxwellian energy distribution at an electron temperature $T > T_0$ and would also tend to establish temperature equilibrium with the bound electrons. This is counteracted by the lattice vibrations which try to maintain equilibrium with the bound electrons at temperature T_0 . These two opposing effects acting on the bound electrons determine their number density and consequently also that of the free electrons. These effects can be discussed in terms of the following processes:

Process 1, in which a free electron having a kinetic energy greater than the donor ionization energy can ionize a donor and create an additional free electron.

Process 2, in which a bound electron is ionized by the absorption of a lattice quantum of energy greater than the donor ionization energy.

† Even though the calculation of this paper is referred to n-type germanium, the results obtained are valid for any covalent semiconductor, provided the ionization energy of donors is less than Θ (Θ = Debye temperature).

In order to satisfy the principle of detailed balancing the reverse of these processes must occur. These reverse processes relate to the capture of a free electron by a donor. These two processes, each with its reverse, are taken into account in §3 in order to determine the free electron density as a function of the lattice and electron temperatures. In §4 we obtain the expression for the current density, by considering the effect of the field on both the mobility and the density of the free electrons. The results obtained in §4 are discussed and compared with experiment in §5. The necessary preliminary discussion for the development of the theory is given in §2.

§ 2. PRELIMINARY CONSIDERATIONS

Fröhlich has considered the effect of an electric field on the energy distribution of the electrons in a series of papers. (Fröhlich 1947 a, Fröhlich 1947 b, Fröhlich and Paranjape 1956). He has shown that the electron-electron interactions play a very important role in determining the energy distributions of electrons in the presence of an electric field. By considering a simple free electron model (i.e. without inter-electron interactions) he and Stratton (1957) have shown that for a field F however small, the sufficiently fast electrons continuously gain energy from the field and would be indefinitely accelerated leading to a non-stationary energy distribution. This can only be avoided by considering electron-electron interactions which bring about a stationary distribution. These authors show that the energy gained from the field is randomized as a result of electron-electron interactions. The average energy of the free electrons which exceeds the vibrational energy of the lattice can therefore be represented in terms of an electron temperature T . Stratton has treated in detail the problem of inter-electronic collisions in semiconductors by considering various ranges of the electron density. He has concluded that even at low densities when the influence of inter-electronic collisions may not be predominant the field dependence of the average energy and of the mobility of electrons is practically the same as that obtained by using the electron-temperature concept. In this paper although we are dealing with very low electron densities, the use of electron-temperature concept will not therefore introduce any serious error in our calculations. To determine T we proceed as follows: We denote the rate of gain of energy by the free electrons from the field by A and the rate of loss of energy by the electrons to the lattice by B . For the steady state the condition

$$A = B \quad \text{.....(2.1)}$$

must be satisfied. On the basis of the electron-temperature concept Stratton has calculated A and B and has obtained an explicit form of Eqn (2.1) which read

$$A = F^2 e n(T) \mu(T) = \frac{32}{3\pi} \frac{n(T) e s^2}{\mu_L(T_0)} \left[\frac{T}{T_0} \right]^{3/2} \left[1 - \frac{T_0}{T} \right] = B \quad \text{.....(2.2)}$$

where $n(T)$ is the free electron density at electron temperature T and $\mu(T)$ is the effective mobility of the electrons at T . Eqn (2.2) is called the energy balance equation and is used to determine T for a given field F . When the field F is increased T would also increase and this would in general affect the electrical properties of the crystal. In this section we consider the effect of electron temperature on the mobility of electrons. For any mechanism of electron scattering, if we know the mobility of an electron of a given energy then the corresponding average mobility at electron temperature T can be obtained by the

usual procedure of averaging. It can be shown that the variation with T of mobility, due solely to scattering by the acoustical modes of the lattice is given by

$$\mu_L(T) = \mu_L(T_0) \left(\frac{T_0}{T} \right)^{1/2} \quad \dots\dots (2.3)$$

The corresponding expression for the mobility $\mu_I(T)$ due to the ionized impurity scattering, which can be obtained with the help of the Conwell and Weisskopf (1950) formula, is

$$\mu_I(T) = \mu_I(T_0) \left[\frac{T}{T_0} \right]^{3/2} \frac{n_I(T_0)}{n_I(T)} \quad \dots\dots (2.4)$$

where $n_I(T)$ is the number density of the ionized impurity at T . It should be remembered that (2.4) is an approximate formula, since we have neglected the terms varying slowly with energy in the Conwell and Weisskopf formula.

Using (2.1) if we eliminate T from (2.3) and (2.4) we will get the expression for the mobility variation with the field. This procedure can be applied in a straightforward manner to lattice scattering; it results in relation (1.1). But for ionized impurity scattering elimination of T is not possible at the present stage since we do not know the electron temperature dependence of $n_I(T)$. We shall derive this quantity in the next section.

§ 3. ELECTRON DENSITY

As a model for our calculations consider a crystal of n-type germanium, containing a donor impurity of N_D per cm^3 and an acceptor impurity of N_A per cm^3 . From the requirement of electrical neutrality one can calculate, using elementary statistical mechanics the number density $n(T_0)$ of free electrons in such a crystal. In this paper we are only interested in low temperature, so low in fact that the density of holes in the valence band is negligible compared with the free electron density.

Defining $n_b(T_0)$ and $n_I(T_0)$ as the density of the bound electrons and the density of ionized donors respectively, then the charge neutrality requires that

$$n(T_0) = n_I(T_0) - N_A \quad \dots\dots (3.1)$$

where

$$n_I(T_0) = N_D - n_b(T_0). \quad \dots\dots (3.2)$$

Relations (3.1) and (3.2) are fundamental and are valid even under the influence of an electric field.

In the absence of an external electric field, there is complete thermal equilibrium between free electrons, bound electrons and the lattice at any temperature T_0 . If we measure the energy ϵ of an electron from the bottom of the conduction band, then the probability $\Phi(\epsilon)$ of finding an electron with a positive or negative value of ϵ obeys the equation

$$\Phi(\epsilon) = \left[\exp \left(\frac{-\xi + \epsilon}{kT_0} \right) + 1 \right]^{-1} \quad \dots\dots (3.3)$$

where ξ is the Fermi energy. For a non-degenerate semiconductor $-\xi \gg kT_0$ (k = Boltzmann's constant), and in terms of $n(T_0)$

$$\exp \left(\frac{\xi}{kT_0} \right) = \frac{n(T_0)h^3}{2(2m\pi kT_0)^{3/2}}.$$

From (3.3) follows

$$n_b(T_0) = N_D \left[\exp \left(-\frac{\xi + I}{kT_0} \right) + 1 \right]^{-1}$$

on the assumption that the donors have a single ionization energy I . Having obtained $n_b(T_0)$ we may determine $n(T_0)$ and $n_i(T_0)$ from Eqns (3.1) and (3.2). Hence the ratio $[n_i(T_0)/n_b(T_0)]$ whose value we require later, is given by

$$\frac{n_i(T_0)}{n_b(T_0)} = \exp\left(-\frac{\xi + I}{kT_0}\right). \quad \dots\dots(3.4)$$

In the presence of an electric field the thermal equilibrium of the crystal is disturbed. However, if the crystal is maintained in a heat bath of temperature T_0 , one may assume that the lattice is maintained at a temperature T_0 while the electron temperature T will be in excess of T_0 .

We denote the energy distribution of free electrons in the conduction band, under the action of the field by $f(\epsilon)$. Since they are assumed to reach equilibrium amongst themselves at temperature T ($T > T_0$), $f(\epsilon)$ can be represented by Fermi-Dirac distribution function at T . This distribution will be valid in the conduction band only for electrons with $\epsilon > 0$. Thus $f(\epsilon) = [\alpha^{-1} \exp(\epsilon/kT) + 1]^{-1}$ where α is a normalizing factor. If $\alpha^{-1} \exp(\epsilon/kT_0) \gg 1$ which is true for non-degenerate semiconductors, we have

$$f(\epsilon) \simeq \exp\left(\frac{-\epsilon}{kT}\right) \quad \dots\dots(3.5)$$

α the normalizing factor, is obtained by using the condition

$$\int_0^\infty f(\epsilon) \rho(\epsilon) d\epsilon = n(T)$$

where $\rho(\epsilon)$ is the density of states per unit range of energy for the free electrons. As is well known $\rho(\epsilon) = 4\pi(2m)^{3/2}(\epsilon)^{1/2}/h^3$ so that

$$\alpha = \frac{n(T)h^3}{2(2m\pi kT)^{3/2}} = \frac{n(T)}{n(T_0)} \left(\frac{T_0}{T}\right)^{3/2} \exp\left(\frac{\xi}{kT_0}\right). \quad \dots\dots(3.6)$$

When $T = T_0$, $\alpha = \exp(\xi/kT_0)$ as is expected.

Since $f(\epsilon)$ as given by (3.5) is only valid for $\epsilon \geq 0$ we cannot determine $n_b(T)$ from it, as we could in the field free case. To determine $n_b(T)$ and hence $n(T)$ and $n_i(T)$ one has to consider in detail the rates of change of $n(T)$ due to processes 1 and 2 introduced in § 1. If we denote the rate of change of $n(T)$ due to process 1 and its reverse by $[dn(T)/dt]_c$ and that due to process 2 and its reverse by $[dn(T)/dt]_L$ then the total rate of change $[dn(T)/dt]_{\text{total}}$ is equal to $[dn(T)/dt]_c + [dn(T)/dt]_L$. For the electron density to be time independent, we must have

$$\left[\frac{dn(T)}{dt}\right]_{\text{total}} = \left[\frac{dn(T)}{dt}\right]_c + \left[\frac{dn(T)}{dt}\right]_L = 0. \quad \dots\dots(3.7)$$

We shall first consider process 1 with its reverse and obtain $[dn(T)/dt]_c$. In process 1 an electron with an energy ϵ greater than the donor ionization energy can ionize a donor and produce an additional free electron. If ϵ is the energy of the initiating electron and the final energies of the resulting electrons are ϵ_1 and ϵ_2 then energy conservation requires that $\epsilon = \epsilon_1 + \epsilon_2 + I$.

Here $[dn(T)/dt]_c$ is expressed as a sum of the rates of increase and decrease of $n(T)$ by the process 1 and its reverse by the equation

$$\left[\frac{dn(T)}{dt}\right]_c = an_b(T) - bn_i(T). \quad \dots\dots(3.8)$$

Using the energy distribution function (3.5) with (3.6) for the electrons at electron

temperature T it can be shown that a and b are related to T by the relation

$$\begin{aligned} \left[\frac{a}{b} \right] &= [\alpha]^{-1} \exp \left[\frac{-I}{kT} \right] \\ &= \left[\frac{n_i(T_0)}{n_b(T_0)} \right] \left[\frac{n(T_0)}{n(T)} \right] \left[\frac{T}{T_0} \right]^{3/2} \exp \left[- \left(\frac{I}{kT} \right) + \left(\frac{I}{kT_0} \right) \right]. \end{aligned} \quad \dots\dots (3.9)$$

The quantities a and b are expressible in terms of the cross section $\sigma_c(\epsilon|\epsilon_1, \epsilon_2)$ for the process 1 and its reverse. If we define an average cross section by

$$\sigma_c(\epsilon) = \int_0^{\epsilon-I} \sigma_c(\epsilon|\epsilon_1, \epsilon_2) \rho(\epsilon_1) d\epsilon_1 \bigg/ \int_0^{\epsilon-I} \rho(\epsilon_1) d\epsilon_1 \quad \dots\dots (3.10)$$

then clearly

$$a = \int_I^\infty f(\epsilon) \sigma_c(\epsilon) v(\epsilon) \rho(\epsilon) d\epsilon \quad \dots\dots (3.11)$$

where $v(\epsilon)$ is the velocity of the electron of energy ϵ . For hydrogen-like impurity (Mott and Massey 1952)

$$\sigma_c(\epsilon) = \frac{0.285\pi e^4}{DI\epsilon} \log \frac{\epsilon D}{0.012I} \quad \dots\dots (3.12)$$

where D is the dielectric constant. Eqn (3.12) is obtained by Born's approximation and is valid for $\epsilon \gg I$, but it gives a fair order of magnitude for $\epsilon \geq I$. Using (3.12) in (3.11) one obtains

$$a = \frac{16\pi}{h^3} \alpha m \sigma_c(I) I k T \exp \left(\frac{-I}{kT} \right) \quad \dots\dots (3.13)$$

where $\sigma_c(I)$ is the ionization cross section for an electron of energy $\epsilon \simeq I$. With the value of a from (3.13) and the ratio $[a/b]$ from (3.9) one can readily obtain

$$b = \frac{16m\pi}{h^3} \alpha^2 \sigma_c(I) I k T. \quad \dots\dots (3.14)$$

We now turn to process 2, in which a bound electron absorbs a lattice quantum of energy $\epsilon + I$; it is thus transferred to the conduction band into a state of energy ϵ . Conversely a free electron of energy ϵ emits a lattice quantum of energy $\epsilon + I$ and is captured. Since this process involves the emission and absorption of a lattice quantum (phonon) the cross section for ionization and recombination respectively can be written as

$$\sigma_{LE}(\epsilon) = \sigma_L(\epsilon) \exp \left(\frac{I+\epsilon}{kT_0} \right) \left[\exp \left(\frac{I+\epsilon}{kT_0} \right) - 1 \right]^{-1} \left. \begin{array}{l} \text{emission of phonon} \\ \text{recombination of an electron,} \end{array} \right\} \quad \dots\dots (3.15a)$$

$$\sigma_{LA}(\epsilon) = \sigma_L(\epsilon) \left[\exp \left(\frac{I+\epsilon}{kT_0} \right) - 1 \right]^{-1} \left. \begin{array}{l} \text{absorption of phonon} \\ \text{ionization of donor,} \end{array} \right\} \quad \dots\dots (3.15b)$$

the quantity $[\exp \{(I+\epsilon)/kT_0\} - 1]^{-1}$ represents the temperature dependence of the number of phonons of energy $\epsilon + I$ which is involved in the interaction. $\sigma_L(\epsilon)$ is independent of T_0 but depends on the properties of the crystal. When $kT_0 \ll I$ (as is the case at liquid helium temperature), $\sigma_{LE}(\epsilon)$ is almost equal to $\sigma_L(\epsilon)$ so that $\sigma(\epsilon)$ can be interpreted as the electron recombination cross section at low temperatures. Here $[dn(T)/dT]_L$ can be written as a sum of the rates of

increase and decrease of $n(T)$ by process 2 and its reverse by

$$\left[\frac{dn(T)}{dt} \right]_{\text{L}} = cn_b(T) - dm_1(T) \quad \text{..... (3.16)}$$

where c and d are related to the cross section $\sigma_L(\epsilon)$ through the following relations

$$c = \int_0^{k\Theta - I} \left[\exp\left(\frac{I + \epsilon}{kT_0}\right) - 1 \right]^{-1} \sigma_L(\epsilon) v(\epsilon) \rho(\epsilon) d\epsilon \quad \text{..... (3.17)}$$

and

$$d = \int_0^{k\Theta - I} f(\epsilon) \exp\left(\frac{I + \epsilon}{kT_0}\right) \left[\exp\left(\frac{I + \epsilon}{kT_0}\right) - 1 \right]^{-1} \sigma_L(\epsilon) v(\epsilon) \rho(\epsilon) d\epsilon. \quad \text{..... (3.18)}$$

To determine c and d it is necessary to know the energy dependence of $\sigma_L(\epsilon)$. Lax (1959) and Frood (1959) have calculated $\sigma_L(\epsilon)$ on the basis of different models and have obtained different results, but both of these authors agree that $\sigma_L(\epsilon)$ should increase as ϵ decreases. Making use of this fact we define $\sigma_L(\epsilon)$ by the relation

$$\sigma_L(\epsilon) = \sigma_L(kT_0) (kT_0/\epsilon)^\beta \quad \text{..... (3.19)}$$

where β is treated as an arbitrary but positive numerical parameter. From (3.5), (3.17), (3.18) and (3.19) it is seen that

$$\frac{c}{d} = (\alpha)^{-1} \left(\frac{T}{T_0} \right)^{\beta-2} \exp\left(\frac{-I}{kT_0}\right) \quad \text{..... (3.20)}$$

provided $I \gg kT_0$ and $k\Theta - I \gg kT$. Substituting the value of α from (3.6) into Eqn (3.20) we get

$$\frac{c}{d} = \frac{n_1(T_0)}{n_b(T_0)} \frac{n(T_0)}{n(T)} \left[\frac{T}{T_0} \right]^{(2\beta-1)/2}. \quad \text{..... (3.21)}$$

From (3.19) and (3.21) we can see that at $T = T_0$

$$\frac{n_1(T_0)}{n_b(T_0)} = \left[\frac{a}{b} \right]_{T_0} = \left[\frac{c}{d} \right]_{T_0}$$

so that

$$\frac{n_1(T_0)}{n_b(T_0)} = \left[\frac{a + c}{b + d} \right]_{T_0}. \quad \text{..... (3.22)}$$

Consider now the integral (3.17) for c . Using Eqn (3.19) we evaluate the integral for c and obtain

$$c = \frac{16m\pi}{h^3} \sigma_L(kT_0) Q \exp\left(\frac{-I}{kT_0}\right) (kT_0)^2 \quad \text{..... (3.23)}$$

where Q is a numerical factor independent of T and is defined by

$$Q = \int_0^{(k\Theta - I)/kT_0} \exp(-x) x^{1-\beta} dx.$$

With the knowledge of the values of the ratio $[c/d]$ from (3.20) and of c from (3.23) the value of d is found as

$$d = [16m\pi/h^3][\alpha][kT_0]^2[\sigma_L(kT_0)Q][T_0/T]^{\beta-2}. \quad \text{..... (3.24)}$$

Substituting the values of a , b , c and d from (3.13), (3.14), (3.23) and (3.24) into (3.8) and (3.16) condition (3.7) can be written as

$$\frac{n_1(T)}{n_b(T)} = (\alpha^{-1}) \left[\frac{\alpha \sigma_c(I) kT \exp(-I/kT) + \exp(-I/kT_0) (kT_0)^2 \sigma_L(kT_0) Q}{\alpha \sigma_c(I) kT + (T_0/T)^{\beta-2} (kT_0)^2 \sigma_L(kT_0) Q} \right]. \quad \text{..... (3.25)}$$

For the sake of convenience we write (3.25) in the form

$$\frac{n_i(T)}{n_b(T)} = (\alpha)^{-1} \left[\frac{a' + c'}{b' + d'} \right] \quad \dots\dots (3.26)$$

where a' , b' , c' and d' stand for the respective terms in (3.25). It should be remembered that a' , b' , c' and d' are obtained from a , b , c and d by the removal of a common factor.

We attempt to solve (3.26) approximately for different ranges of electron temperature T and consider in each range only one predominant term from the numerator and denominator of the right-hand side of the Eqn (3.25). At liquid helium temperature, α is very small so that we expect that a' and b' would be very much smaller than c' and d' respectively for a range of electron temperature $T_0 < T < T_1$ where T_1 is to be determined. On the basis of this and with the known electron temperature dependence of a' , b' , c' and d' we divide the electron temperature T into the following three ranges:

Case I.	$T_0 < T < T_1$	when	$c' \gg a'$	and	$d' \gg b'$
Case II.	$T_1 < T < T_2$	when	$a' > c'$	and	$d' > b'$
Case III.	$T_2 < T$	when	$a' \gg c'$	and	$b' > d'$

The electron temperatures T_1 and T_2 are determined by the conditions $[a']_{T_1} = [c']_{T_1}$ and $[b']_{T_1} = [d']_{T_1}$ respectively.

In case I, we neglect a' and b' from the Eqn (3.26) and writing $n_i(T)$ and $n_b(T)$ in terms of $n(T)$ from (3.1) and (3.2), Eqn (3.26) can be written as

$$\frac{N_A + n(T)}{N_D - N_A - n(T)} = \frac{2(2m\pi kT)^{3/2}}{n(T)h^3} \left[\frac{T}{T_0} \right]^{\beta-2} \exp\left(\frac{-I}{kT_0}\right). \quad \dots\dots (3.27)$$

This quadratic equation in $n(T)$ has the solution

$$n(T) = \frac{1}{2} \{ - (N_A + x) + [(N_A + x)^2 - 4x(N_A - N_D)]^{1/2} \} \quad \dots\dots (3.28)$$

where

$$x = \frac{2(2m\pi kT_0)^{3/2}}{h^3} \left(\frac{T}{T_0} \right)^{(2\beta-1)/2} \exp\left(\frac{-I}{kT_0}\right).$$

Simplifying the relation (3.28) for the condition $x \ll N_A$ and $N_A^2 > 4xN_D$ we obtain

$$n(T) = \frac{2N_D}{N_A} \left[\frac{2m\pi kT_0}{h^3} \right]^{3/2} \exp\left(\frac{-I}{kT_0}\right) \left(\frac{T}{T_0} \right)^{(2\beta-1)/2}.$$

In case II we neglect c' and b' in Eqn (3.26) and solving for $n(T)$ we obtain

$$n(T) + N_A = \frac{N_D [T/T_0]^{\beta-1} [\sigma_c(I)/\sigma_L(kT_0)Q] [I/kT_0] \exp(-I/kT)}{1 + [T/T_0]^{\beta-1} [\sigma_c(I)/\sigma_L(kT_0)Q] [I/kT_0] \exp(-I/kT)}. \quad \dots\dots (3.30)$$

The relation (3.30) can be simplified for the condition

$$1 \gg \left(\frac{T}{T_0} \right)^{\beta-1} \frac{\sigma_c(I)}{\sigma_L(kT_0)Q} \frac{I}{kT_0} \exp\left(\frac{-I}{kT_0}\right) \quad \dots\dots (3.31)$$

giving

$$n(T) + N_A = N_D \left(\frac{T}{T_0} \right)^{\beta-1} \frac{\sigma_c(I)}{\sigma_L(kT_0)Q} \frac{I}{kT_0} \exp\left(\frac{-I}{kT_0}\right). \quad \dots\dots (3.32)$$

For case III, we solve the Eqn (3.26) for $n(T)$ neglecting c' and d' and obtain

$$n(T) = \frac{1}{2} \{ - (N_A + y) + [(N_A + y)^2 - 4y(N_A - N_D)]^{1/2} \} \dots\dots (3.33)$$

where

$$y = [2(2m\pi kT)^{3/2}/h^3] \exp(-I/kT).$$

The relation (3.33) may be simplified to

$$n(T) = \frac{2N_D}{N_A} \left(\frac{2m\pi kT}{h^2} \right)^{3/2} \exp\left(\frac{-I}{kT}\right) \dots\dots (3.34)$$

for the conditions

$$y \ll N_A \quad \text{and} \quad N_A^2 \gg 4yN_D \dots\dots (3.35)$$

§ 4. RESULTS

In this section we make use of the results obtained in the previous sections to derive an expression for the current density J , as a function of F , the applied potential gradient. By definition

$$J = n(T)e\mu(T)F. \dots\dots (4.1)$$

From Eqns (2.3) and (2.4) we therefore have

$$J = n(T_0)e\mu_L(T_0) \left[\frac{n(T)}{n(T_0)} \right] \left[\frac{T_0}{T} \right]^{1/2} F \quad \text{for acoustical mode scattering} \dots\dots (4.2)$$

and

$$J = n(T_0)e\mu_I(T_0) \left[\frac{n(T)}{n(T_0)} \right] \left[\frac{n_I(T)}{n_I(T_0)} \right] \left[\frac{T}{T_0} \right]^{3/2} F \quad \text{for ionized impurity scattering} \dots\dots (4.3)$$

Using (2.2) to eliminate T from (4.2) and (4.3), we shall find J as an explicit function of F . Before carrying out this calculation of J , we first discuss Eqn (2.2) which relates T with F . Unfortunately T is not an experimentally observable quantity so that one cannot confirm the correctness of (2.2) by direct experimental observations. By observing the field dependence of conductivity at temperature 77°K and above Gunn (1957) and several other authors have concluded, that Eqn (2.2) is only qualitatively correct. To get quantitative agreement with experiments the right-hand side of (2.1) must be increased by a factor of the order of 10. Physically this means that the electrons should lose energy to the lattice at a rate ten times greater than that given by B in Eqn (2.2). We do not attempt to give any explanation for this discrepancy but for the purpose of this paper multiply the right-hand side of (2.1) by an arbitrary numerical parameter g and determine its value from higher temperature measurements. If the scattering is due to the acoustical modes then Eqn (2.2) can now be written as

$$F^2\mu_L^2(T_0) = \frac{32}{3\pi} s^2 \left(\frac{T}{T_0} \right)^2 \left(\frac{T - T_0}{T} \right) g. \dots\dots (4.4)$$

When the electric field is large enough to satisfy $F\mu_L(T_0) > \gamma s$ where $\gamma = (32g/3\pi)^{1/2}$, then (4.4) can be simplified to give

$$\frac{T}{T_0} = \frac{F\mu_L(T_0)}{\gamma s} + \frac{1}{2}. \dots\dots (4.5)$$

With the help of (4.5) we may now write the current density J due to acoustical scattering for the three cases defined in § 3.

Case I.

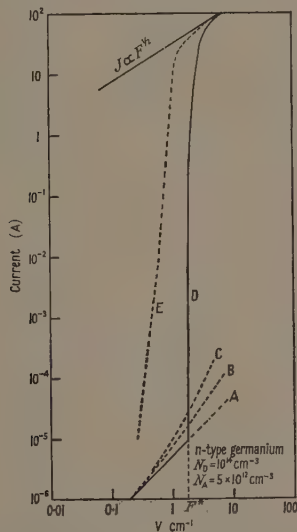
For a field range of $F_1 > F > (\gamma s)/\mu_L(T_0)$ where

$$F_1 = \frac{\gamma s}{\mu_L(T_0)} \left[\frac{T_1}{T_0} - \frac{1}{2} \right] \quad \dots\dots (4.6)$$

we have the current density J as

$$J = [F\mu_L(T_0)e] \frac{N_D}{N_A} \frac{2(2m\pi kT_0)^{3/2}}{h^3} \exp\left(\frac{-I}{kT_0}\right) \left[\frac{F\mu_L(T_0)}{\gamma s} + \frac{1}{2} \right]^{\beta-1} \quad \dots\dots (4.7)$$

provided the conditions for the validity of (3.29) are satisfied.



The variation of the current with the field. Curves A, B and C represent the case I with $\beta=1, 3/2$ and 2 respectively, while the curves D and E represent the cases II and III respectively.

Case II.

For a field range of $F_2 > F > F_1$ where

$$F_2 = \frac{\gamma s}{\mu_L(T_0)} \left[\frac{T_2}{T_0} - \frac{1}{2} \right] \quad \dots\dots (4.8)$$

the current density J is

$$J = [F\mu_L(T_0)e] \left[N_D \left\{ \frac{F\mu_L(T_0)}{\gamma s} + \frac{1}{2} \right\}^{(2\beta-3)/2} \times \frac{\sigma_v(I)}{\sigma_L(kT_0)Q} \frac{I}{kT_0} \exp\left\{ -\frac{I}{kT_0} \left(\frac{F\mu_L(T_0)}{\gamma s} + \frac{1}{2} \right)^{-1} \right\} - N_A \right] \quad \dots\dots (4.9)$$

provided the condition (3.31) is satisfied.

Case III.

For a field range $F > F_2$, the current density J is

$$J = F\mu_L(T_0)e \frac{N_D}{N_A} \frac{2(2m\pi kT_0)^{3/2}}{\hbar^3} \left[\frac{F\mu_L(T_0)}{\gamma s} + \frac{1}{2} \right] \exp \left\{ \left(\frac{-I}{kT_0} \right) \left(\frac{F\mu_L(T_0)}{\gamma s} + \frac{1}{2} \right)^{-1} \right\} \quad \dots (4.10)$$

provided the condition (3.35) is satisfied, which gives the upper limit of F for the validity of (4.10).

An expression for the current density J , when the scattering is due to ionized impurities can be obtained in a similar way. We shall not give the exact expressions here, but derive only approximate results from the cases II and III where the results are interesting. Substituting (2.4) in (2.2), we obtain the relation between T and F as

$$\frac{F^2\mu_I(T_0)\mu_L(T_0)}{s^2\gamma^2} = \frac{n_i(T)}{n_i(T_0)} = \frac{N_A + n(T)}{N_A + n(T_0)}. \quad \dots (4.11)$$

For cases II and III the electron density $n(T)$ varies exponentially with T , so that one can write approximately

$$n(T) = X \exp(-I/kT) \quad \dots (4.12)$$

where X may be assumed to be almost independent of T . Substituting (4.12) in (4.11), we obtain

$$kT = \frac{I}{\log X} - \log \left[\frac{F^2\mu_I(T_0)\mu_L(T_0)\{N_A + n(T_0)\}}{(\gamma s)^2} - N_A \right]. \quad \dots (4.13)$$

This means that kT varies very slowly with F . Using this property we may write J for ionized impurity scattering as

$$J = F^3\mu_I^2(T_0)\mu_L(T_0) e N_A / s^2\gamma^2 \quad \dots (4.14)$$

provided $n(T) < N_A$ and $[F^2\mu_I(T_0)\mu_L(T_0)/s^2\gamma^2] \gg 1$.

When $n(T) > N_A$, the current density J can be expressed as

$$J = Fe\mu_I(T_0)[n(T_0) + N_A] \quad \dots (4.15)$$

so that the current is proportional to the field F . From Eqns (4.14) and (4.15) we can see that no strong field dependence is expected on the basis of this theory when the impurity scattering predominates.

§ 5. DISCUSSION

In § 3 we have obtained expressions for the variation of the free electron density with electron temperature for three separate ranges denoted by cases I, II and III. Each case is defined by considering only one of the two processes by which the ionizations of the donors or the recombinations of the free electrons take place. For case I both the ionization and the recombination is due to the process 2 (lattice interaction) and we obtained a rise in $n(T)$ with T as proportional to $(kT)^{2\beta-1/2}$. For case II, $n(T)$ rises rapidly with T as $\exp(-I/kT)$ when the ionization of the donors is due to process 1 (impact ionization) and the

recombination of the free electrons by process 2. In case III the process 1 completely predominates and is therefore associated with a complete thermal equilibrium of the free and the bound electrons. In this case $n(T)$ increases exponentially till it almost reaches the saturation value of N_D . The transition temperatures T_1 and T_2 can be defined using (3.25) by the following equations

$$\left(\frac{T_1}{T_0}\right)^{\beta-1} \exp\left(\frac{-I}{kT_1}\right) = \frac{N_A \sigma_L(kT_0) Q kT_0}{N_D \sigma_c(I) I} \quad \dots\dots (5.1)$$

and

$$\alpha \sigma_c(I) I k T_2 = \left(\frac{kT_0}{kT_2}\right)^{\beta-2} (kT_0)^2 \sigma_L(kT_0) Q \quad \dots\dots (5.2)$$

respectively.

In § 4, we obtained expressions for the variation of current density J with field F . We illustrate these results graphically for a typical example of a fairly pure n-type germanium crystal having $N_D = 10^{14} \text{ cm}^{-3}$, $N_A = 5 \times 10^{12} \text{ cm}^{-3}$ and with $(I/kT_0) = 25$ (i.e. $T_0 \simeq 4^\circ \text{K}$). Fixing $\gamma = 6$ from the experiments of the field dependence of the conductivity at 77°K , we have drawn for case I three curves for three different values of β . We see that when $\beta = 1$, the current is proportional to the field, which is in agreement with experimental observation by Sclar and Burstein. This value of $\beta = 1$ which lies in the same range as the values obtained theoretically by Lax and Frood, may therefore be the correct value. For cases II and III the current rises very steeply as $\exp(\text{constant}/F)$ for a very narrow range of the field strength F while for higher values of the field the current is proportional to $F^{1/2}$. The $F^{1/2}$ field dependence of the current indicates complete ionization of donors and is therefore consistent with (1.1). The transitional field strength of F_1 , below which the currents are ohmic (case I) and above which the current rises rapidly (case II) is therefore associated with the critical field F^* (the breakdown field, in the terminology of Sclar and Burstein).

F^* is obtained from Eqn (4.6) with the use of (5.1) which determines T_1 the transition electron temperature. $T_1 = 12^\circ \text{K}$ is found if we set $\sigma_c(I) = 10^{-11} \text{ cm}^2$ and $\sigma_L(kT_0)Q = 10^{-12} \text{ cm}^2$ (Lax 1959). From Eqn (4.6) $F^* = 1.8 \text{ v cm}^{-1}$ is then obtained when the mobility of electrons in germanium at 4.2°K is assumed to be $2.7 \times 10^6 \text{ cm}^2 \text{ v}^{-1} \text{ sec}^{-1}$ a value proposed by Sclar and Burstein. F^* has been obtained in agreement with the experimental value, by making use of the experimental value of γ at 77°K and the above values for the cross section and the mobility. In our theory at the field strength F^* the impact ionization (process 1) just begins to surpass ionization by phonons (process 2) while recombination is still predominantly due to phonons. Sclar and Burstein incorrectly neglect the latter, i.e. they consider process 1 for both ionization and recombination according to our case III. This would lead to a much lower field F^* than found by our theory.

ACKNOWLEDGMENTS

The author wishes to thank Professor H. Fröhlich for his guidance at all stages of the work, and Dr. B. K. P. Scaife for his help in the preparation of the manuscript. The financial help from the Electrical Research Association is gratefully acknowledged.

REFERENCES

- BRAY, R., and MENDELSSOHN, K., 1957, *Proc. Phys. Soc. B*, **70**, 889.
CONWELL, E. and WEISSKOPF, V. F., 1950, *Phys. Rev.*, **77**, 388.
FROOD, D. G., 1959, *E.R.A. Technical Report L/T 383*.
FRÖHLICH, H., 1947 a, *Proc. Roy. Soc. A*, **188**, 521.
— 1947 b, *Proc. Roy. Soc. A*, **188**, 532.
FRÖHLICH, H., and PARANJAPÉ, B. V., 1956, *Proc. Phys. Soc. B*, **69**, 21.
GUNN, J. B., 1957, *Progress in Semiconductors*, **2**, 213.
KOENIG, S. H., and GUNTHER MOHR, G. R., 1957, *J. Phys. Chem. Solids*, **2**, 268.
LAX, M., 1959, *J. Phys. Chem. Solids*, **8**, 66.
MOTT, N. F., and MASSEY, H. S. W., 1952, *Theory of Atomic Collisions* (Oxford: Clarendon Press), p. 247.
RYDER, E. J., 1953, *Phys. Rev.*, **90**, 776.
SCLAR, N., and BURSTEIN, E., 1957, *J. Phys. Chem. Solids*, **2**, 1.
STRATTON, R., 1957, *Proc. Roy. Soc. A*, **242**, 335.
SHOCKLEY, W., 1951, *Bell Syst. Tech. J.*, **30**, 990.

Formulae for Non-degenerate Rayleigh-Schrödinger Perturbation Theory in any order

By R. HUBY

Department of Theoretical Physics, University of Liverpool

MS. received 13th February 1961

Abstract. It is shown that Bloch's solution for the n th order perturbation of the energy and the eigenvector in the Rayleigh-Schrödinger perturbation theory of non-degenerate, discrete levels can be expressed in a different form, of a kind suggested by Brueckner, and some advantages of the latter form are presented.

§ 1. INTRODUCTION

THE many-body problem has stimulated interest in the systematic formulation of the higher order terms in Rayleigh-Schrödinger perturbation theory for discrete energy levels, i.e. the determination of the discrete eigenstates and eigenvalues of a Hamiltonian:

$$H = H_0 + H' \quad \dots\dots(1)$$

(the sum of an unperturbed operator H_0 and a perturbing one H') in the form of series in ascending powers of H' . The case most studied has been that of a system of many particles the interactions between which constitute H' , and important perturbation developments appropriate to this particular case have been made (e.g. Goldstone 1957). However, some attention has also been paid to the formulation of the solution to the general problem (1). Bloch (1958) has presented an elegant formulation, which leads to a quite simple expression for the n th order energy or state vector when the problem is 'non-degenerate' (i.e. when we study the shift of a non-degenerate unperturbed energy level). A different prescription for writing down the energy shifts in the first few perturbation orders (again for the non-degenerate problem) had been suggested by Brueckner (1955), but it was not clear how this was to be generalized correctly to any arbitrary order. The purpose of this paper is to show that the prescription of Brueckner for the energy can in fact, with small modifications, be extended up to any arbitrary order; and that it can also be adapted to yield formulae for the state vectors to any order. This is achieved by showing that the formulae proved by Bloch can be expressed alternatively in Brueckner's form.

Brueckner's type of formula has some advantage in the ease with which it can be visualized and applied.

§ 2. BLOCH'S FORMULATION

Let us first summarize the relevant results of Bloch (see also Messiah 1960). We consider some unperturbed, discrete, eigenvalue of H_0 , say E_0 , which in the first instance may perhaps be degenerate, its eigenvectors spanning a g -dimensional

subspace Ω_0 of the total state space. Let P_0 be the operator of projection on to Ω_0 and Q_0 the projector on to the orthogonal sub-space:

$$Q_0 = 1 - P_0. \quad \dots\dots (2)$$

Next, we define the 'energy denominator' operator:

$$\frac{Q}{a} = \frac{1}{E_0 - H_0} Q_0. \quad \dots\dots (3)$$

Now we assume that there are g independent, exact eigenvectors of H which, if the perturbation H' were reduced to zero, would tend to unperturbed vectors lying within the subspace Ω_0 . Let these exact eigenvectors of H be $|\alpha\rangle, |\beta\rangle, \dots (g)$, (all normalized); and let the corresponding eigenvalues of H be $(E_0 + E_\alpha), (E_0 + E_\beta), \dots (g)$. We denote by $|\alpha\rangle_0$ the projection of $|\alpha\rangle$ on to Ω_0 :

$$|\alpha\rangle_0 = P_0 |\alpha\rangle. \quad \dots\dots (4)$$

Bloch works with an operator U , defined so that its product with each of these projections $|\alpha\rangle_0, |\beta\rangle_0, \dots$ is the corresponding exact eigenket of H :

$$|\alpha\rangle = U |\alpha\rangle_0, \quad \dots\dots (5)$$

while the product of U with any vector in the sub-space orthogonal to Ω_0 vanishes. He obtained a perturbation expansion of U :

$$U = \sum_{n=0}^{\infty} U^{(n)}, \quad \dots\dots (6)$$

where

$$U^0 = P_0, \quad \dots\dots (7)$$

and

$$U^{(n)} = \sum' S^{k_1} H' S^{k_2} H' \dots S^{k_n} H' P_0 \quad (n > 0). \quad \dots\dots (8)$$

Here

$$S^0 = -P_0, \quad \dots\dots (9)$$

$$S^k = \left(\frac{Q_0}{a}\right)^k = \left(\frac{1}{a}\right)^k Q_0 \quad (k > 0) \quad \dots\dots (10)$$

and \sum' means a sum taken over all non-negative integers $k_1, k_2, \dots k_n$ which satisfy

$$\sum_{i=1}^n k_i = n \quad \dots\dots (11)$$

and

$$\sum_{i=1}^p k_i \geq p \quad (\text{all } p \text{ from } 1, 2, \dots \text{ to } n-1). \quad \dots\dots (12)$$

In the non-degenerate case ($g=1$) the energy shift can be found immediately with the aid of U . Writing the energy as a perturbation series:

$$E_0 + E_\alpha = E_0 + \sum_{n=1}^{\infty} E_\alpha^{(n)}, \quad \dots\dots (13)$$

we have

$$E_\alpha^{(n)} = \langle 0 | H' U^{(n-1)} | 0 \rangle, \quad \dots\dots (14)$$

where $|0\rangle$ is the *normalized* unperturbed state vector proportional to $|\alpha\rangle_0$. Also the eigenvector of H in a perturbation series (but not normalized to unity), i.e.

$$N|\alpha\rangle = |0\rangle + \sum_{n=1}^{\infty} |\alpha^{(n)}\rangle, \quad \dots\dots (15)$$

is given by

$$|\alpha^{(n)}\rangle = U^{(n)}|0\rangle. \quad \dots\dots (16)$$

Each of the perturbation terms $|\alpha^{(n)}\rangle$ is orthogonal to $|0\rangle$, and so the normalization factor N may be written $\langle 0|\alpha\rangle^{-1}$. N is to be determined, to any chosen perturbation order, after evaluating the right-hand side of (15) to the appropriate order, by calculating the length of this vector.

§ 3. THE FORMULATION AFTER BRUECKNER

We deal only with the non-degenerate case.

It is well known that, if the lowest order non-vanishing correction to the energy in the perturbation series (13) is $E_\alpha^{(n)}$, then this is given by

$$E_\alpha^{(n)} = \langle 0|H' \frac{Q_0}{a} H' Q_0 \frac{Q_0}{a} H' \dots \frac{Q_0}{a} H'|0\rangle \quad \dots\dots (17)$$

(where the bracket contains n factors H'); but on the other hand, if there exist lower order non-vanishing corrections to the energy, then the formula for $E_\alpha^{(n)}$ contains certain additional terms†. When (17) is expanded in terms of the matrix elements of H' , e.g.

$$\langle 0|H' \frac{Q_0}{a} H' \frac{Q_0}{a} H'|0\rangle = \sum_{i,j \neq 0} \frac{\langle 0|H'|j\rangle \langle j|H'|i\rangle \langle i|H'|0\rangle}{(E_0 - E_j)(E_0 - E_i)}, \quad \dots\dots (18)$$

this introduces intermediate unperturbed states $|i\rangle, |j\rangle$, etc., which are all different from the initial state $|0\rangle$. On the other hand, the additional terms that can appear in $E_\alpha^{(n)}$ contain factors in which $|0\rangle$ itself occurs as an intermediate state. For example, the full formula for $E_\alpha^{(3)}$ comprises in addition to (17) the term

$$-\langle 0|H' \frac{Q_0}{a^2} H'|0\rangle \langle 0|H'|0\rangle = - \sum_{i \neq 0} \frac{\langle 0|H'|i\rangle \langle i|H'|0\rangle \langle 0|H'|0\rangle}{(E_0 - E_i)^2}. \quad \dots\dots (19)$$

Brueckner pointed out that, in the first few perturbation orders, the additional terms such as (19) in $E_\alpha^{(n)}$ can be constructed schematically from the basic term of (17) as follows. Writing (19) for instance, as

$$-\langle 0|H' \frac{Q_0}{a} \langle H' \rangle \frac{Q_0}{a} H'|0\rangle,$$

we insert around the inner factors H' in (17) one or more pairs of bra-ket brackets, which signify taking a diagonal matrix element with respect to the state $|0\rangle$ —also a change of sign may be required.

The correct generalization of this procedure to any order is as follows.

Rule 1. To find the n th order energy perturbation of the level E_0 , viz. $E_\alpha^{(n)}$, we first write down the basic matrix element (17). We then add to this all other expressions which can be obtained from it by inserting any number of pairs of bra-ket brackets around the inner H' factors‡. The bra and ket of a pair may be separated

† More precisely, additional terms enter, not in the next higher order above the first non-vanishing one, but only in the next order after that.

‡ By an 'inner' H' factor we mean any H' other than the first or the last.

by any number of link factors

$$H' \frac{Q_0}{a} H' \frac{Q_0}{a} \dots H',$$

and brackets may lie within brackets, but one bra-ket pair may not straddle another, and no brackets may touch. Finally the sign $(-1)^v$ is attached to the expression, where v is the number of bra-ket pairs inserted in it. Each bra-ket pair signifies that we form the expectation value of the operator which it encloses, in the state $|0\rangle$.

Afterwards, any bra-ket pair together with its contents, since they constitute a pure number, may be removed bodily as a factor outside the original expression. As an illustration, $E_a^{(5)}$ is

$$\begin{aligned} E_a^{(5)} = & \langle 0 | H' \frac{Q_0}{a} H' \frac{Q_0}{a} H' \frac{Q_0}{a} H' \frac{Q_0}{a} H' | 0 \rangle \\ & - \langle 0 | H' \frac{Q_0}{a} \langle H' \rangle \frac{Q_0}{a} H' \frac{Q_0}{a} H' \frac{Q_0}{a} H' | 0 \rangle - \dots \\ & - \langle 0 | H' \frac{Q_0}{a} \langle H' \frac{Q_0}{a} H' \rangle \frac{Q_0}{a} H' \frac{Q_0}{a} H' | 0 \rangle - \dots \\ & - \langle 0 | H' \frac{Q_0}{a} \langle H' \frac{Q_0}{a} H' \frac{Q_0}{a} H' \rangle \frac{Q_0}{a} H' | 0 \rangle \\ & + \langle 0 | H' \frac{Q_0}{a} \langle H' \rangle \frac{Q_0}{a} \langle H' \rangle \frac{Q_0}{a} H' \frac{Q_0}{a} H' | 0 \rangle + \dots \\ & + \langle 0 | H' \frac{Q_0}{a} \langle H' \frac{Q_0}{a} \langle H' \rangle \frac{Q_0}{a} H' \rangle \frac{Q_0}{a} H' | 0 \rangle. \quad \dots\dots (20) \\ & \quad \quad \quad (14 \text{ terms}) \\ & = \langle 0 | H' \frac{Q_0}{a} H' \frac{Q_0}{a} H' \frac{Q_0}{a} H' \frac{Q_0}{a} H' | 0 \rangle \\ & - \langle 0 | H' \frac{Q_0}{a^2} H' \frac{Q_0}{a} H' \frac{Q_0}{a} H' | 0 \rangle \langle 0 | H' | 0 \rangle \\ & \quad \vdots \\ & + \langle 0 | H' \frac{Q_0}{a^2} H' | 0 \rangle \langle 0 | H' \frac{Q_0}{a^2} H' | 0 \rangle \langle 0 | H' | 0 \rangle. \end{aligned}$$

The correctness of this prescription is proved in the appendix.

A similar prescription (also proved in the appendix) can be made for the perturbation of the state vector. Let us consider the n th order term in the series (15) for the eigenvector of H . We write down first a 'basic' term (cf. (17))

$$\frac{Q_0}{a} H' \frac{Q_0}{a} H' \dots \frac{Q_0}{a} H' | 0 \rangle, \quad \dots\dots (21)$$

(where there are n factors H'), and this is in fact the correct formula for $|\alpha^{(n)}\rangle$ provided that all the energy corrections of order less than n vanish. Otherwise, however, certain terms must be added to (21). The general rule for formulating these terms is

Rule 2. To find the n th order perturbation of the state vector $|0\rangle$, we first write down the ket that is displayed in (21), and then add to it all the expressions which

can be obtained from it by inserting any number of bra-ket pairs around the H' factors other than the last. The rules for arranging and interpreting the brackets are the same as those in Rule 1, and again the sign $(-1)^v$ is to be attached to an expression, where v is the number of inserted bra-ket pairs.

The perturbed vector thus obtained is the one normalized as in (15) and (16). As an illustration, $|\alpha^{(4)}\rangle$ is

$$\begin{aligned}
 |\alpha^{(4)}\rangle &= \frac{Q_0}{a} H' \frac{Q_0}{a} H' \frac{Q_0}{a} H' \frac{Q_0}{a} H' |0\rangle \\
 &\quad - \frac{Q_0}{a} \langle H' \rangle \frac{Q_0}{a} H' \frac{Q_0}{a} H' \frac{Q_0}{a} H' |0\rangle \\
 &\quad \vdots \\
 &\quad + \frac{Q_0}{a} \langle H' \frac{Q_0}{a} \langle H' \rangle \frac{Q_0}{a} H' \rangle \frac{Q_0}{a} H' |0\rangle. \\
 &\hspace{15em} (14 \text{ terms}) \\
 &= \frac{Q_0}{a} H' \frac{Q_0}{a} H' \frac{Q_0}{a} H' \frac{Q_0}{a} H' |0\rangle \\
 &\quad - \frac{Q_0}{a^2} H' \frac{Q_0}{a} H' \frac{Q_0}{a} H' |0\rangle \langle 0|H'|0\rangle \\
 &\quad \vdots \\
 &\quad + \frac{Q_0}{a^2} H' |0\rangle \langle 0|H' \frac{Q_0}{a^2} H' |0\rangle \langle 0|H'|0\rangle.
 \end{aligned}$$

§ 4. COMMENTS ON THE FORMULATION AFTER BRUECKNER

From (14) and (16) there is a simple relation between $E_\alpha^{(n)}$ and $|\alpha^{(n-1)}\rangle$:

$$E_\alpha^{(n)} = \langle 0|H'|\alpha^{(n-1)}\rangle. \quad \dots\dots\dots (22)$$

This shows that Rule 1 follows directly from Rule 2, the formula for $E_\alpha^{(n)}$ being closely related to that for $|\alpha^{(n-1)}\rangle$ (both, for instance, having the same number of terms).

The formulation given in Rules 1 and 2 is most helpful when the energy corrections vanish below a certain order, say the n th. It is evident from Rule 1 that the necessary and sufficient condition for this is the vanishing of all brackets of the form

$$\langle 0|H' \frac{Q_0}{a} H' \dots H'|0\rangle$$

which contain fewer than n factors H' . This greatly simplifies the construction of the formulae for energies and state vectors of order higher than n : in following Rules 1 and 2 we have simply to exclude all expressions which contain brackets enclosing fewer than n factors H' . For instance, if the lowest non-vanishing energy correction is the third, then $E_\alpha^{(5)}$ is given by

$$\begin{aligned}
 E_\alpha^{(5)} &= \langle 0|H' \frac{Q_0}{a} H' \frac{Q_0}{a} H' \frac{Q_0}{a} H' \frac{Q_0}{a} H' |0\rangle \\
 &\quad - \langle 0|H' \frac{Q_0}{a} \langle H' \frac{Q_0}{a} H' \frac{Q_0}{a} H' \rangle \frac{Q_0}{a} H' |0\rangle. \\
 &\quad \dots\dots\dots
 \end{aligned}$$

Brueckner's original formulation indeed differed slightly from ours of § 3, because he exploited this kind of simplifications as follows. The original problem of (1) is replaced formally by

$$H = \{H_0 + \langle 0|H'|0\rangle\} + u,$$

where

$$u = H' - \langle 0|H'|0\rangle,$$

and u is now treated as the perturbing operator. The unperturbed energy becomes $(E_0 + \langle 0|H'|0\rangle)$, but all the unperturbed states $|i\rangle$ remain unaltered, as does the operator Q_0/a . The first order energy perturbation $\langle 0|u|0\rangle$ now certainly vanishes, and so when the perturbation formulae are written down according to Rules 1 and 2, all expressions containing brackets $\langle u\rangle$ can be excluded.

APPENDIX

Starting from Bloch's formula for $U^{(n)}$ (Eqn. (8)), we assert that this can be constructed by the following Rule:

Rule 3. To find $U^{(n)}$, we first write down

$$\frac{Q_0}{a} H' \frac{Q_0}{a} H' \dots \frac{Q_0}{a} H' P_0, \quad \dots \dots (A.1)$$

(containing n factors H'), and then add to it all the expressions which can be formed from it by inserting any number of bra-ket pairs around the H' factor other than the last. The rules for arranging and interpreting the brackets are the same as those of Rule 1, and again the sign $(-1)^v$ is to be attached to an expression, where v is the number of inserted bra-ket pairs.

Once Rule 3 has been proved, Rules 1 and 2 will follow trivially from it by applying (14) and (16) respectively.

First we show that any single one of the expressions prescribed by Rule 3 is equal to one of the terms in Bloch's series (8). A typical expression in Rule 3 may be written.

$$\begin{aligned} v &= (-1)^v \frac{Q_0}{a} \overset{(1)}{H'} \frac{Q_0}{a} \overset{(2)}{H'} \dots \overset{(i)}{H'} \frac{Q_0}{a} \langle \overset{(i+1)}{H'} \dots \overset{(i+m)}{H'} \rangle \frac{Q_0}{a} \overset{(i+m+1)}{H'} \dots \overset{(n)}{H'} P_0 \\ &\dots \dots (A.2) \\ &\equiv (-1)^v O_1 \langle O_2 \rangle O_3 P_0 = (-1)^v O_1 \langle O_2 \rangle O_3 |0\rangle \langle 0|, \end{aligned}$$

where it is to be understood that the bra beside O_2 is the one closest to the left end of the whole expression and the ket beside O_2 is the proper partner of this bra. That is to say, O_1 contains no bra-ket pairs, but both O_2 and O_3 may do so. Now let us lift out the numerical factor $-\langle O_2 \rangle$ and replace it between $|0\rangle$ and $\langle 0|$ in the last form of (A.2)

$$\begin{aligned} v &= (-1)^{v-1} O_1 O_3 |0\rangle \langle 0| - O_2 |0\rangle \langle 0| \\ &= (-1)^{v-1} O_1 O_3 (-P_0) O_2 P_0 \\ &= (-1)^{v-1} \frac{Q_0}{a} \overset{(1)}{H'} \frac{Q_0}{a} \overset{(2)}{H'} \dots \overset{(i)}{H'} \frac{Q_0}{a_2} \overset{(i+1)}{H'} \dots \overset{(n-m)}{H'} S^0 \overset{(n-m+1)}{H'} \dots \overset{(n)}{H'} P_0. \\ &\dots \dots (A.3) \end{aligned}$$

Comparing this final expression with the first expression in (A.2) the changes can be described as follows:

(i) In the chain of operators (interspersed with brackets)

$$\frac{Q_0}{a} \overset{(1)}{H'} \frac{Q_0}{a} \dots \overset{(n)}{H'},$$

the factor Q_0/a which stood originally just to the right of $\overset{(n-m)}{H'}$ has been shifted leftwards into the place just to the right of $\overset{(i)}{H'}$, converting this factor into Q_0/a^2 , while the place vacated has been refilled with S^0 .

(ii) The number of bra-ket pairs has been reduced by one, and the positions of the remaining brackets have been altered.

(iii) The factor $(-1)^r$ has been altered so as still to correspond to the remaining number of bra-ket pairs. This process is now to be repeated successively, first seeking the nearest complete bra-ket pair to the left end of the expression, and then shifting it to the extreme right end. At each step the number of bra-ket pairs falls by one, and a factor Q_0/a is shifted leftwards, its vacant place being taken by S^0 . Eventually, all the brackets will have gone, and we shall have an expression of the form in (8), which we denote v' :

$$v' \equiv v, \quad \dots\dots (A.4)$$

though it remains to verify that (11) and (12) are satisfied.

Since the total power of $1/a$ in the expression has been conserved, the k 's in v' satisfy (11). The chain of operators in the original expression (A.2) (forgetting for the moment the brackets and sign factor) is of the form of a term in (8), with

$$\sum_{i=1}^p k_i = p.$$

Now in the process of going from v to v' , the shift of factors Q_0/a has always been leftwards; hence the k_i 's in v' satisfy (12).

We proceed to the converse: to show that any single one of the terms in Bloch's formula (8) is equal to one of the expressions prescribed by Rule 3. A typical term in (8) may be rewritten

$$w' = S'^n \overset{(n)}{H'} S'^{n-1} \overset{(n-1)}{H'} \dots S'^1 \overset{(1)}{H'} P_0, \quad \dots\dots (A.5)$$

where, because of (11) and (12)

$$\sum_{i=1}^n l_i = n, \quad \dots\dots (A.6)$$

$$\sum_{i=1}^q l_i \leq q, \quad (\text{all } q \text{ from } 1 \text{ to } n-1). \quad \dots\dots (A.7)$$

We may write

$$\begin{aligned} w' &= -S'^n \overset{(n)}{H'} S'^{n-1} \dots \overset{(i+1)}{H'} \frac{Q_0}{a^{l_i}} \overset{(i)}{H'} \dots H' P_0 \overset{(m)}{H'} \dots \frac{Q_0}{a} \overset{(1)}{H'} P_0 \\ &\equiv -O_4 \frac{Q_0}{a^{l_i}} O_5 P_0 O_6 P_0 = -O_4 \frac{Q_0}{a^{l_i}} O_5 |0\rangle \langle 0| O_6 |0\rangle \langle 0|, \quad \dots\dots (A.8) \end{aligned}$$

where (i) the inner P_0 which has been written down explicitly represents the S^0 nearest to the right end of the expression in (8), (ii) the factor Q_0/a^{l_i} which has been written down explicitly is the factor S^{l_i} nearest to the right end for which $l_i > 1$. Because of (A.7) all the l values contained in O_6 are unity.

Now, let us lift out the numerical factor $\langle 0|O_6|0\rangle$ and replace it between O_4 and O_5 thus:

$$\begin{aligned} w' &= -O_4 \frac{Q_0}{a^{l_i-1}} \langle 0|O_6|0\rangle \frac{Q_0}{a} O_5 |0\rangle \langle 0| \\ &= -S^{(n)}_n H' S^{(i+1)}_{n-1} \dots H' \frac{Q_0}{a^{l_i-1}} \left\langle \frac{(i)}{H'} \frac{Q_0}{a} H' \dots \frac{(i-m+1)}{H'} \right\rangle \frac{Q_0}{a} \frac{(i-m)}{H'} \dots \frac{(1)}{H'} P_0. \\ &\dots\dots(A.9) \end{aligned}$$

Comparing this with the original expression in (A.8), the changes can be described as follows:

- (i) In the chain of operators, from the factor Q_0/a^{l_i} which, having $l_i > 1$, lies nearest to the right end, one factor Q_0/a has been extracted and has been shifted rightwards to replace a S^0 factor, and the remaining S^0 factors right of H' (if any) have been interchanged with some Q_0/a factors.
- (ii) A bracket of the type prescribed in Rule 3 has been inserted to the right of H' .
- (iii) The expression has been multiplied by (-1) .

The process is now to be repeated successively, first lifting out everything to the right of the S^0 factor nearest to the right end (again because of (A.7) this section always contains only a string of Q_0/a factors to first power) and setting it down leftwards inside the first factor Q_0/a^{l_i} from the right end which has $l_i > 1$. This eventually results in the disappearance of all S^{l_i} factors with $l_i \neq 1$, and indeed we get an expression of the type prescribed by Rule 3, which we denote w :

$$w \equiv w'. \quad \dots\dots(A.10)$$

We have now proved that every expression v in Rule 3 equals a term v' in Bloch's (8), and conversely every expression w' in (8) equals a term w in Rule 3. Furthermore, if we follow the first procedure for converting v into v' , and then the second procedure for converting v' back into a Rule 3 type expression, it can be seen that the result obtained is the original v . This is because the second procedure, starting from v' , just reverses step by step the first process which ended in v' . This result finally establishes a 1 : 1 identity between all the individual expressions in Rule 3 and all the terms in (8), so that they both yield the same sum $U^{(n)}$.

REFERENCES

- BLOCH, C., 1958, *Nuclear Phys.*, **6**, 329.
 BRUECKNER, K. A., 1955, *Phys. Rev.*, **100**, 36.
 GOLDSTONE, J., 1957, *Proc. Roy. Soc. A*, **239**, 267.
 MESSIAH, A., 1960, *Mécanique Quantique*, **2**, 615 (Paris: Dunod).

H_2^+ : A Problem in Perturbation Theory

By P. D. ROBINSON

Mathematical Institute, Oxford

*Communicated by C. A. Coulson; MS. received 27th February 1961,
in revised form 17th April 1961*

Abstract. A résumé is given of how accurately perturbation theory (using a ground-state hydrogen-like atom perturbed by a point charge) predicts the $1s\sigma$ and $2p\sigma$ energies of H_2^+ and HeH^{2+} . Corresponding delta-function models are discussed; here it is possible to test the convergence of the perturbation expansions. The models indicate that the series for the $1s\sigma$ energy is divergent for H_2^+ at large values of the internuclear separation R but convergent for HeH^{2+} ; this explains why the H_2^+ series is inaccurate and the HeH^{2+} series accurate. Both series converge for small R . The $2p\sigma$ energies are represented by divergent series which are asymptotically convergent if R is sufficiently large. A 'resonance' correction is justified for the H_2^+ series, giving an accurate $1s\sigma$ energy for all R and an improved $2p\sigma$ energy.

§ 1. INTRODUCTION

EXACT electronic energies of H_2^+ have been found numerically for given values of the internuclear separation R (Bates, Ledsham and Stewart 1953), but it is desirable to express these energies directly as functions of R . An obvious approach is to use a perturbation method and regard the ion as a hydrogen atom perturbed by a proton, but the resulting energies are not accurate even at quite large values of R (Dalgarno and Lewis 1956). This is in contrast to the situation with the heteronuclear ion HeH^{2+} where accurate energies can be obtained using similar techniques, and so H_2^+ poses a problem in perturbation theory.

A physical reason for the poor results with H_2^+ is the so-called 'resonance' degeneracy in the limit of infinite R . To take the simplest case, both the ground state ($1s\sigma$) and the first excited state ($2p\sigma$) of H_2^+ have each to be represented for large R by a $1s$ hydrogen atom perturbed by a proton; the resulting iterated energy cannot be a good approximation to two different exact energies simultaneously, and so the method must be inaccurate for one or both of the states. With HeH^{2+} the nuclei have different charges, and the $1s\sigma$ and $2p\sigma$ energies are represented by two different perturbation expansions.

The central part of this paper is devoted to a mathematical investigation of the conventional perturbation theory approach with the help of a one-dimensional delta-function model for H_2^+ introduced by Frost (1956). Here a transcendental equation for the exact energies is used as a yardstick to test the convergence of corresponding perturbation results. It is, unfortunately, necessary to employ some kind of simplified model, because formulae giving exact energies as functions of R are not available for H_2^+ itself. The reasons for the shortcomings of perturbation theory in the case of Frost's model should be similar to those for the actual ion.

Firstly, however, we give a résumé of the perturbation treatment for the $1s\sigma$ and $2p\sigma$ states of both H_2^+ and HeH^{2+} , and the paper is completed by the justification of a simple 'resonance' correction to the H_2^+ perturbation series. This yields accurate formulae for the $1s\sigma$ energy at all R values and for the $2p\sigma$ energy when R is greater than $4a_0$.

§ 2. PERTURBATION TREATMENT FOR THE $1s\sigma$ AND $2p\sigma$ STATES

The electronic energy of a hydrogen-like atom of nuclear charge Z in its ground state perturbed by a point charge q situated at a distance R away from the nucleus can be formally written

$$E = E_0 + qE_1 + q^2E_2 + O(q^3). \quad \dots\dots(1)$$

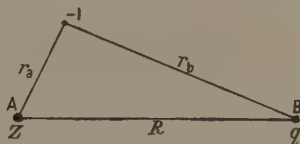


Fig. 1

Here $E_0 = -\frac{1}{2}Z^2$ in ordinary atomic units. Using conventional perturbation theory with $-q/r_b$ as the perturbation to the Hamiltonian (see Fig. 1), it can be shown (Dalgarno and Lynn 1957, Robinson 1958) that if we write

$$t = ZR$$

then

$$E_1 = Z \left[-\frac{1}{t} + \left(1 + \frac{1}{t}\right) e^{-2t} \right],$$

and

$$\begin{aligned} E_2 = & \frac{5}{2t^2} + \left(1 - \frac{1}{t}\right)^2 e^{2t} \text{Ei}^*(2t) - \left(1 + \frac{1}{t}\right)^2 e^{-2t} \text{Ei}(2t) \\ & + \left[1 + \frac{2}{t} - \frac{3}{t^2} + \frac{4}{t} \left(1 + \frac{1}{t}\right) e^{-2t} \right] \text{Ei}^*(2t) \\ & + \left[2 \left(1 + \frac{1}{t}\right)^2 (K + \ln 2t) - 2 - \frac{4}{t} - \frac{5}{t^2} - \left(1 + \frac{1}{t}\right)^2 e^{-2t} \text{Ei}(2t) \right] e^{-2t} \\ & + \left[2 \left(1 + \frac{1}{t}\right)^2 (K + \ln 2t) + 2t + \frac{7}{2} + \frac{4}{t} + \frac{5}{2t^2} \right] e^{-4t}, \end{aligned}$$

K being Euler's constant. It is possible in principle to evaluate further terms in the series (1), but the labour involved in finding even E_3 would be very considerable; good approximations are available for these higher orders (Dalgarno and Lewis 1956, Dalgarno and Stewart 1956b).

In Table 1, the expression $E_0 + qE_1 + q^2E_2$ with $Z=2$ and $q=1$ is compared with the exact $1s\sigma$ energy of HeH^{2+} at different values of R , and the same expression with $Z=1$ and $q=2$ is compared with the exact $2p\sigma$ energy. These exact values were computed by Bates and Carson (1956). It seems likely from the table that the $1s\sigma$ perturbation series converges to the true $1s\sigma$ energy for all values of R . It has been shown by Dalgarno (1956) that the first three terms

of the series do give the true result in the limit of zero R ; this can be verified by considering the limiting values of E_1 and E_2 . We also see from the table that the $2p\sigma$ series is probably asymptotically convergent to the true $2p\sigma$ energy for sufficiently large R .

Table 1. Comparison of Electronic Energies for HeH^{2+}

$R(a_0)$	0	1	2	3	4	5
1s state						
Exact	-4.5	-3.033 35	-2.512 19	-2.335 49	-2.250 60	-2.200 23
Perturbed, $Z=2, q=1$	-4.5	-3.015 30	-2.508 93	-2.335 25	-2.250 58	-2.200 23
Pert. + $\Delta_+\dagger$		-3.018 97	-2.512 02	-2.335 58	-2.250 61	-2.200 23
2pσ state						
Exact	-1.125	-1.338 34	-1.345 18	-1.178 83	-1.031 08	-0.922 54
Perturbed, $Z=1, q=2$	-4.5	-2.755 82	-1.726 13	-1.262 83	-1.038 25	-0.916 26
Pert. + $\Delta_-\dagger$		-1.968 35	-1.546 58	-1.229 11	-1.032 56	-0.915 37

Table 2. Comparison of Electronic Energies for H_2^+

$R(a_0)$	0	1	2	3	4	5
1s state						
Exact	-2.0	-1.451 78	-1.102 62	-0.910 89	-0.796 08	-0.724 42
Pert. + $\Delta_+\dagger$	-2.0	-1.487 66	-1.123 73	-0.918 11	-0.796 63	-0.723 30
Perturbed, $Z=q=1$	-2.0	-1.428 62	-1.042 80	-0.855 72	-0.759 35	-0.704 04
Pert. + $\Delta_-\dagger$	0	-0.653 87	-0.732 34	-0.726 60	-0.704 66	-0.680 66
2pσ state						
Exact	-0.5	-0.564 81	-0.667 53	-0.701 42	-0.695 55	-0.677 29

All energies are expressed in atomic units.

\dagger See § 5.

The results for H_2^+ are displayed in Table 2. This time there is only one 'perturbed' energy, i.e. $E_0 + qE_1 + q^2E_2$ with $Z=q=1$. For large R , this is a good approximation to the *mean* of the $1s\sigma$ and $2p\sigma$ energies (cf. Dalgarno and Lewis 1956), and for small R it again seems likely that the perturbation series converges to the exact $1s\sigma$ energy. It is possible that this also occurs for large R , but if so then the convergence will be slow and many more terms than three in the series (1) will be needed. Dalgarno and Lewis included E_3 and E_4 (in approximate form) without apparent improvement.

If a perturbation expression for the $2p\sigma$ energy is required which is valid for small R , then an unperturbed hydrogenic wave function must be used which

tends to the appropriate 2p function as R tends to zero. We shall not discuss such a problem here as we are primarily concerned with behaviour at large R values.

§ 3. FROST'S DELTA FUNCTION MODELS

(a) *Hydrogen-like atom.* This one-dimensional model of the atom consists of an electron moving along the x axis with a potential of $-\lambda\delta(x)$ replacing the true $-Z/|x|$, $\delta(x)$ being the usual delta-function. This potential is the limiting case of a square well potential centred on the origin, of depth U and width a , as U tends to infinity and a tends to zero whilst the product

$$aU = \lambda$$

is kept constant (see Fig. 2). We call the quantity λ the *strength* of the well, although such a term is sometimes used to mean a^2U . The model has just one bound state with energy

$$E = -\frac{1}{2}\lambda^2, \quad \dots\dots (2)$$

and normalized wave function

$$\psi = \lambda^{1/2} \exp(-\lambda|x|);$$

it is thus analogous to the ground state of the hydrogen-like atom if λ is replaced by Z .

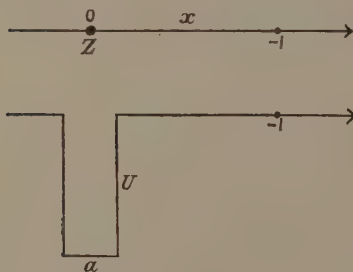


Fig. 2

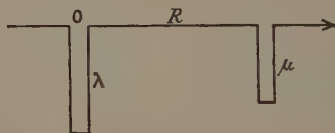


Fig. 3

(b) *Diatomic ion.* The single-nucleus model is extended to represent H_2^+ or HeH^+ by having two delta-function potential wells of strengths λ and μ , the λ well being situated at $x=0$ and the μ well at $x=R$ (see Fig. 3). Two bound state wave functions exist, and are of the form

$$\psi = A \exp(-\gamma|x|) + B \exp(-\gamma|x-R|)$$

where the two possible values for γ are roots of the equation

$$\gamma^2 - (\lambda + \mu)\gamma + \lambda\mu[1 - \exp(-2\gamma R)] = 0. \quad \dots\dots (3)$$

A and B are specified in terms of γ and R , and the energy eigenvalues are given by

$$E = -\frac{1}{2}\gamma^2 \quad \dots\dots (4)$$

in each case.

We denote the two possibilities for γ by γ_1 and γ_2 , where, from (3), γ_1 is the (positive) root of

$$2\gamma_1 = \lambda + \mu + [(\lambda - \mu)^2 + 4\lambda\mu \exp(-2\gamma_1 R)]^{1/2}, \quad \dots\dots (5)$$

and γ_2 is the non-zero root of the similar equation

$$2\gamma_2 = \lambda + \mu - [(\lambda - \mu)^2 + 4\lambda\mu \exp(-2\gamma_2 R)]^{1/2}. \quad \dots\dots (6)$$

We shall suppose, without loss of generality, that $\lambda \geq \mu$. It is clear that γ_1 is the greater value for γ , and thus from (4) yields the ground state of the system. The limiting values of γ_1 as R tends to infinity or to zero are, from (5), respectively λ and $\lambda + \mu$; Eqns (2) and (4) therefore indicate that for large or small R values the ground-state energy approximates to that of a single-well system with strength λ or $\lambda + \mu$ accordingly. This situation is an exact analogue of what happens with the $1s\sigma$ state of the diatomic ion, with the nuclear charges Z and q replaced by delta-function wells λ and μ , and with the limiting cases of ground-state hydrogen-like atoms replaced by single-well systems.

γ_2 gives the only bound excited state of the system. This state can be compared with the first excited state ($2p\sigma$) of the diatomic ion. The behaviour is analogous for large R when γ_2 approximates to μ , showing that the electron is concentrated round the μ well; with the ion the electron is concentrated round the charge q . But the analogy breaks down at small values of R . γ_2 decreases to zero as R decreases to $(\lambda + \mu)/4\lambda\mu$, and is negative when R is less than this value, showing that the model has then only one bound state. However, the model can still be used for testing perturbation theory at large R values.

In §§ 3.1 and 3.2 we give certain series expansions for γ_1 and γ_2 , and in § 3.3 we see to what extent the corresponding energies found from them agree with energies derived from perturbation theory. The case of equal wells is considered in § 3.4.

3.1. *Ground State ('1s'); $\lambda > \mu$*

In order to test the perturbation theory we need an expansion for γ_1 in powers of μ . We see from (5) that γ_1 tends to λ as μ tends to zero, and it can in fact be proved (see Appendix A) that

$$\gamma_1 = \lambda + \mu a_1(\lambda) + \mu^2 a_2(\lambda) + \dots + \mu^n a_n(\lambda) + \dots, \quad \dots\dots (7)$$

where

$$a_n(\lambda) = \frac{\lambda^n}{n!} \left[\frac{d^{n-1}}{d\gamma^{n-1}} \left\{ \frac{1}{\lambda} + \frac{e^{-2\gamma R} - 1}{\gamma} \right\}^n \right]_{\gamma=\lambda} = \sum_{s=0}^n \frac{\lambda^s}{s!(n-s)!} \frac{d^{n-1}}{d\lambda^{n-1}} \left\{ \frac{e^{-2\lambda R} - 1}{\lambda} \right\}^s.$$

The first three coefficients are:

$$a_1(\lambda) = e^{-2\lambda R},$$

$$a_2(\lambda) = [1 - (2\lambda R + 1)e^{-2\lambda R}] \frac{e^{-2\lambda R}}{\lambda},$$

$$a_3(\lambda) = [1 - (4\lambda R + 3)e^{-2\lambda R} + 2(3\lambda^2 R^2 + 3\lambda R + 1)e^{-4\lambda R}] \frac{e^{-2\lambda R}}{\lambda^2}.$$

The radius of convergence ρ of the series (7) is discussed in Appendix A. It is not possible to find ρ explicitly as a function of R , but a partly qualitative graph is shown in Fig. 4. The series converges whenever μ is less than ρ , i.e. under the following circumstances: (a) if $\mu < \nu$, for all values of R ; (b) if $\nu < \mu < \lambda$, for R sufficiently small or sufficiently large, but not in the intermediate region; (c) if $\mu \geq \lambda$, only for R sufficiently small. Thus when

$\lambda > \mu$, (7) will converge for all values of R save possibly for those in some intermediate region. The crucial difference between the cases $\lambda > \mu$ and $\lambda = \mu$ is that in the latter case the series (7) can *never* be convergent for large values of R .

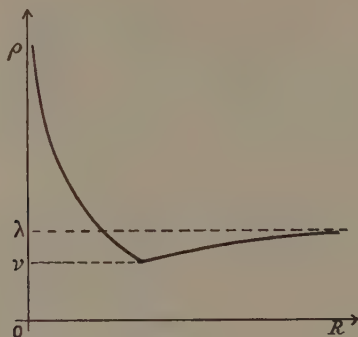


Fig. 4

There is an alternative series expansion for γ_1 in powers of $\exp(-2\lambda R)$ which is valid for large R . Since γ_1 tends to λ as R tends to infinity, (5) gives, by iteration:

$$\gamma_1 = \lambda + \left(\frac{\lambda\mu}{\lambda - \mu} \right) e^{-2\lambda R} - \left[2R + \frac{1}{\lambda - \mu} \right] \left(\frac{\lambda\mu}{\lambda - \mu} \right)^2 e^{-4\lambda R} + 2 \left[3R^2 + \frac{3R}{\lambda - \mu} + \frac{1}{(\lambda - \mu)^2} \right] \left(\frac{\lambda\mu}{\lambda - \mu} \right)^3 e^{-6\lambda R} + O(e^{-8\lambda R}). \quad \dots (8)$$

It is interesting to compare expansions (7) and (8). If (8) is expanded further in ascending powers of μ (permissible since $\mu < \lambda$), then it coincides exactly with (7), correct to order μ^4 .

3.2. Excited State ('2pσ'); $\lambda > \mu$

There is no valid convergent expansion for γ_2 in ascending powers of λ which would correspond to series (7) for γ_1 . We cannot let λ tend to zero in (6), because $\lambda > \mu$. There is, however, an analogue of (8) which will be valid for large R . Since γ_2 tends to μ as R tends to infinity, (6) gives:

$$\gamma_2 = \mu - \left(\frac{\lambda\mu}{\lambda - \mu} \right) e^{-2\mu R} - \left[2R - \frac{1}{\lambda - \mu} \right] \left(\frac{\lambda\mu}{\lambda - \mu} \right)^2 e^{-4\mu R} - 2 \left[3R^2 - \frac{3R}{\lambda - \mu} + \frac{1}{(\lambda - \mu)^2} \right] \left(\frac{\lambda\mu}{\lambda - \mu} \right)^3 e^{-6\mu R} + O(e^{-8\mu R}). \quad \dots (9)$$

(9) is the same as (8) with λ and μ interchanged.

The formal expression

$$\gamma_2 = \mu + \lambda a_1(\mu) + \lambda^2 a_2(\mu) + \lambda^3 a_3(\mu) + O(\lambda^4, e^{-6\mu R}) \quad \dots (10)$$

can be obtained by dividing out the coefficients of the powers of $e^{-2\mu R}$ in (9), but this can never give a convergent series since $\lambda > \mu$. All that can be said for it is that a finite number of its terms give the correct value μ for γ_2 in the limit of infinite R .

3.3. *Perturbation Treatment*

We now treat the two-well model as a single well of strength λ situated at $x=0$ perturbed by a second well of strength μ at $x=R$ (see Fig. 3), and develop an expression for the energy in the form

$$E = E_0 + \mu E_1 + \mu^2 E_2 + \mu^3 E_3 + O(\mu^4). \quad \dots\dots(11)$$

The unperturbed energy and wave function are those of the single-well model, i.e.

$$E_0 = -\frac{1}{2}\lambda^2 \quad \text{and} \quad \psi = \lambda^{1/2} e^{-\lambda|x|},$$

and the perturbation to the Hamiltonian is $-\mu\delta(x-R)$. The first-order correction to the energy is therefore

$$E_1 = - \int_{-\infty}^{\infty} \psi \delta(x-R) \psi dx = -\lambda e^{-2\lambda R}.$$

The sum-rule technique of Dalgarno and Lewis (1955, see also Dalgarno and Stewart 1956a) is employed to evaluate E_2 and E_3 ; details are given in Appendix B. The results are:

$$E_2 = -[1 - (2\lambda R + \frac{1}{2})e^{-2\lambda R}]e^{-2\lambda R},$$

$$E_3 = -[1 - 2(2\lambda R + 1)e^{-2\lambda R} + (6\lambda^2 R^2 + 4\lambda R + 1)e^{-4\lambda R}] \frac{e^{-2\lambda R}}{\lambda}.$$

Substituting these expressions in (11), we have

$$\begin{aligned} E = & -\frac{1}{2}\lambda^2 \left[1 + 2\frac{\mu}{\lambda} e^{-2\lambda R} + 2\left(\frac{\mu}{\lambda}\right)^2 \{1 - (2\lambda R + \frac{1}{2})e^{-2\lambda R}\}e^{-2\lambda R} \right. \\ & \left. + 2\left(\frac{\mu}{\lambda}\right)^3 \{1 - 2(2\lambda R + 1)e^{-2\lambda R} + (6\lambda^2 R^2 + 4\lambda R + 1)e^{-4\lambda R}\}e^{-2\lambda R} + O(\mu^4) \right]. \end{aligned}$$

.....(12)

It can be verified that if series (7) for γ_1 is substituted in $E = -\frac{1}{2}\gamma^2$, then the resulting formula for the energy is identical with (12), to order μ^4 . Thus, on the evidence of the first four terms in the perturbation expansion, the ground-state energy of the two-well model is accurately represented by perturbation theory provided that μ is less than ρ , so that series (7), and therefore also series (11), is convergent.

If the two-well model is regarded as a well of strength μ perturbed by a larger well of strength λ , expression (12) will be obtained with λ and μ interchanged. So the energy predicted for the excited state by perturbation theory will be that derivable from (10); it will only be a poor asymptotic approximation to the true energy for large R , and will be meaningless for small R .

3.4. *The Case of Equal Wells: $\lambda = \mu$*

Here there is just the one perturbation series which has to represent both the '1s σ ' and the '2p σ ' energies, i.e. expression (12) with μ set equal to λ . But in this case series (7) can never be convergent for large R , as we saw in §3.1, and so (12) will not converge for large R either. It is merely a poor asymptotic approximation to both energies. When R is sufficiently small, however, (12) does converge to the true '1s σ ' energy.

With equal wells, Eqns (5) and (6) defining γ_1 and γ_2 degenerate into

$$\gamma/\lambda = 1 \pm e^{-\gamma R},$$

giving the following approximate solutions for large R :

$$\gamma_1/\lambda = 1 + e^{-\lambda R} - \lambda R e^{-2\lambda R} + \frac{3}{2}\lambda^2 R^2 e^{-3\lambda R} \dots, \quad \dots (13)$$

$$\gamma_2/\lambda = 1 - e^{-\lambda R} - \lambda R e^{-2\lambda R} - \frac{3}{2}\lambda^2 R^2 e^{-3\lambda R} \dots \quad \dots (14)$$

(13) and (14) replace (8) and (9), which are no longer valid when $\lambda = \mu$. Unlike (8) and (9), they contain odd powers of $\exp(-\lambda R)$, providing further evidence that series (7), which does not contain such powers, cannot be an accurate representation of γ_1 for large R .

§ 4. RESULTS AND DISCUSSION

If it is permissible to carry over the results derived from the delta-function model to the genuine physical problem, then we can make the following assertions:

HeH^{2+} . In the 1σ state the energy is represented by a perturbation series with $Z=2$ and $q=1$ (cf. $\lambda=2$, $\mu=1$) which is convergent either for all values of R , or possibly for all values of R except those in some 'intermediate' region. For the $2p\sigma$ state, the perturbation series with $Z=1$ and $q=2$ (cf. $\lambda=1$, $\mu=2$) is divergent at any fixed value of R but is asymptotically convergent for sufficiently large R . It can be said to represent the $2p\sigma$ energy only for such values of R . (The asymptotic convergence would seem to be better for HeH^{2+} itself than for the model. Perhaps this is because the contribution to the energy which is *not* exponentially decreasing is less trivial than with the model.)

H_2^+ . The single perturbation series with $Z=q=1$ (cf. $\lambda=\mu=1$) merely converges to the 1σ energy for small values of R . The series is divergent for large R , but it is asymptotically convergent to both the 1σ and the $2p\sigma$ energies.

The question remains as to whether it is possible to 'improve' the perturbation series for H_2^+ . A recent attempt at this has been made by Dalgarno and Lynn (1956). For the ground state they start with the 'best' LCAO wave function

$$\psi_1(\mathbf{r}_a) + \psi_1(\mathbf{r}_b),$$

and improve it with the set of functions

$$\psi_n(\mathbf{r}_a) + \psi_n(\mathbf{r}_b)$$

as a basis for the perturbation expansion, ψ_n being the n th hydrogenic wave function. However their approximations lead to an energy which is not accurate as R tends to zero. In § 5 we attempt to justify a simpler, more accurate formula, which merely adds a 'resonance' term on to the first three terms of the perturbation series (1).

§ 5. A 'RESONANCE' CORRECTION

5.1. A Modified Perturbation Expansion

The primary aim is to find a good approximation to the energy of the 1σ state of H_2^+ for large R . Following Dalgarno and Lynn, and writing

$$A_n = \psi_n(\mathbf{r}_a), \quad B_n = \psi_n(\mathbf{r}_b)$$

(both functions being assumed normalized), we set

$$\psi = A_1 + B_1 + \sum_{n \neq 1} c_n (A_n + B_n)$$

in the wave equation

$$H\psi = E\psi. \quad \dots\dots(15)$$

The Hamiltonian is (see Fig. 1 with $Z=q=1$)

$$H = -\frac{1}{2}\nabla^2 - \frac{1}{r_a} - \frac{1}{r_b} = H^A - \frac{1}{r_b},$$

and as R tends to infinity then

$$E \rightarrow E_0^A;$$

H^A and E_0^A are the Hamiltonian and ground-state energy for an isolated hydrogen atom with nucleus at A . We suppose the coefficients c_n to be small, since c_n tends to zero as R tends to infinity.

If (15) is premultiplied by A_1^* and integrated, and the products of c_n with exponentially decreasing integrals are neglected, it is found that

$$(E - E_0^A)(1 + \langle A_1 | B_1 \rangle) = \left\langle A_1 \left| -\frac{1}{r_b} \right| A_1 \right\rangle + \left\langle A_1 \left| -\frac{1}{r_b} \right| B_1 \right\rangle + \sum_{n \neq 1} c_n \left\langle A_1 \left| -\frac{1}{r_b} \right| A_n \right\rangle. \quad \dots\dots(16)$$

(Here $\langle A_1 | B_1 \rangle$ means $\int A_1^* B_1 d\tau$, $\langle A_1 | -1/r_b | A_n \rangle$ means $\int A_1^* (-1/r_b) A_n d\tau$, etc.) Similarly, if we first premultiply (15) by A_m^* , we obtain

$$c_m = \frac{1}{E - \mathcal{E}_m} \left\langle A_m \left| -\frac{1}{r_b} \right| A_1 + \sum_{n \neq 1} c_n A_n \right\rangle + O(e^{-R}),$$

\mathcal{E}_m being the energy of the hydrogenic function ψ_m . For large R , it follows that

$$c_m \simeq \frac{1}{\mathcal{E}_1 - \mathcal{E}_m} \left\langle A_m \left| -\frac{1}{r_b} \right| A_1 \right\rangle, \quad \dots\dots(17)$$

since E tends to \mathcal{E}_1 ($\equiv E_0^A$) and c_n tends to zero as R tends to infinity.

Substitution of (17) into the last term of (16) gives precisely the second-order perturbation energy E_2^A . Also the first term on the right-hand side of (16) is the first-order energy E_1^A , and so we finally obtain

$$E = E_0^A + \left(E_1^A + E_2^A + \left\langle A_1 \left| -\frac{1}{r_b} \right| B_1 \right\rangle \right) (1 + \langle A_1 | B_1 \rangle)^{-1}. \quad \dots\dots(18)$$

5.2. The 'Resonance' Term

E can be expressed more concisely in terms of a 'resonance' correction, Δ_+ , defined by

$$\Delta_+ = \frac{\langle A_1 + B_1 | H | A_1 + B_1 \rangle}{\langle A_1 + B_1 | A_1 + B_1 \rangle} - \langle A_1 | H | A_1 \rangle.$$

This quantity is the difference in energy caused by having $A_1 + B_1$ rather than A_1 as wave function. Δ_+ simplifies to

$$\{(1 + \langle A_1 | B_1 \rangle)^{-1} - 1\} E_1^A + \left\langle A_1 \left| -\frac{1}{r_b} \right| B_1 \right\rangle (1 + \langle A_1 | B_1 \rangle)^{-1},$$

and using this in (18) we get

$$E = E_0^A + E_1^A + E_2^A (1 + \langle A_1 | B_1 \rangle)^{-1} + \Delta_+. \quad \dots\dots(19)$$

Expression (19) has been derived on the assumption that R is large; the overlap integral $\langle A_1 | B_1 \rangle$ is exponentially decreasing, and so the difference between (19) and

$$E = E_0^A + E_1^A + E_2^A + \Delta_+ \quad \dots\dots (20)$$

will not be very great for large R . (20) has the advantage over (19) in that it correctly represents the $1s\sigma$ energy as R tends to zero, for Δ_+ then also tends to zero. The explicit form of Δ_+ is

$$- \frac{(-1/R + 2R/3)e^{-R} + (1 + 1/R)(1 + R + R^2/3)e^{-3R}}{1 + (1 + R + R^2/3)e^{-R}};$$

it supplies some odd powers of e^{-R} which are lacking in the perturbation series. There was similar trouble with the delta-function model, as we saw in §3.4. Values of (20) are given in Table 2, showing how accurately it represents the $1s\sigma$ energy for all values of R .

The $2p\sigma$ energy of H_2^+ is also quite well represented for large R by

$$E_0^A + E_1^A + E_2^A + \Delta_- \quad \dots\dots (21)$$

where Δ_- is defined as

$$\frac{\langle A_1 - B_1 | H | A_1 - B_1 \rangle}{\langle A_1 - B_1 | A_1 - B_1 \rangle} - \langle A_1 | H | A_1 \rangle,$$

$A_1 - B_1$ being the best LCAO wave function for this state. Values of (21) are also shown in Table 2.

We have expressed the formulae in this section in terms of energies referred to nucleus 'A'. This is purely arbitrary; 'A' and 'B' could be interchanged throughout.

5.3. Resonance in the Heteronuclear Case

It can be shown that the resonance corrections are less significant if the nuclear charges are different. Reverting to Fig. 1 with a charge Z at A and q ($< Z$) at B, the hydrogenic ground-state functions are

$$A_1 = \left(\frac{Z^3}{\pi}\right)^{1/2} \exp(-Zr_a) \quad \text{and} \quad B_1 = \left(\frac{q^3}{\pi}\right)^{1/2} \exp(-qr_b);$$

the best LCAO function is of the form

$$\psi = A_1 + \theta(Z, q, R)B_1,$$

θ being found by minimizing the resulting energy. There are two values for θ , θ_+ (approximating to the $1s\sigma$ state), and θ_- (to the $2p\sigma$ state). The corresponding resonance corrections turn out to be of magnitude

$$\Delta_+ = O(q^4), \quad \Delta_- = O(q^3),$$

if q is sufficiently small. Thus they should not appreciably affect the energy given by (1), where q^3 terms are already neglected. They are calculated for HeH^{2+} , and the difference they make to the perturbed energies is shown in Table 1.

Finally we remark that, as R tends to infinity, θ_+ tends to zero and θ_- tends to infinity provided $Z \neq q$, but $\theta_+ = 1$, $\theta_- = -1$ for all R if $Z = q$. Also if $Z = 1$ and $q = 1 - \epsilon$ where ϵ is small, it can be proved that

$$\theta_{\pm} = \pm 1 - \frac{3\epsilon}{2} \left(\frac{R-1}{2R^2-3} \right) e^R + O(\epsilon^2),$$

showing that, for large R , θ_{\pm} approach their H_2^+ values quite sharply as q gets close to 1. This indicates that the significance of the resonance correction increases markedly as the H_2^+ case is reached.

APPENDIX A

The Series for γ_1 in Powers of μ

Equation (3) can be written

$$\gamma = \lambda + \mu f(\gamma),$$

where

$$f(\gamma) = 1 + [e^{-2\gamma R} - 1] \frac{\lambda}{\gamma},$$

and hence a series in powers of μ can be developed for the root of (3) which tends to λ as μ tends to zero, i.e. for γ_1 . There is in fact a Lagrange's expansion for γ_1 (see, for example, Goursat 1916) of the form (7), where

$$a_1(\lambda) = f(\lambda) \quad \text{and} \quad a_n(\lambda) = \frac{1}{n!} \left[\frac{d^{n-1}}{d\gamma^{n-1}} \{f(\gamma)\}^n \right]_{\gamma=\lambda}.$$

Following Goursat, if $M(r)$ is the greatest value of the function $|f(z)|$ on the circle $|z - \lambda| = r$ in the complex plane, then the radius of convergence ρ of the series (7) is in turn given by the greatest value of the function

$$y(r) = r/M(r), \quad 0 \leq r \leq \infty.$$

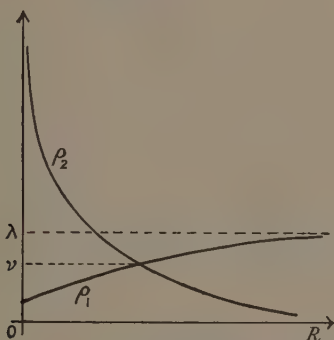


Fig. 5

In our case we obtain

$$y(r) = \frac{r|\lambda - r|}{r + \lambda e^{-2R(\lambda - r)}}.$$

$y(r)$ is never negative, but vanishes when $r=0$, λ and ∞ . It is a continuous function of r with two 'maximum' values, denoted by ρ_1 in the range $0 \leq r \leq \lambda$ and ρ_2 in the range $\lambda \leq r \leq \infty$. ρ itself is the greater of ρ_1 and ρ_2 . It is impossible to find ρ_1 and ρ_2 directly, but analysis shows that:

(i) ρ_1 behaves like $(3 - 2\sqrt{2})\lambda\{1 + 2R\lambda(\sqrt{2} - 1)\}$ for small R , and like $\lambda[1 - 2e^{-\lambda R}]$ for large R ;

(ii) ρ_1 is less than λ for all finite R ;

(iii) ρ_2 behaves like $(1/2R)\ln(1/2R\lambda)$ for small R , and like $0.14/R$ for large R .

We thus arrive at the partly qualitative graphs of ρ_1 and ρ_2 as functions of R shown in Fig. 5, and hence also of ρ , in Fig. 4.

APPENDIX B

The Second- and Third-order Energy Corrections in § 3.3

If μV is the perturbation to the Hamiltonian (here $V = -\delta(x-R)$), and $F(x)$ is a physically acceptable solution of

$$\frac{d^2 F}{dx^2} + 2 \frac{dF}{dx} \frac{d}{dx} (\ln \psi) = V - E_1,$$

then Dalgarno *et al.* showed that the second- and third-order energy corrections are

$$E_2 = 2(\langle \psi | VF | \psi \rangle - E_1 \langle \psi | F | \psi \rangle),$$

$$E_3 = 4(\langle \psi | VF^2 | \psi \rangle - E_1 \langle \psi | F^2 | \psi \rangle - E_2 \langle \psi | F | \psi \rangle).$$

Solving the differential equation for $F(x)$ and applying the necessary finiteness conditions to ψF at $x = \pm \infty$, it is found that

$$F(x) = (C_1 - x) \frac{E_1}{2\lambda} \text{ when } -\infty \leq x < 0;$$

$$F(x) = \left(C_2 + x - \frac{e^{2\lambda x}}{\lambda} \right) \frac{E_1}{2\lambda} \text{ when } 0 < x < R,$$

and

$$F(x) = (C_3 + x) \frac{E_1}{2\lambda} \text{ when } R < x \leq \infty.$$

For continuity at $x=0$ and $x=R$ the constants C_1 , C_2 and C_3 must satisfy the relations

$$C_1 = C_2 - \frac{1}{\lambda} \quad \text{and} \quad C_3 = C_2 - \frac{e^{2\lambda R}}{\lambda};$$

hence just one of the constants is arbitrary. The integrals required for E_2 and E_3 are elementary, and the arbitrary constant cancels out when the results are combined.

ACKNOWLEDGMENTS

I am grateful to Dr. J. T. Lewis and Mr. P. J. Bushell for useful discussions, and to Professor C. A. Coulson for his helpful comments on the manuscript.

REFERENCES

- BATES, D. R., and CARSON, T. R., 1956, *Proc. Roy. Soc. A*, **234**, 207.
 BATES, D. R., LEDSHAM, K., and STEWART, A. L., 1953, *Phil. Trans. A*, **246**, 215.
 DALGARNO, A., 1956, *Proc. Phys. Soc. A*, **69**, 784.
 DALGARNO, A., and LEWIS, J. T., 1955, *Proc. Roy. Soc. A*, **233**, 70.
 ——— 1956, *Proc. Phys. Soc. A*, **69**, 57.
 DALGARNO, A., and LYNN, N., 1956, *Proc. Phys. Soc. A*, **69**, 821.
 ——— 1957, *Proc. Phys. Soc. A*, **70**, 223.
 DALGARNO, A., and STEWART, A. L., 1956 a, *Proc. Roy. Soc. A*, **238**, 269.
 ——— 1956 b, *Proc. Roy. Soc. A*, **238**, 276.
 FROST, A. A., 1956, *J. Chem. Phys.*, **25**, 1150.
 GOURSAT, E., 1916, *A Course in Mathematical Analysis*, Vol. II, Part 1, translated from the French by E. R. HEDRICK and O. DUNKEL (New York: Ginn).
 ROBINSON, P. D., 1958, *Proc. Phys. Soc.*, **71**, 828.

Partial Wave Theory of Positron-Hydrogen Atom Collisions†

BY K. SMITH

Argonne National Laboratory, Argonne, Illinois

MS. received 17th April 1961

Abstract. This paper is concerned with the derivation of the radial equations for positron-hydrogen atom collisions from the continuous state Hartree-Fock equations. The angular coefficients are expressed in terms of vector addition coefficients and Racah coefficients for any angular momentum state of the atomic systems: positronium and atomic hydrogen.

The boundary conditions are written in terms of the S -matrix and expressions are obtained for total and differential cross sections.

§ 1. INTRODUCTION

THE scattering of slow positrons by atomic hydrogen is of interest in connection with the development of approximate methods for the treatment of collision problems. Furthermore, the recent developments of experimental technique associated with the study of positronium formation (Marder *et al.* 1956) focuses additional interest on the fate of a stream of positrons in a gas.

The variational calculations of Moussa (1959) and Spruch and Rosenberg (1960) show that at energies below 5 eV virtual positronium formation has an important effect on the elastic scattering cross section. In particular, Spruch and Rosenberg (1960) found that the positrons are *attracted* to the atom, in contradiction to those calculations which neglect positronium formation (Smith and Burke 1961).

The purpose of this paper is to present a concise formulation of the positron-hydrogen atom collision problem from the eigenfunction expansion point of view. Numerical calculations based on this approach would involve the *exact* solution of the radial equations. These equations are derived from the continuous state Hartree-Fock equations. Calculations, which included positronium formation, should resolve the discrepancy noted above.

When positronium formation is taken into account, the positron problem is more complicated than the electron problem (Percival and Seaton 1957). This is due to the positron-hydrogen atom problem being a two-centre problem.

The effect of electron-positron annihilation to form γ -rays has been neglected.

The radial equations are derived in § 2 and the potentials and kernels are analysed in § 3 and § 4, respectively. The formulae for the cross sections are given in § 5.

§ 2. DERIVATION OF THE RADIAL EQUATIONS

The Schrödinger equation for the positron-hydrogen atom problem cannot be solved exactly. Kohn (1948) has shown that the elements of the S -matrix, from

† Work performed under the auspices of the U.S. Atomic Energy Commission.

which the cross sections are calculated, can be computed to second order in the error in the wave function if the approximate wave function satisfies

$$\iint \Psi^* (H - E) \Psi d\mathbf{r}_1 d\mathbf{r}_2 = 0. \quad \dots (2.1)$$

Since spin-dependent forces will be neglected, the total orbital angular momentum \mathbf{L} and the total spin \mathbf{S} of the system are separately conserved; similarly for their z -components. Thus, a convenient representation to describe the collision process will be one which is diagonal in LM_LSM_S . Let this representation be denoted by

$$\Gamma = \alpha LM_LSM_S \quad \dots (2.2)$$

where α represents all the other quantum numbers required to specify the system: wave numbers and principal atomic quantum number. However, the various types of cross sections are more conveniently discussed in terms of a second representation.

$$\gamma = \alpha l_1 m_1 l_2 m_2 m_1^s m_2^s. \quad \dots (2.3)$$

The two representations are related by a unitary transformation, labelled $(\gamma|\Gamma)$.

The approximate functions considered here are

$$\Psi(1,2) \simeq \sum_{\Gamma} \psi_{\Gamma}(\mathbf{r}_1 s_1, \mathbf{r}_2 s_2) \frac{F_{\Gamma}(r_2)}{r_2} + \sum_{\Delta} \phi_{\Delta}(\boldsymbol{\rho} S, \mathbf{R}) \frac{G_{\Delta}(R)}{R}, \quad \dots (2.4)$$

where Δ is a representation of the Γ -type; $\boldsymbol{\rho}$ is the internal coordinate of positronium, while R is the relative coordinate of positronium and proton.

The continuous state Hartree-Fock equations

$$\iint \psi_{\Gamma}^* (H - E) \Psi d\mathbf{r}_1 d\mathbf{r}_2 = 0 \quad \dots (2.5)$$

$$\iint \phi_{\Delta}^* (H - E) \Psi d\boldsymbol{\rho} d\mathbf{R} = 0 \quad \dots (2.6)$$

are obtained by substituting Eqn (2.4) into Eqn (2.1), with

$$\psi_{\gamma} = \psi_{nl_1 m_1}(\mathbf{r}_1) Y_{l_2 m_2}(\mathbf{r}_2) X(s_1, m_1^s) X(s_2, m_2^s) \quad \dots (2.7)$$

and

$$\phi_{\delta} = \phi_{mp_1 q_1}(\boldsymbol{\rho}) Y_{p_2 q_2}(\mathbf{R}) X(S, M_S). \quad \dots (2.8)$$

ψ_{γ} and ϕ_{δ} are related to ψ_{Γ} and ϕ_{Δ} , respectively, by the unitary transformations, which are given explicitly by Percival and Seaton (1957). Putting $\nu = nl_1 l_2$ and $\mu = mp_1 p_2$, Eqns (2.5) and (2.6) reduce to the radial equations

$$\left[\frac{d^2}{dr_2^2} + k_n^2 - \frac{l_2(l_2+1)}{r_2^2} \right] F_{\nu}(r_2) = \sum_{\nu'} V_{\nu\nu'}(r_2) F_{\nu'}(r_2) + \sum_{\mu'} \int_0^{\infty} K_{\nu\mu'}(r_2, R) G_{\mu'}(R) dR \quad \dots (2.9)$$

and

$$\left[\frac{d^2}{dR^2} + \kappa_m^2 - \frac{p_2(p_2+1)}{R^2} \right] G_{\mu}(R) = \sum_{\mu'} V_{\mu\mu'}(R) G_{\mu'}(R) + \sum_{\nu} \int_0^{\infty} K_{\mu\nu}(R, r_2) F_{\nu}(r_2) dr_2 \quad \dots (2.10)$$

with

$$k_n^2 = \frac{2m}{\hbar^2} (E - E_n) \quad \text{and} \quad \kappa_m^2 = \frac{4m}{\hbar^2} (E - E_m). \quad \dots (2.11)$$

§ 3. THE DIRECT INTERACTIONS V

The function $V_{\nu\nu'}$ is just that which arises in the electron-hydrogen atom problem, but opposite in sign, and has been evaluated by Percival and Seaton (1957).

The direct interaction of positronium with the proton vanishes if only the S -states of positronium are taken into account. In general

$$V_{\mu\mu'} = -\frac{8m}{\hbar^2} \sum_l \delta_{l \text{ odd}} f_l(p_1 p_2, p_1' p_2'; L) y_l(P_{m p_1}, P_{m' p_1'}; 2R), \quad \dots (3.1)$$

where f_l and y_l are defined by Percival and Seaton (1957). For even values of l the direct interaction vanishes.

§ 4. THE KERNELS K

According to Eqns (2.5)–(2.10), the kernels are defined by

$$K_{\nu\mu}(r_2, R) \equiv \frac{16mr_2}{\hbar^2} \iint \left(-\frac{\hbar^2}{4m} \nabla_R^2 + E_m - E - \frac{e^2}{r_1} + \frac{e^2}{r_2} \right) \psi_{\Gamma}^* \phi_{\Delta} R d\mathbf{R} d\mathbf{p}_2 \quad \dots (4.1)$$

where $\nabla_R^2 \equiv \left[\frac{d^2}{dR^2} - \frac{p_2(p_2+1)}{R^2} \right]$

and

$$K_{\mu\nu}(R, r_2) \equiv \frac{32mR}{\hbar^2} \iint \left(-\frac{\hbar^2}{2m} \nabla_2^2 + E_n - E + \frac{e^2}{r_2} - \frac{e^2}{\rho} \right) \phi_{\Delta}^* \psi_{\Gamma} r_2 d\mathbf{p}_2 d\mathbf{R} \quad \dots (4.2)$$

where $\nabla_2^2 \equiv \left[\frac{d^2}{dr_2^2} - \frac{l_2(l_2+1)}{r_2^2} \right]$.

The terms involving the Laplacian will be called the 'kinetic energy' terms, and are analysed in §4.2; the remaining terms will be called the 'potential terms'.

4.1. The Potential Terms

In order to perform the angular integrations the representations will have to be written out explicitly, using Eqns (2.7) and (2.8), and the surface harmonic components of the bound state wave functions will have to be expanded using a theorem given by Moshinsky (1959):

$$\text{Given } \mathbf{r} = \mathbf{x} + \mathbf{y}, \quad \dots (4.3)$$

then

$$r^L Y_{LM}(\mathbf{p}) = \sum_{p,q} \left[\frac{(2L+1)! 4\pi}{(2L-2p+1)! (2p+1)!} \right]^{1/2} \times (pL-pqM-q | LM) Y_{pq}(\hat{\mathbf{x}}) Y_{L-pM-q}(\hat{\mathbf{y}}) x^p y^{L-p}. \quad \dots (4.4)$$

The relation for $L=2$ has been used extensively by Bransden *et al.* (1958) in nucleon-deuteron scattering with tensor forces.

The angular dependence of the radial atomic functions can be extracted by defining the kernels

$$k_{n_l, m p_1}^{\mathcal{L}, i}(r_2, R) = \frac{1}{4\sqrt{2}} \int_{-1}^1 d\eta Q_{n_l}(r_1) Q_{m p_1} \left(\frac{\rho}{2} \right) a^i P_{\mathcal{L}}(\eta) \quad \dots (4.5)$$

where $Q \equiv R/r^i$, and R is the radial function defined by Pauling and Wilson (1935); $\eta \equiv \mathbf{p}_2 \cdot \mathbf{R}$, and

$$r_1 = (4R^2 + r_2^2 - 4Rr_2\eta)^{1/2}, \quad \rho = 2(R^2 + r_2^2 - 2Rr_2\eta)^{1/2}, \quad \dots (4.6)$$

$$a^1 = 1, \quad a^2 = 1/r_1, \quad a^3 = 1/\rho. \quad \dots (4.7)$$

After performing the angular integrations in Eqn. (4.1) the potential contributions to the kernels are

$$K_{\nu\mu}^{\text{pot}}(r_2, R) = \left[\left(-\kappa_m^2 + \frac{4}{r_2 a_0} \right) q_{\nu\mu}^1(r_2, R) - \frac{4}{a_0} q_{\nu\mu}^2(r_2, R) \right], \quad \dots (4.8)$$

where a_0 is the Bohr radius of the H-atom, and

$$\begin{aligned} q_{n_1 l_1, m_1 p_1}^i(r_2, R) &\equiv 4[(2l_1 + 1)!(2p_1 + 1)!(2l_1 + 1)(2l_2 + 1)(2p_1 + 1)(2p_2 + 1)]^{1/2} \\ &\times (-1)^{l_2 + p_2} R r_2^{2v} r_2^{l_1 + p_1} \sum_{v=0}^{l_1} \sum_{u=0}^{p_1} [(2u)!(2v)!(2p_1 - 2u)!(2l_1 - 2v)!]^{-1/2} \\ &\times \left(\frac{R}{r_2} \right)^{u+v} \sum_{\mathcal{L}} k_{n_1, m_1}^{\mathcal{L}, i}(r_2, R) C(L, l_1 l_2, p_1 p_2, uv, \mathcal{L}), \quad \dots (4.9) \end{aligned}$$

and

$$\begin{aligned} C(L, l_1 l_2, p_1 p_2, uv, \mathcal{L}) &\equiv (2\mathcal{L} + 1) \sum_{f, f'} (l_2 l_1 - v 00 | f 0)(p_1 - u \mathcal{L} 00 | f' 0)(p_2 v 00 | f' 0)(\mathcal{L} u 00 | f' 0) \\ &\times W(f' u f p_1 - u; \mathcal{L} p_1) W(v p_2 f p_1; f' L) W(L v l_2 l_1 - v; f l_1). \quad \dots (4.10) \end{aligned}$$

For Eqn (4.2) the potential contributions are

$$K_{\mu\nu}^{\text{pot}}(R, r_2) = 4 \left[\left(-k_n^2 + \frac{2}{r_2 a_0} \right) q_{\nu\mu}^1(r_2, R) - \frac{2}{a_0} q_{\nu\mu}^3(r_2, R) \right]. \quad \dots (4.11)$$

4.2. Kinetic Energy Terms

The first term in Eqn (4.1) can be written as

$$\begin{aligned} K_{\nu\mu}^{\text{k.e.}}(r_2, R) &= -4 \int \int R r_2 d\hat{\mathbf{R}} d\hat{\mathbf{p}}_2 (\gamma | \Gamma)(\delta | \Delta) Y_{l_2 m_2}^*(2) Y_{p_2 q_2}(\hat{\mathbf{R}}) Y_{\mathcal{L} M \mathcal{L}}(2) \\ &\times (\nabla_{R^2})_{r_2} [k_{\nu\mu}^{\mathcal{L}, 1}(r_2, R) Y_{\mathcal{L} M \mathcal{L}}^*(\hat{\mathbf{R}}) r_1^{l_1} Y_{l_1 m_1}^*(\hat{\mathbf{p}}_1) \left(\frac{\rho}{2} \right)^{p_1} Y_{p_1 q_1}(\hat{\mathbf{p}})]. \end{aligned}$$

The solid harmonics, with arguments $\hat{\mathbf{p}}_1$ and $\hat{\mathbf{p}}$ are then expanded using theorem (4.4), and the angular integrations are performed to give

$$K_{\nu\mu}^{\text{k.e.}}(r_2, R) = -q_{\nu\mu}^4(r_2, R), \quad \dots (4.12)$$

where

$$q_{\nu\mu}^4(r_2, R) \equiv \left[\frac{d^2}{dR^2} - \frac{p_2(p_2 + 1)}{R^2} \right] q_{\nu\mu}^1(r_2, R). \quad \dots (4.13)$$

The angular integrations in the kinetic energy term of Eqn (4.2) can be performed to give

$$K_{\nu\mu}^{\text{k.e.}}(R, r_2) = 4q_{\nu\mu}^5(r_2, R), \quad \dots (4.14)$$

where

$$q_{\nu\mu}^5(r_2, R) \equiv \left[\frac{d^2}{dr_2^2} - \frac{l_2(l_2 + 1)}{r_2^2} \right] q_{\nu\mu}^1(r_2, R). \quad \dots (4.15)$$

In conclusion it is seen that the kernels for Eqns (2.9) and (2.10) are given by the sum of Eqns (4.8) and (4.12) and the sum of Eqns (4.11) and (4.14) respectively.

It should be pointed out that spin does not enter into the problem at all, since there is no mechanism present to cause spin flip (which is effected by particle exchange in the corresponding electron problem).

§ 5. CROSS SECTIONS

The formulae for the cross sections for any collision process in which two particles collide and two particles emerge have been given by Blatt and Biedenharn

(1952) and corrected in the phase factors by Huby (1954). The method of Blatt and Biedenharn will be used here to derive the total, and differential, cross sections for transitions from level nl_1 to level $n'l_1'$ of atomic hydrogen and from level nl_1 of atomic hydrogen to level $m'p_1'$ of positronium.

In the asymptotic region the most general wave function (see Eqn (2.4)) with total quantum numbers L and M_L in channel α will have the form

$$\Psi^{LM_L} \approx y_L^{M_L}(\mathbf{r}, \mathbf{r}_\alpha) R_\alpha(r) \{ A_{\alpha}^{LM_L} \exp[-i(k_\alpha r_\alpha - \frac{1}{2} l_\alpha \pi)] - B_{\alpha}^{LM_L} \exp[i(k_\alpha r_\alpha - \frac{1}{2} l_\alpha \pi)] \} / r_\alpha \quad \dots\dots (5.1)$$

with the S -matrix defined by

$$B_{\alpha'}^{LM_L} \equiv \sum_{\alpha} S_{\alpha', \alpha}^L A_{\alpha}^{LM_L}, \quad \dots\dots (5.2)$$

and the real derivative matrix, \mathcal{R} , defined by

$$S \equiv (1 + i\mathcal{R}) / (1 - i\mathcal{R}). \quad \dots\dots (5.3)$$

The analysis proceeds analogously to that of Blatt and Biedenharn to give the differential cross section for excitation of the H atom

$$\frac{d\sigma_{n'l_1', nl_1}(\mathbf{r}_2)}{d\Omega} = \frac{(-1)^{l_1' - l_1}}{4k_n^2(2l_1 + 1)} \sum_v P_v(\cos \theta) B_v(n'l_1', nl_1), \quad \dots\dots (5.4)$$

where

$$B_v(n'l_1', nl_1) \equiv \sum_{Ll_1} \sum_{L'l_1'} T_{n'l_1', nl_1}^{Ll_1} T_{n'l_1', nl_1}^{L'l_1'} Z(l_2' L l_2 \mathcal{L}; l_1 v) Z(l_2' L l_2 \mathcal{L}; l_1' v) \quad \dots\dots (5.5)$$

and the T -matrix and Z -coefficients (without the i -factor (Huby 1954)) are defined by Blatt and Biedenharn.

The total cross section is obtained by integrating Eqn (5.4) over all solid angles to give

$$\sigma_{n'l_1', nl_1} = \frac{1}{k_n^2(2l_1 + 1)} \sum_{Ll_1} T_{n'l_1', nl_1}^L T_{n'l_1', nl_1}^{L*} (2L + 1). \quad \dots\dots (5.6)$$

The total and differential cross sections for positronium formation, into the state $m'p_1'$, $d\sigma_{m'p_1', nl_1}(\mathbf{R})$ and $\sigma_{m'p_1', nl_1}$, respectively, are identical to Eqns (5.4)–(5.6) with $n'l_1'l_2'$ replaced by $m'p_1'p_2'$.

ACKNOWLEDGMENTS

It is a pleasure to thank Drs. R. D. Lawson and M. Peshkin for helpful discussions, and W. J. Cady for reading the manuscript.

REFERENCES

- BLATT, J. M., and BIEDENHARN, L. C., 1952, *Rev. Mod. Phys.*, **24**, 258.
 BRANDEN, B. H., SMITH, K., and TATE, C., 1958, *Proc. Roy. Soc. A*, **247**, 73.
 HUBY, R., 1954, *Proc. Phys. Soc. A*, **67**, 1103.
 KOHN, W., 1948, *Phys. Rev.*, **74**, 1763.
 MARDER, S., HUGHES, V. W., WU, C. S., and BENNETT, W., 1956, *Phys. Rev.*, **103**, 1258.
 MOSHINSKY, M., 1959, *Nucl. Phys.*, **13**, 104.
 MOUSSA, A. H. A., 1959, *Proc. Phys. Soc.*, **74**, 101.
 PAULING, L., and WILSON, E. B., 1935, *Introduction to Quantum Mechanics* (London and New York: McGraw-Hill), p. 132.
 PERCIVAL, I. C., and SEATON, M. J., 1957, *Proc. Camb. Phil. Soc.*, **53**, 654.
 SMITH, K., and BURKE, P. G., 1961, *Phys. Rev.*, **123**, 174.
 SPRUCH, L., and ROSENBERG, L., 1960, *Phys. Rev.*, **117**, 143.

Electron Spin Resonance Studies of Impurity Ions in Magnesium Oxide†

By J. W. ORTON‡§, P. AUZINS§, J. H. E. GRIFFITHS† AND
J. E. WERTZ§

† Clarendon Laboratory, Oxford

§ School of Chemistry, University of Minnesota

MS. received 3rd January 1961

Abstract. The univalent ions Fe^{1+} , Co^{1+} and Ni^{1+} have been produced by ultra-violet or x-irradiation of impure MgO crystals. The electron spin resonance spectra of these ions are compared with those of the isoelectronic ions Co^{2+} , Ni^{2+} and Cu^{2+} which they resemble closely. The spectra of Fe^{1+} , Co^{1+} and Ni^{2+} show line-width effects which may be interpreted as being due to the presence of small distortions in the cubic crystal lattice. A detailed report of the $3d^9$ configuration in a cubic field is given. There is a transition at low temperature from an isotropic to an anisotropic spectrum, presumably due to the 'freezing in' of Jahn-Teller distortions. Observation of hyperfine structure from ^{61}Ni has made it possible to estimate the nuclear moment by comparison with the observed hyperfine structure from Co^{1+} . The ease of formation and stability of these univalent ions is shown to be related to the concentration of positive ion vacancies and to the concentration of trapped hole centres.

§ 1. INTRODUCTION

ELECTRON spin resonance has proved to be a valuable technique for investigating iron-group impurity ions in single crystals of magnesium oxide (Wertz and Auzins 1957, Low 1957b, c, 1958a, b, c). With the exception of titanium and copper, all the iron-group elements have been studied in one or more valence states, and the majority of the results indicate crystalline electric fields having very nearly perfect cubic symmetry. The only ions so far found in non-cubic surroundings are trivalent chromium (Wertz and Auzins 1957, Griffiths and Orton 1959) and iron (Orton, unpublished). Some of these ions are associated with defects (probably positive ion vacancies) in nearest-neighbour or next-nearest-neighbour positive ion sites. There is evidence, however, that some of the 'cubic' ions show very small departures from exactly cubic symmetry (Low 1960a).

There have also been some studies of the effects of irradiation with neutrons (Wertz *et al.* 1957) and with x-rays or ultra-violet light (Wertz *et al.* 1958, 1959) which may aid in the interpretation of optical absorption, photoconductivity and luminescence data. It is apparent that any acceptable theory of the behaviour

† This research was supported in part by the Directorate of Solid State Sciences of the United States Air Force Office of Scientific Research.

|| Now at the Mullard Research Laboratories, Redhill, Surrey.

of MgO under irradiation must take into account the part played by impurity ions. These are important centres for the production and trapping of electrons, and it has not yet proved possible to obtain crystals so pure that impurity effects may be neglected.

The purpose of this paper is threefold: to report the observation of some new resonance spectra in MgO; to present further evidence concerning small departures from exactly cubic surroundings, and to consider some features of the role played by impurity ions in electron transfers due to ultra-violet or x-irradiation.

§ 2. EXPERIMENTAL

The magnesium oxide crystals used in these experiments were obtained from the Norton Company (Canada), the General Electric Company (U.S.A.) and the Infrared Development Company (England). Attempts to diffuse impurities into single crystals of MgO at temperatures up to 1500°C have not led to uniform distribution. In general, only a thin surface layer was obtained, and prolonged heating did little to improve the distribution. The samples containing cobalt were doped in the melt (General Electric Company) and were rose-coloured. For the other impurities it was possible to find crystals which had appropriate concentrations as received, and these crystals were nearly colourless. Some samples used in the Cu^{2+} studies were made from doped powders. Powdered MgO (Fisher, electronic grade) was added to concentrated solutions of CuCl_2 and subsequently dried and heated to the maximum temperature attainable with an oxygen-gas flame.

The electron spin resonance measurements were nearly all made at 9.2 Gc/s; a few were carried out at 6.8 Gc/s and at 23 Gc/s. In some of the work the spectrometer employed bolometer detection in a balanced circuit of the type described by Feher (1957); most of the rest was carried out with transmission cavities with 200 kc/s modulation and crystal detection. The g -values were usually determined with a proton resonance probe, measuring both radio-frequency and microwave frequencies with a Hewlett-Packard 524D counter and its accessories. Samples were irradiated with a low-pressure mercury vapour lamp emitting most of its energy at 4.9 eV (2537 Å) or with x-rays from tubes operated at 50 to 100 kv.

§ 3. THE ELECTRON SPIN RESONANCE SPECTRA

After x- or ultra-violet irradiation of MgO crystals containing iron, cobalt and nickel in divalent form we have detected electron spin resonance spectra which may be attributed to the corresponding univalent ions Fe^{1+} , Co^{1+} and Ni^{1+} . The relevant parameters describing these spectra are collected in the Table together with the corresponding values for the isoelectronic ions, Co^{2+} , Ni^{2+} and Cu^{2+} in the same lattice. The g -values and hyperfine constants A are in all cases isotropic.

The spectra attributed to Fe^{1+} and Ni^{1+} consist of single isotropic lines having widths of order 1 gauss. Co^{1+} shows the expected eight-line hyperfine structure from ^{59}Co ($I=7/2$), the line-width in this case being approximately 20 gauss. At large microwave powers sharp ($\Delta H \sim 1$ gauss) lines appear, superposed on the

Configuration	Ion	Temp. ($^{\circ}\text{K}$)	g	A ($\text{cm}^{-1} \times 10^4$)	Reference
3d ⁷	Co ²⁺	20	4.278 ± 0.001	97.8 ± 0.2	Low (1958 c)
	Fe ¹⁺	20	4.15 ± 0.01	—	This paper
3d ⁸	Ni ²⁺	77	$\dagger 2.2145 \pm 0.0005$	8.3 ± 0.4	This paper
	Co ¹⁺	77	2.1728 ± 0.0005	54.0 ± 0.2	This paper
3d ⁹	Cu ²⁺	77	2.190 ± 0.002	19 ± 1	Hayes (unpubl.) and this paper
	Ni ¹⁺	77	2.1693 ± 0.0005	—	This paper

\dagger Low (1958 b) found $g = 2.227 \pm 0.002$ at 77°K , but we believe this value to be more accurate (see text).

centre of each Co¹⁺ hyperfine component. These may be attributed to double quantum transitions by comparison with the Ni²⁺ spectrum which shows a similar behaviour (Orton, Auzins and Wertz 1960 a), and provide fairly conclusive evidence of the correct assignment of this spectrum to Co¹⁺. It may be mentioned here that the presence of the sharp double-quantum lines enables one to measure the g -values of Co¹⁺ and Ni²⁺ with considerable accuracy. On this account we feel justified in preferring our g -value for Ni²⁺ to that measured previously by Low (1958 b). We may also feel confident of the correct interpretation of the Ni¹⁺ line on account of the low temperature transition discussed in §5.1 and the fact that this spectrum occurs only in crystals showing resonance from Ni²⁺ prior to irradiation.

The assignment of the $g = 4.15$ line to Fe¹⁺ depends on the similarity of g -value and spin lattice relaxation time to those of Co²⁺. In one crystal containing Co²⁺ both spectra were examined together. On increasing the temperature slowly from 20°K the widths of both lines increased rapidly until it was no longer possible to detect resonance. In fact, the new line disappeared first, indicating a slightly shorter T_1 than for Co²⁺ but the difference was very small. The ions most likely to exhibit this behaviour are Fe¹⁺ and Ni³⁺ (V, Cr, Mn, Co and Cu all being ruled out by the absence of hyperfine structure), and the latter may fairly be excluded by the observation of this line in crystals showing no resonance from Ni²⁺ prior to irradiation. It has been detected (with various intensities) in nearly all crystals examined, a fact consistent with the occurrence of iron as an impurity in all crystals available to us.

Further evidence in favour of these interpretations is provided by the results of Bleaney and Hayes (1957), Hayes (1958) and Hayes and Jones (1958) who found the ions Fe¹⁺, Co¹⁺ and Ni¹⁺ after irradiation of NaF crystals containing the corresponding divalent ions. It may be argued that univalent ions would be more stable in NaF than in MgO; however, the question of charge compensation and stabilization will be taken up later.

3.1. Covalent Bonding

For the ions Co²⁺ and Ni²⁺ in MgO, Low (1958 c, b) has shown that there is appreciable covalent bonding between them and the neighbouring oxygen ions. Using the observed g -values of the Table, it is tempting to try to compare the extent of covalency for the univalent ions with their divalent analogues. The

g -values of the three configurations in octahedral crystal field are given by

$$3d^7 \quad g = 3.33 + \alpha k - \frac{15\lambda}{2\Delta} \quad \dots\dots(1a)$$

$$3d^8 \quad g = 2 - \frac{8\lambda}{\Delta} \quad \dots\dots(1b)$$

$$3d^9 \quad g = 2 - \frac{4\lambda}{\Delta}, \quad \dots\dots(1c)$$

where α takes account of the small admixture of 4P states into the 4F ground state of $3d^7$, k is the orbital reduction factor (Stevens 1953), λ is the spin-orbit coupling constant for the ion in the crystal and Δ measures the splitting of the orbital levels by the crystal field. The effects of covalency appear in k and λ (Low 1960 b).

In order to calculate k or λ from the measured g -value, it is obviously necessary to know Δ . It appears probable that Δ may vary appreciably between two isoelectronic ions having different nuclear charges (cf. the cubic field splitting constants of Mn^{2+} and Fe^{3+} in MgO , Low 1957 a) and there is too much uncertainty involved in trying to estimate it. Reliable values may only be obtained from measurements of the appropriate optical spectra and this is also true of α . We have not yet attempted such measurements on the univalent ions as these are present in small concentration ($\sim 10^{-4}$) and their spectra may be confused by much stronger bands from other impurity ions.

Rough calculations using reasonable values of Δ and α seem to indicate that the amount of covalency for each univalent ion is probably about the same as for the corresponding divalent one.

§ 4. SYMMETRY OF THE CRYSTAL FIELD

The isotropic nature of the spectra and the absence of fine structure indicates that the ions Fe^{1+} , Co^{1+} and Ni^{1+} are situated in surroundings having cubic symmetry. The same has been found for several other iron-group ions in MgO , in particular, the corresponding divalent ions from which they are derived (Low 1960 a, Low 1958 b, c). However, the observed line-widths suggest that in several cases there are very small departures from exactly cubic symmetry. We shall discuss the evidence for this provided by the spectra of Ni^{2+} and Fe^{1+} .

In both cases the line-width is found to be dependent on the orientation of the external magnetic field H relative to the crystal axes. For Fe^{1+} the widths with H along the directions [111], [110] and [100] are in the ratios 1:3:6, and for Ni^{2+} the corresponding ratios are 1:1.1:1.5. The precise widths vary from crystal to crystal. With H along the [111] direction, the Fe^{1+} width ranges from 0.8 to 3 gauss at X band and the corresponding Ni^{2+} variation is between approximately 30 and 40 gauss. At K band ($\nu = 23$ Gc/s) the Fe^{1+} widths are approximately 2.5 times greater, suggesting a direct proportionality between ΔH and ν , but in all cases the ratios 1:3:6 for the principal directions are maintained. There is no detectable variation of the Ni^{2+} width with frequency.

4.1. Interpretation of Line-widths for Fe^{1+} and Ni^{2+}

We shall consider three possible causes of these line-width variations: aggregation of impurity ions, Jahn-Teller distortions of the $[MO_6]$ complex (Jahn and Teller 1937) and distortion of the crystal lattice due to dislocations or other faults.

The first possibility, attributing the widths to dipole-dipole interaction, may be disposed of at once on the grounds that it is impossible, in this way, to explain the frequency dependence of ΔH in the Fe^{1+} spectrum. It is also inconsistent with the very small width of the Ni^{2+} double quantum line. The other two possibilities both depend essentially on a distortion of the O^{2-} octahedron surrounding the magnetic centre and may be treated together.

(a) Fe^{1+} .

Consider the simple case of an Fe^{1+} ion in approximately cubic surroundings but with one of its neighbours displaced very slightly so as to produce a small tetragonal component of crystal field. Abragam and Pryce (1951) showed that the g -value of the ground-state doublet will be anisotropic with g_{\parallel} and g_{\perp} lying on either side of g_0 (the value in cubic field) and $g_{\parallel} - g_0 \simeq 2(g_0 - g_{\perp})$. Using this result and taking into account the three ions in unit cell (corresponding to the tetragonal axis being along any one of the cubic axes), we may represent the spectrum along each of the principal directions as shown in Fig. 1. The height

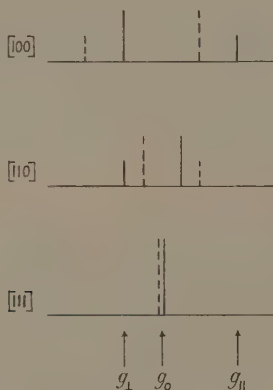


Fig. 1. Reconstruction of the Fe^{1+} line-width along principal directions. The solid lines represent absorption from ions with tetragonal crystal field components of one sign, dotted lines from those of opposite sign.

of a line represents the intensity of absorption, the solid lines arising from tetragonal field of one sign and the dotted ones from opposite sign. It is necessary to include tetragonal components of both signs to account for the observed symmetry of the line shape.

We now postulate a large number of distortions distributed according to a function $f(\Delta g)$ having a maximum value for $\Delta g = 0$ and falling to zero with a half-power width of order $10^{-2}g_0$ (corresponding to $\Delta H \sim 10$ gauss at X band). It may be seen from Fig. 1 that the observed variations of line-width (i.e. the ratios 1:3:6) are reproduced approximately. In particular, the variation of line-width with operating frequency is accounted for since

$$\Delta H \simeq \frac{H_0}{g_0} \Delta g = \frac{\hbar \Delta g}{g_0^2 \beta} \nu. \quad \dots\dots (2)$$

(b) Ni^{2+} .

The occurrence of a small tetragonal component of crystal field will produce small zero-field splittings ΔE between the $S_z=0$ and $S_z=\pm 1$ levels of the Ni^{2+} ground state. By assuming a spread of these values, this situation will give rise to a line-width $\Delta H \sim \Delta E/g\beta$ for $\Delta M=\pm 1$ transitions, while affecting the double quantum transition ($\Delta M=\pm 2$) only by an amount $\sim (\Delta H)^2/H_0$. Taking $\Delta H \sim 50$ gauss, this term is less than 1 gauss at X band; this contribution is less than the commonly observed dipolar width for 3d group ions in MgO and is consistent with the observed double quantum line-width of the order of 1 gauss. That the width of the broad Ni^{2+} line does result from zero-field splittings is supported by two pieces of evidence.

We observe a resonance line at approximately half the field of the main one, having an unusual shape. There is a sharp cut-off at the high field side and much more gradual tailing off to low field. A similar line was observed by Low (1960 a) in the spectrum of Fe^{2+} in MgO and, as he shows, the shape may be explained satisfactorily on the assumption that there is a spread of ground-state splittings. The transition probability for this line is zero in exactly cubic field which accounts for the sharp cut-off on the high field side.

Further evidence is provided by the intensity of absorption in the 'two frequency' double quantum experiment we have already described (Orton, Auzins and Wertz 1960 a). In a three-level system such as this, a double quantum absorption may only be observed if the level separations are in approximately the same ratio as the two frequencies absorbed. Thus, absorption of two quanta at the same frequency requires equally spaced levels and will occur for ions in cubic crystal field. If the frequencies differ, the level spacings must be unequal, which implies the existence of a ground state splitting, and the intensity of absorption obviously depends on the number of ions having the appropriate splitting.

In a series of measurements with the two frequencies ν_A and ν_B differing by increasing amounts we have compared the intensity of absorption I of quanta $h(\nu_A + \nu_B)$ with that of $2h\nu_A$ and $2h\nu_B$ (I_0). The ratios of I/I_0 are represented by

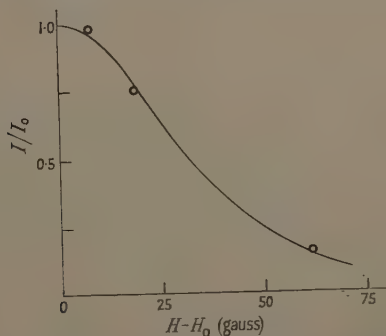


Fig. 2. Results of the 'two frequency' double quantum experiment for three values of $|\nu_A - \nu_B|$. The experimental points show the relative intensity of absorption of quanta $h\nu_A + h\nu_B$ and the solid curve represents the observed shape of the broad Ni^{2+} line.

the experimental points in Fig. 2 where the solid line indicates the shape of the broad Ni^{2+} line. The close agreement between the relative intensity of absorption of $\nu_A + \nu_B$ and the broad line shape provides good evidence for interpreting the latter as arising from a spread of splittings.

(c) *Tetragonal distortions.*

A simple model of tetragonal distortions along the crystal cubic axes would require the line-width along [110] and [111] directions to be much smaller than that observed. The experimental values may be taken as evidence either of the actual symmetry being rhombic, or the axes of distortion not coinciding exactly with [100] type directions (or, possibly, both).

It is not possible to decide with certainty between the Jahn-Teller effect and crystal imperfections as the origin of the proposed distortions, but the weight of evidence is probably in favour of the latter. As the ground-state doublet contains orbital wave-functions, the $3d^7$ configuration might be expected to show a Jahn-Teller distortion but the considerable variation of ΔH from one crystal to another provides fairly strong evidence against its existence in Fe^{1+} . It may also be noted that we have not observed any corresponding line-width variation in the spectrum of Co^{2+} , as might be expected if its origin lay in the Jahn-Teller effect. Finally, one does not expect there to be any appreciable Jahn-Teller distortion for the $3d^8$ configuration, whereas both Ni^{2+} and Co^{1+} spectra show evidence of departure from exactly cubic symmetry.

Perhaps the greatest difficulty with the crystal imperfection theory is that of explaining the occurrence of distortions close to [100] type directions, whereas this could be done in a straightforward fashion in terms of the Jahn-Teller effect. A detailed investigation of specific models may yield a plausible explanation in terms of imperfections but we shall not attempt it here†.

§ 5. JAHN-TELLER EFFECT IN Cu^{2+} AND Ni^{1+}

The theory of the $3d^9$ configuration is complicated by the fact that, in cubic (and trigonal) crystal fields, the ground state is orbitally degenerate. When the spin ($S = \frac{1}{2}$) is included, two Kramers doublets are formed and these are separated only by a tetragonal component of the crystal field. The g -values of these doublets are given by (Abragam and Pryce 1950)

$$(a) \quad g_{\parallel} = 2 - \frac{8\lambda}{\Delta}, \quad g_{\perp} = 2 - \frac{2\lambda}{\Delta}, \quad (b) \quad g_{\parallel} = 2, \quad g_{\perp} = 2 - \frac{6\lambda}{\Delta}, \quad \dots\dots (3)$$

where λ is the spin-orbit coupling constant for the ion in the crystal and Δ is the separation between the ground-state doublet Γ_3 and the next higher level (the triplet Γ_5). The measured g -value depends, of course, on which of the Kramers doublets is lower, i.e. on the sign of the tetragonal field. For ions in cubic (or trigonal) surroundings one expects to find a Jahn-Teller distortion resulting in separation of the doublets (Van Vleck 1939).

5.1. Low Temperature Transitions

Bleaney, Bowers and Trenam (1955) examined a number of cupric salts in which the Cu^{2+} ion is in approximately octahedral surroundings but with a small trigonal distortion. They found that, below a certain temperature (which varied

† The referee of this paper makes the suggestion: "A complex imperfection such as $\text{Fe}^{1+}\text{O}^{2-}\text{Mg}^{2+}\text{O}^{2-}\text{Fe}^{3+}$ would appear quite plausible."

for different salts), the spectrum showed tetragonal symmetry. There were three ions in the unit cell, corresponding to three mutually perpendicular directions of the tetragonal axis. The observed g -values were $g_{\parallel} \simeq 2.45$, $g_{\perp} \simeq 2.10$, indicating that the doublet (a) is lowest. Öpik and Pryce (1957) have shown that this is to be expected in most cases. At these low temperatures it is assumed that the Jahn–Teller distortions are ‘frozen in’. Ludwig and Woodbury (1959) have observed a similar effect in the electron spin resonance spectrum of nickel as an impurity in germanium.

Above the transition temperature they found the g -value to be very nearly isotropic. Abragam and Pryce (1950) explained this as due to a rapid oscillation between the three distorted configurations (each having equal energy), resulting in an average g -value of $2 - 4\lambda/\Delta$. This interpretation is expected to apply to Ni^{2+} and Cu^{2+} in cubic field and leads one to look for a transition temperature below which the Jahn–Teller distortions are ‘frozen in’ as found by Bleaney *et al.*

Both spectra were found to be isotropic at temperatures down to 4°K , but at 1.2°K these were no longer detectable and had been replaced by anisotropic spectra as expected. However, the ‘low temperature’ spectra are not, at the moment, understood. The anticipated model would assume tetragonal distortions occurring along $[100]$ type directions but it does not seem possible to fit this to the experimental results. Further work is planned to analyse these results.

5.2. Line-width of Cu^{2+}

Further evidence for the existence of an oscillating Jahn–Teller effect at temperatures above 4°K is provided by the line-widths of the Cu^{2+} spectrum. The widths of the four hyperfine lines decrease as one goes to higher field (see Fig. 3) and the amplitudes correspondingly increase. A reasonably good fit to the observed spectrum at 77°K was obtained by using a reconstruction of four

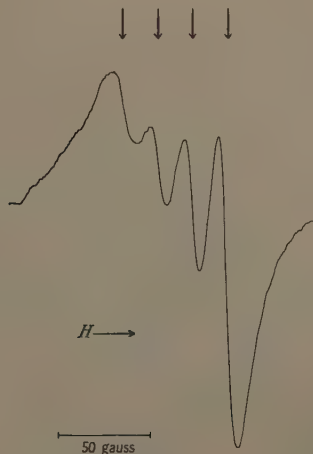


Fig. 3. Derivative of the Cu^{2+} spectrum, showing decrease in width, and consequent increase in amplitude, of the hyperfine components towards higher magnetic field.

Lorentzian lines having equal intensities but differing line-widths (in the ratio 1:1.26:1.57:1.91). The small discrepancies indicate a line shape which is slightly more Gaussian than the pure Lorentz shape chosen. The widths of the components are approximately equal to their separations (~ 20 gauss) so they are not completely resolved from one another.

Very similar observations have been reported for Cu^{2+} ions in solution (McGarvey 1956) and an explanation has been proposed by McConnell (1956). He takes as a model a $[\text{Cu} \cdot 6\text{H}_2\text{O}]$ complex which may be regarded as completely rigid but which undergoes a rapid tumbling motion in the liquid. He assumes the complex to possess an axis of symmetry and shows that the spin Hamiltonian may be written:

$$\mathcal{H} = \mathcal{H}_0 + \mathcal{H}_t, \quad \dots\dots (4)$$

where

$$\mathcal{H}_0 = g\beta H S_z + a\mathbf{I} \cdot \mathbf{S} \quad \dots\dots (5)$$

with

$$g = \frac{1}{3}(g_{\parallel} + 2g_{\perp}) \quad \text{and} \quad a = \frac{1}{3}(A + 2B)$$

and

$$\mathcal{H}_t = (\Delta g \beta H + bI_z)(\cos^2 \theta - \frac{1}{3})S_z + \frac{1}{2}(\Delta g \beta H + bI_z) \sin \theta \cos \theta (S_+ e^{-i\phi} + S_- e^{i\phi}) + \dots, \quad \dots\dots (6)$$

with $b = A - B$ and $\Delta g = g_{\parallel} - g_{\perp}$. The angles θ and ϕ serve to define the direction of the complex axis relative to axes fixed in the laboratory. In consequence of the tumbling motion, θ and ϕ are functions of time. Assuming $\Delta g \beta H \gg b$, McConnell considers the first two terms in (6) and shows that Eqn (6) leads to values of spin-lattice (T_1) and transverse (T_2') relaxation times given by

$$\frac{1}{T_1} \sim \left(\frac{8\pi}{15}\right)^2 (\Delta g \beta H + bI_z)^2 \frac{1}{\hbar^2} \left(\frac{\tau_c}{1 + 4\pi^2 \nu^2 \tau_c^2} \right) \quad \dots\dots (7)$$

$$\frac{1}{T_2'^2} \sim \frac{32\pi}{45} (\Delta g \beta H + bI_z)^2 \frac{1}{\hbar^2} \tan^{-1} \left(\frac{2\tau_c}{T_2'} \right), \quad \dots\dots (8)$$

where τ_c is the correlation time for the tumbling motion and ν is the operating frequency of the spectrometer. The dependence of relaxation times on I_z implies a change of line-width as I_z varies from $-\frac{3}{2}$ to $+\frac{3}{2}$.

The important feature of this theory, from the point of view of the present work, is that it depends on the fact that the angle between H and the $[\text{Cu} \cdot 6\text{H}_2\text{O}]$ axis is constantly changing. Assuming the existence of oscillating Jahn-Teller distortions of the $[\text{CuO}_6]$ complex in MgO , the situation is similar except that, instead of all angles being possible, the 'tumbling' motion now occurs between a number of specific directions. As may be seen from the work of Bloembergen, Purcell and Pound (1948) (on which much of McConnell's theory is based), this will result in changes of relaxation time only through the correlation time τ_c and will not alter the dependence on $\Delta g \beta H + bI_z$.

It is of interest to consider the variation of T_1 and T_2' with τ_c , as given in Eqns (7) and (8). In order to perform some order-of-magnitude calculations we shall neglect b with respect to $\Delta g \beta H$, take $\Delta g \simeq 0.3$, and $\nu \simeq 9 \times 10^9$ c/s. On this basis we arrive at the results shown graphically in Fig. 4. Except for values of τ_c of order 10^{-11} sec or less, $1/T_2'$ is considerably greater than $1/T_1$ and, for $\tau_c > 10^{-8}$ sec $1/T_2'$ is almost constant. Thus, for large values of τ_c , Eqns (7)

and (8) predict that the line-widths will be determined by T_2' and should remain constant, independent of temperature. This is in accordance with observation for temperatures between 77°K and 20°K. Between 20°K and 4°K there are indications of some variation which may be associated with the transition to the 'low temperature' spectrum below 4°K. At 1.2°K when the anisotropic spectrum has replaced the isotropic one, there is no sign of a variation of line-width with I_z , which is consistent with the Jahn-Teller distortions having been 'frozen-in'.

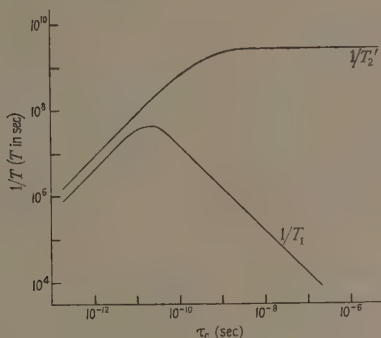


Fig. 4. Variation of $1/T_1$ and $1/T_2'$ with correlation time τ_c as predicted by McConnell's theory.

These conclusions should, of course, be accepted only with reserve, as we have neglected the other contributions to T_1 which may tend to reduce it considerably and the approximation $\Delta g\beta H \gg b$ is of doubtful validity. Also, it should be noted that the value $3 \times 10^9 \text{ sec}^{-1}$ for $1/T_2'$ corresponds to a line-width an order of magnitude larger than that observed. However, spin-lattice relaxation appears to determine the line-width only at temperatures about 77°K, so the above arguments may be correct in principle if not in detail. From the observed line-width at 1.2°K we may estimate $\tau_c > 10^{-7} \text{ sec}$, so values in the range 10^{-8} , 10^{-9} sec do not seem unreasonable for the higher temperature range.

Further evidence supporting the variation of $1/T_2'$ with a term of the type $\Delta g\beta H + bI_z$ is provided by measurements at a microwave frequency of 6.8 Gc/s. As $\Delta g\beta H$ is proportional to ν , we expect the line-width ΔH to be a function of ν also and this is confirmed experimentally.

We may write the ratio of the widths of first and fourth hyperfine lines as

$$\frac{\Delta H_1}{\Delta H_4} = \frac{\Delta g\beta H + \frac{3}{2}|b|}{\Delta g\beta H - \frac{3}{2}|b|} = \frac{x+c}{x-c} = R,$$

where x is proportional to ν . If we take the amplitude D of the line derivative to be proportional to $1/(\Delta H)^2$, we have

$$\frac{D_1}{D_4} = \frac{1}{R^2} = R'.$$

At 9.2 Gc/s, $R_1 = 1.91$, giving $x/c = 3.20$. At 6.8 Gc/s this leads to $x/c = 2.36$ and, hence, to $R_2 = 2.47$. Thus $R_2/R_1 = 1.29$ and, therefore, $R_2'/R_1' = 1/(1.29)^2 = 0.60$, which agrees surprisingly well with our experimental value $R_2'/R_1' = 0.68 \pm 0.10$. In fact, it is not strictly correct to take $D \propto 1/(\Delta H)^2$ on account of the hyperfine

lines being only partially resolved from one another. Allowing for this increases the theoretical ratio R_2'/R_1' slightly, making the agreement even better. This quantitative success may be somewhat fortuitous but the variation of line-width with microwave frequency appears to be established fairly satisfactorily.

The width of the single Ni^{1+} line below 77°K is approximately 2 gauss, which is the usual spin-spin width observed for many other ions in MgO . Why there should be this difference between Ni^{1+} and Cu^{2+} is not clear.

§ 6. NUCLEAR MOMENT OF ^{61}Ni

The sharpness and intensity of the double quantum line in the Ni^{2+} spectrum (at microwave powers of 100 mw and greater) have enabled us to detect for the first time, in an unenriched sample of nickel, hyperfine structure from the ^{61}Ni isotope (Orton, Auzins and Wertz 1960 b). The nuclear spin of ^{61}Ni was found by Woodbury and Ludwig (1958) to be $3/2$, so we expect four hyperfine lines from ^{61}Ni nuclei. Each of these should have an intensity 0.31% of that of the main line from ^{58}Ni and ^{60}Ni (^{61}Ni having a natural abundance of 1.25%).

Careful investigation of the Ni^{2+} spectrum at high microwave power levels shows the presence of two weak, isotropic lines in the wings of the double quantum line and symmetrically disposed about it. They have the same width as the central line and show a similar dependence of intensity on microwave power, i.e. it varies as the square of the power rather than linearly. We assume that these are the outermost components of the hyperfine quartet, the inner pair being lost under the main line. Confirmation is provided by measurement of the weak line intensity with respect to the main one, the ratio being $(0.38 \pm 0.10)\%$ in satisfactory agreement with the anticipated value of 0.31%.

As described in § 3, the Co^{1+} spectrum consists of eight hyperfine components of width of the order of 20 gauss spaced approximately 55 gauss apart. At large microwave powers a sharp double quantum line appears at the centre of each broad one.

The spin Hamiltonian for this system in cubic field may be written:

$$\mathcal{H} = g\beta\mathbf{H} \cdot \mathbf{S} + A\mathbf{I} \cdot \mathbf{S} \quad \text{with} \quad S=1 \text{ and } I=7/2,$$

where g and A are both isotropic. The corresponding energy eigenvalues of \mathcal{H} are given by:

$$W_{M,m} = Mg\beta H + MmA + \frac{1}{4} \frac{A^2}{g\beta H} \{ [S(S+1) - M(M-1)][I(I+1) - m(m+1)] \\ - [S(S+1) - M(M+1)][I(I+1) - m(m-1)] \}, \quad \dots \dots (9)$$

where $M=1, 0$ or -1 and $m=7/2, 5/2 \dots -7/2$. From (9) we may obtain an expression for the positions of the eight double quantum lines, as follows:

$${}^2H_m = H_0 - m \frac{A}{g\beta} - \frac{A^2}{2g^2\beta^2 H_0} [I(I+1) - m^2]$$

where $H_0 = h\nu/g\beta$.

Using this expression and the measured values of 2H_m we can evaluate g and A . The positions of the $\Delta M=1, \Delta m=0$ transitions are given by

$${}^1H_m = H_0 - m \frac{A}{g\beta} - \frac{A^2}{2g^2\beta^2 H_0} [I(I+1) - m^2 \pm m]. \quad \dots \dots (10)$$

This shows they are expected to lie on either side of the double quantum lines and separated from them by $\pm A^2 m / 2g^2 \beta^2 H_0$ gauss, which amounts to 3.3 gauss for $m = \pm 7/2$ (i.e. at the ends of the hyperfine pattern) and decreasing toward the centre. In our case, the separation is much less than the line-width of the $\Delta M = 1$ transitions and is not observable.

One important feature of the discovery of Co^{1+} is that it enables us to calculate a fairly reliable value for the nuclear moment of ^{61}Ni by comparison between the two hyperfine splitting constants $A(^{59}\text{Co})$ and $A(^{61}\text{Ni})$, making use of the relation $A = \gamma \beta \beta_N (\bar{I}/r^3)$. The result of this calculation gives $\mu^{61} = 0.31R$ n.m., where R is the ratio

$$\left(\frac{I}{r^3}\right)(\text{Co}) / \left(\frac{I}{r^3}\right)(\text{Ni})$$

(Orton, Auzins and Wertz 1960 b). To gain some idea of the probable size of R , we calculated it for the parallel case of V^{2+} and Cr^{3+} in MgO and found $R \simeq 0.98$. This led us to suggest a value of $\mu^{61} = 0.30 \pm 0.02$.

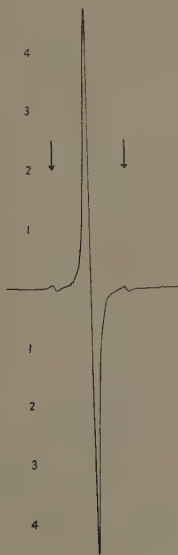


Fig. 5. Hyperfine structure from ^{57}Fe in the spectrum of Fe^{3+} . The lines shown result from the $M = -\frac{1}{2} \rightarrow \frac{1}{2}$ transition.

A further check on R may be obtained by comparing the hyperfine doublet from ^{57}Fe in the spectrum of Fe^{3+} in MgO with that from ^{55}Mn in the spectrum of Mn^{2+} . The nuclear spin of ^{57}Fe is $\frac{1}{2}$ (Ludwig, Woodbury and Carlson 1958) and the natural abundance 2.25%, so the hyperfine pattern associated with each fine structure line is expected to consist of two weak lines with intensity about 1% of that of the main one. This structure is clearly seen in Fig. 5 which shows a trace of the central ($M = -\frac{1}{2} \rightarrow \frac{1}{2}$) transition of the Fe^{3+} spectrum. The value

of A^{57} is found to be $(11.4 \pm 0.1) \times 10^{-4} \text{ cm}^{-1}$ and, comparing this with $A^{55} = 81.0 \times 10^{-4} \text{ cm}^{-1}$, we find $\mu^{57} = 0.092 R \text{ n.m.}$ A determination of μ^{57} by Ludwig and Woodbury (1960) from electron-nuclear double resonance of neutral iron atoms in silicon gave the value $0.0903 \pm 0.0007 \text{ n.m.}$ from which we again find $R \approx 0.98$, confirming the values used previously.

§ 7. PRODUCTION AND DECAY OF UNIVALENT IONS

A proper understanding of the production and decay of these univalent ions can only be obtained within the context of a complete study of all electronic changes taking place during different treatments. We have previously published an account of several of these (Wertz *et al.* 1958, 1959) and reference should be made to these papers for further details. Only one or two points will be touched on here.

On x-irradiation of MgO crystals, it is usually found that the intensity of the Fe^{3+} spectrum increases, indicating the liberation of electrons from Fe^{2+} ions. Another source of electrons in many cases is the production of hole centres at O^{2-} ions. These two processes may be represented by the equations:



The electrons may be trapped by other impurity ions such as (in this case) Fe^{2+} , Ni^{2+} and Co^{2+} to form the corresponding univalent ions or by Cr^{3+} to give Cr^{2+} .

The annealing behaviours of Fe^{1+} , Ni^{1+} and Co^{1+} are very similar. They are all fairly stable at room temperature in the dark but decay in a matter of a few days on exposure to daylight. Fe^{1+} and Co^{1+} decay very rapidly at 100°C (within $\frac{1}{2}$ hour) though Ni^{1+} decays surprisingly slowly at the same temperature. This behaviour is also very similar to that shown by the positive hole centre O^- and should be contrasted with the much greater stability of Fe^{3+} . It seems reasonable to infer from these observations that electrons released by the decay of Fe^{1+} , etc., are captured by O^- and this is probably the main reaction occurring, though some may be trapped by Fe^{3+} , reversing Eqn (11).

More detailed investigation of the stability of the univalent ions shows that it is dependent on the previous treatment given to the MgO crystals and suggests that the number of positive ion vacancies present in the crystal is of great importance. In the presence of such vacancies, which represent an effective negative charge, the stability of an M^{1+} ion will be less than in their absence, on account of the greater electrostatic potential energy. This suggestion is borne out by the following experiment.

Two MgO samples, containing iron, were cleaved from the same parent crystal and one of them, A, was heated *in vacuo* at 1200°C to reduce the number of positive ion vacancies present, while B was heated in oxygen to induce the opposite effect. They were then given identical doses of x-rays and examined at 20°K . A showed a much stronger Fe^{1+} spectrum than B and it proved to be considerably more stable. On exposure to daylight, the intensity in B was reduced by twenty times in two days, while that in A was reduced by only a factor of four after a week. Further evidence is provided by the fact that a sample which had been additively coloured, by heating in magnesium vapour, still showed an Fe^{1+} line some three years later, a remarkable increase in stability over untreated crystals.

The only impurity ions which have been detected in non-cubic crystal fields are Fe^{3+} and Cr^{3+} (Wertz and Auzins 1957, Griffiths and Orton 1959, Orton, unpublished) and these spectra have been interpreted as arising from ions associated with positive ion vacancies. Conversely, it is expected that univalent ions will be situated as far as possible from positive ion vacancies and this suggests that they will be likely always to occur in cubic field. This appears to be the case, experimentally.

Several papers (Weber 1951, Clarke 1957, Day 1953, Soshea, Dekker and Sturtz 1958, Peria 1958, Haxby 1957) have been published on studies of optical absorption, photoconductivity, and thermo-luminescence spectra of MgO crystals. The results have been interpreted in terms of a system of energy levels between the valency and conduction bands. Peria (1958) has criticized the interpretations suggested by earlier workers, finding that both positive and negative charge-carriers are involved. The recent work has been concentrated on interpreting the spectra in terms of iron-group impurity ions and points to the importance of iron. In particular, Peria postulated the existence of Fe^{1+} following x-irradiation.

The magnetic resonance results support these general conclusions and allow us to locate the different impurity levels in the MgO energy gap with rather more certainty. We have proposed an approximate order for several of them in an earlier paper (Wertz *et al.* 1958). It is of importance to try to put these results on a quantitative footing and we have made preliminary measurements on the univalent ions Fe^{1+} , Co^{1+} and Ni^{1+} . They decay under the influence of light from a tungsten filament lamp which appears to locate them all within 4 eV of the conduction band. By the use of suitable optical filters, we estimate the appropriate energies for Fe^{1+} , Co^{1+} and Ni^{1+} to be in the approximate region 2–3.5 eV. This is in agreement with the value for Fe^{1+} suggested by Peria from his photoconductivity results.

§ 8. CONCLUSIONS

(i) The ions Fe^{1+} , Co^{1+} and Ni^{1+} have been studied in irradiated MgO crystals containing the corresponding divalent ions. The stability of these centres is dependent on the concentration of positive ion vacancies in the crystal.

(ii) The electron spin resonance spectra of the univalent ions are very similar to their isoelectronic divalent analogues, Co^{2+} , Ni^{2+} and Cu^{2+} .

(iii) Evidence is presented that, in some cases, the crystal field shows small departures from exactly cubic symmetry.

(iv) The spectra of Cu^{2+} and Ni^{1+} indicate the existence of Jahn–Teller distortions which may be ‘frozen-in’ at low temperatures.

(v) The nuclear moment of ^{61}Ni is estimated as 0.30 nuclear magneton.

ACKNOWLEDGMENTS

It is a pleasure to acknowledge helpful comments made by Dr. John Owen (Oxford). Dr. Richard Hansler of the General Electric Company, Cleveland, Ohio, and Dr. G. K. Finlay of the Norton Company, Chippawa, Ontario, have kindly supplied some of the magnesium oxide crystals used. We are particularly indebted to Mr. R. Pontinen who performed the measurements in the liquid helium range.

REFERENCES

- ABRAGAM, A., and PRYCE, M. H. L., 1950, *Proc. Phys. Soc. A*, **63**, 409.
 — 1951, *Proc. Roy. Soc. A*, **206**, 173.
 BLEANEY, B., BOWERS, K. D., and TRENAM, R. S., 1955, *Proc. Roy. Soc. A*, **228**, 157.
 BLEANEY, B., and HAYES, W., 1957, *Proc. Phys. Soc. B*, **70**, 626.
 BLOEMBERGEN, N., PURCELL, E. M., and POUND, R. V., 1948, *Phys. Rev.*, **73**, 679.
 CLARKE, F. P., 1957, *Phil. Mag.*, **2**, 607.
 DAY, H. R., 1953, *Phys. Rev.*, **91**, 822.
 FEHER, G., 1957, *Bell Syst. Tech. J.*, **36**, 449.
 GRIFFITHS, J. H. E., and ORTON, J. W., 1959, *Proc. Phys. Soc.*, **73**, 948.
 HAXBY, B. V., 1957, *Ph.D. Thesis*, University of Minnesota.
 HAYES, W., 1958, *Disc. Faraday Soc.*, **26**, 58.
 HAYES, W., and JONES, D. A., 1958, *Proc. Phys. Soc.*, **71**, 503.
 JAHN, H. A., and TELLER, E., 1937, *Proc. Roy. Soc. A*, **161**, 220.
 LOW, W., 1957 a, *Phys. Rev.*, **105**, 792.
 — 1957 b, *Phys. Rev.*, **105**, 793.
 — 1957 c, *Phys. Rev.*, **105**, 801.
 — 1958 a, *Ann. N.Y. Acad. Sci.*, **72**, 69.
 — 1958 b, *Phys. Rev.*, **109**, 247.
 — 1958 c, *Phys. Rev.*, **109**, 256.
 — 1960 a, *Phys. Rev.*, **118**, 1130.
 — 1960 b, *Paramagnetic Resonance in Solids, Solid State Physics*, Suppl. 2 (New York: Academic Press), p. 101.
 LUDWIG, G. W., and WOODBURY, H. H., 1959, *Phys. Rev.*, **113**, 1014.
 — 1960, *Phys. Rev.*, **117**, 1286.
 LUDWIG, G. W., WOODBURY, H. H., and CARLSON, R. O., 1958, *Phys. Rev. Letters*, **1**, 295.
 MCCONNELL, H. M., 1956, *J. Chem. Phys.*, **25**, 709.
 MCGARVEY, B. W., 1956, *J. Phys. Chem.*, **60**, 71.
 ÖPIK, U., and PRYCE, M. H. L., 1957, *Proc. Roy. Soc. A*, **238**, 425.
 ORTON, J. W., AUZINS, P., and WERTZ, J. E., 1960 a, *Phys. Rev. Letters*, **4**, 128.
 — 1960 b, *Phys. Rev.*, **119**, 1691.
 PERIA, W. T., 1958, *Phys. Rev.*, **112**, 423.
 SOSHEA, R. W., DEKKER, A. J., and STURTZ, J. P., 1958, *J. Phys. Chem. Solids*, **5**, 23.
 STEVENS, K. W. H., 1953, *Proc. Roy. Soc. A*, **219**, 542.
 VAN VLECK, J. H., 1939, *J. Chem. Phys.*, **7**, 72.
 WEBER, H., 1951, *Z. Phys.*, **130**, 392.
 WERTZ, J. E., and AUZINS, P., 1957, *Phys. Rev.*, **106**, 484.
 WERTZ, J. E., AUZINS, P., GRIFFITHS, J. H. E., and ORTON, J. W., 1958, *Disc. Faraday Soc.*, **26**, 66.
 — 1959, *Disc. Faraday Soc.*, **28**, 136.
 WERTZ, J. E., AUZINS, P., WEEKS, R. A., and SILSBEE, R. H., 1957, *Phys. Rev.*, **107**, 1535.
 WOODBURY, H. H., and LUDWIG, G. W., 1958, *Phys. Rev. Letters*, **1**, 16.

Electrical Breakdown of Gases: Ionization Growth in Air at High Pressures

By J. DUTTON, F. LLEWELLYN JONES AND R. W. PALMER†

Department of Physics, University College of Swansea

MS. received 22nd February 1961

Abstract. The experimental conditions which have to be satisfied in order to measure ionization coefficients accurately at high values of the parameter pd (pressure \times gap distance) are assessed. In an apparatus designed to fulfil these conditions, precision measurements were carried out for uniform electric fields E in air at values of the parameter pd up to 2300 mm Hg cm, which corresponds to a sparking potential of about 80 kv, thus extending the range so far investigated by Llewellyn Jones and Parker in 1950 and 1952. The results show that pre-breakdown ionization growth in air is due to the action of primary (α) and secondary (ω) ionization processes modified by the process of attachment a , and that significant space charge effects were absent. At a value of pd of 2300 mm Hg cm the sparking potential calculated (81 ± 1.5 kv) from the criterion (expressed in terms of the ionization and attachment coefficients) which gives the static sparking potential was in agreement, within the experimental error, with that (79 ± 0.7 kv) observed. It was also shown that the state of the cathode surface had a marked influence on the secondary ionization even at these higher values of pd .

For $35 \leq E/p \leq 40$ v cm⁻¹ (mm Hg)⁻¹ and pressures between 400 and 1000 mm Hg, the apparent secondary ionization coefficient $\omega/(\alpha - a)$ was found to be a function of E/p alone, whereas the apparent primary ionization coefficient $(\alpha - a)/p$ showed a small, just detectable decrease with increasing pressure at a given value of E/p .

§ 1. INTRODUCTION

THE use of increasingly higher voltages for the transmission of electrical power and in nuclear particle accelerators has stimulated considerable interest in recent years in the subject of the electrical breakdown of gases at pressures of an atmosphere and greater; the electrical properties of air are of particular interest because of its wide-spread use as an insulator. An understanding of the initiation, control or suppression of an electric spark can be achieved by a consideration of the basic physical processes leading to breakdown, and investigations of these fundamental processes are therefore of technological as well as of intrinsic interest. It is the purpose of this paper to describe and discuss accurate measurements of ionization coefficients in air for values of pd (pressure \times electrode separation) up to those corresponding to breakdown in a 3 cm gap at atmospheric pressure for which the static sparking potential V_s is about 80 kv. This extends the range by a factor of about 3 above that previously

† Now at The English Electric Company, Chelmsford.

investigated in this Department (Llewellyn Jones and Parker 1950, 1952; both to be referred to as I).

It has been shown in the earlier investigations that, provided the parameter E/p (E the electric field and p the gas pressure) is maintained constant to at least 0.1%, the spatial growth of a pre-breakdown externally maintained ionization current for values of pd up to 760 mm Hg cm in a uniform field in air is in accord with the well-known equation

$$I = \frac{I_0 e^{\alpha d}}{1 - (\omega/\alpha)(e^{\alpha d} - 1)} \quad \dots\dots (1)$$

In this equation I_0 is a small ($\sim 10^{-13}$ A) externally maintained initial current from the cathode, α is the Townsend primary ionization coefficient and ω/α is a generalized secondary ionization coefficient which can be expressed as the linear sum of coefficients representing the action of many possible secondary ionization processes (Llewellyn Jones 1957, Chap. 4).

Equation (1) leads to the Townsend breakdown criterion expressed by equating the denominator of the right-hand side of (1) to zero. Using values of the coefficients α and ω valid over the whole range of current at the particular value of E/p , values of V_s calculated from this criterion for air have been found to agree with those experimentally observed, in that electrical breakdown could be produced for values of the applied potential exceeding V_s , but not when $V < V_s$ within the limits of experimental measurement.

Air having been considered, investigations were extended to other gases, nitrogen, (Dutton, Haydon and Llewellyn Jones 1952) and hydrogen (Crompton, Dutton and Haydon 1956, Davies, Dutton and Llewellyn Jones 1958), in which the detailed contribution of the various possible secondary ionization processes could be more readily assessed. In the course of these investigations the measuring techniques had been continuously improved, and in the present investigation these improved techniques were used both to repeat some of the early measurements (in order to obtain more accurate values of the ionization coefficients), as well as to extend measurements to higher gas pressures and sparking potentials.

As the value of the spark parameter pd_s (and therefore of V_s) increases, the value of the parameter E/p at sparking $= (E/p)_s$ decreases, so that the mean energy of the electrons also decreases (Llewellyn Jones 1957, Chap. 2). As a result of this decrease, the process of attachment of electrons to gas molecules can become important relative to the process of ionization of gas molecules by electron impact, and Eqn (1) is modified as shown by Penning (1938) and Geballe and Reeves (1953). If, as is likely to be the case in air, attachment occurs by one of the low energy processes such as three-bodied, collision stabilized or dissociative attachment (Massey 1950), the equation for ionization growth may be written

$$I = I_0 \left[\frac{\alpha}{\alpha'} \exp(\alpha' d) - \frac{a}{\alpha} \right] / \left[1 - \frac{\omega}{\alpha'} \{ \exp(\alpha' d) - 1 \} \right] \quad \dots\dots (2)$$

In this equation a is the coefficient of attachment defined, in exact analogy with the ionization coefficient α , such that the number of electrons attaching to neutral gas molecules when n electrons move a distance dx in the direction of the field is $nadx$; $\alpha' = \alpha - a$ is the apparent primary ionization coefficient and ω/α' is the apparent secondary ionization coefficient. It can be seen that this equation is analytically similar to Eqn (1), the only significant difference being the additive

constant $-a/\alpha'$ in the numerator which gives rise to a downward curvature of the $(\log(I/I_0), d)$ graph at small values of d ; moreover, the breakdown criterion, which becomes

$$1 - \frac{\omega}{\alpha'} [\exp(\alpha'd) - 1] = 0, \quad \dots, (3)$$

is analytically identical with the criterion valid in the absence of attachment, the apparent primary and secondary ionization coefficients α' and ω/α' replacing the coefficients α and ω/α in the Townsend criterion. The results of the present investigation are analysed in § 4 in terms of Eqns (2) and (3).

§ 2. CONSIDERATIONS UNDERLYING THE EXPERIMENTAL INVESTIGATION

2.1. Physical Significance of the $(\log(I/I_0), d)$ Curves

Measurements of the spatial growth of pre-breakdown ionization currents are conveniently expressed as graphs of $(\log(I/I_0), d)$, and the shape of such curves when determined accurately gives information concerning the mechanism by which ionization develops to set the criterion for determining the static breakdown potential.

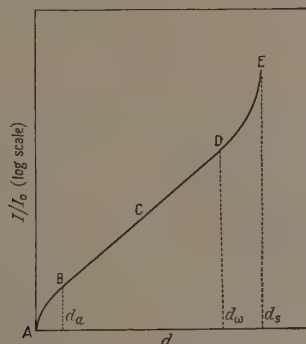


Fig. 1. The growth of ionization current represented by Eqn (2) when $a < \alpha$ and $\omega \ll \alpha$.

When the growth is due to the action in a uniform electric field of both primary and secondary ionization processes modified by attachment, the corresponding coefficients α' , ω/α' and a are determined from the relation (2) which gives the form of the growth. When the coefficients a and ω are small compared with α' , the main portion of the graph is nearly linear and the form of Eqn (2) is as given in Fig. 1. (The part BCD cannot, of course, be exactly linear when the coefficients a and ω are finite.) At values of $d < d_a$, $(\omega/\alpha') [\exp(\alpha'd) - 1] \ll 1$, and the term a/α' becomes significant compared with $(a/\alpha') \exp(\alpha'd)$; the graph here shows a downward departure from linearity as indicated by AB. At large values of d , where $(\omega/\alpha') [\exp(\alpha'd) - 1]$ increases to approach unity, the current increases more rapidly with distance and the graph curves up as shown by DE. The form of this increase gives a critical value d_s of d thus giving the static sparking potential $V_s = Ed_s$; the values of d_s , α' and ω then all satisfy the breakdown criterion (2) at the particular value of E/p .

On the other hand, if the criterion for the static sparking potential were set by a *kanal* or 'streamer' mechanism (Loeb and Meek 1941, Raether 1939, 1959) the form of the $(\log(I/I_0), d)$ graph would then be different at the larger values of d from that considered above. The criterion would be set by the sudden (in distance) attainment of a critical space charge field which would so enhance photo-ionization in the gas as to produce an extremely sharp increase of current. The $(\log(I/I_0), d)$ graph experimentally obtained should then be linear for gap distances d almost up to the critical sparking distance d_s , at which there would be almost a discontinuity, as I becomes larger extremely quickly.

As the gas pressure increases, in the usual experimental arrangements (see I), the ionization density increases due to a decrease in diffusion, so that any mechanism based on space charge distortion is more likely to be operative at high values of the gas pressure than at low values. It is clearly of interest, therefore, to extend measurements of $(\log(I/I_0), d)$ curves to still higher values of the parameter pd in order to investigate when and how any change occurs in the nature of the $(\log(I/I_0), d)$ curve up to the attainment of the sparking potential; such measurements would disclose any change in the basic mechanism by which the criterion giving the sparking potential is set as the parameter pd is increased.

2.2. Choice of Experimental Conditions for Air

In order to obtain information concerning attachment and secondary ionization processes in a particular case it is clearly necessary to choose the experimental conditions so that the regions of curvature AB and DE of the $(\log(I/I_0), d)$ curve can be fully investigated. For air at the values of the parameter pd_s under consideration in the present work, the value of $(E/p)_s$ is about $35 \text{ v cm}^{-1} (\text{mm Hg})^{-1}$. Some published experimental data on ionization coefficients for this value of E/p are: $a/p \simeq 5 \times 10^{-3}$ (Harrison and Geballe 1953); $\alpha'/p \simeq 6.0 \times 10^{-3}$ (Masch 1932, Sanders 1932), $\omega/\alpha' \sim 10^{-5} (I)$; values of α' and a of the same order were published by Prasad (1959). Insertion of these values in Eqn (3) gives a value of pd_s of 2000 mm Hg cm corresponding to $E_s/p = 35 \text{ v cm}^{-1} (\text{mm Hg})^{-1}$. On the assumption that ionization currents could be measured to within 5%, Eqn (2) shows that experimental detection and measurement of ω/α' is possible only for values of $pd > 1500 \text{ mm Hg cm}$, and measurement of a only when $pd < 350 \text{ mm Hg cm}$. If information concerning the secondary ionization is required, it is clear, therefore, that measurements have to be made within the range $1500 < pd < 2000 \text{ mm Hg cm}$ since 2000 is the upper limiting value of pd corresponding to spark breakdown. This range is indicated by the region d_ω to d_s in Fig. 1.

In the apparatus used in the present work the maximum gap distance d was 3 cm, so that a gas pressure of about 700 mm Hg cm was necessary to obtain values of pd up to 2000 mm Hg cm. Since a was only measurable when pd was less than 350 mm Hg cm, the detection and measurement of a was limited at a pressure of 700 mm Hg to gap distances less than 0.5 cm. However, no precise measurements could be made at distances below 0.3 cm because the error in setting these small distances in the large apparatus used would give a possible error in E/p larger than 0.1%, which was considered to be the largest permissible error in this parameter if accurate results were to be obtained. Hence, at the high gas pressures (700 mm Hg) which are essential to obtain the values of pd necessary for the

determination of ω/α' , only an extremely small section ($0.3 < d < 0.5$ cm) of the measured curve was available for the detection and measurement of a , and reliable evidence concerning this coefficient could not be obtained from such measurements alone. For these reasons, then, one single curve giving $(\log(I/I_0), d)$ from small values right up to $d = d_s$ is not itself sufficient to obtain accurate values of α , ω and a . On the other hand, when the gas pressure is low, it is possible to choose the pressure so that the initial curved section AB of the $(\log(I/I_0), d)$ graph together with a sufficient part BC of the linear section can be explored with the required accuracy as the gap distance d is increased up to 2 or 3 cm.

It was necessary in the present work, therefore, to study the current growths in two sets of conditions: first, at high pressures (400 mm Hg to 1000 mm Hg) to obtain the apparent primary ionization coefficient α' and the apparent secondary ionization coefficient ω/α' , and then at low pressures (100 mm Hg to 300 mm Hg) at the same value of E/p to obtain the attachment coefficient a . Preliminary determinations of the coefficient a at low pressures have already been published (Dutton, Llewellyn Jones and Palmer 1959); work on the determination of the attachment coefficients in air and other gases is still in progress and will form the subject of a future paper. The present paper gives the detailed results of the determination of the apparent ionization coefficients α' and ω/α' carried out at high pressures.

2.3. Method of Analysis

It is perhaps advisable to point out here that the accurate experimental determination of coefficients such as α' , ω and a depends not only on the use of cathode surfaces and samples of gas which have constant properties throughout the experiments and the employment of a sufficiently accurate technique of experimental measurement, but also on the soundness of the method of analysis used to deduce the coefficients from the experimental curves for $(\log(I/I_0), d)$ obtained. The method of analysis used in the present investigation will therefore now be considered.

At values of $d > d_a$, when $a/\alpha' \ll (\alpha/\alpha') \exp(\alpha'd)$, Eqn (2) reduces to

$$I = I_0 \left(\frac{\alpha}{\alpha'} \right) \exp(\alpha'd) / \left[1 - \frac{\omega}{\alpha'} \{ \exp(\alpha'd) - 1 \} \right]. \quad \dots\dots (4)$$

In theory it is possible to obtain the constants α' and ω/α' of this equation for any value of E/p from measurements of gas-amplified ionization currents at three suitable gap separations, provided I_0 remains constant throughout the measurements. As stated previously (Crompton, Dutton and Haydon 1956), the short-term stability of the ultra-violet light source used by them to produce the initial current I_0 was good (fluctuations $< 1\%$) over a period of minutes, but the long-term stability over a period of hours was not better than 10% . To take advantage of the accuracy now possible in the measurement of the ionization current (error $\sim 1\%$), it was therefore necessary to measure, in the present work, the initial externally maintained current as well as the gas-amplified current to which it gave rise, within a few minutes of one another. In practice it was found that in air, as in hydrogen, the (I, V) curve at a constant value of d did not attain a saturation value to give a constant value of I_0 . It was therefore necessary to obtain a measure of I_0 by measuring the current I_c flowing at a low value of $E/p = (E/p)_c$. At this low

value of $(E/p)_c$ no amplification took place in the gas and because of back scattering the magnitude of the current I_c was some fraction c of I_0 . From measurements of the ratio I/I_c at three different electrode separations it is possible by means of a method of successive approximations to calculate accurate values of the coefficients α' and ω/α' .

§ 3. APPARATUS AND EXPERIMENTAL PROCEDURE

Much of the apparatus used was the same as that used in previous investigations of current growth carried out in this Department; the voltage measuring system was, for example, that described in I, while the power supplies and current measuring system were those used by Crompton, Dutton and Haydon (1956). However, since the range of pressure investigated was increased to values somewhat above atmospheric, changes in the design of the ionization chamber and vacuum system were necessary and these will now be outlined.

3.1. Ionization Chamber and Vacuum System

The ionization chamber, which is shown diagrammatically in Fig. 2, was of the same general design as that described in I. The main differences from the earlier chamber were that the seals between the borosilicate glass chamber E and the anode support and base plate were such as to enable investigations to be made at

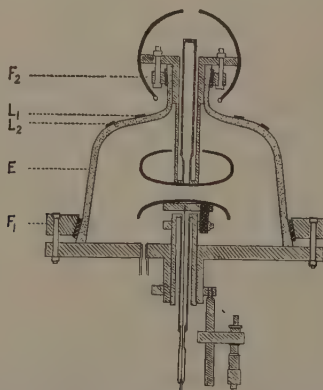


Fig. 2. Diagram of the ionization chamber for use at gas pressures greater than atmospheric.

gas pressures somewhat larger than atmospheric without leakage of the air from the chamber to the atmosphere. These seals were maintained by pulling the glass on to the metal, which was coated with Apiezon M grease, by means of steel flanges F_1 and F_2 . The electrodes used were also different from those of I and were machined and polished to a profile suggested by Bruce (1947) to ensure that the field would be uniform and a maximum over the central section of the electrodes. The purpose of the metal strips L_1 and L_2 on the borosilicate glass chamber is discussed in § 3.2.

The vacuum system was similar to that used previously, and as in I; the usual care was taken to avoid contamination due to mercury and other condensable

vapours by placing a cold trap adjacent to the ionization chamber. This trap was always maintained at liquid air temperature when the ionization chamber was connected to the rest of the system. The main modification to the vacuum system was the use of special spring-loaded glass taps in all those parts of the system which were subjected to internal pressures greater than atmospheric.

The air, which was supplied by the British Oxygen Company as free from CO_2 (< 1.0 volumes per million), water vapour ($< 0.00056 \text{ g m}^{-3}$) and SO_2 (nil), was admitted to the chamber very slowly, passing over P_2O_5 and through two cold traps maintained at the temperature of liquid air. The pressure was measured by a mercury manometer connected to the rest of the system through two cold traps maintained at liquid air temperatures. As a further precaution, the gauge was evacuated only through its own system and no flow of gas from gauge to ionization chamber took place.

3.2. Experimental Procedure

The ionization chamber was evacuated by an oil diffusion pump for several hours through cold traps maintained at the temperature of liquid air. The room temperature was stabilized with thermostats and electric heaters in order to specify accurately the density of the gas sample admitted.

The high resistances (10^7 to $10^{11} \Omega$) in the current measuring system were calibrated to within 1%.

The electrode separation was set at a predetermined value and the ratio I/I_c was measured in the following way. A voltage, chosen to make the value of $E/p = (E/p)_c$, was applied across the electrodes from a stable (fluctuations about 1 in 10^5) 6 kv supply, and the current I_c then measured. The actual values of I_0 which were obtained in the experiments are given in Fig. 4 in terms of I_c ; the ratio I_0/I_c lay between about 1.6 and 4 depending on the value of $(E/p)_c$. The area of cathode irradiated was about 0.25 cm^2 , so that the initial current densities J_0 were about $10 I_c \text{ A cm}^{-2}$. I_c was of the order of 10^{-13} A . The effects of the very small residual fluctuations in the voltage supply were eliminated by means of a circuit similar to that previously described (Dutton, Haydon and Llewellyn Jones 1952). It was found necessary to maintain the metallic strip guard rings L_1 and L_2 on the outside of the chamber at earth potential during this measurement, otherwise movement of charge over the surface due to the application of a potential to the anode gave rise to induced currents in the measuring system. After measuring I_c , the voltage applied to the electrodes was then changed to give the required value of E/p , and the gas-amplified current I was then measured within about two minutes of the measurement of I_c . Since I (10^{-12} to 10^{-8} A) was larger than I_c it was possible to use a 100 kv supply (Crompton, Dutton and Haydon 1956) with a slightly lower stability (fluctuations 1 in 10^4) for this measurement. At these higher voltages it was not practicable to earth the metal strips L_1 and L_2 because of their proximity to the high tension terminal, but then any induced currents due to the movement of charge on the glass walls were negligible compared with the comparatively large gas-amplified current. After the measurements of the gas-amplified currents the strips L_1 and L_2 were again earthed and the whole procedure repeated. An experimental check was always made to make sure that the application of the high voltage required for the measurement of the gas-amplified current I did not affect the subsequent measurement of the much

smaller I_c . It was usually found that it was necessary to wait for a period of about ten minutes after earthing L_1 and L_2 until induced currents became negligible compared with I_c . Having obtained several values for I/I_c at a particular gap separation, the gap distance d was then changed and the above procedure repeated.

It was considered that the employment of the above experimental technique was necessary and sufficient in order to obtain accurate and reproducible data.

§ 4. RESULTS AND DISCUSSION

4.1. Preliminary Results

In order to ascertain whether the apparatus was working satisfactorily a preliminary set of measurements was carried out using a value of E/p of $45 \text{ v cm}^{-1} (\text{mm Hg})^{-1}$ for a gas pressure of 200.3 mm Hg (all pressures are corrected to 20°C throughout this paper), and using an aluminium cathode. The curve obtained is shown in Fig. 3 where it is compared with the results given in I.

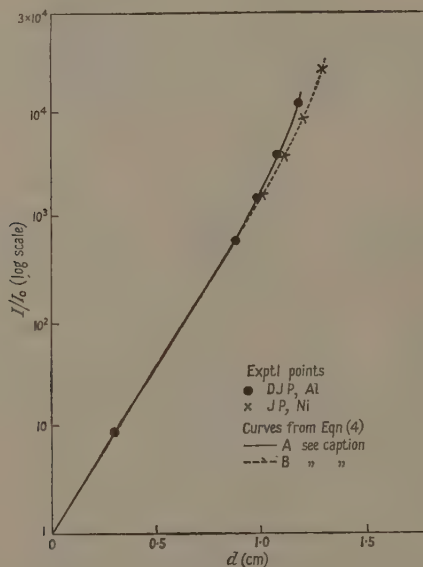


Fig. 3. Experimental and theoretical ($\log(I/I_0)$, d) curves for air at $E/p = 45 \text{ v cm}^{-1} (\text{mm Hg})^{-1}$ and $p = 200 \text{ mm Hg}$ using Ag and Ni cathodes. DJP, present work with Al cathode; JP, Llewellyn Jones and Parker (1952) with Ni cathode; A, $\alpha'/p = 3.53 \times 10^{-2}$, $\omega/\alpha' = 160 \times 10^{-6}$; B, $\alpha'/p = 3.45 \times 10^{-2}$, $\omega/\alpha' = 84 \times 10^{-6}$.

It can be seen that the growth was well represented by Eqn (4) with values of α'/p and ω/α' of 3.53×10^{-2} and 1.6×10^{-4} respectively. The value of α' is thus in agreement (within $2\frac{1}{2}\%$) with that obtained in I, viz. 3.45×10^{-2} , but the value of ω/α' is nearly double that (0.84×10^{-4}) obtained in I using a nickel cathode. The secondary ionization coefficient clearly depends on the nature of the cathode surface, and this indicates that secondary ionization processes acting at the cathode

play an important role in breakdown at these values of pd (~ 250 mm Hg cm), a fact which was later confirmed at even higher values of pd (see § 4.3).

Although it was possible to make a significant analysis of the curve shown in Fig. 3, a certain effect was noted at the larger distances which was similar to that observed in the previous experiments in air (I) and nitrogen (Dutton, Haydon and Llewellyn Jones 1952); this effect was the gradual increase of the gas-amplified current with the time (some minutes) during which it was allowed to flow. In the present experiments with $E/p = 45$ v cm⁻¹ (mm Hg)⁻¹ the effect, however, was very small, but in further experiments at $E/p = 40$ v cm⁻¹ (mm Hg)⁻¹ and $p = 400$ mm Hg it was found that a gas-amplified current of 2×10^{-9} A increased by as much as 40% if allowed to flow for one minute. Measurement of the initial current before and after the passage of the gas-amplified current showed that the externally maintained current had increased by about 15%. The previous investigations in this laboratory of such effects had shown them to be due to the presence of oxide layers on the cathode surface, and in nitrogen it had been found possible to remove the effect altogether by a glow discharge treatment of the electrode in that gas. Clearly, in the present experiments in air, glow discharge treatment in the same gas would only thicken the oxide layer. Glow discharge treatment in another gas, e.g. H₂, which could remove the oxide layer, was also thought to be undesirable because of the adsorption of that gas on surfaces and its subsequent desorption as an impurity into the air being investigated.

Accordingly, the aluminium cathode was changed for one of silver on which any oxide layer so formed is much less tenacious. Experiment showed that this silver cathode was completely satisfactory, confirming the above view of the cause of the effect, and no increase of ionization current with time was observed even at currents of the order of 10^{-7} A. The apparatus was then considered to be in a state where reliable information about the ionization coefficients and mechanism of breakdown could be obtained.

4.2. Detailed Results

Measurements were made, using the silver cathode, for $35 \leq E/p \leq 40$ v cm⁻¹ (mm Hg)⁻¹ for pressures between about 400 and 1000 mm Hg and values of pd up to 2300 mm Hg cm. About fifty ($\log(I/I_c), d$) curves were obtained and a selection of typical curves covering the range of values of pressure and E/p used is given in Fig. 4 (a)–(d). The form of all these curves is in agreement with Eqn (4), and this is consistent with the view that the growth was in all cases due to the action of primary and secondary ionization processes in the absence of any significant space charge effects. Accordingly, values of the appropriate coefficients α'/p and ω/α' can be found from the curves; these values are given in Fig. 4 for the respective graphs.

Numerical analysis of the experimental results on the growth of currents was carried out for the data obtained for a single sample of gas at a given pressure and also for the data for different samples at the various pressures. Typical results are given in Table 1. From this table it can be seen that the various values of α'/p relating to a given gas sample all agreed to within $\pm 2\%$ but that the agreement between the values of α'/p from different samples was only to within $\pm 12\%$. These samples of gas were not all at the same pressure so that some of this variation may well be due to a pressure effect probably involving a (see § 4.3), but at a given pressure the variation is attributable to slight differences in the composition of the

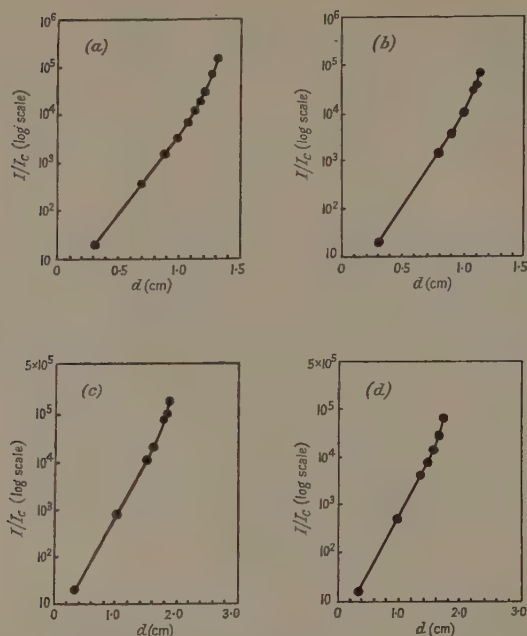


Fig. 4. Typical $(\log(I/I_c), d)$ curves in air using an Ag cathode: the points represent experimental values and the full line curve is calculated from Eqn (4) with the values of α'/p and ω/α' given below.

- (a) $E/p = 40 \text{ v cm}^{-1} (\text{mm Hg})^{-1}$, $p = 402 \text{ mm Hg}$, $\alpha'/p = 19 \times 10^{-3}$,
 $\omega/\alpha' = 33 \times 10^{-6}$, $I_c \sim 5 \times 10^{-13} \text{ A}$.
- (b) $E/p = 38 \text{ v cm}^{-1} (\text{mm Hg})^{-1}$, $p = 700 \text{ mm Hg}$, $\alpha'/p = 12.6 \times 10^{-3}$,
 $\omega/\alpha' = 30 \times 10^{-6}$, $I_c \sim 3 \times 10^{-13} \text{ A}$.
- (c) $E/p = 36 \text{ v cm}^{-1} (\text{mm Hg})^{-1}$, $p = 700 \text{ mm Hg}$, $\alpha'/p = 7.6 \times 10^{-3}$,
 $\omega/\alpha' = 26 \times 10^{-6}$, $I_c \sim 5 \times 10^{-13} \text{ A}$.
- (d) $E/p = 35 \text{ v cm}^{-1} (\text{mm Hg})^{-1}$, $p = 1008 \text{ mm Hg}$, $\alpha'/p = 5.1 \times 10^{-3}$,
 $\omega/\alpha' = 65 \times 10^{-6}$, $I_c \sim 2 \times 10^{-13} \text{ A}$.

$J_0 \simeq 10I_c \text{ A cm}^{-2}$. (The cathode in (d) had been affected by the passage of a high voltage spark.)

samples, which are shown up in this work. In former investigations on air (Paavola 1929, Masch 1932, Sanders 1932, Hochberg and Sandberg 1942, Llewellyn Jones and Parker 1950, 1952, Harrison and Geballe 1953, Prasad 1959) the error in determining α' was probably about 5 to 10% so that the degree of variation disclosed in the present work would not have been readily detectable in the previous work. However, it is interesting to note that the mean values of α'/p obtained from sample to sample in the present investigation are in general agreement with previous results, as is shown in Fig. 5 which gives all published results for comparison.

In order to make a significant comparison between the values of the secondary ionization coefficient ω/α' obtained at various values of E/p and at various gas pressures, it is clearly necessary not only to measure α'/p to a sufficient order of

Table 1. Experimental Values of α'/p

$E/p=35$		$E/p=36$		$E/p=38$		$E/p=40$	
p	$\alpha'/p \times 10^3$	p	$\alpha'/p \times 10^3$	p	$\alpha'/p \times 10^3$	p	$\alpha'/p \times 10^3$
1002	5.0	1002	7.1				
995	$\begin{cases} 4.6 \\ 4.6 \end{cases}$			995	12.1		
1008	5.1	1003	7.1				
1008	5.0	1006	$\begin{cases} 7.4 \\ 7.1 \end{cases}$				
1007	4.9						
1005	4.7						
704	$\begin{cases} 5.6 \\ 5.7 \end{cases}$			704	$\begin{cases} 12.5 \\ 12.4 \end{cases}$		
700	5.4	700	7.7	700	12.6	700	19.0
		701	7.6	701	12.0		
702	4.9	700	7.6	704	11.9		
712	5.0	708	7.6	706	11.5		
708	5.5			705	12.0		
700	5.4			703	11.7		
704	5.5			702	11.2		
	$\begin{cases} 5.4 \\ 5.5 \\ 5.6 \end{cases}$						
708							
703	5.2						
704	5.2						
		402	7.5	402	13.1	402	19.0
		401	7.9	403	12.6	403	19.0

p in mm Hg; α'/p in $\text{cm}^{-1} (\text{mm Hg})^{-1}$; E/p in $\text{v cm}^{-1} (\text{mm Hg})^{-1}$.

In this Table the values of α'/p apply to the *same* gas sample only for those cases when the pressure is the same; for all other cases the gas sample is different for each determination of α'/p .

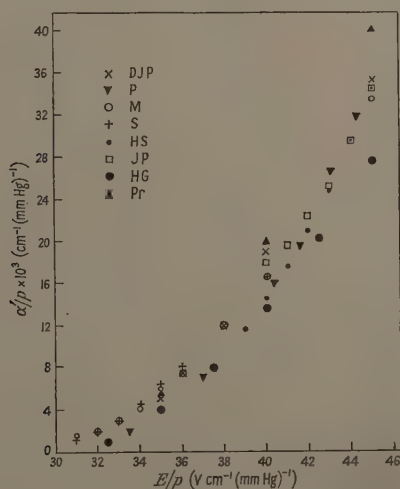


Fig. 5. Comparison of present experimental results in air for the apparent primary ionization coefficient with those obtained by other workers. DJP, present work, mean values; P, Paavola 1929; M, Masch 1932; S, Sanders 1932; HS, Hochberg and Sandberg 1942; JP, Llewellyn Jones and Parker 1952; HG, Harrison and Geballe 1953; Pr, Prasad 1959, mean values from Table 1).

accuracy to allow the determination of ω/α' to within the required limits of say 20%, but also to consider samples of gas for which the primary coefficient is as nearly as possible the same. A suitable set of results for this purpose is given in Table 2 which will now be discussed.

Table 2. Experimental Values of α'/p and ω/α' together with Calculated Values of pd_s for Air with a Silver Cathode

E/p	p	$(\alpha'/p) \times 10^3$	$(\omega/\alpha') \times 10^8$	$(pd_s)_{\text{calc.}}$	sequence
40	402	19.0	33	544	2
	700	19.0	27	552	7
38	402	13.1	21	862	3
	700	12.6	30	820	6
	995	12.2	30	859	5
36	401	7.9	22	1349	4
	700	7.6	26	1398	1
	1006	7.4	21	1464	9
35	708	5.6	12	2022	8
	1008	5.1	65	1896	10

E in v cm^{-1} , p in mm Hg , α' in cm^{-1} , d_s in cm .

(Note: a spark occurred between run 9 and run 10—see text.)

4.3. Ionization Coefficients and Gas Pressure

It can be seen from Tables 1 and 2 that although the gas pressure was changed by more than a factor of 2 from 400 mm Hg to 1000 mm Hg there were only small changes in the values of either α'/p or ω/α' at a given value of E/p .

Thus at $E/p = 35 \text{ v cm}^{-1} (\text{mm Hg})^{-1}$ the mean value for the determinations of α'/p at pressures of about 700 mm Hg was 5.3×10^{-3} , while the mean for determinations at pressures of about 1000 mm Hg was 4.8×10^{-3} (see Table 1). Again at $E/p = 36 \text{ v cm}^{-1} (\text{mm Hg})^{-1}$ the mean value of α'/p from measurements at about 700 mm Hg is 7.6×10^{-3} , while that from measurements at about 1000 mm Hg is 7.2×10^{-3} . These results are consistent with the view that there is a small, just detectable variation of α'/p with pressure, but that this variation is very nearly within the limits of the experimental error when different samples of gas are involved. Thus a dependence of α/p on pressure can not be eliminated, and as such a dependence is significant when considering the type of attachment process occurring in these conditions this effect will be considered in fuller detail elsewhere.

Considering now the secondary ionization coefficient, it can be seen from Table 2 that there is no significant variation of ω/α' with pressure. This result is in marked contrast to the case of hydrogen, in which gas it has been shown (Davies, Dutton and Llewellyn Jones 1958) that ω/α is strongly dependent on gas pressure as well as on E/p . The observed reduction of ω/α with increasing pressure in hydrogen has been shown to be due to the decrease in photoelectric emission as a result of the greater destruction of excited molecules in collision with neutral gas molecules at higher gas pressures. Since no such marked

dependence of ω/α' on gas pressures occurs in air, it is concluded that *either* photoelectric effects in air at high values of pd are negligible, *or* that the cross section for the destruction of excited molecules in collisions of the second kind is very small.

These are some indications, however, from other investigations (Dutton, Haydon, Llewellyn Jones and Davidson 1953) that the photoelectric effect at the cathode plays an important role in ionization growth in air at pressures of about one atmosphere, so that it is reasonable to conclude that the cross section for collisions of the second kind in air is small.

4.4. Secondary Ionization and the State of the Cathode Surface

It has been shown in §4.1 that the nature of the cathode surface plays an important role in the growth of ionization in air at $pd_s \sim 250$ mm Hg cm. Since it has been established (Dutton, Haydon and Llewellyn Jones 1952, Davies, Dutton and Llewellyn Jones 1958) that the occurrence of a spark can have profound local effects in changing the properties of the cathode surface, care was taken in this work to try to avoid the production of a spark throughout the course of the investigation of current growth. On one occasion (at the end of run 9, Table 2), however, an inadvertent reduction of pressure established the conditions for sparking, and a short discharge occurred which, however, was quickly quenched by the voltage drop in the $5\text{ M}\Omega$ limiting resistor. Use was made of this event to investigate the effects of the resulting change in the cathode at the highest values of pd_s used in this work.

It can be seen at once from Table 2 that there is a significant difference between the value of ω/α' obtained at the two different gas pressures at $E/p = 35\text{ v cm}^{-1} (\text{mm Hg})^{-1}$, although there is no evidence from the other results of a dependence of ω/α' on gas pressure. It seemed likely, therefore, that this change in ω/α' was due to a change in the state of the cathode surface due to the spark between run 9 and run 10. That this was in fact the case was confirmed by two further experiments. First, using the cathode which had been sparked in air, measurements were carried out at $E/p = 35\text{ v cm}^{-1} (\text{mm Hg})^{-1}$ at a pressure of 703.8 mm Hg; the results showed a high value of ω/α' (58×10^{-6}) characteristic of the sparked surface. The cathode was then removed and cleaned and another set of results obtained using the cleaned cathode at a pressure of 701.6 mm Hg; in this case the value of α'/p was found to be 4.9×10^{-3} and of ω/α' was 12×10^{-6} , i.e. the low value characteristic of the polished surface before sparking.

It has previously been pointed out (I) that investigation of ionization discharges in air involves complications due to the oxidation of the electrode in the process. This causes difficulty even in measuring extremely small pre-breakdown currents, as the electrical properties of the cathode are greatly influenced by the presence of thin oxide films (Llewellyn Jones and Morgan 1953). In the original work in air (I) two effects of the oxidation of the cathode were found. One was the change of secondary emission attributed to the presence of positive ions on an oxide layer, and the other effect (important in growth experiments) was due to the reduction of the photoelectric efficiency of the cathode and the consequent reduction of the magnitude of the current I_0 maintained by the external radiation. Even when care was taken to maintain and monitor the intensity of the radiation from the stabilized arc, the emission I_0 was considerably reduced during the course of the experiments by oxidation of the cathode surface; indeed, cases have been previously reported (I) in which the photoelectric effect had been practically eliminated. These effects were considerable at pressures less than atmospheric

but on account of the occurrence of higher current densities at the higher pressures, the effects are likely to be greatly enhanced at the high gas pressures used in the present work. For these reasons, as has been previously mentioned, care was taken to avoid the production of an electric spark, and therefore the experimental determination of the sparking potential was not undertaken until the other work was completed, in order to preserve the consistency of the electrode properties during the growth experiments. On completion of the final ($\log(I/I_c)$, d) curve mentioned in § 4.4, the gap distance was gradually increased (adjusting the voltage to keep the ratio E/p constant at $35 \text{ v cm}^{-1} (\text{mm Hg})^{-1}$) until a spark occurred, as observed visually and also by the anode voltage collapse. The current, however, was not allowed to rise beyond a few μA and was quickly quenched by the presence of a $5 \text{ M}\Omega$ resistor in the anode circuit. The sparking potential obtained experimentally in this way was $79 \pm 0.7 \text{ kv}$. This value agreed well with the value of $81 \pm 1.5 \text{ kv}$ at a $pd_s = 2300 \text{ mm Hg cm}$ calculated by inserting the measured values of the ionization coefficients in Eqn (3). A subsequent determination would have served little purpose in these circumstances because ω/α' would have changed significantly as shown in Table 2. Thus it can be seen that, even at the highest value of the parameter pd_s so far investigated, the growth of pre-breakdown ionization, and the subsequent setting of the criterion for the static sparking potential of air in uniform fields, is a consequence of the action of primary and secondary ionization processes, modified by the process of attachment, in accordance with the Townsend-type equations (3) and (4).

§ 5. CONCLUSIONS

Measurements of pre-breakdown ionization currents show that the spatial growth of pre-breakdown ionization at values of pd_s up to 2300 mm Hg cm is a consequence of the action of primary, α , and secondary ionization, ω , processes in the absence of significant space charge, but modified by the process of attachment a . This extends the upper limit of the value of pd_s previously investigated in this way. Using the values of α' ($=\alpha-a$) and ω/α' deduced from the observed growth of pre-breakdown ionization currents at a value of $E/p = 35 \text{ v cm}^{-1} (\text{mm Hg})^{-1}$ in the theoretical sparking criterion (Eqn (3)), the sparking potential $(E/p)pd_s$ was calculated for uniform fields and was found to be equal to that measured within the limits of the experimental error. This is consistent with the view that the criterion which sets the static sparking potential is the consequence of the same ionization and attachment processes which led to the spatial growth, and there is no evidence from these results of the introduction of any new process (i.e. one not conforming to Eqn (4)) for setting the sparking potential in air within the full range of pd_s up to 2300 mm Hg cm .

It is also shown that while both the ionization coefficients α'/p and ω/α' are almost solely dependent on the parameter E/p alone in the range $400 < p < 1000 \text{ mm Hg cm}$ (in that within this range any pressure dependence is small), there appears to be a small decrease of α'/p with increasing pressure which is just greater than the experimental error. The dependence of ω/α' on E/p alone indicates that the destruction of excited molecules in collisions of the second kind does not appear to be an important process in ionization growth in air as it is in hydrogen.

Even at these high values of pd_s in air, the state and nature of the cathode surface have considerable influence on the apparent secondary ionization coefficient. This

indicates that the production of secondary electrons at the cathode can play an important role in the mechanism setting the criterion for breakdown even at voltages up to about 80 kv.

ACKNOWLEDGMENTS

The authors acknowledge with gratitude the assistance which has been provided by the Electricity Supply Research Council in the provision of apparatus. We should also like to thank F. M. Harris for assistance with the experimental work in the later stages of the investigation. One of us (R.W.P.) is grateful to the University College of Swansea for the award of a Postgraduate Scholarship 1955-59 which enabled him to take part in the investigation.

REFERENCES

- BRUCE, F. M., 1947, *J. Instn Elect. Engrs*, **94**, 138.
 CROMPTON, R. W., DUTTON, J., and HAYDON, S. C., 1956, *Proc. Phys. Soc. B*, **69**, 2.
 DAVIES, D. K., DUTTON, J., and LLEWELLYN JONES, F., 1958, *Proc. Phys. Soc.*, **72**, 1061.
 DUTTON, J., HAYDON, S. C., and LLEWELLYN JONES, F., 1952, *Proc. Roy. Soc. A*, **213**, 203.
 DUTTON, J., HAYDON, S. C., LLEWELLYN JONES, F., and DAVIDSON, P. M., 1953, *Brit. J. Appl. Phys.*, **4**, 170.
 DUTTON, J., LLEWELLYN JONES, F., and PALMER, R. W., 1959, *Proc. 4th Int. Conf. on Ionization Phenomena in Gases, Uppsala* (Amsterdam: North-Holland), p. 137.
 GEBALLE, R., and REEVES, M. L., 1953, *Phys. Rev.*, **92**, 867.
 HARRISON, M. A., and GEBALLE, R., 1953, *Phys. Rev.*, **91**, 1.
 HOCHBERG, B., and SANDBERG, E., 1942, *J. Tech. Phys., Moscow*, **12**, 65.
 LLEWELLYN JONES, F., 1957, *Ionization and Breakdown in Gases* (London: Methuen).
 LLEWELLYN JONES, F., and MORGAN, C. G., 1953, *Proc. Roy. Soc. A*, **218**, 88.
 LLEWELLYN JONES, F., and PARKER, A. B., 1950, *Nature, Lond.*, **165**, 1960.
 ——— 1952, *Proc. Roy. Soc. A*, **213**, 185.
 LOEB, L. B., and MEEK, J. M., 1941, *Mechanism of the Electric Spark* (Stanford, California: University Press).
 MASCH, K., 1932, *Arch. Elektrotech.*, **26**, 589.
 MASSEY, H. S. W., 1950, *Negative Ions* (Cambridge: University Press).
 PAAVOLA, M., 1929, *Arch. Elektrotech.*, **22**, 443.
 PENNING, F. M., 1938, *Ned. Tijdschr. Natuurk.*, **5**, 33.
 PRASAD, A. N., 1959, *Proc. Phys. Soc.*, **74**, 33.
 RAETHER, H., 1939, *Z. Phys.*, **112**, 464.
 ——— 1959, *Proc. 4th Int. Conf. on Ionization Phenomena in Gases, Uppsala* (Amsterdam: North Holland), p. 105.
 SANDERS, F. H., 1932, *Phys. Rev.*, **41**, 667.

On Resonant Charge Transfer in Ionized Dense Gases

By IOVITZU POPESCU

Physics Institute of the RPR Academy, Bucharest

MS. received 22nd February 1961

Abstract. When a feebly ionized gas is compressed until the mean distance between atoms decreases down to approximately less than ten times an atomic radius, the positive charge is not carried by the ion in motion but rather jumps resonantly from atom to atom. This statement is arrived at by comparing the mean time of flight of the positive ion between two collisions with the resonant transfer time of the electron from the atom to the next positive ion.

THE simple hypothesis (Sena 1946) concerning the special role of the resonant charge transfer in the kinetics of positive ions through parent gases, seems to be sufficiently tested†. The relations derived from the corresponding model of ions moving in 'relays' generally hold true only for relatively small densities N of gas atoms, when the mean distance $N^{-1/3}$ is much larger than the radius of the effective collision region $(Q/\pi)^{1/2}$, Q being the transfer cross section.

The present paper briefly analyses the case $N^{-1/3} \simeq (Q/\pi)^{1/2}$; accordingly, a qualitatively different picture concerning the motion of positive charge in gases will occur.

Suppose a relatively small number of singly ionized atoms in the parent gas to be scattered. The positive charge will jump resonantly from one atom to the other with a frequency so high that the configuration of the atoms ought to be practically considered as frozen. If we use the simple model of the hydrogen molecule ion (Pauling and Wilson 1935) for the system consisting of two neighbouring ions and the electron interchanging between them, the corresponding lapse of time of the jump will be

$$\tau = \hbar / |\Delta E| \quad \dots\dots (1)$$

ΔE being the energy difference between the symmetric and antisymmetric combination of the wave functions localized on each ion; now, for our purpose, it will be sufficient to use the asymptotic expression ($R \gg a_0$)

$$\Delta E = -\frac{4}{3} \left(\frac{137^2}{mc^2} \right)^{1/2} \alpha^3 (2I)^{3/2} \frac{R}{a_0} \exp \left[-\alpha \left(\frac{137^2 \times 2I}{mc^2} \right)^{1/2} \frac{R}{a_0} \right] \dots\dots (2)$$

where R is the distance between the two ionic centres, I the first ionization

† For further literature about this problem see Badareu and Popescu (1959), Dalgarno (1958), Kagan (1958), Kushnir, Paliuh and Sena (1959), and Badareu, Popescu and Iova (1960).

energy, a_0 the radius of the first Bohr orbit, c the velocity of light in vacuum, m the rest mass of the electron, and α a correction factor of the hydrogen-like wave function, used in this computation, which is consistent with the different experimental data of the transfer cross section (Popescu and Ionescu 1960).

The relations (1) and (2) lead to a practically exponential dependence of τ on R , such that the transition of the positive charge occurs with the greatest probability at the nearest atom. Once the starting point has been selected, the charge will travel a well-determined path, the mean distance between atoms being minimal and equal to $\beta N^{-1/3}$ all along the path. The empirical value of β , determined by means of models, in the three-dimensional case is approximately 0.56. A typical spatial model used consists of 400 'atoms' (plasticine balls a few millimetres in diameter, suspended by threads at a distance z from the x, y plane), arranged randomly in a volume of $90 \times 90 \times 90 \text{ cm}^3$; the coordinates x, y, z were extracted from an urn containing 90 numbers. In the two-dimensional case the minimal mean distance between atoms is approximately $0.75 N^{-1/2}$ and in the one-dimensional case obviously it is N^{-1} .

Without entering into further details, we shall in the following approximate the real situation replacing R by $0.56 N^{-1/3}$.

In order to estimate the limit beyond which the movement of the positive charge in gases is better described by the model above than by that generally used (according to which the positive charge is accompanied all along by the atomic rest) we shall compare τ with the mean time

$$\tau_1 = 1/vQN, \quad \dots\dots(3)$$

the latter being the time of flight of the positive ion between two successive collisions, where the transfer cross section decreases slowly with the increase of the relative ion-atom velocity v (Popescu and Ionescu 1960). Hence, an orientative quantitative picture is given in the Table, in which, for a series of gases at 300°K and vapours, are given the distances R_1, R_{10}, R_{50} and the corresponding pressures p_1, p_{10}, p_{50} , for which τ_1/τ has the values 1, 10, 50 respectively (R is given in units of the corresponding atomic radius a ; this is defined as the radius of the sphere which contains 75% of the external electron cloud and is computed with the help of the hydrogen-like wave function corrected consistently by means of experimental charge transfer cross section data, as shown by Popescu and Ionescu (1960); the correcting factor α , used in the computation of both τ and a , is given in the third column of the Table).

The result is that, as a general feature, for a given $\tau_1/\tau \geq 1$, R/a has almost the same value for all the gases and vapours shown in the Table. At the same time, R/a may be compared with the corresponding radius of the transfer cross section $(Q/\pi a^2)^{1/2}$. Should the condition $\tau_1 \simeq \tau$ hold, then the quantitative description of the movement of the positive charge is hampered by its travelling along the path, partially carried by the ion and partially jumping; for $\tau_1 \gtrsim 10\tau$, however, the conduction of the positive charge is in many ways similar to that which seems to occur on semiconductor impurities at low temperatures.

Thus, for pressures of $p > p_{10}$ approximately, the diffusion coefficient $D = R^2/3\tau$ and the mobility, using Einstein's relation, increases practically exponentially with decrease of R :

$$\mu = 0.1e/kTN^{2/3}\tau. \quad \dots\dots(4)$$

Atom	I (ev)	α	$a \times 10^8$ (cm)	$(Q/\pi a^2)^{1/2}$	R_1/a	p_1 (atm)	R_{30}/a	p_{10} (atm)	R_{60}/a	p_{30} (atm)	300°K
He	24.5	0.70	1.10	3.2	6.6	16.8	4.8	45.0	3.0	190.0	}
Ne	21.5	0.68	1.20	3.4	7.2	10.1	5.4	23.8	3.8	70.0	
A	15.7	0.71	1.36	3.8	7.1	7.2	5.4	16.4	3.8	46.4	
Kr	14.0	0.72	1.42	4.0	7.2	6.1	5.4	14.1	4.0	36.2	
Xe	12.1	0.69	1.59	4.1	7.1	4.5	5.4	10.3	4.0	25.5	
Hg	10.4	0.66	1.78	4.2(960°K)	7.0	10.0(790°K)	5.1	24.0(900°K)	3.5	100.0(1070°K)	
K	4.3	0.60	3.10	4.2(1100°K)	6.5	3.8(1190°K)	4.4	13.5(1380°K)	—	—	
Cs	3.9	0.42	4.60	3.2(1000°K)	6.7	0.8(960°K)	4.7	3.0(1130°K)	3.0	10.0(1420°K)	

The mobility μ_1 which the positive ion might have under these conditions is negligibly small:

$$\mu_1 = e / (2\pi M k T)^{1/2} Q N, \quad \dots\dots (5)$$

where M is the ion mass, k Boltzmann's constant and T the absolute temperature (Badareu and Popescu 1959).

Finally one may say that the customary treatment of the movement of positive ions in parent gases can no longer be applied to concentrations of gas atoms greater than approximately $(0.56/R_{10})^3$. The crude model outlined above may, under these conditions, be considered as a first approximation.

ACKNOWLEDGMENTS

The author is greatly indebted to Acad. Prof. Dr. Eugen Badareu for most helpful discussions on this matter; thanks are due also to the *Proceedings of the Physical Society* referee for valuable comments.

REFERENCES

- BADAREU, E., and POPESCU, I., 1959, *Stud. Cercet. Fiz.*, **4**, 689 (English translation, 1960, *Rev. Phys. Acad. RPR*, **1**, 41).
 BADAREU, E., POPESCU, I., and IOVA, I., 1960, *Rev. Phys. Acad. R.P.R.*, **3-4**, 287.
 DALGARNO, A., 1958, *Phil. Trans. Roy. Soc. A*, **250**, 426.
 KAGAN, YU. M., 1958, *Izv. Akad. Nauk S.S.S.R., Phys. Ser.*, **22**, 702.
 KUSHNIR, R. M., PALIUH, B. M., and SENA, L. A., 1959, *Izv. Akad. Nauk S.S.S.R., Phys. Ser.*, **23**, 1007.
 PAULING, L., and WILSON, E. B., 1935, *Introduction to Quantum Mechanics* (New York: McGraw Hill).
 POPESCU, I., and IONESCU, N., 1960, *Proc. Phys. Soc.*, **75**, 807.
 SENA, L. A., 1946, *J. Exp. Theor. Phys.*, **16**, 734.

Measurements of Rotational Energy Distributions in Ionic Collisions

BY E. M. REEVES† AND R. W. NICHOLLS

Department of Physics, University of Western Ontario, London, Canada

MS. received 28th July 1960, in final form 27th April 1961

Abstract. The measured rotational intensity distribution of N_2^+ First Negative bands excited by 1 mev protons indicates that the rotation of the molecules is not greatly affected by the collisions. Measured rotational temperatures compare favourably with laboratory temperatures. Similar observations on N_2^+ bands excited by 1 to 3 kev Li^+ ions show that these collisions appear to cause a marked departure from Boltzmann distribution of rotational energies. Energy levels of high and of low quantum numbers are enhanced in population.

§ 1. INTRODUCTION

THE rotational energy distribution of molecules in a gas is determined by the environment to which they are subjected. In principle it is possible to learn something of the environment, and of the collision processes taking place in the gas, by measuring the rotational energy distribution of the molecules. One convenient means of doing this is through the measurement, in emission or absorption, of the intensity distribution in rotational lines in band spectra of the molecules concerned.

It is well known (Herzberg 1950) that if thermal equilibrium exists, and if there is no significant amount of self-absorption in the gas, that the intensity $I_{K'K''}$ of the $K'K''$ line of an emission band is given by

$$I_{K'K''} = \text{const. } S_{K'} \nu_{K'K''}^4 \exp \left[- \frac{hcB_{K'} K' (K' + 1)}{kT_{\text{rot}}} \right] \quad \dots (1)$$

and thus that a plot of $\log I_{K'K''}/S_{K'}$ against $K'(K' + 1)$ will be linear and of slope $-hcB_{K'}/kT_{\text{rot}}$ from which the rotational temperature T_{rot} may be found. T_{rot} may also be inferred from the value of K' at the line of maximum intensity of the band (Johnson 1952). Should the plot be non-linear its shape will nevertheless be determined by the collision processes which cause a departure from the Boltzmann distribution.

Such simple ideas have been used extensively to study excitation processes in the aurora from intensity distributions in bands of N_2^+ (Vegard 1956, Vegard, Tönsberg and Kvifte 1951, Petrie 1953, Sheppard and Hunten 1955, Vallance-Jones and Harrison 1955, Vallance-Jones and Hunten 1960). A number of laboratory experiments have also been performed in recent years in which spectroscopic observations have been made upon 30 to 150 kev ion and electron

† Now at Harvard College Observatory, Cambridge, Massachusetts.

beams in various gases (Vegard 1924, Branscomb, Shalek and Bonner 1954, Fan 1956, Carleton 1957, Roesler, Fan and Chamberlain 1958) in order to understand more of the collision processes which give rise to luminosity in the beams and in the aurora. In many of these experiments, temperatures have been inferred from the intensity distribution of rotational levels of N_2^+ bands.

In the present paper, measurements upon N_2^+ bands excited by low energy (1–3 kev) lithium ions and high energy (0.5–1.5 mev) protons and other hydrogenic ions (H_2^+ , H_3^+) are discussed.

§ 2. EXPERIMENTAL

2.1. H^+ , H_2^+ , H_3^+ Ion Beams

Measurements of rotational temperatures of N_2^+ produced by the passage of ion beams of 0.5 to 1.5 mev through N_2 were made in collaboration with Dr. D. A. Bromley using the facilities of the 3 mev Van de Graaff accelerator at Atomic Energy of Canada Ltd., Chalk River. The ion beam was collimated by a series of 1/16 in. apertures which also acted as baffles in a differential pumping system. The experimental arrangements have been described elsewhere (Reeves, Nicholls and Bromley 1960). The nitrogen gas target pressure in the collision chamber was maintained at $58 \mu\text{Hg}$ as previous work had shown that intensities of N_2^+ features varied linearly with pressure up to this pressure.

The luminous beam was focused upon the slit of a Bausch and Lomb 1.5 m grating spectrograph and the (0, 0) $\lambda 3914 \text{ \AA}$ band of the N_2^+ First Negative system photographed on Kodak 103aF film at a reciprocal dispersion of 15 \AA mm^{-1} . The emulsion response in 15 \AA region of the band head was determined using the internal calibration available from the 2.1 intensity alternation between adjacent lines of the R branch.

2.2. Li^+ Ion Beams

Lithium ion beams of 1–3 kev were produced thermionically in an accelerator which has been described in greater detail elsewhere (Pleiter 1956, Nicholls and Pleiter 1956, Reeves 1960). Luminous beams in N_2 were focused upon the slit of an f/3.5 Applied Research Laboratories Raman 3 prism spectrograph, and the $\lambda 4278$ (0, 1) N_2^+ First Negative band photographed in each case on Kodak 103aF film at a reciprocal dispersion of 12 \AA mm^{-1} in about 10 hours. The response of the emulsion was determined with the aid of a density wedge. Earlier experiments had shown that band intensities increased linearly with pressure up to the pressure of $25 \mu\text{Hg}$ at which the collision chamber was maintained.

§ 3. RESULTS

3.1. 0.5 to 1.5 MeV Beams of H^+ and H_3^+ in N_2

A typical $\log I_{K'K''}/K'$ against $K'(K'+1)$ plot for R-branch lines of the (0, 0) N_2^+ First Negative band excited by 1.0 mev protons in N_2 is shown in Fig. 1. Compensation has been made for intensity alternation between adjacent spectrum lines so as to obtain a single plot for the whole R branch rather than two parallel plots for even and odd K' respectively. The linearity of the plot in Fig. 1 suggests the existence of a Boltzmann distribution in the rotational

energy levels of the upper ($B^2\Sigma_u^+$) state of the transition. The rotational temperature $276 \pm 10^\circ\text{K}$ derived from the slope agrees well with the laboratory temperature of 291°K .

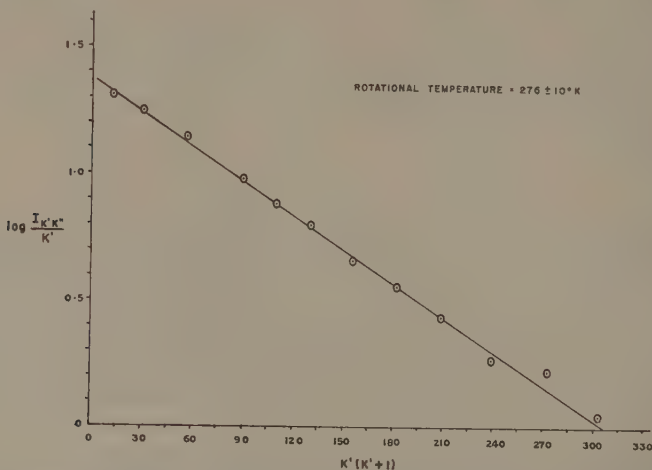


Fig. 1. Variation of $\log I_{K'K''}/K'$ with $K'(K'+1)$ for lines of the $(0, 0) N_2^+$ First Negative band (λ 3914 Å) excited by a beam of 1 mev protons in N_2 at a pressure of 50 μHg .

Temperatures of $301 \pm 80^\circ\text{K}$ were also inferred from the K' value of the line of maximum intensity, of the same band, excited by 0.5 mev protons and 1.5 mev H_3^+ ions. The uncertainty of $\pm 80^\circ\text{K}$ was due to an uncertainty of ± 1 in K' .

The linearity of Fig. 1 together with the good agreement between laboratory and rotational temperatures indicate that hydrogenic ion excitation of N_2^+ at energies of about 1 mev has little apparent effect upon the rotational energy distribution of the target molecules.

This does not necessarily appear to hold in less energetic ionization collisions by heavier ions as pointed out below.

3.2. 1–3 keV Beams of Li^+ in N_2

A microdensitometer trace of the rotational structure of the N_2^+ First Negative $(0, 1) \lambda 4278$ band excited in a 2 keV Li^+ beam in N_2 is shown in Fig. 2. It is typical of results obtained in the 1–3 keV energy range. The first two rotational lines of the R branch are obscured by the $Li\ I$ line at 42 723 Å. Marked differences in profile are observed between traces such as Fig. 2 and those of bands excited by protons. The R branch rises steeply to a maximum at R(6) and falls to zero at R(16) for proton excitation. It is greatly extended in lithium ion excitation and overlaps the $(1, 2)$ band at 4236.5 Å. (A similar effect in unresolved bands has been discussed by Smyth and Arnot (1930) in their comparison between electron and canal-ray excitation of N_2^+ .) The perturbation at $K'=39$ (Childs 1939) caused by the $A^2\Pi$ state of N_2^+ is also seen in Fig. 2 by the displacement of the P(38) line near R(14).

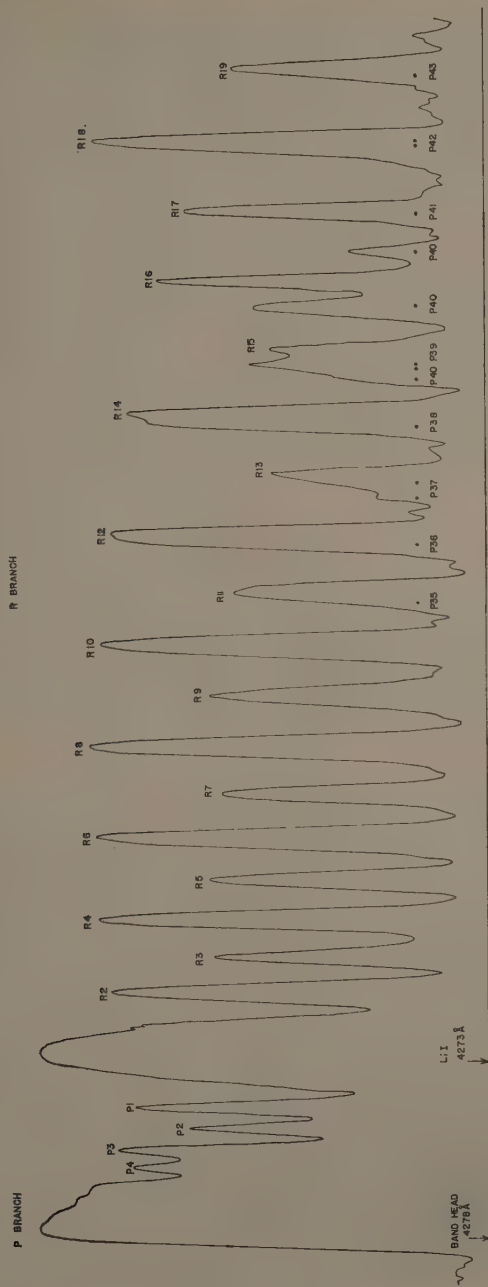


Fig. 2. Microphotometer trace of the $(0, 1)$ N_2^+ first negative band ($\lambda 4278 \text{ \AA}$) excited by a beam of 2 kev lithium ions in N_2 at a pressure of 24 μHg .

Comparative plots are shown in Fig. 3 of $\log I/K'$ against $K'(K'+1)$ for the (0, 1) First Negative band excited by 3.2 kev and 2.0 kev lithium ions. The curves have been arbitrarily set at a point of common tangency at $K'=7$, through which point a straight line is also drawn whose slope is consistent with laboratory temperature. Such a linear plot would be expected if the lithium ion excitation collisions were comparable in all respects with those involving protons and other hydrogenic ions. The departure from thermal equilibrium in a manner which emphasizes high and low quantum numbers is evident in Fig. 3 and the effect appears to be more pronounced for 3.2 kev ions than for 2.0 kev ions.

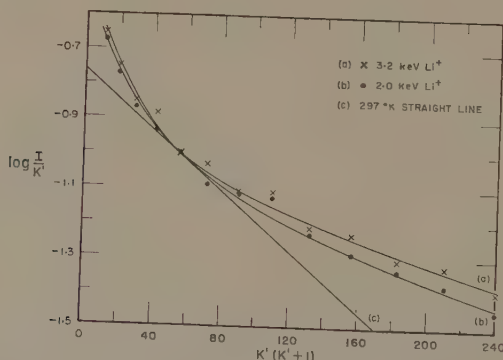


Fig. 3. Variation of $\log I_{K'K'}/K'$ with $K'(K'+1)$ for lines of the (0, 1) N_2^+ First Negative band (λ 4278 Å) excited by beams of (a) 3.2 kev lithium ions and (b) 2 kev lithium ions, in N_2 at a pressure of $24 \mu\text{Hg}$. (c) is a straight line equivalent to the laboratory temperature of 297°K .

§ 4. DISCUSSION

A comparison of Figs 1 and 3 indicates that in the ionization and excitation of N_2 by ionic collision there is a marked difference in the degree of interaction with rotational motion of the target molecules between 1 mev protons and 2 kev lithium ions. The linearity of Fig. 1 implies that the protons interact solely with the electron charge cloud of the target molecule. This results in the formation of $N_2^+(B^2\Sigma_u^+)$ by ionization, and radiation of the First Negative bands. The thermal energy distribution of rotational levels appears to be unaffected in such collisions. Thus the ionization and excitation of N_2^+ by mev protons is quite similar (as might be expected) to excitation by electrons of a few hundred electron volts energy which have about the same velocity.

On the other hand, the departure from linearity of the plots of Fig. 3 indicates that in the less energetic collisions between the target molecules and Li^+ ions, a severe change in the rotational motion of the molecule results in addition to the ionization and excitation of the electron charge cloud. The effect appears to become more pronounced with increase in energy of the ion beam, and the high ($K' \sim 10$) and the low ($K' \sim 1$) rotational levels appear to become more highly populated than would be required for a thermal distribution at laboratory temperature.

Similar qualitative observations of Smyth and Arnot (1930) in canal-ray excitation of N_2^+ bands have been referred to above. Oldenberg (1934) specifically cites excitation by ions as one case in which the internal motion of a target molecule may be significantly changed by collisions. He also points out (Oldenberg 1957) that in eccentric atomic collisions, the collision duration may be significantly longer than that predicted by elementary considerations as a result of the effect of the molecular rotation on molecular potentials. The collision duration may in fact be as long as one rotational period of the diatomic molecule temporarily formed during the atomic collision. Extension of his arguments to the case of ion (or atom)-diatomic molecule collisions makes plausible the hypothesis that the duration of the Li^+-N_2 collisions may also extend to one rotational period of N_2 . In these circumstances, the severe perturbation of rotational motion would not be unexpected. This effect would also probably be enhanced when the mass of the ion beam projectile ($Li=6$, $H=1$) is comparable with that of the reduced mass ($N_2=7$) of the molecular target. The enhancement of the relative populations of high and low rotational energies and the apparent dependence of the magnitude of the effect upon energy of the ion beam still awaits a satisfactory detailed theoretical explanation. Further experiments are in progress.

ACKNOWLEDGMENTS

This work was supported in part by contracts with the Air Force Office of Scientific Research, The Air Force Cambridge Research Center, the Office of Naval Research and in part by research grants from the National Research Council of Canada, The Ontario Research Foundation and the Defense Research Board of Canada. One of us (E. M. R.) gratefully acknowledges the award of an Ontario Research Foundation Fellowship.

REFERENCES

- BRANSCOMB, L. M., SHALEK, R. J., and BONNER, T. W., 1954, *Trans. Amer. Geophys. Union*, **35**, 107.
 CARLETON, N. P., 1957, *Phys. Rev.*, **107**, 110.
 CHILDS, W. H. J., 1939, *Proc. Roy. Soc. A*, **137**, 641.
 FAN, C. Y., 1956, *Phys. Rev.*, **103**, 1740.
 HERZBERG, G., 1950, *Spectra of Diatomic Molecules* (New York: D. Van Nostrand).
 JOHNSON, R. C., 1952, *Introduction to Molecular Spectra* (London: Methuen).
 NICHOLLS, R. W., and PLEITER, D., 1956, *Nature, Lond.*, **178**, 1456.
 OLDENBERG, O., 1934, *Phys. Rev.*, **46**, 210.
 ——— 1957, *Amer. J. Phys.*, **25**, 94.
 PETRIE, W., 1953, *J. Atmos. Terr. Phys.*, **4**, 5.
 PLEITER, D., 1956, *Ph.D. Thesis*, University of Western Ontario.
 REEVES, E. M., 1960, *Ph.D. Thesis*, University of Western Ontario.
 REEVES, E. M., NICHOLLS, R. W., and BROMELY, D. A., 1960, *Proc. Phys. Soc.*, **76**, 217.
 ROESLER, F. L., FAN, C. Y., and CHAMBERLAIN, J. W., 1958, *J. Atmos. Terr. Phys.*, **18**, 890.
 SHEPHERD, G. C., and HUNTEN, D. M., 1955, *J. Atmos. Terr. Phys.*, **6**, 328.
 SMYTH, H. D., and ARNOT, E. C. F., 1930, *Phys. Rev.*, **36**, 1023.
 VALLANCE-JONES, A., and HARRISON, A. W., 1955, *J. Atmos. Terr. Phys.*, **6**, 336.
 VALLANCE-JONES, A., and HUNTEN, D. M., 1960, *Canad. J. Phys.*, **38**, 458.
 VEGARD, L., 1924, *Proc. Roy. Akad. Amsterdam*, **27**, 113.
 ——— 1956, *Geofys. Publ.*, **19**, 9.
 VEGARD, L., TÖNSBERG, E., and KVIFTE, G., 1951, *Geofys. Publ.*, **18**, 4.

On the Extra Reflections in Electron Diffraction Patterns from Thin Evaporated Films of Some of the Face-centred Cubic Metals

By KANWAR BHADUR AND P. V. SASTRY

National Physical Laboratory of India, New Delhi

Communicated by D. W. Pashley; MS. received 13th February 1961

Abstract. Polycrystalline thin films of a number of face-centred cubic metals have been prepared by evaporation on to rock-salt, followed by annealing. In a number of cases, transmission electron diffraction patterns show, in addition to the normal face-centred cubic rings, some extra rings which fit well with those which would be expected from a hexagonal close-packed form of the metals. No hexagonal close-packed rings are observed with aluminium films, and this is correlated with the absence of stacking faults on transmission electron microscope images of aluminium films.

MANY workers have reported the presence of extra rings and spots in the transmission diffraction patterns from thin films of some face-centred cubic metals like gold and silver. The earliest observation of these extra reflections in polycrystalline films was made by Finch, Quarrell and Wilman (1935), see also Quarrell (1937). They explained these rings on the hypothesis of 'basal plane pseudomorphism'. Recent electron diffraction studies have proved beyond doubt that the 'basal plane pseudomorphism' hypothesis is not valid (Pashley 1956). Many of the abnormal streaks and spots observed in the diffraction patterns obtained from single crystalline films of these metals have been attributed to twinning of the lattice and these results have been confirmed by a number of workers (Lassen 1934, Kirchner and Lassen 1935, Bruck 1936, Goche and Wilman 1939, Ogawa, Watanabe and Fujita 1955). However, some spots in these patterns also still remain unidentified (Ogawa, Watanabe and Fujita 1955).

We have examined in detail the transmission diffraction patterns from polycrystalline films of some of the face-centred cubic metals and alloys. The films, about 250 Å in thickness, were obtained by evaporating the pure metals (Au, Ag, Cu and Al of 99.99% and Cd of 99.95% purity) in a vacuum of approximately 10^{-4} mm on freshly cleaved rock-salt substrates maintained at temperatures between 150–250°C. These films on rock-salt substrates were subsequently heat treated at the same temperature for one to two hours, without breaking the vacuum. The transmission diffraction patterns in all cases were recorded at room temperature. A typical transmission diffraction pattern from a gold film is shown in the Plate (Fig. 1 (a)). All the extra lines in this pattern fit perfectly into the scheme of closest packed hexagonal structure with its lattice spacing value $a = a^*/\sqrt{2}$ (where a^* is the normal lattice spacing of the face-centred

cubic structure) and $c/a = 1.63$. The d values of these extra reflections are listed in the Table given below. These results are in agreement with the results of Hirsch, Kelly and Menter (1955) obtained from experiments on beaten gold foil.

Extra Diffraction Rings due to Hexagonal Close-packed Lattice
in Thin Evaporated Films of Gold

hkl	d (obs.) (Å)	d (calc.) (Å)
10 $\bar{1}$ 0	2.50	2.52
10 $\bar{1}$ 2	1.70	1.72
10 $\bar{1}$ 3	1.32	1.33
20 $\bar{2}$ 2	1.02	1.00

We have obtained similar results in the case of thin films of silver, copper, α -solid solution of silver-cadmium and the complete solid solution of silver-gold.

It is well known that stacking faults and dislocations can occur in metals of face-centred cubic structure by a slip occurring in the (111) family of planes. These dislocations can be split up into two partials separated by a faulted region which can be regarded as a thin sheet of lattice of closest-packed hexagonal type (Heidenreich and Shockley 1948). Such stacking faults have been observed in electron microscope examination of thin films of gold (Pashley 1959). In view of the above evidence we attribute the extra reflections observed in our diffraction patterns to reflections from those faulted regions having the closest-packed hexagonal structure. We have failed to observe these extra lines in transmission diffraction patterns from polycrystalline films of pure aluminium (Plate, Fig. 1 (b)). This is again in conformity with the electron microscope evidence of the failure to observe the above type of stacking faults in thin films of aluminium (Whelan, Hirsch, Horne and Bollman 1957, Pashley 1959).

ACKNOWLEDGMENTS

We are thankful to Dr. D. W. Pashley, Tube Investments Research Laboratories, England, for his helpful comments and The Director, National Physical Laboratory of India, for permission to publish this note.

REFERENCES

- BRUCK, L., 1936, *Ann. Phys., Lpz.*, **26**, 233.
 FINCH, G. I., QUARRELL, A. G., and WILMAN, H., 1935, *Trans. Faraday Soc.*, **31**, 1051.
 GOCHE, O., and WILMAN, H., 1939, *Proc. Phys. Soc.*, **51**, 625.
 HEIDENREICH, R. D., and SHOCKLEY, W., 1948, *Reports of Conference on Strength of Solids* (London: Physical Society), p. 1.
 HIRSCH, P. B., KELLY, A., and MENTER, J. W., 1955, *Proc. Phys. Soc. B*, **68**, 1132.
 KIRCHNER, F., and LASSEN, H., 1935, *Ann. Phys., Lpz.*, **22**, 65.
 LASSEN, H., 1934, *Z. Phys.*, **35**, 179.
 OGAWA, S., WATANABE, D., and FUJITA, F. E., 1955, *J. Phys. Soc. Japan*, **10**, 429.
 PASHLEY, D. W., 1956, *Advanc. Phys.*, **5**, 173.
 ——— 1959, *Phil. Mag.*, **4**, 324.
 QUARRELL, A. G., 1937, *Proc. Phys. Soc.*, **49**, 279.
 WHELAN, M. J., HIRSCH, P. B., HORNE, R. W., and BOLLMAN, W., 1957, *Proc. Roy. Soc. A*, **240**, 524.

The Michelson Stellar Interferometer : A Phase Sensitive Variation of the Optical Instrument

By R. C. JENNISON

Nuffield Radio Astronomy Laboratories, Jodrell Bank, University of Manchester

*Communicated by A. C. B. Lovell; MS. received 10th June 1960,
in revised form 7th April 1961*

Abstract. A short summary is given of a variation of the Michelson stellar interferometer. This is an adaptation of part of the principle of the radio-frequency phase-sensitive interferometer developed by the author in 1958 and it enables the phase component associated with the structure of the source to be determined. The technique may also be used to determine the correct relative amplitude of the visibility function of the star at two spacings even when phase and amplitude errors are present.

§ 1. INTRODUCTION

IN an original paper on the stellar interferometer Michelson (1890) predicted that the fringes should reverse in the second maximum of the visibility function from a typical symmetrical source. This reversal is not easy to observe in practice, especially when scintillations are present, and it is even more difficult to determine the smaller changes of phase associated with asymmetry in a stellar object. If both the phase and amplitude of the fringes can be measured in all position angles it is possible to obtain a unique solution for the distribution of brightness over the object and hence to determine its structure. This has been achieved in a radio-frequency system where it was necessary to nullify the errors due to variations in attenuation and phase of the limbs of the interferometer (Jennison 1958). The full realization of the radio-frequency technique in an optical instrument would require the incorporation of a phase switching device and an arrangement to continuously rotate the phase of the fringes. These refinements are omitted from the present design in which the main feature of the radio-frequency system, the use of three slit apertures, is applied to an optical telescope.

§ 2. THE OPTICAL ARRANGEMENT

The optical arrangement is shown in Fig. 1 (*a*) and (*b*). The objective of the telescope is preceded by a slotted mask as shown in Fig. 1 (*a*). For higher resolution it may be fitted with a beam and extending mirrors comprising three parallel slits, one in the centre of the system and the other two spaced equally to either side (Fig. 1 (*b*)). The length of the slits is arranged so that the slits form three independent pairs as shown in the end elevation (Fig. 2 (*a*)). The eyepiece of the instrument is a cylindrical lens whose axis is aligned with the length of the objective slits.

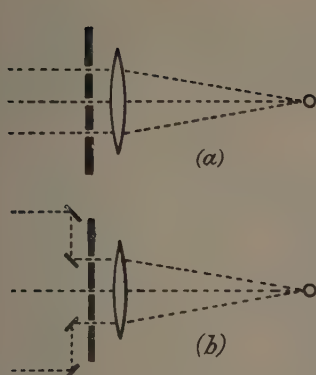


Fig. 1. (a) The ray paths along the axis of the system. The spacing of the slits may be varied by rotating the slit system about an axis through the central slit. (b) The extension of the system by mirrors to form an instrument of wider aperture. The circle on the right represents a cylindrical eyepiece.

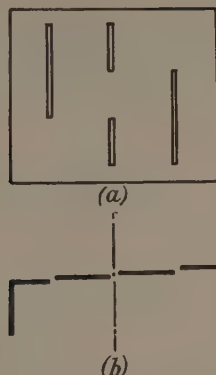


Fig. 2. (a) The arrangement of the slits in the plane of the telescope objective. (b) The arrangement of the slits in echelon to compensate for the foreshortening of the individual slits.

§ 3. PRINCIPLE OF OPERATION

The visibility of the fringe system formed by any pair of slits is in general a complex function given by the component of the Fourier transform of the brightness distribution across the source at the spacing concerned. Thus, if the angular distribution of the source is $F(\theta)$, the Fourier transform $f(x)$ of the distribution may be expressed as

$$f(x) = \int_{-\infty}^{\infty} F(\theta) \exp(2\pi i x \theta) d\theta,$$

where $f(x)$ is in general complex, having a modulus at any value of x corresponding to the visibility criterion given by Michelson,

$$|f(x)| = \frac{I_{\max} - I_{\min}}{I_{\max} + I_{\min}}$$

and a phase angle $\xi(x)$ corresponding to the rotation of $f(x)$ in the complex plane as a result of the partial resolution of certain features of the source (Jennison 1961). Thus a source consisting of two eccentric components, one of which is broad and the other small but bright, would result in a rotation of the phase angle $\xi(x)$ and a corresponding shift in the position of the fringes as x is extended. Viewed with a conventional Michelson stellar interferometer, the effect is to cause the fringe pattern to become centred on the small source at the value of x where the larger source is resolved. The phase information may therefore be determined in principle by observing the position of the fringes relative to the source at all values of the slit spacing but this operation is neither easy nor accurate. The system of three slits described above enables the phase components to be determined without reference to the absolute position of the source.

Illumination by a point source produces three systems of fringes in the field of view. These systems of fringes are separated along the axis of the cylindrical lens. The fringes are parallel to this axis, and the upper and lower sets occur at twice the spacing and are so phased that their maxima are aligned with alternate maxima of the finer central fringes. This is shown in Fig. 3.



Fig. 3. The appearance in the field of view of the fringe patterns from a point source.

In the general case of an arbitrary distribution of brightness across the star the phase of the fringes will be such that they are not aligned and the phase difference may be determined at the larger spacing relative to the shorter spacings. The expression for the intensity distribution of the image along the x axis, perpendicular to the fringes, when monochromatic light passing through one slit interferes with that through another will be of the form

$$I(x)\{1 + |f(x)| \cos [\omega(x) + \xi(x) + \Delta]\} \quad \dots\dots (1)$$

where $I(x)$ is the intensity in the diffraction pattern of the slits and is only slowly varying with x , $\omega(x)$ is the spatial frequency of the fringe system, Δ is the resultant phase difference of phase errors associated with the two slits and $|f(x)|$ and $\xi(x)$ are, as before, the amplitude and phase components of the Fourier transform of the brightness distribution across the source.

We shall refer to the expression within the square brackets as the argument of the fringe system. Thus, if the three slits A, B and C have associated phase errors δ_A , δ_B and δ_C the argument of the fringes when light from slit A interferes with that from slit B will be

$$\omega(AB) + \xi_{AB} + \delta_A - \delta_B. \quad \dots\dots (2)$$

The argument of the fringes when C interferes with B will be

$$\omega(BC) + \xi_{BC} + \delta_B - \delta_C. \quad \dots\dots (3)$$

The argument of the fringes formed between A and C will be

$$\omega(AC) + \xi_{AC} + \delta_A - \delta_C. \quad \dots\dots (4)$$

Adding expressions (2) and (3), the arguments of the fringe systems AB and BC, we obtain

$$\omega(AB) + \omega(BC) + \xi_{AB} + \xi_{BC} + \delta_A - \delta_C = \omega(AC) + \xi_{AB} + \xi_{CB} + \delta_A - \delta_C. \quad \dots\dots (5)$$

Comparing expressions (4) and (5) it will be seen that they represent the arguments of two fringe systems of identical frequency and relative phase

$$\phi = \xi_{AC} - (\xi_{AB} + \xi_{BC}) \quad \dots\dots (6)$$

and if $AB = BC$

$$\phi = \xi_{AC} - 2\xi_{AB} \quad \dots\dots (7)$$

This result is independent of the phase errors δ_A , δ_B and δ_C .

In the case of a simple symmetrical source distribution, if the spacings AB and BC both lie before the first zero of the Fourier transform, then

$$\xi_{AB} = \xi_{BC} = 0.$$

In these circumstances $\phi = \xi_{AC} = 0$ if AC lies within the first maximum and $\phi = \xi_{AC} = \pi$ if AC lies within the second maximum.

In the general case of a complex source distribution the complete phase function may be mapped by varying the spacings of the apertures and recording the relative phases of the fringe systems. It should be noted that it is not necessary for the spacing AB to equal spacing BC in order to measure the phase, provided that, if $AB \neq BC$, both the fringe systems AB and BC are displayed and this sum is recorded.

The amplitude of the Fourier transform of the source distribution may be obtained in the usual way from the visibility of the fringes and it has been shown (Jennison 1958) that if errors exist in the amplitude function as a result of scintillation or other defects these may be removed in principle by a comparison of the visibilities of the three fringe systems and the simultaneous recording of the intensity from any one of the slits.

The brightness distribution across the source may be reconstructed from the Fourier transform of the amplitude (visibility) function and the associated phase function derived in the manner indicated above.

In a small laboratory instrument the spacing of the apertures is varied by rotating the objective mask about an axis through the central slit. The slits are arranged in echelon to reduce the foreshortening of the individual slits at very small angles of incidence, Fig. 2 (*b*). This arrangement enables the instrument to be used with very short projected slit spacings and hence large angular features may be examined.

Provided that the fringes can be distinguished, the technique enables a unique solution of the source structure to be computed subject only to the limitation of detail imposed by the restriction of maximum spacing. It also provides an analytical method for the removal of the effect of scintillation upon the computed visibility.

REFERENCES

- JENNISON, R. C., 1958, *Mon. Not. R. Astr. Soc.*, **118**, 276.
 — 1961, *Fourier Transforms and Convolutions for the Experimentalist* (London, New York, Paris: Pergamon Press).
 MICHELSON, A. A., 1890, *Phil. Mag.* (5), **30**, 1.

Extension of Series in the First Spectrum of Indium (In I)

By W. R. S. GARTON AND K. CODLING

Department of Physics, Imperial College, London

MS. received 27th March 1961

Abstract. The ultra-violet absorption spectrum of indium vapour has been photographed by means of a 3-metre grating spectrograph. Lines of the series $5^2P_{1/2}^0 - n^2S_{1/2}$ ($n=9$ to 27), $n^2D_{3/2}$ ($n=7$ to 33), $5^2P_{3/2}^0 - n^2S_{1/2}$ ($n=10$ to 29), $n^2D_{3/2}$ ($n=8$ to 19), $n^2D_{5/2}$ ($n=8$ to 34), have been measured against good wavelength standards. A short sixth series is identified as $5^2P_{1/2}^0 - n^2P_{1/2}^0$. The accepted value for the ionization potential has been confirmed. From a consideration of the character of the perturbations in the n^2D series we conclude that the sp^2D term lies above the ionization limit, instead of, as formerly supposed, below.

§ 1. INTRODUCTION

AN earlier paper by one of us (Garton 1954) has dealt with the absorption spectrum of indium vapour, observed by means of 1 metre vacuum-grating and medium-quartz spectrographs, combined with a small carbon-tube furnace as absorption vessel. That paper was concerned mainly with the portion of the absorption spectrum, in the Schumann ultra-violet, due to transitions from the ground doublet $5s^25p^2P^0$ to levels of configurations sp^2 , $spnl$, and with the effects of autoionization. In addition, the paper reported measurements, made at the modest resolution of the medium-quartz spectrograph, on a total of thirty-two lines of the series $5^2P_{1/2}^0 - n^2S_{1/2}$ ($n=13$ to 24) and $5^2P_{1/2}^0 - n^2D_{3/2}$ ($n=11$ to 30).

Since 1954 the instrumental equipment available for studies of ultra-violet absorption spectra has been considerably supplemented in this laboratory, in particular by a very good 3 metre normal incidence vacuum spectrograph and a large King furnace. Aside from extension of such studies to other elements (cf. Garton and Codling 1960, Codling 1961), it has proved profitable to make fresh observations on some of the spectra previously examined at low dispersion, and the present paper concerns one such case. The new photographs show good development of the five strong series $5^2P_{1/2}^0 - n^2S_{1/2}$, $n^2D_{3/2}$, $5^2P_{3/2}^0 - n^2S_{1/2}$, $^2D_{3/2, 5/2}$, and traces of a sixth—presumably $5^2P_{1/2}^0 - n^2P_{1/2}^0$ —series. Though the two series, which locate the $n^2S_{1/2}$, $n^2D_{3/2}$ levels, reported on previously have been extended by only a few further members, the new measurements have been made against better wavelength standards at higher dispersion, and are much more reliable. Also, it has been possible to resolve the $^2D_{3/2, 5/2}$ terms up to $n=33$, as compared with the previous limitation to $n=15$. The series measurements confirm the accepted value for the ionization potential of In I (Paschen 1938). It is believed that the unidentified sp^2D term lies above the series limit, instead of below as hitherto supposed, and gives a curious course to the photo-ionization cross section of the atom.

§ 2. EXPERIMENTAL

The main experimental details are to be found in other papers (Garton and Codling 1960, Codling 1961). In the present case the King furnace was held at a succession of temperatures between 950 and 1300°C, and the absorption spectra were photographed on the background continuum provided by a flash-tube (Garton 1953). Wavelength standards were obtained by means of a copper hollow cathode placed in line with furnace and flash-tube. Though the spectral region of interest lay entirely above 2000 Å, the 3-metre spectrograph was nevertheless evacuated, with the advantages of avoidance of air tremor and of the need for reduction of air wavelengths to vacuum wavenumbers. Measurements of lines on several plates were made on a Zeiss Abbe comparator and our wavelengths are believed good to 0.004 Å.

§ 3. RESULTS AND INTERPRETATION

The results of the measurements on the sharp and diffuse series of In I are listed in Tables 1 to 5. The term values T have been calculated on Paschen's (1938) limit, 46669.93 cm⁻¹, quoted by Moore (1958), and originally derived from the 5²D- n^2 F⁰ series. The Figure shows quantum defect plotted against T .

The $n^2S_{1/2}$ series is very regular, and practically Rydbergian from $n=9$ onward; this provides additional support for the value of Paschen's limit. The members of this term series below $n=9$ not shown in the Figure, exhibit a progressive drop in the Rydberg denominator to the value 2.2185 for $n=5$.

A check on the accuracy of the measurements is provided by the notably good agreement in Tables 1 and 2 between the two values of $n^2S_{1/2}$, and of $n^2D_{3/2}$ in Tables 3 and 4, based respectively on combinations with 5²P_{1/2}⁰, 5²P_{3/2}⁰. Our estimate of measurement error is thus confirmed, viz. 0.004 Å, or about 0.1 cm⁻¹.

Table 1. 5s²5p²P_{1/2}⁰-5s²ns²S_{1/2} Series

n	λ_{vac} (Å)	ν_n (cm ⁻¹)	T (cm ⁻¹)	n^*
9	2340.916	42718.32	3951.61	5.270
10	2278.900	43880.82	2789.11	6.273
11	2242.360	44595.87	2074.06	7.274
12	2218.899	45067.40	1602.53	8.275
13	2202.916	45394.38	1275.55	9.275
14	2191.512	45630.60	1039.33	10.275
15	2183.071	45807.03	862.90	11.276
16	2176.671	45941.72	728.21	12.276
17	2171.686	46047.17	622.76	13.274
18	2167.718	46131.46	538.47	14.276
19	2164.523	46199.56	470.37	15.274
20	2161.898	46255.65	414.28	16.275
21	2159.723	46302.13	367.70	17.275
22	2157.900	46341.35	328.58	18.275
23	2156.351	46374.64	295.29	19.277
24	2155.035	46402.96	266.97	20.274
25	2153.897	46427.48	242.45	21.275
26	2152.911	46448.74	221.19	22.274
27	2152.048	46467.36	202.57	23.275

Table 2. $5s^25p^2P_{3/2}^0-5s^2ns^2S_{1/2}$ Series

n	λ_{vac} (Å)	ν_n (cm $^{-1}$)	T (cm $^{-1}$)	n^*
10	2399.905	41668.32	2789.05	6.273
11	2359.417	42383.35	2074.02	7.274
12	2333.456	42854.89	1602.48	8.275
13	2315.786	43181.88	1275.49	9.276
14	2303.185	43418.14	1039.23	10.276
15	2293.872	43594.41	862.96	11.276
16	2286.801	43729.21	728.16	12.276
17	2281.299	43834.67	622.70	13.275
18	2276.927	43918.84	538.53	14.275
19	2273.394	43987.09	470.28	15.275
20	2270.502	44043.12	414.25	16.276
21	2268.103	44089.71	367.66	17.276
22	2266.099	44128.70	328.67	18.273
23	2264.389	44162.03	295.35	19.276
24	2262.933	44190.44	266.93	20.276
25	2361.679	44214.94	242.43	21.275
26	2260.590	44236.24	221.13	22.276
27	2259.642	44254.80	202.57	23.275
28	2258.808	44271.14	186.23	24.275
29	2258.070	44285.61	171.76	25.276

Table 3. $5s^25p^2P_{1/2}^0-5s^2nd^2D_{3/2}$ Series

n	λ_{vac} (Å)	ν_n (cm $^{-1}$)	T (cm $^{-1}$)	n^*
7	2390.284	41836.03	4833.90	4.765
8	2307.581	43335.42	3334.51	5.737
9	2260.683	44234.42	2435.51	6.712
10	2231.396	44814.99	1854.94	7.692
11	2211.830	45211.43	1458.50	8.674
12	2198.083	45494.19	1175.74	9.661
13	2188.077	45702.23	967.70	10.649
14	2180.754	45860.01	809.92	11.640
15	2174.754	45982.21	687.72	12.632
16	2170.198	46078.74	591.19	13.624
17	2166.549	46156.35	513.55	14.617
18	2163.585	46219.58	450.35	15.610
19	2161.139	46271.90	398.03	16.605
20	2159.096	46315.98	354.25	17.600
21	2157.378	46352.56	317.37	18.595
22	2155.916	46384.00	285.93	19.591
23	2154.666	46410.91	259.02	20.583
24	2153.585	46434.20	235.73	21.576
25	2152.636	46454.67	215.26	22.579
26	2151.811	46472.48	197.45	23.575
27	2151.086	46488.14	181.79	24.569
28	2150.442	46502.07	167.86	25.568
29	2149.868	46514.49	155.44	26.570
30	2149.359	46525.49	144.44	27.563
31	2148.902	46535.39	134.54	28.560
32	2148.489	46544.34	125.59	29.560
33	2148.118	46552.38	117.55	30.554

Table 4. $5s^25p^2P_{3/2}^0-5s^2nd^2D_{3/2}$ Series

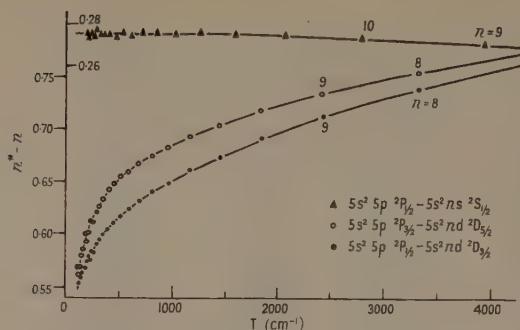
n	λ_{vac} (Å)	ν_n (cm $^{-1}$)	T (cm $^{-1}$)	n^*
8	2431.734	41122.92	3334.45	5.737
9	2379.710	42021.93	2435.44	6.713
10	—	—	—	—
11	2325.639	42998.93	1458.44	8.674
12	2310.452	43281.57	1175.80	9.661
13	2299.396	43489.68	967.69	10.649
14	2291.090	43647.35	810.02	11.639
15	2284.689	43769.63	687.74	12.632
16	2279.657	43866.25	591.12	13.625
17	2275.635	43943.78	513.59	14.617
18	2272.365	44007.02	450.35	15.608
19	2269.662	44059.42	397.95	16.606

$$5^2P_{1/2}^0-5s5p^2\ ^2D_{3/2} \simeq 2026\text{ Å}$$

$$5s5p^2\ ^2D_{3/2} : \nu_n \simeq 49360\text{ cm}^{-1}$$

Table 5. $5s^25p^2P_{3/2}^0-5s^2nd^2D_{5/2}$ Series

n	λ_{vac} (Å)	ν_n (cm $^{-1}$)	T (cm $^{-1}$)	n^*
8	2430.606	41142.00	3315.37	5.753
9	2378.867	42036.82	2420.55	6.733
10	2346.629	42614.32	1843.05	7.717
11	2325.124	43008.46	1448.91	8.703
12	2310.048	43289.14	1168.23	9.692
13	2299.081	43495.64	961.73	10.682
14	2290.836	43652.19	805.18	11.674
15	2284.488	43773.48	683.89	12.667
16	2279.503	43869.21	588.16	13.659
17	2275.497	43946.44	510.93	14.655
18	2272.250	44009.24	448.13	15.648
19	2269.573	44061.15	396.22	16.642
20	2267.352	44104.41	352.96	17.633
21	2265.464	44141.07	316.30	18.626
22	2263.861	44172.32	285.05	19.621
23	2262.492	44199.05	258.32	20.611
24	2261.296	44222.43	234.94	21.612
25	2260.268	44242.54	214.83	22.601
26	2259.359	44260.34	197.03	23.600
27	2258.564	44275.92	181.45	24.592
28	2257.856	44289.80	167.57	25.591
29	2257.228	44302.13	155.24	26.586
30	2256.669	44313.10	144.27	27.580
31	2256.168	44322.92	134.45	28.569
32	2255.714	44331.86	125.51	29.569
33	2255.306	44339.88	117.49	30.561
34	2254.934	44347.20	110.17	31.560



Indium sharp and diffuse series: quantum defect plot.

The course of the quantum defect plots for the diffuse series, in the Figure, is interesting. The rapid fall for higher members of the $^2D_{3/2}$ and $^2D_{5/2}$ series strongly suggests the presence of a perturbing term beyond the series limit (Shenstone and Russell 1932). Of the terms of the $5s5p$ configuration, 4P lies deep (Paschen 1938, Sawyer and Lang 1929, Lansing 1929) 2S and 2P lie well above the ionization limit (Garton 1954); the remaining term 2D , has hitherto been presumed to be deep, but has not been certainly identified. Paschen (1938) argued that the term accepted as 4^2F^0 was actually $5s5p^2^2D$, as follows. In In II and Al II , it is well established that $p^2^1D_2$ has been absorbed into the low members of the snd series, either of the first two members of which can indifferently be thus assigned. By analogy, and because of a large splitting anomaly in the 2D terms between $n=5$ and $n=7$, it might be thought that $5s5p^2^2D$ lay deep amongst $5s^2nd$, except that the quantum defects of the latter series would then acquire unlikely values. Paschen therefore looked elsewhere for $5s5p^2^2D$, and suggested that previous identification of an emission line pair $\lambda\lambda 2518, 2666$, as $5^2P_{1/2}^0, 3/2-4^2F^0$ was incorrect, and rewrote 4^2F^0 as $5s5p^2^2D$. This placing has, however, been questioned by Edlén (Moore 1958), who has stated that the original identification of 4^2F^0 was correct. Confirmation that Paschen indeed wrongly identified $5s5p^2^2D$ is found in the fact that the line pair mentioned is not obtainable in absorption, even at high vapour densities in the furnace. Moreover, a quantum defect plot of the whole 2D series, i.e. an extension of the curves of the Figure to the right (to $n=5$), shows no large perturbation in term position amongst the low series members, though the strong splitting anomaly exists amongst the first few members ($n=5, 6, 7$).

The following seems a likely answer to these difficulties. From the course of the n^2D plots of the Figure we place $5s5p^2^2D$ above the ionization potential, but lying closer to it than do $5s5p^2^2S, ^2P$. Support for this is to be found in the rather curious intensity distribution of the photoionization continuum $5^2P_{1/2}^0-E(s, d)$ which we have photographed in the region between the series limit and the very diffuse group $5^2P^0-5s5p^2^2S, ^2P$. This absorption continuum can be seen on two of the spectra in the plate accompanying the earlier paper (Garton 1954). What is perhaps not so clear on that plate is the fact that the absorption continuum does not set in strongly at or close to the series limit, but increases in strength from there towards shorter wavelengths, to a flat maximum at about 2026 \AA , that is, some 2700 cm^{-1} beyond the limit. It seems probable that we

have here a case of local enhancement of the photoionization cross section, similar to cases observed in Ca, Sr, Ba (cf. Garton and Codling 1960, Garton, Pery-Thorne and Codling 1960), arising from presence of an extremely diffuse term, in the present instance, $5s5p^2D$.

We have yet, however, to explain the splitting anomaly in the diffuse series, already mentioned. The details of this are: $\Delta 5^2D = 23.3 \text{ cm}^{-1}$, $\Delta 6^2D = 49.89$, $\Delta 7^2D = 25.34$. Apparently either $\Delta 5^2D$ is smaller or $\Delta 6^2D$ larger than it would be in absence of a perturbation. It is tempting to try to explain this anomaly in the following way.

In the theory of configuration mixing we distinguish electrostatic and magnetic (spin-orbit) interaction affecting levels of similar parity and identical J -value (Condon and Shortley 1951). For magnetic interaction to occur it is necessary that at least one electron in the two configurations concerned shall have the same value of n , in which case a perturbation can take place between widely separated terms (Shortley 1932)†. On this basis $5s5p^2D$ can interact magnetically with $5s^25d^2D$, but not with $6d$, $7d^2D$ etc., it being remembered that the closed subshell $5s^2$, with $j=0$, has no magnetic moment.

We may be thus inclined to interpret the splitting anomaly in In I in the sense that it is $\Delta 5^2D$ that is reduced, as a result of magnetic interaction with $5s5p^2D$, below the value it would have in the unperturbed series. The general fall in the quantum defect plots of the Figure, for higher members of the diffuse series is, on the other hand, to be ascribed to electrostatic interaction with $5s5p^2D$.

Similar splitting anomalies to that discussed exist in the Al I and Ga I spectra, and may be similarly explicable. However, the above qualitative argument concerning spin-orbit configuration interaction is revealed as too naïve when we proceed to Tl I, in which 6^2D shows no fine-structure anomaly, although $6s6p^2D$ has been located as a very diffuse term at 12740 cm^{-1} above the series limit (Beutler and Demeter 1934). Another distinction between Tl I and the earlier spectra of the same group concerns the relative position of sp^2P . In Al, Ga and In this term lies deep, and close to the first diffuse term. In Tl I, $6s6p^2$ has $^4P_{1/2}$ below and the other two quartet levels slightly above the ionization limit, whereas the term value of 6^2D is about 13000 cm^{-1} . Another, possibly relevant, peculiarity is that in Pb II 6^2D is inverted, for no obvious reason. It is possible that our qualitative argument concerning magnetic interaction of the sp^2 and s^2d configurations has some validity, but should be given proper expression in a more complex form which would involve the sp^2P term. On balance, the evidence seems to point to sp^2D in In I having a position above the series limit, though we are then left with the necessity for proper explanation of the course of the s^2d^2D intervals.

Other perturbations, of less striking nature, for which we cannot offer explanation, are noticeable in the intensities of the $5^2P^0-n^2D$ absorption lines. As shown in Table 4, the $5^2P^0_{3/2}-10^2D_{3/2}$ line is missing altogether. Also, in the series $5^2P_{1/2}^0-n^2D_{3/2}$ the members $n=8$ and 9 are considerably weaker than the members $n=10, 11$.

The sole remaining feature of the absorption spectra needing explanation is the presence of the short sixth series (Table 6), which we have observed at high

† An example of this sort of disturbance is supposed found in the inversion of many of the doublet terms of the alkali arc spectra (Phillips 1933).

Table 6. $5s^25p^2P_{1/2}^0-5s^2np^2P_{1/2}^0$? Series

n	λ_{vac} (Å)	ν_n (cm ⁻¹)	T (cm ⁻¹)	n^*
14	2179.67	45878.5	791.5	11.78
15	2173.99	45998.3	671.6	12.78
16	2169.57	46092.1	577.9	13.78
17	2166.01	46167.9	502.1	14.78
18	2163.10	46230.0	440.1	15.79
19	2160.72	46280.9	389.1	16.79
20	2158.70	46342.2	345.8	17.82
21	2157.03	46360.0	310.0	18.82
22	2155.61	46390.5	279.4	19.82
23	2154.38	46417.1	252.8	20.83

vapour densities. The lines of this series appear as, slightly diffuse, satellites to the short wavelength side of members of $5^2P_{1/2}^0-n^2D_{3/2}$; starting as quite weak absorption lines in the low members, they increase rapidly in strength and eventually merge with, and supplement the intensities of, the higher members of the $^2D_{3/2}$ series. The values of the Rydberg denominator in Table 6 suggest that the lines belong to the forbidden series $5^2P_{1/2}^0-n^2P_{1/2}^0$. We can tentatively attribute the presence of such lines to the occurrence of forced dipole transitions, at the high vapour densities used. Under the same conditions we have seen traces of higher members of yet a seventh series, consisting of lines too feeble for measurement, but having the correct locations for $5^2P_{1/2}^0-n^2P_{3/2}^0$.

ACKNOWLEDGMENTS

The considerable help of several bodies has once again to be acknowledged. We express thanks to the Royal Society for funds towards erection of the 3m spectrograph, and to the University of London for provision, from the Central Research Fund, of King furnace and associated apparatus.

The experiments reported have been made possible by a supporting contract with the Atomic Energy Research Establishment (CTR Division), including provision of a research assistantship for one of us (K.C.).

REFERENCES

- BEUTLER, H., and DEMETER, W., 1934, *Z. Phys.*, **91**, 143.
 CODLING, K., 1961, *Proc. Phys. Soc.*, **77**, 797.
 CONDON, E. U., and SHORTLEY, G. H., 1951, *The Theory of Atomic Spectra* (Cambridge: University Press), Ch. 15.
 GARTON, W. R. S., 1953, *J. Sci. Instrum.*, **30**, 119.
 ——— 1954, *Proc. Phys. Soc. A*, **67**, 864.
 GARTON, W. R. S., and CODLING, K., 1960, *Proc. Phys. Soc.*, **75**, 87.
 GARTON, W. R. S., PERY-THORNE, A., and CODLING, K., 1960, *Proc. 4th International Conference on Ionization Phenomena in Gases*, Vol. I (Amsterdam: North-Holland), p. 206.
 LANSING, W. D., 1929, *Phys. Rev.*, **34**, 598.
 MOORE, C. E., 1958, *Circular Nat. Bur. Stands*, **467**, Vol. III.
 PASCHEN, F., 1938, *Ann. Phys.*, **32**, 148.
 PHILLIPS, M., 1933, *Phys. Rev.*, **44**, 644.
 SAWYER, R. A., and LANG, R. J., 1929, *Phys. Rev.*, **34**, 719.
 SHENSTONE, A. G., and RUSSELL, H. N., 1932, *Phys. Rev.*, **39**, 415.
 SHORTLEY, G. H., 1932, *Phys. Rev.*, **40**, 185.

Van der Waals Forces for Hydrogen and the Inert Gases

By A. DALGARNO AND A. E. KINGSTON

Department of Applied Mathematics, The Queen's University of Belfast

MS. received 6th February 1961

Abstract. Experimental data and theoretical calculations on neon and argon are analysed to yield consistent sets of electric dipole oscillator strengths. The derived oscillator strengths are used with known values for hydrogen and helium to calculate the van der Waals energies between all pairs of atoms selected from hydrogen, helium, neon and argon. The results are summarized in the Table. The probable error is less than 10%.

§ 1. INTRODUCTION

THE magnitudes of the long range forces between pairs of atoms are important parameters in such diverse fields as low energy elastic scattering, transport phenomena, the structure of crystals, the formation of radicals at low temperatures and the collision broadening of spectral lines.

§ 2. THEORY

The leading term in the series representation of the long range interaction energy for a pair of atoms A and B separated by a distance R has the form $-C_{ab}/R^6$ provided the atoms are in states of zero orbital angular momentum. If ϵ_m^a denotes the binding energy of atom A in the m th excited state and ϵ_n^b the binding energy of atom B in the n th excited state, measured in atomic units, the coefficient C_{ab} appropriate to A and B in the ground states may be written

$$C_{ab} = \frac{3}{2} \sum_{m,n \neq 0} \mathbf{S}'_m \mathbf{S}'_n \frac{f_m^a f_n^b}{(\epsilon_0^a - \epsilon_m^a)(\epsilon_0^b - \epsilon_n^b)(\epsilon_0^a + \epsilon_0^b - \epsilon_m^a - \epsilon_n^b)} \quad \dots\dots (1)$$

where f_m^a is the oscillator strength of the electric dipole transition from the ground state of A to the m th excited state and f_n^b is the oscillator strength of the electric dipole transition from the ground state of B to the n th excited state (cf. Margenau 1939).

The problem of evaluating C_{ab} therefore reduces to the determination of the oscillator strengths of the individual atoms. Experimental data on oscillator strengths are scarce and in general theoretical calculations yield values of uncertain accuracy. However, oscillator strengths satisfy various sum rules of the form

$$S(k) = \sum_i \mathbf{S}'_i f_i (\epsilon_0 - \epsilon_i)^k \quad \dots\dots (2)$$

(Dalgarno and Lynn 1957) and it is often possible to determine $S(k)$ accurately by theoretical calculation or by analysis of experimental data. In particular, Dalgarno and Kingston (1960) have analysed the measurements of refractive

indices and of Verdet constants of neon and argon incidentally obtaining $S(k)$ for negative even values of k and they also estimate $S(-1)$. Further $S(0)$ is known for it is equal to the total number of atomic electrons. These sum rules are similar in form to (1) and our procedure consists of selecting oscillator strengths which satisfy the known values of $S(k)$ and substituting them into (1) (cf. Dalgarno and Kingston 1959). Although the accuracy of the oscillator strengths of any individual transition is not high, the control exerted by $S(k)$ prevents serious error entering into the evaluation of (1).

The possible error can be more closely limited in the cases of neon and argon because there exist experimental values of the oscillator strengths of transitions into the continua (Lee and Weissler 1953, 1955, Ditchburn 1960) and theoretical Hartree-Fock calculations of the oscillator strengths of the resonance transitions (Knox 1958, Gold and Knox 1959).

§ 3. RESULTS AND DISCUSSION

We have computed C_{ab} for all pairs selected from hydrogen, helium, neon and argon, using for hydrogen the exact theoretical oscillator strengths and for helium the values derived by Dalgarno and Stewart (1960). The results are shown in the Table. The value for H-H was derived earlier by Pauling and Beach (1935) and the value for He-He supersedes the estimate of Dalgarno and Lynn (1957).

Values of C_{ab} in Atomic Units†				
	H	He	Ne	A
H	6.50	2.82	5.67	20.15
He	2.82	1.46	3.07	9.88
Ne	5.67	3.07	6.63	20.63
A	20.15	9.88	20.63	68.08

† The leading term in the interaction energy between A and B is $\frac{-C_{ab} e^2}{(R/a_0)^6 a_0}$.

We believe that the absolute error in C_{ab} is certainly less than 10% and may be much smaller. The limits claimed are consistent with the available experimental data. For example, Guggenheim and McGlashan (1960) are able to reproduce a wide range of data for two argon atoms by adopting the value of C_{ab} equal to 67.7 recommended by Margenau (1939), which differs from our computed value of 68.08 by less than 0.5%. This close agreement is partly fortuitous since the experimental data do not lead to a unique value of C_{ab} , the derived value depending to some extent on the form adopted for the complete interaction.

We shall not present the detailed oscillator strengths that we have derived, but it is worth noting that our analysis provides no evidence for attaching large oscillator strengths to transitions into the auto-ionizing levels which lie between the neon and argon $^2P_{1/2}$ and $^2P_{3/2}$ series limits. A previous discussion of refractive index data for argon (Koch 1949, Garton 1957) had suggested anomalously large oscillator strengths, but it appears that it did not take proper account of the contribution from transitions into the continuum. This is in harmony with the conclusions of Garton, Pery and Codling (1960) but there remains the problem of explaining the apparently large intensities of lines terminating at auto-ionizing levels that have been observed in absorption studies of the inert gases (Beutler (1935).

ACKNOWLEDGMENT

This work has been partially supported by the United Kingdom Atomic Energy Research Establishment.

REFERENCES

- BEUTLER, H., 1935, *Z. Phys.*, **93**, 177.
- DALGARNO, A., and KINGSTON, A. E., 1959, *Proc. Phys. Soc.*, **73**, 455.
- 1960, *Proc. Roy. Soc. A*, **259**, 424.
- DALGARNO, A., and LYNN, N., 1957, *Proc. Phys. Soc. A*, **70**, 802.
- DALGARNO, A., and STEWART, A. L., 1960, *Proc. Phys. Soc.*, **76**, 49.
- DITCHBURN, R. W., 1960, *Proc. Phys. Soc.*, **75**, 461.
- GARTON, W. R. S., 1957, *Threshold of Space*, Ed. by M. Zelikoff (London: Pergamon Press).
- GARTON, W. R. S., PERY, A., and CODLING, K., 1960, *Ionization Phenomena in Gases*, Vol. 1, Ed. by N. R. Nilsson (Amsterdam: North-Holland).
- GOLD, A., and KNOX, R. S., 1959, *Phys. Rev.*, **113**, 834.
- GUGGENHEIM, E. A., and MCGLASHAN, M. L., 1960, *Proc. Roy. Soc. A*, **255**, 456.
- KNOX, R. S., 1958, *Phys. Rev.*, **110**, 375.
- KOCH, J., 1949, *K. Fysiogr. Sällsk. Lund Förh.*, **19**, 173.
- LEE, P., and WEISSLER, G. L., 1953, *Proc. Roy. Soc. A*, **220**, 71.
- 1955, *Phys. Rev.*, **99**, 540.
- MARGENAU, H., 1939, *Rev. Mod. Phys.*, **11**, 1.
- PAULING, L., and BEACH, J. Y., 1935, *Phys. Rev.*, **47**, 686.

The Absorption Spectrum of the BiF Molecule in the Ultra-violet Region

By K. C. JOSHI†

Physics Department, Allahabad University, India

MS. received 15th February 1961

Abstract. One system of bands comprising thirty-two bands of the BiF molecule has been obtained in absorption in the region $\lambda\lambda 2400\text{--}2180$. Three of these bands were previously observed in emission by Rochester. The bands have been analysed and can be represented by the following formula:

$$\nu_{v'v''} = 44222.0 + 615.0(v' + \frac{1}{2}) - 2.50(v' + \frac{1}{2})^2 - 512.0(v'' + \frac{1}{2}) + 2.25(v'' + \frac{1}{2})^2.$$

A discussion regarding the electronic states involved in the transition shows that the ground state is a triplet state, whereas the upper one a single state and not otherwise as suggested by Rochester.

§ 1. INTRODUCTION

THE spectrum of bismuth fluoride has been the subject of numerous investigations. Howell and Rochester (1934) were the first to observe the spectrum of BiF and BiBr in a high-frequency electric discharge. Later, Howell (1936) made a detailed study and analysed about forty bands occurring in the region $\lambda\lambda 5100\text{--}4200$. He ascribed the two electronic states involved in the production of these bands to A and x states having the following constants (in cm^{-1}):

	ν_e	ω_e	$\omega_e x_e$	$\omega_e y_e$
A	22959.7	381.0	3.00	0.10
x	0	510.0	2.05	—

Morgan (1936), using a long column of BiF₃ vapour heated to 1200°C in an electric furnace and using a 500 watt incandescent lamp as the source of continuum, obtained the same system in absorption. He confirmed the analysis of Howell and identified the x state as the ground state of the molecule. In addition, he also mentioned the occurrence of bands in the near ultra-violet region.

Rochester (1937) made further investigations on the spectrum of BiF in emission and obtained in addition to the known A-x system, fifteen bands, degraded to violet, in the region $\lambda\lambda 3250\text{--}2250$. He classified them into three systems arising from an upper triplet electronic state to the ground state of the molecule. Due to insufficient data and the low dispersion of the instrument used by him, he could mention only the order for the vibrational frequency of the upper state.

No study has, however, been made for this molecule in absorption in the ultra-violet region, though other bismuth halides are known to possess several bands in this region. It was with the object of obtaining more complete information regarding this molecule that the present investigation was undertaken. The spectrum was studied in absorption and thirty-two bands degraded to violet were observed in the region $\lambda\lambda 2400\text{--}2180$. The bands have been analysed into one system and the vibrational constants determined.

† Now at Air Force Cambridge Research Laboratories, Bedford, Massachusetts.

§ 2. EXPERIMENTAL

Pure bismuth fluoride was put inside the graphite tube of the vacuum graphite furnace. The furnace tube was 18 cm long and had an internal diameter of 1 cm. In order to prevent the rapid effusion of the vapours from the tube ends, the furnace chamber was filled with nitrogen gas at a pressure of about 35 cm Hg. A hydrogen discharge lamp manufactured by Thermal Syndicate Ltd., England, was used as the source of ultra-violet continuum. Observations were taken at temperatures ranging from 800°C to 1800°C.

§ 3. RESULTS

Well-defined bands developed at about 1600°C. A few strong bands of Bi₂ along with a couple of atomic lines of bismuth also appeared on the spectrum plate. The spectrum was photographed with a medium quartz spectrograph of Messrs. Carl Zeiss, having an average reciprocal dispersion of about 6 Å mm⁻¹ in the region λλ2392-2193. Ilford N.40 thin plates were used to record the spectrum. A copper arc was employed for the comparison spectrum.

Table 1. Band Head Data for the c-x₁ System of the BiF Molecule

λ _{air} (Å)	Intensity	γ _{vac} (cm ⁻¹)		Analysis v', v''
		obs.	calc.	
2392.6	1	41782	41781	0,5
2385.4	1	41909	41906	1,6
2378.3	1	42034	42030	2,7
2371.2	1	42160	42154	3,8
2365.0	2	42270	42270	0,4
2358.2	2	42390	42391	1,5
2351.5	2	42513	42511	2,6
2344.8	2	42634	42630	3,7
2337.7†	4	42763	42764	0,3
2331.7	4	42885	42880	1,4
2325.0	3	42997	42996	2,5
2318.7	2	43114	43111	3,6
2310.7†	5	43263	43263	0,2
2304.8	5	43374	43374	1,3
2298.8	4	43488	43485	2,4
2293.0	2	43598	43596	3,5
2287.5	2	43702	43706	4,6
2284.1†	6	43767	43766	0,1
2278.6	4	43873	43873	1,2
2273.0	1	43981	43979	2,3
2267.6	1	44085	44085	3,4
2262.4	1	44187	44191	4,5
2258.0†	6	44274	44273	0,0
2252.8	3	44376	44376	1,1
2247.6	6	44478	44478	2,2
2242.5	6	44579	44579	3,3
2237.5	2	44678	44680	4,4
2227.2	4	44885	44883	1,0
2222.5	2	44980	44981	2,1
2217.8	4	45076	45078	3,2
2197.6	2	45489	45488	2,0
2193.3	2	45580	45581	3,1

† Also observed in emission by Rochester.

Table 2. Deslandres Arrangement for the $c-x_3$ System of the BiF Molecule

$v' \backslash v''$	0	1	2	3	4	5	6	7	8
0	44274†	43767†	43263†	42763†	42270	41782			
1	44885	44376	43873	43374	42885	42390	41909		
2	45489	44980	44478	43981	43488	42997	42513	42034	
3		45580	45076	44579	44085	43598	43114	42634	42160
4					44687	44178	43702		

† Also observed in emission by Rochester.

Table 3. Condon Distribution of the Band Intensity for the $c-x_1$ System of BiF

$v' \backslash v''$	0	1	2	3	4	5	6	7	8
0	6	6	5	4	2	1			
1	4	3	4	5	4	2	1		
2	2	2	6	1	4	3	2	1	
3		2	4	6	1	2	2	2	1
4					2	1	2		

The wavelengths, the relative visual intensities of the bands, and the respective wave-numbers are given in Table 1. The last column of the table gives the vibrational analysis and the preceding one the wave-numbers of the band heads calculated on the basis of the proposed formula:

$$\nu_{v',v''} = 44222.0 + 615.0(v' + \frac{1}{2}) - 2.50(v' + \frac{1}{2})^2 - 512.0(v'' + \frac{1}{2}) + 2.25(v'' + \frac{1}{2})^2.$$

In Table 2 all the bands observed have been arranged according to the Deslandres scheme. Table 3 shows the Condon distribution of the intensity of the bands. In Fig. 1 (Plate) the spectrogram showing the bands has been given.

§ 4. DISCUSSION

Altogether thirty-two bands have been observed in this investigation. These include four of the bands obtained in emission by Rochester (1937). The fifteen bands obtained by Rochester have been clasified by him into a triplet system, with wide multiplet separations (4780 cm^{-1} and 7330 cm^{-1}). He attributes these bands as due to transitions between an upper triplet electronic state comprising three components, c_1 , c_2 and c_3 and a lower singlet ground state x . The three bands mentioned above, according to him, are due to the transition c_3-x (Fig. 2(a)).

In the present investigation all the thirty-two bands fit in a single Deslandres scheme, showing that all of them belong to the same system. None of the bands of the c_2-x and c_3-x component systems of Rochester have been observed in absorption, though they are expected to be present. The absence of these two component systems in absorption shows that the ground state is not involved in the transitions. Thus there appears to be some doubt about the nature of the electronic states involved in the above transitions. This doubt may be removed if it is assumed that the ground state is a triplet state, x_1x_2 and x_3 , and the upper state a single level c , as represented in Fig. 2(b). The ground state of BiF is

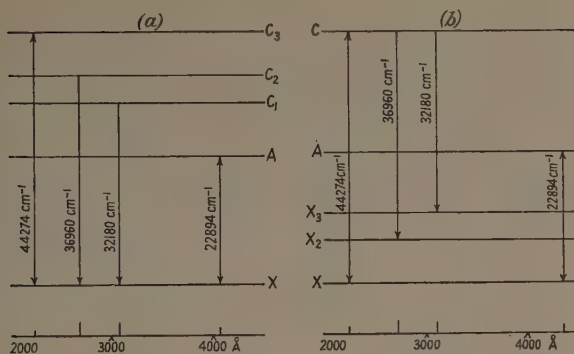


Fig. 2. Energy level diagram of the BiF molecule giving the (0, 0) bands of different systems: (a) observed by Rochester, (b) present investigation.

expected to be a multiplet state, as $\text{Bi}(^4\text{S}) + \text{F}(^2\text{P})$ cannot give rise to a singlet state. If we take the values 4780 cm^{-1} and 7330 cm^{-1} as the multiplet separations of the three components of the ground state, the experimental facts can be accounted for. The absence of the other two component systems in absorption is due to the fact that the states x_2 and x_3 are much too high up and the possibility of transition from them, by absorption of energy, is very small at the temperature of the experiment.

Now the system A-x is known both in emission and absorption with the 0, 0 band at 22894 cm^{-1} . If the ground state x is assumed to be a triplet state, transition between the upper two component levels x_2 and x_3 and the level A may also occur in emission though not in absorption. In the case of A- x_2 , the 0, 0 band would lie at 15564 cm^{-1} ($\lambda 6423.3$) and for A- x_3 , the 0, 0 band would lie at 10784 cm^{-1} ($\lambda 9027.0$). Investigations of the emission spectra in these regions under high dispersion are likely to throw more light regarding the electronic states of the molecule.

ACKNOWLEDGMENTS

The author is deeply indebted to Professor K. Majumdar for his guidance throughout the progress of the work. His thanks are also due to the Council of Scientific and Industrial Research, India, for the award of a Junior Research Fellowship. He is grateful to Professor S. N. Ghosh for making available the facilities of the Physics Department and to Shri R. C. Maheshwari for his helpful suggestions.

REFERENCES

- HOWELL, H. G., 1936, *Proc. Roy. Soc. A*, **155**, 141.
 HOWELL, H. G., and ROCHESTER, G. D., 1934, *Proc. Univ. Durham Phil. Soc.*, **9**, 126.
 MORGAN, F., 1936, *Phys. Rev.*, **49**, 41.
 ROCHESTER, G. D., 1937, *Phys. Rev.*, **51**, 486.

LETTERS TO THE EDITOR

A Note on the Band Spectra of BiF and SbF

The discovery by Joshi (1961) that only one component of the c-x system of BiF is found in *absorption* indicates, as he suggests, that it is the ground state which has the wide multiplet separation and not the upper state as assumed earlier from a study of the same system in *emission*. Whilst the scheme suggested by Joshi is the simplest one, it is not necessarily unique for it has still to be proved that the state c has no inherent multiplet structure. As Joshi points out, a test of his scheme will be to find the same multiplet separation in the A-x system by looking for the A-x₂ and A-x₃ component systems. Here again this simple test will fail unless state A has little structure.

It is of interest to examine whether the same scheme can be applied to the related molecule SbF, the data for which are in some respects more complete than BiF.

Two groups of triplet systems, one occurring in the visible region and another in the ultra-violet, have been observed in emission (Rochester 1937, Howell and Rochester 1939). These band systems occur in the same regions of the spectrum as the systems A-x and c-x of BiF and the SbF bands degrade in the same directions as the BiF bands in the corresponding systems. Moreover, the vibrational constants are such as might be expected for a related molecule like SbF. The following assumptions are therefore made:

- (i) The observed SbF systems correspond to the A-x and c-x systems of BiF.
- (ii) The lowest observed state of SbF, common to all the systems, is the ground state, and, by analogy with BiF, is a triplet.
- (iii) The multiplet structure of state c is small.

With these assumptions it appears that the spectrum of SbF can be explained if state A is also a triplet. Details are as follows:

$$\begin{aligned}\text{Ground State} \quad x_3-x_1 &= 6820 \text{ cm}^{-1} \\ x_2-x_1 &= 1244 \text{ cm}^{-1}\end{aligned}$$

where x_1 is the lowest level.

$$\begin{aligned}\text{State A} \quad A_3-A_1 &= 3471 \text{ cm}^{-1} \\ A_2-A_1 &= 2675 \text{ cm}^{-1}.\end{aligned}$$

The overall separation of the ground state of SbF, that is, 6820 cm^{-1} , may be compared with the corresponding value for BiF, which is approximately 12100 cm^{-1} . The analysis shows that the relative spacings of the multiplet levels of the ground states of BiF and SbF are very different. It also shows that if state A in SbF has been correctly identified, state A in BiF will be a multiplet.

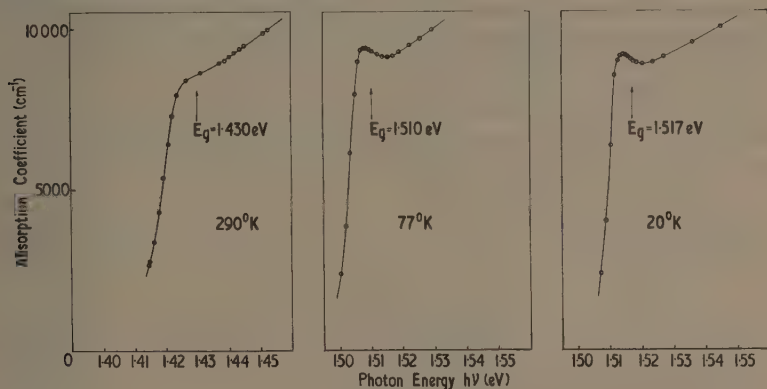
Physics Department,
The Durham Colleges in the University of Durham,
Durham.
28th June 1961.

G. D. ROCHESTER.

HOWELL, H. G., and ROCHESTER, G. D., 1939, *Proc. Phys. Soc.*, **51**, 329.
JOSHI, K. C., 1961, *Proc. Phys. Soc.*, **78**, 610.
ROCHESTER, G. D., 1937, *Phys. Rev.*, **51**, 486.

The Optical Absorption Edge of Gallium Arsenide

The optical absorption edge of semi-insulating gallium arsenide (Gooch, Hilsum and Holeman 1961, to be published) has been investigated at 290, 77 and 20°K. At the lower temperatures the absorption shows a distinct peak followed by a region of slowly increasing absorption. The peak is interpreted as absorption due to direct transitions to bound exciton states at the centre of the Brillouin zone and the slowly increasing absorption as that due to unbound electron-hole pairs. In this respect the absorption is very similar to that of germanium (Macfarlane *et al.* 1958).



By fitting the theoretical absorption curve of Elliott (1957) to the experimental data the band gap and exciton binding energy have been obtained. The band gap is found to be 1.430 (± 0.002) eV at 290°K, 1.510 (± 0.001) eV at 77°K and 1.517 (± 0.001) eV at 20°K.

The measured exciton binding energy is 0.0025 (± 0.0005) eV at 290°K, 0.0027 (± 0.0003) eV at 77°K, and 0.0033 (± 0.0002) eV at 20°K. These values are to be compared with the theoretical exciton binding energy $m^*e^4/2\hbar^2\epsilon^2$, where m^* is the reduced mass and ϵ is the dielectric constant. Using a reduced mass of 0.055 m (Moss and Walton 1959) and dielectric constant of 12.5 (Hambleton, Hilsum and Holeman 1961), this gives an exciton binding energy of 0.0039 eV. Due to the slight non-uniformity of thickness of this specimen ($\sim 6\mu$ thick) the absolute value of the absorption coefficient at the band edge could only be estimated to be of the order of 9000 cm⁻¹.

During the experiment the specimen, prepared by hand grinding and polishing, was freely suspended in an optical cryostat, helium gas being used to ensure thermal equilibrium with the refrigerant. Due to the low transmission with this specimen slits 0.003 eV wide were used. Using slits less than 0.001 eV wide, a slightly more pronounced peak at 77°K was observed but with the same exciton binding energy.

A measurement has also been made on a specimen 4.7 μ thick glued to a glass backing. The temperature was 53°K and the resolution 2.5×10^{-4} eV. The exciton binding energy is 0.0027 (± 0.0002) eV, the mean band gap 1.524 (± 0.001) eV, and the exciton line is split into two main components 0.0040

(± 0.0002) eV apart. The compressive strain in the specimen is calculated from the relative expansion coefficients to be approximately 0.6×10^{-3} . Inserting the data in the formulae of Kleiner and Roth (1959) we find $|D_u'| \simeq 4$ eV and $D_d^c - D_d^v \simeq -10$ eV, the latter in fair agreement with the value -7 eV deduced from the variation of band gap with hydrostatic pressure (Edwards, Slykhouse and Drickamer 1959, Ehrenreich 1960). Here $2D_u'$ is the splitting of the valence band edge due to unit shear in the $[111]$ direction, and D_d^c and D_d^v are the shifts in the band edges due to unit dilatation.

The absorption coefficient at the band edge in this specimen is $8000 (\pm 500) \text{ cm}^{-1}$. From Elliott's formulae we can calculate the oscillator strength for the transition to be $F = -13\hbar^2/2m$. This agrees well with the observed value for m/m^* in the conduction band of 13.8 at 300°K (Moss and Walton 1959).

Measurements at higher resolution over a wide range of temperature and absorption coefficient are continuing.

We would like to thank Dr. C. Hilsum of S.E.R.L., Baldock, for the specimen material, Dr. T. P. McLean and Dr. D. H. Parkinson for advice, and Mrs. C. A. Smith for help with the measurements.

Royal Radar Establishment,
Malvern,
Worcs.
21st July 1961.

M. V. HOBDEN.
M. D. STURGE.

- EDWARDS, A. L., SLYKHOUSE, T. E., and DRICKAMER, H. G., 1959, *J. Phys. Chem. Solids*, **11**, 140.
 EHRENRICH, H., 1960, *Phys. Rev.*, **120**, 1951.
 ELLIOTT, R. J., 1957, *Phys. Rev.*, **108**, 1384.
 HAMBLETON, K. G., HILSUM, C., and HOLEMAN, B. R., 1961, *Proc. Phys. Soc.*, **77**, 1147.
 KLEINER, W. H., and ROTH, L. M., 1959, *Phys. Rev. Letters*, **2**, 334.
 MACFARLANE, G. G., McLEAN, T. P., QUARRINGTON, J. E., and ROBERTS, V., 1958, *Proc. Phys. Soc.*, **71**, 863.
 MOSS, T. S., and WALTON, A. K., 1959, *Proc. Phys. Soc.*, **74**, 131.

Scattering by the Screened Coulomb Potential

The purpose of this Letter is to investigate the accuracy of the second Born approximation to the cross sections for the scattering of particles by a central potential.

We consider the case of the screened Coulomb potential given by

$$V(r) = -Ar^{-1} \exp(-\lambda r)$$

with $A = 2.365$ and $\lambda = 1$, treated in a previous paper by Gerjuoy and Saxon (1954). The values of the partial cross sections Q_l and the total cross section Q for incident particles with wave number $k = 1.816$ obtained by exact numerical integration, by the first Born approximation and by the second Born approximation, are displayed in Table 1.

In the investigation of Gerjuoy and Saxon all terms of the second Born scattering amplitude were retained in calculating Q . This is an inconsistent procedure (Dalitz 1951, Kingston, Moiseiwitsch and Skinner 1960); only terms up to the third order in A should be retained.

In the particular case under consideration we see that though the first Born approximation gives the zero-order partial cross section Q_0 quite accurately, the second Born approximation seriously overestimates it, indicating that the Born expansion is here unsatisfactory. For the higher order partial cross sections, however, the Born expansion converges rapidly towards the correct value.

Table 1. Elastic Scattering of Particles with Wave Number $k=1.816$ by the Screened Coulomb Potential

l	First Partial Cross Section Q_l (in πa_0^2)	Second†	Exact
0	0.905	1.244	0.848
1	0.429	0.522	0.511
2	0.158	0.178	0.179
3	0.0555	0.0596	0.0597
4	0.0192	0.0200	—
5	0.0066	0.0067	—
Total Cross Section Q (in πa_0^2)			
	1.577	2.033	1.627

First = first Born approximation; Second = second Born approximation; Exact = exact numerical integration.

† Only terms up to the third order in A have been retained.

Table 2. Elastic Scattering of Particles with Wave Number $k=1.816$ by the Screened Coulomb Potential

θ	First Differential Cross Section $I(\theta)$ (in a_0^2)	Second†	Exact
0	5.59	6.53	5.30
$\pi/2$	0.097	0.145	0.127
π	0.028	0.044	0.048
Real Part of Scattering Amplitude $f(\theta)$ (in a_0)			
0	2.36	2.56	2.18
$\pi/2$	0.31	0.39	0.078
π	0.17	0.21	-0.053

θ = scattering angle (rad); First = first Born approximation; Second = second Born approximation; Exact = exact numerical integration.

† Only terms up to the third order in A have been retained.

By chance the first Born approximation gives a value $1.577\pi a_0^2$ for the total cross section which is only 3% less than the exact value $1.627\pi a_0^2$, whereas the second Born approximation overestimates the total cross section Q by 25%. However, if the relevant Born zero-order partial cross section is replaced by the exact value, the first Born approximation yields $1.520\pi a_0^2$ for Q which is in error by about 7%, whereas the second Born approximation yields $1.637\pi a_0^2$ for Q which is in error by less than 1%.

It would appear from Table 2 that the second Born approximation gives rise to a fairly satisfactory set of values for the differential cross section $I(\theta)$. This is accidental as can be readily seen by comparing the exact values of the real part of the scattering amplitude $f(\theta)$ with those given by the second Born approximation also displayed in Table 2. Considerable cancellation occurs between the contributions arising from the various partial waves for large angles of scattering θ . Consequently, unless the exact values of the contributions to $f(\theta)$ from the partial waves with l small are used, it is not possible to obtain reliable values for $I(\theta)$.

We conclude, therefore, that a satisfactory method for obtaining cross sections is to carry out an exact numerical integration for the partial waves associated with small values of l and to use the second Born approximation for the remaining partial waves. At sufficiently high impact energies it is, of course, permissible to use the second Born approximation for all the partial waves.

This work has been supported by the United Kingdom Atomic Energy Research Establishment, to whom thanks are due for permission to publish.

Department of Applied Mathematics,
Queen's University,
Belfast, N. Ireland.

B. L. MOISEWITSCH.

24th May 1961.

DALITZ, R. H., 1951, *Proc. Roy. Soc. A*, **206**, 509.

GERJUOV, E., and SAXON, D. S., 1954, *Phys. Rev.*, **94**, 478.

KINGSTON, A. E., MOISEWITSCH, B. L., and SKINNER, B. G., 1960, *Proc. Roy. Soc. A*, **258**, 237.

Plasma Drift Velocity Across a Confining Magnetic Field

The steady drift velocity of fully ionized plasma across a confining magnetic field is usually given as

$$v = -\frac{\eta}{B^2} \nabla p \quad \dots\dots(1)$$

where η is the electrical resistivity and B a steady magnetic field normal to the plasma pressure gradient ∇p (Spitzer 1956).

The above equation is derived from the equation of plasma motion by neglecting the inertia term $(v \cdot \nabla)v$. It is shown, in this note, that the $(v \cdot \nabla)v$ term cannot be neglected if the plasma is bounded by a material wall. However, this does not imply that a plasma cannot be confined by a magnetic field as Slepian (1960) has suggested.

Consider a plasma in a steady state which drifts normal to a magnetic field directed along the z axis of rectangular coordinates. If a plane surface $(0, y, z)$ is drawn in the plasma sufficiently close to and parallel to the material wall on which the charges are recombining, the flow can be considered as one dimensional and the rate of charge generation between this surface and the wall neglected in comparison with the flux of entering charges. The plasma is assumed uniform in the y direction and drifts across the magnetic field with a velocity v in the x direction.

The equations of motion of the plasma fluid are

$$m_i n v \frac{\partial v}{\partial x} = j_y B - \frac{\partial p}{\partial x}, \quad \dots\dots (2)$$

$$\eta j_y = -v B, \quad \dots\dots (3)$$

$$E_x + \frac{1}{ne} \left(\frac{\partial p_e}{\partial x} - j_y B \right) = 0, \quad \dots\dots (4)$$

and

$$nv = n_0 v_0 = \text{constant}, \quad \dots\dots (5)$$

where η is the electrical resistivity, p the plasma pressure, p_e the electron partial pressure, j_y the current density in the y direction, E_x the electric field in the x direction and $n_0 v_0$ the flux of electrons or of ions passing through the surface towards the wall. The electron and ion temperatures T_e and T_i are assumed constant.

It is easily shown from the above equations that

$$(c^2 - v^2) \frac{\partial v^2}{\partial x} = A v^4, \quad \dots\dots (6)$$

where

$$A = \frac{2B^2}{\eta m_i n_0 v_0} \quad \text{and} \quad c^2 = \frac{k(T_e + T_i)}{m_i}.$$

The solution of Eqn (6), using the condition $v = v_0$ at $x = 0$ is

$$\frac{c^2}{v_0^2} \left(1 - \frac{v_0^2}{v^2} \right) - 2 \ln \frac{v}{v_0} = Ax. \quad \dots\dots (7)$$

The presence of a j_y current implies that the B_z field has a gradient in the x direction. This gradient can be neglected provided $\mu_0 c x / \eta \ll 1$. When this condition is violated Eqn (7) takes a different form but the conclusions are unchanged. For simplicity the gradient of B_z is neglected.

The curve v^2 as a function x is sketched in Fig. 1 and it is seen that x has a maximum value when $v = c$.

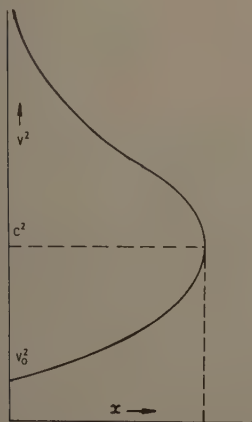


Fig. 1. The plasma velocity v as a function of x .

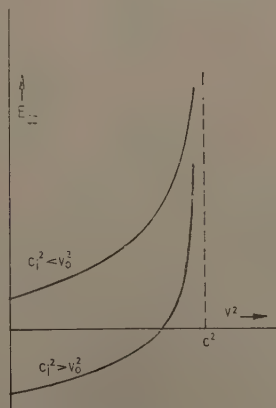


Fig. 2. The electric field E_x as a function of v .

The distribution of E_x is given by

$$E_x = \frac{m_1}{2e} \left(1 - \frac{c_1^2}{v^2} \right) \frac{\partial v^2}{\partial x} \quad \dots\dots (8)$$

where $c_1^2 = kT_1/m_1$. E_x as a function of v^2 is shown in Fig. 2. Now $E_x \rightarrow \infty$ as $v \rightarrow c$ since $\partial v^2 / \partial x \rightarrow \infty$ as $v \rightarrow c$. The appearance of the infinities is due to the assumption that $n_1 = n_e$. If the electrostatic force $e(n_1 - n_e)E_x$ is taken into account the infinities are removed. It has been shown by Tonks and Langmuir (1929) that the plane at which $E = \infty$, following the assumption $n_e = n_1$, marks the formation of a space charge sheath at the plasma boundary. If the sheath thickness is small compared to the plasma dimensions, as is usually the case, the plasma may be assumed to terminate when $v = c$ at the boundary wall.

It is concluded that the velocity of plasma drift transverse to a magnetic field is correctly given by Eqn (1) for an unbounded plasma provided $v^2 \ll c^2$ whereas for a bounded plasma the upper limit to the drift velocity is close to $[k(T_e + T_1)m_1]^{1/2}$ independent of the magnetic field strength. Therefore the $(v \cdot \nabla)v$ term should be taken into account when the drift of a bounded plasma across a confining magnetic field is under consideration.

Two of the authors (S. M. and S. I.) wish to acknowledge their gratitude to Professor Yamamoto for his interest and help in this investigation.

† Faculty of Engineering,
Nagoya University,
Japan.

S. MIYAJIMA,†
S. ITO,†

‡ Atomic Energy Research Establishment
Harwell, Didcot, Berks.

P. C. THONEMANN,‡

26th July 1961.

SPITZER, L., JR., 1956, *Physics of Fully Ionized Gases* (New York: Interscience Publishers), p. 38.

SLEPIAN, J., 1960, *Physics of Fluids*, **3**, 490.

TONKS, L., and LANGMUIR, I., 1929, *Phys. Rev.*, **34**, 896.

Sub-lattice Magnetic Moments in Manganese Ferrite

Hastings and Corliss (1956) found that the ionic distribution in manganese ferrite $MnFe_2O_4$ was $Mn_xFe_{1-x}[Mn_{1-x}Fe_{1+x}]O_4$ with $x \approx 0.8$, where the brackets enclose the ions on octahedral (B) sites in the spinel lattice. Whatever the distribution, with Mn^{2+} and Fe^{3+} ions only (both $3d^5$), ferrimagnetic theory (Néel 1948) predicts a net magnetic moment per molecule of 5 Bohr magnetons (β). Yet the experimental moment was 4.6, in agreement with earlier results (e.g. Guillaud 1951). Gorter (1957) showed that this result would be expected for $x = 0.8$ if all the manganese on B sites were Mn^{3+} ions with an equal number of Fe^{2+} ions for electrostatic balance, but that this did not explain the fact that both B (octahedral) and A (tetrahedral) sub-lattice moments had to be reduced (to 9.2 and 4.6 β respectively) to satisfy the neutron diffraction intensities. At the same time the suggestion was made (Osmond 1957) that these reductions might

be caused by the turning of oxygen p orbitals away from the cube diagonals towards the Mn^{3+} ions in order to make square d^2sp bonds with these $3d^4$ cations, as suggested by Goodenough and Loeb (1955). This interpretation is unsatisfactory since it involves the virtual annulment of some moments of both B and A ions. The existence of some canted spins in both sub-lattices now seems to be a more likely cause of the reduced moments. This note suggests a mechanism by which such canted spins could arise.

A more comprehensive explanation than the square bond theory for the distorting effect of the Mn^{3+} ion is given by ligand field theory (Dunitz and Orgel 1957). The four oxygens at the extremities of the axes of the empty $d_{x^2-y^2}$ cation orbital are drawn closer to this cation than are the two oxygens at the ends of the half-filled d_{xy} orbital. This gives a tetragonal distortion ($c/a > 1$) to this octahedron of surrounding oxygens from which arises the tetragonal spinel structure observed when 60% or more of the B sites are occupied by Mn^{3+} ions (Wickham and Croft 1958, Irani, Sinha and Biswas 1960). Thus for an isolated Mn^{3+} B ion in MnFe_2O_4 the empty $d_{x^2-y^2}$ orbital is directed at four of the six nearest oxygen neighbours, and each lobe of this orbital can temporarily receive a p electron from its own oxygen neighbour if one orbital of the latter is directed at the cation. This orbital is then turned away from the cube diagonal along which, in other circumstances, it might be expected to lie in order to overlap the empty hybrid sp^3 orbital of the A ion. Then in the new arrangement there is less screening by oxygen electrons between the Mn^{3+} ion and two of its nearest B neighbours, so that direct B-B interactions are more possible between each of these neighbours and the Mn ion, as proposed by Wickham and Goodenough (1959). The mechanism suggested is the overlapping of the half-filled d_{xy} cation orbitals. Since the acceptance by such an orbital of an electron from the other cation must entail opposite spins for the two cations there is an impulsion for the Mn^{3+} spin to be reversed relative to that of each of these two B neighbours. Moreover, the second half of each turned p orbital will overlap a half-filled d_{xz} or d_{yz} orbital of the A ion (as pointed out by Wollan 1960). Thus if one p electron goes into the empty $d_{x^2-y^2}$ orbital of the Mn^{3+} ion, with the same spin as that of this ion, the other, with opposite spin, can only go into the half-filled orbital of the A ion if the latter has the opposite spin to that of the electron, i.e. the same spin as the Mn^{3+} ion. This possibility provides a further impulsion for the Mn^{3+} ion to reverse its spin relative to that of the B sub-lattice as a whole (considered to be opposite to that of the A sub-lattice). Alternatively it provides an impulsion for the A ion to reverse its spin. These impulsions may lead to canted spins rather than actual reversals.

With $x = 0.8$ the B sub-lattice should consist of $\text{Mn}_{0.2}^{3+}\text{Fe}_{0.2}^{2+}\text{Fe}_{1.3}^{3+}$ with a Néel moment per molecule of 9.6β . The observed reduction of 0.4 could arise from 0.05 Mn^{3+} ion with reversed spin offset by 0.05 Mn^{3+} ion with normal spin. These values are together well within the maximum possible concentration of isolated B ions of one type which is four per unit cell or 0.5 per molecule. However, it is quite possible that there are no reversed spins, but that for a higher proportion of the Mn^{3+} ions the combination of usual antiparallel A-B interactions with opposed B-B interactions and some reversed A-B interactions leads to canted spins among the Mn^{3+} ions and some or all of their nearest B neighbours. As an extreme case, if all Mn^{3+} ions, supposed isolated, together with all six nearest B neighbours per ion (2/3 of the total Fe^{2+} and Fe^{3+} content) have such

canted spins the net reduction of the moment of these 1.4 ions per molecule is from 6.67 to 6.27. The average angle made by each canted spin with the general spin direction of the B sub-lattice is then $\cos^{-1} 0.94 \approx 20^\circ$. Other spin arrangements, leading to a larger average angle, are of course possible.

Since the A sub-lattice consists of $0.8 \text{ Mn}^{2+} + 0.2 \text{ Fe}^{3+}$ the Néel moment per molecule is 5β . Here the observed reduction of 0.4 is equivalent to the presence of 0.1 Mn^{2+} ion in the low spin state with one unpaired electron, giving a moment of 1β per ion. However, although theoretical reasons and experimental evidence have been given (Sinha 1958, Sinha and Sinha 1957) for the occurrence of such an A ion in Mn_3O_4 , it is unlikely that any would be present with the scattered distribution of Mn^{3+} B ions expected in MnFe_2O_4 . More probably, the presence of some parallel instead of antiparallel A-B interactions, aided by canted B spins, leads to local groups of canted A spins. In the very special case that all four A neighbours of each Mn^{3+} ion linked to it by the oxygens at the ends of its $d_{x^2-y^2}$ orbital have canted spins, and that all these sets of four A ions are independent of each other, the observed reduction in the moment of this total of 0.8 ion per molecule is from 4.0 to 3.6. The average angle made by each canted spin with the general spin direction of the A sub-lattice is then $\cos^{-1} 0.90 \approx 26^\circ$. Other, less ordered canted spin arrangements are of course possible.

Mullard Research Laboratories,
Salfords,
Surrey

W. P. OSMOND.

24th July 1961

- DUNITZ, J. D., and ORGEL, L. E., 1957, *J. Phys. Chem. Solids*, **3**, 20.
 GOODENOUGH, J. B., and LOEB, A. L., 1955, *Phys. Rev.*, **98**, 391.
 GORTER, E. W., 1957, *Proc. Instn Elect. Engrs*, **104B**, Suppl. No. 5, 228.
 GUILLAUD, C., 1951, *J. Phys. Radium*, **12**, 239.
 HASTINGS, J. M., and CORLISS, L. M., 1956, *Phys. Rev.*, **104**, 328.
 IRANI, K. S., SINHA, A. P. B., and BISWAS, A. B., 1960, *J. Phys. Chem. Solids*, **17**, 101.
 NÉEL, L., 1948, *Ann. Phys., Paris*, **3**, 137.
 OSMOND, W. P., 1957, *Proc. Instn Elect. Engrs*, **104B**, Suppl. No. 5, 229.
 SINHA, K. P., 1958, *Nature, Lond.*, **181**, 835.
 SINHA, K. P., and SINHA, A. P. B., 1957, *J. Phys. Chem.*, **61**, 758.
 WICKHAM, D. G., and CROFT, W. J., 1958, *J. Phys. Chem. Solids*, **7**, 351.
 WICKHAM, D. G., and GOODENOUGH, J. B., 1959, *Phys. Rev.*, **115**, 1156.
 WOLLAN, E. O., 1960, *Phys. Rev.*, **117**, 387.

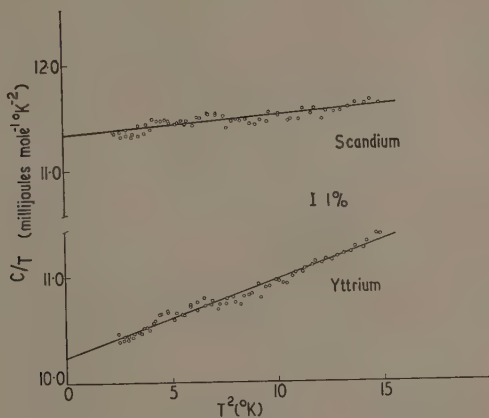
The Low Temperature Specific Heat of Scandium and Yttrium

The electronic structures of scandium, yttrium and lanthanum are of special interest, as each metal is the first member of its respective transition series. Hitherto specific heat measurements below 4°K have been made only on lanthanum (Berman, Zemansky and Boorse 1958), and the purpose of this note is to report similar measurements on the other two metals.

The specimens were obtained from Messrs. Johnson Matthey, in the form of cast cylinders 2.3 cm diameter by 3 cm long. Spectroscopic analysis of the scandium indicated that the chief impurities were about 100 parts per million by

weight of Cu, 70 of Fe, 50 of Pb, and 100 of lanthanides. On metallographic examination the scandium showed a grain size of about 2 mm: there were very few inclusions, although a light precipitate was to be seen at the grain boundaries. However, the yttrium specimen was found to be considerably less pure and according to spectrographic analysis the chief impurity was about 1000 parts per million of Ta. Metallographic examination revealed a grain size of 2–4 mm and there were considerable areas of inclusions of four different types. With an electron probe micro-analyser the major inclusion was shown to be yttrium oxide and the tantalum was found to be associated with one of the minor inclusions.

Specific heat measurements were made between 1.7 and 4.2°K in a calorimeter which will be described in detail elsewhere. The specimen was cooled by a mechanical heat switch similar to that used by Rayne (1956) and exchange gas was used only for the thermometer calibration at the end of the run. The measurements on the scandium were repeated using a different heater and carbon thermometer, and at all temperatures the two determinations agreed to 1%.



$C/T-T^2$ plot for Sc and Y.

The figure shows the experimental data for the two specimens, the curves being displaced to avoid confusion. Scandium has a relatively small cubic term, and measurements at hydrogen temperatures would be needed to obtain a precise value for the Debye temperature. Both metals show large linear components in their specific heats, which rules out the possibility of either being superconductive above 1.7°K. The question arises as to whether these linear terms are a property of the pure elements, or whether they are merely due to impurities. Magnetic impurities such as manganese and iron frequently cause a specific heat curve to turn upwards at the lowest temperatures, but concentrations of the order of 0.5% are required before they can produce a linear specific heat in copper (Zimmerman and Hoare 1960). The present results show no tendency to turn up at low temperatures, and it will be assumed that the linear term is at least predominantly the electronic specific heat of the pure metal.

Values of the electronic coefficients γ and the Debye temperatures are tabulated below, together with overall estimates of random and systematic error. The data for lanthanum derive from the paper by Berman, Zemansky and Boorse (1958).

Element	γ (millijoules mole ⁻¹ °K ⁻²)	θ (°K)
Sc	11.3 ± 0.1	470 ± 80
Y	10.2 ± 0.1	300 ± 10
La	10.1 ± 0.2	142 ± 3

The variation of θ between the elements is typical of transition metal groups (Parkinson 1958), and is due partly to the variation of atomic mass, and partly to the fact that in the earlier members of a group the ionic repulsions are stiffer and hence give rise to higher elastic constants. It is interesting to note that the Debye temperatures of all these metals are much higher than those of the neighbouring elements Ca, Sr, Ba (Parkinson 1958); this is connected with the fact that the latter group of metals have larger atomic volumes than the scandium group. Thus, even a small number of d electrons has a considerable effect upon the atomic binding forces.

The high values of γ bear out a very marked regularity among the early members of each transition series: elements with an odd number of electrons have a high density of states, and elements with an even number have a low density of states. No band structure calculations have been made specifically upon the scandium group, but one can extrapolate to some extent from calculations on calcium. According to Manning and Krutter (1937) the bottom of the 3d band in calcium lies below the 4p band and has a steeply rising $n(e)$ curve: this ensures that any electrons which spill out of the 4s band enter the 3d band and not the 4p. (If this calculation is correct calcium should strictly be regarded as a transition metal, and it is significant that in the alkaline earths $n(e)f$ is four or five times higher than in Group 2b metals such as Zn and Cd (Parkinson 1958).) Now it is unlikely that scandium has fewer 4s electrons than calcium, so that one would expect that the number of 3d electrons in scandium is of the order of unity: this would mean that the 3d band has a high peak in $n(e)$ in the region of 1 electron per atom, and that $n(e)$ falls to a comparatively low value in the neighbourhood of 2 d electrons per atom, corresponding to the case of titanium. The experimental evidence suggests that similar conclusions hold for the 4d and 5d bands.

This general picture predicts that scandium and its analogues should have a high magnetic susceptibility with a negative temperature dependence. The susceptibilities of these metals have been measured by Bommer (1939), whose data on lanthanum have been well confirmed by Lock (1957). In the case of scandium and yttrium the room temperature susceptibility is considerably higher than the Pauli value calculated from the electronic specific heat, as is usually the case in transition metals: in the lanthanum, however, the observed susceptibility is slightly lower than the specific heat value, a fact which is difficult to explain at present. In all three metals the susceptibility has a marked negative temperature dependence, and the susceptibility of scandium falls by 20% between 90°K and 300°K. However, this temperature dependence is much larger than that commonly found among transition metals (Kreissman 1953),

and it is possible that it arises not from band curvature but from other causes such as an antiferromagnetic transition at low temperatures. Measurements are being planned on the magnetic properties of the present samples of scandium and yttrium in order to study this problem further.

Many thanks are due to Mr. A. D. Le Claire and Dr. W. E. Gardner for very useful discussions.

Solid State Physics Division,
Atomic Energy Research Establishment,
Harwell, Didcot, Berks.

H. MONTGOMERY,
G. P. PELLIS.

8th August 1961.

BERMAN, A., ZEMANSKY, M. W., and BOORSE, H. A., 1958, *Phys. Rev.*, **109**, 70.

BOMMER, H., 1939, *Z. Elektrochem*, **45**, 357.

KREISSMAN, C. J., 1953, *Rev. Mod. Phys.*, **25**, 122.

LOCK, J. M., 1957, *Proc. Phys. Soc. B*, **70**, 566.

MANNING, M. F., and KRUTTER, H. M., 1937, *Phys. Rev.*, **51**, 761.

PARKINSON, D. H., 1958, *Rep. Progr. Phys.*, **21**, 226.

RAYNE, J. A., 1956, *Aust. J. Phys.*, **9**, 189.

ZIMMERMANN, J. E., and HOARE, F. E., 1960, *J. Phys. Chem. Solids*, **17**, 52.

The Skeletal Modes of Long-chain Molecules

The torsional oscillations of long-chain paraffin molecules have recently been investigated theoretically by Szigeti (1961). In an infinitely long hydrocarbon chain, torsional waves have a dispersion curve of the form shown in Fig. 1, in

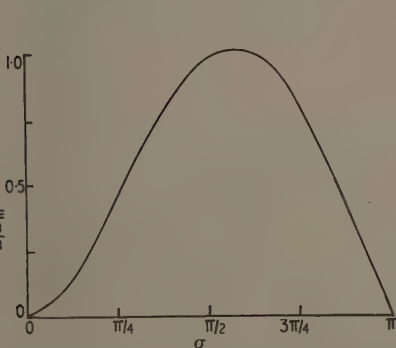


Fig. 1. The variation of frequency ω (maximum value ω_m) with wave-number σ for torsional waves in an infinite, straight, hydrocarbon chain.

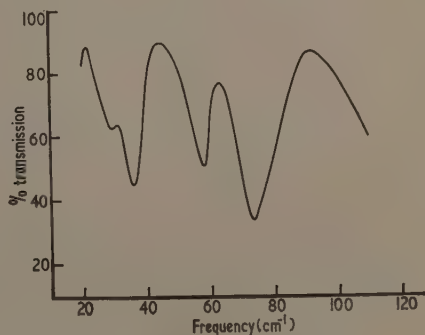


Fig. 2. Spectral transmission through a sample of $(C_{11}H_{23})_2CO$ approximately 0.1 mm thick.

which the frequency reaches a maximum value ω_m near the centre of the zone. The application of the correct boundary conditions for a finite molecule leads to the conclusion that each of the $(L-3)$ torsional modes of a paraffin molecule containing L carbon atoms is a combination of two sinusoidal waves having the same frequency, one having a wave-number greater than that corresponding to ω_m in Fig. 1, and the other with a wave-number smaller than that at ω_m . The corresponding frequencies thus range up to a maximum value close to ω_m . A torsional mode is made up of rotational displacements around each carbon-carbon bond and the characteristic frequencies are, for this reason, directly proportional to the torsional constant, k , of a C-C bond. No entirely satisfactory theoretical account of the resistance to rotation about such a bond is known. If use is made of the value for k determined experimentally for the C-C bond in ethane, i.e. $k = 4.1 \times 10^3$ c.g.s., the value for ω_m is about 5×10^{12} c/s.

These torsional oscillations of a paraffin molecule are not infra-red active, but Dr. Szigeti pointed out to us that the substitution of a C=O group for a CH₂ group, to form the related ketone molecule, would leave the C=O dipole to librate as part of the *skeletal* torsional modes. Associated spectra would then be expected in the range of wavelengths which can be studied using our techniques for the extreme infra-red (Bloor *et al.* 1961) because the value above for the maximum frequency ω_m corresponds to 167 cm^{-1} .

The purpose of this note is to report the observation of absorption spectra, with several solid ketones, which are in accord with the general predictions of Szigeti. Fig. 2 shows the extreme infra-red spectrum of C₁₁H₂₃·CO. C₁₁H₂₃, obtained at 100°K where the lines are more clearly revealed than at room temperature. This is a symmetrical ketone and the central C=O dipole can reveal only the symmetrical modes. Corresponding frequencies for a *paraffin* molecule have been evaluated by Szigeti and his results, increased by a factor 1.2, are recorded in the table together with the observed frequencies for the ketone.

The frequencies, in cm^{-1} , evaluated for CH₃(CH₂)₂₁CH₃ from the computations of Szigeti (using $k = 4.9 \times 10^3$ c.g.s.) and the frequencies of the absorption lines in the range so far studied (from 100 cm^{-1} to 20 cm^{-1})

Computed	37	60	83	115
Observed	37, 28	58	73	115

Additional computed frequencies are at 7.2, 136, 161, 178, 192 and 198 cm^{-1} .

The multiplication by 1.2 amounts to the use of $k = 4.9 \times 10^3$ c.g.s. rather than the ethane value 4.1×10^3 c.g.s., and is made in order to bring the highest line-frequency which we have so far observed (at 115 cm^{-1}) into coincidence with the closest computed frequency. Three other lines are then predicted in the range at present studied, and three are found. The observed frequencies are in reasonable agreement with the computations, bearing in mind the corrections which may be necessary to allow for the loading of the paraffin chain by the oxygen atom, as discussed by Szigeti. The doublet splitting at 37 cm^{-1} in Fig. 2 might be produced by the dipolar interaction between neighbouring molecules which

Szigeti estimates should lie between 1 and 10 cm^{-1} . Similar spectra have been obtained with several other ketones, kindly lent to us by Dr. V. Daniel.

A systematic study of a wide series of ketones is now being made, and the range covered is being extended to reach the maximum frequency expected at about 200 cm^{-1} . Such observations will give a measure of the long-chain torsional constant, of the extent of torsional and rotational motion in the solids and of intermolecular dipole interactions.

Queen Mary College,
(University of London),
Mile End Road,
London, E.1.

S. B. FIELD.
D. H. MARTIN.

2nd August 1961.

BLOOR, D., DEAN, T. J., JONES, G. O., MARTIN, D. H., MAWER, P. A., and PERRY, C. H.,
1961, *Proc. Roy. Soc. A*, **260**, 510.

SZIGETI, B., 1961, *Proc. Roy. Soc. A*, **264**, in the press.

REVIEWS OF BOOKS

Plasma Physics, a course given by S. CHANDRESEKHAR at the University of Chicago. Notes compiled by S. K. TREHAN. Pp. 217. (Chicago: University Press; London: Cambridge University Press, 1960.) 14s.

There is serious need for a comprehensive monograph describing recent developments in the study of plasma dynamics, which are scattered throughout the scientific literature, or more often buried in laboratory or conference reports. Professor Chandrasekhar's lecture notes, while not quite that, do contain a full account of one of the most interesting of these developments. This is the quasi hydrodynamic treatment of a diffuse plasma in a strong magnetic field, which shows how such a plasma may exhibit cohesive hydrodynamic-like behaviour even though the mean free path be extremely large, the localizing feature being the small Larmor radius of particle orbits. In the first few chapters the perturbation theory of particle orbits in slowly varying fields is developed, particular attention being paid to the extremely useful adiabatic invariants of the motion. This theory is then applied to the study of the equilibrium and stability of plasmas confined by magnetic fields, problems in which fields and orbits must be made consistent. The stability of the pinch, a cylinder of plasma confined by a surface current, merits an entire chapter, in which in addition to magneto-hydrodynamic instabilities those produced by anisotropy in the pressure tensor are described. A section on plasma oscillations gives much space to dispersion relations for a non-magnetic plasma and a rather cursory glance at the effect of a magnetic field. A final chapter considers the effect of collisions and the origin of transport processes; of particular interest is the rather spectacular effect on transport processes produced by consideration of a small admixture of neutral gas.

Within a single course of lectures one cannot expect to cover the subject completely, but it is unfortunate that in spite of the space devoted to pinch stability the work of Suydam and Rosenbluth which exposed the artificiality of a stabilized pinch is not mentioned. More serious is the absence of any reference to experiment with which the theory here presented is not always in complete agreement; the flute instabilities which are described and were predicted as diseases of the magnetic mirror have not appeared, although those arising from anisotropy in the pressure tensor have been demonstrated. On the other hand some configurations, especially the 'hard-core' pinch, predicted to be stable have failed to be so. In spite of these limitations, this is the most complete study of the diffuse magnetized plasma yet to have appeared and as such demands the study of all those seriously interested in the field.

W. B. THOMPSON.

Relativity: The General Theory, by J. L. SYNGE. Pp. xv + 505. (Amsterdam: North Holland, 1960.) 110s.

This is a beautiful book. Wherever one turns in it one finds some subject treated in a novel, clear and lucid way, surveyed in a detached and cool fashion. The stress of the whole approach is on the geometrical aspect of general relativity, as might be expected. What is surprising, however, is the success Professor Syngé has had in helping one to visualize highly abstruse geometrical concepts, and part of the joy of reading the book lies in this.

A novel method is employed in dealing with Riemannian geometry, the 'world function' first introduced by Ruse. This is of great help in getting an

intuitive feeling for the theory, because this function is essentially simply the square of the distance between two events. The geometrical aspects of general relativity are firmly in control, guiding, shaping and illustrating the book, but there are also clear and precise references to the observational tests of the theory, right up to the present.

No book of such beauty could possibly have been written had Professor Synge not adopted a well-defined point of view, putting in the forefront the clear and precise notions of geometry, of which he is such an unrivalled master. This has necessarily ruled out detailed attention to the various links between the theory and the rest of physics. It is hard to find beauty (though easy to see fascination) in that odd mixture of compelling argument, half-baked suspicion and wide-open mystery that is characteristic of many of these connections.

The book ranges far and wide. Chapters like those on integral conservation laws and on gravitational waves take one deep into active fields of research. The bibliography of 60 pages forms an extremely valuable part.

The book can be heartily recommended to all who are interested in general relativity. However, the knowledgeable reader will find much that is new to him. For the novice his taste must decide whether this should be his first book on general relativity or whether he prefers to start with the physics, in which case this is an ideal second book for him.

The book is beautifully produced and is a pleasure to own.

H. BONDI.

Solid State Physics, Vol. 11, *Advances in Research and Applications*, Supplement 2, *Paramagnetic Resonance in Solids*, by W. LOW. Edited by F. SEITZ and D. TURNBULL. Pp. viii+212. (New York: Academic Press; London: Academic Books, 1960.) 60s.

As its title and membership of the excellent 'Solid State Physics' series might suggest, this book sets out to point the importance of paramagnetic resonance techniques in the armoury of the solid state physicist. It cannot be claimed that there is great originality of presentation or context. However, the book is to be welcomed as it synthesizes many ideas scattered in the literature in such a way that the basic features of paramagnetic resonance in solids may be understood. The theory of the crystalline field is first developed and followed by a detailed exposition of its application to the iron, rare-earth and uranium groups. A section on relaxation times and line width leads to a short discussion of solid state devices. There are also brief notes on paramagnetic resonance studies of colour centres and defects in crystals. The short final section is concerned with the experimental side of paramagnetic resonance spectrometry. Throughout the whole text many useful references to original articles are given as footnotes.

R. STREET.

Quantum Theory of Atomic Structure, Vol. 1, by J. C. SLATER. Pp. xii+502. (New York, Toronto, London: McGraw-Hill, 1960.) 85s. 6d.

This is the first of a two-volume text on atomic structure, which is itself the first of a series that the author hopes to write on the application of quantum mechanics to the structure of atoms, molecules, solids and the physical and chemical properties of matter.

The approach is very elementary. The book starts with a fifty-page historical introduction to quantum theory, leading in a purely heuristic way to the Schrödinger equation, for a single particle in a potential. Rules of thumb

are then given for writing down the Schrödinger equation in more general circumstances. Matrices are introduced as expectation values in the Schrödinger representation.

The book then gets down to the restricted field implied by the title including a discussion of the hydrogen atom, the Hartree self-consistent field, the determinantal method and the theory of multiplet structure. Angular momentum including spin is treated rather superficially.

Professor Slater has built up for himself a great reputation as a pedagogue, and, as one would expect, everything in this book is explained with his usual clarity. The latter half of the book which starts to deal with atomic structure is excellent, but the first half is disappointing and rather old fashioned. It is perhaps significant that Dirac is not mentioned along with Heisenberg and Schrödinger among the great pioneers of the subject.

The two-volume text will no doubt become a standard work for those primarily interested in atomic structure, but this first volume by itself is not, as the author hopes, suitable as an introductory text in quantum mechanics for those with wider interests in quantum physics, or a desire to gain in physical terms an understanding of the general structure of quantum theory as we now understand it.

P. T. MATTHEWS.

Progress in Nuclear Physics, Vol. 8, edited by O. R. FRISCH. Pp. vii+304. (Oxford: Pergamon Press, 1960.) 90s.

The articles in the eighth volume of this well-known series, with one exception, have a strong inclination towards high energy physics. The exception is the chapter 'Collective motion in nuclei' by D. M. Brink, which provides firstly a brief review of the whole subject and then a more detailed treatment of recent work on pairing correlations and coupling schemes. The collective model is clearly becoming more intelligible theoretically, although it has hardly gained in simplicity.

The volume opens with an interesting account of 'The composition of the primary cosmic radiation' by C. J. Waddington. This is a subject of perpetual interest because the energies involved reach out beyond the applicability of present theories. The article is primarily experimental and deals in detail with the charge spectrum of the heavy incoming particles. One of the techniques which, like the nuclear emulsion method, has found a place both in cosmic ray studies and in high energy physics in the laboratory is Cherenkov counting. In a stimulating and informative article on 'Cherenkov detectors' G. W. Hutchinson continues from existing reviews of the subject into the design and application of new forms of counter, many of which have interesting possibilities so far largely unexploited. Instrumentation for cosmic ray research in satellites will clearly be much aided by these devices.

Laboratory studies in medium and high energy nuclear physics receive attention in the articles by E. J. Squires on 'The interaction of polarized nucleons with nuclei' and by E. H. Bellamy on 'The photoproduction of pions'. The former is a valuable account of a subject in which interest is rapidly increasing following the development of polarized ion sources and targets. A full account of the available experimental material and a clear presentation of the relevant theory are given. The latter article is a readable account of the main experimental techniques and results in photo-pion physics, with emphasis on high energy photon interactions with nucleons. The theoretical

treatment of these results is outlined and the reader cannot fail to notice the frequency with which reference is made to calculations of excitation functions and angular distributions based on dispersion relations. It is therefore fortunate that this volume provides what is perhaps the first attempt to describe the present status of this subject to a general audience, in the chapter 'Dispersion relations for elementary particles' by J. Hamilton. The relation between absorption and scattering processes is a very general one and embraces many physical phenomena; in the present article the somewhat complicated field-theoretic results are approached via several interesting and immediately tangible classical examples.

The volume under review makes perhaps more demands of the reader than some of its predecessors because of its high theoretical content, but this is inevitable if the subjects presented are to be treated adequately. The material discussed is that which was available at about the middle of 1959, and most of the references are dated within the decade 1950-60. The standard of production is high, although rather more misprints and errors in spelling than usual have crept through the proof-reading.

W. E. BURCHAM.

Studies in Theoretical Physics: The Proceedings of the Summer School of Theoretical Physics held at Mussoorie, India on 22nd May-18th June 1959, Part 3. Pp. 341+535. (New Delhi: Government of India Ministry of Scientific Research and Cultural Affairs, 1959.) Rs. 5.

The papers contained in this part of the *Proceedings* are listed in three sections: Chemical physics, Astrophysics and magneto-hydrodynamics, and Selected topics, which include papers on the exact solution of the equations of charged particles in a plane electromagnetic radiation field and the Compton scattering, the theory of distributions and its applications to field physics, fundamentals of function algebra, relativistic cosmology and Einstein's field equations.

Proceedings of the 1960 Annual International Conference on High Energy Physics at Rochester, edited by E. C. G. SUDARSHAN, J. H. TINLOT and A. C. MELISSINOS. Pp. xxv+890. (Rochester, N.Y.: The University of Rochester; New York: Interscience, 1960.) \$13.50.

The Conference consisted of sessions of three different types—four main sessions on Strong interactions of pions and nucleons (experimental), Strong interactions of pions and nucleons (theoretical), Strong interactions of strange particles, and Weak interactions, at which invited papers were presented; four sessions on the same group of subjects, in which summarized reports of associated work were given; and three sessions devoted to subjects of general interest, Structure of elementary particles, New results at superhigh energies, and Theories of elementary particles.

Annual Review of Nuclear Science, Vol. 10, edited by E. SEGRÈ, G. FRIEDLANDER and W. E. MEYERHOF. Pp. vii+617. (California: Annual Reviews Inc., 1960.) \$7.50.

This volume, the tenth of a series of Annual Reviews of Nuclear Science, contains chapters on the following subjects: Neutrino interactions, Nuclear interactions of heavy ions, Cosmic ray showers, Bubble chambers, Optics of high-energy beams, Nuclear structure effects in internal conversion, Recoil

techniques in nuclear reaction and fission studies, Labelling of organic compounds by recoil methods, Nucleon-nucleon scattering experiments and their phenomenological analysis, Theoretical interpretation of the energy levels of light nuclei, Nuclear methods for sub-surface prospecting, Experiments on cosmic rays and related subjects during the International Geophysical Year, and Cellular and vertebrate radiobiology.

Some Ionospheric Results obtained during the International Geophysical Year, Proceedings of a Symposium organized by the URSI, AGI Committee, Brussels, 1959, edited by W. J. G. BEYNON. Pp. xi+399. (London, Amsterdam, New York, Princeton: Elsevier, 1960.) 72s.

During the International Geophysical Year scientific observation was coordinated throughout many countries and outstanding advances resulted in many fields.

One of the fields in which the most intensive research was carried out was that of the ionosphere. The results of this research were discussed at a symposium organized by the International Scientific Radio Union, more usually known as U.R.S.I.

During the course of the International Geophysical Year many millions of radio observations were made. These have been scrutinized for interpretation but more information will no doubt be obtained in future scrutinies of the same material. As the Editor and Chairman of the International Geophysical Year Special Commission say in their Preface to the volume, a comment of the late Lord Rutherford is relevant, "This is a grand subject because there is so much in it we do not know".

A large number of articles on various aspects of the ionosphere will encourage workers to seek further explanation of the material available. The book is divided into eight sections: F2 layer phenomena, High altitude studies, Disturbance phenomena, Ionospheric irregularities, $N(h)$ profiles, Absorption, Drifts, Noise: whistlers, rockets, satellites.

Elektronenbeugung, by ERNST BAUER. Pp. 233. (Munich: Verlag Moderne Industrie, 1960.) DM. 32.

There are few books on the subject of electron diffraction. The principal texts are still those of Thomson and Cochrane (1939), von Laue (1944) and Pinsker (1949). Since the publication of these books there has been a massive growth of the subject of electron microscopy. The application of the methods of this new technology has transformed the subject of electron diffraction, and the appearance of a book which takes account of these developments is therefore timely.

About a quarter of the present book is devoted to the basic theory of the subject. The presentation of this is competent but not outstanding. Much more satisfactory is the section of 84 pages dealing with the constructional details and theoretical limitations of electron diffraction apparatus and the preparation of specimens. A general description of some half dozen commercial instruments from different countries serves to illustrate the discussion of the desirable electron optical and mechanical features of the diffraction camera. The author has given a good general description of the methods available for the preparation of specimens, and the numerous references to published papers enable the reader to obtain readily any further details he may need.

A section on the interpretation of electron diffraction patterns leads naturally to a discussion of the applications of electron diffraction in the metallurgical, chemical and optical industries. The only fault I have to find with an admirably comprehensive treatment is that no indication is given of the difficulty of some of the techniques, so that a reader without prior knowledge of the subject can hardly judge which details of the structure of a specimen are immediately evident in an electron diffraction pattern, and which are brought to light only after prolonged study.

A few pages near the end deal briefly with the diffraction of low energy electrons, and the combination of electron diffraction with electron microscopy. The book concludes with a valuable bibliography of 589 references and—an unusual feature—the addresses of a number of firms in eight countries which manufacture complete instruments or component parts.

The text is marred by numerous errors in references to figures and page numbers; it is to be hoped that these blemishes in an otherwise admirable book will be remedied in later editions.

T. B. RYMER.

Theoretical Physics in the Twentieth Century : A Memorial Volume to Wolfgang Pauli, edited by M. FIERZ and W. F. WEISSKOPF. Pp. x+328. (New York: Interscience, 1960.) 72s.

This volume of articles was originally intended to celebrate the sixtieth birthday of Pauli. His death converted it into a memorial volume instead. As the editors say themselves, no collection of articles could do justice to the memory of Pauli's work and his impact on modern physics, for only further progress in physics carried out in his spirit can ever serve as a true memorial. Nevertheless, this volume is a fitting tribute that leads the reader again and again to marvel at the influence that Pauli had throughout his active life. One tends to think of Pauli as the conscience of theoretical physics, expressing in unmistakable terms his profound abhorrence of any argument not founded upon the strictest mathematical rigour. Indeed he was that; but he was also a physicist of deep intuitive insight who could see through the complexities of atomic spectra to the need for the exclusion principle long before his restless demand for rigour eventually enabled him to set it upon an adequate mathematical framework, and who predicted the existence of the neutrino long before that most elusive of particles was prepared to vindicate him.

There are two different kinds of article in this memorial volume. The first kind concentrates on the exciting days of the discovery of quantum mechanics, filling in the background without which it would be impossible to understand Pauli's own contributions at that time. The other kind traces the development of subjects up to the present day in which Pauli had at some stage a special interest. Quite apart from its other many virtues, this is one of the best accounts I have ever read of the early days of quantum mechanics, giving a vivid description of the many profound difficulties which arose and the part that each of the great physicists of those days played in their eventual resolution. It would have been so easy, and so understandable, to overdo the part of Pauli in all this; but then the result would have been a lesser, not a greater, tribute to one to whom exactness and simplicity of expression were always paramount.

B. H. FLOWERS.

An Introduction to Astro-Dynamics, by R. M. L. BAKER Jr. and M. W. MAKESON. Pp. xiv+358. (New York: Academic Press, 1960.) \$7.50.

The advent of space science has demanded a greatly increased activity in those branches of theoretical astronomy that are concerned with the motions of planets, satellites and interplanetary particles, whether these be artificial or natural. The celestial mechanical principles on which such theory is based are well known, having been developed since the time of Newton. However, methods of applying them to the extensive high speed requirements of space science are now being devised and improved. To cope with these advances special study courses are needed supported by suitable textbooks. This new science of celestial mechanics applied to contemporary problems of space vehicles is called 'Astro-dynamics'.

The book under review provides a very effective introduction to this subject. Its essential aim is to provide the mathematical basis for the practical calculations of space motion. The text is therefore designed for engineers and space scientists rather than astronomers. The reader does not require a knowledge of classical celestial mechanics but will use calculus, vectors and rectangular coordinates. Hamiltonian mechanics is avoided, and spherical and polar coordinates are used only to a restricted extent. The mathematical developments are rather concise. The Table XV is very useful in providing a summary of the combinations of observational data that are likely to be available and indicating those theoretical sections developed elsewhere in the book that should be applied in the various cases. Much attention is given to the application of orbital perturbations to terrestrial and atmospheric problems.

Although the main part of the book is devoted to mathematical utility, there is much that will be useful to the general reader. The early chapters give readable discussions on relevant background subjects such as coordinate systems, general laws, minor planets, comets, and their relations to space science. The value of the book as a reference handbook is enhanced by introducing a chapter in which astrodynamic quantitative concepts are clearly described and the latest numerical values given. There is a very extensive glossary of both terms and symbols.

The book is well printed and has clear efficient notations. It deserves a wide distribution among all who are connected with or interested in space science.

C. W. ALLEN.

Principles of Optics, by M. BORN and E. WOLF. Pp. xvi+803. (London, New York, Paris, Los Angeles: Pergamon Press, 1959.) £6.

The preface to this book explains that it is restricted to "those optical phenomena which may be treated in terms of Maxwell's phenomenological theory". Material media are regarded as continua for which quantities like the dielectric constant are given and the classical molecular optics which occupied about half the space of Born's *Optik* is excluded. Applications of relativity and quantum theory to optics are omitted. This involves the omission of the experiments on moving media, the theory of radiation detectors (including the eye) and the application of information theory to optics. The topics treated include the detailed theory of interference, with special reference to coherence, the theory of diffraction (with an extended treatment of diffraction by ultrasonic

waves) and the theory of optical instruments discussed both in terms of geometrical optics and of wave theory. There is an interesting historical introduction.

One can see that difficult decisions were needed to prevent this book extending to well over 1000 pages and that it was not possible to be strictly logical in deciding what to omit. I wish that moving media had been included and I feel that, since photo-elasticity was included, the electro-optical and magneto-optical effects might also have been treated. The treatment of the diffraction theory of optical instruments is inevitably a little unsatisfactory because discussion of the properties of the receptor and of the ultimate limits of measurement set by noise is excluded. It is thus impossible to show that a loss of transmission in higher spatial frequencies, due to aberration, results in an irretrievable loss of information.

A very large part of this book is concerned with a systematic account of the wave theory of light, including the most recent developments. The treatment is logical and authoritative. To those who are prepared to give concentrated attention to a subject which is not always simple, it is clear and straightforward. All who are concerned with optical theory—and in view of the many applications of wave theory this means all theoretical physicists—are indebted to the authors. The account of optical instruments and of experimental methods is uneven in coverage and in quality. Many topics of interest, such as the sheared-wave interferometer, are very adequately treated. On the other hand, the account of experiments on the velocity of light is inadequate and completely out of date. The choice of material in this part is not very satisfactory; the Lummer-Gehrcke Plate (now mainly of historical interest) is treated at length (6 pages), while there is very little discussion of interference spectroscopy or of optical standards of length.

Let us accept the excellence of the main part of this book and consider the general question of the function of a book of this type in the dissemination of scientific information. If any considerable scientific topic is to be fully discussed in a book, the treatment may become nearly as lengthy as the original papers from which it is derived. Unless the presentation is an advance on the original papers in clarity of exposition, so that the reader obtains a deeper insight, then most people will prefer to have a general introduction together with references to the papers. At a certain point the book must give way to the *Handbuch* or the *Progress Report* containing a series of articles by people who are most expert in restricted fields.

The treatment of coherence in this book is very lengthy, yet I feel that the length is justified because the subject can be seen as a unity (apart from the quantum theory aspects). An endeavour has been made to obtain some of the advantages of the *Handbuch* by calling in a panel of consultant experts (to whom acknowledgment is made in the preface) while retaining the unity which is available when there are one or two authors. Although I would have preferred from these authors a book which omitted much of the experimental and instrumental side and gave a little less space to some theoretical topics which seem to me unimportant, I hope and believe that this book will be very successful. I also hope that its success will not encourage other authors to write at equal length. Every rule may have an exception. Let us regard this as an exception to the rule that a good book should not be too heavy to hold in one's hand.

R. W. DITCHBURN.

Kybernetik, Band 1, Heft. 1—Journal dealing with the transmission and processing of information and with control processes in organisms and automata. Pp. 56. (Berlin, Göttingen, Heidelberg: Springer-Verlag, 1961.) DM. 12.80.

This new journal intends to become a forum on the subjects of information theory, theory of automata, theory of control systems, mathematical foundations of communication theory, sensory processes and micro- and macrophysiology of the central nervous system in relation to information handling, information handling by organisms (including man) and task-oriented groups, and mathematical models for communication and control processes in organisms. This covers to an appreciable degree the scope of the *Journal of Electronics and Control* and the journal *Information and Control*. Judging from the first number we can expect that it will complement them in a happy way because it shows a strong bias towards neurophysiology and biology. Küpfmüller and Jenik contribute a clear and simple article on information processing by neurons. Reichardt sums up his well-known, remarkable investigations on the fungus *Phycomyces*, probably the best explored organism from the point of view of sensory dynamics. Trincker, Sieber and Bartual describe their investigations of eye movements. Vossius gives a mathematical analysis of the efferent-afferent sensory-muscular control circuit. Wenzel gives a most interesting numerical analysis of the reaction times of piano players who read their music. Steinbuch contributes a remarkable article on the learning matrix, with an electro-chemical model. Carson's article on 'Letter constraints within words in printed English' is a further elaboration of one of the classical fields of information theory. Ivo Kohler comes back to Pavlov's equally classical dog.

As always with a new journal, one wonders whether it will be possible to maintain this high level, but this is fairly guaranteed by the distinguished international list of editors. From now on the new journal will have to be followed with attention by everybody working in the various fields which have branched out from information theory.

D. GABOR.

Selected Scientific Papers, by B. VAN DER POL, edited by H. BREMMER and C. J. BOUWKAMP. Vol. I, pp. xiii + 660. Vol. II, pp. 661-1339. (Amsterdam: North-Holland, 1960.) £6 13s. per volume.

We hear frequently these days about scientific radio, but radio has not always been very scientific, and this aspect of physical science has been almost more than any beset by empiricism. Few men have done more than Van der Pol to put radio on a sound scientific basis. Together with his life-long friend Sir Edward Appleton he did much to found and foster the Union Radio Scientifique Internationale. Van der Pol was essentially a theoretician but with a very practical turn of mind. His interests were wide and he made notable contributions to the theory of radio wave propagation, theory of oscillations and the development and applications of operational calculus, to quote only a few of the more important fields in which his researches lay. He was a man of great industry and insight and wrote a great deal that is important in his long and busy life, working right up to the end. The two substantial volumes under review represent only a fraction of his work. We have here, however, a representative selection covering most of the fields in which he made notable contributions and including his most famous papers.

The papers are scattered over a large number of journals and the present collection will make reference much easier for many of those who will, undoubtedly, consult them for a long time to come.

The individual reader may feel that the two volumes are somewhat costly but those who came to know Van der Pol and his work will surely wish to have them as a fitting memorial to one who did so much to give dignity to his subject. Libraries associated in any way with radio research should, of course, have a copy.

The volumes are beautifully produced and the editors, Dr. H. Bremmer and Dr. C. J. Bouwkamp, both of whom were closely associated in his work with Van der Pol, are to be congratulated on the clear presentation and arrangement of the papers. These are introduced by a fitting biographical note by Dr. H. B. G. Casimir.

R. A. SMITH.

The Rotation of the Earth, Cambridge Monograph on Mechanics and Applied Mathematics, by W. H. MUNK and G. J. F. MACDONALD, edited by G. K. BATCHELOR and S. GOLDSTEIN. Pp. xix + 323. (Cambridge: University Press, 1960.) 70s.

This is a delightful book. When one opens a book on an imposing subject, full of uncertainties requiring a tremendous amount of detailed discussion of theories as well as of observations, one expects to find that the authors have undertaken this formidable task in a spirit of duty or as a penance for having added to the confusion of the subject. This expectation is often fulfilled and leads one to anticipate that such a monograph might make heavy reading, but Munk and MacDondald are writers of an entirely different class. They not only love their subject, they positively enjoy writing about it. They convey their pleasure and interest so vividly and in such expressive language that few readers, however little interest the subject may have possessed for them, will be able to resist its fascination.

Phrases like "problems becoming unsolved" and "excursions into the jungle of theory" deserve to become part of the scientific vocabulary.

The range of subjects covered by the authors is tremendous and their mastery is complete at every point. It is most refreshing to find such a degree of healthy scepticism and thorough appreciation of both observational and theoretical difficulties amongst people so deeply immersed in their subject. The full discussion of the various aspects, such as the wobble of the earth's axis and the variations in the length of day, naturally lead the authors deeply into the subject of the evaluation of the observations of the earth's rotation for theories of the structure of the planet. Thus, to use a phrase of theirs, they "make a geophysical asset out of an astronomical nuisance". The treatment is everywhere clear and intelligible to anybody willing to make the effort, and with such fascinating guidance it would require considerable power of will not to make the effort.

The diagrams are particularly intriguing and greatly aid the understanding. Though in some places three-dimensional models might have been more helpful, one can understand the aversion of the publisher to these. My only complaint, if complaint it be, is that glancing through the pages one becomes so attracted by some of the diagrams that, on finding the legend insufficiently informative, one turns to the text to discover just what they refer to, but making a reader read is not really a crime on the part of an author. To anybody interested in

the subject, one of the limited number of possible approaches to a theory of the constitution of the earth, this is an essential book. Few authors, whose work brings them in contact with related disciplines, such as rigid body dynamics, elasticity, plasticity or astronomy, will not benefit from a study of the book and, in addition, will enjoy reading it. The book has been beautifully produced by Cambridge University Press.

H. BONDI.

Complex Variables and the Laplace Transforms for Engineers, by W. R. LE PAGE. Pp. xvii + 475. (London: McGraw-Hill, 1961.) 97s.

Books on the Laplace transform generally fall into two groups: (i) those intended for mathematicians where mathematical concepts and rigour are the matters of primary interest, and (ii) those intended for engineers which are in the main concerned with applications to technical problems, and where only sufficient mathematical analysis is presented to give a reasonable understanding. However, in the more advanced applications a thorough knowledge of the complex variable becomes necessary, and some authors have been content to refer to standard texts. This approach can be wasteful and it is one of the claims of this book that the complex variable theory is presented with applications to engineering problems in mind.

The first seven chapters deal with the development of the appropriate complex variable theory, the subjects including the following: system analysis, analytic functions, conformal mapping, complex integration, Cauchy's integral theorems, infinite series, singularities, residues multivalued functions and a collection of useful theorems.

In Chapter 8 the author presents the theory of convergence of real integrals. Then follows a short chapter on the Fourier integral where its properties are presented. The next four chapters present the definitions, properties and applications of the Laplace transform, one chapter being on the convolution integral and its implications. Here again strict attention is paid to the question of convergence. The next chapter presents in detail the impulse function and the amount of space is justified on the grounds that engineers find it difficult to believe in this function. The last two chapters are concerned with periodic functions and the Z-transform and its application to sampled data.

All sixteen chapters are followed with a selection of problems designed to augment the text (no answers).

The book has been written by an engineer for engineers and has been developed out of a series of lectures, and the level is set at the final year and first year postgraduate stage.

C. C. RITCHIE.

Proceedings of the International Conference on Nuclear Structure, edited by D. A. BROMLEY and E. W. VOGT. Pp. 990. (Toronto: University Press; Amsterdam: North-Holland, 1960.) 125s.

This book is an account of the International Conference on Nuclear Structure held at Kingston, Ontario, from August 29th to September 3rd, 1960. To all research workers in this field the value of the publication has been greatly enhanced by the exemplary speed with which the editors managed to get this enormous mass of material into print and circulation, there being an interval of only several weeks between the close of the conference and the availability of the *Proceedings*. The material is presented with great clarity and in a form which makes it easy to use for reference.

The rapporteur system was used at the conference and in the *Proceedings* the main talks are reproduced in full. The topics discussed were the physical foundations of nuclear models, the gross properties of nuclear matter, nuclear reaction mechanisms, the properties of individual levels, statistics of nuclear levels, giant dipole resonances and finally fission phenomena as related to nuclear structure. There were also two stimulating talks given by R. E. Peierls and D. H. Wilkinson on open problems in nuclear structure.

In addition to the talks given by the main speakers and the resulting discussions a number of selected research contributions are also printed and abstracts of all other contributed papers are presented as an Appendix.

The editors have been successful in achieving in this volume a balance between the large quantity of experimental data of impressive precision and the astonishingly good theoretical description of these data in terms of nuclear models. As Professor Weisskopf points out in his conference summary, which is a gem of elegant simplicity, that this description is so good is an indication of how little we know about the nucleus.

J. E. BOWCOCK.

Physique Nucléaire, par M. BAYET. Pp. 404. (Paris: Masson, 1960.) 65n.fr.

This French undergraduate textbook of nuclear physics follows the traditional syllabus at a fairly elementary level. The first hundred pages are devoted to the ideas of wave mechanics, classical and quantum statistics, scattering theory, spin, and relativity. Next comes a brief survey of elementary particles and the characteristics of stable nuclei, enough being said about nuclear forces to provide a framework on which to attach the various models of nuclear structure. The treatment of natural radioactivity which follows makes room for some relatively modern developments (such as the regularities in the lifetimes of M4 gamma transitions) but is notably out of date in failing to make any reference to parity non-conservation. There is a long section on the interaction of nuclear particles with matter, leading up to a brief description of particle detectors. The book ends with a short account of neutron physics and of fission and fusion processes.

The book is much less ambitious in scope than the textbooks of R. D. Evans, D. Halliday, and I. Kaplan, on which it is avowedly based. This pruning down to essentials might well prove an advantage to some students, and the writer would certainly recommend it to those who can surmount the language barrier but are appalled at the acres of reading often expected of them by all but the most tolerant of lecturers.

H. R. ALLAN.

Physics of the Atom, by M. RUSSELL WEHR and JAMES A. RICHARDS JR. Pp. xi + 420. (Reading, Massachusetts; London: Addison-Wesley, 1960.) 49s.

This textbook is written at about the level of a first-year university course in this country. It begins with chapters on the atomic view of matter, of electricity, and of radiation; it ends with chapters on nuclear energy, cosmic rays and the fundamental particles. Between these extremes, and making up about two-thirds of the book, is an admirably clear account of elementary atomic structure, relativity, x-rays, matter waves, the solid state, radioactivity, and nuclear physics.

With such a vast syllabus, the treatment is inevitably brief. But it is not scrappy. Some formulae are derived, others simply quoted, but their significance

is always made clear and there are plenty of numerical problems to drive home what has been learned. Each chapter ends with a list of useful references for further reading.

As an indication of the degree of detail attempted we observe that the simple Bohr theory of the hydrogen atom is developed fully, whereas electron spin is mentioned only briefly as a cause of fine structure. The exclusion principle is applied to illustrate the building up of the chemical elements, but we are not taken beyond the first two short periods of the Periodic Table.

Special relativity is given a comparatively full treatment: the Lorentz transformation and mass-energy equivalence are both derived and illustrated numerically. Matter waves are discussed without the use of Schrödinger's equation. Solid state physics, too, has an almost wholly qualitative treatment, directed towards an understanding of transistors. The section on nuclear physics, on the other hand, begins with radioactivity and the equations of radioactive growth and decay; and in the survey of nuclear transmutations there is a detailed presentation of Chadwick's evidence for the existence of the neutron. There is no discussion at all of nuclear models, but reactor physics is dealt with at length.

All in all, a very reasonable balance has been struck between rigour with the fundamentals and concessions to the student's interests with qualitative treatments of practical applications and the more glamorous recent discoveries. This is a very good textbook indeed.

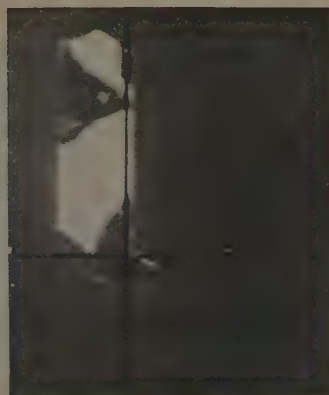
H. R. ALLAN.

Frozen Free Radicals, by G. J. MINKOFF. Pp. ix + 148. (New York and London: Interscience Publishers, 1960.) 36s.

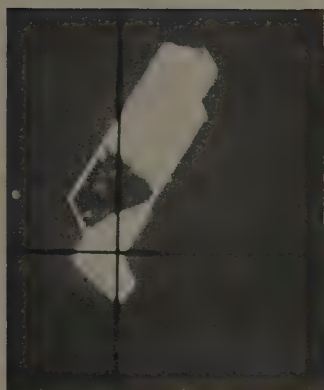
There are few branches of physics and chemistry whose 'early history' can be stated to have ended a mere five years before the present. The rapidly growing field of the stabilization of free radicals at low temperatures is one of these. Admittedly, as is the case for many other low temperature phenomena, Dewar's work in the 1890's provides the first examples, but a systematic study and use of frozen free radicals is less than a decade old.

Such a rapidly growing field, which relies on a careful blending of a variety of techniques, demands a book which can serve both as a guide to the newcomer, and as a quick reference book for the specialist. Dr. Minkoff has aimed high but the result is disappointing. It is true that the table of contents makes impressive reading: experimental methods for the production and trapping of radicals, cryogenic techniques, theoretical work on trapping, and finally, the properties of active atoms and of a large variety of free radicals, are all included. But alas, the treatment is patchy, uneven, and there are some misleading, or trivial, or naïve or useless statements, especially in the chapter on experimental methods. Thus for instance, one wonders whether in describing a method for delivering a gas at a predetermined rate (p. 32), the author refers to the 'recent' discovery of Charles' law, or Poiseuille's law, or of the temperature dependence of viscosity, or of the thermal expansion of solids. Again, to give another example, a sentence on p. 53 might well convey to the uninitiated the idea that the numerical value of the ratio Boltzmann constant/Bohr magneton was not established until 1957. The most charitable explanation for passages like these is that they are the result of hasty and careless composition. One can only hope that the novelty of a subject and the urge to publish a book quickly will not be allowed to become an excuse for such regrettable practices.

N. KURTI.



(a)



(b)



(c)

Fig. 1. Twinned crystal of indium sulphide between crossed polaroids, showing regions in which extinction occurs: (a) specimen axis parallel to vertical crosswire, (b) axis at 30° to vertical crosswire and (c) axis at 60° to vertical crosswire.



Fig. 2. *c* axis rotation photograph of indium sulphide.

PLATE II



(a)



(b)

Fig. 1. (a) Transmission diffraction pattern of gold film. The arrows indicate the position of the extra rings; (b) transmission diffraction pattern of aluminium film.

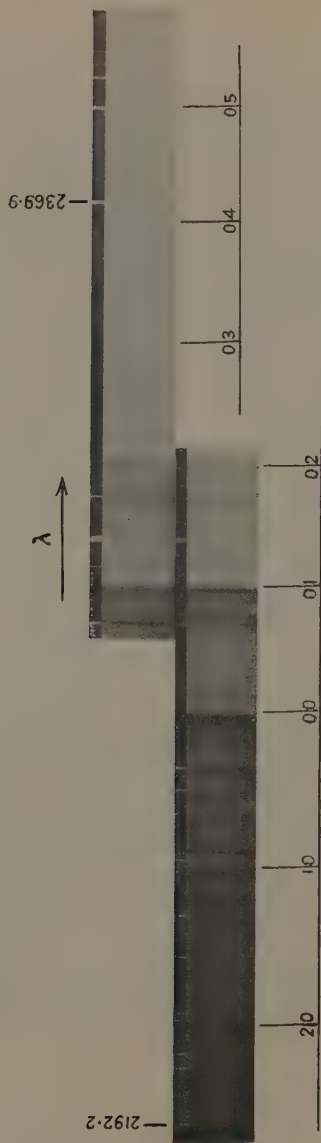


Fig. 1. Spectrogram of BiF molecule.

Direct Interaction with Strong Coupling in Nuclear Collisions II. E2 Excitations

By C. B. O. MOHR

Physics Department, University of Melbourne

MS. received 14th April 1961

Abstract. The work of a previous paper on the effect of coupling between elastically and inelastically scattered waves for the case of E0 excitations of the nucleus throughout its volume has been extended to E2 excitations. The inclusion of coupling causes inelastic cross sections to deviate even more from the distorted wave values for E2 excitations than for E0 excitations. The effect is greater for a volume interaction than for a surface interaction of equivalent strength.

§ 1. INTRODUCTION

SINCE direct interaction is the main mechanism in nuclear collisions at the higher energies of impact, many calculations of total cross sections and angular distributions have been carried out with the distorted wave approximation. Unfortunately, various complicating effects such as exchange and spin-orbit forces can cause as much change in calculated angular distributions as permissible adjustments in the nuclear potential, and have therefore to be taken into account.

The further complication of coupling between elastically and inelastically scattered waves also seems to be of importance whenever the inelastic cross section is comparable with the geometric cross section. Solution of the coupled equations for light nuclei has been carried out for a surface interaction (Yoshida 1956), also for a volume interaction by using a perturbation approximation to a standing wave solution (Yoshida 1958).

In this paper the coupled equations are solved for a light nucleus, for a volume interaction with a simplified model neglecting spin, in an attempt to gain physical insight into the problem, the work of a previous paper on E0 excitations (Mohr 1959, to be referred to as I) being extended to E2 excitations. The extent of the difference in the value of partial cross sections obtained with and without strong coupling is systematically followed as the coupling is increased to give the maximum cross section. The results are compared with those for the simpler case of a surface interaction.

§ 2. THEORY

We shall adopt and extend the notation of I. The ingoing and elastically scattered particles have wave number $k/2\pi$, energy $E = k^2\hbar^2/8\pi^2M$, wave function $F_0(\mathbf{r})$, and move in a potential $-V_{00}(\mathbf{r})$. For the inelastically scattered particles the corresponding quantities are $k_1/2\pi$, $E_1 = k_1^2\hbar^2/8\pi^2M$, $F_1(\mathbf{r})$ and $-V_{11}(\mathbf{r})$. Then, putting $\gamma = 8\pi^2M/\hbar^2$, the coupled equations take the form

$$(\nabla^2 + \gamma E + \gamma V_{00})F_0(\mathbf{r}) = -\gamma V_{01}(\mathbf{r})F_1(\mathbf{r}), \quad \dots\dots (1a)$$

$$(\nabla^2 + \gamma E_1 + \gamma V_{11})F_1(\mathbf{r}) = -\gamma V_{10}(\mathbf{r})F_0(\mathbf{r}), \quad \dots\dots (1b)$$

where $-V_{01}(\mathbf{r})$ is the transition potential, or potential energy of the direct interaction between the incident particle and the nuclear particle excited in the collision averaged over the transition density of the nuclear particle. If this interaction is taken to be of short range, $V_{01}(\mathbf{r})$ has approximately the form of $\psi_0^*(\mathbf{r})\psi_1(\mathbf{r})$.

We consider the frequently occurring case of the nucleus being raised from a 0^+ ground state to a 2^+ excited state by the collision, in which case $\psi_0(\mathbf{r})$ is spherically symmetrical and $\psi_1(\mathbf{r})$ depends on angle as $Y_{2,M}(\theta, \phi)$. We may then write

$$V_{01}(\mathbf{r}) = V_{01}(r)Y_{2,M}(\theta, \phi). \quad \dots\dots (2)$$

Taking the z axis along the incident beam, and putting

$$F_0(\mathbf{r}) = r^{-1} \sum_l F_0^l(r) Y_{l,0}(\theta, \phi), \quad \dots\dots (3a)$$

$$F_1(\mathbf{r}) = r^{-1} \sum_l F_1^l(r) Y_{l,m}(\theta, \phi), \quad \dots\dots (3b)$$

the coupled equations (1) become

$$\sum_l \left(\frac{d^2}{dr^2} + \gamma E + \gamma V_{l0} - l(l+1)r^{-2} \right) F_0^l Y_{l,0} = \sum_{l'} \gamma V_{01}(r) F_1^{l'} Y_{2,M} Y_{l',m'}, \quad \dots\dots (4a)$$

$$\sum_l \left(\frac{d^2}{dr^2} + \gamma E_1 + \gamma V_{l1} - l(l+1)r^{-2} \right) F_1^l Y_{l,m} = \sum_{l'} \gamma V_{01}(r) F_0^{l'} Y_{2,-M} Y_{l',0}. \quad \dots\dots (4b)$$

Since the equations hold for all ϕ , we have $m = -M = m'$. On the right-hand side of (4a) we expand $Y_{2,M} Y_{l',-M}$ as a series of $Y_{L,0}$'s with different values of L , and for (4b) likewise we have a series of $Y_{L,M}$'s with particular M (Rose 1957). From the properties of the Clebsch-Gordan coefficients occurring in the expansion, there are only three terms in the series, with $L = l' + 2$, l' , $l' - 2$. Equating coefficients of corresponding Y 's we obtain

$$\left(\frac{d^2}{dr^2} + \gamma E + \gamma V_{00} - l(l+1)r^{-2} \right) F_0^l = -\gamma V_{01}(r) (a_{l+2,M} F_1^{l+2} + a_{l,M} F_1^l + a_{l-2,M} F_1^{l-2}), \quad \dots\dots (5a)$$

$$\left(\frac{d^2}{dr^2} + \gamma E_1 + \gamma V_{11} - l(l+1)r^{-2} \right) F_1^l = -\gamma V_{01}(r) (b_{l+2,M} F_0^{l+2} + b_{l,M} F_0^l + b_{l-2,M} F_0^{l-2}), \quad \dots\dots (5b)$$

the a 's and b 's denoting numerical coefficients. We have to solve the complete set of equations for a particular value of M and different values of l , noting that all the even order waves are coupled together, similarly all the odd order waves.

At a given energy E the waves $F_0^l(r)$ and $F_1^l(r)$ have appreciable values inside the nuclear radius for only a limited number of orders l , so that the set of equations (5) is limited in number. Suppose there are $2n$ equations in the even (or odd) set, n of type (5a) and n of type (5b). A single differential equation for a given F_0^l or F_1^l may be obtained by eliminating all the other F 's, this equation having $2n$ regular solutions which may be denoted by $F_{0,\nu}^l$ or $F_{1,\nu}^l$, with $\nu = 1, 2, \dots, 2n$.

The most general set of solutions of (5) consists of linear combinations of the $F_{0,\nu}^l$ or $F_{1,\nu}^l$ and may be written

$$F_0^l = \sum_{\nu=1}^{2n} c_{\nu} F_{0,\nu}^l, \quad F_1^l = \sum_{\nu=1}^{2n} c_{\nu} F_{1,\nu}^l, \quad \dots\dots (6)$$

the c 's being arbitrary (complex) coefficients. They must join smoothly on to the exterior solutions, which for neutrons have the form

$$F_0^l = (2l+1)^{1/2} (4\pi)^{-1/2} i^l (kr) j_l(kr) + i\alpha_{l,M} kr h_l^{(1)}(kr), \quad \dots (7a)$$

$$F_1^l = (2l+1)^{1/2} (4\pi)^{-1/2} i^{l+1} \beta_{l,M} k_1 r h_l^{(1)}(k_1 r), \quad \dots (7b)$$

where j_l is a spherical Bessel function and $h_l^{(1)}$ a spherical Hankel function of the first kind. For charged particles the corresponding Coulomb wave functions are of course used. The c 's, α 's and β 's form a set of $4n$ undetermined quantities, which may be found by fitting the $2n$ interior solutions on to the corresponding exterior solutions so that both the functions and their derivatives are continuous across the boundary. The α 's and β 's are thus obtained for a particular value of M , and the whole process is repeated for all of the M values $0, \pm 1, \pm 2$. $|\alpha_{l,M}|^2$ and $|\beta_{l,M}|^2$ are the probability of elastic and inelastic scattering respectively for particles with a given l and M and, after averaging over all M values, have the maximum values of 1 and $k_1/4k$ given by the conservation theorem.

The differential cross sections for elastic and inelastic scattering are given by

$$\sigma_{el}(\Theta) = (4\pi/5) k^{-2} \sum_{M=-2}^2 |\sum_l (2l+1)^{1/2} \alpha_{l,M} Y_{l,M}(\Theta, 0)|^2, \quad \dots (8a)$$

$$\sigma_{in}(\Theta) = (4\pi/5) k_1 k^{-3} \sum_{M=-2}^2 |\sum_l (2l+1)^{1/2} \beta_{l,M} Y_{l,M}(\Theta, 0)|^2, \quad \dots (8b)$$

and the corresponding total cross sections by

$$\sigma_{el} = (4\pi/5) k^{-2} \sum_{M=-2}^2 \sum_l (2l+1) |\alpha_{l,M}|^2, \quad \dots (9a)$$

$$\sigma_{in} = (4\pi/5) k_1 k^{-3} \sum_{M=-2}^2 \sum_l (2l+1) |\beta_{l,M}|^2. \quad \dots (9b)$$

The factor $1/5$ comes from averaging over the five values of M , i.e. from averaging over all orientations of the quadrupole moment in $V_{01}(\mathbf{r})$.

The effect of coupling in E1 excitations may in principle be considered in a similar way, but odd and even order waves are now all coupled together, so that at a given energy the labour of the calculation is greatly increased.

§ 3. CALCULATIONS

For simplicity a square well was taken for $V_{00} = V_{11}$, with depth 47 mev and radius $R = 2.9$ fermi, as in I, corresponding to a carbon nucleus for which the principal energy loss of 4.4 mev corresponds to an E2 excitation from the 0^+ ground state. The incident neutron energy was taken to be 18 mev, for which energy the $l=4$ and higher order waves are small inside the nuclear radius. Then there are only two equations of type (5a) and two of type (5b) for the even order waves, similarly for the odd order waves. The energy loss in the collision was neglected in comparison with the incident energy, so that $k_1 = k$, an approximation which greatly reduces the work without affecting the general conclusions.

3.1. Solution of the Coupled Equations

For $M=0$ each b in (5b) is equal to the corresponding a in (5a)—a considerable simplification. Then, taking $E_1 + V_{11}$ to be equal to $E + V_{00}$, Eqns (5) clearly have two types of solution, viz.

$$F_{1,\nu}^l = \pm F_{0,\nu}^l. \quad \dots (10)$$

Then the equations to be solved for $F_{0,\nu}^l$ are of the form

$$F_{0,\nu}^{1''} + (K^2 - 2r^{-2})F_{0,\nu}^1 = \mp (p_1 F_{0,\nu}^1 + p_3 F_{0,\nu}^3), \quad \dots\dots (11a)$$

$$F_{0,\nu}^{3''} + (K^2 - 12r^{-2})F_{0,\nu}^3 = \mp (q_1 F_{0,\nu}^1 + q_3 F_{0,\nu}^3), \quad \dots\dots (11b)$$

for the odd order waves, all upper signs being taken together or all lower signs. The modifications in the equations for the even order waves $F_{0,\nu}^0$ and $F_{0,\nu}^2$ are obvious. K is 2π times the interior wave number. The p 's and q 's contain the factor $V_{01}(r)$ and so are functions of r .

The equations (11) may be rewritten in the form

$$F_{0,\nu}^{1''} + (s_1 - 2r^{-2})F_{0,\nu}^1 = pF_{0,\nu}^3, \quad \dots\dots (12a)$$

$$F_{0,\nu}^{3''} + (s_3 - 12r^{-2})F_{0,\nu}^3 = qF_{0,\nu}^1. \quad \dots\dots (12b)$$

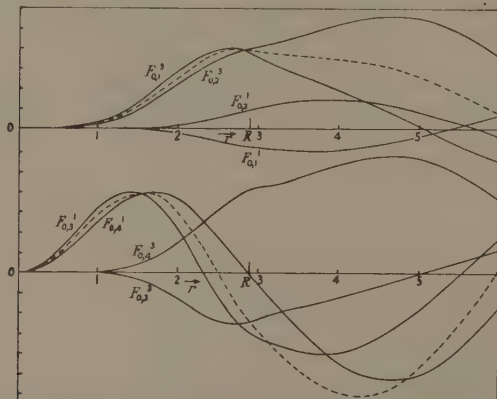


Fig. 1. Graphs of the wave functions $F_{0,\nu}^l$ ($\nu=1, 2, 3, 4$) for ingoing and elastically scattered neutron waves of order l which are solutions of the coupled equations (11). The distance r is in fermis. The neutrons have energy $E=18$ mev, and are scattered by a square well of radius $R=2.9$ fermi and depth $V_{00}=47$ mev. The transition potential $V_{01}(\mathbf{r})=0.2(E+V_{00})Y_{2,0}(\theta, \phi)$ for $r < R$; 0 for $r > R$. The broken curves have the form $Krj_l(Kr)$ for $r < R$, with $l=3$ and 1 for the top and bottom curves respectively, where $K^2=8\pi^2M(E+V_{00})/\hbar^2$.

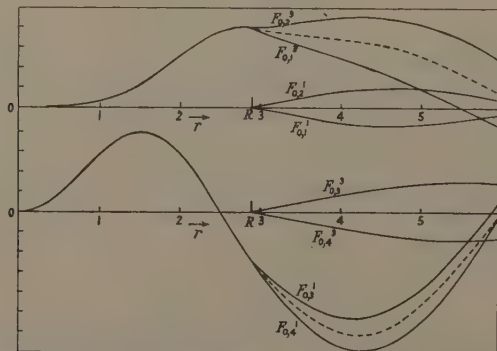


Fig. 2. As for Fig. 1, but with the transition potential V_{01} concentrated at the nuclear surface.

$$\frac{8\pi^2MV_{01}(\mathbf{r})}{\hbar^2} = v\delta(r-R)Y_{2,0}(\theta, \phi) \text{ with } v=0.2K.$$

Eliminating one of the quantities $F_{0,\nu}^{-1}$ and $F_{0,\nu}^{-3}$ gives for the other quantity a fourth-order differential equation which has two regular solutions. Since p and q may be both positive or both negative, we obtain four regular solutions for $F_{0,\nu}^{-1}$ and four corresponding regular solutions for $F_{0,\nu}^{-3}$, i.e. ν takes the values 1, 2, 3, 4.

There are two extreme forms for V_{01} for easiest solution of the coupled equations: (a) a square well of radius R , (b) a Dirac δ -function at $r=R$, corresponding to (a) a simple form of volume interaction, and (b) a surface interaction. Form (b) is often used for the great simplicity it introduces in solving the coupled equations. Form (a) is our main concern, but the results given by form (b) are also presented for comparison.

(a) *Square well for V_{01} .* This makes s_1, s_3, p and q constant for $r < R$. Then the fourth-order differential equation obtained by eliminating $F_{0,\nu}^{-1}$ or $F_{0,\nu}^{-3}$ from (12) may readily be solved by expanding the solution in a power series in r . The indicial equation has roots differing by an integer, and therefore the regular solution for $F_{0,\nu}^{-1}$ and for $F_{0,\nu}^{-3}$ starting with the higher positive power of r contains an additional power series multiplied by $\ln r$. This series is laborious to calculate to many terms, so the solution is calculated in this way for small r only, and extended to $r=R$ by numerical solution of the coupled equations. The power series for the other solution may be used at $r=R$ without much labour. Pairs of solutions for F_0^{-2} and F_0^{-4} are found in exactly the same way. The numerical relation between the magnitudes of corresponding pairs of solutions $F_{0,\nu}^{-1}$ and $F_{0,\nu}^{-1+2}$ is found from one of the two coupled equations.

While the solutions are required only near $r=R$, for fitting on to the exterior solutions (7), the form of the interior solutions is of interest, and we now refer to Fig. 1. $F_{0,3}^{-1}$ and $F_{0,4}^{-1}$ correspond to the upper and lower sign respectively in (10) and (11), and as V_{01} tends to zero they merge together into the form $Krj_1(Kr)$. The amplitudes of the corresponding functions $F_{0,3}^{-3}$ and $F_{0,4}^{-3}$ approach exact proportionality to V_{01} as V_{01} tends to zero, and so get smaller and smaller (in comparison with $F_{0,3}^{-1}$ and $F_{0,4}^{-1}$). Vice versa, $F_{0,1}^{-3}$ and $F_{0,2}^{-3}$ merge together into the form $Krj_3(Kr)$ as V_{01} tends to zero, while $F_{0,1}^{-1}$ and $F_{0,2}^{-1}$ get smaller in comparison. For $r > R$, V_{00} and V_{01} are zero, and the form of the curves is that of a linear combination of $krj_l(kr)$ and $kn_l(kr)$.

Similar principles apply for $M = \pm 1, \pm 2$, but the corresponding a 's and b 's in (5) are no longer equal, and detailed calculations are more complicated.

(b) *Dirac δ -function for V_{01} .* We take

$$V_{01}(r) = v\delta(r-R). \quad \dots\dots (13)$$

The p 's and q 's in (11) are also of form $\delta(r-R)$, so that the right-hand sides of (11a) and (11b) are zero for $r < R$. It follows, from the form of the solutions for case (a), that for $r < R$, $F_{0,3}^{-1}$ and $F_{0,4}^{-1}$ are of form $Krj_1(Kr)$; $F_{0,1}^{-3}$ and $F_{0,2}^{-3}$ are of form $Krj_3(Kr)$; $F_{0,3}^{-3}$, $F_{0,4}^{-3}$, $F_{0,1}^{-1}$ and $F_{0,2}^{-1}$ are zero.

At $r=R$, the right-hand sides of (11a) and (11b) suddenly rise and fall, hence the F 's suddenly change slope by an amount proportional to v . For $r > R$, the same remarks apply as for case (a), but the amplitudes of $F_{0,1}^{-1}$, $F_{0,2}^{-1}$, $F_{0,3}^{-3}$ and $F_{0,4}^{-3}$ are now exactly proportional to V_{01} .

The curves in Fig. 2 may usefully be compared with the corresponding curves in Fig. 1. In Fig. 1 the difference between two curves corresponding to different signs in (11) gradually increases from $r=0$ to $r=R$, whereas in Fig. 2 the difference occurs suddenly at $r=R$. The four $F_{0,\nu}^{-3}$ curves for $r > R$ are similar

for the two forms of potential (the similarity would have been still closer for a more carefully chosen value of v); but the four $F_{0,v}^1$ curves are less similar for the two forms of potential, for with potential (a) they start rising at smaller values of r than the $F_{0,v}^3$ curves.

The modification required for $M \neq 0$ is fairly easily carried out, but to explain it in detail here would take a disproportionate amount of space.

(c) *General form for V_{01} , V_{00} and V_{11} .* More realistic forms for these potentials should be adopted than (a) or (b). The solution of the coupled equations would then be started off at small r by assuming the V 's to be constant, and then extended to larger r by numerical integration. If there are co-operative effects from equivalent particles in the nucleus, the magnitude of V_{01} will be increased accordingly.

3.2. Determination of $\alpha_{l,0}$ and $\beta_{l,0}$

The neatest way of fitting together the complete interior solutions (6) and the exterior solutions (7), and the way least liable to numerical error, is to proceed as follows. The phase shifts at infinity η_v^l of each of the component waves $F_{0,v}^l$ are determined by fitting each at $r=R$ to a linear combination of $kRj_l(kR)$ and $kRn_l(kR)$, so that we may write

$$F_{0,v}^1 \sim \sin(kr - \frac{1}{2}l\pi + \eta_v^1), \quad \dots\dots (14a)$$

$$F_{0,v}^3 \sim f_v \sin(kr - \frac{1}{2}l\pi + \eta_v^3), \quad \dots\dots (14b)$$

the four $F_{0,v}^1$ being normalized to unit amplitude at large r , and the amplitudes of the corresponding four $F_{0,v}^3$ determined through (11a) and denoted by f_v . The four arbitrary constants to be taken with the four pairs $F_{0,v}^1$, $F_{0,v}^3$ are introduced in taking linear combinations of the F 's as in (6), these constants being denoted by c_1 , c_2 , c_3 and c_4 .

The asymptotic forms of the exterior F_0^l and F_1^l as given by (7) are well known, and involve the functions $\sin(kr - \frac{1}{2}l\pi)$ and $\cos(kr - \frac{1}{2}l\pi)$. We now equate the two asymptotic forms for F_0^1 , F_1^1 , F_0^3 and F_1^3 , and for their derivatives, obtaining eight simultaneous algebraic equations containing the eight unknowns c_1 , c_2 , c_3 , c_4 , $\alpha_{1,M}$, $\beta_{1,M}$, $\alpha_{3,M}$ and $\beta_{3,M}$. The α 's and β 's are then given by the quotients of pairs of 8×8 determinants. The rows of each determinant are added and subtracted in pairs to eliminate the quantity kr , and the determinants are then readily reduced to give

$$\begin{aligned} 2i\alpha_{1,0} = & [1 - \{\sum f_1 f_2 \exp[-i(\eta_1^3 + \eta_2^3)] \cos(\eta_3^1 - \eta_4^1) \\ & + i(\frac{2}{3})^{1/2} \sum f_1 \exp[-i(\eta_1^3 + \eta_2^1)] \sin(\eta_2^1 - \eta_4^1)\}] \\ & \div \{\sum f_1 f_2 \exp[-i(\eta_1^3 + \eta_2^3 + \eta_3^1 + \eta_4^1)]\}, \quad \dots\dots (15a) \end{aligned}$$

$$\begin{aligned} -2\beta_{1,0} = & \{\sum f_1 f_2 \exp[-i(\eta_1^3 + \eta_2^3)] \sin(\eta_3^1 - \eta_4^1) \\ & - (\frac{2}{3})^{1/2} \sum f_1 \exp[-i(\eta_1^3 + \eta_3^1)] \sin(\eta_2^1 - \eta_4^1)\} \\ & \div \{\sum f_1 f_2 \exp[-i(\eta_1^3 + \eta_2^3 + \eta_3^1 + \eta_4^1)]\}, \quad \dots\dots (15b) \end{aligned}$$

where \sum denotes the sum of four terms in which the lowered suffixes 1, 2, 3 and 4 are changed in cyclic order, while \sum' denotes a similar expression with the second and fourth terms subtracted from the sum of the first and third terms. The expressions for $2i\alpha_{3,0}$ and $-2\beta_{3,0}$ are obtained from (15) by interchanging the raised suffixes 1 and 3, and replacing the quantities f_1 , f_2 , f_3 , f_4 and $(\frac{2}{3})^{1/2}$ by their reciprocals. The expressions for $2i\alpha_{0,0}$ and $-2\beta_{0,0}$ are obtained from (15) by

replacing the raised suffixes 1 and 3 by 0 and 2 respectively, and replacing the factor $(\frac{2}{3})^{1/2}$ by $5^{1/2}$ (remembering that the f 's now have different numerical values). The expressions for $2i\alpha_{2,0}$ and $-2\beta_{2,0}$ are then obtained by interchanging the raised suffixes 0 and 2, and replacing the f 's and the quantity $5^{1/2}$ by their reciprocals.

The expressions for the case of $M \neq 0$ are necessarily more complicated.

3.3. α_l and β_l for E0 Excitations

It makes a useful comparison to apply the method of § 3.2 to the much simpler case of E0 excitations. With the simplification of $k_1 = k$ and $V_{11} = V_{00}$ previously adopted, we have

$$F_0^l = c_1 F_{0,1}^l + c_2 F_{0,2}^l, \quad \dots (16a)$$

$$F_1^l = c_1 F_{1,1}^l + c_2 F_{1,2}^l, \quad \dots (16b)$$

with

$$F_{1,1}^l = F_{0,1}^l, \quad F_{1,2}^l = -F_{0,2}^l, \quad \dots (17)$$

and

$$F_{0,1}^l \sim \sin(kr - \frac{1}{2}l\pi + \eta_1^l), \quad \dots (18a)$$

$$F_{0,2}^l \sim \sin(kr - \frac{1}{2}l\pi + \eta_2^l), \quad \dots (18b)$$

where η_1^l and η_2^l are the l th-order phase shifts produced by square wells of radius R and depths $V_{00} + V_{01}$ and $V_{00} - V_{01}$ respectively. It is not difficult to show, by equating the asymptotic forms of the exterior solutions (7) with $M = 0$ and the asymptotic forms (18) of the interior solutions (16), (17), that

$$4i\alpha_l = \exp(2i\eta_1^l) + \exp(2i\eta_2^l) - 2, \quad \dots (19a)$$

$$4i\beta_l = \exp(2i\eta_1^l) - \exp(2i\eta_2^l). \quad \dots (19b)$$

As V_{01} tends to zero, $F_{0,1}^l$ and $F_{0,2}^l$ inside the nuclear radius merge into the form $Krj_l(Kr)$, while η_1^l and η_2^l merge into the phase shift η^l produced by a potential well of depth V_{00} . Then

$$2i\alpha_l = \exp(2i\eta^l) - 1, \quad \dots (20a)$$

$$2\beta_l = \eta_1^l - \eta_2^l, \quad \dots (20b)$$

where (20a) is the result of the usual partial wave analysis for elastic collisions, and $\eta_1^l - \eta_2^l$ in (20b) reduces to the value given by the distorted wave method for inelastic collisions.

§ 4. RESULTS AND DISCUSSION

4.1. E0 Excitations

For $V_{01} = 0$, $\eta_1^l = \eta^l = \eta_2^l$. As V_{01} increases, η_1^l increases and η_2^l decreases, so that $\eta_1^l - \eta_2^l$ increases through the value $\pi/2$ (except for sufficiently large l). Hence, from (19b), $|\beta_l|^2$ rises to a maximum value of $\frac{1}{4}$ and falls again. Including an imaginary component in V_{01} —and hence in η_1^l and η_2^l —to allow for absorption, reduces the value of $\exp(i\eta_1^l)$ and $\exp(i\eta_2^l)$, and hence reduces $|\beta_l|^2$. These general results were exhibited in curves given in I for the variation of $|\beta_l|^2$ with V_{01} .

4.2. E2 Excitations

The above simple feature of each $|\beta_{l,0}|^2$ rising regularly to the same maximum value is no longer to be expected for E2 excitations, since (15b) is much more complicated than (19b); and the curves shown in Figs 3 and 4 confirm this.

The maximum values reached are usually less than $\frac{1}{2}$, possibly much less, and in one curve an unexpected twist occurs. The same general features are to be expected for the β 's with $M \neq 0$.

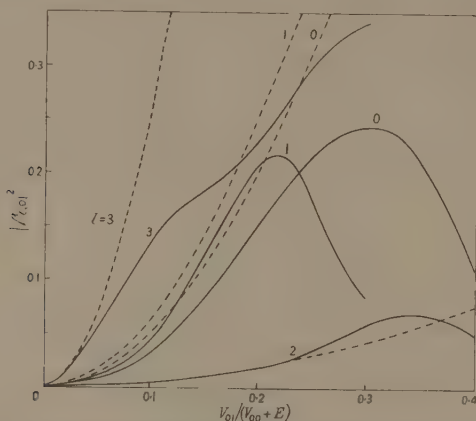


Fig. 3. $|\beta_{l,0}|^2$, the probability of inelastic scattering of l th order neutron waves, is plotted as a function of the transition potential V_{01} , which is taken to be constant for $r < R$ and to have angular dependence $Y_{2,0}(\theta, \phi)$. The other parameters have the same numerical values as for Fig. 1. The broken curves are for the distorted wave approximation.

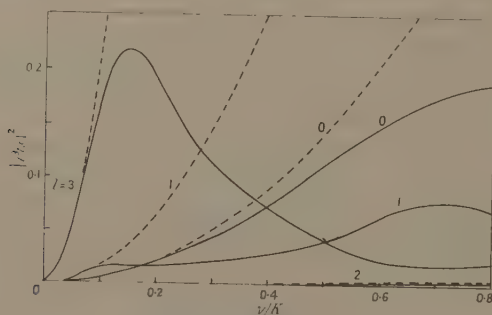


Fig. 4. As for Fig. 3, but with $\frac{8\pi^2 M V_{01}(\mathbf{r})}{h^2} = \tau \delta(r-R) Y_{2,0}(\theta, \phi)$. K is 2π times the interior wave number.

This irregular behaviour of the curves is more marked for the volume interaction (Fig. 3) than for the surface interaction (Fig. 4). Furthermore the curves for $l=1$ and 3 in Fig. 3 were found to be particularly sensitive to the values of the nuclear parameters for the larger values of V_{01} , and were terminated because of insufficient accuracy in the calculations.

The increased sensitivity in the case of E2 excitations may readily be understood. If we regard the right-hand side of (11a) as a perturbation of a wave originally distorted only by the potential V_{00} , then for E0 excitations we have only the perturbation term $p_1 F_{0,\nu}^1$, and its magnitude rises and falls in step with the wave $F_{0,\nu}^1$ itself. But for E2 excitations the extra perturbation $p_3 F_{0,\nu}^3$ is involved,

and this may be large at places where $F_{0,\nu}^{-1}$ is small, causing a particularly marked effect on $F_{0,\nu}^{-1}$ at larger r . We can likewise expect considerable sensitivity to the values of V_{00} and R .

A remark is necessary about the maximum possible value of $|\beta_{l,0}|^2$ in (15b). At first sight it would appear possible to obtain large values by adjusting the terms in the denominator so that they nearly cancel out, but the f 's and η 's are not independent quantities. Fig. 3 shows values of $|\beta_{3,0}|^2$ exceeding $\frac{1}{4}$, but this does not contradict the conservation theorem, which requires only that the value of $|\beta_{l,M}|^2$ averaged over all M values may not exceed $k_1/4k$. Allowing for absorption by taking V_{00} complex, would be expected to reduce the magnitude of the β 's, though this point has not been checked on account of the much greater amount of work involved.

For values of V_{01} large enough to produce inelastic cross sections comparable with the geometric cross section, the relative contributions of the different partial cross sections to the differential cross section will clearly be quite different in strong coupling and in the distorted wave approximation. Thus, in the present calculation, the contribution from the $l=3$ wave will be reduced below the distorted wave value by a far greater amount than the contribution from the other waves. A further difference arises because the ratio of the real and imaginary parts of each β depends markedly on V_{01} in strong coupling, whereas the ratio is independent of V_{01} in the distorted wave approximation.

Since these differences are in general greater for E2 than for E0 excitations, the differences in calculated angular distributions will also be greater; and the differences obtained in I for E0 excitations were already notable in some instances.

To calculate angular distributions for a more realistic form for V_{01} than those used here, and to include other complicating effects of importance, particularly spin-orbit forces, would seem a formidable undertaking, especially if one has to consider more than two channels. In addition, to vary nuclear parameters in an effort to obtain close—and unique—fits with experimental angular distributions would seem almost a hopeless task. On the other hand, efforts to obtain close fits using the distorted wave approximation seem of doubtful value, for the agreement may be completely spoilt by the effect of strong coupling.

REFERENCES

- MOHR, C. B. O., 1959, *Proc. Phys. Soc.*, **73**, 894.
 ROSE, M. E., 1957, *Elementary Theory of Angular Momentum* (New York: John Wiley), p. 61.
 YOSHIDA, S., 1956, *Proc. Phys. Soc. A*, **69**, 668.
 ——— 1958, *Progr. Theor. Phys., Japan*, **19**, 169.

Knock-on Electrons and Direct Electron Pair Production by Cosmic-ray Muons

By P. H. STOKER, C. HOFMEYR† AND C. H. BORNMAN

Department of Physics, Potchefstroom University, South Africa

MS. received 1st February 1961, in revised form 26th April 1961

Abstract. Knock-on electrons and direct electron pair creation by cosmic-ray muons in thin lead plates were investigated with a multiplate cloud chamber. The muons traversing the cloud chamber were classified into two energy intervals, viz. 450 to 1700 mev and higher than 1700 mev. By comparing the experimental results with theoretical predictions which were derived for the knock-on process, an effective range-energy relationship was found for electrons in lead with energies up to about 200 mev. The experimental distributions of the knock-on production as a function of the energy transfer compare well with theoretical distributions calculated from Bhabha's formula for muons in both of these energy ranges. The comparison between the theoretical and experimental results is also satisfactory for the energy distribution for direct pair production by muons with energy above 1700 mev. The theoretical distribution was calculated from a formula deduced anew from the differential cross section given by Murota, Ueda and Tunaka. The experimental results favour a value between 1 and 2 for the indefinite constant α of the theory.

§ 1. INTRODUCTION

MANY experiments have been performed with nuclear emulsions and Wilson cloud chambers to investigate the knock-on secondaries produced by fast electrons and muons. The experimental results are in accordance with theory (cf. Fowler and Wolfendale 1958). Much work has also been done to investigate the process of direct electron pair production by fast electrons in emulsions, the so-called trident process (cf. Roe and Ozaki (1959) for references). The direct electron pair production by muons has received much less attention. Goldsack and Kannangara (1953) analysed 11 pairs produced in nuclear emulsions exposed underground to muons and classified them into the various cases covered by Bhabha's theory. Walker (1953) found two electron pairs in 13 000 traversals by cosmic-ray muons with energy above 1500 mev of a 1 inch carbon plate, against 3.5 pairs predicted by Bhabha's theory. Avan and Avan (1957) have exposed nuclear emulsions at several depths underground and examined the direct pair production by muons in the emulsion. Good agreement with theoretical predictions was obtained for the meson groups with mean energies of 60 and 120 gev. In cloud chamber experiments Roe and Ozaki (1959) and Gaebler, Hazen and Hendel (1961) recently investigated the pair production by energetic muons in lead plates having thicknesses of 0.6 cm and 0.32 cm respectively. They both found an electron pair cross section of a factor about 2 less than the value predicted

† Bursar of the South African Atomic Energy Board.

by the calculations of Murota, Ueda and Tunaka (1956), taking the indefinite constant $\alpha=2$.

The present experiment was set up to investigate the process of direct pair production by cosmic-ray muons as a function of the energy transfer. An analysis of the knock-on electrons produced will provide information on the method and reliability of the experimental procedure, and on the absorption of the electrons in the lead plates.

The theory for the direct pair production is based on quantum electrodynamics and assumes point interaction of the muon with the Coulomb field of the nucleus. A discrepancy may therefore be expected between theory and experiment for large energy transfer in the centre-of-mass system. The same would be true for the collision process between a muon and an electron. Because of the relatively small mass of the electron, the energy transferred in the centre-of-mass system by a relativistic muon to an electron at rest will always be much less than the energy transferred in the laboratory system. The validity of the electrodynamical theory describing muon-electron collisions may therefore be assumed up to high energy transfers in the laboratory system.

§ 2. THE EXPERIMENTAL SET-UP

In order to reduce the amount of absorption of the secondary electrons, thin lead plates were exposed to the cosmic-ray muons. The four upper lead plates in the cloud chamber were 1.5 mm thick, the next four were 3.3 mm, while the bottom plate was 13.3 mm. Thus the observed rate of production of secondary electrons in the two sets of thin plates may be compared, and the energy of an electron may be estimated roughly from its range or from the shower initiated by it. The thick bottom plate facilitates energy estimations, since it allows an electron shower to develop.

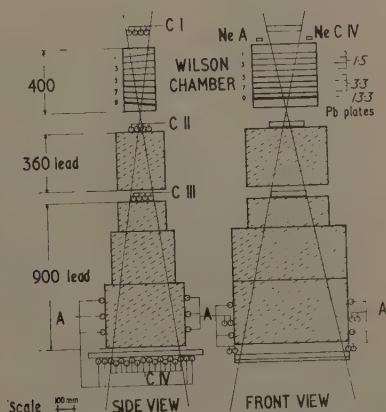


Fig. 1. The experimental set-up.

The cloud chamber was triggered by a triple coincidence between the counter layers C I, C II and C III. The layer of counters C IV and the group of side counters A were both hodoscoped in coincidence with the triple coincidence pulse.

The hodoscope glowlamps NeCIV and NeA, for the respective groups of counters, were photographed together with the cloud chamber. Using Sternheimer's calculations (Sternheimer 1959) for the range of muons in lead, the first layer of lead (377 g cm^{-2}) determined a minimum energy of 450 mev for the triggering of the cloud chamber. If all the lead (1354 g cm^{-2}) was traversed, the hodoscope lamp NeCIV lit up, indicating a minimum energy of 1700 mev. All photographs in which the lamp NeA glowed were rejected.

The illuminated region of the cloud chamber was $400 \text{ mm} \times 400 \text{ mm} \times 200 \text{ mm}$. The nine lead plates were covered with bright aluminium plates, 0.5 mm thick, to prevent sagging of the thin lead plates, and to improve the illumination of the region between the plates. The effect of these aluminium coverings was taken into account when the absorption and the production of knock-on electrons were considered (knock-on probability is proportional to Z/A). It was not taken into account for direct pair production, because of the Z^2/A proportionality of this process.

The cloud tracks were photographed stereoscopically by means of a front silvered mirror placed at right angles to the front window of the cloud chamber. Both the direct view and the mirror view were recorded on a single frame of 35 mm Ferrania microfilm by a camera with a slightly tilted $f/2.8$ lens. The chamber was illuminated by the discharge of $800 \mu\text{F}$ condensers at 2000 v through two Mullard LSD 18 linear quartz flash tubes. In the chamber argon and a water-alcohol mixture were used. The size and front windows were kept fog free by thin heating wires across the windows. To prevent the heated gas from drying the upper part of the chamber, a tray with water was placed on top of the chamber, thus cooling the top by evaporation of the water to a fraction of a degree below room temperature. This assured uniform condensation along the tracks of the charged particles.

§ 3. SELECTION OF THE PHOTOGRAPHS

Only those photographs were selected for analysis in which (i) one muon traversed the chamber in a direction determined by the counter layers CI and CIII (as proved by stereoscopic reconstruction), and (ii) the muon track was clearly visible between all the plates in both the direct and the mirror views. Furthermore, the diffuseness of the droplets along the track had to be consistent with the delay time of the flash light trigger. Secondaries to the muon were accepted only when (i) the same secondary was visible on both the views, (ii) the points of origin of the secondary corresponded on both views to the same position in the lead plate in line with the muon track, and (iii) the diffuseness of the droplets corresponded to the age of the droplets of the muon track.

§ 4. THE ABSORPTION OF KNOCK-ON ELECTRONS IN LEAD

The probability that a muon with energy E will produce a knock-on electron with energy between ϵ and $\epsilon + d\epsilon$ on traversing $dx \text{ g cm}^{-2}$ of material is given by the Rutherford formula when only Coulomb interaction is considered, and by the Bhabha formula when additional terms due to spin-orbit and spin-spin interactions are taken into account (Rossi 1952). In order to calculate the probability that a knock-on electron produced in the lead will emerge from the plate, the absorption of the electrons in the lead plate must be taken into consideration when Bhabha's

formula is integrated. No empirical results are available for the effective range of energetic electrons in lead. For aluminium the simple Feather rule

$$R = 530 \epsilon - 106 \text{ mg cm}^{-2} \quad \dots\dots (1)$$

holds for electrons of energy ϵ ranging from 2.5 to about 20 mev (Katz and Penfold 1952). From the absorption curves of Husain and Putman (1957) it appears that the maximum range in mg cm^{-2} for ^{32}P beta-particles is more or less

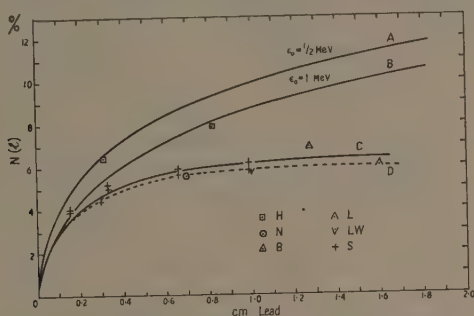


Fig. 2. The mean number of knock-on electrons emerging from a lead plate on the traversal of an energetic muon is represented as a function of the lead thickness. The solid curves were deduced from theory, taking into account absorption in the plate. The results of experiments with working conditions comparable with those of the present experiment are also represented: H, Hopkins, Nielsen and Nordheim (1939); N, Nassar and Hazen (1946); B, Brown, McKay and Palmatier (1949); L, Lovati *et al.* (1954 b); LW, Lloyd and Wolfendale (1959); S, present work. The lower crosses represent our results for all muons with energy above 450 mev, and the upper crosses the results for all muons with energy above 1700 mev.

independent of the material investigated, ranging from beryllium to gold. Let it be assumed that the Feather rule holds good for the mean range of low energy electrons in lead. By integrating Rutherford's formula and assuming a low energy limit determined by the Feather rule, the number of knock-on electrons that will emerge from lead plates of different thicknesses when energetic cosmic-ray muons traverse the plates, can be obtained. Curves A and B in Fig. 2 represent the results of these calculations for a minimum energy of $\frac{1}{2}$ and 1 mev, respectively, at emergence from the lead plate. The angle between the muon direction and that of the knock-on electron at production was also taken into account, but the scattering of the electron off its direction was neglected. Curves A and B will therefore underestimate the number of electrons.

Our present results for knock-on production by muons with energy above 450 mev and above 1700 mev are also represented in the Figure. These results were corrected for absorption and production of knock-on electrons in the aluminium covering plates. Although the cloud chamber contains only 0.15 and 0.33 cm lead plates, the mean number of knock-on electrons from thicker plates can be deduced by considering the number traversing one or more of the plates. Curve C in Fig. 2 was made to fit the experimental results for muons of energy higher than 1700 mev. It is obvious from Fig. 2 that energetic electrons are absorbed much more strongly than given by the Feather rule, Eqn (1). For thin lead plates our results are not inconsistent with the absorption relationship (1) if

the effective minimum energy at emergence from the lead plates is 1 mev. Taking the energy loss of 0.5 mev in the aluminium covering plate into account, this figure is reasonable as a low energy limit.

In order to arrive at an absorption relationship from which the experimental results can be deduced let us rewrite the Feather rule, Eqn (1):

$$\epsilon = \frac{R(\text{cm})}{K} + 0.25 \text{ mev.} \quad \dots\dots(2)$$

From Eqn (1), K would be equal to $0.048 \text{ cm mev}^{-1}$ for lead. By considering K as a parameter, it is possible to arrive at an effective range-energy relationship.

Taking

$$K(l) = 0.0455 (1 - 0.58l) \exp(-0.58l), \quad \dots\dots(3)$$

we arrived at the curve C in Fig. 2, integrating the Rutherford formula. Curve D was traced to fit the experimental points for muons of energy above 450 mev, but was not found by calculation. In this case it would be necessary to integrate the Bhabha formula.

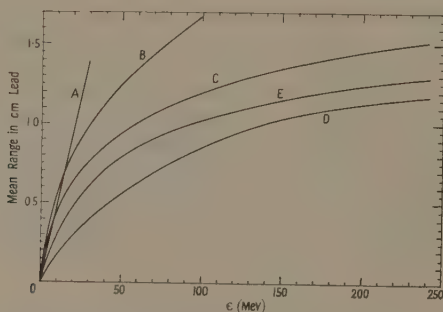


Fig. 3. The range of electrons in lead plotted against the energy in mev. Curve B is taken from Bethe and Heitler (1934), C and D are from Wilson's Monte Carlo calculations (Wilson 1951) while E represents Eqn (2) with K defined by (3). Curve A is the Feather rule, Eqn (2), with $K = 0.048 \text{ cm mev}^{-1}$.

The curve E in Fig. 3 represents the range-energy Eqn (2) with K substituted from Eqn (3). Curves C and D give the average range of the electrons for lead as calculated by Wilson (1951) using the Monte Carlo method. For curve C multiple scattering was not considered, while for curve D it was assumed that the electrons will proceed in the original direction until a critical energy (7.25 mev for lead) is reached, whereafter the electrons will diffuse in a random manner. When comparing curves D and E the scattering correction used by Wilson is presumably too strong.

§ 5. DISCUSSION OF THE RESULTS OF OTHER EXPERIMENTS ON KNOCK-ON ELECTRONS

The value given by Lloyd and Wolfendale (1959) for the number of knock-on electrons produced from a 1 cm lead plate by cosmic-ray muons with energy above 500 mev, is consistent with our results as represented by curve D (Fig. 2). The result obtained by Nasser and Hazen (1946) for electrons of 1 mev and higher

energy, produced in 0.7 cm lead, is also consistent with the curve, and so is the value obtained by Lovati, Mura and Succi (1954a) at 55 m water equivalent underground. The values of Hopkins, Nielsen and Nordheim (1939) are too high. If their iron filter for the cosmic radiation had been beneath the cloud chamber, it would have defined a minimum traversal energy of 450 mev for muons traversing the chamber. Presumably the iron was on top of the chamber, and their large production values may be due to secondary rays from the iron. The value found by Brown, McKay and Palmatier (1949) is also too large. Their experimental set-up defined a minimum energy of 270 mev for the muons traversing the cloud chamber. The results of other experiments (Hazen 1943, Lovati, Mura and Succi 1954b, Naranan *et al.* 1957, Seren 1942, Starr 1938, Tiffany and Hazen 1950, Trumpy 1938, Walker *et al.* 1951, Wilson 1938) are not considered, because the conditions set for these experiments differ from the conditions of the present experiment.

§ 6. THE ENERGY SPECTRUM FOR KNOCK-ON ELECTRONS

In order to arrive at an energy spectrum for the knock-on electrons, an average energy was ascribed from the empirical range curve E (Fig. 3) to each knock-on electron which traversed the lead plates without multiplication. It was estimated that the effective points of production and absorption of a knock-on electron are about one third of the thickness of a lead plate from the surface where the electron leaves the plate in which it is produced, or where it enters the plate in which it is absorbed. The energy of electrons which initiated cascade showers in the lead plates, was estimated from those transition curves of Wilson (1952) that include multiple Coulomb scattering (cf. also Roe and Ozaki 1959).

Table 1

Theoretical and experimental numbers of knock-on electrons produced in different energy ranges in the two sets of lead plates by (a) 1849 cosmic-ray muons in the energy ranges 450 to 1700 mev and (b) 2344 muons with energy above 1700 mev.

(1)		1-20	20-60	60-150	150-350	350-1000
(2)	(a)	482	9.6	0.88	0.033	0
	(b)	513	19.5	4.8	1.5	0.50
(3)	(a) Theor.	609	12.1	1.1	0.03	0
	Exp.	269	8	2	1	0
	(b) Theor.	824	31.3	7.7	2.4	0.81
	Exp.	348	13	7	7	3
(4)	(a) Theor.	1004	20.0	1.8	0.048	0
	Exp.	237	22	3	0	0
	(b) Theor.	1357	51.7	12.7	4.0	1.3
	Exp.	313	36	11	5	1

(1) Knock-on energy range (mev); (2) mean number per muon $\times 10^4$ ($\text{cm}^2 \text{g}^{-1}$); (3) total number of knock-on electrons in four 0.15 cm Pb plates (1-4); (4) total number of knock-on electrons in three 0.33 cm Pb plates (5-7).

The number of knock-on electrons found and the number expected from theoretical calculations are given in Table 1. The secondary production in the eighth plate was not considered, since energy determination for electrons from this plate was difficult. The experimental numbers of single electrons emerging

from the lead plates were corrected for the number of knock-on electrons produced in the aluminium coverings on both surfaces of the lead plates, as was calculated from Bhabha's formula by integration, using the Feather rule, Eqn (1). Only single electrons emerging from the plates were considered, since a rough estimate showed that the number of knock-on electrons appearing as pairs or multiples below a plate is more or less compensated by the number of directly produced electron pairs appearing as single electrons. The number of pairs due to double knock-on production was calculated from the experimental number of single emerging electrons and was found to be equal, within statistical limits, to the observed number of pairs for a total energy less than 20 mev. Hence most of the directly produced electron pairs with total energy less than 20 mev must have appeared as single electrons. The mean numbers of knock-on electrons for the energy ranges considered are also represented in Table 1 for cosmic-ray muons in the two energy ranges. For calculating the mean values, Rossi's differential intensity spectrum (Rossi 1948) of the cosmic-ray muons in the energy range of 450 to 1700 mev was approximated by $(-0.0011 E + 3.5) dE$, and by the power law $E^{-1.83} dE$ (Allkofer 1960) for energies higher than 1700 mev.

In Fig. 4 the theoretical spectra for the knock-on electrons produced by the muons in the two energy ranges are represented as histograms together with the experimental results for the seven lead plates as summarized in Table 1. The

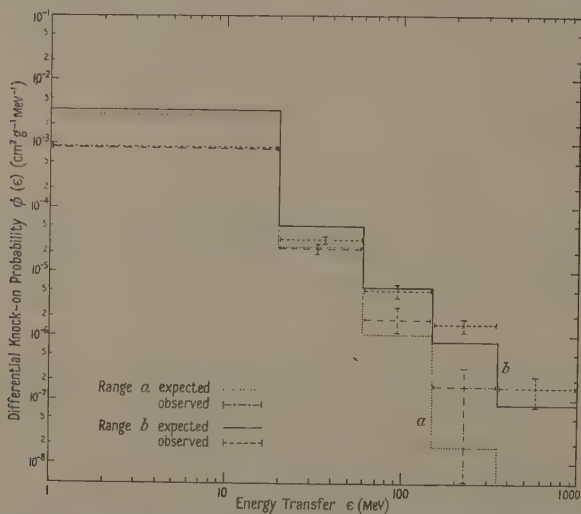


Fig. 4. The theoretical and experimental spectra for knock-on electrons produced in lead by cosmic-ray muons in the energy ranges: *a*, 450 to 1700 mev, *b* above 1700 mev.

statistical limits of the experimental points were calculated from the number of events found in each of the energy intervals and do not include variations due to fluctuations in range and in shower production of electrons (cf. Heitler 1954, Wilson 1952).

The number of low energy electrons found experimentally is much less than that predicted by the theory due to absorption of the lead plates. For the other

energy ranges the agreement between the theoretical and experimental results is satisfactory. The larger number of electrons found for the high energy ranges may be attributed to fluctuations in range and shower production of the electrons.

§ 7. THE ENERGY SPECTRUM FOR DIRECT PAIR PRODUCTION

For energy transfer of more than 20 mev the probability for pair production by a muon in the lead plates of the cloud chamber is much larger than the probability for two knock-on electrons to be produced in the same lead plate, and the number of pairs observed may easily be corrected for double knock-on production. The probability of a pair produced by a gamma ray from a muon in the lead plates can be neglected. No heavy materials were directly above the cloud chamber. The chamber itself was constructed of aluminium.

The theoretical and experimental results are compared in Fig. 5 and in Table 2. The theoretical distributions were calculated from the formula (Stoker and Haarhoff 1960)

$$\phi = \frac{4N}{3\pi A} (Z\alpha')^2 r_e^2 \left[\ln \frac{\alpha\epsilon}{(1+R^2)^{1/2}} - 1 \right] \left[(2+3R^2) \ln \left(1 + \frac{1}{R^2} \right) - 3 + \frac{1}{1+R^2} \right] I(1+C) \frac{d\epsilon}{\epsilon} \text{ cm}^2 \text{ g}^{-1}, \quad \dots\dots(4)$$

where

$$R = \frac{\epsilon}{2mc^2} \frac{\mu c^2}{E} \simeq 100 \frac{\epsilon}{E},$$

α' and r_e are, respectively, the fine structure constant and the classical radius of the electron. α is an undetermined parameter of the order of unity (Murota, Ueda and Tunaka 1956) and $I(1+C)=P$ is the energy partition factor (Stoker and Haarhoff 1960). To arrive at the mean distribution function for pairs produced by muons with energy above 1700 mev, as represented in Table 2 and Fig. 5, extreme values of 1.3 and 1.0 were accepted for the energy partition factor in

Table 2

Predicted and observed number of electron pairs produced in the two sets of lead plates by 2344 cosmic-ray muons with energy above 1700 mev. The true theoretical number must be between the extreme values for the energy partition factor $P=I(1+C)$.

(1)	20-45	45-200	200-1000	Sum	P	α
(2)	1.4	1.25	0.39		1.3	1
	1.04	0.96	0.30		1.0	1
(3)	2.2	2.0	0.63	4.8	1.3	1
	1.7	1.5	0.48	3.7	1.0	1
	3.4	2.6	0.78	6.8	1.3	2
	2.6	2.0	0.60	5.2	1.0	2
	2	2	2	6	Obs.	
(4)	3.6	3.3	1.03	7.9	1.3	1
	2.8	2.5	0.79	6.1	1.0	1
	5.6	4.3	1.28	11.2	1.3	2
	4.3	3.3	0.97	8.6	1.0	2
	3	2	6	11	Obs.	

(1) Energy transfer (mev); (2) mean number per muon $\times 10^4$ ($\text{cm}^2 \text{ g}^{-1}$); (3) total number of pairs in four 0.15 cm lead plates (1-4); (4) total number of pairs in three 0.33 cm lead plates (5-7).

order to facilitate the integration of the function ϕ with respect to the energy spectrum of the cosmic-ray muons. It was not possible to approximate the cosmic-ray muon spectrum for muon energy above 1700 mev by a simple power law, because muons with energy well above 10 gev still contribute appreciably to the pair production rate in spite of reduced intensity. Because of the strong dependence on the muon spectrum, the function ϕ was integrated numerically for the muon intensity spectrum recorded by Ashton *et al.* (1960), and is represented as the histogram *b* in Fig. 5. The experimental points for the two sets of lead plates are represented separately.

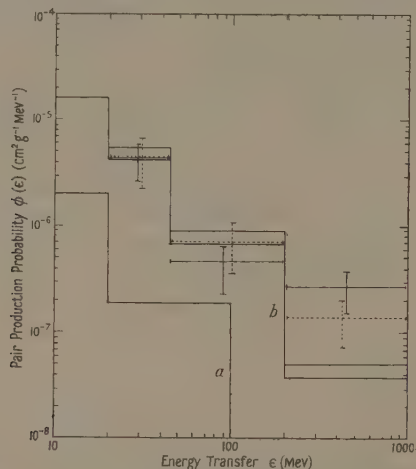


Fig. 5. The theoretical and experimental spectra for electron pairs produced in the lead plates by cosmic-ray muons. Histograms *b* represent the expected distributions for muons in the energy range above 1700 mev and energy partition factors $P=1.3$ and 1.0 , and histogram *a* the energy range 450 to 1700 mev, both for $\alpha=1$. The broken line points are the experimental results for the four 0.15 cm lead plates and the solid line points the results for the three 0.33 cm lead plates.

The histogram *a* represents the expected distribution for the lower muon energy range. This histogram was calculated, in fact, from the figures of Stoker and Haarhoff (1960) for the spectral distribution for 1500 mev muons, because this distribution lies between the mean distributions for the extreme values of 1.0 and 1.3 for the energy partition factor P , for muons in the 450 to 1700 mev range.

The 1849 muons traversing the cloud chamber in this energy range should have produced in the first 7 lead plates 0.5 pairs of energy ranging from 20 to 100 mev. Six pairs, however, with an estimated energy between 20 and 100 mev were found. It is possible that the energy ascribed to most of these pairs is too high due to fluctuation phenomena.

The experimental results represented in Table 2 and Fig. 5 were corrected for double knock-on production but not for absorption of one or both components of a pair. This is believed to be small for high energy transfer in the thin lead plates, notwithstanding the preferentially asymmetric energy partition between the pair electrons when the energy transfer is large. This asymmetric energy partition is obvious in the experimental results and is also brought out by the calculations of Stoker and Haarhoff (1960).

§ 8. DISCUSSION OF THE RESULTS AND CONCLUSION

The experimental distributions for knock-on electrons agree within statistical limits with the theoretical distributions for the energy ranges considered. The results for the pair production agree with the theory with $\alpha = 1$ for the lower energy ranges, but then too many events were observed in the highest electron energy ranges for both the muon energy ranges. Fluctuations in range and shower production of electrons should tend to flatten the spectral distribution, an effect also observed for the knock-on electron distributions. Gaebler, Hazen and Hendel (1961) also found an increase in the number of pairs observed with the energy transfer with respect to the expected distribution. According to R. F. Deery (quoted by Gaebler *et al.* (1961)) knock-on and pair production cross sections might be larger for interactions at small distances. Better statistics and theoretical evaluations are required to settle this point. Both Roe and Ozaki (1959) and Gaebler *et al.* (1961) found the electron pair cross section a factor 2 less than predicted by the calculations of Murota, Ueda and Tunaka (1956), taking $\alpha = 2$. The formula (4) for the pair production cross section, which we have used, led to cross sections at least a factor 2 less than given by the formula of Murota *et al.* (Stoker and Haerhoff 1960).

The total number of pairs that we have observed with energy above 20 mev and produced by muons with energy above 1700 mev, agrees with theory if $\alpha = 2$. Our results seem to favour a value for α between 1 and 2.

ACKNOWLEDGMENTS

Thanks are due to Mr. J. P. van der Walt for technical assistance and to Messrs. G. P. de Beer, J. Kruger and J. P. van der Merwe, who helped with the experimental set-up, the analysis and calculations. This experiment was performed with the financial assistance of the South African Council for Scientific and Industrial Research.

REFERENCES

- ALLKOFER, O. C., 1960, *Z. Phys.*, **158**, 274.
 ASHTON, F., *et al.*, 1960, *Nature, Lond.*, **185**, 364.
 AVAN, M., and AVAN, L., 1957, *Nuovo Cim.*, **6**, 1500.
 BETHE, H., and HEITLER, W., 1934, *Proc. Roy. Soc. A*, **146**, 83.
 BROWN, W. W., MCKAY, A. S., and PALMATIER, E. D., 1949, *Phys. Rev.*, **76**, 506.
 FOWLER, G. N., and WOLFENDALE, A. W., 1958, *Progress in Elementary Particles and Cosmic Ray Physics*, Vol. IV, Ed. by J. G. WILSON and S. A. WOUTHUYSEN (Amsterdam: North-Holland).
 GAEBLER, J. F., HAZEN, W. E., and HENDEL, A. Z., 1961, *Nuovo Cim.*, **19**, 265.
 GOLDSACK, S. J., and KANNANGARA, M. L. T., 1953, *Phil. Mag.*, **44**, 811.
 HAZEN, W. E., 1943, *Phys. Rev.*, **64**, 7.
 HEITLER, W., 1954, *The Quantum Theory of Radiation* (Oxford: University Press).
 HOPKINS, J. I., NIELSEN, W. M., and NORDHEIM, L. W., 1939, *Phys. Rev.*, **55**, 233.
 HUSAIN, S. A., and PUTMAN, J. L., 1957, *Proc. Phys. Soc. A*, **70**, 304.
 KATZ, L., and PENFOLD, A. S., 1952, *Rev. Mod. Phys.*, **24**, 28.
 LLOYD, J. L., and WOLFENDALE, A. W., 1959, *Proc. Phys. Soc.*, **73**, 178.
 LOVATI, A., MURA, A., and SUCCI, C., 1954 a, *Nuovo Cim.*, **11**, 92.
 LOVATI, A., MURA, A., SUCCI, C., and TAGLIAFERRI, 1954 b, *Nuovo Cim.*, **12**, 531.
 MUROTA, T., UEDA, A., and TUNAKA, H., 1956, *Progr. Theor. Phys. Japan*, **16**, 482.
 NARANAN, S., RAMANAMURTY, P. V., SAHIAR, A., and SREEKKANTAN, B. V., 1957, *Nuovo Cim.*, **5**, 1773.

- NASSAR, S., and HAZEN, W. E., 1946, *Phys. Rev.*, **69**, 298.
ROE, B. P., and OZAKI, S., 1959, *Phys. Rev.*, **116**, 1022.
ROSSI, B., 1948, *Rev. Mod. Phys.*, **20**, 537.
—— 1952, *High Energy Particles* (New York: Prentice-Hall).
SEREN, L., 1942, *Phys. Rev.*, **62**, 204.
STARR, M. A., 1938, *Phys. Rev.*, **53**, 6.
STERNHEIMER, R. M., 1959, *Phys. Rev.*, **115**, 137.
STOKER, P. H., and HAARHOFF, P. C., 1960, *Nucl. Phys.*, **14**, 512.
TIFFANY, O. L., and HAZEN, W. E., 1950, *Phys. Rev.*, **77**, 849.
TRUMPY, B., 1938, *Z. Phys.*, **111**, 338.
WALKER, W. D., 1953, *Phys. Rev.*, **90**, 234.
WALKER, W. D., HAMMEL, J. E., SINCLAIR, R. M., and SORREL, J. D., 1951, *Phys. Rev.*, **83**, 655.
WILSON, J. G., 1938, *Nature, Lond.*, **142**, 73.
WILSON, R. R., 1951, *Phys. Rev.*, **84**, 100.
—— 1952, *Phys. Rev.*, **86**, 261.

A Schematic Model for the Impact Excitation of Atoms

By B. L. MOISEWITSCH

Department of Applied Mathematics, The Queen's University of Belfast

MS. received 18th January 1961, in revised form 17th April 1961

Abstract. The third-order approximation is used to derive simple analytical expressions for the partial cross sections corresponding to the scattering of high-energy charged particles by a schematic model atom involving matrix elements having a r^{-2} radial dependence.

§ 1. INTRODUCTION

RECENTLY Kingston, Moiseiwitsch and Skinner (1960) and Kingston and Skinner (1961) have calculated the cross sections for the 1s-2s excitation of hydrogen atoms by electron and proton impact and for the elastic scattering of electrons by hydrogen atoms, respectively, using an approximate expression for the cross section which includes terms up to the third order in the interaction potential between the incident particle and the hydrogen atom and neglects all terms of higher order. In the case of the 1s-2s excitation by proton impact, by neglecting coupling to all states other than the initial and final states, they obtained good agreement with the calculations of Bates (1959) who employed an impact parameter treatment together with the distortion approximation.

In the present paper the third-order approximation is used to investigate the scattering of charged particles by atoms by employing a schematic model, first introduced by Seaton (1955), which involves matrix elements having a radial dependence of the form r^{-2} .

§ 2. WEAK COUPLING APPROXIMATIONS

The theory of the scattering of particles by hydrogen atoms involves the solution of an infinite set of coupled equations which have the form (Massey 1956)

$$[\nabla^2 + k_n^2]F_n(\mathbf{r}) = \sum_m U_{nm}(\mathbf{r})F_m(\mathbf{r}) \quad \dots\dots(1)$$

where

$$U_{nm}(\mathbf{r}_1) = \frac{2M}{\hbar^2} \int \phi_n^*(\mathbf{r}_2)V(\mathbf{r}_1, \mathbf{r}_2)\phi_m(\mathbf{r}_2) d\mathbf{r}_2 \quad \dots\dots(2)$$

and

$$k_n^2 = \frac{2M}{\hbar^2} (E - \epsilon_n). \quad \dots\dots(3)$$

M is the reduced mass and E is the total energy of the system, ϕ_n is the eigenfunction and ϵ_n is the eigenenergy of the n th state of a hydrogen atom, and $V(\mathbf{r}_1, \mathbf{r}_2)$ is the interaction potential between the incident particle and the atom.

If we denote the initial and final states of the atom by 1 and 2 respectively and if the coupling to all other states is neglected, the infinite set of equations (1) reduces to the pair of coupled equations

$$[\nabla^2 + k_1^2 - U_{11}(\mathbf{r})]F_1(\mathbf{r}) = U_{12}(\mathbf{r})F_2(\mathbf{r}) \quad \dots\dots(4)$$

$$[\nabla^2 + k_2^2 - U_{22}(\mathbf{r})]F_2(\mathbf{r}) = U_{21}(\mathbf{r})F_1(\mathbf{r}) \quad \dots\dots(5)$$

where F_1 and F_2 have the asymptotic forms for large r

$$F_1(\mathbf{r}) \sim \exp(ik_1\mathbf{n}_0 \cdot \mathbf{r}) + r^{-1} \exp(ik_1r)f_1(\theta, \phi) \quad \dots\dots(6)$$

$$F_2(\mathbf{r}) \sim r^{-1} \exp(ik_2r)f_2(\theta, \phi), \quad \dots\dots(7)$$

\mathbf{n}_0 being a unit vector in the direction of the incident beam of particles.

Consider the weak coupling approximation known as the *method of distorted waves* which assumes that the back coupling term $U_{12}F_2$ on the right-hand side of Eqn (4) can be neglected. Then the pair of coupled equations (4) and (5) reduce to

$$[\nabla^2 + k_1^2 - U_{11}(\mathbf{r})]F_1(\mathbf{r}) = 0 \quad \dots\dots(8)$$

$$[\nabla^2 + k_2^2 - U_{22}(\mathbf{r})]F_2(\mathbf{r}) = U_{21}(\mathbf{r})F_1(\mathbf{r}) \quad \dots\dots(9)$$

and so

$$f_2(\theta, \phi) = -\frac{1}{4\pi} \int \mathcal{F}_2(\mathbf{r}', \pi - \Theta') U_{21}(\mathbf{r}') F_1(\mathbf{r}') d\mathbf{r}' \quad \dots\dots(10)$$

where the function $\mathcal{F}_2(\mathbf{r})$ satisfies the equation

$$[\nabla^2 + k_2^2 - U_{22}(\mathbf{r})]\mathcal{F}_2(\mathbf{r}) = 0 \quad \dots\dots(11)$$

with the asymptotic form for large r

$$\mathcal{F}_2(\mathbf{r}) \sim \exp(ik_2\mathbf{n}_0 \cdot \mathbf{r}) + r^{-1} \exp(ik_2r)f_2(\theta, \phi) \quad \dots\dots(12)$$

and

$$\cos \Theta' = \cos \theta \cos \theta' + \sin \theta \sin \theta' \cos(\phi - \phi'). \quad \dots\dots(13)$$

Expanding F_1 and \mathcal{F}_2 in the forms

$$F_1(\mathbf{r}) = \frac{1}{r} \sum_{l=0}^{\infty} i^{l(2l+1)} \exp(i\eta_{1,l}) \phi_{1,l}(r) P_l(\cos \theta) \quad \dots\dots(14)$$

$$\mathcal{F}_2(\mathbf{r}) = \frac{1}{r} \sum_{l=0}^{\infty} i^{l(2l+1)} \exp(i\eta_{2,l}) \phi_{2,l}(r) P_l(\cos \theta), \quad \dots\dots(15)$$

\mathbf{n}_0 being chosen in the direction of the polar axis, and assuming that U_{11} , U_{22} and U_{12} are spherically symmetrical, as for s states, we obtain

$$\frac{d^2 \phi_{n,l}}{dr^2} + \left\{ k_n^2 - U_{nn}(r) - \frac{l(l+1)}{r^2} \right\} \phi_{n,l} = 0 \quad (n=1, 2) \quad \dots\dots(16)$$

where $\phi_{n,l}$ has the asymptotic form for large r

$$\phi_{n,l}(r) \sim \frac{1}{k_n} \sin(k_n r - \frac{1}{2}l\pi + \eta_{n,l}). \quad \dots\dots(17)$$

Then

$$f_2(\theta, \phi) = - \sum_{l=0}^{\infty} (2l+1) P_l(\cos \theta) \exp \{i(\eta_{1,l} + \eta_{2,l})\} \\ \times \int_0^{\infty} \phi_{2,l}(r) \phi_{1,l}(r) U_{21}(r) dr \quad \dots\dots (18)$$

and so, to the distorted waves approximation, the cross section for the excitation of the state 2 from the state 1 of the target atomic system is given by

$$Q(1 \rightarrow 2) = \frac{k_2}{k_1} \int_0^{\pi} \int_0^{2\pi} |f_2(\theta, \phi)|^2 \sin \theta d\theta d\phi \quad \dots\dots (19)$$

$$= 4\pi \frac{k_2}{k_1} \sum_{l=0}^{\infty} (2l+1) \left| \int_0^{\infty} \phi_{2,l}(r) \phi_{1,l}(r) U_{21}(r) dr \right|^2 \quad \dots\dots (20)$$

It may be shown that the distorted waves method, which neglects the back coupling term $U_{12}F_2$ in Eqn (4), gives rise to an error of the order of $(U_{12})^3$ in the scattering amplitude f_2 and thus an error of the order of $(U_{12})^4$ in the cross section $Q(1 \rightarrow 2)$.

If only terms up to the third order in the interaction potential are retained in the expression (20) for the cross section we obtain the *third-order approximation*. Now the solution of Eqn (16) with asymptotic form (17) can be written in the integral equation form

$$\phi_{n,l}(r) = \cos \eta_{n,l} j_l(k_n r) + k_n r \int_0^{\infty} j_l(k_n r') n_l(k_n r') U_{nn}(r') \phi_{n,l}(r') r' dr' \quad \dots\dots (21)$$

where

$$\sin \eta_{n,l} = -k_n \int_0^{\infty} r' j_l(k_n r') \phi_{n,l}(r') U_{nn}(r') dr', \quad \dots\dots (22)$$

j_l and n_l being spherical Bessel and Neumann functions respectively and $r_<$, $r_>$ being the lesser and greater of r , r' . Hence to the first order in the interaction energy we have

$$\phi_{n,l}(r) = r j_l(k_n r) + k_n r \int_0^{\infty} j_l(k_n r') n_l(k_n r') U_{nn}(r') j_l(k_n r') r'^2 dr' \quad \dots\dots (23)$$

and so the third-order approximation to the cross section is given by

$$Q(1 \rightarrow 2) = 4\pi \frac{k_2}{k_1} \sum_{l=0}^{\infty} (2l+1) \{1 + 2(\alpha_{1,l} + \alpha_{2,l})\} \\ \times \left[\int_0^{\infty} U_{21}(r) j_l(k_2 r) j_l(k_1 r) r^2 dr \right]^2 \quad \dots\dots (24)$$

where

$$\alpha_{n,l} = \frac{k_n \int_0^{\infty} \int_0^{\infty} U_{21}(r) j_l(k_m r) j_l(k_n r') n_l(k_n r') j_l(k_n r') U_{nn}(r') r^2 r'^2 dr dr'}{\int_0^{\infty} U_{21}(r) j_l(k_2 r) j_l(k_1 r) r^2 dr} \quad \dots\dots (25)$$

with $n=1$, $m=2$ or $n=2$, $m=1$.

If we reject the third-order terms and retain only the second-order terms, expression (24) reduces to the *first Born approximation* formula

$$Q(1 \rightarrow 2) = 4\pi \frac{k_2}{k_1} \sum_{l=0}^{\infty} (2l+1) \left[\int_0^{\infty} U_{21}(r) j_l(k_2 r) j_l(k_1 r) r^2 dr \right]^2. \quad \dots (26)$$

To obtain the *second Born approximation* to the cross section we expand f_2 to the second order in the interaction potential. This gives

$$f_2(\theta, \phi) = - \sum_{l=0}^{\infty} (2l+1) P_l(\cos \theta) \{1 + \alpha_{1,l} + \alpha_{2,l} + i(\beta_{1,l} + \beta_{2,l})\} \\ \times \int_0^{\infty} U_{21}(r) j_l(k_2 r) j_l(k_1 r) r^2 dr \quad \dots (27)$$

where

$$\beta_{n,l} = -k_n \int_0^{\infty} U_{nn}(r') \{j_l(k_n r')\}^2 r'^2 dr', \quad \dots (28)$$

so that to the second Born approximation

$$Q(1 \rightarrow 2) = 4\pi \frac{k_2}{k_1} \sum_{l=0}^{\infty} (2l+1) \{ (1 + \alpha_{1,l} + \alpha_{2,l})^2 + (\beta_{1,l} + \beta_{2,l})^2 \} \\ \times \left[\int_0^{\infty} U_{21}(r) j_l(k_2 r) j_l(k_1 r) r^2 dr \right]^2. \quad \dots (29)$$

Thus some terms of the fourth order in the interaction potential have been retained in deriving this approximation to the excitation cross section. Referring to Eqns (18) and (27) we see that the term $(\beta_{1,l} + \beta_{2,l})^2$ in (29) arises from the expansion of the phase factor $\exp\{i(\eta_{1,l} + \eta_{2,l})\}$ to the first order in the interaction potential and is exactly cancelled if the expansion is carried out to a higher order. It should therefore be rejected from the second Born approximation. Other terms of the fourth order in the interaction potential have also been neglected in deriving the second Born approximation expression (29) and so the most consistent procedure is to employ the third-order approximation (24) which includes all terms up to the third order in the interaction potential and neglects all higher order terms. The Schwinger variational method for the scattering amplitude with plane wave trial functions also neglects some terms of the fourth order and so the same criticisms may be applied to it as have been applied above to the second Born approximation.

§ 3. SCHEMATIC MODEL

In the case of the scattering of particles by hydrogen atoms in the ground 1s state a useful approximation is to include coupling to all the states of principal quantum number $n \leq 2$, viz. 1s, 2s, $2p_0$, $2p_{+1}$, $2p_{-1}$ and to neglect the coupling to all states with $n > 2$ and the continuum states. Then the infinite set of coupled equations (1) reduces to the set of five coupled equations

$$[\nabla^2 + k_1^2 - U_{1s, 1s}(r)] F_{1s}(\mathbf{r}) = U_{1s, 2s}(r) F_{2s}(\mathbf{r}) + \sum_{m=0, \pm 1} U_{1s, 2p_m}(r) F_{2p_m}(\mathbf{r}) \\ \dots (30)$$

$$[\nabla^2 + k_2^2 - U_{2s, 2s}(r)]F_{2s}(\mathbf{r}) = U_{2s, 1s}(r)F_{1s}(\mathbf{r}) + \sum_{m=0, \pm 1} U_{2s, 2p_m}(r)F_{2p_m}(\mathbf{r}) \quad \dots\dots (31)$$

$$[\nabla^2 + k_2^2 - U_{2p_0, 2p_0}(r)]F_{2p_0}(\mathbf{r}) = U_{2p_0, 1s}(r)F_{1s}(\mathbf{r}) + U_{2p_0, 2s}(r)F_{2s}(\mathbf{r}) + \sum_{m=\pm 1} U_{2p_0, 2p_m}(r)F_{2p_m}(\mathbf{r}) \quad \dots\dots (32)$$

$$[\nabla^2 + k_2^2 - U_{2p_{\pm 1}, 2p_{\pm 1}}(r)]F_{2p_{\pm 1}}(\mathbf{r}) = U_{2p_{\pm 1}, 1s}(r)F_{1s}(\mathbf{r}) + U_{2p_{\pm 1}, 2s}(r)F_{2s}(\mathbf{r}) + U_{2p_{\pm 1}, 2p_0}(r)F_{2p_0}(\mathbf{r}) + U_{2p_{\pm 1}, 2p_{\mp 1}}(r)F_{2p_{\mp 1}}(\mathbf{r}) \quad \dots\dots (33)$$

where, for electron impact, the matrix elements $U_{nm}(\mathbf{r})$ have the asymptotic forms for large r

$$\left. \begin{aligned} U_{1s, 1s}(r) &\sim -\frac{2}{a_0} \frac{1}{r} \exp(-2r/a_0), \\ U_{2s, 2s}(r) &\sim -\frac{2}{a_0} \frac{1}{r} \exp(-r/a_0), \\ U_{2p_0, 2p_0}(r) &\sim -\frac{2}{a_0} \frac{1}{r} \exp(-r/a_0) + \frac{24a_0}{r^3} P_2(\cos \theta), \\ U_{2p_{\pm 1}, 2p_{\pm 1}}(r) &\sim -\frac{2}{a_0} \frac{1}{r} \exp(-r/a_0) - \frac{12a_0}{r^3} P_2(\cos \theta), \\ U_{1s, 2s}(r) &\sim \frac{\sqrt{2}}{a_0^3} \left(\frac{2}{3}\right)^2 r \exp(-3r/2a_0), \\ U_{1s, 2p_0}(r) &\sim 8\sqrt{2} \left(\frac{2}{3}\right)^5 \frac{1}{r^3} P_1(\cos \theta), \\ U_{1s, 2p_{\pm 1}}(r) &\sim 8\sqrt{2} \left(\frac{2}{3}\right)^5 \frac{1}{r^3} \frac{1}{\sqrt{2}} P_1^1(\cos \theta) e^{\pm i\phi}, \\ U_{2s, 2p_0}(r) &\sim -\frac{6}{r^2} P_1(\cos \theta), \\ U_{2s, 2p_{\pm 1}}(r) &\sim -\frac{6}{r^2} \frac{1}{\sqrt{2}} P_1^1(\cos \theta) e^{\pm i\phi}, \\ U_{2p_0, 2p_{\pm 1}}(r) &\sim \frac{12a_0}{r^3} \frac{1}{\sqrt{2}} P_2^1(\cos \theta) e^{\pm i\phi}, \\ U_{2p_{\mp 1}, 2p_{\pm 1}}(r) &\sim \frac{6a_0}{r^3} P_2^2(\cos \theta) e^{\pm 2i\phi}, \end{aligned} \right\} \dots\dots (34)$$

the polar axis of the coordinate system being chosen in the direction of the incident beam of particles.

In the present investigation we are concerned with the use of a schematic model to examine the effects of distortion and polarization on the scattering of

particles by atoms. The schematic model replaces the matrix elements (34) by

$$\left. \begin{aligned}
 U_{1s, 1s}(r) &= -\frac{A_1}{r^2}, \\
 U_{2s, 2s}(r) &= -\frac{A_2}{r^2}, \\
 U_{2p_0, 2p_0}(r) &= -\frac{A_2}{r^2} + \frac{2B}{r^2} P_2(\cos \theta), \\
 U_{2p_{\pm 1}, 2p_{\pm 1}}(r) &= -\frac{A_2}{r^2} - \frac{B}{r^2} P_2(\cos \theta), \\
 U_{1s, 2s}(r) &= \frac{A_{1s, 2s}}{r^2}, \\
 U_{1s, 2p_0}(r) &= \frac{A_{1s, 2p}}{r^2} P_1(\cos \theta), \\
 U_{1s, 2p_{\pm 1}}(r) &= \frac{A_{1s, 2p}}{r^2} \frac{1}{\sqrt{2}} P_1^1(\cos \theta) e^{\pm i\phi}, \\
 U_{2s, 2p_0}(r) &= -\frac{A_{2s, 2p}}{r^2} P_1(\cos \theta), \\
 U_{2s, 2p_{\pm 1}}(r) &= -\frac{A_{2s, 2p}}{r^2} \frac{1}{\sqrt{2}} P_1^1(\cos \theta) e^{\pm i\phi}, \\
 U_{2p_0, 2p_{\pm 1}}(r) &= \frac{B}{r^2} \frac{1}{\sqrt{2}} P_2^1(\cos \theta) e^{\pm i\phi}, \\
 U_{2p_{\mp 1}, 2p_{\pm 1}}(r) &= \frac{\frac{1}{2}B}{r^2} P_2^2(\cos \theta) e^{\pm 2i\phi}.
 \end{aligned} \right\} \dots\dots (35)$$

These matrix elements have the same dependence on the angular coordinates θ, ϕ and the same signs as the matrix elements (34) for large r if all the coefficients A and B are chosen to be positive constants for incident particles of negative charge, e.g. electrons, and negative constants for incident particles of positive charge, e.g. positrons, protons, and α -particles.

In order to obtain simple analytical expressions for the third-order approximation to the partial cross section we also put $k_1 = k_2 = k$.

3.1. Method of Distorted Waves

In this section we neglect coupling to all states except the initial and final states and, in addition, neglect back coupling.

We first consider the *elastic scattering* of particles by the ground $1s$ state of the model atom. Then we require the solution of the equation

$$[\nabla^2 + k^2 - U_{1s, 1s}(r)]F_{1s}(r) = 0 \quad \dots\dots (36)$$

where F_{1s} has the asymptotic form (6) for large r .

Expanding F_{1s} in the form (14) we obtain

$$\left[\frac{d^2}{dr^2} + k^2 - \frac{l(l+1) - A_1}{r^2} \right] \phi_{1,l} = 0. \quad \dots\dots (37)$$

Hence

$$\phi_{1,l}(r) = r j_{l_1}(kr) \quad \dots\dots (38)$$

where

$$l_1(l_1+1) = l(l+1) - A_1 \quad \dots\dots (39)$$

i.e.

$$l_1 = \frac{1}{2}[-1 + \{(2l+1)^2 - 4A_1\}^{1/2}]. \quad \dots\dots (40)$$

In order that $r^{-1}\phi_{1,l}(r)$ should be finite at the origin we require that $l_1 \geq 0$. This is always satisfied if $A_1 \leq 0$ i.e. for positively charged particles. However, if $A_1 > 0$ then $l_1 \geq 0$ only if $A_1 \leq l(l+1)$. A difficulty occurs in the latter case when $l=0$ for then $l_1 < 0$. Nevertheless, provided that $A_1 < \frac{1}{4}$, i.e. $l_1 > -\frac{1}{2}$, an expression for the cross section can still be obtained even though the solution is unbounded at the origin (Mott and Massey 1949).

Now

$$\eta_{1,l} = \frac{1}{2}\pi(l - l_1) \quad \dots\dots (41)$$

and so it follows from (40) that

$$\eta_{1,l} = \frac{1}{4}\pi(2l+1) \left[1 - \left\{ 1 - \frac{4A_1}{(2l+1)^2} \right\}^{1/2} \right]. \quad \dots\dots (42)$$

Since

$$f_{1s}(\theta) = \frac{1}{k} \sum_{l=0}^{\infty} (2l+1) \exp(i\eta_{1,l}) \sin \eta_{1,l} P_l(\cos \theta) \quad \dots\dots (43)$$

we see that the l th order partial cross section for elastic scattering is given by

$$Q_l(1s \rightarrow 1s) = \frac{4\pi}{k^2} (2l+1) \sin^2 \eta_{1,l}. \quad \dots\dots (44)$$

Hence the third-order distortion approximation to the elastic partial cross section is

$$Q_l(1s \rightarrow 1s) = \frac{\pi^3}{k^2} \frac{A_1^2}{2l+1} \left\{ 1 + \frac{2A_1}{(2l+1)^2} \right\}. \quad \dots\dots (45)$$

To the second order in A this reduces to the first Born approximation expression

$$Q_l(1s \rightarrow 1s) = \frac{\pi^3}{k^2} \frac{A_1^2}{2l+1}. \quad \dots\dots (46)$$

Because the partial cross sections fall off as l^{-1} for large l the sum of the series of partial cross sections diverges for the schematic model. We shall therefore confine our investigations to the individual partial cross sections only.

We now consider the $1s-2s$ excitation case for which we require the solution of the pair of equations

$$[\nabla^2 + k^2 - U_{1s,1s}(r)]F_{1s}(\mathbf{r}) = 0 \quad \dots\dots (47)$$

$$[\nabla^2 + k^2 - U_{2s,2s}(r)]F_{2s}(\mathbf{r}) = U_{2s,1s}(r)F_{1s}(\mathbf{r}), \quad \dots\dots (48)$$

where F_{2s} has the asymptotic form (7) for large r .

Referring to § 2 we see that $f_{2s}(\theta)$ is given by (18) where

$$\phi_{2,l}(r) = r j_{l_2}(kr) \quad \dots\dots (49)$$

with

$$l_2 = \frac{1}{2}[-1 + \{(2l+1)^2 - 4A_2\}^{1/2}] \quad \dots\dots (50)$$

and

$$\eta_{2,l} = \frac{1}{4}\pi(2l+1) \left[1 - \left\{ 1 - \frac{4A_2}{(2l+1)^2} \right\}^{1/2} \right]. \quad \dots\dots (51)$$

Hence

$$f_{2s}(\theta) = -A_{2s, 1s} \sum_{l=0}^{\infty} (2l+1) P_l(\cos \theta) \exp \{i(\eta_{1,l} + \eta_{2,l})\} \int_0^{\infty} j_{l_1}(kr) j_{l_2}(kr) dr \quad \dots\dots (52)$$

giving for the 1s-2s excitation l th order partial cross section

$$Q_l(1s \rightarrow 2s) = 4\pi(2l+1)(A_{2s, 1s})^2 \left[\int_0^{\infty} j_{l_1}(kr) j_{l_2}(kr) dr \right]^2. \quad \dots\dots (53)$$

Since (Watson 1944)

$$\int_0^{\infty} j_{l_1}(kr) j_{l_2}(kr) dr = \frac{\sin(l_1 - l_2)\frac{1}{2}\pi}{k(l_1 - l_2)(l_1 + l_2 + 1)} \quad (l_1 + l_2 + 1 > 0) \quad \dots\dots (54)$$

it follows that, to the distorted waves approximation,

$$Q_l(1s \rightarrow 2s) = 4\pi(2l+1)(A_{2s, 1s})^2 \times \left[\frac{1}{k(A_2 - A_1)} \sin \frac{1}{4}\pi(2l+1) \left\{ \left(1 - \frac{4A_1}{(2l+1)^2}\right)^{1/2} - \left(1 - \frac{4A_2}{(2l+1)^2}\right)^{1/2} \right\} \right]^2. \quad \dots\dots (55)$$

The third-order distortion approximation is obtained by expanding to the third order in A and is given by

$$Q_l(1s \rightarrow 2s) = \frac{\pi^3}{k^2(2l+1)} (A_{2s, 1s})^2 \left\{ 1 + \frac{2(A_1 + A_2)}{(2l+1)^2} \right\} \quad \dots\dots (56)$$

while the first Born approximation has the form

$$Q_l(1s \rightarrow 2s) = \frac{\pi^3}{k^2} \frac{(A_{2s, 1s})^2}{2l+1}. \quad \dots\dots (57)$$

We now turn our attention to the 1s-2p₀ excitation case which involves the solution of the pair of equations

$$[\nabla^2 + k^2 - U_{1s, 1s}(r)]F_{1s}(\mathbf{r}) = 0 \quad \dots\dots (58)$$

$$[\nabla^2 + k^2 - U_{2p_0, 2p_0}(\mathbf{r})]F_{2p_0}(\mathbf{r}) = U_{2p_0, 1s}(\mathbf{r})F_{1s}(\mathbf{r}) \quad \dots\dots (59)$$

where F_{2p_0} has the asymptotic form for large r given by (7). From Eqn (10) it follows that

$$f_{2p_0}(\theta) = -\frac{1}{4\pi} A_{2p_0, 1s} \int \mathcal{F}_2(r', \pi - \Theta') F_{1s}(\mathbf{r}') P_1(\cos \theta') \frac{1}{r'^2} d\mathbf{r}'. \quad \dots\dots (60)$$

In the first instance let us neglect the term involving $P_2(\cos \theta)$ in $U_{2p_0, 2p_0}$. Then it can be readily shown that

$$f_{2p_0}(\theta) = -iA_{2p_0, 1s} \sum_{l=0}^{\infty} \exp(i\eta_{2,l}) P_l(\cos \theta) \times \left[(l+1) \exp(i\eta_{1,l+1}) \int_0^{\infty} \phi_{2,l}(r) \phi_{1,l+1}(r) \frac{1}{r^2} dr - l \exp(i\eta_{1,l-1}) \int_0^{\infty} \phi_{2,l}(r) \phi_{1,l-1}(r) \frac{1}{r^2} dr \right]. \quad \dots\dots (61)$$

Using the integral (54) we find that to the third order in A

$$Q_0(1s \rightarrow 2p_0) = \frac{\pi}{k^2} (A_{2p, 1s})^2 \{1 + A_1 - A_2\} \quad \dots\dots (62)$$

and

$$Q_l(1s \rightarrow 2p_0) = 0 \quad (l \neq 0). \quad \dots\dots (63)$$

Similarly for the case of the $1s \rightarrow 2p_{\pm 1}$ excitation we obtain

$$\begin{aligned} f_{2p_{\pm 1}}(\theta, \phi) = & iA_{2p, 1s} \sum_{l=1}^{\infty} \exp(i\eta_{2, l}) \frac{1}{\sqrt{2}} P_l^1(\cos \theta) e^{\mp i\phi} \\ & \times \left[\exp(i\eta_{1, l+1}) \int_0^{\infty} \phi_{2, l}(r) \phi_{1, l+1}(r) \frac{1}{r^2} dr \right. \\ & \left. + \exp(i\eta_{1, l-1}) \int_0^{\infty} \phi_{2, l}(r) \phi_{1, l-1}(r) \frac{1}{r^2} dr \right] \end{aligned} \quad \dots\dots (64)$$

if the term involving $P_2(\cos \theta)$ in $U_{2p_{\pm 1}, 2p_{\pm 1}}$ is neglected. To the third order in A this gives

$$Q_0(1s \rightarrow 2p_{\pm 1}) = 0 \quad \dots\dots (65)$$

and

$$Q_l(1s \rightarrow 2p_{\pm 1}) = \frac{\pi}{k^2} (A_{2p, 1s})^2 \frac{2l+1}{2l(l+1)} \left\{ 1 + \frac{A_2 - A_1}{l(l+1)} \right\} \quad (l \neq 0). \quad \dots\dots (66)$$

These partial cross sections reduce to the first Born approximation expressions if only terms up to the second order in A are retained. They are in agreement with the formula for the first Born partial cross section $\sum_{m=0, \pm 1} Q_l(1s \rightarrow 2p_m)$ derived by Seaton (1955) in the limit of large k .

For the $1s \rightarrow 2p_0$ excitation the partial cross section vanishes to the third order in A for all positive integral values of l while in the case of the $1s \rightarrow 2p_{\pm 1}$ excitation the partial cross section vanishes for $l=0$, attains a maximum value for $l=1$, and then decreases with increasing l .

3.2. Distortion-polarization Approximation

We now turn our attention to the effect of polarization resulting from coupling to states which are neither the initial nor the final state, and to the effect of the terms involving $P_2(\cos \theta)$ in $U_{2p_0, 2p_0}(\mathbf{r})$ and $U_{2p_{\pm 1}, 2p_{\pm 1}}(\mathbf{r})$. The analysis is of an elementary nature involving integrations of products of spherical Bessel and Neumann functions all of which can be evaluated in closed form (Watson 1944). However, the analysis is too lengthy to reproduce here so we shall only quote the final results. When coupling to all the states $1s, 2s, 2p_0, 2p_{+1}, 2p_{-1}$ is taken into account to the third order in A and B , we obtain the third-order distortion-polarization approximation (Kingston, Moiseiwitsch and Skinner 1960). To this approximation the l th order partial cross sections are given by

$$Q_l(1s \rightarrow 1s) = \frac{\pi^3}{k^2} \frac{A_1^2}{2l+1} \left[1 + \frac{2A_1}{(2l+1)^2} + \frac{2(A_{2s, 1s})^2}{A_1} \frac{1}{(2l+1)^2} + \frac{(A_{2p, 1s})^2}{A_1} \delta_{0l} \right], \quad \dots\dots (67)$$

$$Q_l(1s \rightarrow 2s) = \frac{\pi^3}{k^2} \frac{(A_{2s, 1s})^2}{2l+1} \left[1 + \frac{2(A_1 + A_2)}{(2l+1)^2} + \frac{A_{2p, 2s} A_{2p, 1s}}{A_{2s, 1s}} \delta_{0l} \right], \quad \dots\dots (68)$$

$$Q_0(1s \rightarrow 2p_0) = \frac{\pi}{k^2} (A_{2p, 1s})^2 \left[1 + A_1 - A_2 + \frac{A_{2p, 2s} A_{2s, 1s}}{A_{2p, 1s}} - B \right], \quad \dots\dots (69)$$

$$Q_l(1s \rightarrow 2p_0) = 0 \quad (l \neq 0), \quad \dots\dots (70)$$

$$Q_0(1s \rightarrow 2p_{\pm 1}) = 0, \quad \dots\dots (71)$$

$$Q_l(1s \rightarrow 2p_{\pm 1}) = \frac{\pi}{k^2} (A_{2p, 1s})^2 \frac{2l+1}{2l(l+1)} \times \left[1 + \frac{A_2 - A_1}{l(l+1)} - \frac{A_{2p, 2s} A_{2s, 1s}}{A_{2p, 1s}} \frac{1}{l(l+1)} + \frac{1 - 4\delta_{ll}}{l(l+1)} B \right] \quad (l \neq 0). \quad \dots\dots (72)$$

The quantities involving the coefficient B in expressions (69) and (72) arise from two sources. The $(2B/r^2)P_2(\cos\theta)$ term of $U_{2p_0, 2p_0}(\mathbf{r})$ introduces the quantity $-\frac{1}{3}B$ while the coupling to the $2p_{+1}$ and $2p_{-1}$ states introduces $-\frac{2}{3}B$. Together they give rise to the quantity $-B$ within the square brackets of expression (69) thus resulting in a contribution to the partial cross section for the $1s \rightarrow 2p_0$ excitation having the same sign as that due to the $-A_2/r^2$ term of $U_{2p_0, 2p_0}(\mathbf{r})$.

In the case of the $1s \rightarrow 2p_{\pm 1}$ excitation the $-(B/r^2)P_2(\cos\theta)$ term of $U_{2p_{\pm 1}, 2p_{\pm 1}}(\mathbf{r})$ introduces within the square brackets of expression (72) the quantities $-B/6$, $-B/30$ and $B/l(l+1)$ for $l=1, 2$ and $l \geq 3$ respectively, while the coupling to the $2p_0$ and $2p_{\mp 1}$ states introduces $-4B/3$, $B/5$ and 0 for $l=1, 2$ and $l \geq 3$ respectively. Together they give rise to $B(1-4\delta_{ll})/l(l+1)$ which, for $l > 1$, has the same sign as the contribution from the $-A_2/r^2$ term of $U_{2p_{\pm 1}, 2p_{\pm 1}}(\mathbf{r})$.

§ 4. DISCUSSION

In the special case of exact resonance for which $k_1 = k_2 = k$, $U_{11} = U_{22}$ and $U_{12} = U_{21}$, the pair of equations (4) and (5) can be rewritten in the uncoupled form (Massey 1956)

$$[\nabla^2 + k^2 - (U_{11} \pm U_{12})]F^{\pm}(\mathbf{r}) = 0 \quad \dots\dots (73)$$

where

$$F^{\pm}(\mathbf{r}) = F_1(\mathbf{r}) \pm F_2(\mathbf{r}). \quad \dots\dots (74)$$

Putting

$$U_{11} = -\frac{A}{r^2} \quad \dots\dots (75) \quad \text{and} \quad U_{12} = \frac{A_{12}}{r^2} \quad \dots\dots (76)$$

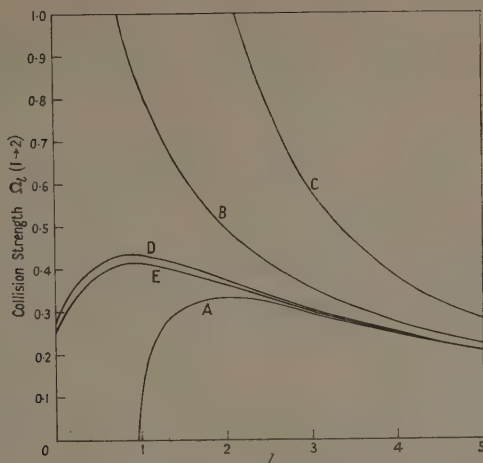
it can be readily shown, using the method of § 3.1, that

$$Q_l(1 \rightarrow 2) = \frac{\pi}{k^2} (2l+1) \sin^2(\eta_l^+ - \eta_l^-) \quad \dots\dots (77)$$

where

$$\eta_l^{\pm} = \frac{1}{4}\pi(2l+1) \left[1 - \left\{ 1 - \frac{4(A \pm A_{12})}{(2l+1)^2} \right\}^{1/2} \right]. \quad \dots\dots (78)$$

In order to assess the accuracy of the various approximations to the partial cross section we assign numerical values to A and A_{12} . A suitable choice of values is $A = -2$ and $A_{12} = -\frac{1}{2}$ which corresponds to the scattering of positively charged particles. In the Figure a comparison is made between the exact values of the collision strength $\Omega_l = (k^2/\pi)Q_l$ and the values of Ω_l obtained with the first and second Born approximations, the third-order approximation and the distorted waves approximation. Very good agreement is obtained between the distorted



Collision strength Ω_l ($l=2$). A, third-order approximation; B, first Born approximation; C, second Born approximation; D, distorted waves approximation; E, exact calculation.

waves approximation and the exact calculations for all l since $A_{12} = -\frac{1}{2}$ gives rise to weak coupling. The first Born approximation is decidedly inferior to the third-order approximation for $l \geq 2$ while for $l=0, 1$ both approximations are unsatisfactory since $A/(2l+1)^2$ is not sufficiently small for $A=2$ and $l \leq 1$. The second Born approximation is unsatisfactory for all l as was predicted in § 2.

In the absence of exact resonance it is no longer possible to obtain an exact analytical expression for the partial cross section. However, the type of effect to be expected from distortion and polarization can still be determined by examining the third-order approximation expressions (67) to (72) for the partial cross sections.

If we again consider the case of the scattering of positively charged particles all the coefficients A and B will be negative in sign. Then it can be readily verified from expression (67) that the effect of distortion on the elastic scattering partial cross section is to reduce it below that given by the first Born approximation. This is in accord with the calculations of Kingston and Skinner (1961) on the elastic scattering of positrons by hydrogen atoms. Referring to the asymptotic expressions (34) we see that the range of the actual potential $U_{1s, 1s}$ is less than that of the actual potentials $U_{2s, 2s}$, $U_{2p_0, 2p_0}$ and $U_{2p_{\pm 1}, 2p_{\pm 1}}$. Hence in the case of excitation we are justified in omitting the effect of the distortion due to the $1s$ state by putting $A_1=0$. It follows from (68) that the effect of distortion on the $1s$ - $2s$ excitation partial cross section is to reduce it below the value given by the first Born approximation in agreement with the calculations of Smith (1960) and of Kingston, Moiseiwitsch and Skinner (1960).

To the third-order approximation all the partial cross sections for the $1s$ - $2p_0$ excitation of the schematic model atom vanish except for the zero-order partial wave. From (69) it can be seen that the effect of distortion on $Q_0(1s \rightarrow 2p_0)$ is to increase it above the first Born approximation. Bates (1961) finds that all the partial cross sections for the proton impact $1s$ - $2p_0$ excitation of atomic

hydrogen are non-vanishing but there exists agreement between his calculations and those based on the schematic model in so far as he obtains an increase in the $1s \rightarrow 2p_0$ excitation cross section at high energies. Referring to (72) we see that distortion decreases the partial cross sections for the $1s \rightarrow 2p_{\pm 1}$ excitation below the first Born approximation for $l \geq 3$. For $l \leq 2$ the effect of the $-A_2/r^2$ term of $U_{2p_{\pm 1}, 2p_{\pm 1}}$ is opposite in sign to that arising from the $-(B/r^2)P_2(\cos \theta)$ term. Bates (1961) obtains a decrease in the total cross section for the proton impact $1s \rightarrow 2p_{\pm 1}$ excitation of atomic hydrogen and since large values of l provide the dominant contribution to the total cross section this is in accord with the schematic model result. In addition Bates finds that $Q_l(1s \rightarrow 2p_{\pm 1})$ vanishes for $l=0$, passes through a maximum and then decreases with increasing l . This is in qualitative agreement with the behaviour of $Q_l(1s \rightarrow 2p_{\pm 1})$ which was found using the schematic model (cf. § 3.1).

The polarization arising from coupling to the $2s$ state results in a decrease in the elastic scattering partial cross section below the first Born approximation in agreement with the calculations of Kingston and Skinner (1961). From (69) and (72) we see, also, that $Q_0(1s \rightarrow 2p_0)$ is decreased and $Q_l(1s \rightarrow 2p_{\pm 1})$ is increased by the coupling to the $2s$ state.

Only the zero-order partial cross sections for elastic scattering, the $1s \rightarrow 2s$ excitation and the $1s \rightarrow 2p_0$ excitation, and the $l=1, 2$ partial cross sections for the $1s \rightarrow 2p_{\pm 1}$ excitation are affected by coupling to the $2p$ states. From expressions (67) to (72) we see that $Q_0(1s \rightarrow 1s)$, $Q_0(1s \rightarrow 2s)$ and $Q_2(1s \rightarrow 2p_{\pm 1})$ are decreased below the first Born approximation and $Q_0(1s \rightarrow 2p_0)$ and $Q_1(1s \rightarrow 2p_{\pm 1})$ are increased above the first Born approximation by the polarization due to the $2p$ states. However, since the partial cross sections for large values of l determine the behaviour of the total cross section it is unlikely that these trends will be reflected in the total cross sections. Thus, although Kingston and Skinner (1961) find that coupling to the $2p$ states decreases the total cross section for the elastic scattering of positrons by hydrogen atoms, Kingston, Moiseiwitsch and Skinner (1960) obtain an increase in the total cross section for the $1s \rightarrow 2s$ excitation of hydrogen atoms by proton impact.

ACKNOWLEDGMENTS

It is a pleasure to acknowledge the hospitality of Professor W. A. Rense of the University of Colorado where the work reported in this article was largely carried out.

It was supported by the National Science Foundation of the U.S.A. under Contract NSF-Y/22.8/329 IGY.

REFERENCES

- BATES, D. R., 1959, *Proc. Phys. Soc.*, **73**, 227.
 — 1961, *Proc. Phys. Soc.*, **77**, 59.
 KINGSTON, A. E., MOISEWITSCH, B. L., and SKINNER, B. G., 1960, *Proc. Roy. Soc. A*, **258**, 237, 245.
 KINGSTON, A. E., and SKINNER, B. G., 1961, *Proc. Phys. Soc.*, **77**, 724.
 MASSEY, H. S. W., 1956, *Handb. d. Phys.*, **36** (Berlin: Springer), p. 11.
 MOTT, N. F., and MASSEY, H. S. W., 1949, *Theory of Atomic Collisions*, 2nd edn (Oxford: Clarendon Press).
 SEATON, M. J., 1955, *Proc. Phys. Soc. A*, **68**, 457.
 SMITH, K., 1960, *Phys. Rev.*, **120**, 845.
 WATSON, G. N., 1944, *Theory of Bessel Functions*, 2nd edn (Cambridge: University Press).

Coherent and Incoherent Scattering of X-rays by H_2 and He

By G. E. KILBY

Department of Physics, The University, Sheffield

Communicated by N. H. March; MS. received 13th April 1961

Abstract. An electron density map calculated by Rollett from an accurate function of James and Coolidge has been used to obtain the coherent x-ray scattering from molecular hydrogen. The results given by the Coulson self-consistent field function are also presented, and it is shown that there is excellent agreement with the James-Coolidge results and with earlier calculations of Carter, March and Vincent.

In addition a more careful study of the incoherent scattering has been made than has previously been attempted. By considering two correlated wave functions, that of Eckart and Hylleraas for helium and that of Gurnee and Magee for hydrogen, previous approximations are shown to lead to somewhat high estimates of the total scattered intensity. For hydrogen, a maximum reduction of about 4% brings theoretical results to within 1% of the experimental values of Wollan.

The momentum distribution and the corresponding shapes of the Compton lines have also been considered for hydrogen and helium. It is suggested from the results obtained for molecular hydrogen that more accurate measurements of the Compton profile might afford a useful method of studying bonding electrons.

§ 1. INTRODUCTION

RECENTLY a theoretical study of the x-ray scattering to be expected from molecular hydrogen was carried out by Carter, March and Vincent (1958, to be referred to as CMV). These workers used a number of approximate wave functions, the most accurate of which was that due to Gurnee and Magee (1950, see also Hurley 1954), which leads to a binding energy of 4.2 ev. However, more recently the electron density in H_2 has been computed by Dr. J. S. Rollett (private communication) using the very accurate 5-term wave function (binding energy 4.5 ev) due to James and Coolidge (1933). In view of this, and with access to an electronic computer, it now proves possible to examine how the approximations made by CMV affect the charge distribution and the coherent x-ray scattering. As the calculation of the incoherent scattering requires the full wave function, not only the electron density, it becomes impractical to use the James and Coolidge function to determine this incoherent component. However by use of the Gurnee and Magee function and appeal to the simpler two-electron problem, the helium atom, two checks are afforded of the approximations used by CMV in their calculation of the incoherent scattering.

In addition to information on the electron density in direct space, we also felt it of interest to consider the momentum distribution in H_2 and the corresponding shape of the Compton line in x-ray scattering. Again a comparison with the He results proves somewhat illuminating.

§ 2. CHARGE DISTRIBUTIONS AND X-RAY SCATTERING

The expressions of Waller and Hartree (1929) for the total and coherent intensities may be written for gaseous hydrogen and helium,

$$\frac{I_T}{I_e} = 2 + 2 \iint |\psi(\mathbf{r}_1, \mathbf{r}_2)|^2 \frac{\sin \kappa r_{12}}{\kappa r_{12}} d\tau_1 d\tau_2 \quad \dots\dots (1)$$

$$\frac{I_{coh}}{I_e} = f^2(\kappa) = 4 \iint \rho(\mathbf{r}_1) \rho(\mathbf{r}_2) \frac{\sin \kappa r_{12}}{\kappa r_{12}} d\tau_1 d\tau_2 \quad \dots\dots (2)$$

where I_e is the Thomson scattering intensity for a single electron, $\psi(\mathbf{r}_1, \mathbf{r}_2)$ is the spatial part of the wave function and $\rho(\mathbf{r})$ the electron density, both normalized to unity and $\kappa = 4\pi(r_{12}/\lambda) \sin \frac{1}{2}\theta$ where θ is the angle of scattering.

The expected form of $f^2(\kappa)$ for H_2 has been calculated using electron densities derived from the James and Coolidge wave functions and also from the self-consistent field wave function of Coulson (1938, binding energy 3.6 eV). Since $\rho(\mathbf{r})$ is not spherically symmetric Eqn (2) was evaluated by the method developed by Banyard and March (1957) in which the electron density is first expanded in spherical harmonics. CMV showed that the s term alone largely determines the coherent scattering of H_2 over the range in which this is a significant part of the

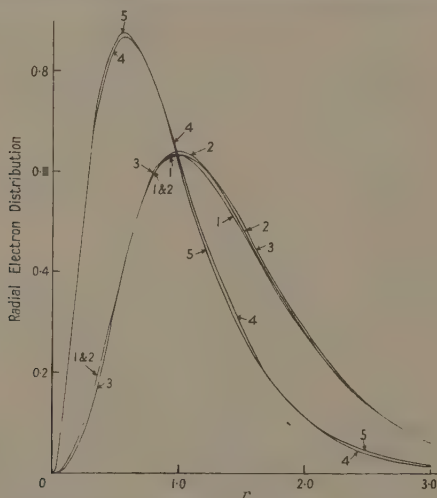


Fig. 1. Radial electron distributions for helium and the hydrogen molecule (atomic units used). Hydrogen: 1, from Rollett's map of the James-Coolidge electron density; 2, from Coulson's self-consistent field function; 3, from the Gurnee and Magee function. Helium: 4, from the self-consistent field function; 5, from the Eckart-Hylleraas function.

total scattered radiation. The radial electron distributions† from the James and Coolidge electron density, the self-consistent field and the Gurnee and Magee functions are shown in Fig. 1. It is seen that to graphical accuracy the first two curves are almost identical. The two $f^2(\kappa)$ curves corresponding to these functions are also almost identical, even when the d terms in the expansion of

† The definition of radial electron distributions adopted here is $r^2 \int \int \rho(\mathbf{r}) \sin \theta d\theta d\phi$.

$\phi(\mathbf{r})$ are also included in the calculation. Whilst these two d terms differ to a greater extent than the corresponding s terms they are still very similar and also in good agreement with those obtained earlier by CMV for the Gurnee and Magee and the LCAO molecular orbital wave functions†. The d terms in fact make only a very small contribution to the scattering factor curves.

The two sets of results for $f^2(\kappa)/4$ agree to within ± 2 in the third decimal place and lie on or between the curves obtained by CMV from the Gurnee and Magee and the LCAO molecular orbital functions. Since the James and Coolidge density is expected to give almost the exact form of $f^2(\kappa)$ these results show that the calculation of $f^2(\kappa)$ by CMV is essentially correct. It follows that the discrepancy (about 5% around $\kappa = 1.6$ A.U. between the results of CMV and the experimental results of Wollan (1931) for the total scattering is not due to the calculation of the coherent component.

Apart from the use of approximate wave functions CMV made a further approximation in their calculation of I_T , namely the one involved in the use of the formula (see, for example, Herzog 1931),

$$I_{\text{inc}}/I_e = 2 - \frac{1}{2}f^2(\kappa) \quad \dots\dots (3)$$

for the calculation of the incoherent intensity. Only if the exact wave function for hydrogen had the form $\phi(\mathbf{r}_1)\phi(\mathbf{r}_2)$ would the difference between Eqns (1) and (2) reduce to the expression (3). Of course the self-consistent field, the LCAO molecular orbital and the 'best' spherical molecular orbital wave functions have this simple form and if they are used in the calculation of I_T then Eqn (3) follows. Although CMV used the correlated wave function of Gurnee and Magee they also assumed the validity of Eqn (3).

It was decided to test Eqn (3) by comparing results from this expression with the difference between Eqns (1) and (2) for some correlated wave functions. Inspection of (1) shows that the full wave function is required in the determination of I_T/I_e ; on grounds of practical difficulty this ruled out the use of the James and Coolidge wave function.

In the light of this difficulty a test of Eqn (3) has been made for hydrogen using the Gurnee and Magee function. Also, in order not to generalize from one instance, a similar test has been made in the case of helium using the correlated wave function of Eckart (1930) and Hylleraas (1929). In both cases I_T has been obtained directly from (1) and also from (2) in conjunction with (3)†.

The Eckart-Hylleraas function is

$$\psi(\mathbf{r}_1, \mathbf{r}_2) = N \{ \exp(-ar_1) \exp(-br_2) + \exp(-br_1) \exp(-ar_2) \}$$

where N is a normalizing constant, $a = 2.1832$, $b = 1.1886$, these values being those obtained by Shull and Löwdin (1956). In this case,

$$\frac{I_T}{I_e} = \frac{4}{\frac{1}{64}a^{-3}b^{-3} + (a+b)^{-6}} \left[\frac{4ab}{(4a^2 + \kappa^2)^2(4b^2 + \kappa^2)^2} + \frac{(a+b)^2}{\{(a+b)^2 + \kappa^2\}^4} \right] \quad \dots\dots (4)$$

$$\frac{I_{\text{coh}}}{I_e} = \frac{4}{[\frac{1}{64}a^{-3}b^{-3} + (a+b)^{-6}]^2} \left[\frac{a}{8b^3(4a^2 + \kappa^2)^2} + \frac{b}{8a^3(4b^2 + \kappa^2)^2} + \frac{1}{(a+b)^2[(a+b)^2 + \kappa^2]^2} \right]^2 \quad \dots\dots (5)$$

† The ordinates of Fig. 3 of CMV have been incorrectly labelled. They should be divided by 4π .

‡ The usual relativistic correction (see, for example, Pirenne 1946, p. 34) corresponding to a value of λ of 1.34 A.U. has been applied to all curves shown in Fig. 2.

The expression (5) agrees with the result of Hurst, Miller and Matsen (1958), but to our knowledge (4) has not previously been recorded.

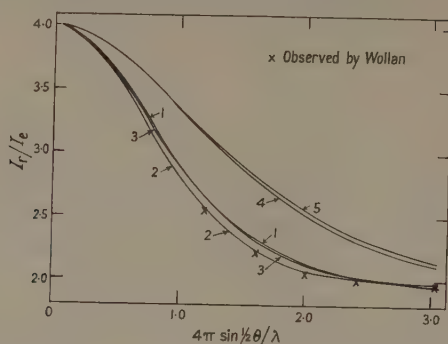


Fig. 2. Total intensities for x-ray scattering by helium and the hydrogen molecule (atomic units used). Hydrogen: 1, calculated from the Gurnee and Magee electron density using expression (3); 2, calculated from the Gurnee and Magee wave function using expression (1); 3, calculated from the self-consistent field function and the James-Coolidge electron densities using expression (3). Helium: 4, calculated from the Eckart-Hylleraas wave function using expression (1); 5, from the Eckart-Hylleraas electron density using expression (3).

In the two instances (see Fig. 2) the values of I_T from Eqn (1) are lower than those obtained by use of the approximate expression (3). Comparison of the two sets of results for helium shows them to agree to within 1.5%. The use of the approximate expression leads to a slightly too high value for all κ , with the maximum discrepancy occurring at $\kappa = 2.4$ A.U. but the two agree for high and low κ . In the case of H_2 the use of (1) leads to values of I_T which are, in the region around $\kappa = 1.7$ A.U., some 3 to 4% lower than the results obtained by CMV. In fact, using the Gurnee and Magee function and making no further approximation almost resolves the discrepancy between theory and experiment noted by CMV. Whilst, in view of the approximate nature of the Gurnee and Magee function, some slight reservation must still be made it seems from the present results for He and H_2 that the use of correlated wave functions in (1) will lead to values of I_T somewhat lower than those obtained from uncorrelated functions. In particular the eventual use of the James-Coolidge wave function is very likely to remove the discrepancies which have previously existed between the experimental results of Wollan and the theoretical scattering curves.

§ 3. MOMENTUM DISTRIBUTION AND COMPTON PROFILE

The momentum distribution function $I(p)$ is defined such that $I(p)dp$ is the probability of finding an electron with momentum magnitude between p and $p+dp$. It is determined by a knowledge of the first order, spinless density matrix in direct space:

$$I(p) = \frac{p^2}{2\pi^2} \iint G(\mathbf{r}, \mathbf{r}') \frac{\sin p|\mathbf{r} - \mathbf{r}'|}{p|\mathbf{r} - \mathbf{r}'|} d\tau d\tau' \quad \dots\dots (6)$$

where

$$G(\mathbf{r}, \mathbf{r}') = \int \psi^*(\mathbf{r}_1 \sigma_1, \dots, \mathbf{r}_n \sigma_n) \psi(\mathbf{r}_1' \sigma_1, \dots, \mathbf{r}_n \sigma_n) d\sigma_1 d\sigma_2 \dots d\sigma_n; \dots\dots (7)$$

σ represents the spin coordinate and \mathbf{x} a space and spin coordinate. If ψ is normalized to unity so is $I(p)$.

It becomes practical to evaluate the integrals involved in (6) if $G(\mathbf{r}, \mathbf{r}')$ is a product or a sum of products of the form $\phi(\mathbf{r})\phi(\mathbf{r}')$, in which case the method of Banyard and March (1957) may be used. The necessary integrals have been evaluated for H_2 using the self-consistent field function to give an approximation

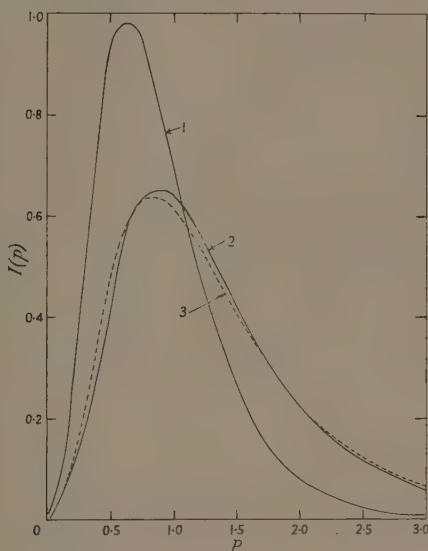


Fig. 3. Momentum distribution functions for helium and the hydrogen molecule (atomic units used). Hydrogen: 1, from Coulson's self-consistent field wave function. Helium: 2, from the self-consistent field wave function; 3, from the Eckart-Hylleraas wave function.

to $G(\mathbf{r}, \mathbf{r}')$ (see Fig. 3). The corresponding calculation using the James and Coolidge function is too lengthy to have been undertaken. For helium similar calculations have been completed, based on the self-consistent field function of Wilson and Lindsay (1935) and the Eckart-Hylleraas function (see Fig. 2). Use of the latter function leads to an analytic expression for $I(p)$:

$$I(p) = \frac{p^2}{4\pi \left[\frac{1}{64} a^{-3} b^{-3} + (a+b)^{-6} \right]} \left\{ \frac{a^2}{b^3(a^2+p^2)^4} + \frac{16ab}{(a+b)^3(a^2+p^2)^2(b^2+p^2)^2} + \frac{b^2}{a^3(b^2+p^2)^4} \right\}.$$

These momentum distribution functions may be used to determine the shape of the Compton profiles to be expected in the incoherent x-ray scattering by gaseous hydrogen and helium (see, for example, Dumond 1933). The shape of this profile is most conveniently expressed in terms of the function $J(q)$ (Duncanson and Coulson 1945) which is independent of the scattering angle and wavelength.

For a system of randomly oriented scatterers

$$J(q) = \int_a^\infty \frac{I(p)}{p} dp. \quad \dots (8)$$

The line shapes corresponding to the $I(p)$ functions discussed above are shown in Fig. 4. Again the Eckart-Hylleraas function leads to an analytic expression,

$$2J(q) = \frac{1}{4\pi \left[\frac{1}{64} a^{-3} b^{-3} + (a+b)^{-6} \right]} \left\{ \frac{a^2}{3b^3(a^2+q^2)^3} + \frac{b^2}{3a^3(b^2+q^2)^3} + \frac{16ab}{(a+b)^3} \left[\frac{a^2+b^2+q^2}{(a^2+q^2)(b^2+q^2)(a^2-b^2)^2} + \frac{2}{(a^2-b^2)^3} \ln \frac{b^2+q^2}{a^2+q^2} \right] \right\}.$$

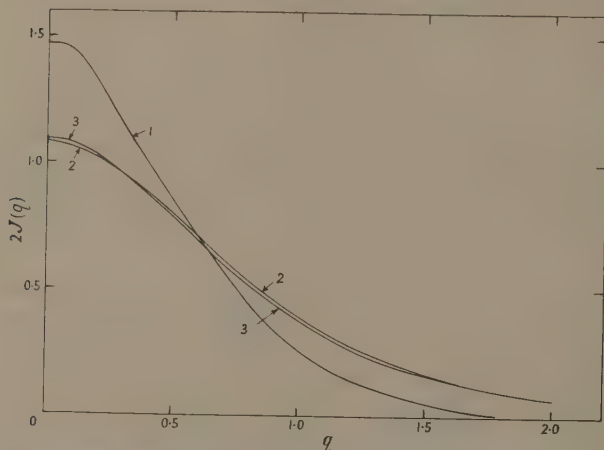


Fig. 4. Compton half-profiles for helium and the hydrogen molecule (atomic units used). Hydrogen: 1, from Coulson's self-consistent field wave function. Helium: 2, from the self-consistent field wave function; 3, from the Eckart-Hylleraas wave function.

Although the two $I(p)$ curves obtained for He differ appreciably in comparison with the differences in the corresponding electron densities, the two $J(q)$ curves do not differ to an extent which would be experimentally significant. The half-widths of the $J(q)$ curves† corresponding to the Eckart-Hylleraas and self-consistent field functions are 1.52 A.U. and 1.58 A.U. respectively. These results agree with the experimental ones of Dumond and Kirkpatrick (1937, half-width 1.5 A.U.). They also agree with the calculated results of Hicks (1937) who obtained a half-width of 1.50 A.U. and also found that his better wave functions gave smaller half-widths.

The half-width obtained here for hydrogen is 1.09 A.U. This is to be compared with the experimental value of Hughes and Starr (1938) of 1.3 A.U. obtained by electron scattering, the theoretical results of Hicks (1937) of 1.17 A.U. and the half-width for atomic hydrogen 1.02 A.U. Here, in contrast to the above result, the better function of Hicks (binding energy 4 eV) leads to a broader Compton profile than the self-consistent field function (binding energy 3.6 eV).

† In the approximation used here the Compton profile is symmetric about $q=0$, for this reason only half-profiles are shown in Fig. 4.

This difference between atomic and molecular wave functions may be observed in other calculations. Duncanson and Coulson (1945) calculated the half-width of the $J(q)$ curves for atomic helium and neon; in both cases these are greater than the experimental values (see Duncanson and Coulson 1945). Yet it seems to be generally true that experimental half-widths, where they exist, for solids and molecules are significantly greater than calculated values. As the $J(q)$ curve weights the low momentum part of $I(p)$, a $J(q)$ curve which is too narrow indicates the use of a wave function which over-estimates the probability of finding an electron with small momentum.

§ 4. CONCLUSION

The calculation, based on the James and Coolidge density map of Rollett, of the coherent x-ray scattering for hydrogen and its comparison with similar calculations based on other functions shows that the effect of correlations on this scattering is small. From this it follows that if the use of Eqn (3) is allowed in the evaluation of the incoherent component then this also must be equally insensitive to correlation. However, use of two correlated functions, the Eckart-Hylleraas function for helium and the Gurnee and Magee function for hydrogen, in Eqn (1) shows that expression (3) leads to an over-estimate of the total intensity in these cases by up to 1.5 and 4% respectively. It thus seems quite possible that the use of the James and Coolidge function in (1) to determine I_T would resolve the discrepancy hitherto thought to exist between theory and Wollan's experimental scattering curve.

To provide additional information on the influence of electronic correlation, results for densities in momentum space have been considered for helium and hydrogen. There is some indication that correlations show up rather more here than in direct space; in the case of helium the effects on x-ray scattering are quite small but for H_2 the influence seems rather more marked. Comparison of the half-width of the Compton profile of H_2 obtained here from the self-consistent field function with that of Hicks and the experimental result of Hughes and Starr suggests that correlation effects may lead to a profile some 10 per cent greater than ours.

It was pointed out at the end of §3 that the shape of the central part of the Compton profile, in particular how rapidly it falls off, is fairly sensitive to the low momentum region of the $I(p)$ curve. This suggests that an accurate measurement of the Compton profile might be a useful method of studying bonding electrons.

ACKNOWLEDGMENTS

I am greatly indebted to my supervisor, Dr. N. H. March, for suggesting the work and for his unfailing help and encouragement. I would also like to thank Dr. J. S. Rollett for supplying his unpublished electron density map of the hydrogen molecule. Thanks are due to Mr. P. H. Blundell for allowing the use of the Ferranti PEGASUS computer which is available to the University Computation Laboratory. I also wish to acknowledge that Dr. A. M. Murray made available some computer programmes, and that Miss M. Barlow helped in the preparation of the manuscript. The work was carried out during the tenure of a Research Studentship from the Department of Scientific and Industrial Research.

REFERENCES

- BANYARD, K. E., and MARCH, N. H., 1957, *J. Chem. Phys.*, **26**, 1416.
CARTER, C., MARCH, N. H., and VINCENT, D., 1958, *Proc. Phys. Soc.*, **71**, 2.
COULSON, C. A., 1938, *Proc. Camb. Phil. Soc.*, **34**, 204.
DUMOND, J. W. M., 1933, *Rev. Mod. Phys.*, **5**, 1.
DUMOND, J. W. M., and KIRKPATRICK, H. A., 1937, *Phys. Rev.*, **52**, 419.
DUNCANSON, W. E., and COULSON, C. A., 1945, *Proc. Phys. Soc.*, **57**, 190.
ECKART, C., 1930, *Phys. Rev.*, **36**, 878.
GURNEE, E. F., and MAGEE, J. L., 1950, *J. Chem. Phys.*, **18**, 142.
HERZOG, G., 1931, *Z. Phys.*, **70**, 590.
HICKS, B., 1937, *Phys. Rev.*, **52**, 437.
HUGHES, A. L., and STARR, M. A., 1938, *Phys. Rev.*, **54**, 189.
HURLEY, A. C., 1954, *Proc. Roy. Soc. A*, **226**, 179.
HURST, A. P., MILLER, J., and MATSEN, F. A., 1958, *Acta Cryst.*, **11**, 320.
HYLLERAAS, E. A., 1929, *Z. Phys.*, **54**, 347.
JAMES, H. M., and COOLIDGE, A. S., 1933, *J. Chem. Phys.*, **1**, 825.
PIRENNE, M. H., 1946, *The Diffraction of X-rays and Electrons by Molecules* (Cambridge: University Press).
SHULL, H., and LÖWDIN, P. O., 1956, *J. Chem. Phys.*, **25**, 1035.
WALLER, I., and HARTREE, D. R., 1929, *Proc. Roy. Soc. A*, **124**, 119.
WILSON, W. S., and LINDSAY, R. B., 1935, *Phys. Rev.*, **47**, 185.
WOLLAN, E. O., 1931, *Phys. Rev.*, **73**, 862.

Gamma Radiation from the Medium Energy Proton Bombardment of Lithium, Beryllium, Boron, Carbon and Nitrogen

By A. B. CLEGG, K. J. FOLEY, G. L. SALMON AND R. E. SEGEL†

Clarendon Laboratory, Oxford

MS. received 15th February 1961

Abstract. Measurements are presented of the gamma radiation produced when lithium, beryllium, boron, carbon and nitrogen are bombarded with 150 mev protons, and the results are discussed with reference to the information they provide about the structure of the nuclei involved. The results include measurements of the residual states produced in $(p, 2p)$ and (p, pn) reactions, which are, to a first approximation, measurements of the parentage of the ground state of the bombarded nucleus. These results are not consistent with a simple jj -coupling model of these nuclei and in one case where calculations are available, are consistent with an intermediate coupling model. It is shown that inelastic scattering cross-sections are determined by the same matrix element as radiative transitions so that inelastic scattering is a powerful tool for picking out strong radiative transitions to nuclear ground states.

§ 1. INTRODUCTION

IN recent years many measurements have been made on the outgoing charged particles from nuclear reactions induced by protons of 100–200 mev. In particular, studies of (p, p') (Strauch and Titus 1956 a, b, Dickson and Salter 1957, Tyrén and Maris 1957 a, b, 1958) and $(p, 2p)$ reactions (Tyrén, Hillman and Maris 1958, Gooding and Pugh 1960) cast much light on nuclear structure problems. In the work described in this paper measurements have been made of the yield of gamma radiation from excited states of residual nuclei produced in the bombardment of p -shell nuclei with 140 mev protons. This work complements the charged particle results by providing what are, in effect, measurements with better energy resolution than is possible by observing charged particles alone. In particular, it is possible to make measurements of the fine structure of the pronounced peaks seen in the excitation spectra of residual nuclei in $(p, 2p)$ reactions (Tyrén, Hillman and Maris 1958, Gooding and Pugh 1960) and in the mirror (p, pn) reactions.

§ 2. EXPERIMENTAL METHODS

A proton beam of energy 153 mev from the Harwell synchrocyclotron is focused by quadrupole magnets on to a target at approximately 17 metres from the cyclotron. The protons travel in vacuum up to a point about 50 cm in

† Now at Aeronautical Research Laboratories, Wright-Patterson Air Force Base, Ohio, U.S.A.

front of the target. A beam intensity (time average) of 1 to 3×10^5 protons/sec has been found adequate for this work (the duty ratio being approximately 2%).

The beam is monitored by a thin ionization chamber placed 50 cm in front of the target; this monitor is calibrated by comparing measurements of the production of ^{11}C (Crandall *et al.* 1956) and the elastic scattering of protons from ^{12}C at forward angles (Dickson and Salter 1957) with the known cross sections; these two normalizations agreed.

The targets were usually about 20 or 40 mev thick and were normally of natural isotopic abundance. We were fortunately also able to borrow targets of separated ^6Li and $^{10}\text{B}^\dagger$. These enabled us not only to make measurements on these isotopes but also to correct the results for natural lithium and natural boron to obtain the cross sections for ^7Li and ^{11}B . For a ^{14}N target liquid nitrogen was contained, for different runs, in a 'Styrofoam' box and in a vacuum-jacketed target. The small concentrations of ^{13}C in carbon and ^{15}N in nitrogen were ignored.

The gamma-ray counter was a thallium-activated sodium iodide crystal, 12.5 cm in diameter and 15 cm long, viewed by an EMI photomultiplier type 9530 run at 900 volts. The pulses produced were transmitted by a cathode follower through fifty yards of cable to the counting room where they were amplified and displayed on a hundred-channel pulse-height analyser, which was gated to count only during the cyclotron beam pulse. With this system there was no evidence for any appreciable gain shift due to counting rate: this was checked both by observing the same gamma ray at different beam intensities, and also by comparing the 4.43 mev gamma ray from the $^{12}\text{C}(\text{p}, \text{p}') \text{ reaction}$ and a much lower counting rate from a polonium-beryllium source. Thus it was possible to use calibration sources (^{22}Na , radiothorium, polonium-beryllium) in between runs to identify the observed gamma rays. In every case the energy corresponding to the experimental peak (determined with an accuracy ranging from $\pm 1\%$ to $\pm 5\%$ depending on how well the peak stands out from the background) agreed with the energy of a gamma ray that would be expected from the reaction under study.

The gamma-ray counter was shielded by 10 cm of lead on all sides except towards the target and there was approximately 4 m of concrete between the counter and the cyclotron. With this shielding, the background with no target was between one-quarter and one-tenth, depending on the pulse height, of the counting rate due to the target; this background was smooth with no indication of any peaks. The spectrum due to a target was made up of peaks due to gamma rays superimposed on a smooth background due presumably to neutrons produced in the target. The yield of a gamma ray was obtained by continuing the smooth background under the peak so that the residual gamma-ray spectrum had the proper shape, as determined by comparison with gamma rays from calibration sources. The counter efficiency was then obtained from calculated tables (Miller, Reynolds and Snow 1958) and the cross section for production of the gamma ray calculated. In the case of the $^{11}\text{B}(\text{p}, \text{p}') \text{ reaction}$ where our cross section can be compared with those obtained by integrating proton angular distributions (adjusted to our energy by assuming the differential cross section to vary as a function of $\theta E^{1/2}$, E being the kinetic energy of the incident proton) the agreement is excellent.

† The ^{10}B was lent by Mr. B. Rose of the Atomic Energy Research Establishment, Harwell, and the sample containing ^6Li was lent by Mr. P. A. White of the Atomic Weapons Research Establishment, Aldermaston.

One has to be careful that the peaks observed are due to gamma rays produced in the target and not due to neutrons interacting in the crystal or in surrounding material. This was checked by inserting lead between the target and the crystal. All peaks at 0.7 mev and above were attenuated suitably and are thus ascribed to gamma rays produced in the target. Below that energy peaks at about 0.45 and 0.63 mev were produced by all targets and were found not to be attenuated by the inserted lead. Thus it is impossible to study gamma radiation of less than 0.7 mev in this work.

§ 3. GAMMA-RAY DATA

A list of gamma rays observed is given in Table 1 with assignments to nuclear transitions and observed cross sections (the information on nuclear energy levels is taken from Ajzenberg-Selove and Lauritsen 1959). Upper limits on the cross section for producing a few gamma rays of particular interest are quoted; these gamma rays were not observed in this work and the upper limit quoted refers to an intensity which would have been evident. Pulse-height spectra corresponding to the gamma rays observed are shown in the figures listed in Table 1. In all cases measurements were made at both 90° and 135° with respect to the proton beam: no evidence was seen for any departure from isotropy of the order of magnitude of the errors quoted on the cross sections. The errors are largely due to the uncertainties in subtracting backgrounds.

In the cases of gamma-ray transitions between states in ^{10}B and ^{14}N both cascades and cross-over transitions are involved. The feeding of states to produce the observed gamma-ray intensities are given in Table 2 for ^{10}B and Table 3 for ^{14}N . For some entries no positive result is recorded: these cross sections were taken to be zero in calculating the remainder.

As will be seen from Figs 5 and 6, the gamma-ray spectra from bombardment of ^{12}C are rather complicated in three energy regions. The energy of the peak at 2 mev is found to be 2.00 ± 0.02 mev. This accuracy was obtained by using the 4.43 mev gamma ray from inelastic scattering on the same run as a calibration; in this way there could be no question of a gain shift between run and calibration. Thus the strongest gamma ray present in the 2 mev region is the transition from the first excited state of ^{11}C at 1.99 mev. However the peak is asymmetric, the asymmetry being consistent with the presence of gamma rays of 2.13 mev from the first excited state of ^{11}B and 2.15 mev from the state of that energy in ^{10}B . Using the spectrum shapes of known gamma rays we find the ratio of intensities of 2.13 plus 2.15 mev to 1.99 mev to be 0.40 ± 0.05 . Taking the cross section for the 2.15 mev gamma ray to be 0.3 ± 0.18 mbn (see Table 2) we find the cross section for production of the first excited state of ^{11}B to be 0.8 ± 0.3 mbn and for production of the first excited state of ^{11}C to be 2.8 ± 0.4 mbn, a ratio of 0.29 ± 0.13 .

The spectrum corresponding to the 4.43 mev gamma ray from inelastic scattering in ^{12}C is very evident in Figs 5 and 6. However there is definite evidence for the presence of higher energy gamma rays around 4.85 mev. That this higher energy tail is not due to pile-up or some similar experimental effect is seen by comparing the ^{12}C spectrum with that due to a 4.43 mev gamma ray produced in the bombardment of ^{14}N shown in Fig. 8, where the high energy side of the 4.43 mev spectrum falls steeply and continuously to the background. These data were taken under the same conditions with the same counting rate. The intensity of the 4.43 mev gamma ray from carbon has been estimated from

Table 1. Gamma Rays Observed, with Assignments and Cross Sections

(1)	(2)	(3)	(4)	(5)	(6)
⁶ Li	149	3.56	⁶ Li 3.56 → 0	0.7 ± 0.3	—
⁷ Li	138	3.56	⁶ Li 3.56 → 0	1.5 ± 0.3	1
⁹ Be	138	0.98	⁸ Li 0.98 → 0	2.4 ± 0.4	—
¹⁰ B	148	0.72	¹⁰ B 0.72 → 0	1.8 ± 0.9	2
	148	1.02	¹⁰ B 1.74 → 0.72	1.0 ± 0.3	2
	148	1.43	¹⁰ B 2.15 → 0.72	0.7 ± 0.3	2
	148	2.15	¹⁰ B 2.15 → 0	1.0 ± 0.4	—
¹¹ B	148	0.72	¹⁰ B 0.72 → 0	12.0 ± 1.6	3
	148	1.02	¹⁰ B 1.74 → 0.72	8.0 ± 1.0	3
	148	1.43	¹⁰ B 2.15 → 0.72	3.5 ± 0.9	3
	148	2.15	¹⁰ B 2.15 → 0	1.8 ± 0.6	—
	148	2.86	¹⁰ B 3.58 → 0.72	< 1.0	—
	148	3.37	¹⁰ Be 3.37 → 0	3.0 ± 0.6	—
	148	4.46	¹¹ B 4.46 → 0	3.8 ± 0.6	—
	148	5.03	¹¹ B 5.03 → 0	< 0.5	—
	148	6.8	¹¹ B 6.76, 6.81 → 0	1.3 ± 0.7	—
¹² C	133	0.72	¹⁰ B 0.72 → 0	4.5 ± 0.5	4
	133	1.02	¹⁰ B 1.74 → 0.72	1.8 ± 0.2	4
	133	1.43	¹⁰ B 2.15 → 1.74	0.6 ± 0.2	4
	143	1.99	¹¹ C 1.99 → 0	3.9 ± 0.4	4, 5
	143	2.86	¹¹ B 2.13 → 0		
			¹⁰ B 3.58 → 0.72	0.9 ± 0.4	5, 6
			¹² C 4.43 → 0	6.6 ± 1.0	5, 6
	143	4.43	¹¹ B 4.46 → 0		
			¹¹ C 4.25 → 0		
			¹² C 4.75 → 0	2.3 ± 1.0	5, 6
	143	4.85	¹¹ B 5.03 → 0		
			¹¹ C 6.50, 6.77 → 0	2.1 ± 0.7	6
	143	6.5 ± 0.3	¹¹ B 6.76, 6.81 → 0		
			¹² C 15.11 → 0	≤ 0.1	—
¹⁴ N	120	0.72	¹⁰ B 0.72 → 0	3.0 ± 0.5	—
	120	1.02	¹⁰ B 1.74 → 0.72	1.0 ± 0.2	7
	120	1.6	¹⁴ N 3.95 → 2.31	0.4 ± 0.1	7
			¹¹ C 1.99 → 0	2 ± 1	7
	120	2.15	¹¹ B 2.13 → 0		
			¹⁰ B 2.15 → 0		
	120	2.31	¹⁴ N 2.31 → 0	0.6 ± 0.2	7
	120	3.09	¹³ C 3.09 → 0	< 0.5	8
	120	3.68	¹³ C 3.68 → 0	≤ 1.6	8
	120	4.43	¹² C 4.43 → 0	20 ± 5	8

(1) Target nucleus; (2) mean proton energy (MeV); (3) gamma-ray energy (MeV); (4) assignment; (5) cross section (mbn); (6) figure number.

the height of the steep fall-off on the high energy side. On then subtracting the spectrum due to this gamma ray the remainder was found to correspond to a gamma ray or gamma rays of about 4.85 MeV; it is ascribed to transitions from the 4.75 MeV state of ¹¹C and the 5.03 MeV state of ¹¹B. The 4.43 MeV spectrum presumably also contains counts due to a 4.25 MeV gamma ray in ¹¹C and a 4.46 MeV gamma ray in ¹¹B; our cross section of 6.6 ± 1.0 mbn for 4.4 MeV gamma rays is higher than those found by integrating angular distributions from the ¹²C(p, p') reaction. Such cross sections, adjusted to our energy, are 5.0 mbn (Dickson and Salter 1957) and 4.8 mbn (Garron *et al.* 1960). Experiments are in progress.

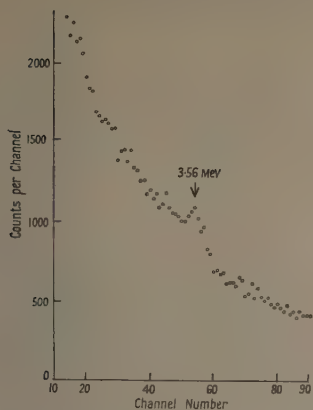


Fig. 1. Pulse-height spectra corresponding to γ -rays of energy 3.56 MeV from proton bombardment of natural lithium.

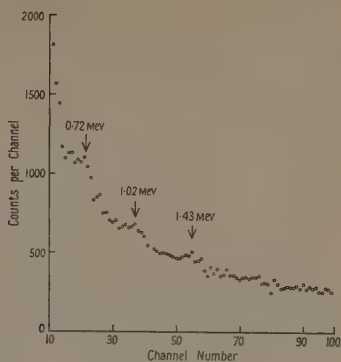


Fig. 2. Pulse-height spectra corresponding to γ -rays of energies 0.72 to 1.43 MeV from proton bombardment of ^{10}B .

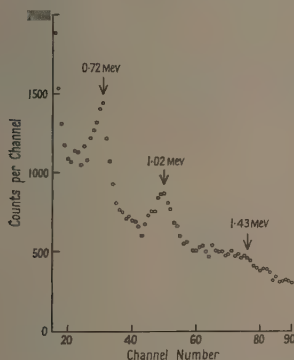


Fig. 3. Pulse-height spectra corresponding to γ -rays of energies 0.72 to 1.43 MeV from proton bombardment of natural boron.

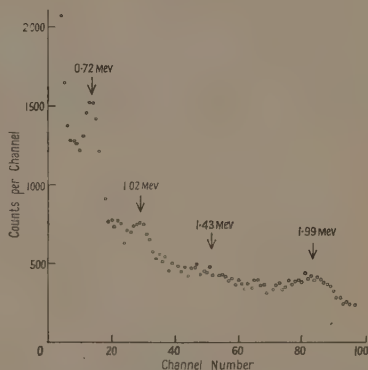


Fig. 4. Pulse-height spectra corresponding to γ -rays of energies 0.72 to 2.13 MeV from proton bombardment of natural carbon.

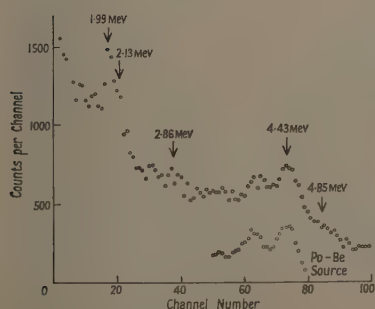


Fig. 5. Pulse-height spectra corresponding to γ -rays of energies 1.99 to 5.03 MeV from proton bombardment of natural carbon.

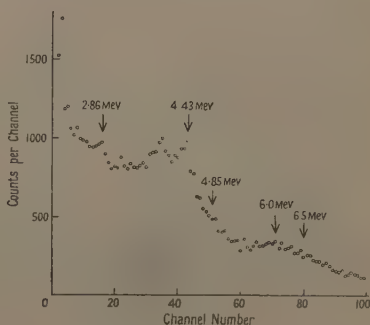


Fig. 6. Pulse-height spectra corresponding to γ -rays of energies 2.86 to 6.8 MeV from proton bombardment of natural carbon.

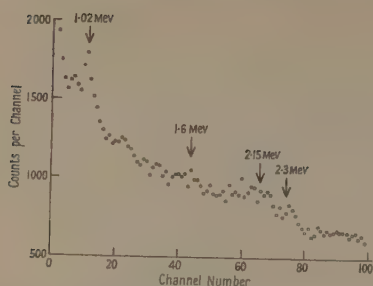


Fig. 7. Pulse-height spectra corresponding to γ -rays of energies 1.02 to 2.31 mev from proton bombardment of natural nitrogen.

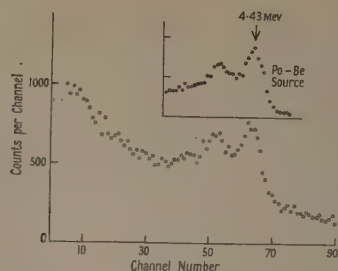


Fig. 8. Pulse-height spectra corresponding to γ -rays of energies 3.09 to 4.43 mev from proton bombardment of natural nitrogen.

to measure the individual yields of these gamma rays by observing coincidences between low energy protons and gamma rays produced in both proton and neutron bombardment of carbon. The broad peak at 6.5 mev is presumably due to transitions from states of ^{11}C at 6.50 and 6.77 mev and from states of ^{11}B at 6.76 and 6.81 mev. There may be a small contribution from ^{16}O impurity in the target, as this produces a spectrum peaked at about 6.1 mev with a cross section of about 30 mbn, due to the (p, pn) and (p, 2p) reactions (A. B. Clegg, P. S. Fisher, K. J. Foley, D. J. Rowe and G. L. Salmon 1960, unpublished work); however

Table 2. Cross Sections (mbn) for Feeding States in ^{10}B in Various Reactions

State in ^{10}B (mev)	$^{10}\text{B} + \text{p}$	$^{11}\text{B} + \text{p}$	$^{12}\text{C} + \text{p}$	$^{14}\text{N} + \text{p}$
3.58	—	<1.7	1.5 \pm 0.7	—
2.15	2.1 \pm 0.65	7.3 \pm 1.5	1.0 \pm 0.55	—
1.74	0.4 \pm 0.4	5.6 \pm 1.1	1.5 \pm 0.3	1.0 \pm 0.2
0.72	0 \pm 1.1	1.1 \pm 2.0	1.5 \pm 0.55	2.0 \pm 0.55

Table 3. Cross Section for Feeding States in $^{14}\text{N}(\text{p}, \text{p}') \text{ Reaction}$

State (mev)	2.31	3.95
Cross section (mbn)	0.2 \pm 0.22	0.4 \pm 0.1

the bulk of the peak in Fig. 6 is above this energy and is thus due to ^{12}C . Our limit of 0.1 mbn for the production of a 15.1 mev gamma ray is consistent with the result of 0.06 mbn found at this energy by Waddell (1957) but inconsistent with the result of 1.8 mbn of Garron *et al.* (1960).

The inelastic scattering from the 4.46 mev state of ^{11}B has been studied by Tyrén and Maris (1958). Integrating their angular distribution, and adjusting to our energy, we find 3.7 mbn in excellent agreement with our result of 3.8 \pm 0.6 mbn.

An excitation function of the 4.43 mev gamma ray produced in the bombardment of ^{14}N has been measured, the proton energy being degraded by carbon absorbers placed approximately 30 cm in front of the target and well shielded from the gamma-ray counter by lead. The relative cross sections are given in Table 4, accurate to $\pm 10\%$.

Table 4. Relative Cross Sections for Production of 4.43 mev Gamma Ray in $^{14}\text{N} + \text{p}$ Reaction

Mean proton energy (mev)	Relative cross section
85	1.3
105	1.2
125	1.1
145	1.0

§ 4. ACTIVATION DATA

Several activation cross sections have been measured as a complement to the gamma-ray work. The sample was irradiated for one to two half-lives in a known proton beam and then carried to the counting room where the resulting gamma rays (positron annihilation quanta in the cases of ^{11}C and ^{13}N and gamma rays in ^{10}B in the case of ^{10}C) were counted with a thallium-activated sodium iodide crystal for several half-lives.

The samples used were

^{12}C : natural carbon;

^{14}N : both liquid nitrogen and boron nitride (the latter for ^{13}N activation only).

The yields of the individual activities were then found by separating the decay curve by a least squares method into exponentials of known half-lives, using the Ferranti MERCURY computer of the Computer Laboratory, Oxford. The results are shown in Table 5.

Table 5. Results of Activation Measurements

Reaction	$\text{p} + ^{12}\text{C}$	$\text{p} + ^{14}\text{N}$	
Mean proton energy (mev)	143	145	
Activity	^{10}C	^{13}N	^{11}C
Yield (mbn)	2.6 ± 1.3	14 ± 1	7.0 ± 1.5

The only results with which these can be compared are those of Symonds, Warren and Young (1957) who used protons of 420–980 mev. To make a comparison we assume that cross sections for (p, pn) reactions fall off in the same way as in the $^{12}\text{C}(\text{p}, \text{pn})$ reaction: if this assumption is made the agreement between the $^{14}\text{N}(\text{p}, \text{pn})$ result presented here and those of Symonds, Warren and Young is good. Symonds *et al.* find an approximately constant cross section as the proton energy varies for the production of ^{10}C from $^{12}\text{C} + \text{p}$. Our result suggests this constancy extends down to 140 mev. Our cross section for the production of ^{11}C from $^{14}\text{N} + \text{p}$ is apparently about half of what it is at the higher energies.

Symonds, Warren and Young (1957) suggest that the lower cross section for the $^{14}\text{N}(\text{p}, \text{pn})$ reaction compared with that for the $^{12}\text{C}(\text{p}, \text{pn})$ reaction, as measured by activation methods, is because there is only one bound state in ^{13}N while there are approximately eight in ^{11}C . This explanation obviously does not hold at our energy as the gamma-ray data show that most of the production of ^{11}C in the $^{12}\text{C}(\text{p}, \text{pn})$ reaction is direct production of the ground state, so that the cross section for production of the ground state of ^{11}C is approximately 2.5 times that for the production of the ground state of ^{13}N . This difference presumably reflects a difference in the structures of ^{12}C and ^{14}N .

§ 5. DISCUSSION OF KNOCKOUT REACTION RESULTS

On the usual direct interaction model of the reactions $A(p, 2p)$ or $(p, pn) A-1$ we are measuring the parentage of nucleus A (Lane and Wilkinson 1955), when we measure the relative populations of states of nucleus $A-1$ produced in these reactions. In measurements of the energies of the outgoing protons in $(p, 2p)$ reactions in the p -shell it has been found (Tyrén, Hillman and Maris 1958, Gooding and Pugh 1960) that the excitation spectra in nuclei $A-1$ show pronounced peaks implying strong excitation of one or a few states in the residual nuclei. These peaks have been interpreted using a simple jj -coupling shell model, which interpretation would seem to conflict with the intermediate coupling picture which has been based on a wide range of work at lower energies (e.g. Inglis 1953, Kurath 1956, Lane 1953, 1955). In the work described here some details of the excitation spectra have been investigated in somewhat more detail and show lack of support for the jj -coupling interpretation; in the one case where calculations are available there is agreement with the intermediate coupling picture.

One has to be careful in applying the simple knockout model and not use it in cases where multiple collisions are important: for example, they are probably important in determining the polarization of neutrons produced in proton bombardment (Squires 1958a). However the main effect of a second collision would be to evict further nucleons so our observation of bound states in nucleus $A-1$ should select events where only a single collision has taken place; similarly the angular correlations of Gooding and Pugh (1960) should not be perturbed by multiple collisions as they restrict their attention to low excitation in ^{11}B . The main causes of disturbance should be inelastic scattering of the incident nucleon before the knockout collision exciting nucleus A to an excited state and the inelastic scattering of either of the outgoing nucleons after the knockout collision exciting nucleus $A-1$ to a bound excited state. One can argue qualitatively that such processes would only contribute a very small amount to the $(p, 2p)$ and (p, pn) reactions, as typical cross sections for inelastic scattering leaving nuclei in bound excited states are about 6 mbn to be compared with typical total reaction cross sections of about 250 mbn (we ignore elastic scattering as this does not change the ratio of states produced), so we can hope that they will not change our main conclusions. However detailed calculation of these effects would be valuable.

Now let us consider specific reactions, starting with ^{12}C for which most detail is available, both experimental and theoretical. The cross section for producing ^{11}C in its bound states is 44 mbn (Crandall *et al.* 1956) and of this the $^{12}\text{C}(p, d)$ cross section is 4 mbn (Cooper and Wilson 1960) so the $^{12}\text{C}(p, pn)$ cross section is 40 mbn; for both these reactions the ratio of population of states in ^{11}C should be the same. For production of bound excited states we find: 1.99 mev, 3 mbn; 4.8 mev, 2 mbn; 6.5 mev, 2 mbn, leaving 37 mbn for the ground state. This agrees with the $^{12}\text{C}(p, d)$ measurements where only a group to the ground state is seen; weak groups of the relative strength seen here would not have been noticed in the (p, d) measurements. So we find for the ratio of population of first excited state ($J=1/2^-$) to ground state ($J=3/2^-$) in ^{11}C a result 0.08 ± 0.03 . This agrees with neither the result for jj -coupling wave functions of zero nor the LS -coupling result of 0.5. Comparing with unpublished intermediate

coupling calculations by Kurath† we find this result implies an intermediate coupling parameter of $a/K = 6.4 \pm 1.0$ (see Fig. 9), which is consistent with the values ($a/K \approx 5.5$) found in the lower energy work. Our result that most of the $^{12}\text{C}(p, pn)$ reaction feeds the ground state of ^{11}C agrees with the result that the ground state of ^{11}B is the main state fed in the mirror $(p, 2p)$ reaction (Tyrén, Hillman and Maris 1958, Gooding and Pugh 1960).

Gooding and Pugh quote 16 ± 4 mbn for the total cross section for the $^{12}\text{C}(p, 2p)$ reaction leaving ^{11}B in low states. This is in agreement with the $^{12}\text{C}(n, 2n)^{11}\text{C}$ cross sections that have been measured as averages over neutron spectra peaked at various energies in this range (see for example results quoted by Rosenfeld, Swanson and Warshaw 1956). We have measured the ^{11}C production in the $^{12}\text{C}(n, 2n)$ reaction for a neutron spectrum with a peak at 130 mev and a maximum energy of 155 mev. If one assumes the $(n, 2n)$ cross section to vary with energy in the same way as the (p, pn) cross section the results correspond to a $^{12}\text{C}(n, 2n)^{11}\text{C}$ cross section at 143 mev of 17 ± 3 mbn. This agreement with the $(p, 2p)$ result of Gooding and Pugh confirms their assumption that there is no major contribution to the cross section from angular regions they have neglected. This gives a ratio of $\sigma(p, 2p)/[\sigma(p, pn) + \sigma(p, d)] = 0.36 \pm 0.06$ in agreement with our result of 0.29 ± 0.13 for the relative production of the first excited states of ^{11}B and ^{11}C , thus lending support to the model discussed here. Finally we note that the ratio $\sigma(p, 2p)/\sigma(p, pn) = 0.40 \pm 0.06$ to be compared with a ratio of 0.56 for the corresponding free-nucleon cross sections (Hess 1958).

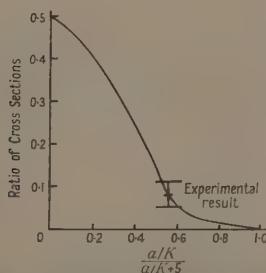


Fig. 9. Ratio of cross sections for producing first excited state and ground state in the $^{12}\text{C}(p, pn)^{11}\text{C}$ reaction as a function of $(a/k)/(a/k+5)$.

One could argue that, as the relative feeding of the excited states is small, the main reaction is a simple feeding of the ground state, as predicted for jj -coupling wave functions, with weak excitation of excited states due to inelastic scattering before and after the knockout collision. In this case, inelastic scattering before knockout would produce the four states of the $p_{3/2}^4 p_{1/2}$ configuration, and on knocking out a $p_{3/2}$ nucleon one gets ten states, so that each of them would be fed by a cross section of only a fraction of a millibarn (an estimate based on typical inelastic scattering cross sections). Inelastic scattering after knock-out should produce the same states as the $^{11}\text{B}(p, p')$ reaction and we see from the measurements presented here that the first excited state is fed weakly, if at all, compared

† We are indebted to Dr. Kurath for his permission to quote his unpublished results.

to the second excited state, in this reaction. Thus it seems unlikely that it would be possible to explain the observed feeding in this way, starting from *jj*-coupling wave functions.

For the ^{11}B ground state in *jj*-coupling there are four parent states. Writing them as (J, T) the relative feeding of these states in ^{10}B is: $(3, 0)$, $7/16$; $(1, 0)$, $3/16$; $(0, 1)$, $1/16$; $(2, 1)$, $5/16$ †. As the 0.72 and the 2.15 mev states have $J = 1$, $T = 0$, while the 1.74 mev state has $J = 0$, $T = 1$, we see that no *jj*-coupling assignment to these states will give agreement with cross sections found in this work. It would be interesting to be able to compare the experimental results with intermediate coupling calculations.

In the other $(p, 2p)$ and (p, pn) reactions observed in this work there are no actual ratios of states to compare with predictions for *jj*-coupling wave functions. It is interesting however to compare the cross sections found with the total cross sections for the *p*-shell estimated from a simple model where the cross section for ejecting a $p_{3/2}$ nucleon is taken to be the number of $p_{3/2}$ neutrons or protons present, multiplied by the corresponding free-nucleon cross section (Hess 1958) and a nuclear absorption factor taken to be $\exp(-kA^{1/3})$. The value of k is found by taking 44 mbn for the cross section for $^{12}\text{C}(p, pn)$ and $^{12}\text{C}(p, d)$ and 16 mbn for the cross section for $^{12}\text{C}(p, 2p)$. (Such a model agrees quite well with the relative cross sections found by Tyrén, Hillman and Maris (1958) if we assume their results to be the same sample of the angular correlations in each case.) For such a model we find:

$^7\text{Li}(p, pn)^6\text{Li}$ $\sigma_{\text{tot}} \sim 28$ mbn,
ratio 3.56 mev state/total; experiment, 0.05; prediction of model†, 0.21

$^9\text{Be}(p, 2p)^8\text{Li}$ $\sigma_{\text{tot}} \sim 9$ mbn,
ratio 0.98 mev state/total; experiment, 0.27; prediction of model†, assuming $J = 1 +$ (which is more likely), 0.10; assuming $J = 3 +$, 0.23

$^{14}\text{N}(p, 2p)^{13}\text{C}$ $\sigma_{\text{tot}} \sim 15$ mbn.

Three states with $J = 1/2^-$, $3/2^-$, $5/2^-$ should be formed with relative intensities 1:2:3. The $J = 3/2^-$ state should thus be formed with a cross section of 5 mbn. One would expect this state to be the $3/2$ state at 3.68 mev for which the cross section is found to be less than or equal to 1.5 mbn.

Thus in all of the three cases there are large discrepancies. Such a simple model cannot be accurate but one would be surprised if there were such large departures from it as would be needed to produce the ratios predicted for *jj*-coupling wave functions. Added to the direct evidence from the $^{12}\text{C}(p, pn)$ and $^{11}\text{B}(p, pn)$ reactions it does not seem that the simple *jj*-coupling interpretation is valid. One can speculate that the very localized excitation found in the residual nuclei in these reactions displays some particular property of the intermediate

† These have been calculated by taking the ground state of ^5Li to be the sole parent of the corresponding states in ^6Li and using the relation between particles and holes given by Lane (1960), his formula (71). A further factor of $1/3$ for the $T = 1$ states comes from the coupling of the isotopic spins.

‡ In calculating the predicted ratios the fractional parentage coefficients of Edmonds and Flowers (1952) were used. In the case of ^9Be the relation between particles and holes (Lane 1960) was also needed.

coupling wave functions. A similar simplicity is seen in the inelastic scattering reactions at these energies as is discussed in § 6 where it is suggested that inelastic scattering picks out certain states with particular properties in intermediate coupling. Perhaps similarly some particular states are picked out in the (p, pn) and (p, 2p) reactions.

The high yield of 4.43 mev gamma rays from the bombardment of nitrogen is probably due to the $^{14}\text{N}(p, pn)$ reaction producing an excited state or states of ^{13}N which decay an appreciable part of the time by emitting a proton and leaving the first excited state of ^{12}C . From the $^{14}\text{N}(p, 2p)$ measurements (Tyrén, Hillman and Maris 1958), it is known that states around 7.5 mev in ^{13}C are produced strongly in this reaction, so presumably mirror states are produced at the same energy in ^{13}N in the $^{14}\text{N}(p, pn)$ reaction. Such states in ^{13}N can decay leaving ^{12}C in either its ground state or first excited state (the states in ^{13}C at this energy can decay only to the ground state of ^{12}C). Thus it is not surprising that these states apparently decay about half the time to leave ^{12}C in its first excited state, thus producing the 4.43 mev gamma ray seen in this work. The alternative is that it is just one of the states that is formed when two nucleons are ejected by the incident proton from ^{14}N ; it would however seem surprising that there would be such a large cross section for producing one particular state in ^{12}C . The difficulty in the former hypothesis is that one would expect negative parity states to be produced in ^{13}C and ^{13}N and there are no recorded states of negative parity at an excitation of about 7.5 mev in these nuclei. However this is also a problem in understanding the results of Tyrén, Hillman and Maris, and we can only conclude that not all the states in this energy range in these nuclei are known. It would be interesting to search for these states; it would seem that the $^{14}\text{N}(p, d)$, ($^3\text{He}, \alpha$) or (t, α) reactions would be suitable if sufficient energy were available.

One can make some remarks about other knockout reactions observed in this work. For reactions where two nucleons are ejected from the target nucleus, for example the production of ^{10}B from ^{12}C , one would expect that one contributing process would be a (p, 2p) or (p, pn) process followed by one of the outgoing nucleons interacting with another nucleon and ejecting it. If this process was the only one responsible for the ejection of two nucleons one would expect that, as the ground states of ^{11}B and ^{11}C are produced approximately 0.81 of the time in the $^{12}\text{C}(p, 2p)$ and $^{12}\text{C}(p, pn)$ reactions, the relative feeding of states of ^{10}B produced in the bombardment of ^{12}C would be much the same as the relative feeding produced in bombardment of ^{11}B . From Table 2 one sees that this is definitely not so, implying that other processes must also contribute, for example the interaction of the incident proton with two-nucleon correlations in the nucleus.

§ 6. DISCUSSION OF INELASTIC SCATTERING REACTIONS

This work also provides some inelastic scattering cross sections which would be hard to measure otherwise. It is easy to show that the matrix elements determining radiative transition rates of electric multipole transitions are approximately the same as the direct interaction inelastic scattering matrix elements for these transitions. For radiative transitions the decay rate is given by

$$T = \frac{8\pi(l+1)}{l[(2l+1)!]} \frac{1}{\hbar} \left(\frac{E_\gamma}{\hbar c} \right)^{2l+1} \frac{|\langle I_f || M(l) || I_i \rangle|^2}{2I_i + 1}$$

while the differential cross section for inelastic scattering for small momentum transfer in the plane-wave approximation is

$$\frac{d\sigma}{d\Omega} = \frac{k_f}{k_i} (|M_0|^2 + \lambda |M_1|^2) \left[\frac{(q)l}{(2l+1)!} \right]^2 (2l+1)^{-1} \frac{|\langle I_f || M(l) || I_i \rangle|^2}{2I_i + 1}$$

where $\langle I_f || M(l) || I_i \rangle$ is the reduced matrix element for the transition from state of spin I_i to state of spin I_f corresponding to the interaction operator

$$M(l, \mu) = \sum_k r_k^l Y_{l\mu}(\theta_k, \phi_k),$$

the summation being over protons for the radiative decay and over all nucleons for the inelastic scattering (one presumes this difference is unimportant in the 1p-shell). M_0 , M_1 are the matrix elements of the nucleon-nucleon interaction corresponding to no-spin-flip and spin-flip respectively and λ is the ratio of the nuclear spin-flip and no-spin flip matrix elements (Kerman, McManus and Thaler 1959). $\mathbf{q} = \mathbf{k}_i - \mathbf{k}_f$ is the momentum transfer in the inelastic scattering.

One can attempt to relate these matrix elements quantitatively, as has been done by Squires (1958b) who showed that the matrix element for exciting the 4.43 mev state of ^{12}C in the $^{12}\text{C}(\text{p}, \text{p}')$ reaction is the same as the radiative matrix element determined by Coulomb excitation (Morpurgo 1956) but to do this the amount of calculation is considerable. Here we attempt a simpler analysis taking ratios of inelastic scattering cross sections to equal the corresponding ratios of radiative decay rates. We can expect this might work if we choose pairs of transitions of the same multipolarity, where the angular distributions are closely similar, and in the same shell, where the change in cross section is going from the plane-wave approximation to the true distorted-wave theory should be much the same. We follow Wilkinson (1956) in quoting $|M|^2$, the ratio of the experimental decay rate to Weisskopf's extreme single particle result. Thus from the known mean life of the 4.43 mev state of ^{12}C , corresponding to $|M|^2 = 1.74$ (all the gamma-ray data used here are taken from Ajzenberg-Selove and Lauritsen (1959) except where other references are given), and the inelastic scattering cross sections for exciting the 4.43 mev state of ^{12}C and the 4.46 mev state of ^{11}B , we find for the electric quadrupole decay of the ^{11}B state: $|M|^2 = 4.5$. To compare with this we find the rate of electric quadrupole decay of this state from the known rate of decay, which is largely magnetic dipole, and the E2/M1 ratio of the order of 0.05 determined from angular distributions in the $^7\text{Li}(\alpha, \gamma)$ reaction (Jones, Johnson and Wilkinson 1959), finding for the electric quadrupole radiative decay of the 4.46 mev state of ^{11}B : $|M|^2 = 6.7$. This agreement is remarkable, particularly when one considers the uncertainty in extracting E2/M1 ratios from angular distributions. A similar comparison of the measured lifetimes of the 4.43 mev state of ^{12}C and the $J=2^+$ state of ^{16}O at 6.92 mev predicts an inelastic scattering cross section of 2.8 ± 0.85 mbn for the latter to be compared with the observed 1.5 mbn (Clegg *et al.* 1960, unpublished). Thus one sees that with this naïve method one can apparently, from inelastic scattering cross sections, determine electric multipole radiative widths of states within an accuracy of a factor or two†. A more refined analysis would be desirable taking into account

† A similar relation between inelastic scattering cross sections and radiative transition rates has been noted in the inelastic scattering of 23 mev protons from medium-weight nuclei (Cohen and Rubin 1958).

the absorption of protons in the inelastic scattering, which must cause the inner parts of the nucleus to be weighted less in the inelastic scattering matrix elements than they are in the radiative matrix elements.

We apply this procedure to the electric quadrupole transition from the 2.15 MeV state of ^{10}B to the ground state comparing its excitation with the 4.43 MeV state of ^{12}C , for which both the inelastic scattering cross section and the radiative lifetime are best determined, finding an estimate for the radiative decay of this state of $|M|^2 = 11$ corresponding to a radiative width of 9.7×10^{-4} ev. From the known branching ratios of transitions from this state one then finds radiative widths for the magnetic dipole transitions to the 0.72 and 1.74 MeV states, giving $|M|^2 = 0.66$ for the transition to the 1.74 MeV state and $|M|^2 = 0.02$ for the transition to the 0.72 MeV state, which are very respectable results for magnetic dipole transitions in the 1p-shell (Wilkinson 1956)†. From the known mean life of the radiative transition from the 0.72 MeV state of ^{10}B we estimate a cross section of 0.3 mbn for the excitation of this state in inelastic scattering which does not disagree with our measurements.

The excitation of the 3.95 MeV state of ^{14}N is due to both the monopole and quadrupole matrix elements. The latter presumably contributes most strongly to the total inelastic scattering cross section, as the former will only contribute to the angular distribution at forward angles. Making this assumption the electric quadrupole radiative width of this state corresponds to $|M|^2 = 0.57$.

One sees that inelastic scattering apparently provides a method for picking out these states which make strong electric multipole radiative transitions to the ground state and one can ask what are the particular properties of the states so selected. It is found that these results fit well with a distorted nucleus model of the 1p-shell where states in the rotational band based on the ground state are strongly excited in inelastic scattering while rotational bands based on excited states are not. This model, which is presumably an approximation to the procedures of Kurath and Pičman (1959) and thus an aspect of the intermediate coupling shell model, is described fully elsewhere (Clegg 1961).

ACKNOWLEDGMENTS

We wish to thank B. Rose and all members of the Atomic Energy Research Establishment cyclotron group for their considerable help to us, which it is impossible to detail, and the Director, Atomic Energy Research Establishment, Harwell, for permission to use the cyclotron. We also wish to thank P. S. Fisher and D. J. Rowe for their help in the latter part of this work. Finally we would like to thank Professor D. H. Wilkinson for his encouragement during this investigation.

REFERENCES

- AJZENBERG-SELOVE, F., and LAURITSEN, T., 1959, *Nucl. Phys.*, **11**, 1.
 CLEGG, A. B., 1961, *Phil. Mag.*, in the press.
 COHEN, B. L., and RUBIN, A. G., 1958, *Phys. Rev.*, **111**, 1568.
 COOPER, P. F., and WILSON, R., 1960, *Nucl. Phys.*, **15**, 373.
 CRANDALL, W. E., MILLBURN, G. P., PYLE, R. V., and BIRNBAUM, W., 1956, *Phys. Rev.*, **101**, 329.

† These results can be compared with $|M|^2 = 1.7$ for the former and $|M|^2 = 0.005$ for the latter calculated for intermediate coupling wave functions by Kurath (1957).

- DICKSON, J. C., and SALTER, D. C., 1957, *Nuovo Cim.*, **6**, 235.
- EDMONDS, A. R., and FLOWERS, B. H., 1952, *Proc. Roy. Soc. A*, **214**, 515.
- GARRON, J. P., JACMART, J. C., MASSONET, L., RIOU, M., and RUHLA, C., 1960, *J. Phys. Radium*, **21**, 317.
- GOODING, T. J., and PUGH, H. G., 1960, *Nucl. Phys.*, **18**, 46.
- HESS, W. M., 1958, *Rev. Mod. Phys.*, **30**, 368.
- INGLIS, D. R., 1953, *Rev. Mod. Phys.*, **25**, 390.
- JONES, G. A., JOHNSON, C. M. P., WILKINSON, D. H., 1959, *Phil. Mag.*, **4**, 796.
- KERMAN, A. K., McMANUS, H., and THALER, R. M., 1959, *Ann. Phys.*, N.Y., **8**, 551.
- KURATH, D., 1956, *Phys. Rev.*, **101**, 216.
- 1957, *Phys. Rev.*, **106**, 975.
- KURATH, D., and PiČMAN, L., 1959, *Nucl. Phys.*, **10**, 313.
- LANE, A. M., 1953, *Proc. Phys. Soc. A*, **66**, 977.
- 1955, *Proc. Phys. Soc. A*, **68**, 197.
- 1960, *Rev. Mod. Phys.*, **32**, 519.
- LANE, A. M., WILKINSON, D. H., 1955, *Phys. Rev.*, **97**, 1191.
- MILLER, W. F., REYNOLDS, J., and SNOW, W. J., 1958, *Argonne National Laboratory Report*, ANL-5902.
- MORPURGO, G., 1956, *Nuovo Cim.*, **3**, 430.
- ROSENFELD, A. H., SWANSON, R. A., and WARSHAW, S. D., 1956, *Phys. Rev.*, **103**, 413.
- SQUIRES, E. J., 1958 a, *Proc. Phys. Soc.*, **72**, 433.
- 1958 b, *Nucl. Phys.*, **6**, 504.
- STRAUCH, K., and TITUS, F., 1956 a, *Phys. Rev.*, **103**, 200.
- 1956 b, *Phys. Rev.*, **104**, 191.
- SYMONDS, J. L., WARREN, J., and YOUNG, J. D., 1957, *Proc. Phys. Soc. A*, **70**, 824.
- TYRÉN, H., HILLMAN, P., and MARIS, TH. A. J., 1958, *Nucl. Phys.*, **7**, 10.
- TYRÉN, H., and MARIS, TH. A. J., 1957 a, *Nucl. Phys.*, **3**, 52.
- 1957 b, *Nucl. Phys.*, **4**, 637.
- 1958, *Nucl. Phys.*, **6**, 82.
- WADDELL, C. N., 1957, *University of California Radiation Laboratory Report*, UCRL-3901.
- WILKINSON, D. H., 1956, *Phil. Mag.*, **1**, 127.

The Importance of Conservation Conditions in Distorted Wave Calculations

BY W. B. SOMERVILLE

Department of Physics, University College, London

Communicated by M. J. Seaton; MS. received 29th May 1961

Abstract. Some recent results of Vainstein, using the distorted wave approximation for the 3s–3p transition in electron–sodium atom collisions are modified on the basis of a method introduced by Seaton in 1961 which ensures that the conservation condition is satisfied. The resulting cross sections lie much closer to those obtained by experiment.

IN a treatment of a collision process based on an analysis of the motion of the incident particle in terms of its partial wave components, the cross sections for the individual partial waves should satisfy the condition for conservation of flux; any formulation which gives large departures from the conservation condition cannot be expected to give reasonable agreement with experimental results. This matter has recently been discussed by Seaton (1961), and reference is made to his paper for fuller details of the analysis.

For the transition in which an atom is excited from state α to state α' , the total cross section is

$$Q(\alpha, \alpha') = \frac{1}{\omega k^2} \sum_{l' L} (2L+1) |T(\alpha l L, \alpha' l' L)|^2, \quad \dots\dots (1)$$

in units of πa_0^2 , where ω is the statistical weight of state α , k is the initial wave number of the colliding particle and l and l' its initial and final angular momentum quantum numbers, respectively, and L is the total angular momentum. T is an element of the transmission matrix \mathbf{T} , and the conservation condition requires that

$$\sum_{\alpha' \neq \alpha} \sum_{l'} |T(\alpha l L, \alpha' l' L)|^2 \leq 1. \quad \dots\dots (2)$$

For the special case of excitation from an S-state, $\omega = 1$ and $L = l$, and the condition on the l th partial cross section becomes

$$\sum_{\alpha' \neq \alpha} \sum_{l'} Q(\alpha l, \alpha' l') \leq \frac{2l+1}{k^2}, \quad \dots\dots (3)$$

summed over all energetically possible excitations.

Percival (1960) and Seaton (1961) have described in detail two approximations which satisfy the conservation condition, based on the use of the reactance matrix \mathbf{R} . If the results of some approximate calculation, 'approximation I', which do not necessarily satisfy (3) are given by

$$\mathbf{T}_I = -2i\mathbf{R}, \quad \dots\dots (4)$$

we consider the alternative approximations

$$T_{II} = \frac{-2iR}{1-iR}, \quad \dots\dots (5)$$

$$T_{III} = 1 - e^{2iR}; \quad \dots\dots (6)$$

these yield cross sections which automatically obey (3). If the results Q_I already satisfy the conservation condition, the results Q_{II} and Q_{III} are usually only slightly smaller. In cases where conservation is violated in approximation I, approximations II and III should afford better agreement with experiment.

Recently, Vainstein (1960) has reported extensive calculations, using the Born and non-exchange distorted wave approximations for a variety of electron-induced transitions in several atoms and ions. In certain cases, Vainstein provides graphs of the first few partial wave cross sections, which may be examined from the point of view of conservation violation. For the 3s-3p transition in sodium in the distorted wave approximation (the total cross section is reproduced in the Figure), several of the partial wave cross sections do not satisfy the conservation condition; most notably, the spurious maximum at $k^2=0.21$ is largely due to the $l \rightarrow l'=0 \rightarrow 1$ cross section, which has a value at this point of about $68\pi a_0^2$, whereas condition (3) requires that it should not be greater than $4.76\pi a_0^2$.

The results for the first seven partial waves have been modified by introducing approximation II. In this case, considering only coupling between the (3s, l) and (3p, $l \pm 1$) states, the reactance matrix is a 3×3 matrix and Eqns (4) and (5) give the new partial cross section

$$Q_{II}(l \rightarrow l') = Q_I(l \rightarrow l') \left[1 + \frac{k^2}{4(2l+1)} \{Q_I(l \rightarrow l-1) + Q_I(l \rightarrow l+1)\} \right]^{-2}, \quad l' = l \pm 1, \quad \dots\dots (7)$$

where Q_I is Vainstein's result. The new total cross section is obtained from the relation

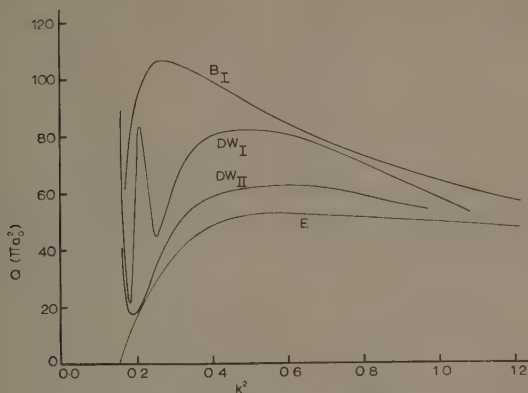
$$Q_{II} = Q_I - \sum_{l=0}^6 \sum_{l'} \{Q_I(l \rightarrow l') - Q_{II}(l \rightarrow l')\}. \quad \dots\dots (8)$$

The results are presented in the Figure, which contains also Vainstein's results (approximation I) for the total Born and total distorted wave cross sections and the experimental curve of Haft (1933) and Christoph (1935). A substantial improvement has been effected by the introduction of approximation II; there is fairly close agreement with experiment over most of the range and the maximum at $k^2=0.21$ has disappeared. The other sharp maximum, just above threshold, persists and is therefore not entirely associated with conservation violation; it is made up of the $1 \rightarrow 0$ and $2 \rightarrow 1$ cross sections only. The presence of this maximum would appear to be in agreement with the measurements of Michels (1931), who reported sharp peaks at threshold for this and other transitions in sodium; however, he obtained vanishing cross sections for energies between these threshold regions for successive excitations, and so his results are generally disregarded (cf. Bates, Fundaminsky, Leech and Massey 1950). A sharp maximum very close to threshold could be consistent with Haft's measured points; more experimental work in the region of threshold is required before a definite conclusion can be reached.

Approximation III, based on Eqn (6), gives in this case results which for all values of k are very close to those of approximation II.

From the work of Salmona and Seaton (1961) on the Bethe cross section for this transition in approximation II, it appears probable that approximation II

to the Born cross section will be very similar to that obtained using distorted waves, but apparently without the initial maximum.



Cross sections for the Na(3s-3p) transition. B_I and DW_I are Vainstein's results using the Born and distorted wave approximations respectively, DW_{II} is approximation II to the distorted wave cross section and E is the experimental curve. k is in atomic units, so that $13.6k^2$ is the incident energy in electron volts.

ACKNOWLEDGMENTS

I am indebted to Dr. M. J. Seaton for valuable discussions. Thanks are due to Dr. Vainstein for sending us a copy of his paper in advance of publication.

This work is supported by the Atomic Energy Research Establishment, Harwell, and permission to publish is gratefully acknowledged.

REFERENCES

- BATES, D. R., FUNDAMINSKY, A., LEECH, J. W., and MASSEY, H. S. W., 1950, *Phil. Trans. Roy. Soc. A*, **243**, 93.
 CHRISTOPH, W., 1935, *Ann. Phys., Lpz.*, **23**, 51.
 HAFT, G., 1933, *Z. Phys.*, **82**, 73.
 MICHELS, W. C., 1931, *Phys. Rev.*, **38**, 712.
 PERCIVAL, I. C., 1960, *Proc. Phys. Soc.*, **76**, 206.
 SALMONA, A., and SEATON, M. J., 1961, *Proc. Phys. Soc.*, **77**, 617.
 SEATON, M. J., 1961, *Proc. Phys. Soc.*, **77**, 184.
 VAINSTEIN, L., 1960, *Effective Cross Sections for the Excitation of Atoms by Electron Impact*.
 I. Neglecting Exchange, Lebedev Physics Institute, Moscow, Report A-33.

Observations on Lattice Rotations in Tabular Silver Bromide Grains

By G. C. FARNELL, R. B. FLINT AND E. PITTS

Research Laboratories, Kodak Limited, Wealdstone, Harrow, Middlesex

MS. received 13th April 1961

Abstract. In pure silver bromide emulsions containing tabular grains some are found in which one part appears to have been rotated with respect to the other about an axis perpendicular to the large (111) faces. To ascertain whether such grains were genuine, possible angles of rotation and their frequency relative to one another were deduced on a simple theoretical basis. Similarity in calculated and observed angles, and in the calculated and observed relative frequencies of occurrence, as well as the simple fact that the angles fall into well-defined groups, show without doubt that such grains are not artefacts but special forms of mis-orientation. It is shown that the distribution of photolytic silver is profoundly different in such grains from that observed in normal grains.

§ 1. INTRODUCTION

IN the course of photographic studies involving silver bromide emulsions with tabular grains, occasional instances have been observed where one half of a grain appeared to be rotated with respect to the other half about an axis perpendicular to a large (111) face. A carbon replica electron micrograph of such a grain is shown in Fig. 1 (Plate I). Until recently there had been some tendency to dismiss such entities as being produced simply by the chance overlapping of one grain by another, perhaps occurring during specimen preparation, though it must be admitted that their reality was strongly suggested by the observation of Evans and Mitchell (1955) that the fraction of such grains could be deliberately increased by the use of turbulent conditions in dilution of saturated ammoniacal solutions of silver bromide. It became clear, however, that there was a considerable similarity in the angles of rotation between the two halves among many specimens encountered, and that the two parts were usually similar in size, as though they were not the result of chance but represented single grains. A systematic study of such entities was therefore made with the aim of confirming this point.

The first step was to deduce by a simple theoretical analysis the possible angles of rotation, about an axis perpendicular to the (111) plane of silver bromide, which could represent metastable states. The ratio of the number of ions in normal lattice positions following rotation to the total number of ions in the (111) plane was also deduced for the various possible angles. It was argued that this ratio should indicate the relative frequencies of occurrence of the various angles and in turn provide a further test of whether the observed entities were genuine

single grains. Micrographs of a number of such grains were then made from which the apparent angles of rotation could be determined. These angles were then compared in value and frequency with those expected on theoretical grounds. In this way it was possible to conclude that all entities studied represented single grains in a metastable state. No attempt will be made here to relate the observations to the much wider field of grain growth.

§ 2. THEORETICAL CONSIDERATIONS

The normal arrangement of ions in adjacent (111) planes of Ag^+ and Br^- ions in silver bromide is shown in Fig. 2. Let it be assumed that other arrangements of the Ag^+ lattice on top of the Br^- lattice are such that some, at least, of the former ions occupy positions which are normal lattice sites with respect to the

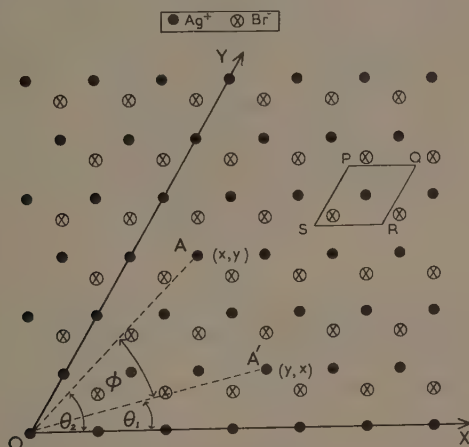


Fig. 2. Diagram showing the normal arrangement of the Ag^+ ion lattice with respect to the Br^- ion lattice in adjacent (111) planes of silver bromide, and illustrating the simple theory whereby permissible angles of rotation may be deduced.

Br^- ions. Such an arrangement would be obtained if for example the plane of ions were rotated about O until the ion labelled A coincided with the site A'. This basic argument is identical with that proposed by Wilman (1951) in his discussion of rotational slip, while our method of calculation broadly resembles his. Since there are certain subtleties in the derivation of possible angles and the associated ratios of ions in normal lattice positions to the total number of ions in the plane of rotation, it was considered worth while to present our calculations and conclusions therefrom in some detail.

All of the arrangements of the Ag^+ ion lattice on the Br^- ion lattice may be derived systematically by choosing any site and performing a rotation until it again coincides exactly with a previous lattice position. If we use coordinates as shown in Fig. 2 and suppose that the coordinates of A are in general (x, y)

then the rotation is such that this site finally occupies the coordinate position (y, x) . Elementary geometry shows that

$$\tan \Theta_1 = \frac{x\sqrt{3}}{2y+x} \text{ and } \tan \Theta_2 = \frac{y\sqrt{3}}{2x+y}.$$

Hence the angle of rotation ϕ , i.e. $\Theta_2 - \Theta_1$ is given by the expression

$$\tan \phi = \frac{(y^2 - x^2)\sqrt{3}}{y^2 + 4yx + x^2}. \quad \dots (1)$$

By dividing both the numerator and denominator of (1) by x^2 , it is obvious that $\tan \phi$ depends on the ratio y/x , and hence rotations will only differ when y and x are relatively prime.

There is a further reason which makes many of the rotations calculated from (1) essentially equivalent. Suppose in Fig. 2 that the y axis is rotated towards the x axis through an angle (corresponding to the rotation A to A'). An essentially equivalent rotation would be obtained by turning the x axis towards the y axis through an angle $(60 - \phi)^\circ$. It is clear that if the two rotations add to make 60° , they are equivalent. From (1) the value of $\tan(60 - \phi)^\circ$ is readily obtained, and let it be supposed that this corresponds to the rotation of (x_1, y_1) to the position (y_1, x_1) . This gives the equation

$$\frac{2xy + x^2}{2y^2 + 2xy - x^2} = \frac{y_1^2 - x_1^2}{y_1^2 + 4x_1y_1 + x_1^2},$$

from which

$$\frac{y_1}{x_1} = \frac{y + 2x}{y - x}.$$

This shows that the rotation corresponding to $(y + 2x)/(y - x)$ is equivalent to a rotation corresponding to a given ratio y/x . In Table 1 the angles of rotation which are essentially different have been listed for values of x and y up to 12 and 11 respectively. In all cases angles less than 30° have been tabulated, rather than the angle greater than 30° which is the complement with respect to 60° .

Table 1. Calculated Permissible Angles of Rotation in the (111) Plane

$y \backslash x$	1	2	3	4	5	6	7	8	9	10	11	12
1												
2												
3		21° 47'										
4			13° 10'									
5				9° 26'	16° 25'							
6					7° 20'							
7						6° 0'	11° 0'	15° 11'	18° 44'		24° 26'	26° 45'
8							5° 5'				19° 16'	
9								4° 24'	8° 15'	11° 38'	14° 37'	17° 14'
10									3° 54'		10° 25'	
11										3° 29'	6° 37'	
											3° 9'	
												2° 53'

After any rotation some of the ions will be in normal lattice sites, while the remainder are displaced. It is reasonable to suppose that at large angles, at least, the ratio of ions in normal sites to the total number will provide some indication of the relative frequency of occurrence of various angles. Consideration of the threefold symmetry of the lattice shows that after a rotation such that A moves to A', the ions at the vertices of a regular hexagon of which OA' is one side will

be in correct positions, together with the ion at the centre of this hexagon. An ion at each vertex is shared between three such hexagons, and hence the total number of ions in their correct positions is $6(\frac{1}{3}) + 1$, i.e. 3 for each hexagon. The number of ions in the hexagon is found by dividing its area by the area associated with each ion, namely PQRS. In terms of the unit length PQ, this area is $\sqrt{3}/2$ and if OA is L units of PQ, the area of the large hexagon is $3L^2\sqrt{3}/2$. There are thus $3L^2$ ions in all, 3 of which are in their correct positions. In terms of these coordinates (x, y) of A, the ratio

$$\frac{\text{ions in correct lattice positions}}{\text{total number of ions}} = \frac{1}{L^2} = \frac{1}{y^2 + xy + x^2} \dots\dots (3)$$

In using this result the equivalence of many rotations corresponding to apparently different choices of y and x must be remembered. Rotations differ only when y and x are relatively prime; if they possess a common factor this must be removed before (3) is used. Further, the rotation corresponding to y/x is equivalent to that corresponding to $(y+2x)/(y-x)$. It may happen that although y and x are relatively prime, $y+2x$ and $y-x$ have a common factor. For example, if $y=7$ and $x=4$, then the ratio $(y+2x)/(y-x)$ is equivalent to the ratio 5:1. The former values give $1/L^2 = 1/93$, while the latter gives $1/L^2 = 1/31$.

In all such cases a little consideration will show that one must choose the smaller value of L^2 as the correct one. The larger value results from counting only one third of the ions which are situated at normal sites. Values of $1/L^2$ with account taken of these rules are shown in Table 2, corresponding to the essentially different rotations in Table 1.

Table 2. Ratio of Ions in Normal Sites to Total Number of Ions in (111) Plane for Lattice Rotations shown in Table 1

$y \backslash x$	1	2	3	4	5	6	7	8	9	10	11	12
1												
2		1:7										
3			1:19		1:13							
4				1:37	1:49		1:79	1:97				
5					1:61		1:31		1:133			
6						1:91	1:109	1:43	1:151		1:67	1:229
7							1:127				1:223	
8								1:169	1:193	1:73	1:247	1:277
9									1:217		1:91	
10										1:271	1:301	
11											1:331	1:397

Taking the view that the frequency with which a rotation occurs decreases with decreasing ratio of ions in correct lattice positions to the total number of ions, we find that the angles most likely to be encountered in order of decreasing frequency will be $21^\circ 47'$, $27^\circ 48'$ and $13^\circ 10'$.

§ 3. OBSERVATIONS AND DISCUSSION

The majority of observations were made using an electron microscope (Metropolitan Vickers EM-2). Specimens of the emulsion were first treated with enzyme (Gelatase 'C'), to remove the gelatin, and then placed in a vacuum chamber. After gold-palladium alloy had been evaporated at an angle of 45°

on to the slide carrying the grains, carbon was evaporated normal to the surface of the specimen. Photomicrographs prepared in previous work were also studied for any occurrence of apparently rotated grains. Many thousands of grains from silver bromide emulsions of tabular grain shape were scanned in the electron microscope, and records made of any grain which appeared to represent a rotation of the two halves.

Table 3. Summary of Measured Angles of Rotation
All emulsions were of the neutral pure silver bromide type

(1)	(2)	(3)	(4)	(5)
1	~2.5	A†	3	23° 20'
2	~1.2	B†	3	27° 50'
3	~1.0	C	3	22° 20'
		D	3	21° 10'
		E	3	21° 20'
		F	3	23°
		G	3	27° 20'
		H	3	27° 50'
		I	3	13° 40'
		J	3	27° 40'
4	~2.0	K†	3	15° 40'
		L	3	21°
		M	6	21° 15'
		N	3	21° 30'
		O	3	13°
		P	6	21° 45'
		Q	3	21° 20'
5	~5.0	R†	3	15° 20'
		S†	3	13° 30'
		T†	3	22°
		U†	3	27° 30'

† Photomicrographs. The remainder were on electron micrographs.

(1) Emulsion number; (2) mean grain size (μ^2); (3) specimen; (4) number of angles measured; (5) average value of rotation.

The first emulsion specifically examined (No. 4 in Table 3) had a mean grain projective area of the order of $2.0\mu^2$. Approximately one grain in 10^5 appeared to possess a rotation. When it did occur it took the form of two hexagons rotated with respect to one another with their centres on the same axis. Fig. 1 is an example of a rotation found in this emulsion. Certain other grains were found in this emulsion growing out of the rotated state to form grains of less distinctive shape. An example of this form is shown in Fig. 3 (Plate I).

This growth out of the rotated state suggested that rotations might be found more frequently in an emulsion of smaller grain size. Examinations were therefore made of a second emulsion (No. 3 in Table 3) having a mean grain projective area of $1.0\mu^2$. Here about one grain in 2×10^4 was found to exhibit lattice rotations, but the effect differed in character to that observed in the previous emulsion. The general form was of a triangle rotated with respect to a hexagon,

again the centres being on a common axis. An example of a grain from this emulsion exhibiting lattice rotation is shown in Fig. 4 (Plate II).

Angles of rotation were measured on all examples encountered of this effect, and are summarized in Table 3, the smaller of the two possible angles being measured. Individual angles were determined to within $\pm \frac{1}{2}^\circ$ on electron micrographs but on light micrographs it was usually only possible to determine angles to within $\pm 1^\circ$.

The mean value of angles around 22° (11 in all) is $21^\circ 49'$ which compares well with the theoretical value for $(x=2, y=1)$ of $21^\circ 47'$. The mean of those near 28° (5 in all) is $27^\circ 38'$, which is in good agreement with the theoretical value of $27^\circ 48'$ for $(x=5, y=2)$. From the information presented in Table 2 this would be expected to be the next most frequently occurring angle of rotation. On the basis of the simple theory the angle of third highest frequency should be that of $13^\circ 10'$ for $(x=3, y=2)$ and indeed 3 values close to this, having a mean of $13^\circ 23'$ were observed. This accounts for all but two angles having a mean value of $15^\circ 30'$. This is close to the theoretical value of $15^\circ 11'$ for $(x=8, y=5)$, but in view of the fact that the two experimental values were obtained from light micrographs another possibility is a correspondence to $16^\circ 25'$ for $(x=5, y=3)$. Uncertainties in experimental determination are considered to be responsible for the small deviations from theoretical values for the angles of rotation in the other comparisons based mainly on electron micrographs. From the close grouping of the angles of rotation, the agreement between calculated and observed values for rotation and the reasonable consistency between frequency of occurrence and that expected from the value of the ratio for ions in normal lattice positions to the total number of ions in the plane of rotation, there can be no doubt that the entities examined represent single grains.

In the course of recent examinations of print-out silver distribution in emulsion grains of the type examined in this work, it has been found that in grains having a lattice rotation there is a marked difference in the manner in which photolytic silver is deposited. In the usual type of grain heavy print-out exposure produces a distribution of small specks on an internal (111) plane. In a grain possessing lattice rotations, however, far larger masses of silver are formed, and associated mounds of halide are extruded, while a system of etch pits due to halogen evolution appears around the mounds. An ordinary silver bromide grain and one possessing a lattice rotation which were given equal print-out exposures in the absence of bulk gelatin are compared in Figs 5 and 6 (Plate III). This difference in response to print-out exposure provides further evidence that the grains under consideration are not simply chance combinations of two ordinary tabular silver bromide grains. The significance of the protrusions of silver halide produced under these conditions of photolysis had been discussed recently by Hamilton and Brady (1960).

§ 4. CONCLUSIONS

(a) Grains in tabular silver bromide emulsions in which one half appears rotated with respect to the other half about an axis perpendicular to their (111) faces are single grains and not a consequence of overlapping of one grain by another. The proportion obviously possessing such rotations in the emulsions examined is quite small (1 in 10^4 – 10^5).

(b) On the supposition that stable lattice arrangement other than the normal require some ions to be in their normal positions, it is possible to account for all

the observed angles with quite high precision. Moreover the relative frequency of occurrence of the various possible angles of rotation is substantially that expected from this concept.

(c) The inherent instability of grains possessing these lattice rotations is demonstrated by the observation of a number of grains in course of transition to other tabular forms.

(d) The presence of a lattice rotation in a grain profoundly modifies the distribution of photolytic silver.

REFERENCES

- EVANS, T., and MITCHELL, J. W., 1955, *Report of the Conference on Defects in Crystalline Solids held at the H. H. Wills Physical Laboratory, Bristol, July 1954* (London: Physical Society).
- HAMILTON, J. F., and BRADY, L. E., 1960, *J. Appl. Phys.*, **31**, 609.
- WILMAN, H., 1951, *Proc. Phys. Soc.*, **64**, 329.

Time Resolved Absorption Studies in a Shock Tube: A New Band System of BaO

By W. H. PARKINSON†

Department of Chemical Engineering, Imperial College, London

Communicated by A. G. Gaydon; MS. received 24th April 1961

Abstract. Time resolved absorption studies have been carried out through the hot gas behind reflected shock waves during their interaction with powdered barium compounds. A capillary-type flash tube with a short pulse duration and high brightness temperature was used as the background source.

A new system of BaO, probably resulting from a $B(^1\Pi)-X^1\Sigma$ transition, has been found in absorption, and vibrationally analysed. The constants derived for the upper state of the system were $T_e = 32\,866.4\text{ cm}^{-1}$, $\omega_e = 488\text{ cm}^{-1}$ and $\omega_e x_e = 3.6\text{ cm}^{-1}$.

A band of zinc oxide possibly due to a polyatomic emitter has been recorded in emission from the luminosity produced during the shock excitation of powdered zinc compounds.

§ 1. INTRODUCTION

SPECTROSCOPIC emission studies of the luminosity which results during the shock excitation of powdered solids have shown that the shock tube is particularly suitable as a laboratory source of high temperature atomic and molecular spectra (Nicholls and Parkinson 1957). In addition, absorption spectra similar to those observed in some cool stars have been recorded during the interaction of shock waves with astrophysically important metallic oxides (Parkinson and Nicholls 1959). A further investigation of the production of diatomic and polyatomic molecular spectra has been made in emission and in absorption. Time resolved absorption spectra were taken through the gas behind reflected shock waves using the continuum from a high intensity, short duration, flash tube. The absorption experiments were carried out on a number of solid barium compounds and a new barium oxide system was found. Emission studies were also made on the luminosity resulting from shock excited hydroxide and oxide compounds of copper, magnesium, barium, iron, manganese and zinc.

This paper reports the vibrational analysis of the new band system of barium oxide and discusses a band of zinc oxide which is due possibly to a polyatomic emitter resembling those found with the alkaline earths.

§ 2. EXPERIMENTAL

The shock waves were produced in a conventional shock tube consisting of a three-foot copper driving section separated by an aluminium diaphragm from a nine-foot copper low pressure section. The low pressure section or channel was closed at one end with a short section, $1\frac{1}{2}$ feet in length, which held two fused quartz windows through which the luminosity behind the reflected shock waves was observed transverse to the flow direction.

† Now at Harvard College Observatory, Cambridge, Massachusetts.

The aluminium diaphragm was broken by the excess pressure of the hydrogen driver gas. Argon was normally used as the carrier gas but a small percentage of oxygen or hydrogen was added to the argon in particular experiments.

The powdered materials were positioned in the channel of the shock tube about 12 in. before the closed end. A small sample was placed either on a steel platform protruding across the diameter of the channel or on a $\frac{1}{2}$ in. wide strip of 'Kleenex' tissue clamped in the channel union near the window. The impurities in the spectra resulting from the 'Kleenex' consisted only of sodium and calcium resonance lines but the intensity of the important features in the spectrum was much higher than with the platform mounting.

In addition to emission studies, absorption spectra were taken through the hot gas behind the reflected shock waves at various times. The background continuum was produced from a high current density quartz-capillary flash tube filled with 10 cm pressure of tank argon. The flash tube was connected in series with two $1\mu\text{F}$ condensers at 7 kv and a hydrogen thyratron. It was fired by an amplified pulse arriving at the thyratron grid from an amplifier and variable delay circuit. The initiating pulse was produced from a platinum heat transfer gauge in the end of the shock tube.

The light pulse from the flash tube falls to one half of its peak intensity in about $5\mu\text{sec}$ whereas the light from the shock wave lasts for approximately $1500\mu\text{sec}$. In order to obtain useful absorption spectra it was necessary to keep the light from the shock wave from masking the absorption. This was accomplished by using a fuse-fired shutter similar to that described by Wurster (1957). The shutter, which consisted of a piece of black electrical tape over a blast channel, is opened (or closed) by the blast from an exploding 5 amp lead fuse strip. The fuse strip was in series with a hydrogen thyratron and a $0.5\mu\text{F}$ condenser at 5 kv. The shutter opened or closed in $35 \pm 5\mu\text{sec}$.

The pulse from the heat transfer gauge in the shock tube was divided and delayed so that one pulse fired the flash tube while the other pulse fired the shutter. Absorption pictures could be taken from 0 to $200\mu\text{sec}$ after the reflection of the shock wave. An additional 0 to $50\mu\text{sec}$ delay was used with the main delay to allow for the opening or closing time of the shutter.

The spectra from the shock tube were recorded by a medium quartz prism spectrograph or a 2 metre concave grating spectrograph with a reciprocal dispersion of about $5\text{\AA}/\text{mm}$. The arc spectra of barium and zinc were recorded by a 2 metre Littrow-mounted plane grating with a reciprocal dispersion of $0.8\text{\AA}/\text{mm}$ in the second order. Ilford Zenith and H.P.S. plates were used.

§ 3. RESULTS

3.1. Barium Oxide in Absorption

Absorption spectra of shocked barium peroxide were taken through the gas behind the reflected shock wave at $100\mu\text{sec}$ intervals over a range of incident Mach numbers from 4 to 6 in argon at 40–60 mm pressure. Plates I a to I f show spectra recorded at times 100, 200, 400, 800 and $1000\mu\text{sec}$ during the flow. From this plate it can be seen that for about the first $200\mu\text{sec}$ the spectra consisted of atomic lines of Ba I, Ba II and impurity lines of Ca I, Na I, Cu I and Al I in absorption. After $200\mu\text{sec}$ the bands of the $\Lambda^1\Sigma-x^1\Sigma$ system of BaO (Mahanti 1934), the

polyatomic band of BaOH (4870, 5120 Å) and Ba₂O₂ (?) (4800, 5020, 5500 Å) and a new band system in the 2900–3800 Å region appeared with the atomic lines. The molecular absorption increased until it reached maximum intensity at about 1000 μsec with the intensity of atomic lines then reduced.

Plates 1*g* and 1*i* show absorption spectra obtained with BaCl₂ and BaO₂ respectively in the shock tube. The bands in the 2900–3800 Å region and the A¹Σ–x¹Σ system were recorded only when both barium and oxygen were present.

The new bands appeared weakly in emission in the shock tube and also were photographed after a 30 minute exposure using the outer 'flame' from barium peroxide or barium nitrate on the poles of a carbon arc (Plate 1*h*).

The wave number data for the band heads are shown in the Deslandres table (Table 1). Table 2 lists the wavelength and eye-estimated intensities of the band heads.

Table 1

$v' \setminus v''$	1	2	3	4	5	6	7	8	9	10	11
0 —	—	—	—	30112	29464	28819	28176	27537	26907	26274	25643
1 —	—	31855	31202	30542	29891	29244	28621	27972			
2 —	—	32293	31640	30982				28410	27778		
3 34055	33390	32732	32078								
4 —	33808	33145									
5 —	34206										

Table 2

λ (Å)	<i>I</i>	v', v''	λ (Å)	<i>I</i>	v', v''
3898.6	2	0, 11	3273.2	5	1, 4
3805.0	2	0, 10	3226.8	7	2, 4
3715.4	3	0, 9	3204.0	6	1, 3
3630.4	4	0, 8	3159.6	8	2, 3
3599.0	1	2, 9	3138.3	3	1, 2
3574.0	2	1, 8	3116.5	8	3, 3
3548.1	5	0, 7	3095.8	3	2, 2
3518.9	1	2, 8	3054.2	10	3, 2
3492.9	2	1, 7	3016.2	4	4, 2
3468.9	7	0, 6	2994.0	5	3, 1
3418.5	3	1, 6	2957.0	9	4, 1
3393.0	8	0, 5	2935.6	4	3, 0
3344.5	7	1, 5	2922.6	7	5, 1
3320.0	4	0, 4			

Weak bands were also observed at 2900, 2866, 2776, 2765, 2738, 2711, 2686, 2638 and 2615 Å but the diffuse nature of the bands and the presence of overlapping bands of the O₂ Schumann-Runge system in absorption did not permit the use of these heads in the vibrational analysis. The uncertainty in precisely locating the relatively weak heads of the bands of this system made the assignment of the vibrational quantum number difficult. The ground state of the system however appeared to be the same ground state as in the transition A¹Σ–x¹Σ which results in the orange bands of BaO. The vibrational constants from the array are shown in Table 3 together with the constants of the A¹Σ–x¹Σ system of BaO (Lagerqvist, Lind and Barrow 1950).

Table 3

State	T_e	ω_e	$\omega_e x_e$	
B($^1\Pi$)	32866.4	488	3.6	(present work) band head
A $^1\Sigma$	16807.7	498.8	1.5	band origin
x $^1\Sigma$	0	670.2	1.95	(present work) band head
		669.8	2.05	band origin

The bands of the B-x $^1\Sigma$ system were investigated at a reciprocal dispersion of 0.8 Å/mm on a 2 metre plane grating but the low intensity of the bands and background radiation did not permit a rotation analysis. The rotational line distribution did appear however to consist of at least three branches. It is suggested therefore that the system comes from transitions between an excited $^1\Pi$ state and the x $^1\Sigma$ ground state.

3.2. Polyatomic Spectra in Emission

The diatomic molecular spectra of calcium, magnesium, strontium and barium oxides (which are observed in arcs and flames containing salts of these compounds) are well known in emission and have been analysed for some time. In addition to their diatomic spectra, however, there has been considerable work done on the polyatomic oxides and hydroxide spectra.

Gaydon and co-workers have studied the spectra of CaOH, CaOD (Gaydon 1955), MgOH, MgOD (Charton and Gaydon 1956), SrOH, SrOD, BaOH and BaOD (Pescic and Gaydon 1959) excited in a 'vacuum' arc in water and heavy water vapour. In addition, when salts of the alkaline earths were excited in an arc in air, complex systems were observed and it has been suggested that these may be due to polyatomic oxides.

The correspondence in spectral region of the polyatomic hydroxide and oxide spectra of these metals with their diatomic fluoride spectra has been pointed out by Charton and Gaydon (1956) and by James and Sugden (1955). These researches have also reported the excitation of hydroxide bands of copper and manganese in oxygen-hydrogen flames.

Emission spectra were recorded from the luminosity produced during the interaction of shock waves with powdered Cu(OH) $_2$, MgO, Mg(OH) $_2$, BaO $_2$, Ba(OH) $_2$, Fe, Fe(OH) $_2$, Mn, Mn(OH) $_2$ and Zn, ZnO and Zn(OH) $_2$.

The hydroxide spectra of copper, magnesium, barium, iron and manganese were obtained as well as the polyatomic oxide spectra of magnesium and barium.

When powdered zinc oxide was subjected to shock-excitation at primary Mach numbers from 4 to 6 in argon, a narrow, red degraded band was observed at 3435 Å. The addition of 5-10% oxygen to the argon, in the same range of Mach numbers, increased the intensity of the band. The intensity decreased with a corresponding addition of hydrogen but the bands of ZnH at 4301 Å, 4240 Å etc. appeared.

Egerton and Rudrakanchana (1954) have reported a weak red-degraded band at this wavelength in the spectrum of zinc dimethyl burning as a diffusion flame.

Spectra taken in the 'flame' of a zinc arc in air gave the same band with considerable background radiation. Plate I *i* shows the band recorded in the second order of a Littrow-mounted plane grating.

Only one band was obtained from shock excited zinc oxide. Since oxygen was required to produce the band in all of the sources this appears to rule out Zn $_2$ as

the emitter. The unresolved rotational structure suggested either a diatomic oxide molecule of ZnO with high multiplicity or a polyatomic oxide of the metal. One would expect however to be able to resolve the rotational structure of a band ZnO of triplet multiplicity, since other diatomic molecules of similar reduced mass and multiplicity have been well analysed. It is suggested therefore that the band at 3435 Å is due to a polyatomic zinc oxide which is similar to the polyatomic oxide spectrum of the alkaline earth metals (Charton and Gaydon 1956).

§ 4. DISCUSSION

The vibrational constants of the ground state of the new system corresponded to those of the ground state of the $A^1\Sigma-x^1\Sigma$ BaO system (Herzberg 1950). It is possible that the present system arises through a $^1\Sigma-^1\Sigma$ transition but a $^1\Pi-^1\Sigma$ transition seems more probable in view of the complex rotational structure. In either case an intercombination system is possible through a transition to the $A^1\Sigma$ state. One would expect a red degraded band system in the region of 6280 Å. The spectrum in this region however was masked with the BaO $A^1\Sigma-x^1\Sigma$ system and it was not possible to identify an intercombination system.

The time resolved absorption spectra showed that molecular absorption was not present over the full flow time but began at about 200 μ sec and increased until reaching a maximum 1000 μ sec after the incident shock wave had been reflected. The atomic absorption however began early in the first 50 μ sec but after 200 μ sec was greatly reduced with the molecular absorption at a maximum. Earlier spectroscopic observation in emission and microscopic and x-ray powder photographs of the shocked powder samples (Parkinson and Nicholls 1959) indicated a high concentration of atoms early in the interaction between the shock wave and the powder particles. It was suggested that the atoms were either the result of severe atomic ablation or dissociation of diatomic molecules from the original powdered particles. The present observation supports these suggestions.

ACKNOWLEDGMENTS

The author would like to express his gratitude to Dr. A. G. Gaydon for his many helpful discussions and suggestions and for providing the experimental facilities for these investigations. Particular appreciation goes to Dr. Ian R. Hurlle for his help in constructing the flash tube and associated electronics.

The author is also very grateful to the National Research Council of Canada for the award of a post-doctoral overseas fellowship.

REFERENCES

- CHARTON, M., and GAYDON, A. G., 1956, *Proc. Phys. Soc.*, **69**, 520.
EGERTON, Sir ALFRED C., and RUDRAKANCHANA, S., 1954, *Proc. Roy. Soc. A*, **224**, 427.
GAYDON, A. G., 1955, *Proc. Roy. Soc. A*, **231**, 437.
HERZBERG, G., 1950, *Spectra of Diatomic Molecules* (New York: Van Nostrand).
JAMES, C. G., and SUGDEN, T. M., 1955, *Nature, Lond.*, **175**, 333.
LAGERQVIST, A., LIND, E., and BARROW, R. F., 1950, *Proc. Phys. Soc. A*, **63**, 1132.
MAHANTI, P. C., 1934, *Proc. Phys. Soc.*, **46**, 51.
NICHOLLS, R. W., and PARKINSON, W. H., 1957, *J. Chem. Phys.*, **26**, 423.
PARKINSON, W. H., and NICHOLLS, R. W., 1959, *Sc. Rep. No. 1. A.F.* 19 (604)-4560.
PESIC, D., and GAYDON, A. G., 1959, *Proc. Phys. Soc.*, **73**, 244.
WURSTER, W. H., 1957, *Rev. Sci. Instrum.*, **28**, 1093.

The Dependence of Capture Rate on Electric Field and the Possibility of Negative Resistance in Semiconductors

By B. K. RIDLEY AND T. B. WATKINS

Mullard Research Laboratories, Salfords, nr. Redhill, Surrey

MS. received 9th May 1961

Abstract. It is pointed out that the rate of capture of electrons and holes by charged centres should depend markedly on electric field strength when this is high enough to produce hot electrons. In particular the capture rate for an attractive centre should decrease while the rate for a repulsive centre should increase as the field rises. Each effect will alter the steady state density of carriers. For the case of repulsive centres a decrease in carrier density will occur and the possibility of using this phenomenon to produce a negative resistance state in the semiconductor is discussed. Suitably compensated n-type germanium crystals containing copper, nickel or gold appear to have the requisite properties for exhibiting negative resistance at temperatures low enough for the thermal ionization rate of the centre to be small. It is pointed out that the long time constants involved in the process preclude the use of short pulse fields.

§ 1. INTRODUCTION

THE rate of capture of an electron (or hole) by an impurity centre in a semiconductor is generally dependent on the energy of the electron. Since an electric field can increase the energy of an electron the capture rates must generally depend on the electric field strength. As a consequence the steady state density of electrons can change as the field is increased (Conwell 1961, Ridley and Watkins, to be published) and in some cases this effect may give rise to negative resistance effects (Ridley and Watkins 1961), a necessary condition being that the capture rate must increase with field (leading to de-ionization). Such an increase in capture rate with field ought to occur when the traps present a repulsive Coulomb force to the electron so that the electron must surmount a potential barrier before capture is possible. An increase of the field allows more electrons to have the necessary energy to surmount the barrier and hence the capture rate increases. If the lattice temperature remains constant and no impact ionization occurs the generation rate does not change with field and the net result is a drop in electron density. For copper, nickel and gold in germanium, barriers up to 0.2 eV have been measured (Battey and Baum 1955, Shulman and Wyluda 1956, Johnston and Levinstein 1960).

To obtain an idea of the order of magnitudes involved in the change of capture cross section for charged impurities the following argument may be followed. For low energy electrons the charge on an impurity centre has a great effect, e.g. impurity scattering becomes important at low temperatures. As the electron energy rises the effect of the charge lessens and in the limit the centre appears

to the electron virtually as a neutral centre. For repulsive centres the capture cross section for thermal electrons is of the order of 10^{-22} cm² and for attractive centres it can be as high as 10^{-12} cm², while for neutral centres it is about 10^{-17} cm². Changes in cross section with mean electron velocity over five orders of magnitude are therefore possible. The actual maximum change will, of course, depend on the structure of the particular centre and also on the temperature, but it is clear that large changes of carrier density can occur.

§ 2. CAPTURE RATE FOR REPULSIVE CENTRE

Consider the case of an extrinsic n-type semiconductor in which the extrinsic electrons derive from thermal ionization of an impurity level in the upper half of the forbidden band. We shall assume that the impurity after losing an electron to the conduction band is nevertheless negatively charged. Many of the deep level acceptors in n-type germanium behave in this way (see, for example, Woodbury and Tyler 1957). We shall also assume that the lattice temperature is low enough to make all effective thermal generation rates other than rate of generation from the impurity level so low that they can be neglected. Consequently all other effective capture rates can be neglected since these are equal to the effective thermal generation rates at equilibrium. The density of electrons in the conduction band is then governed solely by the rates of transition associated with the impurity level. The rate of increase of electron density is then

$$\frac{dn}{dt} = gN^- - BnN^0 \quad \dots\dots(1)$$

where n is the density of electrons in the conduction band, N^- is the density of filled traps, N^0 is the density of unfilled traps, and g and B are the thermal ionization and capture rates respectively averaged over the electron distribution and are, in general, field dependent.

Denoting thermal equilibrium (low field) values by suffix zero we have

$$g_0N_0^- - B_0n_0N_0^0 = 0$$

from which

$$g_0 = B_0n_1$$

where

$$n_1 = 2 \left(\frac{2\pi m^* kT}{h^2} \right)^{3/2} \exp \left(- \frac{E_t}{kT} \right)$$

and E_t is the trap activation energy measured from the conduction band edge. The generation rate depends solely on the lattice temperature. Assuming this to be constant for all fields we have at the steady state

$$B_0n_1N^- - BnN^0 = 0. \quad \dots\dots(2)$$

If Δn is the increase in electron density due to the field, we obtain, by substituting

$n = n_0 + \Delta n$, $N^- = N_0^- - \Delta n$, and $N^0 = N_0^0 + \Delta n$

$$\Delta n = \frac{1}{2} \{ [(N_0^0 + n_0 + \gamma n_1)^2 - 4n_0N_0^0(1 - \gamma)]^{1/2} - (N_0^0 + n_0 + \gamma n_1) \} \quad \dots\dots(3)$$

where $\gamma = B_0/B$. For a repulsive centre $\gamma \leq 1$.

Eqn (3) can be simplified for the special case when the doping is such that at absolute zero the density of occupied levels is less than or of the same order as the density of unoccupied levels. This means that at zero temperature the Fermi level lies on or below the impurity level but never above, so that at

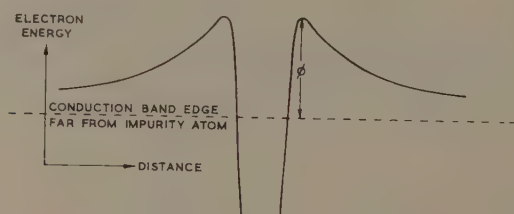
all temperatures a substantial density of unoccupied levels is available for electron capture. This, in fact, is the usual degree of compensation attainable in practice. At a temperature when only about 10% of the electrons are in the conduction band we can put $n_0 \lesssim n_1 \ll N_0^0$. Since $\gamma \leq 1$, γn_1 will also be negligible and Eqn (3) simplifies to give

$$\Delta n = -n_0(1 - \gamma). \quad \dots\dots(4)$$

Since the empty centre is negatively charged the density of electrons in the immediate vicinity of the trap will be different from the average density by a factor $\exp(-\phi/kT)$ at thermal equilibrium (Pekar 1950), neglecting any density of states contribution. ϕ is the potential barrier presented to the electrons (see Figure). If β_0 is the capture rate of thermal electrons which have surmounted the barrier the measured capture rate B_0 is given by

$$B_0 = \beta_0 e^{-\phi/kT}.$$

At high fields the electron distribution function changes from the Maxwellian f_0 to f_F , and $B = \beta f_F(\phi)$ where β , in general, is a function of the field.



Schematic diagram of potential around a negatively charged impurity centre.

§ 3. NEGATIVE RESISTANCE

The condition for negative resistance when electrons change from one state with mobility μ_a to another state with mobility μ_b is (Ridley and Watkins 1961)

$$\left[\left(\frac{\mu_a - \mu_b}{\mu_a + f\mu_b} \right) \left(-\frac{F}{n_a} \frac{dn_a}{dF} \right) - p \right] > 1, \quad \dots\dots(5)$$

where n_a is the density of electrons in the first state, F is the electric field, f is n_b/n_a where n_b is the density of electrons in the second state, and p arises from the assumption that the mobilities are proportional to F^p .

When the second state is a localized state, μ_b is zero, provided impurity conduction is negligible, and the first bracket in the inequality is unity. With phonon scattering predominant, p is negative, thus negative resistance is possible if the field induces de-ionization.

The condition when Eqn (4) is applicable becomes, with $n_a = n_0 + \Delta n$,

$$\frac{F}{B} \frac{dB}{dF} - p > 1. \quad \dots\dots(6)$$

In the most demanding case for lattice scattering, that is, when $p = -\frac{1}{2}$, the above condition is satisfied if the capture rate increases more rapidly than the square root of the field (i.e. $(F/B) dB/dF > \frac{1}{2}$)—not a very stringent condition.

For potential barriers greater than kT the term which varies most rapidly with field is likely to be the distribution function $f_F(\phi)$. In the region of field strengths where $p = -\frac{1}{2}$ to a reasonable approximation the distribution function f_F is of the form (Yamashita and Watanabe 1954) $f_F = \exp\{-a(\epsilon/kT_e)^2\}$, where ϵ is electron energy, the electron temperature T_e is proportional to field strength, and $\frac{2}{3}kT_e$ is defined as the mean kinetic energy of the electrons thus making $a = 0.243$. Condition (6) becomes, with $T_e = \text{const.} \times F$ and $B = \beta_0 \exp\{-a(\phi/kT_e)^2\}$,

$$\frac{\phi}{kT_e} > 1.01. \quad \dots\dots(7)$$

Since the mean energy of the hot electrons is roughly three or four times the thermal equilibrium mean energy in this region an approximate condition is $\phi/kT > 5$. For trap activation energies of the order of 0.1 ev the condition that thermal generation is not too high to make Eqn (4) inapplicable means that $kT \lesssim 0.01$ ev and so $\phi > 0.05$ ev. Observed values for the barrier satisfy this condition easily.

Since the interaction between carrier and trap charge has to be substantial it means that an appreciable energy variation over a free carrier wavelength can occur and hence the concept of bending of the conduction band near the centre, which is used to obtain the density factor in §2, is scarcely valid. The quantitative condition for the barrier height given above must therefore be regarded as a rough estimate.

When the electron temperature is high enough to excite optical phonons the drift velocity becomes independent of field ($\mu \propto F^{-1}$, therefore $p = -1$) and any increase of capture rate with field will produce negative resistance. If the barrier is less than or of the same order as the optical phonon energy the variation of β becomes important and without knowing how this varies with field it is impossible to predict whether negative resistance will occur. All the measured barriers are, however, much greater than $\hbar\omega_{\text{opt}}$ in germanium so that a considerable increase of capture rate ought to occur in the current saturation region.

§ 4. DISCUSSION

It must be emphasized that these considerations apply to the steady state. The time constants involved in transitions between 'repulsive impurity' states and the conduction band can be of the order of seconds at low fields and still of the order of tens of microseconds at high fields. The use of short field pulses of the order of $1\mu\text{sec}$ would merely show the mobility variation with field since the carrier concentration would not vary much in $1\mu\text{sec}$ (unless the impurity concentration were extremely high); d.c. fields are therefore desirable but heating effects must be avoided since the thermal generation rate must be kept low. Heating effects can be delayed to high fields by working at a low temperature. At too low a temperature however impurity conduction may become an appreciable factor. At high fields millisecond pulses may be adequate since the time constant for trapping should be much reduced from the thermal equilibrium value.

As regards material, germanium, containing as impurity any one of copper, silver, gold, platinum, iron, cobalt or nickel, and suitably doped with a shallow level donor, should be adequate. Copper, for instance, gives three acceptor

levels in germanium. Enough donor should be present to compensate completely the two lower levels and about half-fill the uppermost level.

Impact ionization, of course, will destroy any negative resistance effects. An electron to produce impact ionization must not only surmount a higher barrier, since the filled trap will have an extra negative charge, but must have sufficient energy left over to ionize the centre. This effect, if present, will occur at higher fields than those necessary to affect the capture rate, so that its influence will be to reduce the range of fields over which negative resistance is possible rather than to eliminate the possibility altogether. The centre may have excited localized levels which can be significantly populated at temperatures which make the thermal ionization rate low. This increases the probability of impact ionization. It may be expedient, therefore, to work at lower temperatures and excite the electrons in the centre optically. The same conditions for the height of the barrier apply and are even more easily satisfied at lower temperatures. If the temperature is below about 20°K, trapping of the optically excited electrons by the empty donor levels will occur and this will delay the onset of the negative resistance region to fields sufficient to cause substantial impact ionization of the donors.

The influence of the donor levels in this case emphasizes the fact that in this paper we have neglected the effect of other impurity centres, and also the interband transitions. This neglect should be justified at low temperatures when the activation energies of the other levels are greater than the activation energy of our repulsive centre by a few times kT for then the effective transition rates associated with these levels will be very small and can be ignored in Eqn (1). The donors, however, have smaller activation energies and high capture rates. They are positively charged, so that the effect of the field on the capture rate will be to cause ionization, the reverse of the case of repulsive centres. This, coupled with the relative ease with which impact ionization takes place, makes it certain that donors will contribute electrons to the conduction band as the field is increased. There is therefore a tendency to oppose the effect of the field on the repulsive centres unless saturation of the electron concentration due to donor ionization occurs fairly rapidly. But this tendency will have little effect above about 20°K since very few donor levels will be occupied to begin with. Thus, the condition for Eqn (1) to hold when other levels are present is that these levels must be either substantially filled or substantially empty. The breakdown of this condition does not necessarily rule out the possibility of negative resistance; it merely complicates the process.

§ 5. CONCLUSION

In this paper we have shown that the achievement of the negative resistance state by making use of the electric field dependence of capture rate is feasible. The idea of relating the capture rate to the density of electrons in the immediate vicinity of the trap rather than to the average density has led us to the prediction that the effective capture rate for attractive centres should decrease with field, while the opposite effect should occur for repulsive centres when the energy of the carriers is low compared with the energy of interaction between carrier and centre. A necessary condition for obtaining negative resistance in this way is to have repulsive traps present in the crystal.

REFERENCES

- BATTEY, J. F., and BAUM, R. M., 1955, *Phys. Rev.*, **98**, 923; **100**, 1634.
- CONWELL, E. M., 1961, *J. Phys. Chem. Solids*, **17**, 342.
- JOHNSTON, L., and LEVINSTEIN, H., 1960, *Phys. Rev.*, **113**, 1191.
- PEKAR, S. T., 1950, *Z. Exp. Theor. Phys.*, **20**, 267.
- RIDLEY, B. K., and WATKINS, T. B., 1961, *Proc. Phys. Soc.*, **78**, 293.
- SHULMAN, R. G., and WYLUDA, B. J., 1956, *Phys. Rev.*, **102**, 1455.
- WOODBURY, H. H., and TYLER, W. W., 1957, *Phys. Rev.*, **105**, 84.
- YAMASHITA, J., and WATANABE, M., 1954, *Progr. Theor. Phys.*, **12**, 443.

On the Change of Activation Energy with Impurity Concentration in Semiconductors

By J. F. BARNES AND R. H. TREDGOLD

Department of Physics, University College of North Wales, Bangor

MS. received 15th May 1961, in revised form 8th June 1961

Abstract. The existing theories of change in activation energy with impurity concentration are discussed and their limitations pointed out. The ionization energy of a pair of impurities in a dielectric medium is calculated as a function of impurity separation. Assuming a random distribution of impurities, an averaging process is employed to calculate the mean change in activation energy with concentration. This approximation should be poor for high impurity densities but good for low densities. Specific calculations have been made for the case of phosphorus impurities in silicon and satisfactory agreement is obtained with experimental results.

§ 1. INTRODUCTION

THE work of Pearson and Bardeen on silicon (1949) and Debye and Conwell (1954) on germanium shows that, for low concentrations of impurity atoms, the donor or acceptor atoms behave as isolated independent centres having electrons or holes bound to them with definite activation energies. However, as the concentration is increased, the activation energies decrease continuously and become zero at about 10^{17} centres/cm³ in germanium, and at about 10^{19} /cm³ in silicon. More recent work on germanium and silicon by Fritzsche (1955), Blakemore (1959) and Atkins, Donovan and Walmsley (1960), who took measurements to very low temperatures, shows that the conductivity is of the form

$$\sigma = \sigma_1 \exp(-\epsilon_1/kT) + c_2 \sigma_2 \dots\dots (1)$$

where the first term represents the ordinary semiconductor process of activation of donor electrons into the conduction band and ϵ_1 is the activation energy, which depends strongly on impurity concentration. This term is dominant at high temperatures. The second term is dominant at low temperatures ($< 10^\circ\text{K}$) and is dependent on temperature and impurity concentration. This term is said to be due to conduction in an impurity band.

This impurity band conduction can be explained on the model proposed by Mott (1956) and Conwell (1956) who assume that there are both donor and acceptor atoms present with densities N_D and N_A respectively where $N_D - N_A \gg N_A$. At low temperatures all the acceptor states will be filled by donor electrons and the overlap of the donor atoms is great enough for a hole on an ionized donor to jump to a neighbouring neutral donor, and the theoretical predictions of this model agree reasonably well with experiment.

If there are no acceptor impurities present, the number of electrons in the impurity band just equals that of the donor impurity atoms and, as pointed out by Mott (1956), correlation effects will inhibit band conduction unless there is a large overlap of the orbitals associated with adjacent impurity atoms. Erginsoy

(1952) has suggested that the excited states and not the ground states form the impurity band, and this should account for the finite slope of the resistivity curve at low temperatures, but the calculations of the lower band edges of the excited states for hydrogen-like impurities by Erginsoy (1952) and Baltensperger (1953) show that the excited states bands are close to the edge of the conduction band, giving too large an activation energy for the conduction process. Also there is a further objection; Fritzsche (1955) showed that conduction in an excited states band would be extremely small as the excited states cannot be treated as ordinary acceptor states. An excited state can only be occupied if the ground state of the impurity atom is empty. This limits considerably the number of excited states available for conduction as at low temperatures most of the atoms are in their ground state.

Most work on impurity band theory assumes that the impurity atoms are distributed regularly throughout the material, whereas in practice the impurities are quite randomly distributed, but Aigrain (1954) has shown that randomness makes the band approximation valid for a much lower density of impurities.

Pearson and Bardeen (1949) attempted to explain the variation of activation energy (ϵ_1) with impurity concentration by interpreting the decrease to be due to the electrostatic attraction of other ionized donors for an electron which has escaped from its own donor. This potential energy of attraction reduces the energy required for activation. However, on this model it is the density of ionized donors which controls the reduction and not the density of impurity donors (ionized or not) as required by the experimental results.

Pincherle (1951) and Lehmann and James (1955) have considered the effect of the free carriers (electrons from ionized donors) on the activation energy. The free carriers will tend to screen the field around the impurity centres, and the greater the number of free carriers the greater is the screening effect. The number of carriers available for screening depends on the impurity concentration and on the temperature. As the temperature is reduced, the number of carriers is reduced and the activation energy tends to the unscreened value. At relatively high temperatures (above 150°K) the reduction is almost constant and quite large, but does not account for all the reduction in activation energy observed.

A minor contribution to the lowering of the activation energy is due to polarization effects. A free electron in an impure material gives rise to a larger polarization than in the pure material due to the higher dielectric constant caused by the neutral donors. This has the effect of lowering the edge of the conduction band and hence the activation energy. Approximate calculations by Castellan and Seitz (1951) show the effect to be very small.

§ 2. THE MODEL CONSIDERED HERE

In this paper, we calculate the effect of the interaction of impurity atoms in pairs. If a slight overlap exists between the orbitals of adjacent impurity atoms and one of these atoms becomes ionized, the remaining electron will spread out over both impurity centres and thus its kinetic energy will be lowered. This reduction in kinetic energy must be subtracted from the ionization energy of a single impurity atom in order to find the ionization energy of the pair.

To calculate the magnitude of this effect, we thus have to obtain: (i) the energy of a hydrogen molecular ion in a medium of dielectric constant κ for a series of inter-nuclear distances; (ii) the energy of a hydrogen molecule in a similar medium

also for a series of internuclear distances. In (2) we assume a random orientation of spins at temperatures of interest and thus obtain a mean energy by taking three-quarters of the triplet energy and a quarter of the singlet energy. Fortunately, this second correction term need not be known with such accuracy as the first quantity.

We shall consider the case of phosphorus impurities in a medium of silicon, where the normal activation energy is 0.045 eV and the dielectric constant is 11.7.

A phosphorus atom has one more positive charge than a silicon atom, so it can be considered as a single positive charge embedded in a continuous medium with an electron bound to it. When the electron is far from its parent impurity atom, it will be moving slowly and it will polarize the surrounding medium, and the effective dielectric constant will be the static one (κ). When it is near to its parent atom, it will be moving quite rapidly and will only partially polarize the surrounding medium and the effective dielectric constant will be much less. Therefore, for the potential between the impurity atom and its donor electron, we use an expression of the form:

$$V = -\frac{e}{\kappa r} [1 + (\kappa - 1)e^{-\gamma r}] \quad \dots\dots (2)$$

where r is the distance between atom and electron, and γ is some suitable damping factor chosen so that the activation energy will have the correct value. The medium will also reduce the effective mass of the electron m^* and in this case $m^* = 0.25m$ (which is the accepted value for silicon).

We use modified atomic units throughout the calculations: the unit of length $r_0 = \hbar^2/m^*e^2 = 2.12 \text{ \AA}$, the unit of charge $e = 4.80 \times 10^{10} \text{ e.s.u.}$, the unit of energy = $e^4 m^* / \hbar^2 = 6.8 \text{ eV}$. The Schrödinger equation for a single impurity atom becomes

$$\left[-\frac{1}{2}\nabla^2 - \frac{1}{\kappa r} (1 + (\kappa - 1)e^{-\gamma r}) \right] \psi = E\psi \quad \dots\dots (3)$$

where we choose ψ of the form

$$\psi = \frac{a}{\pi^{1/2}} \exp(-r) + \frac{b}{(\pi\kappa^3)} \exp(-r/\kappa). \quad \dots\dots (4)$$

The values of a and b are found by a variational process and the value of γ for the correct activation energy is $\gamma = 1.3$.

§ 3. HYDROGEN MOLECULAR ION IN A DIELECTRIC

Let the two atoms A and B be separated by a distance R , and let the distance of the electron from the atoms be r_A and r_B , then the Schrödinger equation of the system is

$$\left\{ -\frac{1}{2}\nabla^2 + \frac{1}{\kappa R} - \frac{1}{\kappa r_A} [1 + (\kappa - 1)\exp(-\gamma r_A)] - \frac{1}{\kappa r_B} \right. \\ \left. \times [1 + (\kappa - 1)\exp(-\gamma r_B)] \right\} \psi = E_{H_2} + \psi. \quad \dots\dots (5)$$

Dickinson (1933) found for the case of the ordinary hydrogen molecular ion that the energy of the system was given fairly accurately by assuming the wave function was made up of 1s and 2p functions. In this case we take a wave function of the form

$$\psi = c_1(\psi_1(r_A) + \psi_1(r_B)) + c_2(\psi_2(r_A) + \psi_2(r_B)) \quad \dots\dots (6)$$

where $\psi_1(r_A)$ and $\psi_1(r_B)$ are the solutions to the hydrogen atom in a medium of variable dielectric constant given by (4) and

$$\psi_2(r) = \frac{\alpha^{3/2}}{\pi^{1/2}} r \cos \theta \exp(-\alpha r) \quad \dots\dots (7)$$

where θ is the angle between \mathbf{r} and \mathbf{R} .

The spread parameter α is varied to give the minimum value of the energy of the system. Ideally, there ought to be a variable parameter in the S functions, but the correct S function for minimum energy will only be slightly different from the function given in (4), the variation in the p function being the greatest.

The minimum value of the energy in terms of α was then found analytically, and then the energy was minimized with respect to α numerically for a series of values of R . Values of the energy were computed for values of R between 10 and 50 modified atomic units and an approximate expression for the energy of the system E_{H^+} is given by

$$E_{H^+}(R) = E_\infty + 0.0159 \exp(-0.197R) - 0.00277 \exp(-0.0409R). \quad \dots\dots (8)$$

E_∞ is the energy of an isolated impurity atom.

The last term on the right-hand side of (8) is larger than the second term for values of $R > 12$ atomic units, and hence in all realistic values of R , the electron will be more tightly bound than in the case of an isolated impurity atom.

§ 4. THE HYDROGEN MOLECULE IN A DIELECTRIC

Labelling the atoms A and B, and the electrons 1 and 2, r_{A1} and r_{B1} are the distances of the first electron from atoms A and B respectively. r_{A2} and r_{B2} are the distances of the second electron from A and B respectively, and r_{12} and R are the separation of the two electrons and the separation of the two atoms.

We evaluate the energy of the hydrogen molecule in a medium of variable dielectric constant using the model of Heitler and London (1927), using wave functions of the form

$$\Psi = A[\psi(r_{A1})\psi(r_{B2}) + \psi(r_{A2})\psi(r_{B1})] \quad \dots\dots (9)$$

$$A^2 = 1/(2 + 2\Delta^2) \quad \dots\dots (10)$$

$$\Psi_A = B[\psi(r_{A1})\psi(r_{B2}) - \psi(r_{A2})\psi(r_{B1})] \quad \dots\dots (11)$$

$$B^2 = 1/(2 - 2\Delta^2) \quad \dots\dots (12)$$

$$\text{where} \quad \Delta = \int \psi(r_{A1})\psi(r_{B1}) d\tau. \quad \dots\dots (13)$$

Here the one-electron wave functions are given by Eqn (4). The Hamiltonian of the system is taken to be

$$-\frac{1}{2}(\nabla_1^2 + \nabla_2^2) + \frac{1}{\kappa R} + V(r_{12}) - V(r_{A1}) - V(r_{A2}) - V(r_{B1}) - V(r_{B2}) \quad \dots\dots (14)$$

$$\text{where} \quad V(r) = \frac{1}{\kappa r} [1 + (\kappa - 1) \exp(-\gamma r)]. \quad \dots\dots (15)$$

Using these two wave functions ((9) and (11)) we get two values of the energy E_S and E_A corresponding to the symmetrical and antisymmetrical space wave functions

$$E_S = 2E_\infty + \frac{1}{\kappa R} + \frac{E_{11} + E_{12}}{1 + \Delta^2} \quad \dots\dots (16)$$

$$E_A = 2E_\infty + \frac{1}{\kappa R} + \frac{E_{11} - E_{12}}{1 - \Delta^2} \quad \dots\dots (17),$$

where $E_{11} = \iint \psi^2(r_{A1})\psi^2(r_{B2})[V(r_{12}) - V(r_{A2}) - V(r_{B1})] d\tau_1 d\tau_2, \dots (18)$

$$E_{12} = \frac{1}{2} \iint \psi(r_{A1})\psi(r_{A2})\psi(r_{B1})\psi(r_{B2}) \\ \times [2V(r_{12}) - V(r_{A1}) - V(r_{A2}) - V(r_{B1}) - V(r_{B2})] d\tau_1 d\tau_2; \dots (19)$$

E_S is a singlet state and corresponds to an attraction between the two atoms and E_A is a triplet state and gives rise to a repulsion between the atoms at all values of R . The integrals containing $V(r_{A1})$, $V(r_{A2})$, $V(r_{B1})$ and $V(r_{B2})$ are easily evaluated from the table of two-centre integrals tabulated by Coulson (1942). The integral in $V(r_{12})$ for the coulombic term E_{11} is evaluated by standard methods.

The part of the exchange term in r_{12} is

$$\iint \psi(r_{A1})\psi(r_{A2})\psi(r_{B1})\psi(r_{B2})V(r_{12}) d\tau_1 d\tau_2 \\ = \frac{1}{K} \iint \frac{1}{r_{12}} \psi(r_{A1})\psi(r_{A2})\psi(r_{B1})\psi(r_{B2}) d\tau_1 d\tau_2 + \frac{K-1}{K} \iint \frac{1}{r_{12}} \psi(r_{A1})\psi(r_{A2})\psi(r_{B1})\psi(r_{B2}) \\ \times \exp(-\gamma r_{12}) d\tau_1 d\tau_2. \dots (20)$$

The first term contains 16 integrals which can be evaluated by the method of Sugiura (1927) by changing to elliptic coordinates and expanding r_{12} in terms of the associated Legendre functions. The second term cannot be evaluated analytically, but its contribution to E_{12} is very small ($< 1\%$ of E_{12}) and can be roughly estimated from the relative values of the two terms in the integral

$\iint \psi^2(r_{A1})\psi^2(r_{B2})V(r_{12}) d\tau_1 d\tau_2$. As in the case of the molecular ion, values of the energy were computed for values of R between 10 and 50 modified atomic units, and an approximate expression for the energy in these units is

$$E_{H_2}(R) = 2E_\gamma + 0.0717 \exp(-0.0255R) + 0.0219 \exp(-0.133R). \dots (21)$$

The electrons are not so tightly bound, in this case, as an electron on an isolated atom. The energy required to remove an electron from the molecular system will be

$$E_{H_2^+} - E_{H_2} = -E_\infty + 0.0159 \exp(-0.197R) - 0.00277 \exp(-0.0409R) \\ - 0.0717 \exp(-0.255R) - 0.0219 \exp(-0.133R). \dots (22)$$

When computing the amount of reduction in activation energy, it is necessary to consider all the pairs a given atom can make, therefore we must integrate over all possible pairs. Assuming that the impurity atoms are distributed with constant density throughout the material, the reduction in activation energy ΔE is given by

$$\Delta E = 8.4 \times 10^{-20} \rho \text{ ev} \dots (23)$$

where ρ is the density (centres/cm³) of impurity atoms.

This model of considering the impurities in pairs will only hold at low concentrations, when the probability of finding two centres close together in a region of the material is much greater than the probability of finding three centres close together. The linear variation of ΔE with ρ predicted by (23) contrasts with the $\rho^{1/3}$ law arising from the theory of Pearson and Bardeen (1949). However, the experimental results published by them are not sufficiently detailed to determine the power law in the low density region. The results of Debye and Conwell (1954) are also insufficiently detailed in this region to make a comparison possible.

§ 5. DISCUSSION

At 10^{17} centres/cm³ the reduction in activation energy is 0.008 eV which compares with 0.009 eV in the case of Pearson and Bardeen, and the activation energy becomes zero at about 5×10^{17} centres/cm³ on this simple model. However, this approximation can only be considered valid at low densities and will always give values that are high. At high densities, when one electron is excited in a given region of the material, it is not correct to look upon the reduction in activation energy as the spreading of an electron over two centres, but rather to the spreading of $x-1$ electrons over x centres, where x at high densities is much greater than 2. As the density is reduced, the two-centre model will be more correct. At low concentrations using this model, the reduction in activation energy agrees approximately with the results of Pearson and Bardeen (1949) although more recent results show that their zero concentration activation energy is too high.

Hence, at low concentrations, the reduction in activation energy can probably be regarded as due to a combination of the effect discussed here with the screening effect of Pincherle (1951), and at high densities, as a combination of screening and the formation of an impurity band.

REFERENCES

- AIGRAIN, P., 1954, *Physica*, **20**, 978.
ATKINS, K. R., DONOVAN, R., and WALMSLEY, R. H., 1960, *Phys. Rev.*, **118**, 411.
BALTENSPERGER, W., 1953, *Phil. Mag.* (Series 7), **44**, 1355.
BLAKEMORE, J. S., 1959, *Phil. Mag.* (Series 8), **4**, 560.
CASTELLAN, G. W., and SEITZ, F., 1951, *Semiconducting Materials* (London: Butterworths).
CONWELL, E. M., 1956, *Phys. Rev.*, **103**, 51.
COULSON, C. A., 1942, *Proc. Camb. Phil. Soc.*, **38**, 210.
DEBYE, P. P., and CONWELL, E. M., 1954, *Phys. Rev.*, **93**, 693.
DICKINSON, B. N., 1933, *J. Chem. Phys.*, **1**, 317.
ERGINSOY, C., 1952, *Phys. Rev.*, **88**, 893.
FRITZSCHE, H., 1955, *Phys. Rev.*, **99**, 406.
HEITLER, W., and LONDON, F., 1927, *Z. Phys.*, **44**, 455.
LEHMANN, G. W., and JAMES, H. M., 1955, *Phys. Rev.*, **100**, 1698.
MOTT, N. F., 1956, *Canad. J. Phys.*, **34**, 1356.
PEARSON, G. L., and BARDEEN, J., 1949, *Phys. Rev.*, **75**, 865.
PINCHERLE, L., 1951, *Proc. Phys. Soc. A*, **64**, 663.
SUGIURA, Y., 1927, *Z. Phys.*, **45**, 484.

Some Physical Properties of the γ and δ Phases in the U-Zr System

By R. D. BARNARD†

University of Nottingham

Communicated by L. F. Bates; MS. received 10th May 1961

Abstract. Electrical resistivity and magnetic susceptibility measurements are reported for U-70 and 74 at. % Zr in both the γ and δ phases. Negative temperature coefficients of resistivity were found in the metastable γ phase of U-70 at. % Zr, and also in the δ phase of both alloys between 90° and 870°K. The Pauli weak spin paramagnetism, exhibited by both specimens, always increased with temperature.

The results support the view that the δ phase is primitive hexagonal and not an ordered form of the body-centred cubic γ phase. The anomalous resistivity behaviour may be a consequence of the band structure of the alloy.

§ 1. INTRODUCTION

RECENT measurements of the resistivity of metastable γ body-centred cubic U-Mo and U-Nb alloys (Chandrasekhar and Hulm 1958, Berlincourt 1959, Bates and Barnard 1961a, b) have shown an abnormal feature between 4.2 and 500°K, namely, a monotonic decrease of resistivity with increasing temperature. The accumulation of additional data (Hall effect, electronic specific heat, and magnetic susceptibility) particularly for the U-Mo system has furthered our understanding of the electronic structure of these alloys, and a collective electron model now seems appropriate for their description. With this model the resistivity behaviour may be explained, provided that the density of states at the Fermi surface is a sensitive function of energy. The existence of similar resistivity behaviour in γ U-Nb alloys (Bates and Barnard 1961 b), despite the difference in the conventional valency of Nb and Mo, has led to a similar conclusion about the position of the Fermi surface in the density of states-energy spectrum.

This behaviour is not unique in metastable uranium alloys; alloys of Ti-V (Brotzen *et al.* 1955), Ti-Mo (Yoshida and Tsuya 1956), and Ti-Nb (Ames and McQuillan 1954) also show this phenomenon in the quenched body-centred cubic phase, and again no explanation in terms of localized electrons is appropriate. Similar anomalous behaviour has also been reported in other alloy systems; some Fe-Cr (Newmann and Stevens 1959) and Th-Ce (Newmann 1958) alloys exhibit negative temperature coefficients of resistivity over small temperature ranges, but they are thought to be associated with the scattering of electrons by localized moments. Such alloys also show anomalies in the magnetic susceptibility in the same temperature ranges.

The extension of magnetic and electrical observations to the U-Zr system arose naturally from the previous investigations on uranium alloys, for once again the γ phase can be retained at room temperature by quenching alloys of suitable

† Now at E.R.A. Research Laboratories, Cleve Road, Leatherhead, Surrey.

composition. A further investigation of the same properties of the δ phase was performed in the hope of resolving the conflicting views held concerning its crystal structure.

§ 2. THE CRYSTALLOGRAPHY OF THE γ AND δ PHASES

The phase diagram of the U-Zr system is now well established, although disagreement exists between various authors on some of its finer details. There is, however, complete agreement that solid solution exists between γ body-centred cubic uranium and β body-centred cubic zirconium, and the stability of the δ phase is now established (Holden and Seymour 1957). The γ phase can be stabilized at room temperature by quenching alloys in a composition range between about 50 and 80 at. % Zr, but the rapidity with which the δ phase forms often results in two-phase mixtures. Solubility limits of the δ phase have been variously reported; Knapton (1957, unpublished) reports a solubility range of 63–79.5 at. % Zr at 600°C, but Duffey and Bruch (1958) give the limits as 66 and 72 at. % Zr. Studies in this region are complicated by the pronounced effects of oxygen and nitrogen on the δ phase solubility limits, and by the nature of the γ - δ transformation. The δ phase was first thought to be an ordered structure of the γ form (Mueller 1955), but Boyko (1957) considers the structure to be more appropriately indexed as primitive hexagonal. This structure is partly ordered with zirconium atoms located at the (0, 0, 0) positions, while zirconium and uranium atoms are located randomly at $(\frac{1}{3}, \frac{2}{3}, \frac{1}{2})$ and $(\frac{2}{3}, \frac{1}{3}, \frac{1}{2})$ positions. The random distribution of uranium and zirconium atoms allows a considerable range of composition. For U-70 at. % Zr, the δ γ phase change temperature is about 605°C (878°K).

§ 3. EXPERIMENTAL DETAILS

Two alloys of composition U-70 and 74 at. % Zr were used in this investigation, both being within the δ solubility limits. The alloys were prepared at the Atomic Energy Research Establishment, Harwell, in an argon arc furnace from uranium and zirconium samples whose principal impurities are shown in the Table.

Chief Impurity Contents (parts per million) of Uranium and Zirconium

	C	Fe	Al	Si	N ₂	Cr	Mn	H ₂	O ₂	Cu	Ni	W	As
Uranium	800	100	65	25	20	5	10	10	50	—	—	—	—
Zirconium	—	—	—	—	50	4	3	300	200	150	10	200	50

The alloys were homogenized for two weeks, at 1000 °C, in the γ phase region and then rapidly water-quenched to retain the γ phase in metastable equilibrium. Metallographic observations performed on the two alloys after the susceptibility and resistivity examinations showed U-74 at. % Zr to be mainly δ phase and U-70 at. % Zr, though predominantly δ phase, contained considerable amounts of impurity, especially at the grain boundaries.

Details of the apparatus for the measurement of magnetic susceptibility and electrical resistivity over the ranges 293–1200°K and 90–1200°K respectively have been described elsewhere (Barnard 1960).

§ 4. EXPERIMENTAL RESULTS

4.1. Electrical Resistivity

The resistivity-temperature relation of U-70 at. % Zr is shown in Fig. 1. Observations were first taken with temperature increasing from 90°K with the specimen in the metastable γ state; the onset of precipitation of the δ phase is clearly indicated at 375°K, where there is a marked discontinuity in the slope of the resistivity-temperature curve. Readings were continued as the temperature and degree of precipitation increased until, at about 878°K, the γ phase was re-established with a discontinuous decrease of resistivity. Of course, little value can be attached to the observations taken while the γ phase was decomposing, as these were time-dependent as well as temperature-dependent, and they are

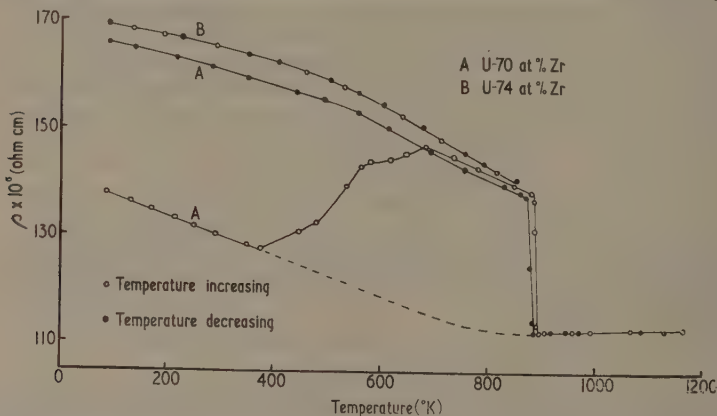


Fig. 1. Electrical resistivity plotted against temperature of U-70 at. % Zr in the metastable γ , stable γ and δ phases and U-74 at. % Zr in the δ phase.

included in Fig. 1 merely to show the marked effect of δ precipitation. In the stable γ region, where the resistivity was almost temperature-independent, the heating and cooling curves were identical, showing that equilibrium was established in this phase. A tentative interpolation shown by the broken line in Fig. 1 has been made between the metastable and stable γ regions of the resistivity curve, thus giving the probable variation between 90 and 1200°K of γ -U-70 at. % Zr. Slight temperature hysteresis was observed on cooling through the γ - δ phase change temperature, after which further cooling was accompanied by a steady increase in resistivity down to 90°K.

It was at first thought that this remarkable behaviour might have been due to insufficient time being allowed for the phase change γ - δ to be completed. It was therefore decided to follow the resistivity changes of U-74 at. % Zr at 875°K while the γ phase decomposed to the δ phase. Between 5 and 30 hours after the decomposition was started by reducing the temperature from 900 to 875°K no change in the resistivity occurred, and so the δ phase was considered to be in equilibrium. Resistivity values were then taken as the temperature was reduced to 90°K. The variation is shown in Fig. 1 together with values taken on heating afterwards. Cooling and heating curves are identical.

From information on the thermal expansion of U-70 at. % Zr in the δ phase (Knapton 1959, private communication), corrections were calculated for the resistivity values, but their effect was so small that the graphs are here plotted without correction. The similarity between the forms of the resistivity variations of δ U-70 at. % Zr and U-74 at. % Zr seems to indicate that the δ phase was in equilibrium in the former case also.

The absolute value of the resistivity of δ phase U-70 at. % Zr at 273°K was $161 \pm 2 \times 10^{-6}$ ohm cm, compared with the value $184 \pm 2 \times 10^{-6}$ obtained by Loasby (1958) who also investigated the same properties of the δ phase but only over the limited temperature range 90–293°K. However, Loasby observed a similar temperature dependence of resistivity. The greater purity of materials in the present alloys may account for the lower resistivity.

4.2. Magnetic Susceptibility

Figure 2 shows the temperature variation of the susceptibility of U-70 at. % Zr in the metastable γ , stable γ and δ phases and also of the δ phase of U-74 at. % Zr. The observations on the former specimen were taken, like those of the resistivity, first in the metastable γ and then in the stable γ region. The variation for U-70 at. % Zr shown in Fig. 2 indicates that in the stable γ region the susceptibility is only weakly dependent on temperature, whilst strong temperature

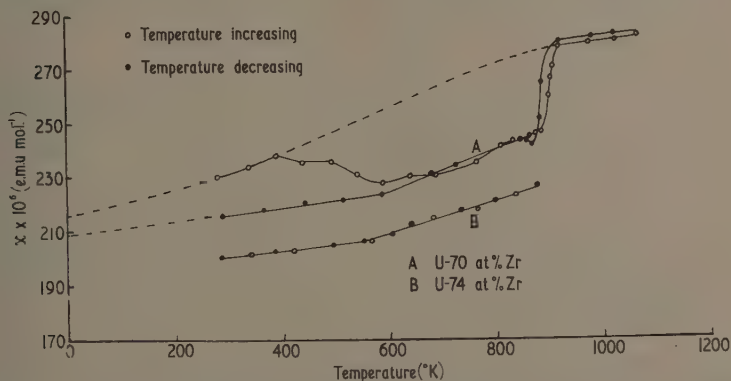


Fig. 2. Magnetic susceptibility plotted against temperature of U-70 at. % Zr in the metastable γ , stable γ and δ phases and U-74 at. % Zr in the δ phase.

dependence holds for the metastable γ state. In this respect the behaviour is similar to that of the uranium-rich γ U-Mo and U-Nb alloys. The effect of precipitation of the δ phase is clearly accompanied by a decrease in susceptibility; this precipitation in the metastable γ U-Zr alloys is much more rapid than with U-Mo or U-Nb alloys, and marked effects occurred in the present sample at temperatures as low as 100°C.

With U-70, 74 at. % Zr in the δ phase there appears to be an increase in slope of the susceptibility-temperature graph at about 560°K. This is at precisely the temperature where the resistivity-temperature curves of the δ phase alloys show a decrease in slope (Fig. 1). These effects are considered later in the discussion of the δ phase.

§ 5. DISCUSSION

Both the susceptibility and resistivity behaviours of γ U-70 at. % Zr are qualitatively similar to those previously reported with the uranium-rich γ U-Mo and U-Nb alloys (Bates and Barnard 1961 a, b). With no other physical property data on γ U-Zr alloys available for correlation purposes, it is hazardous to discuss the possible electronic structure of these alloys. However, the properties presented here seem to indicate that a collective electron model, with a band structure at the Fermi surface at least qualitatively similar to those of the U-Mo and U-Nb alloys is appropriate. It is to be noted that a negative temperature coefficient of resistivity in γ U-Mo alloys is found up to 30 at. % Mo, and with γ U-Nb alloys up to 60 at. % Nb, but this behaviour is present in a γ U-70 at. % Zr specimen. The extension of the anomalous behaviour may well be associated with decreasing electronic contributions from the solute atoms (Mo, Nb, Zr have conventional valencies of 6, 5, 4 respectively).

As far as the author knows, this is the first example of the persistence of a negative coefficient of resistivity characteristic of the δ phase over a wide range of temperature of some 800°K in a metallic alloy in an equilibrium phase. Between liquid oxygen temperature and 800 K there is a 17% decrease in resistivity; this property may have useful applications in low resistance circuits whose total resistance is required to be constant with temperature. Thermal conductivity measurements on the δ phase may be extremely interesting in view of an anomalous scattering mechanism.

Loasby (1958) investigated the resistivity and susceptibility properties of the δ phase at low temperatures and suggested that these were consistent with an almost full Brillouin zone with a small population of an overlapping zone. The effect of temperature was then to transfer electrons from the first zone to the second, thereby increasing the number of current carriers. Another possibility is that discussed by Blatt (1961), in which the first and second derivatives of the density of states with respect to energy at the Fermi surface govern the unusual resistivity behaviour. When Hall effect data are available on the δ phase it will be possible to decide which of these explanations is appropriate. In the former case, the Hall coefficient should decrease strongly with temperature, while a small increase should be observed in the latter.

The resistivity behaviour of U-70 at. % Zr shown in Fig. 1 clearly indicates that the δ phase is characterized by a higher resistivity at a given temperature than the γ phase, and this is hardly typical of a superlattice structure. However, it is theoretically possible, although unusual in practice, for a superstructure to exhibit a higher resistivity than the parent disordered structure. For, if the increase in order of the superlattice which alone results in a lower resistivity is accompanied by a sufficiently large decrease in the number of effectively free electrons, produced possibly by the new faces of the Brillouin zone, then a higher resistivity will ensue. In the present instance, this situation appears improbable, since the near equality of the susceptibilities of the δ and γ phases at 0°K is indicative that no severe electronic change takes place although, obviously, a small change must take place to give the different temperature dependences of susceptibility. It seems, therefore, that the physical properties so far investigated favour the hexagonal structure rather than the superstructure description of the δ phase.

The change of slope exhibited by the δ phase resistivity-temperature and susceptibility-temperature graphs at 560°K is probably a direct consequence of

the increased rate of expansion of the lattice also observed above 560°K (Knpton 1959, private communication). The increased lattice constants modify the volume of the Brillouin zones and could increase the number of effectively free electrons, thus leading to the observed resistivity behaviour. Alternatively, the expansion could change the average mean free path of the current carriers. One expects, on general grounds, an expansion of the lattice to produce as well an increase in the density of states at the Fermi surface, and this could account for the increased slope in the susceptibility-temperature curve.

Finally it may be mentioned that the susceptibility-temperature behaviour of the δ and γ phases could be connected with the presence of antiferromagnetic order in these alloys with high Néel points, although no such order is found in the pure elements uranium or zirconium. Neutron diffraction measurements with these abnormal alloys would probably be very helpful.

ACKNOWLEDGMENTS

The author is indebted to Professor L. F. Bates for valuable discussion and for supervision of the work, to Dr. A. Knpton of Associated Electrical Industries, Aldermaston, for the thermal expansion data and to Dr. W. E. Gardner of the Atomic Energy Research Establishment, Harwell, for the provision of the alloys and much helpful discussion. Thanks are also due to the Director of the Atomic Energy Research Establishment, Harwell, for permission to publish the results.

REFERENCES

- AMES, S. L., and McQUILLAN, A. D., 1954, *Acta Metallurgica*, **2**, 831.
BARNARD, R. D., 1960, *Thesis*, University of Nottingham.
BATES, L. F., and BARNARD, R. D., 1961 a, *Proc. Phys. Soc.*, **77**, 691.
—— 1961 b, *Proc. Phys. Soc.*, **78**, 361.
BERLINCOURT, T. G., 1959, *J. Phys. Chem. Solids*, **11**, 12.
BLATT, F. J., 1961, *J. Phys. Chem. Solids*, **17**, 177.
BOYKO, E., 1957, *Acta Cryst.*, **10**, 712.
BROTZEN, F. R., HARMAN, E. L., and TROIANO, A. R., 1955, *Trans. Amer. Inst. Min. (Metall.) Engrs*, **203**, 413.
CHANDRASEKHAR, B. S., and HULM, J. K., 1958, *J. Phys. Chem. Solids*, **7**, 259.
DUFFEY, J., and BRUCH, C., 1958, *Trans. Amer. Inst. Min. (Metall.) Engrs*, **212**, 17.
HOLDEN, A. N., and SEYMOUR, W. E., 1957, *Trans. Amer. Inst. Min. (Metall.) Engrs*, **209**, 515.
LOASBY, R. G., 1958, *Proc. Phys. Soc.*, **72**, 425.
MUELLER, M. H., 1955, *Acta Cryst.*, **8**, 849.
NEWMANN, M., 1958, *Thesis*, University of Nottingham.
NEWMANN, M., and STEVENS, K. W. H., 1959, *Proc. Phys. Soc.*, **74**, 290.
YOSHIDA, S., and TSUYA, Y., 1956, *J. Phys. Soc. Japan*, **11**, 1206.

Magnetostriction in Antiferromagnetic Nickel Oxide

By L. ALBERTS† AND E. W. LEE

Department of Physics, The University, Sheffield

MS. received 1st May 1961

Abstract. Measurements of magnetostriction on a single crystal of antiferromagnetic nickel oxide were made in fields up to 21 kilo-oersteds. The order of magnitude of the magnetostriction is the same as that for ferromagnetic materials, viz. about -20×10^{-6} and a square law relation, with field, is obeyed up to several thousand oersteds before a gradual saturation tends to set in. The dependence of strain on field and measuring directions is described with respect to axes that constitute cylindrical symmetry.

§ 1. INTRODUCTION

NICKEL oxide, NiO, is an antiferromagnetic substance with a Néel temperature of 523°K (La Blanchetais 1951). Above 523°K it has a cubic structure of the NaCl type. In the antiferromagnetic state below this temperature the spins are ordered in such a way that within a given (111) plane the spins are all parallel, but are antiparallel to those in adjacent (111) planes. This ordering results in a slight contraction of the [111] axis which is normal to the planes containing the spins (Slack 1960, Roth 1960). The unit cell can then be regarded as rhombohedral with a rhombohedral angle of 90°4' at room temperature. As a result of this distortion a crystal having spins in different sets of octahedral planes will be twinned. These twin boundaries can normally be permanently removed by application of mechanical stresses or large fields (Slack 1960, Roth 1960), thereby reducing the crystal to one with all the spins in a single set of parallel octahedral planes. Indeed, it appears from Slack's and Roth's work that it requires rather careful heat treatment and subsequent handling to produce and maintain these twin boundaries in single crystals of NiO.

There appears to be no, or at least very small, inherent anisotropy with the (111) planes containing the spins (Roth and Slack 1960) and the antiferromagnetic domain orientation must be essentially determined by internal stresses, lattice imperfections etc. In the presence of a magnetic field the lowest energy state is one in which the spin-alignment axis is perpendicular to the field and consequently the domains can be aligned in moderate fields without significantly affecting the antiparallel ordering within the domains themselves. Exceedingly large magnetic forces will be required to rotate the spins appreciably out of the octahedral planes.

If a spontaneous magnetostriction exists within the domains, alignment of the latter will result in an overall strain of the crystal. Because the spin directions are confined to a plane the longitudinal and transverse strains within this plane will be equal and opposite provided that there is a random distribution of domains and that the volume magnetostriction is negligible. Since this is the case in ferromagnetic substances where the nature of the spin interaction is similar such an assumption seems quite reasonable.

† On leave from Department of Physics, University of the Orange Free State, South Africa.

Magnetostriiction in polycrystalline NiO has been reported by Belov and Levitin (1959). The strains they observed were very much smaller than those reported here in comparable field strengths and this might be responsible for the fact that they observed an effect only when a certain threshold field had been exceeded. Measurements on CoO crystals by Nakamichi and Yamamoto (1961) show that the magnetostriiction increases steadily as the applied field is increased from zero. They also reported a variation of magnetostriiction, in single crystals of NiO, with field direction, similar to that found here.

§ 2. EXPERIMENTAL PROCEDURE AND RESULTS

The crystal was kindly supplied by Dr. K. Hoselitz of Mullard Research Laboratories. It was approximately 6 mm square and 1 mm thick. X-ray analysis showed that the two parallel flat surfaces lay in a (227) plane. This is the plane ABC in Fig. 1 with $OA = OB$ and $\theta = 22^\circ$ (where OB is perpendicular to AB).

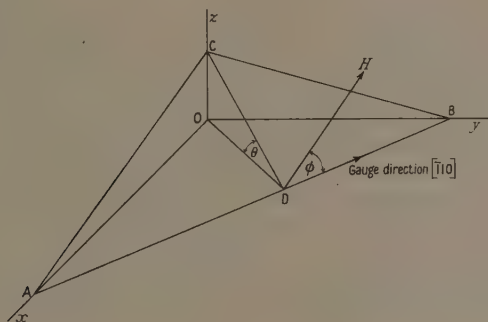


Fig. 1

The magnetostriiction was determined by the usual strain gauge technique. The sensitivity and stability of the arrangement was such that the strain of 10^{-7} could be measured. A small strain gauge (Tinsley, Type 20A, Special) was fixed along the direction AB, i.e. in the $[\bar{1}10]$ direction. The crystal was mounted with the plane ABC horizontal so that the magnetic field, when the electromagnet was turned about a vertical axis, also rotated in this plane.

The experimental results are shown in Figs 3 and 4 and will be discussed separately.

§ 3. THEORETICAL CONSIDERATIONS

The observation of a strain in a NiO crystal on application of a magnetic field could, in principle, be due to (a) movement of twin boundaries, (b) the alignment of antiferromagnetic domains within the octahedral planes and (c) rotation of the spins out of the octahedral planes. Of these (a) can be ruled out immediately since it would give rise to a magnetostriictive strain which would be (1) negative, (2) irreversible and (3) would commence only in fields greater than about 5 kilo-oersteds (Slack 1960). However, preliminary x-ray analysis showed the crystal used here to be untwinned and a subsequent investigation using the high resolution afforded by Kössel lines due to fluorescence from the nickel atoms

confirmed this. (These x-ray determinations were kindly carried out by Dr. P. Gaunt.) With regard to (c), bearing in mind that the transverse susceptibility of NiO is certainly not greater than 10^{-4} , an elementary calculation shows that the corresponding strain would be smaller than that actually observed by several orders of magnitude. The magnetostriction which we observed was positive, completely reversible and increased continuously as the field was increased from zero. These facts, coupled with the absence of twin boundaries lead to the conclusion that the observed magnetostriction must be due to movement of antiferromagnetic domains in which the spins are confined within the octahedral planes. Since the inherent crystal anisotropy in an octahedral plane is very small and the local 'easy directions' are presumably determined by internal stresses the type of domain movement which we envisage is different from that which occurs in a single crystal of, say, iron and is more akin to the situation in cold-worked nickel where the local easy directions are determined by local internal stresses and magnetization is believed to occur by coherent rotation of quite large groups of spins.

In order to test these views the variation of the measured strain with the direction of the applied field was calculated as follows. A certain (111) plane was selected and the component of the applied field in this plane, $H \cos \xi$, was calculated as a function of the azimuthal angle ϕ in the plane ABC. Since the field applied in the rotation experiment (11.6 kilo-oersteds) was well within the square law relation of magnetostriction against field (see Fig. 3) the strain in any direction in the given (111) plane may be taken to be proportional to the square of the field component in that plane. Thus the fraction of the spins that set themselves perpendicular to $H \cos \xi$ will be proportional to $H^2 \cos^2 \xi$. The direction cosines of these spins can then be found as a function of ϕ . The ultimate octahedral plane selected to give the best fit with experiment was the $(\bar{1}\bar{1}\bar{1})$ plane.

By geometry it may be shown that

$$\cos^2 \xi = \frac{\frac{1}{3}\lambda^2 + \frac{2}{3}\tan^2 \theta + (\sqrt{\frac{2}{3}})\lambda \tan \theta + 1}{\lambda^2 + \tan^2 \theta + 1} \quad \dots\dots (1)$$

where

$$\lambda = \left(\frac{2 + \tan^2 \theta}{1 + \cos^2 \theta} \right)^{1/2} \cot \phi$$

and $\theta = 22^\circ$ as determined by x-rays. The direction cosines of the aligned spins (perpendicular to $H \cos \xi$) are

$$(1 - \lambda - \sqrt{2} \tan \theta)s, \quad -(\lambda + 1 + \sqrt{2} \tan \theta)s, \quad -2s, \quad \dots\dots (2)$$

where $s = \{6 + 2(\lambda + \sqrt{2} \tan \theta)^2\}^{-1/2}$. These equations neglect the very small rhombohedral distortion as may be readily justified. The spins are parallel to the $(\bar{1}\bar{1}\bar{1})$ plane and this may be taken as the base of a cylinder with the $[\bar{1}\bar{1}\bar{1}]$ direction as axis. The strain in such a case is given by (Carr 1959)

$$\frac{dl}{l} = k_0 + k_1\beta_3^2 + (k_2 + k_3\beta_3^2)\alpha_3^2 + k_4(\alpha_1\beta_1 + \alpha_2\beta_2)^2 + k_5(\alpha_1\beta_1 + \alpha_2\beta_2)\alpha_3\beta_3 \quad \dots\dots (3)^{**}$$

where the α 's and β 's are the direction cosines of the spins and the measuring direction with respect to a set of orthogonal axes such that $\alpha_3 = 1$ corresponds to

the cylinder axis and the k 's are constants. If now the $[1\bar{1}2]$ direction in the $(\bar{1}1\bar{1})$ plane is taken as the direction $\alpha_2 = 1$ (see Fig. 2), then it may be shown that

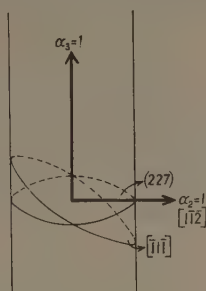


Fig. 2

those spins which are aligned by the applied field (i.e. which are perpendicular to it) have direction cosines

$$\alpha_2 = \{1 + \frac{1}{3}(\lambda + \sqrt{2} \tan \theta)^2\}^{-1/2},$$

$\alpha_1 = (1 - \alpha_2^2)^{1/2}$ and $\alpha_3 = 0$. Also $\beta_1 = 0$, $\beta_2 = 1/\sqrt{3}$ and $\beta_3 = \sqrt{\frac{2}{3}}$. Substituting these values into Eqn (3) and remembering that the field dependent part of the strain must be multiplied by $\cos^2 \xi$ we obtain

$$\frac{dl}{l} = k + (k_0 + \frac{1}{3}k_4\alpha_2^2) \cos^2 \xi \quad \dots\dots (4)$$

where k is a constant. This equation has been plotted in Fig. 4 with $k = 4.55 \times 10^{-6}$, $k_0 = 1.4 \times 10^{-6}$ and $k_4 = 27.3 \times 10^{-6}$. It must be borne in mind that these values are applicable only for a particular field.

§ 4. DISCUSSION AND CONCLUSIONS

The agreement between Eqn (4) and the experimental values shown in Fig. 4 is satisfactory and would seem to confirm the basic premise that the observed magnetostriction is solely due to rotation of the spins within a set of (111) planes.

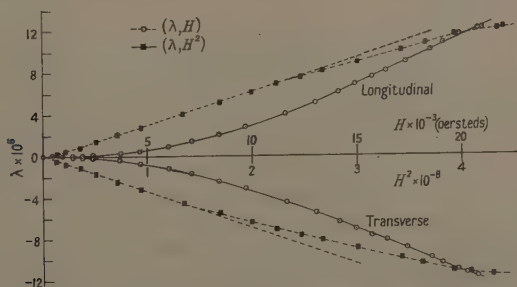


Fig. 3. Variation of longitudinal and transverse magnetostriction with field.

Fig. 3 shows that the longitudinal magnetostriction λ_L is proportional to H^2 up to 15 kilo-oersteds. For the transverse measurement λ_T the departure from

the square law relation sets in about 12 kilo-oersteds. Within the square law region one may write

$$\lambda_L = a H^2 \cos^2 \xi_L$$

and

$$\lambda_T = a H^2 \cos^2 \xi_T$$

where a is a constant and $\cos \xi_L$ and $\cos \xi_T$ are to be obtained from Eqn (1). For a given value of H , therefore, $\lambda_L/\lambda_T = \cos^2 \xi_L/\cos^2 \xi_T$, which for the crystal used here is equal to 0.302. The measured value of 0.90 can be accounted for by the presence of a preferred domain orientation similar to that frequently observed in ferromagnetic materials.

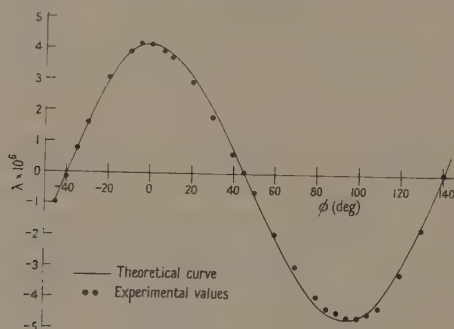


Fig. 4. Variation of magnetostriction with azimuthal angle ϕ in the plane of the crystal: magnetic field 11.6 kilo-oersteds.

As Fig. 2 shows, the magnetostriction shows a tendency towards saturation in the highest fields that were attainable.

An attempt to deduce the saturation value by fitting the high-field end of the longitudinal magnetostriction curve to the equation $\lambda = \lambda_s - c/H$ yielded the value $\lambda_s = 26 \times 10^{-6}$ but this is necessarily uncertain since an equation of this form is usually valid only in the region very close to saturation. Visual inspection of the curve leads to a value $\lambda_s \sim 20 \times 10^{-6}$. This means that there is a spontaneous magnetostriction in NiO which is roughly -20×10^{-6} in the direction of the antiferromagnetic axis.

The maximum strain we observed corresponds to about half the saturation value and this implies that about half the domains are aligned in a field of 21 kilo-oersteds. Now the pressure on a domain wall is $\frac{1}{2}(\chi_{\perp} - \chi_{\parallel})H^2$, where χ_{\perp} and χ_{\parallel} are the transverse and parallel susceptibilities. If we take 10^{-5} as a reasonable figure for $\chi_{\perp} - \chi_{\parallel}$, the pressure in a field of 21 kilo-oersteds is about 2×10^5 dyn cm $^{-2}$, which is roughly the same as that which would be experienced by a 90° wall in iron in a field of about 100 oersteds. Alternatively since 100 oersteds is a field which would be required to magnetize a typical ferromagnetic substance to half its saturation value this implies that the restoring force on a domain wall in our crystal is of the same order of magnitude as that in many ferromagnetics. In polycrystalline NiO, on the other hand, the observed magnetostriction is smaller by an order of magnitude (Belov and Levitin 1959) which implies that the restoring force on the domains walls are greater by a similar factor. Thus although movement of anti-ferromagnetic domain walls will give rise to a change in Young's modulus at the

Néel temperature as observed, for example, by Street and Lewis (1951) in polycrystalline NiO, it is very difficult to account for the magnitude of the changes they observed (a factor of about two) in terms of the same domain wall movement that is responsible for the magnetostriiction which we observe. Our measurements suggest that such a mechanism could not give rise to an effect in NiO which is significantly greater than that observed in ferromagnetics. A more likely explanation is that the change in Young's modulus (which in NiO is a maximum at the Néel point whereas in nickel it occurs at the temperature of minimum anisotropy) is a consequence of the discontinuous changes in the thermal expansion coefficient and specific heat which accompany a second-order phase transition.

ACKNOWLEDGMENTS

It is a pleasure to thank Professor W. Sucksmith for putting all possible departmental facilities at our disposal and Dr. P. Gaunt for generous help and useful discussions in connection with the x-ray determinations.

REFERENCES

- BELOV, K. P., and LEVITIN, Z., 1959, *Zhur. Eksp. i teor. Fiz.* **37**, 565. (English translation 1960, *Soviet Physics-JETP*, **37** (10), 400.)
CARR, W. J., 1959, *Magnetic Properties of Metals and Alloys*, Ch. 10 (Cleveland, Ohio : Amer. Soc. Met.).
LA BLANCHETAIS, C. H., 1951, *J. Phys. Radium*, **12**, 765.
NAKAMICHI, T., and YAMAMOTO, M., 1961, *J. Phys. Soc. Japan*, **16**, 126.
ROTH, W. L., 1960, *J. Appl. Phys.*, **31**, 2000.
ROTH, W. L., and SLACK, G. A., 1960, *J. Appl. Phys.*, **31**, 352 S.
SLACK, G. A., 1960, *J. Appl. Phys.*, **31**, 1571.
STREET, R., and LEWIS, B., 1951, *Nature, Lond.*, **168**, 1036.

The Electric Breakdown of Sodium Chloride

BY R. COOPER AND W. A. SMITH

Electrical Engineering Laboratories, University of Manchester

MS. received 25th November 1960, in revised form 30th May 1961

Abstract. Experiments are described which establish that the electric strength of sodium chloride decreases slowly with increase in specimen thickness. Flat topped impulses were used and the time lag to breakdown of each specimen was measured. The mean statistical time lag depended on the nature of the cathode, and it rapidly decreased with increase in the size of voltage increment. The characteristics of breakdown are similar to those predicted by the single avalanche theory of Seitz according to which disruption results from the passage of an electron avalanche exceeding a critical size.

§ 1. INTRODUCTION

CURRENT theories of intrinsic electric breakdown in solid dielectrics have been comprehensively reviewed by Stratton (1961), who concluded that the collective electron mechanism of Fröhlich and Paranjape (1956) and not the single avalanche mechanism (Seitz 1949) is applicable to the alkali halides.

In collective breakdown it is assumed that the initial density of free electrons is sufficiently great for the inter-electron collisions to determine the electron energy distribution. This is Maxwellian but the electron temperature exceeds the lattice temperature by an amount that increases with the applied field. No steady state is possible if the field exceeds a critical value and the material is rapidly destroyed. The critical field is the intrinsic electric strength of the material and it is independent of the specimen size.

In avalanche breakdown, destruction of the material results from the passage of an electron avalanche exceeding a certain size. This avalanche grows from a single electron injected at the cathode. The critical size is determined by considering the energy balance in the cylindrical volume containing the avalanche, and estimating the electron density required to melt the material at the head of the avalanche near to the anode. The criterion of breakdown is similar to that of the streamer theory of gas breakdown (Loeb and Meek 1940) and as in gas breakdown statistical time lags are predicted with the distribution $N_t = N_0 \exp(-t/T)$. Here N_t is the number of time lags in excess of t , N_0 the total number of time lags and T is the mean statistical time lag. This is equal to the reciprocal of the product of the probability P_1 of electron injection and the probability P_2 of the electron growing into an avalanche in excess of the critical size. The mean statistical time lag depends on the cathode and decreases rapidly when the field increases beyond a certain value. A further prediction of the single avalanche theory is that the electric strength decreases with increase in specimen

thickness. This distinguishes the avalanche theory from the collective electron theory because in the latter case a chance fluctuation may give rise to the necessary high density of free electrons and therefore the observation alone of statistical time lags (Cooper and Grossart 1956) is indecisive.

The predicted thickness effect is small in the range generally found convenient for intrinsic strength investigations using alkali halide crystals. It has not yet been detected but it could be obscured by the spread often observed in comparable values of electric strength (Cooper and Wallace 1956). Stratton (1961) drew his conclusion from a comparison of results obtained by Calderwood and Cooper (1953) and by Kawamura and Ryu (1954) but the validity of this comparison is questionable. There is a dearth of experimental evidence both about statistical time lags and about the influence of thickness on the breakdown of alkali halide crystals and the question of the operative mechanism is still open.

§ 2. METHOD

The specimens were of the plane-recessed type, prepared from (100) plates by the method of Calderwood, Cooper and Wallace (1953). The ranges of specimen thickness extended from about 0.01 cm to about 0.07 cm. This was determined by the necessity of using economically the available parent crystals. Specimens thinner than about 0.01 cm are easily cracked and specimens thicker than about 0.1 cm require much material to provide adequate flashover distances. The surfaces of the specimens were highly polished with a commercially available plastic polish, and then they were annealed at about 10 deg C below the melting point for several hours. This treatment makes the group more homogeneous by removing strains produced in preparing the specimens. It also renders a previously polished surface translucent (Smith 1956). Therefore, upon completion of annealing, the surfaces of each specimen were repolished so that it could be examined with transmitted light in a polarizing microscope. The minimum thickness of each specimen was measured to within $\pm 3\%$. A dial gauge micrometer calibrated in divisions of 10^{-4} in. was used and the method was such that no spring pressure was applied to the specimen during the measurement.

The electric strength of each specimen was determined by applying a series of 0.8:8000 μ sec voltage impulses. The amplitude of each impulse exceeded that of the preceding one by the same percentage and the wave was displayed on a cathode-ray oscilloscope and photographed. The time lag from the peak of the wave to the collapse of voltage at breakdown was measured from an enlargement of the oscillogram, and it was the sum of the formative time and the statistical time lag. The former is believed to be less than 10^{-7} sec (Whitehead 1951) and this estimation is confirmed by the present investigation (see § 3). The estimated error in time lag measurement was 0.2 μ sec.

The impulses were obtained from a single-stage impulse generator and the amplitude of each impulse was determined by multiplying the charging voltage by the efficiency of the generator. The charging voltage was stabilized and the ripple was less than 0.02% of the mean voltage. An irradiated 6.25 cm diameter sphere gap was used for standardization purposes. The estimated error in voltage measurement was within $\pm 4\%$. The electrode system was similar to that described by Calderwood, Cooper and Wallace (1953) and the ambient was silicone oil.

§ 3. TIME LAGS

The results illustrated in Fig. 1 show that the time lag distribution is influenced by the nature of the cathode. Curves *a* and *b* were obtained from specimens whose surfaces had been polished, and the cathode material was deposited on to the residue of this operation. In the former case the cathode material was sodium, deposited after baking the specimens in a vacuum for two days at 150°C, and backed by an evaporated layer of base metal to give protection against oxidation. The cathodes used in the experiment of curve *b* were colloidal graphite. Curve *c* was also obtained by using specimens with colloidal graphite cathodes but they were deposited on to the translucent crystal surfaces produced by the annealing treatment, i.e. the second polishing of the crystal surfaces was omitted.

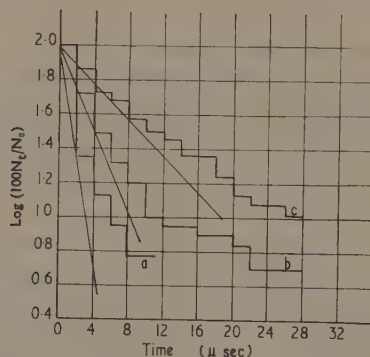


Fig. 1. Effect of cathode on time lag distribution. *a*, 67 specimens with sodium cathodes applied to polished surfaces. $T_{av}=1\ \mu\text{sec}$, $S=1.5\ \mu\text{sec}$; *b*, 100 specimens with graphite cathodes applied to polished surfaces. $T_{av}=3.2\ \mu\text{sec}$, $S=4.5\ \mu\text{sec}$; *c*, 66 annealed specimens with graphite cathodes applied to unpolished surfaces. $T_{av}=11\ \mu\text{sec}$, $S=17\ \mu\text{sec}$.

The average time lag T_{av} and the standard deviation S are quoted in Fig. 1 for each group. Lags exceeding ten times the quoted average value were neglected in the calculation and consequently the values of T_{av} and S are not influenced by the few exceptional results. The size of the groups determined the sensitivity of the investigation. This was limited by the work involved in preparing specimens. A reasonable criterion of significance is that the difference between sample means should be greater than three times the standard error of the difference. With random sampling, this is likely to happen by chance in less than 1% of the trials. The differences between the average time lags quoted in Fig. 1 are significant, according to this standard.

Experiments were also performed with specimens possessing cathodes of evaporated gold, and silver, deposited on to polished crystal surfaces. The time lag distributions were similar to that illustrated in Fig. 1, curve *b*, and in both cases T_{av} was about $3\ \mu\text{sec}$.

In order to determine if T_{av} was influenced by the initial state of strain, the specimens used to obtain Fig. 1, curve *b*, were divided into two sub-groups. One

sub-group consisted of 65 specimens and with these the annealing treatment was omitted. The difference between T_{av} for the two sub-groups was less than $0.5 \mu\text{sec}$ and this is not significant. Values of electric strength are quoted in §4. The small differences in the sizes of comparable groups in Tables 3 and 4 are due to occasional recording omissions.

Table 1. Influence of Voltage Increment on Mean Time Lag

(1)	(2)	(3)	(4)	(5)
Graphite applied to polished surface	1	29	14.5	17
Graphite applied to polished surface	4	95	3.2	4.5
Graphite applied to unpolished surface	4	63	11.0	17
Graphite applied to unpolished surface	12	42	2.2	4.1

(1) Cathode; (2) voltage increment (%); (3) number; (4) T_{av} (μsec);
(5) standard deviation S .

The influence of the voltage increment on T_{av} is illustrated by the results quoted in Table 1. Appreciable error is possible in the measurement of time lags less than $1 \mu\text{sec}$ and therefore the scale of the distribution for 12% voltage increments was extended by using specimens with their surfaces left unpolished after annealing. The results illustrated in Fig. 1, curves *b* and *c*, together with the measured value of $2.2 \mu\text{sec}$ for T_{av} suggest about $0.8 \mu\text{sec}$ is appropriate for specimens with polished surfaces, when they are broken down using 12% voltage increments. This estimation is supported by the fact that wavetail breakdown was not observed when a single $0.5:500 \mu\text{sec}$ impulse of peak voltage sufficient to produce a stress of 1.5 mv cm^{-1} was applied to polished specimens of NaCl. It is evident that T_{av} diminishes with increase in the voltage increment.

With respect to the formative time lag in the breakdown of alkali halide crystals, the result illustrated in Fig. 2 (Plate) is of interest. This is a photograph of the discharge damage caused during the intrinsic breakdown of an annealed specimen of KCl. A single impulse, producing a peak electric stress of 1.5 mv cm^{-1} , was applied to the specimen. The voltage wave increased approximately linearly, and reached the peak value in about $0.03 \mu\text{sec}$. The voltage across the specimen collapsed after another $0.03 \mu\text{sec}$ from the peak of the wave, when it had decayed to about 95% of the peak value. A value about 1.0 mv cm^{-1} may be assumed for the electric strength of the specimen, measured with $1:5000 \mu\text{sec}$ waves (Cooper, Grossart and Wallace 1956) and therefore the stress applied to the above specimen exceeded this value for about $0.04 \mu\text{sec}$. Referring to Fig. 2, a partly completed discharge track can be seen to the left of the main discharge channel. It extends from the anode into the body of the specimen and terminates half way to the cathode. This is a suppressed discharge (Meek and Craggs 1953) and its presence indicates the formative time to be less than $0.04 \mu\text{sec}$. Experiments have shown (Cooper, Higgin and Smith 1960) that the behaviour of KCl with

respect to time lags is similar to that of NaCl. The formative time lag is a negligible fraction of the measured time.

§ 4. ELECTRIC STRENGTH

Average, maximum, and minimum values of electric strength, obtained from the groups of specimens used in the time lag studies, are compared in Table 2

Table 2. Influence of Cathode on Electric Strength of Sodium Chloride

	(1)	(2)	(3)	(4)	(5)	(6)	(7)	(8)
(1)	graphite	polished	4	0.78	1.06	1.31	0.0186	37
(2)	graphite	not polished	4	0.74	1.01	1.38	0.0182	73
(3)	sodium	polished	4	0.70	0.99	1.45	0.0403	68
(4)	gold	polished	4	0.76	1.12	1.54	0.0413	29
(5)	silver	polished	4	0.74	0.98	1.35	0.0248	33
(6)	graphite	polished	1	0.80	0.98	1.26	0.0099	31
(7)	graphite	not polished	12	0.80	0.98	1.15	0.0106	32
(8)	graphite	polished specimens not annealed	4	0.85	1.20	1.65	0.0214	71

Columns: (1) cathode; (2) surface; (3) voltage increment (%); (4)–(6) electric strength (MV cm^{-1}): (4) minimum, (5) average, (6) maximum; (7) variance; (8) number.

and the significant minimum values, for annealed specimens, are constant to within $\pm 6\%$ of 0.74 MV cm^{-1} . The electric strength of sodium chloride is independent of the cathode material. Apart from the cathode, the 240 specimens used to obtain the information stated in rows (1) to (5) of Table 2 were similar, and they were broken down in the same way. The range of specimen thickness

Table 3. Influence of Specimen Thickness on Electric Strength Annealed Specimens with 4% Voltage Increment

	(1)	(2)	(3)	(4)	(5)	(6)	(7)	(8)
(1)	$t < 0.0254$	0.82	1.12	1.49	0.0321	27	0.0193	0.4
(2)	$0.0254 < t < 0.0303$	0.76	1.05	1.38	0.0307	34	0.0279	0.4
(3)	$0.0303 < t < 0.0355$	0.76	0.97	1.54	0.0398	46	0.0332	0.4
(4)	$0.0355 < t < 0.0406$	0.74	1.03	1.32	0.0206	57	0.0355	0.4
(5)	$0.0406 < t < 0.0456$	0.74	0.91	1.16	0.0151	39	0.0437	0.4
(6)	$0.0456 < t < 0.0508$	0.72	0.84	1.04	0.0078	26	0.0557	0.4
(7)	$t > 0.0508$	0.70	0.83	1.02	0.0111	11	0.0581	0.4
(8)	$0.0500 < t < 0.0650$	0.72	0.80	0.97	0.0046	18	0.0568	0.7

Columns: (1) thickness range (cm); (2)–(4) electric strength (MV cm^{-1}): (2) minimum, (3) average, (4) maximum; (5) variance; (6) number of specimens; (7) t_{\min} (cm); (8) radius of recess R (cm).

extended from 0.01 cm to 0.06 cm and the result of dividing, according to thickness, the above group into seven sub-groups is stated in Table 3. Comparable values of electric strength decrease as the thickness of the specimens in the sub-groups increases. The effect is smallest for the minimum values of electric strength. The product moment correlation coefficient obtained from these values of electric

strength (column (2), Table 3) and the corresponding specimen thickness (column (7), Table 3) is -0.94 and Student's ' t ' test shows that the probability of this value occurring by chance is less than 1% and nearly 0.1%. Evidence is thus provided of a decrease in the electric strength of NaCl with increase in specimen thickness.

The field distribution in a plane-recessed specimen depends upon the ratio of cavity radius R to specimen thickness t . Assuming breakdown occurs when the maximum stress (at the surface of the recess) becomes equal to a thickness-independent intrinsic electric strength, the effect of decreasing the ratio R/t on the measured electric strength (i.e. mean stress at breakdown) can be estimated (Loeb and Meek 1940). The effect is very small in the range of R/t used in this investigation. This is confirmed by comparing the values of electric strengths quoted in rows (7) and (8) of Table 3. The thickness effect cannot be accounted for by changes in the field distribution due to varying the specimen thickness t and not keeping the ratio R/t constant.

Corroboration of the thickness effect is provided by the behaviour of the variances, stated in column (5) of Table 3, which become small when the average electric strength of the group decreases below about 0.9 MV cm^{-1} . This can be explained by considering the interaction of the mechanical and electrical phenomena, which may occur in measuring the electric strength of alkali halide crystals (Cooper and Wallace 1956). If the electric field applied to annealed NaCl exceeds about 0.9 MV cm^{-1} , the Coulomb force between the electrodes is sufficient to cause plastic deformation of the crystals. The electric strength ultimately achieved is determined by the work hardening characteristic, which is not the same for apparently similar annealed specimens. This is the cause of the large spread in values of electric strength (Table 2). The above value is independent of specimen thickness between 0.012 cm and 0.045 cm , where observations have been made. If the electric strength of the specimens falls below 0.9 MV cm^{-1} the spread in comparable values should approach that expected from known experimental errors and this is the case. In the final group, row (8), of Table 3 only one specimen possessed electric strength exceeding 0.9 MV cm^{-1} and the spread about the average of the remainder was less than $\pm 10\%$.

§ 5. SECONDARY FACTORS

An apparent decrease of electric strength with increase in specimen thickness is observed when breakdown results from damage caused by ambient discharges (Whitehead 1932). Also in this circumstance, the apparent electric strength depends on the time of application of voltage because the breakdown results from cumulative damage and the longer the application of voltage the lower is the apparent electric strength. In the experiments described previously about ten $0.8 : 8000 \mu\text{sec}$ impulses were applied, on average, to each specimen and the application of twenty impulses was rare. The absence of injurious discharges is established if it can be shown that the electrode system yields values of electric strength independent of the number of impulses applied. The experiment was carried out as follows.

The impulse generator was charged from a constant voltage source and it was tripped automatically every 30 seconds, the total number of impulses being recorded with an electromechanical counter. The specimens were provided

with graphite electrodes. The electrode system was similar to that used in the experiments previously described and it was immersed in silicone oil. The initial voltage applied to each specimen was adjusted to produce not less than 0.70 MV cm^{-1} in the region of minimum thickness. One thousand impulses of the same amplitude were applied, and then the amplitude was increased by 4%, and another 1000 impulses of fixed amplitude were applied, and so on until the specimen broke down. A resistance of about 100 ohms was connected in series with the specimen to provide some protection against damage and to produce, upon breakdown, a voltage to operate a relay and switch off the generator. Fifteen specimens in the thickness range 0.038 cm to 0.050 cm were broken down. Five failed due to discharge damage at the edges of the colloidal graphite electrode. The minimum apparent electric strength in this group was 0.75 MV cm^{-1} and the specimen withstood 1177 impulses. The maximum apparent electric strength was 0.89 MV cm^{-1} and the specimen withstood 5613 impulses. The average number of impulses for this sub-group was 2957 and the average electric strength was 0.83 MV cm^{-1} . The puncture in the remaining ten specimens was at the bottom of the recess and the values of electric strength ranged from 0.75 MV cm^{-1} to 1.1 MV cm^{-1} . The numbers of impulses applied to these two extreme cases were respectively 2100 and 11 107. The range of electric strengths obtained in this experiment is similar to that stated in Table 3 for specimens of comparable thickness, and obtained by applying on average about ten impulses. Therefore, there is no reason to believe that ambient discharges had influenced the measurements described previously.

The apparent electric strength may decrease with specimen thickness if space charges occur, because the applied voltage is dropped over relatively thin layers of crystal near to the electrodes. There has been speculation in the past about the effect of ionic migration upon the measurement of the electric strength of the alkali halides. These materials conduct by the transport only of positive ions at the temperatures generally used in the study of electric breakdown and the possibility must be considered of both thermal and space charge effects. The influence of ionic conductivity upon the electric strength of NaCl measured at room temperature, using $1:8000 \mu\text{sec}$ impulses, and specimens similar to the ones used in the present investigation, has recently been determined by Cooper, Higgin and Smith (1960). The ionic conductivity was controlled by the addition of small amounts of CdCl_2 and it was found that the electric strength of NaCl at 20°C was not changed by increasing the ionic conductivity up to sixty-fold. Previous investigators have claimed (e.g. Caspari 1955) that the electric strength of alkali halide crystals depends upon the cathode material. The effect has been attributed to electronic space charges created by field emission, the rate of which was assumed dependent on the cathode material. The present experiments provide no evidence of this since there is no correlation between corresponding values of average time lag and average electric strength. When a cathode effect has been claimed, the evidence usually consists of apparent differences between the average electric strengths of very small groups of unannealed specimens and may be doubted for statistical reasons.

§ 6. DISCUSSION

The characteristics of electric breakdown established for sodium chloride are similar to those predicted by the single avalanche theory. The deviation (see

Fig. 1) from the theoretical time lag distribution law $N_t = N_0 \exp(-t/T)$ follows from the manner of performing the experiments. This law is based on the assumption that the probability of a suitable avalanche remains constant but this was not the case throughout each experiment. Using solids, the minimum peak voltage required to cause breakdown in the time permitted by the form of the voltage wave cannot be determined, as a preliminary to the experiment, because of the destructive nature of this test. Fixed voltage increments were applied to each specimen but the overvoltage at breakdown measured relative to the above voltage was not known and it was most unlikely to be the same for all of the specimens in each group. A number of excessively long time lags are to be expected from those specimens in a group that break down with relatively small overvoltages and the effect is to raise the tail of the distribution above the theoretical curve in the way illustrated by Fig. 1. The form of the voltage wave also contributed to this effect since the probability of a suitable avalanche decreased as the voltage decreased from the peak value.

The initiating electrons in avalanche breakdown are assumed to be provided by field emission at the cathode. The rate of emission for the various cathodes cannot be determined because the average time lag depends also on the probability of an electron growing into a suitable avalanche. It is evident however that several electrons per microsecond must have been provided in the active region of the specimen, which probably was a cylinder of diameter 0.1 cm and length equal to the specimen thickness. With these assumptions, the emission must have amounted to about 10^{-11} A cm^2 or greater. Little appears to be known about the cold emission of electrons into solid dielectrics but Geller (1956) has obtained currents exceeding 10^{-10} A cm^2 in crystals of KBr. This material is similar to NaCl in its behaviour with respect to time lags. Geller found the rate of emission was not very sensitive to the metal used as cathode but it was effected by the treatment applied to the crystal surface. These results are not inconsistent with the ones obtained in the present investigation. The difference between the average time lags of $3.2 \mu\text{sec}$ and $11 \mu\text{sec}$, obtained respectively from specimens with polished and unpolished crystal surfaces and using graphite cathodes in both cases, is attributed to a difference in the composition of the contaminated surface layers of the crystals.

There are various difficulties in the calculation of electric strength, according to the avalanche theory and these have been discussed by Stratton. The predicted effect of thickness for sodium chloride in the range of 0.02 to 0.06 cm amounts to a decrease in electric strength of from about 1.0 to about 0.85 MV cm^{-1} . The observed decrease was from 0.8 to 0.7 MV cm^{-1} . The critical avalanche according to Seitz's criterion will cause melting of the material in the region of maximum electron density and the processes causing propagation of the molten channel back from the anode to the cathode are speculative.

ACKNOWLEDGMENTS

We wish to acknowledge the kindness of Dr. R. Stratton who provided a copy of his review paper before its publication and the help of Dr. D. T. Grossart in making preliminary measurements using a specimen with sodium cathodes. The photograph of Fig. 2 was obtained in this laboratory by Dr. A. Fernandez.

APPENDIX

The electric strength of annealed KBr is low, and the mechanical force between the electrodes is insufficient to deform plastically the crystal before electrical breakdown occurs. The spread in values of electric strength obtained from comparable annealed specimens of KBr is mainly determined therefore by the random errors of measurement, although some variation must still arise from relatively small structural differences which remain after annealing. Fewer specimens than in the case of NaCl are required to establish the thickness effect in the breakdown of KBr. The result of this experiment is stated in Table 4.

Table 4. Influence of Thickness on Electric Strength of KBr

(1)	(2)	(3)	(4)	(5)	(6)
0.018-0.030	0.50	0.58	0.69	0.0033	14
0.053-0.061	0.44	0.48	0.55	0.0014	12

(1) Thickness range (cm); (2)-(4) electric strength (mv cm⁻¹): (2) minimum, (3) average, (4) maximum; (5) variance; (6) number.

The method was similar to that used for NaCl and the electrodes were colloidal graphite applied to polished crystal surfaces. In the absence of large spread due to mechanical work hardening, average values of electric strength provide a better comparison than do minimum values. Student's 't' test indicates that the difference between the average values stated in Table 4 is significant at the 0.1% level. Similar values of electric strength were obtained from specimens of KBr using voltages that increased approximately linearly at the rate of 2 kv sec⁻¹ (approx).

REFERENCES

- CALDERWOOD, J. H., and COOPER, R., 1953, *Proc. Phys. Soc. B*, **66**, 73.
 CALDERWOOD, J. H., COOPER, R., and WALLACE, A. A., 1953, *Proc. Instn. Elect. Engrs*, Pt. IIa, **100**, 105.
 CASPARI, M. E., 1955, *Phys. Rev.*, **98**, 1679.
 COOPER, R., and GROSSART, D. T., 1956, *Proc. Phys. Soc. B*, **69**, 1351.
 COOPER, R., GROSSART, D. T., and WALLACE, A. A., 1956, *Proc. Phys. Soc. B*, **70**, 169.
 COOPER, R. and WALLACE, A. A., 1956, *Proc. Phys. Soc. B*, **69**, 1287.
 COOPER, R., HIGGIN, R. M., and SMITH, W. A., 1960, *Proc. Phys. Soc.*, **76**, 817.
 FRÖHLICH, H., and PARANJPE, B. V., 1956, *Proc. Phys. Soc. B*, **69**, 866.
 GELLER, M., 1956, *Phys. Rev.*, **101**, 1685.
 KAWAMURA, H., and RYU, T., 1954, *J. Phys. Soc. Japan*, **9**, 438.
 LOEB, L., and MEEK, J. M., 1940, *The Mechanism of the Electric Spark* (Oxford: University Press).
 MEEK, J. M., and CRAGGS, J. D., 1953, *Electric Breakdown of Gases* (Oxford: University Press), Chap. IV.
 SEITZ, F., 1949, *Phys. Rev.*, **73**, 550.
 SMITH, W. A., 1956, *Proc. Phys. Soc. B*, **69**, 848.
 STRATTON, R., 1961, *Progress in Dielectrics* (London: Heywood), in the press.
 WHITEHEAD, S., 1932, *Breakdown of Solid Dielectrics* (London: Benn).
 ——— 1951, *Dielectric Breakdown of Solids* (Oxford: Clarendon Press).

Photofluorescence Decay Times of Organic Phosphors

By T. D. S. HAMILTON†

Department of Physics, Rhodes University, Grahamstown, South Africa

MS. received 15th March 1961

Abstract. An accurate and convenient method for measuring photofluorescence decay times in the nanosecond region is described. Results are given for a number of organic compounds and reasons for differences with previous results are discussed. For anthracene, a value of 24.2 nsec has been measured for a 1 cm cube crystal. Some previous results for quantum efficiencies are corrected on the basis of these measurements and apparent inconsistencies examined with regard to the mean free path of excitons in very thin crystals.

§ 1. INTRODUCTION

PHOTOFLUORESCENCE decay times of organic phosphors have been measured by a number of workers (Hanle *et al.* 1951, Liebson 1952, Birks and Little 1953), but a comparison of the results (Table 1) shows large differences. To measure these decay times, which fall in the range 10^{-7} to 10^{-9} sec, a number of methods have been used, as detailed in the references above. The methods

Table 1. Photofluorescence Decay Times

Phosphor	(1)	(2)	(3)	(4)	(5)	(6)	(7)
Anthracene	6.4(a)	24.2(c)	3.5(g)	14.0(g)	17.0(g)	15.0(e)	13.0(g)
Anthracene	3.1(b)	12.6(d)	3.5(g)	14.0(g)	17.0(g)	25.0(f)	13.0(g)
<i>p</i> -Terphenyl	5.5	5.5	—	3.8	11.0	—	—
<i>z</i> -Stilbene	3.9	4.8	1.7	3.0	3.1	6.0	—
Diphenyl acetylene	—	4.9	—	3.0	2.5	15.0	—

- (1) Microcrystal decay time, present work.
- (2) Thick crystal decay time, present work.
- (3) Microcrystal decay time, Birks and Little (1953).
- (4) Thick crystal decay time, Birks and Little (1953).
- (5) Thick crystal decay time, Liebson *et al.* (1950).
- (6) Thick crystal decay time, Hanle *et al.* (1951).
- (7) Thick crystal decay time, Schmillen *et al.* (1953).
- (a) Microcrystal deposited from pure solvent.
- (b) Microcrystal deposited from impure solvent.
- (c) Freshly cleaved surface.
- (d) Surface long exposed to the atmosphere.
- (e) Pure specimen.
- (f) Commercial grade (Merck).
- (g) State of crystal unspecified.

depend in general on the measurement of phase differences at high frequencies (of the order tens of Mc/s). This necessitates the calibration of a phase changer at these frequencies which is difficult to do with great accuracy. The method to be

† Now at The Physical Laboratories, The University, Manchester 13.

described in the present paper depends on the calibration of a d.c. galvanometer which can be carried out much more easily and accurately.

§ 2. OUTLINE OF METHOD

The present method is based on that originally suggested by Tumerman (1941) and the development of this by Bailey and Rollefson (1953). If we consider the excitation of a phosphor by light modulated at a high frequency, then, due to the finite decay time, there will be a phase difference between the exciting and fluorescent light. Tumerman showed that the phase difference ϕ was related to the decay time τ by the equation

$$\tan \phi = \omega \tau \quad \dots\dots (1)$$

where ω is the angular frequency of modulation of the exciting light. This equation is the basis of the methods previously used. It may be shown (§ 3) that there is also a relation between the relative degree of modulation of the exciting and fluorescent light and the decay time. This forms the basis of the present method. The degree of modulation is the ratio of the varying to the steady component of the signal. In measuring the relative modulation of the two signals the varying components are made equal, by adjusting the intensity of the incident light, so that any non-linearity in the r.f. detector is eliminated. The relative modulation is then just the ratio of the two steady components.

§ 3. THEORY OF THE METHOD

Consider a phosphor excited by light, the intensity of which will be represented by a Fourier series to allow for harmonic components. The basic assumption made in all measurements of photofluorescence decay times is that the decay is exponential. This is to be expected theoretically for a monomolecular process, but it does not necessarily hold when there is re-absorption in the phosphor. This case is discussed in § 4. Following Bailey and Rollefson, the differential equation relating the fluorescence intensity I to the exciting intensity $J(t)$ is

$$\frac{dI}{dt} = -k_1 I + k_2 J(t) \quad \dots\dots (2)$$

where k_1 and k_2 are constants and the decay time $\tau = 1/k_1$. The intensity of the exciting light will be represented by

$$J(t) = \frac{1}{2}a_0 + \sum_n [a_n \cos(n\omega t) + b_n \sin(n\omega t)] \quad \dots\dots (3)$$

where $n = 1, 2, 3 \dots$, a_n and b_n are constants depending on n and $\frac{1}{2}a_0$ is the average intensity of the exciting light. The equation obtained by substituting (3) in (2) is easily solved to give

$$I = \frac{a_0 k_2}{2k_1} + k_2 \sum_n \left[\frac{a_n \cos(n\omega t - \phi_n)}{(k_1^2 + n^2\omega^2)^{1/2}} + \frac{b_n \sin(n\omega t - \phi_n)}{(k_1^2 + n^2\omega^2)^{1/2}} \right] + C \exp(-k_1 t) \quad \dots\dots (4)$$

where the phase angle ϕ_n is given by

$$\tan \phi_n = \frac{n\omega}{k_1} = n\omega\tau \quad \dots\dots (5)$$

which corresponds to the result of Tumerman. The final term is an initial perturbation and becomes negligibly small as t becomes large compared with $1/k_1$, i.e. $tk_1 \gg 1$. Since $1/k_1 = \tau$ is of the order of 10^{-8} sec in the present work this

term will very soon vanish. The intensity I of fluorescence thus contains terms corresponding to each term in the expression (3) for the exciting light $J(t)$. The relation between modulation and decay time is most easily seen if we simplify the expression for $J(t)$. If we have a suitable detector we need consider only one frequency component, i.e. for all terms with $n > 1$, $a_n = b_n = 0$, and, by a proper choice of time scale, either a_1 or b_1 can be made zero. We then have

$$J(t) = \frac{1}{2}a_0 + b_1 \sin(\omega t) \quad \dots\dots(6)$$

$$I = \frac{k_2 a_0}{2k_1} + \frac{k_2 b_1 \sin(\omega t - \phi)}{(k_1^2 + \omega^2)^{1/2}}. \quad \dots\dots(7)$$

The degree of modulation of the exciting light m_e is given by

$$m_e = 2b_1/a_0 \quad \dots\dots(8)$$

and of the fluorescent light by

$$m_f = \frac{2b_1}{a_0} \frac{k_1}{(k_1^2 + \omega^2)^{1/2}}. \quad \dots\dots(9)$$

The ratio of these two is

$$M = \frac{m_f}{m_e} = \frac{k_1}{(k_1^2 + \omega^2)^{1/2}} \quad \dots\dots(10)$$

or in terms of τ , the decay time

$$\tau = \frac{1}{k_1} = \frac{(1 - M^2)^{1/2}}{\omega M}. \quad \dots\dots(11)$$

Thus if M can be measured, τ may be calculated since ω is known. In practice the amplitudes of the r.f. components of the exciting and fluorescent light are made equal so that M is then just the ratio of the steady components.

§ 4. EXPONENTIAL DECAY OF FLUORESCENCE

Since the present as well as previous methods of measuring decay times depend on the assumption that the decay is exponential, this factor requires investigation. It has been found by Holstein (1947, 1951) that in the case of gases the decay of resonance fluorescence is exponential. This case, however, concerns very narrow emission and absorption bands and a much larger overlap than in organic

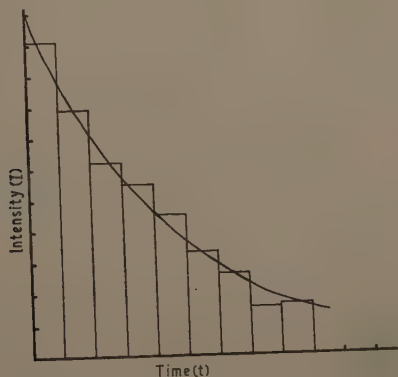


Fig. 1. Calculated decay of fluorescence.

phosphors. As well as affecting the shape of the decay, re-absorption could lead to variations of the decay time over the emission spectrum. The effects in anthracene are shown by the spectra of Fig. 4 which shows how re-absorption reduces the microcrystal spectrum to that for a thick specimen (1 cm thick). The absorption spectrum is obtained from Kortum and Finckh (1942).

The case of anthracene has been investigated by means of a Monte Carlo technique with the result shown in Fig. 1. The histogram shows the calculated decay. The exponential is given by $I = I_0 \exp(-t/\tau)$, with τ as the average of all the lifetimes and I_0 obtained by equating the area under the exponential to that under the histogram. Actual results will not be given here, as the calculation was rather coarse in using only 10 equally probable regions, and it is to be repeated with a larger number of regions. The fit is quite good and justifies the assumption of exponential decay in this case.

§ 5. EXPERIMENTAL

A block diagram of the apparatus is shown in Fig. 2. A crystal controlled power oscillator PO drives an air discharge tube DT to produce the modulated exciting light. The discharge was struck between two pointed electrodes about 1 cm apart by reducing the pressure, after which it was raised to about 5 cm Hg.

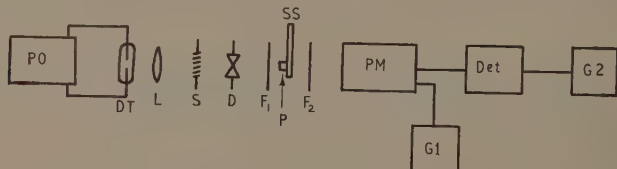


Fig. 2. Block diagram of the apparatus.

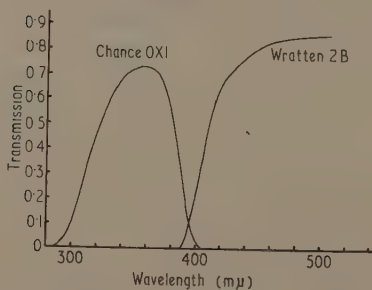


Fig. 3. Filter transmission characteristics.

The pressure at which the tube was operated was a compromise between light output, which decreases, and modulation, which increases with increase of pressure. The light is focused on to the specimen P by a quartz lens L through a shutter S, an iris diaphragm D and a filter F_1 . The specimen is mounted on a sliding stage SS so that the detector, an RCA 5819 photomultiplier PM, can view either the exciting or fluorescent light. The filter F_1 (Wood's glass) only transmits light

below 4000 Å and the filter F_2 (Wratten 2B) only transmits above 4000 Å so that when the phosphor is being excited only the fluorescent light (above 4000 Å) and no exciting light reaches the multiplier. F_2 is attached to SS and is removed from the light path when the exciting light is being examined. The transmission curves of the two filters, as determined on a Beckman model DU spectrophotometer, are shown in Fig. 3. The Wood's glass was 2 mm thick and the Wratten 2B as normally supplied. In practice a double layer of Wratten 2B was used.

The detector Det was a heterodyne unit consisting of crystal oscillator, harmonic amplifier, mixer, i.f. amplifier and detector. The r.f. signal from the photo-multiplier anode was fed directly into the mixer and the rectified output from the detector was measured by galvanometer G2. The d.c. component of the multiplier output was measured by galvanometer G1.

The choice of modulation frequency should be made as far as possible so that $(1 - M^2)^{1/2} = M$, as τ will then depend mainly on ω which is accurately known. For the range of τ encountered (3 to 30×10^{-9} sec) this gives a frequency range of 30 to 6.6 Mc/s. In practice the second harmonic component of the light source was used as this effectively eliminated pickup, but in a well-shielded apparatus this should not be necessary. Since the two signals differ in phase and the pickup is of fixed phase, the pickup cannot be simply subtracted and must therefore be reduced to a negligible value. It appeared in practice that the second harmonic was present in the light output from the discharge tube but not in the driving oscillator. A suitable oscilloscope was not available so that a direct investigation could not be made.

The phosphors used were obtained from a number of sources (see Birks and Cameron 1959) and were of the highest purity available. The microcrystalline layers were deposited on glass slips by evaporation from solution and were about 0.1μ thick. The solvents used were spectroscopically pure (Hopkin and Williams Ltd. and Eastman Kodak Co.). It may be noted that an alternative method with some advantages is described by Northrop and Simpson (1956).

§ 6. CHECK RESULTS AND ACCURACY

It is necessary to test the filters themselves for fluorescence. If F_2 is fluorescent, then the degree of modulation of the fluorescent light from the specimen will be altered. This effect will not be cancelled out since the specimen and F_2 are removed when measuring the exciting light. The fluorescence of F_1 has no direct effect as it will be present in both cases. It will, however, tend to reduce the modulation of the exciting light and thus the accuracy and sensitivity of the apparatus. The filters were tested for fluorescence by comparing the degree of modulation of the exciting light with and without the filter. No significant differences were found, but it should be noted that a number of the filters tested, particularly those heat treated to obtain the required characteristics were strongly fluorescent.

It was also necessary to determine whether the modulation of the light from the discharge tube varied with wavelength, because of the wavelength dependence of specimen absorption, filters and multiplier response. This was done by measuring the modulation through filters transmitting different spectral regions. Some small variations were found, but mainly at long wavelengths whose effects were negligible.

A convenient check on the operation of the apparatus is the measurement of a known decay time. In the past most work has been done on organic dye solutions, and for some of these the decay times appear to be well known. One immediately available in pure form, eosin, was therefore used as the check. The result of this measurement, together with the results of two other investigators are given in Table 2 (Kirchoff 1940, Maercks 1938).

Table 2. Decay Time of Eosin

Phosphor Eosin (10^{-4} g cm $^{-3}$ solution in water)	Present	Decay times (nsec).	
		Kirchoff (1940)	Maercks (1938)
	4.73	4.70	4.70

The linearity of the photomultiplier is the main source of uncertainty in the results. This is a difficult factor to check but they are claimed by the manufacturers to be accurately linear within a specified current range and they were always used well within the range. Frequencies were all crystal controlled and known to within one part in 10^3 . The d.c. galvanometer was checked against standard resistors and found to be linear to better than 1%. For materials on which a number of measurements were made the statistical error was found to be about 1%. For the more important materials up to 100 measurements were made on a number of specimens. From these considerations the accuracy of measurement is estimated to be about 2%.

§ 7. RESULTS

The results obtained have been previously published (Hamilton 1957, Birks and Cameron 1959). There is however a correction to be applied to the microcrystal decay time for anthracene and a number of differences with the results of other workers to be considered. Some results are therefore repeated in Table 1 which also lists the corresponding results of other workers. The two rows for anthracene give the results for pure (upper) and for contaminated specimens (lower), except in the cases marked (g). For these the state of the specimen was unspecified, so that the same value has been entered in both rows. The differences between the present results and those of Birks and Little have already been discussed (Hamilton 1957). The differences were shown to be due to impurities or to probable oxidation of the surface. An instructive experiment showing the oxidation effect is carried out as follows. One face of a long exposed 1 cm cube anthracene crystal was cleaved off. With this new face towards the exciting light the value (c) (Table 1) was obtained. On inverting the crystal, so that an old surface was now towards the exciting light, the value (d) was obtained.

The results of Liebson and Schmillen *et al.* for anthracene appear to lie between the values (c) and (d) and so could be due to an intermediate period of exposure to the atmosphere. The result of Hanle *et al.* (e) is thought to differ from (c) due to a different cause. A reasonable explanation may be based on the fact that their measurements were made by examining the 'reflected' fluorescence from a thick crystal. It is known that the 'reflected' fluorescence spectrum is considerably different from the transmitted spectrum (Birks and Wright 1954), due to decreased self-absorption. This will diminish the effective decay time of the crystal.

Taking rough measurements of the relative areas of the spectra from the above paper, we find the ratio of the reflected to the transmitted to be 0.5. Using the relation (14) (see below) with $\tau_0 = 24.2$ nsec and $K = 0.5$, we find for the 'reflected' decay time the value of 12.1 nsec. Since the spectra are approximate and the exact value will depend on the angle of incidence, this value agrees well enough with (e). The value (f) cannot be considered to be in agreement with (c) since it was also measured by reflection and so underestimated and it is probably influenced by some impurity. Differences for other phosphors are probably due to one or more of the causes discussed for anthracene.

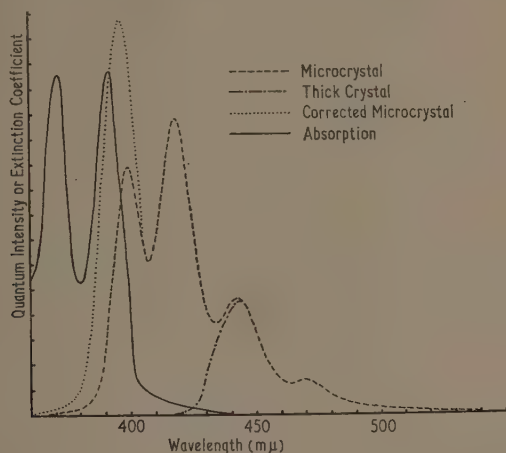


Fig. 4. Absorption and fluorescence spectra for anthracene.

Table 3. Corrections to Anthracene Decay Times

Specimen	K_1	τ_{m1}	K_2	τ_{m2}	K_3	τ_0	τ_{m3}	τ_m
A	0.293	6.55	0.796	5.22	0.234	24.1	5.64	5.43
B	0.340	6.85	0.792	5.42	0.233	22.5	5.25	5.34
C	0.331	6.64	0.755	5.02	0.228	23.9	5.45	5.24
D	0.311	6.58	0.761	5.01	0.236	23.3	5.50	5.26
Means	0.319	6.65	0.776	5.17	0.233	23.5	5.46	5.31

K_1 = ratio of thick to uncorrected micro spectrum.

τ_{m1} = measured micro decay time.

K_2 = ratio of uncorrected to corrected micro spectrum.

$\tau_{m2} = \tau_{m1} \cdot K_2$

K_3 = ratio of thick to corrected micro spectrum.

τ_0 = measured thick decay time.

$\tau_{m3} = \tau_0 \cdot K_3$

τ_m = mean of τ_{m2} and τ_{m3} .

Birks and Cameron (1959) have found from spectral measurements that even in the microcrystalline layers used in the present measurements (the specimens were the same ones) there was some residual re-absorption. They have made a correction to the spectrum for this which is shown in Fig. 4. The improved agreement of the K values shown under K_3 (Table 3) compared with the measured

values under K_1 adds confirmation to this correction. This re-absorption will also affect the decay time.

The decay time ratio for anthracene $\tau_c/\tau_m = 3.8$ is quite close to the ratio of the areas of the spectra after normalization at long wavelengths (Fig. 4: ratio = 4.3). This approximate agreement is to be expected on Birks' photon cascade theory (Birks 1953) for high quantum efficiency q . If p and k are the radiative and the non-radiative transition probabilities and K the spectral area ratio:

$$K = \frac{\text{area of thick crystal spectrum}}{\text{area of microcrystal spectrum}}$$

Then

$$\frac{\tau_m}{\tau_c} = \frac{pK+k}{p+k} \quad \dots\dots (12)$$

and

$$q = \frac{p}{p+k} \quad \dots\dots (13)$$

If $q=1$ then $k=0$ and

$$\frac{\tau_m}{\tau_c} = K \quad \dots\dots (14)$$

If these considerations are to be used to obtain a corrected decay time, a value of $q=1$ has to be used to obtain even the agreement shown in Table 3. Since q is found to be less than 1 (§ 8), it would appear that there is possibly some other process in operation which has been neglected. This is considered in § 8.

§ 8. QUANTUM EFFICIENCIES

Wright (1955) has given a method for measuring photofluorescence quantum efficiencies q from measurements of the decay times and fluorescence spectra of thick and microcrystal specimens. He shows that

$$q = \frac{1 - \tau_m/\tau_c}{\delta + K - \delta K} \quad \dots\dots (15)$$

where δ is an escape coefficient. Wright gave a result for anthracene using (15) but he used a value of $\tau_c = 18.0$ nsec and $\tau_m = 6.7$ nsec and incorrect spectral data. These values were obtained by the method described above but before the effects of oxidation and re-absorption were fully realized. Using the results for the specimens of Table 3 ($\tau_m = 5.31$, $\tau_c = 23.5$, $K = 0.23$) we get $q = 1.12$ with $\delta = 0.1$ as given by Wright or $q = 1.00$ with $\delta = 0$.

If the theory is correct, then these values indicate that there is some error in the measurement or that some other process is operating that has not been taken into account. This is because the efficiency should be somewhat less than 1.0 at room temperature, as it has been found to increase with decrease in temperature (Kuchero v and Faidysh 1956). Note that the values given by Kuchero v and Faidysh are technical efficiencies Q related to the quantum efficiency q by (Wright 1955):

$$Q = \frac{qK}{1 - q + qK} \quad \dots\dots (16)$$

At room temperature $Q = 0.64$ (Kuchero v and Faidysh, Fig. 3, for room temperature) and with $K = 0.23$ we obtain $q = 0.9$. If τ_m is calculated from (15) with $\delta = 0$ and $q = 0.9$, we get $\tau_m = 7.5$ nsec.

It has been suggested that the true molecular lifetime of anthracene may be somewhat higher than the value given in Table 1, and that the reason for the lower value actually measured is the approach of the microcrystal size to the mean free path of the excitons in the microcrystal (Kuchеров and Faidysh 1956, Simpson 1956). The excitons, representing the excitation energy, move through the crystal until de-excitation occurs. If the mean free path is limited, in this case by the size of the microcrystals, de-excitation occurring at crystal boundaries, then the decay time will be reduced. The thickness of the specimens used in the present measurements (0.1μ) is approximately equal to the mean free path reported in the above references, so that some decrease in lifetime may be expected. The approximate lifetime calculated above indicates that this may be what is occurring especially as a more realistic calculation would probably increase rather than decrease the calculated value.

The results of Kallman and Brucker (1957) appear to support this idea but there are a number of corrections required and there are several possible sources of error. Firstly, a correction has to be made for the transit-time spread in the photo-multiplier which has been measured to be about 6 nsec (Hamilton and Wright 1956) for the same type of multiplier (RCA 5819). Small variations in the times can make large variations in the final result, and since this correction has to be made twice (for equipment rise time also, already included in the values tabulated) there is a possibility of large corrections. Scintillation lifetimes are also generally thought to be slightly longer than photofluorescence lifetimes (see for example Brooks 1956). There are also a number of criticisms of the measurements themselves. The thin flakes were 0.01 to 0.02 mm thick whereas re-absorption is still important in anthracene 0.001 mm thick. The flakes were prepared by heating and sublimation but the vessel was apparently not evacuated. The specimens were therefore probably oxidized. A value of 12.6 nsec has been obtained (Table 1) for a 1 cm crystal which has been long exposed to the atmosphere. This value corresponds very closely to the values given by Kallman and Brucker and adds to the doubt about their values.

The evidence in any case does indicate the possibility of a decrease of lifetime due to the limitation of the exciton mean free path, but further experiments on crystals of various thicknesses will be required to establish this. Measurements on various compounds will also be required, as *p*-terphenyl, which has negligible spectral overlap, does not show a decrease. This may be due to a shorter mean free path for excitons in this material.

ACKNOWLEDGMENTS

Part of this work was done under the direction of Dr. G. T. Wright. I wish to thank Dr. J. B. Birks for discussions, and Dr. A. J. W. Cameron for his close co-operation. I also wish to thank the South African Council for Scientific and Industrial Research for maintenance and research grants.

REFERENCES

- BAILEY, E. A., and ROLLEFSON, G. K., 1953, *J. Chem. Phys.*, **21**, 1315.
- BIRKS, J. B., 1953, *Scintillation Counters* (London: Pergamon Press).
- BIRKS, J. B., and CAMERON, A. J. W., 1959, *Proc. Roy. Soc. A*, **249**, 297.
- BIRKS, J. B., and LITTLE, W. A., 1953, *Proc. Phys. Soc. A*, **66**, 921.
- BIRKS, J. B., and WRIGHT, G. T., 1954, *Proc. Phys. Soc. B*, **67**, 657.

- BROOKS, F. D., 1956, *Progr. Nucl. Phys.*, **5**, 252.
HAMILTON, T. D. S., 1957, *Proc. Phys. Soc. B*, **70**, 144.
HAMILTON, T. D. S., and WRIGHT, G. T., 1956, *J. Sci. Instrum.*, **33**, 36.
HANLE, W., KOTSCHAK, O., and SCHARMAN, A., 1951, *Z. Naturf.*, **6a**, 202.
HOLSTEIN, T., 1947, *Phys. Rev.*, **72**, 1212.
—— 1951, *Phys. Rev.*, **83**, 1159.
KALLMAN, H., and BRUCKER, G. J., 1957, *Phys. Rev.*, **108**, 1122.
KIRCHOFF, W., 1940, *Z. Phys.*, **116**, 115.
KORTUM, G., and FINCKH, B., 1942, *Z. Phys. Chem. B*, **52**, 263.
KUCHEROV, I. IA., and FAIDYSH, A. N., 1956, *Izvest. Akad. Nauk SSSR, Ser. fiz.*, **22**, 29.
(English translation: 1958, *Bull. Acad. Sci. U.R.S.S., Phys. Ser.*, **22**, 27.)
LIEBSON, S. H., 1952, *Nucleonics*, **10**, No. 7, 14.
LIEBSON, S. H., BISHOP, M. E., and ELLIOTT, J. O., 1950, *Phys. Rev.*, **80**, 907.
MAERCKS, O., 1938, *Z. Phys.*, **109**, 685.
NORTHROP, D. C., and SIMPSON, O., 1956, *Proc. Roy. Soc. A*, **234**, 124.
SCHMILLEN, A., SCHMILLEN, E., and ROHDE, F., 1953, *Z. Naturf.*, **8a**, 213.
SIMPSON, O., 1956, *Proc. Roy. Soc. A*, **238**, 402.
TUMERMAN, L. A., 1941, *J. Phys. (USSR)*, **4**, 151.
WRIGHT, G. T., 1955, *Proc. Phys. Soc. B*, **68**, 241.

The Crystalline Field Parameters for Dysprosium Ethyl Sulphate

BY M. J. D. POWELL† AND R. ORBACH‡§

† Atomic Energy Research Establishment, Harwell, Didcot, Berks.

‡ Clarendon Laboratory, Oxford

Communicated by B. Bleaney; MS. received 18th May 1961

Abstract. The four crystalline field parameters of the Dy^{3+} ion in the ethyl sulphate, V_2^0 , V_4^0 , V_6^0 and V_6^6 are fitted at 4.2°K and 58°K to give the known level splittings and g values. It is found that $V_2^0 \sim 125 \text{ cm}^{-1}$, $V_4^0 \sim -26 \text{ cm}^{-1}$, $V_6^0 \sim -31 \text{ cm}^{-1}$, and $V_6^6 \sim 490 \text{ cm}^{-1}$, and there exists a slight variation with temperature between 4°K and 58°K . These values are, however, in serious disagreement with those obtained by the extrapolation procedure of Elliott and Stevens. In particular, V_2^0 is extraordinarily large, in agreement with the previous work of Judd on europium ethyl sulphate. An empirical variation of V_n^m with atomic number is given which is in marked contrast to that predicted by Elliott and Stevens.

§ 1. INTRODUCTION

THE recent work of Gramberg (1960) has now made it possible to obtain unequivocally the four crystalline field parameters V_2^0 , V_4^0 , V_6^0 , and V_6^6 (Elliott and Stevens 1953 a) for the dysprosium $3+$ ion in the ethyl sulphate. Up to now, only a few ions in the first half of the rare earth series have been examined in the ethyl sulphate in great detail. In fact, only for the single salt, europium ethyl sulphate (Judd 1959 a), have there been enough data to fit the crystalline field parameters unambiguously. The investigation of these parameters for the dysprosium $3+$ ion is of the utmost significance because of its position well along in the rare earth series, and because it contains an odd number of $4f$ electrons. The elegant work of Elliott and Stevens (1952, 1953 b) which systematized the crystalline field description of the rare earth trivalent ions assumed that V_n^m varied as $(Z-55)^{-n/4}$, where Z is the atomic number. This followed from the observed empirical variation of the spin-orbit coupling constant (proportional to $\langle r^{-3} \rangle$ where $\langle r \rangle$ is the mean radius of an f electron) with atomic number in the rare earth series, and the added assumption that the $4f$ wave functions were approximately hydrogenic in nature. No great weight was given to this procedure, but it did serve as a starting point in their analysis. As they had previously fitted the four parameters to the one salt about which there appeared to be sufficient experimental data, cerium ethyl sulphate, they were able to use the extrapolation procedure (1953 b) to approximate the coefficients for the rest of the trivalent rare earth ions in the ethyl sulphate lattice. In general, rather good agreement with the experimental results, as they were then known, was

§ National Science Foundation Postdoctoral Fellow, now at Division of Engineering and Applied Physics, Harvard University.

found. Since their work a few other salts have given enough experimental data for better fits to be attempted, specifically the non-Kramers salts (an even number of 4f electrons) praseodymium (Baker and Bleaney 1958) and europium ethyl sulphate (Judd 1959a). As a result of the fit we shall present for Dy^{3+} ethyl sulphate, and those for Pr^{3+} and Eu^{3+} in the ethyl sulphate, we find it necessary to question some aspects of the Elliott and Stevens extrapolation procedure. We believe the apparent agreement between their extrapolated parameters and the experimental data to be due to comparing rather insensitive quantities. We shall first, however, present our results for dysprosium ethyl sulphate, and then go on to the analysis of the variation of the crystalline field parameters from ion to ion.

§ 2. THE FIT TO DYSPROSIUM ETHYL SULPHATE

The ground multiplet of the dysprosium $3+$ ion is a $4f^9$, $^6\text{H}_{15/2}$ state. This is split by the ethyl sulphate's crystalline field (having C_{3h} symmetry) into eight levels all doubly degenerate owing to time reversal symmetry. The susceptibility has been measured at helium temperatures (de Haas, van den Handel and Gorter 1933, Cooke *et al.* 1959) and it is found that $g_{\parallel} = 10.8$, $g_{\perp} \sim 0$ which indicates a

Table 1. The Experimental Results of Gramberg (1960) for Dysprosium Ethyl Sulphate

Level	J_z values	4.2°K			58°K Energy splitting Δ_{14}
		Energy splitting Δ_{14} (cm^{-1})	g_{\parallel}	g_{\perp}	
I	$\pm 9/2, \mp 3/2, \mp 15/2$	—	10.76 ± 0.1	0	—
II	$\pm 7/2, \mp 5/2$	16.03 ± 0.05	5.60 ± 0.2	7.28 ± 0.6	16.1 ± 0.2
III	$\pm 11/2, \mp 1/2, \mp 13/2$	21.20 ± 0.1	12.50 ± 0.2	3.90 ± 0.6	20.4 ± 0.2
IV	—	—	—	—	58.9 ± 0.2
V	—	—	—	—	68.1 ± 0.2

combination of $J_z = \pm 9/2, \mp 3/2, \mp 15/2$ levels lowest. Magnetic resonance measurements were performed on the first excited level (Baker and Bleaney 1958) and these together with the temperature independent susceptibility in the perpendicular direction indicate a splitting of 22°K and give $g_{\parallel} = 5.86 \pm 0.10$ and $g_{\perp} = 8.4 \pm 0.5$ in the dilute salt (Dy^{3+} in yttrium ethyl sulphate). This shows the first excited doublet to be a combination of $J_z = \pm 7/2, \mp 5/2$ levels ($\equiv \cos \theta |\pm 7/2\rangle - \sin \theta |\mp 5/2\rangle$). Because the g_{\parallel} and g_{\perp} are related for such a level ($g_{\parallel} = \frac{4}{3}[7 \cos^2 \theta - 5 \sin^2 \theta]$, $g_{\perp} = \frac{4}{3}\sqrt{55} \sin 2\theta$) we cannot fit unambiguously the four crystalline field parameters. Because of Gramberg's (1960) recent optical measurements, however, and his success in identifying three of the eight levels at 4.2°K and five of them at 58°K , we are now assured of enough data with which to fit the crystalline field parameters. His results are listed in Table 1. It is to be noted that the splitting of the second and third levels from the ground doublet, Δ_{12} and Δ_{13} respectively, seems to vary slightly with temperature. This has caused us some trouble in fitting the data and we shall present separate lists of parameters we expect to be appropriate to the liquid helium ($\sim 4^\circ\text{K}$) and the higher ($\sim 58^\circ\text{K}$) temperature regions. In attempting to fit the data in the higher temperature region, we have had no choice but to fit solely to the level splittings given by Gramberg because no g values are known for measurements at that

temperature. The fit is thus in reality just a solution of four simultaneous equations in the four parameters. The results are given in Table 2. It is to be noted that the g values are not very different from those found at helium temperatures. The very significant point about the fit is the size of V_2^0 . Far from lying between about 0 and -5 cm^{-1} , as would be guessed from the extrapolation scheme of Elliott and Stevens, it is much larger. This would imply, if the extrapolation procedure of Elliott and Stevens were in fact valid, and $V_2^0 \propto (Z-55)^{-1/4}$, a value of 238 cm^{-1} for cerium ethyl sulphate. (They found a value of approximately -15 cm^{-1} .) This large positive value however hardly seems reasonable at present.

The fitting at 4.2°K is more difficult, strangely enough, because we have seven independent experimental numbers with which to work, five of them relating to g values. The trouble lies in the fact that for small changes in the V_n^m the g values

Table 2. The Theoretical Spectrum of Dysprosium Ethyl Sulphate from a Fit to the Crystalline Field Splittings Δ_{12} to Δ_{15} of Gramberg (1960) at 58°K

Level	Wave function	Energy splitting (cm^{-1})	g_{\parallel}	g_{\perp}
I	$0.058 \pm 15/2 \rangle - 0.267 \pm 3/2 \rangle + 0.962 \pm 9/2 \rangle$		10.75	0
II	$-0.869 \pm 7/2 \rangle + 0.495 \mp 5/2 \rangle$	16.10	5.41	8.51
III	$0.104 \pm 13/2 \rangle - 0.200 \pm 1/2 \rangle + 0.974 \mp 11/2 \rangle$	20.40	13.68	1.86
IV	$-0.994 \pm 15/2 \rangle + 0.069 \pm 3/2 \rangle + 0.079 \mp 9/2 \rangle$	58.90	19.72	0
V	$-0.983 \pm 13/2 \rangle + 0.129 \pm 1/2 \rangle + 0.131 \mp 11/2 \rangle$	68.10	16.52	1.64
VI	$0.495 \pm 7/2 \rangle + 0.869 \mp 5/2 \rangle$	148.89	2.75	8.51
VII	$0.088 \pm 15/2 \rangle + 0.961 \pm 3/2 \rangle + 0.262 \mp 9/2 \rangle$	201.76	3.03	0
VIII	$0.151 \pm 13/2 \rangle + 0.971 \pm 1/2 \rangle + 0.183 \mp 11/2 \rangle$	242.18	1.16	10.45
$V_2^0 = 123.7 \text{ cm}^{-1}$ $V_4^0 = -26.35 \text{ cm}^{-1}$ $V_6^0 = -31.02 \text{ cm}^{-1}$ $V_6^6 = 492.26 \text{ cm}^{-1}$				

change very little. Hence, a fit to the g values gives an enormous error in the splittings even for a small experimental error in the g values. That is, the g value error may be small, but the resulting error in the level splittings is not. We thus had to weight the values of Δ_{14} and Δ_{15} to keep them near those found by Gramberg at 58°K , and fit them, together with the g_{\parallel} values given by Gramberg for the lowest two states and the known splittings Δ_{12} and Δ_{13} . This allows for the slight change of Δ_{14} and Δ_{15} with temperature from 58 to 4.2°K . A computer programme was written for the fitting procedure which calculated the weighted sum of the squares of the differences between the observed and the calculated data. The programme then found the values of the parameters which minimized the weighted sum. The method of finding the minimum is rather more effective than the method of steepest descents and will be described elsewhere (Powell, to be published). The true minimum was assumed to be reached when a change of $\pm 0.01\%$ in any one parameter caused the weighted sum to increase. The parameters which gave a good fit to the g_{\parallel} values of the two lowest levels and to the splittings Δ_{12} and Δ_{13} , and for which the energy splittings Δ_{14} and Δ_{15} differed only slightly from those observed at 58°K , are given in Table 3.

There are, however, discrepancies between the results of Table 3 and those of Gramberg in Table 1. The g_{\perp} values do not seem to be in agreement for levels 2 and 3, and the g_{\parallel} for level 3 is also in disagreement. A reason for the first two discrepancies may be that Gramberg used fields so large that the Zeeman splitting

was no longer linear in the field H , but also contained terms proportional to H^3 , and his extrapolation to zero field was in error. Because the perpendicular temperature-independent susceptibility is so high and the levels connected by a perpendicular field so close, it is entirely possible that this may be the case. The reasons for error in the g_{\perp} of the third level may also be due to the proximity of the next $J_z = \pm 13/2, \pm 1/2, \mp 11/2$ level ($\Delta_{15} - \Delta_{13} = 48 \text{ cm}^{-1}$). We feel that Gramberg must certainly be in error for level 2 because of consistency requirements between g_{\parallel} and g_{\perp} which we have previously indicated. Gramberg's results do not fulfil the required relation. Further, the g_{\parallel} given by Baker and Bleaney (1958) is roughly that of Gramberg, whereas their (consistent) g_{\perp} is

Table 3. The Theoretical Spectrum of Dysprosium Ethyl Sulphate from a fit to the experimental data (see text) at 4.2°K

Level	Wave function	Energy splitting (cm^{-1})		
		g_{\parallel}	g_{\perp}	
I	$0.053 \pm 15/2 \rangle - 0.261 \pm 3/2 \rangle + 0.964 \mp 9/2 \rangle$	—	10.82	0
II	$-0.872 \pm 7/2 \rangle + 0.489 \mp 5/2 \rangle$	16.04	5.50	8.43
III	$0.096 \pm 13/2 \rangle - 0.195 \pm 1/2 \rangle + 0.976 \mp 11/2 \rangle$	21.22	13.76	1.73
IV	$-0.995 \pm 15/2 \rangle + 0.071 \pm 3/2 \rangle + 0.074 \mp 9/2 \rangle$	60.40	19.74	0
V	$-0.984 \pm 13/2 \rangle + 0.129 \pm 1/2 \rangle + 0.123 \mp 11/2 \rangle$	69.59	16.58	1.61
VI	$0.489 \pm 7/2 \rangle + 0.872 \mp 5/2 \rangle$	144.80	2.84	8.43
VII	$0.088 \pm 15/2 \rangle + 0.963 \pm 3/2 \rangle + 0.256 \mp 9/2 \rangle$	198.24	3.08	0
VIII	$0.150 \pm 13/2 \rangle + 0.972 \pm 1/2 \rangle + 0.179 \mp 11/2 \rangle$	238.82	1.18	10.46

$$V_2^0 = 119.24 \text{ cm}^{-1} \quad V_4^0 = -26.22 \text{ cm}^{-1} \quad V_6^0 = -31.24 \text{ cm}^{-1} \quad V_6^6 = 473.49 \text{ cm}^{-1}$$

much different. To check our conclusions we have also computed the effects of admixtures from the $J = 13/2$ excited multiplet. In all cases we have found a trivial correction, less than 1%, to the ground multiplet g values.

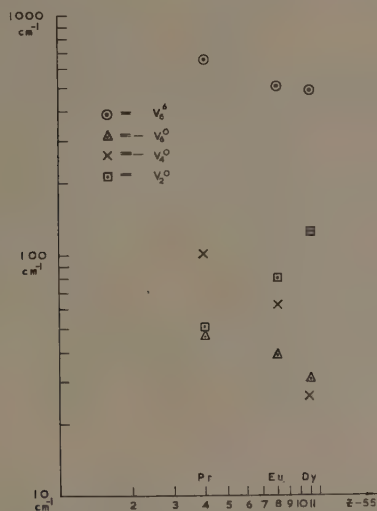
In addition, we have also calculated the temperature-independent susceptibility in both the parallel and perpendicular directions expected in the liquid helium range. We find 0.0181 per mole and 1.104 per mole respectively. The former is in reasonable agreement with the value 0.0152 found by Becquerel *et al.* (1936). The latter agrees well with the value of $1.05_6 \pm 0.02$ found by Cooke *et al.*

It is interesting to note that V_2^0 , V_4^0 , V_6^0 and V_6^6 change by only about 4, < 1, < 1, and 4% respectively between 4.2° and 58°K . This is a weak variation, being practically within the experimental uncertainty.

§ 3. THE EXTRAPOLATION PROCEDURE

We now plot the four crystalline field coefficients for dysprosium, europium, and praseodymium ethyl sulphate against $Z - 55$ to determine their functional variation with this quantity. The results are shown in the Figure. The interesting features of this Figure are two-fold. First, if we demand that $V_n^m \propto (Z - 55)^p$ then we see that p is roughly independent of m as V_6^0 and V_6^6 appear to have similar slopes. This agrees with Elliott and Stevens (1953b). Secondly, $p = +0.8, -1.4$ and -0.33 for $n = 2, 4$ and 6 whereas Elliott and Stevens have taken $p = -0.5, -1.0$ and -1.5 . Clearly something is wrong. Judd (1959b) has discussed the possibility of screening and has reached the conclusion that such may be quite significant, involving higher configurations of the ionic state. There

is as yet, however, no quantitative or even qualitative estimate of this effect. It is intriguing to note that the crystalline field coefficients for these three salts do seem to vary empirically with atomic number in a simple manner (see Figure). For instance, for samarium ethyl sulphate ($4f^5, {}^6H_{5/2}$), we would find $V_2^0 \sim 77 \text{ cm}^{-1}$, $V_4^0 \sim -48 \text{ cm}^{-1}$, $V_6^0 \sim -39 \text{ cm}^{-1}$, $V_6^6 \sim 550 \text{ cm}^{-1}$. To first order in perturbation theory this gives $\Delta_{12} \sim 59 \text{ cm}^{-1}$, $\Delta_{13} \sim 65 \text{ cm}^{-1}$ in rough agreement with the



A log-log plot of the crystalline field parameters, V_2^0 , V_4^0 , V_6^0 and V_6^6 , for praseodymium, europium and dysprosium ethyl sulphate against $Z-55$, where Z is the atomic number.

values of 53.8 cm^{-1} and 63.6 cm^{-1} respectively given by L  mmerman (1958) from optical measurements. These splittings are much better than those found by Elliott and Stevens (1953b) via their extrapolation procedure ($\Delta_{12} \sim 5 \text{ cm}^{-1}$ and $\Delta_{13} \sim 22 \text{ cm}^{-1}$) while they also gave an incorrect ordering for the three levels, viz. $I = |\pm 1/2\rangle$, $II = |\pm 5/2\rangle$, $III = |\pm 3/2\rangle^\dagger$.

Our values for V_n^m give, in agreement with the experimental results of L  mmerman (1958), $I = |\pm 1/2\rangle$, $II = |\pm 3/2\rangle$, and $III = |\pm 5/2\rangle$ in the ground ($J = 5/2$) multiplet.

As good as the agreement may seem in this particular case, however, the dangers of extension to other salts are so great in light of past experience as to make us loath to present any general conclusion other than the following. It is clear on the one hand that in complete agreement with what Judd found for europium ethyl sulphate, V_2^0 is much larger than previously supposed. And, on the other hand, this large value of V_2^0 does not appear to be a function of whether the ion contains an even or odd number of $4f$ electrons, in disagreement with his conjecture.

[†] In fairness to Elliott and Stevens these discrepancies may have arisen from their attempt to fit the very peculiar behaviour of the magnetic susceptibility (van den Handel, unpublished). The recent optical measurement of L  mmerman (1958) have solved this dilemma by showing the susceptibility results to be in error.

Thus, the Elliott-Stevens extrapolation formula appears to be in some error for the rare earth salts about which we have sufficient data to fit the crystalline field parameters. In the future, as we obtain more experimental information on the rare earth salts, we may be able to make some sense of their variation with atomic number. In any case, we now see that the hydrogenic approximation may be in very serious error and treatment of the shielding factor seems all-important.

ACKNOWLEDGMENTS

The authors wish to thank Professor B. Bleaney for his interest and encouragement and Professor K. W. H. Stevens and Dr. W. P. Wolf for their reading of the manuscript and helpful suggestions.

REFERENCES

- BAKER, J. M., and BLEANEY, B., 1958, *Proc. Roy. Soc. A*, **245**, 156.
BECQUEREL, J., DE HAAS, W. J., and VAN DEN HANDEL, J., 1936, *Physica*, **3**, 1133.
COOKE, A. H., EDMONDS, D. T., MCKIM, F. R., and WOLF, W. P., 1959, *Proc. Roy. Soc. A*, **252**, 246.
ELLIOTT, R. J., and STEVENS, K. W. H., 1952, *Proc. Roy. Soc. A*, **215**, 437.
—— 1953 a, *Proc. Roy. Soc. A*, **218**, 553.
—— 1953 b, *Proc. Roy. Soc. A*, **219**, 387.
GRAMBERG, G., 1960, *Z. Phys.*, **159**, 125.
DE HAAS, W. J., VAN DEN HANDEL, J., and GORTER, C. J., 1933, *Phys. Rev.*, **43**, 81.
JUDD, B. R., 1959 a, *Mol. Phys.*, **2**, 407.
—— 1959 b, *Proc. Roy. Soc. A*, **251**, 134.
LÄMMERMAN, H., 1958, *Z. Phys.*, **150**, 551.

Space Correlation and Energy Levels in an Einstein Solid†

By T. LUKES

Department of Physics, Northampton College of Advanced Technology, London

Communicated by R. Firth; MS. received 27th April 1961

Abstract. It is shown that the space correlation function of any space-dependent atomic property may be used to estimate the degree of order in a solid. The correlation function is evaluated for an Einstein solid and is shown to have both long-range order and short-range order components. The thermal scattering and band structure of an Einstein solid is treated by means of time-dependent perturbation theory on the loose-binding approximation, and it is shown that the scattering matrix is related to the spectrum of the potential, the short-range and long-range components giving rise to thermal scattering and energy gaps respectively.

The width of the gaps is found to decrease exponentially with temperature; for a one-dimensional model of sodium the temperature coefficient is found to be about 10^{-3} per degree. On a Mott-type one-dimensional model of liquid sodium this implies a 20% contraction of all energy gaps on melting.

§ 1. INTRODUCTION

THE work reported in the present paper may be divided into two, related, parts. The first of these consists in presenting a method, differing from those hitherto used, for measuring the degree of order in a lattice. The method is applied to the particular case of a lattice subjected to thermal vibration on the Einstein model and has the particular feature that the same function enables the degree of long-range and short-range order to be estimated.

The second part of the paper is a discussion, on the basis of the loose-binding approximation, of the energy levels and scattering in an Einstein solid. The particular feature of the method used is that both the energy levels and thermal scattering emerge from the same treatment, a temperature-dependent energy gap being obtained. The scattering matrix contains expressions which are evaluated in the first part of the paper, and it is found that terms corresponding to the thermal scattering and energy levels can be associated with the degree of short and long range order respectively.

§ 2. DEFINITIONS OF STATISTICAL FUNCTIONS

If $y(x)$ is a scalar function in an infinite, one-dimensional space the degree of statistical dependence between the value of y at the points x , $x + \chi$, may be measured by the autocovariance function

$$A(\chi) = \lim_{L \rightarrow \infty} \frac{1}{L} \int_{-L/2}^{L/2} y(x)y(x+\chi) dx \quad \dots\dots (1)$$

† Part (abridged) of the author's thesis for the Ph.D. degree of the University of London (1960). An account of part of this work was presented at the Physical Society's Conference on Electron-Phonon Interaction in Solids, held at Oxford in December, 1959.

where the limit is assumed to exist. In the cases to be considered the function $y(x)$ will be identified with a space-dependent property of the atom (such as the atomic potential) and will be a function of some random parameters (such as the displacement of the atoms from their equilibrium positions). If, in this case, a particular record $y^m(x)$ of the function is obtained, and the corresponding autocovariance $A^m(\chi)$ computed, this will be a function of such random parameters. The value of $A^m(\chi)$ averaged over these parameters will then be denoted by $\langle A^m(\chi) \rangle$. The present discussion will be confined to ergodic, stationary processes and for these the values of $\langle A^m(\chi) \rangle$ and of $A(\chi)$ are, for physical purposes, identical. The correlation function, or normalized autocovariance, is given by

$$\rho(\chi) = \frac{A(\chi)}{A(0)}. \quad \dots\dots(2)$$

The record $y^m(x)$ over a length L may be represented by a Fourier integral

$$y^m(x) = \int_{-L/2}^{L/2} Y(K) e^{2\pi i K x} dK. \quad \dots\dots(3)$$

The spectrum $G(K)$ defined by the equation

$$G(K) = \lim_{L \rightarrow \infty} \frac{1}{L} \langle |Y^m(K)|^2 \rangle \quad \dots\dots(4)$$

is then related to the autocovariance by the Wiener-Khinchine relation

$$A(\chi) = \int_{-\infty}^{\infty} G(K) \cos 2\pi K \chi dK. \quad \dots\dots(5)$$

For a three-dimensional solid the following analogous definitions hold:

$$A(\rho) = \int_{-\infty}^{\infty} y(\mathbf{r}) y(\mathbf{r} + \rho) d\mathbf{r} \quad \dots\dots(6)$$

$$y^m(\mathbf{r}) = \int_{-\infty}^{\infty} Y^m(\mathbf{K}) e^{2\pi i \mathbf{K} \cdot \mathbf{r}} d\mathbf{K} \quad \dots\dots(7)$$

$$G(\mathbf{K}) = \lim_{L^3 \rightarrow \infty} \frac{1}{L^3} \langle |Y^m(\mathbf{K})|^2 \rangle. \quad \dots\dots(8)$$

§ 3. THE CORRELATION FUNCTION AND SPECTRUM OF AN EINSTEIN SOLID

It will be shown in the present section that the space correlation function may be used to estimate the degree of order, on the atomic scale, which exists in an Einstein solid. For this purpose a physical property, such as the atomic potential, is chosen and the corresponding correlation function computed. In general, we denote by $y_0(x)$ a property of the atom which is independent of the interatomic distance. The function $y^m(x)$ defined over a chain of $2N+1$ atoms occupying a length L is then given by

$$y^m(x) = \sum_{r=-N}^{r=N} y(x - r q_0 - x_r) \quad \dots\dots(9)$$

where q_0 is the interatomic distance and the x_r are the displacements of the atoms from their equilibrium positions. Taking the Fourier transform of (9), multiplying by the complex conjugate and averaging, we find

$$\langle |Y^m(K)|^2 \rangle = |Y_0(K)|^2 \left\langle \sum_{r=-N}^{r=N} \sum_{s=-N}^{s=N} \exp [2\pi i K \{(r-s)q_0 + (x_r - x_s)\}] \right\rangle \quad \dots\dots(10)$$

where $Y_0(K)$ is the Fourier transform of $y_0(x)$. For $r=s$ the value of the sum is clearly $2N+1$. On the Einstein model, the x_r are assumed to be independently

distributed with a distribution $z(x_r)$. Defining the characteristic function of the distribution by

$$Z(K) = \int_{-\infty}^{\infty} z(x_r) \exp(-2\pi i K x_r) dx_r \quad \dots\dots\dots (11)$$

it follows that the characteristic function of the distribution of $x_r - x_n$ is just $|Z(K)|^2$. The spectrum may therefore be written

$$G(K) = \lim_{L \rightarrow \infty} |Y_0(K)|^2 \left[2N + 1 + |Z(K)|^2 \sum_{r=-N}^{r=N} \sum_{s=-N}^{s=N} \exp\{2\pi i K(r-s)q_0\} \right].$$

If the term for $n=m$ were included, the double summation would have the value $\sin \pi K(2N+1)q_0 / \sin \pi Kq_0$. As $N \rightarrow \infty$ this function is infinite at the values $K = n/q_0$ and zero at all others; it may therefore be represented as a delta function of strength $(2N+1)/q_0$. Writing L as $2Nq_0$ for large N and taking the limit, one obtains for the spectrum

$$G(K) = \frac{|Y_0(K)|^2}{q_0} \left[1 - |Z(K)|^2 + \frac{|Z(K)|^2}{q_0} \sum_{r=-\infty}^{r=\infty} \delta\left(K - \frac{r}{q_0}\right) \right]. \quad \dots\dots\dots (12)$$

The evaluation of the spectrum for the three-dimensional case offers no new problems, and the expression is given by

$$G(\mathbf{K}) = \frac{|Y_0(\mathbf{K})|^2}{\Omega_0} \left[1 - |Z(\mathbf{K})|^2 + \frac{|Z(\mathbf{K})|^2}{\Omega_0} \sum_{s=-\infty}^{\infty} \delta(\mathbf{K} - \mathbf{R}_s) \right] \quad \dots\dots\dots (13)$$

where Ω_0 is the volume of the unit cell and \mathbf{R}_s is a reciprocal lattice vector.

The correlation function may be evaluated by the use of Eqn (5). For a specific example we consider the one-dimensional case; take $y(x)$ to be the electrical potential, and choose the potential function $y_0(x)$ of a single, isolated atom to be of the Kronig-Penney type, with height h and width s_0 . If the atom, of mass M , is represented as a simple harmonic oscillator of frequency ν_E the distribution function $z(x_r)$ is, in the classical limit of continuous levels, Gaussian with variance σ^2 given by

$$\sigma^2 = \frac{kT}{4\pi^2 M \nu_E^2}. \quad \dots\dots\dots (14)$$

The expression for the spectrum then takes the form

$$G(K) = \frac{h^2 \sin^2 \pi K s_0}{q_0 \pi^2 K^2} \left[1 - \exp(-4\pi^2 K^2 \sigma^2) + \frac{\exp(-4\pi^2 K^2 \sigma^2)}{q_0} \sum_{r=-\infty}^{r=\infty} \delta\left(K - \frac{r}{q_0}\right) \right]. \quad \dots\dots\dots (15)$$

Substituting into Eqn (5) we obtain the correlation function as $A(\chi)/A(0)$, where

$$\begin{aligned} A(\chi) = & \frac{h^2}{q_0} \left[\frac{2\sigma}{\pi^{1/2}} \exp\left(-\frac{\chi^2}{4\sigma^2}\right) - |\chi| \operatorname{erfc} \frac{|\chi|}{2\sigma} - \frac{\sigma}{\pi^{1/2}} \exp\left(-\frac{(\chi+s_0)^2}{4\sigma^2}\right) \right. \\ & + \frac{|\chi+s_0|}{2} \operatorname{erfc} \frac{|\chi+s_0|}{2\sigma} - \frac{\sigma}{\pi^{1/2}} \exp\left\{-\frac{(\chi-s_0)^2}{4\sigma^2}\right\} + \frac{|\chi-s_0|}{2} \operatorname{erfc} \frac{|\chi-s_0|}{2\sigma} \left. \right] \\ & + \frac{h^2 s_0^2}{q_0^2} + 2h^2 \sum_{r=1}^{\infty} \exp\left(-\frac{4\pi^2 r^2 \sigma^2}{q_0^2}\right) \sin^2 \frac{\pi r s_0}{q_0} \cos \frac{2\pi r \chi}{q_0} \quad \dots\dots\dots (16) \end{aligned}$$

$$\begin{aligned} A(0) = & \frac{h^2}{q_0} \left[\frac{2\sigma}{\pi^{1/2}} - \frac{2\sigma}{\pi^{1/2}} \exp\left(-\frac{s_0^2}{4\sigma^2}\right) - s_0 \operatorname{erfc}\left(\frac{s_0}{2\sigma}\right) \right] + \frac{h^2 s_0^2}{q_0^2} \\ & + 2h^2 \sum_{r=1}^{\infty} \exp\left(-\frac{4\pi^2 r^2 \sigma^2}{q_0^2}\right) \sin^2 \frac{\pi s_0 r}{q_0} \quad \dots\dots\dots (17) \end{aligned}$$

It is seen that the correlation function consists of essentially two terms whose

relative magnitude is determined by the variance σ^2 . The first has appreciable magnitude for an interval χ of the order of the interatomic distance; the second is a periodic function. These may be interpreted as reflecting, respectively, the degree of short-range and long-range order in the system. In the limit of vanishing thermal fluctuations only the periodic component remains, while in the limit $\sigma \gg q_0$ —hardly realizable in a solid—the periodic component vanishes and the correlation function and spectrum have the same shape as for a single, isolated atom. The result obtained in this limit is the same as if the distribution of the atoms on the line was of the Poisson type (Carson 1931, Lukes 1961 a).

§ 4. THERMAL SCATTERING AND ENERGY LEVELS IN AN EINSTEIN SOLID

The effect of thermal vibration on the band structure of semiconductors has been discussed by Fan (1951) using second-order stationary perturbation theory; applying his theory to the case of germanium and silicon, he obtains an energy gap which decreases linearly with temperature, a result which is in good agreement with experiment. A treatment of the energy levels in a short-range order system, corresponding to a one-dimensional model of a liquid, again using second-order stationary perturbation theory, has, since the completion of the present work, been published (Sah and Eizenschitz 1960). For the case of periodic lattices, the results of the loose-binding approach are well known (Sommerfeld and Bethe 1934); for the one-dimensional case, this leads to energy gaps of magnitude $2|V_r|$ situated about values of electron wave number given by $k = \pm \pi r_s/q_0$, where V_r is the r th Fourier coefficient of the potential.

In the present method, the interaction of electrons with the atoms of an Einstein solid is investigated, using time-dependent perturbation theory. As the unperturbed wave functions are taken to be those of free electrons this amounts to using the first Born approximation. The object is to obtain a unified approach from which both the thermal scattering and the energy levels can be derived and, in particular, to see the effect of thermal vibration on the band structure.

We consider, as in the previous section, atoms along a line of length L , vibrating about equilibrium positions on the Einstein model, and take as the unperturbed wave functions

$$\psi(k) = L^{-1/2} e^{ikx}. \quad \dots\dots(18)$$

Treating k as a continuous variable the expression for the probability of a transition per unit time dp/dt from state k to state k' is given by (Landau and Lifshitz 1959)

$$\frac{dp}{dt} = \frac{2\pi}{\hbar} D(E) |V_{kk'}^m|^2 \delta(E_k - E_{k'}) \quad \dots\dots(19)$$

where $V_{kk'}^m$ is the matrix element for a particular 'frozen in' sequence of atomic positions, given by

$$V_{kk'}^m(k - k') = L^{-1} \int_{-L/2}^{L/2} \exp(ikx) v^m(x) \exp(-ik'x) dx \quad \dots\dots(20)$$

and $D(E)$ is the density of states; $v^m(x)$ is the potential field for this particular sequence. The average probability of scattering is given by averaging $|V_{kk'}^m|^2$ over all atomic positions. Taking for the density of states the free electron value, the average probability of scattering takes the form

$$\left\langle \frac{dp}{dt} \right\rangle = \frac{4\pi^2}{\hbar^2} \left(\frac{m}{2E} \right)^{1/2} \lim_{L \rightarrow \infty} \langle |V_{kk'}^m(k - k')|^2 \rangle \delta(E_k - E_{k'}) \quad \dots\dots(21)$$

where

$$V^m(k-k') = LV_{kk'}^m(k-k').$$

The term $\lim_{L \rightarrow \infty} \langle |V^m(k-k')|^2 \rangle$ which occurs in Eqn (21) is simply the spectrum of the potential, expressed as a function of $(k-k')/2\pi$, and may therefore be obtained from Eqn (12). In this way one obtains after some calculation

$$\left\langle \frac{dP}{dt} \right\rangle = \frac{4\pi^2}{\hbar^2} \left(\frac{m}{2E} \right)^{1/2} \frac{|V_0(k-k')|^2}{q_0} \left[1 - \exp\{-\sigma^2(k-k')^2\} \right. \\ \left. + \exp\{-\sigma^2(k-k')^2\} \sum_{r=-\infty}^{\infty} \delta\left(\frac{k-k'}{2\pi} - \frac{r}{q_0}\right) \right] \delta(E_k - E_{k'}). \quad \dots\dots (22)$$

The contributions of the terms in square brackets must be separately considered. The term $1 - \exp\{-\sigma^2(k-k')^2\}$ (where, in the one-dimensional case, $k = -k'$) can clearly be associated with thermal scattering in the lattice; if the exponential is expanded to first order in σ^2 , this is exactly equivalent to the usual procedure of calculating the effect of thermal scattering by expanding the potential in a Taylor series, since

$$\left\langle \left| \int_{-\infty}^{\infty} \exp(ikx) \frac{d}{dx} v_0(x) \exp(-ik'x) dx \right|^2 \right\rangle = (k-k')^2 |V_0(k-k')|^2. \quad \dots\dots (23)$$

Our expression for scattering is, however, also valid for large displacements and for $\sigma k \gg 1$ the expression coincides with that which would be obtained if the atoms were arranged completely at random; since for the case of an alkali metal (to which one would expect a loose-binding approximation most nearly to apply) the Fermi level is given by $k = \pi/2q_0$ this is a case hardly realizable in a solid.

Considering the contribution of the terms in the sum in (22), the conditions specified by the two delta functions can be simultaneously satisfied only if

$$k = -k' = \frac{\pi r}{q_0}. \quad \dots\dots (24)$$

Thus the effect of the summation term in (22) is to ensure certain reflection for values of k given by (24), and the procedure of representing the unperturbed wave function by the incident wave breaks down. Instead, we assume as a first approximation that transitions only occur between the two degenerate states and therefore represent the wave function by a superposition of the incident and reflected waves,

$$\psi(x) = L^{-1/2} \{c_1 \exp(ikx) + c_2 \exp(-ikx)\}. \quad \dots\dots (25)$$

Solving for the energy in the usual way by equating the determinant of the coefficients to zero we obtain for the change of energy produced by the perturbation

$$\Delta E_r = V_0(0) \pm \left| V_0 \left(\frac{2\pi r}{q_0} \right) \right| \exp \left(- \frac{2\pi^2 r^2 \sigma^2}{q_0^2} \right). \quad \dots\dots (26)$$

It follows that there is an energy gap of magnitude $E_g(r)$ where

$$E_g(r) = 2 \left| V_0 \left(\frac{2\pi r}{q_0} \right) \right| \exp \left(- \frac{2\pi^2 r^2 \sigma^2}{q_0^2} \right). \quad \dots\dots (27)$$

Comparison of the result with the usual treatment for a periodic lattice shows that the energy gaps differ by a factor of $\exp(-2\pi^2 r^2 \sigma^2 / q_0^2)$; the effect of taking thermal vibrations into account is therefore seen to be an energy gap which decreases in width exponentially with temperature.

Comparison of the results with those of §3, shows that the terms in the scattering matrix which give rise to thermal scattering and energy gaps are precisely those which, in the expression for the spectrum of the potential, Eqn (12), are associated respectively with short- and long-range order.

The expression for the probability of scattering in three dimensions shows no new features and follows from Eqn (13). Assuming the solid to be isotropic, we obtain

$$\left\langle \frac{d\rho}{dt} \right\rangle = \frac{4\pi^2}{\hbar^2} \left(\frac{m}{2E} \right)^{1/2} |V_0(\mathbf{k}-\mathbf{k}')|^2 \left[1 - \exp(-|\mathbf{k}-\mathbf{k}'|^2\sigma^2) + \frac{1}{\Omega_0} \exp(-|\mathbf{k}-\mathbf{k}'|^2\sigma^2) \sum_s \delta\left(\frac{\mathbf{k}-\mathbf{k}'}{2\pi} - \mathbf{R}_s\right) \right]. \quad \text{..... (28)}$$

The summation term of Eqn (28) shows that the approximation breaks down at values of k given by

$$\mathbf{k}-\mathbf{k}'=2\pi\mathbf{R}_s. \quad \text{..... (29)}$$

Following the same procedure as before we see that the results for the periodic lattice may be taken over if the term $|V_0(2\pi\mathbf{R}_s)|$ which occurs in the periodic lattice expression is replaced by $|V_0(2\pi\mathbf{R}_s)| \exp(-2\pi^2|\mathbf{R}_s|^2\sigma^2)$.

As regards the thermal scattering term, if the probability of scattering per unit time is denoted by $P(k, k')$ it is well known that, for a spherically symmetrical potential, this is a function of the scattering angle θ only. Subject to certain simplifying assumptions (Mott and Jones 1958) the probability of scattering may be related to the relaxation time τ by the equation

$$\frac{1}{\tau} = \int (1 - \cos\theta) P(\theta) dS \quad \text{..... (30)}$$

where the integral is taken over the Fermi surface of which dS is an element. The relaxation time τ is in turn related to the conductivity σ by the equation

$$\sigma = \frac{ne^2\tau}{m}. \quad \text{..... (31)}$$

Eqns (30) and (31) assume the validity of the Boltzmann equation in deriving the electrical conductivity; it appears, however, that, at least at high temperatures, more modern approaches yield the same result (Lukes 1961 b).

From Eqns (28) and (30) the relaxation time is given by

$$\frac{1}{\tau} = \frac{16\pi^2 m^2 k_F}{\hbar^3 \Omega_0} \int_0^\pi |V_0(\theta)|^2 \left[1 - \exp\left(-4k_F^2 \sin^2 \frac{\theta}{2} \sigma^2\right) \right] \sin^3 \frac{1}{2} \theta \cos \theta d\theta. \quad \text{..... (32)}$$

§ 5. DISCUSSION OF RESULTS

The results of the last section predict a decrease of energy gap with temperature as a result of thermal vibration. We estimate the magnitude of this change for the one-dimensional case, taking the case of sodium as an example, since it is to this metal that the free electron approximation is known most nearly to apply. In order to calculate the value of σ^2 we take the Debye temperature as an approximation to the Einstein temperature; however, some doubt appears to exist as to the correct value for this in the case of sodium (Blackman 1961, Bradshaw and Pearson 1956). Taking $\theta_D = 150^\circ\text{K}$ as a reasonable value the quantity $2\pi^2\tau^2\sigma^2/q_0^2$ turns out to be about 1×10^{-3} per degree for the first energy gap. For small temperatures, using Eqn (27) we may therefore write for the first gap

$$E_g(T) = E_g(0)[1 - aT]$$

where a is of the order of 10^{-3} per degree; inspection of Eqn (28) shows that this order of magnitude is not altered in three dimensions.

The method presented here has not been applied to a short-range order system, such as a liquid, since it is believed that (as in the case of the Einstein solid) the first Born approximation is not valid near the band edges. An equivalent conclusion appears to have been reached by Sah and Eisenschitz (1960). Since, for a short-range system, the reflected electrons are spread over a much wider range of k values some modification of the present method would be required. An approximate approach to liquids is, however, provided by Mott's theory of the electrical properties of liquid metals (Mott 1934).

On this theory—originally applied to the resistivity of liquid metals—a liquid metal near the melting point is treated as an Einstein solid with an Einstein temperature lower than that of the solid; the Einstein temperature of the liquid is obtained from that of the solid on the assumption that no change of structural entropy takes place on melting. Taking θ_E for the solid sodium as 150°K its value for the liquid is about 113°K . For the one-dimensional model, melting then results in a contraction of all energy gaps by about 20%.

ACKNOWLEDGMENTS

I wish to thank Dr. R. Fürth, of Birkbeck College, for his interest and encouragement during the course of this work. I am indebted to Dr. N. Cusack, of Birkbeck College, for a number of discussions on liquid metals.

REFERENCES

- BLACKMAN, M., 1951, *Proc. Phys. Soc. A*, **64**, 681.
 BRADSHAW, F. J., and PEARSON, S., 1956, *Proc. Phys. Soc. B*, **69**, 441.
 CARSON, J. R., 1931, *Bell Syst. Tech. J.*, **10**, 374.
 FAN, H. Y., 1951, *Phys. Rev.*, **82**, 900.
 LANDAU, L. D., and LIFSHITZ, E. M., 1959, *Quantum Mechanics* (London: Pergamon Press).
 LUKES, T., 1961 a, *Proc. Phys. Soc.*, **78**, 153.
 — 1961 b, *Physica*, **27**, 319.
 MOTT, N. F., 1934, *Proc. Roy. Soc. A*, **146**, 465.
 MOTT, N. F., and JONES, H., 1958, *The Theory of the Properties of Metals and Alloys* (New York: Dover Publications).
 SAH, P., and EISENSCHITZ, R., 1960, *Proc. Phys. Soc.*, **75**, 700.
 SOMMERFELD, A., and BETHE, H., 1934, *Handb. d. Phys.*, **24**, Part 2.

The Stopping Power for Alpha Particles of Ethyl Alcohol and Carbon Tetrachloride in the Liquid and Vapour States

By R. B. J. PALMER

Department of Medical Physics, Royal Free Hospital School of Medicine,
8 Hunter Street, London, W.C.1

MS. received 1st May 1961

Abstract. Range-energy relations for 8.78 mev alpha particles in ethyl alcohol and carbon tetrachloride in the liquid and vapour states have been determined experimentally using nuclear emulsion and scintillation counting techniques. The range in liquid alcohol was found to be greater than the value previously published. The stopping power for both liquids was found to be different from that of the corresponding vapour, and it is suggested that polarization of the absorbing medium is mainly responsible.

§ 1. INTRODUCTION

RANGE-ENERGY relations for alpha particles in liquid water and water vapour have previously been determined experimentally (Palmer and Simons 1959). The range values obtained for alpha particles of various energies in liquid water were higher than earlier published values (de Carvalho and Yagoda 1952, Aniansson 1955). The differential stopping power of liquid water relative to air was also found to be lower than the values published (Appleyard 1951, McNally 1956) and lower than the differential stopping power of water vapour, particularly at low energies. It was suggested that this might be due to a low energy 'density effect', and it seemed desirable to obtain range-energy relations in other materials in the liquid and vapour phases for comparison. For this purpose ethyl alcohol and carbon tetrachloride were selected.

§ 2. EXPERIMENTAL METHODS

Each range-energy relation involved two different types of experiment: a measurement of the total range of 8.78 mev alpha particles from ThC in the medium concerned and a measurement of residual particle energy after a series of known path lengths in the medium had been traversed.

For range-energy determinations in the vapour phase the apparatus previously described for measurements with air was used (Palmer and Simons 1959). In this apparatus 8.78 mev alpha particles traversed a fixed path length in vapour at known pressures and were recorded in nuclear emulsions. Vapour at the required pressure was introduced into the apparatus by including in it a known volume of liquid inside a sealed capsule which could be punctured after the apparatus had been evacuated. Measurements were made at twenty-two different pressures for both alcohol and carbon tetrachloride vapours. The mean residual track length corresponding to each vapour pressure was calculated from

at least 80 track lengths. The graphs of residual track length against vapour pressure are shown in Fig. 1.

For the determination of the total alpha particle range in vapour the photographic emulsion was replaced by a silver-activated zinc sulphide screen and

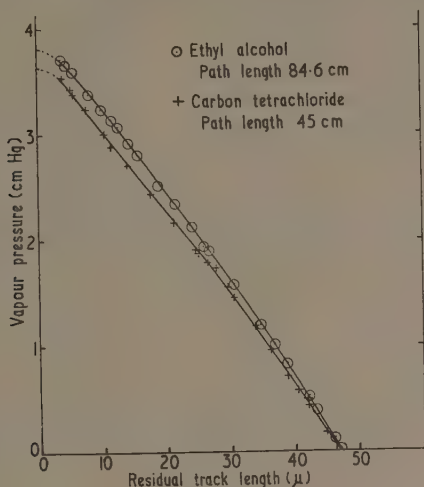


Fig. 1. Relation between vapour pressure throughout an absorbing path of fixed length and residual alpha particle track length in emulsion

photomultiplier, and the change in counting rate was observed as the pressure of the vapour in the apparatus was reduced. Assuming the Bragg-Kleeman rule to hold for vapours within the limits of pressures used in these experiments, the alpha particle range in vapour could be deduced at any required pressure within these limits. Great care was taken to ensure that the alcohol used was dry, and for this reason experiments were carried out using three different drying agents in the vapour chamber: 'Hi-drite', freshly heated calcium oxide and silica gel. Fourteen 'stopping pressure' values obtained using the first two drying agents were all within $\pm 1.2\%$ of their mean value. The values obtained using silica gel as drying agent were all between 1.2% and 2.0% higher than this mean, and since this could have been due to the presence of traces of water vapour these results were rejected. Seven separate determinations of the 'stopping pressure' were made for carbon tetrachloride vapour. The values were all within $\pm 0.7\%$ of their mean value. Increased amplification of the pulses from the photomultiplier had no significant effect on the 'stopping pressure' value obtained, so it was assumed that the alpha particles were being detected by the scintillator when at the extreme end of their range. Typical graphs of counting rate against pressure are shown in Fig. 2.

The relations between alpha particle residual energy and the corresponding path length traversed in liquid ethyl alcohol and carbon tetrachloride were determined by a nuclear emulsion technique previously described for liquid water (Palmer and Simons 1959). They were compiled from approximately 260 track measurements in each of five plates for liquid alcohol and from similar

measurements in seven plates for carbon tetrachloride. Results are shown in Fig. 3.

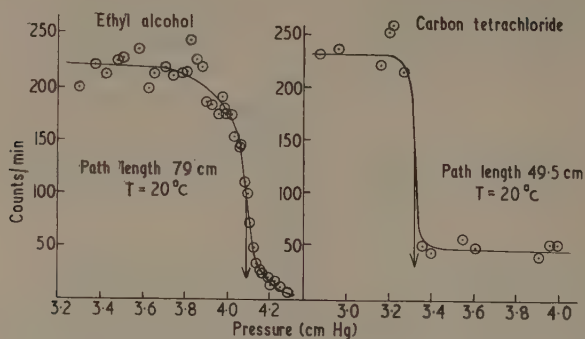


Fig. 2. Typical graphs obtained in the determination of the stopping pressure for alpha particles traversing a fixed path length in a vapour.

The apparatus used for the determination of the total range of alpha particles in the liquid state is shown in Fig. 4. The source holder A was attached to the spindle of a micrometer screw gauge which was calibrated to measure movements with an accuracy to 0.2μ . Alpha particles from the ThC source at B passed through

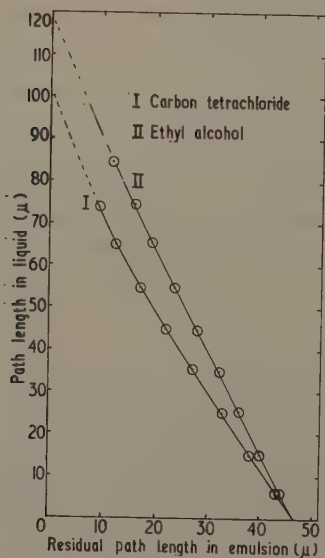


Fig. 3. The relation between the path length traversed by alpha particles in liquid ethyl alcohol and carbon tetrachloride and the residual path length in C2 emulsion.

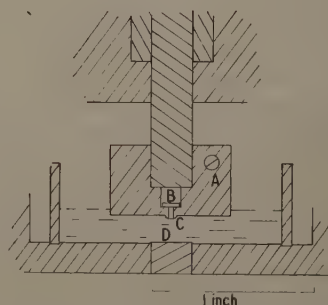


Fig. 4. Apparatus for measuring the range of alpha particles in liquids.

1.4 mm of air and through the Formvar film C into the liquid and were detected by the scintillator at D. The scintillator was a 'Perspex' disk surfaced with small crystals of silver-activated zinc sulphide. The crystals were inset in the Perspex by compressing them between the Perspex and a piece of flat glass at about 120°C . By this means a scintillator was obtained which was flat within $\pm 1\mu$ over an area of several square millimetres. Results obtained using several different scintillators prepared separately in this way did not differ significantly.

The source holder was lowered into the liquid and the counting rate was observed as the source approached the scintillator. A low background counting rate was observed until the distance d between the Formvar-liquid interface and the detector was equal to the total range L in the liquid of the alpha particles emerging from the Formvar, and from this position the counting rate began to increase as the source holder was lowered due to the increasing number of alpha particles reaching the scintillator. If I is the number of alpha particles emitted per second from the exposed area of the source, and r is the total distance between

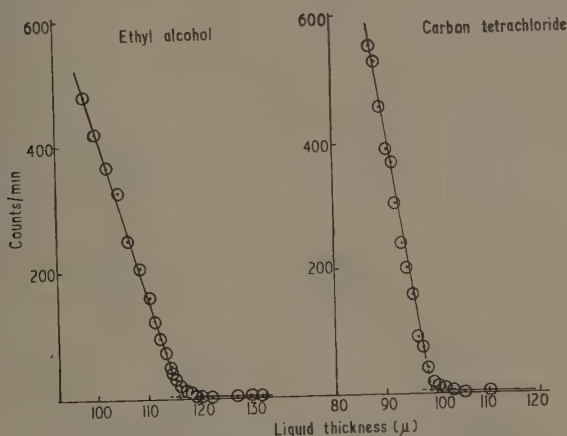


Fig. 5. Typical graphs obtained in the determination of the total range of alpha particles in liquids.

the source and detector it can be shown that the alpha particle counting rate is $I(L-d)/2r$ for values of $L-d$ which are small compared with L . The counting rate was found to vary with the thickness of the liquid layer d as shown in Fig. 5, the non-linear part of the graph being caused by straggling. The straight line part of the graph was extrapolated to the level of the background counting rate and the value of d at the point of intersection was taken as the mean range of alpha particles in the liquid. A correction was made for absorption in the air and the Formvar film. The measurements were carried out at three different pulse amplifications and there was found to be no significant difference in the range values obtained. Mean values taken from eleven measurements with ethyl alcohol and ten measurements with carbon tetrachloride gave range values of $119 \pm 2\mu$ and $100 \pm 1\mu$ respectively for the two liquids. A mean of nine separate measurements carried out with water as the absorbing medium gave

a range of $101 \pm 2 \mu$ which is higher than the value of $96.6 \pm 1.7 \mu$ obtained in previous experiments using a nuclear emulsion technique (Palmer and Simons 1959).

§ 3. RESULTS

The range-energy relations for alpha particles in ethyl alcohol and carbon tetrachloride in the liquid and vapour states are shown in Figs 6 and 7. The range indicated for alpha particles of 5.3 MeV energy in liquid alcohol is seen to be very much higher than the value of 46.5μ obtained by Aniansson (1955).

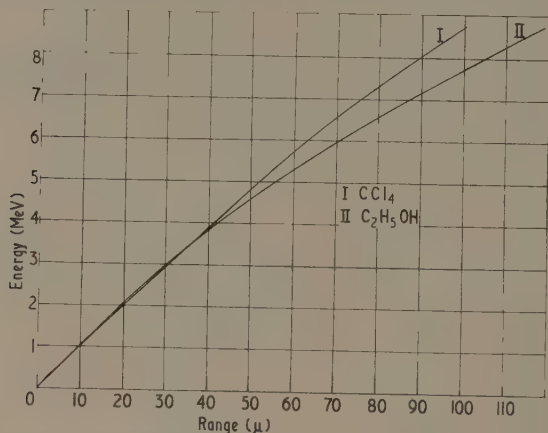


Fig. 6. Range-energy relations for alpha particles in liquid ethyl alcohol and carbon tetrachloride.

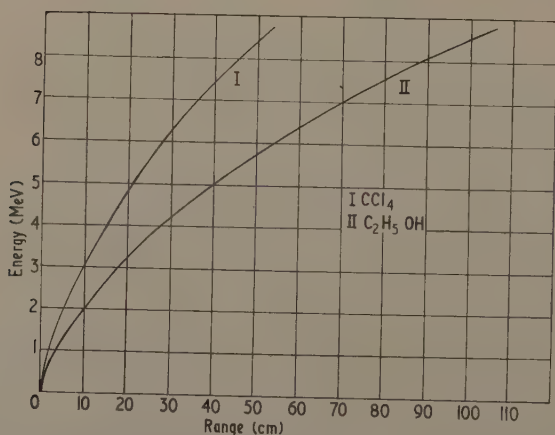


Fig. 7. Range-energy relations for alpha particles in ethyl alcohol and carbon tetrachloride vapour at 3 cm Hg pressure and 15°C.

The Stopping Powers of Liquids and the Corresponding Vapours at Various Energies

Energy (mev)	$\text{C}_2\text{H}_5\text{OH}$				CCl_4				H_2O			
	$\left(\frac{dE}{dx}\right)_L \times 10^3$	$\left(\frac{dE}{dx}\right)_V \times 10^3$	s_L	s_V	$\left(\frac{dE}{dx}\right)_L \times 10^3$	$\left(\frac{dE}{dx}\right)_V \times 10^3$	s_L	s_V	$\left(\frac{dE}{dx}\right)_L \times 10^3$	$\left(\frac{dE}{dx}\right)_V \times 10^3$	s_L	s_V
8	5.4	5.2	4.1	3.9 ₃	7.2	6.2	9.0	7.8	6.3	6.5	1.48	1.53
7	5.7	6.0	3.7	3.9	7.7	7.0	8.3	7.5	7.2	7.7	1.44	1.54
6	6.5	6.8	3.9	4.1	8.4	8.6	8.2	8.4	7.7	8.2	1.41	1.50
5	6.9	7.8	3.7	4.1	9.2	10.0	8.1	8.8	8.4	9.4	1.38	1.53
4	7.6	9.0	3.7	4.3	9.2	10.5	7.3	8.4	9.2	10.3	1.36	1.52
3½	8.3	10.7	3.6	4.7	9.2	11.2	6.6	8.1	10.2	11.6	1.37	1.56
3	9.0	11.8	3.3	4.3	9.4	12.3	5.6	7.4	11.5	14.4	1.29	1.61
2½	9.6	12.8	3.0	4.0	9.6	14.0	4.9	7.2	12.3	17.0	1.18	1.63
2	10.0	13.6	2.6	3.6	9.7	15.2	4.3	6.5	13.0	20.4	1.06	1.66

The specific energy loss in liquids $(dE/dx)_L$ and in their vapours at the same density $(dE/dx)_V$ are given in mev cm^{-1} . The differential stopping powers in liquids s_L and in the corresponding vapours s_V are calculated per molecule relative to one 'atom' of air.

The specific energy losses at various alpha particle energies in ethyl alcohol and carbon tetrachloride in the liquid and vapour phases have been determined from the range-energy relations and are shown in the Table. Values for water previously determined (Palmer and Simons 1959) are given for comparison. In each case the experimental value for the specific energy loss in the vapour phase has been multiplied by the ratio of the molecular densities in the liquid and vapour phases under experimental conditions, so that the value given for the vapour is 'corrected' to the same density as the liquid. The differential stopping powers relative to air, s_L and s_V have been derived from these values of $(dE/dx)_L$ and $(dE/dx)_V$ and from the range energy relation for air previously published (Palmer and Simons 1959). The main source of error in the values of specific energy loss arise in constructing the line through the experimental points. This may give rise to errors of $\pm 2\%$ in the specific energy loss at medium and high energies. At low energies the errors may be greater than this as they will be augmented by errors in the total range determination.

It can be seen that the stopping powers of all three liquids relative to air decrease with decreasing energy. The stopping powers of the vapours vary to a much smaller extent with energy and in differing ways. At high energies there is no significant difference in the stopping power of liquid alcohol and alcohol vapour. The stopping power of carbon tetrachloride vapour appears to be significantly lower than that of the liquid at 7 MeV and above. At energies below 5 MeV the stopping power of the vapour is significantly higher than that of the liquid for all three compounds, and the ratio s_V/s_L increases with decreasing alpha particle energy.

§ 4. CONCLUSIONS

It would appear from these results that several factors may be responsible for the different absorbing properties of liquids and vapours. At high energies the stopping power of carbon tetrachloride is less in the vapour than in the liquid phase, and this may be due to differences in the electronic binding energies in the two phases. At low energies a shielding effect due to polarization of the medium by the alpha particles could account for the lower values of the stopping power in the liquid phase. This effect has been discussed by Palmer and Simons (1959) with particular reference to the difference in the molecular stopping power of water and water vapour. At very low energies the rate of energy loss may be further complicated by the capture of electrons by the alpha particles. Neufeld (1954) considers this problem with particular reference to condensed media, and concludes that the mean alpha particle charge will be greater in a condensed medium than in the corresponding vapour. If this is so, the increased probability of electron loss in a condensed medium should tend to counteract the effect of polarization of the medium and to decrease the ratio s_V/s_L at very low energies. The relative importance of these two effects will depend on the liquids concerned, but at alpha particle energies above 2 MeV the polarization effect would seem to be the overriding factor.

ACKNOWLEDGMENTS

The author would like to thank Dr. H. A. B. Simons for helpful discussion concerning this work and Mr. F. R. Dennis for constructing most of the apparatus required.

REFERENCES

- ANIANSSON, G., 1955, *Phys. Rev.*, **98**, 300.
APPLEYARD, R. K., 1951, *Proc. Camb. Phil. Soc.*, **47**, 443.
DE CARVALHO, H. G., and YAGODA, H., 1952, *Phys. Rev.*, **88**, 273.
MCINALLY, M., 1956, *Proc. Roy. Soc. A*, **237**, 28.
NEUFELD, J., 1954, *Phys. Rev.*, **96**, 1470.
PALMER, R. B. J., and SIMONS, H. A. B., 1959, *Proc. Phys. Soc.*, **74**, 585.

LETTERS TO THE EDITOR

Antiferromagnetic Resonance in the Extreme Infra-red

The magnetic ions in a simple antiferromagnetic crystal like MnF_2 are aligned by exchange interactions so that they form two interpenetrant and equivalent sub-lattices which are spontaneously magnetized in opposite directions. There is a preferred crystallographic axis to which the sub-lattice magnetizations are bound by anisotropic forces arising from dipole-dipole interactions and from crystal field effects. If an alternating magnetic field is applied perpendicularly to the preferred axis the sub-lattice magnetizations will undergo precessional motion which, at 0°K , should be resonant at the frequency below, as deduced by Kittel (1951) and by Nagamiya (1951).

$$\nu = \frac{\gamma}{2\pi} \{ [2H_A(H_E + H_A)]^{1/2} \pm H \}.$$

H_A and H_E are *effective* fields representing the forces constraining the sub-lattice magnetizations to the preferred axis. H_A measures the anisotropy force and H_E the exchange force which is exerted on each ion by the ions forming the other sub-lattice. γ is $ge/2mc$, where g is the g -factor of the ions and will be close to the spin-only value, 2. H is a static externally applied field in the preferred direction whose application leads to two resonant conditions rather than one.

Keffer (1952) has derived theoretical values for H_A and H_E for manganous fluoride. He finds 8.8×10^3 oersteds for H_A and 5.4×10^5 oersteds for H_E . In zero applied field resonance is therefore predicted at 273 Gc/s, or 9.10 cm^{-1} , which corresponds to a wavelength of 1.1 mm. There are two ways in which the resonance frequency can be reduced below this value so that resonance can be observed by microwave methods, which normally do not extend to frequencies as high as 273 Gc/s. The first is to raise the temperature, when both H_A and H_E fall towards zero at the Néel point. The second is to apply a sufficiently large magnetic field for the branch of lower frequency in the equation above to become accessible to measurement. Both methods have been used by Johnson and Nethercot (1959) to study the resonances of manganous fluoride. In this note we report the use of special *infra-red* techniques to observe zero-field low temperature resonances in MnF_2 . The measured resonance frequencies are in good agreement with the theoretical values and with the values obtained by the extrapolation of Johnson and Nethercot's values to zero field and zero temperature.

A grating monochromator was used, with a mercury discharge lamp as source and with a superconducting bolometer as detector, permitting measurements to be made to wavelengths exceeding 1.4 mm (Bloor, Dean, Jones, Martin, Mawer and Perry 1961). The fractional transmission through a crystal of MnF_2 is shown in Fig. 1 as a function of wavelength and for three temperatures. The depth of the absorption lines is about 15% and the two sets of points for 16°K were obtained using different bolometers. The frequencies at which the minima in transmission occurred are as follows:

$$\begin{aligned} &8.77 \pm 0.16 \text{ cm}^{-1} \text{ at } 5.5 \pm 0.3^\circ\text{K} \\ &8.55 \pm 0.16 \text{ cm}^{-1} \text{ at } 16.0 \pm 1.0^\circ\text{K} \\ &7.20 \pm 0.25 \text{ cm}^{-1} \text{ at } 42.5 \pm 1.0^\circ\text{K}. \end{aligned}$$

The last of these temperatures overlaps the lowest temperature at which Johnson and Nethercot detected zero-field resonance. We have plotted their data together with ours in Fig. 2. The curve drawn in the figure is the modified Brillouin curve which should fit the experimental points if the sub-lattice spontaneous magnetization M_s varies with temperature in the manner suggested by the simple molecular field model of Néel (1936) and of Van Vleck (1941), and if both H_A and H_E are proportional to M_s . Johnson and Nethercot extrapolated their zero-field frequencies to zero temperature and their low temperature frequencies to zero

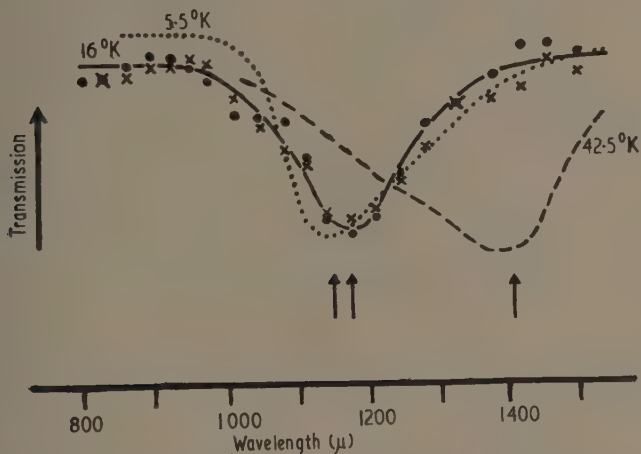


Fig. 1. The relative transmission of MnF_2 as a function of wavelength and temperature.

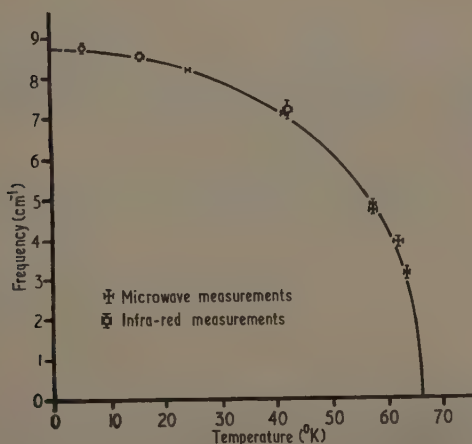


Fig. 2. The temperature dependence of resonance frequency as determined by microwave methods (Johnson and Nethercot) and the infra-red methods.

field, and obtained the value 8.73 cm^{-1} for the zero-field resonance frequency at 0°K . Our most probable value for 0°K is between $\frac{1}{2}\%$ and 1% higher than this, but this difference is within the estimated uncertainty of our determinations. The arrows in Fig. 1 indicate the points at which Johnson and Nethercot's extrapolation procedure would suggest the transmission minima should appear. The results are clearly in good agreement with Keffer's calculations.

The curves of Fig. 1 are unlikely to provide a true measure of the line-breadths. The superconducting bolometers are sufficiently sensitive for the resolution to be limited, not by the available energy, but by the $6 \text{ in.} \times 6 \text{ in.}$ grating in the monochromator. A perfect echelette grating of this size with a 20° groove angle has a resolution of 0.1 cm^{-1} , and defects in our gratings probably limit the resolution attainable to about 0.3 cm^{-1} . It is possible, too, that optical interference effects and non-uniformity of temperature in the sample introduced apparent broadening.

The present measurements at 1140μ , together with the recently reported detection of resonance in MnO at 364μ by Keffer, Sievers and Tinkham (1961) and in NiO at 274μ by Kondoh (1960), show that the techniques of the extreme infra-red are now sufficiently well developed to allow the detection of many of the magnetic resonance phenomena which may be expected in this spectral region.

We are very grateful to Dr. R. Stevenson of the University of Aberdeen, who provided us with a magnificent crystal of MnF_2 .

Queen Mary College,
(University of London),
Mile End Road,
London, E.1

D. BLOOR.
D. H. MARTIN.

9th August 1961

- BLOOR, D., DEAN, T. J., JONES, G. O., MARTIN, D. H., MAWER, P. A., and PERRY, C. P., 1961, *Proc. Roy. Soc. A*, **240**, 510.
JOHNSON, F. M., and NETHERCOT, A. H., 1959, *Phys. Rev.*, **114**, 705.
KEFFER, F., 1952, *Phys. Rev.*, **87**, 608.
KEFFER, F., SIEVERS, A. J., and TINKHAM, M., 1961, *J. Appl. Phys. Suppl.*, **32**, 65S.
KITTEL, C., 1951, *Phys. Rev.*, **82**, 565.
KONDOH, K., 1960, *J. Phys. Soc. Japan*, **15**, 1970.
NAGAMIYA, T., 1951, *Progr. Theor. Phys., Japan*, **6**, 350.
NÉEL, L., 1936, *Ann. Phys., Lpz.*, **5**, 232.
VAN VLECK, J. H., 1941, *J. Chem. Phys.*, **9**, 85.

Hall Effect in Plutonium

Many low temperature properties of plutonium have been interpreted in terms of electronic structural changes at temperatures below 150°K . To explore this possibility further, the Hall effect has been measured in specimens of α -plutonium (maximum impurities 1000 parts per million) and δ -plutonium (stabilized at room temperature by the addition of $3.4 \text{ at. } \%$ Al) at 77°K and 293°K .

Conventional d.c. equipment was used incorporating a permanent magnet of 4.4 kOe field strength. Preliminary measurements on samples of silver, uranium and thorium gave results in good agreement with published data, and additionally a value for thorium at 77°K of $-9.8 \pm 0.6 \times 10^{-11} \text{ m}^3 \text{ c}^{-1}$ was obtained. The results for plutonium are shown in the following table; in each case the value given is the mean of 15–20 observations on each of three samples. The errors quoted arise principally from uncertainty in the specimen thickness.

Temperature (°K)	$R_H (\text{m}^3 \text{ c}^{-1}) \times 10^{11}$	
	$\delta\text{-Pu}$	$\alpha\text{-Pu}$
293	$+11.1 \pm 1.0$	$+6.9 \pm 0.5$
77	$+16.2 \pm 1.5$	-9.5 ± 0.6

All three $\alpha\text{-Pu}$ samples showed a continuous increase in R_H (up to $-18.0 \pm 1.2 \times 10^{-11} \text{ m}^3 \text{ c}^{-1}$) if held at 77°K for up to six hours. After warming to room temperature and remaining there for twelve hours or more, the tabulated values were invariably obtained both at 293°K and initially at 77°K. No time-dependent effect was observed in $\delta\text{-Pu}$.

The large temperature-dependent variation in $\alpha\text{-Pu}$ (opposite in direction to that for $\delta\text{-Pu}$), involving a change in sign, may be analogous to the behaviour of some rare earths (Kevane, Legvold and Spedding 1953) in the region of their magnetic ordering temperatures, although the large effect in dysprosium occurring around the Néel temperature (Liu, Behrendt, Legvold and Good 1959) is in the opposite direction to that in $\alpha\text{-Pu}$.

The observed time dependence in $\alpha\text{-Pu}$ may be related to the detailed thermal cycling reported by Sandenaw and co-workers in specific heat measurements (Sandenaw, Olsen and Gibney 1961) and effects of a similar kind are also shown in some rare earths (McHargue and Yakel 1960). However, we would not exclude the possibility of the effect being due, in this case, to strains remaining in the α samples from the various mechanical and thermal processes of their history.

Projected measurements of the temperature dependence and possible field dependence of the Hall coefficient together with an extension to liquid helium temperatures should enable a more detailed analysis of the effect to be made.

Atomic Weapons Research Establishment,
Aldermaston,
Berks.

R. G. LOASBY.
J. C. TAYLOR.

27th September 1961.

- KEVANE, C. J., LEGVOLD, S., and SPEDDING, F. H., 1953, *Phys. Rev.*, **91**, 1372.
 LIU, S. H., BEHRENDT, D. R., LEGVOLD, S., and GOOD, R. H., 1959, *Phys. Rev.*, **116**, 1464.
 MCHARGUE, C. J., and YAKEL, H. L., 1960, *Acta Metall.*, **8**, 637.
 SANDENAW, T. A., OLSEN, C. E., and GIBNEY, R. B., 1961, *Plutonium 1960*, Mem. No. 42 (London: Cleaver-Hume).

CORRIGENDUM

Explanation of Some 'Forbidden' Transitions in Paramagnetic Resonance, by B. BLEANEY and R. S. RUBINS (*Proc. Phys. Soc.*, 1961, **77**, 103).

We are indebted to Mr. F. I. B. Williams of the Clarendon Laboratory for drawing our attention to some third-order terms omitted from Eqn (7) of this paper. The last term of this equation includes only the contributions arising from terms off-diagonal in the nuclear magnetic quantum number; the omitted terms are diagonal in this quantum number, and arise from the modification of the value of $\langle S_z \rangle$ through admixtures to the state $|M\rangle$ by the crystal field operator. The last term in Eqn (7) should be replaced by

$$\left\{ \frac{D \sin 2\theta}{4g\beta H} \right\}^2 \left\{ \frac{2Am}{M} \right\} \{ [M^2 - S(S+1)]^2 - M^2 \} \\ + \left\{ \frac{D \sin^2 \theta}{4g\beta H} \right\}^2 2AmM \{ 2M^2 + 1 - 2S(S+1) \}.$$

This change does not affect Eqn (8), but Eqn (9) etc. should read

$$\Delta H = x(y \cos^2 \theta - z \sin^2 \theta) \sin^2 \theta \quad \dots\dots (9)$$

where $\delta = (Am/4g\beta H) \{4S(S+1) + 1\}$ and $z = 1 + (Am/g\beta H) = 1 + \epsilon$. Eqn (10) becomes

$$\delta H = x \left\{ z + \frac{y^2}{4(y+z)} \right\} \quad \dots\dots (10)$$

which, for small values of $(Am/g\beta H)$, reduces to

$$\delta H = \left(\frac{25x}{9} \right) \left\{ 1 - \frac{32\delta - 13\epsilon}{45} \right\}.$$

REVIEWS OF BOOKS

Electronic Processes in Solids, by P. R. AIGRAIN, R. J. COELHO and G. ASCARELLI.
Pp. x+67. (London: John Wiley, 1961.) 32s.

In 1957, Professor Aigrain was Visiting Professor at the Massachusetts Institute of Technology and gave a course of lectures in which he examined the foundations of the currently accepted methods of treating transport processes in solids. Starting from the complete crystal Hamiltonian, the various stages leading to transport theory, such as the Born-Oppenheimer approximation, and the solutions of the resulting nuclear and electronic equations were developed. Scattering theory and various scattering mechanisms were considered and led to a discussion of transport theory.

This book was prepared by the authors from notes taken at these lectures, and according to the preface they have extended some of the topics and have presented others in a slightly different way. Their declared object in doing so was to reach a wider audience possessing a "fair background in calculus and in elementary wave mechanics".

It must be admitted that the question of what is a fair background is one of the most difficult ones to answer before writing a book on any advanced topic and the answer tends to vary greatly from one individual to another. Making due allowance for this, however, I still think that the authors have tried to squeeze too much into a book of only sixty-two pages (small ones at that). A comparatively small increase in length, used to include arguments by which one equation is derived from another and to provide general continuity, would have been very well worth while. It would have given the reader a much easier task in attempting to follow the mathematical arguments. As things stand, I very much doubt whether this can be done with the present book unless the reader already knows a good deal about the subject and is thoroughly familiar with quantum mechanics. Even in this case, the attempt is likely to be confused by the absence of an adequate explanation of symbols and by the presence of numerous misprints in the book.

To quote a few examples, in the first equation on page 2, the summation sign appears in both primed and unprimed form with no explanation of the distinction between the two. On page 3, the first equation contains a very confusing misprint (H_r instead of H). A few lines further along a symbol V_a is introduced without any explanation of its significance. On page 6, ω_k should appear as ω_k^2 on the left-hand side of Eqn (3.4). An integral sign is missing in Eqn (6.3). The lack of continuity between sections 6 and 7 is particularly bad. In the former the electronic wave equation is formulated and in the latter the solution is given, but it is practically impossible to see that the same equation is being dealt with in both cases.

These are the sort of things which occur in all lecture notes. It is well known that such notes are usually unintelligible to anyone except the person who has taken them. This book suffers from this fault. A little more care in editing and a little more explanation would have done much more justice to the subject and to Professor Aigrain's treatment of it.

J. R. DRABBLE.

Röntgenstrahl-Interferenzen, by MAX VON LAUE. Pp. x+476. (Frankfurt: Akademische Verlagsgesellschaft, 1960.)

The character of this third edition is essentially the same as that of its predecessors. The original aim of Professor von Laue's book was to form a bridge between crystallography and wave mechanics, and in this it succeeds admirably. This is not a book on methods of structure analysis; it deals with the basic physical and optical principles of x-ray diffraction. The most detailed part of the book concerns the treatment of the dynamical theory of x-ray diffraction from crystals. This section has been brought up to date by a thorough discussion of the anomalous absorption effect, and of the path of the x-rays in the crystal. There is no doubt that Professor von Laue's treatment of all aspects of dynamical theory remains the most comprehensive and authoritative work on this subject.

In preparing this third edition Professor von Laue was conscious of the considerable progress made in our knowledge and understanding of crystal defects. He therefore included a discussion of 'paracrystals', a selection which was no doubt influenced by the fact that this particular topic was developed in his institute.

Although this book also contains the basic principles of structure analysis, calculations of atomic scattering factors, an account of temperature diffuse scattering and of several other topics, to the reviewer this work stands out as the classical exposition of dynamical theory by the father of x-ray diffraction.

P. B. HIRSCH.

An Introduction to Celestial Mechanics, by T. E. STERNE. Pp. xi+206. (New York, London: Interscience, 1960.) 34s.

Celestial mechanics has not been promoted as vigorously during the last few decades as it was last century. Thus we find students are somewhat unprepared for the exacting demands of the new space science which presents a wide range of celestial mechanical problems requiring quick and accurate answers. The basic mathematics is known but not very readily available to those with limited background knowledge and limited time to press further. The interscience tract under review should go far to help this situation.

Any author attempting to deal with the dynamical problems of the space age has to consider whether his approach will be through classical methods or whether suitable progress can be made without them. The present work does take the classical line. It is intended for students at about young graduate level and with a physics or engineering background. The non-astronomer may acquire his basic information on orbital problems from the first three chapters. The serious dynamics begins in chapter 4 where the author takes one quickly, although systematically, through Lagrange's equation, the Hamiltonian form, contact-transformations, the Hamilton-Jacobi equation. All of these steps lead up to the solution of perturbed systems and thus to the orbital variations of space science. There are two treatments of the problem of satellite revolution around a non-spherical planet, one of which might be considered standard, and the other a new treatment with certain advantages in application. The atmospheric density in relation to resistance to the motion and the life of a satellite is also treated fully. Finally, there is a useful chapter on numerical methods of integrating differential equations.

This introduction could be used as a textbook or for ancillary training. It is also useful as a reference source of formulation in dynamics. It should be available in all libraries dealing with mechanics and many private copies will be sought.

C. W. ALLEN.

Plasma Physics and the Problem of Controlled Thermonuclear Reactions, Vol. II, edited by M. A. LEONTOVICH. Pp. vi + 457. (London, New York, Paris, Los Angeles: Pergamon Press, 1960.) £8.

As mentioned in the review of Vol. III (*Proc. Phys. Soc.*, 1960, **76**, 591), the four volumes contain translations of Russian reports dealing with work on controlled thermonuclear fusion from 1951 to 1958. The general comments in the previous review are relevant; for example, the reports are written for the specialist, cover a wide range of topics, and include both theoretical and experimental work.

There are twelve purely theoretical papers in the present volume, of which eight deal with cylindrical plasma columns with steady and time-varying internal and external magnetic fields, axial currents, etc. These include two on the conditions for hydromagnetic stability. Of the four other theoretical papers, one is on nuclear reaction rates, one on bremsstrahlung, and two on relativistic plasmas with sections on relativistic beams.

The experimental papers include three dealing with neutron and x-ray production in cylindrical deuterium discharges, one on current and electric field distributions within the discharge as obtained by using magnetic probes, and one on electrical conductivity in a low frequency (270 c/s) high current linear discharge.

The remaining three papers are concerned with a particular plasma experiment, in which a ring current is induced in a low pressure gas in an apparatus rather similar to a betatron. The ring is then collapsed to form a ball of plasma. This is discussed experimentally in detail following a brief theoretical account.

The volume will repay careful study by all those engaged on research into the properties of plasmas.

R. LATHAM.

Electromagnetic Structure of Nucleons, by S. D. DRELL and F. ZACHARIASEN. Pp. 111. (London: Oxford University Press, 1961.) 12s. 6d.

This little book arrived for review at about the same time as I had undertaken to give a lecture on electromagnetic nucleon structure; it was therefore subjected to rather more than the first quick reading that many books must get from their reviewers. I found it immensely informative and helpful at just the level I required, and surprisingly self-contained. The first chapter defines with great clarity what is meant by the form factors. The second chapter sets about the analysis of experiments from which form factors may be obtained. The third chapter deals with the calculation of form factors by means, in the main, of dispersion theory which it starts off by explaining without being at all frightening. The fourth and final chapter briefly considers the validity of quantum electrodynamics. The book is an excellent addition to a series which is already commanding great respect. Although the subject of the book is expanding fast, so that in detail it may quickly be out of date, there is sufficient in it of substance that it is likely to remain useful for a good many years.

B. H. FLOWERS.

Kinematics of Nuclear Reactions, by A. M. BALDIN, V. I. GOL'DANSKII and I. L. ROZENTHAL. Pp. xiii + 303. (London, New York, Paris, Los Angeles: Pergamon Press, 1960.) 42s.

An adequate and lucid translation of a book originally published in Russian and dealing with a very useful subject from a practical point of view is always welcome. One has to spend so much time calculating tricky kinematical factors that to find almost every conceivable one written down, together with many useful diagrams and tables, is a great relief, particularly to the more indolent theoretician. It is therefore even more to be deplored that the translation was obviously not checked before publication by a competent physicist who could easily have put right so much of the translator's phraseology. Although such defects do not always obscure the meaning completely, they certainly do not help the reader. One example should suffice, dealing with three-body reactions which are considered as the limits of two-body ones: "These limiting cases are, in point of fact, different variants of the substitution of a one-act formation of many particles by several acts, in each one of which up to two particles is formed."

B. H. FLOWERS.

The Theory of Transition-metal Ions, by J. S. GRIFFITH. Pp. x + 455. (London: Cambridge University Press, 1961.) 95s.

This book is concerned with the theory of metal ions having a partly filled d-shell, and particularly with the theoretical properties of these ions in solids when they are under the influence of a crystalline or ligand field. This subject is of considerable current interest having been much investigated during the past few years, especially in the areas of paramagnetic resonance and optical absorption in paramagnetic crystals.

Chapters 1 to 6 deal with mathematical techniques and include a detailed chapter on the structure of free atoms and ions, and also a chapter on groups and their matrix representation. Chapters 7 to 9 then give the theoretical methods used for calculating the properties of complex ions in solids, the cases of weak and strong ligand fields each being dealt with very thoroughly. The last three chapters, 10 to 12, apply the theory to the behaviour of paramagnetic substances and include discussions of susceptibility, optical absorption spectra and paramagnetic resonance. There are a number of appendices which include many useful tables of theoretical and experimental data. All of the above refers to transition group ions with partly filled 3d, 4d or 5d shells—those with partly filled 4f or 5f shells are not treated.

The book will be very valuable to theoretical workers in the field, particularly for the treatment of calculations of energy levels of complex ions. These are necessary, for example, for understanding optical absorption spectra. It is also a useful reference book with many energy level diagrams and tables of theoretical and experimental parameters as well as original references. The treatment throughout tends to be rather formal and mathematical, and the book might have reached a wider audience had there been, in places, a little more simple physical discussion and explanation. Also, some topics are, surprisingly, omitted. For example, in the long chapter (58 pages) on paramagnetic resonance there is barely a mention of hyperfine structure from ligand nuclei, yet one would

have thought that this was one of the most direct applications of this technique to the study of the structure of complex ions. However, these are small criticisms of a good book which gives what is probably the best formal introduction to ligand field theory at present available.

J. OWEN.

The Hall Effect and Related Phenomena, by E. H. PUTLEY. Pp. viii + 263. (London: Butterworths, 1960.) 50s.

I have heard it said that Dr. Putley has measured more Hall voltages than any other scientist. Whether or not this is true, he is well qualified to write this book.

The subject of the book is transport phenomena in semiconductors and it is written from the experimentalists' viewpoint. Methods of measurements are described and various transport equations are derived which in some other publications are only quoted. This makes the book particularly useful for the final year undergraduate who is interested in semiconductors, and for anyone who is beginning research in this field.

The first chapter of 21 pages on 'Conduction processes in semiconductors' provides the standard introductory discussion. There follows 40 pages in which the various thermo-galvanomagnetic effects are defined and the methods of measurement described. Amongst other things, this is a good place for looking up the signs, a feature which will be welcomed by many readers other than those already referred to. Either the right hand or the left hand can be used for turning the pages!

Chapter 3 is called 'Conduction in an isotropic solid'. Here the equations for the various transport effects are derived. Chapter 4 is the best chapter in the book, containing a detailed discussion of the transport properties of, primarily, germanium and silicon. There are some traps for students though. For instance, after a paragraph on carrier scattering by the acoustic modes of atomic vibrations the author writes: "In addition to the longitudinal vibrations of the lattice, transverse modes are possible . . . These are the optical modes . . ." The author gives the impression that the two types of atomic vibrations are: acoustical (longitudinal) and optical (transverse). One would not have expected this from the Royal Radar Establishment where one would have thought that T.A. and L.O. were, so to say, everyday words.

In the final chapter the work on other semiconductors is summarized. This is of necessity brief and is the chapter which suffers most from the continued rapid development of the subject. A major criticism here is that references are not given for the values quoted in the comprehensive Table 5.2 and it is frequently not possible to decide, with the aid of the text, whose value is being quoted. It is also misleading to speak of 'the hexagonal' form of silicon carbide when many hexagonal varieties exist, each a particular stacking fault in the zinc blende structure. Perhaps the data about the 0.25 eV difference in the band gaps of two of the hexagonal modifications were not available at the time of writing, nevertheless it was a gross simplification to write of 'the hexagonal' form.

These are points indicating a certain untidiness of detail. The book as a whole can be recommended to final year undergraduates and to anyone starting research on these topics.

At £2 10s. it seems to me expensive and I should have thought that, in view of the potential undergraduate and research student market, a paper backed edition at half the price would be welcome.

E. W. J. MITCHELL.

Modern Aspects of the Vitreous State, Vol. 1, edited by J. D. MACKENZIE. Pp. viii + 226. (London: Butterworths, 1960.) 50s.

The subjects dealt with in this edited symposium on the properties of glass include discussions of the results of x-ray diffraction, nuclear magnetic resonance, infra-red and high-temperature studies of the vitreous state, and fundamental discussions of crystallization kinetics and the formation of glasses and of the 'glass transition'. There is also a chapter on the constitution of phosphate glasses. Although the book is labelled Volume One, there is no indication as to what future volumes will contain, so that it is difficult to comment on the scope of the present volume.

It is true, as the editor states in his introductory remarks, that "the structure of glassy materials has long been a topic of much controversy" and that "... comparatively little scientific progress was made in the last three decades". Unfortunately, the contents of this symposium, which sets out to survey the modern aspects of the vitreous state, are extremely variable both in quality and outlook. There are three excellent chapters: by D. Turnbull and M. H. Cohen, P. J. Bray and A. H. Silver, and I. Simon; four chapters which, though worthy, are not at all modern in outlook, and one which is simply eccentric. If the editor has attempted to co-ordinate or reconcile the contributions, he has not succeeded. In the present dearth of literature on glass this volume would be a useful source book of references for the active worker in the field, but of little use to the beginner, or the outsider.

G. O. JONES.

CORRIGENDUM

Selected Scientific Papers, by B. VAN DER POËL, edited by H. BREMMER and C. J. BOUWKAMP (*Proc. Phys. Soc.*, 1961, **78**, 636).

The price is £6 13s. for both volumes together, and not £6 13s. per volume as stated.



Fig. 1. Tabular silver bromide grain ($\times 10\,000$) possessing a lattice rotation of $21^{\circ} 30'$ and corresponding to specimen N in Table 3.



Fig. 3. A grain ($\times 13\,000$) from the same emulsion as those grains in Fig. 1, but in course of transition to another tabular form.

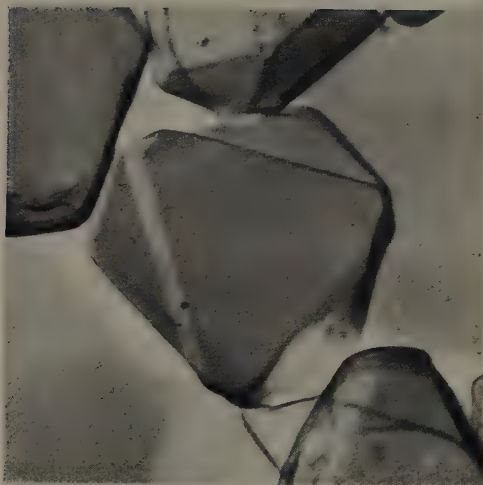


Fig. 4. A tabular silver bromide grain ($\times 14\,000$) from an emulsion of smaller mean grain projective area than the grains shown in Figs 1 and 3. It possesses a lattice rotation of $27^{\circ} 20'$ and corresponds to specimen G in Table 3.

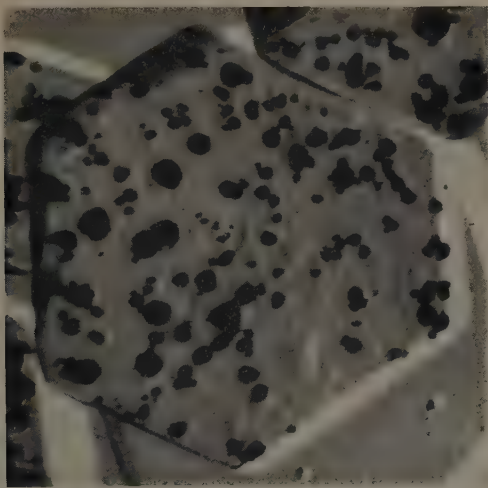


Fig. 5. Tabular silver bromide grain ($\times 14\,000$) of normal form showing the distribution of internal photolytic silver formed on heavy exposure.

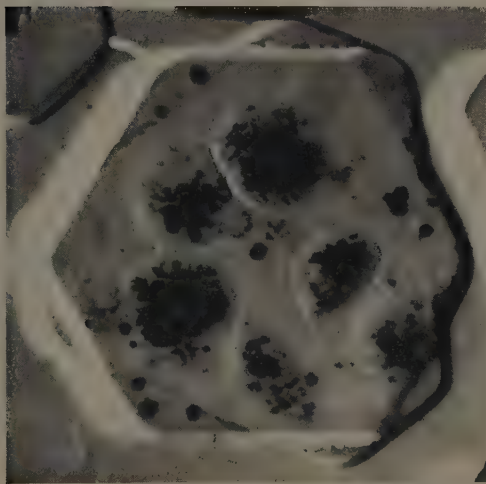
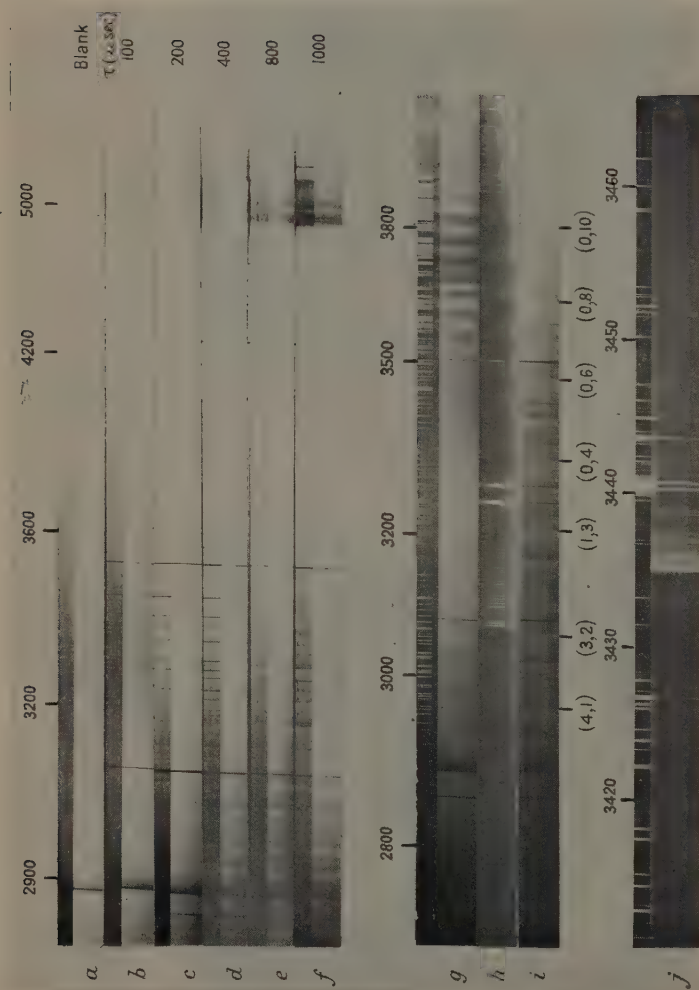


Fig. 6. The modified distribution of internal photolytic silver formed on heavy exposure in a tabular silver bromide grain ($\times 14\,000$) possessing a lattice rotation.



a. Background continuum from flash tube.
 b, c, d, e and f. Barium peroxide in shock tube; absorption behind reflected shock wave at 100, 200, 400, 800 and 1000 μ sec.
 g. Barium chloride in shock tube; absorption behind reflected shock wave at 1000 μ sec. Fe arc above.
 h. Barium nitrate in arc in air.
 i. Barium peroxide in shock tube; absorption behind reflected shock wave at 1000 μ sec.
 j. Zinc oxide in shock tube; emission behind reflected shock wave.

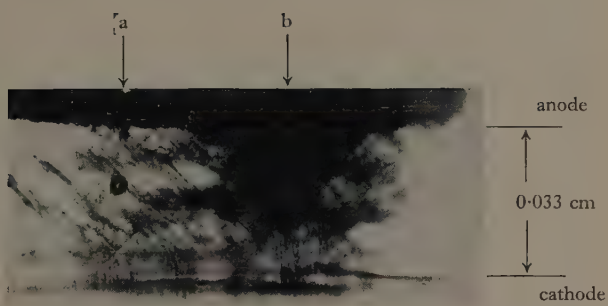


Fig. 2. Suppressed discharge in potassium chloride. *a*, suppressed discharge, *b*, main discharge. Specimen viewed through a plane at right angles to the plane of the cathode.

An Investigation into the Mechanism of Self-quenching Geiger-Müller Counters containing Argon with Small Quantities of Xenon, Oxygen and Nitrogen

By A. J. L. COLLINSON, I. C. DEMETSPOULLOS AND J. M. ZARZYCKI

Borough Polytechnic, London, S.E.1

MS. received 14th April 1961, in revised form 8th June 1961

Abstract. The time distribution of spurious pulses in counters with treated and untreated cathodes was studied by pulse interval analysis, and plateau characteristics, charge per pulse and Geiger threshold potential are plotted as functions of the xenon concentration. In all the counters investigated, the presence of a minimum threshold indicates an optimum xenon concentration of 3.5%. Measurements of the corona threshold with argon and argon-xenon filling mixtures show a pressure dependent increase in gas multiplication with addition of xenon. This increase in ionization is tentatively explained by the hypothesis of two-body collisions between xenon atoms and argon excited molecules leading to the formation of the molecular ion AXe^+ . Mobilities obtained from transit time measurements identify the ions involved as A_2^+ ($1.82 \text{ cm sec}^{-1} (\text{v cm}^{-1})^{-1}$), possibly NO^+ ($2.45 \text{ cm sec}^{-1} (\text{v cm}^{-1})^{-1}$) this ion appearing after the counters have been in continuous discharge, and an ion of mobility $1.64 \text{ cm sec}^{-1} (\text{v cm}^{-1})^{-1}$, which is not inconsistent with the postulated AXe^+ molecular ion.

§ 1. INTRODUCTION

GEIGER-MÜLLER counters containing simple gases (e.g. argon, oxygen, hydrogen, air, etc.), generally designated as 'slow', have been little used for many years. With these fillings the discharge produced by an ionizing event has a strong probability of producing a further discharge which has to be suppressed by inserting a very high value resistor ($\sim 10^9$ ohms) in the anode or by the use of an external quenching circuit, otherwise the counter runs virtually into continuous discharge. Consequently such counters have been largely superseded in favour of those containing polyatomic vapour or halogen which do not require external quenching.

The basic mechanism of Geiger counter action, namely the quenching of the discharge by the slow moving positive ion sheath formed close to the anode, was first explained by Montgomery and Montgomery (1940) who attributed the train of secondary discharges after each discharge in a slow counter to positive ions releasing electrons on arrival at the cathode. This explanation seems to have had fairly general acceptance (Korff 1958), although the work of Ramsey (1951) on argon-oxygen counters indicated that some secondary discharges arose before the positive ion sheath reached the cathode.

The counters which are the subject of the present investigation containing xenon ($\sim 3.5\%$), oxygen ($\sim 0.3\%$), nitrogen ($\sim 1\%$) with argon to a total pressure of about 700 mm Hg were discovered by Shore (1949) and are remarkable in that while the filling gases are those normally associated with slow counters, the characteristics are typical of organically quenched counters. That is, they have flat plateaux obtainable with only a small anode series resistor. The present authors have mainly confirmed Shore's findings and this work has already been briefly reported (Collinson, Demetsopoulos, Dennis

and Zarzycki 1960). The object of the present work was to investigate the performance of the counters in more detail, particularly as to the part played by the xenon. The present investigation does not cover the role of the nitrogen which is subsidiary (Collinson *et al.* 1960).

§ 2. APPARATUS AND EXPERIMENTAL PROCEDURE

2.1. Counters and Filling Procedure

The counters mainly used in this investigation were of the 'gamma' type, glass bodies with cylindrical cathodes 2 cm diameter and tungsten anodes 0.127 mm or in some cases 0.075 mm diameter. The active length of the counters was 20 cm. Cathode materials of copper, nickel, stainless steel, chrome iron, lead and silver have been used.

A conventional, all-glass vacuum system was used including a glass mercury vapour diffusion pump and every precaution was taken to exclude mercury from the system by the use of appropriate cold traps. The argon used was of 99.95% commercial grade but no attempt was made to remove the main impurities, oxygen (0.0005%) and nitrogen (0.05%), as these were normally present in much larger quantities in the filling mixtures. Water vapour and other condensible impurities were removed by passing the argon slowly through a liquid oxygen trap. The other gases used were of 'spectrally pure' quality, the xenon containing not more than 0.5% krypton as an impurity.

The counters were normally baked at 350 °C before filling which was not carried out unless the pressure in the system had previously held to less than 1×10^{-4} mm Hg overnight with pumps shut off.

2.2. Measurements of Plateau Characteristics and Charge per Pulse

When measuring plateau characteristics the anode e.h.t. was fed via a 4.7 megohm resistor and a linear feedback amplifier of gain variable from 25 to 400 was used, the higher gain being sometimes necessary to ensure that all pulses were counted, particularly with counters having poor plateaux, when a large number of small, possibly spurious pulses occurred.

Two methods were employed for measurement of the charge per pulse of the counters. In the first, a standard capacitor was connected between the counter cathode and earth, the potential difference across the capacitor resulting from a known number of counts being determined by an electrometer valve circuit. Provided the count rate was low enough for the chance of a discharge taking place with the positive ion sheath (or part of it) from the previous discharge still in the counter to be small, and that the number of spurious pulses was small, this method was quite satisfactory. However, spurious discharges, if present, gave rise to a smaller charge and the method described above yielded values lower than those represented by a normal discharge. A second method was therefore employed which consisted in measuring the height of the voltage pulse at the anode of the tube by an oscilloscope, the arrangement being calibrated by injecting a known charge from a pulse generator via a small capacitor. Graphs of charge per pulse against voltage obtained from both methods coincided at low overvoltages, the latter being defined as the excess of the operating voltage over the threshold voltage, but diverged at the end of the plateau, as would be expected. In practice both methods were used, the capacitor method yielding more accurate results at or near the counter threshold.

2.3 Time Distribution of Spurious Pulses

Spurious pulses occurring in the various gas mixtures were investigated by the method of pulse interval analysis originally used by Putman (1948) and also by Beretta and Rostagni (1949), for argon-alcohol Geiger counters.

A modified version of the circuit due to Putman (1948) was used to measure I , the rate of arrival of pulse intervals between t and $t + \delta t$. The spurious pulse distribution was determined by comparing the measured interval distribution with that expected from a truly random distribution where the number of intervals recorded in unit time is $n^2 \exp(-nt)\delta t$, by the Poisson law, n being the mean count rate.

The transit time of the positive ion sheath across the counter was measured for the various mixtures at different overvoltages by observation of the current pulse due to the discharge. The latter was viewed by connecting an oscilloscope to the cathode of the counter, a resistor R_K being connected from cathode to earth. The pulse (see figure 1) rises to a maximum value in a few microseconds after the initiation of the

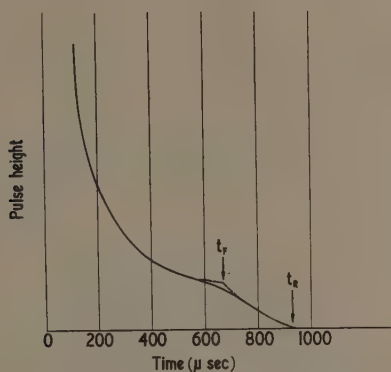


Figure 1. Typical cathode pulse shape.

discharge and then falls away more slowly, a discontinuity where the current starts to fall more rapidly being present at a few hundred microseconds. The positive ion sheath as it moves across the counter distends under the action of its own field. The observed discontinuity corresponds to the time t_F when the front of the sheath reaches the cathode, and the time t_R , the recovery time when all ions are cleared from the counter, is given by the time at which the pulse returns to zero.

§ 3. EXPERIMENTAL RESULTS

3.1. Preliminary Experiments

Observations were made using counter fillings of argon alone and then argon and xenon (3.54%) the total pressure in each case being 700 mm Hg. With both these fillings no Geiger region was observed, the discharge passing abruptly from the proportional to the corona region. In neither case were any pulses recorded when a quenching probe was used. Using a ^{137}Cs source the proportional pulses were observed with an amplifier of a maximum gain of 10^6 and an oscilloscope. With both fillings it was clear

that the onset of the corona region was due to photon-cathode action similar to the observations of Colli and Facchini (1952) with pure argon. In neither case were the familiar pulses, typical of build-up along the anode with positive ion space charge quenching, observed. The chief difference between the two fillings was that the corona threshold was reduced by 500–600 volts by the presence of the xenon.

Although no accurate measurements were made of the gas multiplication, it was clear it increased more rapidly with the argon-xenon mixture than with the argon alone. Just before the respective corona thresholds, the pulse heights in the case of the argon-xenon mixture were about ten times those from the argon alone.

The addition of small quantities of oxygen to either argon or argon-nitrogen mixtures altered the character of the discharge entirely, Geiger pulses typical of discharge build-up along the anode with positive ion space charge quenching being seen on the oscilloscope

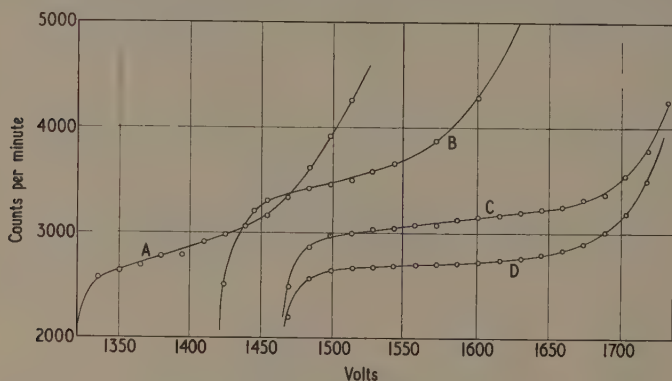


Figure 2. Plateau curves for different cathodes: A, silver, slope 0.17% per volt; B, chrome iron, slope 0.11% per volt; C, stainless steel, slope 0.053% per volt; D, oxidized copper, slope 0.025% per volt. Mixture 2.2% xenon, 0.35% oxygen, 1.1% nitrogen; total pressure, 706 mm Hg.

with many spurious pulses. Mixtures containing 0.3% and 3% of oxygen respectively with total pressures of 700 mm Hg were investigated, plateaux being non-existent. Good plateaux were, however, obtained with both these mixtures using a quenching probe, plateau slopes and lengths being somewhat better with the lower oxygen concentration.

The counters were next filled with several mixture compositions, fairly close to the optimum amounts recommended by Shore, behaving as self-quenching counters and having plateaux varying in length between 60 and 180 volts and in slope between 0.03% and 0.15% per volt, for the various mixtures and cathodes used; silver was an exception in that the plateau slopes could be as high as 1.2% per volt. It was found that not only the type but also the state of the cathodes affected the performance. This was particularly so with copper cathode counters which after being filled, used and refilled several times gave an improved and consistent performance. This was attributed to a slow oxidation and conditioning of the cathode surface. A number of typical plateaux are shown in figure 2. It was also established during these experiments that for a stable cathode the plateau slope increased with the oxygen concentration, the optimum value of the latter being about 0.3%.

From the pulse interval analysis curves obtained with the different counters and mixtures it was clear that the spurious pulses fell into two categories as far as time incidence was concerned. If the voltage was set so that the counter was working on the plateau then a small number of spurious pulses were detected and these were fairly uniformly spread between the dead time and the recovery time. With the counter voltage set beyond the end of the plateau, the incidence of the spurious pulses was a maximum at the end of the dead time and fell away towards the recovery time. Typical curves illustrating these effects are shown in figure 3 (curves A and B) for a stainless

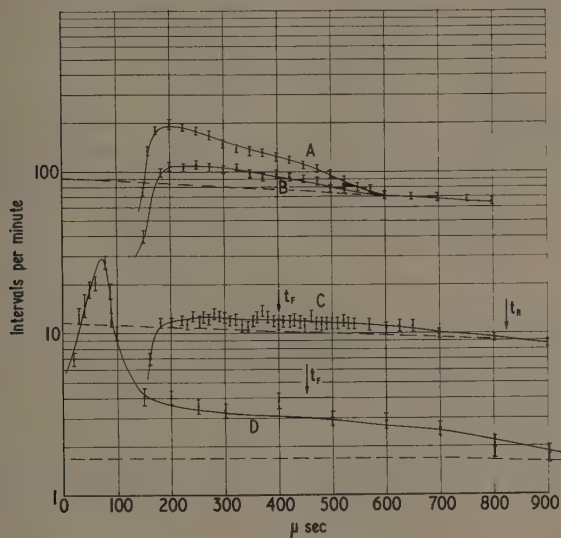


Figure 3. Pulse interval analysis curves for oxidized cathodes: A and B, stainless steel cathodes, overvoltages 175 and 100 volts, xenon concentration 2.23%; C, copper cathode, overvoltage 120 volts, xenon concentration 3.5%; D, copper cathode, overvoltage 6 volts, xenon concentration 0.10%. Dotted lines here and in figure 7 refer to the theoretical Poisson distribution, $I = n^2 \exp(-nt)\delta t$.

steel counter. From the many curves obtained, it was concluded that with these mixtures and cathodes spurious pulses due to ion-cathode effect were not present in any significant quantity otherwise a peak at the positive ion transit time would have been observed.

3.2. Variation of Xenon Concentration

Using two counters with copper cathodes of identical construction the counter characteristics were studied as the xenon concentration was varied from zero to 7%, the other constituents being maintained constant, oxygen at 0.3% and nitrogen at 1.1% with argon to a total pressure of 700 mm Hg. The variation of starting voltage, plateau slope and length are shown in figure 4, the optimum value of xenon concentration being obviously about 3.5%. Curves of m against overvoltage for the different mixtures are shown in figure 5, where m is the ratio of the charge per pulse to the

static charge on the wire, and $m = 2Q \log(b/a)V$, V being the anode potential, b and a the cathode and anode diameters respectively, and Q the charge in the ion sheath per unit length of the wire. Plotted in this form the curves are almost straight lines

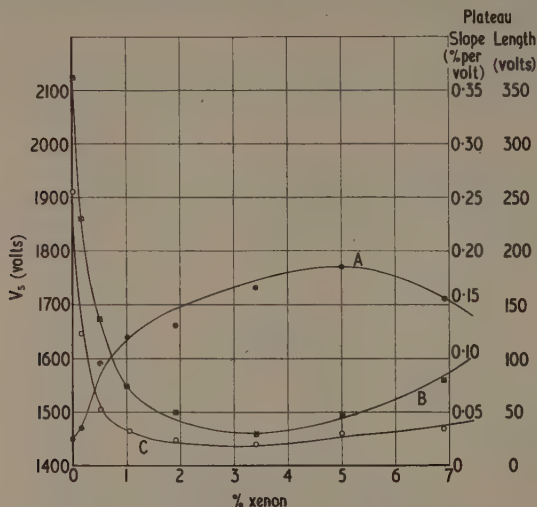


Figure 4. Variation of plateau length (curve A), plateau slope (curve B) and threshold voltage (curve C) for different xenon concentrations. Oxygen concentration 0.3%, nitrogen 1.2%, total pressure 700 mm Hg.

where m is less than unity. In the one case where the plateau is long enough for m to be greater than unity the curve changes slope abruptly at this point. This behaviour is also typical of alcohol-quenched counters (Fenton and Fuller 1949) and has been

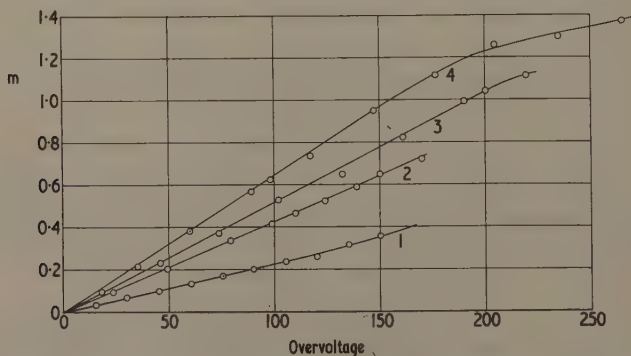


Figure 5. Variation of m with overvoltage for xenon concentrations 0.5% (curve 1), 1.07% (curve 2), 1.91% (curve 3), 3.44% (curve 4).

explained by Wilkinson (1948). It will be observed that the slopes of the charge per pulse-overvoltage curves increase rapidly with admission of xenon varying from 0.24 per 100 volts to 0.66 per 100 volts.

Pulse interval analysis curves obtained with these mixtures showed similar characteristics to those obtained in the preliminary experiments. However, at xenon concentrations less than 1% the dead times were much shorter as spurious pulses from curves taken just at the end of the very short plateau had a maximum incidence at 30 to 50 μsec , whereas with the larger concentrations dead-times were of the order of 150 to 200 μsec . Two typical curves are shown in figure 3, curves C and D, one for the mixture with 0.16% xenon and the other with 3.5% xenon.

From the measured values of the transit times of the front of the ion sheath, the mobility of the fastest ions could be calculated and hence, it was hoped, the ions identified. For this a formula due to Wilkinson (1952) was used, namely

$$r^2 - a^2 = \frac{2kVt(1+mf)}{\log(b/a)} \quad (1)$$

where k is the mobility of the ions and f is the fraction of Q , the charge per unit length in the sheath behind radius r at time t . From this it follows that the transit time of the front of the sheath is, assuming $b^2 \gg a^2$,

$$t_F = \frac{b^2 \log(b/a)}{2kV(1+m)} \quad (2)$$

and of the back of the sheath is

$$t_R = \frac{b^2 \log(b/a)}{2kV}. \quad (3)$$

These expressions were derived assuming that the field due to the charge $-Q_a$ per unit length induced at the anode is negligible and this will be true if $m \ll 1$. In order to correct the expression (2) to take this into account for larger values of m , an approximate correction was derived as follows.

The charge induced on the anode per unit length

$$-Q_a = \int_{R'}^R \frac{\log b - \log r}{\log(b/a)} \frac{d(fQ)}{dr} dr \quad (4)$$

where R is the radius of the front of the sheath and R' that of the back and from (1), $R' = R/(1+m)^{1/2}$. To evaluate (4) substitute df/dr obtained from (1) and integrate giving

$$-Q_a = \frac{QR^2}{4ktV(1+m)} \log \left\{ \left(\frac{b}{R} \right)^2 \frac{e}{(1+m)^{1/m}} \right\}. \quad (5)$$

From (1) putting $r^2 - a^2 = R^2$ and $f = 1$ and substituting in (5) we find

$$-Q_a = \frac{Q}{2 \log(b/a)} \log \left\{ \left(\frac{b}{R} \right)^2 \frac{e}{(1+m)^{1/m}} \right\}, \quad (6)$$

e being the base of the Napierian logarithms.

The velocity of the front of the ion sheath is given by

$$\frac{dR}{dt} = \frac{2k}{R} \left\{ Q_0 + Q - \frac{Q}{2 \log(b/a)} \log \left[\left(\frac{b}{R} \right)^2 \frac{e}{(1+m)^{1/m}} \right] \right\} \quad (7)$$

where Q_0 is the static charge on the anode per unit length and equal to $V/2 \log(b/a)$.

Integrating (7) gives the transit time of the front of the ion sheath to radius R

$$t(R) = \frac{1}{X} \frac{[\log(b/a)]^2}{kVm} \{\overline{\text{Ei}}(\log R^2 X) - \overline{\text{Ei}}(\log a^2 X)\} \quad (8)$$

where

$$X = \frac{(1+m)^{1/m}}{b^2 e} \left(\frac{b}{a}\right)^{2+2/m}$$

Substituting $R = b$ in (8), expanding the exponential functions and neglecting small terms gives

$$t_F = \frac{b^2 \log(b/a) C}{2kV(1+m)} \quad (9)$$

where

$$C = \frac{1 + [m^{-1} \log(1+m) + [2(1+m)m^{-1}] \log(b/a) - 1]^{-1}}{1 - [m - \log(1+m)]/2(1+m) \log b/a}$$

Thus the expression (2) requires correction by the factor C above. In practice this correction increases with m and was about 7% at $m = 1$. Plotting $1/t_F$ against $V(1+m)/C$ gave, except in the case for the mixture with zero xenon concentration, a straight line passing through the origin from which the mobility was calculated. However, the accuracy could not be expected to be better than $\pm 5\%$ owing to the error in measurement of t_F . A typical graph (xenon concentration 1.07%) is shown in figure 6.

During the transit time measurements, a curious effect was observed in that after the counter voltage had been increased beyond the end of the plateau all the transit

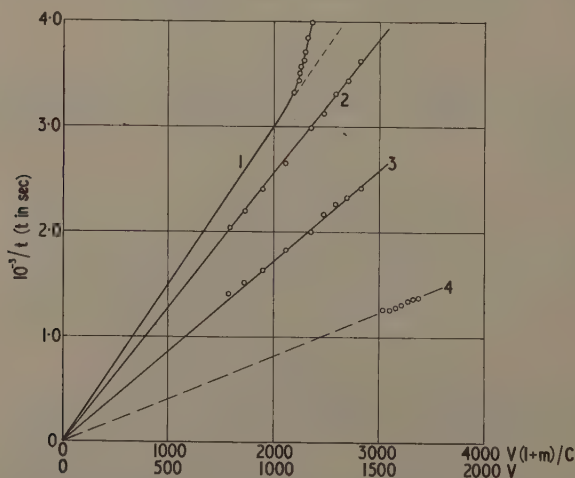


Figure 6. Plot of $1/t_F$ against $V(1+m)/C$ for xenon concentrations, zero (curve 1), 1.07%, mixture in state B (curve 2), 1.07%, mixture in state A (curve 3). Plot of $1/t_R$ against V , xenon concentration 3.44% (curve 4).

times were significantly reduced and a new set of values was obtained. Furthermore, the transit times were found to be similarly changed in the other counters on the manifold. Hence it was clear that a change had occurred in the mixture, although there appeared to be no significant change in the plateau or charge per pulse characteristics. Also, the change in the mixture appeared to be permanent. For purposes of discussion the first phase of the mixture will be referred to as state A and the second as state B. The effect was found to take place in nearly all the mixtures investigated and generally the change was quite sudden having taken place as a result of a sharp corona discharge at high overvoltage, this being observed on the oscilloscope as a burst of multiple pulses followed by a temporary blacking out of the trace. In practice, it was found difficult to avoid the mixture changing to state B but in the case of three of the mixtures a complete set of transit time measurements was made for state A. In a few cases, the mixture was found to be in state B when the transit times were first measured, the changeover presumably having taken place during other measurements.

The values of the mobilities for state B, excluding the mixture with zero xenon concentration, were found to be constant within $\pm 5\%$, after reduction to 760 mm Hg pressure at 0°C , and to zero xenon concentration using the expression for mobility in mixtures (Blanc 1908). No correction was made for the presence of the nitrogen and oxygen as the concentrations were small. The mean value obtained was $2.46\text{ cm sec}^{-1}(\text{v cm}^{-1})^{-1}$. The set of transit time measurements obtained for three of the mixtures in state A (xenon concentrations 1.07%, 0.498% and 3.44%) yielded straight lines through the origin, the mobilities corrected as above having a mean of $1.82\text{ cm sec}^{-1}(\text{v cm}^{-1})^{-1}$.

The transit time measurements for the mixture containing zero concentration of xenon did not yield a straight line through the origin (see figure 6), t_F decreasing more rapidly than expected from the change in charge per pulse. The inference from this was that, although a plateau was obtained, the discharge did not, even at the highest overvoltage where a measurement was made, spread completely along the anode wire, so that the effective m was higher than that measured. The value of the mobility of the ion could only be obtained in this case by extrapolation of the transit time to zero charge per pulse whence substitution in (2) gave the mobility as $3.0\text{ cm sec}^{-1}(\text{v cm}^{-1})^{-1}$.

Although measurements of t_R could not be made with the same accuracy as t_F , there was evidence from such measurements of the existence of a slower ion. It was found that measurements of t_R were more accurate when the counters were in state A as the point at which the cathode pulse returned to zero was better defined. A plot of $1/t_R$ against V is shown for one of the mixtures in state A in figure 6, which, using expression (3), gives a value of the mobility, after correction, of $1.64\text{ cm sec}^{-1}(\text{v cm}^{-1})^{-1}$.

As the ions spend most of the time in the low field towards the cathode, the values of mobility will correspond to those at low X/p . If argon ions are present in the space charge, they will, at these pressures, most certainly be molecular ions A_2^+ . The mobility of such ions at low X/p has been measured by Lauer (1952), Schütt (1955) and Maushart (1958) whose values, reduced to 0°C , are 1.81, 1.81 and $1.84\text{ cm sec}^{-1}(\text{v cm}^{-1})^{-1}$ respectively. The ion detected in state A is thus most likely to be A_2^+ .

The faster ion detected in state B has the same mobility as the oxygen ion O_2^+ which has been measured by Maushart (1958) who gives the value as $2.46\text{ cm sec}^{-1}(\text{v cm}^{-1})^{-1}$. However, it seems unlikely to be O_2^+ since, if it were, there is no valid reason why it should not appear from the first. The most likely possibility seems to be that the ion is NO^+ which, as its mass is only slightly less than that of the oxygen molecular ion, would have a mobility only slightly greater, and certainly the difference would not be resolved by these measurements. A small quantity of nitric oxide is likely to be formed, possibly fairly slowly during the normal operation of the counters but

rapidly when the counter suffers a sharp discharge as described above. In order that the NO^+ ion should appear, charge transfer should take place between this ion and the argon molecular ion, a necessary condition being that the ionization potential of the nitric oxide should be less than that of the argon molecule by, at least, the latter's dissociation energy. The last two values are not known but the appearance potential of the argon molecular ion has been determined from its formation from argon excited states (Hornbeck and Molnar 1951) as between 14.3 and 15.22 volts. The ionization potential of the nitric oxide is lower than that of oxygen (O_2^+), the values being 9.2 and 12.2 volts respectively so that if the argon (A_2^+) ionization potential is about 14 volts and its energy of dissociation about 2 volts, then this would explain the formation of the NO^+ ion.

3.3 Cathode-Ion Effects

The entire absence of any effect attributable to release of electrons by positive ions at the cathode was somewhat surprising, so an attempt was made to produce such effects by suitable conditioning of the cathodes. Four new counters were used for this of identical construction, two with nickel and two with copper cathodes. On filling with the mixture corresponding to the optimum of figure 4 (concentration of xenon 3.5%), plateaux of length of about 120 volts were obtained. The cathodes in this case had been exposed to air and were likely to be slightly oxidized, the cathode-ion effect being absent. The system was now evacuated and the cathodes heated to red heat for some minutes by induction heating. The counters were then refilled when it was found that the plateau had almost disappeared being 8 volts in length for the nickel cathodes and 15 volts for the copper cathodes. Threshold voltages were almost the same for the two types of cathode but lower by a few volts than the previous filling. Pulse interval analysis curves showed that nearly all the spurious pulses occurred after the transit time t_F . In this case measurement of transit time showed that the mixture was in state B and the pulse interval analysis curves showed a small peak just after t_F followed by a larger peak. Presumably, the small peak is due to the NO^+ ions and the larger due to the A_2^+ ions. Two such curves for overvoltages of 4 volts and 20 volts are shown in figure 7. As there is only a suggestion of a peak corresponding to the faster ion for the lower overvoltage it is possible that the mixture had not changed to state B when these measurements were taken. The counters were evacuated and refilled with the same mixture and pulse interval analysis curves obtained at low counting rates in order to avoid, if possible, transition to state B. The curve so obtained is shown at C in figure 7; the transit time t_F measured from the cathode pulse corresponded to the A_2^+ ion and also to the beginning of the single peak.

The interval analysis also afforded a confirmation of the existence of a slower ion mentioned in § 3.2. The width of the peaks was greater than would be expected if a single ion were present. Taking the back edge of the peak as corresponding to the transit time of the slower ion and substituting in equation (3) gave a mean value, from a number of determinations, of the mobility as $1.64 \text{ cm sec}^{-1} (\text{v cm}^{-1})^{-1}$, in agreement with that obtained previously. The cathodes were reoxidized by induction heating in oxygen, at a pressure of a few mm Hg, and the counters were evacuated and refilled with the same mixture proportions. It was found that the counter characteristics improved steadily with operation, the plateau length in a typical case increasing from 9 to 180 volts after operating the counter at a high count rate for several days, the threshold rising by 12 volts.

During this series of experiments the threshold voltages were remarkably constant and changed little with the state or material of the cathode.

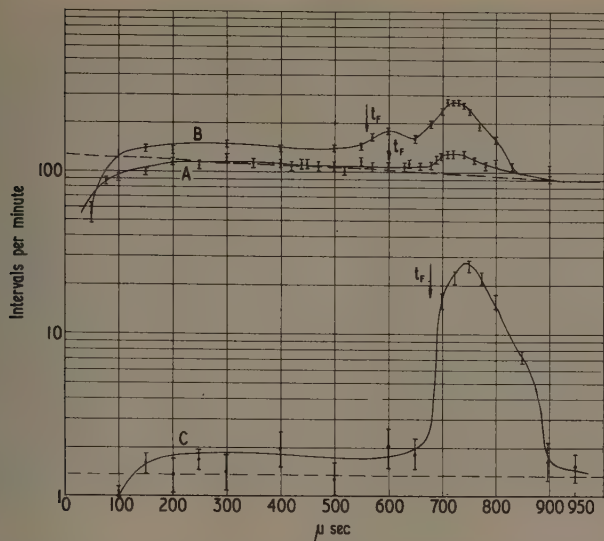


Figure 7. Pulse interval analysis curves after cleaning of cathodes by induction heating in vacuo. A and B, copper cathode, mixture in state B, overvoltages 2 v and 17 v. C, copper cathode, mixture in state A, overvoltage 22 v.

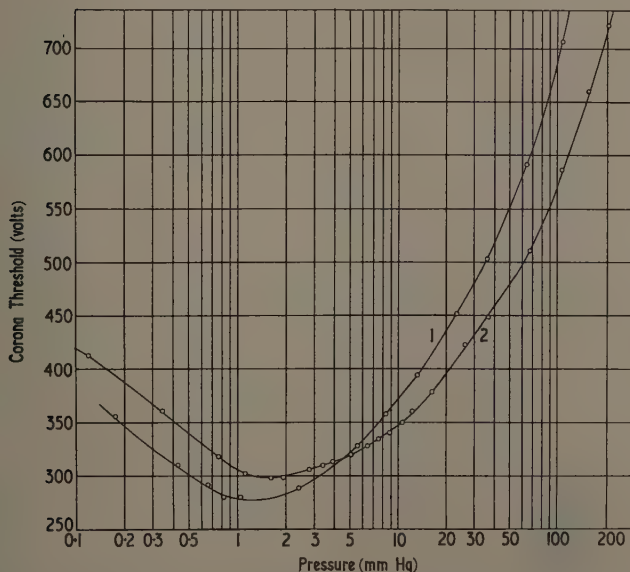


Figure 8. Corona threshold voltages plotted against pressure for argon (curve 1) and argon + 2% xenon (curve 2).

3.4. Variation with Total Pressure

Plateau slopes and lengths were next investigated maintaining the partial pressures of xenon, oxygen and nitrogen constant at the same values as in the experiments described in § 3.3, but varying the argon pressure. It was found, confirming the results of Shore (1949), that the plateau lengths became rapidly shorter and the plateau slopes increased at pressures below 300 mm Hg, the values at 100 mm Hg being 27.5 volt and 0.56% per volt respectively.

These results raised the question as to whether the effect of the xenon in lowering the corona threshold voltage and at the same time raising the gas multiplication is a pressure-dependent effect, particularly as it was reported by Penning (1928) that the addition of 0.03% xenon to argon at 14 mm Hg pressure raised the breakdown potential. Accordingly, a counter was filled first with argon alone and afterwards with argon + 2% xenon, and the voltage for corona discharge and the pulse height just before the onset of corona were measured for a series of total pressures. The results of the corona voltage measurements, below 200 mm Hg, are shown in figure 8 where it will be observed that the curves converge and finally cross over at about 4.5 mm Hg pressure. The ratios of the pulse height fell with pressure, the pulses from the argon-xenon mixture being about a factor of five greater than with the argon alone at 200 mm Hg but approximately equal to 10 mm Hg.

§ 4. DISCUSSION OF RESULTS

4.1. Effect of Xenon

It is apparent from the experiment on the argon-xenon mixture that one of the effects of the addition of xenon is to increase the gas multiplication and at the same time reduce the number of those photons in the avalanches which give rise to secondary electrons. This latter point is clear from the observation that the gas multiplication was much higher at the corona threshold after the addition of xenon. This increase in ionization, which effectively means an increase in α , the first ionization coefficient, is most surprising, as it would have been expected that addition of xenon would lower the electron temperature in the avalanches and thus raise the Geiger threshold voltage. In fact there are clearly two competing processes present as shown by the existence of the threshold minimum of the curve in figure 4. The possibility of argon metastable excited atoms being quenched by collision with xenon atoms and giving rise to ionization in a manner similar to the well-known Penning effect in neon-argon mixtures is ruled out as energetically impossible, as the ionization potential of xenon is 12.127 volts and the metastable potentials of the 3P_2 and 3P_0 levels of argon are 11.53 and 11.72 volts respectively. It is therefore necessary to look for some other mechanism which would give rise to ionization. It has been shown (Colli and Facchini 1952) for pure argon that, at these pressures, the photons which give rise to photoelectrons at the cathode are mainly those which arise from the decay of the excited molecule A_2^* rather than by resonance photons. Higher excited states above the metastable and resonance levels only rarely decay directly to the ground state but usually through some intermediate state by the emission of photons of about 4 eV. The decay of the metastable excited states of argon take place through either two or three body collisions (Phelps and Molnar 1953), the decay probability being given by $A\rho + B\rho^2$ where $A = 40 \text{ sec}^{-1} \text{ mm}^{-1}$ and $B = 9 \text{ sec}^{-1} \text{ mm}^{-2}$. The second process is predominant at the pressures used in this investigation and leads to the formation of the A_2^* excited molecules which have a decay

time of $3.4 \mu\text{sec}$ giving a photon of about 10 eV energy (Colli 1954). This photon has a very small cross section for absorption by either oxygen or nitrogen (Weissler and Lee 1952) and will not be absorbed by either argon or xenon. Consequently any process which is postulated for the action of the xenon must account for the large reduction in the production of the 10 eV photons so that the possibility that the additional ionization due to the xenon is brought about by collision with the higher excited states of argon is unlikely. One possibility is a three-body collision involving two xenon atoms and an excited metastable state of argon leading to the formation of a xenon molecular ion Xe_2^+ but this seems unlikely in view of the fairly small xenon concentrations involved.

This leaves the possibility that the xenon atoms interact with the argon metastable states, or with the argon excited molecules A_2^* , to produce ions and the only way in which this could occur would be by the formation of an argon-xenon molecular ion. In view of the pressure dependence of the action of the xenon, mentioned in § 3.4, it would appear that the interaction is more likely to be with the A_2^* molecule as the formation of this is itself pressure dependent. It will be observed from figure 8 that the crossover of the two curves occurs at a pressure corresponding to $Ap \simeq Bp^2$, that is when the probability of decay of the argon metastable states by the two alternative processes are equal. A possible reaction would therefore be



This suggestion is put forward very tentatively in view of the strong theoretical objections to the existence of such an ion. Bearing in mind the unreliability of identifying ions from their mobilities, nevertheless the existence of the slow ion of mobility $64 \text{ cm sec}^{-1} (\text{V cm}^{-1})^{-1}$ is not inconsistent with this hypothesis. Assuming that the mobility varies as $(1 + M_{\text{atom}}/M_{\text{ion}})^{1/2}$ in accordance with the Langevin expression, this gives, based on the value of 1.84 for the A_2^+ ion, a figure of 1.66 for the AXe^+ ion, 1.715 for the Xe^+ ion and $1.62 \text{ cm sec}^{-1} (\text{V cm}^{-1})^{-1}$ for the Xe_2^+ ion, so that the observed ion could be any of these three, considering the accuracy of the measurements and the not too close agreement of the Langevin expression with experiment.

Consider now the two types of spurious pulses which are found with the counters with oxidized cathodes. Both types obviously arise as a result of the photon-cathode effect, those which occur at the end of the plateau being due to delayed photons which increase in number with the charge per pulse and whose effect becomes significant when the dead-time has shortened sufficiently. For zero and very low xenon concentrations the dead-times and consequently the plateaux are very short.

The incidence of the other type of spurious pulses which appear on the plateaux is early proportional to the charge per pulse as the plateaux are straight. They are probably due to the formation of oxygen negative ions from the photoelectrons arising during and immediately after the discharge. The fact that the plateau slopes increase with oxygen concentration and that the spurious pulses appear more or less uniformly between dead-time and recovery time support this view. Also, the addition of xenon reduces the plateau slope because of its effect in quenching the excited argon molecules which would otherwise decay to emit the 10 eV photons producing the photoelectrons.

If N_0 is the number of metastable argon atoms produced during the discharge and the number at any subsequent time t , the decay can be expressed by

$$N = N_0 \exp(-\beta t)$$

where $\beta = Ap + Bp^2$, assuming that the probability of decay through collision with

nitrogen or oxygen molecules is small. For the pressure used in these experiments the value of Ap is $2.52 \times 10^3 \text{ sec}^{-1}$ and Bp^2 is $4.77 \times 10^6 \text{ sec}^{-1}$, so the predominant mode of decay of the metastable states of the argon atoms is to produce the metastable molecules. If N' is the number of such molecules in the discharge at time t , then

$$\frac{dN'}{dt} = Bp^2 N_0 \exp(-\beta t) - N' \left(\frac{1}{\tau_m} + cx \right) \quad (10)$$

where τ_m is the mean lifetime of the metastable molecules, equal to $3.4 \mu\text{sec}$ and cx is the probability of destruction by collision with xenon atoms for a xenon concentration x .

Integration of (10) gives

$$N' = \frac{Bp^2 N_0}{\beta - (1/\tau_m + cx)} \left\{ \exp \left[-t \left(\frac{1}{\tau_m} + cx \right) \right] - \exp(-\beta t) \right\}. \quad (11)$$

The number of photoelectrons released per discharge is

$$\gamma_p \int \frac{N'}{\tau_m} dt = \frac{\gamma_p Bp^2 N_0}{(1 + \tau_m cx)\beta} \quad (12)$$

by integration after substitution from (11); γ_p is the probability that a photon will release a photoelectron at the cathode. If it is assumed that the number of metastable states N_0 is approximately equal to the number of ions produced then $N_0 = Q/e_0$ where Q is the charge per pulse and equal to kV_0 , k being a constant for a particular mixture, V_0 the overvoltage, and e_0 the electronic charge.

The number of spurious pulses per discharge can be written from (12) as

$$N_{sp} = \frac{\gamma_n \gamma_p Bp^2 k V_0}{(1 + \tau_m cx)\beta e_0} \quad (13)$$

where γ_n is the probability that a photoelectron will produce a spurious pulse after capture to form an oxygen negative ion. The plateau slope S is given by N_{sp}/V_0 so substituting in (13) gives

$$\frac{1}{c\tau_m} + x = \frac{\gamma_n \gamma_p Bp^2}{\beta c \tau_m} \frac{k}{Se_0}.$$

A plot of k/Se_0 against x is shown in figure 9 using the values of k , S and x , obtained from the experiments described in § 3.2, yielding a fairly reasonable straight line. This gives support to the assumption of a two-body interaction leading to the AXe^+ molecular ion rather than the three-body interaction leading to the Xe_2^+ ion as the latter case would yield a straight line only when k/Se_0 is plotted against x^2 . The intercept on the x axis is $1/c\tau_m$ giving an approximate value of $c = 2.4 \times 10^8 \text{ sec}^{-1}$. This means that at a xenon concentration of 2% the number of photoelectrons produced is reduced by a factor of about 20 as is clear from equation (12). The value of c above yields a cross section for destruction of the excited states of the argon molecules as approximately $1.9 \times 10^{-16} \text{ cm}^2$. Also from the slope of the graph a value of $\gamma_n \gamma_p = 5 \times 10^{-11}$ is obtained. It was reported by Colli and Facchini (1954) that the value of γ_p for the 10 eV argon photons for nickel and brass cathodes is of the order of 10^{-3} and was not strongly dependent upon the condition of the cathode surface. Assuming similar values for the copper cathodes used in these experiments, this means that γ_n is of the order of 10^{-8} .

It should be pointed out however that the evidence in favour of the two-body as against the three-body interaction is not necessarily conclusive because it has been assumed above that the small concentrations of xenon do not affect the value of γ_n . It is not clear to what extent the presence of xenon will affect the electron temperature and therefore the probability of photoelectron attachment to form O_2^- ions.

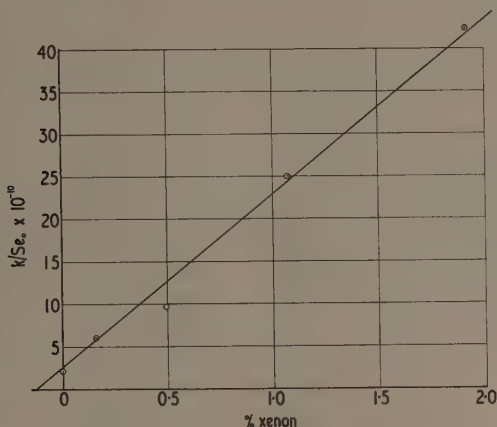


Figure 9. Variation of k/Se_0 with xenon concentration.

4.2. Spread of the Geiger Discharge

It is clear that the presence of oxygen is a necessary condition for the spread of the Geiger discharge along the anode wire. The propagation of this type of discharge is generally attributed to secondary electron production in the quenching gas by photoionization from the high energy photons of the main gas. Huber (1955) has shown that this mechanism explains the formation of the Geiger discharge when a small quantity ($\sim 1\%$) of oxygen is added to nitrogen. However, some difficulties arise if this mechanism alone is postulated to explain the action of the oxygen in the counters described in this paper, because the argon resonance photons have insufficient energy to cause photoionization in the oxygen. The comparatively few photons of higher energy (~ 14 eV) arising from the decay of the upper excited levels of argon will have mean free paths for photoionization of about 1.5 cm in the oxygen at the partial pressures (3.5 mm Hg) employed in these counters (Wainfan, Walker and Weissler 1955). This possibly explains the results obtained with mixtures of zero and low xenon concentrations. The discharge would probably be propagated in rather large steps and not fully developed, resulting in incomplete quenching and very short dead times (figure 3, curve D). The addition of larger amounts of xenon (concentrations greater than 0.5%) assists in the propagation of the discharge inasmuch as the latter now becomes a true Geiger discharge similar to that observed in organically quenched counters. The argon metastable states have mean lifetimes of $1/Bp^2$ ($\sim 0.2 \mu\text{sec}$) against the formation of metastable excited molecules, and these in turn have lifetimes against formation of ions by collision with xenon atoms of $1/cx$, the total time being about $0.3 \mu\text{sec}$. It is therefore suggested that further avalanches are formed in a small zone surrounding the wire by the diffusion of the excited atoms and molecules. The part

played by photon action at the cathode in the spreading of the discharge is only subsidiary because the threshold voltage appears to be little affected by the type or condition of the cathode as shown in § 3.3.

§ 5. CONCLUSION

Counters containing mixtures of argon, xenon, oxygen and nitrogen in appropriate proportions will, provided the cathodes are oxidized, behave similarly to organically quenched counters. This behaviour is attributed to the presence of the xenon. When the latter is not present the Geiger discharge is followed by many spurious discharges caused mainly by the emission of 10 eV photons from the decay of excited argon molecules. When xenon is added, the excited argon molecules are quenched to produce ions instead of photons resulting in a lowering of the threshold voltage. The nature of the interaction, which is pressure-dependent, is either by three-body collisions involving two xenon atoms and an argon excited metastable atom leading to the formation of Xe_2^+ molecular ion, or by two-body collisions involving a xenon atom and an argon excited molecule, and leading to the formation of AXe^+ molecular ion, the evidence appearing to favour the latter. The presence of the xenon also enables the full realization of the Geiger discharge for which, however, the presence of the oxygen as a vehicular gas is necessary.

ACKNOWLEDGMENTS

The authors wish to thank their colleagues Messrs. T. L. Watkins, B. R. Hookway and A. K. M. Haque for their generous assistance; Mr. E. R. Kerkin for valuable work in construction of apparatus and Mr. R. K. Munn for help in preparation of the diagrams; also Dr. J. E. Garside, Principal of the Borough Polytechnic and Mr. V. Pereira-Mendoza, in whose department the work was carried out, for their encouragement and interest.

REFERENCES

- BERETTA, E., and ROSTAGNI, A., 1949, *Nuovo Cim.*, **6**, 391.
 BLANC, A., 1908, *Bull. Soc. Franç. Phys.*, 156.
 ——— 1908, *J. Phys. Chem.*, **7**, 825.
 COLLI, L., 1954, *Phys. Rev.*, **95**, 892.
 COLLI, L., and FACCHINI, U., 1952, *Phys. Rev.*, **88**, 987.
 ——— 1954, *Phys. Rev.*, **96**, 5.
 COLLINSON, A. J. L., DEMETSOPOULLOS, I. C., DENNIS, J. A., and ZARZYCKI, J. M., 1960, *Nature, Lond.*, **185**, 369.
 FENTON, A. G., and FULLER, E. W., 1949, *Proc. Phys. Soc.*, **62**, 32.
 HORNBECK, J. A., and MOLNAR, J. P., 1951, *Phys. Rev.*, **84**, 621.
 HUBER, E. L., 1955, *Phys. Rev.*, **97**, 267.
 KORFF, S. A., 1958, *Encyclopedia of Physics*, **45**, (Berlin: Springer), p. 52.
 LAUER, E. J., 1952, *J. Appl. Phys.*, **23**, 300.
 MAUSHART, R., 1958, *Ann. Phys., Lpz.*, **7**, 264.
 MONTGOMERY, C. G., and MONTGOMERY, D. D., 1940, *Phys. Rev.*, **57**, 1034.
 PENNING, F. M., 1928, *Z. Phys.*, **46**, 335.
 PHELPS, A. V., and MOLNAR, J. P., 1953, *Phys. Rev.*, **89**, 1202.
 PUTMAN, J. L., 1948, *Proc. Phys. Soc.*, **61**, 312.
 RAMSEY, W. E., 1951, *J. Franklin Inst.*, **252**, 143.
 SCHÜTT, K., 1955, *Z. Phys.*, **143**, 489.
 SHORE, L. G., 1949, *Rev. Sci. Instrum.*, **20**, 518.
 WAINFAN, N., WALKER, W. C., and WEISSLER, G. L., 1955, *Phys. Rev.*, **99**, 542.
 WEISSLER, G. L., and PO LEE, 1952, *J. Opt. Soc. Amer.*, **42**, 200.
 WILKINSON, D. H., 1948, *Phys. Rev.*, **74**, 1417.
 ——— 1952, *Rev. Sci. Instrum.*, **23**, 463.

The Radiative Capture Cross Section of ^{236}U for Neutrons in the Energy Range 0.3 to 4.0 MeV

By J. F. BARRY, J. L. BUNCE AND J. L. PERKIN

Atomic Weapons Research Establishment, Aldermaston, Berkshire

MS. received 1st June 1961

Abstract. The cross section of the reaction $^{236}\text{U}(n, \gamma) ^{237}\text{U}$ has been measured for neutrons in the energy range 0.3 to 4.0 MeV using an activation method. Fission products in the irradiated samples were removed chemically and the ^{237}U produced was determined by counting the γ -ray activity with a sodium iodide scintillation spectrometer. The cross section was found to increase from about 300 mbn at 0.3 MeV to about 400 mbn at 1.1 MeV. It then fell sharply to some 30 mbn at 4 MeV.

The shape of the excitation function for this reaction is typical of that found for other heavy even-even nuclides far from a closed shell. It is due to the competition between the radiative capture process and inelastic scattering from the similar collective level structures of these nuclides.

§ 1. INTRODUCTION

THE MEASURED radiative capture cross sections of heavy even-even nuclides far from a closed shell do not fall with increasing neutron energy according to the orthodox statistical theory. Lane and Lynn (1957) have explained this behaviour in terms of the competition between the radiative capture process and the inelastic scattering of neutrons from the rotational energy level structure of these nuclides.

Two such nuclides have been examined in detail to date, namely ^{232}Th and ^{238}U (Barry, O'Connor and Perkin 1959, Hughes and Schwartz 1958). In these experiments the radiative capture cross section of another heavy even-even nuclide ^{236}U has been measured over the energy range 0.3 to 4.0 MeV. An activation method was used involving the measurement of the ^{237}U (6.75 d) activity produced.

§ 2. NEUTRON IRRADIATIONS

The ^{236}U samples irradiated consisted of some 60 mg of ^{236}U dissolved in 0.2 M HNO_3 . The isotopic composition (atomic %) of this uranium was as follows: ^{236}U (98.46%), ^{235}U (1.1%), ^{238}U (0.42%) and ^{234}U (0.02%). Thin-walled Perspex cells with flat cylindrical cavities (1.74 cm \times 0.076 cm) were used to contain the samples during the neutron irradiations and the ^{237}U determinations described later.

Neutrons for these irradiations were obtained from the p-T reaction. A tritium gas target was contained in a cylinder 2.5 cm long and was bombarded with protons from the Atomic Weapons Research Establishment 6 MeV Van de Graaff accelerator. In order to obtain the high neutron output required the technique described by Nobles (1957) was used to obtain proton beam currents of up to 10 μA into the gas target. In this technique the beam enters the gas target through two thin nickel foils which are cooled by helium gas pumped through the space between them.

The ^{236}U samples were irradiated in the forward direction at a distance of 1.4 cm from the end of the gas target. The neutron flux through the samples was measured with a ^{235}U fission counter which was placed at the back of the Perspex cell. Only the thickness of the walls of the cell and counter separated the ^{236}U sample from the ^{235}U deposit in the counter. The circular areas of the ^{235}U foil and the uranium solution subtended the same angle at the neutron source and they were positioned with their centres on the line of the proton beam.

The fission counter contained about 1.5 mg of ^{235}U and was calibrated by irradiation in a known flux of 14.1 mev neutrons from the d-T reaction. This calibration was carried out by placing the counter at a distance of 20 cm from a thick zirconium tritide target and at an angle of 90° to a deuteron beam of 300 kev. The associated α -particles from the reaction were counted in a known geometry at an angle of 135° . The neutron and α -particle yields with respect to the angle of emission and the incident deuteron energy for thick tritium targets of the type used were evaluated. With this information the neutron flux at the counter position was calculated and the fission counting rate per incident neutron $\text{sec}^{-1} \text{cm}^{-2}$ was found. Experiments with and without cadmium shielding around the counter showed that any errors due to a thermal neutron background were smaller than those due to the fission counting rate statistics.

The efficiency of the counter was calculated at other neutron energies by using the known variation of the ^{235}U fission cross section with energy (R. L. Henkel 1961, private communication, Adams, Batchelor and Green 1961, A. Moat 1961, private communication).

The difference between the mean neutron flux through the uranium samples and that through the uranium foil of the fission counter due to the variation of neutron flux with distance from the source and the scattering and absorption by the sample and holder, was measured experimentally. From the variation of flux with distance, the flux through a sample was found to be between 22 and 11% greater than that measured by the fission counter over the neutron energy range 0.3–4.0 mev. The effect of scattering and absorption was found by measuring the change in neutron flux through the counter when a sample and holder were removed. This change varied from –6% to +5% according to the neutron energy over the range 0.3–0.4 mev.

During the irradiations the neutron flux through the samples was about $2 \times 10^7 \text{ cm}^{-2} \text{ sec}^{-1}$ and the length of the irradiations was about 10 hours.

§ 3. CHEMICAL PURIFICATION

3.1. Procedure

In order to resolve the ^{237}U activity produced it was necessary to remove fission products from the irradiated ^{236}U samples. These fission products originated mainly from ^{236}U when the irradiation was made at neutron energies above the fission threshold for this isotope (~ 0.6 mev). Also present were fission products from the small amounts of the other uranium isotopes in the samples (see § 2) at neutron energies above their respective fission thresholds.

The ^{236}U solution was first evaporated to dryness in a platinum crucible and the residue was redissolved in a solution containing 3 ml of saturated ammonium nitrate and 0.3 ml of 6 M nitric acid. Uranium was then extracted with ether for a period of 30 minutes in an apparatus in which the ether was bubbled through the uranium solution and recirculated by means of a reflux condenser (Wayman and Wright 1945). The etheral solution was evaporated to dryness and a few drops of HClO_4 were added. The

solution was then heated strongly to remove any ruthenium fission products present as these are particularly difficult to remove by any other method.

After dissolving in 2 ml of 6 M HCl the uranium was absorbed on a column of an anion exchange resin and washed with 10 ml of 4 M HCl to remove most of the residual fission products. Uranium was then eluted from the column with 15 ml of 0.5 M HCl. After removal of the hydrochloric acid by evaporation the uranium was redissolved in nitric acid, transferred to a weighed platinum crucible, evaporated to dryness and converted to U_3O_8 in order to determine the chemical yield of the purification procedure.

As the value of this uranium sample was considerable, care was required to minimize losses. The use of platinum and polythene to reduce adsorption, the repeated use of the same apparatus for all the separations performed and the preservation of all the residues enabled a chemical yield of approximately 95% to be achieved for each individual separation.

3.2. Efficiency for removing Fission Products

It was essential that any fission product activity remaining after the purification process should be negligible compared with the lowest ^{237}U activity observed. The greatest number of fissions produced in a sample in these experiments amounted to about 2×10^8 . This occurred in the irradiations with 4 mev neutrons where the ^{236}U fission cross section is 0.95 bn and the capture cross section is low. To determine the efficiency of the chemical separations for removing fission products, a subsidiary experiment was performed with a uranium sample containing fission products from about 10^{10} fissions but with practically no ^{237}U present.

The fission products were obtained by irradiating a small (0.5 mg) sample of enriched (99.9%) ^{235}U in a reactor (HERALD A.W.R.E.). The low percentage of ^{238}U in the sample minimized the production of ^{237}U from the ^{238}U (n, 2n) ^{237}U reaction with fast neutrons in the reactor. Natural uranium was added to the sample after irradiation to make the total weight the same as that of the ^{236}U samples.

The purified sample when counted (see § 4) had an initial activity which was less than the ^{237}U activity of the ^{236}U sample irradiated with 4 mev neutrons even though the original fission product activity present was fifty times greater. It is clear that even if all the residual activity in the subsidiary experiment is due to fission products the amount to be expected in the purified ^{236}U samples is negligible compared with the ^{237}U activity found.

§ 4. DETERMINATION OF THE ^{237}U ACTIVITY

Uranium 237 decays by a complex and low energy β -particle emission. (Rasmussen, Canavan and Hollander 1957). The weight of the ^{236}U samples in these experiments was too large to enable precise measurements to be made of the ^{237}U β -particle activity produced. Consequently the method employed was to measure the γ -ray emission using a cylindrical (5.7 cm diam. \times 5.7 cm) sodium iodide scintillation spectrometer.

The γ -ray spectrum observed from an unirradiated sample of ^{236}U is similar to that shown in figure 1(b). This is a complex spectrum due to the presence of ^{234}U , ^{235}U and ^{238}U and their daughters (see § 2). Above 60 kev the spectrum is due to ^{235}U and its daughter ^{231}Th (25.64 h) and ^{238}U and its daughters ^{234}Th (24.1 d) ^{234}Pa (6.66 h) and $^{234\text{m}}\text{Pa}$ (1.17 min). Using the calculated conversion coefficients of Rose (1958) it can be shown that the peak at about 50 kev is mainly due to the 50 kev ^{232}Th

γ -ray from the decay of ^{236}U although the other nuclides present must also contribute to it. The main features of the spectrum from a ^{237}U source are the ^{237}Np γ -ray peaks at 59 and 203 keV and the 100 keV x-ray peak from the internal conversion of the 203 keV γ -ray. A convenient measure of the ^{237}U activity throughout these experiments was the integrated spectrum between 40 and 250 keV. The stability of this energy 'gate' and the overall efficiency of the spectrometer was periodically checked with standard γ -ray sources in conjunction with a 100 channel pulse height analyser.

Each irradiated and purified ^{236}U sample was redissolved in 0.2 M HNO_3 and returned to a Perspex cell. Sufficient extra ^{236}U to make good any losses in the chemical separations was added to ensure that the γ -ray absorption and scattering properties of the sample were the same as any other. The cell was then clamped in a rigid holder about one millimeter from the flat face of the sodium iodide spectrometer and was counted at different times over a period of three weeks to follow the decay of the ^{237}U .

The absolute efficiency of the counter for ^{237}U activity was found by counting cells containing weighed amounts from a stock solution of ^{237}U prepared by the α -particle decay of ^{241}Pu . This solution was standardized by counting weighed amounts in a 4π proportional counter. In order to simulate the γ -ray self absorption of the ^{236}U samples the same weight of natural uranium was added to the cells used for calibration. The counting rates from these cells were corrected for the activity of the natural uranium.

§ 5. RESULTS

The γ -ray spectrum from an irradiated sample of ^{236}U is shown in figure 1. That part which has decayed after two weeks has the same characteristic spectrum as that from the decay of ^{237}U .

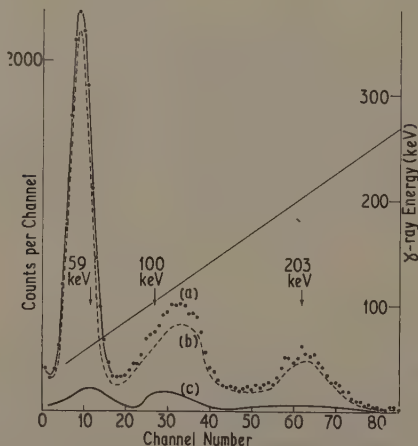


Figure 1. The γ -ray spectrum from a sample of ^{236}U measured (a) 2 days and (b) 13 days, after irradiation with 464 keV neutrons. Curve (c) was obtained by subtracting (b) from (a).

In order to determine the relatively small amount of ^{237}U activity present the gross γ -ray activity between 40 and 250 keV was plotted (figure 2, curve A) as a function of $\exp(-0.693t/T)$, where t is the time elapsed since the end of the irradiation and T is

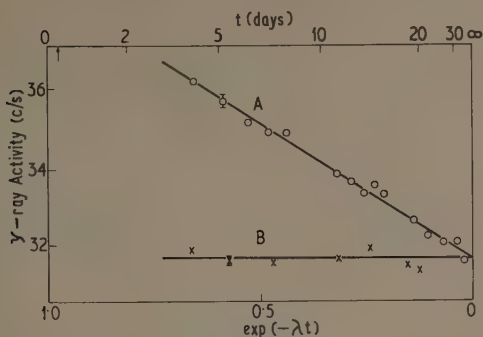


Figure 2. Decay of the γ -ray activity in the energy range 40 to 250 kev from a sample of ^{236}U after irradiation with 560 kev neutrons (curve A). Curve B was obtained with a similar unirradiated sample after chemical purification. The arrow indicates the time at which the chemical separations were performed.

the half-life of ^{237}U (6.75 d). The slope of the resultant straight line gives directly the ^{237}U activity present at the end of the irradiation.

Activity measurements made within about three days after the chemical separations were performed lie a little below a line through the later points, due to the fact that the ^{235}U present did not have sufficient time to re-establish an equilibrium amount of its daughter ^{231}Th . The re-establishment of the daughters of ^{238}U is a much slower process. Measurements made with a chemically purified but unirradiated ^{236}U sample (figure 2, curve B) show however, that this process was not detectable in these experiments and can cause no significant error in the method described for estimating the ^{237}U activity.

The Radiative Capture Cross Section of ^{236}U

E_n (MeV)	0.360	0.464	0.560	0.655	0.705	0.850	0.943
ΔE_n (MeV)	0.070	0.070	0.070	0.070	0.070	0.070	0.075
σ (mbn)	311	308	403	271	301	297	351
Error (mbn)	26	30	32	25	34	29	41
E_n (MeV)	1.063	1.220	1.310	1.585	2.020	2.790	3.970
ΔE_n (MeV)	0.075	0.075	0.080	0.085	0.100	0.120	0.150
σ (mbn)	350	536	196	147	88	68	28
Error (mbn)	43	68	47	30	10	10	10

The calculated values of the (n, γ) cross sections are given in the table and figure 3. Errors quoted for the cross section include counting statistics as well as estimates of errors in the calibration of the counting arrangement, the fission counting rate, fission counter calibration, knowledge of the fission cross section excitation function for ^{235}U , and deduction of the mean neutron flux through the sample from the measured flux at the fission counter. The calculated shape of the energy spectrum for neutrons through the samples varies considerably with the mean neutron energy of the irradiation due to the variation in the energy loss of the proton beam in the target and in the angular distribution of neutrons from the p-T reaction. The energy limits quoted include more than 90% of the neutrons.

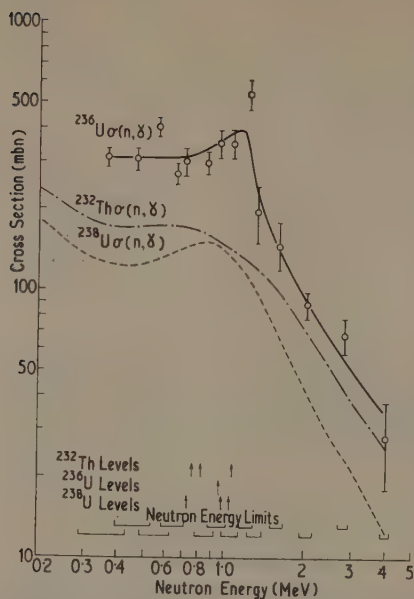


Figure 3. The radiative capture cross section of ^{236}U . The radiative capture cross sections of ^{232}Th and ^{238}U (obtained by drawing smooth curves through the published data) are shown for comparison.

Also shown in figure 3 are the radiative capture cross sections for ^{232}Th and ^{238}U (Barry, O'Connor and Perkin 1959, Hughes and Schwartz 1958). There is an obvious similarity between the shapes of the three excitation functions shown. As seen in the Introduction these shapes are dependent on the level structure of the nucleus concerned.

The positions of the levels found in these nuclei above about 400 keV (Cranberg and Levin 1958, Batchelor and Towle 1959, Durham, Rester and Class 1960, McGowan and Stelson 1960) are shown in the figure. Levels based on the ground state rotational band in this region (Stephens, Diamond and Perlman 1959) have been omitted because of their high spins which make them relatively difficult to excite by inelastic neutron scattering. The fall in the ^{236}U excitation function at about 1 MeV suggests that a group of levels exists in this nucleus similar to that observed in ^{232}Th and ^{238}U .

It can be seen that the absolute value of the cross section for ^{236}U is about double that for ^{238}U and ^{232}Th . The capture cross section in this energy region is proportional to $(\Gamma_\gamma \times \Gamma_n)/(D \times \Gamma)$ in the usual notation (e.g. Kinsey 1957). The ratio Γ_n/Γ is about the same for the three neighbouring nuclei under consideration. Using the method described by Lane and Lynn (1957) the value of Γ_γ/D for a particular neutron energy (400 keV) was calculated for each nucleus. The main factor in these calculations was the dependence of the level spacing D on the neutron binding energy [^{238}U (4.87 keV) ^{232}Th (5.16 MeV) ^{236}U (5.45 MeV)]. The values found for Γ_γ/D for the nuclei in this order were in the ratio of approximately 1 : 1.5 : 3. At 400 keV the corresponding ratio of the observed cross sections is 1 : 1.4 : 2.6 which is in quite good agreement with the theoretical estimate.

Since this work was completed some recent ^{236}U (n, γ) ^{237}U cross section measurements made at the Argonne National Laboratory have been brought to our notice (Stupegia 1961, private communication). These are for neutrons in the energy range 0.3 to 1.5 mev and agree with the present results within experimental error.

ACKNOWLEDGMENT

We are indebted to the United States Atomic Energy Commission for the loan of the ^{236}U enriched uranium.

REFERENCES

- ADAMS, B., BATCHELOR, R., and GREEN, T. S., 1961, *J. Nucl. Energy*, **14**, 84.
BARRY, J. F., O'CONNOR, L. P., and PERKIN, J. L., 1959, *Proc. Phys. Soc.*, **74**, 685.
BATCHELOR, R., and TOWLE, J. H., 1959, *Proc. Phys. Soc.*, **73**, 193.
CRANBERG, L., and LEVIN, J. S., 1958, *Phys. Rev.*, **109**, 2063.
DURHAM, F. E., RESTER, D. H., and CLASS, C. M., 1960, *Proc. Int. Conf. on Nuclear Structure, Kingston, Canada* (Amsterdam: North Holland), p. 594.
HUGHES, D. J., and SCHWARTZ, R. B., 1958, *U.S. Atomic Energy Commission Report*, BNL 325, 2nd Edn (Washington: U.S. Government Printing Office).
KINSEY, B. B., 1957, *Encyclopaedia of Physics*, Vol. XL (Berlin: Springer-Verlag), p. 303.
LANE, A. M., and LYNN, J. E., 1957, *Proc. Phys. Soc. A*, **70**, 557.
MCGOWAN, F. K., and STELSON, P. H., 1960, *Phys. Rev.*, **120**, 1803.
NOBLES, R., 1957, *Rev. Sci. Instrum.*, **28**, 962.
RASMUSSEN, J. O., CANAVAN, F. L., and HOLLANDER, J. M., 1957, *Phys. Rev.*, **107**, 141.
ROSE, M. E., 1958, *Internal Conversion Coefficients* (Amsterdam: North Holland).
STEPHENS, F. S., DIAMOND, R. M., and PERLMAN, I., 1959, *Phys. Rev. Letters*, **3**, 435.
WAYMAN, M. M., and WRIGHT, G. F., 1945, *Industr. Engng Chem. (Anal.)*, **17**, 55.

A Note on the Carr-Purcell Method of Measuring Nuclear Magnetic Resonance Relaxation Times

By H. PURSEY

Basic Physics Division, National Physical Laboratory, Teddington, Middlesex

MS. received 12th July 1961

Abstract. In measuring T_2 by the Carr-Purcell method the number of 180° pulses which can be used in a given sequence is limited by the accumulation of errors in pulse length, which causes a progressive departure of the freely precessing magnetic moments from the equatorial plane. Several methods have been devised to overcome this limitation, but in all cases it is assumed that phase coherence exists between the precessing nuclei and the pulsing radio-frequency field. Under such conditions the errors will accumulate linearly in the orthodox Carr-Purcell experiment, but in fact the order of stability implied in the assumption is unlikely to exist unless special care is taken to obtain it. It has been found experimentally, however, that good Carr-Purcell trains can be obtained in an incoherent system and in the present paper the reasons for this are analysed. It is shown that in such a system the errors add as if they were coplanar vectors of random direction, so that the statistical r.m.s. value of the error after n pulses is proportional to \sqrt{n} . Hence, one would expect to obtain a satisfactory train with up to 10^4 pulses, and it is shown that this is in agreement with observations.

THE 'SPIN-ECHO' method of measuring transverse nuclear magnetic relaxation times was first described by Hahn (1950). In a subsequent paper H. T. Carr and E. M. Purcell (1954) showed that the influence of molecular diffusion on the results obtained by Hahn's method could be virtually eliminated by using a modified technique which is now generally known as the 'Carr-Purcell method'. It consists in applying a 90° radio-frequency pulse to the sample at $t = 0$, followed by a train of 180° pulses at $t = \tau, 3\tau, 5\tau$, etc., 2τ being short compared with the diffusion time constant of the sample. 'Spin-echoes' are produced at $t = 2\tau, 4\tau, 6\tau$, etc. and the envelope of the echo maxima gives the T_2 decay curve of the material under tests.

For samples with short diffusion and long relaxation times it may be necessary to use a large number of 180° pulses to obtain an adequate decay curve, and the problem then arises as to how small errors in the length of the 180° pulses will accumulate. If we assume the magnetic dipoles are always rotated about the same axis relative to the total nuclear magnetic field component in the xy plane (treating z as the axis along the direction of the static field H_0), then errors must accumulate linearly, severely limiting the number of pulses which could be used in any particular train.

Methods of overcoming this limitation have been suggested by Meiboom and Gill (1958), who show that by shifting the phase of the initial (90°) pulse by 90° relative to the succeeding (180°) pulses the errors due to adjacent pulses can be made to cancel, while Shev and Norberg (1960) have shown that a similar improvement can be obtained by applying a linear sweep to the steady field along Oz .

In supposing that each 180° pulse induces rotation of the nuclear magnets about the same axis in the rotating coordinate system it is implied that, for the duration of each pulse train, phase coherence is preserved between the nuclei precessing in H_0 and the

radio-frequency pulses themselves. This implies very high stability (of the order of parts in 10^8) of H_0 relative to the radio-frequency oscillator from which the pulses are derived. In a system where no special care is taken to stabilize H_0 relative to the radio frequency, it is meaningless to talk of rotation about a particular axis in the rotating coordinate system, and each 180° pulse will induce rotation about an axis in the xy plane whose direction is independent of any previous rotations which have occurred.

Observations on such a system show that surprisingly good Carr-Purcell trains can be obtained, using several thousand pulses in each train, without taking any special trouble to ensure that the 180° pulses are of the correct length, and it is the purpose of this paper to show that this is in fact predicted by an analysis based on the Bloch equations.

Now if the pulses are derived from an oscillator whose angular frequency is ω , and if H_0 and H_1 are the respective amplitudes of the static z component and the rotating xy plane component of the magnetic field, we have (neglecting relaxation effects)

$$\dot{M}_x' = (\omega_0 - \omega)M_y' \quad (1)$$

$$\dot{M}_y' = \mu M_z + (\omega - \omega_0)M_x' \quad (2)$$

$$\dot{M}_z = -\mu M_y' \quad (3)$$

where M_x' , M_y' and M_z are the components of nuclear magnetization in a coordinate system rotating about the z axis with angular velocity ω , $\omega_0 = \gamma H_0$, $\mu = \gamma H_1$ and γ is the nuclear gyromagnetic ratio.

From (1), (2) and (3) we derive

$$\ddot{M}_y' = -\{\mu^2 + (\omega_0 - \omega)^2\}M_y' \quad (4)$$

Let us assume for simplicity that $\omega = \omega_0$. Then

$$\ddot{M}_y' = -\mu^2 M_y' \quad (5)$$

whence

$$M_y' = A \sin(\mu t + \phi) \quad (6)$$

and from (3) and (6)

$$M_z = A \cos(\mu t + \phi). \quad (7)$$

Let M be the total nuclear magnetic moment, and let the components of magnetic moment at the start of the n th pulse be P_n in the xy plane and Q_n along Oz .

Then at $t = 0$ we have

$$M_x' = P_n \cos \psi_n$$

$$M_y' = P_n \sin \psi_n = A \sin \phi$$

$$M_z = Q_n = A \cos \phi$$

where ψ_n is the azimuthal angle of M . Let us now apply a pulse such that $\mu t = \pi + \delta$, where δ represents a small error in pulse length.

Then at the end of the pulse we have

$$M_x' = P_n \cos \psi_n$$

$$M_y' = A \sin(\pi + \phi + \delta) = -P_n \sin \psi_n \cos \delta - Q_n \sin \delta$$

$$Q_{n+1} = M_z' = A \cos(\pi + \phi + \delta) = P_n \sin \psi_n \sin \delta - Q_n \cos \delta.$$

Thus

$$Q_{n+1} = -Q_n \cos \delta + (\sin \psi_n \sin \delta) \sqrt{(M^2 - Q_n^2)}.$$

So long as Q_n is small compared with M we have

$$Q_{n+1} \simeq -Q_n \cos \delta + M \sin \psi_n \sin \delta$$

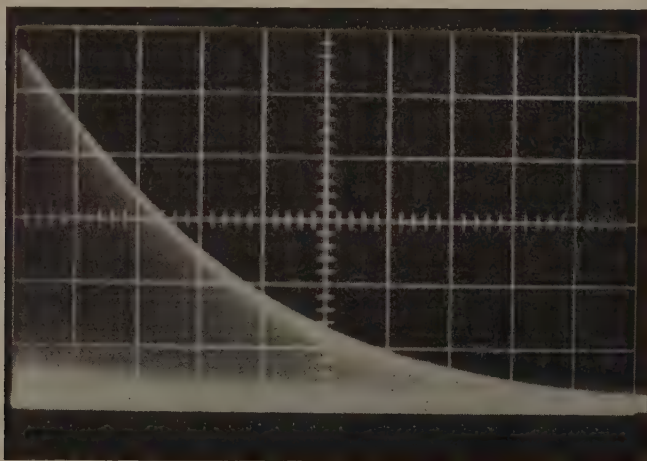
and hence

$$Q_n = (-1)^n Q_0 \cos^n \delta + M \sin \delta \sum_{r=1}^n \sin \psi_{n-r} \cos^{r-1} \delta.$$

If we assume the ψ_{n-r} are a random set then each term of the above summation has a variance of $\frac{1}{2}(\cos \delta)^{2r-2}$, so that the variance of Q_n is

$$\frac{1}{2} M^2 \sin^2 \delta \sum_{r=1}^n (\cos \delta)^{2r-2}.$$

Furthermore, if $\delta \ll 1$ and $n \ll 1/\delta^2$ then the variance of Q_n is approximately $(n/2)M^2 \sin^2 \delta$, so that the r.m.s. value of M_z after n pulses is $(n/2)^{1/2} M \sin \delta$.



This analysis shows that the induction signal will fall off as the square root of n , instead of directly with n as would be the case if phase coherence were preserved. Since the pulse length can be set with an accuracy to about 1% we should expect to obtain satisfactory Carr-Purcell trains containing up to about 10^4 pulses, and this in fact proves to be the case. The figure shows a typical decay curve. The sample is water at room temperature containing a small amount of paramagnetic impurity, so that its transverse relaxation time is about 3.5 sec. The sweep speed is 1 cm sec⁻¹, and the pulse recurrence rate is 1 kc/s, so that the total sweep contains just 10^4 pulses.

In conclusion, it is perhaps worth pointing out that if the magnet instability is increased beyond a certain point a further deterioration of the Carr-Purcell train takes place. This is due to the fact that a phase change will now occur during the time of application of a radio-frequency pulse, so that the resultant nuclear magnetic vectors will no longer be coplanar, but will form a complex figure of eight pattern, as described

by Hahn (1950). Thus the condition under which maximum echo amplitude is obtained, with all the magnetic vectors collinear, will never be completely recovered and it will not be possible to obtain a satisfactory Carr-Purcell train.

ACKNOWLEDGMENTS

Acknowledgment is due to Dr. J. A. Pople and Mr. G. F. Miller for helpful discussion of this problem. The work described in this paper was carried out as part of the research programme of the National Physical Laboratory and is published by permission of the Director of the Laboratory.

REFERENCES

- CARR, H. T., and PURCELL, E. M., 1954, *Phys. Rev.*, **94**, 630.
HAHN, E. L., 1950, *Phys. Rev.*, **80**, 580.
MEIBOOM, S., and GILL, D., 1958, *Rev. Sci. Instrum.*, **29**, 688.
SHEV, A., and NORBERG, R. E., 1960, *Rev. Sci. Instrum.*, **31**, 508.

Zero-field Paramagnetic Resonance of Fe^{3+} in Methylamine Alum

By G. S. BOGLE AND H. F. SYMMONS

Division of Physics, National Standards Laboratory, Commonwealth
Scientific and Industrial Research Organization, Sydney

MS. received 3rd July 1961

Abstract. The splitting of the ground level of Fe^{3+} in $(\text{CH}_3\text{NH}_3)\text{Al}(\text{SO}_4)_2 \cdot 12\text{H}_2\text{O}$ in the absence of a magnetic field has been measured directly. At 90°K the separation of the $S_z = \pm 3/2$ states from the $\pm 1/2$ is equivalent to $12\,227 \pm 5$ Mc/s, and that of the $\pm 5/2$ from the $\pm 3/2$ to $22\,043 \pm 10$ Mc/s. The deduced values of the coefficients in the usual spin-Hamiltonian for the ferric alums are $D = +0.1893 \pm 0.0002$ and $a - F = +0.0171 \pm 0.0001$ cm^{-1} , and it is probable that $a \simeq +0.013$, $F \simeq -0.004$ cm^{-1} . The material is promising for a zero-field maser, with predicted amplifying and pumping frequencies of $12\,290 \pm 15$ and $34\,460 \pm 45$ Mc/s respectively at liquid-helium temperatures.

§ 1. INTRODUCTION

WE HAVE RECENTLY discussed the need for direct measurements of paramagnetic energy level splittings at zero magnetic field, and have described equipment for the range 8 to 18 Gc/s (Bogle *et al.*, 1961). We have now extended our equipment to cover the additional range of 18 to 26 Gc/s (K-band) and this has enabled us to determine the energy level scheme of Fe^{3+} in methylamine alum $(\text{CH}_3\text{NH}_3)\text{Al}(\text{SO}_4)_2 \cdot 12\text{H}_2\text{O}$, at 90.2°K .

§ 2. THE PARAMAGNETISM OF THE FERRIC ALUMS

The paramagnetic resonance of several ferric alums has been studied by Bleaney and Trenam (1954), who have given a full discussion of the crystal structure and the appropriate symmetry of the spin-Hamiltonian. The unit cell of the alums is cubic and contains four Fe^{3+} ions. Each of these is surrounded by six water molecules forming an octahedron. If the octahedron were regular and if the more distant environment were neglected the crystalline electric potential would have the form

$$V = C(\xi^4 + \eta^4 + \zeta^4 - \frac{2}{3}r^4)$$

where ξ , η and ζ are Cartesian coordinates referred to the cubic axes of the octahedron with origin at its centre. With this simplified potential the spin-Hamiltonian would have the form

$$\frac{1}{6}a[S_\xi^4 + S_\eta^4 + S_\zeta^4 - \frac{1}{5}S(S+1)(3S^2 + 3S - 1)]$$

where S_ξ is the ξ -component of the spin operator, and so on, and a is a constant. The levels in zero-field for Fe^{3+} , which has $S = 5/2$, would be a doublet and a quadruplet separated by $3a$.

In the alums, however, the actual electric field consists of the cubic field together with one of axial symmetry, the axis lying in a [111] direction of the octahedron, or, equivalently, a [111] direction (body diagonal) of the unit cell. Each of the four body diagonals is such an axis for one of the four Fe^{3+} sites per unit cell. Calling this axis the z -axis, the additional terms which must be added to the spin-Hamiltonian are

$$D[S_z^2 - \frac{1}{3}S(S+1)] + \frac{1}{180}F[35S_z^4 - 30S(S+1)S_z^2 + 25S_z^2 - 6S(S+1) + 3S^2(S+1)^2]$$

these forms having been chosen so that they transform under rotation like spherical harmonics (Bleaney and Stevens 1953). The complete spin-Hamiltonian in zero field is

$$\mathcal{H} = D(S_z^2 - \frac{3}{12}) + \frac{1}{6}a(S_\xi^4 + S_\eta^4 + S_\zeta^4 - \frac{7}{16}) + \frac{7}{36}F(S_z^4 - \frac{9}{14}S_z^2 + \frac{81}{16}) \quad (1)$$

where for simplicity we have substituted the numerical value of S .

Bleaney and Trenam have made a complete analysis of the spectrum of Fe^{3+} in rubidium sulphate alum and potassium selenate alum, and Meijer has done the same for ammonium sulphate alum. The results are collected on p. 342 of the review article by Bowers and Owen (1955), and it may be seen that, though D varies from 22 to $160 \times 10^{-4} \text{ cm}^{-1}$ for the three materials and is temperature-dependent, $|a|$ varies only from 127 to $134 \times 10^{-4} \text{ cm}^{-1}$ for the three and is temperature-independent. The term F is much smaller, only of the order of $1 \times 10^{-4} \text{ cm}^{-1}$. This behaviour is consistent with the expectation that the cubic component of the crystalline potential, which determines $|a|$, is mainly due to the octahedron of water molecules which surround the Fe^{3+} ion and so is relatively insensitive to changes of constituents outside the octahedron. The results show, too, that the value of D is much more sensitive to such changes.

In the case of methylamine alum, which Bleaney and Trenam also investigated, using the classical paramagnetic resonance technique of fixed frequency and adjustable magnetic fields, the spectrum at 90°K consisted of a very large number of lines. Because the analysis would have been difficult, recourse was had to a process which, in spirit, was a zero-field measurement. The positions of the three lowest-field lines were measured at a series of frequencies in the then available range between 9.0 and 9.9 Gc/s, and the zero-field frequency of each line was found by extrapolation. This process yielded three frequencies, 11.70, 11.76 and 11.88 Gc/s, and in view of the errors ($\pm 300 \text{ Mc/s}$), Bleaney and Trenam concluded that there was probably a single absorption line at $11\,800 \pm 300 \text{ Mc/s}$. Similar measurements at K-band indicated the existence of another absorption line at $22\,200 \pm 300 \text{ Mc/s}$.

In order to fit these results to the spin-Hamiltonian it is necessary to calculate the energy eigenvalues of (1). Before giving the accurate solutions it will be helpful to examine what the states and energies would be if the Hamiltonian were simply $D(S_z^2 - 35/12)$. It may be seen by inspection that the eigenstates would be simply the eigenstates $|M\rangle$ of S_z and that the eigenvalues would be $D(M^2 - 35/12)$. The disposition of energy levels for positive D would be as in figure 1(a). Bleaney and Trenam identified the 22 Gc/s absorption with the $5/2, 3/2$ transition and the 12 Gc/s with the $3/2, 1/2$; this is the most natural identification since it describes methylamine alum as differing from the other alums almost entirely in regard to D , which we know to be structure sensitive, and only slightly in regard to $a - F$ (see below), which we know to be insensitive.

To refine the analysis we now need a more accurate solution of the eigenvalue equation from (1). Bleaney and Trenam (1954) have given the exact solutions; but

when a is small compared with D , as here, the following forms for the differences between the energies (W) are useful:

$$W_{5/2} - W_{3/2} = h\nu\left(\frac{5}{2}, \frac{3}{2}\right) = 4D - \frac{4}{3}(a - F) + \frac{20a^2}{3(18D + a - F)} + O\left(\frac{a^4}{D^3}\right)$$

$$W_{3/2} - W_{1/2} = h\nu\left(\frac{3}{2}, \frac{1}{2}\right) = 2D + \frac{5}{3}(a - F) + \frac{20a^2}{3(18D + a - F)} + O\left(\frac{a^4}{D^3}\right).$$

(2)

Making the simplifying assumption that F was negligible, Bleaney and Trenam calculated the following values of spin-Hamiltonian coefficients at 90 °K (in units of 10^{-4} cm^{-1}):

$$D = (-)1880 \pm 140; \quad a = (-)100 \pm 40.$$

The signs are not determined by this type of measurement, but only the relative signs

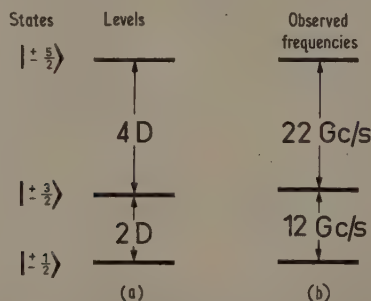


Figure 1. (a) Disposition of the energy levels of Fe^{3+} in methylamine alum with simplified Hamiltonian. (b) Identification of the observed frequencies.

of D and $a - F$ (or D and a if F is negligible). The above signs were inferred on the supposition that a was negative, as it appeared to be in potassium rubidium alum.

One question was not answered conclusively by the above measurements: is there more than one set of splittings for the Fe^{3+} ion? In the alums at room temperature the four Fe^{3+} sites differ only in the directions of their z axes and so should have identical splittings in zero magnetic field. In the 'classical' paramagnetic resonance experiment, i.e. one using a fixed frequency and adjustable magnetic field, a single alum crystal should in general give four distinct spectra because of the different z directions, each spectrum consisting of five strong lines giving a total of twenty. Bleaney and Trenam observed over sixty lines, which seemed too many to be accounted for by the above model even allowing for semi-forbidden lines, and suggested that there might be a change of crystal structure in methylamine alum producing either more than four z directions or more than one set of zero-field levels, or both.

The time is now ripe for a re-appraisal of Fe^{3+} in methylamine alum because of the following subsequent developments:

(i) Cooke, Meyer and Wolf (1956) have measured the Schottky specific heat anomaly of ferric methylamine alum and found good agreement with that calculated for levels separated by 12 and 22 Gc/s, provided that the arrangement is as in figure 1. This shows that D and $a - F$ are positive, contrary to the earlier assignment. It also shows

that, if a multiplicity of level schemes does exist, these schemes do not differ markedly from each other.

(ii) Geschwind (1959) has repeated the experiment on Fe^{3+} in rubidium alum under more favourable conditions than in the earlier work and has found a to be positive. Hence we consider it highly likely that a is positive in all the ferric alums, contrary to the earlier view.

(iii) The new technique of zero-field spectrometry is capable of resolving the question whether or not there are several distinct sets of level arrangements. It can also yield more accurate values of the absorption frequencies, which are important for zero-field maser design as well as for a precise evaluation of D and $a-F$.

We have, therefore, re-measured the zero-field absorption frequencies of Fe^{3+} in methylamine alum; the results are reported below.

§ 3. EXPERIMENTAL METHOD

The only experimental techniques not already described by Bogle *et al.* (1961) are the use of a motor-driven 2K33 klystron to scan the spectrum near 22 000 Mc/s and the provision of frequency-marking pips while scanning (cf. figure 2).

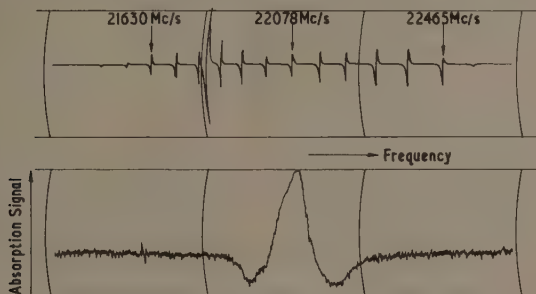


Figure 2. Chart recording of the 22 Gc/s absorption signal of Fe^{3+} in methylamine alum at 80.8 °K. The frequency markers are about 80 Mc/s apart. (The resonance frequency has to be corrected for misalignment of the recorder pens.)

The pips are produced in the following way: part of the microwave power is coupled out of the main waveguide run and led to the entrance iris of a transmission cavity resonator which we call an 'echo tunnel'. This consists of a 150 cm length of standard K-band waveguide short-circuited at each end. Small irises in the short-circuiting diaphragms allow coupling to the external circuitry. When the frequency is such that the echo tunnel length is equal to an integral number of half wavelengths-in-the-guide the tunnel resonates and transmits some power which is detected by a crystal rectifier. The loaded Q is several thousand, and over K-band the interval between resonances varies from 60 to 85 Mc/s.

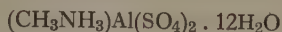
In principle the echo tunnel resonances could be recorded by using d.c. methods; but for higher sensitivity we use a radio-frequency modulation method. The klystron is frequency-modulated at about 500 kc/s, and hence when the microwave frequency is near an echo tunnel resonance the transmitted microwave power is amplitude-modulated at 500 kc/s. The use of a phase-sensitive detector gives the pip shape shown

in figure 2. This method allows the amplification to be done in the 500 kc/s region where crystal detector noise is much lower than at low frequencies.

The echo tunnel resonant frequencies are calibrated in a separate experiment, and are reproducible from day to day to within 1 Mc/s. However, the wavemeter used is not calibrated to better than ± 5 Mc/s. A shorter echo tunnel is simultaneously used to produce more widely spaced pips which aid identification; one such is present on the chart in figure 2. The temperature of the long-echo tunnel is monitored by a mercury-in-glass thermometer strapped to the waveguide.

§ 4. RESULTS

We have used a polycrystalline sample of aluminium methylamine alum



containing nominally one per cent of the corresponding ferric compound.

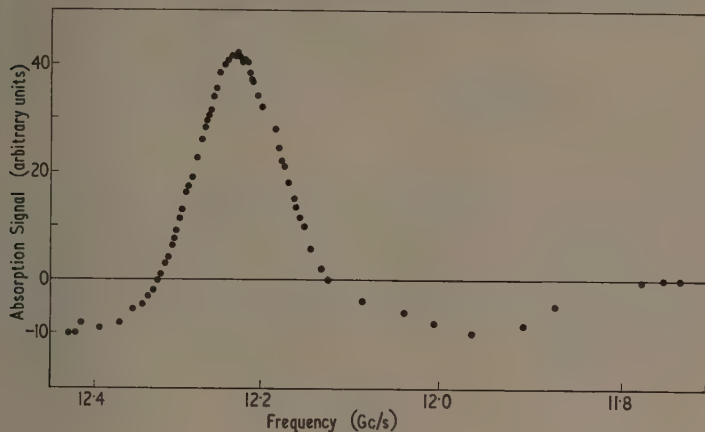
At 90.2°K , the same temperature as used by Bleaney and Trenam, we find a line at $22\,043 \pm 10$ Mc/s (shown in figure 2) and another at $12\,227 \pm 5$ Mc/s. In figure 3 we show (a) the absorption signal of the latter as plotted point by point using a klystron, and (b) the spectrum between 11.8 and 17.5 Gc/s recorded on a chart using a backward-wave oscillator as swept-frequency source. The full width of the 22 Gc/s line at half-height is 75 ± 5 Mc/s, and that of the 12 Gc/s line 135 ± 10 Mc/s. We find no other lines in the range 7.8 to 26.5 Gc/s though we could detect them if they were more than one-tenth as strong as the observed lines.

Using equations (2) we may now deduce the values of D and $a - F$. Our measurements determine the relative signs of D and $a - F$, and Meyer's specific heat measurements, already mentioned, show that D is positive. The second-order term in (2) depends on a^2 which we do not directly determine; but for any reasonable value of a this contributes only -0.0001 cm^{-1} to the computed values of D and $a - F$. Allowing this amount, the values are $D = +1893 \pm 2$; $a - F = +171 \pm 1$ in units of 10^{-4} cm^{-1} .

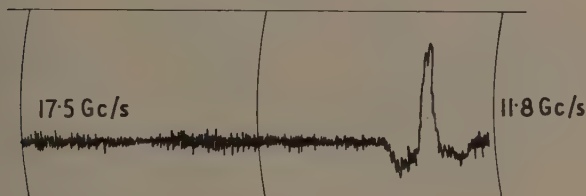
The values of $|a|$ for the three other alums so far studied (Bowers and Owen, 1955, p. 342) are 127, 128 and 134 in the same units, and, as already discussed, the sign is probably positive for all three. Hence we offer, as the best guess for methylamine alum, $a = 130$; $F = -40$ in units of 10^{-4} cm^{-1} . The other alums have $|F|$ about twenty times smaller, but they also have $|D|$ ranging from ten to one hundred times smaller. A definitive theory of the dependence of D and F on the axial crystalline field has not, as far as we know, been worked out; but it does seem reasonable that the stronger axial field in methylamine alum, which makes $|D|$ larger than in the other alums, should have a similar effect on $|F|$.

For zero-field maser design it is desirable to know the frequencies at liquid helium temperatures. We have measured the frequency of the 22 Gc/s line at 81°K ; it is $22\,069 \pm 10$ Mc/s. The uncertainty in the change of frequency between 90.2° and 80.8°K is not as great as may appear at first sight because the absolute error of the wavemeter is not involved. Thus we give the change of frequency as 26 ± 5 Mc/s. The variation of frequency near absolute zero is probably of the form $\nu(T) = \nu_0 + \alpha T^2$, since all temperature coefficients are zero at zero temperature according to the third law of thermodynamics, and we shall make the possibly bold assumption that this form holds even as far as $T = 90^\circ\text{K}$. If so, $d\nu/dT \equiv 2\alpha T \simeq -(26 \pm 5)/10$ Mc/s per degree at 85°K . This determines α , and the frequency at 4°K is predicted to be 123 ± 20 Mc/s

higher than at 90°K : that is, $22\,170 \pm 30$ Mc/s.[†] The temperature dependence of the frequencies is mainly a reflection of that of D , so the other frequency at 12 Gc/s, which involves $2D$ instead of $4D$, should increase by half of 123, i.e. 60 ± 10 , becoming $22\,290 \pm 15$ Mc/s at liquid helium temperatures. It is interesting to notice that Cooke,



(a)



(b)

Figure 3. (a) The 12.2 Gc/s absorption signal of Fe^{3+} in methylamine alum at 90.2°K (modulation 80 gauss). (b) The absorption spectrum between 11.8 and 17.5 Gc/s.

Meyer and Wolf (1956) obtained good agreement between the theoretical and measured specific heats of pure ferric methylamine alum on the assumption that the above frequencies were 21 900 and 12 000 Mc/s. This indicates that there is little change of frequency on dilution with the aluminium salt, confirming Bleaney and Trenam's observations at 90°K .

§ 5. CONCLUSIONS

There is only one type of zero-field energy level scheme for Fe^{3+} in methylamine alum at 90°K . The multiplicity of lines observed for single crystals of the alum in the earlier experiments of the classical paramagnetic resonance type (fixed frequency,

[†] Note added in proof. The measured frequencies at 4°K are $22\,080 \pm 5$ and $12\,230 \pm 5$ Mc/s.

adjustable field) must therefore be due either to the existence of more than the expected four z directions or else to the presence of unexpectedly strong 'forbidden' lines. Now that the spin-Hamiltonian coefficients have been established by zero-field resonance it will be easier to discover the number of distinct z directions by repeating the classical experiment, for we may predict that the highest line will occur for the z direction of magnetic field at a strength of $B = [h\nu + 4D - \frac{4}{3}(a-F)]/g\beta$, where ν is the (fixed) frequency, g is the splitting factor (usually 2.00 for Fe^{3+} in ionic bonding) and β the Bohr magneton (cf. Bowers and Owen 1955, p. 341). For an X-band spectrometer, with $\nu = 9.00$ Gc/s, the highest line will occur at 11.1 kilogauss and will be easily identifiable since it will rise to that field as a maximum as the field direction approaches a z direction.

Methylamine alum is a promising material for a zero-field maser (Bogle and Symmons 1959). At liquid helium temperatures the amplifying frequency, $\nu(\frac{3}{2}, \frac{1}{2})$, is predicted to be $12\,290 \pm 15$ Mc/s, and the pumping frequency, $\nu(\frac{5}{2}, \frac{1}{2})$, to be $34\,460 \pm 45$ Mc/s. The transition probability for pumping is, from p. 15 of the above reference, $10a^2/9D^2$ for polycrystalline material, or 0.006 free-spin units if $a = 0.013$ cm⁻¹ as we have assumed. This is a low transition probability, but in compensation the pumping frequency lies in the well-developed 8 mm-wave radar band for which powerful klystrons are commercially available.

REFERENCES

- BLEANEY, B., and STEVENS, K. W. H., 1953, *Rep. Progr. Phys.*, **16**, 108 (London: Physical Society).
 BLEANEY, B., and TRENAM, R. S., 1954, *Proc. Roy. Soc. A*, **223**, 1.
 BOGLE, G. S., and SYMMONS, H. F., 1959, *Aust. J. Phys.*, **12**, 1.
 BOGLE, G. S., SYMMONS, H. F., BURGESS, V. R., and SIERINS, J. V., 1961, *Proc. Phys. Soc.*, **77**, 561.
 BOWERS, K. D., and OWEN, J., 1955, *Rep. Progr. Phys.*, **18**, 304 (London: Physical Society).
 COOKE, A. H., MEYER, H., and WOLF, W. P., 1956, *Proc. Roy. Soc. A*, **237**, 404.
 GESCHWIND, S., 1959, *Phys. Rev. Letters*, **3**, 207.

Magnetocrystalline Anisotropy and Coercivity in a 'Square-loop' Ferrite Material

By J. R. CHAMBERLAIN

Department of Physics, The University, Sheffield 10†

Communicated by W. Sucksmith; MS. received 11th May 1961, in revised form 18th July 1961

Abstract. It is shown that the first order magnetocrystalline anisotropy constant K_1 of a 'square-loop' ferrite material can be determined from measurements of the approach to saturation of magnetization in a polycrystalline specimen. The energy ($\gamma = 0.20 \text{ erg cm}^{-2}$) and the thickness ($\delta \sim 1.6 \times 10^{-5} \text{ cm}$) of 180° domain boundary walls in a commercial manganese magnesium ferrite, Ferroxcube D.1, are estimated from results obtained in this way. The temperature variation of coercivity in the same material is also discussed in the light of these results, and it is found that the Goodenough theory of domain creation is inapplicable. Pores were observed in the material. Although these have a diameter greater than the estimated domain wall width δ , the experimental results presented are not consistent with the Néel disperse field theory.

§ 1. INTRODUCTION

AT THE TIME that this work was initiated single crystal specimens of 'square-loop' ferrite material had not been prepared, and a method of determining the magnetocrystalline anisotropy constant K with the aid of polycrystalline specimens was required. High values of remanence in this type of material have been shown to be associated with the occurrence of small or zero magnetostriction (Baltzer (1955) Wijn *et al.* (1954)). In this case, the dominant magnetocrystalline anisotropy should be the only agency directing magnetization vectors at remanence, and also impeding the progress of the magnetization to saturation under the action of an applied field. Laws governing the approach to saturation of magnetization have been calculated for several cases. The relevant cases are given below. Under the relatively simple conditions prevailing in the type of material under consideration, it appeared that the use of such laws should give an easy means of determining the required magnetocrystalline anisotropy.

This communication describes experiments in which the approach to saturation of magnetization in a commercial manganese-magnesium ferrite (Ferroxcube D.1) has been measured at different temperatures. From the results of these experiments values of K have been calculated. These values have then been used to estimate the energy and thickness of domain boundary walls and in a discussion of coercivity in the material.

§ 2. MAGNETOCRYSTALLINE ANISOTROPY

2.1. Theory

For the case of a strain-free material with $[111]$ -type easy directions Gans (1932) has given the following law of approach to saturation:

$$I = I_s \left(1 - 0.07619 \left(\frac{K^2}{I_s^2} \right) \frac{1}{H^2} - 0.02362 \left(\frac{K^3}{I_s^3} \right) \frac{1}{H^3} \dots \right) \quad (1)$$

† Now at the National Research Council, Ottawa, Ontario, Canada.

in which I is the magnetization per unit volume of a polycrystalline specimen in a field strength H , I_s is the saturation magnetization and K the first order magnetocrystalline anisotropy constant. The law is valid in relatively high fields and has been tested by Czerlinski (1932) and Polley (1939). An equation calculated on a similar basis for materials with [100]-type easy directions has also been found valid.

If interaction between crystallites is apparent in a given material then equation (1) gives an underestimate of K . This problem has been considered by Holstein and Primakoff (1941) and Néel (1948), who agree that for the case $H \ll 4\pi I_s$, the underestimate in K is $\sqrt{2}$.

For the case of a strained material with negative magnetostriction, Becker and Polley (1940) have calculated

$$I = I_s - \frac{3\lambda^2\sigma_i^2}{5I_sH^2} \quad (2)$$

In this equation, λ is the (isotropic) magnetostriction constant of the material and σ_i the internal stress. This was found valid in strained nickel.

2.2. Experimental

Preliminary measurements showed that in field strengths of 50–180 Oe, at room temperature, the magnetization in a specimen of Ferroxcube D.1 was 0.9 to 0.96 I_s . In this region, equations of the type discussed above should be applicable, so that a relatively simple ballistic galvanometer method was used.

The specimen was a toroid with mean diameter 1.1 cm. This was wound first with a secondary coil, and the primary coil was wound over that. In this way the area turns

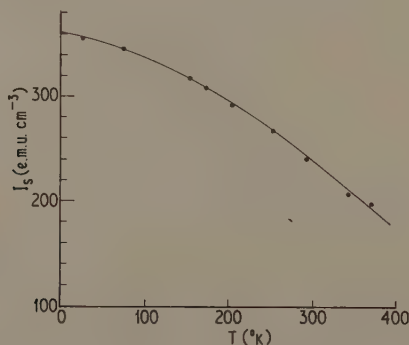


Figure 1. The temperature dependence of the saturation magnetization in Ferroxcube D.1.

in the secondary coil could be estimated more accurately. Some heating of the specimen was observed when larger currents were passed through the primary. This was checked by attaching a thermocouple to the specimen and readings were taken only when the specimen was initially at the temperature of the particular bath in which it was immersed.

The procedure adopted was to observe the deflection of a galvanometer connected across the secondary coil when the current in the primary was reversed. When larger currents were employed, the change in magnetization from the remanent state, on the application of a given field, was determined.

The saturation magnetization of the material was determined as a function of temperature with the aid of a Sucksmith ring-balance. This involved the measurement of the magnetization (per gramme) of an ellipsoidal specimen at a given temperature as a function of applied field, in field strengths up to 12 kOe. After taking account of the demagnetizing factor of the specimen, the magnetization was extrapolated to zero field strength to give σ_0 , the saturation magnetization per gramme. The density of the material was determined by a water displacement method and the volume saturation magnetization determined using this. The saturation magnetization is plotted as a function of temperature in figure 1, and the tabulated results are as follows:

T °K	26	79	153	171	203	250	293	345	373
I_s e.m.u. cm ⁻³	355	345	317	308	292	265	240	208	196

2.3. Results

The experimental results (at room temperature) were compared with equation (1) in the form

$$(I_s - I)H^3 = \Delta IH^3 = \alpha H + \beta \quad (3)$$

where $\alpha = 0.07619(K^2/I_s)$, $\beta = 0.02362(K^3/I_s^2)$. The parameter ΔIH^3 was plotted against H . The straight line given in figure 2 was obtained. The intercept gives a

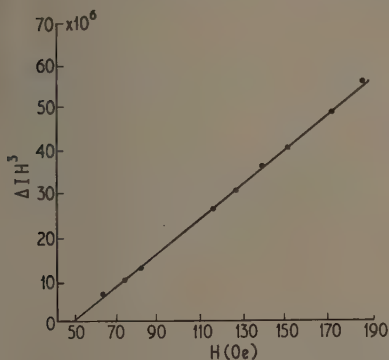


Figure 2. Approach to saturation at room temperature plotted in the form of equation (3).

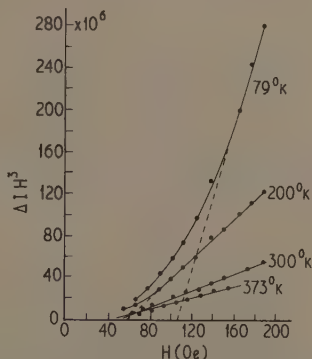


Figure 3. Complete set of results of approach to saturation plotted in the form of equation (3).

negative value of β which in turn depends upon K^3 . This means that K is in fact negative, and the easy directions of magnetization in the material are [111]-type directions, as was assumed. From the gradient and intercept of the line in figure 2 the respective values $K = 3.56 \times 10^4$ and 3.62×10^4 erg cm⁻³ were calculated. These appeared consistent enough to justify extending the experiments to other temperatures. This was done by immersing the specimen in baths of (a) liquid nitrogen (79 °K), (b) crushed solid carbon dioxide in methylated spirits (200 °K), (c) boiling water (373 °K). The approach to saturation was measured at each of these temperatures and the results

plotted in the form of equation (3). A complete set of results is given in figure 3 and the values of K calculated from these are tabulated below. (These have been corrected for the effect of interaction between grains.)

$T (^{\circ}\text{K})$	79	200	296	373
$K_1 \times 10^4 \text{ (ergs cm}^{-3}\text{)}(\alpha)$	17.3	8.5	5.03	3.88
$K_1 \times 10^4 \text{ (ergs cm}^{-3}\text{)}(\beta)$	17.5	8.4	5.1	3.96

2.4. Discussion of Results

The consistency of these results gives confidence in the method. The values of K given above can be compared with a value $K = 3 \times 10^4 \text{ erg cm}^{-3}$ obtained by Standley and Peters (1957) by resonance experiments on a manganese-magnesium ferrite.

It is possible to indicate the effects of stress on the above results with the aid of equations (1) and (2). In the presence of both stress and magnetocrystalline anisotropies the value of K_1 determined above is related to the real value K by

$$K_1^2 = K^2 - \frac{3\lambda^2\sigma_1^2}{5 \times 0.07619}.$$

Hence for $\lambda\sigma_1 \ll K$ and $K_1 \sim K$,

$$\frac{\Delta K}{K_1} \simeq \frac{4\lambda^2\sigma_1^2}{K_1^3}.$$

Using a large value for the stress $\sigma_1 = 3 \times 10^9 \text{ dyn cm}^{-2}$ and $\lambda \simeq 2 \times 10^{-7}$ (Knowles 1959, private communication) with $K_1 = 3.6 \times 10^4 \text{ erg cm}^{-3}$, then $\Delta K/K \sim 10^{-8}$. Unless λ varies violently with temperature, the error incurred from this cause must be infinitesimal. Since the hysteresis loops (see figure 5) do not change in shape to any great extent with temperature variation, one would expect that the relative values of K and $\lambda\sigma_1$ do not vary significantly. It thus seems that the above results must be at least good estimates of the magnetocrystalline anisotropy constant at the appropriate temperatures.

§ 3. EXCHANGE ENERGY AND DOMAIN WALL THICKNESS AND ENERGY IN FERROXCUBE D.1

The results of the saturation magnetization in Ferroxcube D.1 given in figure 1 were fitted to the Bloch equation (Bloch 1930)

$$I_s = I_0(1 - CT^{3/2}) \quad (4)$$

in which I_s is the saturation magnetization in a ferromagnetic material at temperature T , and I_0 the saturation magnetization at the absolute zero. From Herring and Kittel (1951) it can be inferred that the exchange constant A is related to the constant C in equation (5) by

$$A = \left(\frac{I_0}{2\mu_B} \right)^{1/3} \left(\frac{k}{13.3C^{2/3}} \right) \quad (5)$$

where μ_B is the Bohr magneton and k Boltzmann's constant.

Figure 4 shows a plot of I_s against $T^{3/2}$, from which the values $I_0 = 362$ e.m.u. cm⁻³ and $C = 6.79 \times 10^{-5}$ c.g.s. units were obtained. Using these values and $\mu_B = 9.21 \times 10^{-21}$ erg Oe⁻¹, $k = 1.38 \times 10^{-16}$ erg deg⁻¹ in equation (5),

$$A = 2.02 \times 10^{-7} \text{ erg cm}^{-1}.$$

This can be compared with values:

- | | |
|----------------------------------------------------|-----------------------------------------------|
| (i) for iron (Kittel and Galt 1956) | $A = 2 \times 10^{-6} \text{ erg cm}^{-1}$ |
| (ii) for magnetite (Galt 1954) | $A = 1.24 \times 10^{-6} \text{ erg cm}^{-1}$ |
| (iii) for manganese ferrite (Dillon and Earl 1959) | $A = 0.14 \times 10^{-6} \text{ erg cm}^{-1}$ |

and the ferrites containing manganese appear to have lower values of A .

Using the value of A thus calculated, it is possible to estimate the energy γ and thickness δ of domain boundary walls in the material.

In a material with [111]-type easy directions, 71°, 109°, and 180° walls can occur. The thickness of 180° domain walls is determined to a large extent by the magnetostriction of the material. Ferroxcube D.1 has a low magnetostriction and it can be

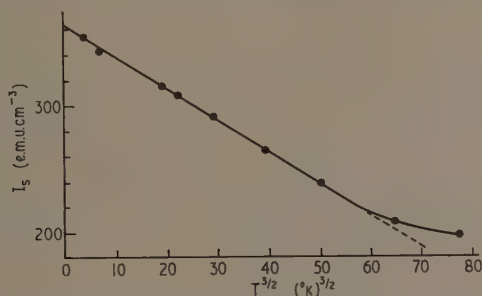


Figure 4. Saturation magnetization in Ferroxcube D.1 plotted against $T^{3/2}$.

shown using Lilley's analysis (Lilley 1950, equation 5.14) that 180° walls can be expected to form only in (112) planes: 180° domain walls in a (110) plane do not have a finite thickness.

The (112)-180° walls then have a thickness $\delta = 7.91(A/K)^{1/2}$ and energy $\gamma = 2(KA)^{1/2}$. Substituting the room temperature value $K = 5.1 \times 10^4$ and A as above, we obtain $\gamma = 0.2$ erg cm⁻¹ and $\delta = 1.6 \times 10^{-5}$ cm. These values will be fairly representative over the whole temperature range as \sqrt{K} varies by a relatively small amount.

90°-type walls will have thicknesses of one quarter to a half of that given above, and energies about a half.

§ 4. COERCIVITY OF FERROXCUBE D.1

Goodenough (1954) suggested that the main process causing reversal of magnetization in 'square-loop' materials is the nucleation of domains of reversed magnetization at grain boundaries. Having been created, these domains expand without impediment to the motion of their walls, and hence give rise to a definite shoulder on the hysteresis

loop. In a theory which should be applicable to all materials which reverse their magnetization through the movement of domain boundary walls, Goodenough defined two critical fields: (i) the field required to create domains of reverse magnetization H_n , and (ii) the field required to move domain walls through the material H_w . The relative magnitudes of H_n and H_w then determine the shape of the hysteresis loop. The sense of H_n is positive or negative depending upon whether domains of reversed magnetization are apparent at remanence, or whether they are created in a reverse field, i.e. a field with the same sense as coercivity. The expressions Goodenough obtained can be summarized in the following:

$$H_c I_s = g\sqrt{K} + f I_s^2 \quad (6)$$

in which g and f are constants. The first term on the right represents the energy required to move domain walls through the material and the second the energy required

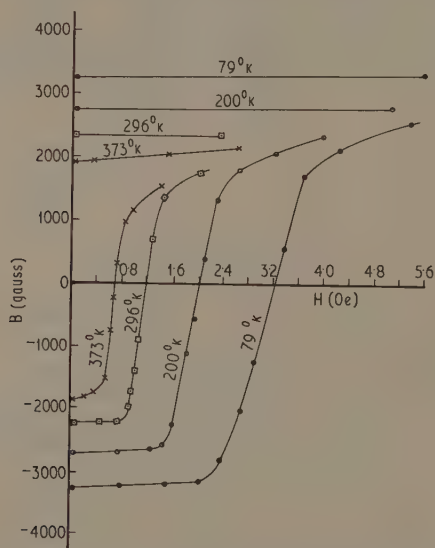


Figure 5. Hysteresis loops of Ferroxcube D.1 at different temperatures.

to create domains of reversed magnetization. The constant f on this basis could take positive or negative values depending upon the conditions outlined above.

Hysteresis loops of Ferroxcube D.1 were determined at the four temperatures used in the previous experiment. These are given in figure 5. The shape of these loops is initially independent of temperature from 79 to 300 °K. The loop taken at the higher temperature does not have quite such a marked 'shoulder', and retentivity I_R/I_s is 0.72 instead of 0.75 in other cases. This would tend to indicate that similar processes are giving rise to reversal of magnetization over most, and possibly the whole, of the temperature range employed.

In figure 6 the parameter $H_c I_s$ is plotted against \sqrt{K} . Attempts were made to fit equation (6) to the curve in figure 6 without any success. The general indication was that an equation of this type would fit only very minor portions of the curve. It was

thus necessary to conclude that reverse domain creation as envisaged by Goodenough does not cause the reversal of magnetization in this material.

It must be noted that in this material, the ratio $2K/I_s \sim 400$ Oe, which is much too large for the possibility of rotations of magnetization vectors to be responsible for the reversal of magnetization.

Micrographic studies of cleaved and polished surfaces of the specimen revealed many pores. These had a diameter of the order of 2×10^{-4} cm. The diameter quoted is a factor of ten larger than the width of domain boundary walls in the material, so

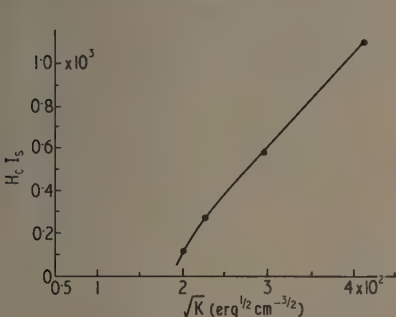


Figure 6. The parameter $H_c I_s$ plotted against \sqrt{K} .

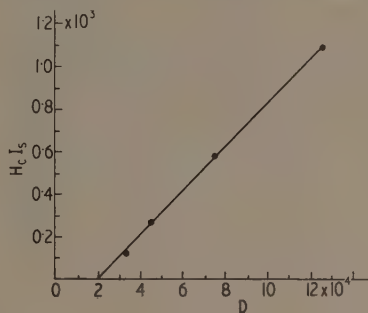


Figure 7. Graph showing variation of $H_c I_s$ with D (see text).

the pores may be expected to influence coercivity. It hence seemed pertinent to compare the results with the Néel disperse field theory (Néel 1949). In its approximate form the theory would predict the following relationship for the coercivity:

$$H_c' \simeq \frac{1}{4} v \frac{\lambda^2 \sigma_1^2}{K I_s} + \frac{K v'}{I_m}. \quad (7)$$

In this equation the first term represents the contribution to the coercive force from islands of free poles, of total fractional volume v , which result from the presence of non-uniform stress in the material. The second term is due to the presence of free poles caused by non-magnetic inclusions of fractional volume v' . Here I_m is the mean magnetization over magnetic and non-magnetic material. Using values $I_m \sim I_s = 240$ e.m.u. cm^{-3} , $\lambda = 2 \times 10^{-7}$, $K = 5 \times 10^4$ erg cm^{-3} and $\sigma_1 \sim 3 \times 10^9$ dyn cm^{-2} , we obtain

$$H_c' \simeq 2 \times 10^{-2} v + 2.1 \times 10^2 v'$$

from which it is obvious that the second term is the dominant one, and on this basis the effect of the pores on the coercivity would be expected to be much larger than any effects of stress.

The complete relationship given by Néel for the case of non-magnetic inclusions is

$$H_c' = \frac{2Kv'}{\pi I_m} \left[0.386 + \ln \left(\frac{2\pi I_m^2}{K} \right)^{1/2} \right]. \quad (8)$$

In figure 7 $H_c I_s$ is plotted against

$$D = \left(\frac{2K}{\pi} \left[0.386 + \ln \left(\frac{2\pi I_s^2}{K} \right)^{1/2} \right] \right).$$

The resulting straight line has a gradient of 10^{-2} and an intercept $D_0 \simeq 2 \times 10^4$. The porosity of the material given by the manufacturers is 2–5%. The gradient is hence reasonably near this value, but the intercept cannot be justified by equation (8). Hence the Néel theory is not obeyed in Ferroxcube D.1.

The reversal of magnetization in a material like Ferroxcube D.1 is expected to occur by some process which gives rise to a very small distribution of coercivities within the material, and in this case one might not expect the Néel theory to apply. However, a process of domain creation appears much more attractive in this respect, since it could quite well explain the shapes of the hysteresis loops, and the reasons for the failure of the Goodenough theory must be questioned. Our present knowledge of domain creation is by no means extensive, and the only experimental work of any significance appears to be that of Bates and Martin (1953, 1956). These authors observed the creation of reverse domains as domain walls passed over non-magnetic inclusions in silicon iron. It hence seems possible that the results given above are not consistent with Goodenough's theory because this theory is specifically concerned with the creation of reverse domains at grain boundaries, and the evidence presented here thus cannot rule out the possibility of domain creation of some other form occurring in Ferroxcube D.1.

§ 5. CONCLUSIONS

It has been found possible to determine the magnetocrystalline anisotropy in a 'square-loop' ferrite by measurements of the approach to saturation in a polycrystalline specimen. The results presented in a linear form of the theoretical equation allow K to be calculated from a gradient and an intercept. The two values obtained in this way were found consistent at the four temperatures used and the method hence appears valid.

The exchange energy constant A in the same material was determined from measurements of the saturation magnetization at low temperatures. Along with the values of K found above, this gave the thickness and energy of domain boundary walls in the material to be 1.6×10^{-5} cm and 0.2 erg cm^{-2} respectively.

Comparison of measured values of coercivity at different temperatures with the relevant parameters determined experimentally shows that the Goodenough theory of domain creation is not applicable to this material. Pores of important size were observed in the material, but the experimental results are not consistent with the Néel disperse field theory.

ACKNOWLEDGMENTS

The author is indebted to his supervisor, Dr. R. Street, for his advice and encouragement. This work was carried out under contract with the Ministry of Supply, and the provision of a maintenance grant is gratefully acknowledged. Specimens of Ferroxcube D.1 were kindly supplied by Dr. K. Hoselitz of Mullard Research Laboratories.

REFERENCES

- BALTZER, P., 1955, *Proceedings of the Boston Conference on Magnetism*.
- BATES, L. F., and MARTIN, D. H., 1953, *Proc. Phys. Soc. A*, **66**, 162.
- 1956, *Proc. Phys. Soc. B*, **69**, 145.
- BECKER, R., and POLLEY, H., 1940, *Ann. Phys., Lpz.*, **5**, 37, 534.
- BLOCH, F., 1930, *Z. Phys.*, **61**, 206.

- ZERLINSKI, E., 1932, *Ann. Phys., Lpz.*, **5**, 13, 80.
- MILLON, J. F., and EARL, H. E., 1959, *J. Appl. Phys.*, **30**, 302.
- GALT, J. K., 1954, *Bell Syst. Tech. J.*, **34**, 1023.
- FRANKS, R., 1932, *Ann. Phys., Lpz.*, **5**, 15, 28.
- WOODENROUGH, J. B., 1954, *Phys. Rev.*, **95**, 917.
- FERRING, C., and KITTEL, C., 1951, *Phys. Rev.*, **81**, 869.
- COLSTEIN, T., and PRIMAKOFF, H., 1941, *Phys. Rev.*, **59**, 388.
- KITTEL, C., and GALT, J. K., 1956, *Solid State Physics*, Vol. 3, 437.
- MILLEY, B. A., 1950, *Phil. Mag.*, **7**, 41, 792.
- NEÉL, L., 1948, *J. Phys. Radium*, **8**, 9, 184.
- NEÉL, L., 1949, *Physica*, **15**, 225.
- COLLEY, H., 1939, *Ann. Phys., Lpz.*, **5**, 36, 625.
- STANDLEY, K. J., and PETERS, J., 1957, *Proc. Instn Elect. Engrs*, **104B**, 206.
- VIJN, H. P. J., GORTER, E. W., ESVELDT, C. J., and GELDERMANN, P., 1954, *Philips Tech. Rev.*, **16**, 49.

A Temperature Dependent Relaxation in a Square Loop Ferrite

By J. R. CHAMBERLAIN

Department of Physics, The University, Sheffield 10†

Communicated by W. Sucksmith; MS. received 11th May 1961, in revised form 18th July 1961

Abstract. Measurements of the initial permeability of a commercial square-loop ferrite (Ferroxcube D.1) as a function of frequency and temperature are reported. These show the presence of a relaxation, which is due to the damping of domain boundary walls in the material by a process of electron diffusion. It is found that all the domain walls in the material are not affected by this process. The presence of the relaxation does not allow the dynamic characteristics of the domain walls, important in conventional pulsed-reversal experiments, to be determined by the method employed here.

MEASUREMENTS have been made of the initial reversible permeability of a square-loop ferrite material (Ferroxcube D.1), as a function of frequency and temperature, using an impedance bridge method. The bridge used was a modification of the Owen inductance bridge (Wilde 1952), in which the specimen is used as the former of a mutual inductance. The impedance presented to the circuit by this inductance is measured in terms of variable air condensers and small carbon resistors.

Figure 1 shows the variation of the real part of the permeability μ' as a function of frequency at room temperature. A similar plot of the imaginary part of the permeability

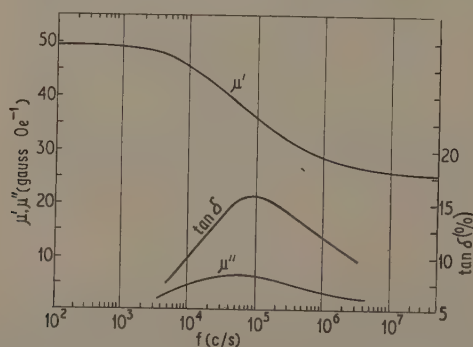


Figure 1. The frequency dependence of the initial permeability in Ferroxcube D.1. at room temperature.

μ'' and the loss angle $\tan \delta$ (μ''/μ') are also given. These have the form of dispersion curves typical of a relaxation phenomenon. However they do not follow normal relaxation curves because of an apparent distribution in the characteristic frequency f_c . This has the effect of broadening the curves over a large frequency range and decreasing

† Now at the National Research Council, Ottawa, Ontario, Canada.

the maximum in μ'' . Ignoring any effect of a distribution in f_c , a curve of the form

$$\mu' - 1 = \frac{\mu_t}{1 + (f/f_c)^2} + \mu_R \quad (1)$$

could be reasonably fitted to figure 1 with f_c taken as the frequency at which μ'' is a maximum. In this equation μ_R represents a frequency independent component of the permeability, and $\mu_R + \mu_t = \mu_0 - 1$ where μ_0 is the d.c. initial permeability. In figure 1 $\mu_R = 26$ gauss Oe⁻¹ and $\mu_t = 22$ gauss Oe⁻¹.

Following Wijn (1953) $\tan \delta$ was determined as a function of temperature at fixed frequencies. The results of these measurements are given in figure 2. For a given

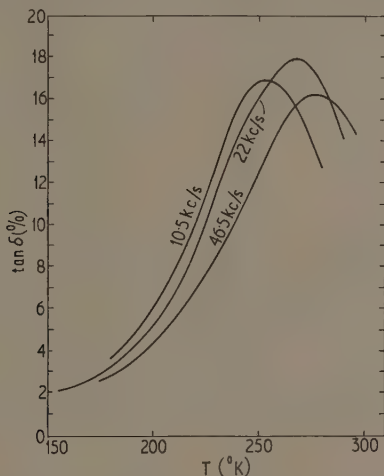


Figure 2. The temperature dependence of the loss angle $\tan \delta$ at frequencies 10.5 kc/s, 22 kc/s and 46.5 kc/s.

frequency the loss angle reaches a maximum at a temperature T_{\max} . Plotting $\log f_c$ against $1/T_{\max}$ gave a straight line which indicated the law of the form

$$f_c = f_\infty \exp(-E/kT)$$

and for the relaxation time $\tau = \tau_0 \exp(E/kT)$. From the results the activation energy $E = 0.37$ eV and the characteristic time $\tau_0 = 5 \times 10^{-12}$ sec were calculated. These values compare with similar results obtained in other ferrites (e.g. Wijn 1953, Galt 1954, Gibbons 1959). The usual explanation is that the relaxation is due to the diffusion of electrons between ions of different valency on similar lattice sites.

The contribution to the initial permeability from rotational processes (Street and Lewis 1958) is

$$\mu_{\text{rot}} = 1 + \frac{2\pi I_s^2}{K} \quad (2)$$

where I_s is the saturation magnetization and K the magnetocrystalline anisotropy constant. For Ferroxcube D.1 at room temperature $K = 5.03 \times 10^4$ erg cm⁻³ and $I_s = 240$ e.m.u. cm⁻³ (Chamberlain 1961), so that $\mu_{\text{rot}} = 8.2$ gauss Oe⁻¹. The contribution to the initial permeability from domain wall motion is hence 39.8 gauss Oe⁻¹.

The effect of electron diffusion in ferrites has been considered by Clogston (1955). In this analysis the diffusing electrons are regarded as free, and are considered to arrange themselves so as to minimize the total free energy of the lattice. This rearrangement causes extra torques which resist changes in the direction of magnetization. The diffusion hence causes an increase in the magnetocrystalline anisotropy constant K and gives a contribution to the domain wall damping parameter β (see, for example, Kittel and Galt 1956). Both of these effects cause a decrease in μ' with frequency. On the basis of Clogston's theory the changes in the rotational contribution to the permeability are less than 1% of μ_{rot} . The fractional change in μ' from this cause is hence negligible. This means that the decrease in permeability is due solely to the damping of domain walls. The residual permeability μ_R (equation (1)) is 26 gauss Oe⁻¹. This is a factor of three greater than μ_{rot} . Hence all the domain boundary walls are not affected by the diffusion process.

The permeability at coercivity and remanence in this material also show a dispersion, indicating the presence of domain boundary walls at these points on the hysteresis loop.

The permeability experiments were initially designed to determine the dynamic characteristics of domain boundary walls in the material for comparison with pulsed remagnetization experiments. In these latter experiments a core of the material is subjected to step-function magnetic fields of sufficient magnitude to take the material around a complete hysteresis loop. Under these conditions the material is observed to reverse its magnetization in about 1 μ sec even at liquid nitrogen temperatures, and the switching coefficient S_w (see for example Menuyk and Goodenough 1955) is fairly insensitive to temperature changes. The relaxation mechanism observed above is hence unimportant in the fast flux reversal that this material experiences in computer applications, except perhaps at higher temperatures where τ is of the same order of magnitude as the time taken to reverse the magnetization in the material.

ACKNOWLEDGMENTS

The author would like to thank Dr. R. Street for his encouragement and Mr. A. C. Lynch for several discussions, and his helpful suggestions on the construction of the bridge network. The work was carried out under contract to the Ministry of Supply and a maintenance grant is gratefully acknowledged. Specimens of Ferroxcube D.1 were kindly supplied by Dr. K. Hoselitz of Mullard Research Laboratories.

REFERENCES

- CHAMBERLAIN, J. R., 1961, *Proc. Phys. Soc.*, **78**, 819.
- CLOGSTON, A. M., 1955, *Bell Syst. Tech. J.*, **34**, 739.
- GALT, J. K., 1954, *Bell Syst. Tech. J.*, **33**, 1023.
- GIBBONS, D. F., 1959, *J. Appl. Phys.*, **28**, 810.
- KITTEL, C., and GALT, J. K., 1956, *Solid State Physics* (New York: Academic Press) Vol. 3.
- MENUYK, V., and GOODENOUGH, J. B., 1955, *J. Appl. Phys.*, **26**, 8.
- STREET, R., and LEWIS, B., 1958, *Proc. Phys. Soc.*, **72**, 604.
- WIJN, H. P. J., 1953, *Thesis*, Leiden University.
- WILDE, H., 1952, *Arch. Elektr. Übertr.*, **6**, 354.

Electron Correlation in the Ground State of Helium

By C. A. COULSON AND A. H. NEILSON

Mathematical Institute, Oxford

MS. received 19th June 1961

Abstract. Formulae are obtained for the distribution function $f(r_{12})$ of the inter-electronic distance r_{12} in the ground state of helium, and for the mean value of any positive integral power of r_{12} . Five different wave functions are considered, showing varying degrees of electron correlation. The greater the degree of correlation the larger is the mean electronic separation. Curves of $f(r_{12})$ are plotted, and from them the size and depth of the Coulomb hole are evaluated. There is a close correlation between the mean value of $1/r_{12}$ and the error in the energy as calculated with these five wave functions.

§ 1. INTRODUCTION

RECENT STUDIES using accurate wave functions for the electrons in atoms and molecules have shown the great importance of electron correlation (for a modern survey see Löwdin 1959). In the case of two-electron atoms the mean value of the interelectronic separation $\langle r_{12} \rangle$ is increased when, by introducing electron correlation into a previously uncorrelated function, we allow the two electrons to avoid being near to each other more frequently than before. Precisely the same situation is found for the two-electron molecule H_2 (Barnett and Coulson 1958) when we pass from the uncorrelated molecular-orbital wave function to the inclusion of configuration interaction.

Electron correlation is of two kinds. In the first we consider electrons of parallel spin. Here the Pauli principle keeps the electrons apart and leads to the Fermi hole. In the case of atoms some calculations of the shape and size of this Fermi hole have been made by Maslen (1956). With metals, however, much more work has been done, and no calculation of cohesive energy is of very great value which does not take explicit account of it. But the second type of correlation involves electrons of different spin, where the Pauli principle exerts no direct influence, and where the effect is due to the classical Coulomb repulsion between the electrons. We may therefore speak of a Coulomb hole.

Practically no numerical calculations have been made of the size of this Coulomb hole. It is, of course, related to the distribution function for the interelectronic distance—which we shall write $f(r_{12})$, and normalize so that

$$\int_0^\infty f(r_{12}) dr_{12} = 1.$$

Any approximate wave function $\psi(1, 2)$ will lead to a corresponding $f(r_{12})$. We shall define the Coulomb hole as the difference between the values of $f(r_{12})$ when the function f is derived (a) from the true wave function, or our best approximation to it, and (b) from the best uncorrelated wave function, i.e. the Hartree-Fock wave function. This definition of the Coulomb hole is entirely analogous to that of the correlation energy, which is the corresponding difference in energy for the same two wave functions. In order to gain information about the Coulomb hole, we have made calculations for the

ground state of helium. The advantages of this choice are several—it is the simplest situation where the hole exists; there is a wide variety of available wave functions embodying varying degrees of electron correlation; and we are not involved in any consideration of the Fermi hole, since our two electrons have opposed spins. In the course of this work it was necessary to evaluate the distribution function $f(r_{12})$ for the same set of approximate wave functions. We were unable to find in the literature any account of this function, and therefore report what we ourselves have done. We hope, in a later paper, to extend this type of discussion to other atoms, having more electrons.

§ 2. THE DISTRIBUTION FUNCTION $f(r_{12})$

In the ground state of the helium atom our wave function will be of the form

$$\psi(1, 2)\{\alpha(1)\beta(2) - \beta(1)\alpha(2)\}/\sqrt{2}.$$

The spin part is totally irrelevant for our analysis, and so we drop it, using only the space part $\psi(1, 2)$ normalized so that $\int \psi^2(1, 2) d\tau_1 d\tau_2 = 1$. In our case it is known

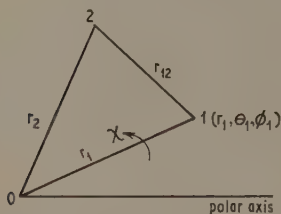


Figure 1. Notation. Numerals 1 and 2 denote the electrons, 0 is the nucleus.

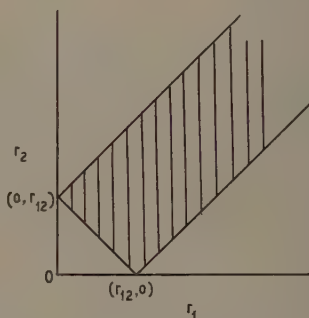


Figure 2. Shaded area represents range of integration in equation (2).

that $\psi(1, 2)$ involves only the three distances r_1, r_2, r_{12} (see figure 1). Then, from the probability interpretation of $\psi^2(1, 2)$ we have

$$f(r_{12}) dr_{12} = \int \psi^2(1, 2) d\tau_1 d\tau_2 \quad (1)$$

where the integration is taken over all positions of the two electrons such that the interelectronic distance lies between r_{12} and $r_{12} + dr_{12}$. Now if we define the direction of 01 by polar angles θ_1, ϕ_1 , and if χ denotes an angle of rotation of the plane 012 around 01 , then

$$d\tau_1 d\tau_2 = r_1 r_2 r_{12} \sin \theta_1 dr_1 dr_2 dr_{12} d\theta_1 d\phi_1 d\chi.$$

Thus in (1) the integrations over the angles are immediate, and

$$f(r_{12}) = 8\pi^2 r_{12} \iint \psi^2(1, 2) r_1 r_2 dr_1 dr_2, \quad (2)$$

r_1 and r_2 being allowed all values compatible with any given r_{12} . This is the shaded

gion in figure 2. Thus (2) may be written

$$f(r_{12}) = 8\pi^2 r_{12} \left\{ \int_{r_{12}}^{\infty} r_1 dr_1 \int_{r_1-r_{12}}^{r_1+r_{12}} r_2 \psi^2(1, 2) dr_2 + \int_0^{r_{12}} r_1 dr_1 \int_{r_{12}-r_1}^{r_{12}+r_1} r_2 \psi^2(1, 2) dr_2 \right\}. \quad (3)$$

the mean value of r_{12}^n is given by

$$\langle r_{12}^n \rangle = \int_0^{\infty} r_{12}^n f(r_{12}) dr_{12}. \quad (4)$$

is often convenient to obtain these mean values from the generating function

$$G(\gamma) = \sum \frac{(-\gamma)^n}{n!} \langle r_{12}^n \rangle = \int_0^{\infty} \exp(-\gamma r_{12}) f(r_{12}) dr_{12} \quad (5)$$

which yields $\langle r_{12}^n \rangle$ for all positive integral n . By combining (2) and (5) we have

$$G(\gamma) = 8\pi^2 \int \exp(-\gamma r_{12}) \psi^2(1, 2) r_1 r_2 dr_1 dr_2 dr_{12}. \quad (6)$$

For states other than the $1S$ states there will be certain angular terms in the integrations (2)–(6).

When evaluating the integrals in (2) and (6) it is often convenient to use the Hylleraas variables $s = r_1 + r_2$, $t = r_2 - r_1$, $u = r_{12}$, for which $-u \leq t \leq u \leq s \leq \infty$, and $r_1 dr_2$ may be replaced by $\frac{1}{2} ds dt$. Equation (2) then becomes

$$f(r_{12}) = \pi^2 r_{12} \int_{r_{12}}^{\infty} ds \int_{-r_{12}}^{+r_{12}} dt (s^2 - t^2) \psi^2(1, 2). \quad (7)$$

With most of the wave functions that we shall use, this leads very simply to an expansion of $f(r_{12})$ in terms of the A_n and B_n functions defined by

$$A_n(\alpha) = \int_1^{\infty} s^n \exp(-\alpha s) ds$$

$$B_n(\alpha) = \int_{-1}^1 t^n \exp(-\alpha t) dt = (-1)^n B_n(-\alpha).$$

Numerical values of A_n and B_n are tabulated by Flodmark (1957).

Similarly, when evaluating (6) it is often convenient to work in terms of the pericentric coordinates used by Pekeris (1958). These are

$$x = r_1 + r_2 - r_{12}, \quad y = r_2 + r_{12} - r_1, \quad z = r_{12} + r_1 - r_2$$

and the volume element $d\tau_1 d\tau_2$ becomes (for wave functions involving only r_1, r_2, r_{12})

$$d\tau_1 d\tau_2 = \frac{1}{4} \pi^2 (x+y)(y+z)(z+x) dx dy dz.$$

The triangular relations implied in figure 1 are now such that all three variables x, y, z range from 0 to ∞ independently.

One small simplification is worth mentioning. If additional correlation is introduced into a function $\psi(1, 2)$ by a factor $g(r_{12})$ so that

$$\psi = \psi(1, 2)g(r_{12})$$

then (2) shows that the new distribution function $f(r_{12})$ is obtained from the old one by a simple multiplication by $\{g(r_{12})\}^2$.

§ 3. WAVE FUNCTIONS USED

We shall be concerned with five distinct wave functions. These are:

I. The Eckart-Kellner function $N \exp\{-c(r_1+r_2)\}$, where N is a normalizing factor (here c^3/π) and c is given the 'best' value $c = 2.5/16 = 27/16$. This is a completely uncorrelated function.

II. The Eckart-Hylleraas function $N\{\exp(-ar_1-br_2)+\exp(-br_1-ar_2)\}$. This allows for 'in-out' correlation since the two electrons may be supposed to be in distinct orbitals. The inner orbital has $a = 2.18$, and the outer orbital has $b = 1.19$.

III. The partly-correlated function $N \exp\{-c(r_1+r_2)\}\{1+\alpha r_{12}\}$ where the presence of the term in brackets tends to increase the weight of those situations where r_{12} is large and so the electrons are well separated.

IV. The Hylleraas function

$$\sum c_{lmn}(r_1+r_2)^l(r_1-r_2)^{2m}r_{12}^n \exp\{-c(r_1+r_2)\}$$

which generalizes (III) and may be made as accurate as we wish by including a sufficient number of terms in the summation. This function has been scaled to satisfy the virial theorem with $2c = 3.636$ and in this case r_1, r_2, r_{12} are written for the transformed vectors $2cr_1, 2cr_2, 2cr_{12}$; the new normalization constant is obtained from the unscaled one by multiplying by $(2c)^3$. In order to avoid undue numerical complexity, which is not justified for our present purpose, we considered the compromise function with six terms. For all practical purposes, however, this may be regarded as giving the exact $f(r_{12})$.

V. The Hartree-Fock function $F(r_1)F(r_2)$. This is the best possible uncorrelated function. The original calculations of $F(r)$ due to Wilson and Lindsay gave $F(r)$ as a numerical table. This is inconvenient. We have therefore used the analytical representation provided by Roothaan, Sachs and Weiss (1960). This is

$$F(r) = \sum_{n,\xi} c_{n,\xi} r^{n-1} \exp(-\xi r)$$

where $n = 1, 2$ and $\xi = 1.40, 3.00$. This four-term function reproduces the self-consistent field function to within 2 or 3 parts in 10^4 , and gives an energy value differing from the full Hartree-Fock value by less than 1 part in 10^5 .

We shall refer to these wave functions by their numbers I-V. More detailed comparison of most of them, together with suitable references, may be found in a paper by Roothaan and Weiss (1960).

§ 4. RESULTS OF CALCULATIONS

In general the expressions for $f(r_{12})$ are too clumsy to be worth transcribing. But the following three formulae are sufficiently simple. (We have used r instead of r_{12} for convenience.)

Wave function I

$$f(r) = \frac{c^3}{6} (3r^2 + 6cr^3 + 4c^2r^4) \exp(-2cr) \quad (8)$$

ave function III

$$f(r) = \frac{4c^5(3r^2 + 6cr^3 + 4c^2r^4)(1 + \alpha r)^2 \exp(-2cr)}{24c^2 + 105\alpha c + 144\alpha^2} \quad (9)$$

ave function IV

$$f(r) = \exp(-2cr) \sum_{p=2}^8 a_p r^p \quad (10)$$

here the a_p are products of the coefficients c_{lmn} in the original wave function. We have shown, in figure 3, curves to represent the variations of $f(r)$ for the functions

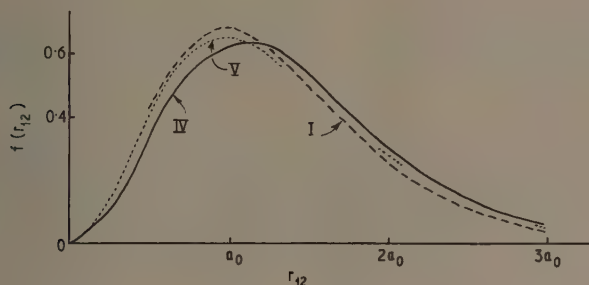


Figure 3. Distribution curves $f(r_{12})$. I Eckart-Kellner wave function, IV Hylleraas 6-term function, V self-consistent field function.

IV and V. The remaining curves are related to these three in a way that follows (see later) from the numerical values in the table.

The two following generating functions $G(\gamma)$ are simple enough to be listed.

ave function I

$$G(\gamma) = \frac{1}{8} \left(1 + \frac{\gamma}{2c}\right)^{-3} + \frac{3}{8} \left(1 + \frac{\gamma}{2c}\right)^{-4} + \frac{1}{2} \left(1 + \frac{\gamma}{2c}\right)^{-5} \quad (11)$$

ave function IV

$$G(\gamma) = \sum_{p=2}^8 p! a_p (\gamma + 2c)^{-(p+1)}, \quad (12)$$

here the notation is the same as in (10).

From the information in (8)–(12), and similar equations for the other wave functions, it is possible to compute the numerical values in the table. All the distances are measured in Bohr radii (a_0). We have verified that in every case except (V)

$$\int_0^\infty f(r_{12}) dr_{12} = 1.$$

In the case of (V) our calculations were not sufficiently extensive for this purpose.

Comparison of Wave Functions for Helium

Wave function	I	II	III	IV	V
$\langle r_{12} \rangle$	1.296	1.394	1.372	1.420	1.311
$\langle 1/r_{12} \rangle$	1.055	0.993	0.974	0.946	1.026
$-E(\text{A.U.})$	2.8476	2.8754	2.8912	2.9032	2.8617
r_{12} at peak of curve	1.0	1.0	1.1	1.1	1.0
$f(r_{12})$ at peak of curve	0.672	0.625	0.649	0.625	0.632
$f(r_{12})$ at $r_{12} = 1.0$	0.672	0.625	0.644	0.616	0.632
2.0	0.258	0.285	0.295	0.311	0.274
3.0	0.039	0.059	0.039	0.058	0.049

Functions I and V have no electron correlation, and their values for $\langle r_{12} \rangle$ are the smallest, and indeed quite similar. The maximum of $f(r_{12})$ occurs for smaller r_{12} , and at large r_{12} the value of $f(r_{12})$ is less than for the highly correlated functions II and IV. The 'in-out' correlated function II and the simple r_{12} -correlated function III give very similar distribution functions. The accurate wave function IV has the largest mean separation $\langle r_{12} \rangle$.

At first sight it may not seem that the spread of values of quantities such as $\langle 1/r_{12} \rangle$ is of great importance. But this is not true. Thus the difference in interelectron repulsion energy between the poorest function I and the best function IV is 0.11 A.U. i.e. 3 e.v. Thus electron correlation has the effect of considerably reducing electron-electron repulsion. But this restriction of motion of the electrons raises their kinetic energy, so that only about one-half of this gain is preserved in the total energy E .

§ 5. THE COULOMB HOLE

We are now in a position to draw the shape of the Coulomb hole. This has been defined in §1 as the difference between $f(r_{12})$ for the true function and the best uncorrelated Hartree-Fock function. In figure 4 we have plotted $\Delta(r_{12})$ as a function of r_{12} , where

$$\Delta(r_{12}) = f(r_{12})_{\text{Hylleraas}} - f(r_{12})_{\text{Hartree-Fock}}. \quad (13)$$

It is clear from the normalization conditions of $f(r)$ that the total area under the Δ -curve is zero. This curve shows that the probability of the two electrons lying anywhere within a distance $1.1 a_0$ from each other is less than it would be without correlation and correspondingly the probability that the electrons are separated by more than $1.1 a_0$ is greater. We could say that $1.1 a_0$ was the radius of the Coulomb hole. The greatest value of $\Delta(r_{12})$ occurs at $r_{12} = 0.52 a_0$, a value which may be compared with the distance $(0.59 a_0)$ from the nucleus at which the radial charge density is maximum. Thus the Coulomb hole is approximately of the same size as the charge-cloud itself. It would be interesting to know whether this occurs with other atoms and other orbitals. Finally the total amount of charge which is moved by the Coulomb hole is equal to the area of the curve in figure 4 between $r_{12} = 0$ and $r_{12} = 1.1 a_0$. This turns out to be only $0.047e$, i.e. approximately one-twentieth of an electron. In this we see how much smaller is the Coulomb hole than the Fermi hole, since in this latter the charge involved is $1.0e$.

In conclusion we would like to draw attention to a curious, but simple, result which is implied in the table. In figure 5 we have plotted the error ΔE in the energy calculated for the five wave functions of § 3 against the mean value $\langle 1/r_{12} \rangle$. It is surprising to see

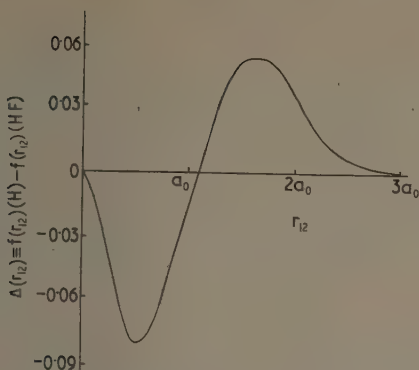


Figure 4. Coulomb hole. (H) = Hylleraas;
(HF) = Hartree-Fock.

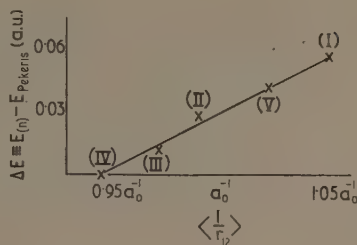


Figure 5. Relation between error
in wave function energy and
mean value of $1/r_{12}$.

that all five points lie so closely on a straight line. Now for any chosen function, when once the various arbitrary parameters have been chosen to minimize the energy, we may suppose that the major part of the remaining error is associated with the extent to which a satisfactory allowance is made for electron-correlation. This is precisely what is borne out by the straight line in figure 5.

ACKNOWLEDGMENT

One of us (A.H.N.) would like to acknowledge the award of a Research Fellowship from the Department of Scientific and Industrial Research.

REFERENCES

- BARNETT, M. P., BIRSS, F. W. and COULSON, C. A., 1958, *Mol. Phys.*, **1**, 44.
 LODMARK, S., 1957, *Table of Molecular A and B Functions* (Stockholm: Institute of Theoretical Physics).
 LÖWDIN, P.-O., 1959, *Advances in Chemical Physics*, Vol. 2 (New York: Interscience), p. 207.
 MASLEN, V. W., 1956, *Proc. Phys. Soc. A*, **69**, 734.
 PETERIS, C. L., 1958, *Phys. Rev.*, **112**, 1649.
 ROOZTHAAN, C. C. J., SACHS, L. M., and WEISS, A. W., 1960, *Rev. Mod. Phys.*, **32**, 186.
 ROOZTHAAN, C. C. J., and WEISS, A. W., 1960, *Rev. Mod. Phys.*, **32**, 194.

Anisotropy of the Electrical Conductivity in Bismuth Telluride

By R. T. DELVES, A. E. BOWLEY,[†] D. W. HAZELDEN
AND H. J. GOLDSMID

The General Electric Company Limited, Central Research Laboratories,
Hirst Research Centre, Wembley, England

MS. received 7th June 1961

Abstract. The anisotropy of the electrical conductivity of Bi_2Te_3 at room temperature has been determined by a four-probe method. The anisotropy ratio for undoped p-type material is close to 3.0; for iodine-doped n-type material it is appreciably higher and increases with the impurity concentration. Measurements of the galvanomagnetic effects in highly doped n-type Bi_2Te_3 have shown that the observed variation of the anisotropy ratio can be interpreted in terms of a change of shape of the equi-energy surfaces in momentum space with increasing density of charge carriers.

§ 1. INTRODUCTION

IN SPITE of the intense study of the semiconductor Bi_2Te_3 during the last few years there have been comparatively few measurements of the anisotropy of its transport parameters. This is due to the fact that such measurements require good single crystals of reasonable size. While it is relatively easy to grow single crystal sheets with dimensions which are large in the plane of the a axes, it is difficult to find samples which have any great thickness in the c direction. Furthermore, many single crystals, which appear at first sight to be perfectly sound, in fact contain deep cracks which are revealed upon etching. Such cracks can give rise to an apparently very large anisotropy ratio for the electrical conductivity and this may explain some of the results reported by Konorov (1956).

Previous measurements of the anisotropy of the electrical conductivity in these laboratories have been confined to a single sample of each conductivity type at room temperature (Goldsamid 1957) and two p-type samples at liquid nitrogen temperatures (Drabble 1958). It was, therefore, thought to be worth while extending these measurements over a wider range of material. Unfortunately all the single crystal p-type material has been undoped and the new observations on such material have merely served to confirm the earlier results. However, n-type crystals of Bi_2Te_3 with differing iodine concentrations have also become available and experiments on these specimens to determine the dependence of the anisotropy ratio on the density of the charge carriers have been carried out.

§ 2. DETERMINATION OF THE ANISOTROPY RATIO BY THE FOUR-PROBE METHOD

The conventional method for measuring the electrical conductivity of a semiconductor requires the application of two large-area current contacts and two intermediate potential probes to a regularly-shaped sample. While such a method can be applied to Bi_2Te_3 without difficulty when current flows along the cleavage planes, it is

[†] Now at the Physics Department, Medical School, Guy's Hospital, London, S.E.1.

much less useful for current flow in the perpendicular direction. In the latter case the most serious disadvantage is the uncertainty as to whether or not the sample is entirely free from cracks, particularly those which may form or deepen during the application of the contacts.

Four-probe electrical conductivity measurements are usually confined to isotropic semiconductors but Airapetyants and Bresler (1959) have shown that they can be used equally well on anisotropic materials. Thus all the present electrical conductivity determinations have been carried out using a four-probe method. By making the inter-probe spacing no more than 0.08 cm it has been possible to work with single crystals having a thickness of only about 0.4 cm in the c direction, though, of course, in such cases it has been necessary to apply corrections due to the finite size of the sample. Moreover, by observing the variation of inter-probe voltage with orientation it has been a simple matter to detect the presence of cracks.

The apparatus will be described in detail elsewhere. It consists essentially of four equally-spaced probes which can be brought into contact with the surface of a crystal Bi_2Te_3 , as shown in figure 1, so that the line joining the probes can make any selected

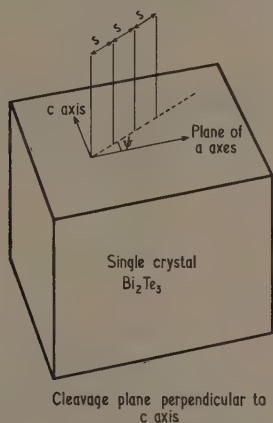


Figure 1. Four-probe arrangement for determining the anisotropy of the electrical conductivity in bismuth telluride.

angle ψ with the cleavage planes. So as to avoid errors due to thermoelectric effects, the direction of the current, which is passed between the two outer probes, is periodically reversed. The voltage appearing between the two inner probes is converted to a single polarity so that it can be measured by a d.c. potentiometer.

The theory of the four-probe method as applied to isotropic conductors has been given by Valdes (1954). The same theory may be used for anisotropic conductors provided that distances measured along each of the principal axes are suitably scaled. The current density \mathbf{J} must satisfy the equations

$$\left. \begin{aligned} J_i &= -\sigma_{ii} \frac{\delta V}{\delta x_i} \\ \text{div } \mathbf{J} &= 0 \end{aligned} \right\} \quad (1)$$

where V is potential and σ_{ii} is the conductivity tensor component along the i th principal

axis. Equations (1) take the same form as for an isotropic conductor of conductivity σ , equal to $(\sigma_{11} \sigma_{22} \sigma_{33})^{1/3}$, if one uses new coordinates X_i such that

$$X_i = \left(\frac{\sigma}{\sigma_{ii}} \right)^{1/2} x_i. \quad (2)$$

In applying this principle to Bi_2Te_3 , which belongs to the crystal class $\bar{3}m$, it should be noted that $\sigma_{11} = \sigma_{22}$ if direction 3 is taken to be parallel to the c axis. Thus, when the probes are brought down on a plane which is perpendicular to the cleavage planes, the inter-probe spacing s must be transformed to S in the new coordinate system where

$$S = \sigma^{1/2} s \left(\frac{\cos^2 \psi}{\sigma_{11}} + \frac{\sin^2 \psi}{\sigma_{33}} \right)^{1/2}. \quad (3)$$

Substituting in Valdes' formula,

$$\frac{V_I}{J_O} = \frac{1}{2\pi\sigma S}$$

where V_I is the voltage between the inner probes and J_O is the current between the outer probes, one finds that

$$\frac{V_I}{J_O} = \frac{(r^{-1} \cos^2 \psi + \sin^2 \psi)}{2\pi\sigma_{11}s} \quad (4)$$

r being the anisotropy ratio σ_{11}/σ_{33} . If one defines an inter-probe resistance R as being equal to the ratio V_I/J_O for any given angle ψ , then

$$\frac{R}{R_a} = (\cos^2 \psi + r \sin^2 \psi)^{-1/2} \quad (5)$$

where R_a is the inter-probe resistance for $\psi = 0$.

Equations (4) and (5) apply strictly only for infinitely large specimens. Valdes showed how corrections could be applied to take into account the close proximity of the probes to the boundaries of the sample. The correction terms for anisotropic media take exactly the same form as given by Valdes provided that effective distances, as defined by equation (2), are employed.

§ 3. RESULTS OF ANISOTROPY MEASUREMENTS AT ROOM TEMPERATURE

Two typical sets of experimental results are shown in figure 2. For the p-type sample all the dimensions were very large compared with the inter-probe spacing and the variation of the inter-probe resistance R with angle ψ followed the form of equation (5) very closely. On the other hand, for the n-type sample, the c dimension was only about 6 times the inter-probe spacing. Thus in this case the variation of R with ψ was found to be appreciably different from that predicted by equation (5).

In figure 3 the measured anisotropy ratio at room temperature is plotted against the electrical conductivity σ_{11} along the cleavage planes. For the p-type samples the mean value of r is 2.95. This is about 10% higher than the value obtained previously at 20 °C (Goldsmid 1957), but agrees quite well with the figure given by Drabble (1958) for 77 °K. The range covered by the p-type samples is too small to allow one to draw any conclusions about the possible variation of anisotropy ratio with carrier concentration.

The observations on iodine-doped n-type samples confirmed the previous determination of the anisotropy ratio r where σ_{11} is equal to $2 \times 10^3 \text{ ohm}^{-1} \text{ cm}^{-1}$. However, they also showed quite clearly that the anisotropy ratio rises with σ_{11} and, for the most heavily doped sample, a value of r equal to 6 is reached. It is suggested that the anisotropy

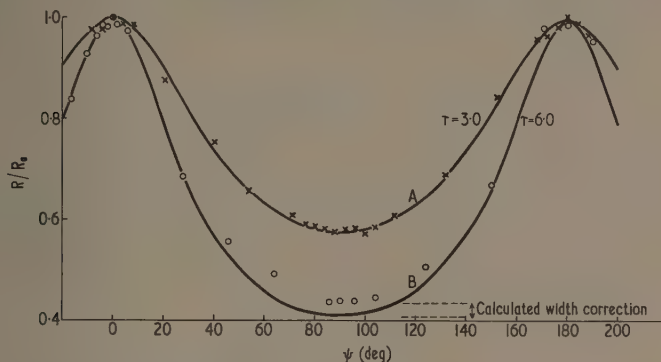


Figure 2. Variation of inter-probe resistance with orientation: A, p-type, $r = 3.0$, large sample; B, n-type, $r = 6.0$, short c dimension; full lines, theoretical curves, $R/R_a = (\cos^2\psi + r \sin^2\psi)^{-1/2}$.

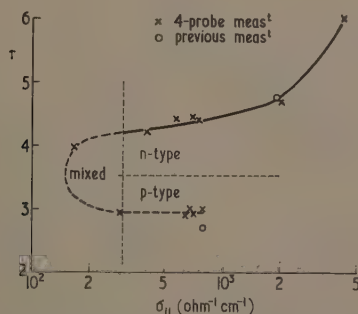


Figure 3. Anisotropy ratio as a function of electrical conductivity measurements at 20 °C.

ratio depends on the carrier concentration because of a variation in the shape of the equi-energy surfaces in momentum space. To test the validity of this suggestion, galvanomagnetic measurements have been made on heavily doped n-type Bi_2Te_3 .

§ 4. GALVANOMAGNETIC EFFECTS IN HIGHLY DOPED N-TYPE Bi_2Te_3

Galvanomagnetic measurements on n-type Bi_2Te_3 , carried out by Drabble, Groves and Wolfe (1958, to be referred to as DGW), indicated the validity of a 6-valley band structure and gave a precise description of the shape and orientation of the equi-energy surfaces, assuming the relaxation time to be a function only of energy. The resistivity ρ_{11} for the material mentioned in DGW at 77 °K was given as $1.46 \times 10^{-4} \text{ ohm cm}$.

The measurements reported here were carried out on single crystal material containing nominally 0.4% by weight of iodine and with a value of 6.57×10^{-5} ohm cm for ρ_{11} at 77 °K. The experimental procedure followed that described in DGW.

The variation of Hall and magnetoresistance effects with orientation of the magnetic field was found for two different experimental arrangements. In case I, shown in

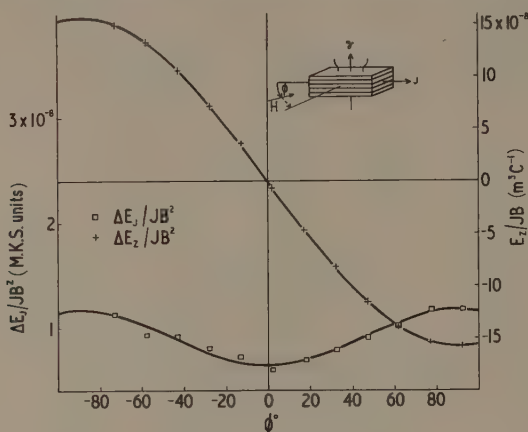


Figure 4. Galvanomagnetic effects in highly doped n-type Bi_2Te_3 —Case I.

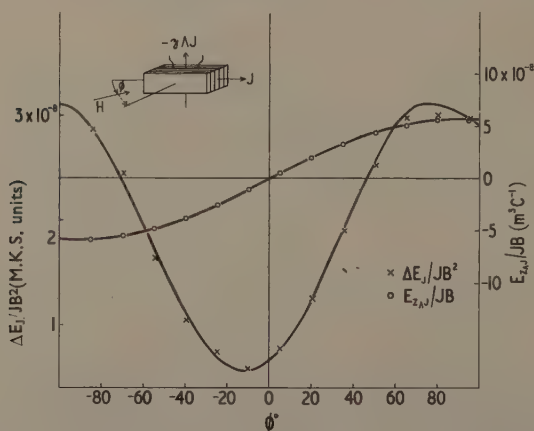


Figure 5. Galvanomagnetic effects in highly doped n-type Bi_2Te_3 —Case II.

figure 4, the magnetic field lay parallel to the cleavage planes. In case II, shown in figure 5, the plane containing the magnetic field lay perpendicular to the cleavage planes. Figures 4 and 5 show that the observed behaviour agreed very well with that expected theoretically from the equations,

$$\text{case I} \begin{cases} \Delta E_J/JB^2 = \rho_{1111} \cos^2 \phi + \rho_{1122} \sin^2 \phi \\ E_z/JB = -\rho_{312} \sin \phi \end{cases} \quad (5a)$$

$$(5b)$$

$$\text{case II} \begin{cases} \Delta E_J / JB^2 = \rho_{1111} \cos^2 \phi + \rho_{1133} \sin^2 \phi + \rho_{1131} \sin 2\phi & (6a) \\ E_{z\wedge J} / JB = \rho_{123} \sin \phi. & (6b) \end{cases}$$

The same terminology as that of DGW has been used and it has been assumed that the Hall effect is linear in magnetic field and that the current flow is parallel to one of the three rotation planes of the crystal. Both these points have been checked under the experimental conditions.

The experimental values of the galvanomagnetic coefficients are given in the second column of the table. In interpreting the results it has been possible to use degenerate statistics. It will be seen that the ratios between the coefficients, shown in the last four rows of the table, do not correspond at all to the values calculated for the parameters m_1/m_2 , m_3/m_2 and $\cos^2 \theta$ of DGW, shown in the third column. Much better correspondence can be achieved if the value of m_3/m_2 is appreciably reduced and the other band parameters altered rather less radically. The results of the calculations for $m_1/m_2 = 1.0$, $m_3/m_2 = 0.05$ and $\cos^2 \theta = 0.06$ are given in the fourth column of the table.

Galvanomagnetic Coefficients of Highly-doped Bi_2Te_3 at 77 °K

The band parameters (a) in the third column satisfy the measurements of DGW on lightly-doped n-type Bi_2Te_3 . The parameters (b) in the fourth column give a better fit to the present measurements.

Coefficient	Exptl value	Calculated values	
		(a)	(b)
$\rho_{11}(\text{ohm m}) \times 10^6$	0.657		
$\rho_{123}(\text{m}^3 \text{C}^{-1}) \times 10^6$	0.058	$m_1/m_2 = 1.21$	$m_1/m_2 = 1.0$
$\rho_{312}(\text{m}^3 \text{C}^{-1}) \times 10^6$	0.156	$m_3/m_2 = 0.093$	$m_3/m_2 = 0.05$
$\rho_{1111}(\text{m.k.s. units}) \times 10^8$	0.66	$\cos^2 \theta = 0.0546$	$\cos^2 \theta = 0.06$
ρ_{1122}	1.18		
ρ_{1133}	3.03		
ρ_{1131}	0.51		
$\rho_{123}^2 / \rho_{11} \rho_{1111}$	0.78	1.67	0.70
$\rho_{123}^2 / \rho_{11} \rho_{1122}$	0.43	1.04	0.39
$\rho_{123}^2 / \rho_{11} \rho_{1133}$	0.17	0.48	0.23
ρ_{312} / ρ_{123}	2.69	2.06	2.70

It must be emphasized that it is impossible to choose a set of band parameters which gives really good agreement with the experimental results. This is in marked contrast to the extremely close correspondence between experiment and theory in DGW. It is thought that the heavy doping of Bi_2Te_3 has not merely made the energy surfaces more prolate; it has also warped them so that they are no longer perfectly ellipsoidal.

The warping of the energy surfaces makes any exact interpretation of their change of shape impossible. However, it seems reasonable to use the band parameters given in the fourth column of the table to make some qualitative predictions about the effect of heavy doping.

In the first place, the anisotropy ratio σ_{11}/σ_{33} corresponding to the new parameters is 4.6 compared with a value of 4.1 obtained by DGW. In other words, the galvanomagnetic measurements on heavily doped material indicate a change in band structure which tends to increase the anisotropy ratio.

Secondly, for the set of band parameters given above, the carrier concentration is given by $n = 0.192/ep_{123}$. This formula leads to an electron density of $2.07 \times 10^{19} \text{ cm}^{-3}$ and a mobility along the cleavage planes at 77°K of $4600 \text{ cm}^2 \text{ v}^{-1} \text{ sec}^{-1}$. For the less heavily doped material of DGW the electron mobility was found to be $8900 \text{ cm}^2 \text{ v}^{-1} \text{ sec}^{-1}$.

The Seebeck coefficients at 77°K for the material of DGW and the highly doped material are -80 and $-22 \mu\text{V deg}^{-1}$ respectively. Supposing that the same scattering law is applicable in both cases, as suggested by magneto-thermoelectric measurements (Bowley, Delves and Goldsmid 1958), the change in Seebeck coefficient represents a $3.6 : 1$ change in the Fermi energy ζ . If the relaxation time for the electrons is a function only of their energy \mathcal{E} , being proportional to $\mathcal{E}^{-\lambda}$ where λ is assumed to be a constant, then the mobility μ obeys the law $\mu \propto \zeta^{-\lambda}$. Thus, on the basis of these assumptions, one would expect the mobility of the heavily doped Bi_2Te_3 to be $3.6^{-\lambda}$ times that of the DGW material. The change of mobility observed experimentally corresponds to a value for λ of 0.52 , the figure for acoustic-mode lattice scattering being 0.5 . It may be objected that a consideration of the change in mobility in the perpendicular direction would give a different result (in fact, the calculated value of λ in this case is 0.61). However, in spite of the uncertainty due to the suspected warping of the energy surfaces, it seems clear that, at the temperature of measurement, acoustic-mode lattice scattering is predominant even for the heavily doped sample.

§ 5. CONCLUSIONS

Four-probe measurements at room temperature have shown that the anisotropy ratio for the electrical conductivity is greater for n-type Bi_2Te_3 than for p-type material. They have also shown that the anisotropy ratio in the n-type case rises with the level of doping with iodine.

Studies of the Hall and magnetoresistance effects at liquid nitrogen temperature have shown that increased doping of n-type Bi_2Te_3 compresses the equi-energy surfaces more strongly in a direction nearly parallel to the three-fold rotation axis of the crystal. Such a change in the band structure tends to increase the anisotropy ratio of the electrical conductivity and, thus, provides a qualitative interpretation of the results of the four-probe measurements.

The galvanomagnetic measurements have supported the hypothesis that acoustic-mode lattice scattering is predominant in Bi_2Te_3 even at high doping levels.

REFERENCES

- AIRAPETYANTS, S. V., and BRESLER, M. S., 1959, *Soviet Physics—Solid State*, **1**, 134.
 BOWLEY, A. E., DELVES, R. T., and GOLDSMID, H. J., 1958, *Proc. Phys. Soc.*, **72**, 401.
 DRABBLE, J. R., 1958, *Proc. Phys. Soc.*, **72**, 380.
 DRABBLE, J. R., GROVES, R. D., and WOLFE, R., 1958, *Proc. Phys. Soc.*, **71**, 430.
 GOLDSMID, H. J., 1957, *Ph.D. Thesis*, University of London.
 KONOROV, P. P., 1956, *J. Tech. Phys., Moscow*, **26**, 1400.
 VALDES, L. B., 1954, *Proc. Inst. Radio Engrs, N.Y.*, **42**, 420.

The Electron Voltaic Effects in Silicon and Selenium Elements†

By E. W. BILLINGTON AND W. EHRENBURG

Department of Physics, Birkbeck College, London

MS. received 12th January 1961, in revised form 1st June 1961

Abstract. The electron and photovoltaic effects in silicon and selenium elements are studied experimentally. It is shown that the response to cathode rays is closely related to their penetration into the cells, and indicates data such as the depth of the barrier and the diffusion length of minority carriers. In particular, it is shown that electrons in grey selenium are mobile, with a diffusion length of about 8 microns.

A brief description is given of some fatigue effects encountered.

§ 1. INTRODUCTION

THE ENERGY of cathode rays impinging on a solid surface is largely dissipated by the production of pairs of electrons and holes within a well-defined distance from the surface. The distance increases rapidly with the voltage of the cathode rays. The Thomson-Whiddington law is a well-known expression for it, but more accurate relations are now available. Cathode rays are easily and within wide limits controlled with respect to energy, duration and intensity, and thus provide a means of studying the effect of ionizing different portions of a semiconductor barrier. This leads to information about the location of the barrier and about the contributions to the voltaic effects (the generation of a circulating current and an e.m.f. by incident radiation) of the carriers generated in different regions.

Studies of this electron voltaic effect were first reported by Becker and Kruppke (1937) for selenium photoelements; by Ehrenberg, Lang and West (1951) and Ehrenberg and Lang (1954) for selenium and copper oxide, and by Rappaport, Loferski and Linder (1956) for germanium barriers. In these papers the basic facts were established. It was found, for example, that in selenium elements, where the barrier is known to be near the surface, the electron voltaic effect commences at very low cathode-ray energies, whereas in copper oxide no effect was observed until the energy was raised to perhaps 70 kev, after some of the surface had been ground off. This confirmed that in copper oxide rectifiers the barrier is situated at the copper-copper oxide interface. But a detailed examination and analysis of the variation of the electron voltaic effect with energy of the cathode rays has not previously been carried out. It is the object of this paper to show, from measurements carried out on silicon and selenium cells, that significant results can be obtained by using cathode rays to probe barriers layers.

§ 2. INSTRUMENTATION

In order to examine the effect of cathode rays, the elements (without protective lacquer!) were placed in a demountable cathode-ray tube of conventional design. Attention was given, however, to minimizing the light coming from the filamentary

† This paper is based on a Ph.D. thesis submitted by E. W. Billington and accepted by the University of London. Some of its contents were presented at the International Conference on Semiconductors (Praha 1960); an abstract is being published in the conference reports.

cathode (and allowing for it). By mildly focusing the beam to a circle of about 1 cm diameter it was assured that it fell within the sensitive region of the elements of 1 in. diameter. By biasing the electron gun, the beam current could be set to any desired value, or it could be pulsed with on and off periods in the millisecond range. The output of the elements could be connected to a galvanometer or to a cathode-ray oscilloscope. The load resistance could be varied over a wide range, and a bias could be applied, but the results obtained with applied bias did not throw new light on the electron voltaic effect.

Measurements with light were carried out using a Philips projection lamp type 13113 C/01 as a source, placed behind a cell through which a copper sulphate solution circulated. Spectral regions were selected by means of Wratten filters. The duration and the intensity of the illumination were controlled by a photographic shutter and by varying the separation of lamp and element. The illumination was measured by substituting a Schwartz thermopile for the element. The calibration provided by the makers (Hilger and Watts Ltd.) was accepted; allowance was made of course for the difference in area of the elements and the pile. The error in the absolute values of the light flux is estimated to 20%.

In measuring the voltaic effects special attention must be given to the load resistance of the elements. According to the elementary theory, the carriers generated in, or diffusing into, the region of changing electric potential drift in the field of the barrier and produce thus a current I in the direction of blocked flow. If the external resistance is sufficiently low, the carriers swept by the field across the barrier constitute the circulating current. I is therefore found by reducing the load to a minimum or by extrapolating to zero load the actual currents i measured at finite load. If the load is not negligible, the current I causes, across the external resistance r , a voltage V in the polarity of easy flow. As all rectifying junctions should satisfy a voltage-current relation of the form $i = i_0[e^{V/b} - 1]$, the net circulating current becomes

$$i = I - i_0[e^{V/b} - 1] \quad (1)$$

where i_0 and b are constants characteristic of the junction, and $V = ir$.

§ 3. SILICON SOLAR CELLS

The silicon 'solar' photovoltaic cell used in our experiments is a disk of p-type silicon, about 25 mm diameter and 0.5 mm thick, with a highly doped n-layer made by diffusion near one of the flat surfaces. In the normal use and in all our experiments, radiation is incident on to the n-type surface. A comprehensive survey of these elements has been given by Kleinman (1961).

For electron bombardment, $I = i_p g(V_p)$; V_p is the energy of the electrons in electron volts and i_p is the current carried by the incident electrons, which in our experiments varied between 4×10^{-10} and 10^{-5} amp; the 'gain' $g(V_p)$ is shown in figure 1. $g(V_p)$ is independent of i_p , and has the same value for steady and pulsed bombardment. Below about 20 kv the gain is small; above, it rises linearly, somewhat less than 5 ev (gross) being required for the creation of a pair.

The ranges of cathode rays in silicon have not been measured, but they should be identical with those in aluminium, if allowance is made for the difference in density. Ranges in aluminium measured by Schonland (1925), Lane and Zaffarano (1954), Young (1956), Holliday and Sternglass (1959) have recently been correlated by King (1960). The corresponding ranges in silicon are also given in figure 1. With increasing voltage

an increasing proportion of the total electron energy is converted into pairs in layers more remote from the surface.

Now in this cell, the barrier is $2.5\ \mu$ behind the surface (personal communication by Mr. A. Bardsley, of Ferranti Ltd.), and so the interesting fact emerges that the *n*-layer is contributing very little to the voltaic effect. This may well be due to a high rate of surface recombination of carriers at the front surface. It has been reported by Harten (1959) that the sensitivity of photoelements can be varied over wide limits by

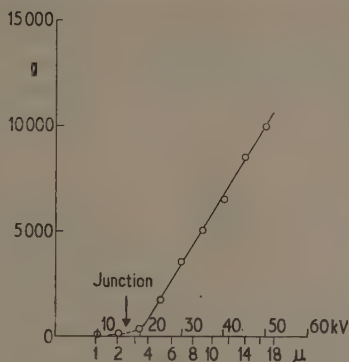


Figure 1. Electron voltaic effect in silicon; gain as function of the energy of the cathode rays and of their penetration. The position of the junction is marked by an arrow.

changing the rate of surface recombination. Surface recombination in silicon elements has also been discussed by Kleinman (1961).

At about 20 kv, pair production in the bulk sets in, and at higher accelerating voltages most of the pair production takes place in the *p*-type silicon.

Electrons can reach the barrier by diffusion if they are generated within a diffusion length from the barrier. It must be concluded that the increase of gain with voltage shown in figure 1 will terminate when the range of electrons exceeds the diffusion length, or, alternatively, the thickness of the cell. The optical analogue of this has been analysed by Harten and Schultz (1955). Here, the accelerating voltage available was not high enough to show this effect.

It is of some interest to compare the electron data with corresponding data for the photovoltaic effect.

Under irradiation with visible light, I is found proportional to the intensity B of illumination, $I = CB$, up to about 10 milliwatts, the highest illumination available after filtering; table 1 gives in the second column observed gross values of C .

Table 1

$\lambda(\mu)$	C (A mw^{-1})	Quantum efficiency
0.44	5.7×10^{-5}	0.23
0.53	11.6×10^{-5}	0.40
0.60	26.5×10^{-5}	0.74

The corresponding values for the quantum efficiency in column 3 are corrected for reflection losses, using the expression for the reflectivities given by Moss (1952).

The values for the quantum efficiency appear to be closely related to the low gain observed with slow electrons; for, according to Dash and Newman (1955), the penetration (reciprocal absorption coefficient) of blue, green and red light is 0.43, 1.2 and 2 microns. The quantum efficiency thus appears to approach unity as the radiation tends to penetrate the *n*-layer, or at least, penetrates the surface region of high recombination.

Equation (1) has been tested by varying the external load at constant irradiation with cathode rays and light. Under all conditions of irradiation equation (1) was found to be satisfied with $b = 0.06$ volt and i_0 about 7×10^{-7} amp. For thin junctions b is calculated to kT/e , approximately 0.026 volt, but silicon junctions normally obey a current-voltage relation of the form $i = i_0[e^{V/b} - 1]$, with $b \simeq 0.05$ volt.

§ 4. SELENIUM

When a selenium cell is suddenly exposed to light, the photovoltaic effect rises in perhaps a millisecond to an 'initial' value and then, normally, decreases, although under extreme conditions the decrease may be replaced by an increase. The extent of this change is not the same for all cells, it strongly depends on the intensity of irradiation. The rate of change is highest at the beginning; after some time it has become a small fraction of its initial value. This phenomenon is known as fatigue, or creep. It is quite as marked for cathode-ray bombardment as it is for irradiation with visible light. The older observations on the electron voltaic effect referred to in the introduction were carried out by exposing the cells to a steady beam of electrons and observing the response of the cells on a galvanometer so that at least a few seconds had lapsed between the commencement of the exposure and the readings. The readings were therefore, to a varying extent, reduced by fatigue.

The fatigue can, however, be completely suppressed if the cathode rays are applied in short pulses. The results given below were accordingly obtained with 6 millisecond square pulses interrupted by 54 msec off periods. Observation of the output on a cathode-ray oscilloscope showed that the rise time of the response is short compared with 6 milliseconds, and the response curve follows closely the primary current pulse; after starting pulsed bombardment no change in the size of subsequent pulses is observed, for the conditions stated. Also, the output current measured by a galvanometer is exactly the mean value of the current measured by the cathode-ray oscilloscope, i.e. 0.1 of the value during the pulse.

For all cells, families of curves were obtained such as are shown in figure 2. The gain I/i_p decreases with increasing electron current. Except for a rather small initial region it increases linearly with voltage up to a critical voltage V_c which depends on the current density, and remains constant for higher electron energies. The penetration of the primary electrons marked on the abscissa is calculated by extrapolating values given by King (1960).

Consider first the curve for $i_p = 10^{-10}$ amp of figure 2. It is the response one would expect to find for a junction situated close to the surface, if the diffusion length of minority carriers in the bulk is about 5 microns. At very low accelerating voltages the ionization is restricted to a very thin layer near the top electrode; the current gain is low because incident electrons carry little energy. As the accelerating voltage increases the primary electrons produce proportionally more pairs, but also the centre of pair production moves away from the front into the junction (which occupies about

(5 μ) and beyond. If the electrons in the bulk selenium were immobile, the gain would then cease to increase with increasing penetration because no contribution to the current would arise from the p-type selenium where the additional carriers are generated. From the observation that the gain still increases with cathode-ray energy, it must be concluded that the electrons released in the bulk diffuse into the junction and thus contribute to the current, just as the minority carriers contribute in the silicon cells. But the gain does cease to increase when at the cathode-ray energy eV_c the

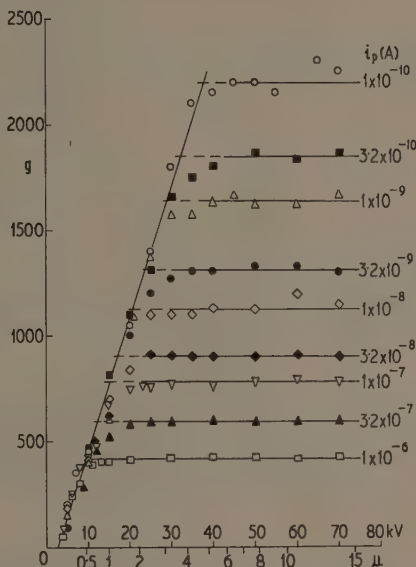


Figure 2. Electron voltaic effect in grey selenium; gain as function of the energy of the cathode rays and of their penetration; the figures beside the curves denote the beam currents.

ionization commences to extend to a depth from which electrons cannot reach the junction by diffusion, i.e. beyond one diffusion length from it. Recent studies by Ehrenberg and King (not yet published) have shown that the ionization caused by cathode rays does not, in the region penetrated, vary much with cathode-ray energy in the range shown in figure 2. This explains why the gain remains approximately constant at energies above eV_c .

The depth of penetration of primary electrons of energy eV_c gives therefore the diffusion length L of the minority carriers. At 10^{-10} amp, the diffusion length L is seen to be about 5 microns. It decreases with increasing density of cathode rays.

In order to extrapolate the diffusion length to zero primary current, consider that the lifetime τ of the carriers should be related to the lifetime τ_0 at zero excitation by

$$\frac{1}{\tau} = \frac{1}{\tau_0} + \frac{1}{\tau_1} \quad (2)$$

where τ_1 would be the lifetime if irradiation were the only cause of decay. Relation (2)

is equivalent to

$$\frac{1}{L^2} = \frac{1}{L_0^2} + f(i_p). \quad (3)$$

By trial and error it was found that the values of V_c or L respectively given in figure 2 (and corresponding sets of values for all other cells examined) satisfy equation (3) closely

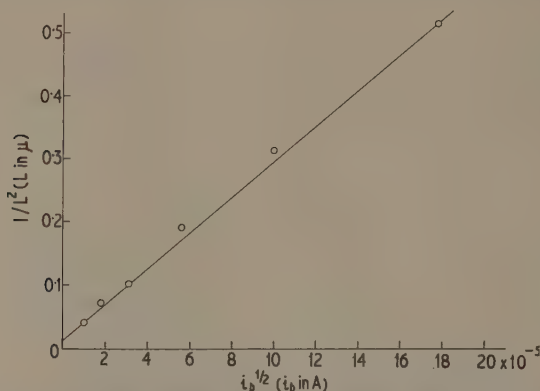


Figure 3. The diffusion length of electrons in grey selenium as a function of the current carried by the cathode rays. The reciprocals of the squares of the diffusion length are plotted against the square root of the current, in units of 10^{-10} amp, for currents below 10^{-7} amp.

if $f(i_p)$ (and therefore $1/\tau_1$) is taken to be proportional to the square root of the primary current density. This is shown in figure 3, the full line representing

$$f(i_p) = 2.8 \times 10^{11} (i_p)^{1/2} \text{ cm}^{-2}.$$

The line cuts the axis at a point corresponding to $L_0 = 9 \times 10^{-4}$ cm (calculated by the method of least squares, $L_0 = 7.5 \mu$). Although in other cells different values of gain and of change of gain with primary current are found, L_0 is always close to 8μ .

Diffusion length L , mobility w and lifetime τ are generally related by

$$L^2 = \frac{wkT}{e} \tau \quad (4)$$

and at 300°K , $kT/e = 2.5 \times 10^{-2}$ volt. This relation can be used to estimate the effective mobility of electrons in grey selenium. An idea of the lifetime of the electrons can be obtained from photoconductivity data. Zworykin and Ramberg (1949) have discussed the variation of photoconductive response of microcrystalline grey selenium with frequency of light pulses. This has one relaxation time of about 0.01 sec and another one of less than 3×10^{-4} sec. If we interpret the longer time as the *total* lifetime τ of the minority carriers, and assume that these data apply to our material we obtain from (4) with $L = L_0 = 8 \times 10^{-4}$ cm for the effective mobility of electrons in grey selenium a value $2.5 \times 10^{-3} \text{ cm}^2 \text{ v}^{-1} \text{ sec}^{-1}$, which is in rather surprising agreement with that given by Spear (1957), viz. $5 \times 10^{-3} \text{ cm}^2 \text{ v}^{-1} \text{ sec}^{-1}$ for electrons in *amorphous* selenium.

According to this interpretation, an electron may undergo many cycles of trapping and release before it finally recombines with a hole or has found its way, by diffusion, to the field of the barrier. The decrease of diffusion lengths with cathode-ray currents indicates a corresponding decrease of total lifetime. It is known that lifetimes can decrease with increasing level of ionization (Hall 1959, 1960, Many and Bray 1958). The relation $\tau_1 \propto i_p^{-1/2}$ may in this connection be of considerable interest.

The numerical values given carry of course a considerable uncertainty. But the consistency of the above results leaves no doubt that the electron voltaic effect brings to light the important fact that the electrons in grey selenium are mobile, and that this mobility plays an important role in the performance of selenium barriers and a decisive role at least in the electron voltaic effect. In this respect the present studies support the view first put forward by Poganski (1953) and Hoffman and Rose (1953) that selenium barriers might have to be considered as p-n junctions rather than as unipolar Schottky barriers (Schottky 1941).

It can also be seen from figure 2, and is confirmed by many other measurements, that for selenium I is proportional to the bombarding current for low voltages up to about 10 kv, but it increases less fast at high voltages. This suggests that the rate of recombination near the surface is not increased by irradiation; this agrees with the well-known fact that at zero external resistance the current generated by visible light is proportional to its intensity; visible light penetrates only very little into selenium, the reciprocal of the absorption coefficient being in the neighbourhood of 0.5 micron (Gillespie 1951).

If for given irradiation the external resistance is varied, equation (1) has always been found to account fairly well for the voltage-current relation, but the parameters a and b depend on irradiation; equation (1) appears also to hold for unilluminated cells or external voltages applied in the forward direction. An examination of a number of cells suggested the figures given in table 2 as representative. The values refer to a surface of 3 cm².

Table 2

	$i_0(\text{A})$	$b(\text{V})$	$I(\text{A})$
Dark cell	7×10^{-7}	0.06	
Cells illuminated with visible light (ft candles)			
(a) 40	3×10^{-6}	0.065	65×10^{-6}
100	4.5×10^{-6}	0.08	154×10^{-6}
(b) 75	4.4×10^{-6}	0.10	190×10^{-6}
160	16×10^{-6}	0.135	400×10^{-6}
Cathode rays of 30 kv			
Beam current (A)			
7×10^{-9}	3.3×10^{-6}	0.07	0.4×10^{-5}
3×10^{-8}	5.6×10^{-6}	0.077	1.4×10^{-5}
1.6×10^{-7}	34×10^{-6}	0.12	5.9×10^{-5}
6×10^{-7}	44×10^{-6}	0.14	11×10^{-5}
1.2×10^{-6}	64×10^{-6}	0.16	16×10^{-5}

In the dark and at low levels of illumination i_0 is near to 10^{-6} A cm⁻² and b is near 0.06 volt. But these parameters increase rapidly with intensity of irradiation. It is an obvious conjecture that the increase of the value of the parameters is due to increased recombination.

§ 5. SOME REMARKS ABOUT FATIGUE

The intriguing and varied phenomena of fatigue have never been satisfactorily explained. Nor have our own quite extensive studies (Billington 1960) led to very definite conclusions. A few aspects may, however, be worth mentioning.

A measure of the fatigue was established as follows. When the irradiation commences, the voltage as observed on a cathode-ray oscilloscope rises rapidly to the initial voltage V_i and then decreases slowly, the rate of change becoming very small after a few seconds. The change of voltage ΔV in 6 seconds is therefore taken as the measure of the fatigue. It was found convenient to measure the incident radiation in terms of V_i , and typical curves showing ΔV as function of V_i (external resistance 1 M Ω) are shown in figure 4 for a number of selenium cells which show the effect strongly. The

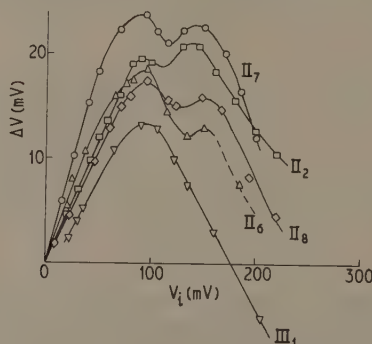


Figure 4. Fatigue of selenium cells under bombardment with 30kv cathode rays. The abscissa is the initial e.m.f., the ordinate the loss in e.m.f. in the first six seconds. Five different cells are represented.

shapes of the curves are essentially the same for cathode rays and light. For cathode rays ΔV increases for a given value of V_i with increasing accelerating voltage; for light the fatigue could not be influenced by varying the humidity of the ambient air. The fatigue decreases slightly from blue to red, i.e. with increasing penetration. An increase of fatigue with wavelengths was observed by Preston (1944, 1946). His studies of fatigue refer, however, to fatigue relaxing within minutes or hours, so that possibly the effects studied previously are not connected with the effect noticed here.

It does not seem possible to explain the shapes of the curves shown in figure 4 by a simple model. But the absence of an ambient effect, and the increase of the effect with increasing penetration of the radiation suggests that the source of the fatigue lies in the interior of the cells, and could be connected with slow surface states situated at grain boundaries.

The silicon cells, as mentioned above, do not fatigue under electron bombardment; nor do they fatigue under illumination if they are kept *in vacuo*. A fatigue develops, however, if the (unvarnished) front is exposed to the atmosphere. The fatigue curves are then similar to those shown in figure 3 with a single broad maximum for $V_i = 275$ mv (at 1 M Ω load).

Harten (1959) has studied the effect of surface recombination on the sensitivity of silicon cells. The comparison with our cells is not straightforward as Harten illuminated his cells from the face opposite the junction. Also he did not look out for fatigue

fects. But Harten did observe large changes in sensitivity on exposing the illuminated surfaces to water vapour, nitrogen or oxygen, and also changes in sensitivity with ambient illumination. The same surface states may be responsible for both Harten's effects and the fatigue we observed.

ACKNOWLEDGMENTS

The authors gratefully acknowledge the receipt of a grant given to one of them (E.W.B.) by the Department of Scientific and Industrial Research. We also wish to thank Messrs. Ferranti Ltd. for letting us have some solar cells, and Messrs. Evans Electric for the supply of selenium elements.

REFERENCES

- BECKER, A., and KRUPPKE, E., 1937, *Z. Phys.*, **107**, 476.
 BILLINGTON, E. W., 1960, *Experimental Studies of the Electron Voltaic Effect*, Thesis, University of London.
 DASH, W. C., and NEWMAN, R., 1955, *Phys. Rev.*, **99**, 1151.
 EHRENBERG, W., and LANG, C. S., 1954, *Physica*, **20**, 1137.
 EHRENBERG, W., LANG, C. S., and WEST, R., 1951, *Proc. Phys. Soc.*, **64**, 424.
 GILLES, M. A., 1951, *J. Chem. Phys.*, **19**, 1291.
 HALL, R. N., 1952, *Proc. Inst. Radio Engrs N.Y.*, **40**, 1512.
 ——— 1959, *Proc. Inst. Elect. Engrs*, **106 B**, Suppl. No. 17, p. 923.
 HARTEN, H. U., 1959, *Philips Res. Rep.*, **14**, 346.
 HARTEN, H. U., and SCHULTZ, W., 1955, *Z. Phys.*, **141**, 319.
 HOFFMANN, A., and ROSE, F., 1953, *Z. Phys.*, **136**, 152.
 HOLLIDAY, J. E., and STERNGLASS, E. J., 1959, *J. Appl. Phys.*, **30**, 1428.
 KING, D. E. N., 1960, *Ph.D. Thesis*, University of London.
 KLEINMAN, D. A., 1961, *Bell. Syst. Tech. J.*, **40**, 85.
 LANE, R. O., and ZAFFARANO, D. J., 1954, *Phys. Rev.*, **94**, 960.
 MANY, A., and BRAY, R., 1958, *Progress in Semiconductors*, Vol. III (London: Heywood), p. 117.
 MOSS, T. S., 1952, *Photoconductivity in the Elements* (London: Academic Press).
 POGANSKY, S., 1953, *Z. Phys.*, **134**, 469.
 PRESTON, J. S., 1944, *Nature, Lond.*, **153**, 680.
 ——— 1946, *J. Sci. Instrum.*, **23**, 173.
 RAPPAPORT, P., LOFERSKI, J. J., and LINDER, E. G., 1956, *R.C.A. Rev.*, **17**, 100.
 SCHONLAND, B. F. J., 1925, *Proc. Roy. Soc. A*, **108**, 187.
 SCHOTTKY, W., 1941, *Z. Phys.*, **118**, 539.
 SPEAR, W. E., 1957, *Proc. Phys. Soc.*, **70**, 13, 669.
 YOUNG, J. R., 1956, *J. Appl. Phys.*, **27**, 1.
 ZWORYKIN, V. K., and RAMBERG, E. G., 1949, *Photoelectricity* (New York: Wiley).

Electrical Properties of Organic Insulating Liquids Containing Fluorescent Solutes

By M. DARVENIZA[†] AND H. TROPPER[‡]

[†] Queensland University

[‡] Queen Mary College, London

MS. received 15th Decemer 1960, in revised form 7th July 1961

Abstract. A new phenomenon is reported which is concerned with the excitation of fluorescent solutes in organic liquid dielectrics when high electric fields are applied. The characteristics of the emitted light have been studied and related to the pre-breakdown conduction current and the electric strength. Dielectric liquids showing this effect have been synthesized by dissolving known concentrations of fluorescent materials in simple organic liquids. These have confirmed the experimental results obtained with more complex transformer oil. Also, experiments are described which show that even highly degassed liquids exhibit a pressure dependence of electric strength if brought into a state of super-saturation by applying tension to the liquid.

§ 1. INTRODUCTION

PREVIOUS WORK in the study of electric breakdown processes in liquids has been fully reviewed elsewhere (Lewis 1959, Darveniza 1959). However, a brief review of relevant luminescence phenomena will be given here, since the reported experimental results link directly for the first time the two fields of electric breakdown and luminescence.

Organic solutions are widely used for the scintillation detection of energetic radiations (Birks 1953). Small amounts of fluorescent materials such as anthracene are dissolved in suitable organic liquids such as benzene, toluene, etc. These solvents absorb the incident radiation and the energy is re-emitted as fluorescence, characteristic of the solute (Kallmann 1950). Various mechanisms for the efficient solvent-solute transfer of energy have been proposed (Northrop and Simpson 1956, Kallmann and Furst 1951, 1954, 1956).

Several workers (Destriau 1947, Payne, Mager and Jerome 1950) have shown that electric fields may produce luminescence when applied to certain inorganic phosphors. Piper and Williams (1955) and Alfrey and Taylor (1955) have made detailed studies of electroluminescence in single crystals of zinc sulphide. A general relationship between the light output L and the applied voltage V has resulted from the experimental work: $L = A \exp(-BV^{-1/2})$ where A and B are constants.

Piper and Williams have considered various mechanisms for electroluminescence and it is generally agreed that the luminescent centres are excited by field-accelerated electrons. All experimental evidence points to the formation of sufficiently high electric fields in localized spots such as fluorescent centres.

§ 2. EXPERIMENTAL APPARATUS

2.1. Test Apparatus

Most of the results described below were obtained with industrial transformer oil conforming to the British Standards Specification B.S. 148: 1951. The oil was of

Peruvian origin and its physical properties may be summarized as follows: colour, pale yellow, slight blue fluorescence; specific gravity, 0.88 at 20 °C; dielectric constant, 2.16 at 20 °C; molecular weight, 310.

The only information available of its chemical properties is the result of an 'm-d-M' analysis: % carbon in aromatics, 8.5; aromatic rings per molecule, 0.3 mean; % carbon in naphthenics, 37.5; naphthenic rings per molecule, 1.8 mean; % carbon in paraffins, 53.7; aromatic compounds, 15% by mass; sulphur compounds, 1.07%, formation unknown; oxygen compounds, traces present, formation unknown.

The impurities which affect the electric strength of insulating liquids are solid particles, moisture and dissolved or entrained air. The oil was purified in a molecular still which utilized a form of flash distillation at reduced pressure and at a temperature sufficiently low to avoid thermal degradation. The still and the test cell formed parts

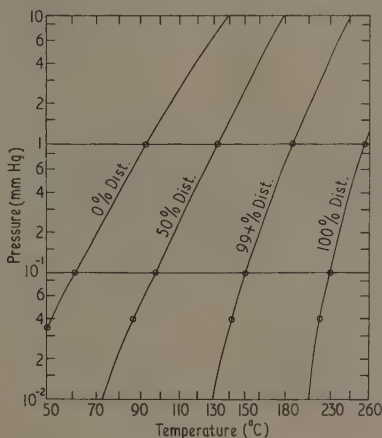


Figure 1. Fractionation of oil as a function of temperature and ambient pressure.

of a totally enclosed all-glass system. Solid particles were removed by filtration through a sintered glass filter of one micron maximum pore size. All parts of the system could be evacuated to a pressure of less than 10^{-4} mm Hg. The distillation technique (Darveniza 1960) enabled the oil to be completely distilled in an atmosphere of air or of nitrogen at pressures between 10^{-2} and 5 mm Hg. Separation of the various fractions of the oil was possible by distillation at suitable temperature and the results are shown in figure 1. It was found that at temperatures approximately 70 °C below that required for complete distillation, only a small fraction of the oil (less than 1%) was not distilled. This consisted mainly of the colouring components of the oil and its separation left the remainder of the oil comparatively clear in appearance.

Experiments were also made using the simple organic liquids hexane and benzene, to which known concentrations of fluorescent materials were added. Spectroscopic grades of these liquids were filtered several times through a fine sintered glass filter under vacuum. After dissolving the fluorescent material the prepared samples were again passed through a filter into the test cell.

The test cell was designed to keep the volume to a minimum. Electrical measurements were made between 1 cm diameter nickel spheres mounted horizontally in the

test cell. The gap spacing could be varied from 50 to 500 microns with an estimated error between $\pm 1.5\%$. Before each test, the electrodes were prepared by mechanical polishing with soft mops and a suitable grease as adopted by Hancox and Tropper (1958). Buffing was continued until no scratches or pits were visible when examined under a metallurgical microscope, magnification 100.

For the variation of the hydrostatic pressure applied to the test liquid two extra-sensitive metal bellows were used. By means of these it was possible to apply tensions equivalent to 350 mm Hg to the test liquid and positive pressures up to 760 mm Hg.

2.2. Electrical Equipment

Direct voltages varying between 600 v and 20 kv were obtained from a stabilized source which incorporated a radio-frequency generator. The measurement of this voltage was considered accurate to within $\pm 1.5\%$. For the tests with impulse voltages a six-stage generator was used. The output voltage was measured by means of a resistance-capacitance divider and a transient oscillograph, with an estimated error of $\pm 3\%$.

During breakdown measurements a diverter was used which by-passed the discharge current in a time less than $0.5 \mu\text{sec}$ after breakdown. This greatly reduced breakdown products and electrode damage and hence the scatter in the measurements.

To permit conduction current to be measured accurately the low voltage electrode of the test cell was fitted with a guard ring and shield. The current was determined by measuring the volt drop across a high resistance with a 'Vibron' electrometer.

Quantitative light measurements were made with an R.C.A. 931-A photomultiplier operated at a total potential of 1100 v. The anode current was measured with a resistive shunt and an electrometer and changes as small as 10^{-9} A could be detected. The spectral range was from 3000 to 6500 Å with a peak in the spectral response at 4000 Å. It is estimated that the cathode collected approximately $\frac{1}{3}$ th of the total light emitted from the test cell.

§ 3. EXPERIMENTAL RESULTS

3.1. Factors affecting Measurements of Electric Strength and Conduction Current

The breakdown strength of the oil before purification was found to be 380 kv cm^{-1} with a coefficient of variation of 8%. After distilling the oil in an atmosphere of nitrogen at a pressure of 10^{-2} mm Hg the strength increased to 1120 kv cm^{-1} and the coefficient of variation was reduced to 4.7%. A marked conditioning process was observed, i.e. an increase in strength with successive breakdowns, and at least 10 conditioning discharges were necessary before a stable electric strength was achieved. Retaining the electrodes but changing the oil sample required a further but much smaller conditioning process and this was also necessary when the liquid in the test cell was allowed to stand undisturbed for periods in excess of twenty-four hours.

The consistency of the breakdown measurements can be seen from table 1 which shows the results of 4 different tests. Before each test the electrodes were freshly prepared by mechanical polishing and degassed in the test cell for at least 12 hours before submersion in the test liquid. It was found that the measurements were independent of the rate of rise of the applied test voltage and of the time interval between successive voltage applications, provided the rate of rise was less than 250 v sec^{-1} and the interval between shots was greater than one minute.

It is well known that electric strength measurements made with short duration impulse voltages are critically dependent on the electrode surface conditions (Hancox and Tropper 1958). The dependence is considered to be due to the time-dependent process of electron emission from the cathode. It was eliminated by brushing the electrodes with grade 2/0 emery cloth. Subsequent impulse strength measurements

Table 1
Consistency of Breakdown Measurements

Test	First breakdown (kv cm ⁻¹)	No. of conditioning shots	Final breakdown strength (kv cm ⁻¹)
A	650	13	1120
B	740	7	1180
C	690	10	1030
D	690	12	1060

with voltage wave-shapes of varying ramp functions (i.e. voltages increasing linearly with time at different rates) resulted in an electric strength independent of time, for times to breakdown in excess of 0.5 μ sec. The strength measured in this manner was similar to that obtained with direct voltages, both in magnitude and scatter.

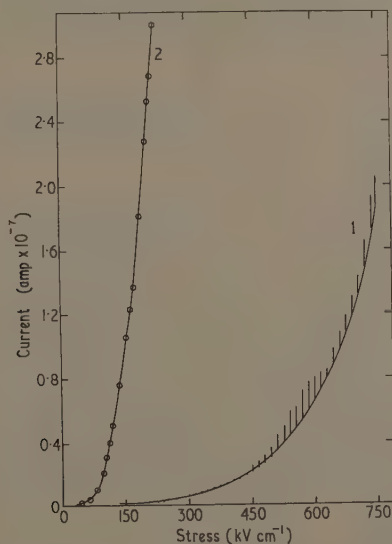


Figure 2. Effect of conditioning on conduction current. Curve 1, before breakdown; curve 2, after spark conditioning of electrodes.

Since most experimental breakdown results were obtained with spark-conditioned electrodes, measurements of pre-breakdown processes were made also with such electrodes. Typical current-electric stress curves for fresh electrodes and spark-conditioned electrodes are shown in figure 2. As with other pre-breakdown processes

the conduction current was much more stable with spark-conditioned electrodes, although the magnitude was at least two orders higher.

In all results of breakdown measurements and of pre-breakdown processes given below, spark-conditioned electrodes were used and only the parameters of the test liquid were varied.

3.2. Dependence of Strength on Gas Content

Breakdown measurements were made on samples of oil distilled in air and in nitrogen, at pressures between 10^{-3} and 5 mm Hg of residual gas. When the gas in use was changed, the oil was flushed with the new gas for at least forty-eight hours. Before each distillation, the oil was allowed to settle into rough equilibrium with the intended still pressure before leaving the gas bubbling chamber. The results obtained are shown in figure 3, the vertical lines indicating the standard deviation. It was found that variation of the nitrogen gas content had no significant effect on the electric strength in the range considered. The electric strength of the oil rose significantly as the partial pressure of air held in solution was raised from 10^{-2} to 1 mm Hg. This result confirms the work reported by Khambanonda (1958).

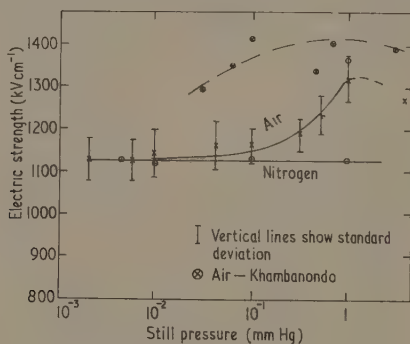


Figure 3. Effect of distillation (i.e. hydrostatic) pressure on electric strength.

Impulse voltage measurements were made, with ramp voltages and scratched electrodes, on oil samples distilled in air and nitrogen pressures of 10^{-2} and 1 mm Hg. The results are given in table 2; the time to breakdown varied between 0.5 and 1.0 μ sec.

Table 2

Electric Strength for Impulse Voltages

Still atmosphere (mm Hg)	Electric strength (kv cm ⁻¹)	Coefficient of variation (%)
Nitrogen, 10^{-2}	1140	5
Nitrogen, 1	1170	4.8
Air, 10^{-2}	1080	6.9
Air, 1	1520	6.7

3.3. Strength of Various Oil Fractions

Samples of oil were distilled at various temperatures in nitrogen at a pressure of 10^{-1} mm Hg and the breakdown results are plotted in figure 4. The electric strength rose as the still temperature was decreased from 210 to 145 °C and thereafter no significant change was observed. Referring to figure 1 it can be seen that the increase in strength is associated with the removal of colouring matter from the oil. The colouring matter was also separated from the oil in a still atmosphere of 1 mm Hg of air and again a significant rise in electric strength was observed.

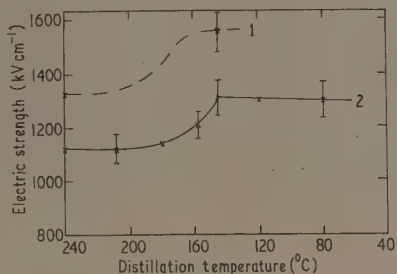


Figure 4. Electric strength of different oil fractions obtained by varying distillation temperature. Curve 1, with air at 1 mm Hg maintained in still; curve 2, with N_2 at a pressure of 10^{-1} mm Hg.

A similar rise in strength was observed with impulse voltages. A strength of 1420 $kV\ cm^{-1}$ with a coefficient of variation of 7.2% was recorded for oil distilled at 140 °C in nitrogen.

3.4. Pressure Dependence of Strength

It is generally agreed that the electric strength of transformer oil shows little dependence on hydrostatic pressure unless the gas in solution is in a state of super-saturation. For highly degassed oil this state cannot be reached by simply reducing the gas pressure above the liquid surface, since the pressure of the head of oil necessary to immerse the electrodes cannot be reduced below about 1 mm Hg. In this work, tensions up to 350 mm Hg were applied to the test fluid through bellows, thus achieving a state of supersaturation. Table 3 shows the pressure dependence of electric strength for highly degassed oil and for oil distilled in nitrogen at a pressure of 1 mm Hg.

Table 3
Pressure Dependence of Electric Strength

Oil sample	Pressure (mm Hg)	Electric strength ($kV\ cm^{-1}$)
Nitrogen (1 mm Hg)	+300	1120
	+ 50	1120
	-100	1100
	-225	1045
	-350	910
Highly degassed oil, 3×10^{-3} mm Hg	+300	1130
	+ 50	1130
	-350	935

The results show a significant reduction in strength when a tension of 350 mm Hg was applied to the test liquid. No significant pressure dependence was observed in the range of 1 to 760 mm Hg of hydrostatic pressure. A similar reduction of electric strength with tension was observed with oil samples distilled in air at 1 mm Hg and oil samples with the colouring fraction removed.

No significant variation in electric strength with tension or pressure was observed with impulse voltages.

3.5. *Light Emission and Conduction Current*

Preliminary experiments showed that the magnitude of conduction current and of pulse activity in transformer oil was several orders higher than that reported of simple hydrocarbon liquids (House 1957). Observation in a completely darkened room showed that visible light was emitted from the highly stressed region of the oil gap for d.c. fields in excess of 600 kv cm^{-1} . It has been found that light emission may be correlated with electric breakdown measurements. Simultaneous records were therefore obtained of electric strength, conduction current and light emission, for each set of experimental conditions.

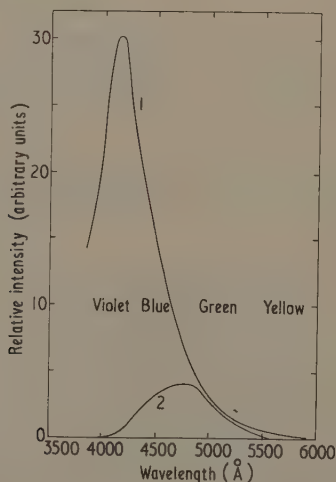


Figure 5. Fluorescence spectrum of transformer oil. Curve 1, emission spectrum; curve 2, eye response to emission spectrum.

The light emitted was blue and similar in appearance to the blue fluorescence obtained by excitation with ultra-violet radiation. The glow appeared if either the voltage across a fixed gap was increased, or if a fixed voltage of 12 kv was applied and the gap decreased from 500 to 100 microns. This showed that the glow was a true high field effect, and that it was not due to spurious corona effects. The fluorescence spectrum of the oil when excited with an ultra-violet source (mercury lamp, OX I filter) was determined and is shown as figure 5. Also shown is the spectrum weighted by the spectral response of the eye. Thus, when viewed by eye, the fluorescence of oil has a peak in the blue region (4800 Å). An Adam Hilger wavelength spectrometer was used to resolve the spectrum of the light emitted due to high electric fields, but

is was very difficult because of the small amount of light emitted. At all stresses, the spectrum appeared to be diffuse. At a stress of 900 kv cm^{-1} , the point of maximum intensity was at 5300 \AA with a visible spread from 4580 to 5600 \AA . The point of peak intensity in the spectrum shifted to shorter wavelengths as the stress increased. At 300 kv cm^{-1} , the peak appeared at 4800 \AA , which corresponds to the peak of fluorescence spectrum as observed by eye (figure 5).

A travelling telescope with a maximum magnification $\times 80$ was used to examine the glow. This appeared to result from filamentary luminous channels which completely bridged the gap from cathode to anode, with no apparent change in intensity along their length. The intensity of light varied from channel to channel, and also with time in each channel, each having a 'flickering' appearance. The filamentary channels occupied a diameter of about three to four times the gap width. As the stress increased above 1100 kv cm^{-1} , the light output became more intense and more diffuse in a localized region about one to two gap widths in diameter. There was some evidence to suggest that it was possible to predict the channel in which final breakdown would occur by choosing the brightest channel at high stress. Photography of the light emission was attempted but even with exposures exceeding 10 minutes and the fastest available film, no record was obtained.

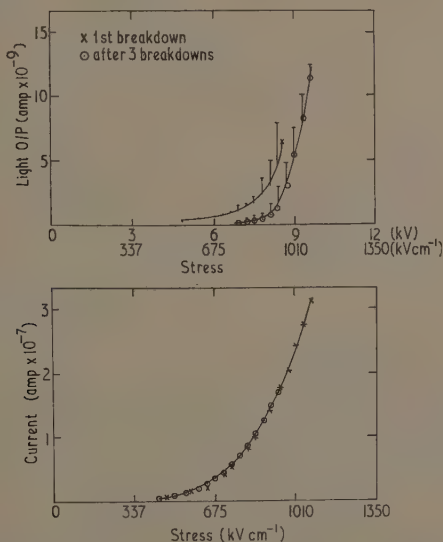


Figure 6. Effect of liquid conditioning on light emission and conduction current. Electrode gap 89μ , oil distilled at 160°C .

3.5.1. Effect of conditioning of test liquid.

Simultaneous conduction current and light output measurements were made on freshly distilled oil and on the same oil after three breakdowns. As can be seen from figure 6, there is no significant change in current in the two cases, but the light intensity over the same range of stress is lower after the three breakdowns. Since the electrodes in both cases were spark-conditioned before the test it must be assumed that a conditioning of the liquid took place during the three breakdowns which had no effect on the conduction current, but resulted in a reduction of light output. This was a

general observation and whenever the test liquid was changed the first few low breakdowns were always preceded by a light output which decreased after subsequent breakdowns as the liquid conditioning proceeded.

3.5.2. Effect of various oil fractions.

Light and current measurements for the various fractions of the oil are given in figures 7 and 8. No breakdowns occurred in the test cell during these tests. The still temperatures were chosen to remove the colouring fraction in steps, and it was found that the light output and the current decreased as more of the colouring fraction was removed. At temperatures below 140 °C, no further significant reduction resulted.

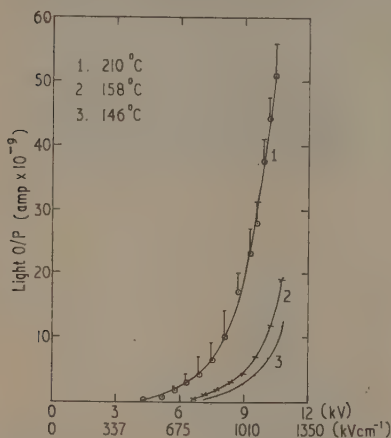


Figure 7. Light emission of different oil fractions. Electrode gap 89 μ . Distillation temperatures as shown.

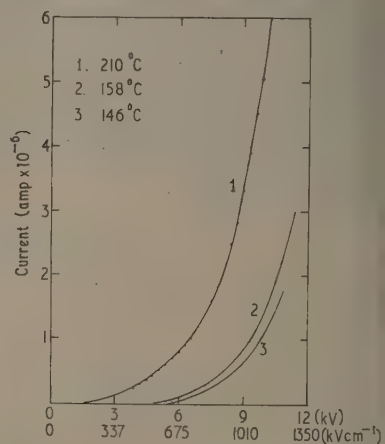


Figure 8. Conduction current of different oil fractions. Electrode gap 89 μ . Distillation temperatures as shown.

3.5.3. Effect of dissolved air and nitrogen.

It was found that the light and current curves did not differ significantly between oils distilled in nitrogen and air atmospheres in the pressure range 10^{-2} and 1 mm Hg. This result was surprising, bearing in mind the pronounced quenching effect (Cohen and Weinreb 1956) of oxygen in liquid organic scintillating liquids, and the marked rise in electric strength obtained with air over this range.

3.5.4. Pressure dependence.

The pressure dependence of light emission and conduction current was determined using an oil sample distilled in air at a pressure of 1 mm Hg. A stress of 1040 kv cm⁻¹ was applied to a 89 micron gap. Fifty alternate readings at +760 mm Hg pressure and -350 mm Hg tension were taken. The averages of the readings are given in table 4.

Table 4
Effect of Pressure on Light Output and Conduction Current

Pressure (mm Hg)	+760	-350
Light output ($A \times 10^{-9}$)	5.1	5.1
Conduction current ($A \times 10^{-7}$)	4.41	4.46

With current a slight increase (1%) was often recorded when tension was applied. This effect is not significant as the conduction current fluctuation during the test was several per cent.

5.5. Confirmatory experiments with hexane and benzene.

The fluorescence of transformer oil is due to unsaturated polycyclic aromatic compounds dissolved in the oil. If these materials cause light emission under the action of high electric fields, it should be possible to synthesize a dielectric which would also emit light. The simple organic liquids, *n*-hexane and benzene were investigated, using dark-conditioned electrodes.

With purified *n*-hexane no visible light was observed at stresses up to 1100 kv cm^{-1} . The hexane was then doped with 1 g l^{-1} of scintillation grade anthracene. Light emission characteristic of anthracene in solution was observed. The electric strength was 610 kv cm^{-1} on the first application of voltage, and increased with succeeding conditioning breakdowns, until an average strength of 955 kv cm^{-1} was obtained. The decrease of light intensity with increase in electric strength is shown in figure 9,

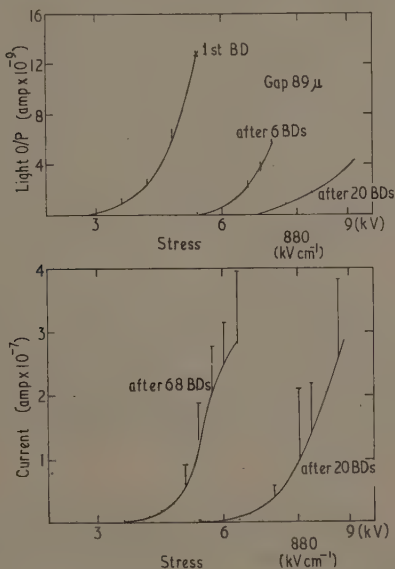


Figure 9. Conduction current and light output of hexane containing 1 g l^{-1} anthracene, after different numbers of breakdowns. Electrode gap 89μ .

but the effect was more pronounced than with transformer oil (figure 8). Samples of hexane were also doped with scintillation grade *p*-terphenyl and again light, characteristic of the fluorescent solute, was emitted when an electric stress was applied.

Commercially pure benzene (extra-pure for molecular weight determination) was filtered and tested without the addition of a fluorescent impurity. Very intense blue light was observed at relatively low electric fields, which was accompanied by a large conduction current. A similar trend of increasing electric strength and decreasing light emission was observed with conditioning breakdown.

Microscopic examination of these samples showed that the filamentary channels were similar to those found in transformer oil, apart from the greatly increased intensity observed in benzene.

§ 4. DISCUSSION OF RESULTS

4.1. *A General Model for Events Leading to Breakdown*

With liquids of high physical purity, the breakdown process is, at least in part, electronic in nature. The events leading to breakdown may be conveniently considered as three separate processes: (i) the production of free electrons in the gap, (ii) the subsequent acceleration of the electrons by the electric field, and their retardation by collisions with liquid or impurity molecules, (iii) the multiplication of charge carriers leading to instability and to final breakdown.

Most workers consider that free electrons are emitted from the cathode and considerable evidence, both experimental and theoretical, indicates that this is so for electric fields of the order 10^5 and 10^6 v cm⁻¹. House (1957) proposed that the dominant process for direct voltages is a Schottky field-aided thermionic emission. For pulse voltages, the availability of free electrons dominates the subsequent breakdown process although Bickley (1958, private communication) has shown that brushing electrodes with emery greatly reduces the statistical time lag for the appearance of an initiating electron.

The free electrons in the gap are then accelerated and are involved in various collision processes with liquid and/or impurity molecules. Loss of energy may be due to: (a) inelastic collisions with the larger liquid molecules, (b) electrons of suitable energy interacting with the vibrational modes in the bonds of the liquid molecules, (c) excitation collision with liquid and impurity molecules in which the excited molecules absorb the energy of the free electrons and are raised into higher electronic excited states which may lead to fluorescence or dissociation, (d) capture of electrons by molecules and the formation of negative ions.

The last process in the breakdown model involves the multiplication of charge carriers in the gap. Formation of positive and negative ions may result from earlier processes and these may in turn influence these processes. However, the decisive event is the multiplication of free electrons in the gap by ionizing collisions. Ionization of molecules is possible in the liquid phase or in a vapour phase such as a micro-bubble.

Of the three processes, each may be described as a necessary but not a sufficient condition for breakdown. According to the experimental conditions, any one may be dominant in determining the electric strength.

4.2. *The Effect of Dissolved Fluorescent Materials*

4.2.1. *Characteristics of light emission.*

The results in § 3.5 show that the light intensity increased in an exponential manner with increasing field, that the intensity of emitted light was associated with the electric strength, and that the spectrum of the light emitted was characteristic of the fluorescent solute. It is significant that these experimental characteristics are similar in nature to the electroluminescence characteristics reported for solid inorganic phosphors. With hexane, known concentrations of anthracene and *p*-terphenyl were introduced; in transformer oil, the constituents which produce the fluorescence are largely unknown. Jezl, Stuard and Ross (1958) have shown that tricyclic and polycyclic aromatics are present in the oil and may constitute up to 1% of the 15% by mass of aromatics present. It is probable that these molecules contribute most to the blue fluorescence and to the yellow colour of the liquid.

The various possible mechanisms for electroluminescence in solid fluorescent materials have been discussed in § 1. A further possibility must be considered here, chemiluminescence due to photochemical action between the dissolved oxygen and fluorescent materials. Chemiluminescence may contribute to the light emission in the doped hexane, but this possibility must be excluded for tests in transformer oil which was highly degassed in the purification system. As in the study of electroluminescence in solid fluorescent materials, it is likely that the fluorescence observed in organic liquids is due to the excitation of the fluorescent materials by electrons accelerated by the high electric field. Since the fluorescent components in transformer oil are largely unknown, no quantitative estimate of the electron energies required for excitation may be made. However, the absorption spectra of anthracene and *p*-terphenyl in dilute solutions are well known. The lower limit of absorption of anthracene is 3800 Å, and this corresponds to a minimum quantum energy of 3.25 eV required for excitation. It is suggested that the emission of light characteristic of the fluorescent material is experimental evidence that free electrons with energies in excess of 3 eV are present in the gap at electric fields below breakdown.

Lewis (1956) and Adamczewski (1957) have demonstrated that the majority of free electrons in the gap are retarded by vibrational collisions with the atomic bonds in the molecule. The bonds usually considered are the C-C and C-H bond, and their vibrational frequencies correspond to quantum energies of 0.11–0.14 eV and 0.36–0.37 eV respectively. It is suggested that a statistically small proportion of the electron population achieves energies in excess of these values and is accelerated by the electric field until excitation collisions occur with fluorescent components of the liquid. Because of the range of fluorescent materials present in transformer oil, it would be expected that materials with lower limits of absorption would be first excited, and that as the field increased the absorption limit would be raised as electrons gained higher energies. This is confirmed by the shift of the emission spectrum in oil to shorter wavelengths as the electric field was increased.

The possibility that the light emission was due to micro-discharges in the oil, rather than to excitation in the liquid phase, may be rejected because the intensity of light emission showed no dependence on hydrostatic pressure, from positive pressures of 760 mm Hg to tensions of 350 mm Hg. Further, fracture of the liquid under tension did not occur with high electric fields, and this indicates that the excitation of the fluorescent materials occurred in the liquid phase.

4.2.2. *Relation between light emission and electric strength.*

Removal, or reduction, of the fluorescent solutes resulted in a marked rise in electric strength, associated with a reduction in the intensity of light emission. Fractional distillation of transformer oil, separating the colouring components, raised the strength from 1100 to 1300 kV cm⁻¹ and reduced the light output by one order. Similarly, the electric strength of hexane was lowered from 1050 kV cm⁻¹ to 700 kV cm⁻¹ by the addition of fluorescent materials, which resulted in light emission.

This relationship between light output and electric strength was also observed during the conditioning of the test liquid. It was found that the strength was low and the light output was high if the oil in the gap was changed. Both were returned to normal by several conditioning sparks. The higher strength after conditioning appears to result from a lower concentration of fluorescent materials in the high stress region. These are probably ionized in the breakdown spark and are swept away to the electrodes by the next application of voltage. It is significant that liquid conditioning was lost if

the oil was allowed to stand undisturbed for long periods, presumably due to the diffusion of the fluorescent materials back into the gap, thus restoring the equilibrium of the solution.

Measurements made with short duration impulses again showed the effect of fluorescent materials on the electric strength of transformer oil. This indicates that these materials affect electronic processes leading to electric breakdown, and that the processes involved are not time-dependent in the range of one microsecond to steady state. Three possibilities are suggested to explain why the presence of these materials and light emission causes a reduction in electric strength: (i) their dissociation gives rise to positive ions which increase electron emission from the cathode as proposed by Green (1956), (ii) photoelectric emission from the cathode due to energetic photons released by the fluorescent process, (iii) the lifetime of an excited fluorescent molecule is about 10^{-8} sec in these liquids, and a definite probability exists for interaction between such a molecule and a low energy electron, with the transfer of the excitation energy to the electron. The chance of such an interaction occurring is greatly increased by the fact that energy transfer may take place between excited fluorescent molecules with a transit time of 10^{-12} sec (Kallmann and Furst 1951, 1954, 1956). Thus, it is possible for electrons to achieve high energies by a mechanism unaffected by vibrational barriers due to liquid molecules. This may be similar to the mechanism outlined by Fröhlich (1939) for ionic crystals containing impurity or imperfection energy levels near the conduction band. It has been shown that if the imperfections are sufficiently numerous to interact with each other the strength will be lowered (von Hippel and Lee 1941).

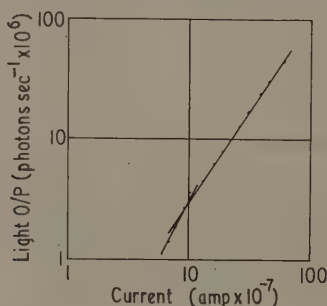


Figure 10. Relation between light output and conduction current.

4.2.3. Light emission, conduction current and stress relationships.

The total light output from the test cell has been plotted against conduction current flowing for transformer oil in figure 10. It shows a linear increase of light output with current, within the limits of observed fluctuations (values were taken from the best curve drawn through the experimental results). A similar relationship was observed for all simultaneous light and current measurements in transformer oil, doped hexane and benzene. It may be shown that the proportion of the total energy absorbed in the gap from the electric field ($V \times I$) which is released by light emission is $1/(3.3 \times 10^9)$. Replotting the light-stress curve for transformer oil in the manner $\log L$ against $E^{1/2}$ gave a straight line. It is significant that the Schottky plots of conduction current and stress reported by House (1957) in *n*-hexane are also linear, and the light output due to electroluminescence in solid inorganic phosphors also follows a similar relation with electric stress.

The experimental results show that fluorescent materials greatly increase the conduction current flowing through the gap at high electric fields. It is well known that the higher molecular weight components of transformer oil (including the colouring fractions) dissociate under the action of daylight, which is sufficiently actinic to produce a noticeable change in the acidity of the oil over a long period. Under the influence of high electric fields, these molecules are dissociated into ions as a result of excitation by energetic electrons moving in the gap, resulting in an increase of charge carriers and to an increase in current.

4.3. Pressure Dependence

Since the light emission and conduction current were unaffected by changes in pressure it is concluded that the first two breakdown processes, outlined above, are not pressure dependent. However, a significant reduction in electric strength measured with direct voltages was observed with the liquid in a state of super-saturation due to the application of tension up to 350 mm Hg. This suggests that the last process, the multiplication of free electrons in the gap by ionization, is affected by hydrostatic pressure. A reduction of electric strength between 12 and 19% due to a change of pressure in this range cannot be explained by a change in density, since the change in volume due to a pressure change of this order is less than $1/10^6$. This suggests that ionization and multiplication of free electrons occurs in a gaseous phase such as a bubble and that it is affected by hydrostatic forces prevailing on the bubble. The fact that no pressure dependence was observed with impulses of short duration indicates that this mechanism is time dependent. This is in agreement with the theory proposed by Seitz (1958) for the growth of bubbles in a supersaturated solution subjected to ionizing radiations.

4.4. Influence of Dissolved Gases

The experimental results show a significant rise in the electric strength of oil with air in solution at an equilibrium pressure of 1 mm Hg. This is in agreement with the results of Sletten (1959) and Khambanonda (1958). This increase is present for direct voltages and impulses of short duration, and it would appear that the air in solution affects electronic processes in the gap. Since nitrogen plays no part, it must be concluded that the effect is due to the presence of oxygen. It is well known (von Hippel and Lee 1941) that oxygen, an electronegative gas, can remove electrons from a discharge by resonance capture of electrons of suitable energy. The mechanism by which oxygen may contribute to the electric strength has been discussed qualitatively elsewhere (Darveniza 1959). Whatever the nature of the liquid state (and there is no generally accepted model), it would be reasonable to expect that dissolved oxygen molecules would be positioned at preferred sites such as holes or vacancies, and that electron acceleration would also be most favoured at these sites. These holes or vacancies are essential to the fluidity of the liquid, making up its free volume. It is suggested that oxygen influences the free electron density in the gap, and so the electric strength, to a degree out of all proportion to its concentration, because the dissolved gas molecules are generally to be found in the very sites in the liquid most suitable for electron acceleration.

§ 5. CONCLUSIONS

It may be concluded from experimental work that dissolved fluorescent materials, such as anthracene, which absorb energy by resonance of electron orbitals into higher states, may be excited in the liquid state by the application of high d.c. electric fields

to organic insulating liquids. Experimental evidence indicates that the presence of these materials and the resultant light emission influences the electric strength of these liquids, both for direct and for impulse voltages. These results suggest that electron processes involved in the breakdown mechanism are influenced by this excitation. Removal of the fluorescent materials was found to decrease the light output, and to increase the strength of the liquid.

The reduction of electric strength, by placing highly degassed liquids in a state of supersaturation by the application of tension, indicates that the breakdown processes must involve, at least in part, a vapour phase which is subject to hydrostatic forces.

ACKNOWLEDGMENTS

Acknowledgments are made to Professor M. W. Humphrey Davies for the provision of facilities, and to colleagues of the dielectrics team at Queen Mary College for encouragement and discussion. The authors wish to thank Professor G. F. J. Garlick of Hull University for the determination of fluorescence spectra.

Finally, one of the authors (M.D.) acknowledges the award in 1956 of a Travelling Research Fellowship by the University of Queensland, Australia.

REFERENCES

- ADAMCZEWSKI, I., 1957, *Zeszyty Nauk Politech.*, **3**, 3.
 ALFREY, J., and TAYLOR, J., 1955, *Proc. Phys. Soc. B*, **68**, 775.
 BIRKS, J. B., 1953, *Scintillation Counters* (London: Pergamon).
 COHEN, S. G., and WEINREB, A., 1956, *Proc. Phys. Soc. B*, **69**, 593.
 DARVENIZA, M., 1959, *Ph.D. Thesis*, University of London.
 — 1960, *J. Inst. Petrol.*, **46**, 84.
 DESTRIAU, G., 1947, *Phil. Mag.*, **38**, 700.
 FRÖHLICH, H., 1939, *Rep. Progr. Phys.*, **6**, 411 (London: Physical Society).
 FROST, D., and McDOWELL, C., 1958, *J. Chem. Phys.*, **29**, 1424.
 GREEN, W., 1956, *J. Appl. Phys.*, **27**, 921.
 HANCOX, R., and TROPPER, H., 1958, *Proc. Instn Elect. Engrs*, **105A**, 250.
 VON HIPPEL, A., and LEE, J., 1941, *Phys. Rev.*, **59**, 824.
 HOUSE, H., 1957, *Proc. Phys. Soc. B*, **70**, 913.
 JEZL, J. L., STUARD, A. P., and ROSS, E. S., 1958, *Trans. Amer. Inst. Elect. Engrs*, **77**, 715.
 KALLMANN, H., 1950, *Phys. Rev.*, **78**, 621.
 KALLMANN, H., and FURST, M., 1951, *Phys. Rev.*, **81**, 853.
 — 1954, *Phys. Rev.*, **94**, 902.
 — 1956, *Symposium on Semiconductors and Phosphors* (Berlin: Springer).
 KHAMBANONDA, A., 1958, *Ph.D. Thesis*, University of London.
 LEWIS, T. J., 1956, *J. Appl. Phys.*, **27**, 645.
 — 1959, *Progress in Dielectrics*, Vol. 1 (London: Heywood).
 NORTHROP, D. C., and SIMPSON, O., 1956, *Proc. Roy. Soc. A*, **234**, 124.
 PAYNE, E. C., MAGER, E. L., and JEROME, C. W., 1950, *Illum. Engr. N.Y.*, **45**, 688.
 PIPER, W., and WILLIAMS, F., 1955, *Brit. J. Appl. Phys.*, **6**, 539.
 SEITZ, F., 1958, *Phys. Fluids*, **1**, 2.
 SLETTEN, A., 1959, *Nature, Lond.*, **183**, 311.

Temperature Effects in Domain Patterns from Single Crystals of Haematite ($\alpha\text{-Fe}_2\text{O}_3$)

By G. KAYE†

Department of Physics, Imperial College, London

Communicated by M. Blackman; MS. received 17th March 1961

Abstract. Electron shadow patterns have been used to study the configuration of domains present in single crystals of haematite ($\alpha\text{-Fe}_2\text{O}_3$) in the temperature range 0 to 700 °C. The observations were made using a furnace designed to fit into the specimen chamber of the electron diffraction camera.

It has been found that once a crystal has been heated to above its Curie temperature the configuration of domains present in the specimen at room temperature is partially stable. Repeated heat treatment of the crystal to above its Curie point leads to a partial 'memory effect' similar to that described by Blackman, Haigh and Lisgarten in 1957 for the low temperature transition in haematite.

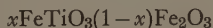
A study of the variation with temperature of the sizes of features in the shadow patterns provides a method of determining the Curie temperature of haematite crystals with an accuracy to 2 to 3 degrees. In this way Curie temperatures between 643 and 688 °C have been observed for crystals from different origins.

Finally an attempt has been made to correlate the Curie temperature of various crystals with their lattice parameters as determined by x-ray powder photographs.

§ 1. INTRODUCTORY REMARKS

THE EXISTENCE of ferromagnetic domains in natural single crystals of haematite was first demonstrated by Blackman, Haigh and Lisgarten (1957) by means of electron shadow patterns. Their results, obtained at room temperature, were consistent with average domain sizes of about $\frac{1}{10}$ mm or more. These observations were later verified by Williams, Sherwood and Rameika (1958). The latter used artificially produced crystals and, employing the magnetic Kerr effect, found domains of a similar size. Part of the present work is concerned with studying the appearance of the electron shadow patterns of the surfaces of natural single crystals of haematite from various localities as the crystals are heated to temperatures above their Curie points and then cooled. In this way information has been gained about the behaviour of ferromagnetic domains in the temperature range 0 to 700 °C.

In addition, it has been known for some time that, under suitable conditions, titanium may be substituted for some of the iron in the haematite crystal lattice. The resulting solid solution series that can be prepared has as its end members haematite and ilmenite (FeTiO_3), so that a typical member of this series can be written



(where x is the molecular proportion of ilmenite in haematite). The properties of the haematite-ilmenite series have been the subject of many investigations; some of the more important of these investigations being by Pouillard (1950), Basta (1953), Ishikawa and Akimoto (1957), Uyeda (1957) and Cox (1958). In all of these cases chemically

† Now at the Morgan Crucible Co., Wandsworth, London.

beam by means of the mechanism G. The heating unit consists of two coaxial cylinders, the inner one H made of silica, the outer one K (the radiation shield) made of stainless steel. Nichrome wire is wound to and fro along the length of the outer surface of the inner cylinder and along the length of the inner surface of the radiation shield. The heating unit is mounted inside the specimen chamber, the supports being constructed principally of Pyrophyllite. The specimen L can be heated to temperatures up to 700 °C. The temperature of the specimen is measured by a chromel-alumel thermocouple (in the form of 'Thermocoax' wire) incorporated in the specimen holder with the hot junction placed immediately behind the specimen. The results of various preliminary experiments showed that the thermocouple recorded the actual temperature of the surface of the specimen.

§ 3. EXPERIMENTAL DETAILS

The experimental arrangement for producing electron shadow patterns of the crystals is similar to that used by Blackman, Haigh and Lisgarten (1959). The electron beam is accelerated in most cases to 40 kv and focused just above the specimen to be examined. In addition, the focus is caused to oscillate at mains frequency by a pair of coils carrying alternating current. The divergent band of electrons so formed is intercepted by the edge of the crystal producing an electron shadow of the surface of the crystal which can be observed on a fluorescent screen or recorded on photographic film. These shadow patterns have been studied as the specimens were heated to temperatures up to 800 °C and then cooled, all experiments being conducted in the earth's magnetic field. In most cases the crystals used had well-formed smooth (00.1) faces. In the case of crystals from Elba and Etna, the faces which were used were the (10.1), (22.3) and (01.4) planes (using hexagonal crystal axes). The specimens were covered with a layer of colloidal graphite, to avoid the possibility of electrostatic charging of inclusions (such as quartz) in the crystals, by the electron beam.

§ 4. RESULTS

4.1. *The Effect of Temperature on the Domain Configurations observed in various Haematite Crystals*

Figure 2 shows a series of shadow patterns of the surface of a typical previously unheated single crystal of haematite from Elba, as the crystal was heated to 700 °C and then cooled in the earth's magnetic field. In these experiments it was found useful to study the variation with temperature of the sizes (denoted by W) of prominent features in the observed shadow patterns. For example figure 3 shows the variation of W with temperature for several prominent features observable in figure 2 as the crystal is heated and then cooled. The experimental results shown in figures 2 and 3 indicate:

(i) That as the crystal is heated the positions of the prominent features in the shadow patterns remain unchanged although their sizes vary; in some cases, however, a few additional features appear as the crystal is heated.

(ii) That the sizes of these features are almost constant up to about 600 °C; from 600 to 680 °C there is a rapid decrease in their sizes, the shadow edge becoming straight at about 688 °C (that is, the shadow is of a purely geometrical nature). This is associated with the disappearance of the ferromagnetism and hence of the magnetic leakage field as the Curie temperature of the crystal is reached.

(iii) That as far as can be estimated from measurements based on the sizes of prominent features, the sizes of all the features in the shadow pattern appear to become zero at the same temperature (see figure 3). These features also appear to vary with temperature in approximately the same way.

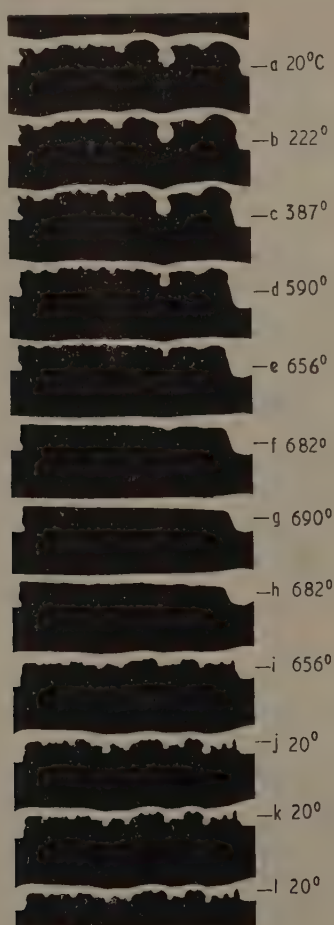


Figure 2. The effect of temperature on the shadow pattern of the surface of a single crystal of haematite, origin Elba. The length of the crystal in the direction perpendicular to the electron beam is 7 mm.

(iv) That, as far as the initial heating of the specimen is concerned, the detail in the shadow pattern observable at room temperature after the crystal has been cooled from above its Curie temperature does not show any similarity to that present in the pattern before the crystal is heated (compare figures 2(a) and (j)). The sizes of the features

n these two patterns are, however, of the same order of magnitude. This can be seen from figure 3 which also shows, for a few features, the variations of feature size with temperature which appear on cooling the crystal from above its Curie point.

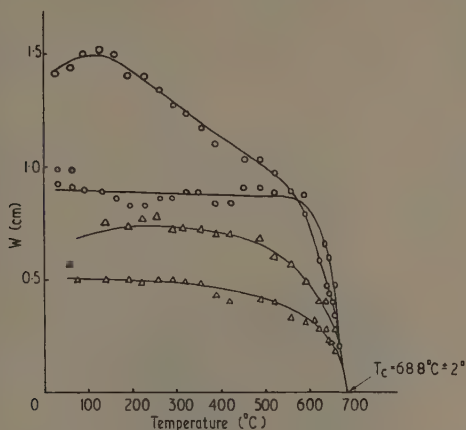


Figure 3. Variation of feature size W with temperature for two prominent features. The lower two curves were obtained during the cooling of the crystal from above the Curie point, the upper curves during heating through the Curie point.

Further experiments in which single crystals of haematite from various localities have been used have shown the following:

(i) The sizes of the features observable in the shadow patterns of different haematite crystals seem to be of the same order of magnitude. Further, these patterns do not appear to be dependent on the type of surface examined (i.e. (00.1), (10.4) etc.).

(ii) When crystals, instead of being heated to their Curie temperature, are heated to, say, 10 °C below this temperature and allowed to cool it is found that the shadow patterns observable before and after heating are identical. The results from an experiment of this type are shown in figure 4.

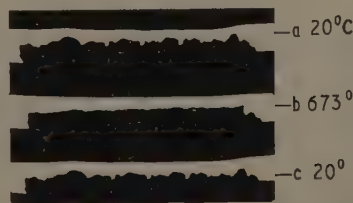


Figure 4. Shadow patterns of a haematite crystal (origin Brazil): (a) at room temperature, (b) at 673 °C (10 deg c below the Curie temperature of 683 °C), (c) at room temperature after the crystal has cooled. The length of the crystal in the direction perpendicular to the electron beam is 7 mm.

(iii) *After the initial heating of the specimen* (to above its Curie point) the shadow patterns which can be seen at room temperature before and after further repeated heating of the specimen showed marked similarities to one another as regards the details. This is also illustrated in figure 2. The crystal of haematite (origin Elba) was heated four times to above its Curie point. The similarity of the details in figures 2(j) to (l) can clearly be seen. However there are some changes in the detail of these patterns during successive heat treatment.

4.2. *The Variation of Curie Temperature in Natural Crystals*

The observation of shadow patterns at high temperatures has been used in § 4.1 to determine the Curie temperature of crystals of haematite. In figure 5 two crystals

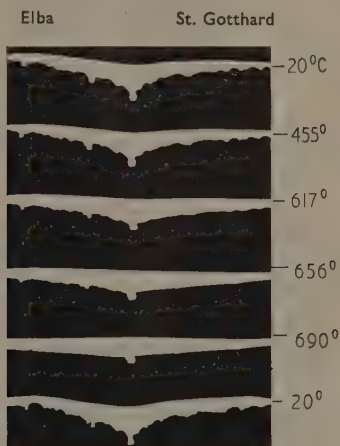


Figure 5. Comparison of the shadow patterns of two natural single crystals of haematite having widely differing Curie points—one (origin Elba) having a Curie point of 688°C , the other (origin St. Gotthard) having a Curie point of 643°C . The length of each of the crystals in the direction perpendicular to the electron beam is 4 mm.

of haematite from different localities (namely Elba and St. Gotthard, Switzerland) were mounted side by side and their shadow patterns observed as the crystals were heated towards their Curie points. The widely differing Curie points of the crystals is clearly seen; a detailed study of the shadow patterns shows these Curie points to be 688°C for the crystal from Elba and 643°C for the other crystal from St. Gotthard. In this way it was found possible to differentiate between haematite crystals having Curie temperatures within 3°C of one another.

Experiments of the type illustrated in figure 5 have been performed using crystals from many different localities. Table 1 indicates the range of Curie temperatures obtained from the various crystals which have been examined. In no case has a Curie temperature of less than 643°C been observed.

Table 1

Curie Temperatures of Natural Haematite Crystals from Various Sources

Specimen No.	Origin	Curie Temp. (°C)
E-H(H)1	Elba	688 ± 2
Et. -H	Mt. Etna, Sicily	688 ± 3
S-H(G-B)D1	Brazil	685 ± 2
S-H(B)20	Brazil	684 ± 2
S-H(E)	Unknown	673 ± 3
S-H(A)1	Unknown	660 ± 3
S-H(G-B)C3, 4	Unknown	659 ± 2
S-H(S-G)A1	St. Gotthard, Switz.	656 ± 3
S-H(S-G)B20	St. Gotthard, Switz.	643 ± 3

Spectrochemical analyses of haematite crystals from various localities have shown (see Kaye 1960) that the variation in Curie temperature shown in table 1 is due, principally, to the various amounts of titanium present as impurity in the crystals. This titanium, when it replaces iron in the haematite crystal lattice, lowers the Curie temperature and slightly increases the size of the unit cell. The change in the lattice parameters was associated with the variation in the Curie temperature in the following way. A number of crystals were first examined by electron shadow pattern methods outlined in § 4.1 to determine their Curie temperatures. A quantity of powder was obtained from each crystal by grinding the surface previously examined. A portion of the powder was analysed by spectrochemical methods, the remainder being used for a determination of the lattice parameters by standard x-ray powder methods.

The information gained in this way for five natural crystals of haematite is shown in table 2, and will be discussed in § 5.

Table 2

Variation of the Lattice Parameters of Haematite Crystals (from various localities) with the Volume of the Hexagonal Unit Cell

Specimen No.	Origin	Major Impurities	Lattice Parameters			Curie Temp. (°C)
			$A_H(\text{\AA})$	$C_H(\text{\AA})$	$V_H(\text{\AA}^3)$	
E-H(H)1	Elba	None	5.0348	13.751	301.87	688
S-H(E)	Unknown	0.3% Ti	5.0357	13.758	302.14	673
S-H(G-B)C1	Unknown	1% Ti	5.0356	13.756	302.08	661
S-H(S-G)A1	St. Gotthard, Switz.	2.5% Ti	5.0362	13.758	302.20	656
S-H(S-G)B1	St. Gotthard, Switz.	3% Ti	5.0362	13.761	302.26	643

V_H is the volume of the hexagonal unit cell. The errors in A_H and C_H are ± 0.0005 and ± 0.002 respectively; the error in V_H is ± 0.13 .

§ 5. DISCUSSION

The interpretation of electron shadow patterns of haematite crystals in terms of the existence of an arrangement of ferromagnetic domains in the crystals is now fairly well established. On this basis one can infer the following from the results described in § 4.1.

The fact that the features in the shadow patterns change very little as the temperature of the crystal is increased to the Curie temperature, implies that the boundaries between the ferromagnetic domains (i.e. the Bloch walls) are, in the main, stable at temperatures below the Curie temperature. The small changes that occur are consistent with the formation of additional domain walls (i.e. the sub-division of large domains).

The variation with temperature of the sizes of the features (figure 3) makes the observation of shadow patterns at high temperatures a reasonably accurate method for the determination of the Curie temperature of haematite crystals. It is possible to measure the Curie point by this method with an accuracy to about 3 deg c.

It should be noted that this Curie point is defined by the vanishing of the magnetic field. This will be higher than the value obtained from the point of inflection of the curve of magnetization against temperature. The latter method gives 675 °c.

The initial heating of a specimen to above its Curie temperature leads, on cooling to room temperature, to an arrangement of domains which is completely different from the original configuration. The new domain boundaries are seen to be at least partially 'pinned down', since subsequent heating and cooling of the specimen produces domain arrangements which show similarities to the arrangement observed on cooling after the first heat treatment (see figures 2 (j) to (l)). There is, therefore, a partial 'memory' effect similar to the memory effect observed by Blackman, Haigh and Lisgarten (1959) for the low temperature transition in haematite. However, in the present case the 'memory' is not nearly so good as for the low temperature transition and appears to vary from specimen to specimen. The experiments in which crystals have been heated to just below the Curie temperature and then cooled show that the magnetic leakage field varies reversibly with temperature provided the Curie temperature is not exceeded.

The results of the present work described in § 4.2 have shown that the lowest Curie temperature observed in natural crystals from many different localities, is 643 °c (as compared with 688 °c for crystals from Elba). Deductions from the spectrochemical analyses of haematite crystals which have a Curie temperature in this region (see Kaye 1960) are consistent with 1.5% titanium at the most being incorporated into the crystal lattice ($x \simeq 0.05$). It seems reasonable, therefore, to assume that this amount of titanium approximates closely to the maximum that can be so accommodated in the haematite lattice at room temperature. Any titanium in excess of the above amount at the time of the formation possibly exsolved out of the lattice as the crystal cooled slowly (assuming the haematite was formed at high temperature). The point is important in connection with the shape of the solvus curve for the haematite-ilmenite series. The present results suggest that the solvus curve should pass through the composition $x \simeq 0.05$ at room temperature. This implies that the solvus relationship determined by Uyeda (1957) should be modified slightly.

The variation of the volume of the hexagonal unit cell with Curie temperature, shown in table 2, is linear to within experimental error. Other investigations of the haematite-ilmenite series, using chemically prepared powders, have not dealt in detail with the region considered in this work, $0 < x < 0.1$, but generally with the entire series. It is not, therefore, possible to compare the results of the present work with those of other investigations.

ACKNOWLEDGMENTS

The author wishes to express his sincere thanks to Professor M. Blackman for suggesting the problem and to Dr. N. D. Lisgarten for his interest and useful dis-

ussions. The author is indebted to the Staff of the Woolwich Outstation Chemistry Department, Atomic Energy Research Establishment, Harwell, for the spectrographic analyses of the samples of haematite, and to Dr. R. G. Davis of the Mineralogy Department, Natural History Museum, for providing facilities for x-ray photographs of some specimens. He would also like to thank the Department of Scientific and Industrial Research for a maintenance grant.

REFERENCES

- BASTA, E. Z., 1953, *Ph.D. Thesis*, University of Bristol.
BLACKMAN, M., HAIGH, G., and LISGARTEN, N. D., 1957, *Nature, Lond.*, **179**, 1288.
— 1959, *Proc. Roy. Soc. A*, **251**, 117.
BLACKMAN, M., and LISGARTEN, N. D., 1957, *Proc. Roy. Soc. A*, **239**, 93.
COX, D. E., 1958, *Ph.D. Thesis*, University of London.
ISHIKAWA, and AKIMOTO, 1957, *J. Phys. Soc. Japan*, **12**, 1083.
KAYE, G., 1960, *Ph.D. Thesis*, University of London.
POUILLARD, E., 1950, *Ann. Chem.*, **5**, 164.
UYEDA, S., 1957, *Jap. J. Geophys.*, **2**, 1.
WILLIAMS, H. J., SHERWOOD, R. C., and RAMEIKA, J. P., 1958, *J. Appl. Phys.*, **29**, 1772.

Magnetothermal Measurements on Gadolinium

By L. F. BATES AND A. J. PACEY

The University, Nottingham

MS. received 25th July 1961

Abstract. The small heat changes accompanying the magnetization of 99.9% pure gadolinium were measured on a rod specimen. The results are analysed, and the principal magnetization processes are identified. Domain wall movement which occurs in low fields is discussed in the light of a theory by Goodenough, and the coercivity which the theory predicts is found to agree fairly well with experiment. Comparison is made with earlier results for cobalt.

§ 1. INTRODUCTION

REASONABLY PURE metallic gadolinium was first prepared by Trombe in 1935. A few months later, Urbain, Weiss and Trombe (1935) showed that the metal was ferromagnetic below about 16 °C. Now, the modern theory (Stoner and Rhodes 1949) of magnetothermal effects is based on the assumption that measurements are made at temperatures well below the Curie point. It is evident, therefore, that magnetothermal measurements on gadolinium must be made at lower temperatures than are usual in such work.

Apart from arrangements for cooling the specimen down to 100 °K, the present experiment followed standard practice (Bates and Sherry 1955). The specimen was in the form of a rod, 20 cm long and 0.31 cm in diameter, and was obtained from Johnson, Matthey and Co. Ltd. It contained less than 0.1% impurities, of which the principal were silicon, aluminium, manganese and iron. Ten thermocouples were tied to the specimen, and it was placed inside the magnetizing solenoid. The magnetic field was changed by successive increments ΔH and the corresponding thermal changes $\Delta Q'$, total and reversible, were measured. By convention, the thermal energy of the system was taken to be zero in the maximum (negative) field used, and a plot of Q' against H for half a cycle was obtained by summing the individual increments of field and thermal energy (figures 1 and 2).

The results were calibrated by making use of the expression

$$(\partial Q'/\partial H)_S = -T(\partial I/\partial T)_H.$$

Values of $-T(\partial I/\partial T)_H$ at $H = 600$ Oe were obtained from the (I, H) measurements over the whole range of temperatures. These were plotted against temperature (figure 3) and the measured deflections which gave $(\partial Q'/\partial H)_S$ were fitted to this graph. It will be seen from figure 3 that $(\partial Q'/\partial H)_S$ is very small at low temperatures, but increases to a high value near the Curie point; above the Curie point, it falls rapidly to a small value.

§ 2. EXPERIMENTAL ERRORS

Following the Stoner and Rhodes theory, the first stage in the analysis of the experimental results is to calculate values of b'' , using the expression,

$$\left[\frac{(\partial Q'_R/\partial H)_S - aI}{H(\partial I_R/\partial H)_T} \right] - a$$

where $a = -(T/I_0)(dI_0/dT)$ and $\partial I_R/\partial H$ is the reversible susceptibility.

Two sources of error in the values of b'' might have been important as a result of making measurements at reduced temperatures. The first of these was the effect of the stability of the system at low temperatures, which meant that low sensitivities had to be used. To estimate this error, it was assumed that the (I, H) measurements were perfectly accurate, the error being entirely in $(\partial Q'/\partial H)_S$, and of magnitude of about $10 \text{ erg cm}^{-3} \text{ Oe}^{-1}$. This represents a 30% error at 100°K , but only 2% error at 223°K ,

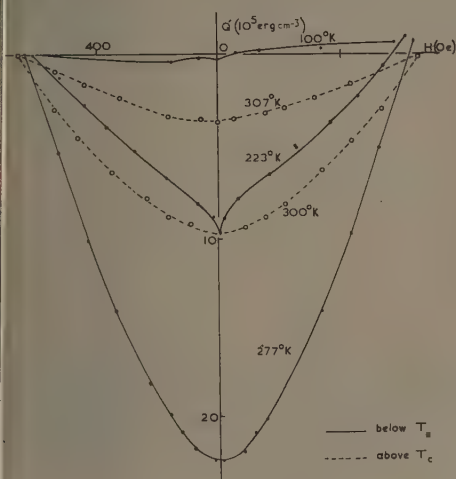


Figure 1. Thermal curves for gadolinium at stated temperatures, those above the Curie point indicated by dotted lines.

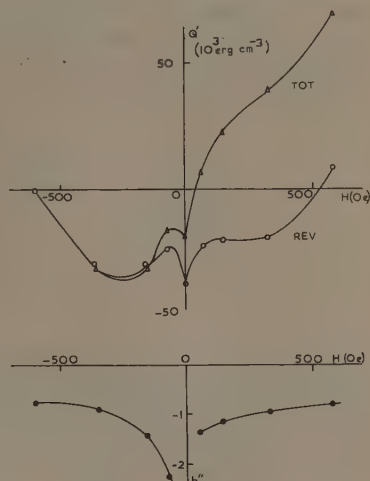


Figure 2. Q' and b'' curves for gadolinium at 100°K .

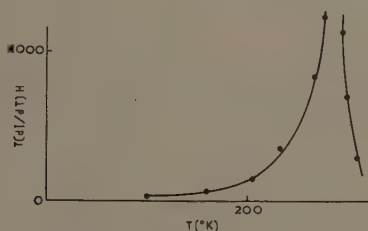


Figure 3. Graph of $-T(dI/dT)_H$ against temperature of the gadolinium specimen.

where $(\partial Q'/\partial H)$ was larger. It will be seen from the expression for b'' that the error in b'' depends on the error in the expression $(\partial Q'/\partial H) - aI$. At 100°K , aI was much greater than $(\partial Q'/\partial H)$, so that the large error in the latter quantity did not have a proportionate effect on b'' . The probable error in b'' was ± 0.2 in all cases.

The second experimental error which may have been important occurs because the temperature at which the thermal measurements were made could not be exactly reproduced when the hysteresis cycle was observed. A Dewar flask which fitted inside the solenoid was arranged to hold liquid oxygen, solid carbon dioxide or ice and salt,

as required. However, the specimen never quite reached the temperature of these materials because of the need to protect it from contact with them by means of a close glass tube. But this precaution, necessary because of the active chemical nature of gadolinium, improved the thermal stability of the system. The effect was probably quite small at 100 °K and 277 °K, but it was estimated that the error was considerable when solid carbon dioxide was used.

Additional errors were to be expected at 277 °K as a result of using the Stoner and Rhodes equation so near to the Curie point. The use of a more general equation involves several estimates, but it seems that b'' should have been about -8.0 instead of -7.5 as found by using the normal method. The several values obtained at different temperatures are given in the table.

Values of b'' and Crystal Anisotropy

$T(^{\circ}\text{K})$	100	223	277	290
K/K_{100}	1.0	0.44	0.23	0.10
$(T/K)(dK/dT)$	-0.7	-1.3	-8.5	—
b''	-0.7	-0.8	-7.5	—

§ 3. ANALYSIS OF RESULTS

In high fields, b'' tends towards a constant value b_1 which should be equal to $(T/K)(dK/dT)$ if rotations are the principal magnetization processes in such fields. In low fields, several magnetization processes may be superimposed. Saunders and Tebble (1960) considered the corresponding thermal effects, and showed from a discussion of the equations given by Teale and Rowlands (1957) that

$$b''H = \sum_{n=1}^N b_n v_n$$

where v_n is the derivative of a free energy function with respect to magnetization, and b_n is a constant, analogous to b_1 , for the n th magnetization process. It is of the form $(T/A_n)(dA_n/dT)$, so that, for example, rotations against strain anisotropy give b_n equal to $(T/\lambda_s)(d\lambda_s/dT)$.

The difficulty with this equation is that there is no way of calculating v_n . However, if only two magnetization processes are superimposed, it is possible to make certain assumptions about v_1 and v_2 which enable estimates of b_2 to be obtained, from both magnetothermal results and coercivity data. We have used the formula (cf. Bates and Pacey 1961†)

$$b_2 = \frac{T}{H_c} \frac{dH_c}{dT} + \frac{T}{I_0} \frac{dI_0}{dT},$$

where H_c is the coercivity. Estimates so obtained for gadolinium appeared to lie between $(T/\gamma)(d\gamma/dT)$ and $(2T/I_0)(dI_0/dT)$. This result suggested that the low field magnetization processes might be those described by Goodenough (1954), who gives an expression for the coercivity of the form

$$H_c \simeq \frac{a_1\gamma}{I_0} + a_2 I_0 \quad \text{with } \gamma = (AK)^{1/2},$$

where a_1 and a_2 are constants for a given material. In figure 4, the measured coercivity

† *Proceedings of International Conference on Magnetism*, Kyoto, Japan.

is compared with that predicted by Goodenough's theory. An absolute value for the value of K at 100 °K, K_{100} , could not be obtained, but it was estimated to be approximately 5×10^5 erg cm⁻³. Using this value, the values of a_1 and a_2 which gave the best fit were, respectively, 1.45×10^4 and 10^{-3} . The agreement is quite good, except that the theory does not give as big a trough at about 210 °K as the experimental points seem to indicate.

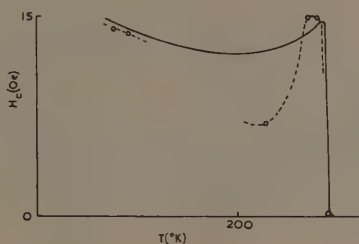


Figure 4. Variation of the coercivity of gadolinium with temperature: full line, theoretical curve; circles, experimental points.

The principal process envisaged by Goodenough is that when domains of reverse magnetization expand, they are controlled by free pole energy and the surface tension of the domain walls. This contributes roughly 13 Oe to the coercivity. The remaining 2 Oe can be accounted for on Goodenough's theory as the effect of grain boundaries.

Before this analysis could be carried out, the temperature dependence of the magnetocrystalline anisotropy had to be measured. A torque magnetometer was used, but as the specimen was polycrystalline, absolute values of K could not be obtained. However, there was sufficient orientation in the specimen to allow satisfactory values of $(T/K)(dK/dT)$ to be found. (As mentioned above, K lay between 10^5 and 10^6 erg cm⁻³ at 100 °K.) Values found for K are given in the table in terms of the value of K at 100 °K. The differences which were found between the measured values of b_1 and $(T/K)(dK/dT)$ were all within the limits of the error suggested in § 2.

Cobalt has a hexagonal crystal structure and a large crystal anisotropy, so that it should behave very much like gadolinium. Data obtained for polycrystalline cobalt by Bates and Sherry (1955) and Tebble and Teale (1957) were examined, and values of b_2 which lay between $(T/\gamma)(d\gamma/dT)$ and $(T/K)(dK/dT)$ were obtained. These specimens were partially annealed and had coercivities of 28 Oe and 34 Oe, respectively. However, Samuel (1928) gives coercivity data for a specimen which was more completely annealed, and from which an estimate of b_2 was obtained in good agreement with $(T/\gamma)(d\gamma/dT)$. The coercivity of this specimen, 11 Oe, was of the order of magnitude predicted by Goodenough's formula.

§ 4. CONCLUSIONS

The magnetothermal measurements described here provided data from which the magnetization processes in polycrystalline gadolinium have been identified. In high fields, the principal magnetization process is rotation against crystal anisotropy. Below about 100 Oe the growth of domains of reverse magnetization, as envisaged by Goodenough, becomes more important. The magnetization processes in annealed, polycrystalline cobalt are substantially the same.

ACKNOWLEDGMENTS

We are indebted to Mr. J. K. Ackers for making the measurements of magnetocrystalline anisotropy. A. J. P. thanks the Department of Scientific and Industrial Research for a maintenance grant.

REFERENCES

- BATES, L. F., and SHERRY, N. P. R., 1955, *Proc. Phys. Soc. B*, **68**, 642.
GOODENOUGH, J. B., 1954, *Phys. Rev.*, **95**, 917.
SAMUEL, M., 1928, *Ann. Phys., Lpz.*, **86**, 798.
SAUNDERS, N. H., and TEBBLE, R. S., 1960, *Proc. Phys. Soc.*, **76**, 282.
STONER, E. C., and RHODES, P., 1949, *Phil. Mag.*, **40**, 481.
TEALE, R. W., and ROWLANDS, G. R., 1957, *Proc. Phys. Soc. B*, **70**, 1123.
TEBBLE, R. S., and TEALE, R. W., 1957, *Proc. Phys. Soc. B*, **70**, 51.
TROMBE, F., 1935, *C. R. Acad. Sci., Paris*, **200**, 459.
URBAIN, G., WEISS, P., and TROMBE, F., 1935, *C. R. Acad. Sci., Paris*, **200**, 2132.

Paramagnetic Resonance of Manganese

By T. P. P. HALL, W. HAYES and F. I. B. WILLIAMS

The Clarendon Laboratory, Oxford

Communicated by B. Bleaney; MS. received 27th July 1961

Abstract. The paramagnetic resonance spectrum of divalent manganese has been investigated in the crystals CdF_2 , KMgF_3 and CdTe which have cubic symmetry, and in the crystals ZnO , MgCl_2 , and CdCl_2 which have axial symmetry. The measured cubic field splitting parameter a is compared with values predicted from recent theoretical work.

§ 1. INTRODUCTION

THE THEORY of Watanabe (1957, 1960) stimulated interest in the splitting of the energy levels of S-state ions by cubic crystal fields. He concluded that the crystal field parameter a should be determined entirely by even powers of the crystal potential V and hence should be positive for both positive and negative values of Dq (for a definition of Dq see McClure 1959). It was subsequently pointed out by Powell, Gabriel and Johnston (1960, 1961, to be referred to as I) that terms odd in V may contribute significantly to a . However, all previous measurements on MnIII ($3d^5, {}^6S_{5/2}$) and the isoelectronic FeIV in cubic environments with both positive Dq (octahedral co-ordination) and negative Dq (fourfold and eightfold co-ordination) have yielded positive values of a . (For a discussion of some recent measurements see Geschwind 1961). In environments with axial symmetry, terms D and F appear in the spin Hamiltonian for d electrons corresponding to axial fields of the second degree (V_2^0) and of the fourth degree (V_4^0). Crystal field mechanisms to account for the second-degree axial term have been proposed by Pryce (1950) and by Watanabe (1957), the first linear in V , and the second quadratic in V (for a review of crystal field theory see Low 1960). Kondo (1960) has extended the theory to include overlap and covalent effects in an attempt to explain observed D values for MnIII in NaCl and LiCl (Watkins 1959).

Because of the general interest in the spectra of S-state ions we have measured the spectra of MnIII present as a substitutional impurity in the cubic crystals CdF_2 , KMgF_3 and CdTe and in the axial crystals CdCl_2 , MgCl_2 and ZnO . CdF_2 has the fluorite structure and cleaves in (111) planes; each cadmium ion is bonded to eight fluorine ions at a distance of 2.33 Å. Crystals of KMgF_3 have the cubic perovskite structure and each magnesium ion is surrounded by six fluorine ions at a distance of 1.994 Å. The CdF_2 and KMgF_3 crystals were grown by the Stockbarger (1949) method. CdTe has the zinc blende structure and cleaves in (110) planes; each cadmium ion is bonded to four tellurium ions at a distance of 2.78 Å. X-ray examination of our CdTe crystals disclosed a high degree of mosaic structure.

CdCl_2 and MgCl_2 have similar structures with $\bar{R}3m$ symmetry and the unit cell dimensions (Wyckoff 1948), with the isomorphous MnCl_2 included for comparison, are given in table 1.

In CdCl_2 the metal ions and the chlorine ions form planes normal to the trigonal axis and the planes of metal ions are separated by two planes of chlorine ions. The bonding

between the adjacent planes of chlorine ions is rather weak (Pauling 1960) and the crystals cleave easily along these planes. For CdCl_2 , the Cd-Cl distance is 2.74 Å, the distance between chlorine ions in the same plane is 3.85 Å and the distance between nearest chlorine ions in neighbouring planes is 3.68 Å, implying a compression along the trigonal axis of the octahedron of chlorine ions surrounding each cadmium ion. From data given by Murray (1955) we find that in MnCl_2 , the Mn-Cl distance is 2.53 Å and the Cl-Cl distance is 3.69 Å and here also we have a compression along the trigonal axis of the chlorine octahedron surrounding the manganese ion. Equivalent data on the atomic spacings in MgCl_2 are not available. The crystals of CdCl_2 and MgCl_2 were grown by dropping an evacuated silica capsule containing the anhydrous chloride powder mixed with 0.1% MnCl_2 through a sharp temperature gradient; they are strongly hygroscopic.

Table 1

	$a_0(\text{\AA})$	α
CdCl_2	6.23	$36^\circ 02'$
MnCl_2	6.20	$34^\circ 35'$
MgCl_2	6.22	$33^\circ 36'$

The ZnO sample, which was kindly supplied to us by Dr. P. B. Dorain, was obtained from a naturally occurring deposit. It contained traces of manganese and was pink in colour due to continuous absorption in the blue region of the spectrum which, presumably, arises from charge transfer transitions associated with impurities. The sample showed the zincite symmetry, $C6mc$, in which the Zn ion is surrounded by a tetrahedron of oxygen ions. The Zn-O distance is 1.95 Å measured along the trigonal axis of the crystal and is 1.98 Å measured along the other axes of the tetrahedron, implying a slight compression of the tetrahedron along the unique axis. The hexagonal unit cell parameters are $a_0 = 3.2426$ Å and $c_0 = 5.1948$ Å (Wyckoff). There are two inequivalent ions in the magnetic unit cell. The measurements were carried out at X and K-band in spectrometers of the type described by Llewellyn (1957).

§ 2. EXPERIMENTAL RESULTS

2.1. Crystals with Cubic Symmetry

The spin Hamiltonian for MnIII in an environment with cubic symmetry may be written

$$\mathcal{H} = g\beta \mathbf{H} \cdot \mathbf{S} + A \mathbf{I} \cdot \mathbf{S} + \frac{1}{6}a[S_\xi^4 + S_\eta^4 + S_\zeta^4 - \frac{1}{3}S(S+1)(3S^2 + 3S - 1)] + \sum_n \mathbf{I}^n \cdot A^n \cdot \mathbf{S}. \quad (1)$$

Neglecting the final term which describes the hyperfine interaction between the magnetic electrons and the nuclei of ligand ions, the positions of the resonance lines are given by

$$\begin{aligned} M = \pm \frac{5}{2} \leftrightarrow \pm \frac{3}{2} & \quad g\beta H = g\beta H_0 \mp 2pa - Am_I - \alpha(\frac{3.5}{4} - m_I^2 \pm 4m_I) \\ M = \pm \frac{3}{2} \leftrightarrow \pm \frac{1}{2} & \quad g\beta H = g\beta H_0 \pm \frac{5}{2}pa - Am_I - \alpha(\frac{3.5}{4} - m_I^2 \pm 2m_I) \\ M = +\frac{1}{2} \leftrightarrow -\frac{1}{2} & \quad g\beta H = g\beta H_0 - Am_I - \alpha(\frac{3.5}{4} - m_I^2) \end{aligned} \quad (2)$$

where $\alpha = A^2/2g\beta H_0$, $p = 1 - 5\phi$, $\phi = l^2m^2 + m^2n^2 + n^2l^2$, and l, m, n are the direction cosines of the magnetic field relative to the principal cubic axes ξ, η, ζ .

In the spectrum of MnIII in CdF_2 the hyperfine interaction with the neighbouring fluorine nuclei may be separated into an isotropic part A_s and an anisotropic part A_p (Inkham 1956). A_s is greater than the cubic field parameter a and the spectrum consists of six manganese hyperfine lines, characterized by m_I , each with a resolved fluorine hyperfine structure, and each of these fluorine lines has a five line fine structure due to the cubic crystal field. A careful investigation of the spectrum was made at X and K-band in the [100], [110] and [111] directions but, because of the great complexity of the spectrum, it was not possible to obtain a precise value for a . It was possible to assign an upper limit of $4 \times 10^{-4} \text{ cm}^{-1}$ to $|a|$ but a value less than half of this is more likely. A re-investigation of the spectrum of MnIII in CaF_2 suggested that the value of $a = +0.6 \times 10^{-4} \text{ cm}^{-1}$ given by Baker, Bleaney and Hayes (1958) should be replaced by an upper limit for $|a|$ similar to that given here for CdF_2 . The measured constants of the spin Hamiltonian are given in table 2. Our measurements on $\text{KMgF}_3\text{:Mn}$ were carried out at X-band only. Our results, which are given in table 2, are in agreement with the measurements of Ogawa (1960) within the quoted experimental errors.

Our measurements on CdTe , given in table 2, were carried out simultaneously with those by Lambe and Kikuchi (1960) and agree with theirs. We find, as they did, that the spin-lattice relaxation time is unusually short. The line width is 50 G at 300°K ; at 10° the fine structure is resolved and the line width is 17 G; at 20° the line width is 3 G and an isotropic interaction A_s with the nearest neighbour cadmium nuclei is observed in the $M_S = +\frac{1}{2} \leftrightarrow -\frac{1}{2}$ transition. The mosaic structure found in all the available samples may explain the failure to resolve the cadmium hyperfine structure in the $\nu_S = \pm\frac{5}{2} \leftrightarrow \pm\frac{3}{2}$ and the $M_S = \pm\frac{3}{2} \leftrightarrow \pm\frac{1}{2}$ transitions. The resolution of a hyperfine interaction with the second nearest neighbours is an indication of the strongly covalent nature of this crystal which has a band gap of 1.5 eV.

The line width and the complexity of the electron spin resonance spectrum often combine to defeat one in trying to find small a values. In an effort to find an alternative method we have examined the relative merits of the electron nuclear double resonance (Fischer 1956) and of the usual electron spin resonance techniques. When the magnetic field is not along a principal cubic axis, cross terms appear in the third and fourth order between the crystal field and the hyperfine structure to give a surprisingly large shift in the energy levels which is linear in the nuclear magnetic quantum number, but with rather a complex dependence on the electronic magnetic quantum number which enables it to be separated from the nuclear quadrupole and Zeeman terms. Bleaney and Rubins (1961) have calculated the effects of some of these cross terms between the hyperfine interaction and a second-degree crystal field with axial symmetry. Calculations are given here for a crystal field of general symmetry. We shall assume a spin Hamiltonian of the form

$$\mathcal{H} = g\beta\mathbf{H} \cdot \mathbf{S} + A\mathbf{I} \cdot \mathbf{S} + V - g_n\beta_n \mathbf{H} \cdot \mathbf{I}$$

where V represents the crystal field and may be written (Baker, Bleaney and Hayes 1958)

$$V = \sum_{n,m} B_n^m O_n^m.$$

The cubic field operator $\frac{1}{6}a[S_x^4 + S_y^4 + S_z^4 - \frac{1}{5}S(S+1)(3S^2 + 3S - 1)]$ of equation (1) becomes $B_4(O_4^0 + 5O_4^4)$ in the notation of Baker, Bleaney and Hayes and the second-degree axial field operator $D[S_z^2 - \frac{1}{3}S(S+1)]$ of equation (5) (see § 3) becomes $B_2^0O_2^0$ in the same notation). This general expression for V is much simplified along the symmetry axes of the crystal, but we shall retain the general form since the effect of

aligning the magnetic field in a general direction will be considered, and it is more convenient to keep the Zeeman interaction diagonal. A discussion of the transformation of these crystal field operators under a general co-ordinate rotation may be found in Baker and Williams (1961). The positions of the electron nuclear double resonance lines are affected by the cubic crystal field through the following mechanisms, where the unperturbed Hamiltonian is $\mathcal{H}_0 = g\beta H_z S_z$

$$(i) |\langle M_S m_I | \mathbf{A} \mathbf{I} \cdot \mathbf{S} | M_S \pm 1, m_I \mp 1 \rangle|^2 \{ \langle M_S \pm 1, m_I \mp 1 | V | M_S \pm 1, m_I \mp 1 \rangle - \langle M_S m_I | V | M_S m_I \rangle \}$$

$$(ii) |\langle M_S m_I | V | M_S + m, m_I \rangle|^2 \{ \langle M_S + m, m_I | \mathbf{A} \mathbf{I} \cdot \mathbf{S} | M_S + m, m_I \rangle - \langle M_S m_I | \mathbf{A} \mathbf{I} \cdot \mathbf{S} | M_S m_I \rangle \}$$

$$(iii) |\langle M_S m_I | V | M_S \pm 1, m_I \rangle|^2 |\langle M_S \pm 1, m_I | \mathbf{A} \mathbf{I} \cdot \mathbf{S} | M_S m_I \pm 1 \rangle|^2.$$

Mechanism (i) reflects the way in which the crystal field helps the Zeeman interaction to decouple the electronic and nuclear spins. Mechanism (ii) shows how the crystal field destroys S_z quantization and hence alters the expectation value of S_z . The last mechanism has been considered by Bleaney and Rubins. These mechanisms contribute to the energy level characterized by (M_S, m_I) as follows:

$$(i) \left(\frac{A}{2g\beta H} \right)^2 \sum_{\pm} \{ S(S+1) - M_S(M_S \pm 1) \} \{ I(I+1) - m_I(m_I \mp 1) \} \\ \times \{ \langle M_S \pm 1, m_I | \sum_n B_n^0 O_n^0 | M_S \pm 1, m_I \rangle - \langle M_S m_I | \sum_n B_n^0 O_n^0 | M_S m_I \rangle \}$$

$$(ii) A m_I \sum_{m \neq 0} \frac{|\langle M_S m_I | \sum_n B_n^{(m)} O_n^{(m)} | M_S + m, m_I \rangle|^2}{m(g\beta H)^2}$$

$$(iii) A m_I \frac{|\langle M_S m_I | \sum_n B_n^1 O_n^0 | M_S m_I \rangle|^2}{8M_S(g\beta H)^2}.$$

It is interesting to note that where $M_S = \pm S$, (ii) and (iii) exactly cancel one another for $m = 1$ in (ii).

A useful figure for comparing the effectiveness of two types of measurement for the determination of a parameter is afforded by the ratio of that parameter's contribution to some observed quantity to the probable error in the measurement of this quantity. To make this more definite, one may define a figure of merit F for an experiment to obtain the value of a parameter x_p by measurement of a quantity s , which is in general a function of all the parameters $x_1, \dots, x_p, \dots, x_n$ of the problem. We assume that we know the value of all these, except x_p , and that our values are in error by $\delta x_1, \dots, \delta x_{p-1}, \delta x_{p+1}, \dots, \delta x_n$. Finally let δs be the probable error in measuring s . Then we define F such that

$$F = x_p \frac{\partial s}{\partial x_p} / \left(\delta s - \sum_{i \neq p} \frac{\partial s}{\partial x_i} \delta x_i \right). \quad (3)$$

It is assumed that the x_i are sufficiently accurately known to justify the neglect of the second term in the denominator of (3). Further, since δs is usually proportional to the line width, it will be replaced by the line width in the ensuing discussion.

Table 2
Parameters of the Spin Hamiltonian for Mn^{III} Ions in Cubic Crystals

Lattice	Temperature (°K)	Line width (gauss)	g	A (10^{-4} cm ⁻¹)	a (10^{-4} cm ⁻¹)	$ A_s $ (10^{-4} cm ⁻¹)	$ A_p $ (10^{-4} cm ⁻¹)
CdF ₂	300	2	2.0026 ± 0.0006	(-) 93 ± 0.2	≤ 4	9.35 ± 0.10	2.4 ± 0.2
KMgF ₃	300	3	2.0015 ± 0.0005	(-) 91 ± 0.5	(+) 6.5 ± 0.5	17.5 ± 0.5	3.5 ± 1.0
CdTe	20	3	2.0075 ± 0.001	(-) 57.1 ± 0.4	(+) 27.0 ± 2	2.6 ± 0.2	

Table 3
Parameters of the Spin Hamiltonian for Mn^{III} Ions in Crystals with Axial Symmetry

Lattice	Temperature (°K)	Line width (gauss)	g	A (10^{-4} cm ⁻¹)	D (10^{-4} cm ⁻¹)	$a-F$ (10^{-4} cm ⁻¹)
ZnO	20	18	2.001 ± 0.001	(-) 75.0 ± 0.05	(-) 229 ± 2	(+) 3.5 ± 2
MgCl ₂	20	18	2.0015 ± 0.001	(-) 82 ± 1	(-) 121 ± 1	≤ 2
	90	18	2.0015 ± 0.001	(-) 82 ± 1	(-) 123 ± 1	≤ 2
	300	—	2.0015 ± 0.0015	(-) 82 ± 1	(-) 131.5 ± 1.5	≤ 2
CdCl ₂	20	15	2.0015 ± 0.0005	(-) 81.5 ± 0.2	(+) 14.8 ± 0.5	≤ 0.5

If in an electron nuclear double resonance experiment the line width Δ_N arises from mechanism (i), i.e. incomplete decoupling of the electronic and nuclear spins, it may be written (Bleaney 1958)

$$\Delta_N = \frac{1}{2} \left(\frac{A}{g\beta H} \right)^2 [S(S+1) - M_S(M_S+1) + 2M_S m_I] \Delta_E$$

if we neglect the nuclear Zeeman term.

The electronic line width Δ_E is assumed to be constant for all transitions, and to be independent of variation of the parameters being measured.

We shall consider measuring the cubic crystal field parameter of MnIII in a crystal with an axial distortion along a $\langle 100 \rangle$ direction. If we neglect the fourth degree axial crystal field term which is usually small then the Hamiltonian with the z axis along a $\langle 100 \rangle$ direction is

$$\mathcal{H} = g\beta \mathbf{H} \cdot \mathbf{S} + A \mathbf{I} \cdot \mathbf{S} + B_2^0 O_2^0 + B_4(O_4^0 + 5O_4^4) - g_n \beta_n \mathbf{H} \cdot \mathbf{I}, \quad (4)$$

where $S = I = \frac{5}{2}$. We then find the most favourable figure of merit for an electron spin resonance determination by measuring the splitting of the $M_S = +\frac{5}{2} \leftrightarrow +\frac{3}{2}$ and the $M_S = -\frac{5}{2} \leftrightarrow -\frac{3}{2}$ lines is

$$F_{\text{ESR}} = \frac{5b_4}{\Delta_E} \quad \text{where} \quad b_4 = 60B_4.$$

The ratios of the above F_{ESR} to the figure of merit F_{ENDOR} for the mechanisms (i), (ii), and (iii) for the $M_S = +\frac{1}{2}$, $m_I = -\frac{3}{2} \leftrightarrow -\frac{5}{2}$ nuclear transition are

(i)

$$\frac{F_{\text{ENDOR}}}{F_{\text{ESR}}} = \frac{40}{13}$$

(ii) + (iii)

$$\frac{F_{\text{ENDOR}}}{F_{\text{ESR}}} = \frac{6}{65} \frac{b_4^1}{b_4^0} \frac{2b_2^1 - b_4^1}{A} \quad \text{for} \quad |m| = 1$$

where $b_4^m = 60B_4^m$ and $b_2^m = 2B_2^m$

(iii)

$$\frac{F_{\text{ENDOR}}}{F_{\text{ESR}}} = \frac{2}{65} \frac{b_4^2}{b_4^0} \frac{3b_2^2 - \frac{1}{5}b_4^2}{A} \quad \text{for} \quad |m| = 2.$$

The first expression does not depend on the parameters of the spin Hamiltonian (4) since we have assumed that the ENDOR line width arises from the same mechanism as this ENDOR shift. The last two expressions vanish if H is aligned in the $[100]$ direction, but if, for example, it lies in a (100) plane at 22.5° to the $[100]$ axis they become

$$\frac{F_{\text{ENDOR}}}{F_{\text{ESR}}} = \frac{6}{13} \frac{(\frac{5}{2}a - 2.82D)}{A} \quad \text{for} \quad |m| = 1$$

$$\frac{F_{\text{ENDOR}}}{F_{\text{ESR}}} = \frac{1}{13} \frac{(0.45D - \frac{1}{2}a)}{A} \quad \text{for} \quad |m| = 2$$

in the a and D notation.

It is apparent that the electron nuclear double resonance technique will begin to yield appreciably more accurate answers than electron spin resonance only when the crystal field splitting exceeds the hyperfine structure (a or $D \gg A$).

2.2. Crystals with Axial Symmetry

The experimental results, summarized in table 3, are interpreted in terms of the spin Hamiltonian (Bleaney and Trenam 1954)

$$\begin{aligned}\mathcal{H} = & g\beta\mathbf{H} \cdot \mathbf{S} + A\mathbf{I} \cdot \mathbf{S} + D[S_z^2 - \frac{1}{3}S(S+1)] \\ & + \left(\frac{a}{6}\right)[S_\xi^4 + S_\eta^4 + S_\zeta^4 - \frac{1}{3}S(S+1)(3S^2 + 3S - 1)] \\ & + \left(\frac{F}{180}\right)[35S_z^4 - 30S(S+1)S_z^2 + 25S_z^2 - 6S(S+1) + 3S^2(S+1)^2].\end{aligned}\quad (5)$$

The axes ξ , η , ζ are the principal axes of the cubic field and the $[111]$ axis, referred to this basis, is the trigonal axis of the crystal and is labelled the z axis. In the case of MgCl_2 and CdCl_2 the hyperfine interaction with the neighbouring chlorine nuclei is not resolved but contributes to the observed line width (see table 3).

The axial terms add to (2) the following expressions for the line positions:

$$\begin{aligned}M = \pm \frac{5}{2} \leftrightarrow \pm \frac{3}{2}, & \quad \mp [2D(3 \cos^2 \theta - 1) + \frac{1}{3}Fq] - 32\delta_1 + 4\delta_2 \\ M = \pm \frac{3}{2} \leftrightarrow \pm \frac{1}{2}, & \quad \mp \left[D(3 \cos^2 \theta - 1) - \frac{5}{24}Fq \right] + 4\delta_1 + 5\delta_2 \\ M = +\frac{1}{2} \leftrightarrow -\frac{1}{2}, & \quad 16\delta_1 - 8\delta_2.\end{aligned}$$

Here θ is the angle between the z axis and the direction of the applied magnetic field, $q = (35 \cos^4 \theta - 30 \cos^2 \theta + 3)$ and the second-order terms due to the axial field are $\delta_1 = (D^2/g\beta H_0) \cos^2 \theta \sin^2 \theta$ and $\delta_2 = (D^2/4g\beta H_0) \sin^4 \theta$.

When measurements are made with the magnetic field either along or perpendicular to the trigonal axis the term $a - F$ occurs in the expression for the line position and it is not possible to determine a and F separately. It is possible to distinguish the effects of the terms in a and F by making measurements in other directions, but the interpretation of the measurements depends on a knowledge of the position of the ξ , η , ζ axes.

In the investigation of MnIII in the hexagonal form of ZnS by Keller, Gelles and Smith (1958) the term in a was dropped from the spin Hamiltonian and a value of $F = -7.5 \times 10^{-4} \text{ cm}^{-1} (-8.1 \text{ G})$ calculated from measurements made in directions parallel and perpendicular to the trigonal axis. From our discussion it would appear that their results indicate a value of $a - F = +7.5 \times 10^{-4} \text{ cm}^{-1}$.

It was not possible to obtain a general orientation of MgCl_2 or of CdCl_2 crystals from the external morphology and x-ray methods were not successful because of the pronounced hygroscopic nature of the crystals. In the case of ZnO the polycrystalline nature of part of the sample imposed a similar limitation. With ZnO there is the further complication that the two ions in each unit cell are inequivalent, the directions of the axes ξ , η , ζ for one being related to ξ' , η' , ζ' for the other by a rotation of 60° about their common trigonal axis. This produces a doublet structure on the $M = \pm \frac{5}{2} \leftrightarrow \pm \frac{3}{2}$ and the $M = \pm \frac{3}{2} \leftrightarrow \pm \frac{1}{2}$ lines except in special directions for which the two spectra coincide. The smallness of a and the large line width of 18 G, which is due to the poor nature of the crystal, account adequately for our failure to observe this effect. We have made measurements at 90° K and at 20° K which are in agreement within the experimental error and the measurements at 20° K are given in table 3. Dorain's (1958) definition of the cubic crystal field term differs from ours and his a values should be multiplied by -3 for comparison with our a values. We then find that his value of a for manganese in ZnO agrees with our value within the experimental error, though his D value does not.

In calculating the line positions for MnIII in MgCl_2 and ZnO it was found necessary to include third-order perturbations terms, e.g. terms proportional to A^2D and, in the perpendicular plane, to D^3 . It was found that all significant third-order contributions were included by expressing the energy denominators in the second-order terms to first order in D and A in place of the zero-order energy differences proportional to $g\beta H_0$. In the perpendicular plane the separation of the extreme lines in the manganese spectrum is $(1/g\beta)[5A + 4D + (a - F)]$ correct to second order in D and A : the third-order corrections are 3.5 G for MgCl_2 and 10 G for ZnO and are clearly significant in comparison with $(1/g\beta)(a - F)$. The large value of D made third-order corrections necessary for calculations on the measurements of the parallel spectrum in ZnO . The fortuitous overlapping of many of the lines in the parallel spectrum in MgCl_2 made it necessary to make use of measurements made in the perpendicular plane in order to obtain sufficient data to evaluate the parameters of the spin Hamiltonian.

Another consequence of the large axial terms, in the case of ZnO , was the appearance of 'forbidden' transitions, corresponding to $\Delta m_I = \pm 1$, of the type discussed by Bleaney and Rubins. These were observed along the parallel direction for which they are expected to vanish; their presence suggested, as was confirmed by x-ray examination, that a considerable proportion, perhaps as much as 20%, of the sample was composed of very small crystals with more or less random orientation.

In all of the crystals examined very weak low field spectra were observed but not measured; their position and appearance was consistent with their being 'forbidden' $\Delta M_S = \pm 2$ transitions. In CdCl_2 there was an additional weak spectrum with a value of D of about $330 \times 10^{-4} \text{ cm}^{-1}$ which is probably due to interstitial MnIII ions.

§ 3. DISCUSSION

If the ground state of MnIII were pure $^6S_{5/2}$ we would not expect an interaction with the crystal field since the crystal field has no direct interaction with the spin. However, spin-orbit coupling will admix other multiplets of the ground configuration, $3d^5$, into the ground state resulting in a small splitting of the $^6S_{5/2}$ manifold into a quartet Γ_8 and a doublet Γ_7 with a separation $3a$. Watanabe in his attempt to calculate this splitting considered the effect of the crystal field, spin-orbit interaction and spin-spin interaction on the sextet and quartet states of the ground configuration of the free ion. He treated the crystal field as a perturbation on the $\sum_{i,j} f(e^2/r_{ij})$ term which describes the electrostatic interaction between the electrons on the MnIII ion. Powell *et al.* (I), who use the same Hamiltonian as Watanabe, point out, however, that the effect of the crystal field is comparable with this term and also show that consideration of the admixture of the doublets of the ground configuration into the ground state by the spin-orbit coupling is essential. Their method of calculating a does not require the crystal field to be small and they conclude that a is most sensitive to the spin-orbit coupling constant λ and to Dq and varies as $\lambda^4(Dq)^n$, where n varies from 3 to 6 over the range of Dq values 700 cm^{-1} to 1500 cm^{-1} . The theory may be applied to crystals with axial symmetry since the cubic and axial parts of the crystal field are separable.

In their initial calculations Powell *et al.* (1960) used a value of 400 cm^{-1} for λ but pointed out subsequently (Powell *et al.* 1961) that a value of about 250 cm^{-1} is more likely in solid environments. The value of λ for iron group ions in solids is found to be about 25% less than the free ion value (Owen 1955, Low 1958, Hall and Hayes 1960) due to screening effects of the ligand electrons (Marshall and Stuart 1961). Variations of λ with environment are therefore to be expected and will be significant since λ occurs to the fourth power in the expression for a .

Table 4 gives a values (kindly supplied to us by Dr. D. F. Johnston) calculated from the theory of Powell *et al.* over a range of Dq and λ values. These values were calculated assuming the Racah (1942) parameter $B = 1000 \text{ cm}^{-1}$ and $C = 3000 \text{ cm}^{-1}$; the values of B and C were arrived at by fitting the field independent $^4\Gamma_1$ level in the crystal at 5000 cm^{-1} and assuming $C/B = 3$ as in the free ion.

Table 4
Calculated Values of a (in 10^{-4} cm^{-1}) for MnIII

$Dq(\text{cm}^{-1})$	$\lambda = 300 \text{ cm}^{-1}$	$\lambda = 270 \text{ cm}^{-1}$	$\lambda = 240 \text{ cm}^{-1}$	$\lambda = 210 \text{ cm}^{-1}$
300	0.14	0.12	0.09	0.06
400	0.47	0.33	0.23	0.15
500	0.93	0.67	0.43	0.29
780	3.40	2.37	1.57	1.00
830	4.17	2.90	1.93	1.23

Powell *et al.* (1960) predict very small negative a values but only for Dq values in the range 0 to $+200 \text{ cm}^{-1}$. Previously measured Dq values for MnIII in crystals with sixfold co-ordination lie in the range $+700$ to $+1000 \text{ cm}^{-1}$ (see table 5) and negative a values are not expected. MnIII and FeIV in cubic crystal fields of positive and of negative Dq and with a variety of ligands have so far always yielded positive a values. It must be emphasized that in the measurements quoted in this paper and in many of the measurements reported in the literature the sign of a is determined relative to the sign of the hyperfine constant A which is assumed to be negative. The sign of A has been measured in some crystals (see, for example, Bleaney and Ingram) and found to be negative and it seems unlikely that environmental effects will change the sign. In the case of symmetries less than cubic, positive values of a have been reported except in KCl:MnIII where Watkins (1959) gives a tentative assignment of $-1 \times 10^{-4} \text{ cm}^{-1}$ to a .

Table 5
 Dq Values of MnIII in Crystal Environments with Sixfold Co-ordination

Crystal	$Dq (\text{cm}^{-1})$	Reference
MnF ₂	780	Stout (1959)
KMnF ₃	780	Hrostowski (private communication via R. G. Shulman)
MnCl ₂	830	Stout (1960)
		Pappalardo (1959, 1960)
MnBr ₂	940	Stout (1960)
		Pappalardo (1959, 1960)
MnO	979	Pratt and Coelho (1959)

The optical absorption spectrum of MnCl₂ (table 5) gives $Dq = 830 \text{ cm}^{-1}$. From table 4 we predict a value of about $2 \times 10^{-4} \text{ cm}^{-1}$ for a if we assume $\lambda = 250 \text{ cm}^{-1}$. It would be interesting to compare this value of a with the a values in CdCl₂:Mn and

$\text{MgCl}_2:\text{Mn}$ but we have been able to determine only values of $a-F$ for these salts. However, since a and F are both fourth-order crystal field terms, we expect F to be considerably smaller than a if it arises from a small perturbation of the cubic field. This is observed to be so in cases for which a and F have been separately determined (e.g. Bleaney and Trenam). If we then assume $a-F \simeq a$, we find that our measured values are smaller than the predicted value for MnCl_2 . A measurement of Dq and a in the same crystal would be advantageous, but, since optical transitions within the ground configuration of MnIII are both spin and parity forbidden the investigation of the optical spectrum is difficult in specimens sufficiently dilute for electron spin resonance measurements. We attempted to grow crystals of $\text{CdCl}_2:\text{Mn}$ in which it would be possible to measure both a and Dq but without success.

Powell *et al.* (1961) using optical data obtained from MnO ($a_0 = 4.435 \text{ \AA}$) (Pratt and Coelho 1959) find that their calculated value of a for MnIII in the isomorphous MgO ($a_0 = 4.203 \text{ \AA}$) is considerably smaller than the measured value (Low 1956) and suggest that the discrepancy may be due in part to the change in lattice parameter affecting Dq and in part to covalency effects. Since fluorine is the most electronegative of the elements, fluoride crystals might be expected to give a better check on the theory. The optical spectrum of MnF_2 (table 5) gives $Dq = 780 \text{ cm}^{-1}$ and the theory of I then predicts a value of about $2 \times 10^{-4} \text{ cm}^{-1}$ for a . The electron spin resonance spectrum of MnIII present as a trace impurity in the isomorphous ZnF_2 has been investigated (Tinkham 1956, Clogston *et al.* 1960) but no value was found for a because of the complexity of the spectrum. Dq in KMnF_3 is 780 cm^{-1} , predicting a value of a which is identical with that predicted for MnF_2 . However, we find $a = 6.5 \times 10^{-4} \text{ cm}^{-1}$ for MnIII in the isomorphous KMgF_3 . Both KMgF_3 and KMnF_3 have cubic symmetry and the lattice parameters are $a_0 = 3.987 \text{ \AA}$ and $a_0 = 4.190 \text{ \AA}$ respectively. The fact that the a value of manganese in KMgF_3 is greater than predicted from measurements in KMnF_3 supports the view of I that the smaller lattice spacing in the diamagnetic crystal may be partly responsible. This view is further strengthened by the fact that the a value of manganese in CdCl_2 is smaller than that predicted from optical measurements on MnCl_2 since in this case the cation-anion distance in the diamagnetic crystal is greater.

Optical data on MnIII bonded with four or eight ligands are scant. Data on other iron group ions are given in table 6 and it is apparent that the crystal field strengths

Table 6

Dq Values of Divalent Iron Group Ions with Fourfold and Eightfold Co-ordination

Ion	Co-ordination	$Dq(\text{cm}^{-1})$	Reference
$\text{ZnO}:\text{Co}$	4	-390	Pappalardo (private communication) See also McClure (1957)
$\text{ZnO}:\text{Ni}$	4	-405	
$\text{ZnO}:\text{Cu}$	4	-500	
CoCl_4^{2-}	4	-375	Orgel (1955) See also Holm and Cotton (1959)
CoBr_4^{2-}	4	-360	
CoI_4^{2-}	4	-290	
$\text{CaF}_2:\text{Co}$	8	-340	Stahl-Brada and Low (1959)

about half those observed with sixfold co-ordination (McClure 1959). We therefore select a Dq value of about 400 cm^{-1} for MnIII with fourfold and eightfold co-ordination. From table 4, an a value of about $0.3 \times 10^{-4}\text{ cm}^{-1}$. We have not been able to put an upper limit on a in the eightfold co-ordinated CaF_2 and CdF_2 because of the complex hyperfine structure but Low and Rosenberger (1960) show that $a < 1 \times 10^{-4}\text{ cm}^{-1}$ in the isomorphous SrCl_2 . The agreement here is reasonable but gets worse as we go to the more covalent ZnO (table 3) and in the very covalent CdTe ($a = 27 \times 10^{-4}\text{ cm}^{-1}$) we find a discrepancy of almost two orders of magnitude indicating the inadequacy of the purely ionic model of I for covalent systems.

The values of a measured for FeIV are in general an order of magnitude larger than the values found for MnIII and Low (1956, 1957) finds in MgO that $a(\text{MnIII}) = +18.61 \times 10^{-4}\text{ cm}^{-1}$ and $a(\text{FeIV}) = +205 \times 10^{-4}\text{ cm}^{-1}$. A reliable value of λ for FeIV is not available but Kotani (1949) suggests that the λ value is only about 10% larger than that for MnIII and should not therefore contribute significantly to the increase in a . The values of Dq for triply charged iron group ions are about twice as large as the Dq values for divalent ions (Holmes and McClure 1957). In an investigation of the variation of a with pressure, Walsh (1961) finds evidence which indicates that a for MnIII and FeIV in MgO varies as $(Dq)^4$ in which case an increase of a factor of two in Dq in passing from MnIII to FeIV would more than account for the observed increase in a .

ACKNOWLEDGMENTS

We would like to thank Professor B. Bleaney and Dr. D. F. Johnston for their comments on the manuscript. We are indebted to Dr. R. W. H. Stevenson for the crystal of CdF_2 , to Dr. P. B. Dorain for the crystal of ZnO and to Professor D. A. Wright and Dr. J. Woods for the crystal of CdTe . The crystal of KMgF_3 was supplied by Mervyn Instruments Ltd. This work was supported by the Board of Admiralty and the United States Air Force. One of us (F.I.B.W.) is indebted to the Rhodes Trust for a Scholarship.

REFERENCES

- BAKER, J. M., BLEANEY, B., and HAYES, W., 1958, *Proc. Roy. Soc. A*, **247**, 141.
 BAKER, J. M., and WILLIAMS, F. I. B., 1961, *Proc. Phys. Soc.*, **78**, in the press.
 BLEANEY, B., 1958, *J. Phys. Radium*, **19**, 826.
 BLEANEY, B., and RUBINS, R. S., 1961, *Proc. Phys. Soc.*, **77**, 103.
 BLEANEY, B., and INGRAM, D. J. E., 1951, *Proc. Roy. Soc. A*, **205**, 336.
 BLEANEY, B., and TRENAM, R. S., 1954, *Proc. Roy. Soc. A*, **223**, 1.
 LOGSTON, A. M., GORDON, J. P., JACCARINO, V., PETER, M. and WALKER, L. R., 1960, *Phys. Rev.*, **117**, 1222.
 DORAIN, P. B., 1958, *Phys. Rev.*, **112**, 1058.
 FEHNER, G., 1956, *Phys. Rev.*, **103**, 500.
 FESCHWIND, S., 1961, *Phys. Rev.*, **121**, 363.
 GALL, T. P. P., and HAYES, W., 1960, *J. Chem. Phys.*, **32**, 1871.
 HOLM, R. H., and COTTON, F. A., 1959, *J. Chem. Phys.*, **31**, 788.
 HOLMES, O. G., and MCCLURE, D. S., 1957, *J. Chem. Phys.*, **26**, 1686.
 KELLER, S. P., GELLES, I. L., and SMITH, W. V., 1958, *Phys. Rev.*, **110**, 850.
 KONDO, J., 1960, *Progr. Theor. Phys., Japan*, **23**, 106.
 KOTANI, M., 1949, *J. Phys. Soc. Japan*, **4**, 293.
 LAMBE, J., and KIKUCHI, C., 1960, *Phys. Rev.*, **119**, 1206.
 LEWELLYN, P. M., 1957, *J. Sci. Instrum.*, **34**, 236.

- LOW, W., 1956, *Phys. Rev.*, **69**, 119.
— 1957, *Phys. Rev.*, **105**, 793.
— 1958, *Phys. Rev.*, **109**, 256.
— 1960, *Paramagnetic Resonance in Solids, Solid State Physics*, Supplement 2 (New York: Academic Press).
- LOW, W., and ROSENBERGER, U., 1960, *Phys. Rev.*, **116**, 621.
MARSHALL, W., and STUART, R., 1961, *Phys. Rev.*, **123**, 2048.
MCCLURE, D. S., 1957, *J. Phys. Chem. Solids*, **3**, 311.
— 1959, *Solid State Phys.*, **9**, p. 407.
- MURRAY, R. B., 1955, *Thesis*, University of Tennessee.
OGAWA, S., 1960, *J. Phys. Soc., Japan*, **15**, 1475.
ORGEL, L. E., 1955, *J. Chem. Phys.*, **23**, 1004.
OWEN, J., 1955, *Proc. Roy. Soc. A*, **277**, 183.
PAPPALARDO, R., 1959, *J. Chem. Phys.*, **31**, 1050.
— 1960, *J. Chem. Phys.*, **33**, 613.
- PAULING, L., 1960, *The Nature of the Chemical Bond*, 3rd edn (Princeton: Cornell University Press).
- POWELL, M. J. D., GABRIEL, J. R., JOHNSTON, D. F., 1960, *Phys. Rev. Letters*, **5**, 145.
— 1961, *Proc. Roy. Soc.*, in the press. Referred to in the text as I.
- PRATT, W., and COELHO, R., 1959, *Phys. Rev.*, **116**, 281.
PRYCE, M. H. L., 1950, *Phys. Rev.*, **80**, 1107.
- RACAH, G., 1942, *Phys. Rev.*, **62**, 438.
STAHL-BRADA, R., and LOW, W., 1959, *Phys. Rev.*, **113**, 775.
STOCKBARGER, D. C., 1949, *J. Opt. Soc. Amer.*, **39**, 731.
STOUT, J. W., 1959, *J. Chem. Phys.*, **31**, 709.
— 1960, *J. Chem. Phys.*, **33**, 303.
- TINKHAM, M., 1956, *Proc. Roy. Soc. A*, **236**, 535, 549.
WALSH, W. M., JR., 1961, *Phys. Rev.*, **122**, 762.
- WATANABE, H., 1957, *Progr. Theor. Phys., Japan*, **18**, 405.
— 1960, *Phys. Rev. Letters*, **4**, 410.
- WATKINS, G. D., 1959, *Phys. Rev.*, **113**, 79.
WYCKOFF, R. W. G., 1948, *Crystal Structures*, Vol. I (New York: Interscience Publishers).

Electron-Phonon Interaction by the Method of Pseudo-potentials

By L. J. SHAM

Cavendish Laboratory, University of Cambridge

Communicated by J. M. Ziman; MS. received 18th August 1961

Abstract. The matrix element is calculated (i) for orthogonalized plane waves assuming that the ion moves rigidly and (ii) for the equivalent plane waves on the assumption that the net effective potential (Hartree-Fock potential plus pseudo-potential) moves rigidly with the ion. It is shown that these two results are equivalent if the pseudo-potential operator can be treated as a localized potential.

§ 1. INTRODUCTION

It is very convenient to regard the conduction electrons in a metal or semiconductor moving in an effective potential field consisting of the Hartree-Fock field and a pulsive potential. The latter arises from the need to orthogonalize the wave functions of the conduction electrons to the wave functions of the core-electrons. By virtue of the near cancellation of these two potentials the wave functions of the conduction electrons can be approximately represented by simple combinations of plane waves. This idea has been justified by Phillips and Kleinman (1959) and Cohen and Heine (1961) for the energy states in crystals. Ziman (1961) has suggested that each ion carries an effective potential around rigidly with it and that the electron-phonon interaction may be calculated as if this were true. We wish to prove this in the following sense. Consider a solid where the ions are slightly displaced from their equilibrium positions. This gives rise to small changes in the actual crystal potential. We can calculate the electron-phonon interaction from first principles by taking matrix elements for the change of potential between electron states of the unperturbed crystal expressed in terms of orthogonalized plane waves. On the other hand, we can let the effective potential take the place of the actual potential and calculate the matrix elements for the change of this potential between electron states, expressed now in *simple* plane waves. We shall show that if the non-local pseudo-potential operator (Cohen and Heine 1961) can be replaced by a local potential function, then these two calculations of the electron-phonon interaction matrix element yield equivalent results.

§ 2. ORTHOGONALIZED PLANE WAVES AND THE PSEUDO-POTENTIAL

We base the whole calculation on the orthogonalized plane-wave method. Consider a finite crystal of N cells, each with volume Ω_0 . For simplicity, we restrict ourselves to one atom per unit cell. The Hamiltonian for one electron is

$$\mathcal{H} = -\nabla^2 + V(\mathbf{r}) \quad (1)$$

where we take the crystal potential in the form

$$V(\mathbf{r}) = \sum_{\mathbf{l}} U(\mathbf{r} - \mathbf{l}), \quad (2)$$

running over the N lattice vectors and $U(\mathbf{r}) = U(\mathbf{r})$.

Following Heine (1957), we take the 'atomic' wave functions of the core-electrons $\phi_i(\mathbf{r})$, as eigenfunctions satisfying

$$[-\nabla^2 + U(\mathbf{r})]\phi_i = \mathcal{E}_i \phi_i. \quad (3)$$

Throughout the calculation we shall assume that $\phi_i(\mathbf{r})$ is negligible outside the Wigner-Seitz cell centred at the origin.

By the tight-binding approximation, the 'crystal' wave functions of the core-electrons are

$$\psi_{i\mathbf{k}}(\mathbf{r}) = \frac{1}{\sqrt{N}} \sum_{\mathbf{l}} \exp(i\mathbf{k} \cdot \mathbf{l}) \phi_i(\mathbf{r} - \mathbf{l}). \quad (4)$$

An orthogonalized plane wave of the form

$$\chi_{\mathbf{k}\mathbf{g}}(\mathbf{r}) = \frac{1}{\sqrt{(N\Omega_0)}} \exp[i(\mathbf{k} + \mathbf{g}) \cdot \mathbf{r}] - \sum_{\mathbf{l}} b_{\mathbf{l}\mathbf{k}\mathbf{g}} \psi_{i\mathbf{l}} \quad (5)$$

where \mathbf{g} is the reciprocal lattice vector and $b_{\mathbf{l}\mathbf{k}\mathbf{g}}$ the orthogonalizing constant given by

$$b_{\mathbf{l}\mathbf{k}\mathbf{g}} = \frac{1}{\sqrt{\Omega_0}} \int_{N\Omega_0} \exp[i(\mathbf{k} + \mathbf{g}) \cdot \mathbf{r}] \phi_i^*(\mathbf{r}) d^3\mathbf{r}. \quad (6)$$

Expanding the wave function of a conduction electron in terms of orthogonalized plane waves, we get

$$\psi_{i\mathbf{k}}(\mathbf{r}) = \sum_{\mathbf{g}} C_{\mathbf{g}} \chi_{\mathbf{g}\mathbf{k}\mathbf{g}}(\mathbf{r}). \quad (7)$$

The clue to our method lies in the matrix element of the determinant, which fixes the energies in the orthogonalized plane wave expansion:

$$\begin{aligned} \langle \chi_{\mathbf{k}\mathbf{g}'} | \mathcal{H} - \mathcal{E} I | \chi_{\mathbf{k}\mathbf{g}} \rangle &= (\mathbf{k} + \mathbf{g})^2 \delta_{\mathbf{g}\mathbf{g}'} + \bar{V}(\mathbf{g}' - \mathbf{g}) \\ &\quad + \sum_{\mathbf{l}} (\mathcal{E} - \mathcal{E}_i) b_{\mathbf{l}\mathbf{k}\mathbf{g}'}^* b_{\mathbf{l}\mathbf{k}\mathbf{g}} - \mathcal{E} \delta_{\mathbf{g}\mathbf{g}'} \end{aligned} \quad (8)$$

where $\bar{V}(\mathbf{g})$ is a Fourier component of $V(\mathbf{r})$, that is,

$$\bar{V}(\mathbf{g}) = \frac{1}{N\Omega_0} \int_{N\Omega_0} V(\mathbf{r}) \exp(-i\mathbf{g} \cdot \mathbf{r}) d^3\mathbf{r}. \quad (9)$$

If we define the transform

$$\begin{aligned} \bar{U}(\mathbf{k}) &= \frac{1}{\Omega_0} \int_{N\Omega} U(\mathbf{r}) \exp(-i\mathbf{k} \cdot \mathbf{r}) d^3\mathbf{r} \\ &= \frac{4\pi}{\Omega_0} \int_0^\infty r^2 U(r) j_0(kr) dr \end{aligned} \quad (10)$$

then

$$\bar{U}(\mathbf{g}) = \bar{V}(\mathbf{g}). \quad (11)$$

Now the effect of orthogonalization manifests itself in the term

$$\sum_{\mathbf{l}} (\mathcal{E} - \mathcal{E}_i) b_{\mathbf{l}\mathbf{k}\mathbf{g}'}^* b_{\mathbf{l}\mathbf{k}\mathbf{g}}.$$

pose the effect can be simulated by a local potential $V_R(\mathbf{r})$ taken in the form

$$V_R(\mathbf{r}) = \sum_{\mathbf{l}} U_R(|\mathbf{r} - \mathbf{l}|) \quad (12)$$

then its Fourier components have to satisfy

$$\bar{U}_R(|\mathbf{g}' - \mathbf{g}|) \simeq \sum_t (\mathcal{E} - \mathcal{E}_t) b_{t\mathbf{k}\mathbf{g}'}^* b_{t\mathbf{k}\mathbf{g}} \quad (13)$$

For our purpose we need the extension

$$\sum_t (\mathcal{E} - \mathcal{E}_t) b_{t\mathbf{k}\mathbf{g}'}^* b_{t\mathbf{k}\mathbf{g}} = \bar{U}_R(\mathbf{k}' + \mathbf{g}' - \mathbf{k} - \mathbf{g}) \quad (14)$$

where the two b 's do not belong to the same \mathbf{k} -vector. Equation (14) follows from equation (13) if we take $U_R(\mathbf{r}) = V_R(\mathbf{r})$ inside the Wigner-Seitz cell and $U_R(\mathbf{r}) = 0$ outside. Then

$$\bar{U}_R(\mathbf{k}) = \sum_{\mathbf{g}} \bar{V}(\mathbf{g}) \frac{1}{\Omega_0} \int_{\Omega_0} \exp[i(\mathbf{g} - \mathbf{k}) \cdot \mathbf{r}] d^3\mathbf{r}.$$

From the Fourier expansion

$$\exp[i(\mathbf{k} - \mathbf{k}') \cdot \mathbf{r}] = \sum_{\mathbf{g}''} \exp(i\mathbf{g}'' \cdot \mathbf{r}) \frac{1}{\Omega_0} \int_{\Omega_0} \exp[i(\mathbf{k} - \mathbf{k}' - \mathbf{g}'') \cdot \mathbf{r}] d^3\mathbf{r}$$

valid inside the Wigner-Seitz cell, we obtain

$$b_{t\mathbf{k}\mathbf{g}} = \frac{1}{\sqrt{\Omega_0}} \int_{\Omega_0} \exp[i(\mathbf{k} + \mathbf{g}) \cdot \mathbf{r}] \phi_t^*(\mathbf{r}) d^3\mathbf{r}$$

($\phi_t(\mathbf{r})$ negligible outside the Wigner-Seitz cell,

$$= \sum_{\mathbf{g}''} b_{t\mathbf{k}'\mathbf{g}+\mathbf{g}''} \frac{1}{\Omega_0} \int_{\Omega_0} \exp[i(\mathbf{k} - \mathbf{k}' - \mathbf{g}'') \cdot \mathbf{r}] d^3\mathbf{r}.$$

Hence

$$\begin{aligned} & \sum_t (\mathcal{E} - \mathcal{E}_t) b_{t\mathbf{k}\mathbf{g}'}^* b_{t\mathbf{k}\mathbf{g}} \\ &= \sum_{\mathbf{g}''} \frac{1}{\Omega_0} \int_{\Omega_0} \exp[i(\mathbf{k} - \mathbf{k}' - \mathbf{g}'') \cdot \mathbf{r}] d^3\mathbf{r} \sum_t (\mathcal{E} - \mathcal{E}_t) b_{t\mathbf{k}\mathbf{g}'}^* b_{t\mathbf{k}'\mathbf{g}+\mathbf{g}''} \\ &= \sum_{\mathbf{g}''} \bar{U}_R(\mathbf{g}' - \mathbf{g} - \mathbf{g}'') \frac{1}{\Omega_0} \int_{\Omega_0} \exp[i(\mathbf{k} - \mathbf{k}' - \mathbf{g}'') \cdot \mathbf{r}] d^3\mathbf{r} \\ &= \bar{U}_R(\mathbf{k}' + \mathbf{g}' - \mathbf{k} - \mathbf{g}) \end{aligned}$$

If we can interpolate the values of $\bar{U}_R(\mathbf{k})$ from equation (13) or, better still, obtain the values from equation (14), we can get, by the Hankel inversion theorem (Sneddon 1951),

$$U_R(\mathbf{r}) = \frac{\Omega_0}{2\pi^2} \int_0^\infty k^2 \bar{U}_R(k) j_0(kr) dk. \quad (15)$$

This provides a practical method for constructing the pseudo-potential using the results of an orthogonalized plane-wave band-structure calculation.

From equations (8) and (13), we see that the matrix element on the left-hand side of equation (8) satisfies

$$\langle \chi_{\mathbf{k}\mathbf{g}'} | \mathcal{H} - \mathcal{E}I | \chi_{\mathbf{k}\mathbf{g}} \rangle = \langle \mathbf{k} + \mathbf{g}' | -\nabla^2 + V + V_R - \mathcal{E}I | \mathbf{k} + \mathbf{g} \rangle \quad (16)$$

where $|\mathbf{k} + \mathbf{g}\rangle$ denotes the plane wave $(N\Omega_0)^{-1/2} \exp i(\mathbf{k} + \mathbf{g}) \cdot \mathbf{r}$. The secular equation

$$\sum_{\mathbf{g}} \langle \chi_{\mathbf{k}\mathbf{g}'} | \mathcal{H} - \mathcal{E}I | \chi_{\mathbf{k}\mathbf{g}} \rangle C_{\mathbf{k}\mathbf{g}} = 0 \quad (17)$$

is equivalent to

$$\sum_{\mathbf{g}} \langle \mathbf{k} + \mathbf{g}' | -\nabla^2 + V + V_R - \mathcal{E}I | \mathbf{k} + \mathbf{g} \rangle C_{\mathbf{k}\mathbf{g}} = 0. \quad (18)$$

This suggests that we may treat the conduction electrons as if they were moving in potential $V + V_R$ and as if their wave functions were combinations of plane waves with the same coefficients as those of corresponding orthogonalized plane waves.

The assumption made in equation (13) can only be justified by a band-structure calculation for a specific metal using the orthogonalized plane-wave method. Note that for our purpose we have chosen the repulsive potential V_R so that (i) it does not involve the wave functions of the conduction electrons and (ii) it does not depend on \mathbf{k} for a given energy.

§ 3. ELECTRON-PHONON INTERACTION FOR ORTHOGONALIZED PLANE WAVES

The next step is to show that the interaction matrix element $\mathcal{J}_{qp}(\mathbf{k}, \mathbf{k}')$ (Ziman 1960, p. 182) based on the rigid ion model is the same whether we calculate it from orthogonalized plane waves in potential V or plane waves in potential $V + V_R$. The details are set out as follows.

We first calculate

$$\mathcal{J}_{qp}(\mathbf{k}, \mathbf{k}') = -Ne_{qp} \int_{N\Omega_0} \psi_{\mathbf{k}'}^* (\nabla U) \psi_{\mathbf{k}} d^3\mathbf{r} \quad (19)$$

where

$$\int_{N\Omega_0} \psi_{\mathbf{k}'}^* \psi_{\mathbf{k}} d^3\mathbf{r} = 1$$

and $\psi_{\mathbf{k}}$ is given by the expansion in orthogonalized plane waves, equation (7).

$$\mathcal{J}_{qp}(\mathbf{k}, \mathbf{k}') = -Ne_{qp} \cdot \sum_{\mathbf{g}\mathbf{g}'} C_{\mathbf{k}'\mathbf{g}'}^* C_{\mathbf{k}\mathbf{g}} \int_{N\Omega_0} \chi_{\mathbf{k}'\mathbf{g}'}^* (\nabla U) \chi_{\mathbf{k}\mathbf{g}} d^3\mathbf{r}. \quad (20)$$

Each term

$$\begin{aligned} & \int_{N\Omega_0} \chi_{\mathbf{k}'\mathbf{g}'}^* (\nabla U) \chi_{\mathbf{k}\mathbf{g}} d^3\mathbf{r} \\ &= \int \left[(N\Omega_0)^{-1/2} \exp[-i(\mathbf{k}' + \mathbf{g}') \cdot \mathbf{r}] - \sum_{\mathbf{t}'} b_{\mathbf{t}'\mathbf{k}'\mathbf{g}'}^* \psi_{\mathbf{t}'\mathbf{k}'}^* \right] (\nabla U) \\ & \quad \times \left[(N\Omega_0)^{-1/2} \exp[i(\mathbf{k} + \mathbf{g}) \cdot \mathbf{r}] - \sum_{\mathbf{t}} b_{\mathbf{t}\mathbf{k}\mathbf{g}} \psi_{\mathbf{t}\mathbf{k}} \right] d^3\mathbf{r} \end{aligned} \quad (21)$$

can be separated into four parts, I + II + III + IV, which we attack in turn.

$$\begin{aligned}
I &= \int [(N\Omega_0)^{-1/2} \exp\{-i(\mathbf{k}' + \mathbf{g}') \cdot \mathbf{r}\}](\nabla U)[(N\Omega_0)^{-1/2} \exp\{i(\mathbf{k} + \mathbf{g}) \cdot \mathbf{r}\}] d^3\mathbf{r} \\
&= \frac{i}{N\Omega_0}(\mathbf{k}' + \mathbf{g}' - \mathbf{k} - \mathbf{g}) \int U \exp[i(\mathbf{k} + \mathbf{g} - \mathbf{k}' - \mathbf{g}') \cdot \mathbf{r}] d^3\mathbf{r} \\
&= \frac{i}{N}(\mathbf{k}' + \mathbf{g}' - \mathbf{k} - \mathbf{g}) \bar{U}(\mathbf{k}' + \mathbf{g}' - \mathbf{k} - \mathbf{g}), \tag{22}
\end{aligned}$$

denoting the Fourier transform of U as in (10).

$$\begin{aligned}
-II &= \int \left[\sum_{t'} b_{t'\mathbf{k}'\mathbf{g}'}^* \phi_{t'\mathbf{k}'}^* \right] (\nabla U) [(N\Omega_0)^{-1/2} \exp\{i(\mathbf{k} + \mathbf{g}) \cdot \mathbf{r}\}] d^3\mathbf{r} \\
&= \frac{1}{N\sqrt{\Omega_0}} \sum_{t'} b_{t'\mathbf{k}'\mathbf{g}'}^* \int \exp[i(\mathbf{k} + \mathbf{g}) \cdot \mathbf{r}] (\nabla U) \phi_{t'}^* d^3\mathbf{r},
\end{aligned}$$

neglecting overlap terms like $\{\nabla U(\mathbf{r})\} \phi_{t'}(\mathbf{r} - \mathbf{l})$ with $\mathbf{l} \neq 0$. From equation (3),

$$\begin{aligned}
(-\nabla^2 + U)\phi_t^* &= \mathcal{E}_t \phi_t^* \\
(-\nabla^2 + U)\nabla \phi_t^* + (\nabla U)\phi_t^* &= \mathcal{E}_t \nabla \phi_t^*. \tag{23}
\end{aligned}$$

Therefore

$$\begin{aligned}
-II &= -\frac{i}{N}(\mathbf{k} + \mathbf{g}) \sum_t \mathcal{E}_t b_{t'\mathbf{k}'\mathbf{g}'}^* b_{t'\mathbf{k}\mathbf{g}} + \\
&\quad + \frac{1}{N\sqrt{\Omega_0}} \sum_{t'} b_{t'\mathbf{k}'\mathbf{g}'}^* \int \exp[i(\mathbf{k} + \mathbf{g}) \cdot \mathbf{r}] (\nabla^2 - U) \nabla \phi_{t'}^* d^3\mathbf{r}. \tag{24}
\end{aligned}$$

Similarly,

$$\begin{aligned}
-III &= \int [(N\Omega_0)^{-1/2} \exp\{-i(\mathbf{k}' + \mathbf{g}') \cdot \mathbf{r}\}](\nabla U) \left[\sum_t b_{t\mathbf{k}\mathbf{g}} \phi_{t\mathbf{k}} \right] d^3\mathbf{r} \\
&= \frac{i}{N}(\mathbf{k}' + \mathbf{g}') \sum_t \mathcal{E}_t b_{t\mathbf{k}\mathbf{g}}^* b_{t\mathbf{k}\mathbf{g}} + \\
&\quad + \frac{1}{N\sqrt{\Omega_0}} \sum_t b_{t\mathbf{k}\mathbf{g}} \int \exp\{-i(\mathbf{k}' + \mathbf{g}') \cdot \mathbf{r}\} (\nabla^2 - U) \nabla \phi_t d^3\mathbf{r}. \tag{25}
\end{aligned}$$

$$\begin{aligned}
IV &= \int \left[\sum_{t'} b_{t'\mathbf{k}'\mathbf{g}'}^* \phi_{t'\mathbf{k}'}^* \right] (\nabla U) \left[\sum_t b_{t\mathbf{k}\mathbf{g}} \phi_{t\mathbf{k}} \right] d^3\mathbf{r} \\
&= \frac{1}{N} \sum_{t't} b_{t'\mathbf{k}'\mathbf{g}'}^* b_{t\mathbf{k}\mathbf{g}} \int \phi_{t'}^* (\nabla U) \phi_t d^3\mathbf{r}
\end{aligned}$$

by equation (4) and 'non-overlapping' assumption

$$= \frac{1}{N} \sum_{t't} b_{t'\mathbf{k}'\mathbf{g}'}^* b_{t\mathbf{k}\mathbf{g}} \int \phi_{t'}^* (\nabla^2 - U + \mathcal{E}_t) \nabla \phi_t d^3\mathbf{r}$$

by equation (23)

$$= \frac{1}{N} \sum_{t't} b_{t'\mathbf{k}'\mathbf{g}'}^* b_{t\mathbf{k}\mathbf{g}} \left[\int \phi_{t'}^* (\nabla^2 - U) \nabla \phi_t d^3\mathbf{r} + \int (\nabla \phi_{t'}^*) (\nabla^2 - U) \phi_t d^3\mathbf{r} \right]. \tag{26}$$

Combining the second term of II and the second term of IV, we get

$$\begin{aligned}
 & -\frac{1}{\sqrt{N}} \sum_{t'} b_{t'k'g}^* \int \left[(N\Omega_0)^{-1/2} \exp\{i(\mathbf{k} + \mathbf{g}) \cdot \mathbf{r}\} - N^{-1/2} \sum_t b_{tkg} \phi_t \right] (\nabla^2 - U) (\nabla \phi_{t'}^*) d^3\mathbf{r} \\
 & = -\frac{1}{\sqrt{N}} \sum_{t'} b_{t'k'g}^* \int (\nabla \phi_{t'}^*) (\nabla^2 - U) \chi_{kg} d^3\mathbf{r}
 \end{aligned}$$

by equation (5), which can be replaced by

$$-\frac{1}{\sqrt{N}} \sum_{t'} b_{t'k'g}^* \int (\nabla \phi_{t'}^*) (-\mathcal{E}_k) \chi_{kg} d^3\mathbf{r} \quad (27)$$

since

$$\begin{aligned}
 & \sum_g C_{kg} \int (\nabla \phi_{t'}^*) (\nabla^2 - U) \chi_{kg} d^3\mathbf{r} \\
 & = \int (\nabla \phi_{t'}^*) (\nabla^2 - U) \psi_k d^3\mathbf{r} \quad \text{by equation (7)} \\
 & = \int (\nabla \phi_{t'}^*) (-\mathcal{E}_k) \psi_k d^3\mathbf{r} \\
 & = \sum_g C_{kg} \int (\nabla \phi_{t'}^*) (-\mathcal{E}_k) \chi_{kg} d^3\mathbf{r}.
 \end{aligned}$$

Similarly, the sum of the second term of III and the first term of IV is replaceable by

$$-\frac{1}{\sqrt{N}} \sum_t b_{tkg} \int \chi_{k'g}^* (-\mathcal{E}_{k'}) (\nabla \phi_t) d^3\mathbf{r}. \quad (28)$$

Expression (27) can be further developed as

$$= \frac{\mathcal{E}_k}{\sqrt{N}} \sum_t b_{t'k'g}^* \int (\nabla \phi_{t'}^*) \left[(N\Omega_0)^{-1/2} \exp\{i(\mathbf{k} + \mathbf{g}) \cdot \mathbf{r}\} - N^{-1/2} \sum_t b_{tkg} \phi_t \right] d^3\mathbf{r}$$

by equation (5)

$$= -\frac{\mathcal{E}_k}{N} i(\mathbf{k} + \mathbf{g}) \sum_t b_{tk'g}^* b_{tkg} - \frac{\mathcal{E}_k}{N} \sum_{t't} b_{t'k'g}^* b_{tkg} \int (\nabla \phi_{t'}^*) \phi_t d^3\mathbf{r} \quad (29)$$

by equation (6).

Similarly, expression (28) becomes

$$\frac{\mathcal{E}_{k'}}{N} i(\mathbf{k}' + \mathbf{g}') \sum_t b_{tk'g}^* b_{tkg} - \frac{\mathcal{E}_{k'}}{N} \sum_{t't} b_{t'k'g}^* b_{tkg} \int \phi_{t'}^* (\nabla \phi_t) d^3\mathbf{r}. \quad (30)$$

For elastic scattering $\mathcal{E}_k \simeq \mathcal{E}_{k'}$ (i.e. phonon energy is assumed negligible)

$$\text{II} + \text{III} + \text{IV} = \frac{i}{N} (\mathbf{k}' + \mathbf{g}' - \mathbf{k} - \mathbf{g}) \sum_t (\mathcal{E}_k - \mathcal{E}_t) b_{tk'g}^* b_{tkg}, \quad (31)$$

making use of equations (24), (25) and (29), (30) and the fact that

$$\int (\nabla \phi_{t'}^*) \phi_t d^3\mathbf{r} + \int \phi_{t'}^* (\nabla \phi_t) d^3\mathbf{r} = 0.$$

ally, from (21), we get

$$\mathcal{J}_{qp}(\mathbf{k}, \mathbf{k}') = -ie_{qp} \cdot \sum_{\mathbf{g}\mathbf{g}'} C_{\mathbf{k}'\mathbf{g}}^* C_{\mathbf{k}\mathbf{g}} (\mathbf{k}' + \mathbf{g}' - \mathbf{k} - \mathbf{g}) \\ \times \left[\bar{U}(\mathbf{k}' + \mathbf{g}' - \mathbf{k} - \mathbf{g}) + \sum_t (\mathcal{E}_{\mathbf{k}} - \mathcal{E}_t) b_{t\mathbf{k}'\mathbf{g}'}^* b_{t\mathbf{k}\mathbf{g}} \right]. \quad (32)$$

Since that equation (32) is exact within the limitation of the orthogonalized plane-wave method and in its derivation the assumption for establishing the pseudo-potential, equation (13) has not been invoked. Observe that transverse phonons as well as longitudinal ones contribute to the scattering, even for N -processes (Collins 1961).

§ 4. ELECTRON-PHONON INTERACTION FOR THE EQUIVALENT PLANE WAVES

In the pseudo-potential model, we regard the ions as carrying around their effective potentials $U + U_R$ so that the wave functions of the conduction electrons are given by

$$\phi_{\mathbf{k}} = \sum_{\mathbf{r}} C_{\mathbf{k}\mathbf{g}} (N\Omega_0)^{-1/2} \exp\{i(\mathbf{k} + \mathbf{g}) \cdot \mathbf{r}\} \quad (33)$$

where $C_{\mathbf{k}\mathbf{g}}$ is given in equation (7). The matrix element is then

$$\mathcal{J}_{qp}(\mathbf{k}, \mathbf{k}') = -Ne_{qp} \cdot \int \phi_{\mathbf{k}'}^* \nabla(U + U_R) \phi_{\mathbf{k}} d^3\mathbf{r} \\ = -ie_{qp} \cdot \sum_{\mathbf{g}\mathbf{g}'} C_{\mathbf{k}'\mathbf{g}'}^* C_{\mathbf{k}\mathbf{g}} (\mathbf{k}' + \mathbf{g}' - \mathbf{k} - \mathbf{g}) \\ \times [\bar{U}(\mathbf{k}' + \mathbf{g}' - \mathbf{k} - \mathbf{g}) + \bar{U}_R(\mathbf{k}' + \mathbf{g}' - \mathbf{k} - \mathbf{g})], \quad (34)$$

following steps similar to those leading to (22).

From equation (14) we conclude that equation (34) is equivalent to equation (32). Thus we have justified the use of the pseudo-potential model in calculating electron-phonon interaction matrix elements. Here it must be emphasized that the corresponding coefficients in the linear combinations of orthogonalized plane waves and plane waves must be the same, namely $C_{\mathbf{k}\mathbf{g}}$ in equation (7), so that when the wave function of the conduction electron is normalized in the expansion of orthogonalized plane waves it will not be so in the expansion of plane waves. This is to be expected since the switch from orthogonalized plane-wave expansion to a plane-wave expansion is not a one-to-one transformation of two state-vector spaces but only a replacement by a cruder mathematical analogue.

Our analysis does not include any contributions to the electron-phonon interaction arising from charge shift of the conduction electrons. This effect can be taken into account formally by a simple extension of Bardeen's method (Bardeen 1937) but there are some difficult technical points concerning the role of correlation and exchange in such a calculation. This problem is being studied further.

In conclusion, we shall show the relation of our calculation to an older calculation, in the case where the cancellation between the crystal potential and pseudo-potential is nearly complete—i.e. $U + U_R$ is nearly constant in $0 < r < r_s$ and zero outside—

single plane waves are good approximations to the wave functions

$$\begin{aligned}\mathcal{J}_{qp}(\mathbf{k}, \mathbf{k}') &= -ie_{qp} \cdot (\mathbf{k}' - \mathbf{k}) C_{\mathbf{k}'0} C_{\mathbf{k}0} \frac{4\pi}{\Omega_0} \int_0^\infty r^2 (U + U_R) j_0(|\mathbf{k}' - \mathbf{k}|r) dr \\ &= -ie_{qp} \cdot (\mathbf{k}' - \mathbf{k}) C_{\mathbf{k}'0} C_{\mathbf{k}0} [U(r_s) + U_R(r_s)] \frac{4\pi}{\Omega_0} \int_0^{r_s} r^2 j_0(|\mathbf{k}' - \mathbf{k}|r) dr \\ &= -ie_{qp} \cdot (\mathbf{k}' - \mathbf{k}) C_{\mathbf{k}'0} C_{\mathbf{k}0} [U(r_s) + U_R(r_s)] \mathcal{G}(|\mathbf{k}' - \mathbf{k}|r_s)\end{aligned}$$

where

$$C_{\mathbf{k}0} = \left(1 - \sum_t |b_{t\mathbf{k}0}|^2 \right)^{-1/2}.$$

Comparing this result with Mott and Jones' calculation based on the rigid ion model using the Wigner-Seitz method (Ziman 1960, p. 185) we see the similarity of the two expressions. $C_{\mathbf{k}'0} C_{\mathbf{k}0} [U(r_s) + U_R(r_s)]$ simply takes the place of $U(r_s) - \mathcal{E}_0$ where \mathcal{E}_0 is the energy at $\mathbf{k} = 0$.

ACKNOWLEDGMENTS

I am deeply indebted to Dr. J. M. Ziman for suggesting this problem and for constant guidance, and to Dr. V. Heine for many stimulating and helpful discussions. I also wish to thank the Master and Fellows of Churchill College for the award of a Research Studentship.

REFERENCES

- BARDEEN, J., 1937, *Phys. Rev.*, **52**, 688.
COHEN, M. H., and HEINE, V., 1961, *Phys. Rev.*, **122**, 1821.
COLLINS, J. G., 1961, *Proc. Roy. Soc. A.*, **263**, 531.
HEINE, V., 1957, *Proc. Roy. Soc. A.*, **240**, 354.
PHILLIPS, J. C., and KLEINMAN, L., 1959, *Phys. Rev.*, **116**, 287.
SNEDDON, I. N., 1951, *Fourier Transforms* (New York: McGraw-Hill), p. 52.
ZIMAN, J. M., 1960, *Electrons and Phonons* (Oxford: Clarendon Press).
— 1961, *Phil. Mag.*, **6**, in the press.

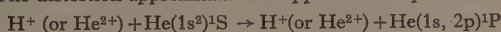
Excitation of Helium to the $(1s, 2p)^1P$ and $(1s, 3p)^1P$ States by Proton and Alpha Particle Impact

By R. J. BELL

Department of Applied Mathematics, The Queen's University of Belfast

MS. received 7th July 1961

Abstract. The distortion approximation is applied to the processes

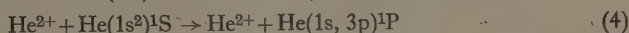
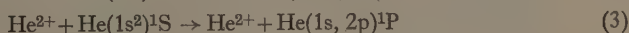
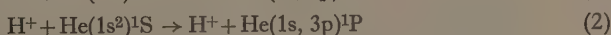
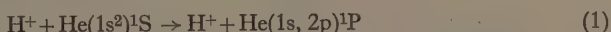


cross sections being obtained for incident proton energies in the range 10 kev to 1000 kev and for incident alpha particle energies in the range 40 kev to 4000 kev. For proton impact the maxima cross sections are found to be $0.18\pi a_0^2$ and $0.035\pi a_0^2$, at 88 kev and 124 kev respectively; and for alpha particle impact they are found to be $0.61\pi a_0^2$ and $0.101\pi a_0^2$ at 511 kev and 935 kev respectively.

§ 1. INTRODUCTION

BATES (1959) has given reasons for expecting that the effect of distortion on inelastic collisions between heavy systems is greater than might at first be supposed. Detailed calculations on atomic hydrogen (Bates 1959, 1961) confirm this expectation.

It was judged desirable to carry out similar calculations on helium, this being the simplest atom which lends itself readily to experimental study. Accordingly the following processes have been treated:



Atomic units are used throughout the paper.

§ 2. THEORY

Let the target system be situated at the origin of coordinates and let the incident system, with position vector \mathbf{R} , move with constant velocity \mathbf{v} in the positive direction along a line distant ρ from the Z axis. It is convenient to choose the zero of time so that $Z = vt$.

The electronic wave function may be represented as

$$\Psi(\mathbf{r}, t) = \sum_m a_m(t) \phi_m(\mathbf{r}) \exp(-i\epsilon_m t) \quad (5)$$

where \mathbf{r} symbolizes the coordinates of electrons, and $\phi_m(\mathbf{r})$ and ϵ_m are the unperturbed eigenfunctions and eigenenergies of the target system in the state indicated by the subscript. The coefficients a_m , as well as being functions of the time, are naturally so dependent upon ρ and v .

Application of time-dependent perturbation theory yields the following set of coupled equations:

$$iv \frac{\partial}{\partial z} a_m(Z) = \sum_s a_s(Z) V_{ms}(\mathbf{R}) \exp(-i\alpha_{sm}Z)$$

with

$$\alpha_{sm} = (\epsilon_s - \epsilon_m)/v$$

and

$$V_{ms}(\mathbf{R}) = \int d\mathbf{r} \phi_m^*(\mathbf{r}) V(\mathbf{r}, \mathbf{R}) \phi_s(\mathbf{r})$$

$V(\mathbf{r}, \mathbf{R})$ being the instantaneous interaction potential. Taking the initial conditions in (6) to be

$$a_0(-\infty) = 1, \quad a_s(-\infty) = 0 \quad (s \neq 0)$$

the probability of excitation from state 0 to state m is

$$\mathcal{P}_{0m}(\rho) = |a_m(\infty)|^2$$

and the cross section describing the transition is given, in units of πa_0^2 , by

$$Q_{0m} = 2 \int_0^\infty \mathcal{P}_{0m}(\rho) \rho d\rho.$$

According to the impact parameter version of the first Born approximation

$$a_m(\infty) = -\frac{i}{v} \int_{-\infty}^{\infty} V_{m0}(\mathbf{R}) \left\{ \exp\left(-\frac{i}{v} \int_0^Z (\epsilon_0 - \epsilon_m) dZ\right) \right\} dZ$$

(Frame 1931); and according to the distortion approximation

$$a_m(\infty) = -\frac{i}{v} \int_{-\infty}^{\infty} V_{m0}(\mathbf{R}) \left\{ \exp\left(-\frac{i}{v} \int_0^Z (\epsilon_0 + V_{00} - \epsilon_m - V_{mm}) dZ\right) \right\} dZ$$

(Bates 1959), in which a complex outside factor of modulus unity has been discarded.

The relationship between the two approximations may be appreciated by observing that ϵ_0 and ϵ_m , the unperturbed eigenenergies appearing in (12), appear in (13) modified by V_{00} and V_{mm} , their first-order corrections under the perturbation $V(\mathbf{r}, \mathbf{R})$. The magnitude of $V_{00} - V_{mm}$ at the origin is about 1.5; for close encounters, at the lowest energy considered, its presence effects a change of the order of π in the phase of the exponential function.† For medium and distant encounters $V_{00} - V_{mm}$ is much smaller than unity and little change of phase is occasioned.

Calculations confirm that, for a selected energy, the effects of distortion upon the probability decrease with increasing impact parameter; and that, for a selected impact parameter, they decrease with increasing energy.

§ 3. CALCULATION AND RESULTS

3.1. The Atomic Wave Functions

The ground state of the target system was described by a product of functions

$$\phi(1s^2; {}^1S|\mathbf{r}) = \psi_0(\mathbf{r}_1)\psi_0(\mathbf{r}_2).$$

† Note that $1/v = 4.997(M/E)^{1/2}$ where M is the mass of the incident proton or alpha particle: on the ^{16}O scale and E is the energy in kev.

The analytic form of the orbitals

$$\psi_0(\mathbf{r}) = N_0[\exp(-\alpha r) + a \exp(-\beta r)] \quad (15)$$

was originally suggested by Löwdin (1953), who obtained values for the parameters by extrapolation from his results for helium-like ions. The following parameters calculated by Green, Mulder, Lewis and Woll (1954) have been chosen as the more accurate: $\alpha = 1.455\,799$, $\beta = 2.911\,598$, $a = 0.60$.

The form adopted for the eigenfunctions of the excited states was

$$\phi(1s, np; {}^1P|\mathbf{r}) = \frac{1}{\sqrt{2}}[\psi_1(\mathbf{r}_1)\psi_n(\mathbf{r}_2) + \psi_n(\mathbf{r}_1)\psi_1(\mathbf{r}_2)]. \quad (16)$$

In this case, the orbitals are due to Morse, Young and Haurwitz (1935) and Goldberg and Clogston (1939). Specifically, these orbitals are given by

$$\psi_1(\mathbf{r}) = N_1 \exp(-\gamma r) \quad (17)$$

with $\gamma = 2.0$,

$$\psi_2(\mathbf{r}) = N_2 r \exp(-\delta r) \cos \theta \quad (18)$$

with $\delta = 0.485$

$$\text{and} \quad \psi_3(\mathbf{r}) = N_3 r [\gamma \exp(-\lambda r) + b \exp(-\mu r)] \cos^2 \theta \quad (19)$$

with $\lambda = \mu = 0.325$ where N_0, N_1, N_2, N_3 are normalization constants; b is chosen to make $\psi_3(\mathbf{r})$ orthogonal to $\psi_2(\mathbf{r})$.

Using the dipole-length formula, these eigenfunctions give oscillator strengths of 0.259 and 0.0728 for the $(1s^2) {}^1S \rightarrow (1s, 2p) {}^1P$ and $(1s^2) {}^1S \rightarrow (1s, 3p) {}^1P$ transitions respectively. These are in satisfactory agreement with the values, 0.255 and 0.0706, obtained by Low (1959) who described the ground state by the six-parameter eigenfunction due to Hylleraas (1929) and the excited states by the eigenfunctions cited above.

3.2. Preliminary Analysis

Some analysis is required to transform (12) and (13) to a form suitable for computation. For the processes considered

$$V(\mathbf{r}, \mathbf{R}) = \mathcal{Z} \left\{ \frac{2}{R} - \frac{1}{|\mathbf{R} - \mathbf{r}_1|} - \frac{1}{|\mathbf{R} - \mathbf{r}_2|} \right\} \quad (20)$$

where \mathcal{Z} is the charge on the incident system. Expansion of (20) in spherical harmonics leads to analytical expressions for the matrix elements involved. We may set

$$V_{np_0, 1s}(\mathbf{R}) = -\frac{1}{2} \mathcal{Z} (\epsilon_{np} - \epsilon_{1s}) \frac{Z}{R} \xi_{np}(R) \quad (21)$$

$$V_{np_{\pm 1}, 1s}(\mathbf{R}) = -\frac{1}{2} \mathcal{Z} (\epsilon_{np} - \epsilon_{1s}) \frac{\rho}{R} \xi_{np}(R) \quad (22)$$

$$V_{np_0, np_0}(\mathbf{R}) - V_{1s, 1s}(\mathbf{R}) = \mathcal{Z} (\epsilon_{np} - \epsilon_{1s}) \left\{ \eta_{np}(R) + \frac{2Z^2 - \rho^2}{R^2} \zeta_{np}(R) \right\} \quad (23)$$

$$V_{np_{\pm 1}, np_{\pm 1}}(\mathbf{R}) - V_{1s, 1s}(\mathbf{R}) = \mathcal{Z} (\epsilon_{np} - \epsilon_{1s}) \left\{ \eta_{np}(R) + \frac{2\rho^2 - Z^2}{R^2} \zeta_{np}(R) \right\} \quad (24)$$

where each state is now labelled according to its highest orbital. Equations (12) and

(13) may then be rewritten to give the Born approximation

$$\mathcal{P}_{1s, n p_0} = \left| \alpha_{np} \mathcal{L} \int_0^\infty \frac{Z}{R} \xi_{np}(R) \sin \alpha_{np} Z dZ \right|^2 \quad (25)$$

$$\mathcal{P}_{1s, n p_{\pm 1}} = \left| \alpha_{np} \mathcal{L} \int_0^\infty \frac{\rho}{R} \xi_{np}(R) \cos \alpha_{np} Z dZ \right|^2 \quad (26)$$

and the distortion approximation

$$\mathcal{P}_{1s, n p_0} = \left| \alpha_{np} \mathcal{L} \int_0^\infty \frac{Z}{R} \xi_{np}(R) \sin \alpha_{np} \{Z + B_{np_0}(\mathbf{R})\} dZ \right|^2 \quad (27)$$

$$\mathcal{P}_{1s, n p_{\pm 1}} = \left| \alpha_{np} \mathcal{L} \int_0^\infty \frac{\rho}{R} \xi_{np}(R) \cos \alpha_{np} \{Z + B_{np_{\pm 1}}(\mathbf{R})\} dZ \right|^2 \quad (28)$$

with

$$\alpha_{np} = \frac{\epsilon_{np} - \epsilon_{1s}}{v} \quad (29)$$

$$B_{np_0}(\mathbf{R}) = \mathcal{L} \int_0^Z \left\{ \eta_{np}(R) + \frac{2Z^2 - \rho^2}{R^2} \zeta_{np}(R) \right\} dZ \quad (30)$$

and

$$B_{np_{\pm 1}}(\mathbf{R}) = \mathcal{L} \int_0^Z \left\{ \eta_{np}(R) + \frac{2\rho^2 - Z^2}{R^2} \zeta_{np}(R) \right\} dZ. \quad (31)$$

$$\epsilon_{2p} - \epsilon_{1s} = 0.7797, \quad \epsilon_{3p} - \epsilon_{1s} = 0.8484. \quad (32)$$

The explicit forms of $\xi_{np}(R)$, $\eta_{np}(R)$ and $\zeta_{np}(R)$ are displayed in the appendix.

3.3. Numerical Procedure and Presentation of Results

The work was done with the aid of a high speed computer. Gaussian quadratures were used to evaluate the integrals in (25) to (28) over the range from 0 to Z_0 where Z_0 is such that for $Z \geq Z_0$, B_{np_0} , $B_{np_{\pm 1}}$ can be taken as constant, and $\xi_{np}(R)$ as proportional to R^{-2} . The range from Z_0 to ∞ remained. Consider

$$\mathcal{J} = \int_{Z_0}^\infty f(Z) \exp(i\alpha Z) dZ. \quad (33)$$

Repeated integration by parts yields the asymptotic series

$$\begin{aligned} \mathcal{J} = \{ & -(i\alpha)^{-1} f^{(0)}(Z_0) + (i\alpha)^{-2} f^{(1)}(Z_0) - (i\alpha)^{-3} f^{(2)}(Z_0) + \\ & \dots + (-i\alpha)^{-p+1} f^{(p)}(Z_0) + \dots \} \exp(i\alpha Z_0) \end{aligned} \quad (34)$$

where bracketed superscripts refer to differentiation with respect to Z . For $Z \geq Z_0$, successive derivatives of $(Z/R)\xi_{np}(R)$ or $(\rho/R)\xi_{np}(R)$ may be computed by recurrence relations based on the properties of Legendre polynomials. This possibility is due to the original expansion of $V(\mathbf{r}, \mathbf{R})$ in spherical harmonics. The method is applicable for all transitions. In the present case, it yields a series whose terms decrease until p exceeds αZ_0 . If the series is truncated before this point is reached, an approximation to \mathcal{J} is obtained which is correct to the order of magnitude of the last term retained.

The results, reckoned to be accurate to within 0.5%, are presented: in diagrams (a) to (f) as graphs of Q_{0m} against E (E is the energy of the ion, in kev, the target system being taken as fixed); in diagrams (g) to (n) as graphs of the coefficients $a_m(\infty)$ against

for selected values of E ; and in diagrams (o) to (r) as graphs of $a_m(\infty)$ against E for selected values of ρ . Curves for processes (3) and (4) are superimposed on a suitably reduced scale for ease of comparison.

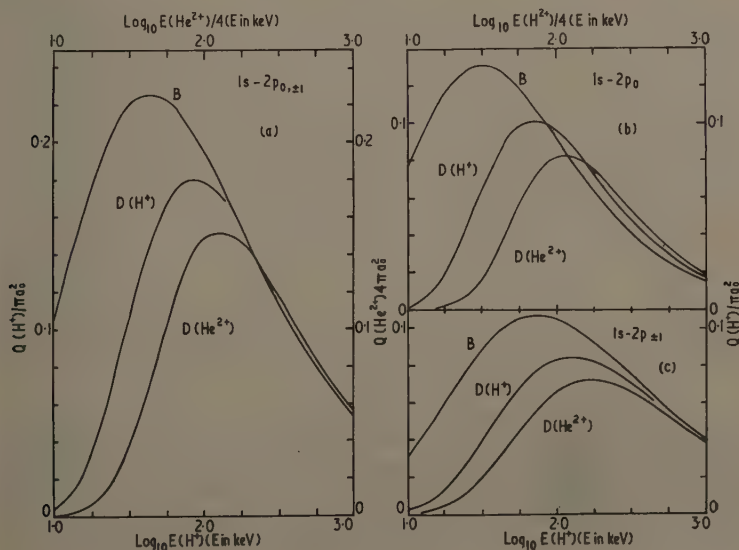
§ 4. DISCUSSION OF RESULTS

Some effects of distortion are understandable from a knowledge of B_{np_0} and $B_{np_{\pm 1}}$. These quantities are comparable with Z near the origin, becoming much smaller than unity for distant encounters. Both are positive with the exception that $B_{np_{\pm 1}}$ becomes negative for very distant encounters, for which the conclusions drawn below must be reversed.

At low energies the presence of B_{np_0} and $B_{np_{\pm 1}}$ accentuates the already sharp oscillation of the trigonometric functions in the integral, reducing probabilities and cross sections.

At high energies, the presence of B_{np_0} shifts the first peak of the sine function closer to the origin. For small ρ the peak is moved closer to, and for large ρ farther from, the maximum of $(Z/R)\xi_{np}(R)$, thus successively increasing or decreasing the integral; and, since the effects of distortion and the probabilities themselves both diminish with increasing ρ , the cumulative effect should be to increase the $1s\text{-}np_0$ cross sections. The presence of $B_{np_{\pm 1}}$, by hastening the initial decay of the cosine function, decreases the magnitude of the corresponding integral. It is doubtful whether the reverse behaviour shown for very distant encounters will ever compensate sufficiently to prevent the $1s\text{-}np_{\pm 1}$ cross sections from being smaller than those given by the Born approximation.

Although distortion reduces the maximum cross sections for processes (2) and (4) more than those for processes (1) and (3), it has not been possible to make any detailed predictions concerning excitation to higher p states. The results are similar in their



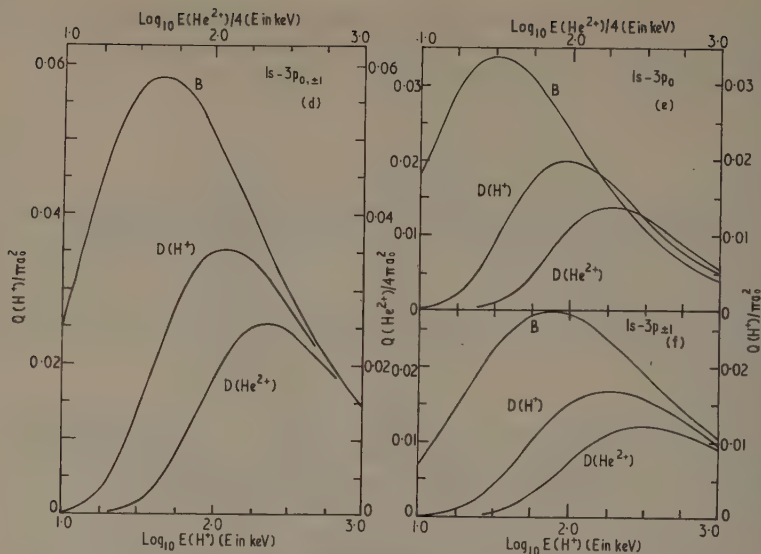


Figure 1. First Born and distortion approximations to the cross sections for:

- (a) $H^+(\text{or } He^{2+}) + He(1s^2)^1S \rightarrow H^+(\text{or } He^{2+}) + He(1s, 2p_{0\pm1})^1P$,
- (b) $H^+(\text{or } He^{2+}) + He(1s^2)^1S \rightarrow H^+(\text{or } He^{2+}) + He(1s, 2p_0)^1P$,
- (c) $H^+(\text{or } He^{2+}) + He(1s^2)^1S \rightarrow H^+(\text{or } He^{2+}) + He(1s, 2p_{\pm1})^1P$,
- (d) $H^+(\text{or } He^{2+}) + He(1s^2)^1S \rightarrow H^+(\text{or } He^{2+}) + He(1s, 3p_{0\pm1})^1P$,
- (e) $H^+(\text{or } He^{2+}) + He(1s^2)^1S \rightarrow H^+(\text{or } He^{2+}) + He(1s, 3p_0)^1P$,
- (f) $H^+(\text{or } He^{2+}) + He(1s^2)^1S \rightarrow H^+(\text{or } He^{2+}) + He(1s, 3p_{\pm1})^1P$.

plotted against $\log_{10} E$ for H^+ impact, or $\log_{10} E/4$ for He^{2+} impact where E is the energy of the incident ion in kev, the target atom being taken as stationary. Curve B of each set of three gives the Born approximation to the cross section for H^+ impact, or 0.25 times the cross section for He^{2+} impact; curve $D(H^+)$ gives the distortion approximation to the cross section for H^+ impact; and curve $D(He^{2+})$ gives 0.25 times the distortion approximation to the cross section for He^{2+} impact. In diagram (a) the curve $D(H^+)$, which is not drawn in full, intersects the curve B when $E(H^+)$ is about 165 kev, intersects the curve $D(He^{2+})$ when $E(H^+)$ is about 255 kev, and lies almost midway between these two curves when $E(H^+)$ is greater than about 450 kev. In diagram (d) the curves B and $D(H^+)$ intersect when $E(H^+)$ is about 750 kev, the curves B and $D(He^{2+})$ intersect when $E(He^{2+})$ is about 3600 kev, and the curves $D(H^+)$ and $D(He^{2+})$ intersect when $E(H^+)$ is about 1000 kev.

pattern of reduction and increase, and for processes (1) and (3) in the magnitude of the reduction at the maxima, to results for the $H(1s) \rightarrow H(2p)$ transition treated by Bates (1961). Arguments given earlier in the section lead one to expect the similarities in pattern to occur for other $s \rightarrow p$ transitions.

The reductions are less marked for all of the above cases than for the $H(1s) \rightarrow H(2s)$ transition (Bates 1959). Bates has already stated (1961) that the distortion approximation to the cross sections should be closer to the Born approximation for optically allowed transitions than for optically forbidden transitions. The difference arises because of the greater dependence of the cross sections for optically allowed transitions on distant encounters where distortion effects are small and because the effects of distortion at

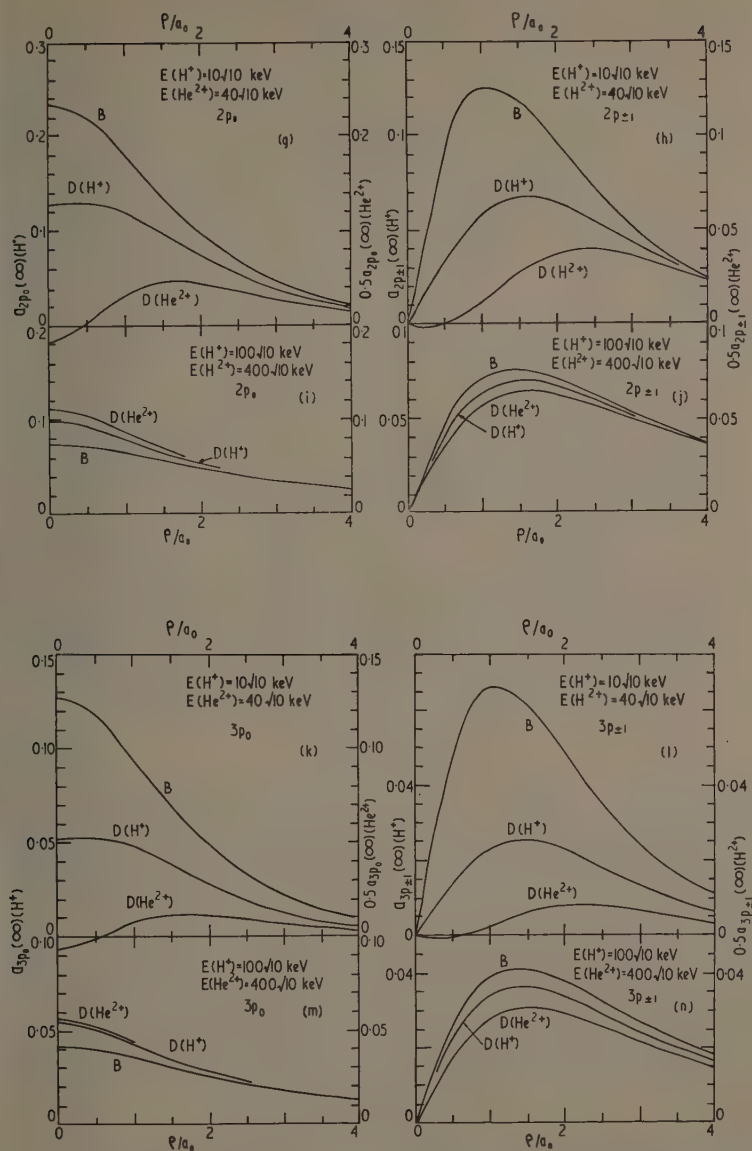


Figure 2. Asymptotic coefficients $a_{np_0}(\infty)$ (diagrams on left) and $a_{np_{\pm 1}}(\infty)$ (diagrams on right) plotted against impact parameter ρ . The energy of the incident ion is as indicated. Diagrams (g) to (j) refer to processes (1) and (3); diagrams (k) to (n) refer to processes (2) and (4). Curve B of each set of three gives the first Born approximation for H^+ impact, or 0.5 times the first Born approximation for He^{2+} impact; curve $D(H^+)$ gives the distortion approximation for H^+ impact; and curve $D(He^{2+})$ gives 0.5 times the distortion approximation for He^{2+} impact.

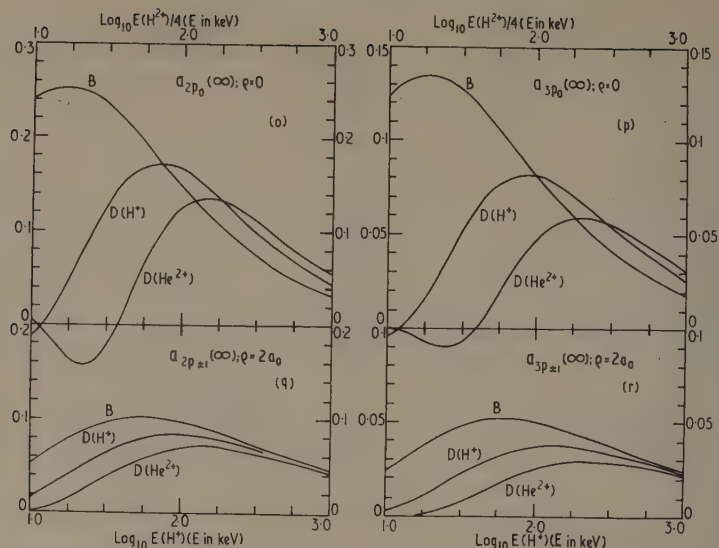
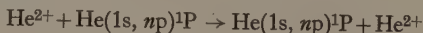
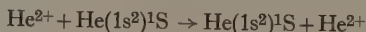


Figure 3. Asymptotic coefficients $a_{np_0}(\infty)$ (diagrams (a) and (p)) and $a_{np_{\pm 1}}(\infty)$ (diagrams (q) and (r)) plotted against $\log_{10} E$ for H^+ impact or $\log_{10} E/4$ for He^{2+} impact; E is the energy of the incident ion in keV, the target atom being taken as stationary. In the np_0 case the impact parameter is chosen to be zero (head-on collision) and in the $np_{\pm 1}$ case it is chosen to be $2a_0$. Diagrams (a) and (q) refer to processes (1) and (3); diagrams (p) and (r) refer to processes (2) and (4). The designations on the curves are as in the preceding figure.

high energies are in opposite senses for the two components of the transition so that cancellation occurs.

Since excitation probabilities for processes (1) to (4) are small,[†] the neglect of back-coupling should not have led to serious inaccuracy. Recent calculations by Skinner (1962, to be published) indicate that the effect of np_0 - $np_{\pm 1}$ coupling is also unimportant. The results may, however, require modification at low energies to allow for the resonance capture processes



and to a lesser extent, to allow for the various non-resonance capture processes which are possible. The cross sections may also be influenced by the effect of polarization.

ACKNOWLEDGMENTS

The author has pleasure in thanking Professor D. R. Bates for suggesting this problem and for his continued assistance throughout the course of the work.

This research has been supported by the Air Force Cambridge Research Center, Geophysics Research Directorate, of the Air Research and Development Command, U.S. Air Force, through its European Office, under Contract No. AF61(052)-131.

[†] $\mathcal{P}_{1s}, n_{p_0}, \mathcal{P}_{1s}, n_{p_{\pm 1}}$ do not exceed 0.03 for proton impact and 0.08 for alpha particle impact.

REFERENCES

- IES, D. R., 1959, *Proc. Phys. Soc.*, **73**, 227.
 — 1961, *Proc. Phys. Soc.*, **77**, 59.
 AME, J. W., 1931, *Proc. Camb. Phil. Soc.*, **27**, 511.
 LDBERG, L. and CLOGSTON, A. M., 1939, *Phys. Rev.*, **56**, 696.
 EEN, L. C., MULDER, M. M., LEWIS, M. N., and WOLL, J. W., 1954, *Phys. Rev.*, **93**, 757.
 LLERAAS, E. A., 1929a, *Z. Phys.*, **54**, 347.
 W, C. H., 1959, *Thesis for the degree of M.Sc.*, The Queen's University of Belfast.
 WDIN, P. O., 1953, *Phys. Rev.*, **90**, 120.
 ORSE, P. M., YOUNG, L. A., and HAURWITZ, E. S., 1935, *Phys. Rev.*, **48**, 948.

APPENDIX

Given below are the explicit forms of $\xi_{np}(R)$, $\eta_{np}(R)$ and $\zeta_{np}(R)$ for $n = 2$ and $n = 3$.
 (i) $n = 2$.

$$\begin{aligned}\xi_{2p}(R) &= R^{-2}\{1.04523 - (1.00838 + 1.00838T_1 + 0.50419T_1^2 + 0.12605T_1^3) \exp(-T_1) \\ &\quad - (0.03685 + 0.03685T_2 + 0.01843T_2^2 + 0.00461T_2^3) \exp(-T_2)\} \\ \eta_{2p}(R) &= R^{-1}\{(1.28251 + 0.96188T_3 + 0.32063T_3^2 + 0.05344T_3^3) \exp(-T_3) \\ &\quad + (1.28251 + 0.64125T_4) \exp(-T_4) - (1.83143 + 0.91571T_5) \exp(-T_5) \\ &\quad - (0.65117 + 0.32559T_6) \exp(-T_6) - (0.08241 + 0.04121T_7) \exp(-T_7)\} \\ \zeta_{2p}(R) &= R^{-3}\{-8.17839 + (8.17839 + 8.17839T_3 + 4.08920T_3^2 + 1.36307T_3^3 \\ &\quad + 0.34077T_3^4 + 0.05679T_3^5) \exp(-T_3)\}\end{aligned}$$

ith

$$T_j = t_j R$$

here

$$\begin{array}{ll}t_1 = 1.940799 & t_4 = 4.0 \\ t_2 = 3.396598 & t_5 = 2.911598 \\ t_3 = 0.97 & t_6 = 4.367397 \\ & t_7 = 5.823196\end{array}$$

(ii) $n = 3$.

$$\begin{aligned}\xi_{3p}(R) &= R^{-2}\{0.488172 - (0.468672 + 0.468672T_8 + 0.234336T_8^2 + 0.048808T_8^3 \\ &\quad - 0.009776T_8^4) \exp(-T_8) - (0.019500 + 0.019500T_9 + 0.009750T_9^2 \\ &\quad + 0.002275T_9^3 - 0.000163T_9^4) \exp(-T_9)\} \\ \eta_{3p}(R) &= R^{-1}\{(1.17868 + 0.98142T_{10} + 0.39208T_{10}^2 + 0.09782T_{10}^3 + 0.01623T_{10}^4 \\ &\quad + 0.00822T_{10}^5) \exp(-T_{10}) \\ &\quad + (1.17868 + 0.58934T_4) \exp(-T_4) - (1.68316 + 0.84158T_5) \exp(-T_5) \\ &\quad - (0.59846 + 0.29923T_6) \exp(-T_6) - (0.07574 + 0.03787T_7) \exp(-T_7)\} \\ \zeta_{3p}(R) &= R^{-3}\{-44.61266 + (44.61266 + 44.61266T_{10} + 22.30633T_{10}^2 + 7.43544T_{10}^3 \\ &\quad + 1.85886T_{10}^4 + 0.34824T_{10}^5 + 0.03843T_{10}^6 + 0.01945T_{10}^7) \exp(-T_{10})\}\end{aligned}$$

here

$$t_8 = 1.780799, \quad t_9 = 3.236598, \quad t_{10} = 0.65.$$

The Radiative Capture of Protons by Neutrons at 50 mev

By N. C. BARFORD, R. B. PALMER AND B. TALLINI†

Imperial College, London

MS. received 31st May 1961

Abstract. By using an internal lithium deuteride target in the Harwell cyclotron, and 'hardening' the resulting scattered neutrons with polythene, a low intensity beam of neutrons with an energy peak at 50 mev was produced. This beam passed through a 9 cm hydrogen bubble chamber and produced in it reactions of the type



which were distinguished by the range-angle distribution of the deuterons from the background of elastic n-p scatters. A cross section of $110 \pm 60 \mu\text{bn}$ was found for the process.

§ 1. INTRODUCTION

NO MEASUREMENTS of the cross section for the radiative capture of neutrons by protons,



have previously been made except at thermal energies (Stooksberry and Crouch 1959). The inverse process of photodisintegration of deuterium has been investigated for protons of a wide range of energies (for example Allen 1955), and, from these results, using detailed balance arguments, one may predict the capture cross section to be $20 \pm 4 \mu\text{bn}$ for 50 mev neutrons (Palmer 1960).

A neutron experiment of such low cross section is feasible even with quite small bubble chambers, because of the absence of beam tracks in the chamber. It was found in preliminary proton experiments with the Imperial College 9 cm hydrogen chamber that simple nuclear reactions could be observed and measured against a background of about 20 beam proton tracks crossing the chamber. For the neutron capture experiment there are, of course, no beam tracks and the only significant background is caused by those proton tracks arising from elastic n-p scatters. At 50 mev the cross section for this is 155 mbn, from which one may show that up to about 500 neutrons per pulse could be allowed to enter the chamber before the scattered proton tracks would give a background equivalent to the 20 beam protons found permissible in the preliminary experiments.

Hence, to observe 100 neutron captures, 36 000 photographs (stereo-pairs) would be required. We may note that a proton experiment of the same cross section would require 900 000 photographs.

§ 2. THE NEUTRON BEAM

The experiment would be best performed with a parallel monoenergetic beam of neutrons. At 50 mev these would form deuterons giving tracks in the liquid hydrogen

† Now at the Department of Physics, Birmingham University.

length 3 cm at angles up to 5° to the beam direction (Palmer 1960). These tracks could be easily observed and distinguished from those of knocked-on protons of the same angular spread whose range would exceed 15 cm.

Such a neutron beam could be obtained from a thin deuterium target placed in an internal proton beam of adequate flux. Unfortunately, this method was impracticable at the Harwell cyclotron.

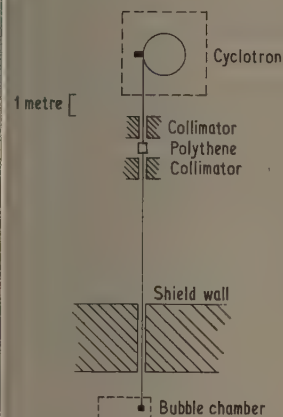


Figure 1

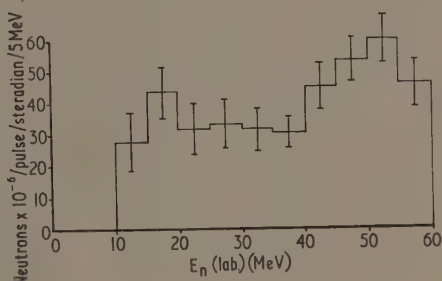


Figure 2

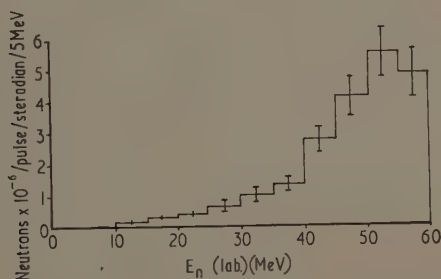


Figure 3

Instead, a lithium deuteride target was used in the circulating beam and neutrons were taken off tangentially (see figure 1). These neutrons were far from monoenergetic. Firstly, the neutrons from the lithium in the lithium deuteride have a wide energy spread, even when the incident protons have a precise energy. Secondly, these protons

do in fact have an energy spread of 15–20 mev caused by radial oscillations in the circulating beam and energy losses in the target itself, which increases with target thickness. A target 20 mm thick was chosen as giving the best compromise between overheating the lithium deuteride and unduly degrading the incident proton energy.

With a circulating beam intensity of approximately 10^{10} protons per pulse the total forward neutron intensity was approximately 4×10^8 neutrons per steradian. The energy spectrum of these neutrons is shown in figure 2. Since the flux was in excess of what the chamber could utilize it was possible to sharpen this energy spectrum by passing the beam through hydrogenous material, thus preferentially scattering out the low energy neutrons. After some trials with various lengths of polythene, a 50 cm length was chosen. The resultant 'hardened' spectrum is shown in figure 3. The total forward flux remaining was then 2×10^7 neutrons per steradian, giving six neutrons per pulse per cm^2 in the chamber. A typical photograph obtained using this flux is shown in figure 4 (plate). The number of tracks is small and well below the number that could be tolerated. The unwanted background illumination was negligible. We were able therefore, to economize both in film and scanning effort by photographing three exposures on each negative. In the example shown in figure 5 (plate) the number of tracks is reasonable and the threefold superposition of optical background quite tolerable. A trial run showed that only when five exposures per negative were used, did the optical background seriously obscure the tracks.

§ 3. CHAMBER OPERATION AND PHOTOGRAPHY

Beam pulses of 100 μsec duration were obtained from the Harwell cyclotron at a rate of 100 per second. This repetition rate was far too great to be matched by the bubble chamber and its camera, which were operated conveniently at 20 cycles per minute. An electronic gating system (Palmer 1960) was used to lock the chamber expansion and photography to one in approximately every 300 of the cyclotron pulses. To avoid the overheating and consequent decomposition of the lithium deuteride target by the unwanted proton pulses, the cyclotron was set to accelerate protons only for a few pulses around the one photographed.

Photographs were taken as stereo pairs on a single reel of 35 mm film, using Dallmeyer 'Serrac' 3 in. lenses. These were 30 cm from the chamber and provided a stereo angle of 15° and demagnification of 1 : 3. With a Siemens SF 7 light source, using 20 joules per flash at 4 kv, good quality photographs were obtained after a bubble growth time of 1 msec.

§ 4. SCANNING AND ANALYSIS

For scanning and measuring the film a simple projection system was used that gave an image $20\times$ magnified of the negative on a horizontal opaque screen. This image was located on the screen by means of fiducial marks and the cartesian coordinates of the ends of the tracks were measured using a pantograph. An estimate of the accuracy of the method was made by measuring 100 proton-proton scatters, whose included angle should be 90° . The overall error, after three-dimensional reconstruction, was found to be equivalent to a measurement error of 10μ on the film or to an uncertainty of 0.3° in the direction of a 3 cm track in the chamber.

In order to determine the neutron spectrum 100 pairs of negatives were selected from the beginning and end of the film, and every track on these was measured without

attempt to identify corresponding pairs in the two stereo views. The coordinates at the ends of the tracks were typed directly on to punched tape; this was later fed into a MERCURY computer, which identified corresponding tracks and reconstructed them in space. A single track image could be measured and typed out in a minimum of 10 seconds and an average of 15 seconds. From the reconstructed tracks, we selected only those satisfying the following conditions: firstly they were required to lie in a rectangular volume $5.6 \text{ cm} \times 7.7 \text{ cm} \times 5.6 \text{ cm}$, which was visible to both cameras; secondly the event represented by the track must have been caused by a beam neutron which, apart from passing through the 6 mm aluminium wall of the bubble chamber vacuum tank, had passed only through the 3 mm copper wall of the chamber itself.

Because of the very small cross section, only one in 7000 of the selected tracks presented a neutron capture event; the rest were scattered protons. It was thus legitimate, in determining the neutron spectrum, to take all tracks to be protons and to calculate an energy distribution of the corresponding neutrons, using known cross sections for elastic n-p scattering (P. H. Bowen *et al.*, to be published). A correction factor, which arose from the restricted selection of proton tracks, was calculated exactly as a function of energy and was then applied to this distribution to give the true neutron energy spectrum, shown in figure 3.

Four thousand pairs of photographs were examined for examples of deuteron formation. Since the directions of deuteron tracks make only small angles with beam neutrons (see § 3), and since the beam was well collimated, we were able to restrict the selection of tracks considerably. Only those were chosen whose images, in both stereo photographs, lay within 10° of the beam direction. This did, however, involve the identification of corresponding images during the scanning. This criterion selects all tracks whose directions in space are within 10° of the beam, as well as a readily calculable proportion of those at greater angles. Consequently, we were able to construct an angular distribution of tracks up to about 30° .

If, as will be shown in § 5, most of these tracks are caused by protons arising from elastic n-p scatters, we would expect the main angular distribution to show a constant number of tracks per steradian (in the centre-of-mass system) at all angles. To show deviation from this we have accordingly divided the number of tracks in each angular interval by $d\Omega_{\text{c.m.}} = 4\pi \sin 2\theta_{\text{lab}} d\theta_{\text{lab}}$ to give the distributions shown in figures 6 (*a*, *b* and *c*). The track length ranges of 0.8–1.8 cm, 1.8–3.1 cm, and 3.1–4.8 cm used for these distributions correspond to energies E_N (lab.) of 10–15 mev, 15–20 mev and 20–25 mev respectively, where E_N (lab.) is that energy of a neutron in the laboratory frame of reference which would elastically scatter a proton having the observed track length. The corresponding values of neutron energy E_N^D (lab.), which would give deuterons in these range intervals are 27–40 mev, 40–54 mev, 54–67 mev.

§ 5. INTERPRETATION

Restricting the discussion for the moment to figure 6(*b*), we can say that particles giving the tracks may arise in one of the following ways. (i) They are deuterons formed by collimated beam neutrons in the energy interval 40–54 mev; figure 3 shows that this interval accounts for about 50% of all beam neutrons. (ii) They are protons knocked-on by collimated beam neutrons in the energy interval 15–20 mev; this includes only 10% of all beam neutrons. (iii) They are protons knocked-on by neutrons not in the collimated beam, which have been scattered out of the beam by the hydrogen or other parts of the apparatus. (iv) They are deuterons formed from such scattered neutrons.

(v) They are charged particles of any kind from interactions of beam neutrons with impurities in the liquid hydrogen.

We should expect the intensity only of the deuterons in category (i) to vary rapidly with angle, since they will all be concentrated within 5° of the beam direction. The intensities of the particles in all the other categories should vary only slowly up to about 30° . Moreover, since the cross section for deuteron production is so small, the deuterons of category (iv) will be negligible in comparison with the protons of category

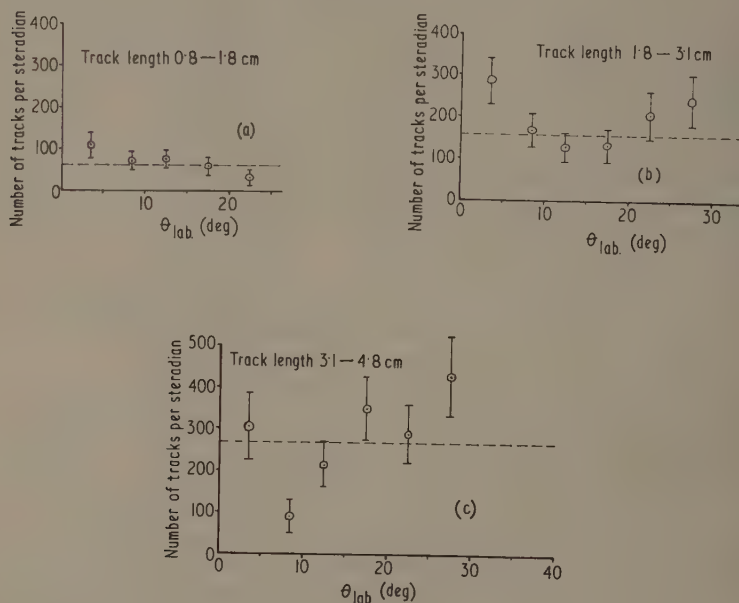


Figure 6

(iii) and, since the impurities in the hydrogen are small ($\sim 0.02\%$ deuterium, for example), particles of category (v) will be negligible in comparison with the protons of category (ii). Consequently, we may expect to see an angular distribution of tracks which varies only slowly up to 30° , arising almost entirely from protons, on which is superimposed a peak below about 5° , caused by deuterons.

The presence of such peaks is evident in figures 6 (a, b and c). One might construct for each histogram a curve through all the points except the first, extrapolate this to the left, and subtract it from the experimental value at the smallest angle to give the magnitude of the peak there. On this basis, for example, practically all the tracks shown at 3.5° in figure 6(c) would represent deuterons. However, no reasonable explanation has been found for the distribution of proton tracks in the range $0 < \theta_{lab} < 30^\circ$ to differ by more than a few per cent from that given by isotropic scattering in the centre-of-mass system. Assuming isotropy, the proton background averaged from the observations is shown as the dotted line in each figure. The resulting estimates of the numbers of neutron captures in each energy range are given in the following table, together with

number of elastic n-p scatters. From these and the cross sections for n-p scattering (H. Bowen *et al.*, to be published), the capture cross sections were derived.

Neutron energy (mev)	27-40	40-54	54-67
Elastic n-p cross section (mbn)	265	170	130
Number of elastic scatters	16 800	31 800	21 700
Number of neutron captures	8 ± 5	20 ± 10	7 ± 15
Capture cross section (μ bn)	126 ± 80	107 ± 50	42 ± 90

A weighted mean of these gives for the neutron capture cross section the value 110μ bn over the range of neutron energies considered, with a statistical error of $\pm 45 \mu$ bn. When the effects of other errors, such as those due to uncertainty in the neutron spectrum, are included, we obtain a final value for the cross section of $110 \pm 60 \mu$ bn. This appears rather high, but the errors are such that no definite discrepancy with theory can be asserted.

In spite of the limited number of photographs examined, the present work establishes the value of the hydrogen bubble chamber for neutron experiments. Events with a cross section in the 10-100 μ bn region can be studied with good statistical accuracy using less than 50 000 photographs.

ACKNOWLEDGMENTS

We are especially indebted to Mr. B. Rose for suggesting this as an experiment to be carried out at the Harwell cyclotron, and for generously providing us with the necessary facilities. Mr. Phillips gave valuable assistance on the theoretical aspects of the problem.

Most members of the Bubble Chamber Group at Imperial College helped to operate the bubble chamber; in this connection we wish particularly to thank Mr. D. L. Reed and Dr. I. Butterworth.

The work was carried out with the support of a Department of Scientific and Industrial Research Special Research Award and, in the case of one of us (R.B.P.), a Research Studentship from the Department of Scientific and Industrial Research.

REFERENCES

- ALLEN, L., 1955, *Phys. Rev.*, **98**, 705.
 ALMER, R. B., 1960, *Ph.D. Thesis*, University of London.
 TOOKSBERRY, R. W., and CROUCH, M. F., 1959, *Phys. Rev.*, **114**, 1561.

On the Momentum Spectrum of Cosmic-ray Muons at Sea Level

By A. L. RODGERS†

Department of Physics, University of Manchester

MS. received 18th April 1961, in revised form 31st May 1961

Abstract. The Manchester spectrum of muons arriving vertically at sea level is discussed in terms of the processes leading to the formation of the sea-level hard component of cosmic radiation. Evidence is presented to show that above a momentum of 20 GeV/c there are particles, probably muons, at sea level which cannot be explained in terms of π - μ decay only.

§ 1. INTRODUCTION

THE Manchester cosmic-ray spectrograph, described by Hyams *et al.* (1950) and Holmes *et al.* (1961a), has been used to measure the momentum spectrum of single muons arriving vertically at sea level in the East-West plane at a latitude of 57°N. The results are described by Owen and Wilson (1955) and Holmes *et al.* (1961b) together they form a continuous momentum spectrum from 0.5 GeV/c to an upper limit in the region of 1000 GeV/c.

In order to ascertain how far a single π - μ decay mechanism explains the observed sea-level variation of muon intensity with momentum, the measured sea-level momentum spectrum is compared with one derived from the accepted primary proton spectrum the Fermi-Landau multiplicity model and a first-order process to describe the diffusion of the mesonic component in the atmosphere. Information is obtained on the primary collision in the primary energy range 10^3 to 10^4 GeV from the comparison in the sea-level momentum range 50 to 500 GeV/c.

It is assumed that the momentum variation in the sea-level spectrum may be adequately defined by the primary proton spectrum alone, the primary charge spectrum, in terms of energy per nucleon, remaining constant with energy. It is however known that the primary alpha-particle spectrum may fall more rapidly with energy than does the proton spectrum. The effect on the conclusions of this investigation is to increase the observed insufficiency of a single π - μ decay process to explain the measured sea-level spectrum at high momentum.

From considerations of the shape of the primary proton spectrum and Fermi-Landau theory of secondary particle production it is expected that beyond a secondary momentum of 5 GeV/c the contribution to the muon generation spectrum from non-primary nucleons and parent mesons other than those arising directly from the primary nucleon-nucleon collision is small, and accordingly, only primary nucleons and first generation mesons are considered. It is expected that the error introduced by this assumption is 3% at 5 GeV and decreases rapidly with increase in energy. The proposal is to some extent substantiated by the fact that the observed maximum in the sea-level charge ratio of muons, which is interpreted as ending the influence of secondary processes, is not much different from 5 GeV/c.

† Now at Atomic Weapons Research Establishment, Aldermaston, Berks.

Because the investigation is indirect the conclusions are subject to the confidence which may be placed in the parameters which occur in the processes leading to the sea-level component. It would seem, however, that the low statistics in present direct observations limit the usefulness of the information which may be gained from them and that a continuous description of the energy dependence in the characteristics of the primary collision may only be afforded by indirect observations of the present type.

§ 2. THE CALCULATED SEA-LEVEL MOMENTUM SPECTRUM

2.1. The Pion Spectrum at Production derived from the Primary Proton Spectrum

The pion spectrum at production is determined from the accepted primary proton spectrum. The experimental primary spectrum is taken from Barrett *et al.* (1952), the slope s of the integral proton spectrum being given by

$$s = 1.35 + 0.04 \ln \frac{E_p}{3.2 \times 10^9} \quad (1)$$

for $E_p \gg 10^9$ ev where E_p (ev) is the proton energy.

It is assumed that high-energy pions are created according to the Fermi-Landau theory of multiple meson production, i.e. the mean number n of pions produced in the primary collision is given by

$$n = kE_p^{1/4} \quad (2)$$

the average energy $E_\pi = KE_p^{3/4}$.

The constant of proportionality in equation (2) is determined by making use of Barrett's observation that muons of mean energy 800 Gev are associated with primaries of mean energy 4×10^4 Gev, viz.

$$E_p = 8.62 \times 10^{10} \left(\frac{E_\pi}{10^{10}} \right)^{4/3}.$$

For a multiplicity process which varies as the fourth root of the primary energy the exponent r of the pion production integral spectrum is related to s by

$$\begin{aligned} r &= \frac{s - \frac{1}{4}}{1 - \frac{1}{4}} \\ &= 1.65 + 0.07 \ln \left(\frac{E_\pi}{10^{10}} \right) \end{aligned} \quad (3)$$

where E_π is measured in ev.

The differential momentum spectrum at production $S'(\pi, p)$ of the pions is accordingly given by

$$S'(\pi, p) dp_\pi = (2.65 + 0.33 \log p_\pi) \exp[-6.1 \log p_\pi + 0.38(\log p_\pi)^2] dp_\pi \quad (4)$$

where p_π (ev/c) is the momentum of the pion.

2.2. The Sea-level Spectrum in terms of π - μ Decay only

An exact analysis leads to a diffusion equation of extreme complexity and the following determination is regarded as a close approximation.

The depth of the atmosphere is taken to be 1000 g cm^{-2} and it is assumed that pions are produced at a unique pressure level of 100 g cm^{-2} below the top of the atmosphere by the total absorption of the primary proton component of geometrically nuclear interaction cross section. Duperier (1951) has shown that such an assumption leads to only a small error in the numbers of mesons surviving to sea level. It is expected that the maximum effect in the whole of the momentum range investigated is less than 10%, the discrepancy being greater at low momentum.

It is assumed that the momentum of the muon is always 0.8 of that of the parent pion and that the subsequent rate of energy loss for muons in excess of 1 Gev is $2.2 \text{ Mev g}^{-1} \text{ cm}^2$.

In the absence of a suitable computer at the time of calculation the process of meson diffusion was treated numerically, the lower 900 g cm^{-2} of the atmosphere being divided into nine equal homogeneous layers, of density corresponding to that of the mean depth of the layer. The variation in density with depth for the Standard Atmosphere is taken from Rossi (1948). This method is considered to be sufficiently accurate in view of the overall uncertainties involved in the analysis.

The rate of capture of pions in the incremental layer $dZ \text{ g cm}^{-2}$ is proportional to $1/\lambda_\pi$ where λ_π is the pion nuclear interaction length in air. The rate of decay of pion in $dZ \text{ g cm}^{-2}$ is proportional to $1/L$ where L is the mean range before decay and is equal to $5.13 \times 10^{-6} p_\pi \text{ cm}$ for pions of momentum $p_\pi \text{ ev/c}$.

For a layer of atmosphere of mean density $\bar{\rho} \text{ g cm}^{-3}$ bounded between the depths Z_1 and $Z_2 \text{ g cm}^{-2}$ the number of pions interacting in the incremental layer $dZ \text{ g cm}^{-2}$ at distance $Z \text{ g cm}^{-2}$ from Z_1 , is $N(\pi, Z) dZ/\lambda_\pi$, and the number decaying is $N(\pi, Z) dZ/L$, where $N(\pi, Z)$ is the number of pions surviving at depth $Z \text{ g cm}^{-2}$.

The fraction of pions lost by decay and interaction is therefore given by

$$-\frac{dN(\pi, Z)}{N(\pi, Z)} = \left(\frac{1}{\lambda_\pi} + \frac{1}{L\bar{\rho}} \right) dZ. \quad (5)$$

The number of pions surviving at Z_2 , $N(\pi, Z_2)$, is found by integrating between the limits Z_1 and Z_2 :

$$N(\pi, Z_2) = N(\pi, Z_1) \exp \left[-(Z_2 - Z_1) \left(\frac{1}{\lambda_\pi} + \frac{1}{L\bar{\rho}} \right) \right]. \quad (6)$$

The pion spectrum at sea level is found by using equation (6) to determine the fraction of pions surviving at the lower boundary of successive homogeneous layers. In terms of the production spectrum $S'(\pi, p)$ the sea level spectrum $S(\pi)$ is

$$S(\pi) = S'(\pi, p) \exp \left[-100 \left(\frac{9}{\lambda_\pi} + \frac{1}{L} \sum_{i=1}^9 \frac{1}{\bar{\rho}_i} \right) \right] \quad (7)$$

where $\bar{\rho}_i$ is the mean density of the i th layer.

The survival probability $P(\pi)$ is, from equation (7),

$$P(\pi) = \frac{S(\pi)}{S'(\pi, p)} = \exp \left[- \left(\frac{900}{\lambda_\pi} + \frac{3.1 \times 10^{11}}{p_\pi + p_0} \right) \right] \quad (8)$$

where $p_0 = 2.2 \times 10^9 \text{ ev/c}$.

Numerical analysis shows that, due to the competing processes of interaction and decay, $S(\pi)$ passes through a maximum at $p_\pi = 100 \text{ Gev/c}$, the absolute value of intensity being dependent on the magnitude of the 'constant' pion cross section for nuclear interaction.

The production spectrum of muons is determined by considering the contribution $N(\mu, dZ)$ from an incremental layer dZ g cm⁻²:

$$dN(\mu, dZ) = N(\pi, Z) \frac{dZ}{L\bar{\rho}}$$

where

$$N(\pi, Z) = N(\pi, Z_1) \exp \left[-(Z_1 - Z) \left(\frac{1}{\lambda_\pi} + \frac{1}{L\bar{\rho}} \right) \right]. \quad (9)$$

The number, $N(\mu, Z_1, Z_2)$, of muons produced by the decay of pions in the layer $Z_1 - Z_2$ g cm⁻² is obtained by integrating equation (9) between the limits Z_1 and Z_2 g cm⁻²:

$$N(\mu, Z_1, Z_2) = \frac{N(\pi, Z_1)}{1 + (L\bar{\rho}/\lambda_\pi)} \left[1 - \exp \left\{ -(Z_1 - Z_2) \left(\frac{1}{\lambda_\pi} + \frac{1}{L\bar{\rho}} \right) \right\} \right]. \quad (10)$$

Rewriting equation (10) in terms of the probability function $P'(\mu)_i$, the muon production spectrum $S'(\mu)_i$ in the i th atmospheric layer is

$$P'(\mu)_i = \frac{S'(\mu)_i}{S'(\pi, p)} = \exp \left[-100 \left(\frac{i-1}{\lambda_\pi} + \frac{1}{L} \sum_{r=1}^{r=i} \frac{1}{\bar{\rho}_i} \right) \right] \left\{ 1 - \exp \left[-100 \left(\frac{1}{\lambda_\pi} + \frac{1}{L\bar{\rho}_i} \right) \right] \right\}. \quad (11)$$

The sea-level muon spectrum is found by summing equation (11) for the nine homogeneous atmospheric layers and correcting for μ -e decay. The sea-level muon spectrum $S(\mu)$, derived from considerations of the pion component only, and a single decay mechanism, is given by

$$S(\mu) = \sum_{i=1}^{i=9} S'(\mu)_i p(\mu) \quad (12)$$

where $p(\mu)$ is the probability of μ -e decay and is given by

$$p(\mu) = \exp \left[-\frac{100}{M} \sum_{r=1}^{r=i} \frac{1}{\bar{\rho}_i} \right]. \quad (13)$$

M is the mean range before decay of muons whose sea-level momentum is 0.8 that of the parent pion, less the momentum lost by ionization in traversing the residual amount of atmosphere to sea level.

§ 3. DISCUSSION AND CONCLUSIONS

The probability functions (8), (11) and (13) are displayed in figures 1, 2 and 3 respectively. Figure 4 shows the calculated ratio of pion flux to muon flux at sea level with momentum on the assumption of a single π - μ decay mechanism. In the absence of information on the interaction of very high energy pions the expected variations appropriate to a pion nuclear interaction cross section of geometric and 0.3 geometric are shown, the corresponding curves being denoted A and B respectively.

It would seem unlikely, however, that the pion is a weakly interacting particle at higher energies, and the discussion is confined mainly to the expectations realized by a nuclear geometrical interacting pion.

The sea-level spectrum $S(\mu, \pi)$ composed of pions and muons only, and derived from the sum of equations (7) and (12) relevant to a constant pion cross section of

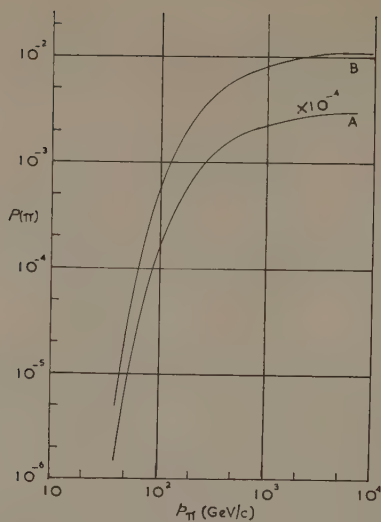


Figure 1. Pion survival probability to sea level.

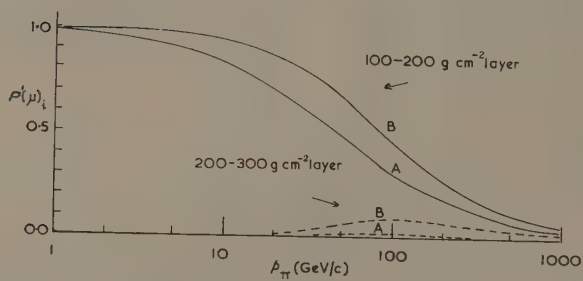


Figure 2. Muon production per layer expressed as a fraction of the muon production spectrum.

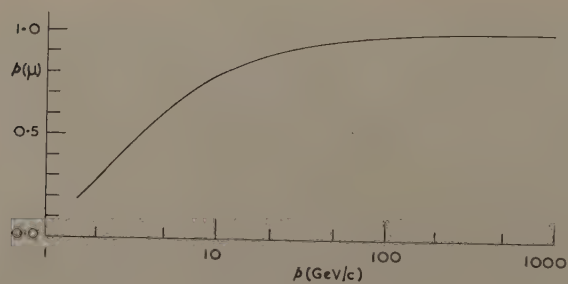


Figure 3. Muon survival probability to sea level.

nuclear geometric, is compared with the measured sea-level spectrum $S(p)$ in figure 5.

For ease of comparison with other workers it is convenient to relate the evidence to the production level. Thus figure 6 shows $S'(\pi, p)$, the pion spectrum derived from the primary proton component, together with $S'(\pi, s)$, the spectrum derived from the measured sea-level spectrum $S(p)$ and the first-order diffusion model. There is good

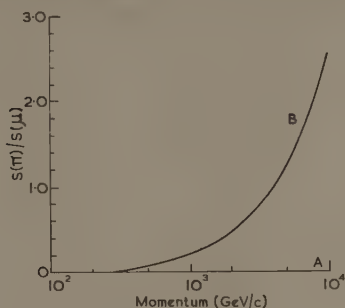


Figure 4. Ratio of pions to muons at sea level from π - μ decay.

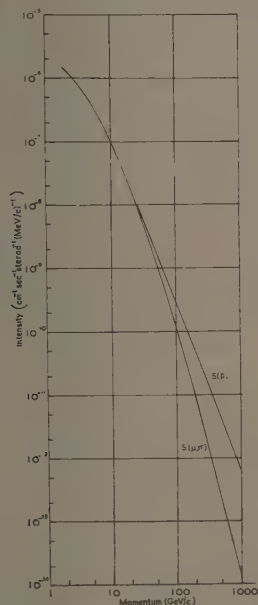


Figure 5. The calculated and observed sea-level spectra, $S(\mu, \pi)$ and $S(p)$.

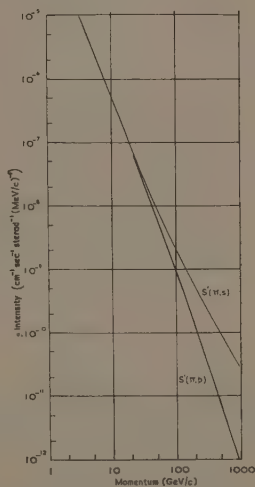


Figure 6. Pion production spectra. $S'(\pi, p)$ is derived from the primary proton component. $S'(\pi, s)$ is derived from the measured sea-level spectrum.

agreement over the momentum range 4 GeV/c to 20 GeV/c. Between 6 GeV/c and 20 GeV/c the two spectra agree to within 1% and at 4 GeV/c the discrepancy is 5%, which is to be expected from the approximations used in the analysis. A comparison of $S'(\pi, p)$ with the results of Puppi (1956) shows good agreement from 3 GeV/c to his upper limit of 40 GeV/c.

The conclusion of the investigation is subject to the validity and approximations of the parameters in the model adopted. Basically two experimentally determined spectra are available which are linked by the statistical model of meson production and a first-order meson diffusion process. However, the good correlation between the two spectra of figure 5 for secondary momenta below 20 GeV/c suggests that, provided the unlikely situation does not exist in which the approximations entering the analysis are completely self-balancing, the observed sea-level spectrum for momenta less than 20 GeV/c is adequately explained in terms of π - μ decay only, the pion cross section for nuclear interaction remaining sensibly nuclear geometric. In particular, the conclusions add some argument in favour of a multiplicity process which does not greatly differ from the predictions of the Fermi theory, and provide some validity for the model adopted in § 2.2, the two inferences being complementary and mutually dependent.

For secondary momenta above 20 GeV/c the evidence suggests that, provided the Fermi theory is still valid and the pion-nuclear interaction remains unchanged from geometric, there are particles surviving at sea level which cannot be explained by the single process of π - μ decay. The excess at sea level is shown in figure 7, where R

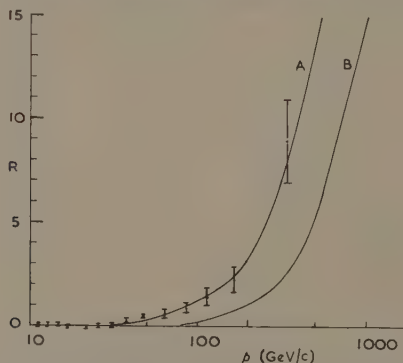


Figure 7. Ratio of the excess muons at sea level to the number expected from π - μ decay only.

is the ratio of the excess particles to those expected on π - μ decay only. The statistical errors in this figure, arising from the measured uncertainties of the sea-level observations, are appropriate to curve A corresponding to nuclear geometric interaction of the pion. Curve B is displayed to show the effect on the excess if the pion becomes less strongly interacting at very high momenta.

If we relate the conclusions to curve A of figure 7 we expect that both high energy proton and pion flux at sea level are small. Provided that the proton interaction cross section remains nuclear geometric it is expected that protons constitute less than 0.1% of the total particles at sea level above 20 GeV/c. This is substantiated by the fact that there is no considerable increase in the charge ratio of particles at sea level (Holmes *et al.* 1961b). Pions at sea level are excluded on the grounds of the probability function, equation (8) (see figure 1), and electrons are eliminated in the spectrograph measurements. Because of the short heavy meson lifetime it is expected that negligible numbers of heavy mesons survive to sea level even if the interaction cross section falls to a small value at high energies. It is concluded, therefore, that the excess particles at sea level are muons arising extraneous to π - μ decay. The inclusion of the expected

primary alpha-particle spectrum would cause an increase in the numbers of excess particles at high energy.

Alternatively, to explain the difference in terms of predominant π - μ decay it is necessary to examine the relevant assumptions which are made in the analysis.

A primary proton spectrum of smaller slope than that given by equation (1), or a proton cross section for nuclear interaction which decreases with increasing energy, could tend to reduce the difference between the observed and calculated spectra. Both effects would, however, have to be considerable to obtain correlation in terms of π - μ decay only. Cudakov *et al.* (1958) have measured the collisional mean free path of very high energy protons in nitrogen nuclei and find that it is substantially nuclear geometric. It would be difficult to reconcile a decreased slope of the primary proton spectrum with the observations at much greater energies.

The evidence in favour of the Fermi theory is that Cocconi (1954) has shown that the characteristics of a large number of relativistic showers in cosmic radiation may be satisfied by the 'tunnel' effect when the Fermi model is used to predict the multiplicity of a single nucleon-nucleon collision. Cocconi concludes that the Heisenberg (1949) model, in which the range of nuclear forces is not limited, would not explain the observed cases of low nuclear excitation. McCusker and Roesler (1957) have confirmed this general agreement with more recent experimental observations.

Referring to the present investigation it is apparent that to explain the measured sea-level spectrum in terms of pion production only beyond 20 gev would imply a multiplicity which decreases with increasing primary energy. Such a process is untenable theoretically, and is experimentally inconsistent with shower observations and the observed sea-level charge ratio variation with momentum.

It is concluded therefore that, conditional upon self-balancing approximations, there are muons surviving to sea level whose origin cannot be explained on the π - μ decay process only. The excess at sea level may be attributed to decays arising from charged heavy mesons, either directly or through an intermediate pion.

Compared with other extended measurements of the sea-level muon spectrum of high upper momentum limit the Manchester spectrum is in agreement with the results of Pine *et al.* (1959) and with Ashton *et al.* (1960) up to a momentum in excess of 100 gev/c.

REFERENCES

- ASHTON, F., BROOKE, G., GARDENER, M., HAYMAN, P. J., JONES, D. G., KISDASAMY, S., LLOYD, J. L., TAYLOR, F. E., WEST, R. H., and WOLFENDALE, A. W., 1960, *Nature, Lond.*, **185**, 364.
 BARRETT, P. H., BOLLINGER, L. M., COCCONI, S., EISENBERG, Y., and GREISEN, K., 1952, *Rev. Mod. Phys.*, **24**, 133.
 COCCONI, S., 1954, *Phys. Rev.*, **93**, 1107.
 CUDAKOV, A. E., *et al.*, 1958, *Nuovo Cim.*, **8**, 737.
 DUPELIER, A., 1951, *J. Atmos. Terr. Phys.*, **1**, 296.
 HEISENBERG, W., 1949, *Z. Phys.*, **126**, 569.
 HOLMES, J. E. R., OWEN, B. G., and RODGERS, A. L., 1961a, *Proc. Phys. Soc.*, **78**, 496.
 — 1961 b, *Proc. Phys. Soc.*, **78**, 505.
 HYAMS, B. H., MYLROI, M. G., OWEN, B. G., and WILSON, J. G., 1950, *Proc. Phys. Soc. A*, **63**, 1053.
 MCCUSKER, C. B. A., and ROESLER, F. C., 1957, *Nuovo Cim.*, **5**, 1136.
 OWEN, B. G., and WILSON, J. G., 1955, *Proc. Roy. Soc. A*, **68**, 409.
 PINE, J., DAVISSON, R. J., and GREISEN, K., 1959, *Nuovo Cim.*, **14**, 1181.
 PUPPI, G., 1956, *Progress in Cosmic Ray Physics*, Vol. 3 (Amsterdam: North-Holland), p. 341.
 ROSSI, B., 1948, *Rev. Mod. Phys.*, **20**, 537.

Existence of Energy Gaps in One-Dimensional Liquids

By R. E. BORLAND

Mathematics Division, National Physical Laboratory, Teddington, Middlesex

Communicated by P. Dean; MS. received 31st August 1961

Abstract. It is shown that a definite energy gap exists in a one-dimensional liquid provided that the maximum deviation of the distance between atoms is less than a critical value. Higher gaps successively appear as the disorder is further reduced.

§ 1. INTRODUCTION

IN A RECENT paper Makinson and Roberts (1960) posed the question whether in an infinite chain of atoms lacking long range order there may be energy gaps in which there are no states whatever, or whether the states are always thinly spread with a density approaching zero as the range of order increases to infinity. In this paper we shall prove that, subject to the usual assumptions, energy gaps exist in a chain lacking long range order provided that the short range order is sufficiently small. We consider a model in which the minimum distance between atoms is of length a and the maximum distance of length $a+b$. No assumptions are made about the type of disorder so that the results derived are valid whether long range order exists or not.

§ 2. CHAIN OF NEGATIVE DELTA FUNCTIONS

To simplify the proof we consider first the special case of a chain of δ -functions of strength $-k_0$. The extension of the argument to a general atomic potential will be discussed later. Hence we are concerned with the eigenvalues E of the Schrödinger equation for an infinite chain

$$\left[-\frac{d^2}{dx^2} - k_0 \sum_i \delta(x-x_i) \right] \psi = E\psi \quad (1)$$

with appropriate boundary conditions, and subject to the condition that

$$a \leq x_{i+1} - x_i \leq a+b.$$

We shall restrict ourselves to positive electron energies and write $E = k^2$.

It has been shown by James and Ginzburg (1953) that the number of eigenstates $N(E)$ per atom with energy less than E is equal to the average phase increase per atom divided by π . The phase ϕ is defined by

$$\tan \phi(E, x) = -\frac{c\psi'(E, x)}{\psi(E, x)},$$

and the condition that ϕ changes continuously with x , c being an arbitrary positive constant. In this case c is chosen as $1/k$ in order that the phase increase from the right of the i th δ -function to the left of the $(i+1)$ th δ -function is equal to $k(x_{i+1} - x_i)$.

The phase ϕ_i' immediately to the right of the i th δ -function can be related to the phase ϕ_i immediately to the left of the δ -function by integrating equation (1) from $x_i - \epsilon$ to $x_i + \epsilon$ and taking the limit as ϵ tends to zero.

We obtain

$$\tan \phi_i' = \tan \phi_i + \alpha \quad (2)$$

where $\alpha = k_0/k$.

We shall now prove that the integrated density of states is equal to unity for the range of k satisfying the inequalities

$$\pi - 2q \leq ka \leq \pi - kb, \quad (3)$$

where q is the principal value of $\arctan \frac{1}{2}\alpha$.

Clearly an integer m exists for which the phase ϕ_i lies either in the interval

$$m\pi - q \leq \phi_i < m\pi + \frac{1}{2}\pi \quad (4)$$

or in the interval

$$m\pi - \frac{1}{2}\pi \leq \phi_i < m\pi - q. \quad (5)$$

For reasons which will become obvious we call the interval (4) a stable phase interval and the interval (5) an unstable phase interval.

Consider first the situation in which ϕ_i lies in the stable interval (4). Using equation (2) it follows that ϕ_i' lies in the interval

$$m\pi + q \leq \phi_i' < m\pi + \frac{1}{2}\pi,$$

since ϕ_i equal to $m\pi - q$ gives ϕ_i' equal to $m\pi + q$. Provided that the inequalities (3) are obeyed ϕ_{i+1} lies in the interval

$$(m+1)\pi - q \leq \phi_{i+1} < (m+1)\pi + \frac{1}{2}\pi$$

and by repeating the argument ϕ_{i+M} lies in the interval

$$(m+M)\pi - q \leq \phi_{i+M} < (m+M)\pi + \frac{1}{2}\pi.$$

Therefore the average phase increase is π per δ -function giving an integrated density of states $N(E)$ equal to unity.

Now consider the alternative that ϕ_i lies in the unstable phase interval (5). In this case there is a tendency for the phases to the left of successive δ -functions to drift into a stable phase interval. To see this it is necessary to consider equation (2). This equation shows that the phase increase $\phi' - \phi$ across a δ -function is a monotonically increasing function of ϕ in an unstable phase interval, and a monotonically decreasing function in a stable interval. Hence any tendency for successive phases to slip back, in the sense that $\phi_{i+1} - \pi < \phi_i$, is accelerated when ϕ_{i+1} lies in an unstable phase interval and retarded in a stable phase interval.

This is of course not a rigorous argument and it is possible to construct chains for which ϕ_i lies in an unstable phase interval for all i . However, even for these unlikely chains the average phase increase is still equal to π if the inequalities (3) are obeyed. For this to be otherwise it would be necessary either that successive phases ϕ_i and ϕ_{i+1} lie in the same unstable phase interval or that at least one empty unstable phase interval separates ϕ_i and ϕ_{i+1} . The former case would require that $ka \leq \pi/2 - q$ and the latter would require that $ka + kb > \pi$. Both these requirements conflict with the inequalities (3).

The inequalities will in general hold over a range of k provided that the ratio of b to a is sufficiently small. For this range of energy $N(E)$ is equal to unity and consequently no states can exist within this range.

By a trivial modification of the argument it follows that energy gaps will exist for all integers n for which the following inequalities hold over a range of k

$$n\pi - 2q \leq ka \leq n\pi - kb.$$

The second and higher energy gaps become smaller or non-existent.

§ 3. GENERALIZATION OF RESULT TO ARBITRARY ATOMIC POTENTIALS

If we take the atoms to be represented by δ -functions of strength $+k_0$ instead of $-k_0$, then similar reasoning applies. Equation (2) becomes instead

$$\tan \phi'_i = \tan \phi_i - \alpha. \quad (7)$$

The phases to the left of succeeding δ -functions drift into and are trapped in the phase intervals

$$m\pi - \frac{1}{2}\pi < \phi_i \leq m\pi + q \quad (8)$$

for the energy ranges for which the following inequalities hold

$$n\pi \leq ka \leq n\pi + 2q - kb. \quad (9)$$

Again these inequalities will hold over a range or ranges of energy provided that the ratio of b to a is sufficiently small.

Finally we consider the general problem in which we have a chain of potentials all identical, which are separated by regions of zero potential which have a maximum deviation of length b . Again the phase ϕ' immediately to the right of an atomic potential will be some function $\phi'(\phi, E)$, where ϕ is the phase immediately to the left of the atomic potential, but ϕ' will of course be a different function from that given by equation (2). However, as we prove in the Appendix, it is always possible for a fixed positive electron energy E to replace the atomic potential by a δ -function surrounded by two regions of zero potential which together have the same transformation properties as the atomic potential upon the wave functions to the right and left of it. Thus the phase increase $\phi' - \phi$ for the substitute atomic potential will be the same function of ϕ as given by the original atomic potential apart from an additive integral multiple of π . This multiple is determined by the condition that the phase is a continuous function of α , and the only consequence of this addition is to alter the integrated density of states by an integer. Thus for a fixed energy a problem involving arbitrary atomic potentials can always be transformed into one involving only δ -function potentials. In the transformed problem the distances between adjacent atoms have to be increased (or decreased) by a constant amount.

It is clear from the foregoing work that if the deviation of the original nearest neighbour distances is sufficiently small it is in general possible to find a range or ranges of energy for which the transformed problems give rise to an integrated density of states equal to an integer. These ranges of energy are therefore forbidden bands.

§ 4. CONCLUSION

The conclusion to be drawn from this work is that forbidden bands in one-dimensional crystals depend essentially upon short range order. Any solution to the wave

uation in the forbidden band has a tendency to adjust itself in order to keep in step with the atoms, so that there is only one node between atoms for the first gap, two nodes between atoms for the second gap, and so on.

ACKNOWLEDGMENT

The work described above has been carried out as part of the research programme of the National Physical Laboratory and this paper is published by permission of the Director of the Laboratory.

REFERENCES

- MES, H. M., and GINZBARG, A. S., 1953, *J. Phys. Chem.*, **57**, 840.
 AKINSON, R. E. B., and ROBERTS, A. P., 1960, *Aust. J. Phys.*, **13**, 437.

APPENDIX

Assume the atomic potential is some function of x between two points x_1 and x_2 , and that there is a region of zero potential to the left of x_1 and to the right of x_2 . The solution of Schrödinger's equation in the region of zero potential to the left of x_1 can be written as

$$\psi_1 = A_1 \exp[ik(x-x_1)] + B_1 \exp[-ik(x-x_1)]$$

and to the right of x_2 as

$$\psi_2 = A_2 \exp[ik(x-x_2)] + B_2 \exp[-ik(x-x_2)].$$

Since the specification of ψ and its derivative at a point is sufficient to determine the solution of a second-order differential equation, and as

$$\begin{pmatrix} \psi_1(x_1) \\ \psi'_1(x_1) \end{pmatrix} = \begin{pmatrix} 1 & 1 \\ ik & -ik \end{pmatrix} \begin{pmatrix} A_1 \\ B_1 \end{pmatrix} \quad (10)$$

it follows that the vector, whose components are the amplitudes of the waves travelling to the right and left, is sufficient to determine the solution.

We can therefore represent the atomic potential from x_1 to x_2 by a transformation matrix as follows:

$$\begin{pmatrix} A_2 \\ B_2 \end{pmatrix} = \begin{pmatrix} T_{11} & T_{12} \\ T_{21} & T_{22} \end{pmatrix} \begin{pmatrix} A_1 \\ B_1 \end{pmatrix}. \quad (11)$$

We wish to show that we can replace the atomic potential by a δ -function surrounded by two regions of zero potential which together give the same transformation matrix. First we need to know the general form of the transformation matrix for an arbitrary atomic potential.

Regarding the atomic potential as a scattering system we have at the point x_1 an incident wave of amplitude A_1 and a scattered wave of amplitude B_1 . Similarly at x_2 we have an incident wave of amplitude B_2 and a scattered wave of amplitude A_2 . We can therefore express the vector of scattered wave amplitudes in terms of the vector

of incident wave amplitudes by means of a scattering matrix for the potential

$$\begin{pmatrix} B_1 \\ A_2 \end{pmatrix} = \begin{pmatrix} S_{11} & S_{12} \\ S_{21} & S_{22} \end{pmatrix} \begin{pmatrix} A_1 \\ B_2 \end{pmatrix}. \quad (1)$$

It is well known that for such a system described by a real Hamiltonian the scattering matrix must be unitary and symmetric as a consequence of conservation of probability and time reversal symmetry. These restrictions give the following relationships between the scattering matrix elements:

$$S_{12} = S_{21} \quad (13a)$$

$$S_{11} = S_{22}^* |S| \quad (13b)$$

$$-S_{12} = S_{12}^* |S| \quad (13c)$$

where the asterisk denotes the complex conjugate and

$$|S| = S_{11} S_{22} - S_{12}^2.$$

On solving equation (12) to obtain equation (11) we find that

$$\begin{aligned} T_{11} &= -\frac{|S|}{S_{12}}, & T_{12} &= \frac{S_{22}}{S_{12}} \\ T_{21} &= -\frac{S_{11}}{S_{12}}, & T_{22} &= \frac{1}{S_{12}}. \end{aligned}$$

Using equation (13c) we find that

$$T_{11} = \frac{1}{S_{12}^*} = T_{22}^*. \quad (14)$$

Equations (13b) and (13c) give

$$T_{21} = \frac{S_{22}^*}{S_{12}^*} = T_{12}^*. \quad (15)$$

One further restriction on the elements of the transformation matrix is imposed by the condition that the determinant of the matrix must be equal to unity, since

$$\begin{aligned} T_{11} T_{22} - T_{12} T_{21} &= \frac{(1 - S_{22} S_{22}^*)}{S_{12} S_{12}^*} \\ &= \frac{(1 - S_{22} S_{11} / |S|)}{S_{12} S_{12}^*} = -\frac{S_{12}^2}{|S| S_{12} S_{12}^*} = 1. \end{aligned}$$

We see therefore that the transformation matrix for an arbitrary atomic potential is of the form

$$\begin{pmatrix} T_{11} & T_{12} \\ T_{12}^* & T_{11}^* \end{pmatrix},$$

where $T_{11} T_{11}^* - T_{12} T_{12}^* = 1$.

Now let us attempt to represent the transformation properties of this atomic potential by a potential which going from left to right consists of a region of zero potential of

length g , a δ -function of strength μ and finally another region of zero potential of length h . The transformation matrix representing a length g of zero potential is

$$\begin{pmatrix} e^{ikg} & 0 \\ 0 & e^{-ikg} \end{pmatrix}.$$

Note the wave function immediately to the right and left of the δ -function by ψ_+ and ψ_- respectively. We have on integrating the wave equation across the δ -function of strength μ and assuming continuity of ψ

$$\begin{pmatrix} \psi_+ \\ \psi_+' \end{pmatrix} = \begin{pmatrix} 1 & 0 \\ \mu & 1 \end{pmatrix} \begin{pmatrix} \psi_- \\ \psi_-' \end{pmatrix}.$$

Using the equation analogous to (10) in both its direct and inverted form we obtain

$$\begin{pmatrix} A_+ \\ B_+ \end{pmatrix} = \frac{i}{2k} \begin{pmatrix} -ik & -1 \\ -ik & 1 \end{pmatrix} \begin{pmatrix} 1 & 0 \\ \mu & 1 \end{pmatrix} \begin{pmatrix} 1 & 1 \\ ik & -ik \end{pmatrix} \begin{pmatrix} A_- \\ B_- \end{pmatrix}. \quad (16)$$

Hence on multiplying the matrices we see that the transformation matrix for the δ -function of strength μ is

$$\begin{pmatrix} 1 - i\mu/2k & -i\mu/2k \\ +i\mu/2k & 1 + i\mu/2k \end{pmatrix}.$$

Therefore the transformation matrix for the combined potential is

$$\begin{pmatrix} e^{ikh} & 0 \\ 0 & e^{-ikh} \end{pmatrix} \begin{pmatrix} 1 - i\lambda & -i\lambda \\ +i\lambda & 1 + i\lambda \end{pmatrix} \begin{pmatrix} e^{ikg} & 0 \\ 0 & e^{-ikg} \end{pmatrix}$$

where $\lambda = \mu/2k$.

On multiplying these matrices we find that the transformation matrix is

$$\begin{pmatrix} (1 - i\lambda) e^{ik(g+h)} & -i\lambda e^{-ik(g-h)} \\ i\lambda e^{ik(g-h)} & (1 + i\lambda) e^{-ik(g+h)} \end{pmatrix}.$$

Now by choosing a value of μ in the range $-\infty$ to 0 or 0 to $+\infty$, the modulus of λ can be made equal to the modulus of T_{12} , and T_{11} and T_{12} can be given their correct phase factors by an independent choice of $g+h$ and $g-h$. Hence we have shown that it is possible to represent the transformation properties of an arbitrary atomic potential by a δ -function surrounded by two regions of zero potential.

The Absorption of Ozone in the Ultra-violet and Visible Regions of the Spectrum

By A. G. HEARN†

Cavendish Laboratory, Cambridge

MS. received 18th May 1961, in revised form 27th July 1961

Abstract. The absorption coefficient of gaseous ozone has been measured for the mercury lines at 2537, 2894, 2967, 3021, 3342, and 5770 Å, by measuring the optical absorption and the pressure as the ozone decays in a sealed quartz absorption tube. This avoids the chemical determination of the ozone. The determination gives independent and absolute values of the absorption coefficients, and their standard deviations are 2½% or less. Previous measurements of the absorption coefficients disagree by as much as 25%, but the present results generally agree within the limits of error with those of Inn and Tanaka.

§ 1. INTRODUCTION

THE ABSORPTION band of ozone in the ultra-violet is of great interest to meteorology but the measurement of the absorption coefficients is difficult because of the unstable nature of gaseous ozone. The absorption coefficients have been measured on several occasions, but the most detailed studies are those by Ny and Choong (1933), Inn and Tanaka (1953) and Vigroux (1953). Their results are illustrated in figure 1. The absolute values disagree by up to 25% and the coefficients throughout the absorption band have been found not to be self-consistent (Vassy 1937, Walshaw 1957). The absorption coefficients at the wavelengths of six mercury lines have been measured to try to resolve the differences between these determinations. The method yields absolute values of the absorption coefficients and the individual measurements are independent.

§ 2. THE PRINCIPLE OF THE DETERMINATIONS

The method is a modification of that used by Läubli (1928). If pure ozone is sealed into an absorption tube and maintained at a constant temperature, then as the ozone decays into oxygen the pressure increases reaching a final pressure one and a half times the original when all the ozone has decayed. The absorption coefficient k is given by

$$k = \alpha L = -\frac{1}{2l} p_0 \frac{T}{T_0} \frac{dD}{dp} (\text{cm NTP})^{-1}$$

where p_0 and T_0 are standard pressure and temperature, p and T are the pressure and temperature of the gas, l is the length of the absorption tube, α is the molecular absorption coefficient, L is Loschmidt's number and D is the optical density measured to the base 10.

So the absorption coefficient may be obtained simply from the rate of change of the optical density with pressure of the gas mixture while the ozone decays.

† Now at the Atomic Energy Research Establishment, Harwell, Berks.

There are several assumptions implicit in the derivation of this relation. Firstly, the absorption coefficient is independent of pressure. This has been investigated by Cassy (1936a), Strong (1941), Barbier and Chalonge (1942) and Vigroux (1953), who found no significant effect of pressure. Secondly, intermediate products must not accumulate during the decay of the ozone. The work of Benson and Axworthy (1957), Heidt (1935) and Heidt and Forbes (1934) show that their lifetimes are very short.

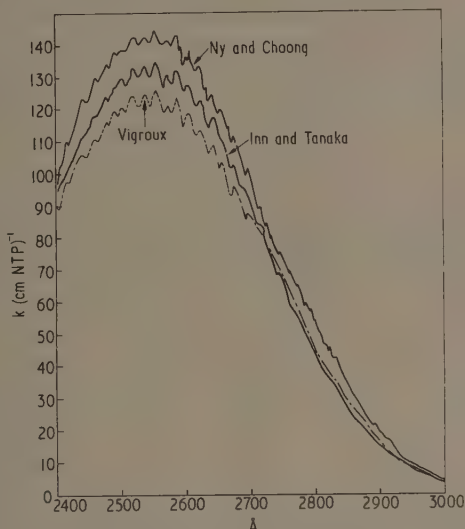


Figure 1. The absorption coefficients measured by Ny and Choong, Vigroux, and Inn and Tanaka.

Thirdly, all the ozone must be converted to oxygen and none must be lost by chemical reaction with the apparatus, which requires the apparatus to be designed so that contact of the ozone with substances such as tap grease is avoided. Fourthly, no ozone must be lost by physical adsorption onto the surface of the apparatus. Preliminary experiments indicated that this was prevented by using absorption tubes made of fused silica.

§ 3. THE APPARATUS

The optical system is shown in figure 2. A mercury vapour lamp was used as the light source and its intensity was stabilized by means of a vacuum photocell controlling the current through the lamp. The lamp was under-run, which reduced the width of the resonance line at 2536 Å to 0.9 Å. The widths of the other lines were less than 0.1 Å. The fine structure of the absorption band of ozone was examined by Chalonge and Jéfebvre (1933) using a six metre concave grating spectrograph in the region from 603 to 3395 Å and they found no structure finer than one or two Ångströms.

The light from the mercury lamp was split into two beams, one of which passed through the absorption tube, and the other was used as a reference beam. The two beams were selected by a rotating shutter and passed, each in turn, into a quartz spectrometer. Their intensities at the required wavelength were compared by means of a

photomultiplier. To reduce the error caused by reflections at the windows of the absorption tube, the beam was allowed to traverse the absorption tube only once. Chance OX7 ultra-violet transmitting filter was placed in front of the mercury lamp so that stray light coming from the visible region would be removed. The spectrograph was a Hilger E1 instrument, which is a quartz Littrow spectrograph with a prism of 4.9 cm base and a focal length of approximately one and a half metres. The plate holder of the spectrograph was replaced by a carriage holding the photomultiplier. The optical system was arranged so that the two beams fell as nearly as possible onto the same portion of the photocathode in order to remove the effects of differential changes in sensitivity across the surface of the photocathode.

The anode current of the photomultiplier was measured by comparing the voltage developed across a ten megohm resistor with a potentiometer using a valve voltmeter.

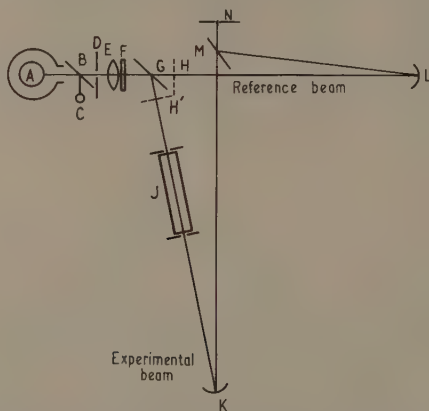


Figure 2. The optical system: *A*, mercury lamp; *B*, quartz plate; *C*, photocell; *D*, diaphragm; *E*, quartz lens; *F*, OX7 filter; *G*, quartz beam splitter; *H*, rotating shutter; *J*, absorption tube; *K*, concave mirror; *L*, concave mirror; *M*, beam splitter; *N*, spectrometer slit.

as a null detector. Two potentiometers were used, one for each beam. The photomultiplier was selected for low dark current, which was sufficiently constant for it to be subtracted from the measurement by adjusting the zero of the valve voltmeter.

A Mazda 27M3 photomultiplier was used, which has a window transmitting down to 2200 Å. The h.t. supply to the photomultiplier was stabilized by the circuit described by Fellgett (1954). The current drawn from the photomultiplier did not exceed 0.1 microamp. In view of the investigations into the linearity of photomultipliers of the 931A and similar types made by Engstrom (1947), Kortum and Maier (1953), and Hermann (1957), there is no reason to doubt the linearity of its response.

The grid current of the valve voltmeter was 10^{-12} A. The faintest intensity measured during the work was represented by an anode current of 10^{-9} A.

Three absorption tubes were used for the measurements. They were made from fused silica and were nominally 15, 10 and 0.75 cm long. The pressure of the mixture of gases in the absorption tube was measured with a small pyrex spiral manometer backed by a conventional mercury manometer. A McLeod gauge was used to calibrate the spiral manometers. Their rotation was measured with a galvanometer mirror.

ached to the free end. The most sensitive spiral had a sensitivity of about 10 cm per Hg pressure at a distance of one metre. The spiral manometers were kindly supplied by the University Chemistry Laboratory in Cambridge.

The decay of ozone releases $34.2 \text{ kcal (g mol)}^{-1}$. To ensure that the temperature of the gas did not rise excessively, a thermocouple was sealed into the absorption tube. The thermocouple was made from two alloys, 10% iridium with 90% platinum and 10% palladium with 60% gold. The calibration remained constant during the experiments indicating that the ozone had no action on it.

The apparatus was housed in a cellar, the temperature of which was thermostatically controlled.

§ 4. THE EXPERIMENTAL PROCEDURE

The ozone was prepared by the method described by Vigroux (1949). Dried cylinder oxygen was passed through a silent discharge ozonizer, and the products liquified in a liquid nitrogen trap. The oxygen was fractionally distilled away by reducing the pressure. There is no evidence of an azeotropic maximum of ozone and oxygen (Jenkins, Di Paolo and Birdsall 1955). Liquid ozone is quite stable at liquid nitrogen temperatures, and was kept in a bulb for several months without appreciable decomposition. The ozone required for an experiment was distilled into an appendix on the absorption tube, which was then sealed. The ozone was allowed to evaporate, filling the absorption tube. By this method contact with grease during the determination was avoided.

Impurities cause an error in the determination only if they decompose during the measurement contributing to a change of pressure or of optical density. The only unstable impurities likely to be present are the oxides of nitrogen which are formed during the ozonizing process from the nitrogen impurity in the oxygen. Except for nitrous oxide, all the oxides of nitrogen are immediately oxidized by the ozone to nitrogen pentoxide. This was estimated by means of its absorption line at 740 cm^{-1} and it was found that the ozone contained less than 0.1% nitrogen pentoxide. This could not cause any significant error.

Preliminary experiments using a pyrex absorption tube indicated that ozone was being desorbed from the walls during the later stages of the determination. This phenomenon had been investigated by Vassy (1936b, 1937). To estimate the desorption of ozone from the quartz absorption tubes, the 0.75 cm absorption tube was filled at nearly atmospheric pressure with ozone, and after an hour the gas was pumped away and the tube sealed. During the following eight hours no evidence of desorbed ozone was found using the large absorption of the mercury resonance line at 2536 \AA . The experiment was first tried with the 10 cm tube, but while the ozone was being pumped away it exploded, completely shattering the absorption tube.

The effect of the desorption of ozone would be most serious for those experiments requiring a low pressure of ozone. For three of the six determinations of the absorption coefficient at 2536 \AA , for which a pressure of only 1 cm Hg was required, a side arm of the absorption tube was filled with quartz wool having a surface area equivalent to five times that of the absorption tube. The difference between the two sets of measurements was not significant, nor is the standard deviation greater in one than the other.

The decay of the ozone in a quartz absorption tube was very slow. Since this is mainly a surface effect, it suggests that the interaction of the ozone with the quartz is much less than with pyrex. The decay was hastened by illuminating the absorption tube with light from two extra mercury lamps. It was necessary to allow time for the heat generated by the decay of the ozone to dissipate.

One of the potentially most serious sources of error in a photometric system is stray light. It was possible to estimate the stray light and to correct for its effect. It could only come from the mercury lines transmitted by the OX7 filter. The absorption coefficient of ozone varies so rapidly between these lines, that the wavelengths shorter than that being measured are heavily attenuated and should not contribute to the stray light; whereas the longer wavelengths are barely attenuated and their contribution to the stray light predominates; and because of the low absorption coefficient, it remains approximately constant over the range of ozone partial pressures used. The effect of the stray light may be calculated if it is independent of the optical density of the ozone and if it is small in intensity compared with that of the required wavelength. If D is the true optical density, D' is the measured optical density and p is the total pressure of the gas in the absorption tube then

$$\frac{dD'}{dp} = \frac{dD}{dp} \left(1 - \frac{S}{I_0} 10^D \right)$$

where I_0 is the intensity of the measuring beam before entering the absorption tube and S is the (constant) intensity of the stray light. So the effect of the stray light is that the measured optical density plotted against the pressure is no longer a straight line. In practice the curvature cannot be detected over the range of optical densities used but the error in the slope of the graph when fitted by least squares is equal to the error determined at the middle point of the optical density range. For most determinations the density range was from 0.2 to 0.8 or 1.0 so that the error due to the stray light is

$$\frac{dD'}{dp} - \frac{dD}{dp} \approx \frac{3S}{I_0} \frac{dD'}{dp}.$$

By starting with a high concentration of ozone, the deviation from the straight line becomes measurable, and the ratio S/I_0 can be deduced, since as the optical density becomes very large, the measured optical density tends towards $\log(S/I_0)$. This estimation of the effect of stray light is only approximate, but the precautions taken reduce the stray light to a level where only an order of magnitude determination of its effect is required. The largest correction required was 0.3%.

§ 5. THE RESULTS

The slope of the optical density and pressure relation was found from the experimental results by the method of least squares. The results of separate determinations were combined by taking the unweighted mean, and these are given with their standard deviations in table 1. The absorption coefficients at some wavelengths were determined using two different absorption tubes, and these are quoted separately.

The determinations at 2967.3 and 3021.5 Å made at high pressures with the shorter absorption tube are much less accurate than those made with the longer absorption tube. There is no significant difference between the mean values. If it is assumed that the pressure dependence of the absorption coefficient is of the form $k_p = k_0(1 + ap)$ where k_p and k_0 are the absorption coefficients at a pressure p and at zero pressure respectively, then the pressure coefficient a is less than 0.002 (cm Hg)⁻¹ at 2967.3 Å and less than 0.0015 (cm Hg)⁻¹ at 3021.5 Å. Because of the poor accuracy of the absorption coefficient determinations at high pressure, this is not a sensitive method of determining the effect of pressure. The two sets of results have not been combined for the

Table 1

Summary of the Experimental Results

Wavelength (Å)	Tube length (cm)	Mean abs. coeff. (cm NTP) ⁻¹	R.M.S. deviation (%)	Number of determinations
2536.5	0.744	133.9	1.05	6
2893.6	10.09	17.2	1.8	2
2967.3	10.09	6.948	0.24	6
2967.3	0.744	6.93	3.2	5
3021.5	10.09	3.308	0.24	6
3021.5	0.744	3.300	2.3	4
3341.5	10.09	0.0498	1.4	13
5769.6	14.991	0.0555	1.6	4

best estimate of the absorption coefficient, but those obtained with the 10 cm tube have been taken by themselves.

Only two determinations were made at 2893.6 Å and the standard deviation given is only an estimate.

In addition to the random error of the mean, there are further errors contributed from the measurement of the length of the absorption tubes and the calibration factors of the McLeod gauge and spiral manometers. These are shown in table 2 together with the total random error of the mean from all sources. Errors due to the variation of the temperature of the ozone-oxygen mixture during the experiment are quite negligible.

In addition to these random errors, there are two sources of systematic error. The errors caused by stray light were estimated and the appropriate corrections to the absorption coefficients are shown in table 3. It was not possible to estimate the effect of the stray light for the determinations at 3341.5 and 5769.6 Å because the absorption coefficient is so small and a sufficiently high optical density could not be obtained. It is probable that the error involved is very small because the main contribution to the stray light comes from light of other wavelengths, and these two lines are particularly strong. A second source of systematic error which affects only the measurements at 3021.5 Å is the presence of companion lines which are unresolved by the spectrometer. This line has three companions at distances of +2.5, +6.5, +9.5 Å. The nearest line has an intensity of one quarter of the principal line, and the other two are less than 1%.

Table 2

Analysis of the Random Errors

Wavelength (Å)	Mean (%)	Tube length (%)	McLeod gauge (%)	Spiral gauge (%)	Total S.D. (%)
2536.5	1.05	0.54	0.81	—	1.4
2893.6	1.8	0.20	—	0.29	1.8
2967.3	0.24	0.20	—	0.29	0.43
3021.5	0.24	0.20	—	0.29	0.43
3341.5	1.4	0.20	—	0.29	1.4
5769.6	1.6	0.00	0.81	0.00	1.8

so that they are negligible. The effect of a companion can be calculated if the ratio of the absorption coefficients at the two wavelengths is known. If k_1 and k_2 are the absorption coefficients for the principal line and the companion respectively, and j is the ratio of the intensity of the companion to the principal line, then the absorption coefficient \bar{k} which is measured by the spectrometer is related to the true absorption coefficient by the relation

$$(j+1)10^{-\bar{k}} = 10^{-k_1} + j10^{-k_2/m}$$

where m is the ratio k_1/k_2 . This ratio obtained from the results of Ny and Choong, Inn and Tanaka, and Vigroux is 1.042, 1.034, and 1.041 respectively. 1.040 was chosen for this ratio and the equation was solved graphically. This correction is also included in table 3.

Table 3
Systematic Errors

Wavelength (Å)	Mean uncorrected abs. coeff. (cm NTP) ⁻¹	Correction for stray light (cm NTP) ⁻¹	Correction for companion (cm NTP) ⁻¹
2536.5	133.9	+0.0	—
2893.6	17.2	—	—
2967.3	6.948	+0.021	—
3021.5	3.308	+0.003	+0.029
3341.5	0.0498	—	—
5769.6	0.0555	—	—

The absorption coefficient at 3021 Å has been published (Hearn, Walshaw and Wormald 1957), but the value given of 3.310 ± 0.009 (cm NTP)⁻¹ did not include this correction for the effect of the companion. There is no other difference between the two results. If a mercury lamp, run under similar conditions to those used for these determinations, is used for the measurement of ozone, then the uncorrected value should be used, since it is the effective absorption coefficient for the line and its companion. The corrected value is the best estimate of the monochromatic absorption coefficient at 3021 Å.

The best estimates of the monochromatic absorption coefficients are given in table 4. For convenience the equivalent molecular absorption cross section is also given.

Table 4
Best Estimates of the Absorption Coefficients

Wavelength (Å)	Absorption coefficient (cm NTP) ⁻¹	Molecular absorption cross section (10 ⁻¹⁹ cm ²)	Temperature (°C)
2536.5	133.9 ± 1.9	114.7 ± 2.4	22
2893.6	17.2 ± 0.3	14.7 ± 0.3	19
2967.3	6.969 ± 0.030	5.971 ± 0.026	22
3021.5	3.340 ± 0.014	2.860 ± 0.011	20
3341.5	0.0498 ± 0.0007	0.0427 ± 0.0006	20
5769.6	0.0555 ± 0.0010	0.0476 ± 0.0009	21

§ 6. DISCUSSION

For comparison the absorption coefficients measured by Ny and Choong, Vigroux, and Inn and Tanaka are shown in table 5. Inn and Tanaka made the measurements photoelectrically and the others photographically. They all used a continuous source, and the values quoted are interpolations from the absorption coefficients measured at maxima and minima. Since no information is available regarding the shape of the absorption bands, the interpolation of these results is rather arbitrary.

Table 5

Other Measurements of the Absorption Coefficients (cm NTP^{-1})

Wavelength (\AA)	Ny & Choong	Vigroux	Inn & Tanaka	Present work
2536.5	142.6	124.3	133.1	133.9
2893.6	21.6	18.2	17.1	17.2
2967.3	8.19	6.83	6.72	6.969
3021.5	3.72	3.29	3.32	3.340
3341.5	0.067	0.058	0.061	0.0498
5769.6	—	0.0553	0.052	0.0555

Inn and Tanaka state that the maximum deviation from the average value of the absorption coefficient was about 5%. The others give no indication of the accuracy of their measurements. The results of Ny and Choong are some 10% higher than the others and possibly this is due to the side reactions in the chemical estimation which are described by Juliard and Silberschatz (1928).

With the exception of 3341.5 \AA , there is no significant difference between the present measurements and those of Inn and Tanaka; whilst for those of Vigroux at 2536.5 and 2893.6 \AA , the differences are significant. The value obtained for 3341.5 \AA is much less than that of any other worker. This discrepancy appears to be due to the difficulty of interpolating the absorption coefficients of Vigroux and Inn and Tanaka. Also, compared with the wavelengths given by Vigroux and Ny and Choong, those given by Inn and Tanaka are 1 \AA wrong. If the interpolation of Inn and Tanaka's coefficients is made with the aid of the values given by Ny and Choong, in which the detail is greater because of the higher resolution of their spectrograph, then it is found that the result is not inconsistent with the present determination. Support for this low value comes from measurements of the infra-red absorption of ozone using the ultra-violet absorption for estimating the ozone (Walshaw 1957).

It appears that for general purposes, the absorption coefficients of Inn and Tanaka are the most accurate and self-consistent. The accuracy which the authors claim for their measurements corresponds to a standard deviation of about 2% in the absorption coefficients. The Cary recording spectrophotometer is designed for measuring the absorption across the ultra-violet band with an accuracy in the wavelength of a few Angström units. The wavelength measurements of Ny and Choong are probably the most reliable, and it seems that the results of Inn and Tanaka could be improved slightly by checking the wavelength calibration against the results of Ny and Choong. For laboratory measurements of ozone, the use of the emission lines of a mercury vapour lamp has the advantage that the wavelength is clearly defined and that an interpolation from continuous measurements of the absorption coefficients is not necessary.

ACKNOWLEDGMENTS

I am very grateful for the advice and encouragement given to me throughout the work by Dr. T. W. Wormell and Dr. C. D. Walshaw, and to the Gassiot Committee of the Royal Society for financial support. The principle of the determination was suggested by Professor R. M. Goody.

REFERENCES

- BARBIER, D., and CHALONGE, D., 1942, *Ann. Phys., Paris*, **17**, 272.
BENSON, S. W., and AXWORTHY, A. E., Jr., 1957, *J. Chem. Phys.*, **26**, 1718.
CHALONGE, D., and LEFEBVRE, L., 1933, *C.R. Acad. Sci., Paris*, **197**, 444.
ENGSTROM, R. W., 1947, *J. Opt. Soc. Amer.*, **37**, 420.
FELLGETT, P., 1954, *J. Sci. Instrum.*, **31**, 217.
HEARN, A. G., WALSHAW, C. D., and WORMELL, T. W., 1957, *Quart. J. R. Met. Soc.*, **83**, 364.
HEIDT, L. J., 1935, *J. Amer. Chem. Soc.*, **57**, 1710.
HEIDT, L. J., and FORBES, G. S., 1934, *J. Amer. Chem. Soc.*, **56**, 2365.
HERMANN, W., 1957, *Z. Naturf.*, **12a**, 1006.
INN, E. C. Y., and TANAKA, Y., 1953, *J. Opt. Soc. Amer.*, **43**, 870.
JENKINS, A. C., DI PAOLO, F. S., and BIRDSALL, C. M., 1955, *J. Chem. Phys.*, **23**, 2049.
JULIARD, A., and SILBERSCHATZ, S., 1928, *Bull. Soc. Chim. Belg.*, **37**, 205.
KORTÜM, G., and MAIER, H., 1953, *Z. Naturf.*, **8A**, 235.
LÄUCHLI, A., 1928, *Helv. Phys. Acta*, **1**, 208.
NY TSI-ZE, and CHOONG, SHIN PIAW, 1933, *Chin. J. Phys.*, **1**, 38.
STRONG, J., 1941, *J. Franklin Inst.*, **231**, 403.
VASSY, E., 1936a, *Suppl. Quart. J. R. Met. Soc.*, **62**, 25.
——— 1936b, *C. R. Acad. Sci., Paris*, **203**, 403.
——— 1937, *Ann. Phys., Paris*, (11) **8**, 679.
VIGROUX, E., 1949, *Bull. Soc. Chim. Fr.*, 402.
——— 1953, *Ann. Phys., Paris*, (12) **8**, 709.
WALSHAW, C. D., 1957, *Quart. J. R. Met. Soc.*, **83**, 315.

The Inversion of Specific Heat Curves

BY R. G. CHAMBERS

H. H. Wills Physics Laboratory, University of Bristol

MS. received 30th June 1961

Abstract. It is shown that the methods proposed by Montroll and Kroll for deriving the lattice frequency spectrum from the experimental specific heat curve will in practice yield only a 'smoothed' spectrum, averaged over a range of 1.6 : 1 or more in frequency. Any practicable improvement in experimental accuracy will reduce this smoothing only slightly. The same smoothed spectrum can be derived more simply by a procedure involving only one quadrature, and a still simpler trial-and-error method is also described and illustrated.

§ 1. INTRODUCTION

NUMBER of authors have considered the problem of determining the lattice vibration spectrum $g(\nu)$ from the specific heat $C_V(T)$, either by approximate methods (Grayson-Smith and Stanley 1950, Katz 1951, Hwang 1954, Barron, Berg and Morrison 1957, Weiss 1959, Barron and Morrison 1960, Hovi and Pautamo 1961) or by formally exact inversion techniques (Montroll 1942, Kroll 1952, Taylor 1956). Several of these methods are reviewed by Blackman (1955). The solutions of Montroll and Kroll both involve two successive quadratures; in this note we derive a solution which involves only one. The 'exact' solution so obtained is of purely formal significance, because the integrand is oscillatory and divergent, but this difficulty can be overcome if we are content to evaluate a smoothed spectrum $\bar{g}(\nu)$, averaged over a certain frequency range. The methods of Montroll and Kroll will in practice only yield a similarly smoothed spectrum, so that the present method will yield the same information with less labour. A still simpler approximate method is also discussed, which is probably adequate for all practical purposes.

§ 2. ANALYTIC METHOD

If the spectrum obtained by inversion is to be of any significance, the specific heat data must first be corrected for the effects of thermal expansion and anharmonicity, and any other extraneous effects, as stressed by Katz and by Barron *et al.* Writing $\epsilon = 1/kT$, $\epsilon = h\nu$, we then have

$$C_V(\beta) = 3R \int_0^\infty g(\epsilon) E(\beta\epsilon) d\epsilon \quad (1)$$

where $kE(\beta\epsilon)$ is the Einstein specific heat function for a single oscillator, and $g(\epsilon)$ is normalized to give

$$\int_0^\infty g(\epsilon) d\epsilon = 1.$$

To derive $g(\epsilon)$, we need to work with some function of E which vanishes at high temperatures, e.g. $(\beta\epsilon)^n E(\beta\epsilon)$, or more generally $F_{m,n}(\beta\epsilon) = (-)^m (\beta\epsilon)^{m+n} d^m E / d(\beta\epsilon)^m$. Writing

$L_{m,n}(\beta) = (-)^m \beta^{m+n} d^m (C_v/3R)/d\beta^m$ and $G_n(\epsilon) = \epsilon^{1-n} g(\epsilon)$, we find from equation (1) dropping the subscripts, that

$$L(\beta) = \int_0^\infty G(\epsilon) F(\beta\epsilon) \frac{d\epsilon}{\epsilon} \quad (2)$$

Changing variables to $\alpha = -\ln \beta$, $\eta = \ln \epsilon$, we can write this in the form

$$L(\alpha) = \int_{-\infty}^\infty G(\eta) F(\alpha - \eta) d\eta \quad (3)$$

so that the measured function $L(\alpha)$ is simply the convolution of the required function $G(\eta)$ with the known function $F(\alpha - \eta)$, as noted by Taylor (1956). The 'unfolding' of $L(\alpha)$ to find $G(\eta)$ is a familiar problem in spectroscopy, where $L(\alpha)$ is the observed line-shape, $G(\eta)$ the true line-shape, and $F(\alpha - \eta)$ the instrumental broadening factor. It has been discussed by many authors (e.g. White and Millington 1928, Shull 1946, Stokes 1948), and it is easily shown that if $L(x)$, $G(x)$ and $F(x)$ are the Fourier transforms of $L(\alpha)$, $G(\eta)$ and $F(\alpha - \eta)$, the solution is $G(x) = L(x)/F(x)$.[†] This is essentially Montroll's solution, which thus requires two quadratures: first to find $L(x)$ from $L(\alpha)$ and then to find $G(\eta)$ from $G(x)$.

If, formally, we define $H(\eta - \alpha)$ as the function whose Fourier transform is $H(x) = 1/F(x)$, then formally the inversion follows at once from a single quadrature:

$$G(\eta) = \int_{-\infty}^\infty L(\alpha) H(\eta - \alpha) d\alpha. \quad (4)$$

Now in fact for large $|x|$,

$$\begin{aligned} F_{m,n}(x) &\simeq \Gamma(m+n+2+ix) \\ &\simeq (2\pi)^{1/2} |x|^{(m+n+1)} \exp(-\tfrac{1}{2}\pi|x|) \exp[ix \ln x - x + \tfrac{1}{2}\pi(m+n+\tfrac{3}{2})] \end{aligned}$$

so that $H(x)$ diverges and this result is of no practical significance. If, less ambitiously, we seek to evaluate not $G(\eta)$ itself but a smoothed spectrum $\bar{G}(\eta)$, formed by the convolution of $G(\eta_1)$ with a weighting factor $W(\eta - \eta_1)$, we need a function H_W such that

$$\bar{G}(\eta) = \int_{-\infty}^\infty G(\eta_1) W(\eta - \eta_1) d\eta_1 = \int_{-\infty}^\infty L(\alpha) H_W(\eta - \alpha) d\alpha. \quad (5)$$

The Fourier transform of equation (5) gives $G(x)W(x) = L(x)H_W(x)$, so that $H_W(x) = G(x)W(x)/L(x) = W(x)H(x)$. Thus if $W(x)$ falls more rapidly than $\exp(-\tfrac{1}{2}\pi|x|)$ for large $|x|$, $H_W(x)$ will tend to zero for large $|x|$, and $H_W(\eta - \alpha)$ will be well-behaved. If for instance $W(x) = \exp(-ax^2)$, $W(\eta) = (4\pi a)^{-1/2} \exp(-\eta^2/4a)$; if $W(x) = 1$ for $|x| \leq x_0$, zero for $|x| > x_0$, $W(\eta) = \sin(\eta x_0)/\pi\eta$. But if $W(\eta)$ has a half-width less than about 0.4 in η , $H_W(x)$ still rises to extremely large values before falling to zero, and correspondingly $H_W(\eta - \alpha)$ becomes a rapidly oscillatory function of very large amplitude. Extreme accuracy would therefore be required in the measured values of $L(\alpha)$ to obtain a close idea of $G(\eta)$ in this way, as we shall see below.

[†] Since $g(\epsilon) \simeq \epsilon^2$ for small ϵ , we need $n < 3$ if $G_n(\eta)$ and $L_{m,n}(\alpha)$ are to remain finite as $\eta, \alpha \rightarrow -\infty$. If $n = 3$, we can avoid singularities in $L(x)$ and $G(x)$ by cutting off $L(\alpha)$ at some large negative α .

If we put $G(\eta) = \delta(\eta)$, equation (3) gives $L(\alpha) = F(\alpha)$, and then equation (5) becomes

$$W(\eta) = \int_{-\infty}^{\infty} F(\alpha) H_W(\eta - \alpha) d\alpha. \quad (6)$$

It also follows at once from $W(x) = F(x)H_W(x)$. Thus H_W is that function which, added with the relatively broad function F , produces the narrower function W . As an alternative to the analytic approach, we can replace H_W by a set of delta-functions of length H_i located at the points $\eta - \alpha = \gamma_i$, and attempt by trial and error to choose H_i and γ_i so that the sum $\sum H_i F(\eta - \gamma_i) = W(\eta)$ is as narrow as possible. It is difficult this way, however, to produce a function W with a half-width less than 0.6 in η , corresponding to a range of 1.8 : 1 in frequency. This is not a great deal less than for F itself: for instance, $F_{0.2}$, $F_{1.1}$ and $F_{1.3}$ have half-widths in η of 1.33, 1.13 and 0.93 respectively. This result merely confirms the conclusion from the analytic approach. Thus the prospect of analytic inversion using equation (5) appears unpromising. Montroll's method, though in principle free from convergence difficulties, will in practice be no more useful, when experimental inaccuracies are taken into account, and since essentially the same limitations apply to all inversion methods it is worth discussing them in a little detail.

§ 3. EFFECT OF EXPERIMENTAL ERROR

Suppose for example that the experimental data consist of N values of C_V , equally spaced over the relevant range of α , and each having a standard error $\sigma(C_V) = sC_V$. For the function $L_{0.1} = C_V/3RkT$ used by Montroll, the resultant standard error in the Fourier transform $L(x)$ is approximately $\sigma(L(x)) \simeq 1.1N^{-1/2}sL(0)$, independent of x . (Here and in what follows, $L(0)$ signifies $L(x=0)$.) But the actual magnitude of $|L(x)/L(0)|$ will fall rapidly with increasing $|x|$; in fact it will be comparable with or less than $|F(x)/F(0)|$, since $G(x) = L(x)/F(x)$ converges. The value of $L(x)$ and so of $G(x)$ will therefore become increasingly uncertain for large $|x|$, and will have to be set equal to zero beyond some point x_0 say. This is precisely equivalent to using a smoothing function $W(\eta) = \sin(\eta x_0)/\pi\eta$, of width $2\pi/x_0$ between zeros, and half-width approximately π/x_0 .

Thus if $N = 100$ and $s = 10^{-2}$, for example, we have $\sigma(L(x)) \simeq 10^{-3}L(0)$, while for the function $F_{0.1}$ we have $|F(x)/F(0)| = 10^{-2}, 10^{-3}, 10^{-4}$ at $|x| \simeq 5.5, 7.4, 9.2$. Thus even if $|L(x)/L(0)|$ falls no faster than this, we shall need to cut off the transform at some point $x_0 \lesssim 7$. The experimental data can therefore only yield a spectrum smoothed over a half-width of at least $\pi/x_0 = 0.45$ in η , i.e. a range of 1.6 : 1 in frequency. If the number and accuracy of the experimental points are increased to $N = 1000$ and $s = 10^{-3}$, we shall still need $x_0 \lesssim 9$, corresponding to only a small decrease in the range of smoothing. Some advantage might be gained by working with the function $L_{1.3}(\alpha)$ instead of $L_{0.1}(\alpha)$, because $F_{1.3}(x)$ and therefore $L_{1.3}(x)$ fall off a little more slowly with $|x|$: for $F_{1.3}$ we have $|F(x)/F(0)| = 10^{-2}, 10^{-3}, 10^{-4}$ at $|x| \simeq 8.3, 10.5, 12.5$. But this advantage will be largely offset by the reduced accuracy of $L_{1.3}(\alpha)$ and hence of $L_{1.3}(x)$, because $L_{1.3}(\alpha)$ involves dC_V/dT rather than C_V .

We need not discuss Kroll's method in detail: it is somewhat similar to Montroll's, and suffers from precisely the same limitations. Finally, it is easily seen that the single-quadrature method of equation (5) involves exactly the same combination of the experimental data as Montroll's method with a cut-off at $|x| = x_0$, so that again the same

limitations apply. In other words, equation (5) will yield exactly the same information as Montroll's method, with the use of only one integration instead of two.

The information obtainable by inversion techniques is of course limited basically by the breadth of the functions F and L . Replacing G by \bar{G} is equivalent to replacing L by a similarly smoothed function \bar{L} :

$$\bar{L}(\alpha) = \int_{-\infty}^{\infty} L(\alpha_1) W(\alpha - \alpha_1) d\alpha_1 = \int_{-\infty}^{\infty} \bar{G}(\eta) F(\alpha - \eta) d\eta = \int_{-\infty}^{\infty} G(\eta) \bar{F}(\alpha - \eta) d\eta,$$

where the last form follows when the smoothing is applied to F instead of G . Clearly it will be impossible to distinguish \bar{G} from G if the resultant smoothed function $\bar{L}(\alpha)$ is experimentally indistinguishable from $L(\alpha)$. Now it is easily shown that the difference $\delta F(\alpha)$ between \bar{F} and F will be imperceptible if the smoothing function $\sin(\eta x_0)/\pi\eta$ has a half-width π/x_0 less than about 0.4. (In fact $|\delta F(\alpha)/F_{\max}(\alpha)| \leq |F(x_0)/F(x=0)|$). Since $L(\alpha)$ is effectively already a 'smoothed' and therefore broadened version of $F(\alpha)$, it will be even more difficult to distinguish $\bar{L}(\alpha)$ from $L(\alpha)$ (corresponding to the fact that $L(x)$ falls off even more rapidly than $F(x)$), and no method of inversion can circumvent this difficulty.

§ 4. TRIAL-AND-ERROR METHOD

Perhaps the most practical method of estimating $G(\eta)$ along these lines is to return to the basic equation (3), and simply attempt by trial and error to find a form for $G(\eta)$ which reproduces the observed $L(\alpha)$. This method, though inelegant, is quite rapid and has the merit that the uncertainties in the resultant spectrum are readily apparent, and more sophisticated techniques may obscure these uncertainties, and give a spurious appearance of accuracy to the results.

Of the possible functions $F_{m,n}$ we choose $F_{1,3}$ because this has the smallest half-width, and because the resultant frequency spectrum $G_3(\epsilon) = g(\epsilon)/\epsilon^2$ gives directly the departures from a Debye spectrum. The corresponding specific heat function $L_{1,3}(\beta) = -\beta^4 d(C_V/3R)/d\beta$ can be derived from the usual plot of the equivalent Debye temperature $\theta(T)$ by using

$$L_{1,3} = (kT)^{-2} \frac{d(C_V/3R)}{d(kT)} = (k\theta)^{-3} \left[1 - \frac{d(\ln \theta)}{d(\ln T)} \right] B\left(\frac{\theta}{T}\right) \quad (7)$$

where the function

$$B\left(\frac{\theta}{T}\right) = -\left(\frac{\theta}{T}\right)^4 \frac{d(C_V/3R)}{d(\theta/T)}$$

gives the value of $(k\theta)^3 L_{1,3}$ for a Debye solid. Values of $B(\theta/T) = B(\beta\epsilon_D)$, derived from Beattie's (1926) table of $C_V/3R$ as a function of θ/T , are given in the table, together with values of $F_{1,3}(\beta\epsilon)$. For a Debye spectrum, $G_3(\epsilon) = 3/\epsilon_D^3$ for $\epsilon \leq \epsilon_D$ and $G_3(\epsilon) = 0$ for $\epsilon > \epsilon_D$, and in equation (7), $k\theta = \epsilon_D$ is independent of temperature, so that from (2) we have $\beta\epsilon_D dB/d(\beta\epsilon_D) = 3F_{1,3}(\beta\epsilon_D)$.

A plot of $L_{1,3}$ against $-\ln \beta = \alpha$ now gives at once, from equation (3), a qualitative indication of the form of $G_3(\eta)$. To proceed further, we rewrite equation (3) in the form

$$L(\alpha) = \sum G_i(\eta_i) F(\alpha - \eta_i) \delta\eta_i \quad (8)$$

in which $G(\eta)$ is approximated by a set of rectangular blocks of height G_i and width

$\beta\epsilon;$ $\beta\epsilon_D$	$F_{1,3}(\beta\epsilon)$	$B(\beta\epsilon_D)$	$\beta\epsilon;$ $\beta\epsilon_D$	$F_{1,3}(\beta\epsilon)$	$B(\beta\epsilon_D)$
1.0	0.151	0.09	7.0	76.950	150.4
1.5	1.015	0.65	7.5	72.381	165.8
1.8	2.299	1.51	8.0	66.048	179.4
2.0	3.627	2.43	8.5	58.738	190.8
2.5	9.011	6.42	9.0	51.030	200.1
3.0	17.594	13.49	9.5	43.445	207.7
3.5	28.971	24.11	10	36.328	213.85
4.0	41.824	38.21	11	24.216	222.45
4.5	54.522	55.22	12	15.286	227.55
5.0	65.501	74.22	14	5.366	232.05
5.5	73.510	94.12	16	1.654	233.30
6.0	78.077	114.0	18	0.461	233.65
6.5	79.075	132.9	20	0.118	233.75

centred on the points η_i , and \bar{F} is the average of F over a range $\delta\eta_i$ about η_i . A set of parameters $G_i(\eta_i)$ satisfying equation (8) can be found quite simply and rapidly by graphical trial-and-error methods; at the same time the latitude in the choice of these parameters can readily be estimated. At low frequencies ($\eta \rightarrow -\infty$), $G_3(\eta)$ tends to

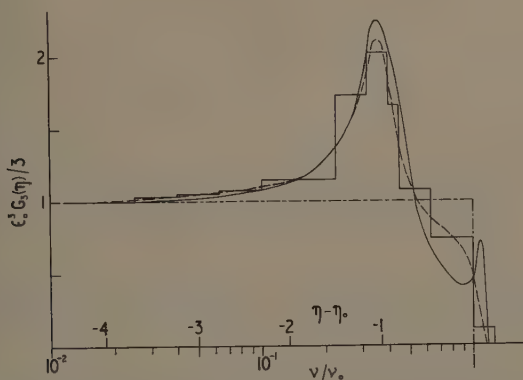


Figure 1. Full line: the spectrum $G_3(\eta)$ for a simple cubic lattice (derived from Blackman 1937). Histogram: approximation to $G_3(\eta)$ derived from Blackman's $\theta(T)$ curve, using equation (8). Dashed curve: smoothed version of histogram. Chain curve: Debye spectrum giving the same low-temperature θ .

the constant value $3/\epsilon_0^3$, where $\epsilon_0 = h\nu_0 = k\theta_0$, and θ_0 is the low-temperature limit of $\theta(T)$. It is convenient to renormalize $G(\eta)$ and $L(\alpha)$ using this factor, and to take as variables $\eta - \eta_0 = \ln(\nu/\nu_0)$ and $\alpha - \eta_0 = \ln(T/\theta_0)$.

To test this method, we have attempted to re-derive a known lattice spectrum from the resultant specific heat curve, using for the purpose the results of Blackman (1937) for the simple cubic lattice. Figure 1 shows the spectrum $G_3(\eta)$ so derived from Blackman's $\theta(T)$ curve, together with Blackman's original spectrum. The low-frequency end is not too badly reproduced, but the narrow peak at the high-frequency end is lost. Unfortunately, when we draw a smooth curve through the histogram and convert from

$G_3(\eta)$ to $g(\epsilon)$, this lack of detail is seen to be disastrous (figure 2). The result would be improved appreciably by enforcing normalization of $g(\epsilon)$ to give

$$\int_0^{\infty} g(\epsilon) d\epsilon = 1;$$

this has not been done here. All inversion techniques will fail in this way, basically because the relevant variable in the inversion procedure is $\ln \nu$ rather than ν itself.

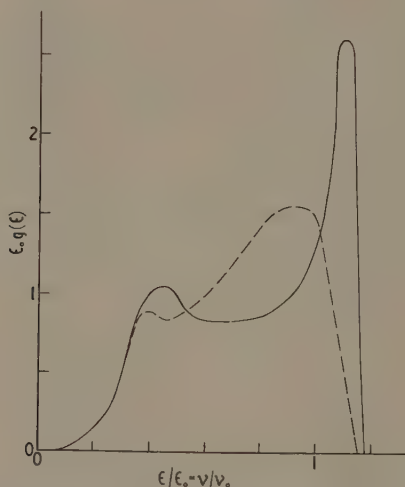


Figure 2. Full line: the spectrum $g(\epsilon)$ for a simple cubic lattice (Blackman 1937). Dashed line: approximation to $g(\epsilon)$ derived from smoothed histogram of figure 1.

and because the function $F(\beta\epsilon) = F(h\nu/kT)$ spreads over a very wide ratio of frequencies. For the same reason, increased accuracy in the experimental measurement of C_V will improve the situation very little.

Most of this work was carried out four years ago, but left unpublished when it was found that Lifshitz (1954) had already derived and discussed the inversion equation (4) and (5). It is published now partly to draw attention to Lifshitz's paper, which is apparently unknown to workers in this field, and partly to point out the limited practical value of inversion techniques generally, and to suggest that the information obtainable in this way may be most simply derived by the trial-and-error method outlined here.

REFERENCES

- BARRON, T. H. K., BERG, W. T., and MORRISON, J. A., 1957, *Proc. Roy. Soc. A*, **242**, 478.
 BARRON, T. H. K., and MORRISON, J. A., 1960, *Proc. Roy. Soc. A*, **256**, 427.
 BEATTIE, J. A., 1926, *J. Math. Phys.*, **6**, 1.
 BLACKMAN, M., 1937, *Proc. Roy. Soc. A*, **159**, 416.
 ——— 1955, *Handb. d. Phys.*, **7/1** (Berlin: Springer), p. 325.
 GRAYSON-SMITH, H., and STANLEY, J. P., 1950, *J. Chem. Phys.*, **18**, 236.
 HOVI, V., and PAUTAMO, Y., 1961, *Proceedings of the Seventh Int. Conf. on Low-temperature Physics* (Toronto: University Press), p. 680.

- HUANG, J.-L., 1954, *J. Chem. Phys.*, **22**, 154.
KATZ, E., 1951, *J. Chem. Phys.*, **19**, 488.
KOLL, W., 1952, *Progr. Theor. Phys.*, Japan, **8**, 457.
LESHITZ, I. M., 1954, *J. Exp. Theor. Phys.*, **26**, 551.
MONTROLL, E. W., 1942, *J. Chem. Phys.*, **10**, 218.
SULL, C. G., 1946, *Phys. Rev.*, **70**, 679.
JONES, A. R., 1948, *Proc. Phys. Soc.*, **61**, 382.
LYLOR, W. J., 1956, *J. Chem. Phys.*, **25**, 721.
WEISS, G., 1959, *Progr. Theor. Phys.*, Japan, **22**, 526.
WHITE, P., and MILLINGTON, G., 1928, *Proc. Roy. Soc. A*, **120**, 701.

Post-arc Temperature Decay

By J. W. S. ALLAN[†], H. EDELS AND D. WHITTAKER

Department of Electrical Engineering, University of Liverpool

MS. received 19th June 1961

Abstract. A method is described for determining the inter-electrode gas temperature at any chosen time following the current interruption of an arc discharge, using a rotating mirror camera to measure the velocity of a shock wave passing through the gas. From a series of such measurements the rate of temperature decay may be found, and results are given for times between 100 μsec and 1 sec after interrupting arcs in air between carbon electrodes. The average rates of decay of the mean core temperature during 1 msec following current interruption were $1.5 \text{ deg } \mu\text{sec}^{-1}$ for an 8 mm gap (10 or 40 A) and $2.8 \text{ deg } \mu\text{sec}^{-1}$ for a 2 mm gap (40 A). The temperature decay subsequent to a 40 A arc has also been calculated from a knowledge of the gas properties and with the assumptions of cylindrical symmetry and energy loss by thermal conduction only.

§ 1. INTRODUCTION

THE TEMPERATURE decay of the inter-electrode gas following the interruption of an arc discharge is of basic interest in the general study of electrode gap properties under varying applied electrical conditions. From a knowledge of the temperature distribution as a function of time assistance is given to the determination of the variation of other properties such as the total electrical conductivity, energy content, and the voltage required for arc re-ignition by either thermal or spark breakdown.

A direct investigation of the decay of arc gas temperature has been carried out by Wienecke (1955, 1956) on a 200 A carbon arc. From the known temperatures of the arc core and the boundaries of aureoles produced by CaO and CN molecules, he was able to record the temperature decay following current interruption by photographing the arc every $4.8 \mu\text{sec}$. Indirect information of temperature decay has been obtained by Crawford and Edels (1960) from their measurements of re-ignition voltage against time; Paschen's law is used to estimate mean axial temperatures at decay times greater than 10 msec when the re-ignition voltage depends on gas density.

The temperature decay measurements described in this paper were obtained from the velocity of a shock wave which passed through the electrode gap. This method has been previously used by Edels and Whittaker (1957) to determine the temperature of the luminous core of a steady arc discharge. The shock wave may be considered as a moving probe whose speed is related to the gas temperature at each point in its path. A rotating mirror camera records the shock propagation which is shown by an increased brightness of the arc; in the non-luminous regions surrounding the arc the shock is displayed by means of a Schlieren system. In order to calculate the temperature, the shock strength as well as the shock speed must be known. The variation of the shock strength with the local gas temperature may be calculated for a plane wave from a theoretical relationship, and the attenuation introduced by the convexity of the wave front may be allowed for empirically.

[†] Now at Atomic Weapons Research Establishment, Aldermaston, Berks.

When applying this shock wave technique to time-dependent temperature distributions it is desirable that the temperature changes are small during the time taken for the high speed 'probe' to traverse the region of interest, so that the derived temperature distribution may be considered as an instantaneous picture. Because the passage of the shock alters the temperature distribution and its subsequent decay it is only possible to obtain one distribution at one chosen time for a given recovering arc. However, by probing a series of recovering arcs at various times after current interruption a set of radial temperature distributions with time as a parameter may be obtained, on the assumption that each arc recovers in the same way.

The steady state radial temperature distribution may be calculated independently of measurements for a given arc current and electrical field strength if the electrical and thermal conductivities of the arc gas are known functions of temperature. The temperature decay following current interruption may then be calculated if the enthalpy and gas density are also known as functions of temperature. This paper describes both the measurement and independent calculation of post-arc temperature decay.

§ 2. SHOCK WAVE THEORY

The analysis by which arc temperatures are obtained from shock velocities has already been treated in detail (Edels and Whittaker 1957), but a summary of this treatment follows.

An arc discharge can be considered to present a series of infinitesimal contact discontinuities to a shock wave travelling normal to the arc axis. At each of these discontinuities the incident shock wave results in the production of a transmitted shock and a reflected shock or rarefaction. The Rankine-Hugoniot shock wave equations and the equation governing the mass flow through a rarefaction wave may be applied in differential form to the interaction. The result of this analysis is a differential equation in terms of the incident shock velocity u , incident Mach number M and local ratio of specific heats γ . This relation fails to satisfy the integrability condition but insertion of typical experimental values shows that the change of γ across the shock front may be neglected. Integration of the remaining terms results in an equation of the form

$$uF(M, \gamma) = 1/c$$

where

$$F(M, \gamma) = \left(1 - \frac{1}{M^2}\right) \left[\left(M^2 + \frac{2}{\gamma-1}\right)^{1/2} + \left(M^2 - \frac{\gamma-1}{2\gamma}\right)^{1/2} \right]^{[2(\gamma-1)/\gamma]^{1/2}} \times \frac{[2\gamma M^2 - (\gamma-1)]^{1/2} - [(\gamma-1)M^2 + 2]^{1/2}}{[2\gamma M^2 - (\gamma-1)]^{1/2} + [(\gamma-1)M^2 + 2]^{1/2}} \quad (1)$$

and c is a constant for a given shock. This relation is shown graphically in figure 1.

The value of c is found for each shock by measurement of its velocity at a point of known temperature outside the arc. The gas temperature at any other point may then be determined by measurement at that point of the velocity of the same shock.

In the original paper it was suggested that the value of γ to be used throughout the analysis was the steady-state value obtaining in front of the shock. However, measurements by Blackman (1956) have shown that the relaxation time of the vibrational degrees of freedom in nitrogen at 5500 °K is 5 μ sec, and extrapolation of his results suggests that this time is reduced to 3 μ sec at a typical steady-state arc temperature of 6500 °K.

This is the value for the relaxation time relating to a high pressure arc in air as the oxygen component is completely dissociated. In the work described in this paper the shock front passed through the arc in $2 \mu\text{sec}$ and hence it would seem reasonable to assume that only processes which occur within $2 \mu\text{sec}$ of the passage of the shock influence the arc temperature measurement. The vibrational degrees of freedom may therefore be considered as inert during the immediate shock transition. Such a consideration applies only to a relatively weak shock, in which the temperature rise across the front is small. In practice, the value of γ chosen is not critical because of the parallelism of the family of γ curves in figure 1 for say m less than 2. Hence the results of Edels and Whittaker are virtually unaffected by the assumption that the vibrational degrees of freedom are immediately active during the shock transition.

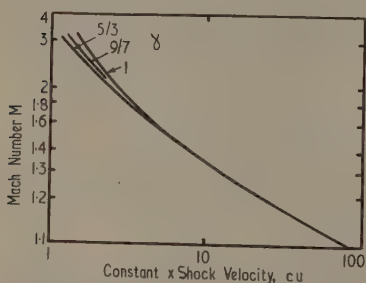


Figure 1. Variation of Mach number with shock velocity.

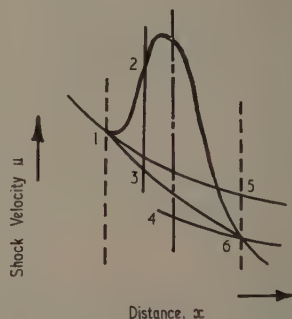


Figure 2. Attenuation of shock passing through arc channel.

The foregoing analysis applies only to the propagation of a shock front which remains plane throughout its passage. It is this planarity which allows the determination of the Mach number and shock velocity at any one point to define directly the value of the constant c at all other points. However, in the practical measurement of an arc temperature by the passage of a shock front through the discharge and its immediate surroundings the wave front becomes convex and the shock strength attenuates. The convexity is set up by normal spherical expansion of the shock front while outside the arc, and also by interaction with the radial temperature distribution of the discharge while within the arc boundaries (Poritsky and Suits 1935).

The attenuation caused by the open-atmosphere expansion of a shock wave can often be represented for many gases at various temperatures and pressures by the empirical relation

$$\log \frac{M_1 - 1}{M_2 - 1} = \frac{x_2 - x_1}{d} \quad (2)$$

where d is a constant of the order of 5 cm (Edels and Whittaker 1957). However, although this equation describes attenuation when the initial Mach number is less than about 2.6, it underestimates the effect at higher shock strengths. Hence an upper limit of $M_1 = 2.6$ was placed on the shock strength used in temperature measurements.

As expected the arc produces additional shock attenuation because of its radial temperature distribution. The effects of attenuation are depicted in figure 2. Thus in a constant-temperature gas, shocks would attenuate according to equation 2 along, for example, line 1, 5 or 4, 6. Within the arc, however, a velocity distance curve 1, 2, 6 is

tained. If now the stream lines which exist in the arc were followed in a constant-temperature gas then some curve such as 1,3,6 would be obtained. If these lines were dotted with the ordinate linear in $\log(M-1)$ then lines 1,5 and 4,6 would be straight and parallel. The exact position of line 1,3,6 will depend on the spatial details of the extra attenuation caused by the arc, but fortunately little error will be produced by an accurate guess and a convenient and not unreasonable assumption is that it too is straight. Hence at point 3 when a fraction f of the distance $x_6 - x_1$ has been traversed, M_3 is obtained from $M_3 - 1 = (M_1 - 1)^{1-f}(M_6 - 1)^f$. As u_3 , M_3 and u_2 are now known the curves of figure 1 may be used to find M_2 and hence the velocity of sound and temperature at point 2. The radial temperature distribution may thus be found by allowing f to vary, and the core value obtained when $f = \frac{1}{2}$.

§ 3. EXPERIMENTAL METHOD AND RESULTS

The increase in density occurring across a shock front which is traversing a self-luminous gas is accompanied by an increase in luminosity. The propagation of this increased luminosity through a horizontally burning d.c. arc is recorded by a rotating mirror camera, as indicated in figure 3. The correction for shock attenuation and the application of the plane wave theory require a knowledge of the shock velocity at two points outside the arc. This information is obtained by the inclusion of a Toepler-Schlieren system, which also serves in the measurement of the shock velocity within the arc when the self-luminosity of the discharge has decayed. The shock wave originates from a spark gap at the back of a shock tube, the mouth of which lies 2 cm from and perpendicular to the arc axis. The arrival of the shock in the arc is synchronized with the correct rotating mirror position by reflection of light from an auxiliary mirror on the main shaft into a photomultiplier PM_1 , the output of which trips the shock-generating spark. The electronic flash tube constituting the Schlieren source is synchronized with the generation of the shock.

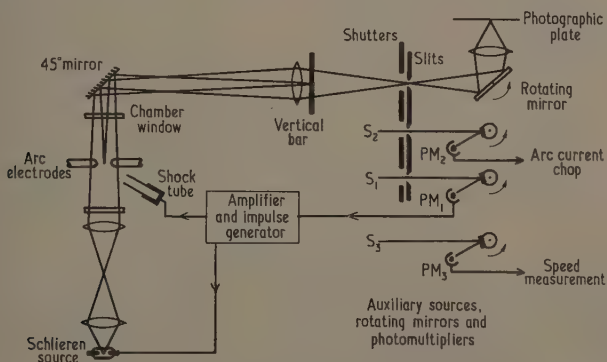


Figure 3. Schematic layout of optical system.

The arc under investigation is initiated by spark breakdown of the inter-electrode space. Current from the d.c. mains supply follows through and an arc discharge is established. After 150 msec of current flow the discharge is interrupted within $5 \mu\text{sec}$ by the diversion of the current through a mercury thyratron connected across the arc. The delay time at which the gas temperature is made is then determined by an electronic

delay unit which is activated by the input pulse to the diverting thyatron. The output of the unit operates the shutter, thereby triggering the shock wave and allowing a single exposure of its passage through the decaying arc plasma. For post-extinction times less than the period of rotation of the mirror (3.3 msec), the delay between arc extinction and shock production is provided by a second photomultiplier PM_2 . This is operated by light reflected from a second auxiliary mirror and the output trips the diverting thyatron. The decay time at which temperature measurements are made is therefore determined by the relative positions of the two auxiliary mirrors on the rotating shaft.

All events in the experimental cycle which do not require precise timing, such as the initiation of the arc and its extinction on the longer delays, are controlled by a rotating cam system.

Temperature measurements are made with the mirror rotating at a predetermined speed. This speed is monitored by a third photomultiplier PM_3 , the output of which is displayed oscillographically against a standard oscillator. Measurement of an angle on the streak photograph and a knowledge of the constants of the optical system give the shock velocity at any point in the field of view.

Figure 4 (plate) shows a set of rotating mirror photographs of the passage of a shock front through the decaying hot gas at various times after interrupting the current of a horizontal 10 A d.c. arc between 4 mm diameter spectroscopic carbon electrodes 8 mm apart in air at one atmosphere pressure. The results presented in figure 5 are mean temperatures across the arc core. They were obtained at the longitudinal mid-points of d.c. arcs burning horizontally between spectroscopic carbon electrodes. No temperature measurements could be made in the range from 5350 °K to 3400 °K as the self-luminosity of the arc was too weak and the Schlieren sensitivity was insufficient at the

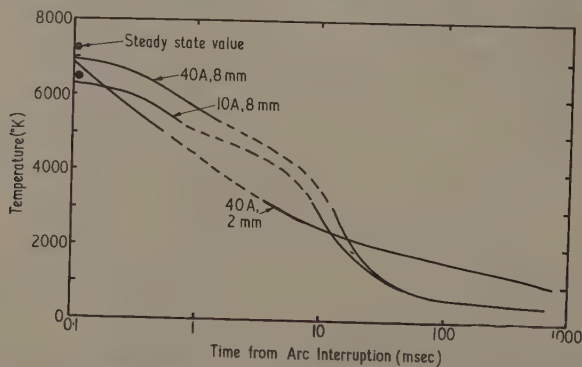


Figure 5. Decay of mean core value of arc gas temperature. Horizontal arc in air at 1 atmosphere pressure between 4 mm diameter spectroscopic carbon electrodes.

low gas densities. As the camera was operating at its optimum performance (Edels and Whittaker 1955) this gap in the measurements could be best filled by increasing the sensitivity of the Schlieren system. The present system can detect only a deflection of about 10^{-2} radian at 3400 °K, which is in accordance with theoretical expectations. It is possible to build a Schlieren system to detect easily angular deflections of 10^{-4} radian, but with the difficult conditions of a steady state arc in the light path this is increased to 10^{-3} radian (Sperling 1950). The sensitivity of the present system could be improved by either increasing the focal length of the second Schlieren lens or reducing the unobscured width of the static Schlieren source image at the knife edge.

This latter method may not be useful because of increasing diffraction effects, although placing the knife edge by a graded filter could help (Holder and North 1953). The estimated errors in the temperature values are $\pm 3\%$ for those lying above 3000°K , $\pm 5\%$ for values between 3000°K and 1000°K and $\pm 10\%$ for values below 1000°K . The error in the measurement of decay time does not exceed $\pm 2\%$ throughout the whole range.

The variation of temperature with radius at any required time may be determined from the rotating mirror photographs by measuring the variation of shock velocity as it passes through the arc. The best records were measured in detail at points corresponding to every 4.5 mm along the arc diameter (0.45 mm on the photographic record), and allowing for shock attenuation as described in § 2 the radial temperature distribution may be obtained. However, the accuracy of these measurements is at present poor compared with the average core temperatures because of the difficulty of measuring shock velocities over short distances on the photographs, and so only the steady state distribution of the axial temperatures of the decaying arc are shown in figure 8.

In order to check that the discharges under investigation had reached complete equilibrium before interruption some steady-state temperature measurements were made both on arcs which had been burning for 150 msec and on arcs which had burned for several seconds. The results obtained for these two arc conditions agreed well with the experimental errors.

§ 4. THEORETICAL TEMPERATURE DECAY

The energy balance equation for a gas which has an electrical input due to an applied field strength E and losses caused by thermal conduction and gas flow may be written

$$\sigma E^2 = -\nabla \cdot k \nabla T + \rho \left(\frac{\partial h}{\partial t} + v \cdot \nabla h \right) - \left(\frac{\partial p}{\partial t} + v \cdot \nabla p \right) \quad (3)$$

where T , ρ , h and p are the gas temperature, density, enthalpy and pressure, $\sigma(T)$ and $k(T)$ are the electrical and thermal conductivities of the gas, and v is the gas velocity.

In a steady-state well-stabilized arc which is convection-free and cylindrically symmetric the arc current I and the tube radius R at a temperature T_R completely determine the radial temperature distribution for a given gas. The axial temperature is a monotonic increasing function of IE , and ER is a slowly varying function of I/R . An analytic solution for the temperature distribution of this model may be obtained from the simplified energy equation which is derived from equation (3) by putting $\partial/\partial t = 0$ and $v = 0$, thus

$$\sigma E^2 = -\frac{1}{r} \frac{d}{dr} \left(r k \frac{dT}{dr} \right). \quad (4)$$

We choose new variables $x = Er$ and $S = \int k dT$ from T_a to T (where T_a is an arbitrary temperature), and take a piecewise linear function to approximate to the actual non-linear relationship between σ and S a solution may be obtained in terms of Bessel functions (Maecker 1959, Goldenberg 1959). Pelzer (1958) calculated for a carbon arc in air that the contribution of radiation to the total energy loss is small, and therefore its omission from equation (4) will not cause a large error.

After current interruption there is no power input, and the gas cools to the ambient temperature. A direct consequence of this cooling is a reduction of pressure towards the axis, which causes gas to flow radially inwards. The pressure gradient necessary

to produce the gas flow is quite small, and may be neglected as far as the association energy is concerned. The equation of the conservation of mass gives the contracting velocity as

$$-v_r = \frac{1}{r\rho} \int_0^r r \frac{\partial \rho}{\partial t} dr$$

where the gas density is related to the temperature on the assumption of constant pressure. The combination of the inward flowing gas and the radial temperature gradient increases the rate of cooling at any given radius. The energy equation becomes for these decaying conditions

$$-\rho \frac{\partial h}{\partial t} = -\frac{1}{r} \frac{\partial}{\partial r} \left(r \frac{\partial S}{\partial r} \right) + \rho v_r \frac{\partial h}{\partial r}.$$

Substituting for v_r from equation (5) the equation in terms of one dependent variable h is

$$-\rho \frac{\partial h}{\partial t} = -\frac{1}{r} \frac{\partial}{\partial r} \left(\frac{r}{\alpha} \frac{\partial h}{\partial r} \right) + \frac{1}{r} \frac{\partial h}{\partial r} \int_0^r \frac{r\rho}{\beta} \frac{\partial h}{\partial t} dr$$

where $\alpha = dh/dS = C_p/k$ and $\beta = -\rho dh/dp$. In this non-linear differential equation we have the three non-linear coefficients α , β and ρ . The equation states that the rate of decay of enthalpy at a given radius equals that due to thermal conduction plus that caused by the gas contracting. If we consider these two effects taking place alternately instead of simultaneously the radial temperature profile shown by curve *a* in figure 6 would change to curve *b* after some small time because of the conduction loss, and the contraction effect would then alter the profile to curve *c*. By use of equation (4) to obtain a steady state profile, the change during a small time interval may be calculated numerically using iterative processes based on equation (7) (Whittaker 1960).

For air at a pressure of 1 atmosphere the values of α , β , ρ and T as functions of h are given in figure 7 (T and ρ from Predvoditelev 1958 and Treanor and Logan 1956).

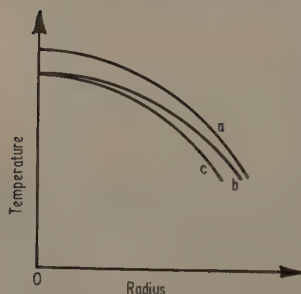


Figure 6. Temperature decay produced by conduction and contraction effects.

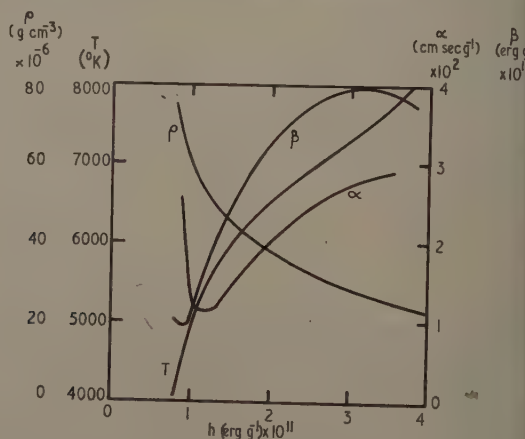


Figure 7. Variation of α , β , ρ and T with h for air at 1 atmosphere pressure.

data for α from Wienecke 1956). In order to compare a calculated temperature with a measured result of § 3 the experimental conditions of the 40 A arc with a length of 8 mm were chosen as best suiting the theoretical assumptions of a cylindrical arc cooled by conduction. A theoretical steady-state radial temperature distribution was calculated to fit the measured temperatures at the axis and at 4.5 mm radius, as shown in figure 8 at time $t = 0$. Normally the variation of electrical conductivity with temperature would be required to draw this curve, but as this data is not well published for air it was necessary to assume a reasonable shape for $n\sigma(T)$, where n is an unknown constant. The total power dissipation is obtainable from the calculated curve, for at any radius where the electrical conductivity is zero we have $\dot{Q} = -2\pi rk \, dT/dr$. As the experimental arc current is known, the field strength, total conductivity of the arc column, and the value of n may be calculated in turn. Temperature profiles subsequent to current interruption are given in figure 8 with time as a parameter.

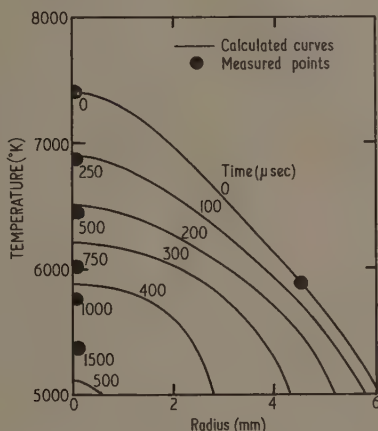


Figure 8. Decay of radial temperature distribution for a 40 A arc in air.

It is appropriate to comment on the importance of the contraction of the gas on the cooling arc, as the solution of equation (7) would be considerably easier if the last term, representing contraction, were omitted. The equation would then be similar to that of the cooling of a solid rod where contraction is negligible and for which series solutions are available. A comparison of the numerical solutions which include and omit this contraction effect for the arc already considered is shown in figure 9. It is seen that the temperature decay at large radii is considerably underestimated when contraction is neglected, and the error at the axis, although initially zero, has become appreciable at 100 μsec .

§ 5. DISCUSSION

Figure 5 shows that for the 8 mm gap length the temperature of the 40 A arc is initially higher than the 10 A arc, and remains higher throughout the decay period. This result is as expected, for both the initial power input and the thermal energy stored in the arc column are higher for the 40 A arc.

Comparison of the 2 mm and 8 mm gap length characteristics of the 40 A arc shows clearly that the initial rate of temperature decay is much more rapid in the 2 mm gap. The average rates of decay for the first millisecond are 2.8 and $1.5 \text{ deg } \mu\text{sec}^{-1}$ respectively. This considerable influence of the proximity of the 4 mm diameter electrode to the whole plasma has also been revealed by work on re-ignition phenomena (Edels and Crawford 1957). Carbon electrodes operate at temperatures in the region of 4000 K. It follows that, in the initial stages of plasma temperature decay, the electrodes help cool the gas by thermal conduction. The shorter the gap, the greater is the influence of the electrodes on the plasma as a whole. Because of the much greater thermal capacity of the electrodes compared with the intervening gas, they cool considerably more slowly. Hence a point will be reached in the decay at which the electrodes begin to slow down the cooling of the inter-electrode space by returning thermal energy to the gas. An intersection of two characteristics of arcs of different gap length is therefore to be expected and is, in fact, revealed in figure 5 at the reasonable gas temperature of 2200 K.

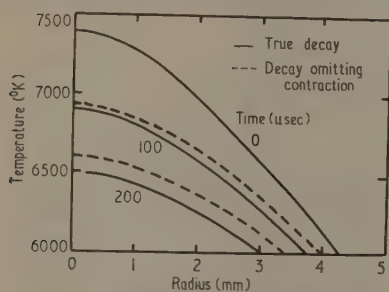


Figure 9. Comparison of temperature decay including and omitting contraction effect.

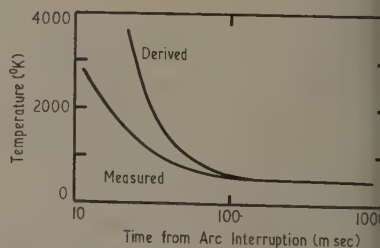


Figure 10. Comparison of measured temperature decay with that derived by Crawford and Edels (1960). (20 A, 8 mm gap, air)

A temperature decay curve derived by Crawford and Edels (1960) from their re-ignition voltage characteristics using Paschen's law is shown in figure 10. There are large differences between this derived curve and that obtained by the shock wave technique for decay times up to 100 msec. This will be mainly due to the shock wave measuring the gas temperature midway between the electrodes, whereas the temperature derived from the re-ignition voltage assumes the gas density is longitudinally uniform and so gives a mean axial temperature. As the gas approaches the ambient temperature these two methods of measurement agree, giving about 600 K at 100 msec and 450 K at 1 sec.

It is not possible to compare the present results with the work of Wienecke (1956) as his initial arc current was so much greater. His photographic method which recorded the radial positions of distinctive aureoles was used to determine the temperature decay of the high temperature gas during the first millisecond after the interruption of a high current arc.

On comparing the theoretical calculations with the experimental results for the 40 A arc, 8 mm gap, figure 8 shows that for the initial fall of the central temperature from 7400 K to 6000 K the theoretical rate of decay is about $4 \text{ deg } \mu\text{sec}^{-1}$ whilst the measured rate is $2 \text{ deg } \mu\text{sec}^{-1}$. This discrepancy would be slightly increased by some effects which have been neglected, for example, the cooling due to radiation and the electrodes. However, the experimental arc was horizontal, and so convection would produce a

considerable flow of hot gas upwards, rather like a hot vertical slab of gas with the heat at near the lower edge, instead of the cylindrical model which was analysed. The theoretical figure of 4 deg μsec^{-1} for a cylinder would possibly be reduced to 3 deg μsec^{-1} for such a slab—the initial rate of decay would be halved at the centre, with smaller variations towards the boundaries. The remaining discrepancy is probably due to measurement errors which would affect both the observed rate of temperature decay and the initial radial temperature profile used for the calculated decay. As reliable data on the electrical conductivity of air is not available it is not possible to check the initial profile against the experimental arc current, and unfortunately the calculated rate of decay depends strongly on this profile.

§ 6. CONCLUSIONS

A shock wave may act as a convenient probe to investigate the temperature of the cooling gas following arc interruption. Mean core temperatures in the range 8000 °K and ambient temperature have been measured. Radial temperature measurements were made with only poor accuracy because of limitations in the resolving power of the optical system and photographic emulsions. From the temperature measurements and theoretical calculations we conclude that the axial temperature decay of a horizontal 40 A carbon arc in air, 8 mm gap length, is from 2 to 3 deg μsec^{-1} during the first 500 μsec after current interruption. The measured rates of decay of the mean core temperature are 1.5 deg μsec^{-1} for the 8 mm gap (10 A or 40 A) and 2.8 deg μsec^{-1} for the 2 mm gap (40 A), averaged over 1 msec following current interruption.

ACKNOWLEDGMENTS

The work was carried out in the Department of Electrical Engineering, University of Liverpool, and the authors wish to thank Professor J. M. Meek for his interest in the work and the facilities placed at their disposal. The financial aid provided by the Central Electricity Research Council is also gratefully acknowledged. Thanks are also due to Mr. J. C. Holmes, who made several independent checks in this Department of the measured rates of temperature decay.

REFERENCES

- BLACKMAN, V., 1956, *J. Fluid Mechanics*, **1**, 61.
- CRAWFORD, F. W., and EDELS, H., 1960, *Proc. Instn Elect. Engrs*, **107 A**, 202.
- EDELS, H., and CRAWFORD, F. W., 1957, *J. Instn Elect. Engrs*, **3**, 88.
- EDELS, H., and WHITTAKER, D., 1955, *J. Sci. Instrum.*, **32**, 103.
- 1957, *Proc. Roy. Soc. A*, **240**, 54.
- GOLDENBERG, H., 1959, *Brit. J. Appl. Phys.*, **10**, 47.
- GOLDER, D. W., and NORTH, R. J., 1953, *Proc. Roy. Photogr. Soc. Centenary Conference* (London: Royal Photographic Society), p. 371.
- LAECKER, H., 1959, *Z. Phys.*, **157**, 1.
- MELZER, H., 1958, *E.R.A. Report G/XT 164*.
- MORITSKY, H., and SUITS, C. G., 1935, *Physics*, **6**, 196.
- REDVODITELEV, A. S., *et. al.*, 1958, *Tables of Thermodynamic Functions of Air* (London: Infosearch).
- PERLING, J., 1950, *Z. Phys.*, **128**, 269.
- REANOR, C. E., and LOGAN, J. G., 1956, *Cornell Aeronautical Laboratory, Report No. AD-1052-A-2*.
- WHITTAKER, D., 1960, *Fourth Int. Conf. Ionization Phenomena in Gases* (Amsterdam: North-Holland), p. 381.
- WIENECKE, R., 1955, *Z. Phys.*, **143**, 118.
- 1956, *Z. Phys.*, **146**, 39.

The Effect of a Thermal Gradient upon Charge Separation between Similar Polyethylene Surfaces

By A. H. BOWLES

The British Cotton Industry Research Association, Manchester 20

MS. received 1st February 1961, in revised form 12th September 1961

Abstract. The apparatus and method are described by which the separation of electrostatic charge between similar polyethylene spheres, initially at different temperatures, during an impulsive contact has been observed.

The amount of such a charge separation varies during a series of observations both progressively and randomly. A component of this charge separation is shown to depend upon the direction of the thermal gradient across the interface. The progressive variation in charge separation with number of impacts is shown to be consistent with a transfer of 'active centres' from one surface to the other. The quantity of charge which separates between two surfaces is also shown to vary with different contact areas on one surface.

§ 1. INTRODUCTION

AN ILLUSTRATIVE theory of charge separation between surfaces not quite in contact, but close enough for charge carriers to pass from one to the other, has been proposed by Henry (1953a), taking account of differences between the two surfaces in affinity for and abundance of, charge carriers, and in temperature.

This model was further developed (Henry 1957), to show that if the surfaces were at different temperatures a component, due to kinetic processes, of the charge density formed over the contact area on separation, would be given by σ where

$$\frac{4\pi e\sigma}{K} = \left[\mu + \frac{V_m - \frac{1}{2}(V_1 + V_2)}{kT} \right] \frac{k\Delta T}{D}$$

in which V_1 , V_2 , V_m are potential energies, relative to an arbitrary zero, of charge carriers at equilibrium on surface 1, surface 2, and at the point of maximum energy between the surfaces respectively, T is the mean temperature of the surfaces, ΔT the temperature difference between the surfaces, D the distance between the surfaces and e the charge on a carrier. μ is a constant of value between $\frac{1}{2}$ and 2, K the effective dielectric constant between the surfaces and k is Boltzmann's constant. Each of these parameters is determined at that instant during the separation of the surfaces when carriers just cease from crossing the gap at a significant rate. (See, e.g., Harper 1951)

The term $\Delta T/D$ in this equation represents a temperature gradient across empty space between two flat surfaces that have been assumed in the model in order to make calculation simple. In reality the two surfaces will not be flat, and the distance between them when carriers are able to cross will be a few ångströms only, comparable with the dimensions of the atoms of which they are made. Under these conditions it is impossible to assign definite positions and temperatures as for the model surfaces, but the notion of a temperature gradient across the interface remains useful. We may suppose that with a more sophisticated model temperature gradient would enter the equation for σ in a similar way to $\Delta T/D$.

This theory was invoked by Henry (1953b) to explain the observation of a separation of charge between like surfaces on being rubbed together. Such a separation has been observed by Shaw (1927), Gruner (1953) and Henry (1953b) between two similar rods rubbed together asymmetrically, that is to say the small contact area of rod A rubbed along the length of rod B and vice versa. The rod contributing the smaller area to the rubbing process was observed to acquire a particular polarity whether it was A or B. On the basis of the above theory the small contact area which during rubbing becomes unbalanced warmer than the other rod is supposed to lose a greater number of charge carriers than it gains. Henry (1953b) further demonstrated that charge also separated between like surfaces rubbed together in an apparently symmetrical manner. In this case the asperities on each surface presumably acquired a higher temperature than the rest of the opposing surface and lost carriers to it.

These observations suggested that a charge separation due to a temperature gradient should be measurable when separated from other effects.

§ 2. DESCRIPTION OF EXPERIMENT

A steep temperature gradient is obtained by bringing two spherical specimens together, initially at different temperatures, for a brief interval. They are mounted as the bobs of two pendula and one is allowed to fall through a pre-determined arc to strike the other once, after which they are kept apart.

Before each collision the spheres are discharged in ionized air. Charge on either sphere is measured by deflecting it into one of two Faraday cylinders connected to a vibrating reed electrometer described by Thomas and Finch (1950) and modified to regenerate external input capacitance. These give a measure of charge repeatable to $\times 10^{-14}$ coulomb; this is about an order of magnitude smaller than the repeatability of the production of charge by a collision.

Polyethylene was chosen as the experimental material on account of its high surface resistivity, chemical simplicity, inertness to water, toughness and easy machinability. It had also been used to demonstrate charging by both asymmetric and symmetric rubbing by Henry (1953b). The material sets a limit on the maximum temperature which may be used on account of variation in the proportions of amorphous and crystalline regions above 80 °C as shown by Bunn and Alcock (1945).

An electrically screened oven below the point of suspension of the pendula allows either bob to be heated to a reproducible temperature when required. In this way the right-hand bob R at room temperature can be drawn aside and released to strike the left-hand bob L hanging inert in the oven, which can be heated or not, or vice versa.

2.1. Apparatus

The essential parts of the apparatus are shown in figure 1. All the apparatus, save only the oven element, insulation, pendulum trunnions and rods, is of brass in order to avoid local electric fields due to contact potential differences, which can cause currents to flow when the air in the apparatus is ionized to discharge the specimens. The pendulum head assemblies are mounted in ball bearings in adjustable supports which allow the axes about which the pendula swing to be made parallel. Each pendulum may be adjusted in length and rotated about its axis to any of eight positions determined by an indent mechanism on the pendulum head assembly. The pendula are adjusted so that on collision their contact areas are perpendicular to the direction of their relative motion, i.e. the bobs collide squarely.

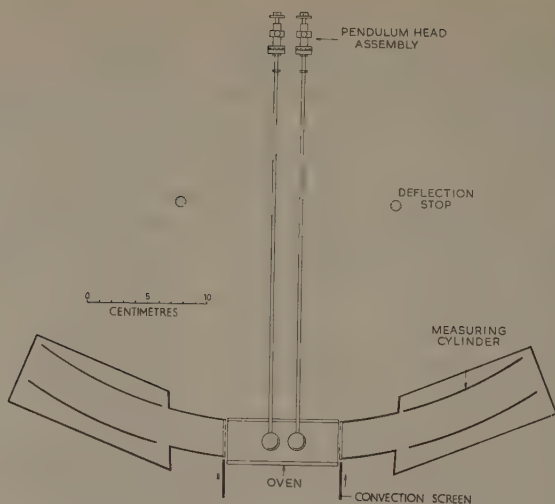


Figure 1. Schematic diagram of apparatus.

The oven has a hard glass tube with a longitudinal slit to allow the passage of the pendula. The tube supports an electrical heating element of a single layer of 'Aquada' and electrodes of 'Burnish Silver' fired on. This element is insulated from a thin brass lining by a sheet of mica as shown in figure 2. This lining is bonded to the earthed brass of the apparatus in order to extend into the oven the equipotential space in which the specimens are discharged. One junction of a thermocouple is soldered to the oven lining and the other held near a brass screen on the apparatus. The e.m.f. generated is measured with a potentiometer to give a measure of the temperature difference between the oven lining and room. At each end of the oven removable brass flaps are fitted to reduce convective cooling of specimens being heated within the oven.

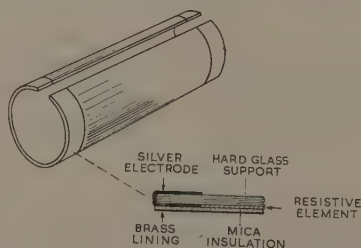


Figure 2. Construction of carbon film oven.

The Faraday cylinders are arcuate brass tubes of circular cross section held on polyethylene supports. They have longitudinal slits to allow the pendulum bobs to enter and are enclosed in earthed brass screens. A well insulated lead is taken from each cylinder to a junction box and thence to the electrometer. The input resistance of the electrometer is kept at a nominal $10^{12}\Omega$ and charge is measured on one of a selection of capacitors of 10 pf or more. The charge on a pendulum bob is measured by observing

change in potential in millivolts across one of these capacitors when the bob is swung into or out from a Faraday cylinder and is recorded in units of 10^{-14} coulomb. The constant of proportionality between the charge on the bob and the charge induced on the measuring capacitor has not been accurately determined, but is not very different from unity.

The duration of contact between the colliding bobs was measured in a separate experiment on the same spheres as were used for the charge separation measurements. A fine copper wire was fused into the surface of each bob near the support tube and a thin opaque film of aluminium was evaporated on *in vacuo*. These films gave a conducting path between a wire and about a third of the equator of each bob. During contact the signal was conveyed from a battery to an oscilloscope where it was compared with the marker pips from a crystal controlled oscillator.

The magnitude of the thermal gradient obtained through the interfacial region on separation may be estimated using the analysis of Carslaw and Jaeger (1947) for semi-infinite bodies at temperatures of $T \pm \Theta$ respectively and brought together at time $t = 0$ over the plane $x = 0$. The thermal gradient is given as $\partial\theta/\partial x$ where

$$\frac{\partial\theta}{\partial x} = \frac{\Theta}{(\pi\kappa t)^{1/2}} \exp\left(-\frac{x^2}{4\kappa t}\right),$$

is the thermal diffusivity of material $1.4 \times 10^{-3} \text{ cm}^2 \text{ sec}^{-1}$ for polyethylene, t the time of separation of bobs $253 \pm 8 \mu\text{sec}$ and 2Θ the difference in temperatures of bobs before contact $= 24 \pm 2 \text{ deg}$.

Substitution gives $\partial\theta/\partial x = 1.0 \times 10^4 \text{ deg cm}^{-1}$ and shows that over 90% of this interfacial value is maintained up to a distance of $3 \times 10^{-4} \text{ cm}$ from the interface.

2.2. Preparation of Samples

With experiments in air, dielectric breakdown of the gap between separating surfaces limits the observed charge density to about $5\text{--}10 \text{ e.s.u. cm}^{-2}$. This corresponds to about one electronic charge per 10^6 \AA^2 of surface area, so clearly a minute amount of active impurity can be of importance. Cleanliness of this order would probably be impracticable for experiments done in the air of a laboratory. In the present work, therefore, the aim has been rather to form surfaces in a reproducible state of ordinary cleanliness. This state has been preserved for as long as possible by enclosing the apparatus in a glass case with a sliding door to allow access. In addition the air around the specimens is kept ionized whenever a charge measurement is not being made in order to dissipate charges and avoid the attraction of matter from the air.

Polyethylene rod as received by us was found to be somewhat molecularly oriented, probably during an extrusion process. This orientation causes distortion of a cut rod as it is softened, thereby showing evidence of internal stresses.

The internal stresses of the polythene to be used for making specimens are first relieved by melting the rod in a container and allowing the melt to cool very slowly. Spheres are then machined out of this material, scrubbed with soap and water, rinsed in tap water and three changes of distilled water and then extracted with ethyl alcohol in a Soxhlet apparatus during about three minutes. These cleaned spheres are then steeped in distilled water for at least an hour and allowed to dry in an ionized atmosphere during several hours. The surface of the sphere is then made smooth by immersing it for a second or two in a small tubular electric oven closed at one end. The walls of the oven are at a temperature of 900°C or thereabouts and the surface of the sphere

melts quickly while the centre remains solid. Surface irregularities and machining marks disappear to leave the sphere glossy and smooth. The above cleansing procedure then repeated.

2.3. Method of Operation

A freshly prepared, or newly cleaned, pair of spheres is mounted on the tubular pendulum arms by means of short lengths of screwed duralumin rod. They are adjusted in position and discharged by ionizing the air around them by means of an 80 μ c radium source for several hours.

The radium source is withdrawn and either pendulum is drawn aside to a deflection stop whence it is released to collide with the other within the oven, which may be heated or not, at a definite velocity. Twenty minutes are allowed for a change in temperature to be established in a sphere and five minutes for a temperature to be restored after an impact and measurement.

A charge on each sphere is measured both before and after a collision. The increment of charge on each sphere due to the collision is recorded, and a mean of the two (with the sign of one reversed) is taken to give the mean charge separated due to the collision. This is arbitrarily given the same polarity as the increment of charge obtained by specimen R and is represented by the charge separations $q_\alpha, q_\beta, q_\gamma, q_\delta$ according to the type of collision (see below). Readings of room temperature and oven thermocouple e.m.f. are also recorded. During the period between observing the charge and the next collision the air around both spheres is ionized by the Ra source for a minimum of three minutes. In this way charge is measured after each of four types of collision between the same pair of spots on the spheres. The types of collision are defined and symbolized by $\alpha, \beta, \gamma, \delta$, where:

- α R strikes L; both at room temperature
- β R strikes hot L; R at room temperature
- γ L strikes R; both at room temperature
- δ L strikes hot R; L at room temperature

where R, L are used to denote the right-hand and left-hand spheres as seen from the front of the apparatus.

3.1. Treatment of Results

It is found that, after having been newly cleaned, a pair of spots suffers a change which progressively alters the charge separation between them for any type of collision. In order to be able to eliminate this effect the types of collision are intermingled successively so far as is practicable. Two successions of collision types are possible and each was used. They are

$\alpha, \gamma, \alpha, \gamma, \beta, \beta, \delta, \delta, \alpha, \gamma, \alpha, \gamma, \beta \dots$

$\gamma, \alpha, \gamma, \alpha, \delta, \delta, \beta, \beta, \gamma, \alpha, \gamma, \alpha, \delta \dots$

It is too time-consuming to intermingle β, δ singly owing to the time taken in establishing a temperature change.

Observations were taken in this manner in groups. Each group contained observations limited to one particular spot on each sphere and is subdivided into a series of runs, each run being made on a different day. The groups are separated by the spheres

ng dismounted from the support tubes, washed, remounted and re-aligned. Thus it is probable that each group represents charge developed between a different pair of points.

The effects of a thermal gradient may conveniently be separated from disturbing effects of comparable magnitude by plotting the observed charge separation against position in the succession of observations. The observations of group 3 run (a) are used to illustrate this in figure 3. In this case the succession of observations was β , β , δ , α , α , γ and so on. Adjacent observations of a given type are then joined by straight lines to form a track. The progressive effect which is then manifest for each type of collision may now be eliminated by forming the quantities $p_{\alpha\beta}$, $p_{\gamma\delta}$ where

$$p_{\alpha\beta} = q_{\beta} - q_{\alpha} = \text{separation between } \beta \text{ and } \alpha \text{ tracks}$$

$$p_{\gamma\delta} = q_{\delta} - q_{\gamma} = \text{separation between } \delta \text{ and } \gamma \text{ tracks}$$

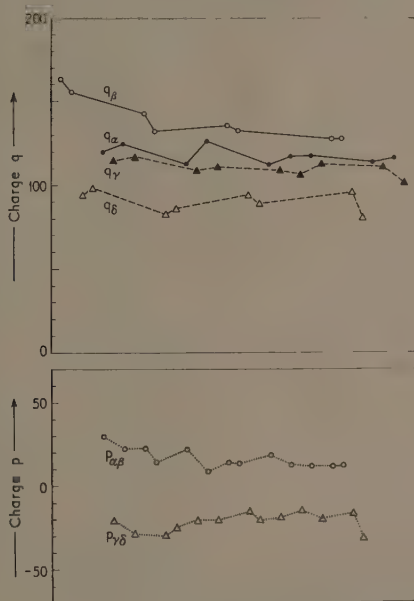


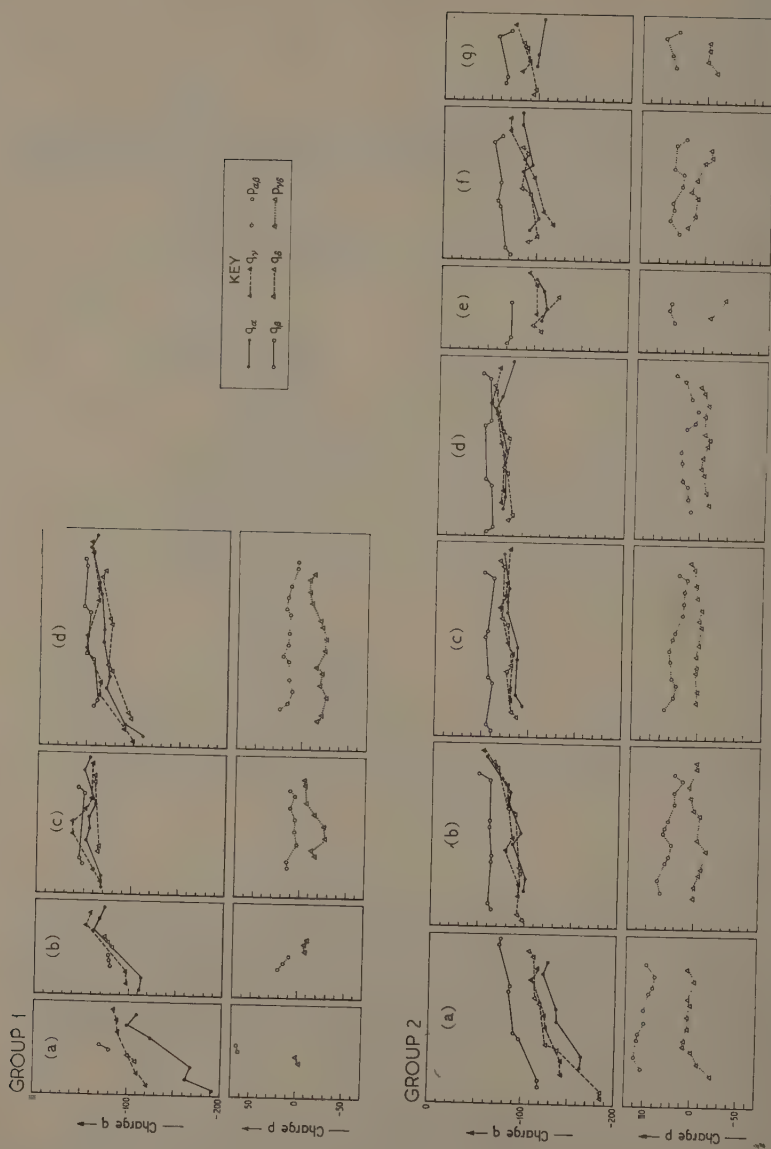
Figure 3. Explanatory diagram of method of displaying the results.

These quantities are then plotted serially in a similar manner to the q 's. The reversible effect due to a temperature gradient is then shown by the lines joining adjacent $p_{\alpha\beta}$ points being more positive than those joining adjacent $p_{\gamma\delta}$ points throughout their run, or vice versa.

3.2. Results and Conclusions

These are presented diagrammatically in figure 4 according to the scheme defined above. From examination of this figure it may be seen that

(i) several factors combine to give the charges measured as q_{α} , q_{β} , q_{γ} , q_{δ} (see Appendix I),



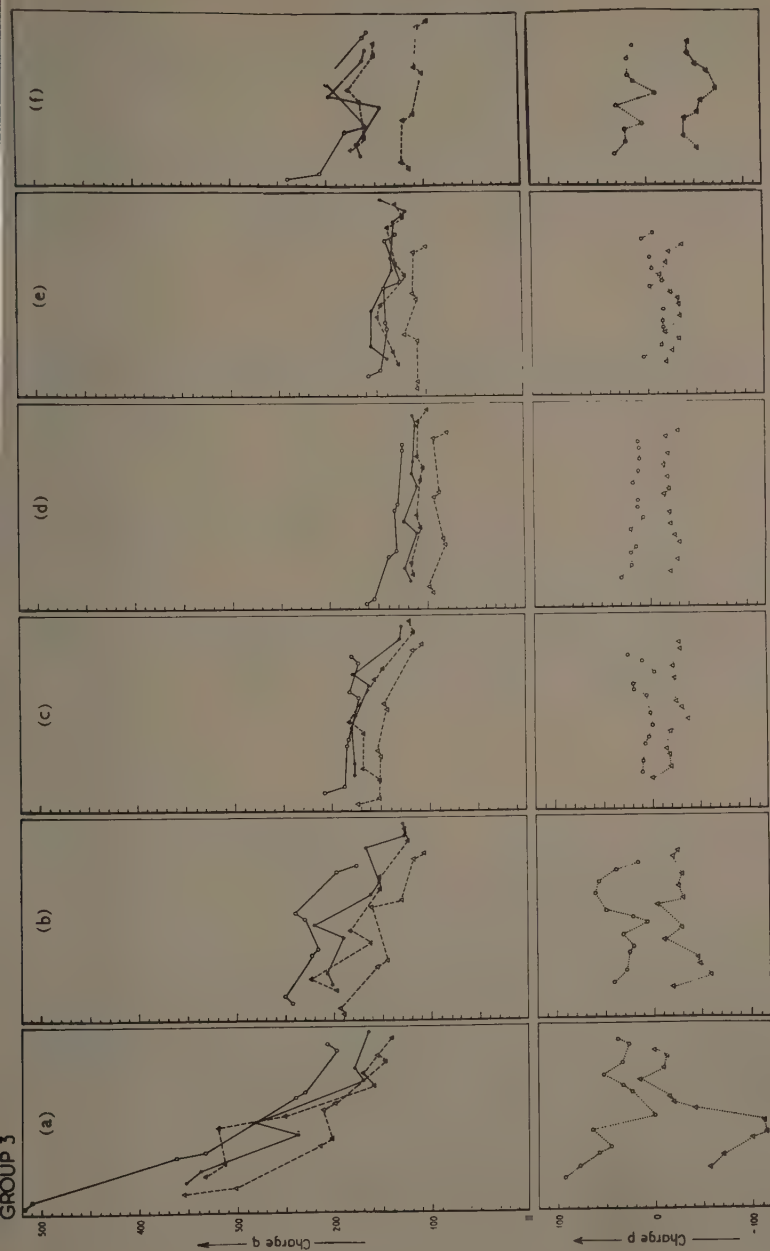


Figure 4. Diagram of the results obtained.

(ii) there is at least one mechanism dependent upon temperature gradient, as shown by $p_{\alpha\beta}$ being more positive than $p_{\gamma\delta}$ in all cases,

(iii) if the mechanism of charge separation is one of thermal diffusion then the carrier responsible for the separation of charge observed are predominantly positively charged (see Appendix I),

(iv) there is an effect which operates to bring q_α , q_β , q_γ , q_δ asymptotically towards separate values as the number of collisions increases. It is this number of impacts which matters rather than, for example, time since cleaning as the charge separation does not show discontinuities during an early overnight rest (e.g. between adjacent runs in group I). This is discussed further in Appendix II.

ACKNOWLEDGMENT

The author wishes to record the valuable discussions and encouragement he has received from Dr. P. S. H. Henry who suggested the problem which led to this paper.

REFERENCES

- BUNN, C. W., and ALCOCK, T. C., 1945, *Trans. Faraday Soc.*, **41**, 317.
 CARSLAW, H. S., and JAEGER, J. C., 1947, *Conduction of Heat in Solids* (Oxford: Clarendon Press) p. 41.
 GRUNER, H., 1953, *Faserforsch. u. Textiltech.*, **4**, 249.
 HARPER, W. R., 1951, *Proc. Roy. Soc. A*, **205**, 83.
 HENRY, P. S. H., 1953a, *Brit. J. Appl. Phys.*, **4**, S6.
 — 1953b, *Brit. J. Appl. Phys.*, **4**, S31.
 — 1957, *J. Text. Inst.*, **48**, 5.
 SHAW, P. E., 1927, *Proc. Phys. Soc.*, **39**, 449.
 THOMAS, D. G. A., and FINCH, H. W., 1950, *Electron. Engng*, **22**, 395.

APPENDIX I

The separation of charge due to a temperature gradient described above may be produced by either of two mechanisms:

- (1) a variation with temperature of the affinity of the surfaces for carriers,
- (2) the thermal diffusion of carriers in the interfacial temperature gradient.

A sure choice can not at present be made between these mechanisms. However, if thermal diffusion is predominant, it is useful to consider the behaviour of free particles in a temperature gradient over areas on two surfaces which come into contact for the period of an impact. Particles are thermally emitted from each surface at a rate dependent upon the temperature of the surface and the energy required to eject the particle. This energy is diminished by the close proximity of another surface so that the thermal emission of particles can proceed at ordinary temperatures.

If we confine ourselves to mobile charged particles, that is to say carriers, they may carry either positive or negative charge so that the rate of loss of charge from a surface due to thermal excitation will be given by a curve from figure 5 according to whether:

- (A) high density of predominantly positive carriers is available at a given temperature,
- (B) lower density of predominantly positive carriers is available at a similar temperature,
- (C) carriers are predominantly negatively charged.

At two particular temperatures T_1 , T_2 the rates of loss of charge from a surface of type A are $(A)_1$, $(A)_2$ respectively denoting the appropriate curve and temperature. Thus if two solids are brought together the initial net rate of loss of charge is given by, for example, $(A)_1 - (B)_1$ for an L sphere with a surface of type A in collision with an R sphere having a surface of type B, both at temperature T_1 .

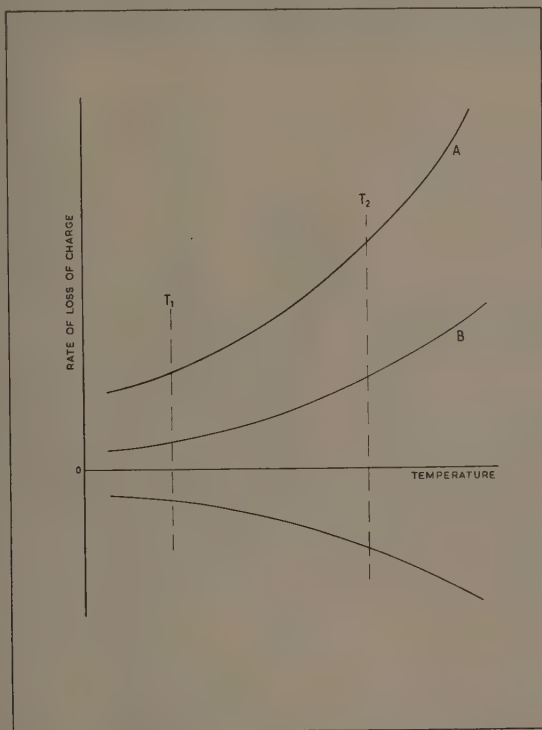


Figure 5. Rate of loss of charge from a surface due to the thermal emission of charged particles.

Charges separate between the surfaces and superimpose an electrostatic field which modifies the A and B curves so that at equilibrium the relevant rates of loss of charge by each surface are the same. It is sufficient for the present purpose to note that whether equilibrium is reached or not the sign of the final charge density is determined by the polarity of the initial current. For simplicity we assume proportionality between the thermally induced parts of the final charge separation and initial current, in which case:

$$\begin{array}{ll} q_{\alpha} \propto (A)_1 - (B)_1 & q_{\beta} \propto (A)_2 - (B)_1 \\ q_{\gamma} \propto (A)_1 - (B)_1 & q_{\delta} \propto (A)_1 - (B)_2 \end{array}$$

hence

$$\begin{array}{l} p_{\alpha\beta} = q_{\beta} - q_{\alpha} = (A)_2 - (A)_1 \\ p_{\gamma\delta} = q_{\delta} - q_{\gamma} = (B)_1 - (B)_2. \end{array}$$

By inspection of figure 5 it is clear that $p_{\alpha\beta}$ and $p_{\gamma\delta}$ are of opposite sign when surfaces A, B collide and of the same sign when surfaces A, C (or B, C) collide. Thus if $p_{\alpha\beta}$ and $p_{\gamma\delta}$ are found to be of opposite sign we conclude that the major part of the thermally induced charge separation is due to carriers of similar polarity from each surface, and vice versa.

In the case of the present experiments $p_{\alpha\beta}$ is seen to lie above $p_{\gamma\delta}$ in all cases, so it is indicated that a positively charged carrier predominates in the thermally induced part of the charge separations observed.

APPENDIX II

From figure 4 it is evident that more than one mechanism is responsible for the amount of charge observed to separate during a collision. There is a significant difference between q_x and q_y , which at first sight should be the same. There is also a progressive variation in any particular q with increasing number of collisions.

It has also been observed that the surface of a sphere is not homogeneous with respect to charge separation. This has been demonstrated by conditioning a particular pair of spots by a series of α -type collisions until q_x remained approximately constant. Pendulum L was then rotated about its longitudinal axis to each of seven other indexed positions. At each position a single value of q_x was obtained, pendulum R remaining in its original position. In this way the conditioned spot on R may act as a proof spot to test the properties of the surface of L in seven unconditioned spots. Observation of q_x with L again in position 1 indicated the stability of the proof spot. The observations are shown in table 1.

Table 1

Position of L	1	2	3	4	5	6	1	7	8
q_x	+4.3	-8.3	-77	-21	-112	-254	+8	-30	-15

Thus it is to be expected that the actual spots used in the principal experiment were probably very different electrically in spite of the consistency of the effect of a temperature gradient.

It is tentatively suggested that the variation in surface properties shown by table 1 may be due to a differing abundance of carriers at different parts of a polyethylene surface. In the neutral state these would be localized near fixed charges of opposite polarity, or active centres. During the collision carriers are rearranged between the two surfaces in contact to give the charge separation observed. In the present experiments the maximum observed charge density is of the order of one electronic unit per $2 \times 10^7 \text{ \AA}^2$ of surface area. Thus the density of easily separated centres and carriers in the polyethylene surface is very small. Before much progress can be made in this subject fair identification of the carriers and centres is necessary.

The transferability of activation centres between surfaces on collision has been studied. It was arranged that, after two spots were conditioned as before, the proof

t on R collided with each of two adjacent spots on L in the following sequence
, 1, 2, 1, 1, 1, 2, 1, 1, 1, 2, 1 . . . and so on.

This provides alternative values for q_α developed with spot 1 under two conditions:

(i) the intermediate collision is with spot 1,

(ii) the intermediate collision is with spot 2.

Spot 2 was chosen as convenient and because q_α with spot 2 was very different from
with spot 1. Runs were made on two separate days with the same spots and gave the
ults shown in table 2.

Table 2

	Mean	Standard deviation	Number of observations
$q_{\alpha 1}$	203	34	57
$q_{\alpha 2}$	462	79	18
δq_S	+9	25	20
δq_D	-20	35	16

here

$q_{\alpha 1}, q_{\alpha 2}$ = value of q_α for collision with spot 1, 2 on L respectively,

δq_S = increment in $q_{\alpha 1}$ with similar contact between,

δq_D = increment in $q_{\alpha 1}$ with dissimilar contact between.

From these results we find that the probability of the observed difference between
 q_S and δq_D being due to chance is less than 1% and deduce that a collision with spot 2
uses the proof spot on R to gain less positive charge when it next collides with spot 1.
so we see that spot 2 on sphere L lost more positive charge to (or gained less positive
charge from) the proof spot on R than does spot 1.

These findings show that a collision with spot 2 on L makes the proof spot more like
spot 2. This is in agreement with the general trend visible in figure 4 where the quantity
charge separating is greater in earlier collisions than later ones during a group of
observations.

Now, since the carriers are neutralized after each observation this means that either
a transfer of active centres between colliding surfaces is possible or (ii) negative ions
collected from the air during neutralization persist and act as active centres.

In the present case (i) is preferred because if (ii) were operative then δq_S and δq_D
could both be negative since $q_{\alpha 1}$ and $q_{\alpha 2}$ are both positive.

Stable Crack Propagation in Plastics

By J. J. BENBOW

Imperial Chemical Industries Limited, Plastics Division,
Welwyn Garden City

MS. received 23rd June 1961

Abstract. A description is given of apparatus designed to measure the crack propagation energy of plastics under conditions where they are brittle. This includes a brief history of the work leading up to the present studies and details of a novel type of instrument suitable for measurements over a range of temperatures. Use of these techniques is illustrated by typical results on Perspex, polystyrene and polythene.

In addition, some of the interesting features found on the surfaces of cracks are described. The patterns found on cracks in polystyrene are illustrated and their possible origins are briefly discussed. Finally the colours found on freshly formed cracks in Perspex are described.

§ 1. INTRODUCTION

THE OBJECT of the paper is to present work done during the past two years on crack propagation in plastics. Most of the measurements were made during short term investigations, and represent a development of work on the physics of fracture started at the Akers Research Laboratories. The paper is not written at the completion of an investigation but is more in the nature of an interim progress report.

To set the work in perspective the history of the subject is briefly summarized and a short discussion is given of the relation between brittle behaviour and specimen size. Apparatus being used at present is described and results on some polymers are given.

Finally, some of the interesting structural features and colour effects found on fracture surfaces are described.

§ 2. THE GRIFFITH THEORY OF FRACTURE

The papers of Griffith (1920, 1924) have exerted a profound influence on the study of fracture processes. Two separate, fundamentally new ideas were contained in his work. One was the idea of 'flaws' or minute defects which act as stress raisers and explain the difference between the observed, macroscopic and relatively low strength of solid materials, and the high strength values predicted from the known strength of chemical bonds.

The other idea originated by Griffith was of an energy balance as the controlling law of crack propagation. He assumed that the balance was between the surface energy (or surface tension) of the newly created fracture surface on the one hand and the elastic energy stored in the stress field on the other. He tested this hypothesis by measuring the bursting strength of glass tubes in which cracks of varying length had first been made.

During the last thirty years or so most of the work done on fracture has been planned with Griffith's ideas in mind, but it is only recently that new and more accurate experiments have been done to test the basic validity of his theory. A review of work up to

These new developments have been given by Orowan (1948). Up to the time covered by Orowan progress had been made in two directions. It was realized that the quantity giving the dimensions of a surface tension, which appears in the Griffith energy balance criterion, may in practice exceed the true specific surface energy by a large factor. This was explained as the effect of a layer of plastically deformed material.

In addition, attempts were made by Mott (1948) to include, in the energy balance, dynamic terms to take into account the stress waves created by the fast moving crack.

§ 3. STABLE FRACTURES

Although some experiments involving stable fractures in mica were made by Preimoff (1930) the explicit introduction of this concept is due to Roesler (1956). In his work on cone cracks he showed under what conditions brittle fracture can be stable (i.e. it can be propagated at an arbitrarily slow speed). His measurements on cone fractures in glass verified the functional form of the energy balance theory, but the numerical value of the fracture energy was found to be larger than a true surface tension can be. This shows that even in brittle materials such as glass the fracture process involves energy dissipation. More recently experiments on cone cracks in fused silica by Benbow (1960) have produced similar conclusions although the precise value of the fracture energy of fused silica has not yet been calculated.

The application of stable fractures to more practically important materials such as plastics was described by Benbow and Roesler (1957). By introducing an auxiliary compressive stress parallel to the crack, its direction and speed can be controlled. Using this technique it is possible to produce stable fractures in sheets or strips of plastics. (At the same time the method has the advantage of using easily available specimens.) The original apparatus has been improved and refined and many more measurements have now been taken. In addition a much simpler instrument based on the same original ideas has been developed which is more suitable for routine measurement of fracture energies rather than for precise tests of the energy balance criterion. Recently Svensson (1961) has described a very similar apparatus, which has been developed independently and he has given results for Perspex and polystyrene over a range of different temperatures.

§ 4. THE EFFECT OF SPECIMEN SIZE ON BRITTLINESS

If the energy balance theory is even approximately valid it has important consequences in the practical use of materials because it predicts that the size of the sample being tested may determine whether a material is brittle or not. The theory predicts that, provided the specimen is large enough, the external stresses at a large distance from the crack tip can be arbitrarily low.

The energy balance theory gives a relation of the same form between the externally applied stress and the specimen size, for all the systems which have been considered. This is:

$$\sigma = \left(\frac{kET}{b} \right)^{1/2} \quad (1)$$

where σ is the applied stress (at which the crack just propagates), E the elastic modulus relevant to the system and T the fracture energy per square centimetre.

The parameter k is a numerical function of the geometry of the system involved and has been given for particular cases in the references quoted. The quantity b is characteristic dimension of the stress field.

In a cleavage experiment of the type which will be described later, b is the width of the sheet and E is Young's modulus of the material. Since, in general, Young's modulus depends on the rate of strain, the value appropriate to the bending of both halves of the split specimen must be used since this determines the stress at the crack tip. If b is small the stress required to propagate a crack may be so large that tough failure occurs before the critical value for fracture is reached. Conversely, if b is very large the tendency for a material to show brittle behaviour will be increased. However, because the critical stress depends on the square root of the characteristic dimension, the transition from tough to brittle behaviour is not likely to be very sharp.

Brittleness measurements are made on plastics for two main purposes, namely to provide a basis of comparing one material with another and to determine the conditions under which a fracture is initiated. These objects are achieved independently from the energy balance theory provided the samples tested are all of a similar size. The importance of the energy balance theory arises in respect to the engineering applications of plastics and the scaling up of tests on small samples to provide data relevant to large structures. Transitions caused by temperature or rate of strain variations are well known in plastics but important transitions can also be achieved by geometrical changes alone. When measuring the properties of materials it is desirable to express the results in terms of quantities which are characteristic of the material and not dependent upon the apparatus or the dimensions of the specimen, although this does not imply that the quantity chosen is necessarily constant under all conditions. In the case of brittleness the specific fracture energy is such a quantity. The instruments which have been developed to test the energy balance theory and to measure the specific fracture energy have resulted in the elimination of several undesirable features which occur in more conventional methods of measuring brittleness. For example, in the case of impact tests it is difficult to avoid much of the measured energy being imparted to the broken specimen in the form of kinetic energy.

§ 5. DEVELOPMENT OF EXPERIMENTAL METHODS

Details of the method used to test the energy balance theory for plastics together with a description of the original apparatus, have already been given by Benbow and Roesler. On the basis of experience gained with this apparatus a second more robust apparatus was made. The principles involved were the same in both cases but in the new apparatus the compression force was applied through heavy ball races. A photograph of this is shown in figure 1. Many different materials have been studied with this instrument; most of these were plastics, but stable fractures have also been measured in plates of glass and cast iron.

To establish the applicability of the energy criterion to plastics it was essential to use a wide range of sample sizes and in particular the width of the specimen b had to be changed as much as possible. Consequently, the size of the apparatus was also rather large and not very suitable for routine measurements since the amount of material is often limited.

Another important factor is that measurements at different temperatures and in different environments cannot be readily obtained with such a large apparatus. On the other hand, the size of the sample can only be reduced to a certain extent because otherwise tough failure will tend to occur rather than brittle fracture. A useful criterion

ensure that $4 > S/b > 1$ where S is the crack length. Bearing these considerations in mind, a new apparatus has been designed which uses specimens 1 in. wide and roughly 6 in. long. The chief difference between this and those previously made is that two symmetrical cracks are produced simultaneously. Diagrammatically the

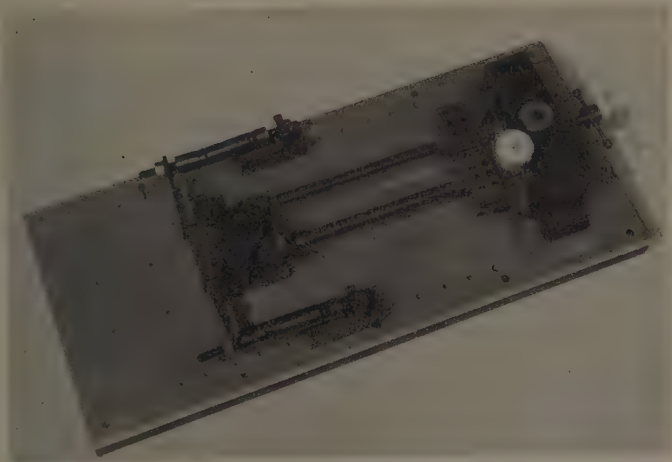


Figure 1

system used is that shown in figure 2. The initially rectangular specimen has a slot cut into it along the centre line parallel to the long edges and extending about 1 in. into each half. Both ends of this slot are cut to a 'swallow-tail' with a fine saw (see figure 2 for details).

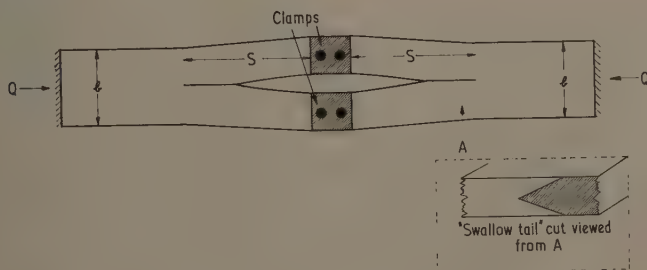


Figure 2

The compression force required to centralize the cracks can now be applied at the free ends, and thus no complicated bearings are required. This feature allows the apparatus to be greatly simplified. Two clamps are fixed to the specimen by 4 B.A. bolts, and are themselves mounted in a slot which allows them to move outwards but prevents rotation. A wedge is screwed between the clamps so that they are forced outwards

by amounts which can be measured in terms of the travel of the wedge. One form of the apparatus is shown in figure 3. This particular apparatus was designed for immersion in a thermostatically controlled vessel with provision for the position of the wedge to be altered and measured externally. This new apparatus is thus in essence the same as the original, but two samples are mounted back to back and cracked simultaneously. The lengths of these cracks are usually measured directly with a steel rule

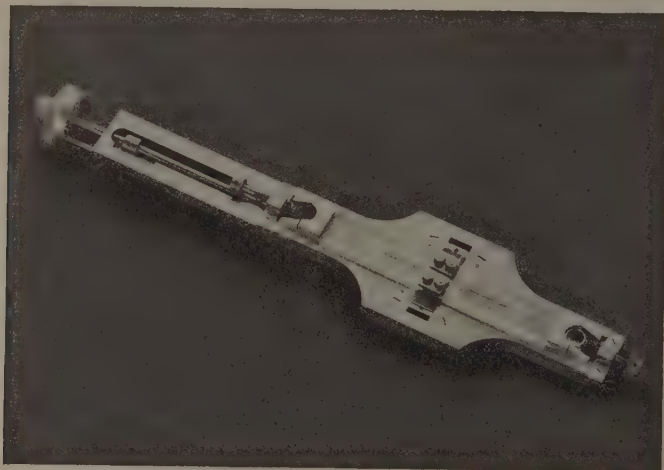


Figure 3

although when making measurements at high temperatures more elaborate techniques are used.

The type of clamping arrangement described is that which has proved most satisfactory. Earlier attempts to use a method in which rotation was permitted at the centre of the specimen were unsatisfactory because if one crack became crazed or did not grow uniformly for some reason, the symmetry of the system was destroyed, and the other crack grew more than it would normally have done. If this system had worked the amount of time spent preparing the samples would have been reduced slightly, but it is doubtful if this is of major significance, since the cutting of the slot takes the greatest amount of time. With the system now used, four holes have to be drilled in each specimen, but these do not affect the results at all, since the lengths of the cracks are measured from the edge of the clamps; the material under the clamps is held rigid by them.

§ 6. RESULTS

6.1. *Acrylics*

Samples of Perspex (polymethylmethacrylate) have been examined at temperatures ranging from 0 to 80 °C in the new symmetrical apparatus. The results are given in table 1 and it will be seen that there is very little change in the fracture energy as the temperature is varied. At the higher temperatures there is a slight tendency for T

increase but the smallness of this change can be seen in perspective by comparing the results obtained for several different polymers, tables 1, 2 and 3.

Table 1

Effect of Temperature on the Fracture Energy of Perspex

Temperature (°C)	3	10	20	32	43	45	50	62	76	80
Fracture energy $\times 10^5$ (dyn cm ⁻¹)	5.7	5.0	4.2	4.3	3.8	4.3	4.7	6.3	6.3	8.0

Table 2

Polystyrenes of Various Molecular Weights

Sample	Mol. Wt.	Type of fracture	Nature of surface	Fracture energy
A	26000	Fast	Rough (Fig. 5(a))	3.0×10^5
		Slow	Laminated	1.9×10^5
B	130000	Fast	Rough (Fig. 5(b))	1.5×10^5
		Slow	Laminated (Fig. 5(a))	6.1×10^5
C	80000	Fast	Rough (Fig. 5(c))	1.5×10^5
		Slow		1.7×10^5
D	60000	Slow	Smooth, mirror-like	$\approx 3.0 \times 10^4$

Table 3

Typical Polythene Results

Type of polythene	Melt index	Density	Fracture energy
High pressure, intermediate density	11.6	0.9317	3.6×10^5
High pressure, low density	20		2.71×10^5
Low pressure process	2.9		1.7×10^5

An interesting effect has been found by wetting the tips of cracks in Perspex with water. In general, cracks in Perspex grow very smoothly with no tendency to jerk. If such a smooth crack is wetted the crack immediately stops growing and the clamped ends of the specimen can be separated by a considerable amount before the crack jumps forward again. When the crack jumps forward it is travelling in dry material and reaches the position it would have had in the absence of water, see figure 4. The apparent fracture energy can be raised to four times that of the dry material by the addition of water. It is well known that the absorption of water in Perspex takes place very slowly but such an immediate effect does appear to have been unknown previously.

6.2. Styrene Polymers

The original work on the propagation of stable cracks in polymers involved a detailed study of commercially available polystyrene sheets. One of the outstanding features of this material is that two types of crack can be produced in it, one slow, the other fast. It was found that the fracture energy of slow cracks was higher than that of Perspex, whereas that for fast cracks was slightly less. Measurements have now been taken on other styrene polymers but particularly interesting results were obtained on four specially prepared specimens (supplied by D. Ridley) having number average molecular weights (determined by osmometry) of 260 000, 130 000, 80 000 and 60 000 respectively. These samples were free from residual stresses and contained virtually

no monomer. The results obtained are summarized in table 2. As the molecular weight falls there is a marked decrease in the fracture energy, a change in the type of fracture surface obtained and the tendency to form fast and slow cracks becomes less marked until with the lowest molecular weight the cracks behave very like those in Perspex when only smooth mirror-like cracks can be obtained without any tendency to form fast and slow cracks.

6.3. Polythenes

Many low density, 'high pressure' polythenes are too tough for cracks to be propagated in them at room temperature. A small number of measurements have been made on high density, high melt index polythenes made by the high pressure process, and

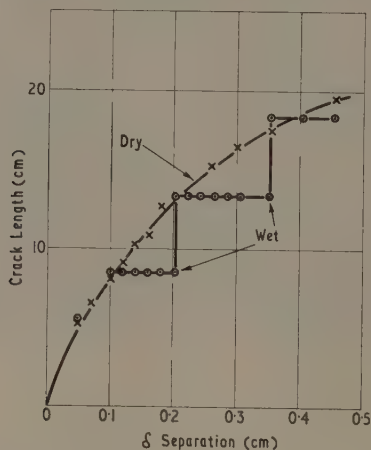


Figure 4

also some high density low pressure materials have been examined. However the number of results is too small to provide more than a few typical results which are useful only for comparison with other polymers (see table 3).

§ 7. FAST AND SLOW CRACKS

Two types of crack can be produced readily in high molecular weight polystyrene and biaxially stretched Perspex. Invariably the cracks of higher velocity have the lowest fracture energy. The physical reason for the two types of crack is not fully understood but their nature does offer an explanation of the fact that the slow cracks have higher fracture energies. The surfaces produced by slow cracks in high molecular weight polystyrene for example, have a number of subsidiary cracks below the main surface and have a flaked appearance (see figure 5(d)). Since the true surface area is many times that deduced from the length of the main crack the *apparent* value of T (slow) will be high even if the *true* value is equal to T (fast). It is possible that the true value of T is the same in both cases. A similar tendency to laminate is found in biaxially stretched Perspex sheet. At low percentage stretch the fracture energy increases with the amount of stretch but above about 50% the fracture energy of fast cracks falls steeply until it is eventually below that of the unstabilized material. However

These high extensions slow cracks can also be produced with laminated surfaces and with apparent fracture energies. Under practical conditions involving sudden impact it is the fast crack which is relevant.

§ 8. SURFACE EFFECTS

The surfaces of freshly cracked specimens of plastics show many interesting features. These can be divided, for convenience, into two main classes, namely surface patterns and colours.

Surface patterns are produced readily when fast cracks are propagated in high molecular weight polystyrenes. Figures 5 (*a, b, c*) show the surfaces of the four polystyrenes already referred to.

At first sight the patterns look like deep ridges but they are in fact well defined alternate regions of smooth and rough patches and are probably Wallner (1939) lines (i.e. periodic marks on the crack faces thought to be caused by interaction between the crack front and ultrasonic stress waves). As the molecular weight decreases the spacing of the lines also decreases, see figures 5 (*a, b, c*). The sample of lowest molecular weight (10 000) showed no surface patterns at all when viewed with low magnification; the surfaces of the cracks were highly polished and similar to those in Perspex.

If it is assumed that a high frequency ($\approx 5\text{--}10$ Mc/s) stress wave is generated by the travelling crack, it is possible to explain the surface patterns formed (Andrews 1959). On the other hand, the fact that the spacing of the lines varies with molecular weight, even though the modulus of elasticity is virtually constant, cannot be easily conciliated with this stress wave theory.

Colour effects are found on the surfaces of stable cracks in polymethyl methacrylate. These second-order colours are seen when the surface is viewed by reflected light and are probably caused by interference since electron microscope photographs of the surfaces show that there is no structure present which could produce diffraction. Somewhat similar effects have been reported by Busse, Orowan and Neimark†, Pollock, Kiess and Newman (1959) and Berry (1960), but when stable cracks are used the colours are uniform in colour over large areas (several square centimetres) and the colours on opposite sides of the crack are identical when the cracks are propagated slowly. Berry reports that he obtains complementary colours on corresponding parts of the crack faces but I have only found this with extruded 'Diakon' sheet in which the crack faces are often rough.

It is quite easy to remove the 'colour' by wiping the crack faces with a dry fabric or by placing the sample in a vacuum. If the sample is cracked, with water filling the crack, no colours appear. If dry Perspex is cracked and then washed, with water, the colours disappear.

Interference colours are also seen when high molecular weight polystyrene sheets are cracked slowly, so that the laminated type of surface is formed. In this case there is interference between the light reflected at the top surface crack and that reflected at sub-surface cracks.

§ 9. CONCLUSIONS

Several points arise out of this work. Some of the more important of these can be conveniently summarized as follows:

1. The brittleness of plastics can be compared without reference to the energy

† *Morphology of Fractures in Polymethyl Methacrylate*, Lecture presented at the American Physical Society, March 1957.

balance theory but results which are characteristic of a material can only be found by introducing the energy criterion.

2. Materials which obey the energy balance criterion can be brittle or not depending on their size, and the concept can be important in the practical application of plastics.

3. The specific fracture energy of plastics can be easily measured in the apparatus which has now been developed.

4. Stable fractures, if necessary produced at arbitrarily slow rates of cracking, provide excellent means of studying surface features on polymer faces. A detailed study of these effects would probably lead to a better understanding of the causes of brittleness in plastics and possibly enable tougher materials to be produced.

ACKNOWLEDGMENTS

I am indebted to Dr. F. C. Roesler of I.C.I. Limited, Billingham Division, for many valuable discussions and to Miss H. M. Bell and Mr. J. G. H. Gray for their assistance with the experimental work.

REFERENCES

- ANDREWS, E. H., 1959, *J. Appl. Phys.*, **30**, 740.
 BENBOW, J. J., 1960, *Proc. Phys. Soc.*, **75**, 697.
 BENBOW, J. J., and ROESLER, F. C., 1957, *Proc. Phys. Soc. B*, **70**, 201.
 BERRY, J. P., 1960, *Nature, Lond.*, **185**, 91.
 GRIFFITH, A. A., 1920, *Phil. Trans.*, **221**, 163.
 — 1924, *Proc. Inst. Engr. Appl. Mech. (Delft)* 55.
 MOTT, N. F., 1948, *Engineering, Lond.* **165**, 16.
 OBREIMOFF, J. W., 1939, *Proc. Roy. Soc. A*, **127**, 290.
 OROWAN, E., 1948-49, *Rep. Progr. Phys.*, **12**, 185 (London: Physical Society).
 ROESLER, F. C., 1956, *Proc. Phys. Soc. B*, **69**, 981.
 SVENSSON, N. L., 1961, *Proc. Phys. Soc.*, **77**, 876.
 WALLNER, H., 1939, *Z. Phys.*, **114**, 368.
 WOLOCK, I., KIESS, J. A., and NEWMAN, S. B., 1959, *Fracture*, Ch. 13, (New York: The Technological Press & John Wiley), p. 262.

The Nature of the Abrasion Process in Plastically Deformable Non-metals

BY J. N. KING AND H. WILMAN

Applied Physics and Chemistry of Surfaces Laboratory,
Chemical Engineering Department, Imperial College, London S.W.7

MS. received 15th June 1961

Abstract. The friction, wear and surface deformation in abrasion of typical very plastic non-metallic materials, AgCl and AgBr, are investigated, on emery papers at 200–500 g load. They are strikingly similar in form and magnitude to those of metals of comparable hardness. The wear rate M is related linearly to the friction coefficient μ when the emery particle diameter D is greater than 20 microns, but on finer abrasive the (M, μ) locus curves to lower μ , as for soft metals.

Optical microscopic study of single abrasion grooves shows the wear to be mainly by a cutting action like that of a lathe tool, but that much plastic flow occurs; and it indicates a high adhesion component of the friction.

Electron diffraction shows a backwardly tilted $\langle 110 \rangle$ orientation in the abraded surface region. Its form, and its preferred azimuthal range, shows its close relation to the rolling texture and to the compression texture when extensive lateral flow is permitted. The correlation between the tilt δ of the orientation axis from the specimen normal and μ is discussed.

§ 1. INTRODUCTION

THE PHYSICAL process of abrasion is important in shaping materials. It is also a prominent cause of friction and wear in machine bearings, where it often arises from adventitious hard abrasive particles (Barwell 1956, Duckworth and Forrester 1957, Burwell 1958) but sometimes from the presence of a hard phase in the bearing metal itself, e.g. perlite in the ferrite matrix in steels (Piggott and Wilman 1957), and often also from the presence of hard oxide or other surface layers which become fragmented under the applied load.

Although many experiments have been made on the friction and wear of metals, little clear evidence has so far been obtained on the behaviour of non-metals, which are now increasingly used in certain kinds of bearings as coatings or impregnating constituents. The experiments described below in § 2 and § 3 show that at least the more highly plastic inorganic non-metallic materials behave in a way closely similar to that of metals during abrasion.

For aluminium and harder metals abraded unidirectionally on bonded abrasives such as emery papers, at load W of the order of 0.2 to 2 kg, the mass loss M (i.e. wear) per centimetre of sliding distance, at the final equilibrium stage of pick-up of abrasive particles, is related linearly to the coefficient of friction μ : $M = kW(\mu - \mu_0)$, where k and μ_0 are constants (Goddard, Harker and Wilman 1959, Avient, Goddard and Wilman 1960). M and μ are practically constant when the abrasive particle diameter D is greater than 70 microns, at least up to 220 microns. Our theoretical results (Goddard, Harker and Wilman 1959, Goddard and Wilman, to be published) account well for these observations, and the quantitative data show that the ploughing component μ_p is

a large part of the total friction, μ . The linear (M, μ) relation indicates that the fraction f_{ee} , of the total load, carried on emery/emery contacts at this equilibrium stage pick-up is practically constant, independent of D .

Further results (Avient and Wilman, to be published) on abrasion of the very soft metals tin, lead and zinc, have also shown a linear (M, μ) relation on emery paper having $D > 20$ microns, but on finer grades the (M, μ) locus curves markedly to lower μ values, indicating that an increasing part of the load is on metal (+oxide)/metal (+oxide) contacts, and a lower f_{ee} applies.

The experiments described below now show for the first time the relation between μ , M and D in abrasion of typical very plastic soft non-metals, namely AgCl and AgBr. We find this is closely similar to that for very soft metals. This exemplifies in a quantitative manner the close analogy between silver halides and metals in their high plasticity which was indeed emphasized by Nye (1949) who referred to AgCl as equivalent to transparent metal.

The nature of the surface deformation caused in the AgCl and AgBr by such unidirectional abrasion is also seen from our electron diffraction observations to involve a high degree of re-orientation. We find, as in metals (Scott and Wilman 1958, Avient, Goddard and Wilman 1960, Wilman 1960) and in graphite (Porgess and Wilman 1960), a pronounced one-degree orientation is developed, the orientation axis being tilted away from the surface normal, back towards the direction from which the abrasive particle came. Comparison of these results for AgCl and AgBr with our recent determinations of their compression and rolling textures (King and Wilman 1961) shows clearly the close relationship of the 'abrasion texture' with both of these.

§ 2. EXPERIMENTAL

The silver chloride and silver bromide were obtained from Messrs. Hopkin & Williams Ltd., and the purity was stated to be 99.8%. Specimens of 1.6 cm diameter and 0.3–0.6 cm height were prepared by melting and resolidifying the halide in glass moulds. Some specimens were also prepared by compression of the original materials (granular, 0.1 to 2 mm diam.) at 32 tons/in² in a steel die 0.5 in. diameter (giving specimens 0.2 to 0.5 cm thick).

The flat surfaces of all the specimens were examined by electron diffraction in a Finch camera, at 50–70 kv and 47 cm camera length. Patterns were recorded before abrasion, then after unidirectional abrasion under about 500 g load for sufficient distance to produce no further change in form of the surface; and at various stages of removal of the abraded surface material by etching in a 0.1% aqueous solution of KCN. This solution etched away the halide at about 2400 Å min⁻¹ when freshly prepared.

The friction and wear experiments were made on the resolidified specimens, sliding on emery papers of various grades as abrasive, since these represent at least approximately defined degrees of surface roughness. Emery papers having a mean particle diameter D of 5, 10, 15, 35, 40, 70, 100 and 150 microns (grades 0000 to 3) were obtained from Messrs J. Oakey and Sons Ltd., and of approximately 15 to 35 microns (grades 000, 00 and 0) from Messrs Hubert. Each 25 cm stroke was over a fresh emery surface. The effect of sliding the silver halides under load on filter paper (Whatman No. 1) was also investigated, at 200 g load and at about 5 cm sec⁻¹. The wear rate M (mass loss/cm) was determined directly by estimation to 0.01 mg, using an Oertling semi-microbalance, the specimens being lightly brushed with a soft brush to remove any loose wear particles before weighing. The frictional force exerted on the specimen to cause non-accelerated

iding at about 5 cm sec^{-1} was determined as simply as possible by the weight required to pull a thread passing over a low-friction pulley. The coefficient of friction μ was measured at the same time as the wear rate, so that the abrasion conditions for the two measurements were identical.

Before determinations of M and μ were made on any grade of emery paper, the halide surface was filed gently to remove any embedded emery particles from previous abrasion on other grades. Friction and wear measurements were made until they attained constant values (after a few hundred centimetres). At this final equilibrium stage of pick-up of emery particles, the mass loss/cm was then the actual rate M of removal of halide by the abrading particles.

The Vickers diamond-indentation hardness number H_D of the resolidified specimens, after dry 4/0 emery abrasion, was determined using a GKN hardness tester, with 30 and 100 g load. For the AgCl, H_D was 9 kg mm^{-2} , and for the AgBr, 10 kg mm^{-2} .

§ 3. RESULTS

3.1. The (μ, D) , (M, D) and (M, μ) Relationships for AgCl and AgBr Abraded Unidirectionally on Dry Emery Papers

Figures 1 and 2 show the friction and wear results for abrasion of resolidified AgCl on dry emery papers under 200 g load, at the final equilibrium stage of pick-up of emery particles by the specimen surface. The friction values and the wear volume rates of AgBr were practically identical with those of AgCl on the same grade of emery. This agrees well with our observations that the hardnesses of the surfaces after abrasion on 4/0 emery paper, were about the same for AgCl and AgBr, namely 9 and 10 kg mm^{-2} respectively.

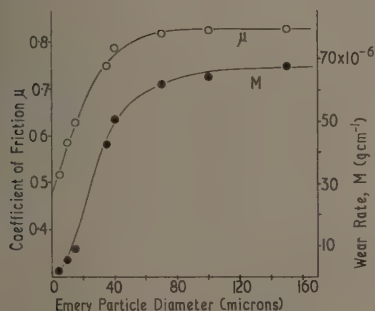


Figure 1. Observed (μ, D) and (M, D) relation for resolidified AgCl abraded on dry emery papers at 200 g load, at the final equilibrium stage of pick-up of abrasive.

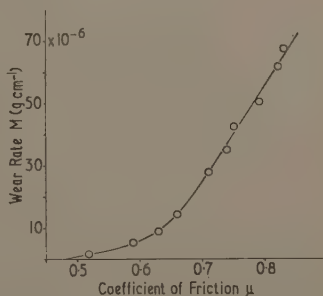


Figure 2. Observed (M, μ) relation for abrasion of resolidified AgCl as stated in figure 1.

μ was practically constant, 0.82, for both halides (see figure 1), on emery grades having $D > 70$ microns. On finer grades μ decreased rapidly with decreasing D to about 0.52 on 4/0 emery paper, due to an increasing proportion of the load being borne on contacts (mainly in the front region of the bearing surface) between the halide specimen and the halide worn-off, which partly clogs the emery paper (cf. Goddard, Harker and Wilman 1959, Avient, Goddard and Wilman 1960). For comparison, the μ of halide on halide was found to be 0.32 for lightly filed surfaces rubbed together until smooth, under a load of a few hundred grammes.

The wear rate varied with D in a roughly similar manner, but still increased slightly at large D . Experiments were also performed using specimens which, after filing, were surfaced by abrasion on the emery grade concerned, wet with propyl alcohol. The dry abrasion of these surfaces on the same grade of emery paper then led to the same final M and μ values as did the dry abrasion directly on the filed surface.

Figure 2 shows that at the final equilibrium a straight-line M/μ locus is observed for emery grades for which $D > 20$ microns. However, for finer grades, the locus curves markedly towards lower μ values.

3.2. *Short-stroke Abrasion Experiments with Silver Halides under 200 g Load*

A very short sliding distance of the order of 2 mm was used to facilitate the examination of individual abrasion grooves in the Vickers projection microscope. The specimens were smoothed by abrasion on 4/0 emery paper wet with propyl alcohol, and then a short abrasion stroke was made at 200 g load, perpendicular to the direction of the initial smoothing, on the particular grade of emery (dry) under consideration.

In the abrasion on relatively coarse emery (e.g. grade 0 or coarser), material was displaced by plastic flow to form lateral ridges at the sides of the grooves created by the ploughing emery particles, as figure 3 (plate I) shows. Also, some of the material was removed in the form of coiled or wavy strips by the emery particles, by a cutting or chiselling process similar to that caused by a lathe tool in a turning operation. Such adherent strips would be removed normally as wear particles during further abrasion.

On the finer emery, little cutting action is observed, but considerable pile-up of material occurs at the sides of the grooves, due to the displacement of material mainly by plastic flow.

Short-stroke sliding experiments were also performed on 'Scotchlite' reflective sheeting, which consists of an almost close-packed array of glass spheres of mean diameter about 125 microns, bonded to a thick paper backing. Figure 4 (plate I) shows a smooth groove of curved cross section, so formed. Some pile-up at the sides is seen, but there is a marked absence of wear debris. Some of the surfacing marks normal to the grooves are still seen traversing the groove, but are curved forward there. Similar forward curvature has been observed for copper and silver (Avient, Goddard and Wilman 1960), but is not observed in polycrystalline graphite (King 1960).

3.3. *Electron Diffraction Examination of the Surface Structure of Unidirectionally Abraded AgCl and AgBr*

After unidirectional abrasion of resolidified AgCl on dry 4/0 emery paper under a load of 500 g, a pattern characteristic of the face-centred cubic AgCl structure was observed, with many extra rings, identified from the ASTM file of x-ray powder pattern data (1955) as due to diasporic, α -AlOOH, which we find is always a component of the emery. Although no orientation of the halide was observed at the freshly abraded surface, a backward-tilted one-degree $\langle 110 \rangle$ orientation was found after etching in 0.1% KCN solution to a few hundred ångströms depth. The mean axis of this orientation was inclined by an angle $\delta \sim 20^\circ$ from the outward normal of the abraded surface, towards the direction from which the abrasive particles came. Figure 5, obtained after etching to 1200 Å, showed the diasporic almost exclusively, indicating partial embedding of the emery in the silver halide surface region. The emery particles themselves (corundum, Al_2O_3 , containing about 15% Fe_2O_3 and other small amounts of impurities) are so large as to be mainly opaque to the electrons, and thus contribute almost nothing to the diffraction pattern.

Abrasion of the halides on emery papers wet with propyl alcohol reduced the pick-up of abrasive particles to a negligible amount. For example, a tilted $\langle 110 \rangle$ 'fibre orientation' with $\delta \sim 8^\circ$ was observed, figure 6 (plate II) (cf. figure 9), from resolidified AgBr abraded on 4/0 emery paper wet with propyl alcohol, and there was no indication of presence of any emery (or diaspore).

Finer abrasion than was caused by 4/0 emery paper was obtained by sliding both compressed and also resolidified specimens of the halides on filter paper (Whatman No. 1). The patterns from these surfaces showed a backwardly inclined $\langle 110 \rangle$ orientation, with $\delta \sim 8^\circ$. The degree of orientation became more pronounced at depths of a few thousand ångströms, exposed by etching and yielding figures 7 and 8 (plate II), but δ remained practically unchanged at about 8° down to 4000 Å. Patterns recorded with the beam in an azimuth 30° from the perpendicular setting showed little change in the relative intensities of the arcs, thus a practically continuous azimuthal range of orientation round the $\langle 110 \rangle$ axis was present. The relative intensities of the arcs in figures 7 and 8, particularly the absence of the 400 arcs at the level at which $h+k=4$ (see figure 9), whereas the 222 arcs are strong, indicates, however, an azimuthal preference such that in the mean either a [001] direction is along the abrasion direction (with more than $\pm 55^\circ$ spread from the mean), or else a direction such as $[1\bar{1}2]$ is along the abrasion direction (with more than $\pm 35^\circ$ spread).

When the electron beam was parallel to the abrasion direction a uniform ring pattern was always obtained, evidently because the beam then grazes also part of the side faces of the grooves, whereas in the perpendicular setting it only penetrates the tips of the edges of the grooves.

§ 4. DISCUSSION

4.1. The (μ, D) , (M, D) and (M, μ) Relations for AgCl and AgBr Abraded on Dry Emery Papers

The variation of both the coefficient of friction μ and the wear rate M , with abrasive particle diameter D , for the silver halides (figure 1) is similar to that observed previously for many metals (Goddard, Harker and Wilman 1959, Avient, Goddard and Wilman 1960) and various graphites (Porgess and Wilman 1960, King 1960). The approximately constant value $\mu_{\max. \text{ equil.}}$ of μ at the final equilibrium, at $D > 70$ microns, is expected for these angular abrasive particles, since theoretically μ is concluded to be independent of D for such particles of conical or pyramidal shape (Goddard, Harker and Wilman 1959, Goddard and Wilman, to be published). The grooves formed by the abrasion of the silver halides are indeed seen to be markedly angular in section.

The value 0.82 found for $\mu_{\max. \text{ equil.}}$ of AgCl and AgBr (for which the hardness $H_D \sim 10$), is close to that for the comparably soft metals such as tin ($H_D \sim 15$ for the 4/0-emery abraded polycrystalline surface; $\mu_{\max. \text{ equil.}} \sim 0.86$). This μ value is larger than μ_{eh} of ploughing emery/halide contacts, because it corresponds to part of the load being carried on emery/emery contacts having $\mu_{ee} \sim 1$ (Goddard and Wilman, to be published). μ_{eh} was estimated to be about 0.76 by sliding a 'tripod' of sparsely distributed groups of emery particles (~ 215 microns diameter) firmly fixed to a metal base with sealing wax, on a relatively smooth surface of silver halide prepared by fusion and resolidification on a flat glass plate. This μ_{eh} value is also similar to the μ_{em} of such emery particles ploughing along a metal of similar hardness, e.g. tin (cf. Avient, Goddard and Wilman 1960).

Since the ploughing component μ_p can be expected to be about the same for materials of the same hardness, it appears that for the emery/halide contacts the adhesion

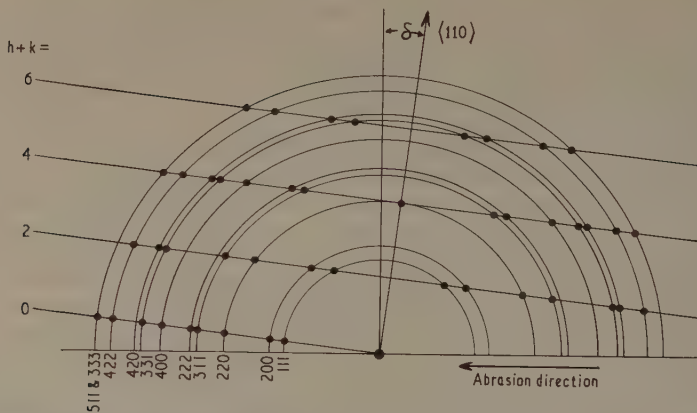


Figure 9. Ring positions and theoretical diffraction positions for face-centred cubic crystals in a one-degree orientation with a $\langle 110 \rangle$ axis inclined at an angle δ away from the surface normal.

component μ_a of the total friction μ_{eh} has a value close to that for the emery/tin (+ oxide) contacts. That the adhesion component is a considerable part of the total μ is indicated by figure 4, showing the pronounced forward drag of the halide by the sliding particle, in this case a glass sphere. The forward drag is rather more than we observed with Cu and Ag (Avient, Goddard and Wilman 1960). In graphite it was negligible, corresponding to the low adhesion friction ($\mu_{gg} = 0.14$) (King 1960).

The μ of halide on halide μ_{hh} is found to be 0.32, and is very similar to the values of approximately 0.3 found for metal (+ oxide)/metal (+ oxide) in the case of Cu and Ag (Avient, Goddard and Wilman 1960) and Sn (Avient and Wilman, to be published), and for Cu_2O on Cu_2O (Porgess 1960). The s/p_m values for these materials (s = shear force/unit area of the shearing contact, and p_m = flow pressure of this shearing region) are thus similar, although these materials have widely different p_m and H_D values; for example, for Cu_2O , $H_D \sim 240$ –260, and for AgCl and AgBr, $H_D \sim 10$. We note, however, that for Cu_2S on Cu_2S , $\mu \simeq 0.5$ (Bowden and Tabor 1950, Porgess 1960).

The slight increase of M with D at $D > 70$ microns, is similar to that observed for tin, lead and zinc (Avient and Wilman, to be published), although for Al and harder metals M was practically constant at $D > 70$ microns (Avient, Goddard and Wilman 1960).

The (M, μ) locus shown in figure 2 is a straight line for $D > 20$ microns, i.e. $M = k(\mu - \mu_0)$, where k and μ_0 are constants and $\mu_0 \simeq 0.62$. However, for finer emery grades ($D < 20$ microns) the locus curves towards lower μ values. Here again the silver halide properties are strikingly similar to those of a metal of similar hardness, because this form of locus is the same as was found for the very soft metals Pb, Sn and Zn (Avient and Wilman, to be published). The curved lower part indicates that in this region the fraction f_{ee} of the load supported on emery/emery contacts is progressively less than the practically constant f_{ee} value which applies over the upper straight region (Goddard and Wilman, to be published). It seems that, for $D < 20$ microns, many of the picked-up emery particles become more or less submerged in the soft halide bearing surface, as was indeed indicated by the electron diffraction photographs from the

surfaces after etching (§ 3.3 and figure 5). This, together with the rapid clogging of the emery paper in these finer grades, leads to more of the load being supported on halide/halide contacts, for which $\mu_{hh} = 0.32$ (see above). One reason why these smaller partly embedded abrasive particles tend more to become submerged than larger particles, is probably that the frictional heating of these particles as they contact the opposing emery sheet over a considerable distance of sliding, must raise their temperature to a higher value than that reached by the larger particles. This will tend to soften the material in which they are embedded, so that deeper embedding of the smaller particles occurs.

The pick-up of emery has the effect of reducing the wear rate and increasing μ compared with the value for an emery-free surface. We have, as yet, however, no estimate of f_{ee} for the silver halides, because of the difficulties caused by the rapidity of pick-up of emery by the surface.

4.2. *The Surface Re-orientation and its Relation to the Compression Texture and the Rolling Texture*

For comparison with the above results we have determined the compression textures of these silver halides (King and Wilman 1961), by x-ray and electron diffraction. The initial granular materials compressed as described in § 2, showed a $\langle 100 \rangle$ texture with axis along the compression axis (together with a moderate proportion of $\langle 110 \rangle$ orientation with axis inclined by up to 30° away from the compression axis). When, however, resolidified specimens in the form of rectangular blocks about $0.5 \times 0.5 \times 0.2$ cm, were compressed between polished, flat stainless steel plates (lubricated with oil) in a vice, only a pronounced $\langle 110 \rangle$ one-degree orientation with axis along the compression axis was observed. The reduction in thickness was more than 80%, i.e. to less than 20% of the initial thickness. The same $\langle 110 \rangle$ texture was also observed in specimens which after compression in a die were further compressed between the steel plates.

Resolidified AgCl rolled from about 0.5 cm diameter and 0.3 cm thickness to about 0.01 to 0.03 cm thickness (in about 20 stages, in the same rolling direction), then showed basically a strong $\langle 110 \rangle$ one-degree orientation, azimuthally limited, and with additional $\{111\}$ twinning. The rolling direction was concluded to be $\langle 1\bar{1}2 \rangle$, in the mean, as in the $\{110\}\langle 1\bar{1}2 \rangle$ rolling texture of face-centred cubic metals.

It is thus clear that the nature of the compression texture depends on the extent to which the material can flow laterally during compression. Compression with freedom for extensive lateral flow is seen to correspond in effect to rolling the material in all radial directions simultaneously. Similarly in abrasion there is extensive laterally directed flow as the material is displaced by the indenting particles, and the $\langle 110 \rangle$ texture developed is in accordance with the $\langle 110 \rangle$ compression and rolling textures.

In the abrasion, the mean azimuthal orientation developed is (like that we find for face-centred cubic metals) with either $\langle 001 \rangle$ or a direction near this, such as $\langle 1\bar{1}2 \rangle$, parallel to the abrasion direction, and is thus probably the same as that in rolling, $\langle 1\bar{1}2 \rangle$. This close correspondence to the rolling texture seems to be due to the indenting emery particles being mostly very obtuse tipped so that in the abrasion the flow under the emery particles is indeed not much different in type and direction to the plastic flow under the roller in rolling. At the final contact with the abrasive particles the flow is then parallel to the groove direction.

The main difference in nature between the conditions in abrasion and rolling is that in abrasion the tangential frictional force (including both the adhesion and ploughing components) is large. The resultant of this force and the normal load is inclined away

from the specimen normal by an amount related to the friction coefficient μ , and the orientation axis of the abrasion texture developed is correspondingly tilted away from the normal by an angle δ .

4.3. The Surface Re-orientation in Relation to the Friction

Previous studies of the relation between δ and μ for the hexagonal metals beryllium and magnesium (Scott and Wilman 1958) and graphite (Porgess and Wilman 1960) showed that the angle of tilt δ of the [001] orientation axis in the abraded surface regions is about equal to $\tan^{-1}\mu$. For face-centred and body-centred cubic metals a backward-tilted $\langle 110 \rangle$ orientation, and a mixed tilted $\langle 100 \rangle + \langle 211 \rangle$ orientation respectively, were observed (Harker 1958, Goddard 1959, Avient, Goddard and Wilman 1960). However, near the surface of these metals the tilt was often considerably less than $\tan^{-1}\mu_{\text{mo-mo}}$, where $\mu_{\text{mo-mo}}$ is the friction coefficient of the metal (+ oxide)/metal (+ oxide) contacts. Etching to several thousand ångströms depth revealed a more tilted $\langle 110 \rangle$ one-degree orientation in the face-centred cubic metals, δ then approximating to $\tan^{-1}\mu_{\text{em}}$, where μ_{em} is the μ of the ploughing emery/metal (+ oxide) contacts, the region of which, near the bottom of the grooves, is then accessible to the electron beam, at this stage of etching.

In the abrasion of the silver halides, μ_{hh} is about 0.32 for the halide/halide contacts, which must occur mainly at the tips of the projections of the rough abraded surface, and must thus be the main region accessible to the electron beam at grazing incidence on the freshly abraded surface. In the regions below the immediate surface, however, δ would be expected to approximate progressively to $\tan^{-1}\mu_{\text{eh}}$. The patterns (similar to figure 5) from the halides abraded on dry 4/0 emery paper and etched to only a few hundred ångströms depth, indeed show that here δ for the $\langle 110 \rangle$ orientation is about 20° , which agrees well with $\tan^{-1}\mu_{\text{hh}}$ (i.e. $\tan^{-1} 0.32$, which is 18°); but it is less than $\tan^{-1}\mu_{\text{eh}}$ and also less than $\tan^{-1}\mu$ (on 4/0 emery). However, no systematic change in δ with depth was observed on etching the surface, and at about 7000 Å depth the halide was in the form of randomly oriented crystals. This evidently indicates that a further factor is present (see below). Furthermore, in the finer abrasion of the silver halides by sliding on filter paper, δ was about 8° near the specimen surface, and also was unchanged down to several thousand ångströms depth. This δ is much less than $\tan^{-1}\mu$ (the observed $\mu \sim 0.3$, thus approximately equal to μ_{hh}), which was about 17° .

This fact, that also for the subsurface regions the observed δ is less than $\tan^{-1}\mu$, must evidently be attributed to the effect of the forward motion of the indenting abrasive particles, additional to the oblique resultant compressive force, and be associated with the forward drag of the material by the adhesive frictional force between the ploughing particles and the halide in the way shown in figure 4. The adhesion causes a tension in the material behind the ploughing particles, and this may cause further deformation with lattice rotation resulting, reducing δ . In the abrasion of graphite, on the other hand, the close agreement of δ with $\tan^{-1}\mu$ (Porgess and Wilman 1960) is evidently associated with the low adhesion between the graphite and the emery particles, as is indicated by the absence of any forward curving of the surfacing striae across rounded grooves caused by sliding graphite on 'Scotchlite' glass spheres as for figure 4 (King 1960).

§ 5. CONCLUSION

The above results show conclusively the extensive and quantitative correspondence of the friction and wear properties of these non-metallic materials in abrasion, to those of metals of comparable hardness. Further results have now also been obtained (Dobson

and Wilman, to be published) showing that this extends also to the case of abrasion of NaCl (both polycrystalline and single-crystal), in spite of its more brittle and cleavable nature. The above results on the nature of the surface re-orientation make clear the dependence of this orientation type on the occurrence of extensive lateral flow of the material displaced by the indenting abrasive particles. Abrasion textures are concluded to be generally largely analogous to the rolling texture, and also closely related to the compression texture which is observed when lateral flow is permitted.

These results thus provide a useful basis for a satisfactory understanding of the friction, wear and surface deformation of such non-metals.

ACKNOWLEDGMENTS

This research was carried out with the financial support of the Atomic Power Division of The English Electric Co. Ltd., Whetstone, nr Leicester. We are also indebted to Messrs J. Oakey and Sons Ltd for specimens of emery, and to the Minnesota Mining & Manufacturing Co. Ltd for samples of 'Scotchlite' reflective sheeting.

REFERENCES

- WILMAN, B. W. E., GODDARD, J., and WILMAN, H., 1960, *Proc. Roy. Soc., A*, **258**, 159.
 WILMAN, F. T., 1956, *Lubrication of Bearings* (London: Butterworths), p. 245.
 WILMAN, F. P., and TABOR, D., 1950, *The Friction and Lubrication of Solids*, (Oxford: Clarendon Press), p. 234.
 WILMAN, J. T., 1958, *Wear*, **1**, 119.
 WILMAN, W. E., and FORRESTER, P. G., 1957, *Proc. Conf. on Lubrication and Wear* (London: Instn Mech. Engrs), p. 713.
 GODDARD, J., 1959, *Ph.D. Thesis*, University of London.
 GODDARD, J., HARKER, H. J., and WILMAN, H., 1959, *Nature, Lond.*, **184**, 333.
 HARKER, H. J., 1958, *Ph.D. Thesis*, University of London.
 WILMAN, J. N., 1960, *M.Sc. Thesis*, University of London.
 WILMAN, J. N., and WILMAN, H., 1961, *Acta Cryst.*, in the press.
 WILMAN, J. F., 1949, *Proc. Roy. Soc. A*, **198**, 190.
 WILMAN, M. R., and WILMAN, H., 1957, *Proc. Conf. on Lubrication and Wear* (London: Instn Mech. Engrs), p. 613.
 WILMAN, P. V. K., 1960, *Ph.D. Thesis*, University of London.
 WILMAN, P. V. K., and WILMAN, H., 1960, *Proc. Phys. Soc.*, **76**, 513.
 WILMAN, V. D., and WILMAN, H., 1958, *Proc. Roy. Soc. A*, **247**, 353.
 WILMAN, H., 1960, *Acta Cryst.*, **13**, 1062.

Radio Wave Scattering from the Lunar Surface

By V. A. HUGHES†

Royal Radar Establishment, Malvern, Worcs.

MS. received 19th May 1961

Abstract. This paper describes some recent measurements on the angular scattering properties of the lunar surface at the wavelength of 10 cm. The scattering law of the surface is shown to be $P(\theta) = \sigma_0 \exp(-10 \cdot 2\theta)$ over the range of θ from 4 to 13° and a comparison with other results shows that it is independent of wavelength up to $\lambda = 1 \cdot 5$ metres. For angles up to 30° the scattering law deviates from an exponential but is still independent of wavelength up to at least $\lambda = 75$ cm. Evidence is given to show that the surface may be considered as rough at radio wavelengths.

§ 1. INTRODUCTION

SINCE the first successful radar contact with the moon by the United States Signal Corps and, independently, by Bay in Hungary in 1946, radar observations have been considerably extended. Most of the original work was carried out with radars developing comparatively low powers and to make it possible to detect the returned signal very long pulses or c.w. were used such that the whole of the lunar surface was illuminated. The c.w. measurements by Kerr, Shain and Higgins (1949) at the wavelength of 15 metres revealed the presence of two fading rates, a large slow period fluctuation together with a much more rapid one. It was suggested that the slow period was produced by Faraday rotation of the linearly polarized waves and Murray and Hargreaves (1954) showed how the moon echo technique could be used to measure the total electron content of the ionosphere. However, the more rapid fluctuations were attributed to the interference between signals scattered from the various regions on the surface which have relative motion due to lunar libration. By a method of pulse-to-pulse correlation Brown *et al.* (1956) determined the frequency spectrum of the fading and by relating this to the expected Doppler shifts Evans (1957) derived the scattering law of the lunar surface. These results showed that at a wavelength of about 1 metre the lunar surface scattered in a very directional manner.

Later measurements with microsecond pulses by Trexler (1958) at a wavelength of about 1·5 metres, by Yaplee *et al.* (1958) and by Hey and Hughes (1959) at a wavelength of 10 cm and more recently by Leadabrand *et al.* (1960) and by Pettengill (1960) at the wavelength of 75 cm, have all confirmed this highly directional scattering and have led to a more detailed study of the variation in echo strength as the pulse moves across the surface of the moon; in fact the higher powered radars at the wavelength of 75 cm have detected the weak scattering that exists out to the limb of the moon.

It has been suggested by Senior and Siegel (1960) that the lunar echo is due to specular reflection from a small number of isolated regions and the term quasi-smooth has been used to describe the surface. However, the signal takes the form of a large number of discrete echoes, each of a duration equal to the pulse length, which fade in

† Now at Radio Research Station, Ditton Park, Slough, Bucks.

a random fashion but with frequencies which are closely related to the expected Doppler shifts. Previous measurements at the wavelength of 10 cm (Hey and Hughes 1959) have shown that no region of the moon with dimensions corresponding to the pulse length of 5 μ sec gives a consistent echo, and this suggested to the author that the results ought to be interpreted as scattering from a rough surface. The later results by Petten-kill (1960) have in fact shown that a very large number of scattering areas exist and that there is no correlation of the 'radar picture' of the moon over intervals of about one minute.

The object of this paper is to describe some measurements on the angular scattering properties of the lunar surface at the wavelength of 10 cm and to show that the results are compatible with reflection from a rough surface which has deviations large in comparison with the wavelength such that a large number of regions will contribute.

§ 2. THE RADAR EQUATION FOR PLANETARY STUDIES

The signal scattered back from a radar target and received at the focus of a radio telescope is given by the well-known radar equation

$$p = \frac{P_T A^2 \sigma}{4\pi \lambda^2 R^4} \quad (1)$$

where P_T is the power transmitted from the aerial, A is the effective aperture of the telescope, R is the range and σ is defined as the effective scattering cross section of the target. In general there will also be losses in the transmission lines and in propagation through the atmosphere but for the present purposes the atmospheric losses which will be small have been ignored. However, the more appreciable transmission line loss α_T will reduce the transmitted power such that if the power developed by the transmitter is P , then that radiated at the aerial is given by $P = \alpha_T P_T$.

The power received at the focus of the telescope will also pass along the transmission line to the receiver and the performance will be measured at the receiver output in terms of the ratio of the signal power to the total noise power. If there were no loss in the transmission line then the noise power at the receiver output would be equivalent to

$$P_N = [(N-1)T_0 + T_A]k\delta f \quad (2)$$

where N is defined as the noise factor of the receiver, k is Boltzmann's constant, δf is the bandwidth of the receiver and T_0 and T_A refer to room temperature (290 °K) and the effective aerial temperature respectively. T_A of course includes both the effective temperature of radiation received from celestial radio sources and that of radiation from the ground and nearby objects. The effect of losses in the transmission line is to degrade the noise factor of the receiver by an amount α_T , and the receiver can then be considered to produce a noise power

$$P_N' = [(\alpha_T N - 1)T_0 + T_A]k\delta f. \quad (3)$$

The signal-to-noise ratio in the simple case is then given by

$$S = \frac{1}{4\pi k} \frac{P}{\alpha_T [(\alpha_T N - 1)T_0 + T_A]} \delta f \frac{A^2}{\lambda^2 R^4} \sigma. \quad (4)$$

In practice, providing there are no large Doppler shifts, the bandwidth is normally chosen such that $\delta f = 1/t_p$ where t_p is the pulse length, and equation (4) becomes

$$S = K_1 P t_p \frac{A^2}{\lambda^2 R^4} \sigma \quad (5)$$

where

$$(K_1)^{-1} = 4\pi k \alpha_T [(\alpha_T N - 1)T_0 + T_A]$$

and the signal-to-noise ratio is proportional to the total energy in the transmitted pulse.

2.1. The Effective Scattering Cross Section

The above derivation of the signal-to-noise ratio assumes that the target or the region of the target that scatters the radiation is small in radial dimension. However, if the target scatters in depth, the power returned will be a function of the pulse length; then for rough surfaces it is more convenient to define an effective scattering cross section per unit area $\sigma_0(\theta)$, which will be a function of aspect angle, or in the case of, say, scattering from the atmosphere a cross section per unit volume. The scattering cross section will then be increased by increase in the pulse length, but at the expense of loss in range resolution. For the case of the moon the scattering cross section is given by integrating over the area of surface A illuminated by the pulse

$$\sigma = \int_A \sigma_0(\theta) dA \quad (6)$$

where θ is the angle of incidence at element dA , and has an upper limit when the pulse illuminates the whole of the surface.

Hence with comparatively low transmitter power but using very long pulse lengths, it was possible in early experiments at metre wavelengths to detect the integrated power scattered back from the whole of the lunar surface. The more recent development of short pulse and higher peak power transmitters at shorter wavelengths has made possible a more detailed study of the scattering mechanism of the lunar surface by making use of the improved range resolution.

2.2. Integration

The previous derivation of signal-to-noise ratio considered the case of a single pulse, but in general the radar will be sending out a train of pulses, so that it is possible to integrate the signal over an appreciable number of pulses. Also if the returned echo is measured over a range interval by means of a range gate it is possible to increase the signal but at the expense of range resolution. Now the noise can be considered as a number of discrete readings each of duration $1/\delta f$, so that if the duration of the range gate is t_g and the pulse repetition frequency is F , during the time constant of integration τ there will be

$$n = t_g \delta f F \tau.$$

independent readings. Hence the uncertainty in the value of the noise power will be reduced by the factor $n^{1/2}$ and the signal-to-noise ratio becomes

$$S = K_3 P t_p \frac{A^2}{\lambda^2 R^4} \sigma (t_g \delta f F \tau)^{1/2} \quad (7)$$

where the constant K_3 contains, besides K_1 , factors which are dependent on the shape of the receiver bandwidth and on the type of integration.

These are the principles that have been used in the design of the equipment for use with the radar for studying lunar echoes.

§ 3. THE RADAR EQUIPMENT

The equipment used for the experimental investigation on lunar scattering was basically as has been described previously (Hey and Hughes 1959), consisting of a radar with the following parameters:

Wavelength $\lambda = 10$ cm, peak pulse power $P = 2 \times 10^6$ w, pulse length $t_p = 5 \times 10^{-6}$ sec, pulse repetition frequency $F = 250$ per sec, receiver noise factor $N = 7.5$, receiver band with $\delta f = 2 \times 10^5$ c/s, aerial diameter $D = 13.7$ metres.

Originally the method of recording was to photograph an intensity modulated time base which was swept slowly across the cathode-ray tube, thus obtaining a range time display with integrated signal amplitude showing as a variation in brightness on the film. However, the method suffered from a number of disadvantages including a restricted dynamic range in signal amplitude, extraneous light produced a shift in the mean level, and despite frequent calibration, the film required careful and controlled development. To improve the method of recording a range gate unit was developed which allowed more accurate measurement of the signal and longer time constants of integration. The unit produced a pulse $20 \mu\text{sec}$ long (corresponding to 3 km of the time base) which sampled the receiver output after each transmitter pulse. The delay between transmitter pulse and range gate could be preset to integral values of $100 \mu\text{sec}$ (15 km) and also automatically swept over a further delay of $700 \mu\text{sec}$ (100 km) in a period of about 1 min. The output from the range gate was passed through an integrating unit, and after amplification was displayed on a recorder on which was also marked the range-gate delay.

With a time constant of integration of 2 sec it was possible to measure signals at levels down to about 3% of the noise power.

During the observation the pointing of the aerial was controlled by means of an analogue computer which converted the celestial coordinates to azimuth and elevation. The computer was set for the correct geocentric latitude and frequent adjustments were made in elevation to correct for lunar parallax in altitude.

§ 4. THE RESULTS

Thirty-one runs were analysed for the period 27th November to 11th December 1959, consisting of about four records obtained on each of a number of days. For each run the delay was set to bring the range gate near to the front of the lunar echo, the automatic swept delay was switched on and a record taken of amplitude against time-base range as the gate moved across the echo; a typical record is shown in figure 1. Owing to the fluctuating nature of the radar return, the time constant of 2 sec was not found to be sufficient and additional smoothing was applied by taking a running mean.

If the area on the surface of a large sphere of radius a illuminated by a short radar pulse of duration equivalent to a range on the time base of r_p is A_p then $A_p = 2\pi ar_p$ and is independent of the distance travelled by the pulse after first contact; hence the amplitude of the echo at any distance from the leading edge will be directly proportional

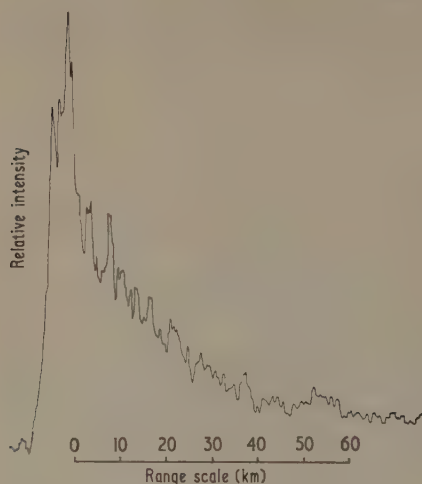


Figure 1. Typical recording of the lunar echo at the output of the integrating unit.

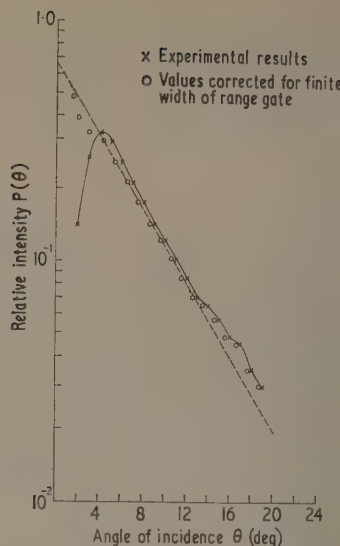


Figure 2. Angular scattering law of the lunar surface at the wavelength of 10 cm. The dashed line corresponds to $P(\theta) \propto \exp(-10.2\theta)$.

to the angular scattering properties of the surface at that point, which we shall call $f(\theta)$. If then the conversion

$$\cos \theta = \frac{a-r}{a} \quad (8)$$

is made where r is the distance behind the leading edge the results obtained will show the angular scattering in terms of the angle of incidence θ .

Each of the 31 records were converted in this way and the mean of all the records is shown in figure 2, together with the straight line corresponding to $\exp(-10.2\theta)$. The agreement is so close that we shall assume that between angles of incidence of at least 4° and 13° the law of scattering of the lunar surface is given by

$$f(\theta) = \exp(-10.2\theta) \quad (9)$$

where θ is in radian measure. For angles of incidence less than 3° , an attempt was made to correct for finite width of the range gate, but owing to the very slow period fading of the front edge of the echo and to the inaccuracies involved in the corrections no great reliance could be placed on this part of the curve. However it appeared that the scattering law for values of θ near to zero might fall slightly below the exponential law.

4.1. Comparison of Results with Short Pulse Observations at the Wavelength of 1.5 Metres

Most of the radar measurements at longer wavelengths have been made with c.w. or very long pulses, apart from those by Trexler (1958) at the wavelength of 1.5 metres. These results for a pulse length of $12 \mu\text{sec}$ are given in terms of percentage of the total energy received as a function of time. To compare the scattering law at the two

wavelengths, the 10 cm results were integrated assuming the scattering law $\exp(-10 \cdot 2\theta)$. The amount of energy returned after time t is then given by

$$P(t) = 2\pi a r_p \int_0^\theta \exp(-10 \cdot 2\theta) d\theta \quad (10)$$

where r_p is the pulse length as defined previously, a is the lunar radius, and

$$\cos \theta = 1 - \frac{ct}{a}$$

$P(t)$ is plotted in figure 3 together with the values derived by Trexler, in terms of range in kilometres after the leading edge. The agreement is not exact, probably due to errors in reducing the values by Trexler, but up to angles of incidence of 14° is sufficient to suggest that the scattering law for small angles of incidence is sensibly independent of wavelength over the range 10 cm to 1.5 metres.

4.2. Comparison with Measurements at 400 Mc/s

More recent measurements by Pettengill (1960 and private communication) at the wavelength of 75 cm and a pulse length of 70 μ sec have shown directly that the scattering from the lunar surface follows an exponential law at the small angles of incidence, but over a range of θ from 7° to approximately 50° may be represented by

$$\sigma_0 \exp(-10 \cdot 5 \sin \theta) + \sigma_D \cos^{3/2} \theta \quad \text{where} \quad \sigma_D = \sigma_0/160; \quad (11)$$

it has been suggested that the term involving σ_D may represent a diffuse scattering component. To determine if the σ_D component is also independent of frequency, the sensitivity of the 10 cm equipment was further improved by increasing the duration of the range gate to 100 μ sec (15 km), by other improvements in the sensitivity of the receiver, and by increasing the range of the automatic sweep of the range gate. It was fully possible to obtain 13 runs during 21st and 22nd December 1960, but the results are shown in figure 4 for values of θ up to 30° together with the empirical law determined by Pettengill. Again the agreement is remarkably good, and though the 10 cm results have not been obtained at all angles of libration, they are sufficient to suggest that any diffuse component of scattering is also independent of wavelength for angles of incidence up to about 30° .

No attempt will be made here to explain why the suggested diffuse component is proportional to $\cos^{3/2} \theta$. This will be discussed in a later paper where it is shown that the theoretical law with the addition of a diffuse scattering term, proportional to $\cos \theta$ can lead to the empirical law of equation (11).

4.3 Comparison of Lunar Scattering with Scattering from Rough Surfaces

A direct comparison can be made between the scattering law as derived from the present experiments with that obtained from various types of surface on the earth. From optical observations the lunar surface appears to have a nearly uniform reflectivity over its surface and measurements on the thermal radiation at radio wavelengths greater than 3 cm show that the surface must have a highly absorbing layer. Hence it is also reasonable to assume that the reflectivity over the surface is constant though small at particular radio wavelength. The closest comparison with terrestrial surfaces from the point of view of angular scattering properties would then be either with desert dunes or with the sea, and for the present purpose a comparison will be made with scattering from the sea.

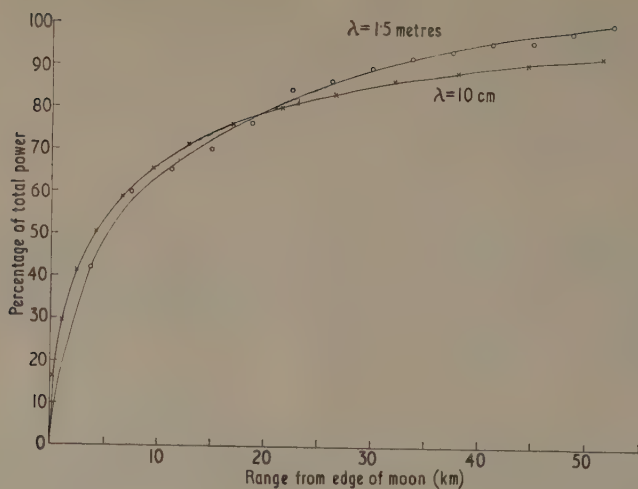


Figure 3. Comparison of results obtained at the wavelength of 10 cm with those by Trexler at the wavelength of 1.5 metres. $\lambda = 10$ cm, pulse length 5 μ sec; $\lambda = 1.5$ m, pulse length 12 μ sec.

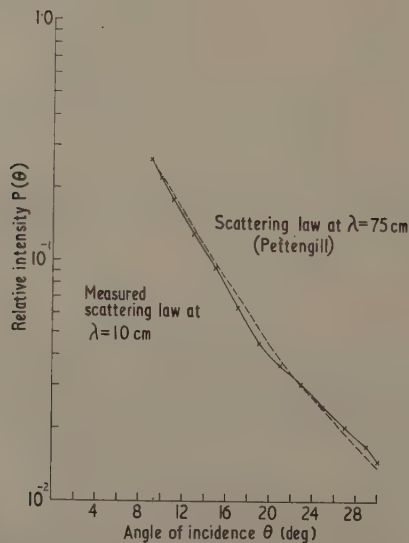


Figure 4. Comparison of angular scattering law at the wavelength of 10 cm with that obtained by Pettengill at the wavelength of 75 cm.

The earliest measurements on sea returns obtained at a wavelength of 3.2 cm have been collected by Goldstein (1951). They show an angular scattering law which varies with the state of the sea, but in general the intensity decreases rapidly at angles away from normal incidence, such that at an angle of 20° the effective scattering area has fallen by a factor of 10–20 dB from the value at normal incidence. The largest decrease corresponds to the case of a 'slight' sea, but even under these conditions the amplitude of waves and ripples is expected to be much greater than the wavelength. The corresponding decrease in scattering area of the moon at an angle of incidence of 20° is about 5 dB. Measurements of the effective scattering area for the average sea at shorter wavelengths have also been made by Grant and Yaplee (1957). They show that over the wavelength range from 8.6 mm to 3.2 cm the scattering law remains sensibly the same and is of a similar form to that obtained for the moon, including the flattening of the curve at comparatively large angles of incidence. Hence the results are in agreement with scattering from a lunar surface which is rough in the same way as the surface of the sea is rough, implying random variation of the surface with amplitude greater than the radar wavelength.

4.4. *Bistatic Radar Measurements on the Moon*

Further indications of a random lunar surface which contributes many reflecting points was obtained in a joint experiment with the University of Texas (Straiton and Tolbert: Hughes 1960). The signals transmitted from Malvern, England, were received at Austin, Texas, after reflection from the moon and at an angle of about 90° to the incident direction, corresponding to the angle subtended at the moon by the Malvern–Austin base-line. In this case the mean level of the signals showed a gradual increase over a distance of about 7 km, in comparison with the initial sharp rise observed at Malvern. This is as would be expected on the rough scattering theory since from considering the geometry of scattering with the short pulse lengths the echo amplitude is proportional to the area of the moon seen to be illuminated from Texas and this increases more gradually. In fact the increase is expected to take place over a distance of about 9 km but the initial rise would be lost in the noise level.

To summarize it is suggested that over representative annular areas of 8000 km², corresponding to the area of the lunar surface from which signals are received at a pulse length of 5 μ sec, the moon would appear to consist of a large number of random scatterers, as for an undulating random surface, and this will be assumed in future discussions. Further evidence that this is consistent will be shown from the theoretical treatment of scattering from rough surfaces in a later paper.

§ 5. VARIATION OF SCATTERING CROSS SECTION WITH WAVELENGTH

To compare the echoing area of the moon at different wavelengths and different pulse lengths the angular scattering law of the surface has to be taken into account. If short pulse lengths are used, then the effective echoing area of the moon is given by

$$2\pi ar_p[\sigma_0 \exp(-10\theta) + \sigma_D \cos^3/2\theta]$$

where $r_p = \frac{1}{2}t_p c$ is half the length in space of the transmitter pulse, a is the lunar radius, σ_0 and σ_D represent the scattering cross section per unit area of the moon for two empirical scattering components and θ is the angle of incidence of the pulse

at the lunar surface. If the moon is illuminated with c.w. then the total echoing area will be given by

$$\begin{aligned}\sigma_T &= 2\pi a^2 \int_0^{\pi/2} [\sigma_0 \sin \theta \exp(-10\theta) + \sigma_D \sin \theta \cos^{3/2} \theta] d\theta \\ &= \pi a^2 [2 \times 10^{-2} \sigma_0 + 8 \times 10^{-1} \sigma_D] \\ &= 2.5 \times 10^{-2} \pi a^2 \sigma_0\end{aligned}\quad (12)$$

where it is assumed that $\sigma_D = \sigma_0/160$. Taking the value $\sigma_0 = 0.85$ for the wavelength of 10 cm which has been corrected from the one previously obtained (Hughes 1960) this yields a figure of

$$\sigma_T = 2.1 \times 10^{-2} \pi a^2. \quad (13)$$

A comparison of the results at different wavelengths, for $\sigma_T/\pi a^2$ and σ_0 is given in the table.

Wavelength (metres)	Pulse length	Reference	$\sigma_T/\pi a^2$	σ_0
0.1	5 μ sec		2.1×10^{-2}	8.5×10^{-1}
0.62	c.w.	(Bleviss & Chapman 1960)	5.0×10^{-2}	2.0
0.7	c.w.	(Fricker <i>et al.</i> 1960)	7.0×10^{-2}	2.8
0.75	70 μ sec	(Pettengill, private communication)	7.0×10^{-2}	2.8
1.0	c.w.	(Trexler 1958)	7.0×10^{-2}	2.8
1.5	c.w.	(Trexler 1958)	8.0×10^{-2}	3.2
2.5	30 msec (c.w.)	(Evans 1957)	1.8×10^{-1}	4.5

Most of the measurements give a value for the integrated scattering cross section for the moon which lie in the region $5-10 \times 10^{-2}$ with the exception of the results obtained at the wavelength of 10 cm. However, since these latter measurements are derived by extrapolating the results obtained for small angles of incidence, and only a small amount of scattering at the large angles could make an appreciable contribution, they may in fact be an underestimate. It may be concluded that though the total scattering cross section may vary slightly with wavelength, the amount of variation is probably small, especially so when it is considered that the accuracy of the readings is probably only $\pm 50\%$.

§ 6. CONCLUSIONS

The main object of this paper has been to describe in more detail the measurements that have been made on radar echoes from the moon at the wavelength of 10 cm. The results show that the scattering law of the lunar surface at least for angles of incidence from about 3 to 13° is sensibly independent of wavelength over the range 10 cm to 1.5 metres, and there is evidence that for angles up to 30° the scattering law at the two wavelengths is sensibly the same. The empirical law would appear to be exponential with argument proportional to θ (or $\sin \theta$) with the addition of a small component proportional to $\cos^{3/2} \theta$ as determined originally by Pettengill. It is not suggested that any physical interpretation may necessarily be applied to these two components, and a theoretical treatment is left to a further paper.

The highly directional form of the scattering law led Senior and Siegel to the conclusion that there must be about 20 or 30 smooth regions on the moon and the term quasi-smooth has been used to describe the surface. However, various factors have been shown to indicate that the results are compatible with scattering from a rough surface, by which is meant one which has deviations large in comparison with the wavelength, and in fact a similarity exists between the scattering law for the lunar surface and the surface of the sea.

An important difference between the quasi-smooth and rough theories arises when an attempt is made to derive the reflectivity of the surface. The quasi-smooth theory predicts that the reflectivity may be obtained by measuring the amplitude of the signal received from the front edge of the moon since this is reflected from a smooth spherical region which is greater than the first Fresnel zone and of radius approximately equal to the lunar radius; on the other hand, as will be seen in a future paper, the rough-surface theory predicts that the reflectivity may only be obtained by integrating the radiation scattered from the whole of the lunar surface. The value of the reflectivity determined from the two theories may differ by as much as 100 times.

ACKNOWLEDGMENTS

The experimental work was carried out at the Ministry of Aviation, Royal Radar Establishment, Malvern, and acknowledgment is made to colleagues who assisted in the construction and operation of the equipment.

REFERENCES

- LEWIS, B. C., and CHAPMAN, J. H., 1960, *J. Res. Nat. Bur. Stand.*, **64D**, 331.
 BROWN, I. C., EVANS, J. V., HARGREAVES, J. K., and MURRAY, W. A. S., 1956, *Proc. Phys. Soc. B*, **69**, 901.
 EVANS, J. V., 1957, *Proc. Phys. Soc. B*, **70**, 1105.
 PICKER, S. J., INGALLS, R. P., MASON, W. C., STONE, M. L., and SWIFT, D. W., 1960, *J. Res. Nat. Bur. Stand.*, **64D**, 455.
 GOLDSTEIN, H., 1951, *M.I.T. Radiation Lab. Series 13* (New York: McGraw Hill), p. 481.
 BRANT, C. R., and YAPLEE, B. S., 1957, *Proc. Inst. Radio Engrs, N.Y.*, **45**, 976.
 REY, J. S., and HUGHES, V. A., 1959, *I.A.U.-U.R.S.I. Paris Symposium on Radio Astronomy* (Stanford: University Press).
 HUGHES, V. A., 1960, *Nature, Lond.*, **186**, 873.
 PERR, F. J., SHAIN, C. A., and HIGGINS, C. S., 1949, *Nature, Lond.*, **163**, 310.
 ADABRAND, R. L., DYCE, R. B., FREDRIKSEN, A., PRESNELL, R. I., and SCHLOBOHM, J. C., 1960, *Proc. Inst. Radio Engrs, N.Y.*, **48**, 932.
 MURRAY, W. A. S., and HARGREAVES, J. K., 1954, *Nature, Lond.*, **173**, 944.
 PITENGLILL, G. H., 1960, *Proc. Inst. Radio Engrs, N.Y.*, **48**, 933.
 SENIOR, T. B. A., and SIEGEL, K. M., 1960, *J. Res. Nat. Bur. Stand.*, **64D**, 217.
 RAITON, A. W., and TOLBERT, C. W.: HUGHES, V. A., 1960, *Amer. Inst. Elect. Engrs Trans.*, Part 1, **79**, 436.
 EXLER, J. H., 1958, *Proc. Inst. Radio Engrs, N.Y.*, **46**, 286.
 YAPLEE, B. S., BRUTON, R. H., CRAIG, K. J., and ROMAN, N. G., 1958, *Proc. Inst. Radio Engrs, N.Y.*, **46**, 293.

Synthesis of Interference Filters

By J. S. SEELEY

Queen Mary College, University of London

MS. received 29th May 1961

Abstract. A method of synthesizing electrical circuit filters to transmit prescribed functions of frequency in a specified pass-band is applied to dielectric interference filters containing up to four half-wave layers. The method relies on an approximation that the half-wave layers are the only parts of the filter which are sensitive to frequency. The reflecting quarter-wave multilayers are described by a single parameter whose values are deduced in the synthesis. The transmission functions are either maximally flat in the pass-band or contain equal ripples. The rate of transition from the pass-band to the stop-band is increased rapidly by increasing the number of half-wave layers.

The synthesis is applied to filters specified to transmit an 8% bandwidth within which the transmissivity is not less than 0.91. The exact transmission characteristics of these examples show excellent agreement in the pass-band with the simple functions.

The method can be applied to the design of filters of moderate bandwidth for any spectral region.

§ 1. INTRODUCTION

ELECTRICAL FILTER networks of lumped inductive and capacitive elements may be synthesized by the classic method of Darlington (1939) to pass a band of frequency following a simple type of transmission function. The method is based on the synthesis of an equivalent low-pass filter consisting of a 'ladder' arrangement of unequal elements. The elements of the band-pass filter are readily deduced from those of the low-pass prototype with a suitable transformation of the frequency variable in the transmission function.

Structures having similar general properties to the ladder networks can be built in distributed circuits by loading an appropriate waveguide with suitably spaced reactive obstacles. The application of the synthesis for band-pass filters to distributed circuits is hindered by the dependence on frequency of the transmission properties of the circuits themselves and by the magnitude and the dependence on frequency of the reflections from the obstacles. Various methods for the approximate synthesis of waveguide filters with a high degree of isolation between the pass-band and stop-band have been described. Their accuracy deteriorates for filters of bandwidth greater than 10%, as discussed by Cohn (1957), Seidel (1957) and Levy (1957) amongst others. The lengths of waveguide which separate the reflecting obstacles are designed to have an effective phase shift of π at the mid-band frequency. These are the principal elements sensitive to frequency and, together with the obstacles, form a cascade of half-wavelength resonant cavities. A Q -factor is associated with each cavity and can be related to the reflectivities of the obstacles. (This expresses the ratio of the resonant frequency to the frequency interval for which more than half the incident power is transmitted, i.e. half-width.) The Q -factors for the cavities are deduced from the lumped elements of a low-pass prototype synthesized by the Darlington method to a simple transmission

unction. The synthesis only predicts behaviour in the fundamental pass-band of the filter and requires that all the cavities should be resonant at the central frequency.

The dielectric multilayer type of interference filter (Polster 1952) is based on the Fabry-Pérot etalon which behaves in a similar manner to the waveguide resonant cavity when the variation of the wave impedance with frequency is considered. It is of interest to apply the Darlington method of synthesis to structures consisting of a cascade of Fabry-Pérot resonant cavities based on dielectric multilayers. In addition to providing a method of designing an interference filter to transmit a prescribed function over a moderate bandwidth the synthesis will indicate how the multilayers which are already used in various spectral regions can be deployed to the best advantage in band-pass filters.

§ 2. THEORY OF THE SYNTHESIS

2.1. External Description of Multi-cavity Filters

The filters are symmetrical arrangements of dielectric multilayers containing more than one half-wave layer (Smith 1958, Turner 1952) as represented in figure 1. We will consider the transmission of a plane wave through this arrangement for normal incidence. All absorption and dispersion in refractive index of the dielectric materials forming the layers will be neglected. The wave impedances of the layers will be normalized with respect to that of the external medium. If this is air the impedances for normal incidence are therefore simply the reciprocals of the refractive indices of the layers.

The amplitudes of the electric and magnetic vectors in the waves crossing the interfaces AA and BB can be written, following for example, Born and Wolf (1959), Heavens (1960) and Weinstein (1954)

$$\begin{bmatrix} \mathbf{E}_{AA} \\ \mathbf{H}_{AA} \end{bmatrix} = [M] \begin{bmatrix} \mathbf{E}_{BB} \\ \mathbf{H}_{BB} \end{bmatrix} = \begin{bmatrix} m_{11} & m_{12} \\ m_{21} & m_{22} \end{bmatrix} \begin{bmatrix} \mathbf{E}_{BB} \\ \mathbf{H}_{BB} \end{bmatrix} \quad (1)$$

where the matrix $[M]$ is the transfer matrix of the structure between AA and BB. The boundary conditions are

$$\begin{aligned} \text{at BB} \quad & \begin{cases} \mathbf{E}_{BB} = \mathbf{E}_e \\ \mathbf{H}_{BB} = \mathbf{E}_e/Z_0 \end{cases} \\ \text{at AA} \quad & \begin{cases} \mathbf{E}_{AA} = \mathbf{E}_i + \mathbf{E}_r = \left(m_{11} + \frac{m_{12}}{Z_0} \right) \mathbf{E}_e \\ \mathbf{H}_{AA} = (\mathbf{E}_i - \mathbf{E}_r)/Z_0 = \left(m_{21} + \frac{m_{22}}{Z_0} \right) \mathbf{E}_e. \end{cases} \end{aligned}$$

The amplitude reflection coefficient at AA when the wave impedance Z_0 is put equal to unity is

$$\frac{\mathbf{E}_r}{\mathbf{E}_i} = \frac{m_{11} + m_{12} - m_{21} - m_{22}}{m_{11} + m_{12} + m_{21} + m_{22}}. \quad (2)$$

The amplitude transmission coefficient at BB is

$$\frac{\mathbf{E}_e}{\mathbf{E}_i} = \frac{2}{m_{11} + m_{12} + m_{21} + m_{22}}. \quad (3)$$

The matrix $[M]$ is the ordered product of the matrices of the individual layers and completely represents the structure. The elements in the matrix of a symmetrical

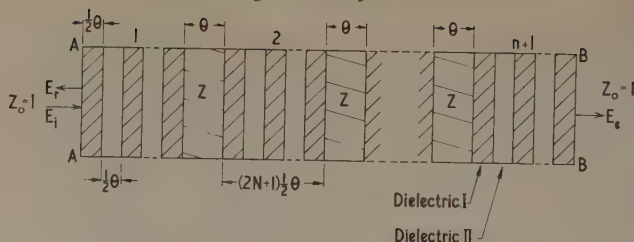


Figure 1. Arrangement of dielectric layers in a generalized filter. There are n half-wave layers of wave impedance $Z/Z_0 = z$. $\theta = \pi\omega/\omega_0$ where ω_0 is the central frequency of the pass-band of the filter. The multilayer systems numbered (1) and $(n+1)$, (2) and (n) etc. are identical. They consist of alternate quarter-wave layers of two dielectric materials. There are $N+1$ layers of the dielectric with the higher refractive index.

structure are related by $m_{11}m_{22} - m_{12}m_{21} = 1$ and $m_{11} = m_{22}$. The transfer matrix of a single layer is

$$\begin{bmatrix} \cos \phi & jz \sin \phi \\ \frac{j \sin \phi}{z} & \cos \phi \end{bmatrix}$$

when there is no absorption, ϕ being the optical thickness and z the normalized wave impedance. z is wholly real for dielectrics without absorption so that $m_{12} = jM_{12}$, $m_{21} = jM_{21}$, m_{11} , M_{12} and M_{21} all being real numbers.

The reflection and transmission coefficients of (2) and (3) can now be expressed more simply in this particular case by

$$\frac{E_r}{E_i} = \frac{j(M_{12} - M_{21})}{2m_{11} + j(M_{12} + M_{21})} \quad \text{and} \quad \frac{E_e}{E_i} = \frac{2}{2m_{11} + j(M_{12} + M_{21})} \quad (4)$$

so that the reflectivity and transmissivity are therefore

$$R = \left| \frac{E_r}{E_i} \right|^2 = \frac{(M_{12} - M_{21})^2}{4m_{11}^2 + (M_{12} + M_{21})^2} = \frac{(M_{12} - M_{21})^2}{4 + (M_{12} - M_{21})^2} \quad (5)$$

$$T = \left| \frac{E_e}{E_i} \right|^2 = \frac{4}{4m_{11}^2 + (M_{12} + M_{21})^2} = \frac{1}{1 + \frac{1}{4}(M_{12} - M_{21})^2} \quad (6)$$

Either (5) or (6) is sufficient to represent the behaviour of the filter because $R + T = 1$ for no absorption. Equation (6) is more convenient to use than equation (5) and the expression for the reciprocal of the transmissivity, $1 + \frac{1}{4}(M_{12} - M_{21})^2$, is widely used in the synthesis of electrical circuit filters free from energy loss. We will use it to predict the behaviour of the arrangement of multilayer resonant cavities shown in figure 1.

2.2. The Transfer Matrix of the Filter

2.2.1. The reflecting multilayers.

The transfer matrix of reflecting multilayers consisting of two dielectric materials I and II is

$$[M'] = \begin{bmatrix} \cos \frac{1}{2}\theta & jz_I \sin \frac{1}{2}\theta \\ \frac{j \sin \frac{1}{2}\theta}{z_I} & \cos \frac{1}{2}\theta \end{bmatrix} \begin{bmatrix} \cos \frac{1}{2}\theta & jz_{II} \sin \frac{1}{2}\theta \\ \frac{j \sin \frac{1}{2}\theta}{z_{II}} & \cos \frac{1}{2}\theta \end{bmatrix} \begin{bmatrix} \cos \frac{1}{2}\theta & jz_I \sin \frac{1}{2}\theta \\ \frac{j \sin \frac{1}{2}\theta}{z_I} & \cos \frac{1}{2}\theta \end{bmatrix} \quad (7)$$

where θ is the optical thickness of the half-wave layers. When the angular frequency ω is equal to the central frequency ω_0 the product $[M']$ reduces to

$$[M'] = \begin{bmatrix} 0 & jz_I \left(\frac{-z_{II}}{z_I} \right)^N \\ \left(\frac{j}{z_I} \right) \left(\frac{-z_{II}}{z_I} \right)^N & 0 \end{bmatrix}. \quad (8)$$

It is convenient to put
$$\frac{1}{z_I} \left(\frac{-z_{II}}{z_I} \right)^N = r. \quad (9)$$

The matrix product of the structure shown in figure 1 must be simplified before equation (6) can be used for synthesis to a prototype transmission function. As a first step we can represent the reflecting multilayers by the matrix of equation (8)

$$\begin{bmatrix} 0 & j/r \\ jr & 0 \end{bmatrix}$$

at all frequencies within the fundamental pass-band of the filter. This approximation ignores two properties of the multilayer. The most important is that the optical thickness is subject to a frequency-dependent phase shift from the central value $(2N+1)\frac{1}{2}\pi$; the other is that the effective transformation ratio only reaches the value r when the phase shift is $(2N+1)\frac{1}{2}\pi$. A multilayer is more accurately represented by (8) for a band of frequencies centred on an angular frequency ω_0 by increasing r . An important consequence of the simplification of (8) is that the optical thicknesses of the half-wave layers become the only elements of the filter which are sensitive to frequency.

2.2.2. The multilayer resonant cavities.

The transfer matrix of a half-wave layer bounded by multilayers represented by the approximate matrix of (8) is

$$[M''] = \begin{bmatrix} 0 & j/r \\ jr & 0 \end{bmatrix} \begin{bmatrix} \cos \theta & jz \sin \theta \\ \frac{j \sin \theta}{z} & \cos \theta \end{bmatrix} \begin{bmatrix} 0 & j/r \\ jr & 0 \end{bmatrix}. \quad (10)$$

The matrix of the half-wave layers must be simplified before the product representing a sequence of resonant cavities can lead to equations in the parameter r which are capable of simple solution. By restricting the fundamental pass-band to about $0.1\omega_0$ we can put $\cos \theta \simeq -1$ in (10) (in fact $\cos \theta$ will vary as about $(1 - \omega/\omega_0)^2 \pi^2/2 - 1$ near ω_0 , $\cos \frac{1}{2}\theta$ in (7) will vary as about $(1 - \omega/\omega_0)\pi/2$). It is also necessary to put $\sin \theta \simeq 0$ in the 21 term in (10) which only increases the half-width of the Fabry-Pérot resonant cavity represented by (10) by a factor of about $r^2/(r^4 - 1)^{1/2}$, involving an error of less than 1% provided that r is greater than 2.5.

The matrix product which we therefore propose for an approximate band-pass synthesis is

$$[M] = \begin{bmatrix} m_{11} & jM_{12} \\ jM_{21} & m_{11} \end{bmatrix} \simeq \begin{bmatrix} 0 & j/r_1 \\ jr_1 & 0 \end{bmatrix} \begin{bmatrix} -1 & jz \sin \theta \\ 0 & -1 \end{bmatrix} \\ \times \begin{bmatrix} 0 & j/r_2 \\ jr_2 & 0 \end{bmatrix} \dots \begin{bmatrix} -1 & jz \sin \theta \\ 0 & -1 \end{bmatrix} \begin{bmatrix} 0 & j/r_{n+1} \\ jr_{n+1} & 0 \end{bmatrix} \quad (11)$$

n is the number of cavities in the filter, $r_{n+1} = r_1$, $r_n = r_2$, etc.

2.3. The Prototype Transmission Functions

Equal ripple (Tchebyshev) and maximally flat (Butterworth) functions are used extensively as transmission functions in the synthesis of electrical filters. The transmission function written in terms of these functions is

$$T = \frac{1}{1 + [f_n(\bar{\omega})]^2} \quad (12)$$

where $\bar{\omega}$ is a transformed frequency variable.

The equal ripple function is

$$f_n(\bar{\omega}) = hT_n(\bar{\omega}) \quad (13)$$

where

$$T_n(\bar{\omega}) = \begin{cases} \cos(n \cos^{-1} \bar{\omega}) & \text{for } |\bar{\omega}| \leq 1 \\ \cosh(n \cosh^{-1} \bar{\omega}) & \text{for } |\bar{\omega}| \geq 1. \end{cases}$$

The Tchebyshev functions $T_n(\bar{\omega})$ are more conveniently expressed as polynomials which are valid for all values of $\bar{\omega}$, as follows

$$\left. \begin{aligned} T_n(\bar{\omega}) &= 1 & \text{for } n &= 0 \\ &= \bar{\omega} & n &= 1 \\ &= 2\bar{\omega}^2 - 1 & n &= 2 \\ &= 4\bar{\omega}^3 - 3\bar{\omega} & n &= 3 \\ &= 8\bar{\omega}^4 - 8\bar{\omega}^2 + 1 & n &= 4 \end{aligned} \right\} \begin{aligned} &T_n(\bar{\omega}) \text{ tends to } 2^{n-1}\bar{\omega}^n \text{ for} \\ &\text{large values of } \bar{\omega}. \end{aligned}$$

The maximally flat function is

$$f_n(\bar{\omega}) = (\bar{\omega}')^n. \quad (14)$$

The two functions are compared in figure 2 which shows $1/T$ plotted against $\bar{\omega}$ for $n = 2, 3$ and 4. The parameter h^2 , which is the amplitude of the ripple, has been set equal to unity for the comparison making $\bar{\omega}'$ equal to $\bar{\omega}$. It should be noted that transmission of the equal ripple type is specified over the bandwidth for which T is not less

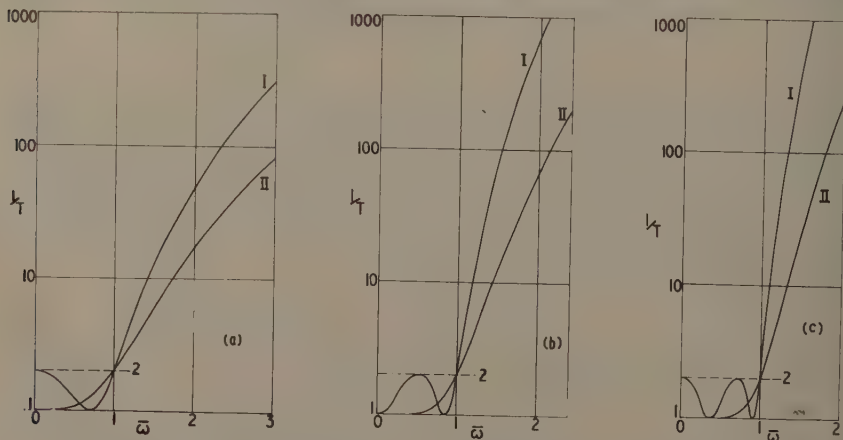


Figure 2. The prototype functions $1/T = 1 + [f_n(\bar{\omega})]^2$, shown for $h^2 = 1$; (a) for $n = 2$, (b) for $n = 3$, (c) for $n = 4$. I, the equal ripple function of equation (13). II, the maximally flat function of equation (14).

than $1/(1+h^2)$, $\bar{\omega}$ having the values of ± 1 at the band edges. The bandwidth of the maximally flat function is specified in the same way but the value of $\bar{\omega}'$ at the band edges depends on the chosen value of h^2 .

The requirements of any particular filter will determine which of the prototype functions is most suitable. If the transmissivity can have a value as low as $1/(1+h^2)$ at any frequency within the pass-band then the equal ripple function should be used since it has a more rapid transition from the pass-band than the maximally flat function. For large values of $\bar{\omega}$, $(T_n(\bar{\omega}))$ is increasing more rapidly than $\bar{\omega}^n$ by a factor of 2^{n-1} . In contrast the maximally flat function always shows complete transmission when $\bar{\omega}' = 0$ and T is nearly equal to unity for a large central part of the pass-band. The number of cavities which are necessary will be determined by the rate at which the transmissivity is required to fall with frequency outside the pass-band.

2.4. Synthesis to the Prototype Functions

The simplified product of (11) has been evaluated for filters consisting of two, three and four cavities; the terms in the matrix $[M]$ being summarized in table 1. Synthesis to the prototype functions requires that

$$\frac{1}{T} - 1 = \frac{1}{4}(M_{12} - M_{21})^2 = [f_n(\bar{\omega})]^2. \quad (15)$$

$(M_{12} - M_{21})$ is a polynomial function containing the terms $\sin^n \theta$, $\sin^{n-2} \theta$, etc. with coefficients in the values of r . Since we have restricted (11) to filters of moderate bandwidth

$$\sin \theta = \sin \frac{\pi(\omega_0 - \omega)}{\omega_0} \simeq \frac{\pi(\omega_0 - \omega)}{\omega_0}. \quad (16)$$

The frequency variable in the equal ripple function $\bar{\omega}$ must equal ∓ 1 when $\omega = \omega_1$ or $2\omega_0 - \omega_1$ where ω_1 defines the edge of the pass-band so that $\bar{\omega}$ can be defined in terms of ω as

$$\bar{\omega} = \frac{\omega - \omega_0}{\omega_0 - \omega_1}. \quad (17)$$

The maximally flat function $(\bar{\omega}')^{2n}$ must have the value h^2 if T is specified to be $1/(1+h^2)$ when $\omega = \omega_1$ or $2\omega_0 - \omega_1$ so that since $\bar{\omega}$, as defined in (17), is equal to ∓ 1 at these frequencies

$$\bar{\omega}' = h^{1/n} \bar{\omega} = h^{1/n} \frac{\omega - \omega_0}{\omega_0 - \omega_1}. \quad (18)$$

$\sin \theta$ can be related to the variables $\bar{\omega}$ and $\bar{\omega}'$

$$\sin \theta \simeq \frac{\pi(\omega_0 - \omega)}{\omega_0} = t \bar{\omega} \text{ or } t' \bar{\omega}' \quad (19)$$

where the scale factors t and t' are given by

$$t = \frac{-\pi(\omega_0 - \omega_1)}{\omega_0} \text{ for the equal ripple function,}$$

$$t' = \frac{-\pi(\omega_0 - \omega_1)}{h^{1/n} \omega_0} \text{ for the maximally flat function.}$$

Table 1
Elements in Simplified Matrix $[M]$ from Product of Equation (11)

Number of cavities	$m_{11} = m_{22}$	M_{12}	M_{21}	$(M_{12} - M_{21})$
2	$r_2 z \sin \theta$	$-\frac{r_2}{r_1^2}$	$r_1^2 r_2 z^2 \sin^2 \theta - \frac{r_1^2}{r_2}$	$\frac{r_1^2}{r_2} - \frac{r_2}{r_1^2} - r_1^2 r_2 z^2 \sin^2 \theta$
3	$1 - r_2^2 z^2 \sin^2 \theta$	$\frac{r_2^2}{r_1^2} z \sin \theta$	$2 r_1^2 z \sin \theta - r_1^2 r_2^2 z^3 \sin^3 \theta$	$\left(\frac{r_2^2}{r_1^2} - 2 r_1^2 \right) z \sin \theta + r_1^2 r_2^2 z^3 \sin^3 \theta$
4	$-\frac{r_2^2}{r_3} z \sin \theta$ $+ r_2^2 r_3 z^3 \sin^3 \theta$ $- r_3 z \sin \theta$	$\frac{r_2^2}{r_1^2 r_3} - \frac{r_2^2 r_3}{r_1^2} z^2 \sin^3 \theta$	$-\frac{r_1^2 r_2^2}{r_3} z^2 \sin^2 \theta$ $+ r_3 \left(r_1^2 z^2 \sin^2 \theta - \frac{r_1^2}{r_2} \right)^2$	$\frac{r_2^2}{r_1^2 r_3} - \frac{r_3 r_1^2}{r_2^2}$ $+ z^2 \sin^2 \theta \left(2 r_1^2 r_3 + \frac{r_1^2 r_2^2}{r_3} - \frac{r_2^2 r_3}{r_1^2} \right)$ $- r_3 r_1^2 r_2^2 z^4 \sin^4 \theta$

Table 2

Simultaneous Equations and Solutions for Parameter r

Number of cavities	Maximally flat	Equal ripple
2	$\pm \left(\frac{r_1^2}{r_2} - \frac{r_2}{r_1^2} \right) = 0$ $\pm \frac{2}{s^2(t')^2} = \pm \frac{\sqrt{2}}{st'}$ $r_1 = \pm \sqrt{r_2}; r_2 = \pm \frac{\sqrt{2}}{st'}$	$\pm \left(\frac{r_1^2}{r_2} - \frac{r_2}{r_1^2} \right) = -2h$ $r_1 = \pm \left(\frac{-2h^2}{st} \right)^{1/2} [h + \sqrt{(1+h^2)}]^{1/4}$ $\pm \frac{4h}{s^2 t^2} = \pm \frac{2\sqrt{h}}{st[h + \sqrt{(1+h^2)}]^{1/2}}$ $r_2 = \pm \frac{2\sqrt{h}}{st[h + \sqrt{(1+h^2)}]^{1/2}}$
3	$\pm \left(\frac{r_2^2}{r_1^2} - 2r_1^2 \right) = 0$ $\pm \frac{2}{s^2(t')^3} = \pm \frac{\sqrt{2}}{st'}$ $r_1 = \pm \left(\frac{r_2}{\sqrt{2}} \right)^{1/2}; r_2 = \pm \frac{\sqrt{2}}{st'}$	$\pm \left(\frac{r_2^2}{r_1^2} - 2r_1^2 \right) = -\frac{6h}{st}$ $r_1 = \pm \left(\frac{-2}{st} \right)^{1/2} \left(\frac{h^{1/3}}{[\sqrt{(1+h^2)} + 1]^{1/3} - [\sqrt{(1+h^2)} - 1]^{1/3}} \right)^{1/2}$ $\pm \frac{8h}{s^3 t^3} = \pm \frac{2\sqrt{h}}{st} \left(\frac{h^{1/3}}{[\sqrt{(1+h^2)} + 1]^{1/3} - [\sqrt{(1+h^2)} - 1]^{1/3}} \right)^{1/2}$ $r_2 = \pm \frac{2\sqrt{h}}{st} \left(\frac{h^{1/3}}{[\sqrt{(1+h^2)} + 1]^{1/3} - [\sqrt{(1+h^2)} - 1]^{1/3}} \right)^{1/2}$
4	$\pm \left(\frac{r_2^2}{r_1^2} - \frac{r_3^2 r_1^2}{r_2^2} \right) = 0$ $\pm \frac{(2 - \sqrt{2})^{1/4}}{\sqrt{(-st')}} = \pm \frac{2^{1/4}}{st'}$ $r_1 = \pm \frac{(2 - \sqrt{2})^{1/4}}{\sqrt{(-st')}} = \pm \frac{2^{1/4}}{st'}$ $\pm \left(2r_1^2 r_3 + \frac{r_1^2 r_2^2}{r_3} - \frac{r_2^2}{r_1^2} \right) = 0$ $r_2 = \pm \frac{2^{1/4}}{st'}$ $\pm \frac{2}{s^4(t')^4} = \pm \frac{\left(\frac{r_2}{r_1} \right)^2}{s^4 t^4}$ $r_3 = \pm \left(\frac{r_2}{r_1} \right)^2$	$\pm \left(\frac{r_2^2}{r_1^2} - \frac{r_3^2 r_1^2}{r_2^2} \right) = 2h$ $r_1 = \pm \left(\frac{-2h}{ktz} \right)^{1/2}$ $\times \left\{ [2 - (1/k)] + [(1/k) - 2]^2 + (k/h)^2 \right\}^{1/4}$ $\pm \left(2r_1^2 r_3 + \frac{r_1^2 r_2^2}{r_3} - \frac{r_2^2}{r_1^2} \right) = -\frac{16h}{s^2 t^2}$ $r_2 = \pm \frac{2\sqrt{k}}{st}$ $\pm \frac{16h}{s^4 t^4} = \pm \frac{16h}{s^4 t^4}$ $r_3 = \pm \frac{16h}{s^4 t^4}$

where $k = (h[\sqrt{(1+h^2)} - h]^{1/2})$

The polynomial functions in $M_{12}-M_{21}$ can now be written in terms of $t(\bar{\omega})$ or $t'(\bar{\omega}')$ by substituting for $\sin \theta$.

Synthesis to the equal ripple function is completed by equating the coefficients of $\sin^n \theta$ etc. with those of $(\bar{\omega}/t)^n$ etc. in the polynomial expansion for $hT_n(\bar{\omega}/t)$ given in (13). Synthesis to the maximally flat function requires that the polynomial function of $\sin \theta$ must equal $(\bar{\omega}')^n$ for all values of $\bar{\omega}'$. The coefficient of $\sin^n \theta$ in $M_{12}-M_{21}$ can therefore be put equal to $1/(t')^n$ and the coefficients of all lower powers of $\sin \theta$ put equal to zero.

The values of the parameter r in the synthesized filter are given in terms of h and t or t' by simultaneous equations obtained from equating the coefficients in (15). The equations and the unique real solutions for r are indicated in table 2 for $n = 2, 3$ and 4. The solutions are no longer simple when n is greater than 4 because the simultaneous equations contain mixed polynomials in r_1, r_2 and r_3 . This problem does not arise in the synthesis of electrical ladder network filters because the values of the circuit elements are deduced from general recurrence formulae such as those given by Belevich (1952) and Orchard (1953); the synthesis of interference filters with more than four cavities requires the development of a general formula for r .

§ 3. APPLICATION OF THE THEORY

The accuracy of the synthesis described in § 2 is illustrated by comparisons between the exact transmission characteristics and the prototype functions of some particular filters. The examples are chosen to transmit an 8% bandwidth with a value of T not less than $1/1.1$ (i.e. $h^2 = 0.1$, $t = -0.04\pi$). Two, three and four cavity filters have been synthesized to the specified equal ripple and maximally flat functions using the equations of table 2. The reflecting multilayers of the example filters have been assumed to consist of single layers. This restriction, as well as simplifying the calculations of the exact transmission characteristics, was imposed to demonstrate the effect of the variation with frequency in the optical thickness of the multilayers. The other approximations

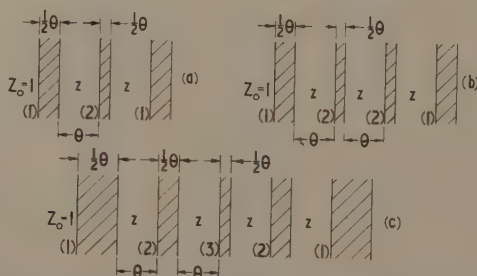


Figure 3. Details of the filters chosen to illustrate the synthesis. T is specified to be not less than $1/1.1$ over an 8% bandwidth. The reflecting systems (1) etc. are assumed to consist of a single dielectric layer, the refractive index of which is given by the values of r_1 etc. shown below. $\theta = \pi \omega/\omega_0$

Filter	Values of r obtained from table 2 for $h^2 = 0.1$, $t = -0.04\pi$					
	Equal ripple			Maximally flat		
	r_1	r_2	r_3	r_1	r_2	r_3
(a) 2 cavities	3.22	7.68		2.50	6.30	
(b) 3 cavities	3.45	10.3		2.33	7.65	
(c) 4 cavities	3.52	11.0	13.4	2.13	7.07	11.0

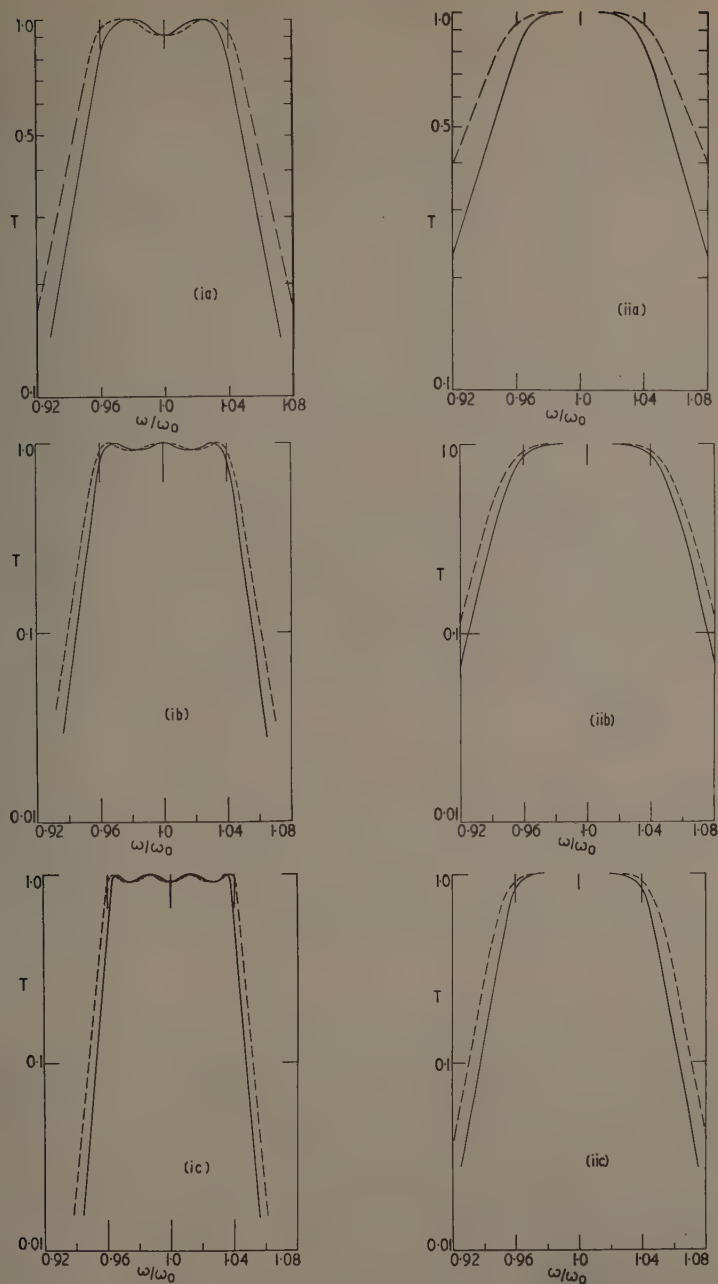


Figure 4. Transmission characteristics of filters chosen as examples, for which $h^2 = 0.1$, $t = -0.04\pi$. (a) 2 cavities, (b) 3 cavities, (c) 4 cavities. Broken line, prototype functions, $T = 1/(1 + [f_n(\bar{\omega})]^2)$, full line, exact transmission of filters represented in figure 3. (i) for equal ripple transmission, (ii) for maximally flat transmission.

in the theory are rigorously tested by the comparatively small value selected for h^2/t . Details of the example filters are illustrated in figure 3; the transmission characteristics are compared with the prototype functions in figure 4.

The exact transmission characteristics shown in figure 4 follow the prototype functions very closely for the greater part of the specified pass-band. The rate at which the transmissivity falls with frequency outside the pass-band also agrees very well with the behaviour of the prototype functions. The only difference between the exact and the simplified characteristics is that the actual bandwidth for which the transmissivity is less than $1/(1+h^2)$ is reduced from the specified value of $-2t/\pi$ in all the examples. The reduction varies from about 18% for the maximally flat two cavity filter to about 7% for the four cavity filters. The width of the transmission characteristic measured at smaller values of transmissivity are reduced by similar percentages. This effect can be associated with the omission from the theory of the variation with frequency in the phase shift across the reflecting multilayers. It can be reduced in any particular case by increasing the value of r either by using a higher order filter or by increasing the value of h^2/t .

It is appreciated that the method of synthesis cannot be applied with the same freedom of choice to interference filters as it is to the design of electrical circuit filters. The parameter r is restricted to combinations of the refractive indices of the dielectrics used in the reflecting multilayers. The situation would be improved considerably if more than two materials were available with refractive indices forming a convenient numerical sequence. The extent to which a particular filter will transmit the specified prototype function will depend on the accuracy with which the required values of r can be achieved with practicable multilayers. For two cavity filters it would be a simple matter to make a reverse calculation of h^2 and t from the values of r which are actually to be used. Filters of higher order will require an iterative calculation to ascertain which practicable values of r will lead to a transmission characteristic nearest to the specification. Decisions of this kind will be assisted by remembering that the transmissivity of any arrangement is easily calculated at $\omega = \omega_0$ by eliminating the half-wave layers. Further, a transmission characteristic intermediate to the equal ripple and maximally flat functions would be expected if the practicable values of r are intermediate to the synthesized values for both functions. The equations of table 2 will provide a quick assessment for the best deployment of quarter-wave layers in a particular filter when, for example, either the overall thickness or the number of layers is fixed.

REFERENCES

- BELEVICH, V., 1952, *Wireless Engr*, **29**, 106.
 BORN, M., and WOLF, E., 1959, *Principles of Optics* (London, New York, Paris: Pergamon Press).
 COHN, S. B., 1957, *Proc. Inst. Radio Engrs*, N. Y., **45**, 187.
 DARLINGTON, S., 1939, *J. Math. and Phys.*, **18**, 257.
 HEAVENS, O. S., 1960, *Rep. Progr. Phys.*, **23**, 12 (London: The Institute of Physics and The Physical Society).
 LEVY, R., 1957, *Proc. Instn Elect. Engrs*, **104C**, 423.
 ORCHARD, H. J., 1953, *Wireless Engr*, **30**, 3.
 POLSTER, H. D., 1952, *J. Opt. Soc. Amer.*, **42**, 21.
 SEIDEL, H., 1957, *Trans. Inst. Radio Engrs*, **MTT-5**, 107.
 SMITH, S. D., 1958, *J. Opt. Soc. Amer.*, **48**, 43.
 TURNER, A. F., 1952, *Technical Reports* 1-6 (New York: Bausch and Lomb).
 WEINSTEIN, W., 1954, *Vacuum*, **4**, 3.

Some Electrical and Optical Properties of InAs-In₂Se₃ and InSb-In₂Se₃ Alloys

By J. C. WOOLLEY AND P. N. KEATING†

Department of Physics, The University, Nottingham

MS. received 9th June 1961, in revised form 27th July 1961

Abstract. Polycrystalline specimens of InAs-In₂Se₃ and InSb-In₂Se₃ alloys have been prepared by suitable annealing of ingots. Measurements have been made of the room temperature values of Hall effect, conductivity, thermoelectric power and infra-red absorption over the whole of the available range of solid solution, and hence values of carrier density n , mobility μ and optical energy gap E_g determined. It is found that the behaviour is similar to that of the corresponding In₂Te₃ alloys in that the alloys rich in A^{III}B^V are n-type and highly degenerate. The observed values of n for the four systems concerned (A^{III}B^V-A₂^{III}B₃^{VI}) are compared, and possible explanations of the results in terms of solubility of tellurium and selenium in the A^{III}B^V compounds, or the band structure of the A^{III}B^V compounds are discussed. The use of thermoelectric power data to give values of the Fermi level is considered, and it is shown that to give consistent results in the composition range where ionized impurity scattering occurs, a scattering relation of the form $\tau \propto E^{+1/2}$ must be used. The results suggest that the InAs-In₂Se₃ system may show a change in conduction band minimum at a composition of low In₂Se₃ content.

§ 1. INTRODUCTION

UNLIKE THE compounds In₂Te₃, Ga₂Te₃ and Ga₂Se₃ which have a defect zinc blende structure, In₂Se₃ has a more complicated structure of lower symmetry. It has however a tendency towards the defect zinc blende structure, as is shown by the relatively large range of solid solution not only in the corresponding A₂^{III}B₃^{VI} compounds but also in the zinc blende type A^{III}B^V compounds such as InAs (Woolley and Keating 1961). Thus these alloys of In₂Se₃ with A^{III}B^V compounds can be conveniently compared with the corresponding alloys between In₂Te₃ and A^{III}B^V compounds and similar alloys of Ga₂Se₃.

The electrical and optical properties of the alloy systems InSb-In₂Te₃ (Woolley, Gillett and Evans 1960, to be referred to as I), InAs-In₂Te₃ (Woolley, Pamplin and Evans 1961, to be referred to as II), and GaAs-Ga₂Se₃ (Nasledov and Fel'tin'sh 1959, Fel'tin'sh 1960) have recently been described. It is found in each case that the addition of a small percentage of A₂^{III}B₃^{VI} to the A^{III}B^V compound produces an alloy which is n-type with a large carrier density ($\sim 10^{18}$ - 10^{20} cm⁻³). In the case of InAs-In₂Te₃, where complete solid solution occurs at all compositions, it has been shown (II) that this large carrier density is retained until some 50 mol % In₂Te₃† is reached, but that for larger In₂Te₃ content the carrier density falls rapidly to a value of the order 10^{12} cm⁻³ for In₂Te₃ itself. The values of electron mobility in alloys of this system show a rapid

† Now at A.E.I. (Woolwich) Limited, Harlow, Essex.

‡ In calculating mol. % in systems composed of one A^{III}B^V compound and one A₂^{III}B₃^{VI} compound, the molecules have been taken as A₃^{III}B₃^V and A₂^{III}B₃^{VI}, i.e. the percentage is strictly the percentage of B^V and B^{VI} atoms on the B sub-lattice.

fall from the value for InAs as small amounts of In_2Te_3 are added and then a slower rate of fall to the low value associated with In_2Te_3 .

In the case of InAs– In_2Se_3 alloys the range of solid solution from 0 to approximately 80 mol % In_2Se_3 enables a comparison to be made between the results obtained with the zinc blende type alloys of this system and those of the InAs– In_2Te_3 system. The InAs– In_2Se_3 results are presented here, together with those for the InSb– In_2Se_3 alloys where only a very limited range of solid solution of In_2Se_3 in InSb occurs (~ 2.5 mol % In_2Se_3).

§ 2. PREPARATION OF SPECIMENS

The details of preparation of the alloys have already been given (Woolley and Keating 1961). The alloys were made by melting together appropriate amounts of the compounds concerned. The In_2Se_3 was prepared from 99.999% purity indium and commercial high purity selenium which had been repeatedly distilled to give better purity, the InAs was of high purity having approximately 10^{16} – 10^{17} carriers/cm³, and the InSb was zone refined material with approximately 3×10^{16} carriers/cm³. All of the ingots were annealed under vacuum in solid form, the InAs– In_2Se_3 alloys for 350 hours at 720 °C and the InSb– In_2Se_3 alloys for 1000 hours at 490 °C, previous investigations having shown that these treatments gave good equilibrium material. The mechanical condition of the ingots varied with composition. Those with small In_2Se_3 content were solid and mechanically sound, containing no blow holes etc. In the InAs alloys the condition of the ingots became worse as the In_2Se_3 content increased, particularly in the range 40 to 60 mol % In_2Se_3 , but the condition in the range close to 75 mol % In_2Se_3 , where some type of ordering appears to occur, was good. With care however suitable specimens for measurement could be cut from the various ingots.

§ 3. METHODS OF MEASUREMENT AND RESULTS

Room temperature values of conductivity and Hall coefficient were obtained for alloys of various compositions, the methods used for the measurements being the same as those described previously for the In_2Te_3 alloys (I and II). For these highly degenerate materials, the electrical results are found to be independent of temperature, and hence the room temperature values were taken to be characteristic of the materials. For the InAs alloys, conductivity values were obtained out to 75 mol % In_2Se_3 , but owing to the low conductivity of the In_2Se_3 -rich alloys, values of Hall coefficient were obtained out to 50 mol % In_2Se_3 only. Similar conductivity and Hall coefficient measurements were made over the 2.5 mol % range of solid solution in the InSb system. The variations of carrier density n (assuming that $R_H = 1/ne$), conductivity σ , and Hall mobility μ ($= \sigma R_H$) obtained from these measurements are shown in figures 1–4.

Optical measurements were also made on various alloys to determine the value of optical energy gap E_g at room temperature, and again the method was the same as described previously (I). The variation of E_g with composition in the two systems is shown in figures 5 and 6.

Measurements were made also of the thermoelectric power Q of the alloys up to the limit of solid solution in each system, using the method described previously (II). In these highly degenerate materials Q would be expected to vary linearly with T . Measurements made in the range 100–400 °K with InAs– In_2Se_3 alloys containing

1 mol %, 10 mol % and 75 mol % In_2Se_3 respectively confirmed that this behaviour was obtained. With the other alloys, the value of Q/T required later was obtained from room temperature measurements only. Figures 7 and 8 show the variation of room temperature thermoelectric power with composition.

It is seen from figures 1-8 that the variation of the parameters n , μ , σ , E_g and Q with composition is very similar to the results for the corresponding In_2Te_3 alloys (I and II). Again for the InSb alloys and in the range 0-60 mol % In_2Se_3 of the InAs alloys, the material is highly degenerate and the results show a considerable filling of the conduction band. Thus in particular the optical results do not give the intrinsic energy gap, but this latter may be obtained in certain cases, if the optical data are combined with the results of the thermoelectric power measurements.

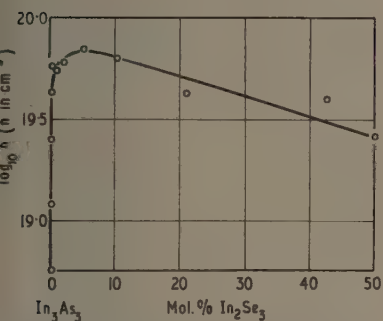


Figure 1. Variation of carrier density n with composition for $\text{InAs-In}_2\text{Se}_3$ alloys.

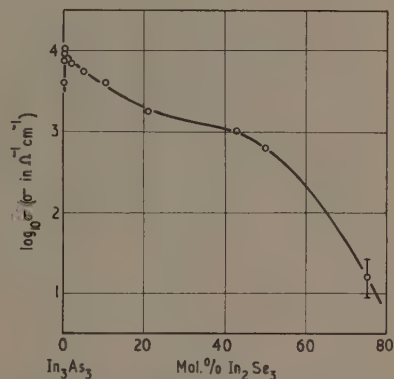


Figure 2. Variation of conductivity σ with composition for $\text{InAs-In}_2\text{Se}_3$ alloys.

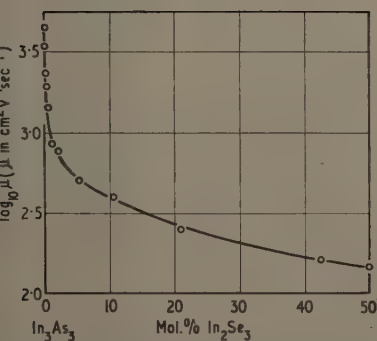


Figure 3. Variation of electron mobility μ with composition for $\text{InAs-In}_2\text{Se}_3$ alloys.

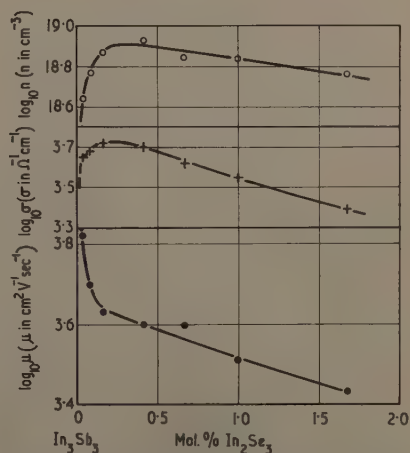


Figure 4. Variation of carrier density n , conductivity σ and electron mobility μ with composition for $\text{InSb-In}_2\text{Se}_3$ alloys.

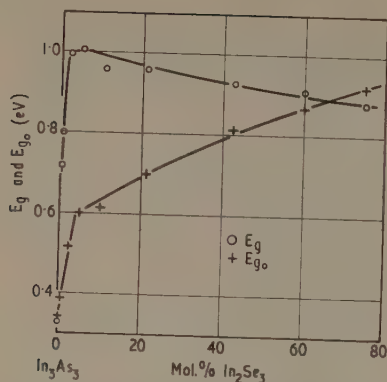


Figure 5. Variation of optical energy gap E_g and intrinsic energy gap E_{g0} with composition for InAs-In₂Se₃ alloys.

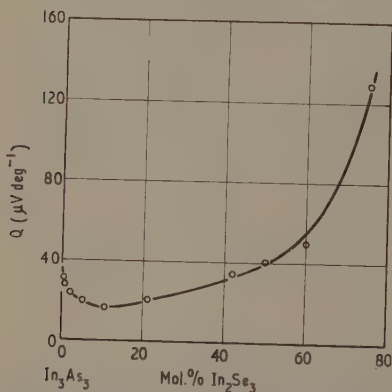


Figure 7. Variation of thermoelectric power Q with composition for InAs-In₂Se₃ alloys.

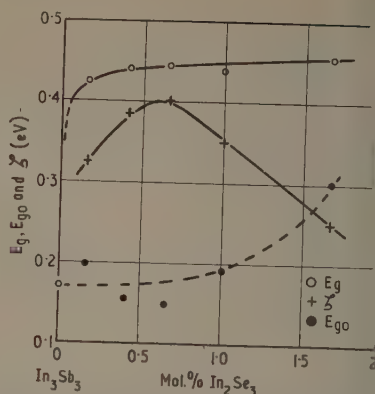


Figure 6. Variation of optical energy gap E_g , Fermi level ζ and intrinsic energy gap E_{g0} with composition for InSb-In₂Se₃ alloys.

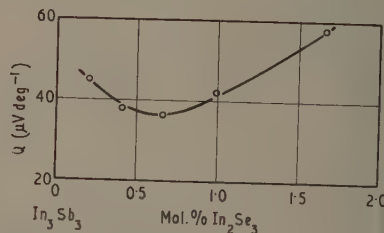


Figure 8. Variation of thermoelectric power Q with composition for InSb-In₂Se₃ alloys.

§ 4. DISCUSSION

If the results for alloys of low In₂Se₃ content are considered, it is seen that these agree with what seems to be a general result that, whenever defect A₂^{III}B₃^{VI} compounds are alloyed with normal zinc blende type A^{III}B^V compounds, a large electron density of the order 10¹⁹–10²⁰ cm⁻³ occurs in the conduction band at very low A₂^{III}B₃^{VI} percentages. It appears that some of the B^{VI} atoms are acting as donors in the B sub-lattice and that the observed high carrier density is probably due to the fact that the number of lattice vacancies occurring in the A sub-lattice is considerably less than the value to be expected from the alloy composition. As indicated in the case of the In₂Te₃ alloys (I and II), the results at very low In₂Te₃ content are the same as those obtained by doping the A^{III}B^V compound with tellurium, and it appears probable that when large amounts of tellurium are added to the A^{III}B^V compound, some lattice vacancies occur similar to those in the A^{III}B^V-In₂Te₃ alloys. The same results are obtained

when $\text{A}^{\text{III}}\text{B}^{\text{V}}\text{-In}_2\text{Se}_3$ alloys are compared with selenium-doped $\text{A}^{\text{III}}\text{B}^{\text{V}}$ compounds. It is assumed that the excess arsenic or antimony atoms are segregated to grain boundaries or lost as a vapour phase, but this has not been experimentally confirmed. Recent work by Parrott (1961)[†] has shown that such behaviour in these alloys is to be expected on the basis of thermodynamic arguments.

As indicated in II, the maximum observed values of n may be determined by one of two factors. One possibility is that this value of n represents the limit of solid solubility of tellurium (or selenium) in the $\text{A}^{\text{III}}\text{B}^{\text{V}}$ compound or the composition at which further addition of In_2Te_3 (or In_2Se_3) produces a stoichiometric number of lattice vacancies. Alternatively it is possible that this observed maximum value of n is determined by the band structure of the $\text{A}^{\text{III}}\text{B}^{\text{V}}$ compound. In this latter case, it would be postulated that solid solution of tellurium (or selenium) continues beyond the value corresponding to n_{max} but that the electrons from these resulting donor atoms enter the conduction band in a region where they have considerably larger effective mass than the electrons in the normal band minimum, and hence would contribute very little to the Hall coefficient and would effectively not be observed. The maximum values of n observed are $9 \times 10^{18} \text{ cm}^{-3}$ for In_2Te_3 in InSb , $9 \times 10^{18} \text{ cm}^{-3}$ for In_2Se_3 in InSb , $5 \times 10^{19} \text{ cm}^{-3}$ for In_2Te_3 in InAs and $7 \times 10^{19} \text{ cm}^{-3}$ for In_2Se_3 in InAs . Although it is possible that the solid solubilities of tellurium and selenium in the $\text{A}^{\text{III}}\text{B}^{\text{V}}$ compound are practically identical for both InAs and InSb , the close agreement in the values of n_{max} for a given $\text{A}^{\text{III}}\text{B}^{\text{V}}$ compound would tend to support the second suggested explanation. As indicated in II, there is some evidence from density measurements to support this also. If, in terms of this band structure explanation, it is assumed that the electrons of larger effective mass are in subsidiary conduction band minima, then the height of the Fermi level above the main conduction band minimum when n is maximum should give some indication of the energy separation of the main and subsidiary conduction band minima. The method of estimating Fermi energies from thermoelectric power data is discussed below.

If the assumption that the observed maximum value of n is due to the effect of a second conduction band minimum is correct, the observed values of E_g at the corresponding composition should give an indication of the height of this minimum above the valence band maximum. The values obtained are:

$\text{InSb-In}_2\text{Te}_3$	0.44 eV	$\text{InSb-In}_2\text{Se}_3$	0.43 eV
$\text{InAs-In}_2\text{Te}_3$	0.85 eV	$\text{InAs-In}_2\text{Se}_3$	1.0 eV

Recent work by Cardona (1961, private communication) indicates that the energy spacing between the valence band maximum and $\langle 111 \rangle$ minima is about 0.5 eV for InSb and 0.8 eV for InAs . This gives very good agreement with the present results, the discrepancy in the $\text{InAs-In}_2\text{Se}_3$ value possibly being due to the effects discussed below.

For degenerate material the thermoelectric power Q is related to the absolute temperature T and the height of the Fermi level above the conduction band minimum, ζ , by the equation (Ehrenberg 1958)

$$Q = -\frac{k}{e} \frac{\pi^2 kT}{2\zeta} \left[1 + \frac{2}{3} \left(\frac{E}{\tau} \frac{d\tau}{dE} \right)_{E=\zeta} \right]$$

and if it is assumed that

$$\tau \propto E^s$$

[†] Reported at the Institute of Physics and Physical Society Conference on Thermoelectricity, Durham, July 1961.

then

$$Q = -\left(\frac{3+2s}{6}\right)\frac{\pi^2 k^2 T}{e\zeta}. \quad (1)$$

The determination of ζ from Q thus requires a knowledge of s , which depends upon the particular scattering mechanism concerned. The two scattering mechanisms expected to predominate in these materials are ionized impurity scattering at low In_2Se_3 content and alloy scattering at higher In_2Se_3 content. The Brooks-Herring (Brooks 1955) and Conwell-Weisskopf (1950) analyses of ionized impurity scattering give $s = \frac{3}{2}$ while Sclar (1956) obtains $s = \frac{3}{2}$, $\frac{1}{2}$ or $-\frac{1}{2}$ under various conditions of concentration etc. For experimental determination of s , with pure semiconductors it is possible to write $E = kT$ and hence mobility-temperature measurements give s . But this method is not valid in the degenerate case. One method of determining s in this latter case is by comparison of thermoelectric and optical data using equation (1). This method has been used by Barrie and Edmond (1955) for InSb heavily doped with tellurium but large discrepancies were found between experiment and theory. Since however, these discrepancies may well be due to the theoretical analysis, it was decided to attempt to use here the comparison of thermoelectric and optical data to find a satisfactory value of s .

A relation between Fermi level ζ and observed optical absorption edge E_g of the form

$$\zeta = E_g + 4kT - E_{g_0}, \quad (2)$$

where E_{g_0} is the intrinsic energy gap, has been assumed as in previous work (Barrie and Edmond 1955, Burstein 1954). The relation will not be accurate, as the $4kT$ term may differ from this value depending on the transition conditions, while the definition of E_g is somewhat arbitrary in the case of polycrystalline materials of unknown reflectivity (Woolley and Evans 1961). In the interpretation of the present optical results for the InSb alloys E_g was taken as the value corresponding to a change in absorption coefficient of 300 cm^{-1} above background, while for the InAs alloys a change of 100 cm^{-1} was used, these values being those required to give the accepted value for E_g in the corresponding pure $\text{A}^{\text{III}}\text{B}^{\text{V}}$ compounds. Even under these conditions it is considered that the inaccuracy in E_{g_0} should be well below 0.1 eV and therefore is sufficient here.

Using the above method for correlating the optical and thermoelectric data, values of E_{g_0} have been calculated for both InSb and InAs alloys containing up to 2 mol. % In_2Se_3 using the various values of s suggested for ionized impurity scattering. It has been assumed that over this range of composition little change in the intrinsic energy gap should occur, and hence the values of E_{g_0} should be close to that for the appropriate $\text{A}^{\text{III}}\text{B}^{\text{V}}$ compound. It is possible that this assumption is invalid in that the presence of an impurity band may greatly affect E_{g_0} or, as indicated by Aigrain (1961), the presence of a high density of donor atoms in the lattice may reduce E_{g_0} . Nevertheless the above assumption has been used to determine the best value of s over this composition range. It is found that for alloys with 10^{19} – 10^{20} carriers/ cm^3 , the use of $s = \frac{3}{2}$ gives values of E_{g_0} very different from the value of the corresponding $\text{A}^{\text{III}}\text{B}^{\text{V}}$ compound, in some cases giving $E_{g_0} \simeq 0$, while the use of $s = -\frac{1}{2}$ gives results which are little better. Good agreement between alloys and compound is obtained however if s is taken as $+\frac{1}{2}$. It appears that within the limits of the assumptions made above $s = +\frac{1}{2}$ is the appropriate value to use for ionized impurity scattering in these alloys. The same result was obtained with the InAs– In_2Te_3 alloys (II). It is perhaps worthy of note that the Sclar resonance method gives $s = +\frac{1}{2}$ and that Domenicali (1960) has treated metal alloys at low temperatures by resonance methods.

For alloys of higher In_2Se_3 content, alloy scattering is assumed to apply. In this case a value of $s = -\frac{1}{2}$ is appropriate (Nordheim 1931, Brooks 1955) but the above method for checking is not available in this case since no values of E_{g_0} are known. However in the case of $\text{InAs-In}_2\text{Te}_3$ the use of $s = -\frac{1}{2}$ for the alloys of higher In_2Te_3 content were found to give consistent results out to the composition where the alloys were non-degenerate and the optical results gave a value of E_{g_0} directly.

For alloys of both the systems $\text{InAs-In}_2\text{Se}_3$ and $\text{InSb-In}_2\text{Se}_3$ values of ζ have been calculated, using $s = +\frac{1}{2}$ at lower In_2Se_3 content and, in the InAs alloys, $s = -\frac{1}{2}$ for higher In_2Se_3 content. These results are shown in figures 6 and 9. In the InSb alloys ionized impurity scattering is dominant throughout the limited range of solid solution, but in the InAs alloys it is apparent that between approximately 2 and 10 mol % In_2Se_3 neither scattering mechanism is dominant, and in this range an interpolated value of ζ is indicated. These values have then been used, together with the optical data, to give values of E_{g_0} from equation (2) and the resulting values of E_{g_0} are shown as a function of composition in figures 5 and 6.

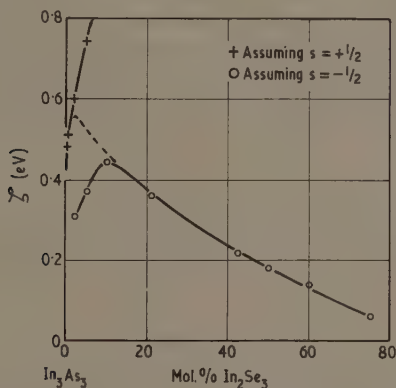


Figure 9. Variation of Fermi level ζ with composition for $\text{InAs-In}_2\text{Se}_3$ alloys.

The form of the E_{g_0} -composition curves are very different for the two In_2Se_3 systems concerned. With the InSb alloys, the value of E_{g_0} stays approximately constant at 0.17 eV to 1 mol % In_2Se_3 and then increases slowly to the limit of solid solution (~2.5 mol %). In the case of the InAs alloys however E_{g_0} rises rapidly from 0.33 eV at InAs to 0.60 eV at 4 mol % In_2Se_3 and then increases slowly up to 0.92 eV at 75 mol % In_2Se_3 , the alloy of largest In_2Se_3 content for which measurements were made. The form of this curve is very similar to that for the Ge-Si system, where a change in slope in the E_{g_0} -composition curve occurs when the lowest conduction band minima change from the $\langle 100 \rangle$ minima characteristic of silicon to the $\langle 111 \rangle$ minima characteristic of germanium. This suggests that possibly a similar band change occurs in the $\text{InAs-In}_2\text{Se}_3$ alloys, where the discontinuity in the E_{g_0} curve at 4 mol. % In_2Se_3 would represent a change in lowest conduction band minimum from the 000 minimum characteristic of InAs to some other set of minima, possibly the $\langle 111 \rangle$ as in germanium. Extrapolation of the curve from compositions above 5 mol % In_2Se_3 would give a value of E_{g_0} for these minima in InAs itself of approximately 0.60 eV, a value rather lower than that quoted above. However, this suggestion that the second conduction band minimum in the $\text{InAs-In}_2\text{Se}_3$ alloys may fall below the 000 minimum is not

inconsistent with the explanation put forward above for the maximum value of n observed with these alloys. Thus even when the 000 minimum is at a slightly higher energy than the other set of minima, provided the electrons in the 000 minimum have a much smaller effective mass, these would be the carriers observed by Hall effect measurements. The discrepancy in the values of E_{g_0} mentioned above could indicate that both sets of conduction band minima were filled to a considerable extent when maximum occurs.

The density of states effective mass m_n is given by the relation

$$n = \frac{8\pi}{3} \left(\frac{2m_n}{\hbar^3} \right)^{3/2} \zeta^{3/2}_5$$

where m_n is related to the effective mass tensor components by the equation

$$m_n = N^{2/3} (m_{ii} m_{jj} m_{kk})^{1/3},$$

N being the number of equivalent minima. This equation, however, only has meaning when electrons in a single type of band minimum are considered. Thus for the InAl alloys this is approximately true only for very low In_2Se_3 content where the 000 minimum is the only minimum appreciably filled, and, assuming the band change postulated above, at large In_2Se_3 content where it may be assumed that the contribution of the 000 minimum is negligible. Using equation (3), in the composition range 0 to 1 mol. % In_2Se_3 the values of m_n are about 0.05–0.06 m_0 in reasonable agreement with the result of Stern and Talley (1955) for InAs, while at 40–50 mol % In_2Se_3 $m_n \simeq 0.30 m_0$ which is rather lower than the value for electrons in the $\langle 111 \rangle$ minima of germanium. Substituting the values for the InSb alloys into equation (3), a value of $m_n \simeq 0.06 m_0$ is obtained at 1.5 mol % In_2Se_3 but the value falls with reduced In_2Se_3 content and extrapolates to a value of 0.035 m_0 for pure InSb.

ACKNOWLEDGMENTS

The authors are indebted to Professor L. F. Bates for the facilities of his laboratory, and to Dr. M. E. Haine of A.E.I. (Woolwich) Limited for a maintenance grant to one of them (P.N.K.).

REFERENCES

- AIGRAIN, P., 1961, *Proc. Int. Conf. on Semiconductor Physics* (Prague: Czechoslovak Academy of Science), p. 404.
 BARRIE, R., and EDMOND, J. T., 1955, *J. Electronics*, **1**, 161.
 BROOKS, H., 1955, *Advances in Electronics and Electron Physics*, **8**, 85.
 BURSTEIN, E., 1954, *Phys. Rev.*, **93**, 632.
 CONWELL, E. M., and WEISSKOPF, V. F., 1950, *Phys. Rev.*, **77**, 388.
 DOMENICALI, C., 1960, *Phys. Rev.*, **117**, 984.
 EHRENBERG, H., 1958, *Electric Conduction in Semiconductors and Metals* (Oxford: University Press).
 FELTIN'SH, I. A., 1960, *Latv. PSR Zinat. Akad. Vestis* (USSR), **9**, 73.
 NASLEDOV, D. N., and FELTIN'SH, I. A., 1959, *Sov. Phys. Solid State*, **1**, 510.
 NORDHEIM, L., 1931, *Ann. Phys., Lpz.*, **9**, 607.
 SCLAR, N., 1956, *Phys. Rev.*, **104**, 1548.
 STERN, F., and TALLEY, R., 1955, *Phys. Rev.*, **100**, 1638.
 WOOLLEY, J. C., and EVANS, J. A., 1961, *Proc. Phys. Soc.*, **78**, 354.
 WOOLLEY, J. C., GILLET, C. M., and EVANS, J. A., 1960, *J. Phys. Chem. Solids*, **16**, 138.
 WOOLLEY, J. C., and KEATING, P. N., 1961, *J. Less Common Metals*, **3**, 194.
 WOOLLEY, J. C., PAMPLIN, B. R., and EVANS, J. A., 1961, *J. Phys. Chem. Solids*, **19**, 147.

Growth and Decay of Luminescence Intensity under Cathode Ray Excitation

By M. SAYER

Department of Physics, University of British Columbia, Vancouver, B.C., Canada

MS. received 9th June 1961

Abstract. Expressions for the growth and decay of cathodoluminescence intensity are derived for phosphors which show exponential decay schemes under ultra-violet excitation. A model is used in which excitation of luminescence centres can take place either by direct interaction with primary electrons or indirectly by transfer of energy from excited lattice electrons. Two systems are considered: (i) with monomolecular recombination in the lattice and monomolecular recombination in the centres, (ii) with bimolecular recombination in the lattice and monomolecular recombination in the centres. Comparison between the theory and published experimental data indicates that such a model with bimolecular recombination in the lattice is compatible with many of the available experimental results.

§ 1. INTRODUCTION

RADIATION is emitted by a luminescent material from luminescence centres situated at specific sites, or impurity atoms, in a host crystal lattice. In general, the number of such centres is a small fraction of the total number of atoms present. If the crystal is illuminated with ultra-violet radiation of a wavelength longer than that corresponding to the absorption edge, energy may be absorbed directly by the luminescence centres with little interaction with the atoms of the host lattice. For many materials such as zinc oxide, tungstates and manganese activated phosphors, this gives rise to a centre recombination process described by monomolecular kinetics, with exponential growth and decay processes of a time constant characteristic of the material.

Cathodoluminescence is again produced by the decay of excited centres, but for a particular phosphor, both the emission spectrum and the growth and decay processes may be altered significantly from those observed under ultra-violet excitation. Simultaneous changes in both emission spectrum and growth and decay processes may be explained in terms of the preferential excitation of different luminescence centres contained in the same material (Froelich 1953). However, a number of phosphors have been reported (Einstein 1957, Feinberg 1959, Arkangel'skaya and Tolstoy 1958) which show a considerable change in the growth and decay processes with no significant change in the emission spectrum. This applies both for a change from optical to electron excitation and for an increase in electron excitation. In the latter case, the primary electrons interact impartially with both lattice atoms and luminescence centres, producing ionization and excitation in both the lattice and the centres. The energy of the excited lattice atoms may be dissipated either by phonon generation, or by transfer to luminescence centres. If the latter process occurs, part of the total emission must be determined by the interaction between the host lattice and the luminescence centres. Thus a phosphor with a monomolecular type of growth or decay process under ultra-violet excitation may be expected to show a more complicated behaviour under cathode

ray excitation. The characteristics to be expected from such a system are the subject of this paper.

2.1. Theory

The situation may be described in terms of a model originally proposed by Bri (1949). Figure 1 shows the transitions possible between energy levels of both the lattice and the centres. Suppose that there are N luminescence centres per cm^3 and a beam of electrons $J \text{ A cm}^{-2}$ is incident on the surface such that an electron density of I electrons per cm^3 is produced over the excited region.

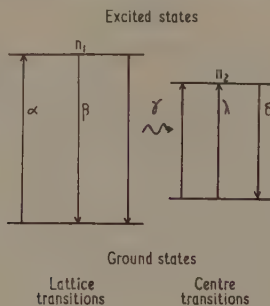


Figure 1. Model for the cathodoluminescence process.

A set of transition probabilities may be defined, viz. α the number of excited lattice atoms per incident primary electron, β the probability that the energy of an excited lattice electron is lost by phonon generation, γ the probability for energy to be transferred from a lattice electron to a centre, λ the number of luminescence centres excited directly by a primary electron and δ the probability for a radiative transition within the centre. To simplify the analysis, the probability for a non-radiative centre transition is assumed to be zero.

It will be assumed that all parameters are uniform over the excited region. This is a reasonable assumption for β , γ , N and δ , but it is less satisfactory for α , λ and I . The electron density I electrons per cm^3 at a distance d cm below the surface is given by an expression $I = (J/R)f(d/R)$ where $J (\text{A cm}^{-2})$ is the primary electron current at the surface, R is the range of electrons in the crystal, and $f(d/R)$ is a function describing the distribution of electrons with depth. Both this expression and those for the excitation probabilities α and λ are complex functions of electron energy, so that an exact calculation of the product αI presents severe difficulties. Errors may therefore be introduced from this source and the analysis can yield no accurate information regarding the luminescence characteristics as a function of electron energy. For changes in current density at constant primary electron energy, it will be assumed that I is proportional to J .

The recombination process in the centres is assumed to remain monomolecular and a lattice recombination of either monomolecular or bimolecular kinetics will be considered.

2.2. Monomolecular Lattice—Monomolecular Centre

Suppose that at a given time t there are n_1 excited lattice electrons and n_2 excited luminescence centres. To simplify the analysis, $n \ll N$ under all conditions.

2.2.1. Rate equations.

$$\frac{dn_1}{dt} = \alpha I - (\beta + \gamma N)n_1 \quad (1)$$

$$\frac{dn_2}{dt} = \lambda I + \gamma N n_1 - \delta n_2. \quad (2)$$

Solving equation (2) for n_1 and substituting

$$\frac{d^2 n_2}{dt^2} + (\delta + \beta + \gamma N) \frac{dn_2}{dt} + \delta(\beta + \gamma N)n_2 = (\alpha I \gamma N + k \lambda I). \quad (3)$$

Writing

$$(\beta + \gamma N) = k \quad \alpha I \gamma N = Z$$

equation (3) has a solution of the form

$$n_2 = \frac{(Z + k \lambda I)}{\delta k} + A \exp(-kt) + B \exp(-\delta t)$$

where A and B are constants.

2.2.2. Growth process.

Inserting boundary conditions and simplifying,

$$t = 0 \quad n_1 = n_2 = 0$$

$$n_2 = \frac{Z}{\delta k} \left[\left\{ 1 + \frac{\lambda k}{\alpha N \gamma} \right\} + \frac{\delta}{(k - \delta)} \exp(-kt) - \left\{ \frac{k}{(k - \delta)} + \frac{\lambda k}{\alpha N \gamma} \right\} \exp(-\delta t) \right] \quad (4)$$

2.2.3. Decay process.

$$t = 0 \quad n_2 = \frac{Z + k \lambda I}{\delta k}$$

$$n_2 = \frac{Z + k \lambda I}{\delta k} \left[\frac{k}{k - \delta} \exp(-\delta t) - \frac{\delta}{k - \delta} \exp(-kt) \right]. \quad (5)$$

The characteristics of the growth and decay processes described by the above equations may be summarized as follows:

(i) The overall process is a combination of two exponential components with time constants δ and $\beta + \gamma N \text{ sec}^{-1}$ respectively.

(ii) For no direct excitation, the proportion of each component is inversely proportional to the time constant. If direct excitation is included, the proportion of the growth process is increased, and the time constant of the growth process is greater than that of the decay process.

(iii) Increase in current density introduces no changes in either the proportions or the time constants of either process.

2.3. Bimolecular Lattice—Monomolecular Centres

2.3.1. Rate equations.

$$\frac{dn_1}{dt} = \alpha I - (\beta + \gamma N)n_1^2 \quad (6)$$

$$\frac{dn_2}{dt} = \lambda I + \gamma N n_1^2 - \delta n_2. \quad (7)$$

2.3.2. *Growth process.*

Solving equation (6) for n_1

$$n_1 = n_0 \tanh n_0 k t$$

where

$$n_0 = \left(\frac{\alpha I}{k} \right)^{1/2} \quad k = (\beta + \gamma N).$$

Substituting in equation (7)

$$\frac{dn_2}{dt} + \delta n_2 = \lambda I + \frac{\gamma N \alpha I}{k} \tanh^2(\alpha I k)^{1/2} t. \quad (8)$$

Writing

$$(\alpha I k)^{1/2} = b \quad \gamma N \alpha I = Z$$

the solution of equation (8) may be reduced to the form

$$n_2 = \frac{\lambda I}{\delta} [1 - \exp(-\delta t)] + \frac{Z}{k} \exp(-\delta t) \int_0^t \exp(\delta t) \tanh^2 b t \, dt. \quad (9)$$

The maximum value of n_2 is given when

$$\delta t = b t = \infty; \quad \tanh^2 b t \rightarrow 1$$

i.e.

$$n_2 = \frac{Z + k \lambda I}{\delta k}.$$

2.3.3. *Decay process.*

Let $I = 0$ in the rate equations and solve (6) for n_1

$$n_1 = \frac{n_0}{1 + n_0 k t}.$$

Substituting into equation (7)

$$\frac{dn_2}{dt} + \delta n_2 = \frac{\gamma N \alpha I}{k} \left[\frac{1}{1 + (\alpha I k)^{1/2} t} \right]. \quad (10)$$

Solving for n_2 and introducing the boundary conditions

$$t = 0 \quad n_2 = \frac{Z + k \lambda I}{\delta k}$$

$$n_2 = \frac{Z}{\delta k} \left[-\frac{\delta}{b(1 + b t)} + \exp(-\delta t) \left\{ \frac{\lambda k}{\gamma N \alpha} + 1 + \frac{\delta}{b} + \frac{\delta^2}{b} \int_0^t \frac{\exp(\delta t)}{1 + b t} dt \right\} \right]. \quad (11)$$

The integrals which occur in equations (9) and (11) have no analytical solution and were computed graphically. The solutions for the growth and decay processes are plotted in figures 2 and 3 respectively, calculated for a fixed value of δ and different values of b and assuming no direct excitation of luminescence centres ($\lambda = 0$).

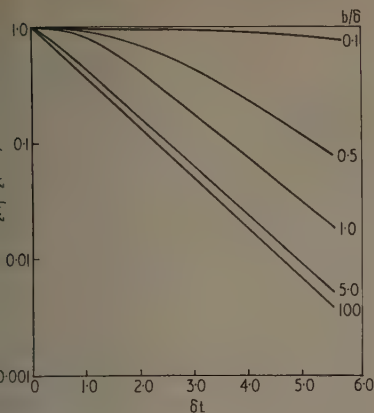


Figure 2. Luminescence growth process for different values of parameter b/δ . Plotted as $n_2(t)/n_2(\max)$. No direct excitation of luminescence centres ($\lambda = 0$).

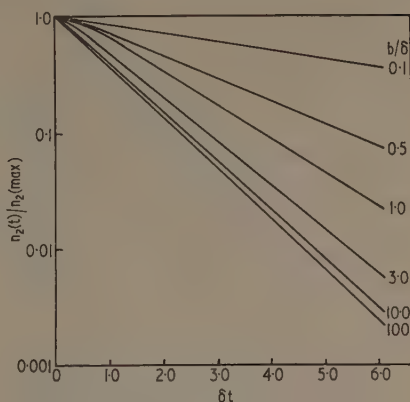


Figure 3. Luminescence decay process for different values of parameter b/δ . No direct excitation of luminescence centres ($\lambda = 0$).

2.4. Summary

The forms of both processes are determined by the relative magnitude of the parameters δ and b . If $b/\delta \gg 1$, both growth and decay are exponential with a time constant which approaches an upper limit δ as $b/\delta \rightarrow \infty$. If $b/\delta \lesssim 1$, the processes are non-exponential, the departure from the exponential form being greatest over the initial part of the curve and being greater for smaller values of b . This is most marked for the growth process and further examination of equation (8) indicates that the beginning of the curve over a small interval of time is proportional to the time squared. At larger times, both processes approximate well to an exponential form with a time constant less than $\delta \text{ sec}^{-1}$. The time constant most often measured experimentally τ , where τ is the time to attain $1/e$ of the maximum value) is shown as a function of b/δ in figure 4. This indicates that the relation between the time constant and the current density is complex, although in the region where $b/\delta \lesssim 1$, the time constants for both processes are proportional to $\log b$ and hence $\log I$. The decay constant is seen to be greater than the growth constant over the same range.

The direct excitation of luminescence centres introduces an extra term

$$(\lambda k/\gamma N\alpha) \exp(-\delta t)$$

to equations (9) and (11). The importance of the additional term is again determined by the magnitude of b/δ . If $b/\delta > 1$, the term is effective over the entire growth and decay, which results in an approximately exponential process of time constant increased above that calculated for the lattice process above. If $b/\delta < 1$, the term is of most importance over the initial part of the growth and decay and if of sufficient magnitude, may replace the initial square law section predicted for the growth process by an exponential process of time constant approaching that of $\delta \text{ sec}^{-1}$. This is shown in figure 5. Note that an increase of electron density I increases the time constant of the lattice process. This may be interpreted experimentally as an increase in the proportion of the process due to direct centre excitation.

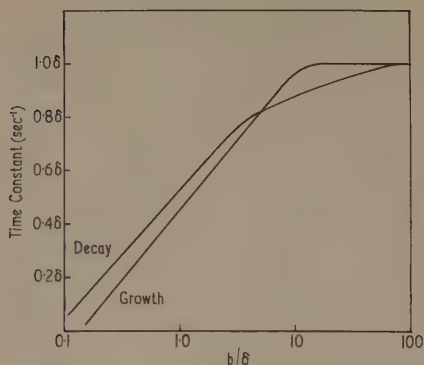


Figure 4. Time constant for growth and decay processes plotted against the parameter b/δ . Time constant measured as $1/\tau$, where τ is time to attain $1/e$ of maximum value. No direct excitation of centres ($\lambda = 0$).

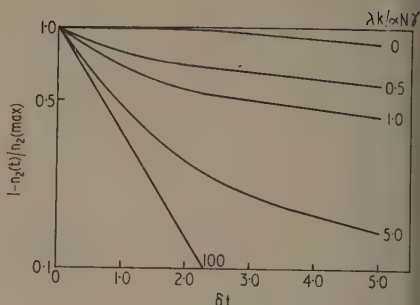


Figure 5. Composite growth process including excitation via the lattice and direct centre excitation. Curves plotted for $b/\delta = 0.1$ and different values of $\lambda k/\alpha N\gamma$.

§ 3. DISCUSSION

Much of the experimental data reported in the literature may be explained in terms of this analysis. Many authors have shown that the growth and decay processes are non-exponential under electron excitation (Arkangel'skaya and Tolstoy 1958). Strange and Henderson (1946) have described the decay schemes of a range of materials in terms of two exponential processes—the A and B processes. On the present analysis, the A process is a result of the direct excitation of luminescence centres by primary electrons, the B process is due to indirect excitation via the lattice. The arbitrary classification of phosphors into two classes used by these authors is explicable if it is assumed that under the conditions of measurement:

Manganese class. ($\delta 10\text{--}10^3 \text{ sec}^{-1}$); $b/\delta \gg 1$, i.e. the overall time constants are fixed at the upper limit $\delta \text{ sec}^{-1}$ and the B process alone is apparent.

Silver class. ($\delta 10^4\text{--}10^6 \text{ sec}^{-1}$); $b/\delta \lesssim 1$, i.e. the value of b/δ is small so that two components are observed. This suggests that the value of $\beta + \gamma N$ is about 10^5 sec^{-1} for most phosphors. The relative proportion of the A process was reported to increase with increased current density. It has been shown in a previous section that such an observation may be due to a change in the effective time constant of the lattice process.

Theoretically the characteristics of both growth and decay processes are determined by the parameter $(\alpha I k)^{1/2}$. The overall lattice transition probability $k = \beta + \gamma N$ appears both in the above expression and in that for the maximum luminescence intensity $Z/\delta k$. Pfahl (1961) has reported experimental data for zinc oxide phosphors which show that an increase in time constants is accompanied by a decrease in luminescence efficiency. Feinberg (1959) and Einstein (1957) have shown that the decay constant is less than the growth constant at low current densities in agreement with theory. Einstein has measured the time constants as a function of current density and has obtained a relation of the form $1/\tau = C i^n$ where C is a constant and n is 0.4 for the growth process and 0.3 for the decay process. An attempt was made to fit these results to theoretical curves but it was not possible to obtain agreement over the entire range of observations.

the theory predicts less of a difference between the exponents n for the growth and decay curves than is observed experimentally. However, at low primary currents where $b/\delta < 1.0$, tangents drawn to the theoretical curves have slopes between 0.2–0.3 which is of the same order as the experimental values.

For the same material, the time constants measured under electron excitation would be less than those under optical excitation. Data published in the literature indicate that this relation is valid for many phosphors, the principal exceptions being certain of the phosphors activated by manganese. In the latter case, increase in current density increases the time constants to values in excess of those obtained either under optical excitation or at low current densities (Garlick and Sayer 1961, Einstein 1957). This may be attributed to an increase in the centre transition probability δ due to increased electron density within the crystal.

Note that the analysis breaks down at very large primary current densities when $\simeq N$. Such a breakdown will be shown experimentally by saturation of the luminescence intensity and will cause the differential equations of § 2 to be non-linear.

§ 4. CONCLUSION

It has been shown that a relatively satisfactory model of the cathodoluminescence process may be set up if the mutual interaction and the recombination kinetics of both the host lattice and the luminescence centres are considered. A satisfactory description of the growth and decay processes as a function of current density is obtained, but a more complex treatment is required for a discussion of the voltage dependence.

ACKNOWLEDGMENTS

The author wishes to thank the National Research Council of Canada for a Postdoctoral Fellowship, and Professor R. E. Burgess for providing facilities.

REFERENCES

- BRANKEL'SKAYA, V. A., and TOLSTOY, N. A., 1958, *Optika i Spectrosk.*, **5**, 415.
 LIL, A., 1949, *Physica*, **15**, 361.
 EINSTEIN, P. A., 1957, *Brit. J. Appl. Phys.*, **8**, 190.
 EINBERG, R., 1959, *Nature, Lond.*, **183**, 1546.
 KOELICH, H. C., 1953, *J. Electrochem. Soc.*, **100**, 496.
 GARLICK, G. F. J., and SAYER, M., 1961, *Enlarged Abstracts, Indianapolis Meeting Electrochem. Soc.* (New York: Electrochemical Society).
 ANHL, A., 1961, *Enlarged Abstracts, Indianapolis Meeting Electrochem. Soc.* (New York: Electrochemical Society).
 RANGE, J. W., and HENDERSON, S. T., 1946, *Proc. Phys. Soc.*, **58**, 368.

Intensity Measurements in Emission on 29 Bands of the O₂ Schumann–Runge System

By G. R. HÉBERT† AND R. W. NICHOLLS

Department of Physics, University of Western Ontario

MS. received 3rd July 1961

Abstract. Relative integrated photoelectric intensity measurements have been made upon each of the $v' = 0, v'' = 9-19$; $v' = 1, v'' = 8-12$; $16-20$; $v' = 2, v'' = 7-9, 15, 16, 19-21$, bands of the Schumann–Runge System. These measurements have been interpreted, with the aid of Franck–Condon factors $q_{v'v''}$ and r -centroids $\bar{r}_{v'v''}$, to determine the variation of electronic transition moment $R_e(r)$ with internuclear separation r as

$$R_e(r) = \text{const.} (1 - 1.1807r + 0.35047r^2); \quad 1.44(\text{\AA}) < r < 1.76(\text{\AA}).$$

A 'smoothed' array of relative vibrational transition probabilities

$$p_{v'v''} = R_e^2(\bar{r}_{v'v''})q_{v'v''}$$

and band oscillator strengths $f_{v'v''}$ have thereby been determined for all bands of the system between 2450 and 5000 Å.

§ 1. INTRODUCTION

THE SCHUMANN–RUNGE band system ($B^3\Sigma_u^- - X^3\Sigma_g^-$) of O₂ and its associated photo-dissociation continuum play an important part in the absorption spectrum of the atmosphere (Goldberg 1954) also in the emission spectrum arising from missile re-entry (Meyerott 1958) and possibly in the spectrum of high altitude nuclear explosions (Griggs and Press 1961) observed over long atmospheric path lengths. It has therefore been thought worth while to make photoelectric intensity measurements in emission on as many bands as are easily accessible in order to obtain an array of relative vibrational transition probabilities for the system.

Owing to the large change $\Delta r_e (\simeq 0.4 \text{ \AA})$ in equilibrium internuclear separation, the band system is very extensive. The bands lie between 1700 Å and 4500 Å and the photo-dissociation continuum lies between 1300 and 1750 Å. The bands are wide and severely overlapped. Their locations and structure are well known. (Lochte-Holtgreven and Dieke 1929, Curry and Herzberg 1934, Knauss and Ballard 1935, Feast 1948, 1949, 1950, Brix and Herzberg 1954, Hébert and Nicholls 1961).

Many of the studies upon the system have involved absorption through cold oxygen, although some work on absorption through hot oxygen (Garton and Feast 1950, Treanor and Wurster 1960) has been done, and studies have also been made on the emission spectrum of O₂ in high voltage high pressure arcs (Feast 1948, 1949, 1950).

Nearly all of the previous work on intensity measurements of the system has been concerned with intensity measurements upon the $v'' = 0$ progression in absorption. Ladenberg and Van Voorhis (1933) measured integrated absorption coefficients of the continuum between 1300 and 1750 Å using photographic photometry. Watanabe, Inn

† Now in Department of Physics, St. Francis Xavier University, Antigonish, Nova Scotia.

and Zelikoff (1953) made photoelectric measurements on absorption from 1050 to 2000 Å in oxygen. They specifically measured partial oscillator strengths of bands between 1750 and 1910 Å and the continuum between 1750 and 1300 Å. Ditchburn and Reddell (1953, 1954) made photographic intensity measurements upon the continuum and also upon the bands of the $v'' = 0$ progression assigning oscillator strengths to each. Bethke (1959) made an accurate photoelectric intensity measurement in absorption of bands lying between 1750 and 2000 Å with pressure broadening. He inferred oscillator strengths for each band and an effective oscillator strength for the whole system. Treanor and Wurster (1960) using flash absorption through shock heated oxygen and photoelectric photometry made oscillator strength measurements upon the bands $v' = 0$, $v' = 10$ –17; $v' = 1$, $v'' = 9$ –12, 16–18; $v' = 2$, $v'' = 9, 15, 16$, and assigned an oscillator strength to the whole system.

Very little work has been done on emission intensity measurements. Keck, Camm, Rivel and Wentink (1959) made photoelectric measurements by a number of repetitive experiments on shock excited air in emission over the wavelength range 3300 to 4700 Å. In view of the strong CN impurity features in their spectra the quantitative aspects of their results must be left in some doubt. They interpreted their measurements using Franck–Condon factors calculated upon the basis of a very crude approximation.

In the present work, photoelectric intensity measurements have been made in emission upon the bands $v' = 0$, $v'' = 9$ –19; $v' = 1$, $v'' = 8$ –12, 16–20; $v' = 2$, $v'' = 7$ –9, 15, 16, 19–21.

The bands studied lie between 2400 and 4500 Å. They are degraded towards the red and exhibit extensive overlapping due to the high gas temperature in the high voltage arc through oxygen at atmospheric pressure in which the system was excited. The triplet splitting of the lines was not resolved at the dispersions used, and the bands appeared to have a $^1\Sigma$ – $^1\Sigma$ structure.

The heavy overlap between adjacent bands precluded the use of simple intensity measurement techniques such as the fractional band intensity method or the method of ‘separation of contour’. Thus the ‘rotational line intensity intercept method’ (Robinson and Nicholls 1961) which is described more fully below was used.

§ 2. THEORY

It is well known that the intensity $I_{v'v''}$ of a band may be represented by

$$I_{v'v''} = DN_v E_{v'v''}^4 R_e^2(\bar{r}_{v'v''}) q_{v'v''} \quad (1)$$

where D is a constant associated with the units and the geometry, N_v is the population of the v' level, $E_{v'v''}$ is the energy quantum of the band, $R_e(r)$ is the electronic transition moment of the system (Fraser 1954), $q_{v'v''}$ is the Franck–Condon factor and $\bar{r}_{v'v''}$ is the r -centroid.

Provided that computed arrays of $\bar{r}_{v'v''}$ and $q_{v'v''}$ and measured values of $I_{v'v''}$ are available this equation may be used:

(i) To infer the variation of electronic transition moment with internuclear separation from plots of $(I_{v'v''}/q_{v'v''}E_{v'v''}^4)^{1/2}$ against $\bar{r}_{v'v''}$ for each v'' progression, with appropriate rescaling to account for the variation of the N_v term.

(ii) To obtain a smoothed array of relative vibrational transition probabilities

$$p_{v'v''} = R_e^2(\bar{r}_{v'v''}) q_{v'v''} \quad (2)$$

for the whole band system.

(iii) In some cases to obtain the variation of $N_{v'}$ with v' from the rescaling factor of (i).

This method has been previously applied to a number of band systems, most of which have exhibited unoverlapped bands so that measurements of $I_{v'v''}$ were not, in principle, difficult to make (see for example Nicholls 1956, 1958, Dixon and Nicholls 1958, Robinson and Nicholls 1958a, b). Bands of the O_2 Schumann–Runge system however overlap strongly and thus recourse has been made in this work to the rotational line intensity intercept method to measure $I_{v'v''}$. The basis of the method is as follows.

The intensity ($I_{K'K''}$) in emission of an individual rotational line of a band is, assuming thermal equilibrium,

$$I_{K'K''} = \text{const} \frac{N_{v'}^4}{Q} \nu_{K'K''}^4 S_{K'K''} R_e^2(\bar{r}_{v'v''}) q_{v'v''} \exp\left(\frac{-E_{\text{rot}}}{kT_{\text{rot}}}\right) \quad (3)$$

where the constant depends upon the geometry and the units employed, Q is the rotational partition function of v' , $\nu_{K'K''}$ is the wave number of the line, E_{rot} is the rotational energy term of the v' , k is Boltzmann's constant and T_{rot} is the rotational temperature. Dividing equations (1) and (3),

$$\frac{I_{K'K''}}{I_{v'v''}} = \frac{S_{K'K''}}{Q} \exp\left(\frac{-E_{\text{rot}}}{kT}\right) \quad (4)$$

if the justifiable approximation $E_{K'K''} = E_{v'v''}$ be made (Fraser 1958). Thus if thermal equilibrium is maintained in the source, a plot of $\ln I_{K'K''}/S_{K'K''}$ against E_{rot} is linear, of slope $-1/kT$ and has a relative intercept on the ordinate axis of $\ln I_{v'v''}/Q$. If such a plot is made for each band of the system (using sufficient line intensity measurements to establish the plot for each band), relative integrated intensities $I_{v'v''}$ may be determined from relative differences on the ordinate scale.

For some band systems it is sufficient to use $B_v K(K+1)$ for E_{rot} in the above plots. For the Schumann–Runge system the more complete expression

$$B_v K(K+1) - D_v K^2(K+1)^2$$

was necessary.

The method has previously been used by Robinson and Nicholls (1958a, b, 1960) for the NO β and BO α , β systems and by Treanor and Wurster (1960) in absorption measurements on Schumann–Runge bands.

§ 3. EXPERIMENTAL PROCEDURES

3.1. Excitation

The band system was excited in a 900–1000 volt a.c. arc between 3/16 in. Pt–Rh electrodes in flowing oxygen at a pressure of a few millimetres above atmospheric in a 1 litre round-bottom flask. Tungsten rods were mounted in ball and socket joints attached at diametrical points to the flask and Pt–Rh tips were attached to the ends of the rods by barrel connectors. The current in the circuit was controlled by a Variac and limited to 400 mA. by a 5000 ohm ballast resistance. At this current the electrode tips became white hot and emitted electrons thermionically. The spectrum was comparable in intensity to that of an iron arc at 2500 °K. The source was similar to that used by Feast (1950).

3.2. Identifications

A complete photographic survey was made of the spectrum of the source prior to making photoelectric intensity measurements on it. A Baird-Atomic 3 metre Eagle mounting grating spectrograph was employed and the spectrum of interest between 80 and 4500 Å photographed in the second and third orders of a 15 000 lines in^{-1} concave grating at a reciprocal dispersion of about 2.7 and 1.7 Å mm^{-1} . They were photographed in three sections: $\lambda 2480\text{--}3000\text{ Å}$, including the 0-10, 11; 1-9, 10, 11, 12; 2-7, 8, 9 bands, $\lambda 3000\text{--}3700\text{ Å}$, including the 0-12, 13, 14, 15, 16; 1-11, 12, 16, 17; 2-15, 16 bands and $\lambda 3700\text{--}4500\text{ Å}$ including the 0-14, 15, 16, 17, 18, 19; 1-16, 17, 18, 19, 20; 2-20, 21 bands.

Identifications of individual lines were made from large scale prints of spectrograms with the aid of the analyses of Lochte-Holtgreven and Dieke (1929) and of Feast (1950). The previously unanalysed band, the (0, 9) at $\lambda 2763.4\text{ Å}$ has been analysed (Hébert and Nicholls 1961).

3.3. Intensity Measurements

After development of a stable source, and a complete identification of all of its spectral features, a calibrated Leeds and Northrup scanning spectrometer (Fastie 1952) was employed to measure relative intensities of lines in each of the bands mentioned in the previous section. The 1P28 photomultiplier of the instrument was sensitive over the wavelength range 2100 to 7000 Å. The instrument had a 10 μ entrance slit and a 20 μ exit slit.

The response of the instrument was calibrated with respect to a Philips tungsten tip filament lamp. Spectral emissivity $E_{\lambda,T}$ data of Larrabee (1959) and of de Vos (1954) were used respectively in the wavelength ranges 3500-4500 Å and 2400-3500 Å. The black body distribution tables of Lowan and Blanch (1940) were also used to rectify the response $R_{K'K''}$ (as read from the trace of the spectrometer record) into line intensity $I_{K'K''}$ through the equation

$$I_{K'K''} = R_{K'K''} E_{\lambda,T} I_{\text{bl}\lambda} / R_{\text{w}\lambda} \quad (5)$$

where $R_{\text{w}\lambda}$ is the response to the emission from the standard lamp at the line wavelength λ .

§ 4. RESULTS

4.1. Line Intensities

The spectral line profiles were planimeted for as many lines per band as were effectively non-overlapped. On the average, twenty to thirty lines per band were accessible. For each line, the resulting area under its profile was multiplied by the $T I_{\text{bl}\lambda} / R_{\text{w}\lambda}$ from equation (5) to give the line intensity $I_{K'K''}$.

4.2. Band Intensities

Semi-logarithmic plots of $\ln I_{K'K''} / S_{K'K''}$ against $B_{v'K'}(K'+1) - D_{v'K'}(K'+1)^2$ were made for each of the 29 bands mentioned in § 1. The $B_{v'}$ and $D_{v'}$ values adopted are those of Curry and Herzberg (1934) and of Feast (1950). That is $B_0' = 0.813\text{ cm}^{-1}$, $B_1' = 0.798\text{ cm}^{-1}$, $B_2' = 0.7845\text{ cm}^{-1}$, $D_{v'} = 4.38 \times 10^{-6}\text{ cm}^{-1}$ for $v' = 0, 1, 2$. $S_{K'} = K$ for the P branch and $K+1$ for the R branch. An example of the disposition of points

on such a plot is shown on figure 1 for (1, 10). It has a clear linear trend. Straight lines could be fitted to the plots for all bands except (1, 16), (2, 16) and (2, 19) for each of which rather few isolated spectral lines could be measured. A best 'least square' straight line was fitted to each of the other 26 bands using an I.B.M. 650 computer programme at the University of Western Ontario, Computation Centre. The slope

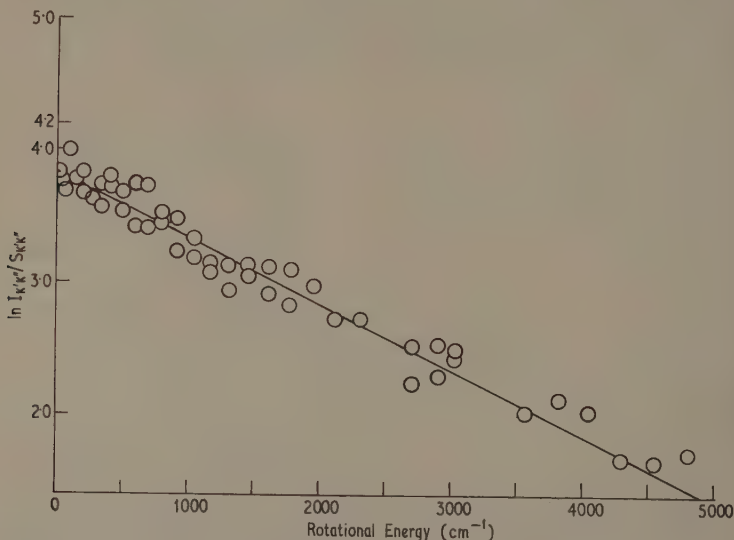


Figure 1. $\ln I_{K'K''}/S_{K'K''}$ against $B_{v'}K'(K'+1) - D_{v'}K'^2(K'+1)^2$ for the (1, 10) band.

were almost identical, consistent with a rotational temperature of 2150 °K existing in the arc. This is some confirmation of the adequacy of the procedure.

In the case of the (1, 16), (2, 16) and (2, 19) bands, severe line overlap prevented measurement of sufficient line intensities to yield enough points for a linear semi-logarithmic plot. The following procedure was therefore adopted. The centroid of the plotted points was calculated in each case and a straight line of the same slope as that determined for the other 26 bands, was placed through it.

The intercepts on the ordinate axis of each of the 29 linear semi-logarithmic plots were then measured and subtracted from that of the most intense (2, 8) band. In this way an array of relative $I_{v'v''}$ values were determined as described in § 2 and these are displayed in table 1. They are integrated relative vibrational intensities determined band by band.

4.3. Electronic Transition Moment and Smoothed Relative Vibrational Transition Probabilities

The set of $I_{v'v''}$ derived band by band in the manner described above can be interpreted as described in § 2 with the aid of the Franck-Condon factors $q_{v'v''}$ and r -centroids $\bar{r}_{v'v''}$ to provide information upon the variation of $R_e(r)$ with r , and thereby by use of equation (3) to provide a smoothed array of relative vibrational transition probabilities $p_{v'v''}$ for the whole band system.

Table 1
Measured Relative Integrated Band Intensities $I_{v'v''}$ for the O₂ Schumann-Runge System

$\frac{v''}{v'}$	7	8	9	10	11	12	13	14	15	16	17	18	19	20	21
0	—	—	71.1	58.3	64.4	48.4	38.2	30.2	16.5	9.70	6.60	2.50	1.58	—	—
1	—	79.4	95.4	89.4	67.2	25.9	—	—	—	3.66	5.74	7.76	3.62	2.44	—
2	58.1	100.0	96.9	—	—	—	—	—	3.13	1.60	—	—	1.32	2.73	2.14

Table 2

Wavelengths $\lambda_{0,v''}$, r-centroids $r_{v',v''}$, Franck-Condon Factors $q_{v',v''}$, Smoothed Relative Vibrational Transition Probabilities $P_{v',v''}$, Intensities at Infinite Temperature I_{∞} , for the O₂ Schumann-Runge Band System

v''	7	8	9	10	11	12	13	14	15	16	17	18	19	20	21
0	(2566.6)	2661.8	2763.4	2870.6	2984.3	3105.1	3233.8	3371.6	3517.6	3674.3	3842.2	4022.3	4215.9	(4469.5)	—
	1.481	1.498	1.516	1.535	1.553	1.573	1.593	1.615	1.636	1.660	1.684	1.710	1.736	1.765	—
	4.72-3	1.25-2	2.80-2	5.36-2	8.67-2	1.21-1	1.46-1	1.53-1	1.38-1	1.07-1	7.21-2	4.16-2	2.05-2	8.60-3	3.04-3
	6.98-2	1.25-1	1.84-1	2.26-1	2.36-1	2.06-1	1.56-1	1.01-1	5.95-2	3.19-2	1.67-2	8.68-3	4.45-3	2.14-3	—
1	9.46-1	1.97	3.36	4.77	5.86	5.99	5.32	4.06	2.85	1.82	1.14	7.09-1	4.39-1	2.67-1	—
	2521.9	2614.7	2712.0	2815.1	2924.2	3040.2	3162.5	3293.7	3433.4	3584.0	3743.3	3913.9	4097.1	4293.6	(4475.8)
	1.473	1.490	1.507	1.525	1.543	1.562	1.582	1.602	1.623	1.646	1.669	1.694	1.720	1.747	1.776
	2.05-2	4.26-2	7.08-2	9.27-2	9.20-2	6.29-2	2.18-2	1.03-4	1.83-2	6.70-2	1.14-1	1.30-1	1.12-1	7.60-2	4.14-2
2	4.59-2	7.51-2	9.73-2	9.69-2	7.27-2	3.69-2	9.37-3	3.26-5	4.40-3	1.26-2	2.14-2	2.07-2	2.05-2	1.85-2	1.51-2
	3.64+1	5.14+1	5.76+1	4.94+1	3.18+1	1.38+1	3.00	8.88-3	1.02-1	2.44	3.01	2.83	2.33	1.74	1.20
	2481.1	2570.0	2664.0	2762.4	2867.6	2979.0	(3092.7)	3223.0	3357.8	3501.0	3651.2	(3837.1)	3988.4	4174.3	4373.8
	1.465	1.482	1.498	1.516	1.534	1.553	1.572	1.592	1.612	1.634	1.656	1.679	1.704	1.730	1.758
3	4.42-2	6.90-2	7.82-2	5.80-2	2.00-2	7.35-7	2.14-2	6.07-2	6.96-2	3.56-2	1.92-3	1.54-2	7.00-2	1.18-1	1.25-1
	1.11-1	1.36-1	1.23-1	6.96-2	1.82-2	4.97-7	1.07-2	2.24-2	6.92-2	7.51-3	3.34-4	2.43-3	1.16-2	2.37-2	3.50-2
	9.33+1	1.00+2	7.79+1	3.83+1	8.62	2.00-4	3.75	6.64	4.85	1.60	6.0-2	3.58-1	1.46	2.50	3.06

Legend: $\lambda(\text{vac})$ band origin (calculated values in parentheses)

$r_{v',v''}$ (A) (Jarman 1960)

$q_{v',v''}$ (Nicholls 1960)

$P_{v',v''}$ (Smoothed)

Note: The positive or negative number in some entries is the power of ten by which the preceding number is multiplied.

Franck-Condon factors $q_{v'v''}$ (Nicholls 1960) for the transition were computed for a Morse model by direct integration of the wave functions using an I.B.M. 704 computer at the U.S. National Bureau of Standards, Computation Laboratory. r -centroids were calculated by W. R. Jarman. Both of these quantities are displayed in table 2.

A plot of $(I_{v'v''}\lambda_{v'v''}^4/q_{v'v''})^{1/2}$ against $\bar{r}_{v'v''}$ was made for bands of the $v' = 0, 1, 2$ progressions. Plots of $\log(I_{v'v''}\lambda_{v'v''}^4/q_{v'v''})^{1/2}$ against $\bar{r}_{v'v''}$ for each progression are shown in figure 2. It will be noted that the curves (one for each progression) are parallel. As is clear from equation (1) they are separated in relative ordinate by a factor which is proportional to $\log N_v^{1/2}$. The curves were 'rescaled' by simple linear displacement on the ordinate axis. The equivalent linear plot of $(I_{v'v''}\lambda_{v'v''}^4/q_{v'v''})^{1/2}$ against $\bar{r}_{v'v''}$ was then made of the rescaled points and is shown in figure 3. A best 'least squares' parabola of the form $R_e(r) = a + br + cr^2$ was fitted to the points and found to be

$$R_e(r) = \text{const}(1 - 1.1807r + 0.35047r^2) \quad 1.44(\text{\AA}) < r < 1.76(\text{\AA}). \quad (6)$$

No superlative accuracy is to be inferred from the large number of significant figures carried in the coefficients. They are required to overcome cancellation.

The array of smoothed relative vibrational transition probabilities

$$p_{v'v''} = R_e^2(\bar{r}_{v'v''})q_{v'v''}$$

or 'band strengths' derived from equation (3) are also displayed in table 2 together, for comparison, with values of intensities at infinite temperatures $I = p_{v'v''}/\lambda_{v'v''}^4$.

The relative displacements ($\log N_v^{1/2}$) of the curves of figure 2, lead to the ratio $N_0 : N_1 : N_2 : 1000 : 57 : 26$, from which an effective vibrational temperature of 1460 °K can be inferred.

§ 5. DISCUSSION

The probable error in measured relative intensity of each band was estimated and the overall effect of this upon the plots leads to probable errors in $p_{v'v''}$ values of 5% for bands on the $v' = 0$ progression, 11% for bands in the $v' = 1$ progression and 12% for bands in the $v' = 2$ progression. Exceptions to these estimates were the (0, 10), (0, 17), (0, 18), (0, 19), (1, 16), (1, 17), (1, 18), (1, 20), (2, 18), (2, 22) bands for which estimated errors (%) are respectively 8, 6, 12, 14, 19, 19, 20, 24, 22, 18. Treanor and Wurster (1960), results of whose photographic photometry on the system are discussed below, estimate their error at 25%.

Treanor and Wurster (1960) inferred $R_{v'v''}^2 = p_{v'v''} = R_e^2(\bar{r}_{v'v''})q_{v'v''}$ in absolute atomic units band by band in $v' = 0, 1, 2$ progressions from heterochromatic photographic absorption measurements upon lines of the Schumann-Runge system in shock heated oxygen. A band oscillator strength $f_{v'v''}$ can be derived from the equations

$$f_{v'v''} = \frac{8\pi^2 mc}{3\hbar e^2} \nu_{v'v''} R_{v'v''}^2 = \frac{8\pi^2 mc}{3\hbar e^2} \nu_{v'v''} R_e^2(\bar{r}_{v'v''})q_{v'v''} \quad (7)$$

$$= \frac{302}{\lambda(\text{\AA})} R_{v'v''}^2 (\text{atomic units})^2. \quad (8)$$

They also took an average value for \bar{R}_e^2 of 0.51 atomic units from the bands which they studied and thereby assigned an 'effective' oscillator strength to the whole system

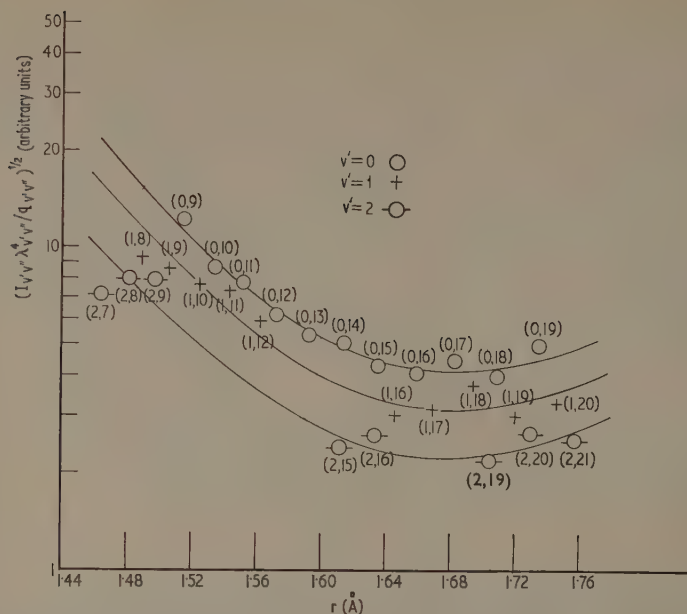


Figure 2. Comparative plots of $\ln(I_{v'v''} \lambda_{v'v''}^4 / q_{v'v''})^{1/2}$ against $\bar{r}_{v'v''}$ for the $v' = 0, 1, 2$ progressions.

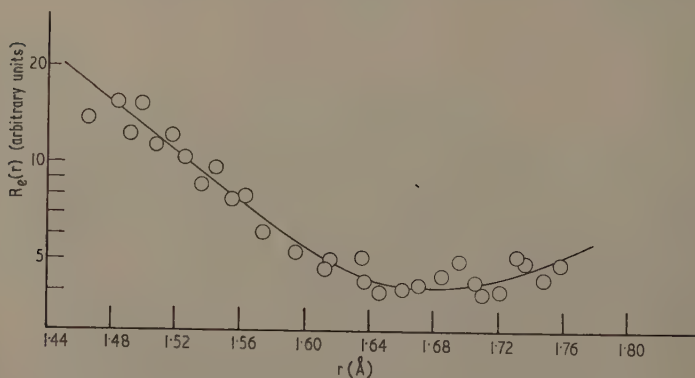


Figure 3. The electronic transition moment $R_e(r)$ as a function of r .

through the equation

$$f = \frac{8\pi^2 mc}{3\hbar e^2} \bar{R}_e^2 = 0.048.$$

The limitations of the concept of an effective oscillator strength for a complete band system which should be treated with great caution and which has also been used by other workers, are discussed below.

A very useful comparison can be made between Treanor and Wurster's absolute values of $p_{v'v''}$, which were obtained band by band, and our smoothed relative values derived from measurements on the whole system. In figures 4, 5 and 6, in which are plotted $p_{v'v''}$ against v'' for $v' = 0, 1, 2$, the two sets of data are compared. Our measurements, on the whole show smooth, undulating variation of $p_{v'v''}$ with v'' as would be expected. Treanor and Wurster's data are a little more fragmentary, but show good

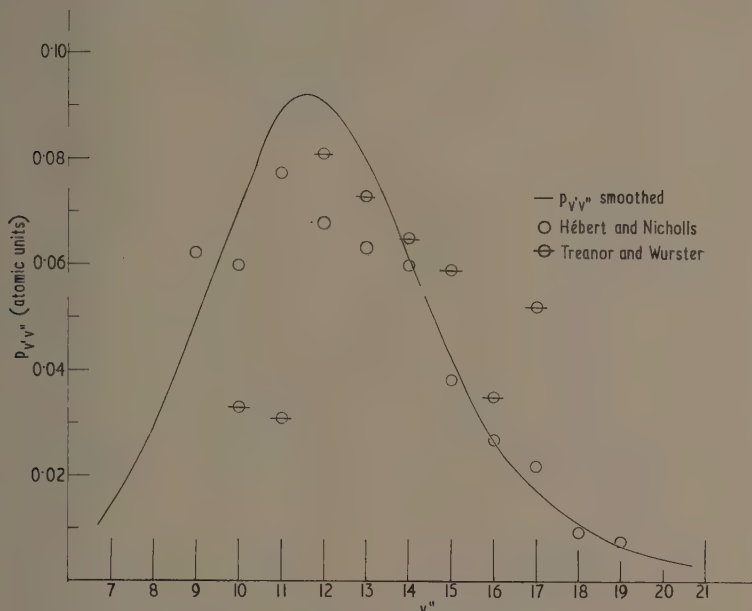


Figure 4. Smoothed relative vibrational transition probability $p_{v'v''}$ against v'' for the $v' = 0$ progression compared with $|R_{v'v''}^2|$ of Treanor and Wurster (1960).

general agreement in trend with ours for the $v' = 0$ progression. Agreement is poorer in the $v' = 1, 2$ progressions. Their points for small values of v'' (corresponding to wavelengths less than about 3000 Å) seem to be consistently low; possibly as an artefact of heterochromatic photographic photometry.

It is possible to make our values absolute by scaling them to agree with Treanor and Wurster's over a large segment of the $v' = 0$ progression. The band oscillator strengths which can be assigned to Treanor and Wurster's measurements are

$$f_{v'v''} = 302R_{v'v''}^2/\lambda(\text{\AA})$$

and the scaling procedure when applied to our data gives smoothed band oscillator strengths

$$f_{v'v''} = 457p_{v'v''}/\lambda(\text{\AA}).$$

In table 3 are displayed the oscillator strengths thereby derived from our measurements scaled onto the $v' = 0$ progression of Treanor and Wurster. Bethke (1959) has made a study in absorption through cold oxygen of intensities of the $v'' = 0$ progression of bands and has also derived a series of oscillator strengths band by band for this progression. His data are also incorporated in table 3.

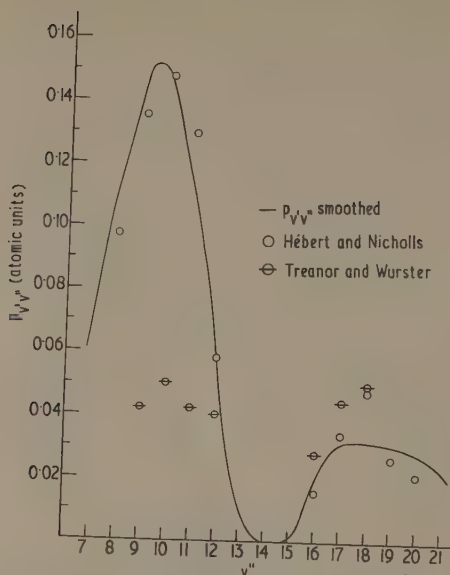


Figure 5. Smoothed relative vibrational transition probability $p_{v'v''}$ against v'' for the $v' = 1$ progression compared with $|R_{v'v''}^2|$ of Treanor and Wurster (1960).

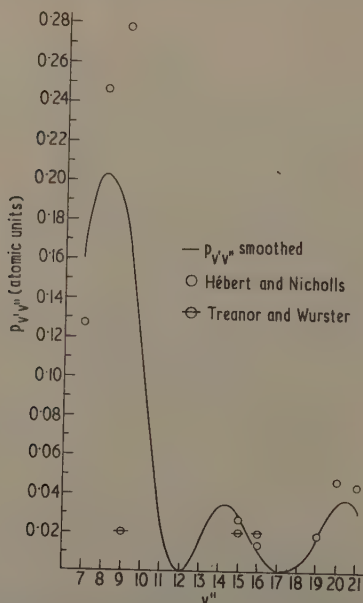


Figure 6. Smoothed relative vibrational transition probability $p_{v'v''}$ against v'' for the $v' = 2$ progression compared with $|R_{v'v''}^2|$ of Treanor and Wurster (1960).

Table 3
Band Oscillator Strengths $f_{v'v''}$ for the O₂ Schumann-Runge Band System

(a) Smoothed $f_{v'v''}$ for the $v' = 0, 1, 2$ progressions

$\frac{v''}{v'}$	7	8	9	10	11	12	13	14	15	16	17	18	19	20	21
0	1.68-3	3.38-3	5.56-3	7.59-3	8.97-3	8.82-3	7.52-3	5.50-3	3.70-3	2.26-3	1.36-3	8.06-4	2.73-4	—	—
1	8.32-3	1.313-2	1.640-2	1.573-2	1.136-2	5.55-3	1.35-3	1.12-5	5.86-4	1.61-3	2.61-3	2.42-3	2.29-3	1.97-3	1.54-3
2	2.045-2	2.418-2	2.110-2	1.151-2	2.90-3	7.62-8	1.58-3	3.18-3	2.61-3	9.80-4	4.18-5	2.89-3	1.33-3	2.60-3	3.66-3

(b) Individual $f_{v'0}$ values of Bethke (1958) for the $v'' = 0$ progression

$\frac{v''}{v'}$	2	3	4	5	6	7	8	9	10	11	12	13	14	15	16	17
0	2.3-8	7.4-8	2.74-7	7.28-7	1.73-6	3.56-5	6.75-5	1.07-5	1.56-5	2.16-5	2.81-5	3.17-5	3.24-5	3.26-5	3.16-5	2.94-5

Note the negative number in each entry is the
 power of ten by which the preceding number is
 multiplied.

It was mentioned above that the results of the increasingly common process of averaging or summing in certain ways band oscillator strengths $f_{v'v''}$ to provide an effective electronic oscillator strength f_{el} for a complete band system, should be treated with some reserve. In such work the assumption is often made that

$$f_{el} = f_{v'v''} E_{00} / q_{v'v''} E_{v'v''}.$$

Weber and Penner (1957), Bethke (1959), Keck, Camm and Kivel (1958), Keck, Camm, Kivel and Wentink (1959) and others have used such a process to assign oscillator strengths to complete band systems in discussions of the molecular contribution to the emissivity of hot gases. The above relation may be formally derived by asserting that

$$f_{el} = \sum_{v'} f_{v'0}$$

performing the summation over v' in equation (7) and dividing equation (7) by the result.

The sweeping assumptions made in such a derivation are (i) constancy of $R_e(r)$ over the whole system, (ii) summability of $f_{v'0}$ and (iii) the adequacy of E_{00} to represent the average energy quantum of the whole transition. We have shown that $R_e(r)$ is by no means constant over the whole system. The adequacy of E_{00} as an average, particularly in extensive systems is also open to question.

Thus although the $f_{v'v''}$ are of great quantitative value in the interpretation of spectral intensities, the applicability of f_{el} to better than a rough order of magnitude guide is open to serious question.

Note added in proof.—It has been pointed out by J. W. Chamberlain of Yerkes Observatory in private conversation that $p_{v'v''}$ could properly be called 'band strength' rather than the cumbersome, dimensionally incorrect though conventional 'relative vibrational transition probability'.

ACKNOWLEDGMENTS

This work has been supported in part by research grants from The National Research Council of Canada and The Ontario Research Foundation and in part by Contracts with the U.S. Air Force Cambridge Research Centre, The Air Force Office of Scientific Research and The Office of Naval Research.

One of us (G.R.H.) has been the recipient of an Ontario Research Foundation fellowship which is gratefully acknowledged.

REFERENCES

- BETHKE, G. W., 1959a, *J. Chem. Phys.*, **31**, 662, 669.
- BRIX, P., and HERZBERG, G., 1954, *Canad. J. Phys.*, **32**, 110.
- CURRY, J., and HERZBERG, G., 1934, *Ann. Phys., Lpz.*, **19**, 800.
- DITCHBURN, R. W., and HEDDLE, D., 1953, *Proc. Roy. Soc. A*, **220**, 61.
- 1954, *Proc. Roy. Soc. A*, **226**, 509.
- DIXON, R. N. and NICHOLLS, R. W., 1958, *Canad. J. Phys.*, **36**, 127.
- FASTIE, W. G., 1952, *J. Opt. Soc. Amer.*, **42**, 9.
- FEAST, M. W., 1948, *Nature, Lond.*, **162**, 214.
- 1949, *Proc. Phys. Soc. A*, **62**, 114.
- 1950, *Proc. Phys. Soc. A*, **63**, 549.
- FRASER, P. A., 1954, *Canad. J. Phys.*, **32**, 515.
- 1958, *Scientific Report No. 4*, Contract AF 9(604)–1718, University of Western Ontario.
- GARTON, W. R. S., and FEAST, M., 1950, *Nature, Lond.*, **165**, 281.

- GOLDBERG, L., 1954, *The Earth as a Planet* (Ed. G. P. Kuiper; Chicago: University Press), Chapter 9.
- GRIGGS, D. T., and PRESS, F., 1961, *J. Geophys. Res.*, **66**, 237.
- HÉBERT, G. R., and NICHOLLS, R. W., 1961, *J. Atmos. Terr. Phys.*, **21**, 213.
- KECK, J., CAMM, J., and KIVEL, B., 1958, *J. Chem. Phys.*, **28**, 723.
- KECK, J., CAMM, J., KIVEL, B., and WENTINK, T., 1959, *Ann. Phys., N.Y.*, **7**, 1.
- KNAUSS, H. P., and BALLARD, S. S., 1935, *Phys. Rev.*, **48**, 790.
- LADENBURG, R., and VAN VOORHIS, C. C., 1933, *Phys. Rev.*, **43**, 315.
- LARRABEE, R., 1959, *J. Opt. Soc. Amer.*, **49**, 619.
- LOCHTE-HOLTGREVEN, W., and DIEKE, G. H., 1929, *Ann. Phys., Lpz.*, **3**, 937.
- LOWAN, A. N., and BLANCH, G., 1940, *J. Opt. Soc. Amer.*, **30**, 937.
- MEYEROTT, R. E., 1958, *Combustion and Propulsion, Third Agard Colloquium* (Ed. S. S. Penner; London: Pergamon) p. 431.
- NICHOLLS, R. W., 1956, *Proc. Phys. Soc. A*, **69**, 741.
- 1958, *Ann. Géophys.*, **14**, 208.
- 1960, *Canad. J. Phys.*, **38**, 1705.
- ROBINSON, D., and NICHOLLS, R. W., 1958a, *Intensity Measurements of Molecular Spectra, Scientific Report No. 5, Contract AF 19(604)-1718*, University of Western Ontario.
- 1958b, *Proc. Phys. Soc.*, **71**, 957.
- 1960, *Proc. Phys. Soc.*, **75**, 817.
- 1961, *J. Quant. Spect. and Rad. Transf.*, **1**, 76.
- TREANOR, C., and WURSTER, W., 1960, *J. Chem. Phys.*, **32**, 758.
- DE VOS, J. C., 1954, *Physica*, **20**, 690.
- WATANABE, K., INN, E. and ZELIKOFF, M., 1953, *J. Chem. Phys.*, **21**, 1026.
- WEBER, D., and PENNER, S. S., 1957, *J. Chem. Phys.*, **26**, 860.

Measurements of Quenching of Ortho-positronium in Gases

By F. F. HEYMANN†, P. E. OSMON‡, J. J. VEIT†§, AND
W. F. WILLIAMS‡

† University College, London

‡ Norwood Technical College, London

MS. received 28th June 1961

Abstract. Three photon annihilations of ortho-positronium in gases as a function of pressure have been investigated using a scintillation spectrometer technique. Quenching rates per atmosphere were determined for argon ($0.035\lambda_0$), neon ($0.024\lambda_0$), helium ($0.014\lambda_0$), oxygen ($3\lambda_0$), nitric oxide ($400\lambda_0$), and carbon dioxide ($0.08\lambda_0$), the last three being only very approximate. λ_0 is the natural annihilation rate of ortho-positronium, $0.7 \times 10^7 \text{ sec}^{-1}$. The high quenching rates in oxygen and nitric oxide are attributed to ortho-to-para conversion by electron exchange. The order of magnitude of the smaller quenching rates is understandable if the positronium atom annihilates with an electron of a gas molecule during collision (pick-off quenching).

§ 1. ANNIHILATION PROCESSES

TWO KINDS of annihilations of positrons emitted into a gas are possible: (i) free annihilations, or annihilations in flight, (ii) bound annihilations, i.e. from the bound states of an electron-positron pair (positronium). In both cases the spins of the pair may be parallel (triplet) or anti-parallel (singlet).

It follows from invariance under charge conjugation that the singlet state of a pair annihilates into an even number of photons and the triplet state into an odd number. Conservation of energy and momentum require that at least two photons are created per annihilation. The probability of annihilation decreases very rapidly the greater the number of photons created. Therefore for all practical purposes singlet states decay into two photons, triplet states into three. The cross section for free singlet annihilations between unpolarized electrons and positrons has been shown (Dirac 1930) to be

$$\sigma_{2\gamma} = \pi r_0^2 \frac{c}{v}$$

for free positrons of non-relativistic velocity v , where r_0 is the classical electron radius.

After allowing for the greater statistical weight it is found (Dirac 1930, Radcliffe 1951) that annihilations from the free triplet state are $1115/3 \approx 372$ times less likely and can therefore be ignored in what follows.

The rate of free annihilations in a gas is therefore

$$\Lambda_1 = n_e \sigma_{2\gamma} v$$

where n_e is the electron density in the path of the positron. If N = Loschmidt's number, p = pressure in atmospheres, and K = effective number of electrons per atom, $n_e = KNp$ and $\Lambda_1 = \pi K p N r_0^2 c$. (High energy positrons are repelled by the field of the

§ Now at Physics Department, University of British Columbia.

om so that $K < Z$, the atomic number; slow positrons polarize the atom so that $K > Z$.)

It is convenient to define λ_f the free annihilation rate per atmosphere of gas

$$\lambda_f = \pi K N r_0^2 c = \frac{\Lambda_f}{p}.$$

The annihilation rates from the bound states of positronium can also be calculated:

(i) From singlet or para-positronium

$$\lambda_p = 4n_e^1 \sigma_{2\gamma} v$$

where n_e is again the density of electrons in the path of the positron, and so

$$\lambda_p = (4|Y_{r=0}|^2)^1 \sigma_{2\gamma} v.$$

For S states with quantum number n this reduces to

$$\begin{aligned} \lambda_p &= \frac{1}{\pi} \left(\frac{me^2}{2n\hbar^2} \right)^3 4\pi r_0^2 \frac{c}{v} v \\ &= 0.8 \times 10^{10} n^{-3} \text{ sec}^{-1}. \end{aligned}$$

(ii) From triplet or ortho-positronium the annihilation rate is 1115 times smaller

$$\begin{aligned} \lambda_0 &= \frac{1}{1115} \lambda_p \\ &= 0.7 \times 10^7 n^{-3} \text{ sec}^{-1}. \end{aligned}$$

In a two-photon annihilation the total energy of the pair is shared equally between the photons. If annihilation is from rest the photons are emitted in opposite directions; alternatively the angle between the emitted photons is a measure of the momentum of the pair before annihilation. In the three-photon case Ore and Powell (1949) have calculated the energy spectrum of the photons, which are coplanar for annihilation from rest.

§ 2. QUENCHING

The term 'quenching' was initially applied to the conversion of ortho-positronium to para-positronium. As the latter, singlet, form has a lifetime so much shorter, this effectively resulted in the destruction or quenching of the positronium. The term is here applied more generally to any process whereby two-photon annihilation replaces three. There are a number of possible quenching processes.

(i) *Exchange quenching.* Atoms and molecules with an unpaired electron (e.g. atomic hydrogen, alkali atoms, nitric oxide) may exchange an electron with a positronium atom during a collision, and in some of these exchanges ortho- to para- will occur. The probability of conversion is one per four collisions (as the statistical weights of triplet and singlet states are in the ratio 3:1) and the cross section for quenching is therefore one quarter of the elastic cross section. (The energy difference between the ground states of ortho- and para-positronium is 8.5×10^{-4} eV which is negligible compared with the kinetic energy of the positronium atom even at thermal energies.) The exchange quenching cross section is therefore energy dependent, increasing rapidly at low positronium energies (Massey and Mohr 1954).

(ii) *Angular momentum processes.* It has been suggested (Gittelmann and Deutsch 1955–1956) that one of the quenching processes effective in oxygen (in addition to exchange) may be triplet–singlet conversion of the positronium atom with a reorientation of the angular momentum of the oxygen molecule.

(iii) *Chemical quenching.* This is the enhanced annihilation rate of ortho-positronium when it is bound to another atom to form a molecule. The observed high quenching cross section of chlorine (Deutsch 1953) is believed to occur in this way. A related process is the attachment of free positrons which is believed to have been observed in freon (CCl_2F_2) (Deutsch 1953).

(iv) *Pick-off quenching.* During any collision between a positronium atom and a gas molecule the positron of the former is temporarily in a region of higher electron density and so is more likely to annihilate. The time spent in the region of higher electron density is inversely proportional to the velocity of the positronium atom (assuming no scattering) and so also, therefore, will be the pick-off quenching cross section, while the quenching rate will be velocity independent. It is possible to make crude estimates of pick-off quenching rates similar to the free annihilation rate estimate above.

(v) *Spin reversal.* Reversal of spin of either component of the positronium atom during a collision by interaction with the magnetic moment of the gas molecule is possible but is expected (Massey and Mohr 1954) to have a cross section at least an order of magnitude smaller than those observed.

A quenching rate $\Lambda_q = Np\sigma_q v$ can be defined for each of the above processes, the rates being additive where more than one process is taking place. For the particular case of pick-off quenching which occurs universally (though it is masked by the much more effective exchange quenching where this occurs) the quenching rate is expected to be nearly independent of positronium energy. Since quenching rate is proportional to gas pressure it is appropriate to express experimental results as quenching rates per atmosphere of gas λ_q .

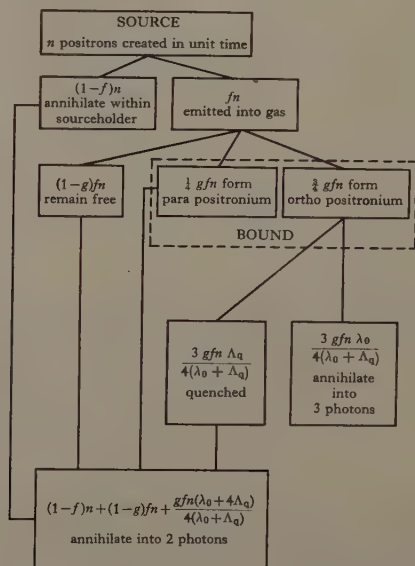


Figure 1. Fate of positrons in a gas (simplified).

For a mixture of gases the quenching contributions from the different gases are additive so that the resulting quenching rate for the mixture is

$$\Lambda_q = p\lambda_q = p_1\lambda_1 + p_2\lambda_2 + \dots$$

where the p 's are the partial pressures in atmospheres of the gases and the λ_q 's their quenching rates per atmosphere.

Figure 1 is a block diagram to show the fates of positrons emitted into a gas.

§ 3. METHOD

The purpose of the observations reported in this paper was to measure quenching rates in a variety of gases in order to provide evidence for the existence of at least two distinct quenching mechanisms.

Two possible distinct methods are available: (A) The multiplicity of the annihilation radiation can be observed either by using counters in coincidence (DeBenedetti and Siegel 1952, Wheatley and Halliday 1952, Pond 1952) or by measuring the energies of the photons (Deutsch 1953, Lewis and Ferguson 1953, Hughes, Marder and Wu 1954). (B) Alternatively the lapse of time between the creation of a positron (which must be marked by the emission of a nuclear gamma ray) and its annihilation can be measured by using counters in delayed coincidence (Deutsch 1953, Lewis and Ferguson 1953, Daniel and Stump 1959). Three mean lifetimes should be distinguishable: (i) the free positron lifetime inversely proportional to gas pressure and equal to Λ_f^{-1} ; (ii) the para-positronium mean lifetime of $\lambda_p^{-1} \sim 10^{-10}$ sec, which is negligibly short for our purposes; (iii) the ortho-positronium mean lifetime $\Lambda_0^{-1} = (\lambda_0 + \Lambda_q)^{-1}$ which is pressure dependent.

Both 'multiplicity' and 'lifetime' methods have been used by other workers. In this paper the work described has all been carried out using the multiplicity method.

The source of positrons was approximately $\frac{1}{4}$ mc of sodium 22 sandwiched between two mica sheets 6 mg cm⁻² thick and 2 cm in diameter and held in the centre of the gas chamber (figure 2). Sodium 22 emits 1.3 mev gamma rays and 560 kev positrons and has a half-life of 2.6 years. Referring to figure 1, if n nuclei decay per second, fn positrons escape into the gas, gfn form positronium, $\frac{2}{3}gfn$ being ortho-positronium, and if a

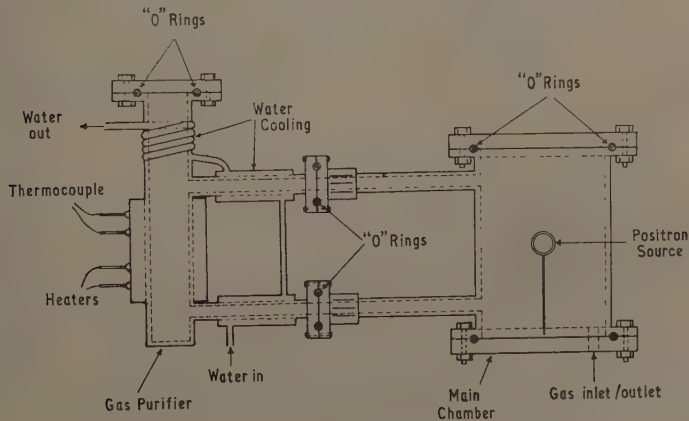


Figure 2. Diagram of the pressure chamber and gas purifier.

proportion η only is detected the rate of three photon annihilations detected by the counter system would be $\frac{3}{4}gfn\eta$ without quenching. When there is quenching at a rate Λ_q the fraction of ortho-positronium annihilating by three-photon emission is

$$\frac{\lambda_0}{\lambda_0 + \Lambda_q} = \frac{\lambda_0}{\Lambda_0}$$

and the observed three-photon rate is

$$R = \frac{3}{4}gfn\eta\lambda_0\Lambda_0^{-1} \\ = \eta A \left(1 + p \frac{\lambda_q}{\lambda_0} \right)^{-1} \quad \text{where } A = \frac{3}{4}gfn.$$

g is constant for a particular gas or mixture of gases; f is constant for the source used; n was effectively constant in these measurements. It follows that

$$\frac{1}{R} = \frac{1}{\eta A} \frac{\lambda_q}{\lambda_0} p + \frac{1}{\eta A}. \quad (1)$$

If η is independent of p a graph of $1/R$ against p should be a straight line with an intercept $-\lambda_0/\lambda_q$ on the pressure axis and intercept $1/\eta A$ on the $1/R$ axis.

The experimental problem is to measure R , i.e. to separate three photon events from the background. The authors employed a sodium iodide scintillation spectrometer technique (block diagram figure 3). The positron source was mounted at the centre of an aluminium alloy cylindrical gas chamber 6 in. long \times 4 in. diameter \times $\frac{1}{8}$ in. wall thickness. The scintillation counter (1 in. thick \times $1\frac{3}{4}$ in. diameter sodium iodide (TI) crystal optically coupled to an EMI 6260 photomultiplier) was placed sufficiently far, 60 cm, from the gas chamber for its detection efficiency for an annihilation event to be sensibly independent of where in the chamber the event occurs. This is necessary in order that η should be independent of p .

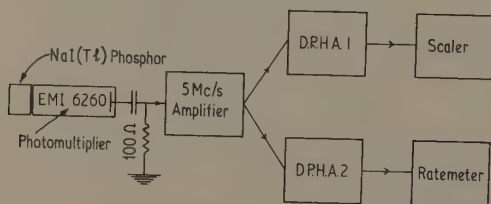


Figure 3. Block diagram of electronics.

Figure 4 shows the observed spectrum. The broken curve is the spectrum when the chamber contained only argon at a pressure sufficient to stop most of the positrons in the gas. The solid curve is the spectrum when sufficient nitric oxide (3%) had been added for exchange quenching to be so strong that there were no three-photon events observed. The accuracy of these measurements was limited only by the stability of the defining voltages of the spectrometer. The second D.P.H.A. shown in figure 3 was arranged to count only pulses occurring in a narrow range halfway up the side of the annihilation line photopeak. Any instability caused a change in ratemeter reading. Series of readings in which such instability occurred were abandoned, the apparatus readjusted, and a fresh series commenced.

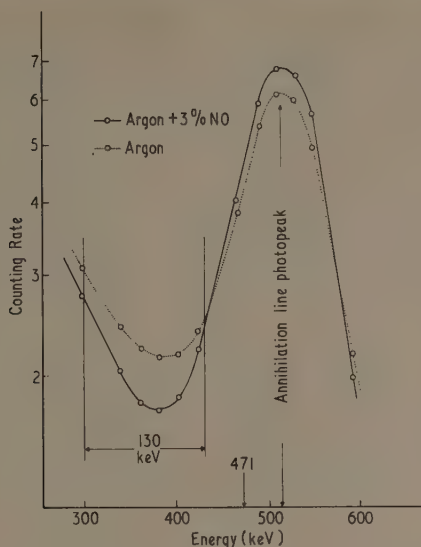


Figure 4. Scintillation spectrum of annihilation radiation.

It is apparent from the two curves that the addition of the nitric oxide has removed three-photon annihilation counts from the region between 300 kev and 440 kev and produced a corresponding increase in the photopeak. The apparatus was adjusted to record only pulses with heights in a range corresponding to 300–440 kev. If R_p is the counting rate in the gas at pressure p and R_0 is the rate in the same gas contaminated with 3% nitric oxide, then $R = R_p - R_0$ is a measure of the amount of ortho-positronium decaying by three-photon emission in uncontaminated gas. Since

$$R_p = \eta_3 A \frac{\lambda_0}{\Lambda_0} + \eta_2 \frac{A}{3} \left(\frac{3\Lambda_q}{\Lambda_0} + 1 \right) + C$$

where η_3 is the efficiency of the counting apparatus for three-photon events, η_2 is the efficiency of the system for two-photon events, and C is the background of other events (free positron annihilations in the gas, annihilations in the walls source and sourceholder, and 1.3 mev nuclear gamma rays) and, with nitric oxide added and all positronium decaying by two-photon events

$$R_0 = \eta_2 \frac{4A}{3} + C$$

we find

$$R = A(\eta_3 - \eta_2) \frac{\lambda_0}{\Lambda_0}$$

which can be stated in the same form as (1) above:

$$\frac{1}{R} = \frac{1}{(\eta_3 - \eta_2)A} \frac{\lambda_q}{\lambda_0} p + \frac{1}{(\eta_3 - \eta_2)A}. \quad (2)$$

The similarity between equations (1) and (2) is to be expected. While quenching does not always result in the loss of a count from the 300–400 kev range (double Compton scattering in the crystal for example will restore some of the possible losses) the change in the counting rate in this range is nevertheless proportional to quenching rate.

§ 4. MEASUREMENT OF QUENCHING IN ARGON AND CARBON DIOXIDE

R_p and R_0 were measured for carbon dioxide for pressures up to twenty atmospheres. The counting rate with the chamber evacuated to a pressure of 10^{-2} mm Hg was also observed and found to agree with R_0 . As effectively all positrons annihilate in the aluminium walls when the chamber is evacuated this confirms the efficacy of the 3% nitric oxide in quenching.

The curve shown in figure 5 is for $1/R$ against p . The minimum in any curve corresponds to a maximum unquenched ortho-positronium decay rate and presumably occurs when all the positrons, or at least most of them, are stopped within the gas. For higher pressures the graph is expected to obey equation (2). The best straight line was fitted to this region. The intercepts $-\lambda_0/\lambda_q$ and $1/A\eta$ provide a value of λ_q in terms of λ_0 and a relative measurement of the amount of positronium formed. In this way we find $(\lambda_q)_{CO_2} = 0.08 \lambda_0$.

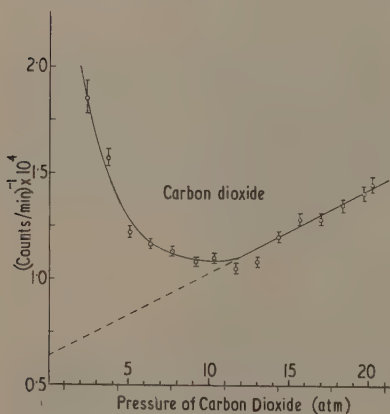


Figure 5. Quenching in carbon dioxide.

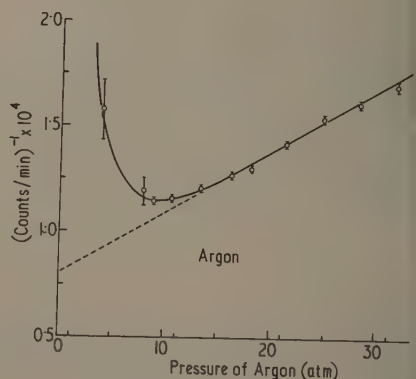


Figure 6. Quenching in argon.

At this stage in the work considerable improvement of the apparatus was carried out. A more stable counting system (enabling the second D.P.H.A. and ratemeter to be dispensed with), better resolution, a strengthened gas vessel (permitting pressures up to 32 atmospheres) and a cleaner system with faster pumping and better ultimate vacuum (less than 5 microns Hg pressure) were developed. With this improved apparatus revised data for argon were obtained and are shown in figure 6. The best straight line was fitted to the points for pressures above 16 atmospheres, and the intercepts calculated by the method of least squares. The standard deviation of the pressure intercept ($\pm 2\%$) was also calculated by the method of least squares giving

$$(\lambda_q)_A = 0.0352\lambda_0 \text{ atm}^{-1} \pm 2\%.$$

§ 5. MEASUREMENT OF QUENCHING IN NEON AND HELIUM

The stopping power of neon for $\frac{1}{2}$ mev positrons is appreciably smaller than that of argon. A quenching rate for neon was therefore extracted from a measured rate for a neon-argon mixture. The mixture was formed of two parts argon and one part neon. The accuracy with which the mixture was formed was estimated to be to about 2%. The results are plotted in figure 7, whence using the later value of $(\lambda_q)_A$ determined above we find

$$(\lambda_q)_{Ne} = 0.024\lambda_0 \text{ atm}^{-1} \pm 40\%.$$

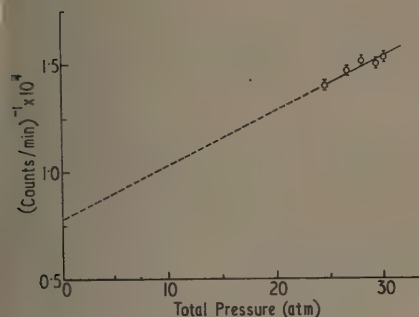


Figure 7. Quenching in neon ($\frac{1}{3}$) argon ($\frac{2}{3}$) mixture.

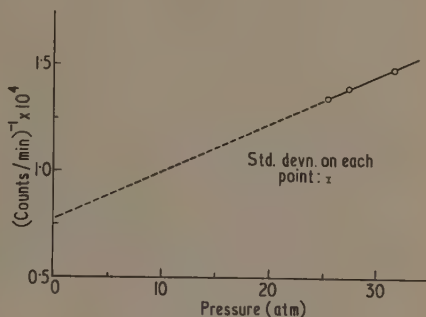


Figure 8. Quenching in helium ($\frac{1}{3}$) argon ($\frac{2}{3}$) mixture.

Similarly quenching by a mixture 2 parts argon, 1 part helium was measured. The results are shown in figure 8 and from the intercepts we find

$$(\lambda_q)_{He} = 0.014\lambda_0 \text{ atm}^{-1} \pm 50\%.$$

§ 6. MEASUREMENT OF QUENCHING IN NITRIC OXIDE AND OXYGEN

Nitric oxide and oxygen quench too powerfully for the same method to be used. Instead very weak constant proportion mixtures of these gases with argon were used. In each case sufficient of the strong quencher was added to argon to reduce the three-photon rate by about one-half (0.03% nitric oxide, 1.6% oxygen). Curves of $1/R$ against p were obtained from these mixtures (figures 9, 10) and quenching rates for the strong quenchers alone extracted from those obtained for the mixtures using the value for argon:

$$(\lambda_q)_{NO} = 400\lambda_0 \text{ atm}^{-1}$$

$$(\lambda_q)_{O_2} = 3\lambda_0 \text{ atm}^{-1}.$$

All the gases used, with the exception of the nitric oxide which was produced in the laboratory, were British Oxygen Company commercial gases.

§ 7. DISCUSSION

The method essentially measures λ_q in terms of λ_0 where λ_0 is the natural or unquenched annihilation rate of ortho-positronium. Ore and Powell (1949) and Radcliffe

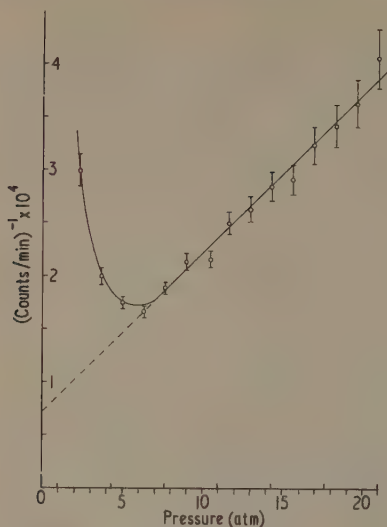


Figure 9. Quenching in argon, nitric oxide (0.03%) mixture.

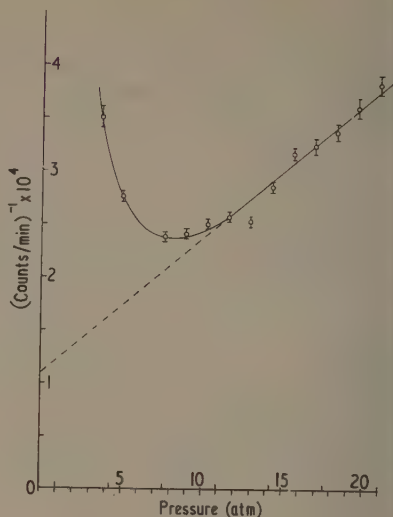


Figure 10. Quenching in argon, oxygen (1.6%) mixture.

(1951) have calculated the natural annihilation rate from the ground state of ortho-positronium (λ_{01}), and if we assume that all our positronium is in the ground state before annihilating we can then use $\lambda_0 = \lambda_{01} = 0.7 \times 10^7 \text{ sec}^{-1}$ and we can write down the absolute value for λ_q . In addition, by making an assumption about the energy distribution of our positronium atoms at annihilation we can deduce a mean cross section for quenching σ_q from λ_q . Assuming that the positronium has reached thermal equilibrium with the quenching gas we can take mean positronium speed to be $6.6 \times 10^6 \text{ cm sec}^{-1}$, leading to the results in table 1.

Table 1

	λ_q	$\sigma_q \times 10^{21} (\text{cm}^2)$
Helium	$0.014\lambda_0$	$0.62 \pm 50\%$
Neon	$0.024\lambda_0$	$1.1 \pm 40\%$
Argon	$0.0352\lambda_0$	$1.55 \pm 2\%$

The helium result is in agreement with that found by Daniel and Stump (1959) using a lifetime method ($0.0093\lambda_0$). The argon quenching rate is appreciably lower than that found with this apparatus in its original form (unpublished) and we believe that the previously higher quenching rate must be attributed to residual oxygen. The fact that we were able to observe the lower quenching rates of helium and neon suggests that any oxygen remaining is having only a very small effect.

The observed increase in quenching rate with atomic size is good evidence in support of the pick-off process as the important quenching mechanism in the inert gases. For more quantitative evidence we need calculations of pick-off quenching cross sections and measurements of the distribution of positronium energies at annihilation.

The results obtained for carbon dioxide, oxygen and nitric oxide are clearly only provisional and give an indication of order only. These measurements are being repeated with the improved apparatus and will be published when complete together with estimates of the relative yields of positronium in the various gases and gas mixtures. Again assuming thermal equilibrium, these provisional results can be summarized as in table 2.

Table 2

	λ_q	$\sigma_q \times 10^{21} (\text{cm}^2)$
Carbon dioxide	$0.08\lambda_0$	3.5
Oxygen	$3\lambda_0$	130
Nitric oxide	$400\lambda_0$	18 000

The quenching rate per atmosphere in nitric oxide is very different (a factor of fifty times less) than that determined by Gittelman and Deutsch (1955–1956). This disagreement is puzzling. However the cross section is clearly large, confirming spin exchange as the mechanism. Quenching in oxygen could also be by spin exchange, or else by the related reorientation of molecular angular momentum process, or both. The quenching rate in carbon dioxide is low enough to suggest that as with the noble gases pick-off is the major process.

ACKNOWLEDGMENTS

The authors wish to thank Professor Sir Harrie Massey for his advice and encouragement and for facilities given in his department. The authors are indebted to the Department of Scientific and Industrial Research and to the London County Council for considerable financial assistance.

REFERENCES

- DANIEL, T. B., and STUMP, R., 1959, *Phys. Rev.*, **115**, 1599.
 DEBENEDETTI, S., and SIEGEL, R. T., 1952, *Phys. Rev.*, **85**, 371.
 DEUTSCH, M., 1953, *Progr. Nucl. Phys.*, **3**, 131.
 DIRAC, P. A. M., 1930, *Proc. Camb. Phil. Soc.*, **26**, 361.
 GITTELMAN, B., and DEUTSCH, M., 1955–1956, *Massachusetts Institute of Technology Progress Report*, June 1955–May 1956, p. 152.
 HUGHES, V. W., MARDER, S., and WU, C. S., 1954, *Phys. Rev.*, **95**, 611.
 LEWIS, G. M., and FERGUSON, A. T. G., 1953, *Phil. Mag.*, **44**, 1011.
 MASSEY, H. S. W., and MOHR, C. B. O., 1954, *Proc. Phys. Soc.*, **67**, 695.
 ORE, A., and POWELL, J. L., 1949, *Phys. Rev.*, **75**, 1696.
 POND, T. A., 1952, *Phys. Rev.*, **85**, 489.
 RADCLIFFE, J. M., 1951, *Phil. Mag.*, **42**, 1334.
 WHEATLEY, J., and HALLIDAY, D., 1952, *Phys. Rev.*, **88**, 424.

Radiation Damage in Well Oriented Pyrolytic Graphites

By L. C. F. BLACKMAN,[†] G. SAUNDERS AND A. R. UBBELOHDE

Department of Chemical Engineering and Chemical Technology,
Imperial College of Science and Technology, London, S.W.7

MS. received 28th March 1961

Abstract. Graphite formed by cracking methane under various conditions has been exposed to neutron irradiation. Changes in electronic properties were measured: (i) after radiation damage by neutron doses of the order 10^{17} neutrons/cm², (ii) after 'mild' annealing around 470 °C, and (iii) after 'strong' annealing at 2200 °C and above. Effects of radiation damage are proportionately greatest in specimens whose properties are initially nearest to those of ideal graphite. Some discrimination can be made between the types of disorder originally present, and the disorder added by irradiation.

Changes of thermoelectric power of graphite in the direction of the *c* axis show 'latent' increases attributed to disorder frozen in until after mild annealing.

§ 1. INTRODUCTION

WELL-ORIENTED pyrolytic graphites have certain properties close to those of ideal crystals. When conventional x-ray methods become insufficiently sensitive to give detailed information about crystal disorder for such near-ideal specimens, various electronic properties still give much information, although effects of disorder can be quite complex. Crystal disorder inherent in graphites prepared at different cracking temperatures has been discussed elsewhere (Blackman, Saunders and Ubbelohde 1961). The present paper deals with the additional disorder introduced in a series of well-oriented specimens by exposure to neutron irradiation.

Previous studies on effects of neutron irradiation on graphite have mainly dealt with polycrystalline specimens (cf. Hennig and Hove 1956). The density of such materials (1.5 to 1.8 g cm⁻³) involves up to 35% porosity and an extensive internal surface. The primary effect of neutron irradiation is to displace carbon atoms from network sites into interstitial positions, leaving network vacancies, but various locations are possible for the displaced atoms. This complicates both structural and electro-magnetic consequences of neutron irradiation in polycrystalline graphites. By using well-oriented graphites, as in the present work, fewer alternative sites are available at intercrystalline boundaries or surfaces of internal pores for the displaced atoms, and the effects of damage are perceptible for much smaller irradiation than is normally used, and should be more readily interpreted. Two main consequences of disorder are the creation of electron traps, and a general increase in scattering of charge carriers. By comparing effects of neutron damage on various electronic properties for a series of specimens of different inherent disorder some discrimination between the main consequences becomes possible in the predominant direction of the *a* axis. As is discussed below, effects in the predominant direction of the *c* axis are at present less easily interpreted partly because a satisfactory theory of electronic properties of graphite in this direction is not yet available.

[†] Now at British Railways Research Department, Muswell Hill, London, N.10.

§ 2. EXPERIMENTAL

Pyrolytic graphites were prepared by cracking gaseous methane at 10 cm Hg pressure, using a flat former of polycrystalline graphite (Morgan EY9A) heated electrically at controlled temperatures in the range 1950–2200 °C. This gives graphites whose crystallites have the predominant direction of their a axes parallel to the flat surface of the former, and of their c axes perpendicular to it. As the temperature of the preparation is raised, various measurements described elsewhere (Blackman, Saunders and Ubbelohde 1961) show that the disorder becomes progressively less. The resistivity can be used as an approximate measure of this disorder. Recrystallization at 2700 °C of pyrolytic deposits formed at 2200 °C gives graphites even nearer to ideal single crystals in their physical and electronic properties.

For electrical measurements in the predominant direction of the a axes, specimens 2 cm \times 0.5 cm \times 0.05 cm were cut from the pyrolytic deposits with three side arms so as to permit measurements of the Hall effect. To minimize mechanical action on the specimens, cutting was effected by a jet of powdered corundum (airbrasive). In the predominant direction of the c axes, circular specimens were cut similarly 0.5 cm \times 0.05 cm; four contact measurements of the resistance and measurements of thermoelectric power were made using methods previously described (Blackman, Mathews and Ubbelohde 1960, Blackman, Dundas and Ubbelohde 1960). Densities were greater than 2.2 g cm⁻³ in all cases which indicates a bulk porosity of less than 3%. At room temperature specific resistances in the direction of the a axis ranged from 33 to 3.8×10^{-5} ohm cm. They are used as an empirical parameter to characterize crystal disorder in what follows, and to display the results in a convenient manner graphically.

Neutron irradiation was carried out in a hollow fuel element in the reactor BEPO for seven days. Specimens sealed *in vacuo* in a silica vessel received a total dose of about 3×10^{17} neutrons cm⁻² (thermal velocity) and 2×10^{17} neutrons cm⁻² (fast, above 1 MeV energy). This amount of irradiation is considered to be approximately equivalent to a dose of 1 Mwd (cf. Hennig and Hove 1956). In accordance with previous findings (Bacon and Warren 1956) the interlayer spacing of a near-ideal specimen increased only slightly from 3.3538 ± 0.0003 Å to 3.3545 ± 0.0005 Å.

In the direction of the a axis measurements of the electrical resistivity, magnetoresistance and Hall coefficient were carried out (cf. Blackman, Saunders and Ubbelohde 1961) at the two temperatures 293 and 77 °K. Measurements of the thermoelectric power were made at various temperatures down to 77 °K. In the direction of the c axis measurements were carried out on electrical resistivity and thermoelectric power.

Annealing operations were carried out under a pressure of less than 10^{-3} mm Hg to minimize any attack by oxygen on carbon atoms made labile by neutron damage (Montet, Hennig and Kurs 1956), and on the graphite network itself. From exploratory trials, it was found that annealing of damaged specimens at around 470° led to changes that reached limiting values in a convenient period of time, about 20 hours. This temperature was therefore used in 'mild' annealing operations; to permit more profound structural reorganization ('strong' annealing), specimens were heated for a few minutes to temperatures above 2000 °C in a rapidly acting induction furnace (Blackman, Dundas, Moore and Ubbelohde 1961). After this treatment only changes in the direction of the c axis could still be measured conveniently, since each successive measurement on the same piece of graphite weakened it mechanically, particularly in the direction of the a axis.

§ 3. RESULTS

For graphites of various initial resistivities, results in the direction of the a axis of the specimens are presented in figures 1, 2 and 3. Measurements of thermoelectric power are given in the table for both crystal directions. The variation of c -axis resistivity with temperature, plotted in the form $\log \rho$ against $1/T$ for a typical sample of well-oriented graphite is given in figure 4.

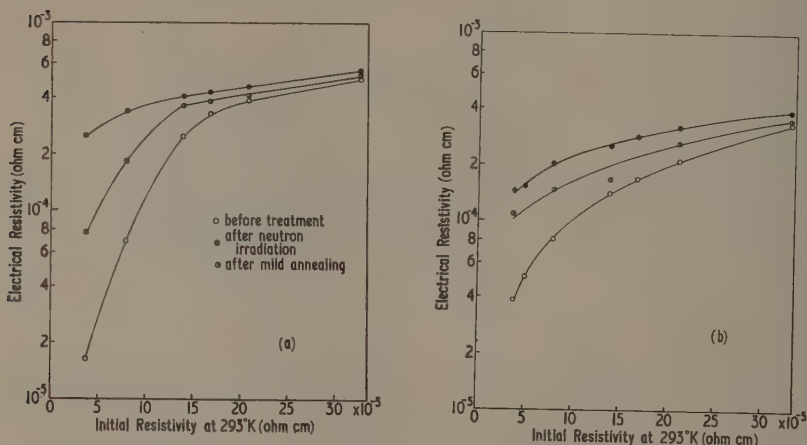


Figure 1. Electrical resistivity of graphites before treatment, after neutron irradiation and after subsequent mild annealing, plotted as a function of the initial room temperature electrical resistivity: (a) at 77 °K, (b) at 293 °K.

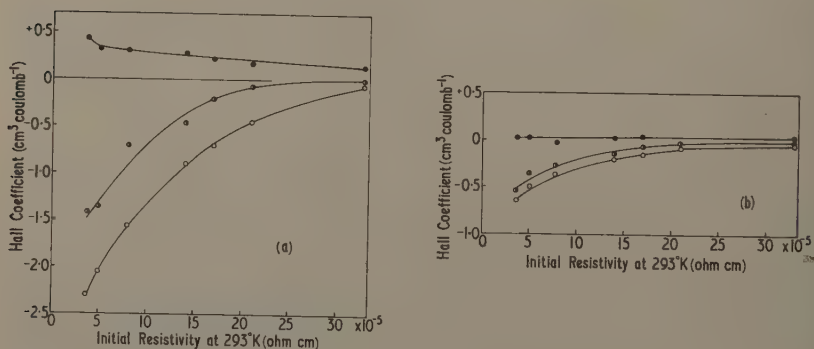


Figure 2. Hall coefficient of graphites before treatment, after neutron irradiation, and after subsequent mild annealing, plotted as a function of the initial room temperature electrical resistivity: (a) at 77 °K, (b) at 293 °K. Key as figure 1.

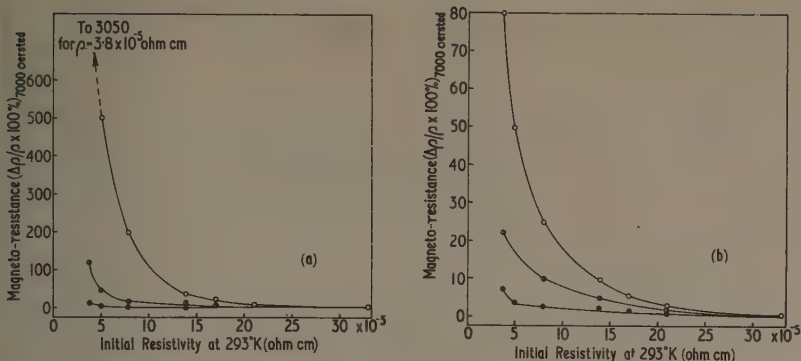


Figure 3. Magneto-resistance of graphites before treatment, after neutron irradiation and after subsequent mild annealing, plotted as a function of the initial room temperature electrical resistivity: (a) at 77 °K, (b) at 293 °K. Key as figure 1.

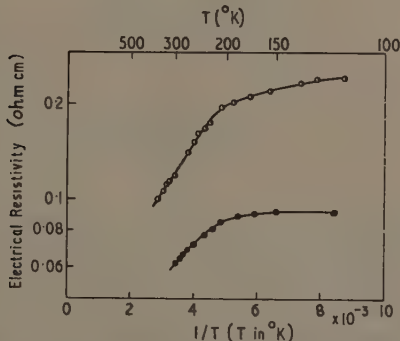


Figure 4. *c*-axis electrical resistivity of a near-ideal graphite (initial *a*-axis resistivity 3.8×10^{-5} ohm cm) measured after neutron irradiation and after subsequent mild annealing, plotted as a reciprocal function of absolute temperature. Key as figure 1.

§ 4. DISCUSSION

For any particular specimen of graphite the sequence of measurements, untreated, annealed after damage and neutron-irradiated, may be expected to give results for increasing defect concentration. The Hall coefficient is affected primarily by the number and sign of the charge carriers. From figure 2 it follows that in the annealed samples the number and sign of the charge carriers must lie quite close to their original values. Radiation damage produces a large increase in positive carriers, but most of these are removed by mild annealing. This increase of defects is most pronounced in the specimens whose resistivity is nearest to ideal graphite, to the left of the figures. From the illustrative example in the table, it will be seen that changes of thermoelectric power in the direction of the *a* axis are reversed by mild annealing in a similar way to

Dependence of Thermoelectric Power of Graphite at 20 °C on Crystal Defects

		<i>c</i> axis direction	
Sample	Treatment		μ v (deg) ⁻¹
Pyrolysis of methane at 1950 °C	Initial		9.60
	After neutron bombardment		11.4
	Anneal 2½ hours at 670 °C		43.35
	Anneal 1 hour at 2200 °C		43.4
	Anneal 30 min at 2800 °C		16.0
Pyrolysis of methane at 2000 °C	Initial		5.7
	After neutron bombardment		7.1
	Anneal 17 hours at 500 °C		45.2
	Anneal 1 hour at 2200 °C		39.9
	Anneal 6 min at 2550 °C		18.35
	Anneal 30 min at 2800 °C		11.45
Pyrolysis of methane at 2150 °C followed by recrystallization at 2750 °C	Initial		4.0
	After neutron bombardment		39.3
	Anneal 2½ hours at 650 °C		34.6
	Anneal 1 hour at 2200 °C		34.1
	Anneal 6 min at 2550 °C		11.9
	Anneal 30 min at 2800 °C		8.4
		<i>a</i> axis direction	
Pyrolysis of methane at 2150 °C	Initial		approx. -8
	After neutron bombardment		approx. +4
	After annealing 17 hours at 470 °C		-2

changes in the Hall effect. Tentatively, it may be thought that the carbon atoms displaced by neutron damage first move to interlamellar sites. Both the interlamellar carbon atoms, and the network holes they leave, then act as electron traps and thus increase the proportion of positive carriers. In this sense an electron trap is any disturbance which reduces the number of mobile carriers in the π band, through alterations in the binding energy where the resonance of ideal graphite is decreased. This includes effects due to buckling of the layers. On mild annealing these traps are reduced in number. A proportion of the interlamellar atoms probably migrates to the edges of the crystallites leaving the network holes, and the remainder return to the original sites thereby closing up network holes.

The electrical resistance of graphite is affected both by changes in the number of carriers, and, to a more marked extent than the Hall effect, by changes in the scattering probability. Inspection of the behaviour of the resistivity (figure 1) shows that scattering makes a marked contribution to the effects of neutron damage in the near-ideal graphites, which is not removed to any great extent by the reduction of traps on mild annealing.

This conclusion is confirmed by measurements of the magneto-resistance which is even more strongly dependent on the scattering probability (approximately as the inverse square according to some theories); figure 3 shows that most of the increased scattering due to neutron damage remains unaffected by the mild annealing.

Before discussing the findings in the direction of the *c* axis, which are less extensive because of physical difficulties in making certain types of measurement with the specimens available, it seems useful to outline a model for damage that could help to interpret results in the direction of the *a* axis. When a carbon atom is displaced from a network

site, the networks will buckle locally (i) to accommodate the interstitial atom between them, and (ii) to allow for any bond rearrangements at a network 'hole' (cf. Ubbelohde 1957).

Figure 5 illustrates schematically that buckling of the network, for example at a network hole, need not involve major pushing aside of the neighbouring networks, since their normal distance of separation (3.4 \AA) is quite large. On the other hand, to accommodate extra atoms between the networks requires a considerable local expansion of the normal separation between networks. Both network holes and interstitial carbon atoms act as traps, but the interstitial atoms are much more labile since their bonding is not stabilized by resonance. On mild annealing, those interstitial atoms which have not been removed too far by neutron damage can return to the original sites and heal the network. Others that are more remote from their origins preferentially migrate to sites where they can form cross links between the edges of macro-aromatic networks,

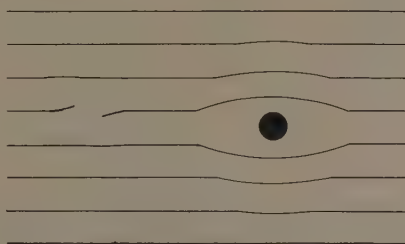


Figure 5. Sketch of buckling of networks around the network hole and an interstitial atom.

with bonding types well known in organic chemistry. Through the removal of the interstitial atoms the number of valency defects (and hence positive carriers) is diminished, but scattering irregularities due to network holes are stabilized. These can only be removed by strong annealing above 2000°C , which permits rearrangements of aromatic C-C bonds.

Types of disorder originally present in the pyrolytic graphites involve disturbances of crystal regularity and the presence of traps, which have been stabilized at the high temperatures of formation. Although consequences of such original disorder are formally similar to those arising from the disorder produced by neutron damage with or without mild annealing, geometrical aspects obviously differ. As the proportion of original defects increases, the distinctive role of neutron damage defects discussed in this paper rapidly becomes less prominent and becomes swamped beyond a limit for initial resistivities greater than about $1.5 \times 10^{-4} \text{ ohm cm}$ (figure 6).

In the direction of the *c* axis, near-ideal samples decrease in resistivity and show a less steep negative temperature coefficient after neutron bombardment (figure 4). The thermoelectric power also becomes more positive (table). If it is assumed that the carriers in this direction are mainly positive these changes are consistent with the model described above; the effect of mild annealing is relatively greater on the resistivity than on the thermoelectric power, but interpretation of this peculiarity awaits a satisfactory band model for the *c*-axis direction in graphite.

Brief comment may also be made about two further aspects of these experimental results.

The table illustrates the fact that for less perfect specimens of pyrolytic graphite the maximum increase in positive thermoelectric power, resulting from neutron damage remains latent until after mild annealing. If the proposed model is used to interpret this unusual result, it would imply that in the direction of the *c* axis scattering effect due to interstitial carbon atoms mask increases in thermoelectric power resulting from

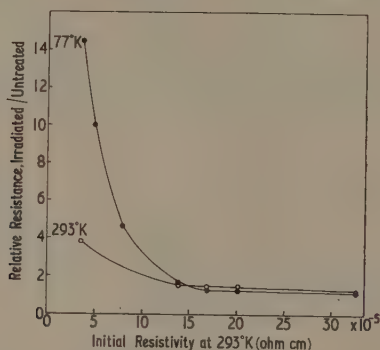


Figure 6. Swamping of neutron damage effects by general disorder in pyrolytic graphites as illustrated by the ratio of the electrical resistance after and before neutron irradiation (plotted as a function of the initial room temperature electrical resistivity).

an increase in positive carriers to an exceptionally strong degree. This could arise if contributions from lattice vibration to thermoelectric power, such as phonon drag and especially Umklapp processes, are particularly prominent in the direction of the *c* axis in graphite. Verification of this suggestion awaits the development of alternative means of studying lattice vibration contributions, such as measurements of thermal conductance which are being made.

Calculations can be made of the approximate number of additional positive carriers created in near-ideal pyrolytic graphite by the production of electron traps, following procedures outlined by McClure (1958). In a typical example, it is found that originally there are 4.5×10^{18} negative and 1.5×10^{18} positive carriers per cm^3 .

After neutron irradiation, the specimen gave a Hall coefficient at 77°K of $0.43 \text{ cm}^3 \text{ coulomb}^{-1}$ which did not vary with field strength. This indicates that conduction is wholly by positive carriers whose concentration is estimated as 17×10^{18} per cm^3 . This may be compared with estimates for neutron damage in polycrystalline graphite made by Hennig (1958), which yield approximately 9×10^{-5} traps per atom or 10×10^{18} traps per cm^3 per Mwd.

ACKNOWLEDGMENTS

Thanks are due to the Research Council of the Electricity Council for their support of this research and to the Atomic Energy Research Establishment, Harwell, for their collaboration in producing samples with neutron damage.

REFERENCES

- BACON, G. E., and WARREN, B. E., 1956, *Acta Cryst.*, **9**, 1029.
- BLACKMAN, L. C. F., DUNDAS, P. P., and UBBELOHDE, A. R., 1960, *Proc. Roy. Soc. A.*, **255**, 293.
- BLACKMAN, L. C. F., DUNDAS, P. H., MOORE, A., and UBBELOHDE, A. R., 1961, *Brit. J. Appl. Phys.*, **12**, 377.
- BLACKMAN, L. C. F., MATHEWS, and UBBELOHDE, A. R., 1960, *Proc. Roy. Soc. A.*, **256**, 15.
- BLACKMAN, L. C. F., SAUNDERS, G., and UBBELOHDE, A. R., 1961, *Proc. Roy. Soc. A.*, **264**, 19.
- HENNIG, G. R., 1958, *Nuclear Sci. Engineering*, **3**, 514.
- HENNIG, G. R., and HOVE, J. E., 1956, *Proc. Int. Conf. on the Peaceful Uses of Atomic Energy*, **7**, 666.
- McCLURE, J. W., 1958, *Phys. Rev.*, **112**, 715.
- MONTET, G., HENNIG, G., and KURS, A., 1956, *Nucl. Sci. Engng*, **1**, 33.
- UBBELOHDE, A. R., 1956, *Nature, Lond.*, **180**, 380.

Determination of the Fierz Interference Term From the K-Capture/ β^+ Ratio for the Pure Gamow-Teller Decay of ^{58}Co

BY B. R. JOSHI AND G. M. LEWIS

Department of Natural Philosophy, The University, Glasgow

MS. received 8th May 1961

Abstract. A direct determination has been made of the Fierz interference term b for the pure Gamow-Teller decay of ^{58}Co . The K/β^+ ratio has been determined by an internal source scintillation counter coincidence method. The value obtained was 4.92 ± 0.09 . This may be compared with the recent predicted value of 4.87. Allowing for the variation in the theoretical value arising from β^+ end point uncertainty this yields a value for b of $(+0.6 \pm 2.3)\%$. Two interpretations of the result are possible on the basis of two-component neutrino theory. If, as is customarily assumed, $C_A = C_A'$, $C_T = -C_T'$, then b should vanish identically; and the small experimental value for b confirms the theory. If alternatively, $C_A = C_A'$, $C_T = +C_T'$ then the experimental result requires that C_T, C_T' be very small.

§ 1. INTRODUCTION

THE SIGNIFICANCE of the Fierz interference term b has changed in recent years, following the introduction of the two-component neutrino theory and the increase in β -decay data. Experimental studies of allowed β -spectral shapes and K/β^+ ratios have shown that b is not large. The subject has been reviewed by Konopinski (1958). Two-component neutrino theory and recent data now demand either that b should vanish identically or that the scalar and tensor coupling constants C_S, C_S', C_T, C_T' should be small.

The expression for b which arises from the combination of different coupling constants can be written

$$b = 2\mathcal{R} \frac{[C_S C_V^* + C_S' C_V'^*]|F|^2 + [C_T C_A^* + C_T' C_A'^*]|G|^2}{[|C_S|^2 + |C_V|^2 + |C_S'|^2 + |C_V'|^2]|F|^2 + [|C_T|^2 + |C_A|^2 + |C_T'|^2 + |C_A'|^2]|G|^2} \quad (1)$$

where F and G are the Fermi and Gamow-Teller matrix elements (cf. De Groot and Tolhoek 1950, Lee and Yang 1956, 1957).

For the determination of b the experimental K/β^+ ratio can be compared with the theoretical value $(K/\beta^+)_{b=0}$ by the relation

$$\frac{K}{\beta^+} = \frac{1+b}{1-\gamma b(1/W)_{av}} \left(\frac{K}{\beta^+} \right)_{b=0} \quad (2)$$

where

$$\gamma = \left\{ 1 - \left(\frac{Z}{137} \right)^2 \right\}^{1/2}$$

and W is the β^+ energy.

Restricting attention at this stage to Gamow-Teller transitions, the experiments by Herrmannsfeldt *et al.* (1958) on ^6He have shown that $[|C_A|^2 + |C_A'|^2]$ is large compared with $[|C_T|^2 + |C_T'|^2]$. For time inversion invariance the coupling coefficients will be real.

For the two-component neutrino theory to hold consistently with polarization experimental data, the relation $C_A = +C_A'$ holds for the dominant coupling coefficients. Both $C_T = -C_T'$ and $C_T = +C_T'$ are consistent with two-component neutrino theory. The combination of the coupling constants in the form $C_A = C_A'$, $C_T = -C_T'$ requires the identical vanishing of b while the form $C_A = C_A'$, $C_T = +C_T'$ does not.

Experimental values of b are therefore necessary to establish the validity of the two-component neutrino theory if $C_T = -C_T'$, or to delimit the maximum magnitude of C_T and C_T' if $C_T = +C_T'$. It is also perhaps relevant to point out that for electron polarization methods designed to determine the validity of the theory, the expression for the electron polarization contains b explicitly (cf. Jackson, Treiman and Wyld 1957). It is therefore desirable, from this view point too, that b be specified experimentally.

The magnitude of b obtained from beta-spectral shape studies is not as closely defined as that from the K/β^+ ratio work. The theoretical K/β^+ ratios have been recalculated by Perlman, Welker and Wofsberg (1958) and, more recently, with second order corrections for the positron wave functions, by Nguyen-Khac (Depommier, Nguyen-Khac and Bouchez 1960). The experimental work on the ratio of orbital capture to positron emission has been reviewed extensively by Perlman, Welker and Wofsberg (1958), Konijn *et al.* (1958), and Depommier, Nguyen-Khac and Bouchez (1960). The majority of the experiments have been done by indirect methods. These generally involve considerable instrumental uncertainties, such as the assessment of detection efficiencies with solid external sources. Further, to estimate the K/β^+ ratio, a knowledge of $(L+M+\dots)/K$ capture ratios has to be presumed. In many cases the Fermi Gamow-Teller admixtures of the nuclei investigated are unknown. In order that the results on b can be readily interpreted it is desirable to consider transitions that are either pure Fermi or pure Gamow-Teller.

The first assessment of b from the K/β^+ ratio for the Gamow-Teller radiator ^{22}Na was made by Sherr and Miller (1954) by an indirect technique. They found b to be $(-2 \pm 4)\%$. A direct observation of the K/β^+ ratio, free from escape effects, was carried out by Drever, Moljk and Scobie (1956) for the Gamow-Teller transition ^{18}F . They used a gaseous source and a wall-less proportional counter technique, and this gave $b = (0.8 \pm 4)\%$. A similar technique was used by Scobie and Lewis (1957). They obtained $b = (-3 \pm 10)\%$ for the predominantly Fermi transition ^{11}C .

A direct experimental measurement of the K/β^+ ratio, free from escape effects, can readily be made for intermediate and high Z nuclei with an internal source scintillation counter technique. This method permits coincidence counting to be used, and this helps to eliminate background effects. The K-capture and β^+ events are separately recorded, and the K/β^+ ratio follows directly. The present paper reports an experiment carried out by this method to measure the K/β^+ ratio for the allowed decay of ^{58}Co which leads directly to the first excited state (810 keV) of ^{58}Fe . The recorded K-capture and β^+ events were observed in coincidence with the 810 keV γ -ray of ^{58}Fe . The result was used to find an upper limit to the value of b .

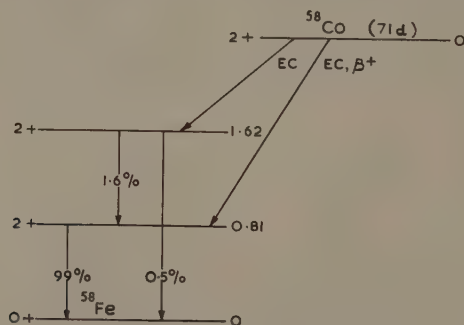
The decay scheme of ^{58}Co is shown in figure 1 (cf. Frauenfelder *et al.* 1956). The predominant decay process which proceeds to the first excited state at 810 keV of ^{58}Fe has been shown to be essentially pure Gamow-Teller by the alignment experiments of Dagley *et al.* (1958), with a Fermi admixture of less than $\frac{1}{2}\%$. The spectrum of positrons for this main branch has been investigated by Deutsch and Elliott (1944) and Cheng, Dick and Kurbatov (1952). They found the positron end-point at 470 ± 15 keV and 472 ± 6 keV respectively. These give a $\log ft$ value of approximately 6.6. The K/β^+ ratio was calculated to be 4.87 by Nguyen-Khac (Depommier, Nguyen-Khac and Bouchez 1960), assuming a 472 keV end point energy. Previous experimental results

on the total electron capture/ β^+ ratio of ^{58}Co by external source methods are shown table 1.

Table 1

Author	Total electron capture to β^+ ratio
Good, Peaslee and Deutsch 1946	5.8 ± 0.2
Cook and Tomnovec 1956	5.9 ± 0.2
Grace, Jones and Newton 1956	6.7 ± 1.3
Konijn <i>et al.</i> 1958	5.67 ± 0.16
Ramaswamy 1959	5.48 ± 0.25

To derive a value for the K/β^+ ratio from these results, it is necessary to use either the predicted value of the ratio of L-capture to K-capture, 0.092 (Brysk and Rose 1958) or the recent measured value of this ratio, 0.108 ± 0.004 (Moler 1961).

Figure 1. Decay scheme of ^{58}Co .

§ 2. EXPERIMENTAL PROCEDURE

The ^{58}Co was prepared by the ^{58}Ni (n, p) reaction, and was supplied by the Amersham authorities as a separated carrier free chloride. The ^{60}Co content was specified as less than 0.5%. In order to establish the purity of the source, the γ -radiations were checked, using an external source and 2 in. diameter \times 2 in. NaI(Tl) scintillation counter with a C.D.C. multichannel pulse height analyser. Aluminium sheet was used to absorb the β^+ radiations, and the source-detector gap kept at 3 in. Except for the two prominent peaks at 810 kev and 510 kev, no other radiations were observed in the region from 100 kev to 2 mev. To confirm still further the absence of ^{60}Co , an external source was examined in a 2 in. diameter \times 2 in. well-type NaI(Tl) crystal. It was found that the ^{60}Co activity was certainly less than 0.1% of the total activity.

In order to analyse the K-capture and β^+ events, a thallium-activated sodium iodide crystal approximately 1 cm diameter \times $1\frac{1}{4}$ cm was grown with a trace of the source by the Bridgman method (1925). Harshaw NaI(Tl) chippings were used. To help to eliminate possible surface effects, the crystal was cut and polished to an area of 4 mm \times 8 mm and a thickness of 2 mm, and mounted in an aluminium container fitted with a thin glass window, with magnesium oxide as reflector. An E.M.I. 9514S phototube

was used. The K capture events produced K x-rays and K Auger electrons which would be almost wholly absorbed in the active crystal. The β^+ particles would be, mostly, wholly absorbed in the crystal. A few per cent of these liberated near the surface would be recorded in the crystal before being absorbed in the crystal assembly. This would not affect the total β^+ counting rate. After amplification in a non-overloading amplifier, the pulses from this counter were fed by delay cable into a gating unit. This gate was controlled by the γ -ray counter described below. Pulses from the activated crystal which were in coincidence with the peak of the 810 kev radiation in the γ -ray counter, were passed to a multichannel kicksorter.

The γ -ray counter consisted of a 2 in. diameter \times 2 in. NaI(Tl) scintillator mounted on another E.M.I. 9514S phototube. A gap of 3 in. lay between this scintillator and the small active crystal. Amplified pulses from the γ -ray counter led to an I.D.L. single-channel kicksorter with the channel set to receive the 810 kev peak. The limits of this channel are shown by the arrows in figure 2. The output of the single channel kicksorter was passed to a univibrator which generated a $5\mu\text{sec}$ gating pulse. Those

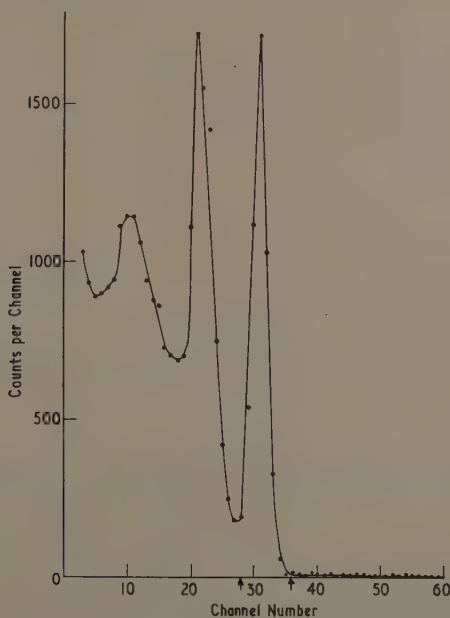


Figure 2. Total gamma ray spectrum of ^{58}Co in a 2 in. diameter \times 2 in. NaI(Tl) crystal obtained in coincidence with K-capture and β^+ events in the thin active crystal.

K-capture and β^+ events from the small crystal which were in coincidence with the 810 kev peak were displayed in separate runs. The stability of the system was checked throughout the runs at regular intervals. This was done by noting the counting rate at the single channel output and by taking the spectrum of the γ -ray gating pulses; no gain shifts were observed.

Typical spectra of K-capture and β^+ events in coincidence with 810 kev radiation are shown in figures 3 and 4 respectively. The β^+ spectrum is of course distorted, in particular by partial absorption in the crystal of the associated annihilation radiation.

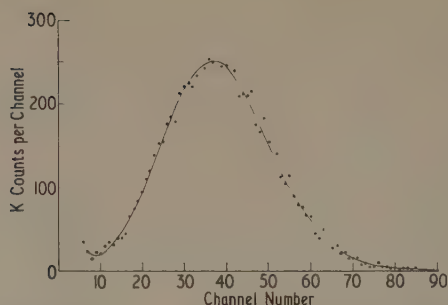


Figure 3. K-capture peak of ^{58}Co (with an internal source) in coincidence with 810 kev gamma ray peak. (1 hour run).

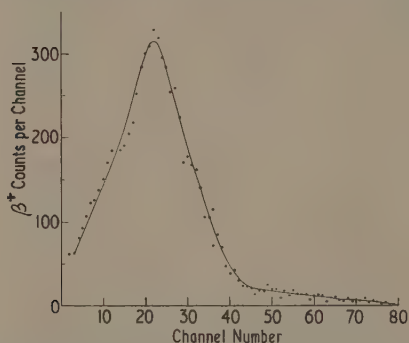


Figure 4. Spectrum associated with β^+ emission from ^{58}Co (with an internal source) in coincidence with 810 kev gamma ray peak. ($4\frac{1}{2}$ hours run).

Several runs were taken, each generally having the order of 10 000–20 000 K-events and 5000 β^+ events and lasting about six hours, over a period of three weeks. The consistency of the runs is shown in table 2. The crystal was cleaned and polished twice during the course of the runs, changing its overall size by about a quarter. The strength of the source in the crystal during the period of measurement fell, due to natural decay and loss of material. The reduction from the loss of material was about a quarter. This, and the consistency of the runs, substantiated the absence of surface effects from the source distribution. The random coincidence count was assessed by inserting appropriate delay cable in the main channel. The random rate was 2% and did not affect the observed ratio. There was no contribution from noise and afterglow effects. There were no losses due to dead time.

Table 2

Observed Uncorrected K/ β^+ Ratio

Run	1	2	3	4	5	6	7	8
K/ β^+ ratio	4.94	4.97	4.95	4.91	4.91	4.93	4.93	4.96

It was necessary to estimate the error arising in the main run owing to the arrival of $\frac{1}{2}$ mev annihilation radiation simultaneously with 810 kev radiation in the γ -ray crystal, which would affect the β^+ contribution. To this end the γ -spectra in coincidence with the K-capture and β^+ events were analysed separately in the 2 in. scintillator by gating with the K-capture peak and the β^+ spectrum in the active crystal respectively, with the counter arrangement otherwise unchanged. The correction for this effect was then determined and found to be small (0.2%).

A small correction arises from the fact that an 810 kev γ -ray associated with a K-capture event can occasionally produce a low energy (10–100 kev) Compton electron in the 2 mm-thick source crystal and a scattered γ -ray which has a chance of recording in the 810 kev gate. Such an event will then be wrongly recorded as a β^+ event. The source was shown by subsidiary measurements to be distributed symmetrically about the appropriate central face of the crystal so that on average the γ -ray traverses 1 mm thickness of crystal. From γ -ray absorption tables, a 1% correction had to be applied for this effect.

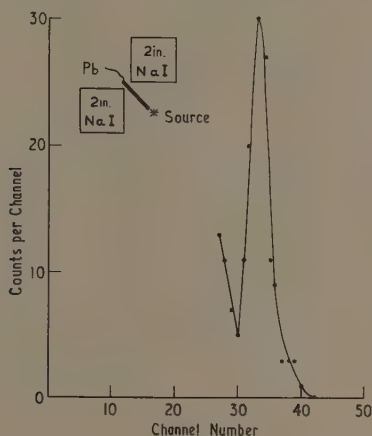


Figure 5. Investigation of the weak capture branch: Peak in the 800 kev region obtained by gamma-gamma coincidence measurements. The inset diagram shows the experimental set-up.

It was necessary to make allowance for the small number of unwanted K-capture γ -rays emitted in the transition to the 1.62 mev level, which would be observed in coincidence with the γ -ray of either of the 810 kev transitions. More accurate data than given in figure 1 were required. This could be readily investigated here because any source strength could be compared with that of the active crystal whose K-capture rate was known. The experimental arrangement for this ancillary measurement is shown in figure 5 (inset). The two counters were fitted with NaI(Tl) crystals, approximately 2 in. diameter \times 2 in. On one side a single-channel kicksorter with the window set at the 810 kev peak was used, and on the other side a discriminator set at 700 kev was employed. The two outputs led to a coincidence unit. Pulses from the coincidence unit operated a gate and the associated spectrum from either side could be displayed on the multichannel kicksorter. Figure 5 shows the spectrum from the counter which had the bias set at about 700 kev. The fraction of the weak electron capture branch to the 1.62 mev state which subsequently proceeded to the 0.81 mev level by γ emission

was found to be $(1.25 \pm 0.1)\%$ of the K electron events in the main branch. Allowing for the L-capture contribution in this weak branch, a correction of 2.2% had therefore to be made in assessing the K/β^+ ratio for the main branch.

§ 3. RESULTS AND DISCUSSION

The experimental value of the K/β^+ ratio after applying the small corrections for the simultaneous arrival of $\frac{1}{2}$ mev and 810 kev radiation in the γ -ray crystal, for the Compton escape, and for the weak branch, all referred to above, was 4.92 ± 0.09 . The error limit was partly associated with statistics, but mainly with the assessment of the low energy end of the K-capture peak. The random rate, as has been mentioned, was low at all energies observed. The rise at low energy is associated with L-capture events. The K-capture peak was fitted by a statistical distribution to assess the scintillation counter efficiency. The L-capture peak expected at 850 ev would then occur in the region of single electron emission from the photocathode; it would contribute to the low energy rise and to the region near the trough of the K-capture peak. (Further confirmation of the validity of this assessment of the K-capture peak was obtained through studies recently made with the same ^{58}Co activated crystal and an E.M.I. photomultiplier having a still better photocathode.)

The experimental value may be compared with the theoretical value of K/β^+ of 4.87 based on the calculation of Nguyen-Khac (Depommier, Nguyen-Khac and Bouchez, 1960). Because of the 6 kev uncertainty in published values for the β^+ end point, the theoretical value of the K/β^+ ratio will become 4.87 ± 0.18 . Inserting the value $(1/W)_a = 0.75$ in equation (2), the Fierz term is found to be $+0.006 \pm 0.023$.

Within the stated limits the value of b is therefore in accord with the two component neutrino theory in the form $C_A = C_A'$ and $C_T = -C_T'$, where b vanishes identically. In this form, the theory will require complete polarization of β -particles at high momentum. If the alternative possibility $C_A = C_A'$ and $C_T = +C_T'$ holds instead, then from relation (1), $0 \leq |C_T/C_A| < 0.015$; and of course at the lower limit the two interpretations are identical.

ACKNOWLEDGMENTS

The authors would like to thank Professor P. I. Dee for his interest in the work. One of us (B.R.J.) is grateful to the Colombo plan authorities for a Research Fellowship and to the Government of Nepal for its sponsorship.

REFERENCES

- BRIDGMAN, P. W., 1925, *Proc. Amer. Acad. Arts Sci.*, **60**, 350.
 BRYSK, H., and ROSE, M. E., 1958, *Rev. Mod. Phys.*, **30**, 1169.
 CHENG, L. S., DICK, J. L., and KURBATOV, J. D., 1952, *Phys. Rev.*, **88**, 887.
 COOK, C. S., and TOMNÓVEC, F. M., 1956, *Phys. Rev.*, **104**, 1407.
 DAGLEY, P., GRACE, M. A., HILL, J. S., and SOWTER, C. V., 1958, *Phil. Mag.*, **3**, 489.
 DE GROOT, S. R., and TOLHOEK, H. A., 1950, *Physica*, **16**, 456.
 DEPOMMIER, P., NGUYEN-KHAC, U., and BOUCHEZ, R., 1960, *J. Phys. Radium*, **5**, 456.
 DEUTSCH, M., and ELLIOTT, L. G., 1944, *Phys. Rev.*, **65**, 211.
 DREVER, R. W. P., MOLJK, A., and SCOBIE, J., 1956, *Phil. Mag.*, **1**, 942.
 FRAUENFELDER, H., LEVINE, N., ROSSI, A., and SINGER, S., 1956, *Phys. Rev.*, **103**, 352.
 GOOD, W. M., PEASLEE, D., and DEUTSCH, M., 1946, *Phys. Rev.*, **69**, 313.

- GRACE, M. A., JONES, G. A., and NEWTON, J. O., 1956, *Phil. Mag.*, **1**, 363.
- HERRMANSSFELDT, W. B., BURMAN, R. L., STAHELIN, P., ALLEN, J. S., and BRAID, T. H., 1958, *Phys. Rev. Letters*, **1**, 61.
- JACKSON, J. D., TREIMAN, S. B., and WYLD, H. W., 1957, *Phys. Rev.*, **106**, 517.
- KONIJN, J., VAN NOOIJEN, B., HAGEDOORN, H. L., and WAPSTRA, A. H., 1958, *Nucl. Phys.*, **9**, 296.
- KONOPINSKI, E. J., 1958, *Proc. Rehovoth Conf. Nucl. Structure*, Ed. by H. J. LIPKIN (Amsterdam: North Holland), p. 319.
- LEE, T. D., and YANG, C. N., 1956, *Phys. Rev.*, **104**, 254.
- 1957, *Phys. Rev.*, **105**, 1671.
- MOLER, R. B., 1961, *Interim Progress Report NSF-G5050, App. IV*, University of Arkansas.
- PERLMAN, M. L., WELKER, J. P., and WOFSEBERG, M., 1958, *Phys. Rev.*, **110**, 381.
- RAMASWAMY, M. K., 1959, *Indian J. Phys.*, **33**, 285.
- SCOBIE, J., and LEWIS, G. M., 1957, *Phil. Mag.*, **2**, 1089.
- SHERR, R., and MILLER, R. H., 1954, *Phys. Rev.*, **93**, 1076.

The Lifetime of the 673 kev Level in ^{132}Xe

By W. D. HAMILTON†

The Department of Physics, The University of Birmingham

Communicated by P. B. Moon; MS. received 13th July 1961

Abstract. The resonant scattering cross section for the 673 kev electric quadrupole transition in ^{132}Xe was directly determined for a particular arrangement of source, scatterer, and detector. The resonant scattering condition was provided by the persistence of nuclear recoil following a preceding transition when the source was in the gaseous phase. The differential cross section for a mean scattering angle of 149° was evaluated as $\sigma(149^\circ) = 1.75 \times 10^{-26} \text{ cm}^2 \text{ sterad}^{-1}$, and the value $\tau = (9.7 \pm 3.0) \times 10^{-12} \text{ sec}$ was found for the mean-life of the level. This result is in good agreement with that obtained from a Coulomb excitation measurement. The enhancement of the E2 transition probability when represented by the ratio $B(\text{E}2; 0 \rightarrow 2)/B(\text{E}2)_{\text{s.p.}}$, has the value 20; this is consistent with the results for even-even nuclei which have characteristic vibrational spectra.

§ 1. INTRODUCTION

THE EVEN-EVEN nuclei in the atomic weight region of xenon are expected to have a well defined spherical equilibrium shape and a spectrum, particularly for the lower excited states characteristic of quadrupole vibrations about this shape. In the review article by Alder, Bohr, Huus, Mottelson and Winther (1956) a general discussion is given on the spectra of such spherical nuclei. The E2 transition probability, as a result of the quadrupole vibrations, is enhanced compared with the single particle estimate, and in the present case the enhancement for the ground-state transition in ^{132}Xe may be estimated from a determination of the mean-life of the 673 kev level. Furthermore, the first excited states of many of the xenon isotopes, including ^{132}Xe , have been Coulomb-excited in experiments by Pieper, Anderson and Heydenburg (1958), and the relative values for the reduced upward transition probabilities, $B(\text{E}2)$, have been determined. It should thus be possible to compare the value of $B(\text{E}2)$ with that obtained from resonant scattering and perhaps to assess the validity of the relative values of the Coulomb excitation results.

The first excited state in ^{132}Xe , which is at 673 kev, is populated by the electron capture transition in ^{132}Cs , and also following the β -decay of ^{132}I . In each case the preceding transition has a greater momentum than the ground state γ -ray and is thus capable of providing the resonant scattering condition. The systematics of E2 transitions in even-even nuclei (Goldhaber and Sunyar 1951) indicate that the order of the mean-life of the 673 kev level will require the resonant radiation to be emitted by nuclei in the gas phase in order to permit the persistence of nuclear recoils free from collisions.

§ 2. CHOICE OF SOURCE

The production of ^{132}Cs by the (p, n) reaction will only proceed to any appreciable extent for bombardment energies exceeding 20 mev, as found by Bhatki, Gupta and Jha (1956) who used 25 mev protons and obtained ^{132}Cs only in low specific activity.

† Now at the Physics Institute, Uppsala University, Sweden.

As an alternative method of production, the (d, α) reaction was tried, and barium oxide was bombarded with 20 mev deuterons in the Nuffield cyclotron at Birmingham University. Cesium carrier was added to the barium target, and after the barium had been removed by the perchlorate method (Saraf 1954) the Cs was precipitated as CsClO_4 . From the trial bombardment only a small fraction of the activity could be attributed to ^{132}Cs and it did not appear possible to produce a source strength of the order 10 mc as would be required, even if a target enriched in the ^{134}Ba isotope was used.

The alternative source, ^{132}I , is the β -decay product of the pile-produced ^{132}Te isotope, which may be obtained in high specific activity. The decay scheme of ^{132}I , which is shown in figure 1, is that proposed by Finston and Bernstein (1954), who confirmed the spin assignment of 2^+ to the first excited state from a measurement of the K-electron internal conversion coefficient. The spin sequence 0^+ , 2^+ , 4^+ and the energy ratio of 2.2 between the second and first excited states are typical of a quadrupole vibrational spectrum.

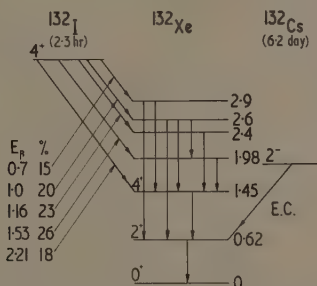


Figure 1. The excited states in ^{132}Xe populated following the β -decay of ^{132}I as proposed by Finston and Bernstein, and the electron capture transition from ^{132}Cs . The percentage intensities of the β -decay modes are listed, and the β - and γ -ray energies are expressed in mev.

The 2.8 hour half-life of ^{132}I was too short for the present resonant scattering experiment, and for convenience the source was maintained in secular equilibrium with its parent, ^{132}Te , which has a half-life of 77 hours. The chemical form of the source was limited by the boiling point and suitability of the tellurium compound and the choice fell upon tellurium tetrachloride which has a boiling point of 414°C at standard temperature and pressure.

The 20 mc source was contained in a conical ampoule of Pyrex glass which had an approximate volume of 3 ml. The ampoule fitted inside a metal container, the temperature of which could be controlled. When the ampoule was being filled 0.1 mM of hydrogen was included, and since ICl_4 readily dissociates when gaseous a large fraction of the source should exist as hydrogen iodide. During the preparation of the source several milligrams of solid material were also unavoidably included in the ampoule. This was believed to be mostly stannous chloride from which any occluded iodine should be easily liberated when the source was heated, while the presence of the additional material was not expected to affect the behaviour of the source.

§ 3. EMISSION LINE PROFILE

The decay of ^{132}I by five β -transitions of comparable intensity, and the many γ -cascades which lead to the 673 kev level will greatly complicate the calculation of the

line shape of the emitted radiation. The enhancement of the E2 transition probabilities will require that the mean-life of the 1.45 mev level be short compared with the collision time when the source is gaseous, and will further increase the difficulties.

In constructing the profile of the broadened emission line, transitions from the upper levels to the 1.45 mev and 673 kev states were considered to have been emitted by nuclei at rest. The recoil momentum distribution in figure 2 then arises from a β - γ cascade, and several γ - γ cascades and single γ -transitions. It was assumed that only the xenon atom accepted the recoil momentum. This would appear to be justified since a large fraction of the source should exist as hydrogen iodide and furthermore since the β - γ cascades have several γ -components it would be expected that the xenon nucleus should be free from any influence of the original TeCl_4 molecule before the final stages of the cascades occurred. The fraction of γ -rays which energetically satisfy the resonant condition has the value $F_0(E) = 6.4 \times 10^{-2} \text{ ev}^{-1}$. This would be slightly reduced if all transitions were considered to contribute to the final recoil distribution.

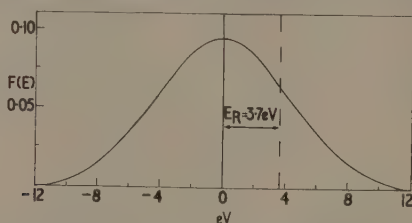


Figure 2. The energy distribution of the emitted 673 kev γ -ray. The absorption line is displaced by 3.7 ev relative to the centre of the emission line as a result of conservation of linear momentum between the γ -ray and the absorbing and emitting nuclei. The area under the curve is normalized to unity and the abscissa $F(E)$ represents the fraction of γ -rays within a unit energy interval.

The effects arising from thermal motion within the source and scatterer can be considered together, and since their contribution to the line broadening will widen the line profile by only a few per cent and have a negligible effect on $F(E)$ in the region of interest, they were neglected in the present case. No account was taken of the angular correlations between the different components of the cascades in view of the other uncertainties; their inclusion could either reduce or increase the fraction of γ -rays which satisfy the resonant condition but probably not to an appreciable extent.

§ 4. EXPERIMENTAL METHOD

The xenon scatterer was the same as that used in previous resonant scattering experiments (Hamilton 1961), but the volume of the xenon gas which was solidified into the container was increased to 12.5 litres at standard temperature and pressure. The intensity of the 673 kev Rayleigh scattered radiation, for which the cross section may be calculated, could not be distinguished above the background with sufficient accuracy to allow it to be compared with that of the resonant scattering, and thus it was impossible to estimate the cross section for the latter from such a comparison. Rather, it was necessary to determine absolutely the number of resonantly scattered γ -rays for a particular geometrical arrangement of source, scatterer and detector. The resonant scattering intensity was obtained from the difference in counting rates when the source was gaseous and solid, since, when the total mean-life of a level is of the order 10^{-11} – 10^{-12} sec,

it is longer than the collision time within a solid source and there will be no significant resonant scattering.

The small change in effective source position, when it was in the gaseous or solid phases, was conveniently determined by using a comparison scatterer. Iodine was a suitable material for this purpose and 65 g of iodine crystals were packed into a copper cylinder which had the same dimensions as the xenon container and which was also covered with styrofoam. No attempt was made to match the scatterers accurately since the amount of xenon which could be solidified varied up to 10% for different runs, although for any particular run the amount of xenon in the container could be accurately estimated. It was impossible to replace the solid xenon by the iodine scatterer since the xenon container was rigidly attached to an associated pumping system, and the scatterers were placed, as shown in figure 3, on each side of the detector and symmetrical with respect to it and the source. The source-scatterer and detector-scatterer separations were 22.5 cm and 11 cm respectively, and the mean scattering angle was 149° . The radiation incident on either scatterer could be cut off by inserting about 6 cm of heavy alloy between it and the source, which permitted in effect the scatterers to be rapidly and conveniently interchanged.

The scattered radiation after passing through a 3 mm lead filter was detected by a NaI(Tl) crystal $1\frac{1}{2}$ in. diameter by 2 in. long mounted on a 6295 DuMont photo-multiplier. A single-channel pulse height analyser selected for recording the radiation which was accepted by a 3 volt wide channel. This channel width which included at least 70% of the photopeak counting rate was also used in the source calibration so that the absolute detection efficiency and source strength were not required.

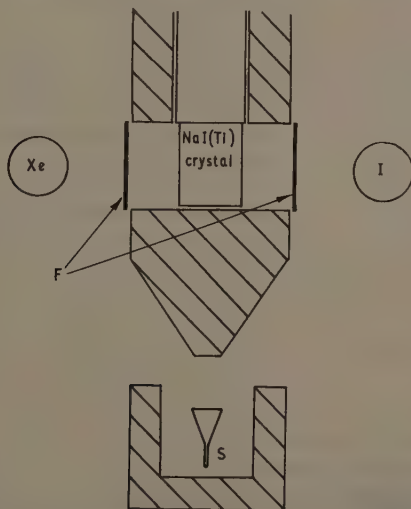


Figure 3. The geometrical arrangement of source S, scatterers, I and Xe, and detector. The shielding about the source and detector is of heavy alloy, and *F* are the lead filters covering the detector.

§ 5. EXPERIMENTAL RESULTS

The mean value of four independent results after correction for source decay and the fraction of xenon scatterer present was 9.6 ± 2.4 resonantly scattered γ -rays per

minute. Each of the results was derived from sets of observations in which the counting rates were recorded for a number of 10 minute periods, when the source was hot and cold, and when the scatterer was alternatively iodine and xenon. The 25% statistical error in the mean value arose because of the large background.

Direct calibration of the source at a distance of 50 cm from the axis of the detector and perpendicular to it, gave a counting rate of 1.48×10^6 counts per min when corrected with respect to source decay; the 3 mm lead filter was in position as before. The relative detection efficiencies corresponding to the source-detector separations at which the source was calibrated, and at which the scattered radiation was detected were determined experimentally since the radiation was perpendicular to the crystal axis and the tabulated theoretical coefficients, which are for a source on the detector axis, were not applicable in the present case. It was found that the resonant scattered counting rate when compared with the source calibration counting rate had to be increased by the factor 1.05 to compensate for the decrease in detector efficiency. A further correction to this counting rate was made for the self-absorption of the resonant scattered radiation within the xenon.

The differential resonant scattering cross section which, for a mean scattering angle of 149° , was determined as

$$\sigma(149^\circ) = 1.75 \times 10^{-26} \text{ cm}^2 \text{ sterad}^{-1}$$

is usually represented by an equation having the form (cf. Metzger 1959).

$$\sigma(\theta) = \sigma_{\max} \frac{\pi}{2} F_0(E) \Gamma \frac{f(\theta)}{4\pi} \text{ cm}^2 \text{ sterad}^{-1}.$$

In the present case the width Γ of the scattering level is the only unknown in the above expression. The maximum cross section σ_{\max} , which occurs for complete overlap of the emission and absorption levels, has the value $2.7 \times 10^{-20} \text{ cm}^2$. The angular distribution function $f(\theta)$ for E2 radiation emitted in the spin sequence $0^+, 2^+, 0^+$ is given by

$$f(\theta) = 1 + 0.357P_2(\cos \theta) + 1.143P_4(\cos \theta),$$

and for a scattering angle of 149° , $f(\theta) = 1.19$. From figure 2 the fraction of γ -rays which have the resonant energy is $F_0(E) = 6.4 \times 10^{-2} \text{ ev}^{-1}$. Following the substitution of these terms in the above equation the level width was evaluated as

$$\Gamma = 6.8 \times 10^{-5} \text{ ev}.$$

The corresponding mean-life of the 673 kev level is then

$$\tau = 9.7 \times 10^{-12} \text{ sec}.$$

This is the total mean-life since there is no competing γ -decay mode to the ground state and internal conversion is insignificant ($\alpha < 3 \times 10^{-3}$). The probable error on the mean-life was set at 30% and it arises principally from the statistics of the recorded counting rates; no account was taken of a possible large error in $F_0(E)$ as it could not readily be assessed.

§ 6. DISCUSSION

In the Coulomb excitation experiments by Pieper, Anderson and Heydenburg (1958) the $B(E2)$ values were determined relative to the assignment of the value $B(E2) = 0.48 \times 10^{-48} \text{ e}^2 \text{ cm}^4$ to the 535 kev transition in ^{130}Xe . They based this assignment

on the systematics of the $B(E2)$ values for even-even nuclei in the region of xenon, and no error was quoted for the results. Their values of $B(E2)$ for ^{131}Xe (364 kev) and ^{132}Xe (673 kev) and the associated downward transition probabilities and mean-lives are given in the table together with the results of the present resonant scattering experiment, and the one previously reported on ^{131}Xe (Hamilton 1961). It was assumed that the total internal conversion coefficient was negligible in each case, and that the transitions were pure E2.

$E_\gamma(\text{kev})$	$B(E2)$	$T(E2; I_i \rightarrow I_f)$	$\tau(E2)$ (sec)	$\tau_{\text{R.S.}}$ (sec)
364(^{131}Xe)	2.07	8.7×10^{10}	1.14×10^{-11}	$(2.0 \pm 0.5) \times 10^{-11}$
673(^{132}Xe)	0.32	1.04×10^{11}	9.6×10^{-12}	$(9.7 \pm 3.0) \times 10^{-12}$

The mean-life from Coulomb excitation of the 364 kev level in ^{131}Xe is some 40% smaller than the experimentally determined value, while for the 673 kev level, there is very good agreement between the values derived from the Coulomb excitation measurements and from the resonant scattering cross section. It perhaps might be a better test if the ratios of the mean-lives as determined by two methods were compared, since this should remove any possible systematic experimental errors in either of the methods. From the values listed in the table it can be seen that these ratios agree to within the error associated with the resonant scattering measurements.

The vibrational spectra have been studied in a number of cases by Coulomb excitation and many of the results have been presented in table V.6 of the review article by Alder *et al.* (1956). In this, for the purpose of comparison, the reduced upward transition probability, $B(E2; 0 \rightarrow 2)$, has been expressed in terms of a single particle transition probability given by $B(E2)_{\text{S.P.}} = 3 \times 10^{-5} A^{4/3} 10^{-48} e^2 \text{cm}^4$. The present result for ^{132}Xe , which yields 20 for this factor, compares favourably with the tabulated values.

It may be considered that the assignment made by Pieper, Anderson and Heydenburg (1958) to the $B(E2)$ value of the 535 kev transition in ^{130}Xe is justified since there is good agreement between the ratios of the mean-lives of levels in ^{131}Xe and ^{132}Xe as obtained from resonant scattering and Coulomb excitation, and since the 673 kev transition probability is consistent with the general features of vibrational spectra in this atomic weight region. It is also to be expected that the value of $F_0(E)$ used in evaluating the mean-life in the present experiment is approximately correct but it is not possible to say to what extent the assumptions which were made, when constructing the emission line profile, are true.

ACKNOWLEDGMENTS

It is a pleasure to record my gratitude to Professor P. B. Moon who supervised the work. I am grateful to Dr. G. F. Pieper of The Johns Hopkins University for enlightening comments on the Coulomb excitation experiments. I am much indebted to Dr. J. D. Jenkins who undertook the preparation of the radioactive source at the Radiochemical Centre, Amersham, and also to Dr. K. F. Chackett who was most helpful with the ^{132}Cs preparation at Birmingham. I gratefully acknowledge the receipt of a Research Studentship from the Ministry of Education for N. Ireland during the course of the above work.

REFERENCES

- ALDER, K., BOHR, A., HUUS, T., MOTTELSON, B., and WINTHER, A., 1956, *Rev. Mod. Phys.* **28**, 432.
- BHATKI, K. S., GUPTA, R. K., and JHA, S., 1956, *Nuovo Cim.*, **4**, 1519.
- FINSTON, H. L., and BERNSTEIN, W., 1954, *Phys. Rev.*, **96**, 71.
- GOLDHABER, M., and SUNYAR, A. W., 1951, *Phys. Rev.*, **83**, 906.
- HAMILTON, W. D., 1961, *Proc. Phys. Soc.*, **77**, 610.
- METZGER, F. R., 1959, *Progr. Nucl. Phys.*, Vol. 7 (Oxford: Pergamon), p. 53.
- PIEPER, G. F., ANDERSON, C. E., and HEYDENBURG, N. P., 1958, *Bul. Amer. Phys. Soc.*, **3**, 38.
- SARAF, B., 1954, *Phys. Rev.*, **94**, 642.

The Lifetime of the 638 kev level in ^{131}Xe

By W. D. HAMILTON†

Department of Physics, The University of Birmingham

Communicated by P. B. Moon; MS. received 13th July 1961

Abstract. A nuclear resonant scattering method was used to estimate the mean-life of the 638 kev level in ^{131}Xe . The result of 4×10^{-13} sec, when compared with the Weisskopf estimate, is consistent with an enhanced E2 transition or a retarded M1 transition. However, in reported Coulomb excitation experiments there is no evidence for an E2 transition probability consistent with the present mean-life, and it is suggested that the transition may be predominantly M1.

§ 1. INTRODUCTION

THE SPIN and parity of the 638 kev level in ^{131}Xe do not yet appear to have been conclusively established. The shell model predictions are not necessarily applicable to a level of such high energy, and indeed, it is thought unlikely that the state could be represented by a single particle configuration (Verster, Nijgh, van Lieshout and Bakker 1951). The level is populated by the 335 kev β -transition from ^{131}I , and has a $\log ft = 6.7$. This value is typical of an allowed or l -forbidden transition for this A-region, and since the ground state of ^{131}I is $7/2^+$, the 638 kev level may have a spin of $5/2$ or $7/2$ and positive parity. There is a wide range of values for the K-electron conversion coefficient and these indicate that the transition could be E1 or E2 as has been mentioned by Bell (1955) in his survey of the many ^{131}I decay scheme studies. The deviations, to a large extent, are removed when account is taken of the relative abundances of the ^{131}I decay modes as used in the different determinations. The results are then in general agreement and indicate that the transition is electric quadrupole.

§ 2. EXPERIMENTAL METHOD

The mean-life was determined from a measurement of the nuclear resonant scattering cross section. The experimental arrangement of source scatterer and detector was the same as that used in the investigation of the resonant scattering of the 364 kev γ -ray also in ^{131}Xe (Hamilton 1961). The resonant scattering condition for the 638 kev γ -ray was provided by the persistence of nuclear recoil following the β -decay which populated the state when the source was gaseous. If it is assumed that the xenon alone accepts the total recoil momentum then the 335 kev β -transition imparts to the nucleus a maximum recoil momentum of 1.32 mc which is adequate to compensate the 1.25 mc lost by the 638 kev γ -ray. The number of γ -rays $F_0(E)$ which have the resonant energy is $4.2 \times 10^{-3} \text{ ev}^{-1}$, but there may be a large error in this value since the absorption line occurs near the extremity of the emission line's energy distribution of which the profile was determined by a graphical method.

It was not possible to make a direct measurement of the number of γ -rays resonantly scattered, since it was not possible to estimate accurately the fraction of emitting nuclei

† Now at the Physics Institute, Uppsala University, Sweden.

which satisfied the resonant scattering condition when the source was gaseous. Rather, since this condition was expected to be the same for both the 364 kev and 638 kev transitions, the intensities of these resonantly scattered γ -rays were compared when the source was solid and gaseous. It was expected that only for the latter condition would the resonant scattering be significant so that the measurement with the solid source should indicate the background. These intensities and the corresponding transition probabilities are proportional to the resonant scattering cross section, and since this has been determined for the 364 kev γ -ray, it might then be obtained for the 638 kev transition.

A 100 mc source of ^{131}I in the form of 4×10^{-3} mM molecular iodine was enclosed together with approximately 0.05 mM of hydrogen in a pyrex glass ampoule, which had a volume of 3.5 ml., and as before it was possible to control its temperature. A mean scattering angle of 119° was selected and all spectra were recorded when a 3 mm lead filter covered the $1\frac{1}{2}$ in. diameter by 1 in. NaI(Tl) crystal. The spectra, which were displayed on a 100-channel analyser, were taken when the source was gaseous and solid, and when the xenon scatterer was alternatively in position and absent. The correction for the change in effective source position when in the different phases was made as described in the earlier experiment. Resonant scattering was found to occur only when the source was gaseous. The areas below the curves representing the 364 kev and 638 kev resonantly scattered γ -rays were corrected for the self-absorption within the scatterer and with respect to the relative abundance and detection efficiency of the transitions which were found from the direct spectrum.

§ 3. RESULTS AND DISCUSSION

The 364 kev resonant scattering intensity after applying the above corrections was found to exceed that of 638 kev by the factor 1.87. The partial mean-life of the 364 kev level had previously been determined as $(2.0 \pm 0.5) \times 10^{-11}$ sec and the corresponding resonant scattering cross section is $\sigma(119^\circ) = 2.4 \times 10^{-26}$ cm² sterad⁻¹. From the intensity ratio of the resonantly scattered γ -rays, the cross section for the 638 kev γ -ray is $\sigma(119^\circ) = 1.08 \times 10^{-26}$ cm² sterad⁻¹. If it is assumed that the 638 kev γ -ray arises from the spin change $\frac{3}{2}^+ \rightarrow \frac{3}{2}^+$ then the peak value of the resonant scattering cross section is $\sigma_{\text{max}} = 12.08 \times 10^{-21}$ cm². The mean-life of the level may be evaluated from an appropriate expression for the differential resonant scattering cross section (cf. Metzger 1959) and has the value $\tau = 3.9 \times 10^{-13}$ sec. If a collision time of $t = 2 \times 10^{-14}$ sec is assumed for the source nuclei when in the solid phase (Ofer and Schwartzchild 1959), then the fraction of recoils persisting after the time $\tau = 4 \times 10^{-13}$ sec is $A = 1 - \exp(t/\tau) \simeq 5\%$, and for the present experiment, resonant scattering should only be observable when the source is gaseous, or possibly liquid for which the collision time may also be sufficiently long.

The statistical error in this determination of the mean-life is less than 30%, but the result cannot be considered to be more than a good estimate since there is a large uncertainty in $F(E)$. Furthermore, the effect of thermal broadening has been ignored, for although small compared with the width of the emission line profile due to β -decay, it should have been included in the total line broadening, since the absorption level overlaps the emission level near its extremity where small effects may not be completely negligible. However, the absence of observable resonance scattering for the solid source does indicate that the mean-life cannot be shorter than about 10^{-13} sec. The transition probability is some 140 times greater than the Weisskopf estimate for a single particle E2 transition.

The Coulomb excitation experiments by Pieper, Anderson and Heydenburg (1958), did not indicate any γ -rays which could be attributed to this transition. A value of $\approx 10^{-13}$ sec for the mean-life of the 638 keV level would give a reduced upward transition probability of $B(E2) = 3.87$, and Dr. Pieper, in a private communication, mentioned that they should have been able to detect 638 keV γ -rays corresponding to 10% of this value for $B(E2)$. A possible explanation for the absence of Coulomb excitation is that the 638 keV level does not de-excite principally by E2 radiation. The E1 multipolarity of the transition may be excluded on the basis of the values for the K electron conversion coefficient. However, α_K and the K/L ratio are not particularly sensitive to an admixture of M1 with the E2 radiation, even to a considerable degree. Such a mixed transition could occur if the spin and parity of the 638 keV level is $\frac{5}{2}^+$. This assignment is in agreement with the β -transition being 1-forbidden ($g_{\frac{7}{2}^+} \rightarrow d_{\frac{5}{2}^+}$), and with $\log ft = 6.7$.

The above value of the mean-life must now be slightly adjusted to take into account the change in the factor which represents the statistical weight of the transition and enters into the expression for σ_{max} through the ratio $(2J_i + 1)/(2J_f + 1)$, where J_i and J_f are respectively the spins of the excited and final states. Also, the angular distribution function of the resonantly scattered radiation is now based on the new spin sequence $\frac{1}{2}^+$, $\frac{5}{2}^+$, $\frac{3}{2}^+$, and should be dependent on the E2:M1 mixing ratio. If it is assumed that the 638 keV level is de-excited by a pure M1 transition, the mean-life then has the value $\approx 3 \times 10^{-13}$. The Weisskopf estimate for a 638 keV M1 transition is 1.4×10^{-13} sec, and if the M1 transition probability is relatively unhindered, the experimentally determined mean-life is also consistent with a large M1 admixture.

Thus, while the mean-life of the level, as would be expected, is not particularly sensitive to the M1 admixture, a value of the order 4×10^{-13} sec may be considered to be a good estimate which is essentially independent of the E2:M1 admixture and spin of the level. This value and the absence of Coulomb excited 638 keV γ -rays suggest an appreciable M1 admixture. It may be hoped that the $L_I:L_{II}:L_{III}$ ratios are more sensitive to the multipolarity of the radiation, but results for such measurements have not yet been reported.

Note added in proof.—The electric hfs alignment of ^{131}I nucleus was made recently by Johnson, Schooley and Shirley (1960), who concluded from their measurements of the γ -ray angular distribution that the 637 keV level had spin $\frac{5}{2}^+$ and de-excited by pure E2 radiation. The latter is inconsistent with the results of Coulomb excitation and the present resonant scattering experiment.

ACKNOWLEDGMENTS

I wish to express my gratitude to Professor P. B. Moon under whose supervision the work was carried out. I am indebted to Dr. G. F. Pieper of The Johns Hopkins University for his helpful comments on the Coulomb excitation experiment and to Dr. J. D. Jenkins at the Radiochemical Centre, Amersham, who prepared the source. I am also pleased to acknowledge the receipt of a Research Studentship from the Ministry of Education for N. Ireland.

REFERENCES

- BELL, R. E., 1955, *Beta- and Gamma-Ray Spectroscopy*, Ch. XXII, Ed. K. Siegbahn, (Amsterdam: North-Holland).
 HAMILTON, W. D., 1961, *Proc. Phys. Soc.*, **77**, 610.
 JOHNSON, C. E., SCHOOLEY, J. F., and SHIRLEY, D. A., 1960, *Phys. Rev.*, **120**, 1777.
 METZGER, R. F., 1959, *Progr. Nucl. Phys.*, **7** (London: Pergamon), p. 53.
 OFER, S., and SCHWARTZCHILD, A., 1959, *Phys. Rev. Letters*, **3**, 384.
 PIEPER, G. F., ANDERSON, C. E., and HEYDENBURG, N. P., 1958, *Bul. Amer. Phys. Soc.*, **3**, No. 1, 38.
 VERSTER, N. F., NIJGH, G. J., VAN LIESHOUT, R., and BAKKER, C. J., 1951, *Physica*, **17**, 637.

LETTERS TO THE EDITOR

New Bands in the Second Negative System of Oxygen

Communicated by P. K. Carroll

The molecular spectrum of O_2^+ consists of two well-known systems: the First Negative system whose strongest bands lie in the visible and infra-red region of the spectrum and the Second Negative system which extends throughout the visible and near ultra-violet. In this laboratory a complete survey of the O_2^+ spectrum from 7000 Å to 400 Å has recently been made in a search for new transitions. No new systems were in fact found; but a considerable extension of the Second Negative system was observed and it was thought worth while reporting briefly the measurements of the new bands.

The source employed in the experiments was a high frequency discharge through pure oxygen. Spectra of the region 2800–400 Å were taken with a new 3-metre vacuum spectrograph (dispersion 2.5 Å mm^{-1}) using Ilford QII plates. The region 7000–2800 Å was photographed on a Hilger E 478 prism spectrograph using both the glass and quartz optics over their appropriate ranges. A complex group of bands at about 4350 Å was photographed in the second order of the 21 ft grating spectrograph. Ilford Zenith and Astra III plates were used in these experiments.

Wavelengths of New Band Heads in the Second Negative System

$v'-v''$	λ	Head	$v'-v''$	λ	Head
23-0	1942†	R ₁	3-10	4182.2	R ₁
22-0	1956†	R ₁		4218.0	R ₂
21-0	1966†	R ₁	11-14‡	4237.0	R ₁
20-0	1977†	R ₁		4271.8	R ₂
	1985†	R ₂	4-11	4313.4	R ₁
19-0	1991.5†	R ₁		4351.0	R ₂
18-0	2005.9	R ₁	2-10	4331.5	R ₁
	2013.7	R ₂	3-11‡	4466.5	R ₁
17-0	2022.0	R ₁	1-10‡	4495.9	R ₁
	2029.9	R ₂		4536.3	R ₂
16-0	2039.8	R ₁	2-11	4636.5	R ₁
	2048.1	R ₂	3-12	4783.8	R ₁
13-1	2187.9	R ₁	3-13	5142.9	R ₁
10-2	2371.8	R ₁	5-14	5154.8	R ₂
11-5	2548.1	R ₁	4-14	5308.6	R ₁
7-3	2602.6	R ₁		5364.2	R ₂
3-8	3727.2	R ₂	4-15	5729.1	R ₂
1-8	3943.6	R ₁	1-13	5736.1	R ₂
	3972.0	R ₂	3-16	6433.0	R ₁
4-10	4050.1	R ₁		6531.8	R ₂
2-9	4059.9	R ₁			
	4092.0	R ₂			

† Vacuum wavelengths. These heads are difficult to locate due to many-line band structure.

‡ Weak and somewhat uncertain bands.

The wavelengths and vibrational assignments of the new bands are given in the table. Previous data on the vibrational structure of the system are due to Johnson (1924) who reported all the stronger bands and Feast (1950) who identified a considerable number of weaker bands. In the same region as the Second Negative system Johnson had observed a number of other features which he attributed to O_3 . Feast however identified most of the ' O_3 ' bands as either new bands of the second negative system or atomic lines of OII .

While the present observations are in agreement with Feast where ' O_3 ' features are identified as weaker O_2^+ bands, they suggest that the identification of some of Johnson's ' O_3 ' bands as OII lines is less certain. Most of these features appear on the present plates with a band-like structure and in some cases they can be identified as further O_2^+ bands. Thus the features reported by Johnson at 4464.7 Å, 4333.3 Å and 4316.5 Å can be identified from the table as the R_1 heads of the 3-11, 2-10 and 4-11 bands respectively while the feature at 4276.9 Å is probably the R_2 head of the 11-14 band. The two features at 378.4 (identified by Feast as the OII line 3377.2 Å) and 3374 appear on the present plates as band heads of moderate strength, although it has not been possible to assign them convincingly to the second negative system. The features at 3284.6 Å and 3278.1 Å, identified by Feast as the OII lines 3287.59 Å and 3277.69 Å respectively, appear as weak and somewhat confused band structure.

An interesting aspect of the present work is the appearance of high members of the $v \rightarrow 0$ progression. It should be pointed out that in this progression the band heads for higher v' values become difficult to locate and the last band which could be identified with any confidence was the 23-0 band at 1942 Å. Beyond this point to about 1870 Å there appeared a considerable amount of close line-like structure. As the dissociation limit for the $A^2\Pi$ state is the same as for the $x^2\Pi$ state, $O(^3P) + O(^4S)$ at 53 600 cm^{-1} , (Watanabe and Marmo 1956) it follows that the structure observed at 1870 Å (53 500 cm^{-1}) must be due to transitions from levels lying very close to the dissociation limit. The investigation of this region under considerably higher resolution should therefore enable a very accurate and direct determination of the dissociation energy of O_2^+ to be made. It would also provide information on the structure of the $A^2\Pi$ state near its dissociation limit. Brix and Herzberg (1954) have observed pronounced changes in the spin splitting of the $B^3\Sigma$ state of O_2 as the dissociation limit is approached. It is possible that an analogous change occurs in the structure of the $A^2\Pi$ state. This could account for the many-lined appearance of the O_2^+ spectrum in the 1870-1950 Å region.

Physics Department,
University College,
Dublin.

J. BYRNE.†

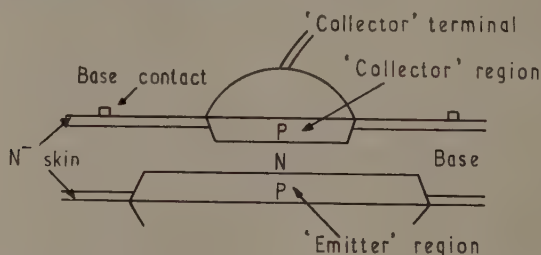
10th August 1960, in final form 8th August 1961.

- BRIX, P., and HERZBERG, G., 1954, *Canad. J. Phys.*, **32**, 110.
FEAST, M. W., 1950, *Proc. Phys. Soc. A*, **63**, 557.
JOHNSON, R. C., 1924, *Proc. Roy. Soc. A*, **105**, 583.
WATANABE, K., and MARMO, F. F., 1956, *J. Chem. Phys.*, **25**, 965.

† Now at Department of Natural Philosophy, University of Edinburgh.

Excess High-frequency Noise in Junction Transistors

For ideal diffusion transistors there is ample experimental evidence to support the accepted theoretical model for low-level noise behaviour at high frequencies (Guggenbühl and Strutt 1957, van der Ziel 1959). A statistical investigation of a large batch of commercial p-n-p alloy-type transistors of normal asymmetrical construction showed, however, that many produced excess noise. Metallurgical cross-sectioning indicated that the excess noise was associated with non-alignment of the emitter-collector axes. In the worst cases a large part of the emitter junction extended beyond the periphery of the collector junction and was therefore opposite the surface of the base adjacent to the collector. It seemed likely that the excess noise was associated with this surface. For proof, the normal roles of emitter and collector of an ideal asymmetrical transistor were interchanged. In this way about half the 'emitter' junction area overlaps the surface of the base around the collector.



Schematic representation of 'reversed' asymmetrical transistor.

Note. P, N used here, corresponding to the normal use p, n.

The transistor chosen was first shown to produce theoretical noise for emitter currents i_E up to 4 mA when connected normally. When reversed the transistor had a cut-off frequency of 1.3 Mc/s and a low frequency near-short-circuit current transfer coefficient in common base of 0.89 at $i_E^\dagger = 1.0$ mA. Measurements of noise figure were made over a wide range of source resistance R_0 for emitter currents from 100 μ A to 5 mA and for frequencies between 100 kc/s and 8 Mc/s. There was little difference between measured noise figure F_m and calculated theoretical noise figure F_t at the lower frequencies.

Excess noise figure, $\Delta F \equiv F_m - F_t$, became detectable below 500 kc/s and increased with frequency thereafter. For 'collector' currents i_C up to 2 mA, ΔF increased as i_C^2 but somewhat less rapidly at higher currents. There was a linear dependence of ΔF on R_0 at high R_0 . Under extreme conditions (high i_C , R_0 and frequency) values of ΔF considerably greater than F_t itself were determined.

As far as device performance is concerned the excess noise figure can be accounted for by an additional noise source represented by a noise current generator i_{cs} in parallel with the normal shot noise generator at the 'collector'-base junction. Above 500 kc/s the spectral density of this additional noise source is invariant with frequency.

The purpose of this letter is to put forward a possible model to account for this extra noise. An N⁻ exhaustion layer is assumed to exist on the surface of the base as shown in the figure. Where the 'emitter' and 'collector' junctions meet the surface

[†] Upper case suffixes refer to direct current components, lower case to small-signal and noise components.

N^- junctions will exist. Only that at the 'collector' need be considered. At the surface the PN^- junction takes up some of the applied 'collector'–base bias voltage; the remainder produces a radial drift field in the N^- surface skin and biases the NN^- junction in reverse. The PN^- 'collector' junction produces full shot noise of the current i_{CN} collected by it. The remainder of the collector current $i_{CS} = i_C - i_{CN}$ flows to the 'collector' terminal through the PN^- junction via the NN^- junction. Hole–electron pairs pass randomly from the base into the N^- region and drift with ambipolar drift velocity towards the PN^- junction at the 'collector'. While drifting they produce concentration–fluctuation noise similar to generation–recombination noise in a filament. The holes which finally reach the PN^- junction carry the current i_{CS} and produce full shot noise. This may be included in the usual way in the shot noise generator at the collector.

The excess noise associated with the concentration fluctuations in the surface skin may be represented by a voltage generator e_s in series with r_s . It should have the spectral form of equation (1)

$$\overline{e_s^2} = Kr_s^2 i_{CS}^2 \frac{\tau}{(1 + \omega^2 \tau^2)}. \quad (1)$$

Here K is a constant, r_s is the resistance of the skin, τ is the lifetime of hole–electron pairs in it and ω is angular frequency. If the ambipolar drift time is comparable with τ , the frequency dependence of $\overline{e_s^2}$ is only slightly modified. Effectively r_s is in series with c_{cs} , the depletion-layer capacitance of the PN^- junction. It is expected that $r_s \ll 1/j\omega c_{cs}$ so that the voltage generator e_s may be replaced by a current generator i_{cs} across c_{cs} , i.e. in parallel with the total collector capacitance c_c . The form of $\overline{i_{cs}^2}$ is

$$\overline{i_{cs}^2} = Kr_s^2 i_{CS}^2 \omega^2 c_{cs}^2 \frac{\tau}{(1 + \omega^2 \tau^2)}. \quad (2)$$

At low frequency ($\omega\tau \ll 1$) this increases as ω^2 and at high frequency ($\omega\tau \gg 1$) is independent of frequency. This can explain the dependence of ΔF on frequency if τ is about $0.5 \mu\text{sec}$, which is a reasonable value. If τ is independent of i_{CS} then $\overline{i_{cs}^2}$ is proportional to i_{CS}^2 . An increase of τ under high-level conditions will weaken this dependence as is required. There will be some correlation between e_s and the 'emitter' noise generator, but in view of the extra transit time for holes at the surface this will be weak and can be ignored to a first order at high frequencies.

It is proposed to test the validity of this model further by controlling the surface conditions using a field electrode and gaseous ambients (Beale, Thomas and Watkins 1958). A low resistivity surface skin should not produce significant excess noise.

Department of Electronic Engineering,
University College of North Wales,
Bangor.

F. J. HYDE.†
H. J. ROBERTS.†

A.E.I. Research Laboratories,
Harlow,
Essex.

B. E. BUCKINGHAM.‡

29th August 1961.

BEALE, J. R. A., THOMAS, D. E., and WATKINS, T. B., 1958, *Proc. Phys. Soc.*, **72**, 910.

GUGGENBUHL, W., and STRUTT, M. J. O., 1957, *Proc. Inst. Radio Engrs*, **N.Y.**, **45**, 839.

VAN DER ZIEL, A., 1959, *Fluctuation Phenomena in Semiconductors* (London: Butterworths).

Cyclotron Resonance at 4 mm Wavelength

Cyclotron resonance absorption from hole carriers has been investigated in high purity p-type germanium at 4.3 mm wavelength over the temperature range 10 to 100 °K. A modified 8 mm microwave spectrometer was employed for these measurements using a substantially non-resonant cavity system with the 4 mm power derived from a crystal doubler. The hole carriers were obtained by thermal ionization of the shallow acceptor impurities ($\sim 3 \times 10^{12} \text{ cm}^{-3}$).

The results obtained with this spectrometer have extended the measurements recently reported by Bagguley, Stradling and Whiting (1961). In particular, the new absorption line found by these authors in the [110] crystallographic direction has been established beyond reasonable doubt as arising from a hole carrier with a true effective mass of $0.265m_e$. The greater resolution which has been obtained at 4.3 mm wavelength has allowed this new absorption line to be observed at temperatures up to 60 °K. These observations verify the suggestion that the absorption line arises from the motion of a classical particle. It is not related to the quantum mechanical fine structure which is found at very low temperatures (Fletcher, Yager and Merritt 1955).

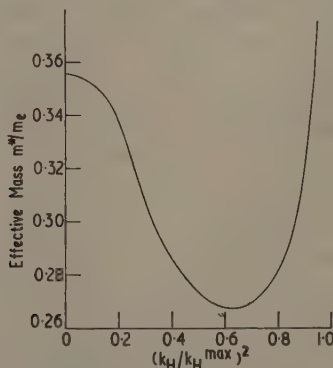


Figure 1. The variation of effective mass in the heavy hole band of germanium calculated as a function of k_H in the [110] direction.

A numerical calculation shows that, for the heavy mass band in the [110] direction, the cyclotron effective mass has a minimum value for those carriers which have a translational energy in the direction of the magnetic field roughly one half of the maximum value possible on any given energy surface. Carriers in this region of wave vector space will have effective masses which are slowly varying functions of the wave vector, k_H , in the direction of the magnetic field. There will be a definite lower limit for the effective mass of these carriers and a spread on the high mass side. This is evident in the recorded absorption line which has a sharp leading edge and a 'tail' on the high field side.

The variation of the effective mass with the wave vector k_H calculated for the [110] direction is shown in figure 1. The values for the constants in the equation for the energy surface

$$E(\mathbf{k}) = Ak^2 \pm [B^2k^4 + C^2(k_x^2k_y^2 + k_y^2k_z^2 + k_z^2k_x^2)]^{1/2}$$

(Dresselhaus, Kip and Kittel 1955) used in this calculation were $A = -13.2$, $|B| = 8.7$, $|C| = 11.6$. These values differ slightly from those given previously by Bagguley, Stradling and Whiting (1961), for the same germanium crystal (G.E.b.1). With the

present values, however, it is possible to fit not only the anisotropy of the heavy-mass hole but also the new absorption line without making any further assumptions. The discrepancy arises because of the approximations involved in relating the measured effective masses to the constants in the energy equation. A numerical calculation shows that the relation given by Dresselhaus, Kip and Kittel (1955) is less accurate than had been anticipated in the [100] direction.

The light-mass hole increases in mass as the temperature increases as shown in figure 2. This increase in mass is in the opposite direction to that which would arise from the decrease in energy gap with temperature, but is in good agreement with the

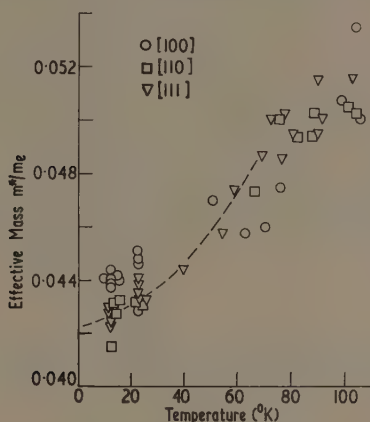


Figure 2. The temperature dependence of the light-mass hole in germanium. ∇ , \square , \circ , experimental points obtained at 4.3 mm wavelength; - - - - mean of the results obtained at 8.5 mm wavelength.

theory of Kane (1956) where the change in mass arises from the change in curvature of the energy bands away from the origin in \mathbf{k} space. From the published curves given by Kane we estimate that the light-mass hole in germanium will have an effective mass of the order

$$\frac{m^*}{m_e} = \frac{1}{24 - 2 \times 10^{-12} k^2}$$

over the temperature range covered by our experiments. This leads to a value of about $0.05 m_e$ at 100 °K in agreement with our results.

We wish to thank Mr. D. C. Handscomb of the Oxford University Computing Laboratory for programming the computer which was used to check our numerical calculations.

The Clarendon Laboratory,
Oxford.

D. M. S. BAGGULEY.
R. A. STRADLING.

3th September 1961.

BAGGULEY, D. M. S., STRADLING, R. A., and WHITING, J. S. S., 1961, *Proc. Roy. Soc. A*, **262**, 340.

DRESSELHAUS, G., KIP, A. F., and KITTEL, C., 1955, *Phys. Rev.*, **98**, 368.

LETCHER, R. C., YAGER, W. A., and MERRITT, F. R., 1955, *Phys. Rev.*, **100**, 747.

KANE, E. O., 1956, *J. Phys. Chem. Solids*, **1**, 82.

Distortion Approximation to Cross Sections for Excitation of 1s-2p Transition of Hydrogenic Ions by Bare Nuclei

Little theoretical work has been done on inelastic collisions between charged atomic systems and no detailed quantal calculations on the cross sections have been reported. This note describes the application of the distortion approximation (Bates 1959) to the study of the excitation of a target hydrogenic ion with nucleus of charge $\mathcal{Z}_t e$ from the 1s to the 2p level by a projectile nucleus of charge $\mathcal{Z}_p e$:

$$A(\mathcal{Z}_t-1)^+(1s) + B\mathcal{Z}_p^+ \rightarrow A(\mathcal{Z}_t-1)^+(2p) + B\mathcal{Z}_p^+. \quad (1)$$

An impact parameter treatment is followed. In spite of the Coulomb repulsion between the target and the projectile it is permissible to suppose that the relative velocity vector does not change appreciably during the encounter unless the relative energy of motion is very low indeed (Bates and Boyd 1962).

Let the target be located at the origin of coordinates and let the projectile, position vector \mathbf{R} , move with constant speed v in the positive direction along a line distant ρ from the Z axis. Expand the complete electronic eigenfunction according to

$$\Psi(\mathbf{r}, t) = \sum_m a_m(Z) \phi_m(\mathbf{r}) \exp \left[-\frac{i\epsilon_m Z}{v} \right], \quad Z = vt \quad (2)$$

where \mathbf{r} is the position vector of the electron, t is the time and $\phi_m(\mathbf{r})$ and ϵ_m are the unperturbed eigenfunctions and eigenenergies of the target in atomic units. Substitution in the Schrödinger equation shows that the expansion coefficient must satisfy

$$i \frac{\partial a_n(Z)}{\partial Z} = \frac{1}{v} \sum_m a_m(Z) U_{nm}(\mathbf{R}) \exp \left[-\frac{i(\epsilon_m - \epsilon_n)Z}{v} \right] \quad (3)$$

where $U_{nm}(\mathbf{R})$ is the matrix element with respect to states m and n , of the interaction potential arising from the projectile. This set of coupled differential equations is effectively exact. A scaling law may be derived which enables results on a family of processes like (1) to be presented compactly.

Introducing

$$\mathbf{R}' = \mathcal{Z}_t \mathbf{R}, \quad Z' = \mathcal{Z}_t Z \quad (4)$$

and noting that the interaction matrix elements may be written

$$U_{nm}(\mathbf{R}) = \mathcal{Z}_t \mathcal{Z}_p U_{nm}'(\mathbf{R}'), \quad (5)$$

where $U_{nm}(\mathbf{R}')$ does not involve \mathcal{Z}_t or \mathcal{Z}_p , and that

$$\epsilon_m = \mathcal{Z}_t^2 \epsilon_m', \quad (6)$$

where ϵ_m' is a constant, it may be seen from (3) that

$$i \frac{\partial a_n(Z')}{\partial Z'} = \frac{\mathcal{Z}_p}{\mathcal{Z}_t} \left(\frac{\mathcal{Z}_t}{v} \right) \sum_m a_m(Z') U_{nm}'(\mathbf{R}') \exp \left[-i(\epsilon_m' - \epsilon_n') Z' \frac{\mathcal{Z}_t}{v} \right]. \quad (7)$$

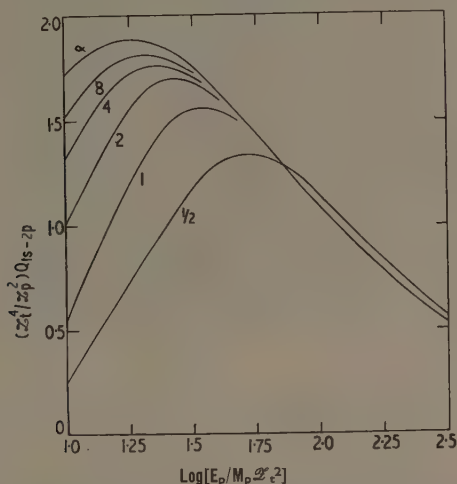
Hence $a_n(\infty)$ depends on $\mathcal{Z}_t \rho$, $\mathcal{Z}_t / \mathcal{Z}_p$ and v / \mathcal{Z}_t only. Since the excitation cross section is given by

$$Q_{0n} = 2\pi \int_0^\infty \rho |a_n(\infty)|^2 d\rho \quad (8)$$

it follows that $\mathcal{Z}_t^2 Q_{0n}$ may be expressed in terms of two parameters $\mathcal{Z}_t / \mathcal{Z}_p$ and v / \mathcal{Z}_t ,

or instead of the latter $E_p/M_p \mathcal{Z}_t^2$ where E_p and M_p are the energy and mass of the projectile.

Using the distortion approximation, the cross section $Q_{1s,2p}$ for (1) was computed for selected values of $\mathcal{Z}_t/\mathcal{Z}_p$ and over a range of values of $E_p/M_p \mathcal{Z}_t^2$ (all such that the effect of the Coulomb repulsion is utterly negligible). The formulae which arise need not be displayed since they are obvious generalizations of formulae contained in an earlier paper on the excitation of the same transition in atomic hydrogen (Bates 1961).



Excitation of the 1s-2p transition in a target hydrogenic ion with nucleus of charge \mathcal{Z}_{te} by a projectile nucleus of charge \mathcal{Z}_{pe} . The value of $\mathcal{Z}_t/\mathcal{Z}_p$ is indicated on each curve. The distortion approximation cross section Q_{1s-2p} is in units of $\pi a_0^2 (8.8 \times 10^{-17} \text{ cm}^2)$; the energy E_p of the projectile nucleus is in kev and the mass M_p is on the chemical (^{16}O) scale.

The results are presented in the figure, the dependent variable being taken to be $(\mathcal{Z}_t^4/\mathcal{Z}_p^2)Q_{1s,2p}$ since this combination depends only on the independent variable $E_p/M_p \mathcal{Z}_t^2$ in the case of the first Born approximation. As would be expected the curves tend to a limit as $\mathcal{Z}_t/\mathcal{Z}_p$ approaches infinity. They do so rather slowly at low energies.

This investigation has been supported by the U.S. Office of Naval Research under Contract No. N.62558-2637. It is a part of Project 'Defender' sponsored by the Advance Research Projects Agency Department of Defence.

Department of Applied Mathematics,
Queen's University,
Belfast,
Northern Ireland.

D. R. BATES.

6th September 1961.

BATES, D. R., 1959, *Proc. Phys. Soc.*, **73**, 227.

— 1961, *Proc. Phys. Soc.*, **77**, 59.

BATES, D. R., and BOYD, ANNE H., 1962, *Proc. Phys. Soc.*, **79**, in the press.

REVIEWS OF BOOKS

The Fundamental Atomic Constants, by J. S. SANDERS. Pp. 88. (London: Oxford University Press, 1961.) 10s.

There is an increasing interest in the values of fundamental atomic constants, among which it is usual to include the velocity of light, because they are now being used in practical applications as standards of measurement. Some of them are related to the units of mass, length and time by direct measurement but others can be obtained only indirectly by combining a number of experimental results. It is the experimental results that are important and in this attractively produced little volume Dr. Sanders gives a most readable and useful introduction to this aspect of the subject.

The methods of measuring the Faraday, e/m , h/e and the Rydberg constant are briefly but clearly outlined. The longest section is devoted to some recent determinations of the velocity of light and fairly full descriptions are given of the measurement of the gyromagnetic ratio of the proton, and the proton magnetic moment.

One of the most difficult problems facing an experimenter is the assessment of the accuracy of his result, but if the values are used as standards of measurement or to assist in the determination of other fundamental constants the question of accuracy is of first importance. Dr. Sanders has chosen not to deal with this problem because, as he explains in the introduction with some justification, it is difficult to decide what the limits represent. In work on the velocity of light, however, authors do explain how they obtain their limits and the methods adopted are so different that they could change the limits by more than 20 to 1. By failing to notice this Dr. Sanders gives a somewhat wrong impression of the relative significance of the various methods of measurement used. The cavity resonator method not only revealed the error in Birge's adopted value but also gave the most accurate value prior to Froome's last determination.

L. ESSEN.

Quantum Theory of Atomic Structure, Vol. II, by J. C. SLATER. Pp. ix + 439. (London: McGraw-Hill, 1960.) £5 15s.

Professor Slater disarms the critic, in his preface to this volume, by pointing out that while the first volume of this book was designed as a textbook, this second one is much more a work of reference for readers already versed in the simpler aspects of atomic theory.

The content of the book extends from an introduction of the Hartree-Fock method to a discussion of hyperfine structure. A lucid treatment of group theory introduces the heavy discussion of combination of angular momenta, and there are chapters on Dirac's theory of spin, the magnetic behaviour of complex atoms and radiation transition probabilities. It might have been profitable to the reader to have had more on density matrix methods, and perhaps some discussion of the effects of perturbing fields of, for example, cubic symmetry. The latter topic belongs more to the theory of the solid state but is illuminating for atomic theory.

This is an easier book in several ways than Condon and Shortley's classic. The author gives much more discussion of the historical motivation for various steps in the theory, and also makes admirable heuristic use of classical arguments wherever these are applicable. The inevitably high price will restrict sales to individuals, but this is a very valuable work of reference. The production, as usual with this series, is excellent.

G. WYLLIE.



Figure 4



Figure 5

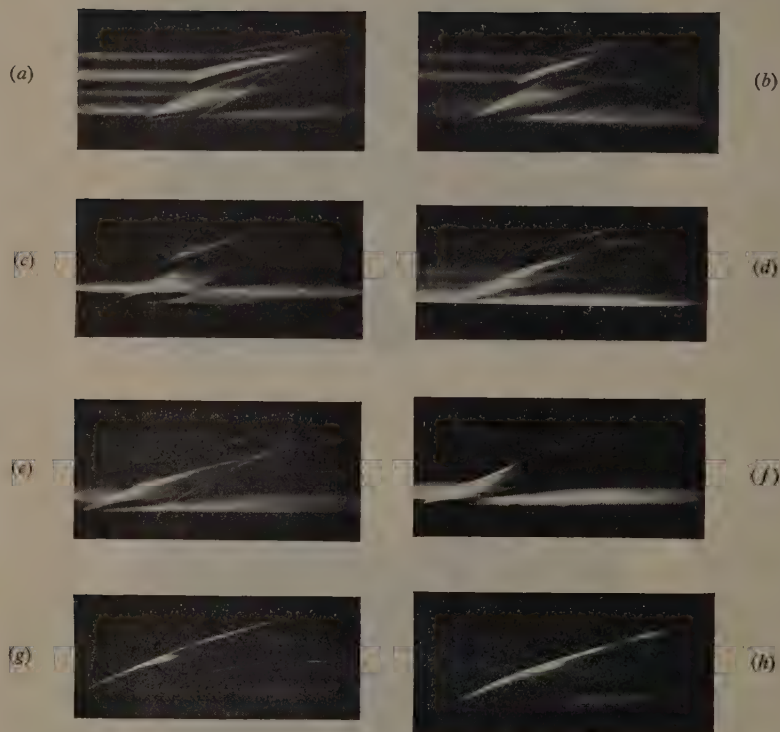
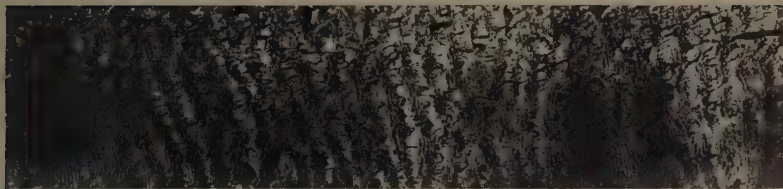


Figure 4. Rotating mirror photographs showing the passage of a shock wave at various times after the interruption of a horizontal 10 A d.c. carbon arc in air. Time scale as abscissa, and direction of shock propagation as ordinate. *a*, steady-state arc; *b*, 0.24 msec; *c*, 0.5 msec; *d*, 7.5 msec; *e*, 13 msec; *f*, 25 msec; *g*, 60 msec; *h*, 810 msec.



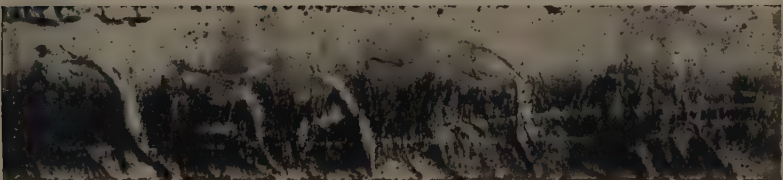
(a)



(b)



(c)



(d)

Figure 5



Figure 3. Resolidified AgBr; one of the grooves (horizontal) caused by a 1-2 mm abrasion on dry 0 emery paper at 200 g total load; note lateral pile-up and also coiled strip being cut out by the ploughing abrasive particle. Vertical fine grooves are due to initial surfacing on wet 4/0 emery paper. 340 \times .

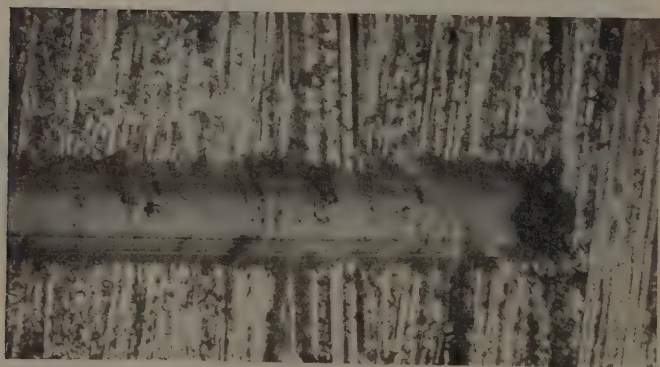


Figure 4. Resolidified AgBr; one of the grooves (horizontal) caused by a glass sphere 125 microns diam., in ~ 1 mm sliding on 'Scotchlite' at 200 g load. Note negligible wear, and the forward curvature of the fine surfacing grooves (vertical) in the main groove. 340 \times .

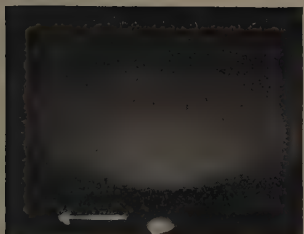


Figure 5. Resolidified AgCl abraded (R to L) on dry 4/0 emery paper at 500 g load; etched to 1200 Å depth.



Figure 6. Resolidified AgBr abraded (R to L) on wet 4/0 emery paper at *c.*500 g load; etched to 1400 Å.

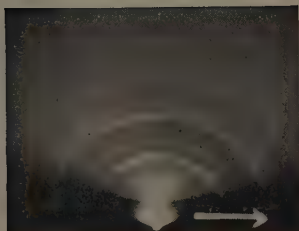


Figure 7. Compressed AgCl abraded (L to R) on filter paper at *c.*500 g load; etched to 4500 Å.

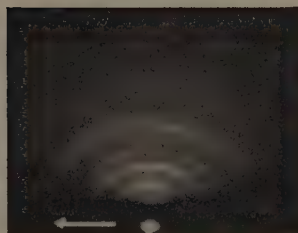


Figure 8. Compressed AgBr abraded (R to L) on filter paper at *c.*500 g load; etched to 2000 Å.

THE RUTHERFORD MEMORIAL LECTURE 1958†

Reminiscences of the Founder of Nuclear Science and of Some Developments Based on his Work

By NIELS BOHR

IT has been a pleasure for me to accept the invitation from the Physical Society to contribute to the series of Rutherford Memorial Lectures in which, through the years, several of Rutherford's closest collaborators have commented on his fundamental scientific achievements and communicated reminiscences about his great human personality. As one who in early youth had the good fortune to join the group of physicists working under Rutherford's inspiration, and owes so much to his warm friendship through the many succeeding years, I welcome the task of recalling some of my most treasured remembrances. Since it is impossible, of course, in a single lecture to attempt a survey of the immense and many-sided life-work of Ernest Rutherford and its far reaching consequences, I shall confine myself to periods of which I have personal recollections and to developments I have followed at close hand.

I

The first time I had the great experience of seeing and listening to Rutherford was in the autumn of 1911 when, after my university studies in Copenhagen, I was working in Cambridge with J. J. Thomson, and Rutherford came down from Manchester to speak at the annual Cavendish Dinner. Although I did not on this occasion come into personal contact with Rutherford I received a deep impression of the charm and power of his personality by which he had been able to achieve almost the incredible wherever he worked. The dinner took place in a most humorous atmosphere and gave the opportunity for several of Rutherford's colleagues to recall some of the many anecdotes which already then were attached to his name. Among various illustrations of how intensely he was absorbed in his researches, a laboratory assistant in the Cavendish was reported to have noted that, of all the eager young physicists who through the years had worked in the famous laboratory, Rutherford was the one who could swear at his apparatus most forcefully.

From Rutherford's own address I especially remember the warmth with which he greeted the latest success of his old friend C. T. R. Wilson who by the ingenious cloud chamber method had just then obtained the first photographs of tracks of α -rays exhibiting clear cases of sharp bends in their usual remarkably straight path. Of course, Rutherford was thoroughly acquainted with the phenomenon which only a few months before had led him to his epoch-making discovery of the atomic nucleus, but that such details of the life history of α -rays could now be witnessed

† The present text is an elaborated version, completed in 1961, of the lecture delivered without a prepared manuscript at a meeting of The Physical Society of London at the Imperial College of Science and Technology on 28th November 1958.

directly by our eyes, he admitted to be a surprise, causing him extreme pleasure. In this connection Rutherford spoke most admiringly of the persistence with which Wilson already during their comradeship in the Cavendish had pursued his researches on cloud formation with ever more refined apparatus. As Wilson later told me, his interest in these beautiful phenomena had been awakened when as a youth he was watching the appearance and disappearance of fogs as air currents ascended the Scottish mountain ridges and again descended in the valleys.

A few weeks after the Cavendish Dinner I went up to Manchester to visit one of my recently deceased father's colleagues who was also a close friend of Rutherford. There, I again had the opportunity to see Rutherford who in the meantime had attended the inaugural meeting of the Solvay Council in Brussels, where he had met Planck and Einstein for the first time. During the conversation, in which Rutherford spoke with characteristic enthusiasm about the many new prospects in physical science, he kindly assented to my wish to join the group working in his laboratory when, in the early spring of 1912, I should have finished my studies in Cambridge where I had been deeply interested in J. J. Thomson's original ideas on the electronic constitution of atoms.

In those days, many young physicists from various countries had gathered around Rutherford, attracted by his genius as a physicist and by his unique gifts as a leader of scientific cooperation. Although Rutherford was always intensely occupied with the progress of his own work, he had the patience to listen to every young man, when he felt he had any idea, however modest, on his mind. At the same time, with his whole independent attitude, he had only little respect for authority and could not stand what he called 'pompous talk'. On such occasions he could even sometimes speak in a boyish way about venerable colleagues, but he never permitted himself to enter into personal controversies, and he used to say: "There is only one person who can take away one's good name, and that is oneself!"

Naturally, to trace in every direction the consequences of the discovery of the atomic nucleus was the centre of interest of the whole Manchester group. In the first weeks of my stay in the laboratory, I followed, on Rutherford's advice, an introductory course on the experimental methods of radioactive research which under the experienced instruction of Geiger, Makower and Marsden was arranged for the benefit of students and new visitors. However, I rapidly became absorbed in the general theoretical implications of the new atomic model and especially in the possibility it offered of a sharp distinction as regards the physical and chemical properties of matter, between those directly originating in the atomic nucleus itself and those primarily depending on the distribution of the electrons bound to it at distances very large compared with nuclear dimensions.

While the explanation of the radioactive disintegrations had to be sought in the intrinsic constitution of the nucleus, it was evident that the ordinary physical and chemical characteristics of the elements manifested properties of the surrounding electron system. It was even clear that, owing to the large mass of the nucleus and its small extension compared with that of the whole atom, the constitution of the electron system would depend almost exclusively on the total electric charge of the nucleus. Such considerations at once suggested the prospect of basing the account of the physical and chemical properties of every element on a single integer, now generally known as the atomic number, expressing the nuclear charge as a multiple of the elementary unit of electricity.

In the development of such views, I was encouraged not least by discussions with George Hevesy who distinguished himself among the Manchester group by his uncommonly broad chemical knowledge. In particular, as early as 1911, he had conceived the ingenious tracer method which has since become so powerful a tool in chemical and biological research. As Hevesy has himself humorously described, he was led to this method by the negative results of elaborate work undertaken as a response to a challenge by Rutherford who had told him that "if he was worth his salt" he ought to be helpful by separating the valuable radium D from the large amount of lead chloride extracted from pitchblende and presented to Rutherford by the Austrian government.

My views took more definite shape in conversations with Hevesy about the wonderful adventure of those Montreal and Manchester years, in which Rutherford and his collaborators, after the discoveries of Becquerel and Madame Curie, had built up the science of radioactivity by progressively disentangling the succession and interconnections of radioactive disintegrations. Thus, when I learned that the number of stable and decaying elements already identified exceeded the available places in the famous table of Mendeleev, it struck me that such chemically inseparable substances, to the existence of which Soddy had early called attention and which later by him were termed 'isotopes', possessed the same nuclear charge and differed only in the mass and intrinsic structure of the nucleus. The immediate conclusion was that by radioactive decay the element, quite independently of any change in its atomic weight, would shift its place in the periodic table by two steps down or one step up, corresponding to the decrease or increase in the nuclear charge accompanying the emission of α - or β -rays, respectively.

When I turned to Rutherford to learn his reaction to such ideas, he expressed, as always, alert interest in any promising simplicity but warned with characteristic caution against overstressing the bearing of the atomic model and extrapolating from comparatively meagre experimental evidence. Still, such views, probably originating from many sides, were at that time lively discussed within the Manchester group and evidence in their support was rapidly forthcoming, especially through chemical investigations by Hevesy as well as by Russell.

In particular, a strong support for the idea of the atomic number as determining the general physical properties of the elements was obtained from spectroscopic investigations by Russell and Rossi of mixtures of ionium and thorium, which pointed to the identity of the optical spectra of these two substances in spite of their different radioactive properties and atomic weights. On the basis of an analysis of the whole evidence then available, the general relationship between the specified radioactive processes and the resulting change of the atomic number of the element was indicated by Russell in a lecture to the Chemical Society in the late autumn of 1912.

In this connection it is interesting that, when after further research especially by Fleck, the radioactive displacement law in its complete form was enunciated a few months later by Soddy working in Glasgow, as well as by Fajans in Karlsruhe, these authors did not recognize its close relation to the fundamental features of Rutherford's atomic model, and Fajans even regarded the change in chemical properties evidently connected with the electron constitution of the atoms as a strong argument against a model according to which the α - as well as the β -rays.

had their origin in the nucleus. About the same time, the idea of the atomic number was independently introduced by van den Broek in Amsterdam, but in his classification of the elements a different nuclear charge was still ascribed to every stable or radioactive substance.

So far, the primary object of the discussions within the Manchester group was the immediate consequences of the discovery of the atomic nucleus. The general programme of interpreting the accumulated experience about the ordinary physical and chemical properties of matter on the basis of the Rutherford model of the atom presented, however, more intricate problems which were to be clarified gradually in the succeeding years. Thus in 1912, there could only be question of a preliminary orientation as to the general features of the situation.

From the outset it was evident that, on the basis of the Rutherford model, the typical stability of atomic systems could by no means be reconciled with classical principles of mechanics and electrodynamics. Indeed, on Newtonian mechanics, no system of point charges admits of a stable static equilibrium, and any motion of the electrons around the nucleus would, according to Maxwell's electrodynamics, give rise to a dissipation of energy through radiation accompanied by a steady contraction of the system, resulting in the close combination of the nucleus and the electrons within a region of extension far smaller than atomic dimensions.

Still, this situation was not too surprising, since an essential limitation of classical physical theories had already been revealed by Planck's discovery in 1900 of the universal quantum of action which, especially in the hands of Einstein, had found such promising application in the account of specific heats and photochemical reactions. Quite independent of the new experimental evidence as regards the structure of the atom, there was therefore a widespread expectation that quantum concepts might have a decisive bearing on the whole problem of the atomic constitution of matter.

Thus, as I later learned, A. Haas had in 1910 attempted, on the basis of Thomson's atomic model, to fix dimensions and periods of electronic motions by means of Planck's relation between the energy and the frequency of a harmonic oscillator. Further, J. Nicholson had in 1912 made use of quantized angular momenta in his search for the origin of certain lines in the spectra of stellar nebulae and the solar corona. Above all, however, it deserves mention that, following early ideas of Nernst about quantized rotations of molecules, N. Bjerrum already in 1912 predicted the band structure of infra-red absorption lines in diatomic gases, and thereby made a first step towards the detailed analysis of molecular spectra eventually achieved on the basis of the subsequent interpretation, by quantum theory, of the general spectral combination law.

Early in my stay in Manchester in the spring of 1912 I became convinced that the electronic constitution of the Rutherford atom was governed throughout by the quantum of action. A support for this view was found not only in the fact that Planck's relation appeared approximately applicable to the more loosely bound electrons involved in the chemical and optical properties of the elements, but especially in the tracing of similar relationships as regards the most firmly bound electrons in the atom revealed by the characteristic penetrating radiation discovered by Barkla. Thus, measurements of the energy necessary to produce the Barkla radiation by electron bombardment of various elements, performed by Whiddington at the time when I was staying in Cambridge, exhibited simple regularities of the kind to be expected from an estimate of the firmest binding

energy of an electron rotating in a Planck orbit round a nucleus with a charge given by the atomic number. From Lawrence Bragg's recently published Rutherford Lecture I have been very interested to learn that William Bragg, then in Leeds, in his first investigation of x-ray spectra, based on Laue's discovery in 1912, was fully aware of the bearing of Whiddington's results on the connection between the Barkla radiation and the ordering of the elements in Mendeleev's table, a problem which through Moseley's work in Manchester soon was to receive such complete elucidation.

During the last month of my stay in Manchester I was mainly occupied with a theoretical investigation of the stopping power of matter for α - and β -rays. This problem, which originally was discussed by J. J. Thomson from the point of view of his own atomic model, had just been re-examined by Darwin on the basis of the Rutherford model. In connection with the considerations mentioned above regarding the frequencies involved in the electron binding in the atom, it occurred to me that the transfer of energy from the particles to the electrons could be simply treated in analogy to the dispersion and absorption of radiation. In this way, it proved possible to interpret the results of the stopping power measurements as additional support for ascribing to hydrogen and helium the atomic numbers 1 and 2 in conformity with general chemical evidence, and in particular with Rutherford and Royds' demonstration of the formation of helium gas by the collection of α -particles escaping from thin-walled emanation tubes. Also for the more complex case of heavier substances, approximate agreement was ascertained with the expected atomic numbers and the estimated values for the binding energies of the electrons, but the theoretical methods were much too primitive to yield more accurate results. As is well known, an appropriate treatment of the problem by modern methods of quantum mechanics was first achieved in 1930 by H. Bethe.

Although Rutherford just at that time was concentrating on the preparation of his great book, *Radioactive Substances and Their Radiations*, he nevertheless followed my work with a constant interest, which gave me the opportunity to learn about the care which he always took in the publications of his pupils. After my return to Denmark I was married in mid-summer 1912 and, on our wedding trip in August to England and Scotland, my wife and I passed through Manchester to visit Rutherford and deliver the completed manuscript of my paper on the stopping problems. Both Rutherford and his wife received us with a cordiality which laid the foundation of the intimate friendship that through the many years connected the families.

II

After settling down in Copenhagen, I remained in close contact with Rutherford, to whom I regularly reported about the development of the work on general atomic problems, which I had started in Manchester. Common to Rutherford's answers, which were always very encouraging, was the spontaneity and joy with which he told about the work in his laboratory. It was indeed the beginning of a long correspondence which lasted over 25 years and which revives, every time I look into it, my memories of Rutherford's enthusiasm for the progress in the field he had opened up and the warm interest he took in the endeavours of every one trying to contribute to it.

My letters to Rutherford in the autumn of 1912 concerned the continued endeavours to trace the role of the quantum of action for the electronic

constitution of the Rutherford atom, including problems of molecular bindings and radiative and magnetic effects. Still, the stability question presented in all such considerations intricate difficulties stimulating the search for a firmer hold. However, after various attempts to apply quantum ideas in a more consistent manner, it struck me in the early spring of 1913 that a clue to the problem of atomic stability directly applicable to the Rutherford atom was offered by the remarkably simple laws governing the optical spectra of the elements.

On the basis of the extremely accurate measurements of the wavelengths of spectral lines by Rowland and others, and after contributions by Balmer and by Schuster, Rutherford's predecessor in the Manchester Chair, the general spectral laws were most ingeniously clarified by Rydberg. The principal result of the thorough analysis of the conspicuous series in the line spectra and their mutual relationship was the recognition that the frequency ν of every line in the spectrum of a given element could be represented with unparalleled accuracy as $\nu = T' - T''$, where T' and T'' are two among a multitude of spectral terms T characteristic of the element.

This fundamental combination law obviously defied ordinary mechanical interpretation, and it is interesting to recall how in this connection Lord Rayleigh had pertinently stressed that any general relationship between the frequencies of the normal modes of vibration of a mechanical model would be quadratic and not linear in these frequencies. For the Rutherford atom we should not even expect a line spectrum since, according to ordinary electrodynamics, the frequencies of radiation accompanying the electronic motion would change continuously with the energy emitted. It was therefore natural to attempt to base the explanation of spectra directly on the combination law.

In fact, accepting Einstein's idea of light quanta or photons with energy $h\nu$, where h is Planck's constant, one was led to assume that any emission or absorption of radiation by the atom is an individual process accompanied by an energy transfer $h(T' - T'')$, and to interpret hT as the binding energy of the electrons in some stable, or so-called stationary, state of the atom. In particular, this assumption offered an immediate explanation of the apparently capricious appearance of emission and absorption lines in series spectra. Thus, in emission processes we witness the transition of the atom from a higher to a lower energy level, whereas in the absorption processes we have in general to do with a transfer of the atom from the ground state, with the lowest energy, to one of its excited states.

In the simplest case of the hydrogen spectrum, the terms are with great accuracy given by $T_n = R/n^2$, where n is an integer and R the Rydberg constant. Thus, the interpretation indicated led to a sequence of decreasing values for the binding energy of the electron in the hydrogen atom, pointing to a steplike process by which the electron, originally at a large distance from the nucleus, passes by radiative transitions to stationary states of firmer and firmer binding, characterized by lower and lower n -values, until the ground state, specified by $n = 1$, is reached. Moreover, a comparison of the binding energy in this state with that of an electron moving in a Keplerian orbit around the nucleus yielded orbital dimensions of the same order as the atomic sizes derived from the properties of gases.

On the basis of the Rutherford atomic model, this view also immediately suggested an explanation of the appearance of the Rydberg constant in the more complex spectra of other elements. Thus it was concluded that we were here

faced with transition processes involving excited states of the atom, in which one of the electrons had been brought outside the region occupied by the other electrons bound to the nucleus, and therefore exposed to a field of force resembling that surrounding a unit charge.

The tracing of a closer relation between the Rutherford atomic model and the spectral evidence obviously presented intricate problems. On the one hand, the very definition of the charge and mass of the electron and the nucleus rested entirely on an analysis of physical phenomena in terms of the principles of classical mechanics and electromagnetism. On the other hand, the so-called quantum postulate, stating that any change of the intrinsic energy of the atom consists in a complete transition between two stationary states, excluded the possibility of accounting on classical principles for the radiative processes or any other reaction involving the stability of the atom.

As we know today, the solution of such problems demanded the development of a mathematical formalism, the proper interpretation of which implied a radical revision of the foundation for the unambiguous use of elementary physical concepts and the recognition of complementary relationships between phenomena observed under different experimental conditions. Still, at that time, some progress could be made by utilizing classical physical pictures for the classification of stationary states based on Planck's original assumptions on the energy states of a harmonic oscillator. In particular, a starting point was offered by the closer comparison between an oscillator of given frequency and the Keplerian motion of an electron around a nucleus, with a frequency of revolution depending on the binding energy.

In fact, just as in the case of a harmonic oscillator, a simple calculation showed that, for each of the stationary states of the hydrogen atom, the action integrated over an orbital period of the electron could be identified with nh , a condition which in the case of circular orbits is equivalent to a quantization of the angular momentum in units $h/2\pi$. Such identification involved a fixation of the Rydberg constant in terms of the charge e and mass m of the electron and Planck's constant, according to the formula

$$R = \frac{2\pi^2 me^4}{h^3}$$

which was found to agree with the empirical value within the accuracy of the available measurements of e , m and h .

Although this agreement offered an indication of the scope for the use of mechanical models in picturing stationary states, of course the difficulties involved in any combination of quantum ideas and the principles of ordinary mechanics remained. It was therefore most reassuring to find that the whole approach to the spectral problems fulfilled the obvious demand of embracing the classical physical description in the limit where the action involved is sufficiently large to permit the neglect of the individual quantum. Such considerations presented indeed the first indication of the so-called correspondence principle expressing the aim of representing the essentially statistical account of quantum physics as a rational generalization of the classical physical description.

Thus, in ordinary electrodynamics, the composition of the radiation emitted from an electron system should be determined by the frequencies and amplitudes

of the harmonic oscillations into which the motion of the system can be resolved. Of course no such simple relation holds between the Keplerian motion of an electron around a heavy nucleus and the radiation emitted by transitions between the stationary states of the system. However, in the limiting case of transitions between states for which the values of the quantum number n are large compared with their difference, it could be shown that the frequencies of the components of the radiation, appearing as the result of the random individual transition processes, coincide asymptotically with those of the harmonic components of the electron motion. Moreover, the fact that in a Keplerian orbit, in contrast to a simple harmonic oscillation, there appears not only the frequency of revolution but also higher harmonics, offered the possibility of tracing a classical analogy as regards the unrestricted combination of the terms in the hydrogen spectrum.

Still, the unambiguous demonstration of the relation between the Rutherford atomic model and the spectral evidence was for a time hindered by a peculiar circumstance. Already twenty years before, Pickering had observed in the spectra of distant stars a series of lines with wavelengths exhibiting a close numerical relationship with the ordinary hydrogen spectrum. These lines were therefore generally ascribed to hydrogen and were even thought by Rydberg to remove the apparent contrast between the simplicity of the hydrogen spectrum and the complexity of the spectra of other elements including those of the alkalis, whose structure comes nearest to the hydrogen spectrum. This view was also upheld by the eminent spectroscopist A. Fowler, who just at that time in laboratory experiments with discharges through a mixture of hydrogen and helium gas had observed the Pickering lines and new related spectral series.

However, the Pickering and Fowler lines could not be included in the Rydberg formula for the hydrogen spectrum, unless the number n in the expression for the spectral terms were allowed to take half integrals as well as integral values; but this assumption would evidently destroy the asymptotic approach to the classical relationship between energy and spectral frequencies. On the other hand, such correspondence would hold for the spectrum of a system consisting of an electron bound to a nucleus of charge Ze , whose stationary states are determined by the same value nh of the action integral. Indeed, the spectral terms for such a system would be given by Z^2R/n^2 , which for $Z=2$ yields the same result as the introduction of half-integral values of n in the Rydberg formula. Thus, it was natural to ascribe the Pickering and Fowler lines to helium ionized by the high thermal agitation in the stars and in the strong discharges used by Fowler. Indeed, if this conclusion were confirmed, a first step would have been made towards the establishment of quantitative relationships between the properties of different elements on the basis of the Rutherford model.

III

When in March 1913 I wrote to Rutherford, enclosing a draft of my first paper on the quantum theory of atomic constitution, I stressed the importance of settling the question of the origin of the Pickering lines and took the opportunity of asking whether experiments to that purpose could be performed in his laboratory, where from Schuster's days appropriate spectroscopic apparatus were available. I received a prompt answer, so characteristic of Rutherford's acute scientific judgment and helpful human attitude, that I shall quote it in full:

March 20, 1913.

Dear Dr. Bohr,

I have received your paper safely and read it with great interest, but I want to look over it again carefully when I have more leisure. Your ideas as to the mode of origin of spectrum and hydrogen are very ingenious and seem to work out well; but the mixture of Planck's ideas with the old mechanics make it very difficult to form a physical idea of what is the basis of it. There appears to me one grave difficulty in your hypothesis, which I have no doubt you fully realise, namely, how does an electron decide what frequency it is going to vibrate at when it passes from one stationary state to the other? It seems to me that you would have to assume that the electron knows beforehand where it is going to stop.

There is one criticism of minor character which I would make in the arrangement of the paper. I think in your endeavour to be clear you have a tendency to make your papers much too long, and a tendency to repeat your statements in different parts of the paper. I think that your paper really ought to be cut down, and I think this could be done without sacrificing anything to clearness. I do not know if you appreciate the fact that long papers have a way of frightening readers, who feel that they have not time to dip into them.

I will go over your paper very carefully and let you know what I think about the details. I shall be quite pleased to send it to the *Phil. Mag.* but I would be happier if its volume could be cut down to a fair amount. In any case I will make any corrections in English that are necessary.

I shall be very pleased to see your later papers, but please take to heart my advice, and try to make them as brief as possible consistent with clearness. I am glad to hear that you are coming over to England later and we shall be very glad to see you when you come to Manchester.

By the way, I was much interested in your speculations in regard to Fowler's spectrum. I mentioned the matter to Evans here, who told me that he was much interested in it, and I think it quite possible that he may try some experiments on the matter when he comes back next term. General work goes well, but I am held up momentarily by finding that the mass of the α -particle comes out rather bigger than it ought to be. If correct it is such an important conclusion that I cannot publish it until I am certain of my accuracy at every point. The experiments take a good deal of time and have to be done with great accuracy.

Yours very sincerely,

E. RUTHERFORD.

P.S. I suppose you have no objection to my using my judgment to cut out any matter I may consider unnecessary in your paper? Please reply.

Rutherford's first remark was certainly very pertinent, touching on a point which was to become a central issue in the subsequent prolonged discussions. My own views at that time, as expressed in a lecture at a meeting of the Danish Physical Society in October 1913, were that just the radical departure from the accustomed demands on physical explanation involved in the quantum postulate should of itself leave sufficient scope for the possibility of achieving in due course the incorporation of the new assumptions in a logically consistent scheme. In connection with Rutherford's remark, it is of special interest to recall that Einstein, in his famous paper of 1917 on the derivation of Planck's formula for temperature radiation, took the same starting point as regards the origin of spectra, and pointed to the analogy between the statistical laws governing the occurrence of spontaneous radiation processes and the fundamental law of radioactive decay, formulated by Rutherford and Soddy already in 1903. Indeed,

this law, which allowed them at one stroke to disentangle the multifarious phenomena of natural radioactivity then known, also proved the clue to the understanding of the later observed peculiar branching in spontaneous decay processes.

The second point raised with such emphasis in Rutherford's letter brought me into a quite embarrassing situation. In fact, a few days before receiving his answer, I had sent Rutherford a considerably extended version of the earlier manuscript, the additions especially concerning the relation between emission and absorption spectra and the asymptotic correspondence with the classical physical theories. I therefore felt the only way to straighten matters was to go at once to Manchester and talk it all over with Rutherford himself. Although Rutherford was as busy as ever, he showed an almost angelic patience with me, and after discussions through several long evenings during which he declared he had never thought I should prove so obstinate, he consented to leave all the old and new points in the final paper. Surely, both style and language were essentially improved by Rutherford's help and advice, and I have often had occasion to think how right he was in objecting to the rather complicated presentation and especially to the many repetitions caused by reference to previous literature. This Rutherford Memorial Lecture has therefore offered a welcome opportunity to give a more concise account of the actual development of the arguments in those years.

During the following months, the discussion about the origin of the spectral lines ascribed to helium ions took a dramatic turn. In the first place, Evans was able to produce the Fowler lines in discharges through helium of extreme purity, not showing any trace of the ordinary hydrogen lines. Still, Fowler was not yet convinced and stressed the spurious manner in which spectra may appear in gas mixtures. Above all he noted that his accurate measurements of the wavelengths of the Pickering lines did not exactly coincide with those calculated from my formula with $Z=2$. An answer to the last point was, however, easily found, since it was evident that the mass m in the expression for the Rydberg constant had to be taken not as the mass of a free electron but as the so-called reduced mass $mM(m+M)^{-1}$, where M is the mass of the nucleus. Indeed, taking this correction into account, the predicted relationship between the spectra of hydrogen and ionized helium was in complete agreement with all the measurements. This result was at once welcomed by Fowler who took the opportunity of pointing out that also in the spectra of other elements series were observed in which the ordinary Rydberg constant had to be multiplied by a number close to four. Such series spectra, which are generally referred to as spark spectra, could now be recognized as originating from excited ions in contrast to the so-called arc spectra due to excited neutral atoms.

Continued spectroscopical investigations were in the following years to reveal many spectra of atoms, from which not only one but even several electrons were removed. In particular, the well-known investigations of Bowen led to the recognition that the origin of the nebular spectra discussed by Nicholson had to be sought not in new hypothetical elements, but in atoms of oxygen and nitrogen in a highly ionized state. Eventually, the prospect arose of arriving, by analysis of the processes by which the electrons one by one are bound to the nucleus, at a survey of the binding of every electron in the ground state of the Rutherford atom. In 1913, of course, the experimental evidence was still far too scarce, and the theoretical methods for classification of stationary states were not yet sufficiently developed to cope with so ambitious a task.

IV

In the meantime, the work on the electronic constitution of the atom gradually proceeded, and soon again I permitted myself to ask Rutherford for help and advice. Thus, in June 1913 I went to Manchester with a second paper which, besides a continued discussion of the radioactive displacement law and the origin of the Barkla radiation, dealt with the ground state of atoms containing several electrons. As regards this problem, I tried tentatively to arrange the electron orbits in closed rings resembling the shell structure originally introduced by J. J. Thomson in his early attempt to account by his atomic model for the periodicity features in Mendeleev's table of the elements.

In Rutherford's laboratory, I met on that occasion Hevesy and Paneth, who told me of the success of the first systematic investigations by the tracer method of the solubility of lead sulphide and chromate, which at the beginning of that year they had carried out together in Vienna. In every way, these repeated visits to Manchester were a great stimulation and gave me the welcome opportunity to keep abreast of the work in the laboratory. At that time, assisted by Robinson, Rutherford was busily engaged in the analysis of β -ray emission and in cooperation with Andrade studied γ -ray spectra. Moreover, Darwin and Moseley were then intensely occupied with refined theoretical and experimental investigations on the diffraction of x-rays in crystals.

A special opportunity to see Rutherford again soon arose in connection with the meeting of the British Association for the Advancement of Science in Birmingham in September 1913. At the meeting, attended by Madame Curie, there was in particular a general discussion about the problem of radiation with the participation of such authorities as Rayleigh, Larmor and Lorentz, and especially Jeans who gave an introductory survey of the application of quantum theory to the problem of atomic constitution. His lucid exposition was, in fact, the first public expression of serious interest in considerations which outside the Manchester group were generally received with much scepticism.

An incident which amused Rutherford and us all was the remark of Lord Rayleigh in response to a solemn request by Sir Joseph Larmor to express his opinion on the latest developments. The prompt reply from the great veteran, who in earlier years had contributed so decisively to the elucidation of radiation problems, was: "In my young days I took many views very strongly and among them that a man who has passed his sixtieth year ought not to express himself about modern ideas. Although I must confess that today I do not take this view quite so strongly, I keep it strongly enough not to take part in this discussion!"

On my visit to Manchester in June I had discussed with Darwin and Moseley the question of the proper sequence for the arrangement of the elements according to their atomic number, and learned then for the first time about Moseley's plans to settle this problem by systematic measurements of the high-frequency spectra of the elements by the Laue-Bragg method. With Moseley's extraordinary energy and gifts of purposeful experimentation, his work developed astonishingly quickly, and already in November 1913 I received a most interesting letter from him with an account of his important results and with some questions regarding their interpretation on the lines which had proved applicable to the optical spectra.

In modern history of physics and chemistry, few events have from the outset attracted such general interest as Moseley's discovery of the simple laws allowing

an unambiguous assignment of the atomic number to any element from its high-frequency spectrum. Not only was the decisive support of the Rutherford atomic model immediately recognized, but also the intuition which had led Mendeleev at certain places in his table to depart from the sequence of increasing atomic weights was strikingly brought out. In particular, it was evident that Moseley's laws offered an unerring guide in the search for as yet undiscovered elements fitting into vacant places in the series of atomic numbers.

Also as regards the problem of the configuration of the electrons in the atom, Moseley's work was to initiate important progress. Certainly, the predominance, in the innermost part of the atom, of the attraction exerted by the nucleus on the individual electrons over their mutual repulsion afforded the basis for an understanding of the striking similarity between Moseley's spectra and those to be expected for a system consisting of a single electron bound to the bare nucleus. The closer comparison, however, brought new information pertaining to the shell structure of the electronic constitution of the atoms.

An important contribution to this problem was soon after given by Kossel who, as the origin of the K, L and M types of Barkla radiation, pointed to the removal of an electron from one of the sequence of rings or shells surrounding the nucleus. In particular he ascribed the $K\alpha$ and $K\beta$ components of Moseley's spectra to individual transition processes by which the electron lacking in the K-shell is replaced by one of the electrons in the L- and M-shells, respectively. Proceeding in this way, Kossel was able to trace further relationships between Moseley's measurements of the spectral frequencies which permitted him to represent the whole high-frequency spectrum of an element as a combination scheme in which the product of any of the terms and Planck's constant was to be identified with the energy required to remove an electron from a shell in the atom to a distance from the nucleus beyond all the shells.

In addition, Kossel's views offered an explanation of the fact that the absorption of penetrating radiation of increasing wavelength practically begins with an absorption edge representing the complete removal in one step of an electron of the respective shell. The absence of intermediate excited states was assumed to be due to the full occupation of all shells in the ground state of the atom. As is well known, this view eventually found its final expression through Pauli's formulation in 1924 of the general exclusion principle for electron binding states, inspired by Stoner's derivation of finer details of the shell structure of the Rutherford atom from an analysis of the regularities of the optical spectra.

V

In the autumn of 1913, another stir among physicists was created by Stark's discovery of the surprisingly large effect of electric fields on the structure of the lines in the hydrogen spectrum. With his vigilant attention to all progress in physical science, Rutherford, when he had received Stark's paper from the Prussian Academy, at once wrote to me: "I think it is rather up to you at the present time to write something on the Zeeman and electric effects, if it is possible to reconcile them with your theory." Responding to Rutherford's challenge, I tried to look into the matter, and it was soon clear to me that in the effects of electric and magnetic fields we had to do with two very different problems.

The essence of Lorentz' and Larmor's interpretations of Zeeman's famous discovery in 1896 was that it pointed directly to electron motions as the origin of

line spectra in a way largely independent of special assumptions about the binding mechanism of the electrons in the atom. Even if the origin of the spectra is assigned to individual transitions between stationary states, the correspondence principle thus led one, in view of Larmor's general theorem, to expect a normal Zeeman effect for all spectral lines emitted by electrons bound in a field of central symmetry, as in the Rutherford atom. Rather did the appearance of so-called anomalous Zeeman effects present new puzzles which could only be overcome more than ten years later when the complex structure of the lines in series spectra was traced to an intrinsic electron spin. A most interesting historical account of this development, to which important contributions were given from various sides, can be found in the well-known volume recently published in memory of Pauli.

In the case of an electric field, however, no effect proportional to its intensity was to be expected for the radiation emitted by a harmonic oscillator, and Stark's discovery therefore definitely excluded the conventional idea of elastic vibrations of electrons as the origin of line spectra. Still, for a Keplerian motion of the electron around the nucleus even a comparatively weak external electric field will through secular perturbations produce considerable changes in the shape and orientation of the orbit. By the study of particular cases in which the orbit remains purely periodic in the external field it was possible, by arguments of the same type as those applied to the stationary states of the undisturbed hydrogen atom, to deduce the order of magnitude of the Stark effect and especially to explain its rapid rise from line to line within the hydrogen spectral series. Yet, these considerations clearly showed that, for an explanation of the finer details of the phenomenon, the methods for a classification of stationary states of atomic systems were not sufficiently developed.

In just this respect a great advance was achieved in the following years by the introduction of quantum numbers specifying components of angular momenta and other action integrals. Such methods were first suggested by W. Wilson in 1915 who applied them to electron orbits in the hydrogen atom. However, owing to the circumstance that on Newtonian mechanics every orbit in this case is simply periodic with a frequency of revolution depending only on the total energy of the system, no physical effects were disclosed. Still, the velocity dependence of the electron mass, predicted by the new mechanics of Einstein, removes the degeneracy of the motion and introduces a second period in its harmonic components through a continual slow progression of the aphelion of the Keplerian orbit. In fact, as was shown in Sommerfeld's famous paper of 1916, the separate quantization of the angular momentum and of the action in the radial motion permitted a detailed interpretation of the observed fine structure of the lines in the spectra of the hydrogen atom and helium ion.

Moreover, the effect of magnetic and electric fields on the hydrogen spectrum was treated by Sommerfeld and Epstein who by a masterly application of the methods for quantization of multiperiodic systems were able, in complete accordance with observations, to derive the spectral terms by the combination of which the resolution of the hydrogen lines appears. The compatibility of such methods with the principle of adiabatic invariance of stationary states, which Ehrenfest had formulated in 1914 in order to meet thermodynamical requirements, was secured by the circumstance that the action integrals to which the quantum numbers refer according to classical mechanics are not modified by a variation of the external field slow compared with the characteristic periods of the system.

Further evidence of the fruitfulness of the approach was derived from the application of the correspondence principle to the radiation emitted by multi-periodic systems, permitting qualitative conclusions regarding the relative probabilities for the different transition processes. These considerations were not least confirmed by Kramers' explanation of the apparently capricious variations in the intensities of the Stark effect components of the hydrogen lines. It was even found possible to account by the correspondence argument for the absence of certain types of transitions in other atoms, beyond those which, as pointed out by Rubinowicz, could be excluded by the conservation laws for energy and angular momentum applied to the reaction between the atom and the radiation.

With the help of the rapidly increasing experimental evidence about the structure of complicated optical spectra, as well as the methodical search for finer regularities in the high-frequency spectra by Siegbahn and his collaborators, the classification of the binding states in atoms containing several electrons continually advanced. In particular, the study of the way in which the ground states of the atoms could be built up by the successive bindings of the electrons to the nucleus led to a gradual elucidation of the shell structure of the electronic configuration in the atom. Thus, although such essential elements of the explanation as the electron spin were still unknown, it became in fact possible within about ten years of Rutherford's discovery of the atomic nucleus to achieve a summary interpretation of many of the most striking periodicity features of Mendeleev's table.

The whole approach, however, was still of largely semi-empirical character, and it was soon to become clear that, for an exhaustive account of the physical and chemical properties of the elements, a radically new departure from classical mechanics was needed in order to incorporate the quantum postulate in a logically consistent scheme. To this well-known development we shall have occasion to return, but I shall first proceed with the account of my reminiscences of Rutherford.

VI

The outbreak of the first world war brought about an almost complete dissolution of the Manchester group, but I was lucky to remain in close contact with Rutherford who in the spring of 1914 had invited me to succeed Darwin in the Schuster Readership of Mathematical Physics. On our arrival in Manchester in early autumn, after a stormy voyage round Scotland, my wife and I were most kindly received by the few of our old friends who remained in the laboratory after the departure of colleagues from abroad and the participation in military duties by most of the British. Rutherford and his wife were at that time still in America on their way back from a visit to their relatives in New Zealand, and it goes without saying that their safe return to Manchester some weeks later was greeted by all of us with great relief and joy.

Rutherford was himself soon drawn into military projects, especially concerning the development of methods of sound tracing of submarines, and teaching the students was almost entirely left to Evans, Makower and me. Still, Rutherford found time to continue his own pioneer work, which already before the end of the war was to give such great results, and showed the same warm interest as ever in the endeavours of his collaborators. As regards the problem of atomic constitution, a new impulse was given by the publication in 1914 of the

famous experiments by Franck and Hertz on the excitation of atoms by electron impact.

On the one hand, these experiments, carried out with mercury vapour, gave most conspicuous evidence of the stepwise energy transfer in atomic processes; on the other hand, the value of the ionization energy of mercury atoms apparently indicated by the experiments was less than half of that to be expected from the interpretation of the mercury spectrum. One was therefore led to suspect that the ionization observed was not directly related to the electronic collisions but was due to an accompanying photoeffect on the electrodes, produced by the radiation emitted by the mercury atoms on their return from the first excited state to the ground state. Encouraged by Rutherford, Makower and I planned experiments to investigate this point, and an intricate quartz apparatus with various electrodes and grids was constructed with the help of the competent German glass blower in the laboratory, who in the earlier days had made the fine α -ray tubes for Rutherford's investigations on the formation of helium.

With his liberal human attitude, Rutherford had tried to obtain permission for the glass blower to continue his work in England in the war time, but the man's temper, not uncommon for artisans in his field, and releasing itself in violent super-patriotic utterances, eventually led to his internment by the British authorities. Thus when our fine apparatus was ruined by an accident in which its support caught fire, there was no help to reconstruct it, and when also Makower shortly afterwards volunteered for military service, the experiments were given up. I need hardly add that the problem was solved with the expected result quite independently by the brilliant investigations of Davis and Gauthier in New York in 1918, and I have only mentioned our fruitless attempts as an indication of the kind of difficulties with which work in the Manchester laboratory was faced in those days, and which were very similar to those the ladies had to cope with in their households.

Still, Rutherford's never failing optimism exerted a most encouraging influence on his surroundings, and I remember how at the time of a serious set-back in the war, Rutherford quoted the old utterance ascribed to Napoleon about the impossibility of fighting the British because they were too stupid to understand when they had lost. To me, it was also a most pleasant and enlightening experience to be admitted to the monthly discussions among a group of Rutherford's personal friends including Alexander, the philosopher, the historian Tout, the anthropologist Elliot Smith, and Chaim Weizmann, the chemist who thirty years later was to become the first president of Israel and for whose distinctive personality Rutherford had great esteem.

A terrible shock to us all was the tragic message in 1915 of Moseley's untimely death in the Gallipoli campaign, deplored so deeply by the community of physicists all over the world, and which not least Rutherford, who had endeavoured to get Moseley transferred from the front to less dangerous duties, took much to heart.

In the summer of 1916 my wife and I left Manchester and returned to Denmark where I had been appointed to the newly created professorship of theoretical physics in the University of Copenhagen. Notwithstanding the ever increasing difficulties of postal communication, a steady correspondence with Rutherford was kept up. From my side, I reported about the progress with the work on a more general representation of the quantum theory of atomic constitution which

at that time was further stimulated by the development as regards the classification of stationary states, already referred to. In that connection, Rutherford took an interest in what news I could give from the continent and in particular of my first personal contact with Sommerfeld and Ehrenfest. In his own letters, Rutherford also gave a vivid description of how, in spite of the increasing difficulties and the pressure of other obligations, he strove to continue his investigations in various directions. Thus, in the autumn of 1916, Rutherford wrote about his intense interest in some surprising results regarding the absorption of hard γ -rays produced by high voltage tubes which had just then become available.

In the next years Rutherford was more and more occupied with the possibilities of producing nuclear disintegrations by means of fast α -rays and already in a letter on 9th December 1917 he writes: "I occasionally find an odd half day to try a few of my own experiments and have got I think results that will ultimately prove of great importance. I wish you were here to talk matters over with. I am detecting and counting the lighter atoms set in motion by α -particles, and the results, I think, throw a good deal of light on the character and distribution of forces near the nucleus. I am also trying to break up the atom by this method. In one case, the results look promising but a great deal of work will be required to make sure. Kay helps me and is now an expert counter." A year later, 17th November 1918, Rutherford in his characteristic manner announced further progress: "I wish I had you here to discuss the meaning of some of my results in collision of nuclei. I have got some rather startling results, I think, but it is a heavy and long business getting *certain* proofs of my deductions. Counting weak scintillations is hard on old eyes, but still with the aid of Kay I have got through a good deal of work at odd times the past four years."

In Rutherford's famous papers in the *Philosophical Magazine*, 1919, containing the account of his fundamental discovery of controlled nuclear disintegrations, he refers to the visit to Manchester, in November 1918, of his old collaborator Ernest Marsden who at the Armistice had got leave from military service in France. With his great experience of scintillation experiments from the old Manchester days when, in collaboration with Geiger, he performed the experiments which led Rutherford to his discovery of the atomic nucleus, Marsden helped him to clear up some apparent anomalies in the statistical distribution of the high-speed protons released by the bombardment of nitrogen with α -rays. From Manchester, Marsden returned to New Zealand to take up his own university duties, but kept in close contact with Rutherford through the years.

In July 1919, when after the Armistice travelling was again possible, I went to Manchester to see Rutherford and learned in more detail about his great new discovery of controlled, or so-called artificial, nuclear transmutations, by which he gave birth to what he liked to call 'modern Alchemy', and which in the course of time was to give rise to such tremendous consequences as regards man's mastery of the forces of nature. Rutherford was at that time almost alone in the laboratory, and as told in his letters, the only help in his fundamental researches, apart from Marsden's short visit, was his faithful assistant William Kay, who by his kindness and helpfulness through the years had endeared himself to everyone in the laboratory. During my visit Rutherford also spoke about the great decision he had had to make in response to the offer of the Cavendish professorship in Cambridge left vacant by the retirement of J. J. Thomson. Certainly, it had not been easy for Rutherford to decide to leave Manchester after the many rich years

there, but of course he had to follow the call to succeed the unique series of Cavendish professors.

VII

From the beginning, Rutherford gathered around him in the Cavendish Laboratory a large and brilliant group of research workers. A most notable figure was Aston who through many years had worked with J. J. Thomson and already during the wartime had started the development of mass spectroscopic methods which was to lead to the demonstration of the existence of isotopes of almost every element. This discovery, which gave such a convincing confirmation of Rutherford's atomic model, was not entirely unexpected. Already in the early Manchester days, it was understood that the apparent irregularities in the sequence of the atomic weights of the elements when they were ordered according to their chemical properties suggested that, even for the stable elements, the nuclear charge could not be expected to have a unique relation to the nuclear mass. In letters to me in January and February 1920, Rutherford expressed his joy in Aston's work, particularly about the chlorine isotopes which so clearly illustrated the statistical character of the deviations of chemical atomic weights from integral values. He also commented humorously on the lively disputes in the Cavendish Laboratory about the relative merits of different atomic models to which Aston's discovery gave rise.

It was a great help in the continuation of Rutherford's own pioneering work on the constitution and disintegrations of atomic nuclei as well as in the management of the great laboratory, that from the very beginning he was joined by James Chadwick from the old Manchester group, who returned from a long detention in Germany where at the outbreak of the war he had been working in Berlin with Geiger. Among Rutherford's collaborators in the early Cambridge years were also Blackett and Ellis, both coming from a career in the defence services, Ellis having been initiated to physics by Chadwick during their comradeship under German imprisonment. A further asset to the group at the Cavendish was the arrival, a few years later, of Kapitza, who brought with him ingenious projects, in particular for the production of magnetic fields of hitherto unheard-of intensities. In this work he was from the start assisted by John Cockcroft, who with his singular combination of scientific and technological insight was to become such a prominent collaborator of Rutherford.

At the beginning, Charles Darwin, whose mathematical insight had been so helpful in the Manchester years, shared with Ralph Fowler responsibility for the theoretical part of the activities at the Cavendish. In collaboration, they made at that time important contributions to statistical thermodynamics and its application to astrophysical problems. After Darwin's departure for Edinburgh, the principal theoretical adviser and teacher in Cambridge right up to the second world war was Fowler, who had become Rutherford's son-in-law. Not only did Fowler with enthusiastic vigour participate in the work at the Cavendish, but he also soon found numerous gifted pupils who benefitted from his inspiration. Foremost among these were Lennard-Jones and Hartree who both contributed, each along his own line, to the development of atomic and molecular physics, and especially Dirac, who from his early youth distinguished himself by his unique logical power.

Ever since I left Manchester in 1916, I had of course tried to use the experience gained in Rutherford's laboratory and it is with gratitude that I recall how Rutherford from the very outset most kindly and effectively supported my endeavours in Copenhagen to create an institute to promote intimate collaboration between theoretical and experimental physicists. It was a special encouragement that already in the autumn of 1920, when the Institute building was nearing completion, Rutherford found time to visit us in Copenhagen. As a token of appreciation, the University conferred upon him an honorary degree, and on that occasion he gave a most stimulating and humorous address which was long remembered by all present.

For the work in the new Institute it was of great benefit that we were joined shortly after the war by my old friend from the Manchester days, George Hevesy, who during the more than twenty years he worked in Copenhagen carried out many of his famous physico-chemical and biological researches, based on the isotopic tracer method. A special event, in which Rutherford took great interest, was the application of Moseley's method by Coster and Hevesy in 1922 to the successful search for the missing element now called hafnium, the properties of which gave strong additional support to the interpretation of the periodic system of the elements. An auspicious start was given to the general experimental work by a visit, at the opening of the laboratory, of James Franck, who during the following months most kindly instructed the Danish collaborators in the refined technique of excitation of atomic spectra by electron bombardment which he had so ingeniously developed together with Gustav Hertz. The first among the many distinguished theoretical physicists who stayed with us for a longer period was Hans Kramers who as a quite young man came to Copenhagen during the war and proved to be such an invaluable asset to our group during the ten years he worked with us until, in 1926, he left his position as lecturer in the Institute to take over a professorship in Utrecht. Shortly after Kramers' arrival in Copenhagen came two promising young men, Oscar Klein from Sweden and Svein Rosseland from Norway, who already in 1920 made their names known by pointing to the so-called collisions of the second kind, in which atoms are transferred by electron bombardment from a higher to a lower stationary state with gain of velocity for the electron. Indeed, the occurrence of such processes is decisive for ensuring thermal equilibrium in a way analogous to the induced radiative transitions which played an essential role in Einstein's derivation of Planck's formula for temperature radiation. The consideration of collisions of the second kind proved particularly important for the elucidation of the radiative properties of stellar atmospheres, to which at that time Saha, working in Cambridge with Fowler, made such fundamental contributions.

The group at the Copenhagen Institute was joined in 1922 by Pauli, and two years later by Heisenberg, both pupils of Sommerfeld, and who, young as they were, had already accomplished most brilliant work. I had made their acquaintance and formed a deep impression of their extraordinary talent in the summer of 1922 during a lecturing visit to Göttingen, which initiated a long and fruitful cooperation between the group working there under the leadership of Born and Franck, and the Copenhagen group. From the early days our close connection with the great centre in Cambridge was maintained especially by longer visits to Copenhagen of Darwin, Dirac, Fowler, Hartree, Mott, and others.

VIII

Those years, when a unique cooperation of a whole generation of theoretical physicists from many countries created step by step a logically consistent generalization of classical mechanics and electromagnetism, have sometimes been described as the 'heroic' era in quantum physics. To everyone following this development, it was an unforgettable experience to witness how, through the combination of different lines of approach and the introduction of appropriate mathematical methods, a new outlook emerged regarding the comprehension of physical experience. Many obstacles had to be overcome before this goal was reached, and time and again decisive progress was achieved by some of the youngest among us.

The common starting point was the recognition that, notwithstanding the great help which the use of mechanical pictures had temporarily offered for the classification of stationary states of atoms in isolation or exposed to constant external forces, it was clear, as already mentioned, that a fundamentally new departure was needed. Not only was the difficulty of picturing the electronic constitution of chemical compounds on the basis of the Rutherford atomic model more and more evident, but insurmountable difficulties also arose in any attempts to account in detail for the complexity of atomic spectra, especially conspicuous in the peculiar duplex character of the arc spectrum of helium.

The first step to a more general formulation of the correspondence principle was offered by the problem of optical dispersion. Indeed, the close relation between the atomic dispersion and the selective absorption of spectral lines so beautifully illustrated by the ingenious experiments of R. W. Wood and P. V. van der Meer on the absorption and dispersion in alkali vapours, suggested from the very beginning a correspondence approach. On the basis of Einstein's formulation of the statistical laws for the occurrence of radiation-induced transitions between stationary states of an atomic system, Kramers in 1924 succeeded in establishing a general dispersion formula, involving only the energies of these states and the probabilities of spontaneous transitions between them. This theory, further developed by Kramers and Heisenberg, included even new dispersion effects connected with the appearance, under the influence of the radiation, of possibilities for transitions not present in the unperturbed atom, and an analogue to which is the Raman effect in molecular spectra.

Shortly afterwards, an advance of fundamental significance was achieved by Heisenberg who in 1925 introduced a most ingenious formalism, in which all use of orbital pictures beyond the general asymptotic correspondence was avoided. In his bold conception, the canonical equations of mechanics are retained in their Hamiltonian form, but the conjugate variables are replaced by operators subject to a non-commutative algorithm involving Planck's constant as well as the symbol $\hbar/2\pi$. In fact, by representing the mechanical quantities by hermitian matrices with elements referring to all possible transition processes between stationary states, it proved possible without any arbitrariness to deduce the energies of these states and the probabilities of the associated transition processes. This so-called quantum mechanics, to the elaboration of which Born and Jordan as well as Dirac from the outset made important contributions, opened the way to a consistent statistical treatment of many atomic problems which hitherto were only amenable to a semi-empirical approach.

For the completion of this great task the emphasis on the formal analogy between mechanics and optics, originally stressed by Hamilton, proved most helpful and instructive. Thus, pointing to the similar roles played by the quantum numbers in the classification of stationary states by means of mechanical pictures and by the numbers of nodes in characterizing the possible standing waves in elastic media, L. de Broglie had already in 1924 been led to a comparison between the behaviour of free material particles and the properties of photons. Especially illuminating was his demonstration of the identity of the particle velocity with the group velocity of a wave-packet built up of components with wavelengths confined to a small interval, and each related to a value of the momentum by Einstein's equation between the momentum of a photon and the corresponding wavelength of radiation. As is well known, the pertinence of this comparison soon received a decisive confirmation with the discoveries by Davisson and Germer and by George Thomson of selective scattering of electrons in crystals.

The culminating event of this period was Schrödinger's establishment in 1926 of a more comprehensive wave mechanics in which the stationary states are conceived as proper solutions of a fundamental wave equation, obtained by regarding the Hamiltonian of a system of electric particles as a differential operator acting upon a function of the coordinates which define the configuration of the system. In the case of the hydrogen atom, not only did this method lead to a remarkably simple determination of the energies of the stationary states, but Schrödinger also showed that the superposition of any two proper solutions corresponded to a distribution of electric charge and current in the atom which on classical electrodynamics would give rise to the emission and resonance absorption of a monochromatic radiation of a frequency coinciding with some line of the hydrogen spectrum.

Similarly, Schrödinger was able to explain essential features of the dispersion of radiation by atoms by representing the charge and current distribution of the atom perturbed by the incident radiation as the effect of a superposition of the proper functions defining the manifold of possible stationary states of the unperturbed system. Particularly suggestive was the derivation on such lines of the laws of the Compton effect which, in spite of the striking support it gave to Einstein's original photon idea, at first presented obvious difficulties for a correspondence treatment, attempting to combine conservation of energy and momentum with a division of the process in two separate steps, consisting in an absorption and an emission of radiation resembling radiative transitions between the stationary states of an atomic system.

This recognition of the wide scope of arguments implying the use of a superposition principle similar to that of classical electromagnetic field theory, which was only implicitly contained in the matrix formulation of quantum mechanics, meant a great advance in the treatment of atomic problems. Still, it was from the beginning obvious that wave mechanics did not point to any less radical modification of the classical physical approach than the statistical description envisaged by the correspondence principle. Thus, I remember how, on a visit of Schrödinger to Copenhagen in 1926, when he gave us a most impressive account of his wonderful work, we argued with him that any procedure disregarding the individual character of the quantum processes would never account for Planck's fundamental formula of thermal radiation.

Notwithstanding the remarkable analogy between essential features of atomic processes and classical resonance problems, it must indeed be taken into account that in wave mechanics we are dealing with functions which do not generally take real values, but demand the essential use of the symbol $\sqrt{-1}$ just as the matrices of quantum mechanics. Moreover, when dealing with the constitution of atoms with more than one electron, or collisions between atoms and free electric particles, the state functions are not represented in ordinary space but in a configuration space of as many dimensions as there are degrees of freedom in the total system. The essentially statistical character of the physical deductions from wave mechanics was eventually clarified by Born's brilliant treatment of general collision problems.

The equivalence of the physical contents of the two different mathematical formalisms was completely elucidated by the transformation theory formulated independently by Dirac in Copenhagen and Jordan in Göttingen, which introduced in quantum physics possibilities for the change of variables similar to those offered by the symmetrical character of the equations of motion in classical dynamics in the canonical form given by Hamilton. An analogous situation is met with in the formulation of a quantum electrodynamics incorporating the photon concept. This aim was first achieved in Dirac's quantum theory of radiation treating phases and amplitudes of the harmonic components of the fields as non-commuting variables. After further ingenious contributions by Jordan, Klein and Wigner, this formalism found, as is well known, essential completion in the work of Heisenberg and Pauli.

A special illustration of the power and scope of the mathematical methods of quantum physics is presented by the peculiar quantum statistics pertaining to systems of identical particles where we have to do with a feature as foreign to classical physics as the quantum of action itself. Indeed, any problem which calls for relevant application of Bose-Einstein or Fermi-Dirac statistics in principle excludes pictorial illustration. In particular, this situation left room for the proper formulation of the Pauli exclusion principle, which not only gave the final elucidation of the periodicity relations in Mendelev's table, but in the following years proved fertile for the understanding of most of the varied aspects of the atomic constitution of matter.

A fundamental contribution to the clarification of the principles of quantum statistics was afforded by Heisenberg's ingenious explanation in 1926 of the duplicity of the helium spectrum. In fact, as he showed, the set of stationary states of atoms with two electrons consists of two non-combining groups corresponding to symmetric and antisymmetric spatial wave functions, respectively associated with opposite and parallel orientations of the electron spins. Shortly afterwards, Heitler and London succeeded on the same lines in explaining the binding mechanism in the hydrogen molecule and thereby opened the way for the understanding of homopolar chemical bonds. Even Rutherford's famous formula for the scattering of charged particles by atomic nuclei had, as was shown by Mott, to be essentially modified when applied to collisions between identical particles like protons and hydrogen nuclei or α -rays and helium nuclei. However, in the actual experiments of large angle scattering of fast α -rays by heavy nuclei, from which Rutherford drew his fundamental conclusions, we are well within the range of validity of classical mechanics.

The increasing use of more and more refined mathematical abstractions to ensure consistency in the account of atomic phenomena found in 1928 a temporary climax in Dirac's relativistic quantum theory of the electron. Thus the concept of electron spin, to the treatment of which Darwin and Pauli had made important contributions, was harmoniously incorporated in Dirac's spinor analysis. Above all, however, in connection with the discovery of the positron by Anderson and Blackett, Dirac's theory prepared the recognition of the existence of antiparticles of equal mass but opposite electric charges and opposite orientations of the magnetic moment relative to the spin axis. As is well known, we have here to do with a development which in a novel manner has restored and enlarged that isotropy in space and reversibility in time which has been one of the basic ideas of the classical physical approach.

The wonderful progress of our knowledge of the atomic constitution of matter and of the methods by which such knowledge can be acquired and interrelated has indeed carried us far beyond the scope of the deterministic pictorial description brought to such perfection by Newton and Maxwell. Following this development at close hand, I have often had occasion to think of the dominating influence of Rutherford's original discovery of the atomic nucleus, which at every stage presented us with so forceful a challenge.

IX

In all the long and rich years during which Rutherford worked with untiring vigour in the Cavendish, I often came to Cambridge, where on Rutherford's invitation I gave several courses of lectures on theoretical problems including the epistemological implications of the development of quantum theory. On such occasions it was always a great encouragement to feel the open mind and intense interest with which Rutherford followed the progress in the field of research which he had himself so largely initiated and the growth of which should carry us so far beyond the horizon which limited the outlook at the early stages.

Indeed, the extensive use of abstract mathematical methods to cope with the rapidly increasing evidence about atomic phenomena brought the whole observational problem more and more to the foreground. In its roots this problem is as old as physical science itself. Thus the philosophers in ancient Greece, who based the explanation of the specific properties of substances on the limited divisibility of all matter, took it for granted that the coarseness of our sense organs would forever prevent the direct observation of individual atoms. In such respect, the situation has been radically changed in our days by the construction of amplification devices like cloud chambers and the counter mechanisms originally developed by Rutherford and Geiger in connection with their measurements of the numbers and charges of α -particles. Still, the exploration of the world of atoms was, as we have seen, to reveal inherent limitations in the mode of description embodied in common language developed for the orientation in our surroundings and the account of events of daily life.

In words conforming with Rutherford's whole attitude, one may say that the aim of experimentation is to put questions to nature, and of course Rutherford owed his success in this task to his intuition in shaping such questions so as to permit the most useful answers. In order that the enquiry may augment common knowledge it is an obvious demand that the recording of observations as well as the

construction and handling of the apparatus, necessary for the definition of the experimental conditions, be described in plain language. In actual physical research, this demand is amply satisfied with the specification of the experimental arrangement through the use of bodies like diaphragms and photographic plates, so large and heavy that their manipulation can be accounted for in terms of classical physics, although of course the properties of the materials of which the instruments, as well as our own bodies, are built up depend essentially on the constitution and stability of the component atomic systems defying such account.

The description of ordinary experience presupposes the unrestricted divisibility of the course of the phenomena in space and time and the linking of all steps in an unbroken chain in terms of cause and effect. Ultimately, this viewpoint rests on the fineness of our senses which for perception demands an interaction with the objects under investigation so small that in ordinary circumstances it is without appreciable influence on the course of events. In the edifice of classical physics, this situation finds its idealized expression in the assumption that the interaction between the object and the tools of observation can be neglected or, at any rate, compensated for.

The element of wholeness, symbolized by the quantum of action and completely foreign to classical physical principles has, however, the consequence that in the study of quantum processes any experimental enquiry implies an interaction between the atomic object and the measuring tools which, although essential for the characterization of the phenomena, evades a separate account if the experiment is to serve its purpose of yielding unambiguous answers to our questions. It is indeed the recognition of this situation which makes the recourse to a statistical mode of description imperative as regards the expectations of the occurrence of individual quantum effects in one and the same experimental arrangement, and which removes any apparent contradiction between phenomena observed under mutually exclusive experimental conditions. However contrasting such phenomena may at first sight appear, it must be realized that they are complementary in the sense that taken together they exhaust all information about the atomic object, which can be expressed in common language without ambiguity.

The notion of complementarity does not imply any renunciation of detailed analysis limiting the scope of our enquiry, but simply stresses the character of objective description, independent of subjective judgment, in any field of experience where unambiguous communication essentially involves regard to the circumstances in which evidence is obtained. In logical respect, such a situation is well known from discussions about psychological and social problems where many words have been used in a complementary manner since the very origin of language. Of course we are here often dealing with qualities unsuited to the quantitative analysis characteristic of so-called exact sciences, whose task, according to the programme of Galileo, is to base all description on well-defined measurements.

Notwithstanding the help which mathematics has always offered for such a task, it must be realized that the very definition of mathematical symbols and operations rests on simple logical use of common language. Indeed, mathematics is not to be regarded as a special branch of knowledge based on the accumulation of experience, but rather as a refinement of general language, supplementing it with appropriate tools to represent relations for which ordinary verbal communication is imprecise or too cumbersome. Strictly speaking, the mathematical formalism

of quantum mechanics and electrodynamics merely offers rules of calculation for the deduction of expectations about observations obtained under well-defined experimental conditions specified by classical physical concepts. The exhaustive character of this description depends not only on the freedom, offered by the formalism, of choosing these conditions in any conceivable manner, but equally on the fact that the very definition of the phenomena under consideration for their completion implies an element of irreversibility in the observational process emphasizing the fundamentally irreversible character of the concept of observation itself.

Of course all contradictions in the complementary account in quantum physics were beforehand excluded by the logical consistency of the mathematical scheme upholding every demand of correspondence. Still, the recognition of the reciprocal latitude for the fixation of any two canonically conjugate variables, expressed in the principle of indeterminacy formulated by Heisenberg in 1927, was a decisive step towards the elucidation of the measuring problem in quantum mechanics. Indeed it became evident that the formal representation of physical quantities by non-commuting operators directly reflects the relationship of mutual exclusion between the operations by which the respective physical quantities are defined and measured.

To gain familiarity with this situation, the detailed treatment of a great variety of examples of such arguments was needed. Notwithstanding the generalized significance of the superposition principle in quantum physics, an important guide for the closer study of observational problems was repeatedly found in Rayleigh's classic analysis of the inverse relation between the accuracy of image-forming by microscopes and the resolving power of spectroscopic instruments. In this connection not least Darwin's mastery of the methods of mathematical physics often proved helpful.

With all appreciation of Planck's happy choice of words when introducing the concept of a universal 'quantum of action', or the suggestive value of the idea of 'intrinsic spin', it must be realized that such notions merely refer to relationships between well-defined experimental evidence which cannot be comprehended by the classical mode of description. Indeed, the numbers expressing the values of the quantum or spin in ordinary physical units do not concern direct measurements of classically defined actions or angular momenta, but are logically interpretable only by consistent use of the mathematical formalism of quantum theory. In particular the much discussed impossibility of measuring the magnetic moment of a free electron by ordinary magnetometers is directly evident from the fact that in Dirac's theory the spin and magnetic moment do not result from any alteration in the basic Hamiltonian equation of motion, but appear as consequences of the peculiar non-commutative character of the operator calculus.

The question of the proper interpretation of the notions of complementarity and indeterminacy was not settled without lively disputes, in particular at the Solvay meetings of 1927 and 1930. On these occasions, Einstein challenged us with his subtle criticism which especially gave the inspiration to a closer analysis of the role of the instruments in the measuring process. A crucial point, irrevocably excluding the possibility of reverting to causal pictorial description, was the recognition that the scope of unambiguous application of the general conservation laws of momentum and energy is inherently limited by the circumstance that any experimental arrangement, allowing the location of atomic

objects in space and time, implies a transfer, uncontrollable in principle, of momentum and energy to the fixed scales and regulated clocks indispensable for the definition of the reference frame. The physical interpretation of the relativistic formulation of quantum theory ultimately rests on the possibility of fulfilling all relativity exigencies in the account of the handling of the macroscopic measuring apparatus.

This circumstance was especially elucidated in the discussion of the measurability of electromagnetic field components raised by Landau and Peierls as a serious argument against the consistency of quantum field theory. Indeed, a detailed investigation in collaboration with Rosenfeld showed that all the predictions of the theory in this respect could be fulfilled when due regard was taken to the mutual exclusiveness of the fixation of the values of electric and magnetic intensities and the specification of the photon composition of the field. An analogous situation is met with in positron theory where any arrangement suited for measurements of the charge distribution in space necessarily implies uncontrollable creation of electron pairs.

The typical quantum features of electromagnetic fields do not depend on scale, since the two fundamental constants—the velocity of light c and the quantum of action h —do not allow of any fixation of quantities of dimensions of a length or time interval. Relativistic electron theory, however, involves the charge e and mass m of the electron, and essential characteristics of the phenomena are limited to spatial extensions of the order h/mc . The fact that this length is still large compared with the ‘electron radius’ e^2/mc^2 , which limits the unambiguous application of the concepts of classical electromagnetic theory, suggests, however, that there is still a wide scope for the validity of quantum electrodynamics, even though many of its consequences cannot be tested by practical experimental arrangements involving measuring instruments sufficiently large to permit the neglect of the statistical element in their construction and handling. Such difficulties would of course also prevent any direct enquiry into the close interactions of the fundamental constituents of matter, whose number has been so largely increased by recent discoveries, and in the exploration of their relationships we must therefore be prepared for a new approach transcending the scope of present quantum theory.

It need hardly be stressed that such problems do not arise in the account of the ordinary physical and chemical properties of matter, based on the Rutherford atomic model, in the analysis of which use is only made of well-defined characteristics of the constituent particles. Here, the complementary description offers indeed the adequate approach to the problem of atomic stability with which we were faced from the very beginning. Thus, the interpretation of spectral regularities and chemical bonds refers to experimental conditions mutually exclusive of those which permit exact control of the position and displacement of the individual electrons in the atomic systems.

In this connection, it is of decisive importance to realize that the fruitful application of structural formulae in chemistry rests solely on the fact that the atomic nuclei are so much heavier than the electrons that, in comparison with molecular dimensions, the indeterminacy in the position of the nuclei can be largely neglected. When we look back on the whole development we recognize indeed that the discovery of the concentration of the mass of the atom within a region so small compared with its extension has been the clue to the understanding

of an immense field of experience embracing the crystalline structure of solids as well as the complex molecular systems which carry the genetic characters of living organisms.

As is well known, the methods of quantum theory have also proved decisive for the clarification of many problems regarding the constitution and stability of the atomic nuclei themselves. To some early disclosed aspects of such problems I shall have occasion to refer in continuing the account of my reminiscences of Rutherford, but it would be beyond the scope of this Memorial Lecture to attempt a detailed account of the rapidly increasing insight in the intrinsic nuclear constitution, brought about by the work of the present generation of experimental and theoretical physicists. This development reminds indeed the elders among us of the gradual clarification of the electronic constitution of the atom in the first decades after Rutherford's fundamental discovery.

X

Every physicist is of course acquainted with the imposing series of brilliant investigations with which Rutherford to the very end of his life augmented our insight into the properties and constitution of atomic nuclei. I shall therefore here mention only a few of my remembrances from those years when I often had occasion to follow the work in the Cavendish Laboratory and learned in talks with Rutherford about the trend of his views and the problems occupying him and his collaborators.

With his penetrating intuition, Rutherford was early aware of the strange and novel problems presented by the existence and stability of composite nuclei. Indeed, already in the Manchester time he had pointed out that any approach to these problems demanded the assumption of forces of short range between the nuclear constituents, of a kind essentially different from the electric forces acting between charged particles. With the intention of throwing more light on the specific nuclear forces, Rutherford and Chadwick, in the first years in Cambridge, performed thorough investigations of anomalous scattering of α -rays in close nuclear collisions.

Although much important new evidence was obtained in these investigations, it was more and more felt that, for a broader attack on nuclear problems, the natural α -ray sources were not sufficient and that it was desirable to have available intense beams of high-energy particles produced by artificial acceleration of ions. In spite of Chadwick's urge to start the construction of an appropriate accelerator, Rutherford was during several years reluctant to embark upon such a great and expensive enterprise in his laboratory. This attitude is quite understandable when one considers the wonderful progress which Rutherford hitherto had achieved with the help of very modest experimental equipment. The task of competing with natural, radioactive sources must also have appeared quite formidable at that time. The outlook, however, was changed by the development of quantum theory and its first application to nuclear problems.

Rutherford himself had as early as 1920 in his second Bakerian Lecture clearly pointed out the difficulties of interpreting α -ray emission from nuclei on the basis of the simple mechanical ideas, which had proved so helpful in explaining the scattering of α -particles by nuclei, since the velocity of the ejected particles was not large enough to allow them by reversal to re-enter the nuclei against the electric repulsion. However, the possibilities of penetration of particles through

potential barriers was soon recognized as a consequence of wave mechanics, and in 1928 Gamow, working in Göttingen, as well as Condon and Gurney in Princeton, gave on this basis a general explanation of α -decay and even a detailed account of the relationship between the lifetime of the nucleus and the kinetic energy of the emitted α -particles, in conformity with the empirical regularities found by Geiger and Nuttall in the early Manchester days.

When, in the summer of 1928, Gamow joined us in Copenhagen, he was investigating the penetration of charged particles into nuclei by a reverse tunnel effect. He had started this work in Göttingen and discussed it with Houtermans and Atkinson, with the result that the latter were led to suggest that the source of solar energy might be traced to nuclear transmutations induced by impact of protons with the great thermal velocities which according to Eddington's ideas were to be expected in the interior of the sun.

During a brief visit to Cambridge in October 1928, Gamow discussed the experimental prospects arising from his theoretical considerations with Cockcroft, who by more detailed estimates convinced himself of the possibility of obtaining observable effects by bombardment of light nuclei with protons of an energy far smaller than that of α -particles from natural radioactive sources. As the result appeared promising, Rutherford accepted Cockcroft's proposal to build a high voltage accelerator for such experiments. Work on the construction of the apparatus was started by Cockcroft at the end of 1928 and was continued during the following year with the collaboration of Walton. The first experiments they made with accelerated protons in March 1930, in which they looked for gamma rays emitted as a result of the interaction of the protons with the target nuclei, gave no result. The apparatus then had to be rebuilt owing to a change of laboratory and, as is well known, production of high-speed α -particles by proton impact on lithium nuclei was obtained in March 1932.

These experiments initiated a new stage of most important progress, during which both our knowledge of nuclear reactions and the mastery of accelerator techniques rapidly increased from year to year. Already Cockcroft and Walton's first experiments gave results of great significance in several respects. Not only did they confirm in all details the predictions of quantum theory as regards the dependence of the reaction cross section on the energy of the protons, but it was also possible to connect the kinetic energy of the emitted α -rays with the masses of the reacting particles which were at that time known with sufficient accuracy thanks to Aston's ingenious development of mass spectroscopy. Indeed, this comparison offered the first experimental test of Einstein's famous relation between energy and mass, to which he had been led many years before by relativity arguments. It need hardly be recalled how fundamental this relation was to prove in the further development of nuclear research.

The story of Chadwick's discovery of the neutron presents similar dramatic features. It is characteristic of the broadness of Rutherford's views that he early anticipated the presence in nuclei of a heavy neutral constituent of a mass closely coinciding with that of the proton. As gradually became clear, this idea would indeed explain Aston's discoveries of isotopes of nearly all elements with atomic masses closely approximated by multiples of the atomic weight of hydrogen. In connection with their studies of many types of α -ray induced nuclear disintegrations Rutherford and Chadwick made an extensive search for evidence concerning the existence of such a particle. However, the problem came to a climax

through the observation by Bothe and the Joliot-Curies of a penetrating radiation resulting from the bombardment of beryllium by α -particles. At first this radiation was assumed to be of γ -ray type, but with Chadwick's thorough familiarity with the multifarious aspects of radiative phenomena he clearly perceived that the experimental evidence was not compatible with this view.

Indeed, from a masterly investigation, in which a number of new features of the phenomenon were revealed, Chadwick was able to prove that one was faced with momentum and energy exchanges through a neutral particle, the mass of which he determined as differing from that of the proton by less than one part in a thousand. On account of the ease with which neutrons, compared with charged particles, can pass through matter without transfer of energy to the electrons and penetrate into atomic nuclei, Chadwick's discovery opened great possibilities of producing new types of nuclear transmutations. Some most interesting cases of such new effects were immediately demonstrated in the Cavendish by Feather, who obtained cloud chamber pictures showing nitrogen nuclei disintegrating under α -particle release by neutron bombardment. As is well known, continued studies in many laboratories along such lines were rapidly to increase our knowledge of nuclear constitution and transmutation processes.

In the spring of 1932, at one of our yearly conferences in the Copenhagen Institute, where as always we were happy to see many of our former collaborators, one of the main topics of discussion was of course the implications of the discovery of the neutron, and a special point raised was the apparently strange circumstance that in Dee's beautiful cloud chamber pictures no interaction whatever was observed between the neutrons and the electrons bound in the atoms. In relation to this point, it was argued that, owing to the dependence in quantum physics of the scattering cross section on the reduced mass of the colliding particles, this fact would not be inconsistent even with the assumption of short range interaction between the neutron and an electron of strength similar to that between the neutron and a proton. A few days later, I got a letter from Rutherford touching incidentally on this point, and which I cannot resist quoting in full:

April 21, 1932.

My dear Bohr,

I was very glad to hear about you all from Fowler when he returned to Cambridge and to know what an excellent meeting of old friends you had. I was interested to hear about your theory of the Neutron. I saw it described very nicely by the scientific correspondent of the Manchester Guardian, Crowther, who is quite intelligent in these matters. I am very pleased to hear that you regard the Neutron with favour. I think the evidence in its support, obtained by Chadwick and others, is now complete in the main essentials. It is still a moot point how much ionization is, or should be, produced to account for the absorption, disregarding the collisions with nuclei.

It never rains but it pours, and I have another interesting development to tell you about of which a short account should appear in *Nature* next week. You know that we have a High Tension Laboratory where steady D.C. voltages can be readily obtained up to 600,000 volts or more. They have recently been examining the effects of a bombardment of light elements by protons. The protons fall on a surface of the material inclined at 45° to the axis of the tube, and the effects produced were observed at the side by the scintillation method, the zinc sulphide screen being covered with sufficient mica to stop the protons. In the case of lithium brilliant scintillations are observed, beginning at about 125,000 volts and mounting up very rapidly with voltage when many hundreds

per minute can be obtained with a protonic current of a few milliamperes. The α -particles apparently had a definite range, practically independent of voltage, of 8 cm in air. The simplest assumption to make is that the lithium 7 captures a proton breaking up with the emission of two ordinary α -particles. On this view the total energy liberated is about 16 million volts and this is of the right order for the changes in mass involved, assuming the Conservation of Energy.

Later special experiments will be made to test the nature of the particles but from the brightness of the scintillations and the trail in a Wilson chamber it seems probable they are α -particles. In experiments in the last few days similar effects have been observed in Boron and Fluorine but the ranges of the particles are smaller although they look like α -particles. It may be, Boron 11 captures a proton and breaks up into three alphas, while fluorine breaks up into oxygen and an alpha. The energy changes are in approximate accord with these conclusions. I am sure you will be much interested in these new results which we hope to extend in the near future.

It is clear that the α -particle, neutron and proton will probably give rise to different types of disintegration and it may be significant that so far results have only been observed in $4n + 3$ elements. It looks as if the addition of the 4th proton leads at once to the formation of an α -particle and the consequent disintegration. I suppose, however, the whole question should be regarded as the result of one process rather than of steps.

I am very pleased that the energy and expense in getting high potentials has been rewarded by definite and interesting results. Actually they ought to have observed the effect a year or so ago but did not try it in the right way. You can easily appreciate that these results may open up a wide line of research in transmutation generally.

We are all very well at home and I start lectures tomorrow. With best wishes to you and Mrs. Bohr.

Yours ever

RUTHERFORD

Beryllium shows some queer effects—still to be made definite.

I shall possibly refer to these experiments in the Royal Society discussion on nuclei on Thursday April 25.

Of course, in reading this letter, it must be borne in mind that my previous visits to Cambridge had kept me acquainted with the work in progress in the Cavendish Laboratory, so that Rutherford had no need to specify the individual contributions of his collaborators. The letter is indeed a spontaneous expression of his exuberant joy in the great achievements of those years and his eagerness in pursuing their consequences.

XI

As a true pioneer, Rutherford never relied merely on intuition, however far it carried him, but was always on the look-out for new sources of knowledge which could possibly lead to unexpected progress. Thus, also in Cambridge, Rutherford and his collaborators continued with great vigour and steadily refined apparatus the investigations of the radioactive processes of α - and β -decay. The important work of Rutherford and Ellis on β -ray spectra revealed the possibility of a clear distinction between intranuclear effects and the interaction of the β -particle with the outer electron system and led to the clarification of the mechanism of internal conversion.

Moreover, Ellis' demonstration of the continuous spectral distribution of the electrons directly emitted from the nucleus raised a puzzling question about energy conservation, which was eventually answered by Pauli's bold hypothesis of the simultaneous emission of a neutrino, affording the basis for Fermi's ingenious theory of β -decay.

By the great improvement of accuracy in measurements of α -ray spectra by Rutherford, Wynn-Williams and others, much new light was thrown on the fine structure of these spectra and their relation to the energy levels of the residual nucleus resulting from the α -decay. A special adventure at an earlier stage was the discovery of the capture of electrons by α -rays which, after the first observation of the phenomenon in 1922 by Henderson, was explored by Rutherford in one of his most masterly researches. As is well known, this work, which brought so much information about the process of electron capture, was to attract new attention a few years after Rutherford's death when, with the discovery of the fission processes of heavy nuclei by neutron impact, the study of the penetration of highly charged nuclear fragments through matter, where electron capture is the dominating feature, came into the foreground.

Great progress both as regards general outlook and experimental technique was initiated in 1933 by the discovery by Frédéric Joliot and Irène Curie of so-called artificial β -radioactivity produced by nuclear transmutations initiated by α -ray bombardment. I need hardly here remind how, by Enrico Fermi's brilliant systematic investigations of neutron induced nuclear transmutations, radioactive isotopes of a great number of elements were discovered and much information gained about nuclear processes initiated by capture of slow neutrons. Especially the continued study of such processes revealed most remarkable resonance effects of a sharpness far surpassing that of the peaks in the cross section of α -ray induced reactions first observed by Pose and to Gurney's explanation of which, on the basis of the potential well model, Gamow at once drew Rutherford's attention.

Already Blackett's observations with his ingenious automatic cloud chamber technique had shown that, in the very process investigated in Rutherford's original experiments on artificial nuclear disintegrations, the incident α -particle remained incorporated in the residual nucleus left after proton escape. It now became clear that all types of nuclear transmutations within a large energy region take place in two well-separated steps. Of these the first is the formation of a relatively long-lived compound nucleus, while the second is the release of its excitation energy as a result of a competition between the various possible modes of disintegration and radiative processes. Such views, in which Rutherford took a vivid interest, were the theme for the last course of lectures which on Rutherford's invitation I gave in 1936 in the Cavendish Laboratory.

Less than two years after Rutherford's death in 1937, a new and dramatic development was initiated by the discovery of the fission processes of the heaviest elements by his old friend and collaborator in Montreal, Otto Hahn, working in Berlin with Fritz Strassmann. Immediately after this discovery, Lise Meitner and Otto Frisch, then working in Stockholm and Copenhagen, and now both in Cambridge, made an important contribution to the understanding of the phenomenon by pointing out that the critical decrease in stability of nuclei of high charge was a simple consequence of the balancing of cohesive forces between the nuclear constituents and the electrostatic repulsion. A closer investigation of the

fission process in collaboration with Wheeler showed that many of its characteristic features could be accounted for in terms of the mechanism of nuclear reactions involving as a first step the formation of a compound nucleus.

In Rutherford's last years he found in Marcus Oliphant a collaborator and friend whose general attitude and working power reminds us so much of his own. At that time new possibilities of research were opened by Urey's discovery of the heavy hydrogen isotope ^2H or deuterium, and by the construction of the cyclotron by Lawrence, who in his first investigations on nuclear disintegrations by deuteron beams obtained a number of new striking effects. In the classical experiments of Rutherford and Oliphant, in which by bombardment of separated lithium isotopes with protons and deuterons they were led to the discovery of ^3H , or tritium, and ^3He , the foundation was indeed created for the vigorous modern attempt to apply thermonuclear reactions to the realization of the full promises of atomic energy sources.

From the very beginning of his radioactive researches, Rutherford was acutely aware of the wide perspectives they opened in several directions. In particular, he early took deep interest in the possibility of arriving at an estimate of the age of the earth and of understanding the thermal equilibrium in the crust of our planet. Even if the liberation of nuclear energy for technological purposes was still to come, it must have been a great satisfaction for Rutherford that the explanation of the hitherto completely unknown source of solar energy as a result of the development he had initiated had come within the horizon in his lifetime.

XII

When we look back on Rutherford's life we perceive it, of course, against the unique background of his epoch-making scientific achievements, but our memories will always remain irradiated by the enchantment of his personality. In earlier Memorial Lectures, several of Rutherford's closest co-workers have recalled the inspiration which emanated from his vigour and enthusiasm and the charm of his impulsive ways. Indeed, in spite of the large and rapidly expanding scope of Rutherford's scientific and administrative activities, the same spirit reigned in the Cavendish as we all had enjoyed so much in the early Manchester days.

A faithful account of Rutherford's eventful life from childhood till his last days has been written by his old friend from the Montreal period, A. S. Eve. Especially the many quotations in Eve's book from Rutherford's astonishingly large correspondence give a vivid impression of his relations with colleagues and pupils all over the world. Eve also does not fail to report some of the humorous stories which constantly grew around Rutherford, and to which I alluded in a speech, reproduced in his book, when Rutherford for the second and last time visited us in Copenhagen in 1932.

Characteristic of Rutherford's whole attitude was the warm interest he took in any one of the many young physicists with whom he came into contact for shorter or longer periods. Thus I vividly remember the circumstances of my first meeting in Rutherford's office in the Cavendish with the young Robert Oppenheimer, with whom I was later to come into such close friendship. Indeed, before Oppenheimer entered the office, Rutherford, with his keen appreciation of talents, had described the rich gifts of the young man, which in the course of time were to create for him his eminent position in scientific life in the United States.

As is well known, Oppenheimer, shortly after his visit to Cambridge, during his studies in Göttingen was among the first who called attention to the phenomenon of particle penetration through potential barriers, which should prove basic for the ingenious explanation of α -decay by Gamow and others. After his stay in Copenhagen, Gamow came in 1929 to Cambridge, where his steady contributions to the interpretation of nuclear phenomena were highly appreciated by Rutherford, who also greatly enjoyed the bizarre and subtle humour which Gamow unfolded in daily intercourse and to which he later gave so abundant expression in his well-known popular books.

Of the many young physicists from abroad working in the Cavendish Laboratory in those years, one of the most colourful personalities was Kapitza, whose power of imagination and talent as a physical engineer Rutherford greatly admired. The relationship between Rutherford and Kapitza was very characteristic of them both and was, notwithstanding inevitable emotional encounters, marked from first to last by a deep mutual affection. Such sentiments were also behind Rutherford's efforts to support Kapitza's work after his return to Russia in 1934, and were from Kapitza's side most movingly expressed in a letter which I received from him after Rutherford's death.

When, in the beginning of the nineteen thirties, as an extension to the Cavendish, the Mond Laboratory was created on Rutherford's initiative for the promotion of Kapitza's promising projects, Kapitza wanted in its decoration to give expression for his joy in Rutherford's friendship. Still, the carving of a crocodile on the outer wall caused comments which could only be appeased by reference to special Russian folklore about animal life. Above all, however, the relief of Rutherford, in Eric Gill's artistic interpretation, placed in the entrance hall, deeply shocked many of Rutherford's friends. On a visit to Cambridge I confessed that I could not share this indignation, and this remark was so welcomed that Kapitza and Dirac presented me with a replica of the relief; installed above the fireplace in my office at the Copenhagen Institute it has since given me daily enjoyment.

When, in recognition of his position in science Rutherford was given a British peerage, he took a keen interest in his new responsibilities as a member of the House of Lords, but there was certainly no change in the directness and simplicity of his behaviour. Thus I do not remember any more severe utterance of his to me than, when at a Royal Society Club dinner in a conversation with some of his friends I had referred to him in the third person as Lord Rutherford, he furiously turned on me with the words: "Do you lord me?"

In the nearly twenty years during which Rutherford, right up to his death, worked with undiminished energy in Cambridge, my wife and I kept in close touch with him and his family. Almost every year, we were hospitably received in their beautiful home in Newnham Cottage at the backs of the old colleges, with the lovely garden in which Rutherford found relaxation and the upkeep of which gave Mary Rutherford much enjoyable work. I remember many peaceful evening hours in Rutherford's study spent discussing not merely new prospects of physical science but also topics from many other fields of human interest. In such conversation one was never tempted to overrate the interest of one's own contributions since Rutherford after a long day's work was apt to fall asleep as soon as the discourse seemed pointless to him. One then just had to wait until he woke up and resumed the conversation with usual vigour as if nothing had happened.

On Sundays, Rutherford regularly played golf in the morning with some close friends and dined in the evening in Trinity College where he met many eminent scholars and enjoyed discussions on the most different subjects. With his insatiable curiosity for all aspects of life, Rutherford had great esteem for his learned colleagues; however, I remember how he once remarked, on our way back from Trinity, that to his mind so-called humanists went a bit too far when expressing pride in their complete ignorance of what happened in between the pressing of a button at their front door and the sounding of a bell in the kitchen.

Some of Rutherford's utterances have led to the misunderstanding that he did not fully appreciate the value of mathematical formalisms for the progress of physical science. On the contrary, as the whole branch of physics, created so largely by himself, rapidly developed, Rutherford often expressed admiration for the new theoretical methods, and even took interest in questions of the philosophical implications of quantum theory. I remember especially how, at my last stay with him a few weeks before his death, he was fascinated by the complementary approach to biological and social problems and how eagerly he discussed the possibility of obtaining experimental evidence on the origin of national traditions and prejudices by such unconventional procedures as the interchange of newborn children between nations.

A few weeks later, at the Centenary Celebrations for Galvani in Bologna, we returned with sorrow and consternation of Rutherford's death, and I went at once to England to attend his funeral. Having been with them both so shortly before and found Rutherford in full vigour and in the same high spirits as always, it was under tragic circumstances, indeed, that I met Mary Rutherford again. We talked about Ernest's great life in which from their early youth she had been so faithful a companion, and how to me he had almost been as a second father. On one of the following days, Rutherford was buried in Westminster Abbey, close to the sarcophagus of Newton.

Rutherford did not live to see the great technological revolution which was to ensue from his discovery of the atomic nucleus and his subsequent fundamental researches. However, he was always aware of the responsibility connected with any increase in our knowledge and abilities. We are now confronted with a most serious challenge to our whole civilization, to see to it that disastrous use of the formidable powers which have come into the hands of man be prevented, and that the great progress be turned into promoting the welfare of all humanity. Some of us, who were called to take part in the war projects, often thought of Rutherford and modestly strove to act in the way which we imagined he himself would have taken.

The memory which Rutherford has left us remains to everyone who had the good fortune to know and come close to him a rich source of encouragement and fortitude. The generations who in coming years pursue the exploration of the world of atoms will continue to draw inspiration from the work and life of the great pioneer.

C. V. BOYS LECTURE

Counter Techniques in High Energy Nuclear Physics: Rare Decays of π - and μ -mesons

BY A. W. MERRISON

Lecture delivered before the Institute of Physics and the Physical Society at the Conference on Nuclear Physics, Birmingham, on 17th April 1961

Abstract. It is shown, with particular reference to the decay $\mu^+ \rightarrow e^+ + \gamma$, how the study of rare decays of pions and muons, by means of counter techniques, has contributed to our understanding of the weak interactions.

IN this talk I want to discuss some of the experiments that have been done, principally by counter techniques, on the unusual modes of decay of π - and μ -mesons. Counter experiments, because of selection criteria which can be built into them, have contributed very largely to this field and I shall in this talk show how the study of these decays has contributed to our knowledge of the weak interactions. I have listed in Table 1 all the known and presently conjectured decay modes of π - and μ -mesons along with their observed or predicted branching ratios and whether any particular mode of decay has any special interest. This last is, to some extent, a personal judgment, but I think there would not be too much divergence of views of high-energy physicists over this. I should point out there exist π^- -decays corresponding to all the π^+ -decays listed here and I have not distinguished neutrinos from anti-neutrinos.

Table 1. Decays of π^\pm and μ -mesons

Decay	Observed	Branching ratio	Interest
$\pi^0 \rightarrow \gamma + \gamma$			
$\gamma + e^+ + e^-$	Yes	1.2×10^{-2}	No
$e^+ + e^- + e^+ + e^-$	Yes	4×10^{-5}	Yes
$\pi^+ \rightarrow \mu^+ + \nu$			
$\mu^+ + \nu + \gamma$	Yes		No
$e^+ + \nu$	Yes	1.2×10^{-4}	Yes
$e^+ + \nu + \gamma$	No	5×10^{-6}	No
$e^+ + \pi^0 + \nu$	No	10^{-8}	Yes
$\mu^+ \rightarrow e^+ + \nu + \nu$			
$e^+ + \nu + \nu + \gamma$	Yes	5×10^{-2}	No
$e^+ + \gamma$	No	?	Yes
$e^+ + e^+ + e^-$	No	?	Yes

Some comments on this table are appropriate. The so-called 'double Dalitz' decay of the neutral pion into 2 electron pairs is of interest in that it makes possible an experiment suggested some years ago by Yang (1950). He pointed out that if the neutral pion is pseudoscalar, then when it decays into two photons their

planes of polarization will be perpendicular, and similarly there will be a correlation between the planes of the two electron pairs. Preliminary results (Plano *et al.* 1959) indicate clearly that the neutral pion is in fact pseudoscalar.

The electron decay mode of the pion is still of interest in that if one looks on the decay of the pion as going through a virtual nucleon-antinucleon state, then the branching ratio $(\pi \rightarrow e + \nu)/(\pi \rightarrow \mu + \nu)$ gives a direct comparison of the axial vector coupling of muons and electrons to nucleons. The most accurate measurements so far (Anderson *et al.* 1960) show that the strengths of the electron and muon couplings to nucleons are identical.

Having declared the field of interest, I shall illustrate what I have to say about counter techniques by discussing in some detail one particular rare, and perhaps non-existent, decay (namely $\mu \rightarrow e + \gamma$) and a particular counter experiment which was made to search for it by a CERN group about two years ago.

DECAYS OF THE μ -MESON

The normal decay mode of the μ -meson is now well established as $\mu \rightarrow e + \nu + \bar{\nu}$, but it is worth looking at the experiments which established this, as they form an interesting background to more recent experiments which establish the existence of other decay modes.

It had been known ever since the first 'mesons' were discovered in the cosmic rays that they normally decayed into a single charged particle of small mass, and without inventing more new particles it seemed reasonable to suppose that this particle was an electron. But it was not until the decisive experiment of Leighton,

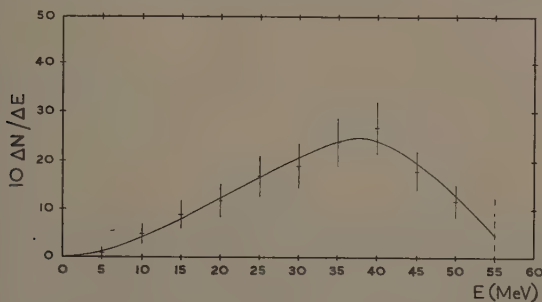


Fig. 1.

Anderson and Seriff (1949) (Fig. 1) that it was established that the electron had a spectrum of energies, so that at least two neutral particles accompanied the emission of an electron. Again, using only *known* light neutral particles one could speculate that the decay was through $\mu \rightarrow e + \nu + \bar{\nu}$, $\mu \rightarrow e + \nu + \gamma$, or $\mu \rightarrow e + \gamma + \gamma$. As it happened, an experiment by Hincks and Pontecorvo (1948) in the previous year had ruled out the possibility that μ -meson decays were accompanied by any substantial fraction of γ -rays. I will spend a little time describing this experiment as it is interesting to compare it with a more recent and, in detail, more complicated experiment which had the same end in view. Cosmic-ray μ -mesons were brought to rest in the block of graphite surrounded by the banks of Geiger counters C and B (Fig. 2). The arrival of a μ -meson was registered by a coincidence AB, and BC coincidences delayed by 0.6 to 5.3 μ sec with respect to AB were looked for. (Note

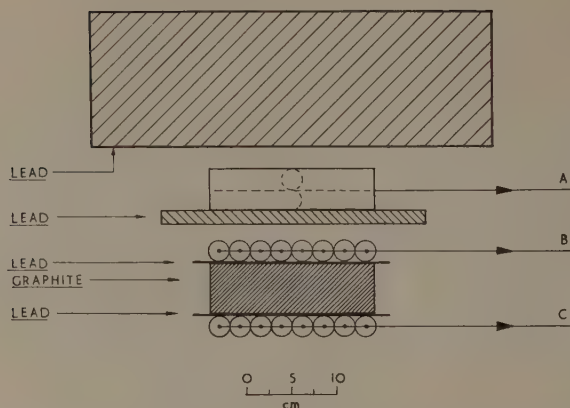


Fig. 2. Apparatus of Hinks and Pontecorvo.

one counter in B must be dead as it has recorded arrival of a μ -meson.) The idea was that the electron from $\mu \rightarrow e + \gamma$ would be detected by either A or B, and the γ -ray by conversion in the lead sheets in front of A and B and by the detection of the resulting pair in A or B.

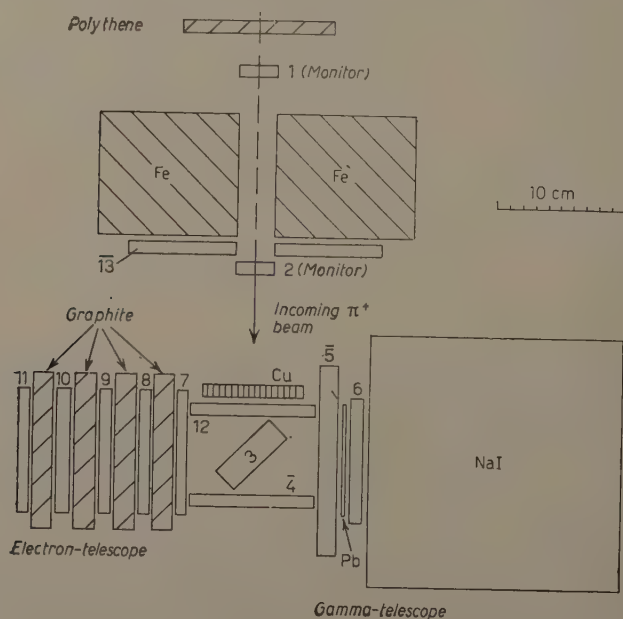


Fig. 3. Schematic diagram of the apparatus.

A modern version of the same experiment is shown in Fig. 3, which shows an experiment carried out by CERN (by Ashkin, Fazzini, Fidecaro, Lipman, Merrison and Paul 1959) specifically to search for the decay $\mu \rightarrow e + \gamma$. This became fashionable at the end of 1958 for the following reasons. The weak interactions can be summed up in the archetypes

$$\mu \rightarrow e + \nu + \bar{\nu}$$

$$n \rightarrow p + e + \bar{\nu}$$

$$\mu + p \rightarrow n + \nu$$

leading to the well-known Puppi triangle (Fig. 4), which sums up the selection rules for the allowed weak interactions, and it is now well-established that one coupling constant is sufficient to account for the rates of all three interactions. An attractive way to account for these facts is to assume that the weak interactions are mediated by a charged vector boson; but this immediately runs into the difficulty that if this boson exists then $\mu \rightarrow e + \gamma$ will have an appreciable decay rate

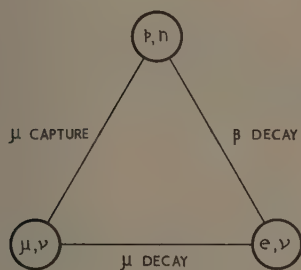


Fig. 4.

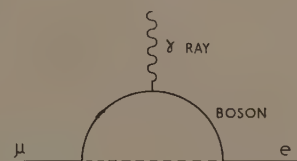


Fig. 5.

through a diagram of the form shown in Fig. 5. One simple calculation (by Feinberg 1958) gives a branching ratio for $(\mu \rightarrow e + \gamma)/(\mu \rightarrow e + \nu + \bar{\nu}) \simeq 10^{-3}$. There are, of course, many ways of reducing or even completely suppressing this mode of decay, and one way, which is receiving a tremendous amount of experimental attention at the moment, is by supposing that the neutrinos associated with electrons and those associated with muons are different. An experiment to test this idea is now in an advanced state of preparation at the CERN laboratories in Geneva. It is a neutrino capture experiment similar to the experiment performed by Reines and Cowan with β -decay neutrinos. A difficulty which seemed to preclude such experiments with muon neutrinos (i.e. neutrinos from $\pi \rightarrow \mu + \nu$) was simply that the available fluxes of such neutrinos are so small. But it was pointed out by a number of people (see Rochester Conference 1960, p. 585) that one could overcome the scarcity of muon neutrinos by making use of the rise of cross section with momentum, which could lead to cross sections of the order of 10^{-38} cm^2 for 1 Gev neutrinos, and counting rates of the order of 1 per ton of detector per day with the fluxes currently available at the CERN proton synchrotron. The experiment would then be to look for the production of *electrons* with these muon neutrinos.

One can take a more simple-minded attitude to the problem, and if a reaction which obeys all the well-established conservation laws does not appear, one can ask experimentally what is its degree of forbiddenness. The search for $\mu \rightarrow e + \gamma$ is made difficult, as has been recently realized, by the existence of the decay $\mu \rightarrow e + \nu + \nu + \gamma$ which provides a background of (e, γ) pairs. The branching ratio of this process compared with the normal decay mode of the muon has been calculated by Fronsda and Uberall (1959) and Kinoshita and Sirlin (1959). The $\mu \rightarrow e + \gamma$ mode, however, can be distinguished because, firstly, the *whole* rest energy of the muon goes into the electron and the γ -ray so that one should observe, as it is a two-body decay, a mono-energetic electron and a mono-energetic γ -ray each of about 53 mev. Secondly, the electron and γ -ray will be emitted at 180° to each other. The bremsstrahlung process, on the other hand, gives continuous spectra for both the electron and γ -ray which are heavily weighted towards low energies, and the angular correlation does not favour 180° emission. So, by searching for high energy electrons and γ -rays at 180° we discriminate strongly against this process.

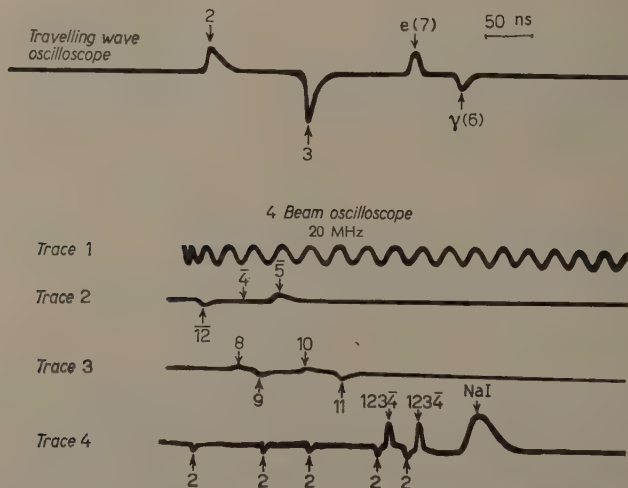


Fig. 6. Examples of traces from the travelling wave and four-beam oscilloscopes.

Of course, the principal difficulty in searching for rare decay modes is to be sure that nothing has been introduced into the design of the apparatus which would obscure the effect one is looking for. For this reason the apparatus was not designed with the idea of rejecting electronically as many unwanted events as possible. We preferred to record during the run also events to be re-examined later, which would show that the apparatus was working properly.

In the CERN experiment the muons were generated by allowing a beam of pions from the 600 mev cyclotron to come to rest and decay in counter 3. So a stopping pion was first identified by a $123\bar{4}$ coincidence. Counter 3 was surrounded on three sides by anticoincidence counters $\bar{12}$, $\bar{5}$, $\bar{4}$. On the fourth side was a coincidence counter telescope 7, 8, 9, 10, 11, with a certain amount of graphite

absorber between the counters, and this served to detect the expected ~ 50 mev electrons. On the opposite side to the electron telescope was a γ -ray telescope formed of the anticoincidence counter $\bar{5}$, the coincidence counter 6 and a lead converter between them, the whole backed by a very large NaI counter which analysed the energy spectrum of γ -rays detected in the electron telescope. Whenever a fast coincidence was recorded in counters 6, 7, 8 and $\bar{5}$ and $\bar{13}$ in anticoincidence† then the pulses from counters 2, 3, 6 and 7 were recorded on a fast oscilloscope.

A typical trace from this oscilloscope with pulses from all four counters present is shown in the top trace of Fig. 6. At the same time we displayed (as shown also in Fig. 6) on a four-beam oscilloscope pulses from counters 4, 5, 12 (on trace 2); from counters 8, 9, 10 and 11 (on trace 3); from counter 2, the NaI counter, and the coincidence pulse 1234 (on trace 4). On trace 1 we displayed a 20 Mc/s calibration signal. Traces 1, 2 and 3 were all run from the same time base. Trace 4 was run from an independent time base having a speed of $2 \mu\text{sec cm}^{-1}$.

The event we searched for was a high-energy electron coming from counter 3, in time coincidence with a high energy γ -ray. This would be characterized by a pair of photographs showing:

(i) pulses from counters 3, 6 and 7 on the fast oscilloscope, present with the proper time relationship for a coincident event, but with either no pulse from counter 2, or with a pulse from counter 2 not in the right position for an incoming pion coincident with the $e\text{-}\gamma$ coincidence;

(ii) pulses from counters 7–11 in the electron telescope (trace 3 of 4-beam oscilloscope, see Fig. 1);

(iii) no pulse present from counter $\bar{5}$ (trace 2). We should also expect no pulses present from counters $\bar{4}$ and $\bar{12}$, because an event originating in the source counter should not trigger these (trace 2);

(iv) a large pulse from the NaI(Tl) counter (trace 4).

For example, the event in Fig. 1 would be accepted as an $e\text{-}\gamma$ event if the time relationship of the pulses in the fast and slow oscilloscopes were correct and if there were no pulses present in counters $\bar{5}$ and $\bar{12}$. Because of the high input rate of pions, many counter 2 and 1, 2, 3, $\bar{4}$ pulses were present on trace 4 of the slow oscilloscopes.

We ran the experiment in its final version for about 50 hours and in this time stopped 7.35×10^8 pions in counter 3, taking a total of 5394 pairs of photographs on the oscilloscopes. We scanned the films first for events with a high energy electron (i.e. pulses from counters 8, 9, 10, 11 present on trace 3 of the slow oscilloscope). Examining the fast oscilloscope, the events which were left could be classified into the following categories:

(a) *Prompts*. These are events with pulses from counters 2, 6 and 7 in prompt coincidence. Such an event could arise from the decay of a neutral pion produced by a charge exchange interaction of an incoming positive pion. Of the resulting two γ -rays, one is converted and triggers the electron telescope, and the other triggers the γ -ray telescope. In most of the prompt events a pulse from counter 12 was present on trace 2 of the 4-beam oscilloscope.

(b) ' $e(7)\gamma(6)$ ' events. Pulses from counters 6 and 7 are present but not from counter 3. This could be a muon decaying with emission of a γ -ray in some place other than counter 3. Some of these events are random; for example, the

† Counter 13 protected the apparatus from showers generated in the lead collimator.

electron from one muon triggers the electron telescope in random coincidence with a γ -ray from another muon.

(c) ' $3e(7)\gamma(6)$ ' events. These are the same as (b) but with a pulse from counter 3. They are essentially the events we are searching for and will be analysed in detail. They will, of course, include random events similar to these described in (b).

(d) ' $3e(7)3\gamma(6)$ ' events. These are a class of random events which contain two separate pulses from counter 3, one in coincidence with a pulse in counter 6 and the other with a pulse in counter 7.

(e) *Random events*. Triggered by a random coincidence circuit and clearly recognizable. We recorded these for the purpose of comparison. These also could be classified into the categories (b), (c), (d) and a few into category (a).

After this analysis we were left with 184 events of the first four categories (associated with a high-energy electron) as shown in Table 2.

Table 2			
Prompt	$e(7)\gamma(6)$	$3e(7)\gamma(6)$	$3e(7)3\gamma(6)$
65	26	72	21

On examination of trace 2 of the slow oscilloscope it was necessary to reject a further 50 of the 72 events $3e(7)\gamma(6)$ because of the presence of 4, 5 or 12 pulses.

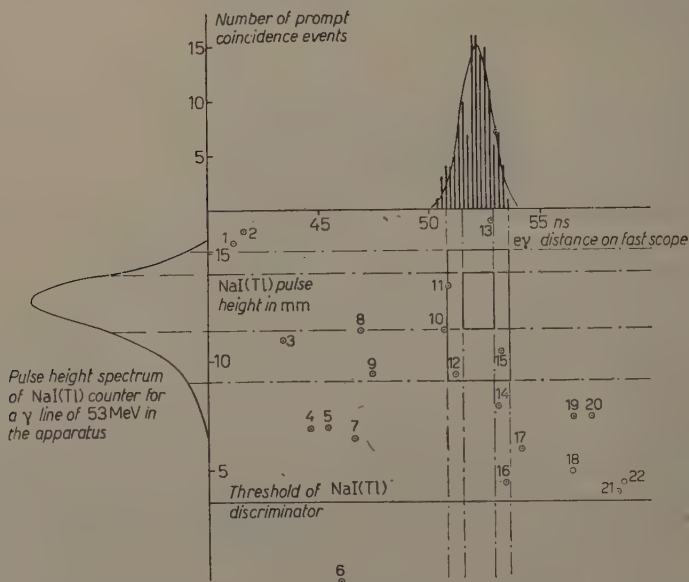


Fig. 7. Time delay and pulse height analysis of the twenty-two observed $e\text{-}\gamma$ events. Abscissa gives the time delay between the $e(7)$ and $\gamma(6)$ pulses; comparison is made with the measured resolution curve for 'prompt' events. The ordinate gives the NaI(Tl) pulse height; comparison is made with a computed curve of the expected pulse height distribution for 53 mev γ -rays incident on the Pb converter.

31 of the rejections were due to a $\bar{5}$ pulse being present. We did not expect the apparatus to record any such events, and in fact it was verified that these were random events which could be recorded only because the time interval for which the anticoincidence counter $\bar{5}$ was rejecting events was not wide enough to cover the whole acceptance time interval of the coincidence circuit.

The remaining 22 events were then subjected to a careful time analysis, and the associated NaI pulse heights were measured in order to select those events which had the correct $e(7)\gamma(6)$ time delay, defined to the closest possible limits, and a γ -ray energy lying within the small range defined by the apparatus.

The total time resolution of the system was determined by measuring 133 prompt events (for which one knows that particles went through counters 6 and 7 in exact coincidence). The result obtained is shown in the top part of Fig. 7. The best-fit Gaussian to the histogram has a standard deviation of 0.70 nsec. This has been used as the defining time resolution curve in the analysis of the $3e(7)\gamma(6)$ events.

Plotted also in Fig. 7 is the expected pulse height distribution from the NaI(Tl) counter for 53 MeV γ -rays emitted from counter 3, and converted with the 3 mm Pb converter. The energy distribution of the electron-positron pair in the Pb converter and counter 6 has been taken into account, together with the experimentally determined NaI(Tl) resolution curve for mono-energetic particles.

The final analysis of the 22 events which had an energetic electron, in terms of the time resolution between electron and γ -ray events and in terms of γ -ray energy, is shown in Fig. 7. We have drawn in this figure the threshold for the NaI discrimination and we would expect to see no events below this. One event (6) has, however, been recorded, and this could be due perhaps to 'pile up' in the slow coincidence circuit or discriminator.

We have drawn on Fig. 7 'boxes' which correspond to 68% of the area under each of the resolution curves and 95% of the area under each curve. It can be seen that no events survive the first criteria and 3 events (11, 12, 15) the second. It is clear from the number of events falling outside the time-resolution curve that we can attribute a certain number of events in the 'boxes' to random events, and this we evaluated to be one event for the larger box. Using the results in the larger box we obtained a final branching ratio

$$\frac{\mu \rightarrow e + \gamma}{\mu \rightarrow e + \nu + \nu} = (1.2 \pm 1.5) \times 10^{-6}.$$

THE DECAY $\pi^+ \rightarrow \pi^0 + e^+ + \nu$

One final word about a reaction in Table 1, so far unobserved, which again looks most interesting: this is the decay $\pi^\pm \rightarrow \pi^0 + e^\pm + \nu$ which looks very much like a nuclear β -decay with the nuclei replaced by pions. The interest in this decay is that a universal coupling scheme, of the sort proposed by Feynman and Gell-Mann (1958), predicts very straightforwardly the rate of this decay. Unfortunately, because of the small momentum-space available (the charged pion is only 4 MeV heavier than the neutral pion) the branching ratio is about 10^{-8} . There is no doubt that technically this is not an impossible thing to look for because the decay of the π^0 into two high energy γ -rays provides a very characteristic 'signature', but with existing pion fluxes the rate of gathering events would be discouragingly small.

REFERENCES

- ANDERSON, H. L., FUJII, T., MILLER, T. H., and TAU, L., 1960, *Phys. Rev.*, **119**, 2050.
ASHKIN, J., FAZZINI, T., FIDECARO, G., LIPMAN, N. H., MERRISON, A. W., and PAUL, H.,
1959, *Nuovo Cim.*, **14**, 1266.
FEINBERG, G., 1958, *Phys. Rev.*, **110**, 1482.
FEYNMAN, R. P., and GELL-MANN, M., 1958, *Phys. Rev.*, **109**, 193.
FRONSDAL, C., and UBERALL, H., 1959, *Phys. Rev.*, **113**, 654.
HINCKS, E. P., and PONTECORVO, B., 1948, *Phys. Rev.*, **73**, 257.
KINOSHITA, T., and SIRLIN, A., 1959, *Phys. Rev.*, **113**, 1652.
LEIGHTON, R. B., ANDERSON, C. D., and SERIFF, A. J., 1949, *Phys. Rev.*, **75**, 1432.
PLANO, R., PRODELL, A., SAMIOS, N., SCHWARTZ, M., and STEINBERGER, J., 1959, *Phys. Rev.*
Letters, **3**, 525.
YANG, C. N., 1950, *Phys. Rev.*, **77**, 242.

The Nuclear Scattering of High Energy Photons

By W. S. C. WILLIAMS†, H. S. CAPLAN‡ AND D. T. STEWART

Department of Natural Philosophy, The University, Glasgow

MS. received 23rd February 1961

Abstract. The scattering from carbon nuclei of photons in the energy range 50–130 mev has been measured by the use of a total absorption Čerenkov spectrometer in conjunction with a counter telescope. The angular range investigated was 90° to 135° . The results have been analysed by means of a simple model of nuclear charge distribution with nucleon polarizability and indicate the presence of some magnetic dipole scattering. A dispersion relation is applied to check the validity of this simple model.

§ 1. INTRODUCTION

THERE are many ways of exploring the structure of atomic nuclei, and each method reveals certain aspects of this structure. Important among these methods are the measurements of differential cross section for the scattering of electrons and of photons by nuclei. The former technique has been extensively used by Hofstadter and his co-workers (Hofstadter 1956) and it yields what is essentially the charge density distribution for the nucleus under study. The scattering of photons can, in principle, yield the same information but it is more influenced by the anomalous structure of the nucleon in the nucleus than is the electron scattering. Thus the existence of the resonant isobar nucleon state will affect the photon scattering whereas it may have no effect on the electron scattering. One of the objectives of the present study is to detect such anomalous effects in the scattering of high energy photons from carbon nuclei.

It is worth noting the main features of the nuclear photon scattering cross section. At energies close to zero (< 1 mev) the cross section is given by the Thomson cross section $\frac{1}{2}(1 + \cos^2 \theta) (Z^2 e^2 / AMc^2)^2$. M is the mass of a single nucleon and other symbols have their usual meaning. As the energy increases in the range 15–40 mev the scattering increases with the giant resonance in the photodisintegration cross section and the scattering total cross section can reach a value of $\sigma_a^2 / 6\pi\lambda^2$, where σ_a is the photon nuclear absorption cross section. Beyond the giant resonance the elastic cross section will fall to a value expected for Z free protons scattering coherently, multiplied by a nuclear form factor f^2 ,

$$\frac{d\sigma}{d\Omega} = Z^2 f^2 \frac{1}{2} (1 + \cos^2 \theta) \left(\frac{e^2}{Mc^2} \right)^2. \quad \dots\dots(1)$$

There will also be a small amount of inelastic scattering. At higher energies the elastic scattering will become negligible except for scattering in the forward direction. The work described in this paper has been done at energies well above the giant resonance but below meson production threshold. Eqn (1) is expected to hold at these energies.

† Now at the Clarendon Laboratory, Oxford.

‡ Now at the Department of Physics, University of Toronto, Canada.

§ 2. EXPERIMENTAL METHOD

2.1. *The Experimental Arrangement*

This experiment was conducted using the bremsstrahlung beam of the Glasgow University Synchrotron. Fig. 1 shows the experimental arrangement to observe photon scattering at 90° from the beam. The peak of the bremsstrahlung spectrum was set at 132 mev in order to exclude the background from γ -rays from π^0 photoproduction. The total scattered γ -ray spectrum was measured and both elastic and inelastic events were accepted. However, in the energy range of interest, from 50 to 130 mev, it is almost certain that the contribution of the inelastic scattering is small.

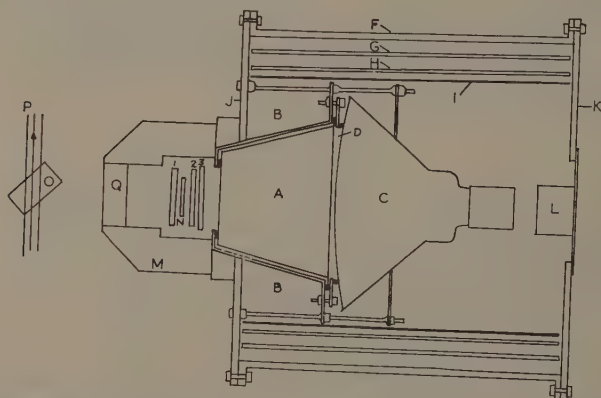


Fig. 1. A horizontal section through the equipment when arranged to measure scattering at 90° . A, lead glass truncated cone; B, magnesium oxide powder; C, DuMont K1258 photomultiplier; D, Perspex light guide; F-H, mild steel screening; I, mu-metal screening; J-K, steel end plates; L, White cathode follower; M, lead shielding; N, lead converter; O, target; P, bremsstrahlung beam; 1, 2 and 3, scintillation counters.

The electrons circulating in the synchrotron were allowed to spiral into a tungsten radiator during a period of approximately $500 \mu\text{sec}$ at peak magnetic field, giving a variation of less than 1% in the bremsstrahlung peak energy during the beam pulse. The beam was collimated and 'scrubbed' by a magnetic field so as to have a diameter of 5 cm at the target. The target, formed of 6 g cm^{-2} of graphite, was set to intercept the entire beam.

2.2. *The Detector and Electronics*

The photon detector must be highly efficient and must also measure the energy of the scattered photon. These requirements were satisfied by a γ -ray telescope followed by a total absorption Čerenkov counter (see Fig. 1). The Čerenkov counter consists of a truncated cone of lead glass (A), 22.5 cm high, 19 cm diameter expanding to 30 cm. This cone was mounted in MgO powder (B) to enhance the light collection, and viewed at its 30 cm diameter face by a 40 cm diameter photomultiplier (C) (DuMont K 1258). The counter was magnetically shielded by a cylinder of mu-metal (I) and three layers (F, G, H) of mild

In order to register a true count, a photon scattered from the target (O) had to pass through the graphite filter, through counter 1 and convert in the lead plate (N). The resulting electron pair then had to pass through counters 2 and 3 and generate a shower in the Čerenkov counter. A block diagram of the associated electronics is shown in Fig. 2. A 6BN6 coincidence unit with a

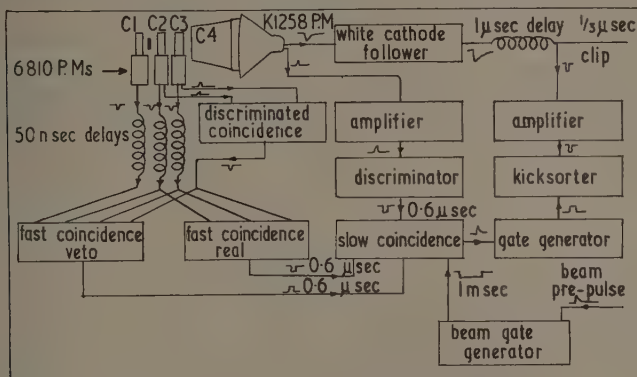


Fig. 2. Block diagram of electronics.

The pulse from the last dynode of the spectrometer photomultiplier was amplified and discriminated. The discriminator level corresponds to a γ -ray depositing 20 mev in the spectrometer. The slow coincidence unit detected coincidences between (*a*) the discriminated output from the spectrometer, (*b*) a gate pulse which surrounded the beam pulse, and (*c*) the real coincidence circuit output, in the absence of an output from the veto coincidence circuit. Thus the slow coincidence unit detected the required [$\bar{1}$, 2, 3 + spectrometer] coincidences occurring during the beam pulse. (This method of specifying a real event was determined by the very high counting rate in counter 1 and reduced the loss of real events due to random anticoincidence to a reasonable level.) The clipped and amplified photomultiplier anode pulse from the spectrometer was examined by a kicksorter gated by the slow coincidence unit. Some early runs employed a camera-oscilloscope combination for pulse height analysis. This arrangement

gave information on 'pile-up' and random background pulses and showed that the experiment could be performed with the present system.

The stability of the spectrometer electronics was checked by injecting standard pulses of various heights into the anode of the spectrometer multiplier. The gain did not change by more than 2% during the 12-hour runs.

2.3. The Calibration of the Spectrometer

The pulse height response of the Čerenkov counter was determined by utilizing a beam of mono-energetic electrons. Electron-positron pairs were produced in a 60 mg cm^{-2} Cu foil placed in the bremsstrahlung beam. The electrons were magnetically analysed and an electron beam with a narrow momentum range was selected by a counter telescope and presented to the Čerenkov counter. That part of the electron orbit which lay within the magnet was enclosed in hydrogen atmosphere in order to minimize the effects of multiple scattering on the momentum definition. This arrangement restricted the momentum spread of the selected electrons to approximately 1%. Pulse height distributions were recorded for electron energies of 50, 100, 150 and 200 mev. Figs 3 and 4 show

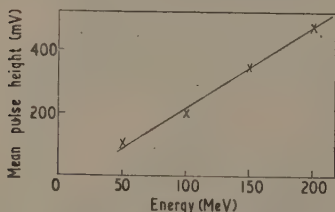


Fig. 3. Čerenkov counter mean output pulse height against incident electron energy.

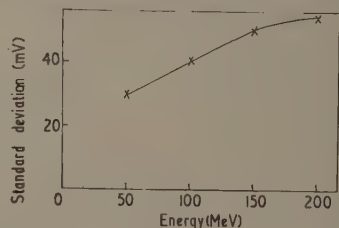


Fig. 4. Standard deviation of Čerenkov output pulse height distribution against incident electron energy.

respectively the mean pulse height and the standard deviation of the distribution, as a function of incident energy. The results correspond to a full width at half height resolution of about 33% at 100 mev and 27% at 200 mev.

2.4. The Efficiency of the System

The efficiency of the system for detection of photons was calculated and the result confirmed by measurement. The calculation involved an analysis of the converter efficiency in conjunction with the counters of the telescope and yielded the curve shown in Fig. 5 showing the detection efficiency against photon energy for a 3.3 gm cm^{-2} converter.

The measurement depends on the fact that the Čerenkov spectrometer alone is very nearly 100% efficient as a detector of photons. The complete system was placed in the bremsstrahlung beam, which was reduced by a factor of 10^7 from its normal intensity, and the number of incident photons recorded by counting the output pulses from the discriminator. At the same time the number of photons giving rise to electron pairs in the converter was measured by counting the gate pulses from the slow coincidence unit. The ratio of these two counts gives the efficiency of the system averaged over the bremsstrahlung beam. The discriminator was set to detect pulse heights corresponding to photons of energy greater than

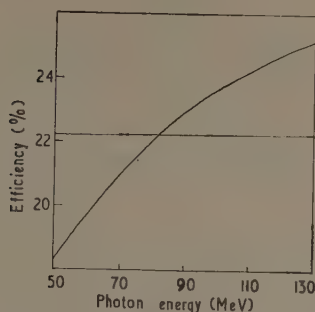


Fig. 5. Calculated photon detection efficiency versus photon energy for 3.3 g cm^{-2} lead converter.

50 MeV giving an energy range of 50–130 MeV. The measured efficiency was 22.2% and as the calculated efficiency, averaged over the same energy interval, was 22%, this result confirms the analysis of the data by the use of the calculated efficiency curve.

2.5. Experimental Procedure

The first part of the experiment was to measure the relative scattering cross sections at angles of 90° , 112° and 135° with a converter of 6.6 gm cm^{-2} . A measurement at a given angle consisted of recording the scattered photon spectrum for a certain value of the integrated beam intensity, followed by a similar run, for the same value of integrated beam with the converter removed. The spectrum due to scattered photons which convert in the lead plate could then be determined. The beam intensity was measured and integrated by the use of Wilson quantameter (Wilson 1957).

The second part of the experiment was the measurement of the absolute cross section at 90° . A number of runs were made with a 3.3 gm cm^{-2} converter in order to reduce the effects of multiple scattering of the electron pairs in the converter. The random anticoincidence rate was found by measuring the ratio of [1, 2, 3] coincidences to real [2, 3] coincidences when the signal from counter 1 was delayed by $5 \times 10^{-8} \text{ sec}$. This measurement was made several times at each angle and the necessary corrections were found to be always less than 10%.

2.6. Analysis of Data

In order to check the operation of the apparatus a comparison was made between the pulse height spectrum generated by the scattered photons with that generated by the incident bremsstrahlung beam when the complete detection system lay in the beam. The expected pulse height spectrum generated by 1000 equivalent quanta of 132 MeV bremsstrahlen was calculated using the calculated detection efficiency and the known resolution and response of the spectrometer. This comparison is shown in Fig. 6 where the predicted spectrum (solid curve) is superimposed upon the observed spectrum (histogram), the two spectra being normalized to the same total number of pulses above 100 millivolts. Next the pulse height spectrum generated by scattered photons at a certain angle for a known number of incident equivalent quanta is compared with the spectrum

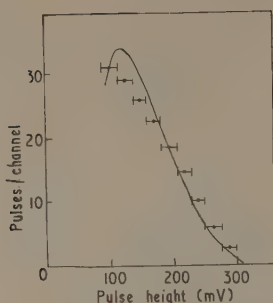


Fig. 6. The predicted (solid line) and observed (points) response of the detection system to 1000 equivalent quanta of 132 mev peak bremsstrahlen.

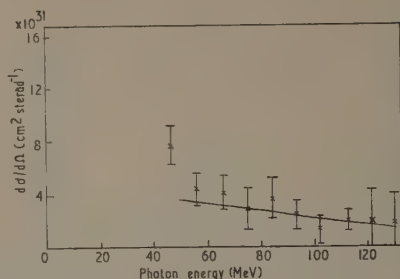


Fig. 7. The observed differential cross section at 90° against photon energy. For details of the solid line, see the text.

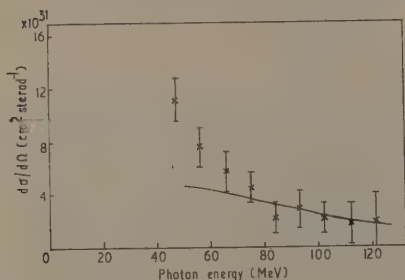


Fig. 8. The observed differential cross sections at 112° against photon energy. For details of the solid line, see the text.

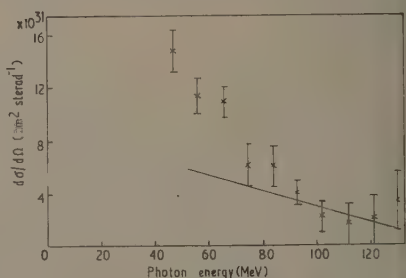


Fig. 9. The observed differential cross section at 135° against photon energy. For details of the solid line, see the text.

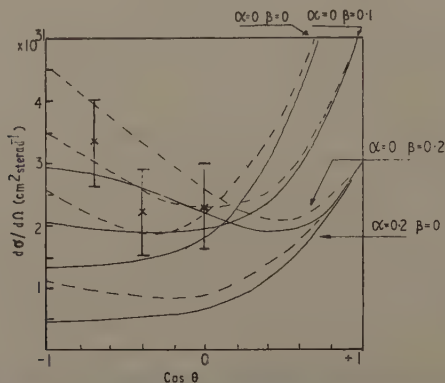


Fig. 10. The differential cross section for the scattering in the range 80-120 mev against $\cos \theta$. For details of the solid lines, see the text.

generated by 1000 equivalent quanta of the incident bremsstrahlen. These two spectra were divided into appropriate energy intervals and the ratio of the number of pulses in corresponding intervals could be multiplied by a known factor, containing the solid angle and target thickness, to give a differential cross section. These results are shown in Figs 7-10. An error of $\pm 10\%$ must be assigned to the vertical scales due to errors arising from the calculation of counter efficiency and the normalization of the observed bremsstrahlung pulse spectrum to the calculated spectrum.

§ 3. DISCUSSION OF THE RESULTS

The following discussion attempts to analyse the results in terms of a classical model of the photon scattering. Each proton in the nucleus gives rise to three scattering amplitudes: the first is due to the pure Thomson scattering, the second due to an induced magnetic dipole, and the third due to an induced electric dipole. Each neutron contributes only to the last two amplitudes and it is assumed that charge independence will cause the proton and neutron polarizability to be equal. The nucleons are assumed to be free but spread out uniformly throughout a sphere of radius $R = 1.2A^{1/3} \times 10^{-13}$ cm, where $A = 12$.

This model cannot be expected to hold below about 70 mev because the giant resonance effects, which are due to nuclear structure, will be reflected by an increase in the scattering at the corresponding energies (Penfold and Garwin 1959). At very low energies it is known that the nuclear scattering is pure Thomson scattering from the entire nucleus (Alvarez, Crawford and Stevenson 1958).

Using the methods developed for the atomic scattering of x-rays (Compton and Allison 1935) it is found that this model leads to the following expression for the differential scattering cross section:

$$\frac{2}{r^2} \frac{d\sigma}{d\Omega} = f^2 \{[(Z - A\alpha)^2 + A^2\beta^2](1 + \cos^2 \theta) - 4A\beta(Z - A\alpha) \cos \theta\} \\ + (1 - f^2) [Z\{(1 - \alpha)^2 + \beta^2\}(1 + \cos^2 \theta) - 4Z(1 - \alpha)\beta \cos \theta \\ + N\{\alpha^2 + \beta^2\}(1 + \cos^2 \theta) + 4N\alpha\beta \cos \theta]. \quad \dots\dots(2)$$

f , Z and N have the usual meaning, r is the classical electric radius of the proton, F is the nuclear form factor given by

$$f = \frac{3}{K^3 R^3} \{\sin KR - KR \cos KR\}, \quad \dots\dots(3)$$

K being the momentum transfer in units of reciprocal length,

$$K = \frac{2 \sin \theta/2}{\lambda}. \quad \dots\dots(4)$$

The symbols α and β stand for the amplitudes (relative to the Thomson amplitude) due to the electric and magnetic polarizability of a nucleon. If $\gamma = E/Mc^2$, E being the photon energy, then α/γ^2 and β/γ^2 are the nuclear polarizabilities in units of $(e^2/\hbar c)(\hbar/Mc)^3 = 6.8 \times 10^{-44}$ cm³ (Baldin 1960).

The differential cross section receives contributions from two parts: the first, proportional to f^2 , is the coherent scattering from the nucleus; the second, proportional to $1 - f^2$, is the contribution due to incoherent scattering, i.e. inelastic scattering. The Pauli exclusion principle and other effects due to nuclear binding reduce this inelastic scattering by an unknown factor and so we shall

consider two cases, the first in which it is present and the second in which it is absent.

The solid lines on Fig. 10 are plots of $d\sigma/d\Omega$ against $\cos\theta$ at 100 mev, for different values of α and β . Superimposed on the curves are the observed cross sections which are the average of the observations in the range 80–120 mev. The presence of α decreases the scattering at all angles as the electric dipole amplitude interferes destructively with the Thomson amplitude at all angles. On the other hand, β decreases the scattering in forward directions and enhances the scattering in the backward direction. It is evident that the data are not sufficiently accurate to determine α and β with any confidence. However, Figs 11 and 12 show the two sets of contours of equal total square deviation on an α - β

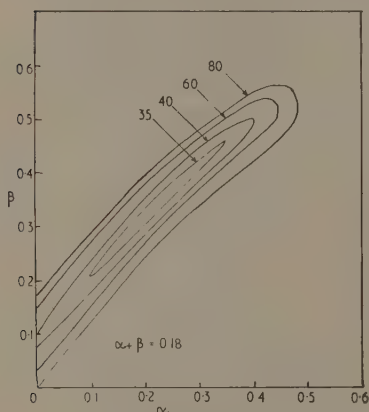


Fig. 11. Contours of equal total square deviations of cross section on α - β plane for coherent plus incoherent scattering. Units of square deviation are $1.38 \times 10^{-64} \text{ cm}^4$.

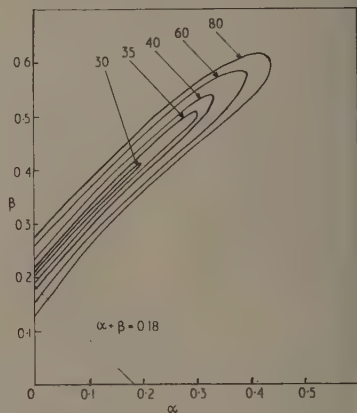


Fig. 12. Contours of equal total square deviations of cross section on α - β plane for coherent scattering alone. Units of square deviations are $1.38 \times 10^{-64} \text{ cm}^4$.

plane, the deviation being that between the observed and the predicted cross section. One set is for the coherent plus incoherent scattering (Fig. 11), the other for the coherent alone (Fig. 12). If $\alpha=0$, the curves suggest $\beta=0.2$ or 0.1 for the cases of coherent or coherent and incoherent scattering respectively. An increase in α requires a corresponding increase in β . The two values mentioned correspond to a polarizability of 1.2 or $0.6 \times 10^{-42} \text{ cm}^3$. The solid lines of Figs 8–10 show $d\sigma/d\Omega$ given by Eqn (1) for coherent scattering alone and $\beta=0.2$, $\alpha=0$. The agreement is as good as can be expected at higher energies. At the lower energies the experimental points lie above the line, presumably due to the effect of the tail of the giant resonance. The line for $\alpha=0$, $\beta=0.1$ and coherent plus incoherent scattering would be very close to that for the conditions stated above.

Dispersion relations can also be applied to photon scattering but, in general, only at a scattering angle of 0° . Fuller and Hayward (1956) give a dispersion relation which gives the total scattering cross section at low energies, assuming dipole scattering alone. At our energies it cannot be applied other than at 0°

and the relevant expression is

$$\frac{d\sigma}{d\Omega}(\theta=0^\circ) = [D(\omega)]^2 + [A(\omega)]^2 = \left[\frac{\omega^2}{2\pi^2} P \int_0^\infty \frac{\sigma_a(\omega')}{\omega'^2 - \omega^2} d\omega' + D(0) \right]^2 + \left[\frac{\omega \sigma_a(\omega)}{4\pi} \right]^2. \quad \dots\dots (5)$$

$D(0)$ is the nuclear scattering amplitude at 0° and zero energy: this is just the Thomson amplitude $= -Z^2 e^2 / AMc^2 = -(3\sigma_T / 8\pi)^{1/2}$. $D(\omega)$ and $A(\omega)$ are the real and imaginary parts of the 0° scattering amplitude, ω is the photon energy in units of reciprocal length and $\sigma_a(\omega)$ is the total cross section for all processes at the energy ω .

The data used to evaluate the dispersion integral were as follows. The total cross section for photons undergoing nuclear effects in carbon in the energy range 15 to 60 mev was obtained from the measurements of Wyckoff and Koch (1960). Above these energies the total cross section is assumed to be due to quasi-deuteron photodisintegration. The cross section for the absorption of a photon which leads to this process is $\sigma \simeq \sigma_D(3NZ/A)$ (Stein *et al.* 1960), where σ_D is the total deuteron photodisintegration cross section. (An escape factor has been dropped from their quasi-deuteron formula as it is irrelevant to the absorption of the incident photon.) The data for the deuteron photodisintegration cross section σ_D were obtained from the work of Galey (1960). Meson photo-production also contributes to the total cross section and from the data given by Marshak (1952) was assumed to be constant at 0.8 mbn between 200 and 400 mev. The results are

$$A(\omega) \simeq 2.4 \times 10^{-16} \text{ cm},$$

$$D(\omega) \simeq -1.5 \times 10^{-15} \text{ cm},$$

at $\omega = 100 \text{ mev}$.

Hence

$$\frac{d\sigma}{d\Omega}(\theta=0^\circ) = 2.3 \times 10^{-30} \text{ cm}^2 \text{ sterad}^{-1}.$$

The uncertainties in the evaluation of $D(\omega)$ and $A(\omega)$ are considerable due to the uncertainties in the total cross section. The real part of the dispersion calculated forward scattering amplitude $D(\omega)$, calculated from the dispersion formula, is expected to be larger (in magnitude) than the value calculated from our model. This latter amplitude is real and for $\alpha=0$, $\beta=0.2$ has the value $-4.7 \times 10^{-16} \text{ cm}$. It is -7.2×10^{-16} for $\alpha=0$, $\beta=0.1$, and -1.3×10^{-15} for $\alpha=\beta=0$. Any increase in α increases (in a positive sense) the amplitude from these values. The difference between $D(\omega)$ and the amplitude of our model is least when $\alpha \simeq \beta \simeq 0$ and thus the dispersion theory suggests that there is no magnetic scattering. This could be because the meson photo-production contribution to the dispersion integral has been underestimated whereas the giant resonance contribution has been overestimated. It is the former which should be the source of expected magnetic contribution because the magnetic polarizability is mesonic in origin. However, the forward scattering amplitude, calculated from dispersion theory, is greater in magnitude than that calculated from our model and that is all that was required.

Dispersion relations can also be applied to give an estimate of the upper limit of nucleon electric plus magnetic polarizability (Goldansky *et al.* 1960).

This value is $11 \times 10^{-43} \text{ cm}^3$ and corresponds to the straight line drawn on Figs 11 and 12, $\alpha + \beta = 0.18$.

The conclusions are that the observed scattering is consistent with Thomson scattering from nucleons possessing a degree of magnetic polarizability in nuclear matter spread over a radius of $1.2 A^{1/3} \times 10^{-13} \text{ cm}$. This result is not in agreement with the measurements of Goldansky *et al.* (1960) who find for the free proton 70 mev that the magnetic polarizability is $2 \pm 2 \times 10^{-43} \text{ cm}^3$ and the electric polarizability is $9 \pm 3 \times 10^{-43} \text{ cm}^3$. However, it is not obvious that the free proton polarizabilities will be observed in nuclei. Our results are in general agreement with the results of Pugh *et al.* (1957).

ACKNOWLEDGMENTS

The authors are indebted to Professor P. I. Dee for his interest and encouragement, and to Dr. W. McFarlane and the synchrotron crew for providing the photon beam.

REFERENCES

- ALVAREZ, L. W., CRAWFORD, F. S., and STEVENSON, M. L., 1958, *Phys. Rev.*, **112**, 1267.
 BALDIN, A. M., 1960, *Nucl. Phys.*, **18**, 310.
 COMPTON, A. H., and ALLISON, S. K., 1935, *X-rays in Theory and Experiment*, 2nd edn (New York: Van Nostrand).
 FULLER, E. G., and HAYWARD, E., 1956, *Phys. Rev.*, **101**, 692.
 GALEY, J. A., 1960, *Phys. Rev.*, **117**, 763.
 GOLDANSKY, V. I., KARPUKHIN, O. A., KUTSENKO, A. V., and PAVLOVSKAYA, V. V., 1960, *Nucl. Phys.*, **18**, 473.
 HOFSTADTER, R., 1956, *Rev. Mod. Phys.*, **28**, 214.
 MARSHAK, R. E., 1952, *Meson Physics* (London, New York: McGraw-Hill).
 PENFOLD, A. S., and GARWIN, E. L., 1959, *Phys. Rev.*, **114**, 1324.
 PUGH, G. E., GOMEZ, R., FRISCH, D. H., and JANES, G. S., 1957, *Phys. Rev.*, **105**, 982.
 STEIN, P. C., ODIAN, A. C., WATTENBURG, A., and WEINSTEIN, R., 1960, *Phys. Rev.*, **119**, 348.
 WILSON, R. R., 1957, *Nucl. Instrum.*, **1**, 101.
 WYCKOFF, J. M., and KOCH, H. W., 1960, *Phys. Rev.*, **117**, 1261.

Differential Energy Loss and Ranges of Ne, N and He Ions

By D. I. PORAT† AND K. RAMAVATARAM‡

The Physical Laboratories, The University, Manchester

MS. received 27th April 1961

Abstract. The rate of energy loss for ^{20}Ne and ^{14}N ions in the energy region of 0.4 to about 6 mev has been measured in C, Al, Ni, Ag and Au. The ranges of the ions in the above elements were calculated by integrating the differential energy loss taking into account scattering and energy losses due to nuclear collisions. The rate of energy loss for ^4He ions up to 2 mev kinetic energy is reported and range curves in Al, Ni, Ag and Au up to 3 mev are presented. Results on the energy loss of deuterons in Ag are used to extend the data at present available for protons to lower energies. The relative accuracy of the stopping power data is about 1% and the absolute accuracy to better than 5%.

§ 1. INTRODUCTION

SOME low-energy nuclear physics experiments require information on the state of a heavy, slow ion which had traversed a target material. The differential energy loss, the range or the charge state may be of interest. These were subject to detailed investigations (Livingston and Bethe 1937, Bohr 1948, Bohr and Lindhard 1954) and the results are generally applicable to ion velocities $v \gg v_0$, where $v_0 = e^2/\hbar$ is the classical velocity of an electron in a hydrogen atom. Bohr has also shown the complementarity of the classical and quantum mechanical treatments of the subject.

At low ion velocities, where $v \sim v_0$, the problem of energy loss for heavy ions is complicated by charge exchange phenomena and by nuclear collisions in screened fields. The continual capture and loss of electrons not only modifies the interaction because of a changing effective charge of the ion, but also constitutes in itself one mode of energy loss.

Data on energy losses of He, C, N and O ions were reported earlier (Porat and Ramavataram 1959, 1960). The present paper reports results obtained with He ions and additional data with N and He ions. Several values on the $(dE/dx, E)$ curve for deuterons in Ag were also measured.

§ 2. EXPERIMENTAL

A detailed description of the method of measurement as well as an error analysis was given in an earlier paper (Porat and Ramavataram 1959). In brief, ions are accelerated by a 6mv Van de Graaff generator and are selected in velocity to 1 part in 10^4 , with the help of a magnetic analyser. A 90° cylindrical electrostatic analyser is used to measure the kinetic energy E_1 of the ion beam. A thin

Now at Cambridge Electron Accelerator, Harvard University, Cambridge, Mass., U.S.A.
Now at Physics Department, Osmania University, Hyderabad, India.

foil Δx is then interposed in the path of the ions at the object point of the electrostatic analyser and the reduced ion energy E_2 is measured. In the limit

$$\frac{E_1 - E_2}{\Delta x} = dE/dx \quad \Delta x \rightarrow 0.$$

The foils were obtained by evaporation and their surface density was measured by absorption of alpha particles. The measuring techniques were described in detail elsewhere (Ramavataram and Porat 1959), while the calibration of the instrument for measuring surface densities of the foils also yielded air equivalents for Al, Ni, Ag and Au at 3.72 and 4.33 mev alpha-particle energy. The surface densities of the foils used in the present experiments were in the region of 20 to 500 $\mu\text{g cm}^{-2}$, depending on the ion, its energy and the stopping element in a particular measurement. Up to twelve different foils were used to establish a curve of $(dE/dx, E)$ for any one combination of ion and stopping element. The comparatively large amount of foils used, together with frequent calibrations of the electrostatic analyser using the $^{19}\text{F}(\text{p}, \alpha\gamma)^{16}\text{O}$ resonance reactions at 874.5 and 935.1 kev (Hunt and Firth 1955) ensured relative values of dE/dx and E with an accuracy to 1% and absolute values with an accuracy to 5% or better.

§ 3 RESULTS

The experimental points for Ne ions are plotted in Fig. 1 and are based on 148 independent measurements. The values in Table 1 were taken from free-hand curves of Fig. 1 representing a best fit to the experimental points. In the lower energy region one has to take into account energy losses from nuclear collisions

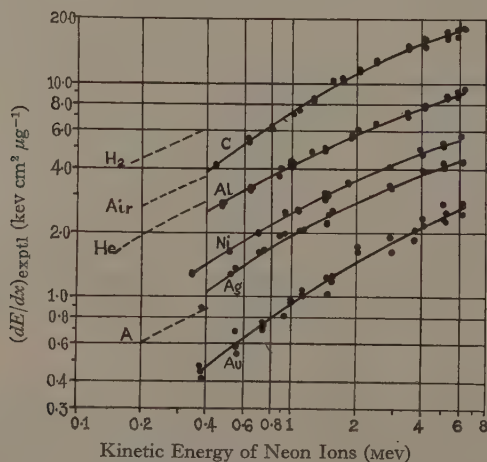


Fig. 1. Stopping power for neon ions. ——— present experiment ——— Weyl (1953).

$(dE/dx)_n$ in addition to the electronic stopping $(dE/dx)_e$. The measured energy losses include $(dE/dx)_e$ and only part of $(dE/dx)_n$, since instrument geometry

excludes detection of those particles which suffered large energy losses and large angular deflections as a result of close, nuclear collisions. An estimate of the contribution of such collisions to the total stopping power was made using the same arguments as in an earlier paper (Porat and Ramavataram 1959). The values under columns (a) in Table 1 refer to electronic stopping power and include a small correction based on the arguments above concerning nuclear large angle scattering. Columns (b) list the nuclear energy loss $(dE/dx)_n$ which was calculated on the basis of Bohr's (1948) theory of nuclear collisions in screened fields. As $(dE/dx)_n$ is only a small fraction of $(dE/dx)_e$, any correction to $(dE/dx)_{\text{exptl}}$ should introduce negligible errors in the final value of $(dE/dx)_e$, even though these corrections are based on an approximate theory. No previous measurements of the differential energy loss for neon ions in solids are available for comparison. The

Table 1. Stopping Power for Neon Ions

Velocity v/v_0	Carbon		Aluminium		Nickel		Silver		Gold	
	(a)	(b)	(a)	(b)	(a)	(b)	(a)	(b)	(a)	(b)
0.899	3.65	0.411	2.39	0.338	1.33	0.270	0.95	0.189	0.441	0.123
1.10	5.05	0.300	3.05	0.250	1.75	0.204	1.39	0.146	0.626	0.099
1.27	6.23	0.239	3.64	0.201	2.11	0.166	1.70	0.120	0.784	0.084
1.42	7.26	0.200	4.12	0.169	2.41	0.140	1.94	0.103	0.920	0.073
1.55	8.24	0.176	4.52	0.145	2.68	0.121	2.14	0.091	1.05	0.064
1.68	9.10	0.155	4.90	0.129	2.93	0.108	2.31	0.081	1.15	0.057
1.79	9.92	0.139	5.22	0.115	3.15	0.097	2.47	0.074	1.25	0.052
1.90	10.4	0.126	5.52	0.105	3.36	0.089	2.63	0.068	1.34	0.048
2.00	11.0	0.114	5.79	0.097	3.54	0.082	2.76	0.062	1.43	0.045
2.10	11.6	0.106	6.02	0.090	3.72	0.076	2.90	0.058	1.52	0.042
2.20	12.1	0.099	6.24	0.084	3.89	0.071	3.01	0.054	1.61	0.039
2.28	12.7	0.093	6.45	0.078	4.01	0.067	3.13	0.051	1.68	0.037
2.37	13.1	0.087	6.65	0.074	4.13	0.063	3.24	0.048	1.75	0.035
2.45	13.6	0.081	6.83	0.070	4.25	0.060	3.33	0.045	1.83	0.033
2.61	14.3	0.074	7.20	0.066	4.49	0.054	3.51	0.041	1.96	0.030
2.76	15.0	0.067	7.55	0.057	4.69	0.049	3.70	0.038	2.08	0.028
2.90	15.7	0.062	7.85	0.053	4.87	0.045	3.84	0.035	2.19	0.026
3.04	16.3	0.057	8.11	0.049	5.02	0.042	3.98	0.032	2.30	0.024
3.17	16.7	0.053	8.37	0.046	5.20	0.040	4.10	0.030	2.40	0.023
3.30	17.2	0.050	8.59	0.043	5.53	0.037	4.21	0.028	2.48	0.021
3.41	17.5	0.047	8.81	0.040	5.44	0.035	4.31	0.027	2.55	0.020
3.52	17.9	0.044	9.05	0.038	5.54	0.033	4.40	0.026	2.64	0.019

(a) Electronic stopping power $(dE/dx)_e$ in $\text{kev cm}^2 \mu\text{g}^{-1}$.

(b) Nuclear stopping power $(dE/dx)_n$ in $\text{kev cm}^2 \mu\text{g}^{-1}$.

broken lines in Fig. 1 refer to measurements by Weyl (1953), using gases as absorbers. On plotting dE/dx in units of ev cm^2 per atom one would expect a monotonic increase in dE/dx with the atomic number of the stopping element. This is true for solid absorbers as a group as well as for the gaseous stopping media. However, the curves for gaseous absorbers are as a group displaced towards the lower rates of energy loss suggesting that the time between collisions in a gas of low pressure is sufficient for atomic de-excitation of the moving ion to take place, which in turn causes a low effective charge and hence lower rates of energy loss in gases than in solids of comparable atomic number.

The ranges of neon ions in the five stopping elements were calculated by numerical integration of the differential energy loss and are shown in Fig. 2. Thus

$$\text{Range, } \bar{R} = \int_{E_{\text{final}}}^{E_{\text{initial}}} \{ (dE/dx)_e + (dE/dx)_n \}^{-1} dE. \quad \dots (1)$$

The trapezium rule was used for integration at intervals of 100 keV and an extrapolated value of $(dE/dx)_e$ was used in the lower energy region. No accuracy is therefore claimed for ranges below about 400 keV. Powers (1960) measured ranges of N, Ne, A and Kr ions of 500 keV kinetic energy and below in the following targets: Be, B, C and Al. It is of interest to compare his results with the semi-empirical ranges of the present work, where these data are in overlapping energy regions. The comparison is drawn in Table 2 and provides an indication of the accuracy of the results for Ne and N ions in the extrapolated (low energy) region.

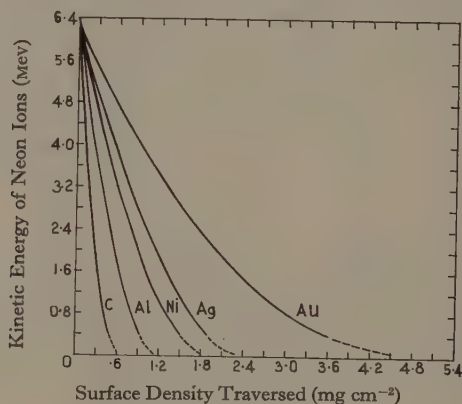


Fig. 2. Ranges of neon ions.

Table 2. Ranges of Ne and N Ions

(1)	(2)	(3)	(4)	(5)
Ne in C	200	75.6 ± 3.7	68.0 ± 7.0	80
Ne in C	500	143.6 ± 8.8		
N in C	200	70.2	28.5	32
N in C	300	98.7		
N in Al	200	117.6 ± 12.8	111.5 ± 15	111
N in Al	500	229.1 ± 16.2		

(1) Ion and target; (2) kinetic energy (keV); (3) range ($\mu\text{g cm}^{-2}$) (Powers); (4), (5) differential range ($\mu\text{g cm}^{-2}$) from 500 keV to 200 keV; (4) Powers, (5) present work.

The measurements on the stopping power for nitrogen ions, reported earlier (Porat and Ramavataram 1959), were extended to higher energies and an additional stopping element, namely carbon, has been included. The experimental points presented in Fig. 3 are based on 108 independent measurements. Table 3 lists the electronic and nuclear stopping powers under columns (a) and (b) respectively. Corrections due to large-angle scattering were applied as in the case of neon ions, above.

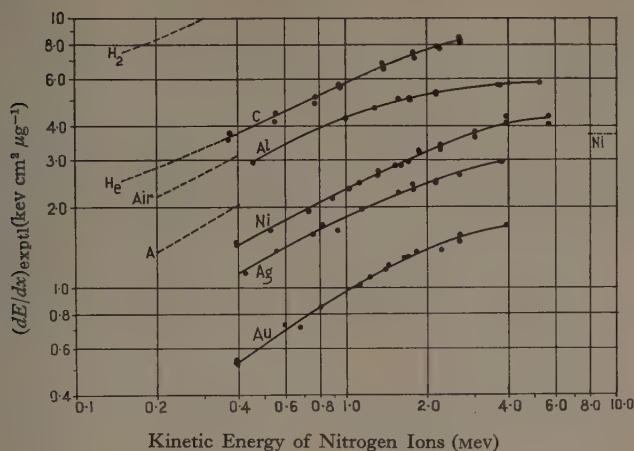


Fig. 3. Stopping power for nitrogen ions. ——— present work, - - - Weyl (1953), - · - · - Reynolds, Scott and Zucker (1954).

Table 3. Stopping Power for Nitrogen Ions

Velocity v/v_0	Carbon		Aluminium		Nickel		Silver		Gold	
	(a)	(b)	(a)	(b)	(a)	(b)	(a)	(b)	(a)	(b)
1.01	3.52	0.175	—	—	—	—	—	—	—	—
1.07	3.71	0.162	2.72	0.133	1.41	0.107	1.11	0.076	0.518	0.051
1.31	4.46	0.117	3.38	0.097	1.77	0.080	1.41	0.057	0.688	0.040
1.51	5.13	0.093	3.89	0.077	2.06	0.064	1.65	0.047	0.830	0.033
1.69	5.72	0.077	4.29	0.065	2.31	0.054	1.83	0.040	0.956	0.020
1.85	6.20	0.067	4.50	0.056	2.52	0.047	2.00	0.035	1.07	0.024
2.00	6.65	0.059	4.79	0.050	2.70	0.042	2.14	0.031	1.18	0.022
2.14	7.02	0.053	4.97	0.045	2.87	0.037	2.25	0.028	1.26	0.020
2.27	7.33	0.048	5.11	0.041	3.05	0.034	2.38	0.025	1.34	0.018
2.39	7.60	0.043	5.23	0.037	3.20	0.031	2.48	0.023	1.40	0.017
2.51	7.83	0.040	5.34	0.034	3.33	0.029	2.56	0.021	1.46	0.016
2.62	8.04	0.037	5.40	0.032	3.48	0.027	2.62	0.020	1.50	0.015
2.73	8.25	0.035	5.46	0.030	3.58	0.025	2.69	0.019	1.54	0.014
2.83	—	—	5.49	0.028	3.68	0.023	2.73	0.018	1.58	0.013
2.93	—	—	5.56	0.026	3.78	0.022	2.79	0.017	1.61	0.012
3.12	—	—	5.64	0.024	3.94	0.020	2.88	0.015	1.66	0.011
3.30	—	—	5.70	0.022	4.07	0.018	2.96	0.014	1.70	0.010
3.47	—	—	5.74	0.020	4.16	0.017	—	—	—	—
3.63	—	—	5.78	0.018	4.22	0.016	—	—	—	—
3.78	—	—	5.82	0.017	4.26	0.014	—	—	—	—
3.86	—	—	5.83	0.016	—	—	—	—	—	—
4.00	—	—	—	—	4.30	0.013	—	—	—	—

(a) Electronic stopping power $(dE/dx)_e$ in $\text{keV cm}^2 \mu\text{g}^{-1}$.

(b) Nuclear stopping power $(dE/dx)_n$ in $\text{keV cm}^2 \mu\text{g}^{-1}$.

Reynolds, Scott and Zucker (1954) measured the range of 8 to 29 mev nitrogen ions in nickel from which one can deduce $dE/dx = 3.7 \text{ kev cm}^2 \mu\text{g}^{-1}$, nearly constant over this energy range. Their results as well as Weyl's (1953) results for nitrogen ions in gases up to 400 kev are indicated in Fig. 3. The values deduced from the range measurements of Reynolds *et al.* appear to be some 12% lower than an extrapolation of the present curves would indicate. However, a differentiation of a range curve cannot yield great accuracy especially at the low-energy end. Also, the value of $dE/dx = 3.7 \text{ kev cm}^2 \mu\text{g}^{-1}$ is an average over an energy interval in which the $(dE/dx, E)$ curve reaches its maximum and from then on assumes a negative slope. The remarks concerning the differences of differential energy

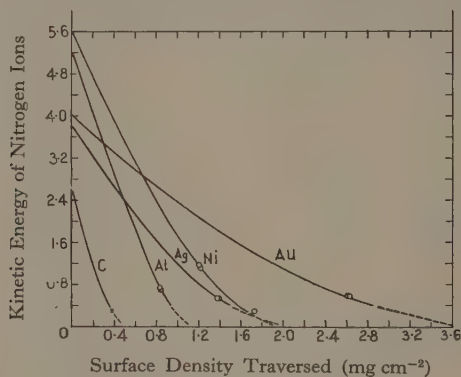


Fig. 4. Ranges of nitrogen ions.

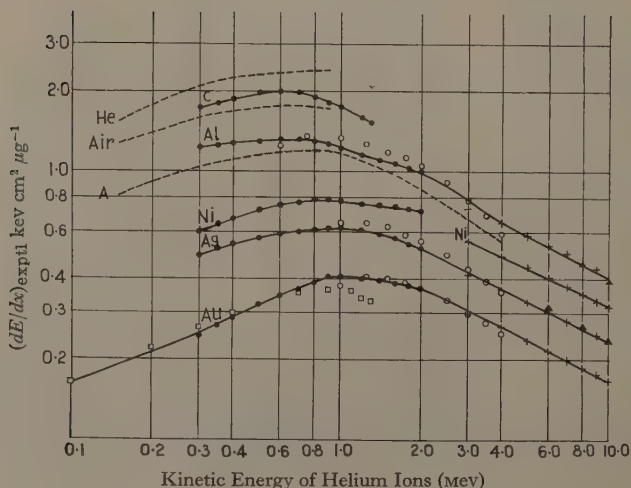


Fig. 5. Stopping power for helium ions. — present work; -- Weyl and Burgy (1957, private communication); o Whaling (1958) calculated from Gobeli's (1956) work; + Rosenblum (1928); ▲ Aron *et al.* (1949); □ Wilcox (1948).

loss in gases as compared with solids made in connection with neon ions are equally applicable here.

The ranges of nitrogen ions in the five absorbers are presented in Fig. 4. The curves are seen to start at different energy values according to the highest energy for which dE/dx has been obtained in a particular stopping element (see Fig. 3). The circles indicate experimental values of ranges obtained with 'thick' absorbers.

Former measurements of dE/dx for helium ions (Porat and Ramavatham 1959) have now been extended to 2 mev and are shown in Table 4 and in Fig. 5 together with the results obtained by others (Aron, Hoffman and Williams 1949, Gobeli 1956, Rosenblum 1928, Weyl and Burgy 1957 (private communication from S. K. Allison), Wilcox 1948). Whaling (1958) calculated dE/dx for helium ions from Gobeli's measurements of air equivalents for alpha particles in various foils. These values seem several per cent higher than the present dE/dx in Al and Ag absorbers.

Table 4. Stopping Power for Helium Ions

Energy (kev)	Velocity v/v_0	Stopping Power dE/dx (kev cm ² μ g ⁻¹)				
		Carbon	Aluminium	Nickel	Silver	Gold
300	1.73	1.73	1.23	0.60	0.49	0.243
350	1.87	1.80	1.25	0.64	0.52	0.266
400	2.01	1.87	1.28	0.67	0.54	0.285
500	2.24	1.98	1.30	0.72	0.57	0.320
600	2.46	2.00	1.32	0.75	0.59	0.345
700	2.66	1.99	1.32	0.77	0.60	0.366
800	2.84	1.90	1.30	0.79	0.61	0.386
900	3.01	1.81	1.27	0.79	0.62	0.406
1000	3.18	1.75	1.22	0.78	0.62	0.406
1200	3.48	1.60	1.16	0.76	0.61	0.400
1400	3.76	1.54†	1.11	0.75	0.59	0.395
1600	4.01		1.07	0.74	0.57	0.383
1800	4.26		1.04	0.725	0.54	0.377
2000	4.49		1.00	0.715	0.52	0.369

† at 1300 kev.

One could use Whaling's summary of stopping power for comparison with the present results since

$$\left(\frac{dE}{dx}\right)_{\text{He}} = \left(\frac{Z_{\text{He}}}{Z_{\text{H}}}\right)^2 \left(\frac{dE}{dx}\right)_{\text{H}} \quad \dots\dots (2)$$

at equal ion velocities. However, the helium ion in the energy region of 0.4 to 2 mev has an effective charge lower than 2 (Rutherford 1924, Dissanaik 1953) which results in a lower rate of energy loss than expected from Eqn (2). Conversely, one may calculate the effective charge of the helium ion as a function of velocity. The calculation is possible where dE/dx data for protons of the same velocities are available. As the cross sections for capture and loss of electrons are only weak functions of the atomic number of the stopping material one can use dE/dx data for He and protons in different materials to obtain an average value of Z_{eff} of the helium ion. The results are presented in Fig. 6 and should be useful in estimating the stopping power for slow helium ions in various media if the stopping powers for protons in these materials have been measured.

Ranges of helium ions have been obtained by integration of the differential energy loss and are shown in Fig. 7. It should be noted that here the abscissa now represents the range of a particle of given energy rather than the thickness of target traversed as in Figs 2 and 4. This representation was possible because the constant of integration is known from experimental range measurements of alpha particles. The curves of Fig. 7 are thus extensions into the low energy region of the information on alpha-particle ranges compiled by Whaling (1958). The cross-over of the range curves for Ag and Au at the low energy end is of interest and can also be observed in the case of heavy ions if one plots the atomic stopping power (dE/dx in units of $\text{ev cm}^2/\text{atom}$) against energy. At low velocities of C, N, O and

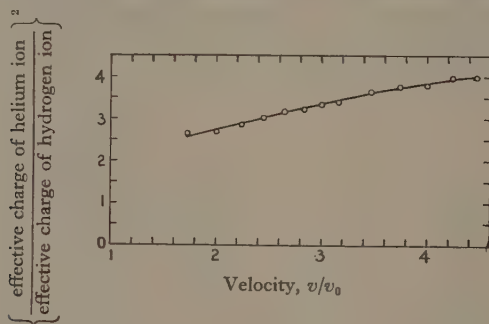


Fig. 6

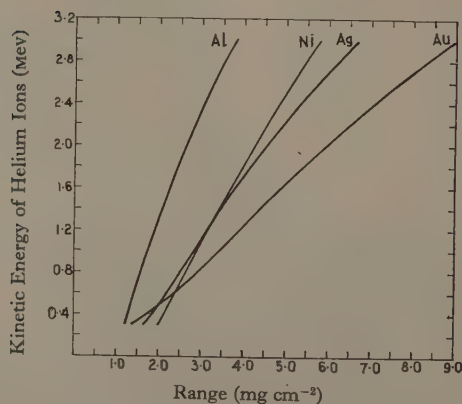


Fig. 7. Ranges of helium ions.

Ne ions one finds the atomic stopping power in gold to be lower than in silver. At higher ion velocities dE/dx increases monotonically with the atomic number of the stopping element, a fact which is also observed in protons and which is in accordance with theory, where applicable. The 'anomaly' of lower atomic stopping power in Au as compared with Ag is interpreted as being due to the lower effective charge of the ion in the heavier stopping element. This lower effective charge of the ion in materials of high Z is expected from Bohr's (1948) theory and

was substantiated in the case of light and heavy fission fragments (Lassen 1955) as well as with protons (Phillips 1955).

The differential energy loss for deuterons in silver in the energy range of 400 to 1000 kev has been measured. The data are useful to extend the curves at present available for dE/dx of protons in Ag to lower energies. The assumption is made that isotopes of equal velocities suffer the same energy loss in a given stopping medium. Table 5 summarizes the results which are presented in terms

Table 5. Stopping Power for Deuterons in Silver

Energy (kev)	400	500	600	700	800	900	1000
dE/dx (kev cm ² μ g ⁻¹)	0.185	0.172	0.162	0.154	0.146	0.138	0.130

of deuteron energy losses. Green *et al.* (1955) measured dE/dx for protons in silver in the energy interval of 0.4 to 1.0 mev by means of the apparent shift in energy of lithium and fluorine (p , γ) resonances. Thus a comparison of their results with the present work is possible in the energy interval of 0.4 to 0.5 mev. Such a comparison shows dE/dx for protons in silver as obtained by Green *et al.* to be about 4% lower than in the present work. This discrepancy is well within the experimental errors of both measurements.

REFERENCES

- ARON, W. A., HOFFMAN, B. G., and WILLIAMS, F. C., 1949, UCRL-121 (University of California Radiation Laboratories).
 BOHR, N., 1948, *Math.-fys. Medd.*, **18**, No. 8.
 BOHR, N., and LINDHARD, J., 1954, *Math.-fys. Medd.*, **28**, No. 7.
 DISSANAIKE, G. A., 1953, *Phil. Mag.*, **44**, 1051.
 GOBELI, G. W., 1956, *Phys. Rev.*, **103**, 275.
 GREEN, D. W., COOPER, J. N., and HARRIS, J. C., 1955, *Phys. Rev.*, **98**, 466.
 HUNT, S. E., and FIRTH, K., 1955, *Phys. Rev.*, **99**, 786.
 LASSEN, N. O., 1955, *Math.-fys. Medd.*, **30**, No. 8.
 LIVINGSTON, M. S., and BETHE, H. A., 1937, *Rev. Mod. Phys.*, **9**, 245.
 PHILLIPS, J. A., 1955, *Phys. Rev.*, **97**, 404.
 PORAT, D. I., and RAMAVATARAM, K., 1959, *Proc. Roy. Soc. A*, **252**, 394.
 ———, 1960, *Proc. Phys. Soc.*, **77**, 97.
 POWERS, D., 1960, *Report of the Third Symposium on Nuclear and Radiochemistry, Chalk River*.
 RAMAVATARAM, K., and PORAT, D. I., 1959, *Nucl. Instrum.*, **4**, 239.
 REYNOLDS, H. L., SCOTT, D. W., and ZUCKER, A., 1954, *Phys. Rev.*, **95**, 671.
 RUTHERFORD, E., 1924, *Phil. Mag.*, [6], **47**, 277.
 ROSENBLUM, S., 1928, *Ann. Phys., Paris*, **10**, 408.
 WHALING, W., 1958, *Handb. d. Phys.*, **34**, Ed. E. Flügge (Berlin: Springer).
 WEYL, P. K., 1953, *Phys. Rev.*, **91**, 289.
 WILCOX, H. A., 1948, *Phys. Rev.*, **74**, 1743.

The Depolarization of Negative Muons in Light Elements

By A. ASTBURY†, P. M. HATTERSLEY, M. HUSSAIN‡, M. A. R. KEMP§,
H. MUIRHEAD AND T. WOODHEAD

Nuclear Physics Research Laboratory, University of Liverpool

MS. received 8th May 1961

Abstract. A measurement of the polarization retained by negative muons in light elements is described. For elements with spin 0 the muon is found to retain about 17% of its initial polarization.

§ 1. INTRODUCTION

MEASUREMENTS of the angular distribution of the decay electrons, appearing when polarized muons are brought to rest in matter, have shown that the asymmetry coefficient α is much smaller for negatively charged muons than for their positive counterparts (see for example Garwin, Lederman and Weinrich 1957).

The distribution of the decay electrons is of the form $1 + \alpha \cos \theta$ where θ represents the angle between the direction of the muon entering the target assembly and that of the outgoing decay electron. The difference in the magnitude of α for the two types of charge may be attributed to the difference in the degree of polarization of the muons when brought to rest. The term α may be written as

$$\alpha^+ = P^+ a^+ \quad \alpha^- = P^- a^- \quad \dots\dots (1)$$

where P^+ and P^- represent the polarization of the positive and negative muons respectively. If the neutrino appearing in μ -decay is massless, then current theories predict that

$$a^- = a^+ = -0.33.$$

The measurement of the term α is of interest for two reasons. Firstly, there is the intrinsic interest of a contribution to the understanding of the mechanism of the capture of muons by atoms; secondly, an evaluation of the polarization factor P^- is necessary for certain experiments involving the nuclear capture of muons (Astbury *et al.* 1959) and for experiments which attempt to measure the helicity of muons by detecting the circular polarization of the μ -mesic x-rays.

In the present paper an account is given of the measurement of the parameter α of a number of elements between carbon and sulphur in the periodic table.

§ 2. EXPERIMENTAL METHOD

The apparatus used in the experiment is shown in Fig. 1. Muons in the negative meson beam of the University of Liverpool synchrocyclotron were slowed by a polythene absorber, and brought to rest in the target material. The polythene absorber also filtered out negative pions from the muons in the beam. The

† Now at Lawrence Radiation Laboratory, Berkeley, California, U.S.A.

‡ Now at the Physics Department, University of Dacca, Pakistan.

§ Now at the Rutherford Laboratory, National Institute for Research in Nuclear Science, Harwell, Berks.

electron contamination in the beam was removed by the use of a lead radiator, in the manner indicated in a previous communication from this laboratory (Astbury *et al.* 1958).

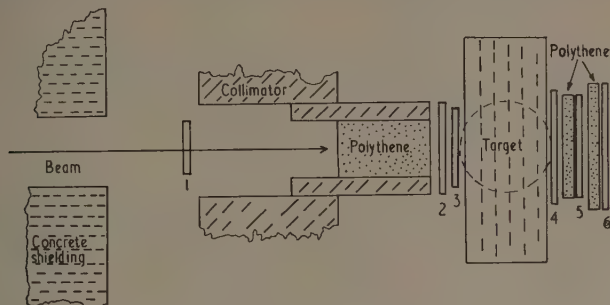


Fig. 1. Arrangement of target and counters.

The principle used in the determination of the asymmetry parameter has already been described by Cassels *et al.* (1957). If polarized muons are brought to rest in matter, and if a magnetic field H is applied at right angles to the plane defined by the muon and electron telescopes, then the number of decay electrons observed at an angle θ is given by the expression

$$\begin{aligned} N(t) &= e^{-\lambda t} (1 + \alpha \cos \theta) \\ &= e^{-\lambda t} \{1 + \alpha \cos (\omega t + \delta)\} \end{aligned} \quad \dots\dots (2)$$

where

$$\omega = g \frac{e}{2mc} H$$

and t represents the time between the arrival of the muon in the target and the appearance of the decay electron. The other symbols have the usual significance. In the present experiment $\delta = 0$, and a magnetic field of 200 gauss was used.

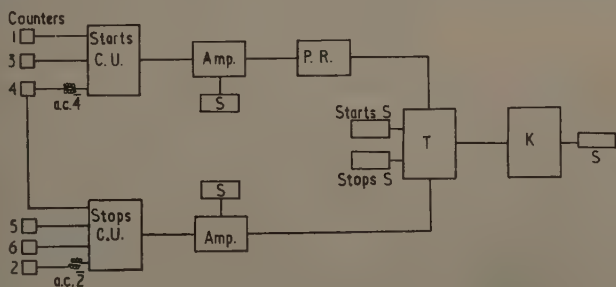


Fig. 2. Block diagram of electronics: C.U., coincidence unit; Amp., amplifier; S, scaler; P.R., pulse rater; T, timesorter; K, kicksorter.

The arrival of the muons in the target was indicated by a coincidence between counters 1 and 3 and an anti-coincidence from counter 4 (134 in the normal notation). Decay electrons were detected by the sequence 2456. Two slabs of polythene of total thickness 1 inch were inserted between counters 4, 5 and 6.

The polythene was present to eliminate Compton electrons arising from γ -rays; the latter can appear during the muon capture process.

The time interval between the arrival of the muon and the appearance of the decay electron was measured by a time to pulse height converter ('timesorter' of Fig. 2), and the information recorded on a kicksorter. A blocking circuit ('pulse rationer' of Fig. 2) was included in the electronic equipment. Its presence ensured that an interval of at least 40 microseconds occurred between successive analyses by the timesorter, thus allowing the instrument adequate time in which to recover.

§ 3. RESULTS

As a check on the apparatus a run was first made with positive muons. These were brought to rest in graphite. The data was analysed by the method of least squares and solutions were obtained for λ and α^+ . The value of α^+ was observed to decrease slowly as a function of time. An effect of this type was expected since the magnetic field in the region of the target was not completely uniform, and hence the precession frequency $\omega/2\pi$ (Eqn (2)) is not quite the same in all parts of the target. This effect vanishes at zero time, i.e. when the time interval between the muon and electron pulses is zero.

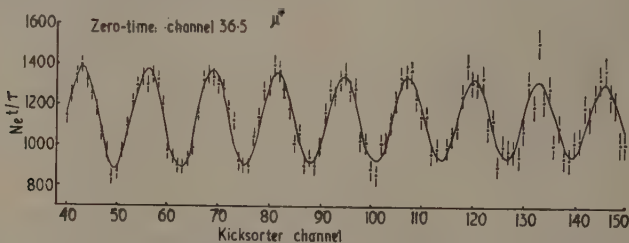


Fig. 3. Asymmetry in electrons from μ^+ on a carbon target.

The results for positive muons are shown in Fig. 3; the data have been plotted in the form

$$N(t)e^{\lambda t} = 1 + \alpha^+ \cos \omega t$$

and includes an empirical correction for the decrease in the magnitude of α^+ with increasing time. After allowance was made for this effect the value obtained for α^+ was 0.23 ± 0.01 ; this result compares favourably with a previous determination reported by this laboratory (Cassels *et al.* 1957).

A negative muon beam of identical momentum was then substituted for the positive muon beam, and a series of runs on carbon, magnesium, silicon, sulphur and lead fluoride was made. Although the last material is a compound, the disappearance rate of muons stopping in lead is so much greater than that in fluorine, that the decay spectrum of electrons from each element could easily be separated.

The results are shown in Table 1. The data include corrections for the solid angle subtended by the counters, and for the variation of α with electron energy (the apparatus would not detect electrons of low energy owing to the thickness of the absorbers). Both corrections are small and tend to cancel. No attempt was made to observe an asymmetry coefficient in lead.

Table 1

Element	$-\alpha^-$
Carbon	0.069 ± 0.011 (a)
	0.040 ± 0.005 (b)
	0.054 ± 0.006 (c)
Fluorine	0.011 ± 0.010 (a)
Magnesium	0.053 ± 0.009 (a)
	0.058 ± 0.008 (b)
Silicon	0.046 ± 0.009 (a)
Sulphur	0.040 ± 0.006 (a)
	0.042 ± 0.006 (b)

(a) This experiment, (b) Ignatenko *et al.* (1959), (c) Prepost *et al.* (1960).

§ 4. DISCUSSION

The results given in Table 1 show a satisfactory agreement with the data of the Dubna group.

The measured asymmetry coefficients may be used to determine the amount of depolarization of negative muons in different elements. This depolarization occurs during the process of de-excitation from a high mesic orbit to a K shell (the period for this transition is negligible compared with the muon lifetime, hence virtually all the muons reach the atomic K shell). The observed asymmetry coefficient may be written as

$$\alpha^- = P^- a^- = P_1^- P_2^- a^-$$

where P_1^- is the polarization of the negative muons arriving at the target and P_2^- is the polarization retained by the muons in the target, i.e. $1 - P_2^-$ represents the depolarization produced in the target. Similarly, we may write

$$\alpha^+ = P_1^+ P_2^+ a^+$$

for positive muons.

Since the conditions for production of positive and negative muons are identical, it would seem reasonable to write $P_1^+ = P_1^-$ so that

$$\frac{\alpha^+}{\alpha^-} = \frac{P_1^+ P_2^+ a^+}{P_1^- P_2^- a^-} = \frac{P_2^+}{P_2^-}$$

or

$$P_2^- = \frac{\alpha^-}{\alpha^+} P_2^+, \quad \dots\dots (3)$$

In the conditions of our present experiment α^+ and P_2^+ refer to a graphite target. The polarization retained by the negative muons can then be determined if the polarization retained by the positive muons in the graphite target is known. Lynch, Orear and Rosendorff (1960) quote a value of 0.79 ± 0.07 for this quantity. The present experiment then leads to the values given in Table 2 for the polarization retained by the negative muon for various elements.

Calculations of the magnitude of P_2^- have been made by Shmushkevich (1959), Dzhrbashyan (1959) and Mann and Rose (1961). Briefly the following physical processes can occur. Firstly, the muons are captured into states with high values for the quantum numbers n and l . In the initial capture, the calculations indicate that the muon retains about $\frac{1}{3}$ of its polarization. The mu-mesic atom then

Table 2

Element	P_2^-	
Carbon	$24 \pm 4\%$	$14 \pm 4\%$ (a)
Magnesium	$18 \pm 4\%$	$20 \pm 5\%$ (a)
Silicon	$16 \pm 4\%$	
Sulphur	$14 \pm 3\%$	$15 \pm 4\%$ (a)
Fluorine	$4 \pm 4\%$	

(a) Ignatenko *et al.* (1959).

reaches states with $n \sim 3$ or 4 by a series of Auger transitions. Radiative transitions then follow the Auger transitions, and on the average the muon loses 50% of its residual polarization, by the radiative process, before reaching the K shell. Thus the residual polarization is approximately $\frac{1}{3} \times \frac{1}{2} \sim 17\%$ of its initial value.

It can be seen that the figure of 17% is in good accord with the data of Table 2, with the exception of fluorine. A result of this nature was expected for fluorine, however, since it possesses a nuclear spin of $\frac{1}{2}$, whereas all the other elements in Table 2 have spin 0.

If a nucleus possesses non-zero spin then a spin-spin interaction can take place whilst the muon is in the K shell leading to further depolarization. A number of workers (Uberall 1959, Lubkin 1960) have shown that in a nucleus of spin I the polarization is reduced by a factor $\frac{1}{3} [1 + 2/(2I + 1)^2]$; for a nucleus of spin $\frac{1}{2}$ the polarization retained by the muon would be expected, therefore, to be of the order of 8%. The result for fluorine is compatible with this figure.

ACKNOWLEDGMENTS

We should like to thank B. Halliday and the cyclotron crew for their cooperation during the course of this experiment.

REFERENCES

- ASTBURY, A., BLAIR, I. M., HUSSAIN, M., KEMP, M. A. R., MUIRHEAD, H., and VOSS, R. G. P., 1959, *Phys. Rev. Letters*, **3**, 476.
 ASTBURY, A., KEMP, M. A. R., LIPMAN, N. H., MUIRHEAD, H., VOSS, R. G. P., ZANGGER, C., and KIRK, A., 1958, *Proc. Phys. Soc.*, **72**, 494.
 CASSELS, J. M., O'KEEFFE, T. W., RIGBY, M., WETHERELL, A. M., and WORMALD, J. R., 1957, *Proc. Phys. Soc.*, **70**, 543.
 DZHRBASHYAN, V. A., 1959, *Soviet Physics-JETP*, **9**, 188.
 GARWIN, R. L., LEDERMAN, L. M., and WEINRICH, M., 1957, *Phys. Rev.*, **105**, 1415.
 IGNATENKO, A. E., EGOROV, L. B., KHALUPA, B., and CHULTEM, D., 1959, *Soviet Physics-JETP*, **8**, 792.
 LUBKIN, E., 1960, *Phys. Rev.*, **119**, 815.
 LYNCH, G. R., OREAR, J., and ROSENDORFF, S., 1960, *Phys. Rev.*, **118**, 284.
 MANN, R. A., and ROSE, M. E., 1961, *Phys. Rev.*, **121**, 293.
 PREPOST, R., HUGHES, V. W., PENMAN, S., MCCOLM, D., and ZIOCK, K., 1960, *Bull. Amer. Phys. Soc.*, **5**, 75.
 SHMUSHKEVICH, I. M., 1959, *Soviet Physics-JETP*, **9**, 449.
 UBERALL, H., 1959, *Phys. Rev.*, **114**, 1640.

Capture Rates for Negative Muons in Light Elements

By A. ASTBURY†, I. M. BLAIR, M. HUSSAIN‡, M. A. R. KEMP§ AND
H. MUIRHEAD

Nuclear Physics Research Laboratory, University of Liverpool

MS. received 8th May 1961

Abstract. Measurements are reported on the capture rates of negative muons in certain light elements. Agreement with other experimental data is found, but a discrepancy between the calculated and experimental values of the capture rate in fluorine is noted.

§ 1. INTRODUCTION

THE results obtained with the apparatus described in the previous paper (Astbury *et al.* 1961) may be used to evaluate the capture rates for negative muons in various light elements.

After background was removed the data recorded on the screen of the kicksorter were of the form

$$N(t) = e^{-\lambda t} (1 + \alpha \cos \omega t).$$

The symbol λ represents the disappearance rate of negative muons in the target material; its magnitude was found by integrating the data over an even number of complete cycles of the term $\cos \omega t$, starting at $t = \pi/2\omega$. The data were then split into two equal time intervals of length T . The total number of counts in the first and second intervals, n_1 and n_2 respectively, were related by the expression

$$n_1/n_2 = e^{\lambda T}$$

and hence λ can be determined.

The term λ represents the sum of the rates for decay λ_d and capture λ_c :

$$\lambda = \lambda_d + \lambda_c.$$

The value of λ_d was taken to be equal to that of the free muon, since Coulomb effects have a negligible influence on the decay rate of negative muons stopped in light nuclei (Astbury *et al.* 1959, Yovanovitch 1960). Hence λ_c can be calculated.

§ 2. RESULTS

The results of the experiment are shown in the Table.

It can be seen that the experimental data from different laboratories are in agreement. The theory of Primakoff (based on a Universal Fermi Interaction) appears to fit the data with the exception of fluorine. The nuclear part of the muon capture process was calculated by Primakoff using a closure approximation. A similar approach was made by Burkhardt and Caine (1960), who used more detailed shell model wave functions than Primakoff.

† Now at Lawrence Radiation Laboratory, Berkeley, California, U.S.A.

‡ Now at the Physics Department, University of Dacca, Pakistan.

§ Now at the Rutherford Laboratory, National Institute for Research in Nuclear Science, Harwell, Berks.

Element	Capture rates $\times 10^5$ (sec ⁻¹)		Theoretical
	Present experiment	Other results	
Carbon	0.3 ± 0.1	0.44 ± 0.1 (a)	0.43 (f)
		0.36 ± 0.04 (b)	
		0.373 ± 0.011 (c)	
Fluorine	2.5 ± 0.4	2.54 ± 0.22 (a)	1.51 (f)
		2.72 ± 0.20 (d)	2.02 (g)
		3.70 ± 0.54 (e)	
Magnesium	5.0 ± 0.2	5.07 ± 0.20 (a)	5.2 (f)
Sulphur	13.5 ± 0.5	13.9 ± 0.9 (a)	14.0 (f)

(a) Sens (1959), (b) Stannard (1960), (c) Reiter *et al.* (1960), (d) Astbury *et al.* (1958), (e) Bertram (1960), (f) based on work of Primakoff (1959) and data of Sens (1959), (g) Burkhardt and Caine (1960).

In view of the excellent agreement of the theory of Primakoff with experimental data (Astbury *et al.* 1958, Sens 1959) for a large number of nuclei between beryllium and lead, the discrepancy noted in the Table for fluorine probably can be attributed to nuclear effects specific to this element.

ACKNOWLEDGMENTS

The authors wish to thank Mr. Halliday and the crew of the cyclotron for its steady operation, and Mr. P. M. Hattersley for assistance with the computations.

REFERENCES

- ASTBURY, A., HATTERSLEY, P. M., HUSSAIN, M., KEMP, M. A. R., MUIRHEAD, H., and WOODHEAD, T., 1961, *Proc. Phys. Soc.*, **78**, 1144.
 ASTBURY, A., HUSSAIN, M., KEMP, M. A. R., LIPMAN, N. H., MUIRHEAD, H., VOSS, R. G. P., and KIRK, A., 1959, *Proc. Phys. Soc.*, **73**, 314.
 ASTBURY, A., KEMP, M. A. R., LIPMAN, N. H., MUIRHEAD, H., VOSS, R. G. P., ZANGGER, C., and KIRK, A., 1958, *Proc. Phys. Soc.*, **72**, 494.
 BERTRAM, W. J., 1960, *Ph.D. Thesis*, Carnegie Institute of Technology.
 BURKHARDT, G. H., and CAINE, C. A., 1960, *Phys. Rev.*, **117**, 1375.
 PRIMAKOFF, H., 1959, *Rev. Mod. Phys.*, **31**, 802.
 REITER, R. A., ROMANOWSKI, T. A., SUTTON, R. B., and CHIDLEY, B. G., 1960, *Phys. Rev. Letters*, **5**, 22.
 SENS, J. C., 1959, *Phys. Rev.*, **113**, 679.
 STANNARD, F. R., 1960, *Phys. Rev. Letters*, **4**, 523.
 YOVANOVITCH, D. D., 1960, *Phys. Rev.*, **117**, 1580.

A Measurement of the Total Cross Section for the Production of Neutral Pions in Proton-Proton Collisions at 383 Mev

By A. ASTBURY†, M. A. R. KEMP†, H. MUIRHEAD, R. G. P. VOSS§ AND T. WOODHEAD

Nuclear Physics Research Laboratory, University of Liverpool

MS. received 8th May 1961

Abstract. A value of $(59 \pm 9) \mu\text{bn}$ has been obtained for the total cross section for the production of π^0 -mesons in proton-proton collisions at 383 Mev.

§ 1. INTRODUCTION

THE total cross section for the reaction $p + p \rightarrow p + p + \pi^0$, which we shall denote by the symbol σ_{pp}^0 , is characterized by its comparatively small size near threshold, and the rapid rise in its value as the energy of the incoming proton is increased. In nucleon-nucleon collisions at energies not too far from threshold, the most important transition in the production of pions is that which leaves the final nucleons in an S state relative to each other, and the meson in a p state with respect to the centre of mass of the system (an Sp transition in the notation of Rosenfeld (1954)). This transition is enhanced by the $(\frac{3}{2}, \frac{3}{2})$ resonance in the pion-nucleon interaction. This transition is allowed for the production of charged mesons in proton-proton collisions, but is forbidden for π^0 mesons for the following reason.

The two final protons in the π^0 production process exist predominantly in the S state at low energies. This state has $J=0$ because of the Pauli principle, and even parity. If the meson is emitted in a p state, the final state of the meson and protons has $J=1$ and even parity. The initial state of the two protons must have zero spin in states of even parity because of the Pauli principle, so that J must equal L and hence be an even integer. There is no initial state of two protons which has $J=1$ and even parity, and hence the Sp transition cannot occur in the production of π^0 mesons in proton-proton collisions. The absence of this transition amplitude explains the smallness of the π^0 production cross section just above the threshold.

Mather and Martinelli (1953) have pointed out that, in addition to the type of transition described above, there can also exist 'displaced transitions'. Let us consider the Ss transition. In this case one of the final nucleons and the pion can be partly in the $(\frac{3}{2}, \frac{3}{2})$ resonance state whilst the complete system has zero overall angular momentum. This is termed a 'displaced S state transition'. Similarly for production into a Sd state there could be a 'displaced D state

† Now at Lawrence Radiation Laboratory, Berkeley, California, U.S.A.

‡ Now at the Rutherford Laboratory, National Institute for Research in Nuclear Science, Harwell, Berks.

§ Now at C.E.R.N., Geneva.

transition'. In Table 1 the variation of the cross section σ_{pp}^0 with η is given for the different transitions, where η is the maximum momentum of the pion, in the centre-of-mass system, in units of μc , where μ is the pion mass.

Table 1

Transition	Ss	Sp	Ps	Pp	Displaced-S	Displaced-D
σ_{pp}^0	η^2	Forbidden	η^6	η^8	η^8	η^8

Mandelstam (1958) has developed a semi-phenomenological theory for the production of a single pion in nucleon-nucleon collisions. In this theory he assumes that all pion production takes place in such a manner that the outgoing pion is in a $(\frac{3}{2}, \frac{3}{2})$ resonant state with one of the nucleons. A theory of this type cannot be very accurate immediately above threshold, but should give good agreement with experiment in the energy ranges where kinematic conditions favour the $(\frac{3}{2}, \frac{3}{2})$ resonance. The form of the cross section σ_{pp}^0 predicted by Mandelstam is

$$\sigma_{pp}^0 = (0.040\eta^6 + 0.047\eta^8) \times 10^{-27} \text{ cm}^2. \quad \dots (1)$$

The most recent experimental results (Dunaitzev and Prokoshkin 1959) have been analysed in conjunction with the Mandelstam resonance model. These authors conclude that a term $(0.032 \pm 0.007)\eta^2 \times 10^{-27} \text{ cm}^2$ must be added to (1) in order to fit the experimental points below 400 mev. This term gives the contribution to the cross section from the non-resonant Ss transition. The final form of the excitation function suggested by Dunaitzev and Prokoshkin is

$$\sigma_{pp}^0 = (0.032 \pm 0.007)\eta^2 + 0.040\eta^6 + 0.047\eta^8 \times 10^{-27} \text{ cm}^2. \quad \dots (2)$$

The present experiment is a measurement of the total cross section in the 383 mev proton beam of the Liverpool synchrocyclotron. The result at this energy serves as a further check on whether a non-resonant term must be added to the Mandelstam formula (1).

§ 2. EXPERIMENTAL METHOD

The experimental arrangement is shown in Fig. 1. The external proton beam of the synchrocyclotron is focused on to a target of liquid hydrogen. The protons travel to the target in a vacuum pipe, and enter and leave the liquid hydrogen container through thin mylar windows. The π^0 mesons are registered by the detection of one of their decay photons. These pass through the anticoincidence counter 1 and materialize in the lead radiator. The electron or positron then gives a triple coincidence in counters 2, 3, 4. The ion chamber was used as a monitor to measure beam intensity. The proton flux which could be used in the experiment was limited by the high counting rate in counter 1, due to protons scattered into it from proton-proton collisions in the liquid hydrogen.

In order to determine the number of γ -rays incident on the counter telescope due to the decay of the π^0 mesons produced in the liquid hydrogen, four runs were made. These were as follows: one with liquid hydrogen and a lead radiator ($\text{H}_2 \text{ Pb}$), one with liquid hydrogen but no radiator ($\text{H}_2 [\text{Pb}]$), one with an empty target, but with the radiator ($[\text{H}_2] \text{ Pb}$), and finally a run with no liquid hydrogen

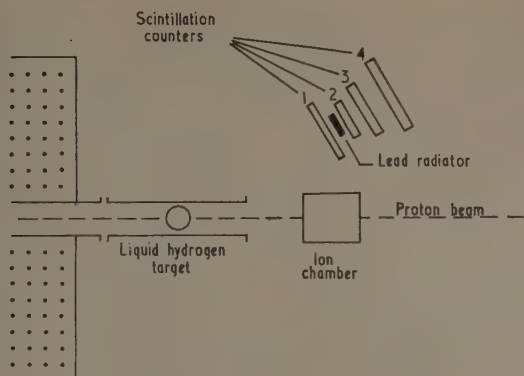


Fig. 1. Experimental arrangement.

and no radiator ($[H_2][Pb]$). By the following subtraction:

$$(H_2 Pb - H_2 [Pb]) - ([H_2] Pb - [H_2] [Pb]) = N_{H_2} \quad \dots\dots (3)$$

we obtain the counts from the liquid hydrogen per monitor count from the ion chamber. N_{H_2} was measured for different thicknesses t of lead radiator. It was necessary to take account of electrons multiply scattered in the lead and hence not detected in the telescope. This was done by extrapolating the $(N_{H_2}/t, t)$ plot to $t=0$ as shown in Fig. 2. We obtain from this intercept and the value of the pair production cross section in lead, the number of γ -rays produced per monitor count.

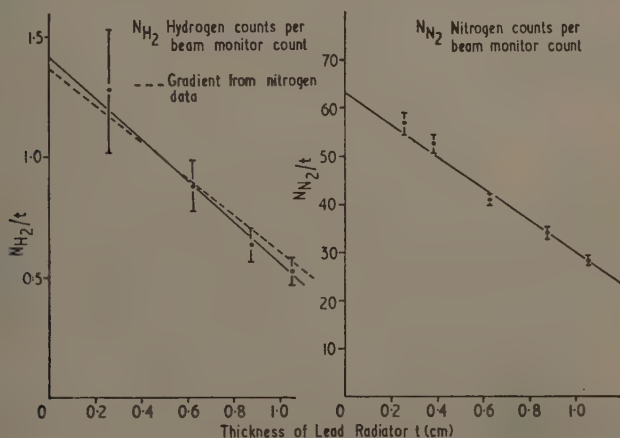


Fig. 2. Comparison of data from nitrogen and hydrogen.

A preliminary experiment was performed with liquid nitrogen in the target. In this case the counting rate due to γ -rays from π^0 decay is increased by a factor of the order of 40, because of the increased production cross section for π^0 mesons in nitrogen. The results of these runs are also plotted in Fig. 2. It was originally

intended to use the gradient from the nitrogen points for extrapolating the hydrogen data. In this way the nitrogen runs would have served to calibrate the γ -ray telescope. Such a method involves the assumption that the spectrum of γ -rays incident on the telescope from the liquid nitrogen is the same as that from the liquid hydrogen. In this case the gradients of the two graphs would be equal implying the same multiple scattering in the radiators for the two experiments. The two gradients obtained do in fact agree within the rather poor counting statistics of the hydrogen runs. However the errors quoted in the final result are those found from a best fit to the hydrogen points alone. Thus the nitrogen data was used only as a check on the procedure for extrapolating back to zero lead thickness.

The angular distribution of the π^0 in the centre-of-mass system of the colliding protons may be expanded as a polynomial in powers of $\cos \theta$

$$F(\theta) = a + b \cos \theta + c \cos^2 \theta \quad \dots\dots (4)$$

where θ is the angle of emission of the π^0 with respect to the direction of the incoming proton. At an incident proton energy of 383 mev the highest power expected in the polynomial is $\cos^2 \theta$, since transitions involving final states with an orbital angular momentum quantum number $l > 1$ are unlikely at this energy. Since the reaction is symmetric with respect to the two colliding protons it is apparent that $b = 0$. Thus Eqn (4) becomes

$$F(\theta) = a + c \cos^2 \theta.$$

It may then be shown (Tiapkin 1956) that the corresponding angular distribution of the γ -rays takes the form

$$F(\theta) = A + C \cos^2 \theta.$$

This distribution possesses the convenient property that the intensity of the γ -rays at angles $\bar{\theta} = \cos^{-1} \pm \sqrt{\frac{1}{3}}$ is related to the total yield of γ -rays in a manner which is independent of the parameters a and c (Tiapkin 1956). In fact at the 'isotropic angles' $\bar{\theta}$, the differential cross section for the γ -ray production $d\sigma^\gamma(\bar{\theta})/d\Omega$ is related to the total cross section for π^0 production as follows

$$\sigma^0_{pp} = 2\pi \frac{d\sigma^\gamma(\bar{\theta})}{d\Omega}. \quad \dots\dots (5)$$

The differential cross section for γ -ray production was measured at laboratory angles of 37° and 102° which correspond to the 'isotropic angles' in the centre-of-mass system for 383 mev protons. The ratio of the counting rates at these two angles may be calculated from the kinematics of the reaction and compared with the experimental value in order to check the validity of the above assumption used for the measurement of the total cross section. The results were

$$\frac{\text{Counting rate } 37^\circ}{\text{Counting rate } 102^\circ} = \frac{2.63 \text{ (calculated value)}}{2.8 \pm 0.6 \text{ (experimental value)}}.$$

In view of this result the two measurements of the γ -ray differential cross section were used to give independent determinations of the total cross section for π^0 production.

§ 3. RESULTS

The values of the total cross section σ^0_{pp} from the measurements at 37° and 102° respectively are $(62 \pm 12)\mu\text{bn}$ and $(58 \pm 10)\mu\text{bn}$. The sources of error in the experiment are given in Table 2.

Table 2

Sources of error	Percentage error
(a) Counting statistics	14.5 (37°) 9 (102°)
(b) Correction for π^0 produced in vacuum vessel of hydrogen target	6.5 (37°) 3 (102°)
(c) Pair production cross section	10
(d) Ion chamber calibration	5
(e) Target thickness and solid angle correction	3

In (b) the errors arise due to the fact that some of the protons in the beam were scattered by the liquid hydrogen and produced π^0 mesons in the aluminium vacuum vessel of the target. These could be detected by the γ -ray telescope and comprised 22% of the total effect at 37°, and 9% at 102°. No account has been taken of the γ -ray background due to protons scattered from the empty target. It has been estimated that this gives a correction of the order of 0.5%, which was neglected in the face of larger errors.

The pair production cross sections were taken from the theory of Bethe and Heitler, and the empirical correction derived by Davies, Bethe and Maximon (1954) applied. This correction is based on experimental results which are accurate to about 2%. The remainder of the error in (c) is due to integrating the cross sections over the spectrum of γ -rays incident on the radiator. The shape of this spectrum, and hence the final pair production cross section used in the calculation, depends on the angular distribution and energy distribution of the π^0 . The assumptions made were those of an angular distribution of the form $(\frac{1}{3} + \cos^2 \theta)$ and the energy distribution derived by Gell-Mann and Watson (1954) for a Pp transition.

The magnitude of the pair production cross section resulting from these calculations is not very sensitive to the shape of the γ -ray spectrum. Values were obtained for four different spectra, three of which corresponded to angular distribution of the π^0 mesons of the form $\cos^2 \theta$, $\frac{1}{3} + \cos^2 \theta$ and isotropic. The fourth was a non-physical case of a square γ -ray spectrum between the upper and lower limits of energy allowed by the kinematics of the reaction. The values showed a spread of about 6% about a mean of about 30 barns.

The value of the total cross section, resulting from the combination of the two measurements at the 'isotropic angles', is $(59 \pm 9) \mu\text{bn}$. In Table 3 this value is compared with other experimental results in the same energy region.

Table 3

Incident proton energy (MeV)	$\sigma_{pp}^0 (\mu\text{bn})$	Measured cross sections
408	81 ± 22	Stallwood <i>et al.</i> (1958)
383	33 ± 17	
367	25 ± 12	
360	30 ± 8	
374	40 ± 10	Dunaitzev & Prokoshkin (1959)
400	90 ± 20	
383	59 ± 9	Present experiment

If the appropriate value of η (0.863 for incident protons of 383 mev) is substituted into Eqn (2), then the experiment gives a further check on the excitation function of Mandelstam, with the addition of the empirical correction of Dunaitsev and Prokoshkin. The results are shown in Table 4.

Table 4

Expected contributions to the cross section		Experiment
$(0.047\eta^6 + 0.047\eta^8) \times 10^{-27} \text{ cm}^2$ (theory of Mandelstam)	31 μbn	
Empirical correction for non-resonant Ss transition (Dunaitsev & Prokoshkin) $0.032\eta^2 \times 10^{-27} \text{ cm}^2$	24 μbn	
Total	55 μbn	(59 \pm 9) μbn

It is clear that at the rather low proton energy of 383 mev the Mandelstam resonance theory cannot account for all the production of π^0 mesons, and a non-resonant Ss transition, introduced through the empirical correction term, can account for the discrepancy.

REFERENCES

- DAVIES, H., BETHE, H. A., and MAXIMON, L. C., 1954, *Phys. Rev.*, **93**, 788.
 DUNAITSEV, A. F., and PROKOSHIN, YU.D., 1959, *Soviet Physics-JETP*, **9**, 1179.
 GELL-MANN, M., and WATSON, K. M., 1954, *Ann. Rev. Nucl. Sci.*, **4**, 219.
 MANDELSTAM, S., 1958, *Proc. Roy. Soc.*, **244**, 491.
 MATHER, J. W., and MARTINELLI, E. A., 1953, *Phys. Rev.*, **92**, 780.
 ROSENFELD, A. H., 1954, *Phys. Rev.*, **96**, 139.
 STALLWOOD, R. A., SUTTON, R. B., FIELDS, T. H., FOX, J. G., and KANE, J. A., 1958, *Phys. Rev.*, **109**, 1716.
 TYAPKIN, A. A., 1956, *Zh. Eksper. Teor. Fiz.*, **30**, 1150.

Low Energy Elastic Scattering of Neutrons by Deuterons

BY J. W. HUMBERSTON

Department of Physics, University College, London

Communicated by Sir Harrie Massey; MS. received 1st June 1961

Abstract. Neutron-deuteron scattering phases are evaluated at five energies below 8 MeV for two ranges of a central Yukawa interaction. The dependence of the phases on the range is found to be very slight. Considerable differences are found between these results and those given by Haas and Robertson in 1959 who used the same form of interaction with the shorter of the two ranges considered here. The results and subsequent discussion resolve some previously inexplicable differences between the scattering lengths obtained with various potential shapes.

§ 1. INTRODUCTION

A THEORETICAL investigation of low energy neutron-deuteron scattering has been performed by Haas and Robertson (1959, to be referred to as HR) assuming a central two-body internucleonic interaction with symmetric exchange and Yukawa shape,

$$V(r) = V_0 \frac{\exp(-r/\lambda)}{r/\lambda}. \quad \dots\dots(1)$$

They ignored any distortion of the deuteron by the incident neutron and represented the deuteron ground state by the Hulthén wave function

$$\chi(r) = \frac{\exp(-\alpha r) - \exp(-\beta r)}{\eta r}, \quad \dots\dots(2)$$

where η is the normalization constant. Their results agree quite well with those of Christian and Gammel (1953), who also used a Yukawa potential, but differ significantly from those of Buckingham, Hubbard and Massey (1952) and Burke and Robertson (1957) who assumed exponential and Gaussian shapes respectively. However, as mentioned by Massey (1960), exponential and Yukawa shapes would be expected to give similar results and there is no *a priori* reason why they should be very different from those obtained using a Gaussian shape. In view of these discrepancies, the S phase shifts are calculated for five neutron energies in the range 0–8 MeV using two different values of the range λ in the interaction (1). Of the two ranges considered, the shorter, used by HR, is consistent with all two-body data whilst the longer range is appropriate in binding energy calculations for light nuclei. The values assumed by the parameters for the two interactions have been determined by Burke (1956) and are given in Table 1.

Table 1. Values of the Parameters occurring in Eqns (1) and (2)

	Interaction A	Interaction B
V_0 (Mev)	-68.01	-33.8
λ (10^{-13} cm)	1.18	1.78
α (10^{13} cm $^{-1}$)	0.22315	0.22302
β (10^{13} cm $^{-1}$)	1.615	1.170

In the notation used by HR, the integro-differential equation describing the scattering in a state of orbital angular momentum $l\hbar$ is

$$\frac{d^2 f_l(r)}{dr^2} + \left(k^2 - \frac{l(l+1)}{r^2} - \alpha U(r) \right) f_l(r) = \int_0^\infty \left(\beta q_l(r, r') + \gamma \left[p_l(r, r') + \left(1 + \frac{E_n}{E_d} \right) n_l(r, r') \right] \right) f_l(r') dr', \quad \dots (3)$$

where the potential function $U(r)$, the kernels $q_l(r, r')$, $p_l(r, r')$ and $n_l(r, r')$, and the values of α , β and γ for the two spin states are as defined by HR. The solution of this equation satisfies the boundary conditions $f_l(0) = 0$, $f_l(r) \sim \sin(kr - \frac{1}{2}l\pi + \delta_l)$ where δ_l is the phase shift.

§ 2. METHOD OF SOLUTION

Equation (3) was solved numerically on the University of London's Ferranti MERCURY computer for the case of $l=0$ using a method due to Robertson (1956). It involves calculating the kernels for values of r and r' ranging from 0 to 21 fermis at a constant interval of 0.3 fermi, and tabulating the results in the form of square matrices so that the element p_{nm} of the kernel matrix $p(r, r')$ is equal to $p(r=0.3n, r'=0.3m)$ etc., r and r' being measured in units of 10^{-13} cm. All integrands in the kernel functions are singular at the lower limit of angular integration when $r=2r'$ and $r'=2r$, the integrands in $q_0(r, r')$ also being singular at the upper limit when $r=r'$. Removal of these singularities by means of appropriate substitutions enables the kernels to be evaluated accurately for all values of r and r' .

The contour diagrams of the kernels $q_0(r, r')$ and $n_0(r, r')$ obtained using the A interaction agree well with those of HR but that of $p_0(r, r')$ differs from theirs in the vicinity of the lines $r=2r'$ and $r'=2r$. This, however, is probably due to errors in drawing the contours and the fact that, owing to the rapid variations of the kernel in these regions, their interpolation method of calculating the elements on these lines is not accurate. Similar diagrams are obtained for the B interaction but, because of its longer range and the smaller value of the deuteron wave function parameter β , the kernels die away more slowly.

§ 3. RESULTS

Values of the phases for both interactions are given in Table 2 and the corresponding Blatt-Jackson curves are plotted in the Figure. From the zero energy intercepts on the $k \cot \delta$ axis the following two sets of scattering lengths are obtained

$$\left. \begin{aligned} a_4 &= 5.6 \times 10^{-13} \text{ cm} \\ a_2 &= 4.0 \times 10^{-13} \text{ cm} \end{aligned} \right\} \text{ for the A interaction,}$$

$$\left. \begin{aligned} a_4 &= 5.9 \times 10^{-13} \text{ cm} \\ a_2 &= 3.9 \times 10^{-13} \text{ cm} \end{aligned} \right\} \text{ for the B interaction.}$$

These are to be compared with HR's values

$$a_4 = 6.9 \times 10^{-13} \text{ cm}, \quad a_2 = 1.4 \times 10^{-13} \text{ cm},$$

and the two experimentally permissible sets,

$$a_4 = 2.4 \times 10^{-13} \text{ cm}, \quad a_2 = 8.3 \times 10^{-13} \text{ cm}, \quad (\text{i})$$

$$a_4 = 6.2 \times 10^{-13} \text{ cm}, \quad a_2 = 0.8 \times 10^{-13} \text{ cm}. \quad (\text{ii})$$

Table 2. S Phases

$k \times 10^{13} \text{ (cm}^{-1}\text{)}$	Quartet			Doublet		
	A	B	HR(0.8)	A	B	HR(0.8)
0.4	-88.030	-77.782	+75.868	-78.010	-81.019	-60.038
0.3	-76.765	-77.480		-62.323	-63.817	
0.2	-59.729	-62.509	-63.173	-42.836	-42.790	-28.594
0.12	-38.076	-40.047	-43.206	-26.389	-25.711	-13.596
0.075	-24.001	-25.264	-28.498	-16.879	-16.283	-6.467

S phases are given in degrees. Columns A and B contain the phases using interactions A and B respectively. Haas and Robertson's final results are given in columns headed HR(0.8).

The results seem to favour set (ii) rather than (i) although good agreement exists only for the quartet scattering lengths.

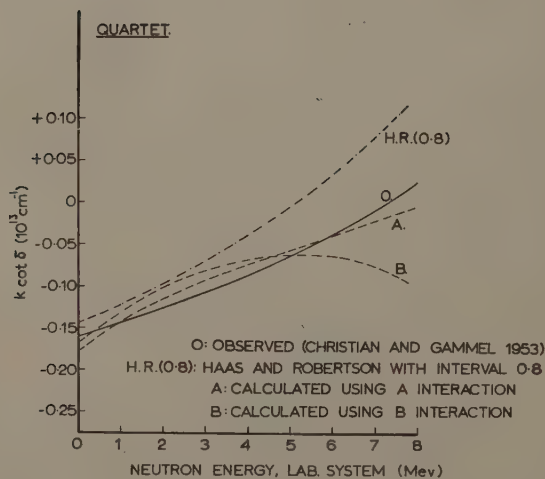
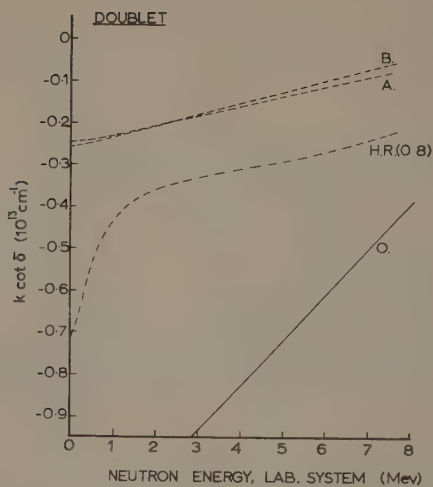
It would appear that the quartet phases are more sensitive to the range of the interaction than are the doublet phases. But, as mentioned previously, the longer range of the B interaction increases the tails of the long range kernels so that they are no longer negligibly small at 21 fermis. This is particularly important for quartet states since the coefficient γ multiplying the long range kernels in Eqn (3) then has the value +1 whereas it is only $-\frac{1}{2}$ for the doublet states. Consequently the error introduced by neglecting the kernels beyond 21 fermis has a greater effect on the quartet phases. In fact most of the difference between the two sets of quartet phases is probably due to this error, which may also be partly responsible for the slight difference in the doublet phases.

It is therefore concluded that the dependence of both quartet and doublet phases on the range of the interaction is very slight.

Table 3. S Phases

$k \times 10^{13} \text{ (cm}^{-1}\text{)}$	Quartet		Doublet	
	(11.4)	HR(0.4)	(11.4)	HR(0.4)
0.4	+83.017	+87.953	-74.773	-75.591
0.3	-72.616		-62.007	
0.2	-45.159	-38.371	-47.055	-47.250
0.12	-24.857	-19.220	-30.727	-30.341
0.075	-14.832	-10.741	-19.813	-19.427

S phases are given in degrees. The columns (11.4) contain the phases using the A interaction with neglect of the kernels beyond $r, r' = 11.4$ fermis. The columns HR(0.4) contain the results of Haas and Robertson using a constant interval of 0.4 fermi and neglecting the kernels beyond $r, r' = 11.6$ fermis.



Comparison of 'observed' and calculated zero-order phase shifts.

In order to explain the considerable differences between the results of HR and the present ones, the A interaction phases have been recalculated using exactly the same method as before but neglecting the kernels beyond 11.4 fermis. Since HR performed very similar calculations using a constant interval of 0.4 fermi with the kernels extending to 11.6 fermis, agreement between the two sets of phases would be expected. They are contained in Table 3 and are seen to agree as well as can be expected in view of the slight differences in the interval and extent of the kernels and the possible errors in $p_0(r, r')$, mentioned previously,

§ 4. DISCUSSION

Comparison of the results in columns (11.4) of Table 3 and the A interaction phases of Table 2 indicates that, contrary to the conclusions of HR, neglect of the tails of the long range kernels does not affect the doublet phases to any great extent although it has a serious influence on the quartet phases. The doublet phases, however, are more sensitive to the interval of integration, making it essential to use as small an interval as possible.

Buckingham, Hubbard and Massey, using a symmetric exchange interaction of exponential shape, obtained similar results to the present ones, the agreement being particularly good in doublet states. Although the calculations of Burke and Robertson, who used a Gaussian shape with various ranges, are not in such good agreement, evidence exists in their paper to suggest that, had they used smaller intervals of integration and extended the kernels further, they would have obtained results closer to the present ones with less dependence on the range. This similarity of the results using three different shapes and a variety of ranges suggests that for central interactions with Serber and symmetric exchange, the phases are almost independent of the form of the interaction provided that, for a given range, the depth is chosen so as to give the correct deuteron binding energy. It is therefore unlikely that any purely central interaction will provide doublet phases in better agreement with experiment without an explicit inclusion of deuteron polarization.

Recently, variational techniques have been used to investigate the effect of polarization on the phases, but the results are not altogether satisfactory. Thus Burke and Haas (1959) and Sartori and Rubinow (1958), using the Kohn and Rubinow methods respectively, concluded that the effect was small for quartet and doublet phases, whereas Efimov (1959), who also used the Rubinow method but considered a more complicated trial function, obtained results contrary to this. He obtained the scattering lengths

$$a_4 = 6.3 \times 10^{-13} \text{ cm}, \quad a_2 = 1.1 \times 10^{-13} \text{ cm},$$

both of which are in good agreement with experiment.

A disadvantage of both variational methods discussed above is that they fail to give either an upper or lower bound on the scattering lengths. Therefore, it is not possible to infer that, because Efimov obtains results close to set (ii), this set is necessarily correct. Only if one of the two possible experimental values were larger than the result of a calculation of the upper bound on the scattering length could the experimental set containing the larger value be definitely rejected. A variational method which does lead to an upper bound on the scattering lengths has been devised by Spruch and Rosenberg (1960) but no numerical results have yet been obtained using it. The authors claim, however, that the conversion

of Efimov's calculations to the form used in their method reduces the value of the scattering lengths so that Efimov's results are in fact upper bounds. As the doublet scattering length of set (i) is larger than the value of the upper bound it follows that the correct set is (ii).

This conclusion is only justified if the equivalent central potential is an accurate approximation to the true potential, but there is very little evidence that this is so. A more realistic approximation is a mixture of central and tensor potentials, and the neutron-deuteron scattering problem with such an interaction has been formulated by Bransden, Smith and Tate (1958). Using this formulation, a recent determination at University College London of the doublet scattering length yielded the result $a_2 = 8.3$ fermis which agrees with set (i). A Gaussian shape was assumed for the central and tensor components and the exchange mixtures were taken to be Serber for the central part and, in the notation of Bransden, Smith and Tate, $w' = \frac{1}{3}$, $m' = \frac{2}{3}$ for the tensor part. The numerical values of all other parameters are given by Massey (1960). A more detailed report of this work will be published later.

Despite the good agreement with set (i), no firm conclusions can be reached until the quartet scattering length has also been calculated. Furthermore, no allowance has been made for distortion of the deuteron which is expected to be a predominantly doublet effect. It is therefore intended to apply the method of Spruch and Rosenberg to the tensor force problem.

ACKNOWLEDGMENTS

I am indebted to Professor Sir Harrie Massey for suggesting the investigation, to the Department of Scientific and Industrial Research for a Research Studentship and to the University of London Computer Unit for the extensive use of its facilities.

I would also like to thank Mr. B. Pardoe for communicating the results of the tensor force calculations prior to publication.

REFERENCES

- BRANDSEN, B. H., SMITH, K., and TATE, C., 1958, *Proc. Roy. Soc. A*, **247**, 73.
 BUCKINGHAM, R. A., HUBBARD, S. J., and MASSEY, H. S. W., 1952, *Proc. Roy. Soc. A*, **211**, 183.
 BURKE, P. G., 1956, *Thesis*, University of London.
 BURKE, P. G., and HAAS, F. A., 1959, *Proc. Roy. Soc. A*, **252**, 177.
 BURKE, P. G., and ROBERTSON, H. H., 1957, *Proc. Phys. Soc. A*, **70**, 779.
 CHRISTIAN, R. S., and GAMMEL, J. L., 1953, *Phys. Rev.*, **91**, 100.
 EFIMOV, Y. N., 1959, *Soviet Physics-JETP*, **8**, 98.
 HAAS, F. A., and ROBERTSON, H. H., 1959, *Proc. Phys. Soc. A*, **73**, 160.
 MASSEY, H. S. W., 1960, *Proceedings of the International Conference on Nuclear Forces and the Few Nucleon Problem, London, July, 1959* (London, New York, Paris: Pergamon Press), p. 345.
 ROBERTSON, H. H., 1956, *Proc. Camb. Phil. Soc.*, **52**, 538.
 SARTORI, L., and RUBINOW, S. I., 1958, *Phys. Rev.*, **112**, 214.
 SPRUCH, L., and ROSENBERG, L., 1960, *Nucl. Phys.*, **17**, 30.

The Transfer and Exchange Transfer of Nucleons between ^{16}O and ^{27}Al

By R. F. COLEMAN AND J. L. PERKIN

Atomic Weapons Research Establishment, Aldermaston, Berks.

MS. received 17th May 1961

Abstract. Cross sections for the following reactions with 36 meV ^{16}O ions have been measured:

Neutron transfer	$^{27}\text{Al}(^{16}\text{O}, ^{15}\text{O})^{28}\text{Al}$	$\leq 7 \mu\text{bn}$
Proton transfer	$^{27}\text{Al}(^{16}\text{O}, ^{17}\text{F})^{26}\text{Mg}$	$210 \pm 50 \mu\text{bn}$
Neutron-proton exchange transfer	$^{27}\text{Al}(^{16}\text{O}, ^{16}\text{F})^{27}\text{Mg}$	$0.7 \pm 0.4 \mu\text{bn}$

The mechanism of the exchange transfer reactions is discussed in terms of the single transfer reactions. There is some evidence to suggest that an exchange reaction is not composed of two single transfer reactions.

§ 1. INTRODUCTION

THE only work on neutron-proton exchange transfer reactions previously reported is that of Pinajian (1960) who found that the cross section of the $^{27}\text{Al}(^{14}\text{N}, ^{14}\text{O})^{27}\text{Mg}$ reaction is $2.2 \pm 1 \mu\text{bn}$ for nitrogen ions of 27.6 meV. This result is consistent with the prediction by Goldansky (1958) that the magnitude of neutron-neutron exchange transfer reactions are of the order of 1 to $10 \mu\text{bn}$. Goldansky obtained this value by calculating the relative probabilities for neutron transfer and neutron-neutron exchange transfer for the 'tunnelling' model of these reactions and comparing these with the geometrical cross section and experimentally determined neutron transfer reaction cross sections (see also Breit 1959).

The aim of the present experiments was to examine a neutron-proton exchange transfer reaction where it was possible to measure the cross sections of the two single transfer reactions of which it was composed. The $^{27}\text{Al}(^{16}\text{O}, ^{16}\text{F})^{27}\text{Mg}$ reaction was chosen for this purpose. An activation method involving the chemical separation of the reaction products was used to measure the cross sections. The products measured for the neutron, proton and exchange transfer reactions were ^{15}O (2 min) ^{17}F (1.1 min) and ^{27}Mg (9.5 min) respectively.

As the activities measured in this work were so small, it was essential to ensure a very good chemical separation of these products from the products of other reactions. It was also important to show either experimentally or by inference from other work on transfer reactions that the transfer products observed could not have been produced in any other way. These points are discussed in the following sections.

§ 2. EXPERIMENTAL DETAILS

2.1. Irradiation of the Aluminium Targets

Currents of the order of $0.1 \mu\text{A}$ of magnetically analysed ^{16}O $5+$ and $6+$ ion beams with energies up to 38 meV were obtained with the Atomic Weapons Research Establishment Tandem Van de Graaff (Allen *et al.* 1959). Thick

(9 mg cm⁻²) targets of aluminium foil were irradiated by placing them across the end of a Faraday cup. Irradiation times were of the order of the half-life of the particular reaction product examined.

2.2. Separation of Magnesium from Aluminium

It was found that after irradiation most of the activity in the aluminium foils consisted of some 10^5 disintegrations per second of ³⁸K (7.7 min). In order to ensure that no trace of this activity was counted with any ²⁷Mg activity present the following procedure was adopted.

The irradiated aluminium was dissolved in 6N sodium hydroxide containing 300 µg of magnesium carrier. The magnesium hydroxide was centrifuged off and washed. This precipitate was dissolved in dilute acid, about 1 mg of iron carrier was added and then precipitated with ammonia. Ammonium phosphate was added to the supernate and the solution made strongly ammoniacal to precipitate magnesium phosphate which was then redissolved and re-precipitated as a further purification step. The efficiency of the scheme for eliminating potassium was measured in a separate experiment by adding ⁴²K tracer to unirradiated aluminium. The fraction of potassium remaining was found to be less than 3×10^{-7} . This was sufficient to ensure that the observed magnesium activity was uncontaminated.

The final precipitate was slurried on to a plastic foil for counting in a 4π gas flow proportional counter. Activities of the order of a few counts per second decaying with the half-life of ²⁷Mg were observed. An anticoincidence ring of Geiger counters was used to reduce the background of this counter to 0.3 c/s.

After counting, the source was dissolved in dilute acid and the yield of magnesium was determined by a micro-titration using ethylene-diamine-tetra-acetic acid.

2.3. Separation of Fluorine from Aluminium

In this separation special care was taken to remove ³⁰P (2.5 min) found in the irradiated aluminium foils which, because of its mode of decay (positron) and its half-life, was likely to cause errors in the measurements of the ¹⁷F activity produced.

The foil was dissolved in 1 ml of sodium hydroxide solution containing 15 mg of fluorine carrier. The solution was scavenged twice with 200 µg of zirconium and then 2 ml of saturated barium hydroxide solution was added. The resulting barium fluoride was washed and then the tube and precipitate were placed in a counter to measure the positron activity from ¹⁷F. Counting commenced about three minutes after the end of the irradiation. The chemical yield of the separation scheme was measured by titrating the fluoride with a standard thorium nitrate solution.

Positrons were detected by means of two cylindrical (5.7 cm × 5.7 cm) sodium iodide scintillation counters on opposite sides of the source. Pulses from the positron annihilation photo-peaks in the two counters were counted when in coincidence in order to discriminate against any γ-ray background from traces of other reaction products remaining after the chemical separation. The overall efficiency of this counting arrangement (~10%) was found by calibration with a solution containing ¹⁸F which has been standardized by counting weighed amounts in a 4π proportional counter.

2.4. The Separation of Oxygen from Aluminium

The irradiated aluminium was dissolved in 1 ml of 6N sodium hydroxide and then transferred to a small still. The water was rapidly boiled off under reduced pressure and then condensed in a tube surrounded by liquid air. The distillate was melted and the decay of the positron activity from ^{15}O was measured in the same counter used for the ^{17}F determinations. The yield was measured by weighing the water. About three minutes elapsed between the end of the irradiations and the commencement of the counting. No activity was detected in any of these experiments.

§ 3. PRODUCTION OF TRANSFER REACTION PRODUCTS BY OTHER REACTIONS

3.1. Magnesium 27 from Reactions with Impurities

The possibility that the ^{27}Mg activity observed was produced by compound nucleus or transfer reactions between ^{16}O ions and impurities in the aluminium targets was investigated. Thick targets of carbon, nitrogen, oxygen, sodium, magnesium, silicon, phosphorus and sulphur, in a suitable form, were irradiated with 38 mev ^{16}O ions and the yields of ^{27}Mg were determined. By means of a procedure described in a previous paper (Coleman *et al.* 1961) these results were used to calculate the yield which would be obtained from one part per million of each of these elements in an aluminium target.

This yield was found to be not more than 7×10^{-16} per ^{16}O ion for all the elements examined with the exception of carbon. As the total amount of impurity in the aluminium was not more than 0.1% the total yield of ^{27}Mg from impurities other than carbon in the aluminium must be not more than 7×10^{-13} per ^{16}O ion which is negligible compared with that observed (Table 1).

The yield for one part per million of carbon impurity in aluminium was 56×10^{-16} per ^{16}O ion and this fell to 36×10^{-16} per ^{16}O ion when measured at 30 mev. In contrast the observed yield from the aluminium targets was reduced by a factor of at least 50 over this energy range (Table 1). Thus the amount of carbon either present in the aluminium target or deposited on the surface of the target (from traces of oil vapour in the accelerator vacuum system) was too small to cause any significant error in the determination of the yield of ^{27}Mg in these experiments.

3.2. Magnesium 27 from the $^{27}\text{Al}(n, p)^{27}\text{Mg}$ Reaction

When two identical aluminium foils were placed in close contact and irradiated together it was found that the foil that was shielded from the ^{16}O beam contained about half the ^{27}Mg activity contained in the foil in which the beam was stopped (Table 1). The activity in the shielded foil was due to the $^{27}\text{Al}(n, p)^{27}\text{Mg}$ reaction caused by neutrons from $^{27}\text{Al}(^{16}\text{O}, xn)$ reactions in the target. The flux in this foil was calculated to be 77% of that in the foil in the beam. An isotropic distribution of neutrons was assumed as it was found that the correction for any anisotropy due to the centre-of-mass motion could be neglected. The yield from the shielded foil can be used therefore to correct the yield of the foil in the ^{16}O beam for the effect of the neutron background. A similar correction was made by Pinajian (1960) in his determination of the $^{27}\text{Al}(^{14}\text{N}, ^{14}\text{O})^{27}\text{Mg}$ exchange transfer reaction cross section.

3.3. Fluorine 17 from Reactions with Impurities

The possibility that the observed yield of ^{17}F in the aluminium targets (see § 4) could be due to reactions between ^{16}O and any impurities in targets was considered. It is energetically possible in these experiments to produce ^{17}F from compound nucleus reactions with light elements up to and including boron. The cross section for the production of ^{17}F is some fraction of the total cross section for the formation of the compound nucleus, which is of the order of 1 barn (Thomas 1959). An analysis of the aluminium targets showed however that there was less than 0.01% of each of these elements present. Therefore no significant contribution to the ^{17}F activity observed could come from this source.

This conclusion also applies to transfer reactions with any impurities as the largest section observed for this type of reaction (Zucker 1960) is of the order of 50 mbn.

§ 4. NUCLEAR EMISSION FROM TRANSFER PRODUCTS

There is a possibility that the ^{27}Mg activity observed is derived from the proton decay of ^{28}Al produced in an excited state from the $^{27}\text{Al}(^{16}\text{O}, ^{15}\text{O})^{28}\text{Al}$ reaction. The possibility also exists that some of the single transfer products ^{15}O and ^{17}F are formed with sufficient excitation energy to emit nucleons (most probably protons in these cases) and escape detection in these experiments. Excitation energies of about 13, 10 and 6 mev for ^{28}Al , ^{15}O and ^{17}F respectively were required before proton emission was possible. An estimate can be made of the cross sections of transfer reactions which result in products with these excitation energies. This can be done by reference to the general trend of transfer cross sections with the energy 'available' at the moment of transfer, 'available' energy being defined as: the incident energy in centre-of-mass coordinates – the barrier height + $Q/2$. It has been found that when (^{14}N , ^{13}N) neutron transfer reaction cross sections are plotted in this way (Halbert *et al.* 1957) the curves, although differing in magnitude of cross section, all have a similar shape. Cross section measurements for other transfer reactions show a similar dependence on 'available' energy (^{14}N , ^{15}O) Reynolds and Zucker 1956 and Reynolds *et al.* 1956; (^{19}F , ^{18}F) recent unpublished work by the present authors).

The excitation energies required for proton emission from the various transfer products in the present work reduce the effective 'available' energy. The corresponding reduced cross sections for reactions involving proton emission can be inferred from the curves already described. In this way it is found that only about 1% of the neutron transfer product ^{15}O formed will escape detection by proton emission and that less than about 1% of the neutron-proton exchange transfer product ^{27}Mg could have been produced by proton emission from ^{28}Al from the $^{27}\text{Al}(^{16}\text{O}, ^{15}\text{O})^{28}\text{Al}$ reaction. The correction for the loss of the proton transfer product ^{17}F due to proton emission is about 20%, which is about the experimental error of the measured cross section (see § 5).

§ 5. RESULTS

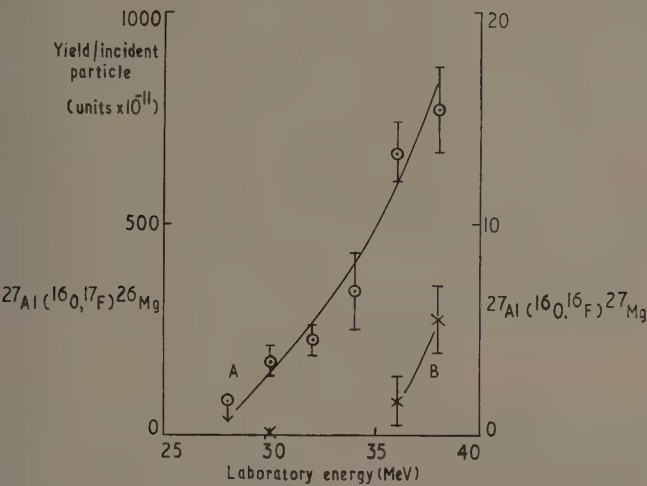
Since ^{15}O activity from the reaction $^{27}\text{Al}(^{16}\text{O}, ^{15}\text{O})^{28}\text{Al}$ was not detected it was possible to estimate an upper limit of 2×10^{-10} per ^{16}O ion for the yield of this reaction at 36 mev. The results for the $^{27}\text{Al}(^{16}\text{O}, ^{17}\text{F})^{26}\text{Mg}$ reaction are shown in the Figure; those for the $^{27}\text{Al}(^{16}\text{O}, ^{16}\text{F})^{27}\text{Mg}$ reaction are given in the Figure and Table 1.

Table 1. Thick Target Yield of ^{27}Mg per ^{16}O Ion (units 10^{-11})

Energy of ^{16}O ion (mev)	30	36	38
Thick target yield in aluminium Y_1	≤ 0.15	8.7 ± 0.9	12.5 ± 1
Yield in neutron background foil Y_2 †	—	7.1 ± 0.8	7.0 ± 1.3
Yield from the $^{27}\text{Al}(^{16}\text{O}, ^{16}\text{F})^{26}\text{Mg}$ reaction			
$Y_1 - Y_2$	≤ 0.15	1.6 ± 1.2	5.5 ± 1.6

† Normalized to the neutron flux in the foil in the oxygen beam.

The cross sections of these reactions at 36 mev were calculated using the expression $\sigma = \epsilon dY/dE$ where ϵ is the atomic stopping power of ^{27}Al for ^{16}O ions at this energy. A value of $2.2 \times 10^{-13} \text{ ev cm}^2$ for this stopping power was taken.



Thick target yield of: A, the $^{27}\text{Al}(^{16}\text{O}, ^{17}\text{F})^{26}\text{Mg}$ reaction, and B, the $^{27}\text{Al}(^{16}\text{O}, ^{16}\text{F})^{27}\text{Mg}$ reaction.

from a previous paper (Coleman *et al.* 1961). The slope of the yield curve dY/dE was assumed to be the same for all three reactions and equal to that for the $^{27}\text{Al}(^{16}\text{O}, ^{17}\text{F})^{26}\text{Mg}$ reaction obtained by drawing a tangent to the curve A in the Figure at 36 mev. The results are given in Table 2.

Table 2

Neutron transfer cross section	$^{27}\text{Al}(^{16}\text{O}, ^{15}\text{O})^{26}\text{Al}$	$\leq 7 \mu\text{bn}$
Proton transfer cross section	$^{27}\text{Al}(^{16}\text{O}, ^{17}\text{F})^{26}\text{Mg}$	$210 \pm 50 \mu\text{bn}$
Neutron-proton exchange transfer cross section	$^{27}\text{Al}(^{16}\text{O}, ^{16}\text{F})^{27}\text{Mg}$	$0.7 \pm 0.4 \mu\text{bn}$

The estimated errors are almost entirely due to the poor counting statistics. Uncertainties associated with the identification of these reactions have been discussed in §§ 3 and 4.

§ 6. DISCUSSION

The transfer of single nucleons has been found to take place between nuclei in Rutherford orbits where the closest distance of approach is about the sum of

their respective radii (Zucker 1960). The cross section of this process can be considered simply as the product of the average Rutherford scattering cross section σ_R , over the small angular region in which products from these reactions have been found to be emitted, and the probability P that a neutron n , or proton p , will transfer from one nucleus to the other. Thus provided that P_n and $P_p \ll 1$, the neutron transfer cross section is given by $\sigma_n \sim \sigma_R P_n$ and similarly $\sigma_p \sim \sigma_R P_p$.

If the neutron-proton exchange transfer reaction is considered as two independent single transfers then $\sigma_{np} \sim \sigma_R P_n P_p \sim \sigma_n \sigma_p / \sigma_R$. The calculated value of σ_R for 36 MeV ^{16}O ions on ^{27}Al is about 400 mbn. This value together with the measured cross sections for σ_n and σ_p in Table 2 enables σ_{np} to be evaluated. The value found is not greater than $0.004 \mu\text{bn}$ which is much smaller than the measured cross section of $0.7 \mu\text{bn}$. Agreement with the magnitude of the measured value would have been obtained if both the single nucleon transfer reaction cross sections had been found to be of the order of 1 mbn. This was the assumption made by Goldansky in his estimate of the exchange transfer cross section mentioned in the Introduction. The magnitude of the proton transfer cross section measured in these experiments is similar to that of (^{14}N , ^{13}N) neutron transfer cross sections at the same 'available' energy (see §4). On the other hand the upper limit obtained for the present neutron transfer cross section is much lower than these values. The very high neutron binding energy of ^{16}O is responsible presumably for this difference.

One explanation of the present results is that the exchange reaction is a two-stage process in which the probability of the second transfer is enhanced by the first one. However, a more likely explanation is that the exchange reaction results from a close 'grazing incidence' reaction. Kaufmann and Wolfgang (1961) have proposed this type of reaction to account for the fact that although the angular distributions they observed for single nucleon transfer reactions have the characteristic peak due to the 'tunnelling' mechanism, this was not the case with all the multi-nuclear transfer reactions they examined. With these reactions the angular distributions were peaked in the forward direction. Some angular distribution measurements on exchange transfer reactions would therefore be of considerable interest, but would be difficult to perform.

ACKNOWLEDGMENTS

We would like to acknowledge the assistance given by Mr. D. N. Herbert and Mr. B. J. Gardner during these experiments.

REFERENCES

- ALLEN, K. W., JULIAN, F. A., ALLEN, W. D., PYRAH, A. E., and BLEARS, S., 1959, *Nature, Lond.*, **184**, 303.
 BREIT, G., 1959, *Handb. d. Phys.*, **41**, 375 (Berlin: Springer).
 COLEMAN, R. F., HERBERT, D. N., and PERKIN, J. L., 1961, *Proc. Phys. Soc.*, **77**, 526.
 GOLDANSKY, V. I., 1958, *Nucl. Phys.*, **9**, 551.
 HALBERT, M. L., HANDLEY, T. H., PINAJIAN, J. J., WEBB, W. H., and ZUCKER, A., 1957, *Phys. Rev.*, **106**, 251.
 KAUFMANN, R., and WOLFGANG, R., 1961, *Phys. Rev.*, **121**, 192, 206.
 PINAJIAN, J. J., 1960, *Nucl. Phys.*, **17**, 44.
 REYNOLDS, H. L., SCOTT, D. W., and ZUCKER, A., 1956, *Phys. Rev.*, **102**, 237.
 REYNOLDS, H. L., and ZUCKER, A., 1956, *Phys. Rev.*, **101**, 166.
 THOMAS, T. D., 1959, *Phys. Rev.*, **116**, 703.
 ZUCKER, A., 1960, *Ann. Rev. Nucl. Sci.*, **10**, 27.

The Elastic Scattering of Positrons by Atomic Hydrogen and Helium

BY D. C. S. ALLISON, H. A. J. MCINTYRE AND
B. L. MOISEWITSCH

Department of Applied Mathematics, The Queen's University of Belfast

MS. received 15th June 1961

Abstract. The variational methods of Kohn and Hulthén are employed to calculate the scattering lengths for elastic collisions between positrons and hydrogen and helium atoms. Allowance is made for the dipole polarizability of the target atom by using a trial function which includes a term corresponding to the first-order perturbation of the atom due to the electric field of the positron.

The effect of allowing for the dipole polarizability of the atom is to change the sign of the scattering lengths for both hydrogen and helium in agreement with the variational calculations of Spruch and Rosenberg for hydrogen. In the case of hydrogen the total elastic cross section at zero impact energy is increased when allowance is made for polarization, but in the case of helium it is decreased from $0.72\pi a_0^2$ to $0.10\pi a_0^2$. The experimental cross section derived by Teutsch and Hughes for 18 eV positrons in helium is still smaller, being only $0.023 \pm 0.006\pi a_0^2$.

§ 1. INTRODUCTION

BY analysing the experimental data of Marder, Hughes, Wu and Bennett (1956) on the slowing down of positrons in the inert gases, Teutsch and Hughes (1956) derived momentum transfer cross sections for positrons in helium, neon and argon. They obtained very small cross sections. For example, in the case of helium they found $0.023 \pm 0.006\pi a_0^2$ at a mean positron energy of approximately 18 eV. This is much smaller than the value $0.53\pi a_0^2$ for the elastic cross section corresponding to 13.6 eV positrons obtained by Massey and Moussa (1958) by numerical integration of the appropriate differential equations employing a Hartree self-consistent field.

Massey and Moussa (1958) also carried out variational calculations on the elastic scattering of positrons by hydrogen atoms using the trial function that Massey and Moiseiwitsch (1951) found to be satisfactory in the case of the elastic scattering of electrons by hydrogen atoms. They obtained the values $0.512a_0$ and $0.582a_0$ for the scattering length with and without allowance for polarization. Subsequently Moussa (1959) used a trial function allowing for the polarization due to the virtual formation of positronium. Again, only a small effect was found, the zero-order phase shift being increased as a result of polarization from -0.264 radian to -0.211 radian for positrons having 3.4 eV energy. This decreased the elastic cross section from $1.09\pi a_0^2$ to $0.70\pi a_0^2$.

Recently Spruch and Rosenberg (1960) have carried out variational calculations on the elastic scattering of positrons by hydrogen atoms employing a similar trial function to that used by Moussa (1959) with allowance for virtual positronium formation. They obtained an upper bound $-1.397a_0$ to the

scattering length and a lower bound $7.80\pi a_0^2$ to the elastic cross section for positrons of zero energy. Their value for the scattering length is rather larger in absolute magnitude and opposite in sign to that found by Moussa demonstrating that the effect of polarization is in fact considerable and results in an increased elastic cross section for the case of atomic hydrogen.

The surprisingly small value for the elastic cross section obtained by Teutsch and Hughes (1956) for the scattering of positrons by helium atoms therefore still remains unexplained. It is the purpose of the present paper to investigate this case further.

§ 2. THEORY

We first consider the elastic scattering of positrons by hydrogen atoms. The wave function $\Psi(\mathbf{r}_1, \mathbf{r}_2)$ of the total system satisfies the Schrödinger equation

$$[H - E]\Psi = 0 \quad \text{..... (1)}$$

where E is the total energy and the Hamiltonian is given by

$$H = -\frac{\hbar^2}{2m}(\nabla_1^2 + \nabla_2^2) + \frac{e^2}{r_1} - \frac{e^2}{r_2} - \frac{e^2}{r_{12}}, \quad \text{..... (2)}$$

\mathbf{r}_1 and \mathbf{r}_2 being respectively the position vectors of the incident positron and the atomic electron relative to the proton, and r_{12} being the distance between the positron and the electron. In the case of the elastic scattering of positrons with zero energy and zero angular momentum by hydrogen atoms in the ground state, the wave function has the asymptotic form for large r_1

$$\Psi(\mathbf{r}_1, \mathbf{r}_2) \sim \psi_0(r_2)r_1^{-1}(a - r_1) \quad \text{..... (3)}$$

where a is the scattering length and $\psi_0(r)$ is the wave function of the 1s state of atomic hydrogen.

It can be shown by using perturbation theory (Dalgarno and Lewis 1955) that the wave function of a hydrogen atom in the Coulomb field of a positron is given to first order by

$$\psi_0(r_2) \left[1 + \sum_{m=1}^{\infty} \frac{1}{r_1^{m+1}} \left\{ \frac{r_2^{m+1}}{m+1} + \frac{a_0 r_2^m}{m} \right\} P_m(\cos \Theta_{12}) \right] \quad \text{..... (4)}$$

where $\mathbf{r}_1 \cdot \mathbf{r}_2 = r_1 r_2 \cos \Theta_{12}$. The $m=1$ term of this expression arises from the dipole polarizability of the hydrogen atom. Hence allowance may be made for the dipole polarizability of the atom by choosing the trial function

$$\Psi_t(\mathbf{r}_1, \mathbf{r}_2) = \psi_0(r_2) \{1 + \gamma f(\mathbf{r}_1, \mathbf{r}_2)\} F(r_1) \quad \text{..... (5)}$$

where

$$f(\mathbf{r}_1, \mathbf{r}_2) = r_1^{-2} \left\{ 1 - \exp\left(-\frac{\delta r_1}{a_0}\right) \right\}^3 \left(\frac{1}{2} r_2^2 + a_0 r_2 \right) \cos \Theta_{12}, \quad \text{..... (6)}$$

$$F(r_1) = r_1^{-1} \left[\left\{ \alpha + \beta \exp\left(-\frac{r_1}{a_0}\right) \right\} \left\{ 1 - \exp\left(-\frac{r_1}{a_0}\right) \right\} - r_1 \right], \quad \text{..... (7)}$$

and $\alpha, \beta, \gamma, \delta$ are arbitrary parameters.

The trial function (5) has the asymptotic form (3) for large r_1 and behaves properly in the limits of vanishing r_1 and r_2 . The value of the parameter δ determines the rate at which f tends to zero as r_1 becomes small.

Spruch and Rosenberg (1960) have shown that

$$a \leq \alpha + \frac{1}{4\pi} \left(\frac{2m}{\hbar^2} \right) L_t \quad \text{..... (8)}$$

where

$$L_t = \int \Psi_t(\mathbf{r}_1, \mathbf{r}_2)(H-E)\Psi_t(\mathbf{r}_1, \mathbf{r}_2) d\mathbf{r}_1 d\mathbf{r}_2. \quad \dots\dots (9)$$

The optimum value of the right-hand side of (8) may be obtained by using Kohn's variational method which involves the solution of the equations

$$\frac{\partial L_t}{\partial \alpha} = -4\pi \left(\frac{\hbar^2}{2m} \right) \quad \dots\dots (10)$$

and

$$\frac{\partial L_t}{\partial \beta} = \frac{\partial L_t}{\partial \gamma} = \frac{\partial L_t}{\partial \delta} = 0. \quad \dots\dots (11)$$

Alternatively, we may use Hulthén's variational method which determines the parameters α , β , γ , δ by employing the equations (11) together with

$$L_t = 0 \quad \dots\dots (12)$$

in place of (10). Because Hulthén's method imposes a restriction on L_t the value of the scattering length given by its application will always be inferior to that obtained with Kohn's method.

Since it is not possible to derive an exact unperturbed helium wave function it is necessary to use an approximate function in order to investigate the elastic scattering of positrons by helium. We have chosen the variational wave function obtained by Green, Mulder, Lewis and Woll (1954) which is a close approximation to the Hartree-Fock wave function for helium.

It has the form

$$\psi_0(r_2, r_3) = u(r_2)u(r_3) \quad \dots\dots (13)$$

where

$$u(r) = N \left\{ \exp\left(\frac{-Zr}{a_0}\right) + c \exp\left(\frac{-2Zr}{a_0}\right) \right\} \quad \dots\dots (14)$$

with $Z=1.4558$ and $c=0.6$. N is a normalizing factor given by

$$N = 2.96847 / (4\pi a_0^3)^{1/2}.$$

The trial function of the system of incident positron and helium atom was taken to have the form

$$\Psi_t(\mathbf{r}_1, \mathbf{r}_2, \mathbf{r}_3) = \psi_0(r_2, r_3) \{1 + \gamma f(\mathbf{r}_1, \mathbf{r}_2, \mathbf{r}_3)\} F(r_1) \quad \dots\dots (15)$$

where

$$f(\mathbf{r}_1, \mathbf{r}_2, \mathbf{r}_3) = r_1^{-2} \left\{ 1 - \exp\left(\frac{-\delta Z r_1}{a_0}\right) \right\}^3 \{ r_2 \cos \Theta_{12} (p_0 a_0 + p_1 r_2) + r_3 \cos \Theta_{13} (p_0 a_0 + p_1 r_3) \} \quad \dots\dots (16)$$

and $\cos \Theta_{ij} = \hat{\mathbf{r}}_i \cdot \hat{\mathbf{r}}_j$. The constants p_0 and p_1 were chosen so that for large r_1 , $\psi_0(r_2, r_3)f(\mathbf{r}_1, \mathbf{r}_2, \mathbf{r}_3)$ should be the first-order correction to the wave function of the helium atom arising from the dipole term of the perturbation due to the positron. Calculations by Dalgarno (private communication) give $p_0=0.242$ and $p_1=0.395$.

§ 3. DISCUSSION OF RESULTS

If polarization is neglected the scattering length a may be readily calculated by numerical integration of the appropriate differential equation. It is found that $a=0.582a_0$ and $0.422a_0$ for hydrogen and helium atoms respectively in

close accord with the values, given in Tables 1 and 2, of the scattering length calculated using variational methods with γ taken to be zero in the trial functions (5) and (15).

Table 1. Elastic Scattering of Positrons by Hydrogen Atoms
Values of the scattering length a and the parameters γ and δ calculated using variational methods

Kohn's variational method			Hulthén's variational method			
	γ	δ	a	γ	δ	a
(i)	0	—	0.58 ₄	0	—	0.58 ₄
(ii)	1	0.55 ₃	-0.77 ₄	1	0.54 ₅	-0.62 ₈
(iii)	1.08 ₃	0.49 ₁	-0.78 ₅	1.09 ₈	0.48 ₄	-0.63 ₇

Table 2. Elastic Scattering of Positrons by Helium Atoms
Values of the scattering length a and the parameters γ and δ calculated using variational methods

Kohn's variational method				Hulthén's variational method			
	γ	δ	a		γ	δ	a
(i)	0	—	0.42 ₅		0	—	0.42 ₅
(ii)	1	0.56 ₇	-0.16 ₀		1	0.56 ₃	-0.10 ₃
(iii)	1.05 ₈	0.51 ₈	-0.16 ₃		1.06 ₇	0.51 ₀	-0.11 ₀

Row (i): $\gamma=0$, α and β varied.

Row (ii): $\gamma=1$, α , β and δ varied.

Row (iii): α , β , γ and δ varied.

By comparing the coefficient of $F(r_1)$ in the trial function (5) with the polarized hydrogen atom wave function given by expression (4) we see that the parameter γ should be close to unity. Similarly the parameter γ arising in the trial function (15) for the case of helium should also be approximately unity. The values of the scattering length obtained with Kohn's and Hulthén's variational methods, putting $\gamma=1$ in the trial functions (5) and (15), are displayed in Tables 1 and 2 for hydrogen and helium respectively. It is evident that the effect of polarization is very important, the sign of the scattering length being reversed in both cases. This means that the overall field of the atom is attractive towards the positron. If γ is now permitted to vary the value of the scattering length is not greatly altered, the value of γ corresponding to the optimum value of a being just slightly greater than unity.

When polarization is neglected there is very close agreement between the values of the scattering length obtained with Kohn's and Hulthén's variational methods. With allowance for polarization the agreement between the two variational methods becomes less satisfactory. This implies that the form of trial function which was chosen to describe the system of incident positron and atom is inadequate in some way for small r_1 . In the case of hydrogen, Spruch and Rosenberg (1960) obtained $-1.397a_0$ as an upper bound to the scattering length. This is considerably smaller than the best value $-0.785a_0$ obtained

with the trial function (5). Spruch and Rosenberg made allowance for virtual positronium formation. This must therefore make a greater contribution to polarization effects than allowance for the dipole polarizability of the atom. However it is clear that in a full treatment of the problem both types of polarization effect should be taken into account.

In the case of the elastic scattering of positrons by helium atoms, the effect of dipole polarizability is to change the sign of the scattering length as for hydrogen. However, the absolute magnitude of the scattering length is decreased. Noting that the total elastic cross section for incident particles of zero energy is given by

$$Q(0) = 4\pi a^2 \quad \dots\dots (17)$$

we see from Table 2 that $Q(0)$ is decreased from $0.72\pi a_0^2$ to $0.10\pi a_0^2$ as a result of polarization. The latter value is about four times larger than the experimental cross section $0.023 \pm 0.006\pi a_0^2$ derived by Teutsch and Hughes (1956) for 18 eV positrons in helium. Allowance for virtual positronium formation will increase $Q(0)$ above $0.10\uparrow$. Consequently, unless the elastic cross section decreases considerably with increasing energy, there is discord between theory and experiment for helium.

ACKNOWLEDGMENTS

It is a pleasure to thank Professor A. Dalgarno for his interest in this investigation.

This work has been supported by the United Kingdom Atomic Energy Research Establishment, to whom thanks are due for permission to publish.

REFERENCES

- DALGARNO, A., and LEWIS, J. T., 1955, *Proc. Roy. Soc. A*, **233**, 70.
 GREEN, L. C., MULDER, M. M., LEWIS, M. N., and WOLL, J. W., 1954, *Phys. Rev.*, **93**, 757.
 MARDER, S., HUGHES, V. W., WU, C. S., and BENNETT, W., 1956, *Phys. Rev.*, **103**, 1528.
 MASSEY, H. S. W., and MOISEWITSCH, B. L., 1951, *Proc. Roy. Soc. A*, **205**, 483.
 MASSEY, H. S. W., and MOUSSA, A. H. A., 1958, *Proc. Phys. Soc.*, **71**, 38.
 MOUSSA, A. H. A., 1959, *Proc. Phys. Soc.*, **74**, 101.
 SPRUCH, L., and ROSENBERG, L., 1960, *Phys. Rev.*, **117**, 143.
 TEUTSCH, W. B., and HUGHES, V. W., 1956, *Phys. Rev.*, **103**, 1266.

\uparrow However, it should be noted that the existence of a bound to the scattering length has been rigorously established only when exact atomic wave functions are employed.

Electron Spin Resonance Absorption for Polycrystalline Substances: II

By J. W. SEARL†, R. C. SMITH‡ AND S. J. WYARD‡§

† Mathematics Department, Northampton College, London, E.C.1

‡ Physics Department, Guy's Hospital Medical School, London, S.E.1

MS. received 19th May 1961

Abstract. Calculations have been made of the electron spin resonance line shapes for polycrystalline substances showing uniaxial g -value anisotropy. The calculations have been made for the Lorentzian and Gaussian line shapes of various line widths. Empirical rules are given for determining g_{\parallel} , g_{\perp} and the line width from the experimental line shapes. Line shapes calculated to fit experimental curves from irradiated deuterium peroxide are given.

CALCULATIONS of the line shapes for a random polycrystalline assembly of uniaxial crystals have been reported in part I (Searl *et al.* 1959). The following assumptions were made for these calculations:

- (i) The absorption line shape for the single crystal is the Lorentzian||

$$I = \frac{AK}{1 + \pi^2 K^2 (x - c)^2}.$$

- (ii) The line width for the single crystal is independent of orientation in the magnetic field.

- (iii) The variation of c with the crystal orientation in the magnetic field, angle θ , is given by $c = (c_{\parallel} - c_{\perp}) \cos^2 \theta + c_{\perp}$, where $c = g$ for sweeping with frequency, or $c = 1/g$ for sweeping with field.

- (iv) The total absorption A is independent of θ .

Searl *et al.* (1960) have also performed calculations using the same assumptions but with the Gaussian line shape

$$I = \pi^{1/2} AK \exp [-(x - c)^2 \pi^2 K^2]$$

(the factor $\pi^{1/2}$ is introduced to ensure that the total absorption is the same for both the Lorentzian and the Gaussian). The calculation must then be performed numerically.

The assumptions (iii) and (iv) above have been altered to improve the accuracy of the calculations as follows:

- (iii) The variation of g with angle θ obeys the formula derived by Bleaney (1951) for a uniaxial crystal, $g^2 = g_{\parallel}^2 \cos^2 \theta + g_{\perp}^2 \sin^2 \theta$.

- (iv) Bleaney (1960) has shown that a variation of factor A with g occurs. For a linearly polarized oscillatory field he finds that A is proportional to

$$\frac{1}{2} g_{\perp}^2 \left[\left(\frac{g_{\parallel}}{g} \right)^2 + 1 \right].$$

This variation is used in the calculations below.

The integration

$$\mathcal{J} = \int_0^{\pi/2} I \sin \theta d\theta$$

§ Now at Biophysics Laboratory, Stanford University, Stanford, California.

|| In part I, a factor of 4π was included in error.

can still be performed exactly for the Lorentzian but, because of the complicated nature of the result, it has been found more convenient to evaluate both line shapes numerically. The calculations can be performed for sweeping with either frequency or field. A set of curves thus obtained is given in Fig. 1, where they are shown as the first derivative $d\mathcal{J}/dx$ for sweeping with field. The calculations were made for both single crystal line shapes, using the same g_{\parallel} and g_{\perp} throughout. In Fig. 1 the calculated polycrystalline line shapes for the two different line shapes are compared for three different line widths.

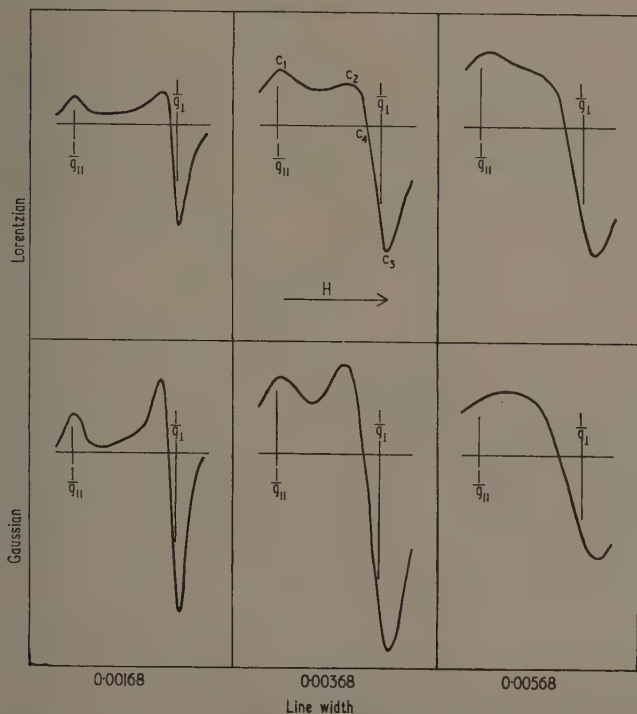


Fig. 1. First derivatives of absorption in polycrystalline substances. The curves are shown for sweeping with field. For all the curves $g_{\parallel}=2.039$ and $g_{\perp}=2.006$. The line widths are in units of $1/g$.

It is seen that peaks 1 and 3 correspond to g_{\parallel} and g_{\perp} respectively. A general rule for the fitting of these peaks is that the closest fit occurs for c_{\parallel} or c_{\perp} whichever has the lower value. Thus for the curves of Fig. 1, c_1 is very close to $1/g_{\parallel}$, except for the Gaussian of the widest line width. The location of $1/g_{\perp}$ to c_3 is less close and for the range of curves shown $1/g_{\perp} = c_3 - \lambda\Delta x$, where Δx is the single crystal line width and λ is a constant of value 0.15 for the Lorentzian, and 0.2 for the Gaussian. The distance $c_3 - c_4$ is related to the single crystal line width. For the curves of Fig. 1, $\Delta x = \mu(c_3 - c_4)$, where μ is a constant of value 2.28 for the Lorentzian and 1.80 for the Gaussian.

Even though these calculations have been described for a random arrangement of uniaxial crystallites, they would hold equally well for a random arrangement of free radicals showing uniaxial symmetry in a magnetic field. Such an arrangement of free radicals would be expected in a glass or similar material.

Calculations have also been made to fit the shapes of spectra recorded experimentally. Fig. 2 (a) and (b) shows the results for spectra obtained from irradiated deuterium peroxide (Smith and Wyard 1960). For the sample heavily irradiated

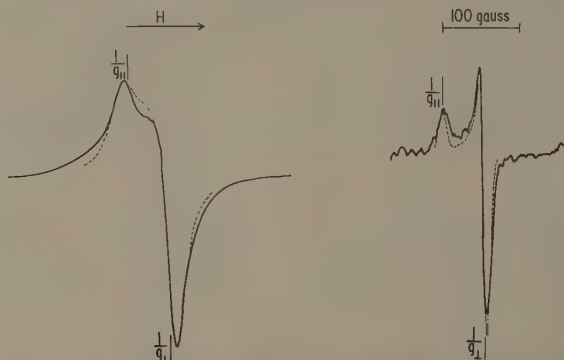


Fig. 2. Experimental and calculated electron spin resonance line shapes from irradiated deuterium peroxide: (a) irradiated with 15 mev deuterons at 90°K to produce a free radical concentration of 3.6×10^{-1} M. Calculated shape uses $g_{||} = 2.039$, $g_{\perp} = 2.0045$, and $\Delta x = 38.0$ gauss for a frequency of 9.35 Gc/s. The single crystal line shape is Lorentzian; (b) irradiated with ultra-violet light and warmed to 133.5°K to produce a free radical concentration of less than 5×10^{-3} M. Calculated shape uses $g_{||} = 2.039$, $g_{\perp} = 2.006$ and $\Delta x = 11.2$ gauss. The single crystal line shape is Gaussian.

with 15 mev deuterons a fit was found using a Lorentzian line shape, but for the warmed sample a Gaussian line shape had to be used. Both curves showed the same $g_{||}$ and g_{\perp} within the experimental error.

Kneubühl (1960) has extended the basic ideas of this type of calculation to crystals showing three different g -values, $g_1 \neq g_2 \neq g_3$. In his paper, Kneubühl derives various relations for the calculation of polycrystalline line shapes and, using the formulae he derives, calculations as above could be performed.

ACKNOWLEDGMENTS

The numerical integrations described above were performed on the 'Pegasus' at Northampton College, and we wish to express our thanks to the members of the Computer Section of the Mathematics Department for their assistance in this work. One of us (R.C.S.) acknowledges a grant from the British Empire Cancer Campaign.

REFERENCES

- BLEANEY, B., 1951, *Phil. Mag.*, **42**, 441.
- 1960, *Proc. Phys. Soc.*, **75**, 621.
- KNEUBÜHL, F. K., 1960, *J. Chem. Phys.*, **33**, 1074.
- SEARL, J. W., SMITH, R. C., and WYARD, S. J., 1959, *Proc. Phys. Soc.*, **74**, 491.
- 1960, *Bulletin Ampère*, fasc. spécial, 9th year, 236.
- SMITH, R. C., and WYARD, S. J., 1960, *Bulletin Ampère*, fasc. spécial, 9th year, 224.

Characteristic Electron Energy Loss Spectra of the Noble Metals and their Neighbours

By J. L. ROBINS†

Department of Physics, University of Western Australia, Nedlands, Western Australia

MS. received 24th April 1961

Abstract. The characteristic electron energy loss spectra of the elements Zr, Pd, Ag, Au, Zn and Cd have been obtained using the reflection technique and primary electron energies of 1500 and 800 eV. It is observed that in the second group of transition metals, the relation between the observed plasma losses and the theoretical values is not quite the same as that found previously for the first group of transition metals, in that the observed values are here greater than the theoretical near the beginning of the series. The spectra of the noble metals are complex and show few similarities to one another. The two elements Zn and Cd, which follow noble metals in the periodic table, have very similar spectra and it is obvious that plasma oscillations involving their two valence electrons are still influenced by the recently filled d band.

§ 1. INTRODUCTION

CHARACTERISTIC electron energy loss spectra represent the energy distribution of electrons which have been scattered both elastically and inelastically in a given material, and the positions of the peaks in the energy distribution, when measured back from the intense peak which is due to elastically scattered electrons, indicate the principal values of energy lost by the electrons during the scattering process. The magnitude of these losses has been found to be characteristic of the scattering material and independent of the primary energy.

It was suggested by Pines and his co-workers (Pines and Bohm 1952, Pines 1956, Nozières and Pines 1958, 1959) that the excitation of plasma oscillations would be the dominant loss process in elements where the outer or valence electrons are loosely bound and the core electrons are tightly bound, and this has been verified experimentally (Powell 1960). However, in elements such as the transition metals, the electrons in the incompletely filled d band can neither be considered as 'free' valence electrons nor 'bound' core electrons and the spectra are much more complex.

In a recent study of the characteristic electron energy loss spectra of the elements of the first group of transition metals, Ti to Cu (Robins and Swan 1960), it was found that the experimental value of the plasma loss agreed with the theoretical value, assuming all 3d and 4s electrons to be 'free', for the first two elements of the series but fell below the predicted value in the following elements. Terminating the transition series of each long period are the noble metals, which are generally considered to have the outermost d level full and one s electron.

† Now at National Research Council, Ottawa, Canada.

The binding energy of the electrons within the d band increases when this stage is reached. The plasma loss in Cu, however, is still not equal to the theoretical value, assuming only one free electron, which quite obviously indicates that the d electrons cannot be considered to be 'tightly bound' at this stage.

The present work was intended to extend the measurement of characteristic energy loss spectra to elements in the other series of transition metals which are terminated by noble metals, and also to study the elements following the noble metals in order to determine whether the d electrons can be considered as 'bound' for these elements.

It was considered desirable that the elements should be studied under as nearly identical conditions as possible, and that these conditions should be the same as those used for the previous work. This was to allow a more valid comparison between the results obtained and any theory which considers the elements as a unified series. In the previous work, target surfaces were prepared by evaporation *in situ*, and the spectra obtained immediately after the deposition of a new layer were considered to be representative of a clean surface of the metal.

In the second group of transition metals the only metals suitable for deposition as clean target surfaces by evaporation within the vacuum were Zr, Pd and Ag. Although only three in number, they fortunately represent both ends of the series and it was felt that they might indicate whether similar trends occur in this series to those seen in the first group of transition metals, particularly the relationship between the observed plasma losses and their theoretical values.

In the third group of transition metals, only the last two elements, Pt and Au, were available and suitable for study in the form of evaporated target surfaces. The element Pt has already been studied by Powell (1960), using the same equipment as used in this present work.

The elements following the noble metals Cu, Ag and Au, are Zn, Cd and Hg respectively. Zinc and cadmium were suitable for study and their spectra were recorded although Cd had also been investigated previously by Powell.

§ 2. EXPERIMENTAL PROCEDURE

The characteristic electron energy loss spectra of these elements were obtained using the reflection technique whereby electrons which have been elastically and inelastically scattered through 90° at the target surface are collimated and analysed with a 127° electrostatic energy analyser. The equipment and procedure were the same as previously described (Robins and Swan 1960). Primary energies of both 1500 and 800 eV were used with each metal to investigate changes in the relative intensities of the peaks.

Targets were prepared by vacuum evaporation *in situ*, and were examined immediately after deposition. With each metal studied the observed spectrum changed with time after the deposition of a clean surface and the change was particularly rapid with Zr, Zn and Cd. This change was generally slowed down by 'gettering' the chamber with prior evaporations of the metal concerned. Many evaporations and observations were made with each element, scanning in both directions along the energy scale, and spectra were found to be reproducible provided they were recorded directly after a new evaporation and thus may be considered characteristic of the clean metals.

The change with time is attributed to oxidation of the target surface but no attempt has been made to verify this, and there is also the possibility that it is due to gas adsorption. In an earlier study (Powell, Robins and Swan 1958) under somewhat different conditions, it was observed that the main effect of the adsorption of gas on tungsten was to alter slightly the characteristic loss values for that metal without seriously altering the spectrum. Thus a radical alteration of the spectra tends to indicate a chemical change rather than gas adsorption, but it should be noted that elements such as zirconium and titanium do adsorb gas rapidly. With liquid air in the cold trap around the target no trouble due to the formation of carbonaceous contamination was experienced.

Spectrographically pure metals obtained from Johnson, Matthey and Co. Ltd. were used for the evaporation of all the metals except Cd. The Cd was obtained from the Imperial Smelting Corporation Ltd., and was stated to be of 99.98% purity. The Zr was evaporated from multi-strand tungsten helical coils whilst the remaining elements were evaporated from single or multi-strand conical baskets. A system of buckets and hoppers allowed the evaporating furnaces to be reloaded in the vacuum in the cases where basket-type filaments were used. The pressure was normally less than 2×10^{-6} mm Hg though it rose above this value during evaporation.

The energy distribution curves presented in this work have all been normalized to compensate for the inherent variation of the effective aperture of the analyser with energy, though this effect is small over the energy ranges involved. The intensity scales are arbitrary and have been adjusted so that the intensities of the 25 eV peaks in the Ag spectra are six units whilst those of the dominant peaks in the Zn and Cd spectra and the 18 to 25 eV peaks in the remaining spectra are eight units. The spectra for Pd, Ag and Au were not extended beyond about 40 eV loss due to technical difficulties. The intense peak at zero energy loss, due to elastically scattered electrons, is not shown, but its width at half maximum intensity was about 1.8 and 2.0 eV at primary energies of 800 and 1500 eV respectively.

§ 3. RESULTS

The characteristic energy losses observed in Zr, Pd, Ag, Au, Zn and Cd are presented in Table 1, where the values quoted are the means of measurements made on a number of different spectra taken for each element and the errors shown are the probable errors of the means. Where possible, allowance has been made for the slope of the background when locating the positions of the peaks. The numbers in parentheses indicate the number of measurements used in the determination of the particular loss value.

Zirconium

The element Zr comes near the beginning of the second group of transition metals in the periodic table and occupies the same position in that series as Ti occupies in the first group of transition metals. Difficulty was experienced both in the evaporation of Zr and in obtaining a spectrum of the clean surface before some change, presumably oxidation, occurred. Similar difficulties had been experienced with Ti (Robins and Swan 1960).

The spectra obtained at the two primary energies are shown in Fig. 1, and the similarity between the general form of these spectra and that of Ti is striking.

There is no record of a previous study of this element. The 18.2 eV loss is interpreted as the plasma loss. No lowered plasma loss is observed and this is difficult to explain though the reason may possibly be connected with the extremely rapid rate of oxidation of the surface of this metal. The 3.4 eV loss was not clearly defined in many of the spectra and was rarely observed with a primary energy of 1500 eV. It could be a modified lowered plasma loss but is more likely to be due

Table 1. Characteristic Energy Losses as Found in the Present Work (in eV)

The numbers in parentheses indicate the number of measurements used in the determination of the particular loss value. The suggested identification of the energy losses is as follows: LP lowered plasma, P plasma, C combination, I ionization, U unidentified.

Zr	3.4 ± 0.1 (10) I	18.2 ± 0.2 (28) P	32.2 ± 0.4 (13) I	41.6 ± 0.3 (23) U	57.1 ± 0.4 (17)
Pd	6.8 ± 0.2 (43) LP	16.0 ± 0.3 (38) U	20.2 ± 0.4 (33) U	25.5 ± 0.2 (39) P	31.9 ± 0.3 (39)
Ag	4.1 ± 0.1 (68) U	7.3 ± 0.2 (67) LP	17.2 ± 0.3 (59) U	25.0 ± 0.2 (65) P	33.5 ± 0.4 (57)
Au	6.3 ± 0.2 (44) LP	16.0 ± 0.4 (40) U	25.8 ± 0.2 (43) P	32.6 ± 0.3 (39) C	
Zn	8.6 ± 0.1 (74) LP	17.0 ± 0.3 (70) P			
Cd	7.5 ± 0.1 (39) LP	15.1 ± 0.2 (39) P	68.2 ± 0.4 (7) I		

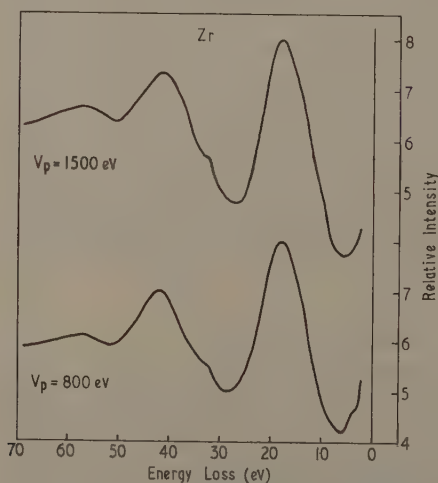


Fig. 1. Characteristic energy loss spectra of zirconium for primary electron energies of 1500 and 800 eV.

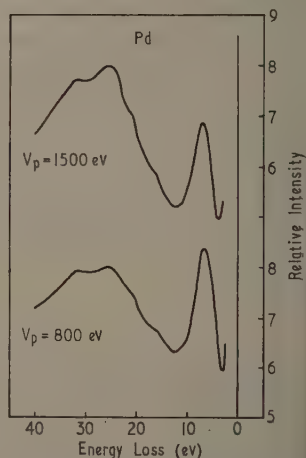


Fig. 2. Characteristic energy loss spectra of palladium for primary electron energies of 1500 and 800 eV.

to an intraband transition or to ionization of the $O_{4,5}$ band. The losses of 32.2 and 57.1 eV are fairly definitely due to ionization of the $N_{2,3}$ and N_1 levels respectively. These values are somewhat greater than would be expected from the x-ray energy-level data (Sandström 1957) but the x-ray values for this element seem slightly low when compared with the values for the neighbouring elements. In addition it should be noted that the ionization values observed in characteristic energy loss work have been found to be systematically greater by a few electron volts (Robins and Swan 1960) than the energy level values which are based on

x-ray absorption edges. In x-ray absorption the transition is to the first vacancy above the Fermi surface, whilst in ionization the electron is completely removed from the neighbourhood of the atom.

The broad intense loss peak of 41.6 eV is in many ways similar to the 48.3 eV loss in Ti and no doubt it has a similar origin. Peaks such as these have been observed in a number of other metals and will be discussed in a forthcoming publication (Robins and Best 1962).

Palladium

The spectrum for Pd, as observed with both primary energies, is shown in Fig. 2. The peaks at 6.8, 25.5 and 31.9 eV loss are much more intense and more clearly defined than those at 16.0 and 20.2 eV, which appear on the steep slope of the 25.5 eV loss peak. Our observed loss values, together with those of Marton and Leder (1954) and Gauthé (1958), are shown together in Table 2 for comparison. The agreement with Marton and Leder is not good as they only observe peaks corresponding to our two least intense peaks. The agreement with Gauthé is better for the more intense peaks, especially as it appears from his published spectrum that a peak near 6 or 7 eV may be present although not resolved from his intense peak of elastically scattered electrons.

Table 2. Characteristic Energy Losses in Palladium as Found in the Present Work and by Other Authors (in eV)

Present work	6.8	16.0	20.2	25.5	31.9	
Marton and Leder (1954)		15.7	21.5			
Gauthé (1958)				23.1	34.5	56 (?)

The peak at 6.8 eV could possibly be explained as a lowered plasma loss, and the fact that its intensity is relatively greater for the lower primary energy is in agreement with this interpretation (Powell 1960). The peaks at 16.0 and 20.2 eV loss remained unexplained. The other two intense peaks show a similarity to the form of the spectra observed for the later elements in the first group of transition elements. If we consider the 25.5 eV loss to be the plasma loss, then the 31.9 eV loss corresponds, within the limits of error, to a combination of the plasma and lowered plasma losses. It would, of course, also be possible for it to be interpreted as resulting from an interband transition.

Silver

The spectrum obtained for Ag, as shown in Fig. 3, is unlike that of any of the other transition metals studied in that it contains two very intense, narrow peaks at small energy loss values. Silver has been studied by a large number of workers and their results are compared with our own in Table 3. There appears to be good general agreement amongst these results if one allows that some experimenters may not have been able to resolve the 17.2 and 25.0 eV loss peaks.

A comparison of this spectrum with those of other transition metals (Robins and Swan 1960) would lead to the interpretation that the 25.0 eV loss is the plasma loss. Based on similar considerations, the 7.3 eV loss could be the lowered plasma loss and the 33.5 eV loss could be due to the combination of plasma and lowered

plasma losses. This leaves the 17.2 and 4.1 eV losses unexplained. Evidence which has recently been put forward to suggest that the loss of about 4 eV might be the plasma loss will be discussed later.

Table 3. Characteristic Energy Losses in Silver as Found in the Present Work and by Other Authors (in eV)

Present work	4.1	7.3	17.2	25.0	33.5	
Rudberg (1930)	4.6	7.4		24.8		
Turnbull and Farnsworth (1938)	3.9	7.3				
Ruthemann (1948)				22.6		45.3
Kleinn (1954)	4.5			22.8		
Watanabe (1954)				22		
Marton and Leder (1954)			16.0			
Marton <i>et al.</i> (1955)	3.4	7.0	16.7	24.8		
Gauthé (1955)		5.7		22.1	33	43
Gauthé (1956)		7.3		22.2	26	35
Jull (1956)	3.3	6.8	14.3	23.8		44.8
Watanabe (1956)	3.4	8	17.5	25	34	
Haberstroh (1956)				22.7		
Gauthé (1958)		7.5		22.1	26	36
Fert and Pradal (1958)				24.4		60
Steinmann (1960)	3.59	7.4	17.0	25.5		

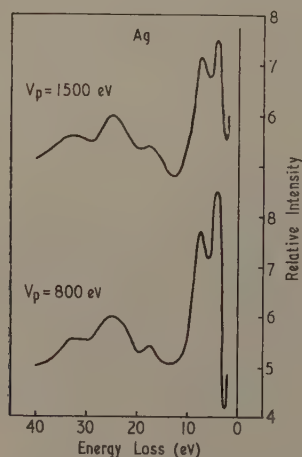


Fig. 3. Characteristic energy loss spectra of silver for primary electron energies of 1500 and 800 eV.

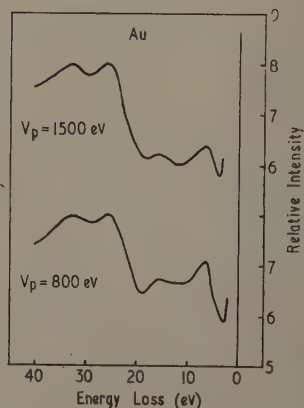


Fig. 4. Characteristic energy loss spectra of gold for primary electron energies of 1500 and 800 eV.

Gold

The spectrum for Au, as observed with the two primary energies, is given in Fig. 4. The suggested interpretation is that the 6.3 and 25.8 eV losses are a lowered plasma and a plasma loss respectively, whilst the 32.6 eV loss could be due to a combination of the two. No explanation of the 16 eV loss can be offered. Our results are compared in Table 4 with those of the many other workers who have studied gold.

Zinc

Extreme difficulty was experienced in obtaining spectra representative of the clean metal surface of Zn. Rapid oxidation, which causes the growth of an intense peak at 18.5 eV loss, made the positioning of the relatively weak peak at 17.0 eV very difficult. However, the curves presented in Fig. 5 are considered representative of the clean metal surface. The agreement between our values and those of other workers, as shown in Table 5, is poor, but this is understandable when the difficulty of maintaining a clean surface is considered. Although Gauthé's values show some agreement, the shape of his curve is completely different and is similar to the spectra of our oxidized target.

Table 4. Characteristic Energy Losses in Gold as Found in the Present Work and by Other Authors (in eV)

Present work	6.3	16.0	25.8	32.6		
Rudberg (1930)	7.3	10.1	25.9	35.2		
Möllenstedt (1949)		15		30	45	60
Watanabe (1954)	6.5	17.5	25	34	49	
Marton and Leder (1954)		16.5	21.5			
Marton <i>et al.</i> (1955)	5.2	14.4	23.9	32.0		
Gauthé (1955)	7.2		21.9	31	42.7	
Gauthé (1956)	6.6	15.5	19.7	23.4	35	44
Jull (1956)	5.5	16.1		24.0	32.2	47.0
Watanabe (1956)	6.5	17.5		25	34	50
Fert and Pradal (1958)	7.5			29		58
Gauthé (1958)	6.6	15.5	20.4	23.8	35	44

Table 5. Characteristic Energy Losses in Zinc as Found in the Present Work and by Other Authors (in eV)

Present work	8.6	17.0	
Kleinn (1954)	6.2		23.1
Gauthé (1959)	5.0	13.8	17.8

The 17.0 and 8.6 eV losses are considered to be the plasma and lowered plasma losses respectively. This interpretation is reasonable when it is considered that the influence of the not too tightly bound d electrons will be more likely to shift the plasma loss to a value which is greater, rather than less, than the value of 13.2 eV which is predicted theoretically by assuming only the two s electrons to be free. Another argument against assuming the 8.6 eV loss to be the plasma loss, with the 17.0 eV loss as a multiple, is the width of the peak, as it has been found (Robins 1962) that plasma peaks are rarely narrow except when they occur close to their theoretically predicted positions. A very slight peak at about 13.9 eV loss was observed in a number of the measured spectra and might possibly be due to $M_{4,5}$ shell ionization.

Cadmium

The spectrum of cadmium, as shown in Fig. 6, is extremely similar to that of Zn, and the interpretation of the peaks is based on the same considerations as those discussed for that metal. The 15.1 and 7.5 eV losses are interpreted as the plasma and lowered plasma losses respectively. A peak observed at 68.2 eV loss

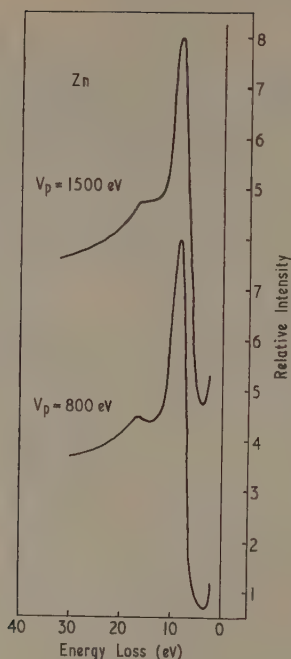


Fig. 5. Characteristic energy loss spectra of zinc for primary electron energies of 1500 and 800 eV.

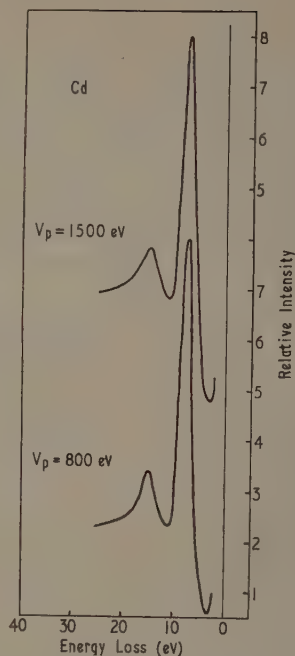


Fig. 6. Characteristic energy loss spectra of cadmium for primary electron energies of 1500 and 800 eV.

Table 6. Characteristic Energy Losses in Cadmium as Found in the Present Work and by Other Authors (in eV)

Present work	7.5	15.1	68.2
Möllenstedt (1949)	9	21.5	
Marton and Leder (1954)		14.5	
Kleinn (1954)	3.9	20.7	
Leder <i>et al.</i> (1956)	4.4	8.1	18.7
Gauthé (1959)			19.2
Powell (1960)	7.8	15.2	23.4

could be due to $N_{2,3}$ shell ionization, and another barely detectable peak at 12.3 eV loss, which appeared in a few of the spectra, might possibly be associated with ionization of the $N_{4,5}$ shell. These results are compared with those of previous workers in Table 6. The results of Powell (1960) were taken with the same equipment as that used in the present work.

§ 4. DISCUSSION

As mentioned previously, it was found that in the first group of transition metals, Ti to Cu, the plasma loss agreed with the theoretical value for the first two elements Ti and V, and then fell below the theoretical value for later elements

in the series, assuming all the 3d and 4s electrons to be 'free'. This was not in agreement with the prediction of Pines (1956) and Nozières and Pines (1958) who reasoned that the effect of interband transitions would cause the experimental values to be higher than the theoretical values at the beginning of the transition group and then to become less than them as one proceeds through the series.

In this present study of some of the elements in the second group of transition metals, it is found that the plasma loss in Zr, an element near the beginning of the series, is 18.2 eV which is considerably higher than the theoretical value of 15.3 eV. The last two elements, Pd and Ag, have plasma losses notably lower than the theoretical values of 30.7 and 29.8 eV respectively. Here, of course, all the 4d and 5s electrons are considered 'free' as in the discussion of Nozières and Pines.

Although it would have been more satisfactory to have been able to study under similar conditions more elements of the series, the present work definitely indicates a difference in the case of these two transition groups. The 'accidental cross-over', as Nozières and Pines term it, will occur later in the second group than in the first. This is possibly related to the fact that the binding energies of the 4d electrons in the second group are relatively higher than those of the 3d electrons in the first group, and this fact may have more significance than a mere consideration of the number of d electrons. It is realized that the elements Nb(Cb) and Mo, which follow Zr in the periodic table, have previously been studied by other workers, but they are not considered here as our aim has been to compare the theory with a set of results taken with the same equipment and under as nearly identical conditions as possible. A consideration of the tables in this and the previous paper will indicate the considerable variation in the results obtained with different techniques, apparatus and experimental procedure.

Interest in the study of silver has been heightened recently by a number of correlated studies. Some time ago, from a consideration of its optical properties, Fröhlich and Pelzer (1955) predicted a loss of about 4 eV in this metal and they implied that this should be the plasma loss, although this is much lower than the values of 9.0 or 29.8 eV which are predicted by the unmodified plasma theory (Pines 1956) if either one or eleven electrons per atom respectively are considered to be 'free'. More recent optical work by Taft and Philipp (1961) leads to the prediction of two energy losses, one at 3.75 eV which could be associated with collective oscillations and another at about 8 eV. Added to this, Steinmann (1960) and Brown, Wessel and Trounson (1960) have observed photon radiation from silver films under electron bombardment, which is considered to arise from plasma oscillations within the metal and this work also indicates a plasmon energy of 3.75 eV.

This would lead to the conclusion that the 4.1 eV loss which is observed in the spectrum of silver in the present work is the plasma loss. The general shape of the spectrum however does not tend to confirm this. If the 4.1 eV loss is the plasma loss, this would represent the only case so far recorded in which the plasma loss peak in the characteristic energy loss spectrum of a pure element is narrow and well defined when its position does not agree fairly closely with the loss value predicted by the unmodified plasma theory. Also, comparison of the spectrum of silver with the spectra of other noble and transition metals tends to indicate that the 25.0 eV loss would be the plasma loss.

Quite obviously some very pronounced phenomenon with an excitation energy of about 3.75 eV does occur in silver, but we feel that the question still remains as to whether this is indeed the same collective oscillation of the free electrons which is generally described by the term 'plasma oscillation'. For example, Hubbard (1955) indicates that there can be more than one frequency at which energy can be absorbed from the incoming electrons.

Following the procedure of Gauthé (1958) some correlation was previously found (Robins and Swan 1960) between the fine structure of x-ray absorption edges and certain characteristic losses in some metals of the first transition group. A similar comparison was attempted with Pd, Ag and Au but no correlation could be found with the x-ray data quoted by Gauthé.

For the elements following the noble metals, namely Zn and Cd, two factors are immediately apparent. Firstly, the inner d electrons are obviously still having an effect on the two outer valence electrons, causing the plasma losses to be shifted from their theoretically predicted values of 13.2 and 11.3 eV for Zn and Cd respectively, assuming only the two valence electrons to be 'free'. This is understandable as the binding energies of the d electrons in these metals are approximately the same as the plasma excitation energies. Secondly, the relative intensity of the lowered plasma loss in each of these elements is exceptionally large. It may be significant that the relative intensity of the peak interpreted as the lowered plasma loss peak increased in the later elements of the first group of transition metals leading up to Zn and again may be considered to increase relatively from Pd through Ag to Cd.

Nozières and Pines (1959) have pointed out that a large increase in the optical transmissivity with increasing frequency is to be expected at the plasma frequency and this has been observed in a number of elements where the plasma loss agrees with the theoretical value (Robins and Swan 1960, Powell 1960, Robins 1962). For the elements Ag, Au and Cd, however, Walker, Rustgi and Weissler (1959) have reported that transmissivity values greater than 0.1 to 0.3% could not be obtained in the ultra-violet. This is interesting as the observed plasma losses in these elements are not in agreement with the theoretically predicted values and the two phenomena may be related.

§ 5. CONCLUSION

The characteristic electron energy loss spectra of the elements Zr, Pd, Ag, Au, Zn and Cd have been obtained using the reflection technique and primary energies of 1500 and 800 eV. It is observed that in the second group of transition metals, the relation between the observed plasma losses and the theoretical values is not quite the same as that found previously for the first group of transition metals in that the observed values are here greater than the theoretical near the beginning of the group. The degree of agreement is probably related to the binding energies of the electrons in the incompletely filled d band rather than the number of electrons in that band.

The spectrum of silver was examined in the light of recent related studies which indicate the plasmon energy in that metal to be 3.75 eV. Although a loss peak is observed at 4.1 eV, it is felt that this loss does not have all the characteristics which it would be expected to have if it were indeed the plasma loss. In general, the spectra of the noble metals are complex and show few similarities to one

another. The two elements Zn and Cd, which follow noble metals in the periodic table, have very similar spectra and it is obvious that plasma oscillations involving their two valence electrons are still influenced by the filled d band.

ACKNOWLEDGMENTS

The author wishes to express his thanks to Professor C. J. B. Clews and Dr. J. B. Swan for their encouragement and interest in the work and also to acknowledge the tenure of a Commonwealth Postgraduate Award. The work was financed by the Research Grants Committee of the University of Western Australia.

REFERENCES

- BROWN, R. W., WESSEL, P., and TROUNSON, E. P., 1960, *Phys. Rev. Letters*, **5**, 472.
FERT, C., and PRADAL, F., 1958, *C.R. Acad. Sci., Paris*, **246**, 252.
FRÖHLICH, H., and PELZER, H., 1955, *Proc. Phys. Soc.*, **68**, 525.
GAUTHÉ, B., 1955, *C.R. Acad. Sci., Paris*, **241**, 188.
— 1956, *C.R. Acad. Sci., Paris*, **242**, 2634.
— 1958, *Ann. Phys., Paris*, **3**, 915.
— 1959, *Phys. Rev.*, **114**, 1265.
HABERSTROH, G., 1956, *Z. Phys.*, **145**, 20.
HUBBARD, J., 1955, *Proc. Phys. Soc. A*, **68**, 976.
JULL, G. W., 1956, *Proc. Phys. Soc. B*, **69**, 1237.
KLEIN, W., 1954, *Optik, Stuttgart*, **11**, 226.
LEDER, L. B., MENDLOWITZ, H., and MARTON, L., 1956, *Phys. Rev.*, **101**, 1460.
MARTON, L., and LEDER, L. B., 1954, *Phys. Rev.*, **94**, 203.
MARTON, L., LEDER, L. B., and MENDLOWITZ, H., 1955, *Advances in Electronics and Electron Physics* (New York: Academic Press), **7**, 183.
MÖLLENSTEDT, G., 1949, *Optik, Stuttgart*, **5**, 499.
NOZIÈRES, P., and PINES, D., 1958, *Phys. Rev.*, **109**, 1062.
— 1959, *Phys. Rev.*, **113**, 1254.
PINES, D., 1956, *Rev. Mod. Phys.*, **28**, 184.
PINES, D., and BOHM, D., 1952, *Phys. Rev.*, **85**, 338.
POWELL, C. J., 1960, *Proc. Phys. Soc.*, **76**, 593.
POWELL, C. J., ROBINS, J. L., and SWAN, J. B., 1958, *Phys. Rev.*, **110**, 657.
ROBINS, J. L., 1962, *Proc. Phys. Soc.*, **79**, in the press.
ROBINS, J. L., and BEST, P. E., 1962, *Proc. Phys. Soc.*, **79**, in the press.
ROBINS, J. L., and SWAN, J. B., 1960, *Proc. Phys. Soc.*, **76**, 857.
RUDBERG, E., 1930, *Proc. Roy. Soc. A*, **127**, 111.
RUTHEMANN, G., 1948, *Ann. Phys., Lpz.*, **2**, 113.
SANDSTRÖM, A. E., 1957, *Handb. d. Phys.*, Vol. 30, edited by S. Flügge (Berlin: Springer-Verlag), p. 57.
STEINMANN, W., 1960, *Phys. Rev. Letters*, **5**, 470.
TAFT, E. A., and PHILIPP, H. R., 1961, *Phys. Rev.*, **121**, 1100.
TURNBULL, J. C., and FARNSWORTH, H. E., 1938, *Phys. Rev.*, **54**, 509.
WALKER, W. C., RUSTGI, O. P., and WEISSLER, G. L., 1959, *J. Opt. Soc. Amer.*, **49**, 471.
WATANABE, H., 1954, *J. Phys. Soc. Japan*, **9**, 920.
— 1956, *J. Electronmicroscopy*, **4**, 24.

The Luminescence of CsBr(Tl) and CsI(Tl) as a Function of Temperature

BY J. C. ROBERTSON, J. G. LYNCH AND W. JACK

Department of Natural Philosophy, University of Glasgow

MS. received 29th December 1960, in revised form 10th April 1961

Abstract. The luminescent efficiencies and decay times of CsBr(Tl) and CsI(Tl) have been studied as a function of temperature in the range -150°C to 150°C . Protons of energy 14 mev, and alpha particles of energy 5.3 mev were used as the exciting radiation. In general, at any one temperature, the luminescence appears to consist of the sum of a fast and a slow exponential component. It is shown that for optimum particle discrimination by pulse shape analysis, there is no advantage to be obtained by maintaining the crystal of CsI(Tl) or CsBr(Tl) at temperatures other than room temperature.

Activation energies for the electron traps in the crystal corresponding to the decay time components τ_i have been obtained.

§ 1. INTRODUCTION

IT has been shown, (Storey, Jack and Ward 1958) that the decay time of the luminescence produced in CsI(Tl) by ionizing particles is dependent on the ionization density produced by the exciting particle. Robertson and Ward (1959) have used this effect to discriminate between different particles entering a CsI(Tl) crystal, and Robertson and Lynch (1961) have shown that of the commonly available inorganic crystals CsI(Tl) and CsBr(Tl) are most suitable for use with this technique. The present measurements on CsI(Tl) and CsBr(Tl) were made in the hope that a more favourable particle discrimination might be obtained at temperatures other than room temperature. The behaviour of the decay times and efficiencies of the luminescence as a function of temperature is also important when the mechanism of the luminescence is considered. Measurements of this type have been made by Bonanomi and Rossel (1952), Hahn and Rossel (1953) and Enz and Rossel (1958) in pure CsI, and by Knoepfel, Loepfe and Stoll (1957) in pure and thallium-activated CsI.

§ 2. EXPERIMENTAL METHOD

The CsI(Tl) and CsBr(Tl) crystals were obtained from the Harshaw Chemical Company, the thallium concentration in each case being 0.1% molar.

The particles producing high and low ionization density in these measurements were respectively, alpha particles of energy 5.3 mev from ^{210}Po , and protons of energy 14 mev from the reaction $^3\text{He}(d, p)^4\text{He}$.

It was necessary to mount the crystals *in vacuo* to avoid condensation of water vapour on the crystal at low temperatures. The assembly used is shown in Fig. 1. It consists of a cylinder of stainless steel (1/32 in. thick and 2 in. in diameter) lined with aluminium foil reflectors. The ^{210}Po source was mounted inside the

cylinder, while the protons entered by a thin (2 mg cm^{-2}) nickel window N in the detachable brass top plate B of the cylinder. The base of the cylinder was closed with a disk of lucite L which was optically coupled to an RCA 6810 photomultiplier with silicone grease. A thin aluminium foil (0.2 mg cm^{-2}) backed the crystal X which was clamped between two copper rings R both of which had aluminized surfaces. The lower ring was attached to a copper rod C which protruded through the wall of the vessel where it could be cooled with liquid nitrogen or heated with an electrical element EI as required.

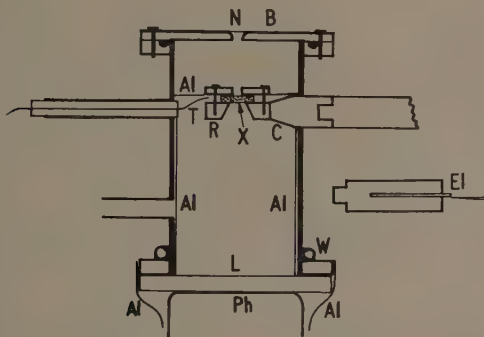


Fig. 1. Crystal mounting.

A thermocouple T was used to measure the crystal temperature. All heating and cooling was carried out slowly and no hysteresis effect was observed. The range of temperatures obtainable was -160°C to $+160^{\circ}\text{C}$. Finally, water cooling pipes W ensured that the temperature of the photo-cathode Ph remained constant.

The current pulses from the photomultiplier were integrated with a leakage time constant of $205 \mu\text{sec}$. These 'voltage' pulses were displayed on a Tektronix type 541 oscilloscope and photographed at fixed temperature intervals.

§ 3. ANALYSIS

The decay of the luminescence was obtained by the method described by Storey, Jack and Ward (1958). Photographs of the voltage pulses were projected and traced on fine graph paper, and after slight correction for the finite leakage time constant ($\tau = 205 \mu\text{sec}$) the pulses were carefully differentiated to obtain the original 'current' pulse. This provides a consistent method of averaging the statistical fluctuations in the current pulse. The analysis of the decay of the luminescence of CsBr(Tl) at 20°C , irradiated with protons of 14 mev , is shown in Fig. 2. From Fig. 2(a) it appears that an exponential component of time constant $\tau = 23 \mu\text{sec}$ is present. Having estimated the lifetime and contribution of this component from Fig. 2(a), we subtracted it from a pulse on a shorter time scale, Fig. 2(b). The resulting points are in reasonable agreement with a pure exponential of time constant $\tau = 2.6 \mu\text{sec}$.

In general, at any one temperature, the decay of the luminescence of CsI(Tl) and CsBr(Tl) may be described by the sum of a fast and a slow exponential component. Fig. 3 shows one of the exceptional cases where three exponential components appear to be present in the luminescence produced by fast proton irradiation of CsBr(Tl).

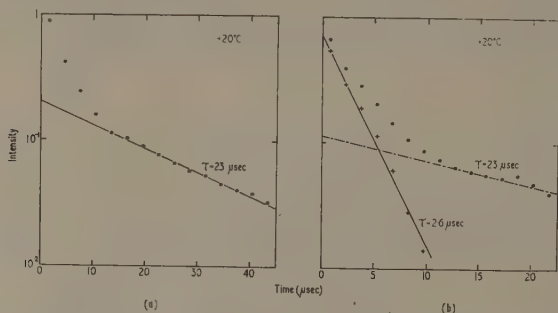


Fig. 2. The decay curves of the luminescence produced by 14 mev protons in CsBr(Tl) at +20°C.

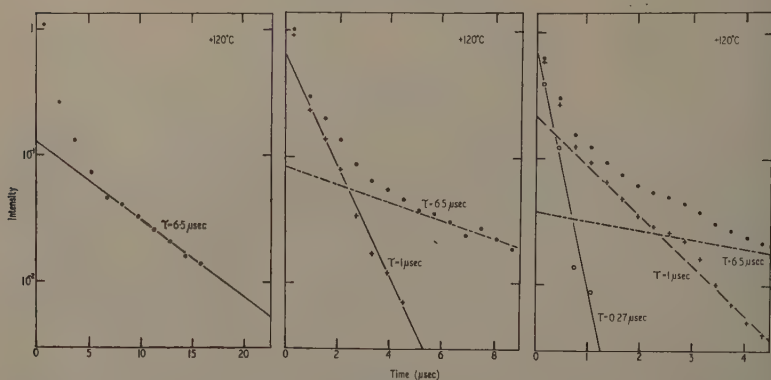


Fig. 3. The decay curves of the luminescence produced by 14 mev protons in CsBr(Tl) at +120°C.

In CsI(Tl) the contribution from the slow exponential component is small over most of the temperature range. Accordingly, the pulse has been analysed by an alternative method which assumes that the decay of the luminescence is a pure exponential at times short compared with the lifetime of the slow exponential component. Values derived by this method are denoted by τ' . The subscripts α and p denote excitation of the crystal by alpha particles and protons respectively.

§ 4. RESULTS

If the logarithm of the decay time components is plotted against the reciprocal of the absolute temperature (Figs 4(a), (b) and 5(a), (b)) it is seen that the components obtained by the above analysis are not distributed randomly, but, in

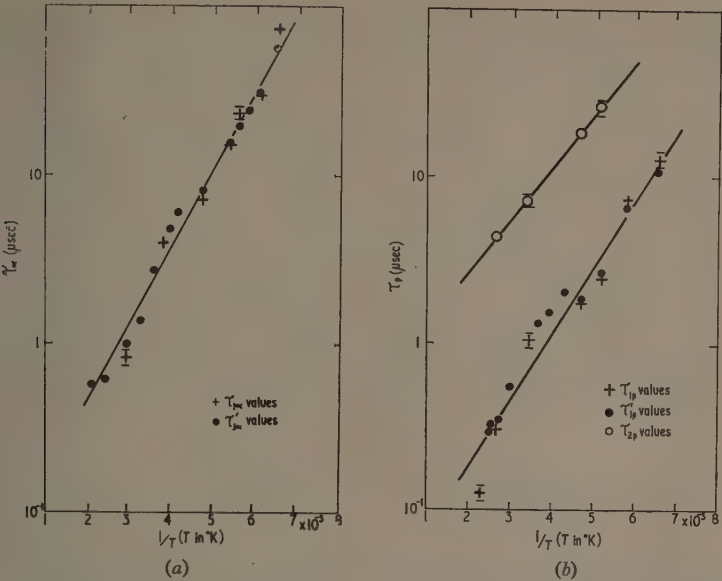


Fig. 4. (a) Alpha-particle excitation of CsI(Tl). Decay time component $\tau_{1\alpha}$ as a function of $1/T$. (b) Proton excitation of CsI(Tl). Decay time components τ_{1p} and τ_{2p} as a function of $1/T$.

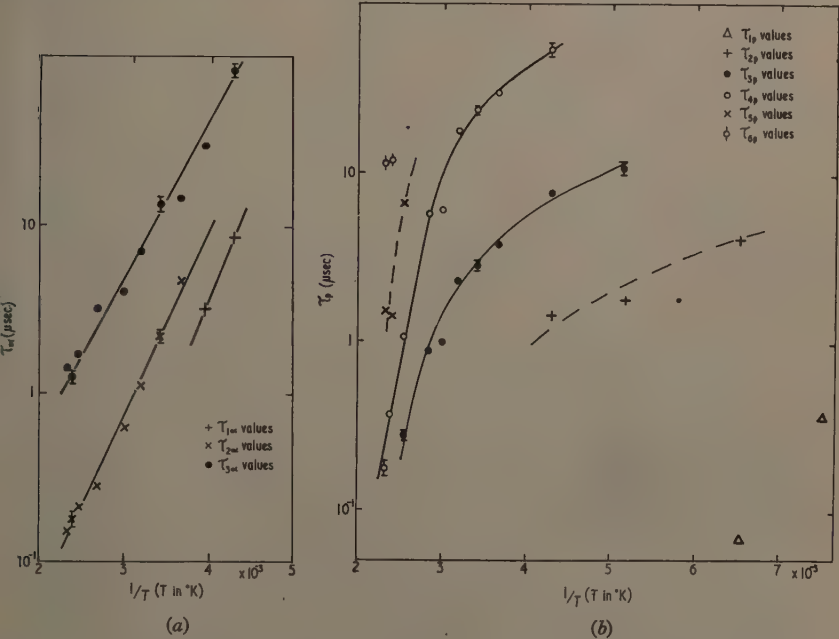


Fig. 5. (a) Alpha-particle excitation of CsBr(Tl). Decay time components $\tau_{1\alpha}$ as a function of $1/T$. (b) Proton excitation of CsBr(Tl). Decay time components τ_{dp} as a function of $1/T$.

general, follow exponential laws. In order to discriminate between the different components present in the decay, the components have been numbered according to the line on which they lie.

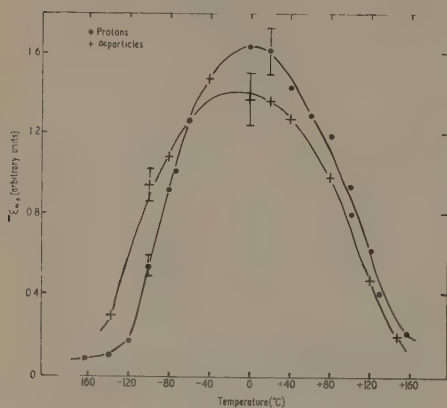


Fig. 6. The efficiency of alpha-particle and proton produced luminescence in CsI(Tl).

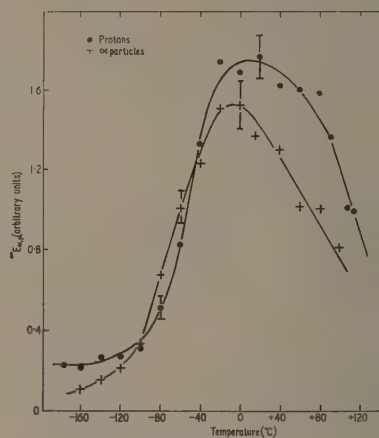


Fig. 7. The efficiency of alpha-particle and proton produced luminescence in CsBr(Tl).

Table 1. Values of R for Excitation of CsI(Tl)

(a) Alpha-particle excitation.

Temp. (°C)	-80	-40	0	+20	+80	+146
R_1	1	1	0.86	0.75	1	1
R_2	—	—	0.14	0.25	—	—

(b) Proton excitation.

Temp. (°C)	-120	-100	-80	-60	+20	+100	+155.5
R_1	1	1	0.32	0.39	0.55	0.93	1
R_2	—	—	0.68	0.61	0.45	0.07	—

Table 2. Values of R for Excitation of CsBr(Tl)

(a) Alpha-particle excitation.

Temp. (°C)	-40	-20	0	+20	+40	+60	+100	+130	+147
R_1	0.19	0.16	—	—	—	—	—	—	—
R_2	—	—	0.23	0.72	0.48	0.56	0.58	0.69	0.74
R_3	0.81	0.84	0.77	0.28	0.52	0.44	0.42	0.31	0.26

(b) Proton excitation.

Temp. (°C)	-120	-80	-40	0	+20	+40	+60	+80	+120	+147	+156.5
R_1	0.26	—	—	—	—	—	—	—	—	—	—
R_2	0.74	0.51	0.18	—	—	—	—	—	—	—	—
R_3	—	0.49	0.16	0.37	0.42	0.47	0.42	0.37	0.27	—	—
R_4	—	—	0.66	0.63	0.58	0.53	0.58	0.63	0.35	0.39	0.18
R_5	—	—	—	—	—	—	—	—	0.38	0.37	0.46
R_6	—	—	—	—	—	—	—	—	0.24	0.37	—

The variation with temperature of the pulse height per unit energy or luminescent efficiency $\propto \mathcal{E}_{\alpha, p}$ is shown in Figs 6 and 7. In these efficiency measurements it was assumed that all the components contributing to the light output were observed. The results have been corrected for the effect of the electronic differentiation time constant of the pulses.

Tables 1 (a), (b) and 2 (a), (b) give the values of R_1 , R_2 etc., the ratios of the light present in components 1, 2 etc. to the total light output observed.

§ 5. DISCUSSION AND CONCLUSIONS

The temperature dependence of the ratio $\tau_{1p}/\tau_{1\alpha}$ for CsI(Tl) is shown in Fig. 8. It can be seen from this figure that, for particle discrimination, there is no advantage in maintaining the crystal at temperatures above room temperature, since, although the ratio $\tau_{1p}/\tau_{1\alpha}$ increases slightly, the efficiencies $\propto \mathcal{E}_{\alpha, p}$ show a marked decrease. A similar type of behaviour is observed in CsBr(Tl).

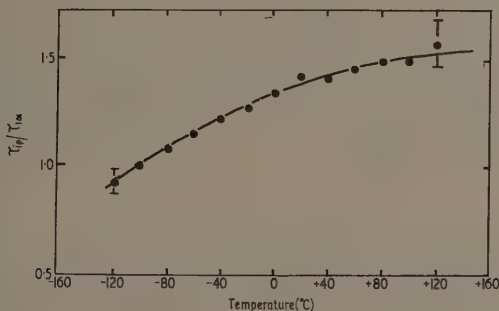


Fig. 8. Variation of the ratio $\tau_{1p}/\tau_{1\alpha}$ with temperature in CsI(Tl).

The variation with temperature of the ratio $\tau_{1p}/\tau_{1\alpha}$ in CsI(Tl) is not in accord with the hypothesis advanced by Storey, Jack and Ward (1958). These authors suggested that the differing values of τ_{1p} and $\tau_{1\alpha}$ might be explained by an increased effective temperature in the material surrounding the particle track for particles of high ionization density. This interpretation would lead one to expect that the ratio $\tau_{1p}/\tau_{1\alpha}$ would increase as the crystal temperature was lowered.

In Figs 6 and 7, it is seen that the luminescent efficiencies of CsI(Tl) and CsBr(Tl) have a maximum value in the neighbourhood of room temperature. An interesting feature is the temperature range -70°C to -140°C in CsI(Tl) where the luminescent efficiency for alpha-particle excitation is greater than that for proton excitation. This effect is also observed to a lesser degree in CsBr(Tl).

We must conclude that there is no advantage to be gained from the point of view of particle discrimination by pulse shape analysis by maintaining the crystal at temperatures other than room temperature.

From Figs 4 (a) and 5 (a) for the alpha-particle excitation of the crystals, it appears that the decay time components in these cases have an exponential dependence on $1/T$, where T is the absolute temperature. It is customary

(Bonanomi and Rossel 1952, Enz and Rossel 1958) to derive from these plots a value for the activation energies of the electron traps associated with the luminescence. The assumption is made that the probability of a luminescent transition is proportional to $e^{-E/kT}$ where E is the electron trap activation energy and k is Boltzmann's constant. For CsI(Tl) we obtain $E_{1a} = 0.092 \pm 0.01$ ev, while CsBr(Tl) yields values $E_{2a} = 0.22 \pm 0.02$ ev and $E_{3a} = 0.19 \pm 0.02$ ev. Although the decay time components for proton excitation of CsI(Tl) τ_{1p} and τ_{2p} show an approximately exponential dependence on $1/T$ yielding electron trap activation energies $E_{1p} = 0.079 \pm 0.01$ ev and $E_{2p} = 0.062 \pm 0.02$ ev, there is no evidence of this exponential behaviour in the proton excitation of CsBr(Tl). This throws doubt on the validity of the above simple picture in the case of proton excitation of the crystals.

It is possible that the phenomena which account for the variation of decay time τ with ionization density due to the particle producing the luminescence also account for the dissimilar behaviour of τ with $1/T$ for different types of particle.

ACKNOWLEDGMENTS

The authors are indebted to Professor P. I. Dee for his interest in this work. Two of us (J. C. R. and J. G. L.) wish to acknowledge the receipt of Research Studentships from the Department of Scientific and Industrial Research. The crystal mounting was an improved version of one designed by G. D. Wells in this department.

REFERENCES

- BONANOMI, J., and ROSSEL, J., 1952, *Helv. Phys. Acta*, **25**, 725.
ENZ, H., and ROSSEL, J., 1958, *Helv. Phys. Acta*, **31**, 25.
HAHN, B., and ROSSEL, J., 1953, *Helv. Phys. Acta*, **26**, 803.
KNOEPFEL, H., LOEPFE, E., and STOLL, P., 1957, *Helv. Phys. Acta*, **30**, 521.
ROBERTSON, J. C., and LYNCH, J. G., 1961, *Proc. Phys. Soc.*, **77**, 751.
ROBERTSON, J. C., and WARD, A., 1959, *Proc. Phys. Soc.*, **73**, 523.
STOREY, R. S., JACK, W., and WARD, A., 1958, *Proc. Phys. Soc.*, **72**, 1.

The Electronic Band Structure of a Model of a Cubic Crystal

BY L. PINCHERLE AND P. M. LEE

Bedford College, University of London

MS. received 9th May 1961

Abstract. The electronic band structures of a simple cubic and a face-centred cubic array of square potential wells were calculated by a plane wave method for various depths of the potential wells. Certain features of the band structure depend only on the symmetry of the crystal and not on the details of the potential: in a simple cubic monatomic substance an s-type band has its minimum at $\mathbf{k}=0$ and its maximum at $\mathbf{k}=(1, 1, 1)$; a p-band has its minimum at $\mathbf{k}=(1, 0, 0)$ and almost certainly its maximum at $\mathbf{k}=(1, 1, 0)$. In a face-centred monatomic crystal an s-band has its minimum at $\mathbf{k}=0$, while its maximum may be at any of several positions, such as $\mathbf{k}=(2, 1, 0)$, $\mathbf{k}=(1, 0, 0)$, or intermediately. A p-band has its minimum at $\mathbf{k}=(1, 1, 1)$ with a secondary minimum at $\mathbf{k}=(1, 0, 0)$, and its maximum at $\mathbf{k}=0$. Various methods of band structure calculation were compared on the example of the lowest level at $\mathbf{k}=0$ for any depth of the potential wells for the face-centred structure. Plane wave methods gave reliable results with least labour.

§ 1. INTRODUCTION

WHEREAS much effort and ingenuity has been directed to the development of powerful and precise methods for evaluating the electronic band structure of a crystal starting from a given field, less attention has been given to the question of how far and in what respects the calculated band structure depends on the choice of a particular field. This point is important in view of the difficulty of achieving complete self-consistency in any calculation of this kind, and the present paper is an attempt at examining the problem in a simple case. That is, we have investigated the effect of changes in the potential on the band structure of a model of a cubic crystal (both simple cubic and face-centred). The general aim was to determine for each crystal structure the possible distributions of energy levels, to see whether some general features are independent of the particular field; and also to study the effect of various characteristics of the potential in displacing levels of a certain symmetry with respect to others. The philosophy of the present approach is thus similar to that of investigations such as Callaway's (1959) on the d-bands of transition metals and Howland's (1958) on the energy bands of KCl. That the crystal structure is fundamental in determining the electronic energy levels is indicated by the fact that a hypothetical sodium with the diamond structure would have bands very similar to those of silicon (Bassani 1959) and that a hypothetical face-centred carbon would be a standard metal (Casella 1958).

Another aim of the investigation was to compare on a simple model the various methods available for band structure calculation, in order to ascertain how

quickly they converge to the correct result and how justifiable it is to stop at a certain approximation.

§ 2. MODEL

The model consists of a simple, or face-centred cubic array of square potential wells. That is, in each Wigner-Seitz cell the potential is taken to be constant and equal to $-\phi$, for $r \leq b$, b having any value less than the radius of the inscribed sphere, and zero otherwise. This model was first considered by Engelmann (1956) and was chosen to facilitate calculations with certain methods. Several procedures for band evaluation are designed for a potential which is constant outside atomic spheres; and matters are drastically simplified if inside such spheres the potential is spherically symmetric.

If a is some fundamental lattice distance to be used as unit of length, the characteristics of the model are expressed through the two dimensionless parameters $R_0 = b/a$; $V_0 = 2ma^2\phi/\hbar^2$. The energy W will also be expressed through the dimensionless quantity $E = 2ma^2W/\hbar^2$ (for $a = 2.5$ atomic units, $= 1.3 \text{ \AA}$, $E = 1$ corresponds to $W \approx 2.2 \text{ eV}$) and the wave vector \mathbf{q} through $\mathbf{k} = a\mathbf{q}$.

If nearest neighbours are at $(2, 0, 0)$ in the simple cubic lattice and at $(2, 2, 0)$ in the face-centred lattice, the radius of the sphere inscribed in the Wigner-Seitz cell is 1 for the former and $2^{1/2}$ for the latter. For the simple cubic lattice the first Brillouin zone is a cube (Fig. 1), k_x, k_y, k_z varying between $-\frac{1}{2}\pi$ and $\frac{1}{2}\pi$; for the face-centred structure it is a truncated octahedron (Fig. 2), the centres of the square faces being at points such as $(\frac{1}{2}\pi, 0, 0)$.

The (E, \mathbf{k}) relation, for the first few bands, was determined for the two structures for a number of values of V_0 . Since a and ϕ enter through the combination $a^2\phi$, one obtains in principle the effect of the variation of both the lattice distance and the depth of the potential wells, but in fact, to study the effect of a change in lattice distance alone, one must vary also R_0 . Here instead R_0 was taken in all cases equal to the radius of the sphere inscribed in the Wigner-Seitz cell: the study of the effect of variations of this quantity, for constant V_0 , did not seem of much physical significance. Attention was mainly concentrated on the determination of the values of V_0 at which the various energy gaps appear and of the position in \mathbf{k} -space of the corresponding band edges. The model is thus relevant to the theory of semiconductors, but not to that of metals, where the details of the often very complicated Fermi surfaces depend generally on the characteristics of the potential.

Similar calculations on more realistic models may serve as a guide to the possible band structures of real crystals, especially to the variation of the band structure along a series of similar crystals or in mixed crystals; for instance, one might study the effect of deviations of the potential from spherical symmetry on the position of the various levels in diamond and zincblende type crystals.

§ 3. LIMITING CASES

The energy levels are known exactly in the two limiting cases of $V_0 = 0$ and $V_0 = \infty$. In the first case (completely free electrons) $E_n(\mathbf{k}) = |\mathbf{k} + \mathbf{K}_n|^2$, \mathbf{K}_n being any fundamental vector of the reciprocal lattice; these fundamental vectors are therefore used to label the free electron bands. In the other limiting case (infinite square well potential) the levels can be labelled as in well-known nuclear models.

The energies of the lowest levels, independent of \mathbf{k} , measured from the bottom of the well, are

Level	1s	1p	1d	2s	1f	2p
ER_0^2	9.87	20.19	33.22	39.48	48.83	59.68

In the general case, if the crystal is without glide planes or screw axes, the energy levels at any point in \mathbf{k} -space are classified according to the irreducible representations of the group of the corresponding \mathbf{k} -vector. Each \mathbf{k} -point of prominent symmetry is traditionally denoted by a Greek or Latin capital letter,

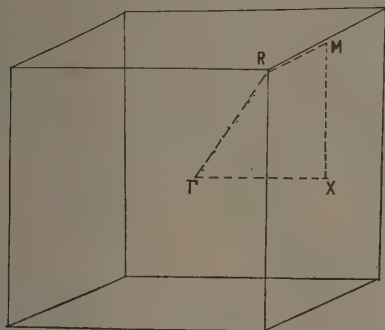


Fig. 1. Brillouin zone for the simple cubic lattice, with prominent symmetry points and path along which the (E, \mathbf{k}) relations were evaluated.

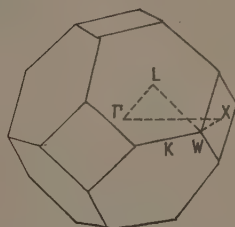


Fig. 2. Brillouin zone for the face-centred cubic lattice, with prominent symmetry points and path along which the (E, \mathbf{k}) relations were evaluated.

indicated in Figs 1 and 2. The various representations will be denoted by the spectroscopic suffices s, p, d . . . , indicating the first term of the expansion in spherical harmonics of the corresponding wave function (Bell 1954). p, p', p'' . . . will be used when there is more than one representation which is predominantly p-type, etc. The methods of group theory permit one also to decide to which of the free electron or tightly bound levels the various states reduce in the two limiting cases.

§ 4. METHOD OF CALCULATION

It would be desirable to have a single method of calculation applicable for all values of V_0 ; but clearly at one end of the scale ($V_0 \rightarrow 0$) plane wave methods must be vastly superior, while at the other end ($V_0 \rightarrow \infty$) the tight binding procedure will yield the energy values with least labour. However a complete calculation was carried out only with the method of simple plane waves, because the region of relatively small values of V_0 seemed physically the most interesting. The tight binding formalism may then be used, particularly for fairly large V_0 , to interpolate results calculated at \mathbf{k} -points of prominent symmetry, and also, with additional assumptions, to extrapolate results to $V_0 \rightarrow \infty$. Application of these methods is described in § 7.

In the method of plane waves, the wave function is expanded in a Fourier series. Enough terms were inserted to obtain the correct ordering of the levels at each point, though not enough to ensure a convergence of the eigenvalues better than about 0.1 (0.2 eV for a lattice spacing, in the simple cubic lattice, of 2.6 Å). The convergence becomes worse, as one would expect, on increasing V_0 .

The function of the correct symmetry for any irreducible representation j of the group of a \mathbf{k} -vector was obtained by standard methods using the projection operator

$$\Psi_{\text{sym}}^{(j)} = \sum_R [D^{(j)}R]_{ii} R\psi$$

where $\Psi_{\text{sym}}^{(j)}$ is the symmetrized function; $[D^{(j)}R]_{ii}$ is the ii th element of the matrix for the representation in question (which is the character if the representation is one-dimensional), and R are the symmetry operations of that particular group. ψ is normally a simple plane wave $\exp\{i(\mathbf{k} + \mathbf{K}_n) \cdot \mathbf{r}\}$. These linear combinations were used to form the energy matrix, the order of the matrix being related to the number of \mathbf{K} -vectors considered. The other quantities in the energy matrix are the Fourier coefficients $V(\mathbf{K}_n)$ of the potential $V(\mathbf{r})$

$$V(\mathbf{K}_n) = \frac{1}{\Omega} \int_{\text{unit cell}} V(\mathbf{r}) \exp(-i\mathbf{K}_n \cdot \mathbf{r}) d\mathbf{r} = -\frac{4\pi V_0}{\Omega K_n^3} [\sin K_n R_0 - K_n R_0 \cos K_n R_0]$$

where Ω is the volume of the Wigner-Seitz cell.

The roots of the energy matrix were obtained using an iterative method, the matrix being first inverted in order to obtain the first few roots without wasting time over higher levels which often were not required. The calculations were performed on the University of London 'Mercury' computer. The largest matrix used was of order 12, but at many points convergence was good with smaller number of waves. At some points, particularly on the zone boundary the wave functions were almost plane waves, whilst at other points they were more atomic like, and at such points the convergence was poorer.

§ 5. RESULTS FOR SIMPLE CUBIC LATTICE

Figures 3, 4 and 5 give the lowest bands, along the directions in \mathbf{k} -space indicated in Fig. 1, for the simple cubic lattice and for $V_0 = 0$ (free electrons), 10, and 25 respectively. All energies are measured from the bottom of the potential well. The various broken lines indicate bands of different symmetry.

A point that immediately emerges is that the quasi free-electron ordering of the levels persists up to relatively high values of V_0 , a circumstance often noted in real crystals (see, for instance, Callaway's (1956) discussion for body-centred cubic crystals). Deviations occur mainly because bands of the same symmetry cannot cross. From results obtained for a few values of V_0 , it is possible to interpolate in the whole range $0 \leq V_0 \leq \infty$, since the relative displacement of the various levels occurs quite smoothly. With the tight binding interpolation procedure it is also possible to plot the bands along other directions in \mathbf{k} -space. At $V_0 = 25$ (Fig. 5), the two lowest bands have already almost exactly the form given by the simplest tight binding calculation.

Thus in a simple cubic crystal the lowest band, s-type, has its lowest energy at $k = 0$ and its highest at the corners of the cubic Brillouin zone. No reasonable form of the potential could lead to any other result. The first and second band

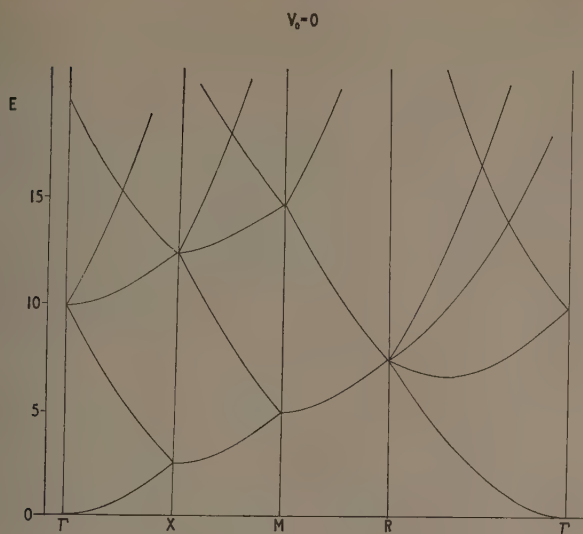
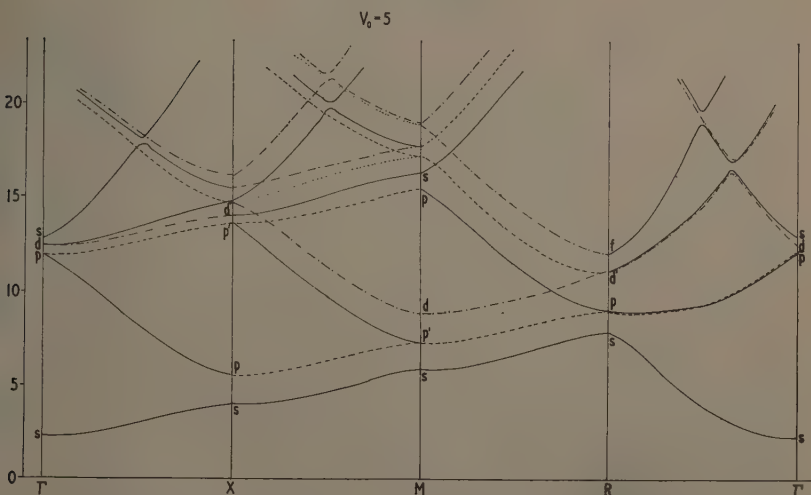


Fig. 3. Free electron bands for the simple cubic lattice.

Fig. 4. The lowest bands in the simple cubic lattice for $V_0=5$.

become separated at $V_0=11.4$. The lowest level of the second (p-type) band is at X, as indicated both by the free electron and by the tight binding models, and again this may be considered a general property of simple cubic crystals. When the second energy gap first appears, at about $V_0=18.6$, the level M_p (non-degenerate) has the highest energy. Now, according to the simplest tight

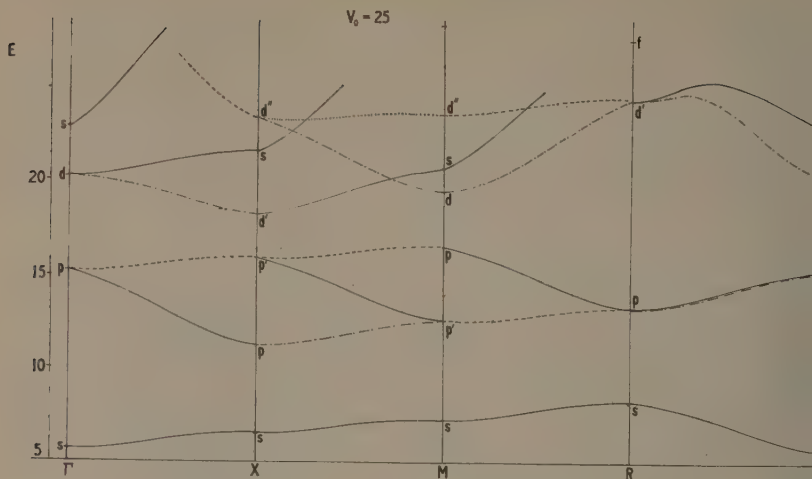


Fig. 5. The lowest bands in the simple cubic lattice for $V_0 = 25$.

binding approximation, the energy of this band is given by

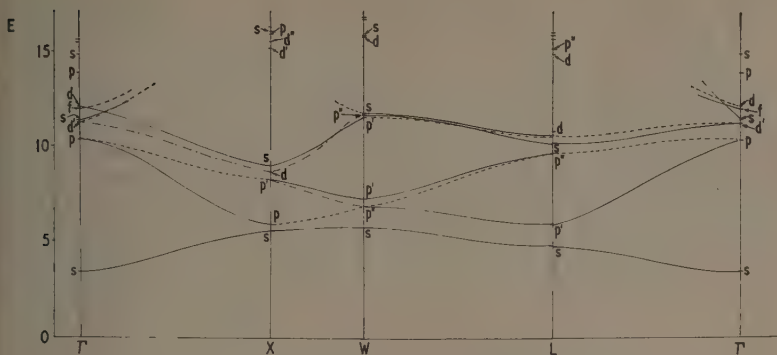
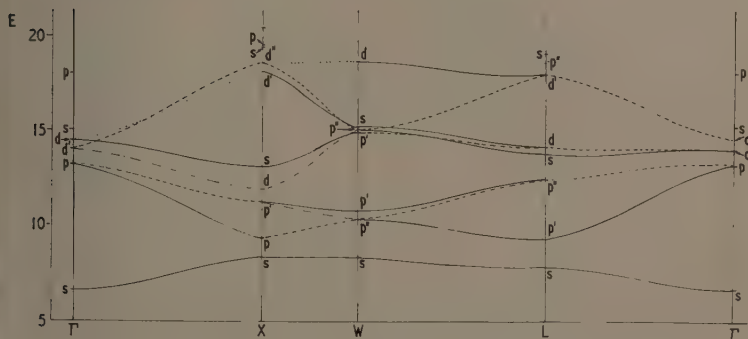
$$E = E_0 + A^2 \cos k_x - B^2 (\cos k_y + \cos k_z),$$

indicating that the top level is at M ($\cos k_x = 1$, $\cos k_y = \cos k_z = -1$) also for $V_0 \rightarrow \infty$; therefore it seems unlikely that intermediate values of V_0 will lead to any other result. There thus seems strong evidence that the positions of the edges of the p-band are also determined by symmetry. No monatomic substance crystallizes in the simple cubic structure, and the only known such structures are the low temperature modifications of CsCl, CsBr, CsI. As is well known, the presence of two atoms in the Bravais lattice brings substantial modifications of the band structure. However the Brillouin zone and the type of bands are the same. The valence band of these substances is a p-band of the type just considered, and thus one would forecast, as far as the present model may apply, that positive holes in these halides would be situated at the twelve equivalent points M of \mathbf{k} -space. The conduction band would be s-type and, unless there were a strong interaction with d-type levels, its bottom would be at $\mathbf{k} = 0$.

The lowest level of the third (d-type) band, when an energy gap first appears between the second and third band, is at M; but this d-type level moves upwards rapidly on increasing V_0 and for V_0 greater than 25 the lowest level is at X. For higher levels the worsening convergence of the results does not warrant any firm conclusion. As the bands become increasingly separated, all levels in a band tend to become predominantly s, or p, or d . . . according to the type of level to which the band reduces for $V_0 \rightarrow \infty$.

§ 6. RESULTS FOR FACE-CENTRED CUBIC LATTICE

Figures 6 and 7 show results for the face-centred lattice for, respectively, $V_0 = 5$ and $V_0 = 10$. In this case the bands were calculated only at Γ , X, W, L and have been sketched in what seemed a reasonable way at intermediate points.

$V_0 = 5$ Fig. 6. The lowest bands in the face-centred cubic lattice for $V_0 = 5$. $V_0 = 10$ Fig. 7. The lowest bands in the face-centred cubic lattice for $V_0 = 10$.

For $V_0 = 10$ the d-band has been sketched as though it were already separated from higher bands.

Again the free electron ordering of the levels is seen to persist to a considerable extent. The ordering of the levels at Γ , X, L is the same as that found by Casella (1958) with the orthogonalized plane waves method for a hypothetical face-centred carbon. The lowest band has its minimum at $k=0$ and its maximum at W, but a second maximum of about the same height exists at X. At the point K, at the end of the (1, 1, 0) direction, the energy is also found not to be much lower. Thus in this case the characteristics of the potential must be the deciding factor. In the tight binding approximation, considering interaction with nearest neighbours only, the energies at X and W, and at all points along the diagonals of the square faces of the Brillouin zone, are the same. Interaction with second nearest neighbours makes W higher. In face-centred solid He, a recent calculation has in fact given the top level at W (Simcox and March, private communication).

An energy gap between the first and second band first appears at $V_0 = 5.4$. The lowest level of the second (p) band is found at L, as for free electrons. The tight binding procedure, with interaction with nearest neighbours only, gives L as the lowest level, with another minimum at X. With second neighbours interaction, X may become the lowest state. The highest state is at $k = 0$ in all approximations, so that this may be considered a general property of monatomic face-centred cubic crystals. A secondary maximum is at L. One must remember that, in an actual substance, the states of the valence band must be orthogonal to all core states, and this may alter quite markedly the order of the levels (see, for instance, Herman and Skillman 1960). This interaction, dealt with generally by the method of orthogonalized plane waves, could be taken into account in the present

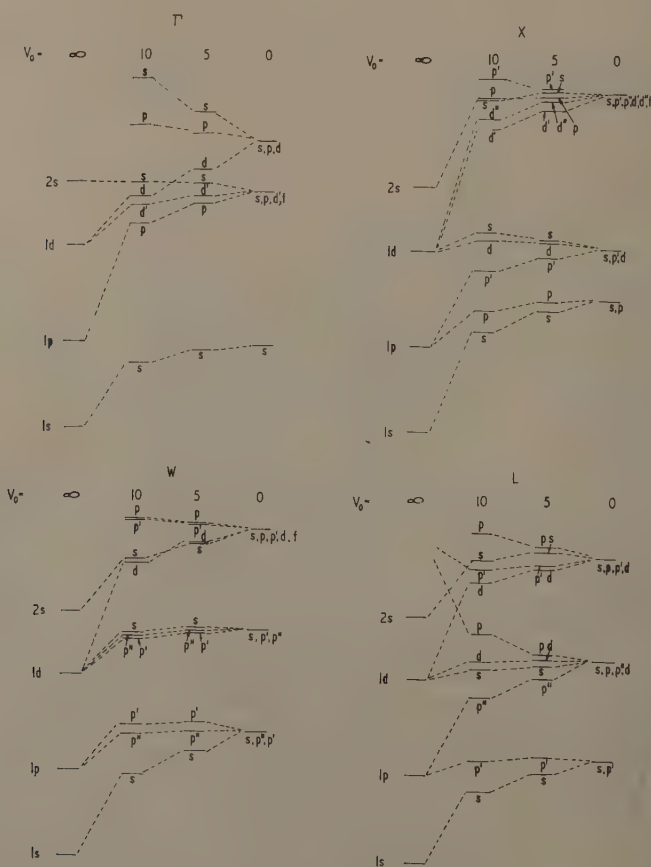


Fig. 8. Displacement of levels with varying V_0 at prominent k -points for the face-centred cubic lattice.

model through a 'pseudo-potential' (Phillips 1958). One would think however that even this effect would not invalidate the conclusion that the topmost level of a p-type band in a face-centred structure must be at $k=0$. Experimentally, this is the case for semiconductors with either the diamond or the zinc blende structure: these structures have the face-centred cubic Bravais lattice. For NaCl structures, also with the face-centred Bravais lattice, the present model cannot be expected to give any firm indication. The maximum of the p-type valence band has been found by various calculations (Bell *et al.* 1953 (on PbS), Howland 1958 (KCl), Grimley 1958 (NaCl), Kucher 1958 (KCl)) to be along the (1, 1, 0) direction. This would appear a further instance of a band characteristic being determined by the crystal structure. However, in PbS and PbTe magnetoresistance measurements (Allgaier 1960) seem to indicate that the edges of both the valence and conduction bands are along the (1, 1, 1) direction.

Almost all monatomic face-centred cubic substances are metals, whose band structure does not deviate much from the free electron scheme. Aluminium is one whose band structure has been particularly well examined theoretically and experimentally (Heine 1957, Harrison 1960, and references). As already remarked, a much finer tool than the present model is necessary in the case of metals. One may however observe that at the most interesting \mathbf{k} -point, the point W, the lowest level in Al is W_p , while W_s is above both W_p and W_{p^*} . In a calculation this arises through the orthogonalization of the wave functions of these states to the core eigenfunctions. Since the effect of orthogonalization may be expressed through a pseudopotential, one can in fact say that such features are determined by the detailed behaviour of the potential. At infinite separation the W_s level must be the lowest.

The third (d) band has its minimum at X. This, and the form of the sub-bands along the (1, 0, 0) direction, agree well with the calculation of Fletcher and Wohlfarth (1951) for Ni (Fletcher 1952). By extrapolation, an energy gap first appears between the second and third band at $V_0 \approx 11.5$. For higher levels, again results are not very reliable and it thus appears unwarranted to make detailed comparison with what is known on the d-bands of transition metals. Fig. 8 indicates schematically the relative positions of the various levels at the \mathbf{k} -points Γ , X, W and L for $V_0 = 0, 5, 10, \infty$. It is clear that for the lowest bands, where there is no crossing of levels, perturbation methods starting from either of the two limiting cases must lead to satisfactory results.

§ 7. COMPARISON OF DIFFERENT METHODS OF CALCULATION

Figure 9 gives the energy, over the bottom of the potential well, of the lowest state at $\mathbf{k}=0$, for the face-centred structure, in the whole range of variation of V_0 for convenience the abscissa is $\log_{10}(1 + V_0)$, as calculated with the most important available procedures. Curve 1 (exact) gives the lowest energy for an isolated well. Curve 2 gives the energy obtained by applying to the crystal the method of tight binding, taking into consideration only the interaction with nearest neighbours (Slater and Koster 1954). Curve 3 gives the results obtained by using the Kohn-Rostoker (1954) procedure based on the Green function formalism. For the level in question the actual formula was given explicitly by Raychaudhuri (1957). Curve 4 gives the energy according to the cellular method in its simplest form, that is substituting equivolume spheres to the actual Wigner-Seitz cells and

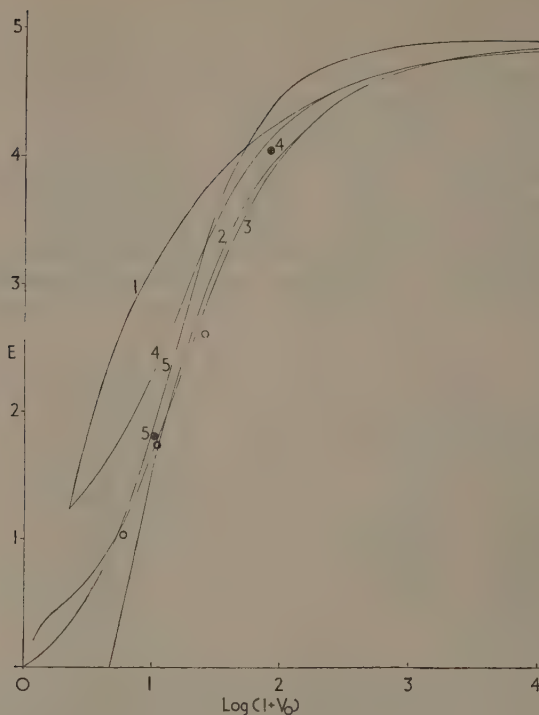


Fig. 9. Energy of lowest level at $\mathbf{k}=0$ in the face-centred cubic lattice as function of $\log_{10}(1+V_0)$. Curve 1: isolated well, exact. Curve 2: tight binding method (nearest neighbours only). Curve 3: *S*-matrix method, spherically symmetric term only. Curve 4: cellular method, matching at equivolume sphere. Curve 5: augmented plane wave (one wave only). Circles: results of main calculation. For other points, see text.

satisfying the boundary conditions at the surface of such spheres using only the spherically symmetric term. The point marked 4 refers to an application of Kohn's (1952) variational procedure for the cellular method, with two terms in the expansion of the wave function. The results of the plane wave calculation are marked with circles. Curve 5 gives the energy according to the augmented plane wave procedure (Saffren and Slater 1953) with one single augmented plane wave. A value obtained with two augmented plane waves is also given (point marked 5).

While all methods, pushed to high approximations, would give the same result, the advantage of using the more appropriate methods in the region of almost free electrons and in that of strongly bound ones respectively is very clear. The simple cellular procedure is not very good, except for strongly bound electrons, and the complications over the boundary conditions make it cumbersome to push it to higher approximations. The augmented plane wave method is very good for almost free electrons, but has the drawback that, with

one wave, the asymptotic behaviour of the energy for $V_0 \rightarrow \infty$ is wrong, a displeasing feature in view of the fact that this is the only approximation that one can immediately extend to the non-periodic case (energy levels in liquids).

In this artificial and oversimplified example the results given by the Green function (or scattering matrix, Korringa 1947) formalism are quite good with very little labour, but the labour increases tremendously at other points in \mathbf{k} -space and for other forms of potential. With plane wave methods, on the other hand, different \mathbf{k} -points and different potentials are taken into account much more readily.

In conclusion, this example confirms that in cases of practical interest the methods more likely to lead to reliable results without the necessity of pushing them to a high approximation are those based on the use of plane waves, orthogonalized or augmented, or on one of the variations and extensions of such methods.

ACKNOWLEDGMENTS

Warm thanks are extended to the Director and Staff of the University of London Computer Unit for the facilities provided, and to Dr. N. H. March and Mr. L. N. Simcox for communicating to us their results. One of us (P. M. L.) is indebted to the Department of Scientific and Industrial Research for a research grant, and the other (L. P.) to the Central Research Fund of the University of London for providing a desk calculating machine.

REFERENCES

- ALLGAIER, R. S., 1960, *Proc. Int. Conf. on Semiconductor Physics, Prague* (Prague: Czechoslovak Academy of Sciences).
- BASSANI, F., 1959, *J. Phys. Chem. Solids*, **8**, 375.
- BELL, D. G., 1954, *Rev. Mod. Phys.*, **26**, 311.
- BELL, D. G., HUM, D. M., PINCHERLE, L., SCIAMA, D. W., and WOODWARD, P. M., 1953, *Proc. Roy. Soc. A*, **217**, 71.
- CALLAWAY, J., 1956, *Phys. Rev.*, **103**, 1219.
- 1959, *Phys. Rev.*, **115**, 346.
- CASELLA, R. C., 1958, *Phys. Rev.*, **109**, 54.
- ENGELMANN, F., 1956, *Z. Phys.*, **145**, 430.
- FLETCHER, G. C., 1952, *Proc. Phys. Soc. A*, **65**, 192.
- FLETCHER, G. C., and WOHLFARTH, E. R., 1951, *Phil. Mag.*, **42**, 106.
- GRIMLEY, T. B., 1958, *Proc. Phys. Soc.*, **71**, 749.
- HARRISON, W. A., 1960, *Phys. Rev.*, **118**, 1182.
- HEINE, V., 1957, *Proc. Roy. Soc. A*, **240**, 340, 354, 361.
- HERMAN, F., and SKILLMAN, S., 1960, *Proc. Int. Conf. on Semiconductor Physics, Prague* (Prague: Czechoslovak Academy of Sciences).
- HOWLAND, L. P., 1958, *Phys. Rev.*, **109**, 1927.
- KOHN, W., 1952, *Phys. Rev.*, **87**, 472.
- KOHN, W., and ROSTOKER, N., 1954, *Phys. Rev.*, **94**, 1111.
- KORRINGA, J., 1947, *Physica*, **13**, 392.
- KUCHER, T. I., 1958, *Zh. Eksper. Teor. Fiz.*, **34**, 394; **35**, 1049.
- PHILLIPS, J. C., 1958, *Phys. Rev.*, **112**, 685.
- RAYCHAUDHURI, A., 1957, *Z. Phys.*, **148**, 435.
- SAFFREN, M. M., and SLATER, J. C., 1953, *Phys. Rev.*, **92**, 1126.
- SLATER, J. C., and KOSTER, G. F., 1954, *Phys. Rev.*, **94**, 1498.

The Efficiency of Production of Characteristic X-radiation in Thick Targets of a Pure Element

BY M. GREEN AND V. E. COSSLETT

Cavendish Laboratory, University of Cambridge

MS. received 30th March 1961

Abstract. A simple theoretical expression is proposed for K quanta production in directions at large angles to the surface of a thick target, neglecting absorption. Direct and indirect production are calculated and the ratio of indirect to total production is shown to be in agreement with experimental results both in magnitude and in independence of over-voltage U_0 . Total production is expressed as a function of atomic number Z and over-voltage U_0 , and is found to vary as $(U_0 - 1)^{1.67}$. Values for total production are in fair agreement with experimental values.

§ 1. INTRODUCTION

THE efficiency of production of K quanta by monoenergetic electrons incident normally on a thick target of a pure element has been given in graphical form by Worthington and Tomlin (1956) and Archard (1960) for a range of elements. Both papers combine theoretical and experimental evidence in their calculations and use the Bethe energy loss relation. In the present calculation, by using the Thomson-Whiddington energy loss equation, which has been more fully tested than the Bethe form in the range 0–100 keV, an analytic expression is derived for K production before target self-absorption. For a useful range of conditions this absorption is small and total K production before absorption may be approximately equated to production as measured at the target surface. The fluorescent contribution to K production arising from the absorption of the continuous radiation was estimated by Worthington and Tomlin and Archard from experimental evidence. Here it is calculated from a known expression for the efficiency of continuous x-ray production.

§ 2. THE RELATION OF K QUANTA PRODUCTION TO THE TOTAL NUMBER OF K IONIZATIONS

K quanta may be produced by an atom when an electron from the L, M or N shells falls into a vacancy in the K shell caused by ionization. The alternative to the emission of a K quantum is an internal conversion process resulting in Auger electron emission. The relative probability of these two processes is described by the fluorescence yield of the K shell ω_K , the fraction of K ionizations resulting in K quantum emission.

If n_K is the total number of K ionizations caused in a thick target by an electron of initial energy E_0 (kev), then the total number of K quanta per electron is N_K where

$$N_K = \omega_K n_K. \quad \dots (1)$$

In a thick target bombarded by electrons, ionization of the K shell is caused in two ways. The first process is the direct ionization of the atoms of the target material by the incident electron. This gives rise to a component which will be referred to as direct ionization and $n_K(\text{direct})$ is the number of direct ionizations per electron.

Continuous radiation is produced by the deceleration of the incident electrons in the target. Those quanta of the continuous radiation which have energies greater than E_K (kev), the K ionization energy, and which are absorbed in the target, give rise to further K ionizations in the absorption process. This is the indirect ionization component where $n_K(\text{indirect})$ is the number per electron.

Equation (1) may be rewritten

$$N_K = \omega_K [n_K(\text{direct}) + n_K(\text{indirect})]. \quad \dots (2)$$

§ 3. K QUANTA ABSORPTION IN THE TARGET

Calculation of the observed intensities of K quanta production at various angles to the surface of the target is complicated by the penetration of the incident electrons into the target and by the absorption at varying depths of the continuous radiation producing indirect ionization. In general, (2) must be written in a

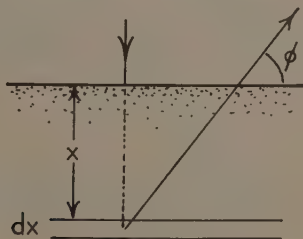


Fig. 1.

differential form for the number of K quanta produced in a layer element of thickness dx :

$$dN_K = \omega_K [dn_K(\text{direct}) + dn_K(\text{indirect})]$$

where $dn_K(\text{direct})$ and $dn_K(\text{indirect})$ are the ionization contributions from the layer element.

Then the number of quanta per unit solid angle per electron at an angle ϕ (defined in Fig. 1) is

$$\frac{1}{4\pi} \int_0^\infty \frac{dN_K}{dx} \{ \alpha \exp(-\mu_\alpha x \csc \phi) + \beta \exp(-\mu_\beta x \csc \phi) \} dx. \quad \dots (3)$$

The assumption is made that only $K\alpha$ and $K\beta$ quanta are emitted and α is the fraction of α quanta and μ_α the $K\alpha$ linear absorption coefficient. Similar definitions hold for $K\beta$ quanta. The quantities $dn_K(\text{direct})/dx$ and $dn_K(\text{indirect})/dx$ are complicated functions of x depending on the electron scattering processes in the target and the angular distribution of the continuous radiation. Even with simple

models of the electron scattering processes in the target, previous authors (Worthington and Tomlin 1956, Archard 1960, Kirkpatrick and Baez 1947) have found that numerical methods are required for the evaluation of integrals similar to (3). Thus an analytic expression for K quanta production can only be found if certain simplifications are made.

In the present work the absorption correction is neglected and the K quanta production $N_K/4\pi$ per electron per unit solid angle at large values of ϕ is written from (2) as

$$\frac{\omega_K}{4\pi} [n_K(\text{direct}) + n_K(\text{indirect})]. \quad \dots\dots (4)$$

This avoids the need for the form of dn_K/dx to be known. Apart from the convenience of producing an analytic expression for K quanta production, this approximation is based on two further considerations. (i) It may be shown from experimental evidence that for $\phi = 45^\circ$, if $ZU_0 < 100$ the absorption correction is less than 10%, which for most elements provides a useful range of E_0 . Here U is the 'over-voltage', i.e. the ratio E/E_K , and $U_0 = E_0/E_K$. (ii) Values of fluorescence yield, ionization cross section and electron energy loss used in all K quanta production calculations are uncertain for many values of Z , making the neglect of the absorption correction a relatively unimportant contribution to the error in the final result.

§ 4. DIRECT IONIZATION CONTRIBUTION

The direct contribution to Eqn (4) may be evaluated by a consideration of the electron paths shown schematically in Fig. 2. The small element of path ds in A is at a point of path length s from the point of entry and an electron traversing

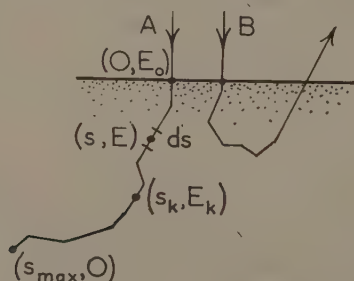


Fig. 2.

the element has an energy E . If $dn_K(\text{direct})$ is the number of direct ionizations per electron in ds , then

$$\int_0^{s_K} \frac{dn_K(\text{direct})}{ds} ds \quad \dots\dots (5)$$

is the total number of direct ionizations per electron for a path of type A where the electron reaches a point where $E = E_K$ and $s = s_K$ without leaving the target material. The path of the electron beyond the point gives rise to no K ionization, as E is now less than E_K .

Relation (5) is true for all electrons which complete their path of length s_K in the material irrespective of the particular shape of the trajectory. Thus the shape factor which makes the evaluation of $dn_K(\text{direct})/ds$ difficult is avoided. However, consideration must be given to paths of the form B where the electron leaves the target through back scattering before its energy has fallen to E_K . Relation (5) is rewritten

$$n_K(\text{direct}) = R \int_0^{s_K} \frac{dn_K(\text{direct})}{ds} ds \quad \dots\dots (6)$$

where R is introduced to allow for this back scattering effect. $1-R$ is the fractional loss of ionization due to back scattering. The fraction of electrons with energies greater than 50 eV back scattered from a thick target is given the symbol η and is found to be nearly constant with respect to variations in E_0 for a particular element. Typical values taken from the work of Sternglass (1954) are 6% for carbon, 29% for copper and 38% for silver. In general, $1-R$ varies with E_0 and is always less than η , as any electron back scattered with an energy less than E_0 has made some contribution to ionization. The energy distribution of back scattered electrons has been investigated by several workers (Sternglass gives many useful references) and from their results $1-R$ may be deduced by a numerical method. In the present work a value of 12% has been found by this method for copper at $U_0=3$, and Kirkpatrick and Baez (1947) quote experimental values taken from the work of Webster, Hansen and Duveneck (1933) of 19% at $U_0=2$ and 21% at $U_0=3$ for a silver target.

Proceeding with the evaluation of (6), $dn_K(\text{direct})/ds$ is written

$$\begin{aligned} \frac{dn_K(\text{direct})}{ds} &= Q_K \times (\text{number of atoms/cm}^3 \text{ in the target material}) \\ &= Q_K \frac{N\rho}{A} \end{aligned}$$

where Q_K is the K shell ionization cross section, N Avogadro's number, ρ the density and A the atomic weight of the target material. Q_K is conveniently given as a function of electron energy and (6) is rewritten

$$n_K(\text{direct}) = -R \int_{E_K}^{E_0} \frac{N\rho}{A} Q_K \frac{ds}{dE} dE \quad \dots\dots (7)$$

to facilitate integration.

§ 5. IONIZATION CROSS SECTION

Bethe's (1930) non-relativistic formula for total ionization cross section is the starting point for finding a suitable form for Q_K . From Bethe's expression, Mott and Massey (1949) write

$$Q_K = \frac{2\pi e^4}{EE_K} b \ln \frac{4E}{B}$$

and conclude

$$B = 1.65E_K, \quad b = 0.35. \quad (a)$$

Worthington and Tomlin (1956) point out that this is only true for large U and use for their numerical integrations

$$B = (1.65 + 2.35 e^{1-U})E_K, \quad b = 0.35 \quad (b)$$

and for their exact integration the limiting value of B in (b) as U tends to unity with b modified to fit the experimental results at $U=3$:

$$B=4E_K, \quad b=0.35 \times 1.73. \quad (c)$$

Three curves of the function $Q_K E_K^2$ produced by the substitution of the values (a), (b) and (c) in the Bethe expression for Q_K are shown in Fig. 3, where they are

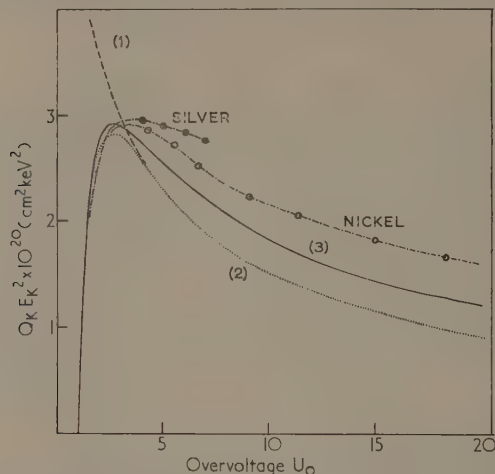


Fig. 3. Comparison of modified forms of the ionization function with experimental values. Curves (1), (2) and (3) are produced by substitution of values (a), (b) and (c) respectively in the Bethe expression for Q_K .

compared with the experimental results of Kirkpatrick and Baez (1947) for silver, and of Pockman *et al.* (1947) for nickel. Values from (c) are seen to agree with experiment as well as values from (b) without the complexity of the latter's form which precludes exact integration. For this calculation values (c) are used leading to

$$Q_K E_K^2 = 7.92 \times 10^{-20} \frac{1}{U} \ln U \text{ (cm}^2 \text{ keV}^2\text{)}. \quad \dots\dots (8)$$

§ 6. ENERGY LOSS RELATION

Worthington and Tomlin use the Bethe (1930) energy loss relation in their calculations. This leads to a form for n_K (direct) involving the logarithmic integral in which the variation of n_K with U_0 and E_K is not easily deducible without reference to tables†.

† Worthington and Tomlin give

$$n_K(\text{direct}) = \frac{b}{Z} \left\{ (U_0 - 1) + \frac{J}{4E_K} \left(\ln \frac{2J}{B} \right) \left[\bar{\text{Ei}} \left(\ln \frac{2E_0}{J} \right) - \bar{\text{Ei}} \left(\ln \frac{2E_K}{J} \right) \right] \right\}$$

where B is constant with respect to U . An examination of the integration would suggest that

$$n_K(\text{direct}) = \frac{b}{Z} \left\{ (U_0 - 1) + \frac{J}{2E_K} \left(\ln \frac{2J}{B} \right) \left[\bar{\text{Ei}} \left(\ln \frac{2E_0}{J} \right) - \bar{\text{Ei}} \left(\ln \frac{2E_K}{J} \right) \right] \right\} \quad \dots\dots$$

is a more correct form.

In this calculation it is proposed to use the experimental Thomson-Whiddington (Whiddington 1912) energy loss relation in the form

$$E_0^2 - E^2 = cpx. \quad \dots\dots (9)$$

c is found to vary with E and Table 1 has been compiled from the experimental values of Whiddington (1912), Terrill (1923), Klemperer (1925) and Klemperer, Thetford and Lenz (1960). The latter authors show that the Bethe formula, which is derived from theoretical considerations, predicts greater energy losses for aluminium (and hence larger values of c when expressed in a suitable form) than the experimental values embodied in the Thomson-Whiddington equation.

Table 1. Constant c in Thomson-Whiddington Energy Loss Equation

E (kev)	1	2	5	10	20	50
c (kev ² cm ² g ⁻¹)	1.0×10^5	1.3×10^5	1.8×10^5	2.3×10^5	2.9×10^5	4.4×10^5

For the purposes of this calculation (9) is required as a function of s the electron path length. Substitution of s for x leads to the given values of c being larger than those appropriate to the new form of the relation, as the path length s is always greater than the penetration x of the electrons measured in a direction normal to the surface. Eqn (9) may be written in a differential form, thus

$$\frac{ds}{dE} = -\frac{2E}{cp} \quad \dots\dots (10)$$

and combined with (7) and (8)

$$\begin{aligned} n_K(\text{direct}) &= \frac{2RN}{Ac} \int_{E_K}^{E_0} 7.92 \times 10^{-20} \frac{1}{E_K^2 U} (\ln U) E dE \\ &= 9.535 \times 10^4 \frac{R}{Ac} \int_1^{U_0} \ln U dU. \end{aligned}$$

$$\text{If } N = 6.02 \times 10^{23}$$

$$n_K(\text{direct}) = 9.535 \times 10^4 \frac{R}{Ac} [U_0 \ln U_0 - (U_0 - 1)] \quad \dots\dots (11)$$

§ 7. INDIRECT IONIZATION

Let $N(\text{cont})$ be the number of continuous quanta per electron with energies greater than the K ionization energy. Then if it is supposed that the continuous radiation is effectively isotropic and that the origin of the continuous radiation is close to the surface of the target compared with the range of the continuous quanta in the target, $\frac{1}{2}N(\text{cont})$ is absorbed in the target. Now if r_K is the ratio of the photoelectric absorption coefficient on the high energy side of the K absorption edge to that on the low side, then the fraction of absorptions which cause K shell ionization is $(r_K - 1)/r_K$. It follows that

$$n_K(\text{indirect}) = \frac{1}{2}N(\text{cont}) \frac{r_K - 1}{r_K}. \quad \dots\dots (12)$$

Dyson (1959) shows that to a close approximation the energy distribution in the continuous radiation may be written

$$I_E = 2.76 \times 10^{-6} Z(E_0 - E) \quad (\text{kev per electron per kev energy interval}).$$

Following the method of Dyson (1956) the number of continuous quanta between E and $E + dE$ is

$$dN_E = 2.76 \times 10^{-8} Z \frac{(E_0 - E)}{E} dE$$

and the number of quanta $E > E_K$ is

$$\begin{aligned} N(\text{cont}) &= 2.76 \times 10^{-8} Z \int_{E_K}^{E_0} \left(\frac{E_0}{E} - 1 \right) dE \\ &= 2.76 \times 10^{-8} Z E_K [U_0 \ln U_0 - (U_0 - 1)]. \end{aligned}$$

Writing $(r_K - 1)/r_K = 0.85$ for all Z involves an error of less than 5% for $30 < Z < 80$, and below $Z = 30$ indirect production is unimportant. Further, $E_K = 1.263 \times 10^{-2} (Z - 2)^2$ kev with little error. Substituting these values in (12), it follows that

$$n_K(\text{indirect}) = 1.46 \times 10^{-8} (Z - 2)^2 Z [U_0 \ln U_0 - (U_0 - 1)]. \quad \dots (13)$$

§ 8. RATIO OF INDIRECT TO DIRECT PRODUCTION

From Eqns (11) and (13) it follows immediately that the ratio of indirectly to directly produced K quanta for a particular value of Z is dependent only on c/R , a very slowly varying function of U_0 . This ratio, following Kirkpatrick and Baez's definition, is $1/P$.

$$\frac{1}{P} = 1.62 \times 10^{-13} (Z - 2)^2 Z \frac{Ac}{R};$$

approximating further,

$$\frac{1}{P} = 3.24 \times 10^{-13} Z^4 \frac{c}{R}. \quad \dots (14)$$

Agreement with experiment both in the magnitudes of the quantities and their relative independence of U_0 is shown in Table 2 giving values of $1/(1 + P)$, the ratio of indirect to total production.

Table 2. Ratio of Indirect to Total Production

Atomic No.	Element	Theory	Experiment
6	Carbon	0.004%	
13	Aluminium	0.02%	
30	Zinc	7%	6% ($U_0 = 2.0$) (1)
47	Silver	44%	35% ($U_0 = 1.5$); 33% ($U_0 = 5$) (2)
79	Gold	89%	82% ($U_0 = 1.5$); 78% ($U_0 = 2.5$) (3)

(1) Castaing (1955); (2) Webster (1928); (3) Stoddard (1935).

Taking values of c smaller than those tabulated, as has been previously suggested would be appropriate, would bring $1/(1 + P)$ more closely in agreement with the experimental values.

§ 9. TOTAL K QUANTA PRODUCTION

The substitution of (11) and (13) in (4) gives

$$\frac{N_K}{4\pi} = \frac{\omega_K}{4\pi} \left(9.54 \times 10^4 \frac{R}{Ac} + 1.46 \times 10^{-8} (Z - 2)^2 Z \right) [U_0 \ln U_0 - (U_0 - 1)] \quad \dots (15)$$

total K quanta per electron per unit solid angle. Duncumb (1957) showed that

a function of the form $[U_0 \ln U_0 - (U_0 - 1)]$ may be expressed as a power of $U_0 - 1$. For the present calculation $[U_0 \ln U_0 - (U_0 - 1)]$ is written as $0.365(U_0 - 1)^{1.67}$ with an error of less than 10% for $1.5 < U_0 < 16$; then

$$\frac{N_K}{4\pi} = \omega_K \left(2.80 \times 10^3 \frac{R}{Ac} + 4.27 \times 10^{-10} (Z-2)^2 Z \right) [U_0 - 1]^{1.67}. \quad \dots (16)$$

Experimental work referred to by Compton and Allison (1935) has yielded values of the power of $U_0 - 1$ of 1.6–1.7, where absorption is unimportant, and this is confirmed by the authors' work.

In Table 3 values are calculated from (16) and compared with five experimental values available for K quanta production in thick targets at large values of ϕ where absorption is less than 10%. The values of ω_K are calculated from the semi-empirical equation of Laberrigue-Frolov and Radvanyi (1956)

$$\omega_K = \frac{(A + BZ + CZ^3)^4}{1 + (A + BZ + CZ^3)^4}$$

where

$$A = -0.0217, \quad B = 0.03318, \quad C = -1.14 \times 10^{-6},$$

R for aluminium is an estimated value.

Table 3. Total K Quanta per Electron per Unit Solid Angle

Element	Z	ω_K	$E(\text{kev})$	U_0	$c(\text{kev}^2 \text{ cm}^2 \text{ g}^{-1})$	R	$N_K/4\pi$	
							Theory	Experiment
Carbon	6	1×10^{-3}	0.849	3	0.8×10^5	1	9.3×10^{-6}	16.3×10^{-6} (1)
Aluminium	13	0.0267	4.68	3	1.6×10^5	0.95	5.2×10^{-5}	5.7×10^{-5} (1)
Copper	29	0.425	27.0	3	2.8×10^5	0.88	2.0×10^{-4}	2.2×10^{-4} (2)
Silver	47	0.810	51.0	2	4.0×10^5	0.81	7.5×10^{-5}	$\begin{cases} 6.4 \times 10^{-5} \text{ (2)} \\ 6.3 \times 10^{-5} \text{ (3)} \end{cases}$

(1) Dolby (1960); (2) Authors (unpublished); (3) Kirkpatrick and Baez (1947).

Figure 4 shows values of $N_K/4\pi$ plotted against Z at $U_0 = 3$. The indirect component which increases rapidly with Z is produced at greater depths in the target than the direct component of the K radiation. Consequently it suffers more absorption and for values of Z greater than 40 at $U_0 = 3$ the condition that the target self-absorption is less than 10% is not satisfied.

§ 10. CONCLUSION

Agreement between theory and experiment may be regarded as satisfactory when consideration is given to the following factors:

- (i) The value of c is an uncertain quantity, particularly for elements of lower atomic numbers at small electron energies. The validity of the Thomson-Whiddington form of the energy loss relation is also uncertain at low energies.
- (ii) The K ionization cross section values are based by extrapolation on only two actual measurements, both on elements of large atomic number compared with aluminium and carbon.
- (iii) The experimental values are few in number and little checking by different workers making similar measurements has been carried out.

- (iv) Values of ω_K for aluminium and carbon have not been checked experimentally and may be considerably in error.
- (v) In the development of the theory, certain approximations have been made.

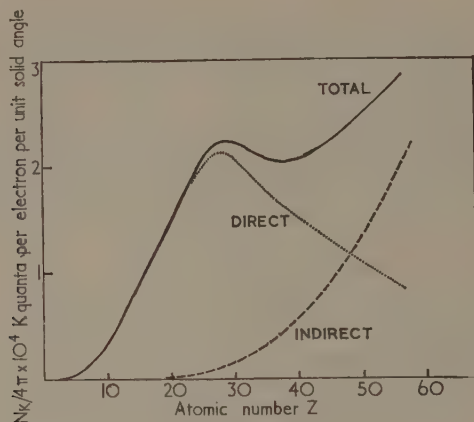


Fig. 4. K quanta per electron per unit solid angle at $U_0=3$.

ACKNOWLEDGMENTS

One of us (M. G.) wishes to thank the Trustees of the Paul Instrument Fund of the Royal Society for financial assistance in carrying out this work.

REFERENCES

- ARCHARD, G. D., 1960, *X-ray Microscopy and X-ray Microanalysis* (Amsterdam: Elsevier).
- BETHE, H. A., 1930, *Ann. Phys., Lpz.*, **5**, 325.
- CASTAING, R., 1955, *J. Phys. Radium*, **16**, 304.
- COMPTON, A. H., and ALLISON, S. K., 1935, *X-rays in Theory and Experiment* (London: Macmillan).
- DOLBY, R. M., 1960, *Brit. J. Appl. Phys.*, **11**, 64.
- DUNCUMB, P., 1957, *Ph.D. Thesis*, University of Cambridge.
- DYSON, N. A., 1956, *Ph.D. Thesis*, University of Cambridge.
- 1959, *Proc. Phys. Soc.*, **73**, 924.
- KIRKPATRICK, P., and BAEZ, A. V., 1947, *Phys. Rev.*, **71**, 521.
- KLEMPERER, O., 1925, *Z. Phys.*, **34**, 532.
- KLEMPERER, O., THETFORD, A., and LENZ, F., 1960, *Proc. Phys. Soc.*, **74**, 705.
- LABERRIGUE-FROLOW, J., and RADVANYI, P., 1956, *J. Phys. Radium*, **17**, 944.
- MOTT, N. F., and MASSEY, H. S. W., 1949, *The Theory of Atomic Collisions* (Oxford: Clarendon Press).
- POCKMAN, L. T., WEBSTER, D. L., KIRKPATRICK, P., and HARWORTH, K., 1947, *Phys. Rev.*, **71**, 330.
- STERNGLASS, E. J., 1954, *Phys. Rev.*, **95**, 345.
- STODDARD, K. B., 1935, *Phys. Rev.*, **48**, 43.
- TERRILL, H. M., 1923, *Phys. Rev.*, **22**, 101.
- WEBSTER, D. L., 1928, *Proc. Nat. Acad. Sci.*, **14**, 337.
- WEBSTER, D. L., HANSEN, W. W., and DUVEINECK, F. B., 1933, *Phys. Rev.*, **44**, 258.
- WHIDDINGTON, R., 1912, *Proc. Roy. Soc. A*, **86**, 360.
- WORTHINGTON, C. R., and TOMLIN, S. G., 1956, *Proc. Phys. Soc. A*, **69**, 401.

A Search for Vibrational Energy Effects in the Dissociation of H_2^+ Ions by Hydrogen Gas

By A. C. RIVIERE AND D. R. SWEETMAN

Atomic Weapons Research Establishment, Aldermaston, Berks.

MS. received 23rd June 1961

Abstract. The dissociation cross section on interaction with hydrogen gas was measured for H_2^+ ions with energies between 280 and 670 kev and with both high and low vibrational excitation. An increase of $7 \pm 4\%$ was found for the cross section for simple dissociation in the case of the more highly vibrationally excited ions. For dissociation into two protons the difference between the cross sections was certainly less.

RIVIERE AND SWEETMAN (1960) have found that the uppermost vibrational levels ($v=17, 18$) of H_2^+ are about five times more populated when the ion is formed by the break-up of an H_3^+ ion than when formed by electron collision in an ion source. Though the results referred to only 0.3 per cent of all the ions, this increased population of the uppermost levels almost certainly corresponds to a higher average excitation. The equilibrium separation of the nuclei in the H_3^+ ion is 1.79 \AA (Hirschfelder 1938), and this is considerably greater than the ground state separation of the H_2^+ ion of 1.06 \AA . Presumably the H_2^+ ion is highly vibrationally excited when formed from H_3^+ at this wide nuclear separation. The absorption cross section for photons by H_2^+ ions calculated by Buckingham, Reid and Spence (1952) would suggest that the cross section for dissociation of H_2^+ ions by gases might depend on the degree of vibrational excitation, and this has been suggested as a possible explanation of the discrepancies between different workers for the value of the latter cross section. The discrepancies may well have a less fundamental experimental origin, but the importance of vibrational excitation has not been established.

For these reasons the dissociation cross section was measured for H_2^+ ions with both high and low vibrational excitation on interaction with hydrogen gas and with energies between 280 and 670 kev.

The equipment and method were identical with those used by Sweetman (1960). In making the comparison it was necessary to ensure that at each energy point the H_2^+ ions of both high and low vibrational excitation were of the same energy. For H_2^+ direct from the source the 3 mev Van de Graaff was set to a voltage E_0 and the ions were selected by a bending magnet whose field was set to a value H_0 . The magnet current was stabilized to 1 part in 10^4 and the field measured by a proton resonance technique. The accelerator was stabilized against the field value by means of a conventional slit system beyond the magnet. Two methods were used to obtain H_2^+ ions of the same energy E ev but which arose from the break-up of accelerated H_3^+ ions. Firstly, a machine voltage of $\frac{3}{2}E_0$ and magnetic field of $\frac{3}{2}H_0$ were set so that H_3^+ ions were selected by the magnet and the H_2^+

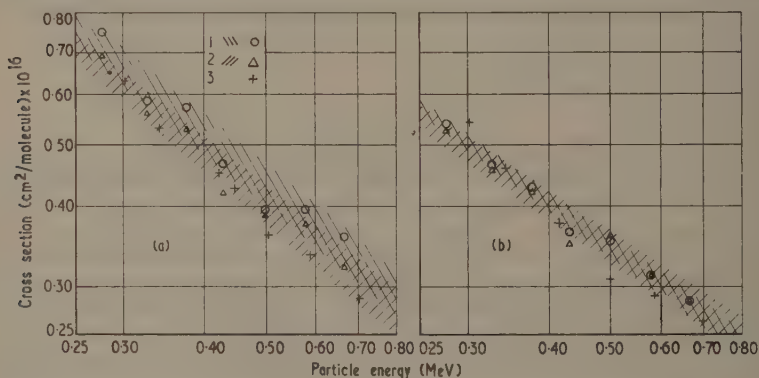
ions were obtained by the break-up of H_3^+ in the drift tube to the apparatus. Secondly, a machine voltage of $\frac{3}{2}E_0$ and magnetic field of H_0 were used so that H_2^+ ions were selected which arose from the break-up of H_3^+ ions before the magnet. No difference was observed between these systems in the results but the second method was preferred since the magnetic field was not changed between measurements. At each energy point a cycle of measurements was made by passing from one type of ion to the other and back. The results are shown in the figure for the processes



and



respectively. The results obtained by Sweetman (1960) for H_2^+ ions direct from the source are also shown. A least squares analysis was carried out for



The cross section for dissociation of H_2^+ ions in hydrogen for the processes (a) $H_2^+ \rightarrow H^0 + H^+$ and (b) $H_2^+ \rightarrow H^+ + H^+$. 1, H_2^+ ions obtained from the break-up of H_3^+ ions; 2, H_2^+ ions obtained direct from the ion source; 3, results of Sweetman (1960) for H_2^+ ions direct from the ion source. Shading indicates region covered by least squares analysis of experimental points.

processes (1) and (2) and for the ions of both low and high vibrational excitation by assuming that the cross section obeyed the law $\sigma = aE^{-b}$. For process (1) the results were

$$\sigma(H_2^+ \text{ direct}) = (15.6 \pm 0.7)E^{-(0.84 \pm 0.05)} \times 10^{-17} \text{ cm}^2$$

and

$$\sigma(H_2^+ \text{ from } H_3^+) = (16.8 \pm 0.9)E^{-(0.84 \pm 0.04)} \times 10^{-17} \text{ cm}^2$$

where E is in units of 10^5 eV.

For process (2) the results were

$$\sigma(H_2^+ \text{ direct}) = (10.5 \pm 0.4)E^{-(0.69 \pm 0.03)} \times 10^{-17} \text{ cm}^2$$

and

$$\sigma(H_2^+ \text{ from } H_3^+) = (11.3 \pm 0.3)E^{-(0.73 \pm 0.02)} \times 10^{-17} \text{ cm}^2.$$

The shaded areas on the figure indicate the regions covered by the results of the least squares analysis.

For process (1) the energy exponents are the same and a direct comparison shows that the cross section for the more highly vibrationally excited ions is $7 \pm 4\%$ greater than that for the other type of ion. For process (2) however this

comparison cannot be made but the difference is certainly less than that for process (1) in the energy range considered. This result could be expected since the energy gap for process (2) of ionization and dissociation is about 13.6 eV greater than that for process (1) if formation of H^0 in excited states is neglected.

The cross section for the dissociation of H_2^+ ions by hydrogen certainly appears to be insensitive to the degree of vibrational excitation, and differences in the degree of excitation cannot account for the discrepancies between the results of different workers.

ACKNOWLEDGMENT

The authors wish to acknowledge the assistance of Mr. D. Coleby in carrying out the observations.

REFERENCES

- BUCKINGHAM, R. A., REID, S., and SPENCE, R., 1952, *Mon. Not. R. Astr. Soc.*, **112**, 382.
HIRSCHFELDER, J. O., 1938, *J. Chem. Phys.*, **6**, 795.
RIVIERE, A. C., and SWEETMAN, D. R., 1960, *Phys. Rev. Letters*, **5**, 560.
SWEETMAN, D. R., 1960, *Proc. Roy. Soc. A*, **256**, 416.

Low Temperature Cloud Chamber Studies on Water Vapour†

By L. A. MADONNA†, C. M. SCIULLI§, L. N. CANJAR|| AND
G. M. POUND*

† Chemical Engineering Department, University of Ottawa, Ottawa, Canada

§ United States Steel Corporation, Pittsburgh, Pennsylvania

|| Chemical Engineering Department, Carnegie Institute of Technology

* Metals Research Laboratory, Carnegie Institute of Technology, Pittsburgh, Pennsylvania

MS. received 27th July 1959, in revised form 9th January 1961

Abstract. The critical supersaturation for the precipitation of water droplets or ice crystals from the vapour was measured between 0°C and -75°C by an expansion-chamber technique. Nitrogen was used as the carrier gas, and measurements were made both in the presence and in the absence of an electric field. The temperature dependence of critical supersaturation was found to be the same in both situations. Thus existing critical supersaturation data for nucleation of water droplets from the vapour in the presence of an electric field probably represent heterogeneous nucleation on ions. Comparison of the data taken in the presence of a field with the Becker-Döring equation for homogeneous nucleation shows fair agreement at the higher temperatures but marked negative deviation at lower temperatures. The precipitate particles appeared to be spherical above -65°C, while at lower temperatures precipitation was in the form of ideomorphic ice crystals.

§ 1. INTRODUCTION

THE rate equation for homogeneous nucleation of droplets from a super-saturated vapour has been derived by Becker and Döring (1935) and by Zeldovich (1942)

$$J = \left(\frac{2\gamma v N^3}{\pi} \right)^{1/2} \left(\frac{p}{kT} \right)^2 \exp \left\{ \frac{-16\pi v^2 \gamma^2}{3kT [RT \ln(p/p_0)]^2} \right\} \dots\dots (1)$$

where v is the molar volume of the liquid, N Avogadro's number, p partial pressure of vapour at supersaturation, p_0 equilibrium vapour pressure and R the gas constant. Inasmuch as the liquid-vapour interface is the only one whose specific free energy γ can be measured directly and accurately, experiments on the nucleation of droplets from vapour provide the best check of nucleation theory (Volmer 1945). It is well known that there is remarkable agreement between critical supersaturations¶ calculated from Eqn (1) and the measurements of Volmer and Flood (1934) on water vapour and a number of organic vapours. In the case of water vapour at 0°C, the critical supersaturation for homogeneous nucleation of droplets is given as 4.2. However, there are reasons to doubt the correctness of this interpretation of the Volmer and Flood results. These

† The research described in this paper was sponsored by the Geophysics Research Division, Air Force Cambridge Research Center, Cambridge, Massachusetts, under Contract No. AF 19(122)-185.

¶ Critical supersaturation is defined as the value of p/p_0 required for appreciable nucleation rate of droplets, a rate of the order of one per cm³ sec.

results are inconsistent with the work of C. T. R. Wilson (1897) and Powell (1928) on water vapour in air. Wilson found that for a terminal temperature of about 0°C the critical supersaturation ratio is 4.2 in the presence of negative ions and about 6 in the presence of positive ions alone. These 'ion limits' were characterized by 'rain-like' condensation, i.e. the concentration of droplets produced was not high and of the order of magnitude of the concentration of ions in the air. He considered that homogeneous nucleation did not occur until the 'fog limit' was reached at a supersaturation of about 8 where a very dense fog of tiny droplets was produced. Wilson did not actually try to measure the critical supersaturation for homogeneous nucleation in the presence of a strong electric field. However, it is difficult to see how he could observe the positive-ion limit (sixfold supersaturation) if it were not below the critical supersaturation for homogeneous nucleation. Further, the present interpretation of Volmer and Flood's results is questionable from a theoretical point of view. There is serious doubt that the macroscopic thermodynamic concepts of surface tension and free energy can be applied to aggregates as small as 100 molecules (Farley 1952, Reiss 1950). Accordingly, it was decided to measure the critical supersaturation of water vapour in very pure nitrogen in the presence of an electric field over a wide range of temperatures and compare the results with the predictions of the Becker-Döring equation. Such a study was undertaken by Sander and Damköhler (1943), but their results at room temperature were sufficiently different from Volmer and Flood's to be considered not entirely conclusive.

§ 2. EXPERIMENTAL PROCEDURES

A full description of the apparatus and its operation has been presented in a previous publication by Madonna (1957). Briefly, gas was purified, humidified and collected in the cloud chamber, which was maintained at a constant low temperature (10°C to -80°C). The cloud chamber was connected by means of a large valve to a vacuum reservoir system. When the valve was suddenly opened, adiabatic expansion of the gas caused a reduction in temperature which produced a supersaturation of the vapour given by

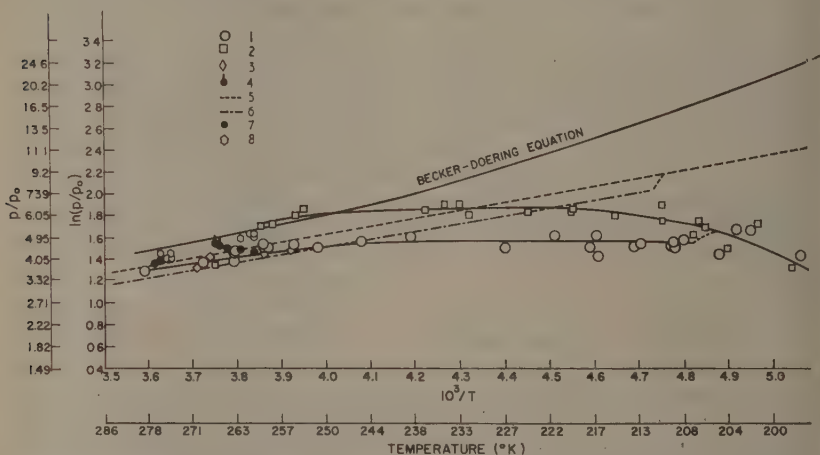
$$S = p/p_0 = p_1 P_2 / p_0 P_1, \quad \dots\dots (2)$$

where p_1 is the partial pressure of vapour prior to expansion and P_1 and P_2 are the initial and final total pressures respectively. That supersaturation which was just sufficient to cause visually observable precipitation was recorded as the critical supersaturation.

The assumption of reversibility and adiabaticity of moderate expansions at ordinary temperatures has been carefully checked by a number of workers (Makower 1903, Sander and Damköhler 1943, Volmer and Flood 1934) and found to be correct within the precision of measurement. However, the present results were checked at both high and low temperatures by varying the conditions of expansion. Changing the size of the vacuum reservoir, cloud-chamber volume and bore of the expansion stopcock did not affect the results. Equilibrium saturation of the carrier gas with water vapour was checked and carefully controlled. The assumption of thermal equilibrium with the thermostat was also checked by means of a thermocouple in a 'dummy' cloud chamber. The presence of a small amount of condensate in the bottom of the cloud chamber and the humidity of the gas in the reservoir had no effect on the results.

§ 3. DISCUSSION OF RESULTS

All of the critical supersaturation data for water vapour obtained in the present work are presented in the Figure, together with the data of Volmer and Flood (1934) and Sander and Damköhler (1943) who used air as the carrier gas. It is seen that there is fair agreement between the present data and those of Volmer and Flood at higher terminal temperatures (around 0°C) regardless of the carrier gas used. However, the data of Sander and Damköhler are appreciably lower at these higher temperatures. Also, over the temperature range down to about -65°C, their gap between critical supersaturations with and without a field is only about $\frac{1}{3}$ of that found in the present work (approximately 1.3). Further, it is seen that there is considerable disagreement of the present data with the results



Assembled critical supersaturation data for water vapour including Madonna-Sciulli-Canjar-Pound data using N_2 carrier gas. 1, Madonna-Sciulli-Canjar-Pound, without field, N_2 ; 2, Madonna-Sciulli-Canjar-Pound, with field, N_2 ; 3, Madonna-Sciulli-Canjar-Pound, without field, O_2 ; 4, Madonna-Sciulli-Canjar-Pound, with field, O_2 ; 5, Sander-Damköhler, with field, air; 6, Sander-Damköhler, without field, air; 7, Volmer-Flood, without field, air; 8, Volmer-Flood, with field, air.

of Sander and Damköhler at low temperatures. This discrepancy cannot be attributed to foreign nuclei, because the ion limits disagree in the same way as do the data taken with an electric field. Accordingly, some difference in technique must be responsible. The writers are not prepared to say that their work is correct and that the other work is wrong. However, some experimental effort was made to resolve the difference. It was considered that their smaller chamber (0.7 l.) might not have been as adiabatic with respect to heat transfer through the vacuum stopcock from the warm room as the 2-litre chamber used in the present work. Accordingly, an apparatus similar to theirs was constructed and tried at low temperatures using nitrogen as the carrier in the absence of a field. This smaller apparatus gave an apparent ion limit which was almost as high as that reported by Sander and Damköhler. Therefore, it is possible that their apparatus was not adiabatic at low temperatures. Possibly the chamber used in the present work

was not entirely adiabatic at low temperatures either. However, this possibility does not affect the general conclusions to be drawn from the present investigation.

The authors feel that the most significant result from both sets of data is that the temperature dependence of critical supersaturation is about the same with or without a field. Although the critical supersaturation for nucleation of droplets on ions has not yet been calculated from theory (Volmer 1945), it seems evident that the temperature dependence should be less than for homogeneous nucleation. Accordingly, one would conclude that the most reasonable explanation of the observations is that nucleation is catalyzed by residual ions even in the presence of an electric field, the higher critical supersaturation being due to a lower ion concentration.

In order to test the applicability of the Becker Döring equation (1) for homogeneous nucleation to the data taken in the presence of a field, theoretically calculated values of critical supersaturation are included in the plot of the Figure. It is seen that there is fair agreement at the higher temperatures but wide divergence at lower temperatures where the calculated values are much higher than those observed. Also, it is evident that the predicted temperature dependence of critical supersaturation for homogeneous nucleation is much higher than that observed. Again, this indicates that the nucleation in the presence of a field was heterogeneous.

In another test of the applicability of homogeneous nucleation theory to the data taken with a field, the specific interfacial free energy was computed from the Becker-Döring equation and the present data. It was found that calculated and measured surface free energies are in fair agreement at the higher temperatures but that there is considerable deviation at lower temperatures. Further, the temperature dependence suggests that the agreement at higher temperatures is fortuitous. Finally, it should be emphasized that the present data, or any other data which represent heterogeneous nucleation on ions, constitute no test of the Becker-Döring equation.

Until a terminal temperature of about -65°C was reached, the precipitate appeared to be in the form of droplets. This does not necessarily mean that they were liquid, because critical supercooling experiments recently conducted on pure water droplets indicated that these 'droplets' may have been frozen to ice balls for terminal temperatures below -41°C (Schaefer 1952). At about -65°C , the appearance of the precipitate exhibited a striking change. A cloud of flickering ice crystals was obtained directly on expansion to all lower terminal temperatures. The scatter of the present data below -65°C (see Figure) is too great to confirm or deny the results of Sander and Damköhler, namely that the effect of the electric field disappears and the slope of the curve increases abruptly at -65°C . However, the present authors are inclined to agree with the conclusion of Sander and Damköhler that the direct nucleation of ice crystals from vapour occurs below terminal temperatures of about -65°C .

§ 4. CONCLUSIONS

1. Existing critical supersaturation data for nucleation of water droplets from the vapour in the presence of an electric field probably represent heterogeneous nucleation on ions.

2. The Becker-Döring equation describes the present data taken in the presence of an electric field using nitrogen as the carrier gas fairly well at the

higher temperatures (-10°C), but there are wide deviations at low temperatures. Further, the temperature dependence suggests a fortuitous agreement at the higher temperatures. However, it is emphasized that the present data, or any other data (including the Volmer and Flood data on water) which represent heterogeneous nucleation on ions, constitute no test of the Becker-Döring equation.

3. In the present work, direct nucleation of ice crystals from the vapour began at -65°C .

REFERENCES

- BECKER, R., and DÖRING, W., 1935, *Ann. Phys., Lpz.*, **24**, 719.
FARLEY, F. J. M., 1952, *Proc. Roy. Soc. A*, **212**, 530.
MADONNA, L. A., 1957, *Canad. J. Technol.*, **34**, 485.
MAKOWER, W., 1903, *Phil. Mag.*, **5**, 226.
POWELL, C. F., 1928, *Proc. Roy. Soc. A*, **119**, 553.
REISS, H., 1950, *J. Chem. Phys.*, **18**, 529.
SANDER, A., and DAMKÖHLER, G., 1943, *Naturwissenschaften*, **31**, 460.
SCHAEFER, V., 1952, *Industr. Engng. Chem.*, **44**, 1300.
VOLMER, M., 1945, *Kinetik der Phasenbildung* (Ann Arbor, Michigan: Edwards), chapter 4.
VOLMER, M., and FLOOD, H., 1934, *Z. phys. Chem. A*, **170**, 273.
WILSON, C. T. R., 1897, *Phil. Trans. Roy. Soc. A*, **189**, 265.
ZELDOVICH, J., 1942, *J. Exp. Theor. Phys.*, **12**, 525.

Vacuum Ultra-violet Spectra of Multiply Ionized Inert Gases

By B. C. FAWCETT, B. B. JONES AND R. WILSON

Atomic Energy Research Establishment, Harwell

MS. received 29th May 1961

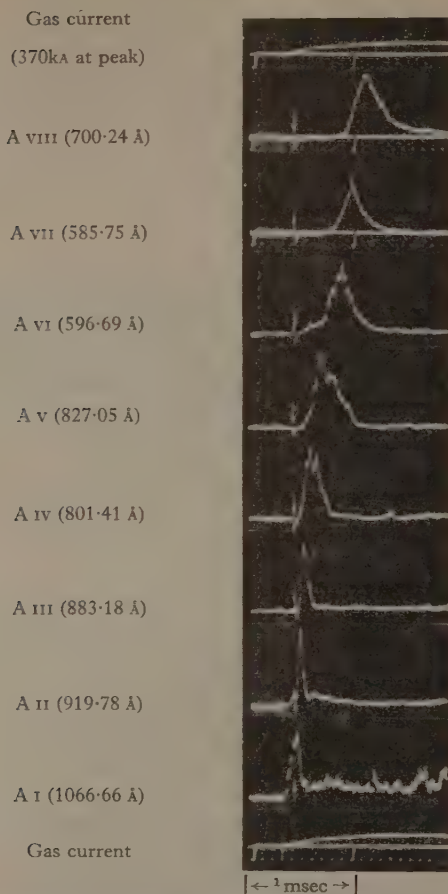
Abstract. The high temperature plasma ($kT_e \simeq 20$ eV) produced in ZETA is a copious source of spectral lines emitted by highly ionized atoms in the vacuum ultra-violet. Spectroscopic investigations in the wavelength range 400–1000 Å have revealed several new lines due to the multiply ionized inert gases Ne, Ar, Kr and Xe. The method of identification is based on the successive appearance of the ionization states of each element, supplemented by isoelectronic calculations which also allowed transitions to be assigned to most lines.

§ 1. INTRODUCTION

ONE of the methods of studying the high temperature deuterium plasma produced in the experimental apparatus ZETA (Butt *et al.* 1958) is the observation of spectral lines emitted by trace elements, deliberately introduced in small quantities into the discharge. Because of their availability in gaseous form, the inert gases are particularly convenient for this purpose, but knowledge of their spectra is limited; for example, the spectra of Kr and Xe are undocumented above the fourth stage of ionization except for three lines of Kr IX in the 100 Å region (Moore 1952). Recent investigations of the ZETA plasma, requiring the use of lines from highly ionized species, have necessitated a limited approach to the problem of spectral line identification, and the purpose of this communication is to present some new observations of the spectra of multiply ionized Ne, Ar, Kr and Xe in the wavelength region 400–1000 Å. Work on the similar discharge apparatus SCEPTRE III has led to the identification of lines due to Ne IV, V, VI and F VI in the quartz ultra-violet (Kaufman *et al.* 1960).

§ 2. METHOD

The line identifications were made as follows. Using a 3-metre normal incidence vacuum spectrograph, having a reciprocal linear dispersion of 2.78 Å mm^{-1} and an aperture of $f/30$, a photograph of the ZETA spectrum was obtained for a discharge in deuterium. This was repeated after the introduction of a small quantity ($\simeq 5\%$) of the inert gas to be studied, and the additional lines observed were then assigned to this element. Typically, 200 discharges are required to give a well exposed spectrogram on Ilford Q2 emulsion. Wavelength values were obtained from the spectrograms, and each line was then monitored during the discharge period using a 1-metre normal incidence vacuum monochromator, equipped with photoelectric recording, giving the variation of spectral line intensity with time. Previous work by Burton and Wilson (1961) has led to a clear interpretation of this type of observation, and has shown that



Temporal variation of the intensities of spectral lines due to A I to A VIII inclusive showing the successive appearance of the ionization states in the ZETA plasma. The argon is introduced as a 5% impurity in deuterium with a total gas pressure of 0.5 millitorr.

for a given element the ascending stages of ionization appear in successive time sequence. This is illustrated by the Figure which reproduces oscillograms of the intensity variations of eight lines due to A I to A VIII inclusive, together with the current waveform. The oscillograms are aligned on a common time scale by means of a timing signal, indicated by arrows and derived from the ZETA firing circuit. Observations of this type enable the spectral lines of the element being studied to be assigned to its various stages of ionization.

By extrapolation along isoelectronic sequences, wavelengths were calculated for several lines of each element expected to appear in the observed region. Comparison between calculated and observed values provided confirmation of the identifications made on the basis of time of appearance, and also allowed the line transitions to be determined.

Newly observed lines of multiply ionized inert gases in the wavelength range 400–1000 Å.

Ion	$\lambda(\text{vac})$	Intensity	Transition
Ne VI	433.17†	2	$2p\ ^2P_{1/2}^0 - 2p^2\ ^2S_{1/2}$
	435.64†	3	$^2P_{3/2}^0 - ^2S_{1/2}$
Ne VI	451.85	1	$2p\ ^4P_{1/2} - 2p^3\ ^4S_{3/2}^0$
	452.75	1	$^4P_{3/2} - ^4S_{3/2}^0$
	454.07	2	$^4P_{5/2} - ^4S_{3/2}^0$
Ne VII	465.21	10	$2s^2\ ^1S_0 - 2p\ ^1P_1^0$
Ne VII	558.6†	3	$2p\ ^3P_1^0 - 2p^2\ ^3P_2$
	559.96	3	$^3P_0^0 - ^3P_1$
	561.38	3	$^3P_1^0 - ^3P_1$
	561.73	4	$^3P_2^0 - ^3P_2$
	562.98	3	$^3P_1^0 - ^3P_0$
	564.52	3	$^3P_2^0 - ^3P_1$
Ne VIII	770.42	8	$2s\ ^2S_{1/2} - 2p\ ^2P_{3/2}^0$
	780.34	4	$^2S_{1/2} - ^2P_{1/2}^0$
Ar VI	754.93	1	$3p\ ^2P_{1/2}^0 - 3p^2\ ^2D_{3/2}$
	767.06	2	$^2P_{3/2}^0 - ^2D_{5/2}$
	767.71	1	$^2P_{3/2}^0 - ^2D_{3/2}$
Ar VIII	700.24	10	$3s\ ^2S_{1/2} - 3p\ ^2P_{3/2}^0$
	713.81	5	$^2S_{1/2} - ^2P_{1/2}^0$
Kr V	472.16	3	—
	708.85	8	—
Kr VI	450.20	2	$4p\ ^2P_{1/2}^0 - 4d\ ^2D_{3/2}$
	465.27	6	$^2P_{3/2}^0 - ^2D_{5/2}$
Kr VI	544.03	5	$4p\ ^2P_{1/2}^0 - 4p^2\ ^2P_{3/2}$
	554.52	5	$^2P_{1/2}^0 - ^2P_{1/2}$
	569.13	5	$^2P_{3/2}^0 - ^2P_{3/2}$
	580.63	2	$^2P_{3/2}^0 - ^2P_{1/2}$
Kr VI	705.84	8	$4p\ ^2P_{1/2}^0 - 4p^2\ ^2D_{3/2}$
	742.83	8	$^2P_{3/2}^0 - ^2D_{5/2}$
Kr VII	585.37	8	$4s^2\ ^1S_0 - 4p\ ^1P_1^0$
	618.67	1	$(4p\ ^3P_2^0 - 4p^2\ ^3P_2)$
Kr VIII	651.57	10	$4s\ ^2S_{1/2} - 4p\ ^2P_{3/2}^0$
	695.91	8	$^2S_{1/2} - ^2P_{1/2}^0$
Xe V	682.56	3	—
Xe VI	599.84	3	—
	800.84	2	—
	880.04	2	—
Xe VII	531.18	1	$5p\ ^3P_1^0 - 5d\ ^3D_2$
	566.04	2	$^3P_2^0 - ^3D_3$
	698.02	10	$5s^2\ ^1S_0 - 5p\ ^1P_1^0$
	723.71	3	$(5p\ ^3P_2^0 - 5p^2\ ^3P_2)$
	995.50	3	$5s^2\ ^1S_0 - 5p\ ^3P_1^0$
Xe VIII	517.00	2	$5p\ ^2P_{1/2}^0 - 5d\ ^2D_{3/2}$
	562.55	2	$^2P_{3/2}^0 - ^2D_{5/2}$
	740.44	7	$5s\ ^2S_{1/2} - 5p\ ^2P_{3/2}^0$
	858.59	3	$^2S_{1/2} - ^2P_{1/2}^0$
Xe IX	658.12	2	—
	661.79	1	—
	686.88	2	—
	700.96	3	—

†These lines are tabulated by Paul and Polster (1941). They are included here because the present observations give significantly different wavelengths.

‡ Blend with Ne vi. Calculated wavelength.

§ 3. RESULTS

The results are shown in the Table. The successive columns give, respectively, the element and degree of ionization, the observed vacuum wavelength, an estimate of the line intensity, and the transition when known. The wavelengths were measured by normal methods, using as standards some of the lines of Ne IV, v and vi previously observed in this region by Paul and Polster (1941) and Boyce (1934). A trace of neon was maintained in the discharge when making measurements of lines due to argon, krypton and xenon. The accuracy of the wavelength values is limited by the shortage of suitable standards and the large Doppler widths of the lines, the latter being caused by the high energies attained by ions in ZETA, of the order of a few hundred electron volts. The probable error of wavelength measurement is estimated to be $\pm 0.03 \text{ \AA}$.

The line intensities were obtained directly from the photographic plates with no attempt to correct for variations of emulsion sensitivity or instrumental transmission with wavelength. They are included only as a guide and are on a linear scale with the strongest tabulated line for each element given arbitrarily as ten. The values give only an approximate indication of the relative intensities of lines of the same element.

Transitions are not tabulated for all lines given in the Table. In some cases either the isoelectronic data was insufficient to establish the identity of the line, or ambiguity occurred due to overlapping of possible multiplets. In two cases, the isoelectronic data predicted the observed wavelength sufficiently accurately but corresponding lines of the same multiplet, expected to be faint, could not be identified. There is therefore some doubt about the classifications in question and they have been bracketed in the table.

The data given in the table are not meant to represent an exhaustive survey of the spectra of the inert gases in the range 400–1000 \AA , and a more complete survey, covering a wider spectral range, may be attempted later. However, the observations are believed to be the first made in the laboratory, although the Ne VIII resonance doublet has been detected in the solar spectrum obtained from rocket flights. (Friedman 1960).

ACKNOWLEDGMENTS

We are grateful for the co-operation of the ZETA Operations Team and the assistance of Mr. R. H. White. The work has benefited from discussions with Mr. W. M. Burton.

REFERENCES

- BOYCE, J. C., 1934, *Phys. Rev.*, **46**, 378.
 BURTON, W. M., and WILSON, R., 1961, *Proc. Phys. Soc.*, **78**, in the press.
 BUTT, E. P., *et al.*, 1958, *2nd Geneva Conference: A/Conf. 15/P/1519*.
 FRIEDMAN, H., 1960, *Astron. J.*, **65**, 264.
 KAUFMAN, A. S., HUGHES, T. P., and WILLIAMS, R. V., 1960, *Proc. Phys. Soc.*, **76**, 17.
 MOORE, C. E., 1952, *Atomic Energy Levels*, National Bureau of Standards Circular **467**.
 PAUL, F. W., and POLSTER, H. D., 1941, *Phys. Rev.*, **59**, 424.

Magnetic Resonance in the Nitrogen Afterglow

By J. M. ANDERSON AND J. N. BARRY†

Department of Physics, University of Toronto, Toronto, Canada

MS. received 17th June 1960, in revised form 5th April 1961

Abstract. The decay of a magnetic resonance absorption in the nitrogen afterglow has been followed and compared with the decay of the afterglow itself. Afterglow was never, in any case, obtained without the presence of this absorption and vice versa. Simultaneous records of the two quantities showed that in all cases the absorption disappeared logarithmically at a rate which did not increase with nitrogen pressure while the afterglow intensity decayed according to an $I^{-1/2}$ law in a somewhat longer time. The rates of both processes are increased by addition of oxygen. The processes involved seem quite independent.

§ 1. INTRODUCTION

PREVIOUS papers (Anderson, Kavadas and McKay 1957, Anderson 1957) have shown that, in the earlier part of the decay of the nitrogen afterglow, the intensity falls off so that $I^{-1/2}$ is linear in time. It was also shown that small percentages of oxygen are necessary for the appearance of this initial decay and that an excitation energy of 900 cm^{-1} must be supplied in the final afterglow collision. The later stages of the afterglow in oxygen-free nitrogen were found to be due to a bimolecular process involving a nitrogen particle in a complex with an impurity presumed to be hydrogen. This complex had a dissociation energy of 5600 cm^{-1} and could show a final logarithmic decay.

In this work a magnetic resonance absorption was studied simultaneously with measurements of decay of the afterglow intensity.

§ 2. APPARATUS

Since simultaneous measurements on afterglow intensity and absorption were required, the magnetic resonance measurements were made in the 10 cm microwave band rather than in the more usual 3 cm band. The lower frequency permitted larger volumes and hence greater afterglow intensities, but also required a larger volume of magnetic field sufficiently uniform to allow magnetic resonance at the same frequency at any point in the glowing gas. To fulfil this requirement a special magnet was constructed giving a field uniform to better than one part in 2000 over a cylindrical volume 4 cm in diameter by 6 cm long. The general design principles used were those described by Daniels (1950).

A block diagram of the apparatus is shown in Fig. 1. The cylindrical microwave cavity was excited in the H_{112} mode by a 707 A/B klystron for the magnetic resonance measurements. A periodic saw-tooth frequency modulation carried the frequency of this source through the cavity resonance frequency with which the magnetic resonance absorption frequency was made to coincide by

† Now at Defence Research Telecommunications Establishment, Ottawa, Canada.

magnetic field adjustments. The cavity with no excitation of the nitrogen was adjusted to be very slightly undercoupled to the 50 ohm coaxial feed line, so that the reflected output of the klystron, studied through the directional coupler, showed a dip almost to zero reflection at the resonance frequency. Using the crystal detector calibration and the amplitude reflected by the cavity at the resonance frequency when completely mismatched, the reflection coefficient of the cavity could be found, not only for the cavity with unexcited gas but also with any degree of added losses due to energy absorption at any time following a discharge. The patterns were photographed using a Tektronix 532 oscilloscope with a dual trace amplifier, type 53/54C using no timebase but a modified Cossor moving film camera as in the previous work. Using the usual equivalent circuit relations it is easily shown that the number of absorbing centres A is proportional to $(\bar{Y} - \bar{Y}_0)(1 - \bar{Y})$ where \bar{Y} and \bar{Y}_0 are amplitude reflection coefficients at the cavity resonance frequency with and without the presence of added losses.

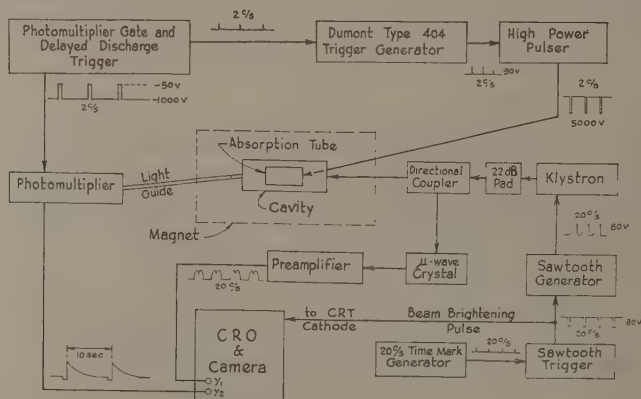


Fig. 1. Block diagram of apparatus.

The nitrogen gas was contained in a cylindrical quartz vessel 4.5 cm long and 4 cm in diameter. Losses due to the quartz were so small that Q 's above 10⁴ were measured for the cavity with no gas excitation. Attempts were made to excite the nitrogen using a pulsed magnetron (100 kw peak) operating in the E_{010} mode of the cavity. This successfully avoided interference in the klystron mode but completely failed to produce active nitrogen. Rather weak glow discharges in the bottle were easily obtained but all attempts to increase the power fed to the cavity to increase the excitation were complete failures. It is suspected that increase in ionization so disturbed the field distributions in the cavity that complete mismatch occurred for the greater part of each pulse. Since this was unsuccessful, tungsten electrodes were inserted in the glass vacuum system well outside the cavity in opposite directions and afterglow was easily excited using the two-microsecond 175 A d.c. pulses from the magnetron supply. Use of electrodes unfortunately made it impossible to assess accurately the purity of the gas and prevented use of the prolonged conditioning found essential in the previous work for exact quantitative study of impurities.

The nitrogen gas as before was prepared by the bromine ammonia method and purified by passage over phosphorus pentoxide, hot copper and sodium. It was impossible to flame the quartz tube in its microwave cavity and purity in this work never reached the levels of the earlier paper. Gas which gave intense but very short afterglows with the radar pulse excitation has been found to show no glow with the continuous wave excitation previously used until much more drastic purification procedures are applied.

The afterglow intensity was followed using a 931A photomultiplier tube as in the earlier work. Light reached this tube which was placed well outside the magnetic field through a light guide made of Pyrex glass tubing wrapped in aluminium foil. This light guide was set in a position to view the afterglow obliquely across the cavity to be sure that only gas in a position to give magnetic resonance could contribute to the afterglow record. With these arrangements it was not possible to follow the glow to nearly such low intensities as in the previous work.

It was found that in the presence of the electrodes the composition of the gas with oxygen impurity added changed rapidly and attained an equilibrium value only after a very large number of discharge pulses. Measurements taken in this equilibrium condition were quite repeatable but the actual behaviour depended somewhat on the previous history of the tube. Measurements at different impurity concentrations were attempted both by adding to the quartz vessel known volumes and pressures of a suitable mixture of oxygen and nitrogen and taking a record after the practical minimum of three discharge pulses and by using a larger number of discharges in each case. The two methods gave results which showed similar behaviour with added oxygen. Duration constants differed by as much as 15% depending on treatment of the tube preceding the readings. Since it was impossible in this case to carry out the prolonged periods of conditioning, found in the earlier work to be essential for obtaining consistent quantitative agreement, the impurity percentages quoted are at best qualitative estimates in which actual impurity content increases monotonically with addition of oxygen but has otherwise little relation to it.

Several sets of measurements made at different times were found to be in close agreement. Due to the presence of the electrodes and the impossibility of proper outgassing procedures the absolute impurity level is quite uncertain but the results serve to establish the trend of the effects with change in molecular nitrogen population.

Measurements of width and exact frequency of the magnetic resonance line were carried out using a small a.c. modulation superposed on the steady magnetic field by a single layer solenoid surrounding the cavity. A phase-sensitive detector was used to measure the energy transmitted by the cavity and hence it was possible to obtain a measure of the first derivative of the absorption with change of field. The line widths were found to be about ten to twelve gauss at the pressures used. They were independent of the strength of the absorption. The centre of the absorption was found to occur at 2.9087×10^9 c/s at a field in which the proton nuclear magnetic resonance frequency was 4.4192×10^6 c/s. The quotient of these results is 658.19 which differs from the much more accurate result 658.1631 of Heald and Beringer (1954) for the nitrogen atom by rather less than our expected reading error. It corresponds equally well with the cyclotron resonance of the free electron.

§ 3. PROCEDURE

Each series of measurements was taken after a preliminary period in which all excitation and sweep procedures were carried out automatically and cyclically while the magnetic field was adjusted so that the microwave absorption frequency coincided with the cavity resonance. This was easily done by watching the oscilloscope pattern of the reflection from the cavity with the time base on. When the field was either too low or too high the absorption dip in the reflected wave was slightly displaced relative to the position on the time base occupied by the dip with no absorption present. The field was easily adjusted so that the dip came at precisely the same point with and without previous excitation of the gas.

Gas conditions were then adjusted for the series desired, the intensity measuring equipment and its gating circuit were checked, the camera film was started, and the cavity completely mismatched to record a reflected wave corresponding to unit reflection coefficient. After a chosen pulse of excitation the excitation pulses were cut off and records of resonance absorption and intensity allowed to run until both effects had completely disappeared. This last part of the magnetic resonance record was used to give the necessary measure of \bar{Y}_0 the reflection coefficient of the cavity with no absorption due to the gas.

In the measurements with impurity added this procedure was varied in two different ways. In the first of these preliminary adjustments were made as above, impurity was added and given time to mix thoroughly, the film was started and after the third discharge pulse recording was carried out as before, more impurity was added and again following the third pulse the record was made, and so forth. In the second method impurity was added and the record made as before but before the next impurity addition twenty discharge pulses were allowed to pass in an attempt to condition the gas.

It was found possible to excite very much more intense afterglows and absorption after prolonged excitation at 20 pulses per second than was obtainable after each regular pulse in the 2 c/s sequence. The rapid repetition rate caused complications with the automatic gating of the photomultiplier so that it was not feasible to get simultaneous recordings of the afterglow intensity. A few measurements were taken of the decay of absorption alone to check the law of decay over a wider range than was possible with the simultaneous measurements.

§ 4. RESULTS

In every case in which afterglow was observed, absorption was also found, and absorption was never found in this work without accompanying afterglow. These statements include many months of work with microwave discharges which produced neither, as well as trials with the d.c. pulse discharge under the widest conditions of pressure, impurity, and discharge intensity. Since impurity content was not under complete control it is impossible to make any statement concerning the cases of very pure gas observed to give no glow in the earlier work.

Results of a series of simultaneous measurements of decay of afterglow intensity and absorption with time for different nitrogen pressures are shown in Fig. 2. Similar series of measurements made at different times agreed qualitatively with this in every way.

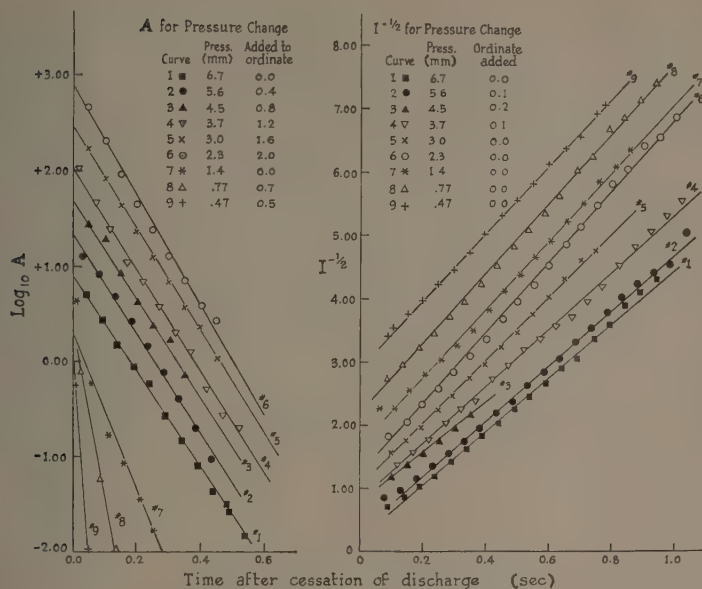


Fig. 2. Decay curves with variation of pressure.

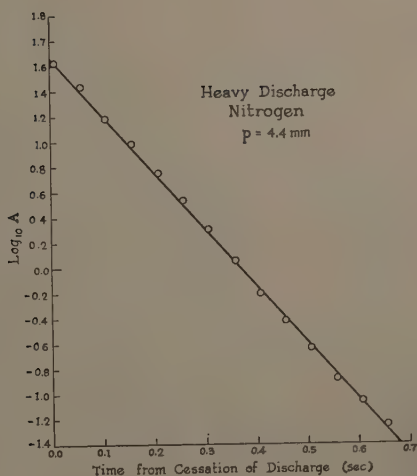


Fig. 3. Decay of absorption with heavy discharge.

It is evident that the afterglow after the first 0.1 second falls off according to the bimolecular law, $I^{-1/2}$ being linear in time with a slope designated hereafter as S , while the absorption falls off logarithmically with time with decay constant K . To be sure that no error was possible, curves of each quantity were plotted on axes corresponding to the other law. In no case was a straight line relation found for reciprocal of absorption plotted against time corresponding to the bimolecular law nor were straight lines found for plots of $\log I$ against time. Special attention was given to those cases in which the experimental points showed an imperfect fit to curves such as those of Fig. 2, but in all cases the plot of the other function showed a still less perfect fit to a linear curve.

Figure 3 shows a plot of the logarithm of absorption against time after a large initial population had been built up by a prolonged series of rapid pulse discharges as described above. The absorption obeys the logarithmic law of decay over a range of three decades.

Results of simultaneous measurements of decay of afterglow intensity and absorption with time as oxygen impurity was added are shown in Fig. 4. Other series by either procedure above were qualitatively the same but again differed in minor quantitative respects. Again $I^{-1/2}$ and logarithm of absorption are linear in time.

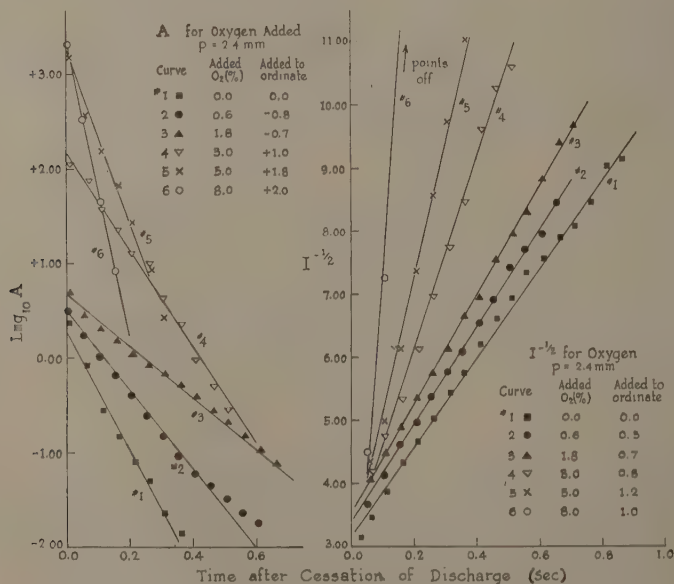


Fig. 4. Decay curves with added oxygen.

§ 5. DISCUSSION

The values of S , the positive slope of the $I^{-1/2}$ curves against time, from Figs 2 and 4 are plotted against pressure and added oxygen in the upper part of Figs 5 and 6 respectively. These slopes are greater by an order of magnitude

than most of the slopes S_1 for the first bimolecular process of the earlier papers. It is believed that the gas used in this work contained at all times an oxygen impurity in the body of the gas falling between or above the final pair of curves of the oxygen series of that paper. This would make all measurements in this work consistent with the previous results and is also consistent with the lower level of purity due to the presence of the electrodes and impossibility of thorough outgassing. It would also explain why the second bimolecular slope of the earlier work was never observed here. This second bimolecular decay disappeared at considerably lower percentages of oxygen. The quoted percentages of oxygen added appear to be an order of magnitude higher in this work but, as pointed out above, the fraction of these additions which appeared in the body of the gas was certainly fairly small and when uncertainties in volumes and concentrations in both this and the earlier work are taken into consideration the two sets of measurements cannot be considered inconsistent.

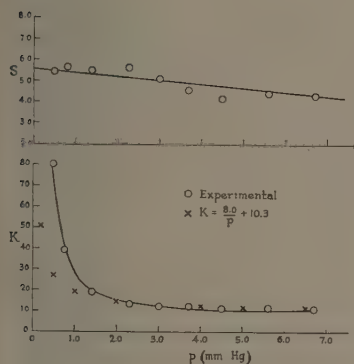


Fig. 5. Variation of slopes with pressure.

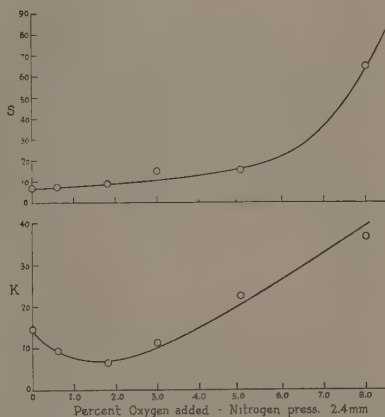


Fig. 6. Variation of slopes with added oxygen.

In Fig. 5 it is seen that S is almost independent of pressure, the small decrease of 20% for a factor of fifteen increase in pressure being probably within the limit of error. Certainly S does not increase with pressure so that it would seem that only the two active aggregates are involved in the afterglow collision and no other nitrogen molecule is involved. The previous work showed a small maximum in S_1 at intermediate pressures and no explanation was found. In consideration of the differences in the two sets of conditions it does not seem possible to come to any conclusion on this point.

The original intention of this work was to study the absorption due to the $^4S_{3/2}$ ground state of the nitrogen atom as a measure of atomic population. The absorption actually recorded falls within our limit of error of the correct frequency but line width and intensity are not consistent with this explanation. Both of these, as well as the frequency measurement, are consistent with cyclotron resonance absorption due to free electrons measured by Jones (1956).

At all times, and for all types of discharge in all gas samples during our measurements free electrons left over from the discharge could be observed by extending the measurements to very short times after the excitation ceased. These always fell below the limit of experimental observation within ten milliseconds after the discharge. This is consistent with the many papers on recombination of ions such as Faire and Champion (1959) and also with the theory of such recombination.

Thus it is evident that the absorption is not caused by free electrons left over from the discharge since no points have been recorded at less than twenty milliseconds and in assessing the results little weight is assigned to points at less than one hundred milliseconds after the discharge ceased. The absorption must be associated with an energy-carrying particle different from that whose bimolecular reaction gives rise to the afterglow since it has been shown that a logarithmic decay is not consistent with the afterglow results while the reciprocal absorption curve is not linear in time.

The negative logarithmic slope of the absorption curves of Figs 2-4 is shown in Fig. 5 to fall rapidly at the lowest pressures and then to become nearly constant as nitrogen pressure is further increased. This curve may indicate an inverse first power dependence on pressure at low pressures indicating a disappearance of the active bodies by diffusion to the walls. At higher pressures this rate of decay becomes small compared with some process occurring within the body of the gas which proceeds at a rate proportional to the active population but independent of nitrogen pressure. Such a process is somewhat difficult to visualize but this behaviour at least indicates that collision with a nitrogen molecule does not affect the particle responsible for the absorption. This would demand that K increase linearly with nitrogen pressure of which there is no sign. Collision with some particle of relatively constant partial pressure is indicated. In view of the equilibrium set up by chemical combination and absorption of oxygen at the electrodes this is not improbable. In view of the result of the earlier work that the slope S_1 does not appear at all unless oxygen is present and in view of the variation of K with added oxygen in Fig. 6 it would seem that this other particle must involve oxygen in some form.

In Fig. 5 the crossed points correspond to the equation $K = (8.0/p) + 10.3$. On the mechanism outlined above, this equation represents $K = D/\lambda^2 p + B$ where D is the diffusion coefficient of the active particle responsible for absorption in nitrogen gas at one millimeter pressure, λ is the diffusion length as in the earlier paper while B is the number of collisions per second made by this energy carrier in the body of the gas which remove its activity in producing absorption. The value of B for the number of collisions per second by a nitrogen molecule in nitrogen at one millimeter pressure is of the order of 5×10^6 . Thus the number of effective collisions in the gas is down by a factor of 5×10^5 below this value. Since the particle necessary for the destructive collision is certainly not nitrogen but is independent of nitrogen pressure this indicates a partial pressure of the required particles which is greater than 2×10^{-6} millimeters and, making an allowance of a factor of 100 for collision efficiency, may be as high as 2×10^{-4} millimeters. Thus the particles in question may occur as an impurity of between 2 and 200 parts per million. This population by comparison with nitrogen at approximately 3×10^{16} molecules per cm^3 could rise as high as 6×10^{12} per cm^3 . This particle presumably containing oxygen is a rather scarce species.

In Fig. 6, K appears to fall with small additions of oxygen and this also occurs in other sets of results. This may possibly be due to the added oxygen inhibiting the destruction of particles at the wall as above. The final rise at higher oxygen addition indicates that the destruction of the active particle is by oxygen collision.

Thus it seems that the early stages of the nitrogen afterglow are due to a bimolecular recombination of two similar particles assumed in previous papers to be nitrogen atoms, one at least of which involves a complex with oxygen. At the same time a different energy carrier exists giving rise to absorption at the free electron frequency, giving no glow, but destroyed logarithmically by collision with oxygen within the gas and only very slowly at the walls. These two energy-carrying particles seem from these measurements to be quite independent since the curves of decay are so regular that common population must be at most extremely small. These observations are consistent with those of Rayleigh (1942) which indicated that the lifetime of the ionization due to active nitrogen was unconnected with the decay of the glow.

ACKNOWLEDGMENTS

The authors wish to acknowledge a grant to one of us (J.M.A.) from the Defence Research Board, Ottawa, Canada, DRB 9512-23 which provided funds for apparatus including the magnet. An operating grant from the National Research Council is also acknowledged. We wish also to thank the Defence Research Telecommunications Laboratory, Ottawa, which granted leave of absence to one of us (J.N.B.) to carry out this work. Thanks are also due to J. H. Dell who assisted in taking some of the later readings.

REFERENCES

- ANDERSON, J. M., 1957, *Proc. Phys. Soc. A*, **70**, 887.
ANDERSON, J. M., KAVADAS, A., and MCKAY, R. W., 1957, *Proc. Phys. Soc. A*, **70**, 877.
DANIELS, J. M., 1950, *Proc. Phys. Soc. B*, **63**, 1028.
FAIRE, A. C., and CHAMPION, K. S. W., 1959, *Phys. Rev.*, **113**, 1.
HEALD, M. A., and BERINGER, R., 1954, *Phys. Rev.*, **96**, 645.
JONES, R. V., 1956, *Ph.D. Thesis*, University of California.
RAYLEIGH, LORD, 1942, *Proc. Roy. Soc. A*, **180**, 140.

The Effect of Particle Streams on Transverse Hydromagnetic Waves†

By E. R. HARRISON

Atomic Energy Research Establishment, Harwell

MS. received 7th November 1960, in revised form 5th May 1961

Abstract. A magnetic field is 'frozen' into a moving conducting fluid when certain conditions are fulfilled, as for example, when the frequency of the fluid disturbance is small compared with the cyclotron frequencies of the fluid particles. If the fluid contains streams of moving particles, parallel to the magnetic field, the magnetic field is also 'frozen' into the streams when there are transverse perturbations. The condition now is that the Doppler shifted frequency of the disturbance must be small compared with the cyclotron frequency of the stream particles. It follows that the phase velocity of transverse hydromagnetic waves is modified if such streams are present. In effect, the momentum flux of the streams reduces the 'tension' of the magnetic flux lines. When the kinetic energy density relative to the centre-of-mass system exceeds the magnetic energy density, the phase velocity in an infinite medium has complex conjugate values and the hydromagnetic wave grows in amplitude. In the case of a stream of finite radius the phase velocity shows dispersion for wavelengths greater than the stream radius and there is an increase in the domain of stability.

§ 1. INTRODUCTION

IN a conducting fluid transverse waves are propagated along a uniform magnetic field with a phase velocity of $(B^2/4\pi\rho)^{1/2}$, as was first shown by Alfvén (1950), where B is the magnetic field strength and ρ is the fluid density. Chandrasekhar, Kaufman and Watson (1958) and others have since shown that if the pressure is anisotropic the phase velocity is modified and under certain circumstances can have complex values.

In plasma physics one finds that the situation is often complicated by the presence of streams of charged particles which are guided along the magnetic lines of force. For example, the streams which produce the auroral effects are in all probability guided along the geomagnetic flux-lines and pass through an atmospheric plasma whilst still at large distances from the Earth. Other examples where such a situation might occur are found in stellar atmospheres, astrophysical objects with a filamentary structure such as the Crab nebula, plasma neutralized accelerators of the kind proposed by Budker (1956), and thermonuclear discharge devices in which a fraction of the electron population is accelerated and forms a circulating stream that is contained by the flux-lines embedded in the plasma. It is shown below that such streams affect the phase velocity of transverse hydromagnetic waves, and in the case of an infinite medium the phase velocity has complex values and the hydromagnetic wave grows in amplitude when the mean kinetic energy density exceeds the magnetic energy density. For a stream of

† This paper was written whilst the author was temporarily at CERN, Geneva.

finite radius the phase velocity is modified for wavelengths which are no longer small in comparison with the radius of the stream. These results are similar in principle to those of Chandrasekhar *et al.* provided one interprets the appropriate part of the anisotropic pressure as a momentum flux.

§ 2. TRANSVERSE WAVES IN AN INFINITE MEDIUM

We commence by assuming that a uniform magnetic field is embedded in an infinite, neutralized, conducting medium of uniform density, and that the medium consists either entirely or partly of streams moving parallel to the magnetic field. Let the uniform field \mathbf{B}_0 and the stream velocities \mathbf{u}_i be parallel to the z axis, and let

$$\mathbf{B} = \mathbf{B}_0 + \mathbf{b}; \quad \mathbf{V}_i = \mathbf{u}_i + \mathbf{v}_i, \quad \dots\dots (1a, b)$$

where \mathbf{b} and \mathbf{v}_i are the perturbations in the field and the velocities transverse to the z axis. Neglecting second-order quantities the equation of motion of the i th stream, of charge density $n_i e_i$ and mass density ρ_i , is

$$\rho_i \left(\frac{\partial}{\partial t} + u_i \frac{\partial}{\partial z} \right) \mathbf{v}_i = n_i \frac{e_i}{c} (\mathbf{E} + \mathbf{V}_i \wedge \mathbf{B}) - \nabla p_i + \sum_k \mathbf{P}_{ik} \quad \dots\dots (2)$$

where the pressure p_i is assumed to be isotropic and \mathbf{P}_{ik} is the rate of momentum transfer from the k th stream due to collisions. Since transverse perturbations do not affect p_i we shall set ∇p_i equal to zero in the usual way (Cowling 1957).

We suppose now that the variables are Fourier analysed in z and t with typical components proportional to $\exp i(\omega t - kz)$, where ω is the frequency and k the wave number. Thus if ξ_b is the displacement of the magnetic flux-lines, then Maxwell's equations for a neutral medium take the form

$$\text{div } \mathbf{E} = 0, \quad \dots\dots (3a)$$

$$\text{div } \mathbf{B} = 0, \text{ or: } \mathbf{b} = B_0 \frac{\partial \xi_b}{\partial z} = -ik B_0 \xi_b \quad \dots\dots (3b)$$

$$\text{curl } \mathbf{E} = -\frac{\partial \mathbf{b}}{\partial t}, \text{ or: } \mathbf{E} \wedge \mathbf{B}_0 = -\frac{\omega}{k} B_0 \mathbf{b} = i\omega B_0^2 \xi_b \quad \dots\dots (3c)$$

$$\text{curl } \mathbf{b} = 4\pi \mathbf{j}. \quad \dots\dots (3d)$$

where \mathbf{E} is the electric field, \mathbf{j} is the current density, and the displacement current is neglected in the usual way.

Equation (2) can be simplified by further supposing that the collision frequencies are small compared with the cyclotron frequencies Ω_i . Thus, if

$$\alpha_i = i(\omega - ku_i)/\Omega_i, \quad \dots\dots (4)$$

the equation of motion now takes the form

$$\alpha_i B_0 \mathbf{v}_i = \mathbf{E} + \mathbf{V}_i \wedge \mathbf{B}.$$

On taking the vector product of this equation with \mathbf{B}_0 , and using Eqns (1), it follows that the velocity components parallel and perpendicular to \mathbf{b} are

$$\mathbf{v}_{i\parallel} = \frac{\mathbf{E} \wedge \mathbf{B}_0 + u_i B_0 \mathbf{b}}{(1 + \alpha_i^2) B_0^2} \quad \dots\dots (5a)$$

$$\mathbf{v}_{i\perp} = \frac{\alpha_i}{1 + \alpha_i^2} \frac{\mathbf{E} + u_i \mathbf{b}}{B_0} \quad \dots\dots (5b)$$

since, according to Eqn (3c), \mathbf{E} has no component parallel to \mathbf{b} . Again, taking the vector product of Eqn (5a) with \mathbf{B}_0 , and using Eqn (5b), it is seen that

$$\mathbf{v}_{i\perp} = -\frac{\alpha_i}{B_0} \mathbf{v}_{i\parallel} \wedge \mathbf{B}_0. \quad \dots\dots (6)$$

Thus, if the Doppler shifted frequency is small compared with the cyclotron frequency, or $\alpha_i \ll 1$, the component of the velocity perpendicular to \mathbf{b} is relatively small. One notices that the contributions to the electric current, which produces the magnetic field perturbation, are proportional to $n_i m_i$, and therefore come mainly from the heavier particles. Combining Eqns (5a) and (5b) one obtains

$$\mathbf{E} + \mathbf{u}_i \wedge \mathbf{b} + (1 + \alpha^2) \mathbf{v}_i \mathbf{B}_0 = 0 \quad \dots\dots (7a)$$

or, when $\alpha_i \ll 1$,

$$\mathbf{E} + \mathbf{v}_i \wedge \mathbf{B}_0 = 0. \quad \dots\dots (7b)$$

In magnetohydrodynamics it is well known that an equation of the form (7b) means that the magnetic field is 'frozen' into a fluid conducting medium. It is less well known, though equally obvious, that when a neutral medium consists of streams of particles with velocities parallel to the magnetic flux-lines, the streams and flux-lines also have identical displacements. This is easily shown, for if ξ_i is the transverse displacement of the i th stream, then

$$\mathbf{v}_{i\parallel} = \frac{d\xi_i}{dt} = \left(\frac{\partial}{\partial t} + u_i \frac{\partial}{\partial z} \right) \xi_i = i(\omega - ku_i) \xi_i.$$

But from Eqn (5a), and using Eqns (3b) and (3c), it also follows that

$$\mathbf{v}_{i\parallel} = \frac{i(\omega - ku_i)}{1 + \alpha_i^2} \xi_b.$$

Hence, if $\alpha_i \ll 1$, then $\xi_i = \xi_b$ + a constant vector, but since the constant must be zero, the i th stream and the field have identical displacements. This means that all streams have equal displacements.

Summing the equations of motion (2) over all particles yields, for a neutral medium,

$$\sum_i \rho_i \left(\frac{\partial}{\partial t} + u_i \frac{\partial}{\partial z} \right)^2 \xi = \mathbf{j} \wedge \mathbf{B}, \quad \dots\dots (8)$$

where all fluid displacements are equal, as shown above. On linearizing the right-hand side of this equation, and using Eqn (3d), we have

$$\mathbf{j} \wedge \mathbf{B} = \mathbf{j}_0 \wedge \mathbf{b} + \frac{B_0^2}{4\pi} \frac{\partial^2 \xi}{\partial z^2} \quad \dots\dots (9)$$

where \mathbf{j}_0 is the electric current of the streams parallel to the uniform field \mathbf{B}_0 .

Strictly speaking, the original assumption that the unperturbed field \mathbf{B}_0 is uniform can only be true when the streams make no contribution, that is $\mathbf{j}_0 = 0$, and the individual streams are themselves neutral or they cancel out each others effect. We shall consider this possibility first.

2.1. Stream Current \mathbf{j}_0 is Zero

The equation of motion of the fluid is now simply

$$\sum_i \rho_i \left(\frac{\partial}{\partial t} + u_i \frac{\partial}{\partial z} \right)^2 \xi = \frac{B_0^2}{4\pi} \frac{\partial^2 \xi}{\partial z^2}, \quad \dots\dots (10)$$

from Eqns (8) and (9). If ρ is the total density of the fluid, $\rho \langle u \rangle$ is the mean momentum, and $\rho \langle u^2 \rangle$ the mean momentum flux, the dispersion equation is

$$\omega^2 - 2 \langle u \rangle \omega k - \left(\frac{B_0^2}{4\pi\rho} - \langle u^2 \rangle \right) k^2 = 0 \quad \dots\dots (11)$$

for a typical Fourier component of $\xi \propto \exp i(\omega t - kz)$. The phase velocity of a disturbance is therefore given by

$$\frac{\omega}{k} = \langle u \rangle \pm \left(\frac{B_0^2}{4\pi\rho} + \langle u \rangle^2 - \langle u^2 \rangle \right)^{1/2}. \quad \dots\dots (12)$$

When the streams have zero velocity we recover from Eqn (12) the Alfvén phase velocity. If all the particles have the same velocity, then $\langle u \rangle^2 = \langle u^2 \rangle$, and the frequency is merely Doppler shifted by an amount uk owing to the mass motion of the medium. However, when the streams have different velocities, unless

$$\frac{B_0^2}{4\pi} > \rho(\langle u^2 \rangle - \langle u \rangle^2), \quad \dots\dots (13)$$

the phase velocity has complex conjugate values and there is transverse or sinuous instability in the form of time or space growing waves. Notice that in terms of momentum flux the pressure parallel to the field is $p_{\parallel} = p + \rho(\langle u^2 \rangle - \langle u \rangle^2)$ in the centre-of-mass system, where $p = p_{\perp} = \Sigma p_i$ is the isotropic pressure of Eqn (2). The stability condition (13) now takes the form

$$\frac{B_0^2}{4\pi} > p_{\parallel} - p_{\perp}, \quad \dots\dots (14)$$

which has been obtained elsewhere (Chandrasekhar, Kaufman and Watson).

One can imagine a simple case in which a neutral stream of charged particles of density ρ_1 , and velocity u_1 , passes through a stationary plasma of density ρ_0 . The phase velocity given by Eqn (13) is now

$$\frac{\omega}{k} = u_1 \frac{\rho_1}{\rho} \pm \left\{ \frac{B_0^2}{4\pi\rho} - u_1^2 \frac{\rho_0\rho_1}{\rho^2} \right\}^{1/2}, \quad \dots\dots (15)$$

where $\rho = \rho_0 + \rho_1$. It is noticed that this is also the phase velocity of small transverse oscillations of a string, of line density ρ_0 and tension $B_0^2/4\pi$, on which beads of line density ρ_1 slide without friction at velocity u_1 . An infinitely flexible tube under tension and containing a moving fluid is an alternative model, and hence the name of 'hose-pipe instability' for complex wave phenomena of this type. The phase velocity has real roots only if

$$\frac{B_0^2}{4\pi} > \frac{\rho_0\rho_1}{\rho} u_1^2, \quad \dots\dots (16)$$

and from either Eqns (13) or (16) we see that there is stability when the magnetic tension $B_0^2/4\pi$ exceeds the 'negative tension' of the momentum flux measured relative to the system in which there is no mass flow (or centre-of-mass system), or, stated in an alternative way, when the magnetic energy density is greater than the kinetic energy density measured in the centre-of-mass system. A similar criterion to (16) in the form of $B_0^2/8\pi > \rho_1 u_1^2$ has been proposed (but without proof) by Finkelstein and Sturrock (1958) as a condition for stabilizing neutralized electron beams in accelerators of the Budker type.

2.2. Stream Current j_0 is Not Zero

So far we have adopted the rather unrealistic assumption that the unperturbed stream current j_0 is zero in the equation of motion (8). In most cases of interest this current is not zero, and in a stream of circular cross section a B_{ϕ} field is superimposed upon the uniform field B_0 and the flux lines are twisted into helices about

the axis of the stream. But if the amount of twist is small per wavelength, or

$$|k^{-1}B_\phi| \ll |aB_0|, \quad \dots\dots (17)$$

where a is the radius of the stream, this effect can reasonably be neglected. In this section boundary conditions are neglected and hence only relatively short wavelengths of $ak \gg 1$ are considered, and therefore the condition (17) should not be difficult to satisfy.

On including the current term \mathbf{j}_0 in the equation of motion (8), but assuming that \mathbf{B}_0 is uniform, it follows that

$$\sum_i \rho_i \left(\frac{\partial}{\partial t} + \mathbf{u}_i \cdot \frac{\partial}{\partial \mathbf{z}} \right)^2 \boldsymbol{\xi} = \mathbf{j}_0 \wedge B_0 \frac{\partial \boldsymbol{\xi}}{\partial z} + \frac{B_0^2}{4\pi} \frac{\partial^2 \boldsymbol{\xi}}{\partial z^2}. \quad \dots\dots (18)$$

Resolving the displacement $\boldsymbol{\xi}$ in the x and y directions, one obtains for $\xi_x \pm i\xi_y$ the dispersion equation

$$\omega^2 - 2\langle u \rangle \omega k - \left(\frac{B_0^2}{4\pi\rho} - \langle u^2 \rangle \right) k^2 \mp j_0 B_0 \rho^{-1} k = 0, \quad \dots\dots (19)$$

and the plus and minus signs correspond to right- and left-hand circularly polarized waves. The force $\mathbf{j}_0 \wedge \mathbf{b}$ twists each flux-line into a helix about the unperturbed flux-line. Using a characteristic value of $B_\phi = 2\pi a j_0$, one sees that the ratio

$$\frac{j_0 B_0 k}{B_0^2 k^2 / 4\pi} \simeq \frac{2B_\phi}{akB_0} \quad \dots\dots (20)$$

is small according to (17). The phase velocity is therefore approximately the same as that given by Eqn (12), and the treatment in §2.1 applies also in those cases when the stream current j_0 is not zero.

§ 3. WAVELENGTHS LARGE COMPARED WITH THE STREAM RADIUS

So far we have considered only wavelengths short in comparison with the stream radius and have regarded the medium as infinitely extended. When the wavelength is comparable with or larger than the stream radius the previous treatment must be modified and the appropriate boundary conditions taken into account.

From Maxwell's equations, one has

$$\nabla^2 \mathbf{E} - 4\pi \frac{\partial \mathbf{j}}{\partial t} = 0 \quad \dots\dots (21)$$

for a neutral medium in which the displacement current is neglected. The right-hand side is determined by using Eqns (5a) and (5b) for the velocity components, and by assuming that $\alpha_i \ll 1$.

$$\begin{aligned} \frac{\partial \mathbf{j}}{\partial t} &= \sum_i n_i \frac{e_i}{c} \frac{\partial}{\partial t} (\mathbf{v}_{i\parallel} + \mathbf{v}_{i\perp}) \\ &= -\frac{j_0}{B_0} \text{curl } \mathbf{E} + \sum_i \frac{\rho_i}{B_0^2} (\omega - k u_i) (i\omega \mathbf{E} - \mathbf{u}_i \wedge \text{curl } \mathbf{E}). \end{aligned}$$

Since the \mathbf{u}_i are constant vectors, and $\mathbf{u}_i \cdot \mathbf{E} = 0$, it follows that

$$\mathbf{u}_i \wedge \text{curl } \mathbf{E} = -(\mathbf{u}_i \nabla) \mathbf{E} = i k u_i \mathbf{E},$$

and Eqn (21) can therefore be written as:

$$\nabla^2 \mathbf{E} + \frac{4\pi}{B_0} j_0 \text{curl } \mathbf{E} + \frac{4\pi}{B_0^2} \sum_i \rho_i (\omega - k u_i)^2 \mathbf{E} = 0. \quad \dots\dots (22)$$

Before proceeding further it should be noticed that this equation neglects all thermal pressure gradients. This can be justified provided the magnetic pressure is large compared with the thermal pressure.

For the E_ϕ component of the electric field let

$$E_\phi = F(r) \exp i(\omega t - kz - m\phi)$$

for a typical wave number k and mode number m . Then in cylindrical polar coordinates, Eqn (22) is equivalent to

$$\frac{\partial^2 F}{\partial r^2} + \frac{1}{r} \frac{\partial F}{\partial r} + \left\{ p_a^2 - \frac{(m \pm 1)^2}{r^2} \right\} F = 0, \quad \dots\dots (23a)$$

$$(r < a): \quad p_1^2 = \frac{4\pi}{B_0^2} \left\{ \sum_i \rho_i (\omega - ku_i)^2 - k^2 \right\} \pm \frac{4\pi}{B_0} j_0 k, \quad \dots\dots (23b)$$

$$(r > a): \quad p_2^2 = \frac{4\pi}{B_0^2} \left\{ \sum_i \rho_i \omega^2 - k^2 \right\}, \quad \dots\dots (23c)$$

where, for $r > a$, the plasma contains only particles which have no streaming motion. Thus, the E_ϕ component is proportional to

$$\exp(-im\phi) \{A_m J_{m \pm 1}(p_a r) + B_m N_{m \pm 1}(p_a r)\}.$$

If there is a conducting boundary, coaxial with the unperturbed stream at $r = R$, then $E_\phi(R) = 0$. Also E_ϕ and its first derivatives are continuous at the boundary of the stream, but as the electric field is proportional to the transverse displacement to a first order, this is equivalent to requiring that E_ϕ and its first derivatives are continuous at $r = a$ for small displacements. These boundary conditions yield

$$\begin{aligned} p_1 J_n'(p_1 a) \{J_n(p_2 a) N_n(p_2 R) - J_n(p_2 R) N_n(p_2 a)\} \\ = p_2 J_n(p_1 a) \{J_n'(p_2 a) N_n(p_2 R) - J_n(p_2 R) N_n'(p_2 a)\}, \dots\dots (24) \end{aligned}$$

where $n = m \pm 1$. For sinusoidal perturbations $m = \pm 1$, and it is sufficient in the present elementary treatment to consider only the zero-order mode of $n = 0$. For small arguments, Eqn (24) reduces to

$$(p_1 a)^2 \ln L/a = 2, \quad \dots\dots (25)$$

where $L = R$. However, when the wavelength is still large in comparison with the stream radius a , but is small compared with R , then approximately $L = k^{-1}$.

Using Eqns (23b) and (25) the dispersion equation is now found to be

$$\sum_i \rho_i (\omega - ku_i)^2 - \frac{B_0}{4\pi} \left\{ k^2 \pm \frac{4\pi}{B_0} j_0 k + \frac{2}{a^2 \ln L/a} \right\} = 0. \quad \dots\dots (26)$$

The last three terms have the proportions

$$ak : 2 \frac{B_\phi}{B_0} : \frac{2}{ak \ln L/a},$$

and for $ak < 1$, $B_\phi < B_0$, the significant term is the last. It follows that for real values of k the phase velocity is therefore

$$\frac{\omega}{k} = \langle u \rangle \pm \left\{ \frac{B_0^2}{2\pi (ak)^2 \rho \ln L/a} + \langle u \rangle^2 - \langle u^2 \rangle \right\}^{1/2}, \quad \dots\dots (27)$$

and ω is real (no time growing waves) when

$$\frac{B_0^2}{4\pi} > \frac{1}{2} (ak)^2 \rho (\langle u^2 \rangle - \langle u \rangle^2) \ln L/a. \quad \dots\dots (28)$$

Comparing this expression with the stability condition (13) it is seen that in

effect the density is reduced approximately to $\rho(ak)^2$ for long wavelengths of $ak \ll 1$. Also, for real values of ω , k is also real (no space growing waves) when

$$\frac{B_0^2}{4\pi} > \frac{1}{2} (a\omega)^2 \rho \left\{ \frac{\langle u^2 \rangle - \langle u \rangle^2}{\langle u^2 \rangle} \right\} \ln L/a. \quad \text{..... (29)}$$

From Eqn (27) it is noticed that the phase velocity is dependent on the wave number k ; however, the group velocity is close to $\langle u \rangle$ when the stability conditions (28) or (29) are satisfied.

§ 4. CONCLUDING REMARKS

In this treatment the non-relativistic approximation has been used but the results are unchanged in form if the appropriate masses are increased by $\gamma_i = (1 - u_i^2/c^2)^{-1/2}$ and the cyclotron frequencies are replaced by Ω_i/γ_i in Eqn (4).

Although there is some justification for omitting the effect of binary collisions it is doubtful whether in many cases the momentum exchange due to collective electrostatic interactions can be neglected (Buneman 1959). In an infinite medium, consisting of electrons and ions of equal temperature, the collective interactions are negligible when the difference of the mean velocities of the electron and ion gases is less than the electron thermal speed (Penrose 1960), or

$$(u_+ - u_-)^2 < \frac{2kT_-}{m} \quad \text{..... (30)}$$

approximately. In many plasmas the conduction electrons drift with a speed of less than $(2kT/m)^{1/2}$, and if the conduction current is parallel to a magnetic field B_0 , there is stability when the current density satisfies

$$j^2 < \frac{B_0^2}{4\pi} \left(\frac{ne^2}{mc^2} \right) = 2.2 \times 10^{-14} n B_0^2 \quad \text{..... (31)}$$

from Eqn (16). For example, for a number of density 10^{14} cm^{-3} , and a field strength of $B_0 = 10^3$ gauss, the maximum stable current density is $1.5 \times 10^4 \text{ A cm}^{-2}$.

Taking the other extreme in the two-stream model, and assuming that the difference between the mean velocities is large compared with the thermal speeds, the dispersion equation for longitudinal electrostatic oscillations is (for example, see Pierce 1947)

$$\frac{\omega_+^2}{(\omega - ku_+)^2} + \frac{\omega_-^2}{(\omega - ku_-)^2} = 1$$

where ω_+ and ω_- are the plasma frequencies of the ions and electrons, u_+ and u_- are the mean ion and electron velocities, and ω and k now refer to longitudinal electrostatic perturbations. For real values of k , the frequencies are real when

$$|u_+ - u_-|k > \omega_- \quad \text{..... (32)}$$

for $\omega \gg \omega_+$. One sees that in an infinite medium there is always a range of wave numbers (corresponding to long wavelengths) for which there is electrostatic instability. However, in a finite cylindrical stream of radius a , the plasma frequency for wavelengths greater than a (that is, $ak \ll 1$) is given by

$$\omega_-^2 = (ka)^2 \frac{2\pi ne^2}{m} \ln \frac{R}{a} \quad \text{..... (33)}$$

where b is the radius of a conducting coaxial boundary (Budker 1956,

Finkelstein and Sturrock 1958). From Eqns (32) and (33) it follows that there is stability when

$$|u_+ - u_-| > a \left(\frac{2\pi n e^2}{m_-} \ln \frac{R}{a} \right)^{1/2}. \quad \dots\dots (34)$$

It can be seen that this condition is also sufficient for wavelengths smaller than the radius of the stream (Harrison 1960). Thus, when the zero temperature approximation is justified, it is still possible under certain conditions to have electron and ion streams freely interpenetrating in the manner assumed in this paper.

ACKNOWLEDGMENTS

The author is indebted to Dr. T. Ohkawa for several discussions and suggestions, and also to Dr. A. Schoch and Dr. Lloyd-Smith for their comments.

REFERENCES

- ALFVÉN, H., 1950, *Cosmical Electrodynamics* (Oxford: University Press). References are given to Alfvén's earlier work.
- BUDKER, G. J., 1956, *CERN Symposium*, **1**, 68.
- BUNEMAN, O., 1959, *Phys. Rev.*, **115**, 503.
- CHANDRASEKHAR, S., KAUFMAN, A., and WATSON, K., 1958, *Proc. Roy. Soc. A*, **245**, 435.
- COWLING, T. G., 1957, *Magnetohydrodynamics* (New York: Interscience).
- FINKELSTEIN, D., and STURROCK, P. A., 1958, *Plasma Physics*, Ed. J. A. Drummond (New York: McGraw Hill, 1961). *CERN Report* PS/Int AR 58-3.
- HARRISON, E. R., 1960, *Nature, Lond.*, **187**, 383.
- PENROSE, O., 1960, *Phys. of Fluids*, **3**, 258.
- PIERCE, J. R., 1947, *J. Appl. Phys.*, **19**, 231.

The Magnetic Susceptibilities of Aluminium-rich Transition Metal Intermetallic Compounds

By M. A. TAYLOR†

Crystallographic Laboratory, Cavendish Laboratory, Cambridge

Communicated by W. H. Taylor; MS. received 29th December 1960, in revised form 24th May 1961

Abstract. In aluminium-rich transition-metal intermetallic compounds the behaviour of transition-metal atoms in an electron-rich environment can be studied. Electron-density maps, prepared from x-ray data, and considerations of Brillouin zones for these compounds have not, up to the moment, yielded accurate information on the state of the transition-metal atoms. The results of the measurements of the magnetic susceptibilities of some such compounds are given: from these measurements information on the 3d state of the transition-metal atoms is derived.

§ 1. INTRODUCTION

RAYNOR (1949) interpreted metallurgical investigations on the aluminium transition-metal intermetallic compounds by assuming that the aluminium-rich phases are analogous to electron compounds and that in the electron-rich surroundings provided by the aluminium atoms the transition-metal atoms will absorb electrons ... "if the electron atom ratios are calculated for these compounds assuming that each aluminium atom contributes three electrons to the structure while each transition-metal atom absorbs electrons to the maximum extent‡ an approximately constant electron atom ratio is maintained, except in the case of FeAl_3 :

CrAl_7	MnAl_6	FeAl_3	Co_2Al_9	NiAl_3
2.05	2.05	1.58	2.12	2.09

This suggests that such compounds are a type of electron compound, whose formation is governed by the attainment of a given electron atom ratio".

This theory enabled many features of a number of phase diagrams to be correlated into a self-consistent scheme and permitted the prediction of the occurrence and stability of several new ternary phases.

Crystallographic research, directed at providing experimental evidence on electron absorption, has resulted in the accurate determination of the structures of the most aluminium-rich compounds, of several binary compounds less rich in aluminium and of several ternary phases. The structures are complex, but several

† Now at Solid State Physics Division, Atomic Energy Research Establishment, Harwell.

‡ The 'maximum extent' corresponds to the number of atomic orbital vacancies of Pauling (1938).

common features have been discovered (e.g. Taylor 1954, Black 1956, Brown 1957). For known crystal structures, electron-density maps have been prepared from the observed x-ray data (e.g. Douglas 1950, Nicol 1953) and it appeared that absorption of electrons by the transition-metal atoms occurred to an extent roughly in agreement with Raynor's negative valency scheme. Black (1955 a), however, showed that due to limitations of the experimental techniques and the theoretical interpretations the existence of electron transfer had not been reliably established.

The relationship of the first Brillouin zone planes to the strong x-ray reflections has been used to calculate the volumes of the zones for certain compounds and hence the effective valencies of the transition-metal atoms (Douglas 1950, Robinson 1953). In general, valencies in approximate agreement with Raynor's absorption hypothesis were obtained. Black (1955 b) then pointed out that for a structure with all interatomic distances approximately equal and with high coordination it can be shown that a set of strong reflections is necessarily observed. Therefore, if the empirical evidence from Brillouin zone calculations is to be significant, it must be shown that individual deviations in the electron/atom ratios correspond to differences in the compositions of the compounds: in most cases this detailed correlation is not found. It must be concluded that the electron absorption suggested by Raynor has not been confirmed experimentally.

Hume-Rothery and Coles (1954) have suggested that the negative valency scheme of Raynor is physically improbable, and have given reasons for this view.

The magnetic measurements described below were undertaken in order to obtain fresh experimental data relevant to this problem.

§ 2. THE APPLICATION OF MAGNETIC SUSCEPTIBILITY MEASUREMENTS

Information on the effectively localized magnetic moments associated with the transition-metal atoms may be obtained from magnetic susceptibility measurements over a temperature range. The magnetic susceptibility of an aluminium transition-metal alloy is made up of the following contributions:

- (i) the orbital diamagnetism of the electrons localized on aluminium ions;
- (ii) the orbital diamagnetism of the electrons localized on transition-metal ions;
- (iii) the Pauli paramagnetism of the conduction electrons (this may be enhanced by correlation effects);
- (iv) the Landau diamagnetism of the conduction electrons;
- (v) the paramagnetism of the 3d electrons, if any, with unpaired spins effectively localized on transition-metal ions.

Contributions (i) to (iv) give rise to a small approximately temperature independent para- or diamagnetism, the accurate calculation of which is not possible. Effectively localized unpaired spins (v), however, define paramagnetism with Curie-Weiss temperature dependence.

When an effectively localized magnetic moment is associated with a transition-metal atom, the contribution (v) swamps the terms (i) to (iv) and the value of the moment can be deduced from the relationship

$$\chi_A = \frac{N^2 \mu_B^2}{3R(T-\theta)} p_{\text{eff}}^2$$

where χ_A is the molar susceptibility, $p_{\text{eff}} = \{4S(S+1)\}^{1/2}$ (assuming the orbital moments are completely quenched) and θ is a parameter related to the intensity of the internal field.

§ 3. PREVIOUS MAGNETIC MEASUREMENTS

Foëx and Wucher (1954, 1956) reported MnAl_6 , CoAl_4 , $\text{Co}_4\text{Al}_{13}$, CrAl_7 , CrAl_4 , Co_2Al_5 and NiAl_3 to have a small temperature independent para- or diamagnetism and FeAl_3 to have a paramagnetism the temperature dependence of which followed a Curie-Weiss law with $p_{\text{eff}} = 1.67 \mu_B$ and $\theta = -103^\circ\text{K}$. They interpreted these results as showing that in MnAl_6 , CoAl_4 , $\text{Co}_4\text{Al}_{13}$, CrAl_7 , CrAl_4 , Co_2Al_5 and NiAl_3 the transition-metal atoms have full 3d shells and that in FeAl_3 an iron ion has slightly less than nine 3d electrons.

Vogt (1954) also reported MnAl_6 to have a small approximately temperature independent paramagnetism.

§ 4. THE PREPARATION OF SPECIMENS

Aluminium transition-metal intermetallic compounds are in general formed as the result of successive peritectic reactions and Phillips (1943) found that even prolonged annealing is unable to remove completely the coring and inhomogeneity: the Aluminium Laboratories Ltd., Banbury, also reached this conclusion. The possibility of producing by normal methods homogeneous single-phase ingots suitable for magnetic measurements was therefore dismissed.

Attempts were made to measure the susceptibilities of samples of single crystals of MnAl_6 (obtained by electrolytic extraction from an aluminium-rich matrix) packed together in the specimen holder; the value of the susceptibility was not reproducible on removing the crystals and re-packing them into the specimen holder, nor could reproducible results be obtained by powdering the crystals. This behaviour is probably due to the anisotropy of the single crystals.

The specimens for the measurements reported below were prepared by a modification of the powder metallurgical technique used at the Aluminium Laboratories Ltd., Banbury, by Goulding (1958, private communication). Fine powders of the pure metals were thoroughly mixed together in the correct proportions, and the compacts were pressed at 12 tons in 2 for periods of five minutes, fused successively at temperatures of 200, 400, 600 and 700°C *in vacuo* and pressed cold after each reaction. The compacts were then annealed for twenty-four hours at 800°C or at a temperature slightly below the decomposition temperature of the phase in question, whichever was lower. The specimens were examined metallographically and by x-ray powder photographs.

The impurities of the various metals, as quoted by their suppliers, are given in Table 1. Some gas was picked up during the sintering process and a typical analysis of a sample, NiAl_3 , by the British Non-Ferrous Metals Research Association gave the weights per cent of oxygen, nitrogen and hydrogen as 0.15, 0.002 and 0.001 respectively.

§ 5. THE MEASUREMENT OF MAGNETIC SUSCEPTIBILITY

A Sucksmith balance was used to measure magnetic susceptibility between 77 and 293°K . The specimen was cooled with liquid nitrogen, which was then allowed to evaporate, susceptibility measurements being taken over a period of four hours as the temperature of the specimen rose to room temperature. The balance was calibrated with tantalum (Hoare and Walling 1951). The absolute accuracy of any susceptibility measurement was to $\pm 3\%$, and the relative accuracy of points on a given temperature run corresponded to an error in the susceptibility

of 10^{-8} e.m.u. g^{-1} . The absolute accuracy of the temperature measurement was to $\pm 1\%$.

The aluminium-iron intermetallic compounds contained traces of ferromagnetic impurities: the effects of these were eliminated by means of Honda-Owen plots.

§ 6. RESULTS

The results of the measurements of the magnetic susceptibilities of the aluminium transition-metal intermetallic compounds are given in Table 2.

Table 2. The Magnetic Susceptibilities of Aluminium Transition-metal Intermetallic Compounds

The first line in each entry gives $10^6\chi$ with χ in e.m.u. g^{-1} and the second line T in $^{\circ}K$.

VAI_{10}	0.89 77	0.88 130	0.85 163	0.82 189	0.82 214	0.80 234	0.80 256	0.77 268	0.75 291
V_7Al_{45}	1.35 77	1.33 133	1.33 139	1.30 187	1.30 209	1.27 235	1.26 255	1.25 293	
V_4Al_{23}	0.60 77	0.55 146	0.52 180	0.49 205	0.45 233	0.44 260	0.41 293		
VAI_3	0.36 77	0.28 127	0.28 160	0.26 215	0.24 272	0.22 294			
V_5Al_8	1.71 77	1.68 129	1.68 142	1.65 159	1.64 179	1.63 188	1.61 212	1.61 224	1.61 231
V_5Al_8	1.59 257	1.59 262	1.57 282	1.55 293					
Cr_2Al_{11}	1.10 77	0.97 135	0.96 173	0.96 198	0.96 218	1.04 255	1.12 296		
$CrAl_7$	0.40 77	0.43 131	0.45 147	0.46 185	0.46 203	0.46 225	0.48 243	0.50 298	
$CrAl_4$	1.82 77	1.82 157	1.82 184	1.83 217	1.83 262	1.83 296			
$MnAl_8$	0.91 77	0.90 132	0.88 158	0.82 224	0.81 232	0.80 247	0.79 268	0.76 295	
$MnAl_4$	9.9 77	8.7 110	8.6 117	8.3 131	7.8 147	7.4 165	7.1 181	6.6 207	6.3 225
$MnAl_4$	6.1 238	6.0 249	5.9 257	5.8 269	5.6 290				
μ (AlMn)	14.3 77	12.4 130	12.1 145	11.4 163	10.8 180	10.1 206	9.7 220	8.9 241	8.3 259
Mn_3Al_{10}	17.1 77	13.1 115	11.1 143	10.4 155	9.7 173	7.7 219	7.4 233	6.4 293	

Mn ₄ Al ₁₁	12.6 77	10.4 122	10.1 133	9.6 144	9.1 157	8.8 168	8.2 186	7.7 207	
Mn ₄ Al ₁₁	7.2 225	7.0 236	6.7 255	6.2 293					
Fe ₄ Al ₁₃	9.7 77	8.9 119	8.4 149	8.0 177	7.6 202	7.4 227	7.0 260	6.7 288	
Fe ₂ Al ₅	33.7 77	28.2 114	25.2 140	23.3 163	21.4 185	19.8 207	18.3 231	17.2 260	16.0 288
FeAl ₂	12.3 77	8.5 117	7.2 150	6.6 205	6.1 227	5.8 243	5.2 278	5.0 290	
Co ₂ Al ₉	0.11 77	0.13 164	0.14 213	0.14 234	0.15 253	0.15 293			
Co ₄ Al ₁₃	1.03 77	1.10 137	1.06 166	0.95 213	0.90 244	0.82 295			
CoAl ₃	0.50 77	0.60 141	0.68 156	0.73 185	0.75 207	0.78 232	0.89 297		
NiAl ₃	0.35 77	0.34 124	0.30 157	0.27 188	0.25 213	0.23 227	0.22 247	0.21 294	
Ni ₂ Al ₃	1.09 77	1.09 142	1.10 167	1.13 197	1.14 211	1.18 257	1.18 297		
Al	0.73 77	0.72 97	0.70 122	0.69 142	0.68 169	0.68 188	0.67 209	0.66 226	0.65 254
								0.63 271	0.62 291

Table 3. The Effective Magnetron Numbers, Curie-Weiss Temperatures and Spin Quantum Numbers for Aluminium-rich Transition-metal Inter-metallic Compounds

	p_{eff}	$\theta(^{\circ}\text{K})$	S	No. unpaired electron spins
MnAl ₄	1.77	-163	0.51	1.02
Mn ₃ Al ₁₀	1.66	-120	0.47	0.94
Mn ₄ Al ₁₁	1.59	-50	0.44	0.88
Fe ₄ Al ₁₃	2.37	-300	0.79	1.58
Fe ₂ Al ₅	2.47	-103	0.83	1.66
FeAl ₂	1.32	-80	0.33	0.66

The compounds may be divided into two groups on the basis of their susceptibilities: the compounds of the first group (VAl₁₀, V₇Al₄₅, V₄Al₂₃, VAl₃, V₅Al₈, Cr₂Al₁₁, CrAl₇, CrAl₄, MnAl₆, Co₂Al₉, Co₄Al₁₃, CoAl₃, NiAl₃ and Ni₂Al₃) show a small approximately temperature independent paramagnetism (see Fig. 1); the compounds in the second group (MnAl₄, Mn₃Al₁₀, Mn₄Al₁₁, Fe₄Al₁₃, FeAl₂ and

Fe_2Al_5) show large susceptibilities obeying the Curie-Weiss law; however, $\mu(\text{AlMn})$ ($\sim \text{Mn}_{11}\text{Al}_{40}$ (Taylor 1960)) (see Fig. 2), has a large temperature dependent paramagnetism which does not obey the Curie-Weiss law.

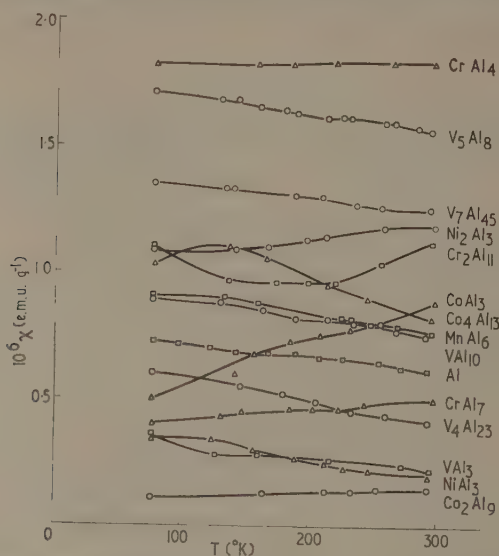


Fig. 1. The temperature dependence of the magnetic susceptibility of some aluminium-rich transition-metal intermetallic compounds.

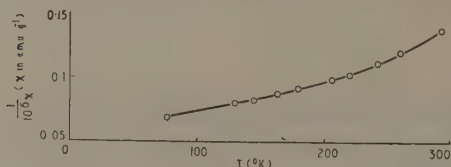


Fig. 2. The reciprocal of the temperature dependence of the magnetic susceptibility of $\mu(\text{AlMn})$.

Table 3 gives, for the compounds obeying the Curie-Weiss law, the values of the effective magneton numbers p_{eff} , the Curie-Weiss temperatures θ , the total spin quantum numbers of the atoms S and the numbers of unpaired electron spins. These have been derived from plots of the reciprocal of the susceptibility against

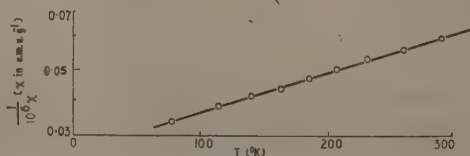


Fig. 3. The temperature dependence of the reciprocal of the magnetic susceptibility of Fe_2Al_5 .

temperature (Fig. 3). The magneton numbers have been derived on the assumption that no moments are localized on the aluminium ions, and orbital contributions to the moments of the transition-metal ions have been neglected.

Ideally, one should subtract contributions (i) to (iv) (§2) from the observed susceptibility; since these contributions cannot be accurately calculated this has not been done. In the case of, for example, MnAl_3 , neglect of a temperature independent paramagnetism of 10^{-6} c.m.u. g^{-1} would introduce errors, relative to the values given in Table 3, in p_{eff} and θ of 12% and 23°K respectively.

The paramagnetism of $\mu(\text{AlMn})$ is anomalous; it is relatively large and the temperature dependence is marked but does not follow a Curie-Weiss law. It is possible that the multiplet intervals are comparable with kT so that the treatment of narrow multiplets is not applicable: then the Boltzmann distribution of the various states would produce striking departures from a Curie-Weiss law (as, for example, in samarium and europium). Another possibility is that θ and/or p_{eff} varies with temperature.

The Curie-Weiss θ gives an indication of the freedom of a spin to orientate in an applied magnetic field. The values of θ (see Table 3) lie between -50 and -300°K and indicate that the spins are relatively free to orientate themselves. The absence of a strong temperature dependent susceptibility in Al-Ni, Al-Co, Al-Cr and Al-V compounds and in MnAl_3 shows that either no effectively localized moments occur in these alloys or the spin interactions are very strong ($\gg kT$).

§ 7. DISCUSSION

The results of Taylor, Burger and Wucher (1959) on dilute solution of V, Cr and Mn in Al are readily explained in terms of the Friedel concept of virtual bound states. Since this treatment is applicable only when the transition-metal atoms are sufficiently dilute not to interact strongly it need occasion no surprise if it does not apply to the intermetallic compounds; in $\text{Mn}_3\text{Al}_{10}$, for example, certain manganese atoms are found at a distance of 2.75 \AA apart (Taylor 1959).

The Lomer and Marshall (1958) scheme for the behaviour of transition-metal elements is now well known. This was based on the x-ray counts of Weiss and DeMarco (1958), the neutron diffraction results of Shull and Wilkinson (1953, 1955) and ferromagnetic saturation data on many alloy systems. Since then, however, Batterman (1959) and Batterman, Chipman and DeMarco (1960) have shown the results of Weiss and DeMarco to be incorrect. However, the empirical Lomer and Marshall scheme still provides an excellent classification of the magnetic properties of transition-metal alloys in terms of numbers of effectively localized 3d electrons. It is shown below that the magnetic behaviour of aluminium transition-metal alloys fits into this scheme.

In these intermetallic compounds no effectively localized magnetic moments exist on either the nickel or the cobalt atoms. This might be due to the conduction electrons from the aluminium atoms filling the vacancies in the 3d band: this implies absorption of approximately 0.6 and 1.7 electrons by the Al-Ni and Al-Co bands respectively. Another possibility is that the 3d states are not fully occupied, but that no localized moments occur since Hund's rule is not obeyed (as in the aluminium transition-metal dilute solutions discussed earlier in this section).

The numbers of unpaired spins on the iron and manganese atoms in the Al-Fe and Al-Mn compounds (see Table 3) are as follows:

MnAl ₆	MnAl ₄	Mn ₃ Al ₁₀	Mn ₄ Al ₁₁	Fe ₄ Al ₁₃	Fe ₂ Al ₅	FeAl ₂
0	1.0	0.9	0.9	1.6	1.7	0.7

The differences of the number of spins from one in the case of the manganese compounds (with the exception of MnAl₆) and from two in the case of the iron compounds (with the exception of FeAl₂) are not considered to be significant; these differences might be caused by several factors, such as incomplete quenching of the orbital contribution to the paramagnetism, spin polarization of the conduction electrons, or the neglect of the temperature independent paramagnetism in deducing p_{eff} from the observed data. It is possible, however, that in the case of Fe₄Al₁₃ and Fe₂Al₅ the moment of iron atoms in an aluminium-rich environment is slightly less than two, as was found by Nathans *et al.* (1958) in the case of Fe₃Al. Therefore, with the exception of MnAl₆ and FeAl₂, in these compounds the manganese and iron atoms retain the effectively localized 3d electron configurations of the pure metals (i.e. 1 in Mn and 2 in Fe respectively).

The crystal structures of the phases MnAl₆ (Nicol 1953), Mn₃Al₁₀ (Taylor 1959) and Mn₄Al₁₁ (Bland 1958) show many similarities (the crystal structure of the MnAl₄ phase is unknown). The manganese atoms in all three phases are surrounded by ten aluminium atoms in similar spatial arrays. The striking difference between MnAl₆ and the other two phases, however, is that in MnAl₆ the manganese atom is in very close contact with two aluminium atoms which are not in contact with other manganese atoms. It is suggested, therefore, that strong covalent bonding occurs between the manganese atom and the two aluminium atoms and that the one 3d electron which may be expected to be effectively localized on the manganese atom is involved in the formation of these covalent bonds, giving zero resultant localized spin on the manganese atom. Other possibilities are that the localized 3d state occurs above the Fermi surface and is therefore unoccupied, or that manganese in MnAl₆ behaves as manganese in dilute solution in aluminium.

The crystal structure of FeAl₂ is unknown (the crystal structure reported by Osawa (1932) has been shown by Forsyth (1959) to be incorrect); it is suggested that some anomalous feature exists here also which would account for the difference between the spins on the iron atoms in FeAl₂ and in Fe₄Al₁₃ and Fe₂Al₅.

The absence of any effectively localized magnetic moments on the chromium and vanadium atoms in these compounds shows that the behaviour of chromium and vanadium atoms is approximately the same as in the pure metals: the chromium atoms appear to have lost the small moment ($0.4\mu_B$) which they possess in the pure metal.

The behaviour of transition-metal atoms in compounds with aluminium is very similar to their behaviour in the ferromagnetic binary alloys discussed by Lomer and Marshall. Furthermore, the marked difference in the magnetic properties between the Al-Fe and Al-Co compounds is similar to that observed between the metals Fe and Co in many ferromagnetic binary alloys: the x-ray work of Batterman now shows that the marked change in the electronic distribution between the pure metals Co and Fe suggested by Weiss and DeMarco does not exist.

The discussion by Hume-Rothery and Coles (1954) of the variation in cohesion in alloys of Al with Ni, Co, Fe, seems to be in line with the scheme for the number of effectively localized 3d electrons suggested in this section, although melting

points give only a very rough indication of bond strengths and the contributions of electrons in various states to the cohesion of a metal cannot be analysed.

Lomer and Marshall suggest that the electronic structure is not appreciably affected by the crystal structure and that the crystal structure is chosen to be the most appropriate to the electronic structure rather than vice versa. Some characteristic features of the structures of the aluminium transition-metal intermetallic compounds have been reviewed by Black (1956) who showed that size factor considerations alone could not be responsible for the observed co-ordination numbers and concluded that the co-ordination numbers are influenced by some specific characteristic of the aluminium transition-metal interaction. In the case of MnAl_6 the unusual magnetic behaviour may possibly be explained by a particular structural peculiarity; a similar explanation is put forward for FeAl_2 . But in general the results of the magnetic analysis do nothing to explain the occurrence of the complex crystal structures taken up by these compounds.

§ 8. CONCLUSIONS

1. The behaviour of transition metal atoms in the aluminium transition-metal intermetallic compounds bears some resemblance to that in the pure metals and in the ferromagnetic binary alloys discussed by Lomer and Marshall (see Table 4).

Table 4. The Analogy between Binary Ferromagnetic Alloys and Aluminium Transition-metal Alloys

	Ti	V	Cr	Mn	Fe	Co	Ni
Binary ferromagnetic alloys (Lomer and Marshall)	no moments			low d		high d	
Aluminium transition-metal alloys	no moments			some low d moments		no moments	

2. The absorption hypothesis of Raynor cannot explain the magnetic behaviour of the Al-Fe, Al-Mn, Al-Cr and Al-V compounds.

3. The results of the magnetic analysis do nothing to explain the occurrence of the complex crystal structures taken up by these compounds.

ACKNOWLEDGMENTS

I wish to thank the Department of Scientific and Industrial Research for the award of a Research Studentship. This research forms part of a project supported by the Air Force Office of Scientific Research of the Air Research and Development Command, United States Air Force, through its European Office, under Contract No. AF.61(052)-50. Some of the equipment used was purchased with the help of a generous award from the Government Grants Committee of the Royal Society.

I am greatly indebted to Professor N. F. Mott and Dr. W. H. Taylor for provision of facilities and for their help and encouragement. I should like to thank Dr. J. Crangle of the University, Sheffield, Professors G. Foëx and J. Wucher of

the Laboratoire Pierre Weiss, Strasbourg, and Dr. W. E. Gardner or many valuable discussions. Aluminium Laboratories Ltd., Banbury, kindly gave the super-purity aluminium used in this work, and I am indebted to Metallisation Ltd., Dudley, who prepared the pure metal powders.

REFERENCES

- BATTERMAN, B. W., 1959, *Phys. Rev. Letters*, **2**, 47.
 BATTERMAN, B. W., CHIPMAN, D. R., and DEMARCO, J. J., 1960, *Acta Cryst.*, **13**, 994.
 BLACK, P. J., 1955 a, *Phil. Mag.*, **46**, 155.
 ——— 1955 b, *Phil. Mag.*, **46**, 401.
 ——— 1956, *Acta Met.*, **4**, 172.
 BLAND, J. A., 1958, *Acta Cryst.*, **11**, 236.
 BROWN, P. J., 1957, *Ph.D. Thesis*, University of Cambridge.
 DOUGLAS, A. M. B., 1950, *Acta Cryst.*, **3**, 19.
 FOËX, G., and WUCHER, J., 1954, *C.R. Acad. Sci., Paris.*, **238**, 1281.
 ——— 1956, *J. Phys. Radium*, **17**, 454.
 FORSYTH, J. B., 1959, *Ph.D. Thesis*, University of Cambridge.
 FRIEDEL, J., 1956, *Canad. J. Phys.*, **34**, 1190.
 HOARE, F. E., and WALLING, J. C., 1951, *Proc. Phys. Soc. B*, **64**, 337.
 HUME-ROTHERY, W., and COLES, B. R., 1954, *Advanc. in Phys.*, **3**, 149.
 LOMER, W. M., and MARSHALL, W., 1958, *Phil. Mag.*, **3**, 185.
 NATHANS, R., PIGOTT, M. J., and SHULL, G. C., 1958, *J. Phys. Chem. Solids*, **6**, 38.
 NICOL, A. D. I., 1953, *Acta Cryst.*, **6**, 285.
 OSAWA, A., 1932, *Sci. Reports Tôhoku Univ.*, **22**, 803; *Kinzoku-no-Kenkyu* **10**, 432.
 PAULING, L., 1938, *Phys. Rev.*, **54**, 899.
 PHILLIPS, H. W. L., 1943, *J. Inst. Met.*, **69**, 275.
 RAYNOR, G. V., 1949, *Progr. Met. Phys.*, **1**, 1.
 ROBINSON, K., 1953, *Acta Cryst.*, **6**, 854.
 SHULL, C. G., and WILKINSON, M. K., 1953, *Rev. Mod. Phys.*, **25**, 100.
 ——— 1955, *Phys. Rev.*, **97**, 304.
 TAYLOR, M. A., 1959, *Acta Cryst.*, **12**, 393.
 TAYLOR, M. A., 1960, *Acta Metall.*, **8**, 256.
 TAYLOR, M. A., BURGER, J.-P., and WUCHER, J., 1959, *J. Phys. Radium*, **20**, 829.
 TAYLOR, W. H., 1954, *Acta Metall.*, **2**, 684.
 VOGT, E., 1954, *Appl. Sci. Res.*, **4B**, 34.
 WEISS, R. J., and DEMARCO, J. J., 1958, *Rev. Mod. Phys.*, **30**, 59.

LETTERS TO THE EDITOR

On the Θ Values from the Temperature Dependence of the Laue-Bragg Scattering

The Debye temperature values occurring in the theory of the temperature dependence of the Laue-Bragg scattering can be calculated with the aid of the relation (Blackman 1955)

$$\frac{3}{\Theta_{\infty}^2(\text{x-ray})} = \left(\frac{k}{h}\right)^2 \frac{\int \rho(\nu) \nu^2 d\nu}{\int \rho(\nu) d\nu},$$

which is valid at moderately high temperatures. Here ν is the frequency of the normal modes of the vibration of the crystal, $\rho(\nu)$ is the normalized frequency distribution function, h and k have their usual meanings and the integrals are taken over the whole vibrational spectrum. For aluminium, using $\rho(\nu)$ calculated by Walker (1956 a), the integrals were evaluated graphically and this yielded a value of 402°K for $\Theta_{\infty}(\text{x-ray})$. Walker's spectrum is derived from the measurements at room temperature, for which case the theory should apply quite well.

The computed value of $\Theta_{\infty}(\text{x-ray})$ for aluminium falls between the scattered experimental $\Theta_{\text{D.W.}}$ values. The measurements of James, Brindley and Wood (1929) give $\Theta_{\text{D.W.}} = 410^{\circ}\text{K}$ at 290°K (Lonsdale 1948), whereas the experiments of Owen and Williams (1947) on powdered samples give the room temperature (293°K) value of $\Theta_{\text{D.W.}} = 395^{\circ}\text{K}$. Walker (1956 b) gives 402°K as the value of $\Theta_{\text{D.W.}}$. His value is based on data taken both at low temperatures and at room temperature. As the force constants change appreciably with temperature, his measurements refer to conditions where the spectrum is not constant. The accuracy of the experiments is also limited to some extent by temperature diffuse scattering (Nilsson 1957, Warren 1953, Paskin 1958), extinctions, Compton and fluorescent scattering. Without estimates of errors due to all these factors, a comparison of $\Theta_{\infty}(\text{x-ray})$ with $\Theta_{\text{D.W.}}$ is not quite justified.

It is a pleasure to thank Professor K. Banerjee for his interest and the referees for helpful comments. Acknowledgments are due to the Council of Scientific and Industrial Research for financial support.

Physics Department,
Allahabad University,
Allahabad, India.

S. K. JOSHI.

8th August 1961, in revised form 3rd October 1961.

- BLACKMAN, M., 1955, *Encyclopaedia of Physics*, Vol. 7, Part I, Ed. S. Flügge (Berlin: Springer), 325.
 JAMES, R. W., BRINDLEY, G. W., and WOOD, R. G., 1929, *Proc. Roy. Soc. A*, **125**, 401.
 LONSDALE, K., 1948, *Acta Cryst.*, **1**, 142.
 NILSSON, N., 1957, *Ark. Fys.*, **12**, 247.
 OWEN, E. A., and WILLIAMS, R. W., 1947, *Proc. Roy. Soc. A*, **188**, 509.
 PASKIN, A., 1958, *Acta Cryst.*, **11**, 165.
 WALKER, C. B., 1956 a, *Phys. Rev.*, **103**, 547.
 — 1956 b, *Phys. Rev.*, **103**, 558.
 WARREN, B. E., 1953, *Acta Cryst.*, **6**, 803.

Effect of Variations in the Quantum Counting Efficiency of Detectors on the Mean Wavelength of X-ray Emission Lines

Modern x-ray diffractometers, used to define the position of an x-ray line by means of its centroid, can now be used to obtain results which are reproducible to 1 part in 10^5 or better. Sources of error which can be neglected in methods of lower precision must be taken into account in this work. One such possible source of error is the variation in the mean wavelength of the detected line profile which can be caused by the change, over the range of wavelength used, of the quantum counting efficiency of the detectors. This variation of the quantum counting efficiency with wavelength will cause the fraction of the incident intensity detected to vary with wavelength. The mean wavelength of the detected profile will differ, therefore, from the mean wavelength of the true profile and, in general, from the mean wavelength of the same line recorded by a different detector.

We shall consider first the general case of a true wavelength distribution $I(\lambda)d\lambda$ modified by a factor $f(\lambda)$. The true centroid is

$$\lambda_0 \equiv \frac{\int \lambda I(\lambda) d\lambda}{\int I(\lambda) d\lambda} \quad \dots\dots (1)$$

and the modified centroid

$$\langle \lambda \rangle = \frac{\int \lambda f(\lambda) I(\lambda) d\lambda}{\int f(\lambda) I(\lambda) d\lambda} \quad \dots\dots (2)$$

Near the centroid, $f(\lambda)$ can be expanded as

$$f(\lambda) = f(\lambda_0) + (\lambda - \lambda_0)f'(\lambda_0) + \dots \quad \dots\dots (3)$$

$$= f + (\lambda - \lambda_0)f' + \dots \quad \dots\dots (4)$$

Then

$$\langle \lambda \rangle = \frac{\lambda_0 + \int (\lambda - \lambda_0) [f + (\lambda - \lambda_0)f' + \dots] I(\lambda) d\lambda}{\int [f + (\lambda - \lambda_0)f' + \dots] I(\lambda) d\lambda} \quad \dots\dots (5)$$

$$= \lambda_0 + \frac{Vf'}{f} + \dots \quad \dots\dots (6)$$

where V is the variance of the wavelength. The fractional change in the centroid wavelength is given to the first order by

$$\frac{\Delta \lambda}{\lambda} = \frac{Vf'}{\lambda f} \quad \dots\dots (7)$$

In the specific case of a change caused by variation in quantum counting efficiency the factor f'/f is simply the fractional rate of change of quantum counting efficiency with wavelength. The Table gives values for f'/f for the

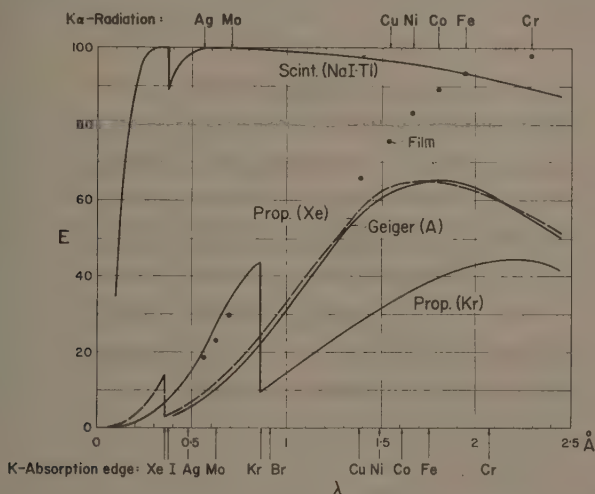
Values of f'/f (\AA^{-1}) for Various Detectors at the Wavelengths of Molybdenum, Copper and Chromium $K\alpha$ Radiations

(1)	(2)	(3)	(4)	(5)	(6)
Mo	+2.80	+2.62	+2.38	+2.78	0
Cu	+0.35	+0.31	+0.88	+0.82	-0.06
Cr	-0.51	-0.45	-0.14	+0.04	-0.13

(1) Radiation; (2)–(6) f'/f (\AA^{-1}) for different detectors: (2) Geiger; (3) proportional (Xe); (4) proportional (Kr); (5) film; (6) scintillation.

most commonly used methods of detection, at the wavelengths of the molybdenum, copper and chromium $K\alpha$ lines. These values were obtained from the Figure.

It is clear that when comparing results obtained by two different detectors the fractional change in wavelength, or in practice the fractional change in lattice spacing, can be found by substituting the difference between the respective values



Calculated quantum counting efficiency E as a function of wavelength λ for four counter tubes. The absorption of Eastman No-screen double-coated x-ray film is indicated by the dots.

Counter	Gas (cm Hg)	Length (cm)	Window thickness (cm)
Geiger	55 cm A	10	Mica 0.0013
Proportional	50 cm Kr	2.2	Mica 0.0013
Proportional	32 cm Xe	2.0	Mica 0.0013 + Be 0.013
Scintillation	(NaI.Tl)	0.1	Be 0.013

(Reproduced by permission of W. Parrish (1962).)

of f'/f in Eqn (7). For the case of copper $K\alpha$ this varies from nearly zero, when comparing results from Geiger and proportional counters, to 3 parts in 10^6 when results from scintillation counters are compared with those obtained from krypton-filled proportional counters. (The variance is taken as one-third of the square of

the peak separation.) Much larger differences can be found in the case of molybdenum $K\alpha$, where a comparison of results obtained by a scintillation counter with those obtained by a Geiger counter can produce differences of 2.5 parts in 10^5 .

The fractional change of the peak wavelength is easily calculated to be $-f'I/\lambda fI''$, where f, I, f', I'' are the values of $f(\lambda), I(\lambda)$ etc. at the peak (Wilson 1958).

Although at the moment this effect is on the fringe of detectability for normal diffractometer techniques, it may well be of importance in the field of x-ray spectroscopy. This will be especially true if, as is hoped, work is done on the line profiles of the more important x-ray emission lines. At the moment, however, this effect is yet another unknown in the determination of x-ray wavelengths.

Viriamu Jones Laboratory,
University College,
Cathays Park,
Cardiff.

A. J. C. WILSON.
B. W. DELF.

16th October 1961.

PARRISH, W., 1962, *Int. Tables for Cryst.*, Vol. 3 (Birmingham: Kynoch).
WILSON, A. J. C., 1958, *Proc. Phys. Soc.*, **72**, 924.

The Structures of NaNbO_3 and $\text{Na}_{0.975}\text{K}_{0.025}\text{NbO}_3$

We have recently determined the structures of pure NaNbO_3 and of a material of composition $\text{Na}_{0.975}\text{K}_{0.025}\text{NbO}_3$, which we have called phase II. Three-dimensional intensity data were used, obtained from Weissenberg and oscillation photographs with $\text{MoK}\alpha$, and the structures were refined using successive differential syntheses. This letter gives preliminary details of the results.

Pure NaNbO_3 has been the subject of several x-ray studies (Wood 1951, Vousden 1951 a, b, Megaw and Wells 1958). There has been some doubt about the space group; Megaw and Wells showed it to be $Pbma$ (No. 57, in the *bca* setting) and this is confirmed by the present work.

Phase II is very closely related to NaNbO_3 . The obvious differences are that it is ferroelectric (Cross 1958) and therefore polar, and that the b dimension of its unit cell is half that of NaNbO_3 (Wells and Megaw 1960), corresponding to $2a_0$ instead of $4a_0$, where a_0 is the cube edge of ideal perovskite. Its space group is $P2_1ma$ (No. 26, in the *cab* setting); its point group is thus $2mm$, while that of NaNbO_3 is mmm .

Cell dimensions and atomic coordinates of the two structures are given in the Table.

Both structures are based on distortions of ideal perovskite. Individual NbO_6 octahedra are only slightly distorted, but are rotated relative to each other about the y axis. The Nb atom in each is displaced by about 0.15 \AA along the x axis, towards the middle of an octahedron edge in the (010) plane; within this plane all Nb displacements are (nearly) in the same direction, and no O is approached by more than one Nb.

The principal difference between the two structures lies in the way in which successive layers of octahedra normal to [010] are arranged. In both structures there are pairs of layers related by a (010) mirror plane, with parallel Nb displacements. But, while in phase II one such pair constitutes the translation

Space group Lattice dimensions (Å)	NaNbO ₃			Phase II		
	Pbma			P2 ₁ ma		
<i>a</i>	5.568			5.582		
<i>b</i>	15.518			7.782		
<i>c</i>	5.505			5.528		
Atomic coordinates	<i>x</i>	<i>y</i>	<i>z</i>	<i>x</i>	<i>y</i>	<i>z</i>
Na ₁	$\frac{3}{4}$	0	0.250	0.771	0	0.272
Na ₂	0.769	$\frac{1}{2}$	0.251	0.734	$\frac{1}{2}$	0.242
Nb	0.261	0.125	0.257	0.260	0.253	0.243
O ₁	$\frac{1}{4}$	0	0.208	0.198	0	0.201
O ₂	0.271	$\frac{1}{2}$	0.290	0.231	$\frac{1}{2}$	0.305
O ₃	0.010	0.121	0.532	0.005	0.231	0.531
O ₄	0.446	0.126	0.972	0.451	0.277	0.969

Note: In phase II the origin is on the screw diad, at a position arbitrarily chosen to give the same *x* coordinate as in NaNbO₃ to the centre of gravity of the O₃O₄ square.

repeat unit, in NaNbO₃ the pairs are operated on by a screw diad along [010], giving an antiparallel array. The Nb arrangement in NaNbO₃ is in essentials that found by Vousden (1951 b).

The suggestion (Wells and Megaw 1960, following Cross 1958) that phase II is probably identical with the polar phase ('forced ferroelectric') produced by the application of a strong electric field to NaNbO₃ at room temperature (Cross and Nicholson 1955) has received strong support from the recent work of Wood and Miller (1962), who showed in a very elegant way that the forced ferroelectric phase also has a *b* dimension of $2a_0$.

There are, of course, points of detail—for example, departures from perfect regularity of the octahedra (different for NaNbO₃ and phase II) and differences in the polyhedra around Na—whose significance needs further consideration. These will be discussed more fully in the detailed report now in preparation.

One of us (M.W.) is grateful to the Royal Commission for the Exhibition of 1951 for the award of a Senior Studentship, during the tenure of which this work was completed.

Crystallographic Laboratory,
Cavendish Laboratory,
Cambridge.

M. WELLS†.
HELEN D. MEGAW.

3rd October 1961.

CROSS, L. E., 1958, *Nature, Lond.*, **181**, 178.

CROSS, L. E., and NICHOLSON, B. J., 1955, *Phil. Mag.*, [7], **46**, 453.

MEGAW, H. D., and WELLS, M., 1958, *Acta Cryst.*, **11**, 858.

VOUSDEN, P., 1951 a, *Acta Cryst.*, **4**, 375.

— 1951 b, *Acta Cryst.*, **4**, 545.

WELLS, M., and MEGAW, H. D., 1960, *Acta Cryst.*, **13**, 1072.

WOOD, E. A., 1951, *Acta Cryst.*, **4**, 353.

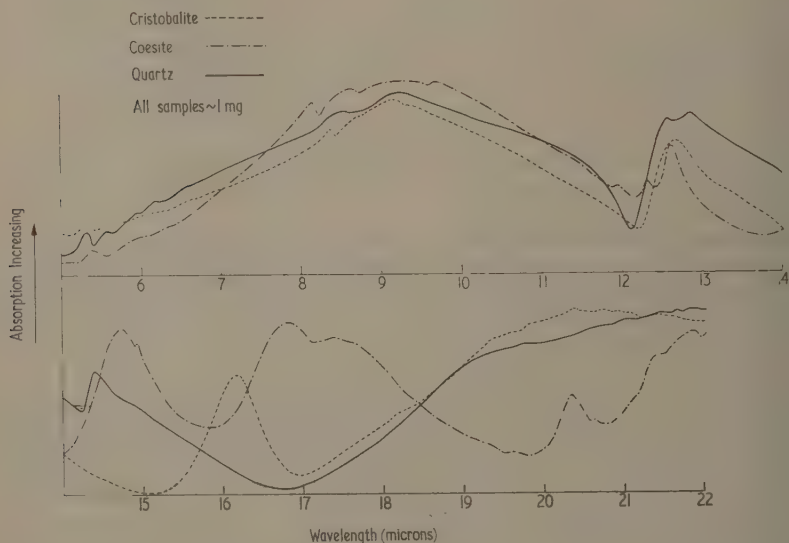
WOOD, E. A., and MILLER, R. C., 1962, *J. Appl. Phys.*, in the press.

† Now at Electronic Computing Laboratory, University of Leeds.

Absorption of Coesite in the Wavelength Region 5-22 Microns

The optical properties of coesite, a dense, high pressure form of silica, are less well known than those of quartz, cristobalite and tridymite, the other members of this family.

Small samples have been made at N.P.I., using a tetrahedral anvil apparatus. Following the data by Boyd and England (1960), a pressure of 42 kilobars and a temperature of 1400°C were used, with finely ground crystal quartz as the starting material. Refractive index and x-ray measurements (Boyd and England 1960) indicated a high yield ($\sim 90\%$) of coesite crystals, approximately 50 microns in diameter.



The infra-red spectrum of coesite shown in the diagram was obtained using the KCl disk technique. Also shown, for comparison, are spectra of cristobalite and α -quartz recorded under similar conditions. The latter shows good agreement with single crystal data (Simon and McMahon 1955, Sevchenko and Florinskaia 1956), thus providing a check on the method.

Structurally, the various forms of silica may be regarded as SiO_4 tetrahedra linked by their corners in different ways. Comparative studies of the various polymorphs of silica (Sevchenko and Florinskaia 1956, Haccuria 1953), silicates (Matossi 1949) and silicic esters (Weiler 1933) have shown that the bands in silica near 8.4, 9.2, 12.6 and 20-22 microns may be associated with the four fundamental vibrations of the SiO_4 group. Except for the last band, these wavelengths are relatively insensitive to the form of the lattice coupling the tetrahedra. Additional bands which appear in the region 13-18 microns are specific to each polymorph.

The spectrum of coesite is consistent with this general view. The marked differences, which occur between coesite and the other polymorphs, are in the fundamental region 20–22 microns and the region 13–18 microns.

Basic Physics Division,
National Physical Laboratory,
Teddington,
Middlesex.

I. G. AUSTIN.
H. A. GEBBIE.
I. MORIN.

10th October 1961.

- BOYD, R. F., and ENGLAND, J. L., 1960, *J. Geophys. Res.*, **65**, 749.
HACCURIA, M., 1953, *Bull. Soc. Chim. Belg.*, **62**, 428.
MATOSI, F., 1949, *J. Chem. Phys.*, **17**, 679.
SEVCHENKO, N. A., and FLORINSKAIA, V. A., 1956, *Soviet Physics-Doklady*, **1**, 508.
SIMON, I., and McMAHON, H. O., 1955, *J. Chem. Phys.*, **21**, 23.
WEILER, J., 1933, *Z. Phys.*, **80**, 617.

Anisotropy in the Electric Strength of Alkali Halide Crystals

Previous investigations (Cooper, Grossart and Wallace 1957) have shown that KCl is strongly anisotropic but NaCl appears to be isotropic with respect to electric strength. No other members of the alkali halide family have been investigated but the discharge tracks from point electrodes have been extensively studied and they are preferentially directed in NaCl and other crystals. Isotropic electric strength is not easily reconciled with this fact. This work has been reviewed recently in detail (Davisson 1959).

In the previous investigation (Cooper, Grossart and Wallace 1957), apparently similar specimens of NaCl and KCl exhibited great variation in their electric strengths. The work of preparation limited the number of specimens in each group and it was not possible for statistical reasons to detect small differences in average electric strengths. The cause of this difficulty has been determined and it can be eliminated by using specimens appreciably thicker than the ones generally used in the past (Cooper and Smith 1961). Using thick specimens, we have re-investigated the electric strengths of NaCl, added to the previous work with KCl, and investigated KBr. The results obtained are stated below. The experimental method was similar to that adopted previously (Cooper and Fernandez 1958) but on this occasion a series of flat-topped impulses was applied to each specimen until it broke down. The amplitude of each impulse exceeded that of the previous one by not more than 3%. The specimens were all annealed.

The values of electric strengths quoted in Table 1 were obtained at 20°C from groups of NaCl specimens with the applied field in the directions stated. The 'equal component' specimens were cut so that the resolved component of the field was the same in a [100], a [110] and a [111] direction and it amounted to 99% of the applied field. The 25°C specimens were prepared from plates obtained by cutting the parent crystals perpendicularly to the (001) planes and at 25°C to the (100) planes. In Table 2 similar results are stated for KBr. The average electric strength of both materials is least in the [100] direction. The difference between this value for NaCl and the corresponding [110] value is small but application of Student's 't' test indicates it to be significant at the 5% level.

Table 1. Electric Strength of NaCl at 20°C

	Field direction	Electric strength (MV cm ⁻¹)				No.	Track
		Max.	Av.	Min.	Variance		
(a)	[100]	0.87	0.79	0.71	0.0026	24	[100]
(b)	[110]	0.89	0.83	0.74	0.0029	16	[110]
(c)	[111]	0.93	0.88	0.78	0.0032	12	[111]
(d)	25° to [100]	0.98	0.89	0.80	0.0027	28	[110] [100]
(e)	equal component	0.94	0.88	0.78	0.0023	22	[100]

(Carbon electrodes) specimen thickness 0.050-0.070 cm; cavity radius 0.7 cm.

Table 2. Electric Strength of KBr at 20°C

	Field direction	Electric strength (MV cm ⁻¹)				No.	Track
		Max.	Av.	Min.	Variance		
	[100]	0.58	0.48	0.44	0.00142	11	[100]
	[110]	0.68	0.60	0.57	0.00067	12	[110]
	[111]	0.63	0.59	0.54	0.00040	11	[111]
	15° to [100]	0.62	0.56	0.50	0.00027	11	[100]
	15° to [100]	0.63	0.59	0.56	0.00046	10	field direction and [100]
	equal component	0.59	0.55	0.51	0.0011	14	[100]

(Carbon electrodes) specimen thickness 0.050-0.070 cm; cavity radius 0.7 cm.

Discharge tracks in directions other than the applied field were noted in both materials. Consideration of Table 1 and Table 2 indicates that breakdown occurred in the direction in which the resolved component of the applied field is equal to the electric strength. The behaviour of KCl is consistent with this. Previous experiments (Cooper and Fernandez 1958) have shown that the electric strength of unstrained [110] specimens is about $\sqrt{2}$ times that of similar [100] specimens and the discharge tracks in both groups were in [100] directions. In the present investigation an average electric strength of 0.73 MV cm⁻¹ was obtained for thick 'equal component' specimens of KCl and 0.66 MV cm⁻¹ for similar [100] specimens. Only [100] tracks were observed in both groups.

In the case of KBr, experiments were made at -190°C, -100°C, +20°C, +110°C and +130°C to determine if the preferred track direction depended on temperature. 'Equal component', uniform field specimens were used, and also specimens with embedded point electrodes of both positive and negative polarity. In these, breakdown occurred in the absence of ambient discharges. In all cases the discharge tracks were in [100] directions.

The present investigation, combined with that of Cooper, Crossart and Wallace (1957), shows that three members of the alkali halide family are anisotropic, the [100] direction being the weakest. The discharge track in a spherically symmetrical field should be in a [100] direction if it results from the primary electronic instability and not from other secondary processes resulting from this instability. This is the case in KBr and in KCl at low temperatures. Above about 150°C the

conditions of breakdown in KCl may be modified by ionic migration (Cooper, Higgin and Smith 1960). The [100], [110] and [111] tracks were all observed in NaCl by Cooper, Grossart and Wallace (1957). This is attributed to the difficulty in producing a truly spherically symmetrical field in a material that is not very anisotropic.

It would be surprising if other members of the alkali halide family behaved qualitatively differently from KCl, KBr, and NaCl, and limited experiments suggest that NaF, and NaBr are respectively similar to KCl and NaCl. The evidence of isotropic behaviour usually quoted consists of experiments performed using small numbers of unannealed NaCl specimens. It is now evident that such experiments could not yield significant results.

Neither this investigation nor the previous one (Cooper, Grossart and Wallace 1957) has provided evidence of marked temperature dependent transitions in the preferred track direction (Davisson 1959). Caspari's investigation (1955) indicates that these occur when breakdown is initiated by discharges in the ambient near to the anode, a condition which did not arise in the present or previous investigation.

Electrical Engineering Laboratories,
The University,
Manchester, 13.

R. COOPER.
A. FERNANDEZ.

25th September 1961.

CASPARI, M. E., 1955, *Phys. Rev.*, **98**, 1679.

COOPER, R., and FERNANDEZ, A., 1958, *Proc. Phys. Soc.*, **71**, 688.

COOPER, R., GROSSART, D. W., and WALLACE, A. A., 1957, *Proc. Phys. Soc.*, **70**, 169.

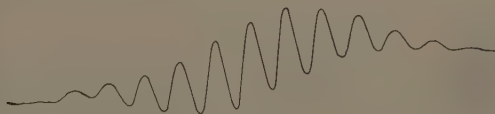
COOPER, R., HIGGIN, R. M., and SMITH, W. A., 1960, *Proc. Phys. Soc.*, **76**, 817.

COOPER, R., and SMITH, W. A., 1961, *Proc. Phys. Soc.*, **78**, 734.

DAVISSON, J. W., 1959, *Progress in Dielectrics*, Vol. 1, *Directional Breakdown in Crystals* (London: Heywood), p. 61.

σ -bonding in $(\text{CuCl}_6)^{4-}$

Paramagnetic resonance methods have been used to investigate the electron distribution in $(\text{CuCl}_6)^{4-}$ complexes present in mixed crystals of $\text{Cu}:\text{CdCl}_2$ with $\text{Cu}:\text{Cd} \sim 1:200$. Extensive hyperfine structures from the Cl nuclei are found which indicate that there are surprisingly strong Cu-Cl σ -bonds. An example is shown in the Figure, where the Cu hyperfine structure is negligible and the Cl structure is particularly well resolved.



Hyperfine structure with H at 45° to x in the xy plane. The structure is from 4 equivalent Cl nuclei, with $B(\text{Cu}) = 0$. The spacing between adjacent lines is 14 gauss.

Previous measurements by Partridge (Orton 1959) have shown that the behaviour of the system is typical of that expected of a trigonally distorted octahedral complex of Cu^{2+} (Abragam and Pryce 1950, Bleaney, Bowers and Pryce 1955). For the present purpose the important point is that at 20°K there are, in addition to the trigonal distortion, frozen-in Jahn-Teller distortions, with the result that the Cu^{2+} ion sees a field of tetragonal symmetry with axis along Cu-Cl bond direction. The ground state is then $d_{x^2-y^2}$ which bonds to four Cl ions. This is the state which has been investigated in detail at 20°K using wavelengths of 1.2 cm and 3.0 cm.

The results may be described by the spin-Hamiltonian

$$\begin{aligned} H_s = & g_{\parallel}\beta H_z S_z + g_{\perp}\beta (H_x S_x + H_y S_y) \\ & + A S_z I_z + B (S_x I_x + S_y I_y) + P [I_z^2 - \frac{1}{3} I(I+1)] \\ & + A' S_x I_x^1 + B' (S_y I_y^1 + S_z I_z^1) + A' S_y I_y^2 + B' (S_x I_x^2 + S_z I_z^2) \\ & + A' S_x I_x^3 + B' (S_y I_y^3 + S_z I_z^3) + A' S_y I_y^4 + B' (S_x I_x^4 + S_z I_z^4), \end{aligned}$$

where $S = \frac{1}{2}$, $I(\text{Cu}) = \frac{3}{2}$, $I(\text{Cl}) = \frac{3}{2}$, z is the distortion axis; the numbers 1, 2, 3 and 4 refer to the Cl ions on the positive and negative x and y axes respectively.

$g_{\parallel} = 2.339 \pm 0.002$, $g_{\perp} = 2.070 \pm 0.002$, $A = 113 \pm 3 \times 10^{-4} \text{ cm}^{-1}$, $B = 0.0 \pm 4 \times 10^{-4} \text{ cm}^{-1}$, $A' = 18.5 \pm 1.0 \times 10^{-4} \text{ cm}^{-1}$, $B' = 5.0 \pm 0.5 \times 10^{-4} \text{ cm}^{-1}$. The limits of B were calculated assuming that the magnitude of P is approximately as found in most other Cu salts ($10 \times 10^{-4} \text{ cm}^{-1}$). In the Cl sub-Hamiltonians the dipolar interaction, the quadrupole interaction and direct effect of the field on the nucleus are omitted because they are negligibly small.

To interpret the Cl hyperfine structure it will be assumed that the distribution of the unpaired electron can be described by the antibonding molecular orbital

$$\Psi_{x^2-y^2} = N[(d_{x^2-y^2} - \alpha_s(s_1 - s_2 + s_3 - s_4) - \alpha_{p_\sigma}(-p_1 + p_2 + p_3 - p_4)],$$

where s and p refer to chlorine $3s$ and $3p_\sigma$ orbitals respectively; N is the normalization constant, and admixture coefficients α_s and α_{p_σ} are expected to consist of an overlap term S plus a covalent bonding parameter λ , $\alpha \sim S + \lambda$ (see Freeman and Watson 1961, who also give earlier references). Overlap with other chlorine orbitals, e.g. $2s$ and $2p_\sigma$, may also be important but will be omitted in order that a simple approximate estimate of the bond strength can be made. The chlorine hyperfine structure constants are then expected to be

$$A_s = \frac{16\pi\gamma\beta\beta_N}{3} N^2 \alpha_s^2 |s(0)|_{3s}^2, \quad A_{p_\sigma} = \frac{4\gamma\beta\beta_N}{5} \langle r_{3p}^{-3} \rangle N^2 \alpha_{p_\sigma}^2,$$

where these are related to the experimentally observed quantities by

$$A' = A_s + 2A_{p_\sigma} \quad B' = A_s - A_{p_\sigma}.$$

Assuming that $|s(0)|_{3s}^2 = 69 \times 10^{24}$ (Hartree and Hartree 1936) and that $\langle r_{3p}^{-3} \rangle = 55.6 \times 10^{24} \text{ cm}^{-3}$ (Sternheimer 1953), the results lead to the values given in the Table.

	$(\text{CuCl}_2)^{4-}$	$(\text{NiF}_6)^{4-}$
$A_s (\text{cm}^{-1})$	9.5×10^{-4}	39.1×10^{-4}
$A_{p_\sigma} (\text{cm}^{-1})$	4.5×10^{-4}	10.9×10^{-4}
$f_s (\%)$	0.67	0.5
$f_{p_\sigma} (\%)$	8.3	4.95

$f_s = N^2\alpha_s^2$ and $f_{p\sigma} = N^2\alpha_{p\sigma}^2$ can be regarded as the effective fraction of unpaired spin in a Cl 3s or 3p_σ orbital, subject to the approximations made above (neglect of 2s, 2p_σ etc.). The nuclear magnetic resonance results of Shulman and Knox (1960) on (NiF₆)²⁻ are also given, where the σ-bonds are between d_{x²-y²} and d_{3z²-r²} Ni²⁺ orbitals and 2s and 2p_σF⁻ orbitals. It is seen that the two sets of results are consistent, in that the ratios of $f_s/f_{p\sigma}$ are much the same in each case, the bonding being stronger for Cl than for F, actually about twice as strong if allowance is made for the fact that in (NiF₆)⁴⁻ d_{3z²-r²}, as well as d_{x²-y²}, can σ-bond to ligands on the x and y axes. The present results thus support these authors, Keffer *et al.* (1959) and Shulman and Sugano (1961), in suggesting that the admixtures in this type of complex are large and apparently much larger than estimates based on overlap effects alone with no covalent bonding.

The values of the parameters for the Cu²⁺ ion, *A*, *B* and *g* given above, also support the general picture of relatively strong bonding as can be seen by comparing the present results for (CuCl₆)⁴⁻ with those of Bleaney, Bowers and Pryce (1955) for Cu²⁺(H₂O)₆. Using the hyperfine structure theory of these authors, we find $p' = 2\gamma\beta\beta_N\langle r^{-3} \rangle N^2 = 212 \pm 15 \times 10^{-4} \text{ cm}^{-1}$, which compares with $p' \simeq 300 \times 10^{-4} \text{ cm}^{-1}$ for Cu²⁺(H₂O)₆ and suggests that $N^2\langle r^{-3} \rangle$ is about 30% smaller in the present case. Similarly, the isotropic s electron contribution is found to be 25% smaller with value $\kappa p' = 73.1 \times 10^{-4} \text{ cm}^{-1}$, where $\kappa = 0.345 \pm 0.015$. Finally, the orbital part of the *g* value, *g* - 2, is reduced in a manner roughly consistent with the other results, but a detailed analysis awaits optical measurements of the splittings of the d orbital levels.

Clarendon Laboratory,
Oxford.

4th October 1961.

J. H. M. THORNLEY.
B. W. MANGUM.†
J. H. E. GRIFFITHS.
J. OWEN.‡

- ABRAGAM, A., and PRYCE, M. H. L., 1950, *Proc. Phys. Soc. A*, **63**, 409.
BLEANEY, B., BOWERS, K. D., and PRYCE, M. H. L., 1955, *Proc. Roy. Soc. A*, **228**, 166.
FREEMAN, A. J., and WATSON, R. E., 1961, *Phys. Rev. Letters*, **6**, 343.
HARTREE, D. R., and HARTREE, W., 1936, *Proc. Roy. Soc. A*, **156**, 45.
KEFFER, F., OGUCHI, T., O'SULLIVAN, T., and YAMASHITA, J., 1959, *Phys. Rev.*, **115**, 1553.
ORTON, J. W., 1959, *Rep. Progr. Phys.*, **22**, 204 (London: Physical Society).
SHULMAN, R. G., and KNOX, K., 1960, *Phys. Rev. Letters*, **4**, 603.
SHULMAN, R. G., and SUGANO, S., 1961, *Phys. Rev. Letters*, **7**, 157.
STERNHEIMER, R., 1953, *Phys. Rev.*, **84**, 244.

† Now at National Bureau of Standards, Washington 25, D.C.

‡ Royal Society Research Fellow (Mr. and Mrs. John Jaffé Donation).

Damping of Sound Waves by an Ideally Rough Surface

A sound wave propagated in a gas confined in a tube has an amplitude attenuation coefficient given by the Helmholtz-Kirchhoff relation (Rayleigh 1894). The majority of experiments using smooth tubes have resulted in attenuations about 15% in excess of the theoretical value. A summary has been given by Lee (1957) and more recent data by Edmonds and Lamb (1958) and by Smith and Wintle

(1960). When tubes with a rough surface are used the attenuation rises but no experiments have been carried out in which the change in attenuation could be compared with a numerical value for roughness.

In the present experiments a sound tube 39.1 cm long and 4.3 cm internal diameter was employed. Each end was closed by a telephone, one of which was fed from a variable-frequency oscillator at about 420 c/s. The amplitude and phase of the voltage output from the second telephone were compared with the input current using an oscilloscope. It can be shown (Zwikker and Kosten 1949) that with poor matching between telephones and gas column and with $\alpha \ll \omega/c$, the transfer impedance Z is given by

$$Z = \frac{E}{I} \propto \operatorname{cosech} ql,$$

using the notation of an earlier paper (Wintle 1960). As the frequency is increased Z executes a dumb-bell figure in the complex plane similar to that of $\operatorname{sech} \frac{1}{2}ql$ (Wintle 1960, Fig. 2). The maximum value of Z is given by

$$\frac{1}{Z_{\max}} \propto \sinh \alpha l \simeq \alpha l,$$

while the phase angle ϕ taken with respect to the position of the maximum is given by

$$\tan \phi \simeq - \frac{2\pi(f - f_n)}{\alpha c},$$

where f_n is the resonance frequency.

The roughness of the sound tube was increased by gluing ball bearings 0.63 cm in diameter to its inner surface. They were placed in rows and arranged randomly along the length of the tube, the least number of rows employed being three. The increase in roughness was presumed to be proportional to the number of balls used. An approximate value for the attenuation due to a sphere placed on the surface of the tube can be calculated by comparing the forces exerted on unit area of the cylindrical surface and on the sphere when subjected to unidirectional Poiseuille flow. The force on the surface is simply $\eta(dv/dx)$, where η is the coefficient of viscosity, v the gas velocity and x the coordinate normal to the surface. The mean velocity past the sphere will be approximately $v(a)$, where a is the radius of the sphere. Since $v(0) = 0$, this becomes $a(dv/dx)$ and the drag given by Stokes' relation is therefore $6\pi\eta a^2(dv/dx)$. With n spheres per unit area the total viscous force is

$$\eta(1 + 6\pi a^2 n) \frac{dv}{dx} = \eta \left(1 + \frac{3a^2 N}{rl} \right) \frac{dv}{dx},$$

where N is the number of balls in the tube, r the radius and l the length of the tube, so the viscous force should be increased in the ratio $1 + 3a^2 N/rl$ compared with that for a perfectly smooth tube. Under oscillatory conditions an increase in attenuation of this order of magnitude must be expected. A graph of α against N should therefore be linear with a slope of about $3\alpha_{\text{HK}} a^2/rl$.

The experimental plot is shown in Fig. 1. The individual values of α are correct to about 3%. The graph is linear as expected, with a slope $3.6 \times 10^{-6} \text{ cm}^{-1}$ per ball to be compared with the calculated value of $1.0 \times 10^{-6} \text{ cm}^{-1}$ per ball. The attenuation with no balls present is three times that expected for a perfectly smooth tube.

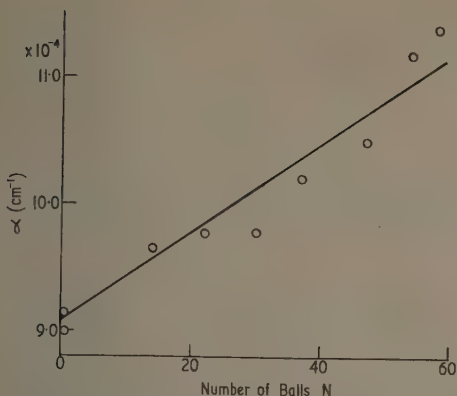


Fig. 1. Graph of attenuation against number of balls in the sound tube.

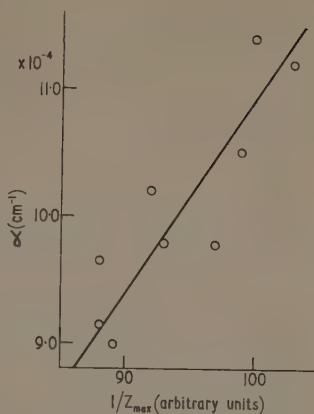


Fig. 2. Graph of attenuation against $1/Z_{\max}$. The straight line passes through the origin, indicating direct proportionality.

A graph of $1/Z_{\max}$ against α is shown in Fig. 2. The straight line is drawn through the mean of the experimental points and the origin and shows that within the experimental error these quantities are in direct proportion, thus establishing the satisfactory operation of the apparatus. It is therefore concluded that the attenuation of sound increases linearly with the numerical measure of the roughness of the tube, and that the magnitude of this increase agrees within a factor of four with that expected upon the basis of an extremely simple approximate theory.

The author wishes to thank the Dean, Royal Military College of Science, for permission to publish this work.

Physics Branch,

Royal Military College of Science,
Shrivenham, Wilts.

H. J. WINTLE.

11th September 1961, in revised form 5th October 1961.

EDMONDS, P. D., and LAMB, J., 1958, *Proc. Phys. Soc.*, **71**, 17.

LEE, T. A., 1957, *Ph.D. Thesis*, University of London.

RAYLEIGH, LORD, 1894, *Theory of Sound* (London: Macmillan).

SMITH, D. H., and WINTLE, H. J., 1960, *J. Fluid Mech.*, **9**, 29.

WINTLE, H. J., 1960, *Proc. Phys. Soc.*, **76**, 772.

ZWICKER, C., and KOSTEN, C. W., 1949, *Sound Absorbing Materials* (Amsterdam: Elsevier).

REVIEWS OF BOOKS

A Degree Physics, Part I: The General Properties of Matter, by C. J. SMITH.
Pp. viii + 732. (London: Edward Arnold, 1960.) 63s.

Dr. Smith accomplishes the task he sets himself with his usual competence. This volume is well written, well produced and a pleasure to read. The price, an important consideration for a students' textbook, is not unreasonable for a book of this bulk.

The tremendous increase of knowledge in the last half century and the fact that students are allowed only three years study for their first degree have together confronted university teachers with the dilemma of the quart and the pint pot. The solution, however unsatisfactory, must be to make space for the fresh brew by rejecting the stale beer. It is with this in mind that Dr. Smith must be criticized; his book fails to fill the requirements of an English university student of physics in the middle of the twentieth century. It treats in great detail many well-established topics but sadly lacks any novelty of approach.

To illustrate this criticism two examples may be chosen. The subject of surface tension is discussed in some seventy pages. Two short paragraphs 'explain' surface tension as a result of intermolecular attraction but no description or explanation of intermolecular forces is given. Nearly two hundred pages are devoted to elasticity and the strength of materials. A description of a method of determining Poisson's ratio for a piece of tubular rubber is given but no account of the elastic properties of a single crystal.

In his preface Dr. Smith regrets that the choice of subject matter is in part fixed by university examination syllabuses. One can sympathize with him, but he alone is responsible for the presentation, and it is difficult to reconcile the above examples with the claim that "the book is written to meet the needs of those who wish to gain a thorough insight into the fundamentals of physics"

To sum up, the book is well written and should be in university libraries as a work of reference for students. The length of the book and its selection of material make it unlikely that it will become a standard textbook. J. A. NEWTH.

Structure and Change: An Introduction to the Science of Matter, by G. S. CHRISTIANSEN and P. H. GARRETT. Pp. xv + 608. (San Francisco, London: Freeman, 1960.) 63s.

This book does not fit into any of the categories of textbooks normally published in this country, but it leaves one with the impression that the general state of scientific education here would be better if such books were less exceptional. After studying it any intelligent person with no previous training in physics or chemistry and with only the most elementary knowledge of mathematics would have a real understanding of the nature of the physical world and of how our understanding of it has been obtained. I should like to see it made compulsory reading for all sixth-form pupils or first-year undergraduates.

The authors have, at the outset, rejected the distinction between physics and chemistry, and the anatomization of these subjects into such moss-encrusted sections as heat, light, sound, properties of matter, and organic, physical and

inorganic chemistry. They discuss in general terms the structure, principles and methods of science, pointing out the relationships between the various stages of observation, generalization, hypothesis, further experiment and modification of hypothesis. My only criticism of this section is that they fail to emphasize how greatly the physical sciences have profited from the possession, in mathematics, of a means of examining rapidly and thoroughly the logical consequences of a postulate.

Part 1 is entitled 'The mechanical view of the physical world', but rightly adds to what is normally called mechanics mechanistic accounts of atomic theory, chemical combination, the behaviour of gases, the concepts of energy and momentum and the nature of solutions. With the same inclusive viewpoint, the authors show in Part 2, 'The electrical view of the physical world', how the principles of electricity and magnetism govern the behaviour of atoms and ions in their chemical behaviour when these principles are taken to include an account of the electrical constitution of matter. All too often students are led to regard physics as the search for general laws governing the *behaviour* of things, and find later with surprise that much of the activity of physicists is concerned with finding ways of describing the *constitution* of things, whether these are nuclei, atoms, solids or stars. A common manifestation of this is a dreadful ignorance of the Periodic Table, a topic returned to several times in this book.

The last part of the book provides a simplified, but not misleading, account of modern physics, including the nature of light, quantum theory, radioactivity, and nuclear reactors, and a final chapter glances rather hastily at some of the most fundamental topics in atomic and cosmic physics. The whole book is well supplied with diagrams which are with very few exceptions clear and helpful, and each chapter is followed by questions which are by no means simply arithmetic and which should help any serious student. Some mathematical operations and some techniques of chemical book-keeping are given in appendices.

Only two criticisms seem worth mentioning. Chapters 15 and 24, The mechanical and chemical views of the earth, by their inevitable differences in approach from those preceding and following them, break the flow of the book, and would be better together at the end; and a chapter on oxidation-reduction reactions serves to introduce some rather arbitrary techniques and terminology (how, in the sense in which the term is defined earlier, does hydrogen increase its valence on being oxidized to water?) which add nothing to an understanding of the constitution or behaviour of matter.

These are minor flaws, and I can think of no better book to recommend to any arts graduate or undergraduate wishing to have a foot in both cultures.

B. R. COLES.

Fourier Transforms: Cambridge Tracts in Mathematics and Mathematical Physics, No. 52, by R. R. GOLDBERG. Pp. viii+76. (London: Cambridge University Press, 1961.) 21s.

This monograph deals directly with mathematical rather than physical theory. Using the ideas of Lebesgue integration, Dr. Goldberg describes the theory of Fourier transforms of integrable-modulus and integrable-square functions so as to provide an introduction to the generalized theory of Fourier transforms on a locally compact group. The latter theory has applications of

physical interest, but these are not discussed in the present work, and indeed the extension beyond transforms on the real line is confined to seven pages of appendix.

After a short first chapter which recalls the necessary definitions and theories on the Lebesgue integral, the second chapter, which is half the book, is devoted to the Fourier transforms of functions in L^1 , that is, functions of integrable modulus. Every such function has a Fourier transform which is continuous on the real line and vanishes at $\pm \infty$. However, not all functions with these two properties are Fourier transforms, and not all Fourier transforms of functions in L^1 lie themselves in L^1 . Inversion then is dealt with by using the convergence factor, $1 - |x|/R$ between $-R$ and R and zero outside that range, then letting $R \rightarrow \infty$. The problem of what sort of functions are Fourier transforms is then discussed, leading up to the remarkable theorem of Wiener that, if the Fourier transform of a function in L^1 is nowhere zero, then any function of L^1 can be constructed as a linear combination of the original function with itself translated by various amounts (more precisely, L^1 is the closure of the set of translates of this function).

A shorter chapter on the transforms on L^2 is followed by a discussion of generalizations of Wiener's theorem, stopping at the point where functional analysis is needed for further progress. There is a final chapter on the Fourier-Stieltjes transform and Bochner's theorem, and a short appendix on abstract harmonic analysis on groups more general than the real line.

This book is very clearly written and makes an admirable guide through the thickets of real variable theory. It is well worth reading even if one has no immediate need to advance into abstract harmonic analysis, but intends rather to turn back from the guided path to a more detailed study of the classical theory.

GEORGE WYLLIE.

The Theory of Neutral and Ionized Gases, edited by C. DEWITT and J. F. DETOEUF.
Pp. 469. (London: John Wiley, 1961.) 140s.

This book is based upon the lectures given at the 1959 Summer School at Les Houches. There were seven lecturers and the scope of their lectures was rather more general than the title suggests. The first article is by E. W. Montroll on modern developments in statistical mechanics, being mainly concerned with the diagrammatic expansions which have recently been applied to equilibrium and to transport problems. There is also an account of random walk problems and the Ising problem. L. van Hove's article is concerned with transport theory and the problem of relating the Pauli and Boltzmann equations to the new closed forms for transport coefficients. The current situation as described by these two articles has enormously clarified in the last few years, but this clarification has amounted to vigorously justifying results already known by other methods. The time should now be ripe for really new ground to be explored, and these articles are a very good introduction to the current situation.

The remaining articles on ionized gases fall into three classes. Those of J. L. Delcroix and A. N. Kaufman and J. F. Denisse on the microscopic properties of plasmas (in French), plasma transport theory and waves in plasmas (in French), respectively, can be regarded as concerned with ideal plasmas, i.e. those properties corresponding to simple physical situations which may be far removed from those obtained in important practical cases. The lectures of M. Kruskal are concerned

with the problems of stability based on hydromagnetic equations. The final article by E. Schatzman (in French) applies plasma theory to astrophysical problems. Again these articles are an excellent introduction to the current situation in plasma theory. The book is rather expensive but it must be admitted that it is beautifully produced.

S. F. EDWARDS.

The Application of Group Theory in Physics. By G. YA. LYNBARKII. Translated from Russian by STEVAN DEDIJER. Pp. ix + 380. (London: Pergamon Press, 1960.) 63s.

This is a translation of a Russian textbook based on the author's lectures at Kharkov University. It commences with a general introduction to groups and their representations, followed by chapters on particular topics. For finite groups the applications are to the theory of small oscillations, second-order phase transitions, crystal properties and the absorption and Raman scattering of light. Of particular interest is the chapter on phase transitions, since apart from a brief discussion in Landau and Lifshitz's book this is not available elsewhere and here it is given in some detail. On infinite groups there are chapters on Clebsch-Gordon and Racah coefficients, on the Lorentz group, relativistic wave equations, and on the application of group theory to nuclear reactions.

The main trouble with books on group theory, and even more so with chapters on group theory in more general books, is that they do not usually go into their subject sufficiently fully for the reader to master an application, before they move on to another field. On the whole this book avoids this trouble, though the Lorentz group for example cannot be thoroughly discussed in thirty pages. Almost any theoretical physicist will find reading this book worth while and probably find some new approach or new application in it. There is however one serious drawback to it: it is quite deplorably printed. It is produced by photolithography direct from a type and handwritten manuscript. Group theoretical formulae usually involve lots of subscripts and superscripts and these are quite often illegible, and these and other symbols are sometimes completely missing. If Pergamon want to produce books this way the least they could do is to buy a decent typewriter and employ a competent proof reader. The reviewer's copy had but half an index; where the other half ought to have been was an apology from the publisher for the state of the book and its price which were excused "with a view to making the information contained in this publication speedily available". In fact group theory cannot be regarded as hot news and one hopes that standard Russian texts will be treated better than this in future.

S. F. EDWARDS.

A Bibliography of The Honourable Robert Boyle, by J. F. FULTON. Pp. 217 + xxvi. (Oxford: The Clarendon Press, 1961.) 50s.

This second edition of the Bibliography of Robert Boyle coincides with the Tercentenary of the Royal Society

Since the first edition of the Bibliography in 1932, a number of fresh studies of Boyle and various aspects of his life and work have become available, and discussion of these is included in the new edition.

Introduction à l'Électrodynamique Quantique, by D. KASTLER. Pp. xii + 333. (Paris: Dunod, 1961.) 68 n fr.

One might expect a Frenchman to be as exact and elegant as possible. Professor Kastler does not disappoint on this score. His book on elementary quantum electrodynamics uses the resources of modern pure mathematics to present an exposition of its subject which is as logically precise as possible. It is the hope hereby unfortunately to enter the minds of physicists, who may be bothered by false difficulties which arise from imprecision of statement and fail to present the subject in a form which is accessible to pure mathematicians without the need of conscious shunning. In this he succeeds, but it seems doubtful to this reviewer that many fruitful consequences will flow from it.

Quantum electrodynamics is in excellent agreement with experiment. The apparent juggling with infinities in the renormalization programme should not be taken too seriously. The difficulties here are really physical rather than mathematical for it seems reasonable to suppose that the quantities would be finite if we understood the details of the theory at short distances. In fact a renormalizable theory is simply one whose low energy behaviour can be predicted without a detailed knowledge of its high energy structure. The real formal difficulties of quantum electrodynamics are largely concerned with the proper formulation of the Lorentz condition and gauge invariance, and within its elementary limits this book gives a good account of them.

The first two chapters are devoted to mathematical preliminaries and then the theory of second quantization is developed. There are chapters dealing with the Klein-Nishina formula and Compton and Møller scattering. The book concludes with the introduction of Feynman graphs and the use of external fields. It does not deal with renormalization theory. Thus the material is as elementary as the style is advanced.

J. C. POLKINGHORNE.

Proceedings of the VIIIth International Conference on Low Temperature Physics, edited by G. M. GRAHAM and A. C. HOLLE HALLITT. Pp. xviii + 725. (Toronto: University Press, Amsterdam: North Holland, 1961.) £5 14s.

No doubt this was a very enjoyable and profitable beano for those who enjoy and profit from such beans. Only I cannot imagine why all those reputable scientists should want to *publish* the scraps of information which they communicated there. Either they had something new and important to say, when it should have been published (i.e. *made public*) in a standard scientific journal, available in any ordinary scientific library, or else it was old, or unimportant, and there was no need to waste print on it. It has been suggested to me that I should compliment the editors and publishers for getting it out so quickly. Certainly, by the usual standards of such publications, eight months is quite expeditious; but may I remark that any physics journal that took so long between receipt of the manuscript and publication would be considered a bit dilatory. The fact is that large expensive miscellanies of this sort are a curse to modern science. Let us all resolve never to make reference to them (it is difficult enough anyway, the title being more a dinner than a mouthful) so that no one ever looks at them, libraries will not buy them, and publishers will refuse to touch them for lack of a profit.

J. M. ZIMAN.

Fundamentos Teóricos de la Física Atómica y Nuclear, by C. SÁNCHEZ DEL RIO.
Pp. vi+167. (Madrid: Servicio de Publicaciones de la J.E.N., 1960.)
175 Pesetas.

The purpose of this book is to provide a qualitative introduction to the theories of the atom, the nucleus and elementary particles. It is meant for two classes of readers: students who are just starting the study of such theories, and engineers and others who are dealing with the technical aspects of atomic energy and want to have at least some notions of current theoretical ideas.

For this second class of readers the book should succeed admirably because the exposition is always as simple as the subject allows it to be and is based on semi-classical arguments, while providing, however, substantially sound information, even on such concepts as 'isotopic spin', 'non-conservation of parity', or 'strangeness'. As for students, one is doubtful. It is certainly an advantage to be introduced without tears to the concepts of modern physics, but in a field in which the point of view, the methods, the approximations, the very mathematical techniques are of paramount importance and are inextricably mixed up with the physical results, an introduction which gives these results in a dogmatic way (even if the doubtful points are fairly stressed) may not lead to the right frame of mind in approaching the subject.

The titles of the eight chapters are: 'Basic ideas on atoms and nuclei', 'Fundamental concepts of quantum theory', 'Structure of the atom', 'Interactions between particles and between particles and radiation', 'Structure of the nucleus', 'Nuclear levels', 'Nuclear reactions', 'Elementary particles'. There are two mathematical appendices, a table of constants and a list of books for further reading. This small volume is well produced and will undoubtedly become very popular in Spanish-speaking countries.

L. PINCHERLE.

Praktische Mathematik für Ingenieure und Physiker, by R. ZURMÜHL. Pp. xiv+548. (Berlin, Göttingen, Heidelberg: Springer, 1960.) DM 29.40.

This book is an introductory reference work for those who, using desk calculators, have frequent occasion to use numerical methods to solve their problems. The inversion of a matrix, eigenvalue problems, questions of numerical integration, the significance of the χ^2 -test are some of the topics treated.

The author gives in most cases a good account of the background theory (without getting lost in it), and then takes off his jacket in order to work through a few numerical examples which illustrate the procedures which he has discussed. This, together with clear diagrams and a lucid style, makes this handbook of numerical analysis very useful. It must be highly recommended as a first reference, with the aid of which one may hope to avoid recourse to a more specialized literature.

The contents include the following: (1) Methods of solving equations of third, fourth or higher order; (2) Linear equations and manipulation of matrices; (3) Interpolation and integration; (4) Statistical methods; (5) Representation of arbitrary functions, including harmonic analysis; (6) Initial and boundary value problems in differential equations.

P. T. LANDSBERG.

The Principles of Nuclear Magnetism: International Series of Monographs on Physics, by A. ABRAGAM. Pp. xvi+599. (London: Clarendon Press, Oxford University Press, 1961.) 84s.

A theoretical argument does not become acceptable to Professor Abragam until he has reproduced it in his own way. Although the subject of nuclear magnetism is a fairly new one, there exists, scattered through the literature, a considerable amount of theory. This has all been brought together in the present volume and presented in a clear, comprehensive and thoughtful way, so that throughout one feels guided by an author who not only has the whole subject at his fingertips but who has also gone to immense trouble to present the arguments in the most instructive ways. Mathematics is not avoided, but it is not indulged in for its own sake, and it is continually reinforced by physical arguments and well-chosen experimental results.

The result is a lengthy but invaluable account of the whole field of nuclear resonance and the associated phenomena of nuclear magnetism, and a book of which the author and publishers can well be proud. Your reviewer is very impressed by the high standard of scholarship maintained throughout, and although one might hesitate to recommend the book as a first introduction to nuclear magnetism, it is obviously a text to which all serious workers in this field will refer repeatedly. As for its contents it is sufficient to say that all the theory is there, even including topics such as cross-relaxation, which can hardly have been discovered when the manuscript first went to press.

K. W. H. STEVENS.

BOOK NOTICES

Contribution A L'Étude Aérothermique d'un Jet Plan Evoluant en Présence d'une Paroi, by J. MATHIEU. Pp. 140. (Paris: Ministère de l'Air, 1961.)

Théorie du Calcul des Cerces, by G. CZERWENKA. Pp. xxi+40. (Paris: Ministère de l'Air, 1961.)

Étude Expérimentale de la Convection de la Chaleur dans un Canal avec Profils de Vitesse Variables, by J. J. C. PICOT. Pp. ix+14. (Paris: Ministère de l'Air, 1960.)

Sur le Calcul des Grilles de Profils, by A. PAPON. Pp. xxvi+62. (Paris: Ministère de l'Air, 1960.)

Équations Intrinsèques du Mouvement à Trois Dimensions des Fluides à Viscosité, by F. J. BOURRIÈRES. Pp. xx+65. (Paris: Ministère de l'Air, 1960.)

Mise en Oeuvre d'un Procédé de Détermination Expérimentale du Domaine Transsonique dans un Écoulement de Type Mixte, by G. CONTIER. Pp. iv+236. (Paris: Ministère de l'Air, 1960.)

Chronophotographie Électronique Application à L'Étude de Phénomènes Aérodynamiques Évolutifs, by G. BATAILLER. Pp. xviii+88. (Paris: Ministère de l'Air, 1960.)

Étude de l'Écoulement d'un Fluide dans un Tunnel Prismatique de Section Trapézoïdale, by E. RODET. Pp. 116. (Paris: Ministère de l'Air, 1960.)

A Direct Measurement of the Proton Total Reaction Cross Section for Copper at 9.3 Mev

By G. W. GREENLEES AND O. N. JARVIS†

Department of Physics, University of Birmingham

MS. received 31st May 1961

Abstract. A value of 930 ± 70 mbn has been obtained for the proton total reaction cross section for copper at 9.3 ± 0.3 mev by a poor geometry transmission method not involving counter coincidence techniques. This result, which is in good agreement with values obtained by indirect methods, is appreciably higher than values predicted by published optical model analyses using a volume absorption term. Differential elastic cross sections are presented for the angular range 30° – 155° (centre of mass). These were obtained using the same target as in the reaction cross section measurement. Good agreement with both the differential cross sections and the reaction cross section can be obtained using an optical model potential with an absorptive term peaked at the nuclear surface.

§ 1. INTRODUCTION

DURING the past few years the measurements of proton–nucleus elastic scattering angular distributions has received considerable attention in the low and intermediate energy regions and considerable success has been achieved in describing the results in terms of the optical model (Glassgold *et al.* 1957, 1958, Melkanoff *et al.* 1957). This model has also been found capable of reproducing the general features of such polarization measurements as have been made (Rosen and Brolley 1958) but, unfortunately, it has been found to be incapable of fitting the available data uniquely, this failure giving rise to the familiar V – R ambiguity relating the possible sets of parameters judged to represent equivalent fits to the data. This ambiguity should be resolvable, at least in part, by a comparison of accurate total reaction cross section measurements with the predictions made by the model for each of the different sets of parameters. As yet, few total reaction cross section measurements have been made in the proton energy range below 100 mev owing to the experimental difficulties involved.

For proton and deuteron energies of only a few mev, the total reaction cross section can be determined as a sum of all the various partial reaction cross sections that are significant. Thus Slaus and Alford (1958) have measured the total reaction cross section for 4 mev deuterons on ^{63}Cu as the sum of the cross sections for the (d, d') , (d, n) , (d, p) , (d, α) and (d, pn) reactions. This procedure is particularly simple when one type of reaction makes the dominant contribution. At higher energies this method becomes less satisfactory owing to the increasing number of reactions that are energetically possible. Recently, however, measurements at 9.85 mev have been reported by Meyer and Hintz (1960) of the proton

† Now at Atomic Energy Research Establishment, Harwell.

total reaction cross sections for copper and zinc. These determinations were made by measuring the total charged particle reaction cross sections and combining the results with existing measurements of the (p, n) cross sections. The results of the work, which are in good agreement with the present determination, will be discussed in some detail in a later section. Finally, Fulmer (1959) has obtained determinations of the proton total reaction cross sections for the uranium isotopes at 23 mev; this is a special case since the fission cross sections make an 80–90% contribution.

Total proton reaction cross sections have been measured by direct transmission methods at several energies above 200 mev, at 134 mev (Cassels and Lawson 1954) and, more recently at 61 and 34 mev (Meyer, Eisberg and Carlson 1960, Gooding 1959). These experiments involve the use of counter coincidence techniques to determine the attenuation of the proton beam on placing the absorber between a set of 'passing' counters and the final detector. At high energies such experiments are not greatly troubled by the energy loss due to ionization in the passing counters and the absorber, but at lower energies the specific ionization increases rapidly and at 10 mev constitutes the dominating feature of this type of measurement.

Because of the short range of protons at 10 mev, the present experiment was designed to use no 'passing' counters to define the beam but to rely on the beam intensity remaining constant over a short time interval whilst the counting rate was determined with and without the absorber in position. The experiment is only practicable using an accelerator providing a continuous beam; in the present work, the Birmingham 60 in. cyclotron was used. The statistics of the experiment are those appropriate to a Poisson distribution so that at least 10^{10} protons must be recorded in order to obtain a 5% result with a copper absorber 0.6 mev thick, since such an absorber gives an attenuation due to non-elastic processes of only 0.02%. Copper was chosen for the present measurement because this element has been the subject of detailed optical model analyses and both angular distribution (Hintz 1957, Greenlees, Kuo and Petravic 1957) and polarization (Rosen and Brolley 1958) data are available; also it is an element for which the optical model is expected to apply using 10 mev protons.

§ 2. EXPERIMENTAL METHOD

As mentioned above, advantage is taken of the fact that the fixed frequency cyclotron is not a pulsed machine and that the beam intensity can be held reasonably constant over short time intervals. With a beam of sufficiently constant intensity it would be possible to measure the total reaction cross section simply by making counting rate determinations with and without the copper absorber in position. In practice, however, the measurements were repeated cyclically with a fairly rapid repetition rate (nearly twice per second) so that any fluctuations in the intensity of the beam averaged out over a sufficient number of cycles. The requirement of a constant intensity was further relaxed by the use of a monitor counter which sampled the beam entering the experimental area. In principle, using a monitor, constancy of beam intensity is no longer important; it does, however, enable higher mean counting rates to be used and this is essential from a practical viewpoint.

The measurement of the beam intensity was made in poor-geometry using a large, accurately defined, acceptance angle subtending a cone of half-angle

θ ($\sim 50^\circ$) at the absorber. A separate experiment was performed to determine the magnitude of the correction term required to allow for the elastic scattering of protons through angles greater than θ . A large acceptance angle was used to reduce the error introduced into the elastic scattering corrections by the uncertainty in this angle. A second correction term was also required to give a measure of those inelastic events occurring in the absorber which give rise to charged particles entering the detector with energies sufficient to overcome the set detector bias (E_{\min}). This term was necessary since it was not possible to bias the detector just below the pulse height corresponding to elastically scattered protons because of the rather poor resolution given by the plastic scintillator used as a detector and because, at the counting rate used throughout the experiment (about 3×10^5 pulses per second), fluctuations in the gain of the electronics must be expected. The bias was set to 50% of the peak height. The magnitude of this non-elastic scattering correction was small and could be estimated from the results of Meyer and Hintz (1960).

Owing to the possibility of the incident protons undergoing nuclear interaction in the scintillation material, as well as in the copper absorber, it was necessary to ensure that the beam energy at the detector be the same for the two counting rate determinations. A comparison absorber of gold, which was chosen so as to give an energy degradation equal to that of the copper, was therefore placed in the beam during the 'no-absorber' measurements. The total reaction cross section for copper was determined from the measurement of the counting rate ratio $R(\theta)$, which gives the relative counting rates with the copper and gold absorbers in the path of the beam. The necessity for introducing this comparison absorber had the unfortunate consequence that the appropriate elastic scattering correction was large, being several times the magnitude of that for the copper absorber. It was therefore necessary to determine this correction accurately. The choice of gold for the comparison absorber was indicated by the small total reaction cross section for 10 MeV protons, this being less than 10% of that for copper owing to the relatively high Coulomb barrier. Since the thickness of the gold absorber (measured in terms of number of nuclei per cm^2) required for the energy compensation was less than one half of that for the copper absorber, it is seen that the total reaction cross section for gold makes only a 4% contribution to the result of the experiment; a rough estimate of its magnitude was therefore sufficient. This was obtained for published optical model predictions based on the results of Hintz (1957) at 9.8 MeV.

The total reaction cross section for copper may be expressed in terms of the measured ratio $R(\theta)$ and the various correction terms mentioned above in the following form

$$\begin{aligned} \sigma_R(\text{Cu}) = & \frac{N_{\text{Au}}}{N_{\text{Cu}}} \left[\int_{\theta}^{\pi} \left(\frac{d\sigma}{d\Omega} \right)_{\text{el, Au}} d\Omega + \sigma_R(\text{Au}) \right] - \int_0^{\pi} \left(\frac{d\sigma}{d\Omega} \right)_{\text{el, Cu}} d\Omega \\ & + \int_0^{\theta} \int_{E_{\min}}^{E_{\max}} \left(\frac{\partial^2 \sigma}{\partial \Omega \partial E} \right)_{\text{non el, Cu}} d\Omega dE - \frac{1}{N_{\text{Cu}}} [R(\theta) - 1] \end{aligned}$$

where N_{Au} , N_{Cu} are the surface densities (number of nuclei per cm^2) for the two absorbers.

§ 3. APPARATUS AND PROCEDURE

3.1. *The Absorption Measurement*

A diagram of the apparatus is shown in Fig. 1. This consisted essentially of a vacuum chamber in which the counting rate determinations were made, and a counting rate monitoring unit which recorded protons elastically scattered from a thin gold foil placed in the path of the collimated beam. The vacuum chamber contained a rotating wheel which placed alternately the copper and the gold absorbers in the path of the beam before the main detector unit. Two sets of scaling units were coupled to each of the two particle detectors and these were gated on and off in synchronism with the rotation of the wheel such that one set was operative when the copper absorber was in the beam and the other set when the gold absorber was in the beam. The gates were opened by pulses from two photomultipliers (not shown in the diagram) attached to the chamber upon which light was allowed to fall each time the wheel passed through two positions; the gates were closed precisely 0.16 sec later by a delayed signal derived from a 1 Mc/s crystal oscillator and a bank of scaling units. In this manner the gate-open periods for the two absorbers were made equal to better than one part in a million.

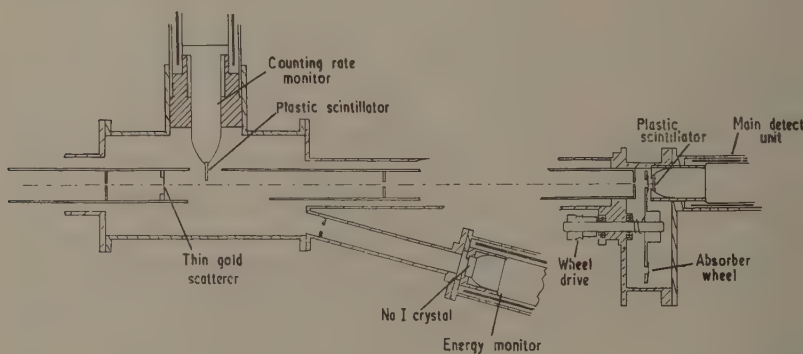


Fig. 1.

A simplified diagram of the electronic system is shown in Fig. 2. This shows that the pulses from the two detectors were first scaled down by a factor of 32 before entering the gating unit. This procedure did not lead to the loss of useful information owing to the very high counting rates used throughout the experiment. The scaling units used were capable of recording at a continuous rate of 20 Mc/s. No electronic counting losses were therefore involved as the cyclotron radio frequency is only 10 Mc/s. The acceleration is such that if two or more protons are accelerated together during the same radio-frequency period the time spread between them will be less than 20 nsec; the scaling units were set so that they would not record such protons separately. Thus, the counting rate correction for the experiment was dependent only on the cyclotron beam intensity and the radio-frequency acceleration period. A pulse sampling system was constructed which accepted a small fraction of those pulses recorded by the input circuit and displayed them on a 100-channel pulse height analyser. This

Petravic 1957). After collimation the beam passed through the target; the scattered beam was detected in a scintillation counter and the unscattered beam was collected in a Faraday cup. The scintillation counter, which was also used as the energy monitor in the absorption measurement, was mounted on the lid of the chamber so that the line joining the centre of the target to the detector made an angle of 15° with the horizontal plane containing the incident beam; as a result of this geometry, scattering angles between 15° and 165° could be studied. Pulses from the detector were displayed on a 100-channel pulse height analyser gated to record until a specific charge had been collected by the Faraday cup. Absolute cross sections could be measured with an accuracy to $\pm 1\%$ using this apparatus.

Table 1. Elastic Scattering of Protons by Cu
Proton Energy (lab) = 9.47 ± 0.05 MeV

$\theta_{\text{c.m.}}$	$(d\sigma/d\Omega)_{\text{c.m.}}$ (mbn sterad $^{-1}$)	$(d\sigma/d\Omega)_{\text{obs}}$ $(d\sigma/d\Omega)_{\text{Ruth}}$	$\theta_{\text{c.m.}}$	$(d\sigma/d\Omega)_{\text{c.m.}}$ (mbn sterad $^{-1}$)	$(d\sigma/d\Omega)_{\text{obs}}$ $(d\sigma/d\Omega)_{\text{Ruth}}$
$32^\circ 50'$	1760 ± 30	0.90 ± 0.017	$76^\circ 20'$	30.8	0.36
$36^\circ 20'$	1235	0.93	$79^\circ 10'$	33.5	0.44
$40^\circ 0'$	830	0.91	$83^\circ 0'$	34.9 ± 1.1	0.54 ± 0.017
$43^\circ 40'$	573	0.87	$87^\circ 0'$	35.2	0.63
$45^\circ 40'$	454 ± 9	0.81 ± 0.017	$90^\circ 30'$	36.3	0.74
$48^\circ 30'$	332	0.75	$94^\circ 40'$	35.0	0.82
$50^\circ 30'$	266	0.70	$95^\circ 40'$	33.3 ± 1.0	0.80 ± 0.025
$52^\circ 10'$	215	0.64	$101^\circ 20'$	30.4	0.87
$54^\circ 10'$	167 ± 5	0.57 ± 0.017	$104^\circ 20'$	27.4	0.85
$56^\circ 30'$	132	0.53	$109^\circ 0'$	23.8	0.83
$58^\circ 0'$	103	0.45	$113^\circ 50'$	18.7 ± 0.7	0.73 ± 0.026
$60^\circ 0'$	78	0.39	$118^\circ 40'$	14.2	0.62
$61^\circ 50'$	69 ± 2	0.38 ± 0.009	$123^\circ 20'$	11.1	0.53
$63^\circ 50'$	53	0.33	$128^\circ 0'$	7.6	0.40
$65^\circ 40'$	44.4	0.31	$137^\circ 20'$	6.2 ± 0.8	0.37 ± 0.040
$67^\circ 30'$	41.4	0.31	$146^\circ 20'$	5.7	0.38
$70^\circ 30'$	34.4 ± 1.0	0.30 ± 0.009	$154^\circ 40'$	8.9	0.64
$73^\circ 20'$	31.2	0.32			

In order to determine the correct elastic scattering corrections it was considered desirable to perform this part of the experiment using targets which presented the same surface density to the beam as those used in the absorption measurement. Consequently, two targets were used for each angular distribution; the first, being set normal to the beam direction, was used for scattering angles θ in the range $30^\circ < \theta < 75^\circ$ and $105^\circ < \theta < 165^\circ$, the second being set at 45° to the beam direction, was used for $75^\circ < \theta < 105^\circ$. The beam energy at which these angular distributions were obtained was determined from the range of protons as measured in a nuclear emulsion (Ilford C2) using the range-energy data of Shapiro (1958). The value so obtained was found to compare well with that obtained from the constants of the scattering chamber and of the Faraday cup beam integrator unit on the assumption that the scattering from gold follows the Rutherford formula exactly for forward scattering angles.

The differential elastic scattering cross sections for gold were found to follow the Rutherford formula closely for scattering angles below 70° and to fall off gradually with increasing angle above this value. The maximum (extrapolated)

deviation from the Rutherford formula was only 10% at 180°. The results for copper are given in Table 1; these measurements are in close agreement with earlier results obtained in this laboratory at a comparable energy (Greenlees, Kuo and Petravic 1957). In order to obtain the elastic scattering correction, the cross section data was integrated numerically over the relevant angular ranges and the energy E was adjusted according to the Rutherford $1/E^2$ relationship so as to be appropriate to the absorption measurements.

§ 4. RESULTS

The absorption apparatus was first tested without the absorbers in position to ensure that there was no asymmetry between the two counting channels. No evidence for such an effect was obtained. A measurement was next undertaken, with the absorbers in position, to discover whether the observed result depended on the bias level of the input circuitry. Bias settings of 25% and 40% of the

Table 2. A Typical Set of Results

Element	Surface density	Energy equiv. at 9.7 Mev
Au	34.8 mg cm ⁻²	0.630 ± 0.006 Mev
Cu	22.6 mg cm ⁻²	0.638 ± 0.006 Mev
Proton energy (lab)		9.30 ± 0.05 Mev
$R(\theta = 48^\circ 30')$		1.000328 ± 0.000016
$\frac{1}{N_{\text{Cu}}} (R(\theta) - 1)$		-1530 ± 70 mbn
$\frac{N_{\text{Au}}}{N_{\text{Cu}}} \int_0^\pi \left(\frac{d\sigma}{d\Omega} \right)_{\text{el, Au}} d\Omega$		+2840 ± 70 mbn
$-\int_0^\pi \left(\frac{d\sigma}{d\Omega} \right)_{\text{el, Cu}} d\Omega$		-420 ± 10 mbn
$\int_0^\theta \int_{E_{\text{min}}}^{E_{\text{max}}} \left(\frac{d^2\sigma}{d\Omega dE} \right)_{\text{non el, Cu}} d\Omega dE$		+29 ± 6 mbn
$\frac{N_{\text{Au}}}{N_{\text{Cu}}} \sigma_{\text{R}}(\text{Au})$		+40 ± 7 mbn
Energy balance correction		+6 ± 4 mbn
Correction for finite beam pencil		+15 ± 3 mbn
Correction for scintillator response variation		-50 ± 25 mbn
Final value for $\sigma_{\text{R}}(\text{Cu})$ averaged over three runs =		930 ± 70 mbn.
Note. Probable errors are quoted in this table.		

peak pulse height gave counting rate ratios $R(\theta)$ which differed from unity by $(33 \pm 2) \times 10^{-5}$ and $(32 \pm 2) \times 10^{-5}$ respectively. These results set an upper limit on the magnitude of any bias dependent effects which might have been present. Unfortunately, the energy monitor was not used in this first experiment and the beam energy was uncertain to ± 150 kev so that an absolute uncertainty of $\pm 9\%$ exists in the resultant value for $\sigma_{\text{R}}(\text{Cu})$. This large error for an uncertainty in energy of ± 150 kev is due to the large Coulomb scattering from the gold (see Table 2).

A second experiment was performed (with a different pair of absorbers) during which the beam energy was monitored using the system described

previously; a result was obtained with a similar statistical uncertainty to that of the previous measurements. After being suitably weighted the several results were combined to give a single cross section. Before a final value for the total reaction cross section for copper can be obtained several corrections must be included. Apart from terms already mentioned, corrections are required for the lack of energy balance between the two absorbers, for the fact that a finite area of the absorbers is illuminated by the proton beam and also for the non-uniformity of response of the scintillator over its surface. The magnitudes of these terms are quoted in Table 2, which is only representative of the three sets of results obtained. The total reaction cross section for copper was found from the weighted mean of three runs to be 930 ± 70 mbn at 9.30 ± 0.30 mev. The total length of machine time required for this measurement was about 100 hours.

§ 5. DISCUSSION

5.1. Proton Total Reaction Cross Section Data near 10 MeV

It has already been mentioned that Meyer and Hintz (1960) have obtained values from the proton total reaction cross section for several elements at 9.85 mev by the addition of the partial cross sections involved. Their cross sections do not include values for the (p, γ) reaction but this is expected to be small (~ 1 –2 mbn). The value quoted by these authors for natural copper is $\sigma_R = 910 \pm 60$ mbn, this result being obtained as a suitable average over the two isotopes. This result is clearly in good agreement with the present measurement of 930 ± 70 mbn at 9.30 mev. The value for σ_R at 9.30 mev would in fact be expected to be less than that at 9.85 mev (by about 30 mbn) owing to the reduced penetrability of the Coulomb barrier, but this could easily be masked by the experimental errors.

The values of the (p, n) reaction cross sections for ^{63}Cu and ^{65}Cu used by Meyer and Hintz were 480^{+90}_{-65} mbn and 819 ± 75 mbn, respectively (the errors represent the spread in the existing measurements). Albert and Hansen (1961) have recently published new measurements for $\sigma(p, n)$ at 9.85 mev. These new values combined with Meyer and Hintz's measurements yield $\sigma_R = 865 \pm 60$ mbn. Benveniste (private communication) has made measurements of the charged particle reaction cross sections for Cu at several energies. These values together with Albert and Hansen's $\sigma(p, n)$ results yield $\sigma_R = 921 \pm 45$ mbn. Combining the several measurements of all the partial cross sections without preference to any particular data we find $\sigma_R = 900 \pm 56$ mbn at 9.85 mev.

Before the experimental values can be compared directly with predictions from optical model analyses, it is necessary to add the contribution to the total reaction cross section appropriate to compound elastic events. The compound elastic cross section for copper is expected to be small on theoretical grounds. Experimentally, the existence of compound elastic scattering is generally assumed (Wall and Waldorf 1957) when the optical model angular distributions fall below the experimental values for large scattering angles where the Coulomb and shape elastic scattering is least and the compound elastic scattering of comparable magnitude. For the even A isotopes of nickel it is indicated that the compound elastic cross section is about 50 mbn (Greenlees and Rolph 1960), but no such effect is found for copper. The presence of compound elastic scattering would, of course, increase the experimental values of σ_R .

5.2. Optical Model Analyses

The elastic scattering angular distribution for copper at 9.75 MeV due to Hintz (1957), was first analysed by Glassgold *et al.* (1957) using an optical model potential for which both the real and imaginary parts were described by the Saxon-Woods form factor (Saxon and Woods 1954). The angular distribution was found to be fitted equally well with several sets of parameters, the values for the total reaction cross section lying in the range 660–790 mbn. In this analysis polarization effects were not considered. Nodvik and Saxon (1960) have repeated the analysis using a potential which includes a spin-orbit term to describe the polarization data of Rosen and Brolley (1958). They found that the inclusion of the spin-orbit term gave rise to only second-order effects in σ_R , the range of values predicted being unaltered. Definite preferred sets of parameters were obtained, however, the set giving the best fit to the data being associated with a value for $\sigma_R = 720$ mbn.

Now that experimental values for σ_R have become available it is clear that the predicted values are too low. In order to obtain values of σ_R from the optical model, which are as much as 200 mbn above the best fit of Nodvik and Saxon, it seems necessary to make some alteration in the form of the potential. There is some theoretical justification for the use of a surface absorption term rather than the volume absorption of the Saxon-Woods form-factor and also for extending the radius of the absorptive part of the potential beyond that for the real part (Shaw 1959, Gomes 1959).

The need for a surface absorption is indicated by the analysis of neutron scattering work by Bjorkland and Fernbach (1958) who found that, in order to obtain a set of optical model parameters which do not change greatly between heavy and light nuclei, it was necessary to use a form-factor for the imaginary part of the potential well which is strongly peaked at the nuclear surface. That this has not so far been necessary in proton scattering is probably due to the influence of the Coulomb potential. It has been indicated on theoretical grounds (Kikuchi 1959) that whereas a surface absorption is probably necessary below 20 MeV its presence above this energy is not very realistic. This is interesting since the reaction cross section measurements for protons at 34 MeV (Gooding 1959) and 61 MeV (Meyer, Eisberg and Carlson 1960) are in reasonable agreement with predictions from optical potentials using only a volume absorption term.

Optical model analyses have recently been carried out by Easlea (1961) using an imaginary potential which combines both volume and surface absorption terms. The effect of varying the relative contributions of these terms was investigated, as was also the effect of increasing the radius for the imaginary part of the potential well relative to that of the real part. The results of this work are published in an accompanying paper and will not be discussed in detail here. The main difficulty in arriving at a unique conclusion was due to discrepancies in the experimental data. Whilst, as discussed earlier in this paper, the reaction cross section measurements available for Cu agree within the experimental errors around 10 MeV, there are significant differences in the differential cross section data. Nevertheless, in order to obtain the required reaction cross section and simultaneously obtain a good fit to any of the differential cross section and polarization data, it is necessary to use an imaginary potential with a peaking in the nuclear surface. To obtain a fit it is not necessary to increase the radius of

the imaginary potential. Since different radii for the real and imaginary potentials introduces an additional parameter it is a step to be avoided unless essential.

Considering only the results (σ_R and differential cross sections) presented in this paper, Easlea was able to obtain an excellent fit to the differential cross section and predict a value of $\sigma_R \sim 900$ mbn using two sets of parameters; one set involved a purely surface imaginary potential of -8.2 mev and gave $\sigma_R = 920$ mbn and the other an imaginary potential with a central value of -2.9 mev and a surface value of -5.8 mev, gave $\sigma_R = 915$ mbn. These are both in good agreement with the present value of 930 ± 70 mbn. Both these sets of parameter give a good fit to Rosen's polarization data (Rosen and Brolley 1958).

In conclusion, the total reaction cross section for Cu obtained in the present work by a direct method, agrees with values obtained by an addition of the partial cross section involved, within the accuracy of the experiments; if such values, which fit the differential cross section data, are to be obtained from an optical model analysis it is necessary to use a surface peaking in the imaginary part of the potential used in the model.

ACKNOWLEDGMENTS

The authors wish to thank members of the Cyclotron Scattering Group for help at various stages of the work and also Mr. B. R. Easlea for providing his results in advance of publication. One of us (O. N. J.) thanks the Department of Scientific and Industrial Research for financial support.

REFERENCES

- ALBERT, R. D., and HANSEN, L. F., 1961, *Phys. Rev. Letters*, **6**, 13.
- BJORKLUND, F. E., and FERNBACH, S., 1958, *Phys. Rev.*, **109**, 1295.
- CASSELS, J. M., and LAWSON, J. D., 1954, *Proc. Phys. Soc. A*, **67**, 125.
- EASLEA, B., 1961, *Proc. Phys. Soc.*, **78**, (next paper).
- FREMLIN, J. H., HARDY, W., and SHAYLOR, H. R., 1959, *J. Sci. Instrum.*, **36**, 390.
- FULMER, C. B., 1959, *Phys. Rev.*, **116**, 418.
- GLASSGOLD, A. E., CHESTON, W. B., STEIN, M. L., SCHULTZ, S. B., and ERICKSON, G. W., 1957, *Phys. Rev.*, **106**, 1207.
- GLASSGOLD, A. E., and KELLOGG, P. J., 1958, *Phys. Rev.*, **107**, 1372.
- GREENLEES, G. W., KUO, L. G., and PETRAVIC, M., 1957, *Proc. Roy. Soc. A*, **243**, 206.
- GREENLEES, G. W., and ROLPH, P. M., 1960, *Proc. Phys. Soc.*, **75**, 201.
- GOMES, L. C., 1959, *Phys. Rev.*, **116**, 1226.
- GOODING, T. J., 1959, *Nucl. Phys.*, **12**, 241.
- HINTZ, N. M., 1957, *Phys. Rev.*, **106**, 1201.
- KIKUCHI, K., 1959, *Nucl. Phys.*, **12**, 305.
- LEWIS, A. D., and COLLINGE, B., 1953, *Rev. Sci. Instrum.*, **24**, 113.
- MELKANOFF, M. A., NODVIK, J. S., SAXON, D. S., and WOODS, R. D., 1957, *Phys. Rev.*, **106**, 793.
- MEYER, V., EISBERG, R. M., and CARLSON, R. F., 1960, *Phys. Rev.*, **117**, 1334.
- MEYER, V., and HINTZ, N. M., 1960, *Phys. Rev. Letters*, **5**, 207.
- NODVIK, J. S., and SAXON, D. S., 1960, *Phys. Rev.*, **117**, 1539.
- ROSEN, L., and BROLLEY, J. E., 1958, *Proc. Second U.N. Int. Conf. on the Peaceful Uses of Atomic Energy*, **14**, 116.
- SAXON, D. S., and WOODS, R. D., 1954, *Phys. Rev.*, **95**, 577.
- SHAPIRO, M. M., 1958, *Handb. d. Phys.*, **45**, 361 (Berlin: Springer).
- SHAW, G. L., 1959, *Ann. Phys.*, N.Y., **8**, 509.
- SLAUS, I., and ALFORD, W. P., 1958, NYO Report 8059, Rochester University.
- WALL, N. S., and WALDORF, W. F., 1957, *Phys. Rev.*, **107**, 1602.

Proton Scattering by Copper at 10 Mev

By B. R. EASLEA†

Institute for Theoretical Physics, University of Copenhagen, Denmark

Communicated by G. E. Brown; MS. received 31st May 1961

Abstract. An optical model analysis is given of the experimental data of Hintz at 9.75 Mev and of Greenlees *et al.* at 9.30 and 9.47 Mev on the scattering of protons by natural copper. A sufficiently general form factor for the imaginary part W of the optical potential is used such that W can have a maximum value lying in any desired region of the nucleus. It is found that the absorption must be peaked at the surface of the nucleus in order to fit not only the polarization and differential elastic cross section, but at the same time to give the correct magnitude of the total reaction cross section. The available experimental data do not at present allow the determination of how much absorption occurs at the centre of the nucleus or whether the maximum of W should lie slightly beyond the half-way radius of the real part of the optical potential.

§ 1. INTRODUCTION

SEVERAL calculations (Verlet and Gavoret 1958, Oda and Harada 1959, Shaw 1959, Gomes 1959) have been carried out to determine the magnitude and radial dependence of the imaginary part W of the optical potential. These calculations have predicted W to have a smaller value at the centre of the nucleus than determined empirically by optical model analyses which use only a volume absorption, i.e. a radial dependence for W given by the Saxon-Woods form factor

$$f(r) = \frac{1}{1 + \exp [(r-R)/a]}. \quad \dots\dots (1)$$

On the other hand none of the theoretical predictions agrees with such a radial distribution. Their prediction is rather that in the surface region W first rises to a maximum value some two or three times greater than its value at the centre of the nucleus before finally falling to zero far enough outside the surface. The calculations assume a nucleon density distribution given by $f(r)$ and predict the peaking of W to take place at, or slightly beyond, the half-way radius R .

Now although one or two of the simplifying approximations made for the surface region in the calculations cannot be justified (Gomes 1959, Weisskopf 1959), nevertheless it is usually assumed that they ought at least to give some guide to the radial dependence of W and accordingly we have chosen a form factor for W in our phenomenological investigations which allows W to follow, if necessary, such a radial dependence.

† The greater part of this work was done while the author was a research student in the Department of Physics, University College London.

We may note here that Björklund *et al.* (Björklund and Fernbach 1958, Björklund, Fernbach and Sherman 1956) have carried out an analysis of elastic scattering and polarization data over a wide range of E and A using either pure volume absorption or pure surface (Gaussian form factor). Their conclusion was that surface absorption seems to fit the available data slightly better up to energies as high as 100 mev. Now a suitable optical model potential must at the same time fit the total inelastic scattering and, with the measurement of such reaction cross sections, it becomes possible to decide quite definitely between the two kinds of radial distribution.

With this consideration in mind we have attempted to fit the available experimental data on proton scattering by natural copper in the energy range 9–10 mev, choosing this particular nucleus and energy region for several reasons. Firstly, the copper nucleus is heavy enough so that compound elastic scattering should be small and the (p, n) thresholds for ^{63}Cu and ^{65}Cu , 4.21 and 2.16 mev respectively (Marion and Fowler 1960), are both well below the energy region of 9–10 mev. Hence one of the main decay channels of the compound nucleus is not blocked. (The author has found that the elastic scattering of protons by ^{58}Ni at approximately 9.5 mev has too much scattering at backward angles to be fitted by the optical model. This is undoubtedly caused by compound elastic scattering since the incident proton energy is only just on the isotope's (p, n) threshold of 9.46 mev. On the other hand, the evidence is that scattering by ^{60}Ni at this energy, (p, n) threshold 7.03 mev, can be fitted much better by the optical model.†) Secondly, the copper nucleus is not deformed so that one can deal with spherical potentials. Finally, its Coulomb barrier is not so high as to prevent protons of low angular momentum from getting into the nucleus at the energies we consider, but is sufficiently high so that, together with the centrifugal barrier, it prevents those of high angular momentum from penetrating. Thus the scattering is very sensitive to the details of the nuclear surface and particularly to the amount of absorption at the surface.

§ 2. THE OPTICAL POTENTIAL AND ITS USE

The optical potential we have used may be written as

$$\begin{aligned} \hat{V}(r) = & -Vf_1(r) - iW \left\{ k f_2(r) - n \frac{df_2(r)}{dr} \right\} \\ & + \left[-\frac{l}{l+1} \right] a_0^2 \frac{1}{r} \left\{ v \frac{df_1(r)}{dr} + iw \frac{df_2(r)}{dr} \right\}, \quad a_0 \equiv 1 \text{ fermi,} \quad \dots (2) \end{aligned}$$

where $f_1(r)$ and $f_2(r)$ may contain different parameters, i.e. $R_1 \neq R_2$ and $a_1 \neq a_2$. The Coulomb potential is obtained by solving Poisson's equation assuming a charge density proportional to $f_1(r)$. V , W , v and w are the absolute magnitudes of the potentials such that $-V$ is an attractive potential, $-iW$ an absorptive one, while the spin up potential ($J = L + \frac{1}{2}$, upper half of square brackets) is attractive and the spin down ($J = L - \frac{1}{2}$, lower half) is repulsive. For w the same sign convention is maintained and thus w effectively accounts for any difference in the density of $J = L + \frac{1}{2}$ and $L - \frac{1}{2}$ levels. At the energies considered w has been found to be very small or zero.

† Optical model analyses on new data for ^{58}Ni and ^{60}Ni confirm these suggestions (G. W. Greenlees, private communication, Brown 1961, Greenlees and Rolph 1960).

We write the form factor for $W(r)$ as

$$g_W(r) = kf_2(r) - n \frac{df_2(r)}{dr}. \quad \text{.....(3)}$$

There are three cases of interest. (i) If $n=0$ then $g_W(r)$ has the radial dependence we refer to as volume absorption. (ii) If $k=0$ then $g_W(r)$ is symmetrical about R_2 . We refer to this as surface absorption. (iii) If k is taken as unity and $n \neq 0$ ($n > a_2$) then W is finite at $r=0$ and rises to a maximum at a value of r slightly less than R_2 . This corresponds to the radial dependence of W calculated

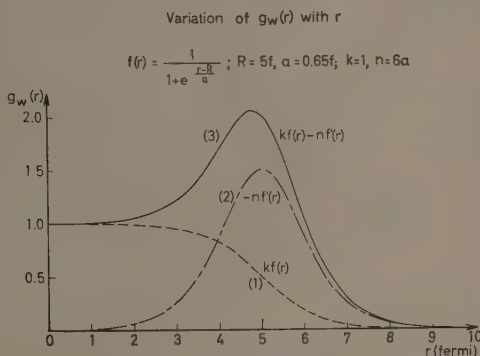


Fig. 1. Curves illustrating the three different radial distributions used for W . Curve (1) shows pure volume absorption, (2) pure surface absorption, and (3) combined volume and surface absorption.

theoretically. Fig. 1 shows $g_W(r)$ plotted for the three different combinations of k and n . They are

$$(1) \ k=1, n=0; \quad (2) \ k=0, n=6a_2; \quad (3) \ k=1, n=6a_2.$$

The third case corresponds to a maximum of W just over twice the value at the centre of the nucleus and lying about $\frac{1}{4}$ fermi inside R_2 .

If we define $W(0) \equiv W_c$, $W(R_2) \equiv W_s$, and $W(r_{\max}) \equiv W_{\max}$ and remember that $R = r_0 A^{1/3}$, we see that $\hat{V}(r)$ may be completely specified by either

$$a_1 a_2 r_{01} r_{02} \text{ (fermi)} \quad VW_c W_s v w \text{ (MeV)} \quad \text{.....(1)}$$

or

$$a_1 a_2 r_{01} r_{\max} \text{ (fermi)} \quad VW_c W_{\max} v w \text{ (MeV)}. \quad \text{.....(2)}$$

If $a_1 = a_2$ and/or $R_1 = R_2$ or r_{\max} , as will usually be the case, then the suffices will be dropped and only one parameter quoted.

The form factor $g_W(r)$ introduces the possibility of using three extra parameters compared with the usual single parameter of pure volume or pure surface absorptive potentials, which is simply the magnitude of W . In general we can have $a_2 \neq a_1$, and we must choose the ratio of W_s/W_c or W_{\max}/W_c as well as the value of R_2 or r_{\max} . However, the advantage of the optical model is that it is able to follow the broad trends of the elastic and polarization data over a wide range of E and A with only regular systematic changes of its, up to now, six

parameters (or seven with Gaussian surface absorption). To fit also the reaction cross section σ_R , both at a particular energy and to follow its energy variation, we do not of course wish to introduce more parameters than seems absolutely necessary. Hence we shall concentrate on keeping $a_2 = a_1$ and R_2 or r_{\max} the same as R_1 . We shall be chiefly interested then in altering the ratio of surface to volume absorption and examining its effect on the elastic scattering and reaction cross section. We have not carried out time-consuming least squares analyses but rather investigated the more general behaviour of the optical model curves. As we shall show, the experimental data are not entirely consistent and while it is possible to draw certain conclusions without a least squares analysis we do not feel that such an analysis could at present decide either between particular choices of form factors or between the experimental data. Furthermore we must suppose that one may not be able to reproduce the data at all angles or the detailed energy variation using such an optical model. In particular the presence of compound elastic scattering, i.e. scattering through compound states, may give rapid energy variations. In such cases we believe that most attention should be paid to fitting data at small angles since the compound elastic scattering is small in this region relative to the scattering by the complex potential which is large at small angles due to coherence from many partial waves. With such theoretical biases we discuss now our analysis of the available experimental data.

§ 3. THE EXPERIMENTAL DATA AND THEIR ANALYSIS

It will be instructive to examine first of all the extensive analysis of Hintz's 9.75 Mev elastic scattering data (Hintz 1957) already performed by Nodvik and Saxon (1960, to be referred to as NS) but with a volume absorption only. Fig. 2 shows both the experimental data (plotted against $\theta_{c.m.}$ as the ratio to the Coulomb

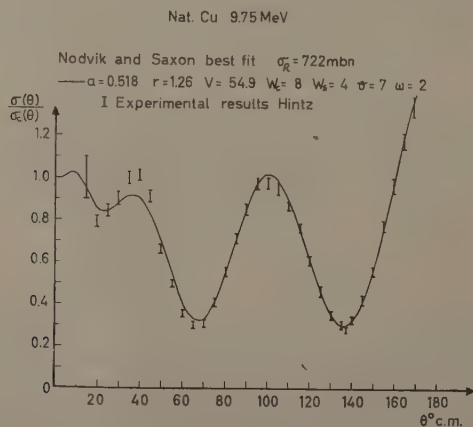


Fig. 2. Curve showing the best fit of Nodvik and Saxon to the elastic scattering data of Hintz.

or Rutherford cross section) and the best fit reported by NS using a radius of $r_0 = 1.26$ fermi. (This curve has been obtained from the author's programme

using the parameters given by NS. The sole difference between the two potentials is due to our use of a Saxon form factor for the charge density distribution.) Nodvik and Saxon noted that, within a range $1.20 \lesssim r_0 \lesssim 1.30$ fermi, almost identical fits to the elastic data could be obtained by making use of the Vr_0^n degeneracy ($n \sim 2.35$) and in Table 1 we reproduce their values relating the

Table 1.

r_0 (fermi)	1.20	1.23	1.26	1.28	1.30
σ_R (mbn)	671	702	725	746	762

total reaction cross section to r_0 . As a consequence of these results Nodvik and Saxon declared that a measurement of σ_R to an accuracy greater than 5% would be necessary to disentangle the Vr_0^n degeneracy. However, we shall see that this ambiguity between V and r_0 is, by itself, insufficient to allow the recently measured values of σ_R to be reached by a volume absorption alone.

In addition, looking more closely at the best fit of NS, we see that for all angles greater than $\theta = 50^\circ$ the fit is excellent but between 20° and 50° there are four experimental points lying above the theoretical curve, the maximum point at 40° being nearly twice the standard deviation above. From our previous considerations this seems somewhat surprising, especially since NS found that there was no combination of parameters which removes the discrepancy between 20° and 50° and at the same time preserves the fit for angles greater than 50° . However, a reasonable fit to the newer *elastic* data of Greenlees and Jarvis (1961) is possible in this region with only a volume absorptive potential. Hence the discrepancy referred to by NS may not be as serious as at first appears. The main point to note from the analysis of NS is that their reaction cross section was 762 mbn with $r_0 = 1.30$ fermi and, since the fit to $\sigma(\theta)$ deteriorated using a larger radius, a value of about 780 mbn effectively represents their maximum reaction cross section. It is this upper bound of 780 mbn to σ_R which is far more worrying.

Values for σ_R have recently been given by Hintz and Meyer (1960) at 9.85 mev, by Albert and Hansen (1961) at the same energy, and by Greenlees and Jarvis at 9.30 mev. Hintz and Meyer measured the cross sections for all reactions in which a charged particle is emitted. When this sum is added to the total (p, n) cross section a lower limit is obtained for σ_R . To this lower limit should be added the values of $\sigma(p, \gamma)$ and $\sigma_{c.e.}$, but Hintz and Meyer claim the former to be of the order of only 1 or 2 mbn and the compound elastic scattering is probably very little greater for the reasons mentioned. (The good optical model fit at backward angles is also an indication of very little compound elastic scattering.) Basing their estimate on rather conflicting measurements for the (p, n) cross sections of ^{63}Cu and ^{65}Cu Hintz and Meyer gave the value of σ_R as 910 ± 60 mbn. Albert and Hansen remeasured these (p, n) cross sections to give σ_R for ^{63}Cu as 875 ± 60 mbn and for ^{65}Cu as 855 ± 60 mbn. A mean value between these isotope cross sections gives the lower bound of σ_R for natural copper as 865 ± 60 mbn.

Greenlees and Jarvis measured σ_R by a somewhat more direct attenuation measurement at the slightly lower energy of 9.30 mev. Essentially they measured

the number of protons absorbed by the copper target by taking the difference in counts between the direct beam with no target absorber present and then with the absorber in place. Their final value for natural copper was $\sigma_R = 930 \pm 70$ mbn. Thus the two measurements of Greenlees and Jarvis and Hintz *et al.* agree within the errors quoted although one might expect σ_R to rise as E increases since the protons are better able to penetrate the Coulomb barrier.

These two values for σ_R of 865 mbn at 9.85 mev and 930 mbn at 9.30 mev show the theoretical upper bound of 780 mbn for σ_R using only volume absorption to be low. For the moment we take the lower value of 865 mbn in analysing Hintz's data and see what can be done to improve matters.

In Fig. 3 we again show the best fit of NS (curve I) as well as one attempt, still using only volume absorption, to fit the forward data better (curve II).

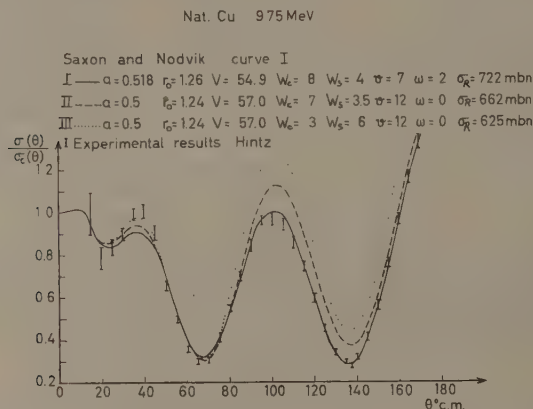


Fig. 3. Curves illustrating the effect of introducing surface absorption on the elastic scattering and reaction cross sections.

However the fit at other angles is destroyed and a decrease in σ_R results. It does not seem possible to increase σ_R for the value of r_0 taken by using pure volume absorption and at the same time to maintain or improve the fit to the elastic data. Hence we introduce a surface absorption (curve III) given by $W_c=3$, $W_s=6$ mev; all other parameters are the same as for curve II. The effect is striking. With the sole exception of the minimum at 70° the elastic scattering is everywhere enhanced, and in particular the maximum at 40° rises to within the experimental limits. But corresponding to the increase in $\sigma(\theta)$ is a large decrease in σ_R from 662 to 625 mbn. At first sight the situation does not look encouraging. We have achieved a fit at forward angles only to lose it elsewhere and we have decreased σ_R when a large effect in the opposite direction is desired. However, since the increase in $\sigma(\theta)$ and the decrease in σ_R are caused solely by putting the absorption at the surface we see that this procedure alone is equivalent to increasing the reflectivity of the absorptive surface. To compensate for this we ought to increase the diffuseness of both real and imaginary surfaces ($a_1=a_2$) both to increase σ_R and to restore the elastic fit at backward angles. Fig 4 (curve I) shows that a large increase from $a=0.5$ to 0.6 fermi is necessary and the

magnitude of V has to be decreased from 57 to 54 MeV to compensate for the increased range of the potential.

This interplay between the diffuseness and the distribution of W brings about welcome improvements. Curve I shows that the fit to $\sigma(\theta)$ is now everywhere

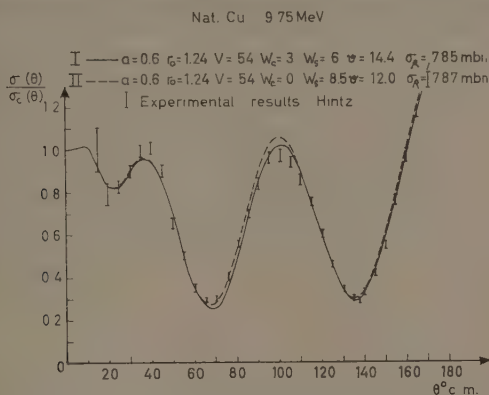


Fig. 4. Two fits to Hintz's elastic data with the absorption peaked at the nuclear surface. Note the increase in σ_R .

very good (note the forward angle fit between 20° and 50°) and, even better, the value of σ_R has increased from 625 to 785 mbn, a value some 70 mbn over an inferior fit to $\sigma(\theta)$ obtainable with only volume absorption. Curve II shows the effect of putting all the absorption at the surface. Both the elastic fit and the value of σ_R are comparable to those of curve I. Provided then that the absorption is peaked at the surface it is evident that the fit to both $\sigma(\theta)$ and σ_R can be improved.

However, while a least squares analysis could now be used to improve even further the fit to $\sigma(\theta)$ we must note that σ_R is still some 80 mbn or so short of the

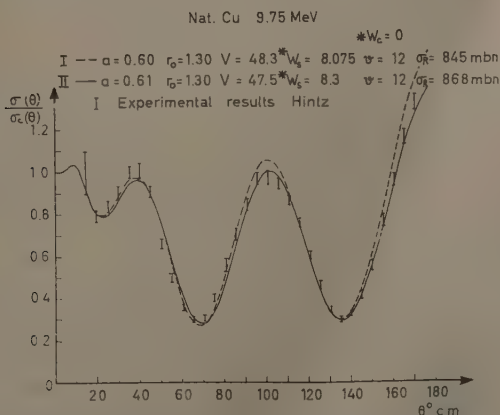


Fig. 5. Two fits to Hintz's elastic data with pure surface absorption and a radius of $r_0=1.30$ fermi. The value of σ_R is now experimentally acceptable.

value given by Albert and Hansen. The only means we have left to push up the value of σ_R is to use the Vr_0^n degeneracy which we achieve by increasing r_0 to 1.30 fermi. This is shown in Fig. 5 with only surface absorption. The fit to $\sigma(\theta)$ remains very good and σ_R has increased from 785 to around 865 mbn. Curve II, with $\sigma_R = 868$ mbn, is perhaps the best overall fit to both $\sigma(\theta)$ and σ_R .

Thus, taking Albert and Hansen's value for the reaction cross section, we see that this extra knowledge both demands the absorption to be peaked at the surface and at the same time removes the Vr_0^n ambiguity by rejecting a radius of 1.24 fermi in favour of the upper limit region around 1.30 fermi.

If however we suppose that σ_R is more in the neighbourhood of 900 mbn (remembering Greenlees and Jarvis's value of 930 ± 70 mbn at 9.30 mev) the question arises as to how we could push up σ_R even further. The fit to $\sigma(\theta)$ deteriorates as r_0 is increased much over 1.30 fermi although this procedure certainly increases σ_R . We can also achieve the same result by increasing a_2 to be about 0.05 fermi greater than a_1 . Finally in Fig. 6 we show the effect of pure

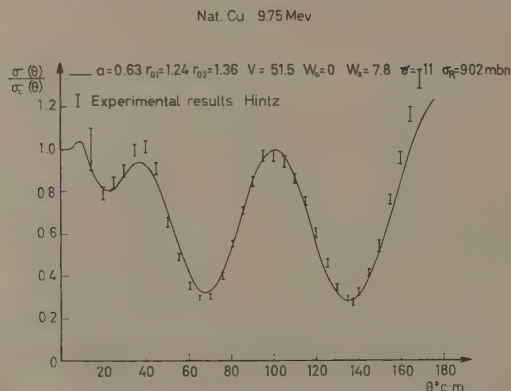


Fig. 6. Effect of extending pure surface absorption beyond the half-way radius used for the real potential.

surface absorption with its peak 0.48 fermi beyond the half-way radius R_1 of V . The diffuseness ($a_1 = a_2$) is now 0.63 fermi and σ_R is up to 902 mbn while the fit to $\sigma(\theta)$ is still acceptable. However, an extra parameter has been introduced and we do not feel that it is worth while to pursue this possibility further until there are strong reasons. In fact we shall show the value of 930 mbn for σ_R given by Greenlees and Jarvis can be obtained quite easily when fitting their corresponding elastic data with a surface absorption.

Before describing the analysis of their data we mention briefly our polarization fits to Rosen's 10 Mev data (Rosen 1959, unpublished Proceedings of the Tallahassee Conference). Curve IV of Fig. 7 shows the best fit of NS which is acceptable at all angles other than between 40° and 70° . However, we prefer to fit this forward angle data better if possible even if it means producing more structure at backward angles. It is reasonable to presume theoretical predictions to show more structure than experimental values especially since the latter quantities are liable to inelastic contamination at backward angles. Thus

we feel curve I probably gives the best all round fit to the data†. It turns out that fits to $\sigma(\theta)$ are not very sensitive to such changes in the value of v .

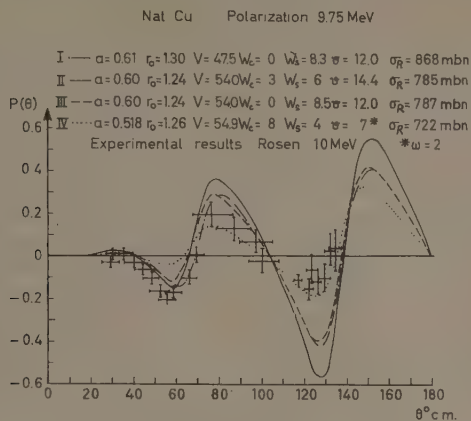


Fig. 7. Typical fits to Rosen's 10 mev polarization data.

In Fig. 8 we have plotted the 9.75 mev elastic scattering data of Hintz together with those of Greenlees, Kuo and Petravic (1957) at 9.37 mev and of Greenlees and Jarvis at 9.47 mev. The two sets of data by Greenlees, Kuo and Petravic and Greenlees and Jarvis agree extremely well with each other between 30 and 120° although there is a rather large difference in the backward angle scattering

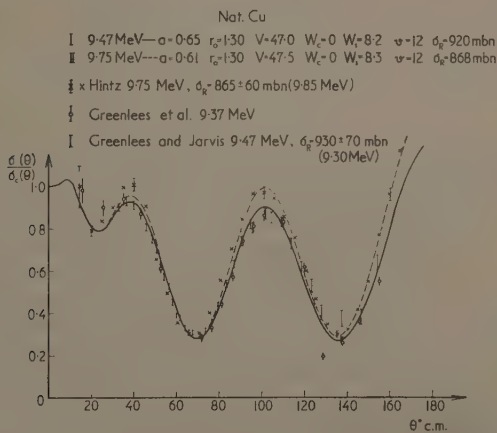


Fig. 8. Comparison of fits to elastic scattering data given by Hintz and by Greenlees, Jarvis *et al.*

† Large polarization at backward angles has been found by Robbins, Grotowski and Greenlees (1961). In fact the polarization predicted using the parameters of curve I, Fig. 8, with $v=12$ mev is in excellent agreement with their data.

beyond 120° . However, as explained earlier, our preference in such cases is to fit the smaller angle scattering and we shall concentrate on the available data between 30° and 120° . As it turns out good fits in this region are about half-way between the two sets of data beyond 120° .

We now compare the experimental data of Greenlees and Hintz between 30° and 120° remembering that one difficulty experienced with Hintz's data was our inability to achieve enough scattering at 40° . In fact the maximum value of $\sigma(\theta)/\sigma_c(\theta)$ obtained using surface absorption and keeping the good elastic fit elsewhere lay at about 0.96 compared with Hintz's value of 1.01 ± 0.03 . Greenlees' data are lower in this region, about 0.92 ± 0.02 , and we shall show that this region can now be fitted very well with surface absorption and almost as well using only volume absorption. Hence this difficulty disappears. Also, however, at 100° Greenlees's results lie again lower than those of Hintz (at 100° Greenlees obtains 0.87 ± 0.025 compared with Hintz's 0.97 ± 0.03). This difference is important because the position of the maximum at 100° determines the amount of diffuseness necessary and on this depends to a large extent the value of the reaction cross section. Because Greenlees's maximum lies lower than that of Hintz, a diffuseness of 0.65 fermi is necessary when surface absorption is used (curve I), and this large diffuseness enables the large reaction cross section of 920 mbn to be reached so easily, combined with an excellent fit to the 9.47 mev elastic data for all angles up to 120° . At the same time the fit to Hintz's 9.75 mev data is likewise good except around 40° (although the theoretical curve is never more than one standard deviation away from the experimental results) and Hintz's value for σ_R of 865 mbn is also fitted well with surface absorption and a diffuseness of 0.61 fermi.

Looking now only at the 9.47 mev data of Greenlees we show in Fig. 9 that volume absorption is completely unacceptable even though the fit to the elastic

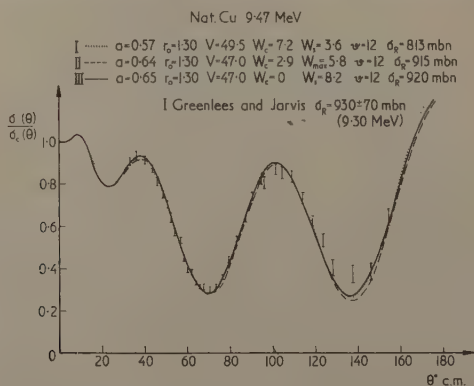


Fig. 9. Three curves illustrating how knowledge of σ_R distinguishes between pure volume absorption and that peaked at the surface.

data is about as good as with surface absorption. This is because σ_R is only 813 mbn which is certainly not high enough for the value of 930 ± 70 mbn by Greenlees and Jarvis. Even if we take the value of 865 ± 60 mbn by Albert and Hansen it is still only just over the lower limit of a lower bound for σ_R . Curve

II shows another good fit to the elastic data using a ratio of surface to volume absorption of 2:1. The maximum of W lies at R_1 and is twice the value of $W(2.9 \text{ MeV})$ at $r=0$. In this case σ_R is 915 mbn. Curve III is the fit with all surface absorption ($\sigma_R=920$ mbn) shown again for comparison. Hence, we see once again that one cannot easily distinguish between a volume and surface absorption fitting only elastic data but that, once reaction cross sections are known, it becomes imperative to place most of the absorption at the surface. Provided the ratio of surface to volume absorption is about 2:1 or greater, equally good fits to both $\sigma(\theta)$ and σ_R can be obtained.

It is of interest to see that the increase in σ_R which results from the combination of surface absorption and large diffuseness comes principally from the partial

Table 2. Partial Wave Contributions to $\sigma_R(l)$ (mbn)

	Volume absorption $W_0=7.2, W_8=3.6$	Volume + surface absorption $W_0=2.9, W_{\max}=5.8$	Surface absorption $W_0=0, W_8=8.2$
$l=0$	66	66	65
$l=1$	159	153	149
$l=2$	273	284	276
$l=3$	217	255	267
$l=4$	75	117	119
$l=5$	22	35	38
$l=6$	1	4	5
$l \geq 7$	0	1	1
σ_R (total)	813	915	920

waves $l=3$ and 4. This is shown in Table 2 where we give the partial wave contributions to σ_R for the three curves of Fig. 9.

§ 4. CONCLUSION

In analysing the available experimental data for protons scattered by natural copper in the energy range 9–10 MeV we have been interested mainly in the changes necessary in the optical potential, if any, which have to be made when fits to σ_R are attempted at the same time as the more usual fits to $\sigma(\theta)$. We found in fact that fits to $\sigma(\theta)$ are not very sensitive to the distribution of W in the nucleus but that fits to σ_R demand W to be peaked in the surface region.

It is difficult to say anything more definite than this. Fits to both σ_R and $\sigma(\theta)$ with either a ratio of surface to volume absorption of 2:1 or with all surface absorption seem equally good. However, since we know theoretically that some absorption does take place well inside the nucleus it is reasonable to assume that the former radial dependence is the more appropriate one. This then agrees with the distribution of W predicted theoretically in the surface region.

The disagreement between the elastic data of Hintz and Greenlees *et al.* seems too great to be due to an energy difference of about 0.3 MeV. Preliminary data by Meyer and Benevise (private communications) in this energy range also appear to be somewhat conflicting in the heights of the two maxima at 4° and 100° . For a more thorough analysis it would be desirable for the elastic data to

agree and for the experimental errors in σ_R to be reduced if possible. For example, consider a possible fit to both Hintz's elastic data and the upper limit of approximately 1000 mbn for σ_R given by Greenlees and Jarvis. Then the difficulty experienced in reaching a value for σ_R as high as 900 mbn makes such a fit appear extremely improbable even with all surface absorption extended beyond the half-way radius of V (Fig. 6). On the other hand if we take the lower limit of 800 mbn as given by Albert and Hansen and try to fit Greenlees' elastic data, then in fact we could do so using only volume absorption. While neither of these extreme cases seems likely the possibility indicates how welcome further experimental clarification would be. If however we take σ_R to lie between 850 and 950 mbn and the elastic data to lie somewhere between those of Hintz and Greenlees *et al.* then the conclusion is unavoidable that W must be concentrated at the surface of the copper nucleus.

ACKNOWLEDGMENTS

It is a pleasure to thank Professor G. E. Brown for suggesting this investigation and for his continual interest and guidance. My thanks are due also to Professor Sir Harrie Massey, Dr. G. W. Greenlees, Mr. L. Castillejo, and Professor N. M. Hintz for interesting conversations, to the staff of the University of London Computer Unit for the many facilities provided and to Mr. M. W. Hansen for drawing the figures. Finally I am grateful to the Department of Scientific and Industrial Research for the award of a Research Studentship and to the Institute for Theoretical Physics, Copenhagen, for hospitality during the time in which this paper was written.

REFERENCES

- ALBERT, R. D., and HANSEN, L. F., 1961, *Phys. Rev. Letters*, **6**, 13.
 BJÖRKLUND, F., and FERNBACH, S., 1958, *Phys. Rev.*, **109**, 1295.
 BJÖRKLUND, F., FERNBACH, S., and SHERMAN, N., 1956, *Phys. Rev.*, **101**, 1832.
 BROWN, G. E., 1961, *Proc. 1960 Int. Conf. on Nuclear Structure, Kingston, Canada*.
 GOMES, L. C., 1959, *Phys. Rev.*, **116**, 333.
 GREENLEES, G. W., and JARVIS, O. N., 1961, *Proc. Phys. Soc.*, **78**, 1275.
 GREENLEES, G. W., KUO, L. G., and PETRAVIC, M., 1957, *Proc. Roy. Soc. A*, **243**, 206.
 GREENLESS, G. W., and ROLPH, P. M., 1960, *Proc. Phys. Soc.*, **75**, 201.
 HINTZ, N. M., 1957, *Phys. Rev.*, **106**, 1201.
 HINTZ, N. M., and MEYER, V., 1960, *Phys. Rev. Letters*, **5**, 207.
 MARION, J. B., and FOWLER, J. L., 1960, *Fast Neutron Physics*, Chapter I.D. (New York: Interscience).
 NODVIK, J. S., and SAXON, D. S., 1960, *Phys. Rev.*, **117**, 1539.
 ODA, N., and HARADA, K., 1959, *Progr. Theor. Phys., Japan*, **21**, 261.
 ROBBINS, A. B., GROTHOWSKI, K. A., and GREENLEES, G. W., 1961, *Proc. Rutherford Jubilee Conf., Manchester* (London: Heywood).
 SHAW, G. L., 1959, *Ann. Phys., N.Y.*, **8**, 509.
 VERLET, L., and GAVORET, J., 1958, *Nuovo Cim.*, **10**, 505.
 WEISSKOPF, V. F., 1959, *Suppl. Progr. Theor. Phys.*, **11**, 52.

On the Reaction $\text{Pt}(n, \alpha)\text{Os}^\dagger$

By M. W. CRESSWELL AND R. R. ROY

Laboratories of Nuclear Physics, College of Chemistry and Physics,
Pennsylvania State University, University Park, Pennsylvania

MS. received 20th March 1961, in revised form 14th July 1961

Abstract. The reaction $\text{Pt}(n, \alpha)\text{Os}$ has been investigated by a nuclear emulsion technique, using the thermal neutron flux of the Pennsylvania State University reactor. A semi-empirical range-energy relationship has been developed for α -particles in platinum and has been used for the evaluation of data. Two groups of alpha particles have been observed with certainty, corresponding to Q -values 6.9 ± 0.3 Mev, and 8.5 ± 0.3 Mev and have been identified with reactions $^{194}\text{Pt}(n, \alpha)^{191}\text{Os}$ and $^{195}\text{Pt}(n, \alpha)^{192}\text{Os}$ respectively. A probable group of alpha particles corresponding to Q -value 12.1 ± 0.3 has been associated with the reaction $^{193}\text{Pt}(n, \alpha)^{190}\text{Os}$.

§ 1. INTRODUCTION

THE aim of the present investigations was to establish the existence of (n, α) reactions for five isotopes occurring in natural platinum by the bombardment with thermal neutrons. The available mass data (Wapstra 1958) for platinum and osmium indicate positive Q -values for (n, α) reactions.

§ 2. EXPERIMENTAL DETAILS

The Pennsylvania State University reactor provided the thermal neutron flux. The natural platinum targets used in the experiment consisted of foils sandwiched between $400\ \mu$ Ilford G5 electron sensitive emulsions. The electron sensitive plates were used in order to detect any beta particles originating from the same point as an alpha particle in the emulsion and would thereby aid in establishing a reaction. In the interests of resolution of the different Q -values, the platinum foil was chosen as thin as possible. However, consideration of the Coulomb barrier indicated a relatively low reaction cross section, and a compromise had to be reached as regards the minimum number of observable events acceptable for measurement. This number was limited by the fact that gamma radiation which blackens the plates was also present in the thermal neutron flux. Consideration of these factors and preliminary trial exposures indicating that a foil thickness of $2.54\ \mu$ was about the optimum under the existing conditions. The plates were placed inside a lead container and exposed for one minute in front of the thermal column, the reactor operating at a power level of 1 kw.

§ 3. MEASUREMENTS AND CALCULATIONS

The plates were examined after development with Leitz Ortholux microscope, By calibrating the microscopes and determining the emulsion shrinkage factors, the ranges R corresponding to energies E_1 (see Fig. 1), of over 1300 alpha particle

† Work supported by U.S. Atomic Energy Commission.

tracks were measured. Only those tracks which entered the emulsion from the surface were taken to be originating in platinum and were considered for measurements. The angles which each track made with the surface of the emulsion were similarly determined.

With this information, the energy E_2 which each particle had or would have had at the centre of the foil, on the trajectory defined by the microscope measurements, was calculated. It was intended to determine the different Q -values by taking the values of E_2 at which peaks in the E_2 spectrum occurred. Particles with E_2 values near to one of these peaks would in general correspond to their being produced in the immediate vicinity of the centre of the foil.

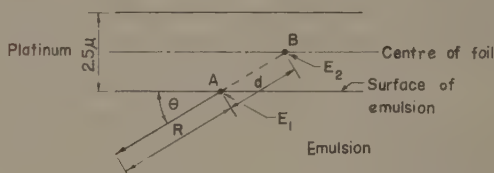


Fig. 1. Schematic representation of the path of an alpha particle.

To determine the energy E_2 it was necessary to develop a range-energy relation for alpha particles in platinum. The passage of a heavy particle through matter is described by the well known relation (Evans 1955):

$$-\frac{dE}{ds} = \frac{4\pi e^4 z^2}{m_0 v^2} NZ \log \left(\frac{2m_0 v^2}{I} \right) \quad \dots\dots (1)$$

where m_0 and e are the electronic mass and charge, ze the charge of the particle, Z the atomic number of the absorber, N the number of atoms per unit volume of the absorber, and I the average excitation potential. The above expression is valid for $2zZ/137\beta \ll 1$ and $\beta \gg Z/137$. By integrating and substituting the parameter values appropriate to the description of the passage of an alpha particle through platinum, Eqn (1) becomes

$$R = 1.084 \text{Ei} (\log 0.470 E^2) \quad \dots\dots (2)$$

where R microns is the range of an α -particle of energy E Mev in platinum and $\text{Ei}(x)$ is the exponential integral

$$\text{Ei}(x) = \int_{-\infty}^x \frac{e^u}{u} du$$

whose values are known (National Bureau of Standards, 1940).

Although the conditions mentioned above are not satisfied for alpha particles of about 10 Mev in platinum, an equation similar to (2) was derived for lead, and the theoretical range values so calculated for α -particles compared favourably with the values given by previous workers (Aron, Hoffman and Williams 1953, Whaling 1958). For this reason, Eqn (2) was taken to be valid for α -particles in platinum.

To determine E_2 a function $K(R)$ was defined by

$$K(R) = \frac{R_{E+1} - R_{E-1}}{R'_{E+1} - R'_{E-1}}$$

where $R_{E \pm 1}$ and $R'_{E \pm 1}$ are the ranges in microns of α -particles of energy $(E \pm 1)$ MeV in emulsion and platinum respectively. The former can be obtained from the data of Rotblat (1951) and the latter from Eqn (2). The function K was constructed empirically in order that once the distance $AB = d$ was determined from the microscope measurements, the equivalent distance Kd , which would represent the distance travelled in the emulsion by an alpha particle between the same two energy limits, E_2 and E_1 , could be obtained. It was found that the function K could approximately be represented by the form $K = 0.0112R + 2.72$ within the limits of R , the range in microns in emulsion of a particle of energy E MeV, which were going to be used. An approach of this type is justified because it is used to determine $E_2 - E_1 = \Delta E$ which is only a small fraction of the energy E_2 .

Accordingly E_2 MeV is the energy of a particle describing a path of length R_2 microns in emulsion where, since K varies only very slowly with R , R_2 is given by

$$R_2 \simeq R + (0.0112R + 2.72)d. \quad \dots (3)$$

The calculation indicated in Eqn (3) was performed for some 1300 tracks measured and the R_2 spectrum obtained.

§ 4. RESULTS AND DISCUSSION

The number of α -particle tracks has been plotted as a function of the corrected range, R_2 , for a total of over 1300 events as shown in Fig. 2.

It can be noted from the figure that there are two maxima of different intensities corresponding to $R_2 = 34.1 \mu$ and 43.9μ . A probable third group of much smaller intensity is observed at $R_2 = 77.8 \mu$. The Q -values derived from the values of R_2 at the maxima are given in the Table together with the values obtained from mass data.

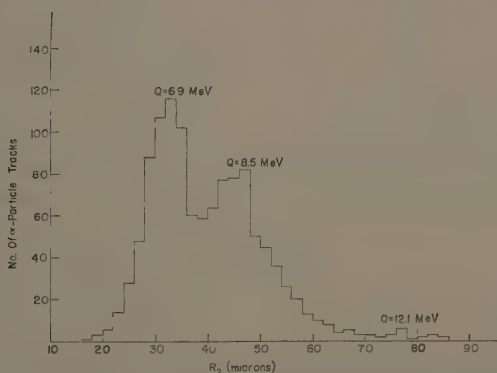


Fig. 2. Corrected range spectrum of 1300 alpha particle tracks.

The experimental Q -values agree well, within experimental error, with the values obtained from mass data. There is no evidence of a peak around 5.24 MeV corresponding to the target nucleus ^{196}Pt at 25.4% relative mass abundance. This, however, can be explained by examining the range-energy relation (2) together with the following fact: in order to make a measurement of the length R of any

Q-values obtained from Experiments and from Mass Data

Reaction	Mass data <i>Q</i> -value (mev)	Observed <i>Q</i> -value (mev)	Relative mass abundance of target
$^{192}\text{Pt}(n, \alpha)^{189}\text{Os}$	9.40	no evidence	0.78%
$^{192}\text{Pt}(n, \alpha)^{190}\text{Os}$	12.12	12.1 ± 0.3	0.1%
$^{194}\text{Pt}(n, \alpha)^{191}\text{Os}$	7.02	6.9 ± 0.3	32.8%
$^{196}\text{Pt}(n, \alpha)^{192}\text{Os}$	8.39	8.5 ± 0.3	33.7%
$^{198}\text{Pt}(n, \alpha)^{193}\text{Os}$	5.24	no evidence	25.4%

track in the emulsion with tolerable error, the minimum range acceptable for measurement was about 20μ . According to the relation (2), a 5.24 mev particle can travel through no more than 0.95μ of platinum before entering the emulsion with sufficient energy to describe a track at least 20μ long and qualify for measurement. This means that a very small number of these tracks would actually be observed in the experiments. Furthermore, those that were counted would originate from a region close to the emulsion surface of the foil and would consequently be overcorrected for their energy loss. Thus, their E_2 values are not truly representative of the actual *Q*-value.

Additional confirmation of the identification of the 6.9 mev peak with the reaction $^{194}\text{Pt}(n, \alpha)^{191}\text{Os}$ was obtained from the fact that the ^{191}Os nucleus is not stable but decays by the emission of a 0.143 mev electron (Rey and Baro 1958). In some fifty cases, beta particle tracks of about this energy were observed originating from the same point as alpha particle tracks. The R_2 spectrum of these particular α -particle tracks indicated fairly well that particles concerned were associated with the experimental *Q*-value of 6.9 mev.

The decay of excited states of medium and heavy elements has been well studied and has been compiled in many review articles (National Research Council Nuclear Data Sheets, 1961, Stroninger, Hollander and Seaborg 1958). No gamma rays of the right energy have been reported that suggest that, within the limits of experimental error, the observed peaks are due to transitions other than to the ground states of different osmium end-products.

The 9.39 mev *Q*-values were not observed in the experiment which might be due to low abundance, 0.78%, of the isotope ^{192}Pt . However, there is an indication of a small peak for the target ^{193}Pt although its mass abundance is of the order of only 0.1%.

REFERENCES

- ARON, W. A., HOFFMAN, B. G., and WILLIAMS, F. C., 1953, *High Energy Particle Data*, UCRL-2426.
- EVANS, R. D., 1955, *The Atomic Nucleus* (New York: McGraw-Hill).
- NATIONAL BUREAU OF STANDARDS, 1940, *Tables of Sine, Cosine and Exponential Integrals*, vol. 2 (Washington D.C.: National Bureau of Standards).
- NATIONAL RESEARCH COUNCIL, WASHINGTON, *Nuclear Data Sheet*, 1961.
- REY, P., and BARO, G. B., 1958, A/CONF. 15/P/1570 (Buenos Aires: Comisión Nacional de Energía Atómica).
- ROTLAT, J., 1951, *Nature, Lond.*, **167**, 550.
- STRONINGER, D., HOLLANDER, J. M., and SEABORG, G. T., 1958, *Rev. Mod. Phys.*, **30**, 585.
- WAPSTRA, A. H., 1958, *Handb. d. Phys.*, **38**, 1, 10.
- WHALING, W., 1958, *Handb. d. Phys.*, **34**, 193.

Multiplet Production by X-rays

By R. R. ROY, C. H. BLANCHARD, E. H. WEBB, H. S. SANDHU
AND R. C. MOHANTY

Nuclear Physics Laboratory, Pennsylvania State University, University Park, Pennsylvania

MS. received 23rd June 1961

Abstract. Ilford G5, 400μ thick nuclear emulsion plates were bombarded by a hardened x-ray beam of energy 5–90 mev. Altogether 54 433 fields of view were examined, the volume of each field of view being $120\mu \times 150\mu \times 220\mu$. A total of 21 887 pairs, 1935 triplets, 106 quartets, 10 quintets and one sextet have been observed. Frequency of occurrence of multiplets, (quartets, quintet and sextet), together with the energy distribution of the small energy partners of the multiplets have been presented. Possible explanations of the origin of multiplets have been discussed.

§ 1. INTRODUCTION

A STUDY of the electron-positron pair and triplet production in nuclear emulsion is being completed at this laboratory. Ilford G5 nuclear emulsion, 400μ thick, was exposed to a hardened x-ray beam from the National Bureau of Standards electron synchrotron. The incident photon spectrum extended from 5 to 90 mev. While these plates were being scanned in search of pairs and triplets, there were observed events in which four, five and six electron tracks originate from the same point. We refer to these many-track events as 'multiplets'. Some examples are reproduced in Fig. 1 (Plate). There was no magnetic field present, and therefore no way to discriminate between positron and electron tracks. In every one of these events most of the energy is shared between two fast particles and the remaining tracks correspond to electrons with energy less than 0.5 mev. There is good reason to believe that the events in question are not examples of multiple pair production, but consist of multiple ionization in single pair production. The ratios of production; pair/triplet/quartet/quintet/sextet, fluctuate strikingly little around a mean value of about 12.5, for the mixture of elements in G5 emulsion for which the average value of Z is 13.3 and the root mean square value of Z is 21.5.

§ 2. RESULTS

Altogether 54 433 fields of view of the microscopes were examined; the volume of each field of view was $120\mu \times 150\mu \times 220\mu$. In the volume of emulsion examined there were observed 21 887 pairs, 1935 triplets, 106 quartets, 10 quintets and 1 sextet.

Fig. 2 gives the distribution of the *sum* of the kinetic energies of the *low* energy tracks of each event. The abscissa is the sum of the two lowest energies for quartets, three lowest energies for quintets and four lowest energies for the sextet.

The ordinate is the number of events in each total-low-energy bin. No distinction is made between different multiplicities or between different photon energies in this figure.

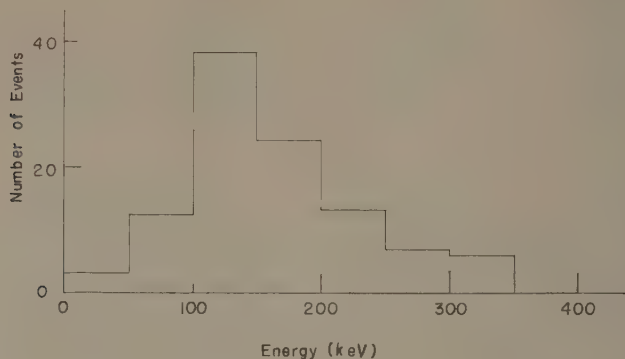


Fig. 2. The ordinate gives the number of events whereas the abscissa represents the sum of the kinetic energies of the small energy partners of multiplets.

§ 3. DISCUSSION

It is necessary to show that the multiplets are not due to the chance occurrence of two or more small energy background electron tracks born at the origin of a pair or of a triplet. Two independent studies were made to estimate such a chance occurrence. The first method consisted of scanning about 900 fields of view from different plates. The aim of this experiment was to determine the number of small energy electrons, pairs and triplets born per field of view of the emulsion and to calculate the probability of a false multiplet due to the chance occurrence of two or more small energy electrons at the origin of a pair or of a triplet. The average number of small energy electrons, pairs and triplets observed per field of view were respectively 31.20, 0.26 and 0.02. With these data it can be shown that the probability of small energy electrons born within 0.4μ (average grain size) of a pair or a triplet thereby giving a false multiplet is indeed very small.

The second method of estimating the chance occurrence of a false multiplet consisted in counting the number of small energy electron tracks ending at the origin of a pair or of a triplet. This number will then give the actual false multiplet, since the probability of a small energy track's ending at the origin of a pair or of a triplet is the same as the probability of its being born at the origin. Some 500 pairs and 100 triplets were specially studied in search of false multiplets. None was observed.

It was therefore concluded that the multiplets observed in the experiment represented the real events.

It seems unlikely that the events under discussion involve multiple pair production, because the ratio of the double pair production cross section to that for single pair production is expected† to be of the order of $(e^2/\hbar c)^2 \simeq (19\,000)^{-1}$.

† W. Heitler (*The Quantum Theory of Radiation*, 3rd edition; Oxford, 1954) gives an estimate on p. 228 which differs from that quoted above. Heitler's incorrect estimate seems to result from an invalid extrapolation (originally suggested by J. E. Hooper and D. T. King, *Phil. Mag.*, **41**, 1194, 1950) of the 'substitution law' to multiple events. Multiple pair production is expected to be even rarer than emphasized by Heitler.

On this estimate we should have seen only about $22\,000/19\,000 \simeq 1$ quartet, whereas we have 106 quartets, an excess of two orders of magnitude. One can perhaps get some feeling for the nature of the effects involved here as follows. Suppose that a pair production takes place in the field of one of the atomic electrons in the K shell, and that the atomic electron thereby acquires a recoil momentum q . The electron will have left the K shell, with a kinetic energy of the order of $E_1 = q^2/2m$, in a time of the order of $T = (a_{\text{Bohr}}/Z)/(q/m)$. Its removal will constitute a pulse of electromagnetic field containing frequencies up to $\omega = 1/T$, and may thus transfer energies as high as $E_2 = (Zq\hbar)/(ma_{\text{Bohr}})$ to the other K electron. For $q \simeq mc$ we have $E_1 \simeq \frac{1}{2}mc^2$ and $E_2 \simeq (Z/137)mc^2$. For the highest Z in emulsion, these energies are seen to be comparable with the observed quartet recoil energies. (This argument is evidently very rough, neglecting relativistic corrections and binding energies, and is intended only as an order-of-magnitude interpretation.)

ACKNOWLEDGMENTS

The authors are indebted to H. W. Koch and J. M. Wyckoff for giving facilities of exposure of the plates with the National Bureau of Standards electron synchrotron and for their help and advice during the exposure. We wish to thank the microscopists, Dorothy Groner, Sylvia Levenson, Judith Loftin, Marie Ventrice and Beverly Wilson for their help in scanning the plates.

Isotope Shift in the CdI Resonance Line λ 2288 Å

By F. M. KELLY AND E. TOMCHUK

Department of Physics, University of Manitoba, Winnipeg, Canada

MS. received 19th June 1961

Abstract. The isotope shifts in the singlet resonance line of CdI have been observed. The line was excited by electron bombardment of an atomic beam and the high resolution was obtained with a Fabry-Pérot interferometer. The shifts measured in this line (λ 2288 Å) are compared with those previously measured in the intercombination resonance line (λ 3261) to show that the specific mass effect is small. Comparisons are made with similar measurements in magnesium, zinc, and strontium.

§ 1. INTRODUCTION

THERE are two causes of isotope shift in atomic spectra, the mass effect and the field or volume effect. In the light elements the observed shifts can be accounted for by the mass effect while in the heaviest elements the shifts are attributed to the field effect. The mass effect can conveniently be separated into the normal mass effect and the specific mass effect (Hughes and Eckart 1930, Bartlett and Gibbons 1933, Vinti 1939, 1940). The normal mass effect is easily determined from a simple reduced mass calculation and thus can be taken into account in all atomic energy levels. The specific mass effect, on the other hand, requires the computation of a number of integrals involving the products of radial wave functions of the atomic levels, and, except in the case of helium, has achieved only moderate success. Both mass effects decrease with increasing atomic number but it is not certain where the specific mass effect can be neglected. It is possible, however, to make an experimental estimate of the specific effect by comparing the shifts in a pair of lines. Such a pair is the singlet and intercombination resonance lines of cadmium.

The singlet resonance line λ 2288 ($5s^2\ ^1S_0-5s5p\ ^1P_1$) and the intercombination resonance line λ 3261 ($5s^2\ ^1S_0-5s5p\ ^3P_1$) have a common lower level. The upper levels arise from the same ($5s5p$) electronic configuration. The field effect shift of either a $p_{1/2}$ or a $p_{3/2}$ electron is small compared to the shift due to an s electron so that the shift arising from the field effect should be the same in both these lines. The specific mass effect, however, predicts that the shifts of these two lines should differ by an amount depending only on $K(5s, 5p)$, one of the specific mass integrals in the notation of Bartlett and Gibbons (1933).

Isotope shifts in λ 3261 have already been reported (Kelly and Tomchuk 1959). The shifts observed in λ 2288 are reported here, and are compared with the shifts in λ 3261. Similar comparisons in lighter elements have been made for zinc (Crawford *et al.* 1950), magnesium (Kelly 1957) and strontium (Hughes 1957).

§ 2. EXPERIMENTAL ARRANGEMENTS

The singlet resonance line was excited in the atomic beam source used for the study of $\lambda 3261$. The collimation of the beam was such that the calculated source line width was 0.002 cm^{-1} . The line was isolated with a Hilger medium quartz spectrograph and the high resolution was supplied with a quartz Fabry-Pérot interferometer mounted externally to the spectrograph. A 10 cm spacer was used. The reflectivity of the aluminium films at $\lambda 2288 \text{ \AA}$ was estimated to be 80% from the measured transmission coefficient in the blue and the curves of Burridge, Kuhn and Pery (1953). The patterns were recorded on Ilford QI and QII plates with exposure times up to two hours.

§ 3. RESULTS

The line $\lambda 2288$ was resolved into three closely spaced components. Twenty-five exposures with structure in two to five orders were measured five times by each of two observers. Microphotometer measurements were not satisfactory due to the curvature of the fringes. The three components are designated A, B and C with A having the highest frequency. The measured separations are

$$\Delta\nu(A, B) = 16.8 \pm 0.3 \times 10^{-3} \text{ cm}^{-1}$$

$$\Delta\nu(B, C) = 12.5 \pm 0.5 \times 10^{-3} \text{ cm}^{-1}.$$

The errors quoted are the average deviations from the mean multiplied by 0.68.

The assignment of component A to a blend of components due to isotopes 110 and 111, component B to a blend of components due to isotopes 112 and 113 and C to isotope 114 is consistent with visually estimated relative intensities.

The unresolved separations of the isotope pairs (110-111) and (112-113) were assumed to be in the ratio found in $\lambda 3261$, and, by Kuhn and Ramsden (1956), in $\lambda 4416$. Then, if we use the relative abundance as a weight factor the separations between even isotopes can be calculated. These calculations give

$$\Delta\nu(110-112) = -17.0 \pm 0.6 \times 10^{-3} \text{ cm}^{-1}$$

$$\Delta\nu(112-114) = -13.2 \pm 1.0 \times 10^{-3} \text{ cm}^{-1}.$$

In this the error has been doubled to allow for the extra uncertainties introduced. We also assumed that the magnetic hyperfine structure in the 1P_1 level is negligible. The negative sign means the lighter isotope has the higher frequency.

A plot of theoretical curves shows that the influence of isotope 116 on the position of isotope 114 is much less than the experimental error.

§ 4. DISCUSSION

The isotope shifts between even isotopes in the singlet ($\lambda 2288$) and the intercombination ($\lambda 3261$) resonance lines may be analysed in a manner similar to that used for the Zn I resonance lines (Crawford *et al.* 1950).

Table 1. Isotope Shift in Cd I (in 10^{-3} cm^{-1})

	2288		3261	
	110-112	112-114	110-112	112-114
Observed shift	-17.0	-13.2	-16.3	-13.5
Normal shift	+ 3.4	+ 3.7	+ 2.7	+ 2.6
Residual shift ($\Delta\nu$)	-20.9	-16.9	-19.0	-16.1
3261-2288 ($\delta(\Delta\nu)$)	+ 1.9	+ 0.8		

The residual shift ($\Delta\nu$) is the observed shift minus the normal mass shift. The differences between the residual shifts are $+1.9 \pm 1.1$ for (110–112) and $+0.8 \pm 1.4$ for (112–114). These two values agree within experimental error and the average is $+1.3 \pm 1.3$.

The difference between the isotope shifts in the triplet and the singlet resonance lines according to the specific mass theory (Bartlett and Gibbons 1933) is

$$\delta(\Delta\nu) \text{ (triplet-singlet)} = -4Rm \left\{ \frac{1}{M_1} - \frac{1}{M_2} \right\} K(ns, np)$$

where R is the Rydberg constant (cm^{-1}), m the electron mass, M_1 , M_2 the nuclear masses ($M_2 > M_1$), and K the specific mass integral which is intrinsically negative. The data for Mg (Kelly 1957), Zn (Crawford *et al.* 1950, Hatley and Littlefield 1958), Sr (Hughes 1957) and Cd for the shifts arising from isotopes differing by two neutrons are summarized in Table 2.

Table 2

n	$\delta(\Delta\nu)$ Triplet-singlet ($\times 10^{-3} \text{ cm}^{-1}$)	$K(ns, np)$
Mg 3	$+57.9 \pm 1.6$	-0.076 ± 0.002
Zn 4	$+10 \pm 1.5$	-0.091 ± 0.014
Sr 5	$+5.6 \pm 1.8$	-0.033 ± 0.024
Cd 5	$+1.3 \pm 1.3$	-0.03 ± 0.03

The value of the specific mass integral $K(ns, np)$ is not very sensitive to the value of the principal quantum number n , and for $n=5$ appears to be decreasing. The factor $\Delta M/M_1 M_2$ in the heavy elements will reduce the resulting specific mass shifts to small values. Consequently in the heavy elements one can expect to obtain specifically nuclear data from the observed isotope shifts.

ACKNOWLEDGMENTS

The research reported here was supported by a grant from the National Research Council of Canada.

REFERENCES

- BARTLETT, J. H., and GIBBONS, J. J., 1933, *Phys. Rev.*, **44**, 538.
 BURRIDGE, J. C., KUHN, H. G., and PERY, A., 1953, *Proc. Phys. Soc. B*, **66**, 963.
 CRAWFORD, M. F., GRAY, W. M., KELLY, F. M., and SCHAWLOW, A. L., 1950, *Canad. J. Res. A*, **28**, 138.
 HATELY, G. F., and LITTLEFIELD, T. A., 1958, *J. Opt. Soc. Amer.*, **48**, 851.
 HUGHES, D. S., and ECKART, C., 1930, *Phys. Rev.*, **36**, 694.
 HUGHES, R. H., 1957, *Phys. Rev.*, **105**, 1260.
 KELLY, F. M., 1957, *Canad. J. Phys.*, **35**, 1220.
 KELLY, F. M., and TOMCHUK, E., 1959, *Proc. Phys. Soc. A*, **74**, 689.
 KUHN, H. G., and RAMSDEN, S. A., 1956, *Proc. Roy. Soc. A*, **237**, 485.
 VINTI, J. P., 1939, *Phys. Rev.*, **56**, 1120.
 ——— 1940, *Phys. Rev.*, **58**, 882.

Rotational Analysis of the E-X System of Silicon Monosulphide

BY R. F. BARROW†, J. L. DEUTSCH†, A. LAGERQVIST‡
AND B. WESTERLUND‡

† Physical Chemistry Laboratory, Oxford University

‡ Institute of Physics, University of Stockholm

MS. received 7th July 1961

Abstract. The rotational analysis of twenty bands of the E-X system of SiS has been carried out. The system arises from a transition $^1\Sigma^+-^1\Sigma^+$, and, unexpectedly, no perturbations have been detected in $E^1\Sigma^+$. Constants (in cm^{-1}) for the state $E^1\Sigma^+$, valid for $0 \leq v \leq 7$ are as follows:

$$T_0 = 41743.8_6, \quad G_v = 406.8_3 \left(v + \frac{1}{2}\right) - 1.95_2 \left(v + \frac{1}{2}\right)^2, \\ B_v = 0.2213_7 - 0.0013_9 \left(v + \frac{1}{2}\right) - 1.7_5 \times 10^{-5} \left(v + \frac{1}{2}\right)^2.$$

It seems probable that the state E is the $^1\Sigma^+$ state arising from the configuration $\dots \pi^3\sigma^2\pi^*$, analogous to the state $B^1\Sigma^+_u$ of the isoelectronic molecule P_2 .

§ 1. INTRODUCTION

PRESENT information about the lower lying electronic states of CO and of similar molecules, such as CS, SiO and SiS, indicates that they arise from the three configurations

$$\dots \pi^4\sigma^2-x^1\Sigma^+ \dots (1)$$

$$\dots \pi^4\sigma\pi^*-^3\Pi_r, ^1\Pi \dots (2)$$

$$\dots \pi^3\sigma^2\pi^*-^1\Sigma^+, ^1\Sigma^-, ^3\Sigma^+, ^3\Sigma^-, ^1\Delta, ^3\Delta. \dots (3)$$

The absorption systems allowed in Hund's cases *a* and *b* are $^1\Pi \leftarrow x^1\Sigma^+$ and $^1\Sigma^+ \leftarrow x^1\Sigma^+$. Rotational analyses of the well-known longest wavelength absorption systems of SiO and SiS have shown that they arise from transitions $^1\Pi \leftarrow ^1\Sigma^+$ (Lagerqvist and Uhler 1953, Barrow 1946), and studies of perturbations in the $^1\Pi$ states (Lagerqvist, Nilheden and Barrow 1952, Nilheden 1955) have provided information about some of the other states which arise from configuration (3).

It was therefore of interest to examine the rotational structure of the second ultra-violet system E-X. For SiO this lies in the Schumann region (Barrow and Rowlinson 1954), but in the case of SiS the most readily observed bands lie between about 2200 and 2500 Å (Vago and Barrow 1946). The present paper is concerned with the rotational analysis of bands of the E-X system of SiS.

Experimental details have already been given. Measurements and analyses were carried out independently in Stockholm and in Oxford.

§ 2. ANALYSIS AND DISCUSSION

All the bands show a simple structure of single R and P branches. Rather surprisingly, by comparison with the $D^1\Pi$ state, no perturbations were detected.

The analyses were straightforward since values of the ground state combination differences $\Delta_2 F''(J)$ were available from earlier work. Constants for the $E^1\Sigma$ state were calculated from those of the ground state, using the relation

$$R(J-1) + P(J) = 2\nu_0 + 2\Delta BJ(J+1) - 2\Delta DJ^2(J^2+1).$$

The results are given in Table 1.

The constants derived in this way for the state $E^1\Sigma^+$ fit well with those obtained for other states believed to arise from the configuration $\dots \sigma^2\pi^3\pi^*$, as may be

Table 1. Constants for Bands of the E-x System of SiS

Band v', v''	$T_{v'}$	$T_{v'}$ mean value	$T_{v'}$ calculated	$B_{v'}$	$B_{v'}$ mean value	$B_{v'}$ calculated
7-1	44481.89	44481.89	44481.98	0.20997	0.20997	0.20996
6-1	102.47	102.40	102.48	0.21165	0.21167	0.21160
6-2	102.30			0.21170		
5-1	43719.19	43719.20	43719.07	0.21321	0.21320	0.21320
5-2	719.24			0.21320		
5-3	719.16			0.21320		
4-1	331.72	331.88	331.76	0.21481	0.21475	0.21476
4-2	331.55			0.21476		
4-3	332.03			0.21476		
4-4	332.37			0.21462		
3-1	42940.61	42940.48	42940.55	0.21621	0.21633	0.21629
3-2	940.42			0.21634		
3-3	940.37			0.21643		
3-4	940.62			0.21628		
2-1	545.04	545.34	545.43	0.21782	0.21779	0.21779
2-2	545.42			0.21781		
2-3	545.47			0.21775		
1-2	146.48	146.45	146.41	0.21925	0.21924	0.21925
1-3	146.43			0.21924		
0-2	41743.86	41743.86	41743.49	0.22067	0.22067	0.22067

(1) The following ground-state constants were used in the calculations: $G_v'' = 749.69 \times (v + \frac{1}{2}) - 2.58(v + \frac{1}{2})^2$, $B_v'' = 0.30363 - 0.00149(v + \frac{1}{2})$; (2) a mean value, $D' = 2.6 \times 10^{-7} \text{ cm}^{-1}$ was used; (3) the calculated values of $T_{v'}$ and of $B_{v'}$ are with $T_0 = 41743.49 \text{ cm}^{-1}$, $G_v = 406.83(v + \frac{1}{2}) - 1.95_2(v + \frac{1}{2})^2$, $B_v = 0.22137 - 0.00139(v + \frac{1}{2}) - 1.7_5 \times 10^{-5}(v + \frac{1}{2})^2$.

Table 2. States of the Configuration $\dots \pi^3\sigma^2\pi^*$

CO				SiS			
State	T_0	ω/ω_x	B/B_x	State	T_0	ω/ω_x	B/B_x
$1^1\Sigma^+$	≤ 66380	≥ 0.48	≥ 0.75	$E^1\Sigma^+$	41915	0.54	0.73
$(1^1\Delta)^+$	≤ 66230	—	≥ 0.83	$1^1\Sigma^-$	≤ 37290	≥ 0.54	≥ 0.70
$e^3\Sigma^-$	64803	0.50	0.66	$F(1^1\Delta)$	37114	0.59	0.75
$d(3^1\Delta)^{\ddagger}$	61824	0.52	0.65	$e^3\Sigma^-$	≤ 35140	≥ 0.54	≥ 0.73
$a'^3\Sigma^+ \ddagger$	55354	0.57	0.70				

\ddagger See references given by Lagerqvist, Nilheden and Barrow (1952).

\ddagger Herzberg and Hugo (1955).

\S Mulliken (1958).

seen from the values given in Table 2. It is probable too that the state E of SiS is analogous to the well-known state $B^1\Sigma_u^+$ of the isoelectronic molecule P_2 (see Table 3).

Table 3.

Molecule	State	T_0	$\omega_e/\omega_e(x)$	$B_e/B_e(x)$
SiS	E $^1\Sigma^+$	41915	0.54	0.73
P_2^\dagger	B $^1\Sigma_u^+$	46943	0.61	0.80
SiS	D $^1\Pi$	35027	0.68	0.88
P_2^\dagger	A $^1\Pi_g$	34515	0.79	0.91

† The data for P_2 are from Douglas and Rao (1958).

At this point some evidence is available for six of the nine electronic states arising from the configurations (1), (2) and (3). Analysis of the visible emission bands of SiS may provide further information, and it might be that a study of the absorption spectrum in the visible region with long paths would reveal the forbidden $^3\Pi-x^1\Sigma^+$ system. Apart from the fact that no state of CO analogous to state E of SiS is yet known, there is no evidence yet to suggest that the lower excited states of SiS are other than similar to those of CO.

REFERENCES

- BARROW, R. F., 1946, *Proc. Phys. Soc.*, **58**, 606.
 BARROW, R. F., and ROWLINSON, H. C., 1954, *Proc. Roy. Soc. A*, **224**, 374.
 DOUGLAS, A. E., and RAO, K. S., 1958, *Canad. J. Phys.*, **36**, 565.
 HERZBERG, G., and HUGO, T. J., 1955, *Canad. J. Phys.*, **33**, 757.
 LAGERQVIST, A., NILHEDEN, G., and BARROW, R. F., 1952, *Proc. Phys. Soc. A*, **65**, 419.
 LAGERQVIST, A., and UHLER, U., 1953, *Ark. Fys.*, **6**, 95.
 MULLIKEN, R. S., 1958, *Canad. J. Chem.*, **36**, 10.
 NILHEDEN, G., 1955, *Ark. Fys.*, **10**, 19.
 VAGO, E. E., and BARROW, R. F., 1946, *Proc. Phys. Soc.*, **58**, 538.

On Perturbation Calculations for the π -Electrons and their Application to Bond Length Reconsiderations in Aromatic Hydrocarbons

By C. A. COULSON AND A. GOŁĘBIEWSKI†

Mathematical Institute, Oxford

MS. received 15th June 1961

Abstract. An alternative method for calculating the atom-atom, atom-bond, bond-bond and other polarizabilities in π -electron molecules, originally due to R. D. Brown, is extended to deal with orbital degeneracy. It is then applied to a new discussion of the bond lengths in certain aromatic hydrocarbons. A simple and partly self-consistent method of calculation is developed, which yields results in satisfactory agreement with recent accurate experimental measurements.

§ 1. INTRODUCTION

ONE of the simplest and relatively powerful methods in quantum chemistry is the LCAO MO theory of π -electrons in planar aromatic hydrocarbons. This method is particularly simple in the Hückel approximation (Hückel 1931, 1932), and all our subsequent theoretical analysis will be in terms of it. Since this standard method is discussed both in papers (e.g. Hückel 1931, 1932, Coulson and Longuet-Higgins 1947 a, b) and in books (e.g. Daudel, Lefebvre and Moser 1959, Coulson 1961) there is no need to do more than recapitulate the notation and a few of the basic equations. Our present paper is concerned with the development of a simple form of perturbation theory within this framework, and its application to the calculation of bond lengths.

The normalized molecular orbital ψ_k of a particular π -electron is approximated, in Hückel's theory, by a linear combination of atomic $2p\pi$ orbitals ϕ_r :

$$\psi_k = \sum_{r=1}^n c_{kr} \phi_r = \mathbf{C}_k^\dagger \boldsymbol{\phi}. \quad \text{.....(1)}$$

In (1) \mathbf{C}_k is a column vector with elements $c_{k1}, c_{k2}, \dots, c_{kn}$; \mathbf{C}_k^\dagger is the transpose of \mathbf{C}_k , and $\boldsymbol{\phi}$ is a column vector with elements $\phi_1, \phi_2, \dots, \phi_n$. The index k enumerates the MO ψ_k , whose energy is ϵ_k . An important concept in this theory is the Hamiltonian matrix \mathbf{H} ; its elements are given by

$$H_{rr} = \int \phi_r^* H \phi_r d\tau = \alpha_r \quad \text{.....(2)}$$

$$H_{rs} = \int \phi_r^* H \phi_s d\tau = \beta_{rs}, \quad r \neq s. \quad \text{.....(3)}$$

It is most frequently assumed in this theory that when dealing with hydrocarbons we may put all Coulomb integrals α_r equal ($\alpha_r = \alpha$ for all r), and all resonance integrals β_{rs} for neighbour carbon atoms equal ($\beta_{rs} = \beta$ for all neighbour

† Now at The Department of Theoretical Chemistry, Jagellonian University, Krakow, Poland.

r, s). The remaining β_{rs} are put equal to zero. We usually take α as the zero of energy and β as the unit in which it is measured.

Let us denote by ξ any perturbation parameter. In a particular case ξ may be a change of one or more Coulomb integrals, or one or more resonance integrals, explicitly or implicitly. Whatever the precise meaning of ξ we have essentially to solve the eigenvalue problem

$$[\mathbf{H}(\xi) - \epsilon_k(\xi)\mathbf{1}]\mathbf{C}_k(\xi) = 0 \quad \dots\dots (4)$$

where

$$\epsilon_k(\xi) = \mathbf{C}_k^\dagger(\xi) \cdot \mathbf{H}(\xi) \cdot \mathbf{C}_k(\xi) \quad \dots\dots (5)$$

$$\mathbf{C}_s^\dagger(\xi) \cdot \mathbf{C}_k(\xi) = \delta_{sk} \quad \dots\dots (6)$$

Eqns (4)–(6) are particularly simple for the unperturbed problem, when $\xi = 0$. Eqn (6) expresses the orthonormality of the MO's.

There are two important situations where the case of $\xi = 0$ has been solved. These are the effect of introducing some heteroatom, such as nitrogen, instead of one of the carbon atoms, and the effect of changing the β_{rs} 's, as in a kind of self-consistent LCAO MO calculation (Coulson, Daudel and Robertson 1951, Pople 1953, Md. Asgar Ali 1960). Both situations could be discussed either *ab initio* or with the use of a perturbation theory (Coulson and Longuet-Higgins 1947 a, b), provided that the perturbation calculations are simple enough. In this paper we shall consider only perturbation calculations, but with a particular regard to their simplicity.

Hitherto perturbation calculations in the LCAO MO theory have usually been based on the concept of atom-atom, atom-bond and bond polarizabilities, introduced by Coulson and Longuet-Higgins (1947 a, b). But unfortunately the calculation of all the polarizabilities needed for any particular problem is usually a tedious task. However Brown and Bassett (1958), independently of the present authors, have pointed out that a more convenient method exists, without depending explicitly on these polarizabilities. In the following section we shall re-discuss this method and remove some of the difficulties which Brown and Bassett found for degenerate levels. Subsequently we shall apply the method to an approximate SCF LCAO MO treatment of conjugated molecules. The object of this application is to reconsider theoretical predictions of bond lengths in butadiene, naphthalene and anthracene. Such reconsideration is desirable in view of new experimental results of high accuracy for these latter two molecules (Unpublished work by Almenningen, Bastiansen and Dyvik, reported in references 6, 7 of Bastiansen and Skancke 1961, Cruickshank and Sparks 1960).

§ 2. GENERAL FORMULATION OF PERTURBATION PROCEDURE

We shall express our analysis in a form that is suitable for calculating the first-order perturbation of any finite Hermitian matrix. The method, therefore, is much more general than the specific use that we shall later make of it. It is necessary, however, to distinguish between degenerate and non-degenerate levels. We deal with them separately.

2.1. Non-degenerate Levels

Equations (4)–(6) are obviously valid for all values of ξ , and it seems reasonable to assume continuity of $\mathbf{C}_k(\xi)$, $\epsilon_k(\xi)$, $H_{rs}(\xi)$ and their first derivatives in the neighbourhood of $\xi = 0$. Differentiating (4)–(6) and letting $\xi \rightarrow 0$, we obtain

$$[\mathbf{H}(0) - \epsilon_k(0) \cdot \mathbf{1}] \mathbf{dC}_k(0) = [\mathbf{d}\epsilon_k \cdot \mathbf{1} - \mathbf{dH}] \mathbf{C}_k(0) \quad \dots\dots (7)$$

where

$$d\epsilon_k = \mathbf{C}_k^\dagger(0) \cdot \mathbf{dH} \cdot \mathbf{C}_k(0) \quad \dots\dots (8)$$

$$(dH)_{rs} = d(H_{rs})$$

$$\mathbf{C}_k^\dagger(0) \cdot \mathbf{dC}_k(0) = 0. \quad \dots\dots (9)$$

Eqns (7)–(9) are effectively the same as those given by Brown and Bassett (1958, to be referred to as BB). According to them it is convenient to look for a solution

$$\mathbf{dC}_k = \mathbf{a}_k + \lambda_k \mathbf{C}_k(0) \quad \dots\dots (10)$$

where \mathbf{a}_k is any particular solution of (7) and where, from (9) and (10),

$$\lambda_k = -\mathbf{C}_k^\dagger(0) \cdot \mathbf{a}_k. \quad \dots\dots (11)$$

The set of equations (7) is easy to solve (in order to get \mathbf{a}_k) because on account of (8) there is no eigenvalue condition, and (7) is therefore a set of simultaneous linear equations.

Having found \mathbf{dC}_k for all occupied orbitals, we can easily obtain the new formal charges $q_u(\xi)$ and the new π -bond orders $p_{uv}(\xi)$. For, if n_k is the occupation number of the MO ψ_k ,

$$q_u(\xi) = q_u(0) + \left(\frac{\partial q_u}{\partial \xi} \right)_0 d\xi \equiv q_u(0) + 2 \sum_k n_k c_{ku} d c_{ku} \quad \dots\dots (12)$$

$$p_{uv}(\xi) = p_{uv}(0) + \left(\frac{\partial p_{uv}}{\partial \xi} \right)_0 d\xi = p_{uv}(0) + \sum_k n_k (c_{ku} d c_{kv} + c_{kv} d c_{ku}). \quad \dots\dots (13)$$

Eqns (7)–(13) show that this type of perturbation calculation is simpler than the repeated solution of the new eigenvalue problem for each $\xi (\neq 0)$. For there is now no eigenvalue condition and, further, the solution of (7) for \mathbf{dC}_k is much simpler than that of the analogous equation for $\mathbf{C}_k(\xi)$. It would, of course, be perfectly possible to express $q_u(\xi)$ and $p_{uv}(\xi)$ of (12) and (13) in terms of the Coulson–Longuet-Higgins polarizability coefficients. But, as BB pointed out, and as we shall see later in our detailed application, the large number of these mutual polarizabilities ($\frac{1}{2}n(n+1)$ for the atom–atom polarizabilities in a molecule containing n carbon atoms) makes the older method less convenient than the new ones.

2.1. Degenerate Levels

So far we have assumed that none of the occupied MO's is degenerate. For degenerate states the method of Brown and Bassett needs special care. This is particularly true if the presence of the perturbation ξ changes the symmetry properties of the molecule. Since our approach for these degenerate levels differs considerably from that of BB, we shall first describe our own method. Then certain differences and contradictions between the two treatments will have to be discussed.

Let us assume that $\epsilon_k(0)$ has a g -fold degeneracy, and $\mathbf{C}_{k1}(0), \dots, \mathbf{C}_{kg}(0)$ are the appropriate eigenvectors, which we assume to be orthonormal. We also suppose that all occupation numbers are the same (usually two, corresponding to a closed-shell molecule). We now have

$$[\mathbf{H}(\xi) - \epsilon_{ki}(\xi) \cdot \mathbf{1}] \mathbf{C}_{ki}(\xi) = 0 \quad \dots\dots (14)$$

$$\mathbf{C}_{ki}^\dagger(\xi) \mathbf{C}_{kj}(\xi) = \delta_{ij} \text{ with } i, j = 1, 2, \dots, g. \quad \dots\dots (15)$$

In general $\epsilon_{ki}(\xi) \neq \epsilon_{kj}(\xi)$ if $i \neq j$, but of course $\epsilon_{ki}(0) = \epsilon_{kj}(0)$ ($= \epsilon_k$ for short). Then by differentiation of (14)–(15) and going to the limit as $\xi \rightarrow 0$:

$$[\mathbf{H}(0) - \epsilon_k \mathbf{1}] \mathbf{dC}_{ki}(0) = [d\epsilon_{ki} \cdot \mathbf{1} - \mathbf{dH}] \mathbf{C}_{ki}(0) \quad \dots\dots (16)$$

$$\mathbf{C}_{ki}^\dagger(0) \cdot \mathbf{dC}_{kj}(0) + \mathbf{C}_{kj}^\dagger(0) \cdot \mathbf{dC}_{ki}(0) = 0 \quad \dots\dots (17)$$

where

$$\mathbf{C}_{ki}(0) = \lim_{\xi \rightarrow 0} \mathbf{C}_{ki}(\xi). \quad \dots\dots (18)$$

Equations (7)–(9) are now replaced by (16)–(18). But certain important differences must be noticed between the two sets of equations. Thus, according to (18), we must start with properly chosen eigenvectors $\mathbf{C}_{ki}(0)$ of the unperturbed problem, and in addition $\mathbf{dC}_{ki}(0)$ is no longer necessarily orthogonal to $\mathbf{C}_{kj}(0)$. However the following theorems simplify the solution of (16)–(18). Their proofs are given in the Appendix.

Theorem 1. If the occupation numbers of all g degenerate levels are equal, so that $n_{k1} = n_{k2} = \dots = n_{kg}$, then without loss of generality it may be assumed that in the calculation of $q_u(\xi)$, $p_{uv}(\xi)$ and $\epsilon_{ki}(\xi)$

$$\mathbf{C}_{ki}^\dagger(0) \cdot \mathbf{dC}_{kj}(0) = 0 \quad \text{for all } i, j. \quad \dots\dots (19)$$

Theorem 2. To avoid inconsistency in the linear set (16) the vectors $\mathbf{C}_{ki}(0)$ must be properly chosen. The necessary and sufficient condition for this proper choice of the zero-order eigenvectors is that

$$\mathbf{C}_{ki}^\dagger(0) \cdot \mathbf{dH} \cdot \mathbf{C}_{kj}(0) = 0 \quad \text{for all } i \neq j. \quad \dots\dots (20)$$

This theorem is proved (see later) on the assumption that the degenerate eigenvectors are orthonormal:

$$\mathbf{C}_{ki}^\dagger(0) \cdot \mathbf{C}_{kj}(0) = \delta_{ij}. \quad \dots\dots (21)$$

Theorem 3. In practice the degeneracy is seldom greater than two. Let us put $g=2$, and take X_{k1} and X_{k2} to be any orthonormal eigenvectors of the unperturbed molecule for the degenerate eigenvalue ϵ_k . Then it follows from theorem 2 that the properly chosen zero-order eigenvectors for the perturbed molecule are given by the following explicit formula.

$$\mathbf{C}_{ki}(0) = \lim_{\xi \rightarrow 0} \mathbf{C}_{ki}(\xi) = aX_{k1} + bX_{k2} \quad \dots\dots (22)$$

where

(i) if $dH_{12}(\xi)$ vanishes in the neighbourhood of $\xi=0$, then

$$a=1, b=0 \text{ or alternatively } a=0, b=1, \quad \dots\dots (23)$$

(ii) if $dH_{12}(\xi)$ does not vanish in the neighbourhood of $\xi=0$, then

$$b/a = -Q \pm (1+Q^2)^{1/2} \quad \dots\dots (24)$$

with—

$$Q = \frac{1}{2} \lim_{\xi \rightarrow 0} \left\{ \frac{dH_{11} - dH_{22}}{dH_{12}} \right\}. \quad \dots\dots (25)$$

Theorem 4. When the proper zero-order eigenvectors have been chosen (according to theorems 2 or 3), and when all the occupation numbers are equal (with the consequences of theorem 1), then the solution of the linear equations (16) can be obtained in a similar way to that in the case of non-degenerate levels:

$$\mathbf{dC}_{ki} = \mathbf{a}_{ki} + \sum_{\text{all } j} \lambda_{ij}^{(k)} \mathbf{C}_{kj}(0), \quad i=1, 2, \dots, g \quad \dots\dots (26)$$

where \mathbf{a}_{ki} is any particular solution of (16) and

$$\lambda_{ij}^{(k)} = -\mathbf{C}_{kj}^\dagger(0) \cdot \mathbf{a}_{ki}. \quad \dots\dots(27)$$

This rather involved discussion of the situation in degenerate levels is essential if we are to deal effectively with molecules such as benzene, where different perturbations affect the molecular symmetry in different ways, as for example in Jahn-Teller distortions in aromatic ions.

Theorems 1 and 4 are different from those given by BB; theorems 2 and 3 are new. The reason for our differences in theorems 1 and 4 lies in BB's claim that with degenerate states a direct solution of (16) in terms of \mathbf{a}_{ki} , $\mathbf{C}_{k1}(0)$, \dots , $\mathbf{C}_{kg}(0)$ is not in general possible, when the perturbation \mathbf{dH} arises from changes in the bond-resonance integrals β . BB say that this arises from an error, usually repeated from Schrödinger, that the vectors \mathbf{dC}_{kj} and \mathbf{dC}_{ki} must be orthogonal for each i and j . But from the proof of our theorem 1 it follows that although such an orthogonality is not really necessary, it can nevertheless be assumed without any lack of generality in calculations of $q_u(\xi)$, $p_{uv}(\xi)$ and $\epsilon_{ki}(\xi)$ if, as is usually the case, the occupation numbers of all the degenerate eigenvectors considered are the same. BB's failure to find the proper solution of (16) may be due either to not having insisted on the proper choice of zero-order functions $\mathbf{C}_{ki}(0)$, $i=1, 2 \dots g$, or to having looked for a solution of the form

$$\mathbf{a}_i + \lambda_1 \mathbf{C}_i^{(1)} + \lambda_2 \mathbf{C}_i^{(2)} + \dots + \lambda_g \mathbf{C}_i^{(g)}, \quad \dots\dots(28)$$

which does not have a sufficient number of indices, as (26) shows.

Our discussion is independent of the kind of degeneracy. This can be either essential (in the case of a high symmetry) or accidental (as in the case of many large polynuclear hydrocarbons).

§ 3. APPLICATION TO HYDROCARBON MOLECULES

We shall now apply this perturbation analysis to develop a simple self-consistent theory for the π -molecular orbitals of an aromatic or condensed hydrocarbon. In the simplest theory (Hückel 1931, 1932) the MO's are only self-consistent with respect to the Coulomb terms α_r (Eqn (2)). For the secular equations are based on the assumption that all β_{rs} (Eqn (3)) are equal. Yet it is then concluded that the π -bond orders p_{rs} are unequal, and hence that the bond lengths are unequal. This should, of course, also imply that the β_{rs} are unequal. Ideally we should now start the cycle of calculations again, using the β 's inferred from the first cycle; and we should continue this iterative procedure till consistency is obtained in the β 's. (Fortunately this process does not spoil the consistency in the α 's.) But we can show that our perturbation analysis enables a satisfactory calculation of almost-consistent bond lengths to be made without any further solution of the secular equations. For this we use the same outlook as Coulson, Daudel and Robertson (1951), though the particular representations (29) and (30) are taken from the successful analysis of bond length alternations in conjugated chain molecules by Longuet-Higgins and Salem (1959) and later papers).

We therefore make the following assumptions concerning the relations between bond lengths R_{rs} , π -bond order p_{rs} and resonance integral β_{rs} :

$$\begin{aligned} (1) \quad \beta_{rs} &= \beta_0 \exp(-\alpha R_{rs}) \quad \text{for neighbours} \\ (2) \quad \beta_{rs} &= 0 \quad \text{for non-neighbours} \end{aligned} \quad \dots\dots(29)$$

(3) $\alpha_r = \text{constant } (\alpha)$ for all r

(4) $R_{rs} = b - cp_{rs}$ (30)

(5) all overlap integrals are zero.

We differ a little from Longuet-Higgins and Salem in our choice of parameters a, b, c . The parameters b and c were fitted by use of the following bond lengths: ethylene 1.337 Å, benzene 1.397 Å, graphite 1.421 Å. (Longuet-Higgins and Salem used 1.350 Å for ethylene. Our value of 1.337 Å is the mean of three recent very accurate measurements: Bartell and Bonham (1957) 1.334 Å, Allen and Plyler (1958) 1.337 Å, Dowling and Stoicheff (1959) 1.339 Å). So we take

$$R_{rs} = 1.517 - 0.180p_{rs}$$

$$\text{i.e. } p_{rs} = \frac{2}{3} - \frac{50}{9}(R_{rs} - 1.397). \quad \text{..... (31)}$$

If this relation were valid down to $p_{rs} = 0$, it would predict that a pure single bond between sp^2 trigonal carbon atoms would have a length 1.517 Å. This is a little longer than is sometimes believed, but not impossibly so. Our change in b and c necessitates changes in a and β_0 . We find

$$\beta_{rs} = \beta_0 \exp(-2.683R_{rs}) \quad \text{..... (32)}$$

where R_{rs} is in Å. The precise value of β_0 is not needed in these calculations.

We have used these relations in a reconsideration of the theoretical bond lengths in butadiene, naphthalene and anthracene, for all of which new accurate experimental results have recently been obtained (Coulson, Daudel and Robertson 1951, Almenningen, Bastiansen and Traetteberg 1958, Bastiansen and Skancke 1961, Cruickshank and Sparks 1960). Our procedure is as follows. Let r_{rs} be the deviation of the final bond length from the benzene value 1.397 Å. Then we have two different approximate relations between p_{rs} and r_{rs} . These are given in (13) and (31). If both are satisfied, we have a self-consistent set of bond orders and lengths. By elimination of p_{rs} we obtain

$$\frac{2}{3} - \frac{50}{9}r_{rs} = p_{rs}(0) + \sum \left(\frac{\partial p_{rs}}{\partial r_{uv}} \right)_0 r_{uv} \quad \text{..... (33)}$$

where $p_{rs}(0)$ denotes the value of p_{rs} calculated with all β_{rs} equal. For different bonds rs this gives a set of linear simultaneous equations whose solution leads at once to the required bond lengths r_{rs} . For large molecules this solution is conveniently obtained by an iterative procedure in which, when finding the n th iterative to r_{rs} we use the $(n-1)$ th iteratives on the right-hand side of (33). A very few iterations are sufficient to give the required values. The numerical values of the various $(\partial p_{rs}/\partial r_{uv})$ can easily be obtained from (13), using the perturbation theory to give each dc_{ku} etc.

§ 4. NUMERICAL VALUES

Accurate comparison of theoretical and experimental bond length has always been beset by one great difficulty—further refinements have frequently made considerable changes in the 'observed' values. Thus the comparison for naphthalene and anthracene which was first made by Coulson, Daudel and Robertson (1951) had to be re-made by Pritchard and Sumner (1955). More recently still, some new different experimental values have been reported by Cruickshank and Sparks (1960) using x-ray methods, and by Almenningen,

Bastiansen and Dyrik. (see Bastiansen and Skancke 1961) using electron-diffraction methods. These latest observed values differ considerably from the earlier observed values, and inspire us to reconsider the theory. It is true that Cruickshank and Sparks have already made some such reconsideration. But they used only x-ray values and did not include the most recent electron diffraction values, nor of course could they include our present calculations. In addition they used for their criterion the root mean square of all bond length deviations. This particular criterion, though probably the most important single one, is disadvantageous to the LCAO method. For it is well known that this method leads to a value for the shortest bond which is usually too great. The Pauling superposition method, on the other hand, generally gives a good value for this bond. Thus in the r.m.s. procedure using LCAO values the bond is weighted highly, so that it is possible to mask a good agreement with other bonds by a poor agreement for this one.

Our results for butadiene, naphthalene and anthracene are given in Tables 1-3. In these tables:

(i) Pauling's superposition method refers to the semi-empirical correlation between bond length and double-bond character, as discussed in the latest edition of Pauling's book (1960).

(ii) Spin states method refers to the use of Slater determinants discussed for example by Daudel, Lefebvre and Moser (1959, pp. 130-134), but using the new experimental values for ethylene, benzene and graphite instead of Table V.10 of their book.

(iii) The LCAO MO method is the original simple Hückel method, using an order-length curve but constant β_{rs} , as described by Coulson (1951).

(iv) The approximate SCF MO method is the result of solving the Eqns (33) of this present paper.

According to Cruickshank and Sparks three independent x-ray estimations of the bond lengths in anthracene gave very close results, but with naphthalene two independent estimates did not agree well. This leads us to trust the anthracene average values more than the naphthalene average values. Fortunately with electron diffraction the situation is reversed. For as Bastiansen and Skancke showed, two different zero-order models for naphthalene gave very close agreement, but not for anthracene. The x-ray and electron-diffraction average values are shown in the Tables. For the purposes of our comparison of theory and experiment, we have used the average of the x-ray and electron-diffraction measurements as the experimental lengths. Since the estimated errors of the two methods are closely similar this is at present the best that can be done.

Table 1. Comparison of Bond Lengths for Naphthalene in (Å)

Method	Bonds				Mean errors		
	1-2	2-3	1-9	9-10	x-ray	e.d.	average
1. Pauling's superposition	1.371	1.422	1.422	1.422	0.005	0.003	0.004
2. Spin states	1.389	1.397	1.417	1.438	0.017	0.014	0.016
3. LCAO MO	1.387	1.408	1.417	1.424	0.010	0.007	0.009
4. Appr. SCF (this paper)	1.382	1.414	1.420	1.419	0.005	0.004	0.004
5. X-ray	1.364	1.415	1.421	1.418	—	0.003	—
6. El. diff.	1.371	1.412	1.422	1.420	0.003	—	—
7. Exp. average	1.368	1.414	1.422	1.419			

Finally the mean error columns in Tables 1-3 require some comment. We have calculated these values as the arithmetic mean of the absolute deviation, but only considering non-equivalent bonds. In this way we hope not to exaggerate the influence of the errors for the shortest bond, already referred to. (It is only for the 1-2 bond of naphthalene that this error is at all serious.)

Table 2. Comparison of Bond Lengths for Anthracene (in Å)

Methods	Bonds					Mean errors		
	1-2	1-11	2-3	9-11	11-12	x-ray	e.d.	average
1. Pauling's superposition	1.361	1.439	1.439	1.394	1.439	0.009	0.019	0.014
2. Spin states	1.389	1.417	1.397	1.408	1.438	0.016	0.009	0.012
3. LCAO MO	1.389	1.421	1.412	1.408	1.430	0.011	0.004	0.007
4. Appr. SCF (this paper)	1.377	1.427	1.420	1.405	1.428	0.005	0.005	0.002
5. X-ray	1.368	1.436	1.419	1.399	1.428	—	0.009	—
6. El. diff.	1.390	1.420	1.419	1.404	1.425	0.009	—	—
7. Exp. average	1.379	1.428	1.419	1.402	1.427			

Table 3. Comparison of Bond Lengths for Butadiene (in Å)

Methods	Bonds		Mean errors		
	1-2	2-3	x-ray	e.d.	average
1. Pauling's superposition	1.337	1.507	0.03	0.012	0.023
2. Spin States	1.362	1.431	0.02	0.038	0.028
3. LCAO MO	1.356	1.436	0.015	0.033	0.023
4. Appr. SCF (this paper)	1.346	1.465	0.005	0.013	0.003
5. X-ray	1.35	1.46	—	0.018	—
6. El. diff.	1.337	1.483	0.018	—	—
7. Exp. average	1.345	1.470			

The following conclusions follow from these three tables.

(1) The poorest agreement with experiment is associated with the approximate spin-states method (which is, however, the simplest).

(2) On average, the Pauling superposition method is about as reliable as the LCAO MO method. It is better by 0.005 Å for naphthalene, but worse by 0.007 Å for anthracene. Cruickshank and Sparks have already drawn attention to the surprising reliability of this simple method.

(3) Our approximate SCF method gives the best results with a mean error for the three molecules of only 0.003 Å. The inclusion of approximate self-consistency reduces the mean error for naphthalene by a factor of two, and for anthracene by a factor of three. Where the x-ray and electron-diffraction data are the same, they are also practically the same as the SCF results, the difference being usually less than 0.003 Å (which is approximately the same as the experimental accuracy of measurement). Where the x-ray and electron-diffraction differ appreciably, our predicted SCF results lie near the average (with the exception of the shortest bond in naphthalene, where the error is 0.014 Å). In all cases the predicted sequence of increasing bond lengths is identical with the experimental average.

It would be interesting to make similar comparison for other aromatic molecules. But this must be done with great care, since the experimental results are usually not known with sufficient accuracy. Thus in coronene, which has

often been used in comparison of theory and experiment, the new electron-diffraction data (as in Bastiansen and Skancke 1961, references 6 and 7) differ from the older x-ray data (Robertson and White 1945) by as much as 0.05, 0.03, 0.023, and 0.008 Å for the various distinct bonds. Until these discrepancies have been elucidated there is no point in attempting a serious comparison with theory.

§ 5. SOME OTHER REFINEMENTS

Pritchard and Sumner (1955) have discussed the influence of some other refinements in the prediction of bond lengths in aromatic molecules:

- (1) Pople's SCF method,
- (2) modified Pople method, with inclusion of compression or extension energy for σ -electrons,
- (3) simple Hückel method with variation of Coulomb integrals,
- (4) SCF MO method with variation of Coulomb integrals,
- (5) as in (4), but with inclusion of compression energy.

Of these only (2) and (4) appear (see also Cruickshank and Sparks 1960) to give significant improvement. We have therefore thought it worth while to compare these two approximations with our own, and with the experimental averages previously described. Tables 4 and 5 show our results.

Table 4. Errors for Bond Lengths in Naphthalene (Å)

	Bonds				Average error
	1-2	2-3	1-9	9-10	
Experimental bond length	1.368	1.414	1.422	1.419	—
LCAO MO	0.019	-0.006	-0.005	0.005	0.009
Approx. SCF (this paper)	0.014	0.000	-0.002	0.000	0.004
Approx. (2)	0.014	0.001	0.001	-0.004	0.005
Approx. (4)	0.011	0.007	0.005	-0.003	0.006

Table 5. Errors for Bond Lengths in Anthracene (Å)

	Bonds					Average error
	1-2	1-11	2-3	9-11	11-12	
Experimental bond length	1.379	1.428	1.419	1.402	1.427	—
Simple LCAO MO	0.010	-0.007	-0.007	0.006	0.003	0.007
Approx. SCF (this paper)	-0.002	-0.001	0.001	0.003	0.001	0.002
Approx. (2)	0.002	0.003	0.003	0.004	-0.003	0.003
Approx. (4)	0.000	0.009	0.011	0.009	0.011	0.008

In the last two lines of these tables we have used the same bond length changes in approximations (2) and (4) as were calculated by Pritchard and Sumner. It would appear from these values that, when the experimental values are taken to be those which we have adopted in this paper, approximation (2) is better than (4), and about equal to our approximate SCF method. But the approximate SCF method is the simpler. In both these two methods the average error is of the same order as the best experimental accuracy that may yet be claimed.

ACKNOWLEDGMENT

We should like to thank Mr. P. N. Skancke for the benefit of valuable discussion, and one of us (A. G.) would like to acknowledge the award of a Rockefeller Fellowship, which has made this work possible.

APPENDIX

Proof of theorem 1. We can obviously expand \mathbf{dC}_{ki} of (16) in the form

$$\mathbf{dC}_{ki} = \sum_{\text{all } m, n} b_{ki, mn} \mathbf{C}_{mn}(0) \quad \dots\dots (A1)$$

where the $b_{ki, mn}$ are at present undetermined. Here, and in (A2) and (A4), the index n enumerates the degenerate orbitals associated with the eigenvalue index m (or k). Inserting (A1) in (16) we find that

$$\begin{aligned} \mathbf{dC}_{ki} = & \sum_{m \neq k, n} \left\{ \frac{\mathbf{C}_{ki}^\dagger(0) \cdot \mathbf{dH} \cdot \mathbf{C}_{mn}(0)}{\epsilon_k - \epsilon_m} \right\} \mathbf{C}_{mn}(0) \\ & + \sum_n b_{ki, kn} \mathbf{C}_{kn}(0). \quad \dots\dots (A2) \end{aligned}$$

Now from (A1) and (17) it follows that

$$b_{ki, kj} = -b_{kj, ki}; \quad b_{ki, ki} = 0. \quad \dots\dots (A3)$$

So the coefficients $b_{ki, kj}$ are antisymmetric in i, j . On the other hand the charges q_u and bond orders p_{uv} and related quantities such as the energy, are symmetric in i, j . This follows from (12) and (13). Thus the second summation in (A2) can at least formally be neglected. Therefore, if all occupation numbers of the degenerate orbitals are equal ($n_{k1} = n_{k2} = \dots = n_{kg}$), in all calculations of q_u, p_{uv} , etc. it is sufficient to take

$$\mathbf{dC}_{ki} = \sum_{m \neq k, n} \left\{ \frac{\mathbf{C}_{ki}(0) \cdot \mathbf{dH} \cdot \mathbf{C}_{mn}(0)}{\epsilon_k - \epsilon_m} \right\} \mathbf{C}_{mn}(0). \quad \dots\dots (A4)$$

Theorem 1 follows immediately from (A4) and the orthogonality of \mathbf{C}_{mn} and \mathbf{C}_{kj} for $m \neq k$.

Proof of theorem 2. This is really the familiar theorem concerning the correct zero-order functions in degenerate first-order perturbation theory. To prove the necessity of (20) we take the product of (16) with $\mathbf{C}_{kj}^\dagger(0)$. The left-hand side vanishes and so also does the first part of the right-hand side. The rest is (20) with i and j interchanged. Also, if (20) holds, then $\mathbf{dH} \cdot \mathbf{C}_{ki}(0)$ must be some multiple of \mathbf{C}_{ki} . There is then no difficulty in solving (16) without the possibility of any inconsistency. Condition (20) is therefore both necessary and sufficient.

Proof of theorem 3. This is a simple application of theorem 2 Eqn (20), when i and j can only take the values 1 and 2.

Proof of theorem 4. When theorems 1-3 are satisfied, (A4) does in fact give the solution for \mathbf{dC}_{ki} . Alternatively, if we can find one particular solution $\mathbf{dC}_{ki} = \mathbf{a}_{ki}$, then the linearity of (16) shows that the full solution must be

$$\mathbf{dC}_{ki} = \mathbf{a}_{ki} + \sum_{\text{all } j} \lambda_{ij}^{(k)} \mathbf{C}_{kj}(0)$$

where, to preserve the orthogonality condition (19), the λ_{ij} must satisfy (27) Eqn (A4) shows that this solution is unique.

REFERENCES

- ALI, MD. ASGAR, 1960, *D. Phil. Thesis*, University of Oxford.
- ALLEN, H. C., and PLYLER, E. K., 1958, *J. Amer. Chem. Soc.*, **80**, 2673.
- ALMENNINGEN, A., BASTIANSEN, O., and TRÆTTEBERG, M., 1958, *Acta Chem. Scand.*, **12**, 1221.
- BARTELL, L. S., and BONHAM, R. A., 1957, *J. Chem. Phys.*, **27**, 1414.
- BASTIANSEN, O., and SKANCKE, P. N., 1961, *Advances in Chemical Physics*, Vol. 3 (New York and London: Interscience), p. 323.
- BROWN, R. D., and BASSETT, I. M., 1958, *Proc. Phys. Soc.*, **71**, 724.
- COULSON, C. A., 1961, *Valence*, 2nd edn (Oxford: University Press).
- COULSON, C. A., DAUDEL, R. and ROBERTSON, J. M., 1951, *Proc. Roy. Soc. A*, **207**, 306.
- COULSON, C. A., and LONGUET-HIGGINS, H. C., 1947 a, *Proc. Roy. Soc. A*, **191**, 40.
- 1947 b, *Proc. Roy. Soc. A*, **192**, 16.
- CRUICKSHANK, D. W. J., and SPARKS, R. A., 1960, *Proc. Roy. Soc. A*, **258**, 270.
- DAUDEL, R., LEFEBVRE, R. and MOSER, C., 1959, *Quantum Chemistry* (New York and London: Interscience), p. 52.
- DOWLING, J. M. and STOICHEFF, B. D., 1959, *Canad. J. Phys.*, **37**, 703.
- HÜCKEL, E., 1931, *Z. Phys.*, **70**, 204.
- 1932, *Z. Phys.*, **76**, 628.
- LONGUET-HIGGINS, H. C., and SALEM, L., 1959, *Proc. Roy. Soc. A*, **251**, 172.
- PAULING, L., 1960, *The Nature of the Chemical Bond*, 3rd edn (Ithaca: Cornell University Press).
- POPLE, J. A., 1953, *Trans. Faraday Soc.*, **49**, 1375.
- PRITCHARD, H. O., and SUMNER, F. H., 1955, *Trans. Faraday Soc.*, **51**, 457.
- ROBERTSON, J. M., and WHITE, J. G., 1945, *J. Chem. Soc.*, 607.

The Band Structure of Body-centred Cubic Transition Metals

By C. A. BATES AND K. W. H. STEVENS

Department of Physics, University of Nottingham

MS. received 19th April 1961

Abstract. The theory of the magnetic properties of iron put forward by Mott and Stevens made a number of assumptions about the band structures of the body-centred cubic 3d transition metals. The purpose of the present paper is to give an account of a theoretical study which has been made to see what could reasonably be expected on fairly general grounds about the band structures. It then becomes possible to see more clearly what innovations are required for the Mott and Stevens theory. The method used is essentially a tight binding method, with the feature that the functions used are not located at lattice sites but are on the links joining nearest neighbour lattice points. It leads to an 8×8 matrix for the lattice potential for each value of \mathbf{K} . A discussion of the diagonalization of this 8×8 matrix is given for a number of symmetry points and directions in \mathbf{K} -space, and it is shown that a good deal of valuable information can be obtained from relatively simple ideas. It is also shown that the band structure so obtained is incomplete because two of the d-functions are omitted, and these are then included by perturbation methods. The Mott and Stevens model of iron is shown to follow from assumptions about the results of this perturbation treatment. A discussion is given of the ground state determinantal functions for vanadium, chromium and iron which it is hoped will be of use in interpreting the physical properties of these elements. Apart from the value the theory may have in its application to the above metals, the algebraic treatment provides an elegant example of the effects of symmetry on band structures, previously thoroughly discussed in terms of groups by Bouckaert, Smoluchowski and Wigner.

§ 1. INTRODUCTION

THE study of the properties of transition metals and alloys has proved to be of considerable experimental interest, and theoreticians have long been under pressure to produce theories which can be used to interpret the observations. As it is not possible to give complete theoretical treatments of the enormously complicated many-body problems involved, approximations are always made. It is not our purpose to review the types of approximations which have been made (see Herring 1960) but it seems worth emphasizing that it is highly desirable that all such approximations should be recognized as such and subjected to close examination.

In an earlier paper one of the present authors, in collaboration with Professor Mott, put forward a theory of the above sort to account for the magnetic properties of iron (Mott and Stevens 1957). This theory has been subjected to a close examination by a number of workers (Marshall and Weiss 1959, Slater, unpublished†, Slater and Wood unpublished‡) as well as by ourselves, and it has been

† *Solid State and Molecular Theory, Group Quarterly Progress Report*, No. 34, p. 11, 1959, Massachusetts Institute of Technology.

‡ *Solid State and Molecular Theory, Group Quarterly Progress Reports*, Nos. 27-38, 1958-1960, Massachusetts Institute of Technology.

criticized quite strongly, mainly on theoretical grounds. In order to have as clear a picture as possible of what may be happening in iron, and also to understand the criticisms in detail, we have been examining, from a general point of view, the band structure which might be expected for a body-centred transition metal. To this we have added special assumptions which lead to the Mott and Stevens model.

§ 2. NON-MATHEMATICAL DESCRIPTION OF MODEL

A body-centred cubic lattice can be regarded as composed of two interpenetrant simple cubic lattices. Although all the atoms in the lattice are identical, it is convenient to refer to them as A or B atoms according to the simple cubic sublattice A or B on which they lie (see Fig. 1). Suppose now that the crystal is

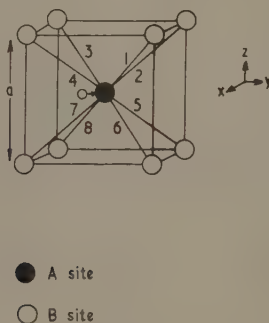


Fig. 1. Body-centred cubic lattice showing the labelling of the links joining an (A site) atom at 0 to its eight nearest neighbours (B site) atoms.

regarded as a large covalently bonded molecule in which each A (or B) atom is linked by a bond to each of its eight neighbouring B (or A) atoms. Such a bond will be said to lie on a link, a link being the line joining two nearest neighbour atoms. To construct such bonds we may proceed as follows. At each A (or B) atom eight orbitals, formed by hybridizing suitable atomic orbitals, are constructed, so that each one is, in turn, directed principally towards a nearest neighbour B (or A) atom. Then consider a typical AB link. Along it there will be an orbital ϕ_A located at the A atom and directed towards the B atom, and at the B atom there will be a similarly shaped orbital ϕ_B directed towards the A atom. The two orbitals may then be combined symmetrically and antisymmetrically, thus:

$$\psi_s = \frac{\phi_A + \phi_B}{\{2(1+S)\}^{1/2}}, \quad \psi_a = \frac{\phi_A - \phi_B}{\{2(1-S)\}^{1/2}} \quad \dots\dots (1)$$

where S is the overlap integral. S will probably not be negligible. ψ_s and ψ_a are orbitals which encompass both atoms and, in the language of theoretical chemistry, ψ_s may be called a bonding orbital and ψ_a an antibonding orbital. This nomenclature arises because although they are both constructed from ϕ_A

and ϕ_B , ψ_a vanishes on the plane which bisects the link at right angles. Thus if they were both eigenstates a higher energy would normally be associated with ψ_a , and the probability of its occupation would be less than that of ψ_s . This is because the charge density associated with ψ_s is less localized than that associated with ψ_a (both charge densities are normalized to unity) since that of ψ_a certainly vanishes on a plane.

Having constructed pairs of such orbitals on each link of the crystal the method of construction is now largely forgotten, for we proceed as if the ψ_s and ψ_a are the basic orbitals. The general principles of band theory require the one-electron wave functions to be orthogonal to one another, and although bonding and antibonding orbitals on the same link are orthogonal, pairs on different links are not, in general, orthogonal. To move in the direction of obtaining fully orthogonal functions it is necessary to pass from the localized bonding and antibonding orbitals to non-localized Bloch functions. This is readily accomplished by following the usual prescription (Bloch 1928). Each Bloch function is characterized by a propagation vector \mathbf{k} and two such functions with differing \mathbf{k} are automatically orthogonal. Further, any single particle operator which has the same periodicity as the lattice has zero matrix elements between Bloch functions of differing \mathbf{k} 's. Thus as well as obtaining orthogonal functions progress is made towards diagonalizing the approximate Hamiltonian. As eight links end on each atom and on each link there are two localized orbitals, sixteen Bloch functions can be formed for each value of \mathbf{k} (assuming the A atoms are different from the B atoms, so that the lattice symmetry is that of a simple cube). Actually the A and B atoms are identical and in the detailed theory it will be shown that the sixteen can be decomposed into two groups of eight.

In a complete treatment one would have to use an infinite number of Bloch functions for each \mathbf{k} , and one would then have to find linear combinations of them to diagonalize the Hamiltonian. Once the Hamiltonian is diagonalized the linear combinations are automatically orthogonal. The approximation we make is that of selecting sixteen functions of each \mathbf{k} , and diagonalizing the associated 16×16 sub-matrix of the Hamiltonian, the assumption being that matrix elements from these sixteen to the rest of the infinite set are negligible. In fact, for a given value of \mathbf{k} it is usually not possible to diagonalize the 16×16 matrix unless the lattice potential is given explicitly, though it is always possible to reduce the problem to that of diagonalizing two 8×8 matrices. However a good deal of progress can be made with a general Hamiltonian for special values of \mathbf{k} , and it is with these values that we shall mostly be concerned.

The method we use appears to be similar to that described by Hall (1958) and used for the diamond lattice. It appears to differ from that used by Hall (1952, 1953 a, b) for a body-centred cubic lattice (though see Slater and Koster 1954).

§ 3. CONSTRUCTION OF THE ORBITALS

At each lattice point eight equivalent orthogonal directed orbitals are to be set up, each directed towards a different nearest neighbour atom. A simple application of group theory shows that this can be achieved by hybridizing functions which transform according to the Γ_1 , Γ_{15} , Γ_{25}' and Γ_2' irreducible representations of the cubic group (the notation of Bouckaert, Smoluchowski and Wigner (1936), to be referred to as B.S.W. will be used throughout). The specification need be no more detailed than this, but in order to be on familiar ground we may

suppose that the Γ_1 function is similar to the normalized 4s orbit of the free atom, Γ_{15} to $4p_x, 4p_y$ and $4p_z$, $\Gamma_{25'}$ to $3d_{xy}, 3d_{yz}$ and $3d_{zx}$, and $\Gamma_{2'}$ to $4f_{xyz}$, where O*x*, O*y* and O*z* are taken parallel to the cube edges (Fig. 1). The hybridized function which is directed primarily along the (1, 1, 1) direction, or link 1 in Fig. 1, is similar to

$$\phi_A = \frac{1}{\sqrt{8}} \{4s + 4p_x + 4p_y + 4p_z + 3d_{xy} + 3d_{yz} + 3d_{zx} + 4f_{xyz}\}.$$

The others may be obtained from this by suitable rotations of axes and, for example, the function directed along the (1, -1, 1) direction is similar to

$$\frac{1}{\sqrt{8}} \{s + p_x - p_y + p_z - d_{xy} - d_{yz} + d_{zx} - f_{xyz}\}$$

where the principal quantum numbers have been omitted. It is not possible to demonstrate the degree of directivity achieved without making assumptions about the radial parts of the atomic wave functions. If however we assume that at some value of the radius all the radial functions are equal, then the values of ϕ_A in the (1, 1, 1), (1, 0, 0), (-1, -1, -1), (-1, 1, 1) and (1, 1, 0) directions are proportional to 9.85, 2.73, -0.10, -1.26 and 5.39 respectively. The next step is to construct the bonding and antibonding orbitals as described by Eqns (1), to obtain new functions which are strongly concentrated on the links.

§ 4. THE BLOCH FUNCTIONS

The eight links which meet on an A atom are labelled from 1 to 8 as shown in Fig. 1. Any link orbital can then be specified by a number which describes the link to which it is parallel and similarly directed, a letter a or b according to whether it is antibonding or bonding and the coordinate of the midpoint of the link on which it is situated. Thus $|1, b, \mathbf{r}_n\rangle$ is the normalized bonding orbital which parallel to link 1 and centred at \mathbf{r}_n . $|1, a, \mathbf{r}_n\rangle$ is the corresponding antibonding orbital. Sixteen nearly normalized Bloch functions are then formed, thus:

$$|s, b\rangle = \frac{1}{\sqrt{N}} \sum_{\mathbf{r}_n} \exp(i\mathbf{k} \cdot \mathbf{r}_n) |s, b, \mathbf{r}_n\rangle \quad \dots\dots (2)$$

$$|s, a\rangle = \frac{1}{\sqrt{N}} \sum_{\mathbf{r}_n} \exp(i\mathbf{k} \cdot \mathbf{r}_n) |s, a, \mathbf{r}_n\rangle \quad \dots\dots (3)$$

where s takes values from 1 to 8, N is the number of A atoms in the lattice, \mathbf{r}_n depends on s , and \mathbf{k} is a vector of the first Brillouin zone of the simple cubic lattice. In practice little confusion arises if the \mathbf{k} dependence is not always given explicitly, and this has been anticipated on the left-hand sides of Eqns (2) and (3) where the \mathbf{k} dependence has been omitted.

We now recognize that the A and B atoms are identical, so that the full symmetry is body-centred cubic, not simple cubic. Then the orbitals which, for example, have been labelled as 1 and 8 are seen to be identical in shape and orientation, but differently placed in the lattice. Suppose then we consider the linear combinations of Bloch functions:

$$\frac{1}{\sqrt{2}} \{|1, b\rangle + |8, b\rangle\} \quad \dots\dots (4A)$$

and

$$\frac{1}{\sqrt{2}} \{|1, b\rangle - |8, b\rangle\} \quad \dots\dots (4B)$$

The first can be written as

$$\frac{1}{\sqrt{(2N)}} \left\{ \sum_{\mathbf{r}_{n_1}} \exp(i\mathbf{k} \cdot \mathbf{r}_{n_1}) |1, \mathbf{b}, \mathbf{r}_{n_1}\rangle + \sum_{\mathbf{r}_{n_8}} \exp(i\mathbf{k} \cdot \mathbf{r}_{n_8}) |8, \mathbf{b}, \mathbf{r}_{n_8}\rangle \right\}$$

or as

$$\frac{1}{\sqrt{(2N)}} \sum_{\mathbf{R}_n} \exp(i\mathbf{k} \cdot \mathbf{R}_n) |18, \mathbf{b}, \mathbf{R}_n\rangle$$

where the summation of \mathbf{R}_n refers to both 1 and 8 orbitals. To write the second expression (4B) in a similar form it is necessary to introduce a new vector \mathbf{K} such that

$$\exp(i\mathbf{k} \cdot \mathbf{r}_{n_1}) = \exp(i\mathbf{K} \cdot \mathbf{r}_{n_1})$$

but

$$\exp(i\mathbf{k} \cdot \mathbf{r}_{n_8}) = -\exp(i\mathbf{K} \cdot \mathbf{r}_{n_8}).$$

Then (4B) becomes

$$|\beta, 1\rangle = \frac{1}{\sqrt{(2N)}} \sum_{\mathbf{R}_n} \exp(i\mathbf{K} \cdot \mathbf{R}_n) |18, \mathbf{b}, \mathbf{R}_n\rangle. \quad \dots\dots (5)$$

The simplest form for \mathbf{K} is $\mathbf{K} = \mathbf{k} + \mathbf{k}_j$, where \mathbf{k}_j is one of $(\pi/a)(\pm 1, \pm 1, 0)$ or $(2\pi/a)(\pm 1, 0, 0)$. Then as \mathbf{k} ranges over the first Brillouin zone of the simple cubic lattice, \mathbf{K} ranges over the volume external to this but internal to the first Brillouin zone of the body-centred cubic lattice. This point is illustrated in Fig. 2, in which the first Brillouin zone of the simple cubic lattice has been shaded. If now \mathbf{K} is allowed to range over the whole of the inside of the first Brillouin zone

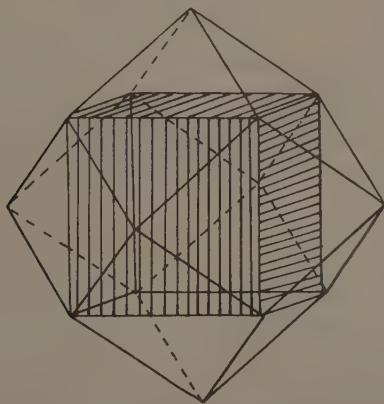


Fig. 2. Brillouin zone of a body-centred cubic lattice showing the inscribed cube corresponding to the Brillouin zone of the simple cubic lattice.

of the body-centred cubic lattice the expression (5) for $|\beta, 1\rangle$ includes both linear combinations (4A) and (4B). A similar argument can be given for the other link directions and for the antibonding orbitals, though for the latter it may be noted that it is the antisymmetric combination,

$$|\alpha, 1\rangle = \frac{1}{\sqrt{2}} \{ |1, a\rangle - |8, a\rangle \}$$

which corresponds to \mathbf{K} inside the first Brillouin zone of the simple cubic lattice. For each value of \mathbf{K} there are now eight Bloch functions. The approximate

Hamiltonian which is used in band theory has the lattice periodicity, body-centred cubic, and it will have no matrix elements between Bloch functions of differing \mathbf{K} 's. For general values of \mathbf{K} no further progress seems possible

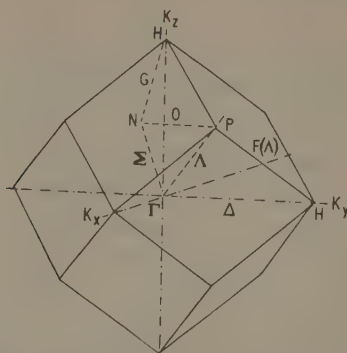


Fig. 3. Brillouin zone of a body-centred cubic lattice showing the axes and points of symmetry as used in the text.

unless the approximate Hamiltonian and the orbitals are given in much greater detail. For special values of \mathbf{K} (Fig. 3) a number of valuable results can be obtained.

§ 5. THE POINT Γ , or $\mathbf{K}=(0, 0, 0)$.

With $\mathbf{K}=0$ rotations which leave the lattice invariant permute the Bloch functions amongst themselves, and they are found by inspection to group naturally as follows:

$$\begin{array}{ll} \Gamma_1; & s; |\beta(1+2+3+4)\rangle \\ \Gamma_{15}; & \begin{cases} p_x; |\alpha(1-2-3+4)\rangle \\ p_y; |\alpha(1+2-3-4)\rangle \\ p_z; |\alpha(1+2+3-4)\rangle \end{cases} \end{array} \quad \begin{array}{ll} \Gamma_{25}'; & \begin{cases} d_{yz}; |\beta(1+2-3-4)\rangle \\ d_{zx}; |\beta(1-2-3+4)\rangle \\ d_{xy}; |\beta(1-2+3-4)\rangle \end{cases} \\ \Gamma_2'; & f_{xyz}; |\alpha(1-2+3-4)\rangle \end{array}$$

where the un-normalized function $[|\beta, 1\rangle \pm |\beta, 2\rangle \pm |\beta, 3\rangle \pm |\beta, 4\rangle]$ is denoted by $|\beta(1 \pm 2 \pm 3 \pm 4)\rangle$ etc. On rotation a state in one set either turns into a multiple of itself or into another state in the same set. Thus they can be used as bases for irreducible representations of the cubic group, as specified by the Γ 's. The s , p_x , p_y etc. denote atomic orbitals which transform in the same ways. As no irreducible representations occur more than once the Hamiltonian has no matrix elements between the sets, as indeed is readily seen by considering the effects of suitable rotations and reflections. Also the states in a given set have the same energies, so we see that at Γ there are two triplets and two singlets.

It is now of interest to consider the physical characteristics of these states. Consider the state denoted by Γ_1 . It is formed entirely from bonding orbitals, and in the neighbourhood of any nucleus it has local Γ_1 symmetry. The s atomic orbitals also have this symmetry, as does one of the g atomic orbitals. However

as 5g is likely to have a much higher energy than 4s it seems likely that near any nucleus Γ_1 will be dominantly s-like, with possibly a small amount of g-like symmetry. (One might imagine it as mainly spherical with extensions in the directions of nearest neighbours.) As $\mathbf{K}=0$ this local symmetry is repeated at each nucleus, as shown schematically in Fig. 4. Similarly the states in Γ_{15} will locally be predominantly p-like, the states in Γ_{25}' will be locally like d_{yz} , d_{zx} and d_{xy} , and the state Γ_2' will be locally like f_{xyz} . If we now wish to infer something about the relative energies of these states we note first that the s- and d-like states

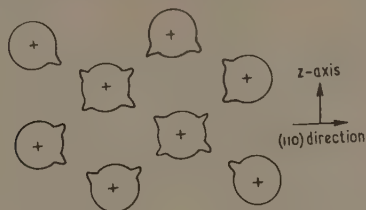


Fig. 4. Schematic diagram showing the local character in the plane containing the 1, 3, 6 and 8 links at the point Γ in the Brillouin zone for the state having Γ_1 -type symmetry. (Allowance for possible g-type orbit has been made by distortions which point towards nearest neighbours, superimposed on a spherical s-type orbit).

are of the bonding type, whereas the p- and f-like are antibonding. Thus as the atoms come together to form a solid we may expect that the s- and d-like orbitals will have their energies reduced, whereas the p- and f-like orbitals will have their energies increased. It is probable that the p- and f-like orbitals will not be occupied by electrons, so we are unlikely to be very interested in them. It is, however, important to decide on the order of the s- and d-like orbitals. This cannot, strictly, be decided without a detailed calculation. However all calculations seem to agree in putting the s-like function lowest, and we shall assume that this is so in our problem. Thus, in order of increasing energy the levels occur as Γ_1 , Γ_{25}' , Γ_{15} and Γ_2' .

§ 6. THE POINT H, or $\mathbf{K}=(0, 2\pi/a, 0)$

The point H lies on the boundary of the Brillouin zone of the body-centred cubic lattice, but corresponds to $\mathbf{k}=(0, 0, 0)$ in the simple cubic zone scheme. Thus H has the full cubic symmetry. The states can again be grouped according to the irreducible representations of the cubic group, thus:

$$\begin{aligned} H_1: & \quad s : |\alpha(1+2-3-4)\rangle \\ H_{15}: & \quad \begin{cases} p_x: |\beta(1-2+3-4)\rangle \\ p_y: |\beta(1+2+3+4)\rangle \\ p_z: |\beta(1+2-3-4)\rangle \end{cases} \quad \begin{cases} H_{25}': & \begin{cases} d_{yz}: |\alpha(1+2+3+4)\rangle \\ d_{zx}: |\alpha(1-2+3-4)\rangle \\ d_{xy}: |\alpha(1-2-3+4)\rangle \end{cases} \\ H_2': & f_{xyz}: |\beta(1-2-3+4)\rangle \end{cases} \end{aligned}$$

It may seem strange that a state such as $|\beta(1+2+3+4)\rangle$ appears as a singlet at the point Γ but belongs to a triplet at H. The reason is that the various orbitals in the Bloch functions are centred at different places, so that, if one considers, for example, the contribution near a given nucleus from $|1, b\rangle$ and $|8, b\rangle$ they add when $\mathbf{K}=(0, 0, 0)$ but subtract when $\mathbf{K}=(0, 2\pi/a, 0)$. Again no irreducible

representation occurs more than once, so the Hamiltonian is diagonal. The state denoted by H_1 has the same local symmetry as the state denoted by Γ_1 . However, on moving from the vicinity of one nucleus to that of a neighbouring nucleus the same function is obtained only with its sign reversed. This is indicated in Fig. 5, from which it is also clear that H does have full cubic symmetry. Similarly H_{15} is locally p-like, with a reversal in sign on passing to a neighbouring nucleus, H_{25}' is locally like d_{yz} , d_{zx} and d_{xy} , and H_2' is like f_{xyz} . In considering the energies it is now the locally s- and d-like states which are antibonding and the p- and f-like states which are bonding. There is thus the

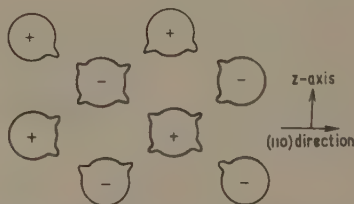


Fig. 5. Schematic diagram showing, for the $[1, 3, 6, 8]$ plane, the local characters of the H_1 -type state at the point H $(0, 2\pi/a, 0)$. The local character is shown to be mainly of s-type modified by a small amount of a g-type orbit. Note the alteration in sign in the y direction.

possibility that the antibonding d-like states will be above the bonding p-like states, and at one time we thought that such an arrangement might help to reduce the amount of d-character in the electronic distribution, as seemed to be required. However, it now seems that the d-character is not greatly different from that of the free atom and in any case such an ordering did not reduce the d-character as much as was apparently needed. There is thus no experimental requirement that H_{15} be below H_{25}' , and a number of theoretical calculations predict the reverse order. We therefore assume that the levels, in order of increasing energy are H_{25}' , H_{15} , H_1 and H_2' . It is possible that the order of H_1 and H_2' is wrong, but this is of no importance since these levels are not occupied by electrons.

§ 7. THE LINE JOINING Γ AND H

Any point on the line Δ which joins Γ and H has $\mathbf{K} = (0, K, 0)$. Except at the points Γ and H , the only rotations of the lattice which permute the Bloch functions are rotations which leave \mathbf{K} unaltered. These are rotations through multiples of $\pi/2$ about the line having direction cosines $(0, 1, 0)$. Reflections in symmetry planes through $(0, 1, 0)$ also permute the Bloch functions. The states can now be conveniently grouped thus:

$$\begin{aligned} \Delta_1: & |\beta(1+2+3+4)\rangle \\ \Delta_1: & |\alpha(1+2-3-4)\rangle \\ \Delta_5: & \begin{cases} |\beta(1-2+3-4)\rangle \\ |\beta(1+2-3-4)\rangle \end{cases} & \Delta_5: & \begin{cases} |\alpha(1-2-3+4)\rangle \\ |\alpha(1+2+3+4)\rangle \end{cases} \\ \Delta_2': & |\beta(1-2-3+4)\rangle & \Delta_2': & |\alpha(1-2+3-4)\rangle \end{aligned}$$

where the Δ_1 , Δ_5 etc. denote the irreducible representations in this smaller group of rotations and reflections. Δ_1 , Δ_5 and Δ_2' each occur twice, so the Hamiltonian is not completely diagonalized by this choice. However, forgetting for the

moment off-diagonal elements, it is instructive to follow the state $|\beta(1+2+3+4)\rangle$ as \mathbf{K} moves along Δ from Γ to H. At Γ this state is the same as Γ_1 , and is s-like locally and bonding. At H it belongs to H_{15} and is locally p_y -like, but still bonding. For some intermediate value of \mathbf{K} the local function is, symbolically,

$$\cos(\tfrac{1}{2}aK)\{s\} + i\sin(\tfrac{1}{2}aK)\{p_y\}$$

and its square modulus, the local charge distribution, gradually becomes more and more elongated in the $\pm y$ direction as K increases. From this it is to be expected that the energy will increase as K increases. However, it must also be remembered that on passing from one nucleus to a neighbouring nucleus, the local function changes by $\exp(i\mathbf{K}\cdot\mathbf{r})$, in this case $\exp(\pm iKa/2)$ for all neighbours. Thus the situation in a region where the local distributions overlap is complicated and difficult to picture. The other level of Δ_1 symmetry, $|\alpha(1+2-3-4)\rangle$, is antibonding f-like at Γ and antibonding s-like at H. The diagonal elements of the two Δ_1 states are unlikely to become equal, so we may expect that the off-diagonal elements, which in any case vanish at Γ and H, will generally have a negligible effect on the states and their energies. Similar considerations hold for all the other states, and the results so far may be summed up diagrammatically as in Fig. 6. Various comments can be made. There is

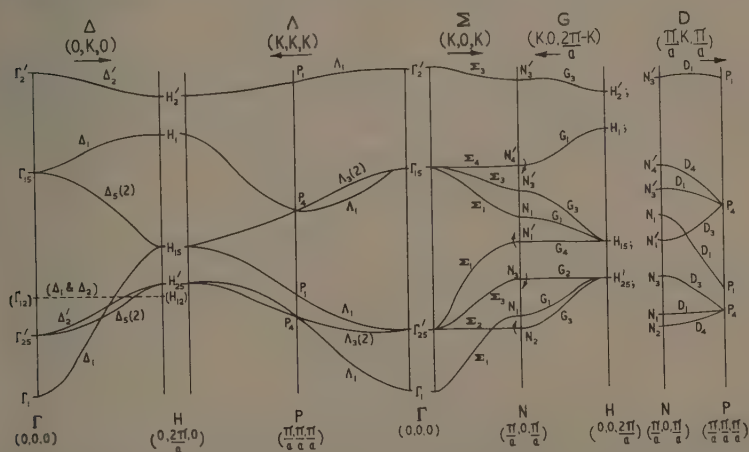


Fig. 6. The predicted energy band structure for a typical body-centred cubic transition metal for various directions in \mathbf{K} space. The doublet e_g band has been inserted only in the Δ direction for clarity and states of the same symmetry have been allowed to cross. Provided that a cross-over does not occur at the Fermi level this approximation has no effect on the ground state determinantal wave-function.

no level of s-like local symmetry throughout which overlaps the other bands, although one frequently reads that in the transition metals there is a broad s-band overlapping the d-band. The broad overlapping band, which does exist, is s-like at Γ , but p-like at H. There are no energy gaps below H_1 . The d_{yz} , d_{zx} and d_{xy} -like states at Γ go into similar states at H, which is consistent with three narrow bands having local d-like symmetry throughout.

§ 8. THE POINT P AND THE LINES JOINING IT TO Γ AND H

Suppose we now choose \mathbf{K} to lie on the line which joins Γ to P, the point $(\pi/a, \pi/a, \pi/a)$. Then $\mathbf{K} = (K, K, K)$. The \mathbf{K} vector is unaltered by rotations about the (1, 1, 1) direction, but the lattice symmetry requires that such rotations be restricted to multiples of $2\pi/3$. Consider that rotation which takes 2 into 4, 4 into 6 and 6 into 2 in Fig. 1. Then $|\beta, 2\rangle$ goes into $|\beta, 4\rangle$, $|\beta, 4\rangle$ into $|\beta, 3\rangle$ and $|\beta, 3\rangle$ into $|\beta, 2\rangle$. There is a slight difference for the α -type states, for $|\alpha, 3\rangle$ and $|\alpha, 4\rangle$ go into $-|\alpha, 2\rangle$ and $-|\alpha, 3\rangle$ respectively, while $|\alpha, 2\rangle$ goes into $|\alpha, 4\rangle$. It is therefore natural to group the states as

$$\begin{aligned}\Lambda_1: & |\beta, 1\rangle \\ \Lambda_1: & |\alpha, 1\rangle \\ \Lambda_1: & |\beta(2+3+4)\rangle \\ \Lambda_1: & |\alpha(2-3+4)\rangle\end{aligned}\quad \begin{aligned}\Lambda_3: & \begin{cases} |\beta(2+\omega 3+\omega^2 4)\rangle \\ |\beta(2+\omega^2 3+\omega 4)\rangle \end{cases} \\ \Lambda_3: & \begin{cases} |\alpha(2-\omega 3+\omega^2 4)\rangle \\ |\alpha(2-\omega^2 3+\omega 4)\rangle \end{cases}\end{aligned}$$

where $\omega = \exp(2\pi i/3)$.

They do not completely diagonalize the Hamiltonian, but show that it gives rise to four singlet and two doublet levels. The singlets are linear combinations of $|\beta, 1\rangle$, $|\alpha, 1\rangle$, $|\beta, 2+3+4\rangle$ and $|\alpha(2-3+4)\rangle$ and if one of the states in a doublet is

$$\lambda|\beta(2+\omega 3+\omega^2 4)\rangle + \mu|\alpha(2-\omega 3+\omega^2 4)\rangle$$

the other is

$$\lambda|\beta(2+\omega^2 3+\omega 4)\rangle + \mu|\alpha(2-\omega^2 3+\omega 4)\rangle.$$

At Γ , which is the special point (0, 0, 0) on (K, K, K) , there are two triplets and two singlets. To understand the relation of these to the above states we can, for example, form the following linear orthogonal combinations of the states in Γ_{25}' :

$$\begin{aligned}d_{xy} + \omega^2 d_{xz} + \omega d_{xy} \\ d_{zy} + \omega d_{xz} + \omega^2 d_{xy} \\ d_{zy} + d_{xz} + d_{xy}.\end{aligned}$$

Inspection shows that they are the same as

$$\begin{aligned}2|\beta(2+\omega 3+\omega^2 4)\rangle \\ 2|\beta(2+\omega^2 3+\omega 4)\rangle \\ 3|\beta, 1\rangle - |\beta(2+3+4)\rangle\end{aligned}$$

respectively. The first two form a special case of a Λ_3 doublet, with $\lambda=1$, $\mu=0$, and the third is a special case of a Λ_1 singlet. Thus as Γ is approached from the (K, K, K) direction, a Λ_3 doublet and a Λ_1 singlet move into coincidence. The extra symmetry operations available at Γ can then be used to interchange the three states as required for a Γ_{25}' representation. Similarly the states in Γ_{15} can be combined as

$$p_x + \omega p_y + \omega^2 p_z, \quad p_x + \omega^2 p_y + \omega p_z, \quad p_x + p_y + p_z$$

which are respectively the same as

$$-2|\alpha(2-\omega^2 3+\omega 4)\rangle, \quad -2|\alpha(2-\omega 3+\omega^2 4)\rangle \quad \text{and} \quad 3|\alpha, 1\rangle + |\alpha(2-3+4)\rangle$$

and the states in Γ_1 and Γ_2' can clearly be written as Λ_1 singlets.

Results of this type can be obtained quite generally by the methods of B.S.W. but it has seemed of value to derive them by the above algebraic considerations

because the results of group theory are sometimes made clearer by such an investigation. In the notation of B.S.W., Γ_{25}' and Γ_{15} would both be said to be compatible with Λ_3 and Λ_1 , whereas Γ_2' and Γ_1 would both be compatible only with Λ_1 .

It is at first sight surprising that a similar analysis can be given for the states at H, for H does not lie in the (K, K, K) direction. This statement however does not take into account the peculiar structure of the Brillouin zones, as is shown by consideration of what happens if one proceeds along the (K, K, K) direction, through $P(\pi/a, \pi/a, \pi/a)$ to the point $(2\pi/a, 2\pi/a, 2\pi/a)$. In the simple cubic zone scheme this point would be equivalent to $(0, 0, 0)$, but in the body-centred lattice we have seen that both Γ and H correspond to $(0, 0, 0)$ for the simple cubic lattice. It transpires that $(2\pi/a, 2\pi/a, 2\pi/a)$ does in fact correspond to H, and not to Γ . Thus a point equivalent to H lies on (K, K, K) at $(2\pi/a, 2\pi/a, 2\pi/a)$. We shall call this point H'. It is necessary to distinguish between H and H' because of the definitions of our states, which involve terms like $\exp(i\mathbf{K} \cdot \mathbf{R}_n)$. Inspection of our definitions shows that

$$\begin{aligned} |\beta, 1, H\rangle &\equiv -|\beta, 1, H'\rangle, & |\beta, 2, H\rangle &\equiv +|\beta, 2, H'\rangle \\ |\beta, 3, H\rangle &\equiv +|\beta, 3, H'\rangle, & |\beta, 4, H\rangle &\equiv -|\beta, 4, H'\rangle \end{aligned}$$

where the occurrence of H or H' indicates that the corresponding value of \mathbf{K} has been used.

Similar results hold for α -type states. Then, for example, expressing the states at H_{15} in the notation for H', thus:

$$\begin{aligned} p_x &: -|\beta(1+2-3-4)\rangle \\ p_y &: -|\beta(1-2-3+4)\rangle \\ p_z &: -|\beta(1-2+3-4)\rangle \end{aligned}$$

we see that the linear combinations

$$\begin{aligned} p_y + \omega p_x + \omega^2 p_z \\ p_y + \omega^2 p_x + \omega p_z \\ p_y + p_x + p_z \end{aligned}$$

are the same as

$$\begin{aligned} -2|\beta(2+\omega^2 3+\omega 4)\rangle \\ -2|\beta(2+\omega 3+\omega^2 4)\rangle \\ -3|\beta, 1\rangle + |\beta(2+3+4)\rangle \end{aligned}$$

respectively. The value of this result lies in the observation that usually the energy is a reasonably smooth function of \mathbf{K} , so that if we know the energies at Γ and H it is likely that the energies at P will be intermediate between suitable pairs from Γ and H.

At P certain additional symmetry elements can be used, for the local function becomes multiplied by $\exp(i\mathbf{K} \cdot \mathbf{r})$, where $\mathbf{K} \equiv (\pi/a, \pi/a, \pi/a)$ and $\mathbf{r} \equiv \frac{1}{2}a(\pm 1, \pm 1, \pm 1)$, on moving from a given nucleus to a neighbouring nucleus. For neighbours at positions 1, 3, 5 and 7 the factor is $-i$, while for neighbours at 2, 4, 6 and 8 the factor is $+i$. All rotations and reflections which leave the [1357]

tetrahedron invariant can thus be used, and by inspection the states can be grouped thus:

$$\begin{aligned}
 P_1: & -s + if_{xy} & : & |\beta(1-2-3-4)\rangle \\
 P_2: & -f_{xy} + is & : & |\alpha(1+2-3+4)\rangle \\
 P_4: & \begin{cases} -d_{yz} + ip_x & : |\beta(1-2+3+4)\rangle \\ -d_{zx} + ip_y & : |\beta(1+2+3-4)\rangle \\ -d_{xy} + ip_z & : |\beta(1+2-3+4)\rangle \end{cases} \\
 P_4: & \begin{cases} -p_x + id_{yz} & : |\alpha(1+2+3-4)\rangle \\ -p_y + id_{zx} & : |\alpha(1-2+3+4)\rangle \\ -p_z + id_{xy} & : |\alpha(1-2-3-4)\rangle \end{cases}
 \end{aligned}$$

showing that at P there are two singlets and two triplets, the states being suitable linear combinations of the above states, which, as written, do not diagonalize the Hamiltonian completely. The P_1 states are readily seen to be compatible with Λ_1 and the P_4 sets are each compatible with Λ_3 and Λ_1 , as follows, for example, because

$$X + \omega Y + \omega^2 Z, \quad X + \omega^2 Y + \omega Z, \quad X + Y + Z$$

are respectively the same as $2|\alpha(2 - \omega^2 3 + \omega 4)\rangle$, $2|\alpha(2 - \omega 3 + \omega^2 4)\rangle$ and $3|\alpha, 1\rangle - |\alpha(2 - 3 + 4)\rangle$ where $(-p_x + id_{yz})$ has been written as X etc.

If we now study the behaviour of the states as **K** moves from Γ through P to H and require that states of the same symmetry do not cross (for there will always be off-diagonal elements to prevent crossing) it follows that the Λ_1 state which leaves Γ_1 must finish at H_{25}' , and Λ_3 which leaves Γ_{25}' must also end at H_{25}' . However, at P, this Λ_3 must coincide with a Λ_1 , which can only be the Λ_1 coming from Γ_1 . The P_4 triplets are, in their local properties, linear combinations of d_{yz} , d_{zx} and d_{xy} with, respectively, p_x , p_y and p_z . We may expect that the lower of the two P_4 triplets will be dominantly d-like. If it is pure d-like its energy is likely to be intermediate between that of Γ_{25}' and H_{25}' . To allow for small admixtures of p-like states we may suppose that its energy is lower than that for pure d-type; that is, its energy is less than the mean energies of Γ_{25}' and H_{25}' . This is indicated in Fig. 6. It is important now to note that the s-like state at Γ becomes dominantly d-like at P, which is quite different from the usual assumption in transition metals that there is a broad overlapping band of predominantly s-character. We may expect that in going from Γ to P its energy will change appreciably, because of the change in local character. In going from P to H the change in character is much less and we might expect that the Λ_1 and Λ_3 states will here remain quite close in energy. By a similar argument, the Λ_3 doublet which leaves Γ_{15} must end at H_{15} , where it is joined by a Λ_1 singlet. This Λ_1 can only come from Γ_{25}' . Also, at P this Λ_3 doublet is coincident with a Λ_1 singlet, which can only be the singlet joining Γ_{15} to H_1 . Further, the states in Γ_{15} and H_{15} are p-like, the Λ_3 which joins them is predominantly p-like, so we may suppose that the energy of this P_4 is slightly greater than the mean energies of Γ_{15} and H_{15} . It is to be noted that the Λ_1 from Γ_{15} remains mainly p-like to P, and thus remains fairly close to the Λ_3 doublet from Γ_{15} to P_4 . However, the energy change for this singlet from P_4 to H_1 is likely to be appreciable, as the local symmetry is changing. The rest of the energy level structure for Γ -P-H can now be readily deduced as the Λ_1 singlet from Γ_2' can only end at H_2' .

Thus it is seen that from a knowledge of the relative states and energies at Γ and H it is possible to deduce a good deal about the behaviour from Γ to P and then from P to H, which is equivalent to the edge of the first Brillouin zone. This edge is denoted by F (B.S.W.) and as might now be expected, its symmetry properties are the same as those for Λ . This explains why the energy bands joining P to H in Fig. 6 have been labelled by Λ rather than the customary F.

In the first Brillouin zone of the body-centred cubic lattice there is one point labelled Γ , but there are six points equivalent to H, namely $(\pm 2\pi/a, 0, 0)$, $(0, \pm 2\pi/a, 0)$, $(0, 0, \pm 2\pi/a)$. It is immaterial which of the six directions Γ to H are considered, as the energy against $|K|$ curves will be the same for each. The states are not identical except at Γ and H. Similarly the directions from Γ to the four points equivalent to P,

$(\pi/a, \pi/a, \pi/a)$, $(-\pi/a, -\pi/a, \pi/a)$, $(-\pi/a, \pi/a, -\pi/a)$, $(\pi/a, -\pi/a, -\pi/a)$,

give identical curves. The states are only identical at the four equivalent points and at Γ . The same curves are obtained for the lines joining Γ to the other four points equivalent to P,

$(-\pi/a, -\pi/a, -\pi/a)$, $(\pi/a, \pi/a, -\pi/a)$, $(\pi/a, -\pi/a, -\pi/a)$, $(-\pi/a, \pi/a, \pi/a)$,

and the states at these four points are identical but different from those at the other set of four. Most writers on band theory choose the points H, P and N in the positions used by B.S.W. In the present paper we do the same for H and P (though we prefer to use right-handed axis in \mathbf{K} space), but for N it is convenient to make a different choice. The curves for Γ to N will be unaffected by our different choice.

§ 9. THE POINT N and the LINES JOINING IT TO Γ , H and P

We now consider the direction $(K, 0, K)$ and the point $N = (\pi/a, 0, \pi/a)$. For a general value of K the symmetry operations which permute the Bloch functions are rotations through multiples of π about $(1, 0, 1)$ and reflections in the symmetry planes through this line. The functions group naturally as:

$$\begin{aligned}\Sigma_1: |\beta(1+4)\rangle, & \quad \Sigma_1: |\alpha(1+4)\rangle, & \quad \Sigma_1: |\beta(2+3)\rangle \\ \Sigma_3: |\beta(1-4)\rangle, & \quad \Sigma_3: |\alpha(1-4)\rangle, & \quad \Sigma_3: |\alpha(2-3)\rangle \\ \Sigma_2: |\beta(2-3)\rangle, & & \quad \Sigma_4: |\alpha(2+3)\rangle\end{aligned}$$

All the levels will be non-degenerate, there being three Σ_1 -type bands with the states compounded from the three above Σ_1 states, three Σ_3 bands, one Σ_2 and one Σ_4 band. At Γ , which is a special point on this line, $|\beta(2-3)\rangle$ is locally the same as $[d_{yz} - d_{xy}]/\sqrt{2}$, which is a typical d-like function but so orientated that it is perpendicular to the $(1, 0, 1)$ direction. This result is also obtained for a general K , except that the local function changes by $\exp(i\mathbf{K} \cdot \mathbf{r})$ on moving from one nucleus to another. However, if it is assumed that the local d-function is more or less confined to the $[2367]$ plane it is to be expected that because \mathbf{K} is perpendicular to this plane, the energy variation with K will be small. This has been emphasized in Fig. 6 by drawing Σ_2 as if its energy were independent of K . In fact at Γ it is entirely bonding and at N it has some antibonding features

so it is probable that its energy increases slightly from Γ to N . A somewhat similar picture emerges for Σ_4 , which is locally p-like with the p-axis perpendicular to K . It is presumably more sensitive to K , for p-functions are less planar than d's, and we would thus expect the Σ_4 state which leaves Γ_{15} to decrease slightly in energy as N is approached, where it is more bonding. At N extra symmetry arises because on moving to a neighbour in the 2, 3, 6 or 7 direction the local function is unaltered, whereas for neighbours in the 1, 5, 8 and 4 directions the local function is reversed. The functions can now be grouped as:

$$\begin{array}{lll} N_1 : s + d_{xy} & : |\alpha(1+4)\rangle & N_1 : s - d_{xy} : |\beta(2+3)\rangle \\ N_1' : p_x + p_z & : |\beta(1+4)\rangle & \\ N_2 : -d_{xy} + d_{yz} & : |\beta(2-3)\rangle & \\ N_4' : p_z - p_x & : |\alpha(2+3)\rangle & \\ N_3 : d_{xy} + d_{yz} & : |\alpha(1-4)\rangle & \\ N_3' : p_y - f_{xyz} & : |\alpha(2-3)\rangle & N_3' : f_{xyz} + p_y : |\beta(1-4)\rangle \end{array}$$

It can easily be seen that N_1 and N_1' are both compatible with Σ_1 , N_3 and N_3' are both compatible with Σ_3 , N_4' with Σ_4 and N_2 with Σ_2 . Now consider $|\alpha(1-4)\rangle$. This is a d-like function locally, lying in the [1485] plane. On moving to a neighbouring site in this plane, the local function reverses, so that as far as this particular plane is concerned the function is the same as one which can be constructed from the three antibonding d-functions in H_{25}' . There is a difference between the two functions on moving to neighbours in the [2376] plane, for at N there is no change in the local function, whereas at H the local function is reversed in sign. If then it is assumed that the d-like function is confined to the [2376] plane the energy of N_3 will be the same as that of H_{25}' . This result is indicated in Fig. 6, though in fact because N_3 is more bonding than H_{25}' it will be slightly lower in energy than H_{25}' . This result may also be deduced by considering the direction $G = (K, 0, 2\pi/a - K)$ which joins $H(0, 0, 2\pi/a)$ to $N(\pi/a, 0, \pi/a)$, for the [1485] plane is perpendicular to this direction. N_3 is compatible with Σ_3 , which is compatible with Γ_{25}' , so we expect to have a Σ_3 level joining Γ_{25}' and N_3 . Similarly $|\beta(1+4)\rangle$ is a p-like function with its axis in the [1485] plane, and it bears the same relation to one of the states in H_{15} as $|\alpha(1-4)\rangle$ does to one of the states in H_{25}' . The p-like functions will be less planar than the d-like functions, so we expect N_1' to be slightly higher in energy than H_{15} . Compatibility requires that this level be joined to Γ_{25}' by a Σ_1 level. The only other state of physical importance is the Σ_1 state which leaves Γ_1 , and becomes N_1 at N . It will be a linear combination of $|\alpha(1+4)\rangle$ and $|\beta(2+3)\rangle$ at N . Now $\{|\alpha(1+4)\rangle + |\beta(2+3)\rangle\}$ is locally s-like, with four bonding and four antibonding neighbours, so its mean energy is likely to be intermediate between that of Γ_1 and H_1 . Similarly $\{|\beta(2+3)\rangle - |\alpha(1+4)\rangle\}$ is locally the same as $\{|\beta(2+3)\rangle - |\beta(1+4)\rangle\}$ at Γ . That is, it is locally like d_{xz} , with four bonding and four antibonding neighbours. Its mean energy will therefore lie between Γ_{25}' and H_{25}' . This energy is probably less than the energy of

$$\{|\alpha(1+4)\rangle + |\beta(2+3)\rangle\}$$

so we infer that the Σ_1 level which leaves Γ_1 arrives at N (where it is denoted by N_1) with an energy somewhat less than the mean energy of Γ_{25}' and H_{25}' . Thus we are able to deduce a good deal about the direction $(K, 0, K)$ from a

straightforward study of the local character of the respective states. On continuing along Σ beyond N, the point $(2\pi/a, 0, 2\pi/a)$, which belongs to Γ in both the simple cubic and body-centred Brillouin zone schemes, is reached. As the energy levels at N are all singlets, the energy versus \mathbf{K} curves are horizontal at N.

At this stage we have dealt with all the points in the Brillouin zone of high symmetry, and the lines joining these to Γ and also the line P to H. The lines N to H and N to P can be investigated using similar methods, though for the behaviours of the bands it is enough to know the compatibility relations. The results of such a study are given in Fig. 6.

It may be noted that there is no implication that covalent bonds occur in b.c.c. transition metals, for the properties of the symmetric and antisymmetric 'link' functions, which might be termed bonding and antibonding, are removed when Bloch functions are formed.

§ 10. THE e_g BANDS

The above discussion began with a model which seemed to incorporate the idea of covalent bonds between neighbouring atoms and then went over into a band description. It might therefore be thought to be satisfactory as it incorporates a number of features which seem to be needed. It is however deficient in one very important respect. From the point of view of symmetry operations it would have been desirable, in building the initial directed orbitals, to have used states which transform according to all the irreducible representations of the cubic group. In fact a number of irreducible representations were not used, namely Γ_2 , Γ_{12} , Γ_{15}' , Γ_1' , Γ_{12}' and Γ_{25} . To see whether anything important has been omitted we may ask what atomic orbitals transform according to these representations. Without going into full details the answer is that Γ_{12} is spanned by the $x^2 - y^2$, $3x^2 - r^2$ orbitals, but that none of the others occur with principal quantum number less than 4. The latter are unlikely to be important in the 3d transition group and can safely be ignored. $3d_{x^2-y^2}$ and $3d_{3x^2-r^2}$ cannot, however be ignored.

In attempting to incorporate $d_{x^2-y^2}$ and $d_{3x^2-r^2}$ there is no reason to introduce hybridization, and the first step is to form Bloch functions from them in the standard way, with the orbitals centred on lattice points. We should now go back to the beginning in our problem of finding the eigenfunctions, and work with ten Bloch functions for each \mathbf{K} . That is, the eight we have discussed at length above, and the two new ones from $d_{x^2-y^2}$ and $d_{3x^2-r^2}$, which are usually referred to as e_g bands. This however is unnecessary if the matrix elements between the original eight and the two new ones are small compared with the energy differences, for we can then use perturbation theory. Our first step is to show that there is good reason to suppose that the matrix elements are indeed small. They are not small compared to the energy differences for all values of \mathbf{K} , for on neglecting them levels of the same symmetry will cross for certain values of \mathbf{K} . At these points there will be a good deal of mixing of the levels, but if the matrix elements are small this mixing will be confined to very limited regions in \mathbf{K} space and, as will be shown later, can probably be neglected as far as physical properties are concerned.

The reason we suppose that the matrix elements are small is that, in their evaluation, it is necessary to determine the matrix elements of the lattice potential between $d_{x^2-y^2}$ and $d_{3x^2-r^2}$ orbitals located on lattice sites and bonding or

antibonding functions located on links. From simple symmetry arguments all such matrix elements are zero if the lattice site is at one end of the link. The only contributions come from lattice sites and links for which the link does not join up to the lattice site in question. Thus the magnitudes depend on the radial extents of the $d_{x^2-y^2}$ and $d_{3z^2-r^2}$ orbitals and the localization of the bonding and antibonding orbitals. But the important observation is that the elements which might have been expected to give the major contribution do in fact give zero for symmetry reasons. Further, there is no reason to suppose, in a cubic environment, that the radial parts of the $d_{x^2-y^2}$ and $d_{3z^2-r^2}$ functions (which will be identical) will be the same as the radial parts of d_{xy} , d_{yz} and d_{zx} . We suggest that, possibly because of the bonding which takes place, the interatomic spacing is determined so that the radial extent of d_{xy} , d_{yz} and d_{zx} is expanded in the metal compared with that in the free atom but that the radial extent of $d_{x^2-y^2}$ and $d_{3z^2-r^2}$ is much the same as in the atom; this does, in fact, make the latter 'inner' orbitals in the metal. Any tendency in this direction decreases the matrix elements between the eight and the two, and leads to the concept of pure $d_{x^2-y^2}$ and $d_{3z^2-r^2}$ or e_g bands. (In accord with common usage, the $d_{x^2-y^2}$ and $d_{3z^2-r^2}$ atomic orbitals are referred to as e_g orbits instead of Γ_{12} , the B.S.W. notation used elsewhere in this paper). The variation in energy with \mathbf{K} of these bands is determined by overlap of functions on different nuclei, and the more 'inner' these orbitals are the less the energy will vary with \mathbf{K} . Also xy etc. at Γ_{25}' have lower energies than in the atoms whereas xy etc. at Γ_{25}' have higher energies than in the atoms. We therefore expect the $3d_{x^2-y^2}$ and $3d_{3z^2-r^2}$ bands to be narrow and lie between these limits. In an exaggeration of the expected situation and for clarity, we have drawn the two extra bands in the direction Δ only, with energy independent of \mathbf{K} , and have allowed states of the same symmetry to cross (Fig. 6). It may be noticed that no concept of crystal field splitting has been used.

It is difficult to compare directly the band structure calculations discussed here with previous work due to the nature of, and the many differences in, the approximations and assumptions made. Many previous discussions and calculations on the band theory of iron have been published (Manning 1943, Slater 1953, Slater and Koster 1954, Callaway 1955, Stern 1959) and a detailed study has been undertaken at the Massachusetts Institute of Technology (Wood 1960, Slater and Wood†).

The forms of the energy bands deduced here from simple physical consideration are supported by the much more detailed calculations of Wood for the same symmetry directions.

§ 11. THE ELECTRONIC ARRANGEMENT

Having obtained a band structure for a number of points and directions in \mathbf{K} space it is possible, by interpolation, to infer something about the density of states curve. However, recent thinking suggests that the independent electron model is not perhaps the best way of viewing the situation, and we shall therefore be concerned first with the ground state of the many electron system, and then excited states which are only slightly above the ground state in energy. To obtain the ground state, we have to place the electrons in suitable states to give the minimum possible energy and we assume that this can be done in some cases to a good approximation, by filling up the band scheme with paired-off electrons to

† see footnote to p. 1321.

Fermi level. The many-electron wave function is then a single determinantal function.

The low temperature phase of titanium is close-packed hexagonal, so it would seem appropriate to begin our discussion of the transition metals with vanadium, which is body-centred cubic and has five electrons outside the argon core. An examination of the energies up to H_{25}' shows that, ignoring the e_g bands, there are three complete bands starting from Γ_{25}' and part, probably about one half, of the band which starts from Γ_1 . Thus up to energy H_{25}' , we might expect to be able to accommodate about seven electrons even without using the e_g bands. In vanadium it would seem that the five electrons can be accommodated in the single band from Γ_1 and the three bands from Γ_{25}' filled up to a level which is somewhere between Γ_{25}' and H_{25}' in energy, and which is probably nearer to H_{25}' than to Γ_{25}' , since the number of states with a given $|\mathbf{K}|$ increases with \mathbf{K} in regions away from the zone boundaries. We assume that the e_g bands are above this level and are unoccupied. The Hall constant of vanadium has been measured by Foner (1957) who reports that it is positive. To account for this we need to study the slightly excited states which may not be single determinantal states, at least in our representation. It is, however, interesting to note that, on the independent electron model, the electrons at the top of the distribution in the bands from Γ_{25}' probably have $\partial^2 E / \partial K^2$ negative and so behave as positive charge carriers. The electrons in the band which starts at Γ_1 may not act as positive charge carriers, in which case the question arises as to whether their mobilities are less than or greater than those of the positive holes. In the direction Γ to P it is seen that although the band from Γ_1 starts as s-like it is d-like at P, and we suggest that there is no real reason to suppose that the mobilities of the electrons at the Fermi level in the band from Γ_1 will be substantially different from those of the holes in the other bands. The hole contribution to the Hall effect will then outweigh the electron contribution.

Chromium, the next body-centred cubic metal, has six electrons per atom to be accommodated. They can be accommodated below H_{25}' without using the e_g levels, but it may be that some of the electrons are in the e_g levels. However, chromium is known to be antiferromagnetic, so our use of a simple determinantal function to describe the ground state cannot be correct, and it is not entirely clear how to proceed. One observation though may be important; states near H_{25}' are now being used and an electron in one of these is aware of the crystal structure, since the wavelength of its Bloch function is comparable with the lattice parameter. It may be that this property helps to stabilize an antiferromagnetic structure (Friedel, Leman and Olszewski 1960, private communication). (It may also have a bearing on the alloying properties of chromium.)

Above H_{25}' the band structure has the special feature that an electron has a very limited choice of levels. Below H_{25}' , and for any line through Γ , there will, in general, be several states of the same energy. Above H_{25}' (but below H_{15}) there will only be one state. Thus on moving to the next metal, manganese, the extra electrons, one per atom, will either have to go into levels of appreciably higher energy or they will have to go into the e_g levels, assuming these are energetically suitable. The interesting fact is that manganese does neither of these things, for it does not have a body-centred cubic lattice, suggesting either that e_g is not available (in which case it is probably not available in chromium either)

or that, having put electrons into e_g , the lattice undergoes a Jahn-Teller type of distortion (Griffith and Orgel 1958).

The next metal, iron, with eight electrons per atom outside the argon core, is body-centred cubic at low temperatures, and is ferromagnetic. Mott and Stevens (1957) explain this by postulating that the ground state is approximately one in which the extra two electrons above chromium (for which it can be assumed that e_g is empty) are in the e_g bands with their spins parallel. If the e_g bands are regarded as consisting of + spin and - spin bands, the bands of + spin are completely full, whereas the - spin bands are empty. The + spins do not take part in electrical conduction etc., because the + band is full. Further, by using a well-known theorem (Wannier 1937) an equivalent description can be given in terms of localized Wannier functions. In this description it is then seen that the energy associated with the determinantal state is not simply that given by summing the energies of all the occupied single electron states, but that there is likely to be an important contribution from the so-called exchange interactions between parallel spins on the same lattice site. There are other smaller energy terms as well; the importance of this intra-atomic energy is that it provides an explanation of why a ground state with a large spin moment is energetically favoured. It is further postulated that the low-lying excited states are like spin-wave states in which spin-deviations of unity are propagating through the lattice. States which consist dominantly of determinantal functions in which electrons have either been removed from e_g and placed at the Fermi level, or have been taken from the Fermi level and placed in the empty e_g - spin bands are supposed to be appreciably higher in energy.

A number of further refinements can be added, though these are more easily described physically than mathematically. In atoms it is known that the energies of outer unpaired electrons are spin dependent when there are unpaired electrons in inner shells. That is, the spins of outer electrons have a tendency to set parallel to the spins of inner electrons. In the model of iron it therefore seems reasonable to suppose that the conduction bands (that is, all the bands except e_g) should also be regarded as composed of separate + and - spin bands, and that, due to the localized moments, the K^+ states will be lower in energy than the K^- , at least near the Fermi level. On filling to a Fermi level there will then be a spin polarization in the conduction band. As this polarization is due to the localized moments and is in an electron distribution which conducts, there is the further desirable effect that, through it, the localized moments are indirectly coupled. There is also a more subtle effect, as follows. It has been assumed that there are no matrix elements of the lattice potential between the e_g bands and the other bands. Suppose now that this is not true, and that there are small off-diagonal elements. When these are included the e_g bands and the conduction bands will be repelled slightly. But the e_g + bands are filled and are below the Fermi level. Thus a + spin conduction state near the Fermi level will have its energy increased. On the other hand the e_g - bands are empty and are thus above the Fermi level, so that a - spin conduction state at the Fermi level has its energy reduced. Anderson (1960, private communication) argues that the net result of this effect and the direct spin polarization effect is to give almost a cancellation, which helps to remove the difficulty of accounting for the relatively small spin polarization actually observed in the conduction bands.

Having lifted the assumption that there are no matrix elements between the e_g and the conduction bands a further step is possible, particularly where bands could otherwise cross. Consider an $e_g K^+$ state which has almost the same energy as a K^+ conduction state. If we assume that both of these states contain electrons then the determinantal function is unaltered by using the correct linear combinations to diagonalize the sub-matrix. The same argument can be given for t_{2g} spin states which cross, except that now neither state will contain electrons. Thus the neglect of the off-diagonal elements is not an approximation provided that both the states involved either do or do not contain electrons. The possibility that, with such a pair of states, one does and the other does not contain electrons seems unlikely with small off-diagonal matrix elements.

There are no other body-centred cubic metals in the first transition group, so it seems appropriate to end our discussion of the implications of the band structure which we have deduced, at this point. There are, of course, many properties of vanadium, chromium and iron which we have not considered, some of which seem to support our band scheme and some of which are difficult to interpret. It is our hope, though, that the rather lengthy discussion which we have given will improve the accuracy of some of the criticisms which have been levelled at the Mott and Stevens theory of iron, by providing a better target.

ACKNOWLEDGMENTS

The authors wish to thank Professor N. F. Mott for stimulating discussions and correspondence and one of us (C.A.B.) is indebted to the Department of Scientific and Industrial Research for financial support.

REFERENCES

- BLOCH, F., 1928, *Z. Phys.*, **52**, 555.
 BOUCKAERT, L. P., SMOLUCHOWSKI, R., and WIGNER, E., 1936, *Phys. Rev.*, **50**, 58. (referred to as B.S.W.)
 CALLAWAY, J., 1955, *Phys. Rev.*, **99**, 500.
 FONER, S., 1957, *Phys. Rev.*, **107**, 1513.
 GRIFFITH, J. S., and ORGEL, L. E., 1958, *Nature, Lond.*, **181**, 170.
 HALL, G. G., 1952, *Phil. Mag.*, **43**, 338.
 ——— 1953 a, *Phys. Rev.*, **90**, 317.
 ——— 1953 b, *Proc. Phys. Soc. A*, **66**, 1162.
 ——— 1958, *Phil. Mag.*, **3**, 429.
 HERRING, C., 1960, *J. Appl. Phys.*, **31**, 3S.
 MANNING, M. F., 1943, *Phys. Rev.*, **63**, 190.
 MARSHALL, W., and WEISS, R. J., 1959, *J. Appl. Phys.*, **30**, 220S.
 MOTT, N. F., and STEVENS, K. W. H., 1957, *Phil. Mag.*, **2**, 1364.
 SLATER, J. C., 1953, *Rev. Mod. Phys.*, **25**, 199.
 SLATER, J. C., and KOSTER, G. F., 1954, *Phys. Rev.*, **94**, 1498.
 STERN, F., 1959, *Phys. Rev.*, **116**, 1399.
 WANNIER, G. H., 1937, *Phys. Rev.*, **52**, 191.
 WOOD, J. H., 1960, *Phys. Rev.*, **117**, 714.

Electron Spin Resonance in Two Salts containing Gadolinium

By J. M. BAKER AND F. I. B. WILLIAMS†

Clarendon Laboratory, Oxford

MS. received 1st June 1961

Abstract. The electron spin resonance spectra of Gd^{3+} have been measured in gadolinium hexa-antipyrene iodide (HAPI), lanthanum HAPI, and cadmium fluoride. In CdF_2 the Gd^{3+} ions are sometimes in sites of cubic and sometimes in sites of tetragonal symmetry. In the latter the zero field splitting is remarkably small, being about 0.05 cm^{-1} . In the HAPI there is a large zero field splitting, about 0.98 cm^{-1} overall, and even in the undiluted salt the line width is only about 230 gauss, so that it may be suitable for a zero field maser. An Appendix gives a discussion of the general problem of rotation of the frame of reference in which the crystal field is described so that the spin Hamiltonian may be written in a form diagonal in the applied magnetic field. The coefficients have been tabulated for the polynomials involved in the general rotation matrix for the operator equivalents. The polynomials have been plotted as a function of angle. There is also a table of factors to relate some of the untabulated matrix elements of the operator equivalents to the Wigner 3- j symbols.

§ 1. INTRODUCTION

THE trivalent gadolinium ion, which is in an S state, is the natural one to choose to investigate the symmetry of the crystalline electric field about a site for lanthanon ions in a host crystal. The electron spin resonance spectrum is normally visible at liquid air temperatures, if not above, and the symmetry of the spin Hamiltonian reflects that of the crystal field.

There is also the possibility, as the eightfold degeneracy of the ground state is partially raised by high-order effects of the crystal field, that the magnitude of the zero magnetic field splittings may be such as to make the crystal a useful maser element.

The gadolinium spectrum has been studied in two salts, cadmium fluoride, and gadolinium hexa-antipyrene iodide both pure and diluted with the lanthanum salt. The former material was kindly grown from the melt by Dr. R. W. H. Stevenson of Aberdeen University; the latter is easily grown from aqueous solution following the recipe given by Marsh (1951).

Cadmium fluoride belongs to the O_h^5 space group, and is isomorphous with calcium fluoride, but its lattice constant is slightly smaller— 5.40 \AA as compared with 5.45 \AA . It is of interest to compare the spectra of gadolinium in these two salts. In calcium fluoride one sometimes finds that the symmetry of the gadolinium site is cubic like that of the calcium which it replaces, and sometimes it is tetragonal (Friedman and Low 1960). Low has shown that the two forms are interconvertible by the appropriate heat treatment. The tetragonal symmetry is thought to be due to an interstitial fluorine ion in a site near the trivalent ion; whether such ions have a chance to diffuse to this energetically favoured site, or get trapped in other parts of the lattice, depends upon the way in which the melt is cooled.

† Now at Institut d'Astrophysique, Cointe-Selessin, Belgium.

The hexa-antipyrene iodides (HAPI) are of interest because they are very magnetically dilute. The chemical formula $[\text{Ln}(\text{C}_{11}\text{H}_{12}\text{ON}_2)_6]\text{I}_3$ indicates that there are a large number of diamagnetic atoms between the paramagnetic ones. One might thus expect to find narrow electron spin resonance lines even in a material which has not been diluted with the isomorphous diamagnetic lanthanon salt. This in itself would be a great convenience in preparing samples for maser use. The HAPI are also of interest because they form a homologous series throughout the lanthanon group in which it might be possible to study the effects of a uniform crystal environment on all of the lanthanon ions. The results of this complete investigation are discussed in the following paper (Baker and Rubins 1961, to be referred to as II).

Preliminary investigations by x-ray methods of the crystal structure of gadolinium HAPI have been made independently by Dr. G. Garton of the Clarendon Laboratory and Dr. J. W. Jeffery of the University of London. They find that the space group is $R\bar{3}$ and that the symmetry at the lanthanon site is probably $\bar{3}$. This symmetry is confirmed by the electron spin resonance measurements. Dr. Garton also measured the hexagonal unit cell dimensions obtaining $a = 13.5 \text{ \AA}$ and $c = 33.5 \text{ \AA}$; there are three molecules in this cell, all three metal ions having identical magnetic properties.

§ 2. THE SPIN HAMILTONIAN

For both crystals the spin Hamiltonian takes the same form

$$\mathcal{H} = \beta \mathbf{H} \cdot \mathbf{g} \cdot \mathbf{S} + \sum_0^2 B_2^m O_2^m + \sum_0^4 B_4^m O_4^m + \sum_0^6 B_6^m O_6^m,$$

where the O_n^m are operator equivalents in the notation of Baker, Bleaney and Hayes (1958). These O_n^m are present in the sums which transform in the same way as the symmetry operations of the point symmetry of the lanthanon site. For the cubic form in cadmium fluoride

$$\mathcal{H} = \beta \mathbf{H} \cdot \mathbf{g} \cdot \mathbf{S} + B_4(O_4^0 + 5O_4^4) + B_6(O_6^0 - 21O_6^4),$$

and the tetragonal form may be written in the following way so that the departure from cubic symmetry is apparent:

$$\mathcal{H} = \beta \mathbf{H} \cdot \mathbf{g} \cdot \mathbf{S} + B_2^0 O_2^0 + B_4(O_4^0 + 5O_4^4) + B_4^0 O_4^0 + B_6(O_6^0 - 21O_6^4) + B_6^0 O_6^0.$$

For the hexa-antipyrene iodides the spin Hamiltonian may be written in terms of the z axis parallel to the hexagonal crystal axis as

$$\mathcal{H} = \beta \mathbf{H} \cdot \mathbf{g} \cdot \mathbf{S} + B_2^0 O_2^0 + B_4^0 O_4^0 + B_4^3 O_4^3 + B_6^0 O_6^0 + B_6^3 O_6^3 + B_6^6 O_6^6.$$

The hyperfine structure terms have been omitted in all of these spin Hamiltonians.

When the external field is not directed along the axis in terms of which the operator equivalents have been defined it is often convenient to work in terms of a set of axes rotated so that the new z axis is parallel to the applied field. In this representation the Zeeman term in the spin Hamiltonian, which is usually the largest, is diagonal and the effects of the crystalline field may be treated by perturbation theory. The way in which the operator equivalents transform under such a rotation is discussed in the Appendix.

§ 3. CADMIUM FLUORIDE

Two batches of crystals were grown from powders of different origins. Both were grown from the melt by the same method. The first batch, A, had about 0.05% Mn^{2+} impurity, while the other, B, had less than 0.01%. Crystals of batch A, containing 4, 0.5 and 0.03% gadolinium to cadmium, gave only cubic spectra except that the most concentrated one showed numerous weak lines (more than 50) of other symmetries, but these were too weak to analyse. Crystals of batch B, containing 1, 0.1 and 0.03% gadolinium to cadmium, all had about 40% of these impurity ions in cubic sites and the other 60% in three non-equivalent tetragonal sites whose principal axes corresponded with those of the cubic ones.

The spin Hamiltonians for both these cases were given in the last section. The values of the parameters of these Hamiltonians are listed below and compared with those for calcium fluoride. All our measurements were made at room temperature and with 1.4 cm microwaves.

Table 1

Diluent Symmetry parameter	Cadmium fluoride		Calcium fluoride	
	Cubic	Tetragonal	Cubic (Low 1958)	Tetragonal (Sierro & Lacroix 1960)
$3B_0^0$	—	42 ± 3	—	$+1488 \pm 5$
$60B_4^0$	47.4 ± 0.3	45.2 ± 1.0	$+46.25 \pm 0.5$	30.4 ± 2.0
$60B_4^0$	—	1.5 ± 0.3	—	-7 ± 3
$1260B_6^0$	0.0 ± 0.3	0.0 ± 0.3	-1.0 ± 0.5	0.1 ± 0.3
$1260B_6^0$	—	0.2 ± 0.5	—	1 ± 2
g	1.992 ± 0.002	1.992 ± 0.002	1.991 ± 0.002	1.993 ± 0.003

Table 2. Spin Hamiltonian Parameters for Gd HAPI

	Undilute 300°K	300°K	Dilute 90°K
g_{\parallel}	1.990 ± 0.002	1.991 ± 0.003	1.9931 ± 0.0005
g_{\perp}	—	1.989 ± 0.003	—
$3B_0^0$	711 ± 5	$702.7^{+2.5}_{-0.2}$	$827^{+2.5}_{-0.2}$
$60B_4^0$	1.72 ± 0.35	1.3 ± 1.6	2.8 ± 1.6
$[3B_4^0]$	—	—	8.0 ± 1.8
$1260B_6^0$	-0.8 ± 0.5	-0.8 ± 1.0	-1.1 ± 1.0
$[36B_6^0]$	—	—	0.8 ± 1.4
$1260B_6^0$	†	7.3 ± 0.9	6.9 ± 0.5

The B_4^0 and B_6^0 terms are $\sim 15^\circ$ out of phase. All B_n^m are given in units of 10^{-4} cm^{-1} .

† Too small to be measured, sixfold variation within the line width.

The signs are only relative except those of Low. All crystal field parameters are in units of 10^{-4} cm^{-1} .

The doubling reported by Ryter (1957) and Horai (1960) for the cubic spectrum of the calcium fluoride when the magnetic field was not along a principal axis was not seen here.

§ 4. HEXA-ANTIPYRENE IODIDE

Measurements were made on both the undiluted salt and on a crystal of the lanthanum salt containing 0.3% Gd. As the crystal field splitting is large measurements were made at K-band (~ 23 Gc/s). The parameters of the spin Hamiltonian are listed in Table 2. The values of g_{\parallel} , B_2^0 , B_4^0 , B_6^0 were obtained from the spectrum when the magnetic field was parallel to the crystal axis. When it is in the plane perpendicular to this axis the spin Hamiltonian becomes

$$\mathcal{H} = g_{\perp} \beta H S_z - \frac{1}{2} B_2^0 O_2^0 + \frac{3}{8} B_4^0 O_4^0 - \frac{5}{16} B_6^0 O_6^0 + \frac{1}{16} B_6^6 \cos 6\alpha O_6^0 \\ + \frac{3}{2} B_2^2 O_2^2 + \frac{15}{32} B_6^6 O_6^2 \cos 6\alpha + \dots,$$

where other terms are too small to give significant contributions and α is the rotational angle in the plane (see Appendix, Euler angles α , $\pi/2$, 0). Thus one observes a sixfold rotational symmetry from which the B_6^6 term may be found. The B_4^3 and B_6^3 coefficients were found by comparing the spectra on either side of the crystal axis in a plane containing it. For a given angle β to the axis the even coefficients will give the same contribution on both sides of the axis, but the odd terms will change sign. Thus upon a rotation (α , β , 0) O_4^3 becomes

$$\frac{1}{8} \sin^3 \beta \cos \beta O_4^0 \cos 3\alpha + \dots,$$

and O_6^3 becomes $\frac{1}{16} \sin^3 \beta \cos \beta (11 \cos^2 \beta - 3) O_6^0 \cos 3\alpha + \dots$. The largest O_4^0 term occurs at $\beta = 60^\circ$ and the largest O_6^0 term at $\beta = 39^\circ$, and the size of B_4^3 and B_6^3 were obtained from measurements at these two angles to the axis of the crystals.

There are small changes in the parameters for the dilute salt between room temperature and 90°K . The signs in the table are relative only. It was not possible to determine the absolute signs as this requires going to temperatures sufficiently low that the population differences between the various states give rise to noticeable intensity differences between the lines, and at these temperatures the crystal structure has undergone a change in which the number of ions in the unit cell changes, and the point symmetry at the gadolinium site is rhombic (see II). In this distorted low temperature state the spectrum is very complicated and there are a large number of overlapping lines so no measurements were made in this temperature region.

Above the transition the narrowest lines observed in the lanthanum salt containing small quantities of Gd^{3+} or Ce^{3+} (see II) are 10 gauss wide, suggesting that this is the line width due to nuclei in the material. This indicates that there are some protons which are near neighbours to the lanthanon ions; the other nuclei in the antipyrene molecule would not give such a large line width at likely interatomic distances of about 2\AA .

In the undiluted salt the central line of the Gd^{3+} spectrum, measured with the external field parallel to the crystal axis, is 230 ± 10 gauss wide. This is greater than the root mean square line width calculated from the theory of Van Vleck (1948) for dipolar interaction between similar ions, and this theory would give too high an estimate as ions in different states cannot be regarded as similar. The other transitions have broader lines indicating that there is some spread of crystal field splitting over the ions in the crystal. This effect is frequently observed in the Gd^{3+} spectrum in other host crystals; also in other HAPI salts there is evidence (see II) that even above the transition there is incipient distortion of the C_{3v} point symmetry at the lanthanon site.

§ 5. DISCUSSION

Above its transition temperature (about 90°K for the undiluted salt and 15°K when diluted with the lanthanum salt) the HAPI has some interest as a maser material as it has a large zero field splitting, about 0.98 cm^{-1} overall. It also has only one type of magnetic ion in the unit cell, is easy to prepare as large specimens and the lines in the undiluted salt are narrow compared with other undiluted lanthanon salts so far investigated by electron spin resonance. It has of course the disadvantage that it is water soluble; it appears otherwise to be fairly stable, but it does tend to crack after many successive coolings to low temperatures. It compares favourably in stability with potassium cobaltcyanide which has been used extensively as a maser material.

Cadmium fluoride, doped with gadolinium, is a more stable material as it is grown from the melt and has no water of crystallization. However, its small crystal field splitting, even in the tetragonal crystal field, makes it of no use as a low field maser.

It is of interest to compare the crystal field parameters for Gd^{3+} in CdF_2 with those for CaF_2 . When the crystal field is cubic the parameters in the two host crystals are nearly equal. This is to be expected as the lattice constants are little different, and also because the gadolinium ion is larger than the ion it replaces, it probably influences the position of its ligands more than the host lattice. However, the tetragonal crystal fields in the two host lattices are quite different. In CdF_2 the axial terms are much smaller and also the B_4 and B_6 terms are approximately the same as they are in the cubic field. There is evidence that when some trivalent ions are incorporated in CaF_2 charge compensation is achieved by an interstitial fluorine $\frac{1}{2}a$ along the $\langle 100 \rangle$ direction from the trivalent ion; this causes the tetragonal terms in the crystal field (see, e.g. Baker, Hayes and O'Brien 1960). It seems reasonable to suppose that this is the mechanism for Gd^{3+} in CaF_2 in view of the large effect. If the charge compensation mechanism is the same in both CaF_2 and CdF_2 and the large differences in B_2^0 arise because this term is extremely sensitive to the differences between lattice constants, one expects this term to be very temperature sensitive. A rough experiment cooling CdF_2 to 90°K shows that this term increases by only $23 \pm 6\%$. B_4 in the cubic sites increases by $7 \pm 3\%$. The strain produced by cooling CaF_2 to 90°K is about 0.4%; that produced in CdF_2 will probably be somewhat smaller, about $\frac{1}{3}$ the change in lattice parameter between CaF_2 and CdF_2 . Hence it is possible that there may be a different mechanism in CdF_2 which gives rise to the smaller tetragonal departure from the cubic field. Whatever the mechanism it must be due to an effective additional negative charge situated along the $\langle 100 \rangle$ direction. It is possible that the Ca^{2+} ion distant a is replaced by a monovalent ion, or that there is an F^- ion in the interstitial site $1\frac{1}{2}a$ away. There are objections to both of these possibilities but there is no direct evidence from which the details of the mechanism may be deduced.

In the absence of a complete theory relating the parameters of the crystal field in the spin Hamiltonian to the crystalline electrostatic potential for S state ions one cannot make further deductions from these comparisons or from the absolute values of the measured parameters. This material is the only one so far investigated where the B_2^0 term, when it exists, is smaller than other terms; in all other salts, including the HAPI the B_2^0 term is by far the biggest.

ACKNOWLEDGMENTS

The authors wish to thank Dr. R. W. H. Stevenson for growing the specimens of CdF_2 , Professor Bleaney for his many helpful suggestions, Mr. R. S. Rubins and Dr. W. Hayes for advice, Mr. J. Hurrell and Miss C. Dorlet for making some of the measurements, and Dr. L. Fox for the use of the Oxford University computer. One of the authors (F.I.B.W.) is indebted to the Rhodes Trust for a Scholarship.

REFERENCES

- BAKER, J. M., BLEANEY, B., and HAYES, W., 1958, *Proc. Roy. Soc. A*, **247**, 141.
 BAKER, J. M., HAYES, W., and O'BRIEN, M. C. M., 1960, *Proc. Roy. Soc. A*, **254**, 273.
 BAKER, J. M., JONES, D. A., and POPE, D. F. D., 1959, *Proc. Phys. Soc.*, **74**, 249.
 BAKER, J. A., and RUBINS, R. S., 1961, *Proc. Phys. Soc.*, **78**, 1353.
 EDMONDS, A. R., 1960, *Angular Momentum in Quantum Mechanics* (Princeton: University Press).
 ELLIOTT, R. J., and STEVENS, K. W. H., 1953, *Proc. Roy. Soc. A*, **219**, 387.
 FRIEDMAN, E., and LOW, W., 1960, *J. Chem. Phys.*, **33**, 1275.
 HORAI, K., 1960, *Mem. Fac. Sci. Kyūsyū Univ.*, **B3**, 1.
 JUDD, B. R., 1955, *Proc. Roy. Soc. A*, **227**, 552.
 LOW, W., 1958, *Phys. Rev.*, **109**, 265.
 MARSH, J. K., 1951, *J. Chem. Soc.*, p. 1337.
 ORBACH, R., 1961, *Proc. Roy. Soc. A*, **264**, 458.
 ROTENBERG, M., BIVINS, R., METROPOLIS, N., and WOOTEN, K. J., 1959, *The 3-j and 6-j Symbols* (Cambridge, Massachusetts: Massachusetts Institute of Technology).
 RYTER, C., 1957, *Helv. Phys. Acta.*, **30**, 353.
 SIERRO, J. and LACROIX, R., 1960, *Compte Rendu du 9^e Coll. AMPERE* (Geneva: Groupe-ment AMPERE) p. 194.
 STEVENS, K. W. H., 1952, *Proc. Phys. Soc. A*, **65**, 209.
 VAN VLECK, J. H., 1948, *Phys. Rev.*, **74**, 1168.
 WIGNER, E. P., 1959, *Group Theory and its Applications to the Quantum Mechanics of Atomic Spectra* (New York: Academic Press).

APPENDIX

The most convenient way to find the eigenvalues of the spin Hamiltonian is to use perturbation theory. Often the largest term is the interaction of the magnetic field with the electronic magnetic moment, so that the representation in which this interaction is diagonal is chosen. The crystalline electric field is normally expressed as a series of terms with the symmetry of the spherical harmonics in terms of spherical polar axes determined by the symmetry axes of the crystal structure. We want to re-express this crystal field in terms of a z axis parallel to the direction of the magnetic field.

An expression will be given for the matrix elements of this crystalline field—a real combination of spherical harmonics—within a constant angular momentum manifold for a direction of quantization along the z axis of a set of axes which has been rotated by Euler angles (α, β, γ) from that in which the field is known.

Define

$$\begin{aligned}\Theta_{lm} &= \frac{1}{2} \left(\frac{4\pi}{2l+1} \right)^{1/2} [Y_{lm} + (-1)^m Y_{l-m}] \\ &= (-1)^m \left(\frac{(l-m)!}{(l+m)!} \right)^{1/2} P_l^m(\cos \theta) \cos m\phi \quad \dots\dots (A1)\end{aligned}$$

$$\Theta_{lm}^{(-)} = \frac{1}{2} \left(\frac{4\pi}{2l+1} \right)^{1/2} [Y_{lm} - (-1)^m Y_{l-m}]. \quad \dots\dots (A2)$$

The P_l^m and Y_{lm} are as defined by Edmonds (1960). The Euler angles also correspond to those of Edmonds: α about the original z axis, β about the new y axis and γ about the newer z axis. A positive rotation is one which advances right-hand screw in a positive direction along the axis. Stevens (1952) has given a rule for calculating these matrix elements by using an operator equivalent. Their form and values have been tabulated for most cases usually met (Stevens 1952, Elliott and Stevens 1953, Judd 1955, Baker, Bleaney and Hayes 1955, Baker, Jones and Pope 1959).

The matrix elements of these operators $-O_l^m$ in the notation of Baker, Bleaney and Hayes (1958) are related to those of the Θ_{lm} and to the Wigner 3- j symbols as follows:

$$\begin{aligned}\langle j\mu|\Theta_{lm}|j\mu'\rangle &= \frac{F(l,j)}{K(\gamma,l,j)} f(l,m) \langle j\mu|\Theta_{lm}|j\mu'\rangle \\ &= F(l,j) f(l,m) \left\{ (-1)^{j-\mu} \begin{pmatrix} j & l & j \\ -\mu & m & \mu' \end{pmatrix} + (-1)^{m+j-\mu} \begin{pmatrix} j & l & j \\ -\mu & -m & \mu' \end{pmatrix} \right\} \\ &\quad \dots\dots (A3) \\ f(l,m) &= (-1)^m \left(\frac{(l+m)!}{(l-m)!} \right)^{1/2} / (\text{R.F. of } P_l^m(\cos\theta))\end{aligned}$$

where R.F. means rational factor, γ denotes a dependence on other quantum numbers, j is the angular momentum of the manifold and μ is the projection of j on the z axis.

Using the rotation matrices for the spherical harmonics (e.g. Edmonds 1960, Wigner 1959) and letting $P_{(\alpha,\beta,\gamma)}$ symbolize the rotation of the coordinate system, one finds in the new system that:

$$\begin{aligned}\langle j\mu|P_{(\alpha,\beta,\gamma)}\Theta_{lm}|j\mu'\rangle &= \langle j\mu|d_{lm}^l(\beta) \cos m\alpha \Theta_{l0} \\ &+ \sum_{m'=1}^l \{ d_{m'm}^l(\beta) \exp[\mp i(m\alpha + m'\gamma)] \\ &+ (-1)^{m'} d_{-m'm}^l(\beta) \exp[\pm i(m\alpha - m'\gamma)] \} \Theta_{lm'}|j\mu'\rangle, \dots\dots (A4)\end{aligned}$$

where

$$\begin{aligned}d_{m'm}^l(\beta) &= (-1)^{l-m'} d_{-m'm}^l(\beta - \pi) = \left(\frac{(l+m')!(l-m')!}{(l+m)!(l-m)!} \right)^{1/2} \\ &\times \sum_s \binom{l+m}{l-m'+s} \binom{l-m}{s} (-1)^{l-m'-s} \left(\cos \frac{\beta}{2} \right)^{2s+m'+m} \left(\sin \frac{\beta}{2} \right)^{2l-2s-m'-m}.\end{aligned}$$

The top signs are used for $\mu' > \mu$ and the bottom ones for $\mu > \mu'$

since

$$\langle j\mu|\Theta_{lm}^{(-)}|j\mu \pm m\rangle = \mp \langle j\mu|\Theta_{lm}|j\mu \pm m\rangle.$$

γ may often be chosen arbitrarily—as, for example, in our case since the magnetic field is axially symmetric—to simplify the expression.

There are two special cases of particular interest. (i) One wants to know the diagonal matrix elements to see how a spectrum should behave to first order

under a general rotation of the magnetic field. These are simply proportional to the Legendre polynomials. In terms of the O_l^m ,

$$\langle j\mu | P_{(\alpha, \beta, \gamma)} O_l^m | j\mu \rangle = \frac{\text{R.F. of } P_l^0(\cos \theta)}{\text{R.F. of } P_l^m(\cos \theta)} P_l^m(\cos \beta) \times \cos m\alpha \langle j\mu | O_l^0 | j\mu \rangle. \dots (A5)$$

(ii) One wants to rotate the magnetic field (and with it the quantization axis) in a plane perpendicular to the z axis of the coordinates in which the field is known. Here the solution for all the matrix elements is quite simple. It may be shown that, for $(-1)^l = 1$,

$$\begin{aligned} \langle j\mu | P_{(\alpha, \frac{1}{2}\pi, \gamma)} O_{lm} | j\mu' \rangle &= \langle j\mu | d_{0m}^l(\tfrac{1}{2}\pi) \cos m\alpha \Theta_{l0} \\ &+ 2 \sum_{m'=1}^l [\delta_{(-1)^{m-m'}} \cos m\alpha \exp(\mp im'\gamma) - \delta_{(-1)^{m-m'}, -1} \sin m\alpha \\ &\times \exp[\mp i(m'\gamma + \tfrac{1}{2}\pi)] d_{m'm}^l(\tfrac{1}{2}\pi) \Theta_{lm'} | j\mu' \rangle \dots (A6) \end{aligned}$$

where δ_{mn} is the Kronecker delta. These matrix elements have been tabulated for all even l and m up to $l=6$ by Baker, Jones and Pope (1959). Their results are obtained by putting $\gamma = \pi/2$ which should make all their matrix elements real.

NUMERICAL CALCULATION OF THE MATRIX ELEMENTS UNDER A GENERAL ROTATION

For $\gamma=0$, Eqn (A4) may be written in terms of the O_l^m as follows:

$$\begin{aligned} \langle j\mu | P_{(\alpha, \beta, 0)} O_l^m | j\mu' \rangle &= \langle j\mu | D_{0m}^l \cos m\alpha O_l^0 + \sum_{m'=1}^l \{ D_{m'm}^{l+} \cos m\alpha \\ &\pm i D_{m'm}^{l-} \sin m\alpha \} O_l^{m'} | j\mu' \rangle, \end{aligned}$$

where again the top sign is used for $\mu' > \mu$ and the bottom one for $\mu > \mu'$. These $D_{m'm}^{l\pm}$ have been calculated at 5° intervals for $\beta=0^\circ$ to 90° on the Oxford University Mercury computer. They are plotted in Figs (1) to (11) for $m=0, 2, 3, 4, 6$ and $l=2, 4, 6$.

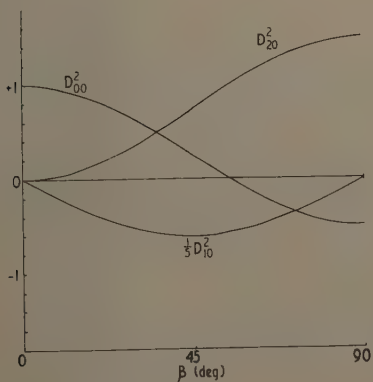


Fig. 1

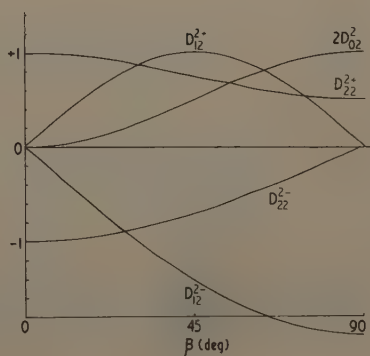


Fig. 2

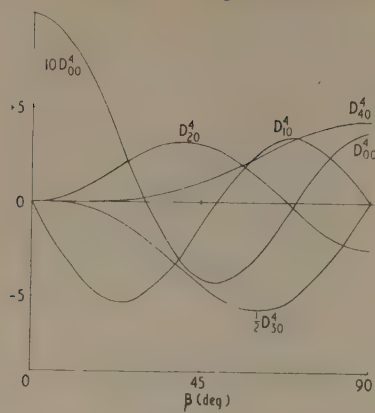


Fig. 3

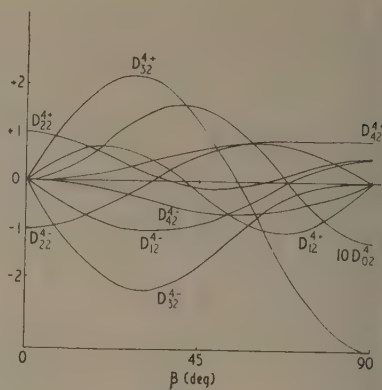


Fig. 4

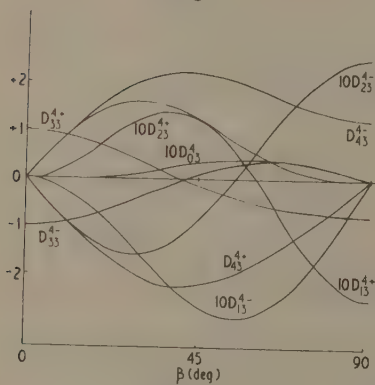


Fig. 5

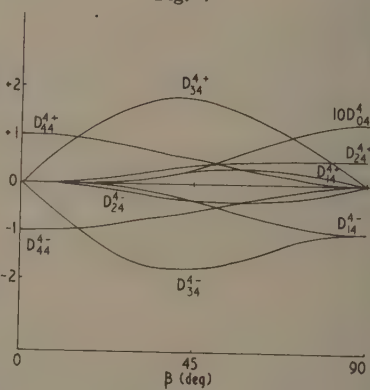


Fig. 6

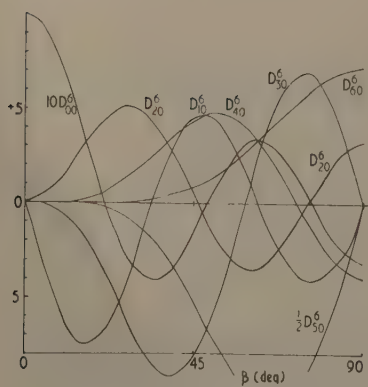


Fig. 7

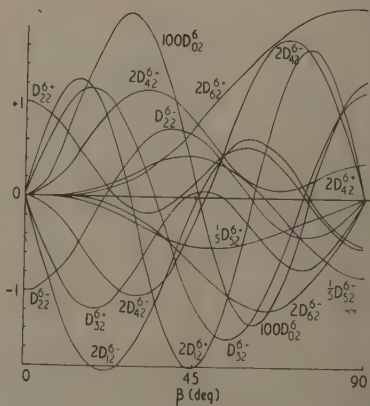


Fig. 8

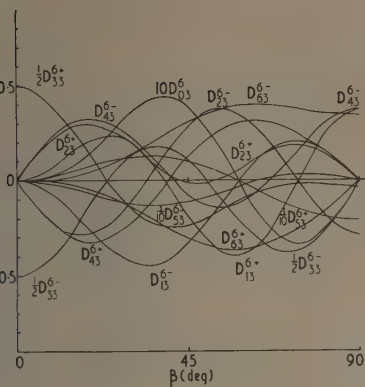


Fig. 9

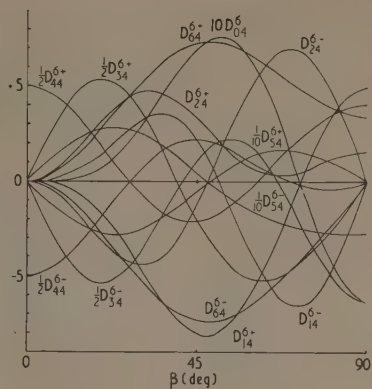


Fig. 10

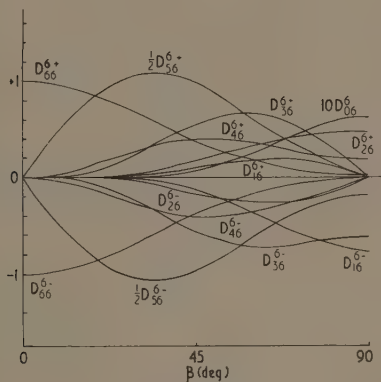


Fig. 11

These $D_{m'm}^{l\pm}$, like the $d_{m'm}^l(\beta)$, may be written as a homogeneous polynomial of order 21 in $\sin(\beta/2)$ and $\cos(\beta/2)$. Specifically,

$$D_{0m}^l = \sum_{n=0}^{2l} B_n \left(\cos \frac{\beta}{2} \right)^n \left(\sin \frac{\beta}{2} \right)^{2l-n}$$

$$D_{m'm}^{l\pm} = \sum_{n=0}^{2l} B_n \left[(-1)^{l+n} \left(\sin \frac{\beta}{2} \right)^n \left(\cos \frac{\beta}{2} \right)^{2l-n} \pm \left(\cos \frac{\beta}{2} \right)^n \left(\sin \frac{\beta}{2} \right)^{2l-n} \right].$$

The B_n , which are functions of l , m and m' only, are tabulated in Tables 3(a)-(c).

MATRIX ELEMENTS OF $O_2^1 O_4^1 O_6^1$ AND O_6^5

Since these are proportional to the Wigner 3- j symbols, which are tabulated up to $j=8$ (Rotenberg *et al.* 1959), only the factors of proportionality have been given—the $F(l, j)f(l, m)$ of Eqn (A3). They are in Table 4. Orbach (1961) has tabulated the explicit forms of these operators.

Table 3(c). Table of B_n [illegible]

Table 4. Factors relating some Operator Equivalents to the Wigner 3- j Symbols

Operator equivalent	O_a^1	O_b^1	O_c^1	O_d^6
j			$F(l, j)f(l, m)$	
1/2				
1	*201			
3/2	* <u>1</u> 11			
2	*1111,	*1401,		
5/2	* <u>1</u> 011,	*2411,		
3	*1211,	*1411, 1	*3420, 11	*4320, 01
7/2	* <u>0</u> 211,	*3411, 1	*4421, 11	*5321, 01
4	*1111, 1	*1411, 11	*3531, 11	*4431, 01
9/2	*1210, 1	*2402, 11	*7431, 11	*8331, 01
5	*2210, 11	*1412, 11	*5431, 111	*6331, 011
11/2	* <u>1</u> 011, 11	*5411, 11	*6621, 111	*7521, 011
6	* <u>2</u> 111, 11	*2411, 111	*5521, 1111,	*6421, 0111,
13/2	*2111, 01	*3411, 111	*7530, 1111,	*8430, 0111,
7	*0011, 011	*2401, 1111,	*4631, 1111,	*5531, 0111,
15/2	*1211, 001	*4411, 0111,	*5431, 2111,	*6331, 1111,
8	*0210, 0011,	*2412, 0111,	*4421, 2111, 1	*5321, 1111, 1

The n th digit represents the power of the n th prime starting with 2 and it is understood that the square root of the product is to be taken. An asterisk denotes that the negative square root is to be used and a line underneath indicates that the power is negative. This convention follows that of Rotenberg *et al.* (1959).

Electron Spin Resonance in Two Groups of Lanthanon Salts

BY J. M. BAKER AND R. S. RUBINS†

Clarendon Laboratory, Oxford

MS. received 1st June 1961

Abstract. Electron spin resonance measurements have been made on lanthanon ions in the hexa-antipyrene iodide (HAPI) salts and also in lanthanum trifluoride. At room temperature the HAPI have trigonal symmetry with one lanthanon ion per unit cell but at low temperatures there is a change of crystal structure. For all ions except Ce^{3+} and Gd^{3+} electron spin resonance is observed only at temperatures below the transition. The lanthanon ion in the HAPI at low temperatures and in the trifluoride have rhombohedral point symmetry and there are several ions in the unit cell. Not all ions with Kramers degeneracy exhibited resonance in both salts, and the few non-Kramers cases investigated also exhibited no resonance. In both salts the most extensive measurements were made on Ce^{3+} . In the HAPI Ce^{3+} has a remarkably long relaxation time and the spectrum is visible at 90°K . The measurements on Ce^{3+} in LaF_3 are correlated with the theoretical discussion given by Van Vleck and Hebb in 1934.

§ 1. INTRODUCTION

SOME of the most interesting results of electron spin resonance studies of the lanthanon ions have come from homologous series of salts. In such salts the crystalline electric field varies from one lanthanon ion to the next mainly because of the change in the radial dependence of the 4f electron wave function, and not because of a change of surroundings. For example in the thyl sulphates (Elliott and Stevens 1952) it has been possible to find the parameters which describe the crystal field from the electron spin resonance spectrum of one of the ions. Approximate extrapolation to neighbouring lanthanon ions could then be refined from a detailed knowledge provided by the electron spin resonance spectrum.

This paper describes measurements on two similar series: the hexa-antipyrene iodides (HAPI), a truly homologous series, and lanthanum fluoride containing about 0.3% of the other lanthanons as impurities (incorporation of this small quantity has been found possible in spite of the fact that the trifluorides do not form a homologous series throughout the whole group).

Either of these series might be of interest as maser elements. They contain no water of crystallization and so may be expected to withstand successive coolings to low temperatures without cracking (in fact the HAPI crystals do sometimes crack at low temperatures). Exchange interactions between lanthanon neighbours are likely to be small as the 4f electrons are deep seated in the ion, and it

† Now at Department of Physics, The Hebrew University, Jerusalem.

may be possible to work with quite a high concentration of paramagnetic ions, indeed the HAPI may be sufficiently dilute without the addition of the diamagnetic salt as the lanthanon ions are about 8 Å apart.

§ 2. THE LANTHANON HEXA-ANTIPYRENE IODIDES

The hope that one might be able to make an extrapolation of the crystal field from one lanthanon ion to the next in the group was frustrated by a crystallographic transition at low temperatures. The simple C_{3v} symmetry with one magnetically distinguishable ion in the unit cell, which was found morphologically and by x-ray analysis by both Dr. G. Garton and Dr. J. W. Jeffery (both unpublished), becomes distorted below the transition temperature into a symmetry with more than one ion in the unit cell.

The transition temperatures in the various lanthanon salts have been studied by observing the spectrum of about 1% Gd^{3+} incorporated into each of them. The results of these experiments are shown in Table 1. The transition is seen to depend on the size of the lanthanon ion; in particular the upper temperature limit of the transition varies in an approximately linear manner with ionic radius.

Table 1. Transition Data for Hexa-antipyrene Iodides

Metal ion	Radius	Upper limit of the transition ($^{\circ}K$)	Approximate range of transition	No. of ions per unit cell at $20^{\circ}K$
Yb^{3+}	1.00	130		
Er^{3+}	1.04	125		
Y^{3+}	1.06	120	125–20	12
Dy^{3+}	1.07	120	120–20	12
Tb^{3+}	1.09	100		
Gd^{3+}	1.11	80	100–20	12
Nd^{3+}	1.15	60		
Pr^{3+}	1.16	60	60–25	6
Ce^{3+}	1.18	40	60–25	6
La^{3+}	1.23	15	40–15	3
			15–5	1

Note a. At $20^{\circ}K$ resonance lines from Yb^{3+} obscure those from Gd^{3+} .

Note b. Below $90^{\circ}K$ Gd^{3+} lines broaden to about 100 gauss $\frac{1}{2}$ width.

Note c. Lines are too broad for detailed investigation.

With the exceptions of Ce^{3+} and La^{3+} HAPI, investigations were not taken below $14^{\circ}K$.

By measuring the resonant frequency of a cavity containing the crystal it was established that there is no large change in dielectric constant at the transition. Nuclear resonance of the protons in a crystal of NdHAPI showed no change of line width between room temperature and $14^{\circ}K$, indicating that the transition does not arise because of the freezing out of hindered rotations of large molecular groups. It thus seems most likely that the transition is related to small movements of the molecular groups surrounding the lanthanon ion.

2.1. Resonance Results

Most of the measurements were made on the Ce^{3+} ion, as it is the only ion apart from Gd^{3+} (Baker and Williams 1961, to be referred to as I) which is observable both above and below the transition. Resonance was also observed (Rubins 1961) in the Nd^{3+} , Er^{3+} and Yb^{3+} salts at $4^{\circ}K$ but the rhombic g -tensors do not uniquely define the ground state. No resonance was observed in the Dy^{3+} salt, although in a rhombic crystal field one is expected. In the Nd^{3+} salt diluted with

the La^{3+} salt, no resonance was observed; this may be due to a very small value of g_{\perp} , but this is unlikely to be the reason in other cases. In ions without Kramers degeneracy transitions are unlikely as all the states are probably singlets in a rhombic field; no resonance was observed in Tb^{3+} or Pr^{3+} , the only two such ions studied.

The cerium spectrum is remarkable in that it can be observed at 90°K . This indicates a considerably longer spin-lattice relaxation time than that found in cerium salts previously. Line width measurements show that T_1 is approximately 3.5×10^{-10} sec at 90°K and greater than 10^{-9} sec at 20°K . The spectrum has been observed in the undiluted salt and also in the lanthanum and neodymium salts containing 1% Ce^{3+} . The spin Hamiltonian for each ion is:

$$\mathcal{H} = g_x \beta H_x S_x + g_y \beta H_y S_y + g_z \beta H_z S_z \quad \dots\dots (1)$$

where g_x , g_y and g_z are the principal values of the g -tensor and $S = \frac{1}{2}$. The g -values and number of ions in the unit cell are given in Table 2. Where there is one ion in the unit cell the symmetry is axial; and when there are more than one it is orthorhombic. In the latter case the principal direction of the g -tensor corresponding to the largest principal value g_z lies very close to the crystal axis; the angle θ in the table is that between these two directions. Changes in the g -value are seen to occur over a much wider range than that of the transition region. At temperatures too low for spin-lattice relaxation to contribute, the line width in both dilute (see I) and undiluted salts in the parallel direction is about that expected from dipolar interaction; but in the perpendicular direction it is much greater. This is probably due to a spread of values of g_{\perp} due to the incipient distortion.

The only other ion which was measured completely is neodymium. Resonance is observed at 4.2°K and below. There are three ions in the unit cell with g -values $g_x = 0.51 \pm 0.01$, $g_y = 0.77 \pm 0.02$, $g_z = 4.34 \pm 0.05$; the angle between the z axis and the crystal axis is 10° .

2.2. Discussion

The g values of Ce^{3+} above the transition cannot be fitted to any ground state within $J=5/2$ in a field of C_{3v} symmetry. They can be fitted with admixtures to the ground state from the $J=7/2$ state, but there are too many parameters for unambiguous fitting. The rhombic g -values below the transition are also easily fitted by a suitable admixture of states by the rhombic terms, but here again there are too many parameters for unambiguous assignment.

It is hoped that additional information might become available about the excited levels from susceptibility or infra-red absorption measurements, or about the crystal field when the surroundings of the lanthanone ion are completely determined by x-ray analysis. If complete information were obtained it would be of considerable interest to attempt to explain theoretically the spin-lattice relaxation in view of the great difference between the relaxation time in this salt and that in other cerium salts.

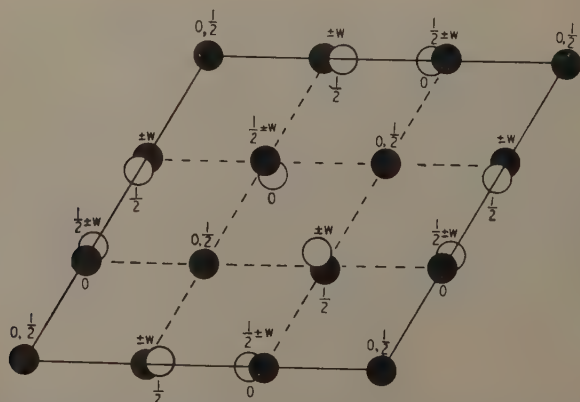
§ 3. LANTHANUM TRIFLUORIDE

Two slightly different crystal structures have been proposed for LaF_3 . One has a bimolecular unit cell with $C6/mmc$ symmetry, the other a hexamolecular cell with $C6/mcm$ symmetry (see Wyckoff 1951); the latter is derived from the

Table 2. g -values of Ce^{3+} in HAPI Salts

Diluent metal ion	La^{3+}	Ce^{3+}	Nd^{3+}
Temperature			
90°K		$2.62 \pm 0.01(1)$ $g_{\perp} = 0.553 \pm 0.002$	
60°K	$2.664 \pm 0.005(1)$		
20°K	$2.686 \pm 0.001(1)$ $g_{\perp} = 0.5281 \pm 0.0003$	$2.649 \pm 0.002(6)$ $g_{\parallel} = 0.51 \pm 0.01$ $g_{\perp} = 0.55 \pm 0.01$ $\theta = 3 \pm 1$	$2.619 \pm 0.003(6)$ $\theta = 5 \pm 1$
14°K	$2.687 \pm 0.002(1)$		
4°K	$2.692 \pm 0.004(3)$ $\theta = 5 \pm 1^{\circ}$		

former by very slight displacements of the lanthanon ions. The electron spin resonance results on Gd^{3+} in LaF_3 favoured the hexamolecular structure as three magnetically distinct ions were observed in the unit cell; the six ions in the hexamolecular unit cell being magnetically equivalent in pairs. The present results on other lanthanon impurities also favour the hexamolecular cell. The Figure is a sketch of the positions of the F^{-} and La^{3+} ions in this hexamolecular structure. The surroundings of a lanthanon ion have orthorhombic symmetry. In non-S-state ions with Kramers degeneracy the crystalline electric field will give rise to a ground doublet with a rhombic g -tensor. Two of the principal values of this tensor lie in the plane perpendicular to the crystal axis and the overall hexagonal symmetry of the crystal requires that the six ions in the unit cell fall into three groups of two, the two ions in each group being identical and the g -tensors of the three groups being the same except for 120° rotations about the crystal axis: this is the situation in Gd^{3+} .



Plan of the hexamolecular unit cell of CeF_3 . The shaded circles are F^{-} ions and the unshaded ones Ce^{3+} ions. Numbers above the circles are the coordinates of the F^{-} and those below the circles refer to Ce^{3+} ; $w = 0.175$.

The measurements on Ce^{3+} are compared with the interpretation by Van Leck and Hebb (1934) of the susceptibility of CeF_3 and the Faraday rotation in pysonite, where it was necessary to postulate 3 or 6 ions in the unit cell, each in rhombic crystal field of the type described in the last paragraph.

3.1. Resonance Results

The crystals used for this work were grown from the melt by Dr. D. A. Jones in Aberdeen. The details of the method used are described by Jones, Baker and Pope (1959).

Resonance lines from those ions which have Kramers degeneracy have been observed either at 20 or 4°K. There are six ions in the unit cell with identical but differently oriented g -tensors. These are derived from one another by 120° rotations about the crystal axis and reflection in the plane perpendicular to it. The spin Hamiltonian for each ion is given by Eqn (1) in § 2.1 if hyperfine structure is neglected. One Cartesian axis, chosen to be the y axis, lies in the plane perpendicular to the crystal hexad axis. This plane is easily determined in LaF_3 , as it is a cleavage plane which reflects light in an almost metallic manner. The other two Cartesian axes bear no obvious relationship to the external crystal faces; of these, the z axis is assumed to make an angle θ with the crystal axis. The resonance results which are set out in Table 3, show that in general the spectra are strongly rhombic.

Table 3. Resonance Results for Rare Earth Ions in Lanthanum Trifluoride

Ion	Temp. (°K)	g					HFS(gauss)
		g_z	g_x	g_y	θ		
$\text{Ce}^{3+} 4f^1$	20	2.608 ± 0.005	0.32 ± 0.01	0.90 ± 0.02	14 ± 1		
$\text{Nd}^{3+} 4f^3$	4.2	3.11 ± 0.03	1.356 ± 0.006	1.092 ± 0.005	45 ± 2		
$\text{Dy}^{3+} 4f^9$	4.2	13.8 ± 0.5	7.0 ± 0.5	1.5 ± 0.1	9 ± 3		
$\text{Er}^{3+} 4f^{11}$	20	10.89 ± 0.05	2.99 ± 0.05	4.91 ± 0.04	44 ± 1		$73.5 \pm 2.0 \dagger$
	14	11.09 ± 0.04	2.98 ± 0.03	4.91 ± 0.03	$45 \pm \frac{1}{2}$		
$\text{Yb}^{3+} 4f^{13}$	20	1.210 ± 0.005	3.76 ± 0.03	5.20 ± 0.01	10 ± 3		$586 \pm 20 \ddagger$

Note 1. In the results for Dy^{3+} , the large error quoted for g_z arises from the extrapolation method used to determine this quantity, that for g_x arises from the large line width at this orientation, and that for g_y from the large effect on the g -value of a slight misorientation of the crystal.

Note 2. θ was generally obtained by measuring the angle of rotation of the magnet between the z -direction and the parallel direction. For Er^{3+} , however, θ was determined by measuring g_{\parallel} and using the relation $g_{\parallel}^2 = g_x^2 \sin^2 \theta + g_z^2 \cos^2 \theta$

† cf. 71.5 ± 0.4 in LaCl_3 (Hutchison and Wong 1958) and 72 ± 1 gauss in CaF_2 (see Orton 1959).

‡ cf. 572.0 ± 5 in yttrium acetate (Cooke and Park 1956).

No resonance lines were observed from the crystal containing Pr^{3+} when experiments were conducted at 20°K or 14°K with both the steady and microwave magnetic field directed parallel to the crystal axis. The negative result is not

surprising as one would expect a singlet state to lie lowest in a 'non-Kramers' ion situated in a crystalline field of such low symmetry. For this reason no experiment at 4.2°K was carried out.

3.2. *g*-values of Cerium—Discussion

In view of the rhombic spectrum which is observed in Ce^{3+} , it is convenient to begin by assuming the ground doublet to be of the form

$$a|\frac{5}{2}, \pm \frac{5}{2}\rangle + b|\frac{5}{2}, \pm \frac{1}{2}\rangle + c|\frac{5}{2}, \mp \frac{3}{2}\rangle$$

where admixtures from the $J=7/2$ level are neglected.

The principal *g*-values are then given by:

$$\begin{aligned} g_z &= 6(5a^2 + b^2 - 3c^2)/7 \\ \frac{1}{2}|g_x + g_y| &= 6(2\sqrt{5ac} + 3b^2)/7 \\ \frac{1}{2}|g_x - g_y| &= 6(4\sqrt{2bc})/7 \end{aligned}$$

where $a^2 + b^2 + c^2 = 1$.

The best set of values for *a*, *b* and *c* is $a=0.717$, $b=0.604$, $c=-0.216$ which give *g*-values $g_x=0.33$, $g_y=0.93$ and $g_z=2.71$. The differences between the theoretical and experimental values are small and may be accounted for in terms of admixtures from the higher $J=7/2$ level, which is only some 2240 cm^{-1} (Lang 1936) above the ground state.

It is of interest to compare these values for *a*, *b* and *c* with those obtained by Van Vleck and Hebb (1934). Using the measurements of Becquerel and de Haas (1934) on the Faraday rotation in Tysonite, and the susceptibility of CeF_3 powder (de Haas and Gorter 1930), they inferred that $g_{\parallel}=2.36$ and $g_{\perp}=1.44$, and obtained for the ground state parameters $a=0.762$, $b=0.525$, $c=-0.379$.

For comparison of these *g*-values our *g*-tensor has a value $g_{\parallel}=2.53$ along the crystal axis and $g_{\perp}=0.81$ as an average in the perpendicular plane. The discrepancies between these two results may be due to (i) other paramagnetic impurities contributing to the Faraday rotation (ii) differences between the lattice spacing of Tysonite and lanthanum trifluoride leading to different *g*-values.

3.3. *g*-values of Ytterbium—Discussion

In Yb^{3+} the ground state is a $J=7/2$ level and is separated by 10300 cm^{-1} from the excited $J=5/2$ level (Gobrecht 1938). In view of the large separation, admixtures from the excited level should be negligible. Thus if the crystal field is of rhombic symmetry it should be possible to fit the experimentally determined *g*-values exactly to a ground state of the form:

$$a|\frac{7}{2}, \pm \frac{7}{2}\rangle + b|\frac{7}{2}, \mp \frac{3}{2}\rangle + c|\frac{7}{2}, \mp \frac{1}{2}\rangle + d|\frac{7}{2}, \mp \frac{5}{2}\rangle$$

where $a^2 + b^2 + c^2 = 1$. The principal *g*-values are given by

$$\begin{aligned} g_z &= 8(7a^2 + 3b^2 - c^2 - 5d^2)/7 \\ \frac{1}{2}|g_x + g_y| &= 8(2\sqrt{7ad} + 2\sqrt{15bc})/7 \\ \frac{1}{2}|g_x - g_y| &= 8(2\sqrt{12bd} + 4c^2)/7. \end{aligned}$$

Fairly close agreement is obtained by taking $a=\pm 0.13$, $b=\mp 0.73$, $c=0.64$, $d=\pm 0.20$ which gives principal *g*-values $g_z=1.2$, $g_x=3.6$, $g_y=5.0$. The agreement is close but not exact, suggesting that the crystal field may not be one of purely rhombic symmetry.

3.4. Discussion

The measurements on Ce^{3+} in LaF_3 are in essential agreement with the theory of Van Vleck and Hebb but give more detailed information about the ground state of the ion than the experiments on which their theory was based. Our results go further in that they suggest six rather than three ions in the unit cell: from the measurements on bulk properties it was not possible to distinguish between these two possibilities.

Unlike the measurements on Gd^{3+} in LaF_3 the present results indicate even lower point symmetry at the lanthanon site than that suggested by the crystallographic arrangement described in § 1. To explain the present results one needs further distortion of the surroundings of the lanthanon ion, or a displacement of the lanthanon ion out of the plane of the diagram in the Figure. In order to maintain the overall crystal symmetry it would be necessary to displace some ions upwards and some downwards, hence making all six ions magnetically nonequivalent. In a site of such low symmetry one would need to know a great deal about the excited states as well as the ground state of a lanthanon ion before the crystal field acting on it could be determined. As one cannot therefore interpret the g -tensors of the various impurities in terms of the crystal field one cannot say how much the crystal field varies from ion to ion. However, the fact that the symmetry for Gd^{3+} is entirely different from that of the other ions suggests that the crystal field does depend upon the nature of the impurity ion. Thus, although our results support the hexamolecular unit cell structure, the electron spin resonance data from which this support is derived is all taken from impurity sites in mixed crystals, so that one cannot positively infer that the hexamolecular cell is also appropriate for the pure lanthanum trifluoride.

§ 4. CONCLUSION

Although some results of interest have come out of this investigation as described in the previous sections, the low point symmetry of the lanthanon sites and the large number of ions in the unit cell in both crystal structures makes the salts of little general interest. For this reason the measurements were not extended to other specimens. For the same reason they would not make useful maser elements with any paramagnetic ion except gadolinium. The properties of the gadolinium salts as maser elements have been discussed by Jones, Baker and Pope (1959) and by Baker and Williams (Paper I).

ACKNOWLEDGMENTS

It is with great pleasure that we acknowledge the untiring assistance given to us by Dr. D. A. Jones of Aberdeen University in preparing the lanthanon trifluoride specimens. We wish to thank Professor B. Bleaney for the interest he has shown in this work and the many helpful suggestions he has made. We are indebted to Dr. G. Garton and Dr. J. W. Jeffery for allowing us to quote some of the results of their crystal structure determinations. We are grateful to Professor R. V. Jones for providing the crystal growing facilities, and to the Board of Admiralty and the U.S. Air Force for financial support.

REFERENCES

- BAKER, J. M., and WILLIAMS, F. I. B., 1961, *Proc. Phys. Soc.*, **78**, 1340.
BECQUEREL, J., DE HAAS, W. J., and VAN DEN HANDEL, J., 1934, *Physica*, **1**, 383.
COOKE, A. H., and PARK, J. G., 1956, *Proc. Phys. Soc. A*, **69**, 282.
ELLIOTT, R. J., and STEVENS, K. W. H., 1952, *Proc. Roy. Soc. A*, **215**, 437.
GOBRECHT, H., 1938, *Ann. Phys., Lpz.* **31**, 755.
DE HAAS, W. J., and GORTER, C. J., 1930, *Proc. Acad. Sci. Amst.*, **33**, 349.
HUTCHISON, C. A., and WONG, E., 1958, *J. Chem. Phys.*, **29**, 754.
JONES, D. A., BAKER, J. M., and POPE, D. F. D., 1959, *Proc. Phys. Soc.*, **74**, 249.
LANG, R. J., 1936, *Canad. J. Res.*, **14**, 127.
ORTON, J. W., 1959, *Rep. Progr. Phys.*, **22**, 204 (London: Physical Society).
RUBINS, R. S., 1961, *Thesis*, University of Oxford.
VAN VLECK, J. H., and HEBB, M. H., 1934, *Phys. Rev.*, **46**, 17.
WYCKOFF, R. W. G., 1951, *Crystal Structures*, Vol. II (New York: Interscience).

The Lorenz Parameter in Dilute Silver-Manganese Alloys at Liquid Helium Temperatures

By M. S. R. CHARI

National Physical Laboratory of India, New Delhi, India

MS. received 14th February 1961, in revised form 23rd June 1961

Abstract. Thermal conductivity data at liquid helium temperatures, on polycrystalline rods of three dilute silver alloys (containing respectively 0.55, 0.32 and 0.14 at. % of manganese in solid solution) in magnetic fields ranging from 0 to 25 kilogauss, have been analysed afresh. The electronic and lattice components of the thermal conductivity are separated by the method of Grüneisen and de Haas. It is inferred that the electronic Lorenz parameter L_e (i) is independent of the magnetic field but varies with the temperature in the liquid helium region, (ii) exhibits a minimum at a temperature which increases with the increase in manganese content, and (iii) is much smaller than the normal 'Sommerfeld' value, but seems to extrapolate to that value at about 1°K.

This behaviour of L_e is explained on the basis of inelastic scattering of the conduction electrons by the magnetic impurity centres having closely spaced energy states, for such an inelastic scattering would contribute considerably to the electronic thermal resistivity while making only a small contribution to the electrical resistivity. Further, since such a scattering cannot occur at 0°K, L_e should approach the normal value at the lowest temperatures.

§ 1. INTRODUCTION

Low temperature electrical resistivity measurements (Gerritsen and Linde 1951a) on silver alloys containing small amounts of manganese in solid solution, showed that instead of attaining a temperature-independent 'residual' resistivity at low temperatures, each of them exhibited a resistance minimum somewhat below liquid hydrogen temperatures, followed by a maximum T_m at still lower temperatures. The electrical magnetoresistance was also found (Gerritsen and Linde 1951b) to be anomalous, being negative, below a temperature T_1 (T_1 being somewhat higher than T_m). Korringa and Gerritsen (1953) made a close study of such behaviour in a number of noble metal alloys containing a small amount of transitional metal in solid solution, and suggested that this behaviour could be due to a re-arrangement scattering of the electrons from the impurity, with resonance close to the Fermi level. They visualized electron states localized near the impurity ion and split by the magnetic interaction so as to lie just above and below the Fermi level.

Owen *et al.* (1957) and Van Itterbeek, Peelaers and Steffens (1960) studied the magnetic susceptibility of such alloys around about these temperatures and concluded that they exhibited a slow transition to anti-ferromagnetism, with indications of ferromagnetism as well. The specific heat C of such alloys at helium temperatures showed an anomalous behaviour, the $(C/T, T)$ curve exhibiting a pronounced 'hump' (de Nobel and du Chatenier 1959, Zimmermann and Hoare 1960).

Schmitt and Jacobs (1956, 1957) discussed their experimental data on the electrical and magnetic behaviour of dilute copper-manganese alloys. They suggested that some form of cooperative magnetic transition occurred in these alloys; and, below the temperature of transition, the spin degeneracy of each impurity ion is removed and the scattering which involves spin-flips of the conduction electron and the ion becomes inelastic. This inelastic scattering would not occur at 0°K . Yosida (1957) and Brailsford and Overhauser (1960) have also discussed the scattering by impurity centres having closely spaced energy states.

Thermal conductivity measurements on three silver-manganese alloy specimens, containing respectively 0.55, 0.32 and 0.14 at. % manganese, showed (Chari 1956, Chari and de Nobel 1959a) an anomalous behaviour at liquid helium temperatures, in a zero magnetic field. This anomaly consisted in the (λ, T) curve† exhibiting a 'knee'. In other words, the lower portion (below 2.3°K) of the (λ, T) curve had higher values than should follow from a simple extension of the higher temperature part (*viz.* that above 2.8°K) of the curve. The $(\lambda/T, T)$ curve exhibited this anomaly in the form of a 'dip' at about 2.8°K followed by a 'hump' near 2.3°K . The thermal magnetoresistance was also anomalous, being negative.

The shape of the (λ, T) curves was not significantly altered even in strong magnetic fields of about 25 kilogauss. It was therefore suggested that this anomaly might be due to an *extra* contribution to the *lattice* thermal conductivity, owing probably to a partial uncoupling of the longitudinal and transverse phonons (Chari 1956, Klemens 1954, 1956, 1958).

In the present paper, our thermal conductivity data at liquid helium temperatures have been analysed afresh and information is obtained regarding the variation of the Wiedemann-Franz-Lorenz parameter for electronic conduction (referred to, in the rest of this paper, as the Lorenz parameter) with respect to temperature and magnetic fields.

In §2, we explain the full significance of assuming the Wiedemann-Franz relation to be valid. The method of Gruneisen-de Haas for the separation of λ_e and λ_g , without a specific assumption of the validity of this relation, is discussed in §3. A possible explanation for the behaviour of the electronic Lorenz parameter with respect to temperature, as derived by this method, is discussed in §4.

§ 2. THE WIEDEMANN-FRANZ RELATION

It has been mentioned above that the thermal conductivity of certain alloys measured by us was anomalous at liquid helium temperatures. Following the procedure usually employed in the case of non-superconducting alloys, we then

† The symbols λ , w , σ and ρ will be used to represent respectively the thermal conductivity, thermal resistivity, electrical conductivity and electrical resistivity; and, where necessary, the qualifying subscripts *e*, *o* and *g* respectively to signify electronic, residual and lattice. λ will be expressed in $\text{w cm}^{-1} \text{deg}^{-1}$, and ρ in ohm cm .

separated the measured λ into its components, λ_e and λ_g , employing the Wiedemann-Franz relation $\lambda_e = L_n T / \rho_0$, where L_n is the normal 'Sommerfeld' value of the Lorenz parameter in a zero field. The anomaly in λ was thus attributed wholly to the lattice component.

This assumption of the validity of the Wiedemann-Franz relation implied (i) that the Lorenz parameter L_e for electronic conduction is a constant, independent of temperature, at any rate, for the liquid helium region, and (ii) that L_e has the normal value ($2.45 \times 10^{-8} \text{ w } \Omega \text{ deg}^{-2}$) in zero magnetic field. It was also difficult to anticipate how L_e would vary with the strength H of the magnetic field, in these alloys, although this is known in the case of zinc (Alers 1956) and tungsten (de Nobel 1957).

Dilute Ag-Mn alloys exhibit antiferromagnetism, with indications of ferromagnetism (Owen *et al.* 1957), in this temperature region, and their anomalous electrical resistivity in a zero field can be simply attributed to a temperature-dependent relaxation time for elastic-inelastic impurity scattering of the conduction electrons (Schmitt 1956). Since it was shown by Kohler (1941) that the Lorenz parameter should be independent of temperature for elastic scattering of the electrons, such an assumption of the validity of the Wiedemann-Franz relation seems questionable in the case of these anomalous alloys.

§ 3. THE METHOD OF GRÜNEISEN AND DE HAAS

We have now analysed (Chari 1961a) our experimental data on the thermal and electrical conductivity of dilute silver-manganese alloys at liquid helium temperatures in transverse magnetic fields (ranging from 0 to 25.5 kilogauss), employing the method of Grüneisen and de Haas (see, for instance, Kohler 1949). This method has been employed earlier by de Haas, Gerritsen and Capel (1936) and Reddemann (1934) for bismuth, Rausch (1947) for antimony, Grüneisen and Adenstedt (1938) for tungsten and beryllium, Grüneisen and Erfling (1940) for beryllium, and de Haas and de Nobel (de Haas and de Nobel 1938, de Nobel 1949) for tungsten at liquid hydrogen temperatures. White and Woods (1958) applied it to their data on antimony at liquid air temperatures.

We have $\lambda = \lambda_e + \lambda_g = \sigma L_e T + \lambda_g$. Here, L_e is looked upon simply as the quotient $\lambda_e / \sigma T$, at temperature T , without making any specific assumptions as to its behaviour. If λ and σ are measured for a few values of the magnetic field H , then, for any particular value of T , we can write $\lambda_{[H]} = \sigma_{[H]} L_e T + \lambda_g$. The subscript $[H]$ here signifies measurements in a magnetic field; we actually used transverse fields of the respective strengths 0, 12, 19 and 25.5 kilogauss. This assumes, firstly, that λ_g is unaffected by magnetic fields. Even though, at these temperatures, λ_g is supposed, in normal alloys, to be limited principally by the conduction electrons, and the paths of the electrons are affected by the magnetic fields, it was shown (Makinson 1938) that the electron-lattice interaction depends solely on the equilibrium constants of the lattice, provided no electric current is flowing (Sondheimer and Wilson 1947). One would thus be justified in assuming λ_g to be unaffected by H .

The other assumption is that L_e is independent of H . This would only be justified if $\lambda_{[H]}$ against $\sigma_{[H]} T$ turns out to be a straight line graph, at fixed T . Figs 1, 2 and 3 show that this is indeed the case, within the experimental uncertainties, for the dilute silver-manganese alloys at liquid helium temperatures.

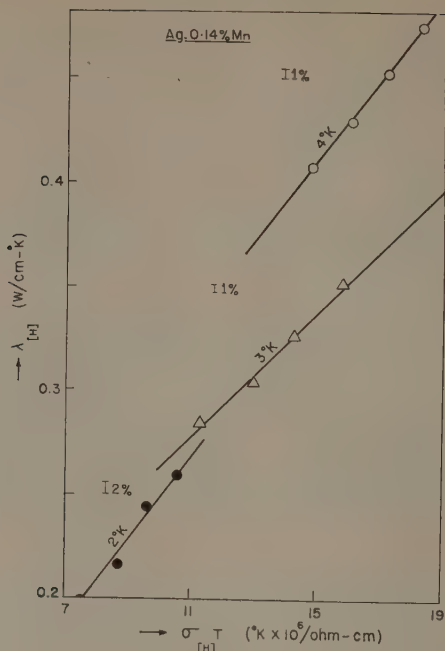


Fig. 1. $\lambda_{[H]}$ plotted against $\sigma_{[H]}T$, for the Ag-0.14% Mn specimen.

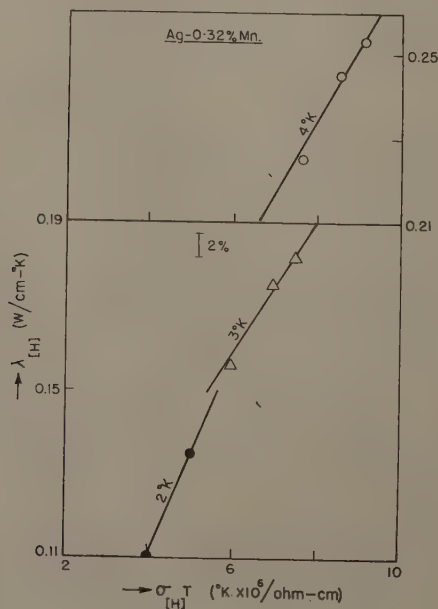


Fig. 2. $\lambda_{[H]}$ plotted against $\sigma_{[H]}T$, for the Ag-0.32% Mn specimen.

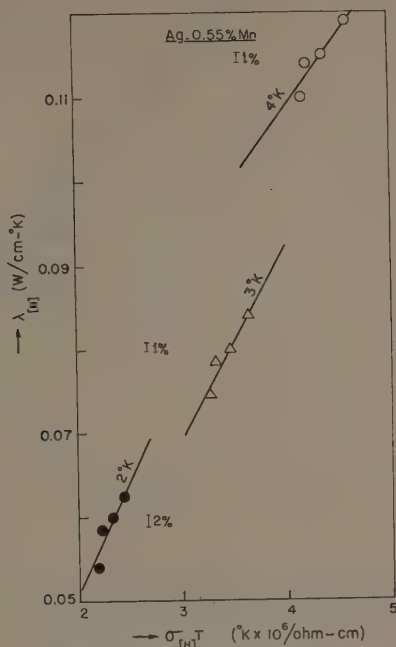


Fig. 3. $\lambda_{[H]}$ plotted against $\sigma_{[H]}T$, for the Ag-0.55% Mn specimen.

In order to avoid confusion, the plots for 1.5, 2.5 and 3.5°K are omitted from these figures. The slope of each of these straight lines gives the value of L_e at that temperature.

Plotting L_e against T (Fig. 4), we find (i) that L_e is smaller than the Sommerfeld value L_n and probably attains that value near about 1°K; (ii) that L_e has a minimum value (at a temperature T_{\min}); we direct attention to the similarity with the results of Rosenberg (1955) for pure iron, and Roder, Powell and Hall (1959) for 'high purity' copper; (iii) that T_{\min} varies with the manganese content c , shifting to a higher value with increasing c ; and (iv) that the depth of the minimum is reduced by increase of c .

We wish to emphasize that two circumstances have made it possible to derive information regarding the behaviour of L_e with temperature and magnetic field, in the silver-manganese specimens: (i) the large (though negative) magnetoresistance, especially the thermal magnetoresistance, and (ii) the rectilinearity of the $\lambda_{[H]}$ against $\sigma_{[H]}T$ curves, indicating an L_e more or less independent of H . In the case of alloys which have a normal (that is, positive), magnetoresistance, the magnitude (especially of the thermal magnetoresistance) is quite small. In fact, our measurements on a Ag-0.24% In specimen (Chari 1956, Chari and de Nobel 1959a) gave a positive electrical magnetoresistance of about 1%, while the thermal magnetoresistance was of about the same order of magnitude as our accuracy of measurement.

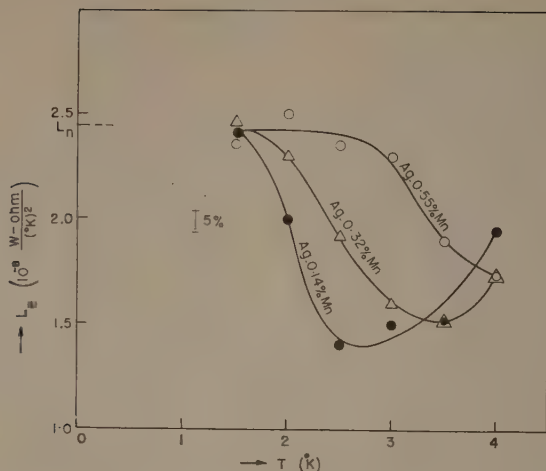


Fig. 4. The electronic Lorenz parameter L_e plotted against T for the silver-manganese alloys.

As regards the criterion (ii) mentioned above, L_e is generally not independent of H , so that the plot of $\lambda_{[H]}$ against $\sigma_{[H]}T$ would not be a straight line, and the method of Grüneisen and de Haas can not be applied for the separation of the lattice and electronic components of the thermal conductivity. Hence, in general, information regarding L_e in alloys would be difficult to obtain.

§ 4. DISCUSSION

4.1. The 'Dip' in the Value of L_e , below the Normal Value L_n

The law of Wiedemann-Franz-Lorenz is known to hold at high temperatures ($T \gg \theta$), where the change in energy of the conduction electron by the emission or absorption of a phonon would be very much less than kT ; and also at sufficiently low temperatures, where the predominant scattering of the conduction electrons is due to static, irregular imperfections or impurity centres. This is because, in both these cases, the scattering can be considered to be effectively elastic, and the relaxation times for electrical and thermal conduction would be identical. In the intervening range of low temperatures, the phonons available for scattering of the electrons would be of long wavelength and the angle of scattering of the conduction electrons small. Such small-angle scattering, whether elastic or otherwise, can make only a small contribution to the electrical resistivity. But inelastic small-angle scattering can contribute substantially to the heat resistivity. In other words, in the presence of the latter type of electron scattering, the electronic Lorenz parameter L_e would fall significantly below the normal value L_n (see Makinson 1938, Fig. 3).

The question arises as to how inelastic impurity scattering would show itself out, in the temperature region where the electrons are scattered predominantly by the impurity centres. Could the 'dip' in the value of L_e (Fig. 4) be due to inelastic electron scattering?

Schmitt (1956) and Schmitt and Jacobs (1957) made specific reference to such a scattering, for interpreting their experimental data on the electrical resistivity of copper-manganese alloys at low temperatures, where (as in the case of our dilute silver-manganese alloys) the resistivity decreased with fall of temperature. The transition to antiferro/ferromagnetism of these alloys (Owen *et al.* 1957, Schmitt and Jacobs 1956, van Itterbeek, Peelaers and Steffens 1960) could remove the spin degeneracy of the ground state of the manganese ion. The scattering of the conduction electrons by the impurity centres, each of which could occupy one or the other of the energy states, could give rise to inelastic scattering (apart from elastic scattering). This inelastic scattering would be temperature-dependent not only because of varying occupation of the states by the ions, but also because the availability of states into which the electrons can be scattered will vary with temperature.

Ziman (1960, see also Kohler 1949) has pointed out that the critical test for the existence of inelastic scattering would be in the thermal resistivity. The 'vertical' transitions of the electrons (wherein the electrons gain or lose energy without suffering a significant change in direction), to which heat conductivity is very sensitive, would result in an anomalous 'hump', provided the electronic thermal resistivity is limited predominantly by the inelastic impurity scattering. In our graphs of $w_e T$ against T (Fig. 5) and w_e against T , we find evidence for such an extra term in the electronic thermal resistivity; in the former, this shows as a pronounced 'peak'.

Starting from the assumption that the anomalous fall of electrical resistivity with fall of temperature arises specifically from the magnetic character of the

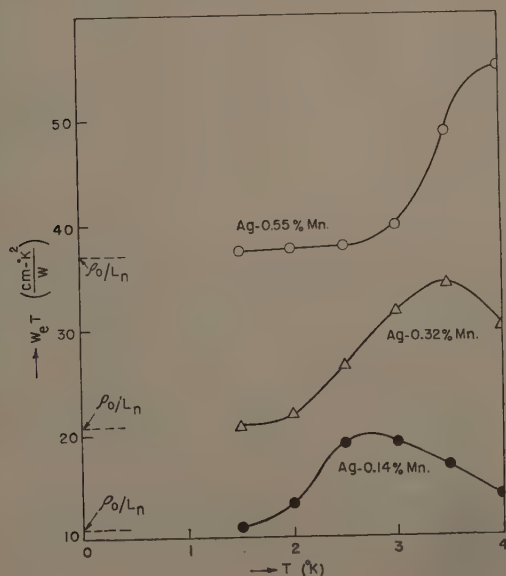


Fig. 5. T times the electronic thermal resistivity, plotted against T .

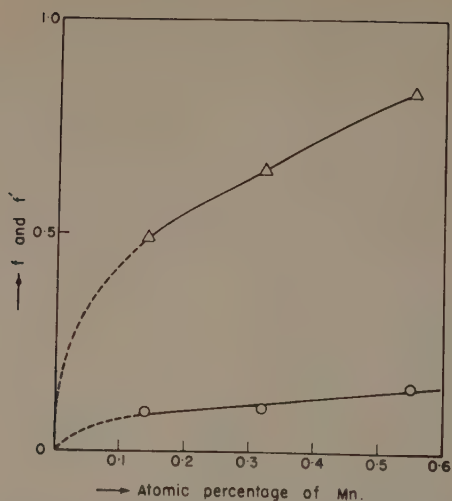


Fig. 6. f (lower curve) and f' (upper curve), the maximum contributions of inelastic impurity scattering expressed as fractions of ρ_0 and $(v_0 T)_0$ respectively plotted against the atomic percentage of manganese.

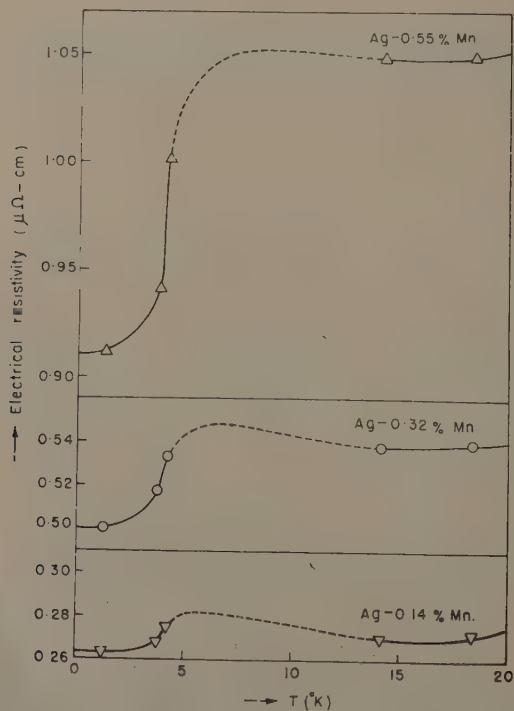


Fig. 7. Electrical resistivity ρ plotted against T (Chari 1956).

impurity metal, Schmitt and Jacobs (1957) find, in the case of their copper-manganese alloy specimens, that spin-flip scattering processes contribute, in the paramagnetic limit, about 10% of the residual electrical resistivity. Following them, we put $f = [(\rho_m/\rho_0) - 1]$ (where ρ_m is the electrical resistivity at the 'hump' of the ρ - T curve at low temperatures, and ρ_0 is the value at $T \rightarrow 0$), and find that in our silver-manganese specimens also, the contribution of inelastic impurity scattering processes, at the hump, amounts to a fraction $f \approx 0.1$ of ρ_0 . There may even be a slight variation of f with the manganese concentration, as indicated in the lower curve of Fig. 6. However, we must emphasize (i) that these estimates of ours are based on interpolation to the temperature region between liquid helium and liquid hydrogen temperatures (Fig. 7), and (ii) that these ignore any temperature-dependent contribution from elastic scattering by the impurity (solute) ions.

We make a similar estimation in the case of the electronic thermal resistivity, writing $f' = [(w_e T)_m / (w_e T)_0] - 1$. Here, $(w_e T)_m$ and $(w_e T)_0$ are the values at the peak and at $T \rightarrow 0$, respectively. Using the values of these from Fig. 5, we obtain $f' \approx 0.5, 0.6_5$ and 0.8_3 , in the order of decreasing manganese content. Thus the contribution of inelastic impurity scattering processes, at the 'peak', amounts to a large fraction of the value of $(w_e T)_0$. This is shown graphically in the upper curve of Fig. 6.

The fact that inelastic impurity scattering makes such a large contribution to the electronic thermal resistivity of these alloys at liquid helium temperatures, while making only a comparatively small contribution to the electrical resistivity, accounts for the 'dip' in the value of L_e (Fig. 4) with respect to the normal value L_n (Chari 1961b). The further result that L_e seems to approach L_n at temperatures close to absolute zero (below about 1°K) is explained by the fact that this inelastic scattering cannot occur at 0°K. Scattering which would involve loss of energy by the electron is not permitted since there are no lower electronic states available; scattering which would involve gain of energy by the electron is also not possible since, at 0°K, there are no ions in the excited states to transfer energy to the electron.

4.2. The Energy Difference between the Split States

Ziman (1960) has pointed out that, if the scattering of the electron is such that the differential scattering cross section has a large forward lobe, and the inelastic scattering contributes the predominant portion of the electronic thermal resistivity, there should be an anomalous 'hump' around about a temperature T_2 given by $kT_2 \approx \frac{1}{4}\Delta E$ (where ΔE is the energy difference between the resolved degenerate levels of the impurity ion, and k the Boltzmann constant). Assuming these criteria to be satisfied in the case of our dilute silver alloys, and taking the values of T_2 from the occurrence of humps in the plot of w_e against T , we obtain $\Delta E/k \approx 10, 11$ and 14.4°K , in the order of increasing manganese content.

We refer now to the model due to Korringa and Gerritsen (1953); this was postulated to account for the electrical resistivity maximum in a zero magnetic field (the position as well as the prominence of this maximum being dependent on the transitional ion content only) and also the negative (electrical) magnetoresistivity. (Magnetic susceptibility and other data on such alloys were forthcoming only in 1956.) From their analysis of the electrical resistivity data of

Gerritsen and Linde, on the dilute alloys Ag-Mn, Cu-Mn, Au-Mn and Au-Cr, the above authors found the relation $\epsilon = 1.54 k T_m$ satisfied. Here, as elsewhere in this paper, T_m represents the temperature of occurrence of the electrical resistivity maximum; $\pm \epsilon$ is the energy separation of the resolved local energy state with respect to the Fermi level. Substituting the values of T_m estimated by us (by interpolation between the liquid hydrogen and liquid helium temperatures in Fig. 7) into this relation, we obtain $\epsilon/k \approx 9.2, 10.8$ and 13.9°K , in the order of increasing manganese content. This is in satisfactory agreement with the above-mentioned values for ΔE obtained from our thermal conductivity data.

§ 5. CONCLUSION

In the present method of analysis, which employs the method of Grüneisen and de Haas, w_e is considered an exact counterpart of the Gerritsen-Linde anomaly in the electrical resistivity at low temperatures. This leads to an electronic Lorenz parameter which is more or less unaffected by the magnetic fields, but presents a marked minimum within the liquid helium region itself.

Apparently, the transition of these alloys to antiferro/ferromagnetism in the region of helium temperatures, which can account for the anomalous fall of their electrical resistivity with fall of temperature (at the lowest temperatures), is also responsible for the anomalous behaviour of L_e with respect to temperature in the helium temperature region.

ACKNOWLEDGMENTS

The author is grateful to the late Sir K. S. Krishnan, F.R.S., for the benefit of valuable discussions, to Dr. P. G. Klemens (of the Westinghouse Research Laboratories, United States of America) for some useful correspondence and to Dr. K. G. Ramanathan and Mr. R. Sundaram for helpful suggestions.

The experimental work on these alloys was done during 1955-56, while the author was a Research Fellow at the Kamerlingh Onnes Laboratory, Leiden, Holland. Grateful acknowledgment is made of the interest taken by Professor C. J. Gorter and Dr. J. de Nobel.

REFERENCES

- ALERS, P. B., 1956, *Phys. Rev.*, **101**, 41.
- BRAILS福德, A. D., and OVERHAUSER, A. W., 1960, *J. Phys. Chem. Solids*, **15**, 140.
- CHARI, M. S. R., 1956, *Thesis*, University of Leiden.
- 1961 a, *Nature, Lond.*, **189**, 824.
- 1961 b, *Nature, Lond.*, **190**, 994.
- CHARI, M. S. R., and DE NOBEL, J., 1959 a, *Physica*, **25**, 60; Leiden Comm. No. 313b.
- 1959 b, *Physica*, **25**, 84; Leiden Comm. Suppl. No. 114b.
- GERRITSEN, A. N., and LINDE, J. O., 1951 a, *Physica*, **17**, 573; Leiden Comm. No. 285c.
- 1951 b, *Physica*, **17**, 584; Leiden Comm. No. 285d.
- GRÜNEISEN, E., and ADENSTEDT, H., 1938, *Ann. Phys., Lpz.*, **31**, 714.
- GRÜNEISEN, E., and ERLING, H.-D., 1940, *Ann. Phys., Lpz.*, **38**, 399.
- DE HAAS, W. J., and DE NOBEL, J., 1938, *Physica*, **5**, 449; Leiden Comm. No. 251d.
- DE HAAS, W. J., GERRITSEN, A. N., and CAPEL, W. H., 1936, *Physica*, **3**, 1143; Leiden Comm. No. 247c.
- KLEMENS, P. G., 1954, *Aust. J. Phys.*, **7**, 57.
- 1956, *Handb. d. Phys.*, **14**, 198 (Berlin: Springer).
- 1958, *Solid State Physics*, **7**, 87 (New York: Academic Press).

- KOHLER, M., 1941, *Ann. Phys., Lpz.*, **40**, 601.
- 1949, *Ann. Phys., Lpz.*, **5**, 181; **6**, 18.
- KORRINGA, J., and GERRITSEN, A. N., 1953, *Physica*, **19**, 457; Leiden Comm. Suppl. No. 106.
- MAKINSON, R. E. B., 1938, *Proc. Camb. Phil. Soc.*, **34**, 474.
- DE NOBEL, J., 1949, *Physica*, **15**, 532; Leiden Comm. No. 278b.
- 1957, *Physica*, **23**, 349; Leiden Comm. Suppl. No. 113a.
- DE NOBEL, J., and DU CHATENIER, F. J., 1959, *Physica*, **25**, 969; Leiden Comm. No. 317c.
- OWEN, J., BROWNE, M. E., ARP, V., and KIP, A. F., 1957, *J. Phys. Chem. Solids*, **2**, 85.
- RAUSCH, K., 1947, *Ann. Phys., Lpz.*, **1**, 190.
- REDDEMANN, H., 1934, *Ann. Phys., Lpz.*, **20**, 441.
- RODER, H. M., POWELL, R. L., and HALL, W. J., 1959, *Phys. Rev.*, **115**, 314.
- ROSENBERG, H. M., 1955, *Phil. Trans. A*, **247**, 441.
- SCHMITT, R. W., 1956, *Phys. Rev.*, **103**, 83.
- SCHMITT, R. W., and JACOBS, I. S., 1956, *Canad. J. Phys.*, **34**, 1285.
- 1957, *J. Phys. Chem. Solids*, **3**, 324.
- SONDHEIMER, E. H., and WILSON, A. H., 1947, *Proc. Roy. Soc. A*, **190**, 435.
- VAN ITTERBEEK, A., PEELAERS, W., and STEFFENS, F., 1960, *Appl. Sci. Res., Hague, B*, **4**, 337.
- WHITE, G. K., and WOODS, S. B., 1958, *Phil. Mag.*, **28**, 342.
- YOSIDA, K., 1957, *Phys. Rev.*, **107**, 396.
- ZIMAN, J. M., 1960, *Electrons and Phonons* (Oxford: Clarendon Press).
- ZIMMERMAN, J. E., and HOARE, F. E., 1960, *J. Phys. Chem. Solids*, **17**, 52.

Dispersion Relations for Superconductors

By A. W. B. TAYLOR

Department of Theoretical Physics, University of Liverpool

Communicated by H. Fröhlich; MS. received 31st May 1961

Abstract. The general macroscopic description of the electromagnetic behaviour of superconductors and normal conductors is developed and dispersion relations for the frequency dependent material functions are rigorously established. From these dispersion relations expressions similar to the usual sum rules of electromagnetic theory are derived. Using these, Ferrell's proof that the Meissner effect is a consequence of the energy gap is shown to be unsound. Using the complex surface impedance it is shown macroscopically that as a consequence of the Meissner effect the area under the absorptivity curve for a superconductor is less than for the normal state.

§ 1. INTRODUCTION

THE dispersion relations which relate the real and imaginary parts of the frequency dependent material functions describing a system's electromagnetic behaviour, e.g. the complex conductivity, provide a possible means of relating in a completely macroscopic manner the zero frequency behaviour of the system to its electromagnetic absorption properties. This is of interest when the system is superconducting for then the energy gap in the superconducting state reduces the superconducting absorptivity below its normal state value for frequencies less than the gap frequency. We therefore have a possible means of relating macroscopically the energy gap or at least the effects of the energy gap to the zero frequency behaviour viz. the Meissner effect.

In §§2 and 3 the electromagnetic behaviour of linear isotropic systems is described by means of space-time dependent material functions and criteria to distinguish the zero frequency behaviour of superconductors and normal conductors are rigorously established.

In §4 the dispersion relations applicable to superconductors and normal conductors for these functions are rigorously derived. These dispersion relations lead directly to an expression which relates the Meissner effect to the difference between the normal state and superconducting state values of the integral over all frequencies of the real part of the transverse conductivity. This relation is similar to the well-known optical sum rule. This however cannot be used to relate the Meissner effect to the absorption properties. Ferrell's proof (1959) that the Meissner effect is a consequence of the energy gap which is based on a similar expression is unsound.

The frequency dependent material function which is directly related to the electromagnetic absorptivity is the complex surface impedance. Assuming the Meissner effect and also that the high frequency behaviour is the same in both

superconductors and normal conductors, we have shown macroscopically by means of rigorously established dispersion relations that the total area under the absorptivity curve for the superconducting state is reduced below its normal state value. This is verified experimentally.

This however does not follow from the mere existence of an energy gap unless an additional assumption about the absorptivity for frequencies greater than the gap frequency is made. Such an additional assumption is certainly needed to distinguish the superconductor from the insulator which also has an energy gap but does not of course exhibit the Meissner effect.

§ 2. ISOTROPIC LINEAR SYSTEMS

In the following all space-time functions $f(\mathbf{r}, t)$ are transformed to Fourier space by

$$f(\mathbf{q}, \omega) = (2\pi)^{-4} \int d^3r dt f(\mathbf{r}, t) \exp(i\mathbf{q} \cdot \mathbf{r} + i\omega t). \quad \dots (2.1)$$

If $f(\mathbf{r}, t)$ is real then

$$f(-\mathbf{q}, -\omega) = f^*(\mathbf{q}, \omega). \quad \dots (2.2)$$

If $f(\mathbf{q}, \omega)$ is a vector $\mathbf{f}(\mathbf{q}, \omega)$ then its longitudinal component $\mathbf{f}^l(\mathbf{q}, \omega)$ and its transverse component $\mathbf{f}^t(\mathbf{q}, \omega)$ are defined by

$$\mathbf{f}(\mathbf{q}, \omega) = \mathbf{f}^t(\mathbf{q}, \omega) + \mathbf{f}^l(\mathbf{q}, \omega) \quad \mathbf{q} \wedge \mathbf{f}^l(\mathbf{q}, \omega) = \mathbf{q} \cdot \mathbf{f}^t(\mathbf{q}, \omega) = 0. \quad \dots (2.3)$$

From the identity

$$q^2 \mathbf{f}(\mathbf{q}, \omega) = \mathbf{q} \mathbf{q} \cdot \mathbf{f}(\mathbf{q}, \omega) - \mathbf{q} \wedge (\mathbf{q} \wedge \mathbf{f}(\mathbf{q}, \omega)) \quad \dots (2.4)$$

it follows that

$$\mathbf{f}^l(\mathbf{q}, \omega) = \frac{\mathbf{q} \mathbf{q} \cdot \mathbf{f}(\mathbf{q}, \omega)}{q^2}, \quad \mathbf{f}^t(\mathbf{q}, \omega) = -\frac{\mathbf{q} \wedge (\mathbf{q} \wedge \mathbf{f}(\mathbf{q}, \omega))}{q^2}. \quad \dots (2.5)$$

Now Eqns (2.3) are invariant under the transformation

$$\mathbf{f}^t \rightarrow \mathbf{f}^t + \mathbf{G} \quad \mathbf{f}^l \rightarrow \mathbf{f}^l - \mathbf{G} \quad \dots (2.6)$$

where \mathbf{G} is a function of \mathbf{q} and ω satisfying

$$\mathbf{q} \cdot \mathbf{G} = \mathbf{q} \wedge \mathbf{G} = 0 \quad \text{i.e.} \quad \mathbf{G} \propto \mathbf{q} \delta(|\mathbf{q}|). \quad \dots (2.7)$$

Therefore, since $\mathbf{G} = 0$ for $|\mathbf{q}| \neq 0$ but is indeterminate for $|\mathbf{q}| = 0$ it follows that a vector in Fourier space can only be decomposed uniquely into its longitudinal and transverse components when $|\mathbf{q}| \neq 0$.

Maxwell's equations in Fourier space are

$$\mathbf{q} \wedge \mathbf{E}(\mathbf{q}, \omega) = -\frac{\omega}{c} \mathbf{B}(\mathbf{q}, \omega) \quad \mathbf{q} \cdot \mathbf{B}(\mathbf{q}, \omega) = 0 \quad \dots (2.8)$$

$$i\mathbf{q} \wedge \mathbf{H}(\mathbf{q}, \omega) = -\frac{4\pi}{c} \mathbf{J}(\mathbf{q}, \omega) + \frac{i\omega}{c} \mathbf{D}(\mathbf{q}, \omega) \quad i\mathbf{q} \cdot \mathbf{D}(\mathbf{q}, \omega) = 4\pi\rho(\mathbf{q}, \omega) \quad \dots (2.9)$$

and the continuity equation is

$$4\pi\mathbf{q} \cdot \mathbf{J}(\mathbf{q}, \omega) = i\omega\mathbf{q} \cdot \mathbf{D}(\mathbf{q}, \omega). \quad \dots (2.10)$$

Longitudinal equations. From (2.5), (2.8), (2.9), (2.10) the longitudinal field equations are

$$\mathbf{B}^l(\mathbf{q}, \omega) \equiv 0 \quad 4\pi\mathbf{J}^l(\mathbf{q}, \omega) = i\omega\mathbf{D}^l(\mathbf{q}, \omega) = -4\pi\omega\rho(\mathbf{q}, \omega)\mathbf{q}/q^2. \quad \dots (2.11)$$

so that all longitudinal magnetic quantities are zero and there are two equations connecting the four quantities \mathbf{E}^l , \mathbf{D}^l , \mathbf{J}^l , ρ . Therefore, for a complete and unique description of the longitudinal behaviour two additional relations are required. For an isotropic linear system we take them to be

$$-i\omega \mathbf{J}^l(\mathbf{q}, \omega) = S(\mathbf{q}, \omega) \mathbf{E}^l(\mathbf{q}, \omega), \quad \mathbf{D}^l(\mathbf{q}, \omega) = \epsilon^l(q, \omega) \mathbf{E}^l(\mathbf{q}, \omega) \quad \dots\dots (2.12)$$

where $S(q, \omega)$, $\epsilon^l(q, \omega)$ are complex scalar functions of $q = |\mathbf{q}|$ and ω .

Defining the complex longitudinal conductivity, $\sigma^l(q, \omega)$ by

$$\mathbf{J}^l(\mathbf{q}, \omega) = \sigma^l(q, \omega) \mathbf{E}^l(\mathbf{q}, \omega) \quad \dots\dots (2.13)$$

$$\text{we have from (2.12)} \quad S(q, \omega) = -i\omega \sigma^l(q, \omega). \quad \dots\dots (2.14)$$

Transverse equations. From (2.5), (2.8), (2.9) the transverse field equations are

$$\mathbf{q} \wedge \mathbf{E}^t(\mathbf{q}, \omega) = -\frac{\omega}{c} \mathbf{B}(\mathbf{q}, \omega), \quad i\mathbf{q} \wedge \mathbf{H}(\mathbf{q}, \omega) = -\frac{4\pi}{c} \mathbf{J}^t(\mathbf{q}, \omega) + \frac{i\omega}{c} \mathbf{D}^t(\mathbf{q}, \omega). \quad \dots\dots (2.15)$$

Now $\mathbf{J}^t(\mathbf{q}, \omega)$, $\mathbf{D}^t(\mathbf{q}, \omega)$ appear in these equations only in the combination

$$\frac{4\pi}{c} \mathbf{J}^t(\mathbf{q}, \omega) - \frac{i\omega}{c} \mathbf{D}^t(\mathbf{q}, \omega)$$

so that there are two equations connecting the four transverse fields, \mathbf{B} , \mathbf{H} , \mathbf{E}^t , $4\pi \mathbf{J}^t/c - i\omega \mathbf{D}^t/c$. Therefore, for a complete and unique description of the transverse behaviour two additional relations are required. For an isotropic linear system we take these to be

$$\mathbf{B}(\mathbf{q}, \omega) = \mu(q, \omega) \mathbf{H}(\mathbf{q}, \omega) \\ \frac{4\pi}{c} \mathbf{J}^t(\mathbf{q}, \omega) - \frac{i\omega}{c} \mathbf{D}^t(\mathbf{q}, \omega) = \frac{K(q, \omega) i\mathbf{q} \wedge \mathbf{B}(\mathbf{q}, \omega)}{q^2} \quad \dots\dots (2.16)$$

where $\mu(q, \omega)$, $K(q, \omega)$ are complex scalar functions of $q = |\mathbf{q}|$ and ω . $\mu(q, \omega)$ is the conventional magnetic permeability.

Substituting (2.16) in the second equation of (2.15), we obtain the differential equation satisfied by $\mathbf{B}(\mathbf{q}, \omega)$ in Fourier space as

$$L(q, \omega) \mathbf{B}(\mathbf{q}, \omega) = -q^2 \mathbf{B}(\mathbf{q}, \omega) \quad \dots\dots (2.17)$$

where

$$L(q, \omega) = K(q, \omega) - q^2 \left[1 - \frac{1}{\mu(q, \omega)} \right]. \quad \dots\dots (2.18)$$

Substituting (2.16) in the first equation of (2.15) gives

$$c^2 K(q, \omega) = -4\pi i\omega \sigma^t(q, \omega) - \omega^2 \epsilon^t(q, \omega) \quad \dots\dots (2.19)$$

where $\sigma^t(q, \omega)$, $\epsilon^t(q, \omega)$ are the conventional complex transverse conductivity and dielectric constant respectively, introduced by

$$\mathbf{J}^t(\mathbf{q}, \omega) = \sigma^t(q, \omega) \mathbf{E}^t(\mathbf{q}, \omega), \quad \mathbf{D}^t(\mathbf{q}, \omega) = \epsilon^t(q, \omega) \mathbf{E}^t(\mathbf{q}, \omega) \dots\dots (2.20)$$

Hence $\sigma^t(q, \omega)$ and $\epsilon^t(q, \omega)$ are not defined separately in terms of $K(q, \omega)$, which is sufficient to describe the transverse behaviour completely. $\sigma^t(q, \omega)$ and $\epsilon^t(q, \omega)$ separately therefore overdescribe the transverse behaviour of the system.

The most usual ways of removing this ambiguity (cf. Fröhlich 1958) are:

(i) to put $\sigma^t(q, \omega) = 0$ and use only a complex dielectric constant defined by

$$c^2 K(q, \omega) = -\omega^2 \epsilon_a^t(q, \omega), \quad \dots\dots (2.21a)$$

(ii) to put $\epsilon^t(q, \omega) = 1$ and use only a complex conductivity defined by

$$c^2 K(q, \omega) = -4\pi i \omega \sigma_b^t(q, \omega) - \omega^2, \quad \dots\dots (2.21b)$$

(iii) to use only a real dielectric constant and a real conductivity defined by

$$c^2 K(q, \omega) = -4\pi i \sigma_c^t(q, \omega) - \omega^2 \epsilon_c^t(q, \omega). \quad \dots\dots (2.21c)$$

These representations evidently provide equivalent macroscopic descriptions of the transverse behaviour and are connected by the well-known equation

$$4\pi \sigma_b^t(q, \omega) = i\omega(1 - \epsilon_a^t(q, \omega)). \quad \dots\dots (2.22)$$

Now for a conducting system $\lim_{\omega \rightarrow 0} \sigma^t(q, \omega)$ is non-zero and finite and (2.22) then implies that $\lim_{\omega \rightarrow 0} \epsilon^t(q, \omega)$ diverges. For example the Drude theory of an electron gas gives

$$\epsilon^t(q, \omega) = 1 - \frac{\omega_p^2}{\omega^2 + i\tau\omega} \quad \dots\dots (2.23)$$

where ω_p, τ are real positive constants.

i.e.

$$\lim_{\omega \rightarrow 0} \epsilon^t(q, \omega) = (1 - \omega_p^2/\tau) + i\infty \quad \dots\dots (2.24)$$

and

$$\lim_{\omega \rightarrow 0} \sigma^t(q, \omega) = \omega_p^2/4\pi\tau. \quad \dots\dots (2.25)$$

Representation (i) above is therefore inconvenient for conducting systems in the stationary limit $\omega = 0$. In the following representation (ii) will always be used.

Therefore from Eqns (2.16), (2.21b)

$$-4\pi i \omega \mathbf{J}^t(\mathbf{q}, \omega) = \{c^2 K(q, \omega) + \omega^2\} \mathbf{E}^t(\mathbf{q}, \omega). \quad \dots\dots (2.26)$$

Eqns (2.26), (2.12) and the first equation of (2.16) are the constitutive equations which we shall use with the Maxwell equations, to give a complete and unique description of the electromagnetic behaviour of a linear isotropic system.

Combining with (2.26), (2.12) gives

$$-4\pi i \omega \mathbf{J}(\mathbf{q}, \omega) = \{c^2 K(q, \omega) + \omega^2\} \mathbf{E}^t(\mathbf{q}, \omega) + 4\pi S(q, \omega) \mathbf{E}^l(\mathbf{q}, \omega) \quad \dots\dots (2.27)$$

the constitutive equation relating the total electric current to the electric field.

Now from (2.6) and (2.7), $\mathbf{E}^t(\mathbf{q}, \omega)$ and $\mathbf{E}^l(\mathbf{q}, \omega)$ are not uniquely defined for $q = 0$. Therefore in order that (2.27) provide a unique description in the limit $q = 0$ we shall require

$$\lim_{q \rightarrow 0} \{c^2 K(q, \omega) + \omega^2\} = \lim_{q \rightarrow 0} 4\pi S(q, \omega), \quad \dots\dots (2.28)$$

for then (2.27) is in the limit $q = 0$

$$-4\pi i \omega \mathbf{J} = \{c^2 \lim_{q \rightarrow 0} K + \omega^2\} \mathbf{E} = 4\pi \lim_{q \rightarrow 0} S \mathbf{E} \quad \dots\dots (2.29)$$

which is of course unique as it involves only the total field and the total current.

An alternative notation for the transverse equations is to define a magnetization vector $\mathbf{M}(\mathbf{q}, \omega)$ and a magnetization current $\mathbf{J}_m(\mathbf{q}, \omega)$ by

$$4\pi \mathbf{M}(\mathbf{q}, \omega) = \mathbf{B}(\mathbf{q}, \omega) - \mathbf{H}(\mathbf{q}, \omega) \quad \mathbf{J}_m(\mathbf{q}, \omega) = -c i \mathbf{q} \wedge \mathbf{M}(\mathbf{q}, \omega). \quad \dots\dots (2.30)$$

The transverse equations then become

$$\mathbf{q} \wedge \mathbf{E}^t(\mathbf{q}, \omega) = -\frac{\omega}{c} \mathbf{B}(\mathbf{q}, \omega); \quad i c \mathbf{q} \wedge \mathbf{B}(\mathbf{q}, \omega) = -4\pi \{\mathbf{J}^t(\mathbf{q}, \omega) + \mathbf{J}_m(\mathbf{q}, \omega)\} + i\omega \mathbf{D}^t(\mathbf{q}, \omega) \quad \dots\dots (2.31)$$

$$-4\pi\{\mathbf{J}^t(\mathbf{q}, \omega) + \mathbf{J}_m(\mathbf{q}, \omega)\} + i\omega\mathbf{D}^t(\mathbf{q}, \omega) = cL(q, \omega)i\mathbf{q} \wedge \mathbf{B}(\mathbf{q}, \omega)/q^2, \quad \dots\dots (2.32)$$

where $L(q, \omega)$ is defined by (2.18).

In this notation we define a complex conductivity $\sigma_m(q, \omega)$ by

$$c^2L(q, \omega) = -4\pi i\omega\sigma_m(q, \omega) - \omega^2 \quad \dots\dots (2.33)$$

and therefore from (2.18), (2.25), (2.32)

$$\mathbf{J}^t(q, \omega) + \mathbf{J}_m(\mathbf{q}, \omega) = \sigma_m(\mathbf{q}, \omega)\mathbf{E}^t(\mathbf{q}, \omega). \quad \dots\dots (2.34)$$

§ 3. SUPERCONDUCTORS AND NORMAL CONDUCTORS

$$\text{If we define} \quad L(q) = \lim_{\omega \rightarrow 0} L(q, \omega) \quad \text{and} \quad S(q) = \lim_{\omega \rightarrow 0} S(q, \omega) \quad \dots\dots (3.1)$$

then we shall prove below that

$$L(q), S(q) \text{ are real and finite} \quad \dots\dots (3.2)$$

for superconductors and normal conductors, and that

$$\left. \begin{array}{l} \text{for normal magnetism} \quad \lim_{q \rightarrow 0} L(q) = 0 \\ \text{for Meissner effect} \quad \lim_{q \rightarrow 0} L(q) > 0 \end{array} \right\} \quad \dots\dots (3.3)$$

$$\left. \begin{array}{l} \text{for normal conduction} \quad S(q) = 0 \\ \text{for perfect conductors} \quad S(q) \neq 0 \end{array} \right\}. \quad \dots\dots (3.4)$$

Now Eqn (A8) of the appendix gives λ , the penetration depth of a stationary magnetic field into a semi-infinite system, as

$$\lambda = \frac{2}{\pi} \int_0^\infty \frac{dq}{q^2 + L(q)}. \quad \dots\dots (3.5)$$

For normal magnetic behaviour λ is infinite, i.e. the integral in (3.5) diverges and consequently $\lim_{q \rightarrow 0} L(q) = 0$. For the Meissner effect λ is finite and non-zero; i.e. the integral converges to a positive, non-zero limit and consequently we require $\lim_{q \rightarrow 0} L(q) > 0$. Eqn (3.3) is thus proved.

Consider now the longitudinal equations (2.12)

$$-i\omega\mathbf{J}^l(\mathbf{q}, \omega) = S(q, \omega)\mathbf{E}^l(\mathbf{q}, \omega) \quad \dots\dots (3.6)$$

in the stationary limit $\omega = 0$.

We have $\lim_{\omega \rightarrow 0} \mathbf{J}^l(\mathbf{q}, \omega) \neq 0$ and finite and hence

$$\lim_{\omega \rightarrow 0} S(q, \omega)\mathbf{E}^l(\mathbf{q}, \omega) = 0. \quad \dots\dots (3.7)$$

Perfect conduction means that stationary longitudinal currents flow in the absence of a (macroscopic) longitudinal electric field, i.e. when

$$\lim_{\omega \rightarrow 0} \mathbf{E}^l(\mathbf{q}, \omega) = 0.$$

From (3.7) the necessary and sufficient condition for this is $\lim_{\omega \rightarrow 0} S(q, \omega) \neq 0$ and finite.

For normal conduction $\lim_{\omega \rightarrow 0} \sigma^l(q, \omega)$ is finite so that from (2.14)

$$\lim_{\omega \rightarrow 0} i\omega\sigma^l(q, \omega) = -\lim_{\omega \rightarrow 0} S(q, \omega) = 0. \quad \dots\dots (3.8)$$

(3.4) is thus proved.

From (3.5) $L(q)$ is finite for both superconductors and normal conductors since the penetration depth λ is non-zero. From (3.4) $S(q)$ is also finite for both superconductors and normal conductors. Therefore, from the reality conditions (2.1)

$$S(q, -\omega) = S^*(q, \omega), \quad L(q, -\omega) = L^*(q, \omega) \quad \dots\dots (3.9)$$

and $L(q)$, $S(q)$ are also real. This proves (3.1).

For example the second London equation for superconductors (London 1950) is given by

$$L(q) = \frac{1}{\lambda_L^2} = \text{constant} \quad \dots\dots (3.10)$$

For then (2.17) becomes

$$-q^2 \mathbf{B}(\mathbf{q}) = \frac{\mathbf{B}(\mathbf{q})}{\lambda_L^2} \quad \dots\dots (3.11)$$

which is the second London equation in Fourier space.

The 'non-local' theory of Pippard (1953) on the other hand requires a q -dependent $L(q)$

$$L(q) = \frac{3\xi}{2\lambda_L^2 \xi_0 (\xi q)^3} \{ (1 + \xi^2 q^2) \arctan \xi q - \xi q \} \quad \dots\dots (3.12)$$

where ξ , ξ_0 are positive constants and λ_L is the London constant of (3.10) above.

Here

$$\lim_{q \rightarrow 0} L(q) = \frac{\xi}{\lambda_L^2 \xi_0} \quad \dots\dots (3.13)$$

and by (3.3) we do have a Meissner effect.

§ 4. DISPERSION RELATIONS

Define

$$S^\infty(q) = \lim_{\omega \rightarrow \infty} S(q, \omega), \quad L^\infty(q) = \lim_{\omega \rightarrow \infty} L(q, \omega). \quad \dots\dots (4.1)$$

For infinitely high frequencies the current carriers of the system will behave as if free so that $S^\infty(q)$, $L^\infty(q)$ can both be assumed real.

We shall now show that for both superconductors and normal conductors the functions $S(q, \omega) - S^\infty(q)$, $L(q, \omega) - L^\infty(q)$ satisfy the conditions of the well-known Titchmarsh theorem (Titchmarsh 1948), namely that they are square integrable with respect to ω and that their Fourier transforms with respect to ω vanish for all negative times.

Now, by definition (4.1)

$$\lim_{\omega \rightarrow \infty} \{S(q, \omega) - S^\infty(q)\} = 0 \quad \dots\dots (4.2)$$

and by (3.2)

$$\lim_{\omega \rightarrow 0} \{S(q, \omega) - S^\infty(q)\} \text{ is real and finite} \quad \dots\dots (4.3)$$

for both superconductors and normal conductors.

Equations (4.2), (4.3) are necessary conditions for square integrability of $S(q, \omega) - S^\infty(q)$. If we assume that $S(q, \omega)$ is not infinitely discontinuous for any finite ω then conditions (4.2), (4.3) are also sufficient.

Performing a Fourier transformation of Eqn (2.12) which defines $S(q, \omega)$ one finds

$$\frac{\partial}{\partial t} \mathbf{J}(\mathbf{r}, t) = (2\pi)^{-4} \int d^3 r' \int_{-\infty}^{+\infty} dt' S(|\mathbf{r} - \mathbf{r}'|, t - t') \mathbf{E}(\mathbf{r}', t') \quad \dots\dots (4.4)$$

where $\mathbf{J}(\mathbf{r}, t)$, $\mathbf{E}(\mathbf{r}, t)$, $S(|\mathbf{r}|, t)$ are Fourier transforms of $\mathbf{J}(\mathbf{q}, \omega)$, $\mathbf{E}(\mathbf{q}, \omega)$, $S(q, \omega)$ respectively. Eqn (4.4) relates the longitudinal current response at time t to the values of the longitudinal electric field at *all* times t' . Causality requires that the field at time t' should have no effect on the response at earlier times $t \leq t'$. The limits of the t' integration in (4.4) therefore become $(-\infty, t)$. This is evidently equivalent to putting

$$S(|\mathbf{r}|, t) = 0 \text{ if } t < 0. \quad \dots\dots (4.5)$$

Therefore the Fourier transform of $S(q, \omega)$ and hence also of $S(q, \omega) - S^\infty(q)$ with respect to ω vanishes for all negative times.

$S(q, \omega) - S^\infty(q)$ and similarly $L(q, \omega) - L^\infty(q)$ thus satisfy the conditions of the Titchmarsh theorem from which follow the Hilbert conjugate relations

$$\left. \begin{aligned} \mathcal{R}S(q, \omega) - S^\infty(q) &= \frac{1}{\pi} \int_{-\infty}^{+\infty} \frac{\mathcal{I}S(q, z) dz}{z - \omega} \\ \mathcal{I}S(q, \omega) &= -\frac{1}{\pi} \int_{-\infty}^{+\infty} \frac{\mathcal{R}S(q, z) dz}{z - \omega} \end{aligned} \right\} \quad \dots\dots (4.6)$$

and similarly for $L(q, \omega)$.

Applying the reality conditions (2.2)

$$\mathcal{R}S(q, z) = \mathcal{R}S(q, -z) \quad \mathcal{I}S(q, z) = -\mathcal{I}S(q, -z) \quad \dots\dots (4.7)$$

to convert the limits of the z integration in (4.6) to $(0, \infty)$ gives the dispersion relations

$$\mathcal{R}L(q, \omega) - L^\infty(q) = \frac{2}{\pi} \int_0^\infty \frac{\mathcal{I}L(q, z) z dz}{z^2 - \omega^2} \quad \dots\dots (4.8)$$

$$\mathcal{I}L(q, \omega) = -\frac{2}{\pi} \int_0^\infty \frac{\mathcal{R}L(q, z) \omega dz}{z^2 - \omega^2} \quad \dots\dots (4.9)$$

$$\mathcal{R}S(q, \omega) - S^\infty(q) = \frac{2}{\pi} \int_0^\infty \frac{\mathcal{I}S(q, z) z dz}{z^2 - \omega^2} \quad \dots\dots (4.10)$$

$$\mathcal{I}S(q, \omega) = -\frac{2}{\pi} \int_0^\infty \frac{\mathcal{R}S(q, z) \omega dz}{z^2 - \omega^2} \quad \dots\dots (4.11)$$

where the principal value of the integrals is implied.

Taking the limit $\omega = 0$ in (4.8), (4.10) and using (2.14), (2.33)

$$\left. \begin{aligned} \int_0^\infty \mathcal{R}\sigma_m(q, z) dz &= \frac{1}{8} c^2 \{L^\infty(q) - L(q)\} \\ \int_0^\infty \mathcal{R}\sigma^1(q, z) dz &= \frac{1}{2} \pi \{S^\infty(q) - S(q)\} \end{aligned} \right\} \quad \dots\dots (4.12)$$

We now compare these equations with the sum rules

$$\left. \begin{aligned} \int_0^\infty \mathcal{R}\sigma_m(q, z) dz &= \frac{1}{8} c^2 L^\infty(q) \\ \int_0^\infty \mathcal{R}\sigma^1(q, z) dz &= \frac{1}{2} \pi S^\infty(q) \end{aligned} \right\} \quad \dots\dots (4.13)$$

which obtain their familiar form with the values

$$S^\infty(q) = \frac{c^2 L^\infty(q)}{4\pi} = \frac{ne^2}{m} \quad \dots\dots (4.14)$$

where n is the electron density (cf. Buckingham 1957).

Comparing these sum rules, (4.13) with (4.12), it is seen that, since by (3.3), (3.4), $L(q)$ and $S(q)$ are non-zero and finite for superconductors the sum rules (4.13) are not obeyed by superconductors.

Now the sum rules (4.13) can be derived from the Kramers-Kronig dispersion relations for $\sigma_m(q, \omega)$ and $\sigma^l(q, \omega)$ in a similar fashion to the derivation of (4.12) from the dispersion relations (4.8) to (4.11) (Ferrell and Glover 1958). However, the Kramers-Kronig dispersion relations for $\sigma_m(q, \omega)$ and $\sigma^l(q, \omega)$ are not obeyed by superconducting systems. For

$$\left. \begin{aligned} \lim_{\omega \rightarrow 0} \sigma_m(q, \omega) &= -\lim_{\omega \rightarrow 0} \frac{c^2 L(q, \omega)}{4\pi i \omega} \simeq i\infty \\ \lim_{\omega \rightarrow 0} \sigma^l(q, \omega) &= -\lim_{\omega \rightarrow 0} \frac{S(q, \omega)}{i\omega} \simeq i\infty \end{aligned} \right\} \dots\dots (4.15)$$

and $\sigma_m(q, \omega)$ and $\sigma^l(q, \omega)$ will therefore not be square integrable with respect to ω unless it is postulated that

$$\mathcal{I} \sigma_m(q, \omega) \simeq \delta(\omega), \quad \mathcal{I} \sigma^l(q, \omega) \simeq \delta(\omega) \text{ for } \omega \rightarrow 0. \quad \dots\dots (4.16)$$

But then the second condition of the Titchmarsh theorem is violated, for the delta functions will give non-vanishing time independent contributions to the Fourier transforms of $\sigma_m(q, \omega)$ and $\sigma^l(q, \omega)$, i.e. the Fourier transforms will not vanish for negative times. The Titchmarsh theorem is therefore not applicable to $\sigma_m(q, \omega)$ and $\sigma^l(q, \omega)$ for superconducting systems. This is the formal reason for the inapplicability of (4.13) to superconducting systems.

Now one may postulate that the high frequency behaviour of a system in the superconducting state is identical to its high frequency behaviour in the normal state. This is in accord with experiment (e.g. Serin 1956)

$$\text{i.e. } \Delta_{ns} L^\infty(q) \equiv L^\infty(q)_{\text{normal}} - L^\infty(q)_{\text{supercond.}} = 0. \quad \dots\dots (4.17)$$

Therefore from (4.12)

$$\Delta_{ns} \int_0^\infty \mathcal{R} \sigma_m(q, z) dz = -\frac{1}{8} c^2 \Delta_{ns} L(q), \quad \dots\dots (4.18)$$

and from (3.3) the Meissner effect implies

$$\lim_{q \rightarrow 0} \Delta_{ns} \int_0^\infty \mathcal{R} \sigma_m(q, z) dz > 0, \text{ finite.} \quad \dots\dots (4.19)$$

Evidently if one could prove that Eqns (4.18) and (4.19) hold for some particular system denoted by the subscript s then this system will exhibit the Meissner effect.

Now Ferrell (1959) has in fact derived an equation equivalent to (4.18) for a system of electrons by applying perturbation theory to evaluate the system's current response to an external magnetic field.

In an attempt to deduce (4.19) he makes the assumption that the electron system possesses an energy gap in the one-electron energy spectrum. This energy gap will therefore annul the electron system's electromagnetic absorptivity for frequencies less than the gap frequency and if one now assumes in addition that (i) for frequencies greater than the gap frequency the absorptivity is the same as in the normal state, (ii) $\lim_{q \rightarrow 0} \mathcal{R} \sigma_m(q, \omega)$ is proportional to the electromagnetic absorptivity for frequency ω (Ferrell's Eqn (13)), then (4.19) follows

immediately from (4.18), i.e. the electron system exhibits the Meissner effect as a consequence of the energy gap and assumptions (i) and (ii) above.

However, assumption (i) is clearly an additional assumption which does not follow from the existence of an energy gap alone. Further, it would have to be shown that it does not contradict the assumption of an energy gap (cf. Buckingham 1957). Nevertheless such an additional assumption as (i) is required physically to distinguish the system from an insulator which also has an energy gap but which does not exhibit the Meissner effect.

Assumption (ii) is equivalent to the neglect of the spatial dispersion of the electromagnetic field by the system. For, from the well-known energy integral of Maxwell's equations the absorptivity is proportional to

$$\int_0^\infty \Re \sigma_m(q, \omega) |\mathbf{E}^t(\mathbf{q}, \omega)|^2 dq$$

which is proportional to $\lim_{q \rightarrow 0} \Re \sigma_m(q, \omega)$ only when $|\mathbf{E}^t(\mathbf{q}, \omega)|^2 \simeq \delta(q)$, i.e. when the electric field is assumed uniform in space. One cannot make this assumption since it is the very nature of the spatial dependence of the electromagnetic field which characterizes the Meissner effect.

We conclude that Ferrell's derivation of the Meissner effect is unsound.

§ 5. ELECTROMAGNETIC ABSORPTION

Consider a transverse electromagnetic wave normally incident on a system which may be in the superconducting or normal state. We assume that the radii of curvature of the surface of the system are everywhere sufficiently large to neglect the tangential derivatives of the fields (e.g. plane surface).

Hence, if we take the x axis as the inward normal at the surface with the origin lying on the surface, we can write the Maxwell induction relation as

$$\frac{\partial}{\partial x} E_z(x, t) = \frac{1}{c} \frac{\partial}{\partial t} B_y(x, t) \quad \dots\dots (5.1)$$

where the electric field $E_z(x, t)$ is in the z direction and the magnetic induction $B_y(x, t)$ is in the y direction. Fourier transforming with respect to time t

$$\frac{\partial}{\partial x} E_z(x, \omega) = -\frac{i\omega}{c} B_y(x, \omega). \quad \dots\dots (5.2)$$

Define a real function of time $Z(t)$ by

$$E_z(0, t) = \int_{-\infty}^t Z(t-t') B_y(0, t') dt'. \quad \dots\dots (5.3)$$

$Z(t-t')$ thus relates $E_z(0, t)$, the electric field on the surface at time t to $B_y(0, t')$, the magnetic induction on the surface at all previous times t' .

Performing a Fourier transformation on Eqn (5.3) with respect to time

$$E_z(0, \omega) = Z(\omega) B_y(0, \omega) \quad \dots\dots (5.4)$$

where

$$Z(\omega) = (2\pi)^{-1} \int_0^\infty Z(t) e^{i\omega t} dt. \quad \dots\dots (5.5)$$

$Z(\omega)$ is the complex surface impedance. It provides in (5.4) a boundary condition to the Maxwell equation (5.2).

Since $Z(t)$ is real,

$$Z(-\omega) = Z^*(\omega). \quad \dots\dots (5.6)$$

By its definition (5.4), $Z(\omega)$ is square integrable with respect to ω since $E_z(0, \omega)$ and $B_y(0, \omega)$ are necessarily square integrable. Also by (5.5) the Fourier transform of $Z(\omega)$ vanishes for all negative times. $Z(\omega)$ therefore satisfies the conditions of the Titchmarsh theorem.

The surface impedance $Z(\omega)$ is important because it is directly related to the electromagnetic absorptivity $A(\omega)$ by (Dingle 1953)

$$A(\omega) = \frac{4\Re Z(\omega)}{|1 + Z(\omega)|^2}. \quad \dots\dots (5.7)$$

Therefore for a normal conductor $Z(\omega) \simeq b\omega^2$ as $\omega \rightarrow 0$ (5.8)
where b is a positive finite constant (Landau and Lifshitz 1960).

Now the penetration depth of a stationary magnetic field into the system is defined by

$$\lambda = \lim_{\omega \rightarrow 0} \int_0^\infty \frac{B_y(x, \omega) dx}{B_y(0, \omega)}. \quad \dots\dots (5.9)$$

From (5.2), (5.4)

$$\lambda = \lim_{\omega \rightarrow 0} \frac{cE_z(\infty, \omega)}{i\omega B_y(0, \omega)} + \lim_{\omega \rightarrow 0} \frac{cZ(\omega)}{i\omega}. \quad \dots\dots (5.10)$$

By (5.2) the first term is proportional to the magnetic induction at $x = \infty$ in the stationary limit $\omega = 0$. For a bulk superconducting system this will vanish because of the Meissner effect. Therefore the superconducting penetration depth is related to the surface impedance by

$$\lambda_s = \lim_{\omega \rightarrow 0} \frac{cZ(\omega)}{i\omega} \quad \dots\dots (5.11)$$

i.e. for superconductors $Z(\omega) \sim ic\lambda_s\omega$ as $\omega \rightarrow 0$ (5.12)

Having described the main properties of the surface impedance we now wish to formulate the dispersion relations for the complex function $F(\omega)$ defined by

$$F(\omega) = \left[\frac{Z_n(\omega)}{|1 + Z_n(\omega)|^2} - \frac{Z_s(\omega)}{|1 + Z_s(\omega)|^2} \right] \frac{i\omega}{A_n(\omega)} \quad \dots\dots (5.13)$$

where the subscripts s, n refer to the same bulk system when in the superconducting state and when in the normal state respectively.

From (5.7), (5.8), (5.11)

$$\lim_{\omega \rightarrow 0} F(\omega) = \frac{\lambda_s}{b} \text{ real, finite and positive} \quad \dots\dots (5.14)$$

also

$$\lim_{\omega \rightarrow 0} F(\omega) = 0 \quad \dots\dots (5.15)$$

since the high frequency behaviours of superconducting state and normal state are identical.

Equations (5.14) and (5.15) are necessary conditions for the square integrability of $F(\omega)$. Since by definition $A_n(\omega) > 0$ for finite ω it is seen from definition of $F(\omega)$, (5.13), and definition of $Z(\omega)$, (5.4), that $F(\omega)$ has no infinite discontinuities for finite ω . (5.14) and (5.15) are therefore also sufficient conditions of square integrability. $F(\omega)$ is therefore square integrable with respect to ω .

Now, as $Z(\omega)$ satisfies the conditions of the Titchmarsh theorem it is an analytic function of ω in the upper half of the complex ω plane. By definition, $A_n(\omega)$

has no zeros in the upper half plane. Therefore from (5.13) $F(\omega)$ is an analytic function in the upper half plane and so satisfies the condition of Titchmarsh's theorem that it be analytic.

$F(\omega)$ therefore satisfies the conditions of the Titchmarsh theorem and the Hilbert conjugate relations follow.

From (5.6), (5.13)

$$F(-\omega) = F^*(\omega) \quad \dots\dots (5.16)$$

so that the dispersion relations relating the real and imaginary parts of $F(\omega)$ follow immediately from the Hilbert conjugate relations.

One of the dispersion relations is

$$\mathcal{R}F(\omega) = \frac{2}{\pi} \int_0^\infty \frac{\mathcal{I}F(z)z dz}{z^2 - \omega^2} \quad \dots\dots (5.17)$$

Now from (5.7), (5.13)

$$\mathcal{I}F(\omega) = \frac{[A_n(\omega) - A_s(\omega)]\omega}{4A_n(\omega)} \quad \dots\dots (5.18)$$

and therefore (5.17) gives

$$\int_0^\infty \frac{A_n(z) - A_s(z)}{A_n(z)} dz = \lim_{\omega \rightarrow 0} 2\pi \mathcal{R}F(\omega). \quad \dots\dots (5.19)$$

Therefore from (5.14)

$$\int_0^\infty \frac{A_n(z) - A_s(z)}{A_n(z)} dz > 0 \text{ and finite.} \quad \dots\dots (5.20)$$

This result, correlating the normal and superconducting absorptivities, is a rigorous consequence of the Meissner effect and the assumption that the high frequency behaviours in normal and superconducting states are identical. Eqn (5.20) has been verified experimentally (Biondi and Garfunkel 1959, Richards and Tinkham 1960).

ACKNOWLEDGMENTS

The author is indebted to Professor H. Fröhlich, who suggested this investigation, for his patient guidance and help. He also acknowledges receipt of a research studentship from the Senatus of Edinburgh University.

APPENDIX

In this appendix we derive an expression for the penetration depth of a stationary magnetic field into a system occupying the half space $x \geq 0$. The magnetic field is taken in the y direction and will be a function of x only.

We assume that the electrons are specularly reflected at the boundary $x=0$ of the system. This assumption simplifies the mathematics, but is unlikely to affect the results since we make the same assumption for both normal and superconducting systems and the results are only used in §§ 3 and 4 to compare the two.

Specularly reflected electrons correspond to electrons coming from a system in $x \leq 0$ which has the same field distribution as the system in $x \geq 0$ except that the magnetic field (and hence the Lorentz force) is reversed. In other words the system filling $x \geq 0$ can be represented by an infinite system with the discontinuity

$$B_y(x=0+) = -B_y(x=0-) \quad \dots\dots (A1)$$

in the magnetic induction.

We can therefore Fourier analyse with respect to x by (2.1) and use the relations of §2 if we take this discontinuity into account.

The differential equation satisfied by the magnetic induction in Fourier space, (2.17), becomes

$$L(q)B_y(q) = -q^2 B_y(q) + \frac{iqB_y(x=0+)}{\pi}, \quad \dots\dots (A2)$$

e.

$$B_y(q) = \frac{iqB_y(x=0+)}{\pi[q^2 + L(q)]}. \quad \dots\dots (A3)$$

Therefore

$$\int_0^\infty B_y(x)dx = \int_0^\infty dx \int_{-\infty}^{+\infty} dq B_y(q) e^{-iqx} \quad \dots\dots (A4)$$

$$= \frac{B_y(x=0+)}{\pi} \int_{-\infty}^{+\infty} \frac{dq}{q^2 + L(q)}, \quad \dots\dots (A5)$$

since

$$\int_0^\infty dx e^{-iqx} = \pi\delta(q) - P\frac{i}{q}, \quad \dots\dots (A6)$$

where P denotes principal value.

The penetration depth λ is defined by

$$\lambda = \int_0^\infty \frac{B_y(x)dx}{B_y(x=0+)}. \quad \dots\dots (A7)$$

Therefore from (A5)

$$\lambda = \frac{1}{\pi} \int_{-\infty}^{+\infty} \frac{dq}{q^2 + L(q)} = \frac{2}{\pi} \int_0^\infty \frac{dq}{q^2 + L(q)} \quad \dots\dots (A8)$$

the last step following since $L(q)$ is even in q .

REFERENCES

- BIONDI, M. A., and GARFUNKEL, M. P., 1959, *Phys. Rev.*, **116**, 853.
 BUCKINGHAM, M. J., 1957, *Nuovo Cim.*, **5**, 1763.
 DINGLE, R. B., 1953, *Physica*, **19**, 311.
 FERRELL, R. A., 1959, *Bull. Amer. Phys. Soc.* [II], **4**, 225.
 FERRELL, R. A., and GLOVER, R. E., 1958, *Phys. Rev.*, **109**, 1398.
 FRÖHLICH, H., 1958, *Theory of Dielectrics* (Oxford: Clarendon), p. 161.
 LANDAU, L. D., and LIFSHITZ, E. M., 1960, *Electrodynamics of Continuous Media* (London: Pergamon), p. 191.
 LONDON, F., 1950, *Superfluids*, Vol. 1 (New York: Wiley).
 PIPPARD, A. B., 1953, *Proc. Roy. Soc. A*, **216**, 547.
 RICHARDS, P. L., and TINKHAM, M., 1960, *Phys. Rev.*, **119**, 575.
 SERIN, B., 1956, *Handb. d. Phys.*, **15**, (11) (Berlin: Springer), p. 210.
 TITCHMARSH, E. C., 1948, *Theory of Fourier Integrals* (Oxford: Clarendon), Theorem 95, p. 128.

Electronic Conduction in Polar Semiconductors

By B. DURNEY

Department of Theoretical Physics, University of St. Andrews, Scotland

*Communicated by R. B. Dingle; MS. received 22nd March 1961,
in revised form 7th June 1961*

Abstract. The Boltzmann equation for polar semiconductors is solved formally as a series expansion. The form of the collision operator used is that derived by Howarth and Sondheimer. The method of solution is based on an iteration procedure analogous to Neumann's series solution for an integral equation. The solution has been computed numerically as a function of electron-energy-phonon-energy for certain typical combinations of values of the temperature and degeneracy parameters. Guided by these 'control solutions' algebraic equations are derived which approximate to the Boltzmann equation in important limiting cases. From these algebraic equations the conductivity and the thermoelectric power are deduced.

§ 1. INTRODUCTION

THE distinctive feature of the electronic conduction phenomena in polar semiconductors is the predominant role played by the optical branch of the lattice vibrations in scattering conduction electrons. As a first approximation these vibrations can be treated as having a common frequency ν_0 . In this limit the Boltzmann integral equation reduces to a second-order finite difference equation. Howarth and Sondheimer (1953) have shown how this difference equation can be solved, in successive approximations, using a variational principle. Delves (1959) has obtained some accurate numerical values of transport coefficients by numerical integration of the Boltzmann equation.

In the present paper the problem is re-examined along the following lines. The Boltzmann difference equation, for each of the two formal times of relaxation (Dingle 1956), can be considered as the limit of an integral equation when the vibrational spectrum of the polarization waves tends to a delta function. This suggests that the relevant solutions of the difference equations can be defined as the limit of appropriate Neumann series. Such definition avoids the difficulty that the solution of the difference equation itself is not unique; the general solution being $w_1 u_1 + w_2 u_2 + v$, where u_1 and u_2 are a fundamental system of solutions of the homogeneous equation, w_1 and w_2 are arbitrary functions of appropriate period and v is a particular solution of the complete equation (cf. Milne-Thompson 1960).

A digital computer has been used to calculate this solution to the Boltzmann equation for combinations of values of the temperature and degeneracy parameters typical of the cases of (i) no degeneracy, high temperatures, (ii) no degeneracy, low temperatures, (iii) degeneracy, high temperatures, (iv) degeneracy, low temperatures. Guided by these 'control solutions', it is possible to simplify the difference equation and thereby obtain approximate solutions in closed

algebraic form. (The results could, of course, be further improved in accuracy by successive approximations.) The results obtained reduce to well-known ones whenever the two formal times of relaxation turn out to be slowly varying functions; this is to be expected, for in these circumstances the precise form of the trial function inserted in the variational principle is not critical. However there is marked disagreement when the two formal times of relaxation are rapidly varying functions, as in the degenerate limit at low temperatures.

§ 2. FORMAL SOLUTIONS OF THE DIFFERENCE EQUATIONS

2.1. General Considerations

It is convenient for the present purposes to express the electrical conductivity and thermoelectric effects in the following notation:

$$\sigma = e^2 K_1, \quad \mathcal{G} = (K_2 - \zeta K_1)/K_1 T \quad \dots\dots (2.1)$$

where

$$K_1 = -\frac{8Ma^3\nu_0^3}{3e^4} \int_0^\infty \xi^{3/2} \tau_1(\xi) \frac{\partial f_0}{\partial \xi} d\xi, \\ K_2 = -\frac{8Ma^3\nu_0^4 h}{3e^4} \int_0^\infty \xi^{3/2} \tau_2(\xi) \frac{\partial f_0}{\partial \xi} d\xi. \quad \dots\dots (2.2)$$

Here M is the reduced mass of the ions, a is the interionic distance, $\xi = E/h\nu_0$, where E is the electron energy and $h\nu_0$ the optical phonon energy, ζ is the Fermi energy level and $f_0 = 1/\{\exp[(h\nu_0\xi - \zeta)/kT] + 1\}$ is the Fermi function. The two formal times of relaxation, $\tau_r(\xi)$ with $r = 1, 2$, satisfy the following finite difference equations

$$\xi^{r-1/2} = \frac{(N+1)f_0\{h\nu_0(\xi+1)\}}{f_0(h\nu_0\xi)} [\tau_r(\xi) \sinh^{-1}\xi^{1/2} \\ - \tau_r(\xi+1)\{(1+\frac{1}{2}\xi^{-1}) \sinh^{-1}\xi^{1/2} - \frac{1}{2}(1+\xi^{-1})^{1/2}\}] \\ + h(\xi-1) \frac{Nf_0\{h\nu_0(\xi-1)\}}{f_0(h\nu_0\xi)} [\tau_r(\xi) \cosh^{-1}\xi^{1/2} \\ - \tau_r(\xi-1)\{(1-\frac{1}{2}\xi^{-1}) \cosh^{-1}\xi^{1/2} - \frac{1}{2}(1-\xi^{-1})^{1/2}\}] \quad \dots\dots (2.3)$$

where $N = 1/\{\exp(h\nu_0/kT) - 1\}$ and $h(\xi-1)$ is the step function defined by $h(\xi-1) = 0$ for $\xi < 1$, $h(\xi-1) = 1$ for $\xi \geq 1$. If $\tau_2(\xi) = \xi\tau_1(\xi)$, a universal time of relaxation can be defined by $\tau = Ma^3(h\nu_0)^{3/2}\tau_1/\{2\pi e^4(2m)^{1/2}\}$; the integrals (2.2) are easily seen to go over into their usual expressions for this case.

With

$$f_+(\xi) = \frac{(N+1)f_0\{h\nu_0(\xi+1)\}}{f_0(h\nu_0\xi)}, \quad f_-(\xi) = \frac{Nf_0\{h\nu_0(\xi-1)\}}{f_0(h\nu_0\xi)} \quad \dots\dots (2.4)$$

$$D(\xi) = f_+(\xi) \sinh^{-1}\xi^{1/2} + h(\xi-1)f_-(\xi) \cosh^{-1}\xi^{1/2}, \\ \xi^{r-1/2}/D(\xi) = d_r(\xi) \quad \dots\dots (2.5)$$

$$k_+(\xi) = (1+\frac{1}{2}\xi^{-1}) \sinh^{-1}\xi^{1/2} - \frac{1}{2}(1+\xi^{-1})^{1/2} \\ k_-(\xi) = (1-\frac{1}{2}\xi^{-1}) \cosh^{-1}\xi^{1/2} - \frac{1}{2}(1-\xi^{-1})^{1/2} \quad \dots\dots (2.6)$$

$$K_+(\xi) = f_+(\xi)k_+(\xi)/D(\xi), \quad K_-(\xi) = f_-(\xi)k_-(\xi)/D(\xi). \quad \dots\dots (2.7)$$

(2.3) can be written

$$\tau_r(\xi) - K_+(\xi)\tau_r(\xi+1) - h(\xi-1)K_-(\xi)\tau_r(\xi-1) = d_r(\xi). \quad \dots\dots (2.8)$$

2.2. The First Order Difference Equation

All the essential features of the solution are present in the first-order difference equation obtained from (2.8) for $\xi < 1$ and $r = 1$

$$\tau(\xi) - \left\{ \frac{k_+(\xi)}{\sinh^{-1}\xi^{1/2}} \right\} \tau(\xi+1) = \frac{\xi^{1/2}}{f_+(\xi) \sinh^{-1}\xi^{1/2}} = f(\xi) \quad \dots\dots (2.9)$$

and thus, this equation will be dealt with first.

Consider the set of integral equations

$$\tau_y(\xi) - \int_0^\infty K_y(x, \xi) \tau_y(x) dx = f(\xi) \quad \dots\dots (2.10)$$

where $K_y(x, \xi) \rightarrow \{k_+(\xi)/\sinh^{-1}\xi^{1/2}\} \delta\{x - (\xi+1)\}$ for $y \rightarrow \infty$. The limit of these integral equations is the difference equation (2.9).

If the Neumann's series is absolutely and uniformly convergent the solution of (2.10) will be given by

$$\tau_y(\xi) = f(\xi) + \int_0^\infty K_y(x, \xi) f(x) dx + \int_0^\infty \int_0^\infty K_y(x, t) K_y(t, \xi) f(x) dt dx + \dots$$

..... (2.11)

For $y \rightarrow \infty$

$$\begin{aligned} \tau_y(\xi) \rightarrow \tau(\xi) = f(\xi) + \frac{k_+(\xi)}{\sinh^{-1}\xi^{1/2}} f(\xi+1) \\ + \frac{k_+(\xi)k_+(\xi+1)}{\sinh^{-1}\xi^{1/2} \sinh^{-1}(\xi+1)^{1/2}} f(\xi+2) + \dots \quad \dots\dots (2.12) \end{aligned}$$

which is a solution of (2.9). The proof that (2.12) is convergent presents no difficulty. Comparison of (2.12) with the general solution of a first-order difference equation (cf. Milne-Thomson 1960, p. 329) shows that it is determined by assigning the value ∞ to the arbitrary constant and 0 to the arbitrary periodic function.

2.3. The Second Order Difference Equations

The same method can be applied to the second-order difference equations (2.8). In a symbolic notation the solutions can be written

$$\begin{aligned} \tau_r(\xi) = d_r(\xi) + [K_+(\xi)0_+ + h(\xi-1)K_-(\xi)0_-]d_r(\xi) \\ \dots + [K_+(\xi)0_+ + h(\xi-1)K_-(\xi)0_-]^n d_r(\xi) + \dots \quad \dots\dots (2.13) \end{aligned}$$

where $0_+ F(\xi) = F(\xi+1)$ and $0_- F(\xi) = F(\xi-1)$, $F(\xi)$ being an arbitrary function of ξ .

$[K_+(\xi)0_+ + h(\xi-1)K_-(\xi)0_-]d_r(\xi)$ is thus defined by

$$[K_+(\xi)0_+ + h(\xi-1)K_-(\xi)0_-]^{n-1} [K_+(\xi)0_+ + h(\xi-1)K_-(\xi)0_-]d_r(\xi)$$

and

$$[K_+(\xi)0_+ + h(\xi-1)K_-(\xi)0_-]d_r(\xi) =$$

$$K_+(\xi)d_r(\xi+1) + h(\xi-1)K_-(\xi)d_r(\xi-1).$$

The properties of the series (2.13) can best be visualized by the use of a graphical representation. If we plot the integers on the x axis and ξ on the y axis, $K_+(\xi)$ is represented by a line joining (p, ξ) and $(p+1, \xi+1)$ and $K_-(\xi)$ by a line joining (p, ξ) and $(p+1, \xi-1)$, where p is an arbitrary integer. Thus

every term of the series (2.13) has a definite corresponding path, as seen in Fig. 1, where the terms $K_-(\xi)K_-(\xi-1)K_+(\xi-2)K_+(\xi-1)K_-(\xi)K_+(\xi-1)d_r(\xi)$ and $+(\xi)K_+(\xi+1)K_+(\xi+2)K_+(\xi+3)K_-(\xi+4)d_r(\xi+3)$ have been represented. It is clear that the terms in $d_r(\xi)$ contain $2n$ ($n=0, 1, 2, \dots$) products of the form $+(\xi')K_-(\xi'+1)$. On the other hand the terms in $d_r(\xi+p)$ contain p unpaired

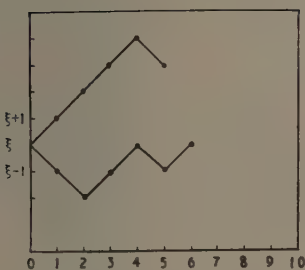


Fig. 1. Graphical representation of terms of the series (2.13).

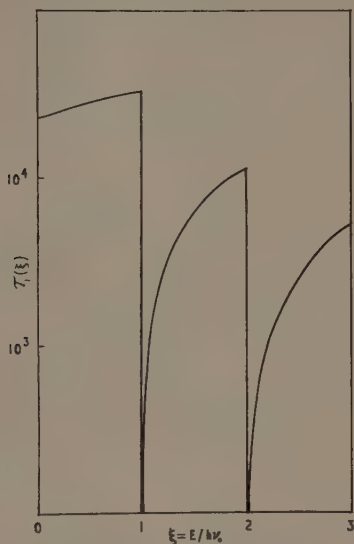


Fig. 3. Exact solution for $h\nu_0/kT=10$, $\zeta/kT=-20$

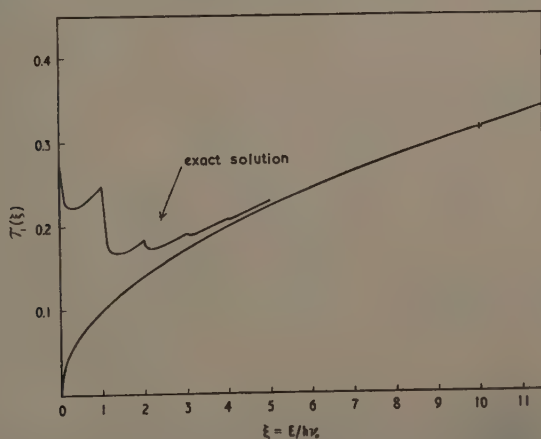


Fig. 2. Exact and approximate solutions for $h\nu_0/kT=0.1$, $\zeta/kT=-20$. The + is a value of the exact solution.

$K_+(\xi')$. These facts suggest how the convergence of the series (2.13) can be established; it is sufficient to find an upper limit small enough for $K_+(\xi')K_-(\xi'+1)$ and $K_+(\xi')$. This topic is further discussed in the Appendix.

Values of $\tau_1(\xi)$ for some typical cases have been calculated with the help of a digital computer; these are plotted in Figs 2 to 5. For low temperatures the main feature of these curves is a strong oscillation with period one.

For high temperatures the oscillations rapidly disappear with increasing ξ and, for large ξ , $\tau_1(\xi)$ tends to a universal relaxation time.

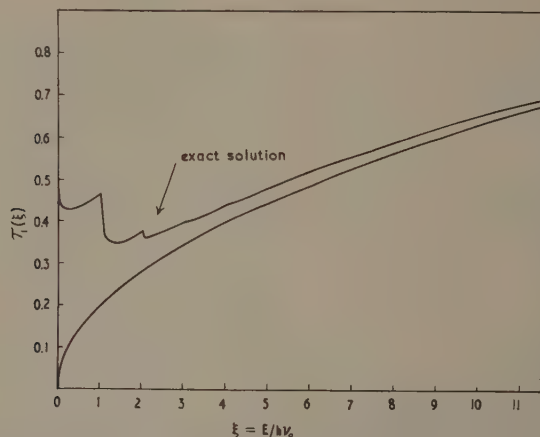


Fig. 4. Exact and approximate solutions for $h\nu_0/kT=0.2$, $\zeta/kT=4$.

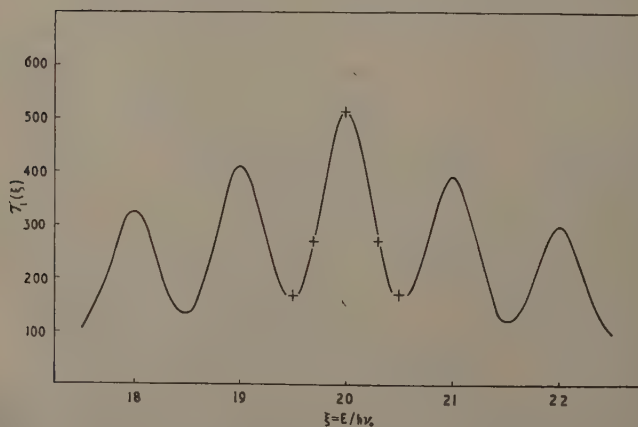


Fig. 5. Exact solution for $h\nu_0/kT=6$, $\zeta/kT=120$. The + 's are values of the approximate solution (3.9).

§ 3. LIMIT EXPRESSIONS FOR THE CONDUCTIVITY

3.1. The Non-degenerate Limit

The conductivity in this case is given by

$$\sigma = \frac{8Ma^3\nu_0^4h \exp(\zeta/kT)}{3e^2kT} \int_0^\infty \tau_1(\xi) \xi^{3/2} \exp(-h\nu_0\xi/kT) d\xi. \quad \dots\dots (3.1)$$

If the variation of $\tau_1(\xi)$ with ξ is neglected the integrand has a maximum for $\xi = 3kT/2h\nu_0$; this suggests that at high temperatures only values of $\xi \gg 1$ contribute significantly to the conductivity, whereas at low temperatures only the range $\xi \ll 1$ is important. These conclusions are indeed confirmed by the resultant expressions.

As $-\zeta/kT$ is large and positive,

$$f_+(\xi) \sim (N+1) \exp(-h\nu_0/kT)$$

and

$$f_-(\xi) \sim N \exp(h\nu_0/kT).$$

For high temperatures, $\tau_r(\xi)$ is a slowly varying function of ξ for moderate values of ξ (see Fig. 2). It follows from (2.3) that $\tau_r(\xi) \sim \xi^{r-1/2}/(N+\frac{1}{2})$. In Fig. 2 the exact solution for the high temperature case $h\nu_0/kT = 0.1$, $\zeta/kT = -20$ has been plotted together with the above approximate expression, both for $r = 1$; agreement is excellent for $\xi \gg 1$, the range required. By (3.1) the conductivity is

$$\sigma = \frac{16Ma^3\nu_0k^2T^2 \exp(\zeta/kT)}{3e^2h^2} \{\exp(h\nu_0/kT) - 1\} \quad \dots\dots (3.2)$$

in agreement with Howarth and Sondheimer's result. As $\tau_2(\xi) = \xi\tau_1(\xi)$, a universal time of relaxation exists in this case.

For low temperatures only the range $\xi \ll 1$ is important and an approximate expression for $\tau_1(\xi)$ can be obtained from the following relations (cf. 2.8) valid for $\xi < 1$:

$$\begin{aligned} \tau_1(\xi+1) - K_+(\xi+1)\tau_1(\xi+2) - K_-(\xi+1)\tau_1(\xi) &= d_1(\xi+1) \\ \tau_1(\xi) - K_+(\xi)\tau_1(\xi+1) &= d_1(\xi). \end{aligned} \quad \dots\dots (3.3)$$

Eliminating $\tau_1(\xi+1)$,

$$\begin{aligned} \tau_1(\xi)[1 - K_+(\xi)K_-(\xi+1)] \\ = d_1(\xi) + K_+(\xi)[K_+(\xi+1)\tau_1(\xi+2) + d_1(\xi+1)] \\ \sim d_1(\xi) + K_+(\xi)d_1(\xi+1) \end{aligned} \quad \dots\dots (3.4)$$

since $K_+(\xi)K_+(\xi+1)\tau_1(\xi+2) < \tau_1(\xi+2)$ can be neglected in comparison with $d_1(\xi) \sim d_1(0) \sim \exp(h\nu_0/kT) - 1$ (see Fig. 3 where $\exp(h\nu_0/kT) - 1 = 22025$). For small ξ , as $K_+(0) = \frac{2}{3}$,

$$K_+(\xi)d_1(\xi+1) \sim \frac{2}{3}[\exp(-h\nu_0/kT) \sinh^{-1}(\xi+1)^{1/2} + \cosh^{-1}(\xi+1)^{1/2}]^{-1}$$

and in particular $K_+(0)d_1(1) \sim \frac{3}{4} \exp(h\nu_0/kT)$. This latter term is not small in comparison with $d_1(0) \sim \exp(h\nu_0/kT)$ (cf. 3.4). Nevertheless $K_+(\xi)d_1(\xi+1)$

decreases rapidly with the increase of $\cosh^{-1}(\xi+1)^{1/2}$ and for not too small values of ξ , $K_+(\xi)d_1(\xi+1)$ can be neglected. The rapid decrease of $K_+(\xi)d_1(\xi+1)$ can be appreciated from the following figures:

$$(h\nu_0/kT=10, \quad \zeta/kT=-20, \quad d_1(\xi) \sim d_1(0) \sim 22025)$$

ξ	0	10^{-5}	10^{-4}	10^{-1}
$\tau_1(\xi)$	44046	22235	22093	23340.

To calculate the conductivity the further approximation

$$\tau_1(\xi) \sim d_1(0) \sim \exp(h\nu_0/kT) - 1$$

can be made as only small values of ξ make a significant contribution. Thus

$$\sigma = \frac{2\pi^{1/2}a^3(v_0kT)^{3/2}}{e^2h^{3/2}} \{\exp(h\nu_0/kT) - 1\} \exp(\zeta/kT) \dots\dots (3.5)$$

in agreement with Howarth and Sondheimer's expression.

The same approximations are valid for $\tau_2(\xi)$, resulting in

$$\tau_2(\xi) \sim d_2(\xi) \sim \xi \{\exp(h\nu_0/kT) - 1\} \sim \xi \tau_1(\xi)$$

and again a universal time of relaxation exists.

3.2. The Degenerate Limit

For simplicity only the case $g = \zeta/h\nu_0 \gg 1$ will be considered.

For high temperatures

$\tau_r(\xi) \sim \xi^{r-1/2}/(N + \frac{1}{2}) \sim \xi^{r-1/2} \{\exp(h\nu_0/kT) - 1\}$ is a valid approximation as in the non-degenerate case. In Fig. 4, $\xi^{1/2}/(N + \frac{1}{2})$ has been plotted together with the exact solution for $h\nu_0/kT = 0.2$, $\zeta/kT = 4$. Agreement is good for $\xi \gg 1$. Inserting $\tau_1(\xi) \sim \xi^{1/2} \{\exp(h\nu_0/kT) - 1\}$ in the expression (2.2) for the conductivity

$$\begin{aligned} \sigma &\sim - \frac{8Ma^3\nu_0^3 \{\exp(h\nu_0/kT) - 1\}}{3e^2} \int_0^\infty \xi^2 \frac{\partial f_0}{\partial \xi} d\xi \\ &\sim \frac{8Ma^3\nu_0^3 \xi^2 \{\exp(h\nu_0/kT) - 1\}}{3e^2h^2} \\ &\sim \frac{8Ma^3\nu_0^2 \xi^2}{3e^2hkT} \dots\dots (3.6) \end{aligned}$$

in agreement with Howarth and Sondheimer's result.

In the limit of low temperatures the integrals (2.2) need only to be evaluated between for example $g - \frac{1}{2}$, and $g + \frac{1}{2}$, since $\partial f_0/\partial \xi$ has a sharp maximum for $\xi = g$. An approximate expression for $\tau_r(\xi)$, in this region, can be obtained from the following relations (cf. 2.8).

$$\begin{aligned} \tau_r(\xi+1) - K_+(\xi+1)\tau_r(\xi+2) - K_-(\xi+1)\tau_r(\xi) &= d_r(\xi+1) \\ \tau_r(\xi) - K_+(\xi)\tau_r(\xi+1) - K_-(\xi)\tau_r(\xi-1) &= d_r(\xi) \dots\dots (3.7) \\ \tau_r(\xi-1) - K_+(\xi-1)\tau_r(\xi) - K_-(\xi-1)\tau_r(\xi-2) &= d_r(\xi-1). \end{aligned}$$

For large values of $h\nu_0/kT$ the following relations hold (with $X = \exp[(h\nu_0\xi - \zeta)/kT]$)

$$K_+(\xi) \sim \frac{k_+(g)}{(1+X) \sinh^{-1} g^{1/2}}, \quad K_-(\xi) \sim \frac{k_-(g)}{(1+X^{-1}) \cosh^{-1} g^{1/2}} \quad \dots\dots (3.8a)$$

$$K_+(\xi-1) \sim k_+(g)/\sinh^{-1} g^{1/2}, \quad K_-(\xi+1) \sim k_-(g)/\cosh^{-1} g^{1/2} \quad \dots\dots (3.8b)$$

$$d_r(\xi) \sim \frac{\xi^{r-1} \exp(h\nu_0/kT)}{(1+X)(1+X^{-1}) \sinh^{-1} \xi^{1/2}}, \quad K_+(\xi+1) \sim K_-(\xi-1) \sim 0 \quad \dots\dots (3.8c)$$

$$d_r(\xi-1) \sim \frac{(\xi-1)^{r-1}(1+X)}{\sinh^{-1}(\xi+1)^{1/2}}, \quad d_r(\xi+1) \sim \frac{(\xi+1)^{r-1}(1+X^{-1})}{\sinh^{-1}(\xi+1)^{1/2}} \quad \dots\dots (3.8d)$$

As $k_+(\xi)/\sinh^{-1} \xi^{1/2}$ and $k_-(\xi)/\cosh^{-1} \xi^{1/2}$ are slowly varying functions of ξ , their values at $\xi=g$ have been taken. Also since ξ is large $\cosh^{-1} \xi^{1/2}/\sinh^{-1} \xi^{1/2}$ has been approximated to one. If the expressions (3.8) are substituted into (3.7) these equations can be solved giving

$$\tau_r(\xi) \sim \frac{\xi^{r-1/2}}{\{1-k^2(g)\} \sinh^{-1} \xi^{1/2}} \left[\frac{\exp(h\nu_0/kT)}{(1+X)(1+X^{-1})} + k(g)(1+X^{-1}) \right] \quad \dots\dots (3.9)$$

where $k^2(g) = k_+(g)k_-(g)/\{\cosh^{-1} g^{1/2} \sinh^{-1} g^{1/2}\}$. Values of (3.9) are plotted in Fig. 5 for $h\nu_0/kT=6$, $\zeta/kT=120$, and agreement is seen to be excellent.

In this approximation a universal time of relaxation exists since $\tau_2(\xi) = \xi \tau_1(\xi)$.

The main contribution to the conductivity comes from the first term of (3.9). Neglecting the variation of $\xi^2/\sinh^{-1} \xi^{1/2}$ near g , it is found that

$$\sigma = \frac{4Ma^3\nu_0\zeta^2 \exp(h\nu_0/kT)}{9e^2h^2\{1-k^2(\zeta/h\nu_0)\} \sinh^{-1}(\zeta/h\nu_0)^{1/2}} \quad \dots\dots (3.10)$$

This result differs markedly from Howarth and Sondheimer's corresponding expression. It is therefore important to calculate the thermoelectric effects explicitly. The thermoelectric power is given by

$$\begin{aligned} \mathcal{G}/k &= (K_2 - \zeta K_1)/kK_1T \sim \frac{6}{kg^3T} \left[h\nu_0 \int_0^\infty \frac{\xi^3 x}{(1+X)^4} dx - \zeta \int_0^\infty \frac{\xi^2 x}{(1+X)^4} dx \right] \\ &= \frac{12kT}{\zeta} \int_{-\infty}^{+\infty} \frac{t^2 e^{2t}}{(1+e^t)^4} dt \quad \dots\dots (3.11) \end{aligned}$$

with $\xi = g + kT \log x/h\nu_0$. The integral K_1 , in the denominator of \mathcal{G}/k has been calculated as in the conductivity (cf. 3.10), and in the numerator the variation of $\sinh^{-1} \xi^{1/2}$ near g has been neglected. The integral in (3.11) can be evaluated as follows

$$\begin{aligned} \int_{-\infty}^{+\infty} \frac{t^2 e^{2t}}{(1+e^t)^4} dt &= \frac{\partial^2}{\partial \alpha^2} \left[\int_{-\infty}^{+\infty} \frac{e^{t(1+\alpha)}}{(1+e^t)^4} dt \right]_{\alpha=1} = \left[\frac{\partial^2}{\partial \alpha^2} \int_0^\infty \frac{u^\alpha}{(1+u)^4} du \right]_{\alpha=1} \\ &= \frac{1}{3!} \frac{\partial^2}{\partial \alpha^2} \left[\Gamma(\alpha+1)\Gamma(3-\alpha) \right]_{\alpha=1} = \frac{1}{3} \left(\frac{\pi^2}{6} - 1 \right). \quad \dots\dots (3.12) \end{aligned}$$

The thermoelectric power is then given by

$$\frac{\mathcal{G}}{k} = \frac{4kT}{\zeta} \left(\frac{\pi^2}{6} - 1 \right). \quad \dots\dots (3.13)$$

ACKNOWLEDGMENTS

The author is indebted to Professor R. B. Dingle for many helpful discussions and to Mr. J. Humberston and Dr. B. Pardoe for programming the series (2.13) on the University of London computer.

APPENDIX

It is possible to prove without difficulty that the series (2.13) is convergent, if

$$K_+(\xi) < ab, \text{ with } a < \frac{1}{2}, b < 1 \text{ for large } \xi \quad \dots\dots (A1a)$$

$$K_-(\xi)K_+(\xi-1) < c^2 < \frac{1}{4} \text{ for } \xi \geq 1. \quad \dots\dots (A1b)$$

(A1a) is immediate, (A1b) holds for $\xi/h\nu_0 < 1$. The proof is somewhat lengthy and will be omitted.

The series (2.13) can be written collecting the terms in $d_r(\xi \pm p)$

$$\tau_r(\xi) = A_{-m}d_r(\xi-m) + A_{-m+1}d_r(\xi-m+1) + \dots + A_0(\xi)d_r(\xi) + \dots + A_p d_r(\xi+p) + \dots \quad \dots\dots (A2)$$

where m is the largest integer smaller than ξ . With the help of Stirling's formula the series A_0 is easily seen to be convergent. Comparing A_p with A_0 and using (A1) it can be shown that $A_p d_r(\xi+p) < C b^p d_r(\xi+p)$, where C is a constant independent of p . (A.2) is thus convergent as $C b^p d_r(\xi+p)$ is the general term of a convergent series.

The inequalities (A1) are sufficient conditions for the convergence of (2.13), but far from necessary; in fact it seems very likely that this series will always converge.

REFERENCES

- DELVES, R. T., 1959, *Proc. Phys. Soc.*, **73**, 572.
 DINGLE, R. B., 1956, *Physica*, **22**, 698.
 HOWARTH, D. J., and SONDHEIMER, E. H., 1953, *Proc. Roy. Soc. A*, **219**, 53.
 MILNE-THOMSON, L. M., 1960, *The Calculus of Finite Differences* (London: Macmillan).

The Infra-red Faraday Effect in Germanium

By A. K. WALTON AND T. S. MOSS

Radio Department, Royal Aircraft Establishment, Farnborough, Hants.

MS. received 5th May 1961, in revised form 22nd June 1961

Abstract. Measurements of the infra-red Faraday effect have been made in n-type, p-type and intrinsic germanium. The Faraday rotations observed are interpreted as being due to free electrons in n-type germanium, valence to conduction band transitions in intrinsic germanium, and light and heavy holes and intervalence band transitions in p-type germanium. The rotations obtained for variously doped n-type specimens are used in conjunction with Hall effect measurements on the same specimens to evaluate the Hall scattering constant as a function of the impurity content. In p-type material the rotations obtained are used to estimate the relative population of the light and heavy hole states.

§ 1. INTRODUCTION

IN recent years a great deal of interest has been revived in the Faraday effect. This has occurred because measurements of the infra-red Faraday rotation and Hall coefficient in a suitably doped semiconductor yield accurate values of the effective mass of the free carriers. The first experiments of this nature were carried out by Moss, Smith and Taylor (1959). Their results for variously doped InSb specimens were used to obtain the (E, k) relationship for the conduction band edge of this material. Good agreement was obtained with the theoretical (E, k) curve derived by Kane (1957). The Faraday effect method has subsequently been applied to obtain the effective mass of conduction band electrons in GaAs (Moss and Walton 1959 a), InP (Moss and Walton 1959 b), Ge (Walton and Moss 1959 a) and Bi_2Te_3 (Austin 1960).

The present paper describes a detailed investigation of the infra-red Faraday effect in germanium. In n-type germanium where the electron effective mass is accurately known from alternative (cyclotron resonance) experiments (Dresselhaus, Kip and Kittel 1955, Lax, Zeiger and Dexter 1956), the results are used to evaluate the Hall scattering constant. For intrinsic germanium the rotation has been measured into the absorption edge and a reversal of sign observed. In p-type germanium the observed Faraday rotation is a complex function of the wavelength and is interpreted as being due to light and heavy holes and intervalence band transitions.

A recent paper by Hartmann and Kleman (1960) presents some interesting Faraday results for intrinsic and n-type germanium, but reports no observable rotation in p-type germanium.

§ 2. THEORY

The Faraday effect is the rotation of the plane of polarization of a beam of electromagnetic radiation when a magnetic field is applied along the direction

of propagation. The rotation is given by

$$\theta = \frac{\omega l}{2c} (n_R - n_L) \quad \dots\dots (1)$$

where ω is the pulsance, l the specimen thickness, c the velocity of light and n_R and n_L are the refractive indices for the right and left circularly polarized components into which the plane polarized beam may be resolved. Here, right and left circularly polarized components are defined respectively as the components whose electric vectors describe right and left helices in space at any fixed time. A positive value of θ corresponds to a clockwise rotation for a wave propagated along the direction of the magnetic field away from the observer.

At infra-red wavelengths, the magnetic dispersion for a semiconductor may be due to either free or bound carriers. A simple classical treatment shows that the rotation due to free carriers (Mitchell 1955, Moss 1959) is given by

$$\theta = \frac{e^3 B N \lambda^2 l}{8 \pi c^3 \epsilon_0 n (m^*)^2} \quad \dots\dots (2)$$

in rationalized units, provided that

$$\omega^2 \tau^2 \gg 1, \quad \omega^2 \gg \omega_c^2, \quad k^2 \ll n^2 \quad \dots\dots (3)$$

where N is the carrier concentration, e the electronic charge, B the magnetic induction, λ the wavelength corresponding to pulsance ω , ϵ_0 the permittivity of free space, n the refractive index, m^* the effective mass, τ the relaxation time, $\omega_c = eB/m^*$, the cyclotron resonance pulsance, and k the absorption index. The requirements of Eqn (3) are readily met beyond the absorption edge of semiconductors. Thus, in semiconductors, the infra-red free carrier Faraday rotation should be proportional to wavelength squared and the magnetic induction. Such dependences have been verified for several materials. The most important feature of Eqn (2) is, however, that the rotation is inversely proportional to effective mass squared so that the effect provides a potentially accurate method of determining effective mass.

A more detailed treatment of the free carrier Faraday effect by Stephen and Lidiard (1958) starting from the Boltzmann transport equation yields an expression identical to that given in Eqn (2) provided that m^* is interpreted correctly according to the band structure. It should be noted in passing however that the sense of rotation is given incorrectly in their paper. The rotation due to free electrons is clockwise for a wave propagated along the direction of the magnetic field away from the observer (Walton 1960), i.e. is that of the current in the coils which produce the magnetic field. The rotation due to free holes is of course in the opposite sense.

Now the equi-energy surfaces for electrons in the conduction band of germanium are four ellipsoids of revolution along the [111] directions (Dresselhaus *et al.* 1955, Lax *et al.* 1956 and Herman 1955). For such ellipsoidal energy surfaces, whatever the degeneracy of the electrons, the infra-red free carrier Faraday rotation is (Lax and Zwerdling 1960)

$$\theta = \frac{Ne^3 B \lambda^2 l}{8 \pi^2 c^3 n \epsilon_0} \cdot \frac{K(K+2)}{3m_l^2} \quad \dots\dots (4)$$

where $K = m_l/m_t$ is the ratio of the longitudinal to the transverse effective mass.

In the valence band of germanium there are two types of carrier, that is both light and heavy holes. It readily follows that in this case the infra-red free

carrier Faraday rotation is given by

$$\theta = -\frac{e^3 B \lambda^2 l}{8 \pi^2 c^3 n \epsilon_0} \left[\frac{p}{m_p^2} + \frac{q}{m_q^2} \right] \quad \dots\dots (5)$$

where q and p are the light and heavy hole concentrations and m_q and m_p are the light and heavy hole masses. The ratio q/p is theoretically equal to the density of states ratio which is $(m_q/m_p)^{3/2}$ so that the few light holes should contribute more than the heavy holes to the free carrier Faraday rotation. The ratio of the contributions of the light and heavy holes is in fact $(m_p/m_q)^{1/2}$ amounting to $\sqrt{8}$ in germanium.

Application of simple classical theory to the bound electrons shows (e.g. Moss 1959) that the rotation due to these electrons is

$$\theta = \frac{Ne^3 \omega^2 B l}{2 n c \epsilon_0 (\omega_0^2 - \omega^2)^2 m^2} \quad \text{for } \omega \gg \omega_c \quad \dots\dots (6)$$

where ω_0 is the resonant pulsance of the bound electrons. Thus, in general, infra-red Faraday rotations due to free and bound charges are different functions of wavelength and consequently can be separated.

§ 3. FARADAY EFFECT APPARATUS

The apparatus was developed from that described by Smith *et al.* (1959) and is shown schematically in Fig. 1. Radiation from the source S passed through the polarizer P_1 and was focused by the mirrors M_1 and M_2 on to the germanium specimen situated at the centre of the electromagnetic gap. The source S was

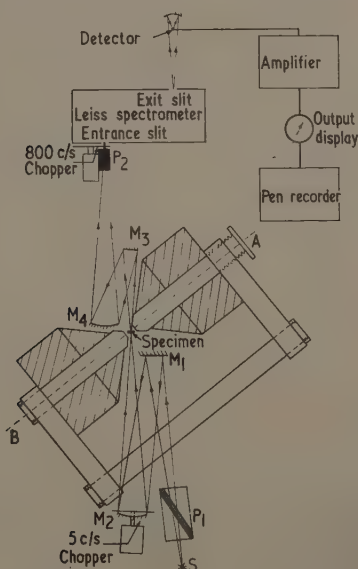


Fig. 1. Schematic diagram of Faraday effect apparatus. (Note that the beam of radiation is deflected in the vertical plane by M_4 on to P_2 which reflects horizontally into the entrance slit of the spectrometer.)

either a tungsten filament lamp with a sapphire window or a Nernst filament according to the wavelength range required. Both sources were suitably stabilized.

A pile of polyethylene plates set at the Brewster angle constituted the polarizing element P_1 . Twelve plates each five microns thick were used. With these very thin plates sufficient transmission was obtained between the polyethylene absorption bands to allow Faraday rotations to be measured at selected wavelengths from 13 microns down to 1.5 microns.

The germanium specimen was orientated so that a normal to its surface made an angle of 50° in the horizontal plane with the geometric axis of the magnet. Because of the high refractive index of the germanium, the approximately normally incident radiation was refracted to traverse the specimen accurately normal to its surface. Thus the Faraday rotations observed corresponded to the magnetic field resolved through 50° . The magnet was always used in the saturated condition so that the magnitude of the field was unaltered (by hysteresis) upon reversing its direction. The magnitude of the required resolved component of the magnetic induction was measured directly with the aid of a search coil mounted on the same support that had carried the specimen. In this way the difficulty of measuring the orientation of the specimen with respect to the magnetic axis was avoided. Resolved fields up to 13 000 gauss were used.

For the n- and p-type specimens, the absorption was such that the radiation was considerably attenuated in a single traverse of the specimen thickness. This loss, together with the attenuation at each reflection, meant that multiple internal reflections were negligible and the Faraday rotation appropriate to only a single traverse of the specimen thickness was measured. In the measurements on intrinsic germanium, where transmission losses were rather low, multiple internal reflection effects were avoided by using slightly non-parallel specimens (see §6). Specimens were prepared by lapping with carborundum powder and then polishing with diamond paste on photographic paper.

After leaving the specimen, the radiation was brought to a second focus at the entrance slit of the spectrometer by the mirrors M_4 , M_3 and P_2 . P_2 was the analyser, constructed from polished single-crystal silicon set at its Brewster angle. The theoretical characteristics of this reflection analyser show that the polarization for a 10° wide beam incident at the Brewster angle is 99%. Since the optics of the spectrometer caused significant polarization ($\sim 3:1$), the analyser P_2 was arranged to polarize in the same plane as the spectrometer and the polarizer P_1 made rotatable. Accordingly M_4 and P_2 deflected the beam in the vertical plane, the radiation finally entering the spectrometer horizontally. P_1 was made in the form of a transmission polarizer to prevent the image of the source moving on rotation.

The spectrometer was a Leiss double monochromator containing either NaCl, CaF_2 or LiF prisms according to the wavelength range and resolution radiation was chopped at 800 c/s, the detector being either a gold doped focused onto a suitable detector T. In the n-type germanium experiments the detector was a vacuum thermopile with a KRS-6 window and the radiation was chopped at 5 c/s. For the p-type and intrinsic germanium experiments the radiation was chopped at 800 c/s, the detector being either a gold doped germanium or indium antimonide cell cooled to 77°K . The detected signal was amplified, rectified, smoothed and fed to a pen recorder.

Measurements were made by slowly rotating the polarizer P_1 through the crossed position with the magnetic field in a given direction and recording the detected signal. A contact breaker marked every degree on the record. This process was then repeated with the magnetic field reversed. Records of two symmetrical minima were obtained in this way and half the angular difference between the two minima was the required Faraday rotation. The minimum of each record was found in the following way. The mean of the two angles at which the signal had a given value was found for various signal levels at which the signal was changed rapidly with angle and the average value taken as the angle corresponding to the minimum. An accuracy to better than $\pm 0.2^\circ$ was obtained by this method.

Measurements of the Faraday rotation were made at room temperature and at 77°K . In the latter case specimens were situated in a demountable liquid nitrogen cryostat which had CaF_2 windows.

§ 4. MEASUREMENT OF CARRIER CONCENTRATION BY FARADAY ROTATION

For semiconductors where the effective mass is known accurately from other magneto-optical experiments, the free carrier Faraday effect provides a new method of determining the carrier concentration N (see Eqn (2)). This method of obtaining N has two advantages over the Hall effect method, namely: (i) The interpretation of the results does not depend on a knowledge of the scattering mechanism since the infra-red free carrier Faraday rotation is independent of scattering. (ii) No electrical contacts are required, which is important since suitable contacts are difficult to provide for many materials.

Disadvantages of the Faraday effect method are: (a) The effective mass must be known. (b) In practice only a limited range of carrier concentration can be measured in this way. For pure materials the rotation is too small while for extremely impure materials the optical transmission is too low because of the low mobility.

Faraday rotations measured in variously doped single-crystal n-type germanium specimens are shown plotted against wavelength squared in Fig. 2.

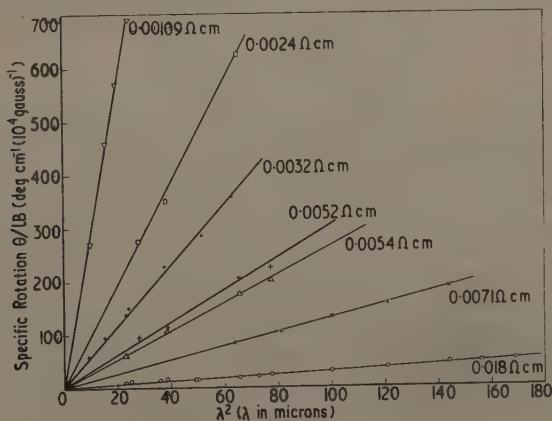


Fig. 2. Faraday rotation in variously doped n-type germanium specimens.

For each specimen, the experimental points fit a straight line through the origin extremely well. The sense of the rotations is that of the current in the coils which produces the magnetic field as expected for free electrons (see §2).

The carrier concentration for each germanium specimen was calculated from the observed Faraday rotation as follows. Rewriting Eqn (4) we have that the carrier concentration in n-type germanium is given by

$$N = \frac{8\pi^2 c^3 n \epsilon_0 (m^*)^2 \theta}{e^3 B \lambda^2 l} \quad \dots\dots (7)$$

where

$$m^* = [3/K(K+2)]^{1/2} m_1. \quad \dots\dots (8)$$

The slopes of the straight lines of Fig. 2 give $\theta/lB\lambda^2$ for each specimen. Now the conduction band of germanium should be parabolic due to the high density of states, so that m^* is a constant, independent of N , and may be calculated from cyclotron resonance data (Dresselhaus *et al.* 1955, Lax *et al.* 1956) to be $0.134m_1$. Using the refractive index data of Salzberg and Villa (1958) with allowance for free carrier dispersion, it is found that $n=3.99$ for the doped germanium of the present experiment over the wavelength range involved. Values obtained for the carrier concentration N on inserting the above data into Eqn (7) are given in Table 1.

These experiments show that the Faraday effect method of determining N is practicable in germanium over the range $N=10^{16}$ – 10^{19} cm⁻³. The higher concentrations of this range are difficult to determine by the Hall effect method since the Hall voltages are very small and the Hall scattering constant is particularly difficult to evaluate theoretically when neither the non-degenerate nor the degenerate statistical approximation applies to the conduction band electrons.

§ 5. DETERMINATION OF THE HALL SCATTERING CONSTANT IN n-TYPE GERMANIUM

In addition to measuring N by the Faraday effect method described above, measurements of the low field Hall coefficient and resistivity were made on the same n-type germanium specimens. The Hall coefficient in n-type germanium at low magnetic field strengths is given by (Brooks 1955)

$$A_{H0} = \frac{r}{Ne} [3K(K+2)/(2K+1)^2]. \quad \dots\dots (9)$$

Accordingly, the Hall scattering constant r was calculated from this equation for each specimen by inserting the cyclotron resonance value of the mass ratio K , the measured low magnetic field limit of the Hall coefficient A_{H0} and the corresponding carrier concentration N obtained from the Faraday rotation. Values obtained for r are presented in Table 1. It will be seen that r depends on the impurity content of the specimens as expected. Jones (1951) has treated the problem of the effect of mixed lattice and impurity scattering on the scattering constant r and has presented his theoretical results in the form of a plot of r against μ/μ_1 , where μ and μ_1 are respectively the actual mobility and the mobility that would arise if only impurity scattering were present. In order to facilitate comparison of the present experimental results with the theory of Jones, the parameter μ/μ_1 has been evaluated for each specimen. The mobility μ was calculated from the carrier concentration N and the measured resistivity. Now the

nobility μ_L , when scattering is by lattice vibrations only, is known to be $8800 \text{ cm}^2 \text{ sec}^{-1} \text{ v}^{-1}$ from drift experiments (Prince 1953) on near intrinsic germanium. Thus μ/μ_L was known and μ/μ_I found from the theoretical curve of Conwell (1952).

Figure 3 shows the experimental values of r plotted against μ/μ_I , together with the theoretical curve of Jones. It will be seen that Jones's theory fits the experimental results for $\mu/\mu_I < 0.5$. At larger values of μ/μ_I it does not fit. However, in his treatment Jones assumed non-degenerate statistics to apply throughout, whereas in germanium at room temperature N exceeds 10^{19} cm^{-3} when $\mu/\mu_I < 0.8$ so that degenerate statistics apply. Thus, at large values of μ/μ_I , r is expected to approach unity somewhat as shown by the broken lines of Fig. 3.

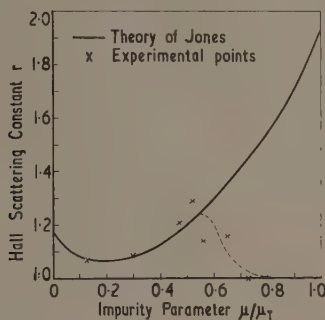


Fig. 3. Hall scattering constant r in n-type germanium as a function of the parameter μ/μ_I .

Table 1. Carrier Concentrations by Faraday and Hall Effect Methods and Values obtained for the Hall Scattering Constant r

Resistivity (ohm cm)	A_{H0} ($\text{cm}^2/\text{c}^{-1}$)	N/r^\dagger (cm^{-3})	N^\ddagger (cm^{-3})	r	μ ($\text{cm}^2 \text{ sec}^{-1} \text{ v}^{-1}$)	μ/μ_I
0.0180	34.4	1.39×10^{17}	1.49×10^{17}	1.07	2330	0.13
0.00710	8.54	$5.7(5) \times 10^{17}$	$6.2(7) \times 10^{17}$	1.09	1400	0.30
0.00536	4.59	1.07×10^{18}	1.29×10^{18}	1.21	900	0.47
0.00519	4.30	1.14×10^{18}	1.47×10^{18}	1.29	820	0.52
0.00315	2.01	2.45×10^{18}	2.80×10^{18}	1.14	710	0.56
0.00244	1.24	$3.9(8) \times 10^{18}$	$4.6(3) \times 10^{18}$	1.16	550	0.65
0.00109	0.368	1.34×10^{19}	1.34×10^{19}	1.00	430	0.73

† Calculated from A_{H0} ; ‡ calculated from Faraday rotation.

The experimental error in a determination of r is approximately $\pm 6\%$ since r depends linearly on θ , B and A_{H0} (compared with the square root dependence of m^* on these measured quantities where the errors are halved).

Another way of determining the scattering constant r is from the low and high magnetic field limits of the Hall coefficient which are given by:

$$A_{H0} = \frac{r}{Ne} \frac{3K(K+2)}{(2K+1)^2}; \quad A_{H\infty} = \frac{1}{Ne}$$

so that

$$A_{H0}/A_{H\infty} = \frac{3K(K+2)r}{(2K+1)^2}. \quad \dots\dots (10)$$

Geballe and Kunzler (1959) have measured the ratio $A_{H0}/A_{H\infty}$ accurately for 20 Ω cm n-type germanium at 77°K and have obtained $r = 1.16$ in close agreement with the theoretical value of $3\pi/8$. To determine $A_{H\infty}$ a magnetic field strength H is required such that $\mu H \gg 1$. Thus to find r by this method for highly doped n-type germanium, where the mobility is low owing to impurity scattering, inconveniently high magnetic fields would be required. This method and the Faraday rotation method of finding r are thus complementary, the former being applicable to pure materials and the latter to impure.

It is suggested that the data of Fig. 3 should be of general use in determining carrier concentrations in n-type germanium from Hall effect measurements.

§ 6. THE INFRA-RED FARADAY EFFECT IN INTRINSIC GERMANIUM

The Faraday rotation was measured in 'intrinsic' germanium (60 Ω cm p-type) over the wavelength range of 1.6 to 5.0 microns at temperatures of 300°K and 77°K. The results of these measurements are shown in Fig. 4. At wavelengths long compared with that of the absorption edge, the rotation is independent of temperature, inversely proportional to wavelength squared and is in the same sense as the current in the coils producing the magnetic field in agreement with classical theory for bound electrons (Walton 1960). However, near the absorption edge the rotation becomes temperature-dependent, rapidly deviates from the inverse square law and soon changes sign.

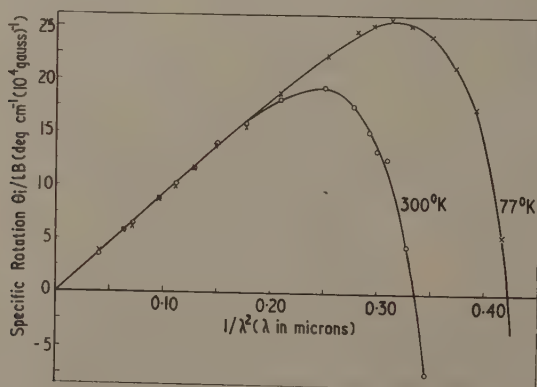


Fig. 4. Faraday rotation in intrinsic germanium at 300°K and 77°K.

The specimens used in these measurements on intrinsic germanium were deliberately made slightly non-parallel (an angle of 1° between transmitting faces) to avoid multiple internal reflection effects. In plane parallel specimens, where multiply reflected components were detected, rotations were about 13% larger than in the non-parallel specimens. Calculations show that the rotation can be as much as 23% too large.

In the original classical treatment, it was shown by Becquerel (1897) that the specific rotation is

$$\frac{\theta}{lB} = -\frac{e\lambda}{2mc} \frac{dn}{d\lambda} \quad \dots\dots(11)$$

where $dn/d\lambda$ is the dispersion in the absence of the magnetic induction B and m is the free electron mass. This equation may be rewritten

$$\frac{\theta}{lB} = \frac{e}{mc\lambda^2} \frac{dn}{d(1/\lambda^2)} \quad \dots\dots(12)$$

Now at wavelengths long compared with that of the absorption edge, $dn/d(1/\lambda^2)$ is a constant in germanium, as shown by the data of Salzberg and Villa (1958) which are plotted in Fig. 5. Thus this theory predicts that the specific rotation should vary as λ^{-2} , as is indeed found experimentally (Fig. 4). Furthermore, the absolute magnitude of the rotation expected can be found from Eqn (12) using the dispersion data of Fig. 5. From the slopes of the straight lines in Figs 4 and 5 we find that the observed rotation is 65% of that predicted—a remarkable degree of agreement for such a simple theory with no adjustable parameters. Recent results by Hartmann and Kleman (1960) give a similar figure, namely that the rotation is 60% of that predicted by Eqn (12).

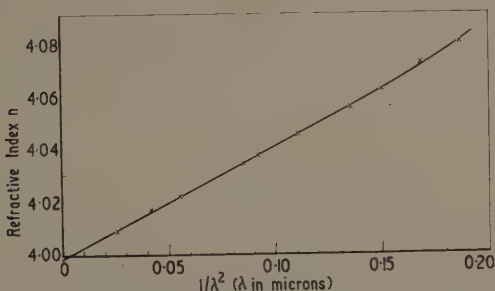


Fig. 5. Dispersion in intrinsic germanium (Salzberg Villa 1958).

The dispersion has not been measured accurately at wavelengths below 2.3μ . However by using the fact that the refractive index and absorption are inter-related (Moss 1959) it can be shown that n will reach a maximum in the neighbourhood of the absorption edge and then fall. Thus the dispersion, and hence the Faraday rotation, should fall to zero and then become negative. Since the absorption edge shifts to shorter wavelengths on cooling, the Faraday rotation is expected to change sign at shorter wavelengths for the cooled material.

This simple classical dispersion theory is seen to give good qualitative (and reasonable quantitative) explanations of the rotation due to bound charges. A full theoretical treatment of the intrinsic effect would need to consider virtual transitions between quantized energy levels in the region of the band edge. This type of treatment has been outlined by Lax and Zwerdling (1960) but it has not yet been developed to the state where it can explain the form and magnitude of the observed behaviour.

§ 7. THE INFRA-RED FARADAY EFFECT IN p-TYPE GERMANIUM

The infra-red Faraday rotation was measured in p-type germanium both at room temperature and at 77°K. Plane parallel specimens of 0.0278 and 0.0100 Ω cm resistivity were used and the measurements extended over the wavelength range of 2 to 6.3 microns, that is, right through the absorption bands (Briggs and Fletcher 1953, Kaiser *et al.* 1953) at 3.5 and 4.5 microns due to intervalence band transitions $h\nu_{13}$ and $h\nu_{23}$ (see Fig. 6). In the room temperature measurements the specimens were sufficiently opaque to avoid multiple internal reflection effects. However in the case of the results at 77°K, the measured rotations have been reduced by 13% at wavelengths where the specimen was transparent, to allow for multiple reflections.

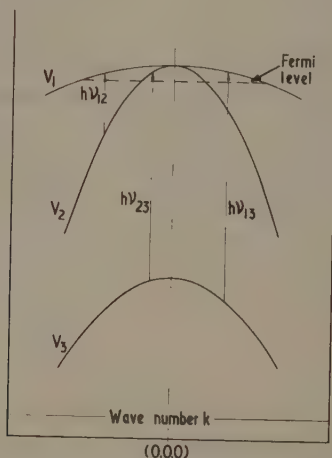


Fig. 6. Transitions causing complex absorption spectra beyond the main absorption edge in p-type germanium.

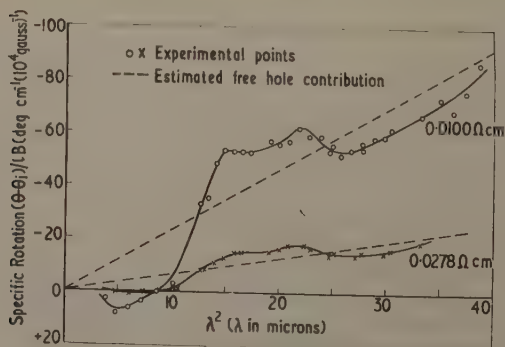


Fig. 7. Faraday rotation in excess of the intrinsic contribution in p-type germanium at 300°K.

In order to eliminate the bound carrier rotation associated with transitions between the valence and conduction bands, the rotation in intrinsic germanium the measurements of which are described in § 6) was subtracted from the rotation obtained in each p-type specimen. Figs 7 and 8 show the resulting rotations plotted against wavelength squared. In each case the rotation is a complicated function of wavelength but is of the sign expected for a rotation due to free holes, i.e. is in the *opposite* sense to that of the current in the coils which produce the magnetic field.

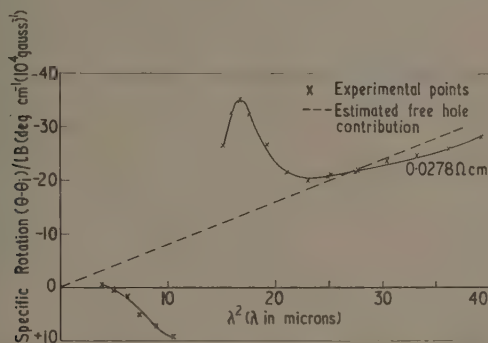


Fig. 8. Faraday rotation in excess of the intrinsic contribution in p-type germanium at 77°K.

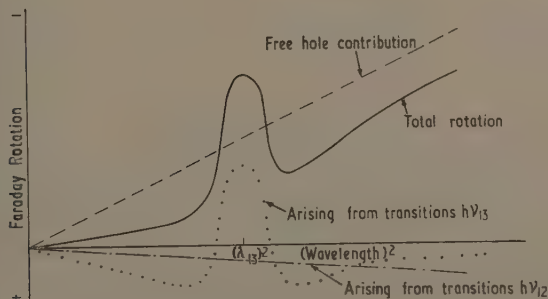


Fig. 9. Theoretical wavelength dependence of the infra-red Faraday rotation in excess of the intrinsic contribution in p-type germanium.

The rotation shown in Figs 7 and 8 is interpreted as arising from free holes and intervalence band transitions. It is suggested that the theoretical wavelength dependence of the rotation in p-type germanium in excess of that in intrinsic germanium should be of the form shown by the continuous line of Fig. 9. The broken lines show the various contributions:

(i) The free hole contribution which will be proportional to wavelength squared.

(ii) The contribution arising from the dispersion associated with the transition $h\nu_{13}$. The wavelength dependence of this contribution has been taken as that of the dispersion associated with a classical oscillator centred at the frequency ν_{13} . In §6, this technique has been shown to give reasonable results when applied to the valence to conduction band transitions in germanium. It follows that, well below the resonant wavelength λ_{13} , the rotation is directly proportional to λ whilst at wavelengths long compared with λ_{13} , the rotation is inversely proportional to λ^2 . The sign of this contribution has been taken to be the same as that of the rotation due to valence to conduction band transitions in germanium.

(iii) Absorption due to transitions $h\nu_{23}$ is weak compared with that due to transitions $h\nu_{13}$. Accordingly, the transitions $h\nu_{23}$ should contribute a relatively small rotation with a wavelength dependence similar to that of (ii) above. This small contribution has been omitted from Fig. 9 for the sake of clarity. However, it may cause an additional peak in the total rotation near the wavelength λ_{23} .

(iv) Proceeding as in (ii), the transitions $h\nu_{12}$ give a contribution roughly proportional to λ^2 in the region of interest where $\lambda \ll \lambda_{12}$.

The experimental results of Figs 7 and 8 are seen to fit the above simple qualitative analysis fairly well. The rotation peaks at wavelengths not far removed from λ_{13} , λ_{23} . Further, the departure of the experimentally observed rotation from a quadratic dependence on wavelength is approximately proportional to carrier concentration and 'sharpens' on cooling. These features are also in accord with what one would expect if the dispersion due to transitions $h\nu_{12}$, $h\nu_{23}$ could be approximated by that of a classical oscillator.

§ 8. THE RELATIVE POPULATION OF THE FAST AND SLOW HOLE STATES IN p-TYPE Ge

The magnitude of the infra-red free carrier Faraday rotation when two occupied hole states exist is given by Eqn (5), namely

$$\theta = - \frac{e^3 \lambda^2 B l}{2 \pi c^3 \epsilon_0 n} \left[\frac{p}{m_p^2} + \frac{q}{m_q^2} \right]. \quad \dots (13)$$

Cyclotron resonance experiments (Dresselhaus *et al.* 1955, Lax *et al.* 1956) have yielded accurate values for the effective mass parameters m_p and m_q . With allowance for warping of the energy surfaces (Lax and Zwerdling 1960), the values of m_p and m_q to be used in Eqn (13) are $0.35m$ and $0.044m$ respectively.

Now the slow hole concentration p can be obtained from Hall effect measurements. At sufficiently high magnetic fields to saturate the fast holes but not the slow holes (i.e. when $\mu_q H \gg 1 \gg \mu_p H$ where μ_q and μ_p are the mobilities of the fast and slow holes respectively) the Hall coefficient is given to a good approximation by

$$A_H' = \frac{r}{pe}.$$

Thus a determination of the infra-red free carrier Faraday rotation allows q to be calculated on inserting the values of p , m_p and m_q into Eqn (13). Since the fast holes contribute much more than the slow holes to the free hole Faraday rotation (see §2), this is a potentially accurate method of measuring the relative population q/p of the two occupied hole states.

However, beyond the absorption edge of p-type germanium, the Faraday rotation is not simply proportional to wavelength squared and is composed of contributions due to free holes and intervalence band transitions as discussed in §7. Thus isolation of the free hole contribution required is difficult. Nevertheless, since the interband transitions should produce a negative rotation in the middle of the band (i.e. near λ_{13} , λ_{23}) and a positive rotation outside it, a straight line giving the free hole contribution may be drawn fairly accurately as shown in Figs 7 and 8. It is assumed here that the contribution to the rotation due to transitions $h\nu_{12}$ is negligible. Such a contribution, being approximately proportional to λ^2 , would be inseparable from the free hole contribution.

From the free hole contribution to the Faraday rotation, estimated as described above, the quantity $[p + qm_p^2/m_q^2]$ was calculated using Eqn (13). The data of Salzberg and Villa (1958), with allowance for free carrier dispersion, was taken for n . The results are shown in Table 2.

In order to determine the slow hole concentration p in the specimens used for the Faraday effect measurements, the Hall coefficient was determined as a function of magnetic field both at room temperature and at 77°K. However, saturation of the fast holes could not be achieved with the magnetic field available and consequently A_H' and hence p could not be obtained directly. This was thought to be due to the low value of the fast hole mobility in these impure materials. Theoretically, although the ratio of the fast to slow hole mobility $a = m_p/m_q = 8$ for lattice scattering, as the doping increases 'a' falls until $a = (m_p/m_q)^{1/2} = 2.8$ for impurity scattering (Brooks 1955). Further, the slow hole mobility itself falls as the doping increases.

Now as the magnetic field increases, the Hall coefficient is expected to fall from the low field value of

$$A_{H0} = (p + a^2q)r/(p + aq)^2e \quad \dots\dots(14)$$

to the high field value

$$A_H' = r/pe. \quad \dots\dots(15)$$

Since $aq \ll p$, it follows that as the impurity content increases, the fall in Hall coefficient caused by saturating the fast holes in a high magnetic field should decrease. With between 2% and 5% of the holes in the low mass state, A_H'/A_{H0} should be approximately 0.95 when impurity scattering is dominant compared with approximately 0.5 for lattice scattering. This point was tested experimentally by measuring the magnetic variation of the Hall coefficient in variously doped p-type germanium specimens at 300°K. The results of these measurements are shown in Fig. 10. It is seen that A_H'/A_{H0} is 0.65 for the purest material but as the impurity content increases the change in Hall coefficient on saturating the fast holes decreases. Although actual saturation of the fast holes could not be achieved in the 0.01 Ω cm and 0.0278 Ω cm materials which were used in the Faraday work, it was estimated from the results of Fig. 10 and the theoretical value of A_H'/A_{H0} for impurity scattering, that A_H' was 0.90 A_{H0} for the 0.0278 Ω cm at 300°K and 0.95 A_{H0} at 77°K. For the 0.01 Ω cm material A_H' was taken to be 0.95 A_{H0} . Clearly A_H' is close to A_{H0} in these impure materials, so that errors involved in finding A_H' from A_{H0} must be small. Table 2 gives the values obtained in this way for A_H' and also the values of p calculated using equation (15) and taking r to be 1.1.

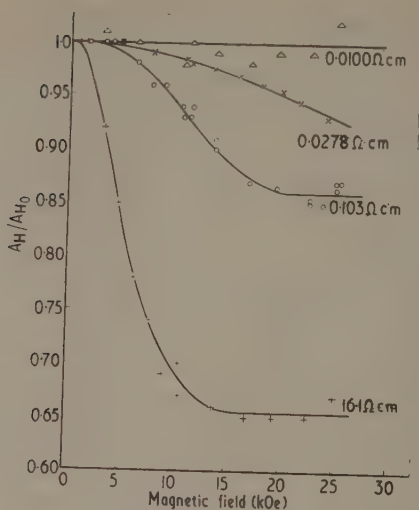


Fig. 10. Magnetic variation of the Hall coefficient in p-type germanium at 300°K.

Table 2. The Relative Population of Light and Heavy Hole States in p-type Germanium calculated from Measurements of the Faraday Rotation and Hall Coefficient

(1)	(2)	(3)	(4)	(5)	(6)	(7)
0.0100	300	7.5×10^{18}	5.4	5.1	1.35×10^{18}	0.07
0.0278	300	2.1×10^{18}	20.0	18.0	3.8×10^{17}	0.07
0.0278	77	2.6×10^{18}	24.3	23.1	3.0×10^{17}	0.12

(1) Specimen resistivity at 300°K (Ω cm); (2) temperature (°K); (3) $p + (m_p/m_q)^2 q$ from Faraday rotation (cm^{-3}); (4) A_{H0} (cm^3 coulomb $^{-1}$); (5) A_H (cm^3 coulomb $^{-1}$); (6) p (cm^{-3}); (7) q/p .

The last column of Table 2 gives the ratio of the fast to slow hole concentration obtained by combining columns three and six of the table. Both specimens give $q/p = 7\%$ at room temperature. This value is rather large compared with the theoretical estimate of $(m_q/m_p)^{3/2}$ which amounts to about $4\frac{1}{2}\%$, and it appears to increase even further on cooling to 77°K. Galvanomagnetic (Willardson *et al.* 1954) and photomagnetic (Walton and Moss 1959b) experiments have yielded $q/p = 2\%$ which is somewhat less than the theoretical estimate.

The values obtained for q/p from the present Faraday and Hall effect experiments are tentative since the interpretation of the Faraday rotation is difficult due to the rotations associated with intervalence band transitions. In the analysis of the results, rotations arising from transitions $h\nu_{12}$ were assumed negligible. However if this contribution to the total rotation is appreciable and of the sign indicated in Fig. 9, the values deduced for q/p are too small! It is possible that the wrong sign has been attributed to the contribution by transitions $h\nu_{12}$. For example, the rotation arising from transitions between the valence and conduction

band of InSb is of the correct wavelength dependence but the opposite sign to that of a classical oscillator (Smith *et al.* 1959, Brown and Lax 1959). This difference of sign for the bound carrier contribution is accounted for by the large negative g -factor of the conduction band electron in InSb (Roth *et al.* 1959). Thus it is possible that too large a value of the free hole rotation has been estimated from the experimental data and consequently too large a value of q/p obtained.

In other materials, where absorption bands due to intervalence transitions may lie at more convenient wavelengths, it may well be possible to get accurate values of the relative population of the light and heavy hole states by Faraday and Hall effect measurements as described in this paper.

ACKNOWLEDGMENTS

The authors are indebted to Dr. E. W. J. Mitchell, Reading University, for helpful discussions and to Miss D. Webber and Mr. D. Newberry for assistance with the experiments. Single crystal germanium was kindly supplied by Dr. A. F. Gibson of the Royal Radar Establishment, Mr. S. E. Bradshaw of The General Electric Co. Ltd., and Mr. R. L. Rouse of Associated Electrical Instruments Ltd.

REFERENCES

- AUSTIN, I. G., 1960, *Proc. Phys. Soc.*, **75**, 169.
 BECQUEREL, H., 1897, *C.R. Acad. Sci., Paris*, **125**, 679.
 BRIGGS, H. B., and FLETCHER, R. C., 1953, *Phys. Rev.*, **91**, 1342.
 BROOKS, H., 1955, *Advances in Electronics and Electron Physics*, **7**, 85.
 BROWN, R. N., and LAX, B., 1959, *Bull. Amer. Phys. Soc.*, [II], **4**, 133.
 CONWELL, E. M., 1952, *Proc. Inst. Radio Engrs, N.Y.*, **40**, 1327.
 DRESSSELHAUS, G., KIP, A. F., and KITTEL, C., 1955, *Phys. Rev.*, **98**, 368.
 GEBALLE, T. H., and KUNZLER, J. E., 1959, see *Semiconductors*, by N. B. Hannay (New York: Reinhold), p. 354.
 HARTMANN, B., and KLEMAN, B., 1960, *Ark. Fys.*, **18**, 75.
 HERMAN, F., 1955, *Proc. Inst. Radio Engrs, N.Y.*, **43**, 1703.
 JONES, H., 1951, *Phys. Rev.*, **81**, 149.
 KAISER, W., COLLINS, R. J., and FAN, H. Y., 1953, **91**, 1380.
 KANE, E. O., 1957, *J. Phys. Chem. Solids*, **1**, 249.
 LAX, B., ZEIGER, H. J., and DEXTER, R. N., 1956, *Phys. Rev.*, **104**, 637.
 LAX, B., and ZWERDLING, S., 1960, *Progress in Semiconductors*, **5**, 221.
 MITCHELL, E. W. J., 1955, *Proc. Phys. Soc. B*, **68**, 973.
 MOSS, T. S., 1959, *Optical Properties of Semiconductors* (London: Butterworths Scientific Publications; New York: Academic Press).
 MOSS, T. S., SMITH, S. D., and TAYLOR, K. W., 1959, *J. Phys. Chem. Solids*, **8**, 323.
 MOSS, T. S., and WALTON, A. K., 1959 a, *Proc. Phys. Soc.*, **74**, 131.
 — 1959 b, *Physica*, **25**, 1142.
 PRINCE, M. B., 1953, *Phys. Rev.*, **92**, 681.
 ROTH, L. M., LAX, B., and ZWERDLING, S., 1959, *Phys. Rev.*, **114**, 90.
 SALZBERG, C. D., and VILLA, J. J., 1958, *J. Opt. Soc. Amer.*, **47**, 244.
 SMITH, S. D., MOSS, T. S., and TAYLOR, K. W., 1959, *J. Phys. Chem. Solids*, **11**, 131.
 STEPHEN, M. J., and LIDIARD, A. B., 1959, *J. Phys. Chem. Solids*, **9**, 43.
 WALTON, A. K., 1960, *Thesis*, University of Reading.
 WALTON, A. K., and MOSS, T. S., 1959 a, *J. Appl. Phys.*, **30**, 951.
 — 1959 b, *Proc. Phys. Soc.*, **73**, 692.
 WILLARDSON, R. K., HARMAN, T. C., and BEER, A. C., 1954, *Phys. Rev.*, **96**, 1512.

Thermally Stimulated Emission and Conductivity Peaks in the Case of Temperature Dependent Trapping Cross Sections

By P. N. KEATING

Associated Electrical Industries Limited, Harlow Research Laboratory, Essex

MS. received 15th June 1961

Abstract. The original theory of thermally stimulated emission is extended to include the effect of a temperature dependent trapping cross section. A method is proposed whereby the ionization energy and temperature dependent capture cross section of a set of identical trapping states may be determined from the half-width and shape of a thermally stimulated emission peak obtained from a single experiment. The method is also applicable to thermally stimulated current peaks if the free electron lifetime varies only slowly with temperature.

§ 1. INTRODUCTION

IN recent years investigation of the fundamental properties of phosphors and photoconductors has intensified and methods of studying trapping states and recombination centres have thus gained in importance. The measurements of thermally stimulated emission and current are powerful methods of investigating the properties of trapping centres in these materials.

Since the original theory of Randall and Wilkins (1945), a number of theoretical treatments have been published and several methods of analysis of the two types of peak exist; these methods are discussed in detail in § 6. In the earlier theories, the escape frequency factor (given by the product $N_c S v$ where N_c is the effective density of states in the conduction band, S is the trapping cross section and v is the electron thermal velocity) has been considered as temperature independent; recently Bube (1960) and subsequently Haering and Adams (1960) have considered S to be temperature independent whilst N_c and v vary as $T^{3/2}$ and $T^{1/2}$ respectively.

According to one theoretical model (Lax 1960), S can vary with temperature more rapidly than T^{-3} whilst Bemski (1958) has shown experimentally that the capture of a charge carrier by an oppositely charged gold centre in silicon can have a cross section which varies as T^{-4} . Thus, in general, the assumption that the capture cross section of a trap does not vary with temperature is invalid and the theory which follows is intended to indicate how the temperature dependence of S will affect peaks of thermally stimulated emission or conductivity. The theory is employed to derive a method of analysis of such peaks which will give the ionization energy and temperature dependent cross section of a trapping level.

§ 2. BASIC THEORY

The theory to be described is an extension of the work of Randall and Wilkins (1945) and a brief outline of the basic theory will first be given. The model upon which the theoretical analysis is based consists of a number of discrete

trapping levels from which electrons may be thermally excited into the conduction band; recombination of free electrons takes place at deep centres. It is assumed that:

(i) Peaks from different trapping levels do not overlap. Although this is not true in many cases, the peaks may be separated by suitable experimental techniques, e.g. by varying the heating rate or by thermal quenching of the low temperature peak (Hoogenstraaten 1958).

(ii) Transitions directly between trapping states and other centres are negligible.

(iii) The recombination lifetime is so short that $dn_c/dt \ll n_c/\tau$, where n_c is the concentration of electrons in the conduction band. This is almost always a valid assumption for phosphors and photoconductors.

The rate of change of the electron concentration n in a trapping level with an ionization energy E is:

$$\frac{dn}{dt} = -nN_cSv \exp\left(\frac{-E}{kT}\right) + An_c(N-n) \quad \dots\dots(1)$$

where N is the number of states in the level and A is a measure of the retrapping probability.

The rate of change of the electron concentration in the conduction band is

$$\frac{dn_c}{dt} = -\frac{n_c}{\tau} - \frac{dn}{dt}$$

and thus

$$\frac{dn_c}{dT} = -\frac{n_c}{\beta\tau} - \frac{dn}{dT}$$

if $\beta = dT/dt$.

Now since $dn_c/dt \ll n_c/\tau$, as assumed above, then $n_c \simeq -\beta\tau dn/dT$.

Hereafter the theory will be discussed with reference to the emission intensity I but with slight modification it is equally applicable to the conductivity case since the stimulated conductivity is, if μ is the electron mobility,

$$\sigma = n_c e \mu = -e \mu \beta \tau \frac{dn}{dT} = \tau e \mu I$$

since

$$I = \frac{n_c}{\tau} = -\beta \frac{dn}{dT}. \quad \dots\dots(2)$$

It has been assumed that retrapping effects are negligible and it will be shown later that this is a reasonable approximation in most cases. The solution of Eqn (1), with the second term negligible compared with the first, then gives

$$n = n_0 \exp \left\{ - \int_{T_0}^T \frac{N_c S v}{\beta} \exp \left(- \frac{E}{kT} \right) dT \right\}$$

and thus

$$I = n_0 N_c S v \exp \left\{ - \frac{E}{kT} - \int_{T_0}^T \frac{N_c S v}{\beta} \exp \left(- \frac{E}{kT} \right) dT \right\}. \quad \dots\dots(3)$$

§ 3. FURTHER ANALYSIS

The trapping cross section S will be taken to be related to temperature by a simple power law as T^{-a} and, for simplicity of analysis, $N_c S v$ is taken to be BT^b

so that $a=2-b$. Thus, from Eqn (3),

$$\ln \left(\frac{I}{I_0} \right) = b \ln T - \frac{E}{kT} - \frac{B}{\beta} \int_{T_0}^T T^b \exp \left(-\frac{E}{kT} \right) dT \quad \dots (4)$$

where $I_0 = n_0 B$ and is temperature independent. A linear temperature increase has been assumed, i.e. $\beta = \text{constant}$.

Differentiation of $\ln(I/I_0)$ with respect to T yields, at the peak temperature T_g ,

$$\frac{B}{\beta} = \left(\frac{b}{T_g^{b+1}} + \frac{E}{kT_g^{b+2}} \right) \exp \left(\frac{E}{kT_g} \right). \quad \dots (5)$$

The integral in Eqn (4) may be evaluated, to a good approximation, by an asymptotic series which gives

$$\int_{T_0}^T T^b \exp \left(-\frac{E}{kT} \right) dT \simeq \frac{kT^{b+2}}{E} (1-\Delta) \exp \left(-\frac{E}{kT} \right)$$

where $\Delta = (b+2)kT/E$.

The error involved is less than 3% if $E/kT_g > 10$.

Thus Eqn (4) becomes

$$-\ln \left(\frac{I}{I_0} \right) = \frac{E}{kT} - b \ln T + \left(\frac{T}{T_g} \right)^{b+2} \left(1 + \frac{bkT_g}{E} \right) (1-\Delta) \exp \left(\frac{E}{kT_g} - \frac{E}{kT} \right). \quad \dots (6)$$

This equation is now applied to the two cases when $I = I_g/2$, i.e. at temperatures T_1, T_2 ($T_1 < T_2$) and is simplified by writing

$$\frac{T_g - T_1}{T_g} = \alpha_1; \quad \frac{T_2 - T_g}{T_g} = \alpha_2.$$

Hence

$$\begin{aligned} \left(1 + \frac{bkT_g}{E} \right) (1-\Delta) + \ln 2 = -\psi - b \ln(1+x) \\ + (1+x)^{b+2} \left(1 + bk \frac{T_g}{E} \right) (1-\Delta) \exp(\psi) \quad \dots (7) \end{aligned}$$

where x is either $-\alpha_1$ or α_2 and

$$\psi = \frac{E}{kT_g} \left(\frac{x}{1+x} \right).$$

Since $\Delta \ll 1$ for $E/kT > 10$, $(b+2)kT_1/E$ and $(b+2)kT_2/E$, have been taken equal to $\Delta = (b+2)kT_g/E$.

Equation (7) has been solved numerically for α_1 and α_2 for values of $b=0, +2, -2$ and E/kT_g between 10 and 35, i.e. for values liable to be encountered experimentally. The results are summarized in Figs 1 and 2; analysis of these curves shows that E/kT_g can be accurately related to $\alpha (= \alpha_1 + \alpha_2)$ for particular values of the ratio $\alpha_2/\alpha_1 = \gamma$ by an equation which is linear in α :

$$\frac{kT_g}{E} = \alpha(1.2\gamma - 0.54) + 5.5 \times 10^{-3} - \left(\frac{\gamma - 0.75}{2} \right)^2. \quad \dots (8)$$

This equation is an accurate description of the variation of kT_g/E with α and γ for values of E/kT_g between 10 and 35 and γ between 0.75 and 0.9 and its validity should extend some way beyond the limits of this range.

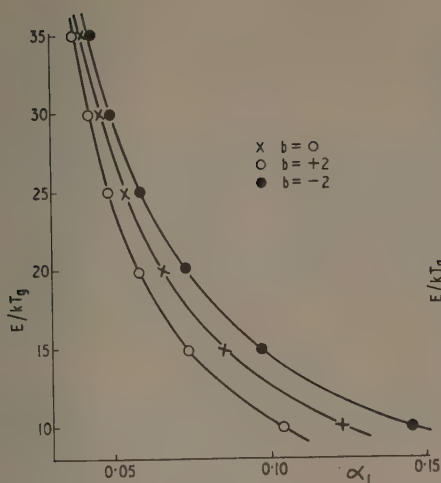


Fig. 1. Variation of E/kT_g as a function of α_1 , for $b=0, +2, -2$.

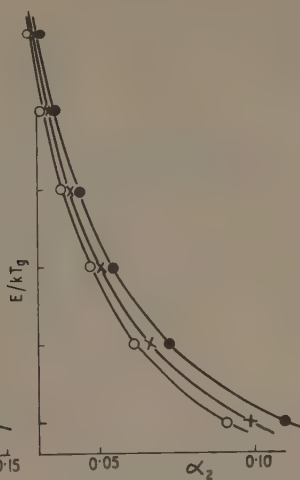


Fig. 2. Variation of E/kT_g as a function of α_2 , for $b=0, +2, -2$.

§ 4. DETERMINATION OF E, a, S FROM EXPERIMENTAL PEAKS

In order to evaluate the ionization energy and $S = CT^{-a}$, where C is a constant, it is necessary to measure four quantities, the peak temperature T_g , the half-width $T_2 - T_1$, the parameter γ which is $(T_2 - T_g)/(T_g - T_1)$, and the heating rate β .

(i) E may be evaluated by substituting α, γ and T_g in Eqn (8).

(ii) The data given in Figs 1 and 2 are replotted in Fig. 3 to enable a to be deduced from the values of E/kT_g and γ .

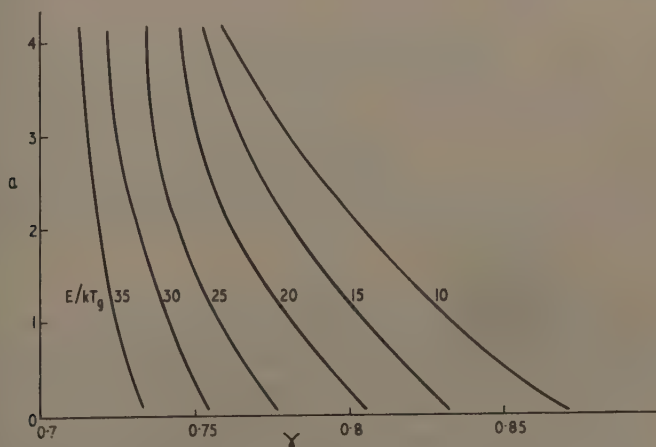


Fig. 3. Variation of a as a function of γ for a number of values of E/kT_g .

(iii) B may be evaluated from Eqn (5) by the substitution of $b=2-a$, T_g and E/kT_g . For negligible retrapping $C=B/K_1K_2$ where K_1, K_2 are given by $N_c=K_1T^{3/2}$, $v=K_2T^{1/2}$. Hence $S=BT^{-a}/K_1K_2$.

§ 5. THE EFFECT OF RETRAPPING

In the limiting case of very fast retrapping when $A(N-n) \gg 1/\tau$, solution of Eqn (1) gives (see Haering and Adams 1960)

$$I = n_0 N_c S v \exp \left\{ -\frac{E}{kT} - \int_{T_g}^T \frac{N_c}{\beta \tau} \exp \left(-\frac{E}{kT} \right) dT \right\}.$$

A similar procedure to that used previously gives, in this case,

$$\begin{aligned} -\ln \left(\frac{I}{I_0} \right) &= \frac{E}{kT} - b \ln T + \left(\frac{T}{T_g} \right)^{7/2} \left(1 - \frac{7kT_g}{2E} \right) \\ &\times \left(1 + \frac{bkT_g}{E} \right) \exp \left(\frac{E}{kT_g} - \frac{E}{kT} \right) \end{aligned} \quad \dots\dots (9)$$

if τ varies but slowly.

(This is to be compared with Eqn (6).)

Thus the result for very fast retrapping is identical with that for no retrapping when $b = \frac{3}{2}$ ($a = \frac{1}{2}$) but Eqns (6) and (9) give differing results for other values of b . This difference will be greatest, for the range of values of b considered, when $b = -2$.

As an example, if $E/kT_g = 20$ and $b = -2$, use of Eqn (9) and the same procedure as before yields $\alpha_1 = 0.067$, $\alpha_2 = 0.050$, $\gamma = 0.745$ and $\alpha = 0.117$. If these two values of γ and α are substituted into Eqn (8), one obtains $E/kT_g = 19.3$, only $3\frac{1}{2}\%$ different. Whilst it does not necessarily follow that, in intermediate cases, the error is between 0 and $3\frac{1}{2}\%$, it is unlikely that a larger error will be introduced by ignoring the effect of retrapping.

§ 6. AN APPRAISAL OF EXISTING METHODS

The main criticism of thermally stimulated current and emission measurements has been that the values of E obtained by the various existing methods sometimes differ by as much as 50%. Part of this error may be attributed to experimental difficulties such as uncertainties in measurement of the true temperature of the specimen and difficulties in achieving a linear temperature increase. In addition, there are three sources of error, some of which are inherent in each of the various methods employed for the analysis of curves, namely (i) variation of the escape frequency factor with temperature, (ii) variations in the initial occupancy of the trapping states, (iii) retrapping.

6.1. Temperature Dependence of the Escape Frequency Factor

Most methods consider the product $N_c S v$ to be independent of temperature and in fact thus imply that $a=2$ since $N_c v$ may be taken to vary as T^2 . In this case, $b=0$ and Eqn (5) becomes

$$\frac{B}{\beta} = \frac{E}{kT_g^2} \exp \left(\frac{E}{kT_g} \right). \quad \dots\dots (10)$$

If b is not equal to zero, errors can be introduced into methods which employ this equation and these may be appreciable. Hoogenstraaten (1958) has used this equation directly by plotting $\ln T_g^2 \beta$ against $1/T$ and if $b = -2$ the error in the value of E so obtained is about 12% for $E/kT_g \simeq 20$ and $T_g \simeq 100^\circ\text{K}$. Booth (1954) has used two heating rates and hence two simultaneous equations to eliminate B from Eqn (10); this is thus similar to the previous method and the same errors are introduced if b is not zero. Garlick and Gibson (1948) have also taken $b=0$ but if this is not valid then their equation should be corrected to $\ln I = b \ln T - E/kT + \text{constant}$, and errors, of the same order as those in the two previous methods, are introduced if this correction is not applied.

Grossweiner (1953) obtained, by approximation methods, an expression which may be written

$$\frac{E}{kT_g} = 1.51 \frac{(1 - \alpha_1)}{\alpha_1};$$

this yields values of E/kT_g which are somewhat larger than the curve shown in Fig. 1. This method is made more inaccurate if the assumption that $b=0$ is invalid since b affects the curve in Fig. 1. Halperin and Branner (1960) have derived a very useful treatment of various recombination conditions but their method of analysing the peaks is rendered somewhat inaccurate by a geometrical approximation, originally due to Lushchik (1955). They assume $b=0$ and, for the conditions assumed in § 2 above, obtain an expression which may be written

$$\frac{E}{kT_g} = \frac{q(1 - \Delta)}{\alpha_2} \quad \dots\dots (11)$$

where q is a quantity related to the shape of the peak (and thus γ) and $\Delta = 2kT_g/E$. This expression gives somewhat different results from those of the theory proposed in this article, e.g. if $\gamma = 0.75$, $q = 1.3$ and for $\alpha_2 = 0.06$, Eqn (11) gives $E/kT_g = 19.5$ instead of 17.9 obtained from Eqn (8)—about 10% difference.

Bube (1960) and Haering and Adams (1960) have taken $N_c v$ to vary as T^2 and have ignored any temperature variation of S . Thus $b=2$ and Eqn (5) becomes

$$\frac{B'}{\beta} = \frac{E}{kT_g} 4 \left(1 + \frac{2kT_g}{E} \right) \exp \left(\frac{E}{kT_g} \right).$$

Bube's equation (1960) is thus in error by the term $2kT_g/E$ which can easily amount to 10%. Haering and Adams (1960) obtained an expression

$$\ln \sigma/\sigma_0 = E/kT + 1,$$

where σ_0 is the product $N_c S v n_0 e \mu \tau$; the error in the value of E obtained by their method is about 8% if $a=4$ for $E/kT_g \simeq 20$ and $T \simeq 200^\circ\text{K}$.

6.2. Initial Trap Occupancy Variations

Several methods (Booth 1954, Hoogenstraaten 1958, Haering and Adams 1960) require a number of measurements at different heating rates and it is always tacitly assumed that the initial occupancy (n_0) of the trapping state is the same for each measurement. But in many phosphors and photoconductors the approach to thermal equilibrium is dependent upon the past history of the specimen and it is extremely difficult to ensure that n_0 is the same for each measurement.

6.3. Retrapping

The values of E derived by methods using a number of heating rates (i.e. Booth 1954, Hoogenstraaten 1958, Haering and Adams 1960) and that of Garlick and Gibson (1948) are unaffected by retrapping but it may give appreciable errors in other methods. The method due to Bube (1955) has been shown by Haering and Adams (1960) to give values of E in error by about 2% for very fast retrapping with larger errors for less retrapping. Halperin and Branner (1960) have considered specific cases but since it is not possible to determine the extent of retrapping, uncertainty is introduced if it is not negligible. Grossweiner's method (1953) ignores retrapping and uncertainty (about 8% for extreme retrapping) again arises when it is appreciable.

All of the methods can be used to evaluate S but if retrapping is not negligible then the value of S obtained is subject to large errors since Eqn (5) is not valid for this case.

§ 7. CONCLUSION

Provided that the three assumptions made in §2 are satisfied, the method summarized in §4 is valid for thermally stimulated emission even when the recombination lifetime varies as a trap empties since I is independent of τ (Eqn (2)). The theory is also valid for thermally stimulated conductivity peaks, provided τ varies only slowly. (It is hoped at a later date to extend the theory to include variations of τ .)

The main advantages of the proposed method are:

(i) The temperature dependence of the trapping cross section is taken into account and, in addition, error in E due to extensive retrapping is small since retrapping is partly corrected for by allowing the effective capture cross section to vary.

(ii) Only one experiment at any one heating rate is necessary for analysis. The values of a and E obtained by the proposed method do not depend on the initial occupancy n_0 .

(iii) The main experimental error is in the measurement of temperature difference and this is about half of that introduced into the somewhat similar methods of Grossweiner (1953) and Halperin and Branner (1960).

As in the other methods, S is subject to large errors if retrapping is appreciable since Eqn (5) is not valid in this case. However, if retrapping can be ignored, S can then be evaluated as a function of temperature whereas previous methods give its value only at the particular temperature at which the peak occurs. The value at the peak temperature can easily differ from the room temperature value by a factor 5 if S varies appreciably with temperature and it is of obvious value to be able to determine S at the temperature at which most measurements are made and at which devices are normally used.

ACKNOWLEDGMENTS

The author wishes to thank Dr. P. D. Fochs and Dr. J. Franks for much helpful criticism and discussion and Dr. M. E. Haine, Director of the Harlow Research Laboratory of Associated Electrical Industries Ltd., for permission to publish this article.

REFERENCES

- BEMSKI, G., 1958, *Phys. Rev.*, **111**, 1515.
BOOTH, A. H., 1954, *Canad. J. Chem.*, **32**, 214.
BUBE, R. H., 1955, *J. Chem. Phys.*, **23**, 18.
——— 1960, *Photoconductivity in Solids* (London, New York: John Wiley), p. 293.
GARLICK, G. F. J., and GIBSON, A. F., 1948, *Proc. Phys. Soc. A*, **60**, 574.
GROSSWEINER, L. I., 1953, *J. Appl. Phys.*, **24**, 1306.
HAERING, R. R., and ADAMS, E. N., 1960, *Phys. Rev.*, **117**, 451.
HALPERIN, A., and BRANNER, A. A., 1960, *Phys. Rev.*, **117**, 408.
HOOGENSTRAATEN, W., 1958, *Philips Res. Rep.*, **13**, 515.
LAX, M., 1960, *Phys. Rev.*, **119**, 1502.
LUSHCHIK, CH. B., 1955, *Dokl. Akad. Nauk SSSR*, **101**, 641.
RANDALL, J. T., and WILKINS, M. H. F., 1945, *Proc. Roy. Soc. A*, **184**, 366.

Spectroscopic Investigations of Plasma Containment in ZETA

By W. M. BURTON AND R. WILSON

Atomic Energy Research Establishment, Harwell, Berkshire

Communicated by R. S. Pease; MS. received 17th April 1961

Abstract. Observations are made of the time variation of the intensities of spectral lines emitted by small quantities of impurity ions in a deuterium discharge in ZETA. A vacuum ultra-violet monochromator which covers the wavelength range 500–2000 Å is used. The observations are interpreted in terms of temporal ionization distributions determined for a partially contained plasma model. The observations are consistent with the model and it is shown that plasma containment in ZETA is violated by two processes: an escape of plasma to the wall represented by a loss rate coefficient $\lambda(\text{sec}^{-1})$, and an injection of atoms in a neutral or low state of ionization represented by an injection coefficient $\Lambda(\text{sec}^{-1})$. The value of λ is effectively independent of the stabilizing magnetic field strength B_z , whereas the injection coefficient varies considerably with this parameter. Both λ and Λ are closely correlated with ϵ , the energy input per unit mass of gas, and over the range of conditions investigated they show a linear increase with ϵ . The ion containment time $1/\lambda$ is about 100 microseconds at $\epsilon = 3 \text{ keV}/m_p$ and at this condition most of the energy input is carried to the walls by the escaping plasma. The net effect of the processes of loss and injection controls the variation of plasma line density, and in general this shows a decrease with time or 'pump-out'. This is measured and related to other discharge phenomena.

§ 1. INTRODUCTION

THE laboratory production of high temperature plasma has received great impetus over the past decade from experiments aimed at producing controlled thermonuclear reactions. At the moment the great need is to understand the basic physical processes which occur in such a plasma and potentially one of the most powerful methods of achieving this is the observation and interpretation of the radiation emitted. This paper deals with one aspect of this field, namely, the spectral line radiation from impurity ions in a deuterium plasma. Emission from highly ionized impurity ions persists after the initial deuterium ionization phase and should therefore give information concerning the physical conditions when the plasma is fully ionized.

The atomic processes governing the state of ionization within a plasma have been established for astrophysical conditions. If the electron density, electron temperature and dimensions of the plasma are known then one can, in principle, determine the quantitative contribution of the different processes. A similar approach can be made to the study of a high temperature laboratory plasma but two important differences emerge. Firstly, the lifetime of the laboratory plasma

is generally short so that the transient phase of the ionization becomes important and must be studied. The second, and more fundamental, difference is that the astrophysicist's assumption of conservation of atoms within his plasma is generally not valid when dealing with the high temperature laboratory plasma. Indeed, one of the primary objectives of thermonuclear research is the conservation of plasma in a suitable magnetic confinement system.

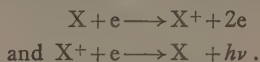
Spectroscopic observations of plasma produced in the laboratory are often interpreted with the assumption that the plasma is fully confined. In the present paper we first describe the ionization processes occurring in such a plasma, and then consider the more realistic case of a partially confined plasma. The non-conservation of atoms is treated empirically. Ions are assumed to escape from the plasma by some loss process represented by a loss-rate coefficient whose reciprocal gives the ion containment time. It is also assumed that some injection process can operate whereby the plasma receives ions, probably from the walls of the confining vessel, in a neutral or low state of ionization.

The mathematical development of this model gives analytical expressions describing the life history of impurity ions in a deuterium plasma, i.e. the temporal frequency distribution of the various states of ionization in terms of the electron density, electron temperature and the parameters describing the processes of loss and gain. The theory is used as the basis for interpreting the observed spectral line transients of impurity ions in the experimental device ZETA. The observations support the model set-up and confirm the existence of the processes of loss and gain in the discharge; indeed, these are the dominant processes governing the ion population in the physical conditions studied.

§ 2. THEORETICAL

2.1. *A Fully Contained Plasma*

We first consider a plasma with neither loss nor injection of atoms. The model is specified by constant uniform electron density n_e and electron temperature T_e , and consists of a deuterium (or hydrogen) plasma containing a small quantity of impurity elements which are present in the neutral state at time $t=0$. The work of Knorr (1958) and McWhirter (1959, 1960) has shown that the dominant atomic processes in a deuterium plasma of the density, temperature and dimensions of ZETA are ionization by electron collision and recombination by radiative capture, as in the solar corona (Woolley and Allen 1948) viz.:



The ionization process for the transition from the n th to the $(n+1)$ th state, is described by the coefficient S_n , given by

$$S_n = \sum \langle Q(v)v \rangle,$$

where the cross section $Q(v)$ at velocity v is averaged over a Maxwellian distribution for an electron temperature T_e and the summation is over all electrons in the n th state ion. Similarly, the radiative recombination coefficient α_n for a transition from the n th to the $(n-1)$ th state of ionization is given by

$$\alpha_n = \sum \langle q(v)v \rangle,$$

where the summation is this time over all energy levels in the n th state ion.

The equations describing the state of ionization of the impurity elements are

$$\frac{1}{n_e} \frac{dx_n}{dt} = x_{n-1} S_{n-1} - x_n [S_n + \alpha_n] + x_{n+1} \alpha_{n+1}, \quad \dots (1)$$

where x_n represents the proportion of each element in the n th state of ionization at time t . The neutral atom is represented by $n=0$ and the fully stripped ion by $n=Z$ where Z is the atomic number. The instantaneous concentration of any ion in the plasma is then given by $n_0 x_n$ where n_0 is the initial concentration of neutral atoms per unit volume. Analytical solutions of (1) are obtainable with the assumption that during the time period that x_n is varying rapidly, only the adjacent states, $n-1$ and $n+1$, have a time varying population, all states lower than $n-1$ having reached a steady state and all states higher than $n+1$ having yet to be populated. Observations of the intensity variation of spectral lines for an ionic sequence show that this is a close approximation. The solutions are

$$x_n = \beta_n \exp[-n_0 S'_n t] - \beta_{n-1} \exp[-n_0 S'_{n-1} t] + \gamma_n, \quad \dots (2)$$

where

$$S'_n = S_n + \alpha_n + \alpha_{n+1},$$

$$\beta_n = 1 - \sum_0^n \gamma_n,$$

and γ_n is the steady state value of x_n given by

$$\frac{\gamma_n}{\gamma_{n+1}} = \frac{\alpha_{n+1}}{S_n} \text{ and } \sum_0^Z \gamma_n = 1.$$

These satisfy the following boundary conditions:

$$t=0; \quad x_n=0, \quad x_0=1,$$

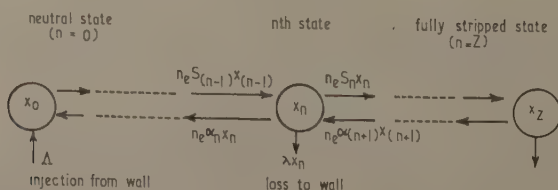
$$t=\infty; \quad x_n=\gamma_n,$$

$$\sum_0^Z x_n = \sum_0^Z \gamma_n = 1.$$

2.2. A Partially Contained Plasma

Into the model described above, two new processes are introduced: (a) a loss of ions from the plasma at a rate $\lambda x_n n_c$, where the loss rate coefficient $\lambda(\text{sec}^{-1})$ represents an inverse containment time, and (b) an injection of atoms from the wall at a rate Δn_0 , where the injection coefficient $\Delta(\text{sec}^{-1})$ represents an inverse time for injecting into the plasma the initial concentration n_0 .

The model can be represented schematically as follows where the concentrations are all expressed as fractions of n_0 .



Since the injection is associated with the walls of the confining vessel, the injected material will be 'cold' and is indicated in the diagram as being in the neutral state, although it is sufficient to suppose that the injected atoms are in a

lower state of ionization than those considered. It is assumed that the coefficients λ and Λ are constant in time and apply, not only to the impurity elements, but also to the parent deuterium plasma. Consequently, the chemical composition of the plasma remains unchanged although its density may vary with time. Spatial uniformity and constant T_e are still assumed.

The differential equations describing this system can be written as

$$\frac{1}{n_e} \frac{dx_n}{dt} = x_{n-1} S_{n-1} - x_n \left[S_n + \alpha_n + \frac{\lambda}{n_e} \right] + x_{n+1} \alpha_{n+1} \quad \dots\dots (3)$$

These are similar to the Eqns (1) describing the fully contained model, but the boundary conditions are quite different and n_e is no longer a constant but becomes a time-varying function depending on λ and Λ . Since we are dealing with a small concentration of impurity ions in a deuterium plasma, we can neglect the contribution of the impurities to the electron density and equate n_e to the number density of the deuterons. Further, as we are interested in the higher stages of ionization of the impurities, we can ignore the initial deuterium ionization phase and assume, as before, that the deuterium is fully ionized throughout. Putting n_0 equal to the initial deuterium number density, we therefore obtain the following equation in n_e :

$$\frac{dn_e}{dt} = n_0 \Lambda - \lambda n_e, \quad \dots\dots (4)$$

which is easily solved to give

$$n_e = n_0 \left[\left(1 - \frac{\Lambda}{\lambda} \right) e^{-\lambda t} + \frac{\Lambda}{\lambda} \right]. \quad \dots\dots (5)$$

Substitution for n_e in Eqns (3) gives a set of differential equations for which analytical solutions are derived with the same approximations as used above. They are:

$$\begin{aligned} x_n = e^{-\lambda t} \left[\beta_n \left(1 - \frac{\Lambda}{n_0 \Lambda S'_n / \lambda + \lambda} \right) \exp \left\{ - \frac{n_0 S'_n}{\lambda} \left(1 - \frac{\Lambda}{\lambda} \right) (1 - e^{-\lambda t}) - \frac{\Lambda}{\lambda} n_0 S'_n t \right\} \right. \\ \left. - \beta_{n-1} \left(1 - \frac{\Lambda}{n_0 \Lambda S'_{n-1} / \lambda + \lambda} \right) \exp \left\{ - \frac{n_0 S'_{n-1}}{\lambda} \left(1 - \frac{\Lambda}{\lambda} \right) \right. \right. \\ \left. \left. \times (1 - e^{-\lambda t}) - \frac{\Lambda}{\lambda} n_0 S'_{n-1} t \right\} + \gamma_n \right] + \Gamma_n, \quad \dots\dots (6) \end{aligned}$$

where Γ_n is the steady state value of x_n given by

$$\Gamma_n = \Lambda \left[\frac{\beta_n}{n_0 \Lambda S'_n / \lambda + \lambda} - \frac{\beta_{n-1}}{n_0 \Lambda S'_{n-1} / \lambda + \lambda} + \frac{\gamma_n}{\lambda} \right].$$

The solutions satisfy the following boundary conditions:

$$\begin{aligned} t=0; \quad x_n=0, \quad x_0=1 \\ t=\infty; \quad x_n=\Gamma_n \\ \sum_0^Z x_n = \left(1 - \frac{\Lambda}{\lambda} \right) e^{-\lambda t} + \frac{\Lambda}{\lambda}. \end{aligned}$$

The expressions (6) are quite general and reduce to the fully contained case (2) when λ and Λ tend to zero.

2.3. Relation to Observed Spectral Line Intensities

The observable quantity is I_n , the intensity of a spectral line emitted by the n th ion as a function of time. To relate I_n to x_n requires a solution of the

equation of radiative transfer for Doppler broadened spectral lines emitted from the model plasma. The problem is identical with that for solar prominences (Ambartsumyan 1958) and the solution can be expressed in the form

$$I_n = n_0 x_n^* d \epsilon \left(1 - \frac{\tau_0}{2! \sqrt{2}} + \frac{\tau_0^2}{3! \sqrt{3}} - \dots \right),$$

where d is the diameter of the plasma, x_n^* is the fraction of x_n populating the lower level of the transition, and ϵ is the atomic line emission coefficient. The optical depth τ_0 at the frequency of the line centre is given by

$$\tau_0 = \frac{\pi^{1/2} e^2}{mc} \frac{n_0 x_n^* d f}{\Delta \nu_D},$$

where f is the oscillator strength of the spectral line and $\Delta \nu_D$ is its Doppler width in frequency units.

The simplest relation between I_n and x_n is the proportionality which exists when the plasma is optically thin at the frequency of the observed spectral line, i.e. when the higher terms in the expression for I_n are negligible. The condition for this is $\tau_0 \ll 2! \sqrt{2}$ which is satisfied for the resonance lines to be observed. An upper limit to τ_0 can be estimated by putting $x_n^* = 1$, and then, using the observed values for the other parameters we get $\tau_0 \leq 0.2$.

Since τ_0 is small the excitation processes governing the emission line coefficient ϵ are analogous to those dominating ionization, viz. electron collisional excitation and radiative decay. For constant T_e we therefore have $\epsilon \propto n_e$ and also $x_n \propto x_n^*$. Hence the expression for the observed intensity of a spectral line as a function of time is given by

$$I_n = C_n n_e x_n, \quad \dots (7)$$

where n_e and x_n are given by Eqns (5) and (6) respectively, and C_n is a constant for any one spectral line.

Practical considerations make it convenient to divide this general expression for I_n into two parts: firstly, that part of the distribution resulting from the atoms initially present at $t=0$ and referred to as the 'initial transient'; secondly, that part of the distribution resulting from the injected atoms and referred to as the 'injection tail'. The expression for the initial transient is

$$I_n(t) = C_n n_0 \left[\left(1 - \frac{\Lambda}{\lambda} \right) e^{-\lambda t} + \frac{\Lambda}{\lambda} \right] e^{-\lambda t} \left[\beta_n \exp \left\{ -\frac{n_0 S'_n}{\lambda} \left(1 - \frac{\Lambda}{\lambda} \right) (1 - e^{-\lambda t}) - \frac{\Lambda}{\lambda} n_0 S'_n t \right\} \right. \\ \left. - \beta_{n-1} \exp \left\{ -\frac{n_0 S'_{n-1}}{\lambda} \left(1 - \frac{\Lambda}{\lambda} \right) (1 - e^{-\lambda t}) - \frac{\Lambda}{\lambda} n_0 S'_{n-1} t \right\} + \gamma_n \right]. \quad \dots (8)$$

In the case of the injection tail, we are mainly interested in the steady state value and therefore omit the time varying part of the function to give

$$I_n(\Gamma) = C_n n_0 \frac{\Lambda}{\lambda} \left[\frac{\Lambda \beta_n}{n_0 \Lambda S'_n / \lambda + \lambda} - \frac{\Lambda \beta_{n-1}}{n_0 \Lambda S'_{n-1} / \lambda + \lambda} + \frac{\Lambda}{\lambda} \gamma_n \right]. \quad \dots (9)$$

2.4. The Coefficients of Injection and Loss

Our main concern in this investigation is the determination of the injection Λ and loss rate λ coefficients and we set out here the expressions for these parameters in terms of the observable quantities R_n and Δt_n . The intensity ratio R_n is given by

$$R_n = \frac{I_n(\Gamma)}{I_n(t_p)}, \quad \dots (10)$$

where $I_n(\Gamma)$ is the intensity of the injection tail, given by Eqn (9), and $I_n(t_p)$ is the peak intensity of the initial transient $I_n(t)$ given by Eqn (8). The 'transient lifetime' Δt_n is given by

$$\Delta t_n = \frac{\int_0^\infty I_n(t) dt}{I_n(t_p)}, \quad \dots\dots (11)$$

which is approximately equal to the time duration of the initial transient measured at an ordinate $I_n(t_p)/e$. The parameters $I_n(\Gamma)$, $I_n(t_p)$ and Δt_n are depicted in Fig. 1 which is reproduced from an actual oscillogram.

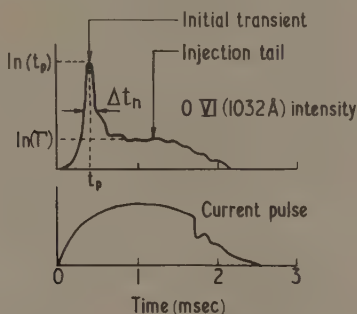


Fig. 1. Typical spectral line intensity and current waveforms showing measured parameters ($P = \frac{1}{2}\mu D_2$, $V_c = 10$ kv, $B_z = 800$ gauss).

When the intensity level in the injection tail is small, i.e. $I_n(\Gamma) \ll I_n(t_p)$, the quantities R_n and Δt_n can be obtained unambiguously from the observed intensity-time distributions. When $I_n(\Gamma)$ becomes large R_n can still be estimated, albeit less accurately, but the initial transient becomes masked by the injection tail. However, it will be shown in § 4 that Δt_n can still be measured under these conditions by using a small quantity of argon, added as a trace element. The injection of argon is very small and therefore reveals the initial transient only (see Fig. 4).

An analysis of Eqns (9), (10) and (11) gives the following approximate expression for the injection coefficient:

$$\Lambda = \frac{2 + 5\Lambda/\lambda + 5(\Lambda/\lambda)^2 R_n}{12(\Lambda/\lambda)^2 \Delta t_n}. \quad \dots\dots (12)$$

The value of the transient lifetime Δt_n depends on n_e , T_e , Λ and λ , and since we know n_e in terms of Λ and λ (Eqn (5)), three unknowns remain. Hence, an independent measurement of T_e would enable us, in principle, to estimate Λ and λ from Eqns (11) and (12). This would not be very satisfactory since it depends on poorly known atomic cross sections and instead we consider the form of Δt_n when n is large. As n increases the ionization rate decreases rapidly, so for any significant value of λ there must be an ionization stage at which the loss rate exceeds the ionization rate, i.e. $\lambda > n_e S_n$. When this occurs an analysis of Eqn (11) shows that Δt_n reaches a constant value which is independent of n_e and T_e and is given approximately by

$$\lim_{n \rightarrow \infty} \Delta t_n \longrightarrow \left(1 + \frac{\Lambda}{\lambda}\right) \frac{e}{2\lambda}, \quad \dots\dots (13)$$

where e is the base of natural logarithms. Thus the asymptotic value of Δt_n when n is large is a function of Λ and λ only. Substitution of the observable quantities R_n and the limiting value of Δt_n in Eqns (12) and (13) allows the determination of Λ and λ without knowledge of the electron temperature or the cross sections of the ionization and recombination processes.

§ 3. EXPERIMENTAL

The plasma studied was produced in the toroidal gas discharge apparatus ZETA 1A which has been described elsewhere by Butt *et al.* (1958) and by Mitchell *et al.* (1959). Since that time modifications have been carried out to replace the 1600 μF capacitor bank by a larger unit with a capacity of 11 000 μF which provides a stored energy of 3 MJ when fully charged to 24 kv. The original 1600 μF capacitor bank charged to about 5 kv is now used as a pre-heat bank to ionize the gas before discharging the main capacitor bank. The main bank is discharged through ignitrons into the primary winding of a pulse transformer with a turns ratio of 4:1. The secondary of the transformer is a single turn discharge in deuterium gas at a pressure of the order of one micron. The discharge is operated at approximately one minute intervals with a current pulse of about 3 msec duration. An axial magnetic field which can be varied up to 1600 gauss was used to increase the stability of the discharge. The range of ZETA operating conditions used during the present observations is summarized below.

Voltage on main capacitor bank	V_c (7 to 15 kv)
Axial magnetic field	B_s (200 to 1600 gauss)
Current (peak value)	I (200 to 600 kA)
Deuterium gas pressure	P ($\frac{1}{4}$ to 2 μm Hg)

The model which was developed in § 2 to describe the life history of impurity ions in a deuterium plasma can only be applied after the deuterium has been fully ionized. Under these conditions most impurity atoms will be multiply ionized. The resonance lines of such ions generally occur with high intensity at wavelengths below 2000 Å in the vacuum ultra-violet region of the spectrum. A vacuum ultra-violet monochromator fitted with a photoelectric detection system was used to select particular lines in the ZETA emission spectrum and to observe the time variation of the intensity of each line throughout the ZETA current pulse. A plan-view diagram of the apparatus is shown in Fig. 2.

The monochromator was coupled to ZETA through a vacuum valve at a port providing a radial view of the plasma at the torus centre axis. A vacuum system on the monochromator enabled the pressure to be reduced to about 10^{-5} mm Hg before the valve to the torus was opened. The path of the observed light was entirely *in vacuo* and it was reflected at near-normal incidence by a concave diffraction grating which was blazed to give a high intensity first-order spectrum at a wavelength of 1500 Å. The grating was a one metre radius aluminized replica (Bausch and Lomb Type No. 372). The emergent first-order wavelength could be varied throughout the range 300–5000 Å by a drive mechanism which rotated the grating and simultaneously displaced it in order to maintain adequate focus†. The exit slit was set to pass the required bandwidth of about 1 Å.

The radiation leaving the exit slit illuminated a thin film of sodium salicylate coated on the inside of a quartz window. This fluorescent surface converted the

† This mechanism was designed by Professor R. W. Ditchburn at the University of Reading, where the monochromator was made.

incident radiation into visible blue light which passed through the window and was detected by a photomultiplier tube (E.M.I. Type: 6256A) placed outside the vacuum system. To limit electrical interference the photomultiplier tube was shielded with 2 cm copper and a balanced output circuit was used to reject in-phase signals. The balanced output signal was displayed on a double-beam oscilloscope (Cawkell Type SC46) and recorded photographically simultaneously with the ZETA current waveform. A remote control motor drive synchro-indicator unit enabled the wavelength setting to be adjusted and displayed.

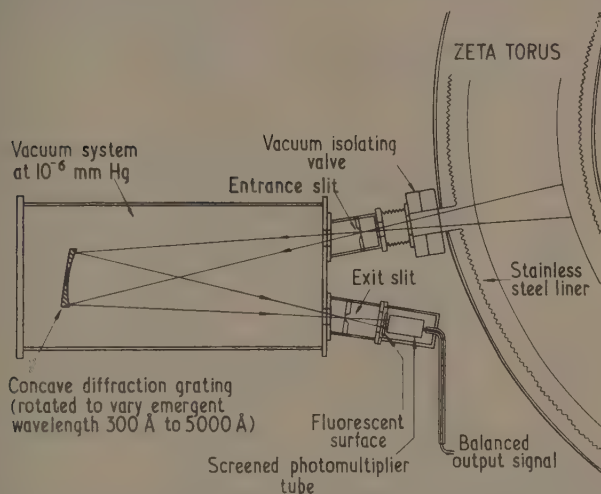


Fig. 2. Schematic diagram of vacuum ultra-violet monochromator fitted to ZETA.

Spectral lines were easily resolved giving signals which were free from electrical interference in spite of the close proximity of the photomultiplier tube to the ZETA primary winding. Experiments were carried out to check that the gain of the detection system did not change significantly during the ZETA pulse, when large stray magnetic fields occur. This was confirmed by observing the signals produced by a separate light source throughout the ZETA pulse. Measurements were made to determine the linearity of the detection system. The light intensity of a laboratory discharge tube was varied by aperture stops reducing the intensity in the ratio 2:1 and the monochromator photomultiplier output signal was found to be proportional ($\pm 5\%$) to the incident light intensity. This proportionality was no longer observed if the output signal exceeded 1.5 volts, and in all subsequent measurements the photomultiplier c.h.t. was adjusted so that the peak output signal was close to 1 volt.

To enable the observation of rapid fluctuations in the light intensity the time constants of the circuit were chosen so that no serious distortion was produced on pulses with durations between 10 msec and $10\mu\text{sec}$. The decay time of the fluorescent sodium salicylate coating is much shorter than the circuit time constant which determined the high-frequency response.

The spectral region covered by the monochromator in this work had previously been photographed using a vacuum spectrograph of similar dispersion (Harding *et al.* 1958). The ZETA spectrum at these wavelengths consists mainly of intense resonance lines of ions of impurity elements including carbon, nitrogen and oxygen which occur at concentrations of about 1%. In addition to these normal impurity ions, a small quantity of argon was usually added to provide an artificial impurity or 'trace' element. The amount of argon added was normally one per cent of the deuterium pressure. This was found to give an adequate signal-to-noise ratio ($\approx 50:1$) and not appreciably to alter the ZETA discharge characteristics. For the subsequent measurements one line of each of the ions to be studied was selected by consideration of intensity and freedom from interfering lines. The lines selected are listed in Table 1.

Table 1. Selected Vacuum Ultra-violet Spectral Lines

Ion	Wavelength (Å)	Classification
CIV	1548.19	2s $^2S_{1/2}$ — 2p $^2P_{3/2}^0$ (a)
NIV	923	2p $^3P^0$ — 2p ² 3P (a)
NV	1238.80	2s $^2S_{1/2}$ — 2p $^2P_{3/2}^0$ (a)
OIV	790.20	2p $^2P_{3/2}^0$ — 2p ² $^2D_{5/2}$ (a)
Ov	629.73	2s ² 1S_0 — 2p $^1P_1^0$ (a)
OVI	1031.91	2s $^2S_{1/2}$ — 2p $^2P_{3/2}^0$ (a)
Av	827.05	3p ² 3P_1 — 3p ² $^3D_2^0$ (b)
AVI	596.69	3p $^2P_{3/2}^0$ — 3p ² $^2S_{1/2}$ (b)
AVII	585.75	3s ² 1S_0 — 3p $^1P_1^0$ (b)
AVIII	700.40	3s $^2S_{1/2}$ — 3p $^2P_{3/2}^0$ (b)

Reference (a) C. E. Moore *An Ultra-violet Multiplet Table* NBS 488(1)

Reference (b) L. W. Phillips and W. L. Parker, *Phys. Rev.*, 1941, **60**, 301.

The experimental results were obtained by selecting the appropriate spectral line of each ion and photographing the intensity and current waveforms for five consecutive ZETA discharges. This was repeated for each ion and for each discharge condition to be studied. Final results were based on the average measurements from each group of five discharges. The transient lifetime values Δt_n were quite reproducible ($\pm 20\%$) but the amplitude measurements $I_n(t_p)$ and $I_n(\Gamma)$ showed greater variation ($\pm 50\%$). These variations make the major contribution to the errors in the final results given in § 5.

Calibration markers were displayed on the oscilloscope immediately following each discharge to facilitate measurement of the waveforms. Amplitude calibration was given by a 1 volt square-wave signal, and timing markers at 100 μ sec and 1 msec intervals were produced by a crystal controlled timing pulse generator. The oscillograms were displayed on a projector and the required measurements of the spectral line intensity transients were determined by direct comparison with the calibration markers.

§ 4. CONFIRMATION OF INJECTION AND LOSS PROCESSES

The equations derived in § 2 can only be applied to the ZETA plasma after the initial deuterium ionization phase, which is completed when the intensity of the Lyman α line decreases following its peak value (McWhirter 1959). Fig. 3 shows the observed intensity-time variation of DL_α and the resonance lines of

the lithium-like impurity ions C IV, N V and O VI. The lines of these ions all reach peak intensity after the deuterium ionization phase is effectively completed, and the criterion was adopted that only ions of state IV and above would be included in the results analysed.

The discharge condition to which the waveforms shown in Fig. 3 refer was selected because of the low level of injection. This enables the initial transient to be observed clearly. The theory given in § 2 predicts that the initial transient will show a rapid rise to a peak value followed by a decrease. This is supported by the observations shown in Fig. 3.

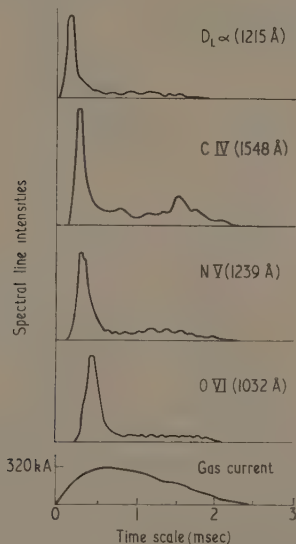


Fig. 3. Spectral line intensity transients of deuterium and the lithium-like impurity ions ($P = \frac{1}{2} \mu D_2$, $V_0 = 10$ kv, $B_0 = 1100$ gauss).

The injection coefficient Λ is given in terms of the observed quantities by Eqn (12). Determined for any ion, it gives the injection rate for that particular element in terms of its initial concentration in the plasma. The value of Λ obtained should therefore be the same for all ions of any one element. This is supported by the observations. The results for a mean of several measurements of the oxygen ionization sequence expressed as a ratio $\Lambda(\text{OIV}) : \Lambda(\text{OV}) : \Lambda(\text{OVI})$ is 1.0:0.9:1.2. This result, which is obtained for several discharge conditions, cannot be explained by atomic processes alone, i.e. by using Eqns (2) for a fully confined plasma.

A further proof that the observed tails in the intensity-time distributions are dynamic steady states caused by the injection of material in a low stage of ionization is afforded by a comparison between observations for those impurities normally present in the plasma (carbon, nitrogen, oxygen, etc.), and deliberately introduced trace elements such as argon which are normally absent. Such a comparison is shown in Fig. 4 which reproduces observed intensity transients of

an Av line ($\lambda 827 \text{ \AA}$) and an Ovi line ($\lambda 1032 \text{ \AA}$) at three different values of B_z . The outstanding feature of the comparison is the presence of a tail in the case of the Ovi transients and its almost complete absence in the case of Av. The Ovi emission persists as an injection tail after the initial transient (which can be identified in the traces) whereas the Av observations show the initial transient

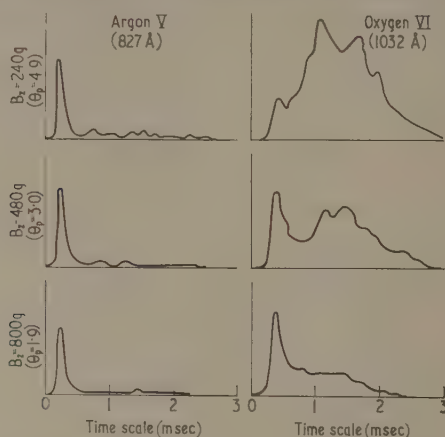


Fig. 4. Argon v and oxygen vi intensity transients showing the effect of an injection process ($P = \frac{1}{2} \mu D_2$, $V_c = 10 \text{ kv}$).

only. This result is typical of observations of a wide range of impurity ions (e.g. carbon, nitrogen, oxygen, silicon) and several argon trace ions (Iv to viii inclusive), and cannot be explained by any known atomic process within the plasma but must be related to the difference in chemical properties of the elements concerned and the nature of the injection process.

Two further points are illustrated by Fig. 4. Firstly, the level of injection is a function of the axial magnetic field B_z , decreasing as B_z increases. Secondly, the intensity in the tail varies through the current pulse, indicating that the injection varies with time. All of these points are dealt with more fully in § 5 below.

The observational test to be applied to establish the existence of a loss process is apparent from a consideration of the transient lifetime Δt_n given by Eqn (11). In a fully confined plasma Δt_n increases rapidly with ionization stage n , becoming infinite (in a plasma of infinite lifetime) for an ionization stage which is heavily populated in the steady state. The existence of a loss process places a 'ceiling' on Δt_n set by the loss rate coefficient λ as expressed in Eqn (13). This is a very specific prediction which is fully supported by the observations, as illustrated by the typical results displayed in Fig. 5. This shows a plot of Δt_n for the argon and oxygen sequences for a selected discharge condition. The abscissa is in terms of t_p , the time at which the initial transient peaks, so that both sequences can be plotted on a common scale.

A high injection will obscure the initial transient from which Δt_n is measured (see Fig. 4). The practical importance of using argon trace ions is now very

apparent, since they show only the initial transient and this allows the measurement of Δt_n and therefore of λ under all conditions of injection. The discharge condition used for Fig. 5 has been selected with high B_z so that the injection is low, enabling Δt_n to be measured for the oxygen sequence as well as for the argon sequence.

The diagram illustrates the existence of a ceiling on Δt_n since the higher stages of ionization all have the same transient lifetime. Further, a common ceiling applies to both the oxygen and argon ions indicating that λ is independent of ion mass and charge and can therefore be inferred from these results for the main plasma constituent, i.e. deuterium.

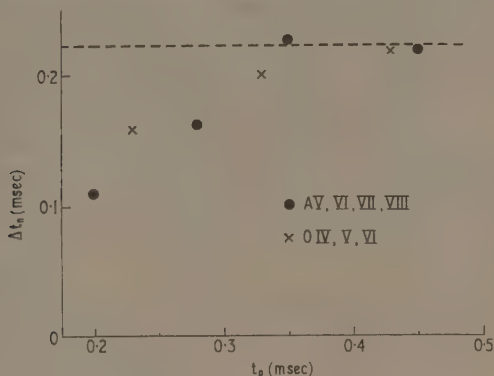


Fig. 5. Variation of transient lifetime Δt_n with state of ionization showing the effect of a loss process ($P = \frac{1}{2}\mu D_2$, $V_0 = 10$ kv, $B_z = 800$ gauss).

The existence of a common ceiling is typical of a wide range of discharge conditions and cannot be explained by atomic processes alone. For the fully contained plasma model described in § 2 the Δt_n values for successive stages of an ionization sequence would increase rapidly. Using the cross sections for electron collisional ionization S_n and radiative recombination α_n given by Elwert (1952), these Δt_n values can be calculated. The values calculated for the sequence argon v-viii in a fully contained plasma at constant temperature $kT_e = 20$ ev (estimated below) are as follows:

Ion	Av	Avi	Avii	Aviii
Δt_n (msec)	0.11	0.57	4.9	33

The results shown in Fig. 5 deviate grossly from these values, and the observed limiting value of Δt_n therefore shows the existence of a loss process.

The coefficients of loss and injection are estimated using expressions (12) and (13) without knowing the electron temperature, and the effect of this parameter will now be considered. It was shown that the shape of the initial transient and therefore Δt_n becomes independent of T_e when $\lambda > n_e S_n$. However, the ordinate scale of the distribution does depend on T_e as can be seen from the expression for x_p , the peak population in the n th stage of ionization:

$$x_p = \frac{n_e(\beta_{n-1}S'_{n-1} - \beta_n S'_n)}{e\lambda} \quad \dots\dots (14)$$

This is derived from Eqns (7) and (8) for the case of constant electron density, i.e. $\Lambda = \lambda$. The dependence of x_n on T_e is expressed by the temperature sensitive parameters β and S' . Hence the ion populations decrease rapidly in successive stages of ionization, although the shape and therefore the value of Δt_n remains constant. Obviously, any estimate of T_e based on ionization distributions derived from atomic processes alone will not be valid in a partially contained plasma.

However, the electron temperature can be estimated approximately from the results shown in Fig. 5. Although the level of the ceiling on Δt_n is controlled by the containment time only, the ionization stage at which it is reached is determined by T_e . If T_e is increased, Δt_n reaches its ceiling at a later stage of ionization, and at an earlier stage if T_e is reduced. From Eqn (11) it can be shown that Δt_n effectively saturates (i.e. within 10%) at the n th stage of ionization when $n_e(S_{n-1} - S_n) \simeq \lambda/5$. For the conditions given in Fig. 5, saturation occurs at about A VII. Using the observed values $\lambda \simeq 9 \times 10^3 \text{ sec}^{-1}$ and $n_e \simeq 10^{14} \text{ cm}^{-3}$ we find the electron temperature $kT_e \simeq 20 \text{ eV}$. This agrees with other determinations of T_e in ZETA using microwave noise measurements and observations of the temperature-sensitive line C V 2271 Å (Butt *et al.* 1958). The method is too crude to determine any variations of T_e but no differences from the above value were detected over the range of conditions investigated.

§ 5. RESULTS

5.1. The Derivation of λ and Λ for Deuterium

It was shown in § 4 that the loss rate coefficient λ has the same value for sequences of argon and oxygen ions which cover an appreciable range in charge and mass. Although this range does not embrace the values of charge and mass for the deuteron, it is reasonable to assume that the value of λ deduced from observations of impurity ions is representative of the deuterons and therefore of the entire plasma.

The injection coefficient Λ was derived for the impurity elements normally present in the plasma, i.e. carbon, nitrogen and oxygen. The value of Λ for deuterium ions, which emit no spectral lines, must then be inferred from the measured injection of these elements. This is done on the basis of the following assumptions. The rate of injection of atoms of any particular element X is assumed to be proportional to the concentration of that element in the adsorbed gas layer on the wall of the discharge tube. This wall concentration is assumed to be related, in turn, to the initial concentration of the element in the gas $(n_0)_X$. In addition the rate of injection will depend on discharge conditions, and these assumptions are expressed as follows:

$$\text{Injection of X (atom sec}^{-1} \text{ cm}^{-3}) = g_X(t) K_X (n_0)_X f(P, B_z, I) \quad \dots (15)$$

where K_X is some equilibrium adsorption factor which is a constant for each element, and $f(P, B_z, I)$ is a function, common to all elements, which is dependent on the discharge conditions only. The factor $g_X(t)$ is included to allow for the time required to establish equilibrium between the gas and the adsorbed layer. When a chemical element is first added to the gas $g_X(t \text{ small})$ is low but it will gradually increase to reach a limiting value of unity when equilibrium is

established. For deuterium and the impurity elements which have been present in the discharge tube for a long period, this equilibrium is assumed to be established and for this case we will put $g_X(t \text{ large}) = 1$.

The absence of an injection tail for argon ions which was shown in Fig. 4 is interpreted as a failure to reach equilibrium during the relatively short time for which argon had been present, so that $g_X(t) \ll 1$. Extended observations of argon ions showed the development of injection tails with $R_{ii} \approx 0.1$ after several hundred discharges. This suggests that the equilibrium time for elements present at about the 1% level is of the order of a few thousand discharges. This time is longer than would be expected if surface adsorption were the only important process. A further possible factor contributing to the low argon injection is that the adsorption factor K_X may be small for the inert gases.

The injection coefficient introduced into the theory given in § 2 was defined by the relation

$$\Lambda_X = \frac{\text{Injection of X (atom sec}^{-1} \text{ cm}^{-2})}{(n_0)_X} \quad \text{.....(16)}$$

Comparing Eqns (15) and (16) and putting $g_X(t) = 1$, we find for the injection coefficient for any element X

$$\Lambda_X = K_X f(P, B_z, I). \quad \text{.....(17)}$$

This relation summarizes the assumptions, which require that the injection coefficients for all elements will be in a constant ratio which is independent of discharge conditions. Fig. 6 shows the observed values of Λ for the impurity

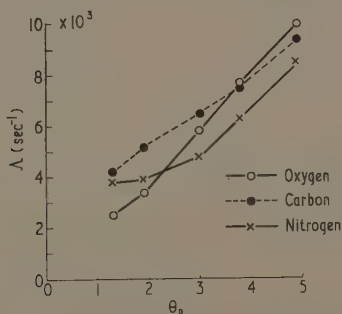


Fig. 6. Variation of injection coefficient with θ_p for different impurity elements ($P = \frac{1}{2} \mu D_z$, $V_0 = 10$ kv).

elements carbon, nitrogen and oxygen, measured with varying values of one discharge parameter, viz. B_z . The values of Λ for the different elements are plotted, not against B_z , but in terms of the magnetic parameter θ (Lees and Rusbridge 1959) which is defined as $\theta = 2I/aB_z$ where I is the current, a is the discharge tube radius, and B_z is the initial value of the axial magnetic field. Physically, θ represents the compression produced by the magnetic pinch forces for an idealized system. The values of θ_p and Λ in Fig. 6 refer to peak current. Although the observed values of Λ vary considerably with θ_p , the ratios of Λ for different elements remain constant within the accuracy of the measurements. The same result is obtained for all discharge conditions investigated, including

variation of gas pressure and current. This provides direct experimental support for Eqn (17).

The deuterium injection coefficient can therefore be expressed by the relation

$$\Lambda_D = K_D f(P, B_z, I) = (K_D/K_X) \Lambda_X.$$

The observed results from which Λ_D is to be calculated are the values of Λ for carbon, nitrogen and oxygen, and we replace Λ_X by Λ_{CNO} , the measured average value of Λ_C , Λ_N and Λ_O for the six lines observed (Table 1). The calculated value of Λ_D is consequently given by the product of Λ_{CNO} and some numerical constant, i.e.

$$\Lambda_D = \sigma \Lambda_{\text{CNO}}. \quad \dots\dots (18)$$

Observations which verify predictions based on Eqn (18) are given in § 5.3 below, and these show that the numerical value of σ is of the order of unity. This is as would be expected if the value of σ , i.e. K_D/K_{CNO} , were determined by physical adsorption of a monolayer, since this would require that $K_D \simeq K_C \simeq K_N \simeq K_O$. Some support for this is given by the observation that $\Lambda_C \simeq \Lambda_N \simeq \Lambda_O$ for each of the discharge conditions shown in Fig. 6.

The derivation of the loss rate and injection coefficients for deuterium from observations of impurity ions enables the remainder of the results to be expressed in terms of the parameters λ and Λ which can now be taken as representative of the entire plasma.

5.2. Variation of λ and Λ with Discharge Conditions

All of the discharge conditions observed are listed in Table 2. The first column gives a number assigned to each condition to which we can refer in the text, and the second column gives the pressure and type of gas in the torus. The third and fourth columns give respectively the potential V_c applied to the capacitor bank and the stored energy E_s . The parameters tabulated in the final three columns will be dealt with in the subsequent text.

Table 2. Selected Results for Discharge Conditions Observed

(1) No.	(2) Gas	(3) V_c	(4) E_s	(5) ϵ	(6) λ	(7) N_c
1	$\frac{1}{2}\mu$ Hg ($D_2 + 1\%$ A)	15	1.2	6.7	15×10^3	6×10^{16}
2	1μ Hg ($D_2 + 1\%$ A)	15	1.2	3.2	8×10^3	5×10^{16}
3	$\frac{1}{2}\mu$ Hg ($D_2 + 1\%$ A)	10	0.52	3.0	9×10^3	6×10^{16}
4	1μ Hg ($D_2 + 1\%$ A)	10	0.52	1.3	5×10^3	5×10^{16}
5	$\frac{1}{2}\mu$ Hg ($H_2 + 1\%$ A)	10	0.52	6.5	15×10^3	7×10^{16}
6	$\frac{1}{2}\mu$ Hg ($D_2 + 5\%$ A)	10	0.52	6.0	14×10^3	(3×10^{16})
7	2μ Hg ($D_2 + \frac{1}{2}\%$ A)	10	0.52	0.6	3×10^3	—
8	$\frac{1}{2}\mu$ Hg ($D_2 + 1\%$ A)	7	0.26	1.5	5×10^3	6×10^{16}
Internal standard error					$\pm 1 \times 10^3$	$\pm 1 \times 10^{16}$

(1) Discharge condition; (2) gas; (3) V_c (kv), capacitor bank voltage; (4) E_s (MJ), energy stored in capacitor bank; (5) ϵ (kev/ m_p), energy input per unit mass of gas; (6) λ (sec $^{-1}$), observed loss rate coefficient; (7) N_c (cm $^{-1}$), critical line density at discontinuity in current waveform.

The values of loss rate coefficient λ and injection coefficient Λ measured at peak current are plotted against θ_p in Fig. 7 for four selected discharge conditions, i.e. (1), (2), (3) and (4) of Table 2. The variation in θ_p is obtained by varying

the axial magnetic field B_z . It will be noticed that the general character of these plots is the same for each condition, except for a change in the scale of the ordinate. The loss rate coefficient λ does not vary appreciably with θ_p and, within the experimental accuracy, can be regarded as constant. The injection coefficient Λ varies linearly with θ_p , becoming equal to λ at about $\theta_p = 5$. These characteristics are true of all the discharge conditions investigated. We can therefore represent each discharge condition by a single measured value—the mean value of λ for all values of θ_p . Then for each condition, we have

Loss rate coefficient $= \lambda$ (constant with θ_p)

Injection coefficient $\Lambda = 0.2\lambda\theta_p$ for $1.2 < \theta_p < 5$.

The upper limit on θ_p is an experimental one above which the discharge becomes grossly unstable, and the lower limit on θ_p represents a minimum in Λ at $\theta_p \approx 1.2$ as is shown by discharge condition 3 in Fig. 7. This effect is reproducible and is observed whenever θ_p falls below 1.2.

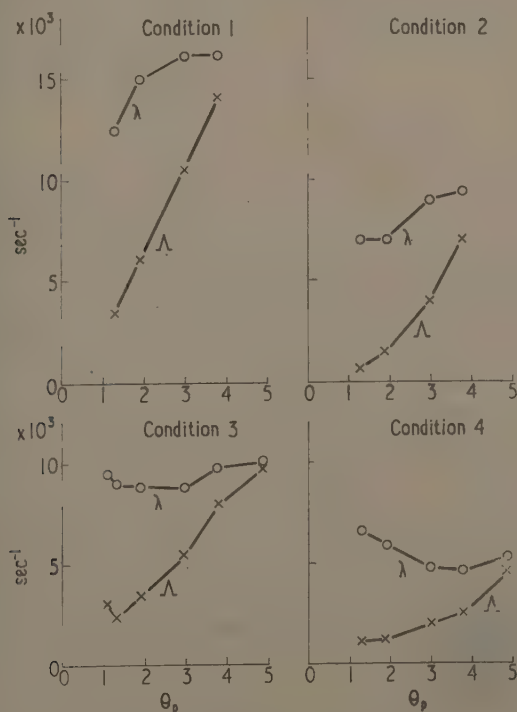


Fig. 7. Variation of injection and loss rate coefficients (Λ and λ) with θ_p for different discharge conditions, numbered as in Table 2. 1: $\frac{1}{2}\mu D_2$, 15 kv; 2: $1\mu D_2$, 15 kv; 3: $\frac{1}{2}\mu D_2$, 10 kv; 4: $1\mu D_2$, 10 kv.

The values of λ representing each discharge condition are tabulated in column (6) of Table 2, where the standard errors are derived solely from the experimental

scatter. Given in column (5) are the values of the parameter ϵ , defined as the energy put into the discharge per unit mass of gas, expressed in $\text{keV } m_p$, where m_p is the proton mass. The energy put into the discharge, which is less than that stored in the capacitor bank, is derived from the electrical characteristics (Butt 1960, private communication) and is given by $\int VI dt$, where V is the volts per turn and I the gas current.

The parameter ϵ is tabulated because of its correlation with the loss rate coefficient λ , as is shown by the plot of these parameters in Fig. 8. The relationship between λ and ϵ is linear over the range of conditions observed and the scatter of the points is consistent with the error of measurement.

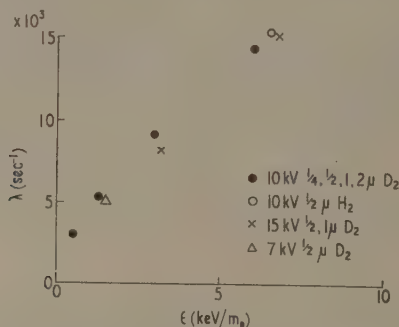


Fig. 8. Variation of loss rate coefficient with ϵ for all observed discharge conditions (ϵ = energy input per unit mass of gas).

The upper limit of ϵ is determined by the present maximum available capacitor voltage $V_c = 15$ kv, and the lower limit is fixed by the lifetime of the plasma itself. The lowest value of ϵ is for condition 7 of Table 2, and gives a value of $\lambda = 3 \times 10^3 \text{ sec}^{-1}$ corresponding to a containment time of about 0.3 msec. This gives a limiting transient lifetime of about 0.8 msec, above which it becomes impossible to establish the ceiling of Δt_n in a pulse length of about 3 msec.

In all but one of the conditions in Table 2 the gas used is deuterium and the range in conditions is obtained by varying the capacitor voltage and the gas pressure. For condition 5 of Table 2, the discharge was operated in hydrogen. Since the gas normally used is deuterium, ZETA was operated in hydrogen for two weeks (approximately 10^4 discharges) prior to this experiment to eliminate possible contamination of the walls with deuterium. A comparison of this hydrogen observation with the corresponding one in deuterium, 3 in Table 2, for which all other parameters are the same, shows that protons escape almost twice as rapidly as deuterons. The slope of the results in Fig. 8 shows that if ϵ is increased by a factor 2, then λ is not doubled but increases by a factor 1.7 which is intermediate between 2 and $\sqrt{2}$. One result of this is that although λ decreases with increasing pressure, the actual loss rate of ions from the plasma remains roughly constant, and in fact increases slightly.

The linear relationship between λ and ϵ appears, on extrapolation, to intercept the λ axis on the positive side. This is clearly inadmissible on energy considerations, and the curve must pass through the origin or make a positive intercept with the ϵ axis.

It is of fundamental interest to consider the energy required to maintain the observed system of injection and loss of particles in the plasma. Gibson and Mason (1961) have shown that the energy lost in the form of radiation is about 20% of the energy input over the range of conditions investigated here. It is easy to show that the rest of the energy can be accounted for by particle loss to the walls.

An energy balance can be carried out by comparing the power input with the power output derived from observed quantities. Thus the power balance equation, per unit length of the discharge, is given by

$$\Omega I^2 = R + N_0 \left(\frac{\Lambda}{\lambda} \right) \left[kT_i + kT_e + \chi_D \right] \lambda,$$

where Ω is the effective discharge resistance per unit length, I is the current, R is the radiated power, N_0 is the initial line density, kT_i is the energy of the ions, kT_e the energy of the electrons and χ_D the deuterium ionization potential. The energy in the impurity atoms is neglected, and it is assumed that the values of λ and Λ observed for ions also applies to the electrons. If we consider this power balance for the time of peak current and for high values of θ_p then λ and Λ are approximately equal. The observations of Gibson and Mason (1961) give $R \simeq 0.2\Omega I^2$, so the above expression reduces to

$$0.8\Omega I^2/N_0 = [kT_i + kT_e + \chi_D]\lambda.$$

Since the left-hand side of the expression is roughly proportional to ϵ we see that to reproduce the gross feature of the correlation in Fig. 8 we need to keep the bracketed terms roughly constant, i.e. any increase in energy input does not substantially increase the temperature.

The largest term on the right-hand side of the expression is kT_i , the energy of the deuterons. The energies of impurity ions, obtained from the Doppler widths of spectral lines, are far in excess of the observed electron temperatures and are of the order of a few hundred electron volts (Butt *et al.* 1958). The energy of the deuterons can be inferred from these observations only when the detailed heating mechanism is understood. An investigation into this is proceeding and preliminary observations (Jones and Wilson, to be published) indicate that the energy of the deuterons is about 100 eV for discharge condition 3 of Table 2. Putting $kT_i \simeq 100$ eV, $kT_e \simeq 20$ eV and $\chi_D = 13.6$ eV, then the power loss due to escape of particles is about 5×10^4 W cm⁻¹ length of discharge at peak current. The power input, derived from the electrical characteristics by Butt (1960, private communication), is 8×10^4 W cm⁻¹. Allowing 20% of this for radiation gives good agreement in the power balance. Over the range of discharge conditions investigated, the major source of energy loss is therefore due to plasma reaching the walls. Direct confirmation of the loss of plasma has been obtained by the detection of thermal electrons in the region near the wall of the torus (Gibson and Mason 1962).

5.3. Variation of Plasma Line Density with Time

The effect of discharge conditions on the loss and injection coefficients measured at peak current is described in the previous section. We will now consider how these processes control the variation of plasma density during a single discharge, and this necessitates the determination of any temporal variation of the respective coefficients.

The values of the loss rate coefficient λ given above were obtained from observations made over the time interval that the ionic sequence Av to AvIII appeared. This time interval varies according to the discharge conditions, but generally it is the period from the end of the deuterium ionization phase to the region of peak current. There is no significant variation in λ over this time period and it is therefore assumed that the measured value of λ applies throughout the current pulse.

The measurements of Λ given above refer specifically to the time of peak current. It was pointed out earlier that the spectral line intensity in the injection tail varies considerably with time, as can be seen from the observations of OVI given in Fig. 4. In determining whether this variation is due to a variation of injection, we apply the test used in §4 when it was shown that the injection coefficients Λ determined at peak current from Eqn (12) for the ionic sequence OIV, OV and OVI, gave the same value within the experimental error. This test was also applied at a time after peak current when the spectral line intensity in the tail had dropped to about 25% of its peak value. The mean of several measurements, normalized to OIV, give $\Lambda(\text{OIV}) : \Lambda(\text{OV}) : \Lambda(\text{OVI}) = 1.0 : 1.0 : 1.2$. The time variation of spectral line intensity in the tail is therefore taken as an injection variation.

The variation of Λ with time is slow compared with $\tau_c = 1/\lambda$. Hence the assumption of constant Λ , made in the original equations, is valid, and to determine the variation of plasma density with time, it is legitimate to replace Λ in Eqn (5) with $\Lambda(t)$, the observed time variation of the injection coefficient. Further, the time variation in plasma density will be dominated by the slow variation in $\Lambda(t)$ and we can therefore equate the $\exp(-\lambda t)$ term to zero for $t > 1/\lambda$. Replacing the number density ($n \text{ cm}^{-3}$) by the density per unit length of discharge ($N \text{ cm}^{-1}$), then this line density at time t is given by

$$\begin{aligned} N(t) &= N_i(t) = N_e(t) \\ &= N_0 \quad (\text{for } t = 0) \\ &= \sigma N_0 \Lambda(t) / \lambda \quad (\text{for } t > 1/\lambda) \end{aligned} \quad \text{.....(19)}$$

where N_0 is the initial line density and σ is the constant given in Eqn (18) which relates the injection coefficients of deuterium and the observed impurity ions. The assumptions on which the application of Eqn (19) depend, i.e. that $\sigma \approx 1$, and that T_e and λ are constant through the pulse, cannot be verified directly. However, since the existence of loss and injection processes has been established, qualitative predictions, based on results derived from Eqn (19), will be correct. Further, quantitative predictions can be tested against other types of observation, and it will be seen in what follows that these assumptions are confirmed.

The calculated values of $N(t)$ at intervals during single pulses at different values of θ_0 in discharge condition 3 of Table 2, are shown in Fig. 9 together with the corresponding current waveforms. The points at which $N(t)$ is measured have been linked by a smooth curve; the broken curves denote the region of interpolation between the earliest measured position and the initial line density.

The general features of the $N(t)$ curves are similar. The line density falls to a minimum, then rises to a maximum in the region of peak current which is followed by a general decrease. This is the result of a loss rate on which is superimposed a slowly varying injection rate. The injection observed during a current pulse shows that Λ is roughly proportional to the current. The minimum in $N(t)$ is

therefore caused by an initial loss which is eventually counteracted by the increase in $\Lambda(t)$, and the final decrease in line density is due to the reduced injection after peak current. In general, the loss rate is greater than the injection rate and the

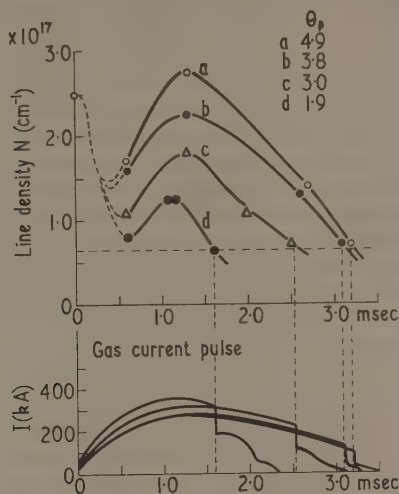


Fig. 9. Measured pump-out during the ZETA pulse ($P = \frac{1}{2} \mu D_2$, $V_c = 10$ kv).

combined effect is to produce a decrease of plasma density with time. This net plasma loss has been named 'pump-out' by Bernstein *et al.* (1957).

An important result of the present work is shown in Fig. 9. It will be noticed that when the line density drops to a critical value ($N_c \approx 6 \times 10^{16} \text{ cm}^{-1}$) there is a sudden drop in the current. The presence of this phenomenon in the current waveform has been known since the earliest operations of ZETA and is accompanied by a sharp burst of x-rays. Using the present result that the discontinuity occurs at a critical line density, Gibson and Mason (1961) have shown that the phenomenon is consistent with a runaway process. The plasma density decreases until the electron drift velocity becomes comparable with the thermal velocity, when the electrons gain energy rapidly from the electric field and strike the walls of the containing vessel to produce the observed x-rays. Quantitative measurements of the energy of the observed x-rays support this interpretation.

The critical line density has been measured for all conditions that the discontinuity is observed and the results are given, for each discharge condition, in Table 2. The standard error at the foot of the column is an internal one. No value is given for condition 7 as the phenomenon is not observed. This is because the high initial pressure of $2 \mu \text{ Hg}$ prevents the density from falling to the critical value. In all cases other than condition 6 the values of N_c are the same within the error of measurement. The accuracy is insufficient to determine whether there is any small variation with pressure or condenser bank voltage. However, the low value of N_c for condition 6 is significant, and is due to the relatively large amount of argon (5%) which had to be used at this low pressure ($\frac{1}{4} \mu \text{ Hg}$) for the argon lines to be observed. It has been known for some time that the discontinuity in the current waveform can be inhibited, and indeed removed

completely, by adding impurities to the gas. Thus the presence of the phenomenon is used as an indication that the discharge is 'clean' and conditioned.

The measured values of critical line density are the same, within the experimental accuracy ($\pm 15\%$), for discharges in hydrogen and deuterium. This provides further corroboration of the runaway theory, since this requires that the critical line density should be independent of the ion mass.

The observed critical line density $N_c \simeq 6 \times 10^{16} \text{ cm}^{-1}$ corresponds to an initial gas pressure of about $\frac{1}{8} \mu \text{ Hg}$. This is the pressure at which the discharge gives breakdown trouble, the current and voltage waveforms showing sharp transients (Butt *et al.* 1958). It is also an observed fact that most pinched discharges have not been maintained in deuterium below a line density of about $5 \times 10^{16} \text{ cm}^{-1}$, independent of tube size (Bickerton 1959).

The discharge conditions can be adjusted so as to reduce the minima shown in Fig. 9 to the critical density value. Such a condition has been observed (Ward 1960, private communication) with $P = \frac{1}{8} \mu \text{ Hg}$ deuterium, $V_c = 15 \text{ kv}$, and $B_z = 1200 \text{ gauss}$. In this condition the current waveform had two different forms which occurred at random with about equal frequency. The first had a normal, smooth, reproducible shape; the second followed the first to a point before peak current, and then broke off to lower values with a jagged unreproducible form. Measurements of the injection and loss rates were made at a time just prior to the break-off point to give a line density of $7 \times 10^{16} \text{ cm}^{-1}$, agreeing within the error of measurement, with the critical value N_c derived above. It should be stressed that only a minimum in the pump-out curve can explain this result. If the injection is sufficient to keep the minimum just above the critical value, the discharge will recover and we get the normal type of current waveform; however if the minimum drops below the critical value then an abnormal current waveform results. The curves shown in Fig. 9 refer to θ_p values greater than 1.9. The discontinuity in the current waveform is not observed at low θ_p values, and the nature of the discharge appears to change below about $\theta_p = 1.3$. This value corresponds to the point of minimum injection shown in condition 3 of Fig. 7. All of the pump-out calculations were made for conditions in which θ_p was greater than this value.

A direct measure of the electron density at one point on the predicted density curve has been obtained by an 8.7 mm microwave transmission experiment (Wort 1960, private communication). The electron densities in ZETA are generally too high for transmission at this wavelength, but the observations predict that n_e will drop to about 10^{13} cm^{-3} at the onset of the discontinuity in the current waveform. This density is below the critical value ($1.5 \times 10^{13} \text{ cm}^{-3}$) for transmission of 8.7 mm microwaves. Observations were made for the case $\theta_p = 1.9$ in Fig. 9, which showed an onset of transmission at about 0.1 msec prior to the discontinuity. This indicated a density of $1.5 \times 10^{13} \text{ cm}^{-3}$ at this time, which is to be compared with the value of $1.3 \times 10^{13} \text{ cm}^{-3}$ predicted by the present work. The agreement shown by these figures may be somewhat better than the uncertainties justify, but the experiment affords a direct quantitative confirmation by an entirely different technique of the pump-out calculations. This result, together with the establishment of an energy balance and the explanation of the current waveform discontinuity, supports the main conclusions of this paper. The interpretation of the processes occurring in ZETA in terms of the partially contained plasma model described above is therefore adequately confirmed.

§ 6. DISCUSSION

The work described above has established the existence of loss and injection processes in ZETA and has also determined the general dependence of these processes on discharge conditions. The results are consistent with the simple plasma model described earlier which assumed uniform electron density in a plasma of fixed dimensions. However, in a pinched discharge a variable degree of compression can occur through the pulse and this should be considered when calculating pump-out curves. The degree of magnetic compression in ZETA has been measured as a function of θ by Lees and Rusbridge (1959). Their results show the radial compression to rise from unity at $\theta = 1$ to a constant value of about two for $\theta > 2$. These compression values are defined in terms of the maximum measured field and are therefore greater than the average compression. The measurements described in this paper were made after the initial deuterium ionization phase and before the end of the current pulse. They therefore cover a limited range in θ and hence a limited variation in compressed plasma diameter. When θ_p exceeds 2.5, maximum compression extends throughout the observed range and the assumption of constant compression made in the model is valid. For lower values of θ_p , the observed range in θ becomes more restricted so that the assumption is again valid within the limits of experimental error (see results for $\theta_p = 1.9$, Fig. 9). Hence corrections to the measured line density ($N_e \text{ cm}^{-1}$) are not necessary, but this is not the case for the number density ($n_e \text{ cm}^{-3}$), and the appropriate compressions have been used in deriving the values of n_e given in the text.

Pump-out has been shown to occur in the Stellarator (Bernstein *et al.* 1957, Spitzer 1958, Ellis *et al.* 1960 a) by direct observation of the electron density measured with a microwave interferometer. This technique cannot be used with ZETA because the electron density is generally too high for transmission of available microwave frequencies. The electron density in the Stellarator shows an initial rise due to the ionization phase, followed by an exponential decrease due to particle loss. Later observations (Ellis *et al.* 1960 b) show that the loss process also occurs during the ionization phase. These results indicate that the loss rate coefficient is constant throughout the ohmic heating pulse, as was assumed in the present ZETA work.

Direct observations of electron density measure the combined effect of the injection and loss processes, whereas the present method measures them separately. The Stellarator workers use the same expression for dn_e/dt as given in Eqn (4) but with the added assumption that the injection is proportional to the loss rate λn_e and to the initial gas pressure. In ZETA these assumptions are clearly invalid, but the observed pump-out curves are quite different in the two devices. Further, these assumptions explain the exponential decay of electron density observed in the Stellarator.

The observed containment times in ZETA and in the Stellarator are of the same order of magnitude (≈ 0.1 msec) and are much shorter than would be expected from classical collisional diffusion theory. Although the two devices use different containment systems, it would not be surprising if the enhanced diffusion of plasma across the confining magnetic fields resulted from the same fundamental process. A possible mechanism has been suggested by Spitzer (1960).

The nature of the injection process is also unknown, but two possible mechanisms—thermal evaporation and unipolar arcs—have been described by

Robson and Hancox (1959). If the heat loading on the discharge tube wall during a current pulse causes the evaporation of only a part of an adsorbed gas layer, then this could account for the observed magnitude and composition of the injected material. If unipolar arcs are the cause of injection, then approximate calculations show that the observed magnitude of the injection could be explained if 10% of the energy input goes into unipolar arcs.

The observations of plasma containment in ZETA show that the loss rate coefficient is roughly independent of the axial magnetic field when this is varied so as to change θ_p from 1 to 5. This is a surprising result since we would have expected some relationship between the loss of plasma across the magnetic field and the configuration of that field. The injection coefficient, however, varies considerably with the axial field, being roughly linear with θ_p but showing a minimum at $\theta_p \simeq 1.2$. When the discharge conditions are changed by varying the current and the pressure and atomic weight of the gas, it is shown that λ is correlated with a single parameter ϵ , the energy input per unit mass of gas. This parameter scales roughly as the square of the Alfvén velocity; however, the apparent scaling of λ with v_A^2 does not extend to variations in v_A caused by varying the axial magnetic field. Further work is required to provide theoretical explanations for the observed properties of the loss and injection processes.

ACKNOWLEDGMENTS

We are grateful for the co-operation of the Zeta Operations Group and for the help of Mr. B. C. Fawcett and Mr. J. G. Firth. The investigation has benefited from many helpful discussions with Mr. R. S. Pease and with other colleagues in the Controlled Thermonuclear Reactions Division.

REFERENCES

- AMBARTSUMYAN, V. A., 1958, *Theoretical Astrophysics* (London: Pergamon Press).
 BERNSTEIN, W., HEALD, M. A., and KRANZ, A. Z., 1957, *U.S.A.E.C. Report No. NYO-7901* (PM-S-31).
 BICKERTON, R. J., 1959, *Proc. Instn Elect. Engrs*, **106A**, Supplement No. 2, 148.
 BUTT, E. P., *et al.*, 1958, *Atomic Energy Conference (Geneva)*, Paper A/CONF.15/P/1519. (Geneva: United Nations).
 ELLIS, R. A., *et al.*, 1960 a, *Phys. Fluids*, **3**, 468.
 — 1960 b, *Bull. Amer. Phys. Soc.*, [II], **5**, 341.
 ELWERT, G., 1952, *Z. Naturf.*, **7a**, 432.
 GIBSON, A., and MASON, D., 1962, *Proc. Phys. Soc.*, **79**, in the press.
 HARDING, G. N., *et al.*, 1958, *Atomic Energy Conference (Geneva)* Paper A/CONF.15/P/1520, (Geneva: United Nations).
 KNORR, G., 1958, *Z. Naturf.*, **13a**, 941.
 LEES, D. J., and RUSBRIDGE, M. G., 1959, *Fourth Int. Conf. on Ionization Phenomena in Gases (Uppsala)*, **II**, 954 (Amsterdam: North Holland).
 MCWHIRTER, R. W. P., 1959, *A.E.R.E. Report No. 2980* (London: H.M.S.O.).
 — 1960, *Proc. Phys. Soc.*, **75**, 520.
 MITCHELL, J. T. D., *et al.*, 1959, *Proc. Instn Elect. Engrs*, **106A**, Supplement No. 2, 74.
 ROBSON, A. E., and HANCOX, R., 1959, *Proc. Instn Elect. Engrs*, **106A**, Supplement No. 2, 47.
 SPITZER, L., 1958, *Phys. Fluids*, **1**, 258.
 — 1960, *Phys. Fluids*, **3**, 659.
 WOOLLEY, R. V. D. R., and ALLEN, C. W., 1948, *Mon. Not. R. Astr. Soc.*, **108**, 292.

Interferometric Measurements of the Electron Density in a Shock Heated Deuterium Plasma

By J. K. WRIGHT, R. D. MEDFORD, A. G. HUNT AND J. D. HERBERT

Atomic Weapons Research Establishment, Foulness, Southend-on-Sea, Essex

MS. received 11th May 1961, in revised form 11th July 1961

Abstract. The first results are reported of experiments new to plasma research, namely time-resolved interferometry in the optical region. It is shown how the electron density distribution of a fast cylindrical pinched discharge may be measured and how the physical conditions in the discharge may be deduced from such measurements.

§ 1. INTRODUCTION

THE experiments in which Alpher and White (1958) and later Ascoli-Bartoli *et al.* (1960) successfully measured electron densities of the order of 10^{17} per cm^3 have shown that the optical interferometer is a powerful tool for the measurement of high density plasmas. Previously microwave transmission methods have been used to measure the electron density of deuterium plasma, but it was found that the highest measurable density was about 10^{13} per cm^3 due to experimental difficulties (Harding *et al.* 1958).

In this paper we describe an experiment to determine the spatial distribution of electrons in an electromagnetically driven electrodeless deuterium discharge (Wright, Eeles and Herbert 1959) using a time-resolved interferometric technique.

§ 2. TRANSMISSION OF ELECTROMAGNETIC WAVES THROUGH A PLASMA

The wave equation for an electromagnetic wave in a plasma is, with certain simplifications, given by Spitzer (1956) as

$$\frac{\partial^2 E_y}{\partial x^2} - \frac{4\pi n_e e^2 E_y}{m_e c^2} = \frac{1}{c^2} \frac{\partial^2 E_y}{\partial t^2} \quad \dots\dots (1)$$

where the 'plasma frequency'

$$\omega_p = \left(\frac{4\pi n_e e^2}{m_e} \right)^{1/2} \quad \dots\dots (2)$$

and n_e is the number of electrons per cm^3 , m_e the electron mass and e the electronic charge (e.s.u.). A possible solution is

$$E_y = E \exp \{i(\beta x + \omega t)\}$$

where

$$\beta \simeq \frac{\omega}{c} \left(1 - \frac{\omega_p^2}{2\omega^2} \right)$$

and $f_p = \omega_p/2\pi = 8.97 \times 10^3 n_e^{1/2}$ from Eqn (2).

If the transmitted wavelength is $\lambda = 2\pi c/\omega$ we obtain

$$\beta = \frac{\omega}{c} (1 - 4.5 \times 10^{-14} n_e \lambda^2).$$

Thus the phase refractivity is $-4.5 \times 10^{-14} n_e \lambda^2$ (3)

Therefore if a light beam from an interferometer is transmitted through x cm of plasma there will be

$$\Delta N = 4.5 n_e 10^{-14} x \lambda \text{ wavelengths shift,} \quad \text{. (4)}$$

i.e. for monochromatic light of wavelength about 5×10^{-5} cm there will be approximately one-fifth of a wavelength shift when the light is transmitted through plasma having a number density of 10^{17} and length 1 cm.

§ 3. EXPERIMENTAL METHOD

A Mach-Zehnder interferometer (Ladenburg and Bershader 1955) is set up to give a pattern of vertical interference fringes across the full width of a cylindrical electrodeless discharge. An image of this is focused on to the horizontal slit of a high speed rotating mirror streak camera and photographed on a fixed length of film. At a suitable part of the camera sweep a high voltage capacitor is discharged into the single copper turn used to form the electrodeless discharge, whilst monochromatic light from a spark discharge is passed through the discharge tube. The result is a streak picture (radius-time curve) of the fringe shift with the self-luminous electrodeless discharge superimposed. More of the experimental detail is given below and a schematic diagram of the optical layout is shown in Fig. 3.

In the Mach-Zehnder interferometer one pair of glass plates is inserted into the working section and the compensating pair is used to give control over the position and the spacing of the fringes, in addition to the other mirror adjustments. It was found that microscope slides split lengthwise and with one half in each beam could be selected to give fringes with little distortion; in this way such pairs were used to provide windows for the discharge tube and the corresponding compensating glasses.

The instrument was finally adjusted to provide a vertical fringe pattern across a diameter of the discharge tube. At this stage of the experiment 10–15 fringes were set up to cover approximately one-half of the diameter.



Fig. 1. Electrodeless discharge tube.

A cylindrical discharge tube 2 inches in diameter and 1.5 inches long was made in $\frac{1}{4}$ inch Perspex; a recessed horizontal slit was cut in each face to accommodate the half microscope slide and these were secured in place with vacuum grease. A $\frac{1}{4}$ inch pipe let into one face led off to a high vacuum pumping unit and gas filling system (see Fig. 1). A single turn coil 3.5 cm wide was wrapped around the centre section and connected to an $8\mu\text{F}$ low inductance condenser consisting of 8 units each of $1\mu\text{F}$ and $1\text{m}\mu\text{H}$ self inductance connected in parallel. Low inductance connections between the units and the model were made with flat copper strips, 6 inches wide, separated by 0.004 inch Melinex insulation. The condensers were discharged into the coil via a low inductance explosive type switch. To ensure reliable breakdown of the deuterium gas on the first half cycle of the discharge it was necessary to pre-ionize with a Tesla coil.

The streak camera includes three photomultiplier units which give out pulses at appropriate parts of the sweep. The first pulse is used to initiate the whole firing sequence through a series of pulse delay units, i.e. the oscilloscopes monitoring the event are triggered and the spark light source is pulsed $1\mu\text{sec}$ before the explosive switch is fired. The other two photomultiplier pulses are recorded on a slow sweep single stroke time base and enable the streaking speed of the camera to be determined. Fig. 2 is a schematic diagram of the synchronizing and firing circuit.

A special high intensity short duration light source was developed from a 'trigatron' valve (pressurized triggered spark gap filled with argon and small percentages of oxygen and nitrogen). A $1\mu\text{F}$ condenser charged to 10 kv and discharged across the gap gave a spark of 5–10 μsec duration and adequate intensity for recording on HPS film. A part of the emitted spectrum was selected with a narrow band interference filter to provide nearly monochromatic light of bandwidth 70 \AA centred on a wavelength of 4670 \AA .

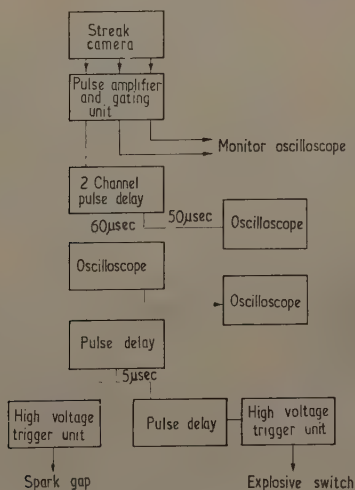


Fig. 2. Synchronizing and firing circuits.

This interference filter was placed adjacent to the spark light source so as not to attenuate the light from the electrodeless discharge.

The streak camera was focused on to a reduced image of the fringe pattern produced by a supplementary lens placed between the Mach-Zehnder interferometer and the camera. This was necessary to give a suitable image size on the recording film. An iris diaphragm placed between the supplementary lens and the exit lens of the Mach-Zehnder interferometer was used to control the amount of light from the discharge entering the camera lens without altering the amount of light from the fringes. By controlling the diaphragm aperture the relative intensities of the discharge and fringe light could be varied over a range sufficient for the present experiment. If the discharge light had been too intense for the diaphragm to give sufficient control, the narrow band interference filter could have been moved from its position close to the spark light to the iris to give a further reduction in the discharge light. A schematic diagram of the optical layout is given in Fig. 3.

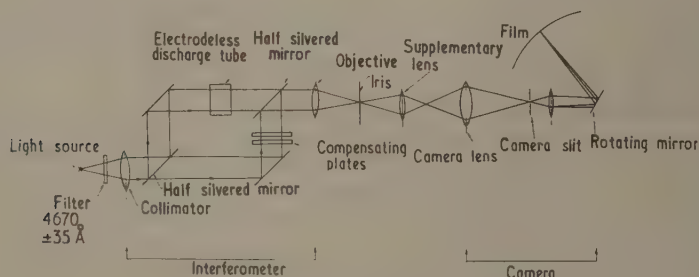


Fig. 3. Layout of optical components.

§ 4. RESULTS

Figures 4, 5 and 6 (Plate) show streak pictures of fringes superimposed on the discharge obtained when the discharge was in deuterium at ambient pressures of 1, 0.5 and 0.3 mm Hg respectively. Fig. 7 (Plate) is a streak picture of the discharge in deuterium at 1 mm Hg without the superimposed fringes. The directions in which the fringes move with increasing electron density are shown by the direction of the arrow at the right of the photograph. The direction of the time axis is from right to left in each photograph.

In each figure the first and second half cycles of the electrodeless discharge are shown. It will be noticed that the fringes are parallel before the first pinch of the discharge is initiated. When the deuterium gas is sufficiently pre-ionized a converging cylindrical shock is formed on the first half cycle of the discharge and when the shock front intersects a fringe the fringe is shifted by an amount proportional to the electron density behind the shock front. Shortly afterwards the current sheet (Wright, Eeles and Herbert 1959) intersects the displaced fringe and the fringe shifts back in the opposite direction to its normal position. Between the first and second half cycle of the discharge the fringes are very nearly parallel again and on the second half cycle the process is repeated.

It will be noticed that the shock formed on the first half cycle of the discharge does not converge on to the axis of the discharge tube because of the trapped magnetic field (Wright, Eeles and Herbert 1959, Medford *et al.* 1960) and the fringes passing close to the axis are undeflected, except in Fig. 4 where the central fringe has a slight kink. The reason for this exception is obvious when Fig. 7 is examined since at this particular gas pressure there is a bright central core of gas inside the self-luminous shell on the axis of the shock tube. The reason for the presence of the bright central core emerges from an analysis of the fringe patterns and will be discussed in §5.

§ 5. ANALYSIS OF THE RESULTS

5.1. Measurement of Percentage of Deuterium Ionized and Swept up

If we put the values of $x = 3.5$ and $\lambda = 4.67 \times 10^{-5}$ cm into Eqn (4) we obtain

$$\Delta N = 7.35 n_e 10^{-18}. \quad \dots (5)$$

This, of course, assumes that along lines parallel to the discharge tube axis n_e is constant and that there are no boundary layer effects.

Ideally fringe shifts should be measured using a microdensitometer but since, in this case, the fringe shifts are large we were able to measure the values of ΔN with a pencil and rule. Values of ΔN measured from Figs 1, 2 and 3 were converted into electron densities by using Eqn (5). From the electron densities obtained it was possible to integrate the number of electrons behind the shock front at any time, and this gave the fraction of the available deuterium swept up and ionized by the shock. We have done this for selected times during the first half cycle of the discharge and the results are given in Table 1. It is seen from

Table 1. Percentage of Gas Swept up and Ionized

Ambient pressure 1 mm		Ambient pressure 0.5 mm		Ambient pressure 0.3 mm	
Time (μ sec)	Ionization (%)	Time (μ sec)	Ionization (%)	Time (μ sec)	Ionization (%)
0.30	17.5	0.26	37	0.43	48
0.41	17	0.35	36	0.53	60
0.52	24.5	0.41	43	0.60	78.5
0.75	20	0.66	57	0.64	85
Theory	13.0	—	30	—	47.0

this table that, as predicted by strong shock theory, (Wright 1960, Niblett, unpublished), the fraction of gas ionized increases with reduced ambient pressure and thus with increasing shock speed, and the quantities are in good agreement with theory during the initial period of implosion.

From Table 1 we see that Fig. 7 corresponds to about 20% ionization behind the shock front. We conclude from this that the bright central core is a result of the trapped magnetic field holding back the ionized particles and allowing the non-ionized particles to implode on to the axis, where the increase of temperature behind the reflected shock causes ionization and the appearance of the bright central core.

5.2. *Calculation of Plasma Resistivity and Electron Temperature at the Current Sheet*

In an idealized shock model we would have expected the electron density to have a step increase to the values given by Wright (1960) and Niblett (unpublished) immediately behind the shock front and a step decrease to zero behind the current sheet. But in our experiment we have not reached sufficiently high shock speeds to give a temperature high enough for the conductivity of the plasma to exclude the driving and the trapped magnetic fields from the plasma. The magnetic fields have obviously penetrated measurable distances into the plasma during the implosion phase and altered the electron distribution.

The relation between the magnetic field strength H in the plasma and the electron number density can be derived from the following equations:

$$\frac{\partial \mathbf{H}}{\partial t} = \text{curl}(\mathbf{V} \wedge \mathbf{H}) + \frac{\eta}{4\pi} \nabla^2 \mathbf{H} \quad \dots\dots (6)$$

$$\rho \frac{d\mathbf{V}}{dt} = -\nabla \left(p + \frac{H^2}{8\pi} \right) \quad \dots\dots (7)$$

where \mathbf{V} is the velocity, p the plasma pressure ρ the plasma density and η the plasma resistivity. Eqn (6) requires η to be constant—not strictly true in our experiment. If the plasma moves with constant velocity \mathbf{V} and if we approximate to the cylindrical electrodeless configuration with a plane geometry, for times taken up to a value where it is felt that errors due to the use of plane geometry become important, the equations become:

$$\frac{\partial H}{\partial t} + \frac{\partial(VH)}{\partial x} = \frac{\eta}{4\pi} \frac{\partial^2 H}{\partial x^2} \quad \dots\dots (8)$$

$$2n_e kT + \frac{H^2}{8\pi} = \text{constant}, \quad \dots\dots (9)$$

and if we put $x = x_1 + Vt$ in Eqn (8), we obtain

$$\frac{\partial H}{\partial t} = \frac{\eta}{4\pi} \frac{\partial^2 H}{\partial x_1^2} \quad \dots\dots (10)$$

Solving this for the boundary conditions

$$H(x_1, t) \rightarrow 0 \text{ as } x_1 \rightarrow \infty$$

and

$$H(x_1, t) \rightarrow H_0 \text{ as } x_1 \rightarrow 0$$

we obtain

$$H(x, t) = H_0 \text{erfc} \left(\frac{x - Vt}{2(\eta t / 4\pi)^{1/2}} \right), \quad \dots\dots (11)$$

and if we change back into cylindrical coordinates we get

$$H(r, t) = H_0 \text{erfc} \left(\frac{a - r}{(\eta t / \pi)^{1/2}} \right), \quad \dots\dots (12)$$

where a is the radius of the current sheet at time t , and $H = H_0$ at the current sheet. From Eqn (9) and the boundary conditions for H together with the condition that when $H = 0$, n_e is a maximum n_m , say, and when $H = H_0$, $n_e = 0$ and assuming that T is constant with respect to time and radius, we obtain

$$n_e(r, t) = n_m \left\{ 1 - \text{erfc}^2 \left(\frac{a - r}{(\eta t / \pi)^{1/2}} \right) \right\}. \quad \dots\dots (13)$$

From the interference fringe patterns it is possible to obtain the variation of electron number density n_e with radius for a fixed value of t , and by using Eqn (13) a fit can be made to the error function curve thus enabling the resistivity η to be computed. The maximum number of experimental points available for curve fitting at any fixed time is only three because the number of fringes is small

Table 2. Plasma Resistivity and Electron Temperature calculated from Fringe Shifts

Ambient pressure	1 mm		0.5 mm		0.3 mm	
Shock speed	2.6 cm μsec^{-1}		3.1 cm μsec^{-1}		3.5 cm μsec^{-1}	
Rankine-Hugoniot temperature ($^{\circ}\text{K}$)	10^4		$1.5 \cdot 10^4$		$1.6 \cdot 10^4$	
Time (μsec)	η (e.m.u.)	T_e ($^{\circ}\text{K}$)	η (e.m.u.)	T_e ($^{\circ}\text{K}$)	η (e.m.u.)	T_e ($^{\circ}\text{K}$)
0.32			$2.63 \cdot 10^6$	$6.0 \cdot 10^4$		
0.34			$2.86 \cdot 10^6$	$5.6 \cdot 10^4$		
0.40					$1.4 \cdot 10^6$	$9.0 \cdot 10^4$
0.45	$0.94 \cdot 10^6$	$1.2 \cdot 10^5$	$0.74 \cdot 10^6$	$1.67 \cdot 10^5$		
0.47	$3.14 \cdot 10^6$	$5.2 \cdot 10^4$				
0.48	$2.27 \cdot 10^6$	$6.5 \cdot 10^4$				
0.49	$3.27 \cdot 10^6$	$5.1 \cdot 10^4$				
0.50			$0.86 \cdot 10^6$	$1.26 \cdot 10^5$		

and only values of η calculated from three experimental points are given. The values of η calculated are given in Table 2 together with the associated values of electron temperature given by Spitzer's formula

$$\eta = 3.80 \times 10^{12} Z \ln(\Lambda) T^{-3/2} \text{ e.m.u.,} \quad \dots\dots (14)$$

where $\ln(\Lambda) = 10$ and $Z = 1$ for deuterium. Also included in Table 2 are the values of temperatures calculated from the measured shock speed and the Rankine-Hugoniot equations excluding the effect of the magnetic fields (see Wright 1960).

It will be noticed that the values of temperature calculated from the interference fringe patterns are generally higher than the temperatures calculated from the shock velocity. This effect has been observed in helium by McLean, Griem, Faneuff and Kolb (1960) and by Wiese, Berg and Griem (1960) in hydrogen and helium. These authors interpret the heating effect as being due to the fact that gas ahead of the shock has been preheated by precursor radiation, but in this case the reason may be that the plasma is still low enough in temperature for Joule heating to be effective (see Wesson 1960).

The following approximate calculation gives the increase in temperature ΔT_e when Joule heating is taken into account.

$$\text{The 'skin depth' at time } t = \delta \simeq 2(\eta t / \pi)^{1/2} \text{ cm.} \quad \dots\dots (15)$$

Therefore the resistance of the skin to azimuthal current is

$$R = \frac{\eta}{10^9} \frac{2\pi a}{3.58} \Omega; \quad \dots\dots (16)$$

the Joule heat is then

$$J = 100I^2 \frac{\eta}{10^9} \frac{2\pi a}{3.58} t \text{ joules} \quad \dots\dots (17)$$

If H_0 is the magnetic field strength external to the plasma, then from Eqn (9) we obtain

$$\frac{H_0^2}{8\pi} = \frac{H^2}{8\pi} + 2nkT = 2n_m kT, \quad \dots\dots (18)$$

and since H_0 is produced by a single turn coil

$$H_0 = \frac{4\pi I}{3.5}, \quad \dots\dots (19)$$

therefore

$$J = 3.5n_m kTa(\pi\eta t)^{1/2} 10^{-7} \text{ joules} \quad \dots\dots (20)$$

Equating this to $\frac{3}{2}nk\Delta T$ erg, where $n \simeq n_m/2$, gives

$$\frac{\Delta T}{T} \simeq \frac{4}{3} 3.5a(\pi\eta t)^{1/2}. \quad \dots\dots (21)$$

If we take values at $t = \frac{1}{2} \mu\text{sec}$ then, from the experimental results, $\eta = 10^8$ e.m.u. and $a = 1.5$ cm, hence

$$\frac{\Delta T_e}{T_e} \text{ is of the order of } 10, \quad \dots\dots (22)$$

and from Table 2 we see that, in general, this is the correct order of magnitude. The accuracy of the value of temperature obtained from the interference fringe patterns would, of course, be improved if the number of fringes were increased.

5.3. *Equilibrium Ionization behind the Shock Front*

It is apparent from an examination of the fringe patterns that the electron number density behind the shock front takes a finite time to reach a maximum. A measure of this rise in time should give information about the ionization process immediately behind the shock front. We are concerned with a strong shock moving at the order of $3 \text{ cm } \mu\text{sec}^{-1}$ into cold deuterium. The first action will be to heat and dissociate the deuterium leaving us with deuterium atoms at a temperature T corresponding to an energy of the order of 3 to 6 eV depending on the actual value of the shock speed. At these low temperatures the atom-atom ionization cross section is very small, but the electron-atom ionization cross sections are appreciable. Petschek (1955) has pointed out that under these conditions the electrons take an appreciable time to heat up. The following approximate calculation gives the time constant for the electron multiplication in the early stages of the process when recombination can be ignored.

If the electronic and atomic masses are m and M respectively, the electron gains a fraction $4m/M$ of the energy of the atom at each collision. Hence if it loses an energy I every time it ionizes an atom, the electron makes on average $MI/6kTm$ elastic collisions with atoms before it is capable of effecting an ionization. The average electron velocity is of the order $(3kT/2m)^{1/2}$ assuming its energy is, on average, half the energy of the atoms. Hence the time constant for

multiplication of electrons is of the order

$$\tau = \frac{MI/6kTm}{N\sigma(3kT/2m)^{1/2}}$$

$$\tau = 0.14 \frac{MI}{N\sigma(kT)^{3/2}m^{1/2}} \quad \dots\dots (23)$$

In this formula N is the number of atoms per cm^3 just behind the shock front and will be of the order of 15 times the number of deuterium molecules per cm^3 just ahead of the shock front. σ is the electron-atom elastic scattering cross section at low energies and will be of the order of $25 \times 10^{-16} \text{ cm}^2$. This is the total elastic cross section—the cross section for appreciable energy exchange will be somewhat less than this. To compensate for this we have taken the lower value of $T(3 \times 10^4 \text{ eV})$ in working out the time constants in Table 3. The agreement with the experimental values is better than could be expected from such a crude treatment.

Table 3. Time Constants for Multiplication of Electrons behind the Shock Front

Ambient pressure 1 mm		Ambient pressure 0.5 mm		Ambient pressure 0.3 mm	
Measured	Calculated	Measured	Calculated	Measured	Calculated
0.04 μsec	0.02 μsec	0.06 μsec	0.04 μsec	0.09 μsec	0.06 μsec

§ 6. CONCLUSIONS

We have found that the optical interferometer technique is one of the most satisfactory tools for the investigation of high density, high temperature plasmas. Using the technique we have measured the spatial distribution of electron density with time and obtained the percentage of deuterium that has been ionized and swept up by the shock. From the fringe patterns we have inferred the penetration depth of magnetic field into the plasma and calculated the electron temperature. The electron temperatures obtained were higher than the temperatures predicted by the Rankine-Hugoniot equations and we have shown how the temperature difference can be caused by Joule heating of the plasma skin.

An approximate theory of the approach to equilibrium ionization behind the shock front has been given and found to agree with the measured time for the increase of electron density behind the front.

It has been particularly satisfying to use a diagnostic technique that has not been subject to electromagnetic interference and enables some of the plasma parameters to be measured without the introduction of large perturbation effects. The disadvantages of the technique, as used in this experiment, are that all effects are integrated along the optical path and boundary effects are not taken into account.

ACKNOWLEDGMENTS

We wish to thank Mr. K. Mead for his help in setting up the Mach-Zehnder interferometer and also Mr. H. E. Bulless for his invaluable assistance in the experiment. We are indebted to the Director of Atomic Weapons Research Establishment for permission to publish this paper.

REFERENCES

- ALPHER, R. A., and WHITE, D. R., 1958, *The Physics of Fluids*, **1**, 452.
- ASCOLI-BARTOLI, U., DE ANGELIS, A., and MARTELLUCCI, S., 1960, *Nuovo Cim.*, **18**, Series 10, 1116.
- HARDING, G. N., *et al.*, 1958, *Second United Nations International Conference on the Peaceful Uses of Atomic Energy*, Vol. 32 (Geneva: United Nations), p. 365.
- LADENBURG, R. W., and BERSHADER, D., 1955, *Physical Measurements in Gas Dynamics and Combustion* (London: Oxford University Press).
- MCLEAN, E. A., FANEUFF, C. E., KOLB, A. C., and GRIEM, H. R., 1960, *The Physics of Fluids*, **3**, 843.
- MEDFORD, R. D., POWELL, A. L. T., HERBERT, J. D., POTTINGER, R. C., and WRIGHT, J. K., 1960, *Nature, Lond.*, **186**, 706.
- PETSCHKE, H. E., 1955, *Ph.D. Thesis*, Cornell University.
- SPITZER, L., 1956, *Physics of Fully Ionized Gases* (New York: Interscience).
- WESSON, J. A., 1960, *Proc. Fourth Int. Conf. on Ionization Phenomena in Gases*, Vol. 11 (Amsterdam: North Holland), p. 648.
- WIESE, W., BERG, H. F., and GRIEM, H. R., 1960, *Phys. Rev.*, **120**, 1079.
- WRIGHT, J. K., 1960, *Proc. Fourth Int. Conf. on Ionization Phenomena in Gases*, Vol. 11 (Amsterdam: North Holland), p. 1105.
- WRIGHT, J. K., EELES, W. T., and HERBERT, J. D., 1959, *Nature, Lond.*, **183**, 1665.

A Low Temperature Adiabatic Calorimeter for Condensed Substances. Thermodynamic Properties of Argon

By P. FLUBACHER†‡, A. J. LEADBETTER†§ AND J. A. MORRISON

Division of Pure Chemistry, National Research Council, Ottawa, Canada

Communicated by M. Blackman; MS. received 25th May 1961

Abstract. An adiabatic calorimeter has been constructed for the study of properties of condensed substances in the temperature range 2° to 300°K . Two resistance thermometers were used, one of platinum for $T > 11^{\circ}\text{K}$ and one of carbon for $T < 11^{\circ}\text{K}$. The carbon thermometer was calibrated on the thermodynamic temperature scale by using the calorimeter vessel as a gas thermometer; subsequent absolute shifts of its resistance on cycling between room temperature and liquid helium temperatures were taken into account by calibrations against the platinum thermometer.

The heat capacities of solid and liquid argon have been measured between 2° and 86°K with estimated accuracies to $\pm 2\%$ at the lowest temperatures, increasing to $\pm 0.2\%$ for $T > 20^{\circ}\text{K}$ but decreasing to $\pm 0.5\%$ at the highest temperatures. In conjunction with these measurements, vapour pressures were measured in the temperature range 66° to 86°K .

The heat of fusion was found to be $284.5 \pm 0.4 \text{ cal mole}^{-1}$, the triple point temperature 83.810°K and the triple point pressure $516.86 \pm 0.02 \text{ mm Hg}$. The amount of impurity in the specimen of argon was estimated to be 3 parts per million from a study of the melting range.

Direct measurement of the heat of vaporization of the liquid gave the result $1563.6 \pm 4.6 \text{ cal mole}^{-1}$ at 85.67°K , which corresponds to $1555.0 \pm 4.6 \text{ cal mole}^{-1}$ at the normal boiling point.

§ 1. INTRODUCTION

BECAUSE of their simple crystal structure and supposed simple interatomic forces, the solids of the inert gas elements have been widely studied from the theoretical point of view. Also, many of their properties have been measured experimentally. Unhappily, much of the theory contains approximations whose consequences are difficult to judge, and much of the experimental information is incomplete. Definitive comparisons between theory and experiment are, therefore, still to be made.

One object of the present work was to provide more complete and more accurate information on the thermodynamic properties of some of the inert gas solids. In part, the work was stimulated by concurrent theoretical calculations by Horton and Leech (1962, to be published), who have obtained accurate numerical values for thermodynamic properties corresponding to models of the

† National Research Council Postdoctorate Research Fellow.

‡ Present address: Schweizerisches Institut für Reaktorforschung, Würenlingen, Switzerland.

§ Present address: Department of Physical and Inorganic Chemistry, The University, Bristol.

inert gas solids based on the Mie-Lennard-Jones potential. The calorimetric method which has been developed can, however, be used quite generally for measurements on condensed substances in the temperature range between 2°K and room temperature. It has, for example, been used to measure heat capacities of ice at low temperatures (Flubacher, Leadbetter and Morrison 1960).

In §2 of this paper we describe the calorimeter assembly, the techniques used to determine the different quantities and the important matter of the temperature scale. In §3 the results of measurements on argon are given. These include the heat capacities of the solid and liquid, heats of fusion and of vaporization and vapour pressures of the solid and liquid. Where possible, comparisons are made with results published by others. Some of the numerical values given here differ slightly from ones contained in a preliminary report (Flubacher, Leadbetter and Morrison 1961). The differences are due to small arithmetical errors which have now been corrected. Equivalent results for krypton are given in the following paper together with a detailed analysis of the properties of solid argon and solid krypton.

§ 2. EXPERIMENTAL

2.1. *The Calorimeter Assembly*

Different types of calorimeters have been developed for heat capacity and other measurements on condensed substances over a wide temperature range below room temperature (see Sturtevant (1949) for a general discussion and references). However, only infrequently have they been used for measurements below solid hydrogen temperatures (i.e. $T < 11^\circ\text{K}$). Generally, measurements in this range are made with somewhat different techniques (see, for example, Hill and Lounasmaa 1959). For our present purposes it was important to obtain the thermodynamic data from temperatures well below 11°K , and also it was desirable to avoid using two calorimeter assemblies. The assembly which we shall now describe accomplishes these objects. It can be used for continuous measurements between 2°K and room temperature. Essentially, it is a conventional adiabatic low temperature calorimeter assembly to which has been added a liquid helium stage.

In basic design the cryostat is similar to one described previously (Morrison, Patterson and Dugdale 1955). Liquid helium is made in the apparatus by means of a Simon expansion bomb (Pickard and Simon 1948), and the cooling of the calorimeter and adiabatic shield below 11°K is accomplished by conduction of heat along the electrical leads, which make thermal contact with the bomb. A photograph of the interior of the cryostat is shown in Fig. 1. The helium bomb C and the adiabatic shield A are hung below the liquid hydrogen container D on nylon cords. In operation, the cryostat is closed by two concentrically arranged metal cans sealed with Wood's metal at X.

The electrical leads into the cryostat are of 36 a.w.g. copper except for inserts of constantan (15 cm of 30 a.w.g.) between C and D and between A and the calorimeter vessel (see below). The junctions between the copper and constantan, although insulated, are brought into good thermal contact with D and C at Y.

The calorimeter filling tube B (1 mm outer diameter, 0.1 mm wall thickness, German silver) is provided with a heater over its entire length from the top of the shield A to the point where it emerges from the top of the cryostat. It is also attached to D through a thermal shunt (10 cm of 28 a.w.g. copper, wound with

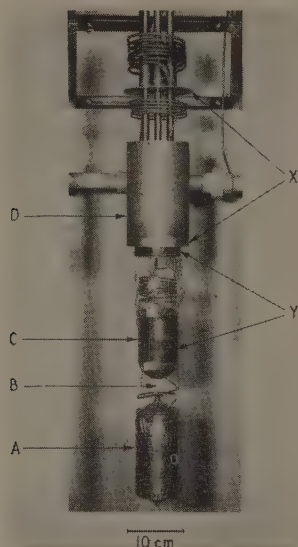


Fig. 1. A photograph of the interior of the cryostat. (For identification of parts, see text.)

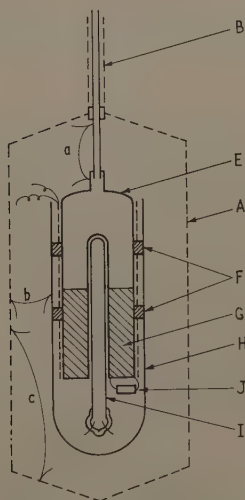


Fig. 2. A sectional view of the calorimeter vessel. (For identification of parts, see text.)

a heating element) whose purpose is to provide a path for heat to be taken from the tube during the experiments at the very low temperatures. The temperature of the point where the shunt is attached to the tube is determined with a thermocouple.

A sectional view of the calorimeter vessel and its associated parts is shown in Fig. 2. The vessel itself, E, (internal volume $\sim 43 \text{ cm}^3$) is made of gold, 0.3 mm thick. It is suspended by means of the filling tube B within the adiabatic shield A. An outer gold plated copper sheath H is attached to the vessel with Wood's metal through copper reinforcing rings F. The calorimeter heater (36 a.w.g. manganin, 160Ω) is wound on the cylindrical side of the calorimeter vessel between the top reinforcing ring and the bottom of the vessel. Heat is distributed inside by means of 8 radial gold vanes G attached to the side and to the re-entrant well, which carries a platinum resistance thermometer I cast in with a thin film of paraffin wax. A carbon thermometer J (Allen Bradley, $\frac{1}{2}$ watt, nominal value $\sim 10 \Omega$) is attached by means of copper lead wires wound several times around the calorimeter vessel. As is mentioned above, lead wires between the calorimeter vessel and the adiabatic shield are of constantan. Their lengths ($\sim 20 \text{ cm}$) were so chosen that the thermal conduction would be high enough for the calorimeter and specimen to be cooled from 11° to 2°K in a reasonable time (5 hours or less), yet low enough for the calorimeter to be not unduly sensitive to the control of the adiabatic shield. Temperature differences within the adiabatic shield are detected with three difference thermocouples: *a*, triple junction chromel-constantan; *b*, single junction Ag, 0.37% Au-Au, 2.4% Co; *c*, single junction chromel-constantan.

2.2. Temperature Scale

As is indicated in the previous section, the calorimeter assembly contains two thermometers, a strain-free capsule-type platinum thermometer and a carbon resistance thermometer. We shall now describe their calibrations.

2.2.1. Platinum thermometer

This thermometer, T-2 (Los and Morrison 1951), was calibrated on the International Temperature Scale down to 90°K . In the temperature range 11° to 90°K it was intercompared with a similar thermometer which had been calibrated on the thermodynamic scale at the National Bureau of Standards (Hoge and Brickwedde 1939). As a check before the present experiments were undertaken, the thermometer was compared with hydrogen vapour pressures by condensing normal hydrogen into the calorimeter vessel. The maximum deviation found in seven comparisons between 14.8° and 20.5°K was 0.006° . It could also be determined that the slope of the platinum thermometer scale was not in error by more than 0.15%.

All of the temperatures given in this and in the following paper (Beaumont, Chihara and Morrison 1961) are based on an ice point of 273.15°K .

2.2.2. Carbon thermometer

When cycled between room temperature and liquid air temperatures or lower, carbon thermometers generally show absolute shifts in resistance. If kept below 90°K the thermometers tend to be stable and reproducible. In order, therefore, to use carbon thermometers for precise work a means of calibrating them *in situ*

needs to be provided, and this is often done by incorporating vapour pressure thermometers into the apparatus. This, however, is not without disadvantages for calorimetry at very low temperatures because heat leaks are increased.

In the present arrangement the carbon thermometer, which was used as the working thermometer for $T < 11^\circ\text{K}$, could be calibrated easily in the temperature range 11° to 20°K by direct comparison with the platinum thermometer. Since the comparison could be made with high precision, the procedure first tried was to use it to determine for each series of experiments the constants in the Clement and Quinell (1952) formula

$$\log R + \frac{K}{\log R} = A + \frac{B}{T}, \quad \dots\dots(1)$$

and so to obtain a carbon thermometer scale for calculating temperatures down to 2°K . Deviations of the carbon thermometer scale from the thermodynamic scale were determined by converting the calorimeter into a gas thermometer and comparing the carbon thermometer with the gas thermometer at a number of points between 2° and 20°K . The deviations were surprisingly small, being a maximum of 0.06° and apparently reproducible to $\pm 0.01^\circ$.

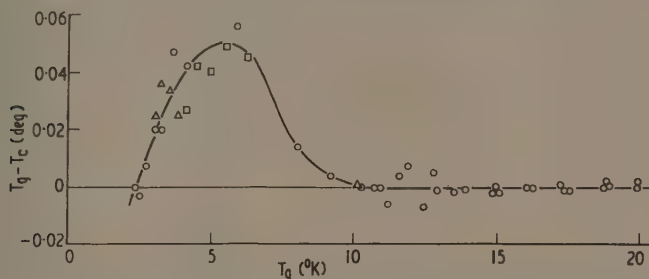


Fig. 3. The deviation of the carbon thermometer scale T_c from the gas thermometer scale T_g as a function of temperature. The different symbols indicate different gas thermometer fillings.

This initial method was almost satisfactory. However, heat capacity measurements repeated after some months deviated systematically from the original ones below 9°K by amounts of as much as two or three times the expected accuracy at the lowest temperatures. It was evident, therefore, that the absolute shifts in the resistance of the carbon thermometer were not being taken into account completely satisfactorily by the calibration procedure. In other words, it became necessary to fix the carbon thermometer scale in some better fashion at the low temperature end if the expected accuracy were to be achieved.

An examination of the shifts in resistance, occurring over a period of a year, showed that at 2°K they were unimportant because of the very large temperature coefficient of resistance at the lowest temperatures (in fact, the maximum shift was equivalent to 0.01°). A constant fixed point, determined with the gas thermometer, was therefore chosen at 2°K , and, with fixed points between 11° and 20° obtained for each series of measurements, was used to calculate a new carbon thermometer scale with the formula

$$\log R + \frac{K}{\log R} + \frac{C}{(\log R)^2} = A + \frac{B}{T}. \quad \dots\dots(2)$$

The deviations of this scale from the thermodynamic scale are shown in Fig. 3. With this modification, the systematic deviations between different sets of heat capacity results either completely disappeared, or at the very least became less than the probable accuracy at all temperatures.

2.3. Heat Capacity Measurements

For all of the heat capacity measurements the calorimeter was operated adiabatically. At the lowest temperatures, temperature increments of about 0.5° were used, and these were increased to about $2\frac{1}{2}^\circ$ at the higher temperatures. Equilibrium times after heating varied from a few seconds at 2°K to 10 to 15 minutes for $T > 50^\circ\text{K}$. When vapour pressures became significant, the calorimeter system was operated with the top of the adiabatic shield slightly warmer (up to 0.05°) than the calorimeter vessel. Tests for condensation in the filling tube were also made periodically by increasing the amount of heat applied to the filling tube and watching for changes in the temperature of the calorimeter vessel and in the pressure.

Under some circumstances, strong temperature gradients in the cryostat produced thermal e.m.f.'s of as much as $3\mu\text{V}$ in the measuring circuits. These were automatically taken into account in the resistance measurements, which were made in the conventional way with a potentiometer, and were too small to have a significant effect on the energy measurements. However, allowance had to be made for them in the difference thermocouple circuits where their effect was to shift the zero point for no heat exchange between the adiabatic shield and the calorimeter vessel.

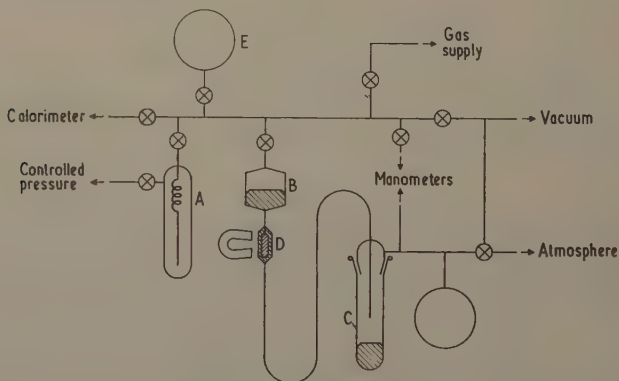


Fig. 4. The calorimeter filling system with additions for measurement of heats of vaporization. (For identification of parts, see text.)

2.4. Measurement of Heat of Vaporization

Heats of vaporization were determined at constant temperature by putting energy into the calorimeter and simultaneously withdrawing vapour into an external system to which the calorimeter was attached. A sketch of the experimental arrangement is shown in Fig. 4. During the vaporization, mercury was withdrawn from the reservoir B into a weighed receiver C under a manually regulated pressure head, at such a rate that the pressure of argon vapour indicated

by the quartz spiral differential manometer A (sensitivity ~ 5 mm displacement per mm Hg) remained substantially constant. Flow of mercury between the reservoir and the receiver could be accurately started or stopped by means of an iron-loaded check valve D operated by means of a magnet. Since the volume of vapour removed was determined directly from a weight of mercury, good accuracy was obtainable with quite small volumes (20 to 50 cm³).

All pressures were measured with a mercury manometer (not illustrated). Heights of the mercury in the two arms were determined from a calibrated steel scale mounted between them, using a comparator which could be read to 0.01 mm. Appropriate corrections were made for capillary depression.

§ 3. THERMODYNAMIC PROPERTIES OF ARGON

3.1. Heat Capacities of the Solid and Liquid

The argon used in the experiments was obtained from the Linde Company and was of a 'spectroscopically pure' grade. The actual specimens were measured out to an accuracy better than 0.1%, using the calibrated volume E (see Fig. 4) of the external system, and then condensed into the calorimeter vessel.

Table 1. The Heat Capacity of Solid Argon at Rounded Values of Temperature

$T(^{\circ}\text{K})$	$C_p(\text{cal mole}^{-1} \text{ deg}^{-1})$	$T(^{\circ}\text{K})$	$C_p(\text{cal mole}^{-1} \text{ deg}^{-1})$
2	0.00468 ₈	35	4.983
3	0.0161 ₁	40	5.387
4	0.0417 ₉	45	5.706
5	0.0881 ₃	50	6.006
6	0.1651	55	6.278
8	0.4237	60	6.528
10	0.7900	65	6.779
12	1.227	70	7.100
15	1.940	75	7.488
20	2.990	80	7.928
25	3.828	83	8.327
30	4.463		

The primary experimental results are given in the Appendix and smoothed values of the heat capacity of the solid in Table 1. Strictly speaking, what was measured was the heat capacity of the solid or liquid in equilibrium with saturated vapour, which is commonly denoted by C_{sat} . This quantity is related to C_p , the heat capacity at constant pressure, by

$$C_{\text{sat}} - C_p = \left[\left(\frac{\partial H}{\partial P} \right)_T - V \right] \left(\frac{\partial P}{\partial T} \right)_{\text{sat}} \dots\dots (3)$$

When numerical values were inserted in Eqn (3) it was found that $C_{\text{sat}} - C_p$ was less than 0.1% of C even at the highest temperatures. The difference $C_{\text{sat}} - C_p$ has therefore been neglected and the results tabulated as C_p , which is the more familiar quantity. The thermochemical calorie ($= 4.184 \text{ abs. J}$) is used throughout.

Above 60°K corrections were necessary for the vaporization of argon which occurred during the heat capacity measurements. The free volume in the calorimeter vessel was calculated using densities of solid argon given by Dobbs, Figgins, Jones, Piercey and Riley (1956) and 1.43 g cm^{-3} for the density of

liquid argon†. Gas imperfection corrections were made using virial coefficients determined by Staveley (1959, private communication) and Kerr (1957).

It is important to assess the accuracy of the experimental heat capacities but it is difficult to make completely satisfactory estimates. For temperatures below 60 K a major limiting factor is the knowledge of the temperature scale. As is indicated in §2.2 the scale used down to 11°K is one from the National Bureau of Standards (Hoge and Brickwedde 1939) which would appear to be reliable to $\pm 0.02^\circ$ at worst (Moessen, Aston and Asch 1954). Resulting inaccuracies in the heat capacities should not exceed about 0.1% . The accuracy of the results at still lower temperatures depends upon the gas thermometry done in conjunction with the heat capacity experiments and is also affected by other factors such as the decreasing sensitivity of the difference thermocouple. Considering these we estimate that the results at the lowest temperatures are accurate to $\pm 2\%$ at worst.

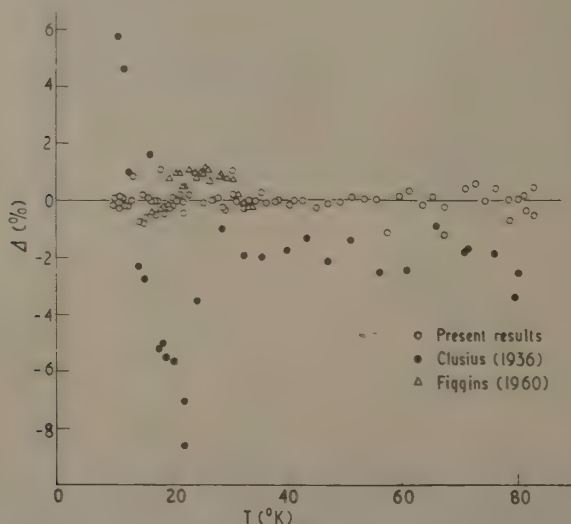


Fig. 5. A comparison of heat capacity results for solid argon.

$$\Delta\% = \frac{C_p(\text{obs}) - C_p(\text{smooth})}{C_p(\text{smooth})} \times 100,$$

where $C_p(\text{smooth})$ is given in Table 1.

Additional factors must be taken into account for $T > 60^\circ\text{K}$, where the absolute values of the heat capacities depend upon knowledge of the densities of the solid and liquid and of the virial coefficients of argon. We have made estimates of the uncertainties in these quantities and conclude that the heat capacities in the region of the triple point should be reliable to $\pm 0.5\%$.

† Recent measurements of van Itterbeek and Verbeke (1960) indicate that the density of the liquid is about 1.40 g cm^{-3} at 86°K . The difference of 2% is not significant in the calculation of the free volumes.

To sum up: we estimate the accuracy of the present measurements to be $\pm 2\%$ at the lowest temperatures, increasing to $\pm 0.2\%$ for $T > 20^\circ\text{K}$ but then decreasing above 60°K to about $\pm 0.5\%$ at the highest temperatures.

Because of its bearing upon the question of accuracy, it is useful to compare the present results with those from other measurements. This is done in Fig. 5 where all of the available results in the region $T > 10^\circ\text{K}$ are plotted as differences from a smooth curve represented by the values given in Table 1. On the whole, the deviations are not large, being 2% or less for all of the results except for those of Clusius (1936) below 25°K . The agreement between the present values and all of those determined by Figgins (1960) in the range 16° to 34°K is just about within the combined estimated accuracies ($\pm 0.7\%$) for both sets. Other measurements of the heat capacity of solid argon between 1.5° and 20°K have been made by Anderson (1960). These will be discussed in the following paper (Beaumont, Chihara and Morrison 1961).

Table 2. Vapour Pressures of Solid and Liquid Argon

$T(^{\circ}\text{K})$	p (mm Hg)	$p - \bar{p}$ (equations of Table 3) (mm Hg)
Solid		
66.129	24.74	+0.12
66.536	26.67	-0.22
67.818	35.30	+0.04
68.468	40.32	+0.02
69.018	45.08	+0.05
69.798	52.60	+0.05
70.081	55.40	-0.14
71.158	68.40	+0.16
71.870	78.04	+0.11
72.554	88.41	+0.09
73.602	106.58	+0.08
74.033	115.00	+0.15
75.430	145.87	+0.06
75.446	146.23	+0.03
76.991	188.24	-0.18
77.046	189.83	-0.25
77.218	194.93	-0.48
78.257	229.99	-0.24
79.606	282.83	-0.22
79.646	284.49	-0.26
80.902	342.76	-0.21
82.302	419.21	+0.10
82.593	436.77	+0.19
83.634	504.44	+0.27
83.639	504.71	+0.24
Liquid		
84.093	533.93	-0.09
85.009	592.26	+0.08
85.578	631.00	+0.19
85.668	637.13	+0.08
85.859	650.91	+0.35
86.693	712.19	-0.49

3.2. Vapour Pressures of the Solid and Liquid

The vapour pressures of the solid and liquid which were measured in conjunction with the heat capacity determinations are tabulated in the second column of Table 2. The pressures are in terms of a mercury column at 0°C and under standard gravity. The precision of the pressure measurements is estimated to be ± 0.03 mm but the accuracy is probably somewhat less than this.

The vapour pressure results were fitted to equations of the form

$$\log p(\text{mm}) = A - \frac{B}{T} \quad \dots\dots(4)$$

by the method of least squares and the resulting coefficients A and B are given in Table 3, where they are compared with values reported by others. The deviations of the actual vapour pressures from the corresponding equations are listed in the last column of Table 2. In doing the least squares analysis, no distinction was made between different series of measurements and all values were given the same weight. The large number of significant figures for A and B is necessary in order to give p to better than 0.05 mm at the higher pressures.

Table 3. Vapour Pressure Equations for Solid and Liquid Argon

A and B are coefficients of the equation $\log p = A - \frac{B}{T}$			
Observers		A	B
	Solid		
Present		7.65590	414.272
Freeman and Halsey (1956)		7.7353	420.9
Clark <i>et al.</i> (1951)		7.54454	404.84
	Liquid		
Present		6.89537	350.484
Freeman and Halsey (1956)		6.9224	352.8
Clark <i>et al.</i> (1951)		6.84451	346

It is evident from the magnitudes of the coefficients in Table 3 that the present results lie in between those of Freeman and Halsey (1956) and of Clark *et al.* (1951). The differences are appreciable: for example, at 80°K, Freeman and Halsey's equation yields a pressure lower than ours by 2.3 mm and the equation of Clark *et al.* a pressure higher by 4.6 mm. There is no simple explanation for the differences other than to say that they must arise from undetected experimental difficulties. Such difficulties were minimized in the present work because the apparent heat capacity was very sensitive to distillation of the argon out of or into the calorimeter vessel.

3.3. Heat of Fusion

The measurements of the heat of fusion are summarized in Table 4, and the average result compared with that obtained by Clusius (1936). In the first

Table 4. The Heat of Fusion of Argon

Amount melted (mole)	Temperature range (°K)	Heat of fusion (cal mole ⁻¹)
0.1534	83.639–84.299	284.4
0.1530	83.634–84.093	284.0
0.1522	83.748–83.850	285.0
	average	284.5 ± 0.4
	Clusius (1936)	280.8

Table 5. The Triple Point of Argon

Fraction melted	$T(^{\circ}\text{K})$	$p(\text{mm Hg})$
0.13	83.8089	516.84
0.36	83.8097	516.89
0.60	83.8098	516.84
0.85	83.8096	—
	average	516.86 ± 0.02
T_{tr} (pure argon)	83.810	
Lovejoy (1962)†	83.816	—
Michels <i>et al.</i> (1957)	83.809 ± 0.001	—
Freeman and Halsey (1956)	83.77	514.1
Clark <i>et al.</i> (1951)	83.78	515.7
Clusius and Staveley (1941)	—	516.85 ± 0.02
Clusius and Weigand (1940)	83.78 ± 0.02	—
Frank and Clusius (1939)	—	516.8 ± 0.2

measurement, the fusion was done in stages and measurements of the equilibrium temperature and pressure made in between. The results are given in Table 5. The triple point of pure argon, given as 83.810°K, was estimated from a plot of the equilibrium temperature against the reciprocal of the fraction melted. The amount of impurity present in the argon was also estimated from the plot and was found to be 3 parts per million. This is in very good agreement with the value of about 1 part per million determined by Lovejoy (1962)† for argon from the same source.

The present result for the triple point temperature of argon is very close to the results of Lovejoy (1962)† and of Michels *et al.* (1957) whose objects were to establish this triple point as a possible thermometric fixed point. The most careful measurements of the triple point pressure which have been made are those of Clusius and Staveley (1941). Our result comes within the limits assigned to theirs.

3.4. Heat of Vaporization

The results of four separate measurements of the heat of vaporization are given in Table 6. They are compared with that calculated from the temperature dependence of the vapour pressure of the liquid, and with a value published by Frank and Clusius (1939). In both comparisons the agreement is well within the assigned uncertainties.

† Note to be submitted to *Nature*.

Table 6. The Heat of Vaporization of Argon at $T=85.67^{\circ}\text{K}$

Amount evaporated (mole)	Heat of vaporization (cal mole ⁻¹)
1.867×10^{-3}	1570.2
2.093×10^{-3}	1566.2
2.135×10^{-3}	1557.5
2.151×10^{-3}	1560.5
average	1563.6 ± 4.6
Calculated from vapour pressures	1555 ± 6
Heat of vaporization at normal boiling point	1555.0 ± 4.6
Frank and Clusius (1939)	1557.5 ± 1.5

§ 4. SUMMARY

In the foregoing sections we have given the results of measurements of the thermodynamic properties of solid and liquid argon. The results are complete in the sense that they are all that can be obtained from the calorimetric and directly associated techniques. In so far as it has been possible, we have assigned probable accuracies to the various quantities measured.

In the following paper (Beaumont, Chihara and Morrison 1961) similar results will be given for solid and liquid krypton. In addition, the vibrational and other properties of solid argon and solid krypton will be discussed in some detail.

ACKNOWLEDGMENTS

We are indebted to Mr. G. Ensell and Mr. R. Reid for valuable assistance with the construction of the calorimeter assembly. We should also like to thank Dr. H. Chihara for much help with the computations.

REFERENCES

- ANDERSON, A., 1960, *Thesis*, University of Oxford.
 BEAUMONT, R. H., CHIHARA, H., and MORRISON, J. A., 1961, *Proc. Phys. Soc.*, **78**, 1462.
 BERG, W. T., and MORRISON, J. A., 1957, *Proc. Roy. Soc. A*, **242**, 467.
 CLARK, A. M., DIN, F., ROBB, J., MICHELS, A., WASSENAAR, T., and ZWIETERING, TH., 1951, *Physica*, **17**, 876.
 CLUSIUS, K., 1936, *Z. phys. Chem. B*, **31**, 459.
 CLUSIUS, K., and STAVELEY, L. A. K., 1941, *Z. phys. Chem. B*, **49**, 1.
 CLUSIUS, K., and WEIGAND, K., 1940, *Z. phys. Chem. B*, **46**, 1.
 DOBBS, E. R., FIGGINS, B. F., JONES, G. O., PIERCEY, D. C., and RILEY, D. P., 1956, *Nature, Lond.*, **178**, 483.
 FIGGINS, B. F., 1960, *Proc. Phys. Soc.*, **76**, 732.
 FLUBACHER, P., LEADBETTER, A. J., and MORRISON, J. A., 1960, *J. Chem. Phys.*, **33**, 1751.
 ——— 1961, *Proc. VIIth Int. Conf. on Low Temperature Physics* (Toronto: University Press), p. 695.
 FRANK, A., and CLUSIUS, K., 1939, *Z. phys. Chem. B*, **42**, 395.
 FREEMAN, M. P., and HALSEY, G. D., 1956, *J. Phys. Chem.*, **60**, 1119.
 HILL, R. W., and LOUNASMAA, O. V., 1959, *Phil. Mag.*, **4**, 785.
 HOGE, H. J., and BRICKWEDDE, F. G., 1939, *J. Res. Nat. Bur. Stand.*, **22**, 351.
 VAN ITTERBEEK, A., and VERBEKE, O., 1960, *Physica*, **26**, 931.
 KERR, E. C., 1957, *Thesis*, Ohio State University.
 LOS, J. M., and MORRISON, J. A., 1951, *Canad. J. Phys.*, **29**, 142.
 MICHELS, A., WASSENAAR, T., SLUYTERS, TH., and DE GRAAFF, W., 1957, *Physica*, **23**, 89.
 MOESSEN, G. W., ASTON, J. G., and ASCAH, R. G., 1954, *J. Chem. Phys.*, **22**, 2096.
 MORRISON, J. A., PATTERSON, D., and DUGDALE, J. S., 1955, *Canad. J. Chem.*, **33**, 375.
 STURTEVANT, J. M., 1949, *Physical Methods of Organic Chemistry*, Part I, 2nd edn, edited by A. WEISSBERGER (New York: Interscience), Chap. XIV.

APPENDIX

Measured Heat Capacities of Solid and Liquid Argon

T (°K)	C_p (cal mole ⁻¹ deg ⁻¹)	T (°K)	C_p (cal mole ⁻¹ deg ⁻¹)	T (°K)	C_p (cal mole ⁻¹ deg ⁻¹)
Series I (0.1580 mole)		72.736	7.352	13.323	1.539
Solid		74.525	7.449	13.837	1.682
17.201	2.410	76.333	7.633	14.309	1.765
18.304	2.648	78.432	7.784	14.806	1.901
19.504	2.884	78.931	7.775	15.314	1.997
20.771	3.139	80.254	7.976	15.820	2.128
22.086	3.372	81.120	8.088	16.389	2.245
23.692	3.642	81.552	8.115	17.514	2.486
25.694	3.919	82.970	8.281	18.727	2.732
26.834	4.076	83.114	8.382	20.063	3.007
27.053	4.103			21.431	3.268
27.900	4.215	Liquid		Series III (0.2404 mole)	
28.792	4.309	84.551	10.378	2.316	0.00740
29.245	4.359	85.434	10.480	2.502	0.00927
30.467	4.565	86.276	10.900	2.777	0.01293
30.759	4.556	Series II (0.1568 mole)		3.011	0.01676
31.223	4.598	2.220	0.00666	3.257	0.02147
32.557	4.745	2.540	0.00985	3.286	0.02219
33.247	4.813	2.693	0.01215	3.510	0.02724
34.446	4.931	3.002	0.01624	3.753	0.03355
35.570	5.029	3.205	0.02155	3.769	0.03401
36.634	5.123	3.467	0.02689	4.013	0.04183
37.978	5.233	3.686	0.03302	4.249	0.05150
38.937	5.312	3.931	0.03971	4.264	0.05049
40.455	5.407	4.191	0.04739	4.478	0.05968
41.225	5.469	4.388	0.05746	4.776	0.07462
42.880	5.572	4.690	0.07227	4.929	0.08246
45.147	5.701	5.158	0.09836	5.711	0.1379
47.219	5.833	5.674	0.1364	6.770	0.2466
49.274	5.961	6.234	0.1895	7.834	0.3970
51.385	6.090	6.761	0.2488	8.845	0.5666
53.403	6.199	7.310	0.3230	9.760	0.7401
55.472	6.318	7.918	0.4114	10.766	0.9482
57.602	6.371	8.826	0.5652	15.227	1.974
59.635	6.520	9.877	0.7658	17.030	2.385
61.596	6.633	10.818	0.9636	18.721	2.723
63.491	6.691	11.333	1.077	20.343	3.051
65.435	6.817	11.839	1.188	21.919	3.331
67.502	6.922	12.374	1.311		
67.529	6.853	12.900	1.438		
70.971	7.205				

Thermodynamic Properties of Krypton. Vibrational and Other Properties of Solid Argon and Solid Krypton

By R. H. BEAUMONT††, H. CHIHARA†§ AND J. A. MORRISON

Division of Pure Chemistry, National Research Council, Ottawa, Canada

Communicated by M. Blackman; MS. received 25th May 1961

Abstract. The calorimetric methods described in the preceding paper have been used to measure thermodynamic properties of solid and liquid krypton. Besides heat capacities and vapour pressures over a range of temperatures, the following were obtained: heat of fusion $= 392.0 \pm 2.3$ cal mole⁻¹, $T(\text{tr. pt.}) = 115.77_6^\circ\text{K}$, $p(\text{tr. pt.}) = 548.7 \pm 0.1$ mm, heat of vaporization at $116.85^\circ\text{K} = 2179.2 \pm 0.9$ cal mole⁻¹ and at the normal boiling point $= 2162 \pm 1$ cal mole⁻¹.

A number of properties of solid argon and solid krypton has been derived, in particular, the apparent Debye characteristic temperatures at 0°K and as a function of temperature, the heats of sublimation at 0°K , the static lattice energies and the zero point energies. The results of the thermal measurements on the solids have been correlated with expansivity and compressibility results and certain inconsistencies resolved. The calorimetric results are shown to be internally consistent.

The shapes of curves of $\Theta_D(T)$ against temperature indicate that anharmonic contributions to the vibrational properties of solid argon and solid krypton are appreciable, particularly in the region $T > \Theta_0/10$.

In the region below the melting points, C_p for both argon and krypton increases rather rapidly with temperature. This is interpreted as an effect of formation of vacancies in the solids. Enthalpies of formation are found to be 1280 ± 130 cal mole⁻¹ for argon and 1770 ± 200 cal mole⁻¹ for krypton. These are about two-thirds of values estimated from theory. An effect of vacancy formation may also be seen in the vapour pressures.

INTRODUCTION

IN the first part of this paper we give the results of measurements of the thermodynamic properties of solid and liquid krypton. The results are analogous to those for argon reported in the preceding paper (Flubacher, Leadbetter and Morrison 1961a). Since the experimental methods used were exactly the same, they require no further description.

† National Research Council Postdoctorate Research Fellow.

‡ Now at Dunlop Rubber Company, Birmingham.

§ Now at Department of Chemistry, Osaka University, Osaka, Japan.

The second and longer part of the paper is concerned with vibrational and other properties of solid argon and solid krypton. The experimental results given here and in the preceding paper are analysed and correlated with other information on these solids so as to obtain derived quantities such as the apparent Debye characteristic temperature, $\Theta_D(T)$, at 0°K and as a function of temperature and the zero point properties, namely, heats of sublimation at 0°K , zero point energies and static lattice energies. A rather long section (§ 2.3) is devoted to the correlation of the thermal properties with existing data on the expansivity and compressibility of solid argon and solid krypton. Here, there are inconsistencies which we have tried to resolve. It would be valuable if our conclusions could be checked by further measurements of expansivities and compressibilities. Because of uncertainties which remain we cannot say very much about the detailed temperature dependence of $\Theta_D(T)$ above 15°K , other than that $\Theta_D(T)$ definitely increases with increasing temperature for both argon and krypton, and that $\Theta_D(T)$ for argon seems to increase more rapidly. Clearly, this behaviour should be ascribed to anharmonicity, but to what extent it is due to zero point energy or to thermal energy cannot be established at present. The fact that the effect seems greater for argon, for which the ratio of zero point energy to lattice energy is greater, suggests that zero point energy is an important factor. The comparison of the experimental properties with those derived from theoretical models corresponding to the inert gas solids is largely left to a theoretical paper by Horton and Leech (1962, to be published).

The heat capacities in the region below the melting point have been analysed so as to obtain estimates of the enthalpies required to form vacancies in solid argon and solid krypton. The results are discussed in § 2.5. The enthalpies found from experiment are only about two-thirds of those computed from models. A further investigation of the discrepancy using expansivity data suggests that the relaxation of surrounding atoms into the vacancy is very much larger than has been estimated by theory.

PART 1. THERMODYNAMIC PROPERTIES OF SOLID AND LIQUID KRYPTON

The following three sections contain the experimental results obtained for krypton and brief accounts of relevant corrections. The krypton used was of a grade similar to that of argon and it also was obtained from the Linde Company. The purity was checked during the determination of the triple point (§ 1.3).

1.1. Heat Capacities of Solid and Liquid Krypton

The measured values of the heat capacity are listed in the Appendix and values for the solid at rounded temperatures in Table 1. The accuracies to be assigned to the results are essentially the same as those applicable to the results for argon. There is, however, a slightly greater uncertainty in the results at higher temperatures. The second virial coefficient of gaseous krypton has not been determined experimentally below room temperature. It was therefore necessary to estimate its value at low temperatures by extrapolation of high temperature results (Beattie, Barriault and Brierly 1952, Whalley and Schneider 1955). The extrapolation was made down to 76°K by a method due to Hirschfelder,

Table 1. The Heat Capacity of Solid Krypton at Rounded Values of the Temperature

$T(^{\circ}\text{K})$	C_p (cal mole ⁻¹ deg ⁻¹)	$T(^{\circ}\text{K})$	C_p (cal mole ⁻¹ deg ⁻¹)
2	0.0105 ₀	50	5.978
3	0.0375 ₃	55	6.140
4	0.0963 ₈	60	6.296
5	0.2039	65	6.451
6	0.3721	70	6.569
8	0.8572	75	6.702
10	1.418	80	6.824
12	1.999	85	6.974
15	2.798	90	7.146
20	3.817	95	7.338
25	4.516	100	7.585
30	4.990	105	7.841
35	5.345	110	8.139
40	5.612	115	8.552
45	5.802		

Curtiss and Bird (1954).† Fortunately, the correction to the heat capacity on account of gas imperfection is rather small, so that the virial coefficients do not need to be known with high accuracy. An uncertainty of 10% in the virial coefficient leads to an uncertainty in the heat capacity of 0.4% at worst. The densities of solid krypton used were those obtained by Figgins and Smith (1960). In correcting the heat capacities of the liquid a single value of the density (2.43 g cm⁻³) was used.

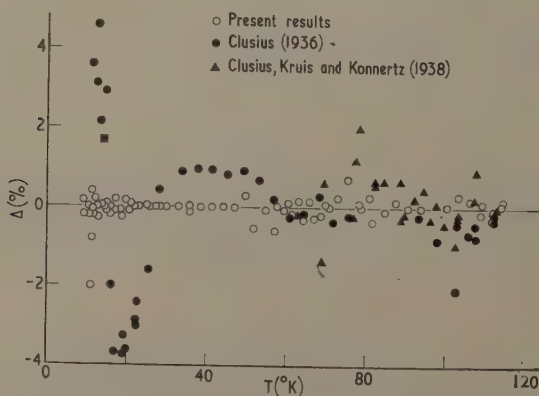


Fig. 1. A comparison of heat capacity results for solid krypton.

$$\Delta(\%) = \frac{C_p(\text{obs}) - C_p(\text{smooth})}{C_p(\text{smooth})} \times 100$$

where $C_p(\text{smooth})$ is given in Table 1.

†The quantum-mechanical correction (de Boer and Michels 1938) was small, amounting to only 0.23% at 116°K.

The measured heat capacities of solid krypton in the region $10^{\circ} < T < T(\text{tr. pt.})$ are compared with earlier results (Clusius 1936, Clusius, Kruis and Konnertz 1938) in Fig. 1. The results are plotted as differences from a smooth curve corresponding to the values given in Table 1. The average deviation of the present results from the smooth curve is less than 0.2%. The other results deviate more strongly, particularly at the lower temperatures.

Table 2. Vapour Pressures of Solid and Liquid Krypton

$T(^{\circ}\text{K})$	p (mm Hg)	$p - \bar{p}$ (Eqn (1)) (mm Hg)
Solid		
83.282	6.07	—
86.319	10.70	—
89.266	17.81	—
89.273	17.89	—
92.603	31.25	-0.03
95.831	50.76	+0.12
98.959	78.42	+0.04
101.984	116.44	-0.14
104.691	162.76	—
104.906	167.42	+0.03
107.651	230.65	-0.34
108.125	243.66	-0.12
110.495	316.81	-0.21
110.836	328.86	-0.13
113.228	423.30	-0.12
113.447	433.27	+0.16
115.112	513.49	+0.69
115.626	539.91	+0.20
115.661	542.04	+0.43
115.758	548.75	—
Liquid		
116.045	560.82	-0.05
116.129	564.68	-0.18
116.240	570.33	+0.20
116.845	598.98	-0.49
117.024	608.15	-0.24
117.045	609.57	+0.14
117.880	652.39	-0.11
117.937	655.73	+0.25
118.923	709.70	+0.14

The heat capacities of solid argon and solid krypton have also been measured between 1.2° and 20°K by Anderson (1960). A comparison of Anderson's results† with ours can be summarized as follows. Over a large part of the temperature region, in particular between 3° and 4°K and above 9°K , the two sets for both argon and krypton agree within their probable accuracies. Between 4° and 9°K Anderson's heat capacities for argon are larger by as much as 4%, and for krypton smaller by as much as 5%. These differences are larger than the estimated accuracy of the present measurements (see §3(a) of Flubacher, Leadbetter and Morrison 1961a). At the lowest temperatures ($T < 3^{\circ}\text{K}$) Anderson's results are consistently higher than ours by up to 3%.

† We should like to thank Dr. Anderson for sending us the tables from his thesis.

1.2. Vapour Pressures of the Solid and Liquid

The vapour pressures of solid and liquid krypton, determined in conjunction with the measurements of the heat capacity, are listed in Table 2. The pressures are of comparable accuracy to those obtained for argon. The results were fitted to the following equations by the method of least squares:

$$\left. \begin{aligned} \text{solid krypton: } \log_{10} p \text{ (mm)} &= 7.70741 - \frac{575.267}{T}, \\ \text{liquid krypton: } \log_{10} p \text{ (mm)} &= 6.96880 - \frac{489.70}{T}; \end{aligned} \right\} \dots\dots(1)$$

the deviations of the actual pressures from the equations are given in the last column of Table 2. The differences, of course, simply reflect the fact that the heats of sublimation and vaporization are temperature dependent. The constants of Eqns (1) are significantly different from those found by Freeman and Halsey (1956), namely 7.7447 and 579.6 for solid krypton, and 6.9861 and 491.9 for liquid krypton. The difference between the two sets of measurements can also be seen in the estimates of the triple point temperature and pressure of krypton (see Table 4).

1.3. The Triple Point of Krypton and the Heats of Fusion and Vaporization

Three determinations of the heat of fusion of krypton were made, and the results are given in Table 3. During the first, the fusion was stopped at intervals for the determination of the triple point pressure and temperature. For this reason the first result may be the least accurate, but on the other hand the amount melted was 40% larger, which would tend to improve the accuracy. In obtaining the average value the three results were given equal weight. The average value agrees well with the result found by Clusius⁽¹⁹³⁶⁾.

Table 3. The Heat of Fusion of Krypton

Amount melted (moles)	Temperature range (°K)	Heat of fusion (cal mole ⁻¹)
0.1550	115.758-116.240	388.6
0.1105	115.661-116.037	393.5
0.1105	115.626-116.129	394.0
	average	392.0 ± 2.3
	Clusius (1936)	390.7

The triple point temperature corresponding to pure krypton was estimated from a plot of the equilibrium temperatures against the reciprocal of the fraction melted. The relevant data are given in Table 4. The amount of impurity was also estimated and the result was 4.5 parts per million. The triple point temperature found here, 115.776°K, lies in between the values given by others. Little can be said about this because the different temperature scales are involved in an absolute way. The triple point pressure does not involve the temperature

Table 4. The Triple Point of Krypton

Fraction melted	$T(^{\circ}\text{K})$	p (mm Hg)
0.20	115.7748	548.90
0.40	115.7756	548.64
0.60	115.7756	548.60
0.80	115.7761	548.66
	average	548.70 \pm 0.10
T_{tr} (pure krypton)	115.776	
Freeman and Halsey (1956)	115.6	538.1
Clusius, Kruis and Konnertz (1938)	115.97 \pm 0.05	548.7 \pm 1.5
Clusius (1936)	116.0 \pm 0.05	549.5 \pm 1.0
Keesom, Mazur and Meihuizen (1935)	115.95 \pm 0.03	549 \pm 1.5

scale and it is interesting to see that our result agrees so well with the values found by Clusius and his colleagues (1936, 1938) and by Keesom, Mazur and Meihuizen (1935). Freeman and Halsey's result is much lower but was probably calculated from a vapour pressure equation.

Table 5. The Heat of Vaporization of Krypton at $T=116.85^{\circ}\text{K}$

Amount evaporated (moles)	Heat of vaporization (cal mole ⁻¹)
7.946×10^{-4}	2178.6
8.167×10^{-4}	2178.4
5.365×10^{-4}	2180.5
Average	2179.2 \pm 0.9
Calculated from vapour pressures	2186 \pm 9
Heat of vaporization at normal boiling point	2162 \pm 1
Clusius, Kruis and Konnertz (1938)	2158 \pm 3

The results of the direct measurement of the heat of vaporization of krypton are given in Table 5, and the average value agrees with that calculated from the vapour pressures to well within the assigned uncertainties. It is also in accord with the average of much more extensive determinations by Clusius, Kruis and Konnertz (1938).

PART 2. VIBRATIONAL AND OTHER PROPERTIES OF SOLID ARGON AND SOLID KRYPTON

2.1. General Remarks

In this second part of the paper our object is to analyse the results of thermal and other measurements on solid argon and solid krypton to see what can be learned about their vibrational properties. For instance, we should like to know to what extent the properties can be described in terms of harmonic vibrations. This is a matter which becomes very important when the experimental results are compared with properties corresponding to models, such as those calculated by Horton and Leech (1962, to be published). Before conclusions about the

interatomic forces can be reached from the agreement or lack of agreement between theory and experiment, effects due to anharmonicity must be clearly understood. While some general conclusions about effects of anharmonicity can be drawn, uncertainties in some of the auxiliary data required are just too great, so that a complete detailed analysis of the thermal measurements cannot be justified at present.

2.2. Zero Point Properties

2.2.1. *The characteristic temperature at 0°K.* An investigation of the low temperature heat capacities of a number of examples has shown (Barron and Morrison 1957) that the expansion

$$C = aT^3 + bT^5 + cT^7 + \dots \quad \dots\dots (2)$$

may be expected to describe experimental results in the temperature region $T < \Theta_0/25$. The apparent Debye characteristic temperature at 0°K, Θ_0 , may be calculated from the first coefficient, i.e.

$$\Theta_0 = \left(\frac{464 \cdot 5}{a} \right)^{1/3}, \quad \dots\dots (3)$$

where a has the units $\text{cal mole}^{-1} \text{deg}^{-4}$. Figs 2 and 3, which are graphs of C_V/T^3

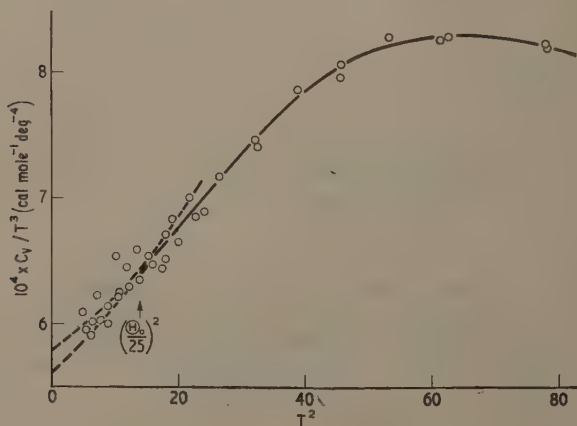


Fig. 2. A graph of C_V/T^3 against T^2 for argon.

against T^2 for the heat capacity results below 9°K, illustrate the estimation of a for argon and krypton. The temperature $\Theta_0/25$ is approximately 4° for argon and 3° for krypton. Since the lowest temperature of the experiments is 2°K, and since the experimental accuracy is least in this region, it is obvious that we cannot conclude from the experimental results whether or not the expansion (Eqn (1)) applies. If, however, we accept the principle of the expansion, we are led to suggest that the dashed lines in the figures represent reasonable limits on the extrapolation of the results to 0°K. The coefficients a so derived correspond

to $\Theta_0 = 93.3 \pm 0.6^\circ$ for argon and $\Theta_0 = 71.7 \pm 0.7^\circ$ for krypton. No attempt has been made to estimate the coefficients b and c . Anderson's heat capacity results (Anderson 1960) yield values of Θ_0 which are about $1\frac{1}{2}\%$ lower.

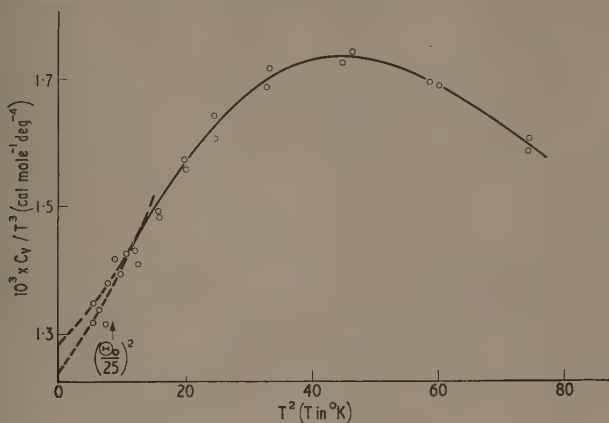


Fig. 3. A graph of C_v/T^3 against T^2 for krypton.

2.2.2. *The heat of sublimation at 0°K .* The thermodynamic properties given in this and in the preceding paper may be used to calculate the heats of sublimation of argon and krypton at 0°K . The relevant thermodynamic expression is a standard one and requires no detailed discussion. It is

$$\Delta H_{\text{sub}}(0^\circ\text{K}) = \Delta H_{\text{sub}}(T) - \int_0^T C_p(\text{gas}) dT + \int_0^T C_p(\text{solid}) dT + RPT^2 \left(\frac{dB_p}{dT} \right). \quad \text{.....(4)}$$

The last term takes account of gas imperfection; the sources of numerical values of the second virial coefficient B_p have been indicated (§ 1.1 above, and § 3.1 of the preceding paper). The results are summarized in Table 6. The estimated uncertainties are also given.

Table 6. Calculation of the Heat of Sublimation at 0°K
(in units of cal mole^{-1})

	Argon	Krypton
Heat of sublimation at $T = T_{\text{tr}}$	1861 ± 5	2579 ± 3
$\int_0^{T_{\text{tr}}} C_p(\text{S}) dT$	391 ± 1	648 ± 2
$-\int_0^{T_{\text{tr}}} C_p(\text{G}) dT$	-416	-575
$RPT^2 \left(\frac{dB_p}{dT} \right)$ at $T = T_{\text{tr}}$	10 ± 1	14 ± 2
Heat of sublimation at $T = 0^\circ\text{K}$	1846 ± 7	2666 ± 7
Dobbs and Jones (1957)	1850 ± 12	—
Walley and Schneider (1955)	1818 ± 40	2589 ± 50

2.2.3. *The static lattice energy.* Recently, Salter (1962) has shown how vapour pressure data for monatomic solids may be analysed to obtain values of the static lattice energy E_0 and the geometric mean frequency ν_g of the lattice frequency distribution. In his paper he uses the vapour pressures of argon and krypton given here to illustrate the method and we shall summarize his results. The numerical values provide a useful test for the consistency of the thermodynamic information. The zero point energy E_z may be obtained as the difference between E_0 , computed from the vapour pressures and the heat of sublimation at 0°K. Alternatively E_z , which is equivalent to the first moment of the lattice frequency distribution, may be estimated through use of the $\nu_D(n)$ function (Barron, Berg and Morrison 1957)

$$\nu_D(n) = \left\{ \frac{1}{3}(n+3) \mu_n \right\}^{1/n}, \quad \dots\dots (5)$$

where μ_n is the n th moment, provided that the general shape of the curve of $\nu_D(n)$ against n can be established. Three values of $\nu_D(n)$, in particular $\nu_D(-3)$, $\nu_D(0)$ and $\nu_D(2)$, can be obtained from Θ_0 , ν_g and Θ_∞ respectively, and since the $\nu_D(n)$ curve should be smooth, interpolation to find $\nu_D(1)$ is not difficult.

Two sets of results calculated from the vapour pressures of argon and krypton are given in Table 7. The uncorrected values refer to direct use of the vapour

Table 7. The Static Lattice Energy and Geometric Mean Frequency Computed from the Vapour Pressures

	E_0 (cal mole ⁻¹)		$10^{-12} \times \nu_g$ (s ⁻¹)	
	Uncorrected	Corrected	Uncorrected	Corrected
Argon	1970 \pm 10	2005 \pm 10	1.06 \pm 0.01	1.15 \pm 0.01
Krypton	2740 \pm 15	2790 \pm 15	0.81 \pm 0.01	0.88 \pm 0.01

pressure data as found experimentally. These give $E_z(\text{argon}) = 124 \pm 17$ and $E_z(\text{krypton}) = 74 \pm 22$ cal mole⁻¹ from E_0 , which are to be compared with 158 ± 5 and 117 ± 5 cal mole⁻¹ from $\nu_D(n)$ curves (not illustrated) based on estimates of Θ_∞ given in §2.4. The differences between the independent estimates of E_z , which are clearly outside the limits shown, turn out to be due to an effect of the presence of vacancies in the lattices at higher temperatures. When an allowance is made for the free energy of formation of vacancies (see §2.5), the corrected results in Table 7 are obtained. These lead to $E_z(\text{argon}) = 159 \pm 17$ and $E_z(\text{krypton}) = 124 \pm 22$ cal mole⁻¹ from E_0 and 171 ± 5 and 134 ± 6 cal mole⁻¹ from $\nu_D(n)$ curves. The agreement is now quite satisfactory.

2.3. The Estimation of $C_p - C_v$

Before the apparent Debye characteristic temperature, $\Theta_D(T)$, at higher temperatures can be calculated it is necessary to know $C_p - C_v$. Estimates of this quantity as a function of temperature have been made for both solid argon (Clusius 1936, Dobbs and Jones 1957) and solid krypton (Clusius 1936), but a

re-examination in the light of more recent experimental and theoretical information turns out to be worth while. The standard expression is

$$C_p - C_v = \frac{\alpha^2 T}{\rho \chi_T} \quad \dots\dots (6)$$

where α is the coefficient of cubical expansion, ρ the density and χ_T is the isothermal compressibility.

2.3.1. *Argon.* Barker and Dobbs (1955) have measured directly the velocities of transverse (v_t) and longitudinal (v_l) lattice waves in solid argon in the temperature range 65° to 80°K, have extrapolated their results to 0°K, and so have obtained estimates of the adiabatic compressibility, χ_s , for the range 0° to 80°K. A check on their extrapolation can be made by using their values of v_t and v_l at 0°K to calculate Θ (elastic), which, assuming harmonic vibrations should be equal to Θ_0 , deduced from the heat capacity data. Barker and Dobbs's results give Θ (elastic) = 80.5°K, which is much smaller than $\Theta_0 = 93.3 \pm 0.6^\circ\text{K}$ (§ 2.2.1). Anharmonicity introduced by zero point energy, which would seem to be the only reasonable cause of a difference between Θ_0 and Θ (elastic), is believed to make Θ (elastic) greater than Θ_0 (Ludwig 1958), and so we conclude that the extrapolation made by Barker and Dobbs cannot be correct.

Velocities of the lattice waves at 0°K have been calculated from theory by Bernades (1960) and Horton and Leech (1962, to be published). The results ($v_t = 0.94 \times 10^4 \text{ cm sec}^{-1}$; $v_l = 1.61 \times 10^4 \text{ cm sec}^{-1}$) lead to Θ (elastic) = 92.6°K, which is in better agreement with Θ_0 . We have therefore calculated χ_s at 0°K from the theoretical wave velocities and have used it with the experimental compressibilities derived by Barker and Dobbs to obtain χ_s as a function of temperature. Fortunately, the values of χ_s at intermediate temperatures are rather close to those tabulated by Dobbs and Jones (1957) (Table III in the appendix to their paper); the maximum difference is 2%.

The density of solid argon has been measured between 20°K and the melting point by Dobbs *et al.* (1956) using x-ray diffraction and volumeter techniques. More recently, Henshaw (1958) has reported a single value of the density at 4.2°K, obtained from neutron diffraction experiments, which is about 3% higher than that given by an extrapolation of the results of Dobbs *et al.* (1956). The difference is disturbingly large, and since there do not appear to be any obvious errors in either the x-ray or neutron diffraction experiments, it is necessary to distinguish between their results using other information.

Theoretical work on the inert gas solids (Barron 1955, Horton and Leech 1962, to be published) suggests that the Grüneisen parameter γ should be only slightly temperature dependent. In particular, the indications are that γ for argon should decrease by probably not more than 10 to 20% when the temperature falls below 50°K. γ is given by

$$\gamma = \frac{\alpha}{\rho \chi_s C_p} \quad \dots\dots (7)$$

We may therefore conveniently test the internal consistency of the quantities on the right-hand side by plotting α/ρ against $\chi_s C_p$. Such a graph is shown in Fig. 4. The points represent smoothed values of α/ρ given by Dobbs *et al.* (1957) at the temperatures 20, 30, 40, 50 and 60°K. The corresponding values of χ_s were taken from the (χ_s , T) relation established as indicated above, and the values of C_p from Table 1 of the preceding paper. The light dashed lines represent

$\gamma = 3.0$ and $\gamma = 2.7$. The points at 20° and 30°K lie well below the dashed lines but the others come nicely in between. If we rely on the theoretical deductions about γ , we are obliged to discard the points at 20° and 30°K and to say that the solid curve in Fig. 4 is what should be used to fix α/ρ below 40°K †. When this is done one finds that the resulting change in the density below 40°K is small. For example, the density at 0°K becomes 1.776 g cm^{-3} compared with 1.770 g cm^{-3} given by Dobbs *et al.* (1956). It seems impossible to make the density value found by Henshaw (1958) consistent with the other data.

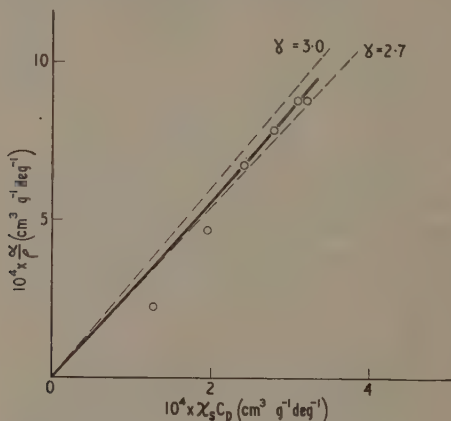


Fig. 4. A graph of α/ρ against $\chi_s C_p$ for argon (see § 2.3.2 of the text).

A summary of the values of α , ρ , χ_s and χ_T used in computing $C_p - C_v$ is given in Table 8. χ_T was calculated from χ_s using

$$\chi_T = \chi_s(1 + \alpha T \gamma). \quad \dots\dots(8)$$

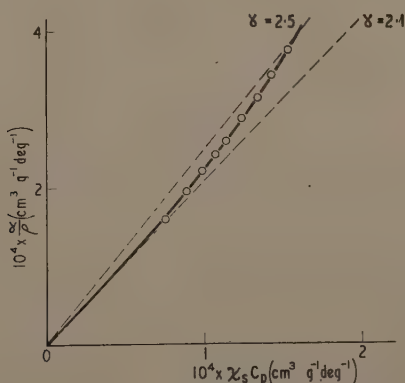
A final check may be made by comparing χ_T so derived at 65° and 77°K with values determined directly by Stewart (1956) using a piston displacement method. The agreement at 65°K is good ($<2\%$) but Stewart's result at 77°K is much higher ($>20\%$). A complicating factor at this higher temperature is that the concentration of thermally created vacancies is appreciable (see § 2.5). The general effect of the vacancies would be to enhance the compressibility as determined by displacement under pressure. It is difficult, however, to construct a quantitative argument. Stewart (1956) has considered other possible reasons, such as errors in density measurements, and shown that they are insufficient to account for the observed difference in χ_T .

2.3.2. Krypton. Figgins and Smith (1960) have measured the density of solid krypton between 20° and 90°K using x-ray diffraction and between 70° and the melting point using a volumeter technique. From the results they have computed the expansivity for the temperature range 20° to 90°K . Very much less information is available for the compressibility of solid krypton. In fact, there

† It will be noted that the measurements at 60°K are represented by two points. One is based on C_p as given in the Table, and the other, which is closer to the ordinate, on C_p corrected for vacancy formation (see § 2.5).

Table 8. Adopted Values for Calculating $C_p - C_v$

$T(^{\circ}\text{K})$	ρ (g cm $^{-3}$)	$10^4 \alpha$ (deg $^{-1}$)	$10^{10} \chi_s$ (cm 2 dyn $^{-1}$)	$10^{10} \chi_T$ (cm 2 dyn $^{-1}$)	$C_p - C_v$ (cal mole $^{-1}$ deg $^{-1}$)
Argon					
0	1.776	0	0.39 ₈	0.39 ₈	—
5	1.776	0.04 ₅	0.40 ₀	0.40 ₀	—
10	1.775	1.5 ₅	0.40 ₂	0.40 ₄	0.003
15	1.773	3.9 ₄	0.40 ₄	0.41 ₀	0.030
20	1.768	6.1 ₀	0.40 ₇	0.42 ₀	0.096
25	1.762	7.9 ₁	0.41 ₁	0.43 ₃	0.196
30	1.755	9.3 ₅	0.41 ₆	0.44 ₈	0.318
40	1.736	11.7 ₀	0.42 ₇	0.48 ₃	0.623
50	1.715	13.5	0.44 ₄	0.52 ₈	0.960
Krypton					
0	3.093	0	0.38 ₈	0.38 ₈	—
5	3.093	0.1 ₀	0.38 ₉	0.38 ₉	—
10	3.092	1.6 ₈	0.39 ₀	0.39 ₁	0.005
15	3.088	3.4 ₉	0.39 ₁	0.39 ₅	0.030
20	3.081	4.9 ₀	0.39 ₂	0.40 ₀	0.078
25	3.073	5.9 ₉	0.39 ₃	0.40 ₆	0.144
30	3.063	6.7 ₇	0.39 ₆	0.41 ₄	0.217
40	3.041	7.8 ₈	0.40 ₄	0.43 ₃	0.378
50	3.015	8.6 ₈	0.41 ₄	0.45 ₆	0.549

Fig 5. A graph of α/ρ against $\chi_s C_p$ for krypton (see § 2.3.2 of the text).

appears to be but a single experimental value of χ_T at 77°K obtained by Stewart (1955). In order to obtain the compressibility of krypton as a function of temperature our only recourse has been to do a type of corresponding states treatment based on the results for argon and using χ_s at 0°K obtained from theory (Horton and Leech 1962, to be published). (The velocities were equivalent to Θ (elastic) = 72.9°K.) The particular method chosen was to use a graph of $\chi_s(T)/\chi_s(0^\circ\text{K})$ against T/T_m , where T_m is the triple point temperature. It is impossible to fix the accuracy of this procedure but it is useful to note that χ_T at 77°K derived using it agreed with Stewart's result to about 3%.

The test for the consistency of the different properties of solid krypton is shown in Fig. 5, which is a graph of α/ρ against $\chi_s C_p$ corresponding to the temperatures 20, 25, 30, 35, 40, 50, 60, 70 and 80°K. In contrast to the example of argon, none of the values of α/ρ needs to be eliminated. All of the points lie close to the solid curve. The only troubling feature is that the magnitude of γ is smaller than is suggested by the calculations from models (Horton and Leech 1962, to be published). This may, of course, simply be caused by a consistent error in the estimation of the compressibility, but on the other hand it could represent a significant departure of experiment from theory. The second part of Table 8 contains the values of $C_p - C_v$ for krypton and of the quantities used in their calculation.

2.4. The Temperature Dependence of $\Theta_D(T)$

Figures 6 and 7 are graphs of $\Theta_D(T)$ as a function of temperature for argon and krypton†. In the calculation of the plotted points, $C_p - C_v$ as given in Table 8

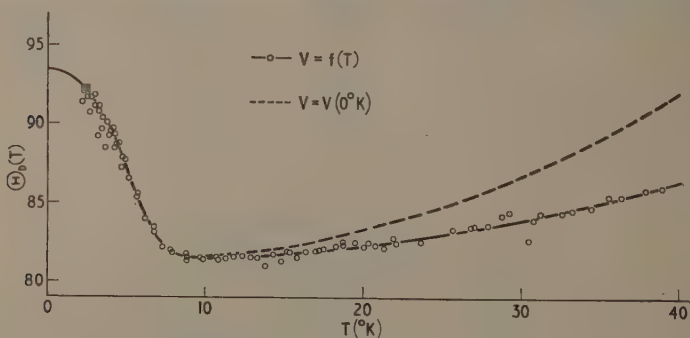


Fig. 6. The apparent Debye characteristic temperature of argon.

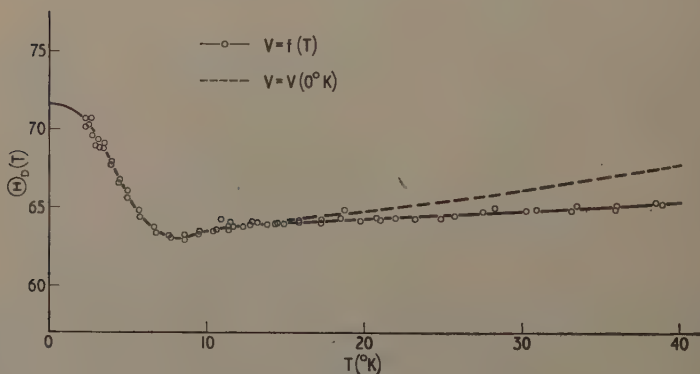


Fig. 7. The apparent Debye characteristic temperature of krypton.

† A graph of $\Theta_D(T)$ against T for argon is contained in a preliminary report (Flubacher, Leadbetter and Morrison 1961 b) and its shape is a little different from that of Fig. 6. It was, however, based on a different estimate of $C_p - C_v$.

was used, and therefore $\Theta_D(T)$ corresponds to a volume which is varying with temperature. What is required for comparison with theory is $\Theta_D(T)$ for a fixed volume. Correction of $\Theta_D(T)$ to the volume of the crystal at 0°K has been made using the expression (Barron, Berg and Morrison, 1957)

$$\Theta_D(V_0) = \Theta_D(V_T) \left(\frac{\rho_0}{\rho_T} \right)^\gamma, \quad \dots\dots (9)$$

and the results are indicated by the dashed curves in Figs 6 and 7. We do not show $\Theta_D(T)$ above 40°K for two reasons. First, above 40°K , $C_p - C_v$ is becoming a large fraction of C_p ($> 11\%$ for argon, $> 7\%$ for krypton), and at best we only know its value to 5% . Second, a non-vibrational contribution to the heat capacity, namely that due to vacancy formation, begins to come in.

While the general shape of the $\Theta_D(T)$ curves in Figs 6 and 7 is rather similar, there are differences in detail. The curve for krypton shows a more pronounced minimum in the vicinity of 8°K , and rises less rapidly at the higher temperatures. The latter feature is displayed more clearly in Fig. 8, where the two curves are compared on a reduced basis using $\Theta_0(\text{argon}) = 93.3^\circ\text{K}$ and $\Theta_0(\text{krypton}) = 71.7^\circ\text{K}$. The difference between the two curves in the region $T/\Theta_0 < 0.15$ is of interest in connection with a comparison with the calculated curves of Horton and Leech (1962, to be published). It turns out that the curve for krypton agrees most

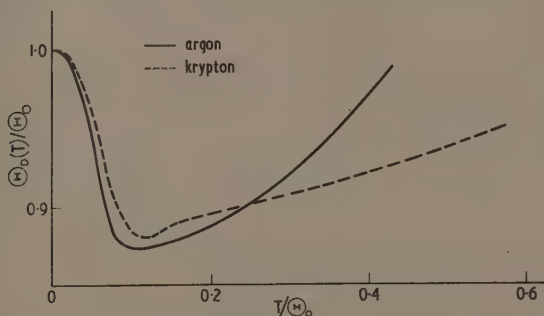


Fig. 8. $\Theta_D(T)$ for argon and krypton on a reduced basis.

closely with one for a central force model including all neighbour interactions, while that for argon agrees better with a model including only first neighbour interactions. Since it is difficult to accept that the nature of the interatomic forces in the two crystals is different in any fundamental way, one is almost obliged to ascribe the difference in the reduced $\Theta_D(T)$ curves to anharmonic effects. Here it is relevant to note that the ratio of zero point energy to the static lattice energy for argon is nearly twice that for krypton, i.e. 0.085 compared with 0.048.

The rise in $\Theta_D(T)$ at the higher temperatures must also be attributed to anharmonicity, and again it appears significant that the effect is much greater for argon. At 40°K , the increase of $\Theta_D(T)$ for argon above the minimum value corresponds to a change of about 4% of C_v , which is outside the combined uncertainties of the experimental heat capacities, of the estimation of $C_p - C_v$ and of the use of Eqn (9). The effect is less certain for krypton where the increase in $\Theta_D(T)$ to 40°K amounts to only 1% of C_v , but the chances are great that it is

real. This being so, it is interesting to note that the behaviour of $\Theta_D(T)$ of argon and krypton at the higher temperatures is quite the reverse of what has been found for other simple crystals such as some alkali halides and diamond structure elements (Berg and Morrison 1957, Flubacher, Leadbetter and Morrison 1959).

Because of the apparent early onset of anharmonic effects (right from 0°K), it is not worth while at this stage to attempt an analysis of the heat capacities to obtain moments and other properties of the lattice frequency distributions. It is even difficult to make an unambiguous choice of Θ_∞ . The best that can be said from inspection of the $\Theta_D(T)$ curves is that Θ_∞ for argon probably lies between 82° and 85°K , and for krypton between 64° and 66°K .

2.5. The Enthalpy to Form Vacancies in Solid Argon and Solid Krypton

The heat capacities of both solid argon and solid krypton show marked upward trends in the temperature region below their melting points. At a few tenths of a degree below the melting points, the heat capacities are about $8.5 \text{ cal mole}^{-1} \text{ deg}^{-1}$ (Tables 1 of this paper and of Flubacher, Leadbetter and Morrison 1961 a). This behaviour might be ascribed to one or more of several causes. For example, it might be due to effects of anharmonicity, to premelting induced by impurities or to the thermal formation of imperfections in the lattices. In the previous section we have seen that anharmonicity is having the opposite effect on the heat capacities of argon and krypton up to 40°K at least, i.e. it is producing a decrease of the heat capacity from that to be expected for harmonic vibrations. The amount of impurity in both the argon and the krypton is known from their behaviour during melting, and its effect on the heat capacity in the region below the melting point can be estimated easily (Sturtevant 1949). It is very small. For example, for argon at 80°K the contribution to the heat capacity is only $0.003 \text{ cal mole}^{-1} \text{ deg}^{-1}$. We conclude therefore, that the major cause of the rise in heat capacity is the thermal creation of imperfections, in particular the creation of Schottky vacancies. The energy (or enthalpy) to form the vacancies has been calculated from theory (Kanzaki 1957, Nardelli and Repanai 1958, 1959), and so it is worth while to obtain estimates from experiment for comparison.

The excess heat capacity due to vacancy formation is (Lidiard 1957)

$$\Delta C_p = \left(\frac{\partial \Delta H}{\partial T} \right)_p = \left(\frac{\partial n_s h_s}{\partial T} \right)_p \quad \dots\dots (10)$$

where n_s , the number of vacancies, is given by

$$n_s = N \exp \left(\frac{s_s}{k} \right) \exp \left(- \frac{h_s}{kT} \right) \quad \dots\dots (11)$$

and N is Avogadro's number, h_s and s_s the enthalpy and entropy of formation. It is obvious that, if $\ln(\Delta C_p \times T^2)$ is plotted against $1/T$, one should get a straight line whose slope is $-h_s/k$.

In order to apply the above, we need only to estimate ΔC_p . This may be done by simply extrapolating a graph of C_p against T smoothly from low temperatures so as to obtain an estimate of the 'normal' heat capacity. We have preferred to use graphs of C_p against $1/T^2$ for this purpose, and the example of argon is shown in Fig. 9. Such a graph foreshortens the high temperature region, and hence makes extrapolation somewhat easier. The broken curves 1, 2, and 3 in Fig. 9 show what seemed to be a reasonable spread of possible extrapolations from the

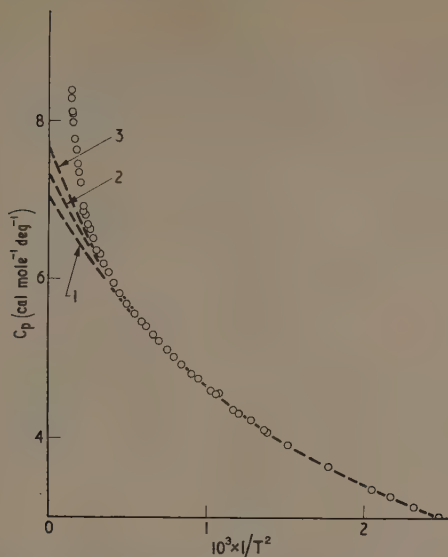


Fig. 9. A graph of C_p against $1/T^2$ for argon. The dashed curves 1, 2 and 3 represent different estimates of the 'normal' heat capacity.

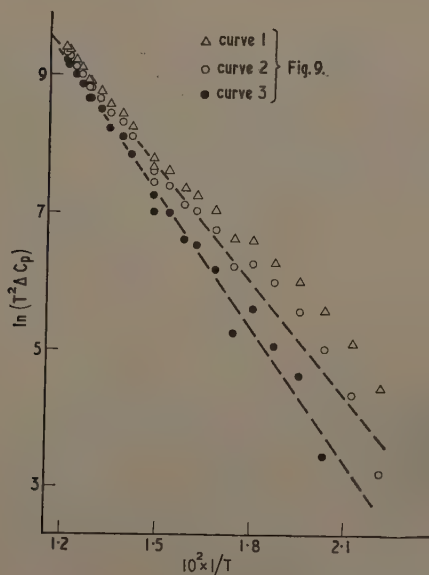


Fig. 10. A graph $\ln(\Delta C_p \times T^3)$ against $1/T$ for argon, based on different estimates of the 'normal' heat capacity.

low temperature region. ΔC_p was determined using each and the resulting graphs of $\ln(\Delta C_p \times T^2)$ against $1/T$ are illustrated in Fig. 10.

There is not too much to choose between extrapolations 2 and 3, although the distribution of points corresponding to 3 around a straight line is better. The slopes for 2 and 3 give $h_s = 1150$ and $1280 \text{ cal mol}^{-1}$ respectively. We therefore

Table 9. The Enthalpy to Form Vacancies in Solid Argon and Solid Krypton

$T(^{\circ}\text{K})$	$h_s \text{ (cal mole}^{-1}\text{)}$ Argon	Reference
Experiment		
45 to 83	1280 ± 130	Present paper
60 to 83	1210	Martin (1957)
Theory		
80	1880	Nardelli and Repanai (1959)
0	2033	Kanzaki (1957)
	Krypton	
Experiment		
60 to 115	1770 ± 200	Present paper
Theory		
109	2740	Nardelli and Repanai (1959)

take the experimental estimate of h_s for argon as $1280 \pm 130 \text{ cal mole}^{-1}$. A similar treatment of the data for krypton gives $h_s = 1770 \pm 200 \text{ cal mole}^{-1}$. These results are compared with the values from theory in Table 9, and we see that the experimental ones are smaller by about one third. It is doubtful that the difference can be ascribed to an erroneous estimate of ΔC_p because, in fact, h_s is not very sensitive to ΔC_p . Also, it should be noted that the value of h_s for argon found by Martin (1957) was obtained using the heat capacity data of Clusius (1936) and a completely different method of extrapolation.

The calculations can be carried further. By using the additional information contained in the intercepts of the lines in Fig. 10, we can obtain explicit expressions for the number of vacancies. These are

$$\frac{n_s}{N} = 30(\pm 20) \exp\left(\frac{-1280(\pm 130)}{RT}\right) \quad \dots\dots (12)$$

for argon, and

$$\frac{n_s}{N} = 30(\pm 20) \exp\left(\frac{-1770(\pm 200)}{RT}\right) \quad \dots\dots (13)$$

for krypton. Having the number of vacancies at any temperature, it is of interest to correlate it with the expansivity, and we shall do this for argon for which expansivities up to the melting point are available (Dobbs *et al.* 1956). At these higher temperatures the densities (and hence the expansivities) were determined by a bulk method, and therefore should be particularly sensitive to the change in volume due to vacancy formation. Indeed, the expansivities of Dobbs *et al.* (1956) show a curl-up in the region $T > 50^{\circ}\text{K}$ (solid curve in Fig. 11). If we assume that the volume of a vacancy is equal to the atomic volume (in other words, assume no relaxation of surrounding atoms into the vacancy) and work out α for a

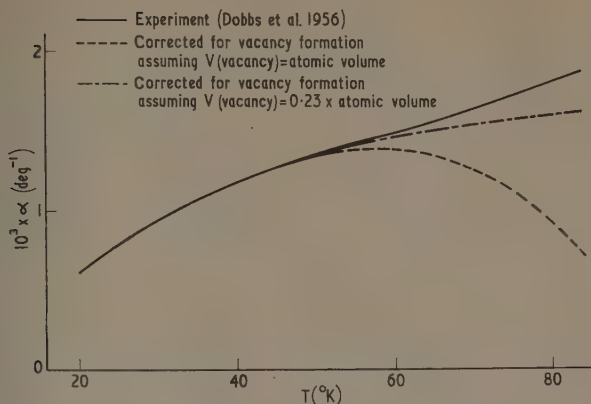


Fig. 11. The expansivity of solid argon.

hypothetical crystal containing no vacancies, we get the result indicated by the dashed curve in Fig. 11 which is completely unreasonable. At worst, α should flatten off at the higher temperatures; it should not decrease. The middle chain curve was calculated assuming that the volume of a vacancy was only 23% of the atomic volume, and this is much more like what should be expected.

SUMMARY

The work which is described in this and in the preceding paper (Flubacher, Leadbetter and Morrison 1961 a) has had the initial object of providing more complete and accurate values of the thermal properties of condensed argon and krypton than have been available heretofore. The experimental results satisfy different tests for internal consistency. For instance, heats of vaporization determined calorimetrically and indirectly from the vapour pressures agree well. Also, zero point energies computed in two ways agree within the uncertainties assigned to the various quantities used.

The latter calculations are of particular interest. In the first place, one of the methods of computation, which uses estimates of certain moments of the lattice frequency distribution, implies harmonic vibrations. The fact that it seems to work suggests that it is not a bad approximation to describe the thermodynamic properties in the low temperature region in terms of an effective harmonic frequency distribution. However, the reduced curves of $\Theta_D(T)$ against temperature (Fig. 8) indicate that anharmonic effects definitely come in at higher temperatures ($T > \Theta_0/10$) and perhaps at all temperatures. A further point about the zero point energy calculations is that they demonstrate the effect of vacancy formation upon the vapour pressures of the solids.

The enthalpies required to form vacancies, determined from the experimental heat capacities for the solids, are quite appreciably smaller than values estimated from theory. The latter are close to the heats of sublimation (compare Tables 6 and 9), and this comes about because energy effects due to relaxation and distortion around a vacancy are taken to be small (Kankazi 1957). However, a comparison

of heat capacity and expansivity results indicates that relaxation of surrounding atoms into a vacancy is probably large. If this were taken into account it would have the effect of reducing the calculated enthalpies of formation.

Perhaps the least satisfactory aspects of the experimental description of the properties of solid argon and solid krypton are the incompleteness of and inconsistencies in some of the expansivity and compressibility data. Further experiments along these lines are clearly desirable. For the time being we have tried to resolve the difficulties here by using certain results of theory and the principle of corresponding states. This must be viewed as a temporary expedient.

ACKNOWLEDGMENTS

Throughout the course of this work we have had as theoretical advisers Dr. T. H. K. Barron, Dr. G. K. Horton, Dr. J. W. Leech and Dr. L. S. Salter. Although they were not always in agreement, their comments and criticisms were valuable, and we should like to thank them for their assistance.

REFERENCES

- ANDERSON, A., 1960, *Thesis*, University of Oxford.
 BARKER, J. R., and DOBBS, E. R., 1955, *Phil. Mag.*, **46**, 1069.
 BARRON, T. H. K., 1955, *Phil. Mag.*, **46**, 720.
 BARRON, T. H. K., BERG, W. T., and MORRISON, J. A., 1957, *Proc. Roy. Soc. A*, **242**, 478.
 BARRON, T. H. K., and MORRISON, J. A., 1957, *Can. J. Phys.*, **35**, 799.
 BEATTIE, J. A., BARRIAULT, R. J., and BRIERLY, J. S., 1952, *J. Chem. Phys.*, **20**, 1613, 1615.
 BERG, W. T., and MORRISON, J. A., 1957, *Proc. Roy. Soc. A*, **242**, 467.
 BERNARDES, N., 1960, *Phys. Rev.*, **120**, 807.
 DE BOER, J., and MICHELS, A., 1938, *Physica*, **5**, 945.
 CLUSIUS, K., 1936, *Z. Phys. Chem. B*, **31**, 459.
 CLUSIUS, K., KRUIS, A., and KONNERTZ, F., 1938, *Ann. Phys., Lpz.*, **33**, 642.
 DOBBS, E. R., FIGGINS, B. F., JONES, G. O., PIERCEY, D. C., and RILEY, D. P., 1956, *Nature, Lond.*, **178**, 483.
 DOBBS, E. R., and JONES, G. O., 1957, *Rep. Progr. Phys.*, **20**, 516 (London: Physical Society).
 FIGGINS, B. F., and SMITH, B. L., 1960, *Phil. Mag.*, **5**, 186.
 FLUBACHER, P., LEADBETTER, A. J., and MORRISON, J. A., 1959, *Phil. Mag.*, **4**, 273.
 ——— 1961 a, *Proc. Phys. Soc.*, **78**, 1449.
 ——— 1961 b, *Proc. VIIth Int. Conf. Low Temperature Physics* (Toronto: University Press), p. 695.
 FREEMAN, M. P., and HALSEY, G. D., 1956, *J. Phys. Chem.*, **60**, 1119.
 HENSHAW, D. G., 1958, *Phys. Rev.*, **111**, 1470.
 HIRSCHFELDER, J. O., CURTISS, C. F., and BIRD, R. B., 1954, *Molecular Theory of Gases and Liquids* (New York: John Wiley), pp. 162–6.
 KANZAKI, H., 1957, *J. Phys. Chem. Solids*, **2**, 107.
 KEESOM, W. H., MAZUR, J., and MEIUIZEN, J. J., 1935, *Physica*, **2**, 669.
 LIDIARD, A. B., 1957, *Handb. d. Phys.*, **20**, part 2, 246.
 LUDWIG, W., 1958, *J. Phys. Chem. Solids*, **4**, 283.
 MARTIN, D. L., 1957, *Report of 2nd Symposium on Melting, Diffusion and Related Topics*, Ottawa, p. 31.
 NARDELLI, G., and REPANAI, A., 1958, *Physica Supplement*, **24**, S182.
 ——— 1959, *Report of Solid State Physics Group, University of Milan*.
 SALTER, L. S., 1962, *Trans. Faraday Soc.*, in the press.
 STEWART, L., 1955, *Phys. Rev.*, **97**, 578.
 STEWART, J. W., 1956, *J. Phys. Chem. Solids*, **1**, 146.
 STURTEVANT, J. M., 1949, *Physical Methods of Organic Chemistry*, 2nd edition, part 1, edited by A. Weissberger (New York: Interscience Publishers), pp. 757–9.
 WHALLEY, E., and SCHNEIDER, W. G., 1955, *J. Chem. Phys.*, **23**, 1644.

APPENDIX

Measured Heat Capacities of Solid and Liquid Krypton

$T(^{\circ}\text{K})$	C_p (cal mole ⁻¹ deg ⁻¹)	$T(^{\circ}\text{K})$	C_p (cal mole ⁻¹ deg ⁻¹)
Series I (0.1586 moles)		Series I (0.1586 moles)	
Solid		Solid	
2.317	0.0163 ₈	81.712	6.844
2.697	0.0257 ₇	84.801	6.961
3.114	0.0420 ₅	87.792	7.081
3.525	0.0616 ₇	90.938	7.179
3.969	0.0927 ₂	94.217	7.316
4.466	0.1389	97.395	7.454
4.957	0.1959	100.472	7.611
5.710	0.3141	103.445	7.783
6.683	0.5159	106.516	7.939
7.643	0.7590	109.481	8.114
8.605	1.016	112.142	8.292
9.555	1.286	114.280	8.488
10.635	1.601	Liquid	
10.905	1.648	116.643	10.325
11.526	1.845	117.491	10.495
11.723	1.916	118.430	10.485
12.307	2.086	Series II (0.1143 moles)	
12.794	2.219	Solid	
13.216	2.328	2.309	0.0166 ₀
13.852	2.507	2.500	0.0209 ₃
14.453	2.660	2.754	0.0287 ₅
14.901	2.776	2.977	0.0373 ₈
15.870	3.001	3.240	0.0484 ₀
17.289	3.307	3.461	0.0593 ₀
18.761	3.584	3.948	0.0918 ₄
20.765	3.940	4.440	0.1378
21.981	4.127	4.938	0.1980
23.239	4.301	5.750	0.3266
24.856	4.502	6.800	0.5502
25.714	4.594	7.743	0.7870
27.529	4.770	8.610	1.031
28.293	4.835	9.497	1.275
30.254	5.012	10.444	1.549
30.941	5.064	11.437	1.844
33.146	5.228	11.443	1.832
33.493	5.246	12.914	2.243
35.960	5.406	14.391	2.646
36.041	5.404	15.890	3.002
38.499	5.538	17.264	3.315
38.881	5.562	18.526	3.550
40.983	5.651	19.799	3.789
41.702	5.682	21.061	3.994
44.497	5.784	64.500	6.420
47.286	5.880	67.237	6.488
50.064	5.999	70.058	6.574
51.976	6.014	72.965	6.670
55.055	6.137	75.775	6.762
57.430	6.179	78.498	6.795
57.969	6.236	81.221	6.874
59.611	6.280	106.171	7.849
60.715	6.325	109.073	8.067
61.712	6.340	111.861	8.250
63.347	6.414	114.444	8.513
66.088	6.489	Liquid	
68.912	6.531	116.538	10.365
71.642	6.619	117.273	10.381
79.059	6.801		

The Specific Heat of Hexagonal Metals at Very Low Temperatures

BY DOUGLAS L. MARTIN

Division of Pure Physics, National Research Council, Ottawa, Canada

Communicated by N. F. Mott; MS. received 26th June 1961

Abstract. The specific heats of cadmium and magnesium have been measured in the temperature range 0.4° to 1.5°K . For cadmium the electronic specific heat coefficient γ is $163.6 \pm 2.6 \mu\text{cal deg}^{-2} (\text{g at.})^{-1}$, the Debye temperature θ is $204 \pm 3 \text{ K}$, and the superconducting transition temperature is $0.52 \pm 0.01^{\circ}\text{K}$. For magnesium γ is $292.7 \pm 2.5 \mu\text{cal deg}^{-2} (\text{g at.})^{-1}$. These results show that a previously reported discrepancy between the elastic and thermal values of θ for the hexagonal metals was due to incorrect interpretation of specific heat data.

§ 1. INTRODUCTION

WOLCOTT (1961) recently drew attention to discrepancies between the values of the Debye characteristic temperature θ for the hexagonal metals derived from elastic constant and specific heat measurements respectively. It follows from the lattice theory of specific heats (see, for example, Blackman 1955) that at very low temperatures, when the thermal vibrations are of long wavelength and the lattice behaves essentially as a continuum, these two values of the Debye temperature should be the same for a given substance. Due to the marked anisotropy of the hexagonal lattice it appears that measurements must be made to much lower temperatures than for cubic lattices with similar θ values, in order to be sure that the continuum region has been reached. In the present paper specific heat results on cadmium and magnesium extending down to about 0.4°K are reported. These results suggest that there is no real discrepancy between the elastic and thermal θ values of the hexagonal metals.

§ 2. EXPERIMENTAL

The measurements were made in a ^3He cryostat using a technique, described elsewhere (Martin 1961 a), in which the sample is stuck to a 'tray' calorimeter with a film of silicone grease.

The cadmium sample was a piece of Tadanac High Purity Cadmium of nominal purity 99.9999%. Some difficulty was experienced at first due to the breaking of the grease bond to the calorimeter on cooling, presumably due to a large differential contraction. This was overcome by sawing the sample into a number of pieces so that the total differential contraction on a given piece was much reduced. The sample then consisted of four pieces, each about 5 cm long and with a contact area of about 1 cm^2 . The pieces were annealed *in vacuo* for one hour at 300°C . The sample weighed 229.768 g.

The magnesium sample was supplied by the Dow Chemical Co. in the form of a rod about 1.3 cm diameter. This material was the same as the Sample No.

28 of Hedgcock, Muir and Wallingford (1960) who quote the following spectrographic analysis: Al <0.001%, Ca <0.01%, Cu <0.001%, Fe <0.001%, In <0.001%, Ni <0.0005%, Pb <0.001%, Si <0.001%, Sn <0.01%, Zn <0.001%. Hedgcock *et al.* found the residual electrical resistance ratio $R_{4.2}/(R_{300} - R_{4.2})$ to be 3.6×10^{-3} , indicating rather a high purity. They also found that this material does not show the anomalous resistance—minimum at low temperatures and therefore specific heat anomalies associated with these phenomena (Martin 1961b) are presumably absent. The magnesium was measured in the same condition as it was received, without any heat treatment. For convenience the calorimeter sample consisted of four pieces of the rod, each about 5 cm long, and weighed 44.300 g.

§ 3. RESULTS

Each sample was measured on two separate occasions, the carbon thermometer in the calorimeter being recalibrated every time it was cooled to low temperatures.

The results have been analysed on the assumption that they may be represented by the equation

$$C = \gamma T + \frac{12\pi^4 R}{5} \left(\frac{T}{\theta} \right)^3$$

where C is the specific heat, γ the electronic specific heat coefficient, R the gas constant and θ the Debye temperature. The values of γ and θ were determined from a least squares analysis of the results from which the 95% confidence limits were also obtained.

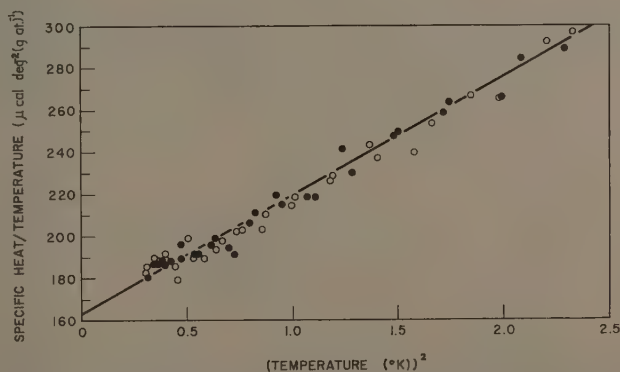


Fig. 1. (Specific heat/temperature) plotted against (temperature)² for the normal state of cadmium.

Results for the normal state of cadmium are shown graphically in Fig. 1 and the derived θ and γ values are given in Table 1. Cadmium becomes superconducting at the lower end of the measurement range and details of the superconducting transition are shown in Fig. 2. The exact temperature of the superconducting transition was determined by taking heating curves through the transition region and noting where the change of slope occurred. By taking

curves at different heating rates, and extrapolating to zero heating rate, the exact transition temperature may be determined. This was done during both sets of measurements on cadmium with the results of $0.519 \pm 0.001^\circ\text{K}$ and $0.519_5 \pm 0.000_5^\circ\text{K}$. The error limits represent the uncertainty on the experimental temperature scale which, as described by Martin (1961 a), is obtained by the us

Table 1. Summary of Specific Heat Results for the Normal State of Cadmium and Magnesium

Cadmium: Atomic weight=112.41		
	$\theta(^{\circ}\text{K})$	$\gamma(\mu\text{cal deg}^{-2} (\text{g at.})^{-1})$
First set	204 ± 4	164 ± 4
Second set	204.5 ± 4	163.5 ± 4
All points	204 ± 3	163.6 ± 2.6
Magnesium: Atomic weight=24.32		
	$\theta(^{\circ}\text{K})$	$\gamma(\mu\text{cal deg}^{-2} (\text{g at.})^{-1})$
First set	442^{+250}_{-75}	294 ± 4
Second set	444^{+210}_{-70}	292 ± 3
All points	440^{+110}_{-56}	292.7 ± 2.5

Note: Indicated errors are 95% confidence limits.
1 calorie=4.186 absolute joules.

of the three constant interpolation formulae of Clement and Quinell (1952) with calibration points at 0.7° , 1.1° and 1.5°K . The temperature scale below 0.7°K was extrapolated due to the difficulty in measuring vapour pressures with sufficient accuracy below this temperature. An estimate of deviations of extrapolated temperature from true temperature may be obtained by examination of specific

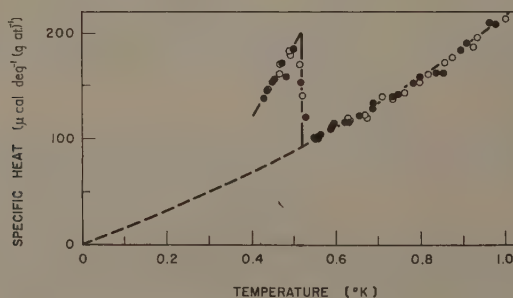


Fig. 2. Details of the superconducting transition for cadmium. The exact position of the transition temperature was determined from heating curves as discussed in the text.

heat results within this region for trends away from results anticipated on the basis of measurements above 0.7°K . On this basis the superconducting transition temperature of cadmium, in the ambient field, is $0.52 \pm 0.01^\circ\text{K}$. The

earth's magnetic field was measured just outside the cryostat and found to be 0.33 gauss. Assuming the same field inside the cryostat, the transition temperature of the cadmium sample would be depressed by about 0.003°K (Smith

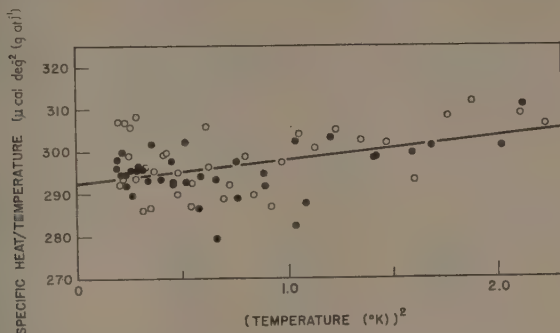


Fig. 3. (Specific heat/temperature) plotted against (temperature)² for magnesium.

and Daunt 1952). The transition width, as determined from the heating curves, was less than 0.001°K .

Results for magnesium are shown graphically in Fig. 3 and the derived θ and γ values are given in Table 1.

§ 4. DISCUSSION

The θ and γ values determined for the normal state of cadmium are compared with those of other workers in Table 2. The only published numerical data of results are the smoothed specific heat values of Smith and Wolcott (1956).

Table 2. Comparison of Results for the Normal State of Cadmium

(1)	(2)	(3)	(4)	(5)
Specific heat results				
Samoilov (1952)	99.95	0.45-0.95	300	170
Smith and Wolcott (1956)	99.99+	1.3-3	188	150
Srinivasan (1959)	99.95	1.3-2.5	189 ± 4	152
This work	99.9999	0.52-1.5	204 ± 3	163.6 ± 2.6
Elastic constant results				
Garland and Silverman (1960)			213 ± 1	

(1) Author; (2) purity of sample (%); (3) temperature range in which θ is assumed constant ($^{\circ}\text{K}$); (4) θ ($^{\circ}\text{K}$); (5) γ ($\mu\text{cal deg}^{-2} (\text{g at.})^{-1}$).

Using the γ value as determined in the present work, values of θ have been calculated from this data and are shown in Fig. 4. If it is assumed that Smith and Wolcott's value at 1.5°K is in error, then it appears that there is satisfactory agreement between the elastic constant and specific heat values of θ . Examination of the θ against T plot for cadmium (Fig. 4) shows that the minimum occurs at an unusually low reduced temperature, $\theta/20$, and the θ value then rises very rapidly

to the value at 0°K. The necessity for making measurements to very low temperatures, in order to obtain the correct limiting value for θ , is therefore quite obvious. Previous discrepancies between the elastic constant and specific heat

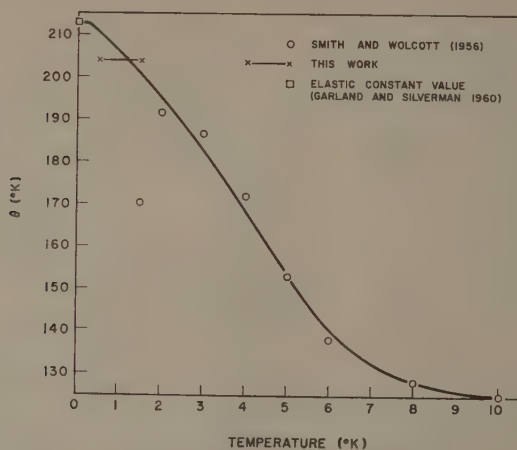


Fig. 4. The Debye temperature of cadmium. The analysis of results for the present work assumes a constant θ value between 0.4 and 1.5°K (see text).

values of θ were because accurate specific heat measurements had not been made to sufficiently low temperatures.

The reported values for the superconducting transition temperature of cadmium cover a wide range, as will be apparent from Table 3. Part of the

Table 3. The Superconducting Transition Temperature of Cadmium

(1)	(2)	(3)
Kürti and Simon (1935)		0.54 \pm 0.02
Goodman and Mendoza (1951)	99.996	0.560
Samoilov (1951)		0.547 \pm 0.005
Steele and Hein (1952)		0.65 \pm 0.02
Smith and Daunt (1952)	99.99	0.602
This work	99.9999	0.52 \pm 0.01

(1) Author; (2) purity of sample (%); (3) superconducting transition temperature (°K).

discrepancy is no doubt due to errors in temperature scales and to the difficulty in ensuring thermal equilibrium at these temperatures. It is also probable that the purity of the sample is an important factor, since it is well known that relatively small amounts of impurity can result in surprisingly large alterations in superconducting transition temperatures (see, for example, Chanin, Lynton and Serin 1959).

The lattice specific heat of magnesium is so small within the temperature range of the present experiments that an accurate value of θ cannot be obtained. However, the value for γ obtained in the present work is significantly lower than previously reported values (Table 4). This suggests that earlier results have either been misinterpreted, due to a lack of data at sufficiently low temperatures, or else the presence of very small amounts of transition metal impurities might

Table 4. Comparison of Results for Magnesium

(1)	(2)	(3)	(4)	(5)
Specific heat results				
Estermann, Friedberg and Goldman (1952)	99.96	1.8-4.2	342	325
Smith (1955)		1.2-4.0	406 \pm 10	315
Rayne (1958)	99.99	1.4-4.2	403 \pm 4	302 \pm 2
This work	99.97 +	0.4-1.5	440 \pm $\frac{110}{56}$	292.7 \pm 2.5
Elastic constant results				
Slutsky and Garland (1957)			388 \pm 3	

(1) Author; (2) purity of sample (%); (3) temperature range in which θ is assumed constant ($^{\circ}\text{K}$); (4) θ ($^{\circ}\text{K}$); (5) γ ($\mu\text{cal deg}^{-2} (\text{g at})^{-1}$).

have resulted in an anomalously high specific heat within the liquid helium temperature region (Martin 1961 b). In either event it is obvious that no published thermal θ values can be accepted as correct. Unfortunately no raw specific heat data for magnesium in the region below 4°K has been published and therefore a re-analysis of earlier data, as has been carried out in this paper for cadmium, is not possible. It therefore seems that establishment of a definite agreement between thermal and elastic θ values for magnesium must await re-measurement of pure magnesium in the range 1.5 to 4°K . However, at the present time there is no reason for supposing that any disagreement exists.

The disagreement between the thermal and elastic constant θ values for another hexagonal metal, zinc, has recently been considered by Garland and Silverman (1961). They showed that the higher temperature specific heat data could be re-analysed on the basis of a new γ value, derived from recent specific heat measurements below 1°K , and a much better agreement between the elastic and thermal θ values was then obtained.

§ 5. CONCLUSION

There is no evidence for discrepancies between the elastic and thermal Debye temperatures of the hexagonal metals, provided that specific heat data at sufficiently low temperatures are used to derive the thermal θ values.

The superconducting transition temperature for pure cadmium was found to be $0.52^{\circ} \pm 0.01^{\circ}\text{K}$.

ACKNOWLEDGMENTS

The pure magnesium sample was kindly supplied by Dr. F. T. Hedgcock of Ottawa University. I am indebted to Dr. D. K. C. MacDonald for his comments on the manuscript, to Mr. R. L. Snowdon for help with the experimental work, to Miss B. A. Cotton for computing assistance and to Messrs. F. W. Richardson and H. J. Broome for the supply of liquid helium.

REFERENCES

- BLACKMAN, M., 1955, *Handb. d. Phys.*, **7**, 325 (Berlin: Springer).
CHANIN, G., LYNTON, E. A., and SERIN, B., 1959, *Phys. Rev.*, **114**, 719.
CLEMENT, J. R., and QUINNELL, E. H., 1952, *Rev. Sci. Instrum.*, **23**, 213.
ESTERMANN, I., FRIEDBERG, S. A., and GOLDMAN, J. E., 1952, *Phys. Rev.*, **87**, 582.
GARLAND, C. W., and SILVERMAN, J., 1960, *Phys. Rev.*, **119**, 1218.
—— 1961, *J. Chem. Phys.*, **34**, 781.
GOODMAN, B. B., and MENDOZA, E., 1951, *Phil. Mag.*, **42**, 594.
HEDGCOCK, F. T., MUIR, W. B., and WALLINGFORD, E., 1960, *Canad. J. Phys.*, **38**, 376.
KÜRTI, N., and SIMON, F. E., 1935, *Proc. Roy. Soc. A*, **151**, 610.
MARTIN, D. L., 1961 a, *Proc. Roy. Soc. A*, **263**, 378.
—— 1961 b, *Canad. J. Phys.*, **39**, 1385.
RAYNE, J. A., 1958, *J. Phys. Chem. Solids*, **7**, 268.
SAMOILOV, B. N., 1951, *Dokl. Akad. Nauk S.S.S.R.*, **81**, 791.
—— 1952, *Dokl. Akad. Nauk S.S.S.R.*, **86**, 281.
SLUTSKY, L. J., and GARLAND, C. W., 1957, *Phys. Rev.*, **107**, 972.
SMITH, P. L., 1955, *Phil. Mag.*, **46**, 744.
SMITH, P. L., and WOLCOTT, N. M., 1956, *Phil. Mag.*, **1**, 854.
SMITH, T. S., and DAUNT, J. G., 1952, *Phys. Rev.*, **88**, 1172.
SRINIVASAN, T. M., 1959, *Proc. Ind. Acad. Sci. A*, **49**, 61.
STEELE, M. C., and HEIN, R. A., 1952, *Phys. Rev.*, **87**, 908.
WOLCOTT, N. M., 1961, *Proc. Phys. Soc.*, **77**, 218.

The Low Temperature Specific Heat of an Aluminium-Manganese Alloy

By DOUGLAS L. MARTIN

Division of Pure Physics, National Research Council, Ottawa, Canada

MS. received 6th July 1961

Abstract. Aluminium-manganese alloys do not show the resistance-minimum phenomena often found in dilute alloys containing transition metals, but anomalous thermoelectric powers are observed. Alloy systems which do show the resistance minimum also have large specific heat anomalies at low temperatures. It was therefore of interest to see whether specific heat anomalies occurred in the aluminium-manganese system.

Measurements of the specific heat of pure aluminium and of an alloy containing 0.045 atomic % manganese were therefore made in the temperature range 0.4° to 1.5°K. In the normal state the specific heats of the two samples are the same. Thus a specific heat anomaly of the type found in systems showing the resistance minimum does not occur. The superconducting transition temperature of the alloy is about 0.84°K (compared with $1.174 \pm 0.002^\circ\text{K}$ for pure aluminium) but the transition remains sharp (width less than 0.001 deg K) and of the second order. The reduced electronic specific heats in the superconducting state $C_{es}/\gamma T_0$, when given in terms of reduced temperature T_c/T , are identical.

§ 1. INTRODUCTION

THE addition of transition metal impurities, in solution, to otherwise pure metals often leads to the resistance-minimum phenomena and associated 'giant' thermoelectric powers (see, for example, review by MacDonald 1956). It is now known that large specific heat anomalies are associated with these phenomena in the following systems: silver-manganese, and copper-manganese (De Nobel and Du Chatenier 1959, Zimmerman and Hoare 1960), copper-iron (Martin and Franck 1960, Franck, Manchester and Martin 1961), copper-cobalt (Crane and Zimmerman 1961), magnesium-manganese (Martin 1961a), copper-chromium, silver-chromium and zinc-manganese (van den Berg, private communication).

Dilute alloys of manganese in aluminium do not show the resistance minimum phenomena (Hedgcock, Muir and Wallingford 1960) but there are anomalous thermoelectric effects (Hedgcock, to be published) similar to those found in systems showing the resistance minimum. It was therefore of some interest to see whether this alloy system showed any specific heat anomalies.

§ 2. EXPERIMENTAL

The measurements were made in a ^3He cryostat using a 'tray' type calorimeter (Martin 1961b). The temperature scale was derived from ^3He vapour pressures (Sydoriak and Roberts 1957).

The aluminium sample was supplied through the courtesy of Dr. Hay of the

Aluminium Company of Canada, Kingston, Ontario, and had a residual electrical resistance at 4.2°K of 1.6×10^{-3} of its room temperature resistance, indicating a high purity. Spectrographic analysis of the sample showed the only impurity to be less than 5 parts per million of copper. In order to measure the sample in, as far as possible, the same physical state as the alloy, it was annealed at 560°C for 2 hours and then water quenched. The sample weighed 74.600 g.

The alloy was a piece of the alloy GKO (nominally 0.045 atomic % Mn) of Hedgcock, Muir and Wallingford (1960), kindly supplied by Dr. Hedgcock. After machining to a suitable shape it was annealed at 560°C for 2 hours in a helium atmosphere and then water quenched to prevent precipitation. A test strip had been rolled from each end of the sample and was similarly heat treated. The residual electrical resistances ($R_{4.2}/(R_{293}-R_{4.2})$) of these strips were 0.1313 and 0.1310. Thus the alloy appeared to be satisfactorily homogeneous with a considerable amount of manganese in solution. The sample weighed 67.391 g and the average atomic weight was taken as 26.985.

§ 3. RESULTS

The specific heat results for pure aluminium and the alloy are shown in Fig. 1 as a plot of specific heat against temperature. The superconducting transition

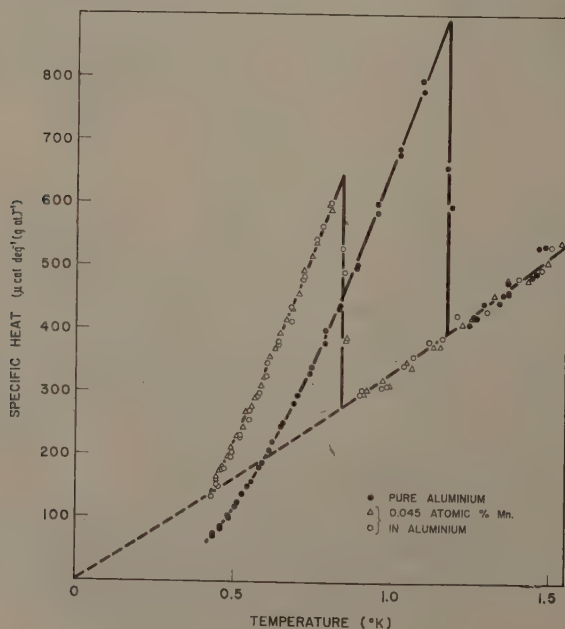


Fig. 1. The specific heats of pure aluminium and of an aluminium-0.045 atomic % manganese alloy.

temperatures were located by heating through the transition at different rates and extrapolating to zero heating current. In all cases the transition was very

sharp, with no latent heat, the transition width being about 0.001 deg K . For pure aluminium the transition temperature was $1.171_5 \pm 0.002^\circ \text{K}$ and for two separate measurements on the alloy values of 0.84 and 0.85°K were obtained. The second figure for the alloy was obtained from an experiment in which the usual apparent dependence of transition temperature on heating rate was not observed. The first figure is therefore considered more reliable and the transition temperature of the alloy will be taken as $0.84 \pm 0.01^\circ \text{K}$. Since the measurements were made in the ambient magnetic field a small correction must be made to obtain the zero field transition temperatures. The local magnetic field outside the cryostat was found to be 0.33 gauss . If it is assumed that the magnetic field on the sample is the same, then, from the known variation of transition temperature with applied field (Daunt and Heer 1949), a correction of around 0.002°K must be applied. The corrected transition temperatures are then taken as $1.174 \pm 0.002^\circ \text{K}$ for pure aluminium and $0.84 \pm 0.01^\circ \text{K}$ for the alloy. (The assumption as to the equality of external and internal field may not be correct since the calorimeter is surrounded by a superconducting lead shield (Martin 1961b) which may affect the internal field (Pippard and Pullan 1952).)

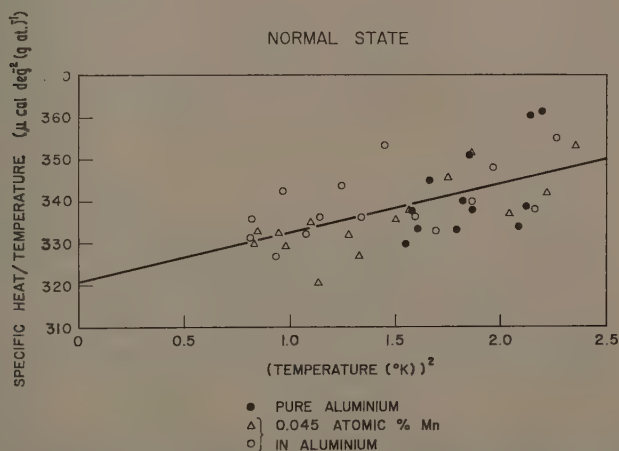


Fig. 2. The normal state specific heat of pure aluminium and an aluminium-0.045 atomic % manganese alloy.

The specific heats in the normal state are shown in Fig. 2 as a plot of specific heat/temperature against the square of the temperature. The line was fitted by a least-squares analysis of the results for the alloy for which the electronic specific heat coefficient γ is $321 \pm 8 \mu \text{ cal deg}^{-2} (\text{g at.})^{-1}$ and the Debye temperature θ is $343^{+70}_{-40}^\circ \text{K}$, where the error limits are 95% confidence limits.

§ 4. DISCUSSION

From the results in the normal state, it is clear that there is no specific heat anomaly of the type found in dilute alloys showing a resistance minimum. The residual resistance measurements show that there is a considerable amount of

the manganese in solid solution, and other measurements (Collings and Hedgcock, to be published) show that manganese ions in solution in aluminium have a magnetic moment. The conditions are therefore similar to those found in the alloys which do show a resistance minimum and associated large specific heat anomaly. A possible explanation for the difference in behaviour is that the splitting of the ground state degeneracy of the manganese ions is either much greater or much smaller than that which occurs in the other systems and consequently the various anomalies are either swamped by other effects or else lie below the present temperature limit of measurement.

However, the anomalous thermoelectric effects in aluminium-manganese alloys (Hedgcock, to be published) occur in a similar temperature range to those found in systems showing a resistance minimum. Thus it might be that the resistance-minimum phenomena and associated specific heat anomalies do not arise from the process causing the anomalous thermoelectric powers.

The value found for γ for the alloy is in good agreement with the result of Phillips (1959) for pure aluminium. The θ value is rather low but is not known accurately due to the smallness of the lattice specific heat. The present results on pure aluminium are also consistent with Phillips's values but due to the very limited range of measurement no accurate estimates of γ or θ can be made for the pure aluminium.

The present value for the superconducting transition temperature of pure aluminium ($1.174 \pm 0.002^\circ\text{K}$) is slightly higher than Phillips's value of 1.163°K . The difference might be due to the differing physical states of the samples, to differences in impurity content (see later) and to differences between the temperature scales employed.

Turning now to the superconducting state the results are shown in Fig. 3 as a plot of $C_{\text{es}}/\gamma T_{\text{c}}$ against T_{c}/T where T_{c} is the superconducting transition temperature and C_{es} is the electronic specific heat in the superconducting state (which has been calculated assuming a Debye θ of 428°K for both pure metal and alloy). Within the experimental accuracy the results for the pure metal and alloy lie on the same curve. The line in Fig. 3 was predicted by the Bardeen, Cooper and Schrieffer (1957) theory to represent results in the low temperature limit but departures from this line apparently occur at very low reduced temperatures (Phillips 1959).

The very considerable depression of the superconducting transition temperature caused by the small amount of impurity is rather striking. Previous work with non-transition metal impurities in tin, indium and aluminium (Lynton, Serin and Zucker 1957, Chanin, Lynton and Serin 1959) had shown that for very dilute alloys the superconducting transition temperature is usually depressed, the depression increasing as the impurity content, and therefore residual resistance is increased. However, for more concentrated alloys the superconducting transition temperature may be raised. Work with transition metal impurities (Matthias and Corenzwit 1955, Matthias *et al.* 1959, Müller 1959) had shown that the superconducting transition temperature was often raised on adding the impurity, but no very dilute alloys were investigated. The results of the present experiment suggest that, in the limit of extreme dilution, there is no essential difference in the effects of transition and non-transition metal impurities on the superconducting transition temperature.

The effect of impurities on the superconducting transition temperature has

been considered theoretically by Pippard (1957), Herring (1958) and Suhl and Matthias (1959). Both experimental and theoretical evidence shows that the effect cannot be due to the magnetic moment of the impurity ions acting in the

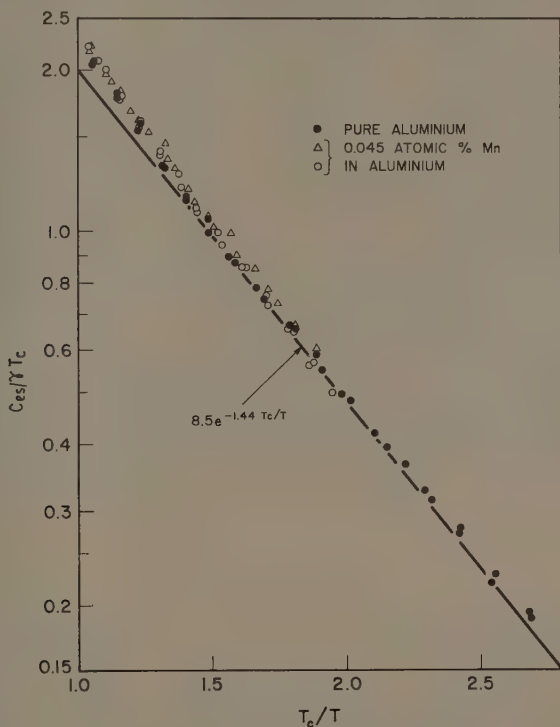


Fig. 3. The electronic specific heat in the superconducting state.

same way as an external field. The dependence, for very dilute alloys, on residual resistivity, and therefore mean free path, suggests that the depression of transition temperature is due to an altered electron-phonon interaction. This alteration apparently has a negligibly small effect on the electronic specific heat.

§ 5. CONCLUSION

For dilute alloys of manganese in aluminium there is no evidence for a specific heat anomaly of the type found in very dilute alloys showing the resistance-minimum phenomena. The presence of 0.045 atomic % manganese in solution in aluminium depresses the superconducting transition temperature by 0.33 deg K.

Note Added in Proof.

Quinn and Budnick (1961) have recently reported that very small amounts of indium, bismuth, or lead dissolved in thallium *raise* the superconducting transition temperature. Thus it appears that the sign of the initial shift of superconducting transition temperature, resulting from the addition of small amounts of impurity, depends on the parent metal.

REFERENCES

- BARDEEN, J., COOPER, L. N., and SCHRIEFFER, J. R., 1957, *Phys. Rev.*, **108**, 1175.
CHANIN, G., LYNTON, E. A., and SERIN, B., 1959, *Phys. Rev.*, **114**, 719.
CRANE, L. T., and ZIMMERMAN, J. E., 1961, *Phys. Rev.*, **123**, 113.
DAUNT, J. G., and HEER, C. V., 1949, *Phys. Rev.*, **76**, 1324.
DE NOBEL, J., and DU CHATENIER, F. J., 1959, *Physica*, **25**, 969.
FRANCK, J. P., MANCHESTER, F. D., and MARTIN, D. L., 1961, *Proc. Roy. Soc. A*, **263**, 494.
HEDGCOCK, F. T., MUIR, W. B., and WALLINGFORD, E., 1960, *Canad. J. Phys.*, **38**, 376.
HERRING, C., 1958, *Suppl. Physica*, **24**, S184.
LYNTON, E. A., SERIN, B., and ZUCKER, M., 1957, *J. Phys. Chem. Solids*, **3**, 165.
MACDONALD, D. K. C., 1956, *Handb. d. Phys.*, **14**, 137 (Berlin: Springer).
MARTIN, D. L., 1961 a, *Canad. J. Phys.*, **39**, 1385.
—— 1961 b, *Proc. Roy. Soc. A*, **263**, 378.
MARTIN, D. L., and FRANCK, J. P., 1960, *Proc. VII Int. Conf. Low Temp. Physics, Toronto*, p. 262.
MATTHIAS, B., COMPTON, V. B., SUHL, H., and CORENZWIT, E., 1959, *Phys. Rev.*, **115**, 1597.
MATTHIAS, B., and CORENZWIT, E., 1955, *Phys. Rev.*, **100**, 626.
MÜLLER, J., 1959, *Helv. Phys. Acta*, **32**, 141.
PHILLIPS, N. E., 1959, *Phys. Rev.*, **114**, 676.
PIPPARD, A. B., 1957, *J. Phys. Chem. Solids*, **3**, 175.
PIPPARD, A. B., and PULLAN, G. T., 1952, *Proc. Camb. Phil. Soc.*, **48**, 188.
QUINN, D. J., and BUDNICK, J. I., 1961, *Phys. Rev.*, **123**, 466.
SUHL, H., and MATTHIAS, B. T., 1959, *Phys. Rev.*, **114**, 977.
SYDORIAK, S. G., and ROBERTS, T. R., 1957, *Phys. Rev.*, **106**, 175.
ZIMMERMAN, J. E., and HOARE, F. E., 1960, *J. Phys. Chem. Solids*, **17**, 52.

Participation of the Electron Gas in Lattice Vibrations

By B. DAYAL AND S. P. SINGH

Department of Physics, Banaras Hindu University, India

MS. received 21st February 1961, in revised form 30th May 1961

Abstract. The vibration spectrum and the specific heats of gold have been studied by two models in order to test whether the electrons participate in the complete vibration spectrum of a crystal. The two models represent the extreme cases given by de Launay, one of which ignores the effect of electrons on the lattice vibration while the other assumes its full participation for all the frequencies. Frequencies have been calculated for the 1000 points of the Brillouin zone and the specific heats have been evaluated by the sampling technique. The choice of this metal for calculation was dictated by the fact that, on account of the large discrepancy in the Cauchy relation, the difference between the lattice frequencies of the two models is expected to be very high. It is found that the central force model does not predict the value of the C_V of the metal at all correctly, while de Launay's model is in qualitative agreement with experiment above 15°K. De Launay's idea that electrons participate only in the non-dispersive region of the spectrum thus appears to be wrong.

§ 1. INTRODUCTION

INVESTIGATIONS on the lattice vibration of metallic crystals by means of the usual Born and Kármán model (1912) meet with one difficulty at the outset. If central forces are assumed to be operative, they necessarily lead to the Cauchy relations, which are not satisfied generally. In the case of cubic metals there is only one Cauchy relation, the equality of the elastic constants c_{12} and c_{44} . Experimental data on elastic constants show that usually this is not obeyed even roughly, the values of c_{12} being in many cases as high as two to three times the other constant. In a well-known work, Fuchs (1935, 1936) gave a probable cause of this discrepancy. According to him certain energies such as the energy of the ground state of the valency electron, the Fermi, the exchange and the correlation energies of the conduction electrons, depend only on the atomic volume. The forces on the displaced ions due to them are not central. They contribute to the compressibility but not to those elastic constants, in the corresponding strains of which the volume changes are absent. Fuchs showed that the constants $c_{11} - c_{12}$ and c_{44} are unaffected by the presence of the electron gas, while the individual values of c_{11} and c_{12} which depend on the compressibility are affected by it. If the contribution of the free electrons to the compressibility is removed, the Cauchy relation would be satisfied.

Fuch's work has greatly influenced all the subsequent calculations of the lattice frequencies of metals. Two different lines of approach have been adopted. In one of these, which owes its inspiration to the work of Fine (1939), and has been developed by Leighton (1948) and Bauer (1953), the presence of the free

electrons has been entirely ignored. The experimental values of the elastic constants are separated into two parts, one of which is assumed to arise from the central interaction of the ions while the other is due to the electron gas. This division is carried out in such a way that the former satisfies the Cauchy relation and at the same time retains the experimental values of $c_{11} - c_{12}$ and c_{44} unchanged. These adjusted constants of the central interaction are then used to calculate the lattice frequencies. Leighton supports this method with the remark "Fuchs result was used in the evaluation of the atomic force constants α and γ because the Born-von Kármán boundary condition which is used in the derivation of the secular determinant requires that the volume of the crystal remains constant so that the conduction electrons have no effect on the motion of the lattice".

In the second method, an electron lattice interaction is explicitly introduced in the setting up of the secular determinant. It has been argued that the ionic vibrations may cause local changes in the volume of the electron gas, even though the total crystal volume remains unchanged and these compressions and rarefactions may greatly alter the numerical values of the frequencies. Force models on these lines have been introduced by de Launay (1953, 1956), Leibfried and Brenig (1953) and Bhatia (1955). The latter has calculated the electron-lattice interaction by means of the Thomas-Fermi model of the atom. If the non-central interaction is put equal to zero, Bhatia's force model does not yield the Cauchy relation as one would expect it to do on the basis of Fuch's investigations. On the other hand we get $c_{11} = c_{44}$ in the case of the body-centred metals and a more complicated relation between elastic constants for the face-centred metals.

Leibfried and Brenig derived a Hooke's constant by considering the change brought about by the ionic displacements on Wigner and Seitz's polyhedra, but confined themselves only to the derivation of certain averages of the powers of the frequencies. De Launay has developed a simple phenomenological approach in which the free electrons are assumed to behave like an ordinary gas supporting a compressional but not a shearing stress. They, therefore, influence the numerical values of the frequencies of the longitudinal wave only. Since the waves traversing the crystal are, in general, neither purely longitudinal nor transverse, they are separated into their longitudinal and transverse components. The former is then corrected for the electron gas by the introduction of new force constants.

De Launay (1956) expressly states that his model applies to the long acoustical waves and has left its applicability to the high frequency thermal waves as an open question. He has discussed two extreme cases. The central force model of Fine and Leighton, in which the effect of the electron gas has been ignored, forms one extreme case. The opposite extreme is represented by his own model, applied to the complete vibration spectrum of the crystal. According to him neither extreme was likely to be correct. He has suggested that "by comparing the results of calculations for both extreme cases, with experiment, one may be able to draw conclusions which will give direction towards a better theory". He has discussed the case of copper and is of the opinion that the participation of the electrons in the long-wave non-dispersive region of lattice vibration is complete, while it is negligible or nearly so in the highly dispersive region. The same conclusion has been reached recently by Overton (1960). In his review article Parkinson (1958) has pointed out that recent experimental data on the specific heats of the alkali metals do not support de Launay's conclusion regarding

electron participation in the non-dispersive part of the spectrum. The specific heats of all the body-centred metals have been calculated in this laboratory under the assumption that de Launay's model is applicable to the complete vibration spectrum of a crystal. A very good agreement has been obtained between the calculated and the experimental values of the specific heats. The results on lithium have already been published (Dayal and Sharan 1960). This would indicate that de Launay's conclusion is erroneous and that the electrons do participate to the same extent in the full vibration spectrum of the metallic crystals.

In copper as well as in the body-centred cubic metals discussed above, the discrepancy from the Cauchy relation is not very large. The calculated frequencies and specific heats for both the extreme cases of de Launay are not likely to differ by large amounts. It is, therefore, possible to ascribe the deviations from the experimental values in either case to the uncertainties in the elastic and the specific heat data. In order to decide the question of electron participation in the lattice vibrations it is obviously necessary to take up a case where the departure from the Cauchy relation is very pronounced. This is so for gold where the elastic constant c_{12} is nearly three and a half times the value of c_{44} . The authors have, therefore, taken up the case of gold, which is a face-centred lattice, for study. The vibration frequencies and specific heats of this metal have been calculated for both the extreme cases of de Launay and the results are being reported in the present paper. Similar cases of lead, aluminium and silver are under study at present and the results will be reported in due course.

§ 2. CHOICE OF WAVE VECTORS

The wave number vectors \mathbf{k} of the permitted vibrations are fixed by Born's cyclic conditions, according to which the vibration pattern repeats itself in a large crystal block of $n \times n \times n = n^3$ cells. Suppose \mathbf{a}_i ($i=1, 2, 3$) are the basic vectors of the unit cell of the direct lattice and \mathbf{a}_i^* those of the reciprocal lattice. The latter are defined by

$$\mathbf{a}_i^* = \frac{\mathbf{a}_j \times \mathbf{a}_k}{V} \quad \dots\dots(1)$$

where V is the volume of the unit cell of the direct lattice. It follows that the wave number vectors \mathbf{k} of the permitted vibrations are the vectors of a miniature reciprocal lattice whose basic vectors are \mathbf{a}_i^*/n (Blackman 1955). These miniature cells are confined within the first Brillouin zone. It is obvious that the zone will contain n^3 lattice points defining a total of n^3 wave vectors.

The unit cell of the face-centred cubic lattice is rhombohedral. The basic vectors of the direct and reciprocal lattice are (Smith 1948)

$$\mathbf{a}_1 = \frac{1}{2}a(0, 1, 1) \quad \mathbf{a}_2 = \frac{1}{2}a(1, 0, 1) \quad \mathbf{a}_3 = \frac{1}{2}a(1, 1, 0) \quad \dots\dots(2)$$

$$\left. \begin{aligned} \mathbf{a}_1^* &= \frac{1}{a}(-1, +1, +1) \\ \mathbf{a}_2^* &= \frac{1}{a}(+1, -1, +1) \\ \mathbf{a}_3^* &= \frac{1}{a}(+1, +1, -1) \end{aligned} \right\} \quad \dots\dots(3)$$

where a is the lattice constant of the cubic cell.

Since the wave number vectors \mathbf{k} are vectors of the miniature reciprocal lattice they are given by

$$\begin{aligned}\mathbf{k} &= \frac{1}{na} [(-p_1 + p_2 + p_3), (p_1 - p_2 + p_3), (p_1 + p_2 - p_3)] \\ &= \frac{1}{na} [p_x, p_y, p_z] \quad \dots\dots (4)\end{aligned}$$

where the p are all integers. It can be easily seen that p_x, p_y, p_z are either all odd or all even.

The boundaries of the Brillouin zone are defined by $p_x = \pm n, p_y = \pm n, p_z = \pm n$ and $p_x \pm p_y \pm p_z = \pm 3n/2$. On account of the cubic symmetry a number of points will correspond to the same values of the frequencies. It is sufficient if we consider only those points of the positive octant for which

$$\left. \begin{aligned}0 \leq p_z \leq p_y \leq p_x \leq n \quad \text{and} \\ p_x + p_y + p_z \leq \frac{3}{2}n.\end{aligned} \right\} \quad \dots\dots (5)$$

Following Kellermann (1940) we have taken n to be ten. There are 48 points defined by (4) and (5) including the origin. These points were also derived by Kellermann, but he missed the point (7, 7, 1), and added an extra-neous point (10, 5, 0) (Dayal and Tripathi 1961). The secular determinants have been solved for each of the 47 points and each frequency has been weighted according to the number of similar points associated with it. The weight of the points on the boundaries of the zone has been taken to be half of the number of similar points (Dayal and Singh 1960). In this way we have been able to get exactly 3000 frequencies including the three zero frequencies corresponding to the origin.

§ 3. FREQUENCY SPECTRUM

Frequencies have been calculated for all the representative points of the Brillouin zone for both the extreme cases, whose secular determinants have been taken from de Launay's article (1956). In one of these, the effect of the electrons has been completely ignored while in the second they participate equally well in all the lattice vibrations. There is a misprint in de Launay's article regarding the definition of ξ which should be given by $(\alpha' - \alpha_1)/\alpha_1$. This has been corrected here.

For the computation of the frequencies we have used the following elastic constants for 0°K , which have been taken from de Launay's review (1956) and refer to measurements made by Goens (1940).

$$\begin{aligned}c_{11} &= 1.94 \times 10^{12} \text{ dyn cm}^{-2} & c_{12} &= 1.62 \times 10^{12} \text{ dyn cm}^{-2} \\ c_{44} &= 0.455 \times 10^{12} \text{ dyn cm}^{-2}.\end{aligned}$$

These constants do not differ substantially from later measurements of Neighbours and Alers (1958). In fact, the numerical values of $c_{11} - c_{12}$ and c_{44} are almost the same in both sets of measurements. As a result, the use of Neighbours and Alers' data would only affect the longitudinal frequencies of de Launay's model by about one or two per cent. The difference is trivial from the point of view of the results of the present paper.

The lattice constant has been taken to be $4.07 \times 10^{-8} \text{ cm}$. It is expected that the calculated values of the frequency are correct to 1%. The frequency

distribution, i.e. the $g(\nu)$ curves for both the cases are shown in Fig. 1. The curves have not been normalized and the units for $g(\nu)$, though the same for both the curves, are arbitrary.

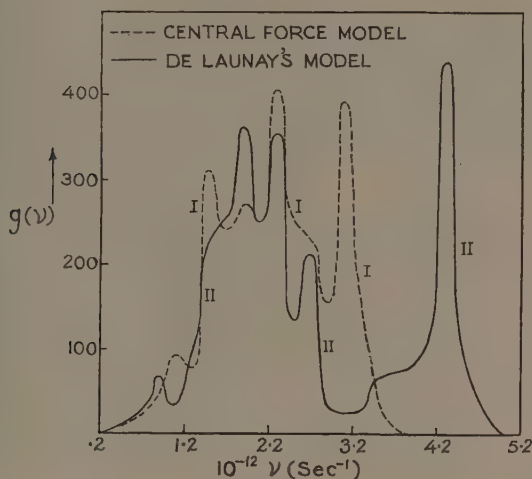


Fig. 1. Frequency distribution curve for gold.

§ 4. EVALUATION OF SPECIFIC HEATS

The specific heats have been calculated by numerical computation by Blackman's sampling technique (Blackman 1937). For this purpose, the vibration spectrum has been divided into intervals of $\Delta\nu = 0.2 \times 10^{12} \text{ sec}^{-1}$. Calculations have not been made below 15°K because the number of frequencies is too small for getting accurate results in this region. The results are shown in the Table and have been compared with the experimental data of Geballe and Giauque (1952). The electronic specific heat has not been subtracted from the experimental results shown in the Table. (θ, T) curves for both the central force and de Launay's models are given in Fig. 2. For presenting θ values below 15°K we have calculated θ_0^3 for both the models from the elastic constants by means of Eqns (11.40) and (11.43) of de Launay's review (1956). These give the following extrapolation formulae for θ for the liquid helium region:

$$\text{Case I} \quad \theta = 156 - 0.064T^2 \quad \dots\dots (6)$$

$$\text{Case II} \quad \theta = 159 - 0.075T^2 \quad \dots\dots (7)$$

These two formulae have been used to extrapolate our calculated (θ, T) curves below 15°K . The experimental values of θ in the range $1-5^\circ\text{K}$ are from the work of Corak *et al.* (1955) and above this range from Geballe and Giauque (1952). It can be seen that the central force model does not show any degree of agreement with the experimental data above 20°K . De Launay's electron gas model shows a much better agreement. The calculated values of θ are, however,

about 6–10% lower than the experimental values. This difference is not large and is obviously due to the general inadequacy of the limited Hooke's law interaction in the case of metals.

There is one feature common to all models based on Hooke's law of forces. Their force constants are selected in such a way that they yield the secular equations of the elastic theory in the long wavelength limit. In the central force model discussed above, this end is achieved by adjustment of the elastic constants. The results given in the Table show that this is not justified. The correspondence between de Launay's model and the elastic theory is, however, exact and it applies to the long acoustic waves in a phenomenological way without any reservation.

The Specific Heats of Gold (cal deg⁻¹ mol⁻¹)

Temp. (°K)	Central force model	de Launay's model	Experimental
15	0.535	0.492	0.354
30	2.380	2.083	1.756
40	3.374	2.972	2.672
50	4.059	3.640	3.396
60	4.528	4.140	3.952
90	5.248	4.990	4.887
120	5.539	5.372	5.296
240	5.847	5.798	5.747

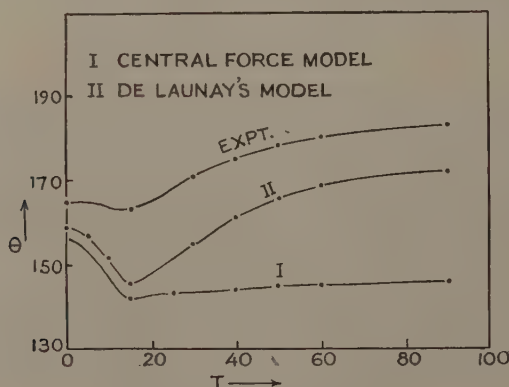


Fig. 2. (θ, T) curves for gold.

It can be seen from the Table that the specific heats given by de Launay's model are always higher than the experimental values. This shows that the actual lattice frequencies for short waves do not lie between the values given by the two models, but are in fact a few per cent higher than those given by de Launay's theory. We are led to conclude that the electrons participate fully in all the vibrations but their effect on the numerical values of the frequencies is slightly greater than that given by the simple phenomenological theory of de Launay.

REFERENCES

- BAUER, E., 1953, *Phys. Rev.*, **92**, 58.
BHATIA, A. B., 1955, *Phys. Rev.*, **97**, 363.
BLACKMAN, M., 1937, *Proc. Roy. Soc. A*, **159**, 416.
—— 1955, *Handb. d. Phys.*, Vol. 8 (Berlin: Springer), p. 338.
BORN, M., and v. KÁRMÁN, TH., 1912, *Phys. Z.*, **13**, 297.
CORAK, W. S., GARFUNKEL, M. P., SATTERTHWAITE, C. B., and WEXLER, A., 1955, *Phys. Rev.*, **98**, 1699.
DAYAL, B., and SHARAN, B., 1960, *Proc. Roy. Soc. A*, **259**, 361.
DAYAL, B., and SINGH, S. P., 1960, *Proc. Phys. Soc.*, **76**, 777.
DAYAL, B., and TRIPATHI, B. B., 1961, *Proc. Phys. Soc.*, **77**, 303.
FINE, P. C., 1939, *Phys. Rev.*, **56**, 355.
FUCHS, K., 1935, *Proc. Roy. Soc. A*, **153**, 622.
—— 1936, *Proc. Roy. Soc. A*, **157**, 444.
GEBALLE, T. H., and GIAUQUE, W. F., 1952, *J. Amer. Chem. Soc.*, **74**, 2368.
GOENS, E., 1940, *Ann. Phys., Lpz.*, **38**, 456.
KELLERMANN, E. W., 1940, *Phil. Trans. Roy. Soc. A*, **239**, 513.
DE LAUNAY, J., 1953, *J. Chem. Phys.*, **21**, 1975.
—— 1956, *Solid State Physics*, Vol. 2 (New York: Academic Press), p. 284.
LEIBFRIED, G., and BRENIG, W., 1953, *Z. Phys.*, **134**, 451.
LEIGHTON, R. B., 1948, *Rev. Mod. Phys.*, **20**, 165.
NEIGHBOURS, J. R., and ALERS, G. A., 1958, *Phys. Rev.*, **111**, 707.
OVERTON, W. C., 1960, *Bull. Amer. Phys. Soc.*, **5**, 199.
PARKINSON, D. H., 1958, *Rep. Progr. Phys.*, **15**, 266 (London: Physical Society).
SMITH, H. J., 1947, *Phil. Trans. Roy. Soc. A*, **188**, 179.

The Excitation of the Vibrational Modes of Ethylene in Homo-molecular Collisions

BY R. HOLMES AND W. TEMPEST

Acoustics Laboratory, Chadwick Physics Laboratory, University of Liverpool

Communicated by H. D. Parbrook; MS. received 15th June 1961

Abstract. Sound absorption and velocity were measured in ethylene at 500 kc/s and 700 kc/s in the ranges 0.07 to 2 atm and -10 to 80°C . All the vibrational modes relaxed out at approximately 1 Mc/s atm, but the assumption of two relaxation times, for the transfer of energy between translational and vibrational motion, fitted the measurements better than the assumption of a single relaxation time. Assuming that the average relaxation time found by fitting single relaxation curves to the measured points was approximately that of the lowest frequency mode, the value of the force constant β in the exponential intermolecular potential was found to be $6.71 \times 10^8 \text{ cm}^{-1}$. This agrees well with the value $4.72 \times 10^8 \text{ cm}^{-1}$ calculated from the Lennard-Jones potential.

§ 1. INTRODUCTION

THE mechanism of the excitation of the internal modes of a gas molecule can be conveniently studied, in many cases, by measurements of the sound propagation constants. Several observers have investigated the excitation of the vibrational modes of ethylene in this way.

Richards and Reid (1934) measured the relaxation time for the transfer of energy between vibrational and translational motion at 15 , 30 and 45°C and investigated the effects of added hydrogen and deuterium in promoting transitions. McCoubrey, Parke and Ubbelohde (1954), McGrath and Ubbelohde (1954) and Arnold, McCoubrey and Ubbelohde (1958) worked at several temperatures between 0 and 25°C and investigated the effects of other added impurities, particularly hydrocarbons. Corran, Lambert, Salter and Warburton (1958) covered the temperature range between 19 and 300°C and found $\ln P_{10}$ to be proportional to $T^{-1/3}$ (P_{10} is the probability of a transition from the first excited state to the ground state per molecule per encounter and T is the absolute temperature). They used the Cottrell and Ream (1955) analysis of vibrational-translational energy exchange to obtain a value for β (the exponent in the intermolecular potential function $V = V_0 e^{-\beta r}$, where r represents the molecular separation), and obtained a value about four times greater than that obtained from viscosity data. Edmonds and Lamb (1958) estimated the relaxation time at 25°C , assuming a single relaxation mechanism, from some low frequency (1 – 10 kc/s) tube absorption measurements. Gravitt (1960) measured absorption in the region of the absorption peak using a tube method at three temperatures between -1.5 and 60°C and fitted single relaxation curves to his results to find the relaxation time and the vibrational specific heat.

The estimates of the relaxation time at a given temperature show a considerable spread; for example, at 25°C the values obtained by the above mentioned workers range from 0.2 μ sec to 0.39 μ sec. This spread may be due to the difficulty of obtaining pure ethylene. All the results published to date are in agreement with the hypothesis of a single relaxation time for vibrational-translational energy transfer, but in most cases only part of the relaxation region has been investigated.

Ethylene has eight vibrational modes with wave numbers between 810 cm^{-1} and 1623 cm^{-1} , a situation which might be expected to give rise to a number of relaxation times close together. This could lead to a broadening of the relaxation peak in the sound absorption curve, which would be easier to detect than the corresponding change in the velocity dispersion curve.

It was therefore decided to make simultaneous absorption and velocity measurements over a wide range of frequency to pressure (f/p) ratios and at several temperatures, the particular objects of the experiments being to reduce the absolute error in the relaxation time measurements and to investigate carefully the possibility of a double or multiple relaxation mechanism. Measurements of the temperature dependence of the relaxation times would give information about the intermolecular force operating in transition-producing encounters.

§ 2. EXPERIMENTAL PROCEDURE

2.1. Apparatus

The absorption and velocity of sound were measured at frequencies between 500 kc/s and 700 kc/s using a pulse technique which has been described in detail elsewhere (Parbrook and Tempest 1957, Holmes, Parbrook and Tempest 1960). The apparatus could be operated at gas pressures between 2.1 and 0.07 atm and covered the range of f/p ratios from 0.24 to 10 Mc/s atm. Measurements were made at temperatures between -10° and $+80^\circ\text{C}$.

2.2. Experimental Accuracy

Individual absorption measurements were estimated to be accurate to $\pm 2\%$ and velocity measurements to $\pm 0.1\%$.

2.3. Gas Supply and Purification

Two sources of ethylene were used in the course of these experiments. Samples of 99.8% stated purity were obtained from the Esso Petroleum Co. Ltd., and a sample of 99.5% stated purity was supplied by Imperial Chemical Industries Ltd. In both cases the main impurity was stated to be ethane.

It is known that water vapour has a considerable effect on the relaxation time in ethylene (Arnold, McCoubrey and Ubbelohde 1958); the gas was therefore dried by passing it slowly through phosphorus pentoxide and magnesium perchlorate.

Work on ethylene-ethane mixtures (Arnold, McCoubrey and Ubbelohde 1958) has shown that the presence of 5.53% ethane shifts the relaxation time in ethylene from 0.32 μ sec to 0.148 μ sec, thus 0.2% ethane should shift it by less than 2%, a change which would not be detected with the present apparatus. For this reason no attempt was made to remove the small quantities of ethane present.

§ 3. THEORY

3.1. *Single Relaxation Mechanism*

Kneser (1933) and Rutgers (1933) calculated expressions for the velocity and absorption of sound in an ideal relaxing diatomic gas, neglecting the effects of viscosity and heat conduction. If it is assumed that binary collisions alone are responsible for the transfer of energy between translational and vibrational motion, the relaxation time τ is related to the pressure by the equation $\tau = K/p$, in which case the velocity and absorption equations take the form:

$$V^2 = \frac{RT}{M} \frac{C_{p0}C_{v0} + 4\pi^2(f/p)^2 K^2 C_{p\infty}C_{v\infty}}{C_{v0}^2 + 4\pi^2(f/p)^2 K^2 C_{v\infty}^2} \quad \dots\dots (1)$$

and

$$\alpha_\lambda = \frac{\pi RC' 2\pi(f/p)K}{C_{p0}C_{v0} + 4\pi^2(f/p)^2 K^2 C_{p\infty}C_{v\infty}}, \quad \dots\dots (2)$$

where T is the absolute temperature ($^{\circ}\text{K}$), M the gramme molecular weight, R the gas constant for one gramme molecule (erg), f the sound frequency (c/s) $= \omega/2\pi$, p the gas pressure (atm), K the relaxation time at 1 atm, C_{v0} the molar specific heat at constant volume (erg) ($\omega\tau \ll 1$), $C_{v\infty}$ the molar specific heat at constant volume (erg) ($\omega\tau \gg 1$), C_{p0} the molar specific heat at constant pressure (erg) ($\omega\tau \ll 1$), $C_{p\infty}$ the molar specific heat at constant pressure (erg) ($\omega\tau \gg 1$), and C' the vibrational specific heat (erg).

$$V_0^2 = \frac{C_{p0}RT}{C_{v0}M} = \text{sound velocity}^2 \text{ (cm/sec)}^2 \quad (\omega\tau \ll 1),$$

$$V_\infty^2 = \frac{C_{p\infty}RT}{C_{v\infty}M} = \text{sound velocity}^2 \text{ (cm/sec)}^2 \quad (\omega\tau \gg 1),$$

$$C_{v0} = C_{v\infty} + C', \quad C_{p0} = C_{p\infty} + C', \quad C_p = C_v + R.$$

The values of K can be obtained from velocity measurement by using the equation

$$4\pi^2 \left(\frac{f}{p} \right)_i^2 K^2 = \frac{C_{v0}^2}{C_{v\infty}^2}, \quad \dots\dots (3)$$

where $(f/p)_i$ is the value of f/p at the point of inflection of Eqn (1).

K can be determined from absorption measurements by using the equation

$$4\pi^2 \left(\frac{f}{p} \right)_M^2 K^2 = \frac{C_{p0}C_{v0}}{C_{p\infty}C_{v\infty}} \quad \dots\dots (4)$$

where $(f/p)_M$ is the value f/p at which α_λ is a maximum.

The equation

$$(\alpha_\lambda)_M = \frac{\pi RC'}{2[C_{p0}C_{v0}C_{p\infty}C_{v\infty}]^{1/2}} \quad \dots\dots (5)$$

where $(\alpha_\lambda)_M$ is the maximum value of the absorption, can be used to evaluate C' .

The above equations are based on the assumption that a single relaxation time can adequately describe the behaviour of the gas. It has been shown by Landau and Teller (1936) that for a diatomic molecule in which anharmonic effects are not appreciable (a situation which applies at 300°K in most gases) there is only a single relaxation time governing energy exchange between translational and vibrational motion. In this case the rate constant k_{10} for $1 \rightarrow 0$

transitions (i.e. from first excited state to ground state) is related to the relaxation time by the equation

$$\frac{1}{\tau} = k_{10} \left[1 - \exp \left(- \frac{h\nu}{kT} \right) \right], \quad \dots\dots (6)$$

where ν is the fundamental vibrational frequency (c/s).

If transitions occur only during collisions and N is the total number of collisions per molecule per second, then the average number of collisions needed for de-excitation, Z , will be N/k_{10} and the probability of de-excitation per collision $P_{10} = 1/Z$.

3.2. Multiple Relaxation

Most polyatomic molecules have several vibrational degrees of freedom appreciably excited at temperatures around 300°K and this gives rise to the possibility of a multiple relaxation process with several relaxation times.

The actual process of de-excitation can occur in a variety of different ways, the two extreme examples of which can be described as 'parallel' and 'series' mechanisms. In the first of these each mode exchanges energy independently with translation and there are as many relaxation times as there are modes. In the second case only one mode (that of lowest frequency) exchanges energy with translation, while the other modes exchange energy internally with this one. In complex molecules there are numerous possibilities which can be described as intermediate between series and parallel.

The theory of multiple relaxation has been developed by Schäfer (1940) who considered two relaxation times and extended by Herzfeld and Litovitz (1959) to cover the case of many relaxation times. A more general treatment has been given by Tanczos (1956) who has derived equations for sound velocity and absorption in the case where all possible transitions (i.e. simple transitions involving energy changes in one mode only and complex transitions involving simultaneous energy changes in two modes) are considered, subject to the condition that transitions can occur only during collisions.

Tanczos's results can be expressed in the form

$$\left(\frac{V}{\bar{V}_0} \right)^2 = 1 + \frac{R}{C_{p0}(C_{v0} - \sum_i C_i')} \sum_i \frac{C_i'' \omega^2 \tau_i''^2}{1 + \omega^2 \tau_i''^2} \quad \dots\dots (7)$$

and

$$2\alpha \left(\frac{V}{\omega} \right) \left(\frac{V}{\bar{V}_0} \right)^2 = \frac{R}{C_{p0}(C_{v0} - \sum_i C_i')} \sum_i \frac{C_i'' \omega \tau_i''}{1 + \omega^2 \tau_i''^2} \quad \dots\dots (8)$$

The C_i'' and τ_i'' are 'apparent' specific heats and relaxation times which can be related to the actual specific heats C_i' and relaxation times τ_i of the molecule. The C_i'' always satisfy the equation

$$\sum_i C_i'' = \sum_i C_i'. \quad \dots\dots (9)$$

The relationships between the C_i'' , τ_i'' and C_i' and τ_i depend on the mechanism of the relaxation process and can be derived from calculations of the various transition probabilities for the molecule. Tanczos (1956) describes how this may be done but the calculation is complex and has so far been carried out for only a few molecules (Tanczos (1956) for chlorinated methanes, Dickens and Linnet (1957) for sulphur dioxide).

3.3. Calculation of P_{10}

Herzfeld and Litovitz (1959) have derived an expression for P_{10} which is applicable to simple transitions involving a change of one in the quantum number of one mode only.

$$P_{10} = \frac{1}{1.017} \left(\frac{r_0}{r_0} \right)^2 \frac{1}{Y(2, 2)} \frac{1}{Z_0} F(M) \left(\frac{\theta'}{\theta} \right) \left(\frac{2\pi}{3} \right)^{1/2} \left(\frac{\theta'}{\bar{T}} \right)^{1/6} \exp \left[-\frac{3}{2} \left(\frac{\theta'}{\bar{T}} \right)^{1/3} + \frac{\theta}{2T} + \frac{\epsilon}{kT} \right], \quad \dots (10)$$

where r_0 , ϵ are Lennard-Jones force constants, $\theta = h\nu/k$, $\theta' = 16\pi^2 \bar{m} \nu^2 / \beta^2 k$, \bar{m} is the reduced mass of the colliding molecules, Z_0 a geometrical factor, r_0 the equilibrium distance for a molecule approaching with a relative velocity V_m , V_m the velocity most likely to cause a transition $(= (4\pi^2 k T \nu / \beta \bar{m})^{2/3})$, $F(M)$ a function of the masses of the molecules and $Y(2, 2)$ the reduced collision cross section.

Equation (10) contains two terms, $\exp(\theta/2T)$ and $\exp(\epsilon/kT)$, which were absent in the earlier derivations of Landau and Teller (1936) and Cottrell and Ream (1955) but the former term was present in the derivation of Schwartz and Herzfeld (1954). These two terms are important in calculating P_{10} and, as pointed out by Milward, McCoubrey and Ubbelohde (1961), their absence in the previous derivations has led to much confusion in the interpretation of relaxation time measurements.

§ 4. RESULTS

Sound velocity and absorption in ethylene were measured at temperatures of $-10, 5, 25, 45, 65$ and 80°C . At each temperature about eighty pairs of measurements were made covering the range of f/p ratios from 0.24 to 10 Mc/s atm. The results at 25 and 80°C only are presented in graphical form and the relaxation times and specific heat values calculated from the results at all the temperatures are set out in tabular form.

4.1. Absorption Results

To obtain a value for the sound absorption due to relaxation alone it is necessary to subtract the viscothermal absorption from the measured value. The viscothermal absorption was calculated using the 'Stokes-Kirchhoff' equation (see, for example, Truesdell 1953),

$$(\alpha_\lambda)_{v+} = \frac{8\pi^2}{3} \left(\frac{f}{p} \right) \frac{1}{\gamma} \left[\eta + \frac{3}{4}(\gamma - 1) \frac{\chi}{c_{p0}} \right], \quad \dots (11)$$

where $(\alpha_\lambda)_{v+}$ is the sound absorption per wavelength (nepers), η the viscosity (poise), $c_{p0} = C_{p0}/M$, $\gamma = C_{p0}/C_{v0}$, χ the thermal conductivity ($\text{erg deg}^{-1} \text{sec}^{-1} \text{cm}^{-2}$).

Values for the viscosity and thermal conductivity were obtained from *International Critical Tables*, (1927), Callear and Robb (1955), *Handbook of Chemical and Physical Constants* (1955), Lambert *et al.* (1955), Kaye and Laby (1956) and Chapman and Cowling (1958).

Figures 1 and 2 show the corrected results of the absorption measurements at 25° and 80°C respectively plotted in the form $\alpha_\lambda(V/V_0)^2$ against $\log(f/p)$. In each case a single relaxation curve (Eqn (2)) and a double relaxation curve (Eqn (8)) have been fitted to the measured points.

The values of C_1'' , C_2'' , K_1'' and K_2'' giving best fit double relaxation curves to the measured absorption at each of the temperatures used are set out in Table 1. The last row of this table gives comparative values of C'/R calculated from spectroscopic data (Sheppard and Simpson 1952).

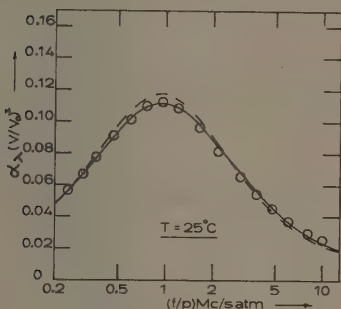


Fig. 1. Ethylene 25°C: sound absorption as a function of frequency/pressure ratio. (Circles, experimental points; full line, calculated double relaxation curve; broken line, calculated single relaxation curve.) Every fifth measured point only is shown.

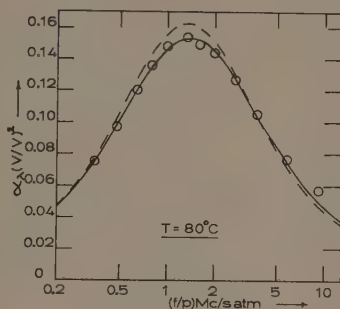


Fig. 2. Ethylene 80°C: sound absorption as a function of frequency/pressure ratio. (Circles, experimental points; full line, calculated double relaxation curve; broken line, calculated single relaxation curve.) Every fifth measured point only is shown.

Table 1

Temperature (°C)	5	25	45	65	80
$K_1'' \times 10^7$ (sec)	2.10	1.88	1.63	1.45	1.31
$K_2'' \times 10^7$ (sec)	1.07	0.91	0.775	0.686	0.608
C_1''/R	0.782	0.931	1.135	1.293	1.410
C_2''/R	0.160	0.210	0.223	0.300	0.372
$(C_1'' + C_2'')/R$	0.942	1.141	1.358	1.593	1.782
C'/R	0.942	1.166	1.397	1.635	1.815

4.2. Velocity Measurements

The measured velocities were 'idealized' by correcting them to zero pressure using the equation

$$\left(\frac{V_m}{V}\right)^2 = \left[1 + \frac{2p}{RT} \left\{ B + \frac{T}{C_{v0}} \frac{dB}{dT} + \frac{1}{2} \frac{T^2 R^2}{C_{p0} C_{v0}} \frac{d^2 B}{dT^2} \right\} \right], \quad \dots (12)$$

where B is the second virial coefficient, V_m the measured sound velocity and V the idealized sound velocity.

Values for the second virial coefficient and its derivatives were taken from Hirschfelder, Curtiss and Bird (1954).

Figures 3 and 4 show the idealized sound velocities, plotted against $\log(f/p)$. The velocities are plotted in the form $(V/V_0)^2 - 1$, where V_0 is the limiting value of the velocity at low f/p ratios. The figures also show calculated single relaxation dispersion curves fitted to the measured points. The double relaxation

curves in Figs 3 and 4 were calculated from the specific heats and relaxation times obtained from the absorption curves at the same temperatures.

The relaxation times (assuming single relaxation) at the various temperatures are set out in Table 2; in this table the values of K_1 are relaxation times at one atmosphere pressure from velocity measurements and the values of K_m are those from absorption measurements.

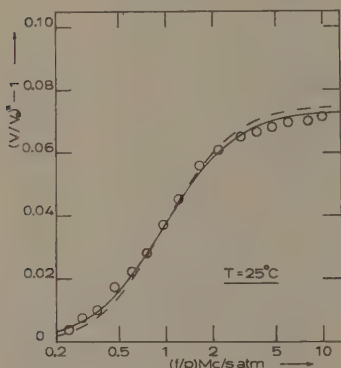


Fig. 3. Ethylene 25°C: sound velocity as a function of frequency/pressure ratio. (Circles, experimental points; full line, calculated double relaxation curve; broken line, calculated single relaxation curve.) Every fifth measured point only is shown.

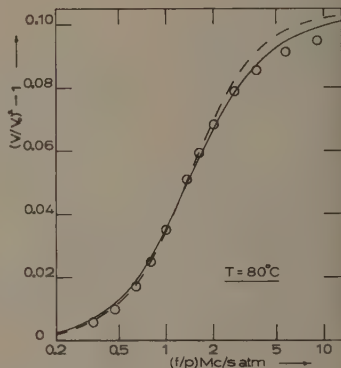


Fig. 4. Ethylene 80°C: sound velocity as a function of frequency/pressure ratio. (Circles, experimental points; full line, calculated double relaxation curve; broken line, calculated single relaxation curve.) Every fifth measured point only is shown.

Table 2

Temperature (°C)	-10	5	25	45	65	80
$K_1 \times 10^7$ (sec)	2.87	2.73	2.26	2.08	1.91	1.83
$K_m \times 10^7$ (sec)	2.64	2.52	2.36	2.19	2.02	1.89

§ 5. DISCUSSION

The present measurements have been considered from two points of view. Firstly, to establish the number of relaxation times necessary to describe the energy exchange mechanism. Secondly, to investigate the temperature dependence of P_{10} of the lowest mode (810 cm^{-1}), assuming that the relaxation time found by fitting single relaxation curves to the results was that of the lowest mode. Using the Herzfeld and Litovitz (1959) expression for P_{10} , a value has been found for the force parameter β , describing the intermolecular force acting in transition-producing encounters.

5.1. Multiple Relaxation

Figures 1 and 2 show that at 25° and 80°C double relaxation curves provide a closer approximation to the measured points than do the single relaxation curves. The same effect was found at the other temperatures. The total specific heat values C' from the double relaxation curves are in good agreement with the

spectroscopic values. As a check against the possibility of an error in the spectroscopic C' the empirical formula for C_{p0} as a function of temperature derived by Din (1956) from the best thermodynamic measurements was used to calculate C' . At all the temperatures of the measurements reported here this formula gave a larger C' , and hence a larger value of $(\alpha_A)_M$ (Eqn (5)), than did the spectroscopic data. A single relaxation absorption curve based on this thermodynamic value of C' would disagree with the experimental curve even more than does the single relaxation curve based on the spectroscopic C' . This indicates that the discrepancy between the single relaxation curve and the experimental curve is genuine. It was therefore concluded that the single relaxation theory is not adequate to describe relaxation in ethylene and that double relaxation theory is a better approximation.

An examination of the vibrational energy level scheme shows that ethylene has several 'low-lying' modes (810 cm^{-1} , 943 cm^{-1} and 949 cm^{-1}) which might be excited independently from translation and also that the higher modes (1027 cm^{-1} , 1236 cm^{-1} , 1342 cm^{-1} , 1444 cm^{-1} and 1623 cm^{-1}) are probably excited easily through the lower modes. The experiment points towards the existence of two distinguishable relaxation times but it would be difficult to assign them to particular transitions without a theoretical analysis similar to that of Tanczos (1956).

5.2. Temperature Dependence of P_{10}

Making the approximation that the average relaxation time found by fitting single relaxation curves to the experimental points is that of the lowest mode, it is possible to estimate the intermolecular force operating in transition-producing encounters.

Equation (6) was used to calculate k_{10} as a function of temperature from the data in Table 2.

The number of collisions per molecule per second at 1 atm was calculated using the Sutherland molecular model,

$$N = 2\sigma^2 n \left(\frac{4\pi kT}{m} \right)^{1/2} \left(1 + \frac{S}{T} \right), \quad \dots\dots(13)$$

where m is the molecular mass, n the molecular density (molecules/cm³) and S the Sutherland constant for ethylene ($=226^\circ\text{K}$).

The Sutherland molecular radius σ was calculated from the experimental viscosity at 0°C using the equation

$$\eta = \frac{5}{16\sigma^2} \left(\frac{kmT}{\pi} \right) \left(1 + \frac{S}{T} \right)^{-1}. \quad \dots\dots(14)$$

Hence $P_{10} = k_{10}/N$ was found as a function of temperature.

A graph of $\ln P_{10} - \ln(1/T)^{1/6} - \theta/2T - \epsilon/kT$ against $(1/T)^{1/3}$ was plotted and from the slope β was found to be $6.71 \times 10^8\text{ cm}^{-1}$ (Fig. 5).

The Lennard-Jones constants for ethylene (calculated from viscosity data) were taken from Hirschfelder, Curtiss and Bird (1954) and a comparative value of β was found by fitting the Lennard-Jones potential to the exponential repulsion by the method given by Herzfeld and Litovitz (1959); this gave

$$\beta = 4.72 \times 10^8\text{ cm}^{-1}.$$

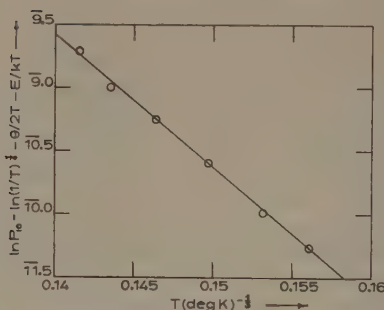


Fig. 5. Graph of $\ln P_{10} - \ln(1/T)^{1/6} - \theta/2T - \epsilon/kT$ as a function of $(1/T)^{1/3}$.

The two values of β agree to within 40%. If the terms $\exp(\theta/2T)$ and $\exp(\epsilon/kT)$ are omitted from the expression for P_{10} then the relaxation time measurements give $\beta = 17.4 \times 10^8 \text{ cm}^{-1}$ which is 4 times greater than the Lennard-Jones value.

§ 6. CONCLUSIONS

Sound absorption and velocity have been measured in ethylene at a series of temperatures between -10 and 80°C . The results suggest that there are two experimentally distinguishable relaxation times governing energy exchange between translational and vibrational motion. The experiment does not permit the relaxation times to be assigned to specific transitions. The value of the exponent in the exponential repulsion potential between colliding molecules found from the temperature dependence of the relaxation time agrees well with the value calculated from the Lennard-Jones potential.

ACKNOWLEDGMENTS

The authors wish to thank Dr. H. D. Parbrook for assistance given to them in the course of this work and to thank the Esso Petroleum Company Ltd. and Imperial Chemical Industries Ltd. for samples of ethylene. One of us (R. H.) is indebted to Imperial Chemical Industries Ltd. for the award of a Research Fellowship.

APPENDIX

VIBRATIONAL SPECIFIC HEATS

The Table below gives the contribution of each vibrational mode of ethylene to the specific heat calculated from the Einstein formula. The values are in units of R .

Wave number (cm^{-1})	Temperature ($^\circ\text{C}$)					
	-10	5	25	45	65	80
810	0.2397	0.2742	0.3193	0.3626	0.4037	0.4330
943	0.1551	0.1839	0.2234	0.2630	0.3021	0.3307
949	0.1519	0.1805	0.2219	0.2590	0.2980	0.3265
1027	0.1157	0.1405	0.1745	0.2115	0.2479	0.2750
1236	0.0532	0.0686	0.0918	0.1176	0.1453	0.1670
1342	0.0351	0.0468	0.0648	0.0856	0.1087	0.1273
1444	0.0232	0.0319	0.0458	0.0624	0.0814	0.0970
1623	0.0110	0.0159	0.0244	0.0350	0.0479	0.0589

REFERENCES

- ARNOLD, J. W., MCCOUBREY, J. C., and UBBELOHDE, A. R., 1958, *Proc. Roy. Soc. A*, **248**, 445.
- CALLEAR, A. B., and ROBB, J. C., 1955, *Trans. Faraday Soc.*, **51**, 630.
- CHAPMAN, S., and COWLING, T. C., 1958, *Mathematical Theory of Non-uniform Gases*, 2nd edn (Cambridge: University Press).
- CORRAN, P. G., LAMBERT, J. D., SALTER, R., and WARBURTON, B., 1958, *Proc. Roy. Soc. A*, **244**, 212.
- COTTRELL, T. L., and REAM, N., 1955, *Trans. Faraday Soc.*, **51**, 1453.
- DICKENS, P. G., and LINNET, J. W., 1957, *Proc. Roy. Soc. A*, **243**, 84.
- DIN, F., 1956, *Thermodynamic Functions of Gases*, Vol. 2 (London: Butterworths).
- EDMONDS, P. D., and LAMB, J., 1958, *Proc. Phys. Soc.*, **72**, 940.
- GRAVITT, J. C., 1960, *J. Acoust. Soc. Amer.*, **32**, 1455.
- Handbook of Chemical and Physical Constants*, 1955, 37th edn (Ohio: Chemical Rubber Publishing Co.).
- HERZFELD, K. F., and LITOVITZ, T. A., 1959, *Absorption and Dispersion of Ultrasonic Waves* (New York: Academic Press).
- HIRSCHFELDER, J. D., CURTISS, C. F., and BIRD, R. B., 1954, *Molecular Theory of Gases and Liquids* (New York: John Wiley).
- HOLMES, R., PARBROOK, H. D., and TEMPEST, W., 1960, *Acustica*, **10**, 155.
- International Critical Tables*, 1929 (New York: McGraw Hill).
- KAYE, G. W. C., and LABY, T. H., 1956, *Tables of Physical and Chemical Constants* (London: Longmans Green).
- KNESER, H. O., 1933, *Ann. Phys.*, **16**, 337.
- LAMBERT, J. D., COTTON, K. J., PAILTHORPE, M. W., ROBINSON, A. M., SCRIVENS, J., VALE, W. R. F., and YOUNG, R. M., 1955, *Proc. Roy. Soc. A*, **231**, 280.
- LANDAU, L., and TELLER, E., 1936, *Phys. Z. Sowjet.*, **10**, 34.
- MCCOUBREY, J. C., PARKE, T. B., and UBBELOHDE, A. R., 1954, *Proc. Roy. Soc. A*, **223**, 155.
- MCGRATH, W. D., and UBBELOHDE, A. R., 1954, *Proc. Roy. Soc. A*, **227**, 1.
- MILWARD, R. C., MCCOUBREY, J. C., and UBBELOHDE, A. R., 1961, *Trans. Faraday Soc.*, **57**, 1472.
- PARBROOK, H. D., and TEMPEST, W., 1957, *Acustica*, **7**, 354.
- RICHARDS, W. T., and REID, J. A., 1934, *J. Chem. Phys.*, **2**, 206.
- RUTGERS, A. J., 1933, *Ann. Phys.*, **16**, 350.
- SCHÄFER, K., 1940, *Z. Phys. Chem. B*, **46**, 212.
- SCHWARTZ, R. N., and HERZFELD, K. F., 1954, *J. Chem. Phys.*, **22**, 767.
- SHEPPARD, N. S., and SIMPSON, D. M., 1952, *Quart. Rev. Chem. Soc., Lond.*, **6**, 1.
- TANCZOS, F., 1956, *J. Chem. Phys.*, **25**, 439.
- TRUESDELL, C., 1953, *J. Rational Mech. and Anal.*, **2**, 643.

The Scattering of Waves by Dislocations

BY F. R. N. NABARRO† AND J. M. ZIMAN‡

† University of the Witwatersrand, Johannesburg

‡ Cavendish Laboratory, Cambridge

MS. received 24th July 1961

Abstract. An exact solution is given for scattering by the potential ρ^{-1} in two dimensions. This is compared with the results of the first and second Born approximations for the same potential in an analysis similar to that of Dalitz for the Coulomb potential r^{-1} in three dimensions. Seeger and Bross have shown that, in the scattering of conduction electrons by an edge dislocation, the second-order terms diverge logarithmically with increase of the radius of the cylinder in which the potential of the dislocation is assumed to act. Similar logarithmic terms appear in the second Born approximations for the potentials r^{-1} and ρ^{-1} , and, following Dalitz, reasons are given for believing that they represent a phase shift produced by the refraction of the incident and scattered waves, and that they do not contribute to the scattered amplitude. The cross sections for scattering by a dislocation are probably never much greater than those given by the first Born approximation, and may even be smaller. It is not possible to deduce the large values suggested by some experimental observations.

§ 1. INTRODUCTION

THE scattering of waves by a straight dislocation line is usually treated in the first Born approximation. The scattering potential is given in cylindrical polar coordinates by $\rho^{-1} \sin \phi$ for an edge dislocation, and there are second-order terms of the form ρ^{-2} for both edge and screw dislocations. It is known that the first Born approximation is only accidentally valid for scattering by the Coulomb potential r^{-1} in three dimensions, and its validity in the case of scattering by a dislocation is in doubt. Both for the scattering of conduction electrons and for the scattering of phonons there are experimental results which are most easily interpreted on the assumption that the true scattering cross section is considerably greater than that estimated by the use of the first Born approximation. Seeger and Bross (1960) have shown that the second-order terms in the wave function of electrons scattered by the potential

$$V = \frac{\hbar^2}{2m} \left(\beta k_F \frac{\sin \phi}{\rho} + \frac{\kappa}{\rho^2} \right), \quad \dots\dots (1)$$

in a cylinder of radius R , are large, of order $\ln k_F R$, although the first-order terms converge for large R . Here m is the mass of the electron, k_F is the wave number at the Fermi surface, assumed spherical, and β and κ measure the strengths of the deformation potentials of the dilatations arising from the linear and the quadratic terms in the elastic equations for a dislocation.

It is not clear whether these terms in $\ln k_F R$ contribute to the scattered amplitude or whether, as Dalitz (1951) showed to be the case for the corresponding term in the Born approximation for scattering by a Coulomb potential, they merely represent a phase shift.

No exact solution has been available for this problem or for a closely related problem which might clarify the physical principles involved. We give here an exact solution for the potential ρ^{-1} . We then summarize Dalitz's discussion of the solution for the potential r^{-1} , develop the first and second Born approximations for the potential ρ^{-1} , and show that the second Born approximation for this potential includes a term of order $\ln kR$ which is to be interpreted as a phase shift. Guided by these two cases for which exact solutions are available, we discuss Seeger and Bross's analysis for the potential (1), and conclude that the terms in $\ln k_F R$ are also to be interpreted as phase shifts which do not contribute to the scattered amplitude.

§ 2. SCATTERING BY THE TWO-DIMENSIONAL POTENTIAL ρ^{-1}

The analysis closely follows Gordon's (1928) analysis for the Coulomb potential r^{-1} , and is therefore given only in outline.

We begin with the wave equation

$$\nabla^2 \psi + k^2 \psi - 2k^2 \alpha \rho^{-1} \psi = 0, \quad \dots\dots (2)$$

and look for solutions in which the coordinate z parallel to the axis of the scattering line does not appear. We introduce new coordinates (x, η) defined by

$$x = x, \quad y = [\eta(2x + \eta)]^{1/2}, \quad \dots\dots (3)$$

so that

$$\eta = \rho - x = 2\rho \sin^2 \frac{1}{2} \theta, \quad \dots\dots (4)$$

where θ is the angle of scattering.

The wave equation (2) now becomes

$$\frac{\partial^2 \psi}{\partial x^2} - \frac{2\eta}{x + \eta} \frac{\partial^2 \psi}{\partial x \partial \eta} + \frac{2\eta}{x + \eta} \frac{\partial^2 \psi}{\partial \eta^2} + \frac{1}{x + \eta} \frac{\partial \psi}{\partial \eta} + \left(1 - \frac{2\alpha}{x + \eta}\right) k^2 \psi = 0. \quad \dots\dots (5)$$

Putting $\psi = \exp(ikx)f(\eta)$, we find

$$\eta \frac{d^2 f}{d\eta^2} + \left(\frac{1}{2} - ik\eta\right) \frac{df}{d\eta} - k^2 \alpha f = 0. \quad \dots\dots (6)$$

The solution of this equation which is appropriate to the present physical problem is given by the confluent hypergeometric function

$$f(\eta) = F(-ik\alpha, \frac{1}{2}, ik\eta). \quad \dots\dots (7)$$

When η is large, this has the asymptotic form

$$F(-ik\alpha, \frac{1}{2}, ik\eta) \sim \frac{\Gamma(\frac{1}{2})(-ik\eta)^{ik\alpha}}{\Gamma(\frac{1}{2} + ik\alpha)} \left[1 + \frac{\Gamma(\frac{1}{2} + ik\alpha)}{\Gamma(-ik\alpha)} (-ik\eta)^{-1/2 - 2ik\alpha} e^{ik\eta}\right]. \quad \dots\dots (8)$$

The complete solution is

$$\psi = e^{ikx} F \sim \frac{\Gamma(\frac{1}{2}) \exp[ik\alpha \ln k(x - \rho)]}{\Gamma(\frac{1}{2} + ik\alpha)} \left\{ e^{ikx} + \frac{\Gamma(\frac{1}{2} + ik\alpha)}{\Gamma(-ik\alpha)} \frac{\exp[-2ik\alpha \ln k(\rho - x)]}{[ik(\rho - x)]^{1/2}} e^{ik\rho} \right\}. \quad \dots\dots (9)$$

The factor outside the braces is the product of a constant term and a variable phase factor of modulus unity. The factor in braces is the sum of the unperturbed incident plane wave $\exp(ikx)$ and of a diverging wave $\exp(ik\rho)$, the amplitude of the latter being the modulus of

$$\frac{\Gamma(\frac{1}{2} + i k \alpha)}{\Gamma(-i k \alpha)} \frac{1}{(2k\rho \sin^2 \frac{1}{2}\theta)^{1/2}}. \quad \dots\dots (10)$$

It is easily shown that

$$\left| \frac{\Gamma(\frac{1}{2} + i k \alpha)}{\Gamma(-i k \alpha)} \right| = (k\alpha \tanh \pi k \alpha)^{1/2},$$

so that the scattered intensity $I(\theta)$ is given by

$$I(\theta) = \frac{\alpha \tanh \pi k \alpha}{2\rho \sin^2 \frac{1}{2}\theta}. \quad \dots\dots (11)$$

When $k\alpha$ is small this leads to the first Born approximation

$$I(\theta) = \frac{\pi k \alpha^2}{2\rho \sin^2 \frac{1}{2}\theta}, \quad \dots\dots (12)$$

which is always greater than the exact value (11).

§ 3. THE COULOMB POTENTIAL r^{-1} IN THREE DIMENSIONS

Before we treat scattering by the potential ρ^{-1} in two dimensions by the first and second Born approximations, we shall discuss Dalitz's analysis of the Born approximations to scattering by the potential r^{-1} in three dimensions. Dalitz found that large matrix elements occurred in the higher Born approximations, and showed that they do not contribute to the scattered intensity, but represent a large change in phase from that corresponding to the first Born approximation. We shall summarize Dalitz's argument and provide some additional support for it.

Dalitz made a detailed study of the scattering by a Coulomb potential of a particle obeying the Schrödinger equation. He took the screened potential

$$V = Ze^2 r^{-1} e^{-r/R}. \quad \dots\dots (13)$$

In addition to confirming the well-known results that in the limit $R \rightarrow \infty$ the differential cross sections calculated by classical mechanics, by the first Born approximation and by an exact solution of the Schrödinger equation, all agree, he calculated the first, second and third Born approximations. He showed that the second approximation involved terms of order $\ln kR$ and the third approximation terms of order $(\ln kR)^2$. Let the first three terms be denoted by B_1 , B_2 and B_3 , write $i\gamma = B_2/B_1$, and consider the expansion of the expression $B_1 \exp i\gamma$ in the form

$$B_1(1 + i\gamma - \frac{1}{2}\gamma^2 + \dots) = B_1 + B_2 - \frac{1}{2}B_1\gamma^2 + \dots \quad \dots\dots (14)$$

Then Dalitz's result is that the term in B_3 which diverges as $R \rightarrow \infty$ is given correctly by the third term of (14), with B_1 equal to the exact scattering amplitude and γ given by

$$\gamma = - \frac{2Ze^2 m}{\hbar^2 k} \ln(2kR \sin \frac{1}{2}\theta). \quad \dots\dots (15)$$

This suggests that the terms which diverge as $R \rightarrow \infty$ represent a phase change of the scattered wave. We shall support this interpretation by showing that the phase shift (15) is asymptotically just that predicted for a particle travelling along the classical orbit. When the particle is far from the scattering centre only its radial motion is important in determining the phase, and its wave equation is approximately

$$\frac{d^2\psi}{dr^2} = \left(-k^2 + \frac{2Ze^2m}{\hbar^2 r} e^{-r/R} \right) \psi \simeq -k^2 \left(1 - \frac{Ze^2m}{\hbar^2 k^2 r} e^{-r/R} \right)^2 \psi. \quad \dots\dots (16)$$

The potential acts once to produce a scattered wave at some distance $r_0 \ll R$ from the centre, and then causes the scattered wave to propagate in a refracting medium in which the wave number is reduced from k to $\tilde{k} - (Ze^2m/\hbar^2 k r) e^{-r/R}$. This introduces a phase advance of

$$- \frac{Ze^2m}{\hbar^2 k} \int_{r_0}^{\infty} e^{-r/R} \frac{dr}{r} \sim \frac{Ze^2m}{\hbar^2 k} \ln \frac{R}{\gamma_0 r_0}, \quad \dots\dots (17)$$

where γ_0 is Euler's constant. The incoming wave suffers an equal phase shift, confirming our interpretation that the logarithmic term in (15) represents the refraction of the incoming and the outgoing waves. This interpretation of the divergent term as a phase shift by refraction is strengthened by the observation that this term arises from intermediate states with wave numbers \mathbf{k}'' which lie very close to \mathbf{k} or to \mathbf{k}' , the wave numbers of the incident and the scattered waves.

§ 4. THE FIRST AND SECOND BORN APPROXIMATIONS FOR THE TWO-DIMENSIONAL POTENTIAL ρ^{-1}

In treating the Born approximations to the solution of (2) we shall use a notation based on that of Seeger and Bross. We represent the projection of the wave vector \mathbf{k} on the z plane by $\tilde{\mathbf{k}}$. We modify the long-range scattering potential $2k^2\alpha\rho^{-1}$ to a cut-off potential $2k^2\alpha\rho^{-1}e^{-\rho/R}$, and introduce the function

$$T(\tilde{\mathbf{k}}, \tilde{\mathbf{k}}') = (2\pi)^{-2} \int_0^\infty \int_0^{2\pi} 2k^2\alpha\rho^{-1} e^{-\rho/R} e^{i\tilde{\mathbf{k}}\cdot\boldsymbol{\rho}} \cos\psi \rho d\psi d\rho. \quad \dots\dots (18)$$

Here K and Φ are defined by

$$\begin{aligned} K \cos \Phi &= \tilde{k} \cos \phi - \tilde{k}' \cos \phi' \\ K \sin \Phi &= \tilde{k} \sin \phi - \tilde{k}' \sin \phi', \end{aligned} \quad \dots\dots (19)$$

and (\tilde{k}, ϕ) and (\tilde{k}', ϕ') are the polar coordinates of the projections of \mathbf{k} and \mathbf{k}' on the z plane.

The matrix element for scattering from the state \mathbf{k} to the state \mathbf{k}' by the potential $2k^2\alpha\rho^{-1}e^{-\rho/R}$ can be expanded in an ascending power series of the form

$$\delta(k - k') \delta(\tilde{\mathbf{k}} - \tilde{\mathbf{k}}') (T_1 + T_2 + \dots), \quad \dots\dots (20)$$

where

$$T_1 = T(\tilde{\mathbf{k}}, \tilde{\mathbf{k}}') \quad \dots\dots (21)$$

and

$$T_2 = \int T(\tilde{\mathbf{k}}, \tilde{\mathbf{k}}'') T(\tilde{\mathbf{k}}'', \tilde{\mathbf{k}}') [(\tilde{k}^2 - \tilde{k}''^2)^{-1} - \pi i \delta(\tilde{k}^2 - \tilde{k}''^2)] d_2 \tilde{\mathbf{k}}''. \quad \dots\dots (22)$$

Seeger and Bross omit the term in $\delta(\tilde{k}^2 - \tilde{k}'^2)$, which makes no contribution to the divergent term in the solution of their problem, but contributes the whole of the divergent term in the case of the symmetrical potentials r^{-1} and ρ^{-1} .

We find that

$$T_1 = \pi^{-1} k^2 \alpha \int_0^\infty J_0(K\rho) e^{-\rho/R} d\rho = \frac{k^2 \alpha R}{\pi(1 + K^2 R^2)^{1/2}}. \quad \dots\dots (23)$$

This converges as $R \rightarrow \infty$ to $T_1 = k^2 \alpha / \pi K$. Since T_1 is multiplied by $\delta(\tilde{k} - \tilde{k}')$, we may write

$$K = 2\tilde{k} \sin \frac{1}{2}\theta \quad \dots\dots (24)$$

and

$$T_1 = k^2 \alpha / 2\pi \tilde{k} \sin \frac{1}{2}\theta. \quad \dots\dots (25)$$

If the wave is incident normal to the z axis, which is the case considered in § 2, we have $\tilde{k} = k$, and $T = k\alpha / 2\pi \sin \frac{1}{2}\theta$. Following Seeger and Bross, we write the amplitude of the scattered wave as

$$\pi^2 \left(\frac{2}{\pi k \rho} \right)^{1/2} T_1 = \left(\frac{\pi k}{2\rho} \right)^{1/2} \frac{\alpha}{\sin \frac{1}{2}\theta}, \quad \dots\dots (26)$$

and again obtain the intensity (12).

As in the problems considered by Dalitz and by Seeger and Bross, we find that the integral (21) converges for large \tilde{k}'' , and that possible divergencies arise only as $\tilde{k}'' \rightarrow \tilde{k}$ and as $\tilde{k}'' \rightarrow \tilde{k}'$. In all of these problems the asymptotic form of the integral for large R may be found by evaluating the contribution to the integral from the neighbourhood of these two singularities. In this way we readily find that when $\tilde{k}' = \tilde{k}$,

$$T_2 = \frac{ik^2 \alpha^2}{\pi \sin \frac{1}{2}\theta} \ln kR. \quad \dots\dots (27)$$

This represents a phase shift

$$\gamma = T_2 / iT_1 = 2k\alpha \ln kR. \quad \dots\dots (28)$$

In the quasi-classical approach which we have used to derive (17) the plane orbits for the potentials r^{-1} and ρ^{-1} are identical, and the ratio of the phase shifts appearing in (28) and (17) is the same as the ratio of the perturbing terms appearing in (2) and (16).

We have thus shown that the exact solutions for the potentials r^{-1} and ρ^{-1} show no divergences as the screening radius R is allowed to tend to infinity, that in each case the second Born approximation contains divergent terms proportional to $\ln kR$, and that in each case this divergent term represents the phase shift due to refraction along the classical orbit.

§ 5. SCATTERING BY AN EDGE DISLOCATION

We now discuss the analysis by Seeger and Bross of the scattering by an edge dislocation, using the potential (1).

The first Born approximation involves the matrix elements $\langle \phi' | V | \phi \rangle$ for scattering from the direction ϕ to the direction ϕ' . The terms in β are given by integrals which oscillate for large values of ρ and, except when $\phi' = \phi$, they are

easily made to converge by using a convergence factor or by cutting off the integration at some large radius R . The matrix element for scattering through small angles diverges like $(\phi - \phi')^{-1}$. The terms in κ converge for large ρ , but an inner cut-off radius ρ_i has to be introduced, within which the assumptions underlying (1) are not valid.

In the next higher approximation, terms arise which are proportional to β^2 , $\beta\kappa$ and κ^2 . The terms in κ^2 may be neglected, but Seeger and Bross show that the terms in β^2 and $\beta\kappa$ include components which are proportional to $\ln k_F R$ and, in practical cases, are considerably larger than the terms linear in β or κ . Of these two terms, that in $\beta\kappa$ predominates. Different methods are used to treat these two second-order terms. That in β^2 is obtained by second-order perturbation theory, while that in $\beta\kappa$ is obtained by applying first-order perturbation theory to the exact solution by phase shift analysis of the two-dimensional Schrödinger equation for the central potential κ . Seeger and Bross assume that the squares of these large second-order matrix elements provide a better estimate of the intensity of the scattering of electrons by a dislocation than do the squares of the first-order elements, and thus a better estimate of the electrical resistivity of a metal containing dislocations. Their method leads, in particular, to the result that if a crystal of large size R contains a single dislocation, this dislocation will make a contribution to the electrical resistance comparable to that of a saw cut of width $(\ln k_F R)^2$ atomic spacings.

We shall now examine these calculations from the standpoint of §§ 3 and 4. We first consider the term in β^2 . Here Seeger and Bross introduce a sharp cut-off radius R , and find a first-order term S_1 , analogous to the T_1 of (21) and given by $S_1 = S(\mathbf{k}, \mathbf{k}')$, where

$$S(\mathbf{k}, \mathbf{k}') = \frac{i}{2\pi} \beta k_F \frac{\sin \Phi}{K} [1 - J_0(KR)]. \quad \dots\dots (29)$$

The second-order term S_2 is analogous to T_2 of (22) and contains a logarithmically divergent term

$$- \frac{1}{8\pi} \frac{\beta^2 k_F^2}{k^2} [1 + \cos(\phi - \phi')] \ln \frac{k_F R}{\gamma_0} \quad \dots\dots (30)$$

We now have to decide whether the terms S_2 and S_1 in this analysis can properly be compared with the terms which we have labelled B_2 and B_1 in Dalitz's analysis, so that the large term S_2 represents a large phase shift but not a change of amplitude. We note first that S_2/S_1 is purely imaginary, as is required by this interpretation. We also observe from the analysis of Seeger and Bross that this logarithmic term arises from two regions in the \mathbf{k}' plane, namely those regions which are very close to \mathbf{k} and those which are very close to \mathbf{k}' .

Moreover, the asymptotic form of (30) is exactly that required by our interpretation. We may calculate the phase shift along the classical orbit by the same method as we calculated the phase shifts (17) and (28). In the present problem the wave incident along ϕ is travelling along the line $-\phi$, and its phase shift in the β potential is asymptotically

$$\gamma_1 = - \frac{\hbar^2 \beta k_F \sin(-\phi)}{2m} \frac{m}{\hbar^2 k} \ln k_F R. \quad \dots\dots (31)$$

For the outgoing wave we have

$$\gamma_2 = - \frac{\hbar^2 \beta k_F \sin \phi'}{2m} \frac{m}{\hbar^2 k} \ln k_F R,$$

giving a total phase shift of

$$\gamma = - (\beta k_F / 2k) (\sin \phi' - \sin \phi) \ln k_F R. \quad \dots\dots (32)$$

It is easily verified that this value of γ satisfies the relation $i\gamma = S_2/S_1$ required by our interpretation.

The comparison with the results of classical dynamics is less encouraging than it is in the Coulomb case. Since the forces are not central, there is no easy way of finding the classical orbits explicitly. In the first-order perturbation the total change of momentum along the path is zero. (This was first observed by Hunter and Nabarro (1953), although their sketch of the classical orbits is incorrect. The orbits of electrons in the neighbourhood of a negative edge dislocation are represented roughly by the conventional drawing of the lattice planes in the neighbourhood of a positive edge dislocation.) An angular deflection occurs only in second-order perturbation, and this singular scattering potential therefore gives in classical mechanics, as in quantum mechanics, differential cross sections proportional to β^2 when β is small. This is true in general for non-singular scattering potentials in three dimensions, but non-singular potentials in two dimensions lead to classical differential cross sections which are linear in the scattering potential. For the present potential the impulse on a particle with initial impact parameter p which is derived from classical second-order perturbation theory is proportional to p^{-2} , so that the differential cross section for scattering through a small angle θ is proportional to $\theta^{-3/2}$, whereas in the quantum mechanical case it is proportional to θ^{-2} .

We now consider the term in $\beta\kappa$ which appears in the second approximation to scattering by the potential (1).

Seeger and Bross obtain a matrix element proportional to $\beta\kappa$ by applying the β potential as a first-order perturbation to the exact quantum mechanical solution for a particle moving in the κ potential. We enquire firstly whether this is a correct use of perturbation theory, and secondly whether the resulting large matrix element represents a change in the scattered amplitude or only in the phase of the scattered wave. The first question is delicate, for the perturbation procedure consists in neglecting terms of order β^2 while calculating those of order $\beta\kappa$. The results shows that the term in $\beta\kappa$ which is obtained is indeed, in practical cases, larger than that in β^2 . Nevertheless this term arises from regions where ρ is large, and in these regions the β potential is larger than the κ potential. In considering the second question, we see that the waves scattered by κ will be expected to show a change of phase as a result of refraction by the β potential analogous to that calculated in §§ 3 and 4. It is easy to see why phase changes of the order of (32) occur in the β^2 term and in the $\beta\kappa$ term, but not in the β term. For if β acts once, it may either scatter through a finite angle or refract. The β term cannot include the refraction of the scattered ray. The phase shift appears to this order only in the undeviated ray, and perturbation theory breaks down just at this angle of scattering.

§ 6. CONCLUSIONS

Our method of argument is to draw an analogy with a hypothesis. There are arguments in favour of the validity of Dalitz's original hypothesis, and in

favour of the validity of our analogy, and there seem to be no compelling arguments against either. We conclude (i) that the problem of the scattering matrix for the potential (1) is still open, (ii) that Seeger and Bross's divergent term in β^2 can be entirely accounted for as a phase shift, and (iii) that a phase shift exists which introduces terms of the same order as their term in $\beta\kappa$. If the present interpretation is correct, (iv) the first Born approximation, supplemented by a correction such as that of Harrison (1958) for scattering by the core of the dislocation, gives the best available estimate of the electrical resistivity produced by undissociated dislocations in a metal. This estimate can hardly be reconciled with the experimental observations on aluminium, although these are still very uncertain.

ACKNOWLEDGMENTS

We are grateful to Professor Seeger for allowing us to see the paper by Seeger and Bross before publication, and for a stimulating discussion which lent support to conclusion (i) above.

REFERENCES

- DALITZ, R. H., 1951, *Proc. Roy. Soc. A*, **206**, 509.
GORDON, W., 1928, *Z. Phys.*, **48**, 180.
HARRISON, W. A., 1958, *J. Phys. Chem. Solids*, **5**, 44.
HUNTER, S. C., and NABARRO, F. R. N., 1953, *Proc. Roy. Soc. A*, **220**, 542.
SEEGER, A., and BROSS, H., 1960, *Z. Naturf.*, **15a**, 663.

Grain Boundary Damping I: Pure Iron

By G. M. LEAK

Department of Metallurgy, University of Manchester

MS. received 21st April 1961

Abstract. Internal friction measurements have been carried out on specimens of high purity iron from which carbon and nitrogen have been removed. A relaxation peak, observed at about 500°C for a frequency of vibration about 1c/s, is associated with the presence of grain boundaries in the specimens. The activation energy Q associated with this damping process is 46 kcal mol⁻¹. The damping appears to be governed by a term, frequency \times (grain size)² exp (Q/RT). The variation of peak damping and background damping is similar to that observed in other pure metals.

§ 1. INTRODUCTION

MECHANICAL and physical properties of metals are markedly affected by the presence of grain boundaries. It is not generally possible, however, to investigate boundary phenomena directly. For example, attempts have been made to extract boundary material for analysis but such techniques entail working on a scale of, at least, microns and have not been very successful in the past. Metallographic evidence suggests that grain boundary thickness must be orders of magnitude smaller. Some success has been obtained by the use of radioactive isotopes, for example, in studying segregation of impurities to boundaries (Thomas and Chalmers 1955). The resolution of the technique is not entirely satisfactory for the solution of many problems. Recent work (Brammar, Honeycombe and Ward 1958, Plateau, Henry and Crussard 1958) using electron microscopy to study surfaces of intergranular fractures has been successful. This technique also has its limitations, particularly in the types of problem which can be tackled. Internal friction measurements (Kê 1947a) give a relaxation peak which is associated with the presence of grain boundaries in the specimen. Very little effort has been devoted to this method, which might, under suitable conditions prove to be a valuable tool for the investigation of grain boundary phenomena. It has one important advantage, that no significant disturbance of the grain boundary material need occur during the experiment. The purpose of this paper is to present results which have been obtained using the internal friction technique to study grain boundaries in pure iron. It represents the initial stages of a programme intended to study the effects of interstitial and substitutional impurity elements in iron.

§ 2. BACKGROUND INFORMATION

Kê observed a damping peak for polycrystalline specimens that was absent in specimens of single crystals (Kê 1947a, b, 1948, 1949). He suggested that this was caused by sliding at grain boundaries. By analogy with flow in other materials, this was called grain boundary viscosity.

Assuming a flat boundary of thickness d , and of linear dimension similar to the grain diameter D , Kê showed that the coefficient of viscosity was given by

$$\eta = dG\tau/D$$

where G is the unrelaxed shear modulus for the material and τ the time for which stress relaxation is allowed to take place. This expression was modified by Smith (1950) without significantly affecting the model of grain boundary sliding to give

$$\eta = 6dG\tau/D. \quad \dots\dots (1)$$

The temperature dependence of η is given by

$$\eta = \eta_0 \exp(Q/RT)$$

where Q is an activation energy. Thus

$$\tau = \frac{D\eta_0}{6dG} \exp(Q/RT). \quad \dots\dots (2)$$

In a damping experiment, the internal friction δ is given by

$$\frac{\delta}{\pi} = \Delta \frac{\omega\tau}{1 + \omega^2\tau^2} \quad \dots\dots (3)$$

where Δ , the relaxation strength of the process, is a constant, ω the frequency of vibration and τ the relaxation time for the mechanism giving rise to the damping. It is assumed that the two values for τ are identical. δ is consequently a function only of $\omega\tau$, that is,

$$\delta = f\left\{\frac{\omega D\eta_0}{6dG} \exp\left(\frac{Q}{RT}\right)\right\}. \quad \dots\dots (4)$$

This point is important for Kê's interpretation of the mechanism. At the peak value of δ , where $\omega\tau$ is unity and the peak temperature is T_p , then plots of $\ln \omega$ against $1/T_p$ for constant grain size D and of $\ln D$ against $1/T_p$ for constant frequency of vibration ω , should both give straight lines of slope Q/R . (It has been assumed that d , G and η_0 are independent of temperature in the region of the damping peak maximum.) Kê's work in fact showed that a variation of grain size was equivalent to a variation of frequency in its effect on peak temperature. Probable atomic mechanisms to account for this damping have been put forward by Mott (1948) and by Kê (1949). Mott considered the boundary as a transition region consisting of islands of good lattice fit between the adjacent grains, separated by regions of bad fit. Slip in the boundary is represented by disordering of atoms around each of the islands. The rate of slip v is then given by

$$v = \frac{\nu a^2 n \sigma w}{kT} \exp\left(\frac{nL}{kT_m}\right) \exp\left(-\frac{nL}{kT}\right) \quad \dots\dots (5)$$

where ν is the frequency of atomic vibration, a the lattice constant, w the area of boundary per atom, σ the shear stress. n atoms are disordered around each island, L is the latent heat of fusion per atom and T_m is the melting point. Kê's results interpreted in this way give n equal to 14, when nL/kT is made equal to the measured activation energy for grain boundary damping. The constant outside the exponent did not give good agreement with experiment. This model,

however, can account for the influence of impurities; if they migrate to boundaries the effective value for nL will be altered.

Kê also assumed that the boundary consisted of regions of good lattice fit but that the slip process involved forcing atoms past one another in a disordered group between the islands of good fit. Then

$$v = \frac{q\gamma\nu\sigma}{kT} \exp\left(\frac{-Q}{kT}\right) \dots\dots (6)$$

where q is the density of disordered groups of atoms, γ the shear strain from the rearrangement of atoms and Q the activation energy for the process. Q would automatically be the same as the activation energy for volume self-diffusion and steady-state creep since his model implied no difference between the type and concentration of imperfections in the boundary and in the grain. Neither of these mechanisms suggests any relationship between the activation energies for grain boundary damping and grain boundary diffusion.

Kê observed grain boundary peaks in several metals of varying purity without systematically studying impurity elements. There was close agreement between the activation energies for grain boundary damping, volume self-diffusion and steady-state creep.

Copper has been studied by several workers. Köster, Bangert and Lang (1955) showed a correlation between the height of the grain boundary damping peak (after subtraction of the background damping) and the grain size, although they did not test the validity of Eqn (4). A similar correlation was obtained between the background damping and grain size. (The background damping was measured at an arbitrary high temperature, remote from the grain boundary peak). The activation energy for the grain boundary peak damping was 32 kcal mol⁻¹. Rotherham and Pearson's (1956) value was 33 ± 3.3 kcal mol⁻¹. Weinig and Machlin (1957) used very high purity copper and found the activation energy to be 40 ± 2 kcal mol⁻¹, whilst less pure copper (OFHC quality) gave a value of 33 ± 2 kcal mol⁻¹. Values quoted in these papers for the activation energy for volume self-diffusion of copper are about 50 kcal mol⁻¹.

Silver specimens (Pearson and Rotherham 1956) gave an activation energy of 22 ± 2.2 kcal mol⁻¹ compared with that for volume self-diffusion of 45.9 kcal mol⁻¹ (Le Claire 1949). Boundary damping has also been observed in zirconium (Bratina and Winegard 1956), titanium (Pratt, Bratina and Chalmers 1954) and molybdenum (Maringer and Schwope 1954).

§ 3. TECHNIQUE AND SPECIMEN PREPARATION

High purity iron was used. This was made by vacuum-melting specially pure Swedish iron following the technique described by Hopkins, Jenkins and Stone (1951). A typical analysis (in wt %) was as follows:

C	N	Si	S	Al	O ₂
0.002	0.001	0.003	0.006	0.001	0.002

The material was forged and rolled down to a diameter of about 6 mm. At this stage the material was given a prolonged anneal in flowing moist hydrogen followed by similar treatment in dry hydrogen. This reduced the carbon and nitrogen to less than 0.0005%, i.e. to below the limits of chemical analysis. The final wire drawing treatment was a reduction of about 90% to a diameter of about

2 mm. This was found essential to produce specimens with a suitable range of grain sizes after recrystallization. The recrystallization anneal, carried out in vacuum, was for 3 hours at 750°C. Grain growth was allowed to occur at 850°C using times up to 3 hours. This gave a series of specimens with grain sizes of 10.6, 14.7, 19.2 and 29.7 grains per linear mm measured transversely.

Grain size determinations were made on the actual specimens used for internal friction experiments. The figures given represent averages for a number of metallographic sections.

Internal friction analyses at this stage showed no carbon or nitrogen interstitial diffusion peaks. This implies that the content of these impurities would be less than 0.0005 wt%.

A torsion pendulum was used with specimens about 20–25 cm long. The equipment was designed to maintain a vacuum of about 1μ Hg with a temperature variation over the specimen of less than $\pm 1\frac{1}{2}^\circ\text{C}$ at about 500°C. Logarithmic decrement was measured from the decay of free vibrations and plotted against temperature of the specimen. This internal friction technique has been described in detail elsewhere (Thomas and Leak 1956).

The grain boundary peaks occurred at temperatures in the neighbourhood of 500°C. Maximum damping was high, even up to a logarithmic decrement of 0.1. Nevertheless it was always possible to locate the peak temperature to within about $\pm 3^\circ\text{C}$. Vibration frequencies in the range 0.3 to 10 c/s were used, damping being recorded visually in the range 0.3 to 2 c/s and photographically for higher frequencies. Frequencies were recorded during experiments. Owing to the high damping it was not possible to measure the frequencies accurately at the temperature of the peak. Consequently frequencies quoted are those measured accurately at room temperature. This does not introduce an appreciable error in the determination of activation energy.

§ 4. RESULTS AND DISCUSSION

A number of curves of internal friction plotted against temperature were taken for each specimen at different frequencies. Within the accuracy of measurement of the peak temperature, the curves for constant frequency were reproducible.

Results are plotted in Fig. 1 in the form of log frequency against inverse temperature.

A typical curve of damping against temperature is shown in Fig. 2. It is worth noting the following characteristics which are different from those reported by Kê (1949) for an iron specimen: (i) the background damping rises more rapidly; (ii) the peak height, after subtraction of the background is lower and the maximum damping observed is higher; (iii) agreement with a theoretical curve, calculated from Eqn (4), is worse. The second point is unlikely to be associated with the technique of measurement or with the equipment since low temperature damping is similar to that reported by Kê and by other workers using the torsion pendulum.

The curves of Fig. 1 form a family of parallel straight lines, each line corresponding to a specific grain size. This is expected if the stress relaxation obeys an Arrhenius equation. The slope of the lines gives the value Q/R from which Q is found to be 46 kcal mol⁻¹. The experimental error for any specific point is

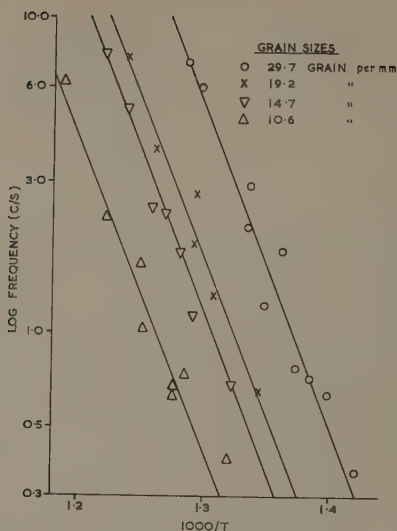


Fig. 1. Variation of peak temperature with frequency of vibration for specimens of various grain sizes.

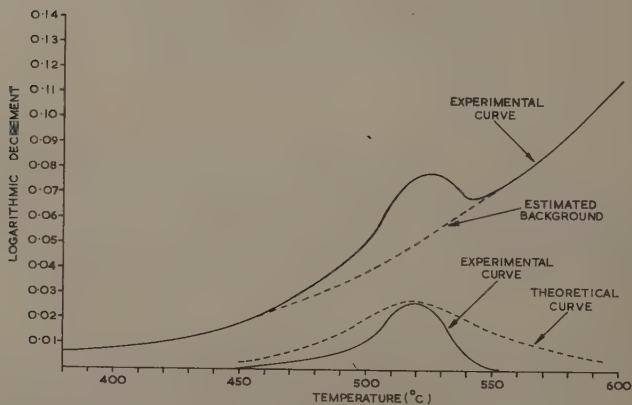


Fig. 2. Typical damping plotted against temperature curves.

high; the estimated error in Q , determined from Fig. 1 is ± 3 kcal mol $^{-1}$. The best fit line was obtained by the least squares method, which gave this uncertainty.

The most probable value for the activation energy for self-diffusion in alpha iron is between 62 and 67 kcal mol $^{-1}$ (Borg and Birchenall 1960). The value of Q for grain boundary damping reported by Kê (1947 b, 1948), for iron, is about 85 kcal mol $^{-1}$. Kê assumed this equal to the current value for the self-diffusion activation energy of 78 kcal mol $^{-1}$. It is possible, however, that the pure iron

used by Kê (1947b, 1948, 1949) contained a small amount of carbon which could markedly alter measured activation energies. Furthermore, if the damping process were that of atoms sliding past each other then agreement could be expected between the activation energies for grain boundary damping and grain boundary self-diffusion. Leymonie, Lacombe and Libanti (1958) using radioactive tracer techniques, give a value of Q for grain boundary self-diffusion equal to 45 kcal mol⁻¹. This agrees closely with the present value for the activation energy for grain boundary damping.

The alternative calculation from Eqn (4) is to consider measurements made at constant frequency for specimens of differing grain diameters. For a frequency of 1 c/s the results give a mean value for Q of 21 ± 5 kcal mol⁻¹. The inaccuracy is a consequence of the narrow range of grain sizes.

Although a variation of grain size does radically alter the temperature of the grain boundary peak, the equivalence of ω and D proposed by Kê is not substantiated. Eqn (4) would give approximately correct values for Q if the term D were replaced by D^2 . Köster, Bangert and Lang's (1955) results for copper also can be interpreted as requiring a D^2 term. Starr *et al.* (1953) found a relationship requiring a term $D^{1.86}$ for aluminium specimens. It is possible that an explanation arises from the formation of a sub-grain structure, when the sub-grain diameter might replace the value for D . However, the present specimens contain no carbon and are in a condition where the sub-structure would be difficult to observe. X-ray back reflection photographs show only recrystallized grains, but no measurable sub-structure.

Some comparisons with other consequences of the theories for this relaxation process can be made.

If we accept the model proposed by Mott the number of atoms which are assumed to take part in boundary sliding will be equal to 13 for a latent heat of melting of 3.63 kcal (g atom)⁻¹. Mott gave n equal to 14 from his interpretation of Kê's measurements on aluminium.

A coefficient of viscosity for the boundary material can be calculated from Eqn (1). For example, taking the figures grain diameter 3.3×10^{-3} cm, frequency of vibration 6.01 c/s, and a peak temperature of 498°C, then the relaxation time is 2.65×10^{-2} sec. The viscosity of molten iron is about 4×10^{-2} poise. Assuming the validity of Andrade's equation and taking Q as 46 kcal mol⁻¹ then we find that the viscosity at 498°C would be 10^6 poise. The shear modulus for iron is 7×10^{11} dyn cm⁻¹ with τ equal to 2.65×10^{-2} sec, then the grain boundary thickness is 3×10^{-8} cm. This is similar to the value calculated by Kê.

Comparison of the experimental curve, Fig. 2, with a curve calculated from Eqn (3) gives poor agreement. This is partly due to the difficulty of estimating a true background damping and partly to the inaccuracies in measuring high damping, and must also be related to the fact that it is not strictly valid to use Eqn (3) in regions where the damping is very high.

After subtraction of the background damping estimated graphically from a series of curves such as Fig. 2, the variation of peak height with grain size can be obtained, Fig. 3. The curves give low peak heights, the accuracy is thus poor and Fig. 3 should be considered only indicative of the trend of results. There is no systematic variation of peak height with frequency of measurement and peak temperature. Fig. 3 could be extended to show zero damping at a large grain diameter, and is then similar to that reported for copper by Köster, Bangert and

Lang (1955). It is not clear how to incorporate this variation of damping with grain size into the theory of the mechanism of damping. Köster *et al.* (1955) observed that the background damping at some arbitrary temperature, above the grain boundary damping peak, changed with grain size in a similar way to the change of grain boundary damping. Fig. 4 shows the changes observed in background damping for iron specimens, taken at 600°C. It has been suggested (Zener 1948) that this damping is the result of deformation at grain corners; certainly it varies with grain diameter and must in some way be associated with the boundaries.

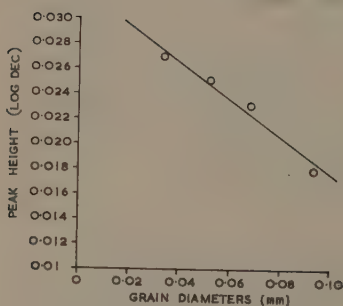


Fig. 3. Variation of intensity of internal friction (peak height) with grain size of specimens.

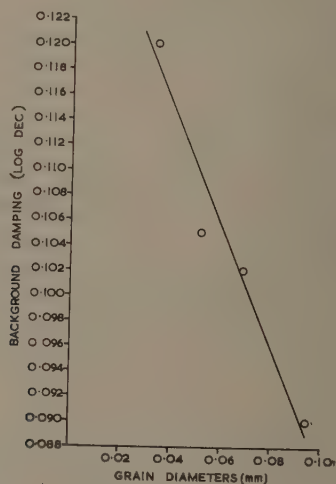


Fig. 4. Variation of background damping with grain size of specimens. (measured arbitrarily at 600°C).

Although the experimental results do not give good agreement with Eqn (3), the results in Fig. 1 imply that one relaxation time does predominate. This will be given by

$$\tau = \tau_0 \exp(Q/RT).$$

Taking Q equal to 46 kcal mol⁻¹, we can calculate the values for τ_0 :

Grain size (mm ⁻¹)	10.6	14.7	19.2	29.7
τ_0 (sec) $\times 10^{14}$	4.23	1.74	0.93	0.31.

There is a trend towards a lower value for τ_0 as the grain size decreases; the significance of this trend cannot be assessed without further data. The original work by Kê gave a value about 10^{-21} sec which is not reasonable for a process involving a single atom jump. The present mean value of 10^{-14} sec nevertheless is a reasonable one for such a unit process. This might suggest an alternative mechanism for the grain boundary damping. Movement of grain boundaries, for example, during growth in recrystallized materials, has an activation energy comparable with that of grain boundary diffusion; it appears to increase as the

impurity content increases. It is possible that grain boundary damping is caused by migration of the grain boundaries, reversibly, into adjoining grains. Boundaries, in the form of dislocation networks, move reversibly under the action of an applied stress (Washburn and Parker 1952). Thus, qualitatively at least, boundary migration could lead to anelastic phenomena. Boundaries will, in general, be irregular and migrations will occur in which one atom or only a few atoms are involved. This mechanism will involve a τ_0 which is comparable with that for single atom jumps and will yield an activation energy corresponding to that for grain boundary diffusion.

The variation of τ_0 , or the frequency factor, with grain size might be dependent on the configurational entropy associated with the atoms taking part in the boundary migration. How such an explanation could be pursued is not clear. The variation of damping with grain size will be dependent on the magnitude of the total grain boundary migration. It should be possible to estimate this dependence.

Clearly, many more experimental results are required to determine the atom movements involved in this contribution to damping. A more accurate determination is required of the shape of the damping curve at the high levels of damping in these experiments.

§ 5. CONCLUSIONS

The results show how the damping peak varies with grain size in the specimens. It is reasonably established that the peak is associated with the presence of grain boundaries in the specimens. The damping appears to be governed by a term $\text{frequency (grain size)}^2 \exp(Q/RT)$.

The value for the activation energy for grain boundary damping in iron is 46 kcal mol⁻¹. This is in disagreement with values reported by previous workers and disagrees with the activation energy for volume self-diffusion and steady-state creep. It is in very good agreement with the activation energy for grain boundary self-diffusion.

It is not possible, from the results on pure iron, to differentiate between the mechanisms which might account for the damping. It is possible that the damping is associated with grain boundary migration in the form of sub-microscopic grain growth.

The variation of peak damping and background damping, with grain size, has been demonstrated.

On the model of Kê it is possible to estimate the coefficient of viscosity for the grain boundary material. When extrapolated to the melting point of iron this gives reasonable agreement with the observed viscosity of molten iron, if a grain boundary thickness of about two atom diameters is assumed. With Mott's model of grain boundary sliding, it appears that the same number of atoms takes part in grain boundary melting in iron and in aluminium.

ACKNOWLEDGMENTS

Much of the experimental work was carried out by Mr. B. Sweeney and Mr. J. H. E. Fox. Analyses were carried out by Mr. K. Speight. The project received considerable help from early discussions with Dr. W. Thomas.

REFERENCES

- ANDRADE, E. N. DA C., 1934, *Phil. Mag.*, **17**, 698.
- BORG, R. J., and BIRCHENALL, C. E., 1960, *Trans. Amer. Inst. Min. (Metall.) Engrs*, **218**, 980.
- BRAMMAR, I. S., HONEYCOMBE, R. W. K., and WARD, R. G., 1958, *Acta Metall.*, **6**, 134.
- BRATINA, W. J., and WINEGARD, W. C., 1956, *Trans. Amer. Inst. Min. (Metall.) Engrs*, **208**, 1.
- HOPKINS, B. E., JENKINS, G. C. H., and STONE, H. E. N., 1951, *J. Iron Steel Inst.*, **168**, 377.
- Kê, T. S., 1947 a, *Phys. Rev.*, **71**, 533.
- 1947 b, *Phys. Rev.*, **72**, 41.
- 1948, *Phys. Rev.*, **73**, 267.
- 1949, *J. Appl. Phys.*, **20**, 274.
- KÖSTER, W., BANGERT, L., and LANG, W., 1955, *Z. Metall.*, **46**, 84.
- LE CLAIRE, A. D., 1949, *Progr. Metal Phys.*, **1**, 306.
- LEYMONIE, C., LACOMBE, P., and LIBANTI, C., 1958, *C.R. Acad. Sci., Paris*, **246**, 2614.
- MARINGER, R. E., and SCHWOPE, A. D., 1954, *Trans. Amer. Inst. Min. (Metall.) Engrs*, **200**, 365.
- MOTT, N. F., 1948, *Proc. Phys. Soc.*, **60**, 391.
- PEARSON, S., and ROTHERHAM, L., 1956, *Trans. Amer. Inst. Min. (Metall.) Engrs*, **206**, 894.
- PLATEAU, J., HENRY, G., and CRUSSARD, C., 1958, *Met. Corrosion Ind.*, **33**, 141.
- PRATT, J. N., BRATINA, W. J., and CHALMERS, B., 1954, *Acta Metall.*, **2**, 203.
- ROTHERHAM, L., and PEARSON, S., 1956, *Trans. Amer. Inst. Min. (Metall.) Engrs*, **206**, 881.
- SMITH, A. D. N., 1950, *R.A.E. Met. Rep.*, 55.
- STARR, C. D., VICARS, E. C., GOLDBERG, A., and DORN, J. E., 1953, *Trans. Amer. Soc. Metals*, **45**, 275.
- THOMAS, W. R., and CHALMERS, B., 1955, *Acta Metall.*, **3**, 17.
- THOMAS, W. R., and LEAK, G. M., 1956, *Metal Treatm.*, **23**, 359.
- WASHBURN, J., and PARKER, E. R., 1952, *J. Metals*, **4**, 1076.
- WEINIG, S., and MACHLIN, E. S., 1957, *Trans. Amer. Inst. Min. (Metall.) Engrs*, **209**, 32.
- ZENER, C., 1948, *Elasticity and Anelasticity of Metals* (Chicago: University Press).

Grain Boundary Damping II: Iron Interstitial Alloys

By G. W. MILES† AND G. M. LEAK‡

† British Iron and Steel Research Association, Sheffield

‡ Department of Metallurgy, The University, Manchester

MS. received 21st April 1961, in revised form 10th July 1961

Abstract. Internal friction measurements of the grain boundary relaxation peak have been carried out on alloys of high purity iron containing carbon or nitrogen. The influence of these impurities on peak height, peak temperature and on the activation energy for the mechanism giving rise to the damping has been determined. The results differ from those reported on the influence of substitutional impurities. The explanation of these effects is discussed qualitatively in terms of the boundary sliding and boundary migration mechanisms.

§ 1. INTRODUCTION

INTERNAL friction measurements show a maximum in the curve of damping against temperature (Leak 1961, to be referred to as Part I) which is associated with the presence of grain boundaries in the specimen. An activation energy can be associated with the process giving rise to the damping. For pure iron this is equal to 46 kcal mol^{-1} . The height for the maximum, after subtraction of the background damping, is dependent upon grain size in a manner shown graphically in Part I. The activation energy is very close to that estimated for grain boundary self-diffusion in alpha iron (Leymonie, Lacombe and Libanti 1958). The coefficient of viscosity for the boundary material has been estimated from Kê's (1947) model of the process. Suitable extrapolation to the temperature of the melting point in iron gives reasonable agreement with the values for viscosity of molten iron, assuming that the grain boundary is two to three atoms wide.

The two principal atomic models for the grain boundary damping process are those proposed by Kê (1949) and by Mott (1948). An advantage of the latter is that account could be taken of the effect of impurities on, for example, the activation energy for the process. This report, based on alloys of high purity iron containing carbon or nitrogen separately shows that interstitial impurities influence the grain boundary damping peak observed with the pure base metal.

Previously published work on the effect of impurities on the grain boundary relaxation peak has referred exclusively to substitutional impurity elements. Weinig and Machlin (1957) investigated alloys of copper containing 0.03 to 1 atomic % of nickel, silicon, aluminium or silver. Addition of the substitutional impurity reduced the height of the original grain boundary peak found with pure copper, called the 'solvent' peak. Simultaneously a new peak, the 'solute' peak, appeared at a much higher temperature and increased in peak height as the amount of the impurity was increased. Small amounts of impurity bring about

these changes; for example the original Cu peak disappeared after the addition of about 0.1 at. % Al or Si. As the solute content increased, the background damping, in the neighbourhood of the solute peak, decreased. The activation energy associated with the solvent peak increased as the solute content increased, e.g. from about 40 kcal mol⁻¹ for pure Cu to 81 kcal mol⁻¹ for Cu 0.1% Al or 0.1% Si. The activation energy of the solute peak decreased, e.g. from 67 kcal mol⁻¹ for 0.1% Al to 50 kcal mol⁻¹ for 0.8% Al or 55 kcal mol⁻¹ for 1% Si. An incidental observation was that there was no significant change in the magnitude of the solute peak as the grain size changed from 0.045 mm to 0.1 mm diameter.

Pearson and Rotherham (Pearson and Rotherham 1956, Rotherham and Pearson 1956) using alloys based on copper and silver as solvents found the activation energy of the solute peaks increased with alloying content, for example to about 44 kcal mol⁻¹ (from 33 kcal mol⁻¹ for pure Cu, presumably of different purity from that quoted by Weinig and Machlin). Their alloys generally contained more than 1% of alloying element. The temperature of the 'solute' peak decreased as the amount of solute increased. Weinig and Machlin (1957) observed the opposite effect, both works reported results for Cu-Si alloys. The activation energy for Cu-Si alloys determined by Weinig and Machlin dropped from 82 to 55 kcal mol⁻¹ as the Si content increased from 0.03 at. % to 1.0 at. %; Rotherham and Pearson's figures are 49 kcal mol⁻¹ at 0.9 at. % and 46 kcal mol⁻¹ at 8 at. %.

Starr *et al.* (1953) using stress-relaxation methods investigated aluminium-based solid solutions and measured activation energies of 38 kcal mol⁻¹, i.e. unchanged from that of pure aluminium. Only with additions of Mg was the activation energy increased to 54 kcal mol⁻¹ for 1.6 at. % Mg.

This brief summary shows the main characteristics of substitutional impurities giving solute and solvent damping peaks. The discussion of the present results will include some comparison of the effects of interstitial and substitutional impurities.

§ 2. SPECIMEN PREPARATION

The basic material used was the high purity iron wire described in Part I. Nitrogen and carbon were removed by prolonged heat treatment in flowing moist hydrogen followed by similar treatment with dry hydrogen (wire diameter about 6 mm).

The wire was reduced in diameter to about 2 mm and given similar recrystallization and grain growth treatments to those described in Part I. Nitrogen was introduced into the specimens by annealing them for 24 hours in a closed system containing known amounts of hydrogen and ammonia at 580°C. Specimens were homogenized by annealing under vacuum at temperatures between 580 and 650°C. The criteria for homogeneity were (a) that chemical analyses should remain constant and (b) that internal friction determination of the Snoek peak should remain constant. This method for introduction of nitrogen did not contaminate the specimens with carbon, above the level of analysis, approximately 0.0005 wt %. Carbon was introduced by heating specimens at 700°C in flowing hydrogen saturated with heptane at room temperature. The treatment lasted between 30–60 minutes according to the level of carbon required in the specimen, and it was followed by an homogenizing anneal, in vacuum, for 70 hours

at 700°C (after removal of the surface deposit of carbon). Experiments showed that the carbon had been introduced uniformly and that the nitrogen content of the specimens was less than 0.001 wt %.

Specimens were wires 20–25 cm long and diameter about 2 mm. A brief survey of the internal friction technique and the references to more complete descriptions are given in Part I.

§ 3. RESULTS

Damping measurements were taken for series of specimens of different grain size and different nitrogen or carbon contents. The specimens were quenched from the temperature of maximum solubility in the α phase, i.e. 580°C for iron–nitrogen specimens and 720°C for iron–carbon specimens. This treatment was adopted in order to give some standard treatment prior to the internal friction experiment. Table 1 gives details of the series of specimens which were prepared. In view of the dependence on grain size observed with specimens of pure iron, two series of iron–nitrogen alloys and one series of iron–carbon alloys were prepared with a fixed impurity content but of varying grain size.

The grain boundary damping peaks were observed at temperatures about 500°C. Precipitation of carbide or nitride would occur as the temperature was raised during the internal friction experiment, followed by re-solution as the temperature was raised further. At the peak temperature all the nitrogen would be in solution except for those alloys containing 0.1%. Carbide would be present for all the iron–carbon alloys with the possible exception of those containing only 0.009% carbon.

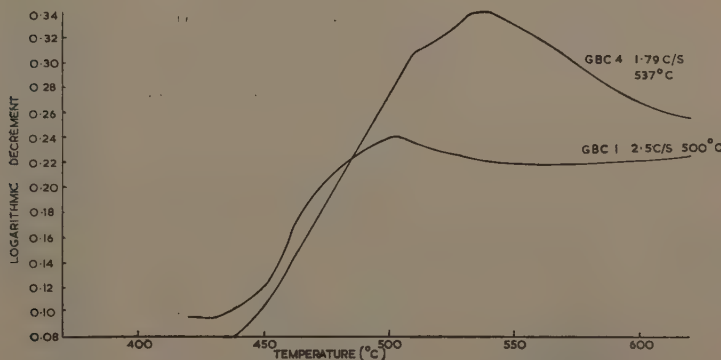


Fig. 1. Typical damping curves for specimens containing carbon.

Figure 1 gives typical damping–temperature curves for the iron–carbon alloys. They are different from those obtained with specimens of pure iron; higher peak damping and higher background damping are observed. Graphically, the peaks agree more closely with the curve calculated theoretically, assuming that the grain boundary stress relaxation takes place with a single relaxation time.

Table 1

Iron-Carbon Alloys			Iron-Nitrogen Alloys		
Series GBC	C content (wt %)	Grain size (No./mm)	Series GBN	N content (wt %)	Grain size (No./mm)
1	0.009	66	10	0.0056	48.8
3	0.022	32	9	0.012	36
4	0.07	32	8	0.016	29
2/1	0.089	30	7	0.018	30
2/2	0.089	11	4/1	0.026	60.5
2/3	0.089	8.6	4/2	0.026	25.2
2/4	0.089	5.8	4/3	0.026	17.2
6	0.16	186	4/4	0.026	10.7
7	0.16	72	3/1	0.0375	70.8
			3/2	0.0375	30.2
			3/3	0.0375	23.0
			1	0.101	80

3.1. Activation Energy: Iron-Carbon Alloys

The activation energy obtained for specimens of pure iron was 46 kcal mol⁻¹ (Part I); grain size variation did not affect the estimation of activation energy Q . Furthermore, it was shown that the damping-temperature relationship was governed by a function which included the term D^2 , where D is the grain diameter. These two aspects were investigated for the iron-carbon alloys containing 0.089% carbon. Fig. 2 shows the results in the form log (frequency) against peak temperature. These temperatures refer to the peaks after the rising background

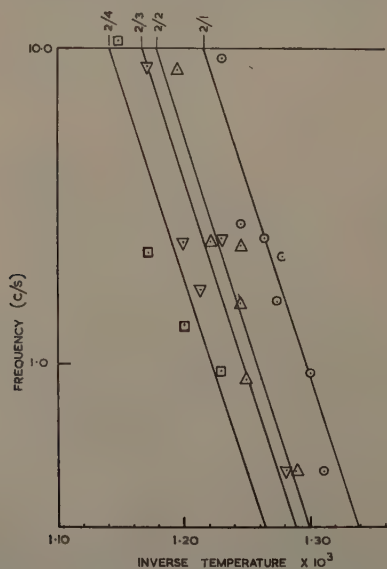


Fig. 2. Damping peak temperatures for iron-carbon specimens plotted as inverse temperature against log (frequency). All specimens containing 0.089% carbon.

damping has been deducted graphically. The two important features are that (a) within the limits of scatter of the result there is no significant change of activation energy with grain size, (b) the activation energy, measured from the slopes of the lines in Fig. 2, gives 60.5 ± 3.5 kcal mol⁻¹ for iron containing 0.089% carbon.

Although there is considerable scatter in these results, the curves in Fig. 2 have been drawn by the method of least squares as parallel straight lines of best fit for each series of specimens. Assuming a constant frequency of vibration, then the activation energy for the process giving rise to the damping should be given by

$$Q = R \frac{(\ln D_1 - \ln D_2)}{1/T_2 - 1/T_1} \quad \dots\dots (1)$$

if there is a simple dependence on D . If, as was found for the pure iron specimens, the dependence is on D^n then the right-hand side of Eqn 2 must be multiplied by n . It is assumed that the relaxation time τ for the process of damping is given by

$$\tau = \tau_0 \exp (Q/RT). \quad \dots\dots (2)$$

The results of this calculation give values varying between 32 and 52 kcal mol⁻¹. The scatter is too great to decide upon a value for n . All that can be concluded is that n lies between 1 and 2, by comparison with the value for Q of 60.5 obtained from frequency variations.

To determine the variation of activation energy with carbon content, series of specimens were carburized to different levels. Results are given in Fig. 3. The

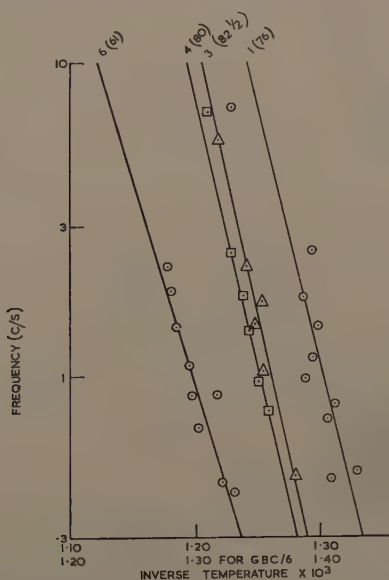


Fig. 3. Damping peak temperatures for iron-carbon specimens plotted as inverse temperature against log (frequency). Each series contains a different level of carbon. The abscissa scale zero is shifted for series GBC/6 to give more clarity.

calculated energies are given in Table 2 together with the value already reported for high purity iron (Part I). The lines in Fig. 3 have been fitted by the method of least squares.

Table 2

Carbon content (%)	0	0.009	0.022	0.07	0.089	0.16
Grain diameter (mm)	—	0.015	0.0313	0.0313	—	0.0054
Activation energy (kcal mol ⁻¹)	46 ± 3	76 ± 2	83 ± 4	80 ± 3	60.5 ± 3.5	61 ± 6

These results are shown graphically in Fig. 4 together with probable errors. Although the number of points on this graph is limited, the marked rise in activation energy with small additions of carbon is definite. Similarly the constancy of activation energy as the carbon content is increased above 0.08% is reasonably certain. The peak temperatures for these specimens are approximately at 500°C, where the carbon solubility is about 0.006% (Wert and Keefer 1957). Fig. 5 shows the variation of peak temperature with carbon content for a constant frequency of vibration and grain diameter. The maximum solubility of carbon in α -iron is about 0.02% at 720°C. The results indicate that the equilibrium solubility of carbon in α -iron grain boundaries must be different from that in the more perfect lattice inside the grains.

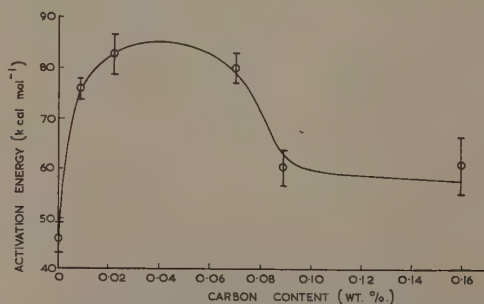


Fig. 4. Variation of activation energy for grain boundary damping with carbon content.

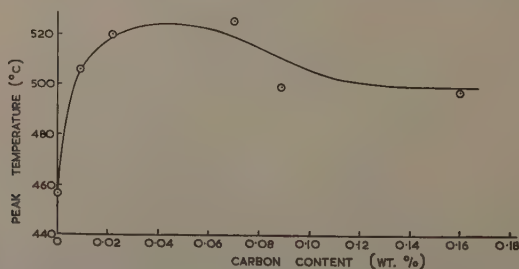


Fig. 5. Variation of grain boundary damping peak temperatures with carbon content.

3.2. Peak Damping: Iron-Carbon Alloys

It was reported in Part I that the height of the grain boundary damping peak and also the background damping decreased linearly with increasing grain diameter for the high purity iron. Marked differences have been observed with iron containing carbon. Despite the scatter in results it is possible to report the various trends.

Within the range of frequencies considered in this report there does not appear to be any significant variation of peak damping, peak height or background damping with frequency.

The variation of damping with grain size, for a series of specimens containing a constant amount of carbon, is given in Table 3.

Table 3. Specimens containing 0.089% Carbon

Grain diameter (mm)	0.0334	0.0908	0.1163	0.1725
Peak damping	0.280	0.273	0.285	0.311
Peak height	0.128	0.095	0.078	0.067
Background damping at 600°C	0.223	0.247	0.262	0.278

These results are shown graphically in Fig. 6; the peak damping increases slightly as the grain diameter increases whilst the background damping rises steadily and to a greater extent. (At 600°C the peak damping does not contribute

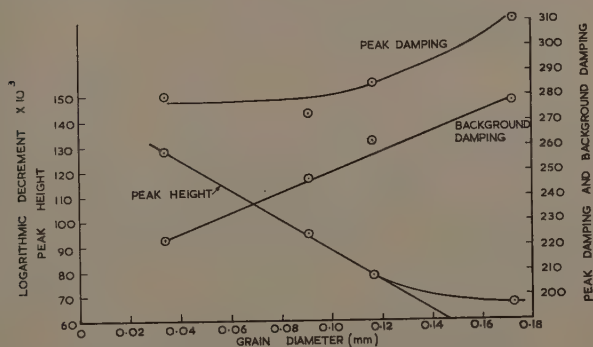


Fig. 6. Variation of peak damping, peak height and background damping with grain size. The background damping is taken arbitrarily at 600°C.

significantly to background damping.) The peak height drops almost linearly with increasing grain diameter. The point corresponding to a grain diameter of 0.1725 mm is probably subject to the greatest error. It has been established that the grain boundary damping peak is no longer detected when the grain size becomes closely comparable with the specimen cross section, although the exact relationship is not known.

Corresponding average values of damping for specimens of varying carbon content are given in Table 4 and Fig. 7.

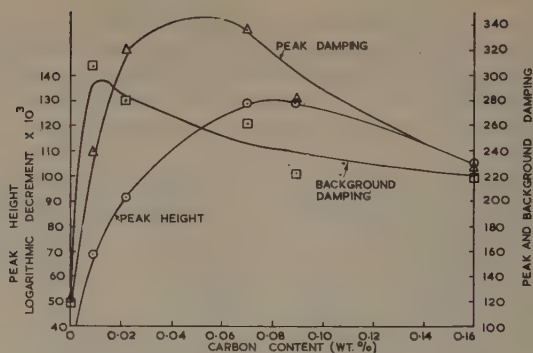


Fig. 7. Variation of peak damping, peak height and background damping with carbon content. The background and damping is taken arbitrarily at 600°C.

Table 4

Carbon content (wt %)	†0	0.009	0.022	0.07	‡0.089	§0.16
Grain diameter (mm)	0.031	0.031	0.031	0.031	0.031	0.031
Peak damping	0.120	0.240	0.320	0.336	0.280	0.230
Peak height	0.028	0.069	0.092	0.129	0.129	0.105
Background damping	0.119	0.308	0.280	0.261	0.221	0.220

† Extrapolated from results in Part I.

‡ Interpolated from experiments reported in Table 3.

§ Interpolated from experiments to be reported elsewhere.

The maximum values of damping for the various criteria plotted occur at widely different levels of carbon content. However, the background damping reaches a maximum corresponding roughly to a carbon content equal to that in equilibrium solid solution at the temperature of measurement (600°C). This conclusion will be significant if the background damping is associated with the movement of dislocations through the grain material in the neighbourhood of the boundaries.

3.3. Activation Energy: Iron-Nitrogen Alloys

One series of iron-nitrogen alloys was studied to determine any variation of activation energy with grain size. These alloys contained 0.0375% nitrogen. The experimental results are given in Fig. 8.

The experimental curves of damping against temperature for iron-nitrogen alloys were not as well defined as those for iron-carbon alloys. There is no apparent reason for this. Scatter in the results was similar to that for the iron-carbon series. However, Fig. 8 shows that there is no significant variation of activation energy (slope of the curves) with varying grain size of the specimens. All the curves have been drawn as parallel straight lines, within the uncertainty of least squares fitting, giving an activation energy of 68.5 kcal mol⁻¹. The probable error in this figure is ± 3 kcal mol⁻¹.

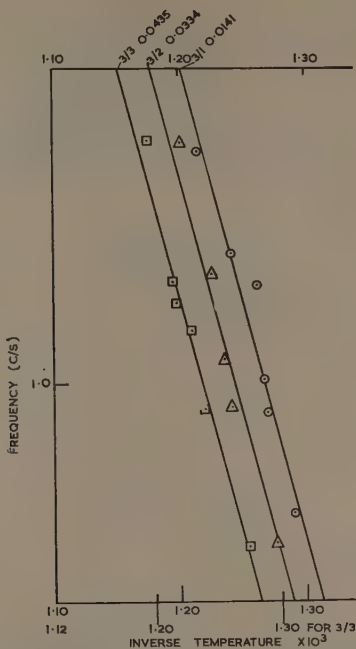


Fig. 8. Damping peak temperatures for iron-nitrogen specimens plotted as inverse temperature against log (frequency). All specimens contain 0.0375% nitrogen.

The activation energy for a constant frequency of vibration, but with varying grain size calculated by the same equation (1) used for the iron-carbon alloys is equal to 75 kcal mol⁻¹, taking the results for series GBN/3/1 and GBN/3/3. The results obtained by including GBN/3/2 give such wide variations that they must be discounted. It is concluded that the results for iron-nitrogen alloys do not require a D^2 term in the factor governing the damping, but a simple proportionality with D .

The variation of activation energy with nitrogen content can be seen from Fig. 9. A summary of the results is given in Table 5 and Fig. 10. The graphs have been drawn using least squares fitting and probable errors calculated from them.

Table 5

Nitrogen content (%)	0	0.0056	0.016	0.018	0.026	0.0375
Grain diameter (mm)	—	0.0225	0.0345	0.0333	0.0165	—
Activation energy (kcal mol ⁻¹)	46 ± 3	56 ± 2.5	66 ± 5	75.5 ± 6	70 ± 5	68.5 ± 3

The same trend is observed as that found with the iron-carbon alloys; the activation energy rises to a maximum then falls to a steady value. The maximum is not so well defined as for the iron-carbon alloys, but it occurs at a nitrogen content of about 0.02%. This is much less than the equilibrium value of the

solubility of nitrogen in α -iron at the temperature of the damping peaks, i.e. about 0.1% at 520°C. A second marked difference between iron-nitrogen and iron-carbon alloys is that the peak height is very small at the maximum level of nitrogen quoted in Table 5. Experiments have been made on alloys containing 0.1% nitrogen, but because the peaks were small and ill-defined, it was impossible to use them to determine an activation energy. The results imply that the grain boundaries become saturated with nitrogen before the grain interiors.

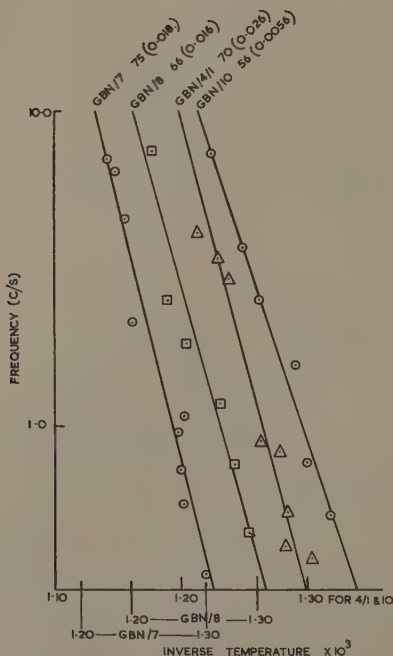


Fig. 9. Damping peak temperatures for iron-nitrogen specimens plotted as inverse temperature against log (frequency). The abscissa zeros have been shifted for series GBN/7 and GBN/8 for greater clarity. Each series of specimens contains a different level of nitrogen.

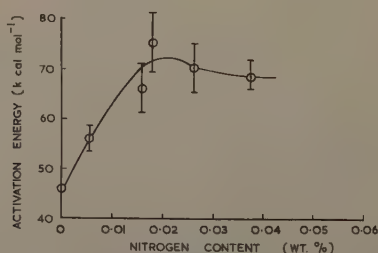


Fig. 10. Variation of activation energy for grain boundary damping with nitrogen content.

3.4. Peak Damping: Iron-Nitrogen Alloys

As with the iron-carbon alloys, no significant trend was observed in variation of peak damping, peak height or background damping, with frequency of vibration. Within the margin of experimental error it has been possible to estimate average values for each series of specimens. The variation of damping with grain size, for a series of specimens containing a constant amount of nitrogen, is shown in.

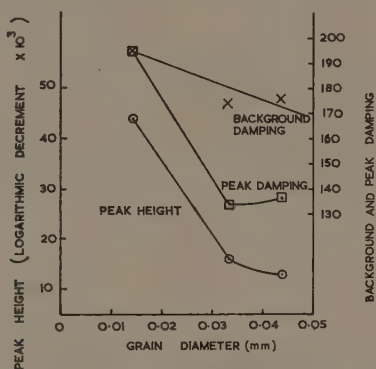


Fig. 11. Variation of peak damping, peak height and background damping with grain size. The background is measured arbitrarily at 600°C.

Table 6 and Fig. 11. Whilst the peak height drops at an approximately linear rate with increasing grain diameter as was observed with the iron-carbon alloys, both background and peak damping also drop. The whole level of damping is generally lower than with the iron-carbon alloys.

Table 6. Specimens containing 0.0375% Nitrogen

Grain diameter (mm)	0.0143	0.0332	0.0435
Peak damping	0.195	0.134	0.137
Peak height	0.044	0.016	0.013
Background damping 600°C	0.196	0.175	0.176

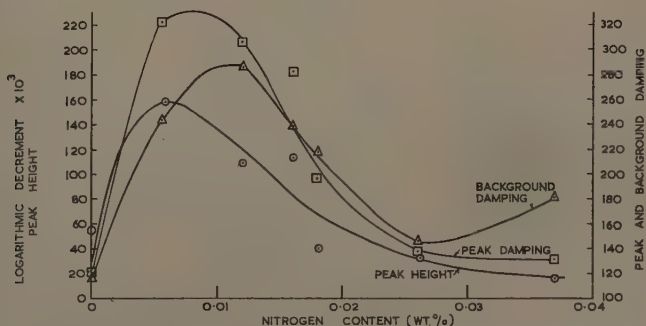


Fig. 12. Variation of peak damping, peak height and background damping with nitrogen contents. The background is measured arbitrarily at 600°C.

Table 7 and Fig. 12 show corresponding results for alloys containing various amounts of nitrogen.

Table 7							
Nitrogen content (wt %)	†0	0.0056	0.012	0.016	0.018	†0.026	†0.037
Grain diameter (mm)	0.031	0.0225	0.0278	0.034	0.033	0.034	0.034
Peak damping	0.120	0.322	0.305	0.282	0.196	0.137	0.134
Peak height	0.028	0.158	0.109	0.113	0.040	0.033	0.016
Background damping	0.119	0.245	0.285	0.239	0.218	0.145	0.180
† Extrapolated from results in Part I.							
‡ Interpolated from results for various grain sizes.							

Some anomalous results have been obtained for higher levels of nitrogen where peaks can sometimes be observed. These are low and inconsistent, and for this latter reason have not been reported.

§4. DISCUSSION

The present results can be discussed in terms of existing theories of grain boundary damping. It is necessary to consider the corresponding influence of substitutional impurities. The brief review of previous work showed that substitutional impurities caused the original solvent damping peak to disappear and a new solute peak to appear at a higher temperature. Both peaks could be observed simultaneously. Kê's (1947, 1949) mechanism of grain boundary sliding must consequently imply the existence of two specific types of boundary; the division of boundaries into these two groups must be caused by the presence of solute atoms. Solute atoms will segregate preferentially to boundaries; their concentration at boundaries will vary according to the misorientation of adjacent grains (McLean 1957). An explanation for the results could then be argued. As solute atoms are added to the alloy, initially some boundaries will be devoid of impurity atoms whilst others will contain varying amounts. This leads to two types of peak. As the solute content is increased all the boundaries will contain some solute atoms and so only one peak will be observed. Increased difficulty in sliding at boundaries in alloys is to be expected; the solute peak will consequently be at a higher temperature. Such an argument would really require a gradual transition in solute peak temperature. This is not observed with substitutional alloys but is observed with interstitial alloys. However, the level of damping in iron-nitrogen alloys was considerably lower than in the iron-carbon alloys. This suggests that less energy was absorbed in the boundaries of iron-nitrogen alloys because a smaller number of interstitial atoms was taking part in the boundary process. The only other explanation would be based on the possibility that less distortion was associated with nitrogen by comparison with carbon atoms. This in turn would imply considerable differences in peak temperatures which were not observed. Theories of boundary segregation cannot yet solve this problem for nitrogen and carbon atoms.

Mott's model of boundary damping gives an expression containing a term $\exp(-nL/kT)$ for the rate of slip at boundaries. n atoms take part in an elementary process of slip at temperature T , L is the latent heat of melting per atom. Whilst this model also cannot satisfactorily explain the existence of solute and solvent peaks it can explain some of the changes observed in activation energy for

the damping process as impurity is added. The changes for substitutional impurities are complex but those for interstitial alloys might be more easily explained. Initially interstitial atoms will add to the value of nL , increasing the observed activation energy. As more impurity is added a stage will be reached in which the number of iron atoms in the group must be reduced. This could allow a decrease in the value of nL . Ultimately the groups of atoms will be saturated with interstitials and the activation energy will become constant. Since carbon introduces greater distortion than nitrogen atoms in the iron lattice, so the general effects of interstitials might be expected to be observed with smaller amounts of carbon than nitrogen. However, Figs 4 and 10 show the opposite trend.

The explanation discussed tentatively in Part I, based on boundary migration, can be extended to explain the present results. The boundary will migrate into an adjacent grain reversibly under the action of an applied stress. It is not necessary to postulate different types of boundary. For substitutional alloys, when the impurity content is low, the boundary atoms will be of two types, solvent and solute. Each type of atom will have its associated energy of activation for jumping from one lattice to the neighbour. Two damping peaks should be observed. As the impurity content is increased all the atom sites favoured for jumping, i.e. all the distorted sites, will be occupied by solute atoms and thus only a solute peak will be observed. Interstitial atoms will occupy distorted interstitial sites in the boundaries. The energy barrier to be overcome by an iron atom in jumping to a neighbouring lattice will now be greater than for the pure metal; extra distortion energy must be supplied. Two peaks will not be observed, merely an increased activation energy for the original solvent peak. This should be identical with the activation energy for iron diffusion in the boundaries of the interstitial alloys. Data for comparison purposes are not available; appropriate measurements are now being made. It is surprising, however, that the measured activation energy for boundary damping in the alloys can rise to a value greater than that for volume self-diffusion.

Unfortunately, calculations of the relaxation time constants τ_0 do not clarify the situation. Eqn (2) is assumed to be valid. Results, calculated for data at 1 c/s, are given in Table 8.

Table 8

Carbon content (wt %)	0.009	0.022	0.07	0.089	0.16
Relaxation constant τ_0 (sec)	5×10^{-23}	3×10^{-24}	3×10^{-23}	10^{-18}	10^{-18}
Nitrogen content (wt %)	0.0056	0.016	0.018	0.026	0.0375
Relaxation constant τ_0 (sec)	3×10^{-17}	10^{-19}	10^{-22}	10^{-20}	5×10^{-20}

The corresponding frequency factors reach maxima at impurity contents similar to those at which the activation energies reach maximum values. None of these frequency factors corresponds to the value to be expected if single atom jumps controlled the damping. This may not be unreasonable when it is realized that impurity atoms segregating to the boundaries alter, considerably, the environment of the iron atoms.

The gradual drop of peak height with increasing solute concentration would be expected as more energy is required to move atoms to the adjacent lattice.

The gradual decrease with increasing grain size is difficult to understand quantitatively. Kê originally suggested that damping should be independent of grain size; this is not substantiated by the present results. Qualitatively as the amount of boundary material present increases so will the amount of energy absorbed, during boundary migration increase.

If the background damping is associated with dislocation movements, for example, in the neighbourhood of the boundaries, then it might be expected to be higher for iron-carbon alloys than for iron-nitrogen alloys. The solubility of carbon is much lower than that of nitrogen; precipitation of iron carbides would take place at temperatures of 500–550°C. This would restrict dislocation movement, but might lead to a greater dislocation density than for the iron-nitrogen alloys.

There are no data in the literature to compare estimations of the viscosity of the iron-carbon and iron-nitrogen alloys from damping measurements with those of experimental viscosity determinations in molten iron. Small changes in the assumptions of boundary thickness could accommodate the sparse viscosity measurements available.

The results presented can be summarized as follows:

- (i) Interstitial impurities raise the temperature of the grain boundary relaxation peak.
- (ii) They alter the activation energy of the damping process which increases to a maximum then decreases to a steady value.
- (iii) The peak height is initially increased, after which it decreases to zero as the impurity content is increased.
- (iv) The background damping and peak damping follow trends similar to each other.
- (v) The explanations put forward by Kê and by Mott cannot adequately explain the damping phenomena in alloys.
- (vi) It is suggested that the mechanism of damping is that of reversible boundary migration on an atomic scale. The observed effects can then be explained at least qualitatively.
- (vii) It is essential to obtain more data on boundary diffusion in order to test this explanation.

ACKNOWLEDGMENTS

Much of the experimental work has been carried out by Mr. J. H. E. Fox. The analyses have been done by Mr. K. Speight.

REFERENCES

- KÊ, T. S., 1947, *Phys. Rev.*, **71**, 533.
 — 1949, *J. Appl. Phys.*, **20**, 274.
 LEAK, G. M., 1961, *Proc. Phys. Soc.*, **78**, 1520.
 LEYMONIE, C., LACOMBE, P., and LIBANTI, C., 1958, *C. R. Acad. Sci., Paris*, **246**, 2614.
 MCLEAN, D., 1957, *Grain Boundaries in Metals* (Oxford: University Press), Chs 2 and 3.
 MOTT, N. F., 1948, *Proc. Phys. Soc.*, **60**, 391.
 PEARSON, J., and ROTHERHAM, L., 1956, *Trans. Amer. Inst. Min. (Metall.) Engrs*, **209**, 894.
 ROTHERHAM, L., and PEARSON, J., 1956, *Trans. Amer. Inst. Min. (Metall.) Engrs*, **209**, 881.
 STARR, C. D., VICARS, E. C., GOLDBERG, A., and DORN, J. E., 1953, *Trans. Amer. Soc. Metals*, **45**, 275.
 WEINIG, S., and MACHLIN, E. S., 1957, *Trans. Amer. Inst. Min. (Metall.) Engrs*, **210**, 32.
 WERT, C. A., and KEEFER, D., 1957, *University of Illinois, Department of Metallurgy, Tech. Rep. No. 11.*

Microwave Measurement of Attachment in Oxygen-Nitrogen Mixtures

BY J. J. LENNON AND M. J. MULCAHY†

Department of Electrical Engineering, The University of Liverpool

MS. received 30th June 1961

Abstract. A microwave cavity method has been used to measure the electron loss rate following a pulsed discharge in oxygen-nitrogen mixtures. Preliminary results indicate that, when suitable pressures of oxygen and nitrogen are chosen, the main mechanism of electron removal in the later afterglow is a three-body attachment process. The three-body coefficient $K = 2.4 \times 10^{-30} \text{ cm}^6 \text{ sec}^{-1}$ is in good agreement with the drift tube measurements, for thermal electrons, of Chanin, Phelps and Biondi.

UP to recent times, experimental difficulties prevented the measurement of attachment rates in electronegative gases at electron energies less than about 1 eV. The advent of microwave and refined drift tube techniques has enabled attachment of electrons at thermal energies (0.04 eV) to oxygen molecules to be studied. Microwave measurements in pure oxygen have indicated a two-body attachment process with a very low cross section (Biondi 1951, Holt 1959, Sexton, Mulcahy and Lennon 1959 a) (10^{-22} cm^2) whilst the drift tube studies of Hurst and Bortner (1959) and Chanin, Phelps and Biondi (1959) have shown that for average electron energies less than 1 eV the process is a three-body one involving the formation of an excited O_2^- ion which is subsequently stabilized by collision with a neutral molecule. The purpose of this note is to give new preliminary results of attachment measurements in oxygen-nitrogen mixtures, using a microwave method.

A resonant microwave cavity method was used which was similar in principle to that used originally by Biondi and Brown (1951) and has already been fully described (Sexton, Mulcahy and Lennon 1959 b). The gas sample being investigated is contained inside the resonant cavity and is ionized by a magnetron pulse. Subsequent deionization is measured by observing the change in resonant frequency of the cavity as a function of time. The detuning of the cavity, caused by the large admittance of the ionized gas, can be related to the average electron density.

As shown by Chanin, Phelps and Biondi (1959) the time rate of change of electron density, for a three-body attachment loss, can be written as

$$\frac{dn_e}{dt} = -\nu_a n_e = -K n^2 n_e$$

where ν_a is the attachment frequency, K is the three-body coefficient and n is the density of captor molecules.

For a binary gas mixture of, say, oxygen and nitrogen this equation can be written as

$$\begin{aligned} \frac{dn_e}{dt} &= -(K_{\text{O}_2} n_{\text{O}_2}^2 + K_{\text{N}_2} n_{\text{N}_2} n_{\text{O}_2}) n_e \\ &= -K' n_{\text{O}_2} n_{\text{N}_2} n_e \end{aligned}$$

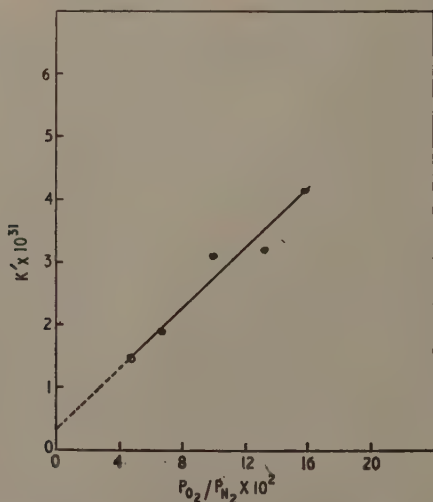
† Now at Associated Electrical Industries (Manchester) Ltd., Trafford Park, Manchester.

where K' is an overall three-body coefficient for the mixture and

$$K' = K_{O_2} \frac{n_{O_2}}{n_{N_2}} + K_{N_2}$$

Thus K' can be calculated from a knowledge of the partial pressures of oxygen and nitrogen and a measurement of dn_e/dt . A three-body attachment process is indicated by a straight line plot of K' against n_{O_2}/n_{N_2} . The slope of this straight line gives K_{O_2} and the intercept on the K' axis gives K_{N_2} which is an indication of the efficiency of nitrogen as a stabilizing agent as compared with oxygen itself.

In an endeavour to resolve the difficulties encountered in interpreting the microwave results in pure oxygen, various mixtures of oxygen and the rare gases have been studied in this Department. While these results give indirect evidence of three-body attachment, it is impossible to extract a coefficient for the process from them. Data on oxygen-helium mixtures have been submitted elsewhere (Mulcahy, Sexton and Lennon†). The present measurements indicate that when suitable pressures of oxygen and nitrogen are chosen, the main mechanism of electron removal in the later afterglow is a three-body attachment process.



Three-body coefficient plotted against oxygen concentration for oxygen-nitrogen mixtures. $P_{N_2} \approx 10$ mm Hg; $P_{O_2} \approx 0.5$ –2 mm Hg; $K_{O_2} = 2.4 \times 10^{-30}$ cm⁶ sec⁻¹; $K_{N_2} = 3.5 \times 10^{-32}$ cm⁶ sec⁻¹.

The Figure shows a plot of K' against the ratio of oxygen to nitrogen pressure. The nitrogen pressure was kept fixed at approximately 10 mm Hg and the oxygen pressure varied from 0.5 to 2 mm Hg. The slope of this line gives a value for K_{O_2} of 2.4×10^{-30} cm⁶ sec⁻¹ and the extrapolated intercept shows that $K_{N_2} = 3.5 \times 10^{-32}$ cm⁶ sec⁻¹. This indicates that a nitrogen molecule is about 70

† Mulcahy, M. J., Sexton, M. C., and Lennon, J. J., Paper submitted to the *Fifth International Conference on Ionization Phenomena in Gases*, held in Munich, August 1961.

times less efficient than an oxygen molecule in stabilizing the newly formed excited negative ion. These figures compare favourably with Chanin's values of $2.8 \times 10^{-30} \text{ cm}^6 \text{ sec}^{-1}$ for K_{O_2} (electron energy 0.04 eV) and a factor of about 50 times smaller than oxygen for K_{N_2} .

For oxygen pressures above 2 mm Hg the value of K' was found to decrease with increase of oxygen partial pressure. This effect could not be pursued to any great extent as the electron loss rate was too fast to permit of accurate measurement for oxygen pressures greater than about 2.7 mm Hg.

The decrease in K' is felt to be due to the onset of collisional detachment by vibrationally excited oxygen molecules as suggested by Nicholls and Hopwood (Craggs 1957) to explain the microwave results in pure oxygen. As the oxygen pressure is reduced below 0.5 mm Hg the calculated value of K' increases rapidly with decrease of oxygen concentration. It is felt that this effect is spurious and may well be due to the loss rate of electrons in mixtures with low oxygen concentrations being comparable with that in pure nitrogen at the same pressure. A similar effect was observed by Hasted, Chantry and Wharmby (1961, private communication) who seem to have confined their measurements to this low oxygen pressure range.

Preliminary results with higher nitrogen pressures indicate a somewhat lower value of K_{O_2} . These results will be reported more fully at a later date.

REFERENCES

- BIONDI, M. A., 1951 a, *Phys. Rev.*, **84**, 1072.
— 1951 b, *Rev. Sci. Instrum.*, **22**, 500.
CHANIN, L. M., PHELPS, A. V., and BIONDI, M. A., 1959, *Phys. Rev. Letters*, **2**, 344.
CRAGGS, J. D., 1957, *Proc. Third Int. Conf. on Ionization Phenomena in Gases, Venice* (Milan: The Italian Physical Society).
HOLT, E., 1959, *Bull. Amer. Phys. Soc.*, [II], **4**, 112.
HURST, G. S., and BORTNER, T. E., 1959, *Phys. Rev.*, **114**, 116.
SEXTON, M. C., MULCAHY, M. J., and LENNON, J. J., 1959 a, *Proc. Fourth Int. Conf. on Ionization Phenomena in Gases, Uppsala* (Amsterdam: North-Holland).
— 1959 b, *Brit. J. Appl. Phys.*, **10**, 356.

The Correction of Signals Distorted by Linear Apparatus†

BY C. P. FLYNN

Department of Physics, University of Illinois, Urbana, Illinois

MS. received 28th October 1960, in revised form 5th June 1961

Abstract. In a previous paper by Flynn and Seymour a technique was developed whereby a type of distortion produced by linear apparatus could be corrected rapidly and efficiently to obtain a 'true' output signal. The distortion considered was not the most general linear distortion, and several cases of practical importance were therefore excluded.

In the present paper, the general linear distortion is examined and equations are developed which permit the rapid correction of distorted output signals into those to be anticipated from the use of ideal apparatus. The procedure is illustrated by means of an example. The accuracy of the corrected signals is then discussed, and it is shown that in some apparatus, as for instance, the magnetic resonance spectrometer, predictable optimum conditions occur under which the form of the true output signal may best be determined.

§ 1. INTRODUCTION

THE desire to obtain more precise data from apparatus output signals has led, particularly in the field of communication engineering, to a continued interest in the relationship between the input and output signals of linear apparatus, both in the presence and absence of apparatus noise. In optics also, much ingenuity has been shown both in the design of components in order to minimize image distortion, and in the development of new techniques whereby inherent distortions may be partially inhibited, as in the case of the 'apodization' of optical instruments (see Dossier and Jacquinot 1950). Nevertheless, it is not possible to produce instruments having infinite resolving power, and rather than deal with the modification of particular apparatus to minimize distortion, our concern will be with the interpretation of the output signal in the inevitable presence of the sources of limited resolution.

In a previous paper (Flynn and Seymour 1960, to be referred to as I) on the correction of output signals, the earlier work of Shull (1946), Stokes (1948) and Tournarie (1957) was considered, and an alternative scheme was presented whereby a simple type of linear distortion could be numerically inverted with a minimum of labour. The present paper contains the extension of this treatment to the general linear distortion, in which case the response of the apparatus is a function of the coordinates of the input signal. It will be appreciated that this

† Supported in part by the U.S. Atomic Energy Commission.

distortion is more complex than that normally encountered in communication apparatus, since the demand of reproducibility in apparatus whose independent variable is time precludes the possibility of the more general distortion occurring. Rather, the present treatment becomes necessary in apparatus having variables other than time, in which event the resolution frequency depends on the position of the input signal.

The application of information theory to transmission systems has resulted in a much wider understanding of the capacity of systems to convey detailed signals from a source to an interpreting device (Shannon 1948, see also Blanc-Lapierre 1953). The theory has been extended by several workers in treatments of optical apparatus (Blanc-Lapierre 1953, Blanc-Lapierre, Perrot and Peri 1955, Toraldo di Francia 1955, Linfoot 1958), and in each case the degrading effect of noise on the quantity of information contained in the output signal has been stressed. It has also been pointed out that in assessing the quality of the output signal in the presence of noise, it is necessary to be pragmatic to the extent of inquiring as to the precise nature of the information required and the manner in which it may be obtained from the output signal, before deciding the appropriate conditions under which an experiment may be performed (see Linfoot 1958). In the present investigation, we are interested in the shape of the input signal, which may only be obtained from the output data by means of a linear processing scheme such as that described in the following pages; our aim in performing an experiment must therefore be to minimize the discrepancy between the input signal and the corrected output signal. In §§ 6 and 7, the standard deviation between the two signals over the interesting section of the output signal is used as a measure of this discrepancy, and in this way simple relationships are obtained which inform the experimentalist as to the apparatus conditions under which the particular structure of interest may best be examined.

Following the notation developed in I, we write $f(x_0)$ for the output signal of a linear apparatus, where x_0 is so chosen as to preserve the order and weight of the output data. This output signal is stimulated by the application to the apparatus of an 'input signal' $g(x_0)$ which may also be considered as a function of x_0 . By virtue of the assumed linearity of the apparatus, the relation between input and output signal of the apparatus may be written

$$f(x_0) = \zeta g(x_0) \quad \text{.....(1.1)}$$

where ζ is some linear operator. It will be demonstrated that ζ is a function of the differential operator d/dx_0 and of x_0 , and that a practical method exists for inverting Eqn (1.1) to yield the apparatus input function

$$g(x_0) = \zeta^{-1} f(x_0). \quad \text{.....(1.2)}$$

The functions $f(x_0)$ and $g(x_0)$ will be assumed to be smooth curves capable of Taylor expansion over a sufficiently wide range of x_0 round any point x . It is true that occasionally an output signal is presented as a set of amplitudes at discrete intervals of x_0 , but it is rare for the input function to be of this form. Thus, the output function will bear more resemblance to the input if modified initially to a smooth curve, and it will be adequate if this case only is considered.

§ 2. THE CORRECTION OPERATOR

As pointed out in I, the relation between $f(x_0)$ and $g(x_0)$ need not wholly be concerned with limiting the resolving power of the apparatus, but may also

result in displacements, differentiations, etc., of the input signal. It is convenient to extract from the operator ζ that part which causes the limited resolution only. This may be performed by simulating an apparatus identical with our real apparatus except for the removal of the source of limited resolving power; that is to say, an apparatus whose response to a δ function input signal is the δ function or one of its derivatives, together with an appropriate constant of proportionality. If we take the response of this apparatus to be

$$f(x_0) = \xi g(x_0) \quad \dots\dots (2.1)$$

and write for our real apparatus

$$f(x_0) = (\zeta \xi^{-1}) \xi g(x_0) = \eta \xi g(x_0) \quad \dots\dots (2.2)$$

where $\eta = (\zeta \xi^{-1})$, then it is evident that we may reduce the distorted output signal to that to be anticipated from the use of an idealized instrument, by means of the correction operator η^{-1} and the relation

$$\eta^{-1} f(x_0) = \xi g(x_0). \quad \dots\dots (2.3)$$

It is clear that as the resolving power of the instrument is increased, η^{-1} tends to unity and the modification of $f(x_0)$ produced by the correction operator tends to zero. In practical correction, this property of η^{-1} is invaluable, since the distortion is normally quite small, and a rapidly convergent expansion of correction terms may therefore be used to obtain an infinitely resolved output signal from the distorted one.

§ 3. THE GENERAL LINEAR APPARATUS

If we supply a δ -function input signal to a real apparatus at $x_0 = x$:

$$g(x_0 - x) = \delta(x_0 - x), \quad \dots\dots (3.1)$$

then we may anticipate some sort of output signal

$$f(x_0 - x) = h(x_0 - x|x) \quad \dots\dots (3.2)$$

in the neighbourhood of $x_0 = x$, tending to zero fairly rapidly as $|x_0 - x|$ increases. It will be noted that in general, the function $h(x_0 - x|x)$ is a function both of the displacement from the position of the input δ -function, and of the position x itself.

By taking account of the linearity of the apparatus, it is evident that in the presence of an input signal $g(x_0)$, the apparatus response will be given by the relation

$$f(x_0) = \int_{-\infty}^{\infty} g(x_0 - x) h(x|x_0 - x) dx. \quad \dots\dots (3.3)$$

By Taylor expansion of the function $g(x_0 - x)h(x|x_0 - x)$ round the point x_0 , it is found that

$$f(x_0) = \int_{-\infty}^{\infty} \sum_{n=0}^{\infty} \frac{(-1)^n}{n!} x^n \frac{d^n}{dx_0^n} \left\{ g(x_0) h(x|x_0) \right\} dx \quad \dots\dots (3.4)$$

$$= \left\{ \sum_{n=0}^{\infty} \sum_{m=n}^{\infty} \frac{(-1)^m}{(m-n)! n!} M_m^{m-n}(h|x_0) \frac{d^n}{dx_0^n} \right\} g(x_0), \quad \dots\dots (3.5)$$

where

$$M_p^q(h|x_0) = \frac{d^q}{dx_0^q} \int_{-\infty}^{\infty} h(x|x_0) x^p dx \quad \dots\dots (3.6)$$

is the q th rate of change, with respect to the position x_0 , of the p th moment of the apparatus response to a δ -function input signal at x_0 . It is now evident from comparison of Eqns (1.1) and (3.5) that the response operator of the real apparatus may be written

$$\zeta = \left\{ \sum_{n=0}^{\infty} \sum_{m=n}^{\infty} \frac{(-1)^m}{(m-n)!n!} M_m^{m-n}(h|x_0) \frac{d^n}{dx_0^n} \right\}. \quad \dots (3.7)$$

The idealized apparatus operator ξ appears when a factor independent of the $M_p^q(h|x_0)$ can be removed from ζ . In the great majority of cases, this factor is simply a constant, but in a few cases, a power of d/dx_0 is common to all terms in ζ as a consequence of the zero value of the first few moments of $h(x|x_0)$. Infrequently, examples may be found, as for instance in the case of a time constant circuit where a more complicated factor occurs, corresponding to a displacement operator.

Let us suppose that the first p moments of $h(x|x_0)$ vanish identically: clearly

$$\xi = \frac{d^p}{dx_0^p}, \text{ leaving}$$

$$\eta = \left\{ \sum_{n=0}^{\infty} \sum_{m=n}^{\infty} \frac{(-1)^{m+p}}{(m-n)!(n+p)!} M_{m+p}^{m-n}(h|x_0) \frac{d^n}{dx_0^n} \right\}. \quad \dots (3.8)$$

Hence by placing

$$M_n(h|x_0) = \sum_{m=n}^{\infty} \frac{(-1)^{m+p}}{(m-n)!(n+p)!} M_{m+p}^{m-n}(h|x_0), \quad \dots (3.9)$$

and

$$\mu_n(h|x_0) = M_n(h|x_0)/M_0(h|x_0), \quad \dots (3.10)$$

$$f(x_0) = \eta \xi g(x_0) = \left\{ M_0(h|x_0) \sum_{n=0}^{\infty} \mu_n(h|x_0) \frac{d^n}{dx_0^n} \right\} \xi g(x_0). \quad \dots (3.11)$$

Equation (3.11) will be used in § 4 as the basis of a technique for correcting the general linear distortion. Before continuing, however, it is useful to note the relationship between the general form (3.8) of the distortion operator and the form found in the particular case studied in I.

Consider the curve

$$\psi(x_0|x_1) = \xi^{-1} h(x_0|x_1). \quad \dots (3.12)$$

Assuming that $\xi = d^p/dx_0^p$, we may relate the moments $M_r^s(\psi|x_1)$ of the curve $\psi(x_0|x_1)$ to the moments $M_r^s(h|x_1)$:

$$M_{r+p}^s(h|x_1) = (-1)^p \frac{r!}{(r+p)!} M_r^s(\psi|x_1). \quad \dots (3.13)$$

Hence, substituting for $M_{m+p}^{m-n}(h|x_0)$ in Eqn (3.8),

$$\eta = \left\{ \sum_{n=0}^{\infty} \sum_{m=n}^{\infty} \frac{(-1)^m(m+p)!}{(m-n)!(n+p)!m!} M_m^{m-n}(\psi|x_0) \frac{d^n}{dx_0^n} \right\}. \quad \dots (3.14)$$

In the event of $h(x|x_0)$ being independent of x_0 , i.e. $h(x|x_0) = h(x)$; $\psi(x|x_0) = \psi(x)$, it may be seen that

$$\eta = \left\{ \sum_{n=0}^{\infty} \frac{(-1)^n}{n!} M_n^0(\psi) \frac{d^n}{dx_0^n} \right\}, \quad \dots (3.15)$$

which is effectively the result derived in I.

§ 4. THE CORRECTION EQUATION

Following the procedure adopted in I, Eqn (3.11) may be inverted to give an equation for $\xi g(x_0)$ in terms of $f(x_0)$ and its horizontal difference at a differencing interval ω . The conventional symbols δ and μ will be used for the differencing operators since there is little chance of confusion between μ and $\mu_n(h|x_0)$.

To be of value, the various terms in $f(x_0)$ in the expression for $\xi g(x_0)$ need to be sorted into an approximate order of decreasing size so that the correction procedure may easily be terminated when a sufficient accuracy is achieved. In order to achieve this, it is useful to make the following reasonable assumptions as to the form of $h(x|x_0)$:

(i) The total distortion is small, in which case

$$\left. \begin{aligned} 1 &\gg \frac{\mu_2(h|x_0)}{\omega^2} \gg \frac{\mu_4(h|x_0)}{\omega^4}, \\ \mu_1(h|x_0) &\gg \frac{\mu_3(h|x_0)}{\omega^2}, \text{ etc.} \end{aligned} \right\} \dots\dots (4.1)$$

(ii) The variation of the $\mu_n(h|x_0)$ over a distance ω is small compared with $\mu_n(h|x_0)$.

(iii) $h(x|x_0)$ is essentially even or odd according to whether p is even or odd. In this event, $\mu_n(h|x_0)$ is small for n odd.

These assumptions are easily justified; the first by the demonstration in §§ 6 and 7 that the maximum information concerning the input signal may be determined only when the distortion is small, and the second and third assumptions are simply observations concerning the output characteristics of many forms of linear apparatus.

Using assumptions (i) to (iii) in order to find the most important terms, the correction equation is found to be

$$\begin{aligned} \xi g(x_0) = & \left[1 - \mu_1(h|x_0) \frac{\mu \delta^1}{\omega} - \left\{ \mu_2(h|x_0) - \mu_1^2(h|x_0) \right\} \frac{\delta^2}{\omega^2} \right. \\ & - \left\{ \mu_3(h|x_0) - \frac{\omega^2}{6} \mu_1(h|x_0) - \mu_1(h|x_0) \mu_2(h|x_0) \right\} \frac{\mu \delta^3}{\omega^3} \\ & \left. - \left\{ \mu_4(h|x_0) - \frac{\omega^2}{12} \mu_2(h|x_0) - \mu_2^2(h|x_0) \right\} \frac{\delta^4}{\omega^4} - \dots\dots \right] f(x_0), \end{aligned} \dots\dots (4.2)$$

where

$$f(x_0) = f(x_0)/M_0(h|x_0). \dots\dots (4.3)$$

It is instructive to compare the general correction Eqn (4.2) with the particular form deduced in I for the case of $M_p^q(h|x_0)$ not dependent on x_0 . In the present notation, the latter equation is

$$\xi g(x_0) = \left[1 - \mu_2(h) \frac{\delta^2}{\omega^2} - \mu_3(h) \frac{\delta^3}{\omega^3} - \left\{ \mu_4(h) - \frac{\omega^2}{12} \mu_2(h) - \mu_2^2(h) \right\} \frac{\delta^4}{\omega^4} \right] f(x_0) \dots\dots (4.4)$$

where the $\mu_n(h)$ are simply proportional to the normalized moments of $h(x_0)$,

$$\text{i.e.} \quad \mu_n(h) = (-1)^{n+p} M_n(h)/(n+p)! M_0(h). \dots\dots (4.5)$$

In the general case, $\mu_1(h|x_0)$ may not be assumed zero, and additional terms are thereby introduced into the correction in passing from (4.4) to (4.2). Further, the $\mu_n(h|x_0)$ are sums of a series of terms in $M_p^q(h|x_0)$ rather than being of the

simpler form (4.5). However, these complications are not very serious, since the terms in $\mu_1(h|x_0)$ are usually small, corresponding to a reasonably symmetrical response function, and the series for $\mu_n(h|x_0)$ converge very rapidly in most cases so that only one or possibly two terms are significant in the correction.

The principal difference introduced by the more general form (4.2) is the dependence of the $\mu_n(h|x_0)$ on x_0 . In the numerical correction procedure, the differences of $f(x_0)$ must then be multiplied by the coefficients appropriate to the point x_0 at which the differences are taken, rather than by a factor whose value is independent of x_0 , as in the case of the more simple distortions.

§ 5. A PRACTICAL EXAMPLE

From the general form of Eqns (3.6), (3.9), (3.10), (4.2) and (4.3), the computation of a corrected output signal may appear a formidable proposition. By means of an example in which a fairly complicated distortion is corrected, it will be shown that this is not the case, and that the correction may be accomplished with efficiency and accuracy.

The apparatus response to an infinitely resolved input $\delta(x_0)$ will be represented by

$$h(x|x_0) = (\beta^2/\pi)^{1/2}(1 + x_0/3) \exp\{-\beta^2 x^2\} \quad \dots\dots (5.1)$$

so that in the range $-3 < x_0 < 3$, the magnitude $M_0(h|x_0)$ of the response varies from 0 to 2, and also, each element of the input is spread into a Gaussian shape with dispersion $(2\beta^2)^{-1/2}$. The distortion represented by (5.1) is therefore a rather exaggerated example of the variation of sensitivity which occurs in many practical instruments. For instance, the wavelength sensitivity of photographic plates and photocell, and the variations of flux with energy in a particle spectrometer lead to this type of distortion. Again, the sensitivity variation may be due to an inherent, though undesired, property of the experiment itself, as are the effects of transition probabilities on bands observed by soft x-ray techniques.

The apparatus input function will be taken as

$$g(x_0) = (\alpha^2/\pi)^{1/2} \exp\{-\alpha^2 x_0^2\} \quad \dots\dots (5.2)$$

and the apparatus response to this input,

$$f(x_0) = \int_{-\infty}^{\infty} g(x_0 - x)h(x|x_0 - x),$$

may be found in the form

$$f(x_0) = (\gamma^2/\pi)^{1/2}(1 + \gamma^2 x_0/3\alpha^2) \exp\{-\gamma^2 x_0^2\} \quad \dots\dots (5.3)$$

where

$$\gamma^2 = \alpha^2 \beta^2 / (\alpha^2 + \beta^2). \quad \dots\dots (5.4)$$

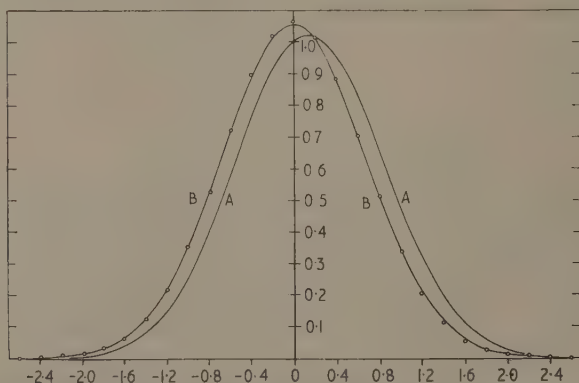
α and β are chosen to be 1 and 3 respectively, in order both that $g(x_0)$ is spread over a wide range of apparatus response and that a fairly severe distortion occurs owing to the width $(\beta)^{-1}$ of the curve $h(x|x_0)$. Using these values, $f(x_0)$ is shown as curve A in the figure and tabulated at intervals of $\omega = 0.2$ in the second column of the Table. $g(x_0)$, the output to be anticipated from an idealized experiment, is shown marked B in the figure. The difference between curves A and B shows the magnitude of the distortion to be large, as could be anticipated from the description of the distortion function.

The moments for use in the correction scheme are found from (5.1) (in practice, they would be experimentally observed or theoretically predicted quantities):

$$\left. \begin{aligned} M_0^0(h|x_0) &= (1+x_0/3), \\ M_1^n(h|x_0) &= 0 \quad \text{for all } n, \\ M_2^0(h|x_0) &= (1/18)(1+x_0/3), \\ M_2^1(h|x_0) &= 1/54 \end{aligned} \right\} \dots\dots (5.5)$$

etc. Using only the moments written above, the values of the $\mu_n(h|x_0)$ are found to be

$$\mu_1(h|x_0)/\omega = -15/108(3-x_0); \quad \mu_2(h|x_0)/\omega^2 = 25/36. \quad \dots\dots (5.6)$$



Plot of distorted curve (A) and infinitely resolved curve (B). The points are derived from curve (A) using the correction scheme.

In column 3 of the Table $f(x_0)$ is transformed to $\mathbf{f}(x_0)$ by division using the value of $M_0(h|x_0)$ appropriate to the x_0 shown in column 1. Columns 4 and 5 are the first and second differences of $f(x_0)$ taken successively from column 3, and column 6 is the corrected curve computed from the relation

$$\chi(x_0) = \mathbf{f}(x_0) - \{\mu_1(h|x_0)/\omega\}\mu\delta^1\mathbf{f}(x_0) - \{\mu_2(h|x_0)/\omega^2\}\delta^2\mathbf{f}(x_0) \quad \dots\dots (5.7)$$

Care must be taken to use the correct sign for the difference 1, and to note that the appropriate values of $\mu\delta^1\mathbf{f}(x_0)$ are the *means of two successive entries* in column 4.

The calculated ideal output signal $\chi(x_0)$ is shown as the points lying almost exactly on the theoretical curve (in fact, the standard deviation of the points is less than 0.3% of the peak height of $g(x_0)$). In view of the large distortion and the brevity of computation, this agreement must be considered very satisfactory. The inclusion of higher order terms in (5.7) would refine the calculation, but is hardly necessary in this case.

It is usual for an apparatus to be used in the measurement of many different input signals. In this event, it is not necessary in practice to recompute the

Numerical Correction of $f(x_0)$ to find $\chi(x_0)$

x_0	$f(x_0)$	$\mathbf{f}(x_0)$	$\delta^1 f(x_0)$	$\delta^2 f(x_0)$	$\chi(x_0)$
2.8	0.001	0.001			0.001
			0.000		
2.6	0.002	0.001		0.002	0.000
			-0.002		
2.4	0.005	0.003		0.003	0.001
			-0.005		
2.2	0.013	0.008		0.005	0.004
			-0.010		
2.0	0.029	0.018		0.010	0.010
			-0.020		
1.8	0.060	0.038		0.016	0.026
			-0.036		
1.6	0.114	0.074		0.026	0.054
			-0.062		
1.4	0.200	0.136		0.032	0.112
			-0.094		
1.2	0.322	0.230		0.035	0.205
			-0.129		
1.0	0.478	0.359		0.032	0.338
			-0.154		
0.8	0.654	0.516		0.013	0.511
			-0.170		
0.6	0.823	0.686		-0.014	0.703
			-0.156		
0.4	0.954	0.842		-0.044	0.883
			-0.112		
0.2	1.018	0.954		-0.066	1.011
			-0.046		
0.0	1.000	1.000		-0.079	1.065
			+0.033		
-0.2	0.903	0.967		-0.069	1.020
			0.102		
-0.4	0.750	0.865		-0.048	0.897
			0.150		
-0.6	0.572	0.715		-0.019	0.722
			0.169		
-0.8	0.401	0.546		+0.009	0.529
			0.160		
-1.0	0.258	0.386		0.027	0.354
			0.133		
-1.2	0.152	0.253		0.034	0.216
			0.099		
-1.4	0.082	0.154		0.031	0.122
			0.068		
-1.6	0.040	0.086		0.027	0.060
			0.041		
-1.8	0.018	0.045		0.018	0.027
			0.023		
-2.0	0.007	0.022		0.011	0.011
			0.012		
-2.2	0.003	0.010		0.006	0.004
			0.006		
-2.4	0.000 ₇	0.004		0.004	0.001
			0.002		
-2.6	0.000 ₂	0.002		0.000	
			0.002		
-2.8	0.000				

moments of the distortion function for each correction: initially the moments may be tabulated, and any number of signals then corrected using the accumulated data. The process correcting an individual curve is then simply the manipulation involved in the Table, needing perhaps an hour of computation on a hand machine. It will be noted also that the scheme is well adapted for programming into a digital computer if available.

§ 6. THE EFFECT OF NOISE ON OUTPUT INFORMATION†

The fact that a signal has been subjected to a transformation does not necessarily imply that information contained in the signal has been dissipated, since the application of the inverse transformation reproduces the original signal. As far as convolutions are concerned, the inverse transformation may always be found provided that all the moments of the response function do not vanish round some point. This may be seen by considering the Fourier transforms of the constituent curves, together with the theorem of resultants. For practical purposes, therefore, the input function is completely defined by the output signal together with the apparatus response operator.

The misconception that a loss in resolution does imply a loss of information about the input signal no doubt arises from experience in cases where the output signal contains noise (random errors). In this event, as will be demonstrated below, a dissipation of information does occur in the presence of any noise which is independent of the apparatus distortion: i.e. more information may be derived from an undistorted signal with this type of noise than is possible from its distorted counterpart having an identical noise content. On the other hand, in the presence of noise which does suffer the apparatus distortion, the signal and noise are indistinguishable to the apparatus, and the application of the inverse operation simply reproduces the input signal plus noise with no loss of information due to the distortion.

The loss of the information may be understood in general terms as follows. The result of the distortion is that the output signal is broader and lower than the input, with the consequence that the percentage uncertainty introduced into the two signals by a standard noise content is greater in the case of the output signal. In reproducing the input signal from the output, not only is this larger percentage error reflected into the input signal, but also some additional enhancement of the noise occurs since, in passing from input to output signals reversibly, the noise should be flattened in precisely the manner found in the case of the true signal. As an example of this type of loss of information, one could cite the example of the nuclear resonance apparatus in which the noise from the input coil does not suffer the modulation distortion evident in the output resonance signal. More generally, this applies to all spectrographs having both finite resolving power and an intrinsic detector noise.

It is of interest to determine the degree to which the input formation is degraded by a noise content of this type since, in this way, conditions are found under which the input signal may best be determined. The relative random errors contained in the corrected and observed curves will therefore be discussed, subject to the assumption that only the first-order correction term is used, as will

† The writer would like to thank Professor N. T. Hamilton, of the University of Illinois, and also the referees, for some helpful comments on this section.

be the case when the distortion is small. As usual, the output signal is written $f(x_0)$ and the corrected output $\xi g(x_0) = \chi(x_0)$. Writing $M_2(\psi)/2\omega^2 = \mu_2$, and reading $\Delta(x_0)$ as 'the error in $f(x_0)$ ', we have

$$\chi(x_0) + \Delta\chi(x_0) = (1 + \mu_2\delta^2)\{f(x_0) + \Delta f(x_0)\}. \quad \dots\dots(6.1)$$

Hence from the first-order correction relation

$$\chi(x_0) = f(x_0) - \mu_2\delta^2 f(x_0) \quad \dots\dots(6.2)$$

it follows that

$$\Delta\chi(x_0) = \Delta f(x_0) - \mu_2\delta^2 \Delta f(x_0). \quad \dots\dots(6.3)$$

If three consecutive differencing ordinates x_1 , x_2 and x_3 have respective errors in $f(x_0)$ of σ_1 , σ_2 and σ_3 , then at the central point it may be shown from (6.3) that

$$\Delta\chi(x_0) = -\mu_2\left\{\sigma_1 - 2\left(1 + \frac{1}{2\mu_2}\right)\sigma_2 + \sigma_3\right\} \quad \dots\dots(6.4)$$

Introducing a mean square value σ_0^2 for each of σ_1 , σ_2 and σ_3 , it follows that the root mean square error in the corrected curve is given by

$$\sigma = \sigma_0\{1 + 4\mu_2 + 6\mu_2^2\}^{1/2}. \quad \dots\dots(6.5)$$

Eqn (6.5) shows that the relative error in the corrected signal increases monotonically as μ_2 and the distortion increase. It is therefore evident that given a distorted curve, the value of the differencing interval ω chosen for the correction procedure should be as large as is consistent with the structure on the curve to be analysed. In this event, the value of μ_2 , and consequently also the value of the random error in the corrected signal, will be reduced to a minimum.

§ 7. THE OPTIMUM APPARATUS CONDITIONS

In many types of linear apparatus the fractional random error in the output signal bears an inverse relation to the distortion. For example, increasing the aperture of an optical apparatus may decrease the resolving power but cause a simultaneous increase in intensity of the output signal. A similar set of circumstances occurs on increasing the modulation amplitude of a magnetic resonance spectrometer. Thus, a decrease in fractional random error occurs which may offset the increase in random error described by Eqn (6.5). The possibility exists, therefore, that conditions may be found under which the form of the input function is best determined.

Before deriving these conditions, it may be advisable to consider the form they can take. The only unit of length with which the moments of the distortion function $f(x)$ can be compared is the differencing interval ω , which, in view of Eqn (6.5) must be chosen as large as possible. The differencing interval, however, is limited by the structure on the curve to be represented, and must not be so large that the chosen points do not give an adequate representation of the curve. Thus the optimum differencing interval relates the moments of the distortion function to the structure of the signals to be corrected.

In the particular case of the magnetic resonance spectrometer, the idealized apparatus operator is proportional to the modulation amplitude and therefore to

$\mu_2^{1/2}$. Similarly in the case of an optical slit the intensity shows the same dependence on $\mu_2^{1/2}$. In both cases, we may therefore simulate the relative error in the corrected output signal by

$$\sigma/\sigma_0 = \mu_2^{-1/2} \{1 + 4\mu_2 + 6\mu_2^2\}^{1/2}, \quad \dots\dots(7.1)$$

rather than by Eqn (6.5) alone.

Equation (7.1) shows that the corrected signal has a minimum in its fractional error when $\sqrt{6\mu_2} = 1$. In terms of the modulation amplitude a , this leads to the condition $a \simeq 1.8\omega$ (see I).

This expression for the optimum modulation amplitude has been used in observing the shape of the copper nuclear resonances at temperatures up to 1300°K, under which conditions the available signal-to-noise ratio is rather poor (Flynn and Seymour 1961). In practice, it was judged that six or seven differencing intervals in the peak-to-peak derivative width of the resonances were needed to give an adequate description of the shapes. The predicted optimum condition of the modulation proved admirable, since the modulation peak-to-peak amplitude was then some two-thirds of the width of the resonance and the signal amplitude therefore approached its maximum value. On the other hand, the maximum first-order correction to the shape was only about 5% of the peak integrated signal amplitude, and the second-order correction was often negligible. Consequently, the additional noise effectively introduced into the corrected signal by the distortion was small, while the relative true noise on the signal was maintained small also. It is therefore considered that equations of the type (7.1) do in fact predict closely the experimental conditions under which the shape of an output signal may best be determined.

§ 8. SUMMARY

A method has been presented whereby signals subjected to a general linear distortion may be corrected to give a more precise measure of the input signal. This technique is particularly efficient in the practical case of small distortion.

The effect of noise on the output signal has been discussed and an analysis has been given of the dissipation of information concerning the input signal, resulting from the presence at the output of noise which does not suffer the apparatus distortion. This led to the prediction of optimum apparatus conditions in the presence of such noise. Noise which undergoes the same distortion as the signal does not give rise to these conditions; the noise is indistinguishable from the signal, and the quantity of input information, including noise, is not affected by the distortion.

In conclusion, it may be remarked that many experimenters are reluctant to subject output data to linear processing either by the use of adequate compensating apparatus or by means of numerical methods. This might appear unreasonable since applying the inverse transformation to a transformed system seems an admirable method of restoring the *status quo*. However, assumptions concerning linearity and reproducibility of apparatus are invoked whatever the method of correction used. The greatest care must therefore be exercised to avoid the production of artificial structure on a signal by the use of linear processing techniques in inappropriate circumstances. It is clear then, that the matter is best left to the skill and discretion of the individual experimentalist.

ACKNOWLEDGMENT

Part of this work was performed at the University of Leeds under the supervision of Dr. E. F. W. Seymour. The writer wishes to thank Dr. Seymour for his helpful criticisms.

REFERENCES

- BLANC-LAPIERRE, A., 1953, *Ann. Inst. Poincaré*, **13**, 245.
BLANC-LAPIERRE, A., PERROT, M., and PERI, G., 1955, *Optica Acta*, **2**, 1.
DOSSIER, B., and JACQUINOT, P., 1950, *J. Rech.*, **12**, 123.
FLYNN, C. P., and SEYMOUR, E. F. W., 1960, *Proc. Phys. Soc.*, **75**, 337.
—— 1961, *Proc. Phys. Soc.*, **77**, 922.
LINFOOT, E. H., 1958, *Physica*, **24**, 476.
SHANNON, C. E., 1948, *Bell Telephone System Monograph* B-1598, 51.
SHULL, C. G., 1946, *Phys. Rev.*, **70**, 679.
STOKES, A. R., 1948, *Proc. Phys. Soc.*, **61**, 382.
TORALDO DI FRANCIA, G., 1955, *Optica Acta*, **2**, 5.
TOURNARIE, M., 1957, *C. R. Acad. Sci., Paris*, **245**, 1301.

OBITUARY NOTICES

Professor W. T. Astbury

William Thomas Astbury, Sc.D., F.Inst.P., F.R.S., who died at the age of 63 on 4th June 1961, was the eldest son of a large family in the potteries district of Staffordshire. There was no advantage of a scholastic or professional background in his origins, yet he rose to a position of world-wide fame in his field. After very successful years at Longton High School he proceeded to Cambridge, gaining his education by winning scholarships. His University degree was in Physics and he graduated in 1921.

He worked with Sir William Bragg from 1921–1928, mostly at the Davy Faraday Laboratory of the Royal Institution. A wonderful new subject, x-ray crystallography, was just beginning. There were the numerous tasks of managing the early fickle x-ray tubes, there was much equipment to devise, even photometers to invent, and any of these jobs could have occupied years. But Astbury wanted results to exercise his mind and he became very quick at settling on sufficient apparatus that would work just neatly and effectively. He soon published papers on tartaric acid and on acetyl acetones among the host of crystals waiting to be done. And with Yardley he had simplified, in the well-known space group tables, the important facts about symmetry in crystals so that these could be readily used by the increasing band of x-ray crystallographers.

With all the choice available to him Astbury chose the most difficult field of all to work in. To others it would seem a great gamble to tackle the structure of fibrous proteins as he did in 1928 when he became lecturer in Textile Physics in the Department of Textile Industries at Leeds University. However, Astbury would scarcely notice the odds against him, so great was his energy and his faith in himself. More important still was the mystery of the unknown. This continued to drive him on; his leading spirit and his success encouraged others to start working in this field.

In the early 1930s Astbury published his great detailed papers on the structure of hair, wool and related fibres, of especial note being that with H. J. Woods entitled 'The molecular structure and elastic properties of hair keratin'[†]. These described the α - β transformation of fibrous proteins and explained this as a reversible intramolecular chain folding. The many original experiments and arguments gave a very clear picture of chains unfolding on stretching to reach a limit about twice their natural length. There were many other original papers on feather keratin, protein denaturation, muscle proteins and muscle itself, nucleic acids, alginic acid; also the two very important Proctor Memorial Lectures on collagen. His work on keratin had been to him a first step in molecular biology—it had revealed the possibility of explaining biological phenomena in molecular terms. Most of these other studies he regarded as adventures to survey and open up the field. He was in great demand to introduce and to give the concluding remarks at scientific meetings both abroad and at home. A notable part of his teaching was done in this way, and he achieved great simplicity of explanation and attractiveness of style.

Over the years many efforts were made to provide a model to explain the α - β transformation, the structure of collagen, the structure of nucleic acids, but

he did not win the race he started in finding acceptable models. He was an outstandingly keen and proud worker and with characteristic cheerfulness and enthusiasm he took up the implications of the planar amide group and applied these to considerations on wool keratin, collagen, cross- β structure and feather keratin.

Astbury had great gifts and he used them well. He was a very eminent man without the slightest shade of grey eminence. He was abundantly friendly and cheerful with the most infectious enthusiasm. He became Professor of Bio-molecular Structure at Leeds in 1945, though he would have preferred the name of Biophysics or Molecular Biology for the field of his studies. He died most actively engaged in this work, and the force of his pioneering efforts will last long after his death.

K. M. RUDALL.

† Astbury, W. T., and Woods, H. J., 1933, *Phil. Trans. A*, **232**, 333.

Guy Barr

Dr. Guy Barr's lifetime researches of 42 years at the National Physical Laboratory will probably best be remembered by the use in science and industry of his standard methods of measuring the viscosity coefficient of Newtonian liquids. At the outbreak of the first world war, Dr. Barr was a Senior Assistant at the N.P.L., the staff of which he joined in 1908, having graduated with first class honours in physics and mathematics at Cambridge University in 1907; he later obtained the D.Sc.(London) degree in 1917.

His work began under Dr. W. Rosenhain, F.R.S., mainly on metallurgical analyses, then on physical-chemical problems arising in aeronautics. He published numerous reports in *Reports and Memoranda of the Advisory Committee for Aeronautics*, 1910-1926.

This work on the development of tests for the hydrogen permeability of balloon fabrics and for the strength and tautness of aircraft fabrics was continued for the Fabrics Co-ordinating Research Committee leading to reports on the waterproofness of 'porous' fabrics and on the deterioration of fabrics during weathering. Parallel researches on the formulation of aeronautical dopes and observations of the deteriorating action of sunlight on doped fabric were made at the Royal Aircraft Establishment under the guidance of Dr. J. E. Ramsbottom when the writer became acquainted with Dr. Barr and his valuable national work. At Farnborough both Dr. F. Aston of isotope fame and Dr. Lindemann, later Lord Cherwell, shared in these wartime researches and it was Dr. Aston who taught us younger chemists to blow Dr. Barr's U-tube viscometers in glass. At that time we were aware of the rheological properties of aircraft dopes, the viscosity being dependent on the rate of shear and so on the design of the viscometer. Dr. Guy Barr using an x-ray method and the writer a sphere suspended over a light pulley demonstrated that the fall of a sphere in pigmented dopes and similar systems was not in accord with Stokes' law. Barr's work on the viscosity of aeroplane dopes led to the development of U-tube viscometers the design of which has been adopted by the British Standards Institution and since 1929 the calibration of such viscometers and of Redwood viscometers (Institute of Petroleum) has been carried out in the N.P.L. Metallurgy division. Barr's

Monograph of Viscometry (Oxford University Press) was printed in 1931 and became a recognized handbook on the subject.

Prior to and during the 1939 war years, Dr. Barr developed methods for measuring the rate of transmission of moisture through wrapping films and proofed cardboard, and tests were made on containers for mortar bombs and other ammunition to assist the Ministry of Supply in the development of improved types. Further work for the same department was done on the best method of sealing lids on tins to withstand immersion in water when supplies were to be landed on beaches. Shortly before his retirement on 31st May 1950, Dr. Barr assisted the Home Office Gas Cylinder and Containers Committee regarding recommendations for the filling ratios, marking and maintenance of gas cylinders. As a P.S.O. in charge of the Chemistry section of the Metallurgy division he assisted in researches on new methods of preparing pure beryllium in the early days of nuclear energy development and was responsible for developing the spectrographic section in the division.

At the World Petroleum Congress organized by the Institute of Petroleum, held at the Imperial College of Science and Technology in July 1933, the measurement of viscosity was discussed at great length and the agreed recommendations were incorporated in the B.S. 188 method for the determination of the viscosity of liquids in c.g.s. units, under the chairmanship of Dr. Guy Barr.

His scholarly, sound and patient work is well shown in this B.S. 188 standard. All his colleagues will miss him and his friendly and sympathetic manner and his ability in solving problems. He was a keen athlete in his younger days and his activity as a scientist is indicated by the imposing number of his official publications.

E. W. J. MARDLES.

Leslie E. C. Hughes

Leslie E. C. Hughes, Ph.D., B.Sc.(Eng.), M.I.E.E., passed away very suddenly on 10th June at the age of 57 and at a time when he was full of enthusiasm for the new tasks he had set himself. Following graduation, Hughes became a demonstrator and later a lecturer in acoustics and telecommunications at the City and Guilds College, South Kensington, and it was during this period that he wrote his well-known textbook *Engineering Acoustics*.

In 1941 Dr. Hughes entered industry and for the next ten years he was engaged in various aspects of electro-acoustics research. However, his interests were turning towards technical writing and he became editor of many technical reference books.

Dr. Hughes had a lively mind and a great love and knowledge of music which stemmed from his early training under Dr. Jolly at St. George's, Hanover Square, where he was a chorister. He was a keen educationalist and maintained an active interest in his old school, the Quintin, and in Convocation of London University. He was also a member of many societies and was a past president of the Institution of Electronics and the first president of the British Sound Recording Association and had been elected vice-chairman of the newly formed H. G. Wells Society. Only a few days before his untimely death he had been appointed editor of a technical journal.

Members of the Acoustics Group of The Institute of Physics and The Physical Society will particularly miss his lively interventions in discussions. R.W.B.S.

Sir K. S. Krishnan

It is with profound regret that we record the sudden death of Sir K. S. Krishnan, F.R.S., Director, National Physical Laboratory, India, on 14th June 1961. Scientific research in India owes much to his contribution and valuable guidance, particularly during the crucial period of scientific and technological progress of the country, and his death is a national loss.

Kariamankam Srinivasa Krishnan was born on December 4, 1898, in the village of Watrap near Srivilliputtur in Madras State. After basic education in Watrap and Srivilliputtur, he studied the Intermediate in American College, Madurai (1914–1916) and joined the Christian College, Madras (1916–1918) for the graduate course. Soon after his obtaining the B.A. degree in Physics he was appointed as a Demonstrator in Chemistry in the same college. But his thirst for higher studies and research led to his joining the Indian Association for the Cultivation of Science, Calcutta in 1923 to work under Professor C. V. Raman. Placed in the proper environment, Krishnan's latent potentialities came to light and soon he shone as an enthusiastic and brilliant investigator and was foremost among Professor Raman's collaborators. Based on the results of his original work, Krishnan was awarded the M.Sc. (1925) and D.Sc. (1932) degrees of the Madras University. He was appointed as a Reader in Physics at the Dacca University in 1928 and in 1933 as Mahendralal Sircar Professor of Physics at the Indian Association for the Cultivation of Science. Subsequently, in 1942, he joined the Allahabad University as the Professor of Physics. When the N.P.L., the first of the chain of new national laboratories of India was opened in 1947, it was but natural that Sir K. S. Krishnan should have been chosen as its first Director, a post which he held until his death.

The research work of Krishnan and his associates extends over diverse branches of physics. During the years 1923–1928 he carried out theoretical and experimental investigations on the scattering of light by liquids and related molecular phenomena in collaboration with Professor C. V. Raman, which culminated in the discovery of the Raman effect. His versatility and deep appreciation of the essential unity underlying several of the physical phenomena and the internal architecture of crystals resulted in Krishnan's becoming interested, while at Dacca, in the magnetic properties of substances. He devised an elegant and ingenious method for the precise determination of the magnetic anisotropy of crystals, and even today the results obtained by him on several paramagnetic and diamagnetic crystals remain the most authoritative in the subject, and valuable correlations were obtained by him and his students connecting the symmetry and configuration of the molecules in crystals, the crystalline field and their magnetic properties. During the period 1933 to 1947 he carried out significant investigations on statistical thermodynamics and quantum theory and at Allahabad he built up an active school of research interested in thermal and electrical properties of metals and alloys. At the N.P.L., besides organizing its multifarious activities, he was concerned with work on the physics of the solid state. His recognition of the interdependence of the different branches of science, both pure and applied, are well illustrated by the problems studied by him and his co-workers during the past decade. In trying to eliminate the difficulties which beset an accurate study of the thermionic properties of metals and semiconductors, he evolved a new technique for a precise determination of not only the thermionic constants but also their temperature coefficients. This

method has been successfully applied to the monovalent and the transition metals. A study of the temperature distribution along an electrically heated filament yielded a new experimental method for the measurement of the thermal conductivity, particularly at high temperatures. The electrical conductivity of metals and alloys is a topic which engaged his attention in relation to the above studies and an elegant theoretical explanation has been given by him and his co-workers for the large increase in resistance of a binary alloy due to alloying. A longstanding controversy about the relative merits of the Lorentz and Drude refraction formulae was also resolved in an extremely simple manner and their mathematical equivalence established. Another recent contribution is the subject of vibrations of ionic crystals and the anharmonicity of some of their normal modes.

In recognition of his distinguished researches Krishnan was elected a Fellow of the Royal Society in 1940 and was knighted in 1946. The Government of India honoured him with Padma Bhushan in 1954 and he was the recipient of the Bhatnagar Memorial Award in March 1961. He was elected a Foreign Associate of the National Academy of Sciences, U.S.A., and was a Fellow of the Royal Society of Arts, the Institute of Physics, the Physical Society and the Institute of Metals, London. He was also a Fellow of the Indian Academy of Sciences and the National Institute of Sciences of India. He was the recipient of the honorary D.Sc. degree from various Indian Universities.

Krishnan was President of the section of Physics, Indian Science Congress in 1940 and its general President in 1949. He was Chairman, Scientific Advisory Committee, UNESCO; Vice-President of the International Council of Scientific Unions and of the International Union of Pure and Applied Physics; Chairman, Indian National Committees URSI and IGY and Chairman, Sub-Commission for co-operation with UNESCO. He was Chairman, Board of Research in Nuclear Science, Member, Atomic Energy Commission, the University Grants Commission and the Standing Board of Astronomy. His association with the Council of Scientific and Industrial Research, India, dates back to its inception and he served the Council in various capacities, as member of the Governing Body, Board of Scientific and Industrial Research, Board of Engineering Research, Editorial Board of the Journal of Scientific and Industrial Research and was a member of several Research Committees.

No sketch of Professor Krishnan's career would be complete without a reference to his extensive travels abroad, which gave him many an opportunity to visit important centres of research in Europe and America and to cultivate personal relations with eminent men of science. He first visited Europe when he was invited to take part in the International Conference on photoluminescence held at Warsaw in 1936. He toured widely throughout Europe and delivered a series of lectures at various important centres including the Royal Institution in London and the Cavendish Laboratory at Cambridge and in many of the continental universities. The Liège University honoured him with the award of the University Medal. He again visited Europe in 1939 to attend the International Conference in Magnetism held at Strasbourg under the auspices of the International Institute of Intellectual Co-operation and of the Service Central de Recherche Scientifique de France. In the summer of 1946 he went to England as one of the Indian delegates to the Empire Scientific Conference organized by the Royal Society. He has since been abroad many times.

Krishnan, who was a physicist of no mean calibre, possessed also other qualities which endeared him to those with whom he came into contact. His love of fundamental research did not blind him either to the need for or to the value of applied physics and technology and he was often able to show up in a striking manner the close relation existing between the two. He had an abiding interest in pure mathematics also and his knowledge of the subject often enabled him to find an elegant solution to physical problems. He was also a learned scholar of Tamil and Sanskrit and one found in him a rare combination of a true scientist, unassuming and simple, and a philosopher with an integrated personality.

R. S. KRISHNAN.

Sydney Marsh

Dr. Sydney Marsh died in London on 14th December 1960 at the age of seventy-six. His death has ended a long career of service to education and to science.

As an undergraduate he studied mathematics and physics at the University College, Cardiff, and obtained first class honours in both these subjects. From the University of Wales he proceeded to postgraduate studies in the Universities of Munich and Göttingen where he worked under the supervision of Professor E. Riecke, and for his investigations on the operation of discharge tubes he was awarded the degree of Ph.D. He continued his interest in this field of research after his return home and, with A. E. Evans, published a paper on 'Electrode Potential Measurements with Direct and Alternating Current Electrolysis', which appeared in the *Proceedings of the Royal Society* in 1922.

For his contribution to physics he was later awarded the degree of D.Sc. in the University of Wales.

He was appointed to the staff of the Battersea Polytechnic in 1909 and after spending two years (1917-19) as head of the Mathematics and Physics Department at the Rutherford Technical College, Newcastle-upon-Tyne, he returned in 1919 as head of the Department of Physics to the Battersea Polytechnic and remained there until his retirement in 1950. He continued his association with the Physics Department at Battersea as a part-time lecturer to the end, and gave his last lecture only two days before his unexpected death.

Marsh was a scholar and a great teacher. It is not too much to say of him that he was one of the most sound, lucid and sympathetic teachers of physics associated with the work of the University of London. He made his department a centre of sound learning and, in the difficult circumstances of busy teaching demands, he encouraged and stimulated research.

His friends and colleagues of the University of London met him most frequently as a member of academic and examining boards upon which he played active and important parts. For many years he acted as a chief examiner for the external special and general honours degrees and his colleagues recognized his sound judgment and sense of fairness in this work. His work on the Joint Matriculation Board was equally recognized on account of his unerring judgment. His own knowledge was wide and deep and in the new branches of physics which are now represented in examination papers he had a rare ability of detecting the superficial and half-understood knowledge from that which was deeper and firmly grasped. He was an excellent examiner

ready to reprove when questions proposed seemed to him unsuitable, and ready to temper the wind of too harsh a marking.

He was a devoted member of the Physical Society and of the Physical Society Club.

His death has brought a feeling of great loss to all his friends and colleagues. Those working with him have always recognized the quality of his contribution to the work they had in common and his sudden departure from their midst has emphasized the reliance they had in him and the regard and affection they felt for him.

H. T. FLINT.

Reprinted from *Nature*, 1st July 1961

J. Walter Ryde, F.R.S.

John Walter Ryde died at Marlborough, Wiltshire, on 15th May, after a short illness. He was sixty-three years old. He was born in Brighton on 15th April 1898 the son of Mr. W. W. Ryde, and was educated at St. Paul's School and in France. Plans for him to continue his studies in Germany and then go to the University of Cambridge were interrupted by the First World War. He returned from Berlin to England just before the outbreak of war and entered the City and Guilds Technical College, Finsbury, where he studied under Professor Sylvanus Thompson and Professor Charles R. Darling.

Ryde joined the Royal Engineers voluntarily in 1916, at the age of eighteen on the completion of his course at City and Guilds, and was trained in anti-aircraft work in Monmouthshire and on the Norfolk coast before being drafted to France during the last few months of the War. He continued to serve in France until his demobilization in 1919.

Ryde joined the Research Laboratories of the General Electric Company, Ltd., as a physicist in 1919, going directly from his war service to the newly established research unit directed by Clifford C. Paterson in the Company's lamp factory at Hammersmith. He was a leading member of the scientific staff of the Laboratories from the start.

In the early days at Hammersmith, and again after the Laboratories had moved to their new premises at Wembley in 1923, the variety of Ryde's research work was indicative of the breadth of interests which was so characteristic of him. They included pure spectroscopy, thermionics and the gaseous electrical discharge. Under his direction the first practical high-pressure mercury vapour lamp was developed—the foundation of a new industry to which he made many subsequent contributions.

His theoretical work on the scattering of light, first applied in the twenties to optical diffusing media in glasses, was extended by him during the Second World War to classic studies of the attenuation and the radar echoes produced by meteorological phenomena at centimetre wavelengths. (A footnote in this paper included the following: "The author (J. W. R.) and Mrs. Ryde were responsible for the theory and calculation of the effects caused by liquid and solid particles, . . .") He was an early worker on crystal valves and quickly recognized the potentialities of germanium as a semiconducting material.

Other researches included velocity modulation tubes, luminescent materials and optical projection systems. He contributed much to various research projects undertaken for the United Kingdom Atomic Energy Authority, and he took part in work on the FIDO fog-dispersal system. It was typical of Ryde to design, in his leisure hours, a pocket illumination chart for use by the Services. It showed levels of illumination, by day and by night, at various latitudes, and was used extensively in military operations.

Ryde was elected a Fellow of the Royal Society in 1948. He was appointed chief physicist at the G.E.C. Research Laboratories—recently named the Hirst Research Centre—in 1950 and chief scientist in 1953. During these recent years he had overall responsibility for the programmes of pure scientific research of the Centre, and his particular interests lay in the fields of new materials, crystal growing and solid state physics.

He was a member of the Royal Institution of Great Britain since 1935 and chairman of the Davy Faraday Laboratory of the Institution since 1951. He served on the Board of Managers of the Institution and always took a great interest in its affairs. He was a Fellow of the Institute of Physics and the Physical Society, a Fellow of the Royal Astronomical Society, and a member of the Geological Association, the Wiltshire Archaeological Society and the Athenaeum.

Ryde married, in 1930, Dorothy Ritchie, daughter of the then chief illuminating engineer of the General Electric Co. There is one son.

The Hirst Research Centre has lost a senior man who earned the admiration and respect not only of his colleagues but also of eminent men both in Great Britain and overseas. He lived his life for science, and his leisure activities were very largely extensions of his life's work. Archaeology was a persistent interest—at an early age he learned to read hieroglyphic writing and ancient scripts. He was a profound student of astronomy but, in recent years, microscopy became a dominant hobby. He was particularly interested in diatoms, and his beautifully mounted specimens are evidence of the elegant experimental skill which he retained to the end.

His memory was prodigious and visual. He never forgot the details of work which he had done and could sketch from memory some experimental arrangement or the detailed shape of a specimen long afterwards. Such a memory, supplemented with the many carefully prepared and indexed note-books which he compiled throughout his working life, made Ryde a powerful authority indeed in the world of science.

In all his work he displayed great ability and unflinching perseverance, together with brilliant insight and inspiration. His colleagues will always remember his patient readiness to discuss and assess the problems of the day, and his helpful elucidation of critical experiments, often elegant in their simplicity, which he designed to solve them.

O. W. HUMPHREYS.

Arthur Mannering Tyndall

Arthur Mannering Tyndall was a man who devoted his life to the University of Bristol and who played a very important part in guiding its growth from a small college to a great university. He was a physicist who was elected into the fellowship of the Royal Society for his work on the mobility of gaseous ions. No

less important was his work in building the Henry Herbert Wills Physical Laboratory, in staffing it and in giving it scientific leadership. He died suddenly at his home on October 29th. His wife, Lilly Tyndall, his son and two daughters survive him.

Arthur Tyndall was born in Bristol on 18th September 1881. He entered the University College, holding the only scholarship offered annually by the City of Bristol for study in that college, and graduated with second class honours in physics in the external London examination in 1903. That year he was appointed assistant lecturer, was promoted to lecturer in 1907, and became lecturer in the University when the university college became a university in 1909. During this time he served under Professor A. P. Chattock, but Chattock retired in 1910 at the age of 50 and Tyndall became acting head of the department. Then, with the outbreak of war, he left the university to run an army radiological department in Hampshire. He was about to go to the Mediterranean when he was summoned back to the university to continue in charge of the physics department, which was in danger of disintegrating without him. It was in 1916 that he first met Henry Herbert Wills, pro-Chancellor and chairman of a special buildings committee, who was planning with the architect the details of the Great Hall of the University. His first contact with him was a letter to Wills as chairman of the General Purposes Committee about a site for a battery of accumulators. Out of this arose a friendship, and with it Harry Wills's ambition to build a truly worthy home for physics. Though his intentions were clear earlier, it was in March 1919 that he announced a gift of £100 000 and as much again a year later. In 1922 he died leaving a further considerable sum to the University for buildings and endowment.

In 1919 Tyndall was elected to the Henry Overton Wills Chair of Physics. The formal opening by Lord Rutherford of the new laboratory was in 1927. The staff then was twelve, including Lennard-Jones, Skinner and Sucksmith; there was ample space in the building—a large room for everyone, as there was in 1933 when the present writer succeeded Lennard-Jones as Professor of Theoretical Physics. For undergraduates too there was plenty of room; there were never before the second war more than six honours students in the final year, sometimes only two.

In fact one of my first recollections of Bristol physics before the war was this spaciousness; the other was, of course, the personality of Tyndall. He was a man who lived for the achievements of his colleagues in the department. Nothing gave him greater pleasure than when they achieved a good piece of research, or any outside recognition. Everyone knew this and it coloured the whole place. Anything less like the tyrannical professor of contemporary legend it would be difficult to imagine. Frequently the whole staff joined him in a Sunday walk over the Somerset hills; and if there were any departmental problems, that was how they were resolved. After the war there was of course a sudden and large expansion in the number of students and of staff but he preserved remarkably the intimate, friendly atmosphere of a small department in which everyone knew and took pride in each other's achievements. Among those who worked with Tyndall before and after the war are E. T. S. Appleyard, C. R. Burch, F. C. Frank, H. Fröhlich, R. W. Gurney, W. Heitler, L. C. Jackson, J. E. Lennard-Jones, H. Jones, H. London, A. C. B. Lovell, S. H. Piper, C. F. Powell, H. W. B. Skinner, W. Sucksmith and the present writer, to mention only a few.

Tyndall was so wrapped up in their achievements that he was too modest about his own personal research, but his work was of real distinction. His principal contributions to physics were in the field of the discharge of electricity in gases. As a young man, working in a small laboratory, he had followed with great attention the early experiments on radioactivity, and he used to describe with what excitement in the early 1900's he used to await the next issue of the *Philosophical Magazine* in which, at that time, Rutherford and his colleagues published much of their work. The study of the ionization produced by radium and its products raised the question of the nature of the ions, and methods for determining their mobility were developed by Rutherford, Langevin, Zeleny and others. In Bristol, Chattock had made extensive studies of the 'electric wind', the small pressure difference established in a gas as a result of a point-discharge. Tyndall took part in some of these experiments; he was led to make independent studies of the nature of the ions, and developed a number of independent methods.

By the early 1920's, measurements of the mobilities of the positive ions had been made in many laboratories, but the results were very discordant. Tyndall realized that this was associated with the presence of traces of impurities in the gas which attached themselves to the original ions, or which led to a change in the constitution of the ions through charge-exchange. In all the earlier apparatus these small traces of impurities could not be excluded, but the great change in vacuum-practice introduced after the first world war gave the possibility of making experiments in much improved conditions, in glass apparatus with metal electrodes which could be baked-out before the introduction of the gas.

Taking advantage of these technical innovations and generators of high-frequency alternating potential based on the use of valves, Tyndall and his colleagues developed a number of elegant methods of determining the mobility of a great variety of positive ions in a number of pure gases. In the course of a few years, a large measure of order was brought into a field which had been the subject of hundreds of investigations over a period of twenty-five years. On this subject he wrote a monograph which was published by the Cambridge University Press.

From 1919-48 he was H. O. Wills Professor of Physics and from 1927-40 Director of the H. H. Wills Physics Laboratory. In 1940-45 and from 1946-47 he was pro vice-chancellor and in 1945 acting vice-chancellor. In 1948 at the age of 67 he retired and was created Emeritus Professor and Honorary Fellow. At that time his portrait, a gift of colleagues, past and present students and friends, was painted by James Gunn and now hangs in the main building of the university. In 1950 he was awarded the C.B.E.; in 1958 the Hon. LL.D. of his own university.

He took a leading part in the scientific committee work of the country. Elected into the fellowship of the Royal Society in 1933, he served on Council from 1941-42 and was vice-president in 1942. He was president of the Institute of Physics in 1946-48 (his photograph is on the staircase at 47 Belgrave Square), he was on the Council of the Physical Society from 1925-29, he was president of the physics section of the British Association in 1952. He was a manager of the Royal Institution, president in 1953 of the Science Masters' Association, chairman from 1946-49 of the executive committee of the National Physical Laboratory. He was from 1940-45 member and sometime chairman of a

Ministry of Education committee on the award of state bursaries and scholarships. In Bristol from 1948 he was a member and for part of the time vice-chairman of the Management Committee of the Southmead Hospital Group. In fact, from the date of his retirement and indeed before, he gave most generously of his time and ability to medical education and the National Health Service.

From the date of his retirement until the day of his death he was an editor of the *Philosophical Magazine*, and indeed a most active one, most of the papers accepted or rejected passing through his hands.

In his early days he played hockey and gained a number of county caps; he was also an active tennis player. He was keenly interested in music and in drama.

Tyndall will be remembered particularly for two things. He presided over part of that phenomenal growth of English physics in the 1930's, when it burst out of its traditional homes at Cambridge and Manchester and flourished all over the country. The generosity of Harry Wills gave him his opportunity and he knew how to take it. If the H. H. Wills Physical Laboratory has achieved anything in the post-war period, all those who worked there know how much they owe, both to that generosity and to Tyndall's wisdom, kindness and uncompromising standards.

He also worked during his whole life for what has become one of our greatest universities. In his department he believed that no effort was too great, no time should ever be grudged in finding out what everyone thought and in seeing that everyone was heard. If Bristol's growth from small beginnings has been happy, and if the university has been relatively free from the strains and frustrations which are occasionally expressed elsewhere, it may be that Tyndall's example has had much to do with it.

N. F. MOTT.

Russell S. Wright

R. S. Wright was probably the last of the instrument makers associated with the manufacture of the old 'gas' x-ray tubes of the pre-First-World-War years. He was for many years the moving spirit in the firm of Newton and Wright which produced surgical x-ray equipment. Another of his loves was the smaller firm of Newton and Co. which had two great distinctions. Firstly, the firm had a continuous existence from the time of Sir Isaac Newton and, secondly, the lantern slides produced by the firm were used to illustrate lectures all over the world.

R. S. Wright was a 'character'. He was Captain of a Boys' Brigade Company for an incredible number of years; he bathed daily, summer and winter, far beyond his youth, in the Highgate Ponds. He regarded his firm as his family, and on retirement took the lay charge of a Presbyterian Church! Every year he was to be found going most carefully round the Physical Society Exhibition. He lived a very full life and enjoyed every minute of it.

A. J. PHILPOT.

REVIEWS OF BOOKS

1960 *Nuclear Data Tables: Part 3. Nuclear Reaction Graphs*, edited by J. B. MARION. Pp. xi+181. (Washington: National Academy of Sciences—National Research Council, 1960). \$1.25.

This volume contains the most comprehensive collection of graphs and data yet published in this field. It should prove to be very useful for the planning and analysis of nuclear reaction experiments.

There is a section on the ranges and energy loss of charged particles in matter, but unfortunately there is little information on the ranges of protons in matter above an energy of about 7 mev. A complete collection of data on gamma-ray detection in NaI(Tl) crystals and some information on neutron source cross sections is included. There is a graph of electron ranges in aluminium, but it is not immediately clear whether the quantity we are looking up is the mean range or the maximum range. Among the many other graphs are some polarization contour maps, energies of elastically scattered particles, and also a silicon diode barrier nomograph.

This is an excellent publication and at a price of 10s. this volume represents very good value for money.

B. H. ARMITAGE.

Advances in Electronics and Electron Physics. Vol. XIII. 1960. Edited by L. MARTON. Pp. x+454. (New York and London: Academic Press.) \$13.50.

One of the chief purposes of the progress review ought to be to keep the non-specialist up-to-date without his having to read the original papers: it ought also to help the specialist by concentrating recent material into a convenient compass and by reminding him of things he might have overlooked. In fact the progress review ought to be one part of the answer to the complaint that it is almost impossible to keep up with the literature in any but the most restricted field. But it ought, too, if a continued publication, to be the sort of volume the informed non-specialist can turn to when he wants to know 'what it is all about' when a new topic attracts his attention. Perhaps, in addition to all this, the ideal review will help in fertilization by attracting attention to new fields and by supplying the worker in one field with ideas borrowed from another.

All of the articles in this volume fulfil some of these purposes and most of them fulfil them all to some extent. It is an admirable publication, consisting of five substantial articles varied in style almost as much as in content. The writing and presentation are good and clear enough throughout to be comprehensible to the non-specialist, except perhaps for P. A. Lindsay's work on 'Velocity distribution in electron streams', which is necessarily and properly mathematical. But here the author specifies clearly in the introduction that he will consider electron flow "in the six dimensions of phase space, consisting of the configuration and momentum spaces joined together".

In an article on 'Inelastic collisions between atomic systems', J. B. Hasted introduces a new and elegant system of notation particularly suitable for dealing with inelastic collisions, where the complexity of state of the particles is so much greater than the complexity of chemical species. There is a balanced

account of developments in experiment and in theory characterized by clear statements of the various questions which arise followed by careful presentation of the information available.

'Field ionization and field ion microscopy' by E. W. Muller makes a strong aesthetic appeal: photographs which actually show atoms sticking up in ordered arrays produce a satisfaction which nothing less direct could provide. Here the introduction is a quite inadequate shop window: surely it should tempt the general reader with some hint that he is to be shown photographs of a tungsten tip at a magnification of 10^6 and that he will be told how they are taken. The account of field evaporation of layers of atoms until site vacancies appeared is particularly fascinating.

Raymond Castaing's account of 'Electron probe microanalysis' deals with a clearly delimited field in a satisfying way, presenting the experimental information, a study of the corrections and limitations, and an account of the applications of the method to scientific research.

The last article in the volume is by P. K. Weimer, on 'Television camera tubes: a research review'. Physicists often want to know how things work, what they can be used for and what their limitations are, without being committed to prolonged study. The present article supplies just this want.

The book is pleasant to handle, the production is excellent and it is to be commended to the general reader as well as to the reader with a specific interest in the topics mentioned in the titles.

W. A. PROWSE.

Plasma Acceleration, edited by S. W. KASH. Pp. vii+117. (London: Oxford University Press; California: Stanford University Press, 1960.) 34s.

This book is based upon the fourth Lockheed Symposium on Magneto-hydrodynamics. The earlier volumes of this series dealt with the theory of ionized gas behaviour and the problems of thermonuclear fusion. Here the temperatures discussed are much lower than those required for fusion and the emphasis is on plasma acceleration as a power source for rocket propulsion. Low level thrusts over a long period, e.g. accelerating 10^6 grams at 1 cm sec^{-2} for several days, are sufficient to manoeuvre a rocket in space.

A number of possible plasma accelerators are discussed both theoretically and experimentally and an article on scaling laws describes a procedure for inter-relating any two experiments. Several methods of acceleration are available, homopolar devices, electrostatic plasma guns and the use of travelling magnetic fields, but the most promising approach seems to be the hydromagnetic plasma gun of Marshall at Los Alamos. Marshall has achieved plasma velocities of 100 km sec^{-1} with an efficiency of 40% but only for a very short time. A practical system may demand continuous running. An interesting proposal is a d.c. accelerator where plasma is fed into a coaxial nozzle which has a suitable configuration of currents, and electric and magnetic fields. The plasma acceleration arises from the interaction between the currents and the magnetic field. The most efficient acceleration is a gentle one with just sufficient Joule heating to maintain the plasma state, and this is achieved when the back e.m.f. produced by the motion of the plasma across the magnetic field is only slightly less than the applied electric field. The book suggests that although the basic requirements are well understood the development of a successful device will take a long time.

H. J. PAIN.

Théorie des Ondes dans les Plasmas, by J. F. DENISSE and J. L. DELCROIX. Pp. xii+167. (Paris: Dunod, 1961.) 16 n fr.

This small book in the Dunod series of monographs gives a fairly exhaustive account of the propagation of waves of small amplitude in a plasma. The spatial and time dependences of physical quantities are assumed to be of the form $A \exp(j\omega t - jkz)$ and a general dispersion relation in the form of a ninth-order determinant is developed. From this, particular modes of oscillation are examined. These include transverse and longitudinal electromagnetic waves and their polarization in the presence of a longitudinal magnetic field. The theory is taken further than the simple cases usually considered in the literature, and many more types of wave are examined here. Inevitably this results in an increased complexity in the formulae, but the authors partly overcome this by confining the more elaborate equations to the appendix and by including many illustrative diagrams to explain the physical processes involved. For example, an explanation of resonances in ordinary and extraordinary transverse electromagnetic waves is made in terms of the gyro-magnetic frequencies of the ions and electrons respectively. There is new work presented in three of the chapters, including a classification of the types of wave in terms of the source of energy for propagation, and the coupling of the modes of oscillation by a transverse magnetic field. It is disappointing to find in the section on electrostatic oscillations no derivation of Landau damping but an inadequate interpretation in terms of electron trapping. This book is within the understanding of the average research student, and will be of use to those in this particular field. M. G. HAINES.

Infra-red Physics: An International Research Journal, Vol. 1, No. 1, edited by W. K. WEIHE, S. PASSMAN, N. MIGEOTTE and T. S. MOSS. Pp. vi+103 +iv. (Oxford, London, New York, Paris: Pergamon Press, March, 1961.) £7 per annum.

This is a new international journal concerned with all aspects of infra-red physics. Whether the introduction of any new journal is justified is always the first question to be asked, and in this case the wide variety of the aspects of the subject as indicated in the first issue certainly suggests that the journal is indeed desirable. The branches of the subject covered by the reports include light sources for optical communication, infra-red photography, infra-red interferometry and a sun-seeker for solar spectroscopy. The printing of the journal, including the reproduction of photographs and diagrams, is of high quality and the editors are to be congratulated on making an excellent start with the new journal. A. JACKSON.

Halbleiterprobleme, edited by F. SAUTER. Pp. vii+343. (Germany: Friedrich Vieweg, 1960.) DM. 48.

The fifth volume of this series, which was up to now edited by W. Schottky, contains an unusual variety of contributions. This feature is, in fact, suggested by the title (for almost anything can be called problems in German), but it might puzzle people here to find articles different in type, as reported below, in one slim volume.

Three of the contributions, occupying about a third of the volume, are of the type of 'progress reports'. All three are excellent and very readable. O. O. Folberth discusses the physical chemistry of $A^{III}B^V$ compounds; O. Madelung

surveys and analyses the behaviour of semiconductors in strong magnetic fields, and D. Geist reports on masers. Another third of the book, or rather more than a third (137 pages), is occupied by a paper on the theory of tarnishing reactions by K. Hauße and W. Schottky. This is a new analysis of the phenomenon, based on a review of older work, a paper such as one would, in this country, expect to find in the *Transactions*, and it should not be missed by anyone working in this field.

The rest of the volume consists of the extended version of a lucid discourse given by J. Jaumann on infra-red absorption spectra of solids; an article by H. Krömer on his new ideas about negative effective masses in semiconductors (published in more detail in *Progress in Semiconductors*, Vol. IV); a discussion, by H. Schmidt, of some aspects of band structure, electron lattice interaction and light absorption in semiconductors; and some supplements to reports published in earlier volumes.

The present volume is a witness of a lively and penetrating approach to semiconductor problems. Although, in the first instance, a record of the semiconductor group of the German physical societies, it deserves a place among the books on solid state physics everywhere.

W. EHRENBURG.

Problems in Quantum Mechanics, by I. I. GOLDMAN and V. D. KRIVCHENKOV. Pp. viii + 275. (London, New York, Paris, Oxford: Pergamon Press, 1961.) 50s.

The problems which are to be found at the back of Abraham and Becker's *Electricity and Magnetism* are prefaced by the phrase "Be ye doers of the word, and not hearers only, deceiving your own selves". Anyone who has ever studied any branch of the exact sciences will appreciate the aptness of this quotation.

The book under review is an excellent translation from Russian, and consists of over 250 problems complete with their solutions. It is designed as a companion volume to the text book 'Quantum Mechanics' by Landau and Lifshitz and covers the same ground, with particular emphasis on matrices and angular momentum. There are collections of specific problems on motion in a magnetic field, the atom, the molecule, and the scattering of a particle in a potential.

The book should be of great value both to lecturers and students. Anyone who has worked through it can be confident that he has both understood the concepts, and mastered the basic techniques, in the topics covered. One's only regret is that it does not go further, into relativistic quantum theory and elementary particle physics. Perhaps a further volume will be forthcoming.

P. T. MATTHEWS.

Quantum Mechanics, by J. L. POWELL and B. CRASEMANN. Pp. x + 495. (Reading, Massachusetts: Addison-Wesley, 1961.) 74s.

This book is an introduction to quantum mechanics. The early chapters are disappointing in that the approach is historical and somewhat old-fashioned, Schrödinger's equation being obtained by a heuristic argument based mainly on the phenomenon of electron diffraction. The notions of linear differential operators, eigenfunctions and eigenvalues do not appear until Chapter 6 and it is only then after 150 pages that a serious effort is made to explain what the subject

is really about. Matrix operators are first introduced in Chapter 9, more than half way through the book. These essentially theoretical chapters are interspersed with fairly standard discussions of one-dimensional motion in simple potentials including the harmonic oscillator, spherically symmetrical systems, phase shift analysis, and (after the chapter on matrices) angular momentum, perturbation theory for bound states and scattering amplitudes, and finally statistics and the exclusion principle.

The best book of this type available during the last ten years has been, by common consent, that of Schiff, and when a new one appears one cannot help asking how it compares. The book as a whole does not stand up to this severe test, but there are some aspects of it which are attractive. A large number of instructive problems are included at the end of each chapter. References to other books on the various topics given at the ends of the chapters are ample and sound. There is a welcome shift towards the use of operator methods, but unfortunately no use is made of the Dirac notation.

It is a book that will be a welcome addition to a college library, but one would probably not advise a student to buy it for himself. P. T. MATTHEWS.

Diffusion and Heat Flow in Liquids, by H. J. V. TYRRELL. Pp. xii + 329. (London: Butterworths, 1961.) 65s.

This book is a very useful addition to the literature concerned with irreversible processes. Of particular value are the description and criticism of various experimental techniques, the detailed analysis of optical methods of measuring diffusion coefficients, and the presentation of some practical solutions to the macroscopic differential equations descriptive of the response of a liquid to thermal and mechanical forces. The author has also included a considerable amount of experimental data and has attempted to show how this data can be interpreted.

In my opinion, the treatment of the macroscopic aspects of diffusion and heat flow is excellent, but the microscopic interpretation is too conventional and, above all, too abbreviated to be adequate. For instance, more space is devoted to the well-known activated state models than to the conceptually more satisfying and much more difficult theory of Kirkwood (the ratio of space is about 8:1). To give some examples, no mention is made of the linear prediction theory and acoustic analysis of Fixman; no space is devoted to the question of how one estimates the friction constant of the molecular theory; the rigid sphere model is mentioned but not analysed in physical terms; no mention is made of the Kubo autocorrelation function formulation. While this book is clearly not intended to be a monograph in statistical mechanics, the omissions are very serious.

In general, then, Tyrrell's book will be extremely useful to those investigators concerned with measuring the diffusion coefficient, Soret coefficient, etc., of a liquid but it will not help them to understand the results in terms of the current molecular theory. That such understanding is pertinent to the matters discussed is best illustrated by the use of the general statistical theory of transport to develop a quantitative theory of the heat of transport of ionic solutions (Helfand and Kirkwood). Although this work appeared too late to be incorporated into the text, it could not be fitted in unless some of the background material I have indicated was omitted were to be added. STUART A. RICE.

Progress in Low Temperature Physics, Vol. III, edited by G. J. GORTER. Pp. xii+495. (Amsterdam: North Holland, 1961.) 96s.

After the second volume appeared in 1957, Professor Gorter wanted to return to 'pondering and reading about questions that fascinate him' rather than edit another book. Fortunately he was persuaded of the usefulness of the series and he has again collected together review articles by a considerable number of authoritative authors. Like its predecessors, Vol. III is fairly evenly divided between the purely low temperature topics—liquid and solid helium and superconductivity—and others. While some people have been debating whether low temperature physics still exists as a subject in its own right, Professor Gorter has increased the fraction of the book devoted to helium and superconductivity to well over half.

Superconductivity is represented solely by a masterly review of recent developments by Bardeen and Schrieffer. They are at pains to discuss the meaning of the present theory as well as describing its application in the interpretation of the many properties which have now been measured. With nearly two hundred and fifty references, this chapter should become a classic in the field.

Liquid helium four is represented by 'Vortex lines in liquid helium II' by Vinen, by 'The nature of the λ -transition' by Buckingham and Fairbank and by 'Helium ions in liquid helium II' by Careri. Vinen gives a very clear account of recent experiments and of their significance in a field to which he and Hall have made notable contributions. Buckingham and Fairbank have taken the opportunity of describing their recent more accurate measurements of the specific heat near the λ -point, made with Kellers, from which they derive the singular term. The behaviour of other properties is analysed, and an experiment to look for a similar specific heat singularity in a superconductor is mentioned.

The increased availability of helium three is reflected in the articles by Grilly and Hammel on 'Liquid and solid ^3He ' and by Taconis on ' ^3He cryostats'. While enough was known about the low temperature properties of ^3He in 1955 for an article to appear in Vol. I, ^3He cryostats were then only just being developed. Nuclear orientation is another subject which has advanced so rapidly that a second article is required, and the developments since the appearance of Vol. II are discussed by Huiskamp and Tolhoek.

The remaining three articles are: 'Electron resonance in metals' by Azbel and Lifshits, 'Solid state masers' by Bloembergen and 'Some solid-gas equilibria at low temperatures' by Dokoupil. One could not hope for more authoritative authors on electron resonance, than two of the Russians who have contributed so much to this subject. In an extremely well produced book, it is unfortunate that the only serious misprints seem to occur in the translated details on some of their figures (≈ 1 for Oe^{-1} , N_0 for Na, and Li-thick for Li-thick).

Although it may be difficult to write high-brow review articles which will be understandable to physicists not engaged in fields related to one's own, the present series shows what can be achieved in broadening the outlook of anyone working in one large branch of physics and having some acquaintance with the concepts used. Now that Professor Gorter has once shown that he can be forced to surrender under sufficient pressure, let us hope that he will continue to edit this series and to derive satisfaction from reading the contributions which are sent to him for further volumes.

R. BERMAN.

Handbuch der Physik, Vol. III, Part 1, *Principles of Classical Mechanics and Field Theory*, edited by S. FLÜGGE. Pp. viii + 902. (Berlin: Springer, 1960.) DM 198.

The first part (225 pages) by J. L. Synge is a complete and elegant account of classical mechanics, including the dynamics of special relativity. The treatment is fairly formal, and obviously not for the beginner, but, as the latest treatise on the oldest and most important branch of applied mathematics, it will stand comparison with its many illustrious predecessors. It is noteworthy for the careful definition of the various abstract 'Spaces' into which the analysis is extended, and for the thorough geometrical interpretations of the formulae. It seems to fulfil perfectly the role expected of such an article in the *Handbuch*.

The remainder, nearly 700 pages, is called 'The Classical Field Theories' and is by C. Truesdell and R. Toupin, with an appendix on 'Tensor Fields' by I. L. Ericksen. This is certainly an unusual work. Not only does it deal with the basic theory of elasticity and hydrodynamics, but also presents an analysis of thermodynamics, and of electromagnetism. These topics are seen entirely from a formal mathematical point of view, as examples of special kinds of tensor fields subject to the fullest rigour of definition and abstraction; every result is proved in the most general form, and only explained in more familiar terms as a trivial special case. Although this abstract mathematical point of view is a perfectly proper and valuable attitude towards physics, it is rather startling to find it carried through with such ruthlessness and erudition over such a wide field. The authors have tried to restate and prove (or, in some cases disprove) every theorem of importance that can be found in the literature, going back more than two centuries for some of their references. They propose quite frankly, to replace some of our crude old-fashioned rules, like Maxwell's equations or the Laws of Thermodynamics, with their own more general principles based upon a more critical study of the mathematical possibilities. In many cases they claim, quite rightly, that the complete account which they give has never been attempted before, so that their work is, in this sense, of the highest originality and interest. I think, myself, that they overrate the importance of mathematical rigour, especially of the algebraic kind, and betray a lack of intuition for the synthetic, geometrical type of proof (how can they write on such a subject at such length with only about one figure per 14 pages of text?) which has always been more fruitful of *new* ideas than the analytical approach. But, as an attempt to reduce all known classical physics to the most abstract and elementary mathematical statements, this book is likely to be extremely valuable as an authority and as a source book, for years to come. The historical notes alone (our old friend Stokes' theorem is really due to Kelvin; or shouldn't it be Thomson, as in 1850 he then was!) are excellent.

It is most unfortunate that such an idiosyncratic work should be published as part of an encyclopaedia. It is too big, and cuts across too many boundaries. The reformulation of Thermodynamics, for example, with entropy as the independent field variable in place of temperature, should have been in Volume III, Part 2. It is a pity that the editor did not, in this case as in others in this series, insist on closer conformity to the general scheme—or else bring all the other contributors into step.

Another reason why Professor Truesdell and his collaborators would have done better to have this work published elsewhere as a separate book is that I

calculate that it could then have been sold for about £8, which would have brought it just within the reach of the ordinary individual applied mathematician or theoretical physicist. At the monstrous price of £18 (according to the current rate of exchange) it will be purchased only by libraries, where it will not have the circulation and influence that it deserves. The new edition of the *Handbuch der Physik* has some good things in it, but it is certainly not worth twice as much per word and symbol as ordinary treatises and textbooks.

J. M. ZIMAN.

Field Theory for Engineers, by PARRY MOON and DOMINA E. SPENCER. Pp. ix+530. (Toronto, New York, London, Princeton, New Jersey: Van Nostrand, 1961.) 96s.

The purpose of the book is stated by the authors to be the application of boundary value techniques to engineering. The field theory approach is dealt with by the technique of separation of variables, and it is thought that this method is of most use for applications of this kind.

Chemical Crystallography, by C. W. BUNN. Pp. xiii+509. (Oxford: Clarendon Press, 1961.) 60s.

This is the second edition of a book first published in 1945. Its scope is essentially the same as that of the first edition, but there are several additions and alterations: these are chiefly in the latter part of the book which is expanded to cover important recent developments in the various methods of structure determination, especially direct experimental methods involving heavy atoms and the use of anomalous scattering effects to determine the phases of different x-ray beams, and indirect interpretative methods involving the concept of the molecular transform.

The Mathematical Theory of Relativity, by A. S. EDDINGTON. Pp. ix+270. (Cambridge: University Press, 1961.) 16s.

The Mathematical Theory of Electricity and Magnetism, by SIR JAMES JEANS. Pp. vii+652. (Cambridge: University Press, 1961.) 25s.

The Mathematical Theory of Non-uniform Gases, by S. CHAPMAN and T. G. COWLING. Pp. xxiii+431. (Cambridge: University Press, 1961.) 17s. 6d.

These three further reprints, at a very reasonable price, of some of the classics of physics are a welcome issue from the Cambridge University Press. They will be most valuable to students in these days of expensive textbooks.

The Collected Works of Irving Langmuir, edited by GUY SUITS (Oxford, London, New York, Paris: Pergamon Press, 1961.) £5 per Vol.

The Collected Works of Irving Langmuir are to be published in twelve volumes. Each volume covers one or more subjects in which Langmuir was interested and contains reprints of papers which he had published in the various scientific journals. Four volumes have been published to date: Volume 3, *Thermionic Phenomena*; Volume 4, *Electrical Discharge*; Volume 5, *Plasma Oscillations*; Volume 6, *Structure of Matter*.

In Volume 12 there is to be a survey of Langmuir's career as a whole; it is of interest that his creative work covered a very wide range of years. Irving Langmuir was the first American industrial scientist to receive a Nobel prize; he was associated with the General Electric Research Laboratory for nearly fifty years.



Quartet



Quintet



Sextet

Fig. 1. Typical examples of some multiplets.

Fig. 4. Streak interferogram at 1 mm ambient pressure.

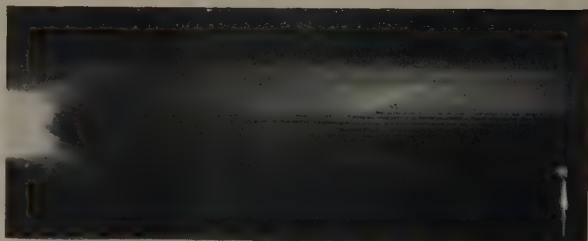


Fig. 5. Streak interferogram at 0.5 mm ambient pressure.

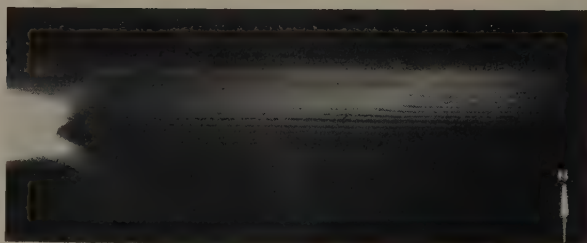


Fig. 6. Streak interferogram at 0.3 mm ambient pressure.

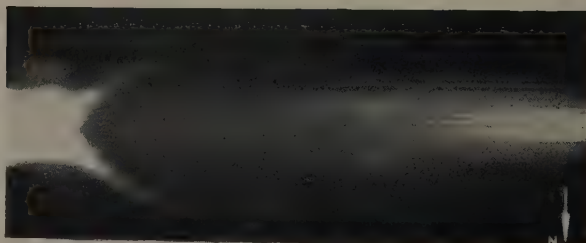


Fig. 7. Streak record at 1 mm ambient pressure showing luminous central core.



PROCEEDINGS OF THE PHYSICAL SOCIETY

1961—VOL. 78

SUBJECT INDEX

	PAGE
Abrasion in plastically deformable non-metals	979
Absorption edge, optical, of GaAs (L)	615
Absorption of coesite in wavelength region 5–22 microns (L)	1260
Absorption spectrum of BaO found in shock excitation	705
Absorption spectrum of BiF molecule, ultra-violet	610
Absorption spectrum, ultra-violet, of indium vapour, extension of series	600
Absorption, ultra-violet and visible, of gaseous ozone	932
Absorption, <i>see also under</i> Electron spin resonance	
Air showers, electron density spectrum at high densities	103
Alloys, Al–Mn, low temperature specific heat	1489
Alloys, dilute Ag–Mn, Lorenz parameter at liquid helium temperatures	1361
Alloys, GaSb–InSb, temperature variation of optical energy gap	354
Alloys, InAs–In ₂ Se ₃ and InSb–In ₂ Se ₃ , electrical and optical properties	1009
Alloys, Ni–Fe, preparation of continuous single-crystal thin films	33
Alloys of high purity iron, internal friction measurements and grain boundaries	1529
Alloys, Pt–Co, ordered, domain structure	225
Alloys, U–Nb, electrical and magnetic properties	361
Alloys, U–Zr, electrical and magnetic properties of γ and δ phases	722
Alpha particles, range–energy relations and stopping power for ethyl alcohol and CCl ₄ in liquid and vapour states	766
Alums, ferric, zero-field paramagnetic resonance	812
Anisotropy in electric strength of alkali halide crystals (L)	1261
Anisotropy of electrical conductivity in Bi ₂ Te ₃	838
Anisotropy, magnetic, <i>see</i> Magnetic anisotropy	
Anisotropy, magnetocrystalline, and coercivity in square-loop ferrite material	819
Antiferromagnetic resonance in extreme infra-red (L)	774
Apparatus, linear, correction of signal distortion	1546
Arc discharge, post-arc temperature decay	948
Argon, liquid, electric strength, influence of cathode and anode surfaces	448
Argon, thermodynamic properties	1449
Atomic spectra, isotope shift in CdI resonance line 2288 Å	1304
Atoms, impact excitation, schematic model	661
Auger effect in semiconductors, phonon-assisted	204
Band spectra, emission, O ₃ Schumann–Runge	1024
Band spectra of BiF and SbF (L)	614
Band spectra, rotational analysis of E–x system of silicon monosulphide	1307
Band spectra, second negative system of oxygen, new bands (L)	1074
Band spectrum, triplet, of CO molecule, Franck–Condon factors and <i>r</i> -centroids	399
Band spectrum of CuAg molecule in visible region	197
Band spectrum, <i>see also</i> Absorption spectrum	
Band structure, electronic, of model of cubic crystal	1195
Band structure of body-centred cubic transition metals	1321
Berthelot tubes, tensile strength of liquids in	133
Beta decay, Fierz interference term for Gamow–Teller decay of ⁵⁸ Co	1056
Biphenyl negative ion, narrowing and broadening of spectrum	370
Bismuth telluride, anisotropy of electrical conductivity	838
Breakdown, <i>see under</i> Ionization	
Breakdown, electrical, <i>see</i> Electrical breakdown	

	PAGE
Calorimeter, low temperature adiabatic, for condensed substances	1449
Calorimetric methods used to determine thermodynamic properties of A and Kr	1462
Capture, radiative, of protons by neutrons at 50 mev	912
Capture rate of negative muons in light elements	1149
Capture, <i>see also</i> Cross section	
Carbon monoxide, ionization and attachment coefficients in uniform fields, measurement	43
Carbon tetrachloride, α -particle stopping power in liquid and vapour states	766
Cathodoluminescence, growth and decay of intensity	1017
Charge separation between similar polyethylene surfaces, effect of thermal gradient	958
Charge transfer, resonant, in ionized dense gases	584
Charles Vernon Boys Lecture—counter techniques in high energy nuclear physics	1116
Circuits, electrical, filters, synthesis	998
Cloud chamber studies, low temperature, on water vapour	1218
Cobalt 58. Gamow-Teller decay, determination of Fierz interference term from K-capture/ β^+ ratio	1056
Coesite, absorption in wavelength region 5–22 microns (L)	1260
Collisions, atomic, positron-hydrogen, partial wave theory	549
Collisions, inelastic, excitation of 1s–2p transition of hydrogenic ions by bare nuclei (L)	1080
Collisions, ionic, measurements of rotational energy distributions	588
Collisions, nuclear, direct interaction with strong coupling—II: E2 excitations	641
Conservation conditions, importance in distorted wave calculations	695
Contact between polyethylene spheres, charge separation and thermal gradient	958
Cosmic-ray muons, <i>see</i> Muons	
Cosmic-ray spectrograph, Manchester	496
Cosmic rays, <i>see</i> Air showers	
Coulomb potential, screened, scattering by (L)	616
Counters, Geiger-Müller, self-quenching, containing A, Xe, O and N, mechanism	785
Counter techniques in high energy nuclear physics	1116
Counting efficiency, quantum, of detectors in x-ray emission work (L)	1256
Coupling between elastically and inelastically scattered waves, effect for E2 excitations	641
Crack propagation in plastics	970
Cross section, proton total reaction, for copper at 9.3 mev, measurement	1275
Cross section, radiative capture, of ^{238}U for neutrons in energy range 0.3–4.0 mev	801
Cross section, total, for production of neutral pions in p-p collisions at 383 mev	1151
Cross section, <i>see also</i> Dissociation	
Crystal, cubic, electronic band structure of model	1195
Crystal, LiF, reflection and polarization of elastic waves	39
Crystal, metal, vibration spectrum, electron participation	1495
Crystal model, simple, surface states	217
Crystal, single, <i>see under</i> Films, thin	
Crystalline field parameters for dysprosium ethyl sulphate	753
Crystals, alkali halide, anisotropy in electric strength (L)	1261
Crystals, $\beta\text{-In}_2\text{S}_3$, twinning	491
Crystals, CsBr(Tl) and CsI(Tl), luminescence as function of temperature	1188
Crystals, ferroelectric, $\text{Na}_{0.975}\text{K}_{0.025}\text{NbO}_3$, structure (L)	1258
Crystals, imperfect cubic, and non-cubic, spin-lattice relaxation	1
Crystals, single, of antiferromagnetic NiO, magnetostriction in	728
Crystals, single, of haematite, temperature effects in domain patterns	869
Crystals, single, of magnetite, anisotropy at low temperatures	17
CuAg, emission spectrum in visible region	197
CuK α radiation, effect of absorption in β filter on mean wavelength, experimental (L)	305
Cyclotron resonance at 4 mm wavelength (L)	1078
Damping of sound waves by ideally rough surface (L)	1265
Debye temperature values of Laue-Bragg scattering (L)	1255
Deformation, surface, in abrasion of plastic non-metals	979

Diamond dodecahedra, micro-disk patterns on	12
Diamond, electronic distribution, theoretical calculation and comparison with experiment	239
Diamonds, insulating, energy levels in forbidden gap	256
Dielectric dispersion, application of Onsager's theory (L)	311
Dielectrics, liquid, electrical breakdown	423
Dielectrics, organic liquid, electrical properties	854
Discharge, arc, <i>see</i> Arc discharge	
Dislocations, scattering of waves by, theory	1512
Dispersion, dielectric, <i>see</i> Dielectric dispersion	
Dissociation cross section for interaction of H_2^+ ions with hydrogen gas	1215
Distorted wave calculations, importance of conservation conditions	695
Distortion approximation and excitation of helium to $(1s, 2p)^1P$ and $(1s, 3p)^1P$ states	903
Distortion approximation to cross sections for excitation of $1s-2p$ transition of hydrogenic ions (L)	1080
Distortion produced by linear apparatus, correction	1546
Domain patterns from single crystals of haematite, temperature effects	869
Domain structure of ordered Pt-Co alloys	225
Domain wall velocity in square loop ferrite	233
Double beta decay (L)	464
Dysprosium ethyl sulphate, crystalline field parameters	753
Einstein solid, space correlation and energy levels in	759
Elastic recovery of conical indentations	169
Elastic waves, reflection and polarization in LiF crystal	39
Elastic waves, <i>see also under</i> Waves	
Electric breakdown of NaCl	734
Electric strength of liquid argon, influence of cathode and anode surfaces	448
Electrical breakdown of gases: ionization growth in air at high pressures	569
Electrical breakdown of liquid dielectrics	423
Electrical conductivity, anisotropy in Bi_2Te_3	838
Electrical resistivities and magnetic susceptibilities of U-Nb alloys	361
Electrical resistivity of γ and δ phases in U-Zr system	722
Electroluminescence and infra-red emission in ZnS phosphors	348
Electron attachment in oxygen-nitrogen mixtures by microwave cavity method	1543
Electron capture, dependence of rate on electric field, and possibility of negative resistance in semiconductors	710
Electron correlation in ground state of helium	831
Electron diffraction patterns from thin films of face-centred cubic metals, extra reflections	594
Electron distribution in $(CuCl_2)^{4-}$ (L)	1263
Electron spin resonance absorption for polycrystalline substances: II	1174
Electron spin resonance absorption spectrum of biphenyl negative ion	370
Electron spin resonance in two groups of lanthanon salts	1353
Electron spin resonance in two salts containing Gd	1340
Electron spin resonance studies of impurity ions in MgO	554
Electronic conduction in polar semiconductors	1384
Electronic structure and spectrum of nitrobenzene	460
Electrons, free, m/e determined by momentum transfer	433
Electrons, knock-on, and direct electron pair production by cosmic-ray muons	650
Emulsions, silver bromide, lattice rotations in tabular grains	698
Energy distributions, rotational, in ionic collisions, measurement	588
Energy gaps, existence in one-dimensional liquids	926
Energy levels and space correlation in Einstein solid	759
Energy levels in forbidden gap of insulating diamonds	256
Energy levels, intersecting, line shapes in	70

	PAGE
Energy levels of magnesium isotopes mass 25 to 28	473
Energy levels, <i>see also</i> Level	
Energy loss, differential, and ranges of Ne, N and He ions	1135
Energy loss of noble metals and their neighbours	1177
Ethyl alcohol, α -particle stopping power in liquid and vapour states	766
Ethylene, excitation of vibrational modes in homo-molecular collisions	1502
Faraday effect in non-degenerate semiconductors	120
Faraday effect, infra-red, in Ge	1393
Ferrite, square-loop, estimation of domain wall velocity	233
Ferrites, square-loop, magnetocrystalline anisotropy and coercivity	819
Ferrites, square-loop, temperature dependent relaxation	828
Field theory, electron-phonon interaction by method of pseudo-potentials	895
Fierz interference term, determination from K-capture/ β^+ ratio for Gamow-Teller decay ^{58}Co	1056
Films, thin, monocrystalline and continuous, of Ni and Ni-Fe alloys, preparation	33
Films, thin, of face-centred cubic metals, extra reflections in electron diffraction patterns	594
Films, thin, single-crystal, of Ni, magnetic anisotropy	25
Filters, electrical interference, synthesis	998
Fluorescence, excitation in organic liquid dielectrics by electric fields	854
Franck-Condon factors and r -centroids for triplet band system of CO molecule	399
Friction, internal, measurements on iron-interstitial alloys	1529
Friction, internal, measurements on pure iron	1520
Friction, <i>see also</i> Abrasion	
Gadolinium, electron spin resonance in salts containing	1340
Gadolinium, magnetothermal measurements	878
Gamma radiation from medium energy proton bombardment of Li, Be, B, C and N	681
Gases, dense ionized, resonant charge transfer	584
Gases, inert, <i>see</i> Inert gases	
Germanium, infra-red Faraday effect	1393
Grain boundary damping I: pure iron	1520
Grain boundary damping II: iron interstitial alloys	1529
Graphites, pyrolytic, well oriented, radiation damage in	1048
Haematite, single crystals, temperature effects in domain patterns	869
Hall effect in monovalent metals at low temperatures (L)	316
Hall effect in plutonium (L)	776
Hartree-Fock method, unrestricted	113
Helium, coherent and incoherent scattering of x-rays by	673
Helium, electron correlation in ground state	831
Helium, excitation to $(1s, 2p)^1P$ and $(1s, 3p)^1P$ states by proton and α -particle impact	903
Hydrocarbons, aromatic, bond length, and perturbation calculations for π -electrons	1310
Hydrogen atoms, scattering of low-energy ortho-positronium by	329
Hydrogen, coherent and incoherent scattering of x-rays by	673
Hydrogen gas, dissociation of H_2^+ ions, vibrational energy effects	1215
Hydrogen, pre-breakdown ionization at low pressures	92
Hydrogen, van der Waals forces	607
Hydromagnetic waves, transverse, effect of particle streams	1236
Hyperfine structure in terbium metal (L)	313
Impurity ions in MgO, electron spin resonance studies	554
Impurity, <i>see also under</i> Semiconductors	
Indentations, conical, elastic recovery	169
Indium alloys, electrical and optical properties	1009
Indium vapour, ultra-violet absorption spectrum, extension of series	600

	PAGE
Inert gases, multiply ionized, vacuum ultra-violet spectra	1223
Inert gases, van der Waals forces	607
Infra-red emission and electroluminescence in ZnS phosphors	348
Infra-red, extreme, antiferromagnetic resonance in (L)	774
Infra-red Faraday effect in Ge	1393
Interaction, electron-phonon, by method of pseudo-potentials	895
Interferometer, Michelson stellar	596
Ionization and attachment coefficients in CO in uniform fields measurement	438
Ionization growth, pre-breakdown, in air at high pressures	569
Ionization, pre-breakdown, in hydrogen at low pressures	92
Ionosphere, F region, analogue solution of continuity equation	409
Ions, ranges, of Ne, N and He, and differential energy loss	1135
Iron alloys, internal friction measurements and grain boundaries	1529
Iron, internal friction measurements and grain boundaries	1520
Isotope shift in CdI resonance line 2288 Å	1304
Krypton, thermodynamic properties	1462
Lanthanum salts, electron spin resonance in	1353
Lattice rotations in tabular silver bromide grains	698
Lattice vibration spectrum, derivation from specific heat curves	941
Lattice vibrations, participation of electron gas in	1495
Level, 6^3P_1 in mercury, g_J value, using double-resonance technique	65
Lifetime of 638 kev level in ^{131}Xe	1071
Lifetime of 673 kev level in ^{132}Xe	1065
Line shapes in method of intersecting energy levels	70
Line shapes, resonance, properties	75
Liquids, one-dimensional, existence of energy gaps in	926
Liquids, tensile strength in Berthelot tubes	133
Lorenz parameter in dilute Ag-Mn alloys at liquid helium temperatures	1361
Low pressures, pre-breakdown ionization in hydrogen	92
Low temperature electric field effects in semiconductors	517
Low temperature specific heat of Al-Mn alloy	1489
Low temperature specific heat of hexagonal metals	1482
Low temperature specific heat of scandium and yttrium (L)	622
Low temperatures, Hall effect in monovalent metals (L)	316
Low temperatures, Lorenz parameter in dilute Ag-Mn alloys	1361
Luminescence, growth and decay of intensity under cathode-ray excitation	1017
Luminescence of CsBr(Tl) and CsI(Tl) as function of temperature	1188
Magnesium isotopes mass 25 to 28, energy levels	473
Magnetic anisotropy and rotational hysteresis in single crystals of magnetite below transition temperature	17
Magnetic anisotropy in single crystal Ni films	25
Magnetic moment, sub-lattice, in manganese ferrite (L)	620
Magnetic properties in nickel (L)	145
Magnetic resonance in nitrogen afterglow	1227
Magnetic resonance, <i>see also under</i> Proton	
Magnetic susceptibilities and electrical resistivities of U-Nb alloys	361
Magnetic susceptibilities of Al-rich transition-metal intermetallic compounds	1244
Magnetic susceptibility of γ and δ phases in U-Zr system	722
Magnetic susceptibility of $\text{MnF}_2\text{-ZnF}_2$ solid solutions (L)	318
Magnetite, single crystals, anisotropy at low temperatures	17
Magnetoelastic constants of nickel	391
Magnetoresistance, quantum theory I: low fields	275
Magnetostriiction in antiferromagnetic NiO	728

	PAGE
Magnetothermal measurements on gadolinium	878
Manganese ferrite, sub-lattice magnetic moments in (L)	620
Manganese, paramagnetic resonance	883
Manganese zinc fluoride solid solutions, magnetic susceptibility (L)	318
Materials, non-metallic, plastic, abrasion process in	979
Mercury, 6^3P_1 level, γ_J value, using double-resonance technique	65
Mesons, π and μ , rare decay, counter techniques for	1116
Mesons, <i>see also</i> Muons, Pions	
Metals, hexagonal, specific heat at very low temperatures	1482
Metals, monovalent, Hall effect at low temperatures (L)	316
Metals, noble, and neighbours, characteristic electron energy loss spectra	1177
Metals, thermoelectricity in, at normal temperatures (L)	306
Metals, <i>see also</i> Terbium	
Metals, transition, <i>see</i> Transition metals	
Microwave cavity method for measurement of attachment in oxygen-nitrogen mixtures	1543
Models, use to determine surface states of crystals	217
Molecular integrals, numerical integration method	53
Molecular liquids, multiple proton magnetic resonance relaxation in	377
Molecules, long-chain, skeletal modes (L)	625
Momentum transfer, used to determine m/e for free electrons	433
Moon, radio wave scattering from	988
Multiplet production by x-rays	1301
Muons, cosmic-ray, direct electron pair production by, and knock-on electrons	650
Muons, cosmic-ray, measurement of momentum spectrum and charge ratio at sea level	505
Muons, cosmic-ray, momentum spectrum at sea level	918
Muons, negative, in light elements, capture rate	1149
Muons, negative, in light elements, depolarization	1144
Negative resistance effects in semiconductors, possibility	293
Negative resistance in semiconductors and dependence of capture rate on electric field	710
Neutrons, low energy elastic scattering by deuterons	1157
Neutrons, radiative capture by protons at 50 mev	912
Nickel and Ni-Fe alloys, continuous single-crystal thin films, preparation	33
Nickel, magnetic properties (L)	145
Nickel, magnetoelastic constants	391
Nickel oxide, antiferromagnetic, magnetostriction in	728
Nitrobenzene, electronic structure and spectrum	460
Nitrogen afterglow, magnetic resonance in	1227
Nitrogen, N v, lines of spectrum in visible and near ultra-violet	201
Nuclear magnetic resonance relaxation times, Carr-Purcell method of measuring	808
Onsager's theory, application to dielectric dispersion (L)	311
Optical absorption, <i>see</i> Absorption, optical	
Optical energy gap, temperature variation for GaSb-InSb alloys	354
Organic liquid dielectrics, electrical properties	854
Ortho-positronium in gases, measurement of quenching rates	1038
Ortho-positronium, low-energy, scattering by H atoms	329
Oxygen, new bands in second negative system (L)	1074
Ozone, gaseous, absorption in ultra-violet and visible	932
Paramagnetic resonance, 'forbidden' transitions, explanation (C)	778
Paramagnetic resonance methods to study electron distribution in $(CuCl_2)_4^{4-}$ (L)	1263
Paramagnetic resonance of manganese	883
Paramagnetic resonance, zero-field, of Fe^{3+} in methylamine alum	812
Particles, charged, effect of streams on transverse hydromagnetic waves	1236

Perturbation calculations for π -electrons and application to bond length reconsiderations in aromatic hydrocarbons	1310
Perturbation theory for predicting $1s\sigma$ and $2p\sigma$ energies of H_2^+ and HeH^{2+}	537
Perturbation theory, non-degenerate Rayleigh-Schrödinger in any order	517
Phonons, effect on Auger recombination in semiconductors	204
Phonons, electron-phonon interaction by method of pseudo-potentials	895
Phosphors, effect of temperature dependent trapping cross sections on thermally stimulated emission	1408
Phosphors, organic, photofluorescence decay times	743
Phosphors, ZnS, infra-red emission and electroluminescence in	348
Photoconductors, effect of temperature dependent trapping cross sections on thermally stimulated emission	1408
Photofluorescence decay times of organic phosphors	743
Photons, high energy, nuclear scattering	1125
Photovoltaic effects in Si and Se elements	845
Pions, neutral, cross section for production in p-p collisions at 383 mev	1151
Plasma containment in ZETA, spectroscopic investigation	1416
Plasma drift velocity across confining magnetic field (L)	618
Plastics, crack propagation in	970
Plutonium, Hall effect in (L)	776
Polycrystalline substances, electron spin resonance absorption: II	1174
Positron-hydrogen atom collisions, partial wave theory	549
Positrons, elastic scattering by atomic hydrogen and helium	1169
Proton bombardment, medium energy, of Li, Be, B, C and N, γ -radiation from	681
Proton magnetic resonance relaxation in molecular liquids	377
Proton scattering, <i>see</i> Scattering	
Pulses, stochastic, statistical properties of sequences	153
Quantum theory of magnetoresistance I: low fields	275
Quenching of ortho-positronium in gases, measurement	1038
γ -centroids and Franck-Condon factors for triplet band system of CO molecule	399
Radiation damage in well oriented pyrolytic graphites	1048
Radio wave scattering from lunar surface	988
Reaction, $^{56}\text{Mn}(d, p)^{56}\text{Mn}$	404
Reaction, $\text{Pt}(n, \alpha)\text{Os}$	1297
Reactions, $^{10}\text{B}(^3\text{He}, d)^{11}\text{C}$ and $^{11}\text{B}(^3\text{He}, d)^{12}\text{C}$	81
Reactions, $(^3\text{He}, d)$, leading to ^{11}C and ^{12}C	81
Reactions, exchange transfer, between ^{16}O and ^{27}Al	1163
Reactions, <i>see also</i> Cross section, Energy levels	
Reflection, horizontal, in three-dimensional stratified medium	46
Relaxation, spin-lattice, in imperfect cubic and in non-cubic crystals	1
Relaxation, spin-lattice, time measurements in dilute $\text{K}_3\text{Fe}(\text{CN}_6)$	180
Relaxation, temperature dependent, in square-loop ferrite	828
Relaxation times, nuclear magnetic resonance, Carr-Purcell method of measuring	808
<i>Reports on Progress in Physics</i> corrigendum to 'Double beta decay' (L)	464
Resistance, negative, <i>see</i> Negative resistance	
Resistivity, electrical, <i>see under</i> Electrical	
Resonance, antiferromagnetic, <i>see under</i> Antiferromagnetic	
Resonance fluorescence from Hg vapour, changes with magnetic field	70
Resonance, line-shape functions, properties	75
Resonance, <i>see also</i> Electron, Nuclear magnetic, Paramagnetic, Proton	
Rotational analysis of E-x system of silicon monosulphide	1307
Rutherford Memorial Lecture, 1958 (Niels Bohr)	1083

	PAGE
Scattering by screened Coulomb potential (L)	616
Scattering, elastic, of positrons by atomic hydrogen and helium	1169
Scattering, Laue-Bragg, Debye temperature values (L)	1255
Scattering, elastic, low energy, of neutrons by deuterons	1157
Scattering, nuclear, of high energy photons	1125
Scattering of low-energy ortho-positronium by H atoms	329
Scattering of waves by dislocations, theory	1512
Scattering, proton, by copper at 10 Mev	1285
Scattering, proton-proton, below 50 Mev	185
Scattering, x-ray, coherent and incoherent, by H ₂ and He	673
Selenium elements, electron voltaic effects	845
Semiconductors, impurity concentration, change of activation energy with	716
Semiconductors, low temperature electric field effects	517
Semiconductors, negative resistance in, and dependence of capture rate on electric field	710
Semiconductors, non-degenerate, Faraday effect in	120
Semiconductors, phonon-assisted Auger effect	204
Semiconductors, polar, electronic conduction in	1384
Semiconductors, possibility of negative resistance effects in	293
Semiconductors, <i>see also</i> Bismuth, Cyclotron resonance, Indium, Selenium, Silicon	
Shock waves, time-resolved absorption in BaO	705
Sigma bonding in (CuCl ₆) ⁴⁻ (L)	1263
Signal distortion produced by linear apparatus, correction	1546
Silica, <i>see</i> Coesite	
Silicon elements, electron voltaic effects	845
Silicon monosulphide, rotational analysis of E-X system	1307
Sound absorption and velocity measurements in ethylene	1502
Sound propagation, underwater, horizontal reflection	46
Sound waves, damping by ideally rough surface (L)	1265
Space correlation and energy levels in Einstein solid	759
Specific heat curves, inversion	941
Specific heat, hyperfine structure in terbium metal (L)	313
Specific heat, low temperature, of scandium and yttrium (L)	622
Specific heat of Al-Mn alloy at low temperatures	1489
Specific heat of hexagonal metals at very low temperatures	1482
Spectra, <i>see under</i> Absorption, Band, Energy loss	
Spectra, ultra-violet, <i>see</i> Ultra-violet	
Spectrograph, high energy magnetic cosmic-ray, Manchester	496
Spectroscopic investigation of plasma containment in ZETA	1416
Spectrum, lines of N v in visible and near ultra-violet	201
Spectrum of biphenyl ion, narrowing and broadening	370
Spin-lattice relaxation, <i>see</i> Relaxation	
Spinel structure, cation-deficient, twinning	491
Structures of NaNbO ₃ and Na _{0.975} K _{0.025} NbO ₃ (L)	1258
Superconductivity in niobium, study by electron tunnelling (L)	309
Surface states of simple crystal model	217
Susceptibility, magnetic, <i>see under</i> Magnetic	
Target, thick, of pure element, efficiency of production of characteristic x-radiation	1206
Temperature variation of optical energy gap for GaSb-InSb alloys	354
Tensile strength of liquids in Berthelot tubes	133
Terbium metal, hyperfine structure in (L)	313
Thermal conductivity of Ag alloys at liquid helium temperatures	1361
Thermodynamic properties of argon	1449
Thermodynamic properties of krypton	1462
Thermoelectricity in metals at normal temperatures (L)	306
Transfer and exchange transfer of nucleons between ¹⁶ O and ²⁷ Al	1163
Transistors, junction, excess high-frequency noise in (L)	1076

	PAGE
Transition-metal intermetallic compounds, Al-rich, magnetic susceptibilities . . .	1244
Transition metals, body-centred cubic, band structure	1321
Trapping cross sections, temperature dependent, effect of thermally stimulated emission and conductivity peaks	1408
Tunnelling, study of superconducting niobium by (L)	309
Ultra-violet absorption spectrum, <i>see</i> Absorption spectrum	
Ultra-violet spectra, vacuum, of multiply ionized inert gases	1223
Ultra-violet, <i>see also</i> Absorption, Spectrum	
Van der Waals forces for hydrogen and inert gases	607
Vibrational energy effects in dissociation of H_2^+ ions by hydrogen gas	1215
Vibrational modes, excitation in ethylene	1502
Water vapour, low temperature cloud chamber studies	1218
Wave functions, unrestricted Hartree-Fock method	113
Waves, elastic and electromagnetic, horizontal reflection in three-dimensional stratified medium	46
Waves, elastic, <i>see also</i> Elastic waves	
Waves, hydromagnetic, transverse, effect of particle streams	1236
Waves, sound <i>see</i> Sound waves	
Wear, <i>see</i> Abrasion	
X-radiation, characteristic, efficiency of production in thick targets of pure element	1206
X-ray diffractometers, sources of error in high precision work (L)	1256
X-ray diffractometry, peak shifts in	249
X-ray emission lines, effect of absorption in β filter on mean wavelength, experimental (L)	305
X-ray emission, variation in quantum counting efficiency of detectors (L)	1256
X-ray reflections in diamond, comparison between theory and experiment	239
X-ray scattering, coherent and incoherent, by H_2 and He	673
X-rays, multiplet production by	1301
Xenon 131, lifetime of 638 kev level	1071
Xenon 132, lifetime of 673 kev level	1065
ZETA, spectroscopic investigation of plasma containment	1416

INDEX TO AUTHORS (WITH TITLES)

	PAGE
Alberts, L., and Lee, E. W.: Magnetostriction in antiferromagnetic nickel oxide .	728
Allan, J. W. S., Edels, H., and Whittaker, D.: Post-arc temperature decay .	948
Allison, D. C. S., McIntyre, H. A. J., and Moiseiwitsch, B. L.: Elastic scattering of positrons by atomic hydrogen and helium .	1169
Anderson, J. C.: Magnetic anisotropy in single-crystal nickel films .	25
Anderson, J. C., with Heavens, O. S., Miller, R. F., and Moss, G. L.: Preparation of continuous single-crystal thin films of nickel and nickel-iron alloys .	33
Anderson, J. M., and Barry, J. N.: Magnetic resonance in nitrogen afterglow .	1227
Andrew, E. R., and Tunstall, D. P.: Spin-lattice relaxation in imperfect cubic crystals and in non-cubic crystals .	1
Astbury, A., Blair, I. M., Hussain, M., Kemp, M. A. R., and Muirhead, H.: Capture rates for negative muons in light elements .	1149
Astbury, A., Hattersley, P. M., Hussain, M., Kemp, M. A. R., Muirhead, H., and Woodhead, T.: Depolarization of negative muons in light elements .	1144
Astbury, A., Kemp, M. A. R., Muirhead, H., Voss, R. G. P., and Woodhead, T.: Measurement of total cross section for production of neutral pions in proton-proton collisions at 383 mev .	1151
Austin, I. G., Gebbie, H. A., and Morin, I.: Absorption of coesite in region 5-20 microns (L) .	1260
Auzins, P., with Orton, J. W., Griffiths, J. H. E., and Wertz, J. E.: Electron spin resonance studies of impurity ions in magnesium oxide .	554
Bagguley, D. M. S., and Stradling, R. A.: Cyclotron resonance at 4 mm wavelength (L) .	1078
Bahadur, Kanwar, and Sastry, P. V.: On extra reflections in electron diffraction patterns from thin evaporated films of some face-centred cubic metals .	594
Baker, J. M., and Rubins, R. S.: Electron spin resonance in two groups of lanthanon salts .	1353
Baker, J. M., and Williams, F. I. B.: Electron spin resonance in two salts containing gadolinium .	1340
Ballentyne, D. W. G.: Infra-red emission and electroluminescence in zinc sulphide phosphors .	348
Barford, N. C., Palmer, R. B., and Tallini, B.: Radiative capture of protons by neutrons at 50 mev .	912
Barnard, R. D.: Some physical properties of the γ and δ phases in U-Zr system .	722
Barnard, R. D., with Bates, L. F.: Electrical and magnetic properties of uranium-niobium system .	361
Barnes, J. F., and Tredgold, R. H.: On change of activation energy with impurity concentration in semiconductors .	716
Barrow, R. F., Deutsch, J. L., Lagerqvist, A., and Westerlund, B.: Rotational analysis of E-X system of silicon monosulphide .	1307
Barry, J. F., Bunce, J. L., and Perkin, J. L.: Radiative capture cross section of ^{238}U for neutrons in energy range 0.3 to 4.0 mev .	801
Barry, J. N., with Anderson, J. M.: Magnetic resonance in nitrogen afterglow .	1227
Bates, C. A., and Stevens, K. W. H.: Band structure of body-centred cubic transition metals .	1321
Bates, D. R.: Distortion approximation to cross sections for excitation of 1s-2p transition of hydrogenic ions by bare nuclei .	1080
Bates, L. F., and Barnard, R. D.: Electrical and magnetic properties of uranium-niobium system .	361
Bates, L. F., and Pacey, A. J.: Magnetothermal measurements on gadolinium .	878
Beaumont, R. H., Chihara, H., and Morrison, J. A.: Thermodynamic properties of krypton. Vibrational and other properties of solid argon and solid krypton .	1462

Bell, R. J.: Excitation of helium to (1s, 2p) ¹ P and (1s, 3p) ¹ P states by proton and alpha particle impact	903
Benbow, J. J.: Stable crack propagation in plastics	970
Bhalla, M. S., and Craggs, J. D.: Measurement of ionization and attachment coefficients in carbon monoxide in uniform fields	438
Billington, E. W., and Ehrenberg, W.: Electron voltaic effects in silicon and selenium elements	845
Birss, R. R., with Lee, E. W.: Magnetoelastic constants of nickel	391
Blackman, L. C. F., Saunders, G., and Ubbelohde, A. R.: Radiation damage in well oriented pyrolytic graphites	1048
Blair, I. M., with Astbury, A., Hussain, M., Kemp, M. A. R., and Muirhead, H.: Capture rates for negative muons in light elements	1149
Blanchard, C. H., with Roy, R. R., Webb, E. H., Sandhu, H. S., and Mohanty, R. C.: Multiplet production by x-rays	1301
Bleaney, B., and Hill, R. W.: Hyperfine structure in terbium metal (L)	313
Bleaney, B., and Rubins, R. S.: Explanation of some 'forbidden' transitions in paramagnetic resonance (C)	778
Bloor, D., and Martin, D. H.: Antiferromagnetic resonance in extreme infra-red (L)	774
Bogle, G. S., and Symmons, H. F.: Zero-field paramagnetic resonance of Fe ³⁺ in methylamine alum	812
Bohr, N.: Rutherford Memorial Lecture 1958: Reminiscences of founder of nuclear science and of some developments based on his work	1083
Bolton, H. C., and Heaton, J. W.: Electronic distribution in diamond and intensities of x-ray reflections	239
Borland, R. E.: Existence of energy gaps in one-dimensional liquids	926
Bornman, C. H., with Stoker, P. H., and Hofmeyr, C.: Knock-on electrons and direct electron pair production by cosmic-ray muons	650
Bowles, A. H.: Effect of thermal gradient upon charge separation between similar polyethylene surfaces	958
Bowley, A. E., with Delves, R. T., Hazelden, D. W., and Goldsmid, H. J.: Anisotropy of electrical conductivity in bismuth telluride	838
Briggs, B. H., and Rishbeth, H.: Analogue solution of continuity equation of ionospheric F region	409
Buckingham, B. E., with Hyde, F. J., and Roberts, H. J.: Excess high-frequency noise in junction transistors (L)	1076
Bunce, J. L., with Barry, J. F., and Perkin, J. L.: Radiative capture cross section of ²³⁸ U for neutrons in energy range 0.3 to 4.0 mev	801
Burton, W. M., and Wilson, R.: Spectroscopic investigation of plasma containment in ZETA	1416
Byrne, J.: New bands in second negative system of oxygen (L)	1074
Canjar, L. N., with Madonna, L. A., Sciulli, C. M., and Pound, G. M.: Low temperature cloud chamber studies on water vapour	1218
Caplan, H. S., with Williams, W. S. C., and Stewart, D. T.: Nuclear scattering of high energy photons	1125
Chamberlain, J. R.: Magnetocrystalline anisotropy and coercivity in 'square-loop' ferrite material	819
Chamberlain, J. R.: Temperature dependent relaxation in square-loop ferrite	828
Chambers, R. G.: Inversion of specific heat curves	941
Chari, M. S. R.: Lorenz parameter in dilute silver-manganese alloys at liquid helium temperatures	1361
Chihara, H., with Beaumont, R. H., and Morrison, J. A.: Thermodynamic properties of krypton. Vibrational and other properties of solid argon and solid krypton	1462
Clegg, A. B., Foley, K. J., Salmon, G. L., and Segel, R. E.: Gamma radiation from medium energy proton bombardment of lithium, beryllium, boron, carbon and nitrogen	681

	PAGE
Codling, K., with Garton, W. R. S.: Extension of series in first spectrum of indium (In I)	600
Coleman, R. F., and Perkin, J. L.: Transfer and exchange transfer of nucleons between ^{16}O and ^{27}Al	1163
Collinson, A. J. L., Demetsopoulos, I., and Zarzycki, J. M.: Investigation into mechanism of self-quenching Geiger-Müller counters containing argon with small quantities of xenon, oxygen and nitrogen	785
Cooper, R., and Fernandez, A.: Anisotropy in electric strength of alkali halide crystals (L)	1261
Cooper, R., with Pearson, R. F.: Magnetic anisotropy and rotational hysteresis in single crystals of magnetite below transition temperature	17
Cooper, R., and Smith, W. A.: Electric breakdown of sodium chloride	734
Cosslett, V. E., with Green, M.: Efficiency of production of characteristic x-radiation in thick targets of pure element	1206
Coulson, C. A., and Golebiewski, A.: On perturbation calculations for π -electrons and their application to bond length reconsiderations in aromatic hydrocarbons	1310
Coulson, C. A., and Neilson, A. H.: Electron correlation in ground state of helium	831
Craggs, J. D., with Bhalla, M. S.: Measurement of ionization and attachment coefficients in carbon monoxide in uniform fields	438
Craik, D. J., and Nuñez, Felicia: Domain structure of ordered platinum-cobalt alloy	225
Cresswell, M. W., and Roy, R. R.: On reaction $\text{Pt}(n, \alpha)\text{Os}$	1297
Dalgarno, A., and Kingston, A. E.: Van der Waals forces for hydrogen and inert gases	607
Dalton, A. W., Parry, G., Scott, H. D., and Swierszczewski, S.: $^{55}\text{Mn}(d, p)^{56}\text{Mn}$ reaction	404
Darveniza, M., and Tropper, H.: Electrical properties of organic insulating liquids containing fluorescent solutes	854
Daw, H., and Harris, F. S.: Determination of m/e for free electrons by momentum transfer	433
Dayal, B., and Singh, S. P.: Participation of electron gas in lattice vibrations	1495
Delf, B. W.: Effect of absorption in β filter on mean wavelength of x-ray emission lines (L)	305
Delf, B. W., with Wilson, A. J. C.: Effect of variations in quantum counting efficiency of detectors on mean wavelength of x-ray emission lines (L)	1256
Delves, R. T., Bowley, A. E., Hazelden, D. W., and Goldsmid, H. J.: Anisotropy of electrical conductivity in bismuth telluride	838
Demetsopoulos, I., with Collinson, A. J. L., and Zarzycki, J. M.: Investigation into mechanism of self-quenching Geiger-Müller counters containing argon with small quantities of xenon, oxygen and nitrogen	785
Deutsch, J. L., with Barrow, R. F., Lagerqvist, A., and Westerlund, B.: Rotational analysis of E-x system of silicon monosulphide	1307
Dodd, J. N.: g_J value of 6^3P_1 level in mercury	65
Donovan, B., and Webster, Janet: Faraday effect in non-degenerate semiconductors	120
Durney, B.: On electronic conduction in polar semiconductors	1384
Dutton, J., Jones, F. Llewellyn, and Palmer, R. W.: Electrical breakdown of gases: ionization growth in air at high pressures	569
Eagles, D. M.: Phonon-assisted Auger effect in semiconductors	204
Easlea, B. R.: Proton scattering by copper at 10 mev	1285
Edels, H., with Allan, J. W. S., and Whittaker, D.: Post-arc temperature decay	948
Ehrenberg, W., with Billington, E. W.: Electron voltaic effects in silicon and selenium elements	845
Evans, J. A., with Woolley, J. C.: Temperature variation of optical energy gas for GaSb-InSb alloys	354
Farnell, G. C., Flint, R. B., and Pitts, E.: Observations on lattice rotations in tabular silver bromide grains	698

Fawcett, B. C., Jones, B. B., and Wilson, R.: Vacuum ultra-violet spectra of multiply ionized inert gases	1223
Fernandez, A., with Cooper, R.: Anisotropy in electric strength of alkali halide crystals (L)	1261
Field, S. B., and Martin, D. H.: Skeletal modes of long-chain molecules (L)	625
Finlayson, D. M., Robertson, I. S., Smith, T., and Stevenson, R. W. H.: Magnetic susceptibility of manganese zinc fluoride solid solutions (L)	318
Fletcher, G. C.: Magnetic properties of nickel (L)	145
Flint, R. B., with Farnell, G. C., and Pitts, E.: Observations on lattice rotations in tabular silver bromide grains	698
Flubacher, P., Leadbetter, A. J., and Morrison, J. A.: Low temperature adiabatic calorimeter for condensed substances. Thermodynamic properties of argon	1449
Flynn, C. P.: Correction of signals distorted by linear apparatus	1546
Foley, K. J., with Clegg, A. B., Salmon, G. L., and Segel, R. E.: Gamma radiation from medium energy proton bombardment of lithium, beryllium, boron, carbon and nitrogen	681
Fraser, P. A.: Scattering of low-energy ortho-positronium by hydrogen atoms	329
Garton, W. R. S., and Codling, K.: Extension of series in first spectrum of indium (In I)	600
Gebbie, H. A., with Austin, I. G., and Morin, I.: Absorption of coesite in region 5-20 microns (L)	1260
Goldsmid, H. J., with Delves, R. T., Bowley, A. E., and Hazelden, D. W.: Anisotropy of electrical conductivity in bismuth telluride	838
Golebiewski, A., with Coulson, C. A.: On perturbation calculations for π -electrons and their application to bond length reconsiderations in aromatic hydrocarbons	1310
Goodyear, J., and Steigmann, G. A.: Twinning in cation-deficient spinel structure	491
Gopaulsingh, K., with Reid, R. J., Page, D. E., Idnurm, M., McCusker, C. B. A., Malos, J., Miller, D. D., and Winterton, G.: Differential electron density spectrum of air showers at high densities	103
Green, M., and Cosslett, V. E.: Efficiency of production of characteristic x-radiation in thick targets of pure element	1206
Greenlees, G. W., and Jarvis, O. N.: Direct measurement of proton total reaction cross section for copper at 9.3 mev	1275
Griffiths, J. H. E., with Orton, J. W., Auzins, P., and Wertz, J. E.: Electron spin resonance studies of impurity ions in magnesium oxide	554
Griffiths, J. H. E., with Thornley, J. H. M., Mangum, B. W., and Owen, J.: σ -bonding in $(\text{CuCl}_2)_4^{4-}$ (L)	1263
Grimley, T. B., and Holland, B. W.: Surface states of simple crystal model	217
Hall, T. P. P., Hayes, W., and Williams, F. I. B.: Paramagnetic resonance of manganese	883
Hallin, R., and Hughes, T. P.: Lines of N v spectrum in visible and near ultra-violet wavelength regions	201
Hamilton, T. D. S.: Photofluorescence decay times of organic phosphors	743
Hamilton, W. D.: Lifetime of 638 kev level in ^{131}Xe	1071
Hamilton, W. D.: Lifetime of 673 kev level in ^{133}Xe	1064
Harris, F. S., with Daw, H.: Determination of m/e for free electrons by momentum transfer	433
Harrison, E. R.: Effect of particle streams on transverse hydromagnetic waves	1236
Hattersley, P. M., with Astbury, A., Hussain, M., Kemp, M. A. R., Muirhead, H., and Woodhead, T.: Depolarization of negative muons in light elements	1144
Haydon, S. C., and Robertson, A. G.: Pre-breakdown ionization in hydrogen at low pressures	92
Hayes, W., with Hall, T. P. P., and Williams, F. I. B.: Paramagnetic resonance of manganese	883

- Hazelden, D. W., with Delves, R. T., Bowley, A. E., and Goldsmid, H. J.: Anisotropy of electrical conductivity in bismuth telluride 838
- Hearn, A. G.: Absorption of ozone in ultra-violet and visible regions of spectrum 932
- Heaton, J. W., with Bolton, H. C.: Electronic distribution in diamond and intensities of x-ray reflections 239
- Heavens, O. S., Miller, R. F., Moss, G. L., and Anderson, J. C.: Preparation of continuous single-crystal thin films of nickel and nickel-iron alloys 33
- Hébert, G. R., and Nicholls, R. W.: Intensity measurements in emission on 29 bands of O_2 Schumann-Runge system 1024
- Herbert, J. D., with Wright, J. K., Medford, R. D., and Hunt, A. G.: Interferometric measurements of electron density in shock heated deuterium plasma 1439
- Heymann, F. F., Osmon, P. E., Veit, J. J., and Williams, W. F.: Measurements of quenching of ortho-positronium in gases 1038
- Hill, Nora E.: Application of Onsager's theory to dielectric dispersion—correction (L) 311
- Hill, R. W., with Bleaney, B.: Hyperfine structure in terbium metal (L) 313
- Hindmarsh, W. R., and Thomas, K. A.: Collision broadening in argon spectrum (C) 145
- Hinds, S., Marchant, H., and Middleton, R.: Energy levels of magnesium isotopes of mass 25 to 28 473
- Hinds, S., and Middleton, R.: Study of (^3He , d) reactions leading to ^{11}C and ^{12}C 81
- Hobden, M. V., and Sturge, M. D.: Optical absorption edge of gallium arsenide (L) 615
- Hofmeyr, C., with Stoker, P. H., and Bornman, C. H.: Knock-on electrons and direct electron pair production by cosmic-ray muons 650
- Holland, B. W., with Grimley, T. B.: Surface states of simple crystal model 217
- Holmes, J. E. R., Owen, B. G., and Rodgers, A. L.: Manchester high energy magnetic cosmic ray spectrograph 496
- Holmes, J. E. R., Owen, B. G., and Rodgers, A. L.: Measurements of momentum spectrum and charge ratio of cosmic ray muons at sea level in momentum range 10 gev/c –1000 gev/c 505
- Holmes, R., and Tempest, W.: Excitation of vibrational modes of ethylene in homo-molecular collisions 1502
- Huby, R.: Formulae for non-degenerate Rayleigh-Schrödinger perturbation theory in any order 529
- Hughes, D. G., and MacDonald, D. K. C.: Some properties of resonance line-shape functions 75
- Hughes, T. P., with Hallin, R.: Lines of N v spectrum in visible and near ultra-violet wavelength regions 201
- Hughes, V. A.: Radio wave scattering from lunar surface 988
- Humberston, J. W.: Low energy elastic scattering of neutrons by deuterons 1157
- Hunt, A. G., with Wright, J. K., Medford, R. D., and Herbert, J. D.: Interferometric measurements of electron density in shock heated deuterium plasma 1439
- Hussain, M., with Astbury, A., Blair, I. M., Kemp, M. A. R., and Muirhead, H.: Capture rates for negative muons in light elements 1149
- Hussain, M., with Astbury, A., Hattersley, P. M., Kemp, M. A. R., Muirhead, H., and Woodhead, T.: Depolarization of negative muons in light elements 1144
- Hyde, F. J., Roberts, H. J., and Buckingham, B. E.: Excess high-frequency noise in junction transistors (L) 1076
- Idnurm, M., with Reid, R. J., Gopaulsingh, K., Page, D. E., McCusker, C. B. A., Malos, J., Millar, D. D., and Winterton, G.: Differential electron density spectrum of air showers at high densities 103
- Ito, S., with Miyajima, S., and Thonemann, P. C.: Plasma drift velocity across confining magnetic field (L) 618
- Iwadare, J.: Proton-proton scattering below 50 mev 185
- Jack, W., with Robertson, J. C., and Lynch, J. G.: Luminescence of CsBr(Tl) and CsI(Tl) as function of temperature 1188

Jain, D. C., with Singh, N. L.: Franck-Condon factors and r -centroids for triplet band system of CO molecule	399
Jarvis, O. N., with Greenlees, G. W.: Direct measurement of proton total reaction cross section for copper at 9.3 mev	1275
Jennison, R. C.: Michelson stellar interferometer: phase sensitive variation of optical instrument	596
Joel, N.: Reflection and polarization of elastic waves in LiF crystal: mode conversion from longitudinal to transverse	38
Jones, B. B., with Fawcett, B. C., and Wilson, R.: Vacuum ultra-violet spectra of multiply ionized inert gases	1223
Jones, F. Llewellyn, with Dutton, J., and Palmer, R. W.: Electrical breakdown of gases: ionization growth in air at high pressures	569
Joshi, B. R., and Lewis, G. M.: Determination of Fierz interference term from K-capture/ β^+ ratio for pure Gamow-Teller decay of ^{58}Co	1056
Joshi, K. C.: Absorption spectrum of BiF molecule in ultra-violet region	610
Joshi, K. C., and Majumdar, K.: Band spectrum of CuAg molecule in visible region	197
Joshi, S. K.: On Θ values from temperature dependence of Laue-Bragg scattering (L)	1255
Kaye, G.: Temperature effects in domain patterns from single crystals of haematite ($\alpha\text{-Fe}_2\text{O}_3$)	869
Keating, P. N.: Thermally stimulated emission and conductivity peaks in case of temperature dependent trapping cross sections	1408
Keating, P. N., with Woolley, J. C.: Some electrical and optical properties of InAs-In ₂ Se ₃ and InSb-In ₂ Se ₃ alloys	1009
Kelly, F. M., and Tomchuk, E.: Isotope shift in CdI resonance line λ 2288 Å	1304
Kemp, M. A. R., with Astbury, A., Blair, I. M., Hussain, M., and Muirhead, H.: Capture rates for negative muons in light elements	1149
Kemp, M. A. R., with Astbury, A., Hattersley, P. M., Hussain, M., Muirhead, H., and Woodhead, T.: Depolarization of negative muons in light elements	1144
Kemp, M. A. R., with Astbury, A., Muirhead, H., Voss, R. G. P., and Woodhead, T.: Measurement of total cross section for production of neutral pions in proton-proton collisions at 383 mev	1151
Kibble, B. P., and Series, G. W.: Line shapes in method of intersecting energy levels	70
Kilby, G. E.: Coherent and incoherent scattering of x-rays by H ₂ and He	673
King, J. N., and Wilman, H.: Nature of abrasion process in plastically deformable non-metals	979
Kingston, A. E., with Dalgarno, A.: Van der Waals forces for hydrogen and inert gases	607
Knowles, J. E.: Estimation of domain wall velocity in 'square-loop' ferrite, and some observations on reversal process	233
Lagerqvist, A., with Barrow, R. F., Deutsch, J. L., and Westerlund, B.: Rotational analysis of E-x system of silicon monosulphide	1307
Leadbetter, A. J., with Flubacher, P., and Morrison, J. A.: Low temperature adiabatic calorimeter for condensed substances. Thermodynamic properties of argon	1449
Leak, G. M.: Grain boundary damping. Part I. Pure iron	1520
Leak, G. M., with Miles, G. W.: Grain boundary damping. Part II. Iron interstitial alloys	1529
Lee, E. W., with Alberts, L.: Magnetostriction in antiferromagnetic nickel oxide	728
Lee, E. W., and Birss, R. R.: Magnetoelastic constants of nickel	391
Lee, P. M., with Pincherle, L.: Electronic band structure of model of cubic crystal	1195
Lennon, J. J., and Mulcahy, M. J.: Microwave measurement of attachment in oxygen-nitrogen mixtures	1543
Lewis, G. M.: Tensile strength of liquids in Berthelot tubes	133

	PAGE
Lewis, G. M., with Joshi, B. R.: Determination of Fierz interference term from K-capture/ β^+ ratio for pure Gamow-Teller decay of ^{58}Co	1056
Lewis, T. J., with Swan, D. W.: Influence of cathode and anode surfaces on electric strength of liquid argon	448
Loasby, R. G., and Taylor, J. C.: Hall effect in plutonium (L)	776
Logie, H. J., the late, with Urlau, R. R., and Nabarro, F. R. N.: Energy levels in forbidden gap of insulating diamonds	256
Lukes, T.: Space correlation and energy levels in Einstein solid	759
Lukes, T.: Statistical properties of sequences of stochastic pulses	153
Lynch, J. G., with Robertson, J. C., and Jack, W.: Luminescence of CsBr(Tl) and CsI(Tl) as function of temperature	1188
McCusker, C. B. A., with Reid, R. J., Gopaulsingh, K., Page, D. E., Idnurm, M., Malos, J., Millar, D. D., and Winterton, G.: Differential electron density spectrum of air showers at high densities	103
MacDonald, D. K. C., with Hughes, D. G.: Some properties of resonance line-shape functions	75
MacDonald, D. K. C., and Pearson, W. B.: Thermoelectricity in metals at normal temperature—query (L)	306
McIntyre, H. A. J., with Allison, D. C. S., and Moiseiwitsch, B. L.: Elastic scattering of positrons by atomic hydrogen and helium	1169
Madonna, L. A., Sciuili, C. M., Canjar, L. N., and Pound, G. M.: Low temperature cloud chamber studies on water vapour	1218
Magnusson, E. A., and Zauli, C.: Evaluation of molecular integrals by numerical method	53
Majumdar, K., with Joshi, K. C.: Band spectrum of CuAg molecule in visible region	197
Malos, J., with Reid, R. J., Gopaulsingh, K., Page, D. E., Idnurm, M., McCusker, C. B. A., Millar, D. D., and Winterton, G.: Differential electron density spectrum of air showers at high densities	103
Mangum, B. W., with Thornley, J. H. M., Griffiths, J. H. E., and Owen, J.: σ -bonding in $(\text{CuCl}_6)^{4-}$ (L)	1263
Marchant, H., with Hinds, S., and Middleton, R.: Energy levels of magnesium isotopes of mass 25 to 28	473
Marshall, W.: Unrestricted Hartree-Fock method	113
Martin, D. H., with Bloor, D.: Antiferromagnetic resonance in extreme infra-red (L)	774
Martin, D. H., with Field, S. B.: Skeletal modes of long-chain molecules (L)	625
Martin, D. L.: Low temperature specific heat of aluminium-manganese alloy	1489
Martin, D. L.: Specific heat of hexagonal metals at very low temperatures	1482
Medford, R. D., with Wright, J. K., Hunt, A. G., and Herbert, J. D.: Interferometric measurements of electron density in shock heated deuterium plasma	1439
Megaw, Helen D., with Wells, M.: Structures of NaNbO_3 and $\text{Na}_{0.975}\text{K}_{0.025}\text{NbO}_3$	1258
Merrison, A. W.: C. V. Boys Lecture: Counter techniques in high energy nuclear physics: rare decays of π^- and μ^- mesons	1116
Middleton, R., with Hinds, S.: Study of $(^3\text{He}, d)$ reactions leading to ^{11}C and ^{12}C	81
Middleton, R., with Hinds, S., and Marchant, H.: Energy levels of magnesium isotopes of mass 25 to 28	473
Miles, G. W., and Leak, G. M.: Grain boundary damping. Part II. Iron interstitial alloys	1529
Millar, D. D., with Reid, R. J., Gopaulsingh, K., Page, D. E., Idnurm, M., McCusker, C. B. A., Malos, J., and Winterton, G.: Differential electron density spectrum of air showers at high densities	103
Miller, R. F., with Heavens, O. S., Moss, G. L., and Anderson, J. C.: Preparation of continuous single-crystal thin films of nickel and nickel-iron alloys	33
Miyajima, S., Ito, S., and Thonemann, P. C.: Plasma drift velocity across confining magnetic field (L)	618
Mohanty, R. C., with Roy, R. R., Blanchard, C. H., Webb, E. H., and Sandhu, H. S.: Multiplet production by x-rays	1301

	PAGE
Mohr, C. B. O.: Direct interaction with strong coupling in nuclear collisions II. E2 excitations	641
Moiseiwitsch, B. L.: Scattering by screened Coulomb potential (L)	616
Moiseiwitsch, B. L.: Schematic model for impact excitation of atoms	661
Moiseiwitsch, B. L., with Allison, D. C. S., and McIntyre, H. A. J.: Elastic scattering of positrons by atomic hydrogen and helium	1169
Montgomery, H., and Pells, G. P.: Low temperature specific heat of scandium and yttrium (L)	622
Morin, I., with Austin, I. G., and Gebbie, H. A.: Absorption of coesite in region 5-20 microns (L)	1260
Morrison, J. A., with Beaumont, R. H., and Chihara, H.: Thermodynamic properties of krypton. Vibrational and other properties of solid argon and solid krypton	1462
Morrison, J. A., with Flubacher, P., and Leadbetter, A. J.: Low temperature adiabatic calorimeter for condensed substances. Thermodynamic properties of argon	1449
Mosley, M. H., with Powles, J. G.: Exchange effects and anisotropy broadening of hyperfine spin resonance spectrum of biphenyl negative ion in solution	370
Moss, G. L., with Heavens, O. S., Miller, R. F., and Anderson, J. C.: Preparation of continuous single-crystal thin films of nickel and nickel-iron alloys	33
Moss, T. S., with Walton, A. K.: Infra-red Faraday effect in germanium	1393
Muirhead, H., with Astbury, A., Blair, I. M., Hussain, M., and Kemp, M. A. R.: Capture rates for negative muons in light elements	1149
Muirhead, H., with Astbury, A., Hattersley, P. M., Hussain, M., Kemp, M. A. R., and Woodhead, T.: Depolarization of negative muons in light elements	1144
Muirhead, H., with Astbury, A., Kemp, M. A. R., Voss, R. G. P., and Woodhead, T.: Measurement of total cross section for production of neutral pions in proton-proton collisions at 383 mev	1151
Mulcahy, M. J., with Lennon, J. J.: Microwave measurement of attachment in oxygen-nitrogen mixtures	1543
Nabarro, F. R. N., with Urlau, R. R., and Logie, H. J., the late: Energy levels in forbidden gap of insulating diamonds	256
Nabarro, F. R. N., and Ziman, J. M.: Scattering of waves by dislocations	1512
Neale, D. J., with Powles, J. G.: Multiple proton magnetic resonance relaxation in number of molecular liquids	377
Neilson, A. H., with Coulson, C. A.: Electron correlation in ground state of helium	831
Nicholls, R. W., with Hébert, G. R.: Intensity measurements in emission on 29 bands of O ₂ Schumann-Runge system	1024
Nicholls, R. W., with Reeves, E. M.: Measurements of rotational energy distributions in ionic collisions	588
Núñez, Feliza, with Craik, D. J.: Domain structure of ordered platinum-cobalt alloy	225
Orbach, R., with Powell, M. J. D.: Crystalline field parameters for dysprosium ethyl sulphate	753
Orton, J. W., Auzins, P., Griffiths, J. H. E., and Wertz, J. E.: Electron spin resonance studies of impurity ions in magnesium oxide	554
Osmon, P. E., with Heymann, F. F., Veit, J. J., and Williams, W. F.: Measurements of quenching of ortho-positronium in gases	1038
Osmond, W. P.: Sub-lattice magnetic moments in manganese ferrite (L)	620
Owen, B. G., with Holmes, J. E. R., and Rodgers, A. L.: Manchester high energy magnetic cosmic ray spectrograph	496
Owen, B. G., with Holmes, J. E. R., and Rodgers, A. L.: Measurements of momentum spectrum and charge ratio of cosmic ray muons at sea level in momentum range 10 gev/c-1000 gev/c	505
Owen, J., with Thornley, J. H. M., Mangum, B. W., and Griffiths, J. H. E.: σ -bonding in (CuCl ₂) ₄ ⁻ (L)	1263

	PAGE
Pacey, A. J., with Bates, L. F.: Magnetothermal measurements on gadolinium	878
Page, D. E., with Reid, R. J., Gopaulsingh, K., Idnurm, M., McCusker, C. B. A., Malos, J., Millar, D. D., and Winterton, G.: Differential electron density spectrum of air showers at high densities	103
Palmer, R. B., with Barford, N. C., and Tallini, B.: Radiative capture of protons by neutrons at 50 mev	912
Palmer, R. B. J.: Stopping power for alpha particles of ethyl alcohol and carbon tetrachloride in liquid and vapour states	766
Palmer, R. W., with Dutton, J., and Jones, F. Llewellyn: Electrical breakdown of gases: ionization growth in air at high pressures	569
Pandeya, D. C., and Tolansky, S.: Micro-disk patterns on diamond dodecahedra	12
Paranjape, V. V.: Low temperature electric field effects in semiconductors	516
Parkinson, W. H.: Time resolved absorption studies in shock tube: new band system of BaO	705
Parry, G., with Dalton, A. W., Scott, H. D., and Swierszczewski, S.: $^{55}\text{Mn}(\text{d}, \text{p})^{55}\text{Mn}$ reaction	404
Paxman, D. H.: Spin-lattice relaxation time measurements in dilute potassium ferricyanide	180
Peacock, T. E.: Electronic structure and spectrum of nitrobenzene	460
Pearson, R. F., and Cooper, R.: Magnetic anisotropy and rotational hysteresis in single crystals of magnetite below transition temperature	17
Pearson, W. B., with MacDonald, D. K. C.: Thermoelectricity in metals at normal temperature—query (L)	306
Pells, G. P., with Montgomery, H.: Low temperature specific heat of scandium and yttrium (L)	622
Perkin, J. L., with Barry, J. F., and Bunce, J. L.: Radiative capture cross section of ^{238}U for neutrons in energy range 0.3 to 4.0 mev	801
Perkin, J. L., with Coleman, R. F.: Transfer and exchange transfer of nucleons between ^{16}O and ^{27}Al	1163
Pincherle, L., and Lee, P. M.: Electronic band structure of model of cubic crystal	1195
Pitts, E., with Farnell, G. C., and Flint, R. B.: Observations on lattice rotations in tabular silver bromide grains	698
Popescu, Iovitzu: On resonant charge transfer in ionized dense gases	584
Porat, D. I., and Ramavataram, K.: Differential energy loss and ranges of Ne, N and He ions	1135
Pound, G. M., with Madonna, L. A., Sciulli, C. M., and Canjar, L. N.: Low temperature cloud chamber studies on water vapour	1218
Powell, M. J. D., and Orbach, R.: Crystalline field parameters for dysprosium ethyl sulphate	753
Powles, J. G., and Mosley, M. H.: Exchange effects and anisotropy broadening of hyperfine spin resonance spectrum of biphenyl negative ion in solution	370
Powles, J. G., and Neale, D. J.: Multiple proton magnetic resonance relaxation in number of molecular liquids	377
Primakoff, H., and Rosen, S. P.: Corrigendum to article 'Double beta decay' in <i>Reports on Progress in Physics</i> (L)	464
Pursey, H.: Note on Carr-Purcell method of measuring nuclear magnetic resonance relaxation times	808
Ramavataram, K., with Porat, D. I.: Differential energy loss and ranges of Ne, N and He ions	1135
Reeves, E. M., and Nicholls, R. W.: Measurements of rotational energy distributions in ionic collisions	588
Reid, R. J., Gopaulsingh, K., Page, D. E., Idnurm, M., McCusker, C. B. A., Malos, J., Millar, D. D., and Winterton, G.: Differential electron density spectrum of air showers at high densities	103
Ridley, B. K., and Watkins, T. B.: Dependence of capture rate on electric field and possibility of negative resistance in semiconductors	710

Ridley, B. K., and Watkins, T. B.: Possibility of negative resistance effects in semiconductors	293
Rishbeth, H., with Briggs, B. H.: Analogue solution of continuity equation of ionospheric F region	409
Riviere, A. C., and Sweetman, D. R.: Search for vibrational energy effects in dissociation of H_2^+ ions by hydrogen gas	1215
Roberts, H. J., with Hyde, F. J., and Buckingham, B. E.: Excess high-frequency noise in junction transistors (L)	1076
Robertson, A. G., with Haydon, S. C.: Pre-breakdown ionization in hydrogen at low pressures	92
Robertson, I. S., with Finlayson, D. M., Smith, T., and Stevenson, R. W. H.: Magnetic susceptibility of manganese zinc fluoride solid solutions (L)	318
Robertson, J. C., Lynch, J. G., and Jack, W.: Luminescence of CsBr(Tl) and CsI(Tl) as function of temperature	1188
Robins, J. L.: Characteristic electron energy loss spectra of noble metals and their neighbours	1177
Robinson, P. D.: H_2^+ : Problem in perturbation theory	537
Rochester, G. D.: Note on band spectra of BiF and SbF (L)	614
Rodgers, A. L.: On momentum spectrum of cosmic-ray muons at sea level	918
Rodgers, A. L., with Holmes, J. E. R., and Owen, B. G.: Manchester high energy magnetic cosmic ray spectrograph	496
Rodgers, A. L., with Holmes, J. E. R., and Owen, B. G.: Measurements of momentum spectrum and charge ratio of cosmic ray muons at sea level in momentum range 10 gev/c-1000 gev/c	505
Rosen, S. P., with Primakoff, H.: Corrigendum to article 'Double beta decay' in <i>Reports on Progress in Physics</i> (L)	464
Roy, R. R., Blanchard, C. H., Webb, E. H., Sandhu, H. S., and Mohanty, R. C.: Multiplet production by x-rays	1301
Roy, R. R., with Cresswell, M. W.: On reaction $Pt(n, \alpha)Os$	1297
Rubins, R. S., with Baker, J. M.: Electron spin resonance in two groups of lanthanon salts	1353
Rubins, R. S., with Bleaney, B.: Explanation of some 'forbidden' transitions in paramagnetic resonance (C)	778
Salmon, G. L., with Clegg, A. B., Foley, K. J., and Segel, R. E.: Gamma radiation from medium energy proton bombardment of lithium, beryllium, boron, carbon and nitrogen	681
Sandhu, H. S., with Roy, R. R., Blanchard, C. H., Webb, E. H., and Mohanty, R. C.: Multiplet production by x-rays	1301
Sastry, P. V., with Bahadur, Kanwar: On extra reflections in electron diffraction patterns from thin evaporated films of some face-centred cubic metals	594
Saunders, G., with Blackman, L. C. F., and Ubbelohde, A. R.: Radiation damage in well oriented pyrolytic graphites	1048
Sayer, M.: Growth and decay of luminescence under cathode ray excitation	1017
Sciulli, C. M., with Madonna, L. A., Canjar, L. N., and Pound, G. M.: Low temperature cloud chamber studies on water vapour	1218
Scott, H. D., with Dalton, A. W., Parry, G., and Swierszczewski, S.: $^{55}Mn(d, p)^{56}Mn$ reaction	404
Searl, J. W., Smith, R. C., and Wyard, S. J.: Electron spin resonance absorption for polycrystalline substances II	1174
Seeley, J. S.: Synthesis of interference filters	998
Segel, R. E., with Clegg, A. B., Foley, K. J., and Salmon, G. L.: Gamma radiation from medium energy proton bombardment of lithium, beryllium, boron, carbon and nitrogen	681
Series, G. W., with Kibble, B. P.: Line shapes in method of intersecting energy levels	70
Sham, L. J.: Electron-phonon interaction by method of pseudo-potentials	895
Simons, S.: Hall effect in monovalent metals at low temperatures (L)	316

	PAGE
Singh, N. L., and Jain, D. C.: Franck-Condon factors and <i>r</i> -centroids for triplet band system of CO molecule	399
Singh, S. P., with Dayal, B.: Participation of electron gas in lattice vibrations	1495
Smith, K.: Partial wave theory of positron-hydrogen atom collisions	549
Smith, R. C., with Searl, J. W., and Wyard, S. J.: Electron spin resonance absorption for polycrystalline substances II	1174
Smith, T., with Finlayson, D. M., Robertson, I. S., and Stevenson, R. W. H.: Magnetic susceptibility of manganese zinc fluoride solid solutions (L)	318
Smith, W. A., with Cooper, R.: Electric breakdown of sodium chloride	734
Somerville, W. B.: Importance of conservation conditions in distorted wave calculations	695
Steigmann, G. A., with Goodyear, J.: Twinning in cation-deficient spinel structure	491
Stevens, K. W. H., with Bates, C. A.: Band structure of body-centred cubic transition metals	1321
Stevenson, R. W. H., with Finlayson, D. M., Robertson, I. S., and Smith, T.: Magnetic susceptibility of manganese zinc fluoride solid solutions (L)	318
Stewart, D. T., with Williams, W. S. C., and Caplan, H. S.: Nuclear scattering of high energy photons	1125
Stilwell, N. A., and Tabor, D.: Elastic recovery of conical indentations	169
Stinchcombe, R. B.: Quantum theory of magnetoresistance I: low fields	275
Stoker, P. H., Hofmeyr, C., and Bornman, C. H.: Knock-on electrons and direct electron pair production by cosmic-ray muons	650
Stradling, R. A., with Bagguley, D. M. S.: Cyclotron resonance at 4 mm wavelength (L)	1078
Sturge, M. D., with Hobden, M. V.: Optical absorption edge of gallium arsenide (L)	615
Sutton, J., with Townsend, P.: Study of superconducting niobium by electron tunnelling (L)	309
Swan, D. W.: Electrical breakdown of liquid dielectrics	423
Swan, D. W., and Lewis, T. J.: Influence of cathode and anode surfaces on electric strength of liquid argon	448
Sweetman, D. R., with Riviere, A. C.: Search for vibrational energy effects in dissociation of H_2^+ ions by hydrogen gas	1215
Swierszczewski, S., with Dalton, A. W., Parry, G., and Scott, H. D.: $^{56}\text{Mn}(\text{d}, \text{p})^{56}\text{Mn}$ reaction	404
Symmons, H. F., with Bogle, G. S.: Zero-field paramagnetic resonance of Fe^{3+} in methylamine alum	812
Tabor, D., with Stilwell, N. A.: Elastic recovery of conical indentations	169
Tallini, B., with Barford, N. C., and Palmer, R. B.: Radiative capture of protons by neutrons at 50 mev	912
Taylor, A. W. B.: Dispersion relations for superconductors	1372
Taylor, J. C., with Loasby, R. G.: Hall effect in plutonium (L)	776
Taylor, M. A.: Magnetic susceptibilities of aluminium-rich transition metal intermetallic compounds	1244
Tempest, W., with Holmes, R.: Excitation of vibrational modes of ethylene in homo-molecular collisions	1502
Thomas, K. A., with Hindmarsh, W. R.: Collision broadening in argon spectrum (C)	145
Thonemann, P. C., with Miyajima, S., and Ito, S.: Plasma drift velocity across confining magnetic field (L)	618
Thornley, J. H. M., Mangum, B. W., Griffiths, J. H. E., and Owen, J.: σ -bonding in $(\text{CuCl}_2)^{4-}$ (L)	1263
Tolansky, S., with Pandeya, D. C.: Micro-disk patterns on diamond dodecahedra	12
Tomchuk, E., with Kelly, F. M.: Isotope shift in CdI resonance line λ 2288 Å	1304
Townsend, P., and Sutton, J.: Study of superconducting niobium by electron tunnelling (L)	309
Tredgold, R. H., with Barnes, J. F.: On change of activation energy with impurity concentration in semiconductors	716

Tropper, H., with Darveniza, M.: Electrical properties of organic insulating liquids containing fluorescent solutes	854
Tunstall, D. P., with Andrew, E. R.: Spin-lattice relaxation in imperfect cubic crystals and in non-cubic crystals	1
Ubbelohde, A. R., with Blackman, L. C. F., and Saunders, G.: Radiation damage in well oriented pyrolytic graphites	1048
Urlau, R. R., Logie, H. J., the late, and Nabarro, F. R. N.: Energy levels in forbidden gap of insulating diamonds	256
Veit, J. J., with Heymann, F. F., Osmon, P. E., and Williams, W. F.: Measurements of quenching of ortho-positronium in gases	1038
Voss, R. G. P., with Astbury, A., Kemp, M. A. R., Muirhead, H., and Woodhead, T.: Measurement of total cross section for production of neutral pions in proton-proton collisions at 383 mev	1151
Walton, A. K., and Moss, T. S.: Infra-red Faraday effect in germanium	1393
Watkins, T. B., with Ridley, B. K.: Dependence of capture rate on electric field and possibility of negative resistance in semiconductors	710
Watkins, T. B., with Ridley, B. K.: Possibility of negative resistance effects in semiconductors	293
Webb, E. H., with Roy, R. R., Blanchard, C. H., Sandhu, H. S., and Mohanty, R. C.: Multiplet production by x-rays	1301
Webster, Janet, with Donovan, B.: Faraday effect in non-degenerate semiconductors	120
Wells, M., and Megaw, Helen D.: Structures of NaNbO_3 and $\text{Na}_{0.975}\text{K}_{0.025}\text{NbO}_3$ (L)	1258
Wertz, J. E., with Orton, J. W., Auzins, P., and Griffiths, J. H. E.: Electron spin resonance studies of impurity ions in magnesium oxide	554
Westerlund, B., with Barrow, R. F., Deutsch, J. L., and Lagerqvist, A.: Rotational analysis of E-x system of silicon monosulphide	1307
Weston, D. E.: Horizontal refraction in three-dimensional medium of variable stratification	46
Whittaker, D., with Allan, J. W. S., and Edels, H.: Post-arc temperature decay	948
Williams, F. I. B., with Baker, J. M.: Electron spin resonance in two salts containing gadolinium	1340
Williams, F. I. B., with Hall, T. P. P., and Hayes, W.: Paramagnetic resonance of manganese	883
Williams, W. F., with Heymann, F. F., Osmon, P. E., and Veit, J. J.: Measurements of quenching of ortho-positronium in gases	1038
Williams, W. S. C., Caplan, H. S., and Stewart, D. T.: Nuclear scattering of high energy photons	1125
Wilman, H., with King, J. N.: Nature of abrasion process in plastically deformable non-metals	979
Wilson, A. J. C.: Note on peak displacements in x-ray diffractometry	249
Wilson, A. J. C., and Delf, B. W.: Effect of variations in quantum counting efficiency of detectors on mean wavelength of x-ray emission lines (L)	1256
Wilson, R., with Burton, W. M.: Spectroscopic investigation of plasma containment in ZETA	1416
Wilson, R., with Fawcett, B. C., and Jones, B. B.: Vacuum ultra-violet spectra of multiply ionized inert gases	1223
Winterton, G., with Reid, R. J., Gopaulsingh, K., Page, D. E., Idnurm, M., McCusker, C. B. A., Malos, J., and Millar, D. D.: Differential electron density spectrum of air showers at high densities	103
Wintle, H. J.: Damping of sound waves by ideally rough surface (L)	1265
Woodhead, T., with Astbury, A., Hattersley, P. M., Hussain, M., Kemp, M. A. R., and Muirhead, H.: Depolarization of negative muons in light elements	1144
Woodhead, T., with Astbury, A., Kemp, M. A. R., Muirhead, H., and Voss, R. G. P.: Measurement of total cross section for production of neutral pions in proton-proton collisions at 383 mev	1151

	PAGE
Woolley, J. C., and Evans, J. A.: Temperature variation of optical energy gap for GaSb-InSb alloys	354
Woolley, J. C., and Keating, P. N.: Some electrical and optical properties of InAs-In ₂ Se ₃ and InSb-In ₂ Se ₃ alloys	1009
Wright, J. K., Medford, R. D., Hunt, A. G., and Herbert, J. D.: Interferometric measurements of electron density in shock heated deuterium plasma	1439
Wyard, S. J., with Searl, J. W., and Smith, R. C.: Electron spin resonance absorption for polycrystalline substances II	1174
Zarzycki, J. M., with Collinson, A. J. L., and Demetsopoulos, I.: Investigation into mechanism of self-quenching Geiger-Müller counters containing argon with small quantities of xenon, oxygen and nitrogen	785
Zauli, C., with Magnusson, E. A.: Evaluation of molecular integrals by numerical method	53
Ziman, J. M., with Nabarro, F. R. N.: Scattering of waves by dislocations	1512

INDEX TO REVIEWS OF BOOKS

	PAGE
Abraham, A.: <i>The principles of nuclear physics: International series of monographs on physics</i>	1274
Aigrain, P. R., Coelho, R. J., and Ascarelli, G.: <i>Electronic processes in solids</i>	779
Ajzenberg-Selove, Fay (Ed.): <i>Nuclear spectroscopy</i> , Parts A and B	146
Allen, W. D.: <i>Neutron detection</i>	328
Allis, W. P., (Ed.): <i>Nuclear fusion—The second Geneva series on the peaceful uses of atomic energy</i>	327
Baker, R. M. L., Jr, and Makeson, M. W.: <i>An introduction to astro-dynamics</i>	634
Baldin, A. M., Gol'danskii, V. I., and Rozenthal, I. L.: <i>Kinematics of nuclear reactions</i>	782
Bauer, Ernst: <i>Electronenbeugung</i>	632
Bayet, M.: <i>Physique nucléaire</i>	639
Beynon, W. J. G. (Ed.): <i>Some ionospheric results obtained during the International Geophysical Year, Proceedings of a symposium organized by the URSI/AGI Committee, Brussels, 1959</i>	632
Born, M., and Wolf, E.: <i>Principles of optics</i>	634
de Broglie, L.: <i>Review of non-linear wave mechanics</i>	147
Bromley, D. A., and Vogt, E. W. (Eds): <i>Proceedings of the international conference on nuclear structure</i>	638
van Bueren, H. G.: <i>Imperfections in crystals</i>	326
Bunn, C. W.: <i>Chemical crystallography</i> , 2nd edn	1576
Chandrasekhar, S.: <i>Plasma physics</i> (a course given at the University of Chicago. Notes compiled by S. K. Trehan.)	628
Chapman, S., and Cowling, T. G.: <i>The mathematical theory of non-uniform gases</i>	1576
The Chemical Society: <i>Annual reports on the progress of chemistry</i> , Vol. LVI	327
Christiansen, G. S., and Garrett, P. H.: <i>Structure and change: an introduction to the science of matter</i>	1268
Collin, R. E.: <i>Field theory of guided waves</i>	471
Crystal growth, discussions of the <i>Faraday Society</i> , No. 5, 1949	149
Denisse, J. F., and Delcroix, J. L.: <i>Théorie des ondes dans les plasmas</i>	1571
Dewitt, C., and Detoeuf, J. F. (Eds): <i>The theory of neutral and ionized gases</i>	1270
Drell, S. D., and Zachariasen, F.: <i>Electromagnetic structure of nucleons</i>	781
Dresner, L.: <i>Resonance absorption in nuclear reactors</i>	325
Eddington, A. S.: <i>The mathematical theory of relativity</i>	1576
Fierz, M., and Weisskopf, W. F. (Eds): <i>Theoretical physics in the twentieth century: a memorial volume to Wolfgang Pauli</i>	633
Flügge, S. (Ed.): <i>Encyclopedia of physics</i> , Vol. IX, <i>Fluid dynamics</i> , Vol. III	150
Flügge, S. (Ed.): <i>Handbuch der Physik</i> , Vol. III, Part 1, <i>Principles of classical mechanics and field theory</i>	1575
Francis, G.: <i>Ionization phenomena in gases</i>	324
Frisch, O. R. (Ed.): <i>Progress in nuclear physics</i> , Vol. 8	630
Fulton, J. F.: <i>A bibliography of the Honourable Robert Boyle: Fellow of the Royal Society</i> , 2nd edn	1271
Goldberg, R. R.: <i>Fourier transforms: Cambridge tracts in mathematics and mathematical physics</i> , No. 52	1269
Goldman, I. I., and Krivchenkov, V. D.: <i>Problems in quantum mechanics</i>	1572
Goodman, R. (Ed.): <i>Annual reviews in automatic programming</i> , Vol. 1	149
Gorter, G. J.: <i>Progress in low temperature physics</i> , Vol. 3	1574

	PAGE
Graham, G. H., and Hallett, A. C. Hollis (Eds): <i>Proceedings of the VIIth international conference on low temperature physics: University of Toronto, Canada</i>	1272
Gray, C. H.: <i>Laboratory handbook of toxic agents</i>	148
Griffith, J. S.: <i>The theory of transition-metal ions</i>	782
Hannan, E. J.: <i>Time series analysis</i>	321
Henry, N. F. M., Lipson, H., and Wooster, W. A.: <i>The interpretation of x-ray diffraction photographs</i> , 2nd edn	151
Herman, R., and Hofstadter, R.: <i>High energy electron scattering tables</i>	468
Hume-Rothery, W.: <i>Atomic theory for students of metallurgy</i>	466
Ivakin, B. N.: <i>Soviet research in geophysics</i> , Vol. 3, <i>Microstructure and macro-structure</i>	323
Jeans, Sir James: <i>The mathematical theory of electricity and magnetism</i>	1576
Jerrard, H. G., and McNeill, D. B.: <i>Theoretical and experimental physics</i>	152
Kahan, Th.: <i>Théorie des groupes en physique classique et quantique</i> , Vol. 1, <i>Structures mathématiques et fondements quantiques</i>	472
Kash, S. W. (Ed.): <i>Plasma acceleration</i>	1570
Kastler, D.: <i>Introduction à l'électrodynamique quantique</i>	1272
Kleber, W.: <i>Angewandte Gitterphysik</i> , 3rd edn	466
Kybernetik, Band 1, Heft 1	636
Landé, A.: <i>From dualism to unity in quantum physics</i>	469
von Laue, Max: <i>Röntgenstrahl-Interferenzen</i>	780
Leontovich, M. A. (Ed.): <i>Plasma physics and the problem of controlled thermonuclear reactions</i> , Vol. II	781
Le Page, W. R.: <i>Complex variables and the Laplace transforms for engineers</i>	638
Levinger, J. S.: <i>Nuclear photodisintegration</i>	322
Lock, W. O.: <i>High energy nuclear physics</i>	323
Low, W. (Eds F. Seitz and D. Turnbull): <i>Solid state physics</i> , Vol. 11, <i>Advances in research and applications</i> , Suppl. 2, <i>Paramagnetic resonance in solids</i>	629
Lynbarskii, G. Ya.: <i>The application of group theory in physics</i>	1271
McGee, J. D., and Wilcock, W. L. (Eds): <i>Photo-electronic image devices</i>	152
Mackenzie, J. D. (Ed.): <i>Modern aspects of the vitreous state</i>	784
Marion, J. B. (Ed.): <i>1960 nuclear data tables</i> , Part 3, <i>Nuclear reaction graphs</i>	1569
Marton, L. (Ed.): <i>Advances in electronics and electron physics</i> , Vol. XII	152
Marton, L. (Ed.): <i>Advances in electronics and electron physics</i> , Vol. XIII	1569
Minkoff, G. J.: <i>Frozen free radicals</i>	640
Moon, Parry, and Spencer, Domina E.: <i>Field theory for engineers</i>	1576
Munk, W. H., and MacDonald, G. J. F. (Eds G. K. Batchelor and S. Goldstein): <i>The rotation of the earth</i> , <i>Cambridge monograph on mechanics and applied mathematics</i>	637
Nilsson, N. R. (Ed.): <i>Proceedings of the fourth international conference on ionization phenomena in gases</i> , Vols I and II	146
Olver, F. W. J. (Ed.): <i>Royal Society mathematical tables</i> , Vol. 7, <i>Bessel functions</i> , Part III, <i>Zeros and associated values</i>	327
Pimentel, G. C., and McClellan, A. L.: <i>The hydrogen bond</i>	470
van der Pol, B. (Eds H. Bremmer and C. J. Bouwkamp): <i>Selected scientific papers</i> , Vols I and II	636
Powell, J. L., and Crasemann, B.: <i>Quantum mechanics</i>	1572
Putley, E. H.: <i>The Hall effect and related phenomena</i>	783

	PAGE
Ratcliffe, J. A. (Ed.): <i>Physics of the upper atmosphere</i>	467
del Rio, C. S.: <i>Fundamentos teóricos de la física atómica y nuclear</i>	1273
Sanders, J. S.: <i>The fundamental atomic constants</i>	1082
Sauter, F. (Ed.): <i>Halbleiterprobleme V</i>	1571
Segrè, E., Friedlander, G., and Meyerhof, W. E. (Eds): <i>Annual review of nuclear science</i> , Vol. 10	631
Seitz, F., and Turnbull, D. (Eds): <i>Solid state physics</i> , Vol. 11	327
Shubnikov, A. V., and Sheftal, N. N. (Eds): <i>Growth of crystals</i> , Vols 1 and 2	150
Slater, J. C.: <i>Quantum theory of atomic structure</i> , Vol. I	629
Slater, J. C.: <i>Quantum theory of atomic structure</i> , Vol. II	1082
Smith, C. J.: <i>A degree physics</i> , Part I, <i>General properties of matter</i>	1268
Sterne, T. E.: <i>An introduction to celestial mechanics</i>	780
<i>Studies in theoretical physics: the proceedings of the Summer School of Theoretical Physics held at Mussoorie, India, on 22nd May-18th June, 1959</i> , Part 3	631
Sudarshan, E. C. G., Tinlot, J. H., and Melissinos, A. C. (Eds): <i>Proceedings of the 1960 annual international conference on high energy physics at Rochester</i>	631
Suits, G. (Ed.): <i>The collected works of Irving Langmuir</i>	1576
Synge, J. L.: <i>Relativity: the general theory</i>	628
Takács, L.: <i>Stochastic processes, problems and solutions</i>	328
Temple, G.: <i>Cartesian tensors: an introduction</i>	326
Townes, C. H. (Ed.): <i>Quantum electronics</i>	148
Tyrrell, H. J. V.: <i>Diffusion and heat flow in liquids</i>	1573
Ubbelohde, A. R., and Lewis, F. A.: <i>Graphite and its crystal compounds</i>	468
Wehr, M. Russel, and Richards, James A., Jr: <i>Physics of the atom</i>	639
Weihe, W. K., Passman, S., Migeotte, N., and Moss, T. S.: <i>Infra-red physics: an international research journal</i> , Vol. 1, No. 1	1571
Yourgrau, W., and Mandelstam, S.: <i>Variational principles in dynamics and quantum theory</i> , 2nd edn	322
Zurmühl, R.: <i>Praktische Mathematik für Ingenieure und Physiker</i>	1273

Printed in England

TAYLOR & FRANCIS, LTD., Red Lion Court, Fleet Street, London, E.C.4